Fourth Edition

Catalytic Asymmetric Synthesis

Edited by:

Takahiko Akiyama • Iwao Ojima

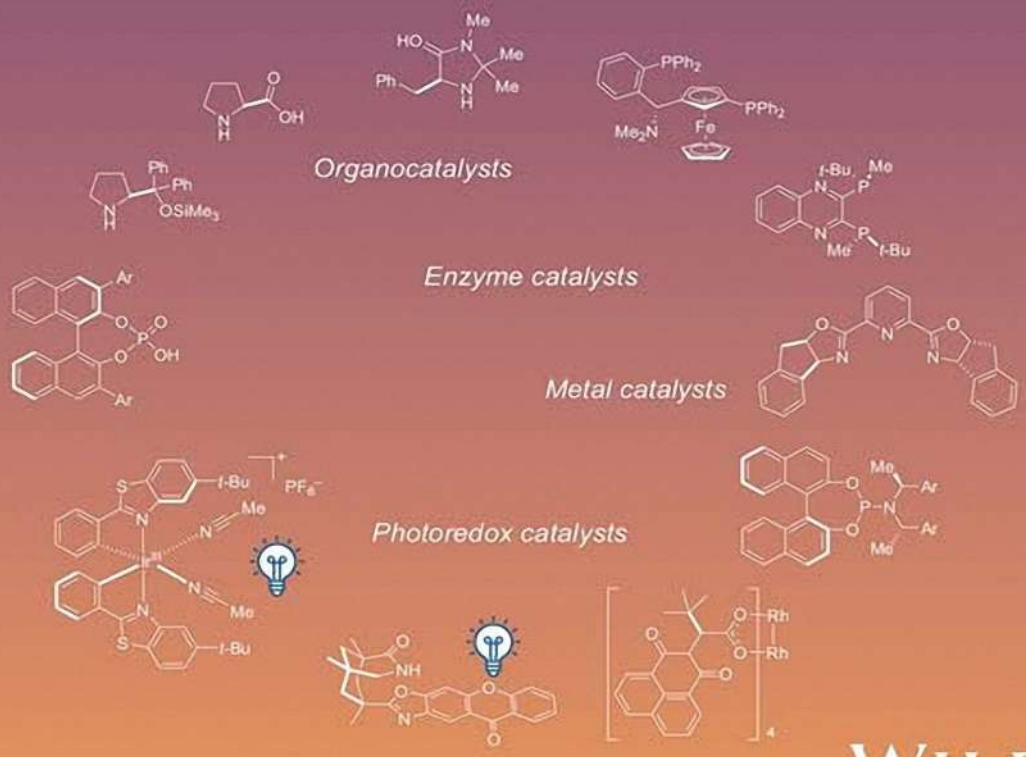

WILEY

CATALYTIC ASYMMETRIC SYNTHESIS

CATALYTIC ASYMMETRIC SYNTHESIS

Fourth Edition

Edited By
TAKAHIKO AKIYAMA
Department of Chemistry
Gakushuin University
Tokyo

IWAO OJIMA
Department of Chemistry
SUNY Stony Brook
New York

WILEY

This fourth edition first published 2022

Edition history
Catalytic Asymmetric Synthesis, 1st Edition, 1995, Ojima. ISBN: 978-0-471-18625-0
Catalytic Asymmetric Synthesis, 2nd Edition, 2004, Ojima. ISBN: 978-0-471-22054-1
Catalytic Asymmetric Synthesis, 3rd Edition, 2010, Ojima. ISBN 978-0-470-17577-4

Registered Office
John Wiley & Sons, Inc., 111 River Street, Hoboken, NJ 07030, USA

Editorial Office
John Wiley & Sons, Inc., 111 River Street, Hoboken, NJ 07030, USA

For details of our global editorial offices, customer services, and more information about Wiley products visit us at www.wiley.com.

Wiley also publishes its books in a variety of electronic formats and by print-on-demand. Some content that appears in standard print versions of this book may not be available in other formats.

Library of Congress Cataloging-in-Publication Data applied for:

Hardback ISBN: 9781119736394

Cover Design: Wiley
Cover Images: © AVIcon/Shutterstock; Courtesy of Takahiko Akiyama

Set in Times Ten 9/11pt by Straive, Pondicherry, India

CONTENTS

PREFACE

The first, second, and third editions of *Catalytic Asymmetric Synthesis* published in 1993, 2000, and 2010, respectively, were warmly received by research communities in academia and industries, from graduate students, research associates, faculty, staff, senior researchers, and others. *Catalytic Asymmetric Synthesis* has become a common tool for the synthesis of enantiopure compounds in both industry and academia.

The Nobel Prize in Chemistry 2001 was given to W. Knowles, K. B. Sharpless, and R. Noyori for their outstanding contributions to the advancement of catalytic asymmetric synthesis, using transition-metal catalysis. Quite recently it was announced that Benjamin List and David MacMillan won the Nobel Prize in Chemistry 2021 for their work on the development of asymmetric organocatalysis, using small organic molecule. This is the second Nobel Prize given to the field of asymmetric catalysis, following the Nobel Prize in Chemistry 2001, which clearly indicates the profound importance of asymmetric catalysis.

More than 10 years have passed after the third edition was published, and 2010s has witnessed revolutionary advancement of asymmetric catalysis. Therefore, the publication of the fourth edition of this book series, capturing the highly innovative progress in this field, deemed in demand and was fully justified. In order to cover the revolutionary advances in the last decade, Takahiko Akiyama joined as the leading editor in this fourth edition.

In the first and second editions, chiral metal-based catalysts played the central roles for the asymmetric synthesis because transition-metal-catalyzed enantioselective reactions were extensively studied, in particular, in the 1980s and 1990s. Organocatalysis, Lewis and Brønsted acids, C–H activation, carbon-heteroatom bond forming reactions, and enzyme-catalyzed reactions were introduced in the third edition.

After 2010, in addition to transition-metal catalyzed reactions, organocatalysis, including Brønsted acids and C–H activation reactions, has been making remarkable advances. Photoredox catalysis emerged as a useful new synthetic reaction mainly after 2008 and has been rapidly growing and has become a critical methodology. Because the chapters in the third edition are still very informative and the methodologies described therein are still inspiring and stimulating even today, those methodologies are considered "classics" in catalytic asymmetric synthesis.

We decided to edit a new book, which would be the most useful desktop reference book by covering new methodologies, but at the same time keeping the progress in the "classics" of the third edition. In order to capture the most significant progress in the 2010s, several new chapters of organocatalysis are introduced, i.e., enamine and iminium catalysis (Chapter 1), acid catalysis (Chapter 2), base catalysis (Chapter 3), phase transfer catalysis (Chapter 4), peptide catalysis (Chapter 5), carbene catalysis (Chapter 6), and hypervalent catalysis (Chapter 7). Photochemical reactions are also introduced, i.e., photoredox catalysis (Chapter 8), photoredox reactions in the absence of photoredox catalysis (Chapter 9), and [2 + 2] cycloaddition reactions (Chapter 10). The asymmetric C–H bond activation reactions are covered by two chapters, i.e., C(sp^2)–H bond (Chapter 11) and C(sp^3)–H bond (Chapter 12).

Asymmetric halogenation reaction, enzyme-catalyzed asymmetric synthesis, asymmetric hydrogenation, and asymmetric polymerization are presented in Chapters 13, 14, 15, and 21. The construction of noncentrochiral compounds are discussed in two chapters, i.e., axially chiral compounds (Chapter 19) and planar chiral and helically chiral compounds (Chapter 20). Finally, applications of continuous flow technology to catalytic asymmetric synthesis, which may dramatically change manufacturing processes for pharmaceutical drugs and chiral materials, is discussed in Chapter 21.

We sincerely hope that this book attracts the interest of broad range of synthetic, organic, medicinal, and material chemists, in particular, among the younger generation researchers in both academia and industry, who can bring in creative ideas and innovative approaches to *Catalytic Asymmetric Synthesis* and advance it to the new height.

Takahiko Akiyama
Iwao Ojima
November, 2021

PREFACE TO THE FIRST EDITION

Biological systems, in most cases, recognize a pair of enantiomers as different substances, and the two enantiomers will elicit different responses. Thus, one enantiomer may act as a very effective therapeutic drug, whereas the other enantiomer is highly toxic. The sad example of thalidomide is well-known. It is the responsibility of synthetic chemists to provide highly efficient and reliable methods for the synthesis of desired compounds in an enantiomerically pure state, that is, with 100% enantiomeric excess (% ee), so that we shall not repeat the thalidomide tragedy. It has been shown for many pharmaceuticals that only one enantiomer contains all of the desired activity, and the other is either totally inactive or toxic. Recent movements of the Food & Drug Administration (FDA) in the United States clearly reflect the current situation in "Chiral Drugs," that is, pharmaceutical industries will have to provide rigorous justification to obtain the FDA's approval of racemates. Several methods are used to obtain enantiomerically pure materials, which include classical optical resolution via diastereomers, chromatographic separation of enantiomers, enzymic resolution, chemical kinetic resolution, and asymmetric synthesis.

The importance and practicality of asymmetric synthesis as a tool to obtain enantiomerically pure or enriched compounds have been fully acknowledged to date by chemists in synthetic organic chemistry, medicinal chemistry, agricultural chemistry, natural products chemistry, pharmaceutical industries, and agricultural industries. This prominence is due to the explosive development of newer and more efficient methods during the last decade.

This book describes recent advances in catalytic asymmetric synthesis with brief summaries of the previous achievements as well as general discussions of the reactions. A previous book reviewing this topic, *Asymmetric Synthesis, Vol. 5—Chiral Catalysis*, edited by J. D. Morrison (Academic Press, Inc., 1985), compiles important contributions through 1982. Another book, *Asymmetric Catalysis*, edited by B. Bosnich (Martinus Nijhoff, 1986) also concisely covers contributions up to early 1984. In 1971, an excellent book, *Asymmetric Organic Reactions*, by J. D. Morrison and H. S. Mosher, reviewed all earlier important work on the subject and compiled nearly 850 relevant publications through 1968, including some papers published in 1969. In the early 1980s, a survey of publications dealing with asymmetric synthesis (in a broad sense) indicated that the total number of papers in this area of research published in the 10 years after the Morrison/ Mosher book, that is, 1971–1980, was almost the same as that of all the papers published before 1971. This doubling of output clearly indicates the attention paid to this important topic in 1970s. Since the 1980s, research on asymmetric synthesis has become even more important and popular when enantiomerically pure compounds are required for the total synthesis of natural products, pharmaceuticals, and agricultural agents. It would not be an exaggeration to say that the number of publications on asymmetric synthesis has been increasing exponentially every year.

Among the types of asymmetric reactions, the most desirable and the most challenging is *catalytic* asymmetric synthesis because one chiral catalyst molecule can create millions of chiral product molecules, just as enzymes do in biological systems. Among the significant achievements in basic research: (i) asymmetric hydrogenation of dehydroamino acids, a groundbreaking work by W.S. Knowles et al.; (ii)

the Sharpless epoxidation by K.B. Sharpless et al.; and (iii) the second-generation asymmetric hydrogenation processes developed by R. Noyori et al. deserve particular attention because of the tremendous impact that these processes have made in synthetic organic chemistry. Catalytic asymmetric synthesis often has significant economic advantages over stoichiometric asymmetric synthesis for industrial-scale production of enantiomerically pure compounds. In fact, a number of catalytic asymmetric reactions, including the "Takasago Process" (asymmetric isomerization), the "Sumitomo Process" (asymmetric cyclopropanation), and the "Arco Process" (asymmetric Sharpless epoxidation), have been commercialized in the 1980s. These processes supplement the epoch-making "Monsanto Process" (asymmetric hydrogenation), established in the early 1970s. This book uncovers other catalytic asymmetric reactions that have high potential as commercial processes. Extensive research on new and effective catalytic asymmetric reactions will surely continue beyond the year 2000, and catalytic asymmetric processes promoted by man-made chiral catalysts will become mainstream chemical technology in the twenty-first century.

This book covers the following catalytic asymmetric reactions: asymmetric hydrogenation (Chapter 1), isomerization (Chapter 2), cyclopropanation (Chapter 3), oxidations (epoxidation of allylic alcohols as well as unfunctionalized olefins, oxidation of sulfides, and dihydroxylation of olefins) (Chapter 4), hydrocarbonylations (Chapter 5), hydrosilylation (Chapter 6), carbon–carbon bond-forming reactions (allylic alkylation, Grignard cross-coupling, and aldol reaction) (Chapter 7), phase-transfer reactions (Chapter 8), and Lewis acid-catalyzed reactions (Chapter 9). The authors of the chapters are all world leaders in this field, who outline and discuss the essence of each catalytic asymmetric reaction. In addition, a convenient list of the chiral ligands appearing in this book, with citation of relevant references, is provided as an Appendix.

This book serves as an excellent reference for graduate students as well as chemists at all levels in both academic and industrial laboratories.

Iwao Ojima
March, 1993

LIST OF CONTRIBUTORS

Lutz Ackermann, Institut für Organische und Biomolekulare Chemie, Georg-August-Universität Göttingen, Göttingen, Germany and Wöhler Research Institute for Sustainable Chemistry (WISCh), Georg-August-Universität Göttingen, Göttingen, Germany

Takahiko Akiyama, Department of Chemistry, Gakushuin University, Tokyo, Japan

Andrés R. Alcántara, Department of Chemistry in Pharmaceutical Sciences, Section of Organic and Pharmaceutical Chemistry, Faculty of Pharmacy, Complutense University of Madrid, Madrid, Spain

Thorsten Bach, School of Natural Sciences, Department Chemie and Catalysis Research Center (CRC), Technische Universität München, Garching, Germany

Eva Bednářová, Department of Chemistry, Columbia University, New York, NY, USA

Jun Kee Cheng, Department of Chemistry, Southern University of Science and Technology, Shenzhen, China

Aurélie Claraz, Institut de Chimie des Substances Naturelles, Université Paris Saclay, Gif-sur-Yvette, France

Uttam Dhawa, Institut für Organische und Biomolekulare Chemie, Georg-August-Universität Göttingen, Göttingen, Germany

Yun E. Du, California Institute of Technology, Pasadena, CA, USA

Jorge Escorihuela, Department of Organic Chemistry, Pharmacy Faculty, University of Valencia, Valencia, Spain

Tyler J. Fulton, California Institute of Technology, Pasadena, CA, USA

Santos Fustero, Department of Organic Chemistry, Pharmacy Faculty, University of Valencia, Valencia, Spain

Luo Ge, Stratingh Institute for Chemistry, University of Groningen, Groningen, The Netherlands

Gonzalo de Gonzalo, Department of Organic Chemistry, University of Seville, Seville, Spain

Arnald Grabulosa, Departament de Química Inorgànica i Orgànica, Facultat de Química, Universitat de Barcelona, Barcelona, Spain, and Institut de Nanociència i Nanotecnologia (IN_2UB), Universitat de Barcelona, Barcelona, Spain

Syuzanna R. Harutyunyan, Stratingh Institute for Chemistry, University of Groningen, Groningen, The Netherlands

Freya M. Harvey, School of Natural Sciences, Department Chemie and Catalysis Research Center (CRC), Technische Universität München, Garching, Germany

Yujiro Hayashi, Department of Chemistry, Graduate School of Science, Tohoku University, Sendai, Japan

Kazuaki Ishihara, Graduate School of Engineering, Nagoya University, Nagoya, Japan

Haruro Ishitani, Green & Sustainable Chemistry Social Cooperation Laboratory, Graduate School of Science, The University of Tokyo, Tokyo, Japan

Loránd Kiss, Institute of Organic Chemistry, Research Centre for Natural Sciences, Budapest, Hungary

Shū Kobayashi, Department of Chemistry, School of Science, The University of Tokyo, Tokyo, Japan and Green & Sustainable Chemistry Social Cooperation Laboratory, Graduate School of Science, The University of Tokyo, Tokyo, Japan

Kazuaki Kudo, Institute of Industrial Science, The University of Tokyo, Tokyo, Japan

Azusa Kondoh, Graduate School of Science, Tohoku University, Sendai, Japan

Jie Li, State Key Laboratory of Fine Chemicals, Dalian University of Technology, Dalian, China

Xiao-Bing Lu, State Key Laboratory of Fine Chemicals, Dalian University of Technology, Dalian, China

Jiyuan Lyu, Institut de Chimie des Substances Naturelles, Université Paris Saclay, Gif-sur-Yvette, France

Dengke Ma, ICIQ – Institute of Chemical Research of Catalonia, Tarragona, Spain

Géraldine Masson, Institut de Chimie des Substances Naturelles, Université Paris Saclay, Gif-sur-Yvette, France

Mercedes Medio-Simón, Department of Organic Chemistry, Pharmacy Faculty, University of Valencia, Valencia, Spain

Paolo Melchiorre, ICIQ – Institute of Chemical Research of Catalonia, Tarragona, Spain and ICREA – Institució Catalana de Recerca i Estudis Avançats, Barcelona, Spain

Edward Miller, University of California, Berkeley, Berkeley, CA, USA

Patrick J. Moon, University of California, Berkeley, Berkeley, CA, USA

Attila M. Remete, Institute of Pharmaceutical Chemistry, University of Szeged, Szeged, Hungary and Interdisciplinary Excellence Centre, Institute of Pharmaceutical Chemistry, University of Szeged, Szeged, Hungary

Antoni Riera, Departament de Química Inorgànica i Orgànica, Facultat de Química, Universitat de Barcelona, Barcelona, Spain and Institute for Research in Biomedicine (IRB Barcelona), The Barcelona Institute of Science and Technology (BIST), Barcelona, Spain

Yonggui Robin Chi, Division of Chemistry and Biological Chemistry, School of Physical and Mathematical Sciences, Nanyang Technological University, Singapore, Singapore and Laboratory Breeding Base of Green Pesticide and Agricultural Bioengineering, Key Laboratory of Green Pesticide and Agricultural Bioengineering, Ministry of Education, Guizhou University, Guiyang, China

Tomislav Rovis, Department of Chemistry, Columbia University, New York, NY, USA

Yuki Saito, Department of Chemistry, School of Science, The University of Tokyo, Tokyo, Japan

Daniel M. Sedgwick, Department of Organic Chemistry, Pharmacy Faculty, University of Valencia, Valencia, Spain

Yangyang Shen, Department of Chemistry, Columbia University, New York, NY, USA

Takanori Shibata, Department of Chemistry and Biochemistry, Faculty of Science and Engineering, Waseda University, Tokyo, Japan

Brian M. Stoltz, California Institute of Technology, Pasadena, CA, USA

Bin Tan, Department of Chemistry, Southern University of Science and Technology, Shenzhen, China

Ken Tanaka, Department of Chemical Science and Engineering, Tokyo Institute of Technology, Tokyo, Japan

Masahiro Terada, Graduate School of Science, Tohoku University, Sendai, Japan

F. Dean Toste, University of California, Berkeley, Berkeley, CA, USA

Muhammet Uyanik, Graduate School of Engineering, Nagoya University, Nagoya, Japan

Xavier Verdaguer, Departament de Química Inorgànica i Orgànica, Facultat de Química, Universitat de Barcelona, Barcelona, Spain and Institute for Research in Biomedicine (IRB Barcelona), The Barcelona Institute of Science and Technology (BIST), Barcelona, Spain

Anton Vidal-Ferran, Departament de Química Inorgànica i Orgànica, Facultat de Química, Universitat de Barcelona, Barcelona, Spain and Catalan Institution for Research and Advanced Studies (ICREA), Barcelona, Spain and Institut de Nanociència i Nanotecnologia (IN_2UB), Universitat de Barcelona, Barcelona, Spain

Hongling Wang, Laboratory Breeding Base of Green Pesticide and Agricultural Bioengineering, Key Laboratory of Green Pesticide and Agricultural Bioengineering, Ministry of Education, Guizhou University, Guiyang, China

Tomasz Wdowik, Institut für Organische und Biomolekulare Chemie, Georg-August-Universität Göttingen, Göttingen, Germany

Thomas Hin-Fung Wong, ICIQ – Institute of Chemical Research of Catalonia, Tarragona, Spain

Shaohua Xiang, Department of Chemistry, Southern University of Science and Technology, Shenzhen, China

Jia-Lei Yan, Division of Chemistry and Biological Chemistry, School of Physical and Mathematical Sciences, Nanyang Technological University, Singapore, Singapore

Xiao Zhang, Department of Chemistry, Columbia University, New York, NY, USA

PART I

ASYMMETRIC ORGANOCATALYSIS

1

ASYMMETRIC ENAMINE AND IMINIUM ION CATALYSIS

Yujiro Hayashi
Department of Chemistry, Graduate School of Science, Tohoku University, Sendai, Japan

1.1. INTRODUCTION

Enamines are key reactive species in many asymmetric organocatalytic reactions. The field of asymmetric catalytic reactions involving an enamine as a reactive intermediate dates back to the seminal work in the 1970s on proline-mediated intramolecular aldol reaction of triketone reported by Hajos and Parrish at Hoffmann-La Roche [1] and Eder, Sauer, and Wiechert at Schering AG [2] (Eq. 1.1). In 2000, List, Lerner, and Barbas reported a proline-mediated intermolecular aldol reaction (Eq. 1.2) [3], in which enamine is a key intermediate. In the same year, MacMillan reported a Diels-Alder reaction catalyzed by a chiral imidazolidinone via an iminium ion as a reactive intermediate (Eq. 1.3) [4]. In these reactions, small organic molecules catalyze reactions enantioselectively. Since these discoveries, chemistry based on organocatalysts involving an enamine and an iminium ion as an intermediate has developed dramatically [5]. There are several advantages to performing reactions with organocatalysts: (i) exclusion of water and air is not necessary, (ii) the product is free from metal contamination, (iii) most of the organocatalysts are nontoxic, (iv) most reactions do not need low temperature or high temperature, and (v) it is easy to carry out the reaction on a large scale. Given these merits, many catalysts and reactions have been developed. In the previous book of this series published in 2010 [6], progress in the field of organocatalysis is nicely summarized up to 2010. In this chapter, a brief introduction to enamine and iminium ion species will be presented, including work before 2010, and more recent developments in this field will be expanded. Reactions using a combination of organocatalyst and photocatalyst, which have been developed recently, will be described in Chapter 9 of this book.

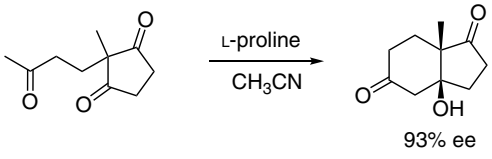

(1.1)

Catalytic Asymmetric Synthesis, Fourth Edition. Edited by Takahiko Akiyama and Iwao Ojima.

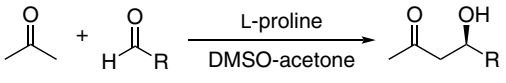

(1.2)

R = 4-$NO_2C_6H_4$, 68%, 76% ee R = *i*-Pr, 97%, 96% ee
R = Ph, 62%, 60% ee

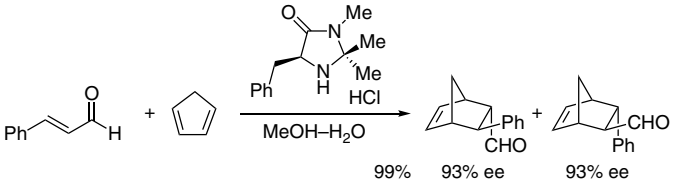

(1.3)

1.2. REPRESENTATIVE ORGANOCATALYSTS

1.2.1. Introduction

Enamines are generated from aldehydes or ketones upon reaction with secondary or primary amines, and the enamine can react with an electrophile to give an α-functionalized derivative of the carbonyl compounds (Eq. 1.4).

α,β-Unsaturated aldehydes or ketones also react with secondary or primary amines to generate an iminium ion, which has lower LUMO (lowest unoccupied molecular orbital) level compared with the parent α,β-unsaturated carbonyl compound. A nucleophile reacts with the iminium ion to afford a β-functionalized derivative of the carbonyl compound (Eq. 1.5).

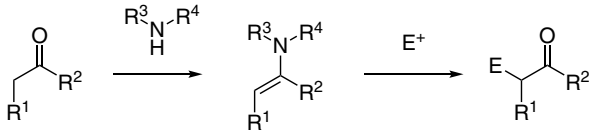

(1.4)

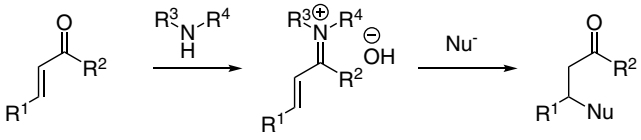

(1.5)

Enamine and iminium ions are reactive species and many reactions involving these intermediates have been developed. Representative organocatalysts that have been used to generate enamines and iminium ions are presented in Figure 1.1.

Proline is a secondary amine catalyst that was first used in the intramolecular aldol reaction in the 1970s (Eq. 1.1). It is a bifunctional catalyst, possessing an amine moiety and an acid moiety (carboxylic acid) *vide infra* [3]. Imidazolidinone catalyst, which was developed by MacMillan, is a secondary amine catalyst prepared from phenylalanine [4]. Diarylprolinol silyl ether [7], which was developed by Jørgensen [8] and Hayashi [9] independently at the same time, is synthesized from proline; it is also a secondary amine catalyst. These two catalysts are not bifunctional catalysts, and do not possess an acid moiety. Cinchona amine-based catalysts [10] are prepared from cinchona alkaloids, which are primary amines. This catalyst has several functional groups, and acts as a bifunctional catalyst.

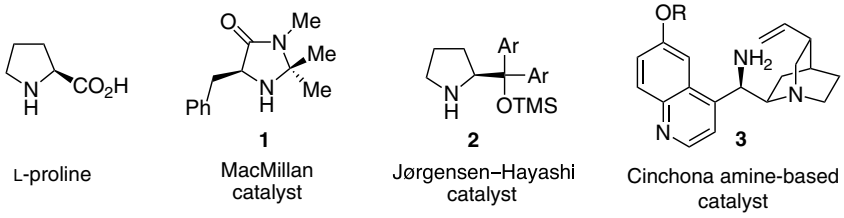

Figure 1.1. Representative organocatalysts.

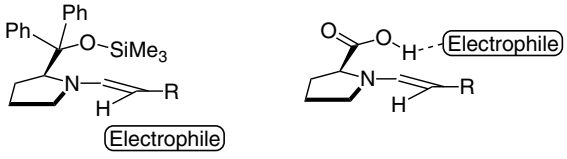

Figure 1.2. The reaction of enamines generated from diphenylprolinol silyl ether and proline.

The design concepts underlying bifunctional and monofunctional organocatalysts are different. Diphenylprolinol silyl ether, a monofunctional catalyst, reacts with an aldehyde to generate an enamine, in which one of the enantiofaces of the enamine is completely shielded by the bulky diphenyltrimethylsiloxymethyl moiety, and an electrophile approaches from the opposite side of this bulky substituent (Figure 1.2). Thus, the steric shielding of one of the enantiofaces is a key for the high enantioselectivity. Irrespective of the electrophile, high enantioselectivity is expected because the enantioface selectivity of the nucleophile is controlled by the catalyst. This is a contrast to bifunctional catalysts such as proline, in which an acid moiety activates the electrophile. Thus, the most suitable catalyst for a given reaction depends on the electrophile.

1.2.2. Reactivity of Diphenylprolinol Silyl Ether Catalyst and MacMillan's Catalyst

Diphenylprolinol silyl ether catalyst and MacMillan's catalyst are widely used in reactions involving enamine or iminium ion intermediates. In this section, the reactivity of these catalysts will be discussed.

Mayr investigated the nucleophilicity (N) of enamines, and the electrophilicity (E) of iminium ions of several pyrrolidines and imidazolidinones (Figure 1.3) [11]. For enamines, the nucleophilicity is evaluated by the reaction with diarylcarbenium ions, and it correlates poorly with the Brønsted basicities. The enamine, which is derived from diphenylprolinol silyl ether catalyst **2**, is almost two orders of magnitude less reactive than the corresponding enamine prepared from pyrrolidine. The reduction of the reactivity is primarily due to the electron-withdrawing inductive effect of the trimethylsiloxybenzhydryl group in diphenylprolinol silyl ether catalyst. The reactivity of the enamine generated from MacMillan's catalyst **1** is another two to three orders of magnitude less reactive relative to the enamine of diphenylprolinol silyl ether catalyst, because of the inductive electron-withdrawing effect of the extra endocyclic amide group in the catalyst, the pyramidalization of the enamine nitrogen, and the steric shielding of both faces of the C=C bond by the two alkyl groups at the 2-position of the imidazolidinone ring.

In the case of iminium ions, the iminium ion generated from diphenylprolinol silyl ether is 20 times more electrophilic than the iminium ion derived from the parent pyrrolidine because of the electron-withdrawing substituents. The iminium ion of MacMillan's catalyst, which is useful for the Diels-Alder reaction, is more reactive than the iminium ion derived from diphenylprolinol silyl ether.

These investigations indicate that MacMillan's catalyst is more electron deficient, and that its iminium ion is reactive because of the lower LUMO level. Diphenylprolinol silyl ether catalyst possesses suitable nucleophilicity and electrophilicity of its enamine and its iminium ion, respectively. Thus, this catalyst is effective for domino reactions (see Figure 1.3).

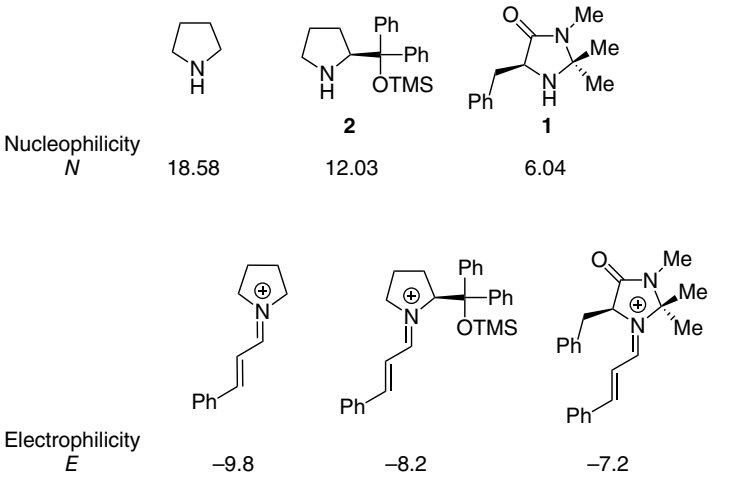

Figure 1.3. Nucleophilicity and electrophilicity of enamines and iminium ions. Source: Based on [11].

1.2.3. Cinchona Amine-Based Catalysts

Some secondary amine catalysts, such as diphenylprolinol silyl ether, are effective catalysts in Michael reactions using an aldehyde as a Michael donor (see Scheme 1.1), but these catalysts are not effective in Michael reactions using a ketone as a Michael donor because generation of an enamine from a ketone using diphenylprolinol silyl ether is hindered by its steric bulk. On the other hand, a primary amine can easily generate an enamine from a ketone. Primary amine catalysts derived from cinchona alkaloids have enabled the stereoselective functionalization of a variety of sterically hindered carbonyl compounds, which cannot be realized by secondary amine catalysts (Scheme 1.1) [10]. Moreover, primary amine catalysts can activate structurally substituted substrates such as α-branched substituted aldehydes and ketones. They also activate α-substituted α,β-unsaturated aldehydes and ketones. The reactions of these substrates using chiral cyclic secondary amine catalysts are difficult.

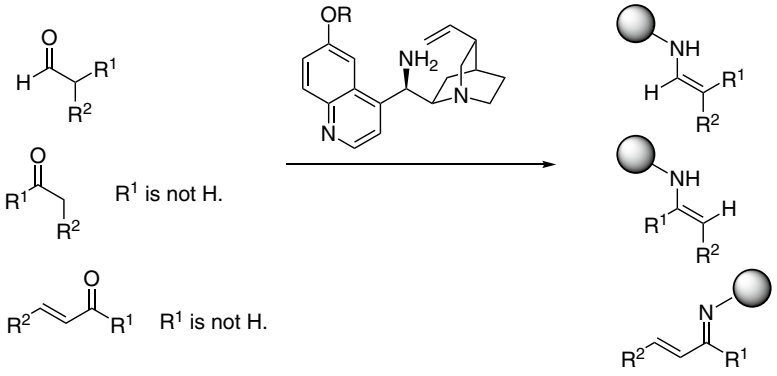

Scheme 1.1. Reactions of cinchona alkaloid catalysts. Source: Based on [10].

Cinchona alkaloid catalysts act as efficient bifunctional catalysts. They possess a primary amine moiety that can react with aldehydes, ketones, and α,β-unsaturated carbonyl compounds to generate enamines and imines. The catalysts have a basic quinuclidine moiety, which acts as a base, and a hydroxy or alkoxy group on C9, which can make a hydrogen-bonding interaction. Thus, they can simultaneously activate both electrophilic and nucleophilic reagents in a reaction.

1.3. ENAMINE

1.3.1. Aldol Reaction

Aldol reaction is one of the most important carbon–carbon bond-forming reactions in synthetic organic chemistry, and the application of organocatalysts in this reaction has been investigated intensively [12]. The basic design of catalysts for aldol reactions is a bifunctional catalyst such as proline, with acid and basic moieties (Figure 1.4) [13]. The amine moiety reacts with a carbonyl group to generate an enamine, while the acid moiety activates the electrophile. Based on this concept, many bifunctional aldol catalysts have been developed.

Although proline is an effective and inexpensive organocatalyst, its solubility in organic solvents is poor; rather large loading of the catalyst is necessary, and applicable aldol reactions are limited. This has driven the development of organocatalysts that are more reactive and selective than proline, and the substrate scope has been expanded greatly. These developments have been nicely summarized in several reviews [12].

In the proline-mediated aldol reactions, the *anti*-isomer was obtained predominantly, which is explained by List–Houk model (Figure 1.4). In most of the aldol reactions catalyzed by organocatalyst, the *anti*-isomer is generated predominantly. The development of *syn*-selective and enantioselective aldol reactions catalyzed by organocatalyst is a challenging problem. Maruoka developed a biphenyl-based axially chiral amine with a triflamide moiety (Eq. 1.6). This catalyst is a *syn*-selective catalyst and gave excellent enantioselectivity [14].

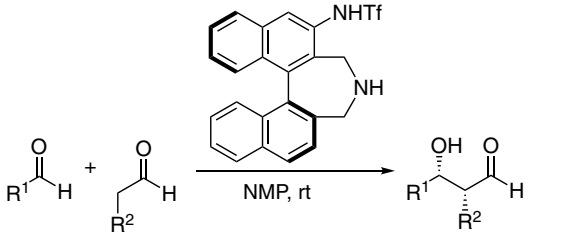

(1.6)

Acetaldehyde is a synthetically useful aldehyde that can act as both a nucleophile and an electrophile. Given its high reactivity, it is difficult to use acetaldehyde as a nucleophile in the aldol reaction even with a metal catalyst. Hayashi developed diarylprolinol, which is an effective catalyst with acetaldehyde as a nucleophile (Eq. 1.7) [15]. This catalyst is also effective in the other cross-aldol reactions of two different aldehydes [16].

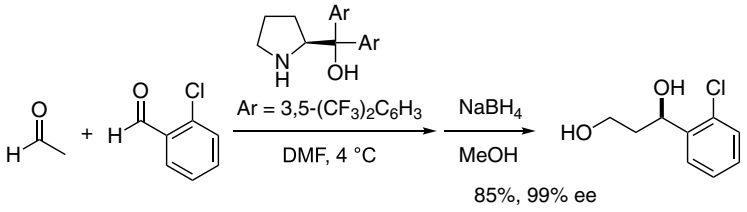

(1.7)

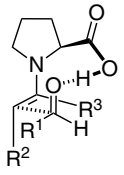

Figure 1.4. Transition state for the aldol reaction catalyzed by proline. Source: Based on [13].

1.3.2. Mannich Reaction

The Mannich reaction is important for the construction of nitrogen-containing molecules. List reported the three-component Mannich reaction of aldehyde, ketone, and anisidine catalyzed by proline in 2000 (Eq. 1.8) [17]. Barbas reported the *syn*-selective Mannich reaction of *N*-PMP-protected α-imino ethyl glyoxylate and an aldehyde, or ketone, in 2002 (Eq. 1.9) [18]. Whereas *syn*-selectivity is explained by the model shown in Figure 1.5, the *anti*-selective Mannich reaction is a challenging task. Nevertheless, an axially chiral sulfonamide, developed by Maruoka, was successfully used to afford *anti*-selective Mannich products [19]. In addition to simple aliphatic aldehydes, an α-amino acetaldehyde as a nucleophile afforded an *anti*-vicinal diamine derivative (Eq. 1.10).

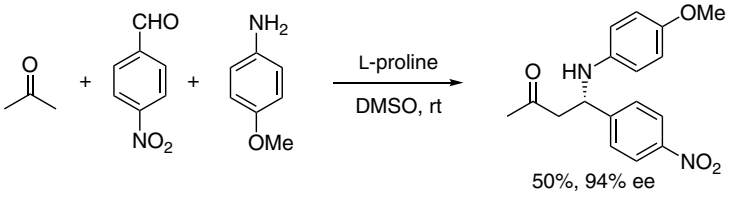

(1.8)

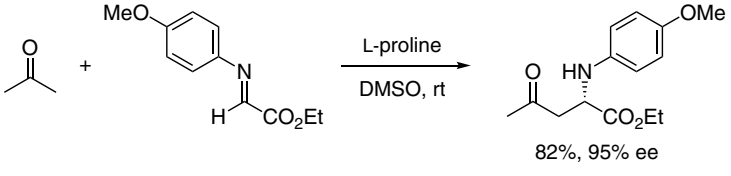

(1.9)

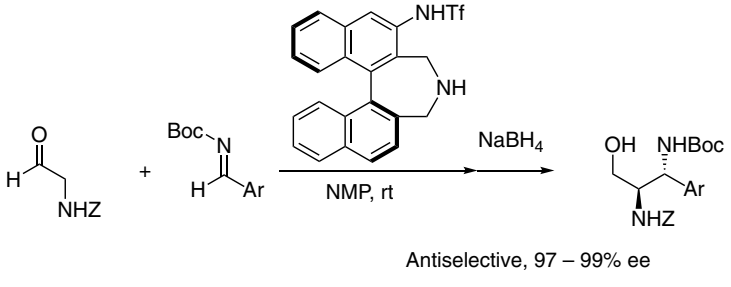

(1.10)

Instead of using a bifunctional catalyst, organocatalysts without an acid moiety, such as diphenylprolinol silyl ether, are effective catalysts in the Mannich reaction to afford the *anti*-product selectively with excellent enantioselectivity (Eq. 1.11) [20].

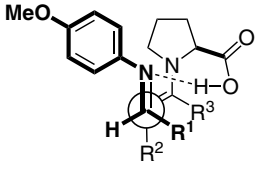

Figure 1.5. Transition state of the Mannich reaction.

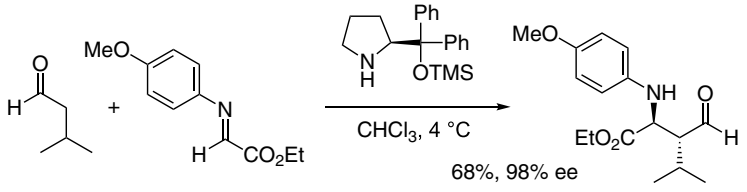

(1.11)

1.3.3. Other Functionalization of the α-Position of Carbonyl Groups

Bifunctional organocatalysts are effective not only for the aldol and Mannich reactions but also for functionalization of the α-position of carbonyl compounds. α-Fluorination [21], α-bromination [22], and α-iodination [23] of aldehydes are successfully carried out by the use of organocatalyst. Azodicarboxylate is used in the α-amination of aldehydes catalyzed by proline [24]. α-Aminoxylation of carbonyls is catalyzed by proline [25] and proline salt [26] using nitrosobenzene as an electrophile. These reactions are summarized in the previous book [6].

1.3.4. Michael Reaction

Organocatalysts are also useful for the addition of carbonyl compounds to electron-deficient alkenes, known as the Michael reaction. The reaction of aldehydes and nitroalkenes catalyzed by organocatalyst is a well-investigated reaction. In 2005, diphenylprolinol silyl ether was applied to this reaction, which afforded a Michael product with excellent diastereo- and enantioselectivity (Eq. 1.12) [9]. It was also found that an acid additive accelerates the reaction, and the effect of the acid has been investigated in detail (Scheme 1.2) [27]. An enamine and a nitroalkene react to afford cyclobutane **A** and dihydro-oxazine N oxide **B** as initial products, which were converted into the Michael product, and acid affects this conversion step.

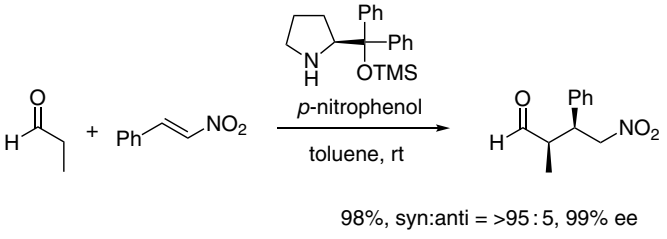

(1.12)

As a Michael acceptor, not only nitroalkene but also vinyl sulfones [28], β-substituted α-nitroacrylates [29], dicyanoalkenes [30], and β-substituted α-cyano α,β-unsaturated esters [31] can be successfully employed to afford the Michael products with excellent diastereo- and enantioselectivity (Eq. 1.13).

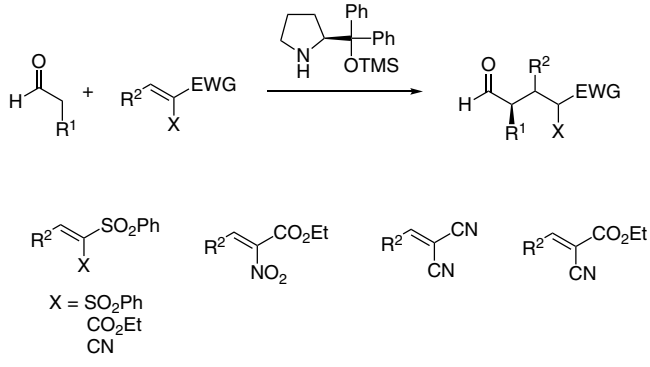

(1.13)

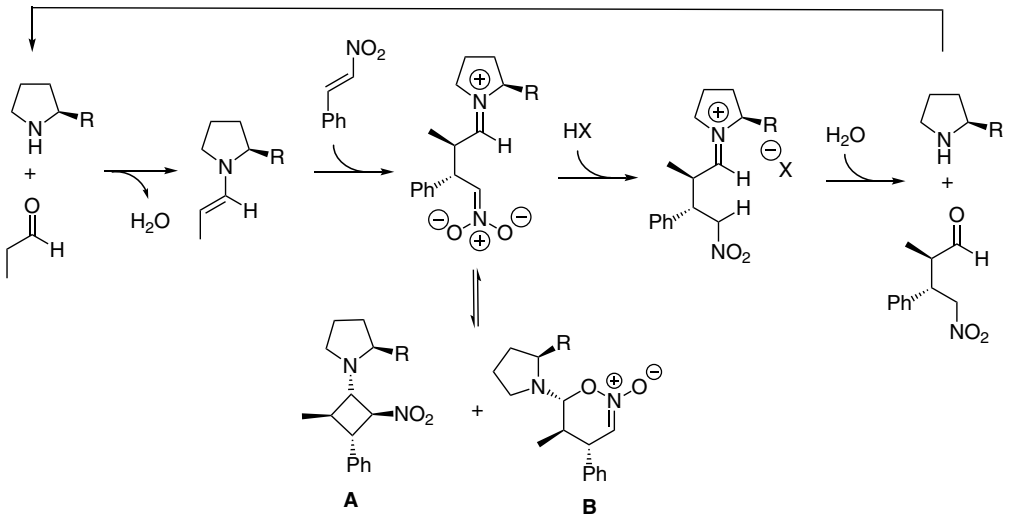

Scheme 1.2. The reaction mechanism of the Michael reaction of aldehyde and nitroalkene. Source: Based on [27].

Low catalyst loading and the development of a reactive catalyst are important issues for the asymmetric synthesis of chiral molecules. For the Michael reaction of aldehydes and nitroalkenes, Wennemers reported a very active tripeptide catalyst H-D-Pro-Pro-Glu-NH_2, which catalyzes the Michael reaction of butanal and nitrostyrene in the presence of only 0.1 mol% of the catalyst (Eq. 1.14) [32]. This catalyst is a bifunctional catalyst, possessing a secondary amine moiety and an acid moiety.

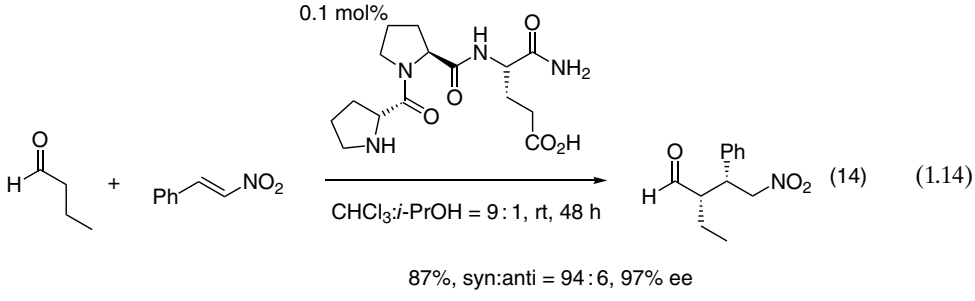

(14) (1.14)

1.3.5. Dienamine and Trienamine as an Intermediate [33]

Enamine chemistry was extended to dienamine chemistry: diarylprolinol silyl ether reacts with an α,β-unsaturated aldehyde to generate an iminium ion, which is further converted into a dienamine. As dienamines are electron-rich, they act as reactive dienes in the Diels-Alder reaction. The 1,4-position of the original aldehyde reacts with a dienophile. Jørgensen reported the reaction of a dienamine with azodicarboxylate, in which only the s-*cis* dienamine from a mixture of s-*cis* and s-*trans* isomers reacts in a concerted fashion (Diels-Alder reaction) to afford the product with excellent enantioselectivity (Eq. 1.15) [34].

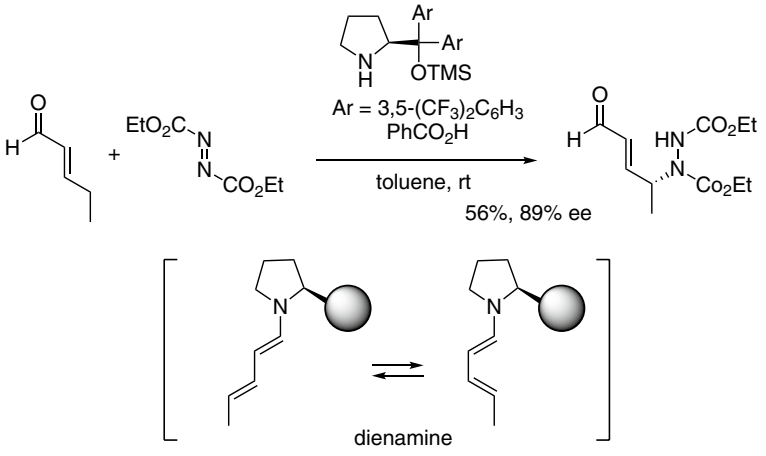

(1.15)

A dienamine is successfully utilized in the enantioselective synthesis of a key intermediate of 14β-steroids by the reaction of an enal with a cyclic dienophile in the presence of diphenylprolinol silyl ether (Eq. 1.16). This reaction allows easy access to an optically active steroid core with a variety of substituents in the A ring in high yields and up to more than 99% ee. (+)-Estrone was efficiently synthesized by using this reaction as a key step [35].

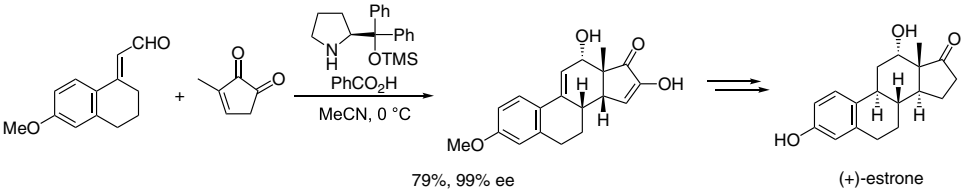

(1.16)

This dienamine system was further extended to trienamine chemistry. Chen and Jørgensen reported the generation of an electron-rich trienamine from a polyconjugated 2,4-dienal. By a reaction with a dienophile, a cycloaddition reaction proceeded to afford a spirocyclic oxindole possessing a cyclohexene moiety with an exclusive β,ε-regioselectivity and excellent stereoselectivity (Eq. 1.17) [36].

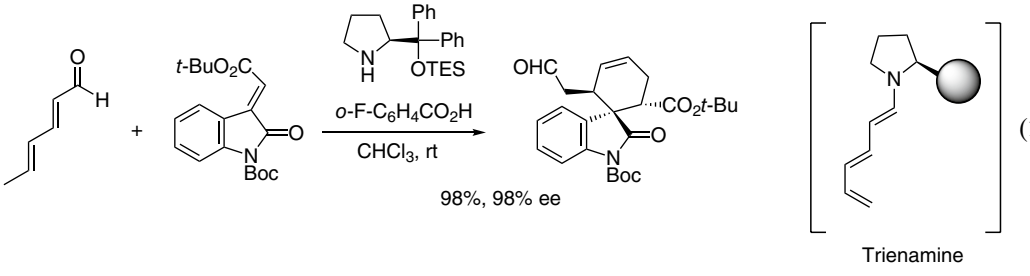

(1.17)

1.4. IMINIUM ION

1.4.1. Introduction of an Iminium Ion

MacMillan reported the Diels-Alder reaction using a chiral imidazolidinone, which reacts with an α,β-unsaturated aldehyde to afford an iminium ion. The iminium ion is a highly electron-withdrawing group; its alkene has a lower LUMO level than the parent α,β-unsaturated aldehyde. Thus, the Diels-Alder

reaction proceeds via the iminium ion intermediate not from the α,β-unsaturated aldehyde. By the appropriate design of the chiral amine moiety, an enantioselective reaction can be realized. In fact, the chiral imidazolidinone catalyst afforded an excellent enantioselectivity (see above; Eq. 1.3) [4]. Many reactions have been developed involving the iminium ion as a key intermediate.

1.4.2. Two Reaction Paths

Two reaction paths, Diels-Alder type reaction and Michael reaction, involve an iminium ion as a reactive intermediate [37]. These two reaction paths will be discussed in the reactions of cinnamaldehyde and cyclopentadiene catalyzed by diarylprolinol silyl ether (Table 1.1).

The Diels-Alder reaction was catalyzed by diarylprolinol silyl ether **6**, with trifluoromethyl groups on the aryl moiety (Figure 1.6) with a combination of a strong acid such as CF_3CO_2H [38]. It should be noted that the *exo*-isomer was obtained predominantly.

On the other hand, when a mixture of cinnamaldehyde and cyclopentadiene was treated with diphenylprolinol silyl ether **5** (Figure 1.6) with a combination of *p*-nitrophenol or NaOAc, Michael products were obtained with excellent enantioselectivity without formation of the Diels-Alder products [39]. Iminium ions are key intermediates in both reactions.

As the pyrrolidine moiety of catalyst **6** is more electron deficient than that of catalyst **5** because of the electron-withdrawing CF_3 group, the LUMO of the iminium ion generated from **6** is lower than that of the iminium ion generated from **5**. The Diels-Alder reaction proceeds smoothly when the LUMO of the dienophile is lower. Thus, the Diels-Alder reaction proceeded in the case of **6** (Scheme 1.3). On the other hand, in the Michael reaction (Scheme 1.4), after the formation of the iminium ion, counterion (OH^-) reacts with *p*-nitrophenol to generate phenoxide, which reacts with cyclopentadiene to generate an anion of cyclopentadiene. This anionic nucleophile reacts with the iminium ion to afford the Michael product. For the generation of anionic nucleophile, the nucleophile is limited to the active methylene compounds, and a strong acid cannot be employed.

TABLE 1.1. The two reaction paths in the reaction of cinnamaldehyde and cyclopentadiene

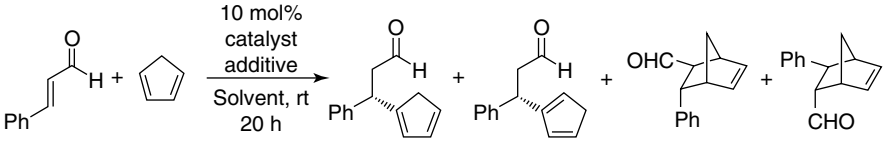

3a **3b** **4-exo** **4-endo**

			3			4		
Catalyst	Solvent	Additive	Yield/%	a:b	ee/%	Yield/%	exo/endo	ee/%
5	MeOH	*p*-nitrophenol	84	70 : 30	92	0		
5	MeOH	NaOAc	81	64 : 36	92	0		
5	toluene		0			0		
6	toluene	CF_3CO_2H	0			80	85 : 15	97/88

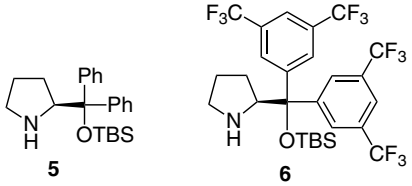

5 **6**

Figure 1.6. Diarylprolinol silyl ether in this study.

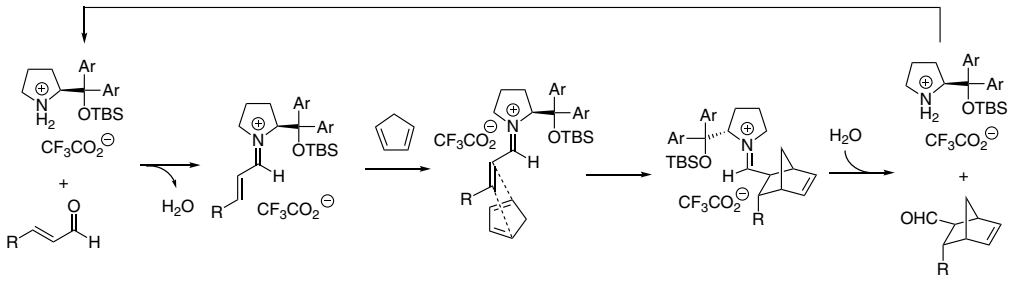

Scheme 1.3. The reaction mechanism of the Diels-Alder reaction.

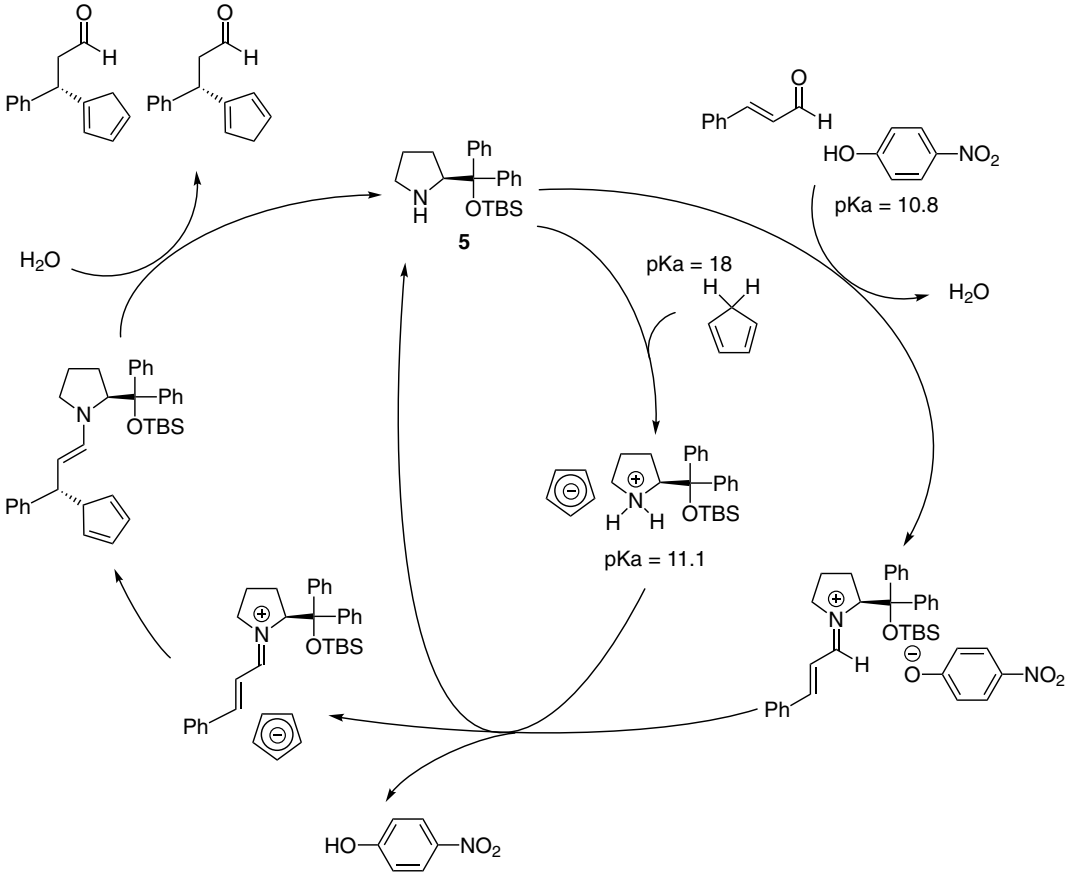

Scheme 1.4. The reaction mechanism of the Michael reaction.

1.4.3. Diels-Alder Type Reaction

The Friedel-Craft reaction belongs to the Diels-Alder type set of reactions, and pyrroles, indoles, and aniline react readily with α,β-unsaturated aldehydes in the presence of MacMillan's catalyst to afford the products with excellent enantioselectivity (Eq. 1.18) [40]. [3+2] Nitrone cycloaddition also belongs to this type of reaction [41].

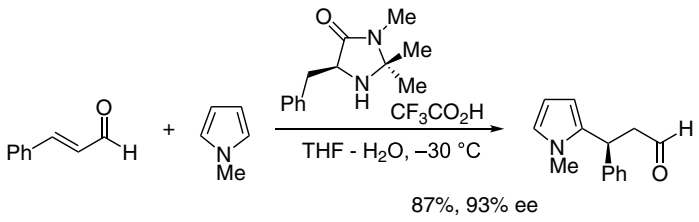

(1.18)

1.4.4. Michael Reaction

Active methylene compounds such as nitroalkanes (Eq. 1.19), malonates, and β-keto esters are suitable Michael donors in the Michael reaction using α,β-unsaturated aldehydes as a Michael acceptor, catalyzed by diphenylprolinol silyl ether catalyst [42].

Oximes, such as benzaldehyde oxime, also act as suitable Michael donors to afford β-hydroxy carbonyl compounds after hydrogenolysis (Eq. 1.20) [43]. Given that asymmetric oxy-Michael reactions are difficult because of the facile retro-Michael reaction, this two-step reaction is synthetically useful.

Thiol is also a good Michael donor and chiral β-thio aldehydes were obtained with excellent enantioselectivity [44].

Aza-Michael reactions were also reported using thiazoles, tetrazoles, and succinimides, and the products were generated with excellent enantioselectivity [45].

Construction of a C–P bond by the Michael reaction was reported. Asymmetric hydrophosphination proceeded by a reaction of diphenylphosphine and α,β-unsaturated aldehydes catalyzed by diarylprolinol silyl ether (Eq. 1.21) [46].

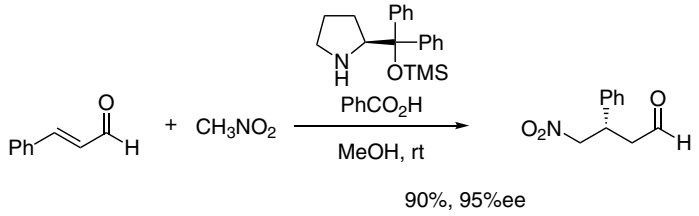

(1.19)

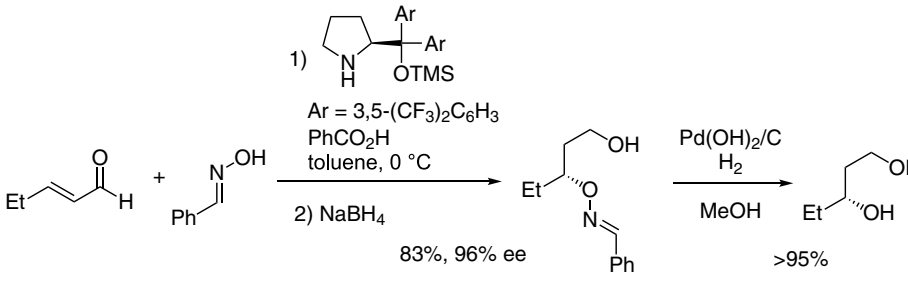

(1.20)

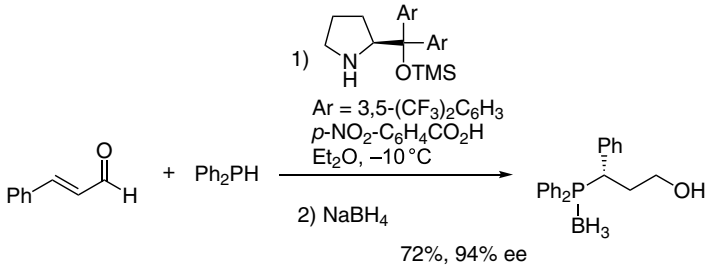

(1.21)

Nonactivated ketones such as cyclohexanone are also employed as Michael donors in the reaction of α,β-unsaturated aldehydes catalyzed by a combination of diphenylprolinol silyl ether and hydroxyproline (or pyrrolidine), to afford the Michael products with excellent enantioselectivity (Eq. 1.22) [47]. The key nucleophile is not an enamine but an enolate, which is generated from a secondary amine by combination with *p*-nitrophenol (Eq. 1.23) [48].

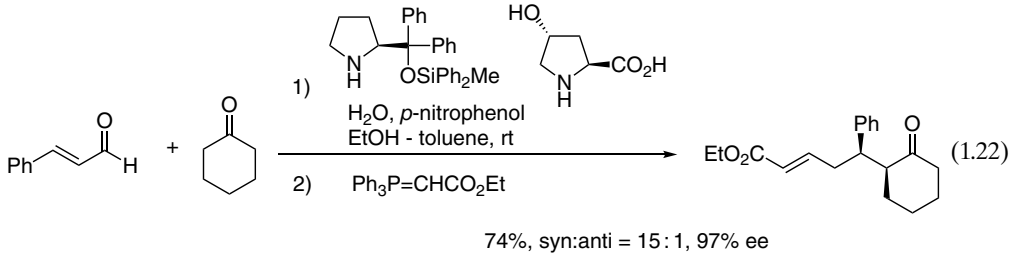

(1.22)

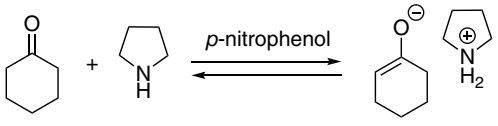

(1.23)

1.5. DOMINO REACTION

1.5.1. Introduction of Domino (Cascade and Tandem) Reactions

Domino reactions offer a powerful way to construct complex structures in a single reaction vessel; each reaction occurs as a consequence of the intermediates generated in previous steps without changing any reaction conditions [49]. Most of the asymmetric domino reactions are composed of two reactions occurring one after the other. Organocatalysts can also be effective in domino reactions [50]. List [51], MacMillan [52], and Jørgensen [44] reported the domino iminium/enamine reaction at the same time in 2005. List reported conjugate reduction–Michael cyclization of enal enones, in which treatment of the enal enone with Hantzsch dihydropyridine in the presence of a catalytic amount of MacMillan's catalyst provided cyclic keto aldehydes with excellent enantioselectivity (Eq. 1.24). MacMillan reported an iminium/enamine domino reaction employing several nucleophiles and electrophiles catalyzed by MacMillan's catalyst (Eq. 1.25). Jørgensen reported that a domino reaction of conjugate addition of thiol and amination, which was catalyzed by diarylprolinol silyl ether, afforded 1,2-aminothiol derivatives in nearly optically pure form (Eq. 1.26).

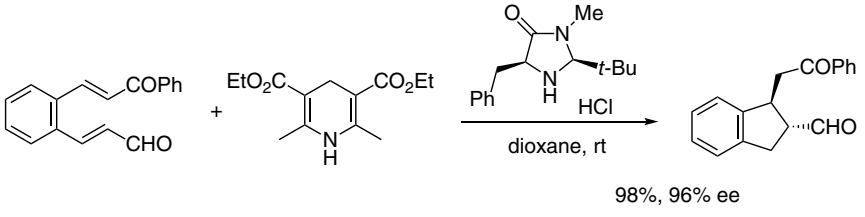

(1.24)

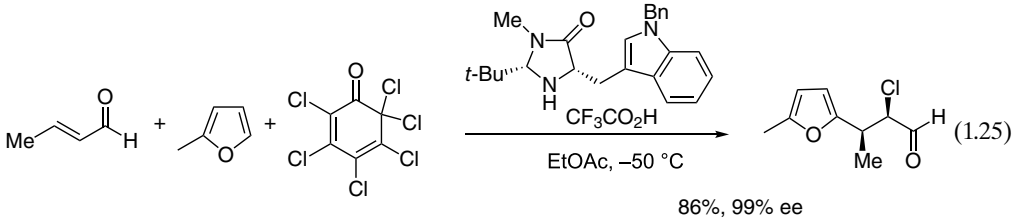

(1.25)

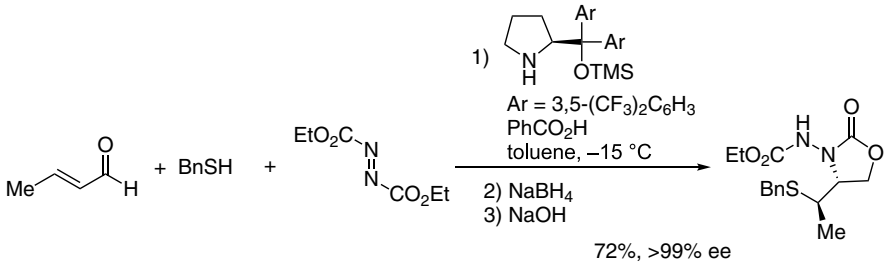

(1.26)

1.5.2. Enders' Work

In 2006, Enders reported a seminal paper on organocatalyst-mediated domino reaction (Eq. 1.27) [53]. He reported an excellent domino reaction catalyzed by diphenylprolinol silyl ether, wherein three reactions such as Michael/Michael/intramolecular aldol condensation reactions take place in one pot to provide cyclohexene carbaldehydes bearing four stereogenic centers with excellent stereocontrol. Rather complex skeletons were synthesized only by mixing the substrates via a domino reaction.

Enders' group reported many useful domino reactions [54]. For instance, functionalized complex tricyclic polyethers were synthesized by one-pot quadruple domino oxa-Michael/Michael/Michael/aldol condensation/hetero-Diels-Alder reaction in nearly enantiomerically pure form (Eq. 1.28) [55]. Tetracyclic pyridocarbazole derivatives were synthesized by the three-component triple cascade reaction such as Diels-Alder/aza-Michael/intramolecular aldol condensation reactions with excellent enantioselectivity (Eq. 1.29) [56].

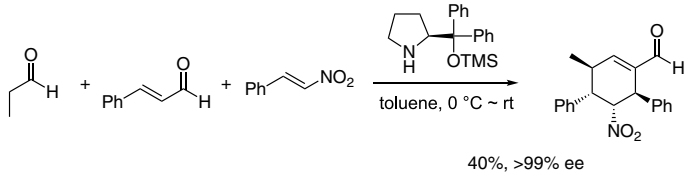

(1.27)

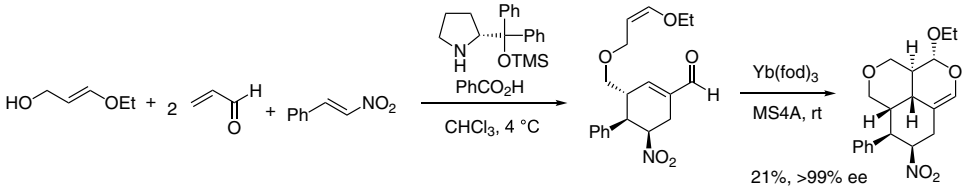

(1.28)

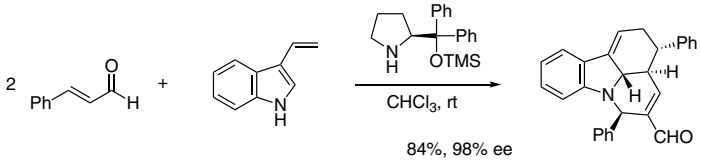

(1.29)

1.6. DOMINO REACTION AND TOTAL SYNTHESIS

Many domino reactions have been developed that use organocatalysts. Domino reaction catalyzed by organocatalysts can generate complex structures in a single reaction vessel. This is a very powerful method for the synthesis of natural products and drugs [57]. Organocatalytic domino reactions have been successfully applied to natural product synthesis. In this section, selected domino reactions will be described with an application to total synthesis.

1.6.1. Steroid Skeleton

Hong reported the synthesis of a steroid skeleton by a one-pot reaction starting from an α,β-unsaturated aldehyde and a nitroalkane (Eq. 1.30). A domino Michael/Michael reaction proceeded, followed by aldol and Henry reaction in a one-pot operation, to afford a steroid skeleton with excellent enantioselectivity [58].

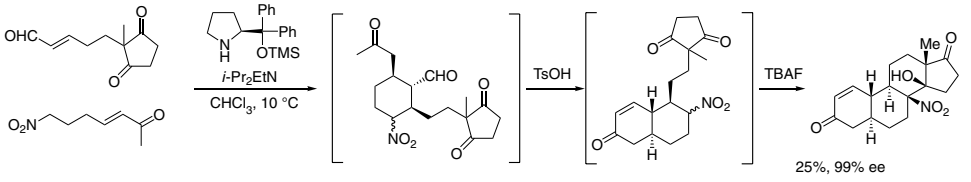

(1.30)

1.6.2. α-Skytanthine and Quinine

Ishikawa reported a domino Michael reaction/hemiacetal formation/dehydration for the synthesis of C4-alkyl substituted chiral piperidines using diphenylprolinol silyl ether (Eq. 1.31) [59]. This is a formal aza [3+3] cycloaddition reaction with aliphatic α,β-unsaturated aldehydes and thioamide derivatives. Thioamide is a reactive nucleophile. The reaction proceeded efficiently, and only 0.1 mol % catalyst loading is sufficient for a multigram-scale synthesis to complete within a suitable reaction time. This reaction was applied to the total synthesis of several alkaloids such as α-skytanthine [59a] and quinine [59b].

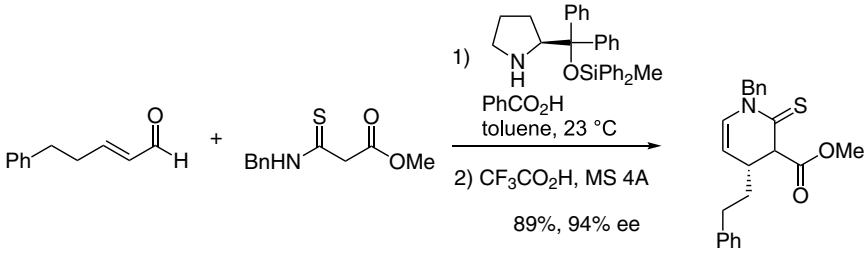

(1.31)

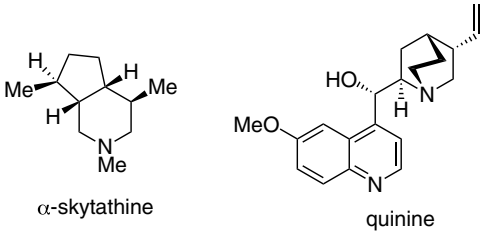

α-skytathine quinine

1.6.3. (+)-Lycoposerramine Z

Bradshaw and Bonjoch reported a domino Michael/aldol (Robinson annulation)/aza-Michael reaction to afford a substituted decahydroquinoline with a high diastereo- and enantioselectivity in a one-pot operation (Eq. 1.32). (+)-Lycoposerramine Z was synthesized from this intermediate [60].

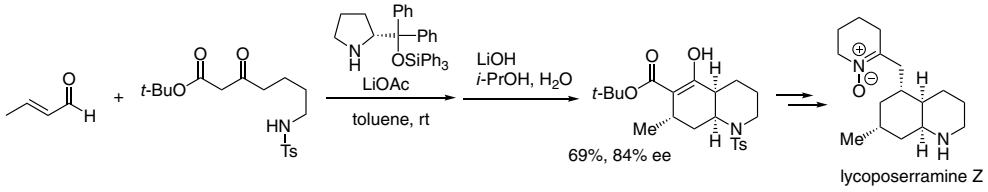

(1.32)

1.6.4. Estradiol Methyl Ether

Bicyclo[4.3.0]none derivatives, which are C and D rings of the steroids, were synthesized as a single isomer with excellent enantioselectivity by diphenylprolinol silyl ether mediated Michael reaction of nitroalkane possessing a diketone moiety and an α,β-unsaturated aldehyde, followed by aldol reaction (Eq. 1.33). This domino reaction was used as a key reaction for the total synthesis of estradiol methyl ether, which was synthesized using five reaction vessels with four purifications [61].

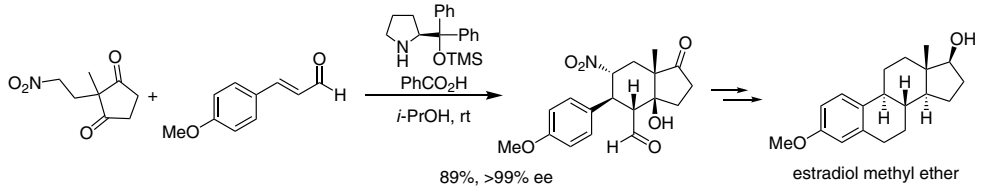

(1.33)

1.6.5. MacMillan's Alkaloid Synthesis

MacMillan reported the domino Diels-Alder reaction/β-elimination of methyl selenide/aza-Michael reaction to afford a spiroindoline intermediate (Eq. 1.34). The first Diels-Alder reaction and the third aza-Michael reaction were catalyzed by the same MacMillan's catalyst via an iminium ion as an intermediate, and an excellent enantioselectivity was obtained. From the intermediate, (-)-strychnine, (-)-akuamicine, (+)-aspidospermidine, (+)-vincadifformine, (-)-kopsinine, and (-)-kopsanone were synthesized efficiently [62].

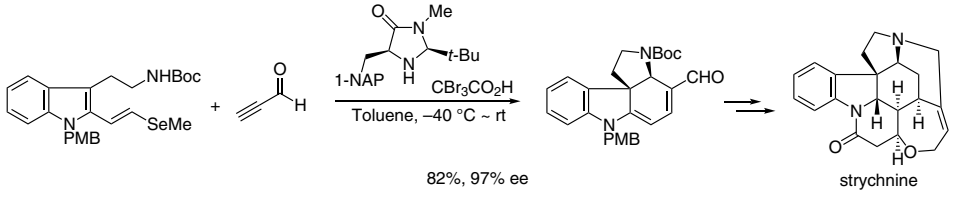

(1.34)

1.6.6. Prostaglandin E_1 Methyl Ester

A domino Michael/Henry reaction of succinaldehyde and nitroalkene in the presence of diphenylprolinol silyl ether proceeded to afford substituted cyclopentanecarbaldehyde, which was further treated with Horner-Wadsworth-Emmons reagent to provide a cyclopentane derivative with excellent enantioselectivity in a one-pot operation (Eq. 1.35). This is a key intermediate for the synthesis of prostaglandin E_1 methyl ester, which was synthesized using a total of three reaction vessels [63].

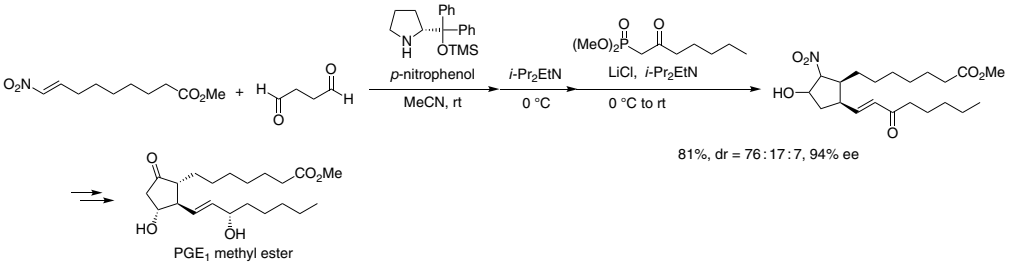

(1.35)

1.6.7. Corey Lactone

Nonactivated ketones are useful Michael donors for the Michael reaction of α,β-unsaturated aldehydes catalyzed by diphenylprolinol silyl ether (see above; Eq. 1.22) [47]. When ethyl 4-oxo-2-pentenoate was employed as a nucleophile, a domino Michael/Michael reaction proceeded to afford a trisubstituted cyclopentanone in nearly enantiomerically pure form (Eq. 1.36). By using this reaction as a key step, a one-pot, 152-minute total synthesis of Corey lactone was realized [64]. Latanoprost [64b] and clinprost [65] were also synthesized by using the same key reaction.

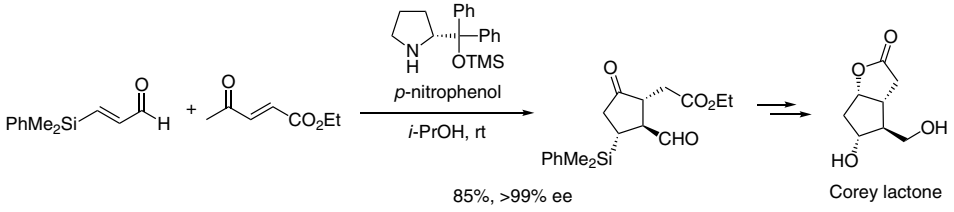

(1.36)

1.7. COMBINATION OF TWO CATALYSTS

In the previous sections, asymmetric reactions using a single chiral organocatalyst were described. By the use of two catalysts, synergistic effects would be expected [66]. A combination of organocatalyst with another catalyst can be used to realize asymmetric reactions, which are difficult to achieve by using a single catalyst. Some of the successful reactions will be discussed in this section.

1.7.1. Combination of Two Organocatalysts

Rovis reported a domino Michael/benzoin reaction of 1,3-diketones and α,β-unsaturated aldehydes by using a combination of diarylprolinol silyl ether and *N*-heterocyclic carbene catalyst (Eq. 1.37) [67]. This is a formal [3+2] cycloaddition reaction that affords highly functionalized cyclopentanone derivatives

with excellent enantioselectivity. When only diarylprolinol silyl ether was employed as a single catalyst, first Michael reaction proceeded to afford the Michael product with lower enantioselectivity, because of the retro-Michael reaction. A combined use of the two catalysts not only provided the formal [3+2] cycloaddition products but also realized excellent enantioselectivity.

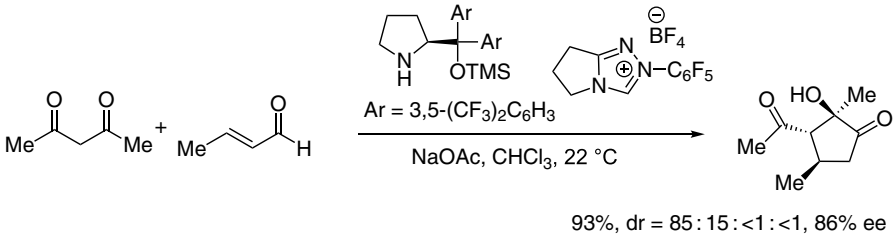

(1.37)

Luo reported a unique two-catalyst cooperative system of a chiral primary amine and a ketone for the asymmetric α-hydroxylation of β-ketocarbonyls with H_2O_2 (Eq. 1.38) [68]. A chiral primary amine not only reacts with β-ketocarbonyl to generate an enamine, it also reacts with 2,2,2-trifluoroacetophenone to generate a chiral ketimine, which reacts further with H_2O_2 to afford an oxaziridine intermediate. The chiral enamine–chiral oxaziridine coupling provided α-hydroxylated β-ketocarbonyls in excellent yield with excellent enantioselectivity.

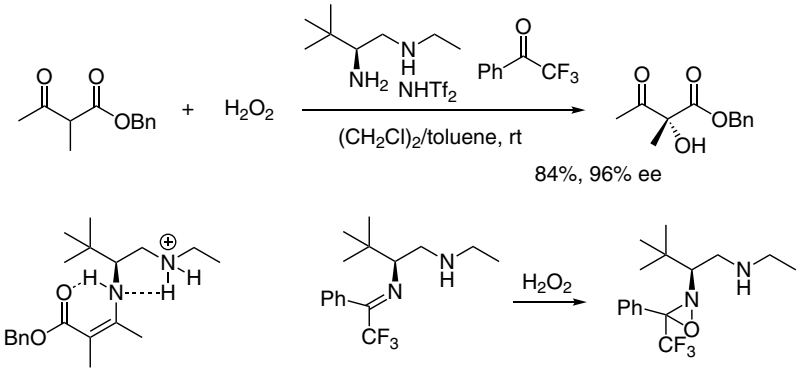

(1.38)

1.7.2. Combination of Organocatalyst and Metal Catalyst

Metal catalysts are widely used in organic synthesis, and a combination of metal catalyst with enamine and iminium ion intermediates opens a new avenue for the synthetic organic chemistry [69]. However, there are limitations to the use of organocatalysts and metal catalysts cooperatively. In organocatalytic reactions involving an enamine as an intermediate, water would be generated in the reaction, and organometallic catalysts have to act efficiently under these reaction conditions. Moreover, the organocatalyst is usually an amine, and metal catalysts also have to catalyze the reaction in the presence of organo amine catalyst. In spite of these limitations, several successful reactions have been developed using a combination of organocatalyst and metal catalyst.

1.7.2.1. Enamine and Metal Catalyst MacMillan reported α-trifluoromethylation (Eq. 1.39) [70], α-arylation (Eq. 1.40) [71], and α-vinylation [72] of aldehydes with iodonium salts catalyzed by a combined use of MacMillan's catalyst and copper catalyst. In the α-trifluoromethylation reaction, Togni's reagent is employed as CF_3 source. In the α-arylation reaction, Cu(I) reacts with diaryliodonium salts

to generate aryl-Cu(III) species, which react with an enamine to generate η^1 iminium organocopper species. Reductive elimination afforded an α-arylated product, and excellent enantioselectivity was obtained.

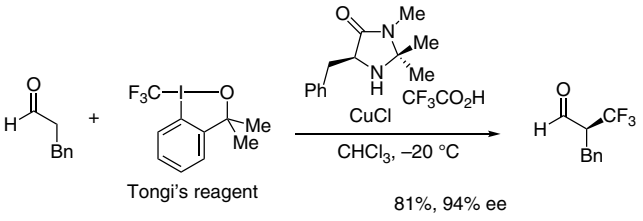

(1.39)

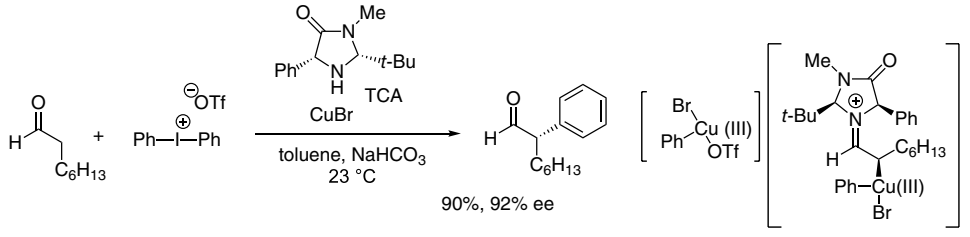

(1.40)

Cordova reported an α-allylation of an aldehyde with an allyl acetate catalyzed by a combination of diphenylprolinol silyl ether and Pd catalyst (Eq. 1.41). A π-allyl complex would be generated from allyl acetate and $Pd(PPh_3)_4$, which reacts with a chiral enamine generated from an aldehyde and organocatalyst [73]. Excellent enantioselectivity was obtained.

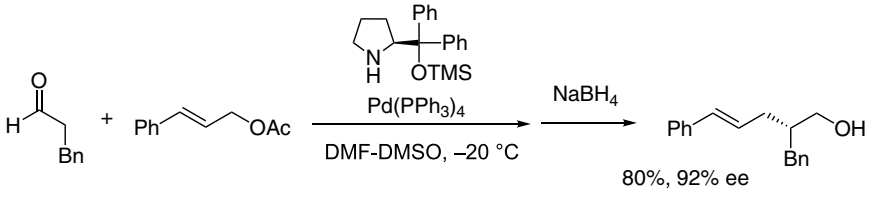

(1.41)

Cozzi reported an asymmetric allylation reaction of an aldehyde and an allyl alcohol catalyzed by a combination of MacMillan's catalyst and a Lewis acid such as $InBr_3$ (Eq. 1.42) [74]. This is an S_N1-type reaction, and the chiral enamine, which is generated from an aldehyde and MacMillan's catalyst, reacts with an allylic carbenium ion, which is generated from an allyl alcohol and $InBr_3$ to afford the product after hydrolysis.

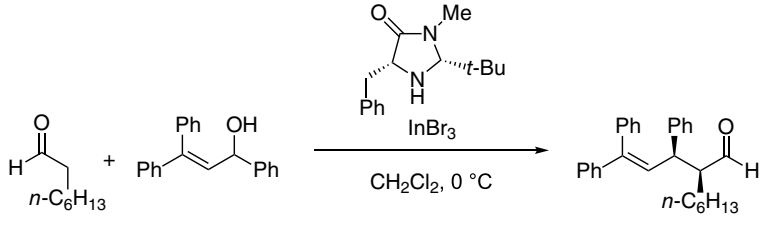

(1.42)

Dixon reported an asymmetric carbocyclization of aldehyde-linked allene by a combined use of diarylprolinol silyl ether and $Pd(OAc)_2$ to afford a substituted cyclopentanecarbaldehyde with good enantioselectivity (Eq. 1.43) [75]. The organocatalyst reacts with an aldehyde to generate a chiral enamine, which reacts with allene activated by Pd(II).

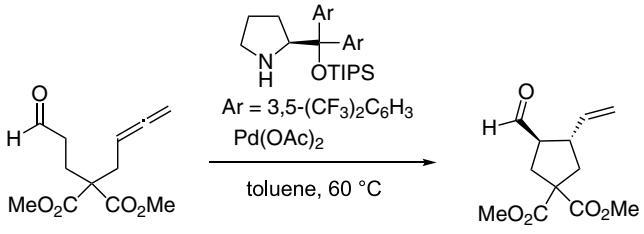

72%, 82% ee (1.43)

Gong reported that diphenylprolinol/Pd(II) cooperative catalysis has enabled a highly enantioselective addition of cyclic ketones to unactivated alkenes (Eq. 1.44) [76]. The reaction includes amide-directed, regioselective activation of alkenes by Pd(II) and enhancing the nucleophilicity of α-carbon of the ketones by enamine catalysis, which provides the γ-addition products with good to high yields and efficient stereochemical control.

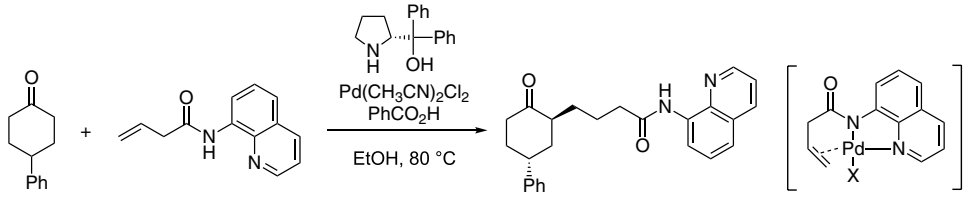

96%, dr = 2.8 : 1, 92% ee, 69% ee (1.44)

Jia reported an enantioselective α-arylative desymmetrization of cyclohexanones using $Pd(OAc)_2$ and proline as a chiral amine catalyst (Eq. 1.45) [77]. Morphan derivatives bearing α-carbonyl tertiary stereocenters were produced in good yields with excellent enantioselectivities. The generated enamine reacts with Ar-Pd-X, and β-hydride elimination affords another enamine, which is hydrolyzed to provide the product (Scheme 1.5).

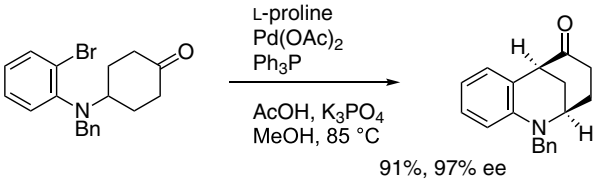

91%, 97% ee (1.45)

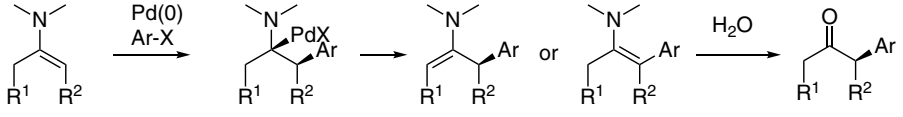

Scheme 1.5. The reaction mechanism.

Nishibayashi reported an enantioselective propargylic alkylation of propargylic alcohols with aldehydes in the presence of a thiolate-bridged diruthenium complex and diarylprolinol silyl ether as a co-catalyst to afford the corresponding propargylic alkylated products in excellent yields with high enantioselectivity (Eq. 1.46) [78]. This is a new type of enantioselective propargylic substitution reaction, wherein the chiral enamines react with the ruthenium–allenylidene complexes, where both the transition metal catalyst (ruthenium complex) and organocatalyst (secondary amine) activate propargylic alcohols and aldehydes, respectively, and cooperatively.

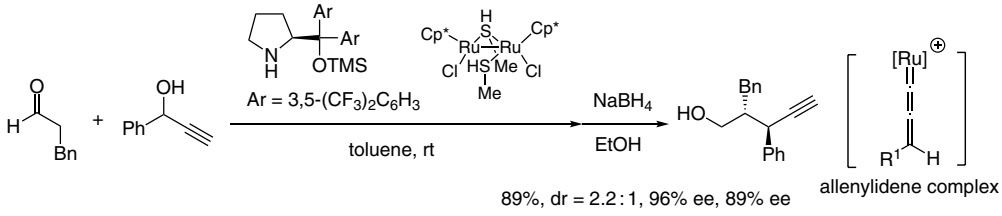

(1.46)

1.7.2.2. Iminium Ion and Transition Metal Catalyst Cordova reported an enantioselective silyl addition to enals using Me_2PhSi-B(pin) as a silyl source, and the reaction is catalyzed by a combination of diphenylprolinol silyl ether and a copper(I) salt (Eq. 1.47) [79]. The copper(I)–silyl intermediate is a nucleophile that reacts with an iminium ion to afford the Michael product with excellent enantioselectivity. The product is a synthetically useful β-silylated aldehyde.

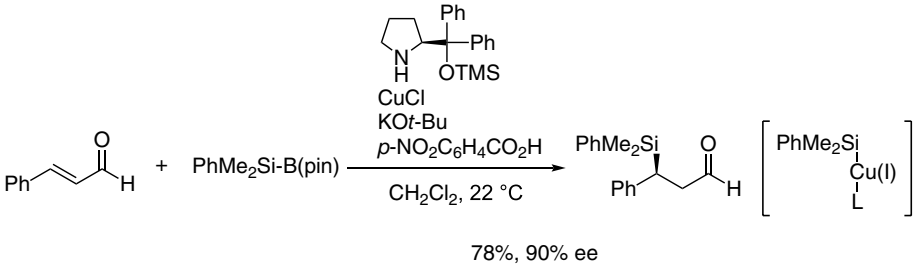

(1.47)

The same group extended the reaction using $B_2(pin)_2$ and dialkyl zinc, respectively, by a combined use of diphenylprolinol silyl ether and $Cu(OTf)_2$ to afford β-borylated aldehydes (Eq. 1.48) [80] and β-alkylated aldehydes [81], respectively, both with excellent enantioselectivity. The β-arylation reaction also proceeded using $ArB(OH)_2$, which is catalyzed by diphenylprolinol silyl ether and $Pd(OAc)_2$ [82].

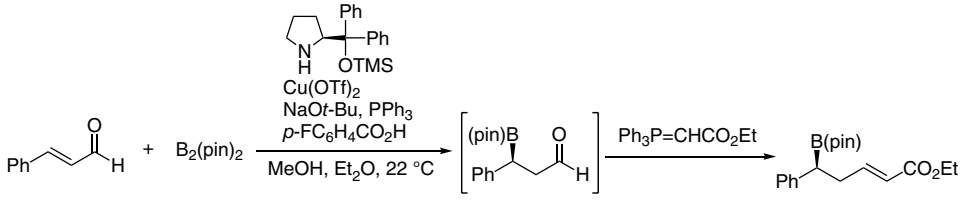

(1.48)

It is known that Hantzsch esters are useful hydride donors for the reduction of α,β-unsaturated aldehydes to saturated aldehydes, and, in 2005, MacMillan reported the asymmetric reduction of β,β-disubstituted α,β-unsaturated aldehydes catalyzed by MacMillan's catalyst (Eq. 1.49) [83].

In 2012, Hori reported an asymmetric hydrogenation of β,β-disubstituted α,β-unsaturated aldehyde, which is catalyzed by a combination of 2-diarylmethylpyrrolidines and heterogeneous $Pd/BaSO_4$ under an H_2 atmosphere (Eq. 1.50) [84]. This reaction is successfully applied to citral. A mixture of *E*- and *Z*-citral in any ratio afforded citronellal with high enantioselectivity. Citronellal is a key synthetic intermediate of *l*-menthol.

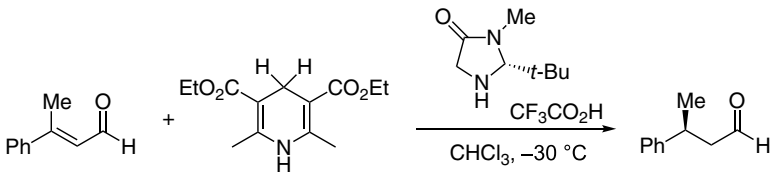

(1.49)

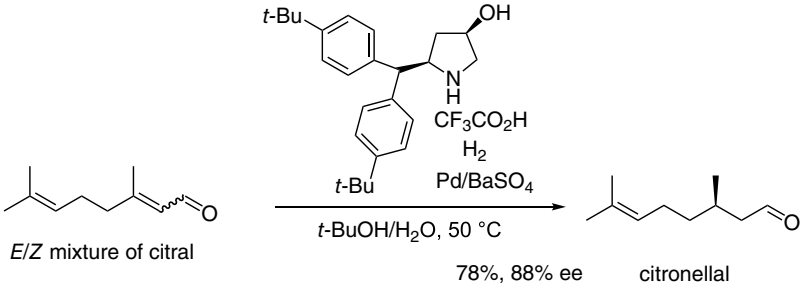

(1.50)

1.7.3. Two Chiral Catalysts

In the synthesis of molecules with two chiral centers, there are four possible isomers. When one chiral catalyst controls one chiral center and the second chiral catalyst controls the second chiral center independently with minimal matched/mismatched interactions, all four isomers can be synthesized with high selectivity. However, the realization of this concept is very difficult. Recently, excellent catalyst systems have been reported for this type of the reaction.

Carreira reported a stereodivergent α-allylation of branched aldehydes by the reaction of allylic alcohols and α,α-disubstituted acetaldehydes (Scheme 1.6) [85]. Products bearing quaternary stereocenters in a vicinal relationship to tertiary stereocenters are obtained in good yields with excellent selectivities. Cinchona-alkaloid-derived primary amine (**A1** and **A2**) and chiral iridium (ligand: **L**) were used as catalysts. The amine catalyst reacts with an aldehyde to generate an enamine, which controls the enantioface selectivity of the aldehyde, while iridium catalyst generates a chiral π-allyl complex in which two distinct and highly face-selective catalytic cycles are merged to provide access to all possible stereoisomers of a target compound in enantiomerically pure form.

The author also extended this reaction to the stereodivergent α-allylation of linear aldehydes with dual chiral iridium catalyst and diphenylprolinol silyl ether catalyst [86].

Dong reported a stereodivergent synthesis of γ,δ-unsaturated aldehydes via alkyne hydrofunctionalization starting from α-branched aldehydes and alkynes using Rh catalyst with a chiral bisphosphine ligand (**L**) and a chiral primary amine catalyst (**A**) (Scheme 1.7) [87]. An alkyne isomerizes into an allene by Rh catalyst and it is further converted into π-allyl Rh complex with a chiral ligand. Chiral amine reacts with an aldehyde to generate a chiral enamine, which reacts with a chiral π-allyl Rh complex. All possible stereoisomers were obtained with high enantio-, diastereo-, and regioselectivity.

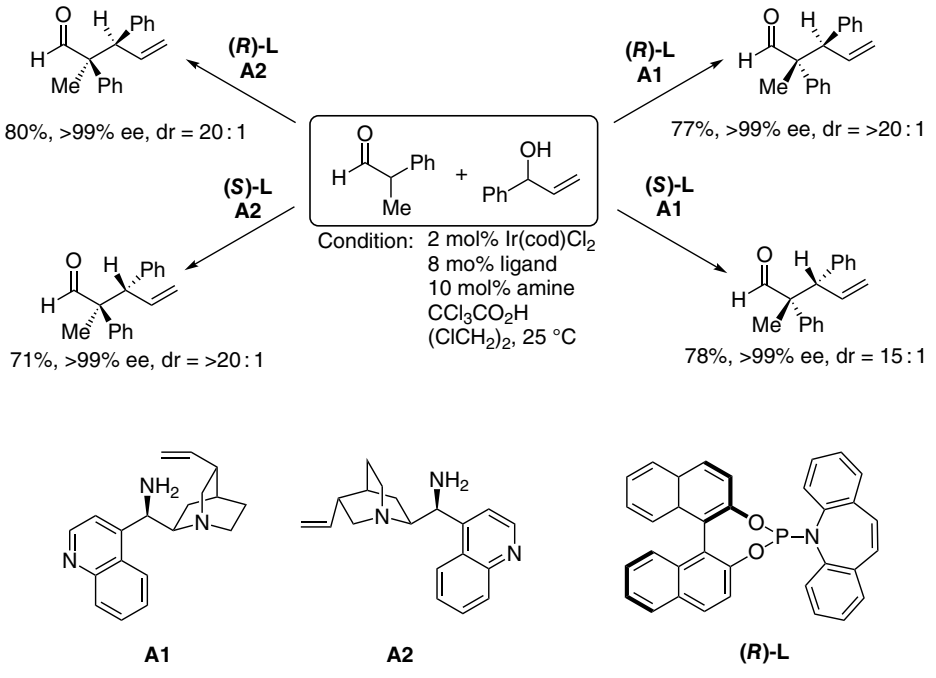

Scheme 1.6. Stereodivergent α-allylation of branched aldehydes using allyl alcohols. Source: [85]/American Association for the Advancement of Science.

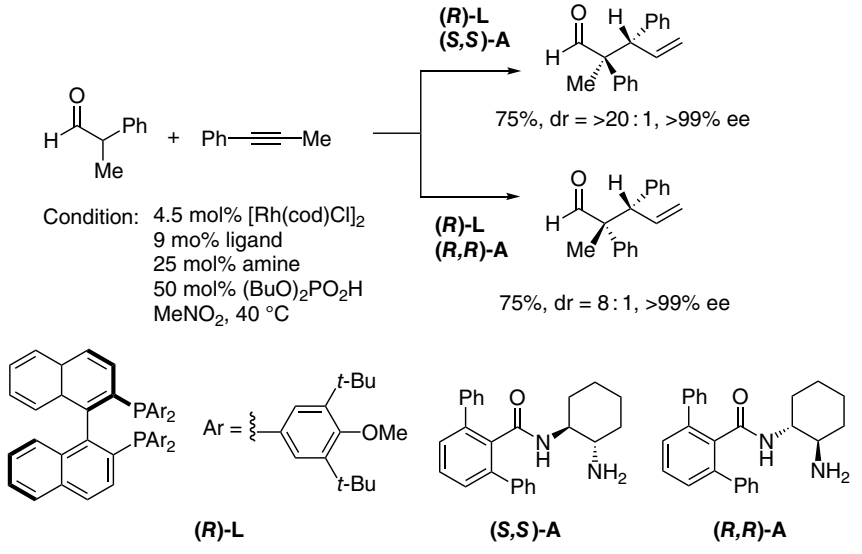

Scheme 1.7. Stereodivergent α-allylation of branched aldehydes using an alkyne. Source: Based on [87].

1.8. CONCLUSION

After the discovery of the proline-mediated intermolecular aldol reaction and organocatalyst-mediated Diels-Alder reaction in 2000, the basic concept of reactions involving an enamine and an iminium ion has become established. Since these first reactions, domino reactions using organocatalysts have developed

dramatically and complex skeletons have been constructed with excellent enantioselectivity in a single pot. The application of organocatalyst-mediated reactions to total syntheses of natural products and drugs is another recent advancement. Combination of organocatalyst and other catalysts is another developing field, and many successful reactions have been reported. Given that enamines and iminium ions are useful intermediates, many reactions involving these intermediates await to be developed. I hope this chapter will encourage further development in organocatalytic reactions.

REFERENCES

1. (a) Hajos, Z. G.; Parrish, D. R. German Patent DE 2102623, **1971**. (b) Hajos, Z. G.; Parrish, D. R. *J. Org. Chem.* **1974**, *39*, 1615–1621.
2. (a) Eder, U.; Sauer, G.; Wiechert, R. German Patent DE 2014757, **1971**. (b) Eder, U.; Sauer, G.; Wiechert, R. *Angew. Chem. Int. Ed.* **1971**, *10*, 496–497.
3. (a) List, B.; Lerner, R. A.; Barbas III, C. F. *J. Am. Chem. Soc.* **2000**, *122*, 2395–2396. (b) Sakthivel, K.; Notz, W.; Bui, T.; Barbas III, C. F. *J. Am. Chem. Soc.* **2001**, *123*, 5260–5267. Review of enamine, see; (c) Mukherjee, S.; Yang, J. W.; Hoffmann, S.; List, B. *Chem. Rev.* **2007**, *107*, 5471–5569.
4. (a) Ahrendt, K. A.; Borths, C. J.; MacMillan, D. V. C. *J. Am. Chem. Soc.* **2000**, *122*, 4243–4244. Reviews of iminium ion: (b) Lelais, G.; MacMillan, D. W. C. *Aldrichimica Acta*, *2006*, 39, 79–87. (c) Erkkilä, A.; Majander, I.; Pihko, P. M. *Chem Rev.* **2007**, *107*, 5416–5470.
5. Selected reviews on organocatalysis: (a) *Asymmetric Organocatalysis 1: Lewis Base and Acid Catalysts*, (Ed.: B. List) Stuttgart: Thieme, **2012**. (b) *Asymmetric Organocatalysis 2: Brønsted Base and Acid catalysts, and Additional Topics* (Ed.: K. Maruoka) Stuttgart: Thieme, **2012**.
6. Watson, A. J. B.; MacMillan, D. W. C. *Catalytic Asymmetric Synthesis*, 3rd ed, (Ed.: I. Ojima). Hoboken, John Wiley & Sons, **2010**, pp. 39–57.
7. Reviews, see: (a) Palomo, C.; Mielgo, A. *Angew. Chem. Int. Ed.* **2006**, *45*, 7876–7880. (b) Mielgo, A.; Palomo, C. *Chem. Asian J.* **2008**, *3*, 922–948. (c) Xu, L. W.; Li, L.; Shi, Z. H. *Adv. Synth. Catal.* **2010**, *352*, 243–279. (d) Jensen, K. L.; Dickmeiss, G.; Jiang, H.; Albrecht, Ł.; Jørgensen, K. A. *Acc. Chem. Res.* **2012**, *4*, 248–264. (e) Wróblewska, A. *Synlett* **2012**, *23*, 953–954. (f) Gotoh, H.; Hayashi, Y. *Sustainable Catalysis* (Eds.: Dunn, P. J.; Hii, K. K.; Krische, M. J.; Williams, M. T.) Hoboken: Wiley, **2013**, pp. 287–316. (g) Donslund, B. S.; Johansen, T. K.; Poulsen, P. H.; Halskov, K. S.; Jørgensen, K. A. *Angew. Chem. Int. Ed.* **2015**, *54*, 13860–13874.
8. Marigo, M.; Wabnitz, T. C.; Fielenbach, D.; Jørgensen, K. A. *Angew. Chem. Int. Ed.* **2005**, *44*, 794–797.
9. Hayashi, Y.; Gotoh, H.; Hayashi T.; Shoji, M. *Angew. Chem. Int. Ed.* **2005**, *44*, 4212–4215.
10. Reviews: (a) Marcelli, T.; van Maarseveen, J. H.; Hiemstra, H. *Angew. Chem. Int. Ed.* **2006**, *45*, 7496–7504. (b) Xu, L.-W.; Luo, J.; Lu, Y. *Chem. Commun.* **2009**, 1807–1821. (c) Melchiorre, P. *Angew. Chem. Int. Ed.* **2012**, *51*, 9748–9770.
11. (a) Lakhdar, S.; Tokuyasu, T.; Mayr, H. *Angew. Chem. Int. Ed.* **2008**, *47*, 8723–8726. (b) Mayr, H.; Lakhdar, S.; Maji, B.; Ofial, A. R. *Beilstein J. Org. Chem.* **2012**, *8*, 1458–1478. (c) Lakhdar, S.; Maji, B.; Mayr, H. *Angew. Chem. Int. Ed.* **2012**, *51*, 5739–5742. (d) An, F.; Maji, B.; Min, E.; Ofial, A. R.; Mayr, H. *J. Am. Chem. Soc.* **2020**, *142*, 1526–1547.
12. (a) List, B. Amine-catalyzed aldol reactions, in: *Modern Aldol Reactions* (Ed.: R. Mahrwald) Weinheim: Wiley-VCH, **2004**, Chapter 4, pp. 161–200. (b) Mase, N.; Hayashi, Y., The aldol reaction: organocatalysis approach, in: *Comprehensive Organic Synthesis*, 2nd ed (Eds.: P. Knochel, G. A. Molander) Amsterdam: Elsevier, **2014**; Chapter 2.07, pp. 273–339. (c) Yamashita, Y.; Yasukawa, T.; Yoo, W. J.; Kitanosono, T.; Kobayashi, S. *Chem. Soc. Rev.* **2018**, *47*, 4388–4480.
13. (a) Bahmanyar, S.; Houk, K. N.; Martin, H. J.; List, B. *J. Am. Chem. Soc.* **2003**, *125*, 2475–2479. (b) Allemann, C.; Gordillo, R.; Clemente, F. R.; Cheong, P. H. Y.; Houk, K. N. *Acc. Chem. Res.* **2004**, *37*, 558–569.
14. Kano, T.; Yamaguchi, Y.; Tanaka Y.; Maruoka, K. *Angew. Chem. Int. Ed.* **2007**, *46*, 1738–1740.
15. Hayashi, Y.; Itoh, T.; Aratake, S.; Ishikawa, H. *Angew. Chem. Int. Ed.* **2008**, *47*, 2082–2084.
16. (a) Urushima, T.; Yasui, Y.; Ishikawa, H.; Hayashi, Y. *Org. Lett.* **2010**, *12*, 2966–2969. (b) Hayashi, Y.; Yasui, Y.; Kawamura, T.; Kojima, M.; Ishikawa, H. *Synlett* **2011**, 485–488. (c) Hayashi, Y.; Yasui, Y.; Kawamura, T.; Kojima, M.; Ishikawa, H. *Angew. Chem. Int. Ed.* **2011**, *50*, 2804–2807. (d) Hayashi, Y.; Yasui, Y.; Kojima, M.; Kawamura, T.; Ishikawa, H. *Chem. Commun.* **2012**, *48*, 4570–4572. (e) Hayashi, Y.; Kojima, M. *ChemCatChem.* **2013**, *5*, 2883–2885. (f) Hayashi, Y.; Kojima, M.; Yasui, Y.; Kanda, Y.; Mukaiyama, T.; Shomura, H.; Nakamura, D.; Ritmaleni, L.; Sato, I. *ChemCatChem.* **2013**, *5*, 2887–2892. (g) Yasui, Y.; Benohoud, M.; Sato, I.; Hayashi, Y. *Chem. Lett.* **2014**, *43*, 556–558. (h) Hayashi, Y.; Watanabe, S.; Yasui, Y.; Umemiya, S. *ChemCatChem.* **2015**, *7*, 1646–1649. (j) Hayashi, Y.; Nakamura, D.; Yasui, Y.; Iwasaki, K.; Chiba, H. *Adv. Synth. Catal.* **2016**, *358*, 2345–2351.
17. (a) List, B. *J. Am. Chem. Soc.* **2000**, *122*, 9336–9337. Review of Mannich reaction, see; (b) Verkade, J. M. M.; van Hemert, L. J. C.; Quaedflieg, P. J. L. M.; Rutjes, F. P. J. T. *Chem. Soc. Rev.* **2008**, *37*, 29–41.
18. (a) Córdova, A.; Notz, W.; Zhong, G.; Betancort, J. M.; Barbas III, C. F. *J. Am. Chem. Soc.* **2002**, *124*, 1842–1843. (b) Córdova, A.; Watanabe, S.; Tanaka, F.; Notz, W.; Barbas III, C. F. *J. Am. Chem. Soc.* **2002**, *124*, 1866–1867.

19. (a) Kano, T.; Yamaguchi, Y.; Tokuda, O.; Maruoka, K. *J. Am. Chem. Soc.* **2005**, *127*, 16408–16409. (b) Kano, T.; Yamaguchi, Y.; Maruoka, K. *Angew. Chem. Int. Ed.* **2009**, *48*, 1838–1840. (c) Kano, T.; Sakamoto, R.; Akakura, M.; Maruoka, K. *J. Am. Chem. Soc.* **2012**, *134*, 7516–7520.
20. (a) A. Córdova, *Chem. Comm.* **2006**, 1760–1762. (b) Hayashi, Y.; Sakamoto, D.; Shomura, H.; Hashizume, D. *Chem. Eur. J.* **2013**, *19*, 7678–7681.
21. (a) Marigo, M.; Fielenbach, D.; Braunton, A.; Kjœrsgaard, A.; Jørgensen, K. A. *Angew. Chem. Int. Ed.* **2005**, *44*, 3703–3706. (b) Steiner, D. D.; Mase, N.; Barbas III, C. F. *Angew. Chem. Int. Ed.* **2005**, *44*, 3706–3710. (c) Beeson, T. D.; MacMillan, D. W. C. *J. Am. Chem. Soc.* **2005**, *127*, 8826–8828.
22. (a) Brochu, M. P.; Brown, S. P.; MacMillan, D. W. C. *J. Am. Chem. Soc.* **2004**, *126*, 4108–4109. (b) Halland, N.; Braunton, A.; Bachmann, S.; Marigo, M.; Jørgensen, K. A. *J. Am. Chem. Soc.* **2004**, *126*, 4790–4791.
23. (a) Bertelsen, S.; Halland, N.; Bachmann, S.; Marigo, M.; Braunton, A.; Jørgensen, K. A. *Chem. Commun.* **2005**, 4821–4823. (b) Kano, T.; Ueda, M.; Maruoka, K. *J. Am. Chem. Soc.* **2008**, *130*, 3728–3729.
24. Bøgevig, A.; Juhl, K.; Kumaragurubaran, N.; Zhuang, W.; Jørgensen, K. A. *Angew. Chem. Int. Ed.* **2002**, *41*, 1790–1793.
25. (a) Brown, S. P.; Brochu, M. P.; Sinz, C. J.; MacMillan, D. W. C. *J. Am. Chem. Soc.* **2003**, *125*, 10808–10809. (b) Zhong, G. *Angew. Chem. Int. Ed.* **2003**, *42*, 4247–4250. (c) Bøgevig, A.; Sundén, H.; Córdova, A. *Angew. Chem. Int. Ed.* **2004**, *43*, 1109–1112. (d) Hayashi, Y.; Yamaguchi, J.; Sumiya, T.; Shoji, M. *Angew. Chem. Int. Ed.* **2004**, *43*, 1112–1115.
26. Hayashi, Y.; Nariyoshi, U.; Hirama, T. *Org. Lett.* **2017**, *19*, 4155–4158.
27. (a) Patora-Komisarska, K.; Benohoud, M.; Ishikawa, H.; Seebach, D.; Hayashi, Y. *Helv. Chim. Acta*, **2011**, *94*, 719–745. (b) Seebach, D.; Sun, X.; Ebert, M. O.; Schweizer, W. B.; Purkayastha, N.; Beck, A. K.; Duschmalé, J.; Wennemers, H.; Mukaiyama, T.; Benohoud, M.; Hayashi, Y.; Reiher, M. *Helv. Chim. Acta* **2013**, *96*, 799–852.
28. (a) Mossé, S.; Alexakis, A. *Org. Lett.* **2005**, *7*, 4361–4364. (b) Landa, A.; Maestro, M.; Masdeu, C.; Puente, A.; Vera, S.; Oiarbide, M.; Palomo, C. *Chem. Eur. J.* **2009**, *15*, 1562–1565.
29. Sakamoto, D.; Hayashi, Y. *Chem. Lett.* **2018**, *47*, 833–835.
30. Hayashi, Y.; Kranidiotis-Hisatomi, N.; Sakamoto, D.; Oritani, K.; Kawamoto, T.; Kamimura, A. *Eur. J. Org. Chem.* **2018**, 6843–6847.
31. Hayashi, Y.; Odoh, A. S.; Kranidiotis-Hisatomi, N. *Chem. Cat. Chem.* **2020**, *12*, 2412–2415.
32. (a) Wiesner, M.; Revell, J. D.; Wennemers, H. *Angew. Chem. Int. Ed.* **2008**, *47*, 1871–1874. (b) Wiesner, M.; Revell, J. D.; Tonazzi, S.; Wennemers, H. *J. Am. Chem. Soc.* **2008**, *130*, 5610–5611. (c) Wiesner, M.; Upert, G.; Angelici, G.; Wennemers, H. *J. Am. Chem. Soc.* **2010**, *132*, 6–7.
33. (a) Arceo, E.; Melchiorre, P. *Angew. Chem. Int. Ed.* **2012**, *51*, 5290–5292. (b) Li, J. L.; Liu, T. Y.; Chen, Y. C. *Acc. Chem Res.* **2012**, *45*, 1491–1500.
34. Bertelsen, S.; Marigo, M.; Brandes, S.; Dinér, P.; Jørgensen, K. A. *J. Am. Chem. Soc.* **2006**, *128*, 12973–12980.
35. Halskov, K. S.; Donslund, B. S.; Barfüsser, S.; Jørgensen, K. A. *Angew. Chem. Int. Ed.* **2014**, *53*, 4137–4141.
36. Jia, Z. J.; Jiang, H.; Li, J. L.; Gschwend, B.; Li, Q. Z.; Yin, X.; Grouleff, J.; Chen, Y. C.; Jørgensen, K. A. *J. Am. Chem. Soc.* **2011**, *133*, 5053–5061.
37. Gotoh, H.; Uchimaru, T.; Hayashi, Y. *Chem. Eur. J.* **2015**, *21*, 12337–12346.
38. (a) Gotoh, H.; Hayashi, Y. *Org. Lett.* **2007**, *9*, 2859–2862. (b) Hayashi, Y.; Samanta, S.; Gotoh, H.; Ishikawa, H. *Angew. Chem. Int. Ed.* **2008**, *47*, 6634–6637.
39. (a) Gotoh, H.; Masui, R; Ogino, H.; Shoji, M.; Hayashi, Y. *Angew. Chem. Int. Ed.* **2006**, *45*, 6853–6856. (b) Gotoh, H.; Ogino, H.; Ishikawa, H.; Hayashi, Y. *Tetrahedron* **2010**, *66*, 4894–4899.
40. (a) Paras, N. A.; MacMillan, D. W. C. *J. Am. Chem. Soc.* **2001**, *123*, 4370–4371. (b) Austin, J. F.; MacMillan, D. W. C. *J. Am. Chem. Soc.* **2002**, *124*, 1172–1173. (c) Paras, N. A.; MacMillan, D. W. C. *J. Am. Chem. Soc.* **2002**, *124*, 7894–7895.
41. Jen, W. S.; Wiener, J. J. M.; MacMillan, D. W. C. *J. Am. Chem. Soc.* **2000**, *122*, 9874–9875.
42. (a) Brandau, S.; Landa, A.; Franzén, J.; Marigo, M.; Jørgensen, K. A. *Angew. Chem. Int. Ed.* **2006**, *45*, 4305–4309. (b) Gotoh, H.; Ishikawa, H.; Hayashi, Y. *Org. Lett.* **2007**, *9*, 5307–5309. (c) Franke, P. T.; Richter, B.; Jørgensen, K. A. *Chem. Eur. J.* **2008**, *14*, 6317–6321. (d) Rueping, M.; Sugiono, E.; Merino, E. *Chem. Eur. J.* **2008**, *14*, 6329–6332.
43. Bertelsen, S.; Dinér, P.; Johansen, R. L.; Jørgensen, K. A. *J. Am. Chem. Soc.* **2007**, *129*, 1536–1537.
44. (a) Dinér, P.; Nielsen, M.; Marigo, M.; Jørgensen, K. A. *Angew. Chem. Int. Ed.* **2007**, *46*, 1983–1987. (b) Jiang, H.; Nielsen, J. B.; Nielsen, M.; Jørgensen, K. A. *Chem. Eur. J.* **2007**, *13*, 9068–9075.
45. (a) Carlone, A.; Bartoli, G.; Bosco, M.; Sambri, L.; Melchiorre, P. *Angew. Chem. Int. Ed.* **2007**, *46*, 4504–4506. (b) Ibrahem, I.; Rios, R.; Vesely, J.; Hammar, P.; Eriksson, L.; Himo, F.; Córdova, A. *Angew. Chem. Int. Ed.* **2007**, *46*, 4507–4510.
46. Hayashi, Y.; Umekubo, N. *Angew. Chem. Int. Ed.* **2018**, *57*, 1958–1962.
47. Umekubo, N.; Terunuma, T.; Kwon, E.; Hayashi, Y. *Chem. Sci.* **2020**, *11*, 11293–11297.
48. Domino reaction, see: (a) Tietze, L. F. *Chem Rev.* **1996**, *96*, 115–136. (b) *Domino Reactions*, (Ed. Tietze, L. F.), Wiley-VCH, Weinheim, **2014**.Cascade reaction, see: (c) Nicolaou, K. C.; Edmonds, D. J.; Bulger, P. G. *Angew. Chem. Int. Ed.* **2006**, *45*, 7134–7186. (d) Nicolaou, K. C.; Montagnon, T.; Snyder, S. A. *Chem. Commun.* **2003**, 551–564.Tandem reaction, see: (e) Denmark, S. E.; Thorarensen, A. *Chem. Rev.* **1996**, *96*, 137–166.
49. Reviews: (a) Grondal, V; Jeanty, M.; Enders, D. *Nature Chem.* **2010**, *2*, 167–178. (b) Albrecht, L.; Jiang, H.; Jørgensen, K. A. *Angew. Chem. Int. Ed.* **2011**, *50*, 8492–8509. (c) Pellissier, H. *Adv. Synth. Catal.* **2012**, *354*, 237–294. (d) Volla, C. M. R.;

Atodiresei, I.; Rueping, M. *Chem. Rev.* **2014**, *114*, 2390–2431. (e) Hong, B. C.; Raja, A.; Sheth, V. M. *Synthesis* **2015**, *47*, 3257–3285. (f) Y. Hayashi, *Chem. Sci.* **2016**, *7*, 866–880. (g) Chanda, T.; Zhao, J. C.-G. *Adv. Synth. Catal.* **2018**, *360*, 2–79.
50. Yang, J. W.; Hechavarria Fonseca, M. T.; List, B. *J. Am. Chem. Soc.* **2005**, *127*, 15036–15037.
51. Huang, Y.; Walji, A. M.; Larsen, C. H.; MacMillan, D. W. C. *J. Am. Chem. Soc.* **2005**, *127*, 15051–15053.
52. Marigo, M.; Schulte, T.; Franzén, J.; Jørgensen, K. A. *J. Am. Chem. Soc.* **2005**, *127*, 15710–15711.
53. Enders, D.; Hüttl, M. R. M.; Raabe, G. *Nature* **2006**, *441*, 861–863.
54. Chauhan, P.; Mahajan, S.; Enders, D. *Acc. Chem. Res.* **2017**, *50*, 2809–2821.
55. Dochain, S.; Vetica, F.; Putreddy, R.; Rissanen, K.; Enders, D. *Angew. Chem. Int. Ed.* **2016**, *55*, 16153–16155.
56. Enders, D.; Joie, C.; Deckers, K. *Chem. Eur. J.* **2013**, *19*, 10818–10821.
57. (a) Reyes-Rodriguéz, G. J.; Rezayee, N. M.; Vidal-Albalat, A.; Jørgensen, K. A. *Chem. Rev.* **2019**, *119*, 4221–4260. (b) Wang, Z. *Molecules* **2019**, *24*, 3412–3450. (c) Parella, R.; Jakkampudi, S.; Zhao, J. C.-G. *ChemistrySelect* **2021**, *6*, 2252–2280.
58. Jhuo, D.-H.; Hong, B.-C.; Chang, C.-W.; Lee, G.-H. *Org. Lett.* **2014**, *16*, 2724–2727.
59. (a) Shiomi, S.; Sugahara, E.; Ishikawa, H. *Chem. Eur. J.* **2015**, *21*, 14758–14763. (b) Shiomi, S.; Misaka, R.; Kaneko, M.; Ishikawa, H. *Chem. Sci.* **2019**, *10*, 9433–9437.
60. Bradshaw, B.; Luque-Corredera, C.; Bonjoch, J. *Org. Lett.* **2013**, *15*, 326–329.
61. (a) Hayashi, Y.; Koshino, S.; Ojima, K.; Kwon, E. *Angew. Chem. Int. Ed.* **2017**, *56*, 11812–11815. (b) Koshino, S.; Kwon, E.; Hayashi, Y. *Eur. J. Org. Chem.* **2018**, 5629–5638.
62. Jones, S. B.; Simmons, B.; MacMillan, D. W. C. *Nature* **2011**, *475*, 183–188.
63. Hayashi, Y.; Umemiya, S. *Angew. Chem. Int. Ed.* **2013**, *52*, 3450–3452.
64. (a) Umekubo, N.; Suga, Y.; Hayashi, Y. *Chem. Sci.* **2020**, *11*, 1205–1209. (b) Umekubo, N.; Hayashi, Y. *Eur. J. Org. Chem.* **2020**, *29*, 6221–6227.
65. Umekubo, N.; Hayashi, Y. *Org. Lett.* **2020**, *22*, 9365–9370.
66. Allen, A. E.; MacMillan, D. W. C. *Chem. Sci.* **2012**, *3*, 633–658.
67. Lathrop, S. P.; Rovis, T. *J. Am. Chem. Soc.* **2009**, *131*, 13628–13630.
68. Cai, M.; Xu, K.; Li, Y.; Nie, Z.; Zhang, L.; Luo, S. *J. Am. Chem. Soc.* **2021**, *143*, 1078–1087.
69. Reviews: (a) Shao, Z.; Zhang, H. *Chem. Soc. Rev.* **2009**, *38*, 2745–2755. (b) Du, Z.; Shao, Z. *Chem. Soc. Rev.* **2013**, *42*, 1337–1378. (c) Chen, D.-F.; Han, Z.-Y.; Zhou, X.-L.; Gong, L.-Z. *Acc. Chem. Res.* **2014**, *47*, 2365–2377. (d) Afewerki, S.; Córdova, A. *Chem. Rev.* **2016**, *116*, 13512–13570. (e) Meazza, M.; Rios, R. *Synthesis* **2016**, *48*, 960–973.
70. Allen, A. E.; MacMillan, D. W. C. *J. Am. Chem. Soc.* **2010**, *132*, 4986–4987.
71. Allen, A. E.; MacMillan, D. W. C. *J. Am. Chem. Soc.* **2011**, *133*, 4260–4263.
72. Skucas, E.; MacMillan, D. W. C. *J. Am. Chem. Soc.* **2012**, *134*, 9090–9093.
73. Afewerki, S.; Ibrahem, I.; Rydfjord, J.; Breistein, P.; Córdova, A. *Chem. Eur. J.* **2012**, *18*, 2972–2977.
74. Gualandi, A.; Mengozzi, L.; Wilson, C. M.; Cozzi, P. G. *Chem. Asian J.* **2014**,*9*, 984–995.
75. Li, M.; Datta, S.; Barber, D. M.; Dixon, D. J. *Org. Lett.* **2012**, *14*, 6350–6353.
76. Shen, H.-C.; Zhang, L.; Chen, S.-S.; Feng, J.; Zhang, B.-W.; Zhang, Y.; Zhang, X.; Wu, Y.-D.; Gong, L.-Z. *ACS Catal.* **2019**, *9*, 791–797.
77. Liu, R.-R.; Li, B.-L.; Lu, J.; Shen, C.; Gao, J.-R.; Jia, Y.-X. *J. Am. Chem. Soc.* **2016**, *138*, 5198–5201.
78. Ikeda, M.; Miyake, Y.; Nishibayashi, Y. *Angew. Chem. Int. Ed.* **2010**, *49*, 7289–7293.
79. Ibrahem, I.; Santoro, S.; Himo, F.; Córdova, A. *Adv. Synth. Catal.* **2011**, *353*, 245–252.
80. Ibrahem, I.; Breistein, P.; Córdova, A. *Angew. Chem. Int. Ed.* **2011**, *50*, 12036–12041.
81. Afewerki, S.; Breistein, P.; Pirttilä, K.; Deiana, L.; Dziedzic, P.; Ibrahem, I.; Córdova, A. *Chem. Eur. J.* **2011**, *17*, 8784–8788.
82. Ibrahem, I.; Ma, G.; Afewerki, S.; Córdova, A. *Angew. Chem. Int. Ed.* **2013**, *52*, 878–882.
83. Ouellet, S. G.; Tuttle, J. B.; MacMillan, D. W. C. *J. Am. Chem. Soc.* **2005**, *127*, 32–33.
84. Maeda, H.; Yamada, S.; Itoh, H.; Hori, Y. *Chem. Commun.* **2012**, *48*, 1772–1774.
85. Krautwald, S.; Sarlah, D.; Schafroth, M. A.; Carreira, E. M. *Science* **2013**, *340*, 1065–1068.
86. Krautwald, S.; Schafroth, M. A.; Sarlah, D.; Carreira, E. M. *J. Am. Chem. Soc.* **2014**, *136*, 3020–3023.
87. Cruz, F. A.; Dong, V. M. *J. Am. Chem. Soc.* **2017**, *139*, 1029–1032.

2

ASYMMETRIC ACID ORGANOCATALYSIS

Takahiko Akiyama
Department of Chemistry, Gakushuin University, Tokyo, Japan

2.1. INTRODUCTION

The advent of chiral Brønsted acids in the early 2000s followed extensive studies on chiral Lewis acid catalysts [1]. While a range of compounds can be considered chiral Brønsted acids (Figure 2.1) [2], including thiourea **1** [3], **2** [4], TADDOL (α,α,α′,α′-tetraaryl-1,3-dioxolane-4,5-dimethanol) **3** [5], 1,1′-bi-2-naphthol (BINOL) derivatives **4** [6], and bis-quinoline acid salt (HQuin-BAM) **5** [7], we will primarily focus on more acidic BINOL-derived phosphorus- and sulfur-containing organic acids, such as phosphoric acid (CPA [chiral phosphoric acid]) **6** [8, 9], dicarboxylic acid **7** [10], disulfonic acid (BINSA) **8** [11], disulfonimide (DSI) **9** [12], imidodiphosphate (IDP) **10** [13], and imidodiphosphorimidate (IDPi) **11** [13]. This chapter will provide a compilation of transformations that have been mediated by chiral Brønsted acids [15, 16], and is organized by the type of reactions starting from nucleophilic reaction, cycloaddition reaction, Michael reaction, reduction, addition to alkenes, substitution, rearrangements, and others.

2.2. FEATURES OF CHIRAL BRØNSTED ACIDS

2.2.1. Acidity of Chiral Brønsted Acids

The pK_as of common chiral Brønsted acids in dimethyl sulfoxide (DMSO) have primarily been interrogated computationally. Cheng found using SMD/M06-2x/6-311++G(2df,2p)//B3LYP/6-31+G(d) method that chiral phosphoric acids and carboxylic acids, derived from BINOL, were the least acidic among those studied, with pK_as of 3.37 and 3.97, respectively, and that bis(sulfonic acid) **8a** was the most acidic (Figure 2.2) [17]. In comparison to CPA **6**, derived from BINOL, those derived from H_8-BINOL **12** [18] and SPINOL **13** [19, 20] are less acidic with pK_as of 4.61 and 4.20, respectively. *N*-Triflyl chiral phosphoramide **14**[21] is much more acidic with pK_a –3.40. Dicarboxylic acid **7** is slightly less acidic than phosphoric acid, whereas sulfonimide **9** is more acidic. These values broadly agree with experimental values of related compounds [22]. A follow-up study revealed that 3,3′-substitution in chiral phosphoric acids enables modulation of acidity by nearly two orders of magnitude: from 2.63 for CPA **6b** with 3,5-$(CF_3)_2C_6H_3$ groups to 4.20 for CPA **6i** with Ph_3Si groups (Figure 2.3).

Catalytic Asymmetric Synthesis, Fourth Edition. Edited by Takahiko Akiyama and Iwao Ojima.

Hydrogen bond catalysts

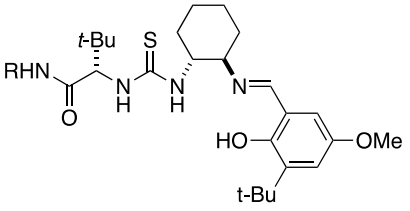

1: Jacobsen [3]

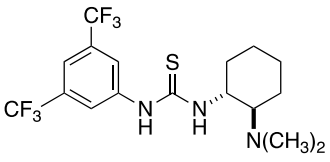

2: Takemoto [4]

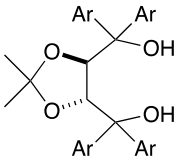

3: Rawal [5]

Relatively weak acids

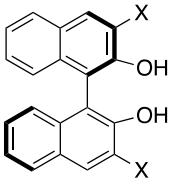

4: Schaus [6]

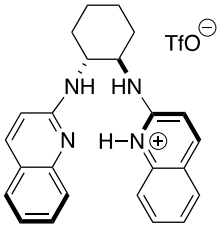

5: Johnston [7]

Relatively stronger acids

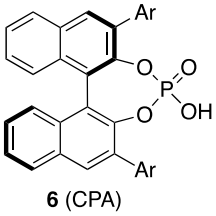

6 (CPA)
Akiyama, Terada [8,9]

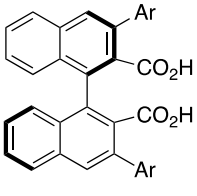

7
Maruoka [10]

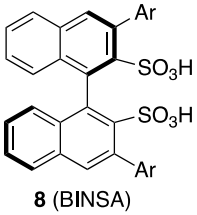

8 (BINSA)
Ishihara [11]

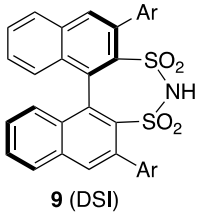

9 (DSI)
List [12]

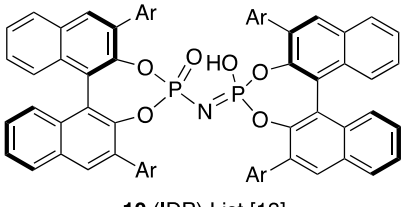

10 (IDP) List [13]

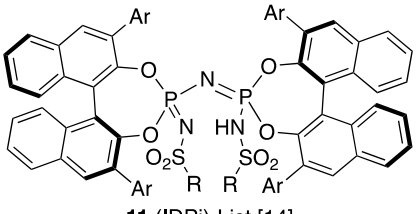

11 (IDPi) List [14]

Figure 2.1. Examples of chiral Brønsted acids.

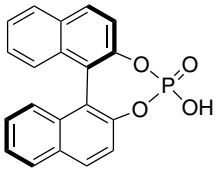

6a: 3.37

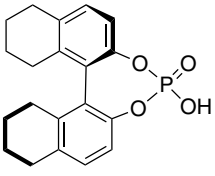

12a: 4.61

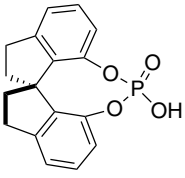

13a: 4.20

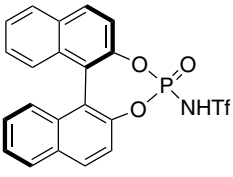

14a: –3.40

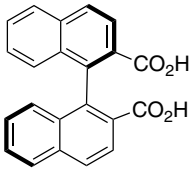

7a: 3.97

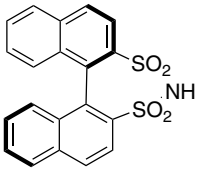

9a: 0.15

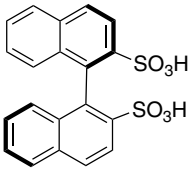

8a: –9.06

Figure 2.2. pK_a values of chiral Brønsted acids in DMSO by calculation. Source: [17].

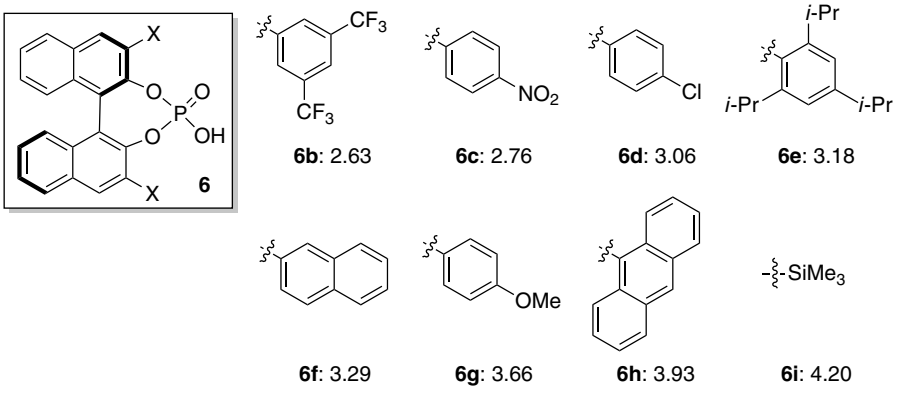

Figure 2.3. Effect of 3,3′-substituents of BINOL-derived phosphoric acid on the pK_a values in DMSO by calculation.

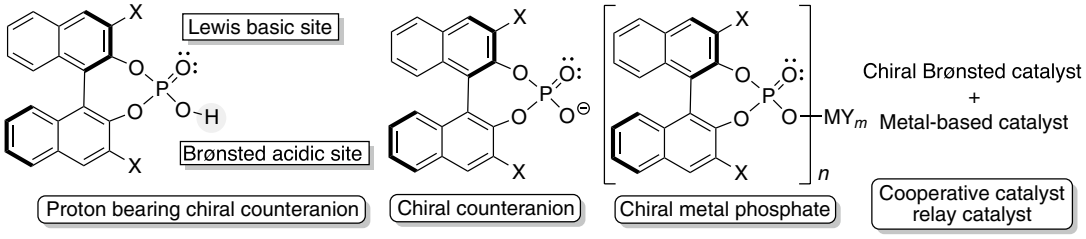

Figure 2.4. Function of chiral phosphoric acid.

2.2.2. Mode of Activation of Chiral Phosphoric Acids and Related Compounds

CPA is, in principle, a Brønsted acid, but the phosphoryl oxygen plays a crucial role as a basic site (Figure 2.4). The bifunctional nature of CPA and other chiral Brønsted acids is, in many cases, critical for the high enantioselectivity and reactivity. CPA is considered to be "proton-bearing chiral counteranion." List expanded the concept of chiral Brønsted acid to "asymmetric counteranion-directed catalysis" (ACDC) [23]. Toste also proposed "chiral anion catalysis" [24]. The concept will be discussed in detail in Chapter 4 [25]. Metal phosphates are also employed as Lewis acid catalysts [26]. Cooperative and/or relay catalyst system of combining chiral Brønsted acids with metal-based catalysts or photoredox catalysts have also attracted much attention lately [27].

2.2.3. Effect of Metal Salts

In addition to CPA per se, metal phosphates function as achiral Lewis acid, and numerous kinds of enantioselective reactions were reported. Examples include Yb triphosphates by Inanaga et al. [28], lithium phosphates by Ishihara et al. [29], calcium phosphates by Masson and Zhu [30], and magnesium phosphates by Antilla [31].

Ishihara conducted a reinvestigation of the report of Terada [9] and pointed out the possible formation and contamination of BINOL-derived phosphoric acid during purification on silica gel (Figure 2.5). They cautioned that such impurities may have a substantial influence on the catalytic activity [32]. Subsequently, Klussmann and List analyzed the impurities of CPA **6e** bearing 2,4,6-(*i*-Pr)$_3$C$_6$H$_2$ groups at 3,3′-positions of BINOL (TRIP) by inductively coupled plasma optical emission spectrometry (ICP-OES) and found that TRIP contained various alkali and alkaline earth metals as major impurities. Because metal phosphates are generated during the preparation of CPA and/or the purification by silica gel chromatography, washing with hydrochloric acid is strongly recommended to obtain free phosphoric acid [33].

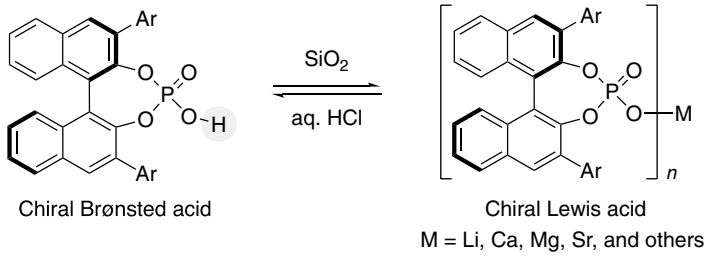

Figure 2.5. Metal salts of chiral phosphoric acid.

2.3. NUCLEOPHILIC REACTIONS

2.3.1. Reactions with Imines and Iminium Salts

BINOL-derived CPA **6a** is available in bulk amounts and is employed as a resolving reagent for amines [34]. In 2004, Akiyama reported a Mannich-type reaction between aldimines bearing the 2-hydroxyphenyl moiety on nitrogen and ketene silyl acetals catalyzed by CPA **6c**, derived from (*R*)-BINOL bearing 4-nitrophenyl groups at 3,3′-positions, which gave β-amino-α-alkyl or α-siloxy amino esters in preference of the *syn* isomer with 81–96% ee (Scheme 2.1a) [8]. The use of aldimines derived from 2-hydroxyaniline is critical for the excellent enantioselectivity. Based on the theoretical study by Yamanaka, the Mannich-type reaction is proposed to proceed through the protonation of imine with CPA followed by the nucleophilic attack via zwitterionic and nine-membered cyclic transition state (TS-1) [35]. Concurrently, Terada reported a direct Mannich reaction between *N*-Boc aldimines and pentan-2,4-dione catalyzed by CPA **6j** to give the adducts with 90–98% ee (Scheme 2.1b) [9].

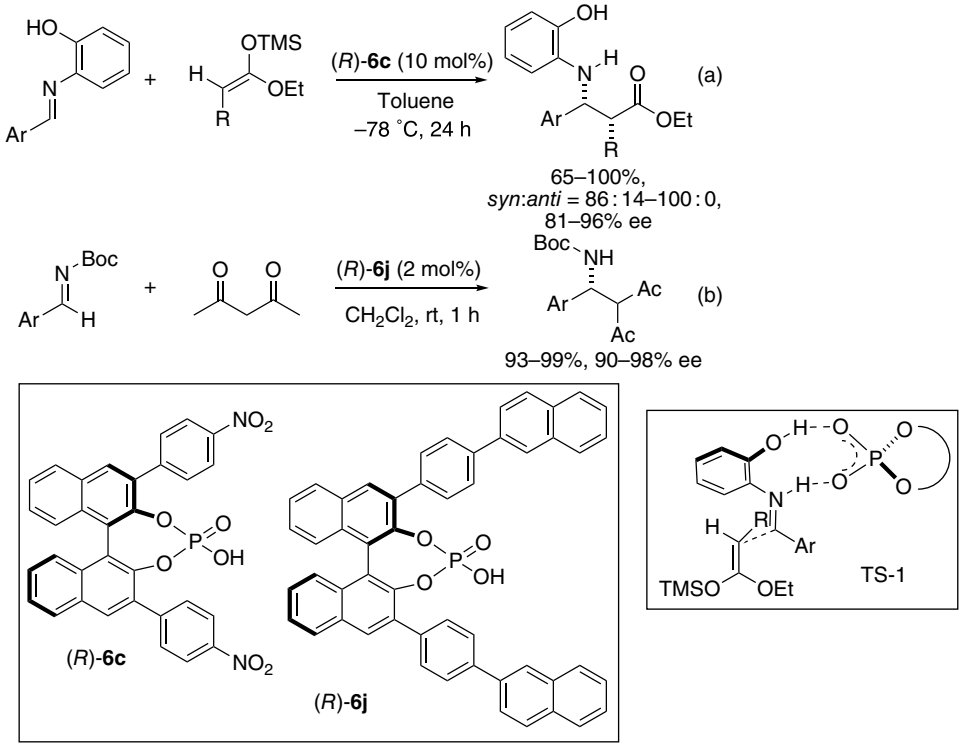

Scheme 2.1. Mannich reaction by Akiyama (a) (Source: Based on [8]), and by Terada (b) (Source: Based on [9]).

Yamamoto reinvestigated the Mannich-type reaction[8] and found that CPA **6k**, bearing 2,4,6-Me_3-3,5-$(NO_2)_2C_6$ moiety, was more effective for the Mannich-type reaction, furnishing β-amino esters with higher enantioselectivity in comparison with CPA **6b** (Scheme 2.2a) [36]. The higher enantioselectivity (up to >99% ee) was ascribed to both steric and electronic effects from the three methyl groups. Furthermore, when phosphoramide **2a** bearing 3,5-(NO_2)-4-$CH_3C_6H_2$ groups was used, *N*-phenyl aldimines were also found to be suitable substrates and use of *N*-2-hydroxyphenyl-substituted aldimine was obviated without compromising the enantioselectivity (Scheme 2.2b).

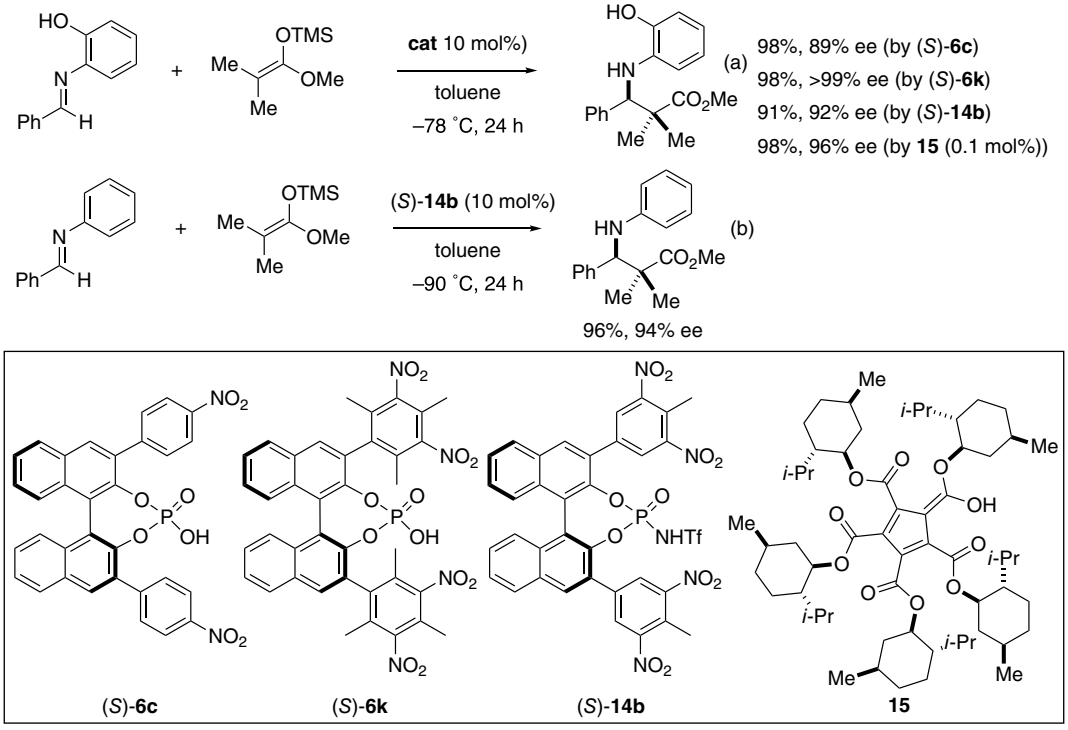

Scheme 2.2. Mannich reaction with *N*-(2-hydroxyphenyl)-imine (a) and with *N*-phenyl imine (b).

Lambert developed a novel chiral Brønsted acid **15**, which is readily prepared from (–)-menthol and 1,2,3,4,5-pentacarbomethoxycyclopentadiene, and reported Mannich-type reaction using as low as 0.01 mol% of **15** (Scheme 2.2a). A chiral anion pathway is proposed. It is noted that **15** can be synthesized inexpensively for about US$4/g because (–)-menthol is a naturally occurring compound [37].

Ishihara developed the chiral bisammonium salt of (*R*)-BINSA (1,1′-binaphthyl-2,2′-disulfonic acid) **8b** as a chiral Brønsted acid for the direct Mannich reaction [38]. Although CPA requires bulky 3,3′-substituents for attaining high enantioselectivity, the BINSA ammonium salt achieved excellent enantioselectivity without 3,3′-substituents using as low as 1 mol% of the catalyst loading (Scheme 2.3).

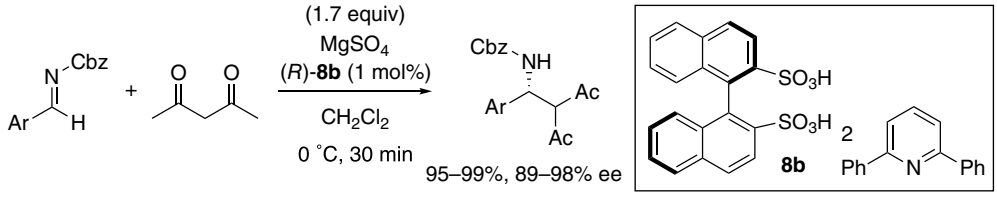

Scheme 2.3. Mannich reaction of 2,4-pentandione and *N*-Cbz-imine.

List recently reported an enantioselective synthesis of unprotected β-amino acids by the reaction between bis-silyl ketene acetal and silylated aminomethyl ether, followed by hydrolytic workup using a confined IDPi **11a** (Scheme 2.4) [39].

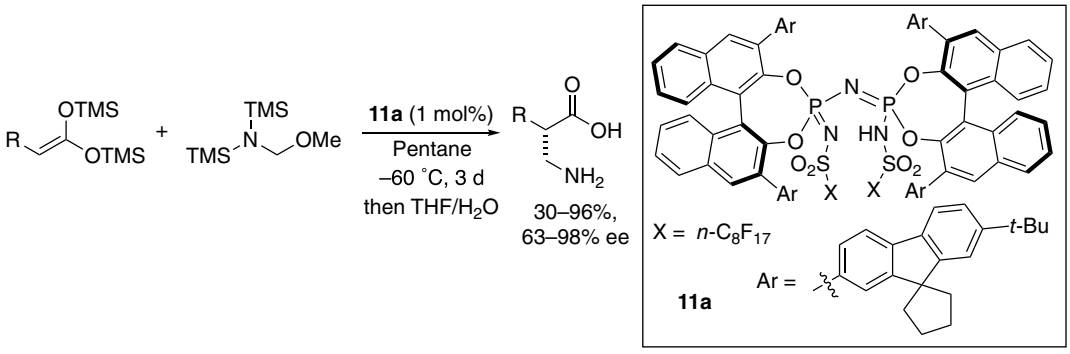

Scheme 2.4. Mannich reaction between bisi-silyl ketene acetal and silylated aminomethyl ether. Source: Based on [39].

In 2006, List reported a Pictet-Spengler reaction between substituted tryptamines and aldehyde catalyzed by CPA (*S*)-**6e**, bearing 2,4,6-(*i*-Pr)$_3$C$_6$H$_2$ moieties at 3,3′-positions, to furnish the corresponding tetrahydro-β-carbolines with 72–99% ee (Scheme 2.5a) [40]. The presence of bisethoxycarbonyl moieties is critical for the reaction. It is noted that CPA **6e** is called TRIP, and is the most frequently used chiral phosphoric acid. You reported a Pictet-Spengler reaction of indolyl dihydropyridines to afford tetrahydro-β-carbolines with 72–99% ee employing SPINOL-derived CPA (*R*)-**13b** (Scheme 2.5b) [41].

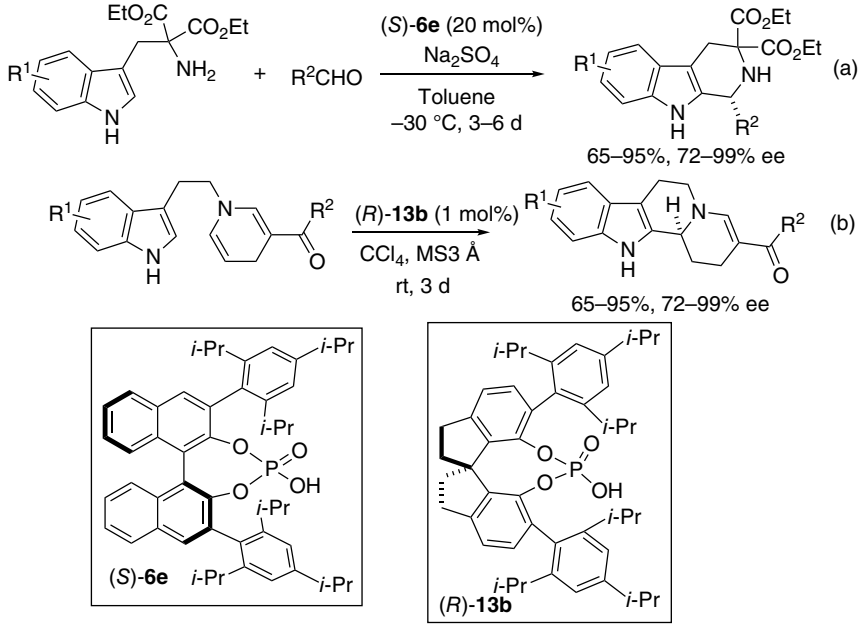

Scheme 2.5. Pictet-Spengler reaction between tryptamine and aldehyde (a) (Source: Based on [40]), and of indolyl dihydropyridines (b) (Source: Based on [41]).

The development of novel synthetic reactions and catalyst designs is normally accomplished by empirical optimization. Denmark demonstrated the utility of machine learning for predicting optimized catalyst CPA **6l** (TCYP) using the addition reaction between thiol and imino ketones. The predicted enantioselectivity correlated strongly with the experimental values. It is noted that this is the first example of the machine-learning-driven catalyst design in the field of asymmetric acid catalysts. The results constitute a potential transformation of empirical selection and optimization of a chiral catalyst by synthetic chemists into a mathematical-guided process (Scheme 2.6) [42].

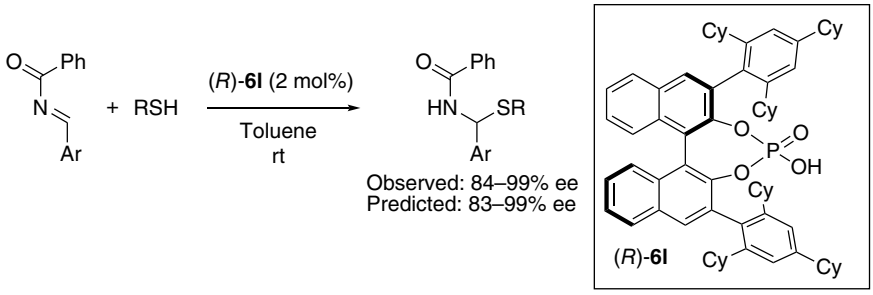

Scheme 2.6. Addition of thiol. Source: Based on [42].

Zhu reported a nucleophilic addition of *N*-monosubstituted hydrazones to *N*-Boc imines catalyzed by (*S*)-**6l**, which gave β-amino *N*,*N*′-dialkyldiazenes in excellent yields, and the obtained β-amino *N*,*N*′-dialkyldiazenes were transformed into vicinal diamines (Scheme 2.7) [43]. *N*-Alkyl hydrazones served as the α-azo carbanion equivalents.

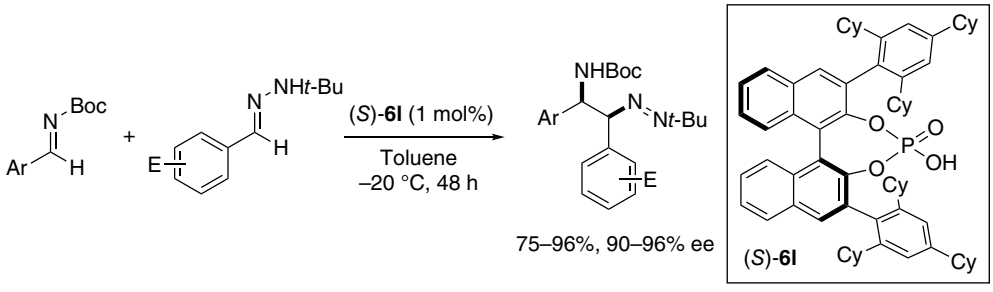

Scheme 2.7. Addition of hydrazone. Source: Based on [43].

Zhao reported a polyene cyclization reaction using BINOL-derived chiral phosphoramide (*R*)-**14b** to furnish fused tricyclic compounds (Scheme 2.8). The cyclization reaction was applied to the total synthesis of (–)-ferruginol [44].

The Friedel-Crafts alkylation reaction between electron-rich heterocycles and imine is an important method for the preparation of chiral indole derivatives. You reported a Friedel-Crafts alkylation reaction between indole and aldimines using BINOL-derived CPA **6f** [45]. Lin synthesized novel CPA from (*S*)-1,1′-spirobiindane-7,7′-diol ((*S*)-SPINOL), and found that **13c**, bearing the 1-naphthyl moiety at 6,6′-positions, exerted similar reactivity and enantioselectivity to BINOL-derived phosphoric acid (Scheme 2.9) [19, 46]. Numerous kinds of Friedel-Crafts alkylation reactions of indoles with aldimines and other electrophiles have been reported to proceed efficiently using organocatalysts [47].

The construction of a quaternary carbon center is a challenging task. Ishihara developed chiral monopotassium binaphthyl disulfonate **8c** as a strong Brønsted acid catalyst and realized Friedel-Crafts alkylation

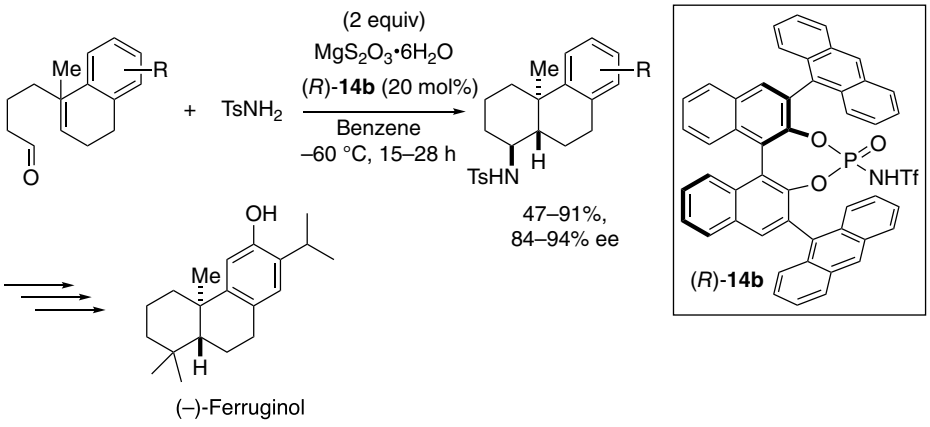

Scheme 2.8. Polyene cyclization.

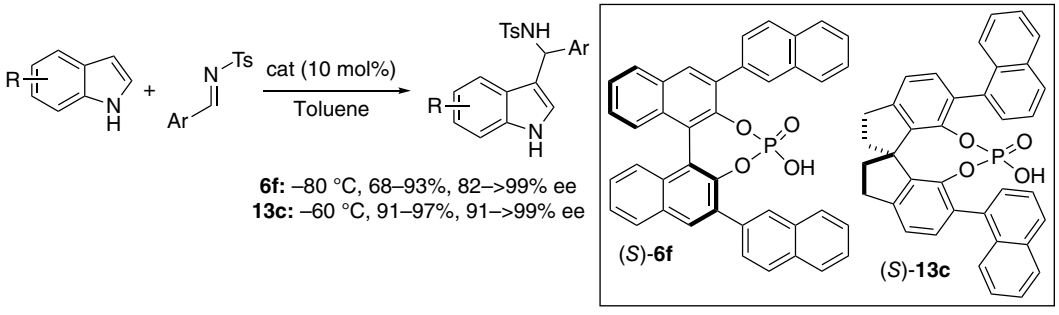

Scheme 2.9. Friedel-Crafts alkylation reaction between indoles and imines. Source: [19, 46].

reaction between indole and ketimine to generate quaternary stereogenic centers (Scheme 2.10a) [48]. Ishihara also developed C_1-symmetric BINOL-derived bisphosphoric acid **16** and achieved a Friedel-Crafts alkylation reaction between 2-methoxyfuran and α-imino esters (Scheme 2.10b) [49]. The bisphosphoric acid **16** exhibited stronger acidity in comparison with monophosphoric acid due to the intramolecular hydrogen bond network. This is an example of the Brønsted acid-assisted Brønsted acid catalysis [50].

In general, *N*-aryl ketimines are stable, whereas *N*-H imines are labile. In contrast, trifluoromethylated *N*-H ketimines are relatively stable. Akiyama reported Friedel-Crafts alkylation reaction between CF_3-substituted *N*-H ketimines and pyrroles using CPA **6e** to furnish 2-pyrrole derivatives with 83–97% ee (Scheme 2.11a) [51, 52]. 4,7-Dihydroindoles also participated in the Friedel-Crafts alkylation reaction with CF_3-subsituted ketimine, and subsequent dehydrogenation with 2,3-dichloro-5,6-di cyano-1,4-benzoquinone (DDQ) furnished 2-substituted indoles with 76–95% ee (Scheme 2.11b) [53].

Ohshima developed C_1-symmetric 3-monosubstituted BINOL phosphoric acid **17** and achieved a highly enantioselective Friedel-Crafts alkylation reaction between *N*-unprotected α-iminoesters and indoles (Scheme 2.12) [54]. Interestingly, use of C_2-symmetric 3,3′-disubstituted BINOL phosphoric acid gave lower enantioselectivity: 93% ee with CPA **17** and 61% ee with CPA **6h**.

Akiyama reported an enantioselective synthesis of tetrahydroquinoline derivatives by the internal redox reaction catalyzed by biphenol-derived CPA **18** [55]. This reaction was proposed to proceed by a [1,5]-H shift to generate a zwitterionic intermediate, followed by a 6-*endo* cyclization to yield tetrahydroquinoline derivatives (Scheme 2.13). An enantioselective C–H activation was proposed.

Radical reactions are an underexplored area in the field of chiral Brønsted acid catalysis. Kim reported a radical addition reaction that used iodoalkane as the radical precursor in the presence of chiral

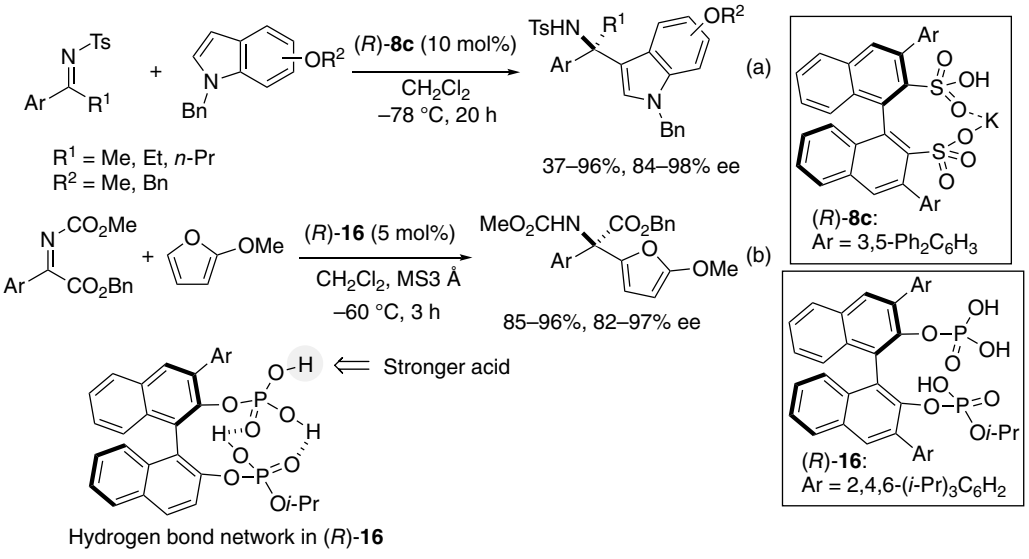

Scheme 2.10. Friedel-Crafts alkylation reaction with ketimines and indoles (a) (Source: Based on [48]) and furans (b) (Source: Based on [49]).

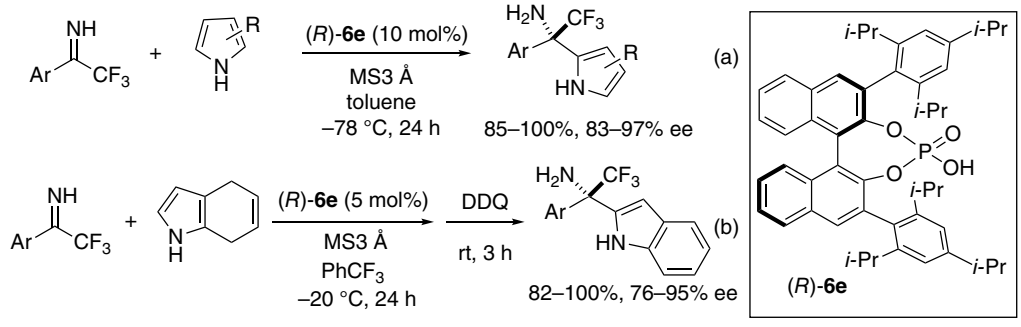

Scheme 2.11. Friedel-Crafts alkylation reaction between *N*-H trifluoromethylated ketimines and pyrroles (a) (Source: [51, 52]) and 4,7-dihydroindole (b) (Source: Based on [53]).

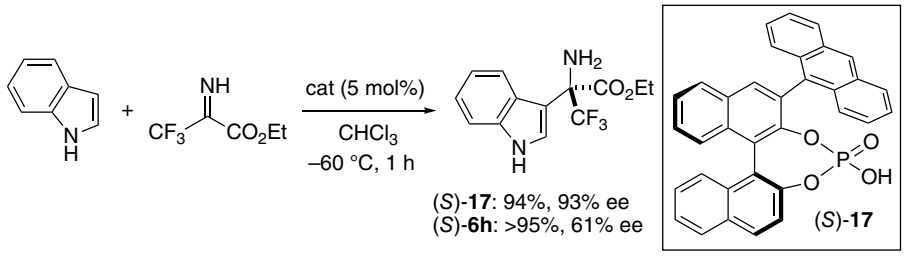

Scheme 2.12. Friedel-Crafts alkylation reaction between indole and *N*-H trifluoromethylated iminoesters. Source: Based on [54].

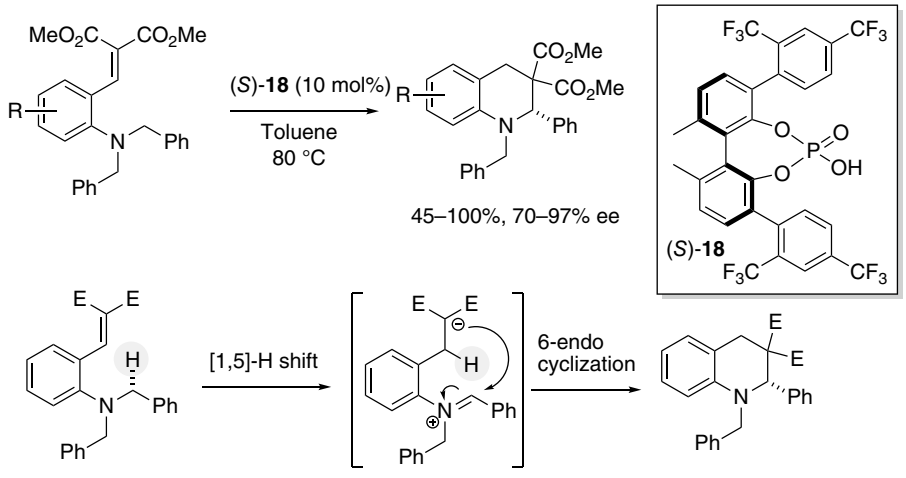

Scheme 2.13. Internal redox reaction.

phosphoramide **14c**, which furnished addition products in good yields and with moderate to good enantioselectivity (73–84% ee) (Scheme 2.14). $(Me_3Si)_3SiH$ (TTMSSH) and Et_3B were employed as initiators [56].

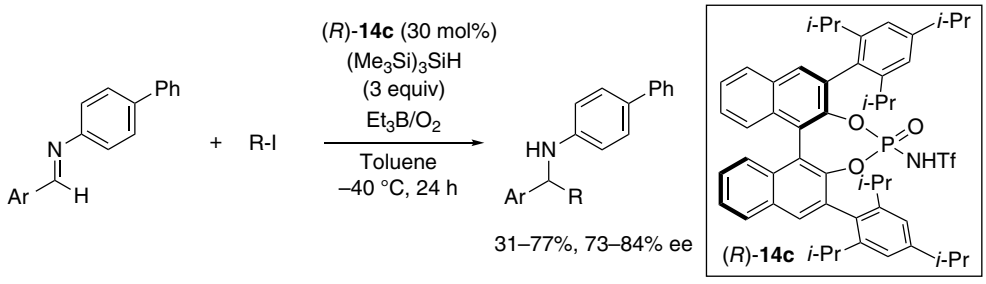

Scheme 2.14. Radical addition to imines.

2.3.2. Reactions with Carbonyl Compounds and Oxonium Salts

List reported a Torgov reaction catalyzed by chiral DSI **9b**, which yielded enantioenriched tri- and tetracyclic dienes. The Torgov reaction is proposed to proceed by the isomerization of alkene followed by the Prins reaction, a subsequent isomerization, and dehydration (Scheme 2.15). The method was successfully applied to a concise synthesis of (+)-estrone [57].

List subsequently attempted to perform Prins cyclization, but chiral DSI **9** was not sufficiently acidic enough to promote the Prins cyclization. List developed confined imino-imidodiphosphates (*i*IDPs) **19a** and **19b** as a new class of highly acidic Brønsted acids and reported the Prins cyclization. Both aliphatic and aromatic aldehydes participated in the reaction successfully to furnish tetrahydropyran derivatives with 80–96% ee (Scheme 2.16) [58].

List reported an intramolecular carbonyl-ene reaction of olefinic aldehyde using confined IDP **10a** as chiral Brønsted acid to afford diverse *trans*-3,4-disubstituted five-membered carbo- and heterocycles in 77–96% yields and with *trans* selectivity (4 : 1 to >20 : 1), and with 84–96% ee (Scheme 2.17) [59].

Rueping reported intermolecular carbonyl-ene reaction of 1,1-disubstituted alkene with ethyl trifluoromethylpyruvate using *N*-triflyl phosphoramide. But the enophile was limited to trifluoromethylpyruvate [60]. In order to achieve carbonyl-ene reaction with wider substrate scope, Terada designed stronger

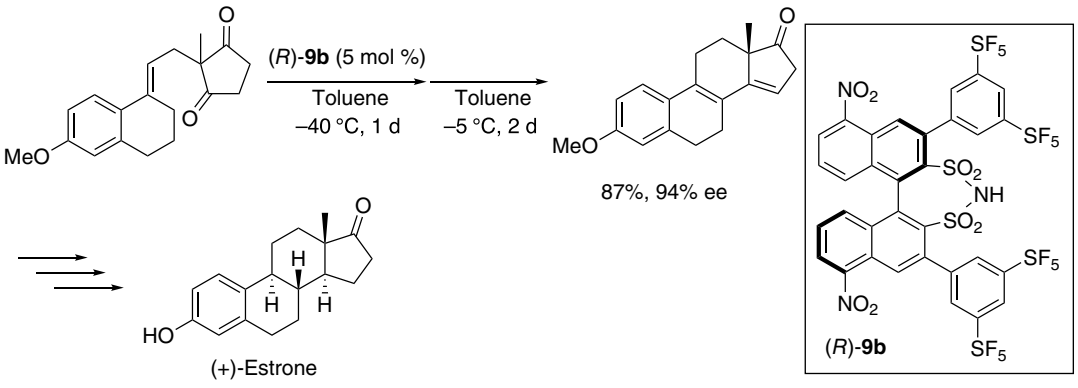

Scheme 2.15. Torgov reaction.

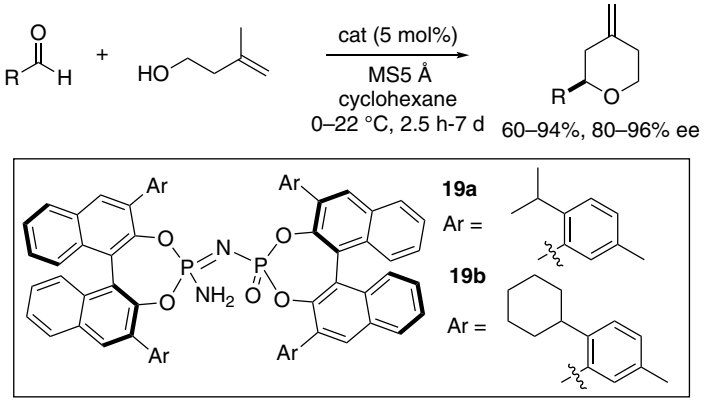

Scheme 2.16. Prins cyclization. Source: Based on [58].

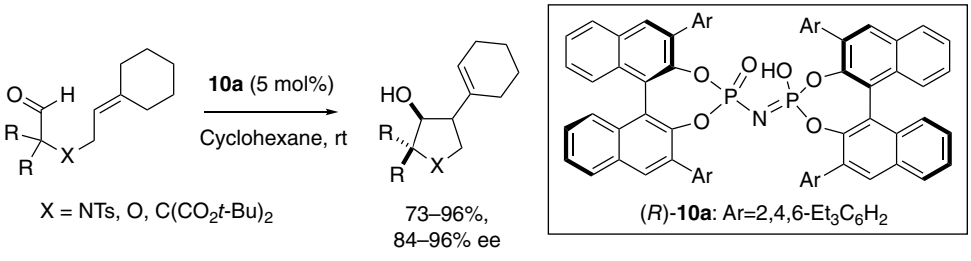

Scheme 2.17. Intramolecular carbonyl-ene reaction. Source: Based on [59].

Brønsted acid by perfluorination of the BINOL moiety. CPA **20**, derived from F_{10}-BINOL, catalyzed the intermolecular carbonyl-ene reaction between exocyclic alkene and ethyl glyoxylate to furnish homoallylic alcohols with 62–93% ee (Scheme 2.18) [61].

In 2010, List independently synthesized chiral phosphoric acids derived from (*S*)-SPINOL. A highly enantioselective kinetic resolution of homoaldols was achieved using CPA **13b** (STRIP), which is derived from (*S*)-SPINOL bearing 2,4,6-(*i*-Pr)$_3$C$_6$H$_2$ groups at 6,6′-positions, to furnish tetrahydrofuran derivatives in a highly enantioselective manner by transacetalization (Scheme 2.19) [20].

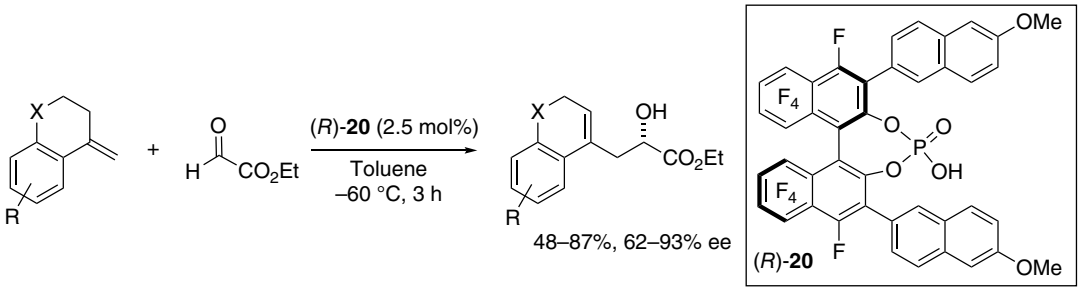

Scheme 2.18. Intermolecular carbonyl-ene reaction. Source: Based on [61].

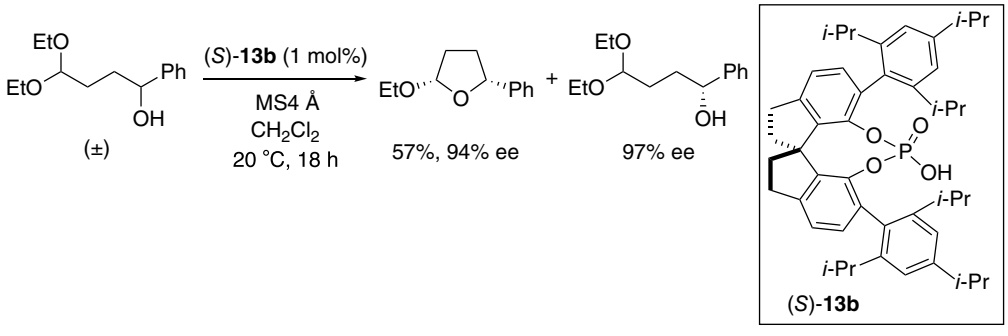

Scheme 2.19. Kinetic resolution of homoaldols. Source: Based on [20].

The enantioselective allylation of aldehyde is an important reaction for the preparation of homoallylic alcohols. Antilla reported an enantioselective allylation of aromatic and aliphatic aldehydes with allylboronate using CPA **6e** to furnish homoallylic alcohols with 73–99% ee (Scheme 2.20a) [62]. Allenyl boronate also participated in the reaction to furnish homopropargyl alcohols in 87–96% yields and with 77–96% ee (Scheme 2.20b) [63]. Based on the density-functional theory (DFT) studies, Goodman [64], and Houk-Antilla [65] independently proposed a transition state model of the allylboration and the propargylation. Phosphoric acid forms a hydrogen bond with boronate pseudo axial oxygen and at the same time, phosphoryl oxygen forms a hydrogen bond with formyl hydrogen (Figure 2.6).

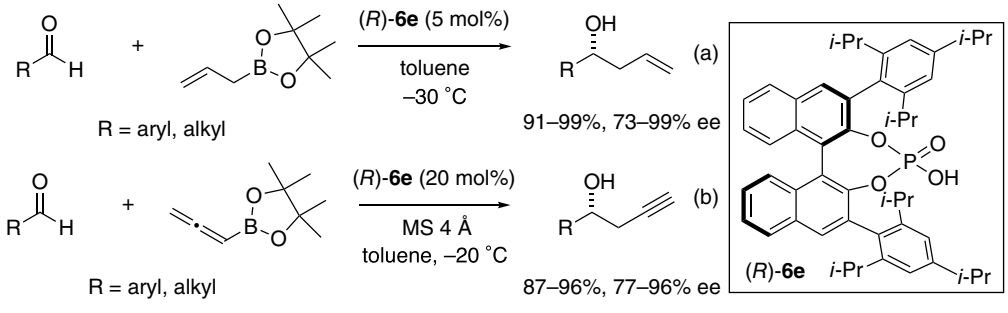

Scheme 2.20. Allylation of aldehyde by allylboronate (a) (Source: Based on [62]), and proparygylation with allenylboronate (b) (Source: Based on [63]).

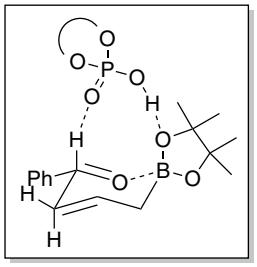

Figure 2.6. Transition state model of the allylation with allylboronate.

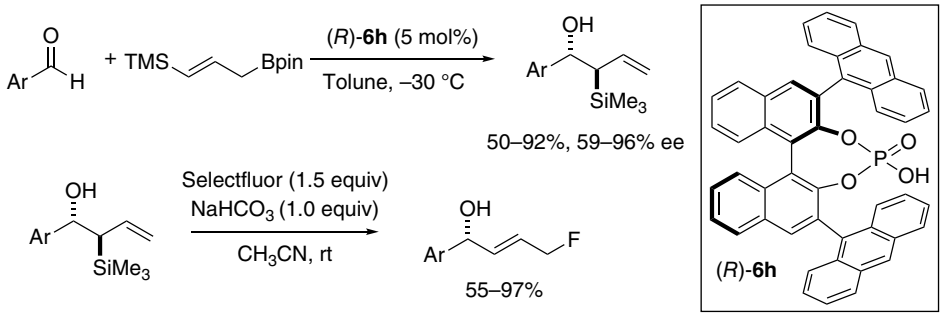

Scheme 2.21. Allylation of aldehyde with γ-silyl boronate.

Barrio employed γ-silyl boronate to form α-silyl homoallylic alcohols with excellent diastereoselectivity and with 59–96% ee catalyzed by CPA **6h** (Scheme 2.21). Subsequent treatment with Selectfluor furnished fluorinated allylic alcohols [66].

Chen reported an enantioselective addition of achiral α-vinyl allylboronate to aldehyde to furnish dienyl homoallylic alcohols with high *Z*-selectivity and with 90–97% ee (Scheme 2.22) [67, 68].

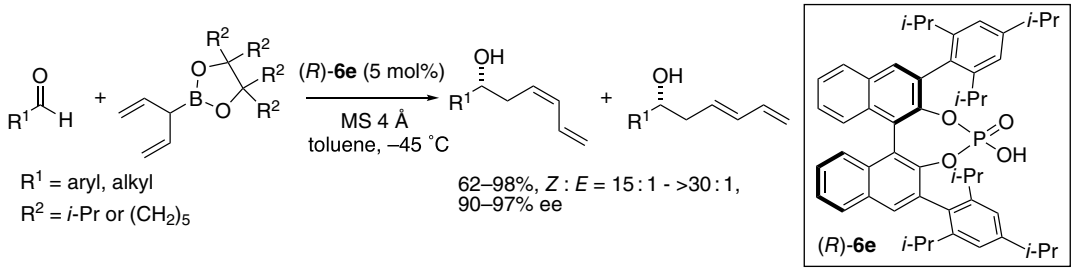

Scheme 2.22. Allylation of aldehydes with α-vinyl allylboronate. Source: Based on [67, 68].

As an extension of the allylation reaction, Murakami combined allylboration and a Pd-catalyzed transposition reaction of homoallylic bisboronate. Treatment of 1,1-di(boryl)alk-2-ene with Pd catalyst generated allylboronate, in situ, which underwent an allylboration reaction with an aldehyde using CPA **6e** to afford *anti*-homoallylic alcohols with high diastereo- and enantioselectivities (Scheme 2.23a) [69]. The same group subsequently reported an enantioselective synthesis of *anti*-1,2-oxaborinan-3-enes from aldehydes and 1,1-di(boryl)alk-3-enes using Ru(II) complex and CPA **6e** (Scheme 2.23b) [70].

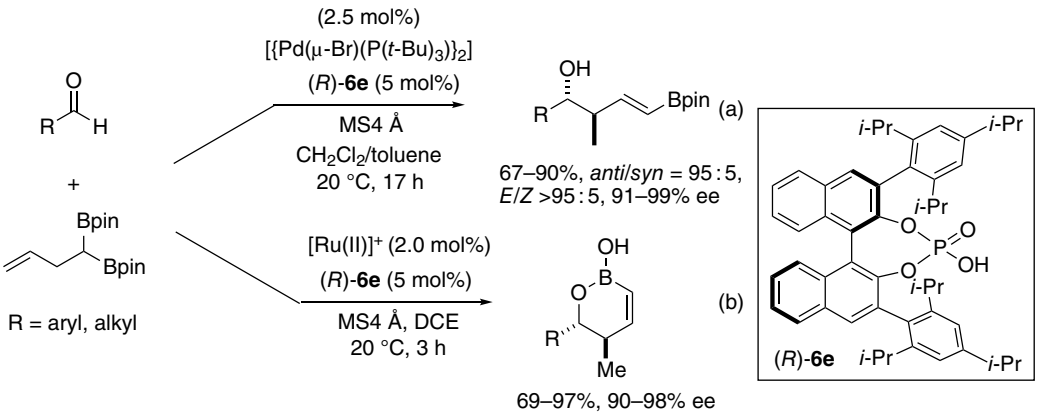

Scheme 2.23. Reaction between di(boryl)butane and aldehyde, leading to the formatinof *anti*-homoallylic alcohols (a) (Source: Based on [69]), and *anti*-1,2-oxaborinan-3-enes (b) (Source: Based on [70]).

With regard to the allylation reaction using allylsilane, List reported the Hosomi-Sakurai allylation reaction between allylsilane and aromatic aldehydes catalyzed by chiral DSI **9c** (Scheme 2.24a) [71]. DSI **9c** acted as a precatalyst, *N*-trimethylsilyl sulfonimide was generated as a chiral Lewis acid catalyst, and sulfonimide anion controlled the enantioselectivity by acting as a chiral counteranion. Subsequently, List developed highly acidic IDPs **11b** and **11c** [14], and reported a catalytic addition reaction between allyltrimethylsilane and aldehydes, which is based on the silylium-based Lewis acid organocatalysis (Scheme 2.24b) [72]. Both aromatic and aliphatic aldehydes were suitable substrates. It is noted that as

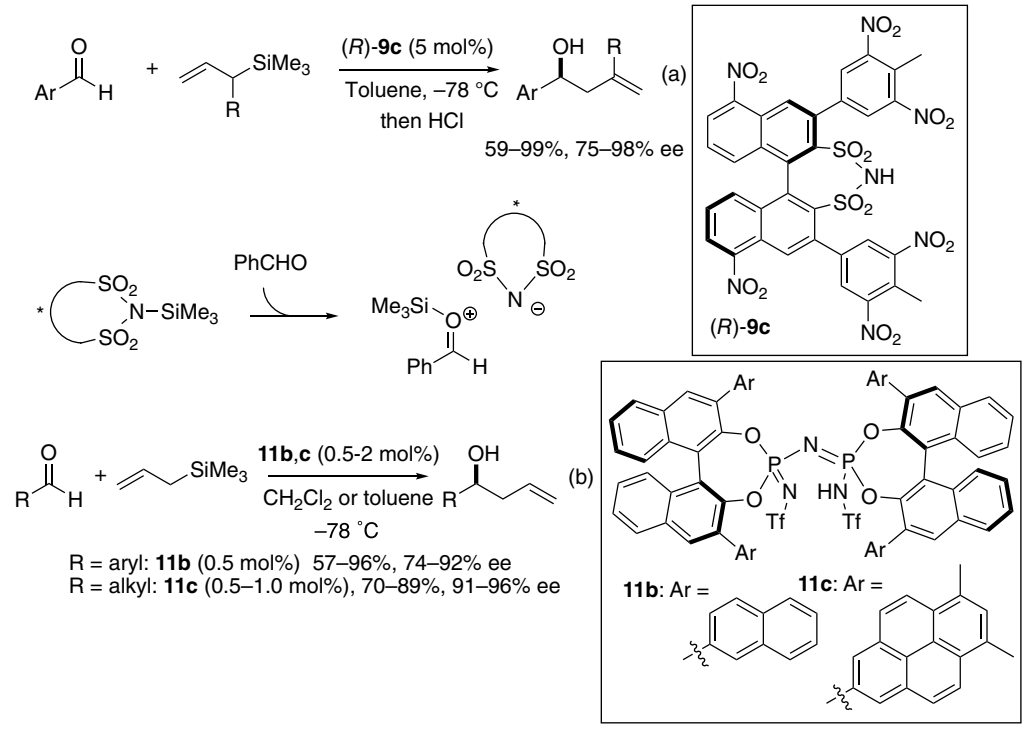

Scheme 2.24. Allylation reaction using **9c** (a) and **11b,c** (b) (Source: Based on [72]).

low as 0.5 mol% of the catalyst promoted the allylation reaction with aromatic aldehyde, and as low as 0.05 mol% of the catalyst could be employed with aliphatic aldehydes.

List reported a catalytic Mukaiyama aldol reaction that uses chiral IDPi **11d** as the catalyst to furnish aldol products with 80–98% ee. The silylium ion is considered to be the actual catalyst. It is noted that parts per million (ppm) levels of catalyst were sufficient for the aldol reaction [73]. In general, aldehyde is more reactive than ketone. They subsequently developed a ketone-selective Mukaiyama aldol reaction catalyzed by **11e** to afford tetrahydrofuran derivatives with high chemoselectivity and with 84–97% ee (Scheme 2.25). The in situ generated silylium ion pair coordinated to sterically less hindered aldehydes and subsequent intramolecular cyclization gave a highly active cyclic oxocarbenium ion intermediate bearing a chiral counteranion, which appears to be responsible for the chemoselectivity (Figure 2.7) [74].

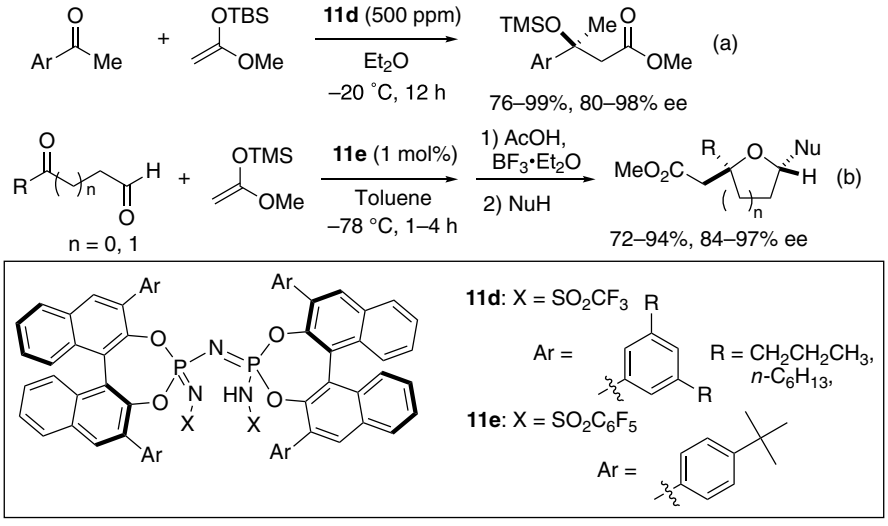

Scheme 2.25. Mukaiyama aldol reaction with ketones (a) and ketone selective Mukaiyama aldol reaction (b).

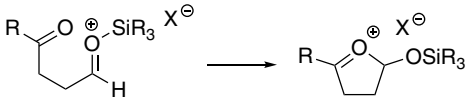

Figure 2.7. Reaction intermediate in the ketone-selective reaction. Source: Based on [74].

Seidel developed an enantioselective synthesis of isoindolinones through the condensation of 2-acylbenzaldehydes with anilines in the presence of CPA **6e** (Scheme 2.26) [75]. They proposed that the tautomerization of the hydroxy-isoindoline intermediate to isoindoline is proposed to be the enantiodetermining step.

Yang developed an efficient method for the synthesis of 4*H*-3,1-benzoxazines by kinetic resolution of 2-amido benzyl alcohols catalyzed by CPA **6i** [76]. A broad range of benzyl alcohols (both tertiary and secondary alcohols) was kinetically resolved, wherein the amide group reacted as the electrophile (Scheme 2.27).

The oxa-Pictet-Spengler reaction was reported by several groups. List employed nitrated confined IDP **10b** as the chiral strong Brønsted acid catalyst for the oxa-Pictet-Spengler reaction between 2-arylethanols and aldehydes to furnish 1-substituted isochromans with 90–99% ee (Scheme 2.28) [77].

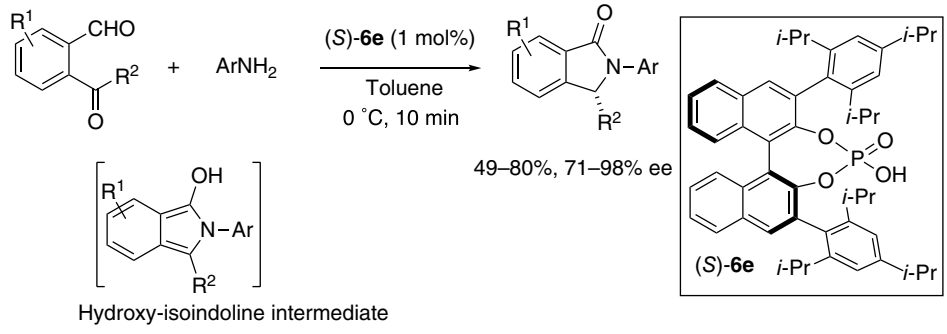

Scheme 2.26. Enantioselective synthesis of isoindolinones. Source: Based on [75].

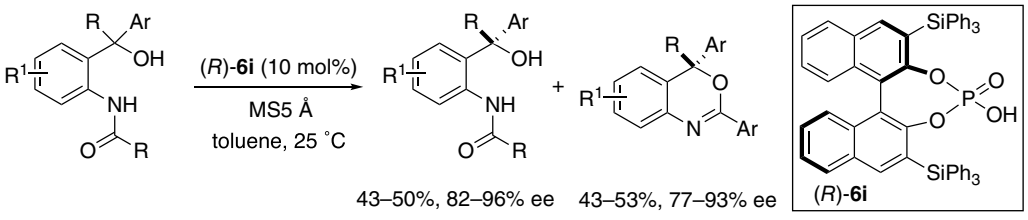

Scheme 2.27. Kinetic resolution of 2-amido benzyl alcohols.

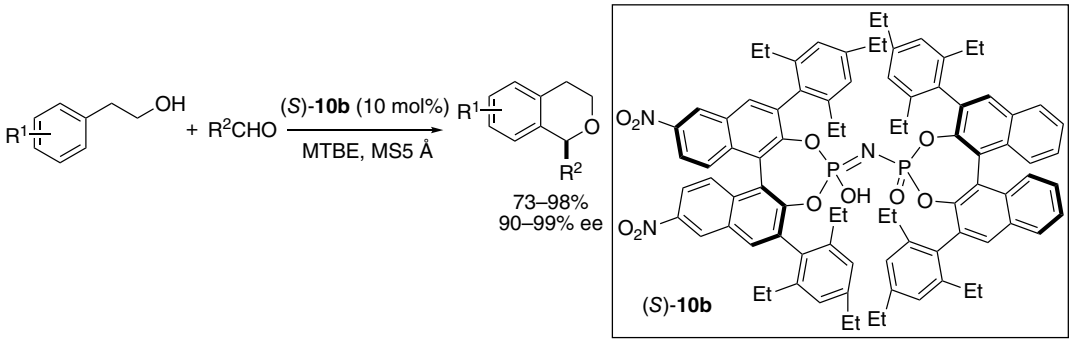

Scheme 2.28. Oxa-Pictet-Spengler reaction of 2-arylethanols. Source: Based on [77].

Subsequently, Scheidt developed a cooperative catalyst system consisting of achiral hydrogen donor **21** and CPA **6b**, and achieved an oxa-Pictet-Spengler reaction (Scheme 2.29). The reaction proceeded via oxocarbenium ions bearing chiral counteranion intermediate [78].

Seidel developed a dual catalyst system employing both chiral amine HCl salt and a chiral bisthiourea to generate oxocarbenium ion intermediate from aldehyde and realized an oxa-Pictet-Spengler reaction between tryptophol and aldehydes (Scheme 2.30) [79].

Seidel was the first to report an oxa-Pictet-Spengler reaction with ketals by developing novel chiral carboxylic acid **24**, bearing a urea moiety derived from 1,2-diaminocyclohexane (Scheme 2.31) [80]. They measured the pK_a value of the catalysts in CH_3CN and found that **24** was one order of magnitude more acidic than CPA **6e**: 12.7 for **24** and 13.6 for CPA **6e**.

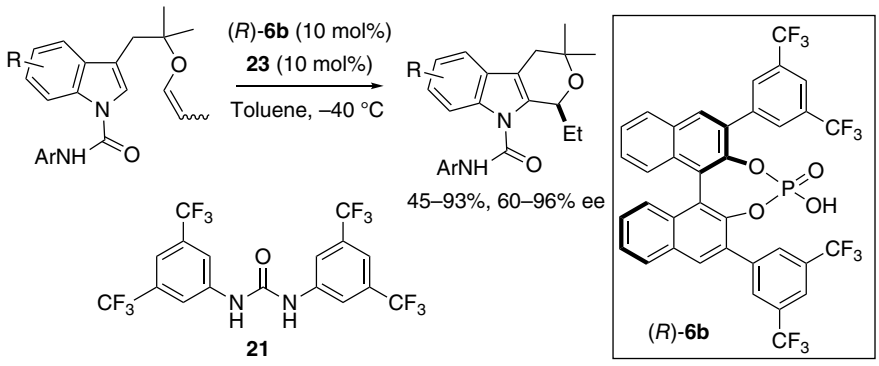

Scheme 2.29. Oxa-Pictet-Spengler reaction. Source: Based on [78].

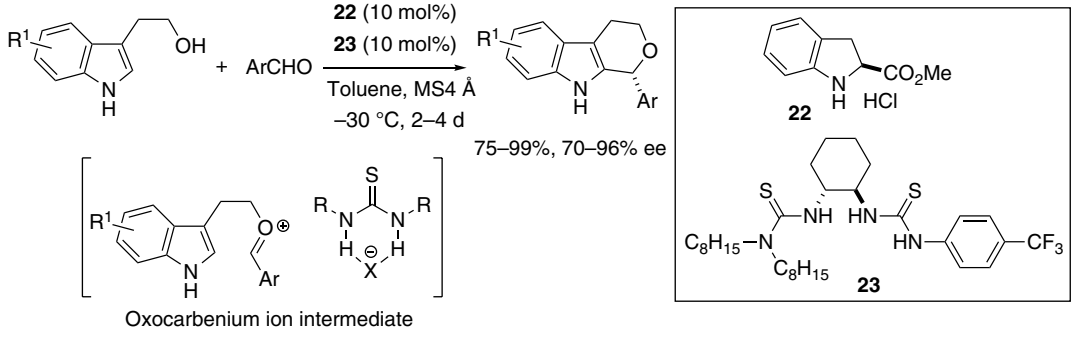

Scheme 2.30. Oxa-Pictet-Spengler reaction between tryptophol and aldehydes. Source: Based on [79].

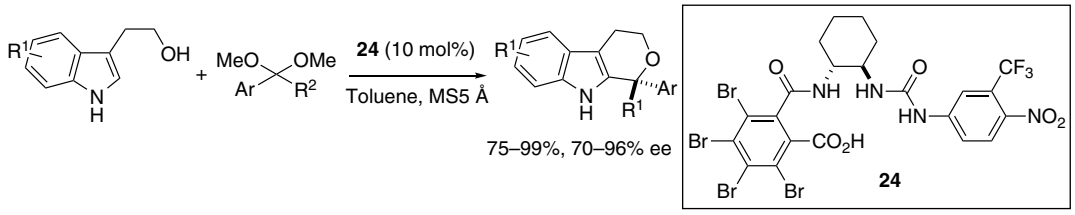

Scheme 2.31. Oxa-Pictet-Spengler reaction with ketal.

2.4. CYCLOADDITION REACTIONS

2.4.1. Diels-Alder Reactions

In comparison with metal-based Lewis acid catalysts, chiral Brønsted acid catalysts had limited application to reactive substrates because of the moderate acidity of phosphoric acid. In order to overcome this drawback, Yamamoto introduced an NHTf moiety in place of the OH moiety of CPA **6** to generate a stronger Brønsted acid in 2006. As shown in Section 2.2.1 (Figure 2.2), acidity of phosphoramide **14** is seven orders of magnitude stronger than CPA **6**. CPA **6** did not promote the Diels-Alder reaction between α,β-unsaturated ketone and siloxydiene. *N*-triflyl chiral phosphoramide **14c** catalyzed the Diels-Alder reaction smoothly to furnish the cycloadducts in 43–>99% yields with 82–92% ee (Scheme 2.32) [21, 81].

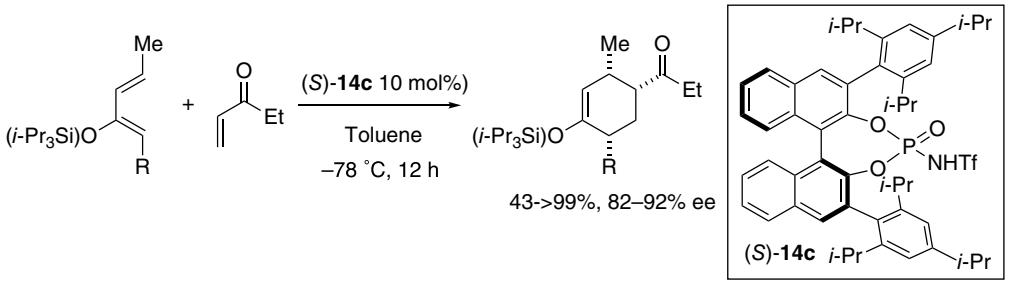

Scheme 2.32. Diels-Alder reaction. Source: [21, 81].

List reported a highly enantioselective Diels-Alder reaction between cyclopentadiene and 9-anthracenylmethyl cinnamates [82]. C-H acid **25** was employed in combination with ketene silyl acetal as the silylating agent (Scheme 2.33). Silylium ion was identified as the chiral Lewis acid catalyst. The reaction was proposed to proceed by way of the silylium binaphthyl-allyl-tetrasulfonate (BALT) anion intermediate (Figure 2.8). Although use of bulky 9-anthracenylmethyl ester was required, List later reported that a simple α,β-unsaturated ester could be employed in the Diels-Alder reaction with cyclopentadienes using IDPi catalysts **11** (Scheme 2.34) [83].

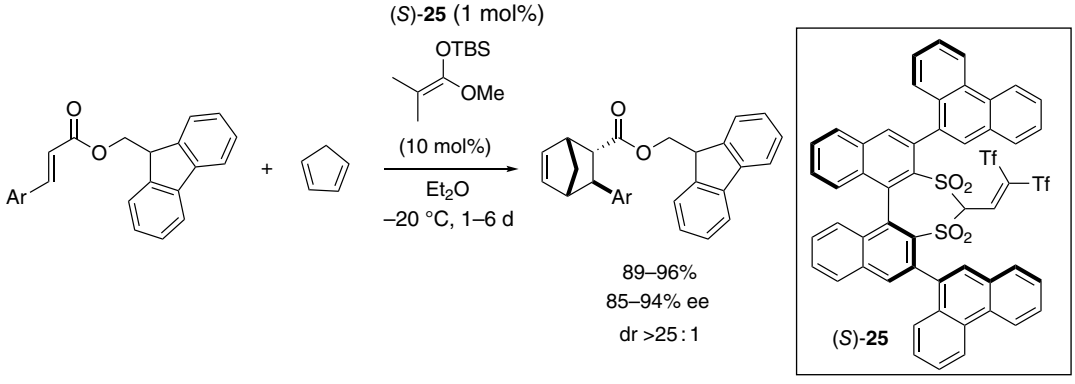

Scheme 2.33. Diels-Alder reaction by C–H acid.

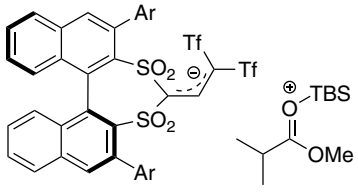

Figure 2.8. Silylium binaphthyl-allyl-tetrasulfonate anion intermediate.

List reported an enantioselective Diels-Alder reaction between cyclopentadiene and enals, which is based on a multisubstrate screening approach [84]. Whereas α-substituted enals gave *exo* adducts selectively, β-substituted enals gave *endo* adducts preferentially catalyzed by **11j** (Scheme 2.35a). List subsequently reported a Diels-Alder reaction between cross-conjugated cyclohexadienones and cyclopentadiene using confined chiral monophosphate **11k**. Up to five stereocenters were constructed in 66–98% yields with high diastereoselectivity and with 84–95% ee (Scheme 2.35b) [85].

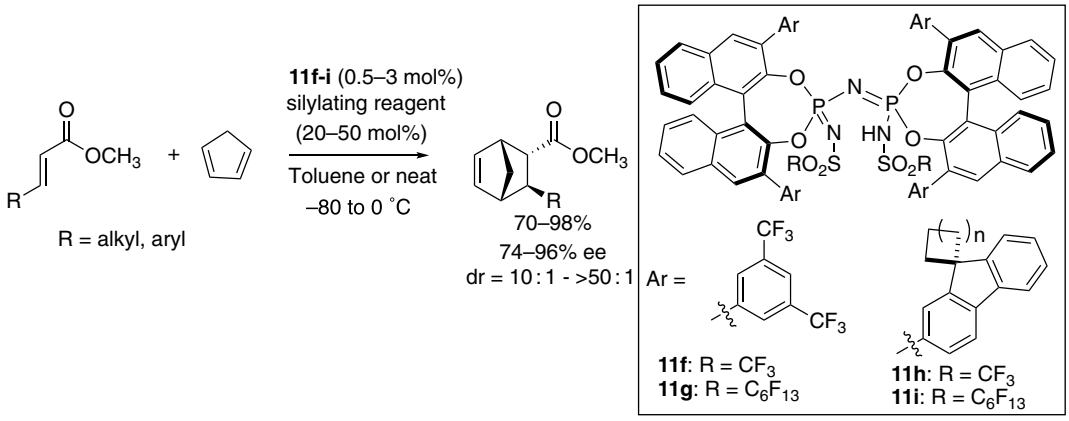

Scheme 2.34. Diels-Alder reaction between simple ester and cyclopentadiene catalyzed by IDPi. Source: Based on [83].

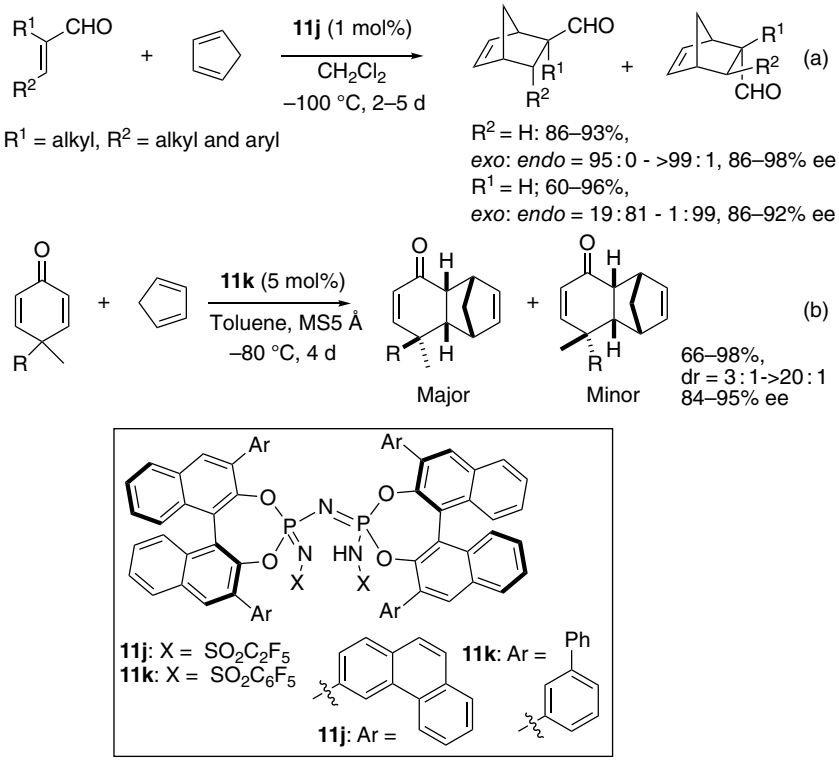

Scheme 2.35. Diels–Alder reaction between cyclopentadien and enals (a), and cyclopentadienone (b) using IDPi (Source: Based on [85]).

Numbers of enantioselective Diels-Alder reactions have been reported, but reactions with unbiased benzoquinones have remained a formidable challenge. Masson developed the Diels-Alder reaction between quinone and diene carbamate to afford dihydronaphthalene-1,4-diols catalyzed by SPINOL-derived CPA **13c** (Scheme 2.36a) [86]. Simply changing the amount of quinone resulted in the selective formation of the redox isomers with high stereoselectivity (Scheme 2.36b).

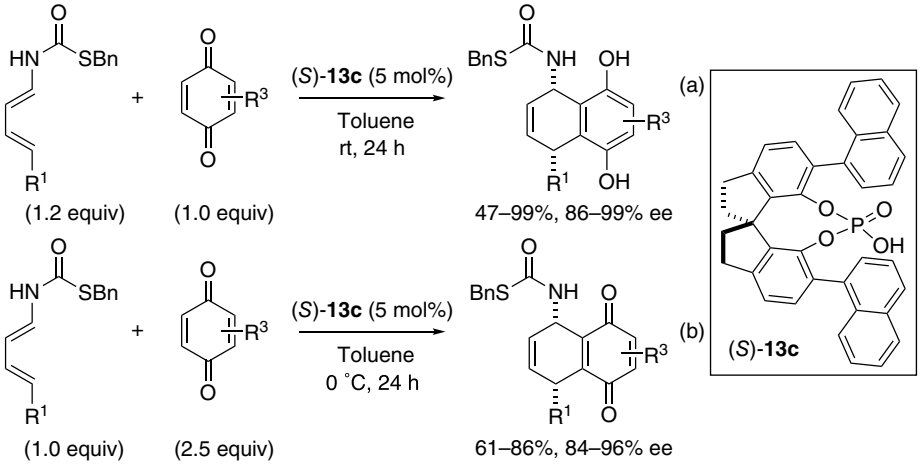

Scheme 2.36. Redox-divergent Diels-Alde reaction leading to dihydronaphthalene-1,4-diols (a) (Source: Based on [86]), and redox isomers (b).

In order to generate a stronger chiral Brønsted acid, Ishihara employed a BBr_3-CPA **6m** complex that is expected to function as Lewis acid-assisted Brønsted acid (LBA) [50], to promote the Diels-Alder reaction between α-substituted acroleins and 1,2-dihydropyridines, which gave cycloadducts with 92–98% ee (Scheme 2.37, Figure 2.9) [87].

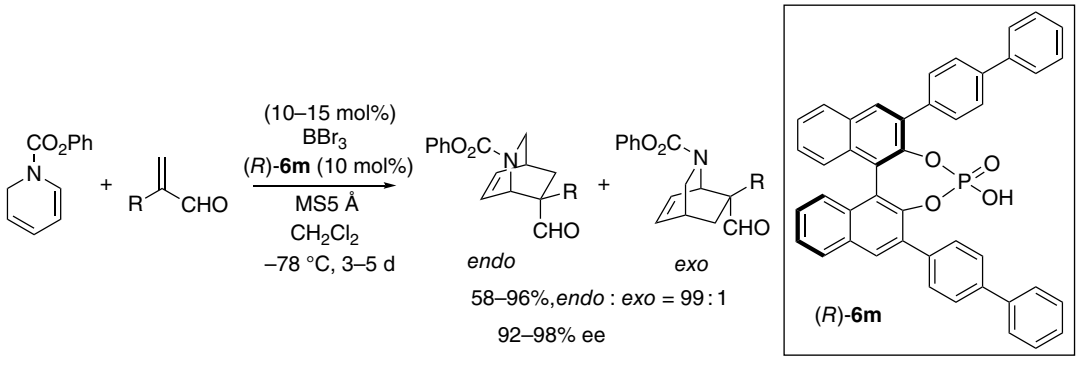

Scheme 2.37. Diels-Alder reaction promoted by Lewis acid-assisted Brønsted acid. Source: Based on [87].

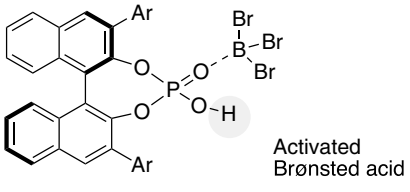

Figure 2.9. Lewis acid-assisted chiral Brønsted acid. Source: Based on [87].

2.4.2. Aza-Diels-Alder Reactions

The Povarov reaction is an inverse electron-demand aza-Diels-Alder reaction and 2-azadiene and electron-rich alkenes. Akiyama reported the Povarov reaction between aldimine bearing a 2-hydroxyphenyl group on nitrogen and electron-rich alkene using CPA **6h** in 2006 (Scheme 2.38a) [88]. Although presence of the 2-hydroxyphenyl group on nitrogen was critical for the Povarov reaction, Zhu and Masson reported a three-component Povarov reaction using enecarbamates as dienophiles catalyzed by **12a** (Scheme 2.38b) [89, 90]. Use of the 2-hydroxyphenyl group was obviated. The mechanism of the Povarov reaction is shown in Figure 2.10. Whereas phosphoryl oxygen formed a hydrogen bond with the 2-OH moiety in the reaction reported by Akiyama, Zhu and Masson proposed that phosphoryl oxygen would form a hydrogen bond with the *N*-H moiety of the enecarbamate.

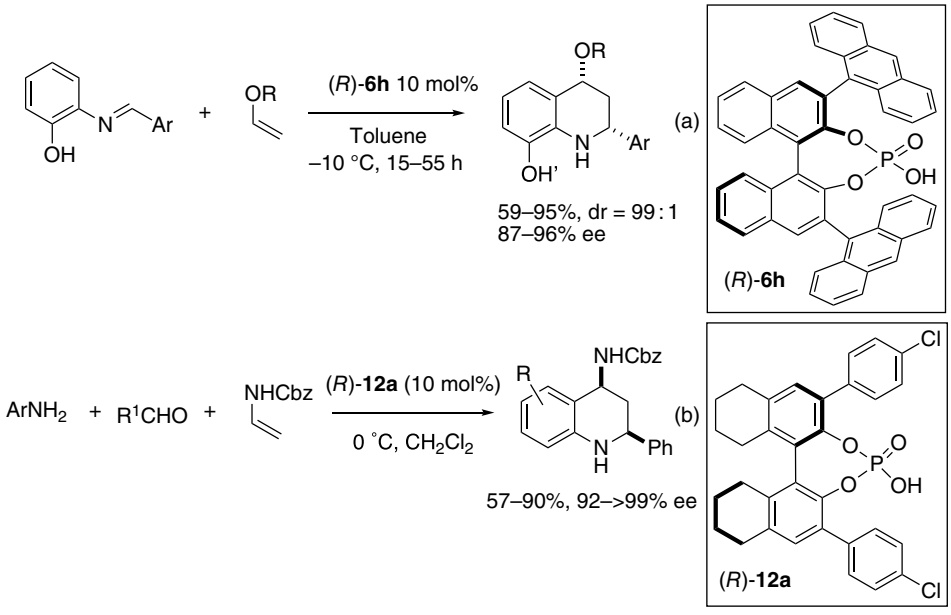

Scheme 2.38. Povarov reaction with *N*-2-hydroxyphenyl imine (a) (Source: Based on [88]) and *N*-phenyl imine (b) (Source: [89, 90]).

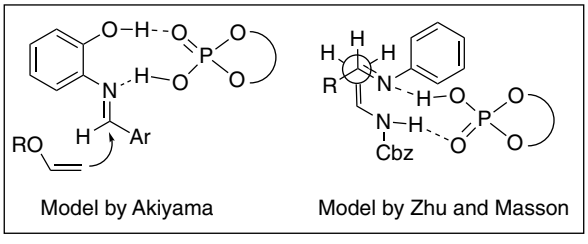

Figure 2.10. Transition state model of the aza-Diels-Alder reaction.

Masson subsequently reported intramolecular Povarov reactions catalyzed by **6e** (Scheme 2.39) [91]. Imines were generated in situ from aldehydes and *o*-hydroxyaniline.

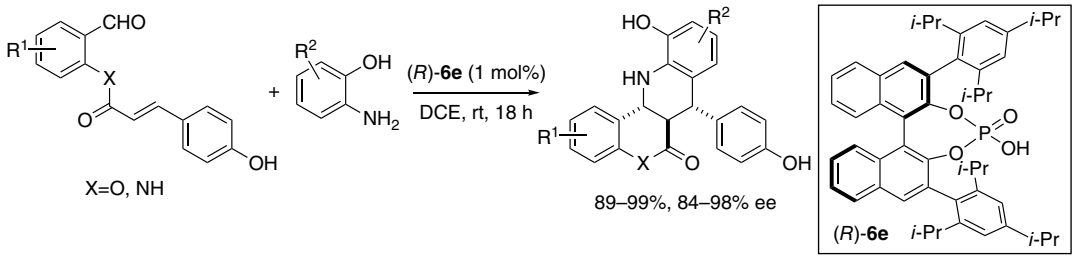

Scheme 2.39. Intramolecular Povarov reaction of azadiene. Source: [91].

Huang succeeded in the construction of tetrahydroquinolines bearing two quaternary stereogenic centers by the reaction between two types of aniline derivatives and pyruvate catalyzed by CPA **12b** (Scheme 2.40) [92]. The Mannich reaction and the subsequent Friedel-Crafts cyclization gave C2-quaternary carbon centers. "Hybrid" Povarov products were obtained from aniline pairs.

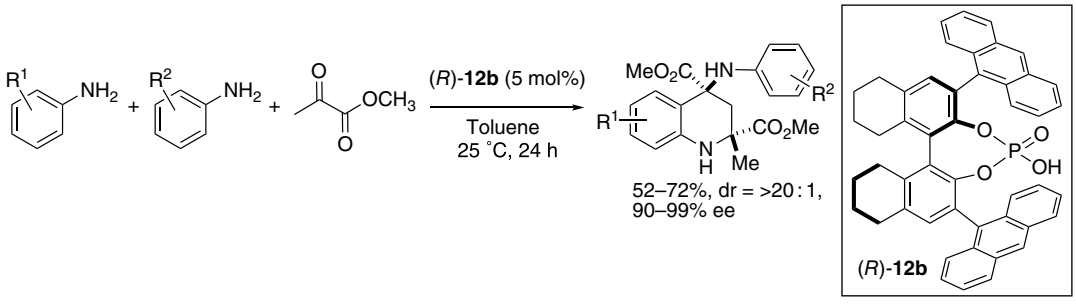

Scheme 2.40. Povarov reaction leading to tetrahydroquinoline with two quaternary stereogenic centers.

Terada reported a hetero-Diels-Alder reaction between azopyridine carboxylate and amidodienes by developing a novel chiral carboxylic acid-monophosphoric acid **26** (Scheme 2.41) [93].

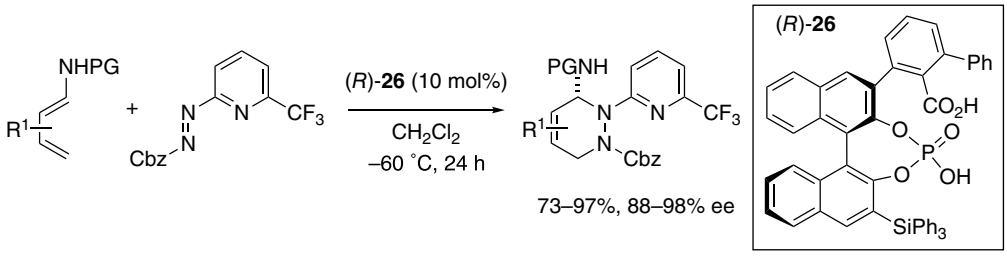

Scheme 2.41. Hetero-Diels-Alder reaction between azopyridine carboxylate and amidodienes. Source: Based on [93].

Schneider reported a hetero-Diels-Alder reaction between enamides and in situ generated aza-*o*-quinone-methide, giving rise to tetrahydroacridines using CPA **6n** [94]. Subsequent transformation gave free hexahydroacridines with a total of three new stereogenic centers (Scheme 2.42).

Ishihara developed a chiral magnesium potassium binaphthyl disulfonate cluster as a chiral Brønsted acid catalyst for the cycloaddition reaction between styrene derivatives and aldimines to afford cyclic carbamates with 79–98% ee (Scheme 2.43) [95]. They obtained a 3 : 1 : 4 aqua complex of (*R*)-**8d**/Mg/K as a crystal and determined the structure of the cluster by X-ray structural analysis and electrospray

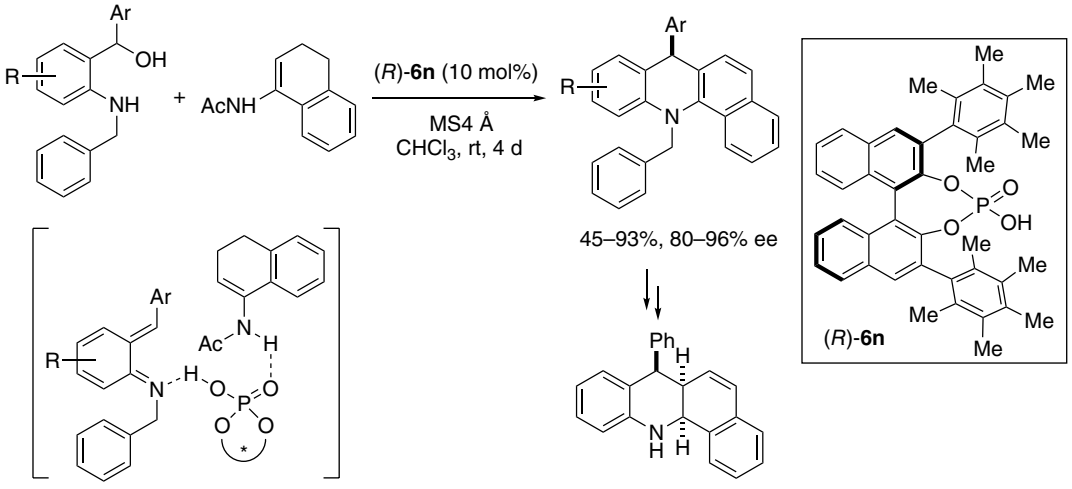

Scheme 2.42. Addition of enamides to *ortho*-quinone methide.

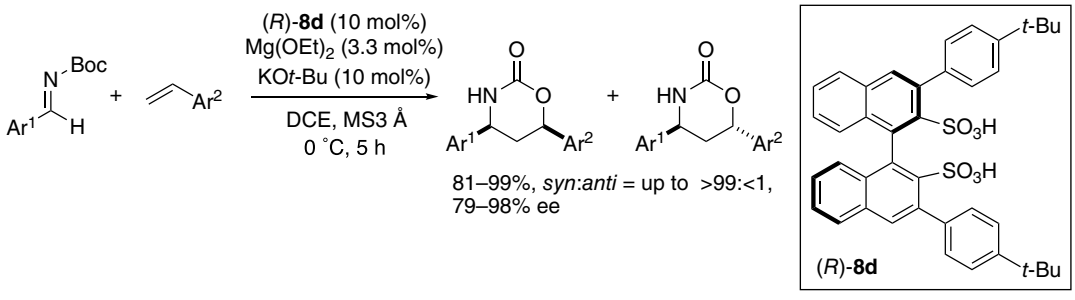

Scheme 2.43. Cycloaddition reaction between styrenes and aldimines. Source: Based on [95].

ionization mass spectrometry (ESI-MS) analysis (Figure 2.11). Although the cluster itself did not exhibit the catalytic activity, the addition of TfOH restored the catalytic activity through H^+ exchange. It was found that the strong acidity of the catalyst dissolved MS3Å and took up leached Mg^{2+} and K^+.

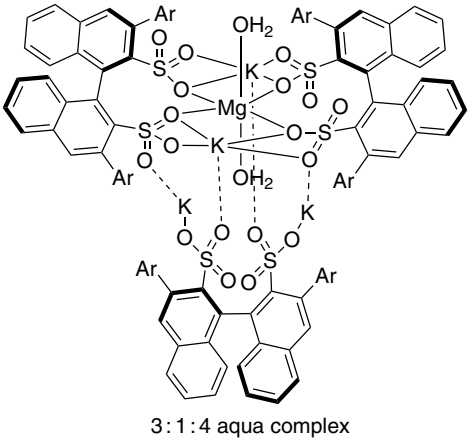

Figure 2.11. 3 : 1 : 4 Aqua complex of (*R*)-**8d**/Mg/K.

Terada reported an enantioselective synthesis of β-amino secondary amides by [4+2] cycloaddition reaction between vinyl azides and *N*-acyl imines using chiral phosphoramide **14c**. The [4+2] cycloaddition was followed by subsequent ring-opening of iminodiazonium ion intermediate, Schmidt-type 1,2-aryl migration, recyclization of the resulting nitrilium ion, and acid hydrolysis (Scheme 2.44) [96].

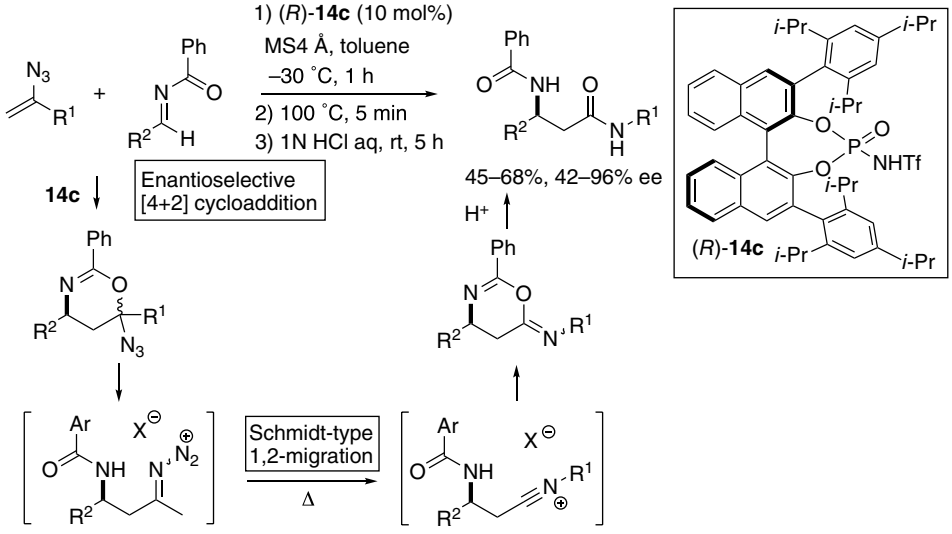

Scheme 2.44. [4+2] cycloaddition reaction between vinyl azides and *N*-acyl imines. Source: Based on [96].

2.4.3. Oxa-Diels-Alder Reactions

Shi reported an inverse electron-demand oxa-Diels-Alder reaction of *ortho*-quinone methide, which was generated in situ from *ortho*-hydroxybenzyl alcohols catalyzed by CPA **6o** (Scheme 2.45) [97]. This is the first example of the oxa-version of the inverse electron-demand Diels-Alder reaction.

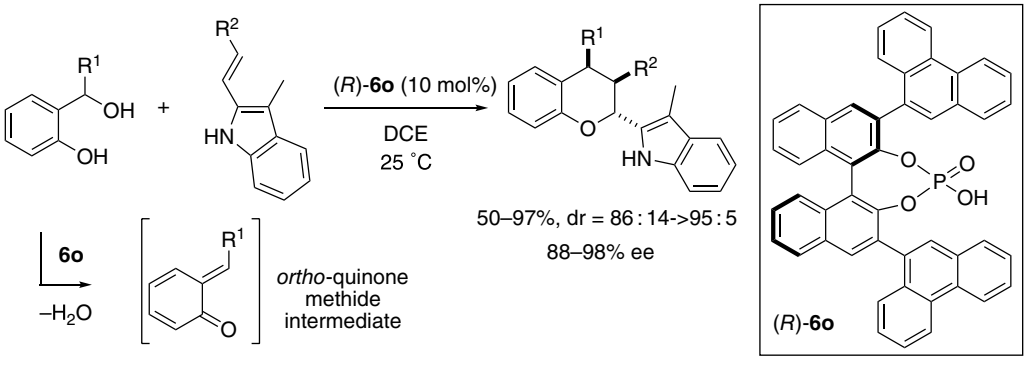

Scheme 2.45. Inverse electron-demand oxa-Diels-Alder reaction of *ortho*-quinone methide. Source: Based on [97].

ortho-Quinone methide intermediate has been employed extensively in numerous transformations. Schneider reported an enantioselective synthesis of 4*H*-chromenes, which involves a conjugate addition of β-diketones to in situ generated *ortho*-quinone methides using **6p**, followed by a cyclodehydration reaction (Scheme 2.46) [98].

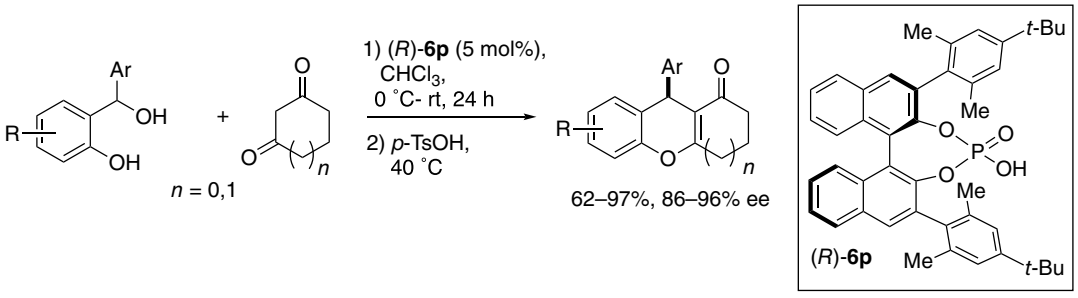

Scheme 2.46. Enantioselective synthesis of 4-aryl-4*H*-chromenes. Source: Based on [98].

Schneider reported a domino-type reaction between diazoesters and *ortho*-quinone methides generated in situ to furnish densely functionalized chromans with three contiguous stereogenic centers. A transition metal and a Brønsted acid catalyst **6b** acted synergistically to produce a transient oxonium ylide and *ortho*-quinone methide, which underwent subsequent coupling in a conjugate-addition-hemiacetalization event to afford chromans (Scheme 2.47) [99].

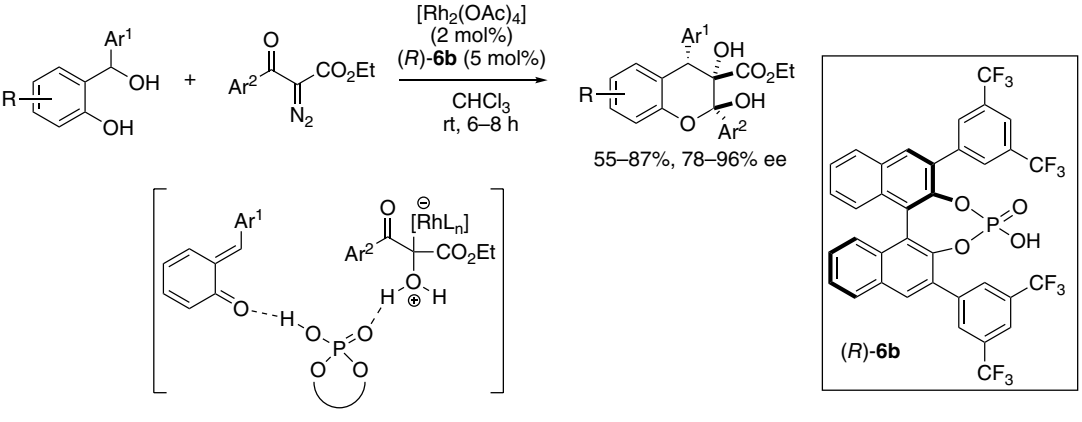

Scheme 2.47. Synergistic rhodium/phosphoric acid catalysis. Source: Based on [99].

2.4.4. Other Cycloaddition Reactions

Shi reported a 1,3-dipolar cycloaddition reaction between azomethine ylide and isatin-derived ketimines to afford a spiro-imidazolidine-2,3′-oxindole framework with a single diastereomer and with 73–94% ee using CPA **6h** (Scheme 2.48) [100].

Shi reported a formal [3+2] cycloaddition reaction of isatin-derived 3-indolylmethanols with 3-methyl-2-vinylindole using CPA **12c** (Scheme 2.49) [101]. Indolylmethanols are useful precursors for the generation of the indolenium ion intermediate and have been extensively investigated for numerous transformations (Scheme 2.50) [102, 103].

Masson reported a [4+3] cycloaddition reaction between indolyl alcohol and 1,3-diene-1-carbamates catalyzed by CPA **6e** (Scheme 2.51) [104].

In addition to 3-indolylmethanol, 2-indolylmethanol was employed successfully. For example, Schneider reported a [3+2] cycloaddition reaction between 2-vinylindoles and in situ generated 2-methide-2*H*-indoles to afford pyrrolo[1,2-a]indoles using CPA **6q** (Scheme 2.52) [105]. Subsequently, Shi reported a similar [3+2] cycloaddition reaction of 3-indolylmethanol [106].

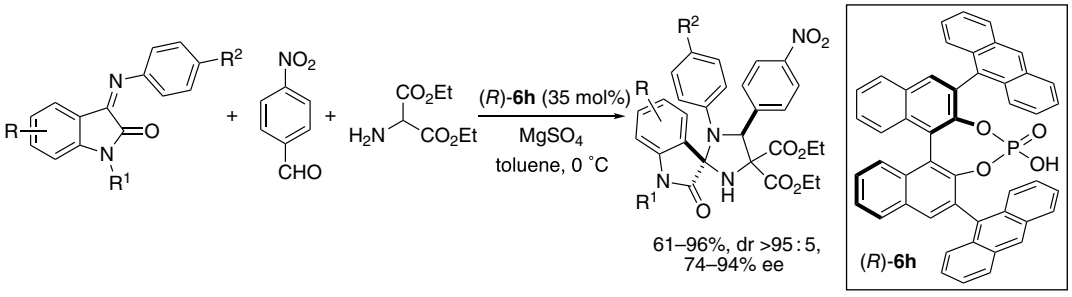

Scheme 2.48. 1,3-Dipolar cycloaddition reaction between azomethine ylide and isatin-derived ketimines. Source: Based on [100].

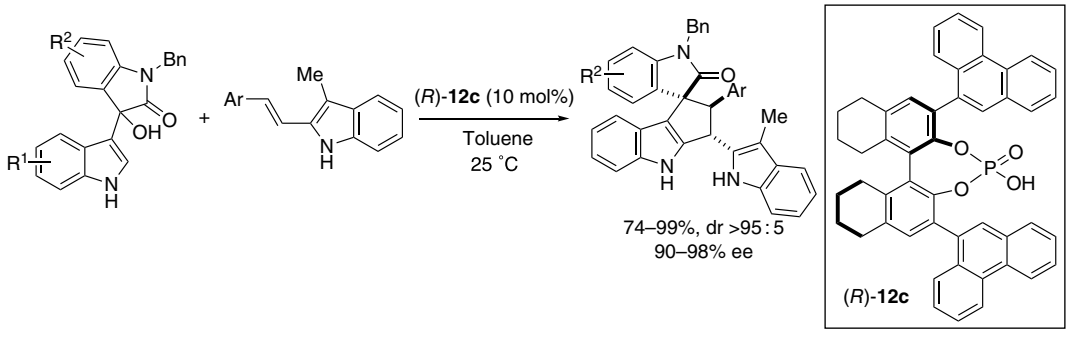

Scheme 2.49. [3+2] Cycloaddition reaction of isatin-derived 3-indolylmethanols. Source: Based on [101].

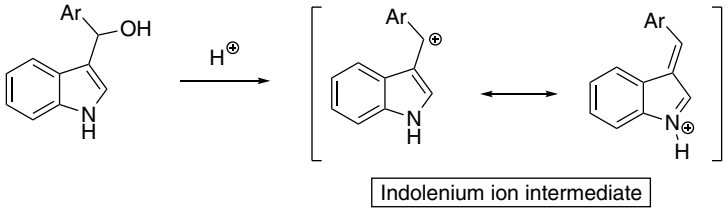

Scheme 2.50. Generation of the indolenium ion intermediate. Source: [102, 103].

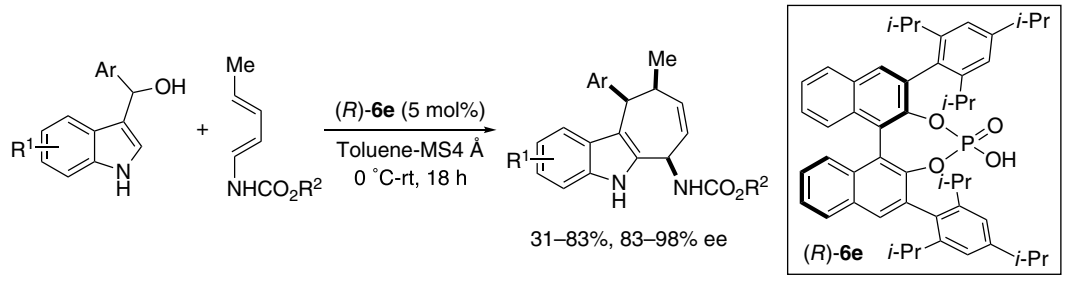

Scheme 2.51. [4+3] Cycloaddition reaction of indolyl alcohol. Source: Based on [104].

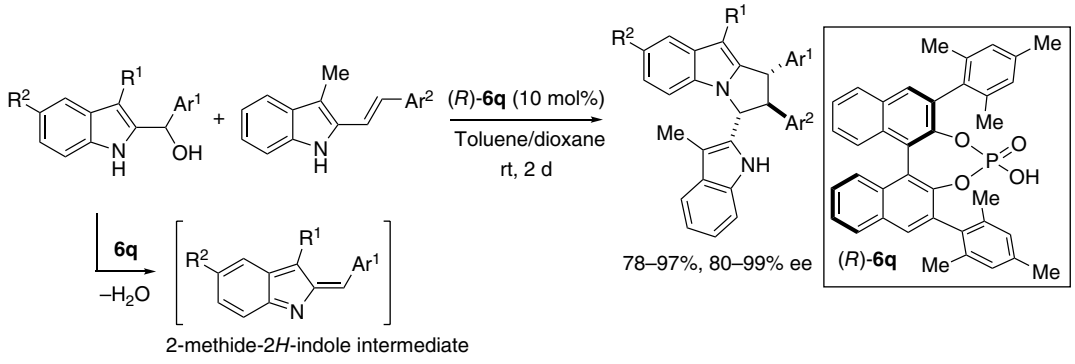

Scheme 2.52. [3+2] Cycloaddition of 2-indolylmethanols. Source: Bera and Schneider [105].

Shi reported a [3+3] cycloaddition reaction between 2-indolylmethanols and azomethine ylides to afford a tetrahydro γ-carboline framework using CPA **12b** (Scheme 2.53) [107]. Presence of diaryl moieties (Ar^1) at the 2′-position is critical for the cycloaddition reaction to proceed. Transition state model is proposed.

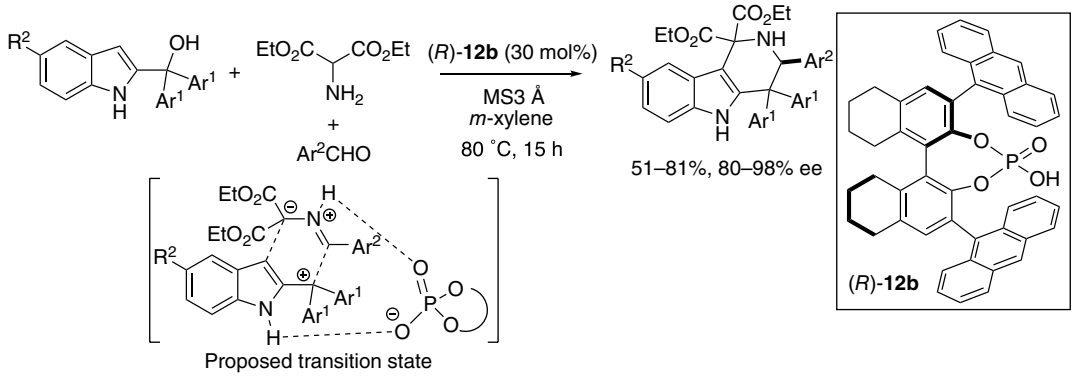

Scheme 2.53. [3+3] Cycloaddition of 2-indolylmethanols. Source: Based on [107].

Schneider reported a [4+3] cycloannulation reaction between *ortho*-quinone methides and carbonyl ylides to furnish functionalized oxa-bridged dibenzooxacines in 56–95% yields and with 82–94% ee in a single synthetic step catalyzed by CPA **6r** (Scheme 2.54). The combination of rhodium complex and CPA **6r** worked cooperatively [108]. Chiral phosphoric acid formed hydrogen-bonded *o*-quinodimethane intermediate starting from *o*-hydroxybenzylalcohol. Carbonyl ylide was generated by Rh-catalyzed decomposition of α-diazoester tethered to an aryl ketone.

Vicario reported [4+3] cycloaddition reaction between furans and oxa-allyl cations, which were generated in situ from allenamides and DMSO as an oxidant, catalyzed by CPA **14d** (Scheme 2.55) [109]. Authors proposed that both hydrogen bond and electrostatic interactions through ion pairing with the oxalyl cation dienophile were involved.

2.4.5. Nazarov Cyclizations

The Nazarov 4π-conrotatory electrocyclization reaction is a useful and powerful method for the construction of cyclopentanones. Rueping reported the first Nazarov cyclization reaction catalyzed by phosphoramide **14** in 2007 [110]. Tius reported a Nazaro cyclization that generated a vicinal all-carbon

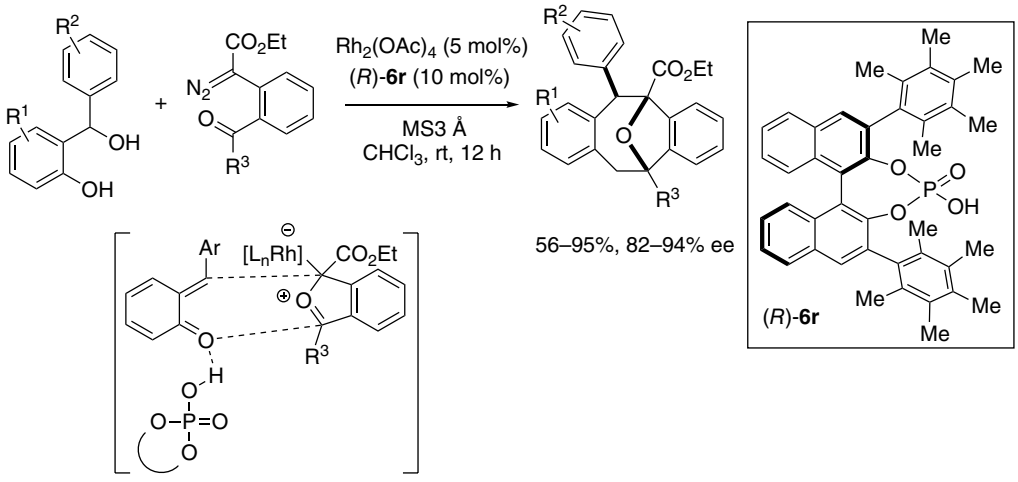

Scheme 2.54. [4+3] Cycloannulation reaction between *ortho*-quinone methides and carbonyl ylides.

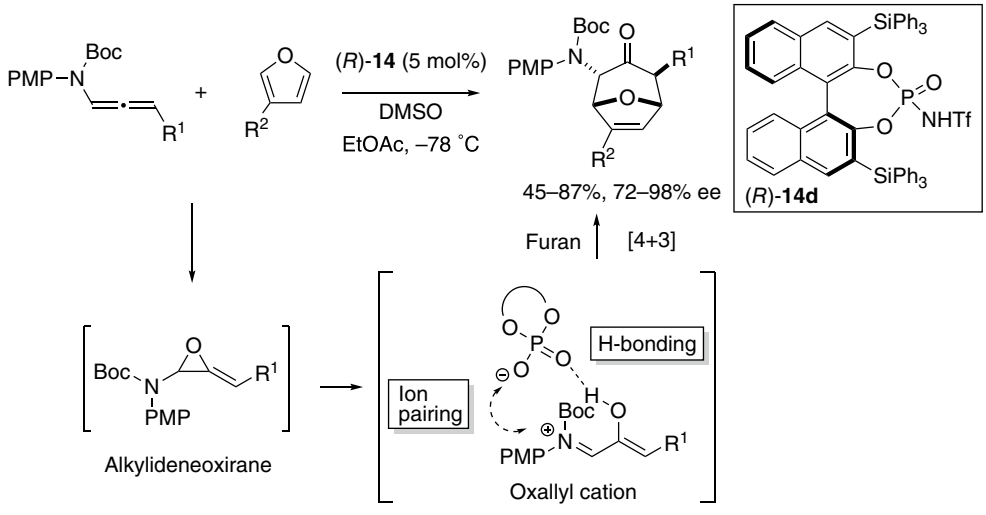

Scheme 2.55. [4+3] Cycloaddition reaction between furans and oxa-allyl cations. Source: Based on [109].

quaternary stereocenter using chiral phosphoramide **14** as the catalyst [111]. Enantioselective Nazarov reactions were limited to activated substrates or cyclic ketones. List reported a Nazarov reaction of simple, acyclic, aliphatic-substituted divinyl ketones using confined IDPi **11l** to furnish 2-methylene cyclopentenone with 92–99% ee (Scheme 2.56) [112].

Chan reported a dehydrative Nazarov-type electrocyclization reaction of electron-rich aryl- and 2-thienyl-β-amino-2-en-1-ols using **14e**. The 4π conrotatory electrocyclization gave a wide variety of 1*H*-indenes and 4*H*-cyclopenta[*b*]-thiophenes (Scheme 2.57) [113].

Tu reported a tandem Nazarov cyclization semipinacol rearrangement reaction using unactivated substrates to furnish spiro[4.4]nonane-1,6-diones using chiral phosphoramide **14f** (Scheme 2.58) [114].

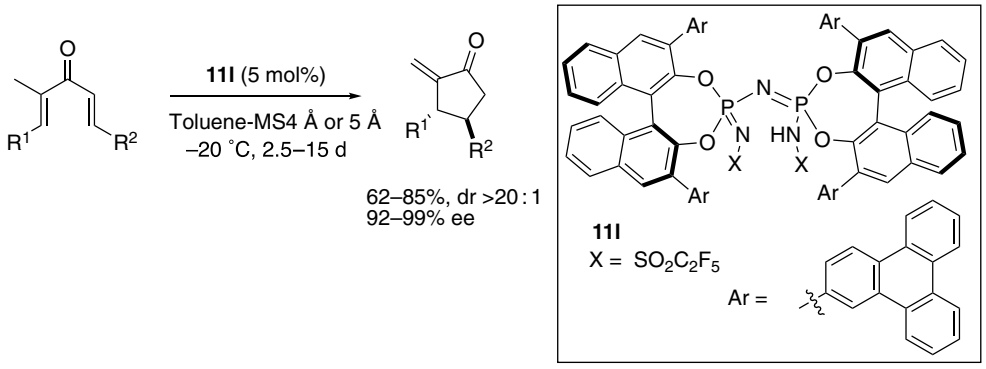

Scheme 2.56. Nazarov reaction of acyclic divinyl ketones. Source: Based on [112].

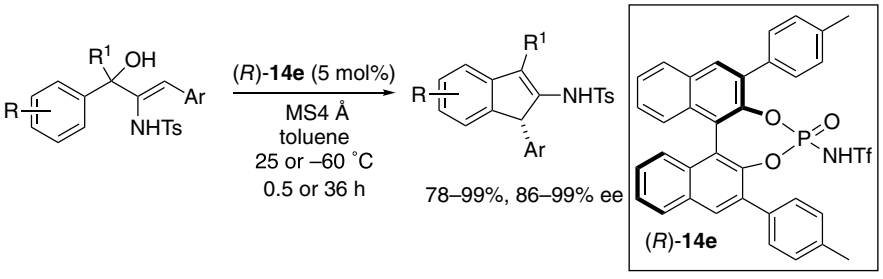

Scheme 2.57. Nazarov-type electrocyclization. Source: Based on [113].

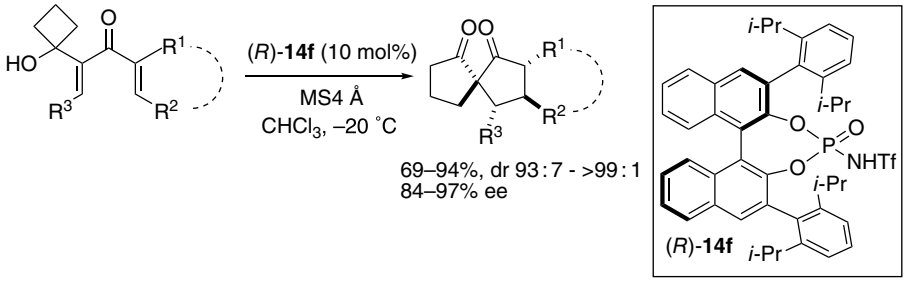

Scheme 2.58. Tandem Nazarov cyclization semipinacol rearrangement reaction. Source: Based on [114].

2.5. MICHAEL REACTIONS

Enamine catalysis may be employed to construct a carbon–carbon bond at the α-substituted position of a ketone using the Michael reaction. However, a stoichiometric amount of enantiopure amine is required for the asymmetric synthesis. List proposed an "enol catalysis," in which CPA **6e** accelerated both enolization and activation of the electrophile and the nucleophile through their Brønsted acidic P–OH and Brønsted basic P=O moieties to furnish α,α-disubstituted cyclohexanone derivatives with 81–96% ee (Schemes 2.59) [115].

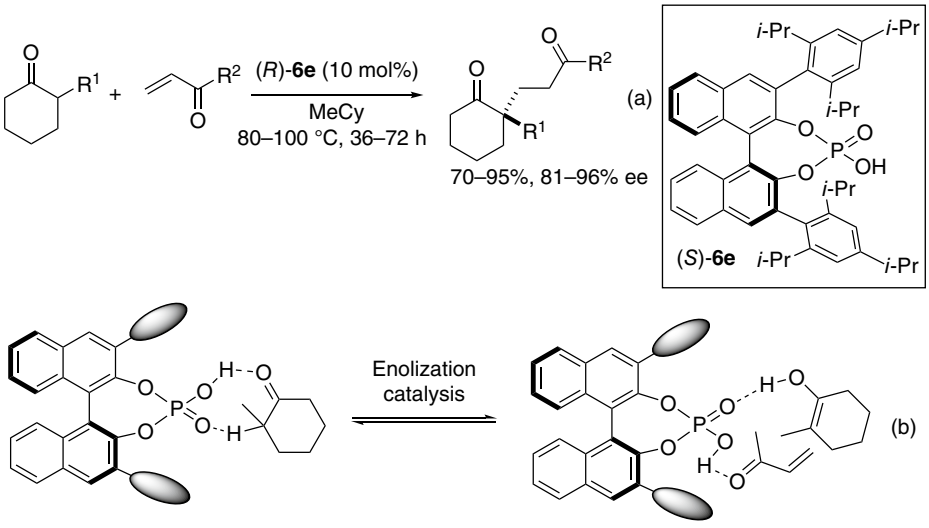

Scheme 2.59. Michael reaction cyclohexanone and enone (a) and enol catalysis (b). Source: Based on [115].

Terada reported aza-Michael-addition reactions of pyrazoles to generate *N*-protected alkenyl benzimidazoles catalyzed by **6s** (Scheme 2.60) [116]. Structural analysis of the transition state revealed that the *N*-protecting group of benzimidazoline as well as the catalyst substituent contributed to the high enantioselectivity.

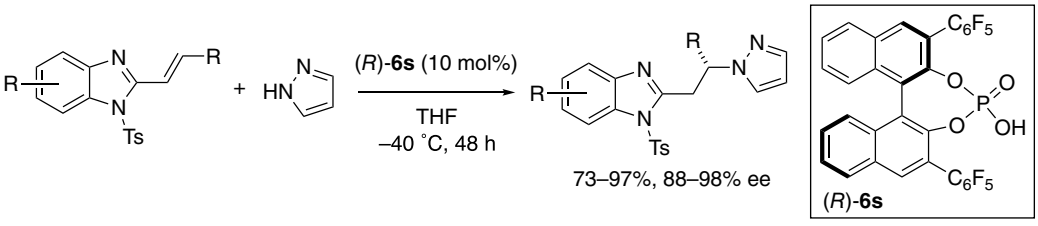

Scheme 2.60. Aza-Michael-addition reactions of pyrazoles. Source: Based on [116].

Ooi developed a chiral phosphonium salt bearing a BArF anion, which was derived from 1,1′-binaphthalene-2,2′-diamine (BINAM), and achieved a sulfa-Michael reaction between aromatic and aliphatic nitroalkene and thiols under the synergistic catalysis by chiral ionic Brønsted acid **27** and 2,6-lutidine (Scheme 2.61) [117].

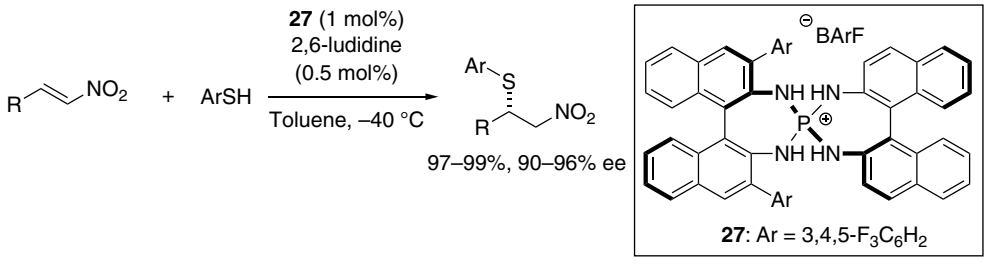

Scheme 2.61. Sulfa-Michael reaction to nitroalkenes. Source: Based on [117].

The Friedel-Crafts-type reaction of heterocycles is useful for the preparation of chiral indole and pyrrole derivatives. A Friedel-Crafts alkylation reaction between indoles and nitrostyrenes was developed by Akiyama in 2008 using CPA **6i** in the presence of MS3Å (Scheme 2.62a) [118]. The use of *N*-H indole is critical, and *N*-methylindole did not undergo the Friedel-Crafts alkylation reaction. In order to construct a quaternary carbon stereocenter, β,β-disubstituted nitroalkenes were employed as substrates for the Friedel-Crafts alkylation reaction using **6e**. Although β-methyl-β-aryl-substituted nitroalkene was found to be not suitable, β-methoxycarbonyl-β-aryl-substituted nitroalkenes reacted with indoles smoothly to afford corresponding adducts bearing quaternary carbon center with 85–94% ee (Scheme 2.62b) [119]. Subsequently, a Friedel-Crafts alkylation reaction between indole and β-trifluoromethyl-β-aryl-substituted nitroalkene was attempted. Although CPA **6e** did not promote the reaction, calcium phosphate catalyzed the Friedel-Crafts alkylation reaction smoothly to afford the corresponding adducts with 82–98% ee (Scheme 2.62c) [120].

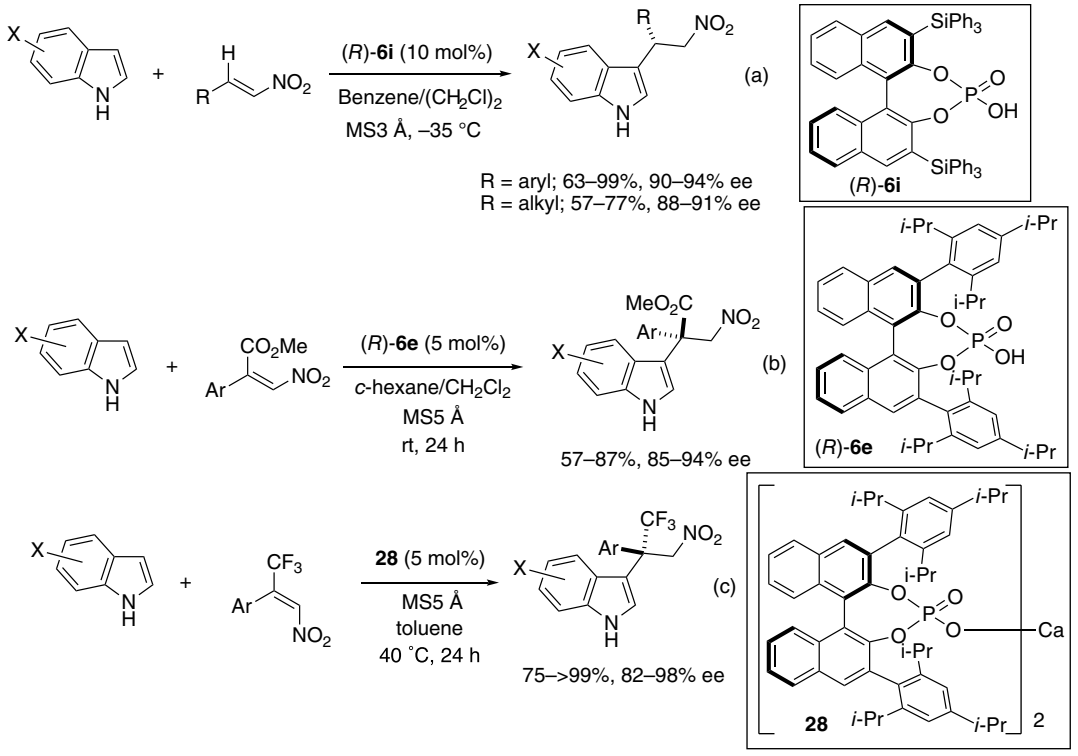

Scheme 2.62. Friedel-Crafts alkylation reaction between indole and nitroalkene (a) (Source: Based on [118]), β-methoxycabonyl-β-aryl-substituted nitroalkenes (b) (Source: Based on [119]), and β-trifluoromethyl- β-aryl- substituted nitroalkenes (c) (Source: Based on [120]).

You developed a Friedel-Crafts alkylation reaction between pyrroles and nitrostyrenes using CPA **6h** to furnish 2-substituted pyrroles with 88–95% ee (Scheme 2.63a) [121]. As an extension of the methodology, they employed 4,7-dihydroindole in the presence of CPA **6h**, followed by dehydrogenation with *p*-benzoquinone to furnish 2-substituted indole derivatives with 88–95% ee (Scheme 2.63b). It is noted that as low as 0.5 mol% of the phosphoric acid promoted the reaction smoothly [122].

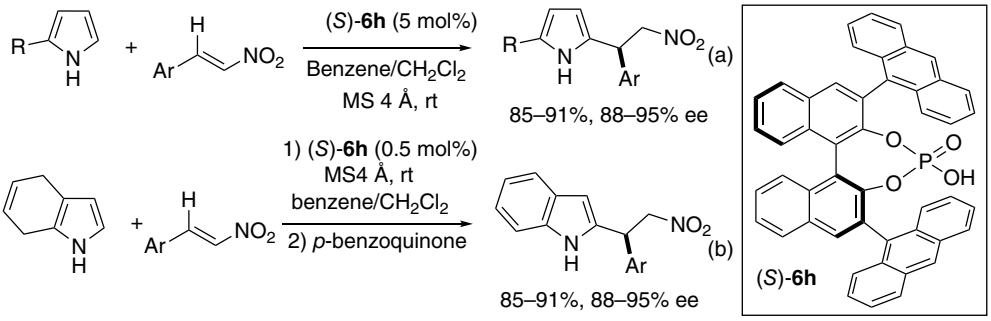

Scheme 2.63. Friedel-Crafts alkylation reaction between nitrostyrenes and pyrroles (a) (Source: Based on [121]), and 4,7-dihydroindole (b) [122].

2.6. REDUCTION

2.6.1. Reduction of Imines

2.6.1.1. Transfer Hydrogenation of Ketimines Rueping et al. [123], List et al. [124], and MacMillan et al. [125] independently reported a transfer hydrogenation of ketimines using CPA as the Brønsted acid and Hantzsch ester as the hydrogen donor, and enzymes and cofactors in the biological system were replaced by small organocatalysts and nicotinamide adenine dinucleotide (NADH) analogues (Scheme 2.64). The combination of CPA and Hantzsch ester was extended to the transfer hydrogenation of numerous kinds of substrates, such as α-imino esters;[126] heterocycles, including pyridines [127], 2-, 3-, 4-substituted quinolines [128], benzoxazines, benzothiazines, benzoxazinones [129], quinoxalines, quinoxalinone [130], indolines [131], and [1,4]benzodiazepines;[132] and others (Figure 2.12) [133].

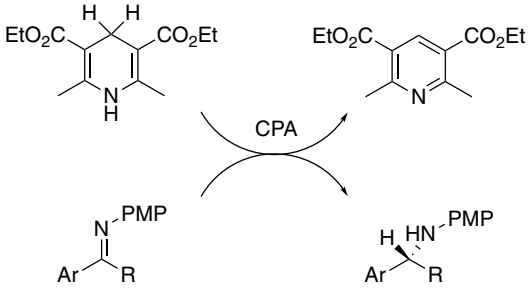

Scheme 2.64. Transfer hydrogenation of ketimines by Hantzsch ester.

Theoretical studies by Goodman [134] and Himo [135] led to the elucidation of the mechanism, wherein hydrogen bond between *N*-H and phosphoryl oxygen is important (Figure 2.13).

One of the drawbacks of the transfer hydrogenation by the combined use of Hantzsch ester and CPA is that a stoichiometric amount of Hantzsch ester is required. In order to resolve the issue, Zhou employed 9,10-dihydrophenanthridine (DHPD) as the hydrogen donor in place of Hantzsch ester and reported transfer hydrogenation of benzoxazinone, quinoxalines, and quinolines by the combined use of CPA **12d**, Ru catalyst, and phenanthridine (**29**), wherein hydrogen gas was employed as the terminal reductant for the regeneration of DHPD (Scheme 2.65) [136].

Xiao reported a direct asymmetric reductive amination reaction between aromatic amines and aryl methyl ketones by the combined use of CPA **6e** and Ir catalyst **30** (Scheme 2.66) [137]. Chiral Ir catalyst bearing phosphate counteranion was generated.

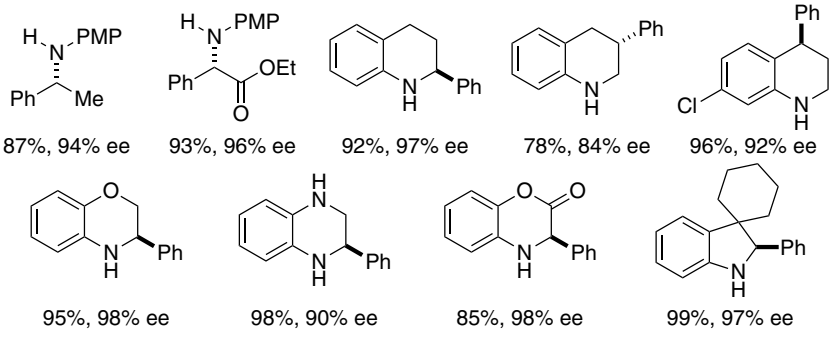

Figure 2.12. Results of the transfer hydrogenation of ketimines. Source: Based on [133].

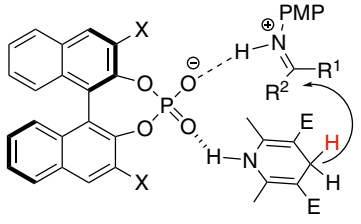

Figure 2.13. Transition state of the transfer hydrogenation with Hantzsch ester.

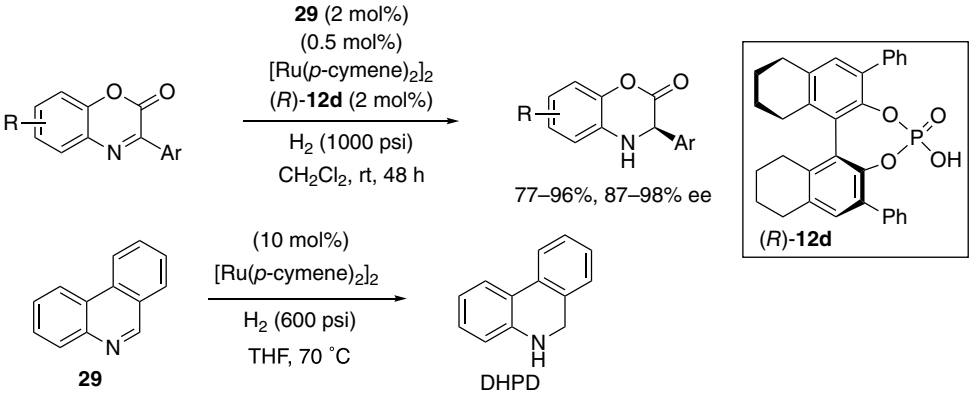

Scheme 2.65. Transfer hydrogenation of benzoxazine using DHPD. Source: Based on [136].

The transfer hydrogenation reaction by the combined use of CPA and Hantzsch ester required use of *N*-aryl ketimines as substrates due to the catalyst deactivation through salt formation with the highly basic amine product. List reported a transfer hydrogenation of *N*-alkyl-substituted ketimine using more acidic chiral DSI **9d**, which was derived from BINOL in the presence of Boc_2O to furnish Boc-protected *N*-alkyl amine. A range of ketimines bearing methyl, ethyl, propyl, butyl, benzyl, allyl, and other alkyl moieties participated in the transfer hydrogenation successfully to furnish corresponding amines with 81–97% ee (Scheme 2.67a) [138]. Subjecting *N*-H ketimines with the combination of DSI **9e** and Hantzsch ester resulted in the reductive condensation reaction of the *N*-H ketimines to afford C_2-symmetric secondary amines (Scheme 2.67b) [139]. List subsequently employed *N*-H ketimine HCl salt as the substrate and achieved an enantioselective reduction efficiently to furnish crystalline primary amines using DSI **9f** (Scheme 2.67c). A kinetic study suggested the bifunctional nature of DSI [140].

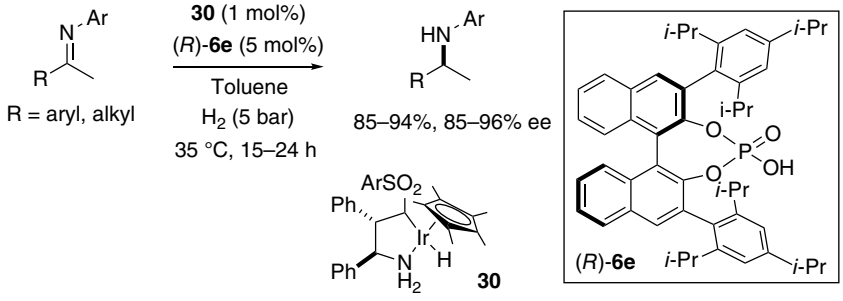

Scheme 2.66. Metal-Brønsted acid cooperative catalysis. Source: Based on [137].

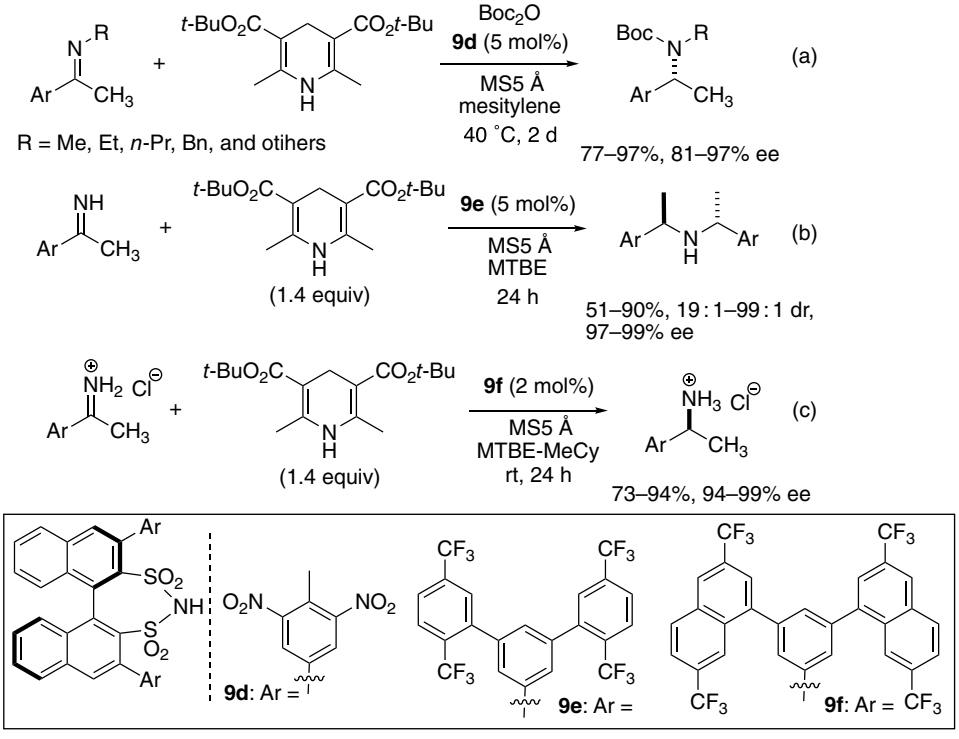

Scheme 2.67. Transfer hydrogenation of *N*-alkyl ketimines (a) (Source: Based on [138]), reductive condensation of *N*-H ketimines (b) (Source: Based on [139]), and transfer hydrogenation of HCl salt of *N*-H ketimines (c) [140].

In addition to Hantzsch ester, benzothiazoline was also found to function as a hydrogen donor in combination with CPA because benzothiazoline releases dihydrogen to generate benzothiazole (Figure 2.14) [141]. A range of ketimines derived from acetophenones [142], propiophenones [143], α-imino esters [144], trifluoromethylated ketimines [145], difluoromethylated ketimines [146], alkynylated ketimines [147], and 1,4-benzodiazepine [148] successfully participated in the transfer hydrogenation (Figure 2.15). The reductive amination also proceeded efficiently [149]. Interestingly, use of 2-aryl-2-deuterated benzothiazoline resulted in the formation of α-deuterated amines with high enantioselectivity [150]. Benzothiazoline sometimes afforded higher enantioselectivity in the transfer hydrogenation of ketimines in combination with CPA in comparison with Hantzsch ester as a hydrogen donor. Theoretical study by Yamanaka elucidated the transition state, wherein hydrogen bond between *N*-H

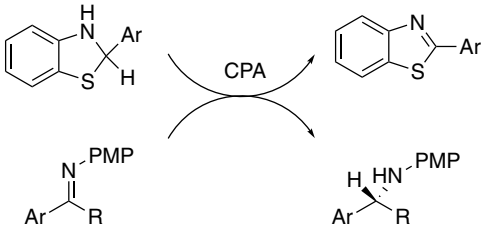

Figure 2.14. Transfer hydrogenation of ketimines by benzothiazoline. Source: Based on [141].

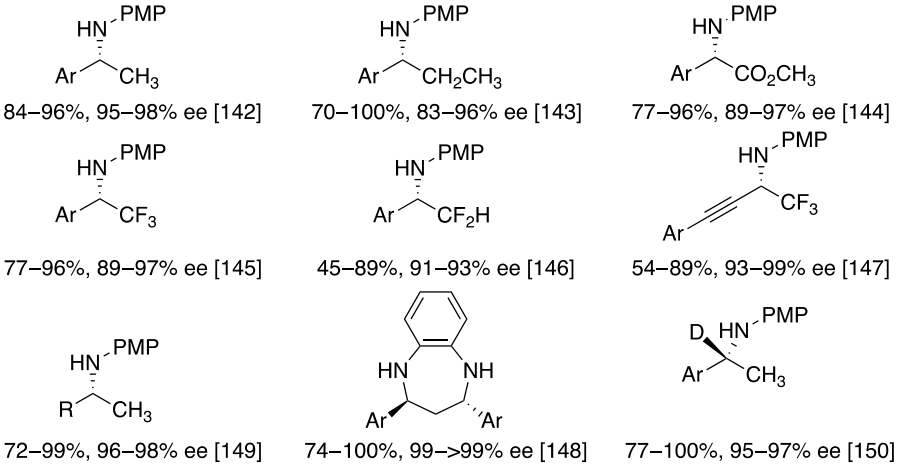

Figure 2.15. Results of the transfer hydrogenation of ketimines by benzothiazoline.

and phosphoryl oxygen is critical [151]. Higher selectivity of benzothiazoline may be ascribed to the position of the transferred hydrogen. Hydrogen at the α-position of nitrogen of benzothiazoline was transferred, whereas γ-hydrogen was transferred in the case of Hantzsch ester (Figure 2.16).

Furthermore, 2-arylindoline also functioned as a hydrogen donor for the transfer hydrogenation of ketimines (Scheme 2.68a) [152]. (*R*)-2-Arylindole reacted much faster than its (*S*)-isomer in combination with (*R*)-BINOL-derived phosphoric acid. Taking advantage of the difference in the reactivity, Akiyama developed oxidative kinetic resolution of 2-substituted indoline. On treatment of 2-substituted indoline with 0.6 equivalent of ketimine in the presence of CPA **6e**, (*R*)-indoline underwent transfer hydrogenation with *N*-3,4,5-$(MeO)_3C_6H_2$-substituted ketimine much faster than (*S*)-indoline, and (*S*)-indoline was recovered in approximately 50% chemical yields with excellent enantioselectivity (Scheme 2.68b) [153]. In particular, 2-arylindolines were obtained with >99% ee.

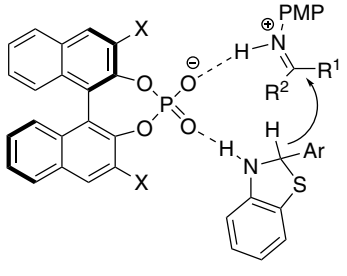

Figure 2.16. Transition state of the transfer hydrogenation with Hantzsch ester.

Subsequently, Akiyama reported a self-redox strategy for the oxidative kinetic resolution of indolines to furnish 2-aryl indolines with 87–99% ee using salicyl aldehyde derivative as the preresolving reagent in place of ketimine catalyzed by CPA **6t**, bearing bulky 9-anthryl-2,6-diisopropylphenyl group at 3,3′-positions. Iminium ion intermediate **31**, which was formed by the condensation of indoline with salicyl aldehyde derivative, was hydrogenated from the 2-aryl indoline (Scheme 2.68c) [154].

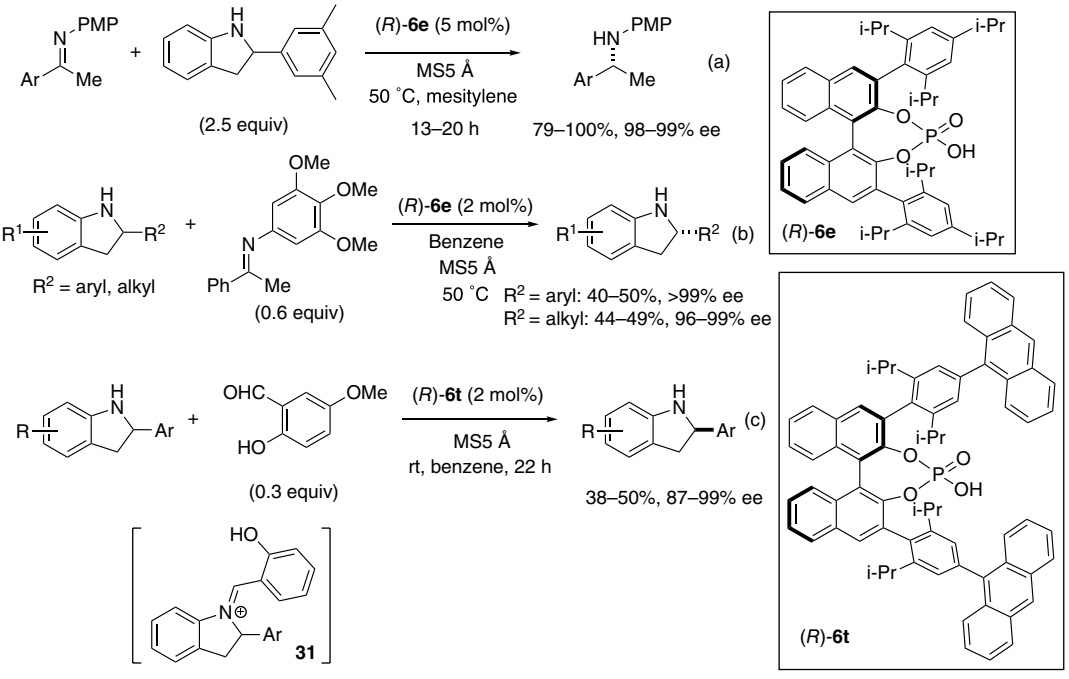

Scheme 2.68. Transfer hydrogenation using indoline as a hydrogen donor (a) (Source: Based on [152]), oxidative kinetic resolution of indolines using ketimine (b) (Source: Based on [153]), and oxidative kinetic resolution of indolines based on self-redox reaction (c) (Source: Based on [154]).

2.6.2. Reduction of Ketones

Antilla reported an enantioselective reduction of ketones using CPA **6h** as the precatalyst. The use of catecholborane as the reducing agent in combination with 4-dimethylaminopyridine (DMAP) gave secondary alcohols with 82–98% ee (Scheme 2.69). Based on the ^{11}B nuclear magnetic resonance (NMR) study, transition state **32** involving a boro-phosphate intermediate was proposed [155].

2.6.3. Reduction of Alkenes

Antilla reported a transfer hydrogenation of *trans*-chalcone derivatives using CPA **6f**, employing borane as the hydride source (Scheme 2.70) [156].

Song developed an efficient method for the reduction of 2-substituted indoles to produce 2-substituted indolines by the combined use of CPA **6q** and catecholborane in the presence of water. The formation of phosphoric acid boron complex **33** was proposed (Scheme 2.71) [157].

Sun accomplished the reduction of 1,1-diarylethenes by a transfer hydrogenation that used a combination of Hantzsch ester and CPA **6i** to afford 1,1-diarylethanes with 75–99% ee (Scheme 2.72) [158].

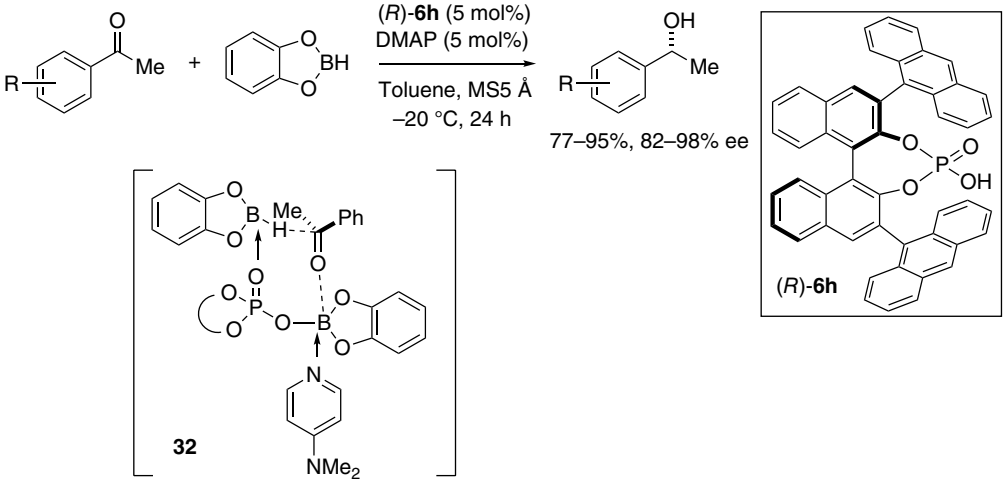

Scheme 2.69. Reduction of ketones by the combined use of catecholborane.

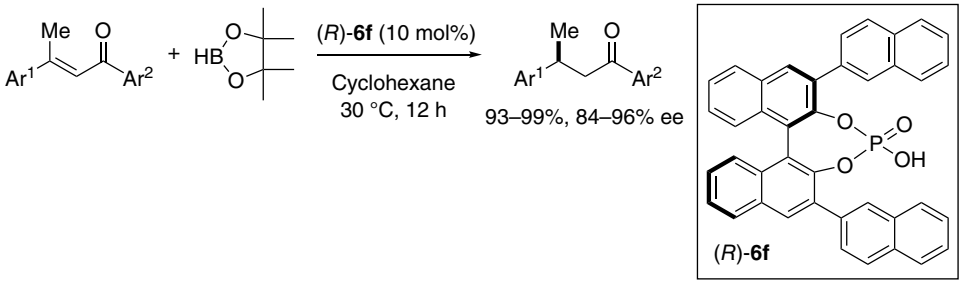

Scheme 2.70. Transfer hydrogenation of chalcone derivatives. Source: Based on [156].

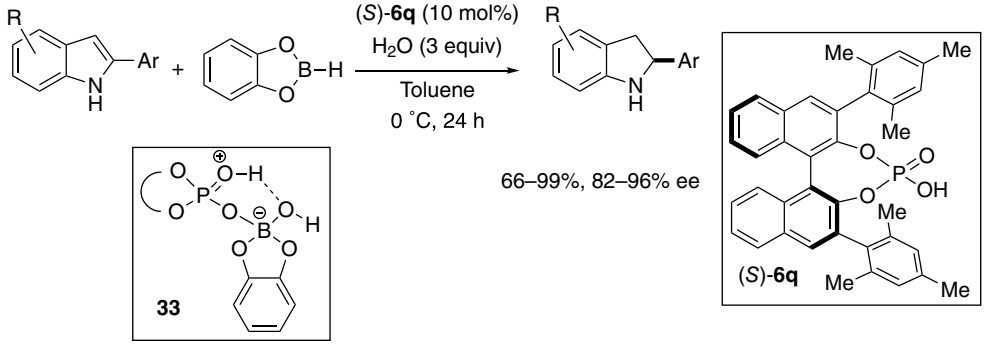

Scheme 2.71. Reduction of indolines. Source: Based on [157].

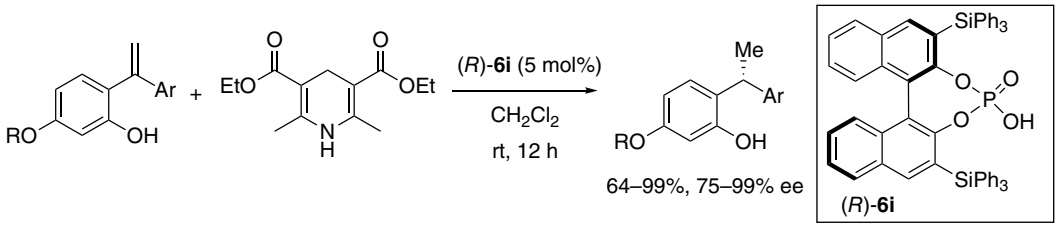

Scheme 2.72. Transfer hydrogenation of 1,1-diarylethenes. Source: Based on [158].

2.7. ADDITION TO ALKENES

In order to attain high enantioselectivity, numerous kinds of chiral Brønsted acids were developed. Regarding CPA, bulky 3,3′-substituents such as 2,4,6-triisopropylphenyl and 2,4,6-tricyclohexylphenyl groups were introduced. In order to realize an extremely sterically demanding cavity, List designed and synthesized confined IDP **10a** on the basis of a C_2-symmetric imidodiphosphoric acid motif, and realized a highly enantioselective spiroacetalization (Scheme 2.73) [13]. Small and functionally unbiased substrates were found to be suitable because of the geometrically constrained bifunctional active site.

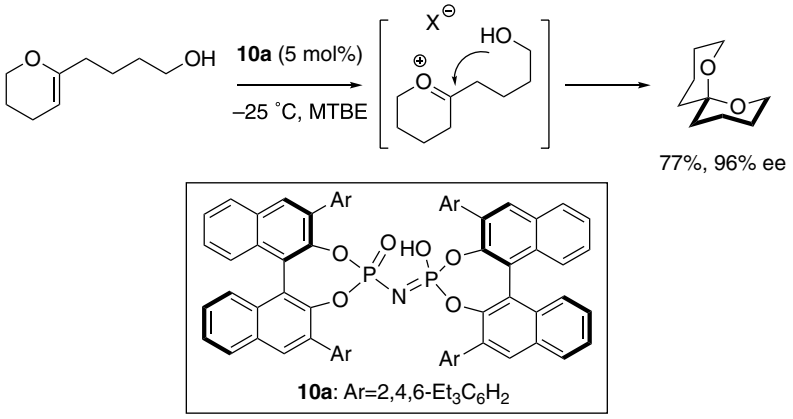

Scheme 2.73. Asymmetric spiroacetalization by confined Brønsted acid. Source: Based on [13].

Nagorny concurrently reported spiroketalization using CPA **6e**, although the use of tertiary alcohols was critical as substrates (Scheme 2.74) [159].

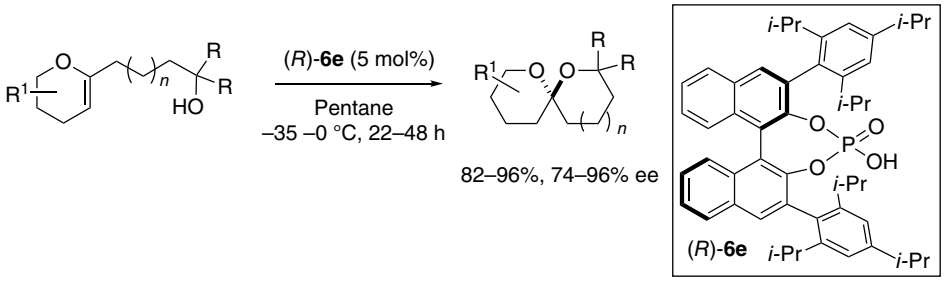

Scheme 2.74. Asymmetric spiroacetalization by TRIP. Source: Based on [159].

Liu reported an intramolecular hydroamination of alkenes using chiral phosphoramide **34** to furnish pyrrolidines with an α-tetrasubstituted carbon stereocenter (Scheme 2.75a) [160]. Liu subsequently applied the methodology for the desymmetrization of *meso* dienes to afford pyrrolidine derivatives bearing two congested tertiary or quaternary stereocenters based on the hydroamination of unactivated alkenes (Scheme 2.75b) [161]. Mechanistic study elucidated the transition state **35**, wherein thiourea moiety was employed both as activating and a directing group through cooperative multiple hydrogen bonds with a Brønsted acid and the double bond.

Sun reported an asymmetric synthesis of 1,1-diarylethanes through a transfer hydrogenation reaction of 1,1-diarylalkenes bearing *o*-hydroxyphenyl moieties and Hantzsch ester using **6i** as shown in

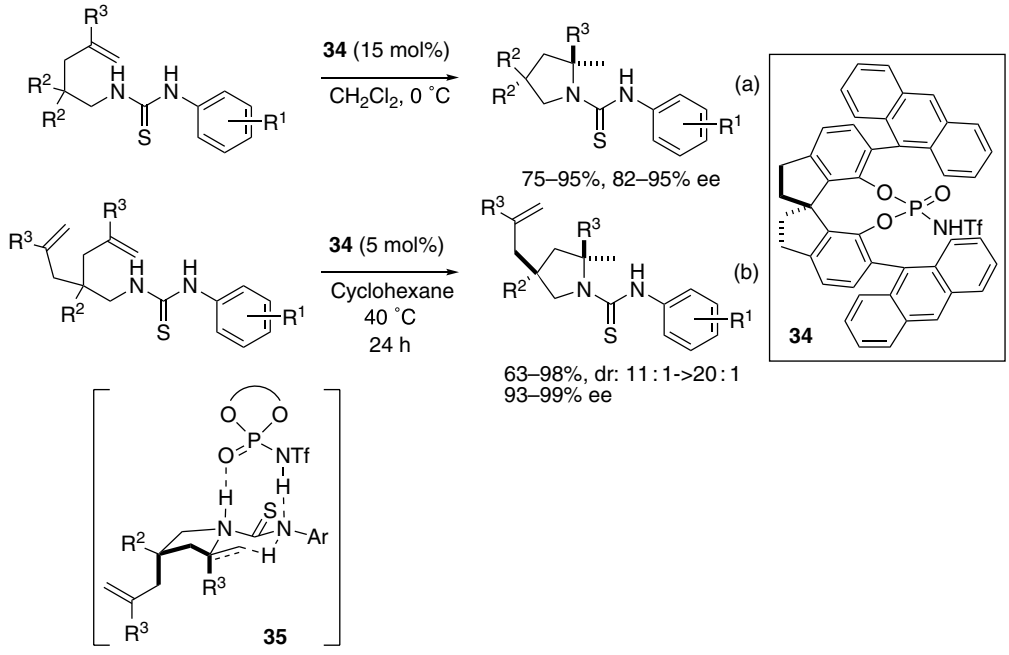

Scheme 2.75. Intramolecular hydroamination of alkenes (a) (Source: Based on [160]), and its application to desymmetrization of meso dienes (b) (Source: Based on [161]).

Scheme 2.72. Indole also participated in the reaction to afford 1,1,1-triarylethanes bearing acyclic all-carbon quaternary stereocenters using **13d** (Scheme 2.76) [158].

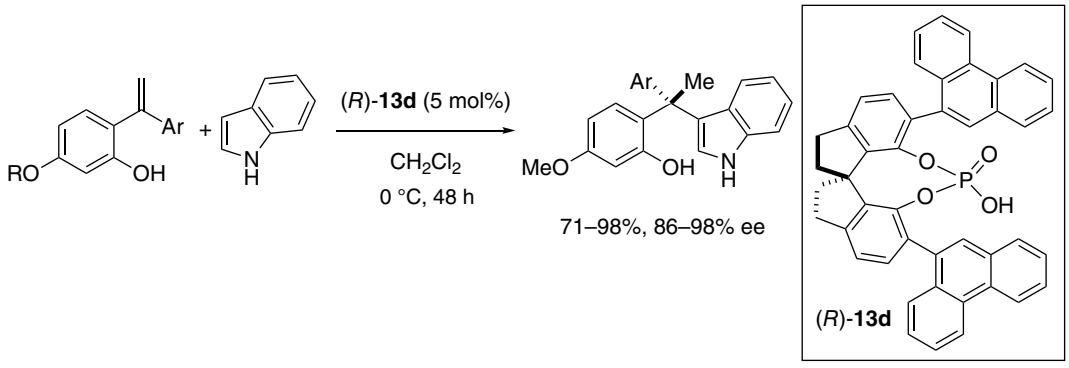

Scheme 2.76. Hydroarylation of 1,1-diarylethenes. Source: Based on [158].

Yamamoto reported a bromocyclization of polyenes using 1,3-dibromo-5,5-dimethylhydantoin as the electrophilic bromine source and chiral phosphoramide **14g** bearing bulk 4-(9-antrhyl)-2,6-diisopropylp henyl moiety at 3,3′-position (Scheme 2.77) [162].

Ackermann reported the first example of the activation of unactivated alkene by CPA **6b**. Intramolecular hydroamination reaction took place to furnish pyrrolidine derivative with 17% ee [163]. A highly enantioselective version of the intramolecular hydroalkoxylation of unactivated alkene was developed by List using confined and strong chiral Brønsted acid [164]. Tetrahydrofuran derivatives with

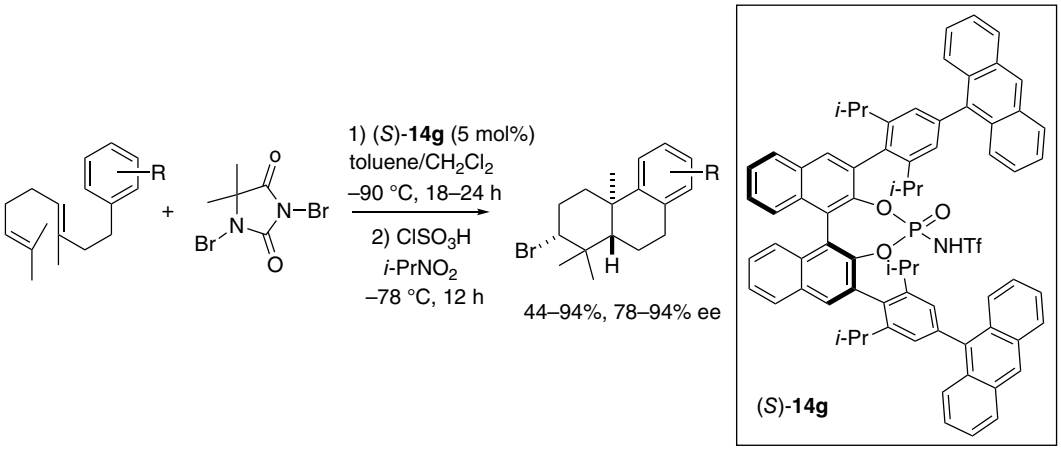

Scheme 2.77. Bromocyclization of polyenes. Source: Based on [162].

the stereogenic center at 2-position and tetrahydropyrans were obtained with 84–97% ee using **11m** (Scheme 2.78b). List recently achieved an intramolecular hydroarylation of unactivated alkenes with indoles catalyzed by a strong and confined chiral Brønsted acid [165]. Both alkyl and aryl-alkenes participated in the reaction successfully to construct a quaternary stereocenter with 68–94% ee using **11n** (Scheme 2.78b).

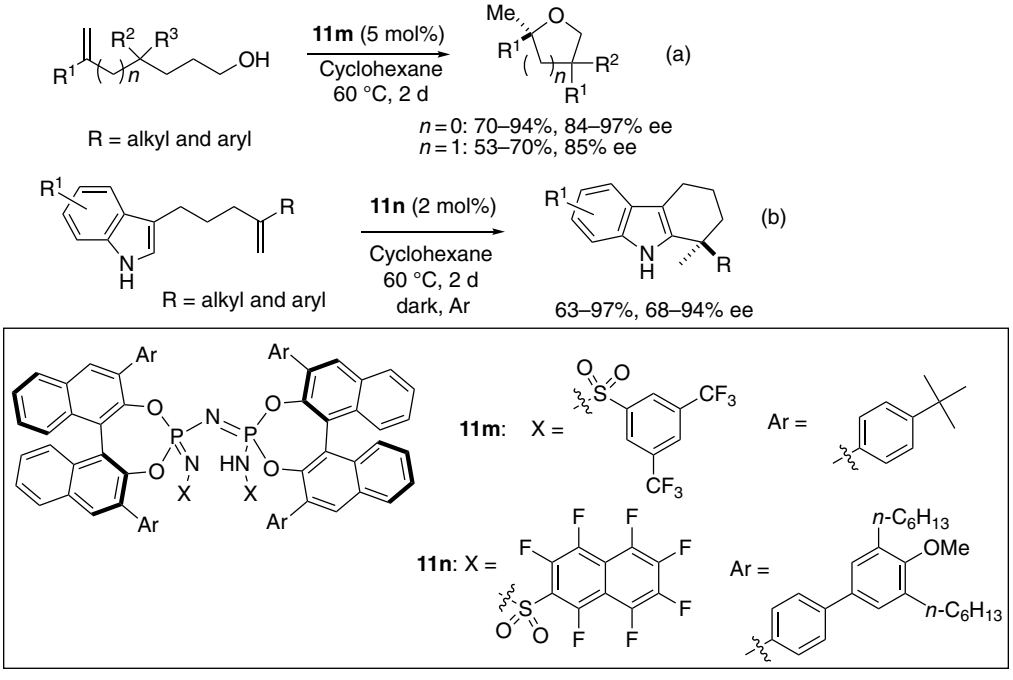

Scheme 2.78. Intramolecular hydroalkoxylation of unactivated alkenes (a) [164], and hydroarylation of unactivated alkenes (b) [165].

2.8. SUBSTITUTION REACTIONS

Sun reported an enantioselective construction of all-carbon quaternary stereocenters from indoles and tertiary alcohol bearing *o*-hydroxyphenyl moieties using SPINOL-derived CPA **13d** (Scheme 2.79) [166]. *o*-Quinone methide intermediate was generated in situ.

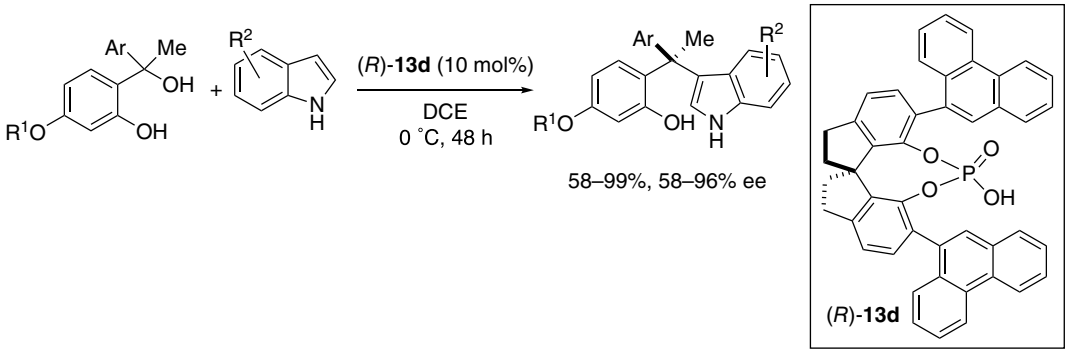

Scheme 2.79. Construction of all-carbon quaternary stereocenters from indoles and tertiary alcohol. Source: Based on [166].

Sun reported the construction of tetraarylmethanes by way of in situ generated *para*-quinone methide or extended iminium intermediates catalyzed by CPA **6l** to afford triaryl(2-pyrrolyl)methane (Scheme 2.80a) and diaryl(2-indolyl)(2-pyrrolyl)methane (Scheme 2.80b) with 83–99% ee and 83–97% ee, respectively [167]. The presence of 2-alkoxy moiety on the phenyl moiety was critical for the excellent enantiocontrol.

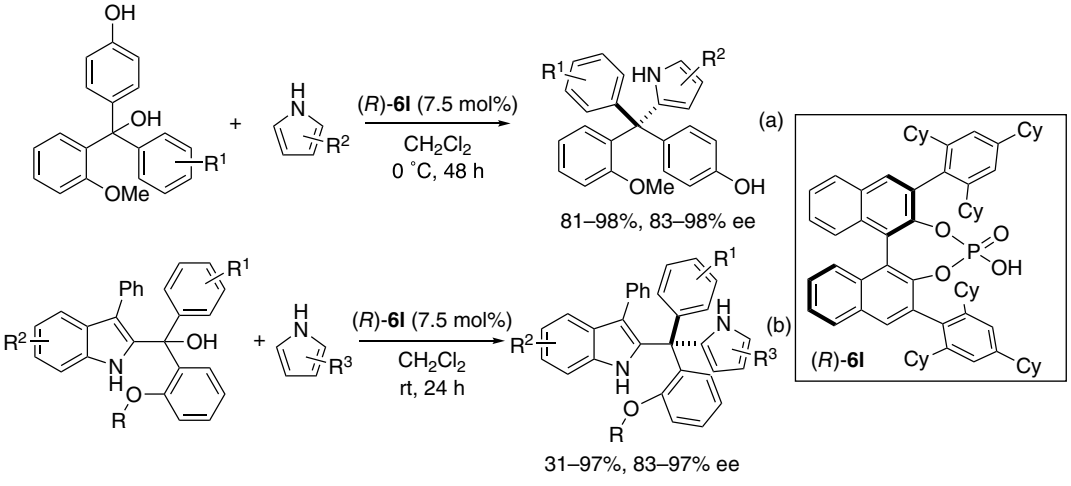

Scheme 2.80. Construction of triarylpyrrolylmethanes (a) and diarylindolylpyrrolylmethanes (b). Source: Based on [167].

2.9. REARRANGEMENT REACTIONS

Terada reported a ring expansion reaction of 1,3-dithianes in the presence of pyrrole using CPA **6u**, forming 1,4-dithiepane derivatives with high enantioselectivity. Indole also participated in the reaction successfully [168]. DFT calculation revealed that an unprecedented enantioselective 1,2-sulfur rearrangement/

stereospecific nucleophilic addition sequence is the concrete mechanism, which is controlled by the chiral counteranion (Scheme 2.81).

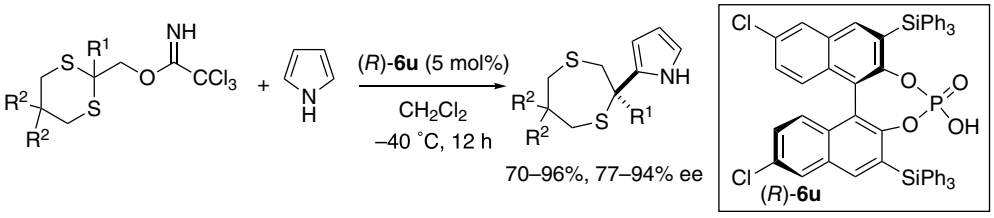

Scheme 2.81. Ring expansion reaction of 1,3-dithianes.

Terada subsequently reported a vinylogous Wagner-Meerwein shift through the activation of trichloroimidate as the leaving group to yield α-vinyl cyclopentanones with high enantioselectivity using chiral phosphoramide **14c** as the chiral Brønsted acid catalyst. Quaternary carbon centers were constructed with 57–95% ee (Scheme 2.82) [169].

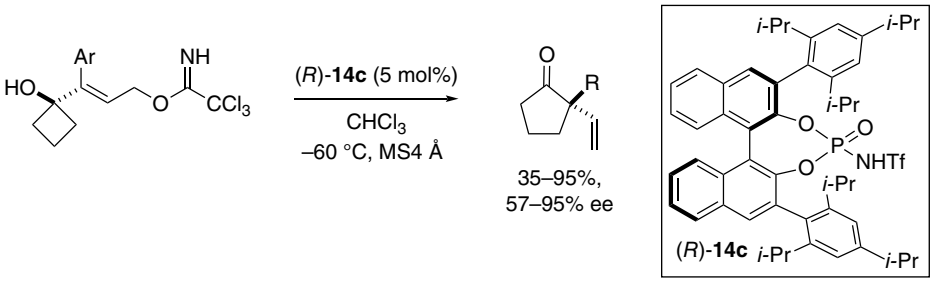

Scheme 2.82. Vinylogous Wagner-Meerwein shift. Source: Based on [169].

Sun reported a House-Meinwald rearrangement of racemic tetrasubstituted oxirane using CPA **6v** or **6w** to afford 2,2-diarylcyclohexanone [170]. Chiral ketones bearing all-carbon quaternary center at the α-position were obtained efficiently with 86–97% ee (Scheme 2.83).

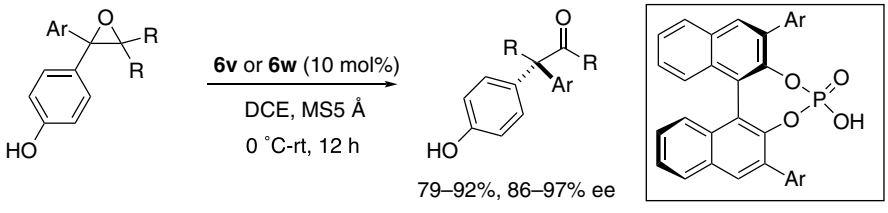

6v: Ar = 1-naphthyl
6w: Ar = 4-(3,5-$(CF_3)_2C_6H_3$)C_6H_5

Scheme 2.83. House-Meinwald rearrangement.

Zhu and co-workers reported pinacol rearrangement of 1,2-tertiary diols to furnish 2-alkynyl-2-arylcyclohexanones catalyzed by *N*-triflyl chiral phosphoramide **14c** (Scheme 2.84a) [171]. They also reported Meinwald rearrangement of spirooxiranes to give 2,2-diarylcyclohexanones (Scheme 2.84b).Both reactions resulted in the formation of quaternary all-carbon stereocenters with 81–94% ee and 72–91% ee, respectively.

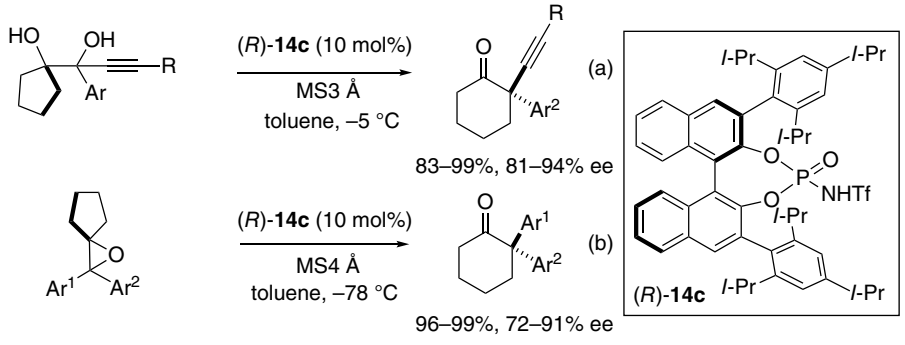

Scheme 2.84. Construction of quaternary stereocenters by Pinacol rearrangement (a) (Source: Based on [171]) and Meinwald rearrangement (b).

2.10. MISCELLANEOUS REACTIONS

List reported a ring-opening reaction of *meso*-aziridine using **6e** and carboxylic acid to afford the ring-opening products with 85–99% ee (Scheme 2.85). They obtained the X-ray crystallographic analysis of heterodimer **36** between CPA **6e** and acetic acid, and proposed the heterodimeric association of a carboxylic acid with CPA as a new activation principle for organocatalysis. The carboxylic acid plays a dual role in the reaction by both accomplishing the ring-opening reaction and protecting the catalyst from degradation [172].

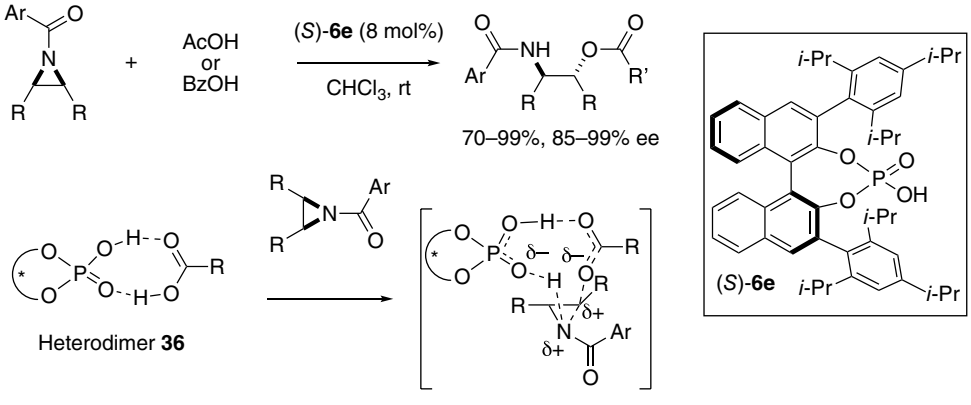

Scheme 2.85. Ring-opening of *meso*-aziridines.

List reported an enantioselective oxidation of sulfide catalyzed by confined Brønsted acid **10a** to furnish sulfoxides with 85–98% ee (Scheme 2.86) [173].

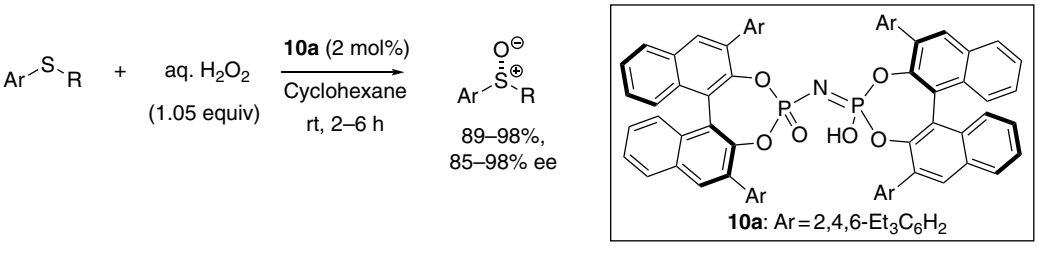

Scheme 2.86. Enantioselective oxidation of sulfides to sulfoxides. Source: Based on [173].

List reported an enantioselective transformation of oxirane to thiiranes using chiral phosphoric acid **6e** in the presence of thioamide. Both oxiranes and thiiranes were obtained with 85–99% ee and 76–95% ee, respectively, by the kinetic resolution (Scheme 2.87). Formation of the initial heterodimer **37** between CPA **6e** and the sulfur donor was proposed [174].

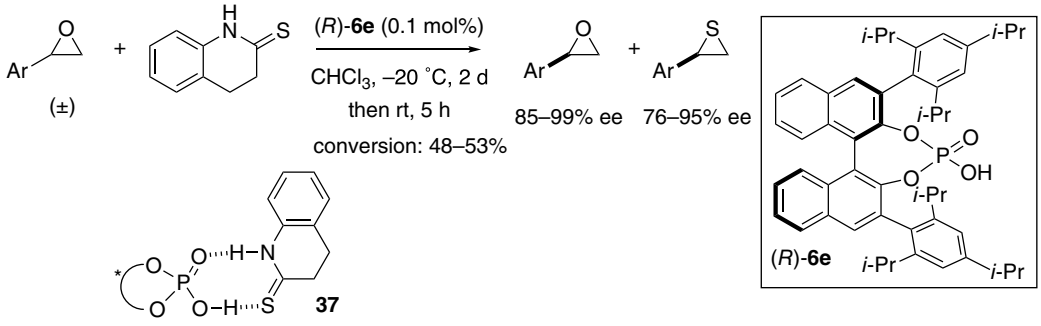

Scheme 2.87. Kinetic resolution of oxiranes by the transformation of oxirane into thiiranes.

2.11. CONSTRUCTION OF AXIALLY, PLANAR, AND HELICALLY CHIRAL COMPOUNDS

There are numerous recent reports on the enantioselective construction of axially chiral [175] and planar chiral compounds recently, but those topics will not be discussed here. Please see Chapter 19 [176] for axially chiral compounds and Chapter 20 [177] for planar chiral compounds.

2.12. COMBINATION WITH TRANSITION METAL CATALYSTS [25–27]

Chiral Brønsted acid may be employed in combination with metal catalysts. Several kinds of combination are reported such as cooperative catalysis and relay catalysis. We already discussed some asymmetric reactions involving the combination of chiral Brønsted acid and metal catalysts in the previous sections, but we will briefly show several representative reactions in this section.

List reported an enantioselective α-allylation of aldehyde by the combined use of CPA and $Pd(PPh_3)_4$. Enamine, generated in situ from aldehyde and allylic amine, reacted with π-allyl palladium intermediate **37** bearing chiral counteranion to afford adducts with 97% ee (Scheme 2.88) [178]. List developed an asymmetric counteranion-directed catalysis (ACDC) strategy [23], and employed chiral phosphate anion as the chiral counteranion for a range of transformations.

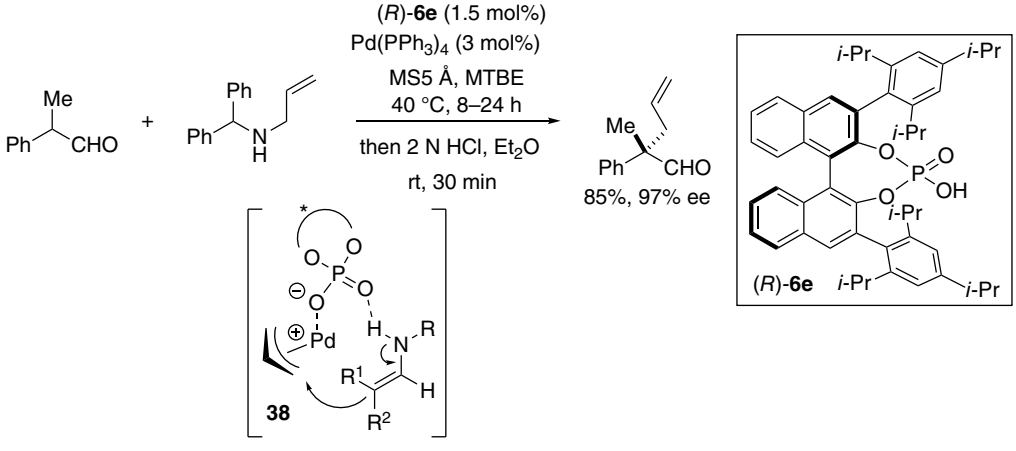

Scheme 2.88. α-Allylation of aldehyde. Source: [178].

You reported enantioselective synthesis of polycyclic indoles, such as tetrahydropyrano[3,4-*b*] indoles and tetrahydro-β-carbolines, through olefin cross-metathesis and subsequent intramolecular Friedel-Crafts alkylation reaction using the dual catalysis system of Ru complex **38** and CPA **6o** (Scheme 2.89) [179]. The use of readily available starting materials can make the synthesis of polycyclic indoles more practical and economical.

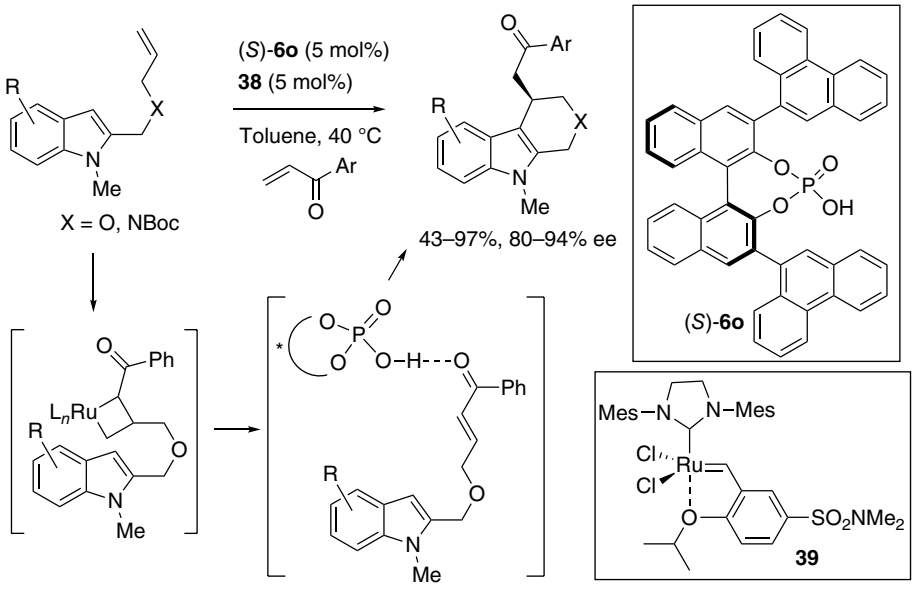

Scheme 2.89. Dual catalysis system of CPA and Ru complex. Source: Based on [179].

Hu and Gong developed a cooperative catalysis system using CPA **6o** and $Rh_2(OAc)_4$ to realize a three-component reaction between diazo ester, alcohol, and imine that generated *syn*-β-amino-α-hydroxy acid with excellent diastereoselectivity and with 93% ee (Scheme 2.90) [180]. This reaction proceeded through the generation of oxonium ylide intermediate **40** from diazo ester and $Rh_2(OAc)_4$ by way of Rh carbene species, and the subsequent reaction with imine, which was activated by CPA [181].

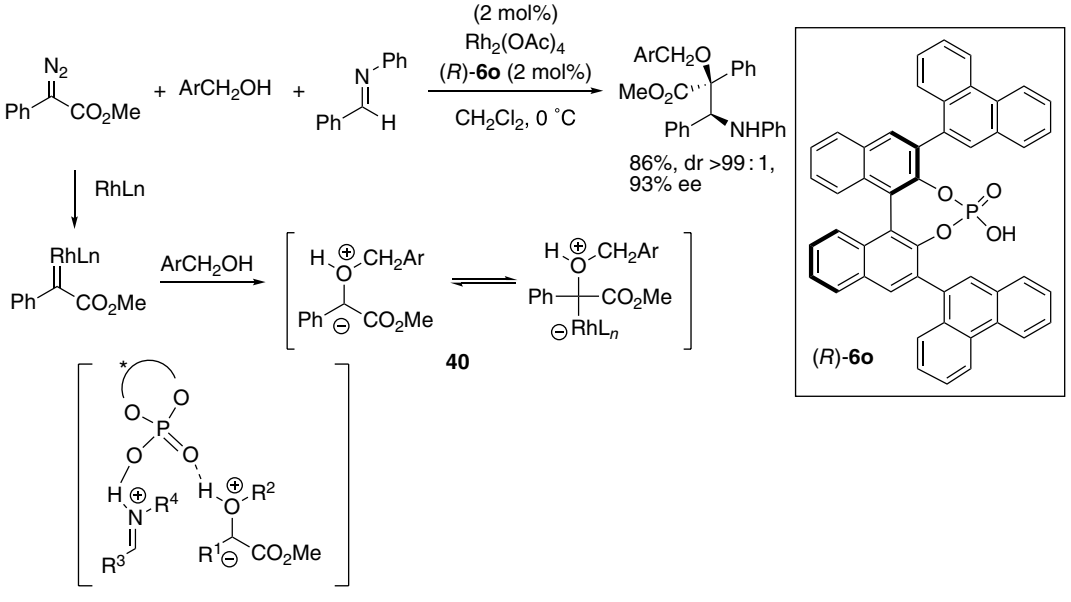

Scheme 2.90. Cooperative catalysis with CPA and $Rh_2(OAc)_4$. Source: Based on [180].

Hu recently reported the fluoroalkyl-substituted *syn*-diamines by the *gem*-difluoro functionalization of 2,2,2-trifluorodiazoethane, which could be efficiently converted into a series of fluoroalkyl-substituted structures by the cooperative system of CPA **6b** and iron porphyrin complex (FeTPPCl) (Scheme 2.91) [182]. Trifluorodiazoethane reacted with FeTPPCl to give the nonconjugated Fe carbene, which reacted with aniline to give free ylide. Subsequent reaction with imine furnished expected product.

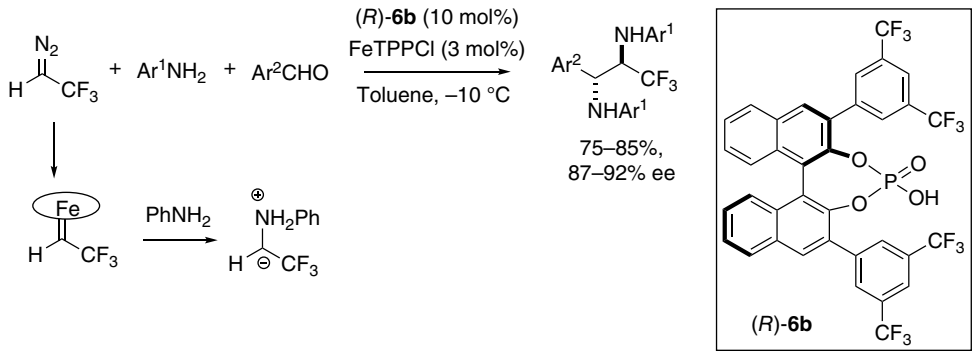

Scheme 2.91. Cooperative catalysis with CPA and Fe complex. Source: Based on [182].

Hu reported a Pd(II)/CPA **6b** catalyzed three-component reaction between aryldiazoacetate, enamines, and imines to afford α-amino-δ-oxo pentanoic acid derivatives (Scheme 2.92a) [183]. Phenyldiazoacetate reacted with Pd salt to form Pd carbene intermediate, which reacted with aniline to generate Pd enolate. Subsequent aza-Michael reaction with iminium salt of chalcone derivatives and hydrolysis furnished the adducts (Scheme 2.92b).

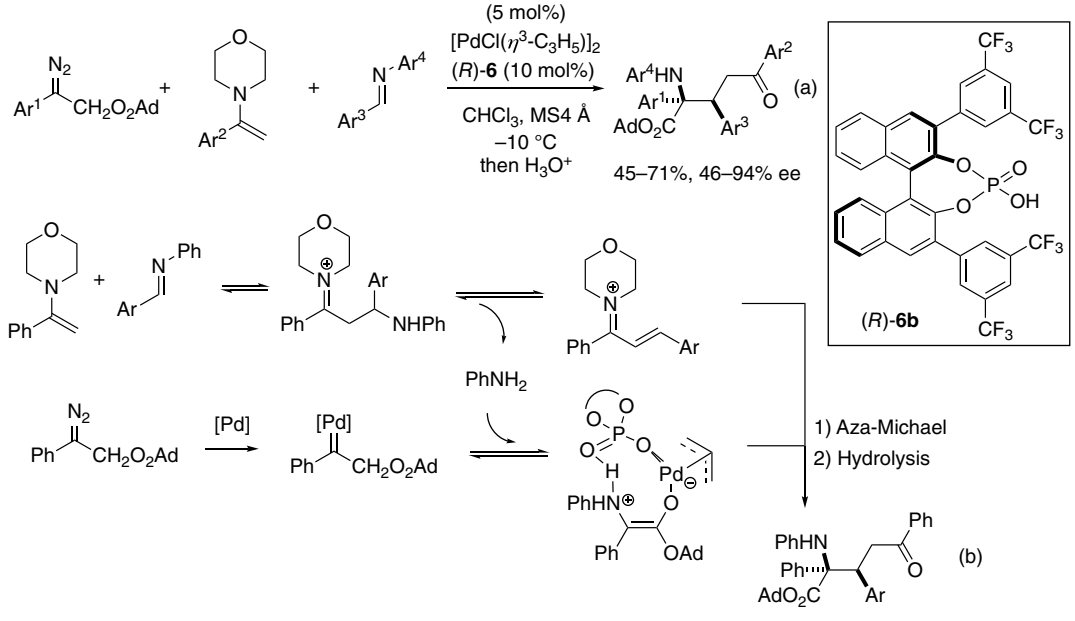

Scheme 2.92. Cooperative catalysis with CPA and Pd(II) complex (a) (Source: Based on [183]), and its mechanism (b).

Hu reported a reaction between diazoacetamides and various imines using $Rh_2(OAc)_4$ and CPA **6i** to furnish chiral oxindole derivatives. The zwitterionic intermediate was trapped by imines (Scheme 2.93) [184].

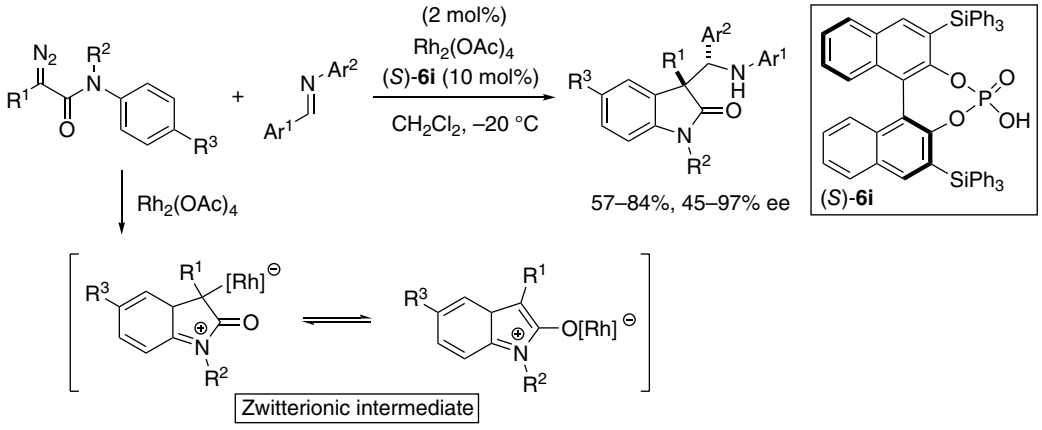

Scheme 2.93. Cooperative catalysis with CPA and $Rh_2(OAc)_4$. Source: Based on [184].

2.13. COMBINATION WITH PHOTOREDOX CATALYST

The merger of chiral Brønsted acid and photoredox catalyst was first reported by Knowles in 2013. The reductive coupling of ketones and hydrazones proceeded in a highly enantioselective manner to furnish *syn*-1,2-amino alcohols with excellent levels of diastereo- and enantioselectivities. The reaction was proposed to proceed *via N*-centered radicals formed by the proton-coupled electron transfer (PCET) activation of sulfonamide *N*-H bonds [185]. A range of enantioselective reactions taking advantage of the combination of photoredox catalysis and chiral Brønsted acid catalysis has been reported [186]. For details, please see Chapter 8 [187].

2.14. CONCLUSION

In summary, development of chiral Brønsted acid catalysis up to 2020 has been discussed in this chapter. Significant advances in this area have emerged in the past decade, and numerous numbers of papers were published. Transformation mediated by chiral Brønsted acid started from the reaction with imines because of the basic nature of imine nitrogen. Functional groups activated by chiral Brønsted acids have been expanded to carbonyl, alkyne, alkene, alcohol, and others. A wide range of asymmetric reactions was catalyzed by the chiral Brønsted acid with high to excellent enantioselectivities. Furthermore, combination with other catalysts such as metal-based catalysts and photoredox catalysts was successfully achieved. Relay catalysis and cooperative catalysis led to formation of complex molecules with high to excellent optical purity in simple operations. Its application to industrial process will be also expected. I hope this chapter will be useful to synthetic organic chemists who are interested in this active area, and will contribute to further advances.

ACKNOWLEDGMENTS

Generous support from JSPS KAKENHI Grant numbers JP20H00380 and JP20H04826 (Hybrid Catalysis) is acknowledged.

REFERENCES

1. Yamamoto, H.; Ishihara, K. eds *Acid Catalysis in Modern Organic Synthesis, Vol. 1, and 2,* Weinheim, Germany: Wiley-VCH. **2008**.
2. (a) Schreiner, P. R. *Chem. Soc. Rev.* **2003**, *32*, 289–296. (b) Pihko, P. M. *Angew. Chem. Int. Ed.* **2004**, *43*, 2062–2064.
3. (a) Sigman, M. S.; Jacobsen, E. N. *J. Am. Chem. Soc.* **1998**, *120*, 4901–4902. (b) Sigman, M. S.; Vachal, P.; Jacobsen, E. N. *Angew. Chem. Int. Ed.* **2000**, *39*, 1279–1281.
4. (a) Wenzel, A. G.; Jacobsen, E. N. *J. Am. Chem. Soc.* **2002**, *124*, 12964–12965. (b) Okino, T.; Hoashi, Y.; Takemoto, Y. *J. Am. Chem. Soc.* **2003**, *125*, 12672–12673. (c) Inokuma, T.; Hoashi, Y.; Takemoto, Y. *J. Am. Chem. Soc.* **2006**, *128*, 9413–9419; (d) For reviews, see: Takemoto, Y. *Org. Biomol. Chem.* **2005**, *3*, 4299–4306. (e) Taylor, M. S.; Jacobsen, E. N. *Angew. Chem. Int. Ed.* **2006**, *45*, 1520–1543. (f) Doyle, A. G.; Jacobsen, E. N. *Chem. Rev.* **2007**, *107*, 5713–5743. (g) Zhang, Z.; Schreiner, P. R. *Chem. Soc. Rev.* **2009**, *38*, 1187–1198. (h) Knowles, R. R.; Jacobsen, E. N. *Proc. Natl. Acad. Sci. USA* **2010**, *107*, 20678–20685. (i) Takemoto, Y. *Chem. Pharm. Bull.* **2010**, *58*, 593–601.
5. Huang, Y.; Unni, A. K.; Thadani, A. N.; Rawal, V. H. *Nature* **2003**, *424*, 146.
6. McDougal, N. T.; Schaus, S. E. *J. Am. Chem. Soc.* **2003**, *125*, 12094–12095.
7. (a) Nugent, B. M.; Yoder, R. A.; Johnston, J. N. *J. Am. Chem. Soc.* **2004**, *126*, 3418–3419. (b) Singh, A.; Yoder, R. A.; Shen, B.; Johnston, J. N. *J. Am. Chem. Soc.* **2007**, *129*, 3466–3467. (c) For a recent example, see: Yousefi, R.; Struble, T. J.; Payne, J. L.; Vishe, M.; Schley, N. D.; Johnston, J. N. *J. Am. Chem. Soc.* **2019**, *141*, 618–625.
8. Akiyama, T.; Itoh, J.; Yokota, K.; Fuchibe, K. *Angew. Chem. Int. Ed.* **2004**, *43*, 1566–1568.
9. Uraguchi, D.; Terada, M. *J. Am. Chem. Soc.* **2004**, *126*, 5356–5357.
10. (a) Hashimoto, T.; Maruoka, K. *J. Am. Chem. Soc.* **2007**, *129*, 10054–10055. (b) Hashimoto, T.; Maruoka, K. *Synthesis* **2008**, 3703–3706.
11. (a) Hatano, M.; Maki, T.; Moriyama, K.; Arinobe, M.; Ishihara, K. *J. Am. Chem. Soc.* **2008**, *130*, 16858–16860. (b) For reviews, see: Hatano, M.; Ishihara, K. *Asian J. Org. Chem.* **2014**, *3*, 352–365. (c) Hatano, M.; Zhao, X.; Mochizuki, T.; Maeda, K.; Motokura, K.; Ishihara, K. *Asian J. Org. Chem.* **2021**, *10*, 360–365
12. (a) García-García, P.; Lay, F.; García-García, P.; Rabalakos, C.; List, B. *Angew. Chem. Int. Ed.* **2009**, *48*, 4363–4366. (b) Ratjen, L.; García-García, P.; Lay, F.; Beck, M. E.; List, B. *Angew. Chem. Int. Ed.* **2011**, *50*, 754–758. (c) For a review, see: James, T.; van Gemmeren, M.; List, B. *Chem. Rev.* **2016**, *115*, 9388–9409.
13. Čorić, I.; List, B. *Nature* **2012**, *483*, 315–319.
14. DSI, IDP, and IDPi are mainly used as precatalyst to generate silylium cation as well as chiral Brønsted acid. For a review on imidodiphosphorimidate (IDPi) catalysis, see: Schreyer, L.; Properzi, R.; List, B. *Angew. Chem. Int. Ed.* **2019**, *58*, 12761–12777.
15. (a) For reviews on chiral Brønsted acid catalysis, Akiyama, T.; Itoh, J.; Fuchibe, K. *Adv. Synth. Catal.* **2006**, *348*, 999–1010. (b) Akiyama, T. *Chem. Rev.* **2007**, *107*, 5744–5758. (c) Terada, M. *Synthesis* **2010**, 1929–1982. (d) Terada, M. *Bull. Chem. Soc. Jpn.* **2010**, *83*, 101–119. (e) Parmar, D.; Sugiono, E.; Raja, S.; Rueping, M. *Chem. Rev.* **2014**, *114*, 9047–9153. (f) Akiyama, T.; Mori, K. *Chem. Rev.* **2015**, *115*, 9277–9306. (g) Parmar, D.; Sugiono, E.; Raja, S.; Rueping, M. *Chem. Rev.* **2017**, *117*, 10608–10620. (h) Maji, R.; Mallojjalaa, S. C.; Wheeler, S. E. *Chem. Soc. Rev.* **2018**, *47*, 1142–1158. (i) Merad, J.; Lalli, C.; Bernadat, G.; Maury, J.; Masson, G. *Chem. Eur. J.* **2018**, *24*, 3925–2943. (j) Li, X.; Song, Q. *Chin. Chem. Lett.* **2018**, *29*, 1181–1192. (k) Xia, Z.-L.; Xu-Xu, Q.-F.; Zheng, C.; You, S.-L. *Chem. Soc. Rev.* **2020**, *49*, 286–300.
16. (a) Maruoka, K. ed. Asymmetric Organocatalysis 2, Brønsted base and acid catalysts, and additional topics. In: *Science of Synthesis*, Stuttgart, Germany, Georg Thieme Verlag KG, **2012**. (b).Rueping, M., Parmar, D., and Sugiono, E. eds *Asymmetric Brønsted Acid Catalysis*, Weinheim, Germany: Wiley-VCH. **2016**.
17. (a) Yang, C.; Xue, X.-S.; Jin, J.-L.; Li, X.; Cheng, J.-P. *J. Org. Chem.* **2013**, *48*, 7076–7085. (b) Yang, C.; Xue, X.-S.; Li, X.; Cheng, J.-P. *J. Org. Chem.* **2014**, *79*, 4340–4351.
18. Guo, Q.-X.; Liu, H.; Guo, C.; Luo, S.-W.; Gu, Y.; Gong, L.-Z. *J. Am. Chem. Soc.* **2007**, *129*, 3790–3791.
19. For a review on SPINOL derived chiral phosphoric acid, see: Rahman, A.; Lin, X. *Org. Biomol. Chem.* **2018**, *16*, 4753–4777.
20. Coric, I.; Müller, S.; List, B. *J. Am. Chem. Soc.* **2010**, *132*, 17370–17373.
21. Nakashima, D.; Yamamoto, H. *J. Am. Chem. Soc.* **2006**, *128*, 9626–9627.
22. (a) Christ, P.; Lindsay, A. G.; Vormittag, S. S.; Neudörfl, J.-M.; Berkessel, A.; O'Donoghue, A. C. *Chem. Eur. J.* **2011**, *17*, 8524–8528. (b) Kaupmees, K.; Tolstoluzhsky, N.; Raja, S.; Rueping, M.; Leito, I. *Angew. Chem. Int. Ed.* **2013**, *52*, 11569–11572.
23. For a review on ACDC, see: Mahlau, M.; List, B. *Angew. Chem. Int. Ed.* **2013**, *52*, 518–533.
24. (a) Phipps, R. J.; Hamilton, G. L.; Toste, F. D. *Nature Chem.* **2012**, *4*, 603–614. (b) See also, Brak, K.; Jacobsen, E. N. *Angew. Chem. Int. Ed.* **2013**, *52*, 534–561.
25. Toste, D. (this issue), Chapter 4 – Asymmetric phase transfer and ion pair organocatalysis. In: Akiyama, T. and Ojima, I. *Catalytic Asymmetric Synthesis*, 4e, Wiley.
26. Parra, A.; Reboredo, S.; Castro, A. M. M.; Alemán, J. *Org. Biomol. Chem.* **2012**, *10*, 5001–5020

27. (a) For reviews, see: Zhong, C.; Shi, X. *Eur. J. Org. Chem.* **2010**, *2010* 2999–3025. (b) Piovesana, S.; Scarpino Schietroma, D. M.; Bella, M. *Angew. Chem. Int. Ed.* **2011**, *50*, 6216–6232. (c) Brière, J.-F.; Oudeyer, S.; Dalla, V.; Levacher, V. *Chem. Soc. Rev.* **2012**, *41*, 1696–1707. (d) Tran, V. T.; Nimmagadda, S. K.; Liu, M.; Engle, K. M. *Org. Biomol. Chem.* **2020**, *18*, 618–637.
28. (a) Inanaga, J.; Sugimoto, Y.; Hanamoto, T. *New J. Chem.* **1995**, *19*, 707–712. (b) Furuno, H.; Hanamoto, T.; Sugimoto, Y.; Inanaga, J. *Org. Lett.* **2000**, *2*, 49–52.
29. Hatano, M.; Ikeno, T.; Matsumura, T.; Torii, S.; Ishihara, K. *Adv. Synth. Catal.* **2008**, *350*, 1776–1780.
30. Drouet, F.; Lalli, C.; Liu, H.; Masson, G.; Zhu, J. *Org. Lett.* **2010**, *13*, 94–97.
31. Ingle, G. K.; Liang, Y.; Mormino, M. G.; Li, G.; Fronczek, F. R.; Antilla, J. C. *Org. Lett.* **2011**, *13*, 2054–2057.
32. (a) Hatano, M.; Moriyama, K.; Maki, T.; Ishihara, K. *Angew. Chem. Int. Ed.* **2010**, *49*, 3823–3826. (b) Hatanoa, M.; Ishihara, K. *Synthesis* **2010**, 3785–3801
33. Klussmann, M.; Ratjen, L.; Hoffmann, S.; Wakchaure, V.; Goddard, R.; List, B. *Synlett* **2010**, 2189–2192.
34. For an example, see: Prashad, M.; Hu, B.; Repi, O.; Blacklock, T. J.; Giannousis, P. *Org. Process Res. Dev.* **2000**, *4*, 55–59.
35. Yamanaka, M.; Itoh, J.; Fuchibe, K.; Akiyama, T. *J. Am. Chem. Soc.* **2007**, *129*, 6756–6764.
36. Zhou, F.; Yamamoto, H. *Angew. Chem. Int. Ed.* **2016**, *55*, 8970–8974
37. Gheewala, C. D.; Collins, B. E.; Lambert, T. H. *Science* **2016**, *351*, 961–965
38. Hatano, M.; Maki, T.; Moriyama, K.; Arinobe, M.; Ishihara, K. *J. Am. Chem. Soc.* **2008**, *130*, 16858–16860.
39. Zhu, C.; Mandrelli, F.; Zhou, H.; Maji, R.; List, B. *J. Am. Chem. Soc.* **2021**, *143*, 3312–3317.
40. Seayad, J.; Seayad, A. M.; List, B. *J. Am. Chem. Soc.* **2006**, *128*, 1086–1087.
41. Wang, S.-G.; Xia, Z.-L.; Xu, R.-Q.; Liu, X.-J.; Zheng, C.; You, S.-L. *Angew. Chem. Int. Ed.* **2017**, *56*, 7440–7443.
42. (a) Zahrt, A. F.; Henle, J. J.; Rose, B. T.; Wang, Y.; Darrow, W. T.; Denmark, S. E. *Science* **2019**, *363*, eaau5631. (b) See also: Reid, J. P.; Sigman, M. S. *Nature* **2019**, *571*, 343–348.
43. Wang, Y.; Wang, Q.; Zhu, J. *Angew. Chem. Int. Ed.* **2017**, *56*, 5612–5615.
44. Fan, L.; Han, C.; Li, X.; Yao, J.; Wang, Z.; Yao, C.; Chen, W.; Wang, T.; Zhao, J. *Angew. Chem. Int. Ed.* **2018**, *57*, 2115–2119.
45. Kang, Q.; Zhao, Z.-A.; You, S.-L. *J. Am. Chem. Soc.* **2007**, *129*, 1484–1485.
46. Xu, F.; Huang, D.; Han, C.; Shen, W.; Lin, X.; Wang, Y. *J. Org. Chem.* **2010**, *75*, 8677–8680.
47. (a) For reviews, see: Zeng, M.; You, S.-L. *Synlett* **2010**, 1289–1301. (b) Terrasson, V.; Marcia de Figueiredo, R.; Campagne, J. M. *Eur. J. Org. Chem* **2010**, 2635–2655.
48. Hatano, M.; Mochizuki, T.; Nishikawa, K.; Ishihara, K. *ACS Catal.* **2018**, *8*, 349–353.
49. Hatano, M.; Okamoto, H.; Kawakami, T.; Toh, K.; Nakatsuji, H.; Sakakura, A.; Ishihara, K. *Chem. Sci.* **2018**, *9*, 6361–6367.
50. For a review on combined acid catalysis for asymmetric synthesis, see: Yamamoto, H.; Futatsugi, K. *Angew. Chem. Int. Ed.* **2005**, *44*, 1924–1942.
51. Miyagawa, M.; Yoshida, M.; Kiyota, Y.; Akiyama, T. *Chem. Eur. J.* **2019**, *25*, 5677–5681.
52. For a review on organocatalytic enantioselective Friedel-Crafts alkylation reactions of pyrroles, see: Gaviña, D.; Escolano, M.; Torres, J.; Alzuet-Piña, G.; Sánchez-Roselló, M.; del Pozo, C. *Adv. Synth. Catal.* **2021**, *363*, 3439–3470.
53. Uchikura, T.; Suzuki, R.; Suda, Y.; Akiyama, T. *ChemCatChem* **2020**, *12*, 4784–4787.
54. Yonesaki, R.; Kondo, Y.; Akkad, W.; Sawa, M.; Morisaki, K.; Morimoto, H.; Ohshima, T. *Chem. Eur. J.* **2018**, *24*, 15211–15214.
55. (a) Mori, K.; Ehara, K.; Kurihara, K.; Akiyama, T. *J. Am. Chem. Soc.* **2011**, *133*, 6166–6169. (b) See also, Mori, K.; Isogai, R.; Kamei, Y.; Yamanaka, M.; Akiyama, T. *J. Am. Chem. Soc.* **2018**, *140*, 6203–6207.
56. Lee, S.; Kim, S. *Tetrahedron* **2009**, *50*, 3345–3348.
57. Prévost, S.; Dupré, N.; Leutzsch, M.; Wang, Q.; Wakchaure, V.; List, B. *Angew. Chem. Int. Ed.* **2014**, *53*, 8770–8773.
58. Liu, L.; Kaib, P. S. J.; Tap, A.; List, B. *J. Am. Chem. Soc.* **2016**, *138*, 10822–10825.
59. Liu, L.; Leutzsch, M.; Zheng, Y.; Alachraf, M. W.; Thiel, W.; List, B. *J. Am. Chem. Soc.* **2015**, *137*, 13268–13271.
60. Rueping, M.; Theissmann, T.; Kuenkel, A.; Koenigs, R. M. *Angew. Chem. Int. Ed.* **2008**, *47*, 6798–6801.
61. Kikuchi, J.; Aramaki, H.; Okamoto, H.; Terada, M. *Chem. Sci.* **2019**, *10*, 1426–1433.
62. Jain, P.; Antilla, J. C. *J. Am. Chem. Soc.* **2010**, *132*, 11884–11886.
63. Jain, P.; Wang, H.; Houk, K. N.; Antilla, J. C. *Angew. Chem. Int. Ed.* **2012**, *51*, 1391–1394.
64. Grayson, M. N.; Pellegrinet, S. C.; Goodman, J. M. *J. Am. Chem. Soc.* **2012**, *134*, 2716–2722.
65. Wang, H.; Jain, P.; Antilla, J. C.; Houk, K. N. *J. Org. Chem.* **2013**, *78*, 1208–1215.
66. Barrio, P.; Rodríguez, E.; Saito, K.; Fustero, S.; Akiyama, T. *Chem. Commun.* **2015**, *51*, 5246–5249.
67. Gao, S.; Duan, M.; Houk, K.; Chen, M. *Angew. Chem. Int. Ed.* **2020**, *59*, 10540–10548.
68. (a) Wang, M.; Khan, S.; Miliordos, E.; Chen, M. *Adv. Synth. Catal.* **2019**, *360*, 4634–4639. (b) Liu, J.; Chen, M. *Org. Lett.* **2020**, *22*, 8967–8972.
69. Miura, T.; Nakahashi, J.; Murakami, M. *Angew. Chem. Int. Ed.* **2017**, *56*, 6989–6993.
70. Miura, T.; Nakahashi, J.; Zhou, W.; Shiratori, Y.; Stewart, S. G.; Murakami, M. *J. Am. Chem. Soc.* **2017**, *139*, 10903–10908.
71. Mahlau, M.; García-García, P.; List, B. *Chem. Eur. J.* **2012**, *18*, 16283–16287.
72. Kaib, P. S. J.; Schreyer, L.; Lee, S.; Properzi, R.; List, B. *Angew. Chem. Int. Ed.* **2016**, *55*, 13200–13203.
73. Bae, H. Y.; Höfler, D.; Kaib, P. S. J.; Kasaplar, P.; De, C. K.; Döhring, A.; Lee, S.; Kaupmees, K.; Leito, I.; List, B. *Nat. Chem.* **2018**, *10*, 888–894.

74. Lee, D. S.; Bae, H. Y.; List, B. *Angew. Chem. Int. Ed.* **2018**, *57*, 12162–12166.
75. Min, D. C.; Lin, Y.; Seidel, D. *Angew. Chem. Int. Ed.* **2017**, *56*, 15353–15357.
76. Rajkumar, S.; Tang, M.; Yang, X. *Angew. Chem. Int. Ed.* **2020**, *59*, 2333–2337
77. Das, S.; Liu, L.; Zheng, Y.; Alachraf, M. W.; Thiel, W.; De, C. K.; List, B. *J. Am. Chem. Soc.* **2016**, *138*, 9429–9432.
78. Maskeri, M. A.; O'Connor, M. J.; Jaworski, A. A.; Davies, A. V.; Scheidt, K. A. *Angew. Chem. Int. Ed.* **2018**, *57*, 17225–17229.
79. Zhao, C.; Chen, S. B.; Seidel, D. *J. Am. Chem. Soc.* **2016**, *138*, 9053–9056.
80. Zhu, Z.; Odagi, M.; Zhao, C.; Abboud, K. A.; Kirm, H. U.; Saame, J.; Lõkov, M.; Leito, I.; Seidel, D. *Angew. Chem. Int. Ed.* **2020**, *59*, 2028–2032.
81. For a review on enantioselective cycloaddition reaction catalyzed by chiral phosphoric acids, see: Held, F. E.; Grau, D.; Tsogoeva, S. B. *Molecules* **2015**, *20*, 16103–16126.
82. Gatzenmeier, T.; van Gemmeren, M.; Xie, Y.; Höfler, D.; Leutzsch, M.; List, B. *Science* **2016**, *351*, 949–952.
83. Gatzenmeier, T.; Turberg, M.; Yepes, D.; Xie, Y.; Neese, F.; Bistoni, G.; List, B. *J. Am. Chem. Soc.* **2018**, *140*, 12671–12676.
84. Kim, H.; Gerosa, G.; Aronow, J.; Kasaplar, P.; Ouyang, J.; Lingnau, J. B.; Guerry, P.; Farès, C.; List, B. *Nat. Commun.* **2019**, *10* 770.
85. Ghosh, S.; Das, S.; De, C. K.; Yepes, D.; Neese, F.; Bistoni, G.; Leutzsch, M.; List, B. *Angew. Chem. Int. Ed.* **2020**, *59*, 12347–12351.
86. Varlet, T.; Gelis, C.; Retailleau, P.; Bernadat, G.; Neuville, L.; Masson, G. *Angew. Chem. Int. Ed.* **2020**, *59*, 8491–8496.
87. Hatano, M.; Goto, Y.; Izumiseki, A.; Akakura, M.; Ishihara, K. *J. Am. Chem. Soc.* **2015**, *137*, 13472–13475.
88. Akiyama, T.; Morita, H.; Fuchibe, K. *J. Am Chem. Soc.* **2006**, *128*, 13070–13071.
89. (a) Liu, H.; Dagousset, G.; Masson, G.; Retailleau, P.; Zhu, J. *J. Am. Chem. Soc.* **2009**, *131*, 4598–4599. (b) Dagousset, G.; Zhu, J.; Masson, G. *J. Am. Chem. Soc.* **2011**, *133*, 14804–14813.
90. For a review, see: Varleta, T.; Masson, G. *Chem. Commun.* **2021**, *57*, 4089–4105.
91. Jarrige, L.; Blanchard, F.; Masson, G. *Angew. Chem. Int. Ed.* **2017**, *56*, 10573–10576.
92. (a) Luo, C.; Huang, Y. *J. Am. Chem. Soc.* **2013**, *135*, 8193–8196. (b) See also: Dai, W.; Jiang, X.-L.; Tao, J.-Y.; Shi, F. *J. Org. Chem.* **2016**, *81*, 185–192.
93. Momiyama, N.; Tabuse, H.; Noda, H.; Yamanaka, M.; Fujinami, T.; Yamanishi, K.; Izumiseki, A.; Funayama, K.; Egawa, F.; Okada, S.; Adachi, H.; Terada, M. *J. Am. Chem. Soc.* **2016**, *138*, 11353–11359.
94. Kretzschmar, M.; Hodík, T.; Schneider, C. *Angew. Chem. Int. Ed.* **2016**, *55*, 9788–9792.
95. Hatano, M.; Nishikawa, K.; Ishihara, K. *J. Am. Chem. Soc.* **2017**, *139*, 8424–8427.
96. Nakanishi, T.; Kikuchi, J.; Kaga, A.; Chiba, S.; Terada, M. *Chem. Eur. J.* **2020**, *26*, 8230–8234.
97. Zhao, J.-J.; Sun, S.-B.; He, S.-H.; Wu, Q.; Shi, F. *Angew. Chem. Int. Ed.* **2015**, *54*, 5460–5464.
98. El-Sepelgy, M. S. O.; Haseloff, M. S. S.; Alamsetti, S. K.; Schneider, C. *Angew. Chem. Int. Ed.* **2014**, *53*, 7923–7927.
99. Alamsetti, S. K.; Spanka, M.; Schneider, C. *Angew. Chem. Int. Ed.* **2016**, *55*, 2392–2396.
100. Wang, Y.-M.; Zhang, H.-H.; Li, C.; Fan, T.; Shi, F. *Chem. Commun.* **2016**, *52*, 1804–1807.
101. Tan, W.; Li, X.; Gong, Y.-X.; Ge, M.-D.; Shi, F. *Chem. Commun.* **2014**, *50*, 15901–15904.
102. For a review on enantioselective reactions of indolylmethanol catalyzed by chiral phosphoric acid, see: Mei, G.-J.; Shi, F. *J. Org. Chem* **2017**, *82*, 7695–7707.
103. For a review on enantioselective reactions of indole-based chiral heterocycles catalyzed by chiral phosphoric acid, see: Zhang, Y.-C.; Jiang, F.; Shi, F. *Acc. Chem. Res.* **2020**, *53*, 425–446.
104. Gelis, C.; Levitr, G.; Merad, J.; Retailleau, P.; Neuville, L.; Masson, G. *Angew. Chem. Int. Ed.* **2018**, *57*, 12121–12125.
105. Bera, K.; Schneider, C. *Chem. Eur. J.* **2016**, *22*, 7074–7078.
106. Zhu, Z. Q.; Shen, Y.; Sun, X. X.; Tao, J. Y.; Liu, J. X.; Shi, F. *Adv. Synth. Catal.* **2016**, *358*, 3797–3808.
107. Sun, X. X.; Zhang, H. H.; Li, G. H.; He, Y. Y.; Shi, F. *Chem. Eur. J.* **2016**, *22*, 17526–17532.
108. Suneja, A.; Loui, H. J.; Schneider, C. *Angew. Chem. Int. Ed.* **2020**, *59*, 5536–5540.
109. Villar, L.; Uria, U.; Martínez, J. I.; Prieto, L.; Reyes, E.; Carrillo, L.; Vicario, J. L. *Angew. Chem. Int. Ed.* **2017**, *56*, 10535–10538.
110. Rueping, M.; Ieawsuwan, W.; Antonchick, A. P.; Nachtsheim, B. J. *Angew. Chem. Int. Ed.* **2007**, *46*, 2097–2100.
111. Jolit, A.; Walleser, P. M.; Yap, G. P. A.; Tius, M. A. *Angew. Chem. Int. Ed.* **2014**, *53*, 6180–6183.
112. Ouyang, J.; Kennemur, J. L.; De, C. K.; Farès, C.; List, B. *J. Am. Chem. Soc.* **2019**, *141*, 3414–3418.
113. Jin, J.; Zhao, Y.; Gouranourimi, A.; Ariafard, A.; Chan, P. W. H. *J. Am. Chem. Soc.* **2018**, *140*, 5834–5841.
114. Yang, B.-M.; Cai, P.-J.; Tu, Y.-Q.; Yu, Z.-X.; Chen, Z.-M.; Wang, S.-H.; Wang, S.-H.; Zhang, F.-M. *J. Am. Chem. Soc.* **2015**, *137*, 8344–8347.
115. Felker, I.; Pupo, G.; Kraft, P.; List, B. *Angew. Chem. Int. Ed.* **2015**, *54*, 1960–1964.
116. Wang, Y.-Y.; Kanomata, K.; Korenaga, T.; Terada, M. *Angew. Chem. Int. Ed.* **2016**, *55*, 927–931.
117. Uraguchi, D.; Kinoshita, N.; Nakashima, D.; Ooi, T. *Chem. Sci.* **2012**, *3*, 3161–3164.
118. Itoh, J.; Fuchibe, K.; Akiyama, T. *Angew. Chem. Int. Ed.* **2008**, *47*, 4016–4018.
119. Mori, K.; Wakazawa, M.; Akiyama, T. *Chem. Sci.* **2014**, *5*, 1799–1803.
120. Ibáñez, I.; Kaneko, M.; Kamei, Y.; Tsutsumi, R.; Yamanaka, M.; Akiyama, T. *ACS Catal.* **2019**, *9*, 6903–6909.

121. Sheng, Y.-F.; Gu, Q.; Zhang, A.-J.; You, S.-L. *J. Org. Chem* **2009**, *74*, 6899–6901.
122. Sheng, Y.-F.; Li, G.-Q.; Kang, Q.; Zhang, A.-J.; You, S.-L. *Chem. Eur. J.* **2009**, *15*, 3351–3354.
123. Rueping, M.; Sugiono, E.; Azap, C.; Theissmann, T.; Bolte, M. *Org. Lett.* **2005**, *7*, 3781–3783.
124. Yang, J. W.; Fonseca, M. T. H.; Vignola, N.; List, B. *Angew. Chem. Int. Ed.* **2005**, *44*, 108–110.
125. Storer, R. I.; Carrera, D. E.; Ni, Y.; MacMillan, D. W. C. *J. Am. Chem. Soc.* **2006**, *128*, 84–86.
126. (a) Li, G.; Liang, Y.; Antilla, J. C. *J. Am. Chem. Soc.* **2007**, *129*, 5830–5831. (b) Kang, Q.; Zhao, Z.-A.; You, S.-L. *Adv. Synth. Catal.* **2007**, *349*, 1657–1660. (c) For corrigendum, Kang, Q.; Zhao, Z.-A.; You, S.-L. *Adv. Synth. Catal.* **2007**, *349*, 2075.
127. Rueping, M.; Antonchick, A. P. *Angew. Chem. Int. Ed.* **2007**, *46*, 4562–4565.
128. (a) Rueping, M.; Antonchick, A. P.; Theissmann, T. *Angew. Chem. Int. Ed.* **2006**, *45*, 3683–3686. (b) Rueping, M.; Theissmann, T.; Raja, S.; Bats, J. W. *Adv. Synth. Catal.* **2008**, *350*, 1001–1006.
129. Rueping, M.; Antonchick, A. P.; Theissmann, T. *Angew. Chem. Int. Ed.* **2006**, *45*, 6751–6755.
130. Rueping, M.; Tato, F.; Schoepke, F. R. *Chem. Eur. J.* **2010**, *16*, 2688–2691.
131. Rueping, M.; Brinkmann, C.; Antonchick, A. P.; Atodiresei, I. *Org. Lett.* **2010**, *12*, 4604–4607.
132. Han, Z.-Y.; Xiao, H.; Gong, L.-Z. *Bioorg. Med. Chem. Lett.* **2009**, *19*, 3729–3732.
133. (a) For reviews on transefr hydrogenation using CPA and Hantzsch ester, see: Rueping, M.; Sugiono, E.; Schoepke, F. R. *Synlett* **2010**, 852–865. (b) Rueping, M.; Dufour, J.; Schoepke, F. R. *Green Chem.* **2011**, *13*, 1084–1105. (c) Zheng, C.; You, S.-L. *Chem. Soc. Rev.* **2012**, *41*, 2498–2518. (d) Phillips, A. M. F.; Pombeiro, A. J. L. *Org. Biomol. Chem* **2017**, *15*, 2307–2340.
134. Simón, L.; Goodman, J. M. *J. Am. Chem. Soc.* **2008**, *130*, 8741–8747.
135. Marcelli, T.; Hammar, P.; Himo, F. *Adv. Synth. Catal.* **2009**, *351*, 525–529.
136. Chen, Q.-A.; Gao, K.; Duan, Y.; Ye, Z.-S.; Shi, L.; Yang, Y.; Zhou, Y.-G. *J. Am. Chem. Soc.* **2012**, *134*, 2442–2448.
137. (a) Li, C.; Villa-Marcos, B.; Xiao, J. *J. Am. Chem. Soc.* **2009**, *131*, 6967–6969. (b) Tang, W.; Johnston, S.; Iggo, J. A.; Berry, N. G.; Phelan, M.; Lian, L.; Bacsa, J.; Xiao, J. *Angew. Chem. Int. Ed.* **2013**, *52*, 1668–1672.
138. Wakchaure, V. N.; Kaib, P. S. J.; Leutzsch, M.; Lis, B. *Angew. Chem. Int. Ed.* **2015**, *54*, 11852–11856.
139. Wakchaure, V. N.; List, B. *Angew. Chem. Int. Ed.* **2016**, *55*, 15775–15778.
140. Wakchaure, V. N.; Obradors, C.; List, B. *Synlett* **2020**, *31*, 1707–1712.
141. Zhu, C.; Saito, K.; Yamanaka, M.; Akiyama, T. *Acc. Chem. Res.* **2015**, *48*, 388–398.
142. Zhu, C.; Akiyama, T. *Org. Lett.* **2009**, *11*, 4180–4183.
143. Saito, K.; Horiguchi, K.; Shibata, Y.; Yamanaka, M.; Akiyama, T. *Chem. Eur. J.* **2014**, *20*, 7616–7620.
144. Zhu, C.; Akiyama, T. *Adv. Synth. Catal.* **2010**, *352*, 1846–1850
145. Henseler, A.; Kato, M.; Mori, K.; Akiyama, T. *Angew. Chem. Int. Ed.* **2011**, *50*, 8180–8183.
146. Sakamoto, T.; Horiguchi, K.; Saito, K.; Mori, K.; Akiyama, T. *Asian J. Org. Chem.* **2013**, *2*, 943–946.
147. Miyagawa, M.; Takashima, K.; Akiyama, T. *Synlett* **2018**, *29*, 1607–1610.
148. Horiguchi, K.; Yamamoto, E.; Saito, K.; Yamanaka, M.; Akiyama, T. *Chem. Eur. J.* **2016**, *22*, 8078–8083.
149. Saito, K.; Akiyama, T. *Chem. Commun.* **2012**, *48*, 4573–4575.
150. Sakamoto, T.; Mori, K.; Akiyama, T. *Org. Lett.* **2012**, *14*, 3312–3315.
151. Shibata, Y.; Yamanaka, M. *J. Org. Chem.* **2013**, *78*, 3731–3736.
152. Saito, K.; Miyashita, H.; Akiyama, T. *Org. Lett.* **2014**, *16*, 5312–5315.
153. Saito, K.; Shibata, Y.; Yamanaka, M.; Akiyama, T. *J. Am. Chem. Soc.* **2013**, *135*, 11740–11743.
154. Saito, K.; Akiyama, T. *Angew. Chem. Int. Ed.* **2016**, *55*, 3148–3152.
155. (a) Zhang, Z.; Jain, P.; Antilla, J. C. *Angew. Chem. Int. Ed.* **2011**, *50*, 10961–10964. (b) See also, Enders, D.; Stöckela, B. A.; Rembiaka, A. *Chem. Commun.* **2014**, *50*, 4489–4491.
156. Na, F.; Lopez, S. S.; Beauseigneur, A.; Hernandez, L. W.; Sun, Z.; Antilla, J. C. *Org. Lett.* **2020**, *22*, 5953–5957.
157. Yang, K.; Lou, Y.; Wang, C.; Qi, L.-W.; Fang, T.; Zhang, F.; Xu, H.; Zhou, L.; Li, W.; Zhang, G.; Yu, P.; Song, Q. *Angew. Chem. Int. Ed.* **2020**, *59*, 3294–3299.
158. Wang, Z.; Ai, F.; Wang, Z.; Zhao, W.; Zhu, G.; Lin, Z.; Sun, J. *J. Am. Chem. Soc.* **2015**, *137*, 383–389.
159. Sun, Z.; Winschel, G. A.; Borovika, A.; Nagorny, P. *J. Am. Chem. Soc.* **2012**, *134*, 8074–8077.
160. Lin, J.-S.; Yu, P.; Huang, L.; Zhang, P.; Tan, B.; Liu, X.-Y. *Angew. Chem. Int. Ed.* **2015**, *54*, 7847–7851.
161. Yu, Z.-L.; Cheng, Y.-F.; Jiang, N.-C.; Wang, J.; Fan, L.-W.; Yuan, Y.; Li, Z.-L.; Gu, Q.-S.; Liu, X.-Y. *Chem. Sci.* **2020**, *11*, 5987–5993.
162. Samanta, R. C.; Yamamoto, H. *J. Am. Chem. Soc.* **2017**, *139*, 1460–1463.
163. Ackermann, L.; Althammer, A. *Synlett* **2008**, 995–998.
164. Tsuji, N.; Kennemur, J. L.; Buyck, T.; Lee, S.; Prévost, S.; Kaib, P. S. J.; Bykov, D.; Farès, C.; List, B. *Science* **2018**, *359*, 1501–1505.
165. Zhang, P.; Tsuji, N.; Ouyang, J.; List, B. *J. Am. Chem. Soc.* **2021**, *143*, 675–680.
166. Zhao, W.; Qian, H.; Li, Z.; Sun, J. *Angew. Chem. Int. Ed.* **2015**, *54*, 1910–1913.
167. Li, X.; Duan, M.; Deng, Z.; Shao, Q.; Chen, M.; Zhu, G.; Houk, K. N.; Sun, J. *Nat. Catal.* **2020**, *3*, 1010–1019.
168. Li, F.; Korenaga, T.; Nakanishi, T.; Kikuchi, J.; Terada, M. *J. Am. Chem. Soc.* **2018**, *140*, 2629–2642.
169. Kayal, S.; Kikuchi, J.; Shimizu, M.; Terada, M. *ACS Catal.* **2019**, *9*, 6846–6850.

170. Ma, D.; Miao, C.-B.; Sun, J. *J. Am. Chem. Soc.* **2019**, *141*, 13783–13787.
171. Wang, H. W.; Zhu, J. *J. Am. Chem. Soc.* **2019**, *141*, 11372–11377.
172. Monaco, M. R.; Poladura, B.; Dias de los Bernardos, M.; Leutzsch, M.; Goddard, R.; List, B. *Angew. Chem. Int. Ed.* **2014**, *53*, 7063–7067.
173. Liao, S.; Čorić, I.; Wang, Q.; List, B. *J. Am. Chem. Soc.* **2012**, *134*, 10765–10768.
174. Liao, S.; Leutzsch, M.; Monaco, M. R.; List, B. *J. Am. Chem. Soc.* **2016**, *138*, 5230–5233.
175. (a) For reviews, see: Shirakawa, S.; Liu, S.; Kaneko, S. *Chem. Asian J.* **2016**, *11*, 330–341. (b) Renzi, P. *Org. Biomol. Chem.* **2017**, *15*, 4506–4516. (c) Wang, Y.-B.; Tan, B. *Acc. Chem. Res.* **2018**, *51*, 534–547. (d) Corti, V.; Bertuzzi, G. *Synthesis* **2020**, *52*, 2450–2468.
176. Xiang, S.; Cheng, J. K.; Tan, B. (this issue). Chapter 19 – Asymmetric synthesis of axially chiral compounds. In: Akiyama, T. and Ojima, I. *Catalytic Asymmetric Synthesis*, 4e, Wiley.
177. Shibata, T. (this issue). Chapter 20 – Asymmetric synthesis of planar-chiral and helically chiral compounds. In: Akiyama, T. and Ojima, I. *Catalytic Asymmetric Synthesis*, 4e, Wiley.
178. (a) Mukherjee, S.; List, B. *J. Am. Chem. Soc.* **2007**, *129*, 11336–11337. (b) Jiang, G.; Halder, R.; Fang, Y.; List, B. *Angew. Chem. Int. Ed.* **2011**, *50*, 9752–9755. (c) Jiang, G.; List, B. *Adv. Synth. Catal.* **2011**, *353*, 1667–1670.
179. Cai, Q.; Zhao, Z.-A.; You, S.-L. *Angew. Chem. Int. Ed.* **2009**, *48*, 7428–7431.
180. Hu, W.; Xu, X.; Zhou, J.; Liu, W.-J.; Huang, H.; Hu, J.; Yang, L.; Gong, L.-Z. *J. Am. Chem. Soc.* **2008**, *130*, 7782–7783.
181. (a) Guo, X.; Hu, W. *Acc. Chem. Res.* **2013**, *46*, 2427–2440. (b) Lv, F.; Liu, S.; Hu, W. Asian J. *Org. Chem.* **2013**, *2*, 824–836.
182. Li, J.; Zhang, D.; Chen, J.; Ma, C.; Hu, W. *ACS Catal.* **2020**, *10*, 4559–4565.
183. Zhang, D.; Zhou, J.; Xia, F.; Kang, Z.; Hu, W. *Nat. Commun.* **2015**, *6*, 5801.
184. Qiu, H.; Li, M.; Jiang, L.-Q.; Lv, F.-P.; Zan, L.; Zhai, C.-W.; Doyle, M. P.; Hu, W.-H. *Nature Chem.* **2012**, *4*, 733–738.
185. (a) Rono, L. J.; Yayla, H. G.; Wang, D. Y.; Armstrong, M. F.; Knowles, R. R. *J. Am. Chem. Soc.* **2013**, *135*, 17735–17738. (b) Gentry, E. C.; Knowles, R. R. *Acc. Chem. Res.* **2016**, *49*, 1546–1556. (c) For a recent example, see: Roos, C. B.; Demaerel, J.; Graff, D. E.; Knowles, R. R. *J. Am. Chem. Soc.* **2020**, *142*, 5974–5979.
186. For a review, see: Yin, Y.; Zhao, X.; Qiao, B.; Jiang, Z. *Org. Chem. Front.* **2020**, *7*, 1283–1296.
187. Masson, G. (this issue). Chapter 8 – Asymmetric visible-light photoredox catalysis. In: Akiyama, T. and Ojima, I. *Catalytic Asymmetric Synthesis*, 4e, Wiley.

3

ASYMMETRIC BASE ORGANOCATALYSIS

Azusa Kondoh and Masahiro Terada
Graduate School of Science, Tohoku University, Sendai, Japan

3.1. INTRODUCTION

Brønsted base catalysis – the catalysis by a small molecule having Brønsted basicity, such as an amine – is one of the most fundamental types of catalysis in organic chemistry. The catalysis enables the direct transformation of starting compounds into desired products in a highly atom-economical fashion under mild reaction conditions and, thus, has been widely utilized in organic synthesis over a long period of time. In particular, the catalysis has recently attracted considerable attention as a family of "environmentally benign" organocatalysis, and the development of enantioselective reactions has been intensively explored by using chiral uncharged organobases as a catalyst [1]. Generally, the catalysis is initiated by the generation of an anionic nucleophile through the direct deprotonation of a pronucleophile by a Brønsted base catalyst (Figure 3.1). Then, the transformation of the anionic nucleophile, such as addition to an unsaturated bond, rearrangement, and isomerization, proceeds to generate a different anionic intermediate. Finally, the protonation of the resulting anionic intermediate with the conjugate acid of the Brønsted base catalyst (or the other molecule of a pronucleophile in some cases) occurs to provide the desired products along with the regeneration of the catalyst (or the anionic nucleophile), completing the catalytic cycle. In the case of enantioselective reactions, the transformation of the anionic nucleophile (and/or the protonation of the anionic intermediate) proceeds in a stereoselective fashion under the influence of the conjugate acid of a chiral Brønsted base catalyst, and an enantio-enriched product can be obtained.

In establishing a new Brønsted base-catalyzed reaction, one must take into account the balance of the acidities of a pronucleophile and a product and the basicity of a catalyst. In other words, both the effective generation of an anionic nucleophile and the efficient regeneration of a catalyst are essential to promote a catalytic reaction efficiently. If the basicity of a catalyst is not high enough to deprotonate a substrate, the reaction does not proceed. Therefore, the range of the pronucleophiles applicable to the reaction is highly dependent on the basicity of the employed catalysts. On the other hand, if the basicity of the anionic intermediate, that is the conjugate base of a product, is not high enough to deprotonate the conjugate acid of a catalyst, the catalyst turnover does not occur, and the reaction does not proceed at least in a catalytic fashion. Furthermore, in the case of catalytic enantioselective reactions, the application of a proper chiral catalyst is also critical to achieve high stereoselectivity. Therefore, the development of chiral catalysts is crucial to accomplish various types of catalytic enantioselective reactions. Indeed, a

Catalytic Asymmetric Synthesis, Fourth Edition. Edited by Takahiko Akiyama and Iwao Ojima.

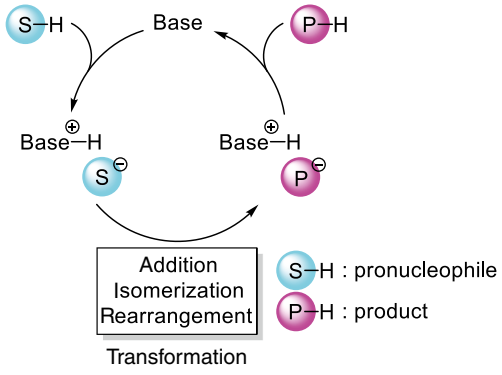

Figure 3.1. General catalytic cycle for Brønsted base catalysis.

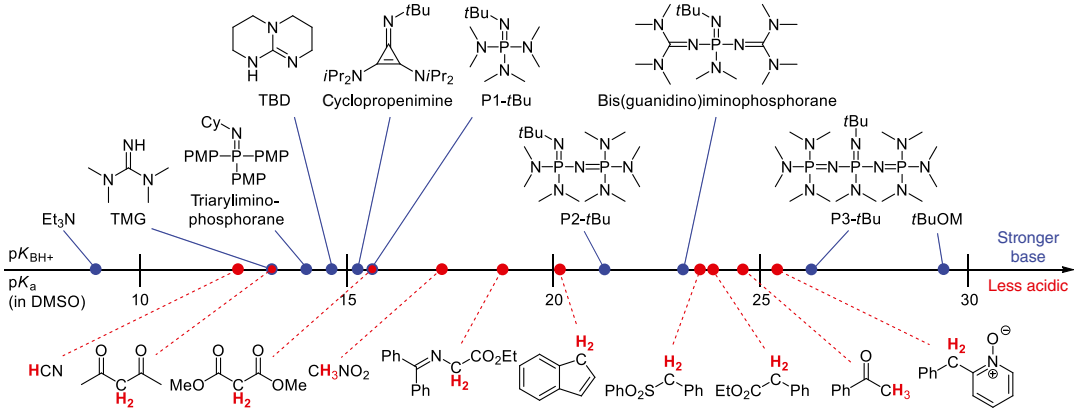

Figure 3.2. Relationship between basicity of uncharged organobases and acidity of representative pronucleophiles (including approximations based on the reported pK_{BH+} in other solvents). Source: Based on [2].

variety of chiral uncharged organobase catalysts has been developed to date, which has broadened the utility of asymmetric Brønsted base catalysis in organic synthesis.

In the field of asymmetric Brønsted base catalysis, chiral tertiary amines have been most widely employed as chiral Brønsted base catalysts. Chiral guanidines have also been used as alternative chiral catalysts over the decades. More recently, chiral organic molecules having a different type of Brønsted base functionality, such as a cyclopropenimine, an iminophosphorane, and a phosphazene (triaminoiminophosphorane), have emerged as efficient chiral Brønsted base catalysts. As a common feature of guanidine catalyst and the new types of organobase catalysts, their basicity is much higher than that of tertiary amine catalysts (Figure 3.2) [2]. Each class of chiral organobase catalysts offers many advantages, and a tremendous amount of applications has been found based on the advantages.

In this chapter, we categorize the chiral organobase catalysts on the basis of their Brønsted base functionalities and present a brief overview of each category with representative catalysts and their selected applications. It should be noted that there are several excellent reviews on chiral tertiary amine catalysts [3], chiral guanidine catalysts [4], and the other chiral organobase catalysts [5]. In particular, the third edition of this book includes the detail of the background of chiral tertiary amine catalysts and their fundamental applications [6]. Therefore, as to the category of chiral tertiary amine catalysts, we here mainly focus on the recent applications. Although the chiral ion-pair type Brønsted base catalysts, such as chiral ammonium betaines [7], and chiral anionic Brønsted base catalysts, such as chiral ureates [8], may also be categorized as a family of chiral organobase catalysts, only chiral uncharged organobase catalysts are discussed in this chapter.

3.2. CHIRAL TERTIARY AMINE CATALYSTS: CHIRAL ACID–BASE BIFUNCTIONAL CATALYSIS

In the field of asymmetric Brønsted base catalysis, one of the most important pioneering works would be a series of studies on enantioselective Michael additions conducted by Wynberg and co-workers, in which cinchona alkaloids were employed as readily available chiral tertiary amine organobase catalysts [9]. For instance, they reported that the addition of aryl thiols to cyclic enones proceeded with moderate enantioselectivities by using cinchonidine (**1a**) as a catalyst (Scheme 3.1) [10]. In the report, the importance of the C9 hydroxy group as a hydrogen bond donor site, namely the bifunctional catalysis, was also suggested [11].

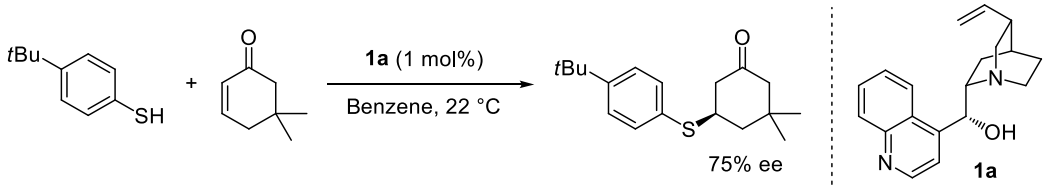

Scheme 3.1. Enantioselective addition of aryl thiols to cyclic enones catalyzed by **1a**. Source: Based on [10].

Cinchona alkaloids are complex small molecules containing five stereogenic centers, a basic quinuclidine nitrogen, a chiral secondary alcohol moiety, and a quinoline unit (Figure 3.3). A highlighted advantage of the use of cinchona alkaloid-based chiral organobase catalyst is the attainability of either enantiomer of desired products owing to the availability of pseudo-enantiomeric pairs, such as cinchonidine (**1a**)/cinchonine (**1b**) and quinine (**1c**)/quinidine (**1d**). Thus, cinchona alkaloids are nowadays not only used directly as a chiral organobase catalyst but also utilized as a versatile chiral scaffold for the development of various chiral organobase catalysts [4].

On the other hand, the prevailing design of chiral tertiary amine catalysts is the "chiral acid–base bifunctional catalyst," in which an additional acidic hydrogen bond donor unit is introduced into a catalyst molecule along with a basic tertiary amine moiety. This catalyst design is based on the idea of dual activation of a pronucleophile and an electrophile; a chiral tertiary amine activates a pronucleophile and a hydrogen bond donor simultaneously activates an electrophile (Figure 3.4a).

There are three common structural motifs utilized widely in the development of chiral acid–base bifunctional catalysts. The first motif is the catalyst consisting of a tertiary amine and a double hydrogen donor unit, such as a thiourea, connected by a chiral two-carbon linker (Figure 3.4b). In 2003, Takemoto

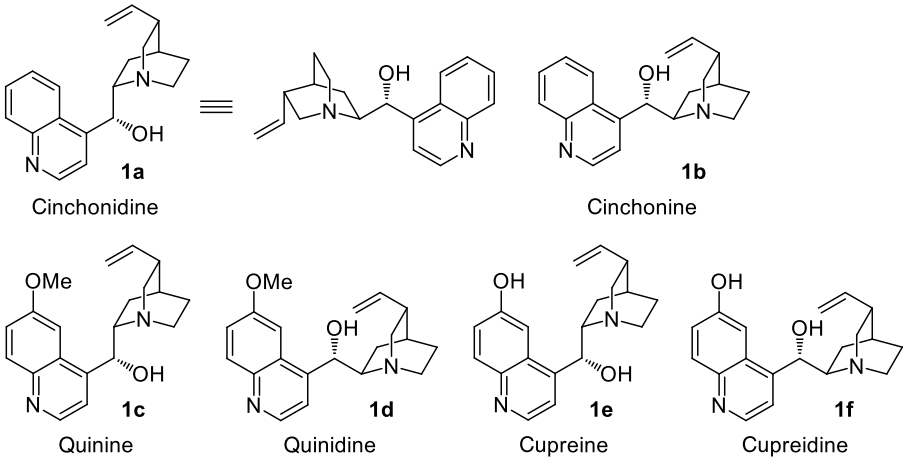

Figure 3.3. Cinchona alkaloids and derivatives.

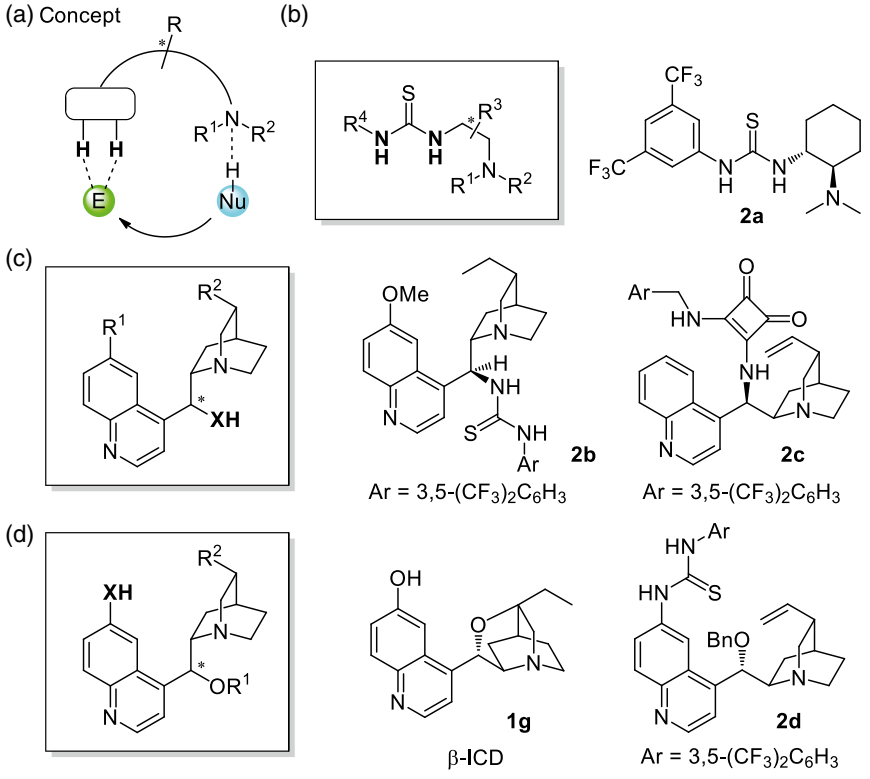

Figure 3.4. Chiral acid–base bifunctional catalysts.

and co-workers developed the seminal amine-thiourea bifunctional catalyst **2a** [12]. They reported that catalyst **2a** efficiently promoted the Michael addition of malonates to nitroalkenes in a highly enantioselective manner (Scheme 3.2).

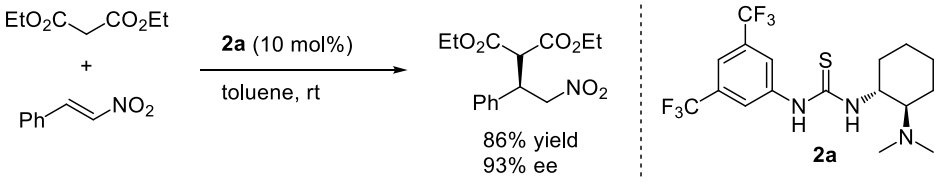

Scheme 3.2. Enantioselective addition of malonates to nitroalkenes catalyzed by **2a.** Source: Based on [12].

It should be noted that the authors originally proposed the reaction mechanism involving the cooperative activation of the pronucleophile and the electrophile by the tertiary amine and the thiourea moieties of the catalysts to account for the significant enhancement in the rate and stereoselectivity of the reaction (ternary complex A in Figure 3.5) [13]. On the other hand, Pápai and co-workers proposed a different mode of activation based on their computational study [14]. In their proposal, the pronucleophile was sequentially activated by the thiourea and the tertiary amine while the electrophile was activated by the resulting ammonium proton (ternary complex B). The study also implied that the proposed mode of activation is not restricted to the Takemoto's catalyst but it is applicable to other bifunctional catalysts having a double hydrogen bond donor unit and a tertiary amine. Later, Takemoto and co-workers conducted the detailed mechanistic study, and the result of the study supported the Pápai's activation model [15].

Based on the design of Takemoto's catalyst, a variety of related catalysts possessing different substituents on the tertiary amine moiety, on the chiral linker, and on the nitrogen of thiourea moiety was

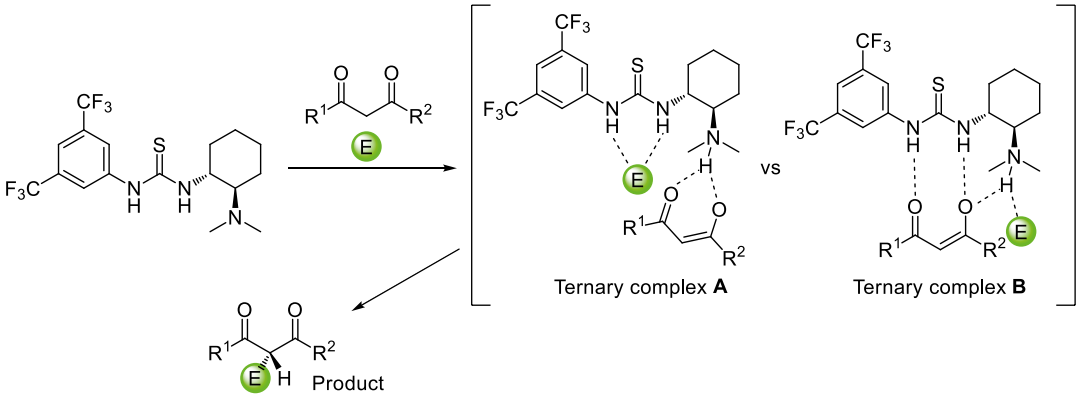

Figure 3.5. Proposed mechanism of the bifunctional amine-thiourea catalyzed reaction.

developed and utilized in a vast number of enantioselective reactions [16]. In addition, highly efficient catalysts having a urea, squaramide, and thiosquaramide as a double hydrogen bond donor unit were also developed, indicating that the replacement of a double hydrogen bond donor unit is the other important option for optimizing the catalyst structure [17].

The second motif is the cinchona alkaloid-derived catalyst having a hydrogen bond donor unit at the C9 position (Figure 3.4c). In 2005, four groups reported enantioselective Michael addition reactions catalyzed by cinchona alkaloids having a thiourea moiety at the C9 position (Scheme 3.3) [18].

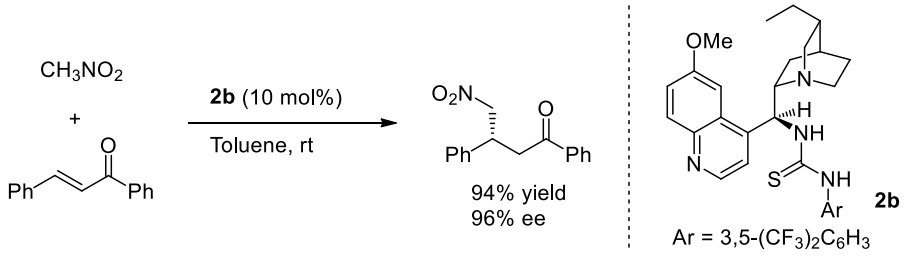

Scheme 3.3. Enantioselective addition of nitromethane to chalcone derivatives catalyzed by **2b**. Source: Based on [18b].

Since the emergence of these catalysts, a variety of catalysts having a different functional group at the C9 position was developed. As an important achievement, in 2008, Rawal and co-workers developed catalyst **2c**, which is the first chiral bifunctional tertiary amine catalyst utilizing a squaramide as a double hydrogen bond donor (Scheme 3.4) [19a]. Since then, squaramides have been widely utilized as an effective alternative to thioureas in the field of chiral tertiary amine catalysis [20].

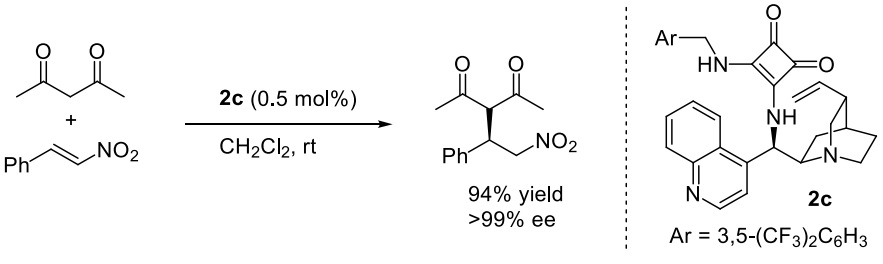

Scheme 3.4. Enantioselective addition of β-ketoesters to nitroalkenes catalyzed by **2c**. Source: Based on [19].

The third motif is the cinchona alkaloid-derived catalyst having a hydrogen bond donor moiety at the C6' position of a quinoline ring (Figure 3.4d). Cupreine (**1e**) and cupreidine (**1f**), which are the demethylated derivatives of quinine and quinidine, possess a phenoxy group at the C6' position. In 2004, Deng and co-workers reported that **1e**, **1f**, and their C9-ether derivatives could serve as chiral bifunctional catalysts in enantioselective addition of malonates and β-ketoesters to nitroalkenes [21]. On the other hand, Jørgensen and co-workers reported the highly enantioselective amination of β-dicarbonyl and related compounds with azodicarboxylates by using β-isocupreidine (β-ICD, **1g**) as a chiral bifunctional catalyst [22]. Deng and co-workers then proposed the transition-state model in their report on the enantio- and diastereoselective addition of β-ketoesters and the related compounds to nitroalkenes, which rationalized the stereochemical outcome (Scheme 3.5 and Figure 3.6) [23]. In the proposed model, the catalyst adopts an anti-open conformation to activate and orient the pronucleophile and electrophile simultaneously by using a network of hydrogen bond interaction.

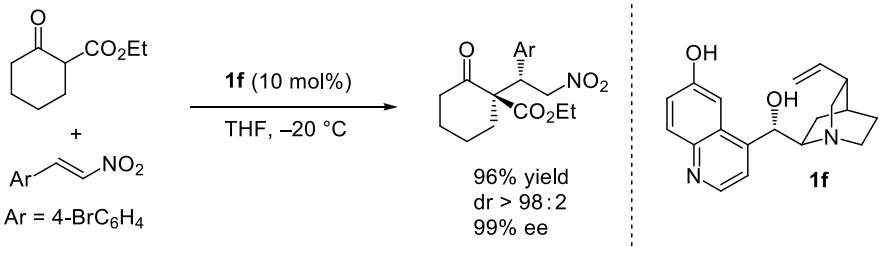

Scheme 3.5. Enantioselective addition of β-ketoesters to nitroalkenes catalyzed by **1f**. Source: Based on [23].

Following from these works, several catalysts having a different C9-ether moiety and a hydrogen bond donor unit, such as **2d**, have been developed [24], although the application of this motif is somewhat limited compared to those of the other two common motifs [25].

3.2.1. Application of Designed Pronucleophiles

Following are the remarkable applications of chiral tertiary amine catalysts selected from our point of view.

The expansion of the scope of pronucleophiles is one of the most important tasks in the field of asymmetric Brønsted base catalysis because it broadens the range of accessible chiral building blocks. To this end, a variety of rationally designed pronucleophiles has been applied to the catalysis, and highly enantioselective reactions have been developed to date.

Barbas and co-workers designed pyrazoleamides **3** as a pronucleophile and developed the enantioselective addition to nitroalkenes by using cinchona alkaloid-urea catalyst **2e** (Scheme 3.6). This is a rare example of the use of amide derivatives as pronucleophiles in chiral tertiary amine catalysis [26]. The pyrazoleamide moiety potentially functions as a good leaving group for further transformations.

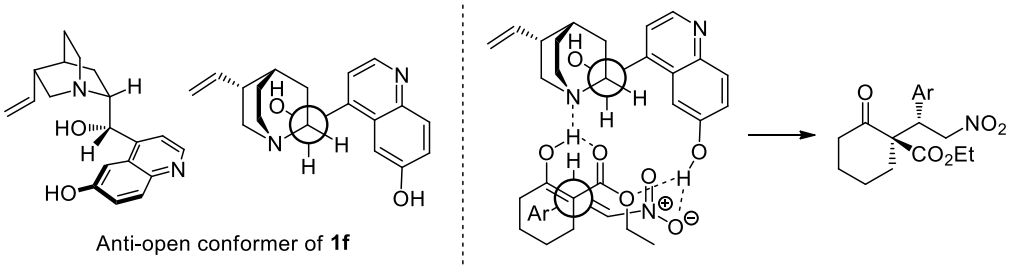

Figure 3.6. Transition-state model of Michael addition catalyzed by **1f**. Source: Based on [23].

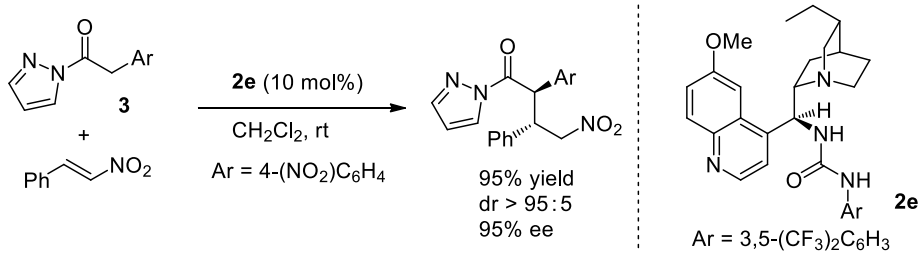

Scheme 3.6. Enantioselective addition of pyrazoleamides **3** to nitroalkenes catalyzed by **2e**. Source: Based on [26].

Malonic acid half thioesters **4** are popular as an (thio)ester enolate equivalent. As a useful application of these compounds in chiral tertiary amine catalysis, List, Song, and co-workers reported the enantioselective decarboxylative aldol reaction with aromatic aldehydes [27]. Cinchona alkaloid-based **2f** having a sulfonamide moiety was the optimum catalyst for the reaction, and the desired products were obtained with high enantioselectivities (Scheme 3.7).

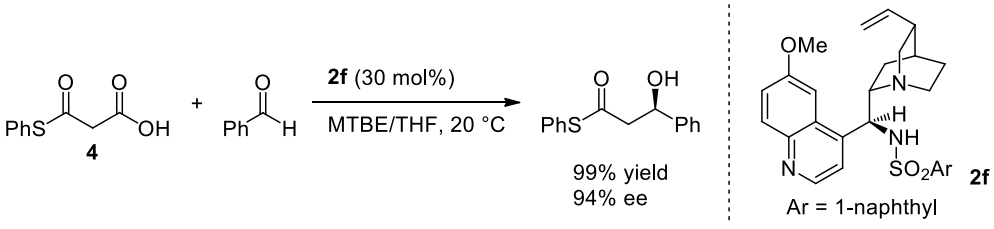

Scheme 3.7. Enantioselective aldol reaction of malonic acid half thioesters **4** catalyzed by **2f**. Source: Based on [27].

On the other hand, Wennemers and co-workers introduced mono-thiomalonates **5** as a thioester enolate equivalent [28]. As a remarkable application of these compounds as a pronucleophile, the enantioselective synthesis of oxindoles possessing adjacent tetrasubstituted stereogenic centers was accomplished [28c]. Cinchona alkaloid-urea catalyst **2g** or Takemoto's catalyst **2a** efficiently promoted the addition of mono-thiomalonates **5** to isatin-derived ketimines to provide the desired oxindoles in high yields with high diastereo- and enantioselectivities (Scheme 3.8).

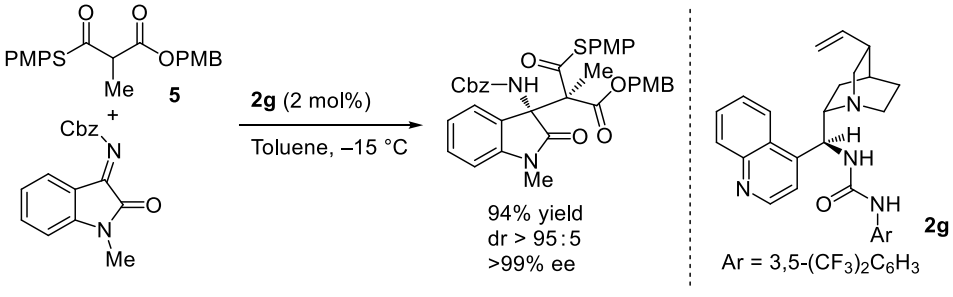

Scheme 3.8. Synthesis of oxindoles possessing adjacent tetrasubstituted stereogenic centers. Source: Based on [28c].

The same group further investigated the enantioselective reactions of fluorinated variants of malonic acid half thioesters **6** and mono-thiomalonates, and successfully developed the decarboxylative aldol reaction and the direct Mannich-type reaction, respectively, by using chiral bifunctional catalysts (Scheme 3.9) [29].

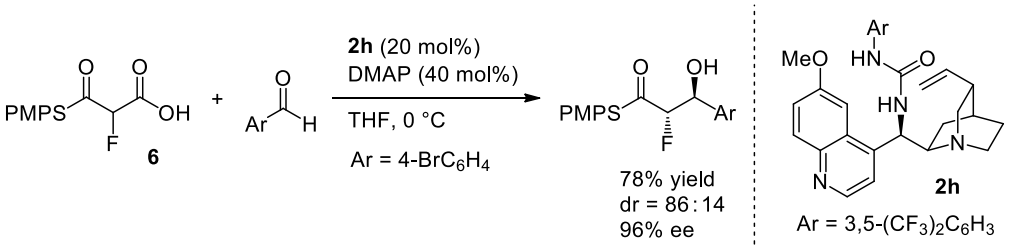

Scheme 3.9. Enantioselective aldol reaction of fluorinated malonic acid half thioesters **6** catalyzed by **2h**. Source: [29].

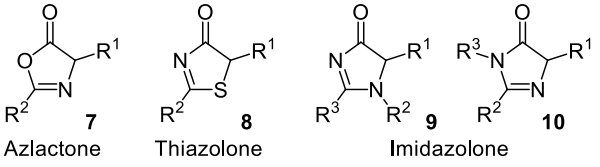

Figure 3.7. *N*-Heterocyclic compounds used as a pronucleophile.

Azlactones **7** are recognized as a useful pronucleophile and widely used in asymmetric synthesis because the hydrolysis of the adducts affords enantio-enriched α,α-disubstituted amino acid derivatives (Figure 3.7) [30]. Palomo and co-workers investigated the enantioselective reactions of the related *N*-heterocyclic compounds that were less explored as a pronucleophile, such as thiazolones **8** and imidazolones **9** and **10** [31]. For instance, the group developed the enantioselective addition of thiazolones **8** to nitroalkenes by using chiral bifunctional catalyst **2i** having a ureidopeptide moiety as a hydrogen bond donor unit (Scheme 3.10) [31a]. The products of the reaction were readily converted to functionalized tertiary thiols otherwise difficult to synthesize.

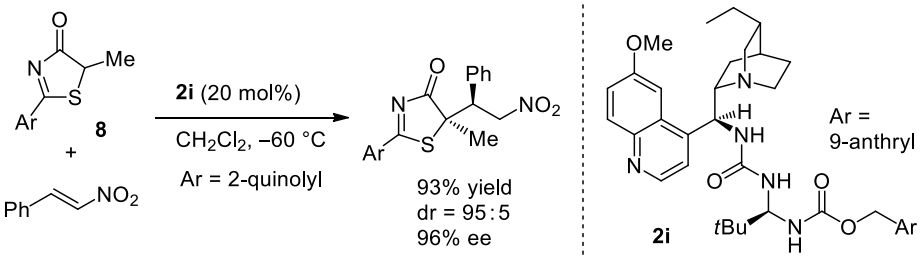

Scheme 3.10. Enantioselective addition of thiazolones **8** to nitroalkenes catalyzed by **2i**. Source: Based on [31a].

Protected hydroxy malononitriles **11**, known as masked acyl cyanide (MAC) reagents, are among the versatile umpolung synthons [32]. Rawal and co-workers successfully applied MAC reagents **11** as a pronucleophile in enantioselective addition to enones [33]. The reaction was efficiently catalyzed by amine-squaramide catalyst **2j** (Scheme 3.11). The method was utilized for the total synthesis of (+)-fornicin C.

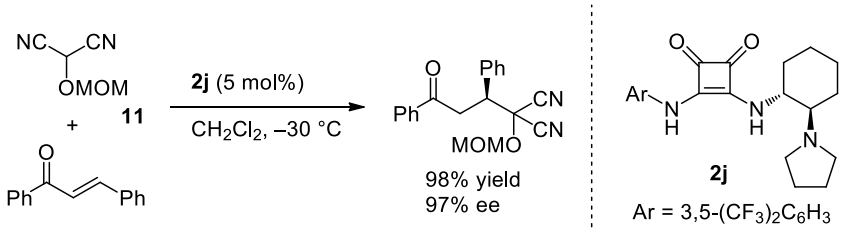

Scheme 3.11. Enantioselective addition of MAC reagents **11** to enones catalyzed by **2j**. Source: Based on [33].

Takemoto and co-workers used glyoxylate cyanohydrins **12**, which have a similar structure to MAC reagents, as a pronucleophile for the first time in enantioselective reactions [34]. Specifically, the group developed the direct Mannich-type reaction of **12** mediated by chiral bifunctional catalysts **2k** and **2l**, both possessing a benzothiadiazine moiety as a strong hydrogen bond donor unit (Scheme 3.12). Interestingly, the tuning of the substituents on the catalysts, namely the choice of **2k** and **2l**, resulted in the diastereodivergent synthesis. The enantio-enriched adducts were readily converted into a series of chiral motifs.

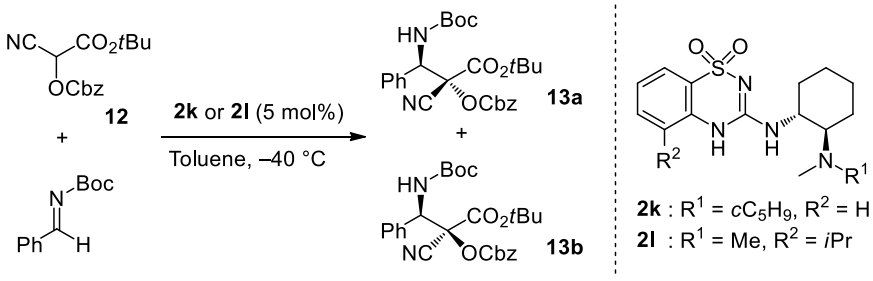

Scheme 3.12. Enantioselective addition of glyoxylate cyanohydrins to imines catalyzed by **2k** and **2l**. Source: Based on [34].

Palomo and co-workers established a new strategy for enantioselective α-functionalization of 2-alkyl azaarenes [35]. The addition of 2-cyanomethylpyridine *N*-oxides **13** to enones proceeded under the influence of amine-squaramide catalyst **2m** to provide the adducts having an all-carbon quaternary stereogenic center in a highly enantioselective manner (Scheme 3.13). In the reaction system, the *N*-oxide moiety played strategic roles as a removable activating group, which enhances the acidity of α-proton, and a stereodirecting group.

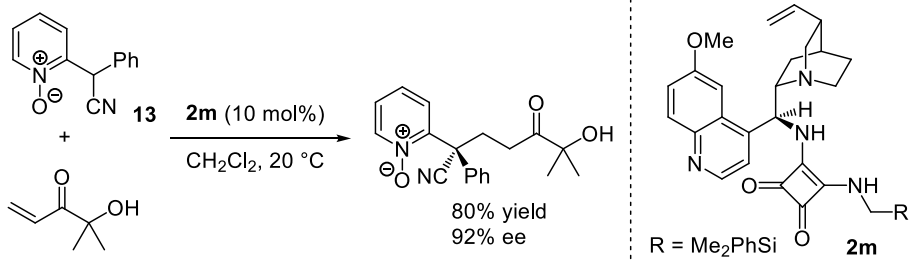

Scheme 3.13. α-Functionalization of 2-alkyl azaarene *N*-oxides **13**. Source: Based on [35].

The same group designed 2-alkylthio-4,6-dioxopyrimidines **14** as barbituric acid equivalents, and developed the enantioselective Michael addition to enones catalyzed by amine-squaramide **2n** (Scheme 3.14) [36]. This is the first example of highly enantioselective synthesis of chiral barbituric acid derivatives with an in-ring tetrasubstituted stereogenic center.

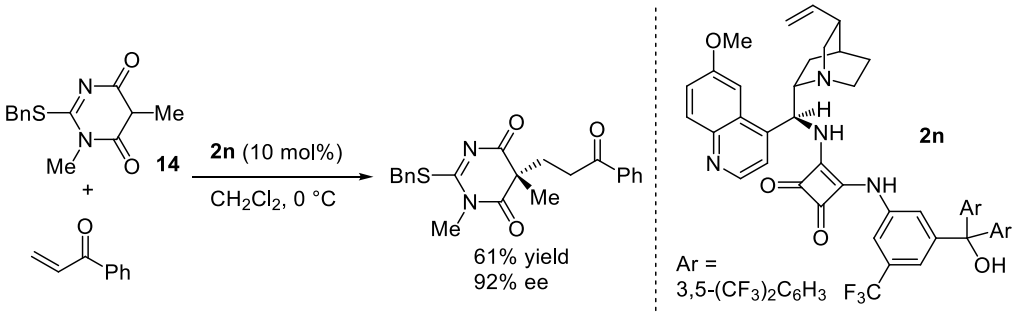

Scheme 3.14. Enantioselective Michael addition of barbituric acid derivatives **14** to enones catalyzed by **2n**. Source: Based on [36].

3.2.2. Carbon-Heteroatom Bond Formations

Enantioselective intramolecular addition of a heteroatom pronucleophile to a carbon–carbon double bond is a powerful strategy for the construction of useful heterocyclic frameworks containing a stereogenic center. Asano and Matsubara reported the enantioselective cycloetherification via oxa-Michael addition mediated by cinchona alkaloid-thiourea catalyst **2h** (Scheme 3.15) [37]. The reaction provided an efficient access to enantio-enriched 2-substituted tetrahydrofurans and tetrahydropyrans in a highly enantioselective manner.

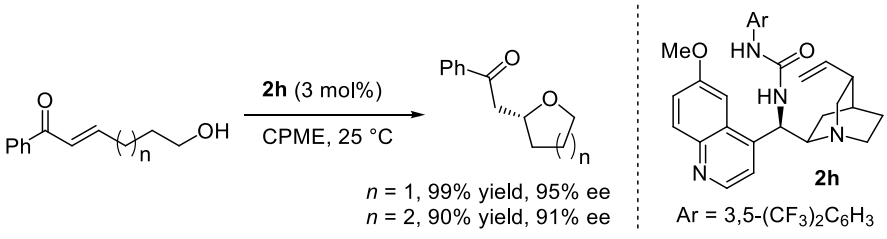

Scheme 3.15. Enantioselective cycloetherification via oxa-Michael addition catalyzed by **2h**. Source: Based on [37].

The same group developed two types of intriguing cascade processes that involve the enantioselective intramolecular oxa-Michael addition. One is the enantioselective synthesis of spiroketals through the intramolecular hemiacetalization followed by oxa-Michael addition catalyzed by Takemoto's catalyst *ent*-**2a** (Scheme 3.16) [38]. The authors suggested that the enantioselectivity of the reaction is largely attributed to the oxa-Michael addition step while the diastereoselectivity is determined through the kinetic resolution of the chiral hemiacetal intermediates.

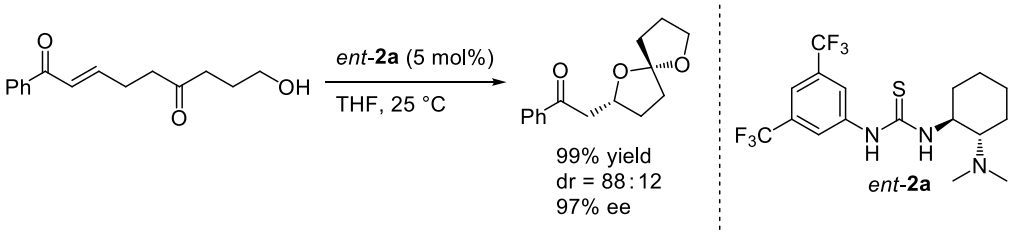

Scheme 3.16. Enantioselective synthesis of spiroketals. Source: Based on [38].

The other process is the enantioselective synthesis of tetrahydropyrans with two stereogenic centers one of which is a tetrasubstituted one [39]. This method features an enantioselective oxa-Michael addition and dynamic kinetic resolution (DKR) involving reversible generation of chiral cyanohydrins **15** (Scheme 3.17). Amine-thiourea **2o** efficiently catalyzed the reaction to furnish the desired products in high yields with high diastereo- and enantioselectivities.

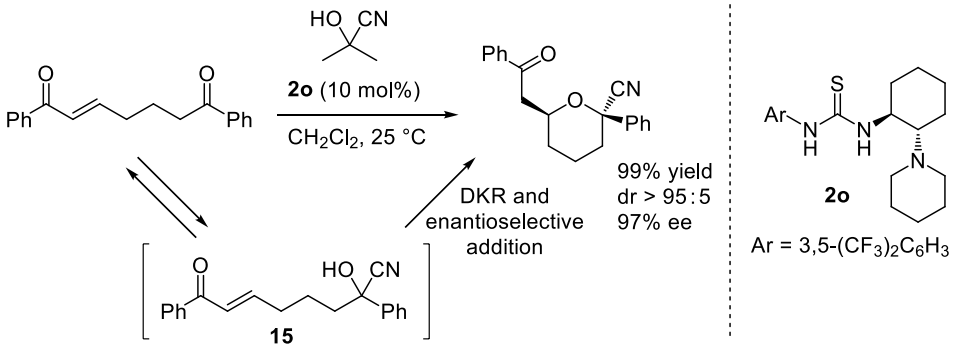

Scheme 3.17. Enantioselective synthesis of tetrahydropyrans with two stereogenic centers. Source: Based on [39].

Takemoto and co-workers investigated the enantioselective intramolecular oxa-Michael addition of α,β-unsaturated amides and esters [40]. Because of the low reactivity of these Michael acceptors, the reaction with the conventional catalysts was rather sluggish. In contrast, catalyst **2p** having a strong hydrogen bond donor unit efficiently promoted the reaction to provide the corresponding isoxazolidines in high yields with high enantioselectivities (Scheme 3.18). This catalyst system was also applicable to the synthesis of dihydrobenzofuran derivatives.

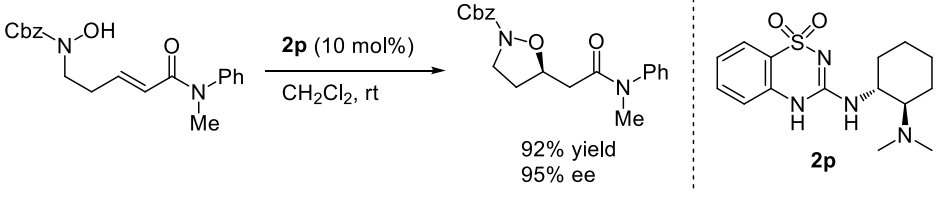

Scheme 3.18. Enantioselective intramolecular oxa-Michael addition of α,β-unsaturated amides catalyzed by **2p**. Source: Based on [40].

Ghorai and co-workers reported the enantioselective intramolecular oxa-Michael addition of 4-hydroxy cyclohexadienones **16** generated in situ via dearomatization of phenols [41]. The reaction was efficiently catalyzed by cinchona-squaramide **2q**, providing enantio-enriched tetrahydrofurans attached to a cyclohexadienone moiety in spiro fashion (Scheme 3.19). The products were easily transformed into chromans without disturbing the enantiomeric purity by treating with a Lewis acid.

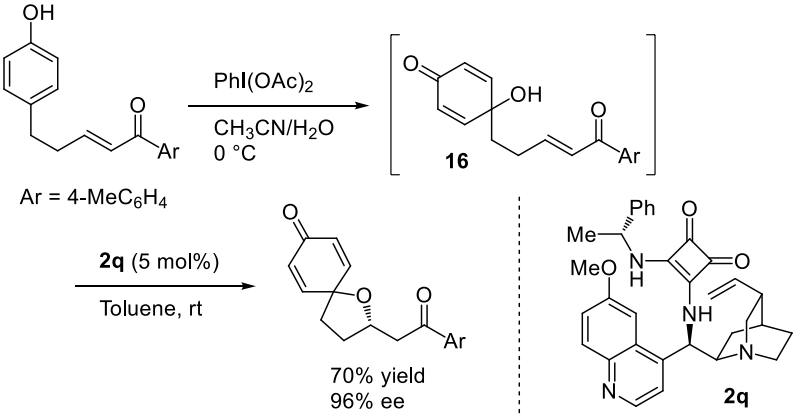

Scheme 3.19. Enantioselective intramolecular oxa-Michael addition of in situ generated 4-hydroxy cyclohexadienone via dearomatization of phenol catalyzed by **2q**. Source: Based on [41].

Chiral bifunctional catalysts can also be applied to aza-Michael addition reactions. For instance, Ghorai and co-workers developed the intramolecular aza-Michael addition of enamines to several Michael acceptors including ketones, esters, thioesters, and Weinreb amide [42]. The reaction proceeded efficiently by using cinchona alkaloid-squaramide **2r** as a catalyst to provide enantio-enriched dihydroisoquinoline derivatives (Scheme 3.20).

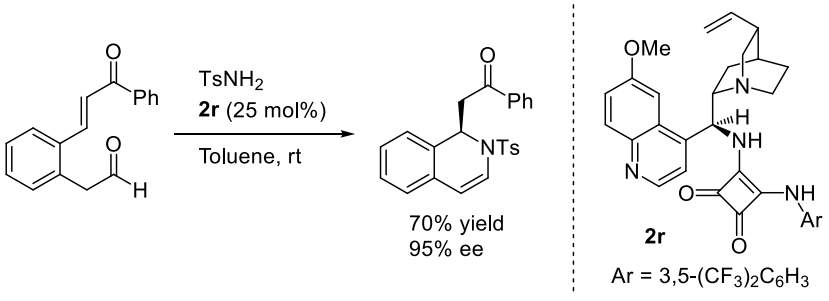

Scheme 3.20. Enantioselective intramolecular aza-Michael addition of enamines catalyzed by **2r**. Source: Based on [42].

On the other hand, Dixon and co-workers developed one-pot catalytic enantioselective synthesis of 2-pyrazolines, which involves the intermolecular aza-Michael addition of hydrazone derivatives (Scheme 3.21) [43]. In this reaction, newly developed cinchona alkaloid-derived **2s**, which possesses a 3,5-dichlorobenzoylamide moiety as a single hydrogen bond donor, was the optimum catalyst.

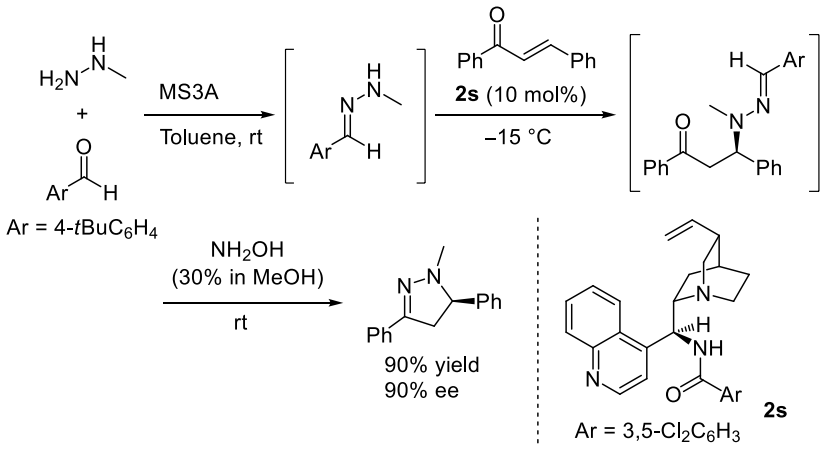

Scheme 3.21. One-pot catalytic enantioselective synthesis of 2-pyrazolines. Source: Based on [43].

As an example of addition reactions of sulfur nucleophiles, Ellmann and co-workers reported the enantioselective addition of thioacids to trisubstituted nitroalkenes catalyzed by cinchona alkaloid-squaramide **2t** (Scheme 3.22) [44]. This transformation constitutes the first example of nucleophilic addition to a trisubstituted nitroalkene followed by the enantioselective protonation.

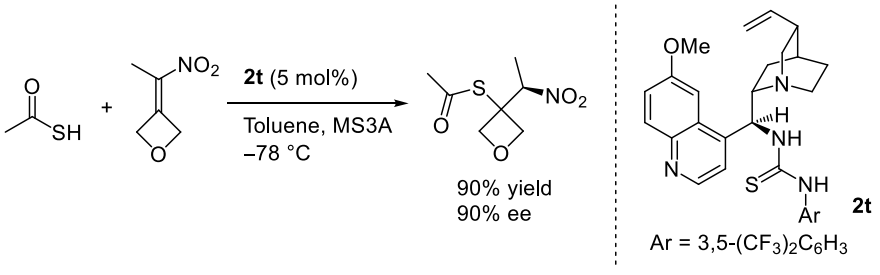

Scheme 3.22. Enantioselective addition of thioacids to trisubstituted nitroalkenes catalyzed by **2t**. Source: Based on [44].

Liu, Li, and co-workers developed the enantioselective addition of thiols to in situ generated *ortho*-quinone methides **17** (Scheme 3.23) [45]. Cinchona alkaloid-squaramide **2u** was employed as a catalyst and water was used as a solvent. The control experiments suggested that water–oil biphase was crucial to achieve both high yields and high stereoselectivity in this reaction.

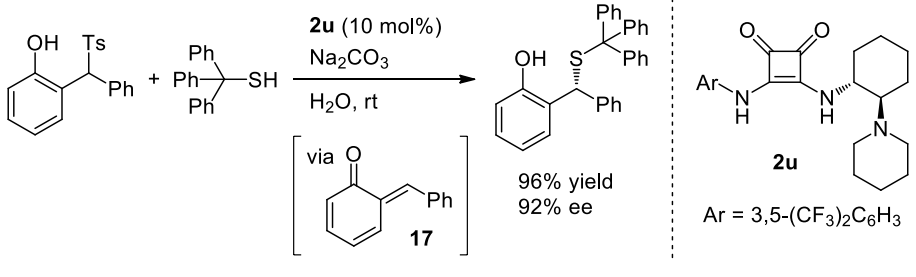

Scheme 3.23. Enantioselective addition of thiols to in situ generated *ortho*-quinone methides catalyzed by **2u**. Source: Based on [45].

3.2.3. Other Applications

Enantioselective cascade reactions under organocatalysis have emerged as a powerful methodology for the efficient synthesis of complex molecules having multiple stereogenic centers in operationally simple protocols by using readily available precursors [46]. Chiral tertiary amine catalysts have also been utilized in a variety of enantioselective cascade reactions [20a]. Following are some selected examples of such reactions. Wang and co-workers developed enantioselective Michael/cyclization reaction sequence for the synthesis of spirooxindoles [47]. The reaction of α-isothiocyanato imides, esters, and lactones with alkylidene oxindoles was promoted by amine-thiourea catalyst **2v** to provide the corresponding spirooxindoles in high yields with high stereoselectivities (Scheme 3.24).

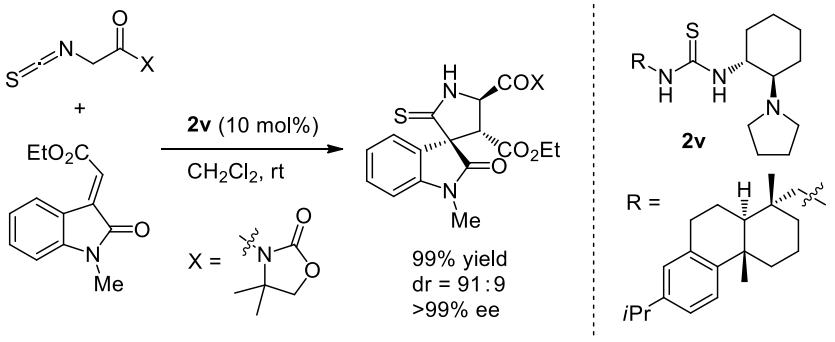

Scheme 3.24. Enantioselective Michael/cyclization reaction sequence catalyzed by **2v**. Source: Based on [47].

On the other hand, Connon and Manoni reported the catalytic enantioselective Tamura cyclization of enolizable anhydrides with alkylidene oxindoles, providing a different type of spirooxindoles (Scheme 3.25) [48]. In this reaction, an unusual temperature-controlled diastereodivergency was observed.

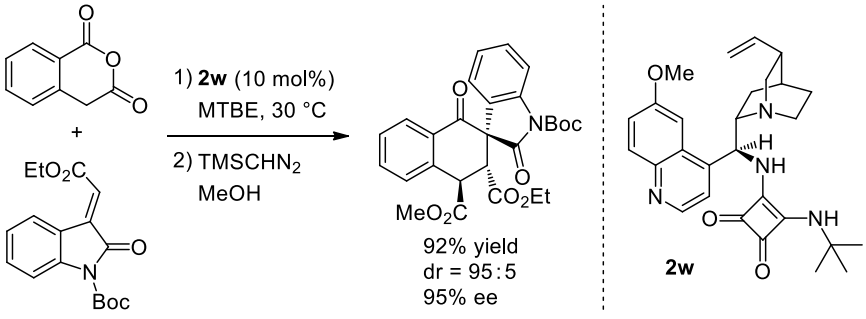

Scheme 3.25. Enantioselective Tamura cyclization catalyzed by **2w**. Source: Based on [48].

The enantioselective formal [3+2] cycloaddition of cyclopropyl ketones with nitroalkenes was developed by Jørgensen and co-workers (Scheme 3.26) [49]. This reaction would involve the ring-opening of a cyclopropane moiety, which would occur through the deprotonation of the α-proton and β-elimination under the influence of amine-thiourea catalyst **2x**, and the following stereoselective intermolecular/intramolecular addition sequence.

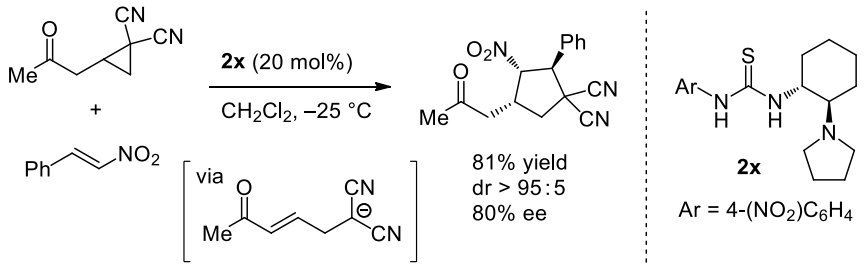

Scheme 3.26. Enantioselective formal [3+2] cycloaddition of cyclopropyl ketones with nitroalkenes catalyzed by **2x**. Source: Based on [49].

Rodriguez, Coquerel, and co-workers established the enantioselective synthesis of benzazocinones by using cinchona alkaloid-squaramide catalyst **2c** [50]. The reaction involves the Michael addition/four-atom ring expansion cascade from activated cyclobutanones and *ortho*-amino nitro styrene derivatives (Scheme 3.27). The resulting benzazocinone products could be further converted into functionalized glutarimide derivatives by 1,8-diazabicyclo[5.4.0]undec-7-ene (DBU) catalyzed ring contraction.

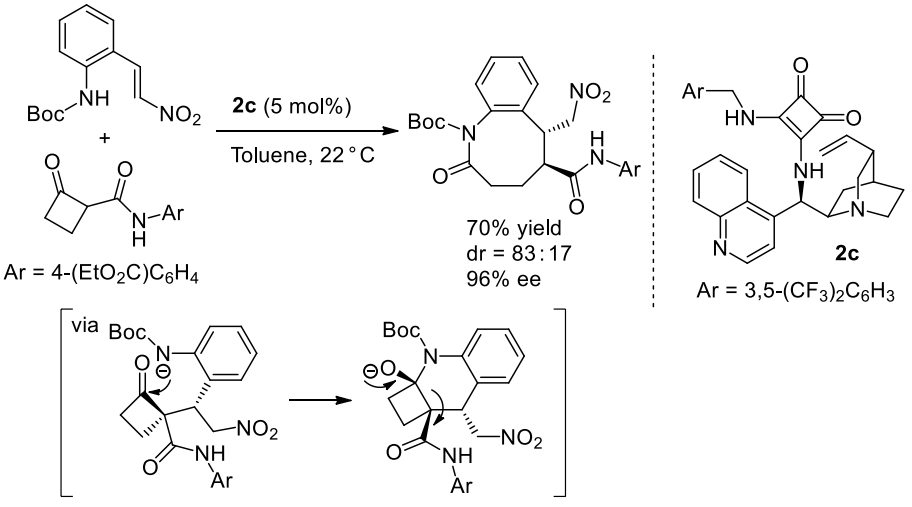

Scheme 3.27. Enantioselective synthesis of benzazocinones. Source: Based on [50].

As a different type of application of the catalysis, Bressy, Bugant, Rodriguez, and co-workers developed an enantioselective synthesis of axially chiral 4-arylpyridine derivatives **19** based on the central-to-axial chirality conversion strategy (Scheme 3.28) [51]. In this synthesis, 4-aryl-1,4-dihydropyridines **18** having a central chirality were first prepared through the enantioselective Michael addition of dimedone to chalcone derivatives catalyzed by Takemoto's catalyst **2a** and the treatment of the resulting Michael adducts with ammonium acetate. Then, the intermediates **18** were converted to the corresponding axially chiral 4-arylpyridines **19** by MnO_2-mediated oxidation with moderate to high conversion percentage (*cp* = %ee of substrate/%ee of product).

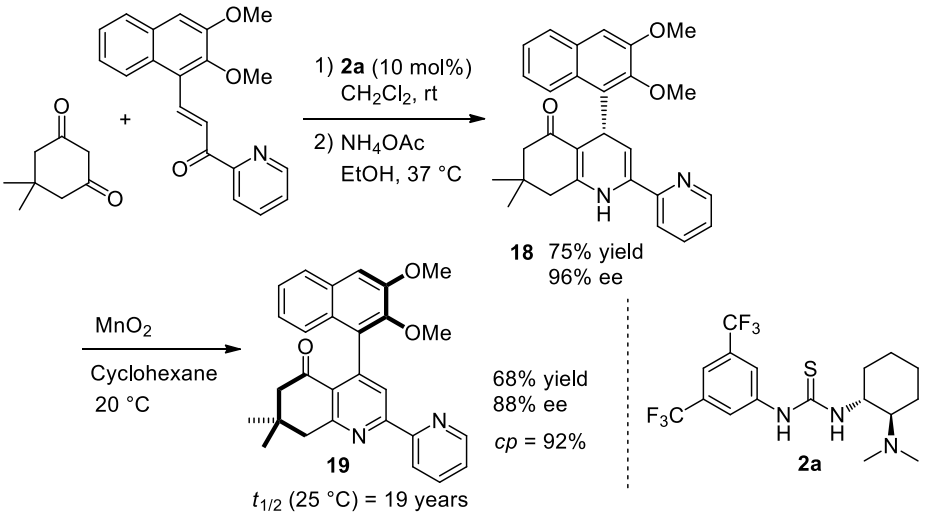

Scheme 3.28. Enantioselective synthesis of axially chiral 4-arylpyridine derivatives based on the central-to-axial chirality conversion strategy. Source: Based on [51].

Later, the same group achieved, for the first time, the synthesis of enantio-enriched atropoisomeric furans based on the central-to-axial chirality conversion strategy (Scheme 3.29) [52].

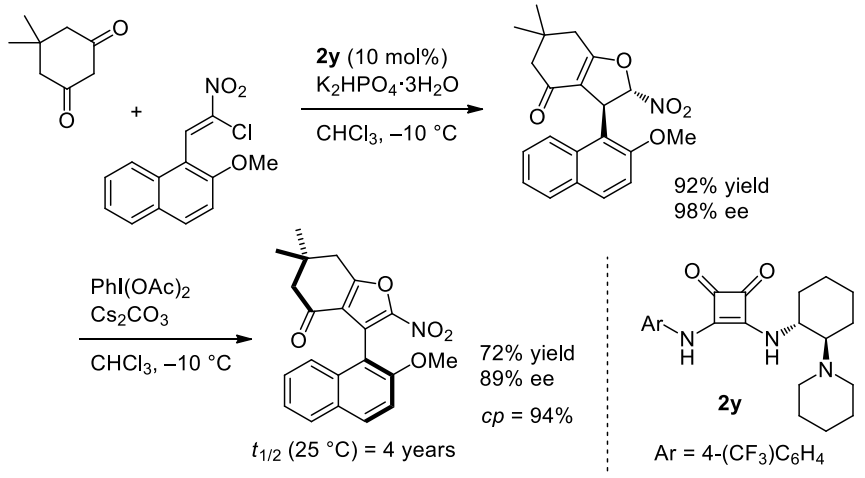

Scheme 3.29. Enantioselective synthesis of atropoisomeric furans based on the central-to-axial chirality conversion strategy. Source: Based on [52].

Yan and co-workers developed the intramolecular [4+2] cycloaddition between in situ generated vinylidene *ortho*-quinone methides **20** and benzofurans (Scheme 3.30) [53]. In the reaction processes, cinchona alkaloid-thiourea catalyst **2t** promoted the enantioselective prototropic rearrangement (tautomerization) of a 2-alkynyl naphthol to generate axially chiral vinylidene *ortho*-quinone methide **20**. Subsequently, the formal inverse electron-demand hetero-Diels-Alder reaction of the vinylidene *ortho*-quinone methide with a benzofuran, driven by both rearomatization and strain release, occurred to provide the cycloaddition product. The same group later achieved the enantioselective construction of axially chiral styrenes based on the strategy utilizing the catalytic generation of axially chiral vinylidene *ortho*-quinone methides by using chiral acid–base bifunctional catalysts [54].

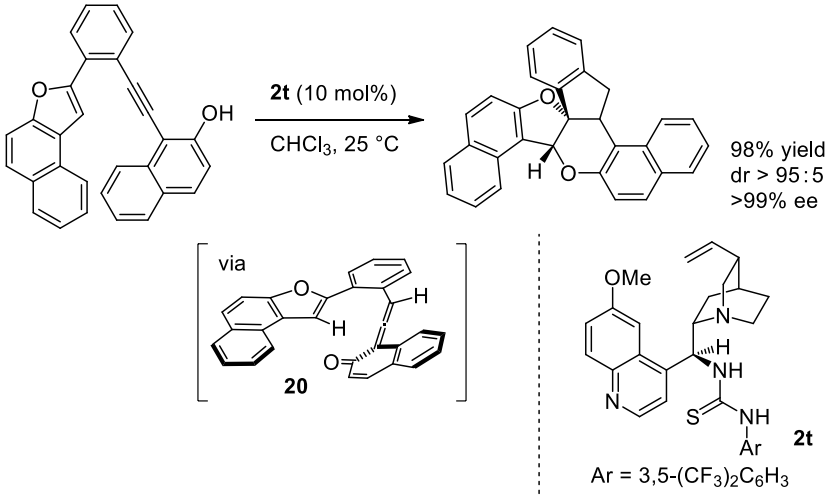

Scheme 3.30. Intramolecular [4+2] cycloaddition between in situ generated vinylidene *ortho*-quinone methides and benzofurans. Source: Based on [53].

3.3. CHIRAL GUANIDINE CATALYSTS

Guanidine is present in a variety of natural products and plays a key role in many biological activities. It can also be found as the side chain of arginine, one of natural amino acids. The intrinsic and distinctive property of guanidine is its strong basicity resulting from the resonance stability in its conjugate acid form, namely guanidinium cation, in which the positive charge can be delocalized over the three nitrogen atoms. In addition, guanidinium cation can interact strongly with anionic species through the combination of hydrogen bonding and ionic bonding, which is widely utilized in molecular recognition [55]. Because of such characteristic features of guanidine and guanidinium cation, chiral guanidine has attracted considerable attention as a promising platform for chiral Brønsted base catalysts in the field of asymmetric synthesis. Indeed, a variety of chiral guanidine catalysts has been developed, and, as a result, various types of useful enantioselective transformations including carbon–carbon bond formations and carbon-heteroatom bond formations have been accomplished over the past two decades, which are comprehensively summarized in the literature based on the types of transformations or those of catalysts [4]. Following are the representative chiral guanidine catalysts with their fundamental and/or remarkable applications.

As a pioneering study of chiral guanidine as a chiral Brønsted catalyst, in 1994, Nájera and co-workers reported the enantioselective nitroaldol reaction albeit with only a modest enantioselectivity [56]. On the other hand, the first highly enantioselective reaction was reported by Lipton and co-workers in 1996 [57]. They developed the enantioselective Strecker reaction catalyzed by chiral guanidine **21** (Scheme 3.31).

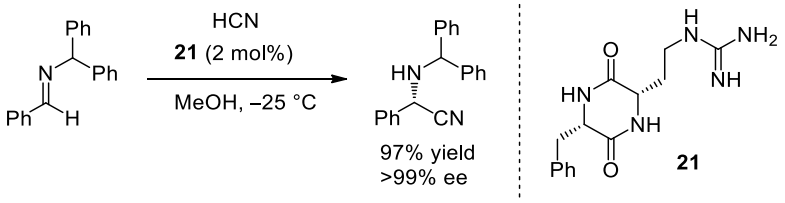

Scheme 3.31. Enantioselective Strecker reaction catalyzed by **21**. Source: Based on [57].

In 1999, Corey and Grogan developed the enantioselective Strecker reaction catalyzed by chiral bicyclic guanidine **22a**, which is the important seminal work in the field of chiral guanidine catalysis (Scheme 3.32) [58].

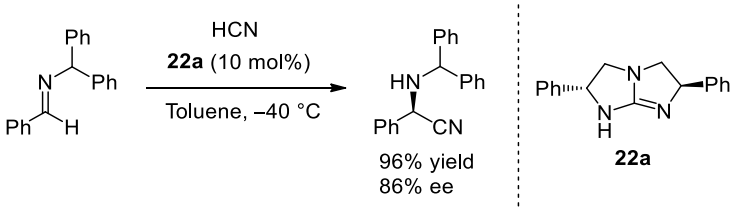

Scheme 3.32. Enantioselective Strecker reaction catalyzed by **22a**. Source: Based on [58].

In the report, the authors proposed the suggestive reaction mechanism (Figure 3.8). First, the deprotonation of hydrogen cyanide (HCN) by the guanidine proceeds to form the guanidinium cyanide complex. The complex can function as a hydrogen bond donor, and thus the activation of the imine electrophile occurs to form the pretransition-state termolecular assembly. Finally, the attack of the cyanide within the ion pair to the hydrogen bond-activated imine occurs to afford the adduct.

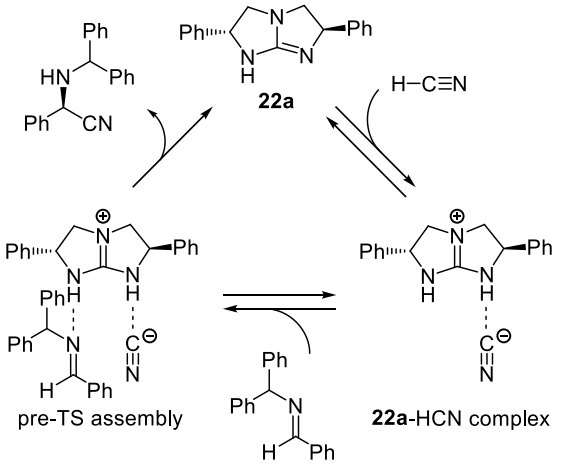

Figure 3.8. Proposed reaction mechanism.

Tan and co-workers intensively studied the enantioselective transformations by using this type of chiral bicyclic guanidines **22**, and successfully developed a lot of highly enantioselective reactions [59]. For instance, a series of enantioselective reactions of anthrones, such as the Diels-Alder reaction with maleimide and the addition to Michael acceptors, was developed [60]. The tandem reaction process involving a Michael addition of thiols followed by a highly enantioselective protonation was also established by using *tert*-butyl substituted **22b** (Scheme 3.33) [61].

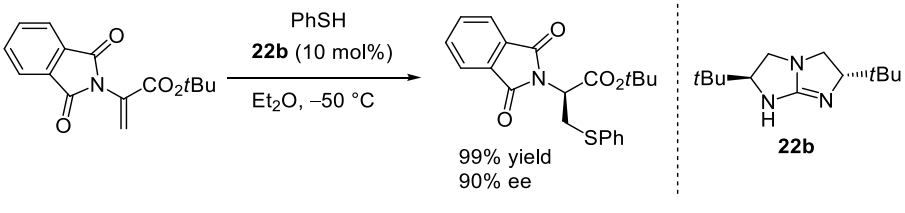

Scheme 3.33. Enantioselective protonation catalyzed by **22b.** Source: Based on [61].

Other remarkable application of chiral bicyclic guanidine **22b** is the enantioselective synthesis of axially chiral allenoates by the enantioselective isomerization of 3-alkynoates (Scheme 3.34) [62].

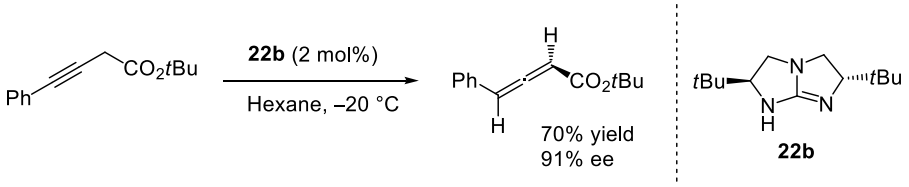

Scheme 3.34. Enantioselective isomerization of 3-alkynoate catalyzed by **22b**. Source: [62].

Ishikawa and co-workers developed chiral monocyclic guanidine **23** having a hydroxy group, and applied the catalyst to the enantioselective Michael addition of glycine imines to acrylates (Scheme 3.35) [63]. The control experiments suggested that the matched relative configuration of the three chiral centers on the catalyst and the existence of the hydroxy group are essential for achieving both high conversion and high enantioselectivity. The catalyst was also applied to the enantioselective oxa-Michael addition for the synthesis of chromane skeletons [64].

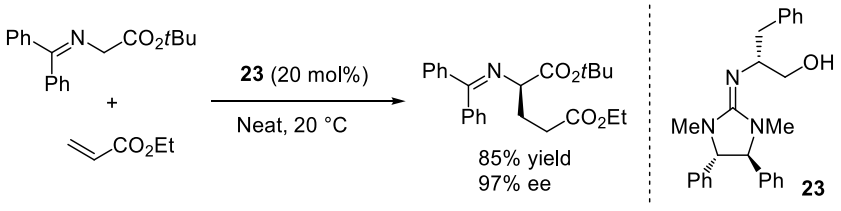

Scheme 3.35. Enantioselective Michael addition of glycine imines to acrylates catalyzed by **23**. Source: [63].

Misaki, Sugimura, and co-workers developed chiral bicyclic guanidine **24** bearing a hydroxy group as a hydrogen bond donor unit. This catalyst was highly effective in a series of enantioselective reactions of 5*H*-oxazol-4-ones as a pronucleophile, such as direct aldol reaction and the 1,4-addition to alkynyl carbonyl compounds (Scheme 3.36) [65].

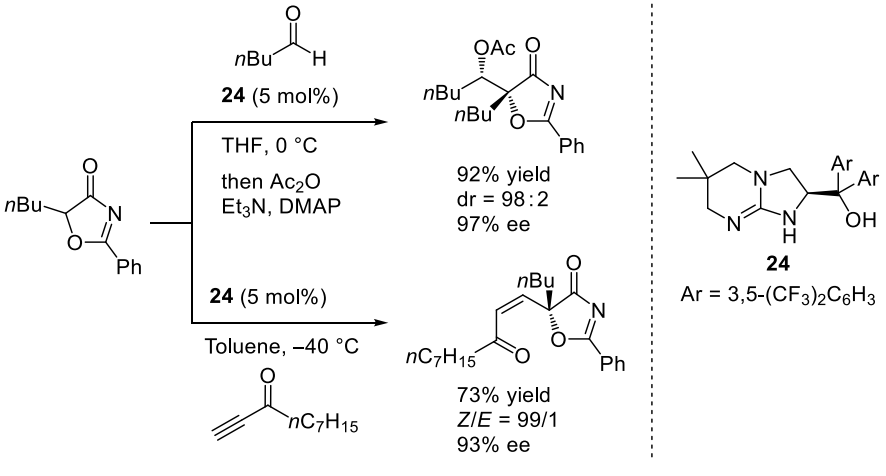

Scheme 3.36. Enantioselective reactions of 5*H*-oxazol-4-ones as a pronucleophile catalyzed by **24**. Source: [65].

Nagasawa and co-workers developed a series of guanidine-(thio)urea bifunctional catalysts **25** having conformationally flexible chiral linkers [66]. The catalyst design was based on the idea of using the formation of a double hydrogen bonding network, where a guanidine and a (thio)urea simultaneously activate a pronucleophile and an electrophile, respectively. The adequacy of the catalyst design was verified by applying them to a variety of enantioselective reactions. For instance, guanidine-bisthiourea catalyst **25a** was successfully utilized in the *ortho*-selective alkylation of phenols through the enantioselective addition with nitroalkenes (Scheme 3.37) [67].

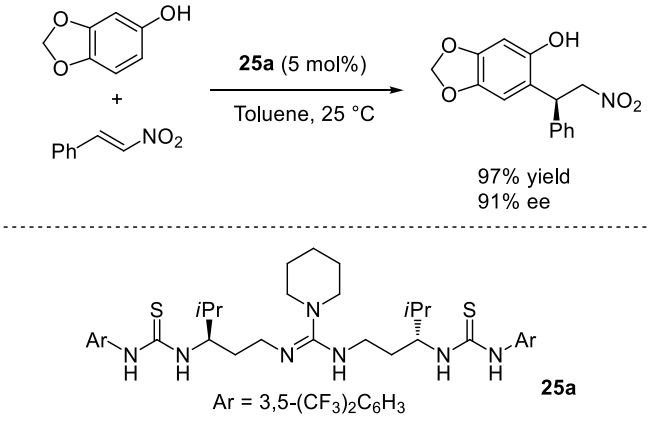

Scheme 3.37. Enantioselective addition of phenols to nitroalkenes catalyzed by **25a**. Source: Based on [67].

On the other hand, the use of guanidine-bisthiourea catalyst **25b** enabled the solvent-dependent enantiodivergent Mannich-type reaction (Scheme 3.38) [68]. The authors concluded that the origin of solvent-dependent stereodiscrimination was controlled by the enthalpy–entropy compensation. This type of catalysts was utilized not only in carbon–carbon bond formations but also in carbon-heteroatom bond formations [69], such as α-hydroxylation of tetralone-derived β-ketoesters [70].

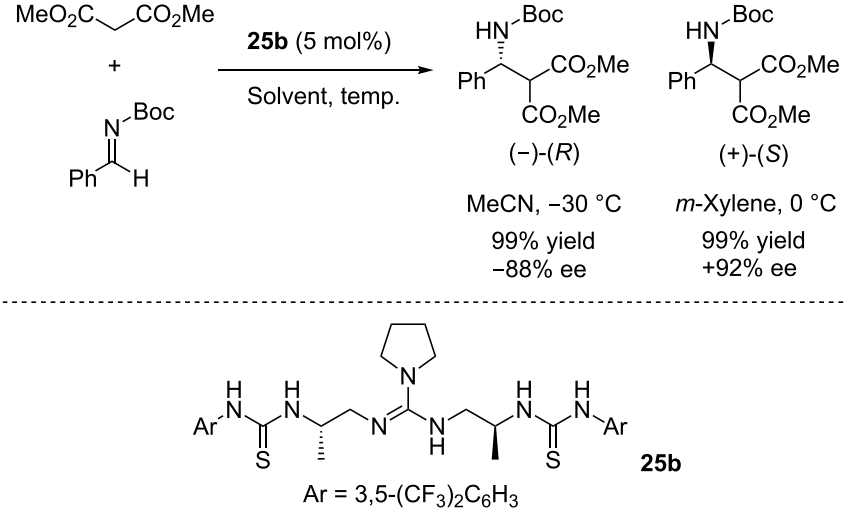

Scheme 3.38. Solvent-dependent enantiodivergent Mannich-type reaction catalyzed by **25b**. Source: Based on [68].

Feng and co-workers designed bifunctional guanidine catalyst **26a** featuring a chiral amino amide backbone, in which an amide moiety functions as a hydrogen bond donor unit [71]. The catalytic activity was demonstrated in the enantioselective addition of β-ketoesters to nitroalkenes (Scheme 3.39).

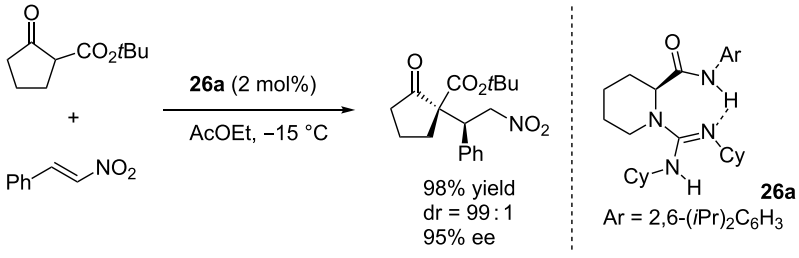

Scheme 3.39. Enantioselective addition of β-ketoesters to nitroalkenes catalyzed by **26a**. Source: Based on [71].

Liu, Feng, and co-workers later developed related guanidine-amide bifunctional catalysts, such as **26b**, **26c**, and **26d**, and successfully utilized them in several enantioselective reactions (Scheme 3.40) [72].

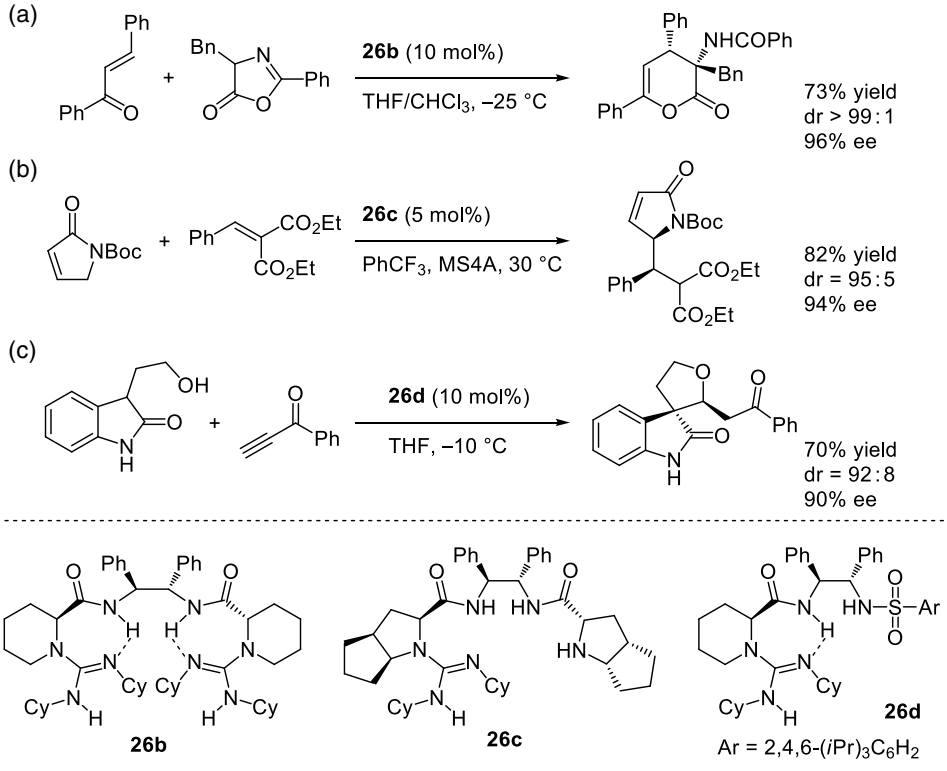

Scheme 3.40. Enantioselective reactions catalyzed by **26**. Source: [72].

Wang, Qu, and co-workers developed tartaric acid-derived seven-membered cyclic chiral guanidine **27**, and utilized the catalyst in the enantioselective α-hydroxylation of β-ketoesters and β-diketones with oxaziridine (Scheme 3.41) [73]. This type of chiral guanidine catalyst was also used in the Michael addition of 3-substituted oxindoles to nitroalkenes [74].

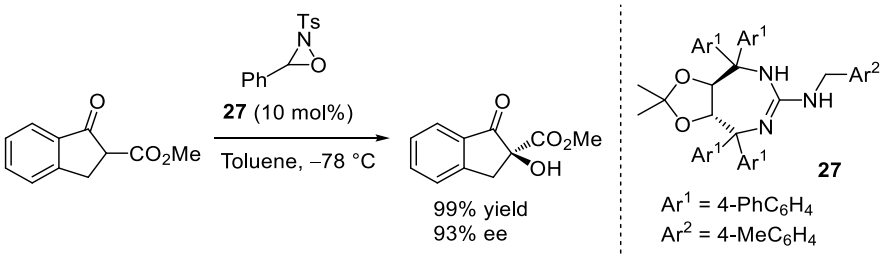

Scheme 3.41. Enantioselective α-hydroxylation of β-ketoesters catalyzed by **27**. Source: Based on [73].

Tan and co-workers developed an aminoindanol-derived chiral guanidine **28**. The catalyst was utilized in the desymmetrization of *meso*-aziridines with thiols and carbamodithioic acids as a pronucleophile, providing the ring-opening products in high yields with high enantioselectivities (Scheme 3.42) [75].

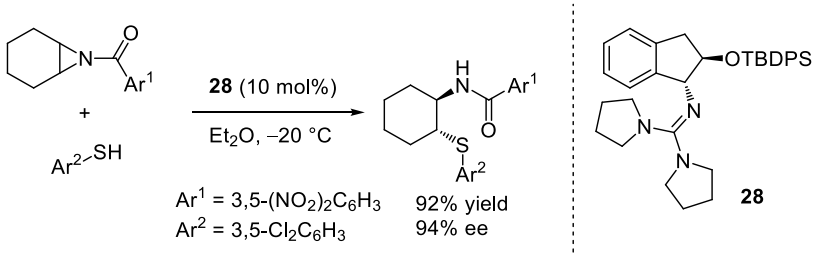

Scheme 3.42. Desymmetrization of *meso*-aziridines with thiols catalyzed by **28**. Source: Based on [75].

Aforementioned all chiral guanidine catalysts control the stereoselectivity of the bond-forming process based on the central chirality of the catalyst molecule. In contrast, Terada and co-workers introduced, for the first time, the methodology based on axial chirality of the catalyst molecule into the field of chiral guanidine catalysis [76]. Specifically, the group designed two types of axially chiral guanidines having an axially chiral binaphthyl backbone (Figure 3.9). One is the nine-membered cyclic guanidines **29**, in which an N-C-N guanidine subunit is involved in the ring structure. The other is the seven-membered cyclic guanidines **30**, in which one nitrogen atom of guanidine is involved in the ring structure.

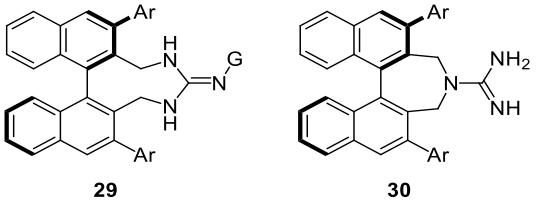

Figure 3.9. Axially chiral guanidine catalysts.

The high catalytic activity of nine-membered **29** was demonstrated in the enantioselective Michael addition of β-dicarbonyl compounds and diphenyl phosphite to nitroalkenes [77]. Both substituents at the 3,3′-positions of binaphthyl backbone (Ar) and that attached on the guanidine nitrogen (G) had a strong impact on the stereoselectivity of the reactions. Chiral guanidine **29a** was also utilized in the enantioselective direct vinylogous aldol reaction of furanones, as well as vinylogous Michael addition of furanones to nitroalkenes, to provide the corresponding adducts in high yields with high enantioselectivities (Scheme 3.43) [78].

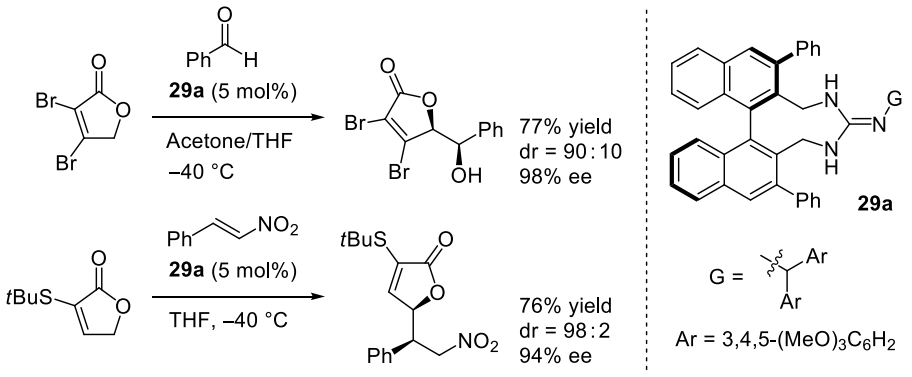

Scheme 3.43. Enantioselective reactions of furanones as a pronucleophile catalyzed by **29a**. Source: [78].

On the other hand, the catalytic activity of seven-membered **30** was confirmed by the highly enantioselective amination of β-dicarbonyl compounds with azodicarboxylate (Scheme 3.44) [79]. In this catalyst design, the reach of the steric demand exerted by the aromatic substituents (Ar) is important to provide an efficient chiral environment around the substrate recognition site at the guanidine moiety. Therefore, the employment of chiral guanidine **30a** with *para*-biphenyl substituents having a bulky *tert*-butyl groups at the 3,5-positions of the terminal phenyl ring was essential to achieve the high level of stereocontrol. This type of chiral guanidine catalyst was also utilized in the enantioselective [3+2] cycloaddition of glycine imines with maleate [80].

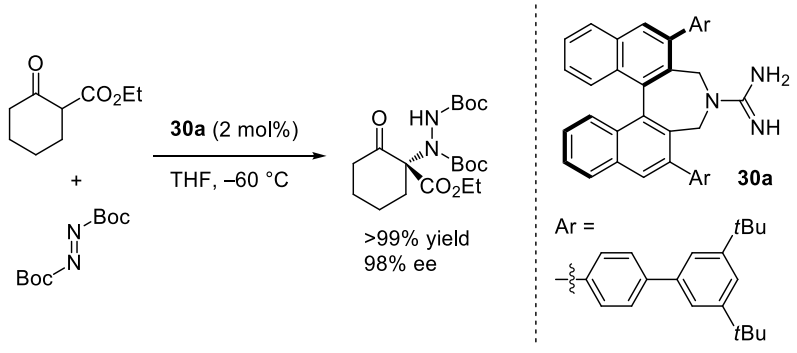

Scheme 3.44. Enantioselective amination of β-dicarbonyl compounds with azodicarboxylate catalyzed by **30a**. Source: Based on [79].

3.4. OTHER CHIRAL UNCHARGED ORGANOBASE CATALYSTS: CHIRAL ORGANOSUPERBASES

As described in the previous section, chiral bifunctional tertiary amine catalysts have been recognized as a particular class of chiral Brønsted base catalysts and have found a vast number of applications. However, the chiral tertiary amine catalysis still possesses inherent critical limitations; high catalyst loadings and long reaction times are often required, and arguably the range of pronucleophiles and electrophiles that are applicable to the reactions is rather narrow, which stem from the low basicity of tertiary amines. Only highly acidic compounds are applicable as pronucleophiles, and thus the resulting anionic nucleophiles only possess moderate nucleophilicity to react with highly electrophilic compounds. In this context, chiral uncharged organobases having higher basicity than chiral tertiary amines have attracted increased

attention. This class of chiral organobases, including conventional chiral guanidines, is often called "chiral organosuperbase" although the definition of the term "organosuperbase" is rather ambiguous [1b]. The application of chiral organosuperbases has significant advantages. Most importantly, the chiral organosuperbases potentially broaden the scope of pronucleophiles to compounds having higher pK_a values. In addition, the chiral organosuperbases increase the concentration of anionic nucleophiles. Consequently, they can dramatically accelerate the bimolecular reactions and decrease the catalyst loading and reaction time. Over the last decade, some new types of chiral organosuperbase catalysts have been developed, which is overviewed in this section.

3.4.1. Chiral Cyclopropenimine Catalysts

In 2012, Lambert and Bandar introduced chiral cyclopropenimines as a powerful class of chiral organobase catalysts for the first time (Figure 3.10) [81].

The basicity of **31** was measured and found to be higher than that of guanidines and comparable to that of P1-phosphazenes. Their high basicity is attributed to the stabilization of the conjugate acid by three nitrogen lone pairs and an aromatic cyclopropenium ion. The superior catalytic activity of **31** was demonstrated in the enantioselective additions of glycine imines to various kinds of Michael acceptors and imines (Scheme 3.45) [82].

The mechanistic rationale was provided based on the experimental results along with computational study (Figure 3.11) [83]. The lowest-energy enantiodetermining transition state involves the (*E*)-enolate hydrogen-bonded to the N-H function of the protonated catalyst, with the acrylate hydrogen-bonded to the catalyst hydroxy group. Interestingly, an unusual intramolecular C-H· · ·O interaction between a hydroxy group and a cyclohexane ring was identified as a key element in transition-state organization.

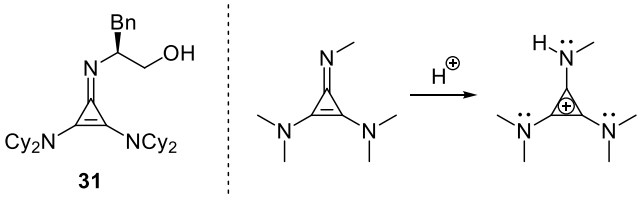

Figure 3.10. Chiral cyclopropenimine catalyst.

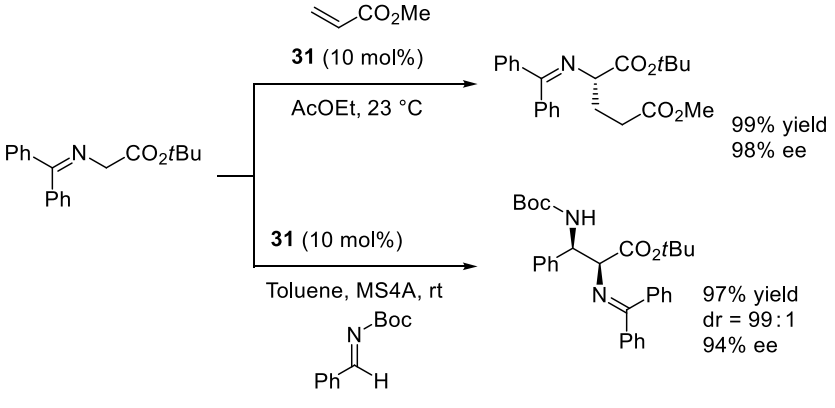

Scheme 3.45. Enantioselective additions of glycine imines catalyzed by **31**. Source: Based on [82]. Source: Based on [81] and [82].

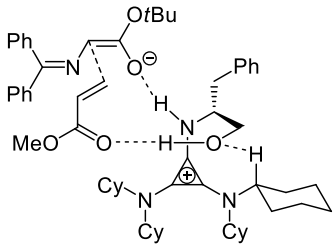

Figure 3.11. Mechanistic rationale. Source: [83].

Jørgensen and co-workers developed the enantioselective [3+2] cycloaddition of glycine imines with 2-acyl cycloheptatrienes by using **31** (Scheme 3.46) [84]. **31** was also utilized in the catalytic enantioselective [2,3]-Wittig rearrangement [85].

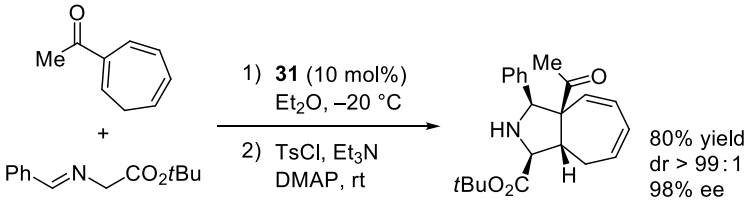

Scheme 3.46. Enantioselective [3+2] cycloaddition of glycine imines with 2-acyl cycloheptatrienes catalyzed by **31**. Source: Based on [84].

3.4.2. Chiral Triaryliminophosphorane Catalysts

Dixon and co-workers designed and developed a series of chiral bifunctional iminophosphorane (BIMP) catalysts **32** based on their idea of the introduction of an enhanced organobase functionality relative to tertiary amines into chiral acid–base bifunctional catalysts (Figure 3.12) [86].

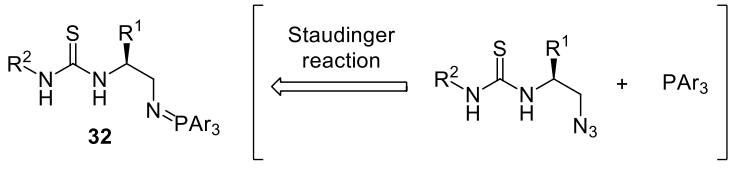

Figure 3.12. Chiral bifunctional iminophosphorane (BIMP) catalysts.

The basicity of *N*-alkyl triaryliminophosphorane was determined to be comparable to that of guanidines. The attractive feature of the catalyst design is high modularity. The catalysts incorporating a variable hydrogen bond donor, chiral amino acid-derived scaffold, and triaryliminophosphorane are readily synthesized via a last step Staudinger reaction of a chiral organoazide and a triarylphosphine. The synthetic potential of this class of catalysts was first demonstrated in the enantioselective addition of nitromethane to ketimines catalyzed by **32a** in 2013 (Scheme 3.47) [87].

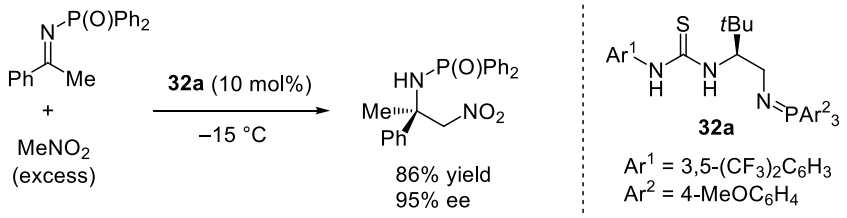

Scheme 3.47. Enantioselective addition of nitromethane to ketimines catalyzed by **32a**. Source: Based on [87].

After that, the BIMP catalysts **32** were successfully utilized in several enantioselective reactions (Scheme 3.48). For instance, a series of enantioselective sulfa-Michael additions including that with α-substituted acrylates was developed (Scheme 3.48a) [88]. On the other hand, the enantioselective synthesis of conjugated cyclohexanones through a facial selective 1,3-proton shift was achieved by using **32c** (Scheme 3.48b) [89]. The related enantioselective 1,3-proton shift was also utilized in the total synthesis of a natural product, (-)-himalensine A [91]. Furthermore, **32d** having a sterically demanding amide moiety efficiently promoted the direct aldol addition of less acidic acetophenone derivatives to α-fluorinated ketones to provide the corresponding adducts in high yields with high enantioselectivities (Scheme 3.48c) [90]. Johnson and co-workers utilized the BIMP catalysts in their development of enantioselective reactions, such as the enantioselective additions of nitroalkanes and alkyl thiols to enone diesters, and the enantioselective three-component coupling reaction of benzylidene pyruvates, aldehydes, and dialkyl phosphites [92].

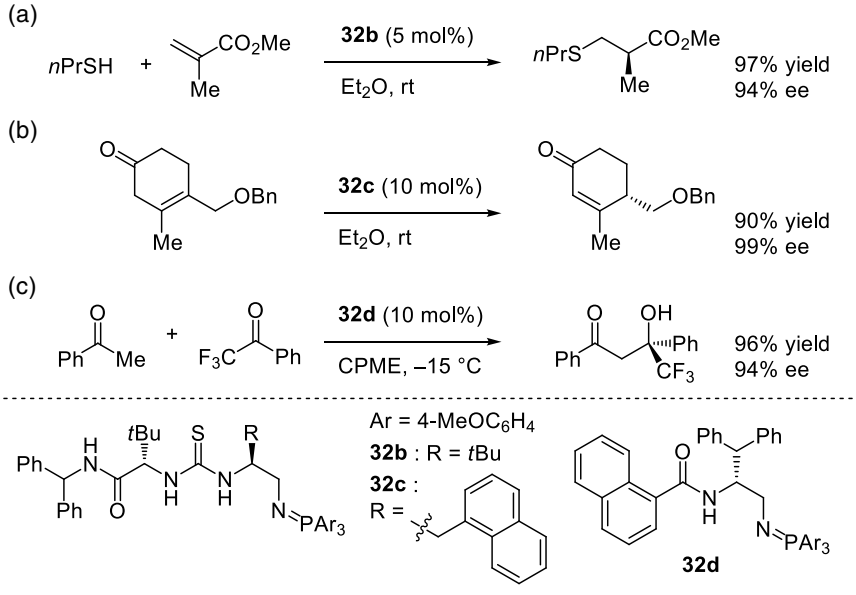

Scheme 3.48. Enantioselective reactions catalyzed by **32**. (a) Source: [88]. (b) Source: Based on [89]. (c) Source: Based on [90].

3.4.3. Chiral P1-Phosphazene Catalysts

Phosphazenes are pentavalent phosphorus compounds possessing a P=N double bond and three P–N single bonds, and are recognized as the strongest uncharged organobases. The basicity of the simplest P1-phosphazenes, which possess secondary amine subunits on the iminophosphorane core, is even higher than that of guanidines. Although this class of compounds was first introduced by Schwesinger and

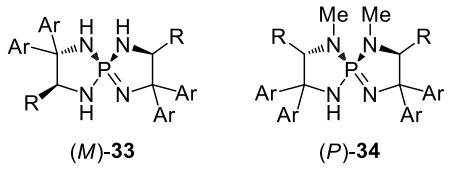

Figure 3.13. Chiral P1-phosphazene catalysts.

Schlemper in 1987 [93], the chiral variants were not prepared and utilized as chiral organobase catalysts until 2007. Ooi and co-workers utilized phosphazenes as a platform for chiral organobase catalysts for the first time [94]. They designed and synthesized chiral P1-phospazene catalysts (*M*)-**33** and (*P*)-**34** containing a pseudo-C_2-symmetric 5,5-membered spirocyclic core structure (Figure 3.13).

The characteristic feature of the structural motif is that the direction of not only substituents on the rigid spirocycles but also N-H protons in the conjugate acid forms can be accurately regulated. In addition, hydrogen bond donor and acceptor sites are arranged side by side around the central phosphorus atom: the nitrogen atom of the iminophosphorane moiety (P=N) functions as a hydrogen bond acceptor, while the N-H moiety attached to the iminophosphorane core functions as a hydrogen bond donor. The high catalytic activity of this class of chiral organobases was demonstrated in a series of the direct Henry reaction [95] and the hydrophosphonylation of aldehydes (Scheme 3.49) [96].

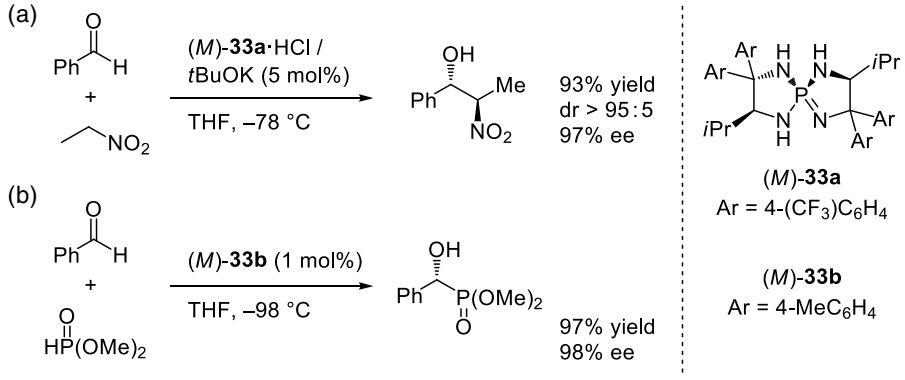

Scheme 3.49. Enantioselective addition of nitroalkanes and dialkyl phosphites to aldehydes catalyzed by (*M*)-**33**. (a) Source: Based on [95]. (b) Source: Based on [96].

The computational study by Simón and Paton suggested the mechanism involving a single catalyst molecule that makes hydrogen bonds with both a nucleophile and an electrophile, transferring a proton to the electrophile preventing the negative charge accumulation (Figure 3.14) [97].

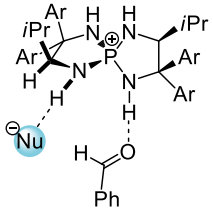

Figure 3.14. Proposed transition-state model.

The chiral P1-phosphazene catalysts (*P*)-**34** exhibited the distinctive feature in the Michael addition reactions involving the multiple selectivity control (Scheme 3.50). For instance, catalyst (*P*)-**34a** promoted the enantioselective addition of 2-benzyloxythiazol-5(4*H*)-ones to β-substituted alkynyl *N*-acylpyrazoles with high *E* selectivity (Scheme 3.50a) [98]. The addition of azlactones to δ-substituted dienyl *N*-acylpyrroles and ζ-substituted trienyl *N*-acylpyrroles proceeded in highly 1,6- and 1,8-selective fashion, respectively, under the catalysis of (*P*)-**34b**, and the corresponding adducts were obtained in high yields with high diastereo- and enantioselectivities (Scheme 3.50b) [99]. Furthermore, (*P*)-**34c** efficiently catalyzed the 1,6-addition of azlactones to enynyl *N*-acylpyrazole and the consecutive γ-protonation of the vinylogous enolate to afford *Z*,*E*-configurated conjugated dienes, while the application of a bifunctional chiral tertiary amine catalyst provided the 1,4-addition products (Scheme 3.50c) [100].

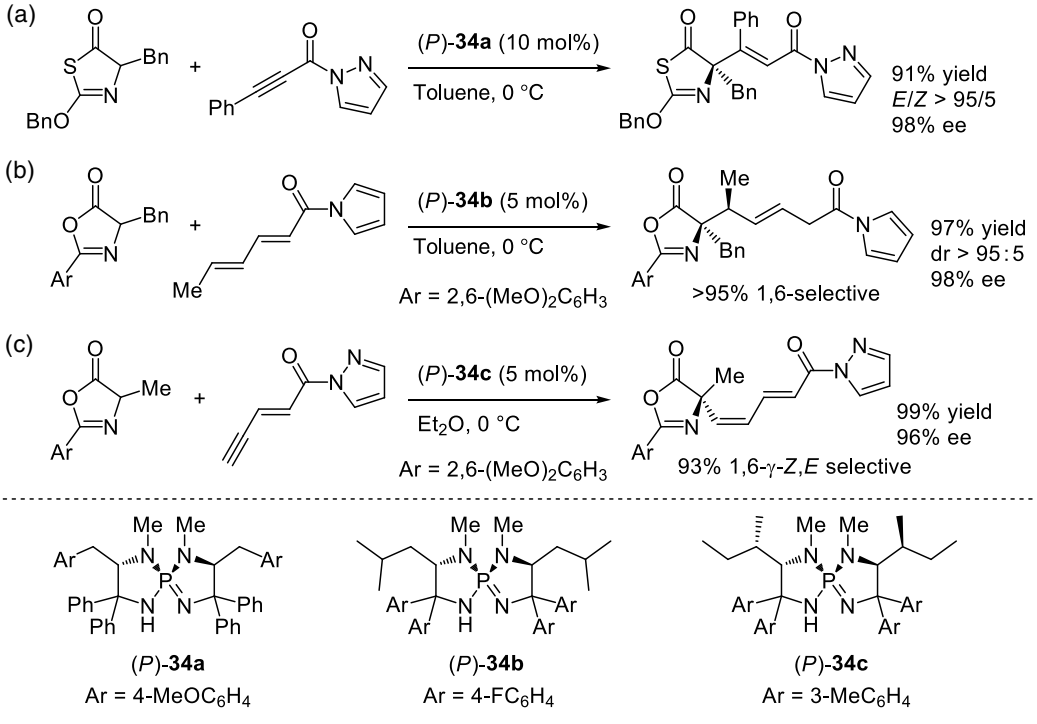

Scheme 3.50. Enantioselective Michael addition reactions catalyzed by (*P*)-**34**. (a) Source: Based on [98]. (b) Source: [99]. (c) Source: Based on [100].

Furthermore, this class of chiral catalysts was successfully utilized in the development of new types of catalytic enantioselective reactions. For instance, Ooi, Johnson, and co-workers developed the enantioselective aldol-type reaction of α-hydroxy phosphonoacetates (Scheme 3.51) [101]. This reaction involves a catalytic generation of the reactive glycolate enolate **36** from an α-hydroxy phosphonoacetate **35** through the [1,2]-phospha-Brook rearrangement and the subsequent enantioselective addition to an aldehyde. The group also reported the related enantioselective three-component coupling reaction of isatin derivatives, aldehydes, and dialkyl phosphites [102].

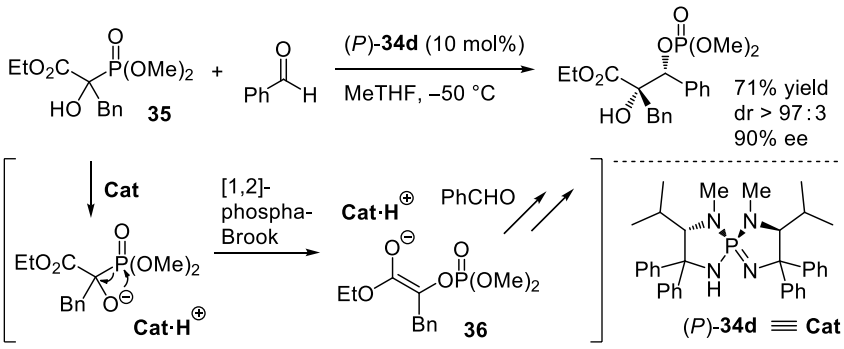

Scheme 3.51. Enantioselective aldol-type reaction of α-hydroxy phosphonoacetates catalyzed by (*P*)-**34d**. Source: Based on [101].

As the other remarkable catalytic enantioselective reaction, Ooi and co-workers developed the enantioselective Payne-type oxidation of *N*-sulfonyl imines based on the combined use of H_2O_2 and trichloroacetonitrile under the catalysis of (*P*)-**34e** (Scheme 3.52) [103]. In this reaction system, the reactive organic peroxy acid **37**, which was catalytically generated in situ, was successfully controlled by the chiral catalyst molecule.

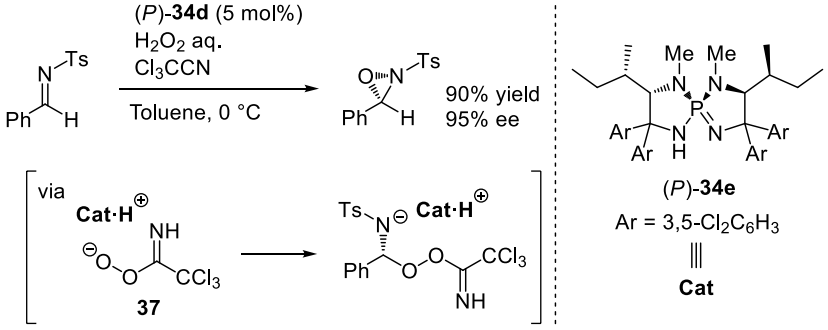

Scheme 3.52. Enantioselective Payne-type oxidation of *N*-sulfonyl imines catalyzed by (*P*)-**34e**. Source: [103].

3.4.4. Chiral Higher-Order Phosphazene Catalysts

As described as well in the previous section, the expansion of the scope of pronucleophiles is one of the most important tasks in the field of asymmetric Brønsted base catalysis. The most direct approach for this purpose is the application of chiral organobases having strong basicity as a catalyst. The recent efforts for the development of chiral organobases with higher basicity than chiral tertiary amines, such as chiral guanidines, cyclopropenimines, triaryliminophosphoranes, and P1-phosphazenes, have substantially advanced the field of asymmetric Brønsted base catalysis as described above. However, even with these chiral organosuperbase catalysts, the applicable pronucleophiles are still mainly limited to the compounds having high acidity because of their insufficient basicity. In order to overcome the intrinsic limitation of pronucleophiles, the development of chiral organobase catalysts possessing much higher basicity than aforementioned chiral organosuperbase catalysts, namely chiral "higher-order" organosuperbase catalysts, is highly anticipated. In this context, Terada and co-workers focused on higher-order phosphazenes as a new platform for chiral organobase catalysts. Higher-order phosphazenes, in which

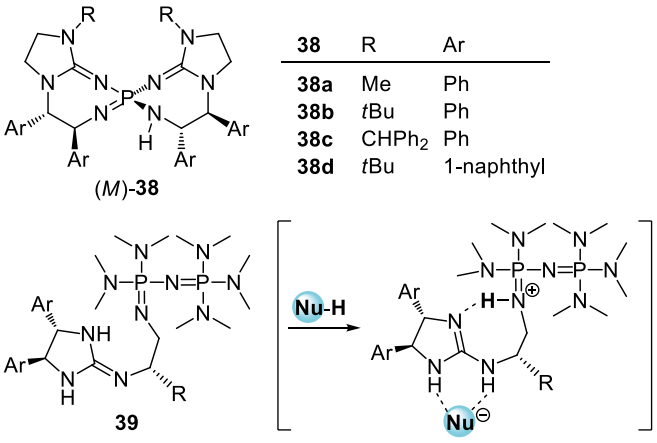

38	R	Ar
38a	Me	Ph
38b	*t*Bu	Ph
38c	$CHPh_2$	Ph
38d	*t*Bu	1-naphthyl

Figure 3.15. Chiral higher-order phosphazene catalysts.

phosphazene or guanidine subunit(s) are introduced to the iminophosphorane core, possess much higher basicity than P1-phosphazenes owing to the better delocalization of the positive charge formed through the protonation. Specifically, Terada and co-workers designed and developed two types of chiral higher-order phosphazene catalysts as a superb class of chiral organosuperbase catalysts that enable the expansion of the scope of pronucleophiles (Figure 3.15).

In 2013, Terada and Takeda developed chiral pseudo-C_2-symmetric bis(guanidino)iminophosphorane catalysts (*M*)-**38**, in which two guanidine subunits are introduced to the central iminophosphorane core [104]. The characteristic feature of chiral bis(guanidino)iminophosphoranes is underscored by their helical chirality based on the 7,7-membered spirocyclic system along with central chirality derived from chiral diamines. In addition, as similar to Ooi's P1-phosphazene catalysts, hydrogen bond donor and acceptor sites are arranged side by side around the central phosphorus atom. The catalytic performance of (*M*)-**38** as chiral "higher-order" organosuperbases was validated in the enantioselective amination of 2-alkyltetralone as a less acidic pronucleophile with azodicarboxylate (Scheme 3.53).

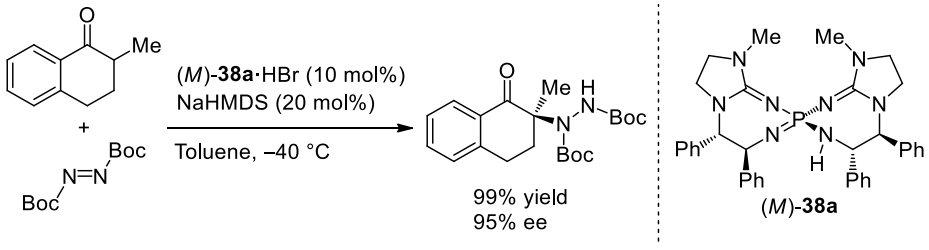

Scheme 3.53. Enantioselective amination of 2-alkyltetralone with azodicarboxylate catalyzed by (*M*)-**38a**. Source: Based on [104].

By taking advantage of the strong basicity of (*M*)-**38**, Terada and co-workers successfully developed a series of enantioselective addition reactions of less acidic pronucleophiles, such as 2-alkoxycarbonyl 1,3-dithianes, α-alkylthionolactones, and 2-benzylpyridine *N*-oxides (Scheme 3.54) [105]. (*M*)-**38** was also applied to the enantioselective protonation through the hydrophosphinylation of 2-vinyl quinoline *N*-oxides [106].

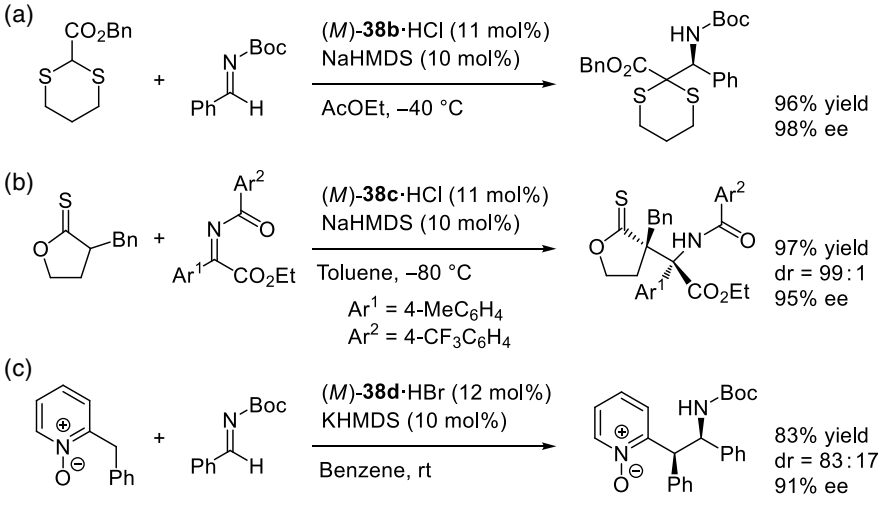

Scheme 3.54. Enantioselective addition reactions of less acidic pronucleophiles catalyzed by (*M*)-**38**. Source: [105].

As the other remarkable application of (*M*)-**38**, Terada and co-workers developed the enantioselective formal [3+2] cycloaddition of epoxysulfones with imines (Scheme 3.55) [107]. This reaction involves the generation of alkoxide intermediate **40** through the ring-opening of epoxide and the subsequent enantioselective intermolecular addition to imine followed by the diastereoselective intramolecular aza-Michael addition of chiral intermediate **41**. In the tandem catalytic processes, the key roles of the chiral organosuperbase are: (i) facilitating the reaction with its high basicity, (ii) controlling the enantioselectivity in the addition of **40** to imine, and (iii) assisting the diastereocontrol of the aza-Michael addition of **41**.

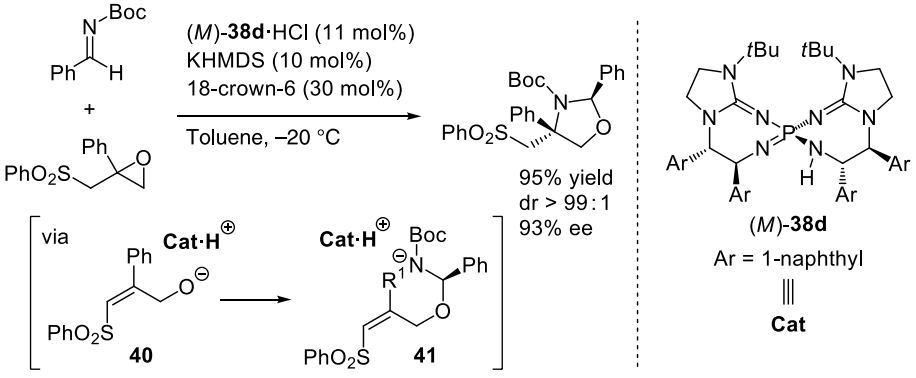

Scheme 3.55. Enantioselective formal [3+2] cycloaddition of epoxysulfones with imines catalyzed by (*M*)-**38d**. Source: [107].

In 2020, Terada and co-workers developed "chiral cooperative binary base catalysts" **39**, which consist of two different organobase functionalities: a P2-phosphazene as an organosuperbase and a chiral guanidine as a hydrogen bond donor unit for substrate recognition [108]. The molecular design is based on a conceptually new idea for a distinctive cooperative function by two organobases in a single catalyst molecule: the formation of a chiral cyclic structure with an intramolecular hydrogen bond between the

two organobase functionalities in the conjugate acid form, which creates an effective chiral environment around the substrate recognition site by limiting the conformational flexibility (Figure 3.15). The prominent catalytic activity of **39** was demonstrated in the enantioselective direct Mannich-type reaction of α-phenylthioacetate as a less acidic pronucleophile (Scheme 3.56a). The P3-phosphazene-based catalyst **42** possessing enhanced basicity was also synthesized based on the molecular design. The catalyst could promote the reaction of much less acidic α-phenylthioacetamide, which did not proceed with P2-phosphazene-based catalyst **39**, albeit in moderate stereoselectivities (Scheme 3.56b).

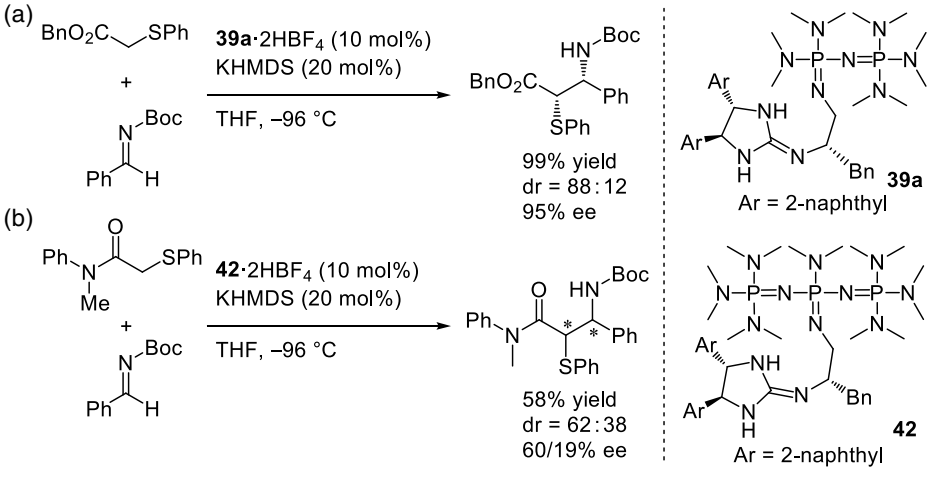

Scheme 3.56. Enantioselective direct Mannich-type reactions catalyzed by chiral cooperative binary base catalysts. Source: Based on [108].

3.5. CONCLUSION AND OUTLOOK

Over the past two decades, the development of enantioselective reactions under asymmetric Brønsted base catalysis has been intensively explored, and fruitful progress has been made in this field. A variety of useful enantioselective transformations has been achieved based on the rational reaction design as well as the suitable choice of a chiral catalyst. In parallel with the development of new enantioselective reactions, various types of efficient chiral uncharged organobase catalysts have been designed and synthesized, which dramatically accelerated the progress. In particular, the new types of chiral organosuperbase catalysts possessing much higher basicity than that of conventional chiral tertiary amine catalysts have substantially expanded the scope of applicable pronucleophiles. Nevertheless, there is still a large room for improvement in this field. For instance, the development of chiral organosuperbase catalysts is still in its infancy, and the development of new catalysts, particularly with unprecedented catalyst design, is highly desirable to accomplish a variety of enantioselective transformations using a much broader range of pronucleophiles. On the other hand, the mechanism and the origin of the stereoselectivity have not been clarified in many reactions. Therefore, detailed mechanistic studies are also needed for a better understanding of the catalysis and the development of next generation of chiral catalysts and reaction systems. Further progress of the asymmetric Brønsted base catalysis is highly anticipated, which will find valuable applications in various fields of organic chemistry, such as natural product synthesis and drug discovery research.

REFERENCES

1. (a) Palomo, C.; Oiarbide, M.; López, R. *Chem. Soc. Rev.* **2009**, *38*, 632–653. (b) *Superbases for Organic Synthesis: Guanidines, Amidines, Phosphazenes and Related Organocatalysts*; Ishikawa, T., Ed.; John Wiley & Sons: Chichester, West Sussex, **2009**. (c) *Comprehensive Enantioselective Organocatalysis*; Dalko, P. I. Ed.; Wiley-VCH: Weinheim, **2013**, pp 343–363.

2. For pK_{BH+} values of organobases: (a) Tshepelevitsh, S.; Kütt, A.; LõKov, M.; Kaljurand, I.; Saame, J.; Heering, A.; Plieger, P. G.; Vianello, R.; Leito, I. *Eur. J. Org. Chem.* **2019**, 6735–3748. (b) Schwesinger, R.; Schlemper, H.; Hasenfratz, C.; Willaredt, J.; Dambacher, T.; Breuer, T.; Ottaway, C.; Fletschinger, M.; Boele, J.; Fritz, H.; Putzas, D.; Rotter, H. W.; Boldwell, F. G.; Satish, A. V.; Ji, G.-Z.; Peters, E. M.; Peters, K.; von Schnering, H. G.; Walz, L. *Liebigs Ann.* **1996**, 1055–1081. (c) Kolomeitsev, A. A.; Koppel, I. A.; Rodima, T.; Barten, J.; Lork, E.; Röschenthaler, G.-V.; Kaljurand, I.; Kütt, A.; Koppel, I.; Mäemets, V.; Leito, I. *J. Am. Chem. Soc.* **2005**, *127*, 17656–17666. Also see, refs 81 and 87.
3. (a) Marcelli, T.; Hiemstra, H. *Synthesis* **2010**, 1229–1279. (b) Yeboah, E. M. O.; Yeboah, S. O.; Singh, G. S. *Tetrahedron* **2011**, *67*, 1725–1762.
4. (a) Leow, D.; Tan, C.-H. *Chem. Asian J.* **2009**, *4*, 488–507. (b) Don, S.; Feng, X.; Liu, X. *Chem. Soc. Rev.* **2018**, *47*, 8525–8540. (c) Chou, H.-C.; Leow, D.; Tan, C.-H. *Chem. Asian. J.* **2019**, *14*, 3803–3822.
5. (a) Krawczyk, H.; Dzięgielewski, M.; Deredas, D.; Albrecht, A.; Albrecht, Ł. *Chem. Eur. J.* **2015**, *21*, 10268–10277. (b) Teng, B.; Lim, W. C.; Tan, C.-H. *Synlett* **2017**, *28*, 1272–1277. (c) Wang, Y.-H.; Cao, Z.-Y.; Li, Q.-H.; Lin, G.-Q.; Zhou, J.; Tian, P. *Angew. Chem. Int. Ed.* **2020**, *59*, 8004–8014.
6. *Catalytic Asymmetric Synthesis*; Ojima, I. Ed.; John Wiley & Sons: New Jersey, **2010**, pp 59–94.
7. (a) Uraguchi, D.; Koshimoto, K.; Ooi, T. *J. Am. Chem. Soc.* **2008**, *130*, 10878–10879. (b) Uraguchi, D.; Oyaizu, K.; Ooi, T. *Chem. Eur. J.* **2012**, *18*, 8306–8309. (c) Zhang, W.-Q.; Cheng, L.-F.; Yu, J.; Gong, L.-Z. *Angew. Chem. Int. Ed.* **2012**, *51*, 4085–4088. (d) Zhou, X.; Wu, Y.; Deng, L. *J. Am. Chem. Soc.* **2016**, *138*, 12297–12302.
8. Kondoh, A.; Ishikawa, S.; Terada, M. *J. Am. Chem. Soc.* **2020**, *142*, 3724–3728.
9. Wynberg, H. *Topics in Stereochemistry* **1986**, *16*, 87–129.
10. Hiemsta, H.; Wynberg, H. *J. Am. Chem. Soc.* **1981**, *103*, 417–430.
11. Grayson, M. N.; Houk, K. N. *J. Am. Chem. Soc.* **2016**, *138*, 1170–1173.
12. Okino, T.; Hoashi, Y.; Takemoto, Y. *J. Am. Chem. Soc.* **2003**, *125*, 12672–12673.
13. Okino, T.; Hoashi, Y.; Furukawa, T.; Xu, X.; Takemoto, Y. *J. Am. Chem. Soc.* **2005**, *127*, 119–125.
14. Hamza, A.; Schubert, G.; Soós, T.; Pápai, I. *J. Am. Chem. Soc.* **2006**, *128*, 13151–13160.
15. Azuma, T.; Kobayashi, Y.; Sakata, K.; Sasamori, T.; Tokitoh, N.; Takemoto, Y. *J. Org. Chem.* **2014**, *79*, 1805–1817.
16. (a) Miyabe, H.; Takemoto, Y. *Bull. Chem. Soc. Jpn.* **2008**, *81*, 785–795. (b) Fang, X.; Wang, C.-J. *Chem. Commun.* **2015**, *51*, 1185–1197. (c) Gandhi, S.; Sivadas, V.; Baire, B. *Eur. J. Org. Chem.* **2021**, 220–234. (d) Han, X.; Kwiatkowski, J.; Xue, F.; Huang, K.-W.; Lu, Y. *Angew. Chem. Int. Ed.* **2009**, *48*, 7604–7607. (e) Probst, N.; Madarász, Á.; Valkonen, A.; Pápai, I.; Rissanen, K.; Neuvonen, A.; Pihko, P. M. *Angew. Chem. Int. Ed.* **2012**, *51*, 8495–8499. (f) Yang, C.; Zhang, E.-G.; Li, X.; Cheng, J.-P. *Angew. Chem. Int. Ed.* **2016**, *55*, 6506–6510.
17. (a) Zhu, Y.; Malerich, J. P.; Rawal, V. H. *Angew. Chem. Int. Ed.* **2010**, *49*, 153–156. (b) Rombola, M.; Sumaria, C. S.; Montgomery, T. D.; Rawal, V. H. *J. Am. Chem. Soc.* **2017**, *139*, 5297–5300. (c) Kimmel, K. L.; Robak, M. T.; Ellman, J. A. *J. Am. Chem. Soc.* **2009**, *131*, 8754–8755. (d) Kimmel, K. L.; Weaver, J. D.; Lee, M.; Ellman, J. A. *J. Am. Chem. Soc.* **2012**, *134*, 9058–9061. (e) Inokuma, T.; Furukawa, M.; Uno, T.; Suzuki, Y.; Yoshida, K.; Yano, Y.; Matsuzaki, K.; Takemoto, Y. *Chem. Eur. J.* **2011**, *17*, 10470–10477.
18. (a) Li, B.-J.; Jiang, L.; Liu, M.; Chen, Y.-C.; Ding, L.-S.; Wu, Y. *Synlett* **2005**, 603–606. (b) Vakulya, B.; Varga, S.; Csámpai, A.; Soós, T. *Org. Lett.* **2005**, *7*, 1967–1969. (c) McCooey, S. H.; Connon, S. J. *Angew. Chem. Int. Ed.* **2005**, *44*, 6367–6370. (d) Ye, J.; Dixon, D. J.; Hynes, P. S. *Chem. Commun.* **2005**, 4481–4483.
19. (a) Malerich, J. P.; Hagihara, K.; Rawal, V. H. *J. Am. Chem. Soc.* **2008**, *130*, 14416–14417. (b) Zhu, Q.; Lu, Y. *Angew. Chem. Int. Ed.* **2010**, *49*, 7753–7756. (c) Ding, M.; Zhou, F.; Liu. Y.-L.; Wang, C.-H.; Zhao, X.-L.; Zhou, J. *Chem. Sci.* **2011**, *2*, 2035–2039. (d) Urruzuno, I.; Mugica, O.; Oiarbide, M.; Palomo, C. *Angew. Chem. Int. Ed.* **2017**, *56*, 2059–2063. (e) Arai, R.; Hirashima, S.; Kondo, J.; Nakashima, K.; Koseki, Y.; Miura, T. *Org. Lett.* **2018**, *20*, 5569–5572.
20. (a) Chauhan, P.; Mahajan, S.; Kaya, U.; Hack, D.; Enders, D. *Adv. Synth. Catal.* **2015**, *357*, 253–281. (b) Mukhopadhyay, S.; Gharui, C.; Pan, S. C. *Asian J. Org. Chem.* **2019**, *8*, 1970–1984. (c) Hou, X.-Q.; Du, D.-M. *Adv. Synth. Catal.* **2020**, *362*, 4487–4512.
21. Li, H.; Wang, Y.; Tang, L.; Deng, L. *J. Am. Chem. Soc.* **2004**, *126*, 9906–9907.
22. Saaby, S.; Bella, M.; Jørgensen, K. A. *J. Am. Chem. Soc.* **2004**, *126*, 8120–8121.
23. Li, H.; Wang, Y.; Tang, L.; Wu, F.; Liu, X.; Guo, C.; Foxman, B. M.; Deng, L. *Angew. Chem. Int. Ed.* **2005**, *44*, 105–108.
24. Marcelli, T.; Haas, R. N. S.; Maarseveen, J. H.; Hiemstra, H. *Angew. Chem. Int. Ed.* **2006**, *45*, 929–931.
25. Xiao, X.; Xie, Y.; Su, C.; Liu, M.; Shi, Y. *J. Am. Chem. Soc.* **2011**, *133*, 12914–12917.
26. Tan, B.; Hernández-Torres, G.; Barbas III, C. F. *Angew. Chem. Int. Ed.* **2012**, *51*, 5381–5385.
27. Bae, H. Y.; Sim, J. H.; Lee, J.-W.; List, B.; Song, C. E. *Angew. Chem. Int. Ed.* **2013**, *52*, 12143–12147.
28. (a) Clerici, P.; Wennemers, H. *Org. Biomol. Chem.* **2012**, *10*, 110–113. (b) Bahlinger, A.; Fritz, S. P.; Wennemers, H. *Angew. Chem. Int. Ed.* **2014**, *53*, 8779–8783. (c) Engl, O. D.; Fritz, S. P.; Wennemers, H. *Angew. Chem. Int. Ed.* **2015**, *54*, 8193–8197.
29. (a) Saadi, J.; Wennemers, H. *Nature Chem.* **2016**, *8*, 276–280. (b) Cosimi, E.; Engl, O. D.; Saadi, J.; Ebert, M.-O.; Wennemers, H. *Angew. Chem. Int. Ed.* **2016**, *55*, 13127–13131.
30. (a) Alba, A.-N. R.; Rios, R. *Chem. Asian J.* **2011**, *6*, 720–734. (b) Marra, I. F. S.; Castro, P. P.; Amarante, G. W. *Eur. J. Org. Chem.* **2019**, 5830–5855.
31. (a) Diosdado, S.; Etxabe, J.; Izquierdo, J.; Landa, A.; Mielgo, A.; Olaizola, I.; López, R.; Palomo, C. *Angew. Chem. Int. Ed.* **2013**, *52*, 11846–11851. (b) Etxabe, J.; Izquierdo, J.; Landa, A.; Oiarbide, M.; Palomo, C. *Angew. Chem. Int. Ed.* **2015**, *54*,

6883–6886. (c) Izquierdo, J.; Etxabe, J.; Duñabeitia, E.; Landa, A.; Oiarbide, M.; Palomo, C. *Chem. Eur. J.* **2018**, *24*, 7217–7227.
32. Nemoto, H.; Kubota, Y.; Yamamoto, Y. *J. Org. Chem.* **1990**, *55*, 4515–4516.
33. Yang, K. S.; Nibbs, A. E.; Türkmen, Y. E.; Rawal, V. H. *J. Am. Chem. Soc.* **2013**, *135*, 16050–16053.
34. Nanjo, T.; Zhang, X.; Tokuhiro, Y.; Takemoto, Y. *ACS Catal.* **2019**, *9*, 10087–10092.
35. Izquierdo, J.; Landa, A.; Bastida, I.; López, R.; Oiarbide, M.; Palomo, C. *J. Am. Chem. Soc.* **2016**, *138*, 3282–3285.
36. Pozo, S.; Vera, S.; Oiarbide, M.; Palomo, C. *J. Am. Chem. Soc.* **2017**, *139*, 15308–15311.
37. Asano, K.; Matsubara, S. *J. Am. Chem. Soc.* **2011**, *133*, 16711–16713.
38. Yoneda, N.; Fukata, Y.; Asano, K.; Matsubara, S. *Angew. Chem. Int. Ed.* **2015**, *54*, 15497–15500.
39. Yoneda, N.; Fujii, Y.; Matsumoto, A.; Asano, K.; Matsubara, S. *Nature Commun.* **2017**, *8*, 1397.
40. Kobayashi, Y.; Taniguchi, Y.; Hayama, N.; Inokuma, T.; Takemoto, Y. *Angew. Chem. Int. Ed.* **2013**, *52*, 11114–11118.
41. Reddy, R. R.; Gudup, S. S., Ghorai, P. *Angew. Chem. Int. Ed.* **2016**, *55*, 15115–15119.
42. Roy, T. K.; Parhi, B.; Ghorai, P. *Angew. Chem. Int. Ed.* **2018**, *57*, 9397–9401.
43. Thomson, C. J.; Barber, D. M.; Dixon, D. J. *Angew. Chem. Int. Ed.* **2019**, *58*, 2469–2473.
44. Phelan, J. P.; Patel, E. J.; Ellman, J. A. *Angew. Chem. Int. Ed.* **2014**, *53*, 11329–11332.
45. Guo, W.; Wu, B.; Zhou, X.; Chen, P.; Wang, X.; Zhou, Y.-G.; Liu, Y.; Li, C. *Angew. Chem. Int. Ed.* **2015**, *54*, 4522–4526.
46. Volla, C. M. R.; Atodiresei, I.; Rueping, M. *Chem. Rev.* **2014**, *114*, 2390–2431.
47. Cao, Y.; Jiang, X.; Liu, L.; Shen, F.; Zhang, F.; Wang, R. *Angew. Chem. Int. Ed.* **2011**, *50*, 9124–9127.
48. Manoni, F.; Connon, S. J. *Angew. Chem. Int. Ed.* **2014**, *53*, 2628–2632.
49. Blom, J.; Vidal-Albalat, A.; Jørgensen, J.; Barløse, C. L.; Jessen, K. S.; Iversen, M. V.; Jørgensen, K. A. *Angew. Chem. Int. Ed.* **2017**, *56*, 11831–11835.
50. Zhou, Y.; Wei, Y.-L.; Rodriguez, J.; Coquerel, Y. *Angew. Chem. Int. Ed.* **2019**, *58*, 456–460.
51. Quinonero, O.; Jean, M.; Vanthuyne, N.; Roussel, C.; Bonne, D.; Constantieux, T.; Bressy, C.; Bugaut, X.; Rodriguez, J. *Angew. Chem. Int. Ed.* **2016**, *55*, 1401–1405.
52. Raut, V. S.; Jean, M.; Vanthuyne, N.; Roussel, C.; Constantieux, T.; Bressy, C.; Bugaut, X.; Bonne, D.; Rodriguez, J. *J. Am. Chem. Soc.* **2017**, *139*, 2140–2143.
53. Wu, X.; Xue, L.; Li, D.; Jia, S.; Ao, J.; Deng, J.; Yan, H. *Angew. Chem. Int. Ed.* **2017**, *56*, 13722–13726.
54. (a) Jia, S.; Chen, Z.; Zhang, N.; Tan, Y.; Liu, Y.; Deng, J.; Yan, H. *J. Am. Chem. Soc.* **2018**, *140*, 7056–7060. (b) Tan, Y.; Jia, S.; Hu, F.; Liu, Y.; Peng, L.; Li, D.; Yan, H. *J. Am. Chem. Soc.* **2018**, *140*, 16893–16898.
55. (a) Schug, K. A.; Lindner, W. *Chem. Rev.* **2005**, *105*, 67–113. (b) Blondeau, P.; Segura, M.; Pérez-Fernández, R.; Mendoza, J. *Chem. Soc. Rev.* **2007**, *36*, 198–210.
56. Chinchilla, R.; Nájera, C.; Sánchez-Agulló, P. *Tetrahedron: Asymmetry* **1994**, *5*, 1393–1402.
57. Iyer, M. S.; Gigstad, K. M.; Namdev, N. D.; Lipton, M. *J. Am. Chem. Soc.* **1996**, *118*, 4910–4911.
58. Corey, E. J.; Grogan, M. J. *Org. Lett.* **1999**, *1*, 157–160.
59. Leow, D.; Tan, C.-H. *Synlett* **2010**, *2010*, 1589–1605.
60. Shen, J.; Nguyan, T. T.; Goh, Y.-P.; Ye, W.; Fu, X.; Xu, J.; Tan, C.-H. *J. Am. Chem. Soc.* **2006**, *128*, 13692–13693.
61. Leow, D.; Lin, S.; Chittimalla, S. K.; Fu, X.; Tan, C.-H. *Angew. Chem. Int. Ed.* **2008**, *47*, 5641–5645.
62. (a) Liu, H.; Leow, D.; Huang, K.-W.; Tan, C.-H. *J. Am. Chem. Soc.* **2009**, *131*, 7212–7213. (b) Xue, H.; Jiang, D.; Jiang, H.; Kee, C. W.; Hirao, H.; Nishimura, T.; Wong, M. W.; Tan, C.-H. *J. Org. Chem.* **2015**, *80*, 5745–5752.
63. (a) Ishikawa, T.; Araki, Y.; Kumamoto, T.; Seki, H.; Fukuda, K.; Isobe, T. *Chem. Commun.* **2001**, 245–246. (b) Ishikawa, T. *Chem. Pharm. Bull.* **2010**, *58*, 1555–1564.
64. Saito, N.; Akemi, R.; Nakanishi, W.; Kumamoto, T.; Ishikawa, T. *Eur. J. Org. Chem.* **2008**, *2008*, 2759–2766.
65. (a) Misaki, T.; Takimoto, G.; Sugimura, T, *J. Am. Chem. Soc.* **2010**, *132*, 6286–6287. (b) Misaki, T.; Kawano, K.; Sugimura, T. *J. Am. Chem. Soc.* **2011**, *133*, 5695–5697.
66. Sohtome, Y.; Nagasawa, K. *Synlett* **2010**, *2010*, 1–22.
67. Sohtome, Y.; Shin, B.; Horitsugi, N.; Takagi, R.; Noguchi, K.; Nagasawa, K. *Angew. Chem. Int. Ed.* **2010**, *49*, 7299–7303.
68. Sohtome, Y.; Tanaka, S.; Takada, K.; Yamaguchi, T.; Nagasawa, K. *Angew. Chem. Int. Ed.* **2010**, *49*, 9254–9257.
69. Hosoya, K.; Odagi, M.; Nagasawa, K. *Tetrahedron Lett.* **2018**, *59*, 687–696.
70. (a) Odagi, M.; Furukori, K.; Watanabe, T.; Nagasawa, K. *Chem. Eur. J.* **2013**, *19*, 16740–16745. (b) Odagi, M.; Furukori, K.; Yamamoto, Y.; Sato, M.; Iida, K.; Yamanaka, M.; Nagasawa, K. *J. Am. Chem. Soc.* **2015**, *137*, 1909–1915.
71. Yu, Z.; Liu, X.; Zhou, L.; Lin, L.; Feng, X. *Angew. Chem. Int. Ed.* **2009**, *48*, 5195–5198.
72. (a) Dong, S.; Liu, X.; Chen, X.; Mei, F.; Zhang, Y.; Gao, B.; Lin, L.; Feng, X. *J. Am. Chem. Soc.* **2010**, *132*, 10650–10651. (b) Yang, Y.; Dong, S.; Liu, X.; Lin, L.; Feng, X. *Chem. Commun.* **2012**, *48*, 5040–5042. (c) Kang, T.; Zhao, P.; Yang, J.; Lin, L.; Feng, X.; Liu, X. *Chem. Eur. J.* **2018**, *24*, 3703–3706.
73. Zou, L.; Wang, B.; Mu, H.; Zhang, H.; Song, Y.; Qu, J. *Org. Lett.* **2013**, *15*, 3106–3109.
74. Zou, L.; Bao, X.; Ma, Y.; Song, Y.; Qu, J.; Wang, B. *Chem. Commun.* **2014**, *50*, 5760–5762.
75. Zhang, Y.; Kee, C. W.; Lee, R.; Fu, X.; Soh, J. Y.-T.; Loh, E. M. F.; Huang, K.-W.; Tan, C.-H. *Chem. Commun.* **2011**, *47*, 3897–3899.
76. Terada, M. *J. Synth Org. Chem.* **2010**, *68*, 1159–1168.

77. (a) Terada, M.; Ube, H.; Yaguchi, Y. *J. Am. Chem. Soc.* **2006**, *128*, 1454–1455. (b) Terada, M.; Ikehara, T.; Ube, H. *J. Am. Chem. Soc.* **2007**, *129*, 14112–14113.
78. (a) Ube, H.; Shimada, N.; Terada, M. *Angew. Chem. Int. Ed.* **2010**, *49*, 1858–1861. (b) Terada, M.; Ando, K. *Org. Lett.* **2011**, *13*, 2026–2029.
79. Terada, M.; Nakano, M.; Ube, H. *J. Am. Chem. Soc.* **2006**, *128*, 16044–16045.
80. Nakano, M.; Terada, M. *Synlett* **2009**, *2009*, 1670–1674.
81. Bandar, J. S.; Lambert, T. H. *J. Am. Chem. Soc.* **2012**, *134*, 5552–5555.
82. Bandar, J. S.; Lambert, T. H. *J. Am. Chem. Soc.* **2013**, *135*, 11799–11802.
83. (a) Bandar, J. S.; Sauer, G. S.; Wulff, W. D.; Lambert, T. H.; Vetticatt, M. J. *J. Am. Chem. Soc.* **2014**, *136*, 10700–10707. (b) Bandar, J. S.; Bathelme, A.; Mazori, A. Y.; Lambert, T. H. *Chem. Sci.* **2015**, *6*, 1537–1547.
84. Lauridsen, V. H.; Ibsen, L.; Bolm, J.; Jørgensen, K. A. *Chem. Eur. J.* **2016**, *22*, 3259–3263.
85. Ošeka, M.; Kimm, M.; Järving, I.; Lippur, K.; Kanger, T. *J. Org. Chem.* **2017**, *82*, 2889–2897.
86. Formica, M.; Rozsar, D.; Su, G.; Farley, A. J. M.; Dixon, D. J. *Acc. Chem. Res.* **2020**, *53*, 2235–2247.
87. Núñez, M. G.; Farley, A. J. M.; Dixon, D. J. *J. Am. Chem. Soc.* **2013**, *135*, 16348–16351.
88. (a) Farley, A. J. M.; Sandford, C.; Dixon, D. J. *J. Am. Chem. Soc.* **2015**, *137*, 15992–15995. (b) Yang, J.; Farley, A. J. M.; Dixon, D. J. *Chem. Sci.* **2017**, *8*, 606–610. (c) Formica, M.; Sorin, G.; Farley A. J. M.; Diaz, J.; Paton, R. S.; Dixon, D. J. *Chem. Sci.* **2018**, *9*, 6969–6974.
89. Golec, J. C.; Carter, E. M.; Ward, J. W.; Whittingham, W. G.; Simón, L.; Paton, R. S.; Dixon, D. J. *Angew. Chem. Int. Ed.* **2020**, *59*, 17417–17422.
90. Thomson, C. J.; Barber, D. M.; Dixon, D. J. *Angew. Chem. Int. Ed.* **2020**, *59*, 5359–5364.
91. Shi, H.; Michaelides, I. N.; Darses, B.; Jakubec, P.; Nguyan, Q. N. N.; Paton, R. S.; Dixon, D. J. *J. Am. Chem. Soc.* **2017**, *139*, 17755–17758.
92. (a) Horwitz, M. A.; Fulton, J. L.; Johnson, J. S. *Org. Lett.* **2017**, *19*, 5783–5785. (b) Fulton, J. L.; Horwitz, M. A.; Bruske, E. L.; Johnson, J. S. *J. Org. Chem.* **2018**, *83*, 3385–3391. (c) Horwitz, M. A.; Zavesky, B. P.; Martinez-Alvarado, J. I.; Johnson, J. S. *Org. Lett.* **2016**, *18*, 36–39.
93. Schwesinger, R.; Schlemper, H. *Angew. Chem. Int. Ed. Engl.* **1987**, *26*, 11617–1169.
94. Uraguchi, D.; Ooi, T. J. *Synth. Org. Chem.* **2010**, *68*, 1185–1194.
95. (a) Uraguchi, D.; Sakaki, S.; Ooi, T. *J. Am. Chem. Soc.* **2007**, *129*, 12392–12393. (b) Uraguchi, D.; Ito, T.; Nakamura, S.; Sakaki, S.; Ooi, T. *Chem. Lett.* **2009**, *38*, 1052–1053. (c) Uraguchi, D.; Nakamura, S.; Ooi, T. *Angew. Chem. Int. Ed.* **2010**, *49*, 7562–7565.
96. (a) Uraguchi, D.; Ito, T.; Ooi, T. *J. Am. Chem. Soc.* **2009**, *131*, 3836–3837. (b) Uraguchi, D.; Ito, T.; Nakamura, S.; Ooi, T. *Chem. Sci.* **2010**, *1*, 488–490. (c) Uraguchi, D.; Ito, T.; Kimura, Y.; Nobori, Y.; Sato, M.; Ooi, T. *Bull. Chem. Soc. Jpn.* **2017**, *90*, 546–555.
97. Simón, L.; Paton, R. S. *J. Org. Chem.* **2015**, *80*, 2756–2766.
98. Uraguchi, D.; Yamada, K.; Ooi, T. *Angew. Chem. Int. Ed.* **2015**, *54*, 9954–9957.
99. (a) Uraguchi, D.; Yoshioka, K.; Ueki, Y.; Ooi, T. *J. Am. Chem. Soc.* **2012**, *134*, 19370–19373. (b) Uraguchi, D.; Yoshioka, K.; Ooi, T. *Nature Commun.* **2017**, *8*, 14793. (c) Yamanaka, M.; Sakata, K.; Yoshioka, K.; Uraguchi, D.; Ooi, T. *J. Org. Chem.* **2017**, *82*, 541–548.
100. Uraguchi, D.; Shibazaki, R.; Tanaka, N.; Yamada, K.; Yoshioka, K.; Ooi, T. *Angew. Chem. Int. Ed.* **2018**, *57*, 4732–4736.
101. Corbett, M. T.; Uraguchi, D.; Ooi, T.; Johnson, J. S. *Angew. Chem. Int. Ed.* **2012**, *51*, 4685–4689.
102. Horwitz, M. A.; Tanaka, N.; Yokosaka, T.; Uraguchi, D.; Johnson, J. S.; Ooi, T. *Chem. Sci.* **2015**, *6*, 6086–6090.
103. (a) Uraguchi, D.; Tsutsumi, R.; Ooi, T. *J. Am. Chem. Soc.* **2013**, *135*, 8161–8164. (b) Uraguchi, D.; Tsutsumi, R.; Ooi, T. *Tetrahedron* **2014**, *70*, 1691–1701. (c) Tanaka, N.; Tsutsumi, R.; Uraguchi, D.; Ooi, T. *Chem. Commun.* **2017**, *53*, 6999–7002.
104. (a) Takeda, T.; Terada, M. *J. Am. Chem. Soc.* **2013**, *135*, 15306–15309. (b) Takeda, T.; Terada, M. *Aust. J. Chem.* **2014**, *67*, 1124–1128.
105. (a) Kondoh, A.; Oishi, M.; Takeda, T.; Terada, M. *Angew. Chem. Int. Ed.* **2015**, *54*, 15836–15839. (b) Takeda, T.; Kondoh, A.; Terada, M. *Angew. Chem. Int. Ed.* **2016**, *55*, 4734–4737. (c) Hu, Q.; Kondoh, A.; Terada, M. *Chem. Sci.* **2018**, *9*, 4348–4351.
106. Das, S.; Hu, Q.; Kondoh, A.; Terada, M. *Angew. Chem. Int. Ed.* **2021**, *60*, 1417–1422.
107. Kondoh, A.; Akahira, S.; Oishi, M.; Terada, M. *Angew. Chem. Int. Ed.* **2018**, *57*, 6299–6303.
108. Kondoh, A.; Oishi, M.; Tezuka, H.; Terada, M. *Angew. Chem. Int. Ed.* **2020**, *59*, 7472–7477.

4

ASYMMETRIC PHASE-TRANSFER AND ION-PAIR ORGANOCATALYSES

EDWARD MILLER, PATRICK J. MOON, AND F. DEAN TOSTE
University of California, Berkeley, Berkeley, CA, USA

4.1. INTRODUCTION

Asymmetric organocatalysis has become a powerful strategy for the construction of chiral functional molecules and materials, providing unique reactivity manifolds compared to traditional metal-catalyzed or enzymatic-based approaches. Within the field, reversible covalent substrate activation or binding with a chiral catalyst (enamine, iminium, or *N*-heterocyclic carbene [NHC] catalysis) has been extensively exploited to achieve highly enantioselective transformations. Conformational analysis of the catalyst-bound intermediates has permitted the rationalization of the origin of enantioselectivity in a number of reactions, which in turn has helped drive catalyst design with relative ease. Another approach involves the use of noncovalent interactions as the basis for substrate activation and asymmetric induction. Within this category, asymmetric phase-transfer and ion-pairing catalyses have proven to be uniquely suited to achieve highly selective reactions involving charged substrates or intermediates (Scheme 4.1). This chapter will cover key historical and recent developments in the area of chiral cation phase-transfer and cation-binding catalyses, in addition to more recent advances in chiral-anion (phase-transfer) and anion-binding catalyses. Additionally, examples featuring transition-metal and phase-transfer dual catalysis will also be highlighted.

4.2. CHIRAL CATION

4.2.1. Chiral Cation Phase-Transfer Catalysis

4.2.1.1. Alkylation In 1984, Dolling reported the enantioselective methylation of an indanone derivative using a cinchoninium salt phase-transfer catalyst (PTC, Scheme 4.2) [1]. While phase-transfer catalysis had already been reported to yield racemic alkylation products, the significance of this landmark study cannot be understated since it demonstrated that chiral information from a catalytically generated ion-pair could be transferred in an alkylation step to achieve high enantiocontrol. Enantioselectivity is rationalized from a composite of electrostatic, hydrogen bonding, and π–π interactions that selectively block one face of the enolate, allowing for selective alkylation. This ensemble of various noncovalent interactions is a key feature of ion-pairing catalysis [2].

Catalytic Asymmetric Synthesis, Fourth Edition. Edited by Takahiko Akiyama and Iwao Ojima.

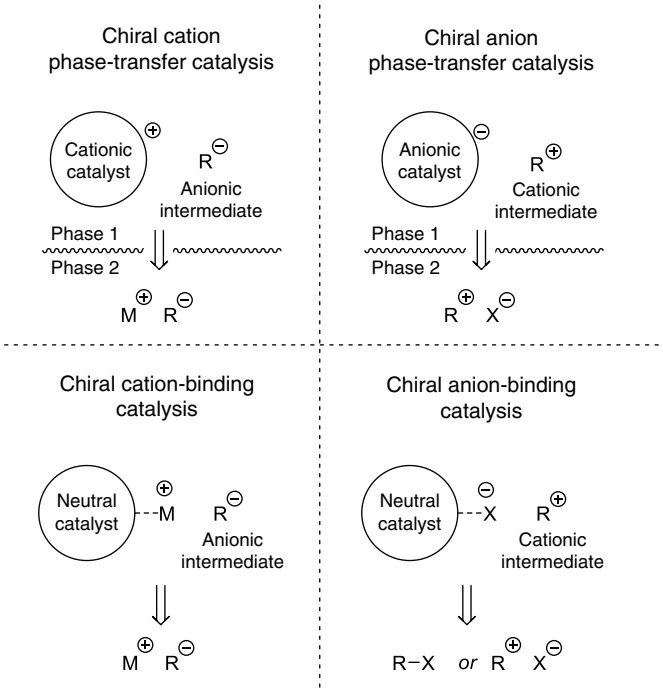

Scheme 4.1. Modes of asymmetric phase-transfer and ion-pair organocatalysis.

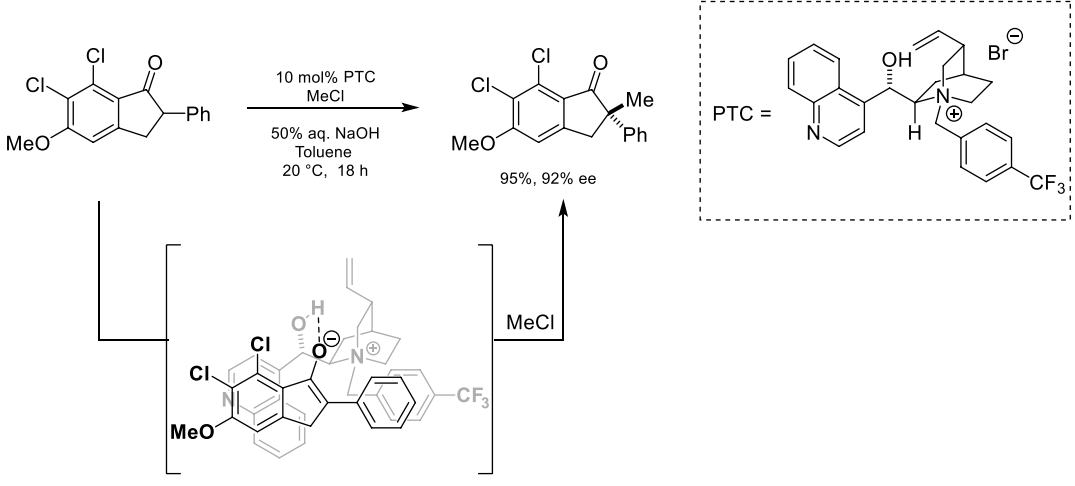

Scheme 4.2. First enantioselective alkylation using chiral cation phase transfer catalysis. Source: Based on [2].

In 1989, another key development in the field was reported by O'Donnell: the enantioselective alkylation of benzophenone protected glycine imines using similar cinchoninium PTC (Scheme 4.3) [3]. This is an operationally simple protocol to access chiral α-amino acid derivatives upon imine hydrolysis.

In the years following these seminal reports, numbers of other chiral cationic organocatalyst architectures were developed for asymmetric alkylation reactions. The benzylation of tert-butyl benzophenone glycine imine has since become a classical reaction to benchmark catalysts (Scheme 4.4). Early efforts focused on modifying the bridgehead nitrogen substituent of the cinchoninium, which proved to have a

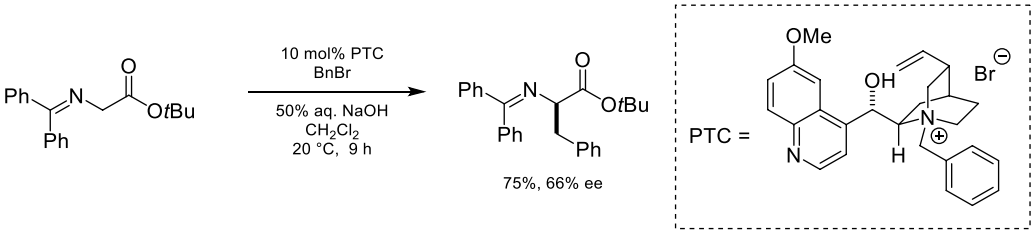

Scheme 4.3. Enantioselective benzylation of glycine imines. Source: Based on [3].

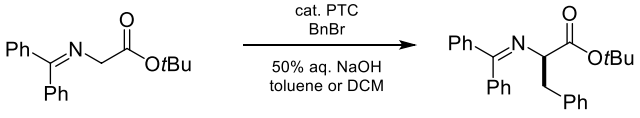

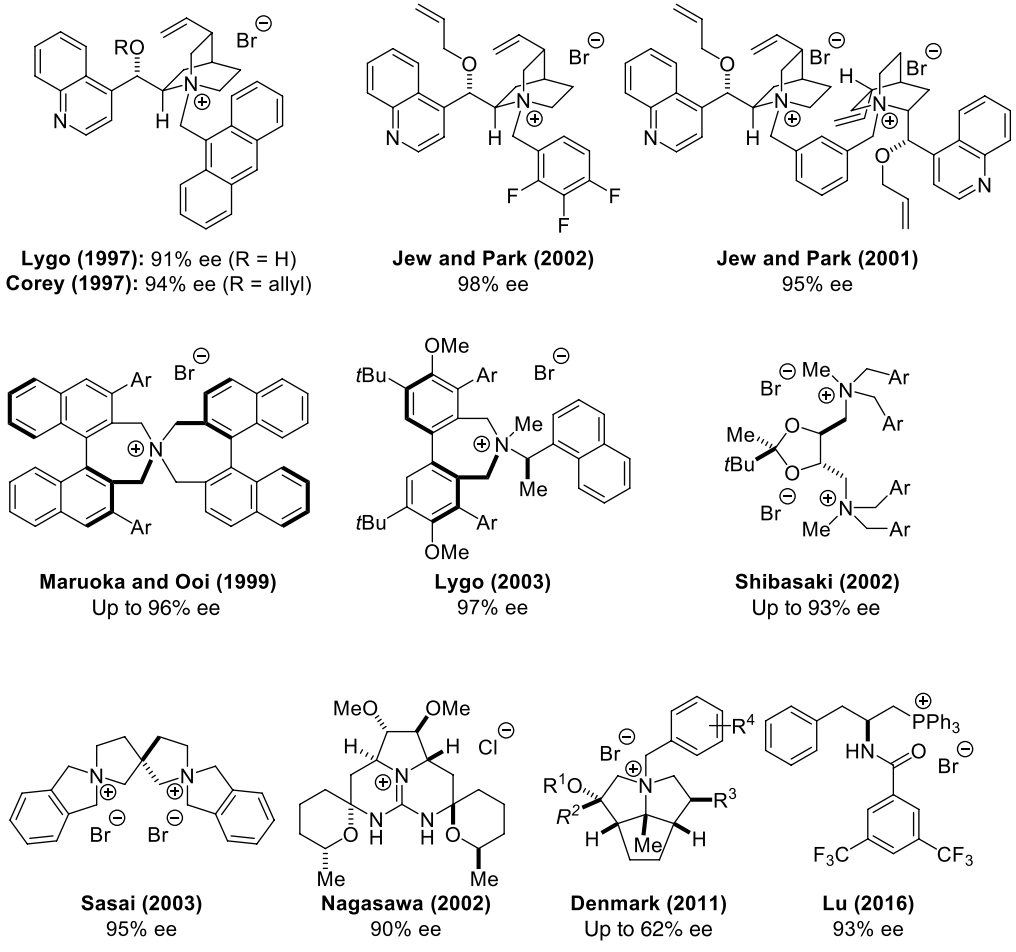

Scheme 4.4. Catalyst development for the enantioselective mono-alkylation of glycine imines.

significant impact on enantioselectivity. In 1997, Lygo [4–6] and Corey [7, 8] independently reported the use of an anthracene-substituted cinchoninium catalyst for the benzylation of glycine imines to achieve higher enantioselectivity (91–94% ee). Jew and Park later disclosed a 2,3,4-trifluorobenzyl substituted cinchoninium catalyst, which further improved enantioselectivity (98% ee) [9]. A dicationic, tethered bis-cinchoninium catalyst was also reported by the same authors as an efficient benzylation catalyst (95% ee) [10, 11].

Concurrently, efforts by a number of groups aimed to explore catalyst architectures that significantly differed from cinchoninium alkaloids. In 1999, Maruoka reported the use of C_2-symmetric chiral ammonium salts derived from binaphthyl backbones [12]. High enantioselectivity (up to 96% ee) was achieved with this family of catalysts and marked the first departure from previously reported cinchoninium catalysts. Later, the same group reported a related catalyst wherein one chiral binaphthyl group is replaced by a more flexible achiral biphenyl group, which also achieved high enantioselectivity (94% ee) [13]. Building on this, Lygo reported in 2003 a structurally distinct chiral ammonium catalyst based on a simple biphenyl backbone, where the chiral element originates from a chiral benzylic amine [14]. Due to the scaffold's modular synthesis and ease of diversification, a small library of ammonium catalysts was synthesized and benchmarked against the enantioselective benzylation of glycine imine. The optimal catalyst featured an α-methylnathphtylamine group and proved to be highly enantioselective (97% ee). In 2002, Shibasaki reported a tartrate-derived bis-ammonium catalyst that proved to be highly enantioselective for the same reaction (93% ee) [15–17]. The hypothesis was that the tert-butyl glycinate anion would preferentially orient itself between both ammonium centers, leading to enantiotopic face discrimination. Monte Carlo molecular mechanics simulations were consistent with this substrate-catalyst binding mode. In 2003, Sasai reported another dicationic bis-ammonium catalyst based on a spirocyclic bis-pyrrolidinium scaffold, which also proved to be highly enantioselective in the same reaction (95% ee) [18]. In 2002, Nagasawa reported pentacyclic guanidine salts as efficient catalysts for the same reaction (90% ee) [19]. Hydrogen bonding interactions with the glycinate anion are proposed, which allow for high levels of enantioinduction. In 2011, Denmark disclosed a family of tricyclic ammonium catalysts that proved to be moderately enantioselective (up to 62% ee) [20]. Most recently in 2016, Lu reported that quaternary phosphonium salts derived from amino acids were highly efficient catalysts for the benzylation of glycine imines (93% ee) [21].

The use of benzophenone-derived imines in the enantioselective phase-transfer catalyzed alkylation reactions described above allowed for exclusive mono-alkylation selectivity over bis-alkylation and avoided product racemization. This is due to the lower C–H acidity (p*K*a~23) of the mono-alkylated benzophenone imine product compared to the nonalkylated starting material (p*K*a~19) [22]. The stark difference in acidity can be rationalized by unfavorable allylic 1,3-strain between the benzophenone imine phenyl group and the α-alkyl substituent, forcing them out of plane and reducing stabilization of the azaallyl anion.

Modification of the benzophenone imine to an aldimine derivative allowed for the formation of α,α-dialkylated products (Scheme 4.5). In 1992, O'Donnell reported the first enantioselective alkylation of α-alkylated amino acid aldimines to from α, α-dialkylated amino acids [23]. Tuning of the catalyst by Lygo et al. [24] and later by Jew and Park [25] allowed improved enantioselectivity for this reaction. Notably, Jew and Park's conditions included more basic RbOH that provided high enantioselectivity (95% ee) for this reaction. Maruoka reported that chiral-bisnaphthyl-derived ammonium catalysts also catalyzed this reaction at impressively low catalyst loadings (as low as 0.05 mol%) while providing very high enantioselectivity (98% ee) [26, 27]. Under similar conditions, Shibasaki reported the use of a tartrate-derived bis-ammonium catalyst that provided high enantioselectivity, however required low temperature (–70 °C) [16].

While α-amino acid imines have arguably been the most explored class of substrates for enantioselective phase-transfer catalysis, enolates derived from ketones, esters, and amides have also successfully been used in such transformations. Furthermore, numbers of different alkyl electrophiles, both activated and unactivated, have been reported in such transformations. These will not be comprehensively discussed in this chapter, but can be found in more detailed reviews on the subject [28]. Overall, successful implementation of enantioselective phase-transfer catalysis for enolate alkylation hinges on controlling mono-alkylation and bis-alkylation, while avoiding product racemization.

Beyond enantioselective enolate C-alkylations described previously, selective O-alkylation can also be achieved via chiral phase-transfer catalysis (Scheme 4.6). In 2017, Smith described a strategy to access

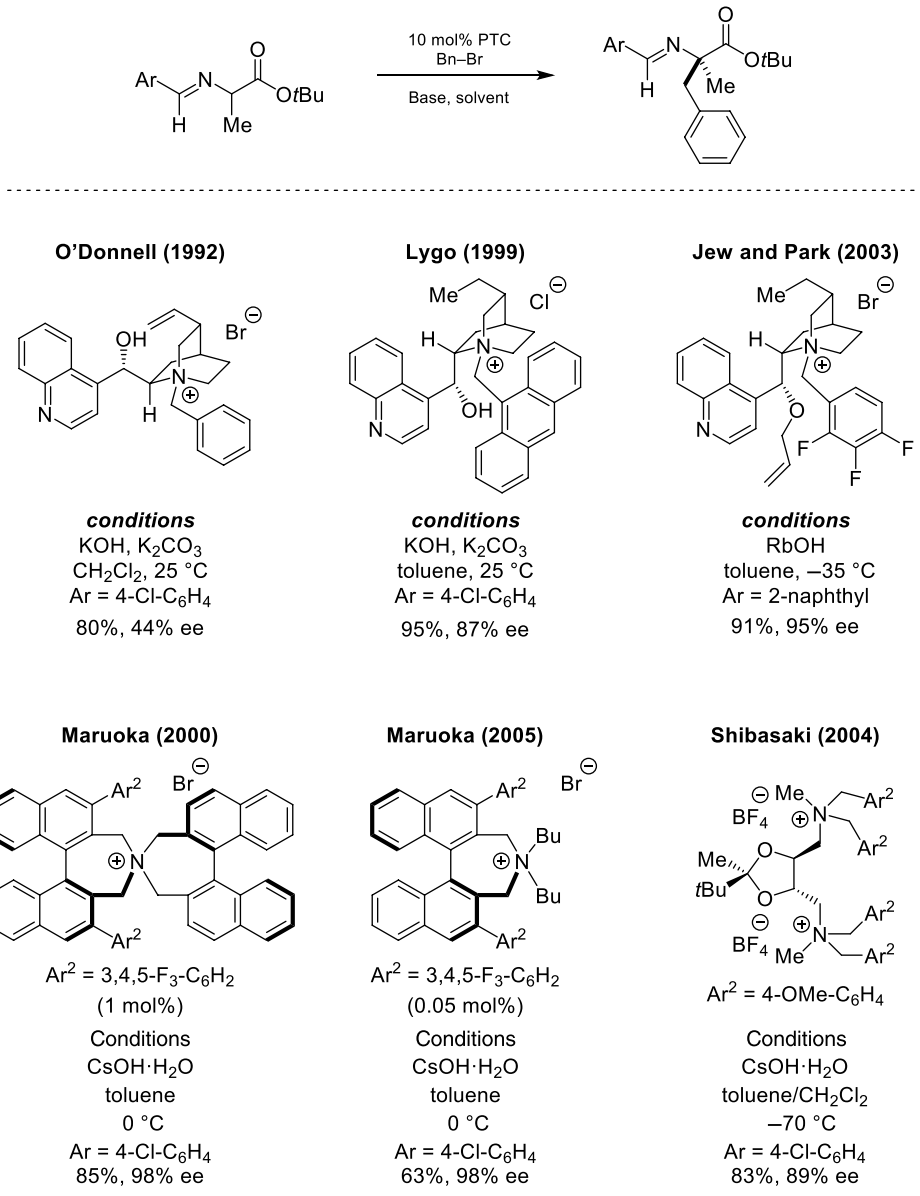

Scheme 4.5. Catalyst development for the enantioselective synthesis **α**,**α**-dialkylated glycine imines.

unsymmetrical 1,1′-bi-2-naphthol (BINOL) derivatives [29]. A chiral cinchoninium catalyst was found to promote the highly atropselective enolate O-alkylation of tetralone derivatives with only traces of C-alkylation observed. Oxidative aromatization with DDQ afforded unsymmetrical BINOL derivatives. An investigation of the mechanism by density-functional theory (DFT) suggests two hydrogen-bonding interactions between the tetralone enolate and the cinchoninium (OH group and benzylic C–H) are involved in the enantiodetermining O-alkylation [30].

4.2.1.2. Addition to Michael Acceptors In the early years of asymmetric cation phase-transfer catalysis, significant focus was dedicated to enantioselective enolate alkylations with alkyl halides. Soon afterward, it was recognized that this strategy had broader potential. Once generated, the enolate/catalyst ion-pair could

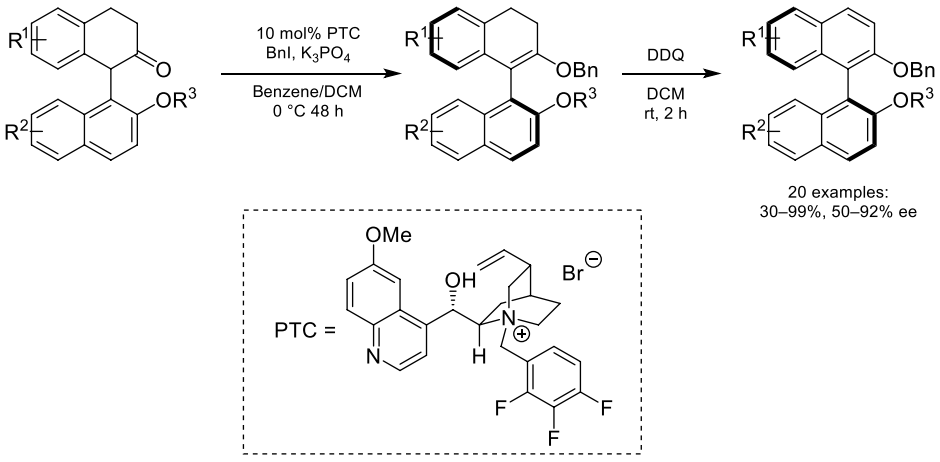

Scheme 4.6. Atropselective enolate O-alkylation.

be matched with a number of other classes of electrophiles, with Michael acceptors being an early example (Scheme 4.7). In 1998, Corey reported the use of an anthracene-functionalized cinchoninium catalyst for the enantioselective addition of a diphenyl glycine ester to acrylates, and later acrylonitrile derivatives [31, 32]. A few years later in 2002, Shibasaki reported the use of a tartrate-derived chiral bis-ammonium catalyst for the same class of reactions [15]. In the same year, Arai and Nishida reported that an N-spirocyclic ammonium catalyst was also a competent catalyst for this reaction, albeit affording moderate enantioselectivity [33]. In recent years, Maruoka reported the use of bifunctional chiral ammonium salts to catalyze the enantioselective addition of nucleophiles to Michael acceptors such as nitroolefins[34–36] and maleimides[37, 38] under neutral conditions. The successful implementation of this base-free phase-transfer strategy hinged on the use of water-rich solvent mixtures proposed to allow formation of the key reactive catalyst-substrate ion-pair. This strategy was later extended for successful asymmetric aldol, chlorination, and sulfenylation reactions [39, 40].

The asymmetric oxidation of α,β-unsaturated carbonyl compounds using phase-transfer catalysis was also extensively studied in the early years of the field as new chiral cationic catalysts were being developed. In 1998, Shioiri and Arai reported the epoxidation of chalcone using aqueous hydroperoxide as the oxidant and a chiral cinchoninium catalyst (Scheme 4.8) [41, 42]. Later, Jew and Park reported that a tethered bis-cinchoninium catalyst could catalyze the same reaction to provide the corresponding epoxide with excellent enantioselectivity [43]. Interestingly, the use and optimization of a surfactant (Span 20) improved both the rate of the reaction and the enantioselectivity, presumably due to increased surface area between the organic and aqueous phases or the formation of micelles. Finally, a chiral cationic aza-crown ether catalyst was shown to promote the same reaction with moderate enantioselectivity [44]. A number of other groups also reported the phase-transfer catalyzed epoxidation of chalcones and related compounds, using alternative oxidants such as hypochlorite salts [45–47].

A related phase-transfer strategy was also used for the enantioselective aziridination of α,β-unsaturated carbonyl compounds, using N-acyl hydroxylamines as the "nitrene equivalent" source. Aires-de-Sousa first reported the aziridination of acrylate derivatives using first-generation chiral cinchoninium catalysts (Scheme 4.9) [48]. This reaction proceeds via the intramolecular rearrangement of the N-acylhydroxylamine anion to an O-acylhydroxylamine anion under basic conditions. Conjugate addition of the ion-paired catalyst/N-acylhydroxylamine to the acrylate electrophile is followed by intramolecular cyclization and liberation of pivalate. Later work by Murugan and Siva demonstrated the use of modified chiral cinchoninium catalysts for the highly enantioselective aziridination of acrylates [49]. Specifically, tosylation of the free alcohol in the ammonium catalyst provided high levels of enantioinduction.

Building on these studies using phase-transfer catalysis to achieve 1,4-conjugate additions with O- and N-based nucleophiles, hydrazide derivatives were later shown to be suitable nucleophiles. In 2010,

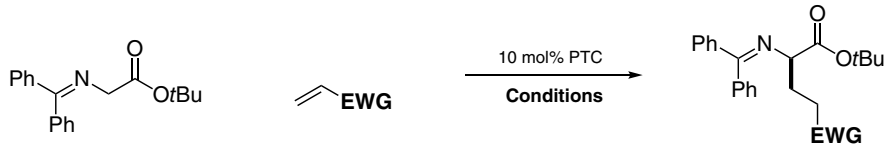

PTC =

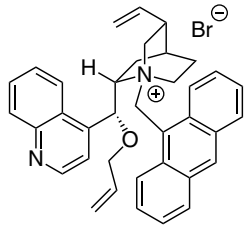

Corey (1998)

EWG = CO_2Me

Conditions
$CsOH{\cdot}H_2O$
CH_2Cl_2, –78 °C
85%, 95% ee

Corey (2000)

EWG = CN

Conditions
50% aq. KOH
CH_2Cl_2, –55 °C
Ar = 4-Cl-C_6H_4
85%, 91% ee

Shibasaki (2002)

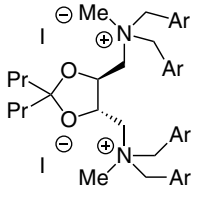

EWG = CO_2Et

Conditions
Cs_2CO_3
PhCl, –30 °C
88%, 82% ee

Ar = 4-Me-C_6H_4

Arai and Nishida (2002)

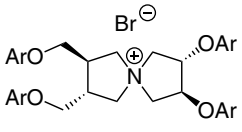

Ar = 4-CF_3-C_6H_4

EWG = CO_2tBu

Conditions
10 mol% $CsOH{\cdot}H_2O$
MTBE, –60 °C
73%, 77% ee

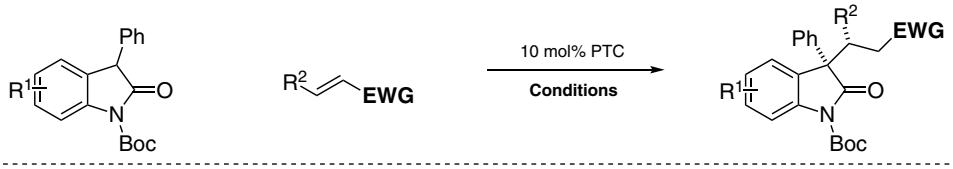

Maruoka (2009)

PTC =

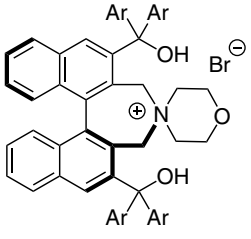

Ar = 3,5-$(CF_3)_2$-C_6H_3

EWG = NO_2

Conditions
1 mol% PTC
10 : 1 H_2O/toluene
0 °C, 2 h

9 examples:
34–99%, 55 : 45–95 : 5 d.r.
20–99% ee

Shirakawa (2017)

PTC =

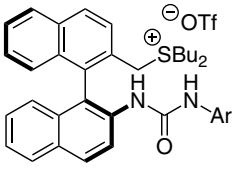

Ar = 4-NO_2-C_6H_4

Electrophile =

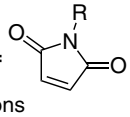

Conditions
5 mol% PTC
10 : 1 H_2O/toluene
25 °C, 24 h

16 examples:
17–85%, 83 : 17–96 : 4 d.r.
83–93% ee

Scheme 4.7. Enantioselective addition of glycine imines to Michael acceptors.

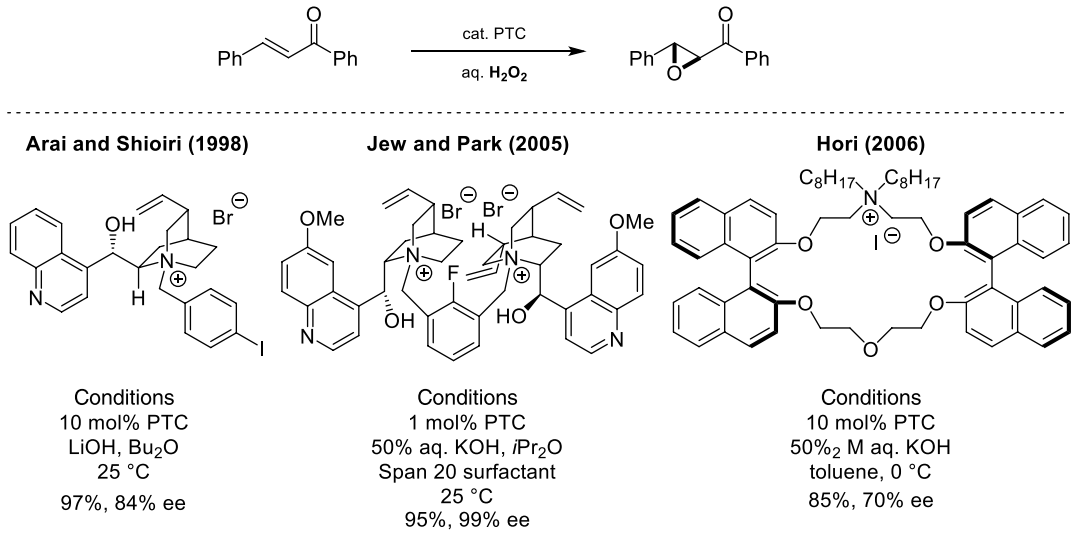

Scheme 4.8. Enantioselective epoxidation of chalcones.

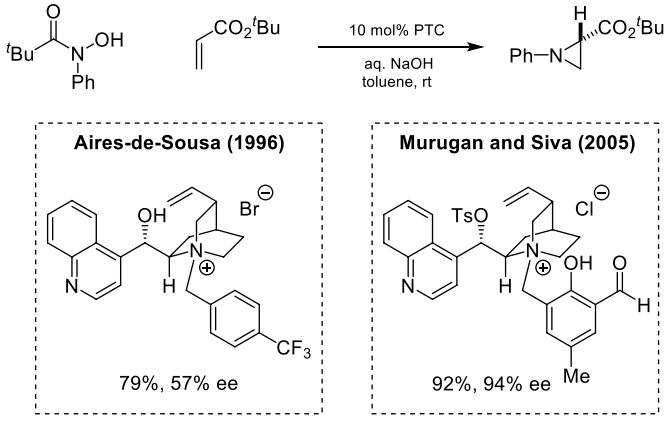

Scheme 4.9. Enantioselective aziridination of α,β-unsaturated esters.

Brière demonstrated the use of a chiral cinchoninium catalyst for the enantioselective synthesis of pyrazolines (Scheme 4.10) [50]. Ion-pairing of a hydrazide anion with the chiral ammonium catalyst allowed the enantioselective aza-Michael addition with chalcones, followed by cyclocondensation to afford the pyrazoline product.

4.2.1.3. Addition to Carbonyls and Imines Compared to alkylation reactions, phase-transfer catalyzed aldol reactions have been comparatively underexplored. In 1991, Miller reported the aldol reaction of diphenyl glycine imine nucleophiles and various aldehydes with chiral cinchoninium-based catalysts (Scheme 4.11) [51]. Unfortunately, these reactions suffered from very low enantioselectivity (3–12% ee). Over the years, improvements using cinchoninium-based catalysts have been reported for related aldol reactions, but still suffered from moderate enantioselectivity (up to 83% ee) [52]. In 2002, Maruoka reported a highly enantioselective phase-transfer catalyzed aldol reaction using chiral N-spiro ammonium catalysts (up to 98% ee) [53, 54]. Mechanistic studies revealed competitive retro-aldol reactions were occurring under first-generation conditions, but this was solved with the use of dilute and catalytic sodium hydroxide and ammonium chloride.

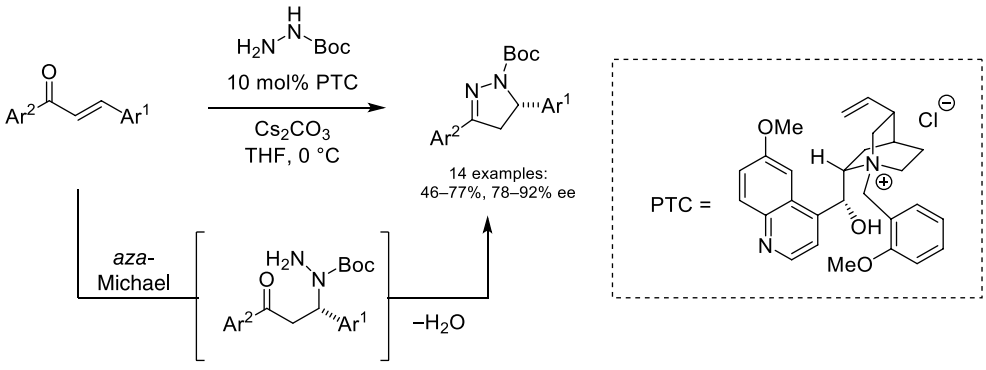

Scheme 4.10. Enantioselective aza-Michael addition of hydrazides to chalcones for the synthesis of pyrazolines.

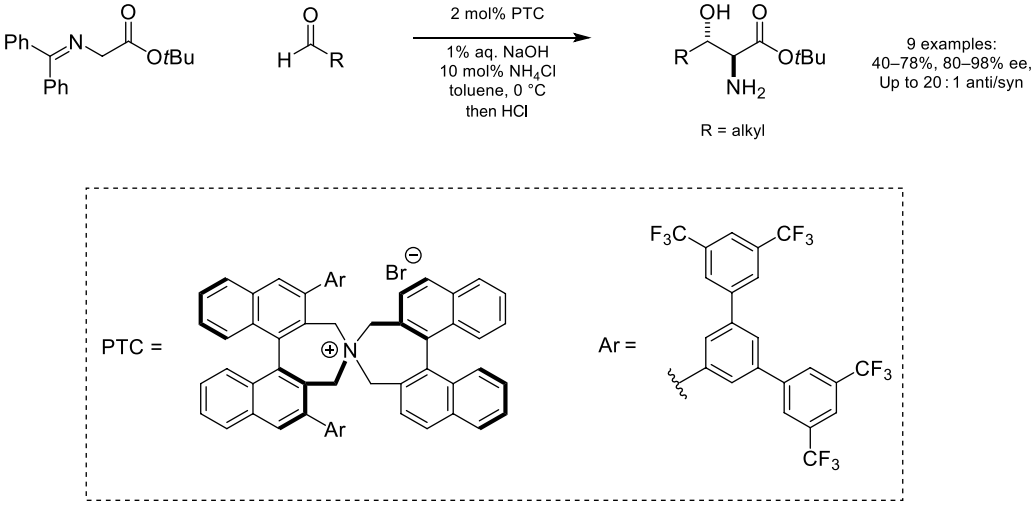

Scheme 4.11. Enantioselective aldol reaction using glycine imines. Source: Based on [51].

The same family of chiral N-spiro ammonium salts was later reported by Maruoka in 2004 as selective phase-transfer catalysts for the related Mannich reaction of a diphenyl glycine ester with a N-PMP protected α-imino-ester (Scheme 4.12) [55]. A year later, Oshima and Shibasaki reported the use of a tartrate-derived chiral bis-ammonium catalyst as an efficient catalyst for the Mannich reactions using Boc-protected aldimines [56].

Asymmetric phase-transfer catalysis has also been exploited successfully for a number of other reactions involving the addition of an enolate to a carbonyl or imine electrophile. For example, the addition of α-halo carbonyl compounds to aldehydes or ketones (Darzens reaction) to yield epoxides was first achieved using chiral phase-transfer catalysis in 1998 by Arai and Shioiri and has since been further developed [57, 58]. Another example is the addition of cyanide nucleophiles to imine derivatives (Strecker reaction) leading to chiral α-amino nitriles, which has been extensively studied; the first highly enantioselective phase-transfer catalyzed version of this reaction was reported by Maruoka in 2006 [59, 60].

4.2.1.4. Arylation In 2005, Jørgensen reported the first enantioselective S_NAr arylation of enolates using chiral phase-transfer catalysis (Scheme 4.13) [61, 62]. β-ketoesters could be arylated with activated aryl fluorides using a cinchoninium-based catalyst. Notably, quaternary carbon centers were formed obviating the potential issue of product racemization.

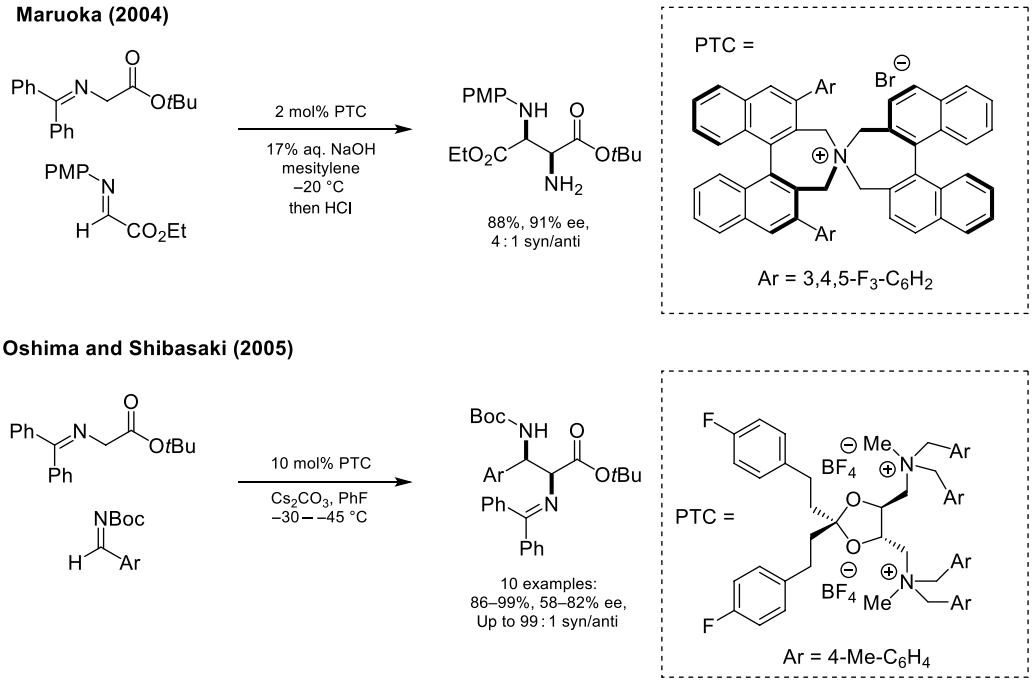

Scheme 4.12. Enantioselective Mannich reaction using glycine imines.

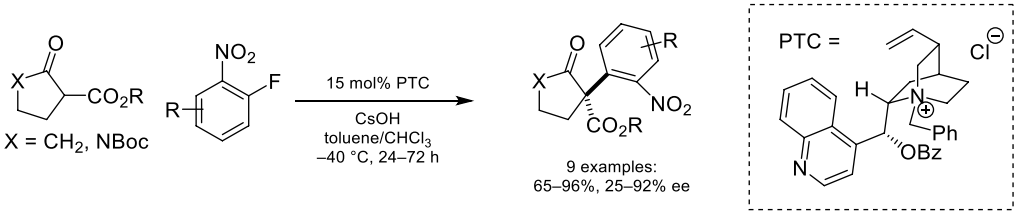

Scheme 4.13. Enantioselective arylation of 1,3-dicarbonyl nucleophiles via nucleophilic aromatic substitution. Source: [61, 62].

In 2014, Maruoka used a similar S_NAr PTC strategy to achieve the enantioselective arylation of glycine imine derivatives (Scheme 4.14) [63]. Here, a chiral ammonium catalyst with a biaryl backbone proved to be optimal. This chemistry was further expanded to use electron neutral and electron-rich aryl electrophiles, activated as $Cr(CO)_3$ complexes [64]. Use of a chiral binaphthyl-derived ammonium catalyst proved to be optimal in this case.

In a further extension of this work, the arylation of oxindoles with activated aryl fluorides was accomplished using a binaphthyl-derived chiral phosphonium catalyst (Scheme 4.15) [65].

In recent years, the atropselective synthesis of biaryl motifs using chiral phase-transfer catalysis has garnered increased attention. In 2014, Smith disclosed the first atropselective S_NAr reaction using a dichloropyrimidine electrophile and a thiophenol nucleophile, wherein restricted rotation around the biaryl linkage in the product gives rise to atropisomers (Scheme 4.16) [66]. Moderate to high enantioselectivity is observed using a first-generation chiral cinchoninium catalyst. Building on this work using the same cinchoninium catalyst and related S_NAr strategy, Gustafson later reported in 2018 the kinetic resolution of pyrolopyrimidines [67].

In 2017, Cai reported a chiral phase-transfer catalyzed atropselective macrocyclization strategy to access (–)-pterocarine and (–)-galeon (Scheme 4.17) [68]. A chiral cinchoninium catalyst was found to

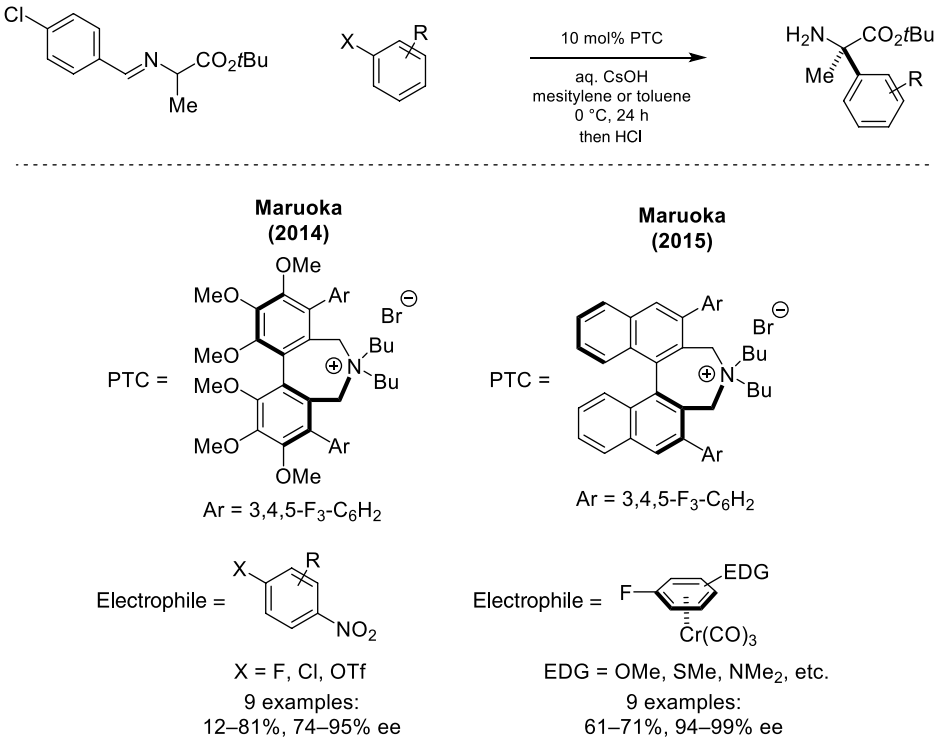

Scheme 4.14. Enantioselective arylation of mono-alkylated glycine imines via nucleophilic aromatic substitution.

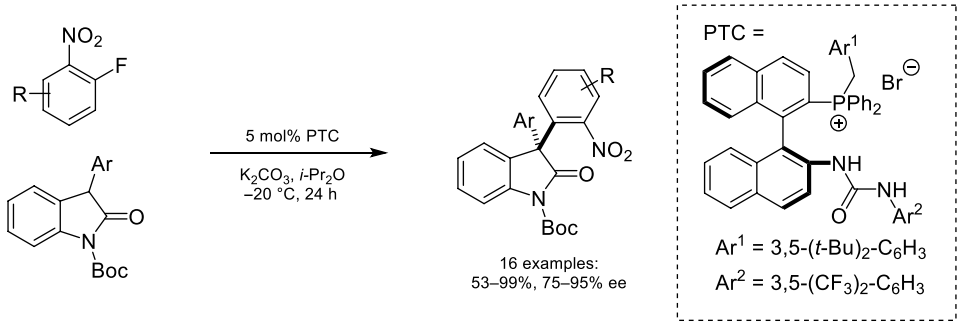

Scheme 4.15. Enantioselective arylation of oxindoles via nucleophilic aromatic substitution. Source: Based on [65].

catalyze the intramolecular S_NAr reaction of a phenol with an activated aryl fluoride to obtain the desired macrocyclic product with moderate to good enantioselectivity.

4.2.1.5. Carbon-Heteroatom (C-X) Bond Formation The importance of enantioselective carbon-heteroatom bond-forming reactions cannot be overstated seeing as C–X (X = halogen, O, N, etc.) bonds are ubiquitous in pharmaceuticals and agrochemicals. Over the years, phase-transfer catalysis has proven to be a privileged strategy to achieve these transformations. Among the most important factors for the successful implementation of such strategies is the development and use of suitable electrophilic heteroatom transfer reagents.

The strategic incorporation of a fluorine atom in drug discovery can directly impact a molecule's lipophilicity, modulate the acidity/basicity of neighboring functional groups, and improve potency [69].

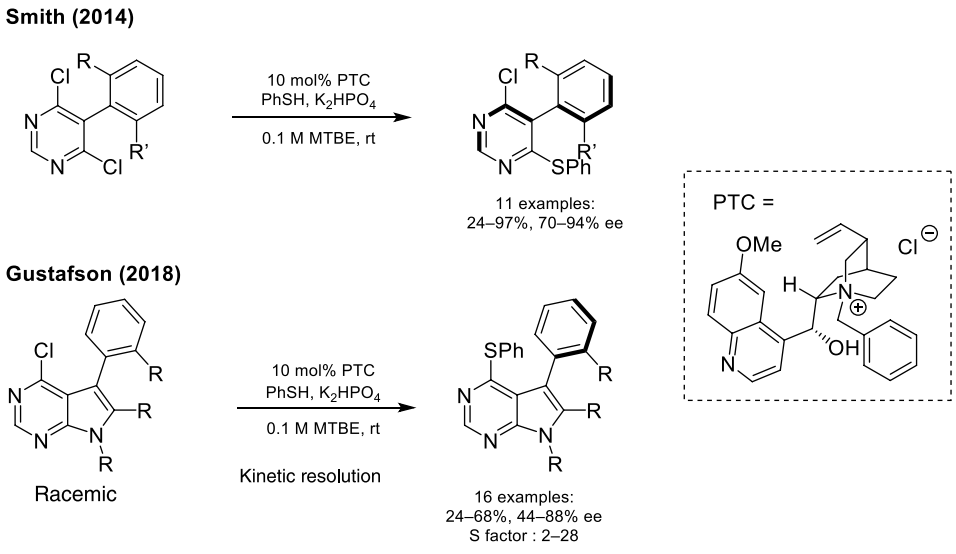

Scheme 4.16. Atropselective synthesis of biaryl motifs via nucleophilic aromatic substitution.

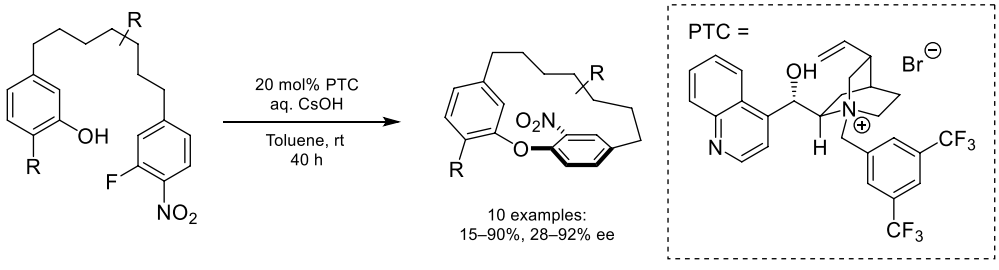

Scheme 4.17. Atropselective macrocyclization via nucleophilic aromatic substitution. Source: Based on [68].

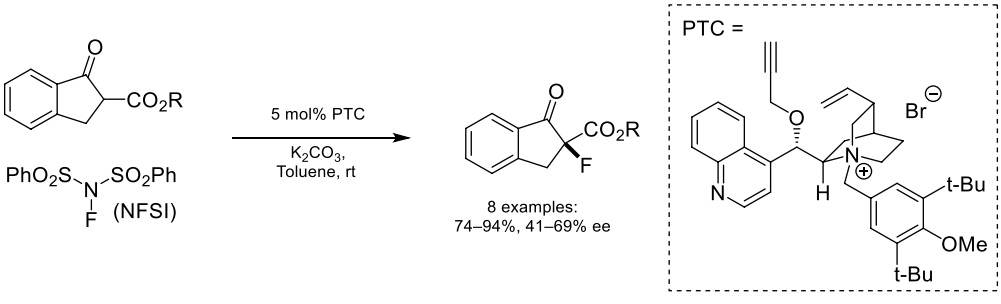

Scheme 4.18. Enantioselective α-fluorination of β-ketoesters. Source: Based on [71].

Asymmetric fluorination reactions have therefore garnered significant attention from the synthetic community over the last 20 years [70]. In 2002, Kim reported the first example of enantioselective α-fluorination of β-ketoesters using phase-transfer catalysis (Scheme 4.18) [71]. A chiral cinchoninium catalyst was found to promote this reaction with moderate enantioselectivity using NFSI as the electrophilic fluorine source.

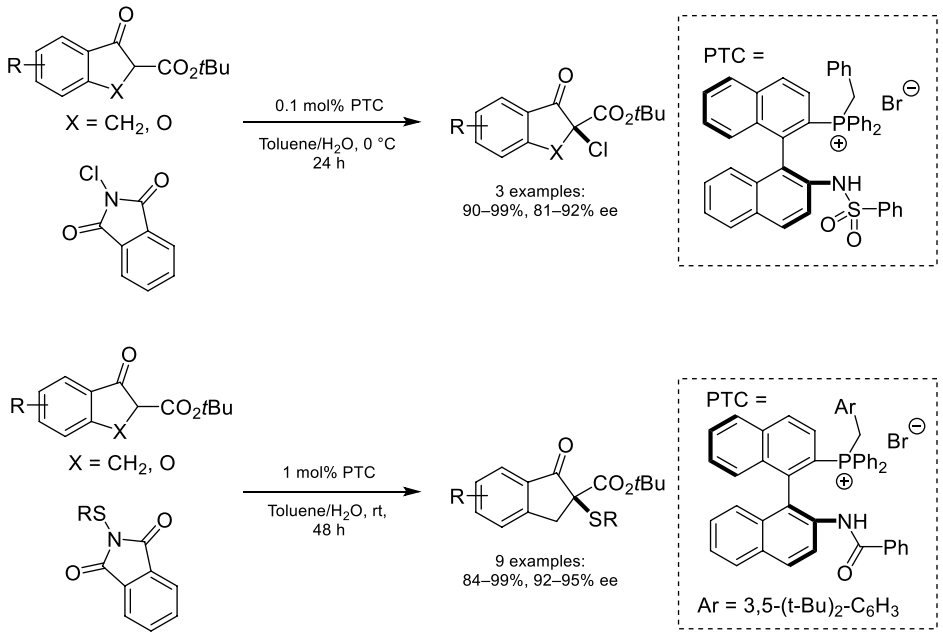

Scheme 4.19. Enantioselective α-chlorination and α-sulfenylation of 1,3-dicarbonyl nucleophiles. Source: Based on [72].

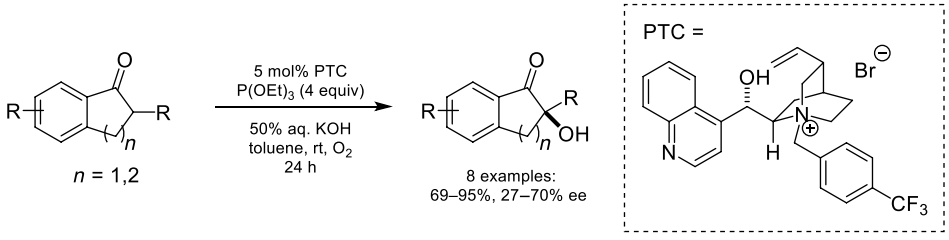

Scheme 4.20. Enantioselective α-hydroxylation of indanones. Source: Based on [73].

The α-chlorination of enolates has also been reported using phase-transfer catalysis, despite attracting less attention than α-fluorination. In 2013, Maruoka reported the first α-chlorination of β-ketoesters using N-chlorophthalimide and a chiral phosphonium-based catalyst (Scheme 4.19) [72]. Incorporation of a sulfonamide group on the binaphthyl backbone of the catalyst proved to be optimal. Interestingly, modification of the sulfonamide for a benzamide on the catalyst allowed the analogous α-sulfenylation to proceed in high enantioselectivity using N-(arylthiol)phthalimides as the electrophilic sulfenylation reagent.

The first example of enantioselective enolate α-oxygenation was reported in 1988 by Shioiri (Scheme 4.20) [73]. A chiral cinchoninium catalyst was found to promote the α-oxygenation of indanones with moderate enantioselectivity from an in situ generated electrophilic hydroperoxide formed from triethylphosphite and molecular oxygen.

In 2008, 20 years after the seminal report by Shiori, Itoh disclosed a related system that proved to be highly enantioselective using an anthracene-functionalized chiral cinchoninium catalyst (Scheme 4.21) [74]. In the years following these reports, numbers of related systems have been reported using other electrophilic oxygenating reagents such as hydroperoxides or oxaziridines [75].

In 2008, Maruoka reported the first example of phase-transfer catalyzed α-amination of enolate derivatives. Specifically, β-ketoesters could be aminated in high enantioselectivity using diazocarboxylates as electrophilic aminating reagents and a chiral tetraalkylphosphonium catalyst (Scheme 4.22) [76]. Notably, this was a pioneering example of the use of a chiral tetraalkylammonium catalyst in phase-transfer

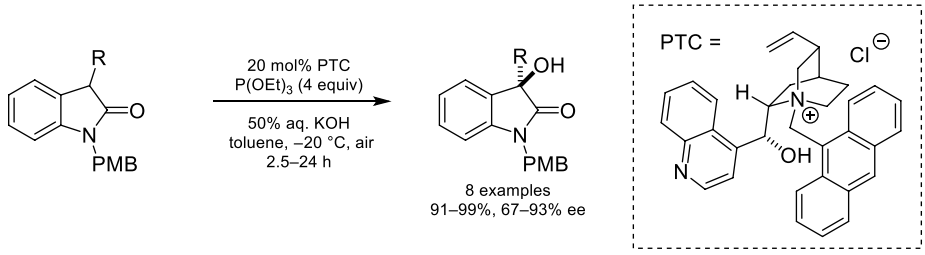

Scheme 4.21. Enantioselective α-hydroxylation of oxindoles. Source: Based on [74].

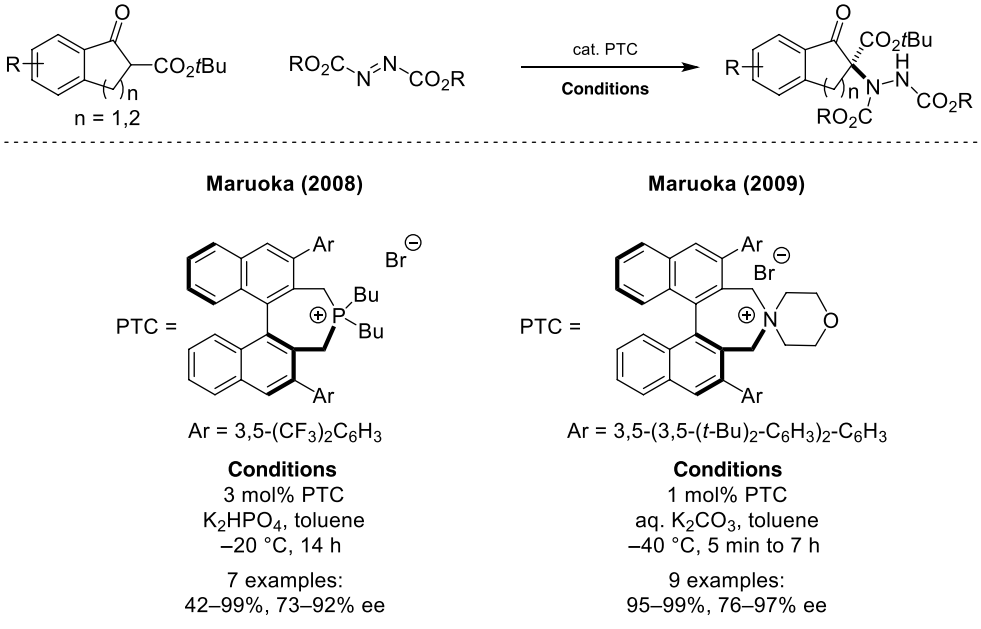

Scheme 4.22. Enantioselective α-amination of β-ketoesters using azodicarboxylates.

catalysis. The same group disclosed a year later that a more selective spirocyclic chiral ammonium catalyst could also promote this reaction at lower catalyst loadings [77]. A similar strategy was disclosed in 2011 by Ma [78] and later in 2019 by Maruoka [79] for the enantioselective amination of oxindoles and benzofuranones (Scheme 4.23). Ma's system used a quaternary phosphonium catalyst and Maruoka's system used a spirocyclic ammonium catalyst, both featuring chiral C2-symetric binaphthyl backbones.

While diazocarboxylates proved to be suitable electrophilic amination reagents for phase-transfer-catalyzed enolate α-amination to form hydrazine derivatives, subsequent reductive N–N bond cleavage is required to unmask the free amine. In 2016, Ooi disclosed an elegant system wherein direct amination is achieved using an electrophilic aminating reagent formed in situ from the corresponding hydroxylamine and trichloroacetonitrile (Scheme 4.24) [80]. Notably, a triazolium-based chiral phase-transfer catalyst was optimal, providing α-aminated oxindoles with high enantioselectivity.

4.2.2. Transition-Metal/Chiral Cation Dual Catalysis

Asymmetric transition-metal catalysis has traditionally relied on the use of chiral ancillary ligands to modulate the metal's primary coordination sphere to directly influence enantioselectivity. In recent years, a distinct strategy has emerged wherein ion-pairing interactions at a metal's secondary coordination

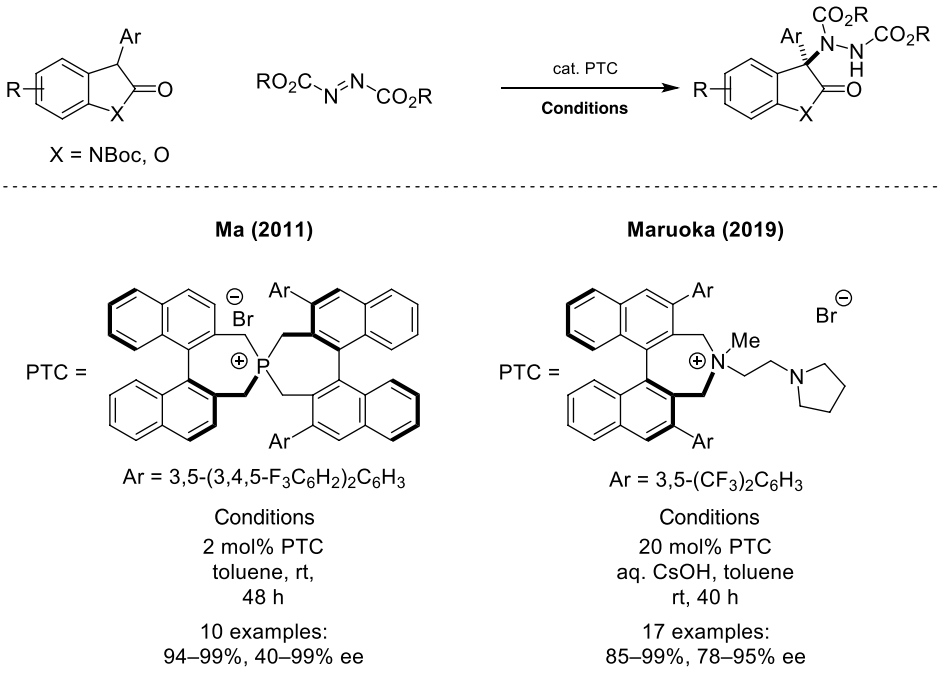

Scheme 4.23. Enantioselective α-amination of oxindoles and lactones using azodicarboxylates.

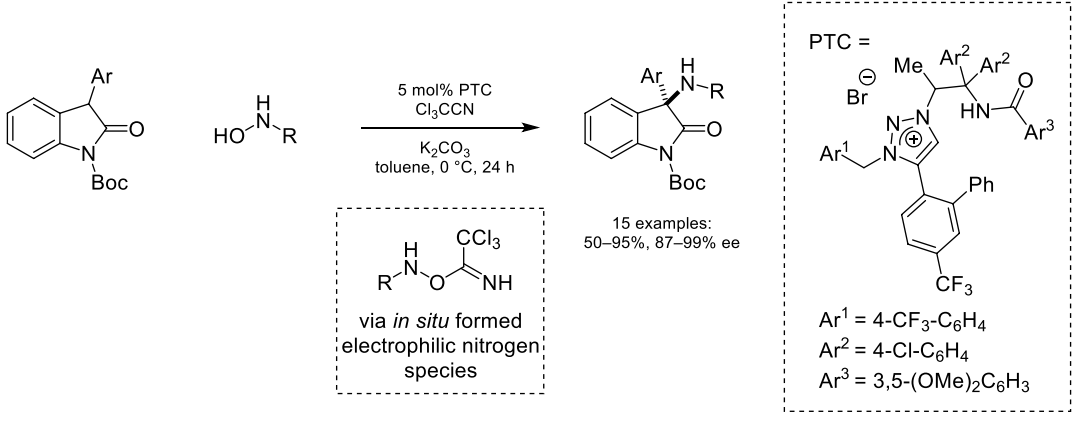

Scheme 4.24. Enantioselective α-amination of oxindoles using hydroxylamines. Source: Based on [80].

sphere can influence enantioselectivity. Given that cationic metal complexes are more common than their anionic counterparts in catalysis, implementation of this strategy using chiral-anions has seen more progress and will be discussed in detail in Section **3.6**. Conversely, ion-pairing between a chiral cation and an anionic metal complex has also been reported. In 2016, Tan reported the use of a dinuclear peroxomolybdate anionic oxidant ion-paired to a chiral bisguanidinium dication catalyst for the enantioselective oxidation of various sulfides to the corresponding sulfoxides (Scheme 4.25) [81]. This proposed catalytically relevant ion-pair was isolable and characterized by single-crystal X-ray diffraction. The same year, a related system was reported by the same group using a tungstate catalyst and the identical chiral bisguanidinium catalyst [82]. Prior to this work, chiral cationic catalysts had been reported to ion-pair with anionic metal complexes such as permanganate anions when used stoichiometrically [83, 84].

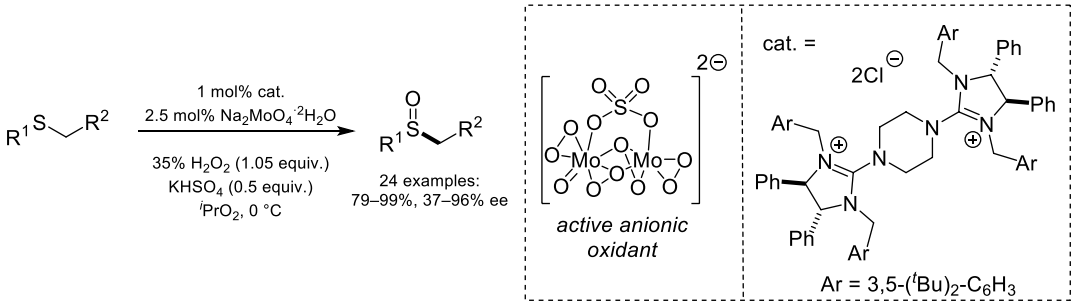

Scheme 4.25. Enantioselective oxidation of sulfides using a peroxomolybdate/chiral cation ion pair catalyst. Source: Based on [81].

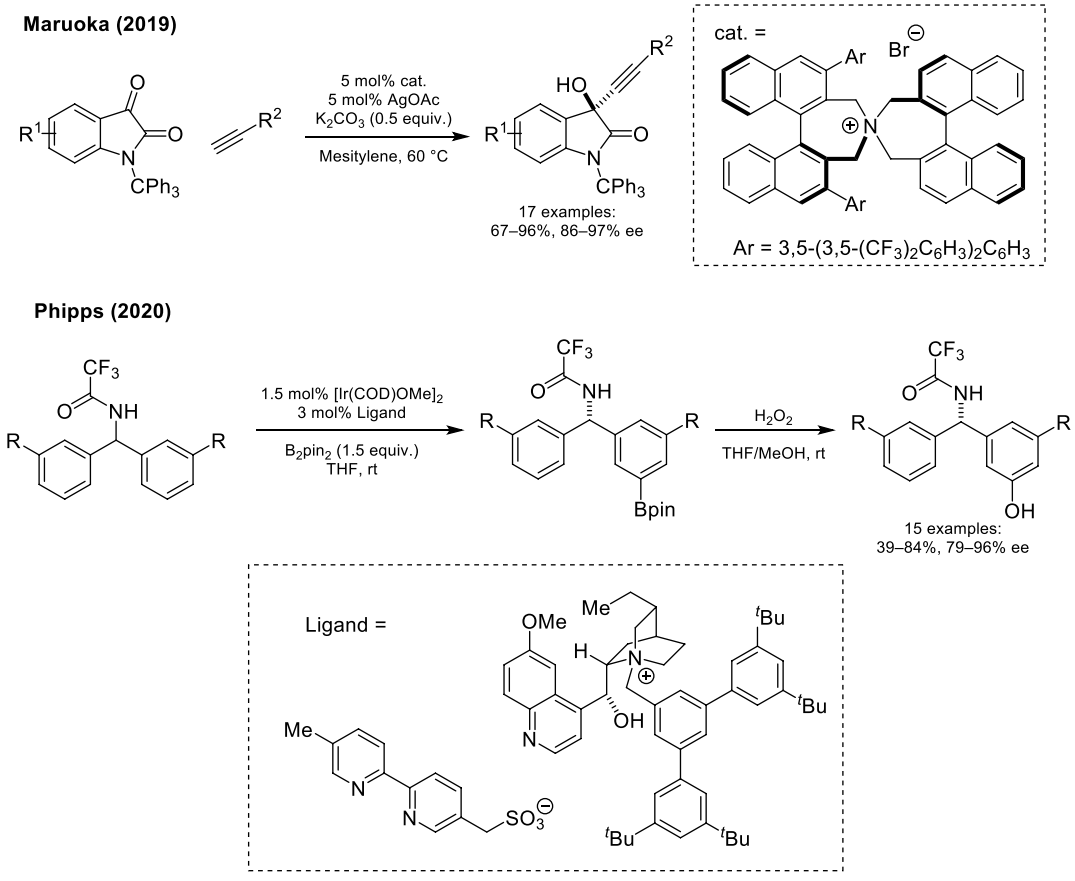

Scheme 4.26. Enantioselective transformations via transition metal/chiral cation ion pairing catalysis.

The asymmetric addition of alkynyl nucleophiles to carbonyl-containing compounds represents a powerful approach to form chiral propargyl alcohols. In 2019, Maruoka demonstrated that a chiral ammonium catalyst could ion-pair with a catalytically generated Ag-alkynylide for the enantioselective addition to isatin derivatives (Scheme 4.26) [85]. While chiral ion-pairing and phase-transfer catalyses have typically involved ion-pairing with an enolate nucleophile, this represents a unique example where an alternative carbon-based nucleophile can be productively used via the use of a transition-metal co-catalyst. In 2020,

the Phipps group disclosed an elegant system for the desymmetrization of geminal diaryl derivatives via enantioselective Ir-catalyzed C–H borylation [86]. The key ion-pairing between a strategically placed sulfonate group on the bipyridine ligand backbone and a chiral cinchoninium cation enables the enantioselective meta-selective borylation of prochiral diaryl substrates. This work is particularly significant as it represents a rare example of remote asymmetric induction, where the site of the newly formed C–B bond is far from the newly formed chiral center. Looking forward, the strategy of incorporating chiral ion-pairing interactions in ligand design for metal-catalyzed transformations is positioned to have significant impact for the development of new reactions with unique selectivity profiles.

4.2.3. Cation-Binding Catalysis

Since the discovery of the cation-binding properties of cyclic polyethers, there has been a desire to utilize this class of compounds to impart enantioselectivity onto a reaction by utilizing a chiral crown ether. The first example of this concept was demonstrated by Cram in 1981, with the asymmetric Michael addition of a cyclic β-keto ester into methyl vinyl ketone (MVK) with a BINOL-derived 22-crown-6 catalyst (Scheme 4.27) [87]. In this example, a chiral crown ether acts as a phase-transfer catalyst for KO*t*Bu. After deprotonation of the substrate, a potassium-bound crown ether cation is ion-paired with an enolate, allowing for enantioselective addition to methyl vinyl ketone (MVK).

Since the initial report by Cram, focus in the field of cation-binding catalysis shifted to utilizing crown ether catalysts derived from carbohydrates. In 1989, a highly symmetric polyether catalyst was reported that catalyzed an asymmetric Michael addition of methyl phenyl acetate to methyl acrylate in high yield and moderate enantioselectivity (Scheme 4.28) [88]. In 1997, the Bakó group reported that an aza-crown ether catalyst derived from D-glucose catalyzed a nitro-Michael reaction in high enantioselectivity [89]. This catalyst architecture proved to be applicable in various asymmetric phase-transfer settings, such as in glycine imine[90] and aminomethylene phosphonate alkylation[91], as well as asymmetric chalcone epoxidation [92].

In 2009, the Song group demonstrated a novel polyether catalyst based on the BINOL scaffold that competently bound and phase-transferred KF (Scheme 4.29) [93]. This catalyst was effective for the kinetic resolution of silyl-protected alcohols via desilylation [94]. A 2015 follow-up publication revealed that this catalyst architecture was competent for the reverse-reaction, where an alcohol was kinetically resolved by silylation with the catalyst [95]. In early 2016, the Yan group applied this system to kinetic resolution via an E1cB-elimination of β-sulfonyl ketones [96]. Over the next several years, numbers of other kinetic resolutions featuring various leaving groups were shown to be compatible with this strategy, such as poly halogenated ketones[97], and aldols [98].

In addition to initiation with KF, in 2012, an organocatalytic asymmetric Strecker reaction was developed utilizing BINOL-derived crown ether with KCN (Scheme 4.30) [99]. The functionalization of α-amidosulfones proved to be a valuable paradigm, as many compatible anions were demonstrated to perform Mannich reactivity in high yields and selectivities. Notable nucleophiles include fluorooxindoles [100], indoles [101], fluoroketones [102], thiocyanato ketones [103], and phthalimides [104]. In addition to kinetic resolutions, this system was also found to be useful for the synthesis of cyclic compounds from unsaturated ketones, such as with nitrones [105], mercaptoacetaldehyde [106], or intramolecular *exo*-trig cyclizations [107].

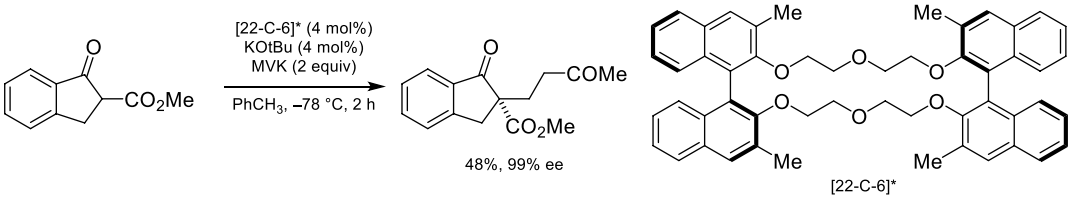

Scheme 4.27. Asymmetric Michael addition via cation binding BINOL-derived ether catalysts. Source: Based on [87].

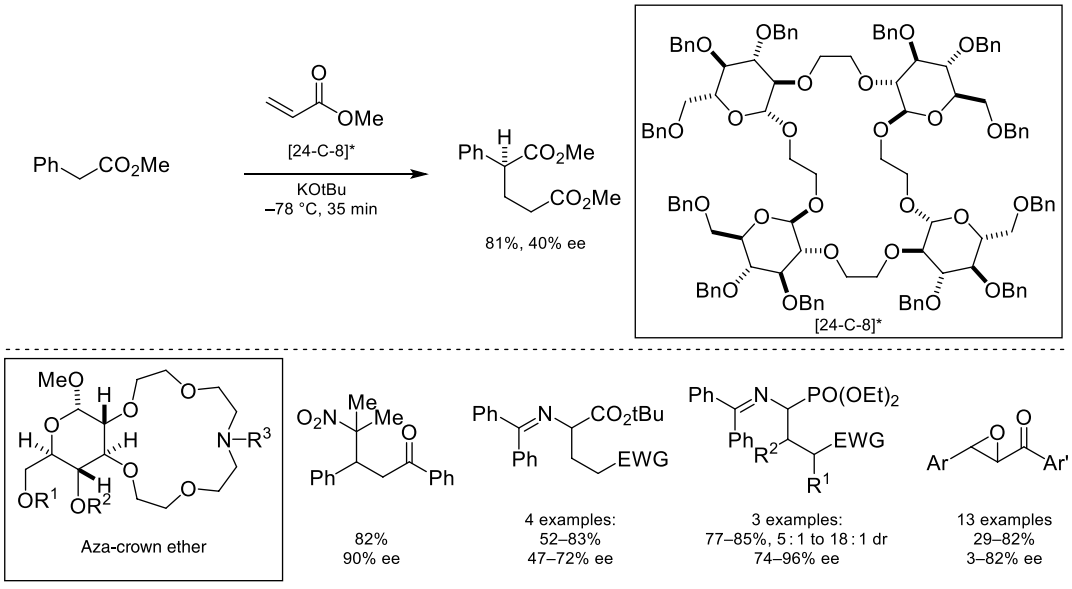

Scheme 4.28. Enantioselective Michael addition via cation binding sugar-derived ether catalysts. Source: Based on [88].

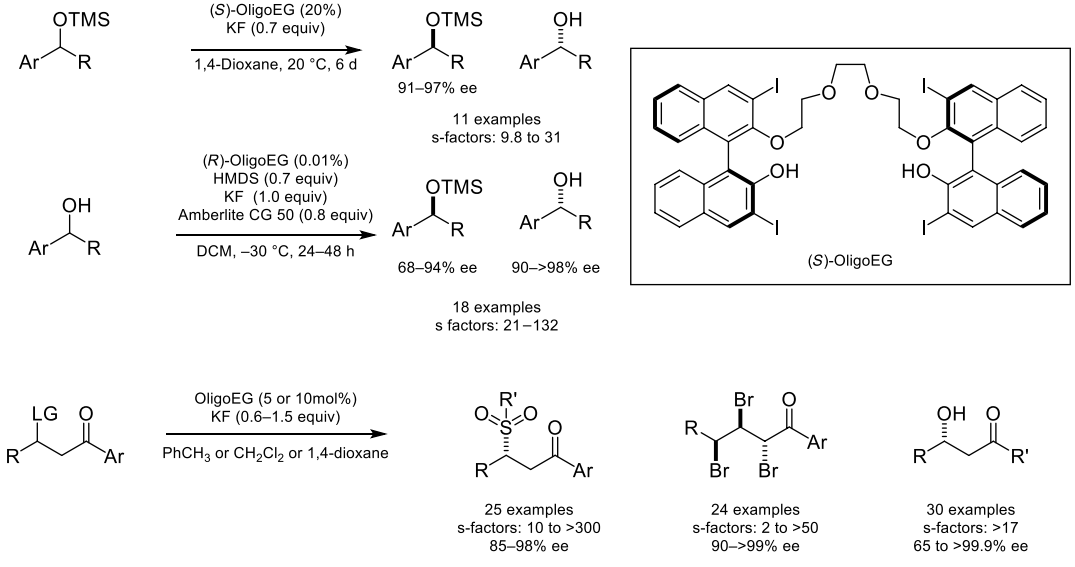

Scheme 4.29. Kinetic resolution of silyl-protected alcohols. Source: Based on [93].

4.3. CHIRAL-ANION

The developments in the field of chiral cation phase-transfer and ion-pairing catalyses have displayed immense advancements for the field of catalysis. Despite the long history of this mode of catalysis, the charged-reversed version, chiral-anion catalysis, has been a significantly more recent development. This mode of activation centers on utilizing chiral-anions to impart enantioselectivity on cationic intermediates and reagents via ion-pairing. One advantage of this strategy is the orthogonal reactivity that can be achieved by focusing on transformations that feature cationic intermediates from relatively unactivated starting materials under mild conditions.

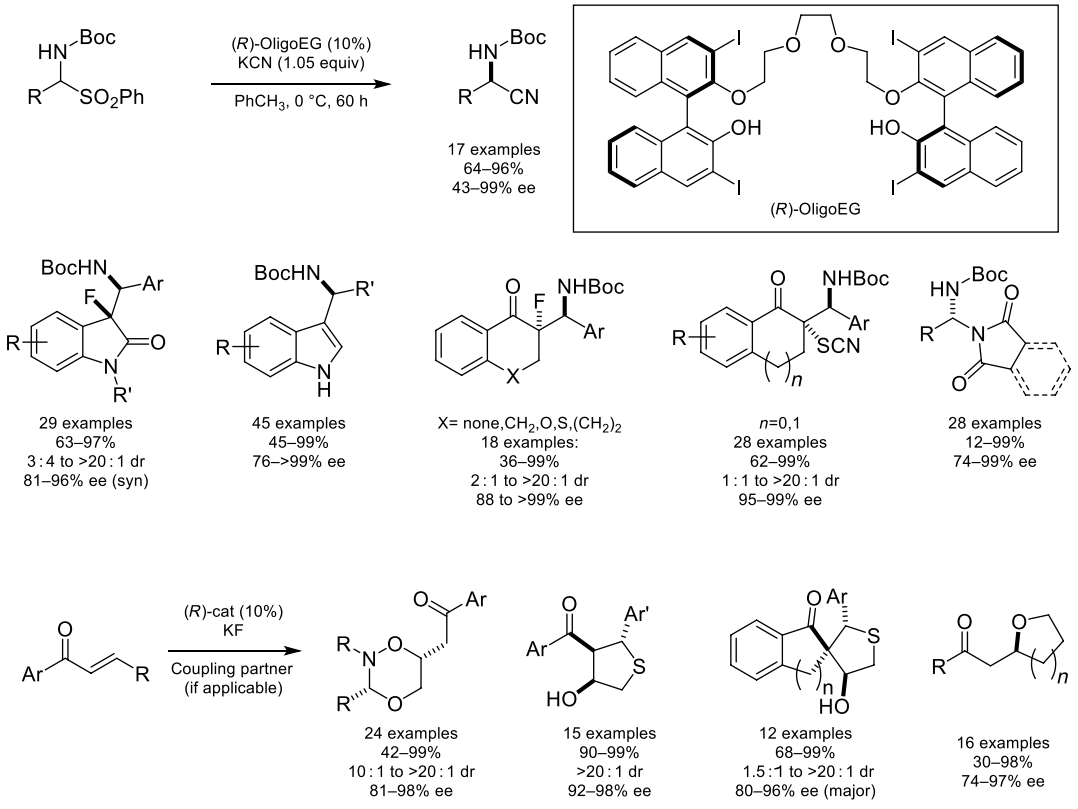

Scheme 4.30. Asymmetric Strecker reaction catalyzed by BINOL-derived crown ether. Source: Based on [99].

4.3.1. Iminium

The first proof of principal example of utilizing ion-pairing catalysis with a chiral-anion was demonstrated by the List group in 2006 (Scheme 4.31) [108]. In this example, an ammonium/chiral phosphate salt would catalyze the enantioselective reduction of enals with Hantzsch ester. The key intermediate for imparting enantioselectivity is the iminium formed from condensation of the achiral ammonium and the enal, which remains ion-paired with a (R)-TRIP counteranion. This ion-pair leads to preferential reduction of one face of the alkene by Hantzsch ester, leading to β-chiral ketones in high yields and enantioselectivities. Following this, the List group utilized this key intermediate for the epoxidation of di- and tetrasubstituted enals by using *t*-butyl hydroperoxide [109]. It was found that the identity of the achiral ammonium had a profound effect on the observed enantioselectivities (24–90% ee), where dibenzylic ammoniums with electron deficient arenes provided the best enantioselectivities. This demonstrates the importance of tuning both components of the ion-pair for cooperatively achieving high selectivities, and is a key feature in many examples of chiral-anion catalysis.

In addition to ammonium/chiral phosphoric acid salts, a variety of catalyst architectures can be utilized for generating iminium intermediates that are amenable to chiral-anion catalysis. In 2013, the Masson group demonstrated that an iminium intermediate could be generated from protonation and subsequent dehydration of γ-hydroxy-γ-lactams by a chiral phosphoric acid (Scheme 4.32) [110]. The resulting iminium intermediate underwent asymmetric C3-arylation with indoles in high yields and enantioselectivities. Other catalysts not based on BINOL phosphoric acids have been demonstrated to be competent for chiral-anion catalysis. Notable examples include a novel conjugate-based stabilized carboxylic acid that catalyzes an enantioselective three-component Povarov reaction[111], and an ammonium/chiral BOROX salt, which activates aldehydes toward an asymmetric three-component Ugi reaction [112].

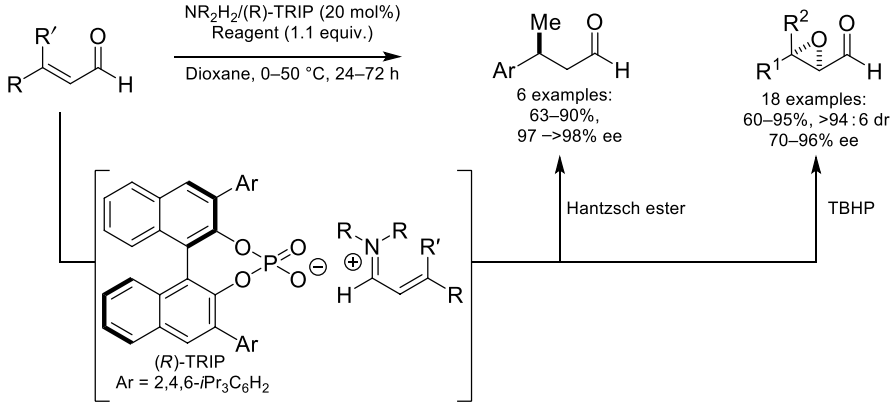

Scheme 4.31. First example of asymmetric counteranion-directed catalysis. Source: Based on [108].

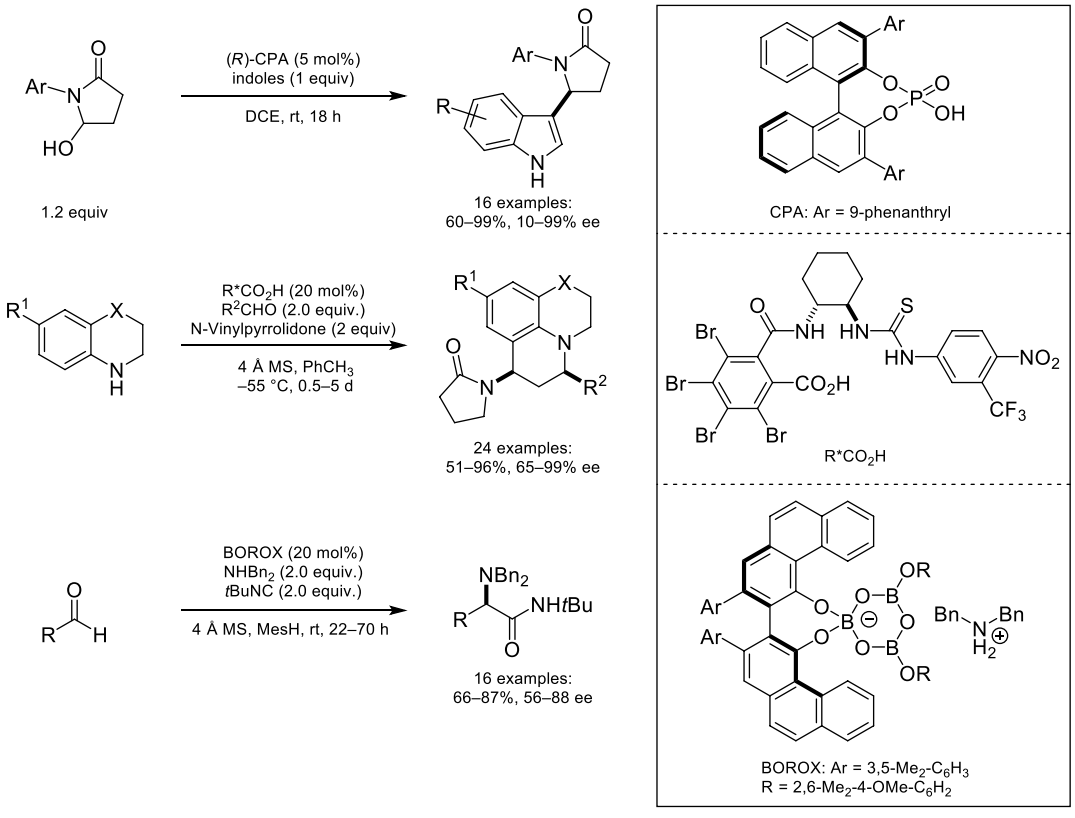

Scheme 4.32. Asymmetric counteranion-directed catalysis involving iminium ion intermediates. Source: Based on [110].

4.3.2. Oxocarbenium

Following the successful demonstration of asymmetric iminium reactivity with chiral-anions, there was an increased interest in expanding this reactivity to other cationic intermediates. In 2007, the List group expanded the scope of ion-pairing catalysis to oxocarbenium intermediates in an asymmetric Mukaiyama aldol reaction by using a highly acidic disulfonimide catalyst (Scheme 4.33) [113]. In a closely related

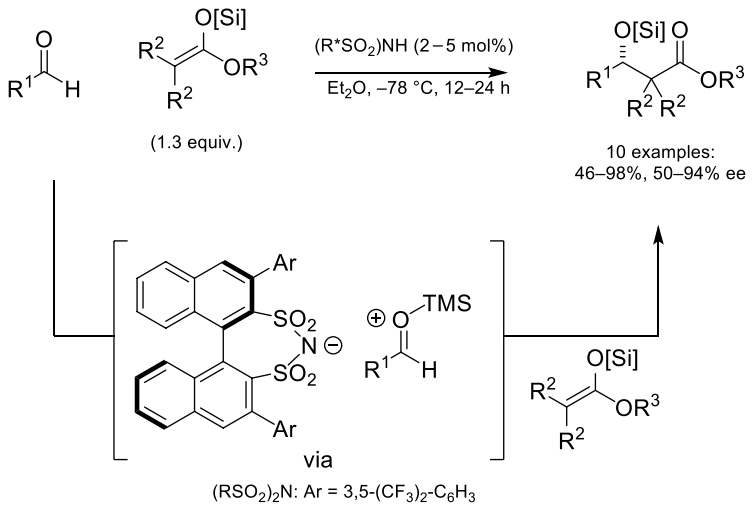

Scheme 4.33. Asymmetric Mukaiyama aldol reaction catalyzed by a highly acidic BINOL-derived disulfonimide. Source: Based on [113].

follow-up publication, the List group demonstrated vinylogous and doubly vinylogous silyl enol ethers as nucleophiles [114].

A variety of stabilized oxocarbenium intermediates has been shown to be compatible with this reaction paradigm. In 2013, the Terada group demonstrated an enantioselective reduction of hydroxy-pyrans via a pyrylium/TRIP chiral ion-pair (Scheme 4.34) [115]. A similar pyrylium intermediate was shown to undergo an enantioselective Diels-Alder via ion-pairing with a chiral phosphate, followed by rearrangement to an exo-cyclic ketone [116]. Nonaromatic oxocarbeniums have also been accessed and utilized in chiral-anion catalysis, as demonstrated by the Nagorny group. In this work, an allyl acetal underwent a Diels-Alder, via the intermediacy of an allylic oxocarbenium ion-paired with a chiral phosphate anion [117].

In order to access oxocarbenium intermediates without stabilizing moieties, more acidic chiral acids were required to favor ionization of the substrate. In 2016, the Thiel, De, and List groups developed an oxa-Pictet-Spengler reaction, catalyzed by a highly acidic imidodiphosphoric acid (Scheme 4.35) [118]. In 2018, Scheidt demonstrated that a similar oxa-Pictet-Spengler reaction could be realized with a less acidic chiral catalyst [119], by introducing exogenous achiral urea to increase the acidity of the catalyst via hydrogen bonding of the phosphate anion. Similarly, a bifunctional catalyst featuring a thiourea moiety to greatly increase the acidity of an intramolecular carboxylic acid was shown to be competent for this reactivity [120].

A potential alternative to the use of stronger chiral acids to access unstabilized oxocarbeniums was demonstrated in 2015 by the Luo group (Scheme 4.36) [121]. In this example, a trityl cation/chiral phosphate salt was shown to activate α-ketoesters toward asymmetric reactivity with a variety of coupling partners. Numbers of transformations were compatible with this system, such as 1,4-addition with indoles, Diels-Alder with cyclopentadiene, and 1,2-addition with α-methyl styrene, which occurred in high yields and selectivities.

4.3.3. Carbocation

A variety of asymmetric intramolecular reactions was developed featuring stabilized carbocations as intermediates. In 2010, the Antilla group demonstrated that chiral phosphoric acids could catalyze the enantioselective semi-pinacol rearrangement of an indolyl diol via intermediacy of the indolyl cation/chiral phosphate ion-pair (Scheme 4.37) [122]. A vinylogous variant of this reaction was reported in 2016 by the Zhu group, forming β,γ-unsaturated ketones in high yields and enantioselectivities [123]. Other intramolecular reactivity was shown in 2018 by the Ariafard and Chan groups, with an enantioselective

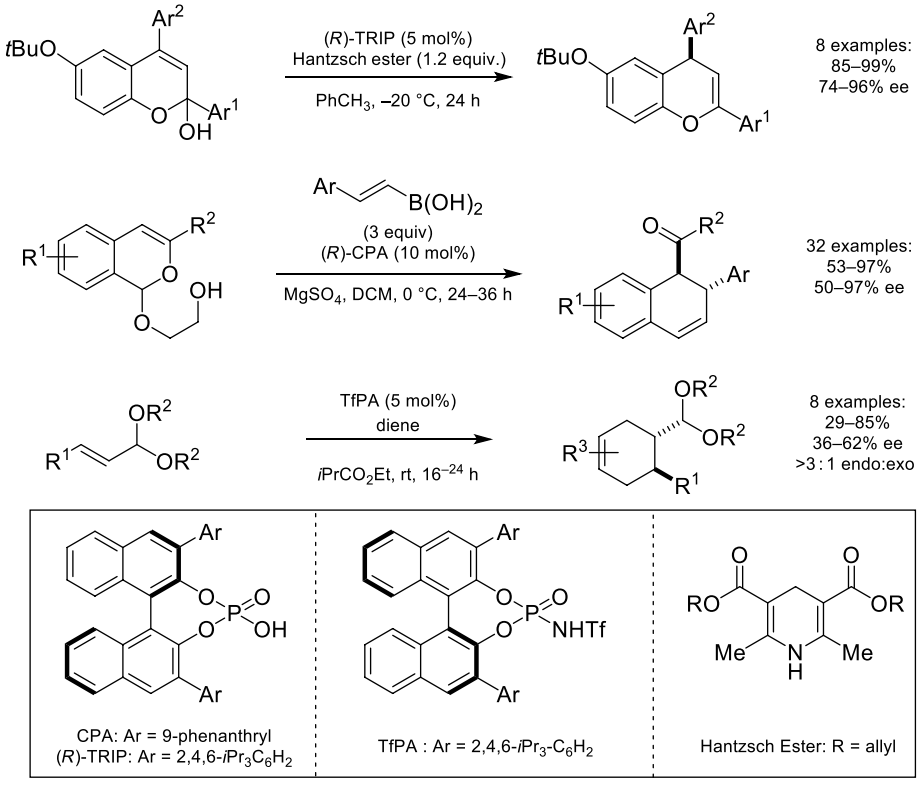

Scheme 4.34. Asymmetric counteranion-directed catalysis involving stabilized oxocarbenium intermediates. Source: Based on [115].

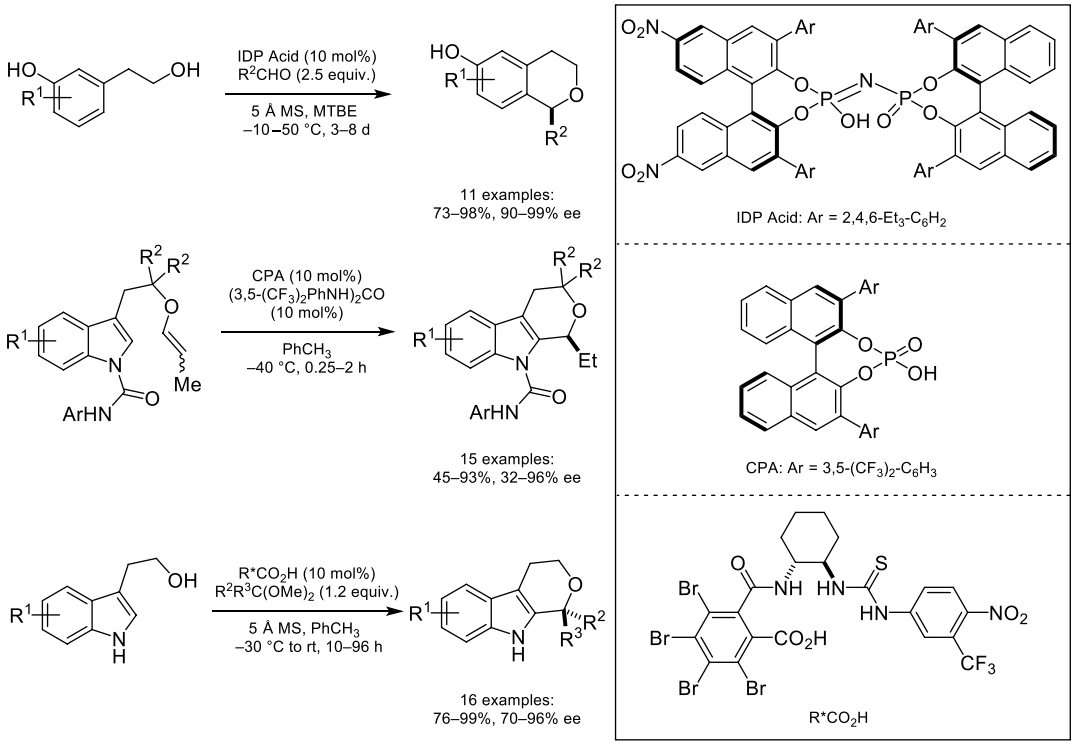

Scheme 4.35. Asymmetric counteranion-directed catalysis with unstabilized oxocarbenium intermediates. Source: Based on [118].

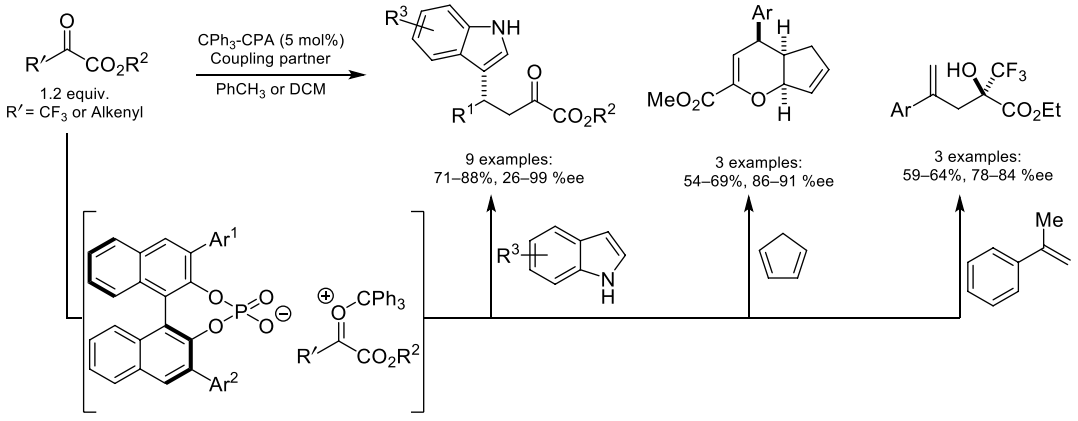

Scheme 4.36. Trityl cation/ chiral phosphate salt activation of α-ketoesters. Source: Based on [121].

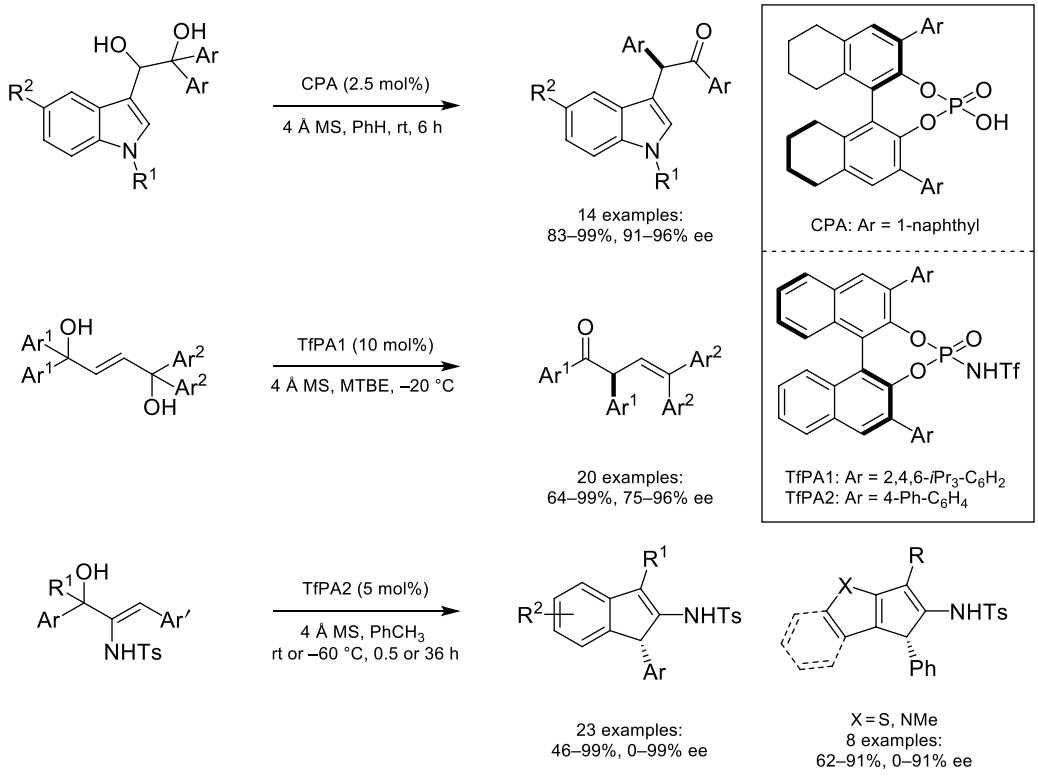

Scheme 4.37. Intramolecular asymmetric counteranion-directed catalysis with carbocation intermediates. Source: Based on [122].

Nazarov-type electrocyclization of allylic alcohols, forming chiral indenes and tricyclic compounds in high yields and enantioselectivities [124].

Intermolecular transformations utilizing carbocations in conjunction with chiral-anions have been of recent synthetic interest. In 2017, the Sun group demonstrated an asymmetric intermolecular reaction involving ion-pairing with carbocations (Scheme 4.38) [125]. In this example, a propargyl alcohol is ionized by protonation/dehydration with *N*-triflylphosphoramide catalysts. This intermediate was then shown to

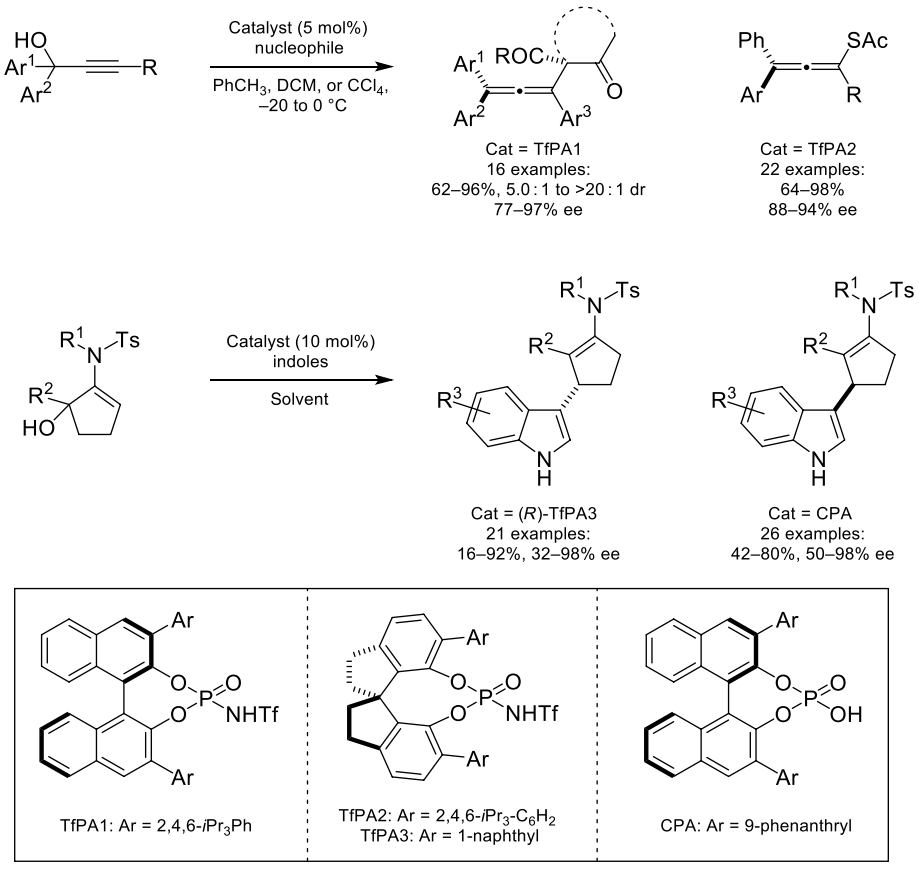

Scheme 4.38. Intermolecular asymmetric counteranion-directed catalysis with carbocation intermediates. Source: Based on [125].

undergo nucleophilic attack by 1,3-diketones and thioacetic acid in high yields and enantioselectivities. Following this, the Peng and Yang groups [126], as well as the Kartika group [127], demonstrated enantioselective intermolecular arylation reactions of allyl alcohols with indoles.

4.3.4. Miscellaneous

A novel ion-pairing strategy was demonstrated in 2008 by Toste and coworkers (Scheme 4.39) [128]. In this example, chiral phosphoric acid or silver phosphate salts would convert amines and sulfides featuring β-leaving groups into the corresponding aziridinium or episulfonium. The chiral-anion would cata-

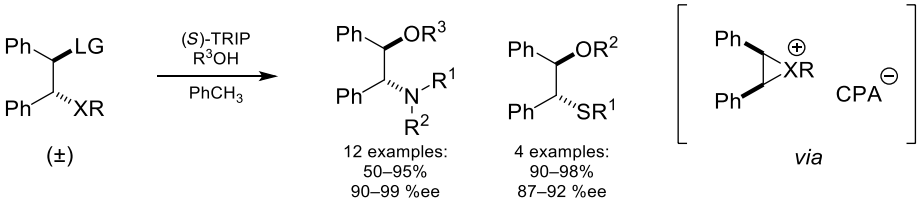

Scheme 4.39. Enantioselective aziridinium and episulfonium ring-opening. Source: Based on [128].

lyze an asymmetric ring opening of these cationic three-membered heterocycles with alcohols, to the corresponding 1,2-amino-alcohols and β-alkoxy sulfides in high yields and enantioselectivities. A computational investigation of the mechanism revealed that a C–H•••O interaction between the three-membered ring's C–H and the phosphate oxygen is key for stabilizing the ion-pair intermediate, and is essential for the enantioselectivity of the reaction [129].

Another novel application of chiral-anion catalysis was demonstrated in 2018 by the Nicewicz group. In this report, a pyrillium/chiral phosphate salt was developed that was catalytically active for a photoredox catalyzed Diels-Alder, providing bicyclic cyclohexene products in good yield and moderate enantioselectivity (Scheme 4.40) [130]. Impressively, the reaction could also be conducted intermolecularly, with a cyclic or acyclic diene. This represents a rare example in chiral ion-pairing catalysis, where the reactivity of radical intermediates is leveraged in an asymmetric fashion.

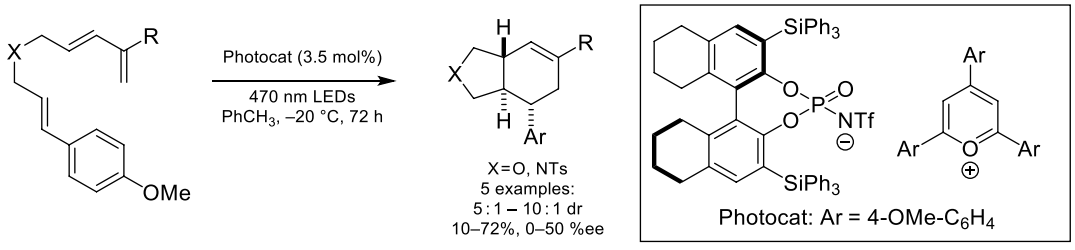

Scheme 4.40. Asymmetric Diels Alder via photoredox/chiral anion dual catalysis. Source: Based on [130].

4.3.5. Chiral-Anion Phase Transfer

4.3.5.1. Halogenation In 2011, the Toste group introduced a novel concept in the field of ion-pairing catalysis, focused on a chiral-anion phase transfer (CAPT) strategy (Scheme 4.41) [131]. The initial report focused on utilizing a catalytically generated SelectFluor/chiral phosphate ion-pair for the asymmetric fluorocyclization of alkenes. In this system, a deprotonated chiral phosphoric acid catalyst undergoes salt metathesis with insoluble SelectFluor, which introduces a chiral environment around the electrophilic fluorine, allowing it to be transferred with high yields and enantioselectivities to a variety of alkenes. In this system, the phosphate anion serves a dual purpose of activating the substrate via hydrogen bonding and ion-pairing with the cationic reagent.

In the decade following the initial report of CAPT catalysis, numbers of enantioselective fluorination reactions have been reported with the chiral phosphoric acid/SelectFluor system (Scheme 4.42). Enantioselective difunctionalization of alkenes constitutes a plurality of this field, and includes enantioselective fluorocyclizations of tryptamines [132], tryptophols [133], and enamides [134], as well as fluorinative semi-pinacol rearrangement with sulfonamides [135] and alcohols [136]. In addition to difunctionalization reactions, enantioselective α-fluorinations have also been demonstrated with this system, such as with enamides [137], phenols [138], and branched cyclohexanones [139]. The final class of transformations promoted by this system is enantioselective allylic fluorinations, with amide- and phenol-directing groups [140]. From this, it was later shown that enantioselective fluorination could be accomplished with allylic [141] and homoallylic alcohols [142], utilizing a condensed boronic-acid-directing group [143].

Catalysts other than chiral phosphoric acids have also been demonstrated to be compatible with the CAPT strategy. The Hamashima group developed a bifunctional catalyst that mimics the dual functional nature of the chiral phosphate phase-transfer catalysts (Scheme 4.43) [144]. This catalyst affected the *endo*-fluorolactonization of 2-styrenal benzoic acids, where the catalyst's free alcohol group serves to hydrogen bond with the substrate, while the carboxylate ion-pairs with the SelectFluor cation. A dimeric version of the catalyst featuring two carboxylates was later developed to synergize with the dicationic nature of SelectFluor. This catalyst was utilized for selective *endo*-fluorocyclization with an amide nucleophile [145], as well as allylic fluorination [146].

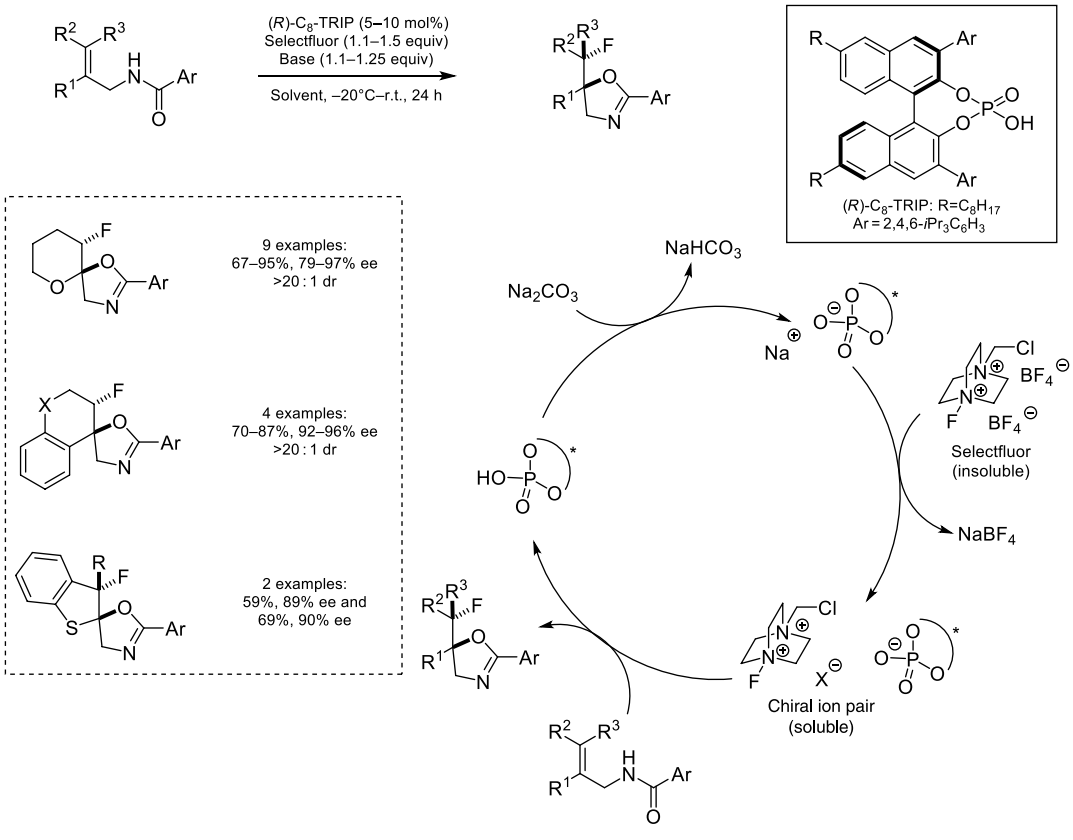

Scheme 4.41. First example of chiral anion phase-transfer catalysis. Source: Based on [131].

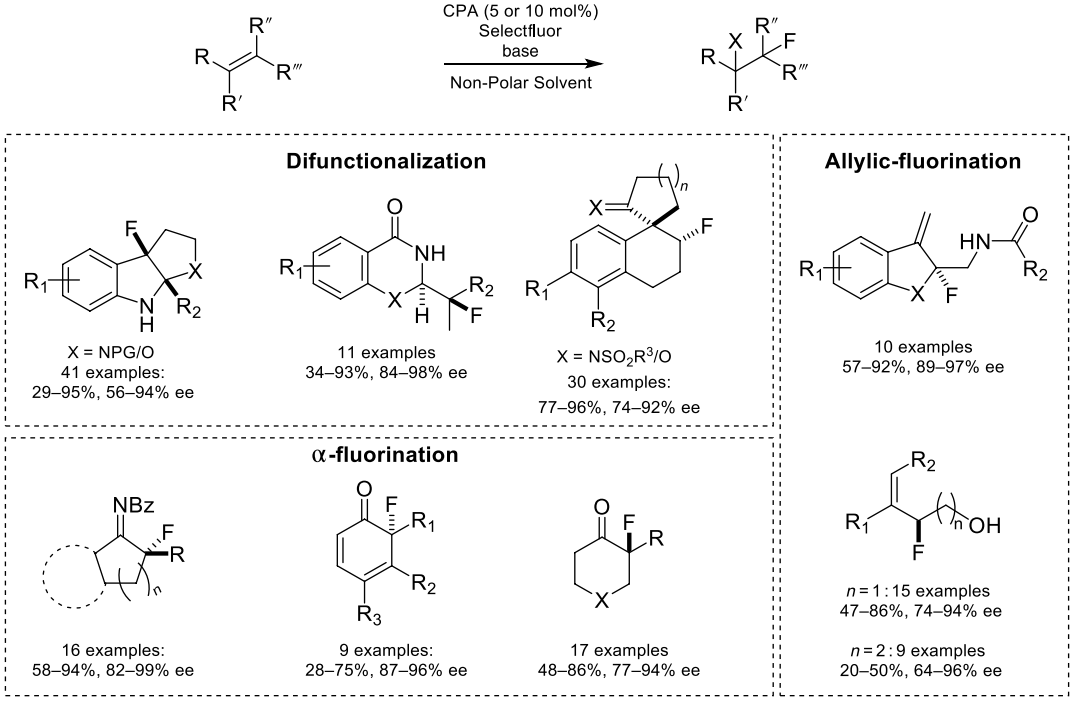

Scheme 4.42. Overview of chiral anion phase-transfer catalyzed fluorination reactions.

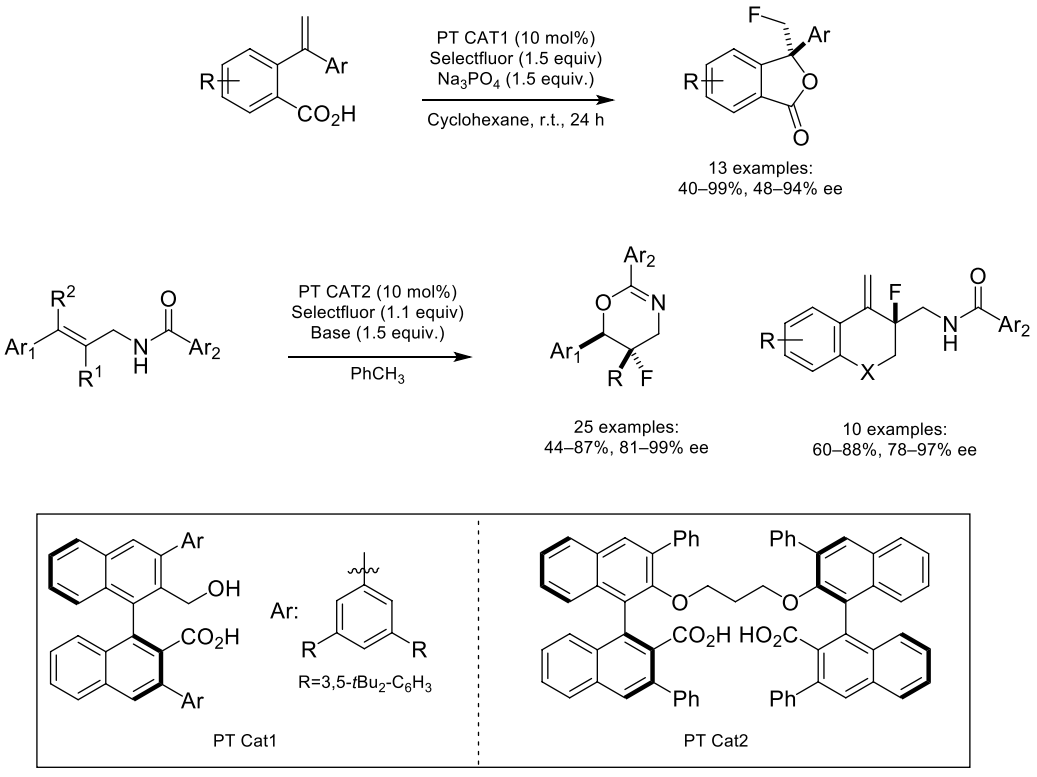

Scheme 4.43. Chiral anion phase-transfer catalyzed fluorination with BINOL-derived carboxylate catalysts. Source: Based on [144].

In addition to fluorination with SelectFluor, CAPT catalysis was adapted to bromo- and iodocyclizations by utilizing DABCOnium-based halogenating reagents (Scheme 4.44) [147]. This was first demonstrated by the Toste group with halocyclization of alkenes with tailored-reagents based on the SelectFluor scaffold. This strategy was found to be applicable to bromocyclization of difluoroalkenes, providing access to tetrasubstituted CF_2Br-containing stereocenters [148]. These compounds were derivatized to a variety of pharmaceutically relevant difluoromethylene-containing moieties, such as difluoromethyl, difluoroester, and difluorophosphonate. The DABCOnium-based brominating reagents have been applied to the enantioselective bromocyclization of other classes of substrates, such as tryptamines [149], tryptophols [150], and indenes [151]. Similarly to asymmetric fluorination, the CAPT bromination and iodination strategies were applicable to reactions outside of halocyclizations, such as halogenative semi-pinacol rearrangements [136] as well as atroposelective bromination [152].

4.3.5.2. Amination Due to the generality of the CAPT strategy, other cationic electrophiles could be deemed asymmetric by amending them to a phase-transfer setting. In 2014, the Toste group demonstrated that aryl diazonium salts were suitable electrophiles for CAPT catalysis, by developing an asymmetric diazenation of tryptamines (Scheme 4.45) [153]. In a 2015 follow-up publication, the strategy was applied to carbonyl-containing nucleophiles to generate quaternary diazenated stereocenters [154].

4.3.5.3. Miscellaneous Transformations In 2013, the Toste group demonstrated the compatibility of oxopiperidinium salts in conjunction with CAPT catalysis for an enantioselective cross-dehydrogenative coupling reaction (Scheme 4.46) [155]. Instrumental to this was the development of novel triazole-containing phosphoric acids, where it was hypothesized that these were engaging in noncovalent interactions with the substrate, leading to high enantioselectivities. A follow-up mechanistic study focusing on a

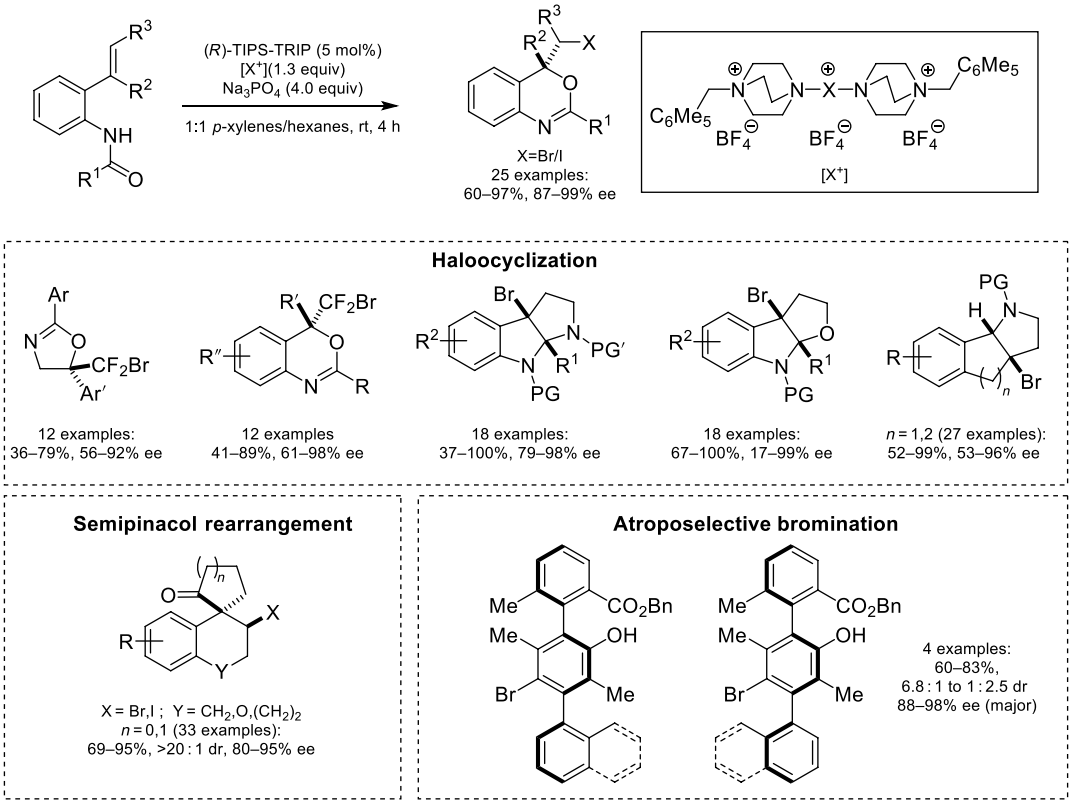

Scheme 4.44. Overview of chiral anion phase-transfer catalyzed bromination and iodination. Source: Based on [147].

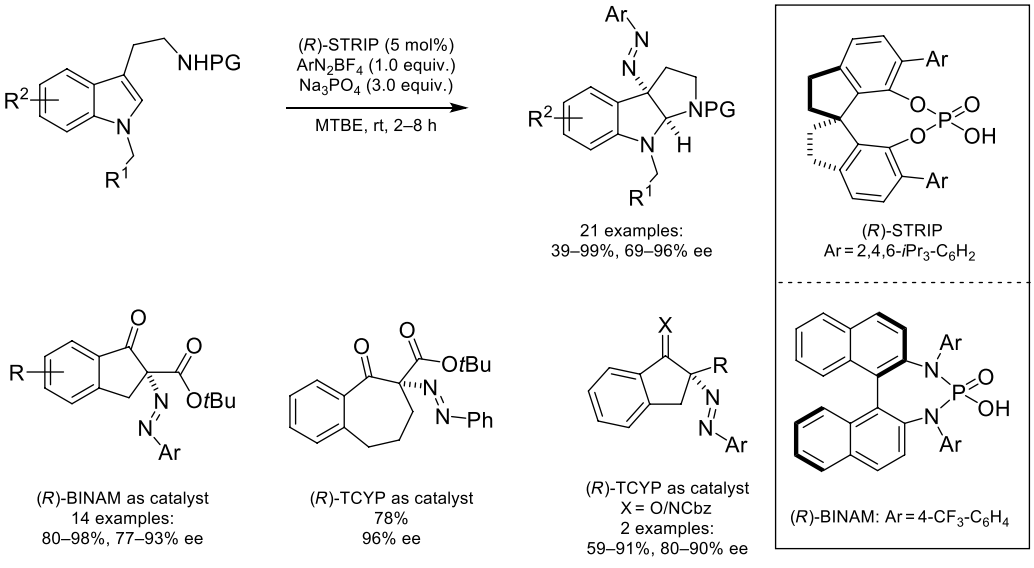

Scheme 4.45. Chiral anion phase-transfer catalyzed diazenation. Source: Based on [153].

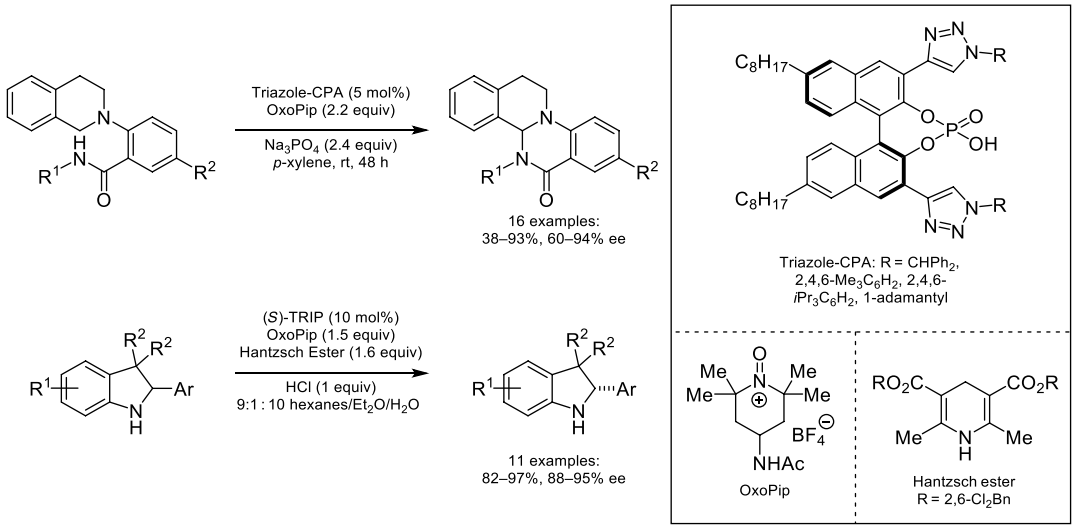

Scheme 4.46. Asymmetric transformations mediated by oxopiperidinium/chiral anion salts. Source: Based on [155].

data-intensive approach revealed that a π-stacking interaction between the triazole and the substrate was the primary factor in controlling enantioselectivity [156]. The oxopiperidinium/chiral-anion system was later utilized in a deracemization reaction of indolines via oxidation to the 3-H indole scaffold proceeding, and subsequent reduction to the indoline [157]. In 2016, the Toste group reported the asymmetric arylation of benzopyrylium with phenols under phase-transfer conditions (Scheme 4.47) [158].

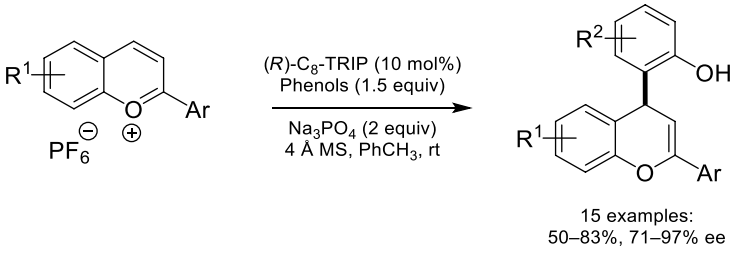

Scheme 4.47. Asymmetric arylation of benzopyrylium with phenols under phase-transfer conditions. Source: Based on [158].

4.3.6. Transition-Metal/Chiral-Anion Dual Catalysis

With the prevalence of cationic transition-metal complexes in catalysis, there was a strong interest in rendering these reactions asymmetric by utilizing ion-pairing with chiral counterions. In 2007, the Toste group demonstrated this principle with an enantioselective Au(I) catalyzed hydro-cyclization of allenes (Scheme 4.48) [159]. The chiral-anion strategy was crucial for success in this system, as the linearity of Au(I) complexes rendered attempts to use chiral ligands for enantioselectivity unsuccessful. By combining an achiral gold complex with a chiral phosphate counter anion, the enantioselective cyclization of alcohols, sulfonamides, and carboxylic acids could be achieved in high yields. Solvent choice was found to be a key factor for achieving selectivity, as more polar solvents resulted in weaker ion-pairing, leading to diminished selectivities. This strategy was later adapted to the desymmetrization of 1,3-diols via intramolecular cyclization of allenes [160]. In the succeeding decade, the robustness of this strategy was demonstrated by the compatibility of chiral-anions with a wide variety of transition-metal-catalyzed reactions.

The combination of Pd catalysis with chiral-anions has led to many asymmetric methodologies. Of particular initial interest was the generation of cationic Pd-allyl complexes with a chiral counteranion for

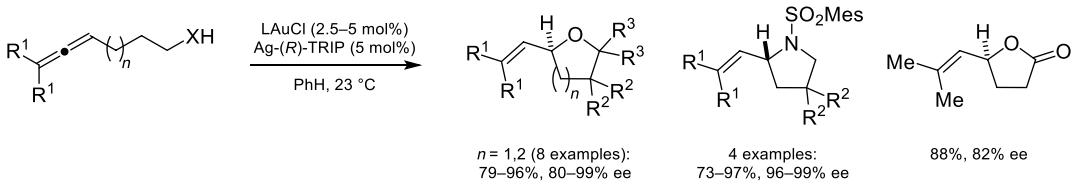

Scheme 4.48. First example of a transition-metal/chiral anion catalyzed transformation. Source: Based on [159].

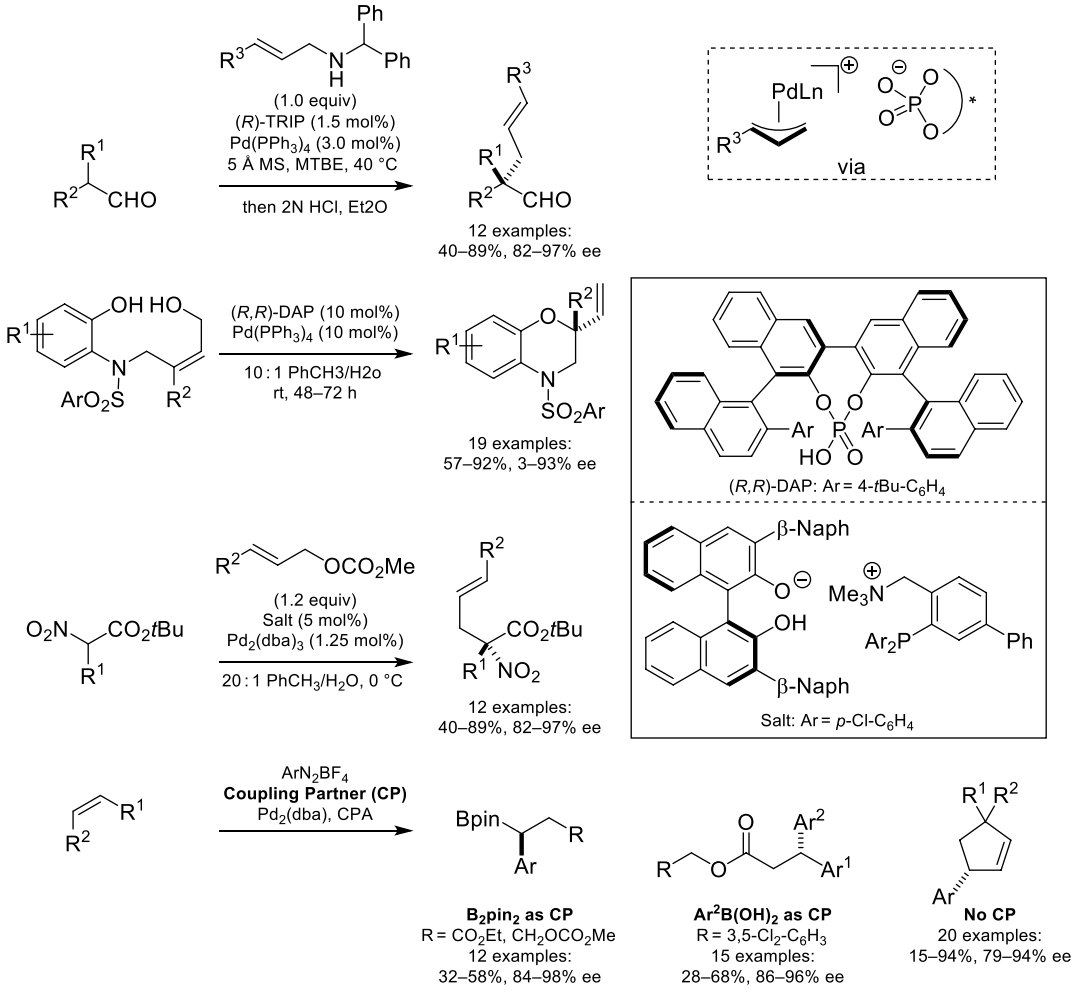

Scheme 4.49. Asymmetric transformations catalyzed by a Pd/chiral phosphate ion pair. Source: Based on [161].

asymmetric Tsuji–Trost-type allylations. This was first demonstrated by the List group in 2007, with an asymmetric α-allylation of aldehydes (Scheme 4.49) [161]. An intramolecular version of this reaction was later reported by the Toste and Sigman labs, where pyrrolidines and benzomorpholines were accessed in high yields and enantioselectivities [162]. In addition to ion-pairing with a cationic transition-metal center, the Ooi lab demonstrated that enantioselectivity can be achieved by utilizing an achiral cationic ligand ion-paired with a BINOL-derived anion [163]. In addition to Pd(II) allyl complexes, the Toste group demonstrated an enantioselective 1,1-arylborylation of alkenes, which proceeds through an

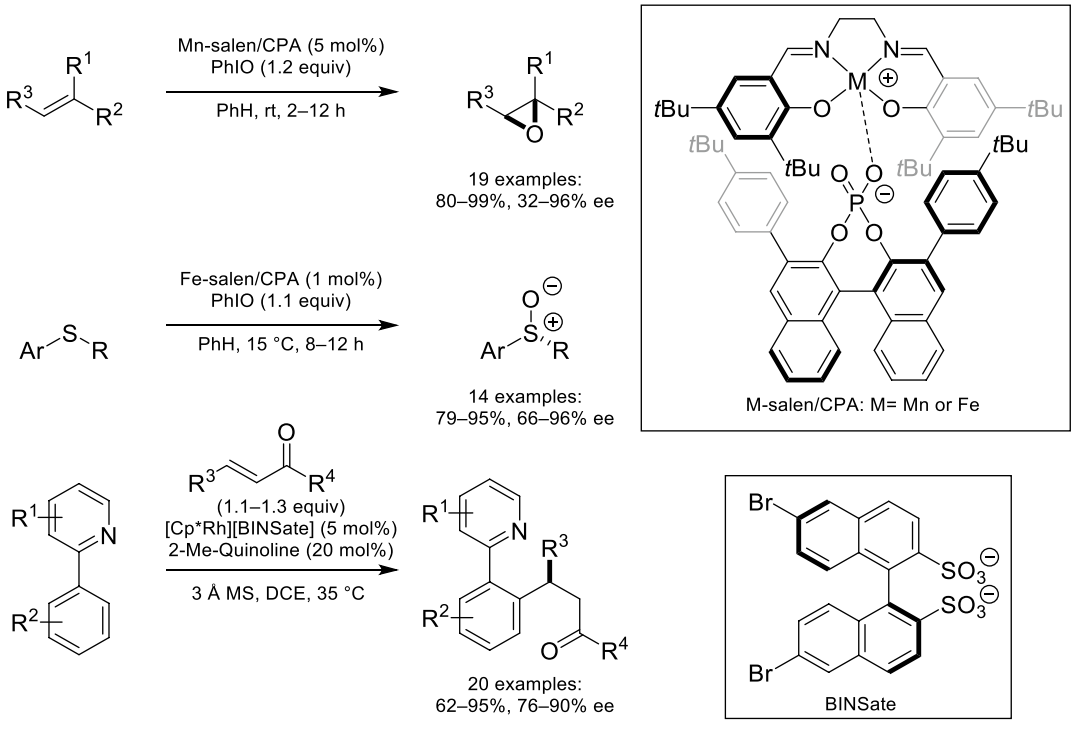

Scheme 4.50. Asymmetric transformations catalyzed by other transition-metals ion-paired with chiral anions. Source: Based on [167].

enantiodetermining migratory insertion, followed by β-hydride elimination and reinsertion [164]. By changing the coupling partner to aryl boronic acids, an enantioselective 1,1-diarylation was achieved [165]. Additionally, exclusion of a coupling partner was found to result in an asymmetric Heck–Matsuda arylation, generating cyclic arylated stereocenters in high yield and enantioselectivity [166].

Expansion to other transition metals and reaction manifolds was successful. One such important contribution came from the List group in 2010, by utilizing an achiral Mn-salen complex in conjunction with a chiral-anion (Scheme 4.50) [167]. The chiral-anion was proposed to stabilize one enantiomorph of the achiral Mn-salen complex, leading to high selectivity for the epoxidation of alkenes. This was later extended to the enantioselective sulfoxidation of sulfides with an Fe-salen complex [168]. In 2018, the Matsunaga group demonstrated an Rh-catalyzed enantioselective C–H functionalization using a binaphthyl-derived bis-sulfate chiral-anion [169].

4.3.7. Anion-Binding Catalysis

Rather than utilizing an anionic chiral catalyst to ion-pair cationic reagents, an alternate strategy was developed that focuses on a neutral chiral catalyst that can bind achiral-anions, forming an in situ chiral-anion.

4.3.7.1. Nonaromatic Cations In 2004, the Jacobsen group demonstrated that an anion-binding catalyst could be used to affect an enantioselective acyl-Pictet-Spengler reaction (Scheme 4.51) [170]. A variant that features activation of a hydroxylactam by trimethylsilyl chloride (TMSCl) was later demonstrated as well [171]. Mechanistically this reaction proceeds by formation of an acyl iminium cation, where the chloride counteranion is hydrogen bound to the chiral urea catalyst. This keeps the chiral information close to the cationic center, allowing selective nucleophilic attack by the indole.

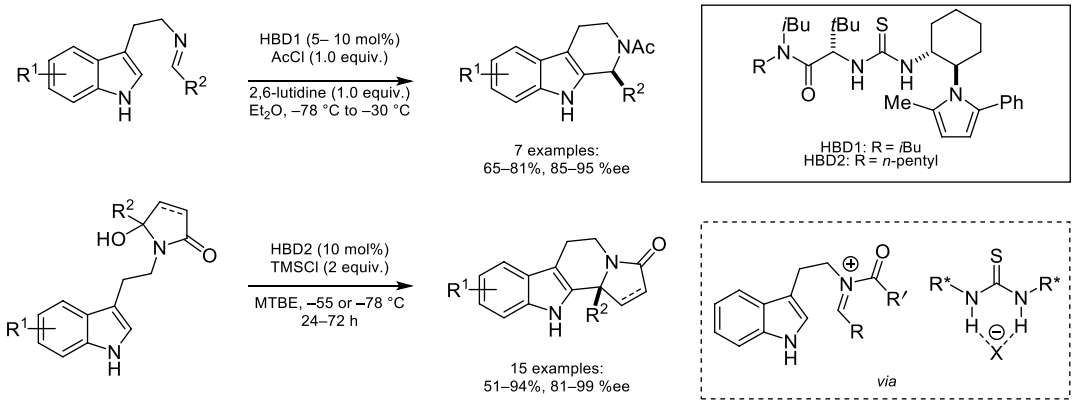

Scheme 4.51. Enantioselective acyl-Pictet-Spengler reaction enabled by anion-binding catalysis. Source: Based on [170].

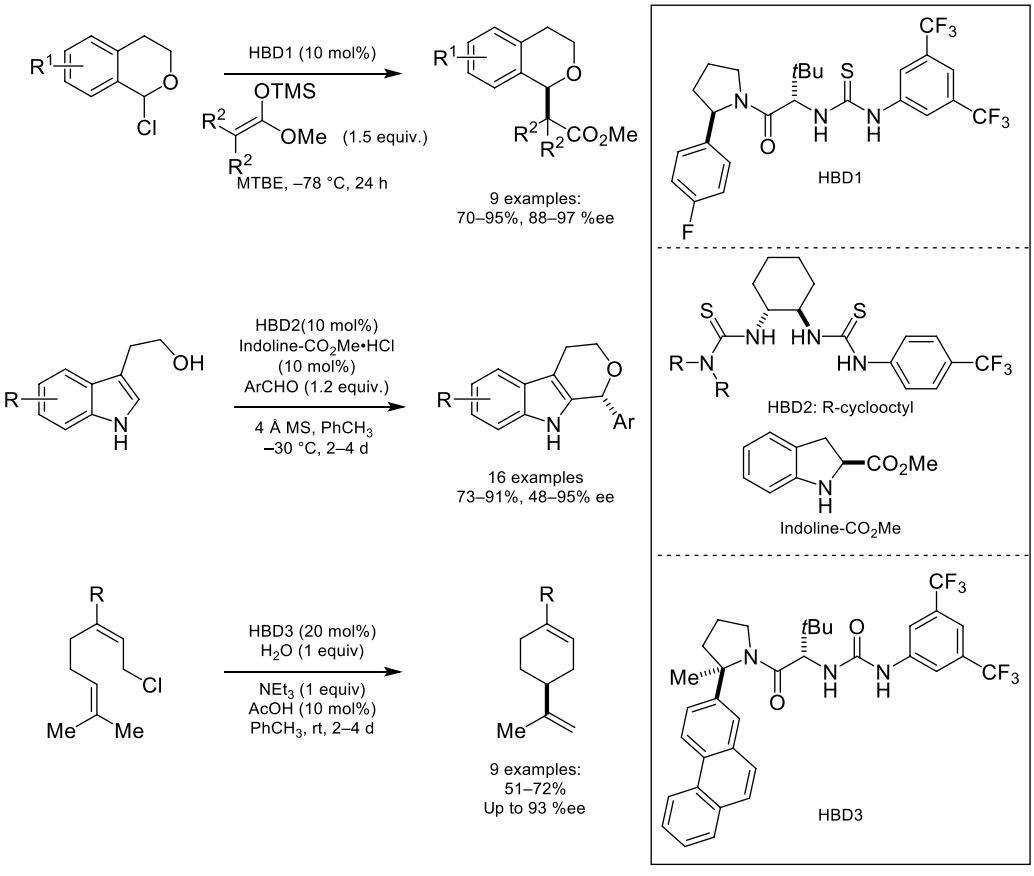

Scheme 4.52. Enantioselective reactions enabled by anion-binding catalysis proceeding through oxocarbenium and carbocation intermediates. Source: Based on [172].

In addition to iminium reactivity, this anion-binding strategy was applicable to the generation and enantioselective transformations of oxocarbeniums. In the first report by the Jacobsen group, chloroisochromans were activated by anion-binding of the chloride, generating an oxocarbenium ion-paired to a chloride-bound chiral catalyst (Scheme 4.52) [172]. The oxocarbenium is then trapped enantioselectively

by silyl ketene acetals in good yield and enantioselectivities. In 2016, the Seidel group demonstrated the first highly enantioselective, catalytic oxa-Pictet-Spengler via anion-binding catalysis [173]. A strong counteranion effect on the enantioselectivity of the reaction reveals the importance of cooperativity between the anion and hydrogen-bond donor. The ionization of alkyl halides could also be accomplished without the aid of an adjacent heteroatom donor. By utilizing neryl chloride analogues, the Jacobsen lab demonstrated an enantioselective tail-to-head cyclization proceeding in high yields and enantioselectivities [174].

4.3.7.2. Cationic Heterocycles In 2009, Seidel demonstrated the first use of anion-binding asymmetric catalysis for the kinetic resolution of amines (Scheme 4.53) [175]. In this system, 4-dimethylaminopyridine (DMAP) is first benzoylated by benzoic anhydride, forming an activated electrophilic cation, and achiral benzoate anion. The benzoate becomes associated to the catalyst by hydrogen bonding, forming a chiral-anion complex. This newly formed chiral ion-pair can then lead to the kinetic resolution, with s-factors between 7.1 and 24 for a variety of benzylic amine substrates. By utilizing variants of a chiral thiourea catalyst, this strategy was found to be applicable to a variety of other amines, such as propargylic amines [176], allylic amines [177], as well as the desymmetrization of *meso*-diamines [178], and kinetic resolution of 1,2-diamines [179]. The choice of achiral DMAP derivative in this chemistry was found to have a profound effect on observed selectivities, highlighting the importance of tuning the achiral cation to achieve good selectivities [180].

In 2011, the Jacobsen group demonstrated the enantioselective benzoylation of cyclic silyl ketene acetal *via* anion-binding catalysis (Scheme 4.54) [181]. In this example, benzoyl fluoride is used with co-catalytic DMAP derivative to generate free fluoride anion, which is hydrogen bound to the thiourea. The fluoride desilylates the substrate, leading to binding of the anionic enolate and subsequent asymmetric benzoylation. This was expanded upon shortly thereafter by the Seidel group, with an enantioselective Steglich rearrangement utilizing a thiourea catalyst [182]. By replacement of the DMAP with quinolines, it was found that nucleophilic attack occurred onto the 2-position of the quinoline, rather than at the carbonyl.

In 2014, the Mancheño group demonstrated chiral helical oligotriazoles as a new class of anion-binding catalysts (Scheme 4.55) [183]. In this reaction, a quinoline undergoes an enantioselective dearomative alkylation-carbonylation. In this transformation, the chloride anion released from nucleophilic attack onto the TrocCl is bound to the anion-binding catalyst. This reaction was found to also work well with isoquinolines with slight modification to the catalyst structure [184]. In addition, silyl ketene thioacetals were also well tolerated as nucleophiles [185]. In addition to fused aromatics, the reaction was found

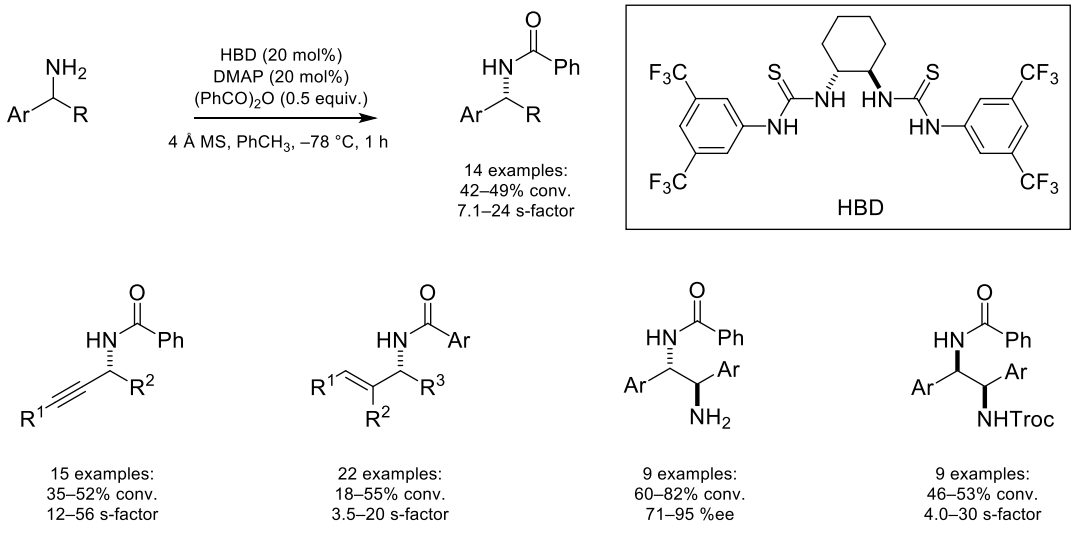

Scheme 4.53. Kinetic resolution of amines via anion-binding catalysis. Source: Based on [175].

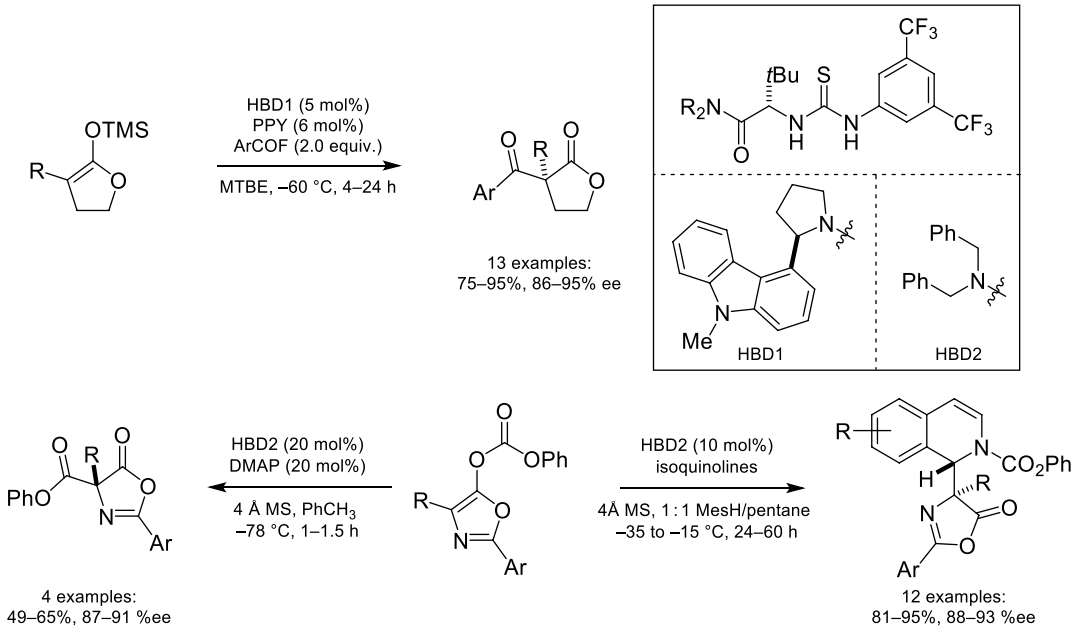

Scheme 4.54. Enantioselective reactions of enol ethers enabled by anion-binding catalysis. Source: Based on [181].

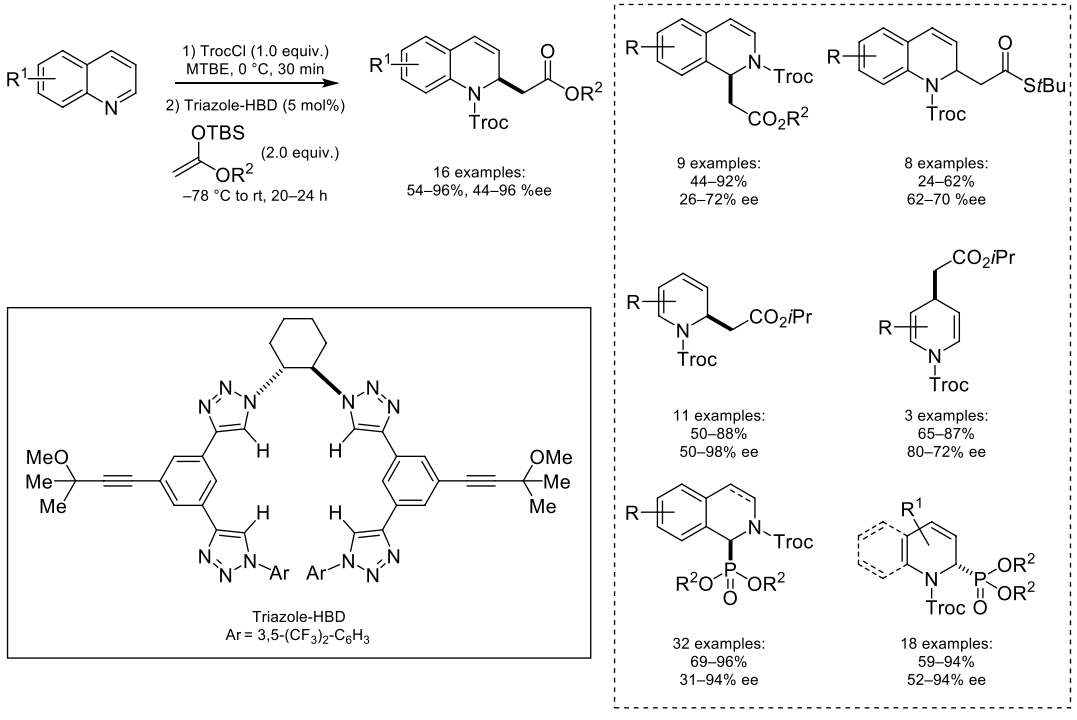

Scheme 4.55. Enantioselective dearomatization of heterocycles enabled by anion-binding catalysis. Source: Based on [183].

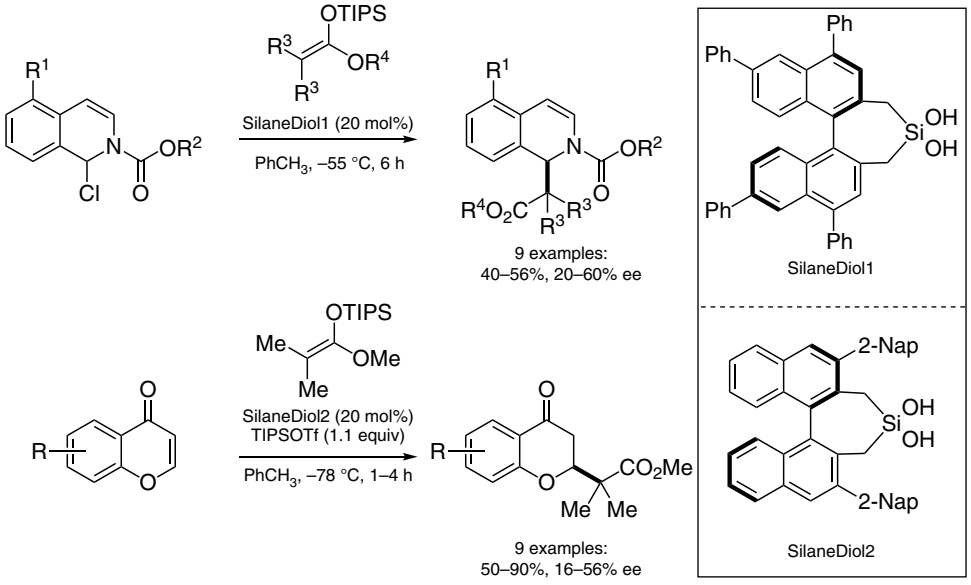

Scheme 4.56. Enantioselective transformations catalyzed by BINOL-derived silane-diols. Source: Based on [191].

to work well with pyridine substrates [186]. Selectivity between alkylation of C-2 and C-4 was mainly controlled by the identity of the substrate, where high yields and enantioselectivities were observed at both sites. This work was expanded to diazines, where similar selectivities were controlled by the substrates [187]. In 2016, the Mukherjee group demonstrated that silyl phosphites were good nucleophiles for this reaction in combination with thioether catalyst [188]. In 2017, the Mancheño group demonstrated similar reactivity with silyl phosphites on quinolines [189]. In addition to (thio)urea and triazole-containing catalysts, the Mattson group developed novel BINOL-derived silanediol, anion-binding catalysts [190]. In 2015, an improved silanediol catalyst was developed that catalyzed the alkylation of isoquinolines in moderate yield and enantioselectivity (Scheme 4.56) [191]. In a follow-up publication, the Mattson group applied this new catalyst system to chromenone functionalization, via pyrilium intermediates [192].

4.3.7.3. Asymmetric Ring Opening of Strained Heterocycles In 2012, the Jacobsen group demonstrated that hydrogen bonding catalysts could affect the asymmetric ring opening of episulfonium cations with indoles (Scheme 4.57) [193]. The source of the enantioselectivity was proposed to be an ensemble of electrostatic, cation-π, and hydrogen-bonding interactions between the anion-bound catalyst, indole, and episulfonium. The Gouverneur lab extended this reactivity to utilizing fluoride as the nucleophile, a notoriously challenging fluorine source for asymmetric fluorination reactions [194]. Other advances in the field include an asymmetric selenocyclization through the intermediacy of a seleniranium ion-pair [195]. It was shown that the seleniranium readily interconverts between two enantiomers via group transfer, allowing for a Curtin-Hammett situation that determines the enantioselectivity of the reaction.

4.4. CONCLUSION

Since the initial reports of chiral cation phase-transfer catalysis, there has been an exponential growth in the number of key strategies available for asymmetric induction of reactions involving ion-pairing. Currently, there is a push to better understand the mechanistic interplay between the chiral ion, its achiral counterion, and the substrate. This has taken the form of utilizing traditional transition state analysis by DFT, as well as newer data-intensive approaches that focus on linear-regression analysis. Another major

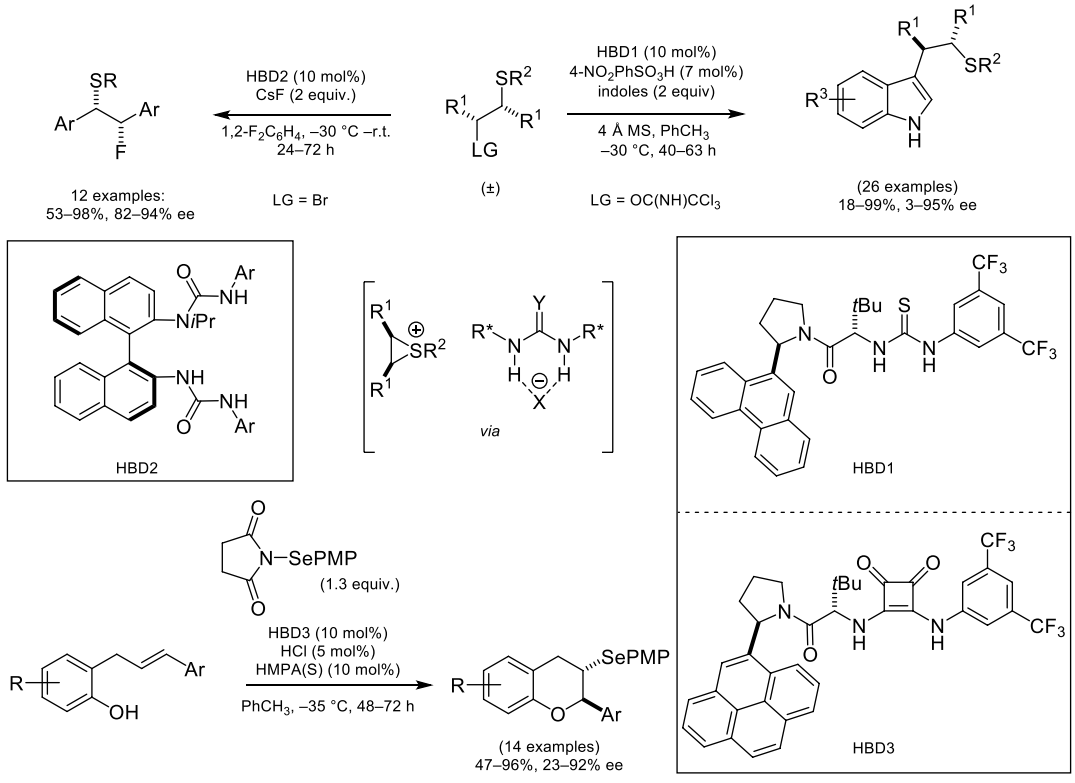

Scheme 4.57. Asymmetric ring opening of strained heterocycles by anion-binding catalysis. Source: Based on [193].

area of current focus is utilizing these interesting noncovalent effects in combination with the unique reactivity of transition-metal catalysis, to yield novel enantioselective methodologies.

REFERENCES

1. Dolling, U. H.; Davis, P.; Grabowski, E. J. J. *J. Am. Chem. Soc.* **1984**, *106*, 446–447.
2. Hughes, D. L.; Dolling, U. H.; Ryan, K. M.; Schoenewaldt, E. F.; Grabowski, E. J. J. *J. Org. Chem.* **1987**, *52*, 4745–4752.
3. O'Donnell, M. J.; Bennett, W. D.; Wu, S. *J. Am. Chem. Soc.* **1989**, *111*, 2353–2355.
4. Lygo, B.; Wainwright, P. G. *Tetrahedron Lett.* **1997**, *38*, 8595–8598.
5. Lygo, B.; Crosby, J.; Lowdon, T. R.; Wainwright, P. G. *Tetrahedron* **2001**, *57*, 2391–2402.
6. Lygo, B.; Andrews, B. I. *Acc. Chem. Res.* **2004**, *37*, 518–525.
7. Corey, E. J.; Xu, F.; Noe, M. C. *J. Am. Chem. Soc.* **1997**, *119*, 12414–12415.
8. Corey, E. J.; Bo, Y.; Busch-Petersen, J. *J. Am. Chem. Soc.* **1998**, *120*, 13000–13001.
9. Jew, S.-S.; Yoo, M.-S.; Jeong, B.-S.; Park, I. Y.; Park, H.-G. *Org. Lett.* **2002**, *4*, 4245–4248.
10. Jew, S.-S.; Jeong, B.-S.; Yoo, M.-S.; Huh, H.; Park, H.-G. *Chem. Commun.* **2001**, 1244–1245.
11. Park, H.-G.; Jeong, B.-S.; Yoo, M.-S.; Park, M.-K.; Huh, H.; Jew, S.-S. *Tetrahedron Lett.* **2001**, *42*, 4645–4648.
12. Ooi, T.; Kameda, M.; Maruoka, K. *J. Am. Chem. Soc.* **1999**, *121*, 6519–6520.
13. Ooi, T.; Uematsu, Y.; Kameda, M.; Maruoka, K. *Angew. Chem. Int. Ed.* **2002**, *41*, 1551–1554.
14. Lygo, B.; Allbutt, B.; James, S. R. *Tetrahedron Lett.* **2003**, *44*, 5629–5632.
15. Shibuguchi, T.; Fukuta, Y.; Akachi, Y.; Sekine, A.; Ohshima, T.; Shibasaki, M. *Tetrahedron Lett.* **2002**, *43*, 9539–9543.
16. Ohshima, T.; Gnanadesikan, V.; Shibuguchi, T.; Fukuta, Y.; Nemoto, T.; Shibasaki, M. *J. Am. Chem. Soc.* **2003**, *125*, 11206–11207.
17. Ohshima, T.; Shibuguchi, T.; Fukuta, Y.; Shibasaki, M. *Tetrahedron* **2004**, *60*, 7743–7754.

18. Sasai, H. (**2003**). Quaternary ammonium salt having spirochirality and its utilization. Mitsubishi Chem. Corp., JP2003335780.
19. Kita, T.; Georgieva, A.; Hashimoto, Y.; Nakata, T.; Nagasawa, K. *Angew. Chem. Int. Ed.* **2002**, *41*, 2832–2834.
20. Denmark, S. E.; Gould, N. D.; Wolf, L. M. *J. Org. Chem.* **2011**, *76*, 4260–4336.
21. Wen, S.; Li, X.; Lu, Y. Asian J. *Org. Chem.* **2016**, *5*, 1457–1460.
22. O'Donnell, M. J. *Tetrahedron* **2019**, *75*, 3667–3696.
23. O'Donnell, M. J.; Wu, S. *Tetrahedron Asymmetry* **1992**, *3*, 591–594.
24. Lygo, B.; Crosby, J.; Peterson, J. A. *Tetrahedron Lett.* **1999**, *40*, 8671–8674.
25. Jew, S.-S.; Jeong, B.-S.; Lee, J.-H.; Yoo, M.-S.; Lee, Y.-J.; Park, B.-S.; Kim, M. G.; Park, H.-G. *J. Org. Chem.* **2003**, *68*, 4514–4516.
26. Ooi, T.; Takeuchi, M.; Kameda, M.; Maruoka, K. *J. Am. Chem. Soc.* **2000**, *122*, 5228–5229.
27. Kitamura, M.; Shirakawa, S.; Maruoka, K. *Angew. Chem. Int. Ed.* **2005**, *44*, 1549–1551.
28. Hashimoto, T.; Maruoka, K. *Chem. Rev.* **2007**, *107*, 5656–5682.
29. Jolliffe, J. D.; Armstrong, R. J.; Smith, M. D. *Nat. Chem.* **2017**, *9*, 558–562.
30. Li, H.; Fan, W.; Hong, X. *Org. Biomol. Chem.* **2019**, *17*, 1916–1923.
31. Corey, E. J.; Noe, M. C.; Xu, F. *Tetrahedron Lett.* **1998**, *39*, 5347–5350.
32. Zhang, F. Y.; Corey, E. J. *Org. Lett.* **2000**, *2*, 1097–1100.
33. Arai, S.; Tsuji, R.; Nishida, A. *Tetrahedron Lett.* **2002**, *43*, 9535–9537.
34. He, R.; Shirakawa, S.; Maruoka, K. *J. Am. Chem. Soc.* **2009**, *131*, 16620–16621.
35. Wang, L.; Shirakawa, S.; Maruoka, K. *Angew. Chem. Int. Ed.* **2011**, *50*, 5327–5330.
36. Shirikawa, S.; Wang, L.; He, R.; Arimitsu, S.; Maruoka, M. *Chem. Asian J.* **2014**, *9*, 1586–1593.
37. Shirakawa, S.; Terao, S. J.; He, R.; Maruoka, K. *Chem. Commun.* **2011**, *47*, 10557–10559
38. Liu, S.; Maruoka, K.; Shirakawa, S. *Angew. Chem. Int. Ed.* **2017**, *56*, 4819–4823.
39. Shirakawa, S.; Ota, K.; Terao, S. J.; Maruoka, K. *Org. Biomol. Chem.* **2012**, *10*, 5753–5756.
40. Shirakawa, S.; Maruoka, K. *Tetrahedron Lett.* **2014**, *55*, 3833–3839.
41. Arai, S.; Tsuge, H.; Shioiri, T. *Tetrahedron Lett.* **1998**, *39*, 7563–7566.
42. Arai, S.; Tsuge, H.; Oku, M.; Miura, M.; Shioiri, T. *Tetrahedron* **2002**, *58*, 1623–1630.
43. Jew, S.-S.; Lee, J.-H.; Jeong, B.-S.; Yoo, M.-S.; Kim, M.-J.; Lee, Y.-J.; Lee, J.; Choi, S.-H.; Lee, K.; Lah, M. S.; Park, H.-G. *Angew. Chem. Int. Ed.* **2005**, *44*, 1383–1385.
44. Hori, K.; Tamura, M.; Tani, K.; Nishiwaki, N.; Ariga, M.; Tohda, Y. *Tetrahedron Lett.* **2006**, *47*, 3115–3118.
45. Allingham, M. T.; Howard-Jones, A.; Murphy, P. J.; Thomas, D. A.; Caulkett, P. W. R. *Tetrahedron Lett.* **2003**, *44*, 8677–8680.
46. Ooi, T.; Ohara, D.; Tamura, M.; Maruoka, K. *J. Am. Chem. Soc.* **2004**, *126*, 6844–6845.
47. Corey, E. J.; Zhang, F.-Y. *Org. Lett.* **1999**, *1*, 1287–1290.
48. Aires-de-Sousa, J.; Lobo, A. M.; Prabhakar, S. *Tetrahedron Lett.* **1996**, *37*, 3183–3186.
49. Murugan, E.; Siva, A. *Synthesis* **2005**, *12*, 2022–2028.
50. Mahé, O.; Dez, I.; Levacher, V.; Brière, J.-F. *Angew. Chem. Int. Ed.* **2010**, *49*, 7072–7075.
51. Gasparski, C. M.; Miller, M. J. *Tetrahedron* **1991**, *47*, 5367–5378.
52. Mettath, S.; Srikanth, G. S. C.; Dangerfield, B. S.; Castle, S. L. *J. Org. Chem.* **2004**, *69*, 6489–6492.
53. Ooi, T.; Taniguchi, M.; Kameda, M.; Maruoka, K. *Angew. Chem. Int. Ed.* **2002**, *41*, 4542–4544.
54. Ooi, T.; Kameda, M.; Taniguchi, M.; Maruoka, K. *J. Am. Chem. Soc.* **2004**, *126*, 9685–9694.
55. Ooi, T.; Kameda, M.; Fujii, J.-I.; Maruoka, K. *Org. Lett.* **2004**, *6*, 2397–2399.
56. Okada, A.; Shibuguchi, T.; Ohshima, T.; Masu, H.; Yamaguchi, K.; Shibasaki, M. *Angew. Chem. Int. Ed.* **2005**, *44*, 4564–4567.
57. Arai, S.; Ishida, T.; Shioiri, T. *Tetrahedron Lett.* **1998**, *39*, 8299–8302.
58. Arai, S.; Shirai, Y.; Ishida, T.; Shioiri, T. *Tetrahedron* **1999**, *55*, 6375–6386.
59. Ooi, T.; Uematsu, Y.; Maruoka, K. *J. Am. Chem. Soc.* **2006**, *128*, 2548–2549.
60. Ooi, T.; Uematsu, Y.; Fujimoto, J.; Fukumoto, K.; Maruoka, K. *Tetrahedron Lett.* **2007**, *48*, 1337–1340.
61. Bella, M.; Kobbelgaard, S.; Jørgensen, K. A. *J. Am. Chem. Soc.* **2005**, *127*, 3670–3671.
62. Kobbelgaard, S.; Bella, M.; Jørgensen, K. A. *J. Org. Chem.* **2006**, *71*, 4980–4987.
63. Shirakawa, S.; Yamamoto, K.; Tokuda, T.; Maruoka, K. Asian J. *Org. Chem.* **2014**, *3*, 433–436.
64. Shirakawa, S.; Yamamoto, K.; Maruoka, K. *Angew. Chem. Int. Ed.* **2015**, *54*, 838–840.
65. Shirakawa, S.; Koga, K.; Tokuda, T.; Yamamoto, K.; Maruoka, K. *Angew. Chem. Int. Ed.* **2014**, *53*, 6220–6223.
66. Armstrong, R. J.; Smith, M. D. *Angew. Chem. Int. Ed.* **2014**, *53*, 12822–12826.
67. Cardenas, M. M.; Toenjes, S. T.; Nalbandian, C. J.; Gustafson, J. L. *Org. Lett.* **2018**, *20*, 2037–2041.
68. Ding, Q.; Wang, Q.; He, H.; Cai, Q. *Org. Lett.* **2017**, *19*, 1804–1807.
69. Gillis, E. P.; Eastman, K. J.; Hill, M. D.; Donnelly, D. J.; Meanwell, N. A. *J. Med. Chem.* **2015**, *58*, 8315–8359.
70. Miller, E.; Toste, F. D. *Asymmetric Fluorination Reactions*, In: *Organofluorine Chemistry* (Eds. K. Szabó and N. Selander), Wiley-VCH, Weinheim, **2021**, pp. 241–280.

71. Kim, D. Y.; Park, E. J. *Org. Lett.* **2002**, *4*, 545–547.
72. Shirakawa, S.; Tokuda, T.; Kasai, A.; Maruoka, K. *Org. Lett.* **2013**, *15*, 3350–3353.
73. Masui, M.; Ando, A.; Shioiri, T. *Tetrahedron Lett.* **1988**, *29*, 2835–2838.
74. Sano, D.; Nagata, K.; Itoh, T. *Org. Lett.* **2008**, *10*, 1593–1595.
75. Schörgenhumer, J.; Tiffner, M.; Waser, M. *Beilstein J. Org. Chem.* **2017**, *13*, 1753–1769.
76. He, R.; Wang, X.; Hashimoto, T.; Maruoka, K. *Angew. Chem. Int. Ed.* **2008**, *47*, 9466–9468.
77. Lan, Q.; Wang, X.; He, R.; Ding, C.; Maruoka, K. *Tetrahedron Lett.* **2009**, *50*, 3280–3282.
78. Zhu, C.-L.; Zhang, F.-G.; Meng, W.; Nie, J.; Cahard, D.; Ma, J.-A. *Angew. Chem. Int. Ed.* **2011**, *50*, 5869–5872.
79. Paria, S.; Kang, Q.-K.; Hatanaka, M.; Maruoka, K. *ACS Catal.* **2019**, *9*, 78–82.
80. Ohmatsu, K.; Ando, Y.; Nakashima, T.; Ooi, T. *Chem.* **2016**, *1*, 802–810.
81. Zong, L.; Wang, C.; Moeljadi, A. M. P.; Ye, X.; Ganguly, R.; Li, Y.; Hirao, H.; Tan, C.-H. *Nat. Commun.* **2016**, *7*, 1–7.
82. Ye, X.; Moeljadi, A. M. P.; Chin, K. F.; Hirao, H.; Zong, L.; Tan, C.-H. *Angew. Chem. Int. Ed.* **2016**, *55*, 7101–7105.
83. Brown, R. C. D.; Keily, J. F. *Angew. Chem. Int. Ed.* **2001**, *40*, 4496–4498.
84. Wang, C.; Zong, L.; Tan, C.-H. *J. Am. Chem. Soc.* **2015**, *137*, 10677–10682.
85. Paria, S.; Lee, H.-J.; Maruoka, K. *ACS Catal.* **2019**, *9*, 2395–2399.
86. Genov, G. R.; Douthwaite, J. L.; Lahdenperä, A. S. K.; Gibson, D. C.; Phipps, R. J. *Science* **2020**, *367*, 1246–1251.
87. Cram, D. J.; Sogah, G. D. Y. *J. Chem. Soc. Chem. Commun.* **1981**, 625 – 628.
88. Vicent, C.; Martín-Lomas, M.; Penadés, S.; *Tetrahedron* **1989**, *45*, 3605–3612.
89. Bakó, P.; Kiss, T.; Töke, L. *Tetrahedron Lett.* **1997**, *38*, 7259–7262.
90. Itoh, T.; Shirakami, S. *Heterocycles* **2001**, *55*, 37–43.
91. Pham, S. T.; Rapi, Z.; Bakó, P.; Petneházy, I.; Stirling, A.; Jászay, Z. *New J. Chem.* **2017**, *41*, 14945–14953.
92. Bakó, P.; Bakó, T.; Mészáros, A.; Keglevich, G.; Szöllosy, Á.; Bodor, S.; Makó, A.; Toke, L. *Synlett* **2004**, *4*, 643–646.
93. Lee, J. W.; Yan, H.; Jang, H. B.; Kim, H. K.; Park, S. -W.; Lee, S.; Chi, D. Y.; Song, C. E. *Angew. Chem. Int. Ed.* **2009**, *48*, 7683–7686.
94. Yan, H.; Jang, H. B.; Lee, J. -W.; Kim, H. K.; Lee, S. W.; Yang, J. W.; Song, C. E. *Angew. Chem. Int. Ed.* **2010**, *49*, 8915–8917.
95. Park, S. Y.; Lee, J. -W.; Song, C. E. *Nat. Commun.* **2015**, *6*, 1–7.
96. Li, L.; Liu, Y.; Peng, Y.; Yu, L.; Wu, X.; Yan, H. *Angew. Chem. Int. Ed.* **2016**, *55*, 331–335.
97. Tan, Y.; Luo, S.; Li, D.; Zhang, N.; Jia, S.; Liu, Y.; Qin, W.; Song, C. E.; Yan, H. *J. Am. Chem. Soc.* **2017**, *139*, 6431–6436.
98. Paladhi, S.; Hwang, I. -S.; Yoo, E. J.; Ryu, D. H.; Song, C. E. *Org. Lett.* **2018**, *20*, 2003–2006.
99. Yan, H.; Oh, J. S.; Lee, J. -W.; Song, C. E. *Nat. Commun.* **2012**, *3*, 1–7.
100. Paladhi, S.; Park, S. Y.; Yang, J. W.; Song, C. E. *Org. Lett.* **2017**, *19*, 5336–5339.
101. Kim, M. J.; Xue, L.; Liu, Y.; Paladhi, S.; Park, S. J.; Yan, H.; Song, C. E. *Adv. Synth. Catal.* **2017**, *359*, 811–823.
102. Vaithiyanathan, V.; Kim, M. J.; Liu, Y.; Yan, H.; Song, C. E. *Chem. Eur. J.* **2017**, *23*, 1268–1272.
103. Yu, L.; Wu, X.; Kim, M. J.; Vaithiyanathan, V.; Liu, Y.; Tan, Y.; Qin, W. L.; Song, C. E.; Yan, H. *Adv. Synth. Catal.* **2017**, *359*, 1879–1891.
104. Park, S. Y.; Liu, Y.; Oh, J. S.; Kweon, Y. K.; Jeong, Y. B.; Duan, M.; Tan, Y.; Lee, J. -W.; Yan, H.; Song, C. E. *Chem. Eur. J.* **2018**, *24*, 1020–1025.
105. Liu, Y.; Ao, J.; Paladhi, S.; Song, C. E.; Yan, H. *J. Am. Chem. Soc.* **2016**, *138*, 16486–16492.
106. Duan, M.; Liu, Y.; Ao, J.; Xue, L.; Luo, S.; Tan, Y.; Qin, W.; Song, C. E.; Yan, H. *Org. Lett.* **2017**, *19*, 2298–2301.
107. Jadhav, A. P.; Oh, J. -A.; Hwang, I. -S.; Yan, H.; Song, C. E. *Org. Lett.* **2018**, *20*, 5319–5322.
108. Mayer, S.; List, B. *Angew. Chem. Int. Ed.* **2006**, *45*, 4193–4195.
109. Wang, X.; List, B. *Angew. Chem. Int. Ed.* **2008**, *47*, 1119–1122.
110. Courant, T.; Kumarn, S.; He, L.; Retailleau, P.; Masson, G. *Adv. Synth. Catal.* **2013**, *355*, 836–840.
111. Min, C.; Mittal, N.; Sun, D. X.; Seidel, D. *Angew. Chem. Int. Ed.* **2013**, *52*, 14084–14088.
112. Zhao, W.; Huang, L.; Guan, Y.; Wulff, W. D. *Angew. Chem. Int. Ed.* **2014**, *53*, 3436–3441.
113. García-García, P.; Lay, F.; García-García, P.; Rabalakos, C.; List, B. *Angew. Chem. Int. Ed.* **2009**, *48*, 4363–4366.
114. Ratjen, L.; García-García, P.; Lay, F.; Beck, M. E.; List, B. *Angew. Chem. Int. Ed.* **2011**, *50*, 754–758.
115. Terada, M.; Yamanaka, T.; Toda, Y. *Chem. Eur. J.* **2013**, *19*, 13658–13662.
116. Qian, H.; Zhao, W.; Wang, Z.; Sun, J. *J. Am. Chem. Soc.* **2015**, *137*, 560–563.
117. Borovika, A.; Nagorny, P. *Tetrahedron* **2013**, *69*, 5719–5725.
118. Das, S.; Liu, L.; Zheng, Y.; Alachraf, M. W.; Thiel, W.; De, C. K.; List, B. *J. Am. Chem. Soc.* **2016**, *138*, 9429–9432.
119. Maskeri, M. A.; O'Connor, M. J.; Jaworski, A. A.; Davies, A. V.; Scheidt, K. A. *Angew. Chem. Int. Ed.* **2018**, *57*, 17225–17229.
120. Zhu, Z.; Odagi, M.; Zhao, C.; Abboud, K. A.; Kirm, H. U.; Saame, J.; Lõkov, M.; Leito, I.; Seidel, D. *Angew. Chem. Int. Ed.* **2020**, *59*, 2028–2032.
121. Lv, J.; Zhang, Q.; Zhong, X.; Luo, S. *J. Am. Chem. Soc.* **2015**, *137*, 15576–15583.
122. Liang, T.; Zhang, Z.; Antilla, J. C. *Angew. Chem. Int. Ed.* **2010**, *49*, 9734–9736.
123. Wu, H.; Wang, Q.; Zhu, J. *Angew. Chem. Int. Ed.* **2016**, *55*, 15411–15414.
124. Jin, J.; Zhao, Y.; Gouranourimi, A.; Ariafard, A.; Chan, P. W. H. *J. Am. Chem. Soc.* **2018**, *140*, 5834–5841.
125. Qian, D.; Wu, L.; Lin, Z.; Sun, J. *Nat. Commun.* **2017**, *8*, 1–9.

126. Rajkumar, S.; Wang, J.; Zheng, S.; Wang, D.; Ye, X.; Li, X.; Peng, Q.; Yang, X. *Angew. Chem. Int. Ed.* **2018**, *57*, 13489–13494.
127. Saputra, M. A.; Nepal, B.; Dange, N. S.; Du, P.; Fronczek, F. R.; Kumar, R.; Kartika, R. *Angew. Chem. Int. Ed.* **2018**, *57*, 15558–15562.
128. Hamilton, G. L.; Kanai, T.; Toste, F. D. *J. Am. Chem. Soc.* **2008**, *130*, 14984–14986.
129. Duarte, F.; Paton, R. S. *J. Am. Chem. Soc.* **2017**, *139*, 8886–8896.
130. Morse, P. D.; Nguyen, T. M.; Cruz, C. L.; Nicewicz, D. A. *Tetrahedron* **2018**, *74*, 3266–3272.
131. Rauniyar, V.; Lackner, A. D.; Hamilton, G. L.; Toste, F. D. *Science* **2011**, *334*, 1681–1684.
132. Liang, X.-W.; Liu, C.; Zhang, W.; You, S.-L. *Chem. Commun.* **2017**, *53*, 5531–5534.
133. Liang, X.-W.; Cai, Y.; You, S.-L. *Chinese J. Chem.* **2018**, *36*, 925–928.
134. Honjo, T.; Phipps, R. J.; Rauniyar, V.; Toste, F. D. *Angew. Chem. Int. Ed.* **2012**, *51*, 9684–9688.
135. Romanov-Michailidis, F.; Pupier, M.; Besnard, C.; Bürgi, T.; Alexakis, A. *Org. Lett.* **2014**, *16*, 4988–4991.
136. Romanov-Michailidis, F.; Romanova-Michaelides, M.; Pupier, M.; Alexakis, A. *Chem. Eur. J.* **2015**, *21*, 5561–5583.
137. Phipps, R. J.; Hiramatsu, K.; Toste, F. D. *J. Am. Chem. Soc.* **2012**, *134*, 8376–8379.
138. Phipps, R. J.; Toste, F. D. *J. Am. Chem. Soc.* **2013**, *135*, 1268–1271.
139. Yang, X.; Phipps, R. J.; Toste, F. D. *J. Am. Chem. Soc.* **2014**, *136*, 5225–5228.
140. Wu, J.; Wang, Y.-M.; Drljevic, A.; Rauniyar, V.; Phipps, R. J.; Toste, F. D. *Proc. Natl. Acad. Sci. U. S. A.* **2013**, *110*, 13729–13733.
141. Zi, W.; Wang, Y.-M.; Toste, F. D. *J. Am. Chem. Soc.* **2014**, *136*, 12864–12867.
142. Coelho, J. A. S.; Matsumoto, A.; Orlandi, M.; Hilton, M. J.; Sigman, M. S.; Toste, F. D. *Chem. Sci.* **2018**, *9*, 7153–7158.
143. Neel, A. J.; Milo, A.; Sigman, M. S.; Toste, F. D. *J. Am. Chem. Soc.* **2016**, *138*, 3863–3875.
144. Egami, H.; Asada, J.; Sato, K.; Hashizume, D.; Kawato, Y.; Hamashima, Y. *J. Am. Chem. Soc.* **2015**, *137*, 10132–10135.
145. Egami, H.; Niwa, T.; Sato, H.; Hotta, R.; Rouno, D.; Kawato, Y.; Hamashima, Y. *J. Am. Chem. Soc.* **2018**, *140*, 2785–2788.
146. Niwa, T.; Ujiie, K.; Sato, H.; Egami, H.; Hamashima, Y. *Chem. Pharm. Bull.* **2018**, *66*, 920–922.
147. Wang, Y. -M.; Wu, J.; Hoong, C.; Rauniyar, V.; Toste, F. D. *J. Am. Chem. Soc.* **2012**, *134*, 12928–12931.
148. Miller, E.; Kim, S.; Gibson, K.; Derrick, J. S.; Dean Toste, F. *J. Am. Chem. Soc.* **2020**, *142*, 8946–8952.
149. Xie, W.; Jiang, G.; Liu, H.; Hu, J.; Pan, X.; Zhang, H.; Wan, X.; Lai, Y.; Ma, D. *Angew. Chem. Int. Ed.* **2013**, *52*, 12924–12927.
150. Liu, H.; Jiang, G.; Pan, X.; Wan, X.; Lai, Y.; Ma, D.; Xie, W. *Org. Lett.* **2014**, *16*, 1908–1911.
151. Wang, H.; Zhong, H.; Xu, X.; Xu, W.; Jiang, X. *Adv. Synth. Catal.* **2020**, *362*, 5358–5362
152. Beleh, O. M.; Miller, E.; Toste, F. D.; Miller, S. J. *J. Am. Chem. Soc.* **2020**, *142*, 16461–16470.
153. Nelson, H. M.; Reisberg, S. H.; Shunatona, H. P.; Patel, J. S.; Toste, F. D. *Angew. Chem. Int. Ed.* **2014**, *53*, 5600–5603.
154. Nelson, H. M.; Patel, J. S.; Shunatona, H. P.; Toste, F. D. *Chem. Sci.* **2015**, 6, 170–173.
155. Neel, A. J.; Hehn, J. P.; Tripet, P. F.; Toste, F. D. *J. Am. Chem. Soc.* **2013**, *135*, 14044–14047.
156. Milo, A.; Neel, A. J.; Toste, F. D.; Sigman, M. S. *Science* **2015**, *347*, 737–743.
157. Lackner, A. D.; Samant, A. V.; Toste, F. D. *J. Am. Chem. Soc.* **2013**, *135*, 14090–14093.
158. Yang, Z.; He, Y.; Toste, F. D. *J. Am. Chem. Soc.* **2016**, *138*, 9775–9778.
159. Hamilton, G. L.; Kang, E. J.; Mba, M.; Toste, F. D. *Science* **2007**, *317*, 496–499.
160. Zi, W.; Toste, F. D. *Angew. Chem. Int. Ed.* **2015**, *54*, 14447–14451.
161. Mukherjee, S.; List, B. *J. Am. Chem. Soc.* **2007**, *129*, 11336–11337.
162. Tsai, C. -C.; Sandford, C.; Wu, T.; Chen, B.; Sigman, M. S.; Toste, F. D. *Angew. Chem. Int. Ed.* **2020**, *132*, 14755–14763.
163. Ohmatsu, K.; Ito, M.; Kunieda, T.; Ooi, T. *Nat. Chem.* **2012**, *4*, 473–477.
164. Nelson, H. M.; Williams, B. D.; Miró, J.; Toste, F. D. *J. Am. Chem. Soc.* **2015**, *137*, 3213–3216.
165. Yamamoto, E.; Hilton, M. J.; Orlandi, M.; Saini, V.; Toste, F. D.; Sigman, M. S. *J. Am. Chem. Soc.* **2016**, *138*, 15877–15880.
166. Avila, C. M.; Patel, J. S.; Reddi, Y.; Saito, M.; Nelson, H. M.; Shunatona, H. P.; Sigman, M. S.; Sunoj, R. B.; Toste, F. D. *Angew. Chem. Int. Ed.* **2017**, *56*, 5806–5811.
167. Liao, S.; List, B. *Angew. Chem. Int. Ed.* **2010**, *49*, 628–631.
168. Liao, S.; List, B. *Adv. Synth. Catal.* **2012**, *354*, 2363–2367.
169. Satake, S.; Kurihara, T.; Nishikawa, K.; Mochizuki, T.; Hatano, M.; Ishihara, K.; Yoshino, T.; Matsunaga, S. *Nat. Catal.* **2018**, *1*, 585–591.
170. Taylor, M. S.; Jacobsen, E. N. *J. Am. Chem. Soc.* **2004**, *126*, 10558–10559.
171. Raheem, I. T.; Thiara, P. S.; Peterson, E. A.; Jacobsen, E. N. *J. Am. Chem. Soc.* **2007**, *129*, 13404–13405.
172. Reisman, S. E.; Doyle, A. G.; Jacobsen, E. N. *J. Am. Chem. Soc.* **2008**, *130*, 7198–7199.
173. Zhao, C.; Chen, S. B.; Seidel, D. *J. Am. Chem. Soc.* **2016**, *138*, 9053–9056.
174. Kutateladze, D. A.; Strassfeld, D. A.; Jacobsen, E. N. *J. Am. Chem. Soc.* **2020**, *142*, 6951–6956.
175. De, C. K.; Klauber, E. G.; Seidel, D. *J. Am. Chem. Soc.* **2009**, *131*, 17060–17061.
176. Klauber, E. G.; De, C. K.; Shah, T. K.; Seidel, D. *J. Am. Chem. Soc.* **2010**, *132*, 13624–13626.
177. Klauber, E. G.; Mittal, N.; Shah, T. K.; Seidel, D. *Org. Lett.* **2011**, *13*, 2464–2467.
178. De, C. K.; Seidel, D. *J. Am. Chem. Soc.* **2011**, *133*, 14538–14541.

179. Min, C.; Mittal, N.; De, C. K.; Seidel, D. *Chem. Commun.* **2012**, *48*, 10853–10855.
180. Mittal, N.; Sun, D. X.; Seidel, D. *Org. Lett.* **2012**, *14*, 3084–3087.
181. Birrell, J. A.; Desrosiers, J. -N.; Jacobsen, E. N. *J. Am. Chem. Soc.* **2011**, *133*, 13872–13875.
182. De, C. K.; Mittal, N.; Seidel, D. *J. Am. Chem. Soc.* **2011**, *133*, 16802–16805.
183. Zurro, M.; Asmus, S.; Beckendorf, S.; Mück-Lichtenfeld, C.; Mancheño, O. G. *J. Am. Chem. Soc.* **2014**, *136*, 13999–14002.
184. Zurro, M.; Asmus, S.; Bamberger, J.; Beckendorf, S.; Mancheño, O. G. *Chem. Eur. J.* **2016**, *22*, 3785–3793.
185. Duong, Q. -N.; Schifferer, L.; Mancheño, O. G. *Eur. J. Org. Chem.* **2019**, 5452–5461.
186. Mancheño, O. G.; Asmus, S.; Zurro, M.; Fischer, T. *Angew. Chem. Int. Ed.* **2015**, *54*, 8823–8827.
187. Fischer, T.; Bamberger, J.; Mancheño, O. G. *Org. Biomol. Chem.* **2016**, *14*, 5794–5802.
188. Choudhury, R. A.; Mukherjee, S. *Chem. Sci.* **2016**, *7*, 6940–6945.
189. Fischer, T.; Duong, Q. -N.; Mancheño, O. G. *Chem. Eur. J.* **2017**, *23*, 5983–5987.
190. Schafer, A. G.; Wieting, J. M.; Fisher, T. J.; Mattson, A. E. *Angew. Chem. Int. Ed.* **2013**, *52*, 11321–11324.
191. Wieting, J. M.; Fisher, T. J.; Schafer, A. G.; Visco, M. D.; Gallucci, J. C.; Mattson, A. E. *Eur. J. Org. Chem.* **2015**, 525–533.
192. Hardman-Baldwin, A. M.; Visco, M. D.; Wieting, J. M.; Stern, C.; Kondo, S.; Mattson, A. E. *Org. Lett.* **2016**, *18*, 3766–3769.
193. Lin, S.; Jacobsen, E. N. *Nat. Chem.* **2012**, *4*, 817–824.
194. Pupo, G.; Ibba, F.; Ascough, D. M. H.; Vicini, A. C.; Ricci, P.; Christensen, K. E.; Pfeifer, L.; Morphy, J. R.; Brown, J. M.; Paton, R. S.; Gouverneur, V. *Science* **2018**, *360*, 638–642.
195. Zhang, H.; Lin, S.; Jacobsen, E. N. *J. Am. Chem. Soc.* **2014**, *136*, 16485–16488.

5

ASYMMETRIC PEPTIDE CATALYSIS

Kazuaki Kudo
Institute of Industrial Science, The University of Tokyo, Tokyo, Japan

5.1. INTRODUCTION

The research on peptide catalysis has made great strides in these two decades. Nowadays, many kinds of reactions are in the sight of peptide catalysts including acid/base, redox, and even radical catalysis.

In general, the asymmetric molecular catalysts consist of two parts. One is a catalytic center that directly interacts with substrates and activates them to make the reactions occur. In some cases, a catalyst molecule may have two or more catalytic centers that cooperatively activate substrates. The other is rest of the catalyst molecule that provides microenvironment by its three-dimensional (3D) shape and several contact points to "pin" the substrates through a variety of intermolecular interactions to ensure the enantioselectivity of the reaction.

Enzymes have large-sized microenvironment made of folded polypeptide chain to realize lock-and-key-like shape complementarity with substrates, which results in strict molecular recognition in the biogenic reactions. Modification of enzyme molecules to purposely designed catalyst may be possible by biotechnological method, but is cumbersome and has a limitation in a catalytic reaction scope. On the other hand, small molecular catalysts are easier to be modified based on established synthetic chemistry. However, their size of the microenvironment is relatively small and sometimes they cannot provide efficient contact points leading to a restriction of substrates and types of catalytic reactions. Peptide catalysts comprise the advantages of the above two because of their molecular size and modular nature, thus three-dimensionally designed enough-sized microenvironment is available by well-established peptide synthesis procedures along with modifiability of amino acid molecules [1].

Within a living organism, some enzymes work as organocatalyst and others as metal-centered catalyst. These two categories can also apply for peptide catalysts. In fact, many reports on "metallopeptide catalysts" have appeared. However, since this chapter is included in the organocatalyst group, and due to the limited space, only the peptides that work as organocatalysts will be addressed here. The development of metallopeptide catalysts is reviewed elsewhere [2, 3].

Historically, asymmetric peptide catalysis started with poly(amino acid)s (PAAs). In the mid-1970s, Inoue and coworkers reported a PAA-catalyzed enantioselective Michael addition of thiols to enones. After several years, Juliá, Colonna, and their coworkers demonstrated asymmetric epoxidation of chalcones catalyzed by helical PAAs. Around the same time, Nonaka and coworkers found electrochemical asymmetric oxidation/reduction mediated by PAA-coated electrodes. On the other hand, asymmetric small-peptide catalysis was first reported by the Inoue's group for hydrocyanation of aryl aldehydes in the late 1970s, and a study on enantiomer-discriminating hydrolysis of esters by Ohkubo and coworkers

Catalytic Asymmetric Synthesis, Fourth Edition. Edited by Takahiko Akiyama and Iwao Ojima.

appeared in the early 1980s. After stagnant growth period, Miller and coworkers disclosed rationally designed peptide catalysts for the acylation of alcohols in the late 1990s. This finding, along with the emergence of asymmetric aminocatalysis by small molecules in 2000, brought renaissance of this research field.

Nowadays, some of the peptide catalysts show versatility for different kinds of catalytic reactions, which is shown in Figure 5.1.

Miller and coworkers have been continuously and intensively working on peptide catalyst **1** with turn structure. In 1998, they utilized peptide **1a** for acylation of secondary alcohols. In 2007 they demonstrated catalytic asymmetric epoxidation of C=C bond with **1b**-related peptide through peracid intermediate, and extended that reaction to a site-selective epoxidation of the substrates with multiple C=C bonds. Then in 2010 they showed the viability of the tetrapeptide **1c** as asymmetric aminocatalyst in atroposelective bromination of biaryls, and the same peptide was further utilized as a catalyst for atroposelective coupling reaction in 2020.

In 2001, the same group developed another peptide catalyst **2** for acylation of hydroxyl group, of which the substrate scope is complementary to **1a**, by means of a library screening method. This catalyst was applicable to other selective OH-derivatization reactions.

In 2005, Wennemers and coworkers showed that an N-terminal prolyl tripeptide **3a** with a turn structure efficiently catalyzes asymmetric intermolecular aldol reaction via an enamine mechanism. Three years later, their group succeeded catalytic asymmetric nitro Michael reaction with structurally related peptide **3b**. For both cases, the side chain carboxylate plays important role in the catalytic process.

In 2008, Schreiner and coworkers developed an asymmetric acylation of 1,2-diols with using a peptide catalyst **4** containing an artificial amino acid with adamantine skeleton. Due to the presence of this residue, the whole peptide chain adopts a restricted conformation to efficiently interact with substrates. This catalyst was later used in asymmetric Dakin-West Reaction.

Also in 2008, Kudo and coworkers presented asymmetric hydrogenation of enals catalyzed by resin-immobilized peptide **5** having turn and helix structures, via an iminium ion intermediate. The polyleucine part was made by the polymerization of *N*-carboxyanhydride. Besides Michael addition to enals with other nucleophiles, this peptide catalyst was also viable to an α-oxyamination of aldehydes, which proceeds via an enamine intermediate.

In 2014, the same group demonstrated that a simple helical peptide **6** can serve as an asymmetric catalyst for the reactions of enones and α-branched aldehydes.

Most of the reactions catalyzed by the peptides in Figure 5.1 show a high degree of selectivity, and some are difficult to be achieved by low-molecular-weight catalysts or enzymes. Those include the enantioselective reactions that control point chirality, axial chirality, and planar chirality. In some cases, even regio- or site-selective reactions are realized.

As can be seen in these examples, the catalytic center is either *N*-terminal amino group or a functional group on a side chain, and even for the latter cases, generally the catalytically active amino acid is placed at N-terminal. This might save the catalytic centers from being buried in folded peptide chain and ensure them to efficiently contact with the substrate molecules. From the viewpoint of catalyst preparation, it is also advantageous to introduce the catalytic center at the N-terminus when the active site is the artificially designed functional group on unnatural amino acid; this can avoid any possible synthetic problems during the peptide elongation process (e.g. epimerization, side reactions), which might be caused by such functional groups.

The other characteristic is that, in most cases, non-natural amino acids including protected ones and D-amino acids are employed. By using such amino acids, purposeful secondary structure can be obtained more easily compared to the peptide with only proteinogenic amino acids.

It should be mentioned that the peptides shown in Figure 5.1 are not always the best catalyst for a given reaction. Rather they should be considered as "lead catalysts" that await an appropriate modification.

Several reviews on asymmetric peptide catalysts have been published [4]. Especially comprehensive are two reviews in a series written by Miller and coworkers in 2007 [4c] and in 2020 [3]. Including these two, most of reviews are arranged by reaction class as organized elements. On these backgrounds, this chapter is intended not to exhaustively introduce every peptide catalysts but rather to summarize focusing on the catalytic center.

Miller and coworkers

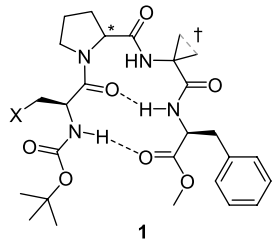

1

1a: X =  *Pmh*

(* = D, † = CH_3 / CH_3)

1b: X = 

(* = D or L, † = CH_2-CH_2)

1c: X =  *Dmaa*

(* = D, † = CH_3 / CH_3)

- acylative kinetic resolution of alcohols
- site selective phosphorylation of *myo*-inositol-derivative
- epoxidation
- pyridine *N*-oxidation
- atropo selective phenol bromination
- fragment coupling to axially chiral biaryls

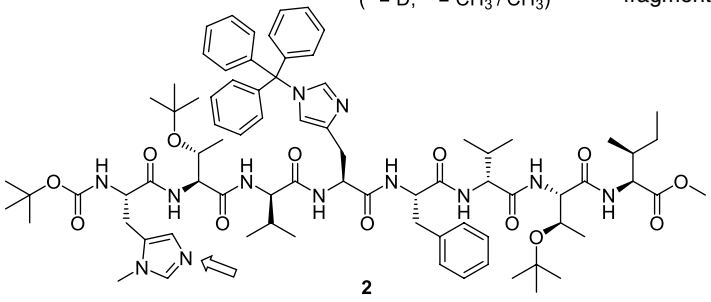

2

- acylative kinetic resolution of alcohols
- dynamic kinetic resolution of sulfinyl chloride
- site selective thiocarbonylation of sugar derivatives

Wennemers and coworkers

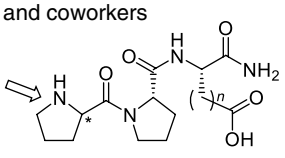

3

3a (* = L, *n* = 1) - cross aldol reaction

3b (* = D, *n* = 2) - nitro Michael addition

Schreiner and coworkers

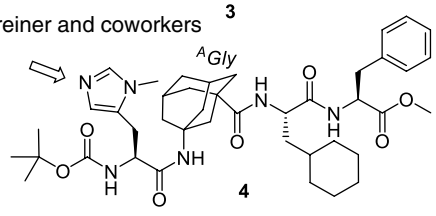

4

- acylative kinetic resolution/ desymmetrization of 1,2-diols
- Dakin-West Reaction

Kudo and coworkers

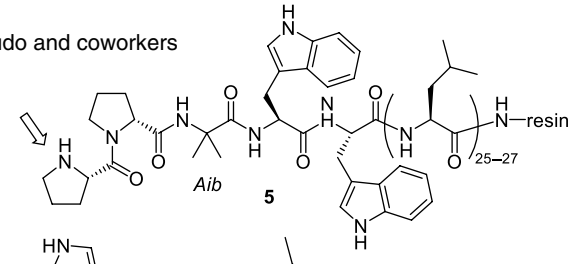

5

- Michael addition to enals
- α-oxyamination of aldehydes

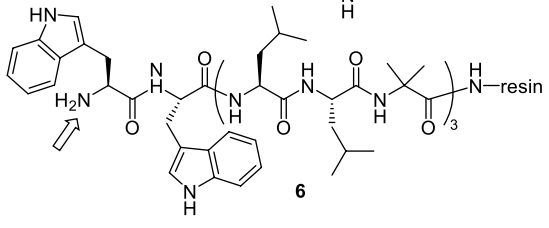

6

- Michael addition to enones
- α-amination of crowded aldehydes

Figure 5.1. Some "standard" peptide catalysts applied to two or more asymmetric reactions. The parts indicated by arrows are main catalytic center. Names in italic are an abbreviation for unnatural amino acids.

5.2. CATALYSIS BY N-TERMINAL AMINO GROUP OF PEPTIDES

In 1975, Inoue and coworkers reported the first peptide-catalyzed asymmetric reaction, which was the conjugate addition of a thiol to an enone (Scheme 5.1). As for the catalyst, helix-forming poly(γ-benzyl L-glutamate), poly(β-benzyl L-aspartate), and poly(alanine) were examined [5]. The enantioselective step of this reaction was a protonation of the intermediate enolate anion, which was thought to be associated by formation of ion pair with a terminal ammonium ion on the peptide chain.

In 1980, Juliá and coworkers reported a helical polyalanine-catalyzed asymmetric nucleophilic epoxidation of chalcone by alkaline hydrogen peroxide with very high enantioselectivity (Scheme 5.2) [6]. A detailed study by Juliá, Colonna, and their coworkers revealed that polyleucine is equally good catalyst [7].

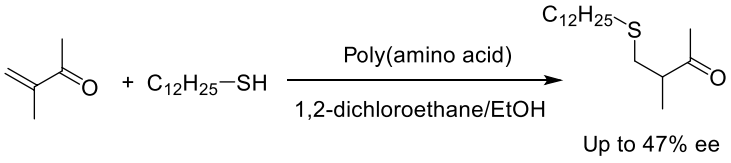

Scheme 5.1. Poly(amino acid)-catalyzed asymmetric Michael addition.

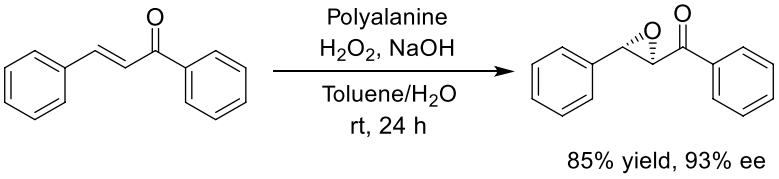

Scheme 5.2. Polyalanine-catalyzed asymmetric epoxidation (Juliá–Colonna epoxidation). Source: Based on [6].

In 2001, Roberts and coworkers showed that in case the terminal amino group of polyleucine is acetylated, methylated, or dimethylated, the enantioselectivity decreases [8]. This indicates that the amino group participates in the catalytic process. The Juliá-Colonna reaction will be discussed at the end of this section.

5.2.1. Enamine Catalysis

Another finding in earlier days related to peptide catalyst is a proline-catalyzed asymmetric intramolecular aldol condensation. In the 1970s, Weickert and coworkers [9] and Hajos and coworkers [10] independently reported proline-catalyzed Robinson annulation to yield a precursor alcohol for Wieland-Miescher ketone with high enantioselectivity (Scheme 5.3). This is a net intramolecular desymmetrization via an aldol reaction.

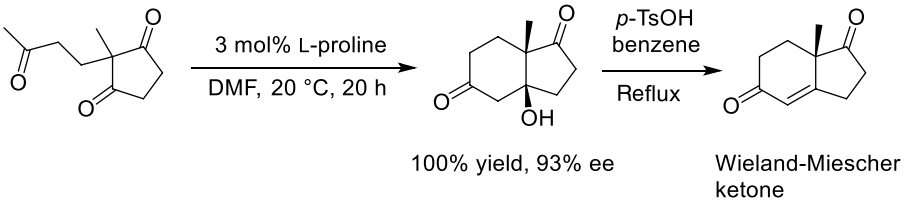

Scheme 5.3. Proline-catalyzed asymmetric Robinson annulation (Hajos–Parrish-Eder–Sauer–Wiechert reaction).

After more than 20 years, a seminal report by List, Lerner, and Barbas appeared in 2000, which describes a proline-catalyzed intermolecular asymmetric aldol reaction of acetone with aryl- or α-substituted alkylaldehydes via enamine intermediate (Scheme 5.4) [11].

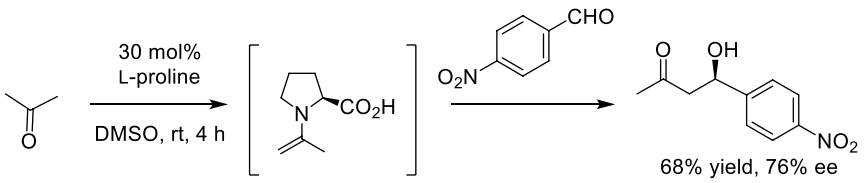

Scheme 5.4. Proline-catalyzed asymmetric cross aldol reaction. Source: Based on [11].

The above finding brought about an explosive spread of this enamine chemistry to utilize wide variety of proline-related compounds as catalysts. Roughly speaking, there were two choices for the improvement of proline catalyst. One is to modify the structure of proline by introducing a substituent or by derivatizing the carboxylate group to other functional groups. The other is to make *N*-terminal-prolyl peptides. Peptide would provide an asymmetric environment similar to that in enzymes to realize a high enantioselectivity in the aldol reaction. In relation with this, further recognition of substrates can potentially lead to site- or chemoselective transformations. From a different aspect, relevance to the prebiotic chemistry is of another interest. To date, more than 60 reports on this reaction with using di- to heptapeptide catalyst have appeared[12–20], most of which are covered in the two reviews by Miller and coworkers with in-depth explanation [3, 4c]. In many of the reports, the reactions of 4-nitrobenzaldehyde (4NBA) with acetone and/or cyclohexanone are demonstrated as benchmarks (Scheme 5.5).

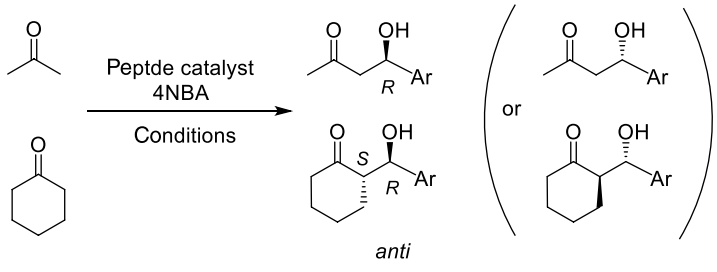

Scheme 5.5. Stereochemical outcome for the peptide-catalyzed asymmetric cross aldol reaction.

Major characteristic points are as follows:

1. Not only the N-terminal prolyl peptides, but alanyl, valyl, or arginyl peptides are also viable catalysts [13]. In some cases, C-terminal is immobilized on resin, other solid material, or dendrimer [14].
2. The reactions were performed not only in organic solvents, but also in aqueous solvents [15], in water [16], or brine [17], and even by ball-milling procedure [18]. Aggregated-state peptide catalysts such as micellar or liquid crystalline form have been also reported [19]. In some reactions in organic solvents, addition of water results in the reversal of enantioselectivity [20].
3. For the reaction of acetone and 4NBA catalyzed by *N*-terminal L-prolyl peptide, the enantioselectivity is roughly as follows: if the peptide catalyst does not contain free carboxylic acid, the major product is *R*-isomer. In case with COOH-containing peptides, some give *S*-product and others give *R*. This indicates the participation of COOH group in the enantiodetermining step.
4. In most cases, the reaction of cyclohexanone and 4NBA gives *anti* product as a major diastereomer.

5. For the two kinds of aldol donors, there is a consistency in the stereochemistry of OH-bound carbon with a small number of exception. Namely, a catalyst that gives *R*-isomer for the reaction of acetone affords (2*S*)-2-[(*R*)-hydroxy(4-nitrophenyl)methyl]cyclohexanone.

In 2003, Reymond and coworkers reported the first peptide catalyst for this reaction [12a]. They used trifluoroacetic acid (TFA) salt of peptide that was in situ neutralized with *N*-methylmorpholine. For the reaction of acetone with 4NBA, several efficient catalysts were found, and the maximum ee value was 66% (*R*) for H-Pro-Glu-Leu-Phe-OH. Soon after, List and coworkers' work was published, and ee of the product was close to the result with proline (77% ee (*R*) for H-Pro-Ser-OH) [12b]. An improvement in enantioselectivity was reported by Gong and coworkers in 2004. They showed that the reaction of hydroxyacetone and 4NBA in THF/H_2O at 0 °C for six days catalyzed by 10 mol% of H-Pro-Phe-Phe-Phe-Phe-OH gave (*R*)-1,4-dihydroxybutan-2-one derivative as a major regioisomer with 87% ee [15a].

As for the benchmark compound acetone, in 2005, Wennemers and coworkers showed that use of 5 mol% of H-Pro-Pro-Asp-NH-resin, an immobilized version of peptide **3a**, gave the product with 90% ee (*S*) when the reaction was conducted at –20 °C [12d]. They also found that another peptide H-Pro-D-Ala-D-Asp-NH-resin also efficiently catalyzed the same reaction to give *R*-product with 81% ee. It is worth to mention that, although both catalyses proceed enamine formation with L-proline part of the peptide, the resulting products show complementarity in their chirality. They found these two peptide catalysts from over 3000 resin-bound tripeptide library including D-amino acids by a high throughput screening, which was based on co-immobilization of catalyst and substrate on a resin; upon the reaction with externally added dye-connected aldehyde, the beads containing catalytically active peptide acquire color, and they can be isolated and subjected to the sequence analysis (Scheme 5.6) [21].

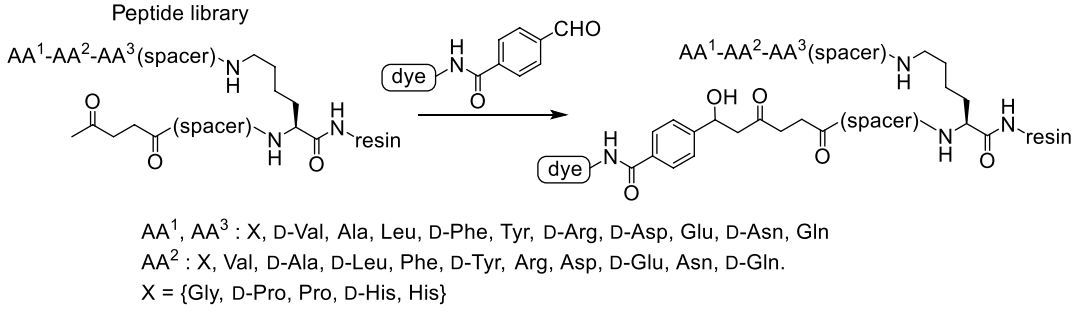

Scheme 5.6. Combinatorial approach for screening of peptide catalyst for cross aldol reaction. Source: Based on [21].

Kudo and coworkers reported the aldol reaction of acetone under aqueous conditions with using a tripeptide catalyst H-D-Pro-Tyr-Phe-NH-resin (quantitative yield, 71% ee (*S*)) [14b]. Five-times reusability of the catalyst was confirmed without any significant loss in catalytic activity or selectivity. They applied this catalyst to two kinds of one-pot sequential reactions in which the first step is an aldehyde-generating reaction. Starting from an acetal, the immobilized acid-catalyzed hydrolysis and the subsequent catalytic asymmetric aldol reaction by the resin-bound peptide proceeded smoothly to give the aldol product without observation of neutralization-based deactivation (Scheme 5.7a) [14d]. The combined resin could be reused for five times. Another solid catalyst-promoted two-step reaction is oxidation/aldol using benzylic alcohol as a substrate (Scheme 5.7b) [14i]. It is interesting to note that the adsorption of cupper ions on the peptide resin did not deteriorate the catalytic activities. Recyclability was also mentioned.

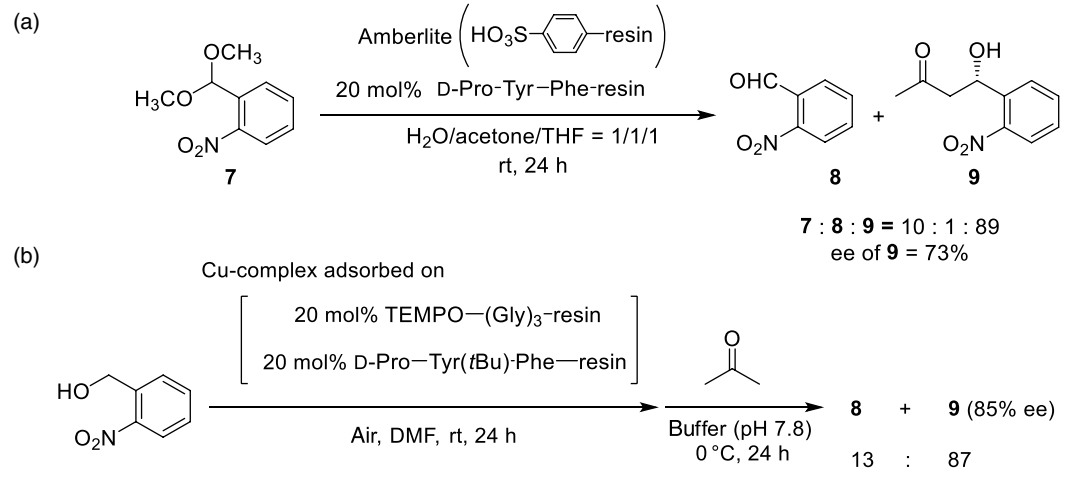

Scheme 5.7. One-pot sequential reactions including peptide-catalyzed asymmetric aldol reaction; a) the reactions starting from acid-catalyzed acetal deprotection, and b) the reactions starting from copper-catalyzed aerobic oxidation of benzylic alcohol. Source: Based on [14d, 14i].

Berkessel and coworkers have shown that the proline-derived catalysts have retro-aldol reaction ability [22]. With focusing on the reversible nature of peptide-catalyzed aldol reactions, Kudo and coworkers utilized the asymmetric aldol reaction chemistry in kinetic resolution of planar chiral compounds (Scheme 5.8) [14p]. Arylaldehydes with ansa cyclophane framework were treated with peptide catalysts to give the corresponding aldol product, and then the reaction mixture was treated with an antipode of the original peptide catalyst to promote retro-aldol reaction. The first step proceeded to give (S_p,*S*)-product as a major isomer with moderate enantioselectivity but high diastereoselectivity. In the second step, retro-aldol reaction of (X_p,*R*)-isomer (*X* = either *R* or *S*) preferentially occurred leading to the increase in the ee of aldols.

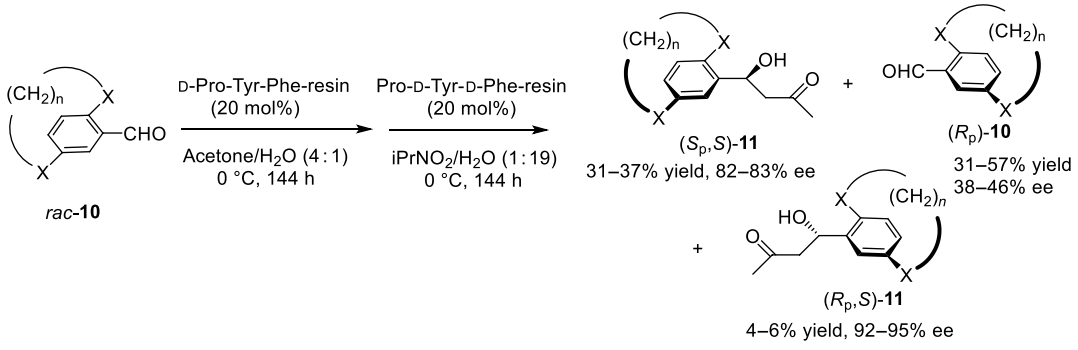

Scheme 5.8. Peptide-catalyzed kinetic resolution of planar chiral ansa cyclophanes. Source: Based on [14p].

Du and coworkers showed that the enantiomer selective dehydration of aldol is possible by using N-terminal valyl peptide catalyst (Scheme 5.9) [23]. The dehydration process was thought to be assisted by the carboxylate group at C-terminus.

Other than aldol reaction, List and coworkers utilized N-terminal prolyl peptide for the conjugate addition of ketones to nitroalkenes, although with low enantioselectivity [24]. Cordova and coworkers showed that H-Ala-Ala-OH-catalyzed nitro Michael addition of cyclohexanone and other six-membered

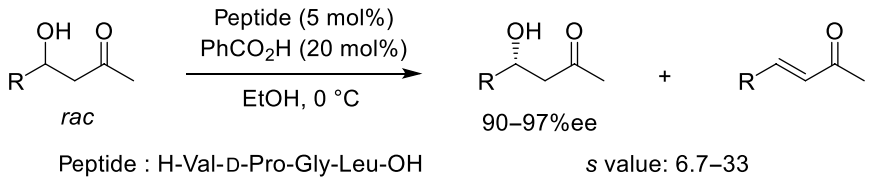

Scheme 5.9. Peptide-catalyzed kinetic resolution of aldols via enantiomer discriminating dehydration. Source: Based on [23].

ring ketones gives the product with high diastereoselectivity (>12 : 1) and enantioselectivity (>90%ee). However, in case the Michael donor is either cyclopentanone or linear ketone, the stereoselectivities were considerably lower (Scheme 5.10) [25].

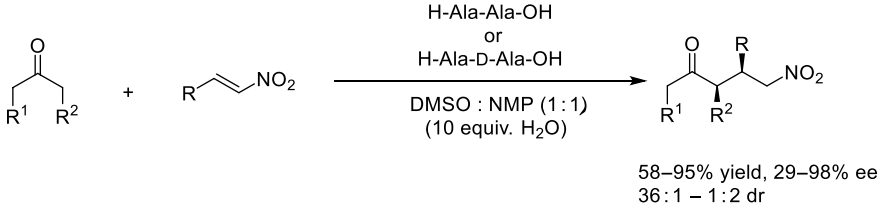

Scheme 5.10. Peptide-catalyzed diastereo-/enantioselective nitro Michael addition of ketones. Source: Based on [25].

Wennemers and coworkers demonstrated that the peptide-catalyzed conjugate addition of aldehydes to nitroalkenes proceeds in a highly enantioselective manner. Starting from the peptide **3a** that was previously found in the aldol reaction, they developed a new catalyst **3b** that gives the Michael adduct with >95% ee (Scheme 5.11a) [26]. This reaction was extended to diastereo/enantioselective version to obtain syn isomer with high ee (Scheme 5.11b) [27]. Worth to mention is this reaction requires only 1% of peptide catalyst. After fine-tuning of the reaction conditions, they showed that the catalyst amount can be reduced to 0.1% [28].

This peptide could be used in immobilized state on resin as heterogeneous catalyst [29]. As high as 30 times recyclability was demonstrated without loss of activity and selectivity. This immobilized catalyst was also applied to continuous flow system with a flow rate of 0.12 ml/min and residence time of 1.8 h to give the corresponding product with 30 : 1 syn/anti ratio and 95% ee in a multigram scale [30].

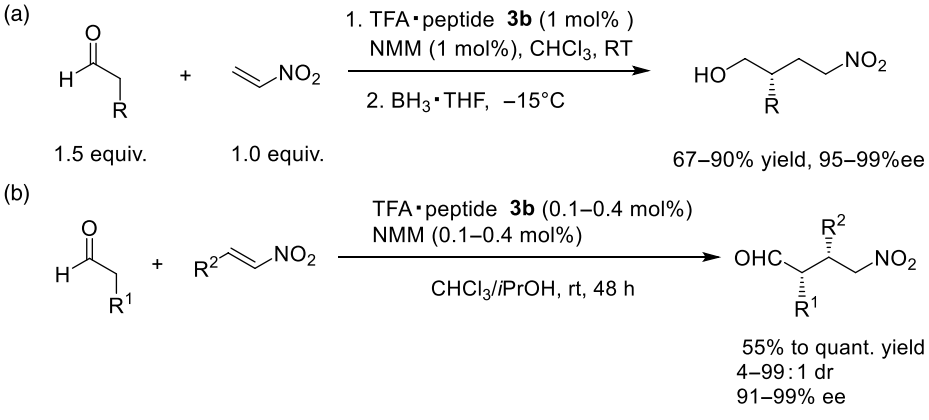

Scheme 5.11. Peptide-catalyzed stereoselective nitro Michael addition of aldehydes; (a) enantioselective reaction, (b) *syn*-diastereoselective and enantioselective reaction. Source: Based on [26, 27].

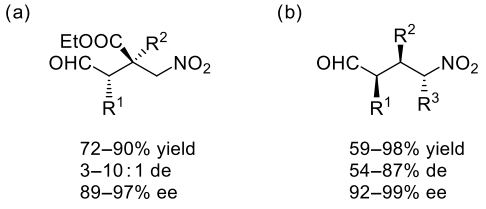

Figure 5.2. Structure of diastereo-/enantioselective nitro Michael adducts; (a) product with an all-carbon quaternary chiral center and (b) product with three contiguous chiral centers.

They extended this reaction to synthetically more challenging stereocontrol in two ways. One is the construction of all-carbon quaternary center [31]. By using (*Z*)-α-ethoxycarbonyl-β-nitrostyrenes, the Michael addition of aldehydes was investigated. Starting from peptide **3b**, the catalyst structure was finally optimized to be H-D-Pro-Pro-NH-(*R*)-CH(Ph)CH_2(*p*-Me)C_6H_4 (Figure 5.2a). The other is control of three contiguous stereogenic centers [32]. The reaction of aldehydes with (*E*)-β-alkyl-β-nitrostyrenes was studied. H-Pro-Pro-D-Gln-OH and H-Pro-Pro-Asn-OH were found to be equally viable catalysts to give mainly 2,3-*syn*-3,4-*anti* product with very high ee (Figure 5.2b).

They systematically compared stereoisomeric tripeptides H-Pro-Pro-Glu-OH and tetrapeptides H-Pro-Pro-Glu-Pro-OH as asymmetric catalyst [33]. It was found that, for the above asymmetric nitro Michael addition, peptide **3b** with DLL stereochemistry was better than tetrapeptide, while the enantioselectivity with other stereoisomeric tripeptides was considerably improved by introducing the "additional" proline at the C-terminals.

Wennemers' group demonstrated that not only nitroolefins but also maleimides are feasible as a Michael acceptor. By using **3b**-related peptide, H-D-Pro-Pro-Asn-NH_2, the corresponding adduct was obtained in high yield and with high diastereomeric/enantiomeric excess [34].

In the field of peptide catalysis, compared to the enantioselectivity control, the diastereoselectivity control has not been well explored. Concerning this, Wennemers and coworkers reported catalyst-controlled *anti*-selective nitro Michael addition [35]. Their strategy was to tune the amino acid structure rather than peptide sequence. By using the **3**-related peptide as a catalyst, *anti* adduct was preferentially formed with quite high ee (Scheme 5.12).

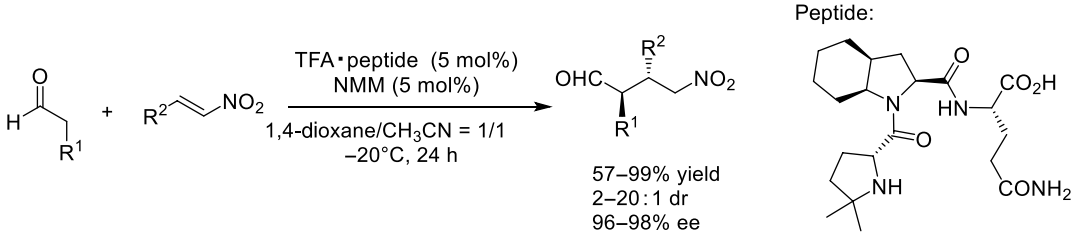

Scheme 5.12. Peptide-catalyzed *anti*-diastereoselective and enantioselective nitro Michael addition of aldehydes.

Other than C–C bond-forming reactions, enamine-mediated α-functionalization of aldehydes catalyzed by peptide **5** was reported by Kudo and coworkers (Table 5.1) [36]. The reaction with TEMPO under oxidizing conditions afforded α-oxyaminated aldehydes with higher ee. For this reaction, they employed peptide catalyst **5**. Use of cupper(I) salt under oxygen atmosphere increased the oxidizing power, hence could be applied to one-pot sequential oxidation/α-oxyamination of alcohols [37]. Instead of the metal salts, laccase could be used for the α-oxyamination. For that case, the reaction was carried out in a buffer, and production of both α-oxyaminated aldehyde and carboxylic acid was possible depending on the presence/absence of detergent in a reaction system [38].

TABLE 5.1. Asymmetric α-oxyaminaton of aldehyde and its variation.

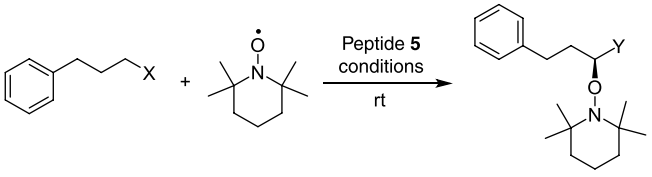

Entry	X	Y	Conditions	Yield (%)	ee (%)	Ref.
1	CHO	CHO	4 equiv. TEMPO, 3 mol% **5**, 10 mol% $FeCl_2 \cdot 4H_2O$, 10 mol% $NaNO_2$, air, 24 h	87	90	[36]
2	CH_2OH	CHO	4 equiv. TEMPO, 20 mol% **5**, 30 mol% CuCl, 30 mol% 2,2'-bipyridine, O_2, 36 h	76	90	[37]
3	CHO	CHO	1 equiv. TEMPO, 20 mol% **5**, laccase, acetate buffer (pH 4.4), air, 1 h	77	86	[38]
4	CHO	CO_2H	1.5 equiv. TEMPO, 20 mol% **5**, laccase, acetate buffer (pH 4.4), air, 0.2 vol% Tween80, 5 h	78	91	[38]

They also presented a peptide-catalyzed asymmetric α-amination of aldehydes, using azodicarboxylate as an electrophilic nitrogen source (Scheme 5.13) [39]. Ten times of catalyst reuse was demonstrated without any loss of selectivity, although efficiency was slightly lowered.

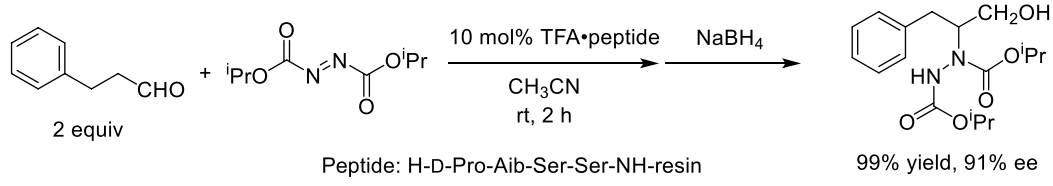

Scheme 5.13. Peptide-catalyzed asymmetric α-amination of aldehydes. Source: Based on [39].

5.2.2. Iminium Ion Catalysis

Besides enamine catalysis, primary and secondary amines are known to have a potential for iminium ion catalysis [40]. In 2000, the concept of iminium ion catalysis was proposed by Macmillan and became prevalent among synthetic chemists [41]. Earlier to this report, in 1994, Yamaguchi and coworkers showed that proline rubidium salt catalyzes asymmetric Michael addition of nitroalkanes to enones (Scheme 5.14) [42]. In their paper, intermediacy of iminium salt was proposed. After 10 years, this reaction was realized with peptides by Tsogoeva and coworkers, using unique oligomers of 4-*trans*-aminoproline with an assistance of *trans*-2,5-dimethylpiperazine [43].

In 2008, Kudo and coworkers reported an enantioselective Michael addition of hydride from Hantzsch ester to enals catalyzed by peptide **5** in aqueous solvents (Scheme 5.15) [44]. Although the catalytic center is N-terminal proline, helical polyleucine part was indispensable for catalyst performance. Infrared (IR) spectral analysis of the catalyst suggested that polyleucine stabilizes the turn structure at the N-terminal end of peptide chain under aqueous conditions.

Peptide catalyst **5** was also applicable to Friedel-Crafts type reaction of indoles and pyrroles to enals [45]. The optimization of the helical chain part of the peptide showed that those with repeated Leu-Leu-Aib sequence (Aib: 2-aminoisobutyric acid), which was developed by Tanaka and coworkers as 3_{10}-helix-inducing structure[46], gave even better result (Table 5.2).

This **5**-related peptide catalyst was also applied to a construction of all-carbon quaternary stereocenter (Scheme 5.16a) [47], a regio- and stereoselective 1,6-addition to dienal (Scheme 5.16b) [48], and a

TABLE 5.2. Effect of helical part of peptide catalyst for enantioselective Friedel-Crafts-type conjugate addition.

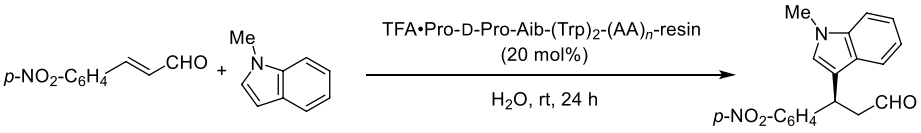

Entry	(AA)*n*	Conv. (%)	ee (%)
1	(Leu)*28.3*	63	86
2	Leu-Leu-Aib	84	82
3	$(Leu\text{-}Leu\text{-}Aib)_2$	92	91
4	$(Leu\text{-}Leu\text{-}Aib)_3$	90	92

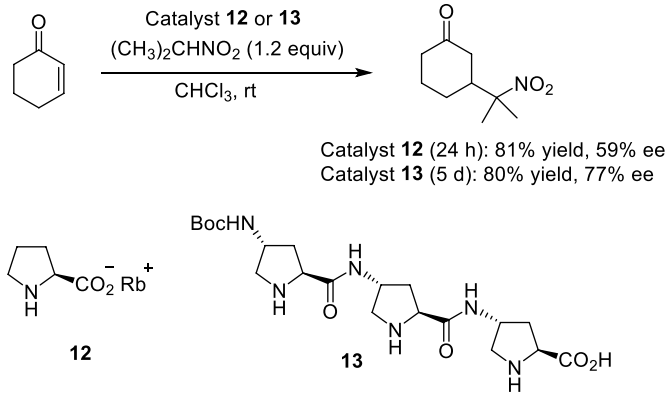

Scheme 5.14. Peptide-catalyzed asymmetric Michael addition of 2-nitropropane to cyclohex-2-en-1-one. Source: [42].

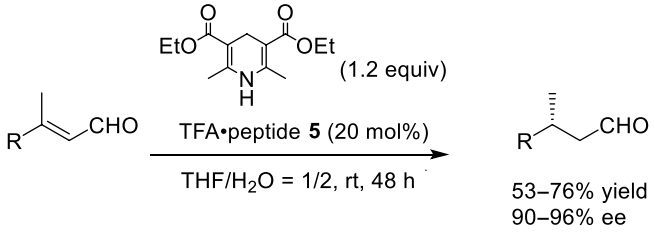

Scheme 5.15. Peptide-catalyzed asymmetric hydride conjugate addition to enals. Source: [44].

kinetic resolution of planar chiral metallocene derivatives (Scheme 5.16c) [49] after slight modification of the sequence. The last reaction could be extended to desymmetrization of 1,2-bis(2-formylviniy)ferrocene [50]. By using Hantzsch ester, monohydrogenated product was obtained in 25% yield, 91% ee, along with its intramolecular Michael addition product in 21% yield, 86% ee. Reaction of dienal was also studied with thiol nucleophiles to give bisadducts in moderate enantioselectivities [51].

Further optimization of **5**-related peptide catalyst was carried out for the Michael addition of malonate to enal by high throughput library screening [52]. Resin-bound N-terminal prolyl peptide library was subjected to the reaction of enal and dye-connected malonate. Conjugate addition to an intermediate iminium ion gives the corresponding enamine, which could be reduced by a borohydride to give the product-bound colored resin. Thus, by picking up the colored beads and by analyzing its sequence, catalytically active peptides could be identified (Scheme 5.17).

This assay method was applied for the library of H-Pro-D-Pro-Aib-X-Y-$(Leu\text{-}Leu\text{-}Aib)_2$-NH-resin, where X, Y = {Arg, Asp, Glu, His, Lys, Orn, Phe, Pro, Ser, Tyr} (Orn: L-ornithine). As a result, X-Y = Phe-His

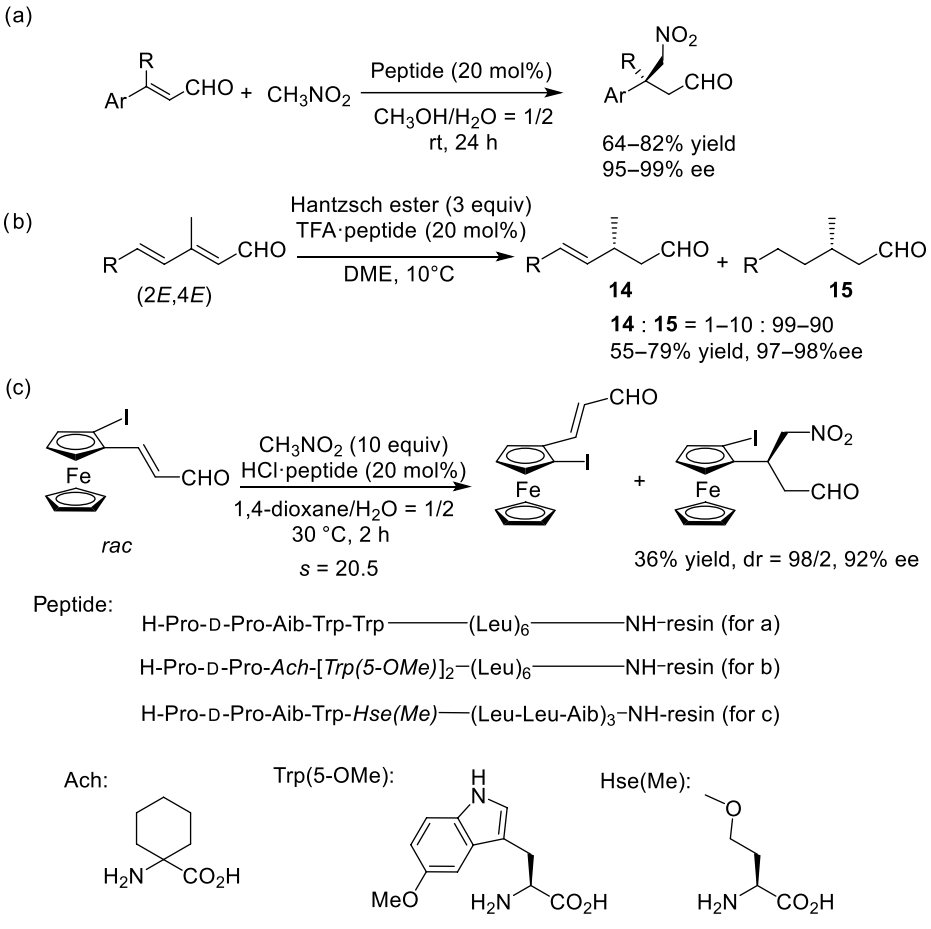

Scheme 5.16. Asymmetric conjugate additions catalyzed by turn-helix peptides; (a) all-carbon quaternary center formation, (b) regioselective 1,6-addition, and (c) kinetic resolution of planar chiral ferrocenes. Source: Based on [47–49].

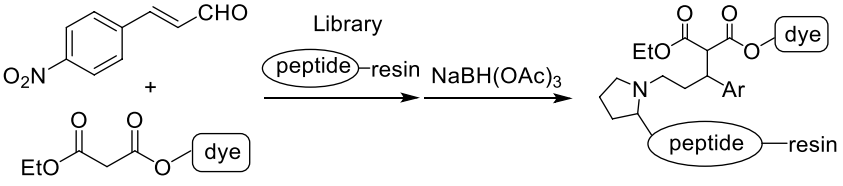

Scheme 5.17. Combinatorial approach for screening of peptide catalyst for Michael addition of dye-labelled malonate to an enal.

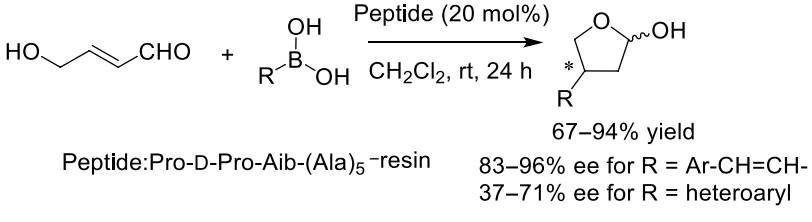

Scheme 5.18. Peptide-catalyzed asymmetric Michael addition of boronic acids to a γ-hydroxy-α, β-unsaturated aldehyde. Source: Based on [53].

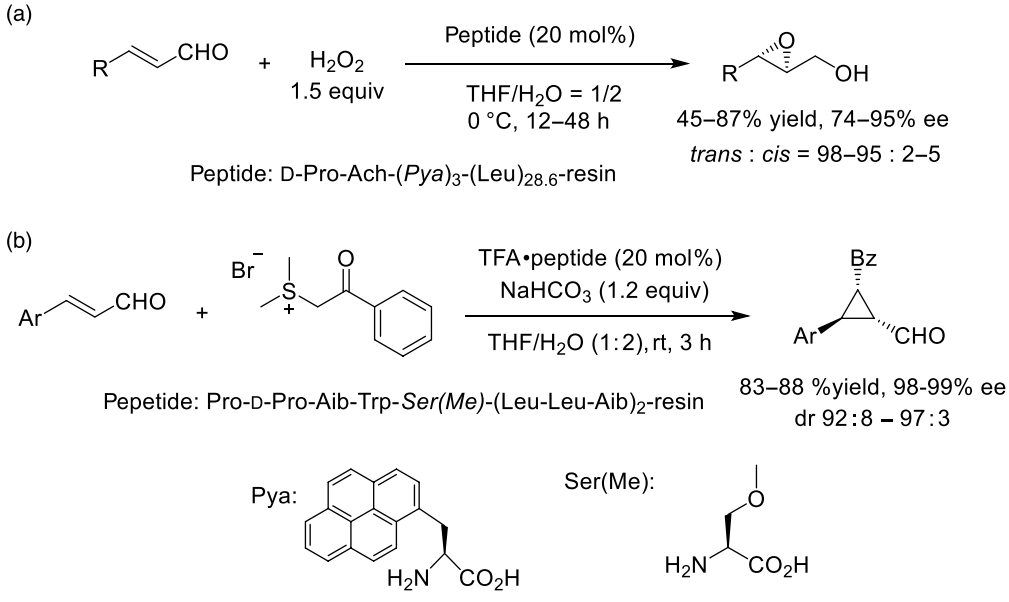

Scheme 5.19. Peptide-catalyzed diastereo-/enantioselective formation of three-membered cycles form enals using nucleophilic-electrophilic reagents; (a) epoxidation with hydrogen peroxide, and (b) cyclopropanation with sulfur ylide. Source: Based on [54].

and Tyr-His were found. The two new peptides gave better results than the parent peptide (X-Y = Trp-Trp), both for catalytic activity and enantioselectivity.

They also developed an asymmetric Michael addition of boronic acids to enals, for which the optimum peptide catalyst somewhat different from **5** was employed (Scheme 5.18) [53].

The conjugate addition to enals was successfully extended to the enantioselective epoxidation (Scheme 5.19a) [54] and diastereo-/enantioselective cyclopropanation [55] of enals, using nucleophiles having zwitterionic characters (Scheme 5.19b). For the latter, the substrate scope was complementary to the result with a chiral 2-carboxydihydroindole catalyst reported by Macmillan and coworkers [56].

With an intention to find a brand-new peptide sequence for catalyst, Kudo and coworkers extended their library study. Two libraries of H-Pro-AA^1-AA^2-AA^3-AA^4-AA^5-AA^6-NH-resin, library A: AA*n* = {Aib, His, Leu, D-Pro, Trp, Tyr} and library B: AA*n* = {Aib, D-Leu, Leu, D-Pro, Trp, Tyr}, were screened [57]. They found consensus sequences for each library, which was then subjected to the second-generation library screening, and finally reached to the peptide catalysts shown in Scheme 5.20. It is interesting to mention that although these two have same amino acids for N-terminal two residues, the enantioselectivity was contrary to each other.

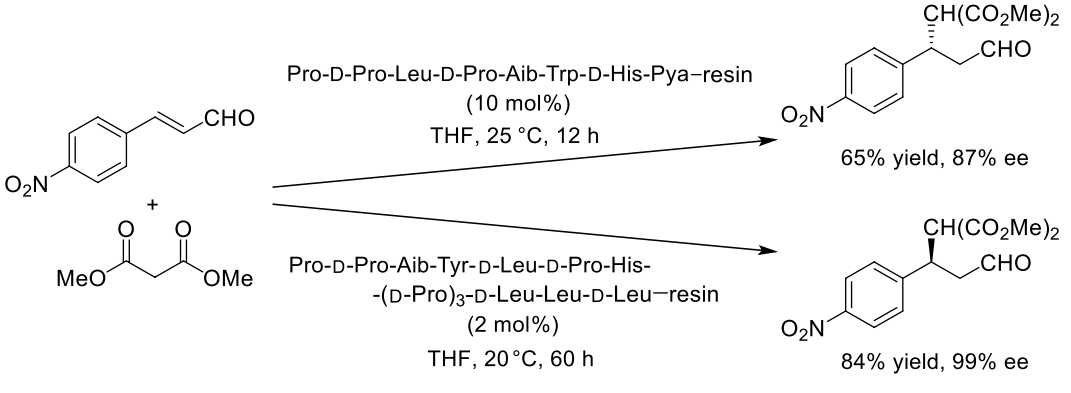

Scheme 5.20. Enantiodivergent Michael addition using peptide catalysts having Pro-D-Pro at their N-terminals.

When the screening was allowed in aqueous media, another unique sequence was obtained (Scheme 5.21) [58]. For this case, the amount of catalyst could be reduced to 0.3 mol%.

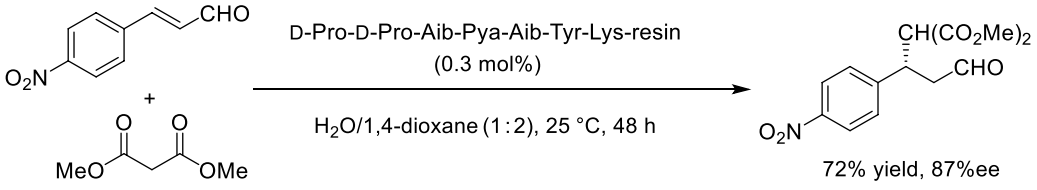

Scheme 5.21. Peptide-catalyzed enantioselective Michael addition of malonate to enal under aqueous conditions. Source: Based on [58].

The same group reported iminium-ion-mediated Michael addition to enones by utilizing peptide catalysts with N-terminal primary amino group. They first found the peptide **6** with helical Leu-Leu-Aib repeating unit as a viable catalyst for the addition of nitromethane and malonate esters (Scheme 5.22a) [59]. This catalyst was applied to a kinetic resolution of planar chiral [2.2] paracyclophane-derived enones after slight modification of peptide sequence (Scheme 5.22b) [60].

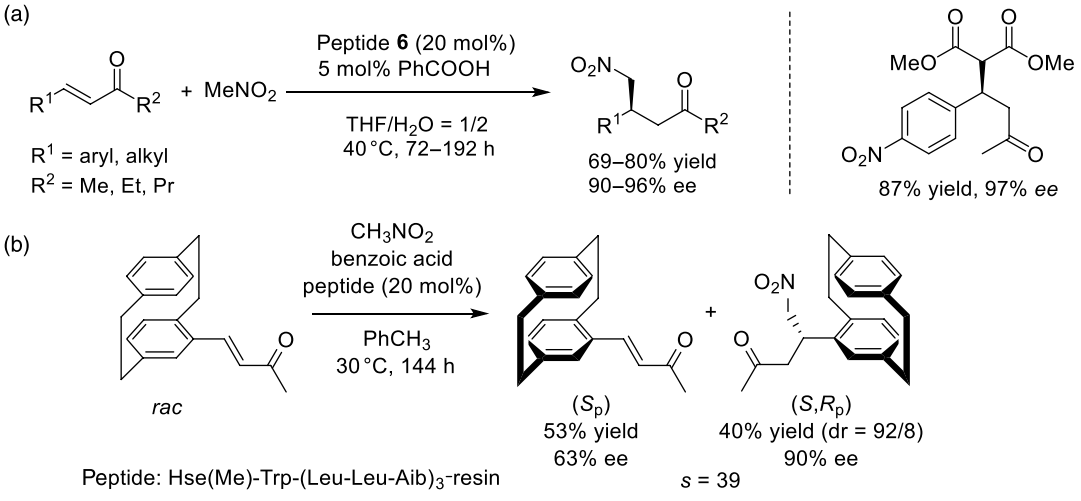

Scheme 5.22. (a) Peptide-catalyzed asymmetric Michael addition of carbon nucleophiles to enones and (b) its extension to kinetic resolution of planar chiral [2.2]paracyclophanes. Source: Based on [59, 60].

The catalyst **6** was also applicable to tandem Michael addition and α-amination (Scheme 5.23) [61].

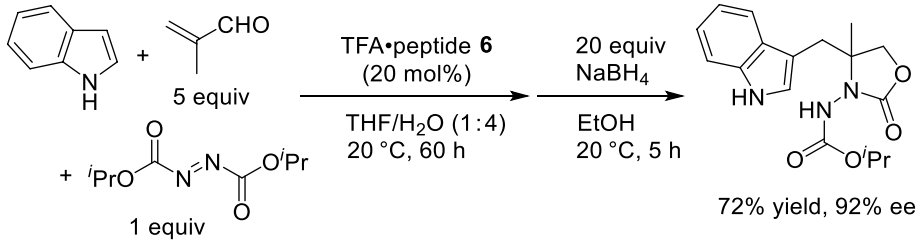

Scheme 5.23. Tandem Michael addition and asymmetric α-oxyamination of an enal catalyzed by immobilized peptide. Source: Based on [61].

Epoxidation of ketone was realized by using a peptide catalyst with terminal 1-pyrenylalanine. This reaction has similarity with Juliá-Colonna epoxidation, because the enantioselectivity is essentially induced by the helical peptide. Interestingly, despite the same right-handed helicity for polyleucine and $(Leu\text{-}Leu\text{-}Aib)_2$, the enantioselectivity was in an opposite sense for these two (Scheme 5.24) [62, 63].

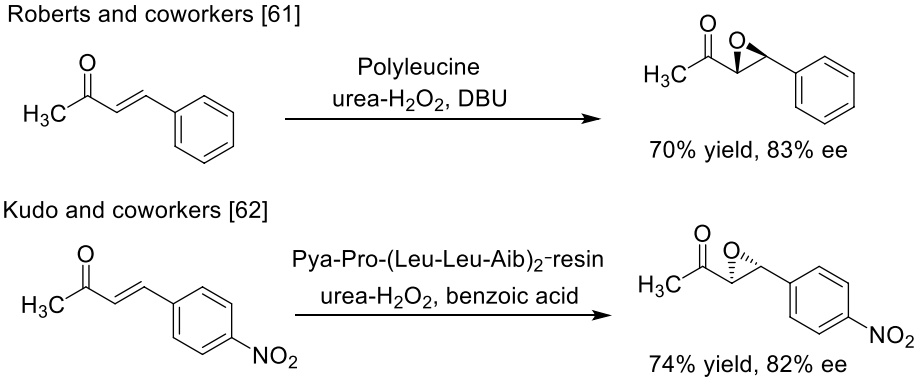

Scheme 5.24. Divergence in enantioselectivity for catalytic asymmetric epoxidation with right-handed-helical peptides. Source: [62, 63].

5.2.3. Other Type of Peptide Catalysts That Utilize Terminal Amino Groups

As mentioned in the beginning of this section, helical polyalanine/polyleucine catalyzes an asymmetric epoxidation of chalcone. For this Juliá-Colonna reaction, detailed review was already published by Miller and coworkers[4c], therefore will be only briefly mentioned here. The reaction was originally carried out in a triphasic system of toluene, water, and gel-state peptide [7]. In 1990, Itsuno and coworkers showed that a resin-immobilized polyleucine is a better catalyst with higher efficiency and reusability [64]. In 1995, Roberts and coworkers developed nonaqueous biphasic system using urea-hydrogen peroxide and DBU [65]. In 2004, Kelly and Roberts had proposed a mechanism of this reaction, which is now broadly accepted, based on accumulated experimental evidence: Fast, reversible, nonenantioselective addition of $^{-}$OOH to chalcone occurs first, and this is followed by slow, enantiomer-discriminating ring closure assisted by polyleucine to give the epoxide in an enantioselective manner [66]. The OOH adduct interacts with the α-helical peptide catalyst at its N-terminal by hydrogen bonding with three amide N-H groups that are not involved in helix-forming hydrogen bond network (Figure 5.3). In such a complex, one of the enantiomers is conformationally fixed so as to enolate π-orbital and O-OH σ*-orbital bond is efficiently overlapped to proceed the epoxide formation. This "triple hydrogen bonding" postulate was

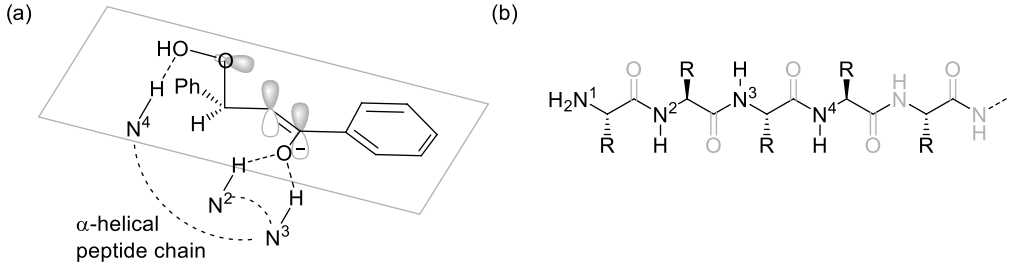

Figure 5.3. (a) Possible reaction intermediate for Juliá-Colonna epoxidation. Source: Based on [66]. (b) Molecular structure of peptide at around N-terminal. Grayed-out functional groups participate in hydrogen-bonding network to construct an α-helical structure.

later experimentally supported by Tanaka and coworkers: the epoxidation catalyzed by 3_{10}-helical peptide, which can serve only two amide N-H groups at the N-terminal for the hydrogen bonding, gave the product with low ee [67]. It should be noted that the terminal amino group, N^1H_2, does not participate in the catalytic process. Nevertheless, there is a clear experimental evidence that the derivatization of this amino group considerably affects the reaction outcome. More detailed mechanistic study might be needed to clarify the role of the terminal amino group.

In 2012, Akagawa and Kudo reported an enantioselective cyanosilylation of benzaldehyde as another polyleucine-catalyzed reaction. The enantioselectivity was positively correlated with the length of peptide chain (Scheme 5.25). Although the detailed mechanism is not clear, the terminal amino group was found to be indispensable for this reaction [68].

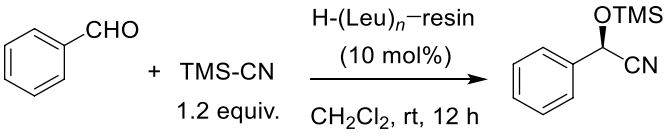

n	ee (%)
8.6	16
19.8	31
40.0	51

Scheme 5.25. Polyleucine-catalyzed asymmetric cyanosilylation. Source: Based on [68].

5.3. CATALYSIS BY SIDE CHAIN FUNCTIONAL GROUP ON PEPTIDES

As the discovery of catalytic ability of proline triggered the studies on prolyl peptide catalysts, the first to appear in this category was an amino acid, histidine. In 1974, Brown and coworkers reported enantiomer-differentiating hydrolysis of Ac-Phe-OPNP (PNP = 4-nitrophenyl), which was catalyzed by micellar *N*-acylated histidine ($k_L/k_D = 3$) [69]. Then, in 1979, Inoue and coworkers reported *cyclo*(Ala-His)-catalyzed asymmetric hydrocyanation of benzaldehyde (9.9% ee) [70]. After these pioneering works, besides the nucleophilic histidine, acidic aspartate/glutamate, basic arginine/lysine, and redox active/nucleophilic cysteine have been utilized as key residues for catalytic activity. In many cases, these amino acids were chemically modified or tuned to make the catalysis highly efficient and selective, rather than used as they are.

5.3.1. Histidine-Based Peptide Catalysis

In 1982, Ohkubo and coworkers reported the highly enantiomer differentiating hydrolysis ($k_L/k_D > 80$) of RCO-Phe-OPNP (R = C_9H_{19} or $C_{13}H_{27}$, PNP = 4-nitrophenyl) promoted by five times larger amount of Cbz-Leu-His-OH at 10 °C [71]. Ueoka and coworkers found that Cbz-Phe-His-Leu-OH in the vesicular system efficiently works at room temperature to give k_L/k_D up to 71 (Scheme 5.26) [72].

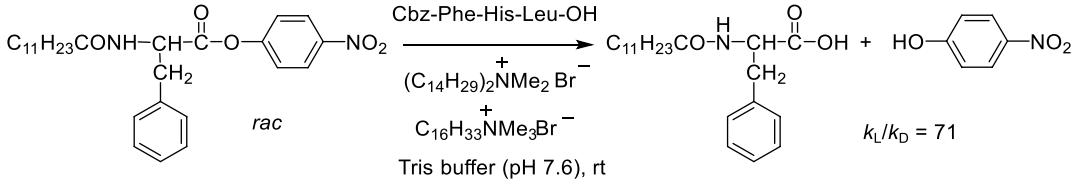

Scheme 5.26. Kinetic resolution in the hydrolysis of activated esters by peptides in a vesicular media. Source: Based on [72].

As for discrete molecular peptide catalysts for hydrolysis, Baltzer and coworkers designed helix-loop-helix 42-mer peptide with six histidines on a same face of the folded peptide chain, and this showed hydrolytic activity for $C_4H_9CH(NH_2)COOPNP$ with $k_2(D)/k_2(L) = 1.4$ [73]. Ueno and coworkers reported an enantioselective hydrolysis catalyzed by the cooperative action of Glu, His, and a peptide-bound β-cyclodextrin on a helical peptide template. The hydrolysis of Boc-D-Ala-OPNP was seven-fold faster

than its antipode [74]. Although not a peptide, Reymond and coworkers developed a hydrolytic dendrimer catalyst containing catalytic-triad element amino acids (His, Ser, Asp) [75]. One enantiomer of active ester of PhMeCHCOOH hydrolyzed faster than the other by a factor of 2. Kudo and coworkers reported a peptide catalyst of which N-terminal Pro and the side chain of His cooperatively promote the hydrolysis of formylphenyl esters [76]. The substrate and Pro give an iminium ion that then acts as activated leaving group. Kinetic resolution of PhMeCHCOO-(*o*-CHO)C_6H_4 was demonstrated.

As for the hydrocyanation catalyzed by cyclic dipeptides, Inoue and coworkers continued their research and finally reached to *cyc*(Phe-His), which showed high enantioselectivities (Scheme 5.27) [77].

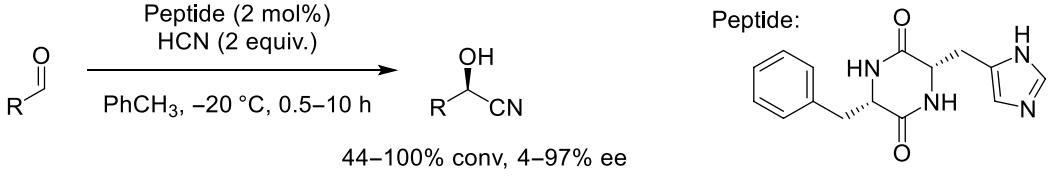

Scheme 5.27. Asymmetric hydrocyanation catalyzed by a cyclic dipeptide. Source: Based on [77].

Other than the catalysis mentioned above, His residue is expected to serve as nucleophilic catalysis for acylation. Concerning this, it has been reported that *N*-alkylimidazole is better catalyst compared to imidazole [78]. Miller and coworkers are the first to present on an asymmetric peptide catalyst having *N*-alkylimidazole active center. In 1998, they reported that 5 mol% of a tripeptide with "His-like" 3-(1-imidazolyl)-(*S*)-alanine successfully catalyzed the acylative kinetic resolution (Scheme 5.28) [79]. This peptide catalyst contains turn-forming Pro-Aib sequence [80,81] along with (*R*)-α-methylbenzylamine (Mba) at C-terminus with an expectation of π-stacking between the activated acyl donor and the aromatic ring at C-terminus to result in a reaction intermediate with rigid 3D structure.

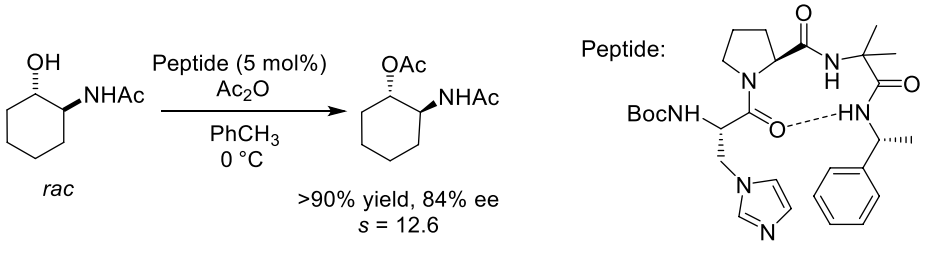

Scheme 5.28. Peptide-catalyzed kinetic resolution in the acylation of secondary alcohol. Source: Based on [79].

The uniqueness of this peptide catalyst was demonstrated for its chemoselectivity. It catalyzed the acetylation of *trans*-2-acetamidocyclohexanol in six times higher rate over 1-(1-naphthyl)ethanol whereas *N*-methylimidazole (NMI) catalyzed the reaction of these two in a same rate. This implies high potential of the peptide catalyst for enzyme-like substrate recognition.

They tried to improve the catalyst by focusing on 3D structural rigidity and reached to the peptide catalyst **1a** having π-methylhistidine (Pmh) [82, 83]. With this catalyst, *s*-value for the above acetylation increased to 28.

Next they carried out high throughput library screening to find an efficient catalyst for enantiomer-discriminating acylation of 1-phenylethanol, which does not have any polar functional groups other than OH (Scheme 5.29) [84]. Photoinduced electron transfer (PET) system was introduced on beads for the solid-phase peptide synthesis, in which the fluorescence from anthracene is quenched by the amino group. In case the resin-immobilized peptide shows catalytic activity, liberated acetic acid forms a salt

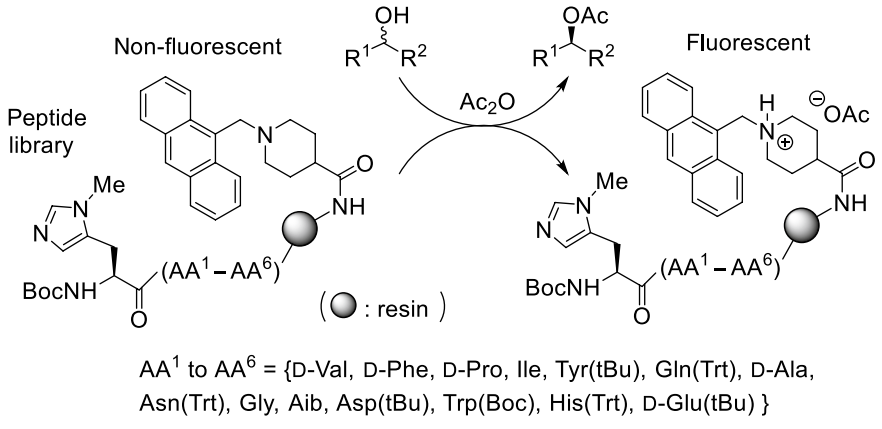

Scheme 5.29. Combinatorial approach for screening of peptide catalyst for acylation of a secondary alcohol. Source: Based on [84].

with the amine leading to inhibition of PET, hence the fluorescence should be observed. Due to the limitation of the amount handled at a time, 100 thousand of beads out of $14^6 = 7.5$ million was screened, and they successfully obtained several kinds of viable peptide catalysts.

Thus found peptide catalysts were then tested and modified, and they finally reached the peptide **2** (Scheme 5.30a). Ellman, Miller, and their coworkers revealed that this peptide was also applicable for dynamic kinetic resolution (DKR) of *tert*-butylsulfinyl chloride (Scheme 5.30b) [85]. This peptide was

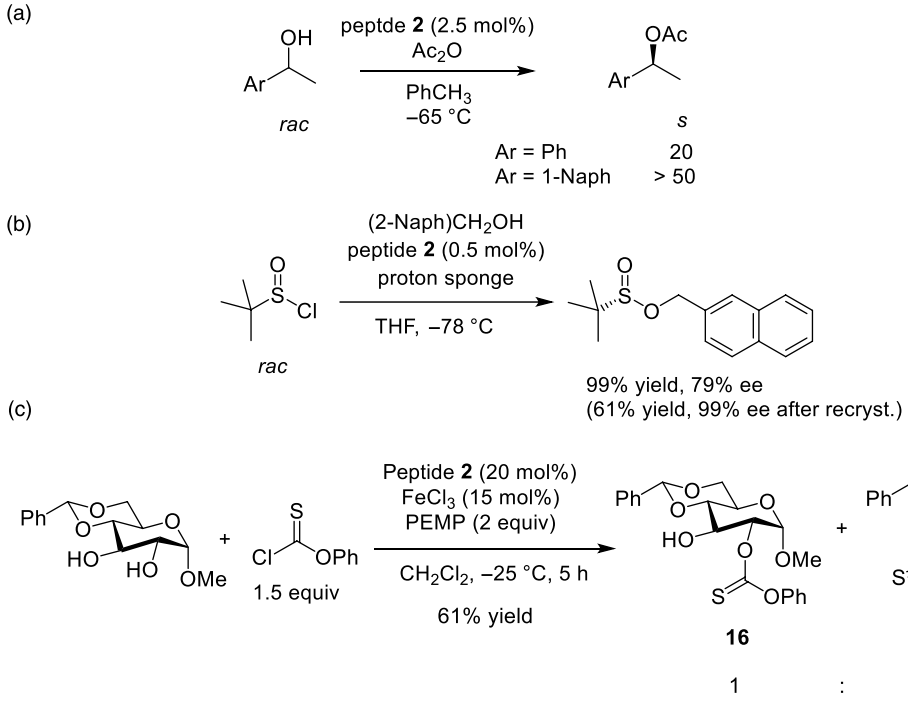

Scheme 5.30. Peptide-catalyzed enantio- or regiodifferentiating reaction in the derivatization of alcohols; (a) kinetic resolution of chiral secondary alcohols, (b) kinetic resolution of chiral sulfinyl chlorides, and (c) regioselective thiocarbonate formation of carbohydrate derivatives. Based on [85, 86].

then utilized to site-selective thiocarbonate formation of partially protected glucose derivative (Scheme 5.30c) [86]. Interestingly, complementary site selectivity was found with **1a**-related Boc-Pmh-D-Pro-Aib-D-Trp(Boc)-D-Phe-OMe (70% yield, **16** : **17** = 22 : 1). The thiocarbonylation was connected to Barton-McCombie reaction to result in the net deoxygenation of sugars.

Miller's group realized a peptide-catalyzed acylative desymmetrization of a 2-*O*-benzylglycerol. After screening 54 kinds of peptides, Boc-Pmh-D-Pro-D-Asp(tBu)-Tyr(Bn)-D-Phe-OMe was found to afford monoacetylated product of 2-*O*-(3,5-dimethoxybenzyl)glycerol in 34% yield and 95% ee [87]. Later, they successfully extended this chemistry to highly challenging bis(phenol) compound [88]. For this reaction the best peptide catalyst among 138 screened was Boc-Pmh-Asn(Trt)-Aib-Ser(tBu)-D-Leu-Phe-OMe. By replacing C-terminal two residues with a chiral diamine TsDPEN, even higher selectivity was attained (Scheme 5.31).

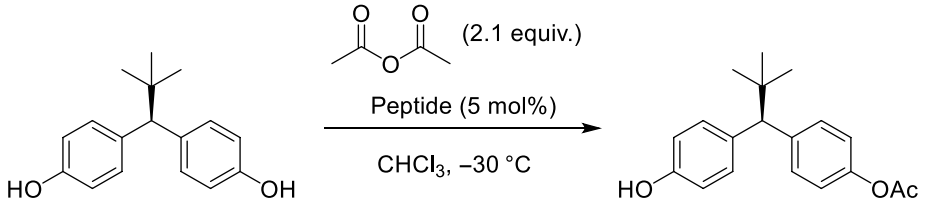

Peptide: Boc-Pmh-Asn(Trt)-Aib-Ser(tBu)-(*R*,*R*)TsDPEN 80% yield, 95% ee

Scheme 5.31. Peptide-catalyzed acylative desymmetrization of a bisphenol-type substrate.

They had also demonstrated that the peptide-catalyzed acylation could be applicable to site-selective reactions for glucosamine and glucose derivatives (Scheme 5.32) [89], erythromycin A (Figure 5.4a) [90], and partially protected vancomycin (Figure 5.4b) [91]. For the reaction of antibiotic vancomycin, peptide catalyst **23** was designed on the basis of the mechanism of action; vancomycin is known to bind to bacterial peptideglycan at Lys-D-Ala-D-Ala C-terminal structure; thus catalytically active Pmh was introduced as its D-form and placed at an appropriate position.

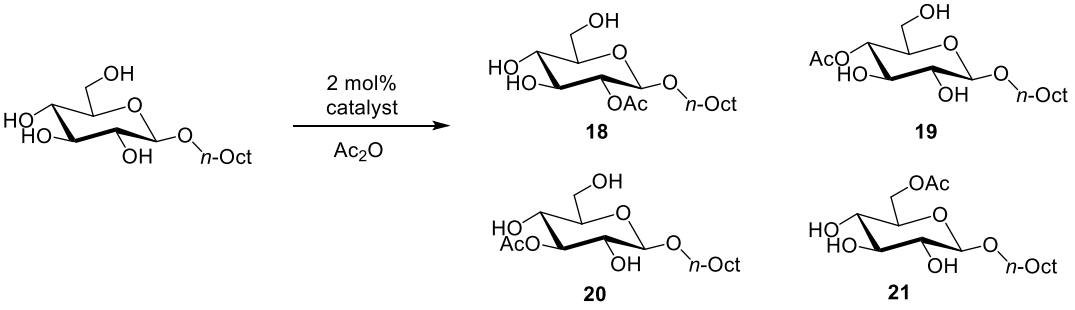

Catalyst:	**18** : **19** : **20** : **21**
NMI	0 : 20 : 16 : 64
Boc-Pmh-His(τ-Bn)-Cha-D-Ala-Phe-OMe	9 : 11 : 58 : 22

Scheme 5.32. Peptide-catalyzed site-selective acylation of a glycoside. Source: [89]/ELSEVIER.

Compared to chiral secondary alcohols, the corresponding amines are much more difficult substrates for kinetic resolution. Miller and coworkers realized this by an indirect approach [92]. They derivatized amines to thioformamides, and then subjected to acylative kinetic resolution with Boc_2O (Scheme 5.33). Thioformyl group and Boc group could be removed under oxidative and acidic conditions, respectively.

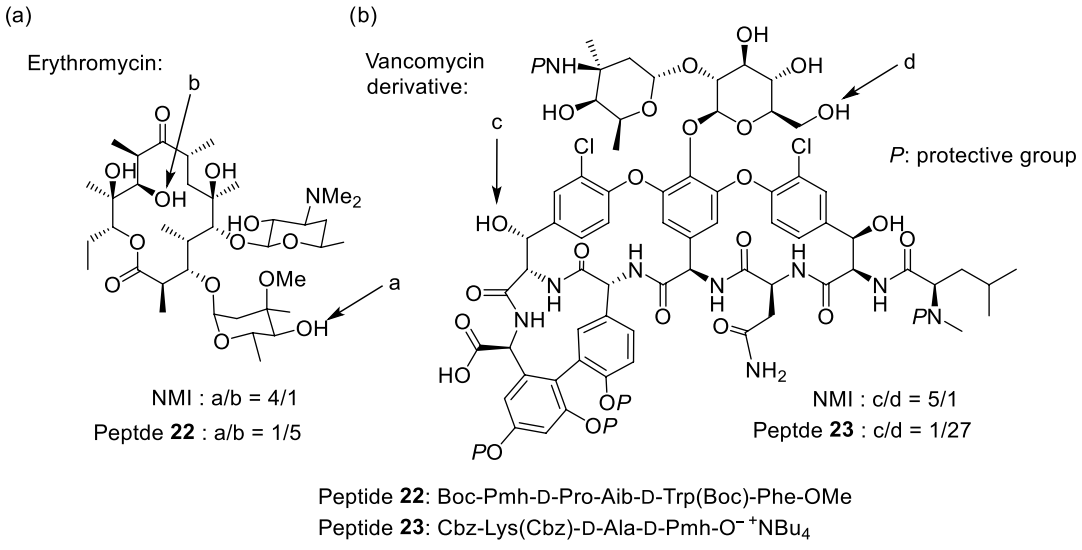

Figure 5.4. Site selectivity for the peptide-catalyzed derivatization of naturally occurring polyol derivatives; (a) monoacetylation of erythromycin A, and (b) thiocarbonylation of vancomycin derivative. Source: Based on [90, 91].

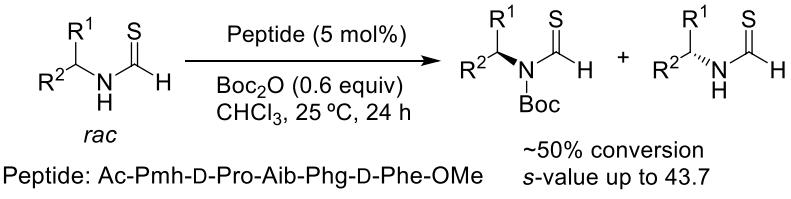

Scheme 5.33. Peptide-catalyzed acylative kinetic resolution of secondary thioamides.

Schreiner and coworkers reported another type of peptide catalyst for acylation. The key is the incorporation of non-natural amino acid, γ-aminoadamantanecarboxylic acid (^{A}Gly), to increase the lipophilicity and rigidity of the catalyst [93]. They used the catalyst for enantioselective acylation of *trans*-1,2-diols (Scheme 5.34) [94]. The peptide catalyst worked very efficiently with low loading, and the five- to eight-membered *trans*-cycloalkane-1,2-diol was successfully converted to monoacylates with *s* value of >50. They also showed that carboxylic acid can be used as an acyl donor with assistance of carbodiimide and 4-dimethylaminopyridine (DMAP).

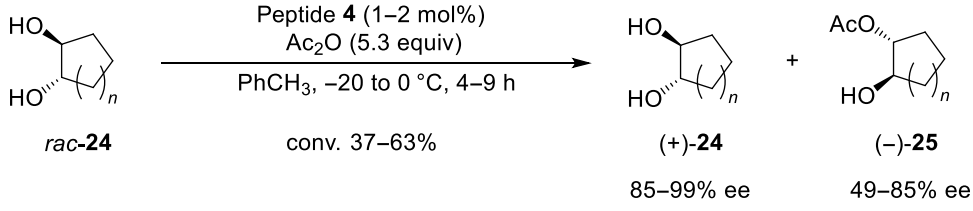

Scheme 5.34. Peptide-catalyzed monoacylative kinetic resolution of *trans*-cycloalkane-1,2-diols. Source: Based on [94].

This peptide was then utilized for the desymmetrization of *meso*-1,2-diols. As the obtained monoacylated diol is well known to proceed 1,2-acetyl migration, the product was immediately oxidized to the corresponding ketones in one pot (Scheme 5.35) [95]. By changing the C-terminal structure of peptide

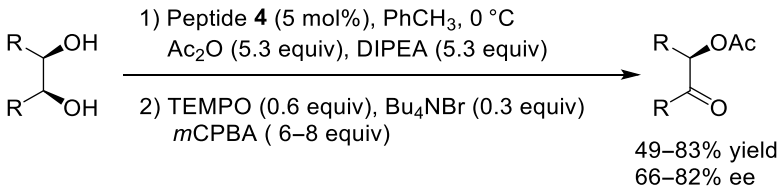

Scheme 5.35. Peptide-catalyzed monoacylative desymmetrization of alkane-1,2-diols. Source: Based on [95].

4 from methyl ester to an amide with 4-amino-TEMPO, they realized a multicatalyst system for this two-step reaction [96]. Using this multicatalyst, they demonstrated that aldehydes [97] and even alcohols [98] can be used as an acyl donor *via* in situ oxidation reactions. On the other hand, by derivatizing C-terminal of peptide **4** as an amide with 2-aminomalonic acid, they made an epoxidation-acylation multicatalyst [99]. With this peptide, starting from *cis*-alkenes, epoxidation-hydration-kinetic resolution sequence was successfully carried out. The key is catalytic peracid formation at the diacid moiety, which was found by Miller and coworkers [100](*vide infra*).

Schreiner and coworkers further applied the ^{A}Gly-containing peptide catalyst to asymmetric Dakin-West reaction, which is a decarboxylative C-acylation of α-amino acids with an intermediacy of isolable 5(4*H*)-oxazolone derivative (Scheme 5.36) [101]. Catalyst screening gave a peptide having Pmh at C-terminal.

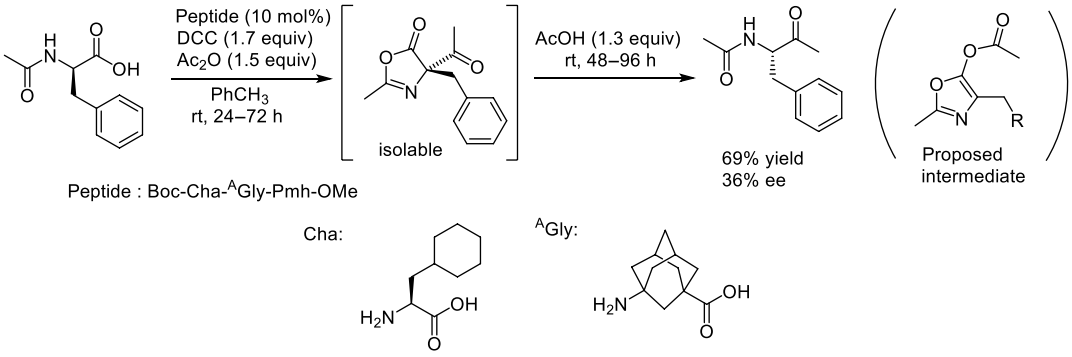

Scheme 5.36. Peptide-catalyzed asymmetric Dakin–West reaction. Source: Based on [101].

Miller and coworkers extended Pmh-based peptide catalyst to other OH derivatization. NMI has been reported as the catalyst for phosphorylation of secondary hydroxyl group in 1990 [102]. The Miller's group successfully developed its asymmetric version of this reaction (Scheme 5.37) [103]. They screened 39 peptides for phosphorylative desymmetrization of 2,4,6-tri-*O*-benzyl *myo*-inositol to find the one that gives *myo*-inositol-1-phosphate. During the selection of the catalyst, they realized that some of the peptide showed the enantioselectivity for the opposite chirality. Then, after screening 178 kinds of peptides in total, they finally reached to highly enantioselective catalyst to give *myo*-inositol-3-phosphate derivative [104].

Phosphorylation chemistry was applied to derivatization of three distinct hydroxy groups of a teicoplanin derivative that selectively underwent the reaction by three kinds of peptide catalysts (Figure 5.5).

They also reported a site-selective sulfonation of alcohols (Scheme 5.38) [105].

Site-selective deoxygenation of erythromycin was realized by intermediate phosphoramide formation (Scheme 5.39) [106].

Pmh-containing peptide was utilized to a catalytic asymmetric Morita-Baylis-Hillman (MBH) reaction in which molecular proline was used as co-catalyst (Scheme 5.40) [107].

On the other hand, a reaction in which τ-alkylhistidine derivative plays an important role has been also reported. With an assistance of chiral amide at C-terminal, a tripeptide was successfully utilized to

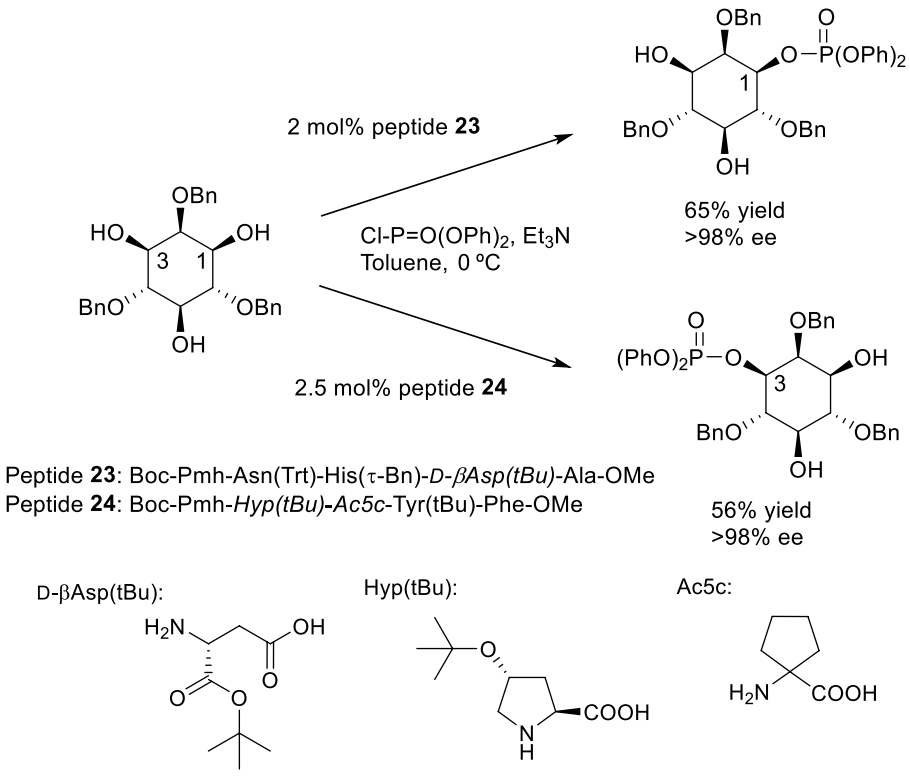

Scheme 5.37. Peptide-catalyzed phosphorylative desymmetrization of a *myo*-inositol derivative. Source: Based on [103].

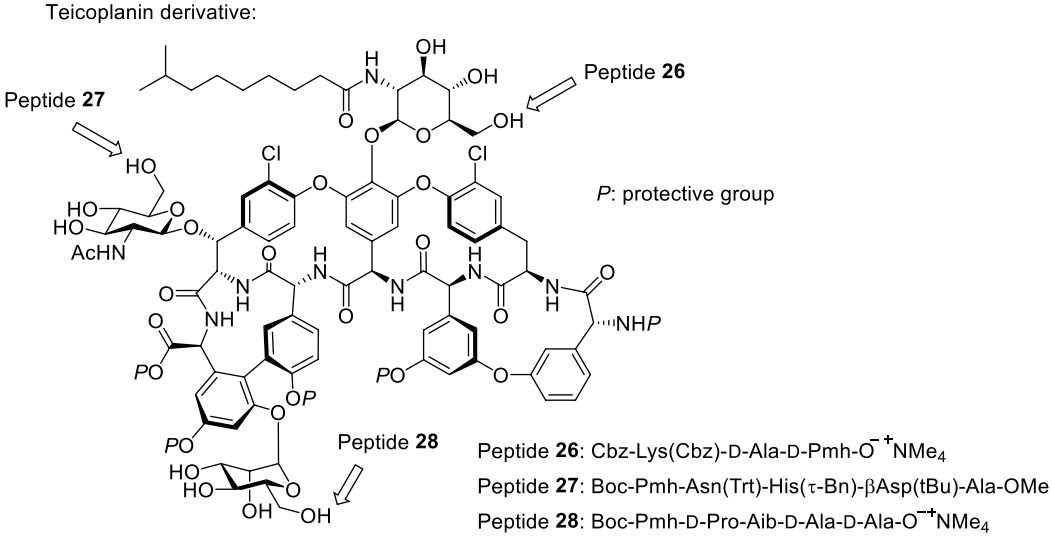

Figure 5.5. Site selectivity for the peptide-catalyzed phosphorylation of teicoplanin derivative.

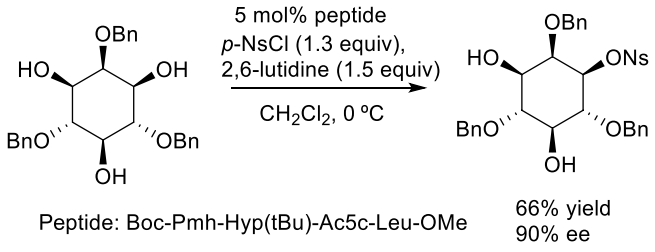

Scheme 5.38. Peptide-catalyzed sulfonylative desymmetrization of a *myo*-inositol derivative. Source: Based on [105].

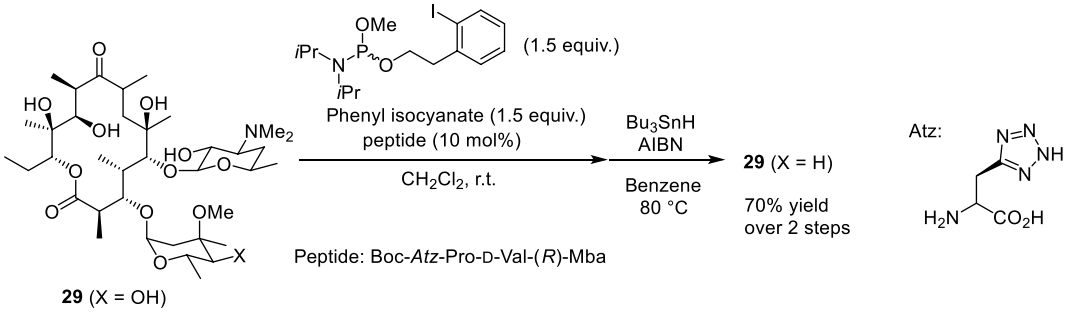

Scheme 5.39. Peptide-catalyzed site-selective derivatization of a polyol compound and the subsequent deoxygenation. Source: Based on [106].

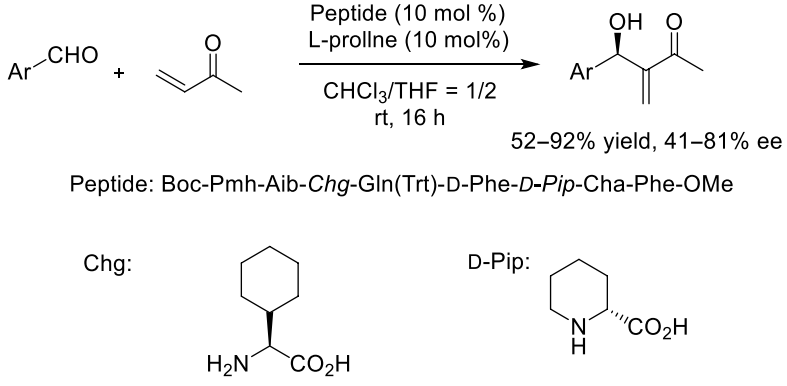

Scheme 5.40. Peptide/proline-cocatalyzed asymmetric Morita–Baylis–Hillman reaction. Source: [107].

catalytic asymmetric azide Michael addition (Scheme 5.41) [108]. For this reaction, accumulation of potentially explosive hydrogen azide could be avoided by a slow addition of the trimethylsilyl azide.

5.3.2. Aspartate/Glutamate-Based Peptide Catalysis

To date, use of aspartate or glutamate in peptide chain solely as a Brønsted acid catalysis has not been reported. This might be due to the low acidity of the COOH group. Instead, as were seen in previous sections, these amino acids have played key role in enhancing peptide-catalyzed reactions and/or raising its selectivity.

Miller and coworkers elegantly utilized Asp-containing peptides as "chiral catalytic peracid" for oxygenation reactions (Scheme 5.42). Peracids are well-known powerful oxidizers that donate oxygen atom to the substrate. However, they have been used only as reagents but not catalysts.

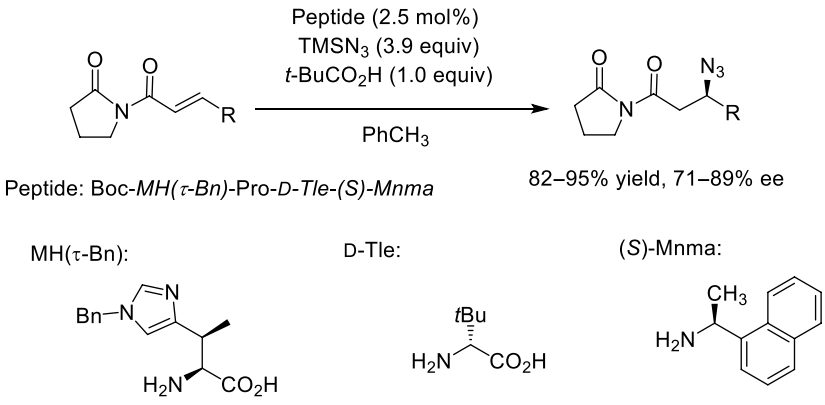

Scheme 5.41. Peptide-catalyzed asymmetric conjugate addition of azide. Source: Based on [108].

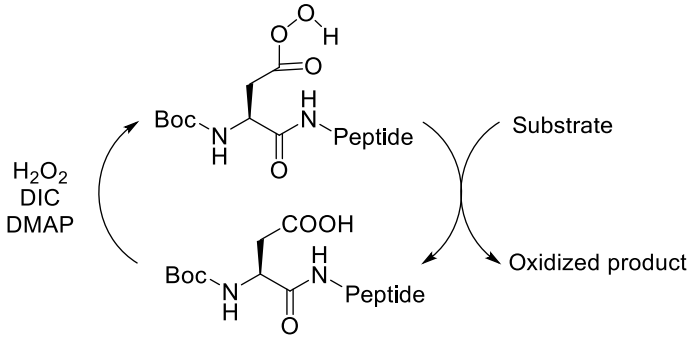

Scheme 5.42. Catalytic cycle for oxidation mediated by Asp-containing peptides.

By using H_2O_2 and condensing agent *N,N′*-diisopropylcarbodiimide (DIC), Miller and coworkers generated peracids in situ from the carboxylate on Asp side chain [100]. They first tested a catalytic olefin epoxidation with 10 mol% of aspartic acid derivative to prove their hypothesis for the catalytic cycle. The key was the use of DMAP as nucleophilic catalyst for the peracid formation. Then, by introducing Asp at N-terminal, enantioselective peptide catalyst for epoxidation of allyl carbamates was realized (Scheme 5.43). Related to this reaction, lipase/carboxylate-catalyzed epoxidation of olefins by H_2O_2 via the intermediacy of peracid has been reported [109]. However, in that paper, application to selective organic synthesis was not explored.

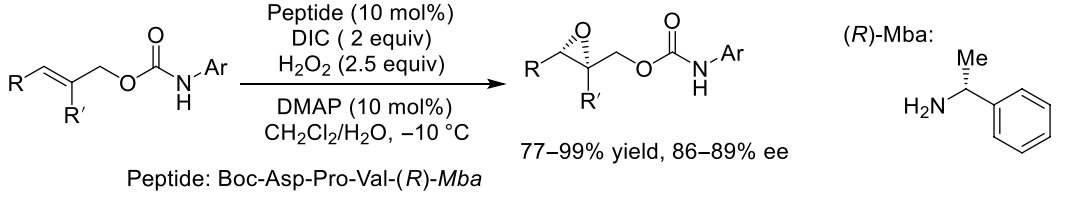

Scheme 5.43. Peptide-catalyzed asymmetric epoxidation of allylic carbamates.

This reaction was applicable to transformation of 3-substituted indoles to synthetically important chiral 3-hydroxy-indolenines via epoxidation of indole ring [110]. Then they applied this oxidation

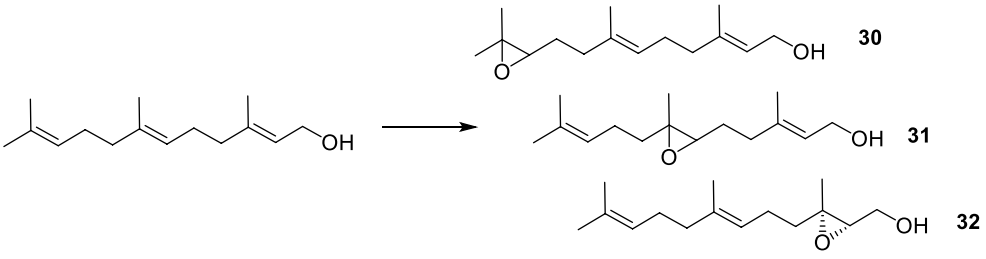

Scheme 5.44. Peptide-catalyzed site-/enantioselective epoxidation of farnesol. Source: [111].

system to site-selective epoxidation of terpene alcohols. After the library screening, they found peptide catalysts for 2,3- and 6,7-selective epoxidation (Scheme 5.44) [111].

The Miller's group tried to apply this Asp-based peracid peptide catalyst to a nucleophilic oxidation, namely, Baeyer-Villiger (BV) oxidation (Scheme 5.45) [112]. For this reaction, slow addition of carbodiimide was found to be necessary in order to avoid the formation of non-nucleophilic acylperoxide that consumes nucleophilic peracid, an actual reactive species with ketone, by the action of excess carbodiimide. Using unsymmetrical cyclic ketones, they succeeded to override the inherent migratory aptitude of the substrates by the catalyst control. In this reaction, parallel kinetic resolution was observed [113].

Then, the substrate having both alkene and ketone functional groups, along with two directing groups that have been used for the oxidation of each functional group, was subjected to Asp-peptide-mediated oxidation [114]. Several "specific" peptide catalysts were found. They explained the result as enzyme-like diversity of peptide catalyst.

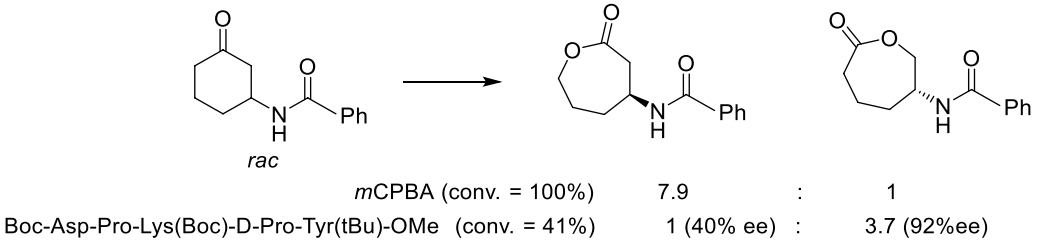

Scheme 5.45. Peptide-catalyst-controlled site-/enantioselective Beayer–Villiger oxidation. Source: [113].

This oxidation system was further extended to the pyridine *N*-oxide formation. C_s-symmetrical di(3-pyridyl)methane was enantioselectively oxidized by the peptide catalyst (Scheme 5.46) [115]. Interestingly, for this reaction, the optimum peptide catalyst has the structure in which the Asp residue was located not at the N-terminal but next to that position.

This chemistry was also applied to the recognition of helical chirality, and achieved dynamic kinetic resolution of Loratadine derivatives (Scheme 5.47) [116]. For this substrate, *N*-oxidation competed with olefin epoxidation and the former was slightly preferred. Starting with the peptide **1c** that showed low enantioselectivity, they optimized the catalyst structure to finally reach Boc-Asp-(α-Me)Pro-Acpc-D-Phe-OMe that gave the helically chiral (+)-*N*-oxide in 40% yield, 86% ee.

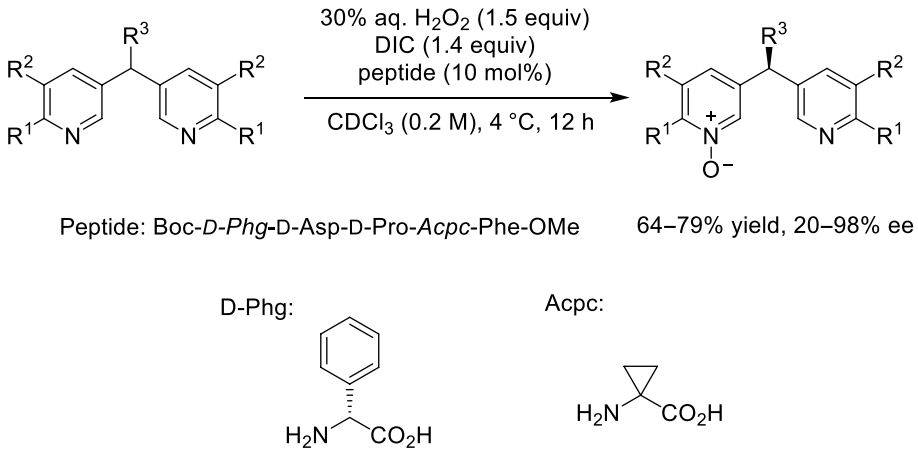

Scheme 5.46. Peptide-catalyst-controlled N-oxidative desymmetrization of dipyridylmethanes. Source: [115].

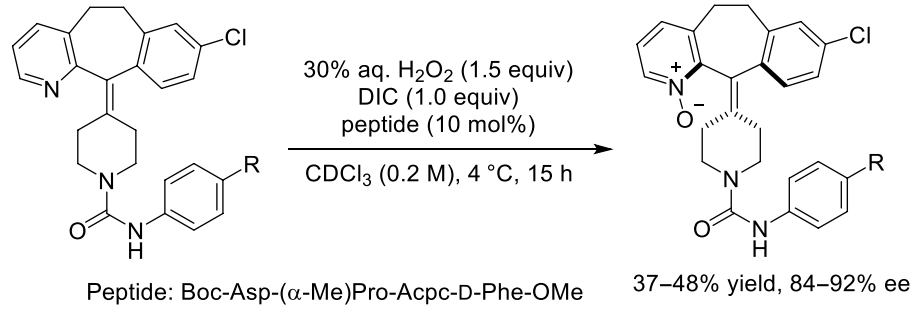

Scheme 5.47. Peptide-catalyzed N-Oxidation of conformationally dynamic substrate to a helically chiral product in an enantioselective manner. Source: Based on [116].

5.3.3. Arg/Lys-Based Peptide Catalysis

In the biological system, lysine plays an important role in the class I aldolases [117]. However, in the peptide catalysis field, lysine has been rarely used as primary catalytic center. Brack and coworkers showed that Lys-rich peptides are viable for the phosphate ester hydrolysis. For the scission of oligonucleotide chain, poly(Leu-Lys) showed higher activity than polylysine [118]. For this reaction, Arg-containing peptides were less efficient, and His-rich peptides showed only very low catalytic power.

On the other hand, if we assume lysine as "chiral base" catalytic center on a peptide, tetramethylene chain between α-carbon and side chain amino group seems unfavorable because of high degree of conformational freedom. Thus, Miller and coworkers focused on utilizing 3-dimethylamino-2-aminopropanoic acid (Dmaa), instead of Lys. Dimethylated amino group may avoid unwanted interactions or reactions during the catalytic process.

In 2014, they reported a highly selective methanolytic dynamic kinetic resolution of oxazolones (Scheme 5.48) [119]. Starting from peptide **1c** that gave the product with 34% ee, they found optimum peptide catalyst that attained the product of >90% ee.

Earlier than this, the Miller's group reported their first usage of Dmaa-containing peptide catalyst for quite unique asymmetric reaction, that is, a phenol tribromination leading to dynamic kinetic resolution of atropoisomeric biaryls (Scheme 5.49) [120]. In this reaction, Dmaa was used as a directing group, which interacts with substrate carboxylic acid moiety to fix the conformation of biphenyl. A turn-structured Dmaa-containing tripeptide with (*R*)-Mba at C-terminal was employed first, and then it was revealed that this chiral amine part can be transposable to dimethylamino group with slight increase in the enantioselectivity.

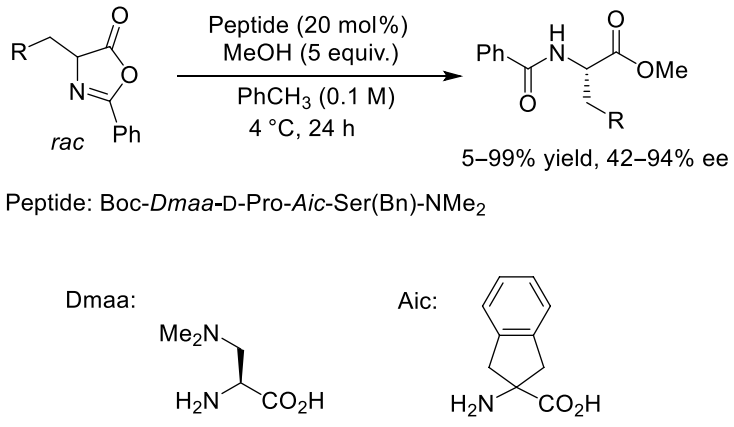

Scheme 5.48. Peptide-catalyzed methanolytic dynamic kinetic resolution of oxazolones. Source: Based on [119].

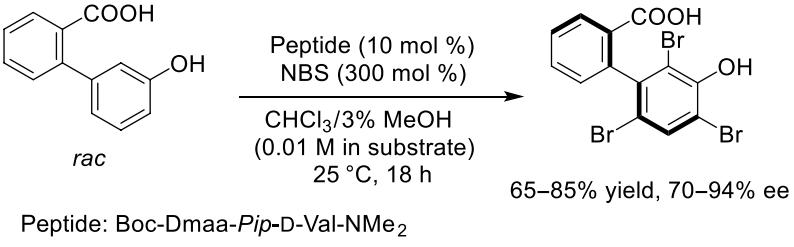

Scheme 5.49. Peptide-catalyzed asymmetric synthesis of axially chiral biphenyls via atroposelective bromination of phenol ring. Source: Based on [120].

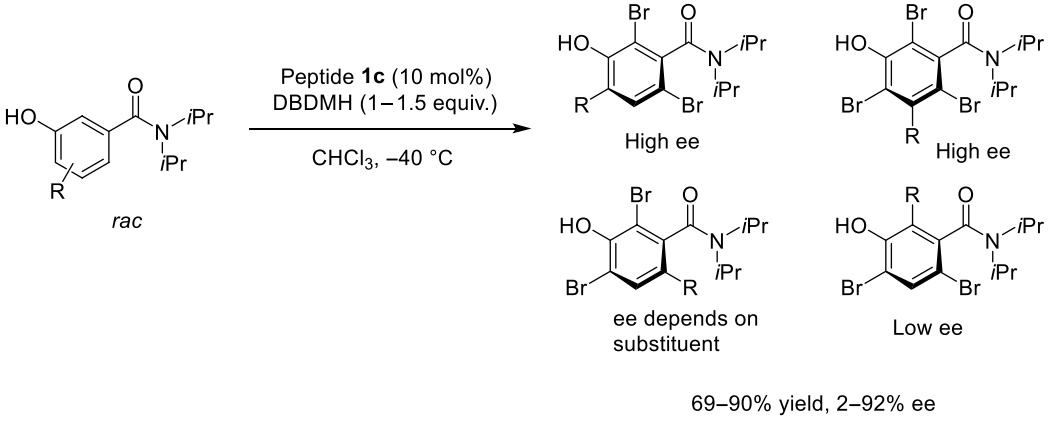

Scheme 5.50. Peptide-catalyzed asymmetric synthesis of axially chiral arylamides via atroposelective bromination of phenol ring.

This reaction was extended to the bromination of "carboxylate free" bulky 3-hydroxybenzamides (Scheme 5.50) in which the role of Dmaa was an activator of phenols [121]. Enantioselectivity of this reaction depended on the kind and position of substituent R in the substrate.

Further substrate scope study found that 3-arylquinazolin-4(3*H*)-ones also undergo atroposelective bromination (Scheme 5.51) [122]. In the report, X-ray crystallographic and two-dimensional nuclear magnetic resonance (2D NMR) analyses of the peptide catalyst were provided.

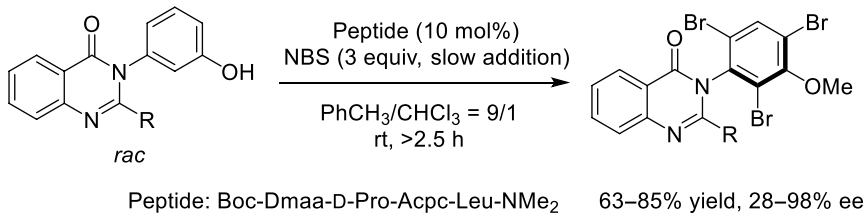

Scheme 5.51. Peptide-catalyzed enantioselective synthesis of 3-arylquinazolin-4(3*H*)-ones via atroposelective bromination. Source: Based on [122].

Subsequently, the relationship of the structure and the performance of peptide catalysts for this reaction was extensively studied. X-ray crystallographic investigation of 35 kinds of **1c**-related peptides were carried out and structural parameters of these peptides were analyzed along with 2D NMR and density functional theory (DFT) calculation of selected peptides [123]. Through this study they found that the conformational space available to simple peptide-based catalysts is more diverse than was supposed. Even a single peptide catalyst, up to three different conformations were found in the crystal structure.

The phenol bromination was further applied to a desymmetrization of bisphenol compounds through monobromination on one of the two substituted phenol rings. With using peptide **1c**, (*S*)-product was obtained with low to fair ee, whereas a peptide catalyst similar to **1c** in which the Aib part was replaced with 1-aminocyclopropanecarboxylic acid (Acpc) showed (*R*)-selectivity with quite high ee.

Yet another approach for peptide-catalyzed formation of axially chiral biaryl was fragment coupling. Inspired by the earlier study on the quinine-catalyzed atroposelective coupling[124], Miller and coworkers conducted Michael addition of 2-naphthol to substituted p-benzoquinone catalyzed by **1c**-related peptide to obtain the product with high ee (Scheme 5.52) [125].

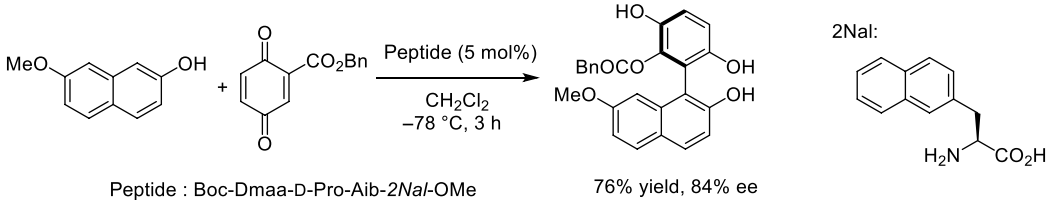

Scheme 5.52. Peptide-catalyzed asymmetric synthesis of chiral biaryls by fragment coupling. Source: Based on [125].

As for the peptide catalyst using arginine and its analogue, in 1996 Lipton and coworkers developed cyclic dipeptide-catalyzed asymmetric Strecker reaction. One methylene shorter analogue of arginine was utilized for this catalyst (Scheme 5.53) [126]. It should be noted that, later in 2005, asymmetric induction by this catalyst was questioned by Kunz and coworkers; they followed the experimental procedure reported by Lipton, including the catalyst synthesis, and found that the Strecker reaction showed no enantioselectivity [127].

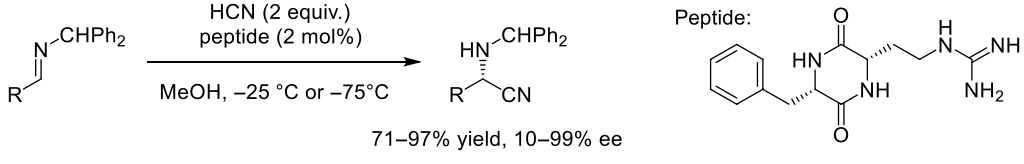

Scheme 5.53. Peptide-catalyzed asymmetric hydrocyanation of imines by cyclic dipeptide having guanydyl group. Source: Based on [126].

In 2004, Tsogoeva and coworkers reported H-Asp-Phe-Arg-OH and H-Asp-Pro-Arg-OH as a catalyst for asymmetric Michael addition of 2-nitropropane to cyclohexanone in the presence of 1 equiv. of *trans*-2,5-dimethylpiperazine up to 73% yield and up to 71% ee [128]. Another type of asymmetric Michael addition that gives chiral quaternary carbon center was reported by Miller and coworkers. They used a peptide having modified arginine and a τ-benzyl histidine, and the corresponding adduct was obtained with moderate ee (Scheme 5.54) [129].

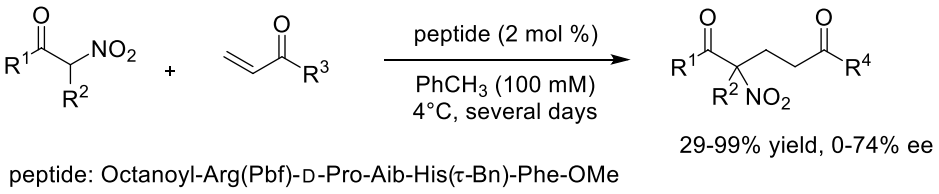

Scheme 5.54. Peptide-catalyzed asymmetric Michael addition of prochiral nucleophile to vinyl ketones. Source: Based on [129].

Toste, Miller, and their coworkers reported tandem catalytic DKR to construct two-axis terphenyl atropisomers, which was realized by sequential use of two peptides each having tetramethylguanidyl group (Scheme 5.55) [130]. For the second DKR, chirality match/mismatch for the substrate and catalyst was observed to some extent. In case the second step reaction is bromination, use of chiral phosphoric acid was more effective than the peptide **34**.

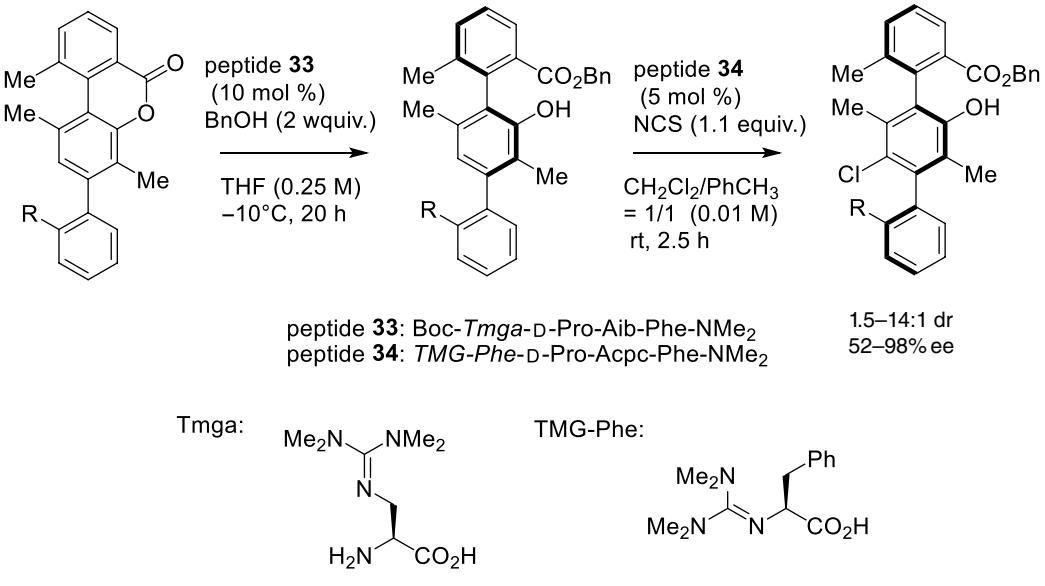

Scheme 5.55. Peptide-catalyzed atroposelective formation of two-axis terphenyls via tandem dynamic kinetic resolutions. Source: Based on [130].

5.3.4. Cysteine-Based Peptide Catalysis

Cysteine is unique among the proteinogenic amino acids because the thiol group on cysteine shows high nucleophilicity, redox reactivity, and also radical stabilizing ability.

Miller and coworkers have first utilized this amino acid, but not peptide, to a catalytic asymmetric reaction. They found that simple *N*-acetylcysteine methyl ester successfully catalyzed enantioselective Rauhut-Currier reactions (Scheme 5.56) [131].

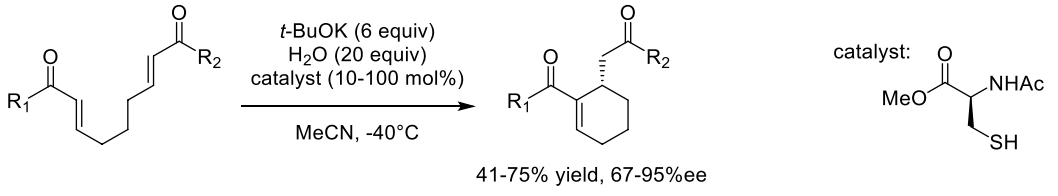

Scheme 5.56. Enantioselective Rauhut–Currier reactions promoted by protected cysteine. Source: Based on [131].

Cysteine-containing tripeptide was elegantly applied to catalytic enantioselective cycloaddition of vinyl-cyclopropanes promoted by photogenerated thiyl radical (Scheme 5.57) [132].

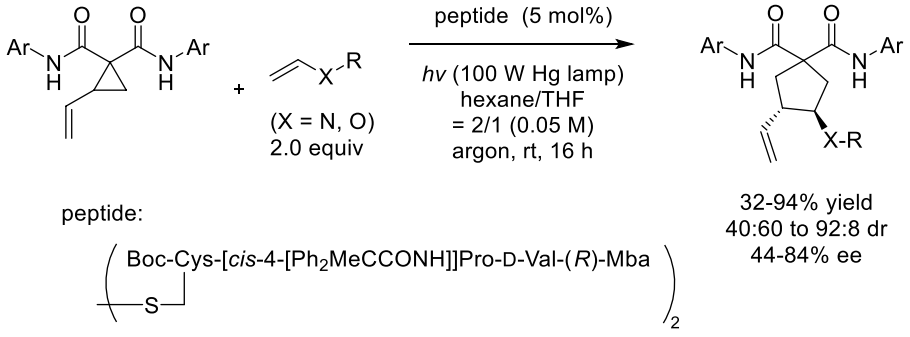

Scheme 5.57. Enantioselective vinylcyclopropane ring-opening/cycloaddition cascade activated by thiyl radical generated via UV light-promoted homolysis of cystine-based peptide dimers. Source: Based on [132].

This radical chemistry was successfully combined with photocatalytic system to realize deracemization of cyclic urea derivatives (Scheme 5.58) [133]. Miller, Knowles, and their coworkers utilized the chiral-discriminating ability of Cys-containing peptide as "chiral hydrogen atom donor." They realized photo-driven deracemization of urea derivative. The system consists of three steps: (i) achiral photocatalyst-mediated electron transfer, (ii) chiral phosphate-base-mediated enantioselective deprotonation, and (iii) peptide-mediated enantioselective hydrogen atom transfer to the intermediate radical. The control experiments using achiral phosphate or thiol indicated that the second step shows up to 86 : 14 enantiomer ratio and the third step 79 : 21. By using chiral phosphate and peptide catalyst, they successfully obtained 96 : 4 enantiomer ratio, which indicates that the two enantioselective steps are independent of each other.

5.4. CATALYSIS BY FUNCTIONAL GROUPS COVALENTLY BOUND TO PEPTIDES

As seen in previous sections, a variety of functional groups on peptide can serve as reaction center. However, as long as relying on those derived from natural amino acids, the scope for the catalytic reaction is still limited. As mentioned in the Introduction, molecular catalysts are composed of a catalytic center and the others. For peptide catalysts, it is possible to externally introduce a catalytic center to peptide. Such a method has been reported from several groups.

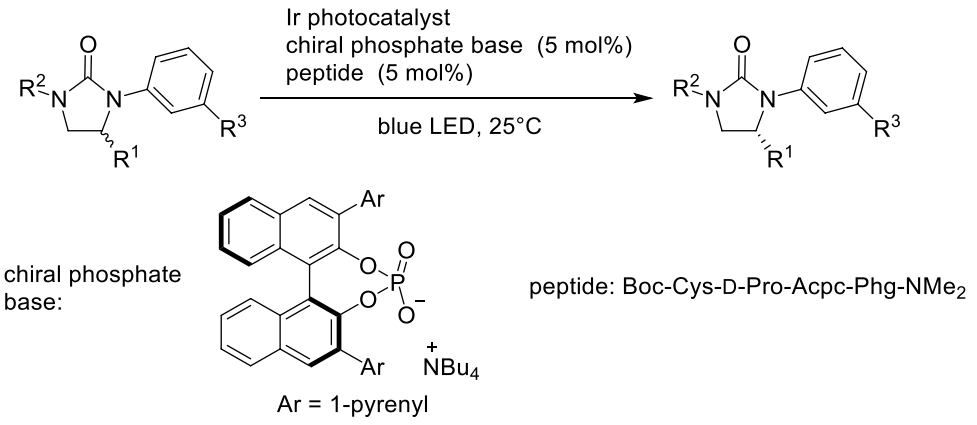

Scheme 5.58. Photo-driven deracemization of urea derivative promoted by a combination of achiral photocatalyst-mediated electron transfer, chiral phosphate-base-mediated enantioselective deprotonation, and the Cys-containing peptide-mediated enantioselective hydrogen atom transfer. Source: [133]/American Association for the Advancement of Science.

5.4.1. Peptide Catalysts That Have Catalytic Center Connected to N-Terminal

In 2012, Miller and coworkers reported a catalytic asymmetric epoxidation of nonfunctionalized olefins. With an assistance of C-terminal (*R*)-Mba amide, a dipeptide having trifluoromethyl ketone moiety in the N-terminal acyl group was demonstrated in the dioxirane-mediated asymmetric catalytic epoxidation of olefins (Scheme 5.59) [134].

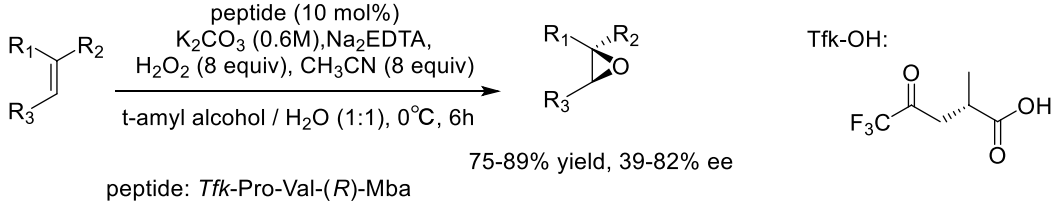

Scheme 5.59. Catalytic asymmetric epoxidation of alkenes mediated by trifluoroacetyl-conjugated peptide. Source: Based on [134].

In 2014, Chimni and coworkers reported catalytic enantioselective ring opening of *meso*-epoxide by using N-terminal thiourea derivatized peptides (Scheme 5.60) [135].

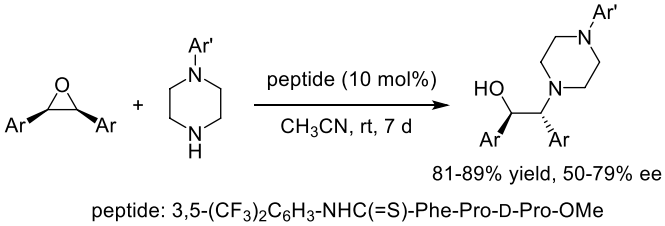

Scheme 5.60. Peptide-catalyzed ring-opening desymmetrization of epoxide. Source: Based on [135].

Hunter and coworkers utilized nucleophilic 4-PPY as a reaction center of peptide to realize acylative kinetic resolution of secondary alcohols (Scheme 5.61) [136].

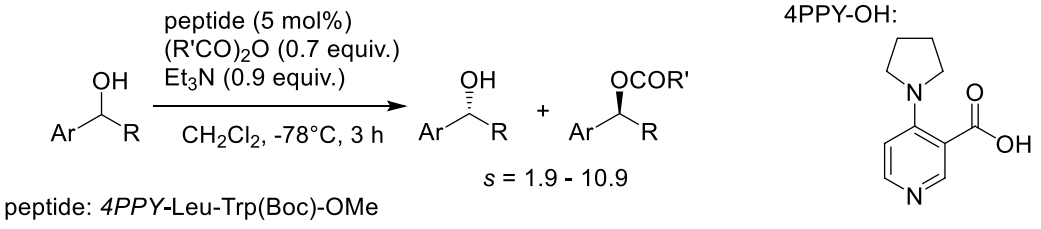

Scheme 5.61. Peptide-catalyzed acylative kinetic resolution of secondary alcohols. Source: Based on [136].

Borhan and coworkers reported peptide-catalyzed asymmetric bromolactonization. The catalytic center is aryl iodide and intermediacy of bromoiodinane species was proposed (Scheme 5.62).

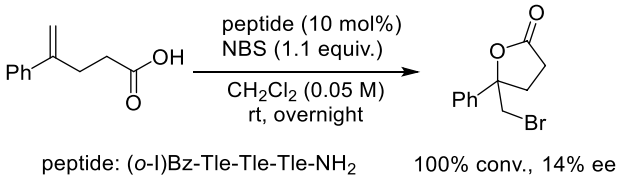

Scheme 5.62. Peptide-catalyzed asymmetric bromolaconization.

Imada and coworkers reported that the peptide with Flavin at *N*-terminus is capable of catalyzing the oxidation of sulfides to sulfoxides and BV oxidation of cyclobutanone (Scheme 5.63) [137]. Interestingly, the competing reaction between the two substrates showed preference to the BV oxidation, while *m*CPBA-mediated reaction prefers the *S*-oxidation.

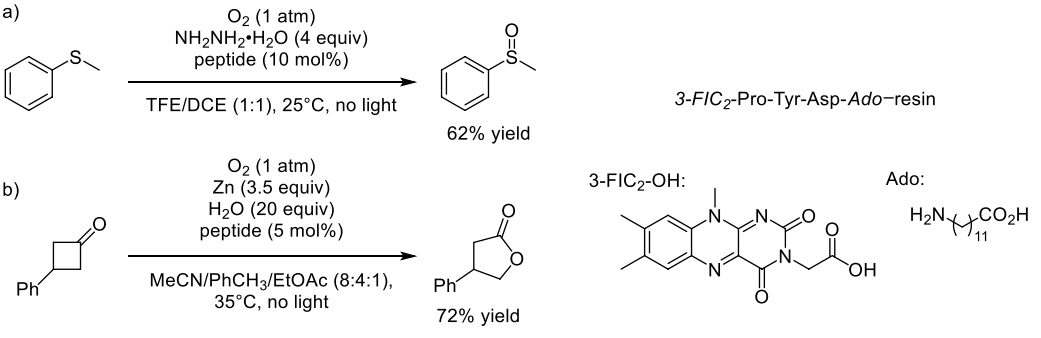

Scheme 5.63 Catalytic oxidation by flavin-conjugated peptide; (a) sulfoxidation, and (b) Baeyer–Villiger oxidation. Source: Based on [137].

An N-terminal TEMPO-bound heptaglycine with (*S*)-1-phenylethyl group on nitrogens successfully catalyzed enantiomer-discriminating oxidation of benzylic alcohols (Scheme 5.64).

5.4.2. Peptide Catalysts That Have Catalytic Center on Side Chain of Amino Acid

Chiral phosphoric acid is definitely one of the organocatalyst with high versatility [138]. Concerning this, Miller and coworkers had successfully demonstrated that phosphothreonine monobenzyl ester (pThr) incorporated in the peptide chain serves as a chiral Brønsted acid or an acid/base cooperative catalyst.

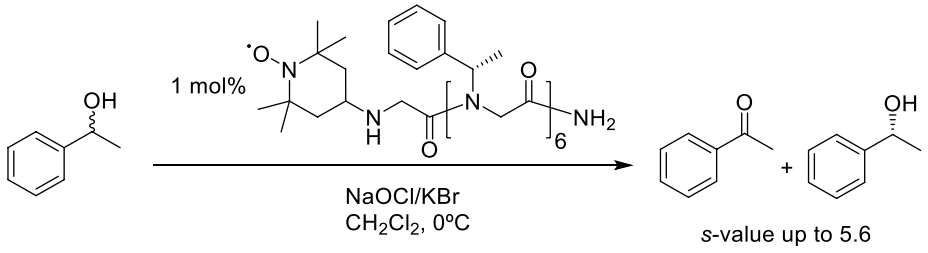

Scheme 5.64 TEMPO-conjugated peptoid-catalyzed oxidative kinetic resolution of a secondary alcohol.

They showed that Hantzsch ester-mediated asymmetric reduction of 2-substituted-8-aminoquinolines is possible with pThr-containing peptide catalyst with **1**-related sequence (Scheme 5.65) [139]. Then, it was extended to the reductive amination of racemic 3-substituted cyclohexanones for kinetic resolution and diastereoselective reduction of imines (Scheme 5.66) [140]. They also utilized this functionality for enantioselective BV oxidation (Scheme 5.67) [141]. In this reaction, the phosphate moiety was explained to interact with both the hydroxyl group and hydroperoxy group of the Criegee intermediate. It is interesting to add that just changing C-terminal L-Dap(Ac) to L-Phe resulted in the inversion of major enantiomer of the product.

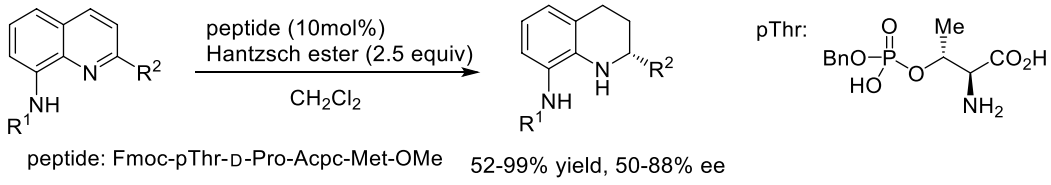

Scheme 5.65. Asymmetric reduction of quinoline derivatives catalyzed by a peptide with phosphorylated threonine. Source: Based on [139].

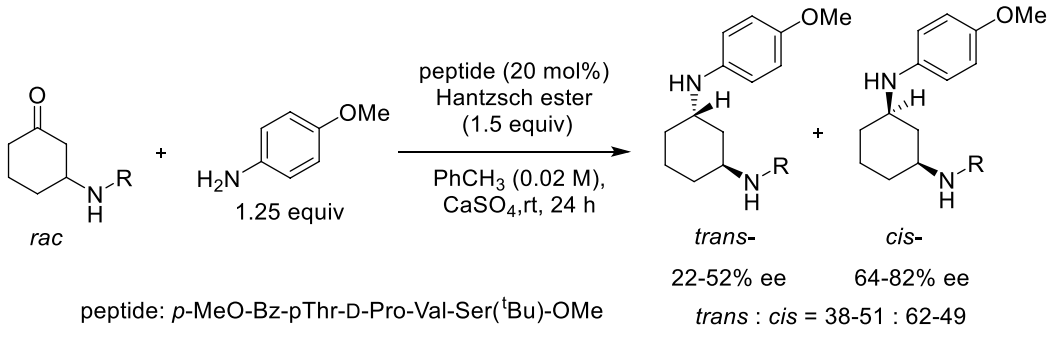

Scheme 5.66. Reductive kinetic resolution of imines catalyzed by a peptide with phosphorylated threonine. Source: Based on [140].

The pThr-containing peptide also found application in the catalytic atroposelective cyclodehydration leading to axially chiral benzimidazoles (Scheme 5.68) [142]. The peptide catalyst showed comparative performance to the C_2-symmetrical BINOL-derived phosphoric acid. High ee was observed with the substrate with 2-monosubstituted phenyl group on nitrogen. Those with 2,6-disubstituted phenyl group gave the products with low enantioselectivity for some cases.

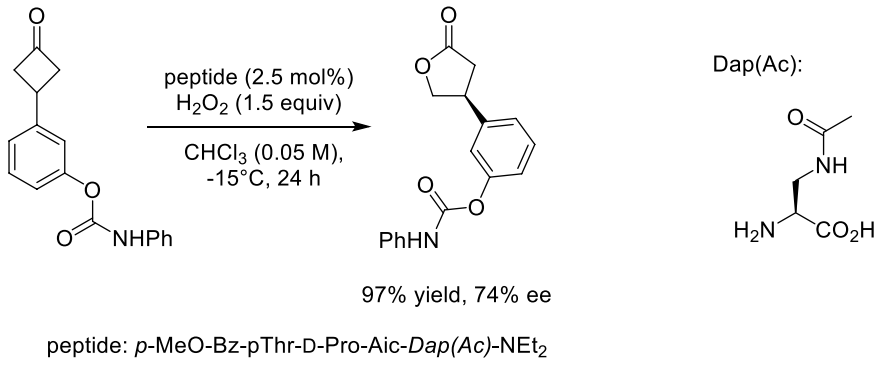

Scheme 5.67. Enantioselective Baeyer-Villiger oxidation controlled by a peptide with phosphorylated threonine. Source: Based on [141].

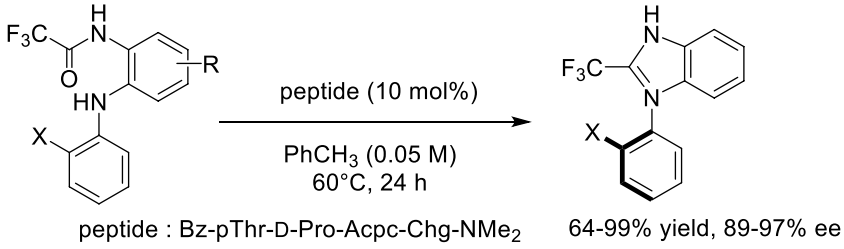

Scheme 5.68. Atroposelective cyclodehydration leading to axially chiral benzimidazoles catalyzed by a peptide with phosphorylated threonine. Source: Based on [142].

In 2021, Miller and coworkers utilized the pThr-containing tetrapeptide to the stereocontrolled dinucleotide synthesis based on a dynamic kinetic asymmetric transformation of phosphoramidite [143]. Phosphoramidite method is a standard in solid-phase oligonucleotide synthesis, and it contains azole-catalyzed displacement of amino group in phosphoramidite by the 5′-hydroxy group of oligonucleotide chain. The role of the azole is widely accepted as both acid and nucleophilic catalyses. The Miller's group envisioned that such a dual catalysis might also be possible with the phosphoric acid derivatives. With using isocyanate as a scavenger for the liberated amine, they successfully realized the catalytic dinucleotide formation by achiral diphenyl phosphate (DPP). By replacing DPP with allothreonine-based tetrapeptide catalyst and with BINOL-based axially chiral (*S*)-phosphate catalyst, they obtained S_P and R_P dinucleotides, respectively, with high ee (Scheme 5.69).

In 2009, Miller and coworkers reported aza-MBH reaction of allenoates by utilizing non-natural 3-(3-pyridiyl)alanine-containing peptide (Scheme 5.70a) [144]. In the catalyst screening stage, they clarified that DMAP or NMI derivative does not work well for this reaction. This allenoate chemistry was then expanded to the control of both point and axial chirality by utilizing racemic axially chiral allenoates (Scheme 5.70b) [145].

In 2016, Kirsch and coworkers reported site-selective acylation using DMAP-connected peptide. The unique point of this catalyst is that the DMAP is connected via Huisgen cycloaddition on a propargyl group connected to main chain nitrogen atom in the middle of the peptide chain (Scheme 5.71) [146]. They prepared 154 kinds of DMAP-containing peptide and screened for the acetylation of 1-phenylethanol, and then those that gave promising result were utilized for the site-selective acylation of sugar derivatives and other polyols. By rigorous screening, they found the appropriate peptide catalyst for each substrate. The peptide catalysts that give the optimum results differ depending on the substrate.

In the field of biocatalysis, functionally highly interesting are the coenzymes. From such viewpoint, peptide catalysts having coenzyme-related reaction center have been prepared and utilized. Imperiali and coworkers reported the peptides that contain amino acids having covalently attached coenzyme on

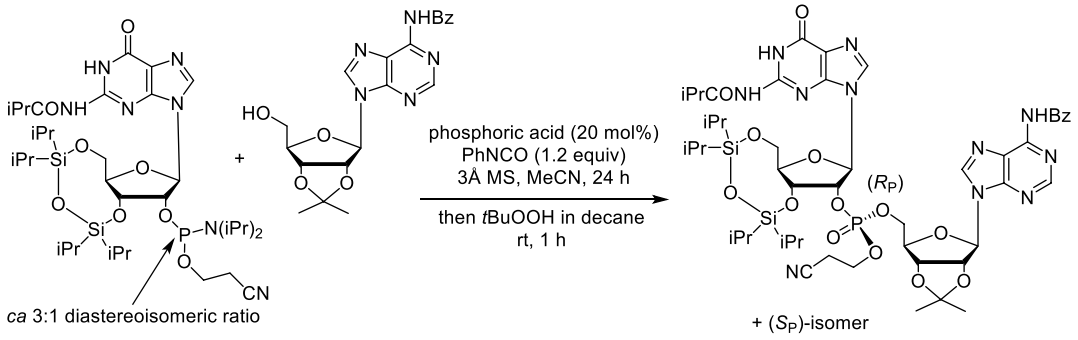

phosphoric acid	result
Bz-*allo-pThr*-D-Pro-Aib-Dap(Ac)-NMe_2	79% yield, 88% ee for (S_P)-isomer
Ar = 2,4,6-tricyclohexylphenyl	63% yield, 98% ee for (R_P)-isomer

allo-pThr:

Scheme 5.69. Diastereodivergent construction *P*(III) chiral center from phosphoroamidite controlled by chiral phosphoric acid catalysts.

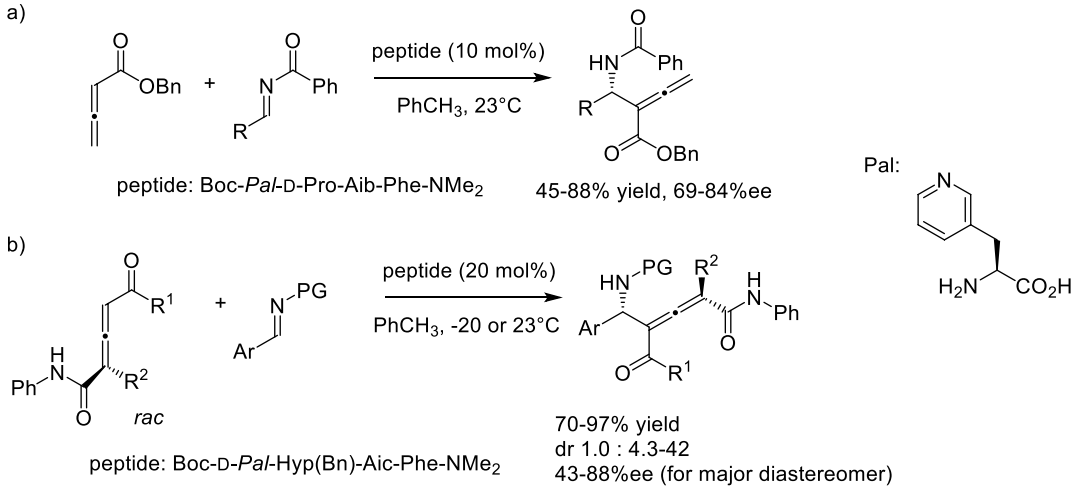

Scheme 5.70. (a) Pyridine-conjugated peptide-catalyzed asymmetric aza-MBH reaction of allenoates and (b) its extension to diastereo-/enantioselective version. Source: Based on [144, 145].

their side chains (Scheme 5.72) [147]. They utilized previously designed 23-residue peptide with ββα supersecondary structure as a template[148], and the Tyr at the sixth position was replaced with pyridoxamine amino acid (Pam). They carried out a transamination between pyruvate and D-phenylalanine to yield enantioenriched alanine [149]. After screening the residues next to Pam, optimal sequence was obtained. Interestingly, the enantiomer preference was affected by the absence/presence of Cu(II) ion. They also prepared thiazolium amino acid (Taz)-containing peptide, and demonstrated that H/D

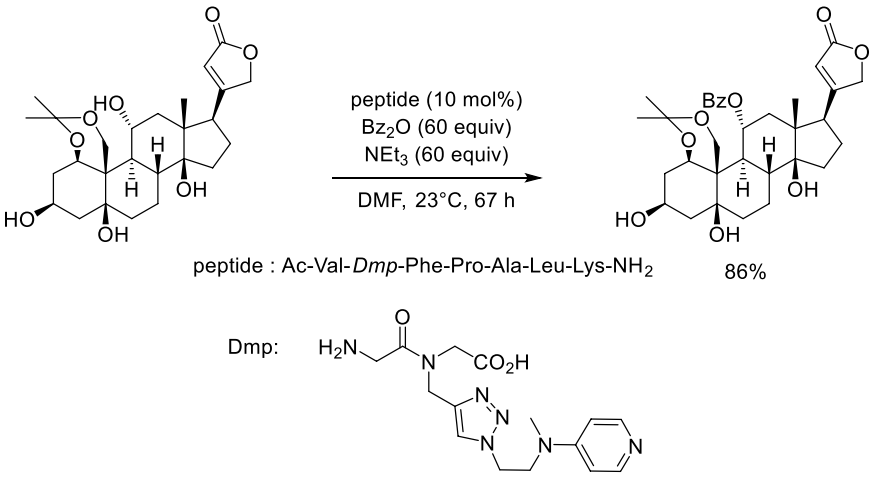

Scheme 5.71. Site-selective acylation using peptide catalyst with DMAP-type side chain. Source: Based on [146].

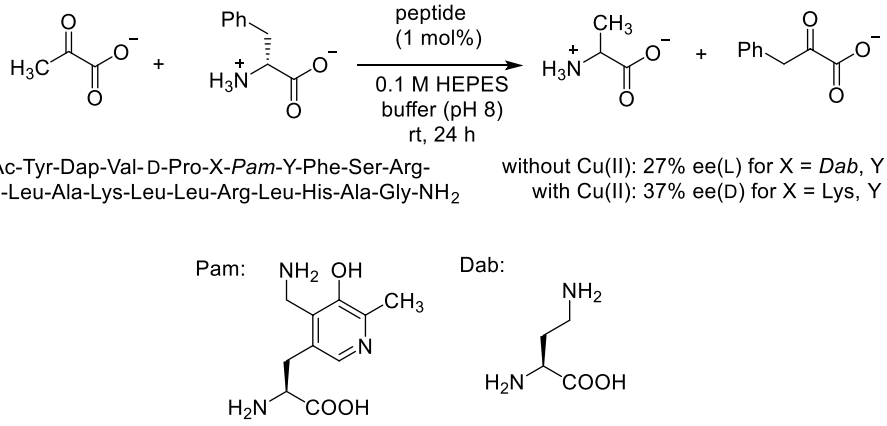

Scheme 5.72. Peptide-catalyzed enantioselective transamination of pyruvate. Source: [147]/Springer Nature.

exchange at 2-position of thiazolium ring was 5–125 times faster than simple thiazolium salt. However, they have not utilized this to asymmetric reactions.

Concerning this, Miller and coworkers showed that Taz-containing peptide can be used as asymmetric catalyst for intramolecular Stetter reaction (Scheme 5.73a) [150]. At first they tried the peptide with **1**-related structure, but ee was lower than 21%. They finally found that shorter peptide gives good result. The same peptide was also viable for the reaction between aldehyde and acylimine (Scheme 5.73b) [151].

Side chain flavin-bound amino acid has been synthesized and the peptide incorporating this residue has been utilized as photodimerized DNA repair[152], however, application of this amino acid to asymmetric reaction has not been reported.

5.5. PEPTIDE CATALYSIS WITH OTHER TYPES OF CATALYTIC CENTERS

In 1983, Nonaka and coworkers reported an electrochemical asymmetric reduction of activated C–C double bond and *gem*-dihalide with polyvaline-coated graphite (Scheme 5.74) [153]. In the next year, they demonstrated an asymmetric anodic oxidation of unsymmetrical sulfide to sulfoxide up to 93% ee on polyvaline-coated Pt electrode (Scheme 5.75). For this reaction, helical peptides such as polyleucine or poly(γ-benzyl L-glutamate) were less effective [154].

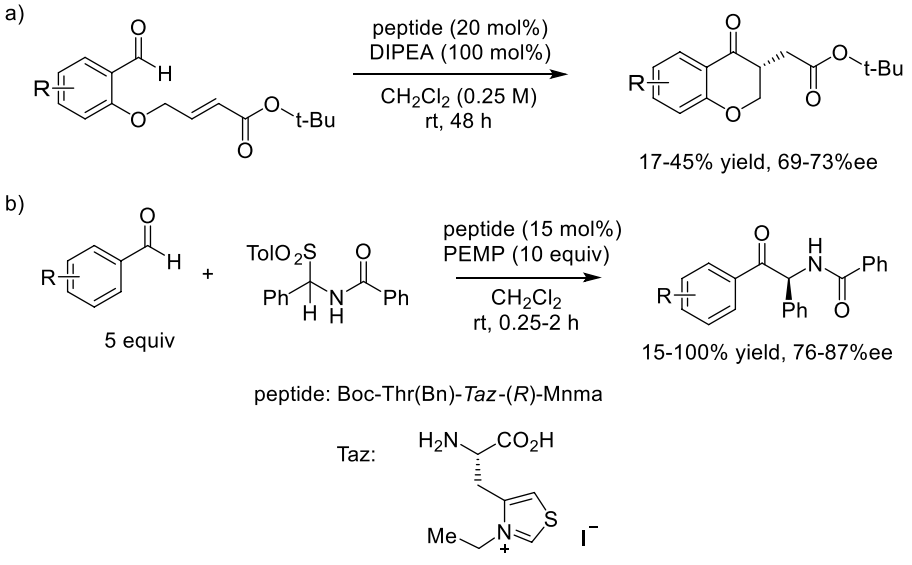

Scheme 5.73. Asymmetric reactions catalyzed by a peptide having thiazolium side chain; (a) intramolecular Stetter reaction, and (b) intermolecular C–C bond formation between aldehyde and acylimine. Source: Based on [150, 151].

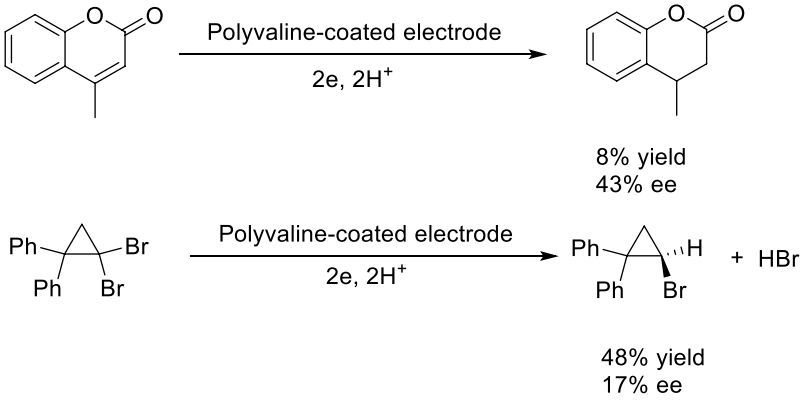

Scheme 5.74. Asymmetric cathodic reduction on polyvaline-coated graphite electrode. Source: Based on [153].

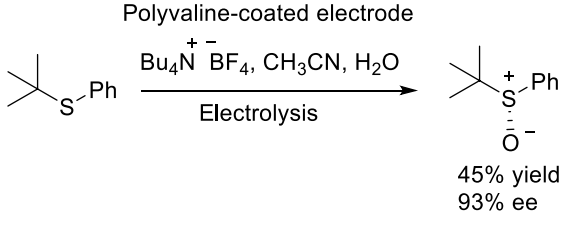

Scheme 5.75. Asymmetric anodic sulfoxidation on polyvaline-coated Pt electrode.

5.6. CONCLUSION

As seen in this chapter, asymmetric peptide catalysts, which were initially positioned as one of the organocatalysts, have since come to the forefront of their uniqueness. This trend will be continued in the future. Considering the relationship with the enzyme, it seems possible to append substrate specificity as

needed, and this may lead to tailor-made catalysts. Highly modular nature of this catalyst enables the use of library screening that can potentially give the brand-new sequence that cannot be even imagined by a simple extrapolation of existing peptides.

In the field of catalytic asymmetric organic synthesis, there are several kinds of "privileged chiral catalysts" [155] that have a common molecular structural framework for realizing high degree of enantioselectivity. As introduced in the beginning of this chapter, we might say that such a kind of core structure has been found to date for the peptide catalysts.

On the other hand, due to quite high conformational freedom, the relationship between the peptide molecular structure and their catalytic performance is still on the way to be understood. Not only the traditional methods, but also an approach from data science may be a possible choice.

REFERENCES

1. Knowles, R. R.; Jacobsen, E. N. *Proc. Natl. Acad. Sci. U. S. A.* **2010**, *107*, 20678–20685.
2. Akagawa, K. Catalysis by peptides. In: Peptide Applications in Biomedicine, Biotechnology and Bioengineering; Koutsopoulos, S., Ed.; Elsevier, **2018**; pp 513–564.
3. Metrano, A. J.; Chinn, A. J.; Shugrue, C. R.; Stone, E. A.; Kim, B.; Miller, S. J. *Chem. Rev.* **2020**, *120*, 11479–11615.
4. (a) Tsogoeva, S. B. *Lett. Org. Chem.* **2005**, *2*, 208–213. (b) Blank, J. T.; Miller, S. J. *Biopolymers* **2006**, *84*, 38–47. (c) Davie, E. A. C.; Mennen, S. M.; Xu, Y.; Miller, S. J. *Chem. Rev.* **2007**, *107*, 5759–5812. (d) Wennemers, H. *Chem. Commun.* **2011**, *47*, 12036–12041. (e) Kudo, K.; Akagawa, K. Peptide-catalyzed asymmetric synthesis. In: Polymeric Chiral Catalyst Design and Chiral Polymer Synthesis; Itsuno, S., Ed.; Wiley, **2011**; pp 91–123. (f) Duschmale, J.; Arakawa, Y.; Wennemers, H. Peptide catalysis. In: Science of Synthesis, Asymmetric Organocatalysis; List, B., Maruoka, K., Eds.; Thieme, **2012**; Vol. *2*, pp 741–786. (g) Giuliano, M. W.; Miller, S. J. *Top. Curr. Chem.* **2016**, *372*, 157–202. (h) Akagawa, K.; Kudo, K. *Acc. Chem. Res.* **2017**, *50*, 2429–2439. (i) Zozulia, O.; Dolan, M. A.; Korendovych, I. V. *Chem. Soc. Rev.* **2018**, *47*, 3621–3639. (j) Metrano, A. J.; Miller, S. J. *Acc. Chem. Res.* **2019**, *52*, 199–215.
5. (a) Fukushima, H.; Ohashi, S.; Inoue, S. *Makromol. Chem.* **1975**, *176*, 2751–2753. (b) Fukushima, H.; Inoue, S. *Makromol. Chem.* **1975**, *176*, 3609–3611. (c) Ueyanagi, K.; Inoue, S. *Makromol. Chem.* **1976**, *177*, 2807–2817.
6. Juliá, S.; Masana, J.; Vega, J. C. *Angew. Chem., Int. Ed.* **1980**, *19*, 929–931.
7. Juliá, S.; Guixer, J.; Masana, J.; Rocas, J.; Colonna, S.; Annuziata, R.; Molinari, H. *J. Chem. Soc. Perkin Trans. 1* **1982**, 1317–1324.
8. Bentley, P. A.; Flood, R. W.; Roberts, S. M.; Skidmore, J.; Smith, C. B.; Smith, J. A. *Chem. Commun.* **2001**, 1616–1617.
9. Eder, U.; Sauer, G.; Wiechert, R. *Angew. Chem. Int. Ed.* **1971**, *10*, 496–497.
10. Hajos, Z. G.; Parrish, D. R. *J. Org. Chem.* **1974**, *39*, 1615–1621.
11. List, B.; Lerner, R. A.; Barbas, C. F. *J. Am. Chem. Soc.* **2000**, *122*, 2395–2396.
12. (a) Kofoed, J.; Nielsen, J.; Reymond, J.-L. *Bioorg. Med. Chem. Lett.* **2003**, *13*, 2445–2447. (b) Martin, H. J.; List, B. *Synlett* **2003**, *2003*, 1901–1902. (c) Shi, L.-X.; Sun, Q.; Ge, Z.-M.; Zhu, Y.-Q.; Cheng, T.-M.; Li, R.-T. *Synlett* **2004**, *2004*, 2215–2217. (d) Krattiger, P.; Kovasy, R.; Revell, J. D.; Ivan, S.; Wennemers, H. *Org. Lett.* **2005**, *7*, 1101–1103. (e) Revell, J. D.; Wennemers, H. *Tetrahedron* **2007**, *63*, 8420–8424. (f) Angelici, G.; Falgiani, A.; Luppi, G.; Kaptein, B.; Broxterman, Q. B.; Tomasini, C. *Synth. Commun.* **2008**, *38*, 1137–1146. (g) Chen, F.; Huang, S.; Zhang, H.; Liu, F.; Peng, Y. *Tetrahedron* **2008**, *64*, 9585–9591. (h) Revell, J. D.; Wennemers, H. *Adv. Synth. Catal.* **2008**, *350*, 1046–1052. (i) Chandrasekhar, S.; Johny, K.; Reddy, C. R. *Tetrahedron: Asymmetry* **2009**, *20*, 1742–1745. (j) Wang, B.; Chen, G.; Liu, L.; Chang, W.; Li, J. *Adv. Synth. Catal.* **2009**, *351*, 2441–2448. (k) Rodriguez-Llansola, F.; Miravet, J. F.; Escuder, B. *Chem. Commun.* **2009**, 7303–7305. (l) Tsandi, E.; Kokotos, C. G.; Kousidou, S.; Ragoussis, V.; Kokotos, G. *Tetrahedron* **2009**, *65*, 1444–1449. (m) Uhlich, N. A.; Darbre, T.; Reymond, J.-L. *Org. Biomol. Chem.* **2011**, *9*, 7071–7084. (n) Milbeo, P.; Maurent, K.; Moulat, L.; Lebrun, A.; Didierjean, C.; Aubert, E.; Martinez, J.; Calmes, M. *Tetrahedron* **2016**, *72*, 1706–1715. (o) Schnitzer, T.; Wiesner, M.; Krattiger, P.; Revell, J. D.; Wennemers, H. *Org. Biomol. Chem.* **2017**, *15*, 5877–5881. (p) Bhowmick, S.; Zhang, L.; Ouyang, G.; Liu, M. *ACS Omega* **2018**, *3*, 8329–8336. (q) Al-Momani, L. A. *Jordan J. Chem.* **2018**, *13*, 179–189. (r) Kon, K.; Kohari, Y.; Murata, M. *Tetrahedron Lett.* **2019**, *60*, 415–418. (s) Du, Z. H.; Tao, B. X.; Yuan, M.; Qin, W. J.; Xu, Y. L.; Wang, P.; Da, C. S. *Org. Lett.* **2020**, *22*, 4444–4450.
13. (a) Tsogoeva, S. B.; Wei, S. *Tetrahedron: Asymmetry* **2005**, *16*, 1947–1951. (b) Córdova, A.; Zou, W.; Dziedzic, P.; Ibrahem, I.; Reyes, E.; Xu, Y. *Chem. Eur. J.* **2006**, *12*, 5383–5397. (c) Wu, F.-C.; Da, C.-S.; Du, Z.-X.; Guo, Q.-P.; Li, W.-P.; Yi, L.; Jia, Y.-N.; Ma, X. *J. Org. Chem.* **2009**, *74*, 4812–4818.
14. (a) Andreae, M. R. M.; Davis, A. P. *Tetrahedron: Asymmetry* **2005**, *16*, 2487–2492. (b) Akagawa, K.; Sakamoto, S.; Kudo, K. *Tetrahedron Lett.* **2005**, *46*, 8185–8187. (c) Revell, J. D.; Gantenbein, D.; Krattiger, P.; Wennemers, H. *Biopolymers* **2006**, *84*, 105–113. (d) Akagawa, K.; Sakamoto, S.; Kudo, K. *Tetrahedron Lett.* **2007**, *48*, 985–987.e) Yan, J.; Wang, L. *Synthesis* **2008**, *2008*, 2065–2072. (f) Yan, J.; Wang, L. *Chirality* **2009**, *21*, 413–420. (g) Zhang, L.; Ding, W. B.; Yu, Y. P.; Zou, H. Bin. *Chin. Chem. Lett.* **2009**, *20*, 1065–1067. (h) Gruttadauria, M.; Salvo, A. M. P.; Giacalone, F.; Agrigento, P.; Noto, R. *Eur. J.*

Org. Chem. **2009**, 5437–5444. (i) Akagawa, K.; Takigawa, S.; Mano, E.; Kudo, K. *Tetrahedron Lett.* **2011**, *52*, 770–773. (j) Uhlich, N. A.; Darbre, T.; Reymond, J.-L. *Org. Biomol. Chem.* **2011**, *9*, 7071–7084. (k) Otvos, S. B.; Mandity, I. M.; Fulop, F. *J. Catal.* **2012**, *295*, 179–185. (l) Jebors, S.; Enjalbal, C.; Amblard, M.; Mehdi, A.; Subra, G.; Martinez, J. *J. Mater. Chem. B* **2013**, *1*, 2921–2925. (m) Szollosi, G.; Csampai, A.; Somlai, C.; Fekete, M.; Bartok, M. *J. Mol. Catal. A* **2014**, *382*, 86–92. (n) Machuca, E.; Granados, G.; Hinojosa, B.; Juaristi, E. *Tetrahedron Lett.* **2015**, *56*, 6047–6051. (o) Bonnefoy, J.; Legrand, A.; Quadrelli, E. A.; Canivet, J.; Farrusseng, D. *J. Am. Chem. Soc.* **2015**, *137*, 9409–9416. (p) Akagawa, K.; Higuchi, J.; Yoshikawa, I.; Kudo, K. *Eur. J. Org. Chem.* **2018**, 5278–5281.

15. (a) Tang, Z.; Yang, Z.; Cun, L.; Gong, L.; Mi, A.; Jiang, Y. *Org. Lett.* **2004**, *6*, 2285–2287. (b) Andreu, C.; del Olmo, M.; Asensio, G. *Tetrahedron* **2012**, *68*, 7966–7972. (c) Bayat, S.; Tejo, B. A.; Salleh, A. B.; Abdmalek, E.; Normi, Y. M.; Abdul Rahman, M. B. *Chirality* **2013**, *25*, 726–734. (d) Bayat, S.; Tejo, B. A.; Abdulmalek, E.; Salleh, A. B.; Normi, Y. M.; Abdul Rahman, M. B. *RSC Adv.* **2014**, *4*, 38859–38868.
16. (a) Zou, W.; Ibrahem, I.; Dziedzic, P.; Sundén, H.; Córdova, A. *Chem. Commun.* **2005**, 4946–4948. (b) Córdova, A.; Zou, W.; Dziedzic, P.; Ibrahem, I.; Reyes, E.; Xu, Y. *Chem. Eur. J.* **2006**, *12*, 5383–5397. (c) Dziedzic, P.; Zou, W.; Háfren, J.; Córdova, A. *Org. Biomol. Chem.* **2006**, *4*, 38–40. (d) Lei, M.; Shi, L.; Li, G.; Chen, S.; Fang, W.; Ge, Z.; Cheng, T.; Li, R. *Tetrahedron* **2007**, *63*, 7892–7898. (e) Psarra, A.; Kokotos, C. G.; Moutevelis-Minakakis, P. *Tetrahedron* **2014**, *70*, 608–615.
17. (a)De Nisco, M.; Pedatella, S.; Ullah, H.; Zaidi, J. H.; Naviglio, D.; Ozdamar, O.; Caputo, R. *J. Org. Chem.* **2009**, *74*, 9562–9565. (b) Huang, W.; Tian, H.; Xu, H.; Zheng, L.; Liu, Q.; Zhang, S. *Catal. Letters* **2011**, *141*, 872–876. (c) Tian, H.; Gao, J.; Xu, H.; Zheng, L.-Y.; Huang, W.-B.; Liu, Q.-W.; Zhang, S.-Q. *Tetrahedron: Asymmetry* **2011**, *22*, 1074–1080. (d) Bisticha, A.; Triandafillidi, I.; Kokotos, C. G. *Tetrahedron: Asymmetry* **2015**, *26*, 102–108. (e) Triandafillidi, I.; Bisticha, A.; Voutyritsa, E.; Galiatsatou, G.; Kokotos, C. G. *Tetrahedron* **2015**, *71*, 932–940. (f) Hu, X.-M.; Zhang, D.-X.; Zhang, S.-Y.; Wang, P.-A. *RSC Adv.* **2015**, *5*, 39557–39564. (g) Vlasserou, I.; Sfetsa, M.; Gerokonstantis, D.-T.; Kokotos, C. G.; Moutevelis-Minakakis, P. *Tetrahedron* **2018**, *74*, 2338–2349.
18. (a) Rodriguez, B.; Bruckmann, A.; Bolm, C. *Chem. Eur. J.* **2007**, *13*, 4710–4722. (b) Hernandez, J. G.; Juaristi, E. *J. Org. Chem.* **2011**, *76*, 1464–1467. (c) Hernandez, J. G.; Juaristi, E. *Tetrahedron* **2011**, *67*, 6953–6959. (d) Machuca, E.; Rojas, Y.; Juaristi, E. *Asian J. Org. Chem.* **2015**, *4*, 46–53. (e) Machuca, E.; Juaristi, E. *Tetrahedron Lett.* **2015**, *56*, 1144–1148.
19. (a) Rodriguez-Llansola, F.; Miravet, J. F.; Escuder, B. *Chem. Commun.* **2009**, 7303–7305. (b) Tena-Solsona, M.; Nanda, J.; Diaz-Oltra, S.; Chotera, A.; Ashkenasy, G.; Escuder, B. *Chem. Eur. J.* **2016**, *22*, 6687–6694. (c) Soares, B. M.; Aguilar, A. M.; Silva, E. R.; Coutinho-Neto, M. D.; Hamley, I. W.; Reza, M.; Ruokolainen, J.; Alves, W. A. *Phys. Chem. Chem. Phys.* **2017**, *19*, 1181–1189. (d) Bhowmick, S.; Zhang, L.; Ouyang, G.; Liu, M. *ACS Omega* **2018**, *3*, 8329–8336. (e) Pelin, J. N. B. D.; Gerbelli, B. B.; Soares, B. M.; Aguilar, A. M.; Alves, W. A. *Catal. Sci. Technol.* **2019**, *9*, 4304–4313. (f) Pelin, J. N. B. D.; Gerbelli, B. B.; Edwards-Gayle, C. J. C.; Aguilar, A. M.; Castelletto, V.; Hamley, I. W.; Alves, W. A. *Langmuir* **2020**, *36*, 2767–2774. (g) Pelin, J. N. B. D.; Edwards-Gayle, C. J. C.; Castelletto, V.; Aguilar, A. M.; Alves, W. A.; Seitsonen, J.; Ruokolainen, J.; Hamley, I. W. *ACS Appl. Mater. Interfaces* **2020**, *12*, 13671–13679.
20. (a) D'Elia, V.; Zwicknagl, H.; Reiser, O. *J. Org. Chem.* **2008**, *73*, 3262–3265. (b) Messerer, M.; Wennemers, H. *Synlett* **2011**, 499–502. (c) Illa, O.; Porcar-Tost, O.; Robledillo, C.; Elvira, C.; Nolis, P.; Reiser, O.; Branchadell, V.; Ortuno, R. M. *J. Org. Chem.* **2018**, *83*, 350–363.
21. Krattiger, P.; Kovasy, R.; Revell, J. D.; Wennemers, H. *QSAR Comb. Sci.* **2005**, *24*, 1158–1163.
22. Rulli, G.; Fredriksen, K. A.; Duangdee, N.; Bonge-Hansen, T.; Berkessel, A.; Gröger, H. *Synthesis* **2013**, *45*, 2512–2519.
23. Du, Z.-X.; Zhang, L.-Y.; Fan, X.-Y.; Wu, F.-C.; Da, C.-S. *Tetrahedron Lett.* **2013**, *54*, 2828–2832.
24. Martin, H. J.; List, B. *Synlett* **2003**, 1901–1902.
25. Xu, Y.; Zou, W.; Sundén, H.; Ibrahem, I.; Córdova, A. *Adv. Synth. Catal.* **2006**, *348*, 418–424.
26. Wiesner, M.; Revell, J. D.; Tonazzi, S.; Wennemers, H. *J. Am. Chem. Soc.* **2008**, *130*, 5610–5611.
27. Wiesner, M.; Revell, J. D.; Wennemers, H. *Angew. Chem. Int. Ed.* **2008**, *47*, 1871–1874.
28. Wiesner, M.; Upert, G.; Angelici, G.; Wennemers, H. *J. Am. Chem. Soc.* **2010**, *132*, 6–7.
29. Arakawa, Y.; Wiesner, M.; Wennemers, H. *Adv. Synth. Catal.* **2011**, *353*, 1201–1206.
30. Arakawa, Y.; Wennemers, H. *ChemSusChem* **2013**, *6*, 242–245.
31. Kastl, R.; Wennemers, H. *Angew. Chem. Int. Ed.* **2013**, *52*, 7228–7232.
32. Duschmalé, J.; Wennemers, H. *Chem. Eur. J.* **2012**, *18*, 1111–1120.
33. Schnitzer, T.; Wiesner, M.; Krattiger, P.; Revell, J. D.; Wennemers, H. *Org. Biomol. Chem.* **2017**, *15*, 5877–5881.
34. Grünenfelder, C. E.; Kisunzu, J. K.; Wennemers, H. *Angew. Chem. Int. Ed.* **2016**, *55*, 8571–8574.
35. Schnitzer, T.; Budinská, A.; Wennemers, H. *Nat. Catal.* **2020**, *3*, 143–147.
36. Akagawa, K.; Fujiwara, T.; Sakamoto, S.; Kudo, K. *Org. Lett.* **2010**, *12*, 1804–1807.
37. Akagawa, K.; Fujiwara, T.; Sakamoto, S.; Kudo, K. *Chem. Commun.* **2010**, *46*, 8040–8042.
38. Akagawa, K.; Kudo, K. *Org. Lett.* **2011**, *13*, 3498–3501.
39. Tanaka, T.; Akagawa, K.; Mitsuda, M.; Kudo, K. *Adv. Synth. Catal.* **2013**, *355*, 294–296.
40. Erkkilä, A.; Majander, I.; Pihko, P. M. *Chem. Rev.* **2007**, *107*, 5416–5470.
41. Ahrendt, K. A.; Borths, C. J.; MacMillan, D. W. C. *J. Am. Chem. Soc.* **2000**, *122*, 4243–4244.
42. (a)Yamaguchi, M.; Shiraishi, T.; Igarashi, Y.; Hirama, M. *Tetrahedron Lett.* **1994**, *35*, 8233–8236. (b) Yamaguchi, M.; Igarashi, Y.; Reddy, R. S.; Shiraishi, T.; Hirama, M. *Tetrahedron* **1997**, *53*, 11223–11236.

43. (a) Tsogoeva, S. B.; Jagtap, S. B.; Ardemasova, Z. A.; Kalikhevich, V. N. *Eur. J. Org. Chem.* **2004**, *2004*, 4014–4019. (b) Tsogoeva, S. B.; Jagtap, S. B.; Ardemasova, Z. A. *Tetrahedron Asymmetry* **2006**, *17*, 989–992.
44. (a) Akagawa, K.; Akabane, H.; Sakamoto, S.; Kudo, K. *Org. Lett.* **2008**, *10*, 2035–2037. (b) Akagawa, K.; Akabane, H.; Sakamoto, S.; Kudo, K. *Tetrahedron: Asymmetry* **2009**, *20*, 461–466.
45. Akagawa, K.; Yamashita, T.; Sakamoto, S.; Kudo, K. *Tetrahedron Lett.* **2009**, *50*, 5602–5604.
46. Demizu, Y.; Tanaka, M.; Nagano, M.; Kurihara, M.; Doi, M.; Maruyama, T.; Suemune, H. *Chem. Pharm. Bull.* **2007**, *55*, 840–842.
47. Akagawa, K.; Kudo, K. *Angew. Chem. Int. Ed.* **2012**, *51*, 12786–12789.
48. Akagawa, K.; Sen, J.; Kudo, K. *Angew. Chem. Int. Ed.* **2013**, *52*, 11585–11588.
49. Akiyama, M.; Akagawa, K.; Seino, H.; Kudo, K. *Chem. Commun.* **2014**, *50*, 7893–7896.
50. Akagawa, K.; Akiyama, M.; Kudo, K. *Eur. J. Org. Chem.* **2015**, *2015*, 3894–3898.
51. Akagawa, K.; Nishi, N.; Sen, J.; Kudo, K. *Org. Biomol. Chem.* **2014**.
52. Akagawa, K.; Sakai, N.; Kudo, K. *Angew. Chem. Int. Ed.* **2015**, *54*, 1822–1826.
53. Akagawa, K.; Sugiyama, M.; Kudo, K. *Org. Biomol. Chem.* **2012**, *10*, 4839–4843.
54. Akagawa, K.; Kudo, K. *Adv. Synth. Catal.* **2011**, *353*, 843–847.
55. Akagawa, K.; Takigawa, S.; Nagamine, I. S.; Umezawa, R.; Kudo, K. *Org. Lett.* **2013**, *15*, 4964–4967.
56. Kunz, R. K.; MacMillan, D. W. C. *J. Am. Chem. Soc.* **2005**, *127*, 3240–3241.
57. Akagawa, K.; Satou, J.; Kudo, K. *J. Org. Chem.* **2016**, *81*, 9396–9401.
58. Akagawa, K.; Iwasaki, Y.; Kudo, K. *Eur. J. Org. Chem.* **2016**, *2016*, 4460–4464.
59. Akagawa, K.; Suzuki, R.; Kudo, K. *Asian J. Org. Chem.* **2014**, *3*, 514–522.
60. Akagawa, K.; Nishi, N.; Yoshikawa, I.; Kudo, K. *Eur. J. Org. Chem.* **2015**, *2015*, 5055–5059.
61. Akagawa, K.; Umezawa, R.; Kudo, K. *Beilstein J. Org. Chem.* **2012**, *8*, 1333–1337.
62. Bentley, P. A.; Bergeron, S.; Cappi, M. W.; Hibbs, D. E.; Hursthouse, M. B.; Nugent, T. C.; Pulido, R.; Roberts, S. M.; Eduardo Wu, L. *Chem. Commun.* **1997**, 739–740.
63. Akagawa, K.; Hirata, T.; Kudo, K. *Synlett* **2015**, *27*, 1217–1222.
64. Itsuno, S.; Sakakura, M.; Ito, K. *J. Org. Chem.* **1990**, *55*, 6047–6049.
65. Bentley, P. A.; Bergeron, S.; Cappi, M. W.; Hibbs, D. E.; Hursthouse, M. B.; Nugent, T. C.; Pulido, R.; Roberts, S. M.; Eduardo Wu, L. *Chem. Commun.* **1997**, 739–740.
66. Kelly, D. R.; Roberts, S. M. *Chem. Commun.* **2004**, 2018–2020.
67. Nagano, M.; Doi, M.; Kurihara, M.; Suemune, H.; Tanaka, M. *Org. Lett.* **2010**, *12*, 1397–1398.
68. Akagawa, K.; Kudo, K. *Tetrahedron Lett.* **2012**, *53*, 5981–5983.
69. Brown, J. M.; Bunton, C. A. *J. Chem. Soc. Chem. Commun.* **1974**, 969–971.
70. Oku, J.; Ito, N.; Inoue, S. *Makromol. Chem.* **1979**, *180*, 1089–1091.
71. Ohkubo, K.; Matsumoto, N.; Ohta, H. *J. Chem. Soc. Chem. Commun.* **1982**, 738–740.
72. Ueoka, R.; Matsumoto, Y.; Moss, R. A.; Swarup, S.; Sugii, A.; Harada, K.; Kikuchi, J. I.; Murakami, Y. *J. Am. Chem. Soc.* **1988**, *110*, 1588–1595.
73. Broo, K. S.; Nilsson, H.; Nilsson, J.; Baltzer, L. *J. Am. Chem. Soc.* **1998**, *120*, 10287–10295.
74. Tsutsumi, H.; Hamasaki, K.; Mihara, H.; Ueno, A. *J. Chem. Soc. Perkin Trans. 2* **2000**, 1813–1818.
75. Esposito, A.; Delort, E.; Lagnoux, D.; Djojo, F.; Reymond, J. L. *Angew. Chem. Int. Ed.* **2003**, *42*, 1381–1383.
76. Akagawa, K.; Kudo, K. *Chem. Lett.* **2016**, *45*, 300–302.
77. Tanaka, K.; Mori, A.; Inoue, S. *J. Org. Chem.* **1990**, *55*, 181–185.
78. Connors, K. A.; Pandit, N. K. *Anal. Chem.* **1978**, *50*, 1542–1545.
79. Miller, S. J.; Copeland, G. T.; Papaioannou, N.; Horstmann, T. E.; Ruel, E. M. *J. Am. Chem. Soc.* **1998**, *120*, 1629–1630.
80. Ravi, A.; Balaram, P. *Tetrahedron* **1984**, *40*, 2577–2583.
81. (a) Miller, S. J.; Grubbs, R. H. *J. Am. Chem. Soc.* **1995**, *117*, 5855–5856. (b) Miller, S. J.; Blackwell, H. E.; Grubbs, R. H. *J. Am. Chem. Soc.* **1996**, *118*, 9606–9614.
82. Copeland, G. T.; Jarvo, E. R.; Miller, S. J. *J. Org. Chem.* **1998**, *63*, 6784–6785.
83. Blank, J. T.; Guerin, D. J.; Miller, S. J. *Org. Lett.* **2000**, *2*, 1247–1249.
84. (a) Copeland, G. T.; Miller, S. J. *J. Am. Chem. Soc.* **1999**, *121*, 4306–4307. (b) Copeland, G. T.; Miller, S. J. *J. Am. Chem. Soc.* **2001**, *123*, 6496–6502.
85. Evans, J. W.; Fierman, M. B.; Miller, S. J.; Ellman, J. A. *J. Am. Chem. Soc.* **2004**, *126*, 8134–8135.
86. Sanchez-Roselló, M.; Puchlopek, A. L. A.; Morgan, A. J.; Miller, S. J. *J. Org. Chem.* **2008**, *73*, 1774–1782.
87. Lewis, C. A.; Sculimbrene, B. R.; Xu, Y.; Miller, S. J. *Org. Lett.* **2005**, *7*, 3021–3023.
88. Lewis, C.A.; Chiu, A.; Kubryk, M.; Balsells, J.; Pollard, D.; Esser, C. K.; Murry, J.; Reamer, R. A; Hansen, K. B.; Miller, S. J. *J. Am. Chem. Soc.* **2006**, *128*, 16454–16455.
89. Griswold, K. S.; Miller, S. J. *Tetrahedron* **2003**, *59*, 8869–8875.
90. Lewis, C. A.; Miller, S. J. *Angew. Chem. Int. Ed.* **2006**, *45*, 5616–5619.
91. Fowler, B. S.; Laemmerhold, K. M.; Miller, S. J. *J. Am. Chem. Soc.* **2012**, *134*, 9755–9761.
92. Fowler, B. S.; Mikochik, P. J.; Miller, S. J. *J. Am. Chem. Soc.* **2010**, *132*, 2870–2871.
93. Mueller, C. E.; Wanka, L.; Jewell, K.; Schreiner, P. R. *Angew. Chem. Int. Ed.* **2008**, *47*, 6180–6183.

94. Mueller, C. E.; Zell, D.; Hrdina, R.; Wende, R. C.; Wanka, L.; Schuler, S. M. M.; Schreiner, P. R. *J. Org. Chem.* **2013**, *78*, 8465–8484.
95. Mueller, C. E.; Zell, D.; Schreiner, P. R. *Chem. Eur. J.* **2009**, *15*, 9647–9650.
96. Mueller, C. E.; Hrdina, R.; Wende, R. C.; Schreiner, P. R. *Chem. Eur. J.* **2011**, *17*, 6309–6314.
97. Hofmann, C.; Schuler, S. M. M.; Wende, R. C.; Schreiner, P. R. *Chem. Commun.* **2014**, *50*, 1221–1223.
98. Hofmann, C.; Schuemann, J. M.; Schreiner, P. R. *J. Org. Chem.* **2015**, *80*, 1972–1978.
99. Hrdina, R.; Müller, C. E.; Wende, R. C.; Wanka, L.; Schreiner, P. R. *Chem. Commun.* **2012**, *48*, 2498–2500.
100. Peris, G.; Jakobsche, C. E.; Miller, S. J. *J. Am. Chem. Soc.* **2007**, *129*, 8710–8711.
101. Wende, R. C.; Seitz, A.; Niedek, D.; Schuler, S. M. M.; Hofmann, C.; Becker, J.; Schreiner, P. R. *Angew. Chem. Int. Ed.* **2016**, *55*, 2719–2723.
102. Kato, N. *J. Am. Chem. Soc.* **1990**, *112*, 254–257.
103. Sculimbrene, B. R.; Miller, S. J. *J. Am. Chem. Soc.* **2001**, *123*, 10125–10126.
104. Sculimbrene, B. R.; Morgan, A. J.; Miller, S. J. *J. Am. Chem. Soc.* **2002**, *124*, 11653–11656.
105. Fiori, K. W.; Puchlopek, A. L. A.; Miller, S. J. *Nat. Chem.* **2009**, *1*, 630–634.
106. Jordan, P. A.; Miller, S. J. *Angew. Chem. Int. Ed.* **2012**, *51*, 2907–2911.
107. (a) Imbriglio, J. E.; Vasbinder, M. M.; Miller, S. J. *Org. Lett.* **2003**, *5*, 3741–3743. (b) Vasbinder, M. M.; Imbriglio, J. E.; Miller, S. J. *Tetrahedron* **2006**, *62*, 11450–11459.
108. Guerin, D. J.; Miller, S. J. *J. Am. Chem. Soc.* **2002**, *124*, 2134–2136.
109. Björkling, F.; Frykman, H.; Godtfredsen, S. E.; Kirk, O. *Tetrahedron* **1992**, *48*, 4587–4592.
110. Kolundzic, F.; Noshi, M. N.; Tjandra, M.; Movassaghi, M.; Miller, S. J. *J. Am. Chem. Soc.* **2011**, *133*, 9104–9111.
111. (a) Lichtor, P. A.; Miller, S. J. *Nat. Chem.* **2012**, *4*, 990–995. (b) Lichtor, P. A.; Miller, S. J. *J. Am. Chem. Soc.* **2014**, *136*, 5301–5308.
112. Peris, G.; Miller, S. J. *Org. Lett.* **2008**, *10*, 3049–3052.
113. Romney, D. K.; Colvin, S. M.; Miller, S. J. *J. Am. Chem. Soc.* **2014**, *136*, 14019–14022.
114. Alford, J. S.; Abascal, N. C.; Shugrue, C. R.; Colvin, S. M.; Romney, D. K.; Miller, S. J. *ACS Cent. Sci.* **2016**, *2*, 733–739.
115. Hsieh, S. Y.; Tang, Y.; Crotti, S.; Stone, E. A.; Miller, S. J. *J. Am. Chem. Soc.* **2019**, *141*, 18624–18629.
116. Stone, E. A.; Cutrona, K. J.; Miller, S. J. *J. Am. Chem. Soc.* **2020**, *142*, 12690–12698.
117. Rutter, W. J.; Rajkumar, T.; Penhoet, E.; Kochman, M.; Valentine, R. *Ann. N. Y. Acad. Sci.* **1968**, *151*, 102–117.
118. Barbier, B.; Brack, A. *J. Am. Chem. Soc.* **1992**, *114*, 3511–3515.
119. Metrano, A. J.; Miller, S. J. *J. Org. Chem.* **2014**, *79*, 1542–1554.
120. Gustafson, J. L.; Lim, D.; Miller, S. J. *Science* **2010**, *328*, 1251–1255.
121. Barrett, K. T.; Miller, S. J. *J. Am. Chem. Soc.* **2013**, *135*, 2963–2966.
122. Diener, M. E.; Metrano, A. J.; Kusano, S.; Miller, S. J. *J. Am. Chem. Soc.* **2015**, *137*, 12369–12377.
123. Metrano, A. J.; Abascal, N. C.; Mercado, B. Q.; Paulson, E. K.; Hurtley, A. E.; Miller, S. J. *J. Am. Chem. Soc.* **2017**, *139*, 492–516.
124. Moliterno, M.; Cari, R.; Puglisi, A.; Antenucci, A.; Sperandio, C.; Moretti, E.; Di Sabato, A.; Salvio, R.; Bella, M. *Angew. Chem. Int. Ed.* **2016**, *55*, 6525–6529.
125. Coombs, G.; Sak, M. H.; Miller, S. J. *Angew. Chem. Int. Ed.* **2020**, *59*, 2875–2880.
126. Iyer, M. S.; Gigstad, K. M.; Namdev, N. D.; Lipton, M. *J. Am. Chem. Soc.* **1996**, *118*, 4910–4911.
127. Becker, C.; Hoben, C.; Schollmeyer, D.; Scherr, G.; Kunz, H. *Eur. J. Org. Chem.* **2005**, 1497–1499.
128. Tsogoeva, S. B.; Jagtap, S. B.; Ardemasova, Z. A.; Kalikhevich, V. N. *Eur. J. Org. Chem.* **2004**, *2004*, 4014–4019.
129. Linton, B. R.; Reutershan, M. H.; Aderman, C. M.; Richardson, E. A.; Brownell, K. R.; Ashley, C. W.; Evans, C. A.; Miller, S. J. *Tetrahedron Lett.* **2007**, *48*, 1993–1997.
130. Beleh, O. M.; Miller, E.; Toste, F. D.; Miller, S. J. *J. Am. Chem. Soc.* **2020**, *142*, 16461–16470.
131. Aroyan, C. E.; Miller, S. J. *J. Am. Chem. Soc.* **2007**, *129*, 256–257.
132. Ryss, J. M.; Turek, A. K.; Miller, S. J. *Org. Lett.* **2018**, *20*, 1621–1625.
133. Shin, N. Y.; Ryss, J. M.; Zhang, X.; Miller, S. J.; Knowles, R. R. *Science* **2019**, *366*, 364–369.
134. Romney, D. K.; Miller, S. J. *Org. Lett.* **2012**, *14*, 1138–1141.
135. Chimni, S. S.; Kumar, V.; Bala, N. *Asian J. Org. Chem.* **2014**, *3*, 700–705.
136. Cozett, R. E.; Venter, G. A.; Gokada, M. R.; Hunter, R. *Org. Biomol. Chem.* **2016**, *14*, 10914–10925.
137. Arakawa, Y.; Yamanomoto, K.; Kita, H.; Minagawa, K.; Tanaka, M.; Haraguchi, N.; Itsuno, S.; Imada, Y. *Chem. Sci.* **2017**, *8*, 5468–5475.
138. (a) Akiyama, T. *Chem. Rev.* **2007**, *107*, 5744–5758. (b) Terada, M. *Chem. Commun.* **2008**, 4097–4112. (c) Xia, Z. L.; Xu-Xu, Q. F.; Zheng, C.; You, S. L. *Chem. Soc. Rev.* **2020**, *49*, 286–300.
139. Shugrue, C. R.; Miller, S. J. *Angew. Chem. Int. Ed.* **2015**, *54*, 11173–11176.
140. Shugrue, C. R.; Featherston, A. L.; Lackner, R. M.; Lin, A.; Miller, S. J. *J. Org. Chem.* **2018**, *83*, 4491–4504.
141. Featherston, A. L.; Shugrue, C. R.; Mercado, B. Q.; Miller, S. J. *ACS Catal.* **2019**, *9*, 242–252.
142. Kwon, Y.; Li, J.; Reid, J. P.; Crawford, J. M.; Jacob, R.; Sigman, M. S.; Toste, F. D.; Miller, S. J. *J. Am. Chem. Soc.* **2019**, *141*, 6698–6705.
143. Featherston, A. L.; Kwon, Y.; Pompeo, M. M.; Engl, O. D.; Leahy, D. K.; Miller, S. J. *Science* **2021**, *371*, 702–707.

144. Cowen, B. J.; Saunders, L. B.; Miller, S. J. *J. Am. Chem. Soc.* **2009**, *131*, 6105–6107.
145. Mbofana, C. T.; Miller, S. J. *J. Am. Chem. Soc.* **2014**, *136*, 3285–3292.
146. Huber, F.; Kirsch, S. F. *Chem. Eur. J.* **2016**, *22*, 5914–5918.
147. Imperiali, B.; McDonnell, K. A.; Shogren-Knaak, M. *Top. Curr. Chem.*, **1999**, *202*, 1–38.
148. Struthers, M. D.; Cheng, R. P.; Imperiali, B. *Science* **1996**, *271*, 342–345.
149. Shogren-Knaak, M. A.; Imperiali, B. *Bioorg. Med. Chem.* **1999**, *7*, 1993–2002.
150. Mennen, S. M.; Blank, J. T.; Tran-Dubé, M. B.; Imbriglio, J. E.; Miller, S. J. *Chem. Commun.* **2005**, 195–197.
151. Mennen, S. M.; Gipson, J. D.; Kim, Y. R.; Miller, S. J. *J. Am. Chem. Soc.* **2005**, *127*, 1654–1655.
152. Carell, T.; Butenandt, J. *Angew. Chem. Int. Ed.* **1997**, *36*, 1461–1464.
153. (a) Abe, S.; Nonaka, T.; Fuchigami, T. *J. Am. Chem. Soc.* **1983**, *105*, 3630–3632. (b) Abe, S.; Fuchigami, T.; Nonaka, T. *Chem. Lett.* **1983**, 1033–1036.
154. Komori, T.; Nonaka, T. *J. Am. Chem. Soc.* **1984**, *106*, 2656–2659.
155. Yoon, T. P.; Jacobsen, E. N. *Science* **2003**, *299*, 1691–1693.

6

ASYMMETRIC CARBENE CATALYSIS: A BRIEF HIGHLIGHT OF DEVELOPMENTS IN THE PAST DECADE

Jia-Lei Yan[1], Hongling Wang[2], and Yonggui Robin Chi[1,2]
[1]*Division of Chemistry and Biological Chemistry, School of Physical and Mathematical Sciences, Nanyang Technological University, Singapore, Singapore*
[2]*Laboratory Breeding Base of Green Pesticide and Agricultural Bioengineering, Key Laboratory of Green Pesticide and Agricultural Bioengineering, Ministry of Education, Guizhou University, Guiyang, China*

6.1. EARLY DEVELOPMENT OF ASYMMETRIC NHC CATALYSIS

The past 20 years have witnessed prosperous development in *N*-heterocyclic carbene (abbreviated as NHC or carbene) organocatalysis. Multiple activation modes have been developed with numerous asymmetric reactions demonstrated. In this chapter, we'll first take a glance at the historical development of NHC catalysis, especially the main progress during the first decade of this century. We'll then summarize the key advancements of this field in the last 10 years. As an important note, this short chapter is by no means complete or comprehensive. It is also hard to avoid biases when these topics are introduced from personal perspectives of the authors.

N-heterocyclic carbene is defined as a heterocyclic species containing a carbene carbon and at least one α-nitrogen atom in the ring structure [1]. Glorius has summarized the general structural features of NHC catalysts in 2014 [2], as shown in Figure 6.1. A variety of synthetic methods have been developed for the preparations of diverse NHC pre-catalysts [3]. The free carbene catalyst is typically generated in situ through deprotonation of the corresponding azolium salt (the NHC pre-catalyst). Therefore, it is important to know the acidities of different NHC precursors [4]. From literature reports, thiazolium and triazolium NHC pre-catalysts are generally more acidic than imidazolium NHC pre-catalysts [5]. The *N*-aryl substituents were found to have significant impact on the acidity of triazolium NHC pre-catalysts [6]. The reactivities of different NHC catalysts in organocatalytic reactions were also systematically studied [7].

6.1.1. Early Discoveries on NHC-Mediated Reactions: Benzoin and Related Reactions via Acyl Anion Intermediates

The modern development of asymmetric NHC catalysis can perhaps be traced back to Ukai's demonstration that thiazolium salts could catalyze the benzoin reaction [8] and Breslow's contribution of its mechanism in 1958 [9]. Enantioselective benzoin reactions were then realized by Sheehan and Hunneman using chiral

Catalytic Asymmetric Synthesis, Fourth Edition. Edited by Takahiko Akiyama and Iwao Ojima.

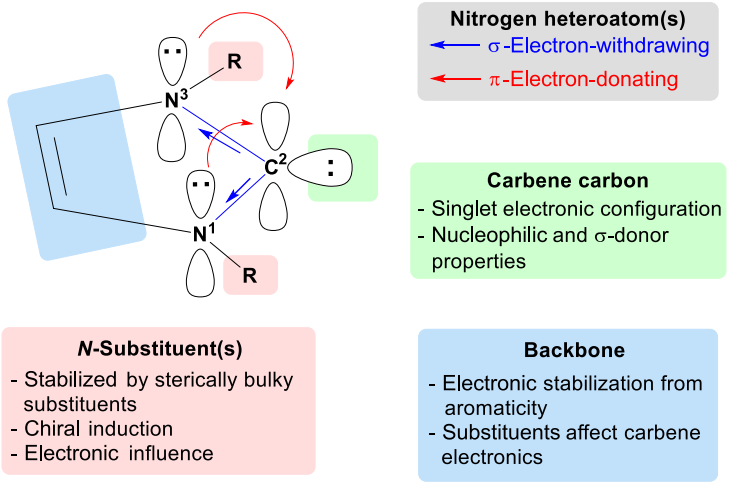

Figure 6.1. General structural features of NHCs.

thiazolium NHC pre-catalysts [10]. Stable free *N*-heterocyclic carbenes were also prepared by Bertrand [11] and Arguengo [12] independently. In the arena of asymmetric benzoin reactions, Enders moved from chiral thiazoliums to triazolium-based NHC catalysts to achieve impressive success [13]. Subsequent development then led to a large number of asymmetric homo- and cross-benzoin reactions [14], aza-benzoin reactions [15], and Stetter reactions [16] using similar acyl anion Breslow intermediates (Figure 6.2).

6.1.2. Moving from Simple Aldehydes to Enals and α-Functionalized Aldehydes: A Key Progress During the First Decade of This Century

6.1.2.1. Activation of Enals via Homoenolate Intermediates It is an important progress in NHC catalysis to get various enal substrates activated instead of the simple aldehydes. The 1,4-conjugated structures in enals provided unexplored activation modes and reaction patterns. In 2004, the groups of Glorius and Bode independently reported that enals could react as homoenolate precursors in the presence of NHC catalysts (Figure 6.3a) [17]. The reaction proceeds via addition of an NHC catalyst to the aldehyde moiety of enals (**2**) to form an α,β-unsaturated acyl anion intermediate (**5a)** that bears a nucleophilic reactive β-carbon (as illustrated by its resonance structure **5b**). This intermediate (also called homoenolate intermediate) then reacts with another aldehyde (**1**) to eventually afford γ-lactones and regenerates the NHC catalyst. Built on this important progress in which the products are formed as racemic mixtures, asymmetric reactions with excellent enantioselectivities were then discovered using aldehydes or activated ketones as the electrophiles (Figure 6.3b) [18].

Imines and ketimines can also be used as suitable substrates in NHC-catalyzed homoenolate activation reactions. In 2005, Bode reported the homoenolate activation of enals with *N*-sulfonyl imines via NHC catalysis to form γ-lactams with good yields and diastereoselectivities [19]. These types of lactam forming reactions have drawn continuous attentions in the following years (Figure 6.4a) [20]. The same class of NHC-bound intermediates have been used in reactions with electron-deficient carbon–carbon double bonds (Michael acceptors) to prepare all-carbon rings and related derivatives (Figure 6.4b). In 2006, Nair reported racemic reactions between enals and α,β-unsaturated ketones to form cyclopentene derivatives [21]. Asymmetric variants of this reaction were reported by the groups of Bode [22], Scheidt [23], Glorius [24], Rovis [25], and others [26].

6.1.2.2. Functionalization of Enals via Enolate Intermediates The β-carbon of NHC-bound homoenolate intermediates can in principle undergo a protonation process to form acyl azolium enolate intermediates for asymmetric reactions. In 2006, Bode reported NHC-catalyzed generation of a highly

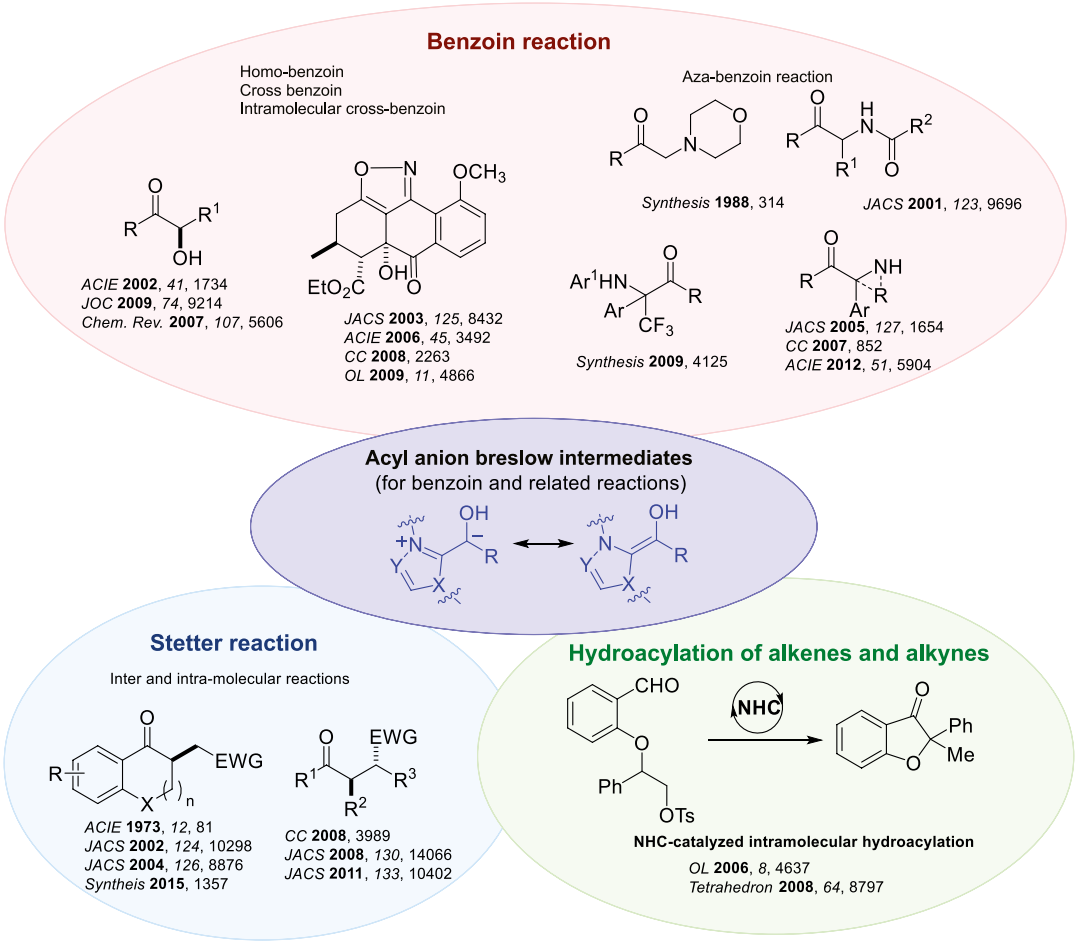

Figure 6.2. Early development of benzoin and related reactions via acyl anion intermediates.

reactive azolium enolate intermediate (**10**) that participated in the hetero-Diels–Alder cyclization with α,β-unsaturated imines (**7**) (Figure 6.5a) [27]. The NHC-bound enolate intermediate can also react with other electrophiles, as demonstrated by the groups of Glorius et al. [18a], Bode et al. [28], Sun et al. [29], Chi et al. [30], and Wang et al. [31]. Both aliphatic and aromatic substituted enals can be used as efficient enolate precursors under mild reaction conditions (Figure 6.5b).

6.1.2.3. Oxidation of Homoenolate to α,β-Unsaturated Acyl Azolium Intermediates The electron-rich homoenolate intermediates generated from addition of NHC catalysts to enals can also be oxidized to give the α,β-unsaturated acyl azoliums for 1,4-addition reactions with nucleophiles (Figure 6.6a). In 2007, Scheidt reported the use of MnO_2 as an oxidant for this oxidative process [34]. In 2010, Studer reported that 3,3′,5,5′-tetra-tert-butyl- 4,4′-diphenoquinone (DQ) can oxidize homoenolates to α,β-unsaturated acyl azoliums [35]. Since then, DQ has been widely used in NHC-catalyzed oxidative reactions. In these two studies by Scheidt and Studer, α,β-unsaturated acyl azolium intermediates reacted with alcohols to form the corresponding esters.

In 2009, Lupton reported the generation of the same α,β-unsaturated acyl azolium intermediates from reaction of NHC catalyst with vinyl esters and acyl fluorides for subsequent racemic annulation reactions with enols [36]. In 2010, Studer reported the NHC-catalyzed asymmetric Michael addition

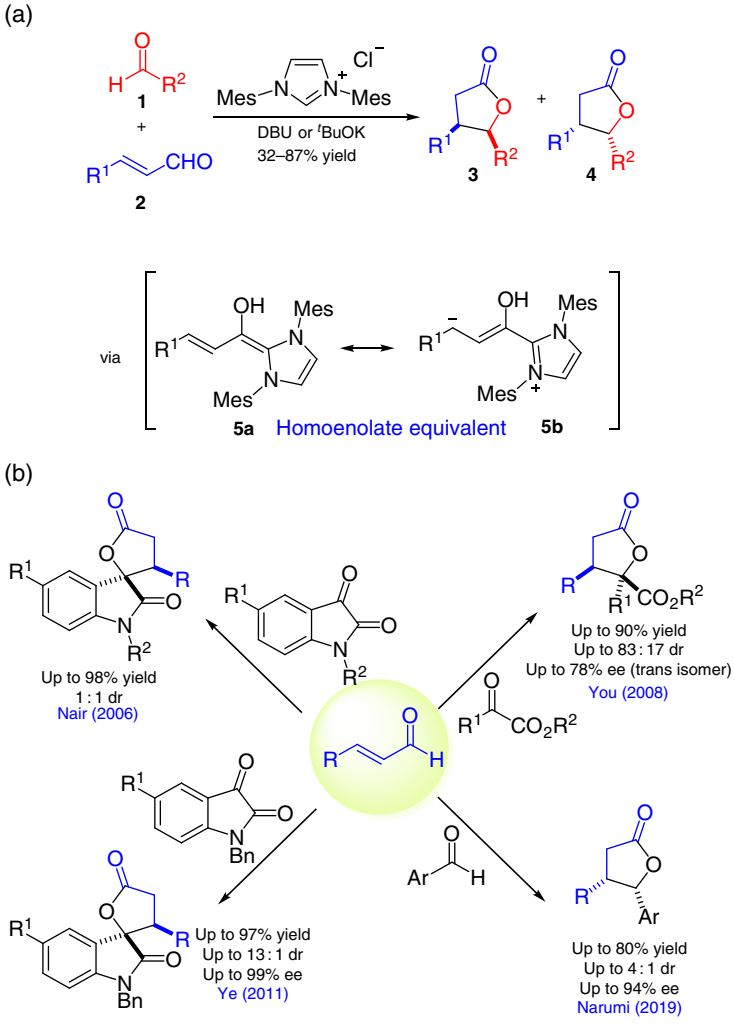

Figure 6.3. Reactions of enals with ketones and aldehydes. (a) NHC-Catalyzed reactions of enals involving homoenolates. Source: [17]. (b) NHC-Catalyzed reactions of enals with ketones and aldehydes. Source: [18].

of 1,3-dicarbonyl compounds to enals via α,β-unsaturated acyl azolium intermediate (Figure 6.6b) [32]. Bode disclosed a [3+3] annulation of the α,β-unsaturated acyl azolium with enamines to prepare dihydropyridinones (Figure 6.6c) [33].

6.1.2.4. Activation of α-Functionalized Aldehydes for Asymmetric Reactions In 2004, Rovis reported the NHC catalyzed intramolecular redox reaction of α-halogen aldehydes to form esters [37]. Since then, α-halogen aldehydes have been explored as acyl azolium enolate precursors for asymmetric reactions. In 2006, Bode reported the generation of chiral enolate intermediates from α-haloaldehydes (**11**) for annulation reactions with Michael acceptors (**12**) to afford chiral dihydropyridinones (**13**) (Figure 6.7a) [38]. In addition to α-halogen aldehydes [42], aryloxyacetaldehydes [39], and α-epoxide aldehydes [40] have also been used as azolium enolate precursors (Figure 6.7b,c). The related α-functionalized enals can be activated by NHC catalysts to form α,β-unsaturated acyl azolium intermediates via self-redox processes. Ye has reported a highly enantioselective [3+3] annulation reaction of α-bromoenals and 1,3-dicarbonyl compounds (Figure 6.7d) [41].

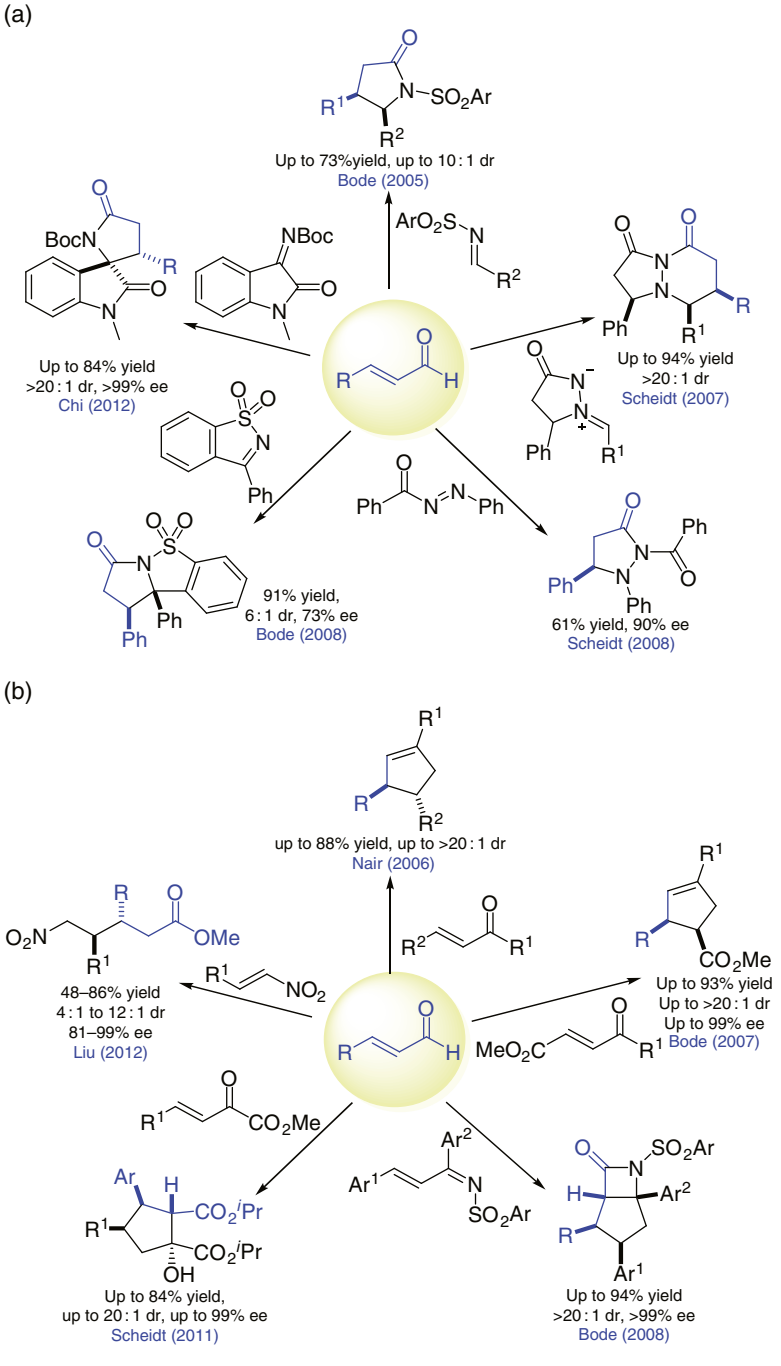

Figure 6.4. Reactions of enals with imines, ketimines, and Michael acceptors. (a) NHC-Catalyzed reactions of enals with imines and ketimines. Source: [20]. (b) NHC-Catalyzed reactions of enals with Michael acceptors.

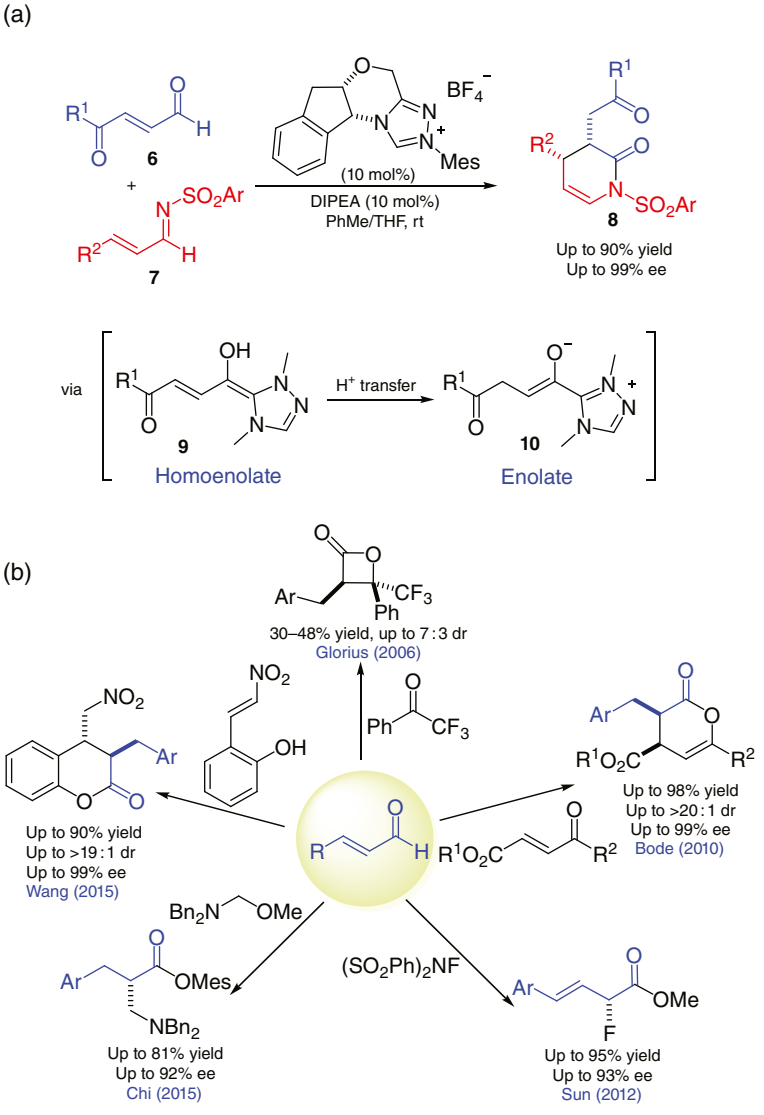

Figure 6.5. Reactions of enals involving NHC-bound enolate intermediates. (a) Bode's hetero-Diels-Alder cyclization with α,β-Unsaturated imines. Source: Based on [27]. (b) Further developments.

6.1.3. Remaining Challenges When the Last Decade Started

The impressive early developments on NHC catalysis have significantly enhanced our understanding of the basic reactivity and reaction patterns of the catalysts and the relevant substrates. However, many potentially fruitful directions have not been truly appreciated or fully recognized at the beginning of the last decade. Examples of these directions may be viewed as the following: (i) the use of NHCs to activate substrates other than aldehydes, and activation of relatively inert substrates and chemical bonds, (ii) single-electron transfer activation and radical reactions, (iii) cooperative catalysis involving NHC organocatalysts and transition metal catalysts, and (iv) NHC-catalyzed strategies for the synthesis of sophisticated (and useful) molecules. In the remainder of this chapter, we'll highlight the NHC catalytic strategies developed in the above four directions.

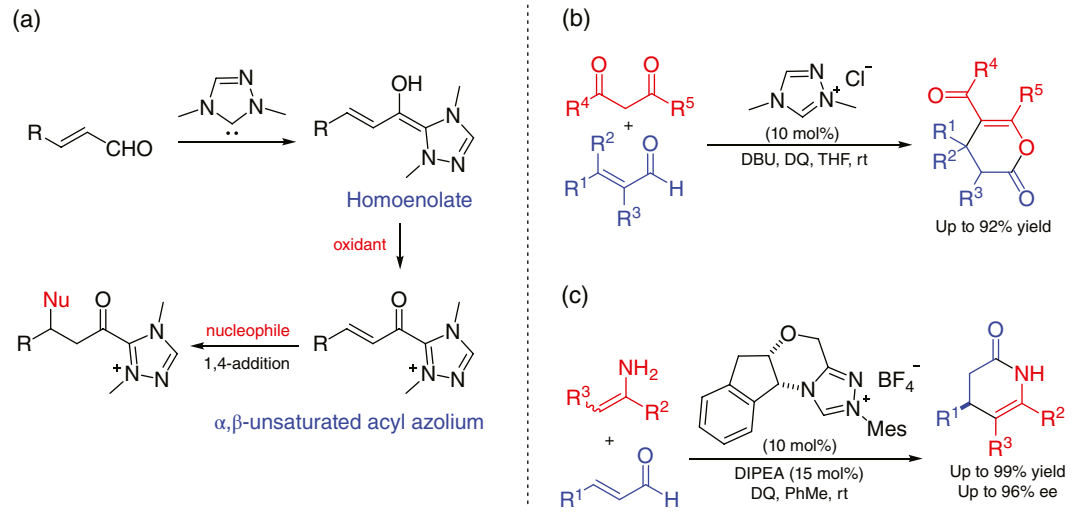

Figure 6.6. Activation of enals under oxidative NHC catalysis. (a) Generation of α,β-unsaturated acyl azolium. (b) Studer's [3+3] annulation with 1,3-diketones. Source: Based on [32]. (c) Bode's [3+3] annulation with enamines. Source: Based on [33].

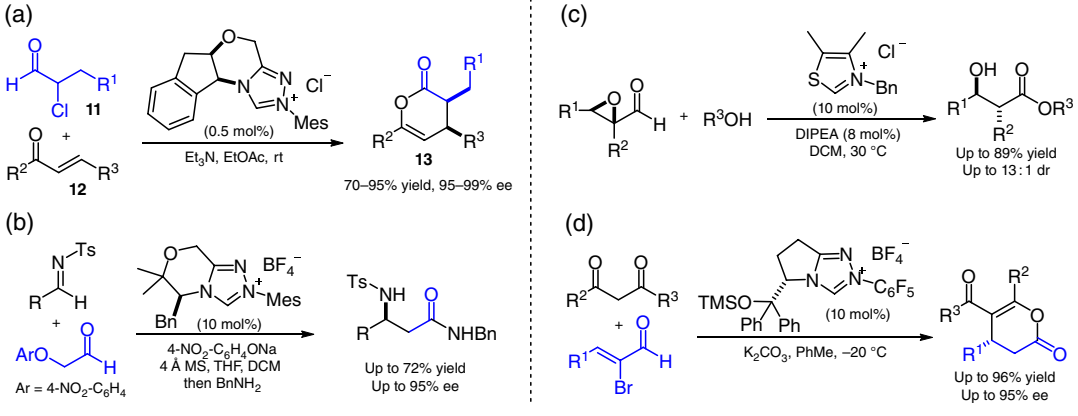

Figure 6.7. NHC-catalyzed reactions of α-functionalized aldehydes. (a) Bode's [4+2] annulation of α-chloroaldehydes with enones. Source: Based on [38]. (b) Scheidt's activation of α-aryloxyacetaldehydes. Source: Based on [39]. (c) Bode's activation of α-epoxide aldehydes. Source: Based on [40]. (d) Ye's activation of α-bromoenals. Source: Based on [41].

6.2. ACTIVATION OF SUBSTRATES BEYOND ALDEHYDES

6.2.1. Activations of Stable Carboxylic Esters

6.2.1.1. α-Carbon Activation of Carboxylic Esters Carboxylic acids and their derivatives such as esters and anhydrides are common starting materials in organic synthesis. Direct transformations of these molecules via asymmetric catalysis to prepare optically enriched functionalized products receive continuous attention. In 2012, Chi disclosed the first NHC-catalyzed generation of an enolate intermediate from stable α-aryl carboxylic esters (Figure 6.8) [43]. The reaction proceeds through a direct addition of NHCs to esters (without formation of the ketene intermediate) to form enolate intermediates (**16**). The NHC-bound enolate intermediates (**16**) then react with α,β-unsaturated imines (**15**) to form the δ-lactams (**17**) with high stereoselectivities. Subsequent studies by the same group revealed that this reaction is general with respect to the carboxylic ester substrates; alkyl substituted carboxylic esters and

acetic acid esters could be used as effective substrates for the asymmetric enolate reactions [44]. The carboxylic acids may also be directly used as the reaction partner through an in situ-activation (e.g. by carbonyldiimidazole) before reaction with the NHC catalysts, as disclosed by Scheidt [45].

6.2.1.2. β-sp²-Carbon Activation of α,β-Unsaturated Carboxylic Esters When α,β-unsaturated esters are used as the substrate, addition of NHC catalyst to the ester moiety can lead to LUMO activation of the β-sp²-carbon to react as an electrophile. In 2013, Chi reported enantioselective reactions between unsaturated esters (**18**) and imines (**19**) to form lactam products (**22**) with high enantioselectivities (Figure 6.9) [46]. The key intermediate in this reaction is an NHC-bound α,β-unsaturated acyl azolium intermediate (**20**). Notably, this intermediate can also be generated from the corresponding enals under oxidative NHC catalysis [34, 47], carboxylic acids with in situ activation [48], or other activated esters and derivatives [49].

6.2.1.3. γ-Carbon Activation of α,β-Unsaturated Carboxylic Esters When the β-sp² carbon of α,β-unsaturated esters are activated by the NHC catalyst, the acidity of the γ-CH is increased. Deprotonation of the γ-CH leads to vinyl enolate intermediate (**27b**) that can then undergo enantioselective reactions with electrophiles such as activated ketones and imines, as reported by Chi in 2013 (Figure 6.10) [50]. The vinyl enolate intermediates can also be generated from α,β-unsaturated carboxylic acid through addition of appropriate dehydrating reagents, such as acid chlorides or peptide coupling reagents [51].

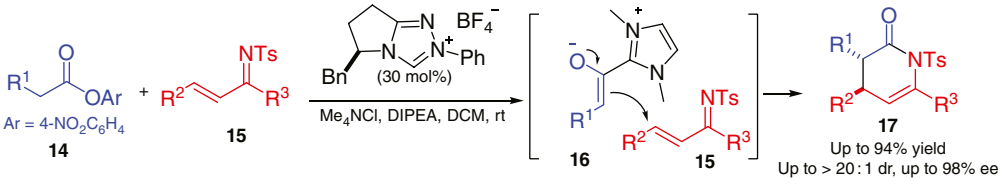

Figure 6.8. α-Carbon activation of stable carboxylic esters. Source: Based on [43].

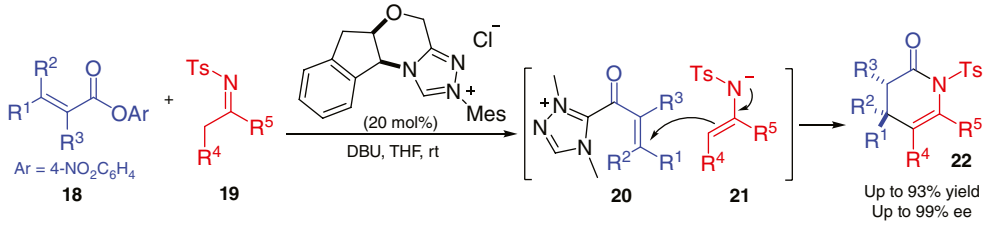

Figure 6.9. β-sp²-Carbon activation of α,β-unsaturared carboxylic esters. Source: [46].

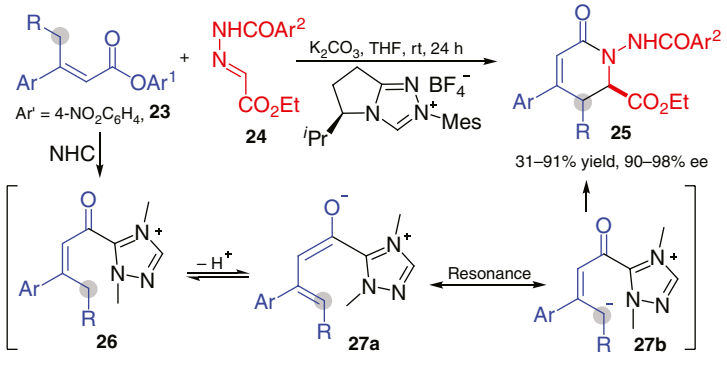

Figure 6.10. γ-Carbon activation of α,β-unsaturared carboxylic esters. Source: Based on [50].

6.2.1.4. β-sp³-Carbon Activation of Saturated Esters The β-sp³-carbon of saturated carboxylic esters are typically inert and difficult to be directly functionalized. In 2013, Chi demonstrated that further deprotonation (on the β-carbon) of the ester-derived azolium enolate intermediate is feasible under mild conditions. This deprotonation yields homoenolate intermediate (**33**) with the β-carbon activated as the nucleophilic carbon. The overall process activates the otherwise inert β-sp³ carbon of the saturated ester and inverts its initial polarity (Figure 6.11a) [52]. With this new mode of activation, the β-sp³-carbon of saturated esters can react with a diverse set of electrophiles to form various products with high optical purities (Figure 6.11b) [52, 53]. The carboxylic esters can also be replaced with other carboxylic acid derivatives such as anhydrides [54].

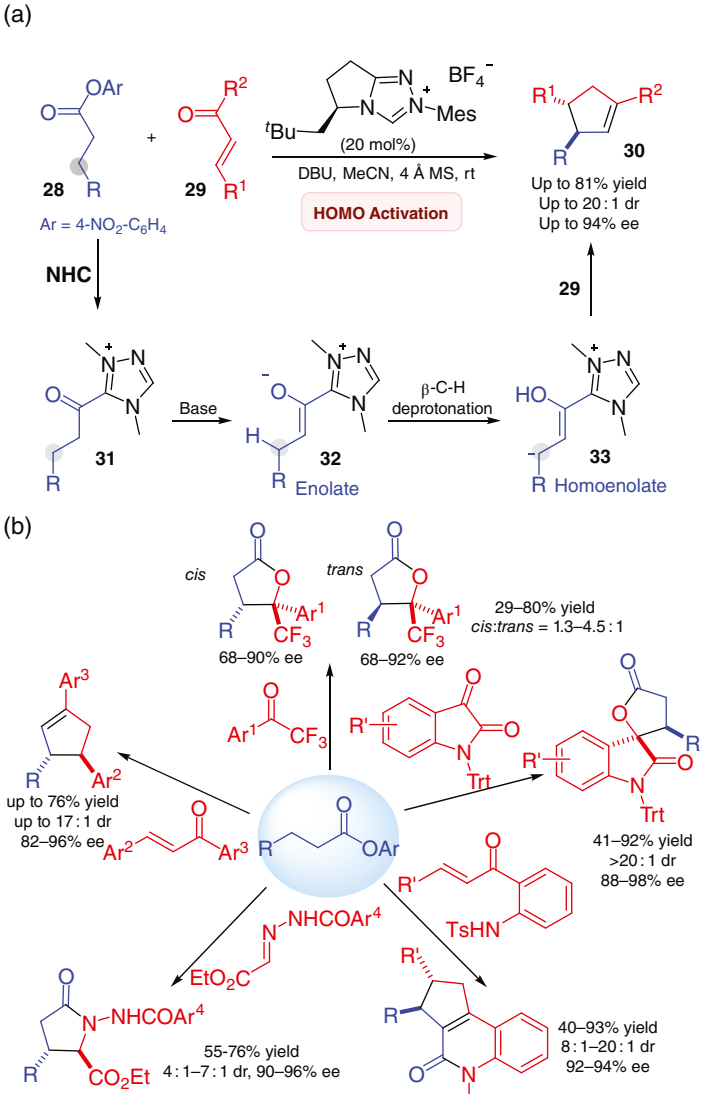

Figure 6.11. NHC-catalyzed β-activation of carboxylic esters. (a) Chi's NHC-catalyzed HOMO activation of esters. Source: Based on [52]. (b) Further developments. Source: [52, 53].

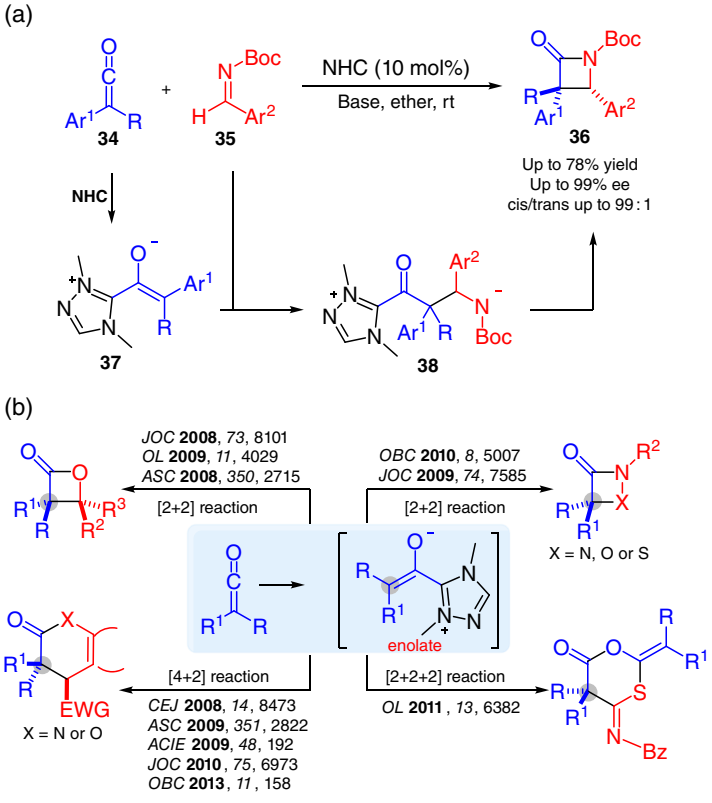

Figure 6.12. NHC-catalyzed activation of ketenes. (a) NHC-catalyzed Staudinger reactions of ketenes with imines. (b) Further developments in NHC-catalyzed annulations of ketenes. Source: [57].

6.2.2. Activation of Ketenes

Ketenes are compounds containing adjacent C=C and C=O double bonds, which can also be activated by NHC catalysts. In 2008, the groups of Ye [55] and Smith [56] independently reported the NHC-catalyzed [2+2] cycloaddition reaction of ketenes (**34**) with *N*-protected imines (**35**) to afford the corresponding lactams (**36**) (Figure 6.12a). In both cases, the key intermediate is a reactive zwitterion (**37**) generated from addition of NHC to the ketene substrate (**34**). The corresponding lactams were afforded in good to excellent yields and stereoselectivities.

The Ye group has also developed NHC-catalyzed asymmetric [2+2], [4+2], and [2+2+2] cycloaddition reactions of ketenes with a variety of electrophiles (Figure 6.12b) [57]. In all these reactions, the corresponding lactone or lactam products are obtained in good to excellent yields with high enantio- and diastereoselectivities.

Additionally, α,β-unsaturated acyl chlorides can also be used in NHC-catalyzed γ-functionalization [58]. Of note, cinchona alkaloids were used as co-catalysts to achieve better enantioselective control [59].

6.2.3. Activation of Imines

In 2008, Hou disclosed the pioneering work on NHC-catalyzed N-S cleavage reactions of *N*-tosylimines (**39**) with aziridines/unsaturated esters, with unexpected tosyl group transfer products (**41**) afforded in moderate to good yields (Figure 6.13a) [60]. Chi disclosed the asymmetric sulfonation of enones (**43**) under the cooperative catalysis of an NHC and a chiral tertiary amine-thiourea multifunctional catalyst

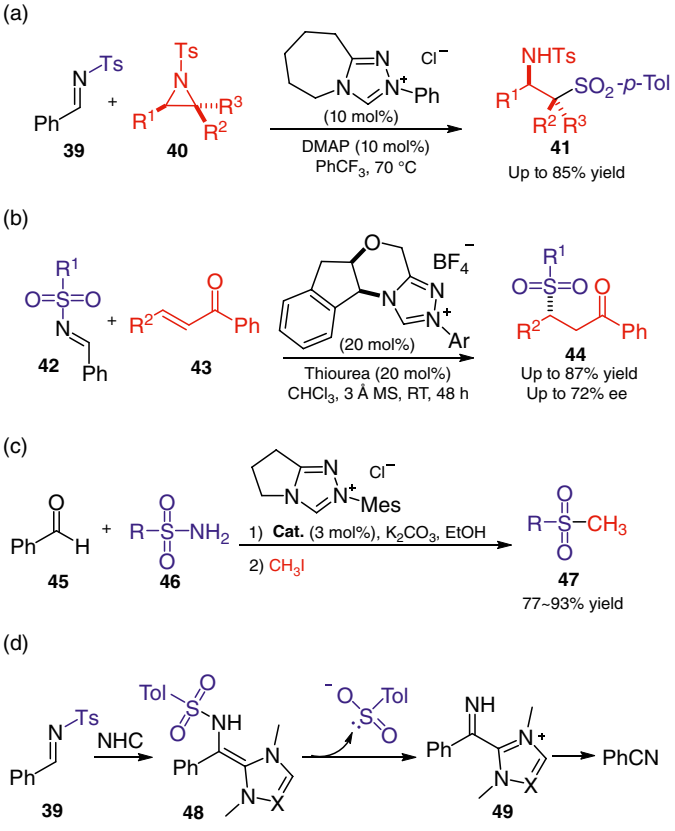

Figure 6.13. NHC-catalyzed activation of sulfonylimines. (a) Hou's NHC-catalyzed reactions of tosylimines with aziridines. Source: Based on [60]. (b) Chi's NHC-catalyzed reactions of sulfonyl imines with enones. Source: Based on [61]. (c) Maloney's NHC-catalyzed reactions of sulfonyl imines. Source: Based on [62]. (d) Proposed mechanism for NHC-catalyzed activation of tosyl imines.

(Figure 6.13b) [61]. Five years later, Maloney successfully applied this strategy to the late-stage functionalization of complex bioactive molecules (Figure 6.13c) [62]. It has been widely accepted that the Ts anion can be released from the aza-Breslow intermediate (**48**) that was generated through addition of the NHC catalyst to the Ts-imine substrate (**39**), with the benzonitrile released as the stoichiometric byproduct (Figure 6.13d). Additionally, Douthwaite reported an intramolecular addition of an NHC to unactivated imines to afford the aza-Breslow intermediates in 2009 [63]. It is worth noting that the Rovis group successfully isolated aza-Breslow products which were confirmed by X-ray crystallography [64].

In 2017, the groups of Biju [65] and Suresh [66] independently disclosed NHC-catalyzed intramolecular aza-Stetter reactions of imines with Michael acceptors to prepare indoles. NHC-catalyzed umpolung activation of imines has been further developed by the groups of Biju [67], Huang [68], and Lupton [69] (Figure 6.14).

Recently, Fu et al [70]. and Chi et al [71]. independently reported a new reaction pathway for NHC-catalyzed activation of imines for the enantioselective synthesis of heterocycles (Figure 6.15). In this reaction, the remote nitrogen atom of (benz)imidazole-derived aldimines (**50**) was activated to form an NHC-bound triaza-diene intermediate (**52**), which then reacted with ketones (**51**) through a concerted asynchronous addition pathway (supported by mechanistic studies and density functional theory [DFT] calculations). A variety of spiro-heterocycles (**53**) were obtained with good to excellent yields and enantioselectivities.

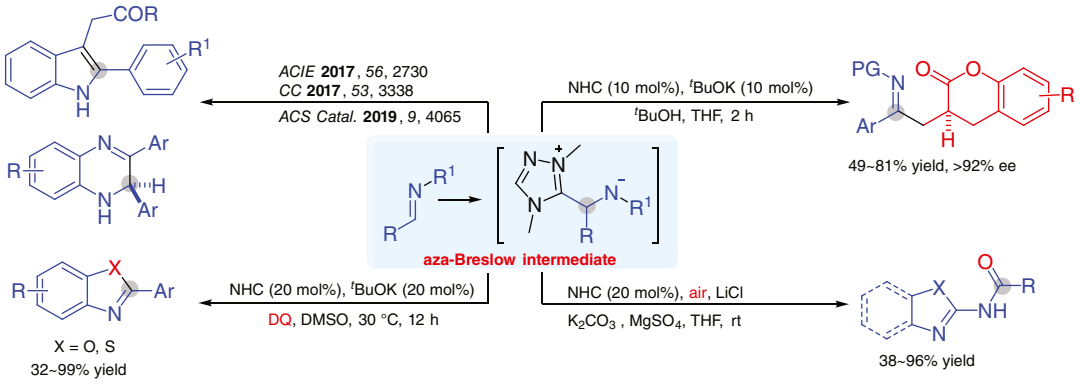

Figure 6.14. NHC-catalyzed umpolung of imines. Source: [67–69].

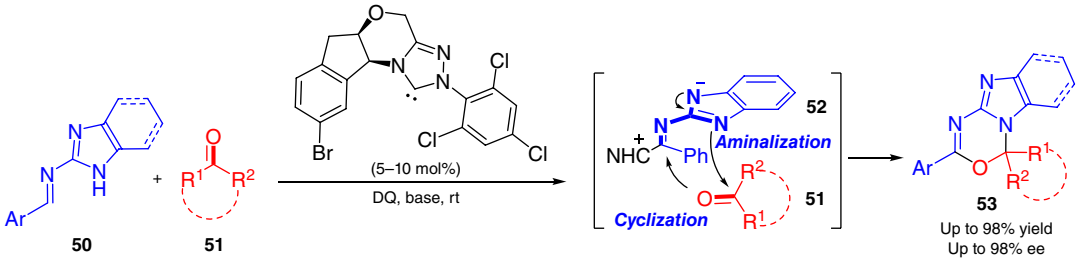

Figure 6.15. NHC-catalyzed activation of remote nitrogen atoms.

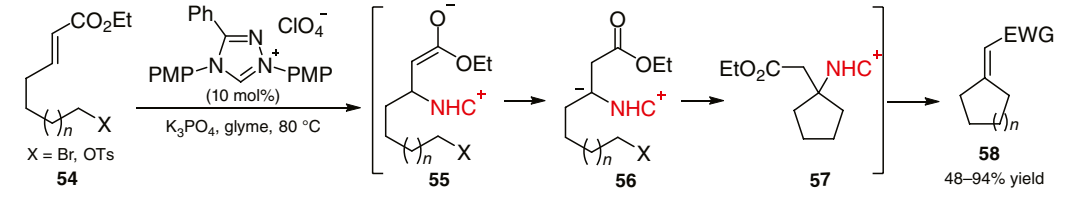

Figure 6.16. NHC-catalyzed β-alkylations of Michael acceptors. Source: Based on [72].

6.2.4. Activation of Other Substrates

Electron-deficient Michael acceptors and styrenes can also be activated by NHC catalysts. In 2006, Fu reported excellent work on NHC-catalyzed umpolung of Michael acceptors (Figure 6.16) [72]. In this case, the NHC catalyst adds to the electrophilic β-carbon of the α,β-unsaturated ester (**54**) to give an enolate intermediate (**55**). The enolate (**55**) undergoes tautomerization to give (**56**), in which the β-carbon is activated as a nucleophilic carbon. After an intramolecular S_N2 cyclization process, intermediate (**57**) was afforded and was quickly transformed to the final product (**58**) with regeneration of the NHC catalyst.

Ye and co-worker reported an NHC catalyzed Morita–Baylis–Hillman reaction in 2007 and 2013 respectively [73]. The groups of Scheidt et al. [74], Matsuoka et al. [75], Glorius et al. [76], and Lupton et al. [77] have also made contributions in the field of NHC-catalyzed umpolung activation of carbon–carbon double bonds.

6.3. SINGLE-ELECTRON TRANSFER ACTIVATION AND RADICAL REACTIONS

6.3.1. Oxidation of Aldehydes to Esters

Single-electron transfer (SET) processes mediated by carbene catalysts have their presence in biological systems. The vitamin B1-mediated decarboxylation of pyruvates in the presence of redox enzymes involves SET of an acyl anion (Breslow intermediate) as a key process. In 2018, Studer reported oxidation of aldehydes (**59**) by TEMPO (**60**) to form the corresponding ester product (**61**) [78]. This reaction is believed to proceed through two SET steps (Figure 6.17).

6.3.2. Reductive Coupling Reactions Involving Nitroalkenes and Nitrobenzyl Bromides

In 2014, Chi demonstrated that the Breslow intermediate could be oxidized by nitroalkenes through a single-electron transfer pathway (Figure 6.18a) [79]. In this process, nitroalkenes can be reductively coupled at the β-carbon through SET radical pathways. Electron paramagnetic resonance (abbreviated as EPR) analysis and radical clock experiments supported the existence of radical intermediates in the key catalytic processes (Figure 6.18b).

The Chi group also showed that 4-nitrobenzyl bromides can behave as a single-electron oxidant [80]. The overall reactions of nitrobenzyl bromides with activated ketones/imines/nitro alkenes constitute a formal reductive coupling process (Figure 6.19). A variety of nitrobenzyl bromides have been extensively explored in NHC-catalyzed radical reactions. They serve as efficient electron acceptors to selectively oxidize the electron-rich Breslow intermediates and generate radical intermediates for SET reactions.

6.3.3. Activation of Enal on β-Carbon via SET for Asymmetric Reactions

When enals were used in SET oxidation under NHC catalysis, the NHC-bound radical cation intermediate could be formed. Electron delocalization could pose radical characteristics on the β-carbon of this intermediate. Since the NHC catalyst is still covalently bound to the radical intermediate, it becomes possible to develop asymmetric β-carbon functionalization reactions via radical reaction pathways. In 2014 and 2015 Rovis [81] and Chi et al. [82], independently reported enantioselective β-hydroxylation of

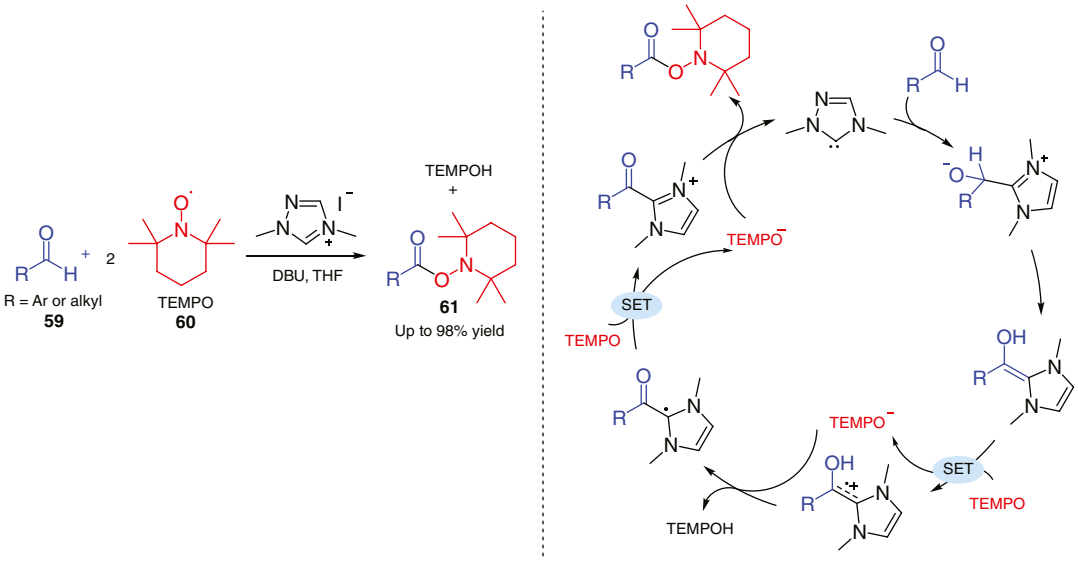

Figure 6.17. Biomimetic NHC-catalyzed oxidations of aldehydes.

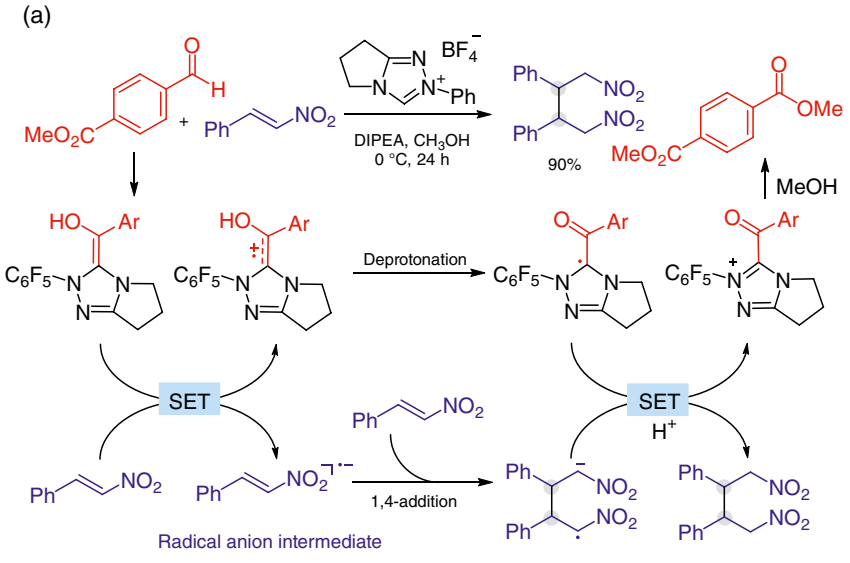

Black line: EPR spectrum of the anionic radical derived from β-isopropyl nitroethylene obtained in methanol at 22(±2) °C.
Red line: Simulated spectrum based on hyperfine coupling constants of 1N = 13.025 G, $1H_a$ = 8.775 G, $1H_b$ = 2.80 G, $1H_c$ = 6.375 G and 6H = 0.275 G, with a line width of 0.15 G.

Figure 6.18. NHC-catalyzed reductive β,β-coupling of nitroalkenes. (a) Chi's reductive β,β-coupling reaction of nitroalkene. Source: Based on [79]. (b) EPR spectrum of key reaction intermediates. Source: [79]/American Chemical Society.

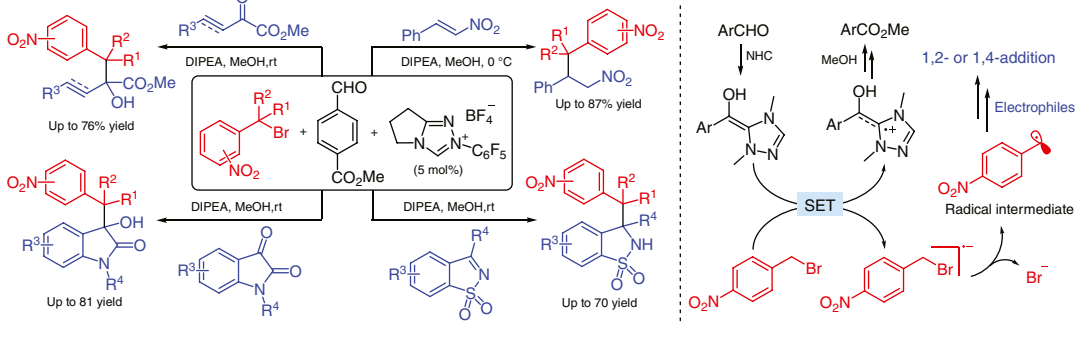

Figure 6.19. NHC-catalyzed reductive coupling of nitrobenzyl bromides.

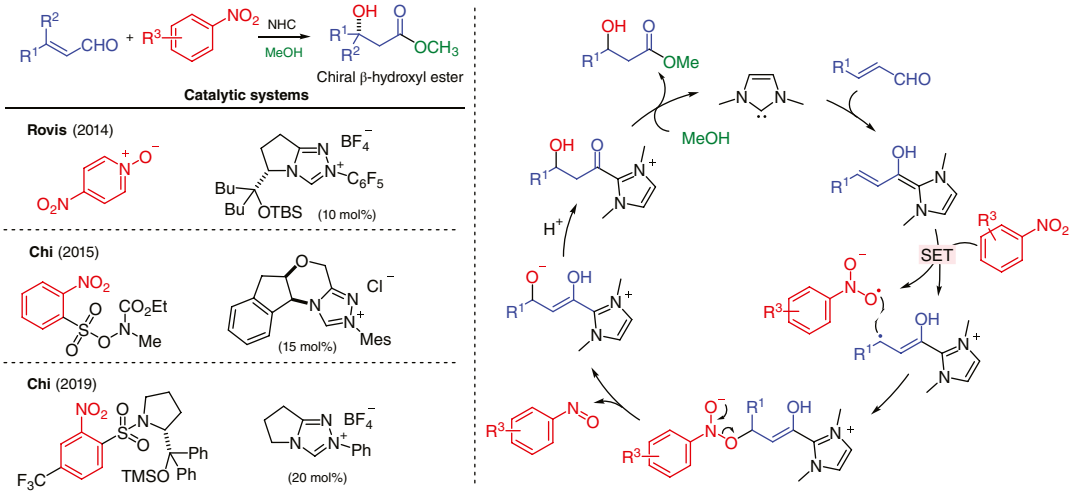

Figure 6.20. Enantioselective β-hydroxylation of enals via SET processes.

enals via NHC-catalyzed radical pathways (Figure 6.20). Rovis has also demonstrated that this NHC-bound radical cation intermediate could react with another equivalent of α,β-unsaturated Breslow intermediate to form 3,4-disubstituted cyclopentanones with excellent stereoselectivities [83]. In 2019, Chi showed that the enantioseletivity of the β-hydroxylation reaction could also be controlled by using chiral oxidants in the presence of an achiral NHC catalyst [84].

It's important to note that some of the NHC-mediated reactions that were thought to proceed via electron-pair transfer pathways may actually involve radical intermediates. One notable study regarding NHC-catalyzed SET reactions is Rehbein's mechanistic examination of NHC-catalyzed benzoin reactions [85]. The use of polyhalides as oxidants in NHC catalysis by Sun [86] and Chi's [87] also likely involves SET processes.

6.3.4. Radical–Radical Coupling via NHC-Catalyzed Activation of Aldehydes

The search for single-electron oxidants and radical reaction partners continues to offer impressive success, although these reactions generate achiral or racemic products. In 2019, Ohmiya demonstrated that NHCs could promote the decarboxylative coupling reaction of aryl aldehydes (**62**) and aliphatic carboxylic acid-derived redox-active esters (**63**) (Figure 6.21a, Eq. 1) [88]. Aryl alkyl ketones were afforded as the final products in these reactions. Recently, Hong reported that the Katritzky pyridinium salts (**65**) can also behave as SET oxidants to generate alkyl radical species (Figure 6.21a, Eq. 2) [89]. The reaction mechanism is depicted in Figure 6.21b. In this process, the Breslow intermediate (**67**) was oxidized to give radical (**69**), which can couple with alkyl radical (**70**) to give the final products (**64** or **66**).

Ohmiya reported that NHCs could also catalyze the vicinal alkylacylation of styrenes [90]. The reaction proceeds via a radical addition to olefins and a following radical–radical coupling relay process, which introduced tertiary alkyl groups and acyl groups to carbon–carbon double bonds with exclusive regioselectivity to produce functionalized ketone derivatives (**71**). Meanwhile, Li presented the multicomponent radical acylfluoroalkylation of olefins in the presence of various aromatic aldehydes and fluoroalkyl reagents to afford fluorinated ketones (**72** or **73**) as the final products [91]. Additional contributions in the NHC-catalyzed radical cross-coupling reaction of aldehydes have come from the groups of Wang et al. [92] and Ohmiya et al. [93], as summarized in Figure 6.22.

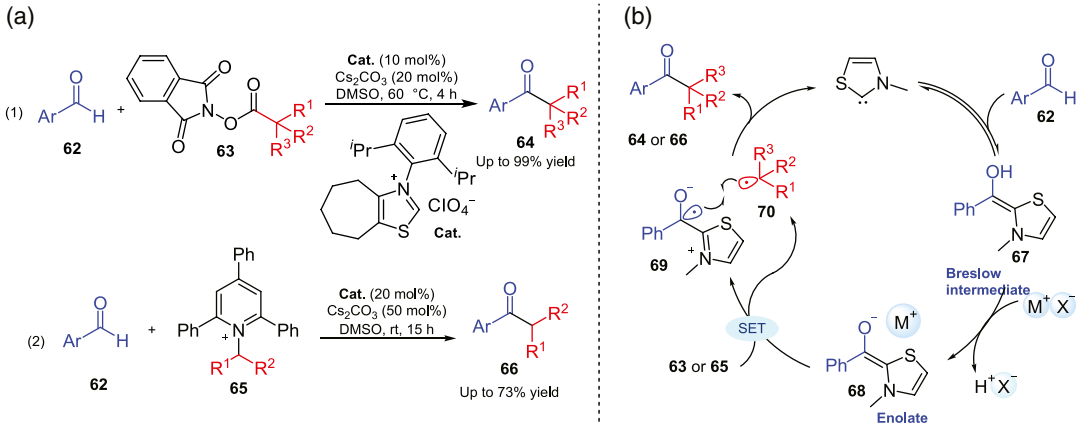

Figure 6.21. NHC-catalyzed alkylation of aldehydes via SET process. (a) NHC-catalyzed radiacl coupling reactions. Source: [88, 89]. (b) Reaction mechanism of the coupling reactions.

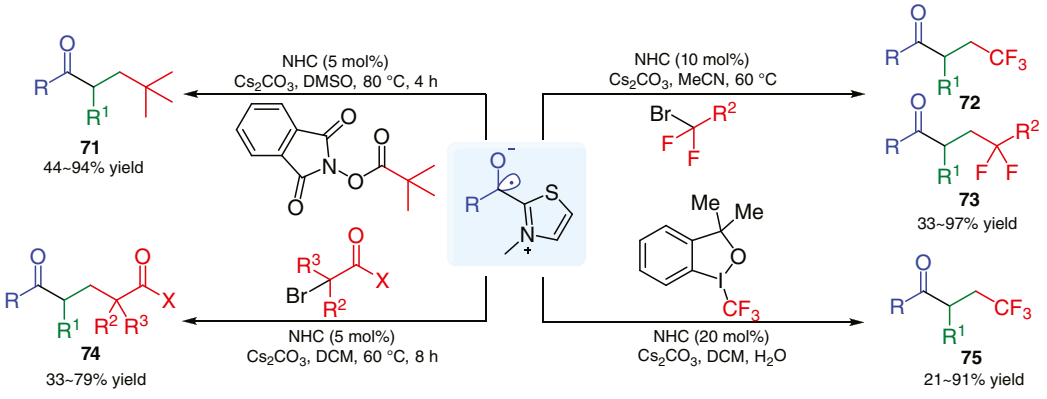

Figure 6.22. NHC-catalyzed SET difunctionalization of olefins.

6.3.5. Visible-Light-Driven Radical Reactions

Light-promoted activation is a promising approach to generate radical intermediates. In 2012, Rovis reported NHC/photoredox co-catalyzed asymmetric umpolung addition of aldehydes to the in situ generated iminium ion from tertiary amines [94]. The iminium ion intermediate formation is believed to proceed through a light-driven radical process. Although it may be argued that the radical intermediate here does not participate in the NHC-mediated process itself, this study clearly demonstrates that light-driven radical process is compatible with the typical NHC catalytic conditions. Light-driven reactions in which the radical intermediates directly reacted with NHC-bound intermediate was reported by Ye in 2019 [95]. Ye's lab showed that the γ- and ε-alkylation of enals through SET radical processes could be achieved under the dual catalysis of a photoredox catalyst and NHC (Figure 6.23). They subsequently reported a photoredox/NHC co-catalyzed ring opening and γ-alkylation reaction of cyclopropanes enals [96] and oxidative Smiles rearrangement of *O*-aryl salicylaldehydes [97].

Recently, Scheidt reported a SET reduction of the NHC-bound acyl azolium intermediate (Figure 6.24) [98]. The catalytically generated azolium radical intermediate (**81**) coupled with an alkyl radical intermediate (**83**) to give the ketone (**78**). Shu presented the direct synthesis of amides from aldehydes and imines by the dual catalysis of photoredox catalyst and NHC [99]. It should be noted that 2,4,5,6-tetrakis (9H-carbazol-9-yl) isophthalonitrile (4CzIPN) was used as metal-free photoredox catalyst in this reaction.

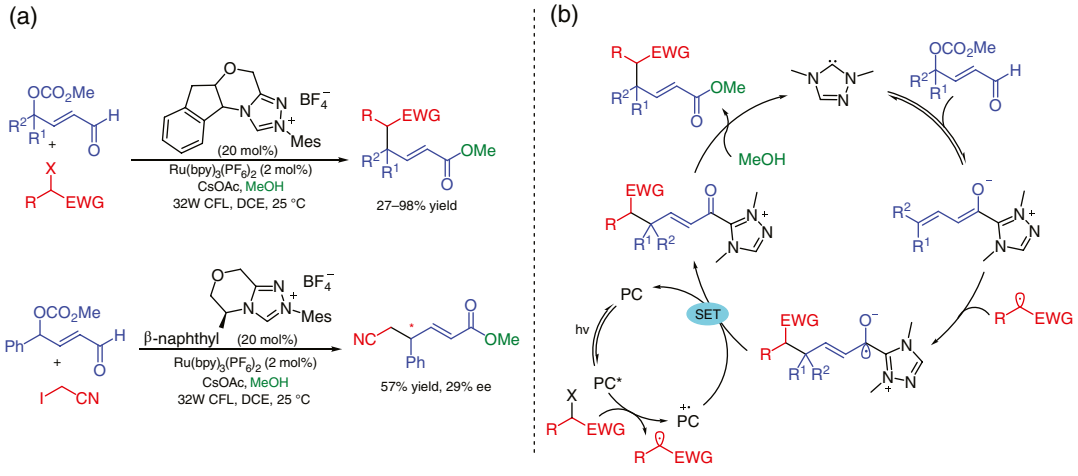

Figure 6.23. Synergistic Ru-photoredox/NHC catalysis. (a) Ye's NHC/photoredox co-catalyzed γ-and ε-alkylation. (b) The reaction mechanism.

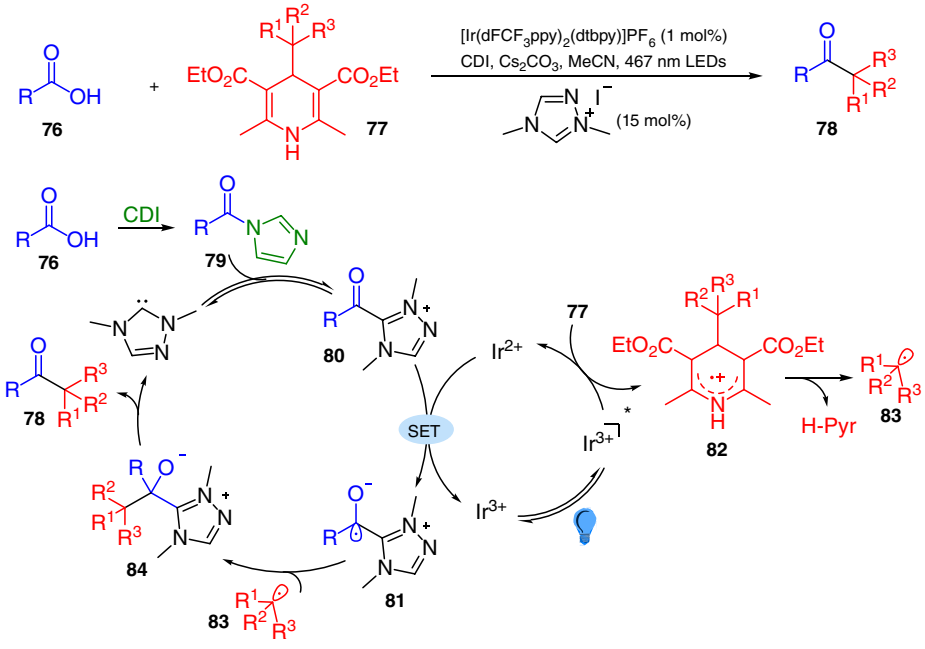

Figure 6.24. Photoredox and carbene catalysis for the generation of ketones. Source: Based on [98].

Light-driven reactions without using photoredox catalysts have also been realized. Hopkinson reported an NHC-catalyzed Diels–Alder reaction of acid fluorides and trifluoroacetophenones without addition of photoredox catalysts (Figure 6.25) [100]. An unprecedented photoenolization/Diels–Alder (PEDA) process was developed in this protocol. In the proposed reaction mechanism, a light-driven 1,5-hydrogen atom transfer gives rise to a triplet dienol biradical which could isomerize to a hydroxy-*o*-quinodimethane (*o*-QDM) species for the sequential Diels–Alder process. In addition, Chen has also reported light-driven photocatalyst-free radical reactions facilitated by the weak interaction of the NHC [101].

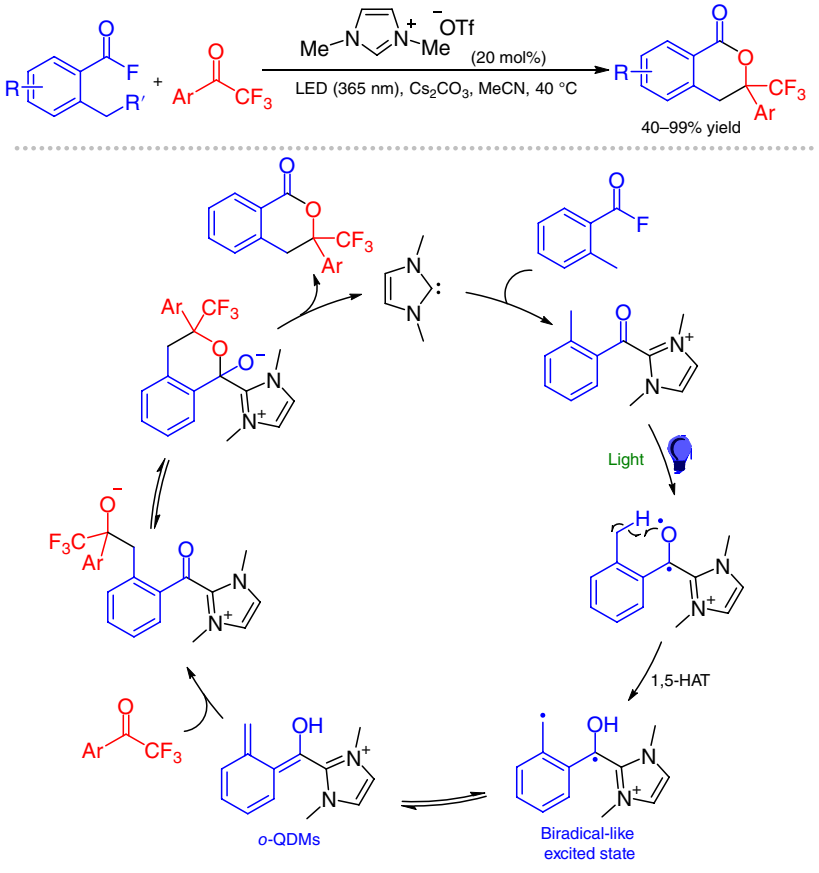

Figure 6.25. Photoenolization/Diels–Alder reaction of acid fluorides. Source: Based on [100].

6.4. NHC AS NON-COVALENT (BRØNSTED BASE) CATALYSTS

NHCs can behave as Brønsted bases and form hydrogen bonds with substrates bearing a lone pair of electrons. In 2005, Movassaghi and co-worker disclosed an NHC-catalyzed amidation of unactivated esters with amino alcohols (Figure 6.26a) [102]. Mechanistic studies reveal that the chemical shift of the proton of the hydroxyl groups increases by 2–5 ppm after mixing with the NHC catalyst. An X-ray structure of the carbene–alcohol complex has also been obtained (Figure 6.26b). The NHC catalyst is believed to act as a Brønsted base to activate the alcohol via hydrogen bond formation. In the same year, Hu reported a theoretical study on the mechanism of the NHC-catalyzed transesterification, which supported the noncovalent catalytic pathway [103].

NHCs can also activate aliphatic esters or ketones to form an NHC-enol complex incorporated with H-bonding interactions. The structure of the key intermediate in the NHC-promoted ester activation was confirmed via single crystal X-ray diffraction by Nolan in their report on NHC-catalyzed Claisen condensations (Figure 6.27a) [104]. In 2008, Song reported an NHC-catalyzed silyl transfer reaction from trialkylsilyl ketene acetals to ketones (Figure 6.27b) [105]. In this case, the ketone is also activated through H-bonding interactions with NHC, and the nucleophilicity of the enol hydroxyl group is increased to facilitate the silyl transfer reaction.

In 2009, Rodriguez reported a conjugate addition reaction enabled by NHCs through a Brønsted base catalytic activation pathway to prepare spirocyclic products (Figure 6.28a) [106]. Later, the authors successfully applied the NHC-catalyzed noncovalent ketone activation strategy in the intermolecular Michael addition reaction [108]. In most cases, aldehydes are usually activated by NHCs through

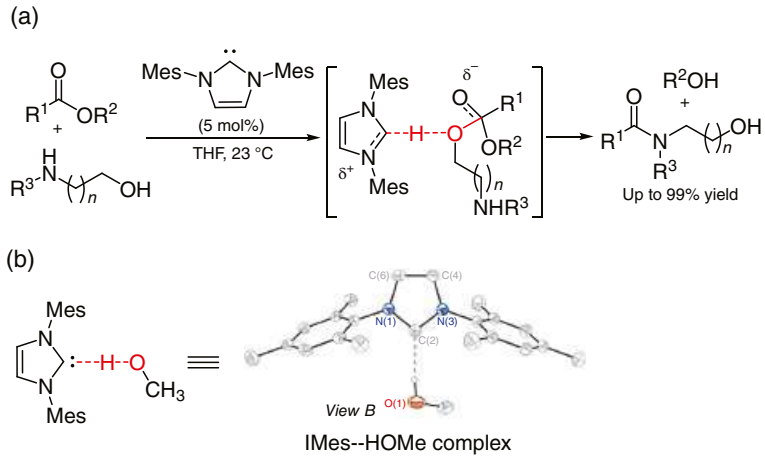

Figure 6.26. NHC-catalyzed amidation of unactivated esters. (a) NHC-catalyzed amidation of unactivated esters with amino alcohols. Source: Based on [102]. (b) The first X-ray structure of a carbene-alcohol complex.

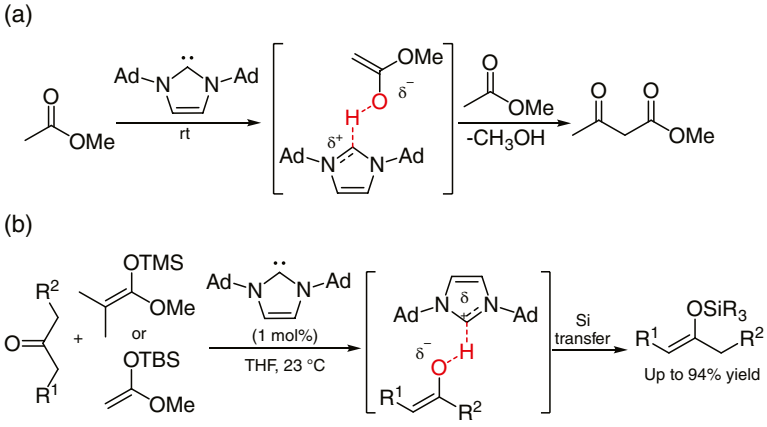

Figure 6.27. Activation of esters and ketones by NHC as Brønsted base. (a) Non-covelent activation of esters for Claisen condensation. Source: Based on [104]. (b) Non-covelent activation of ketones for silyl transfer reactions. Source: Based on [105].

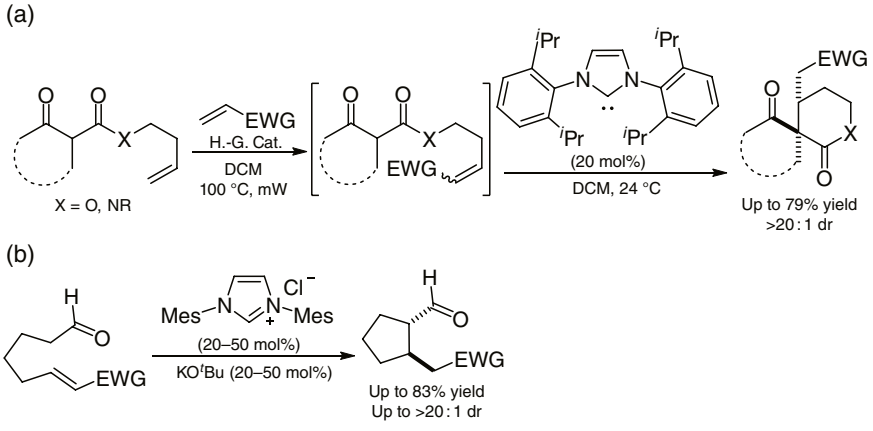

Figure 6.28. Michael additions catalyzed by NHCs through non-covalent pathway. (a) NHC-catalyzed intramolecular Michael addition of diketones. Source: Based on [106]. (b) NHC-catalyzed Michael addition of aldehydes. Source: Based on [107].

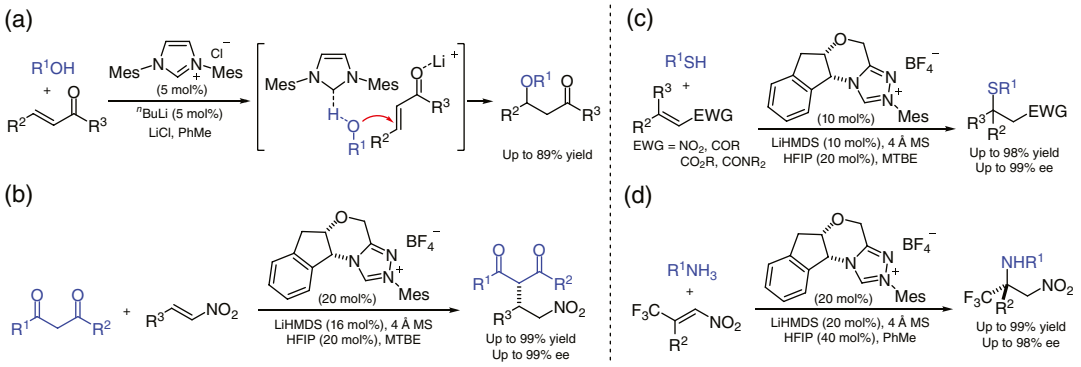

Figure 6.29. NHC as Brønsted base catalyzed Michael additions. (a) Scheidt's oxo-Michael addition. Source: Based on [109]. (b) Huang's asymmetric addition of 1,3-diketones. Source: Based on [110]. (c) Huang's asymmetric sulfa-Michael addition. Source: Based on [111]. (d) Huang's asymmetric aza-Michael addition. Source: Based on [112].

covalent activation pathways. However, Hong found that aliphatic aldehydes could also be activated by NHC catalysts via non-covalent activation mode to form enolate intermediates for tandem Michael addition reactions (Figure 6.28b) [107].

The NHC-catalyzed oxa-Michael reaction via a non-covalent activation mode was disclosed by Scheidt in 2010 (Figure 6.29a) [109]. In the reaction, the alcohol was activated by the NHC catalyst via hydrogen bonding interactions to increase the nucleophilicity of hydroxyl group and facilitated the conjugate addition to the lithium activated enones. Meanwhile, Kang and Zhang [113] disclosed the NHC-catalyzed, noncovalent activation reaction for aza-Michael additions. In 2014, Rodriguez reported the S- and P-Michael additions enabled by NHC-mediated no-covalent activation [114].

In 2014, Huang and Chen disclosed an enantioselective Michael addition via NHC catalyzed noncovalent activation process (Figure 6.29b) [110]. In this reaction, a catalytic amount of hexafluoroisopropanol can dramatically improve the reaction rate and enantioselectivity. This is believed to result from a proton shuttle effect in facilitating the proton transfer process. Later, the same group extended this NHC-catalyzed noncovalent activation mode to an asymmetric thio-Michael addition (Figure 6.29c) [111] and asymmetric aza-Michael addition (Figure 6.29d) [112]. Good to excellent yields and enantioselectivities were obtained in all cases.

6.5. COOPERATIVE CATALYSIS OF NHCs WITH OTHER CATALYSTS

6.5.1. Dual Catalysis of NHC Organocatalysts and Transition Metal Catalysts

Transition metal catalysts are widely explored to accomplish unique activation modes and chemical transformations for the synthesis of functional molecules [115]. It has been envisioned that merging transition metal catalysts with NHCs should provide a powerful strategy in chemical synthesis [116]. Due to the strong-coordinating property of NHC catalysts, both the NHC and the transition metal catalysts might be quenched with each other when combining them in one reaction system. However, extensive investigations have been carried out in the development of the cooperative catalytic reactions with transition metals and NHC organocatalysts during the past decade [117].

6.5.1.1. NHC and Pd In 2006, Hamada reported a one-pot sequential NHC and palladium co-catalyzed reaction (Figure 6.30a) [118]. In this transformation, Pd was employed to catalyze allylic amination, and NHC catalyst was employed to catalyze Stetter reaction. In 2008, Glorius reported the cooperative catalysis of NHC and palladium catalysts to prepare functionalized tertiary homoallylic alcohols (Figure 6.30b) [119]. Shortly after that, She reported an NHC/Pd cooperative catalytic reaction for the synthesis of linear ketone products [120].

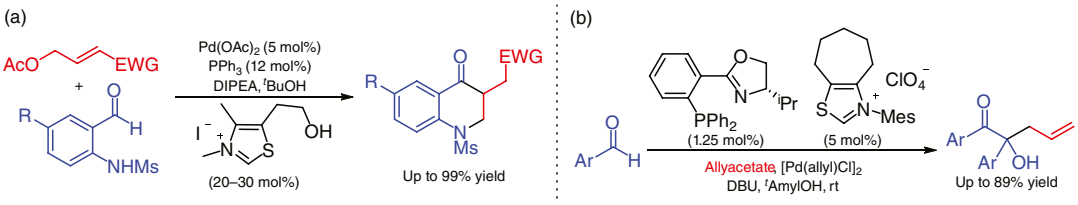

Figure 6.30. Early researches on cooperative NHC/Pd catalysis. (a) Hamada's one-pot sequential NHC/Pd multi-catalysis. Source: Based on [118]. (b) Glorius' NHC/Pd Dual-catalyzed coupling reactions. Source: Based on [119].

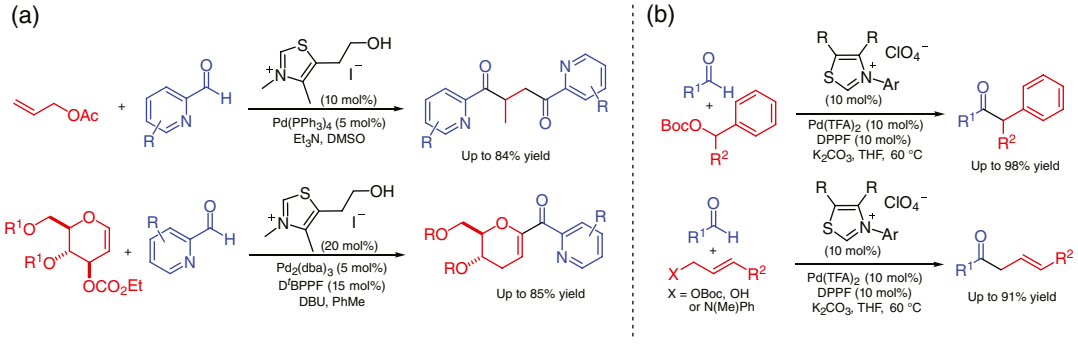

Figure 6.31. NHC/Pd dual-catalyzed reactions of aldehydes. (a) Liu's Pd-NHC dual-catalyzed coupling reactions. Source: Based on [121]. (b) Ohmiya's Pd-NHC dual-catalyzed coupling reactions. Source: [122].

In 2014, Liu reported an NHC/Pd dual catalyzed coupling reaction of (*O*-azaaryl)-carboxaldehyde with allyl acetate (Figure 6.31a) [121]. This reaction involves the coupling of the in situ generated Breslow intermediate and a Pd-π-allyl complex, followed by the mono-coupled intermediate reacting with another Breslow intermediate through a Stetter reaction to give the final product in up to 84% yield. The same group extended the scope of the dual catalyzed reaction to aldehydes and glycals, and developed a novel method for *C*-glycosylation [123]. In the same year, Scheidt also disclosed a cooperative Pd-catalyzed allylation of NHC-activated aldehydes to access 3-allyl dihydrocoumarin derivatives [124]. Recently, Ohmiya reported the NHC/Pd dual-catalyzed reactions of aldehyde acyl anions with diarylmethyl or allylic carbonates [125]. Various functional groups were well tolerated in this transformation, and the corresponding ketone products were afforded in up to 91% yield (Figure 6.31b) [122].

In 2016, Glorius reported the umpolung activation reaction between α,β-unsaturated aldehydes (**86**) and vinyl benzoxazinanones (**85**) with chiral NHC/Pd cooperative catalysis (Figure 6.32a) [126]. In this case, a nucleophilic NHC-bound homoenolate (**89**) and an electrophilic Pd-π-allyl species (**88**) coupled together to form a new carbon–carbon bond. The same group also applied the dual catalysis strategy in an enantioselective [5+2] annulation of enals (**90**) with vinylethylene carbonates (**91**) to prepare seven-membered lactones (**92**) (Figure 6.32b) [126c].

Recently, Walsh disclosed an NHC/Pd dual-catalyzed umpolung 1,4-addition of aryl iodides (**93**) and enals (**94**) (Figure 6.33) [127]. In this reaction, the in situ generated homoenolate intermediate (**97**) attacked the palladium species (**96**) to form a Pd-C complex (**98**), which then goes through a reductive elimination to give the target product (**95**).

6.5.1.2. NHC and Cu Cooperative catalysis of NHCs and copper catalysts remains challenging due to the potential risk of self-quenching interactions between the two catalysts. In 2014, Chi reported a Cu and NHC cooperative catalytic reaction for direct activation of alkynes (Figure 6.34) [128]. This NHC/Cu dual-catalyzed reaction was initiated by the Cu-catalyzed activation of alkyne (**99**) to react with TsN_3 to eventually generate a ketenimine (**102**) as the key intermediate. The ketenimine intermediate (**102**) was

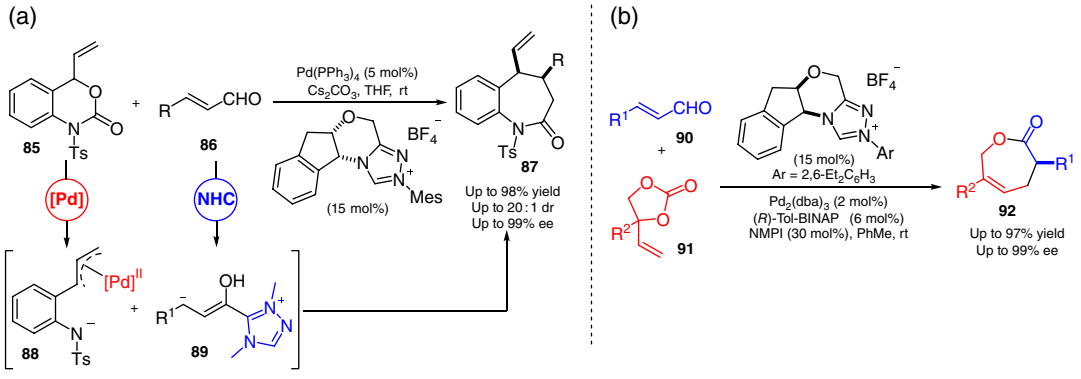

Figure 6.32. NHC/Pd dual catalyzed asymmetric coupling reactions. (a) NHC/Pd dual-catalyzed reactions of enals and benzoxazinanones. Source: [126]. (b) NHC/Pd dual-catalyzed enantioselective [5+2] annulation. Source: Based on [126c].

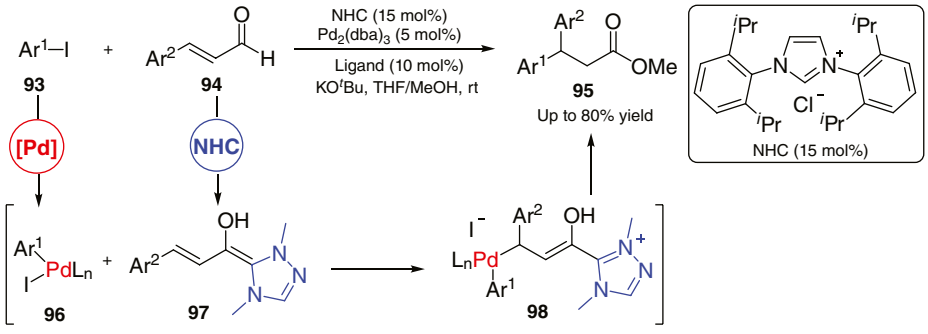

Figure 6.33. NHC/Pd dual catalyzed umpolung 1,4-addition. Source: Based on [127].

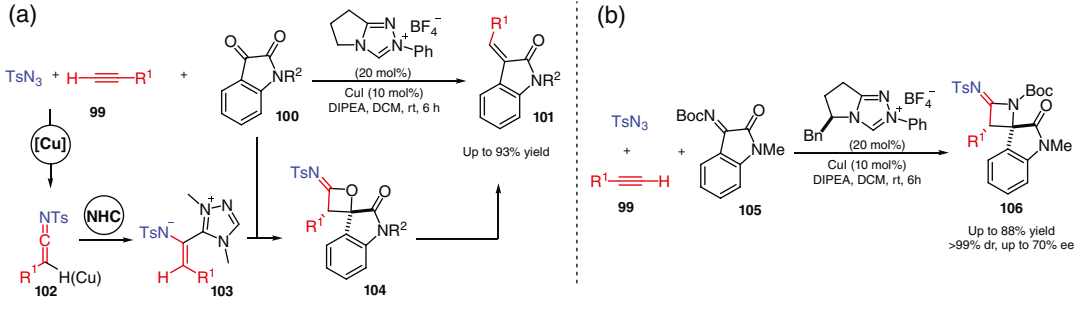

Figure 6.34. NHC/Cu dual-catalyzed activation of alkynes as enolate equivalents. (a) Isatin as electrophiles. (b) Isatin-derived imines as electrophiles. Source: Based on [128].

then activated by the NHC catalyst presented in the same reaction solution to form an azolium enamide intermediate (**103**). The azolium enamide intermediate (**103**) can react with electrophilic substrates such as reactive ketones and imines to form the final product (**101** or **106**).

In 2019, Gong reported the NHC/Cu dual-catalyzed enantioselective [3+3] and [3+4] annulations of isatin-derived enals with ethynylethylene carbonates and ethynyl benzoxazinanones. Spiroxindole derivatives with various substituents and substitution patterns are afforded in good to excellent yields and enantioselectivities (Figure 6.35) [129]. In this case, the in situ generated NHC-bound homoenolate

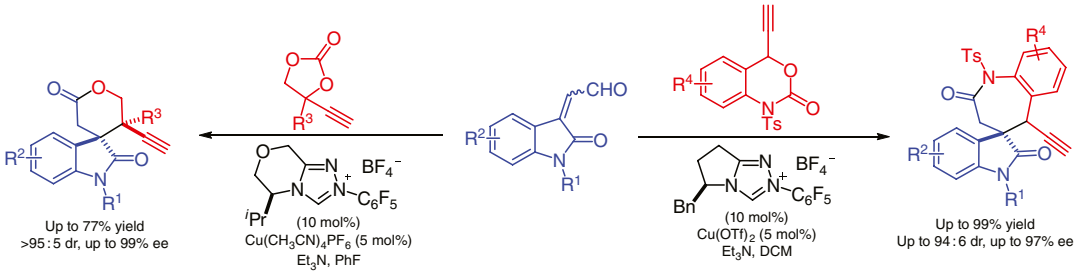

Figure 6.35. NHC/Cu dual-catalyzed enantioselective [3+3] and [3+4] annulations. Source: Based on [129].

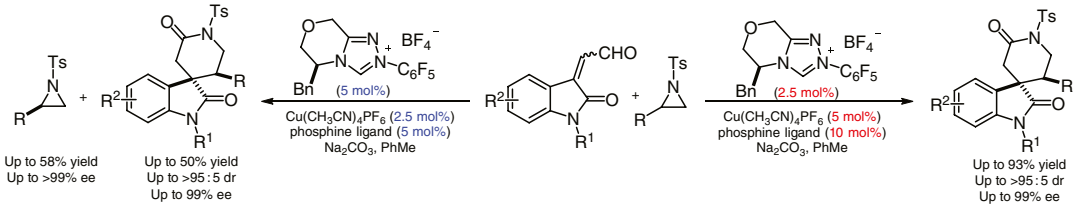

Figure 6.36. Kinetic resolution of aziridines enabled by NHC/Cu dual catalysis. Source: Based on [130].

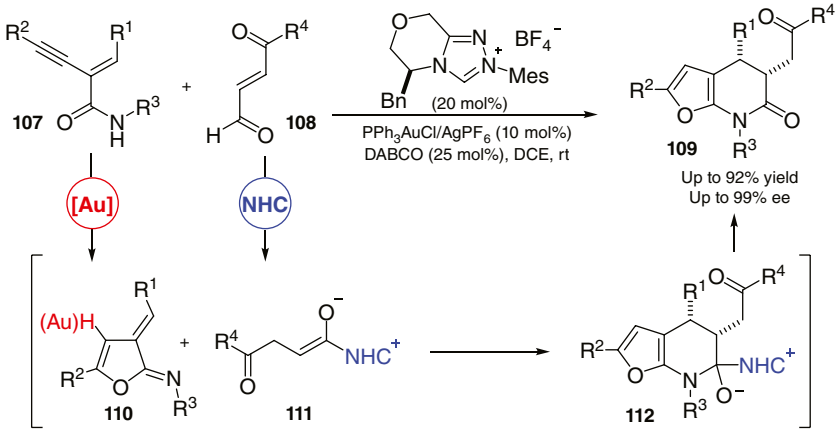

Figure 6.37. NHC/Au dual-catalyzed enantioselective annulation reactions. Source: Based on [133].

intermediates and copper allenylidene intermediates couple together and give the acyl azolium intermediate for further transformations.

Recently, Gong reported an NHC/Cu cooperative catalytic strategy for kinetic resolution of aziridines (Figure 6.36) [130]. In this case, both of the kinetic resolution and dynamic kinetic asymmetric transformation could be realized by adjusting the amount of the NHC and copper catalyst. In the mechanistic study, the authors found that the NHC catalyst not only serve as an organocatalyst to activate the enal but also act as a ligand coordinating to the copper complex.

6.5.1.3. NHC and Au Gold has good affinities to alkynes, arenes, allenes, and even alkenes. Therefore, gold catalysis has become a useful tool in the transformations of various unsaturated molecules [131]. One of the seminal reports in the combined use of gold and NHC catalysts for one-pot tandem reactions was from Suresh in 2011 [132]. In 2020, Chi reported the enantioselective cycloisomerization/cyclization reactions of ynamides and enals enabled by gold and NHC relay catalysis (Figure 6.37) [133]. In this reaction,

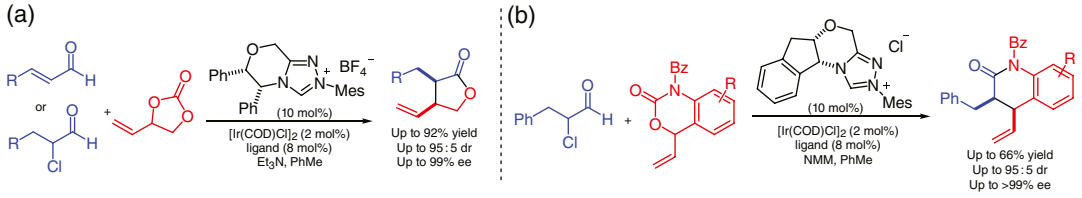

Figure 6.38. NHC/Ir dual-catalyzed [3+2] and [4+2] annulations. (a) NHC/Ir dual-catalyzed [3+2] annulation. Source: Based on [136]. (b) NHC/Ir dual-catalyzed [4+2] annulation.

Au activates the ynamide (**107**) to generate the α,β-unsaturated *N*-sulfonyl ketamine (**110**) as the key intermediate. Concurrently, NHC converts the enal (**108**) to form the Breslow intermediate that undergoes a proton transfer process to form an azolium enolate intermediate (**111**). The cyclization of these two key intermediates gives the desired lactam product (**109**).

6.5.1.4. NHC and Ir Iridium is also a versatile transition metal that can catalyze a variety of transformations in organic synthesis [134]. Success has been achieved in the cooperative NHC/iridium-based photoredox catalyzed reactions [98, 135], as illustrated in Section 6.3.5. Recently, Glorius reported an enantio- and diastereodivergent [3+2] annulation reaction for the synthesis of α,β-disubstituted γ-butyrolactones through cooperative NHC/Ir catalysis (Figure 6.38a) [136]. In this reaction, the iridium catalysis generates an Ir-π-allyl species, while the NHC catalysis generates an enolate intermediate. Nucleophilic attack of the NHC-bound enolate to the Ir-π-allyl intermediate and a sequential lactonization gives the desired product. This strategy can also be used in the synthesis of δ-lactams through asymmetric [4+2] annulation reactions (Figure 6.38b).

6.5.1.5. Other Important Studies Some of the transition metals can also be used as electron carriers in the oxidative NHC organocatalytic reactions. In 2013, Studer reported a cooperative NHC/ruthenium-based redox catalysis for the aerobic oxidation of Breslow intermediates in the oxidative esterification reaction of aldehydes [137]. Iron and ruthenium catalysts have been reported as effective co-catalysts for the aerobic oxidation of the NHC-bound homoenolate intermediates via single-electron transfer process [138]. The dual catalysis of NHC and Ruthenium-based photoredox catalysts has also been reported. This part has already been introduced in Section 6.3.5.

6.5.2. Dual Catalysis of NHC Organocatalysts and Lewis Acid Co-catalysts/Additives

Compared with the strong binding interactions between NHCs and transition metals, the interactions between NHCs and Lewis acids are much weaker. As a result, it would be much easier for the NHC organocatalysts to be compatible with the Lewis acid co-catalysts in one catalytic system. In 2010, Scheidt disclosed the stereoselective homoenolate activation reactions through an NHC/Lewis acid cooperative catalytic process (Figure 6.39) [139]. In this work, the coordinative effect plays an important role in controlling the *cis*/*trans* selectivity. The combined use of chiral titanium Lewis acid and achiral NHC was effective in the enantio- and diastereoselective dimerization of the cinnamyl aldehyde.

The groups of Scheidt [23, 140] and Studer [141] have conducted further research on NHC/Lewis acid dual-catalyzed annulation reactions as summarized in Figure 6.40a. In 2012, Chi reported an NHC/Lewis acid dual catalytic strategy for remote enantioselective control over the oxidative γ-functionalization of enals (Figure 6.40b) [142]. The product enantioselectivities dropped significantly without the addition of the Lewis acid co-catalysts.

NHC/Lewis acid dual catalysis has also been used in the activation of ynals. In 2013, She reported a conjugate umpolung reaction of ynals enabled by cooperative catalysis of NHC and LiCl (Figure 6.40c) [143]. In 2018, Wang reported the NHC/$Mg(OTf)_2$ dual-catalyzed enantioselective [3+3] annulation of cyclic 1,3-diones with ynals for the construction of axially chiral α-pyrone-aryls in moderate to good yields with good to excellent enantioselectivities (Figure 6.40d) [144].

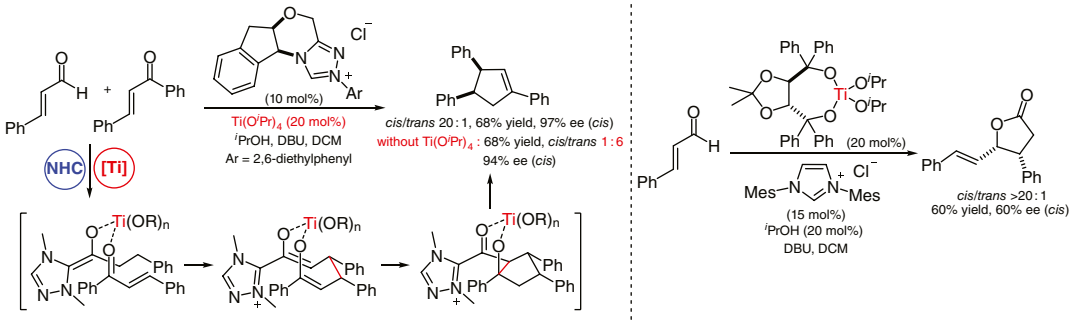

Figure 6.39. NHC/Lewis acid dual-catalyzed annulation with homoenolates. Source: Based on [139].

In 2016, Cheng and co-workers [145] reported that in presence of a titanium Lewis acid, the modified enal-enone multifunctional substrate would go through a different reaction pathway from the previously reported intramolecular cyclization reaction with the same starting material (Figure 6.41) [146]. It's proposed that in Cheng's work, the coordination of titanium could increase the electrophilicity of the carbaldehyde group, which can then react with the nucleophilic β-carbon of the homoenolate intermediate generated from addition of the NHC catalyst and the aldehyde group of another multifunctional substrate molecule.

Furthermore, the groups of Wu et al. [147], Yao et al. [148], Ye et al. [51a], Cheng et al. [149], Huang et al. [150], Wang [151], Huang et al. [68], Du et al. [152], Chi et al. [153], Xu et al. [154], and Tambar [155] have also reported significant progresses on the cooperative catalysis of NHC and Lewis acids.

6.5.3. Dual Catalysis of NHC Organocatalysts and Brønsted Acids

The cooperative catalysis of NHC and Brønsted acid has also been widely explored in NHC organocatalytic reactions. In 2010, Waser reported a novel bifunctional NHC catalyst bearing a (thio)urea moiety to provide H-bonding interaction and applied the catalytic strategy in asymmetric benzoin reactions [156]. Coquerel also reported the synthesis of the bifunctional NHCs incorporated with H-bond donor moieties, which can effectively promote the cyclopentannulation reaction in enantioselective fashion [157].

In 2013, Chi reported the asymmetric sulfonation reaction of enones through a cooperative NHC/thiourea/tertiary amine catalytic strategy (Figure 6.42a) [61]. In this study, the NHC activated the sulfonimines (**113**) to generate sulfinic anions (**116**), which was delivered to the enones (**114**) by the chiral thiourea/amine co-catalyst via H-bonding interactions to furnish the asymmetric conjugate addition reaction. Scheidt developed an NHC/chiral phosphate dual catalytic system for allenolate annulations of alkynals (**118**) and ketones (**119**) to prepare enones (**120**) (Figure 6.42b) [158]. The chiral phosphate is essential in activating the ketones and controlling the enantioselectivities of the catalytic reactions.

NHC/Brønsted acid dual catalysis can also be used in asymmetric protonation process. In 2015, Scheidt disclosed the cooperative NHC/H-bond donor (HBD) catalyzed enantioselective β-protonation reaction of enals (Figure 6.43a) [159]. This dual catalytic system could improve both the reaction yield and enantioselectivity. In 2017, Huang reported an NHC/Brønsted acid dual-catalyzed asymmetric β-protonation of enals (Figure 6.43b) [150a]. Thioesters with a β-chiral center were prepared in a redox-neutral fashion in excellent yields and enantioselectivities.

The enantioselective construction of all-carbon spirocyclic structures has been synthetically challenging. In 2019, Chi disclosed an NHC/thiourea dual-catalyzed cascade strategy to address this issue (Figure 6.44) [160]. This cascade process involves an NHC-catalyzed intermolecular Stetter reaction and an intramolecular aldol reaction. The stereoselectivity was controlled by the chiral NHC. The use of the thiourea co-catalyst is critical to this reaction, since no product was formed in the absence of the thiourea.

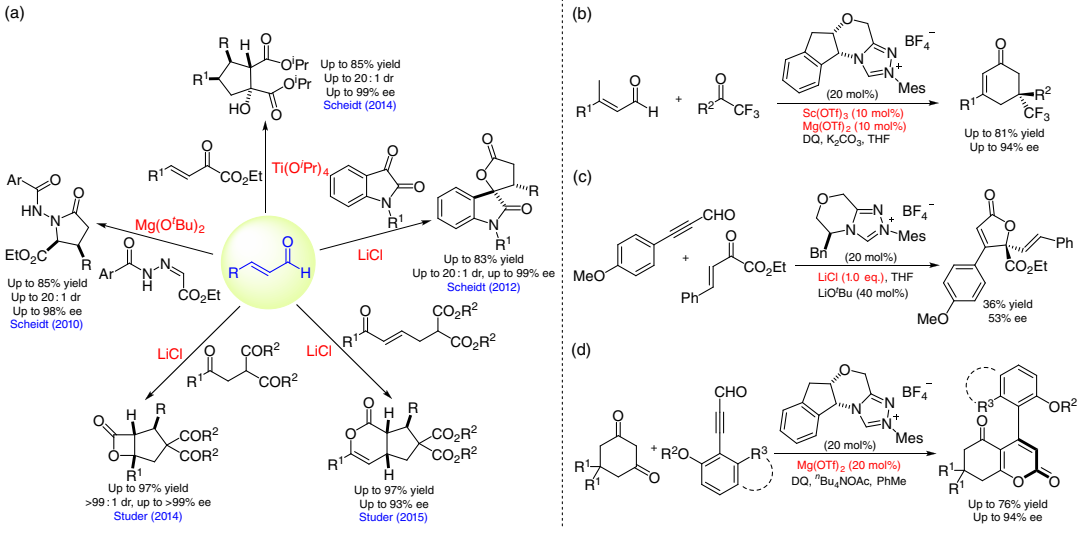

Figure 6.40. NHC/Lewis acid dual-catalyzed reactions. (a) NHC/Lewis acid dual-catalyzed annulations of enals. (b) Chi's annulations involving dienolate. Source: [142]. (c) She's conjugate umpolung reaction of ynals. Source: [143]. (d) Wang's [3+3] annulation involving alkynl acyl azolium. Source: [144].

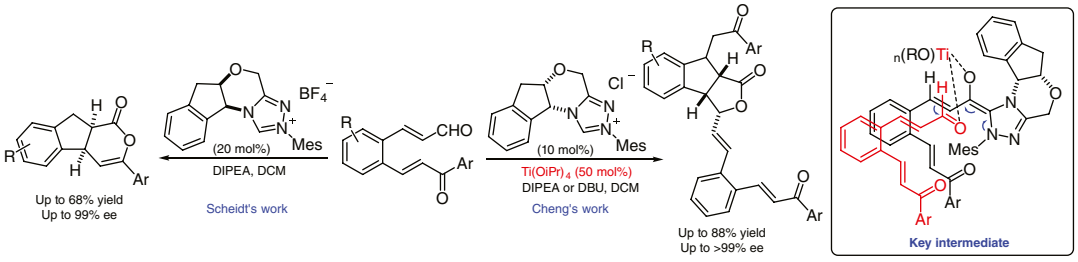

Figure 6.41. A switched reaction pathway enabled by NHC/Lewis acid dual catalysis. Source: Based on [146].

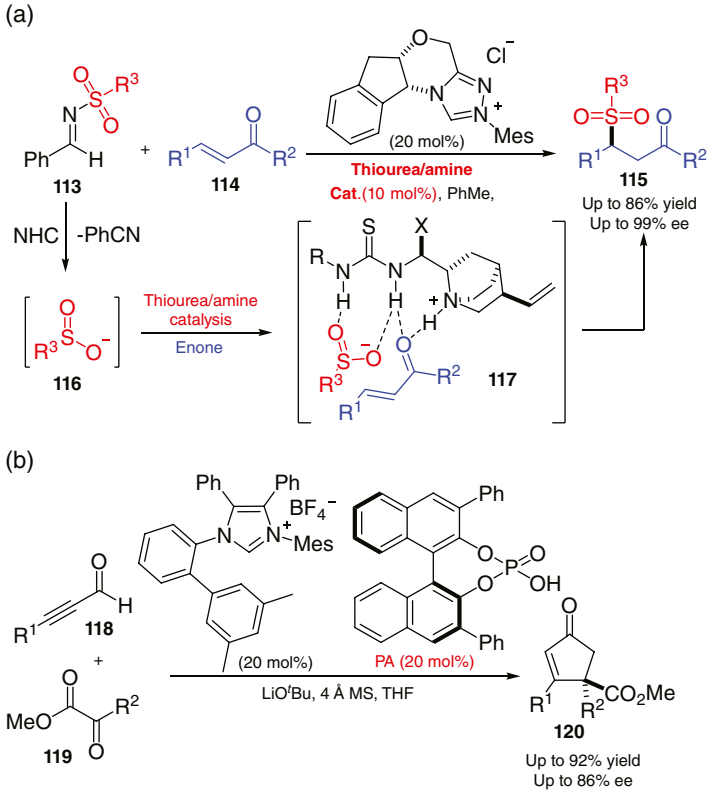

Figure 6.42. Early cooperative catalytic strategies of NHCs and Brønsted acids. (a) Chi's cooperative NHC/thiourea/tertiaryamine multicatalysis. Source: Based on [61]. (b) Scheidt's NHC/chiral phosphate dual-catalyzed annulations. Source: Based on [158].

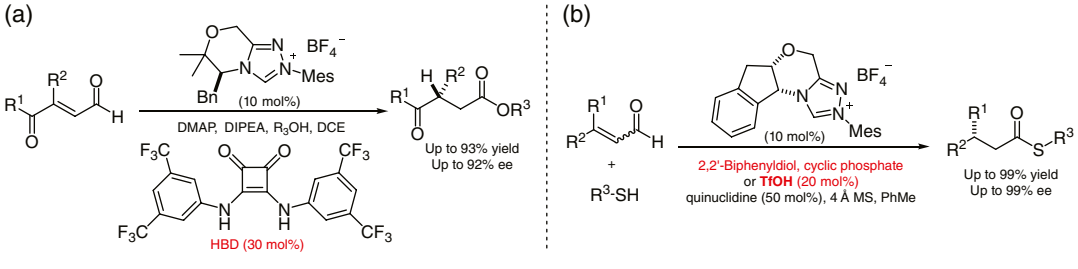

Figure 6.43. NHC/Brønsted acid dual-catalyzed β-protonation of enals. (a) Scheidt's NHC/HBC dual-catalyzed enantioselective β-protonation. Source: [159]. (b) Huang's enantioselective β-protonation via a shuttling strategy. Source: [150a].

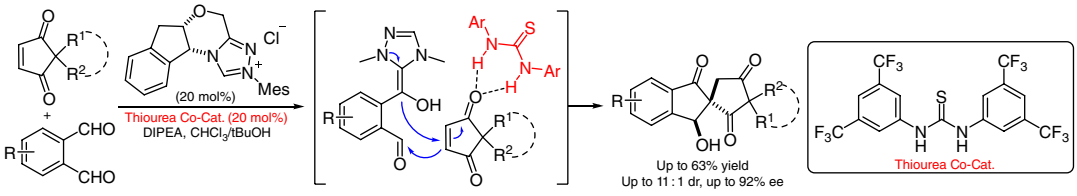

Figure 6.44. NHC/thiourea dual-catalyzed construction of spirocyclic structures. Source: Based on [160].

Scheidt has also reported the NHC/thiourea/Lewis acid cooperative catalysis for lactonization of simple enals and α-ketoesters [140c]. Chi has used in situ generated acetic acid as co-catalyst to activate *o*-hydroxybenzhydryl amine for the access to dihydrocoumarins [161]. In 2007, He reported the use of hexafluoroisopropanol as a H-bond donor co-catalyst for NHC catalyzed sulfa-Michael addition of enals [162]. The groups of Rovis [163] and Wang [164] have also reported significant progress on NHC/Brønsted acid dual-catalyzed reactions.

6.5.4. Dual Catalysis of NHC Organocatalysts and Other Catalysts

In addition to the cooperative catalysis of NHCs with transition metals, Lewis acids, and Brønsted acids, there are also investigations on the dual catalysis of NHCs with other catalysts. In 2014, Youn reported an NHC/cinchonine dual-catalyzed asymmetric synthesis of 3-substituted phthalides (Figure 6.45a) [165]. The cinchonine was used as the chiral Brønsted base catalyst to activate the in situ generated acid and control the stereoselectivity of the intramolecular oxa-Michael addition reaction.

In 2019, Chi disclosed an NHC and sulfinate co-catalyzed Rauhut–Currier reaction for enantioselective access to azepino[1,2-a]indoles (Figure 6.45b) [166]. In this case, the NHC activates the enal and the sulfinate activates the nitrovinyl indole. Both activation processes are realized via covalent additions of the organic catalysts to the electrophilic substrates.

Chi has also used HOBt as the co-catalyst in several NHC catalytic reactions [167]. For example, in 2018, the Chi group reported the NHC-catalyzed oxidative LUMO activation of the β-carbons of saturated carboxylic esters for the formation of lactams and lactones (Figure 6.46) [167a]. The addition of HOBt can significantly improve both of the yields and enantioselectivities.

6.6. SYNTHETIC APPLICATIONS OF NHC CATALYSIS

6.6.1. Kinetic Resolution and Desymmetrization

NHC catalysis is not only a powerful tool for constructing complex molecules, but also a useful method for asymmetric kinetic resolutions (KR), dynamic kinetic resolutions, and desymmetrizations of prochiral molecules [168].

6.6.1.1. NHC-Catalyzed Kinetic Resolutions In 2004, Suzuki reported the kinetic resolution of racemic secondary alcohols via an enantioselective acylation by in situ generated chiral NHC-derived acyl azolium intermediates (Figure 6.47a) [169]. Shortly after that, Maruoka reported an NHC-catalyzed acylative kinetic resolution of racemic alcohols with increased enantioselectivities [171]. The groups of Studer [172] and Yashima [173] have also reported their studies on NHC-catalyzed kinetic resolution of alcohols with chiral NHC-bound acyl azolium intermediates via enantioselective acylation.

In 2013, Zhao reported an example of NHC-catalyzed kinetic resolution of racemic tertiary alcohols (Figure 6.47b) [170]. In this case, the acylative kinetic resolution of 3-hydroxy-3-substituted oxindoles was realized with high efficiency and enantioselectivity in an NHC/Lewis acid co-catalyzed oxidative system. In the same year, an NHC-catalyzed enantioselective kinetic resolution and desymmetrization of cyclic diols and amino alcohols was achieved by Yamada (Figure 6.48a) [174]. In this case, the reaction rate and enantioselectivity could be enhanced by carboxylate additives via H-bond interactions.

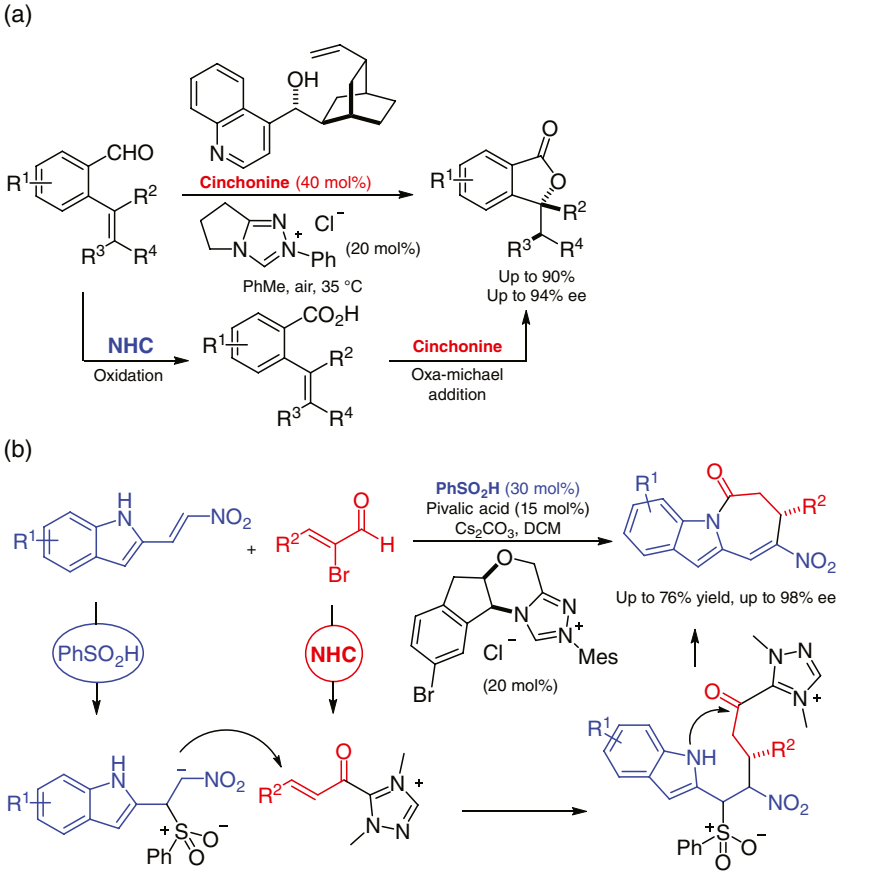

Figure 6.45. Cooperative catalysis of NHCs with other catalysts. (a) Youn's NHC/cinchonine dual-catalyzed lactonization. Source: Based on [165]. (b) Chi's NHC/$PhSO_2H$ dual-catalyzed reactions. Source: Based on [166].

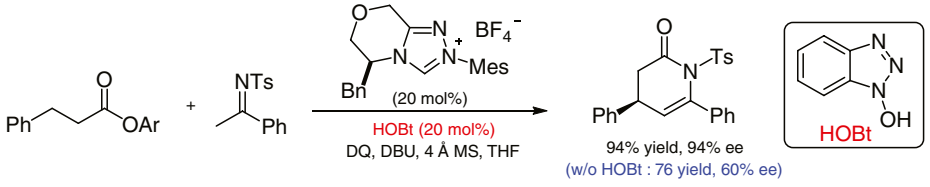

Figure 6.46. Cooperative catalysis of NHCs and HOBt. Source: Based on [167a].

The kinetic resolution of racemic mixtures of axially chiral phenols can also be realized with asymmetric NHC catalysis. In 2014, Zhao reported a highly efficient NHC-catalyzed kinetic resolution of 1,1′-biaryl-2,2′-diols and amino alcohols (Figure 6.48b) [175]. Mechanistic studies with DFT calculation reveal that the in situ generated benzoic acid is crucial in accelerating the proton transfer step by forming H-bonds, which is also responsible for the high enantioselectivities [176].

Amines and imines are also suitable substrates in NHC-catalyzed kinetic resolutions. For example, Bode reported the catalytic resolution of racemic cyclic amines by an enantioselective amidation (Figure 6.49) [177]. This reaction involves an NHC-catalyzed acylation of the chiral hydroxamic acid co-catalyst to form a chiral acylation intermediate, which then participates in the enantioselective resolution of racemic amines.

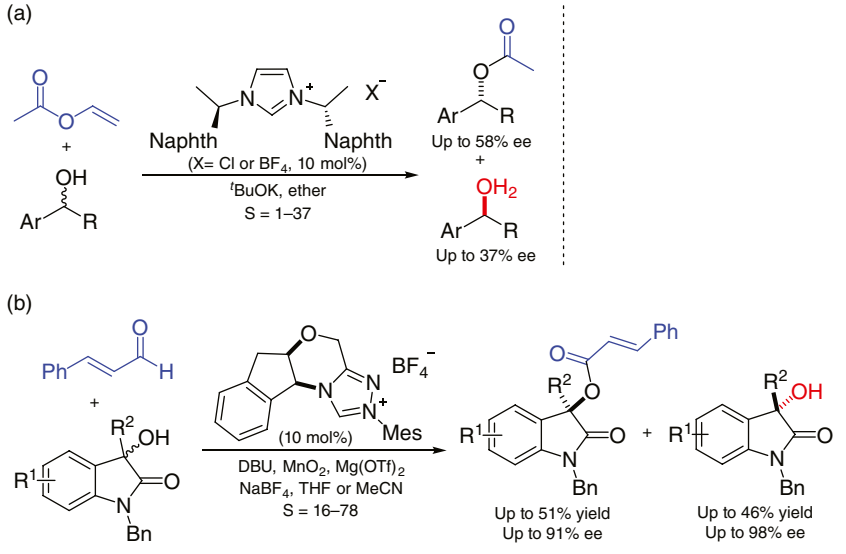

Figure 6.47. Kinetic resolution of secondary and tertiary alcohols. (a) Suzuki's NHC-catalyzed acylative KR of alcohols. Source: Based on [169]. (b) Zhao's NHC-catalyzed acylative KR of tertiary alcohols. Source: [170].

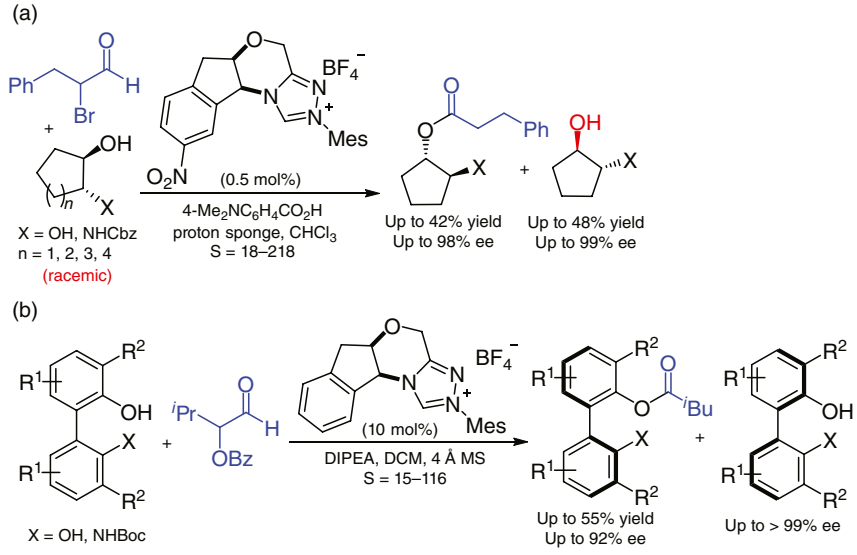

Figure 6.48. Kinetic resolution of alcohols and phenols. (a) Yamada's NHC-catalyzed KR of secondary alcohols. Source: [174]. (b) Zhao's NHC-catalyzed KR of BINOL and NOBIN derivatives. Source: [175].

In 2014, Chi reported an NHC-catalyzed [3+4] cycloaddition of azomethine imines and enals. A kinetic resolution of azomethine imines was achieved in a highly enantioselective manner (Figure 6.50a) [178]. In this case, the substrate chiral center can be well resolved even though it's remote from the NHC-activating moiety. The NHC-catalyzed kinetic resolution of racemic sulfoximines was realized by Bolm (Figure 6.50b) [179]. The enantioselective amidation proceeds smoothly with both enantiomers of the sulfoximines being obtained in excellent optical purities under different catalytic conditions.

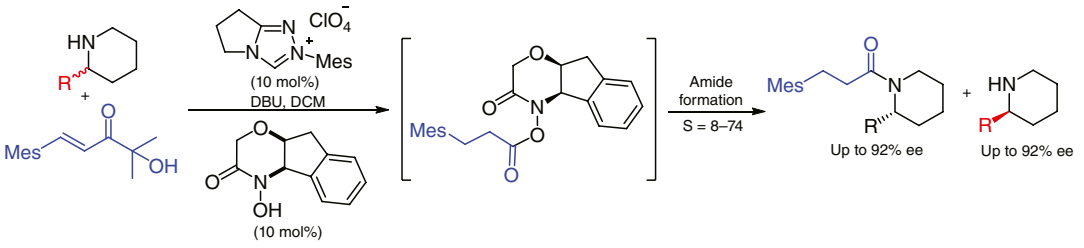

Figure 6.49. NHC-catalyzed kinetic resolution of amines. Source: [177].

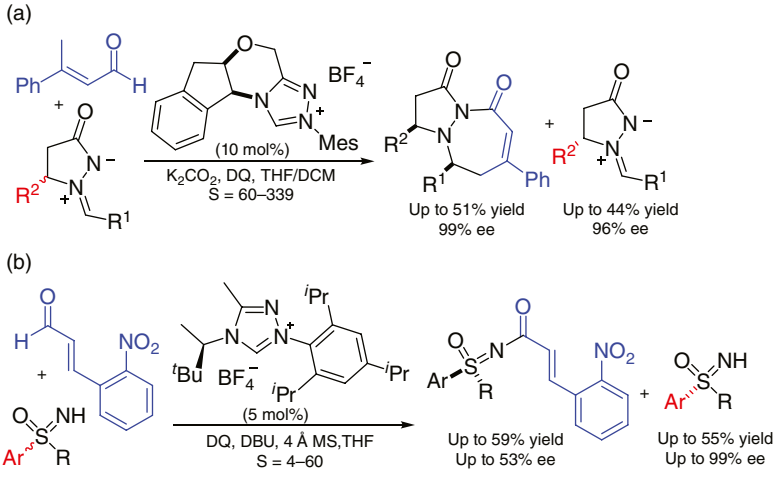

Figure 6.50. NHC-catalyzed kinetic resolution of imines. (a) Chi's NHC-catalyzed KR of 1,3-dipolar azomethine imines. Source: [178]. (b) Bolm's NHC-catalyzed KR of sulfoximines. Source: [179].

In addition, You has achieved the kinetic resolution of amide-containing aldehydes, with a wide range of *cis*-4-formyl-β-lactams formed in good to excellent enantioselectivities [180]. Ye reported the kinetic resolution of enamines/imines enabled by an asymmetric NHC-catalyzed [3+3] annulation process [181]. Recently, Gong developed an NHC/Cu dual-catalyzed method for kinetic resolution of aziridines [130].

6.6.1.2. NHC-Catalyzed Dynamic Kinetic Resolutions Theoretically, kinetic resolution can give optically pure products in up to 50% yield. Therefore, dynamic kinetic resolution (DKR) has been developed as an important method for enantioselective resolutions with theoretical yields increased to 100% [182]. In 2012, Scheidt disclosed an NHC-catalyzed DKR of racemic enals containing β-ketoester motifs (Figure 6.51a) [183]. Under the asymmetric catalytic condition, one isomer of the racemic substrate reacted quickly to afford the cyclized product, whereas the other isomer reacted slowly but could isomerize to its enantiomer due to the strong acidity of the α-C–H bond. As a result, all the substrates were enantioselectively converted to β-lactones or cyclopentenes in good yields and ee values. In 2017, Biju also reported a DKR process involving chiral NHC-bound enolates as the key intermediates [185].

In 2014, Johnson disclosed the DKR of α-keto-β-halo esters via NHC-catalyzed asymmetric cross-benzoin reactions (Figure 6.51b) [184]. In this case, the DKR also proceeded successfully to give the coupling products in high yields and excellent stereoselectivities. Shortly after that, the same group also realized the DKR of α-keto-β-haloesters [186]. In 2015, Wang reported the DKR of α-keto-β-haloesters with NHC-bound dienolate as the key reaction intermediate [187].

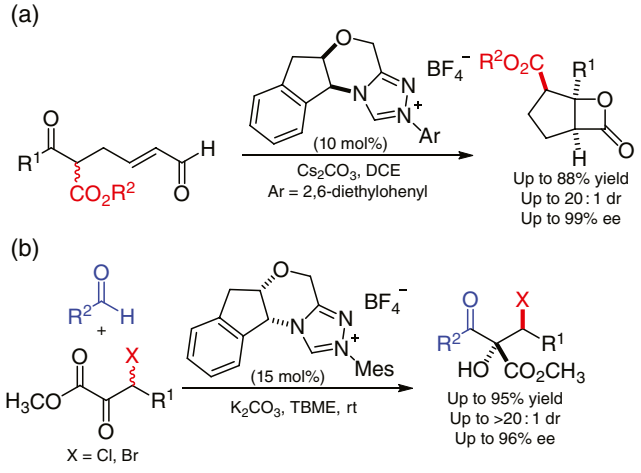

Figure 6.51. NHC-catalyzed DKR of functionalized ketones. (a) Bode's NHC-catalyzed DKR of multifunctional ketones. Source: [183]. (b) Johnson's NHC-catalyzed DKP of α-ketoesters. Source: Based on [184].

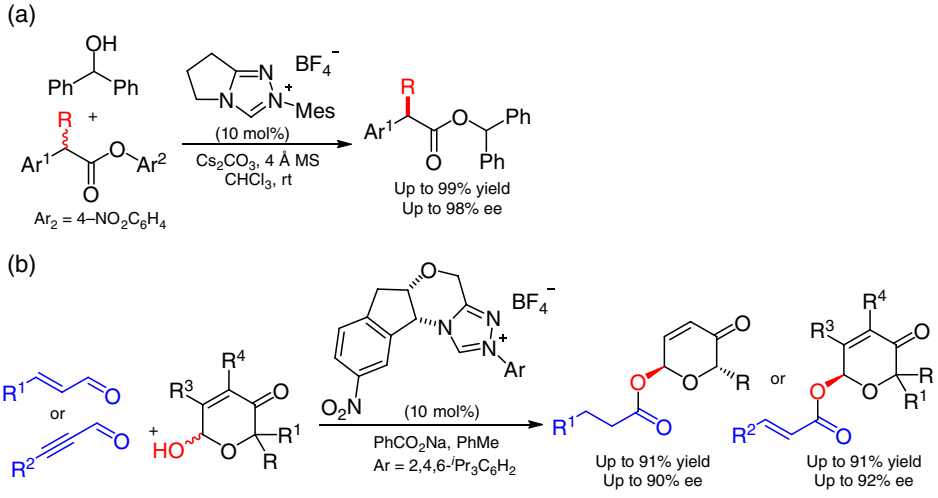

Figure 6.52. NHC-catalyzed DKR of esters and pyranones. (a) Chi's DKR of α,α-disubstituted carboxylic esters. Source: Based on [184]. (b) Wang's NHC-catalyzed DKR of pyranones. Source: Based on [188].

NHC-catalyzed asymmetric acylation reactions can also be applied in DKR processes. In 2016, Chi reported the NHC-catalyzed DKR of α,α-disubstituted carboxylic esters with excellent yields and enantioselectivities (Figure 6.52a) [188]. In the same year, Wang reported the DKR of pyranones by enals or alkynals through an NHC-catalyzed asymmetric redox acylation process (Figure 6.52b) [189].

6.6.1.3. NHC-Catalyzed Desymmetrizations Desymmetrization is a useful method to produce chiral molecules from pro-chiral substrates. The NHC-catalyzed desymmetrization of alcohols mainly relies on asymmetric acylation reactions. In the seminal report by Rovis in 2004, α-haloaldehydes were used as acylation reagents under the catalysis of chiral NHCs in a self-redox fashion (Figure 6.53a) [37a]. In 2007, Scheidt also reported the desymmetrization of *meso*-diols with NHC catalysis [34]. The NHC-catalyzed desymmetrization of 1,3-diols was reported by Chi in 2016 (Figure 6.53b) [190]. In this case, one hydroxyl group of the symmetric 1,3-diols was selectively acylated to afford the chiral esters with high yields and ee values.

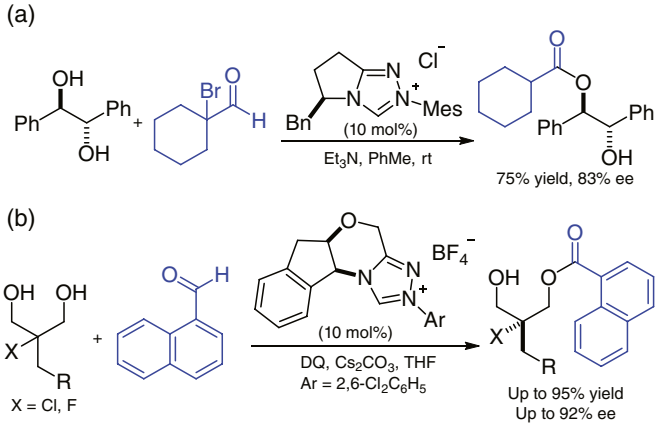

Figure 6.53. Acylative desymmetrization of diols. (a) Rovis's NHC-catalyzed desymmetrization of meso-1,2-diol. Source: Based on [37a]. (b) Chi's NHC-catalyzed desymmetrizations of 1,3-diols. Source: Based on [190].

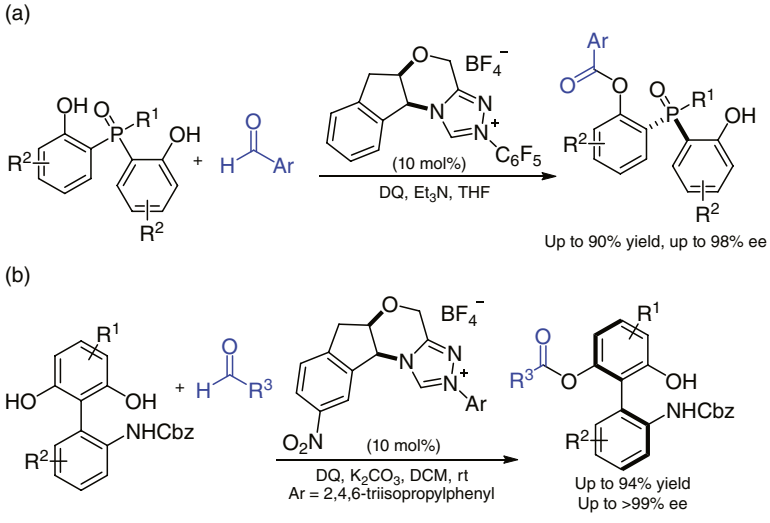

Figure 6.54. Acylative desymmetrization of biphenols. (a) Chi's NHC-catalyzed desymmetrization of phosphorates. Source: Based on [192]. (b) Wang's NHC-catalyzed desymmetrization of biaryl biphenols. Source: Based on [193].

Shortly after that, Wang also reported an example on desymmetrization of 1,3-diols based on an NHC-catalyzed asymmetric acylation process [191].

Pro-chiral phenols can also be desymmetrized via NHC-catalyzed asymmetric acylation. Chi disclosed an NHC-catalyzed desymmetrization of pro-chiral bisphenol compounds bearing P-stereogenic centers in 2016 (Figure 6.54a) [192]. Recently, Wang reported an NHC-catalyzed desymmetrization of pro-chiral biphenols for atropoenantioselective synthesis of axially chiral biaryl amino phenols (Figure 6.54b) [193]. The groups of Zhao et al. [194] and Li et al. [195] have also reported significant progresses on the desymmetrization of prochiral phenols.

In 2009, Ema disclosed the desymmetrizations of cyclic 1,3-diketones via NHC-catalyzed intramolecular cross-benzoin reactions (Figure 6.55a) [14e]. The same group has also provided an intensive study on the substrate scope and transition-state models to explain the enantioselectivity [197]. In 2016, Fang reported a general strategy for the asymmetric desymmetrization of 1,3-diketone via NHC-catalyzed intramolecular benzoin reactions [198]. Stetter reactions can also be applied in the desymmetrizations of

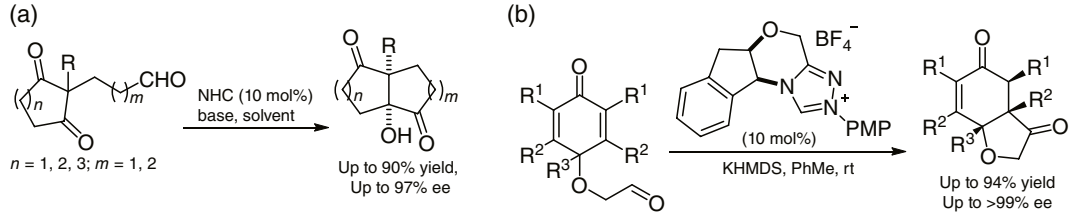

Figure 6.55. Desymmetrization through benzoin and Stetter reactions. (a) Ema's desymmetrization of 1,3-diketones. Source: Based on [14e]. (b) Rovis's desymmetrization of cyclohexadienones Source: Based on [196].

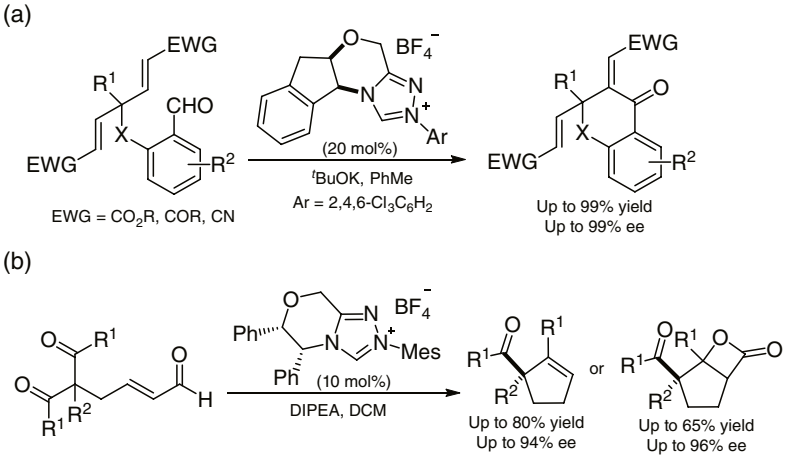

Figure 6.56. Desymmetrization of 1,4-dienes and 1,3-diketones. (a) Fang's NHC-catalyzed desymmetrization of 1,4-dienes. Source: Based on [200]. (b) Scheidt's NHC-catalyzed desymmetrization of 1,3-diketones. Source: Based on [201].

pro-chiral molecules, as disclosed by Rovis in 2006 (Figure 6.55b) [196]. Later, You also reported the desymmetrization of cyclohexadienones via NHC-catalyzed intramolecular Stetter reactions [199].

In 2016, Fang developed an NHC-catalyzed enantioselective intramolecular Stetter reaction for the asymmetric desymmetrization of multi-functional 1,4-dienes (Figure 6.56a) [200]. A wide range of tetralone derivatives and other cyclic ketones with two continuous stereogenic centers were obtained in good yields and enantioselectivities.

NHC-bound enolates can also react as the key intermediates in desymmetrizations. In 2007, Scheidt reported an NHC-catalyzed desymmetrization of 1,3-diketones for access to α,α-disubstituted cyclopentenes (Figure 6.56b) [201]. This reaction involves an enantioselective aldol reaction and a decarboxylation of β-lactone intermediate to afford functionalized carbocycles in moderate yields with excellent enantioselectivities.

6.6.2. NHC Catalysis in Natural Product Synthesis

NHC catalysis is a powerful tool for the construction of complex molecules in highly efficient and enantioselective manners. With rich activation modes and transformation diversities in hand, its applications in natural product synthesis have achieved prosperous success. A large variety of NHC-catalyzed transformations can be found in the total synthesis of natural products.

The benzoin reaction is one of the most widely used reactions in total synthesis. An excellent example was provided by Suzuki during the asymmetric synthesis of (−)-seragakinone A (**126**) in 2011 (Figure 6.57) [202]. In this work, the compound **122** was treated with NHC in the presence of Et_3N to

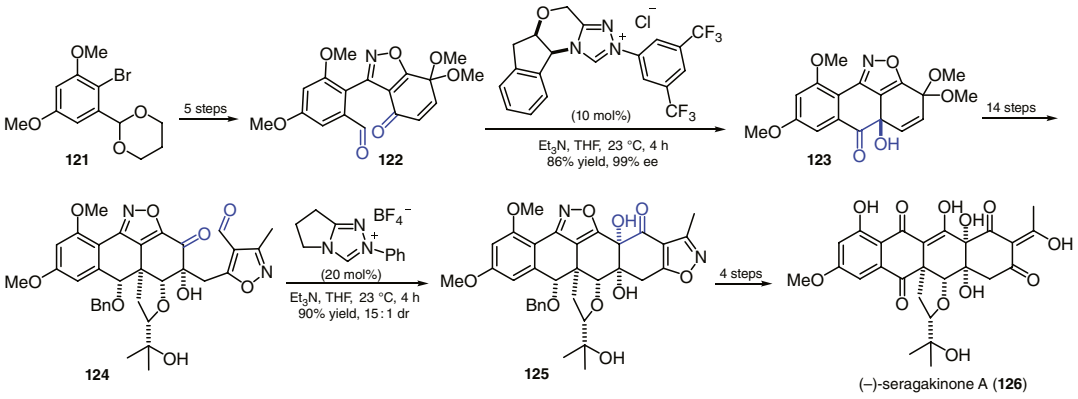

Figure 6.57. Total synthesis of (–)-seragakinone A. Source: Based on [202].

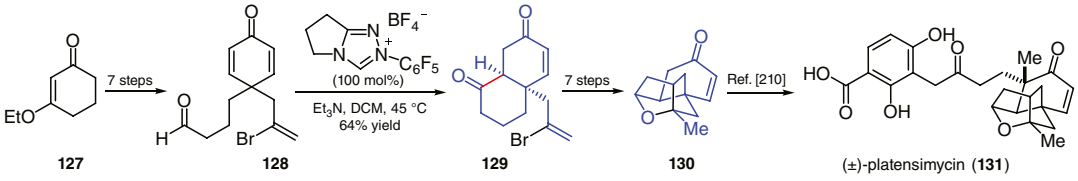

Figure 6.58. Formal synthesis of (±)-platensimycin. Source: Based on [211].

conduct the benzoin cyclization. The benzoin reaction proceeded smoothly with the designed cyclic ketol **123** obtained in an excellent yield and enantioselectivity (86%, 99% ee). After 13 steps, the author employed the benzoin reaction again to construct another α-hydroxyl ketone motif. The benzoin reaction was successful in converting ketoaldehyde **124** to ketol **125** in a 90% yield with excellent diastereoselectivity (d.r. 15 : 1). After an additional 4 steps, the target (–)-seragakinone A (**126**) was prepared in 26 steps with an overall 2% yield.

The benzoin reaction has also been used in the synthesis of other natural products and complex molecules, including *trans*-Resorcylide [203], (+)-Sappanone B [204], Cassialoin [205], Kinamycins C, F, and J [206], Lomaiviticins [207], Pleospdione [208], Inositols [209], and (+)-7,20-Diisocyanoadociane [210].

The Stetter reaction is another representative NHC-catalyzed reaction that has been widely used in natural product synthesis. For example, Nicolaou reported the formal synthesis of (±)-platensimycin (**131**) in 2007 (Figure 6.58) [211]. In this report, the triazolium-derived NHC is used to catalyze the Stetter reaction of aldehyde **128** with the cyclohexadienone moiety and gives the diketone **129** in 64% yield as a single diastereoisomer. This intramolecular Stetter reaction plays a crucial role in constructing the key octahydronaphthone motif in the cage-like core structure of platensimycin. After another 7 steps, the authors produced the key intermediate **130**, which can be easily converted to the final target molecule based on their previously reported procedures [212].

Intermolecular Stetter reactions can also be used in the total synthesis of various complex molecules. For example, in the total synthesis of Roseophilin (**137**) reported by Tius and coworkers, the NHC-catalyzed Stetter reaction was successfully used in the coupling of enone **133** and aldehyde **134** (Figure 6.59). This Stetter reaction was catalyzed by achiral triazolium-derived NHC catalyst, with the *trans* product **135** afforded in 77% yield with an excellent diastereoselectivity. After an additional 6 steps, the target product Roseophilin was produced in 15 steps with an overall 7% yield.

NHC-catalyzed Stetter reactions have also been used in the synthesis of other natural products or complex targets, such as Hirsutic acid C [213], *cis*-Jasmon [214], Dihydrojasmon [214], Atorvastatin [215], *trans*-Sabinene hydrate [216], Monomorine I [217], Indolizidines [217], Haloperidol [218], Englerin

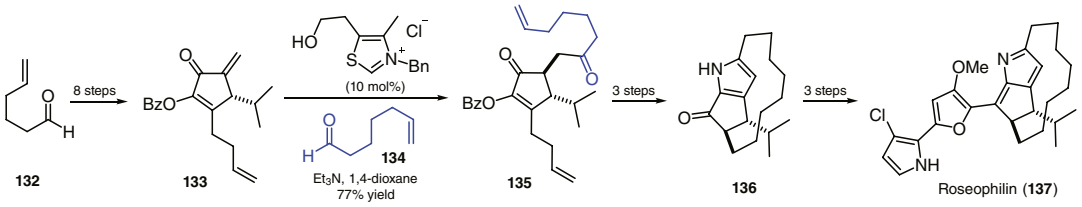

Figure 6.59. Total synthesis of roseophilin.

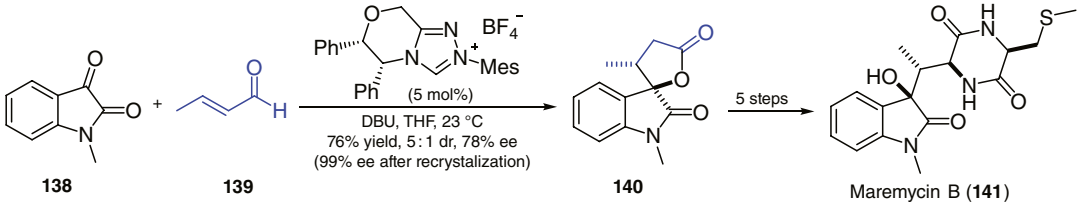

Figure 6.60. Total synthesis of Maremycin B. Source: Based on [140b].

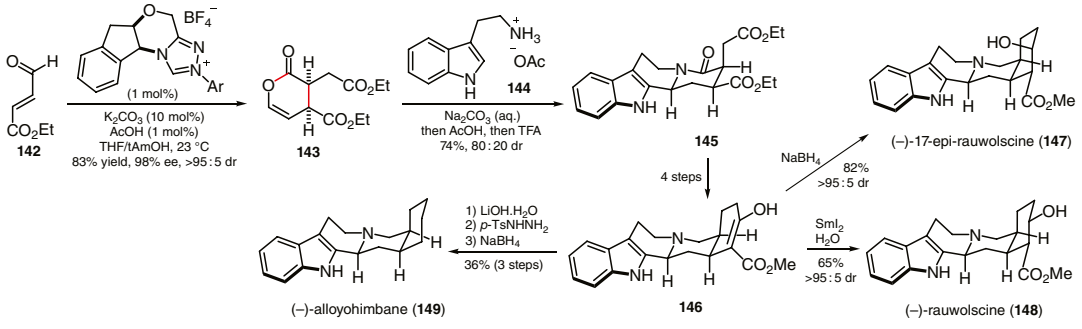

Figure 6.61. Total synthesis of Yohimbine alkaloids. Source: Based on [221].

A [219], and Piperodione [220]. In all cases, the Stetter reactions have played significant roles in the preparations of the target molecules.

NHC-catalyzed homoenolate and enolate activation reactions are also widely used in natural product synthesis. In 2012, Scheidt reported a six-step synthesis of Maremycin B (**141**) involving an NHC-catalyzed [3+2] homoenolate annulation reaction (Figure 6.60) [140b]. In this case, the annulation of *N*-methyl isatin **138** and enal **139** proceeded smoothly to give spiro-oxindole compound **140** in 76% yield with good stereoselectivities (5 : 1 dr, 78% ee, >99% ee after recrystallization). After five more steps, Maremycin B (**141**) was furnished in 17% overall yield without the use of protecting groups.

Recently, Scheidt reported an enantioselective approach for the synthesis of Yohimbine alkaloids (Figure 6.61) [221]. In this work, an NHC-catalyzed [4+2] annulation via enolate intermediate was performed to convert enal **142** to lactone **143**. It was found that the use of 1 mol% NHC catalyst gave the desired product **143** in 83% yield with excellent enantio- and diastereoselectivities. After the following amidation/*N*-acyliminium ion cyclization sequence and an additional 4 steps, the authors accessed a key synthetic intermediate **146**. Three Yohimbine alkaloids can be obtained from the intermediate **146** in one or three steps.

The NHC-catalyzed homoenolate and enolate activation reactions have also been successfully used in the syntheses of Salinosporamide A [222], Bakkenolides I, J, and S [223], Clausenamide [224], Paroxetine [225], Femoxetine [225], Baclofen [52], Rolipram [52], and 3-Dehydroxy Secu'amine A [226].

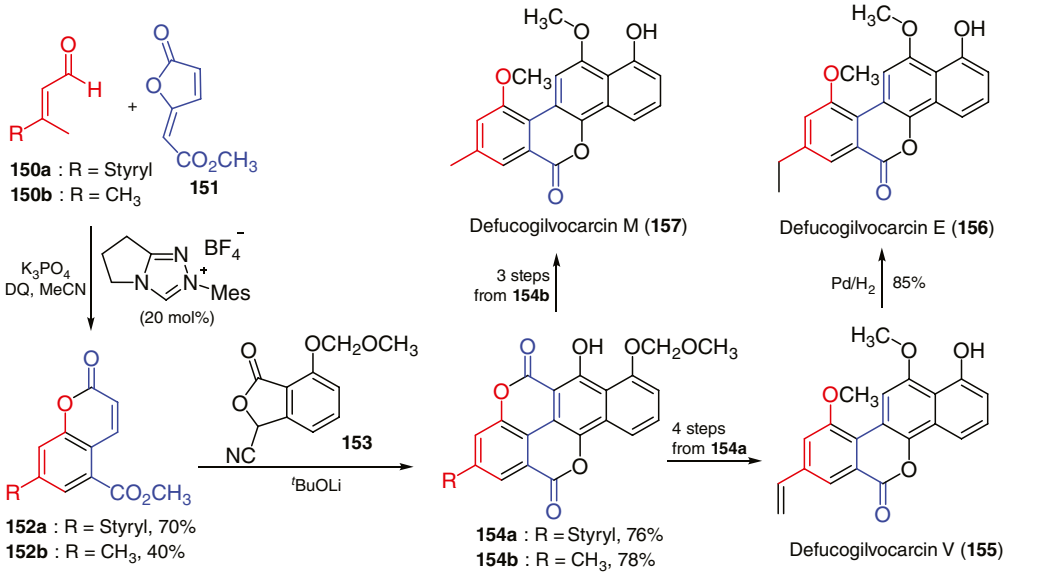

Figure 6.62. Total synthesis of defucogilvocarcins E, M, and V. Source: Based on [227].

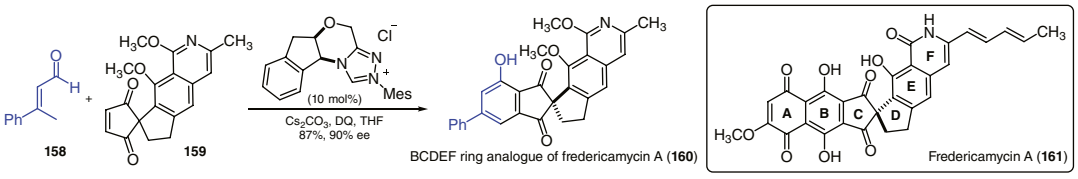

Figure 6.63. Synthesis of BCDEF ring analogue of fredericamycin A. Source: Based on [228].

In 2017, Chi reported an NHC-catalyzed formal [5+5] annulation for coumarin construction and applied this strategy in the total synthesis of defucogilvocarcins M, V, and E (Figure 6.62) [227]. In this work, NHC-catalyzed γ-carbon activation of the enals (**150**) gave rise to the NHC-bound dienolates which then reacted with furanone **151** to afford the lactones (**152**). The Hauser annulation reactions of lactones (**152**) with **153** successfully afforded chartreusin analogues (**154**) which could be further converted to defucogilvocarcins M (**157**, 25% overall yield), V (**155**, 25% overall yield), and E (**156**, 22% overall yield) in three to five steps.

In 2019, Chi reported another annulation reaction of NHC-bound dienolates to form multisubstituted phenols with the simultaneous highly enantioselective installation of a remote all-carbon quaternary chiral center. This strategy was applied in the synthesis of BCDEF ring analogue of the natural antibiotic fredericamycin A with 87% yield and 99% ee (Figure 6.63) [228].

The NHC-bound α,β-unsaturated acyl azolium intermediates are also promising strategies for the construction of complex molecules. In 2019, Lupton reported the enantioselective synthesis of (−)-Δ^9-tetrahydrocannabinol ((−)-Δ^9 THC, **166**) with NHC catalysis (Figure 6.64) [229]. In this work, readily accessible cinnamate **163** (X = OH) was converted into acyl fluoride **164** (X = F), which then participated in the NHC-catalyzed annulation reaction with donor–acceptor cyclobutane **162**. This annulation reaction proceeded smoothly to give the cyclohexyl β-lactone **165** in 45% yield with a 98 : 2 er value as a single diastereoisomer. The target molecule (−)-Δ^9 THC (**166**) can be achieved in 10 steps with a good yield and stereoselectivity.

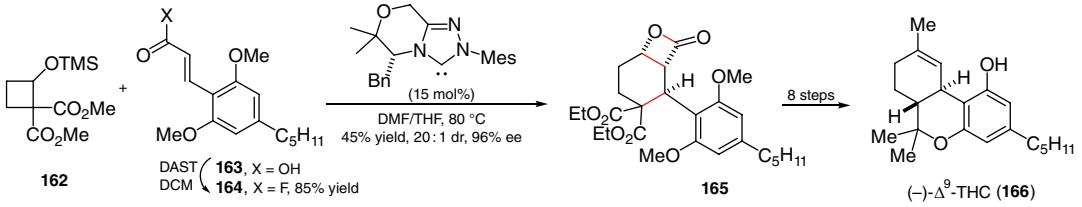

Figure 6.64. Total synthesis of (–)-**Δ**^{9}-tetrahydrocannabinol. Source: Based on [229].

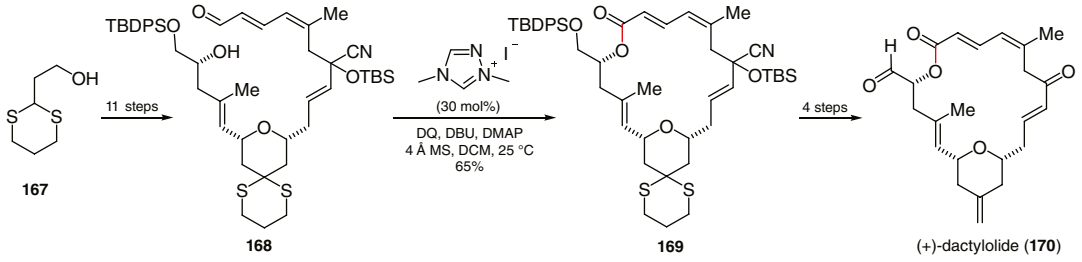

Figure 6.65. Total synthesis of (+)-dactylolide. Source: Based on [230].

The NHC-bound acyl azolium intermediates have already been used for the preparations of ketones, esters, and amides in the synthesis of various natural products. For example, in 2012, Hong applied the NHC-catalyzed oxidative esterification strategy in the late-stage macrolactonization to form the 20-membered macrocyclic core of (+)-Dactylolide (Figure 6.65) [230]. In this study, the aldehyde **168** was treated with triazolium-derived NHC catalyst in the presence of DBU, DMAP, and the oxidant (DQ). The desired macrolactone **169** was afforded in 65% yield without epimerization. After four more steps, compound **169** was converted to the Dactylolide (**170**) in 19 steps in 1.4% (1.9% brsm) yield.

The NHC-catalyzed oxidative esterification strategy has also been applied in the synthesis of other natural products, such as Davanone [231], Gelsemoxonine [189], Tanikolide [232], Cyanolide A [233], Clavosolide A [234], and Bryostatin 7.[235].

There have been other types of NHC-catalyzed reactions employed in natural product synthesis. For example, Lupton applied the NHC-catalyzed rearrangement of α,β-unsaturated enol esters in the total synthesis of (–)-7-Deoxyloganin [236], Suzuki utilized an NHC-catalyzed aroylation strategy to construct the tetracyclic framework in total synthesis of atroviridin [237], Coquerel employed a tandem secondary amine-catalyzed Michael addition/NHC (Brønsted base) catalyzed aldol annulation to form the carbocyclic core of (1*R*)-suberosanone [238]. The above examples demonstrate the utility of NHC catalysis in complex molecule synthesis.

6.7. SUMMARY AND OUTLOOK

The development of NHC catalysis in the last decade has tremendously expanded the scope of organocatalysis. A number of new activation and reaction modes were developed, with rich synthetic transformations and new mechanistic understanding established. In the coming decade, we expect to see an increase in applications of using NHC-catalyzed reactions as key steps in the construction of medicines, natural products, and other molecules. Unprecedented activation modes with NHCs as (key) catalysts, as well as deep and comprehensive understanding of these catalytic reactions, shall also emerge.

REFERENCES

1. (a) Bourissou, D.; Guerret, O.; Gabbaï, F. P.; Bertrand, G. *Chem. Rev.* **2000**, *100*, 39–92. (b) de Frémont, P.; Marion, N.; Nolan, S. P. *Coord. Chem. Rev.* **2009**, *253*, 862–892.
2. Hopkinson, M. N.; Richter, C.; Schedler, M.; Glorius, F. *Nature* **2014**, *510*, 485–496.
3. (a) Benhamou, L.; Chardon, E.; Lavigne, G.; Bellemin-Laponnaz, S.; César, V. *Chem. Rev.* **2011**, *111*, 2705–2733. (b) Flanigan, D. M.; Romanov-Michailidis, F.; White, N. A.; Rovis, T. *Chem. Rev.* **2015**, *115*, 9307–9387.
4. (a) Dröge, T.; Glorius, F. *Angew. Chem. Int. Ed.* **2010**, *49*, 6940–6952. (b) Kim, Y.-J.; Streitwieser, A. *J. Am. Chem. Soc.* **2002**, *124*, 5757–5761. (c) Washabaugh, M. W.; Jencks, W. P. *J. Am. Chem. Soc.* **1989**, *111*, 674–683.
5. (a) Chu, Y.; Deng, H.; Cheng, J.-P. *J. Org. Chem.* **2007**, *72*, 7790–7793. (b) Amyes, T. L.; Diver, S. T.; Richard, J. P.; Rivas, F. M.; Toth, K. *J. Am. Chem. Soc.* **2004**, *126*, 4366–4374.
6. (a) Massey, R. S.; Collett, C. J.; Lindsay, A. G.; Smith, A. D.; O'Donoghue, A. C. *J. Am. Chem. Soc.* **2012**, *134*, 20421–20432. (b) Higgins, E. M.; Sherwood, J. A.; Lindsay, A. G.; Armstrong, J.; Massey, R. S.; Alder, R. W.; O'Donoghue, A. C. *Chem. Commun.* **2011**, *47*, 1559–1561.
7. Maji, B.; Breugst, M.; Mayr, H. *Angew. Chem. Int. Ed.* **2011**, *50*, 6915–6919.
8. Ukai, T.; Tanaka, R.; Dokawa, T. J. *Pharm. Soc. Jpn* **1943**, *63*, 296–300.
9. Breslow, R. *J. Am. Chem. Soc.* **1958**, *80*, 3719–3726.
10. Sheehan, J. C.; Hunneman, D. H. *J. Am. Chem. Soc.* **1966**, *88*, 3666–3667.
11. Igau, A.; Grutzmacher, H.; Baceiredo, A.; Bertrand, G. *J. Am. Chem. Soc.* **1988**, *110*, 6463–6466.
12. Arduengo, A. J.; Harlow, R. L.; Kline, M. *J. Am. Chem. Soc.* **1991**, *113*, 361–363.
13. Enders, D.; Breuer, K.; Teles, J. H. *Helv. Chim. Acta* **1996**, *79*, 1217–1221.
14. (a) Hachisu, Y.; Bode, J. W.; Suzuki, K. *J. Am. Chem. Soc.* **2003**, *125*, 8432–8433. (b) Takikawa, H.; Hachisu, Y.; Bode, J. W.; Suzuki, K. *Angew. Chem. Int. Ed.* **2006**, *45*, 3492–3494. (c) Enders, D.; Niemeier, O.; Balensiefer, T. *Angew. Chem. Int. Ed.* **2006**, *45*, 1463–1467. (d) Li, Y.; Feng, Z.; You, S.-L. *Chem. Commun.* **2008**, 2263–2265. (e) Ema, T.; Oue, Y.; Akihara, K.; Miyazaki, Y.; Sakai, T. *Org. Lett.* **2009**, *11*, 4866–4869.
15. Chen, X.; Wang, H.; Jin, Z.; Chi, Y. R. *Chin. J. Chem.* **2020**, *38*, 1167–1202.
16. Yetra, S. R.; Patra, A.; Biju, A. T. *Synthesis* **2015**, *47*, 1357–1378.
17. (a) Sohn, S. S.; Rosen, E. L.; Bode, J. W. *J. Am. Chem. Soc.* **2004**, *126*, 14370–14371. (b) Burstein, C.; Glorius, F. *Angew. Chem. Int. Ed.* **2004**, *43*, 6205–6208.
18. (a) Burstein, C.; Tschan, S.; Xie, X.; Glorius, F. *Synthesis* **2006**, *2006*, 2418–2439. (b) Li, Y.; Zhao, Z.-A.; He, H.; You, S.-L. *Adv. Synth. Catal.* **2008**, *350*, 1885–1890. (c) Nair, V.; Vellalath, S.; Poonoth, M.; Mohan, R.; Suresh, E. *Org. Lett.* **2006**, *8*, 507–509. (d) Sun, L.-H.; Shen, L.-T.; Ye, S. *Chem. Commun.* **2011**, *47*, 10136–10138.
19. He, M.; Bode, J. W. *Org. Lett.* **2005**, *7*, 3131–3134.
20. (a) Chan, A.; Scheidt, K. A. *J. Am. Chem. Soc.* **2007**, *129*, 5334–5335. (b) Chan, A.; Scheidt, K. A. *J. Am. Chem. Soc.* **2008**, *130*, 2740–2741. (c) Rommel, M.; Fukuzumi, T.; Bode, J. W. *J. Am. Chem. Soc.* **2008**, *130*, 17266–17267. (d) Lv, H.; Tiwari, B.; Mo, J.; Xing, C.; Chi, Y. R. *Org. Lett.* **2012**, *14*, 5412–5415.
21. Nair, V.; Vellalath, S.; Poonoth, M.; Suresh, E. *J. Am. Chem. Soc.* **2006**, *128*, 8736–8737.
22. Chiang, P.-C.; Kaeobamrung, J.; Bode, J. W. *J. Am. Chem. Soc.* **2007**, *129*, 3520–3521.
23. Cohen, D. T.; Cardinal-David, B.; Scheidt, K. A. *Angew. Chem. Int. Ed.* **2011**, *50*, 1678–1682.
24. Guo, C.; Schedler, M.; Daniliuc, C. G.; Glorius, F. *Angew. Chem. Int. Ed.* **2014**, *53*, 10232–10236.
25. White, N. A.; DiRocco, D. A.; Rovis, T. *J. Am. Chem. Soc.* **2013**, *135*, 8504–8507.
26. (a) Nair, V.; Sinu, C. R.; Babu, B. P.; Varghese, V.; Jose, A.; Suresh, E. *Org. Lett.* **2009**, *11*, 5570–5573. (b) Maji, B.; Ji, L.; Wang, S.; Vedachalam, S.; Ganguly, R.; Liu, X.-W. *Angew. Chem. Int. Ed.* **2012**, *51*, 8276–8280.
27. He, M.; Struble, J. R.; Bode, J. W. *J. Am. Chem. Soc.* **2006**, *128*, 8418–8420.
28. Kaeobamrung, J.; Kozlowski, M. C.; Bode, J. W. *Proc. Natl. Acad. Sci. U.S.A.* **2010**, *107*, 20661–20665.
29. Zhao, Y.-M.; Cheung, M. S.; Lin, Z.; Sun, J. *Angew. Chem. Int. Ed.* **2012**, *51*, 10359–10363.
30. Xu, J.; Chen, X.; Wang, M.; Zheng, P.; Song, B.-A.; Chi, Y. R. *Angew. Chem. Int. Ed.* **2015**, *54*, 5161–5165.
31. Wu, Z.; Wang, X.; Li, F.; Wu, J.; Wang, J. *Org. Lett.* **2015**, *17*, 3588–3591.
32. De Sarkar, S.; Studer, A. *Angew. Chem. Int. Ed.* **2010**, *49*, 9266–9269.
33. Wanner, B.; Mahatthananchai, J.; Bode, J. W. *Org. Lett.* **2011**, *13*, 5378–5381.
34. Maki, B. E.; Chan, A.; Phillips, E. M.; Scheidt, K. A. *Org. Lett.* **2007**, *9*, 371–374.
35. De Sarkar, S.; Grimme, S.; Studer, A. *J. Am. Chem. Soc.* **2010**, *132*, 1190–1191.
36. Ryan, S. J.; Candish, L.; Lupton, D. W. *J. Am. Chem. Soc.* **2009**, *131*, 14176–14177.
37. (a) Reynolds, N. T.; Read de Alaniz, J.; Rovis, T. *J. Am. Chem. Soc.* **2004**, *126*, 9518–9519. (b) Reynolds, N. T.; Rovis, T. *J. Am. Chem. Soc.* **2005**, *127*, 16406–16407. (c) Vora, H. U.; Rovis, T. *J. Am. Chem. Soc.* **2010**, *132*, 2860–2861.
38. He, M.; Uc, G. J.; Bode, J. W. *J. Am. Chem. Soc.* **2006**, *128*, 15088–15089.
39. (a) Kawanaka, Y.; Phillips, E. M.; Scheidt, K. A. *J. Am. Chem. Soc.* **2009**, *131*, 18028–18029. (b) Phillips, E. M.; Wadamoto, M.; Roth, H. S.; Ott, A. W.; Scheidt, K. A. *Org. Lett.* **2009**, *11*, 105–108.
40. (a) Chow, K. Y.-K.; Bode, J. W. *J. Am. Chem. Soc.* **2004**, *126*, 8126–8127. (b) Bode, J. W.; Sohn, S. S. *J. Am. Chem. Soc.* **2007**, *129*, 13798–13799. (c) Vora, H. U.; Rovis, T. *J. Am. Chem. Soc.* **2007**, *129*, 13796–13797. (d) Li, G.-Q.; Li, Y.; Dai, L.-X.; You,

S.-L. *Org. Lett.* **2007**, *9*, 3519–3521. (e) Du, D.; Wang, Z. *Eur. J. Org. Chem.* **2008**, *2008*, 4949–4954. (f) Thai, K.; Wang, L.; Dudding, T.; Bilodeau, F.; Gravel, M. *Org. Lett.* **2010**, *12*, 5708–5711. (g) Wang, L.; Thai, K.; Gravel, M. *Org. Lett.* **2009**, *11*, 891–893.

41. Sun, F.-G.; Sun, L.-H.; Ye, S. *Adv. Synth. Catal.* **2011**, *353*, 3134–3138.
42. Ni, Q.; Zhang, H.; Grossmann, A.; Loh, C. C. J.; Merkens, C.; Enders, D. *Angew. Chem. Int. Ed.* **2013**, *52*, 13562–13566.
43. Hao, L.; Du, Y.; Lv, H.; Chen, X.; Jiang, H.; Shao, Y.; Chi, Y. R. *Org. Lett.* **2012**, *14*, 2154–2157.
44. (a) Hao, L.; Chen, S.; Xu, J.; Tiwari, B.; Fu, Z.; Li, T.; Lim, J.; Chi, Y. R. *Org. Lett.* **2013**, *15*, 4956–4959. (b) Chen, S.; Hao, L.; Zhang, Y.; Tiwari, B.; Chi, Y. R. *Org. Lett.* **2013**, *15*, 5822–5825.
45. Lee, A.; Younai, A.; Price, C. K.; Izquierdo, J.; Mishra, R. K.; Scheidt, K. A. *J. Am. Chem. Soc.* **2014**, *136*, 10589–10592.
46. (a) Cheng, J.; Huang, Z.; Chi, Y. R. *Angew. Chem. Int. Ed.* **2013**, *52*, 8592–8596. (b) Fu, Z.; Wu, X.; Chi, Y. R. *Org. Chem. Front.* **2016**, *3*, 145–149.
47. (a) Li, G.-T.; Gu, Q.; You, S.-L. *Chem. Sci.* **2015**, *6*, 4273–4278. (b) Wu, X.; Liu, B.; Zhang, Y.; Jeret, M.; Wang, H.; Zheng, P.; Yang, S.; Song, B.-A.; Chi, Y. R. *Angew. Chem. Int. Ed.* **2016**, *55*, 12280–12284.
48. Chen, X.-Y.; Gao, Z.-H.; Song, C.-Y.; Zhang, C.-L.; Wang, Z.-X.; Ye, S. *Angew. Chem. Int. Ed.* **2014**, *53*, 11611–11615.
49. (a) Zhang, Z.; Zeng, X.; Xie, D.; Chen, D.; Ding, L.; Wang, A.; Yang, L.; Zhong, G. *Org. Lett.* **2015**, *17*, 5052–5055. (b) Mou, C.; Wu, J.; Huang, Z.; Sun, J.; Jin, Z.; Chi, Y. R. *Chem. Commun.* **2017**, *53*, 13359–13362.
50. Xu, J.; Jin, Z.; Chi, Y. R. *Org. Lett.* **2013**, *15*, 5028–5031.
51. (a) Jia, W.-Q.; Zhang, H.-M.; Zhang, C.-L.; Gao, Z.-H.; Ye, S. *Org. Chem. Front.* **2016**, *3*, 77–81. (b) Fang, S.; Jin, S.; Ma, R.; Lu, T.; Du, D. *Org. Lett.* **2019**, *21*, 5211–5214. (c) Que, Y.; Xie, Y.; Li, T.; Yu, C.; Tu, S.; Yao, C. *Org. Lett.* **2015**, *17*, 6234–6237.
52. Fu, Z.; Xu, J.; Zhu, T.; Leong, W. W. Y.; Chi, Y. R. *Nat. Chem.* **2013**, *5*, 835–839.
53. (a) Fu, Z.; Jiang, K.; Zhu, T.; Torres, J.; Chi, Y. R. *Angew. Chem. Int. Ed.* **2014**, *53*, 6506–6510. (b) Xu, J.; Yuan, S.; Miao, M.; Chen, Z. *J. Org. Chem.* **2016**, *81*, 11454–11460.
54. Jin, Z.; Chen, S.; Wang, Y.; Zheng, P.; Yang, S.; Chi, Y. R. *Angew. Chem. Int. Ed.* **2014**, *53*, 13506–13509.
55. Zhang, Y.-R.; He, L.; Wu, X.; Shao, P.-L.; Ye, S. *Org. Lett.* **2008**, *10*, 277–280.
56. Duguet, N.; Campbell, C. D.; Slawin, A. M. Z.; Smith, A. D. *Org. Biomol. Chem.* **2008**, *6*, 1108–1113.
57. (a) He, L.; Lv, H.; Zhang, Y.-R.; Ye, S. *J. Org. Chem.* **2008**, *73*, 8101–8103. (b) Wang, X.-N.; Shao, P.-L.; Lv, H.; Ye, S. *Org. Lett.* **2009**, *11*, 4029–4031. (c) Wang, T.; Huang, X.-L.; Ye, S. *Org. Biomol. Chem.* **2010**, *8*, 5007–5011. (d) Huang, X.-L.; Chen, X.-Y.; Ye, S. *J. Org. Chem.* **2009**, *74*, 7585–7587. (e) Lv, H.; Zhang, Y.-R.; Huang, X.-L.; Ye, S. *Adv. Synth. Catal.* **2008**, *350*, 2715–2718. (f) Jian, T.-Y.; He, L.; Tang, C.; Ye, S. *Angew. Chem. Int. Ed.* **2011**, *50*, 9104–9107. (g) Wang, X.-N.; Shen, L.-T.; Ye, S. *Org. Lett.* **2011**, *13*, 6382–6385. (h) Zhang, Y.-R.; Lv, H.; Zhou, D.; Ye, S. *Chem. Eur. J.* **2008**, *14*, 8473–8476. (i) Lv, H.; You, L.; Ye, S. *Adv. Synth. Catal.* **2009**, *351*, 2822–2826. (j) Lv, H.; Chen, X.-Y.; Sun, L.-H.; Ye, S. *J. Org. Chem.* **2010**, *75*, 6973–6976. (k) Jian, T.-Y.; Chen, X.-Y.; Sun, L.-H.; Ye, S. *Org. Biomol. Chem.* **2013**, *11*, 158–163. (l) Jian, T.-Y.; Shao, P.-L.; Ye, S. *Chem. Commun.* **2011**, *47*, 2381–2383.
58. Shen, L.-T.; Shao, P.-L.; Ye, S. *Adv. Synth. Catal.* **2011**, *353*, 1943–1948.
59. (a) Shen, L.-T.; Sun, L.-H.; Ye, S. *J. Am. Chem. Soc.* **2011**, *133*, 15894–15897. (b) Shen, L.-T.; Jia, W.-Q.; Ye, S. *Angew. Chem. Int. Ed.* **2013**, *52*, 585–588.
60. Chen, D.-D.; Hou, X.-L.; Dai, L.-X. *J. Org. Chem.* **2008**, *73*, 5578–5581.
61. Jin, Z.; Xu, J.; Yang, S.; Song, B.-A.; Chi, Y. R. *Angew. Chem. Int. Ed.* **2013**, *52*, 12354–12358.
62. Fier, P. S.; Maloney, K. M. *J. Am. Chem. Soc.* **2019**, *141*, 1441–1445.
63. Simonovic, S.; Frison, J.-C.; Koyuncu, H.; Whitwood, A. C.; Douthwaite, R. E. *Org. Lett.* **2009**, *11*, 245–247.
64. DiRocco, D. A.; Oberg, K. M.; Rovis, T. *J. Am. Chem. Soc.* **2012**, *134*, 6143–6145.
65. Patra, A.; Mukherjee, S.; Das, T. K.; Jain, S.; Gonnade, R. G.; Biju, A. T. *Angew. Chem. Int. Ed.* **2017**, *56*, 2730–2734.
66. Harish, B.; Subbireddy, M.; Suresh, S. *Chem. Commun.* **2017**, *53*, 3338–3341.
67. (a) Patra, A.; Gelat, F.; Pannecoucke, X.; Poisson, T.; Besset, T.; Biju, A. T. *Org. Lett.* **2018**, *20*, 1086–1089. (b) Das, T. K.; Ghosh, A.; Balanna, K.; Behera, P.; Gonnade, R. G.; Marelli, U. K.; Das, A. K.; Biju, A. T. *ACS Catal.* **2019**, *9*, 4065–4071. (c) Patra, A.; James, A.; Das, T. K.; Biju, A. T. *J. Org. Chem.* **2018**, *83*, 14820–14826.
68. Wang, G.; Fu, Z.; Huang, W. *Org. Lett.* **2017**, *19*, 3362–3365.
69. Fernando, J. E. M.; Nakano, Y.; Zhang, C.; Lupton, D. W. *Angew. Chem. Int. Ed.* **2019**, *58*, 4007–4011.
70. Wang, G.; Zhang, Q.; Wei, C.; Zhang, Y.; Zhang, L.; Huang, J.; Wei, D.; Fu, Z.; Huang, W. *Angew. Chem. Int. Ed.* **2021**, *60*, 7913–7919.
71. Yang, X.; Xie, Y.; Xu, J.; Ren, S.; Mondal, B.; Zhou, L.; Tian, W.; Zhang, X.; Hao, L.; Jin, Z.; Chi, Y. R. *Angew. Chem. Int. Ed.* **2021**, *60*, 7906–7912.
72. Fischer, C.; Smith, S. W.; Powell, D. A.; Fu, G. C. *J. Am. Chem. Soc.* **2006**, *128*, 1472–1473.
73. (a) He, L.; Jian, T.-Y.; Ye, S. *J. Org. Chem.* **2007**, *72*, 7466–7468. (b) Chen, X.-Y.; Xia, F.; Ye, S. *Org. Biomol. Chem.* **2013**, *11*, 5722–5726.
74. Atienza, R. L.; Roth, H. S.; Scheidt, K. A. *Chem. Sci.* **2011**, *2*, 1772–1776.
75. Matsuoka, S.-I.; Ota, Y.; Washio, A.; Katada, A.; Ichioka, K.; Takagi, K.; Suzuki, M. *Org. Lett.* **2011**, *13*, 3722–3725.
76. Biju, A. T.; Padmanaban, M.; Wurz, N. E.; Glorius, F. *Angew. Chem. Int. Ed.* **2011**, *50*, 8412–8415.

77. (a) Scott, L.; Nakano, Y.; Zhang, C.; Lupton, D. W. *Angew. Chem. Int. Ed.* **2018**, *57*, 10299–10303; (b) Bae, S.; Zhang, C.; Gillard, R. M.; Lupton, D. W. *Angew. Chem. Int. Ed.* **2019**, *58*, 13370–13374.
78. Guin, J.; De Sarkar, S.; Grimme, S.; Studer, A. *Angew. Chem. Int. Ed.* **2008**, *47*, 8727–8730.
79. Du, Y.; Wang, Y.; Li, X.; Shao, Y.; Li, G.; Webster, R. D.; Chi, Y. R. *Org. Lett.* **2014**, *16*, 5678–5681.
80. (a) Li, B.-S.; Wang, Y.; Proctor, R. S. J.; Zhang, Y.; Webster, R. D.; Yang, S.; Song, B.; Chi, Y. R. *Nat. Commun.* **2016**, *7*, 12933. (b) Wang, Y.; Du, Y.; Huang, X.; Wu, X.; Zhang, Y.; Yang, S.; Chi, Y. R. *Org. Lett.* **2017**, *19*, 632–635.
81. White, N. A.; Rovis, T. *J. Am. Chem. Soc.* **2014**, *136*, 14674–14677.
82. Zhang, Y.; Du, Y.; Huang, Z.; Xu, J.; Wu, X.; Wang, Y.; Wang, M.; Yang, S.; Webster, R. D.; Chi, Y. R. *J. Am. Chem. Soc.* **2015**, *137*, 2416–2419.
83. White, N. A.; Rovis, T. *J. Am. Chem. Soc.* **2015**, *137*, 10112–10115.
84. Wang, H.; Wang, Y.; Chen, X.; Mou, C.; Yu, S.; Chai, H.; Jin, Z.; Chi, Y. R. *Org. Lett.* **2019**, *21*, 7440–7444.
85. Phan, J.; Ruser, S.-M.; Zeitler, K.; Rehbein, J. *Eur. J. Org. Chem.* **2019**, *2019*, 557–561.
86. Yang, W.; Hu, W.; Dong, X.; Li, X.; Sun, J. *Angew. Chem. Int. Ed.* **2016**, *55*, 15783–15786.
87. Wu, X.; Zhang, Y.; Wang, Y.; Ke, J.; Jeret, M.; Reddi, R. N.; Yang, S.; Song, B.-A.; Chi, Y. R. *Angew. Chem. Int. Ed.* **2017**, *56*, 2942–2946.
88. Ishii, T.; Kakeno, Y.; Nagao, K.; Ohmiya, H. *J. Am. Chem. Soc.* **2019**, *141*, 3854–3858.
89. Kim, I.; Im, H.; Lee, H.; Hong, S. *Chem. Sci.* **2020**, *11*, 3192–3197.
90. Ishii, T.; Ota, K.; Nagao, K.; Ohmiya, H. *J. Am. Chem. Soc.* **2019**, *141*, 14073–14077.
91. Li, J.-L.; Liu, Y.-Q.; Zou, W.-L.; Zeng, R.; Zhang, X.; Liu, Y.; Han, B.; He, Y.; Leng, H.-J.; Li, Q.-Z. *Angew. Chem. Int. Ed.* **2020**, *59*, 1863–1870.
92. Zhang, B.; Peng, Q.; Guo, D.; Wang, J. *Org. Lett.* **2020**, *22*, 443–447.
93. Ota, K.; Nagao, K.; Ohmiya, H. *Org. Lett.* **2020**, *22*, 3922–3925.
94. DiRocco, D. A.; Rovis, T. *J. Am. Chem. Soc.* **2012**, *134*, 8094–8097.
95. Dai, L.; Xia, Z.-H.; Gao, Y.-Y.; Gao, Z.-H.; Ye, S. *Angew. Chem. Int. Ed.* **2019**, *58*, 18124–18130.
96. Dai, L.; Ye, S. *Org. Lett.* **2020**, *22*, 986–990.
97. Xia, Z.-H.; Dai, L.; Gao, Z.-H.; Ye, S. *Chem. Commun.* **2020**, *56*, 1525–1528.
98. Davies, A. V.; Fitzpatrick, K. P.; Betori, R. C.; Scheidt, K. A. *Angew. Chem. Int. Ed.* **2020**, *59*, 9143–9148.
99. Liu, M.-S.; Shu, W. *ACS Catal.* **2020**, *10*, 12960–12966.
100. Mavroskoufis, A.; Rajes, K.; Golz, P.; Agrawal, A.; Ruß, V.; Götze, J. P.; Hopkinson, M. N. *Angew. Chem. Int. Ed.* **2020**, *59*, 3190–3194.
101. (a) Sheng, H.; Liu, Q.; Su, X.-D.; Lu, Y.; Wang, Z.-X.; Chen, X.-Y. *Org. Lett.* **2020**, *22*, 7187–7192. (b) Chen, K.-Q.; Wang, Z.-X.; Chen, X.-Y. *Org. Lett.* **2020**, *22*, 8059–8064.
102. Movassaghi, M.; Schmidt, M. A. *Org. Lett.* **2005**, *7*, 2453–2456.
103. Lai, C.-L.; Lee, H. M.; Hu, C.-H. *Tetrahedron Lett.* **2005**, *46*, 6265–6270.
104. Grasa, G. A.; Singh, R.; Scott, N. M.; Stevens, E. D.; Nolan, S. P. *Chem. Commun.* **2004**, 2890–2891.
105. Song, J. J.; Tan, Z.; Reeves, J. T.; Fandrick, D. R.; Yee, N. K.; Senanayake, C. H. *Org. Lett.* **2008**, *10*, 877–880.
106. Boddaert, T.; Coquerel, Y.; Rodriguez, J. *Adv. Synth. Catal.* **2009**, *351*, 1744–1748.
107. Kim, H.; Byeon, S. R.; Leed, M. G. D.; Hong, J. *Tetrahedron Lett.* **2011**, *52*, 2468–2470.
108. Boddaert, T.; Coquerel, Y.; Rodriguez, J. *Chem. Eur. J.* **2011**, *17*, 2266–2271.
109. Phillips, E. M.; Riedrich, M.; Scheidt, K. A. *J. Am. Chem. Soc.* **2010**, *132*, 13179–13181.
110. Chen, J.; Huang, Y. *Nat. Commun.* **2014**, *5*, 3437.
111. (a) Chen, J.; Meng, S.; Wang, L.; Tang, H.; Huang, Y. *Chem. Sci.* **2015**, *6*, 4184–4189. (b) Yuan, P.; Meng, S.; Chen, J.; Huang, Y. *Synlett* **2016**, *27*, 1068–1072.
112. Wang, L.; Chen, J.; Huang, Y. *Angew. Chem. Int. Ed.* **2015**, *54*, 15414–15418.
113. Kang, Q.; Zhang, Y. *Org. Biomol. Chem.* **2011**, *9*, 6715–6720.
114. Hans, M.; Delaude, L.; Rodriguez, J.; Coquerel, Y. *J. Org. Chem.* **2014**, *79*, 2758–2764.
115. Magano, J.; Dunetz, J. R. *Chem. Rev.* **2011**, *111*, 2177–2250.
116. Du, Z.; Shao, Z. *Chem. Soc. Rev.* **2013**, *42*, 1337–1378.
117. Nagao, K.; Ohmiya, H. *Top Curr Chem (Cham)* **2019**, *377*, 35.
118. Nemoto, T.; Fukuda, T.; Hamada, Y. *Tetrahedron Lett.* **2006**, *47*, 4365–4368.
119. Lebeuf, R.; Hirano, K.; Glorius, F. *Org. Lett.* **2008**, *10*, 4243–4246.
120. He, J.; Tang, S.; Tang, S.; Liu, J.; Sun, Y.; Pan, X.; She, X. *Tetrahedron Lett.* **2009**, *50*, 430–433.
121. Bai, Y.; Xiang, S.; Leow, M. L.; Liu, X.-W. *Chem. Commun.* **2014**, *50*, 6168–6170.
122. (a) Haruki, H.; Yasuda, S.; Nagao, K.; Ohmiya, H. *Chem. Eur. J.* **2019**, *25*, 724–727. (b) Ohnishi, N.; Yasuda, S.; Nagao, K.; Ohmiya, H. Asian J. *Org. Chem.* **2019**, *8*, 1133–1135.
123. Bai, Y.; Leng, W. L.; Li, Y.; Liu, X.-W. *Chem. Commun.* **2014**, *50*, 13391–13393.

124. Liu, K.; Hovey, M. T.; Scheidt, K. A. *Chem. Sci.* **2014**, *5*, 4026–4031.
125. (a) Yasuda, S.; Ishii, T.; Takemoto, S.; Haruki, H.; Ohmiya, H. *Angew. Chem. Int. Ed.* **2018**, *57*, 2938–2942. (b) Takemoto, S.; Ishii, T.; Yasuda, S.; Ohmiya, H. *Bull. Chem. Soc. Jpn.* **2019**, *92*, 937–940.
126. (a) Guo, C.; Fleige, M.; Janssen-Müller, D.; Daniliuc, C. G.; Glorius, F. *J. Am. Chem. Soc.* **2016**, *138*, 7840–7843. (b) Guo, C.; Janssen-Müller, D.; Fleige, M.; Lerchen, A.; Daniliuc, C. G.; Glorius, F. *J. Am. Chem. Soc.* **2017**, *139*, 4443–4451. (c) Singha, S.; Patra, T.; Daniliuc, C. G.; Glorius, F. *J. Am. Chem. Soc.* **2018**, *140*, 3551–3554.
127. Yang, W.; Ling, B.; Hu, B.; Yin, H.; Mao, J.; Walsh, P. J. *Angew. Chem. Int. Ed.* **2020**, *59*, 161–166.
128. Namitharan, K.; Zhu, T.; Cheng, J.; Zheng, P.; Li, X.; Yang, S.; Song, B.-A.; Chi, Y. R. *Nat. Commun.* **2014**, *5*, 3982.
129. Zhang, Z. J.; Zhang, L.; Geng, R. L.; Song, J.; Chen, X. H.; Gong, L. Z. *Angew. Chem. Int. Ed.* **2019**, *58*, 12190–12194.
130. Zhang, Z.-J.; Wen, Y.-H.; Song, J.; Gong, L.-Z. *Angew. Chem. Int. Ed.* **2021**, *60*, 3268–3276.
131. (a) Ma, S.; Yu, S.; Gu, Z. *Angew. Chem. Int. Ed.* **2006**, *45*, 200–203. (b) Alcaide, B.; Almendros, P. *Acc. Chem. Res.* **2014**, *47*, 939–952.
132. Adamo, M. F. A.; Bellini, G.; Suresh, S. *Tetrahedron* **2011**, *67*, 5784–5788.
133. Zhou, L. J.; Wu, X. X.; Yang, X.; Mou, C. L.; Song, R. J.; Yu, S. Y.; Chai, H. F.; Pan, L. T.; Jin, Z. C.; Chi, Y. R. *Angew. Chem. Int. Ed.* **2020**, *59*, 1557–1561.
134. (a) Takeuchi, R.; Kezuka, S. *Synthesis* **2006**, *2006*, 3349–3366. (b) Bower, J. F.; Krische, M. J., Formation of C-C Bonds via Iridium-Catalyzed Hydrogenation and Transfer Hydrogenation. In: *Iridium Catalysis*, Andersson, P. G., Ed. Springer, Berlin, Heidelberg. **2011**, *34*, 107–138. (c) Cheng, Q.; Tu, H.-F.; Zheng, C.; Qu, J.-P.; Helmchen, G.; You, S.-L. *Chem. Rev.* **2019**, *119*, 1855–1969.
135. (a) Meng, Q.-Y.; Döben, N.; Studer, A. *Angew. Chem. Int. Ed.* **2020**, *59*, 19956–19960. (b) Du, D.; Zhang, K.; Ma, R.; Chen, L.; Gao, J.; Lu, T.; Shi, Z.; Feng, J. *Org. Lett.* **2020**, *22*, 6370–6375.
136. Singha, S.; Serrano, E.; Mondal, S.; Daniliuc, C. G.; Glorius, F. *Nat. Catal.* **2020**, *3*, 48–54.
137. Zhao, J.; Mück-Lichtenfeld, C.; Studer, A. *Adv. Synth. Catal.* **2013**, *355*, 1098–1106.
138. (a) Axelsson, A.; Hammarvid, E.; Ta, L.; Sundén, H. *Chem. Commun.* **2016**, *52*, 11571–11574. (b) Wang, Q.; Chen, J.; Huang, Y. *Chem. Eur. J.* **2018**, *24*, 12806–12810.
139. Cardinal-David, B.; Raup, D. E. A.; Scheidt, K. A. *J. Am. Chem. Soc.* **2010**, *132*, 5345–5347.
140. (a) Raup, D. E.; Cardinal-David, B.; Holte, D.; Scheidt, K. A. *Nat. Chem.* **2010**, *2*, 766–771. (b) Dugal-Tessier, J.; O'Bryan, E. A.; Schroeder, T. B. H.; Cohen, D. T.; Scheidt, K. A. *Angew. Chem. Int. Ed.* **2012**, *51*, 4963–4967. (c) Murauski, K. J. R.; Walden, D. M.; Cheong, P. H.-Y.; Scheidt, K. A. *Adv. Synth. Catal.* **2017**, *359*, 3713–3719. (d) Wang, M. H.; Scheidt, K. A. *Angew. Chem. Int. Ed.* **2016**, *55*, 14912–14922.
141. (a) Bera, S.; Samanta, R. C.; Daniliuc, C. G.; Studer, A. *Angew. Chem. Int. Ed.* **2014**, *53*, 9622–9626. (b) Bera, S.; Daniliuc, C. G.; Studer, A. *Org. Lett.* **2015**, *17*, 4940–4943.
142. Mo, J.; Chen, X.; Chi, Y. R. *J. Am. Chem. Soc.* **2012**, *134*, 8810–8813.
143. Qi, J.; Xie, X.; Han, R.; Ma, D.; Yang, J.; She, X. *Chem. Eur. J.* **2013**, *19*, 4146–4150.
144. Zhao, C.; Guo, D.; Munkerup, K.; Huang, K.-W.; Li, F.; Wang, J. *Nat. Commun.* **2018**, *9*, 611.
145. Wang, Z.-Y.; Ding, Y.-L.; Wang, G.; Cheng, Y. *Chem. Commun.* **2016**, *52*, 788–791.
146. Phillips, E. M.; Wadamoto, M.; Chan, A.; Scheidt, K. A. *Angew. Chem. Int. Ed.* **2007**, *46*, 3107–3110.
147. Chen, Z.; Yu, X.; Wu, J. *Chem. Commun.* **2010**, *46*, 6356–6358.
148. Xiao, Z.; Yu, C.; Li, T.; Wang, X.-S.; Yao, C. *Org. Lett.* **2014**, *16*, 3632–3635.
149. Wang, Z.-Y.; Ding, Y.-L.; Li, S.-N.; Cheng, Y. *J. Org. Chem.* **2016**, *81*, 11871–11881.
150. (a) Chen, J.; Yuan, P.; Wang, L.; Huang, Y. *J. Am. Chem. Soc.* **2017**, *139*, 7045–7051. (b) Wang, L. M.; Wang, Q.; Chen, J. A.; Huang, Y. *Acta Chim. Sinica* **2018**, *76*, 850–856.
151. Xie, Y.; Wang, J. *Chem. Commun.* **2018**, *54*, 4597–4600.
152. Cao, J.; Sun, K.; Dong, S.; Lu, T.; Dong, Y.; Du, D. *Org. Lett.* **2017**, *19*, 6724–6727.
153. Liu, C.; Wu, S.; Xu, J.; Chen, L.; Zheng, P.; Chi, Y. R. *Org. Lett.* **2019**, *21*, 9493–9496.
154. He, C.; Li, Z.; Zhou, H.; Xu, J. *Org. Lett.* **2019**, *21*, 8022–8026.
155. Sharique, M.; Tambar, U. K. *Chem. Sci.* **2020**, *11*, 7239–7243.
156. Brand, J. P.; Siles, J. I. O.; Waser, J. *Synlett* **2010**, *2010*, 881–884.
157. Nawaz, F.; Zaghouani, M.; Bonne, D.; Chuzel, O.; Rodriguez, J.; Coquerel, Y. *Eur. J. Org. Chem.* **2013**, *2013*, 8253–8264.
158. Lee, A.; Scheidt, K. A. *Angew. Chem. Int. Ed.* **2014**, *53*, 7594–7598.
159. (a) Wang, M. H.; Cohen, D. T.; Schwamb, C. B.; Mishra, R. K.; Scheidt, K. A. *J. Am. Chem. Soc.* **2015**, *137*, 5891–5894. (b) Wang, M. H.; Barsoum, D.; Schwamb, C. B.; Cohen, D. T.; Goess, B. C.; Riedrich, M.; Chan, A.; Maki, B. E.; Mishra, R. K.; Scheidt, K. A. *J. Org. Chem.* **2017**, *82*, 4689–4702.
160. Zhuo, S.; Zhu, T.; Zhou, L.; Mou, C.; Chai, H.; Lu, Y.; Pan, L.; Jin, Z.; Chi, Y. R. *Angew. Chem. Int. Ed.* **2019**, *58*, 1784–1788.

161. Chen, X.; Song, R.; Liu, Y.; Ooi, C. Y.; Jin, Z.; Zhu, T.; Wang, H.; Hao, L.; Chi, Y. R. *Org. Lett.* **2017**, *19*, 5892–5895.
162. Cong, Z.-S.; Li, Y.-G.; Du, G.-F.; Gu, C.-Z.; Dai, B.; He, L. *Chem. Commun.* **2017**, *53*, 13129–13132.
163. Chen, D.-F.; Rovis, T. *Synthesis* **2017**, *49*, 293–298.
164. Peng, Q. P.; Li, S. J.; Zhang, B.; Guo, D. H.; Lan, Y.; Wang, J. *Commun. Chem.* **2020**, *3*, 177.
165. Youn, S. W.; Song, H. S.; Park, J. H. *Org. Lett.* **2014**, *16*, 1028–1031.
166. Wu, X.; Zhou, L.; Maiti, R.; Mou, C.; Pan, L.; Chi, Y. R. *Angew. Chem. Int. Ed.* **2019**, *58*, 477–481.
167. (a) Liu, B.; Wang, W.; Huang, R.; Yan, J.; Wu, J.; Xue, W.; Yang, S.; Jin, Z.; Chi, Y. R. *Org. Lett.* **2018**, *20*, 260–263. (b) Liu, B.; Luo, G.; Wang, H.; Hao, L.; Yang, S.; Jin, Z.; Chi, Y. R. *Chem. Eur. J.* **2019**, *25*, 12719–12723.
168. (a) Wang, Z.; Pan, D.; Li, T.; Jin, Z. *Chem. Asian J.* **2018**, *13*, 2149–2163. (b) Biju, A. T.; Lu, S.; Poh, S. B.; Ong, J. Y.; Zhao, Y., NHC-Catalyzed Kinetic Resolution, Desymmetrization, and DKR Strategies. In: *N-Heterocyclic Carbenes in Organocatalysis*, Biju, A. T., Ed.; Wiley VCH, **2018**, 287–308.
169. Suzuki, Y.; Yamauchi, K.; Muramatsu, K.; Sato, M. *Chem. Commun.* **2004**, 2770–2771.
170. (a) Lu, S.; Poh, S. B.; Siau, W.-Y.; Zhao, Y. *Angew. Chem. Int. Ed.* **2013**, *52*, 1731–1734. (b) Lu, S.; Poh, S. B.; Siau, W.-Y.; Zhao, Y. *Synlett* **2013**, *24*, 1165–1169.
171. Kano, T.; Sasaki, K.; Maruoka, K. *Org. Lett.* **2005**, *7*, 1347–1349.
172. De Sarkar, S.; Biswas, A.; Song, C. H.; Studer, A. *Synthesis* **2011**, *2011*, 1974–1983.
173. Iwahana, S.; Iida, H.; Yashima, E. *Chem. Eur. J.* **2011**, *17*, 8009–8013.
174. Kuwano, S.; Harada, S.; Kang, B.; Oriez, R.; Yamaoka, Y.; Takasu, K.; Yamada, K.-I. *J. Am. Chem. Soc.* **2013**, *135*, 11485–11488.
175. Lu, S.; Poh, S. B.; Zhao, Y. *Angew. Chem. Int. Ed.* **2014**, *53*, 11041–11045.
176. Maji, R.; Wheeler, S. E. *J. Am. Chem. Soc.* **2017**, *139*, 12441–12449.
177. Binanzer, M.; Hsieh, S.-Y.; Bode, J. W. *J. Am. Chem. Soc.* **2011**, *133*, 19698–19701.
178. Wang, M.; Huang, Z.; Xu, J.; Chi, Y. R. *J. Am. Chem. Soc.* **2014**, *136*, 1214–1217.
179. Dong, S.; Frings, M.; Cheng, H.; Wen, J.; Zhang, D.; Raabe, G.; Bolm, C. *J. Am. Chem. Soc.* **2016**, *138*, 2166–2169.
180. Li, G.-Q.; Li, Y.; Dai, L.-X.; You, S.-L. *Adv. Synth. Catal.* **2008**, *350*, 1258–1262.
181. Chen, K.-Q.; Gao, Z.-H.; Ye, S. *Angew. Chem. Int. Ed.* **2019**, *58*, 1183–1187.
182. (a) Caddick, S.; Jenkins, K. *Chem. Soc. Rev.* **1996**, *25*, 447–456. (b) Stürmer, R. *Angew. Chem. Int. Ed.* **1997**, *36*, 1173–1174. (c) Huerta, F. F.; Minidis, A. B. E.; Bäckvall, J.-E. *Chem. Soc. Rev.* **2001**, *30*, 321–331.
183. Cohen, D. T.; Eichman, C. C.; Phillips, E. M.; Zarefsky, E. R.; Scheidt, K. A. *Angew. Chem. Int. Ed.* **2012**, *51*, 7309–7313.
184. Goodman, C. G.; Johnson, J. S. *J. Am. Chem. Soc.* **2014**, *136*, 14698–14701.
185. Mondal, S.; Mukherjee, S.; Das, T. K.; Gonnade, R.; Biju, A. T. *ACS Catal.* **2017**, *7*, 3995–3999.
186. Goodman, C. G.; Walker, M. M.; Johnson, J. S. *J. Am. Chem. Soc.* **2015**, *137*, 122–125.
187. Wu, Z.; Li, F.; Wang, J. *Angew. Chem. Int. Ed.* **2015**, *54*, 1629–1633.
188. Chen, X.; Fong, J. Z. M.; Xu, J.; Mou, C.; Lu, Y.; Yang, S.; Song, B.-A.; Chi, Y. R. *J. Am. Chem. Soc.* **2016**, *138*, 7212–7215.
189. Zhao, C.; Li, F.; Wang, J. *Angew. Chem. Int. Ed.* **2016**, *55*, 1820–1824.
190. Li, B.-S.; Wang, Y.; Proctor, R. S. J.; Jin, Z.; Chi, Y. R. *Chem. Commun.* **2016**, *52*, 8313–8316.
191. Wu, Z.; Wang, J. *ACS Catal.* **2017**, *7*, 7647–7652.
192. Huang, Z.; Huang, X.; Li, B.; Mou, C.; Yang, S.; Song, B.-A.; Chi, Y. R. *J. Am. Chem. Soc.* **2016**, *138*, 7524–7527.
193. Yang, G.; Guo, D.; Meng, D.; Wang, J. *Nat. Commun.* **2019**, *10*, 3062.
194. Lu, S.; Song, X.; Poh, S. B.; Yang, H.; Wong, M. W.; Zhao, Y. *Chem. Eur. J.* **2017**, *23*, 2275–2281.
195. Li, S.; Liu, B.; Chen, L.; Li, X.; Cheng, J.-P. *Org. Chem. Front.* **2018**, *5*, 1101–1107.
196. Liu, Q.; Rovis, T. *J. Am. Chem. Soc.* **2006**, *128*, 2552–2553.
197. Ema, T.; Akihara, K.; Obayashi, R.; Sakai, T. *Adv. Synth. Catal.* **2012**, *354*, 3283–3290.
198. Li, Y.; Yang, S.; Wen, G.; Lin, Q.; Zhang, G.; Qiu, L.; Zhang, X.; Du, G.; Fang, X. *J. Org. Chem.* **2016**, *81*, 2763–2769.
199. (a) Jia, M.-Q.; You, S.-L. *Chem. Commun.* **2012**, *48*, 6363–6365. (b) Jia, M.-Q.; You, S.-L. *Synlett* **2013**, *24*, 1201–1204.
200. Lin, Q.; Li, Y.; Das, D. K.; Zhang, G.; Zhao, Z.; Yang, S.; Fang, X. *Chem. Commun.* **2016**, *52*, 6459–6462.
201. Wadamoto, M.; Phillips, E. M.; Reynolds, T. E.; Scheidt, K. A. *J. Am. Chem. Soc.* **2007**, *129*, 10098–10099.
202. Takada, A.; Hashimoto, Y.; Takikawa, H.; Hikita, K.; Suzuki, K. *Angew. Chem. Int. Ed.* **2011**, *50*, 2297–2301.
203. Mennen, S. M.; Miller, S. J. *J. Org. Chem.* **2007**, *72*, 5260–5269.
204. Takikawa, H.; Suzuki, K. *Org. Lett.* **2007**, *9*, 2713–2716.
205. Koyama, Y.; Yamaguchi, R.; Suzuki, K. *Angew. Chem. Int. Ed.* **2008**, *47*, 1084–1087.
206. Nicolaou, K. C.; Li, H.; Nold, A. L.; Pappo, D.; Lenzen, A. *J. Am. Chem. Soc.* **2007**, *129*, 10356–10357.
207. Nicolaou, K. C.; Nold, A. L.; Li, H. *Angew. Chem. Int. Ed.* **2009**, *48*, 5860–5863.
208. Takikawa, H.; Ishikawa, Y.; Yoshinaga, Y.; Hashimoto, Y.; Kusumi, T.; Suzuki, K. *Bull. Chem. Soc. Jpn.* **2016**, *89*, 941–954.

209. Kang, B.; Sutou, T.; Wang, Y.; Kuwano, S.; Yamaoka, Y.; Takasu, K.; Yamada, K.-I. *Adv. Synth. Catal.* **2015**, *357*, 131–147.
210. Lu, H.-H.; Pronin, S. V.; Antonova-Koch, Y.; Meister, S.; Winzeler, E. A.; Shenvi, R. A. *J. Am. Chem. Soc.* **2016**, *138*, 7268–7271.
211. Nicolaou, K. C.; Tang, Y.; Wang, J. *Chem. Commun.* **2007**, 1922–1923.
212. Nicolaou, K. C.; Li, A.; Edmonds, D. J. *Angew. Chem. Int. Ed.* **2006**, *45*, 7086–7090.
213. Trost, B. M.; Shuey, C. D.; DiNinno, F. *J. Am. Chem. Soc.* **1979**, *101*, 1284–1285.
214. Stetter, H. *Angew. Chem. Int. Ed.* **1976**, *15*, 639–647.
215. Baumann, K. L.; Butler, D. E.; Deering, C. F.; Mennen, K. E.; Millar, A.; Nanninga, T. N.; Palmer, C. W.; Roth, B. D. *Tetrahedron Lett.* **1992**, *33*, 2283–2284.
216. Galopin, C. C. *Tetrahedron Lett.* **2001**, *42*, 5589–5591.
217. Randl, S.; Blechert, S. *J. Org. Chem.* **2003**, *68*, 8879–8882.
218. Anjaiah, S.; Chandrasekhar, S.; Grée, R. *Adv. Synth. Catal.* **2004**, *346*, 1329–1334.
219. Xu, J.; Caro-Diaz, E. J. E.; Theodorakis, E. A. *Org. Lett.* **2010**, *12*, 3708–3711.
220. Sommerwerk, S.; Kern, S.; Heller, L.; Csuk, R. *Tetrahedron Lett.* **2014**, *55*, 6243–6244.
221. Miller, E. R.; Hovey, M. T.; Scheidt, K. A. *J. Am. Chem. Soc.* **2020**, *142*, 2187–2192.
222. Struble, J. R.; Bode, J. W. *Tetrahedron* **2009**, *65*, 4957–4967.
223. Phillips, E. M.; Roberts, J. M.; Scheidt, K. A. *Org. Lett.* **2010**, *12*, 2830–2833.
224. He, M.; Rommel, M.; Bode, J. W. *Heterocycles* **2012**, *86*, 1689–1696.
225. White, N. A.; Ozboya, K. E.; Flanigan, D. M.; Rovis, T. Asian J. *Org. Chem.* **2014**, *3*, 442–444.
226. ElSohly, A. M.; Wespe, D. A.; Poore, T. J.; Snyder, S. A. *Angew. Chem. Int. Ed.* **2013**, *52*, 5789–5794.
227. Huang, X.; Zhu, T.; Huang, Z.; Zhang, Y.; Jin, Z.; Zanoni, G.; Chi, Y. R. *Org. Lett.* **2017**, *19*, 6188–6191.
228. Zhu, T.; Liu, Y.; Smetankova, M.; Zhuo, S.; Mou, C.; Chai, H.; Jin, Z.; Chi, Y. R. *Angew. Chem. Int. Ed.* **2019**, *58*, 15778–15782.
229. Ametovski, A.; Lupton, D. W. *Org. Lett.* **2019**, *21*, 1212–1215.
230. Lee, K.; Kim, H.; Hong, J. *Angew. Chem. Int. Ed.* **2012**, *51*, 5735–5738.
231. Morrison, K. C.; Litz, J. P.; Scherpelz, K. P.; Dossa, P. D.; Vosburg, D. A. *Org. Lett.* **2009**, *11*, 2217–2218.
232. Nambu, H.; Jinnouchi, H.; Fujiwara, T.; Yakura, T. *Synlett* **2016**, *27*, 1106–1009.
233. Kim, H.; Hong, J. *Org. Lett.* **2010**, *12*, 2880–2883.
234. Baker, J. B.; Kim, H.; Hong, J. *Tetrahedron Lett.* **2015**, *56*, 3120–3122.
235. Lu, Y.; Woo, S. K.; Krische, M. J. *J. Am. Chem. Soc.* **2011**, *133*, 13876–13879.
236. Candish, L.; Lupton, D. W. *Org. Lett.* **2010**, *12*, 4836–4839.
237. Suzuki, Y.; Fukuta, Y.; Ota, S.; Kamiya, M.; Sato, M. *J. Org. Chem.* **2011**, *76*, 3960–3967.
238. Ren, Y.; Presset, M.; Godemert, J.; Vanthuyne, N.; Naubron, J.-V.; Giorgi, M.; Rodriguez, J.; Coquerel, Y. *Chem. Commun.* **2016**, *52*, 6565–6568.

7

ASYMMETRIC HYPERVALENT IODINE CATALYSIS

Muhammet Uyanik and Kazuaki Ishihara
Graduate School of Engineering, Nagoya University, Nagoya, Japan

7.1. INTRODUCTION

Over the past three decades, hypervalent organoiodines (III and V) have attracted great attention due to their mild and chemoselective oxidizing properties and environmentally benign characteristics in contrast to heavy metal-based oxidants [1]. In particular, the reactivities of organoiodines(III) resemble those of Hg(II), Tl(III), and Pb(IV). On the other hand, the development of chiral hypervalent iodine-mediated enantioselective oxidative reactions is one of the most challenging areas in asymmetric synthesis (Scheme 7.1) [2–13]. In 1986, Imamoto and colleagues reported the first example of the chiral hypervalent iodine-mediated enantioselective oxidation reactions [14]. The asymmetric oxidation of sulfides gave sulfoxides with moderate enantioselectivities by using oligomeric chiral iodine(III) species **1**, which was proposed by Koser later [15], generated from iodosobenzene (PhIO) and tartaric anhydride derivatives. After these seminal contributions, a variety of chiral organoiodine(III) reagents **2**–**11** for oxidation of sulfides [16–18], oxidative difunctionalization of alkenes [19–42], oxidative α-functionalization of carbonyls [21, 42–47], and oxidative dearomative cyclization of arenols [48], as well as chiral organoiodine(V) reagents **12**–**18** for oxidation of sulfides [49], oxidative desymmetrization of vicinal diols [50], and hydroxylation of phenols [51–56] were developed (Scheme 7.1).

However, in general, the use of hypervalent iodines as stoichiometric oxidants has been limited because some of them are shock-sensitive or explosive, and/or show poor solubility in organic solvents. Therefore, the catalytic use of hypervalent iodine is strongly demanded from both economic and environmental perspectives [1]. The first catalytic use of both hypervalent organoiodine(III) and organoiodine(V) compounds using chemical oxidants was reported in 2005 [57–59]. In these reactions, iodine(III) or iodine(V) catalytic active species can be generated in situ from the oxidation of the corresponding iodoarenes with suitable stoichiometric oxidants such as *meta*-chloroperbenzoic acid (*m*-CPBA) or oxone (a triple salt, $2KSO_5 \cdot KHSO_4 \cdot K_2SO_4$), respectively (Scheme 7.2) [60–63]. On the other hand, the first chiral hypervalent iodine-catalyzed enantioselective oxidative coupling reaction

Catalytic Asymmetric Synthesis, Fourth Edition. Edited by Takahiko Akiyama and Iwao Ojima.

chiral organoiodines(III)

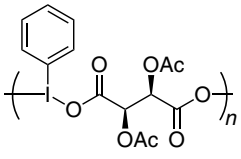

1
Imamoto, **1986** [14]
Koser, **1992** [15]

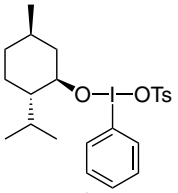

2
Koser, **1990** [16]

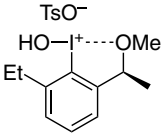

3
Wirth, **1997**, **2001**
[19, 21]

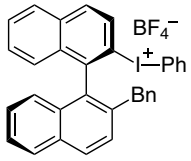

4
Ochiai, **1999** [43]

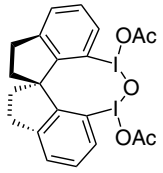

5
Kita, **2008** [48]

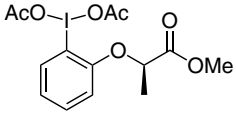

6
Fujita, **2007** [22]

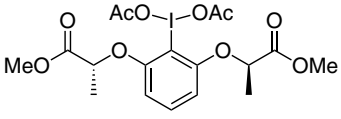

7
Fujita, **2010** [24]

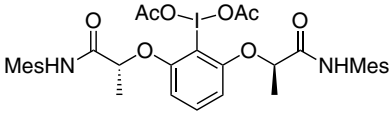

8
Wirth, **2012** [28]

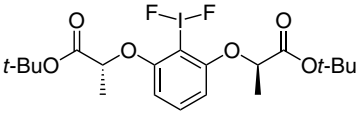

9
Nevado, **2013** [31]

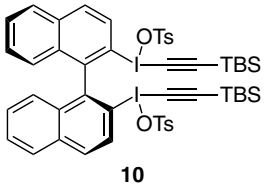

10
Pouységu, Quideau, **2017** [46]

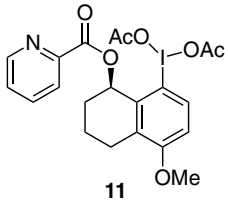

11
Wirth, **2019** [42]

chiral organoiodines(V)

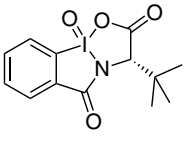

12
Zhdankin, **2000** [49]

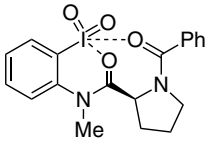

13
Zhdankin, **2006** [50]

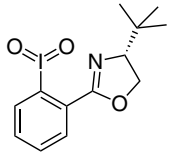

14
Birman, **2009** [51]

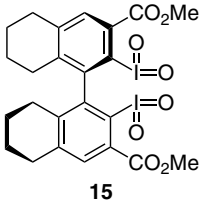

15
Pouységu, Quideau, **2014** [52]

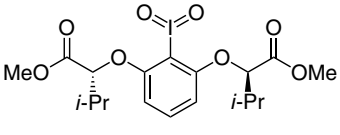

16
Yoshida, **2016** [54]

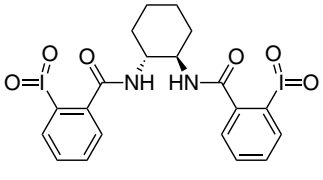

17
Pouységu, Quideau, **2016** [53]

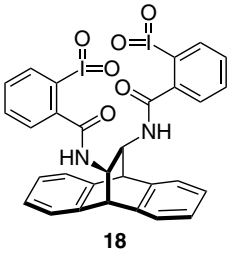

18
Pouységu, Quideau, **2017** [55]

Scheme 7.1. Chiral organoiodine(III and V) reagents.

was reported in 2007 [64]. Since these breakthroughs, rapid progress has been made in the development of enantioselective hypervalent iodine catalysis [2–13]. In the following, we describe the chiral hypervalent iodine-catalyzed enantioselective oxidative coupling reactions in three main topics: oxidative dearomative coupling of arenols, oxidative α-functionalization of carbonyls, and oxidative difunctionalization of alkenes.

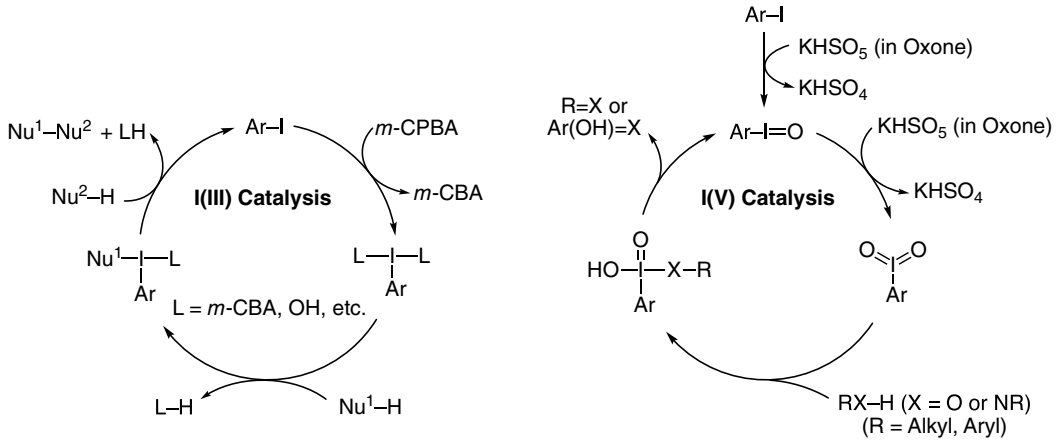

Scheme 7.2. General catalytic cycles of organoiodine(III/I and V/III) catalysis.

7.2. OXIDATIVE DEAROMATIVE COUPLING OF ARENOLS

Oxidative dearomatization of 2- or 4-substituted phenols in the presence of suitable nucleophiles affords the corresponding cyclohexa-2,4- or 2,5-dienones, respectively. Various *O*- or *N*- or *C*-based nucleophiles could be used in either an inter- or intramolecular fashion [65]. In this event, the planar achiral substrates can be transformed into chiral three-dimensional structures through sp^2-to-sp^3 geometry change on one of the sp^2-hybridized carbon centers. The diastereo- or enantioselective control of this process is highly challenging and has attracted substantial attention in recent years [66–69].

The enantioselective oxidative dearomative coupling of arenols is an useful strategy for the synthesis of various biologically active compounds [65]. The development of enantioselective oxidative dearomatization using chiral hypervalent iodine compounds is one of the most challenging areas in asymmetric organocatalysis [70, 71]. Especially, several researchers pointed out that it may be quite difficult to induce asymmetry via a chiral hypervalent iodine reagent because of the exclusive formation of phenoxenium ion via the dissociation of a chiral organoiodine fragment during the reaction (Scheme 7.3) [70–73]. Additionally, one might expect that asymmetric induction would be challenging even for associative pathways due to free rotation of C–O and I–O bonds in the intermediates and transition states.

In 2008, Kita and colleagues overcame these difficulties for the first time [48]. Kita's group succeeded in the first enantioselective oxidative dearomatization of 1-naphthols (oxidative spirolactonization, which was developed originally by Wood [74]). By using chiral μ-oxo-bridged-hypervalent iodine(III) reagent **5**, which has a conformationally rigid 1,1-spirobiindane backbone, the corresponding spirolactones were obtained with high enantioselectivities up to 86% ee as highest enantioselectivity at that time (Scheme 7.4) [48]. The chiral iodine(I) **19**, the reduced form of **5**, could be recovered after the reaction by silica-gel chromatography. Furthermore, the catalytic use of **19** (30 mol% based on iodine) could be achieved in the presence of *m*-CPBA and acetic acid; however, the enantioselectivity was reduced to 69% ee. The enantioselectivity of the products was highly dependent on the solvent polarities under their reaction conditions. A high level of enantioselectivities was observed in halogenated solvents such as chloroform and dichloromethane. In contrast, racemic products were obtained in 1,1,1,3,3,3-hexafluoro-2-propanol (HFIP) as a solvent. Moreover, the oxidation of 4-methoxy-susbtituted 1-naphthol gave the racemic product. These results might be explained by the stabilization of the phenoxenium ion (a dissociative intermediate, see Scheme 7.3) by polarizable solvents such as HFIP or resonance donation of methoxy group.

In order to improve the enantioselectivity, especially for the catalytic conditions, Kita and colleagues designed a new series of *ortho*-functionalized spirobiindane catalysts [75]. By using chiral iodine **20**, the

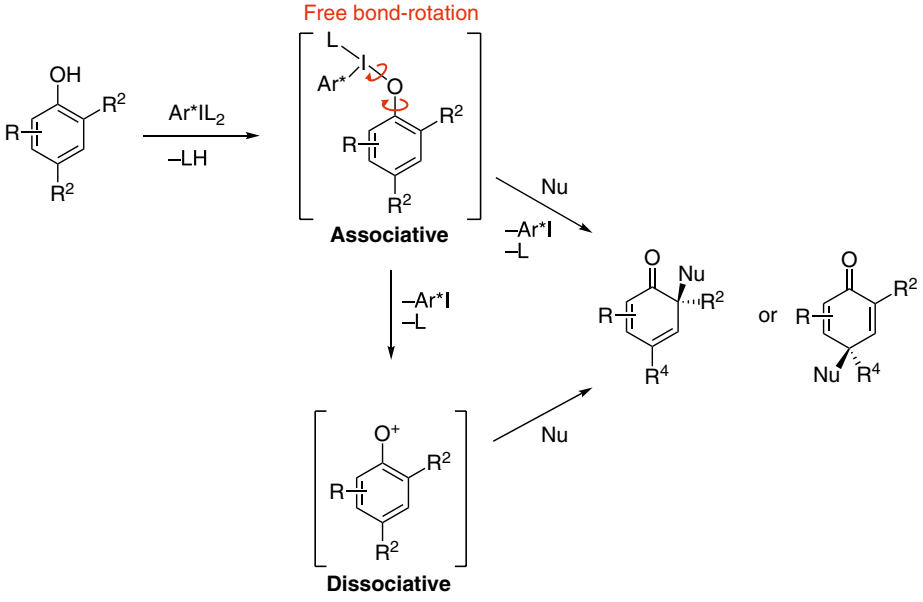

Scheme 7.3. Challenges in the hypervalent iodine-mediated enantioselective oxidative dearomative coupling of arenols. Source: Based on [70–73].

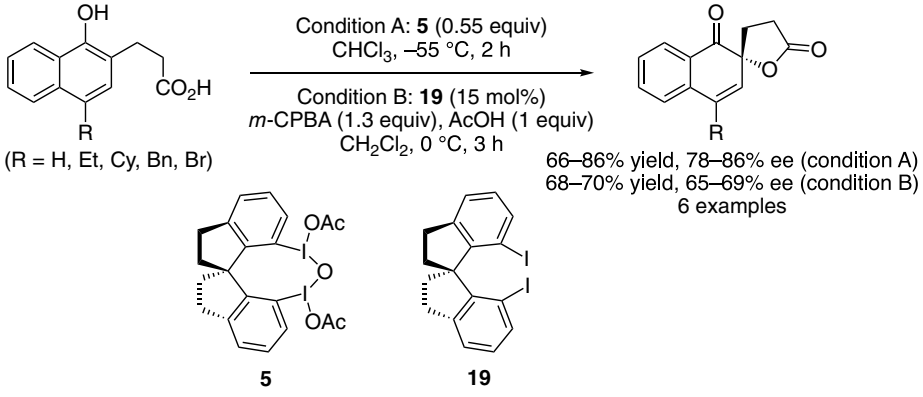

Scheme 7.4. The first enantioselective dearomatization of 1-naphthols using conformationally rigid chiral organoiodines. Source: [48].

enantioselectivity of spirolactones was up to 92% ee (Scheme 7.5). μ-Oxo-bridged-iodine(III) species **21** could be generated in situ from the oxidation of **20** with *m*-CPBA in the presence of acetic acid. Theoretical calculations performed by Houk, Xue, and colleagues revealed that proton transfer from the pendant carboxylic acid of 1-naphthol to the bridging oxygen atom or the ligand of iodine(III) is crucial for the dearomative cyclization by improving both the nucleophilicity of the carboxylate and the nucleofugality of the iodine(III) in intermediates **22** and **24** [76]. In addition, halogen bonding interaction between the resulting carboxylate and the electron-deficient iodine(III) center further stabilizes the intermediates and transition states. Interestingly, although the two iodine(III) centers are both capable of the oxidative dearomative cyclization of 1-naphthols, half-reduced iodine(III) **23** was found to be more reactive but less selective than the μ-oxo-bridged bis-iodine(III) **21**. Therefore, the coexistence of two sequential dearomative cyclization processes in the reaction system may result in lower enantioselectivity.

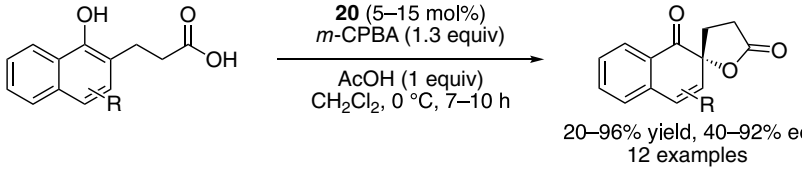

Proposed mechanism based on theoretical calculations:

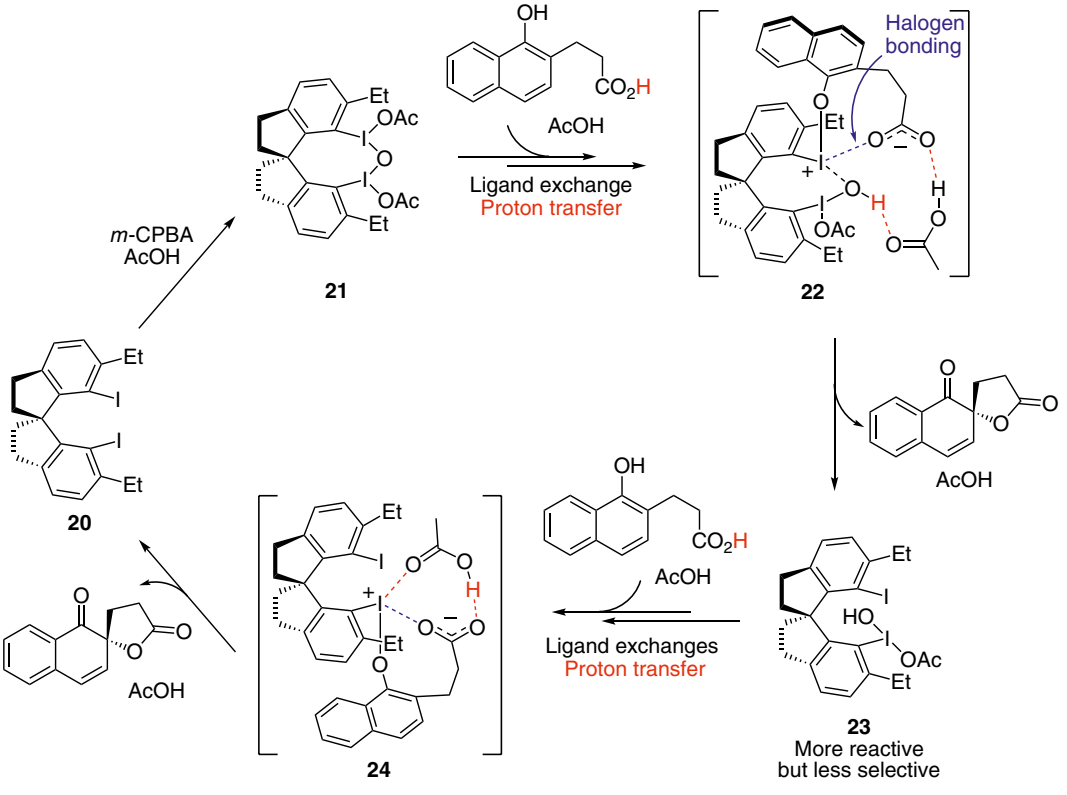

Scheme 7.5. Kita's modified spirobiindane-derived catalyst **20** for highly enantioselective spirolactonization of 1-naphthols. Source: [75, 76].

In sharp contrast to Kita's conformationally rigid design, Ishihara, Uyanik, and colleagues demonstrated the rational design of conformationally flexible hypervalent organoiodines as chiral catalysts based on secondary nonbonding interactions (i.e., intramolecular hydrogen-bonding interactions, etc.) [77]. In 2010, they designed conformationally flexible C_2-symmetric chiral iodoarenes **25** consisting of three units, including an iodoaryl moiety (**A**), chiral linkers (**B**), and subfunctional groups (**C**) (Scheme 7.6). These units could be easily combined to give a wide variety of chiral iodoarenes **25**. Notably, the hypervalent iodines(III) **26** generated in situ from iodoarenes **25** were expected to exhibit intramolecular hydrogen-bonding interactions between the acidic hydrogen of **C** (N*H*Ar) and the ligand (L, such as an acyloxy group, alkoxy group, hydroxy group, etc.) of iodine(III) (**26-I**). Alternatively, intramolecular n–σ* interactions between the electron-deficient iodine(III) center (σ^*_{C-I} orbital) of **A** and the Lewis-basic group of **C** (lone pair n), such as carbonyl groups, might also be generated (**26-II**). Thus, a suitable chiral environment could be constructed around the iodine(III) center of **26** via such non-covalent bonding intramolecular interactions. The Ishihara–Uyanik group used lactate into a chiral linker for their first-generation catalyst design. Notably, in 2007, Fujita and colleagues first introduced lactate as a chiral source for their C_1-symmetric chiral iodines(III) (Scheme 1) [22].

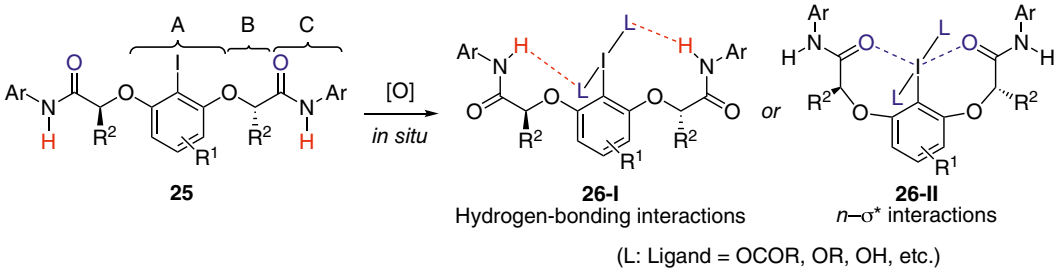

Scheme 7.6. Design of conformationally flexible first-generation chiral organoiodines. Source: [77].

By using chiral iodine **25a** in the presence of *m*-CPBA, oxidative dearomative cyclization of various 1-napthols afforded the corresponding spirolactones in higher enantioselectivity than that of structurally rigid catalysts **19** and **20** (Scheme 7.7) [77, 78]. In addition, notably, in contrast to Kita's results [48, 75], high enantioselectivities were observed regardless of the polarity of the solvent under these conditions.

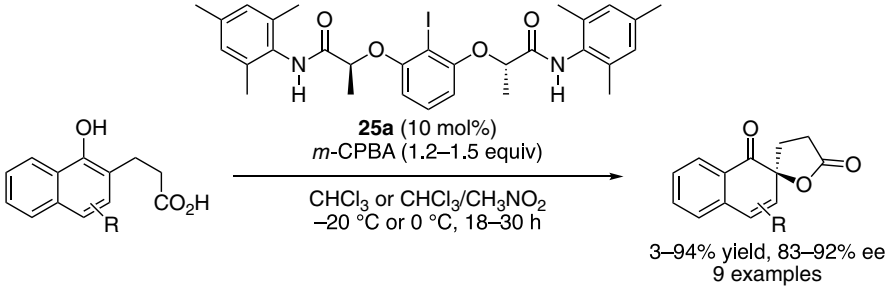

Scheme 7.7. Lactate-derived bis-*sec*-amide **25a**-catalyzed highly enantioselective spirolactonization of 1-naphthols. Source: [77, 78].

However, lactate-derived catalysts **25** were found to be insufficient for the oxidation of phenols, which were less reactive than 1-naphthols, with respect to not only reactivity but also enantioselectivity. To overcome these limitations, Ishihara, Uyanik, and colleagues designed new chiral organoiodines **27**, second-generation catalysts, derived from 2-aminoalcohol instead of lactate as a chiral source (Scheme 7.8) [79]. Because both **25** and **27** consist of 2-iodoresorcinol (**A**) and secondary amide (**C**) units, the acidic hydrogens are the same distance from the iodine center. On the other hand, because sp^2-hybridized carbonyl groups are moved to the outer sides, second-generation catalysts **27** would be much more conformationally flexible. Moreover, **27** would be stereochemically much more stable than **25** for the same reason that the stereocenters are far from the carbonyl groups.

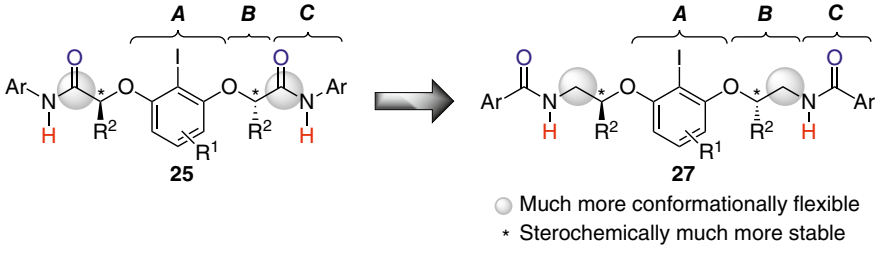

Scheme 7.8. Design of 2-aminoalcohol-derived organoiodines as conformationally flexible second-generation catalysts. Source: [79].

A catalyst loading of 1 to 10 mol% of second-generation catalyst **27a** for the enantioselective oxidative dearomative spirolactonization of a variety of phenols was enough to give the desired spirolactones with excellent enantioselectivities up to 99% ee (Scheme 7.9) [79]. Additionally, various dienophiles (X=Y) could be used for the subsequent [4+2] cycloaddition of cyclohexadienone spirolactones to give the corresponding adducts as single diastereomers. Notably, methanol and HFIP were used as additives for the oxidation of electron-rich and electron-deficient phenols, respectively.

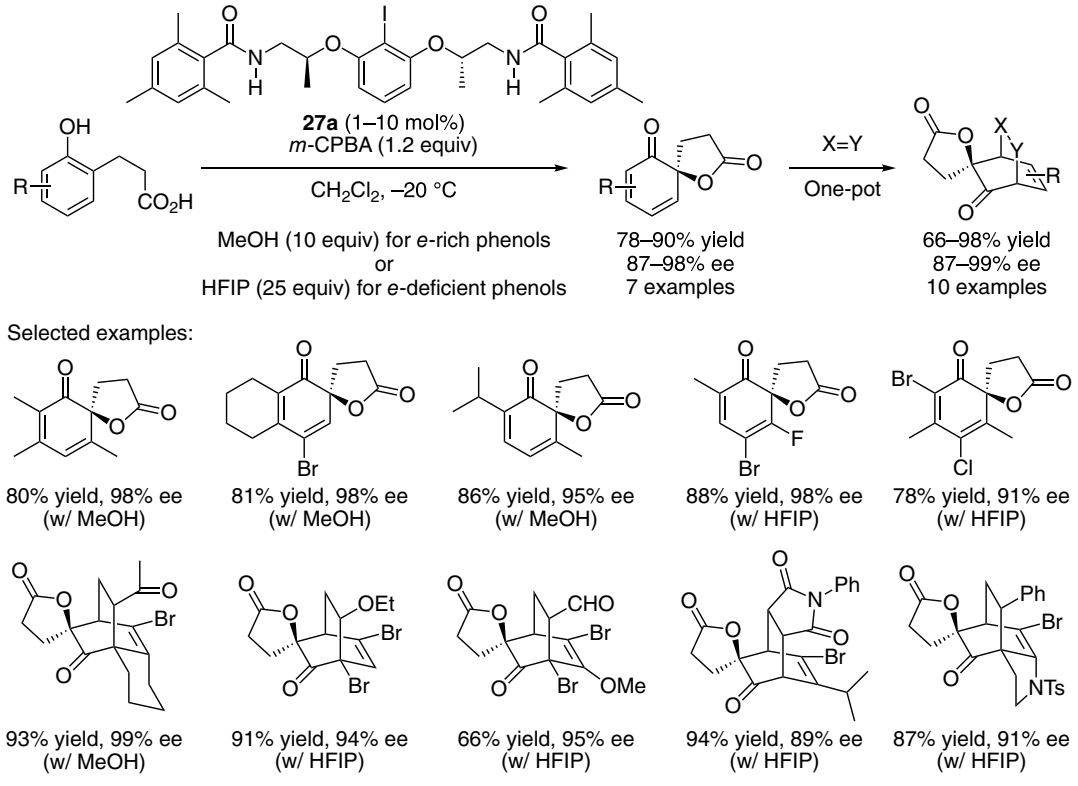

Scheme 7.9. Conformationally flexible iodoarene **27a**-catalyzed enantioselective oxidative dearomatization of phenols. Source: [79].

The additive effect of achiral alcohols such as methanol and HFIP was found to play a crucial role in the enantioselectivity and catalytic activity [79]. A plausible additive effect of methanol for the oxidation of electron-rich phenols is shown in Scheme 7.10. In the presence of excess amounts of methanol, (methoxy)(phenoxy)iodine(III) complex **29** might be generated from (acyloxy)(phenoxy)iodine(III) complex **28** via ligand exchanges under equilibrium. The oxidative cyclization reaction would then occur enantioselectively to produce enantio-enriched spirolactone (*enantioselective path*). In contrast, if the phenoxenium ion **30** is generated through dissociation of the iodoarene moiety ($[Ar^*I(OCOR)]^-$) from **28**, racemic spirolactone might be obtained (*racemic path*). Dissociative intermediate **30** might be generated more preferentially in the oxidation of more electron-rich phenols due to stabilization of the cationic intermediates. The generation of **30** might be suppressed by the formation of **29**, since the leaving ability of an alkoxy ligand would be inferior to that of an acyloxy ligand. In fact, the enantioselectivities were significantly improved with the use of methanol for the catalytic or stoichiometric oxidation of electron-rich phenols [79]. Additionally, control experiments suggested that methanol accelerates the oxidation reaction as a protic polar solvent and improves the enantioselectivity as a ligand of iodine(III). On the other hand, the beneficial effect of HFIP on the reactivity of hypervalent organoiodine-mediated reactions was investigated by Kita and colleagues

[62, 80]. However, the enantioselectivities were significantly dropped for the oxidation of highly reactive 1-naphthols in the presence of HFIP [79]. In sharp contrast, HFIP did not reduce the enantioselectivities for the oxidation of *electron-deficient* phenols (Scheme 7.10). This could be explained by the disfavoring of the dissociative path for electron-deficient phenols under these conditions.

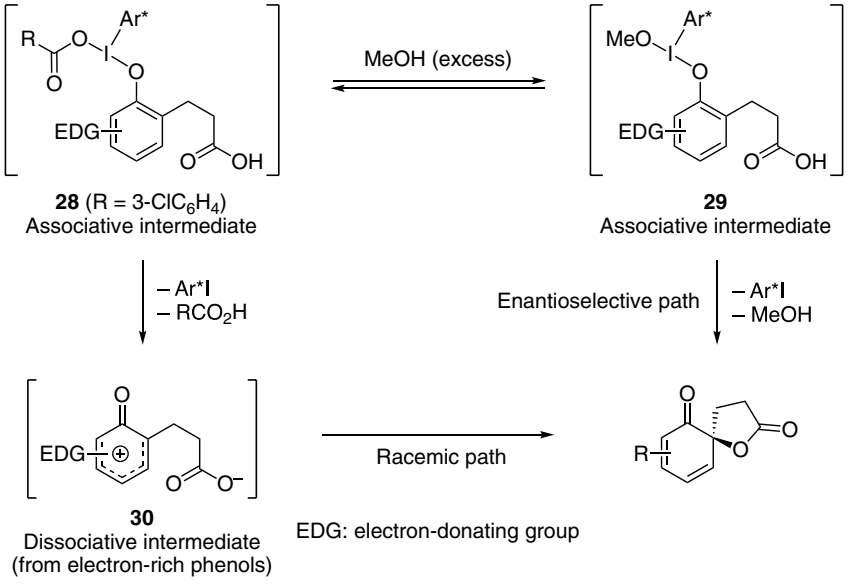

Scheme 7.10. Additional methanol effect on the enantioselective dearomatization of electron-rich phenols. Source: [79].

Furthermore, X-ray diffraction and NOE (Nuclear Overhauser Effect)–NMR analyses of organoiodine(III) **31a** showed that a suitable chiral environment around the iodine(III) center may be constructed via intramolecular hydrogen-bonding interactions (Scheme 7.11) [79]. In contrast, the conformation of **27a** was confirmed to be linear. These findings suggest that intramolecular hydrogen-bonding interactions may play a key role in the high reactivity and excellent enantioselectivity in this conformationally flexible organoiodine catalysis.

By using conformationally flexible organoiodine catalysts **25** or **27**, the first enantioselective oxidative dearomatization of *ortho*- and *para*-hydroquinone derivatives was achieved to give the corresponding masked benzoquinones with high enantioselectivities (Schemes 7.12) [81]. A tether strategy in which phenols were *O*-tethered to an acetic acid or ethanol unit at the *ortho*- or *para*-position realized rapid intramolecular cyclization enantioselectively prior to dissociation of the chiral iodine moiety. Interestingly, the use of slightly modified catalyst **27b** was superior to the use of **27a** for *ortho*-cyclization (Schemes 7.12a). Especially, this remote electronic effect was found to enhance enantioselectivity for the oxidation of phenols in a toluene–buffer (pH 7.0) biphasic solvent.

To achieve high enantioselectivity for the highly challenging *para*-cyclization reaction, in which the developing stereocenter is far from the chiral environment created by phenoxide-bound iodine(III), new lactic acid-derived catalysts **25b** bearing a deeper chiral cavity was designed (Schemes 7.12b) [81]. The remote steric effects of these hydrogen bonding designer organoiodine catalysts enabled the high chemo- and enantioselectivity for the oxidative dearomatization of *para*-hydroquinone derivatives through associative iodine(III)–phenoxide intermediate. Recently, Xiong and colleagues reported an enantioselective cascade *para*-cyclization namely dearomative alkoxy-oxylactonization of 3′-hydroxy-[1,1′-biphenyl]-2-carboxylic acids by using similar lactate-based catalysts **25**, albeit with moderate enantioselectivity up to 56% ee [82].

A highly enantioselective oxidative dearomatization of 2-naphthol derivatives, which are less reactive and selective by using first-generation catalysts **25**, was also achieved by using second-generation catalysts **27** (Scheme 7.13) [83]. Excellent enantioselectivities were also achieved for 1-naphthol derivatives that had previously [77, 78] been obtained with lower enantioselectivities with lactate-based iodoarenes **25**.

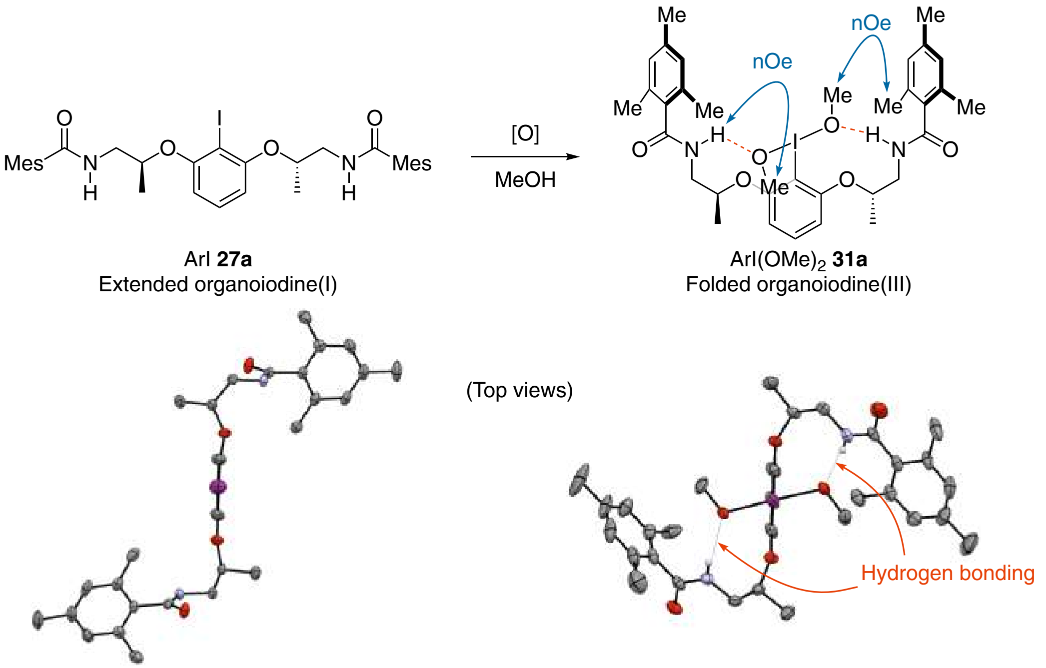

Scheme 7.11. X-ray structures of extended iodine(I) **27a** and folded iodine(III) **31a**, and key NOE correlations of **31a**. Source: [79].

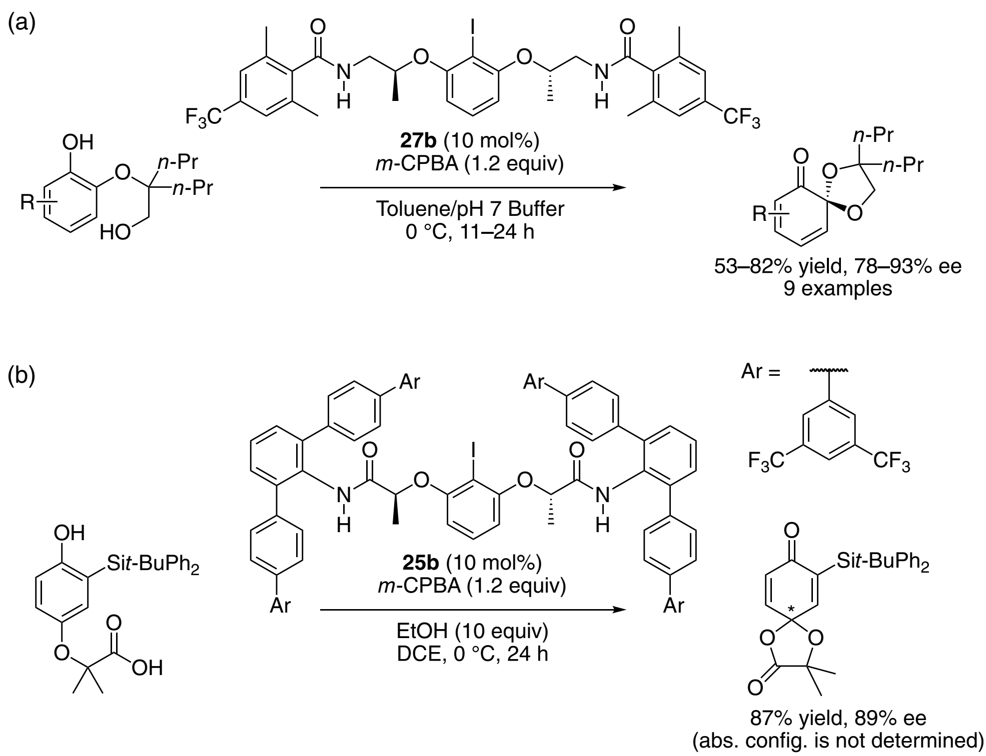

Scheme 7.12. Enantioselective oxidative cyclization of *ortho*- and *para*-hydroquinones. (a) *Ortho*-cyclization. (b) *Para*-cyclization. Source: [81].

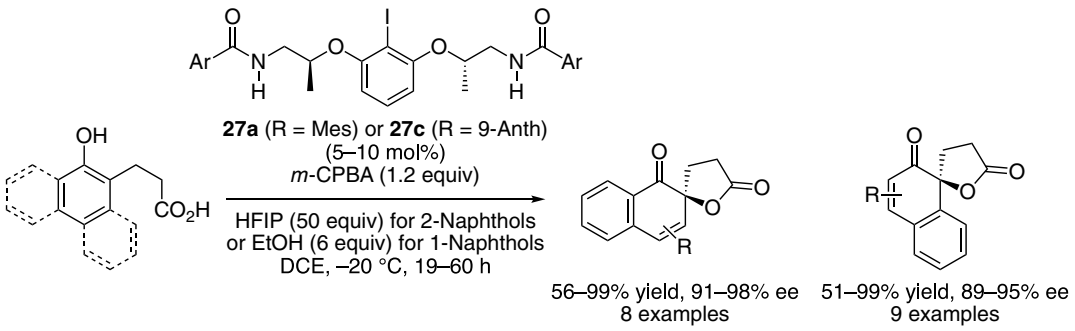

Scheme 7.13. Enantioselective oxidative spirolactonization of 1- and 2-naphthol derivatives using second-generation catalysts **27**. Source: [83].

Interestingly, the use of HFIP and methanol as additives was crucial to induce high enantioselectivity for 2-naphthol and 1-napthols, respectively.

Conformationally flexible organoiodine catalysis has successfully been applied to the asymmetric total synthesis by Suzuki, Kobayashi, Tanino and colleagues (Scheme 7.14) [84]. First, the total synthesis of pestheic acid was achieved based on an intramolecular S_NAr reaction without a nitro group, which has generally been required for the electrophilic substrates for S_NAr reactions. Then, an enantioselective oxidative dearomative spiroketalization of pestheic acid in a sub-gram scale using catalyst *ent*-**27a** in the presence of methanol as an additive gave enantiomerically pure (–)-maldoxin in excellent yield.

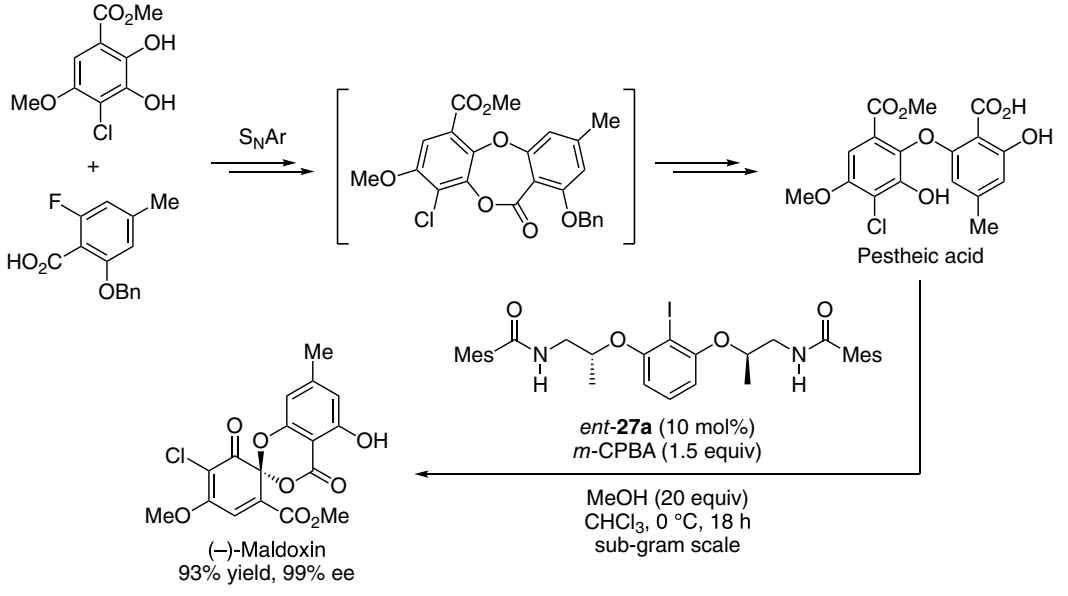

Scheme 7.14. Asymmetric total synthesis of (–)-maldoxin using organoiodine catalysis. Source: [84].

Ciufolini and colleagues have designed 2-amino alcohol-based chiral iodoarenes **32** as structural analogues of **27** (Scheme 7.15). **32a**-Catalyzed enantioselective spiroetherification of 1-naphthol derivatives with *m*-CPBA as an oxidant afforded the corresponding spiroethers with high enantioselectivity [85]. Interestingly catalyst **32a** was superior to **27a** with respect to both stereoselectivity and reactivity for this particular reaction, especially under low catalyst-loading conditions. The same research group has also reported the oxidative kinetic resolution of some 1-naphtholic alcohols using catalyst **32b** with an *S*-factor of up to 19.0 [86]. Recently, the same research group has also applied their

catalyst **32a** to the enantioselective oxidative dearomative spiroamination of 1-naphtholic sulfonamides, albeit in moderate enantioselectivity and low yields [87]. The low chemical yields are attributed to the generation of the intermolecular coupling product with *m*-CBA, a side-product derived from the oxidant used. Interestingly, this dearomatized *ortho*-acyl adduct can be obtained in significantly enantioenriched form.

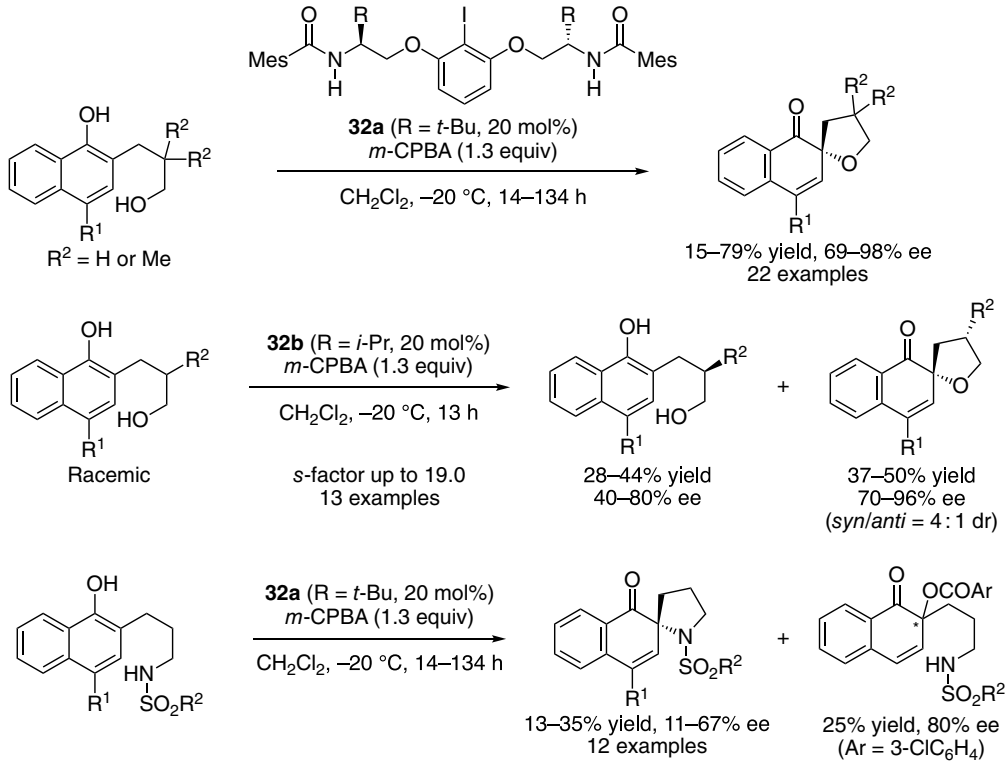

Scheme 7.15. Enantioselective dearomative cyclization using chiral iodoarene catalysts **32** as structural analogues of **27**. Source: [85–87].

Gong and colleagues have first succeeded in the organoiodine-catalyzed enantioselective dearomative C–C coupling reaction to generate an all-carbon spiro-stereocenter [88]. Enantioselective oxidative spirocyclization of 1-hydroxy-*N*-aryl-2-naphthamide derivatives by using chiral iodoarene catalyst **25a** in the presence of *m*-CPBA as an oxidant gave the corresponding spirooxindoles with high enantioselectivity (Scheme 7.16). Interestingly, the use of both trifluoroethanol and water as additives improved both reactivity and enantioselectivity, albeit long reaction times were still required.

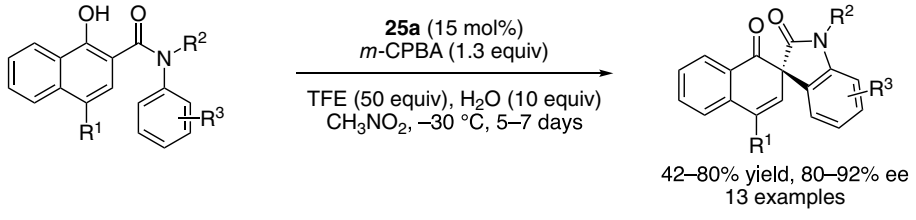

Scheme 7.16. Enantioselective dearomative C–C coupling. Source: [88].

Recently, Nachtsheim and colleagues have designed a new triazole-substituted C_1-symmetric chiral iodoarenes based on the enzymatic kinetic resolution of easily accessible propargylic alcohols (Scheme 7.17) [89–91]. Specifically, *ortho*-modified iodoarene **33** showed remarkable enantioselectivity up to 99% ee in the oxidative spirolactonization of 1-naphthol derivative [91]. Notably, this catalyst can be defined as "omnipotent" since the observed enantioselectivities for mechanistically diverse transformations such as oxidative dearomatization of arenols (both intra- and intermolecular coupling), α-oxidative coupling of carbonyls, and oxidative rearrangement of allyl alcohols (vide infra) were the highest ever reported. A significant role of the triazole unit of **33** was rationalized by DFT calculations as a stabilizing donor both in a potential *N*-bound state (*N*–I interaction) or as a hydrogen-bond acceptor (*N*–HO interaction) in the iodine(III) active species [91]. These secondary interactions may force the geometry of the iodine(III) center into a reactive bent state, "hypervalent twist" [92], with an unusual vertical alignment between the hypervalent bond and the arene ring.

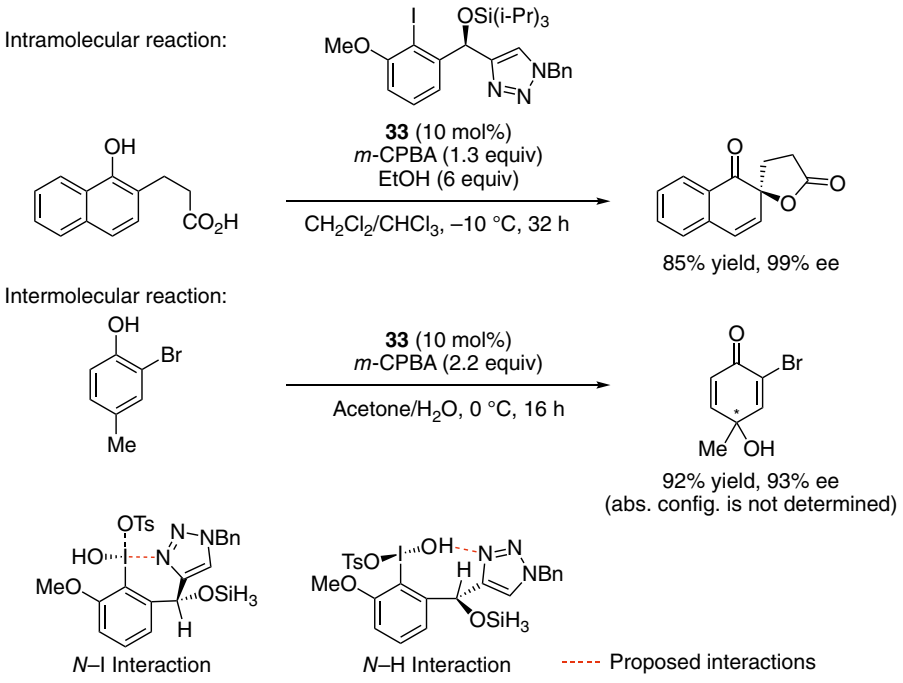

Scheme 7.17. Triazole-derived C_1-symmetric iodoarene **33**-catalyzed enantioselective oxidative dearomatization reactions. Source: [91].

Besides these conformationally flexible modular catalysts described above, several structurally unique iodoarenes **34**–**38** have also been synthesized and applied to the enantioselective oxidative spirolactonization of 1-naphthols as a model benchmark reaction (Scheme 7.18) [93–97].

In general, the development of asymmetric catalysis of intermolecular reactions is much more difficult than that of intramolecular reactions. In 2009, Quideau and colleagues first reported the chiral organoiodine-catalyzed enantioselective intermolecular dearomative coupling of arenols (Scheme 7.19) [98]. Dearomative hydroxylation of 2-methylnaphthol mediated by hypervalent organoiodine species generated in situ from the oxidation of stoichiometric amount of chiral iodoarene **39** with *m*-CPBA gave *ortho*-quinol with 50% ee. On the other hand, when a catalytic amount of **39** was used, a subsequent epoxidation of *ortho*-quinol with *m*-CPBA gave an epoxide, albeit with lower enantioselectivity. The authors proposed that iodine(III) **40** or iodine(V) **41** may be generated in situ by the oxidation of **39** with *m*-CPBA. Based on the ESI-MS analysis, iodine(V) **41** was believed to be active species, which would provide the desired *ortho*-quinol enantioselectively via the proposed intermediate model **42**.

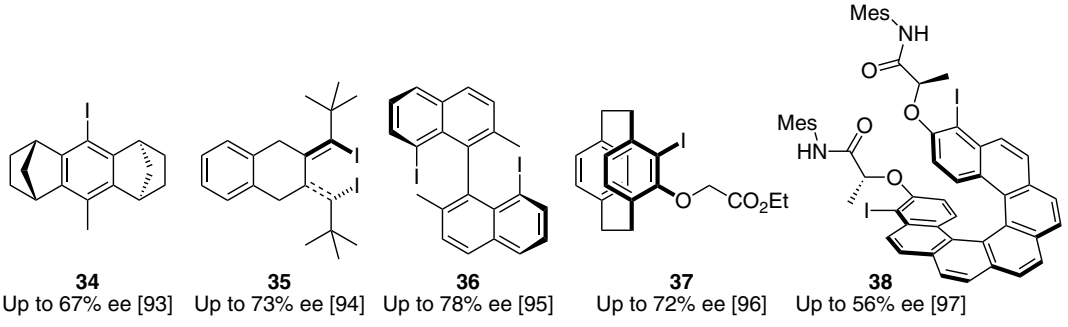

Scheme 7.18. Structurally unique chiral iodoarene catalysts **34**–**38**.

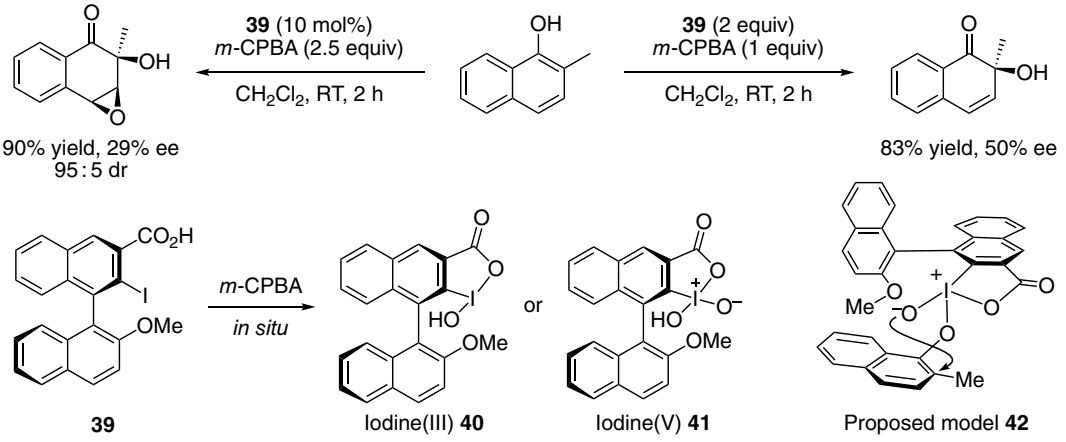

Scheme 7.19. Enantioselective dearomative hydroxylation of 1-napthol using binaphthyl-based chiral iodoarene **39**. Source: [98].

Besides organoiodine catalysis, chiral organoiodine(V) reagents **14**–**18** have also been designed for the enantioselective dearomative hydroxylation of phenols (Scheme 7.1) [51–55]. Especially, C_2-symmetric chiral organoiodines(V) **15**, **17**, and **18** have been successively applied to the enantioselective synthesis of natural products, such as (+)-biscarvacrol [52], (−)-bacchopetiolone [53], and (+)-scyphostatin analogues [55] (Scheme 7.20).

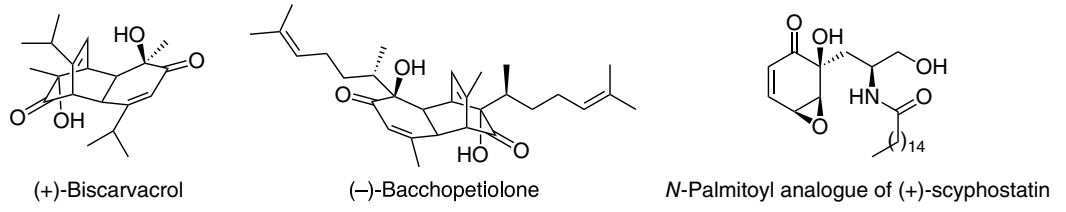

Scheme 7.20. Examples of natural products synthesized by enantioselective hydroxylation of the corresponding phenol precursors using chiral iodine(V) reagents. Source: [52, 53, 55].

The design of enantioselective organoiodine catalysis of oxidative dearomatization at *para*-position would be much more difficult than that of *ortho*-dearomatization, since the developing stereocenter appears to be quite distant from the chiral environment of iodine catalyst. In 2013, based on their molecular modeling studies [70], Harned and Volp designed new chiral iodine catalysts for the first

hydroxylative *para*-dearomatization of phenols (Scheme 7.21) [99]. Iodoarene **43** derived from 8-iodotetralone and tartaric acid could catalyze the oxidation of *para*-alkylphenols in the presence of *m*-CPBA and water to afford the desired *para*-quinols with high enantioselectivity. In this catalyst design, the tetrahydronaphthalene unit might limit the conformational freedom of the chiral information, while the two amidic protons could be used as H-bond donors. The best results were obtained with *ortho*-silyl-substituted phenols, and enantioselectivity is up to 60% ee.

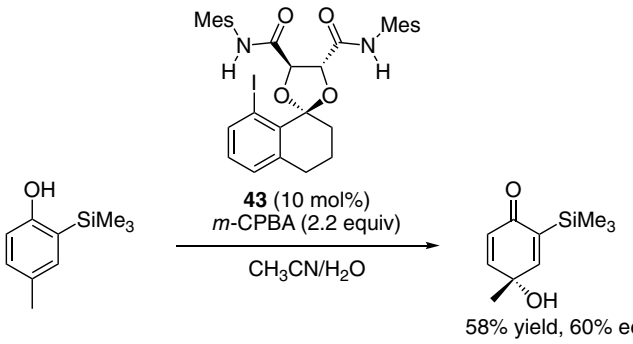

Scheme 7.21. The first organoiodine-catalyzed enantioselective *para*-dearomative hydroxylation. Source: [99].

As reported by Muñiz and Fra in 2017, lactate-based conformationally flexible iodoarenes could also be used for intermolecular oxidative dearomative coupling [100]. Bisamide **25c**-catalyzed dearomative hydroxylation of phenols or aniline at the *para*-position using *m*-CPBA as an oxidant in aqueous acetonitrile gave the corresponding *para*-quinols or imine with moderate enantioselectivity (Scheme 7.22).

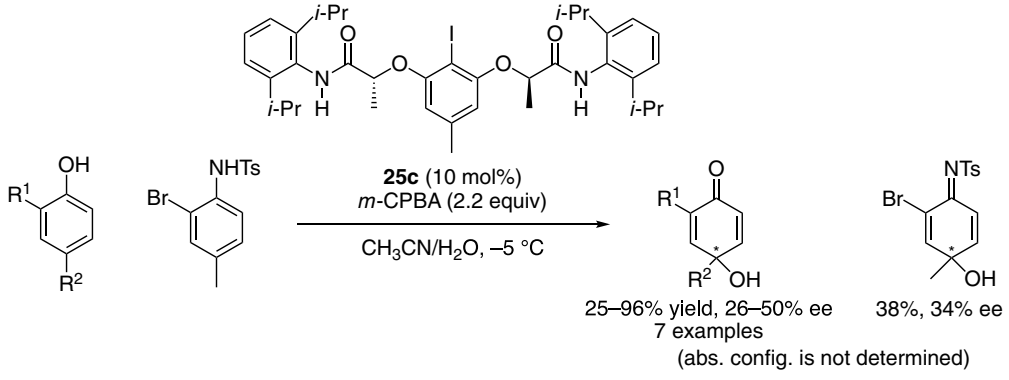

Scheme 7.22. Lactate-derived **25c**-catalyzed enantioselective *para*-hydroxylation of phenols and imines. Source: [100].

In 2018, Maruoka, Hashimoto, and colleagues have developed a new-class of chiral organoiodine catalysts for the intermolecular enantioselective dearomatization of phenols [101]. By using indanol-based catalyst **44** in the presence of *m*-CPBA as an oxidant under aqueous conditions, enantioselective dearomative hydroxylation of 2,4-disubstituted phenols at the *para*-position gave the corresponding *para*-quinols with high enantioselectivity up to 84% ee (Scheme 7.23). Notably, introduction of 2,6-disubstituted aniline-derived lactamide at the *ortho*-position of iodoarene catalyst improves the enantioselectivity remarkably. Recently, the highest reactivity and enantioselectivity (93% ee) of the dearomative *para*-hydroxylation were achieved by Nachtsheim's "omnipotent" catalyst **33** (Scheme 7.17) [91].

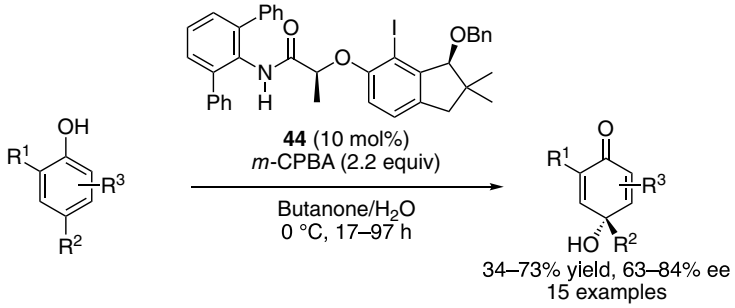

Scheme 7.23. Highly enantioselective *para*-hydroxylation of phenols using indanol-derived iodoarene **44**. Source: [101].

7.3. OXIDATIVE α-FUNCTIONALIZATION OF CARBONYL COMPOUNDS

Carbonyl compounds play a central role in synthetic organic chemistry. The oxidative α-functionalization of carbonyl compounds enables access to a large number of synthetic building blocks and high-value molecules. To date, a number of oxidation systems using transition metal catalysis as well as iodine-based redox organocatalysis have been developed for this purpose [1, 102]. Ochiai and colleagues have reported the first organoiodine(III)-catalyzed α-oxidative coupling of carbonyl compounds [57]. After this seminal report, rapid progress has been made in the development of hypervalent iodine catalysis for α-oxidative coupling reactions. Among them, α-oxysulfonylation of carbonyl compounds with arenesulfonic acids has been studied most extensively [1]. α-Sulfonyloxy carbonyls are utilized extensively to replace lachrymatory and relatively toxic α-halocarbonyls for the synthesis of various heteroaromatics such as thiazoles, oxazoles, imidazoles, pyrazoles, etc. [103]. In 2006, Togo and colleagues have reported the first organoiodine(III)-catalyzed α-oxytosylation of ketones with TsOH by employing iodobenzene as a catalyst and *m*-CPBA as an oxidant [104]. After this report, several organoiodine(III) catalysts have been developed for α-oxysulfonylation of ketones [60–64].

The development of enantioselective α-oxytosylation of ketones using chiral organoiodine(III) reagents has been ongoing for almost a quarter of a century. In 1997, Wirth and colleagues have reported the first enantioselective α-oxytosylation of ketones using chiral hypervalent organoiodine(III) reagents [19]. In 2007, the first catalytic enantioselective α-oxytosylation of ketones was also reported by Wirth's group [64]. By using chiral iodoarene **45** as a catalyst α-tosyloxypropiophenone was obtained with 27% ee (Scheme 7.24). After this pioneering work, a number of structurally varied chiral iodoarene catalysts **46**–**50** have been developed, however, the enantioselectivities are moderate (<70% ee) (Scheme 7.24) [105–112].

The low to moderate enantioselectivity obtained for the α-oxytosylation of ketones may be attributed to the mechanistic pathway proceeding through an S_N2'-type reductive elimination involving an *O*-bonded iodane intermediate **51** generated from the iodine(III)-mediated enolization of the ketone (Scheme 7.25) [113]. In 2015, Legault and colleagues reported a breakthrough in the organoiodine-catalyzed enantioselective α-oxytosylation [114]. The use of enol ester derivatives in place of ketone might prevent passage through the *O*-bonded intermediate pathway and instead would favor proceeding through an α-*C*-bonded iodane intermediate **52** (Scheme 7.25) [113, 115].

Indeed, enantioselective α-oxytosylation of enol esters afforded the corresponding α-tosyloxy ketones with an unprecedented level of enantioselectivity up to 90% ee (Scheme 7.26a) [114]. The use of bis(lactate)-derived tertiary bisamide **53** as a chiral iodoarene catalyst gave the best results. The reaction could be performed under both catalytic and stoichiometric conditions. To simplify the investigation of the substrate scope, the authors focused on the development of stoichiometric reactions, since iodoarene **53** was stable under the oxidative conditions and could be easily recovered (>80%) (Scheme 7.26b). For stoichiometric reactions, the iodine(III) active species can be first prepared by the oxidation of **53** with *m*-CPBA in the presence of TsOH [116]. Several enol acetates could be converted to the corresponding α-tosyloxy ketones in high yields with high enantioselectivity. Under the stoichiometric conditions, products were obtained with the same level of selectivity as the catalytic conditions. The stereochemistry of

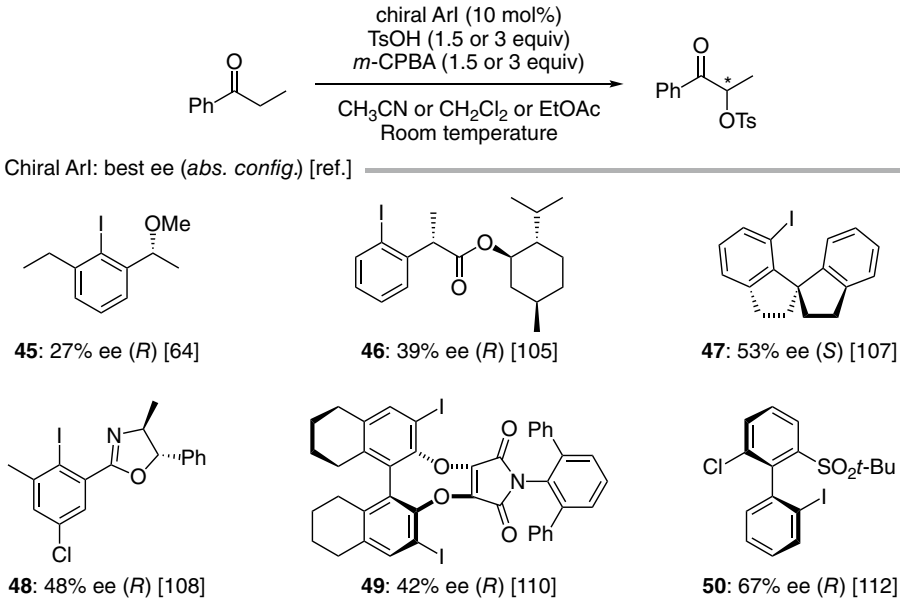

Scheme 7.24. Chiral organoiodine-catalyzed enantioselective α-oxytosylation of propiophenone.

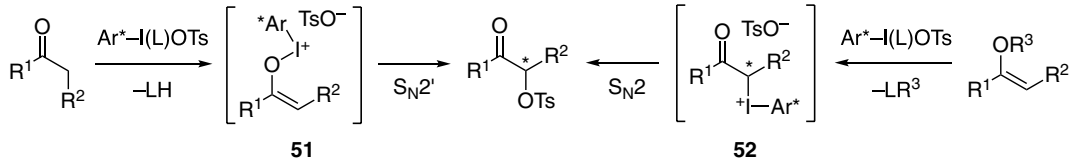

Scheme 7.25. Mechanistic consideration of the enantioselective α-oxytosylation of ketones and enol derivatives. Source: [113–115].

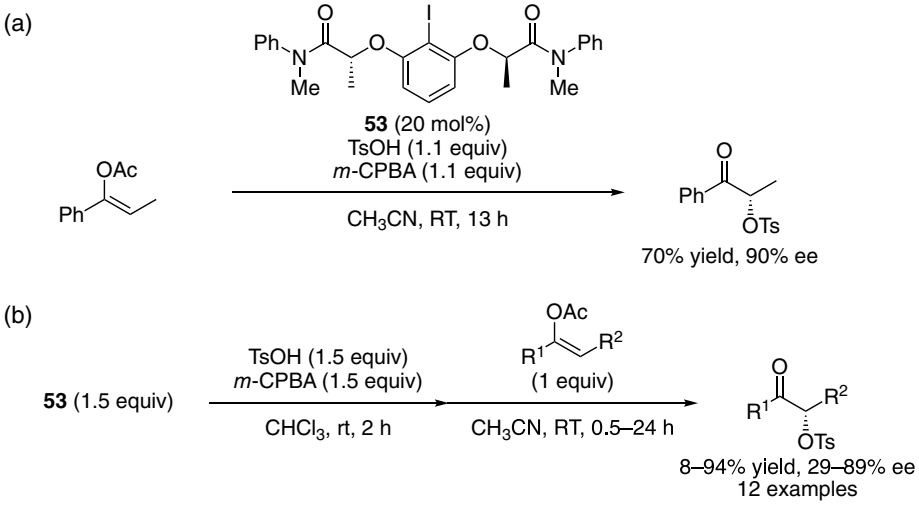

Scheme 7.26. Highly enantioselective α-oxytosylation of enol esters under catalytic and stoichiometric conditions. (a) Catalytic conditions. (b) Stoichiometric conditions. Source: [114].

enol ester was highly important to induce high enantioselectivity. Cyclic substrates having (*E*)-*O*-enol stereochemistry afforded only modest enantioselectivities.

Recently, Nachtsheim and colleagues proved that high stereoinduction could be achieved for the enantioselective α-oxytosylation of ketones using designer organoiodine(III) catalysts [91]. Chiral iodoarene **33** showed remarkable enantioselectivity up to 88% ee in the α-oxytosylation of propiophenone (Scheme 7.27). On the other hand, very recently, Wirth and colleagues introduced C–N axial chiral iodoarenes [117] as new catalysts for the α-oxytosylation of ketones with moderate to high enantioselectivity up to 80% ee [118].

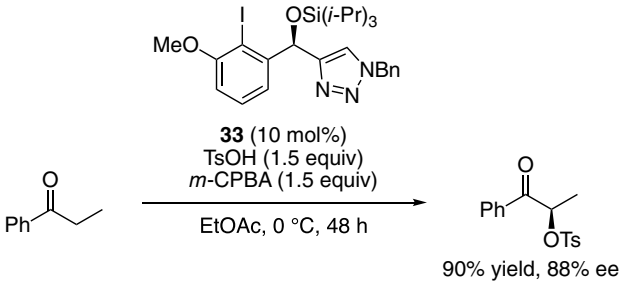

Scheme 7.27. Highly enantioselective α-oxytosylation of propiophenone using **33** as an "omnipotent" catalyst. Source: [91].

In contrast to α-oxysulfonylation reactions, the organoiodine(III)-catalyzed enantioselective intermolecular direct α-oxyacylation of carbonyls has not yet been achieved. Instead, inspired by Legault's enol ester strategy that would favor to proceed the coupling through an α-*C*-bonded iodane intermediate [113–115], recently, Wirth and colleagues achieved the first highly enantioselective α-oxyacylation of enol acetates [119]. By using secondary bis-amide catalyst **25c** in combination with *m*-CPBA as an oxidant and boron trifluoride as an additive in a mixed solvent of acetic acid and dichloromethane, oxidative coupling of several enol acetates derived from aryl ketones provided the corresponding α-acetoxylated products in high yields with generally moderate to high enantioselectivities up to 88% ee (Scheme 7.28).

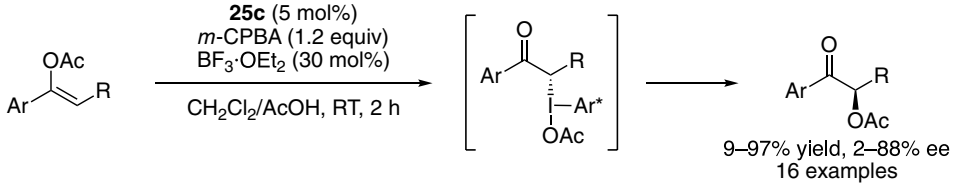

Scheme 7.28. Bis-*sec*-amide **25c**-catalyzed enantioselective α-oxyacylation of enol acetates via α-*C*-bonded iodane intermediates. Source: [119].

A few examples of the catalytic enantioselective α-oxylactonization of ketocarboxylic acids as an intramolecular α-C–O coupling have also been reported. For example, in 2012, Moran and colleagues reported the enantioselective oxylactonization of 5-oxo-5-phenylpentanoic acid using pseudoephedrine-derived iodoarene catalyst **54** in the presence of *m*-CPBA as an oxidant and TsOH as an activator to give γ-benzoyl-γ-butyrolactone with 51% ee (Scheme 7.29) [120]. Again, as in the α-oxytosylation reaction, the highest enantioselectivity up to 81% ee for α-oxylactonization reaction was achieved by Nachtsheim's catalyst **33** (Scheme 7.29) [91].

On the other hand, α-halogenation, especially α-fluorination, of carbonyl compounds has also been extensively investigated using hypervalent iodine(III) reagents such as (difluoroiodo)benzene ($PhIF_2$) [1]. In 2013, Kitamura and colleagues have reported the first organoiodine(III)-catalyzed α-fluorination of 1,3-dicarbonyls using aqueous HF as a fluorine source and *m*-CPBA as a terminal oxidant [121]. The key for this catalytic reaction was the in situ generation of an active species, $ArIF_2$, by the smooth oxidation of iodoarene in the presence of hydrogen fluoride.

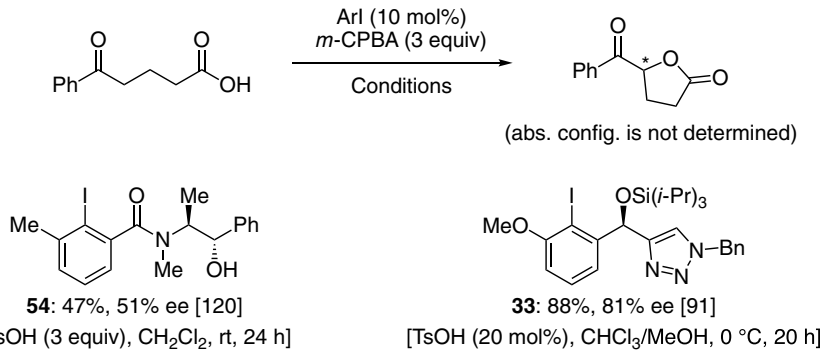

Scheme 7.29. Enantioselective oxylactonization of ketocarboxylic acid.

The highly enantioselective electrophilic α-fluorination of carbonyl compounds was realized by transition metal catalysts or organocatalysts using Selectfluor or NFSI as an expensive electrophilic fluorinating reagent [122]. However, enantioselective nucleophilic α-fluorination of carbonyl compounds has less been studied. In 2014, Shibata and colleagues reported the first chiral organoiodine(III)-catalyzed enantioselective α-fluorination of 1,3-dicarbonyl compounds using HF·pyridine as a nucleophilic fluorinating reagent in the presence of binaphthyl diiodide **55** as a chiral catalyst (Scheme 7.30) [123]. The best selectivities were observed for the α-fluorination of indanone-derived β-keto esters having a sterically demanding adamantyl or *L*-menthyl ester, with 56% ee or 65% de, respectively.

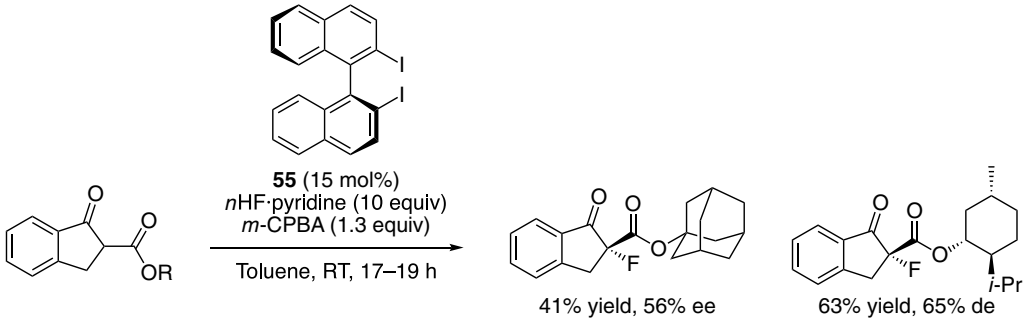

Scheme 7.30. The first chiral organoiodine(III)-catalyzed enantioselective or diastereoselective α-fluorination. Source: [123].

In 2018, Rueping and colleagues reported a highly enantioselective α-fluorination of indanone-derived β-ketoesters catalyzed by lactate-derived C_2-symmetric bisester **56** having electron-withdrawing substituent at *para*-position of the resorcinol unit (Scheme 7.31) [124]. The choice of hydrogen fluoride source was crucial for both chemical yields and enantioselectivity. Commercially available triethylamine pentahydrofluoride ($5HF{\cdot}Et_3N$) provided a compromise between good chemical yield and selectivity. The oxidative α-fluorination reactions tolerated a wide range of functional groups and gave the products with a quaternary stereocenter with high enantioselectivity up to 92% ee. Interestingly, a hydrogen fluoride-containing complex might be crucial for catalytic activity since stoichiometric control reaction with organoiodine(III) **57**, $ArIF_2$, showed only traces of the product in the absence of hydrogen fluoride.

The authors performed DFT calculations to investigate the reaction mechanism in detail (Scheme 7.31). Experimental results reveal the in situ formation and activation of the iodine(III), $ArIF_2$ (**57**), by the HF molecule to give $[ArIF]^+[HF_2]^-$ (**58**) as an active species. The first steps involve the reaction of β-keto ester with **58** to give an *O*-bonded iodine(III) intermediate **59**. The reaction could proceed in a single step to the product through an S_N2'-type reductive elimination via a nucleophilic attack of a fluoride anion to the α-*C* atom of **59**. However, S_N2'-type mechanism would favor the formation of (*S*)-enantiomer of the

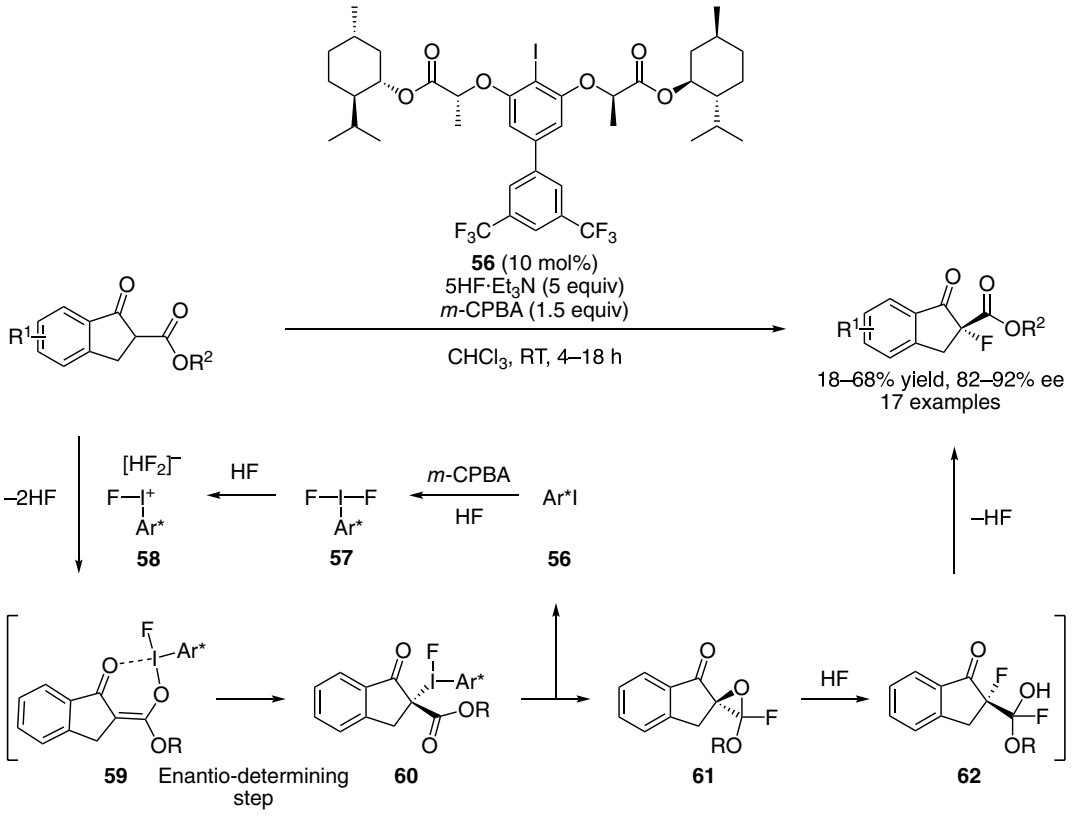

Scheme 7.31. Highly enantioselective α-fluorination of indanone-derived β-keto esters. Source: [124].

product, which was in disagreement with the experimental selectivity of the observed (*R*)-enantiomer. The reaction could more easily proceed *via* transfer of the $[ArIF]^+$ fragment from the *O* atom to the α-*C* atom to give an α-*C*-bonded iodine(III) intermediates **60**. This is the enantioselectivity-determining step, and the formation of the (*R*)-enantiomer of intermediate **60** is favored. The intermediate **60** is found to be very stable and the energy barrier (31.2 kcal/mol) for the reverse reaction from **60** to **59** is too high for the reaction conditions. From intermediate **60**, the reductive elimination of ArI and formation of an epoxide ring occurs to give a hemiacetal intermediate **61** with an inversion of stereochemistry at α-*C* atom. Ring opening of the epoxide **61** by a nucleophilic attack of fluoride anion affords intermediate **62** and restores the (*R*)-configuration at the α-*C* atom. Dissociation of the fluoride leads to (*R*)-enantiomer of product.

Zheng and colleagues developed a novel planar chiral iodoarene **63** based on [2.2]paracyclophane as a catalyst for the enantioselective oxidative α-fluorination of indanone-derived β-ketoesters with high enantioselectivity up to 89% ee (Scheme 7.32) [125]. Notably, α-fluorination of β-ketoamide also proceeded under similar conditions to afford the product with good enantioselectivity. Although this was the first highly enantioselective reaction using organoiodine catalyst with planar chirality, catalyst **63** was inferior to resorcinol-derived catalyst **56** [124] with respect to enantioselectivity.

In 2014, Gong and colleagues reported the first organoiodine(III)-catalyzed enantioselective oxidative α-C–C coupling of carbonyl compounds [126]. The sequential oxidative Friedel–Crafts type spirocyclization of N^1,N^3-diarylmalonamides [127] using lactate-derived bis-*tert*-amide **64** gave the structurally diverse spirooxindoles in good to moderate yields with high enantioselectivity up to 90% ee (Scheme 7.33) [126]. The use of trifluoroacetic acid (TFA) as an activator was crucial to enhance the catalytic activity. Investigation of the side-arms of the resorcinol-derived C_2-symmetric chiral catalysts

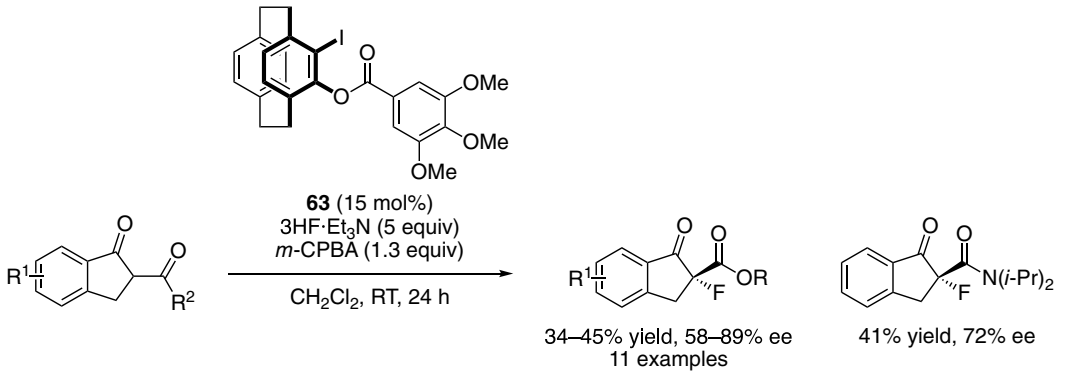

Scheme 7.32. Enantioselective α-fluorination using planar chiral catalyst **63**. Source: [125].

revealed that the tertiary amide rather than secondary amide or carboxylic acid plays a key role in inducing high enantioselectivity. Notably, the use of peracetic acid (AcOOH) as an oxidant instead of *m*-CPBA gave higher chemical yield and enantioselectivity.

Sunoj and colleagues investigated the reaction mechanism of this cascade α-C–C coupling reactions (Scheme 7.33) [128, 129]. The multistep sequential mechanism of oxidative coupling of malonamide derivatives involves α-*C*-bonded iodonium species **65** and **67** as key intermediates with a critical trifluoroacetate counterion. DTF calculations suggested that trifluoroacetate anion offers the energetically most preferred transition state for the Friedel–Crafts type cyclization. Additionally, 1,3-migration of the chiral iodine(III) in the *O*-iodonium enolate **66** to *C*-iodonium enolate **67** was identified as the enantio-determining step in the overall reaction. Several noncovalent secondary interactions (i.e., hydrogen bonding interactions), particularly between amide sidearms and the iodine(III)-bound ligands (TFA), induce a helical fold [79, 130] around the iodine(III) center.

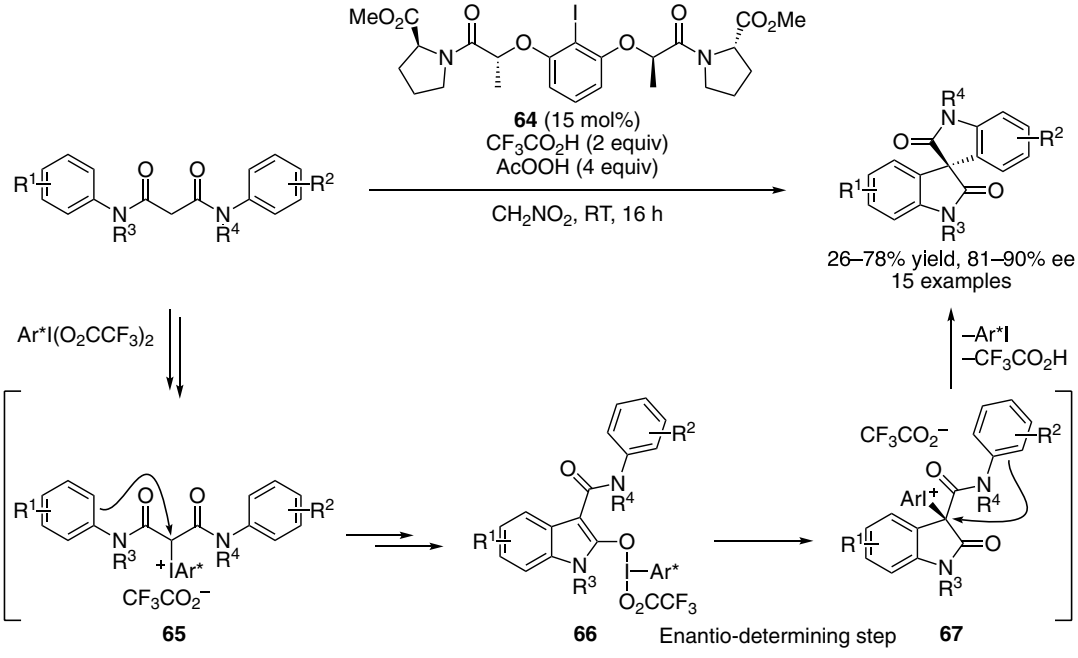

Scheme 7.33. Enantioselective oxidative Friedel–Crafts type spirocyclizations. Source: [126, 129].

As a similar enantioselective cascade oxidative coupling reaction, in 2016, Du and colleagues reported a sequential oxidative spirocyclization of alkyl 3-oxopentanedioate monoamide derivatives catalyzed by a lactate-derived bis-*tert*-amide **68** to give biologically important spirofurooxindoles with high enantioselectivity up to 91% ee (Scheme 7.34) [131]. The reaction conditions were similar to Gong's procedure [126] using an excess amount of TFA as an activator. The reaction was proposed to proceed via oxidative C–O bond formation followed by oxidative C–C bond formation.

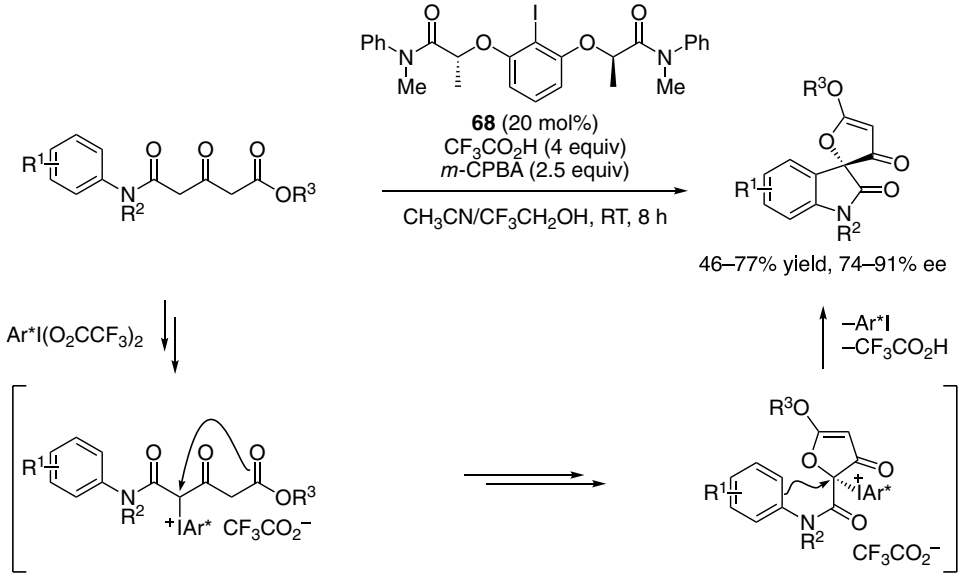

Scheme 7.34. Enantioselective cascade oxidative spirocyclization. Source: [131].

7.4. OXIDATIVE DIFUNCTIONALIZAITON OF ALKENES

Alkenes are one of the most versatile and ubiquitous classes of functional groups, and their functionalization to access a variety of high-value molecules has played a central role in organic synthesis. Traditionally, enantioselective transition-metal catalysis has often been used for alkene difunctionalization [132]. Recently, enantioselective organoiodine(III) catalysis adds the aspect of an environmentally friendly alternative for these oxidative transformations including oxygenations, aminations, and halogenations [133–136]. In general, the electrophilic reactivity of the organoiodines(III) can be enhanced by a Lewis or Brønsted acid additive. As the first example of enantioselective oxidative functionalization of alkenes using chiral organoiodine(III) reagents, in 1997, Wirth and colleagues have reported the oxidative ditosylation of styrene with up to 21% ee, which was later improved to 65% ee with a modified reagent **3** (Scheme 7.35a) [19]. On the other hand, Fujita and colleagues achieved the highly enantioselective diacetoxylation of styrenes using lactate-derived diester-type reagent **7** [24], as one of the representatives of a class of C_2-symmetric organoiodines(III) (Scheme 7.35b) [25]. The Wirth group [20, 21, 28, 29, 34, 35, 39, 41, 42] and the Fujita group [22, 23, 32, 33, 37, 38] have developed an extensive array of enantioselective oxidative functionalization of alkenes using stoichiometric amount of chiral organoiodine(III) reagents.

Alkenes as electron-rich activated functional groups can also react directly with the stoichiometric oxidant used for iodine(I) oxidation. To induce high chemo- and enantioselectivity for organoiodine(III) catalysis, oxidant should be preferentially used for the oxidation of the iodine(I) to iodine(III) over the non-catalyzed background reactions. In 2012, Fujita and colleagues reported the first example of the organoiodine-catalyzed enantioselective difunctionalization of alkenes [137]. By using lactate-derived chiral iodoarene catalyst **69** in the presence of *m*-CPBA and trifluoracetic acid as an oxidant and activator, respectively, enantioselective

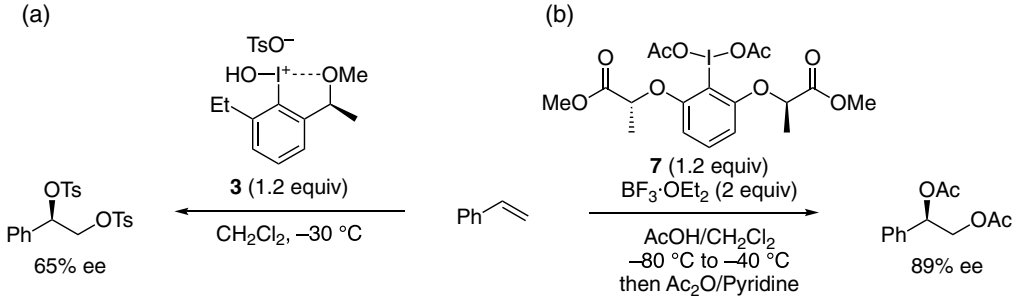

Scheme 7.35. Enantioselective vicinal dioxygenations of styrene using chiral organoiodine(III) reagents. (a) Ditosylation. Source: [19]. (b) Diacetoxylation. Source: [25].

cascade oxidative lactonization/cycloetherification of *ortho*-alkenylbenzoates bearing a pendant hydroxyl group gave the corresponding dihydrofuran-fused isochromanones with up to 91% ee (Scheme 7.36). A catalyst-controlled diastereoselective synthesis of natural products such as (+)-monocerin and 12-hydroxymonocerines could also be achieved from oxidative cyclization of the corresponding optically active substrates under these catalytic conditions [137, 138]. Notably, the stereogenic centers that were preinstalled to the substrates did not dominate the stereochemistry of the oxidative cyclization process.

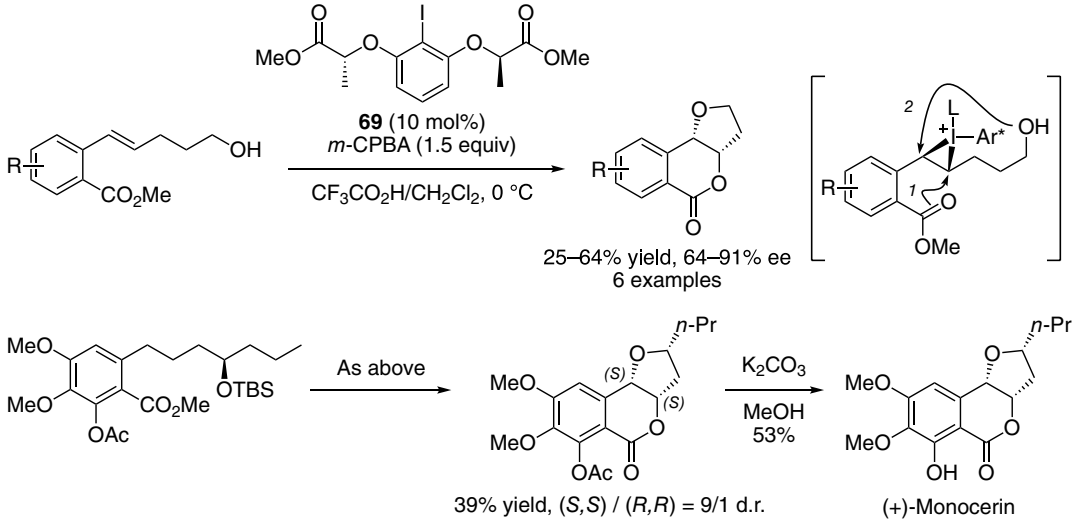

Scheme 7.36. Chiral organoiodine-catalyzed cascade enantioselective oxidative lactonization/cycloetherification. Source: [137, 138].

Fujita and colleagues have also developed diastereo- and enantioselective hydroxylactonization of *ortho*-alkenylbenzoates to 4-hydroxyisochromanones, a core motif in a wide variety of polyketide natural products, by using menthyl-derived bisester **70** as a catalyst (Scheme 7.37) [139]. Under catalytic conditions, four products could be obtained. Chiral organoiodine(III)-mediated process provided the *syn*-addition products with high enantioselectivity and high *endo*/*exo* regioselectivity through Woodward-type mechanism. On the other hand, direct oxidation by *m*-CPBA as a background reaction afforded the racemic *anti*-addition products through Prévost-type mechanism.

In 2014, Wirth and colleagues reported enantioselective intramolecular aminocyclization of homoallylic guanidine and diaminosulfone derivatives (Scheme 7.38) [140]. A novel organoiodine(III) reagent **71** bearing a strongly chelating pyridine moiety, which would allow efficient coordination to the

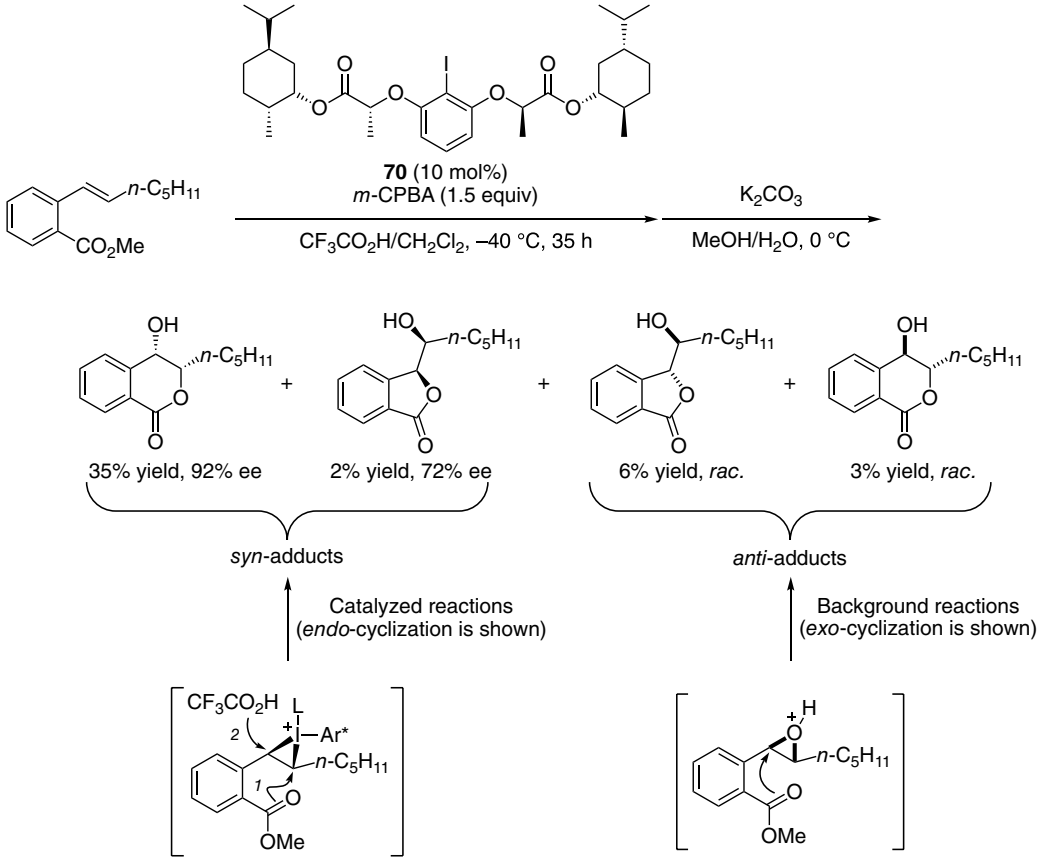

Scheme 7.37. Diastereo- and enantioselective oxylactonization of *ortho*-alkenylbenzoates. Source: [139].

iodine(III) center has been developed to induce high enantioselectivity up to 94% ee. In addition, catalytic oxidative cyclization could be realized by using a catalytic amount of iodoarene **72** in the presence of sodium perborate and acetic acid as an oxidant and activator, respectively. However, compared to stoichiometric reactions, lower enantioselectivities were observed under catalytic conditions, which may due to the higher temperatures and different acid activator used to achieve catalytic efficiency.

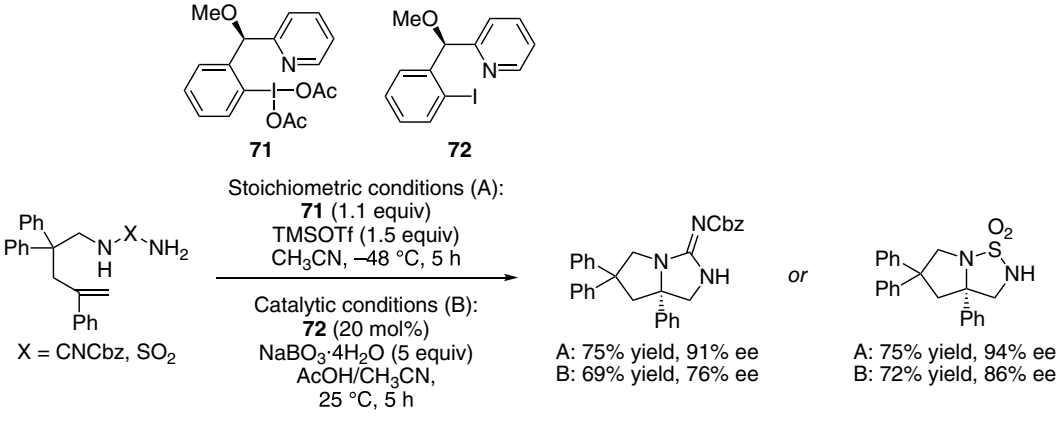

Scheme 7.38. Enantioselective oxidative aminocyclization. Source: [140].

Organoiodine-catalyzed oxidative intramolecular cyclization of alkenes was also applied to the asymmetric synthesis of various heterocycles. For example, in 2015, Moran reported an enantioselective synthesis of isooxazoline and dihydrooxazine by oxidative cyclization of *N*-alkenylamides using bis-*tert*-amide **73** as a chiral iodoarene catalyst in the presence of Selectfluor and TFA as an oxidant and activator, respectively (Scheme 7.39a) [141]. The reaction was proposed to proceed via an intramolecular attack by the amide oxygen followed by an intermolecular nucleophilic substitution of TFA to give the trifluoroacetate adduct as an unstable transient product, which was then hydrolysis by alkaline work-up. Similarly, in 2017, Masson and colleagues reported enantioselective sulfonyl- or phosphoryl-oxylactonization of 4-pentenoic acids with *m*-CPBA using bis-*sec*-amide *ent*-**25a** to give the corresponding sulfonyloxy- or phosphoryloxy-γ-butyrolactones (Scheme 7.39b) [142]. The use of the stoichiometric amount of *ent*-**25a** at lower temperatures gave the products with higher enantioselectivity up to 94% ee.

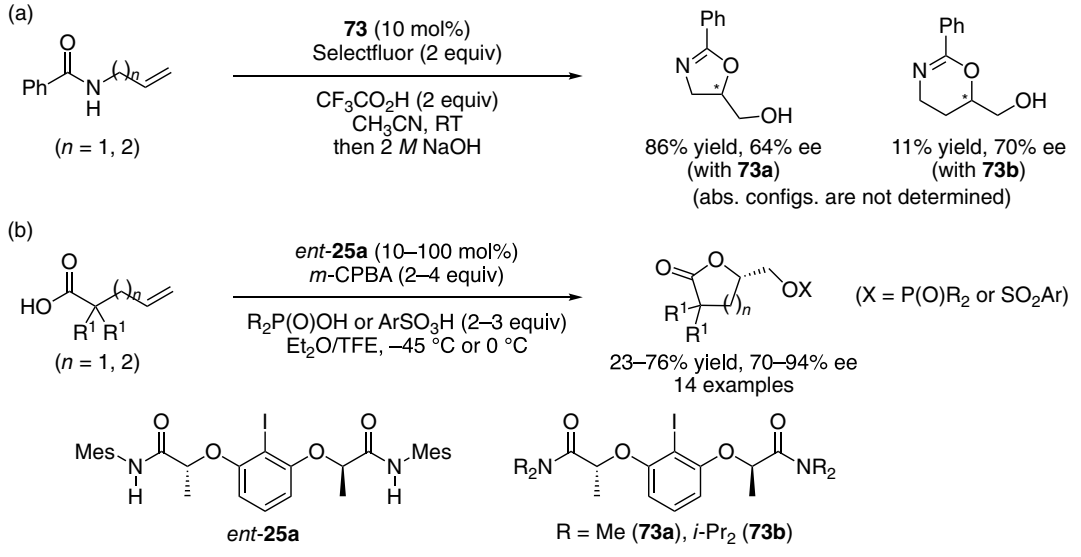

Scheme 7.39. Enantioselective oxidative cyclization of unsaturated amides. (a) Source: [141]. (b) Source: [142].

In 2013, Nevado and colleagues reported the first enantioselective fluorination of alkenes, namely aminofluorination, by using chiral difluoroiodine(III) reagent **9** [31]. In 2014, Shibata, Kita, and colleagues reported the first organoiodine-catalyzed enantioselective fluorination of alkenes by in situ generation of chiral difluoroiodine(III) active species [123]. Intramolecular aminofluorination of ω-amino-alkene using hydrofluoric acid as a nucleophilic fluorinating reagent in the presence of binaphthyl diiodide **55** as a chiral catalyst provided fluoropiperidine in moderate yield with moderate enantioselectivity (Scheme 7.40a).

Jacobsen and colleagues expanded the scope of intramolecular aminofluorination to the β-fluorinated aziridines (Scheme 7.40b) [143]. Lactate-derived bisester **74**-catalyzed enantioselective aminofluorination of cinnamyl sulfonamides using HF-pyridine and *m*-CPBA as the fluoride source and oxidant, respectively, proceeded with complete *syn* diastereoselectivity with excellent enantioselectivity. However, the scope of substrates was limited to ones bearing electron-deficient arene substituents, since electron-rich arenes underwent preferential aryl migration to the 1,1-difluoride products. Very recently, Szabó and colleagues reported the similar enantioselective fluorocyclizations of 1,1-styrenes with pendant nosylamides or alcohols as internal nucleophiles (Scheme 7.40c) [144]. By using a lactate-derived iodoarene catalyst **75**, amino- or oxy-fluorination of electron-deficient styrenes gave the corresponding pyrrolines or tetrahydrofurans bearing tertiary fluoride stereocenters with high enantioselectivity.

Jacobsen and colleagues have also reported fluorolactonization of alkenyl benzoates using lactate-derived catalyst **76** and HF-pyridine as a nucleophilic fluoride source (Scheme 7.41a) [145]. The corresponding 4-fluoro-isochromanones were obtained with high enantioselectivity and *syn* diastereoselectivity. Notably, while fluorolactonization with electrophilic fluorinating reagents such as Selectfluor proceeded

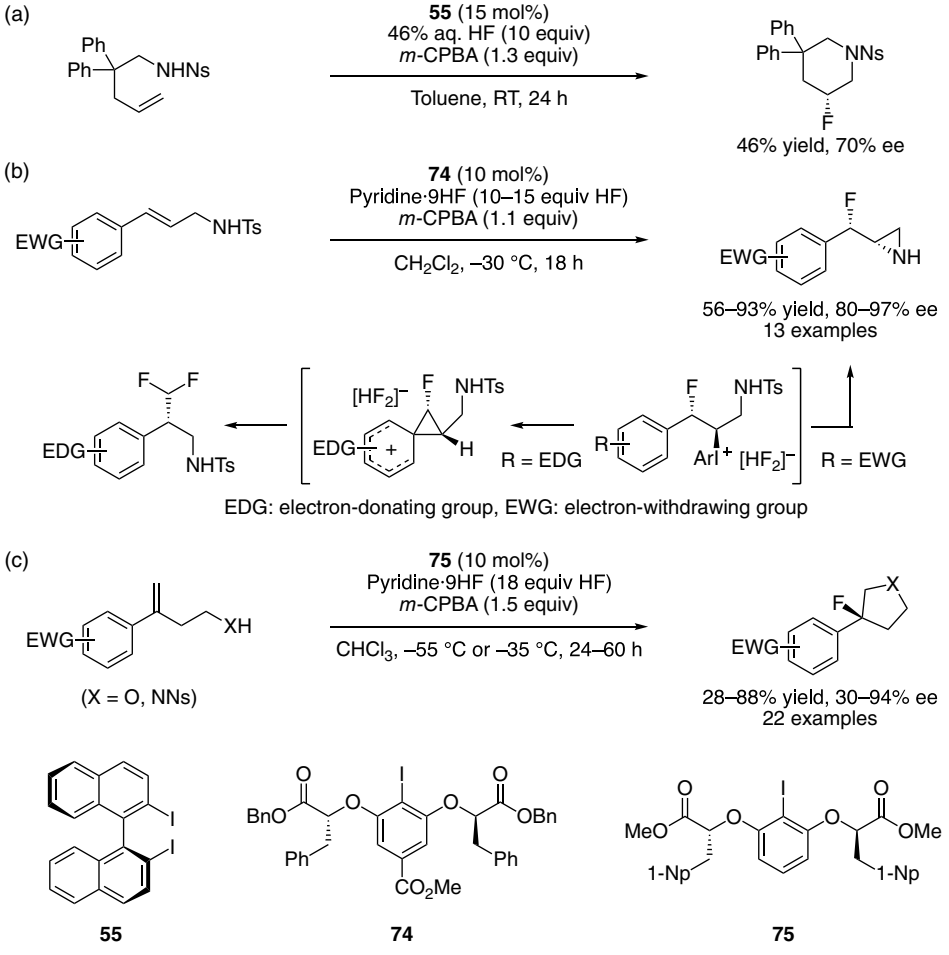

Scheme 7.40. Organoiodine-catalyzed enantioselective oxidative fluorocyclization. (a) Source: [123]. (b) Source: [143]. (c) Source: [144].

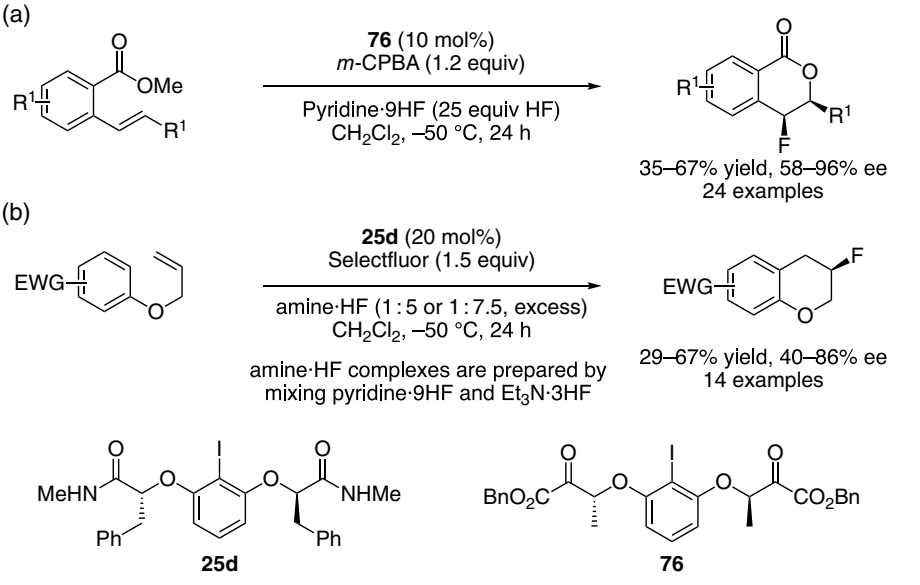

Scheme 7.41. Enantioselective fluorocyclization via C–O and C–C bond formation. (a) Source: [145]. (b) Source: [146].

via *exo*-selective cyclization, organoiodine-catalyzed nucleophilic fluorolactonization provided *endo*-cyclization products exclusively. On the other hand, Gilmour and colleagues have recently reported the chiral bisamide **25d**-catalyzed fluoro-carbocyclization of aryl allyl ethers using Selectfluor as an oxidant to generate 3-fluorochromanes with moderate to good enantioselectivity (Scheme 7.41b) [146]. Notably, the HF-to-amine ratio was important to induce high chemoselectivity of desired Friedel–Crafts-type fluorocyclization over vicinal difluorination. Two conditions were developed, one with a higher HF:amine ratio to increase reactivity and another with a lower HF:amine ratio to increase enantioselectivity.

On the other hand, in 2016, Muñiz and colleagues first demonstrated the feasibility of organoiodine catalysis in enantioselective alkene oxidation under full intermolecular reaction control (Scheme 7.42) [130, 147]. Highly enantioselective oxidative vicinal diacetoxylation of terminal styrenes was achieved by using structurally congested secondary bisamide **25c** as a catalyst. Notably, the choice of peracetic acid as an oxidant was crucial to avoid an undesired background epoxidation. In addition, the catalytic use of triflic acid was also required to activate iodine(III) active species, and to minimize undesired direct epoxidation of the substrate with *m*-CPBA. Two regioisomeric acetoxy alcohols with identical enantioselectivity were generated via hydrolysis of the Woodward-type dioxolane intermediate **77** under the catalytic conditions, and acetylation of the crude reaction mixture afforded the desired diacetoxy products in good yields with high enantioselectivity. As demonstrated by Ishihara and Uyanik previously for their conformationally flexible second-generation catalysis (Scheme 7.11) [78], the folding structures via hydrogen-bonding interactions as well as helical chirality of the corresponding iodine(III) **26c** were confirmed by X-ray structural analysis [130].

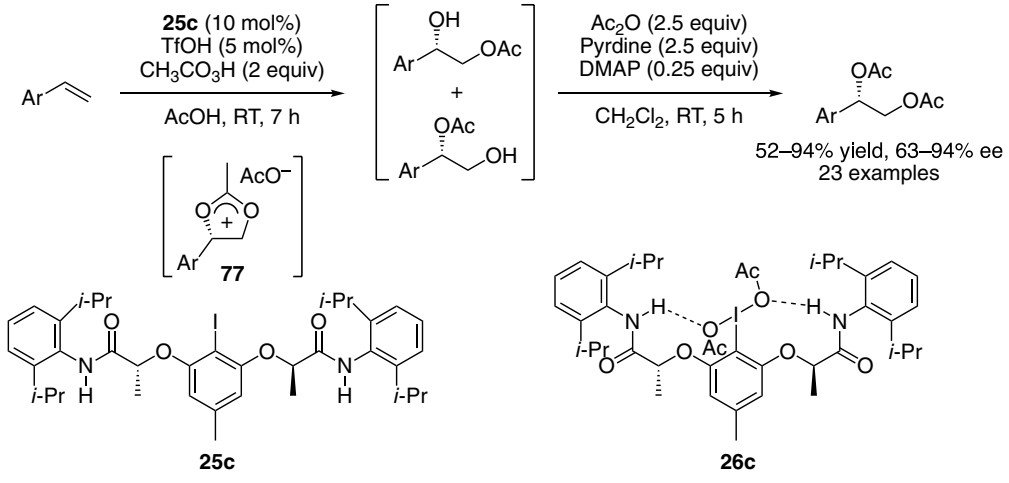

Scheme 7.42. Enantioselective vicinal diacetoxylation of styrenes. Source: [130].

In 2011, Muñiz and colleagues reported the first example of enantioselective intermolecular C–N functionalizations of alkenes using a chiral organoiodine(III) reagent **7** [26]. The formal enantioselective diamination of styrenes proceeded by using bismesylimide as amine equivalents under mild conditions to give the corresponding 1,2-disulfonimides in good yield with high enantioselectivity up to 95% ee. Following this seminal work, in 2017, the same group developed a catalytic version of this reaction (Scheme 7.43) [148]. By using bis-*tert*-amide **78** as a catalyst and *m*-CPBA as an oxidant, a variety of terminal and β-substituted styrenes underwent diamination with excellent enantioselectivity up to 98% ee. As in the stoichiometric oxidative coupling [26], (*E*)-styrenes gave the *anti*-product through presumed anchimeric assistance by the sulfonimide. Direct epoxidation by *m*-CPBA could be minimized through temperature control as well as by using a mixed solvent of *tert*-butyl methyl ether/hexafluoroisopropanol (or trifluoroethanol). Interestingly, a single crystal X-ray structural analysis of the corresponding iodine(III) **79** revealed the double hydrogen bonding via a water molecule, which may provide a useful explanation for the high enantioselectivity observed.

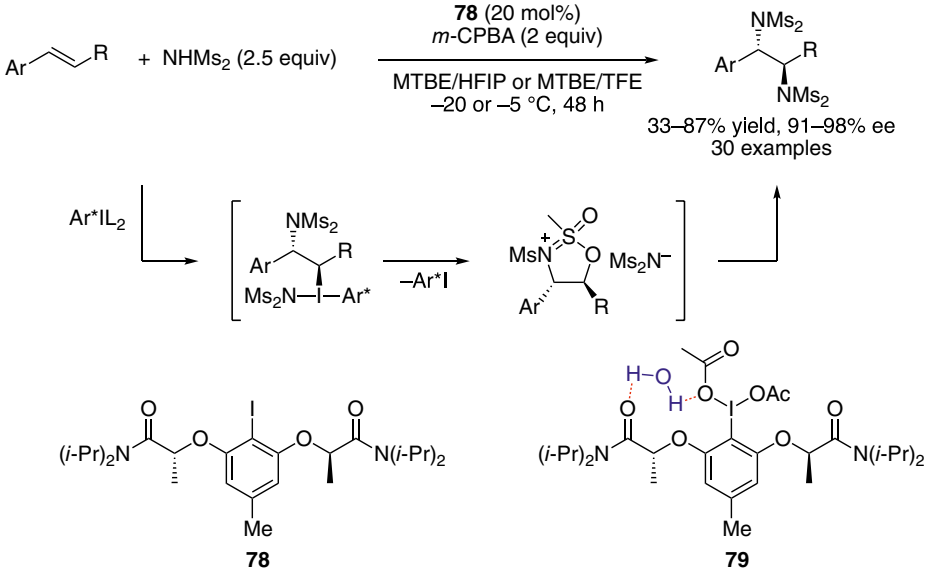

Scheme 7.43. Catalytic enantioselective vicinal diamination of styrenes. Source: [148].

By using a similar bis-*tert*-amide catalyst **80**, very recently, Hashimoto and colleagues developed catalytic enantioselective intermolecular oxyamination of alkenes (Scheme 7.44) [149]. Notably, a key to success was the discovery of a virtually unexplored chemical entity, *N*-(fluorosulfonyl)carbamate, as a bench-stable bifunctional *N*,*O*-nucleophile. The use of both carbamate and its lithium salt was essential to promote the chemoselective reaction. In addition, the judicious choice of an oxidant depending on the electronic properties of substrates was important. While for electronically neutral and slightly electron-poor styrenes, magnesium monoperoxyphthalate hexahydrate (MMPP) was optimal, the use of Selectfluor constantly gave the products in good yields with high enantioselectivities for the electron-deficient or *ortho*-halogenated styrenes as well as terminal aliphatic alkenes. The products could be easily deprotected in one step to reveal free amino alcohols without loss of enantioselectivity.

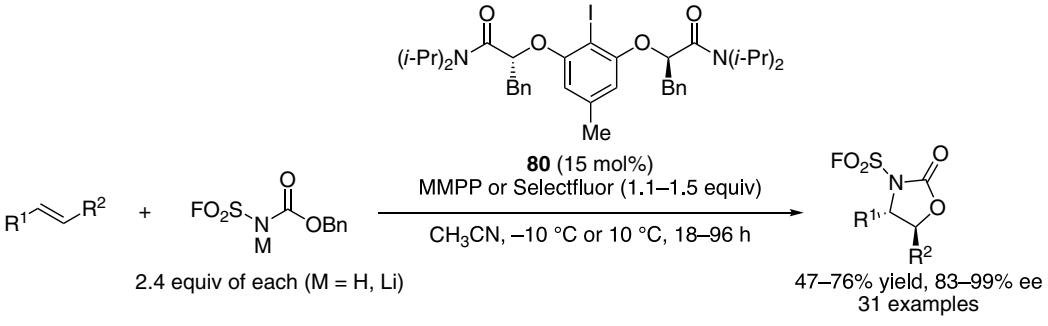

Scheme 7.44. Catalytic enantioselective intermolecular oxyamination of alkenes. Source: [149].

Organoiodine-catalyzed difluorination of alkenes has received a considerable research interest motivated by the interesting conformational properties such as the "gauche effect" of vicinal difluorides [150]. In 2016, groups of Gilmour [151] and Jacobsen [152] independently reported the first organoiodine-catalyzed vicinal difluorination of alkenes. While triethylamine-HF complex and Selectfluor were used in Gilmour's protocol as a fluoride source and oxidant, respectively, pyridine-HF complex and *m*-CPBA

were used in Jacobsen's protocol. In both seminal reports, preliminary enantioselective variants were also disclosed by using lactate-derived chiral iodoarene catalysts with moderate or excellent enantioselectivity, respectively.

In 2018, Gilmour and colleagues followed up their enantioselective catalytic vicinal difluorination by using bis-*sec*-amide catalyst **25e** (Scheme 7.45a) [153]. Electron-deficient styrenes underwent difluorination with up to 88% ee. Interestingly, the HF-to-amine ratio was found to have a dramatic effect on selectivity for the 1,2-difluoride products (*vic*) versus the 1,1- difluoride products (*gem*) that were generated via aryl migration. While the use of the HF:amine ratio of 4.5 : 1 provided the vicinal difluoride with optimal enantioselectivity and high chemoselectivity, increasing the HF:amine ratio to 9.2 : 1 led to a complete reversal to favor the formation of the migration products.

On the other hand, in 2019, Jacobsen and colleagues followed up their enantioselective vicinal difluorination of cinnamamides by using bisester catalyst **74** (Scheme 7.45b) [154]. Several β-alkylcinnamamides underwent vicinal difluorination with up to 98% ee with generally excellent product selectivity. Notably, the incorporation of the *para*-carbomethoxy substituent on the catalyst improved the catalyst stability and yields in the difluorination reactions. Experimental observations revealed that chemoselectivity between the 1,2- and 1,1-difluorination (aryl migration) pathways is based on the competition between phenonium ion formation versus anchimeric assistance by the amide in the breakdown of the alkyl iodine(III) intermediate.

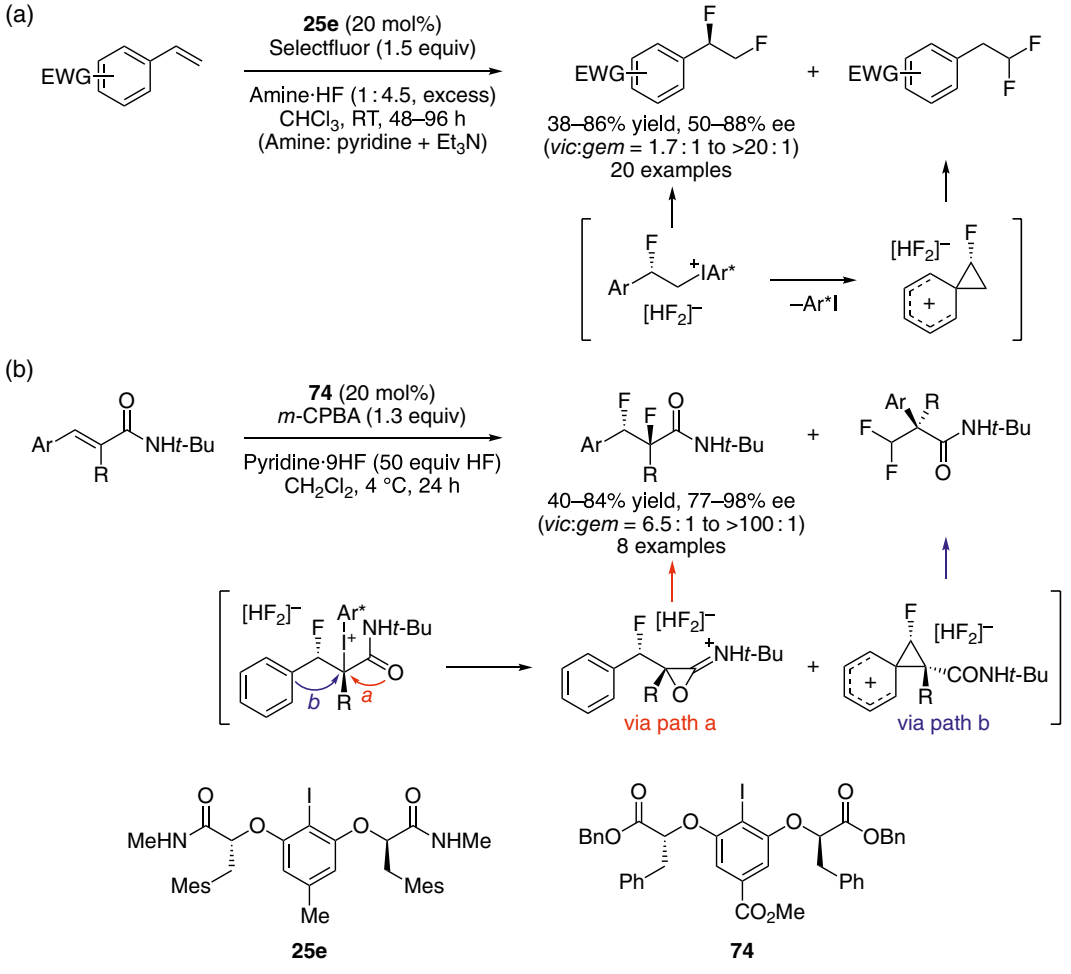

Scheme 7.45. Catalytic enantioselective vicinal difluorination of alkenes. (a) Source: [153]. (b) Source: [154].

Taking advantage of the propensity for β-aryliodine(III) intermediates to undergo rearrangement via phenonium ion formation, as discussed above, Jacobsen and colleagues developed an enantioselective catalytic protocol for the geminal difluorination of alkenes (Scheme 7.46a) [155]. This migration concept was previously introduced by Wirth and colleagues in the enantioselective oxidative rearrangements of chalcones under stoichiometric conditions using chiral organoiodine(III) reagent **8** [29]. By using iodoarene catalyst **74** in the presence of HF-pyridine and *m*-CPBA, a variety of disubstituted cinnamamides and di- and tri-substituted cinnamate esters underwent difluorination with aryl migration to afford the corresponding rearrangement products with high enantioselectivity. Notably, the incorporation of a *para*-methoxycarbonyl group on the iodoarene **74** improved enantioselectivity remarkably, albeit had a minimal influence on the chemical yield. In addition, the introduction of benzylic moieties in the chiral position of the catalyst was crucial for high reactivity and enantioselectivity, due to the decrease in reaction temperature. Theoretical calculations revealed that the formation of alkyliodine(III) intermediates common to both 1,2- and 1,1-difluorination pathways is enantio-determining step and multiple attractive non-covalent interactions in substrate–iodine(III) complex such as C–H-π, C–H-O, and slipped π-π stacking play dominant roles in the enantiodiscrimination [156]. The substrate scope of the geminal difluorination is recently expanded to α-bromostyrenes (Scheme 7.46b) [157]. The rearrangement proceeded via bromonium rather than phenonium ion formation to provide β,β-difluorinated alkyl bromides with high enantioselectivity. Notably, since decomposition of catalyst **74** via alkylation of the ester groups by the bromonium ion intermediate was observed, electron-deficient benzyl ester-derived catalyst **81** was designed to suppress undesired decomposition pathways.

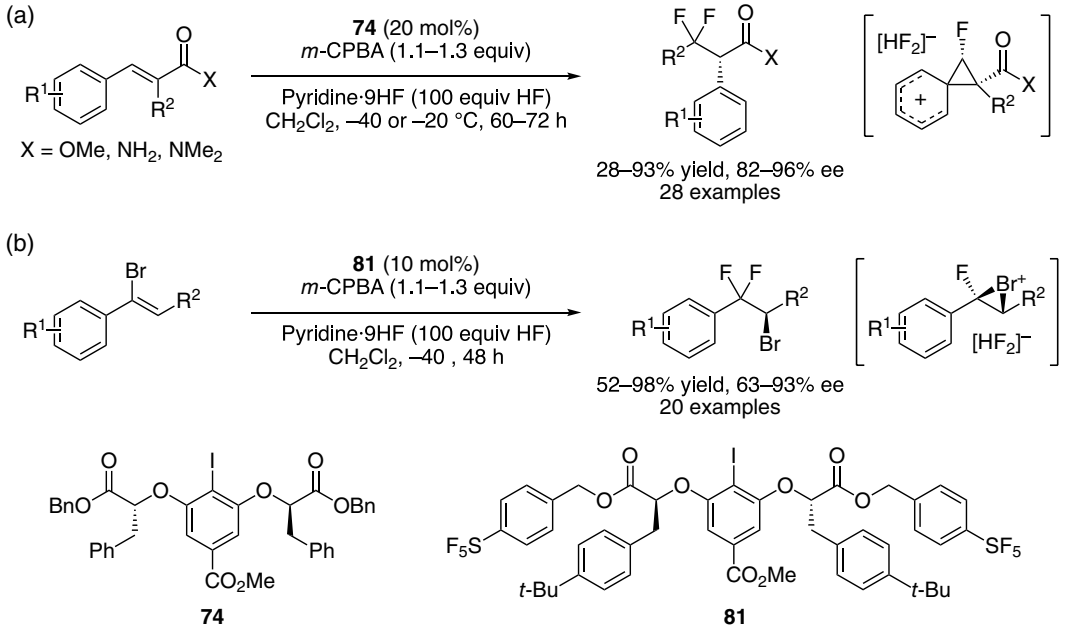

Scheme 7.46. Catalytic enantioselective geminal difluorination of alkenes. (a) Aryl migration (Source: [155]). (b) Bromide migration (Source: [157]).

Jacobsen and colleagues have also reported Wagner–Meerwein rearrangements of β-substituted styrenes involving aryl, alkyl, and hydride migrations (Scheme 7.47) [158]. By using iodoarene catalysts **74** under similar conditions, a variety of 1,3-difluorinated adducts could be obtained in good yields with excellent enantio- and diastereoselectivity. Hammett and kinetic isotope effect studies as well as theoretical calculations revealed the existence of two different mechanisms in these rearrangement reactions depending on the migrating group. In the alkyl group or hydride rearrangements, π-complexation of the

substrate followed by enantio-determining fluoride attack forms the 1,2-fluoroiodinated adduct which then undergoes migration to generate the *syn*-product. On the other hand, π-complexation of the substrate is followed by enantiodetermining intramolecular 1,2-migration prior to fluorination in an aryl rearrangement process to give *anti*-product. Notably, both pathways were operative under the same conditions for closely related substrates, and both were promoted by the same chiral organoiodine catalyst with high enantioselectivity.

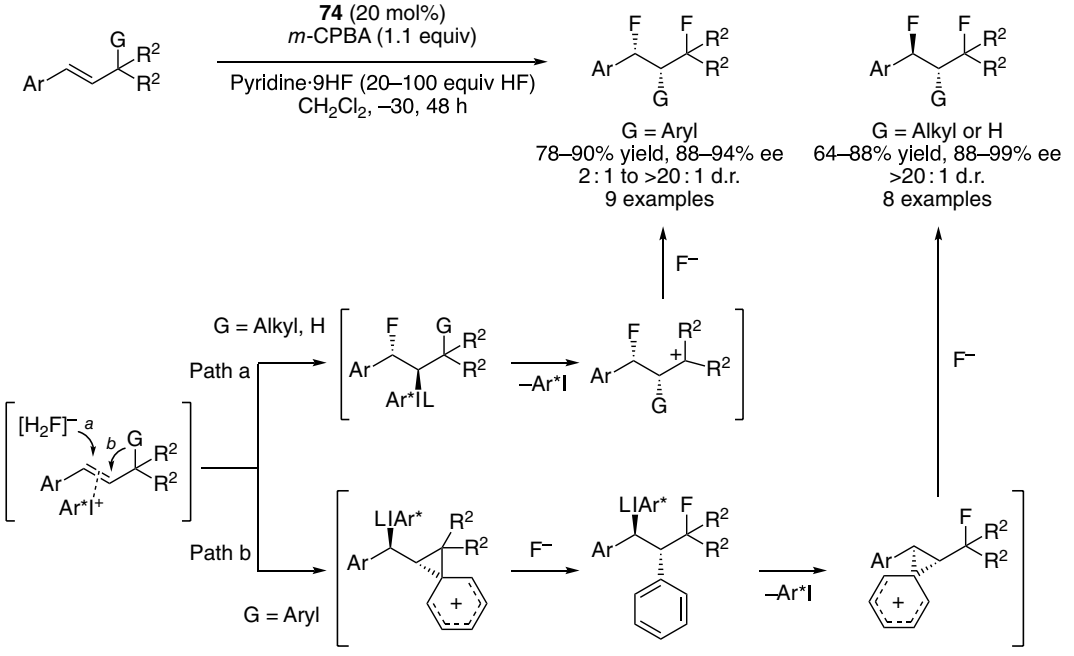

Scheme 7.47. Catalytic enantioselective geminal difluorination of alkenes. Source: [158].

As mentioned above, Wirth and colleagues have reported the first enantioselective oxidative rearrangements of chalcones and 1,1-disubstituted alkenes using chiral organoiodine reagent **8** under stoichiometric conditions [29]. Following from these precedents, in 2019, Gong and colleagues reported the first highly enantioselective catalytic oxidative rearrangement of tertiary allylic alcohols to afford α-carboalkoxy ketones using bis-*tert*-amide catalyst **64** in the presence of Selectfluor and TsOH as an oxidant and activator, respectively (Scheme 7.48) [159]. The reaction was proposed to be initiated by Brønsted acid-catalyzed 1,3-rearrangement of 1,1-diaryl allylic alcohols in the presence of the excess amount of alcohols used as a co-solvent to give the corresponding 3,3-diaryl allyl ethers, which might then be oxidatively rearranged to the corresponding α-aryl ketones with high enantioselectivity. The reaction of substrates bearing two different aryl groups at the allylic position afforded a mixture of regioisomers with modest selectivity. Both products were obtained with high enantioselectivity and major isomer was derived from the migration of the more electron-rich arene.

7.5. CONCLUSION AND OUTLOOK

In this chapter, we reviewed the recent progress on the enantioselective organoiodine catalysis for oxidative transformations. The first organoiodine(III)-catalyzed enantioselective oxidative coupling reaction was reported in 2007 [64]. After the breakthroughs of the development of the lactate-derived C_2-symmetic bisamides or bisesters as chiral organoiodine catalysts in 2010 [24, 77], rapid progress has been made in

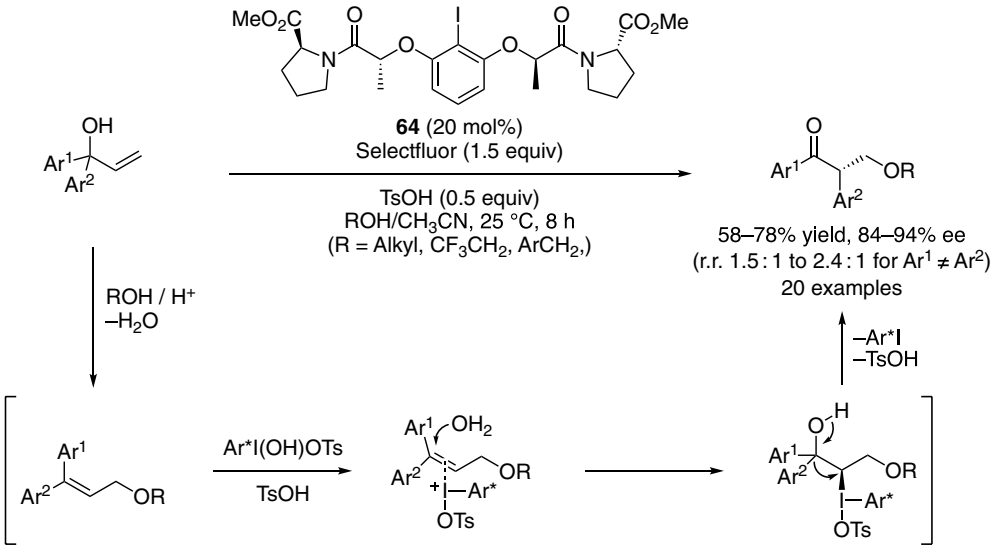

Scheme 7.48. Enantioselective oxidative rearrangement of tertiary allylic alcohols. Source: [159].

the development of enantioselective organoiodine catalysis for oxidative dearomatization of arenols, oxidative α-coupling of carbonyls, and oxidative difunctionalizaiton of alkenes. Suitable catalysts may be found out easily among those both diamide- and diester-type catalysts for further enantioselective oxidative transformations.

However, organoiodine catalysis has some drawbacks. For example, relatively expensive and potentially explosive oxidants such as *m*-CPBA or Selectfluor have often been used in the presence of Lewis or Brønsted acid activators. In addition, side-products such as *meta*-chlorobenzoic acid (*m*-CBA) derived from the oxidants are generated. To overcome these limitations, very recently, organoiodine (III or V) catalysis under aerobic or electro-oxidation conditions has been developed [160–162]. However, no enantioselective variant has been reported to date. On the other hand, in 2010, Uyanik, Ishihara, and colleagues have developed ammonium hypoiodite catalysis, which is not covered in this review, for the oxidative coupling reactions [163]. The hypoiodite salts, catalytic active species, are generated in situ from the corresponding iodides in the presence of relatively inexpensive and mild oxidants such as hydrogen peroxide or alkyl hydroperoxides. In contrast to organoiodine(III) catalysis, this catalytic oxidation system proceeds under milder conditions and water or alcohol is the only side-products derived from the oxidant used. After these findings, rapid progress has been made in the development of inorganic iodine-catalyzed oxidative transformations [164]. However, in contrast to organoiodine(III) catalysis, enantioselective hypoiodite catalysis has so far been explored modestly. Especially, the development of a general and highly enantioselective intermolecular coupling looks to be highly promising, and perhaps this is an area where major further developments might be expected.

REFERENCES

1. Yoshimura, A.; Zhdankin, V. V. *Chem. Rev.* **2016**, *116*, 3328–3435.
2. Lupton, D. W.; Ngatimin, M. *Aust. J. Chem.* **2010**, *63*, 653–658.
3. Liang, H.; Ciufolini, M. A. *Angew. Chem. Int. Ed.* **2011**, *50*, 11849–11851.
4. Uyanik, M.; Ishihara, K. *J. Synth. Org. Chem., Jpn.* **2012**, *70*, 1116–1122.
5. Parra, A.; Reboredo, S. *Chem. Eur. J.* **2013**, *19*, 17244–17260.
6. Berthiol, F. *Synthesis* **2015**, 587–603.
7. Basdevant, B.; Guilbault, A.-A.; Beaulieu, S.; Lauriers, A. J.-D.; Legault, C. Y. *Pure Appl. Chem.* **2017**, *89*, 781–789.
8. Fujita, M. *Heterocycles* **2018**, *96*, 563–594.

9. Claraz, A.; Masson, G. *Org. Biomol. Chem.* **2018**, *16*, 5386–5402.
10. Ghosh, G.; Pradhan, S.; Chatterjee, I. *Beilstein J. Org. Chem.* **2018**, *14*, 1244–1262.
11. Flores, A.; Cots, E.; Bergès, J.; Muñiz, K. *Adv. Synth. Catal.* **2019**, *361*, 2–25.
12. Parra, A. *Chem. Rev.* **2019**, *119*, 12033–12088.
13. Wang, Y.; Yang, B.: Wu, X.-X.; Wu, Z.-G. *Synthesis* **2021**, *53*, 889–903.
14. Imamoto, T.; Koto, H. *Chem. Lett.* **1986**, *15*, 967–968.
15. Ray, D. G.; Koser, G. F. *J. Org. Chem.* **1992**, *57*, 1607–1610.
16. Hatzigrigoriou, E.; Varvoglis, A.; Bakola-Christianopoulout, M. *J. Org. Chem.* **1990**, *55*, 315–318.
17. Ray, D. G.; Koser, G. F. *J. Am. Chem. Soc.* **1990**, *112*, 5672–5673.
18. Tohma, H.; Takizawa, S.; Morioka, H.; Maegawa, T.; Kita, Y. *Chem. Pharm. Bull.* **2000**, *48*, 445–446.
19. Wirth, T.; Hirt, U. H. *Tetrahedron: Asymmetry* **1997**, *8*, 23–26.
20. Hirt, U. H.; Spingler, B.; Wirth, T. *J. Org. Chem.* **1998**, *63*, 7674–7679.
21. Hirt, U. H.; Schuster, M. F. H.; French, A. N.; Wiest, O. G.; Wirth, T. *Eur. J. Org. Chem.* **2001**, *2001*, 1569–1579.
22. Fujita, M.; Okuno, S.; Lee, H. J.; Sugimura, T.; Okuyama, T. *Tetrahedron Lett.* **2007**, *48*, 8691–8694.
23. Fujita, M.; Ookubo, Y.; Sugimura, T. *Tetrahedron Lett.* **2009**, *50*, 1298–1300.
24. Fujita, M.; Yoshida, Y.; Miyata, K.; Wakisaka, A.; Sugimura, T. *Angew. Chem. Int. Ed.* **2010**, *49*, 7068–7071.
25. Fujita, M.; Wakita, M.; Sugimura, T. *Chem. Commun.* **2011**, *47*, 3983–3985.
26. Röben, C.; Souto, J.; González, Y.; Lishchynskyi, A.; Muñiz, K. *Angew. Chem. Int. Ed.* **2011**, *50*, 9478–9482.
27. Deng, Q.-H.; Wang, J.-C.; Xu, Z.-J.; Zhou, C.-Y.; Che, C.-M. *Synthesis* **2011**, 2959–2967.
28. Farid, U.; Wirth, T. *Angew. Chem. Int. Ed.* **2012**, *51*, 3462–3465.
29. Farid, U.; Malmedy, F.; Claveau, R.; Albers, L.; Wirth, T. *Angew. Chem. Int. Ed.* **2013**, *52*, 7018–7022.
30. Röben, C.; Souto, J.; Escudero-Adán, E. C.; Muñiz, K. *Org. Lett.* **2013**, *15*, 1008–1011.
31. Kong, Q.; Feige, P.; Haro, T.; Nevado, C. *Angew. Chem. Int. Ed.* **2013**, *52*, 2469–2473.
32. Takesue, T. Morifumi Fujita, M.; Sugimura, T.; Akutsu, H. *Org. Lett.* **2014**, *16*, 4634–4637.
33. Shimogaki, M.; Fujita, M.; Sugimura, T. *Molecules* **2015**, *20*, 17041–17057.
34. Mizar, P.; Niebuhr, R.; Hutchings, M.; Farooq, U.; Wirth, T. *Chem. Eur. J.* **2016**, *22*, 1614–1617.
35. Brown, M.; Kumar, R.; Rehbein, J. Wirth, T. *Chem. Eur. J.* **2016**, *22*, 4030–4035.
36. Ahmad, A.; Silva, L. F. *J. Org. Chem.* **2016**, *81*, 2174–2181.
37. Shimogaki, M.; Fujita, M.; Sugimura, T. *Angew. Chem. Int. Ed.* **2016**, *55*, 15797–15801.
38. Shimogaki, M.; Fujita, M.; Sugimura, T. *J. Org. Chem.* **2017**, *82*, 11836–11840.
39. Qurban, J.; Elsherbini, M.; Wirth, T. *J. Org. Chem.* **2017**, *82*, 11872–11876.
40. Fujita, M.; Miura, K.; Sugimura, T. *Beilstein J. Org. Chem.* **2018**, *14*, 659–663.
41. Hokamp, T.; Mollari, L.; Wilkins, L. C.; Melen, R. L.; Wirth, T. *Angew. Chem. Int. Ed.* **2018**, *57*, 8306–8309.
42. Hokamp, T.; Wirth, T. *J. Org. Chem.* **2019**, *84*, 8674–8682.
43. Ochiai, M.; Takaoka, Y.; Masaki, Y. *J. Am. Chem. Soc.* **1999**, *121*, 9233–9234.
44. Mizar, P.; Wirth, T. *Angew. Chem. Int. Ed.* **2014**, *53*, 5993–5997.
45. Malmedy, F.; Wirth, T. *Chem. Eur. J.* **2016**, *22*, 16072–16077.
46. Companys, S.; Peixoto, P. A.; Bosset, C.; Chassaing, S.; Miqueu, K.; Sotiropoulos, J.-M.; Pouységu, L.; Quideau, S. *Chem. Eur. J.* **2017**, *23*, 13309–13313.
47. Gao, W.-C.; Xiong, Z.-Y.; Pirhaghani, S.; Wirth, T. *Synthesis* **2019**, *51*, 276–284.
48. Dohi, T.; Maruyama, A.; Takenaga, N.; Senami, K.; Minamitsuji, Y.; Fujioka, H.; Caemmerer, S. B.; Kita, Y. *Angew. Chem. Int. Ed.* **2008**, *47*, 3787–3790.
49. Zhdankin, V. V.; Smart, J. T.; Zhao, P.; Kiprof, P. *Tetrahedron Lett.* **2000**, *41*, 5299–5302.
50. Ladziata, U.; Carlson, J.; Zhdankin, V. V. *Tetrahedron Lett.* **2006**, *47*, 6301–6304.
51. Boppisetti, J. K.; Birman, V. B. *Org. Lett.* **2009**, *11*, 1221–1223.
52. Bosset, C.; Coffinier, R.; Peixoto, P. A.; Assal, M. E.; Miqueu, K.; Sotiropoulos, J.-M.; Laurent Pouységu, L.; Quideau, S. *Angew. Chem. Int. Ed.* **2014**, *53*, 9860–9864.
53. Coffinier, R.; Assal, M. E.; Peixoto, P. A.; Bosset, C.; Miqueu, K.; Sotiropoulos, J.-M.; Laurent Pouységu, L.; Quideau, S. *Org. Lett.* **2016**, *18*, 1120–1123.
54. Yoshida, Y.; Magara, A.; Mino, T.; Sakamoto, M. *Tetrahedron Lett.* **2016**, *57*, 5103–5107.
55. Assal, M. E.; Peixoto, P. A.; Coffinier, R.; Garnier, T.; Deffieux, D.; Miqueu, K.; Sotiropoulos, J.-M.; Laurent Pouységu, L.; Quideau, S. *J. Org. Chem.* **2017**, *82*, 11816–11828.
56. Yoshida, Y.; Kanashima, Y.; Mino, T.; Sakamoto, M. *Tetrahedron* **2019**, *78*, 3840–3849.
57. Ochiai, M.; Takeuchi, Y.; Katayama, T.; Sueda, T.; Miyamoto, K. *J. Am. Chem. Soc.* **2005**, *127*, 12244–12245.
58. Dohi, T.; Maruyama, A.; Yoshimura, M.; Morimoto, K.; Tohma, H.; Kita, Y. *Angew. Chem. Int. Ed.* **2005**, *44*, 6193–6196.
59. Thottumkara, A. P.; Bowsher, M. S.; Vinod, T. K. *Org. Lett.* **2005**, *7*, 2933–2936.
60. Ochiai, M.; Miyamoto, K. *Eur. J. Org. Chem.* **2008**, *2008*, 4229–4239.
61. Dohi, T.; Kita, Y. *Chem. Commun.* **2009**, *45*, 2073–2085.
62. Finkbeiner, P.; Nachtsheim, B. J. *Synthesis* **2013**, *45*, 979–999.

63. Yusubov, M. S.; Zhdankin, V. V. *Res.-Effic. Technol.* **2015**, *1*, 49–67.
64. Richardson, R. D.; Page, T. K.; Altermann, S. M.; Paradine, S. M.; French, A. N.; Wirth, T. *Synlett* **2007**, 538–542.
65. You, S.-L. Ed.; *Asymmetric Dearomatization Reactions*; John Wiley & Sons, Weinheim, **2016**.
66. Magdziak, D.; Meek, S. J.; Pettus, T. R. R. *Chem. Rev.* **2004**, *104*, 1383–1430.
67. Roche, S. P.; Porco, J. A., Jr. *Angew. Chem. Int. Ed.* **2011**, *50*, 4068–4093.
68. Zhuo, C.-X.; Zhang, W.; You, S.-L. *Angew. Chem. Int. Ed.* **2012**, *51*, 12662–12686.
69. Wu, W.-T.; Zhang, L.; You, S.-L. *Chem. Soc. Rev.* **2016**, *45*, 1570–1580.
70. Harned, A. M. *Tetrahedron. Lett.* **2014**, *55*, 4681–4689.
71. Quideau, S.; Pouységu, L.; Peixoto, P. A.; Deffieux, D. Phenol dearomatization with hypervalent iodine reagents. In: *Hypervalent Iodine Chemistry*; Wirth, T. Ed.; Springer: Switzerland, **2016**, pp 25–74.
72. Kürti, L.; Herczegh, P.; Visy, J.; Simonyi, M.; Antus, S.; Pelter, A. *J. Chem. Soc., Perkin Trans. 1* **1999**, 379–380.
73. Pelter, A.; Ward, R. S. *Tetrahedron* **2001**, *57*, 273–282.
74. Drutu, I.; Njardarson, J. T.; Wood, J. L. *Org. Lett.* **2002**, *4*, 493–496.
75. Dohi, T.; Takenaga, N.; Nakae, T.; Toyoda, Y.; Yamasaki, M.; Shiro, M.; Fujioka, H.; Maruyama, A.; Kita, Y. *J. Am. Chem. Soc.* **2013**, *135*, 4558–4566.
76. Zheng, H.; Sang, Y.; Houk, K. N.; Xue, X.-S.; Cheng, J.-P. *J. Am. Chem. Soc.* **2019**, *141*, 16046–16056.
77. Uyanik, M.; Yasui, T.; Ishihara, K. *Angew. Chem. Int. Ed.* **2010**, *49*, 2175–2177.
78. Uyanik, M.; Yasui, T.; Ishihara, K. *Tetrahedron* **2010**, *66*, 5841–5851
79. Uyanik, M.; Yasui, T.; Ishihara, K. *Angew. Chem. Int. Ed.* **2013**, *52*, 9215–9218.
80. Dohi, T.; Yamaoka, N.; Kita, Y. *Tetrahedron* **2010**, *66*, 5775–5785.
81. Uyanik, M.; Sasakura, N.; Mizuno, M.; Ishihara, K. *ACS Catal.* **2017**, *7*, 872–876.
82. Deng, Q.; Xia, W.; Hussain, M. I.; Zhang, X.; Hu, W.; Xiong, Y. *J. Org. Chem.* **2020**, *85*, 3125–3133.
83. Uyanik, M.; Yasui, T.; Ishihara, K. *J. Org. Chem.* **2017**, *82*, 11946–11953.
84. Suzuki, T.; Watanabe, S.; Uyanik, M.; Ishihara, K.; Kobayashi, S.; Tanino, K. *Org. Lett.* **2018**, *20*, 3919–3922.
85. Jain, N.; Xu, S.; Ciufolini, M. A. *Chem. Eur. J.* **2017**, *23*, 4542–4546.
86. Jain, N.; Ciufolini, M. A. *Synthesis* **2018**, *51*, 3322.
87. Jain, N.; Hein, J. E.; Ciufolini, M. A. *Synlett* **2019**, *30*, 1222–1227.
88. Zhang, D.-Y.; Xu, L.; Wu, H.; Gong, L.-Z. *Chem. Eur. J.* **2015**, *21*, 10314–10317.
89. Hempel, C.; Maichle-Mössmer, C.; Pericàs, M. A.; Nachtsheim, B. J. *Adv. Synth. Catal.* **2017**, *359*, 2931–2941.
90. Boelke, A.; Lork, E.; Nachtsheim, B. J. *Chem. Eur. J.* **2018**, *24*, 18653–18657.
91. Abazid, A. H.; Nachtsheim, B. J. *Angew. Chem. Int. Ed.* **2020**, *59*, 1479–1484.
92. Guilbault, A.-A.; Legault, C. Y. *ACS Catal.* **2012**, *2*, 219–222.
93. Murray, S. J.; Ibrahim, H. *Chem. Commun.* **2015**, *51*, 2376–2379.
94. Ogasawara, M.; Sasa, H.; Hu, H.; Amano, Y.; Nakajima. H.; Takenaga, N.; Nakajima, K.; Kita, Y.; Takahashi, T.; Dohi, T. *Org. Lett.* **2017**, *19*, 4102–4105.
95. Dohi, T.; Sasa, H.; Miyazaki, K.; Fujitake, M.; Takenaga, N.; Kita, Y. *J. Org. Chem.* **2017**, *82*, 11954–11960.
96. Wang, Y.; Zhao, C.-Y.; Wang, Y.-P. Zheng, W.-H. *Synthesis* **2019**, *51*, 3675–3682.
97. Antien, K.; Pouységu, L.; Deffieux, D.; Massip, S.; Peixoto, P.; Quideau, S. *Chem. Eur. J.* **2019**, *25*, 2852–2858.
98. Quideau, S.; Lyvinec, G.; Marguerit, M.; Bathany, K.; Ozanne-Beaudenon, A.; Buffeteau, T.; Cavagnat, D.; Chenede, A. *Angew. Chem. Int. Ed.* **2009**, *48*, 4605–4609.
99. Volp, K. A.; Harned, A. M. *Chem. Commun.* **2013**, *49*, 3001–3003.
100. Muñiz, K.; Fra, L. *Synthesis* **2017**, 2901–2096.
101. Hashimoto, H.; Shimazaki, Y.; Omatsu, Y.; Maruoka, K. *Angew. Chem. Int. Ed.* **2018**, *57*, 7200–7204.
102. Smith, A. M.; Hii, K. K. *Chem. Rev.* **2011**, *111*, 1637–1656.
103. Hoffman, R. V. *Tetrahedron* **1991**, *47*, 1109–1135.
104. Yamamoto, Y.; Togo, H. *Synlett* **2006**, 798–800.
105. Altermann, S. M.; Richardson, R. D.; Page, T. K.; Schmidt, R. K.; Holland, E.; Mohammed, U.; Paradine, S. M.; French, A. N.; Richter, C.; Bahar, A. M.; Witulski, B.; Wirth, T. *Eur. J. Org. Chem.* **2008**, 5315–5328.
106. Farooq, U.; Schäfer, S.; Shah, A. A.; Freudendahl, D. M.; Wirth, T. *Synthesis* **2010**, *47*, 1023–1029.
107. Yu, J.; Cui, J.; Hou, X.-S.; Liu, S.-S.; Gao, W.-C.; Jiang, S.; Tian, J.; Zhang, C. *Tetrahedron: Asymmetry* **2011**, *22*, 2039–2055.
108. Guilbault, A.-A.; Basdevant, B.; Wanie, V.; Legault, C. Y. *J. Org. Chem.* **2012**, *77*, 11283–11295.
109. Thérien, M.-È.; Guilbault, A.-A.; Legault, C. Y. *Tetrahedron: Asymmetry* **2013**, *24*, 1193–1197.
110. Brenet, S.; Minozzi, C.; Clarens, B.; Amiri, L.; Berthiol, F. *Synthesis* **2015**, *47*, 3859–3873.
111. Feng, Y.; Huang, R.; Hu, L.; Xiong, Y.; Coeffard, V. *Synthesis* **2016**, *48*, 2637–2644.
112. Levitre, G.; Dumoulin, A.; Retailleau, P.; Panossian, A.; Leroux, F. R.; Masson, G. *J. Org. Chem.* **2017**, *82*, 11877–11883.
113. Beaulieu, S.; Legault, C. Y. *Chem. Eur. J.* **2015**, *21*, 11206–11211.
114. Basdevant, B.; Legault, C. Y. *Org. Lett.* **2015**, *17*, 4918–4921.
115. Basdevant, B.; Legault, C. Y. *J. Org. Chem.* **2015**, *80*, 6897–6902.
116. Yamamoto, Y.; Togo, H. *Synlett* **2005**, 2486–2488.

117. Yang, G.-H.; Zheng, H.; Li, X.; Cheng, J.-P. *ACS Catal.* **2020**, *10*, 2324–2333.
118. Alharbi, H.; Elsherbini, M.; Qurban, J.; Wirth, T. *Chem. Eur. J.* **2021**, *27*, 4317–4321.
119. Hokamp, T.; Wirth, T. *Chem. Eur. J.* **2020**, *26*, 10417–10421.
120. Rodriguez, A.; Moran, W. J. *Synthesis* **2012**, 1178–1182.
121. Kitamura, T.; Muta K.; Kuriki, S. *Tetrahedron Lett.* **2013**, *54*, 6118–6120.
122. Yang, X.; Wu, T.; Phippa, R. J.; Toste, F. D. *Chem. Rev.* **2015**, *115*, 826–870.
123. Suzuki, S.; Kamo, T.; Fukushi, K.; Hiramatsu, T.; Tokunaga, E.; Dohi, T.; Kita, Y.; Shibata, N. *Chem. Sci.* **2014**, *5*, 2754–2760.
124. Pluta, R.; Krach, P. E.; Cavallo, L.; Falivene, L.; Rueping, M. *ACS Catal.* **2018**, *8*, 2582–2588.
125. Wang, Y.; Yuan, H.; Lu, H.; Zheng, W.-H. *Org. Lett.* **2018**, *20*, 2555–2558.
126. Wu, H.; He, Y.-P.; Xu, L.; Zhang, D.-Y.; Gong, L.-Z. *Angew. Chem. Int. Ed.* **2014**, *53*, 3466–3469.
127. Wang, J.; Yuan, Y.; Xiong, R.; Zhang-Negrerie, D.; Du, Y.; Zhao, K. *Org. Lett.* **2012**, *14*, 2210–2213.
128. Sreenithya A.; Sunoj, R. B. *Org. Lett.* **2014**, *16*, 6224–6227.
129. Sreenithya A.; Patel. C.; Hadad, C. M.; Sunoj, R. B. *ACS Catal.* **2017**, *7*, 4189–4196.
130. Haubenreisser, S.; Wöste, T. H.; Martínez, C.; Ishihara, K.; Muñiz, K. *Angew. Chem. Int. Ed.* **2016**, *55*, 413–417.
131. Cao, Y.; Zhang, X.; Lin, G.; Zhang-Negrerie, D.; Du, Y. *Org. Lett.* **2016**, *18*, 5580–5583.
132. Jacobsen, E. N.; Pfaltz, A.; Yamamoto, H. Eds., *Comprehensive Asymmetric Catalysis*. 1st ed. Berlin, Germany: Springer; **1999**.
133. Romero, R. M.; Wöste, T. H.; Muñiz, K. *Chem. Asian J.* **2014**, *9*, 972–983.
134. Fujita, M. *Tetrahedron Lett.* **2017**, *58*, 4409–4419.
135. Li, X.; Chen, P.; Liu, G. *Beilstein J. Org. Chem.* **2018**, *14*, 1813–1825.
136. Lee, J. H.; Choi, S.; Hong, K. B. *Molecules* **2019**, *24*, 2634.
137. Fujita, M.; Mori, K.; Shimogaki, M.; Sugimura, T. *Org. Lett.* **2012**, *14*, 1294–1297.
138. Fujita, M.; Mori, K.; Shimogaki, M.; Sugimura, T. *RSC Adv.* **2013**, *3*, 17717–17725.
139. Shimogaki, M.; Fujita, M.; Sugimura, T. *Eur. J. Org. Chem.* **2013**, *2013*, 7128–7138.
140. Mizar, P.; Laverny, A.; El-Sherbini, M.; Farid, U.; Brown, M.; Malmedy, F.; Wirth, T. *Chem. Eur. J.* **2014**, *20*, 9910–9913.
141. Alhalib, A.; Kamouka, S.; Moran, W. J. *Org. Lett.* **2015**, *17*, 1453–1456.
142. Gelis, C.; Dumoulin, A.; Bekkaye, M.; Neuville, L.; Masson, G. *Org. Lett.* **2017**, *19*, 278–281.
143. Mennie, K. M.; Banik, S. M.; Reichert, E. C.; Jacobsen, E. N. *J. Am. Chem. Soc.* **2018**, *140*, 4797–4802.
144. Wang, Q.; Lübcke, M.; Biosca, M.; Hedberg, M.; Eriksson, L.; Himo, F.; Szabó, K. J. *J. Am. Chem. Soc.* **2020**, *142*, 20048–20057.
145. Woerly, E. M.; Banik, S. M.; Jacobsen, E. N. *J. Am. Chem. Soc.* **2016**, *138*, 13858–13861.
146. Sarie, J. C.; Thiehoff, C.; Neufeld, J.; Daniliuc, C. G.; Gilmour, R. *Angew. Chem. Int. Ed.* **2020**, *59*, 15069–15075.
147. Wöste, T. H.; Muñiz, K. *Synthesis* **2016**, *48*, 816–827.
148. Muñiz, K.; Barreiro, L.; Romero, R. M.; Martínez, C. *J. Am. Chem. Soc.* **2017**, *139*, 4354–4357.
149. Wata, C.; Hashimoto, H. *J. Am. Chem. Soc.* **2021**, *143*, 1745–1751.
150. Molnár, I. G.; Thiehoff, C.; Holland, M. C.; Gilmour, R. *ACS Catal.* **2016**, *6*, 7167–7173.
151. Molnár, I. G., Gilmour, R. *J. Am. Chem. Soc.* **2016**, *138*, 5004–5007.
152. Banik, S. M.; Medley, J. W.; Jacobsen, E. N. *J. Am. Chem. Soc.* **2016**, *138*, 5000–5003.
153. Scheidt, F.; Schäfer, M.; Sarie, J. C.; Daniliuc, C. G.; Molloy, J. J.; Gilmour, R. *Angew. Chem. Int. Ed.* **2018**, *57*, 16431–16435.
154. Haj, M. K.; Banik, S. M.; Jacobsen, E. N. *Org. Lett.* **2019**, *21*, 4919–4923.
155. Banik, S. M.; Medley, J. W.; Jacobsen, E. N. *Science* **2016**, *353* 51–54.
156. Zhou, B.; Haj, M. K.; Jacobsen, E. N.; Houk, K. N.; Xue, X.-S. *J. Am. Chem. Soc.* **2018**, *140*, 15206–15218.
157. Levin, M. D.; Ovian, J. M.; Read, J. A.; Sigman, M. S.; Jacobsen, E. N. *J. Am. Chem. Soc.* **2020**, *142*, 14831–14837.
158. Sharma, H. A.; Mennie, K. M.; Kwan, E. E.; Jacobsen, E. N. *J. Am. Chem. Soc.* **2020**, *142*, 16090–16096.
159. Zhang, D.-Y.; Zhang, Y.; Wu, H.; Gong, L.-Z. *Angew. Chem. Int. Ed.* **2019**, *58*, 7450–7453.
160. Cosio, M. N.; Cardenal, A. D.; Maity, A.; Hyun, S.-M.; Akwaowo, V. E.; Hoffman, C. W. Powers, T. P.; Powers, D. C. *J. Chem. Educ.* **2020**, *97*, 3816–3821.
161. Elsherbini, M.; Wirth, T. *Chem. Eur. J.* **2018**, *24*, 13399–13407.
162. Tang, H. T.; Jia, J.-S.; Pan, Y.-M. *Org. Biomol. Chem.* **2020**, *18*, 5315–5333.
163. Uyanik, M.; Okamoto, H.; Yasui, T.; Ishihara, K. *Science* **2010**, *328*, 1376–1379.
164. Chen, R.; Chen, J.; Zhang, J.; Wan, X. *Chem. Rec.* **2018**, *18*, 1292–1305.

PART II

ASYMMETRIC PHOTOCHEMICAL REACTIONS AND PHOTOREDOX CATALYSIS

8

ASYMMETRIC VISIBLE-LIGHT PHOTOREDOX CATALYSIS

Jiyuan Lyu, Aurélie Claraz, and Géraldine Masson
Institut de Chimie des Substances Naturelles, Université Paris Saclay, Gif-sur-Yvette, France

8.1. INTRODUCTION

Asymmetric catalysis plays a pivotal role in modern synthetic organic chemistry, and the growing demand for enantiopure compounds in the fine chemical, pharmaceutical, and fragrance industries has stimulated an increased interest in identifying and creating new stereoselective catalysts. Visible light has been identified as an inexpensive, abundant, and environmentally benign source of energy for activating chemical transformations under mild conditions. Therefore, combining visible light photocatalysis with asymmetric catalysis affords direct access to efficient and green synthesis of enantiopure complex structural motifs (that are otherwise difficult to construct by non-photochemical synthetic methods alone). However, the development of catalytic enantioselective photochemical reactions has proved to be challenging due to the high reactivity of photoexcited intermediates generated during the processes. In recent years, several approaches have been successfully developed and two main strategies have been adopted: one relies on the use of two separate catalysts, an achiral photocatalyst and a chiral co-catalyst working synergistically in a single organic transformation, and the second one employs a single chiral catalyst connected to a visible photosensitizer. Although recent review articles on the topic of asymmetric photocatalysis have been appeared [1], this tutorial chapter will highlight the recent advances to achieve high efficiency and selectivity in asymmetric photoredox transformations. We divide our discussion in two parts: (i) dual catalysis approach and (ii) single bifunctional catalyst approach. Dual catalytic cross-coupling reactions and biocatalytic approach will not be covered in this chapter.

8.2. DUAL CATALYSIS APPROACH

8.2.1. Lewis Base Catalysis

8.2.1.1. Enamine Catalysis

8.2.1.1.1. SET Reduction of Electrophilic Radical Precursors Enamine catalysis is a well-established method in asymmetric organocatalysis. Activating an aldehyde (or a ketone) with a chiral secondary or primary amine enables the generation of a chiral enamine. The latter features a higher HOMO (highest occupied molecular orbital) than the parent carbonyl compound and can therefore readily react with

Catalytic Asymmetric Synthesis, Fourth Edition. Edited by Takahiko Akiyama and Iwao Ojima.

electrophiles through a HOMO–LUMO (lowest unoccupied molecular orbital) interaction in an asymmetric fashion. A major breakthrough was achieved by MacMillan et al. in 2008 who merged this paradigm with photoredox catalysis allowing the reaction to take place with in-situ generated electrophilic radicals through a HOMO–SOMO (single occupied molecular orbital) interaction [2]. In their seminal works, MacMillan et al. reported the enantioselective α-alkylation of aldehydes **1** with α-bromocarbonyl compounds **2** using $Ru(bpy)_3Cl_2$ $\mathbf{A_1}$ as photosensitizer and imidazolidinone $\mathbf{B_1}$ as chiral organocatalyst (Scheme 8.1). Good yields and excellent enantioselectivities were attained. Importantly, this

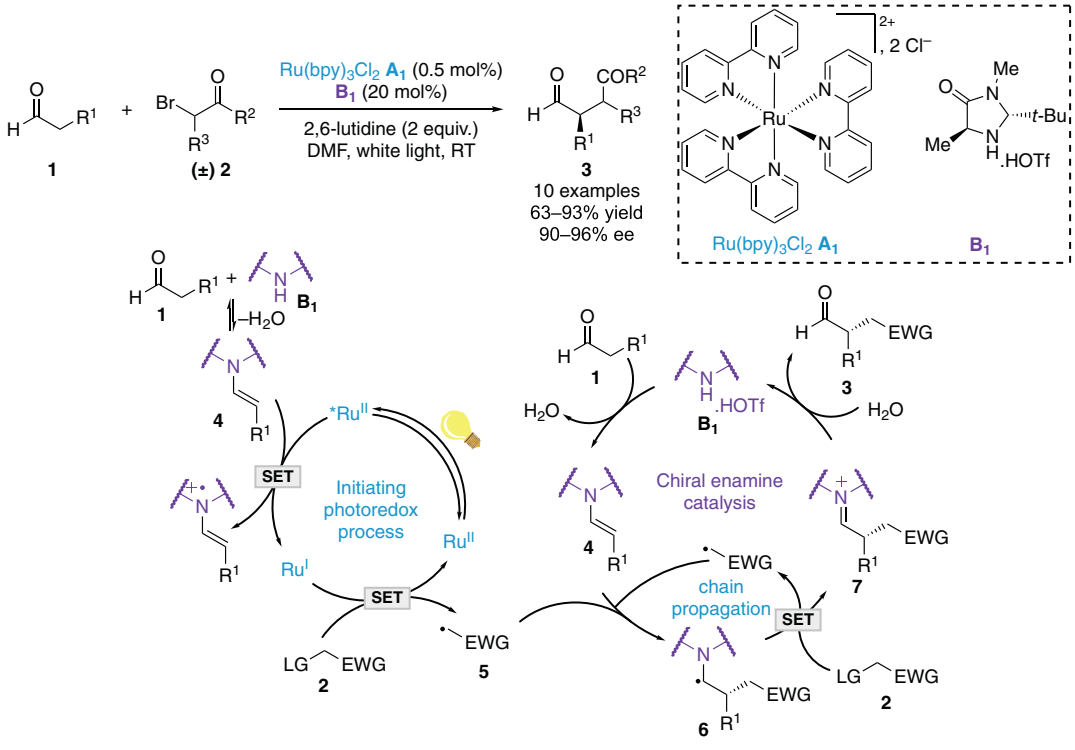

Scheme 8.1. Enantioselective α-alkylation of aldehydes: general mechanism.

transformation was not possible with enamine catalysis alone. The proposed mechanism was initiated by the condensation of organocatalyst $\mathbf{B_1}$ with aldehydes **1** to form a sacrificial amount of enamine **4**. This electron-rich species reductively quenched the $*Ru^{II}$ excited-state ($E_{1/2}$ ($*Ru^{II}/Ru^{I}$) = +0.77 V vs. saturated calomel electrode (SCE) in CH_3CN) to produce the highly reducing Ru^{I} species ($E_{1/2}$ (Ru^{II}/Ru^{I}) = –1.33 V vs. SCE in CH_3CN). The latter reduced **2** and initiated the generation of electrophilic radical **5**. Enantioselective addition of **5** to another molecule of **4** provided enantioenriched α-amino radical **6**. Mechanistic studies undertaken by Yoon et al. supported a chain propagation process (quantum yield Φ = 18) during which electron-rich radical **6** would be oxidized by **2** [3]. Hydrolysis of the resulting iminium ion **7** liberated the desired enantioenriched α-alkyl aldehydes **3** and closed the chiral enamine catalytic cycle. Interestingly, Yoon et al. demonstrated that the efficiency of the radical initiation and thus the overall rate of product formation could be improved by simply adding 0.5 mol% of *N,N*-dimethyl-*p*-toluidine as a more powerful reductive quencher of $*Ru^{II}$ than enamine **4** [2].

Subsequently, this transformation has been expanded to the enantioselective α-perfluoroalkylation [4] and β-cyanation [5] of aldehydes (Scheme 8.2).

The enantioselective α-alkylation of aldehydes has also been developed with other photosensitizers to replace the transition metal ruthenium salt. For instance, Cozzi et al. have used $Fe(bpy)_3Br_2$ [6] and

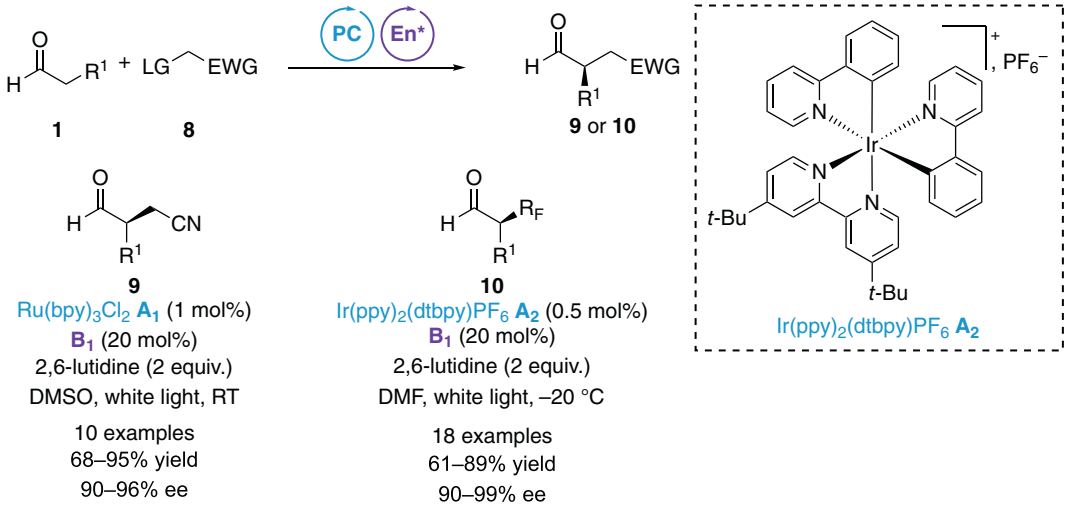

Scheme 8.2. Extension to the enantioselective α-perfluoroalkylation and β-cyanation of aldehydes.

Al(Salen)Cl [7] complexes $\mathbf{A}_3$ and $\mathbf{A}_4$ as alternative photosensitizers based on earth-abundant metals. In these cases, the excited photocatalyst would act as a reductant for initiating the radical chain mechanism. Alternatively, Zeitler and Ferroud et al. have demonstrated the ability of eosin Y $\mathbf{A}_5$ [8, 9] and rose Bengal $\mathbf{A}_6$ [10] as organic dyes sensitizers to perform this transformation under metal-free conditions. In the latter case, an additional catalytic amount of anhydrous LiCl allowed the decreasing of chiral catalyst $\mathbf{B}_1$ loading. Also of note, low-band-gap semiconductors such as $PbBiO_2Br$ [11] and commercially available Bi_2O_3 powder [12] have also been used as heterogeneous photocatalysts (Scheme 8.3).

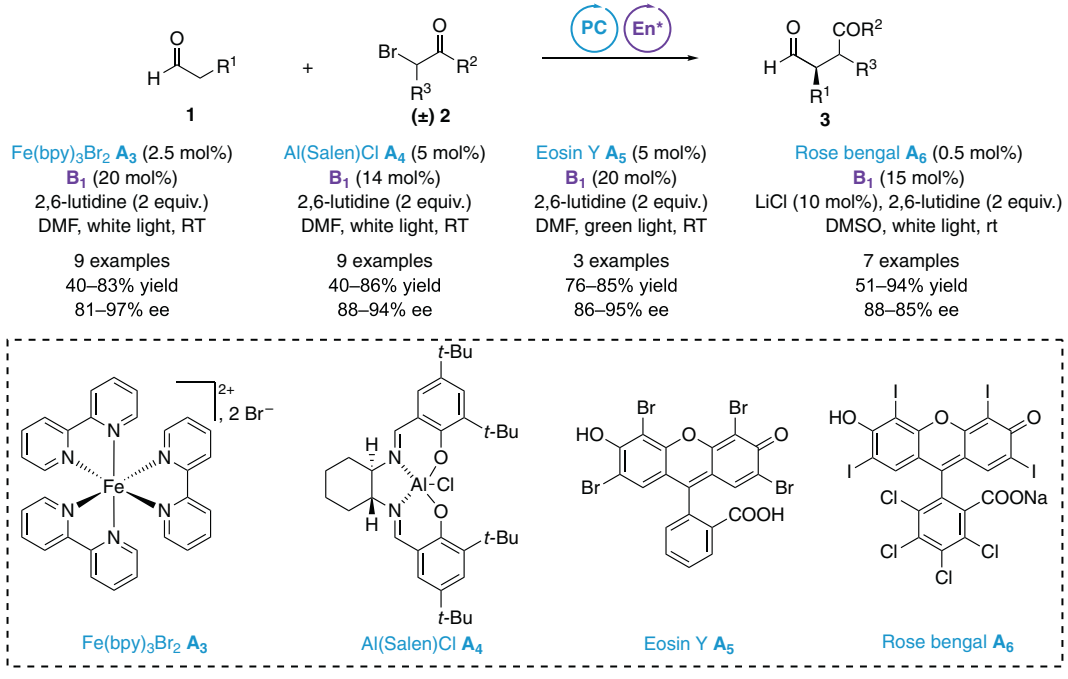

Scheme 8.3. Alternative photosensitizers.

Luo et al. have reported the α-alkylation of β-ketocarbonyl compounds **11** and β-ketoamides **14** by using chiral primary amine $\mathbf{B_2}$ as organocatalyst forging all-carbon quaternary stereocenters with high enantioselectivities. To trap the in-situ liberated HBr, inorganic base $NaHCO_3$ gave better results than the classically used 2,6-lutidine. Interestingly, control experiments revealed that this transformation could also take place under visible light in the absence of any photocatalyst delivering the corresponding product with high enantioselectivity but much lower yield. Such observation suggested that an additional process involving an electron-donor acceptor (EDA) might also proceed but should be minor. To account for the high stereoinductions, the authors proposed critical H-bonding interactions between the protonated tertiary amine of $\mathbf{B_2}$ and the carbonyl group of **12** or **15** to guide the approach of the radical to the chiral enamine (Scheme 8.4) [13].

MacMillan et al. have also accomplished the enantioselective α-benzylation of aldehydes **1** with benzyl bromides **17** having electron-deficient aryl or heteroaryl moieties [14]. Herein, the key electrophilic

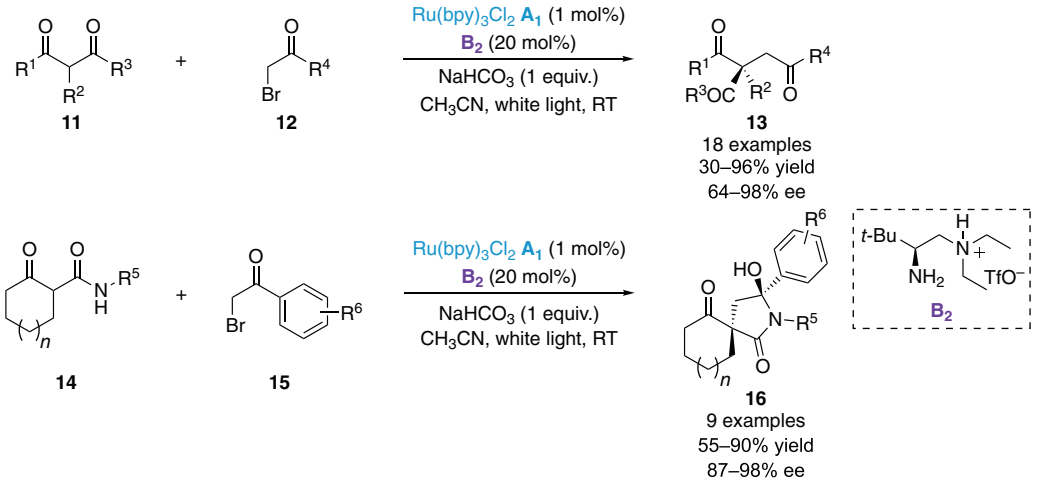

Scheme 8.4. Enantioselective α-alkylation of β-ketocarbonyl compounds and β-ketoamides. Source: [13]/American Chemical Society.

benzylic radical (E^{red} = –0.88 V vs SCE for the HBr salt of 4-bromomethylpyridine) was generated via the oxidative quenching of excited-state **fac*-Ir(ppy)$_3$ $\mathbf{A_7}$ ($E_{1/2}$ (Ir^{IV}/$*Ir^{III}$) = –1.73 V vs SCE in CH_3CN). A high quantum yield (Φ = 12.5) suggested a radical chain propagation mechanism during which the photocatalyst would only serve as an initiator (Scheme 8.5).

Afterwards, MacMillan extended this α-benzylation of aldehydes **1** with heterobenzylic alcohols **19** using Ir^{III} complex $\mathbf{A_8}$ as photocatalyst and organocatalyst $\mathbf{B_2}$ [15]. In the proposed mechanism, the $*Ir^{III}$ excited state reduces the protonated form of **19** to furnish radical **22** and Ir^{IV}. Importantly, it has been

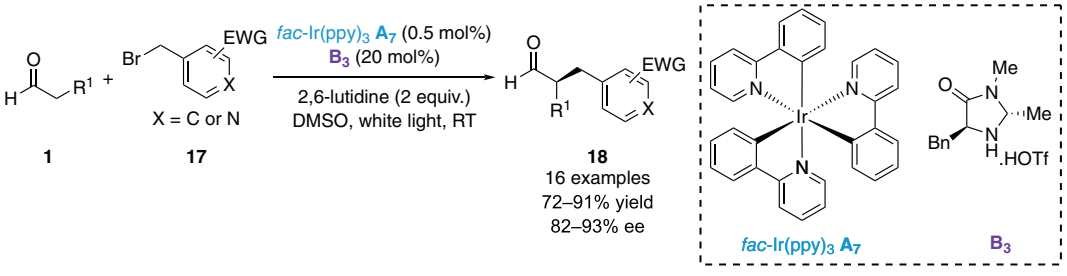

Scheme 8.5. Enantioselective α-benzylation of aldehydes with bromo-derivatives.

shown that a spin center shift (SCS) was required to induce C–O scission with the net loss of water enabling the generation of benzylic radical **23**. Herein, the relative difficult reduction of the protonated heterobenzylic alcohols **19** proscribed their reduction by α-amino radical **24**. As such, a radical chain propagation would not occur (quantum yield $\Phi = 0.071$). Instead, Ir^{IV} oxidized **24** to close the photocatalytic cycle and produce iminium ion **25**. Hydrolysis of the latter species delivered the enantioenriched α-alkyl aldehyde **20** and closed the organocatalytic cycle. To avoid the direct oxidation of the enamine **21** by Ir^{IV}, it is worth pointing out that photocatalyst $\mathbf{A_8}$ was selected for its moderate oxidizing Ir^{IV} state ($E_{1/2}$ (Ir^{IV}/Ir^{III}) = +0.77 V vs SCE in CH_3CN) (Scheme 8.6).

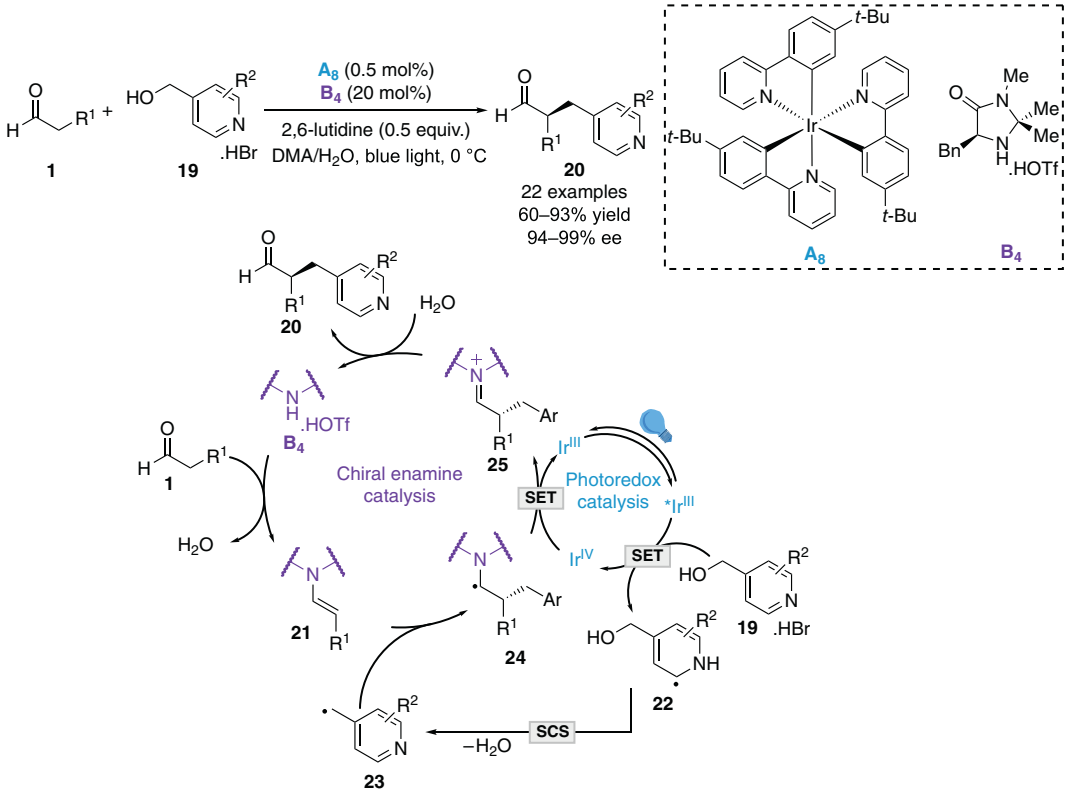

Scheme 8.6. Enantioselective α-benzylation of aldehydes with alcohols.

8.2.1.1.2. SET Oxidation of Chiral Enamine All mentioned above redox neutral photoredox organocatalytic α-alkylations of carbonyl compounds involved the coupling of a chiral enamine with various electrophiles through the generation of an electrophilic radical. In 2017, MacMillan et al. devised a synergistic triple catalytic system to enable the coupling of a chiral enamine with simple olefins as reactive partners through the generation of an α-iminiumyl radical [16]. By merging photoredox, enamine and hydrogen atom transfer (HAT) catalysis, such redox neutral process is an attractive alternative to the previously developed oxidative SOMO-organocatalysis that required an excess of oxidant [17]. Herein, excited-state photocatalyst $*Ir^{III}$ oxidized enamine **30** to form electrophilic chiral iminiumyl radical **31**. Enantioselective nucleophilic addition of olefin **28** generated the secondary nucleophilic radical **32**. HAT with thiophenol catalyst furnished closed-shell iminium species **33** along with thiyl radical. The latter was reduced by in-situ generated Ir^{IV} to close both the photocatalytic and HAT cycles. Concurrently, hydrolysis of iminium **33** concluded the organocatalytic cycle by releasing the desired enantioenriched α-alkyl

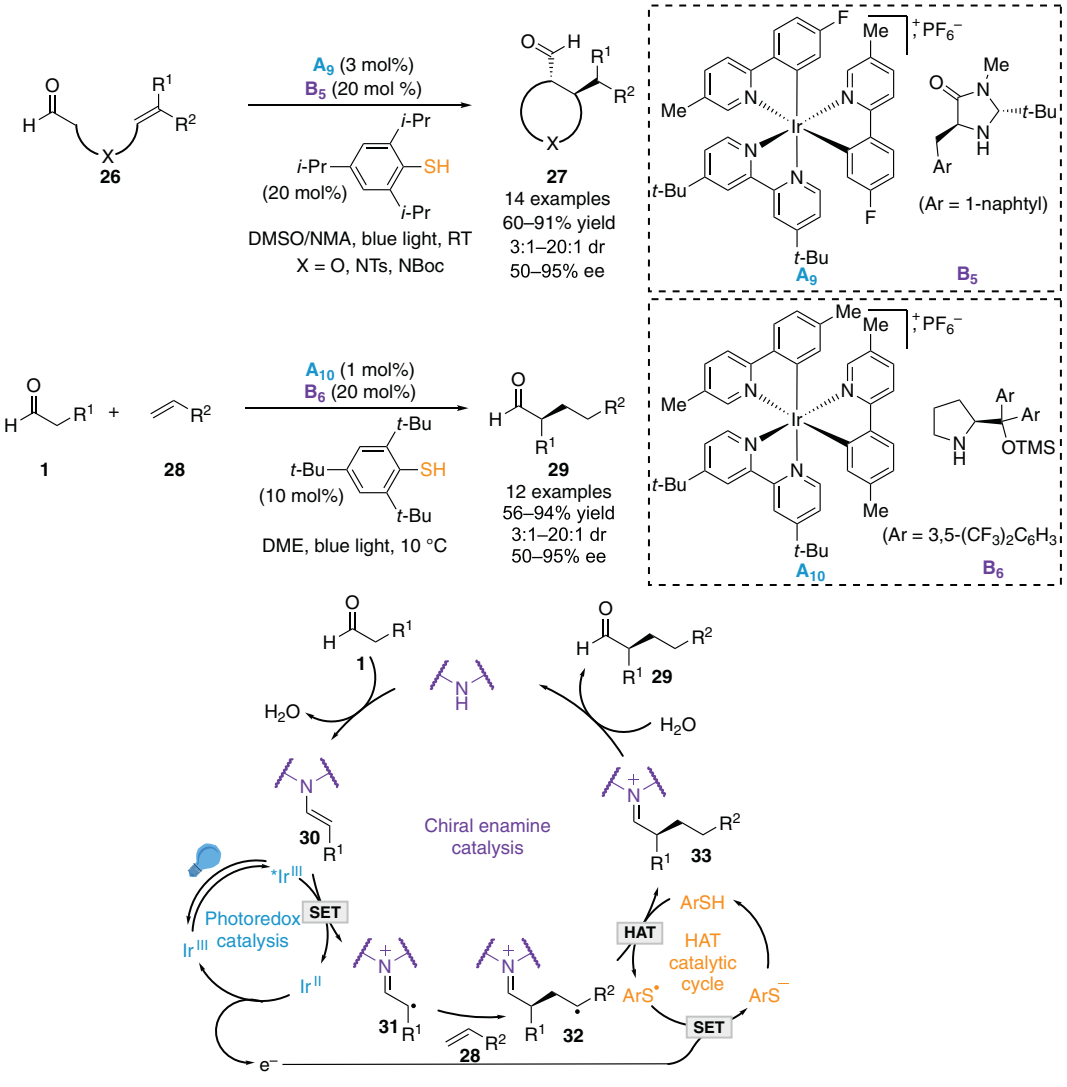

Scheme 8.7. Enantioselective α-alkylation of aldehydes with alkenes.

aldehydes **29** and the chiral organocatalyst. Intra- and intermolecular examples have been described with good yields and high enantioselectivities (Scheme 8.7).

In line with their continued efforts toward the α-functionalization of β-ketocarbonyl compounds, Luo et al. reported the enantioselective decarboxylative coupling of **34** and propiolic acids **35** to yield alkynylation adducts **36** using photocatalyst $Ru(bpy)_3Cl_2$ $\mathbf{A_1}$ and chiral primary amine organocatalyst $\mathbf{B_2}$ [18]. High enantioselectivities were achieved albeit with moderate yields due to the competitive formation of α-alkylation products **37**. Herein, a stoichiometric amount of hypervalent iodine oxidant **38** (BIOH) was required to allow the oxidative quenching of excited-state $*Ru^{II}$ and the generation of oxidizing Ru^{III}. According to the proposed mechanism, this dual catalytic system involved the formation of secondary primary enamine **40**, SET oxidation by Ru^{III}, and deprotonation of the resulting highly acidic secondary enaminyl radical cation **41** to furnish the key α-imino radical **42**. The latter combined with in-situ generated propiolate hypervalent iodine **43** to form α-functionalized imine **44**. Subsequent hydrolysis yielded α-alkynyl products **36** and released the primary amine $\mathbf{B_2}$ and benziodoxole radical **39** to close the chiral amine cycle and trigger a new photoredox process (Scheme 8.8).

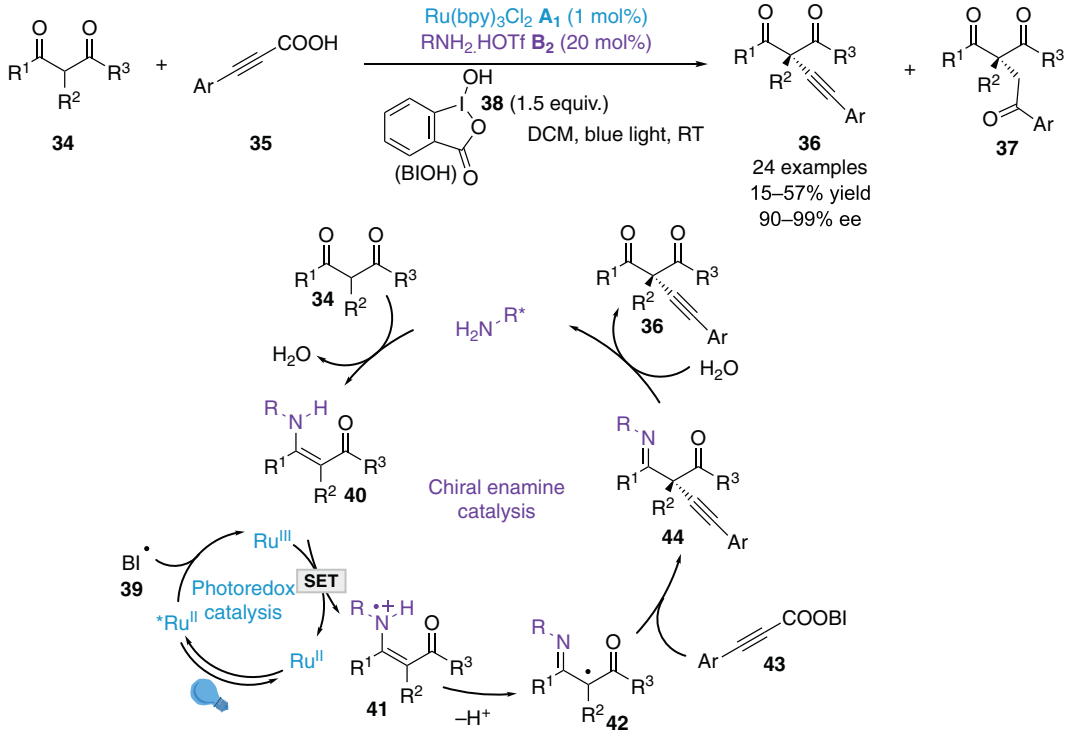

Scheme 8.8. Enantioselective α-alkynylation of β-ketocarbonyl compounds.

8.2.1.1.3. SET Reduction of Electrophilic Radical Precursor and Oxidation of Chiral Enamine The enantioselective β-arylation of cyclohexanone **45** with dicyanobenzene **46** has been demonstrated by MacMillan et al. in 2013 using photocatalyst *fac*-Ir(ppy)$_3$ $\mathbf{A_7}$ and cinchona alkaloid-derived enamine organocatalyst $\mathbf{B_7}$ [19]. Herein, **46** oxidatively quenched the excited-state $^*Ir^{III}$ to generate persistent arene radical anion **48** and Ir^{IV}. The latter oxidized in turn the cyclohexanone-derived chiral enamine **49** to provide secondary enaminyl radical cation **50**. Deprotonation of the resulting highly acidic allylic C–H bond afforded the key nucleophilic chiral allylic radical **51**. Radical cross-coupling of **48** and **51** furnished β-aryl cyclohexanone **47**. Importantly, **46** is sufficiently electron poor to avoid direct reaction with enaminyl radical cation **50** while the corresponding arene radical anion **48** is sufficiently electron rich to prohibit coupling with enamine **49**. Despite moderate enantioselectivity (50%), it is the unique example of enantioselective direct β-functionalization of saturated ketones through dual photoredox enamine catalysis (Scheme 8.9).

8.2.1.1.4. α-Oxygenation The direct enantioselective α-hydroxylation of aldehydes and ketones with molecular oxygen has been reported by Córdova using various amino acids such as L-alanine or chiral secondary amines as organocatalysts and tetraphenylporphyrin (TPP) as organic dye [20–22]. The reaction would proceed through a chiral enamine intermediate which would react with highly reactive singlet oxygen, in-situ generated via photosensitization of the organic dye. Mechanistic studies were further carried out by Gryko et al. to rationalize the influence of the catalyst structure and the reaction conditions on the yields and the obtained configuration of the products [23].

8.2.1.2. Iminium Catalysis Activation of α,β-unsaturated aldehydes or ketones upon condensation with a chiral amine allows the generation of a chiral iminium. The latter exhibits a lower LUMO than the corresponding carbonyl compound which facilitates the enantioselective conjugate addition of various polar nucleophiles. In 2016, such strategy has been extended to radical nucleophiles by Melchiorre et al. through the combination with photoredox catalysis. In the seminal studies, this dual catalytic system has

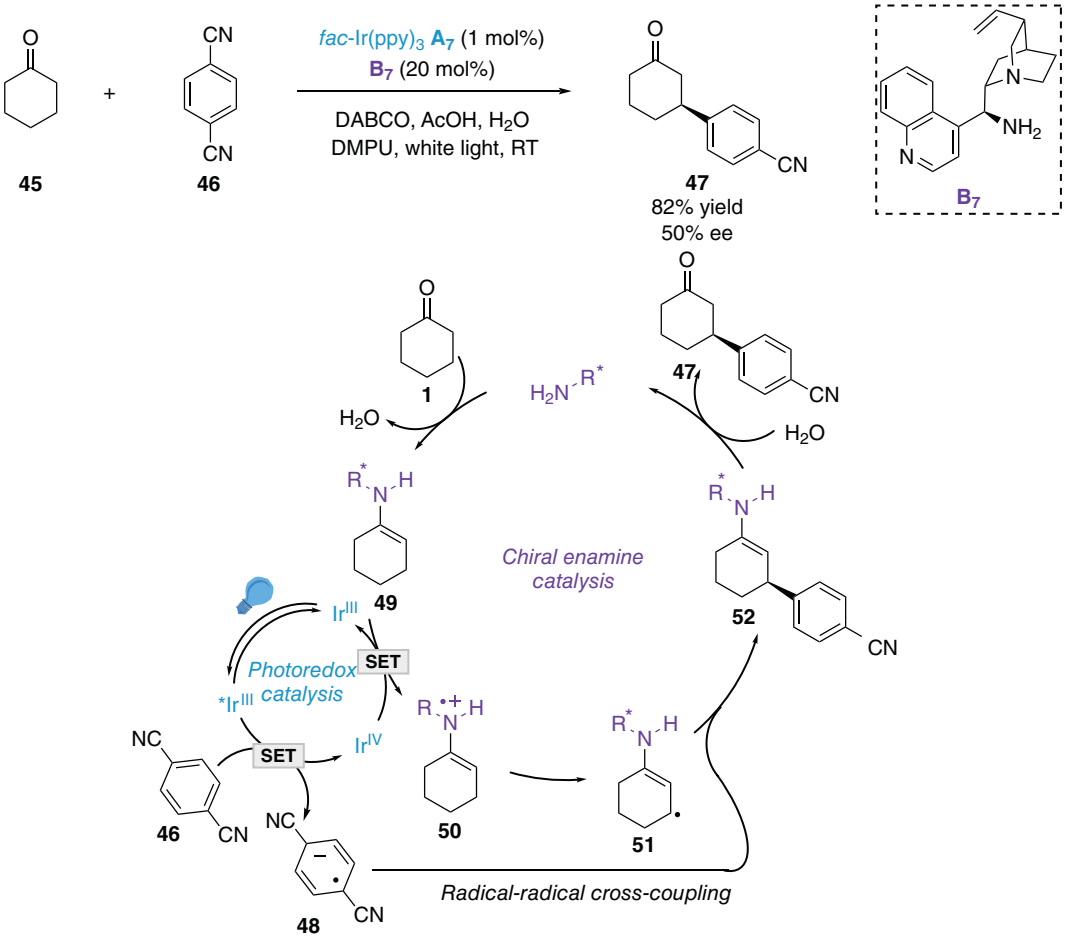

Scheme 8.9. Enantioselective β-arylation of cyclohexanone.

been applied to the conjugate addition of C-centered radical to cyclic enones **53** [24]. Critical to the success of this transformation was the use of a chiral amine catalyst $\mathbf{B}_8$ bearing a redox active carbazole unit. Indeed, after radical addition of the nucleophilic C-centered radical **59** to in-situ generated iminium ion **58**, the resulting α-iminiumyl radical cation **60** would be efficiently reduced by the electron-rich carbazole moiety to avoid the retro-Giese type reaction. Herein, the photocatalytic cycle served both to generate the C-centered radical **59** and to reduce the transiently generated carbazole radical cation **61**. Further mechanistic studies have revealed that this last event was the rate-determining step [25]. Two different photocatalytic cycles have been applied to this system: a HAT mechanism with tetrabutylammonium decatungstate ($(n\text{-}Bu_4N)_4[W_{10}O_{32}]$) TBADT photocatalyst $\mathbf{A}_{11}$ for the introduction of benzodioxoles **54** and a SET mechanism with $Ir[dF(CF_3)ppy]_2(dtbbpy)PF_6$ photocatalyst $\mathbf{A}_{12}$ for the addition of α-amino radicals from tertiary amine **56** (Scheme 8.10).

More recently, this dual iminium photoredox catalysis has been extended to the enantioselective β-hydroacylation of aromatic enals **63** with α-ketoacids **64** [26] and to the enantioselective β-alkylation of aromatic and aliphatic enals **66** with various trimethylsilyl derivatives **67** [27] with $Ru(bpz)_3(PF_6)_2$ $\mathbf{A}_{13}$ and acridinium $\mathbf{A}_{14}$ as photocatalysts respectively. In both cases, chiral free-carbazole amino-organocatalyst $\mathbf{B}_9$ was used. As such, it was assumed that the reduced form of the photocatalyst directly reduced the α-iminiumyl radical cation (Scheme 8.11).

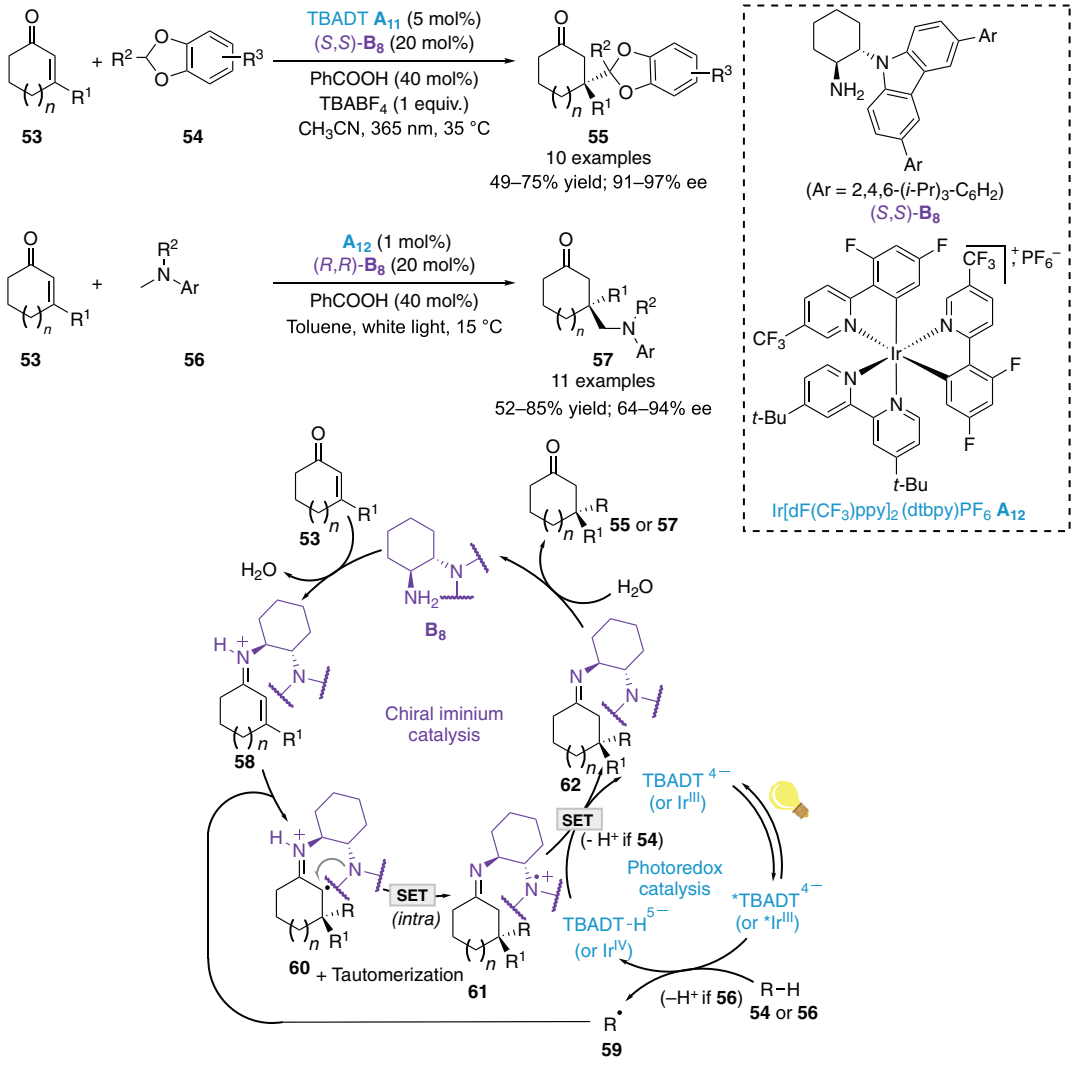

Scheme 8.10. Enantioselective conjugate addition of C-centered radicals to cyclic enones.

8.2.2. Hydrogen-Bonding Catalysis

In 2017, Jiang et al. reported the enantioselective reduction of 1,2-diketones **69** by combining their own dicyanopyrazine (DPZ)-derived photocatalyst $\mathbf{A}_{15}$ and guanidinium salt $\mathbf{B}_{10}$ as H-bonding organocatalyst in the presence of tetrahydroquinoxaline **70** as terminal reductant. According to the proposed mechanism, excited-state *DPZ was quenched by **70** to furnish reduced state DPZ$^{\bullet-}$. The latter performed one SET reduction of **69** leading to ketyl radical **73** which would readily interact with chiral $\mathbf{B}_{10}$ via H-bonding interactions, thanks to its strong basicity. A second SET reduction from **70** generated chiral carbanion complex **74** and triggered a key final enantioselective protonation. The resulting α-hydroxy ketones **71** were obtained in good yields and high enantioselectivities [28]. It is worth mentioning that similar yields and enantioselectivities could be achieved under blue light irradiation in the absence of any photosensitizer suggesting an electron-donor acceptor (EDA) complex between substrates **69** and the sacrificial reductant **70** (Scheme 8.12).

The dual photoredox H-bonding catalysis was further extended to an enantioselective reductive dehalogenation of α-α-dihalogeno aromatic ketones **75** using squaramide $\mathbf{B}_{11}$ as chiral H-bonding catalyst.

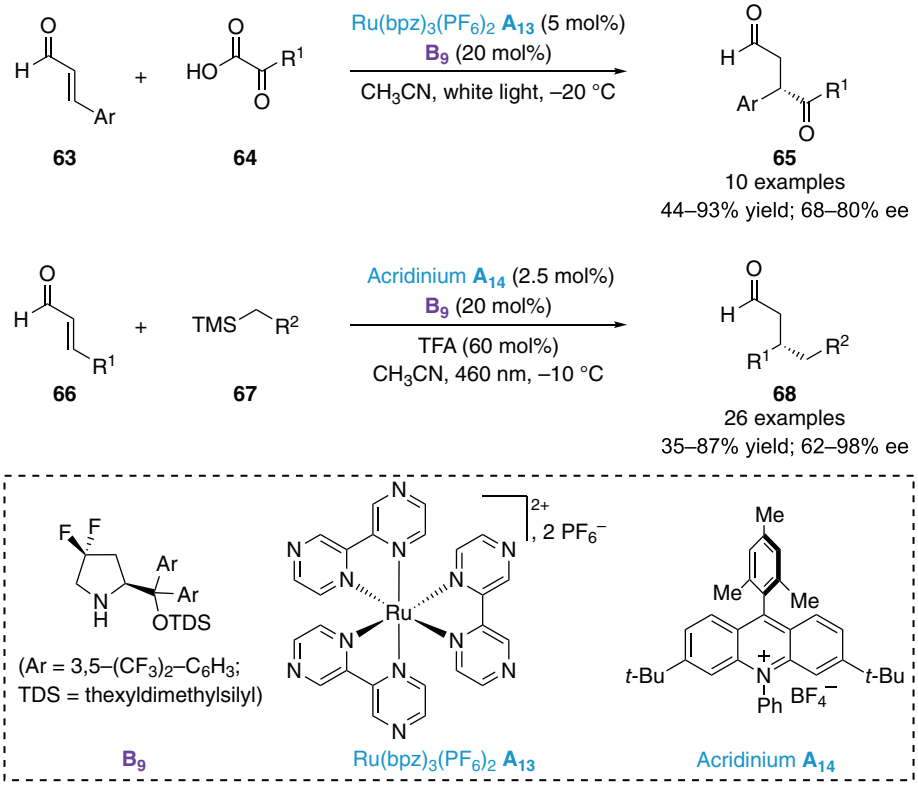

Scheme 8.11. Enantioselective β-hydroacylation and β-alkylation of enals.

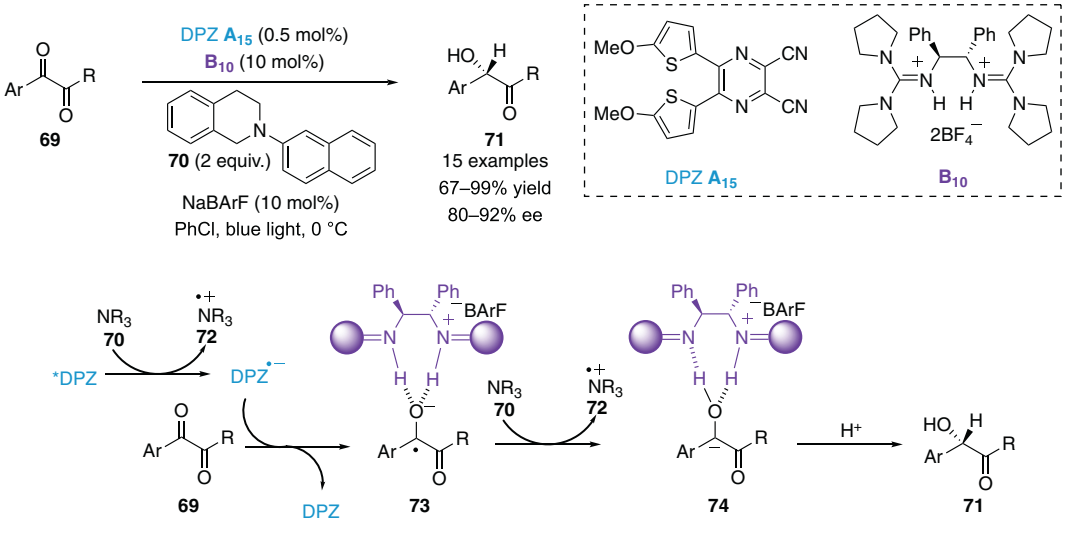

Scheme 8.12. Enantioselective reduction of 1,2-diketones.

Two single electron transfers would also take place furnishing carbanion **77**. The organocatalyst afforded the required chiral environment for the final enantioselective protonation step through H-bonding interactions between the squaramide moiety and the carbonyl group. Highly enantioenriched α-fluoro, α-chloro, and α-bromo aromatic ketones **76** could be obtained in good yields (Scheme 8.13) [29].

It is also worth mentioning that in 2016 Bach et al. have reported a photocatalytic enantioselective addition of α-amino methylradicals to 3-alkylidene indolin-2-ones in the presence of a chiral hydrogen-bonding template. The latter being introduced in a sub-stoichiometric amount (2.5 equiv.), this transformation will not be detailed here [30].

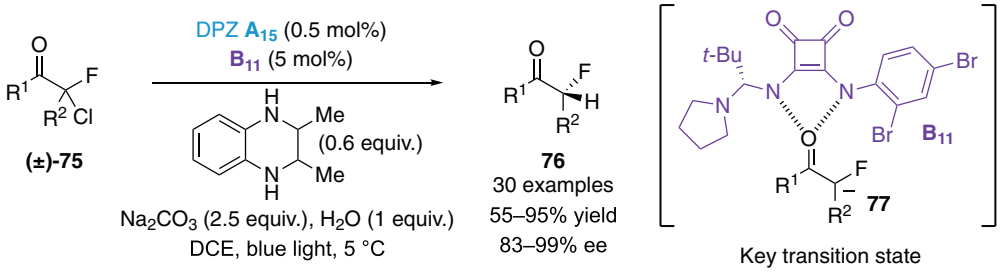

Scheme 8.13. Enantioselective reductive dehalogenation of α–α-dihalogeno aromatic ketones. Source: [29]/Royal Society of Chemistry.

8.2.3. Brønsted Base Catalysis

An enantioselective photocatalytic synthesis of alkoxyamine-substituted pyrroloindolines **81** from tryptophan **78** and TEMPO **79** has been reported by Knowles et al. in 2018 [31]. The best reaction conditions involved *fac*-Ir(ppy)$_3$ $\mathbf{A_7}$ as photocatalyst and H_8 TRIP BINOL phosphate base $\mathbf{B_{12}}$ as chiral organocatalyst in the presence of TIPS-EBX **80** as a sacrificial oxidant. Herein, oxidative quenching of excited-state $^*Ir^{III}$ by **80** produced Ir^{IV} which in turn oxidized the indole-phosphate complex **82**. The resulting indole radical cation–chiral phosphate ion pair **83** combined with the stable nitroxyl TEMPO radical **79** to build the C–O bond in an asymmetric fashion. Intramolecular trapping of the iminium **85** by the amine furnished the desired highly enantioenriched cyclized product **81** along with the phosphoric acid **86**. Deprotonation by in-situ generated benzoate **84** released phosphate $\mathbf{B_{12}}$ to close the asymmetric cycle. As such, in this dual catalytic system, the weak phosphate Brønsted base would play two important roles: (i) it lowered the potential required for indole oxidation through hydrogen bonding interactions which is characteristic of a PCET (proton-coupled electron transfer) process and (ii) it afforded the chiral environment for controlling the enantioselectivity in the C–O bond forming step (Scheme 8.14). It is worth mentioning that the same transformation was further achieved in a photocatalyst-free fashion by Xia et al. highlighting the crucial role of excited-state TEMPO [32].

An enantioselective intramolecular hydroamination of alkenes **87** has also been accomplished by Knowles et al. via a triple catalytic system combining iridium photocatalyst $\mathbf{A_{16}}$, chiral Brønsted base (phosphate) organocatalyst $\mathbf{B_{13a}}$, and hydrogen atom donor (thiol) catalyst [33]. Herein a neutral *N*-centered radical **90** would be generated upon oxidative PCET process with the excited-state $^*Ir^{III}$ photocatalyst and the chiral phosphate base $\mathbf{B_{13}}$. Intramolecular radical addition on the alkene furnished the *exo*-cyclic radical **90** which is trapped by the thiol catalyst to deliver enantioenriched pyrrolidine products **88**. The resulting thiyl radical was subsequently reduced by in-situ generated Ir^{II} in the presence of phosphoric acid to close simultaneously the Brønsted base, photoredox, and HAT catalytic cycles. Mechanistic studies supported noncovalent interactions between the neutral sulfonamidyl radical **89** and the in-situ generated chiral phosphoric acid for controlling selectivity in the enantiodetermining C–N bond forming step. The 1,2,3-triazole cores at the 3,3′-position of the phosphate base were crucial for reaching high enantioselectivities (Scheme 8.15).

A triple photoredox/chiral phosphate Brønsted base/chiral HAT catalysis has also been realized by Miller and Knowles for the deracemization of cyclic ureas **91** using Iridium photocatalyst $\mathbf{A_{17}}$, chiral Brønsted base (phosphate) organocatalyst $\mathbf{B_{13b}}$, and chiral cysteine-derived thiol as hydrogen atom donor

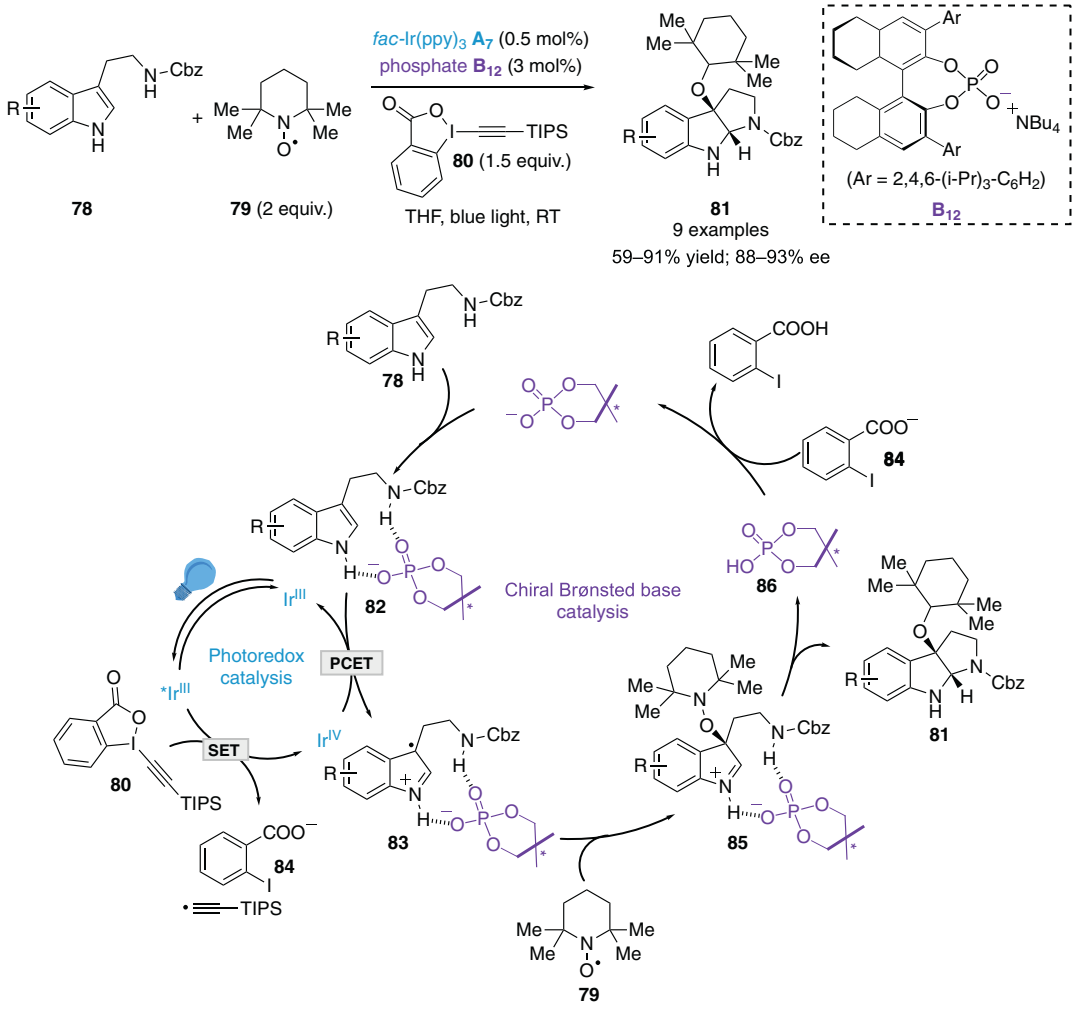

Scheme 8.14. Enantioselective photocatalytic synthesis of pyrroloindolines.

catalyst. In this process, racemic urea was initially oxidized by excited-state $*Ir^{III}$ photocatlyst to form a mixture of aminium radical cation (*R*)- and (*S*)-**92**. The latter underwent a kinetic resolution during which fast-reacting (*S*)-**92** was deprotonated at the highly acidic α-C–H bond by the chiral Brønsted base to deliver α-amino radical **93**. Slower-reacting (*R*)-**92** underwent charge recombination with Ir^{II} to enrich the reaction solution in urea (*R*)-**91**. Concurrently, an enantioselective H-atom transfer between prochiral α-amino radical **93** and the chiral thiol catalyst produced preferentially (*R*)-**91** as well. A final PCET between thiyl radical, Ir^{II} and the protonated Brønsted base regenerated the three catalysts. (*R*)-**91** was obtained in excellent yields and good enantioselectivities (Scheme 8.16) [34].

8.2.4. Brønsted Acid Catalysis

The merger of photoredox and chiral Brønsted acid catalysis was first reported by Knowles et al. in 2013 in the context of an asymmetric intramolecular reductive coupling of ketones and hydrazones [35]. This aza-pinacol cyclization of **94** was realized in the presence of the photoredox catalyst $Ir(ppy)_2(dtbpy)PF_6$ $\mathbf{A_2}$ and chiral phosphoric acid $\mathbf{B_{14}}$ employing Hantzsch ester (HEH) as a stoichiometric reductant.

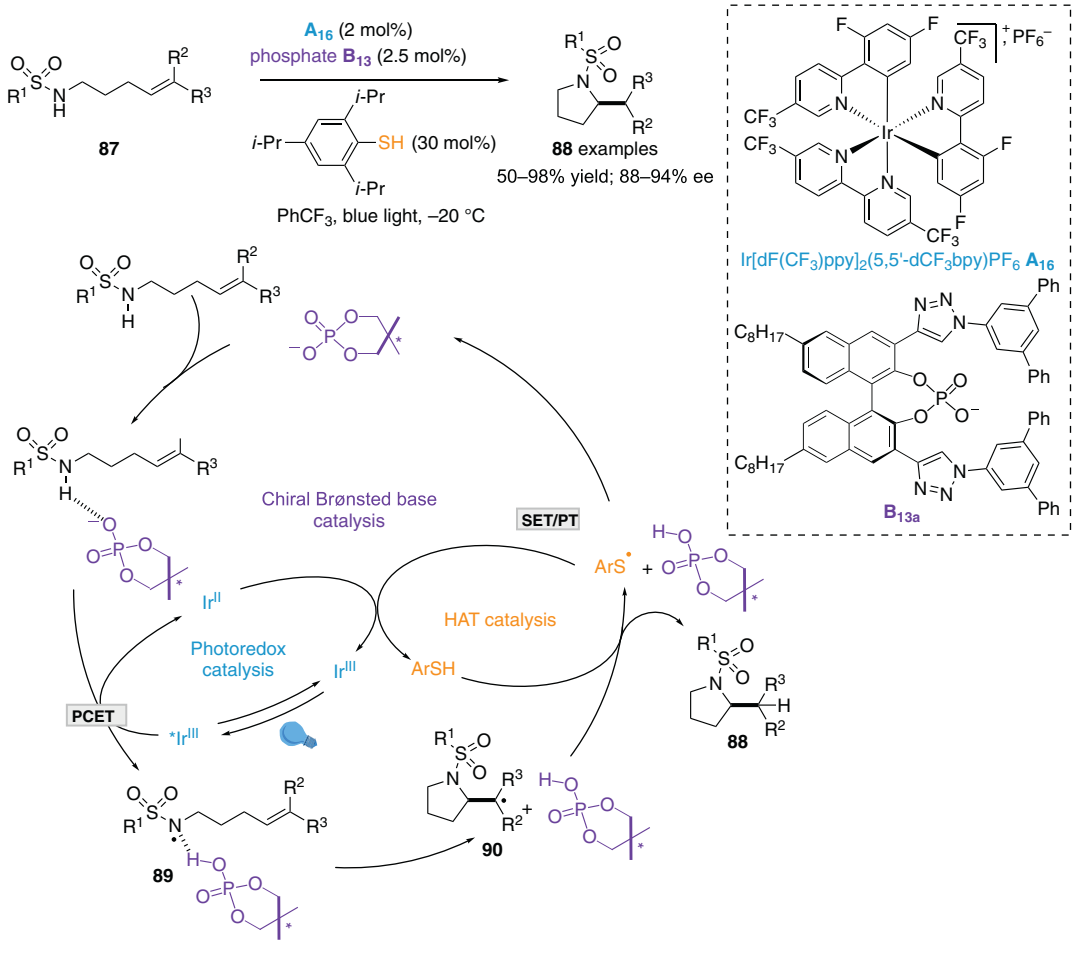

Scheme 8.15. Enantioselective intramolecular hydroamination of alkenes.

This dual catalytic system was supposed to be initiated by the reductive quenching of the excited-state $^*Ir^{III}$ photocatalyst by HEH. SET from the resulting strongly reducing species Ir^{II} to the ketone occurred in concert with a proton transfer from the chiral phosphoric acid $\mathbf{B}_{14}$ (PCET event) to enable the formation of the ketyl radical **96** and close the photocatalytic cycle. Subsequent radical cyclization afforded hydrazyl radical **97** which underwent HAT from HEH to deliver the highly enantioenriched vicinal amino-alcohol **95**. Protonation of the released phosphate anion by the in-situ generated pyridinium py. H^+ closed the Brønsted acid catalytic cycle. Herein the phosphoric acid would (i) enable the generation of the ketyl radical during the PCET and (ii) furnish the chiral environment in the enantiodetermining C–C bond forming step through a non-covalent H-bonded interaction between the neutral prochiral ketyl radical **96** and chiral phosphate anion (Scheme 8.17).

The combination of photoredox and Brønsted acid catalysis has been widely used in the activation of aza-heterocycles. In 2018, Phipps et al. developed an enantioselective Minisci-type addition reaction of α-amino acid-derived redox-active esters (RAE) **99** to pyridines and quinolines **98** in high yields with excellent control of both enantioselectivities and regioselectivities [36]. According to the authors, a sacrificial amount of in-situ generated pyridium phosphate reductively quenched excited-state $^*Ir^{III}$ photocatalyst $\mathbf{A}_{12}$ in an off-cycle process (not shown). A subsequent SET from the resulting Ir^{II} species to RAE **99** furnished the prochiral α-amino radical **101** which added to the protonated heteroarene to forge the new C–C bond and form aminium radical **102**. Deprotonation by the chiral phosphate and oxidation by

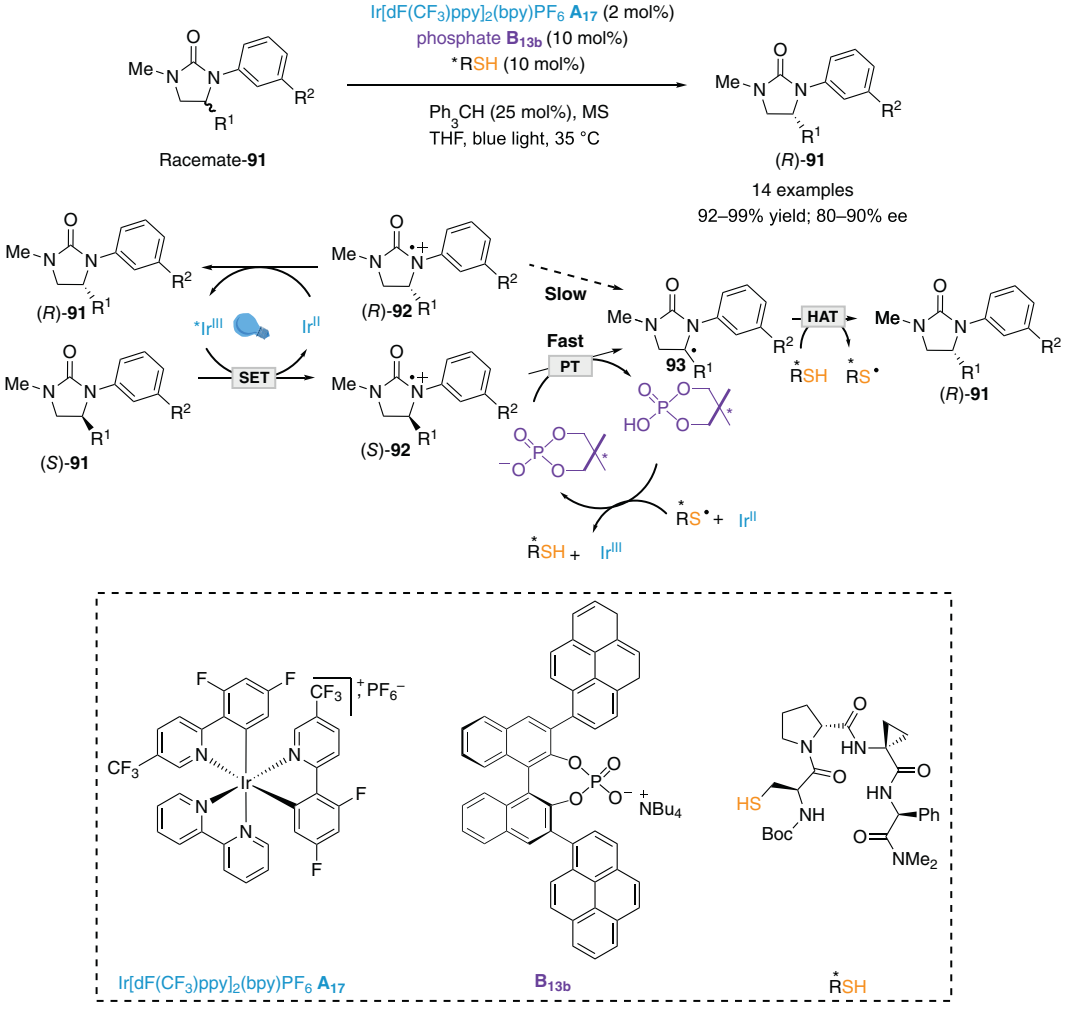

Scheme 8.16. Deracemization of cyclic ureas. Source: [34]/American Association for the Advancement of Science.

the excited-state $*Ir^{III}$ photocatalyst delivered the substituted aza-arenes **100** and closed both the photoredox and the Brønsted acid catalytic cycles. To achieve high enantioselectivities, this asymmetric catalytic system is limited to the addition of α-amino-radical with hydrogen-bond donor allowing an attractive non-covalent interaction between the chiral phosphate anion and aminium radical **102** (Scheme 8.18).

While poor enantioselectivities were obtained on isoquinolines **104** with the reaction conditions developed by Phipps et al., Jiang et al. solved this problem by using SPINOL-derived phosphoric acid $\mathbf{B}_{17}$ as chiral Brønsted acid catalyst. Moreover, the use of DPZ as photosensitizer allowed the reaction to be performed under metal-free conditions (Scheme 8.19a) [37]. Also of note, Studer et al. reported an elegant enantioselective three-component Minisci-type reaction between heterocycles **98**, enamides **107**, and bromoacetates **108**. This transformation was initiated by the reduction of bromoacetate **108** to generate electrophilic radical **110**. Subsequently regioselective radical addition to the electron-rich enamide **107** furnished the requested nucleophilic α-amino radical **111**. As in Phipps' work, the latter reacted with activated aza-arene **98** in an enantioselective fashion, thanks to the chiral phosphoric acid $\mathbf{B}_{15}$ (Scheme 8.19b) [38].

The merger of chiral Brønsted acid and photoredox catalysis has also been used in various conjugate radical additions to vinyl azaarenes. Herein, protonation of the nitrogen atom reduced the energy of the

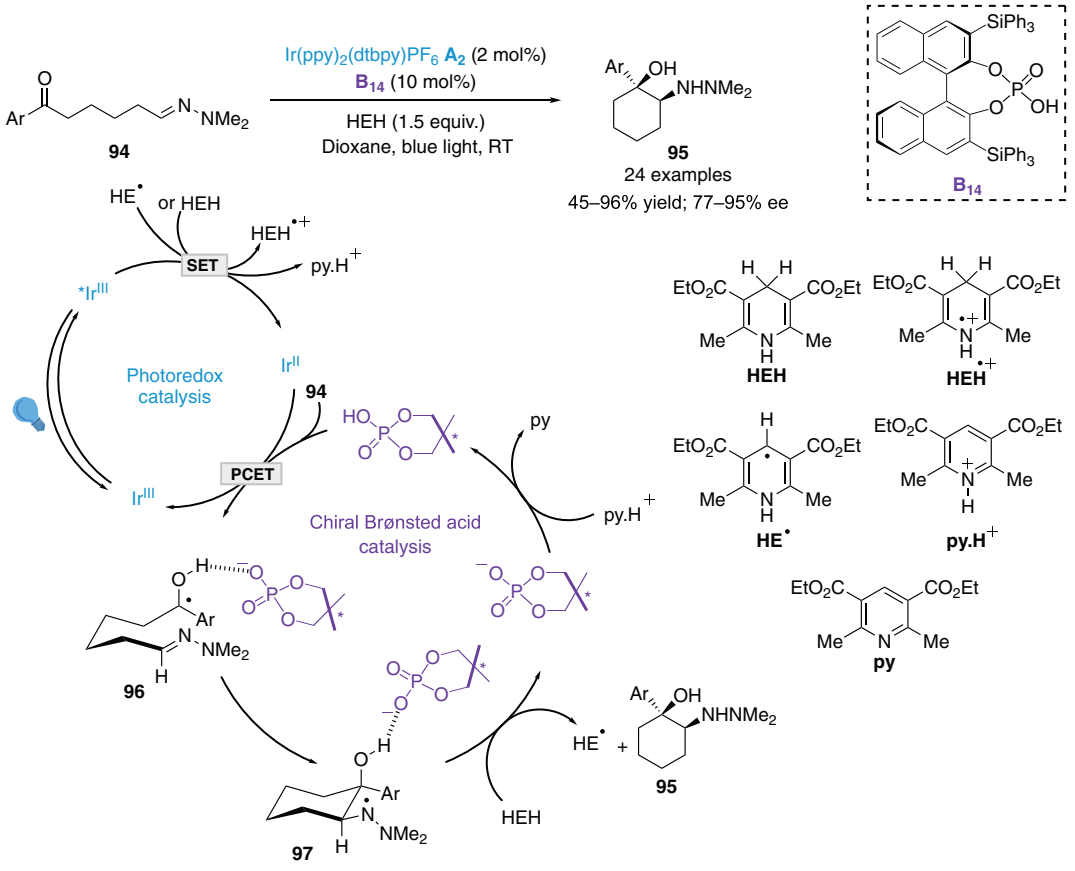

Scheme 8.17. Enantioselective aza-pinacol cyclization.

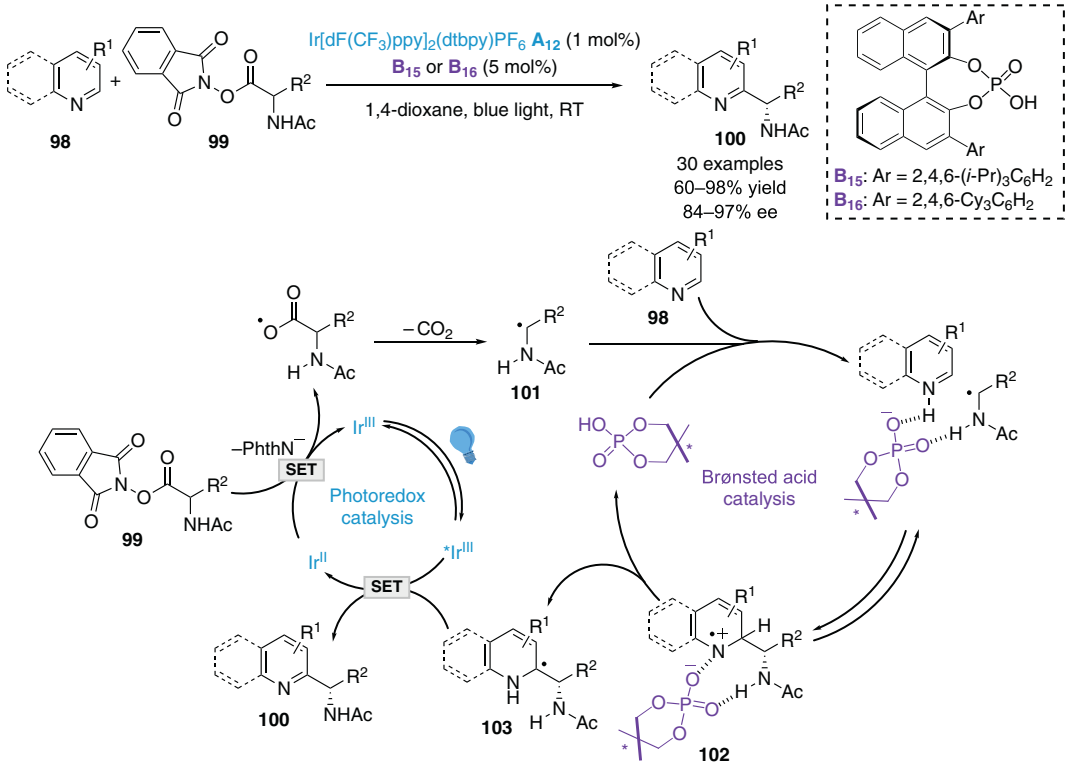

Scheme 8.18. Enantioselective Minisci-type addition reaction of α-amino acid-derived RAE to quinolines.

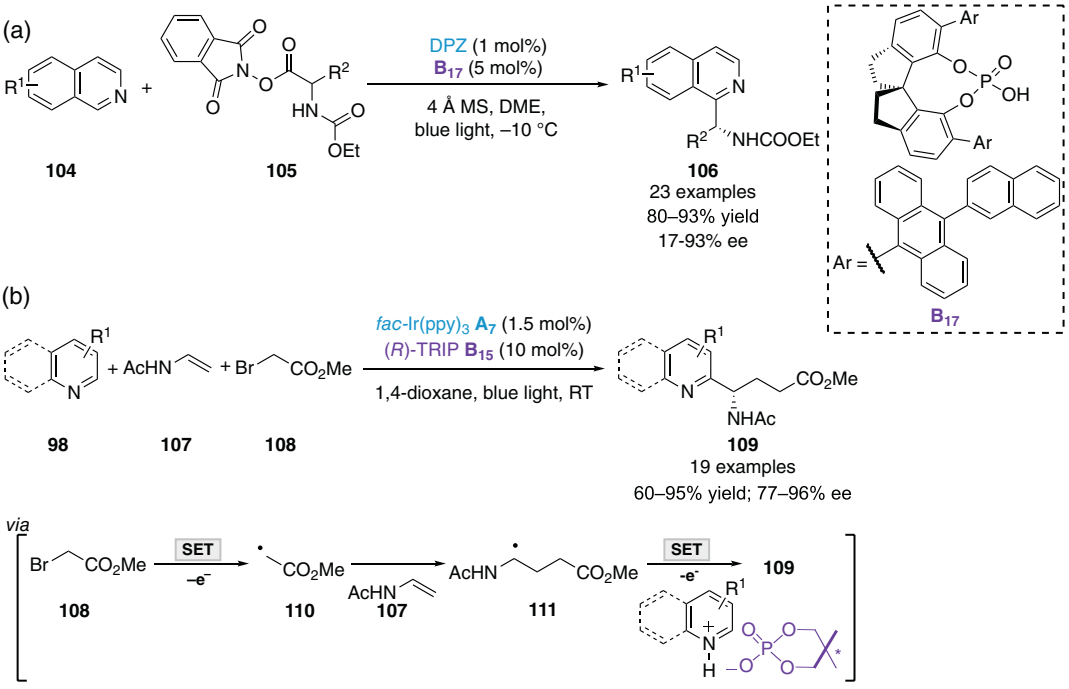

Scheme 8.19. Enantioselective Minisci-type reactions. (a) Isoquinolines as radical acceptors. Source: [37]/American Chemical Society. (b) Three-component reactions. Source: [38]/John Wiley & Sons.

LUMO at the β-carbon atom facilitating the addition of nucleophilic radicals. For instance, Jiang et al. reported in 2018 a conjugate addition/enantioselective protonation of *N*-aryl glycines **113** to α-branched prochiral vinyl azaarenes **112** [39]. Using DPZ as a photosensitizer and chiral SPINOL-derived phosphoric acid $\mathbf{B}_{18}$, this transformation enabled the synthesis of 2-substituted azaarenes **114** with a tertiary stereogenic center in good yields and high enantioselectivities. Reductive quenching of the excite-state *DPZ by **113** furnished non-prochiral primary α-amino radical **115** which undergo conjugate addition to $\mathbf{B}_{18}$-activated azaarene **112**. Subsequent reduction of benzylic radical **116** by the reduced form of the photocatalyst would close the photocatalytic cycle. Enantioselective protonation of the resulting carbanion **117** took place in a chiral environment provided by the chiral phosphoric acid $\mathbf{B}_{18}$ (Scheme 8.20).

Subsequently, Jiang et al. extended this strategy to the reductive photochemical enantioselective conjugate addition of prochiral ketyl radicals to vinyl pyridines **118** using a stoichiometric amount of Hantzsch ester (HEH) **120** as reductant. Herein, prochiral ketyl radicals **122** are generated through PCET reductions of aldehydes or ketones **119** by the reduced form $DPZ^{\bullet-}$. During the enantiodetermining conjugate addition reaction, a dual activation of the prochiral radical species **122** and activated vinyl pyridine was ensured by the chiral phosphoric acid $\mathbf{B}_{19}$ via H-bonding interactions. Importantly, to avoid any disturbance of this chiral H-bonding network, bulky substituents on the Hantzsch ester were crucial. The resulting benzylic radical **123** underwent HAT with HEH to deliver the target products **121** and release the Brønsted acid. Good yields and high enantioselectivities were achieved. A slight modification on the reaction conditions allowed also the use of imines as coupling partners instead of carbonyl compounds (Scheme 8.21) [40]. Using similar dual catalytic system, Melchiorre et al. had also reported in 2016 one example of conjugate addition of a primary α-amino radical to a prochiral β-substituted vinylpyrydine with modest enantioselectivity (35% ee) [41].

Recently, Jiang et al. have developed a formal asymmetric (3+2)-radical cycloaddition between cyclopropylamines **125** and α-branched 2-vinyl azaarenes **124**. Herein, oxidative ring opening of **125** from excited-state *DPZ photosensitizer furnished distonic radical ion **128** featuring a nucleophilic radical moiety and an electrophilic iminium functional group. Radical addition to the protonated vinyl

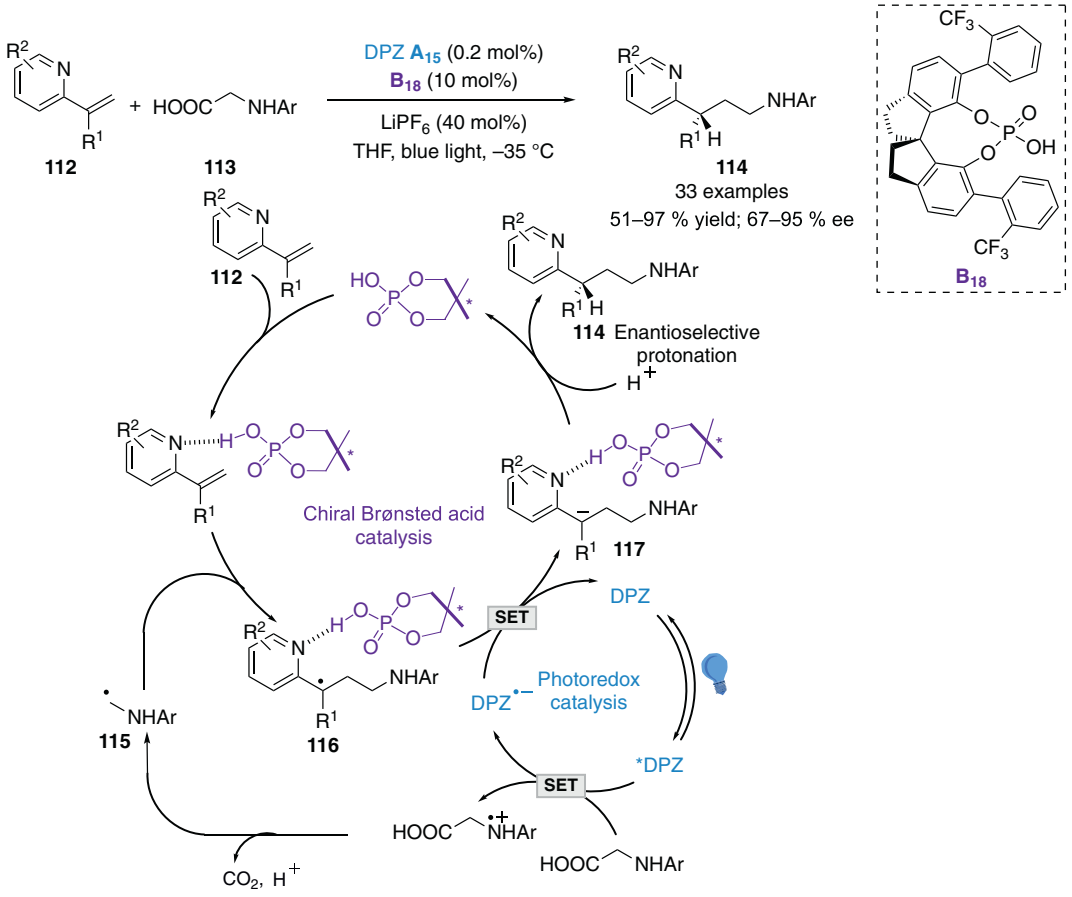

Scheme 8.20. Conjugate addition/enantioselective protonation of *N*-aryl glycines to α-branched prochiral vinyl azaarenes.

azaarene **127** yielded aminocyclopentane **126** with high stereoselectivities. Confined C_2-symmetric imidodiphosphoric acid $\mathbf{B}_{20}$ acted as a bifunctional catalyst through a ternary transition state **129** in the enantiodetermining radical cyclization step (Scheme 8.22) [42].

Jiang et al. also applied the interaction between azaarenes and a chiral Brønsted acid catalyst in the enantioselective photochemical reduction of various 2-azaaryl ketones **130**. A sacrificial stoichiometric amount of tertiary amine **131** was employed to generate the reduced form DPZ$^{\bullet-}$ of the photosensitizer upon reductive quenching. The carbonyl group underwent a first SET reduction facilitated by the chiral Brønsted acid $\mathbf{B}_{18}$ to furnish ketyl radical **133**. Further second SET reduction and subsequent enantioselective protonation took place in a chiral environment provided by the chiral phosphoric acid via two H-bounding interactions to deliver alcohols **132** in high enantioselectivities (Scheme 8.23) [43]. This methodology has been subsequently extended to the α-deuteriation of azaarenes using inexpensive deuterium oxide as the deuterium source [44].

In 2019, You and Zhang et al. reported a dual photoredox-chiral Brønsted acid catalytic system for the asymmetric dearomatization of tryptophols and tryptamines **134** leading to various furoindolines and pyrroloindolines **136** with moderate to high yields and enantioselectivities. Similar to Knowles' work (see Scheme 8.14) [29], this transformation had nevertheless the advantage to be performed under air as a terminal oxidant enabling the introduction of *N*-hydroxycarbamates **135** as nucleophiles on the indoline core. Herein the chiral Brønsted acid would play two important roles: (i) it afforded the chiral environment during the cyclization step (intermediate **137**) and (ii) it facilitated the nucleophilic addition of **135** on the resulting carbocation **139** through electrostatic and H-bonding interactions (Scheme 8.24) [45].

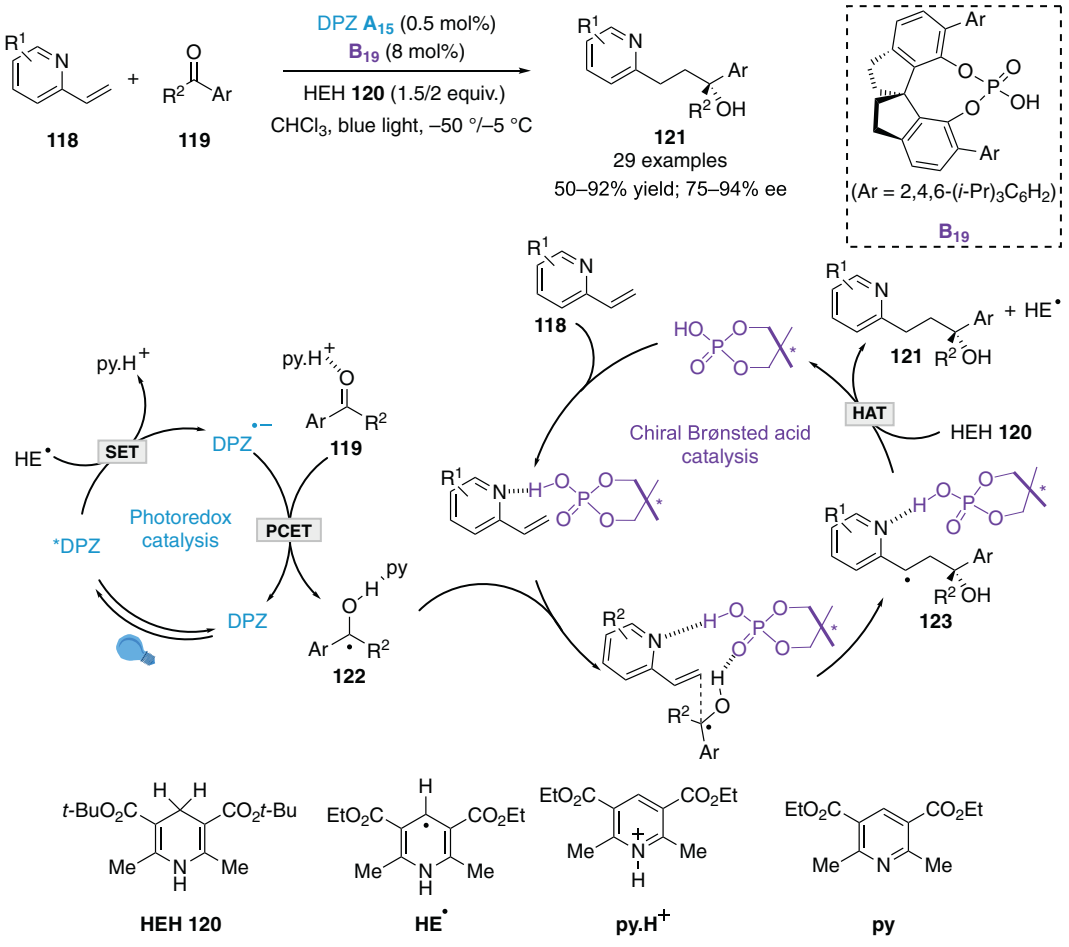

Scheme 8.21. Enantioselective conjugate addition of prochiral ketyl radicals to vinyl pyridines. Source: [40]/American Chemical Society.

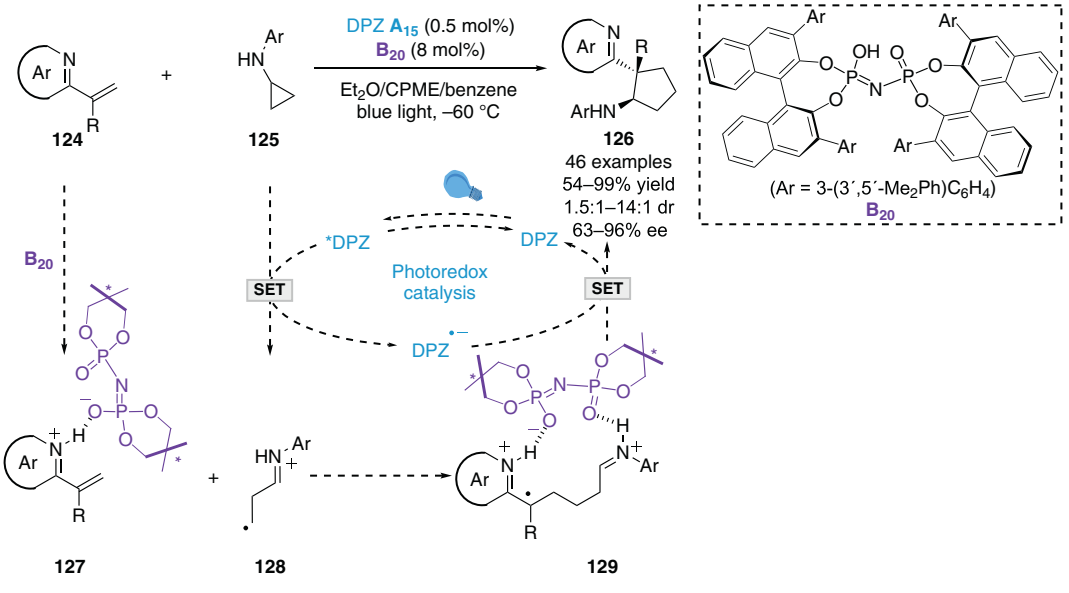

Scheme 8.22. Enantioselective (3+2)-radical cycloaddition between cyclopropylamines and α-branched 2-vinyl azaarenes. Source: [42]/American Chemical Society.

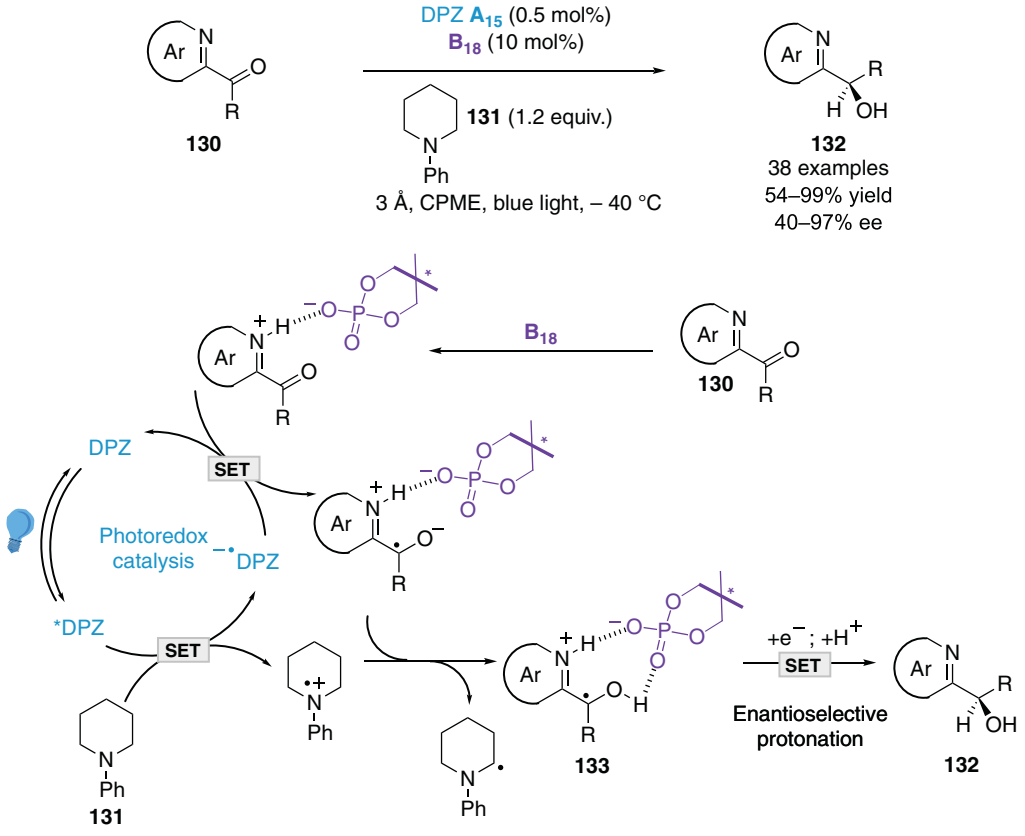

Scheme 8.23. Enantioselective reduction of various 2-azaaryl ketones. Source: [43]/Royal Society of Chemistry.

Wang et al. have recently accomplished a radical conjugate addition/enantioselective protonation of simple alkanes **141** to exocyclic enones **140** using TBADT $\mathbf{A_{11}}$ as HAT photocatalyst and chiral SPINOL-derived phosphoric $\mathbf{B_{21}}$ as chiral Brønsted acid. In this dual catalytic system, triplet excited-state TBADT abstracted a hydrogen of **141** to generate nucleophilic non-prochiral primary alkyl radical **143** which underwent conjugate addition to **140**. Subsequent HAT from the reduced form of the photocatalyst and final enantioselective tautomerization in the presence of the chiral proton-transfer shuttle Brønsted acid catalyst $\mathbf{B_{21}}$ furnished ketones **142** bearing an α-tertiary stereogenic center with good enantioselectivities (Scheme 8.25) [46].

In 2018, Jiang et al. developed a radical cross-coupling between α-bromo ketones **144** and *N*-aryl α-amino acids **145**. During this redox-neutral process, **145** underwent single electron-oxidative decarboxylation by the excited photocatalyst *DPZ to furnish persistent α-amino radical **147**. Subsequently, **144** underwent reductive debromination by reduced form $DPZ^{\bullet-}$ to generate α-keto radical **148**. The following radical cross-coupling took place in a chiral environment provided by the phosphoric acid *ent*-$\mathbf{B_{21}}$. Notably, as poor yield was obtained in the absence of $\mathbf{B_{21}}$, it was assumed that the phosphoric acid would act as a bifunctional H-bonding catalyst to stabilize the electrophilic radical species **148** and activate the nucleophilic α-amino radical **147** (Scheme 8.26) [47]. This transformation has been further extended to the radical cross-coupling of *N*-aryl glycines with 1,2-diketones via the reductive formation of ketyl radicals [48] and with 3-chlorooxindoles via a reductive dechlorination [49].

In 2015, Ooi et al. established an enantioselective radical cross-coupling between *N*-arylaminomethanes **150** and *N*-sulfonylimines **149** by combining photoredox catalyst $\mathbf{A_{18}}$ and chiral

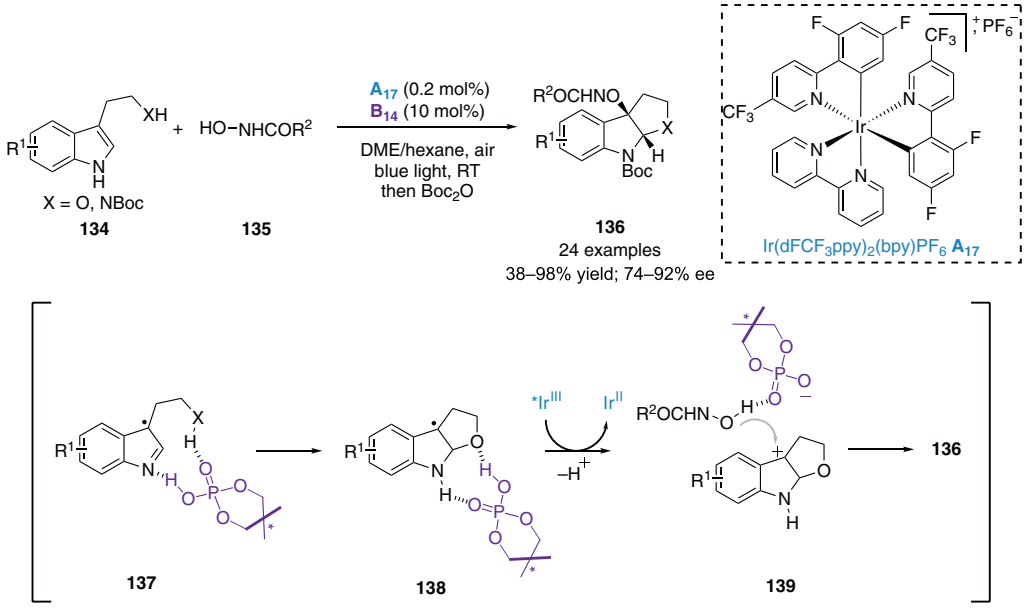

Scheme 8.24. Enantioselective syntheses of furoindolines and pyrroloindolines. Source: [45]/John Wiley & Sons.

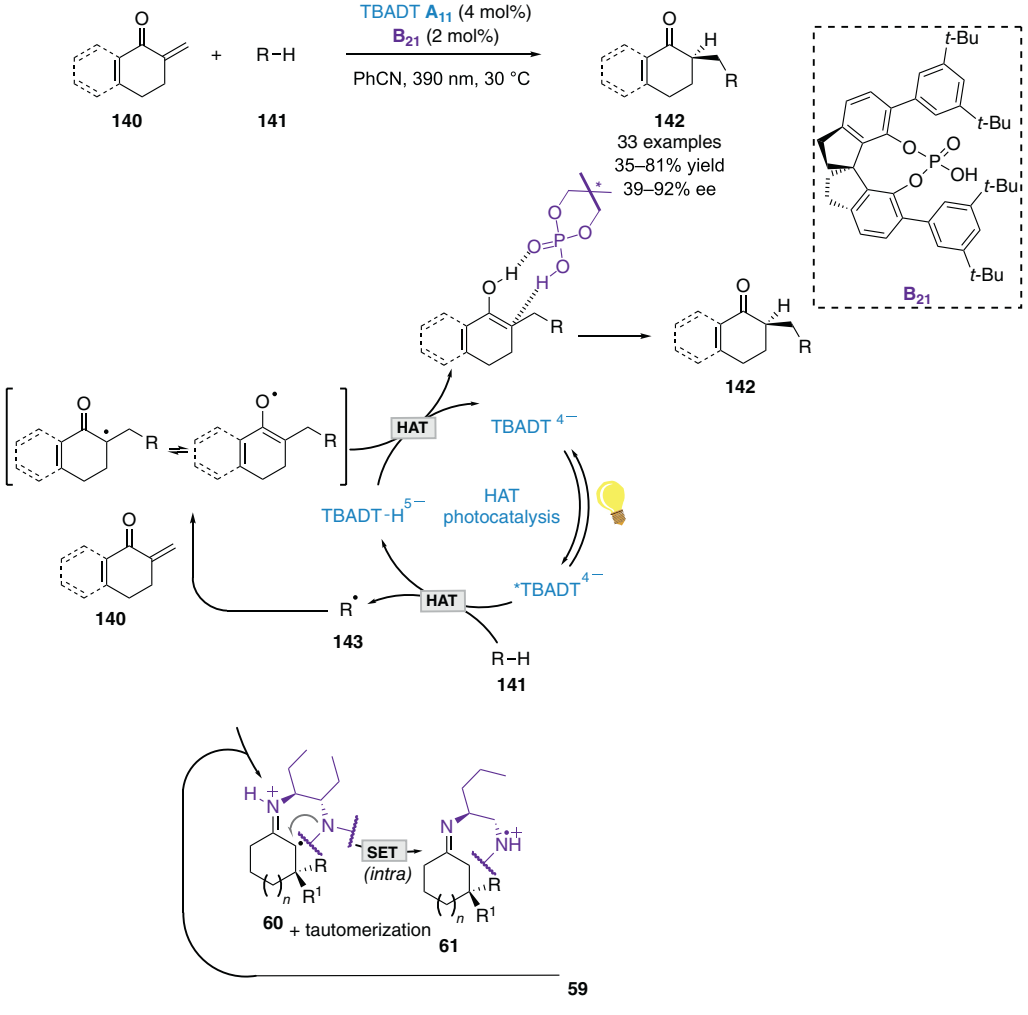

Scheme 8.25. Conjugate addition/enantioselective protonation of simple alkanes **141** to exocyclic enones. Source: [46]/American Chemical Society.

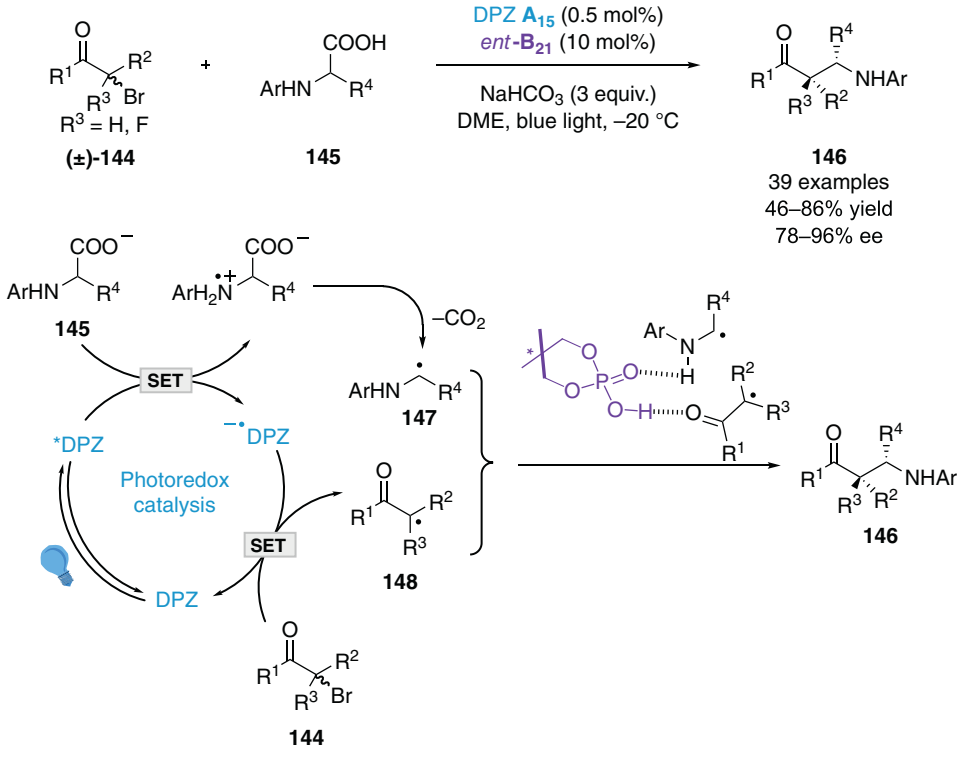

Scheme 8.26. Enantioselective coupling of α-bromo ketones with *N*-aryl α-amino acids. Source: [47]/Springer Nature.

ionic Brønsted acid catalyst $\mathbf{B}_{22}$. The mechanism is similar to the one proposed in the work of Jiang et al. (see Scheme 8.26) [47]. During this redox neutral process, amine **150** was oxidized by excited-state $^*Ir^{III}$ photocatalyst to form persistent aminomethyl radical **153** after deprotonation of cationic radical **152**. Subsequently, imine **149** underwent SET reduction from in-situ generated Ir^{II} to close the photocatalytic cycle and to form anionic radical **154**. Further radical cross-coupling between **153** and **154** yielded 1,2-diamines **151**. Importantly, besides providing the chiral environment, ionic H-bond donor catalyst $\mathbf{B}_{22}$ would prevent the homocoupling of **154** since only pinacolic-type product **155** was obtained with either a tetrabutylammonium salt or a neutral Brønsted acid (e.g. phosphoric acid, benzoic acid, thiourea) instead (Scheme 8.27) [50]. Later the authors reported a modified procedure which was initiated by the oxidative quenching of the photosensitizer using trimethylsilylmethyl amines in place of **150** and *fac*-$Ir(ppy)_3$ $\mathbf{A}_7$ as photosensitizer [51].

Very recently, Wang et al. have reported the asymmetric coupling between glycine ester derivatives **157** and α-bromoketones **156** giving rise to enantioenriched unnantural α-aminoacids **158** bearing β-stereogenic centers with high yields, enantio- and diastereoselectivities. A photoredox neutral catalytic cycle was involved to generate both α-amino ester radicals **160** upon the reductive quenching of excited $^*Ir^{III}$ and α-carbonyl radical **162** through the reductive debromination of **156** by in-situ generated Ir^{II} species. Interestingly, unlike Jiang et al. and Ooi et al., a radical cross-coupling between **160** and **162** was not proposed. A SET oxidation of **160** by excited $^*Ir^{III}$ to form iminium ion **161** was suggested instead. The latter underwent radical addition of **162** to give rise to aminium ion radical **163**. Subsequent reduction by Ir^{II} closed the second photocatalytic cycle and released target product **158**. During the C–C bond formation, a key dual activation of the iminium ion and the carbonyl group provided by the chiral phosphoric acid via H-bonding interactions was proposed to account for the high enantioselectivities (Scheme 8.28) [52].

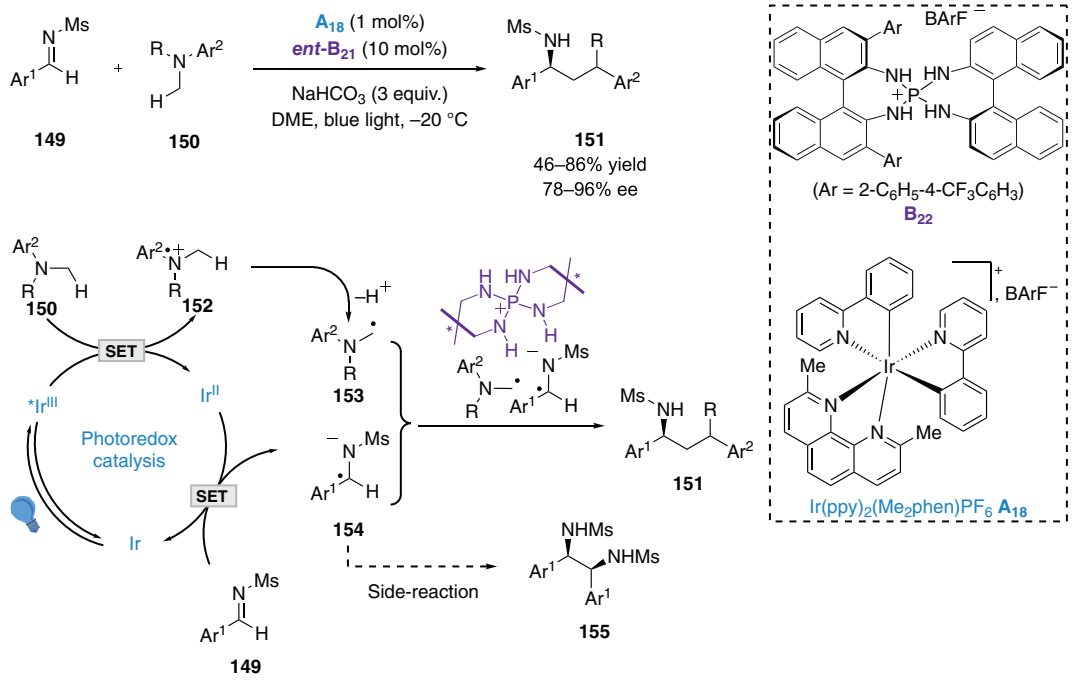

Scheme 8.27. Enantioselective coupling of *N*-arylaminomethanes with *N*-sulfonylimines. Source: [50]/American Chemical Society.

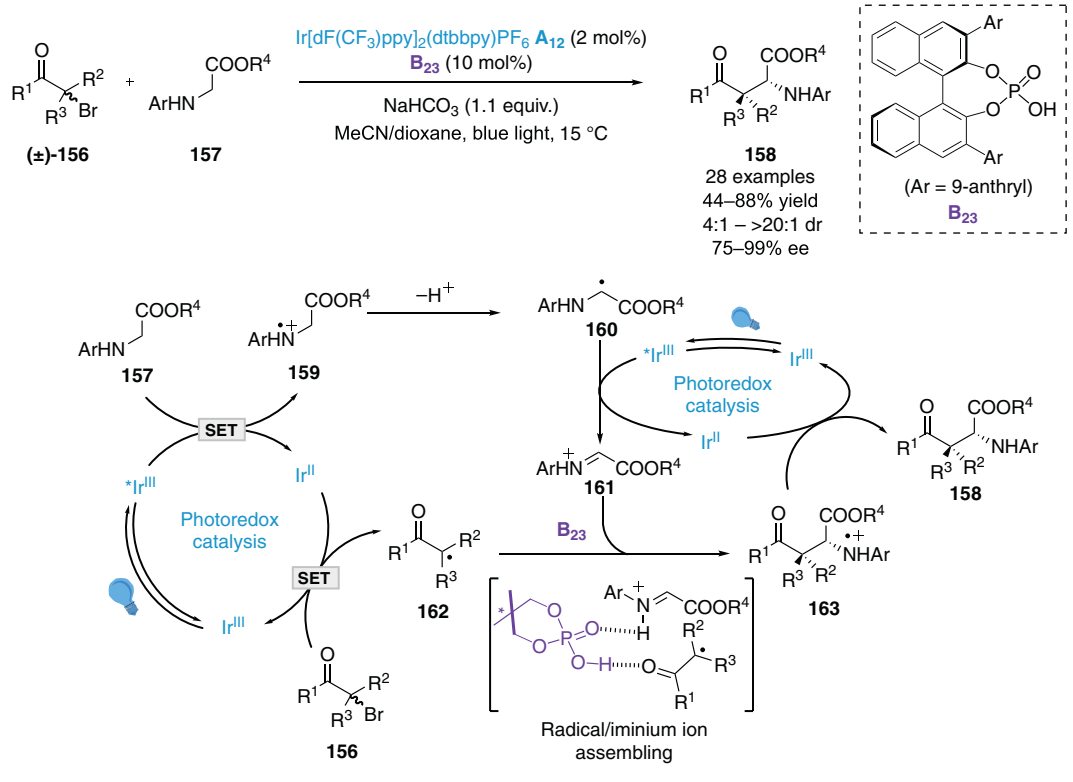

Scheme 8.28. Enantioselective coupling of glycine esters derivatives with α-bromoketones. Source: [52]/John Wiley & Sons.

8.2.5. Lewis Acid Catalysis

Activating organic substrates by a chiral Lewis acid is a well-established method in asymmetric catalysis. Notably, it has found numerous applications in photocatalytic processes. Apart from bringing the chiral environment in the enantiodetermining step, coordination of a Lewis acid to heteroatom-containing molecules can either greatly enhance their electrophilicity or lower their reduction potential. It can also have a dramatic impact on the reaction rate by stabilizing photochemically generated anionic radical intermediates. Such dual photoredox/Lewis acid catalysis has been widely used in enantioselective [2+2]-cycloaddition reactions and will be detailed in another chapter of this book. In this section, other examples are discussed.

8.2.5.1. Activation of Substrates toward Radical Addition Lewis acid co-catalysts can activate electron-deficient organic substrates toward nucleophilic radical addition by increasing their electrophilicity. They have been used in enantioselective photo-Giese-type reactions. A general mechanism is depicted in Scheme 8.29. SET oxidation of an organic substrate **164** from the excited state of a photocatalyst *PC generated a nucleophilic radical **167**. Concurrently, a chiral Lewis acid LA co-catalyst activated a Michael acceptor **165** to form chiral complex **168**. The latter could then readily undergo stereoselective conjugate addition of radical **167** to produce α-carbonyl radical **169**. Subsequent SET reduction by the reduced state of the photocatalyst $PC^{\bullet-}$ regenerated ground-state PC. Final protonation of enolate **170** and ligand exchange delivered the enantioenriched product **166** and release chiral complex **168** to trigger a new dual catalytic system. The Michael acceptors were especially designed to effectively bind the Lewis acid. In these processes, the Lewis acid is not directly involved in the photo-induced electron transfer but it controls the enantioselectivity and accelerates the rate-limiting conjugate addition step.

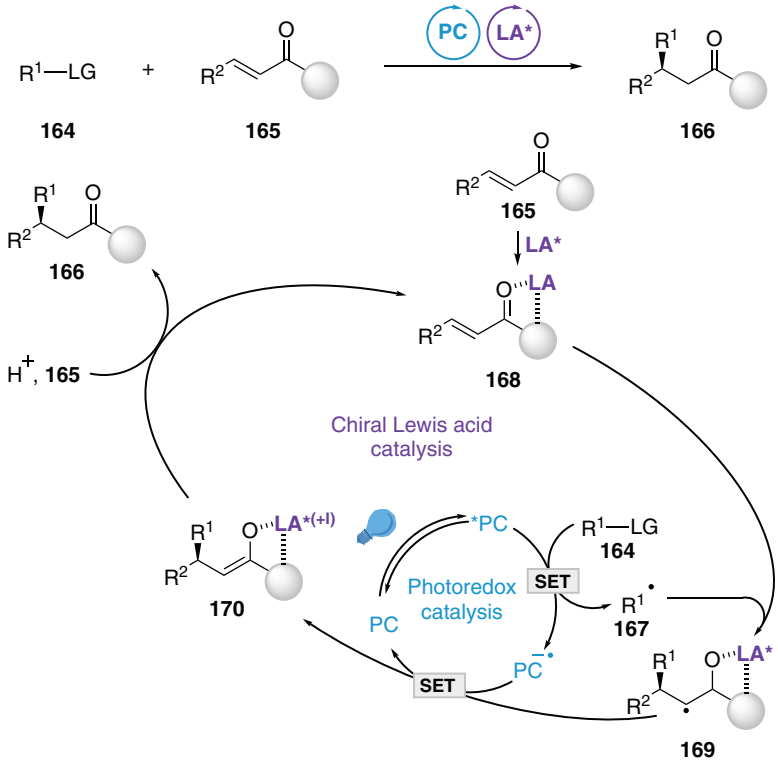

Scheme 8.29. Enantioselective photo-Giese-type reactions: general mechanism.

Such concept has been pioneered by Yoon et al. in 2015 for the addition of α-amino radical, generated from α-silyl amines **171**, to enones **172** using Ru^{II}/chiral Sc^{III} dual catalytic system [53]. Shibasaki et al. have recently engaged α-silyl amines **171** with 7-azaindoline enamides **174** under Ir^{III}/Cu^{I} dual catalysis [54]. The enantioselective additions of simple alkyl radicals to α,β-unsaturated acyl imidazoles **177** with chiral-at-metal rhodium and cobalt-centered octahedral chiral complexes $\mathbf{B}_{26}$ and $\mathbf{B}_{27}$ have been reported by Meggers and Xiao et al. respectively. With acridinium $\mathbf{A}_{19}$ photosensitizer, the former used organotrifluoroborate salts **176** as radical precursors, whereas the latter employed 1,4-dihydropyridines **179**. Remarkably, good yields and enantioselectivities were obtained at very low Lewis acid catalyst loadings (Scheme 8.30) [55–57].

Meggers et al. have subsequently developed three different strategies to generate the required nucleophilic radical for chiral rhodium-based Lewis acid-catalyzed enantioselective photo-Giese-type reaction. A domino sequence involving SET photoreductive generation of alkoxy radical from *N*-alkoxyphthalimides **180** followed by radical translocation via 1,5-HAT afforded remote enantioenriched $C(sp^3)$ functionalized alcohols **182** in good yields and high enantioselectivities. From a mechanistic point of view, a sub-stoichiometric amount (1.5 equiv.) of Hantzsch ester (HEH) was required to reductively quench photoexcited-state $^*fac$-$[Ir(ppy)_3]$ $\mathbf{A}_7$ and produced highly reducing agent fac-$[Ir(ppy)_3]^{\bullet-}$ which was able to transfer an electron to substrate **180**. The radical cascade sequence was ended by hydrogen atom abstraction from in-situ generated Hantzsch ester radical ($HE^{\cdot}$) by α-carbonyl radical **186** (Scheme 8.31a) [58]. A photoredox/Brønsted base/chiral Lewis acid triple catalysis enabled the asymmetric γ-selective $C(sp^3)$–H bond functionalization of amides **187**. This process exploited a PCET oxidation of amide **187** by excited-state photosensitizer $\mathbf{A}_{16}$ and the phosphate base followed by selective 1,5-HAT of the resulting *N*-centered radical (Scheme 8.31b) [59]. Finally, the same group has demonstrated that aliphatic and aromatic aldehydes **192** could be directly used as acyl radical precursors by using neutral eosin Y $\mathbf{A}_5$ as HAT photocatalyst. Such an approach gave rise to enantioenriched 1,4-dicarbonyl compounds **193** upon reaction with activated α,β-unsaturated *N*-acyl-3,5-dimethylpyrazoles **181**. Remarkably, other C–H (e.g. cyclic ethers or tertiary amines) and X–H (e.g. sulfinic acid or hydrophosphine oxide) partners could also be employed instead of aldehydes (Scheme 8.31c) [60].

Alemán et al. established an enantioselective formal (3+2)-cycloaddition between silyl-indole derivatives **194** and α,β-unsaturated *N*-acyl oxazolidinones **195** to access pyrrolo[1,2-*a*]indoles **197** in moderate yields and enantioselectivities under dual Ir^{III}/chiral Yb catalysis. Even though the mechanism was not fully elucidated, notable features of this cascade radical reaction included SET oxidation of **194** by excited-state photocatalyst $^*Ir^{III}$ $\mathbf{A}_{12}$, enantioselective conjugate addition of the resulting α-amino radical **198** to **195** under asymmetric Lewis acid catalysis, and intramolecular radical substitution of the indole core. Excess of ethyl cyanoacetate **196** was employed as terminal oxidant to both regenerate ground-state Ir^{III} and perform the final aromatization of open-shell species **200** yielding target product **197** (Scheme 8.32) [61].

Recently, Ryu et al. reported an enantioselective 1,2-addition reaction of α-aminoalkyl radicals to α,β-unsaturated or aromatic aldehydes **202** under dual Ir^{III}/chiral oxazaborolidinium ion ($\mathbf{B}_{29}$) Lewis acid catalysis. The catalytic cycle was initiated by the reductive quenching of excited-state photosensitizer $^*Ir^{III}$ by α-silyl amine **201**. Subsequent enantioselective nucleophilic radical 1,2-addition of the resulting α-amino alkyl **204** to aldehyde **202** was facilitated by the chiral Lewis acid $\mathbf{B}_{29}$. Herein, a high quantum yield value ($\Phi = 30$) supported a radical chain mechanism comprising SET between α-silyl amine **201** and intermediate **205** to furnish propagating radical **204** and enantioenriched silyl-alcohol **206**. Importantly, classical radical clock control experiment ruled out any formation of a ketyl radical which would be involved in a radical–radical coupling mechanism (Scheme 8.33) [62].

8.2.5.2. Activation of Electron-Deficient Organic Substrates toward Photocatalytic Reduction It has also been demonstrated that chiral Lewis acid co-catalysts can activate electron-deficient organic substrates toward photocatalytic reduction by decreasing their reduction potential and subsequently control the stereochemistry of a further radical bond formation.

Meggers et al. have disclosed an enantioselective coupling between α-silylamines **207** and 2-acyl imidazoles **208** under dual Ru^{II}/chiral Rh Lewis acid catalysis. In this redox neutral process, SET oxidation of α-silylamine **207** by excited-state photocatalyst $^*Ru^{II}$ followed by classical spontaneous extrusion of the trimethylsiliyl group generated persistent α-amino radical **211**. In parallel, chiral Rh Lewis acid $\mathbf{B}_{26}$ activated 2-acyl imidazole **208** to form complex **212**. The latter could then readily undergo SET reduction

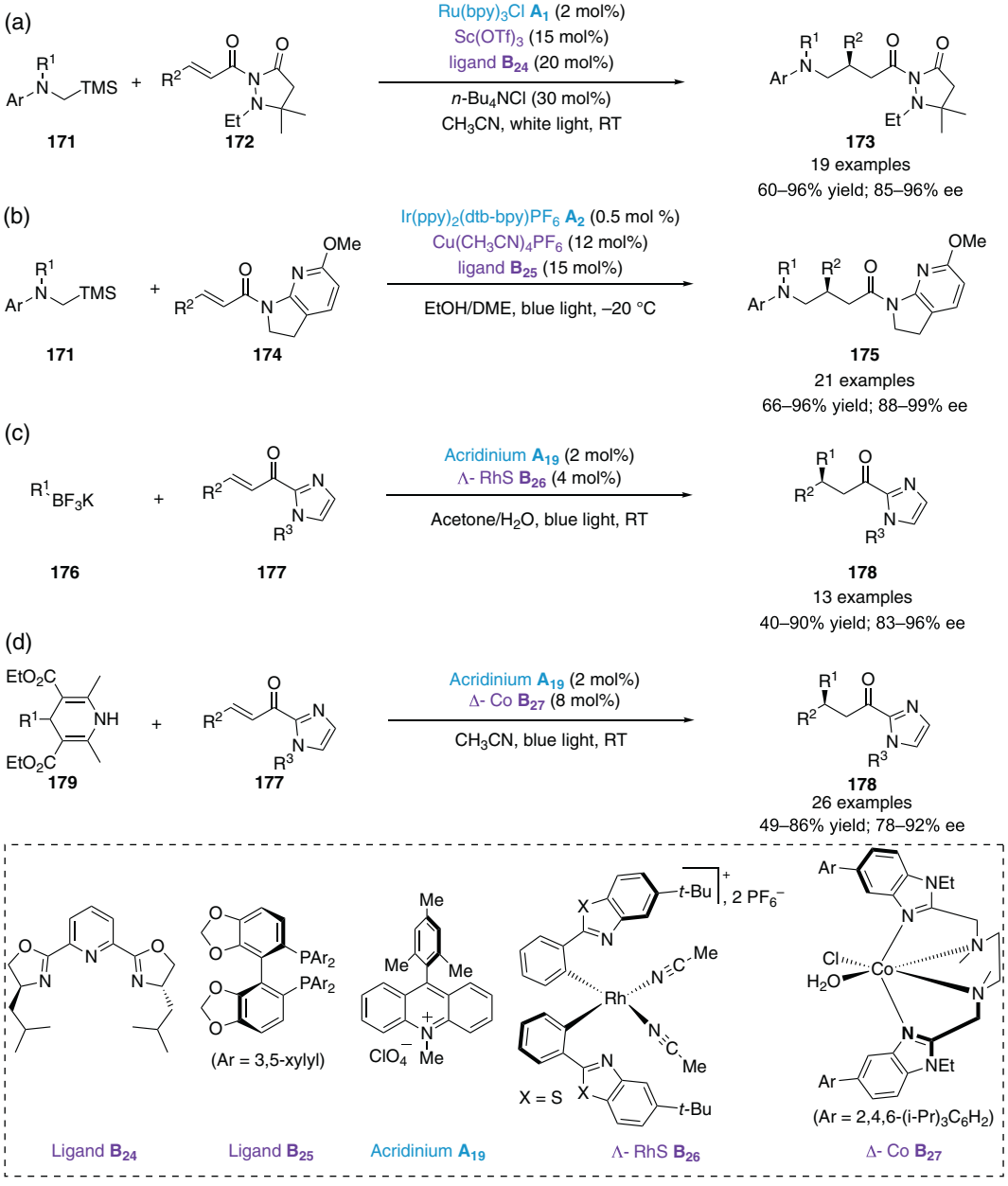

Scheme 8.30. Examples of enantioselective photo-Giese-type reactions. (a) Ru^{II}/chiral Sc^{III}-catalyzed conjugate addition of α-amino radicals [53]. (b) Ir^{III}/chiral Cu^{I}-catalyzed conjugate addition of α-amino radicals [54]. (c) Acridinium/chiral Rh^{III}-catalyzed conjugate addition of alkyl radicals [55–56]. (d) Acridinium/chiral Co^{II}-catalyzed conjugate addition of alkyl radicals [57]. Source: Based on [55–57].

from reduced state photocatalyst Ru^{I} to close the photocatalytic cycle and produce ketyl radical **213**. Radical–radical cross-coupling with **211** under the stereocontrol of $\mathbf{B}_{26}$ and subsequent ligand exchange yielded enantioenriched silylated 1,2-aminoalcohol **215** and initiate a new catalytic cycle. Interestingly, the authors pointed out a crucial role of the released trimethylsilyl group which would act as an additional Lewis acid to activate the rhodium-coordinated 2-acyl imidazole **212** (Scheme 8.34) [63].

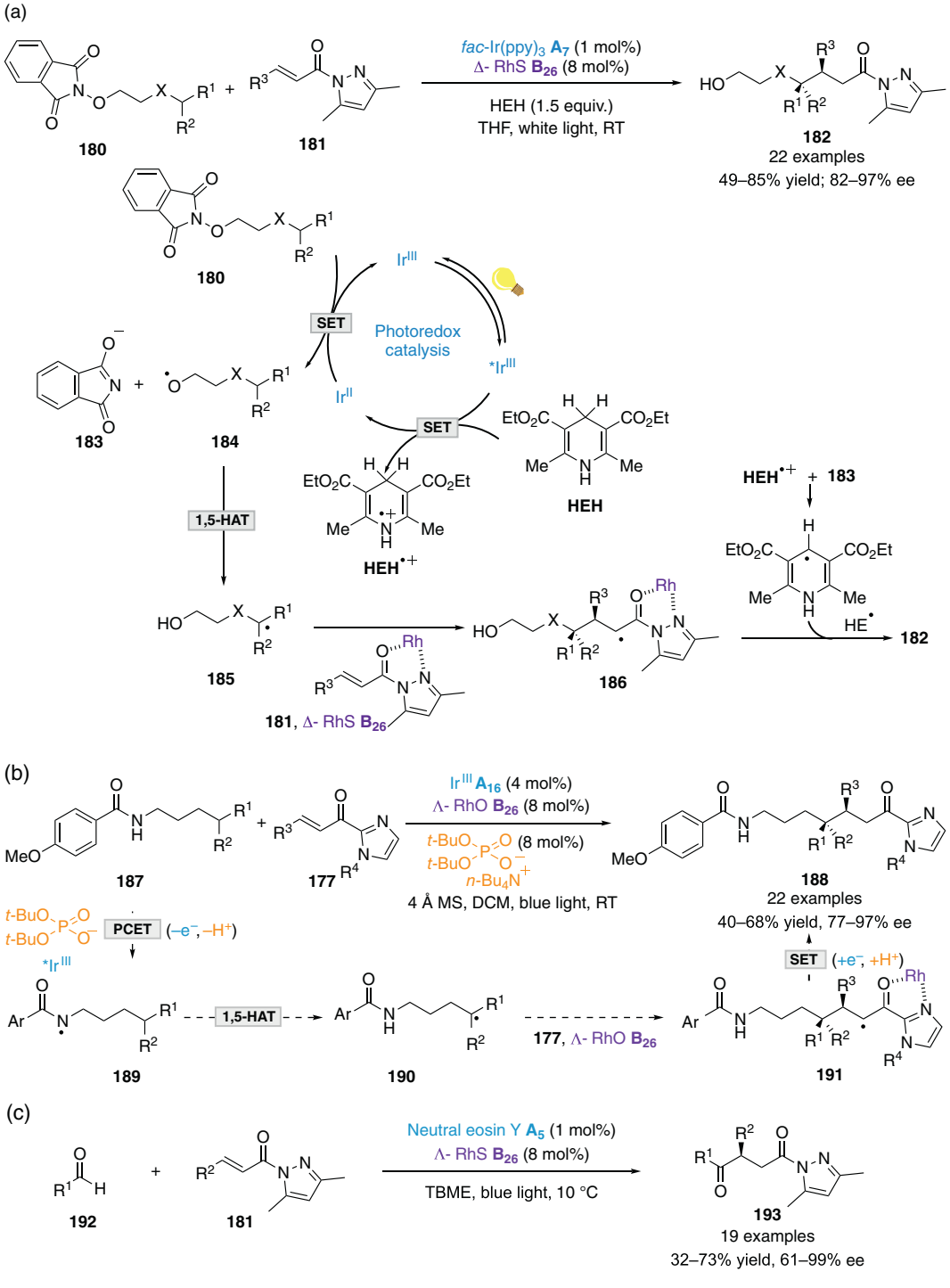

Scheme 8.31. Various strategies of generation of C-centered radicals for enantioselective photo-Giese-type reactions. (a) Alkoxy radical/1,5-HAT/conjugate addition. Source: [58]/John Wiley & Sons. (b) Amidyl radical/1,5-HAT/conjugate addition. Source: [59]/Royal Society of Chemistry. (c) Photoinduced-HAT catalysis. Source: [60]/John Wiley & Sons.

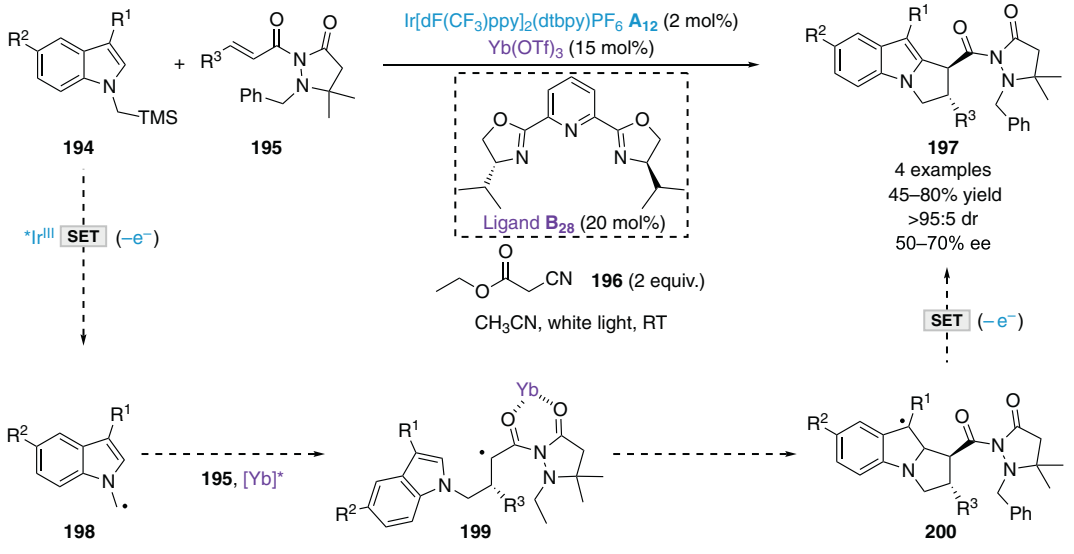

Scheme 8.32. Enantioselective synthesis of pyrrolo[1,2-*a*]indoles. Source: [61]/Royal Society of Chemistry.

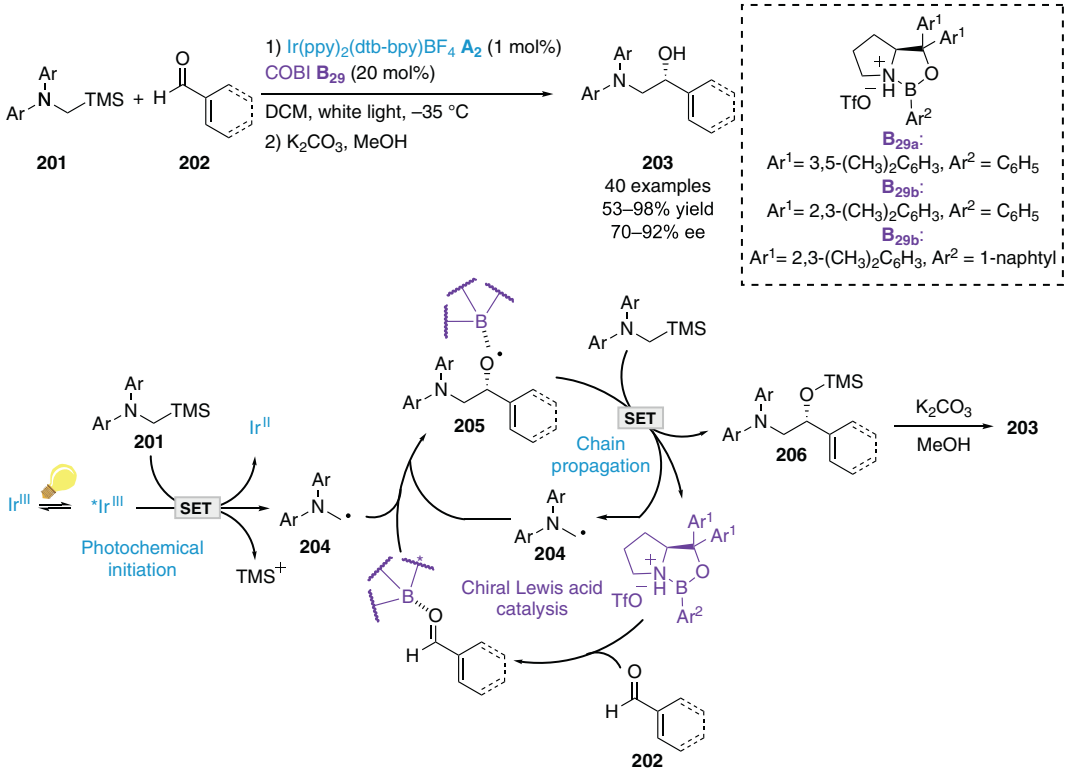

Scheme 8.33. Enantioselective 1,2-addition reactions of α-aminoalkyl radicals to aldehydes. Source: [62]/American Chemical Society.

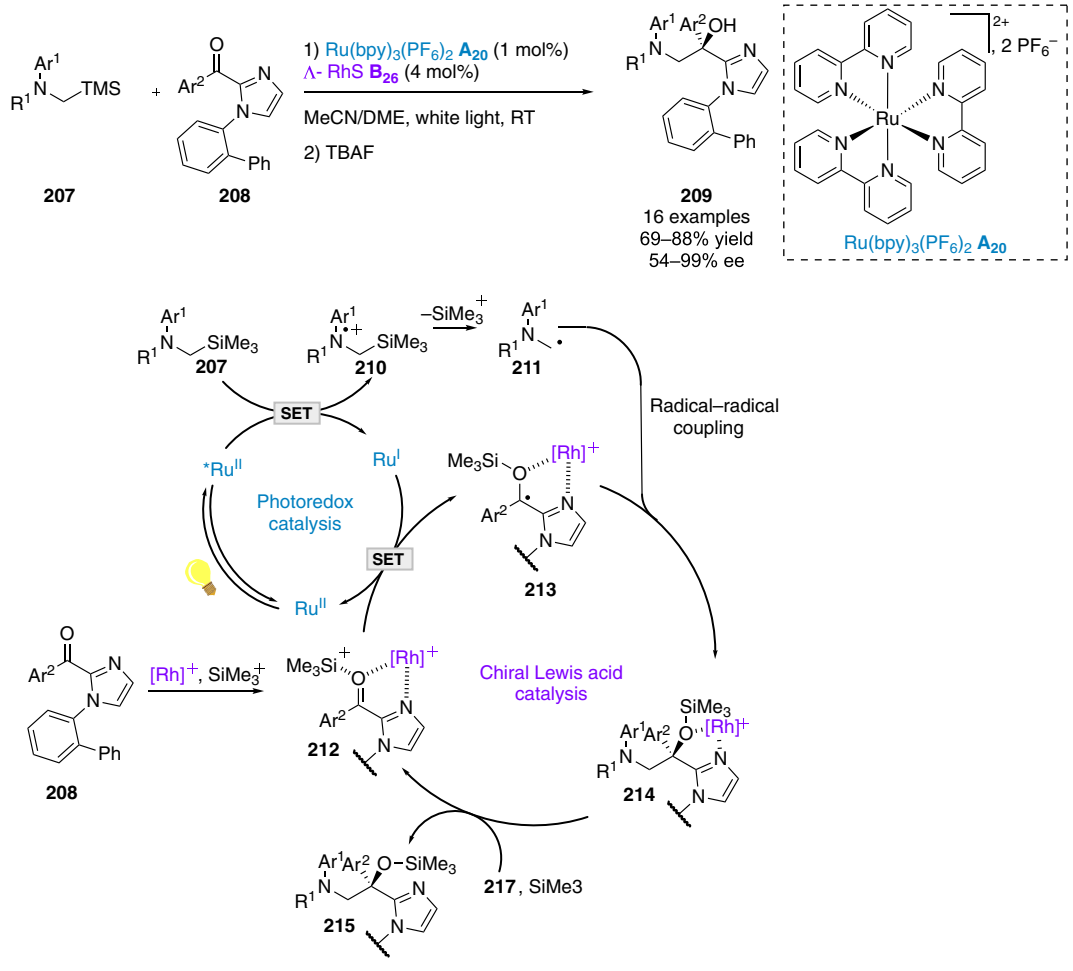

Scheme 8.34. Enantioselective coupling of α-silylamines with 2-acyl imidazoles. Source: [63]/Royal Society of Chemistry.

Subsequently, the same authors reported an enantioselective photoredox neutral coupling between *N*-aryl carbamic esters **216** and α,β-unsaturated 2-acyl imidazoles **217** under Ir^{III}/Brønsted phosphate base/chiral Lewis acid triple catalysis. Herein, a PCET oxidation of phosphate base-activated **216** by exited-state photocatalyst $*Ir^{III}$ generated electron-poor carbamoyl radical **219**. Subsequently, upon complexation with chiral Rh Lewis acid $\mathbf{B}_{26}$, enone **217** could be readily reduced by in-situ generated Ir^{II} to produce persistent electron-rich radical enolate **220**. Stereoselective C–N radical–radical cross-coupling between *N*-centered radical **219** and chiral radical complex **220**, followed by protonation and ligand exchange, afforded β-amino ketones **218** with high yields and excellent enantioselectivities (Scheme 8.35) [64].

More recently, Gong et al. have reported an elegant photoredox neutral regio- and enantioselective C(sp^3)–H functionalization of benzylic and allylic hydrocarbons **224** with imino esters **225** under dual HAT/chiral copper Lewis acid catalysis. Selective hydrogen atom abstraction of **224** from triplet-state HAT organocatalyst $\mathbf{A}_{21}$ generated alkyl radial **227**. Subsequently, chiral copper-activated iminoester **228** could be easily reduced by in-situ generated semiquinone type radical to close the photocalytic cycle and produce persistent radical **229**. Final stereocontrolled radical–radical cross-coupling, protonation and ligand exchange led to the radical-Mannich-type products **226** and triggered a new catalytic cycle. This transformation has also been extended to simple unactivated alkanes as C–H partners (Scheme 8.36) [65].

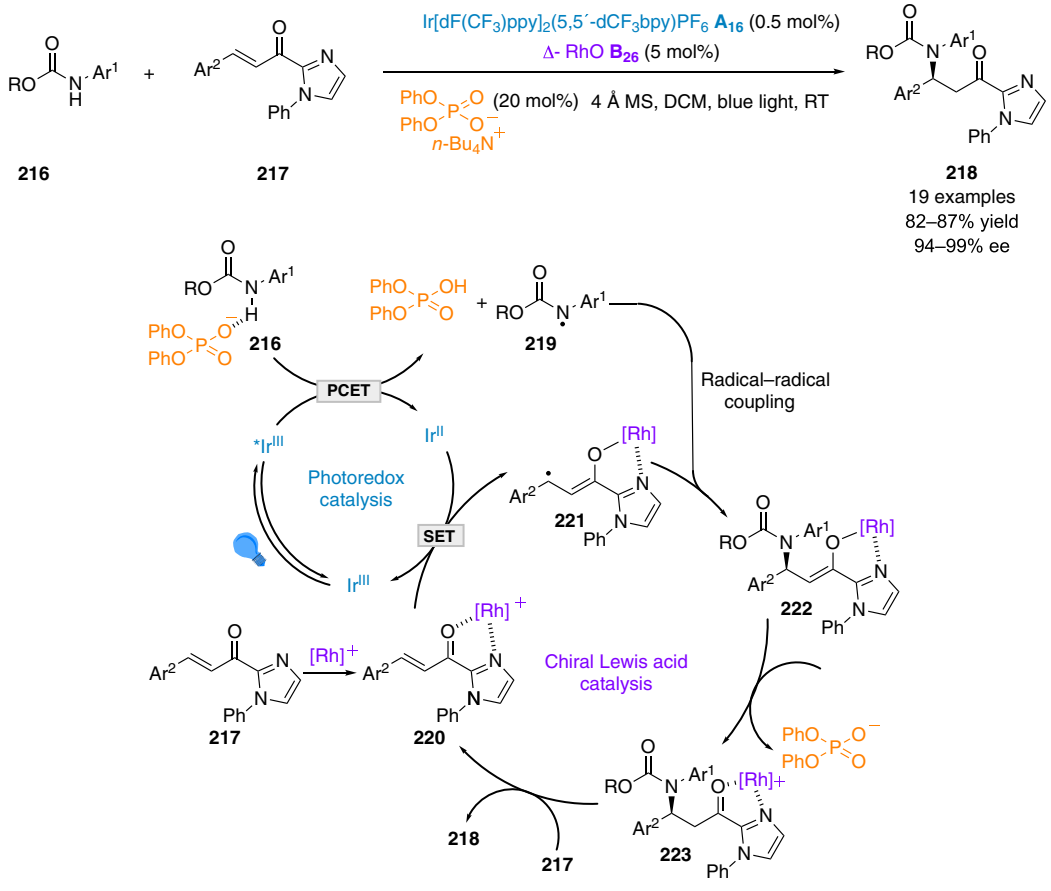

Scheme 8.35. Enantioselective redox-neutral coupling of *N*-aryl carbamic esters with α,β-unsaturated 2-acyl imidazoles. Source: [64]/Royal Society of Chemistry.

Huang et al. have disclosed an enantioselective photoreductive cross-coupling reaction of nitrones **231** with aromatic aldehydes **232** under dual Ru^{II}/chiral Sc^{III} catalysis giving access to vicinal amino alcohols **233** with good yields and enantioselectivities. An excess of tetraethylethylenediamine (TEEDA) was used as reductive quencher. The authors proposed a radical-type Zimmerman–Traxler model involving chiral Sc^{III} Lewis acid, nitrone **231,** and in-situ generated aromatic ketyl radical to account for the reactivity and selectivity. Herein, a radical–radical cross-coupling between a putative α-oxyamino radical (which would be generated upon reduction of nitrones **231**) and the ketyl radical was not considered (Scheme 8.37) [66].

Yoon et al. have established an enantioselective photoreductive formal (3+2)-cycloaddition between aryl cyclopropyl ketones **234** and alkenes **235** under dual Ru^{II}/chiral Gd Lewis acid catalysis. Densely substituted cyclopentanes **236** were obtained in good yields and high enantioselectivities. Diisopropylethylamine (DIPEA) was used as reductive quencher. Key features of this process involved SET photoreduction of chiral Gd-activated cyclopropyl ketones **234** to produce ketyl radicals **238** which spontaneously underwent ring-opening to distonic radical **239**. Formal radical cycloaddition with alkenes **235** afforded enantioenriched cyclopentyl ketyl radical **240**. Electron transfer to another equivalent of substrate led to chain propagation and delivered closed-shell products **236**. Chiral ligand $\mathbf{B_{32}}$ with strong coordinating ability was specially designed to avoid the formation of an inactive adduct between DIPEA and Gd^{3+} (Scheme 8.38) [67].

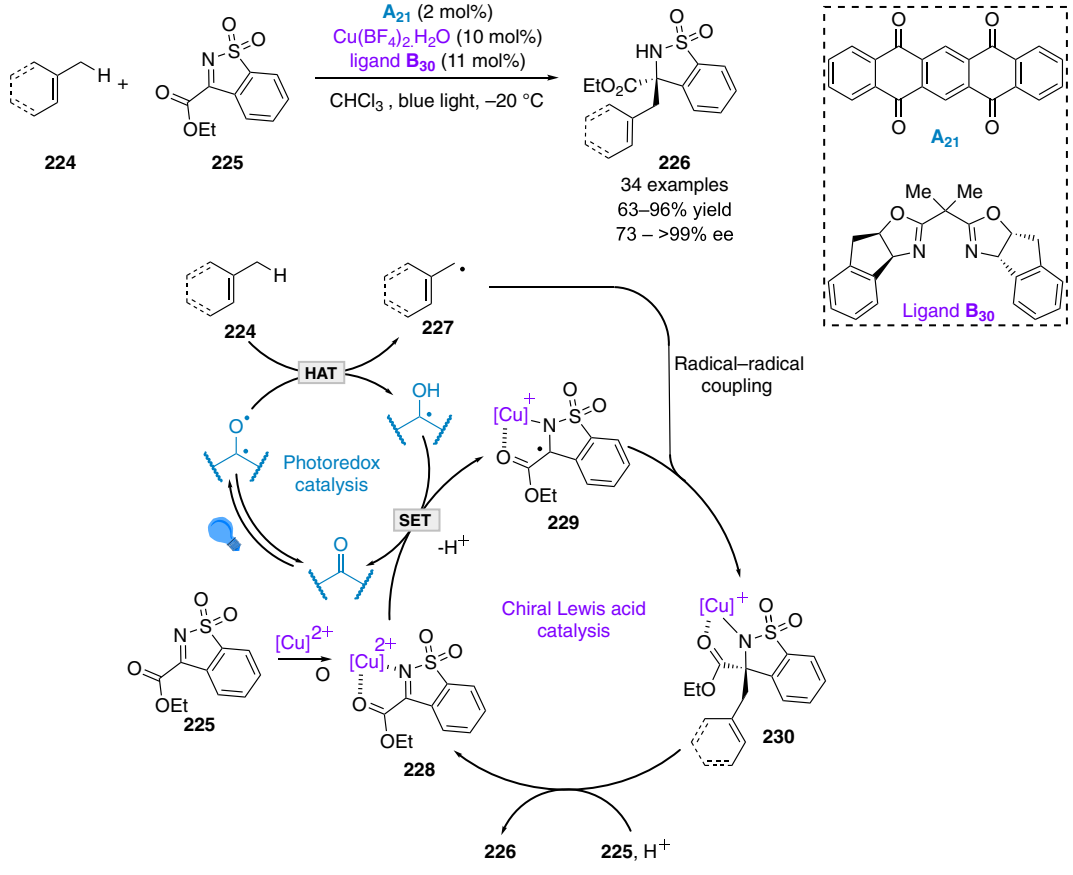

Scheme 8.36. Enantioselective C(sp^3)–H functionalization of hydrocarbons with imino esters. Source: [65]/Springer Nature.

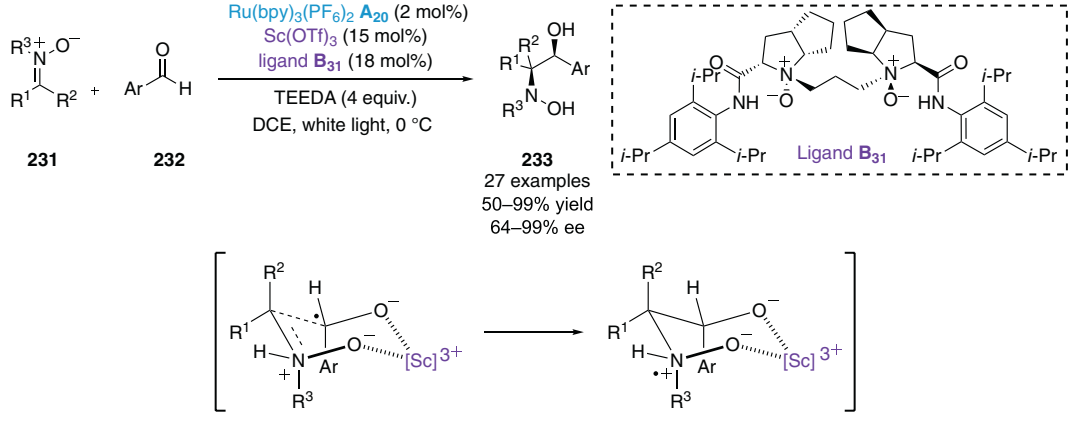

Scheme 8.37. Enantioselective reductive coupling of nitrones with aromatic aldehydes. Source: [66]/Springer Nature.

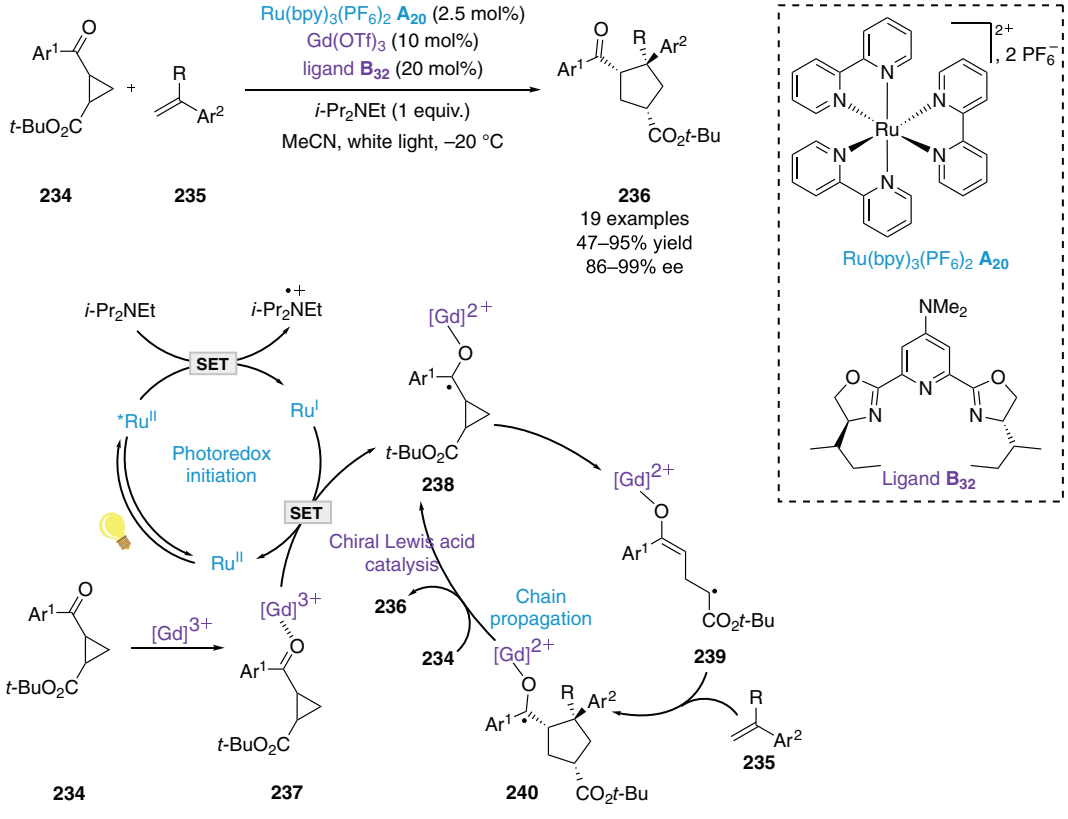

Scheme 8.38. Enantioselective (3+2)-cycloaddition between aryl cyclopropyl ketones and alkenes. Source: [67]/American Chemical Society.

8.2.5.3. Chiral Enolate Complex as Reductive Quencher and Acceptor of Electrophilic Radicals The asymmetric α-functionalization of 2-acyl imidazoles **241** with electrophilic radicals has been realized under dual chiral-at-metal rhodium-based Lewis acid $\mathbf{B_{26}}$/ photoredox catalysis. A general mechanism is depicted in Scheme 8.39. Coordination of carbonyl compound **241** to Lewis acid $\mathbf{B_{26}}$ and deprotonation produced the key electron-rich chiral rhodium-enolate **244** which was able to reductively quench excited-state photocatalyst $*Ru^{II}$. Subsequent SET from the resulting highly reducing agent Ru^{I} to electron-poor substrate **242** generated electrophilic radical **245**. Stereoselective addition of this electrophilic radical to electron-rich chiral enolate **244** furnished ketyl radical **246** which in turn can reductively quench $*Ru^{II}$ to form closed-shell complex **247** and trigger a new photocatalytic cycle. Final ligand exchange delivered enantioenriched α-functionalized products **243** and allowed a new Lewis acid catalytic cycle to take place. A radical chain propagation involving SET from ketyl radical **246** to radical precursor **242** was also proposed. This concept was initially designed by Meggers et al. for the asymmetric α-aminations and α-alkylations using aryl azides **242a** and α-diazo carboxylic esters **242b** with Ru^{II} photocatalyst $\mathbf{A_{20}}$ [69]. It has been later extended to the α-difluoroalkylations with bromodifluoroacetamides **242c** and Ir^{III} photocatalyst $\mathbf{A_2}$ by Xu et al. (Scheme 8.39) [68].

8.2.6. Phase-Transfer Catalysis

Meng et al. have reported an aerobic photocatalytic enantioselective α-hydroxylation of cyclic β-ketoesters **248** under asymmetric phase-transfer catalysis. Tetraphenylporphyrin (TPP) $\mathbf{A_{21}}$ was utilized as a photosensitizer to generate highly electrophilic singlet oxygen by energy transfer. Reaction with

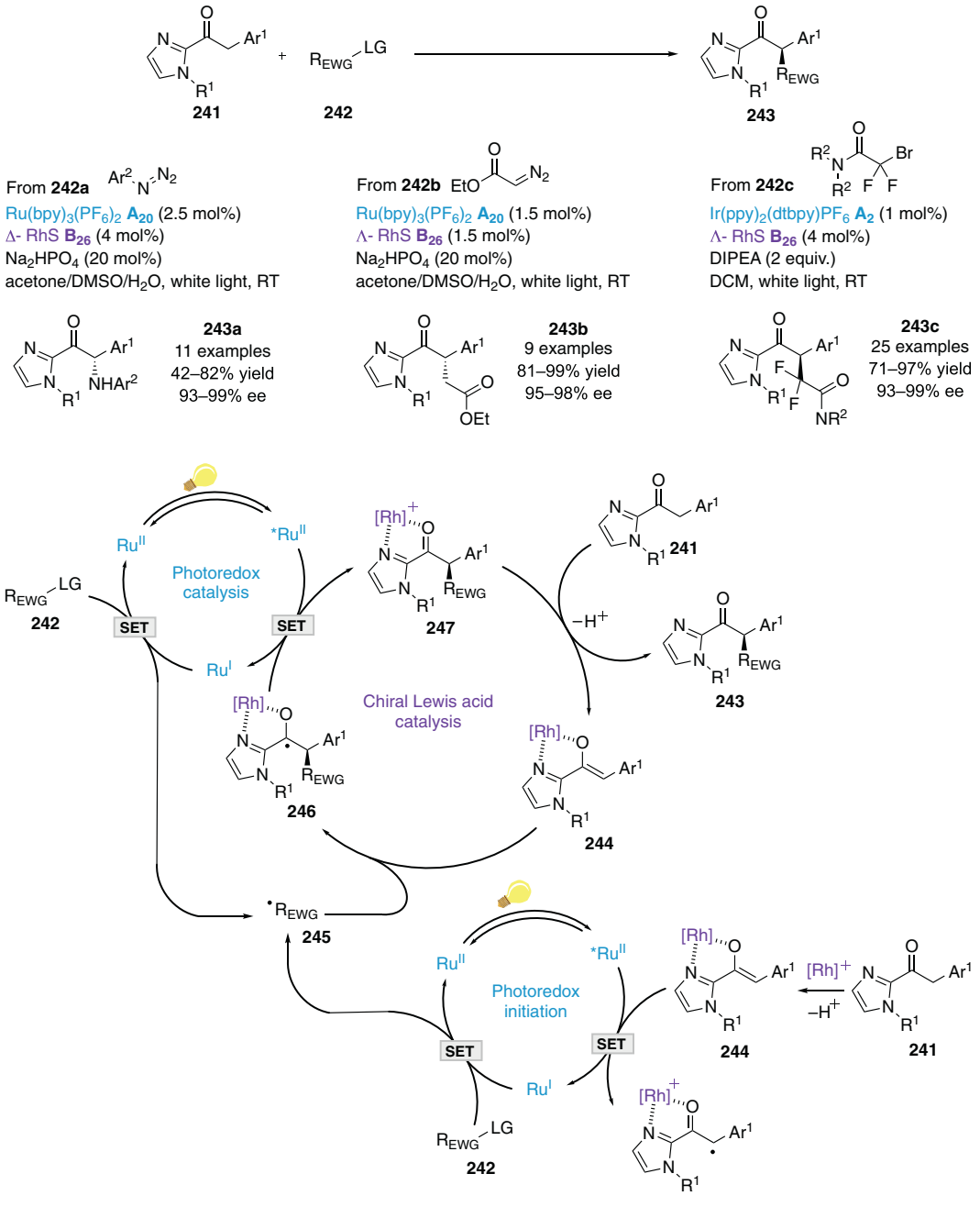

Scheme 8.39. Enantioselective α-functionalization of 2-acyl imidazoles. Source: [68]/American Chemical Society.

chiral ammonium enolate **250** provided α-hydroperoxyde salt **251** which could oxidize another chiral enolate **250** to deliver two molecules of α-hydroxy β-ketoesters **249**. High yields and excellent enantioselectivities were achieved, thanks to the new C-2′ modified cinchonine-derived phase-transfer catalyst $\mathbf{B}_{33}$ [70–72]. Interestingly, the authors subsequently demonstrated that chiral ammonium enolate **250** could act as a photosensitizer to generate singlet oxygen in the absence of TPP (Scheme 8.40) [73].

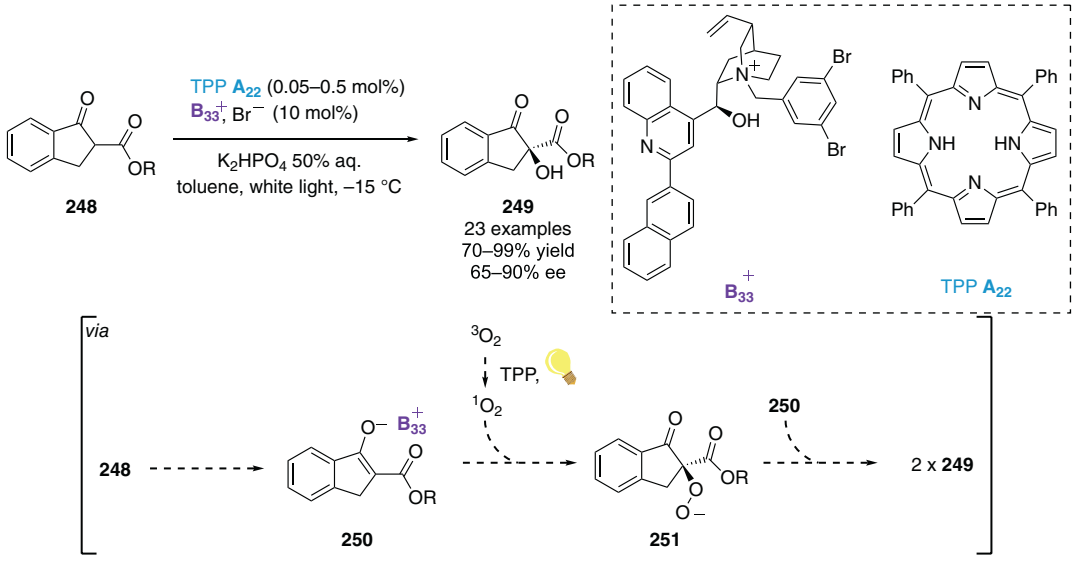

Scheme 8.40. Enantioselective α-hydroxylation of cyclic β-ketoesters. Source: [73]/John Wiley & Sons.

8.3. SINGLE BIFUNCTIONAL CATALYST APPROACH

8.3.1. Chiral Organophotocatalysts

8.3.1.1. Enamine Catalysis As described above, the synergic combination of chiral secondary amines with achiral photocatalysts is a powerful tool for the promotion of asymmetric transformations [2–15]. In 2018, Alemán's group [74] demonstrated that a single chiral photoamino catalyst $\mathbf{A_{22}}$ bearing thioxanthone moiety was also effective for enantioselective α-alkylation of carbonyls with electron-deficient α-bromoalkene compounds **252** (Scheme 8.41). Under optimized conditions, the reaction provided alkylated of aldehydes **253** in high yields and with excellent enantioselectivities (up to 99%). The proposed mechanism was similar to that reported by Macmillan et al. (Scheme 8.1) [2–15], proceeding via a key excited enamine intermediate **254**. The resulting intermediate can reduce the bromoalkane derivative **252** via a SET process to yield radical alkyl **256.** Next, the addition of alkyl radical **256** to the enamine produces α-amino radical **257A.** Finally, the resultant radical can be oxidized by the thioxanthone radical cation and hydrolyzed to produce the desired α-alkylated aldehyde **253**. Through a set of control experiments, the authors note that they cannot rule out the alternative mechanism involving the generation of alkyl radical through an energy transfer.

8.3.1.2. Ion-pair Catalysis In addition, merging ion-pair catalysis with photocatalytic reaction has also emerged as a new platform for developing enantioselective radical transformations. In 2017, Luo et al. [75] were the first to report a single chiral ion pair organophotocatalyst $\mathbf{A_{23}}$ in which a chiral phosphate anion was paired with C_9-mesityl acridinium photocatalyst Fukuzumi's catalyst Mes-Acr$^+$). This new ion pair photocatalyst $\mathbf{A_{23}}$ was efficiently used in asymmetric Nicewicz's hydroetherification of alkenols **258** (Scheme 8.42) [76]. The proposed mechanism involves a reductive quenching of the excited state of the ion-pair acridinium photocatalyst $\mathbf{A_{23}}$* to produce chiral radical cation ion pair **262** after chiral ion-exchange between $\mathbf{A_{24}}$ and **258**. Subsequent cyclization of **262** within the chiral environment produces radical **264** that can abstract a hydrogen atom from 2-phenylmalonitriles **260** to give the desired tetrahydrofurans **259** in excellent yields albeit with moderates enantioselectivities (up to 64% ee). It is interesting to note that authors found a better catalytic activity of ion-pair catalyst $\mathbf{A_{24}}$ than the Fukuzumi;s catalyst Mes-AcrBF$_4$.

Soon after, Nicewicz's group [77] reported a similar approach to develop enantioselective intra- and intermolecular cation-radical Diels–Alder reactions by using a chiral ion-pair photocatalyst $\mathbf{A_{24}}$ generated

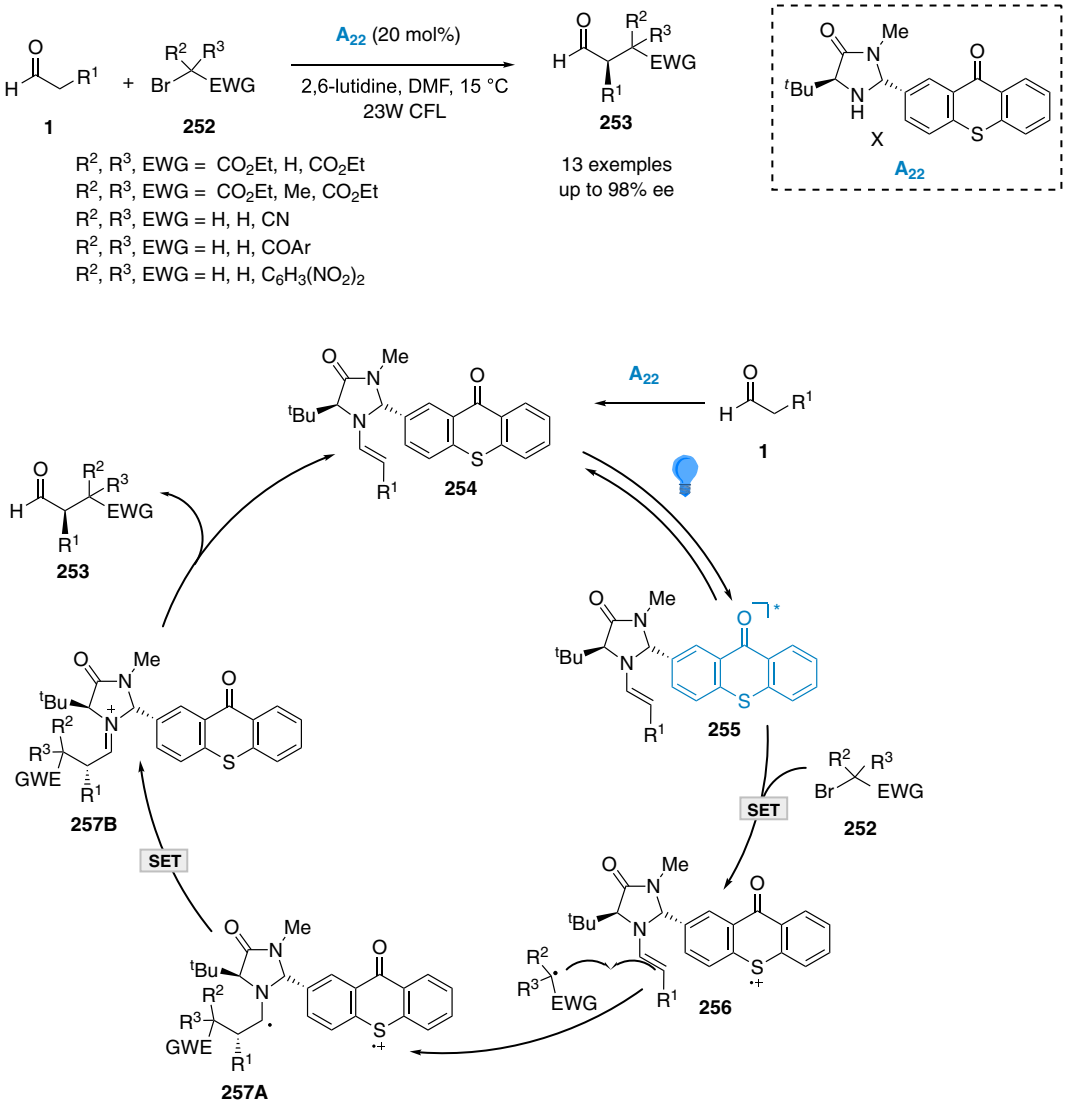

Scheme 8.41. Bifunctional photoamino-catalyzed enantioselective alkylation of aldehydes.

by assembly of a chiral N-triflyl phosphoramide anion and a cationic oxopyrylium (TP^+) photocatalyst (Scheme 8.43). The intramolecular version with various trienes **266** afforded a range of chiral heterocycles **267** with low to moderate yields and enantioselectivities. No better asymmetric induction was achieved in intermolecular Diels–Alder version between styrenes **268** and pentadiene (**269**). The mechanism proposed is similar to that proposed by Luo [75]. Excited chiral ion-pair photocatalyst $\mathbf{A}_{24}$* formed upon blue LEDs irradiation oxidizes the electron-rich olefins to produce a chiral cation radical intermediate **274**. The latter undergoes enantioselective cycloaddition with the dienes and the resulting ion pair **275** is then reduced by **TP•** **276** to complete the catalytic cycles.

Very recently, Ooi et al. conceived a strategic installation of urea as redox-active directing group (DG) onto cyclopropylamines **277** to realize a photoinduced (3+2)-cycloaddition with α-substituted styrenes **278** using chiral photocatalyst $\mathbf{A}_{25}$, an iridium polypyridyl complex Ir^{III+} bearing a weakly coordinating chiral borate counterion as photocatalyst B_x. The DG possessed anionic-recognition ability to bind the chiral anion and effectively fix the photocatalyst to the substrate prior to electron transfer. Upon light irradiation, SET oxidation of **277** by excited-state $*Ir^{III+}$ generated cyclopropyl aminium radical cation

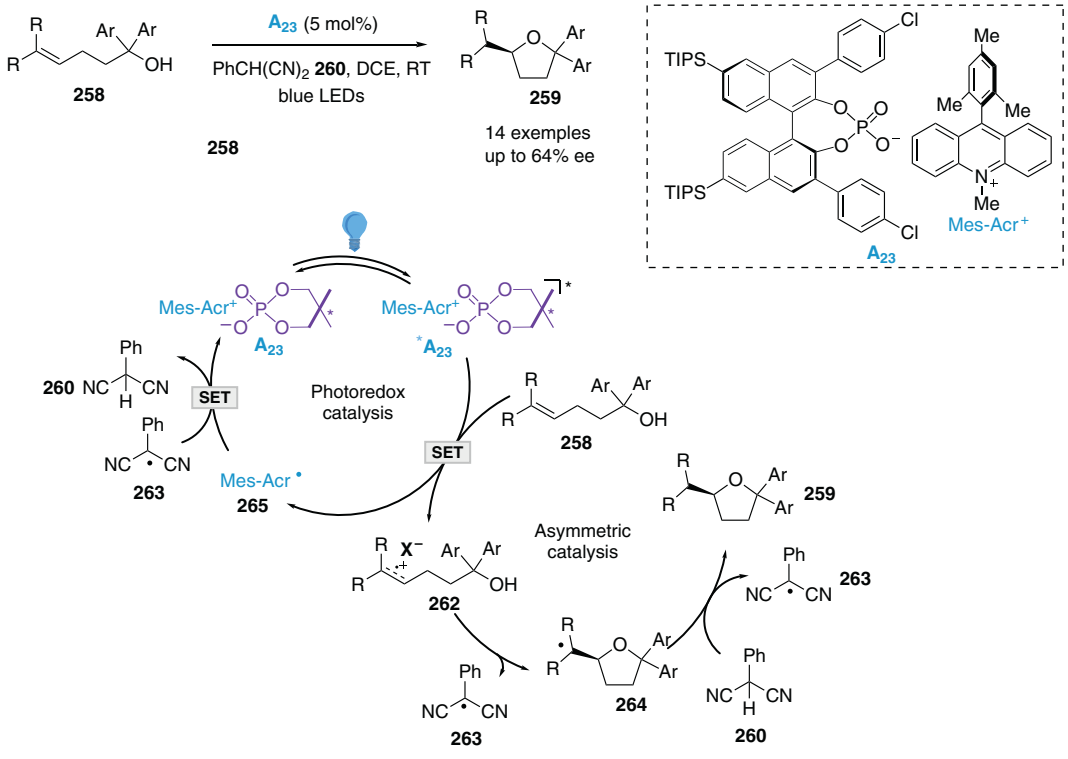

Scheme 8.42. Chiral acridinium salt-catalyzed enantioselective anti-Markovnikov hydroetherification. Source: Based on [76].

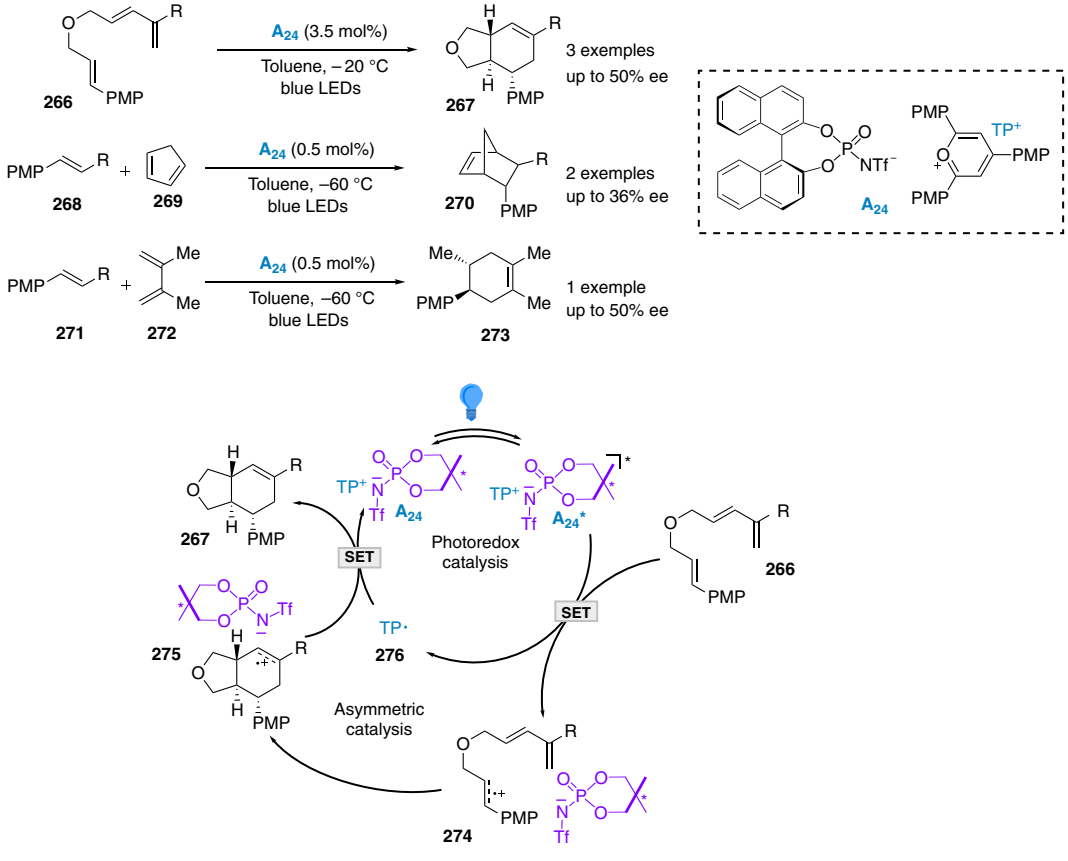

Scheme 8.43. Chiral oxopyrylium salt-catalyzed enantioselective Diels–Alder reactions.

282 which is in equilibrium with distonic iminium radical **281**. The latter regioselectivity added to alkene **278** to form alkyl radical **283**. The selectivity of the subsequent enantio-determining cyclization step was controlled by the anchored chiral anion to furnish chiral cyclopentanyl aminium radical cation **284**. Final SET reduction from Ir^{II+} and ligand exchange with **277** closed the photocatalytic cycle and delivered cyclopentamine **279** with high diastereo- and enantioselectivities. Interestingly, the reaction was very sluggish with PF_6^- (Scheme 8.44) [78]. This transformation has been extended to the synthesis of five-membered alicyclic α-quaternary β-amino acids by using α-substituted acrylates instead of styrenes [79].

8.3.1.3. Chiral Brønsted Acid Catalysis In the past few years, remarkable progress has been made in cooperative photoredox and asymmetric Brønsted catalysis. However, since the pioneering work of Bach [1, 80], few single chiral organo-photocatalysts bearing Brønsted acid moiety have been developed for enantioselective photochemical transformations involving redox processes (Scheme 8.45a). In 2014, Sivaguru et al. demonstrated that binaphthyl-derived thiourea catalysts $\mathbf{A_{27}}$ could be applied to enantioselective intramolecular [2+2]-photocycloadditions of 4-alkenyl-substituted coumarins **287** [81]. The author proposed that the reaction proceeds through an exciplex intermediate formed between the thiourea catalyst $\mathbf{A_{27}}$ and the coumarine substrate **287** which is stabilized by hydrogen bonding (Scheme 8.45b). Later, Bach et al. developed a new family of visible-light-thiourea photocatalysts $\mathbf{A_{28}}$ by linking a

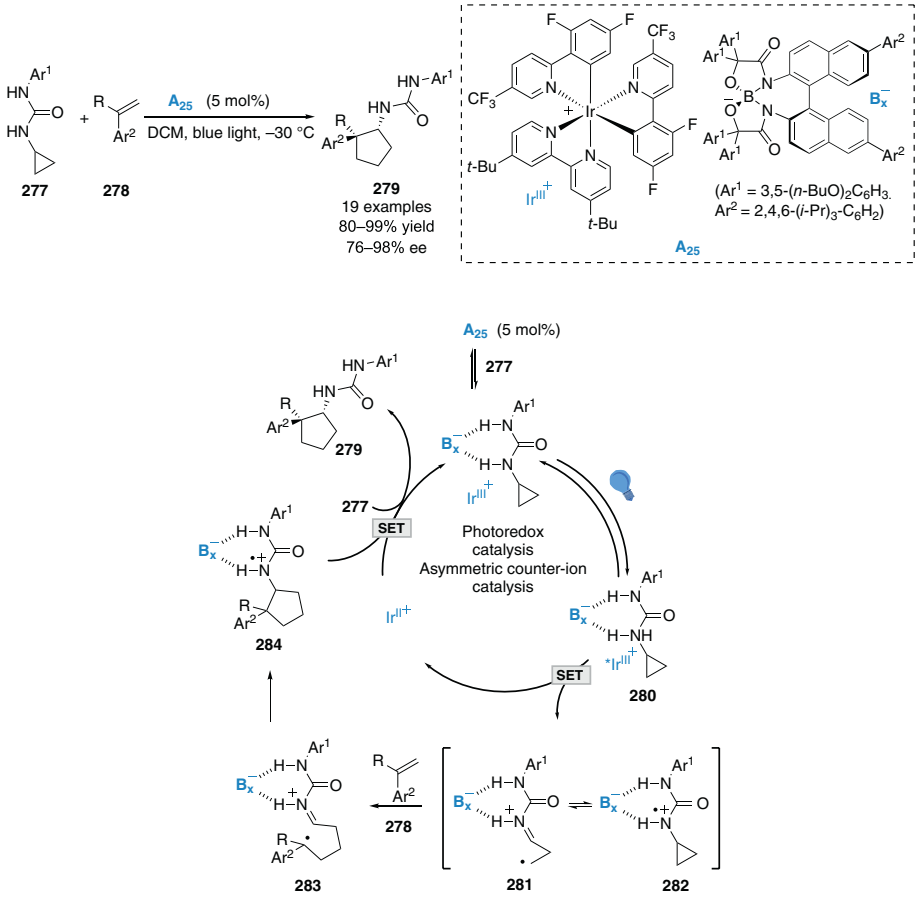

Scheme 8.44. Urea as redox-active directing group for enantioselective (3+2)-cycloaddition of cyclopropylamines with α-substituted styrenes. Source: [78]/American Chemical Society.

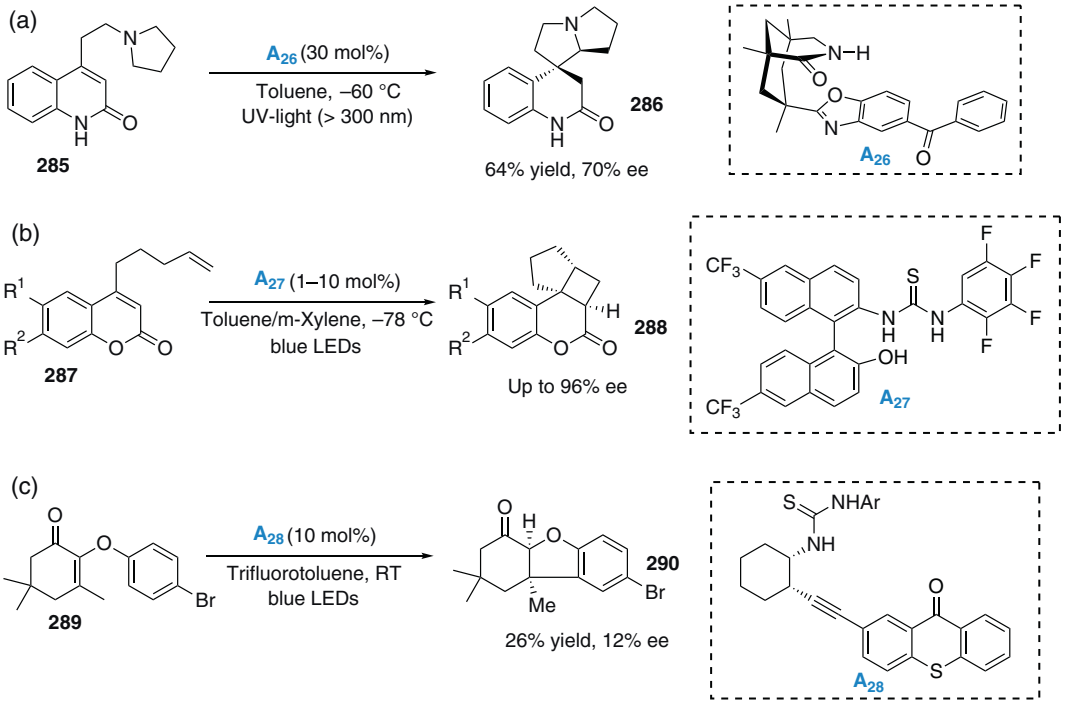

Scheme 8.45 Chiral Brønsted acid-photocatalyzed enantioselective reactions. (a) Enantioselective spirocyclization [1, 80]. (b) Enantioselective intramolecular [2+2] photocycloadditions [81]. (c) Enantioselective photocyclization [82].

thioxanthone motif onto chiral 1-aminocyclohexanes and utilized them for enantioselective photocyclization of a substituted cyclohexanone **289** (Scheme 8.45c). Both yield and enantioselectivity were low [82].

As previously illustrated, the chiral phosphoric acids combined with achiral photocatalysts are proven to be efficient dual catalytic systems for enantioselective photochemical transformations [35–52]. However, it is only recently that phosphoric acids as single chiral photocatalysts have been reported. In 2020, Bach et al. developed chiral organophotocatalysts $\mathbf{A}_{29}$ in which chiral phosphoric acids were attached to two thioxanthone photoactive units at the 3,3′-positions (Scheme 8.46a) [83]. These catalysts were then applied for enantioselective intermolecular [2+2]-photocycloaddition reactions of β-carboxyl-substituted cyclic enones **292** and olefins **291** proceeding via energy-transfer mechanism. Nearly at the same time, independent work from the group of Masson also designed a monosubstituted C1-symmetric photocatalyst derived from chiral phosphoric acid $\mathbf{A}_{30}$ for enantioselective synthesis of 1,2-diamines **297** (Scheme 8.46b) [84]. The reaction provides an efficient access to various disubstituted 1,2-diamine derivatives **297** in high yields with moderate diastereoselectivities and excellent enantioselectivities. The one-pot tandem process is believed to proceed by enantioselective three-component electrophilic amination of enecarbamates, azodicarboxylates, and thiols [85] followed by photocatalyzed Friedel–Crafts reaction of resulting α-carbamoylsulfide intermediates **298** with pyrazoles **296**. The mechanistic studies supported mainly that C–S bond cleavage [86] occurs via an energy-transfer mechanism rather than electron-transfer mechanism.

8.3.2. Chiral Organometallic Photocatalysts

Investigations on metal Lewis acid-catalyzed enantioselective photocatalytic processes have met with great success [87]. Two main strategies have been used to design chiral organometallic photocatalysts. The first involved the use of chiral ligands to confer chirality to a metal complex [88]. The second one

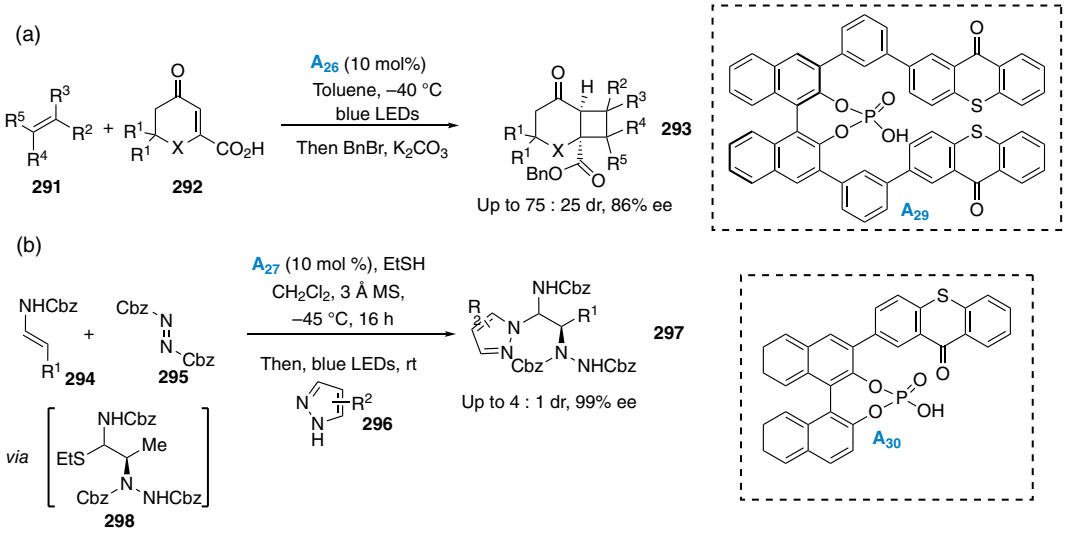

Scheme 8.46. Chiral phosphoric acid-photocatalyzed enantioselective reactions. (a) Enantioselective intermolecular [2+2] photocycloaddition reactions. Source: [83]/John Wiley & Sons. (b) Enantioselective synthesis of 1,2-diamines. Source: [84]/American Chemical Society.

(aspect) is that the chirality is located on the metal which binds two achiral bidentate ligands in a left (Λ)- or right (Δ)-handed propeller-type fashion [89].

8.3.2.1. Chiral-at-Metal Photocatalysts In 2014, Meggers et al. introduced a new class of chiral iridium photocatalysts $\mathbf{A_{31}}$–$\mathbf{A_{34}}$ where the chiral information is exclusively located at the metal center. Iridium (octahedral metal center) is coordinated by two N-(2-pyridyl)-substituted *N*-heterocyclic carbene bidentate ligands and two acetonitrile ligands (Scheme 8.47) [90, 91]. Λ-Ir catalyst $\mathbf{A_{33}}$ proved to be very efficient in the enantioselective α-alkylation of 2-acyl imidazoles **299** with electron-deficient benzyl bromides and phenacyl bromides **300** leading to α-alkylated ketones **301** in excellent yields and enantioselectivities. The author found that $\mathbf{A_{33}}$ was superior catalyst in term of enantioselectivity over Δ -IrO $\mathbf{A_{31}}$. This is due to the longer C–S bond of benzothiazoles compared to the C–O bonds of benzoxazoles, which make the two tert-butyl groups closer to the substrate coordination site. The proposed mechanism begins by the formation of electron-rich iridium enolate **302** between 2-acyl imidazole **299** and chiral iridium complex $\mathbf{A_{33}}$ with the assistance of a weak base. Visible light irradiation excites the bidentate enolate complex **302** into a strong reductant **303**, which performs a single electron transfer (SET) of **300** to generate alkyl radical **307**. Subsequent enantioselective addition of electrophilic radical to **303** produces the ketyl radical **304**. This latter species is oxidized by SET from iridium catalyst to regenerate the photocatalyst **302**. It is important to note that the double coordination between the metal Lewis acid and the N and O of **299** is crucial for an efficient transfer of stereochemical information. Later, the same group extended this photocatalytic process to enantioselective α-trichloromethylations of 2-acyl imidazoles and 2-acyl pyridines [92]. Soon afterwards, an efficient enantioselective perfluoroalkylation of 2-acyl imidazoles with perfluoroalkyl iodides was also developed by Meggers' group using benzothiazole Λ-IrS catalyst $\mathbf{A_{33}}$ [93].

This novel benzothiazole Λ-IrO catalyst $\mathbf{A_{31}}$ could also catalyze the enantioselective radical coupling reaction between 2-acyl imidazoles **308** and α-silyl alkylamines **309** providing a direct access to 1,2-amino alcohols **310** in high yields with moderate to high diastereoselectivities and in most cases excellent enantioselectivities (Scheme 8.48a) [94]. A similar mechanism as described above involving an electron-rich iridium enolate photocatalyst **311** was proposed. Then, the authors study also the ability of the chiral iridium Λ-IrS catalysts $\mathbf{A_{33}}$ to promote the enantioselective coupling of trifluoroacetyl imidazoles **312** with tertiary amines **313** (Scheme 8.48b) [95]. Detailed mechanistic studies suggest that photoactivated iridium-bound trifluoromethyl ketone **315** can oxidize the tertiary amine **313** via a SET to generate an

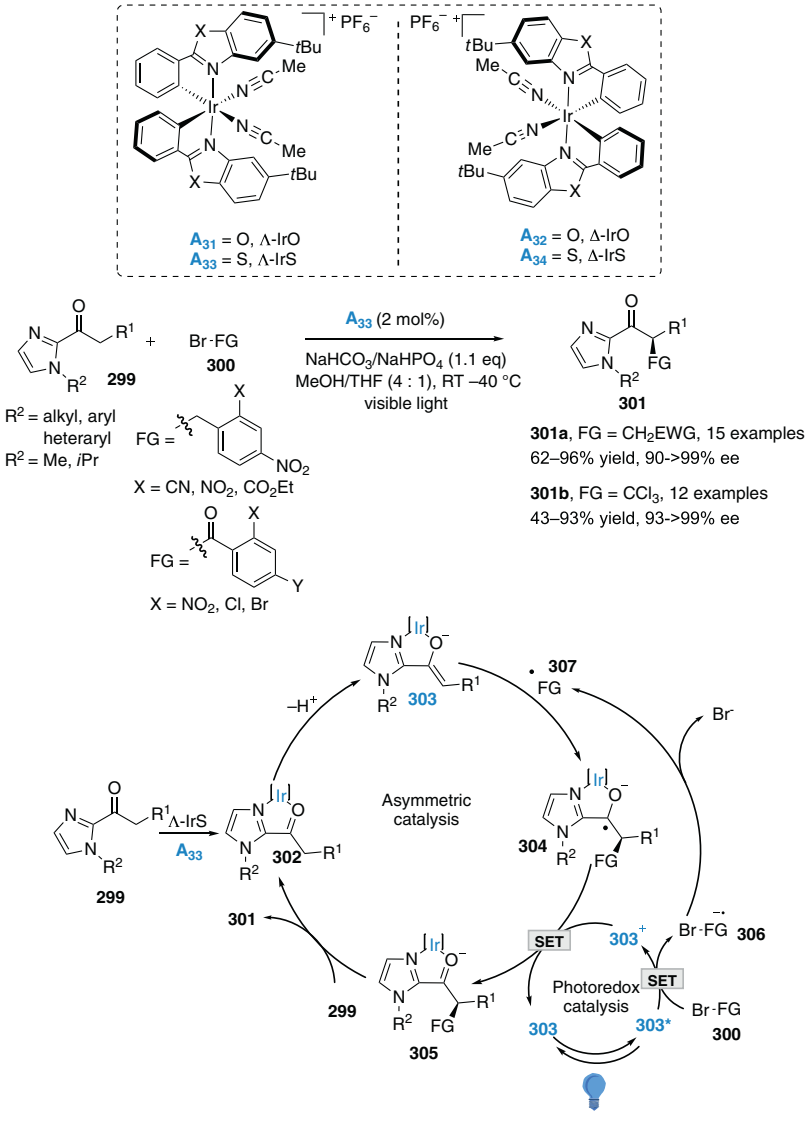

Scheme 8.47. Chiral iridium-catalyzed photoinduced enantioselective alkylation of acyl imidazoles. Source: Based on [90, 91].

iridium-bound ketyl radical **317** and an α-aminoalkyl radical **318**. The two resulting radicals **317** and **318** undergo recombination in a stereoselective manner to provide the enantioenriched 1,2-amino alcohol product **314**. The presence of electron-withdrawing group (CF_3) on **312** was essential to form a photoactive catalyst able to oxidize **313**.

Later, Gong, Meggers et al. designed a novel rhodium(III) photoredox catalyst (Λ-RhO) $\mathbf{A_{35}}$ and proved its catalytic efficiency for the enantioselective catalytic cross-coupling of two Csp_3 center in presence of air (Scheme 8.49a) [96]. The reactions afforded β-amino carbonyl compounds **321** in good yields and with excellent enantioselectivities. The reaction involves the formation of iminium ion **323** generated by oxidation of tertiary amine **319** with photoactivated Rh-enolate complex **322** that reacts with iminium ion **323** to produce the desired product **321**.

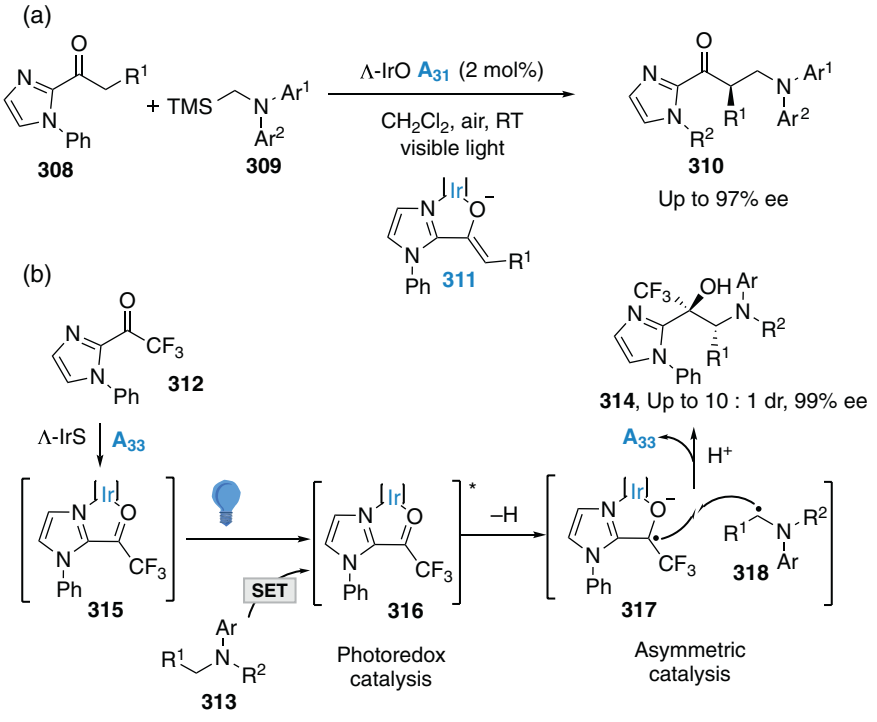

Scheme 8.48. Chiral iridium-catalyzed photoinduced enantioselective alkylation of acyl imidazole derivatives. (a) Enantioselective radical coupling reaction of 2-acyl imidazoles. Source: [94]/John Wiley & Sons. (b) Enantioselective coupling of trifluoroacetyl imidazoles. Source: [95]/John Wiley & Sons.

In 2017, Kang et al. extended applications of chiral-at-rhodium(III) catalyst $\mathbf{A}_{36}$ (Δ-RhO) to enantioselective radical conjugate addition reaction of α-amino radicals to Michael acceptors (Scheme 8.49b) [97]. The reaction provides β-amino carbonyl compounds **327** in good yields with moderate to high diastereoselectivities and excellent *ee* values. A similar mechanism was proposed in which a photoactivated Rh-enolate complex **328** react with the α-amino radical **329**, generated in situ from **325**. Meggers et al. also demonstrated that chiral-at-rhodium complex $\mathbf{A}_{37}$ catalyzed β-alkylation of 2-acyl imidazoles and 2-acylpyridines **332** with α-ketoesters **333**, affording alkylated products in high yields, diastereoselectivities, and *ee* values (Scheme 8.49c) [98]. As shown in Scheme, the photoactivated Rh^{III} enolate complex **334** reduce the α-ketoesters **331** followed by proton transfer and an enantioselective radical–radical cross-coupling reaction between **335** and **334**. In all these three examples, Rh complexes $\mathbf{A}_{35}$–$\mathbf{A}_{37}$ were proved to be superior catalyst over AIrS catalyst $\mathbf{A}_{33}$–$\mathbf{A}_{34}$.

Meggers et al. found that rhodium(III) complex (Λ-RhO) $\mathbf{A}_{35}$ was efficient catalyst for the enantioselective α-amination of 2-acyl imidazoles **337** with 2,4-dinitrophenylsulfonyloxy-*N*-functionalized carbamates **338** (Scheme 8.50) [99]. It is noteworthy that no reaction occurred when the reaction was carried out in the presence of chiral iridium Λ-IrS catalysts $\mathbf{A}_{33}$. The superiority of the rhodium complexes was attributed to much faster ligand-exchange kinetics compared to the iridium complexes. The corresponding products were achieved with high enantioselectivities. The mechanism proposed the formation of enolate rhodium complex **341** which after irradiation leads to the formation of electrophilic aminyl radical **342**. Its subsequent addition leads ketyl radical intermediate **343** which can reduce **341+** to regenerate the ground-state rhodium complex **340**.

In 2018, Meggers et al. also reported an enantioselective β-alkylation of α,β-unsaturated 2-acyl imidazoles **345** with a variety of Hantzsch esters **346** as an alkyl radical source, affording the corresponding products **347** with excellent yields and enantioselectivities (up to 98% ee) [100]. The three-component reaction employed a chiral-at-metal rhodium Λ-RhS catalyst $\mathbf{A}_{38}$ (Scheme 8.51a). The same year, Meggers et al.

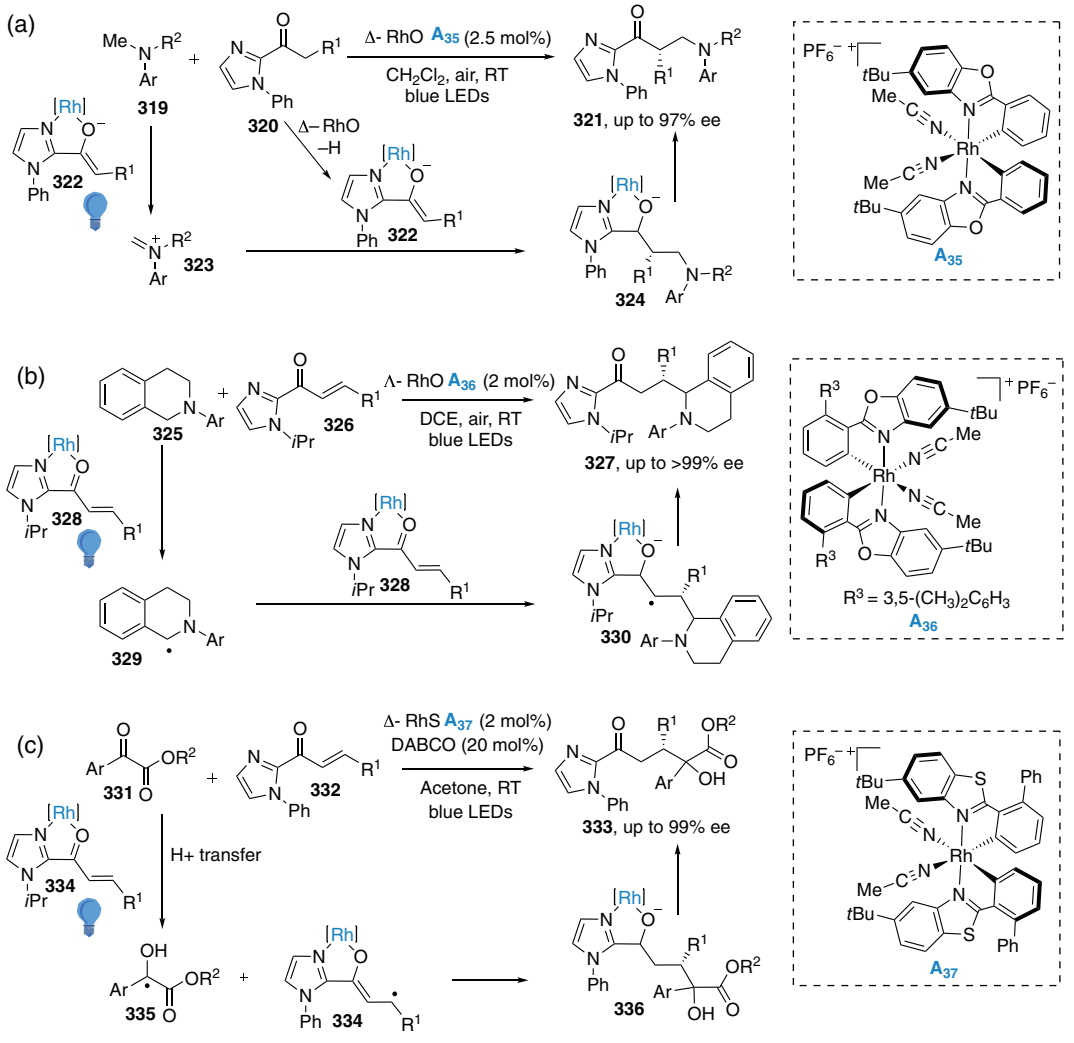

Scheme 8.49. Chiral iridium-catalyzed α-functionalization of acyl imidazole derivatives and conjugate addition of α,β-unsaturated ketone derivatives. (a) Asymmetric dehydrogenative cross-coupling. Source: [96]/John Wiley & Sons. (b) Enantioselective radical conjugate addition reaction. Source: [97]/Royal Society of Chemistry. (c) Enantioselective β-alkylation of 2-acyl imidazoles. Source: [98]/American Chemical Society.

developed enantioselective radical conjugate addition of α-aminoalkyl radicals, generated from phthalimide derivatives **349** to α,β-unsaturated N-acylpyrazoles **348** for the synthesis of β-substituted chiral γ-aminobutyric acid analogues (GABA) **351** [101]. This protocol employs chiral Δ-RhS $\mathbf{A}_{38}$ as a photocatalyst in the presence of Hantzsch ester (HE, **350**) as an external reductant (Scheme 8.51b). The developed catalytic procedure was used for the synthesis of (*S*)-pregabalin, (*R*)-baclofen, (*R*)-rolipram, and (*S*)-nebracetam.

Very recently, the same group developed visible-light-induced enantioselective [3+2]-photocycloaddition of cyclopropyl ketones **352** with a wide range of alkenes **353** or alkynes **355** using chiral Lewis Rh $\mathbf{A}_{38}$ (Scheme 8.52) [102]. This process enabled the synthesis of a wide range of cyclopentanes **354** and cyclopentenes **356** with high enantioselectivity and diastereoselectivity. Herein, the reaction is commenced by the generation radical anion from the cyclopropyl ketone **359** via single electron-transfer reduction by rhodium complex (generated from reduction of **358*** with DIPEA). Then, the radical anion **360** reacts in an intermolecular fashion with alkenes **353**. The chiral-at-metal rhodium-based Lewis acid complex $\mathbf{A}_{38}$

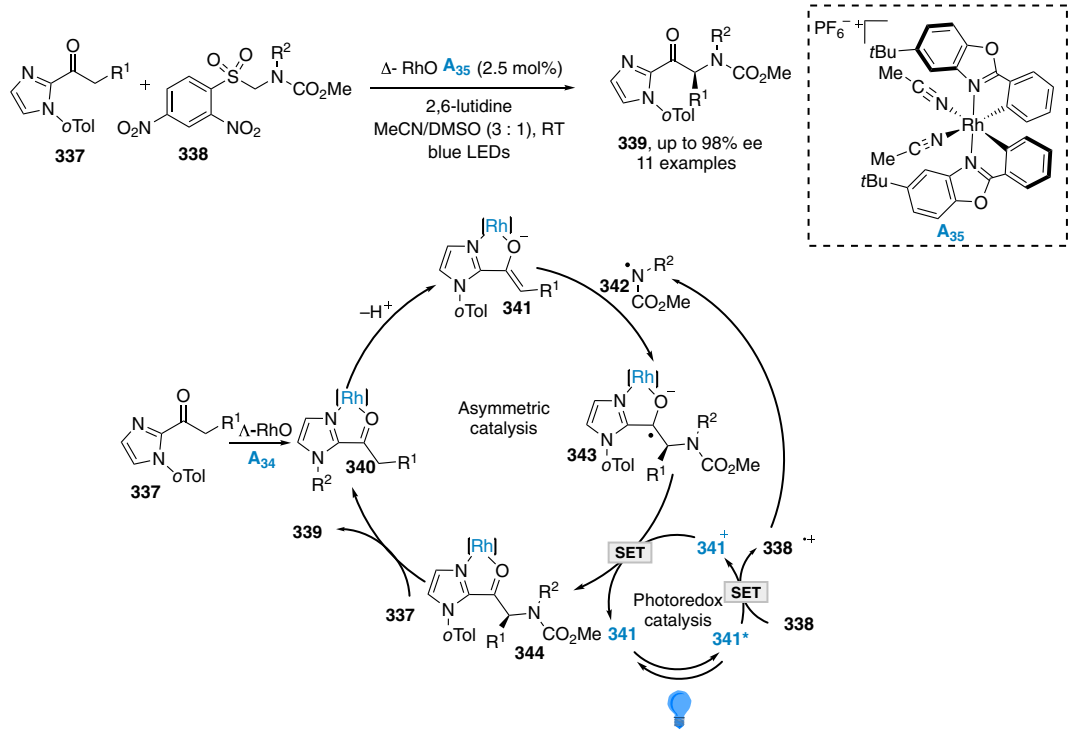

Scheme 8.50. Rhodium photocatalyzed enantioselective amination. Source: [99]/John Wiley & Sons.

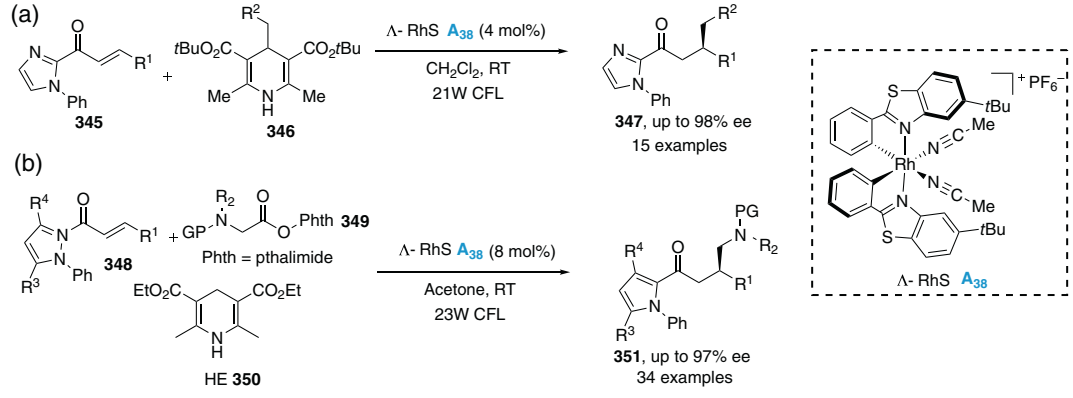

Scheme 8.51 Enantioselective β-alkylation of α,β-unsaturated 2-acyl imidazoles using Hantzsch esters as radical reservoirs. (a) Asymmetric β-alkylation of α,β-unsaturated 2-acyl imidazoles [100]. (b) Enantioselective radical conjugate addition of α-aminoalkyl radicals [101].

controls the enantioselectivity during this step. Then, the resultant radical **361** can donate an electron to the oxidized amine radical cation for the regeneration of DIPEA. Finally, ligand exchange regenerates the enolate complex **357** and liberates the final cycloadduct **354**.

This class of stereogenic-only-at-metal complexes, bis-cyclometalated iridium(III), and rhodium(III) complexes was further recognized as triplet photosensitizers for enantioselective intramolecular [2+2]-p hotocycloadditions [103]. This will be described in the following chapter.

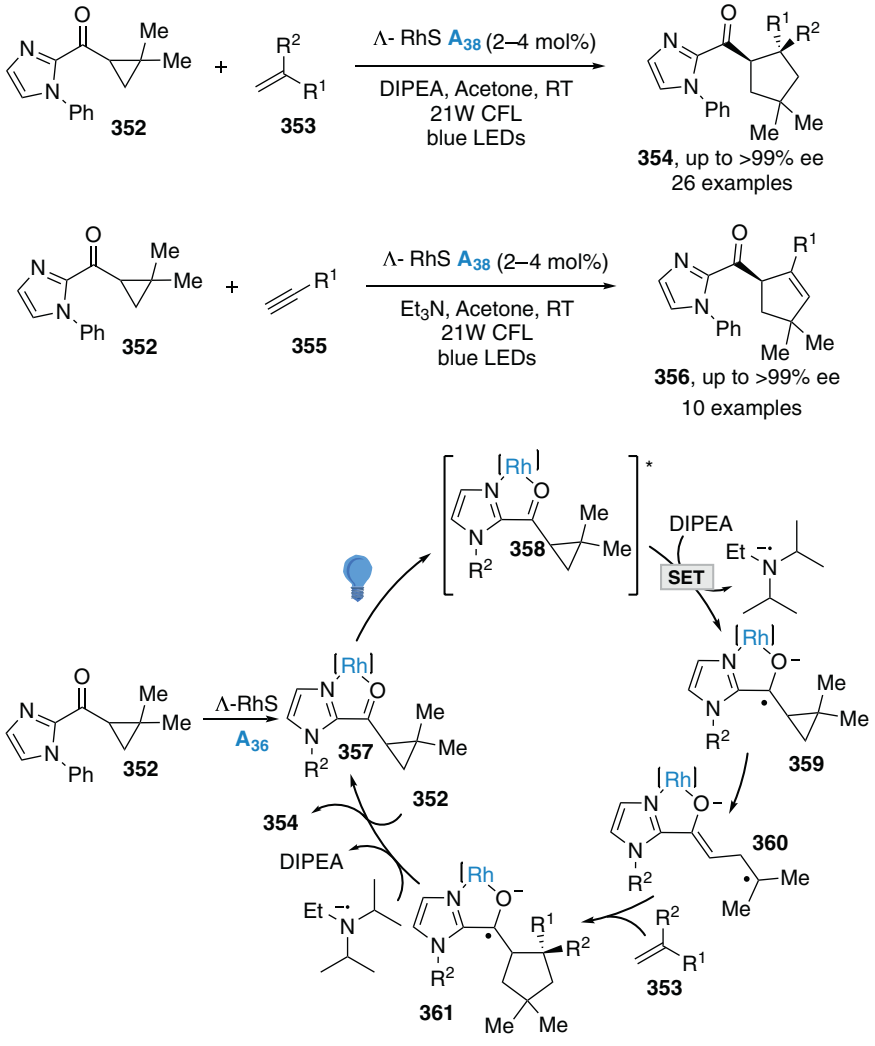

Scheme 8.52. Enantioselective photocatalytic [3+2]-cycloaddition. Source: [102]/John Wiley & Sons.

8.3.2.2. Chiral Ligands and Photocatalysts The use of chiral ligands with metal also turned out to be an effective strategy to develop enantioselective photocatalytic transformations [104]. Recently, copper complexes have emerged as alternative photocatalysts to noble metals because they offer some advantages, namely, high abundance, low price, and low toxicity. Very recently, enantioselective photocatalyzed transformations using chiral Cu complexes as catalysts have been reported. A seminal report by Fu and Peters in 2012 disclosed that the chiral copper(I) spirophosphine complex $\mathbf{A}_{39}$ was a highly efficient photocatalyst for the cross-coupling of racemic tertiary α-haloroamides **362** with carbazoles **363** (or indoles) [105]. The process allows synthesis of a series of valuable chiral amides **365** in high yields with excellent enantioselectivities (Scheme 8.53). Mechanistic studies were consistent with the active catalyst comprising a chiral copper(I) spirophosphine species $\mathbf{A}_{39}$, which was generated in situ from CuCl, chiral spirophosphine **364**, and carbazole **362** (or indole). It was proposed that in the excited state, this complex $\mathbf{A}_{39}$ reduces the alkyl chloride **362** via SET to generate a radical **367** that reacts with nucleophile-bound copper(II)carbazolide **368**. Then, the resulting Cu^{III} intermediate **369** undergoes a reductive elimination to deliver the desired enantioenriched C–N coupling product **365**.

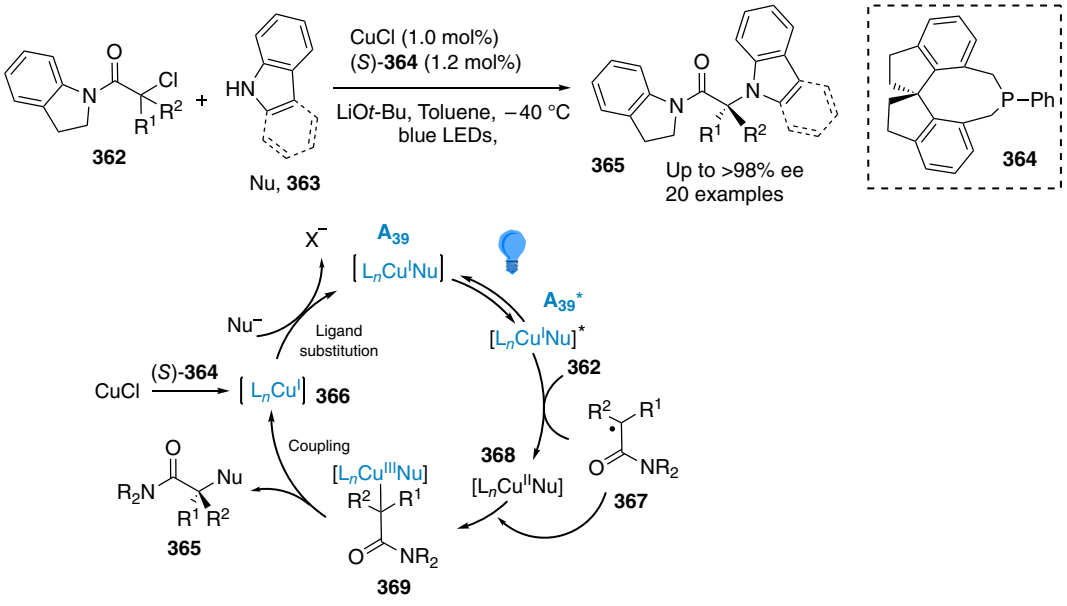

Scheme 8.53. Asymmetric copper-catalyzed C–N cross-couplings.

Since this seminal report, chiral copper complexes have been used in other enantioselective photocatalyzed transformations. In 2018, Gong et al. established that in-situ generated copper(II) bisoxazoline complex (Cu(II)–BOX, $\mathbf{A}_{40}$) was efficient photocatalyst for enantioselective alkylation of *N*-cyclic sulfonylimines **370** with trifluoroborate salt **371** (Scheme 8.54) [106]. This procedure also extended to the enantioselective benzylation of isatin-derived ketimines **374**. Mechanistic studies suggest that a ligand exchange/light-accelerated homolysis process may occur. The chiral Cu(II)–bisoxazoline complex $\mathbf{A}_{40}$ or $\mathbf{A}_{41}$ is alkylated through transmetallation from the corresponding trifluoroborate salt **371**. After irradiating, the resulting excited $\mathbf{A}_{40}$* or $\mathbf{A}_{41}$* generates an alkyl radical **377** and a Cu(I) intermediate **378**. Subsequent addition of radical **377** to the imine coordinated by chiral Cu(II)–bisoxazoline complex **379** gives *N*-centered radical **380**. Then, the Cu(I) transfers a single electron to **380** to produce the alkylated imine **373** or **376** with high enantioselectivity.

Subsequent to this work, the same group reported Ni(II)–DBFOX complex (DBFOX = 4,6-bis((R)-4-phenyl-4,5-dihydrooxazol-2-yl)dibenzo[b,d]furan) catalyzed enantioselective reaction of α,β-unsaturated carbonyl compounds **382** and tertiary/secondary *α*-silylamines **383** affording chiral *γ*-amino carboxylic acid derivatives **385** in high yields and enantioselectivities (Scheme 8.55) [107]. Notably, the Ni(II)–DBFOX catalyst $\mathbf{A}_{42}$ not only serves as photosensitizer but also provides chiral environment for the subsequent radical reaction. The authors propose that the pyrazole is coordinated by a Ni-(II) species $\mathbf{A}_{42}$ and then, in the presence of visible light, a nucleophilic α-amino alkyl radical **387** and Ni-(I)$^{\bullet}$- intermediate is generated. Then, the enantioselective radical conjugate addition of **387** to the complex **388** produces a new radical species **389** followed by its reduction by reductant Ni–(I)$^{\bullet}$- to form the final product **385** after protonation and decomplexation step.

Zhang et al. reported a chiral Cu(I) complex-catalyzed enantioselective difunctionalization of styrenes **392** with alkynes **393** and alkyl or aryl iodides **394** (Scheme 8.56) [108]. The authors propose that the key photoactive species is a copper acetylide complex **A42**, which is generated in situ from CuI, **395** and alkyne **393**. After irradiation, this complex reduces the alkyl or aryl iodide **394** via SET to generate a radical **398**. This latter then adds to styrene **392** to afford benzyl radical **399**, which is further intercepted with Cu(II) complex **400** to deliver Cu(III) intermediate **401**. The subsequent reductive elimination **401** delivers the final product **396** with high enantioselectivity.

Very recently, Wang, Xu et al. reported Cu-catalyzed photoredox enantioselective three-component couplings of styrenes **402**, perfluorinated alkyl iodides **403,** and TMSCN **404** to prepare an array

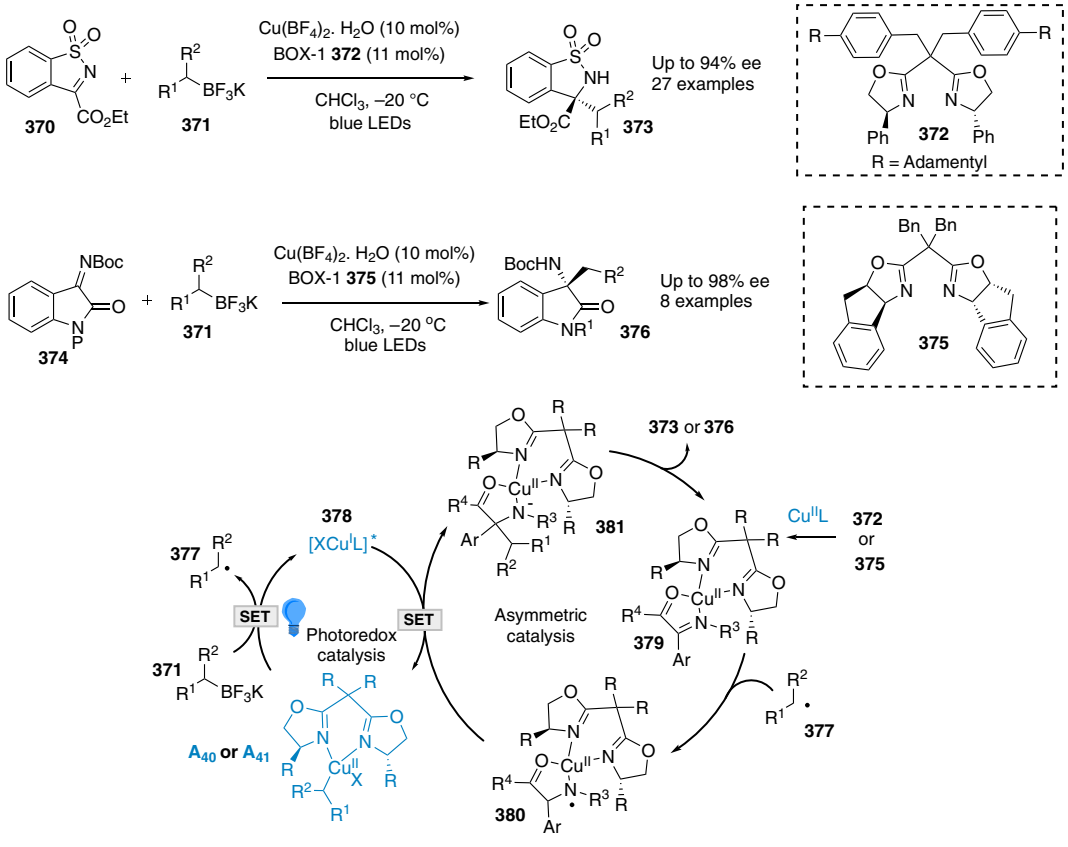

Scheme 8.54. Copper-catalyzed enantioselective alkylation of *N*-cyclic sulfonylimines. Source: [106]/American Chemical Society.

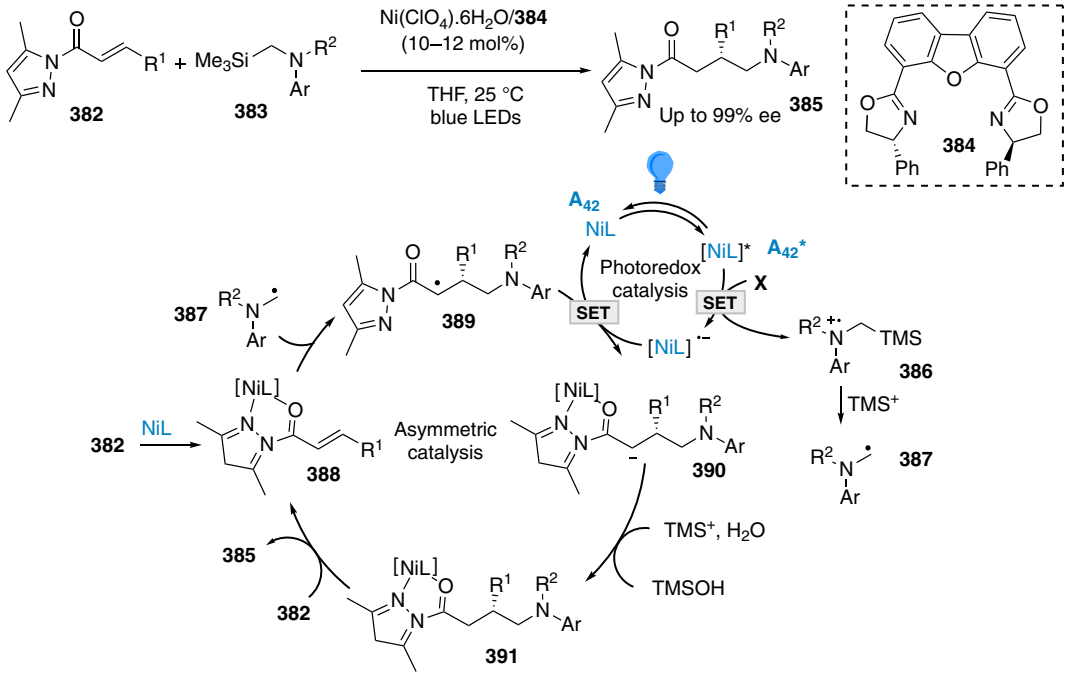

Scheme 8.55 Nickel-catalyzed enantioselective reactions between α,β-unsaturated carbonyl compounds and α-silylamines. Source: [107]/Royal Society of Chemistry.

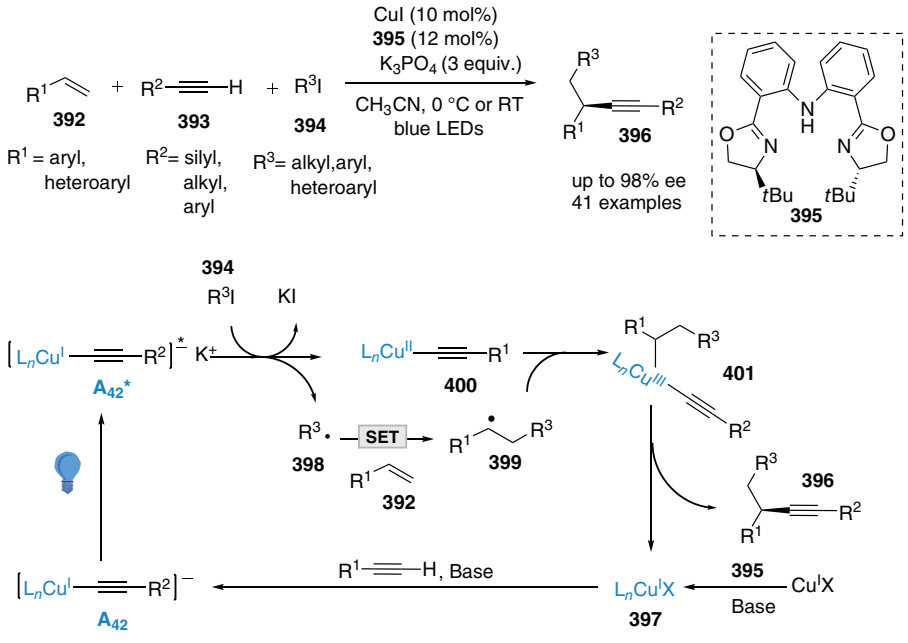

Scheme 8.56 Copper-catalyzed enantioselective difunctionalization of styrenes. Source: [108]/American Chemical Society.

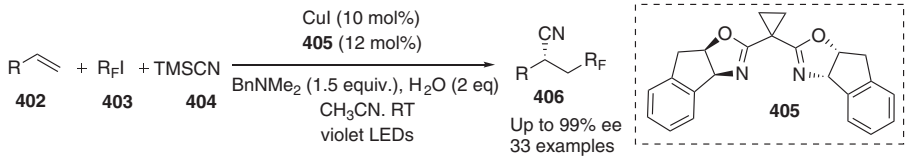

Scheme 8.57. Copper-catalyzed enantioselective cyanoalkylation of styrenes. Source: [109]/American Chemical Society.

of cyanoperfluoroalkylated compounds **406** in good yields with high enantioselectivities (Scheme 8.57) [109]. The author proposes similar mechanism that was described by Fu in which a chiral copper(I) complex generated in situ is active photocatalyst [104].

8.4. CONCLUSION

Significant progress has been made recently in the design and development of chiral photoredox catalysts for asymmetric transformations, as described herein. Both cooperative catalysts and single-bifunctional catalysts have yielded promising chiral induction effects in enantioselective reaction. Despite such great achievements, further research in this area can be conducted to develop versatile photocatalysts with higher reactivities and better selectivities. We hope that this chapter will encourage further research on this field.

REFERENCES

1. (a) Rigotti, T.; Alemán, J. *Chem. Commun.* **2020**, *56*, 11169–11190. (b) Takagi, R.; Tabuchia, C. *Org. Biomol. Chem.*, **2020**, *18*, 9261–9267. (c) Saha, D. *Chem. Asian J.* **2020**, *15*, 2129–2152. (d) Yin, Y. L.; Zhao, X. W.; Qiao, B. K.; Jiang, Z. Y. *Org. Chem. Front.* **2020**, *7*, 1283– 1296. (e) Zhou, Q. Q.; Zou, Y. Q.; Lu, L. Q.; Xiao, W. J. *Angew. Chem. Int. Ed.* **2019**, *58*, 1586–1604. (f) Jiang, C.; Chen, W.; Zheng, W. H.; Lu, H. F. *Org. Biomol. Chem.* **2019**, *17*, 8673–8689. (g) Coote, S. C.; Bach, T. Visible Light Photocatalysis in Organic Chemistry, 1st ed., John Wiley & Sons, **2018**, 335–361. (h) Garrido-Castro, A. F.;

Maestro, M. C.; Alemán, J. *Tetrahedron Lett.* **2018**, *59*, 1286–1294. (i) Wang, C.; Lu, Z. *Org. Chem. Front.* **2015**, *2*, 179–190. (j) Meggers, E. *Chem. Commun.* **2015**, *51*, 3290–3301.
2. Nicewicz, D. A.; MacMillan, D. W. C. *Science* **2008**, *322*, 77–80.
3. Cismesia, M. A.; Yoon, T. P. *Chem. Sci.* **2015**, *6*, 5426–5434.
4. Nagib, D. A.; Scott, M. E.; MacMillan, D. W. C. *J. Am. Chem. Soc.* **2009**, *131*, 10875–10877.
5. Welin, E. R.; Warkentin, A. A.; Conrad, J. C.; MacMillan, D. W. C. *Angew. Chem. Int. Ed.* **2015**, *54*, 9668–9672.
6. Gualandi, A.; Marchini, M.; Mengozzi, L.; Natali, M.; Lucarini, M.; Ceroni, P.; Cozzi, P. G. *ACS Catal.* **2015**, *5*, 5927–5931.
7. Gualandi, A.; Marchini, M.; Mengozzi, L.; Kidanu, H. T.; Franc, A.; Ceroni, P.; Cozzi, P. G. *Eur. J. Org. Chem.* **2020**, *2020*, 1486–1490.
8. Neumann, M.; Füldner, S.; König, B.; Zeitler, K. *Angew. Chem. Int. Ed.* **2011**, *50*, 951–954.
9. Neumann, M.; Zeitler, K. *Org. Lett.* **2012**, *14*, 2658–2661.
10. Fidaly, K.; Ceballos, C.; Falguières, A.; Sylla-Iyarreta, M.; Guy, A.; Ferroud, C. *Green Chem.* **2012**, *14*, 1293–1297.
11. Cherevatskaya, M.; Neumann, M.; Fuldner, S.; Harlander, C.; Kummel, S.; Dankesreiter, S.; Pfitzner, A.; Zeitler, K.; Koenig, B. *Angew. Chem. Int. Ed.* **2012**, *51*, 4062–4066.
12. Riente, P.; Matas Adams, A.; Albero, J.; Palomares, E.; Pericàs, M. A. *Angew. Chem. Int. Ed.* **2014**, *53*, 9613–9616.
13. Zhu, Y.; Zhang, L.; Luo, S. *J. Am. Chem. Soc.* **2014**, *136*, 14642–14645.
14. Shih, H. W.; Wal, M. N. V.; Grange, R. L.; MacMillan, D. W. C. *J. Am. Chem. Soc.* **2010**, *132*, 13600–13603.
15. Nacsa, E. D.; MacMillan, D. W. C. *J. Am. Chem. Soc.* **2018**, *140*, 3322–3330.
16. Capacci, A. G.; Malinowski, J. T.; McAlpine, N. J.; Kuhne, J.; MacMillan, D. W. C. *Nat. Chem.* **2017**, *9*, 1073–1077.
17. Conrad, J. C.; Kong, J.; Laforteza, B. N.; MacMillan, D. W. C. *J. Am. Chem. Soc.* **2009**, *131*, 11640–11641.
18. Wang, D.; Zhang, L.; Luo, S. *Org. Lett.* **2017**, *19*, 4924–4927.
19. Pirnot, M. T.; Rankic, D. A.; Martin, D. B. C.; MacMillan, D. W. C. *Science*, **2013**, *339*, 1593–1596.
20. Sunden, H.; Engqvist, M.; Casas, J.; Ibrahem, I.; Córdova, A. *Angew. Chem. Int. Ed.* **2004**, *43*, 6532–6535.
21. Córdova, A.; Sunden, H.; Engqvist, M.; Ibrahem, I.; Casas, J. *J. Am.Chem. Soc.* **2004**, *126*, 8914–8915.
22. Ibrahem, I.; Zhao, G.; Sunden, H.; Córdova, A. *Tetrahedron Lett.* **2006**, *47*, 4659–4663.
23. Walaszek, D. J.; Rybicka-Jasińska, K.; Smoleń, S.; Karczewski, M.; Gryko, D. *Adv. Synth. Catal.* **2015**, *357*, 2061–2070.
24. Murphy, J. J.; Bastida, D.; Paria, S.; Fagnoni, M.; Melchiorre, P. *Nature.* **2016**, *532*, 218–222.
25. Bahamonde, A.; Murphy, J. J.; Savarese, M.; Brémond, É.; Cavalli, A.; Melchiorre, P. *J. Am. Chem. Soc.* **2017** *139*, 4559–4567.
26. Zhao, J. J.; Zhang, H. H.; Shen, X.; Yu, S. Y. *Org. Lett.* **2019**, *21*, 913–916.
27. Le Saux, E.; Ma, D.; Bonilla, P.; Holden, C. M.; Lustosa, D.; Melchiorre, P. *Angew. Chem. Int. Ed.* **2014**, *53*, 9613–9616.
28. Lin, L.; Bai, X.; Ye, X.; Zhao, X.; Tan, C. H.; Jiang, Z. *Angew. Chem. Int. Ed.* **2017**, *56*, 13842–13846.
29. Hou, M.; Lin, L.; Chai, X.; Zhao, X.; Qiao, B.; Jiang, Z. *Chem. Sci.* **2019**, *10*, 6629–6634.
30. Lenhart, D.; Bauer, A.; Pöhtig, A.; Bach, T. *Chem. Eur. J.* **2016**, *22*, 6519–6523.
31. Gentry, E. C.; Rono, L. J.; Hale, M. E.; Matsuura, R.; Knowles, R. R. *J. Am. Chem. Soc.* **2018**, *140*, 3394–3402.
32. Liang, K. J.; Tong, X. G.; Li, T.; Shi, B. F.; Wang, H. Y.; Yan, P. C.; Xia, C. F. *J. Org. Chem.* **2018**, *83*, 10948–10958.
33. Roos, C. B.; Demaerel, J.; Graff, D. E.; Knowles, R. R. *J. Am. Chem. Soc.* **2020**, *142*, 5974–5979.
34. Shin, N. Y.; Ryss, J. M.; Zhang, X.; Miller, S. J.; Knowles, R. R. *Science*, **2019**, *366*, 364–369.
35. Rono, L. J.; Yayla, H. G.; Wang, D. Y.; Armstrong, M. F.; Knowles, R. R. *J. Am. Chem. Soc.* **2013**, *135*, 17735–17738.
36. Proctor, R. S. J.; Davis, H. J.; Phipps, R. J. *Science* **2018**, *360*, 419–422.
37. Liu, X. Y.; Liu, Y.; Chai, G.; Qiao, B. K.; Zhao, X. W.; Jiang, Z. Y. *Org. Lett.* **2018**, *20*, 6298–6301.
38. Zheng, D. Q.; Studer, A. *Angew. Chem. Int. Ed.* **2019**, *58*, 15803–15807.
39. Yin, Y.; Dai, Y.; Jia, H.; Li, J.; Bu, L.; Qiao, B.; Zhao, X.; Jiang, Z. *J. Am. Chem. Soc.* **2018**, *140*, 6083–6087.
40. Cao, K.; Tan, S.; Lee, R.; Yang, S.; Jia, H.; Zhao, X.; Qiao, B.; Jiang, Z. *J. Am. Chem. Soc.* **2019**, *141*, 5437–5443.
41. Hepburn, H. B.; Melchiorre, P. *Chem. Commun.* **2016**, *52*, 3520–3523.
42. Yin, Y. L.; Li, Y. Q.; Gonçalves, T. P.; Zhan, Q. Q.; Wang, G. G.; Zhao, X. W.; Qiao, B. K.; Huang, K. W.; Jiang, Z. Y. *J. Am. Chem. Soc.* **2020**, *142*, 46, 19451–19456.
43. Qiao, B. K.; Li, C. Y.; Zhao, X. W.; Yin, Y. L.; Jiang, Z. Y. *Chem. Commun.* **2019**, *55*, 7534–7537.
44. Shao, T. J.; Li, Y. J.; Ma, N. N.; Li, C. Y.; Chai, G. B.; Zhao, X. W.; Qiao, B. K.; Jiang, Z. *iScience* **2019**, *16*, 410–419.
45. Cheng, Y. Z.; Zhao, Q. R.; Zhang, X.; You, S. L. *Angew. Chem. Int. Ed.* **2019**, *58*, 18069–18074.
46. Dai, Z. Y.; Nong, Z. S.; Wang, P. S. *ACS Catal.* **2020**, *10*, 4786–4790.
47. Li, J.; Kong, M.; Qiao, B.; Lee, R.; Zhao, X.; Jiang, Z. *Nat. Commun.* **2018**, *9*, 2445–2254.
48. Liu, Y.; Liu, X.; Li, J.; Zhao, X.; Qiao, B.; Jiang, Z. *Chem. Sci.* **2018**, *9*, 8094–8098.
49. Zeng, G. K.; Li, Y. Q.; Qiao, B. K.; Zhao, X. W.; Jiang, Z. Y. *Chem. Commun.* **2019**, *55*, 11362–11365.
50. Uraguchi, D.; Kinoshita, N.; Kizu, T.; Ooi, T. *J. Am. Chem. Soc.* **2015**, *137*, 13768–13771.
51. Kizu, T.; Uraguchi, D.; Ooi, T. *J. Org. Chem.* **2016**, *81*, 6953–6958.
52. Che, C.; Li, Y. N.; Cheng, X.; Lu, Y. N.; Wang, C. J. *Angew. Chem. Int. Ed.* **2021**, *60*, 4698–4704.
53. Espelt, L. R.; McPherson, I. S.; Wiensch, E. M.; Yoon, T. P. *J. Am. Chem. Soc.* **2015**, *137*, 2452–2455.
54. Pagire, S. K.; Kumagai, N.; Shibasaki, M. *Chem. Sci.* **2020**, *11*, 5168–51745.

55. Huo, H.; Harms, K.; Meggers, E. *J. Am. Chem. Soc.* **2016**, *138*, 6936–6939.
56. Ma, J.; Zhang, X.; Huang, X.; Luo, S.; Meggers, E. *Nat. Protoc.* **2018**, *13*, 605–632.
57. Zhang, K.; Lu, L. Q.; Jia, Y.; Wang, Y.; Lu, F. D.; Pan, F. F.; Xiao, W. J. *Angew. Chem. Int. Ed.* **2019**, *58*, 13375–13379.
58. Wang, C.; Harms, K.; Meggers, E. *Angew. Chem. Int. Ed.* **2016**, *55*, 13495–13498.
59. Yuan, W.; Zhou, Z. J.; Gong, L.; Meggers, E. *Chem. Commun.* **2017**, *53*, 8964–8967.
60. Kuang, Y. L.; Wang, K.; Shi, X. C.; Huang, X. Q.; Meggers, E.; Wu, J. *Angew. Chem. Int. Ed.* **2019**, *58*, 16859–16863.
61. Casado-Sánchez, A.; Domingo-Legarda, P.; Cabrera, S.; Alemán, J. *Chem. Commun.* **2019**, *55*, 11303–11306.
62. Kim, J. Y.; Lee, Y. S.; Choi, Y.; Ryu, D. H. *ACS Catal.* **2020**, *10*, 10585–10591.
63. Ma, J. J.; Harms, K.; Meggers, E. *Chem. Commun.* **2016**, *52*, 10183–10186.
64. Zhou, Z.; Li, Y.; Han, B.; Gong, L.; Meggers, E. *Chem. Sci.* **2017**, *8*, 5757–5763.
65. Li, Y. J.; Lei, M.; Gong, L. *Nature Catalysis* **2019**, *2*, 1016–1026.
66. Ye, C. X.; Melcamu, Y. Y.; Li, H. H.; Cheng, J. T.; Zhang, T. T.; Ruan, Y. P.; Zheng, X.; Lu, X.; Huang, P. Q. *Nat. Commun.* **2018**, *9*, 410–419.
67. Amador, A. G.; Sherbrook, E. M.; Yoon, T. P. *J. Am. Chem. Soc.* **2016**, *138*, 4722–4725.
68. Liang, H.; Xu, G. Q.; Feng, Z. T.; Wang, Z. Y.; Xu, P. F. *J. Org. Chem.* **2019**, *84*, 60–72.
69. Huang, X.; Webster, R. D.; Harms, K.; Meggers, E. *J. Am. Chem. Soc.* **2016**, *138*, 12636–12642.
70. Lian, M. M.; Li, Z.; Cai, Y. C.; Meng, Q. W.; Gao, Z. X. *Chem. Asian J.* **2012**, *7*, 2019–2023.
71. Mohammadinejad, R.; Karimi, S.; Iravani, S.; Varma, R. S. *Green Chem.* **2016**, *18*, 20–52.
72. Tang, X. F.; Zhao, J. N.; Wu, Y. F.; Zheng, Z. H.; Feng, S. H.; Yu, Z. Y.; Liu, G. Z.; Meng, Q. W. *Org. Biomol. Chem.* **2019**, *17*, 7938–7942.
73. Tang, X. F.; Zhao, J. N.; Wu, Y. F.; Feng, S. H.; Yang, F.; Yu, Z. Y.; Meng, Q. W. *Adv. Synth. Catal.* **2019**, *361*, 5245–5252.
74. Rigotti, T.; Casado-Sánchez, A.; Cabrera, S.; Pérez-Ruiz, R.; Liras, M.; de la Peña O'Shea, V. A.; Alemán, J. *ACS Catal.* **2018**, *8*, 5928–5940.
75. Yang, Z.; Li, H.; Li, S.; Zhang, M. T.; Luo, S. *Org. Chem. Front.* **2017**, *4*, 1037–1041.
76. (a) Margrey, K. A.; Nicewicz, D. A. *Acc. Chem. Res.* **2016**, *49*, 1997–2006. (b) Hamilton, D. S.; Nicewicz, D. A. *J. Am. Chem. Soc.* **2012**, *134*, 18577–18580.
77. Morse, P. D.; Nguyen, T. M.; Cruz, C. L.; Nicewicz, D. A. *Tetrahedron*, **2018**, *74*, 3266–3272.
78. Uraguchi, D.; Kimura, Y.; Ueoka, F.; Ooi, T. *J. Am. Chem. Soc.* **2020**, *142*, 46, 19462–19467
79. Kimura, Y.; Uraguchi, D.; Ooi, T. *Org. Biomol. Chem.* **2021**, *19*, 1744–1747.
80. (a) Alonso, R.; Bach, T. *Angew. Chem., Int. Ed.* **2014**, *53*, 4457–4460. (b) Hölzl-Hobmeier, A.; Bauer, A.; Silva, A. V.; Huber, S. M.; Bannwarth, C.; Bach, T. *Nature* **2018**, *564*, 240–243.See also, (c) Zou, Y. Q.; Hörmann, F. M.; Bach, T. *Chem. Soc. Rev.* **2018**, *47*, 278–290.
81. Vallavoju, N.; Selvakumar, S.; Jockusch, S.; Sibi, M. P.; Sivaguru, J. *Angew. Chem. Int. Ed.* **2014**, *53*, 5604–5608.
82. Mayr, F.; Mohr, L. M.; Rodriguez, E.; Bach, T. *Synthesis* **2017**, *49*, 5238–5250.
83. Pecho, F.; Zou, Y. Q.; Gramüller, J.; Mori, T.; Huber, S. M.; Bauer, A.; Gschwind, R. M.; Bach, T. *Chem. Eur. J.* **2020**, *26*, 5190–5194.
84. Lyu, J. Y.; Claraz, A.; Vitale, M. R.; Allain, C.; Masson G. *J. Org. Chem.* **2020**, *85*, 20, 12843–12855.
85. Dumoulin, A.; Bernadat, G.; Masson, G. *J. Org. Chem.* **2017**, *82*, 1775–1789.
86. Lebée, C.; Languet, M.; Allain, C.; Masson, G. *Org. Lett.* **2016**, *18*, 1478–1481.
87. Twilton, J.; Le, C.; Zhang, P.; Shaw, M. H.; Evans, R. W.; Macmillan, D. W. C. *Nat. Rev. Chem.* **2017**, *52*, 1–18.
88. (a) Bolm, C.; Gladysz, J. A. *Chem. Rev.* **2003**, *103*, 2761–2762. (b) Jacobsen, E. N.; Pfaltz, A.; Yamamoto, H. In: Comprehensive Asymmetric Catalysis, **1999**, Springer-Verlag, Berlin; Germany. (c) Catalytic Asymmetric Synthesis, 2nd ed. (Ed.: I. Ojima), Wiley-VCH, New York, **2000**. (d) Knowles, W. S. *Angew.Chem. Int. Ed.* **2002**, *41*, 1998–2007. (e) Noyori, R. *Angew. Chem. Int. Ed.* **2002**, *41*, 2008–2022. (f) Sharpless, K. B. *Angew. Chem. Int. Ed.* **2002**, *41*, 2024–2032. (g) Jacobsen, E. N.; Pfaltz, A.; Yamamoto, H. In: Comprehensive Asymmetric Catalysis; Springer-Verlag, Berlin; Germany, **2004**.
89. (a) Bauer, E. B.; *Chem. Soc. Rev.* **2012**, *41*, 3153–3167. (b) Gong, L.; Chen, L. A.; Meggers, E. *Angew. Chem. Int. Ed.* **2014**, *53*, 10868–10874. (c) Zhang, L.; Meggers, E. *Chem. Asian. J.* **2017**, *12*, 2335–2342.
90. Huo, H.; Shen, X.; Wang, C.; Zhang, L.; Röse, P.; Chen, L. A.; Harms, K.; Marsch, M.; Hilt, G.; Meggers, E. *Nature* **2014**, *515*, 100–103.
91. Huang, X.; Meggers, E. *Acc. Chem. Res.* **2019**, *52*, 833–847.
92. Huo, H.; Wang, C.; Harms, K.; Meggers, E. *J. Am. Chem. Soc.* **2015**, *137*, 9551–9554.
93. Huo, H.; Huang, X.; Shen, X.; Harms, K.; Meggers, E. *Synlett* **2016**, *27*, 749–753.
94. Wang, C. Y.; Zheng, Y.; Huo, H. H.; Rose, P.; Zhang, L.; Harms, K.; Hilt, G.; Meggers, E. *Chem. Eur. J.* **2015**, *21*, 1–6.
95. Wang, C. Y.; Qin, J.; Shen, X. D.; Riedel, R.; Harms, K.; Meggers, E. *Angew. Chem. Int. Ed.* **2016**, *55*, 685–688.
96. Tan, Y.; Yuan, W.; Gong, L.; Meggers, E. *Angew. Chem. Int. Ed.* **2015**, *44*, 13045–13048.
97. Lin, S. X.; Sun, G. J.; Kang, Q. *Chem. Commun.* **2017**, *53*, 7665–7668.
98. Ma, J. J.; Rosales, A. R.; Huang, X.; Harms, K.; Riedel, R.; Wiest, O.; Meggers, E. *J. Am. Chem. Soc.* **2017**, *139*, 17245–17248.
99. Shen, X. D.; Harms, K.; Marsch, M.; Meggers, E. *Chem. Eur. J.* **2016**, *22*, 9102–9105.

100. de Assis, F. F.; Huang, X.; Akiyama, M.; Pilli, R. A.; Meggers, E. *J. Org. Chem.* **2018**, *83*, 10922–10932.
101. Ma, J.; Lin, J.; Zhao, L.; Harms, K.; Marsch, M.; Xie, X.; Meggers, E. *Angew. Chem., Int. Ed.*, **2018**, *57*, 11193–11197.
102. Huang, X. Q.; Lin, J. H.; Shen, T. Q.; Harms, K.; Marchini, M.; Ceroni, P.; Meggers, E. *Angew. Chem. Int. Ed.* **2018**, *57*, 5454–5458.
103. (a) Skubi, K. L.; Kidd, J. B.; Jung, H.; Guzei, I. A.; Baik, M. H.; Yoon, T. P. *J. Am. Chem. Soc.* **2017**, *139*, 17186–17192. (b) Huang, X.; Quinn, T. R.; Harms, K.; Webster, R. D.; Zhang, L.; Wiest, O.; Meggers, E. *J. Am. Chem. Soc.* **2017**, *139*, 9120–9123.
104. Nicholls, T. P.; Bissember, A. C.; *Tetrahedron Letters* **2019**, *60*, 150883–150893.
105. Kainz, Q. M.; Matier, C. D.; Bartoszewicz, A.; Zultanski, S. L.; Peters, J. C.; Fu, G. C. *Science*, **2016**, *351*, 681–684.
106. Li, Y. J.; Zhou, K. X.; Wen, Z. R.; Cao, S.; Shen, X.; Lei, M.; Gong, L. *J. Am. Chem. Soc.* **2018**, *140*, 15850–15858.
107. Shen, X.; Li, Y. J.; Wen, Z. R.; Cao, S.; Hou, X. Y.; Gong, L. *Chem. Sci.* **2018**, *9*, 4562–4568.
108. Zhang, Y. J.; Sun, Y. W.; Chen, B.; Xu, M. C.; Li, C.; Zhang, D. Y.; Zhang, G. Z. *Org. Lett.* **2020**, *22*, 1490–1494.
109. Guo, Q. P.; Wang, M. R.; Peng, Q.; Huo, Y. M.; Liu, Q.; Wang, R.; Xu, Z. Q. *ACS Catal.* **2019**, *9*, 4470–4476.

9

ASYMMETRIC PHOTOREDOX REACTIONS WITHOUT PHOTOCATALYSTS

Dengke Ma[1], Thomas Hin-Fung Wong[1], and Paolo Melchiorre[1,2]
[1]*ICIQ – Institute of Chemical Research of Catalonia, Tarragona, Spain*
[2]*ICREA – Institució Catalana de Recerca i Estudis Avançats, Barcelona, Spain*

9.1. GENERAL INTRODUCTION

The stereocontrolled preparation of chiral molecules is a central goal for chemists. Asymmetric catalysis is the most effective and energy-saving way to achieve this target [1]. Over the last 60 years, major advances have been spurred by the identification of a few generic catalytic modes of substrate activation [2], which enabled the development of many enantioselective catalytic processes [3]. The power of a generic mode of catalytic reactivity is that the intermediate formed upon activation of the substrate by the chiral catalyst can participate in many reaction types with consistently high stereoselectivity. The intrinsic limit of this approach is that it allows the design of mechanistically related processes only (Figure 9.1, left panel). Because of these mechanistic constraints and the extraordinary levels of sophistication already reached, it was considered difficult to further broaden the reactivity boundaries of established modes of catalytic activation. This situation changed dramatically when the tools of asymmetric catalysis were combined with photochemical reactivity [4]. Recent studies have demonstrated how the photoexcitation of chiral intermediates can switch on novel catalytic functions unavailable to conventional ground-state asymmetric catalysis (Figure 9.1, right panel). This is because the use of light excitation to bring a molecule from its ground state to an electronically excited state could open new dimensions in chemistry. Compared to the ground state, excited states can react in completely different ways [5]: for example, photoexcitation can enable radical-based processes by promoting electron transfer pathways.

This chapter will describe how combining the classical tools of asymmetric catalysis with photochemistry has enhanced the potential of generic modes of catalytic activation beyond their established ground-state reactivity. Instead of providing an exhaustive list of reactions, we will critically discuss the essential ideas and landmark discoveries that were crucial to expanding the synthetic potential of enantioselective catalysis. A selection of studies will demonstrate how the direct light excitation of intermediates with an established reactivity in asymmetric polar processes switched on new catalytic functions, which enabled mechanistically unrelated radical-based enantioselective pathways.

We will cover methods that exploit the ability of key chiral catalytic intermediates to directly reach an excited state upon light absorption, and to participate in the photochemical activation of substrates without using external photocatalysts. Two main photochemical mechanisms are available for the excitation of chiral intermediates, which allow chemists to switch on reactivity profiles that

Catalytic Asymmetric Synthesis, Fourth Edition. Edited by Takahiko Akiyama and Iwao Ojima.

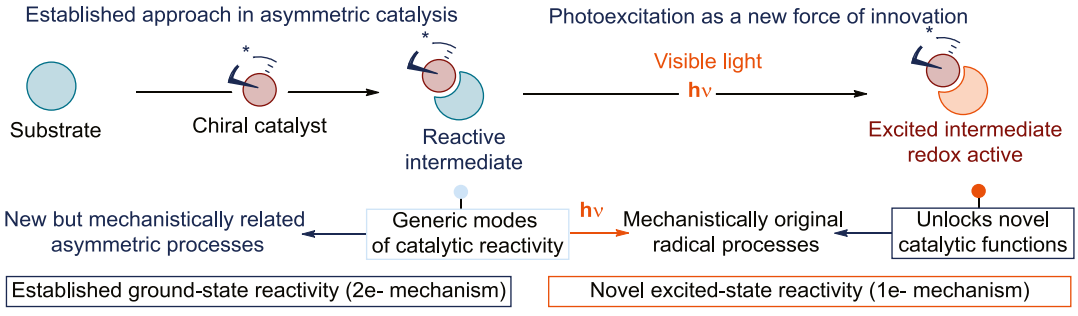

Figure 9.1. Enhancing the potential of generic modes of catalytic reactivity with light. Photoexcitation provides chiral catalytic intermediates with the ability to activate substrates via electron transfer and trigger stereocontrolled radical pathways that diverge from the innate ground-state two-electron reactivity.

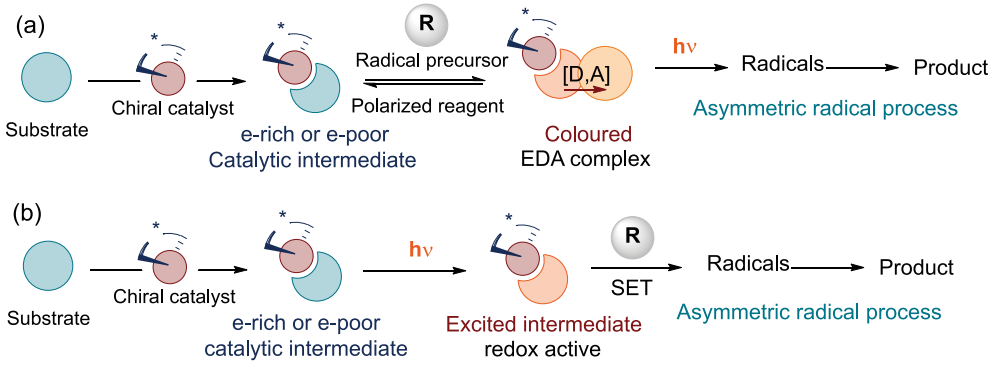

Figure 9.2. The two photochemical mechanisms available to promote asymmetric radical strategies. (**a**) In-situ-generated catalytic chiral intermediates can form an intermolecular EDA complex with a polarized reagent R. (b) The direct excitation of catalytic chiral intermediates triggers an SET event to form radicals. In both approaches, the chiral catalyst ensures effective stereochemical control over the ensuing radical process. R: a polarized reagent that acts as a radical precursor; SET: single-electron transfer; EDA: electron donor-acceptor.

diverge from the established ground-state reactivity and promote asymmetric radical pathways. At the same time, the chiral catalyst ensures effective stereochemical control. The first mechanism relies on the formation of visible-light-absorbing electron donor-acceptor (EDA) complexes [6], generated in the ground state upon association of a chiral catalytic intermediate (which generally has an electron-rich or electron-poor character) with a suitable substrate with a complementary polarization (Figure 9.2a). Irradiation of the colored EDA complex induces an intra-complex single-electron transfer (SET) event that can generate radical intermediates [7]. Recently, the EDA complex photochemistry provided fresh opportunities in synthetic chemistry [8], including asymmetric catalysis. A second mechanism (Figure 9.2b) exploits the ability of a chiral catalytic intermediate to directly reach an electronically excited state upon direct light absorption, and then to act as a potent single-electron reductant or oxidant. The ensuing SET event allows the generation of open-shell intermediates from suitable redox-active substrates, triggering asymmetric radical processes that are inaccessible without photoexcitation.

This chapter discusses recent developments in asymmetric catalytic processes achieved using these two light-induced mechanistic frameworks. We will present examples from the fields of organocatalysis, metal-mediated catalysis, and enzymatic catalysis. We will also briefly discuss a recent approach that relies on the excitation of substrates to generate radicals and its use in asymmetric catalysis.

9.2. PHOTOEXCITATION OF ORGANOCATALYTIC INTERMEDIATES

9.2.1. Enamine Catalysis in EDA Complex Photoactivation

Research in asymmetric organocatalysis [9], and specifically in enamine-mediated catalysis [10], has provided a force for innovation in the fields of enantioselective radical chemistry [11] and photoredox catalysis [12]. Enamines were the first catalytic intermediates to show potential in triggering photochemical processes by forming light-responsive EDA complexes while activating substrates via photoinduced SET mechanisms (Scheme 9.1). A crucial observation about enamines' photoactivity was made during investigations of the direct α-alkylation of aldehydes **1** with electron-deficient alkyl bromides **2** (including benzyl and phenacyl bromides), catalyzed by the chiral secondary amine **3** [13]. Previous studies [12] of similar reactivity established the need for a photoredox catalyst to generate radicals via reductive cleavage of the alkyl bromide **2**. However, a control experiment revealed that, for specific substrates **2**, the reaction could

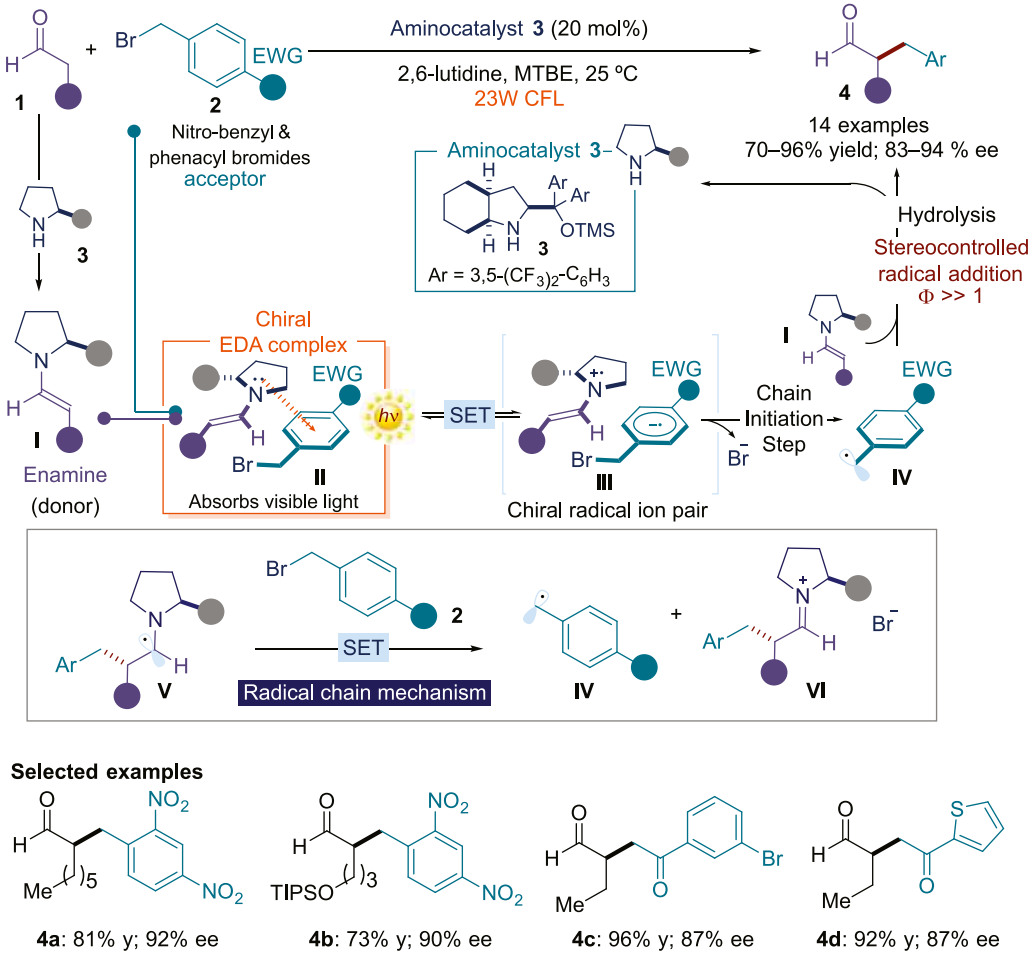

Scheme 9.1. Enantioselective catalytic α-alkylation of aldehydes enabled by irradiation of an enamine-based EDA complex **II**, formed upon association of the transient catalytic chiral intermediate **I** with electron-poor substrate **2**. The inset shows the key step of the radical propagation mechanism. CFL: compact fluorescent lamp; EWG: electron-withdrawing group; TIPS: triisopropylsilyl; MTBE: methyl *tert*-butyl ether; TMS: trimethylsilyl. The filled gray circle represents a bulky substituent on the organic catalyst.

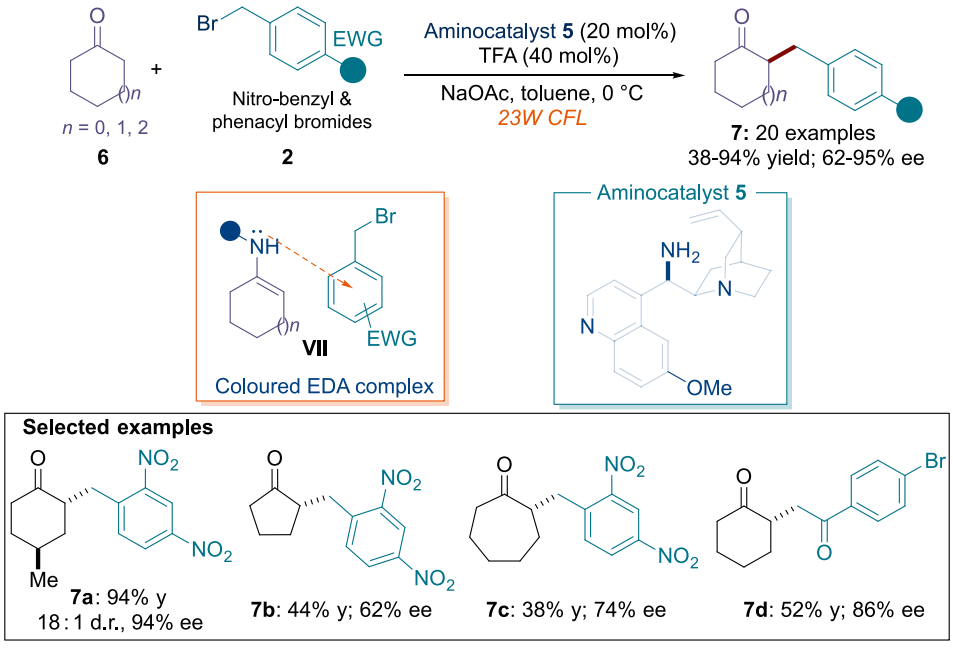

Scheme 9.2. Enantioselective α-alkylation of cyclic ketones via photochemical EDA complex activation. CFL: compact fluorescent lamp; EWG: electron-withdrawing group. The filled circles represent bulky substituents on the chiral organic catalyst.

stereoselectively proceed without the need for an external photoredox catalyst [13]. The chemistry required light irradiation, and evidence was collected supporting a radical mechanism. Mechanistic studies revealed the ability of the electron-rich chiral enamine **I**, generated upon condensation of the amine catalyst **3** with aldehyde **1**, to trigger the formation of visible-light-absorbing EDA complexes (**II**) with electron-deficient dinitro-benzyl and phenacyl bromides **2**. Evidence for the formation of complex **II** was collected via optical absorption spectroscopic studies, since **II** could absorb in visible-frequency regions where the individual components (enamine **I** and bromide **2**) could not. Irradiation of the enamine-based EDA complex **II** induced an intra-complex SET event leading to the chiral radical ion pair **III**. The irreversible cleavage of the carbon-bromine bond within **III** afforded the open-shell intermediate **IV**. Quantum yield measurements [14] established that the reaction proceeded via a self-propagating radical chain mechanism [15]. This implies that the photochemical activity of the enamine-based EDA complex **II** is the initiation event that sustains a chain process (inset in Scheme 9.1). The propagation manifold relied on the ability of the α-aminoalkyl radical **V**, emerging from the trap of radical **IV** from the ground-state chiral enamine **I**, to regenerate **IV** upon SET reduction of organic bromides **2**. Hydrolysis of the iminium ion intermediate **VI** afforded the final product **4** while liberating the amine catalyst **3**.

Nitro-benzyl bromides and phenacyl bromides both formed EDA complexes with the enamine intermediate and were productive reaction partners. Various aldehydes were competent in the photochemical reaction, affording the α-alkylated products **4** in good to excellent yields and enantioselectivity (see selected examples in Scheme 9.1). This study provided a demonstration that catalytic intermediates with an established profile in ionic asymmetric catalysis, such as chiral enamines, can engage in the formation of photoactive EDA complexes and trigger asymmetric radical processes that are not achievable with ground-state organocatalysis. In general terms, this study established that the synthetic potential of organocatalysis could be enhanced when combined with photochemical reactivity to unlock reaction pathways that are inaccessible with thermal activation [16].

The enamine-based EDA complex strategy was expanded to develop mechanistically related enantioselective α-alkylation of cyclic ketones [17]. The electron-rich enamine, generated in situ upon condensation of cyclic ketones **6** and the cinchona-based primary amine catalyst **5**, elicited the formation of a visible-light-absorbing EDA complex **VII** with 2,4-dinitrobenzyl bromide or phenacyl bromides **2**

(Scheme 9.2). A photoinduced electron transfer triggered the formation of radicals while the chiral catalyst **5** secured the stereoselective formation of products **7**. The product yields were moderate to excellent, with high stereocontrol achieved for cyclohexanone-derived substrates. The enantioselectivity decreases somewhat with cyclopentanone (adduct **7b**) or cycloheptanone (**7c**).

9.2.2. Phase Transfer Catalysis in EDA Complex Photoactivation

The above examples relied on the enhanced electron-donor character of chiral enamines to trigger the formation of photoactive EDA complexes and drive asymmetric radical processes. This discovery motivated the quest for other chiral organocatalytic intermediates that could use similar photochemical mechanisms. The electronic similarities with enamines suggested the use of chiral enolates of type **VIII**, generated in situ under phase transfer catalysis (PTC) conditions [18] by deprotonation of cyclic β-ketoesters **8**, as suitable donors to facilitate the formation of ground-state EDA complexes (Scheme 9.3). Perfluoroalkyl iodides ($R_F I$ **9**, where R_F indicates the perfluoroalkyl fragment) served as electron-accepting substrates, leading to the formation of the colored EDA complex **IX** [19]. A visible-light-promoted SET triggered the formation of the perfluoroalkyl radical **X** (R_F•) through the reductive cleavage of the C–I bond within **9**. The electrophilic nature of R_F• allowed the stereoselective trap by the chiral enolate **VIII**, generated using the cinchonine-derived PTC catalyst **11**. The chemistry provided straightforward access to enantioenriched ketoester products **10** bearing a perfluoroalkyl- (adducts **10a**–**c** in Scheme 9.3) or a trifluoromethyl-containing quaternary stereocenter (product **10d**).

9.2.3. Iminium Ion Catalysis in EDA Complex Photoactivation

Iminium ions are classical organocatalytic intermediates that have found extensive use in polar asymmetric catalysis [20]. These electron-poor intermediates are generated from weakly polarized α,β-unsaturated carbonyl substrates upon activation by a chiral amine catalyst. The ground-state electrophilic reactivity of chiral

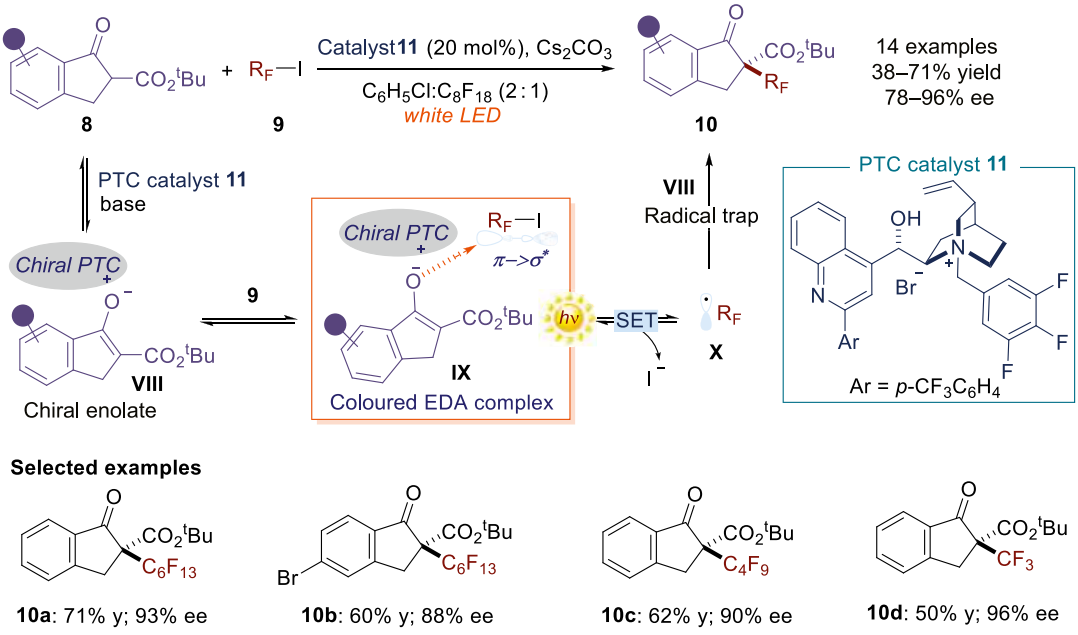

Scheme 9.3. Phase-transfer-catalyzed enantioselective perfluoroalkylation of β-ketoesters, driven by the photochemical activity of the enolate-based EDA complex **IX**. PTC: phase transfer catalyst; LED: light-emitting diode.

iminium ions traditionally accounts for the stereoselective interception of nucleophilic compounds at the β-position. Recent studies demonstrated how the electronic nature of the transient catalytic iminium ion could also be useful to trigger the formation of a photon-absorbing *intramolecular* EDA complex (Scheme 9.4) [21]. Specifically, the use of a chiral amine catalyst **12** adorned with an electron-rich carbazole moiety [22] secured, upon condensation with cyclic enones **13**, the formation of chiral iminium ions that showed a broad absorption band in the visible region. This optical property originated from an *intramolecular* charge transfer π–π interaction between the electron-rich carbazole fragment and the electron-deficient iminium double bond: for example, aliphatic iminium ions can typically only absorb in the ultraviolet (UV) region (below 400 nm).

The formation of the intramolecular EDA complex **XI** was corroborated by X-ray crystallographic analysis, which showed that the interatomic separation between the carbazole nitrogen and the sp^2 α-carbon of the iminium ion (3.10 Å) was significantly shorter than the van der Waals distance. Excitation of the intramolecular EDA complex **XI** at 420 nm promoted an SET process from the carbazole to the iminium ion, furnishing the chiral radical intermediate **XII**. The long-lived carbazole radical cation in **XII** served as an oxidant to generate a radical **XIII** from an easily oxidizable alkyl silane **14**. The resulting radical was then stereoselectively intercepted by the ground-state electron-poor iminium ion. Mechanistic studies established that the process proceeded via a radical chain propagation manifold. The radical conjugate additions to β-substituted cyclic enones enabled the formation of quaternary carbon stereocenters [23] with high stereocontrol using visible-light irradiation. A series of α-silyl carbazoles and anilines were suitable radical precursors, while enones of different ring size reacted smoothly (see selected examples in Scheme 9.4). This study demonstrated that the photoactivity of visible-light-absorbing *intra-*

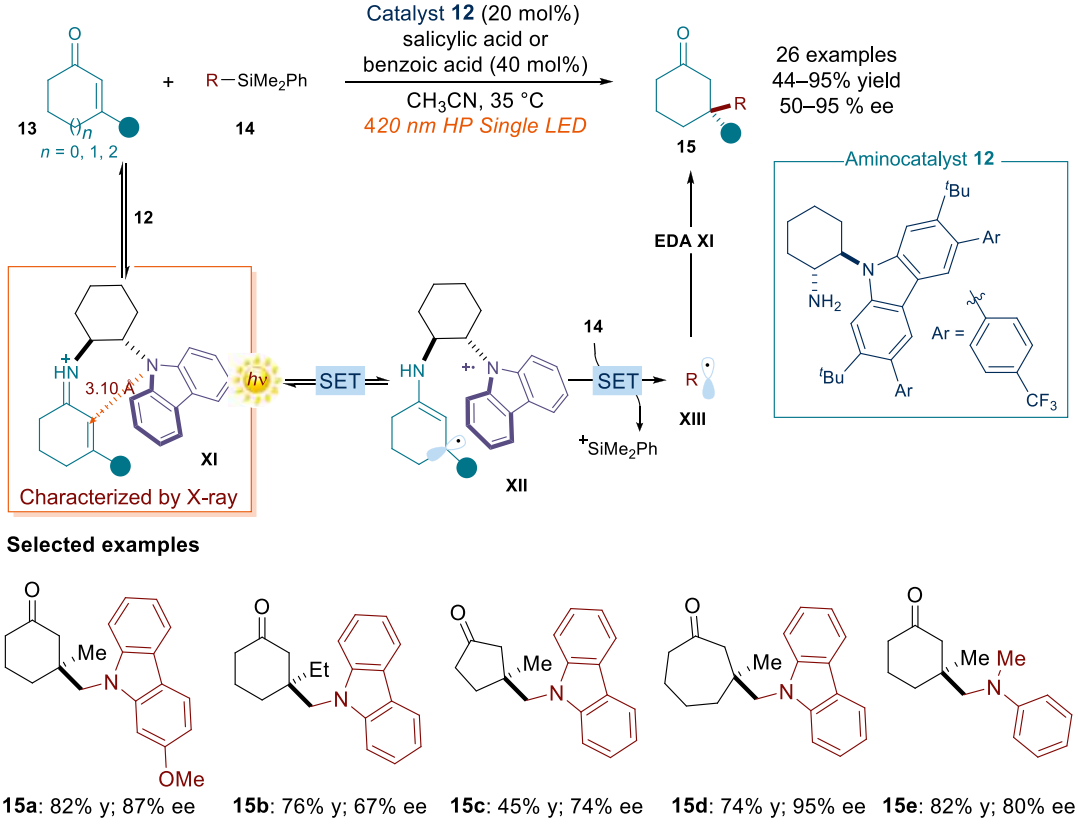

Scheme 9.4. Enantioselective catalytic radical conjugate addition driven by the excitation of an intramolecular iminium-ion-based EDA complex **XI**. HP LED: high-power light-emitting diode. Source: Adapted with permission from [21]/Springer Nature.

molecular EDA complexes can be used to generate radicals under mild conditions. Therefore, the EDA complex activation strategy does not necessarily rely on the excitation of intermolecular aggregates formed upon association of two substrates/intermediates.

Electron-poor iminium ions were also used to form intermolecular EDA complexes with donor substrates (for example α-keto acids) [24]. While this strategy holds great promise for the development of new reactions, its use in asymmetric photochemical processes has not yet been demonstrated. The photochemistry of iminium-ion-based EDA complexes is not only limited to photoredox reactions but is also used to trigger asymmetric [2+2] photocycloaddition processes [25].

9.2.4. Direct Photoexcitation of Enamines

While studying the enamines' ability to engage in the formation of photoactive EDA complexes (see Section 9.2.1), it was found that these chiral catalytic intermediates can use a different photochemical strategy to generate radicals under mild conditions [26]. Specifically, some chiral enamines can absorb light to switch on completely novel catalytic functions. This is because, by bringing enamines into an electronically excited state, irradiation turns a merely nucleophilic intermediate into a strong *reductant*. These excited-state functions can trigger the formation of radicals via SET reduction of suitable substrates, which are otherwise inert toward ground-state organocatalytic reactivity. The possibility of direct photoexcitation of enamines was discovered during studies on the α-alkylation of aldehydes **1** with bromomalonate derivatives **16** catalyzed by the chiral secondary amine **18** (Scheme 9.5a) [26].

Given its similarity with the previous studies on enamine-based EDA complex chemistry discussed in Scheme 9.1 [13], this catalytic method was developed in anticipation of EDA complex formation. However, UV-visible spectroscopy demonstrated that the enamines **XIV** could not form any EDA complex upon aggregation with bromomalonates **16**. Instead, enamine **XIV** was the only compound capable of absorbing light at the wavelength of irradiation needed for the process to proceed (from 365 nm till 400 nm). Mechanistically, upon photoexcitation, the chiral enamine **XIV** acquired the ability to act as a potent SET reductant (reduction potential of **XIV*** estimated as ≈–2.0 V vs Ag/Ag^+ in CH_3CN). SET reduction of the bromomalonate **16** induced the formation of the radical **XV**.

The implication of enamine **XIV**, which could absorb light till about 415 nm, within the photochemical regime was established by Stern-Volmer quenching studies. These experiments showed that the luminescence of the excited enamine **XIV*** was effectively quenched by **16**. Determination of the quantum yield established a value largely exceeding unity ($\Phi_{measured} = 20$), which was congruent with a radical chain mechanism [14]. Upon stereocontrolled addition of the radical **XV** to the chiral ground state **XIV**, the resulting aminoalkyl radical **XVI** abstracts a bromine atom from **16** thereby regenerating the radical **XV** (Scheme 9.5b). The ensuing adduct **XVII** is not stable and evolves to a bromide-iminium ion pair **XVIII**, which eventually hydrolyzes to release the chiral product **17** and the aminocatalyst **18**. The α-alkylation of aldehydes driven by the direct excitation of enamines provided products **17** in moderate to high yields and high enantioselectivities using bromomalonates **16** as the radical precursors (Scheme 9.5c). Functional group tolerance included groups such as free alcohols and olefins (adducts **17b** and **17c**).

These studies demonstrated that light excitation can turn enamines (which behave as nucleophiles in the ground state) into strong reductants and trigger the formation of radicals. At the same time, ground-state enamines control the stereochemical course of the radical trapping event. This strategy was expanded to develop mechanistically related enantioselective α-functionalization reactions (Scheme 9.5d), including amination [27a], and arylsulfonyl alkylation [27b] of aldehydes.

9.2.5. Direct Photoexcitation of Iminium Ions

Recently, it was also established that chiral iminium ions can unlock a rich photochemistry upon light excitation [28]. A crucial aspect is that the condensation of the chiral secondary amine catalyst **19** with aromatic enals **20** converts an achromatic substrate into a colored iminium ion **XIX** (Scheme 9.6). Selective excitation with a violet-light-emitting diode (LED) brings this electron-poor intermediate into an electronically excited state (**XIX***) and thus turns an electrophilic species into a strong SET

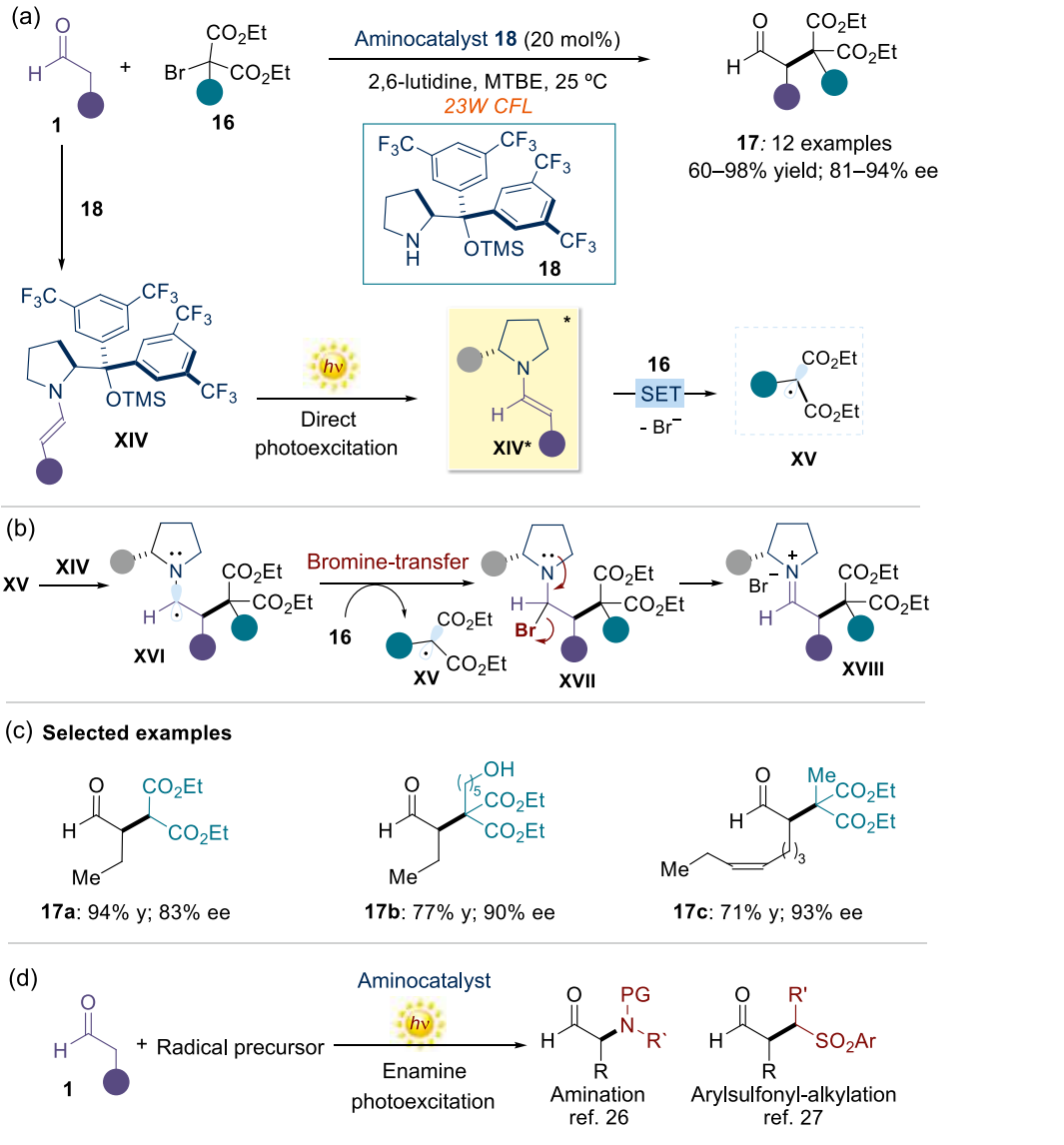

Scheme 9.5. (a) Direct excitation of chiral enamines in the enantioselective α-alkylation of aldehydes with bromomalonates **16**. Source: Adapted with permission from [26]/American Chemical Society. (b) The key step of the chain propagation mechanism. (c) Selected examples. (d) Further synthetic applications for the photochemical stereocontrolled α-functionalization of aldehydes. The filled gray circle represents a bulky substituent on the chiral organic catalyst **18**; EWG: electron-withdrawing group; TMS: trimethylsilyl; PG: protecting group. Source: Based on [27a, 27b].

oxidant [29], which can trigger the formation of radicals through SET oxidation of organic silanes **21**. The latter event furnishes the chiral 5π-electron β-enaminyl radical intermediate **XX** along with the neutral benzyl radical **XXI**, which is generated upon irreversible fragmentation of the carbon–silicon bond in **21**. A stereocontrolled intermolecular coupling of the chiral β-enaminyl radical **XX** and **XXI** then forges the stereogenic center within the β-functionalized aldehyde product **22**. The β-benzylation process was effective for aromatic enals, while alkyl enals were not viable substrates. The scope of silanes included some heteroaromatic ring systems such as indoles (adduct **22d**), and heteroatoms such as sulfur **22e** or nitrogen **22b**.

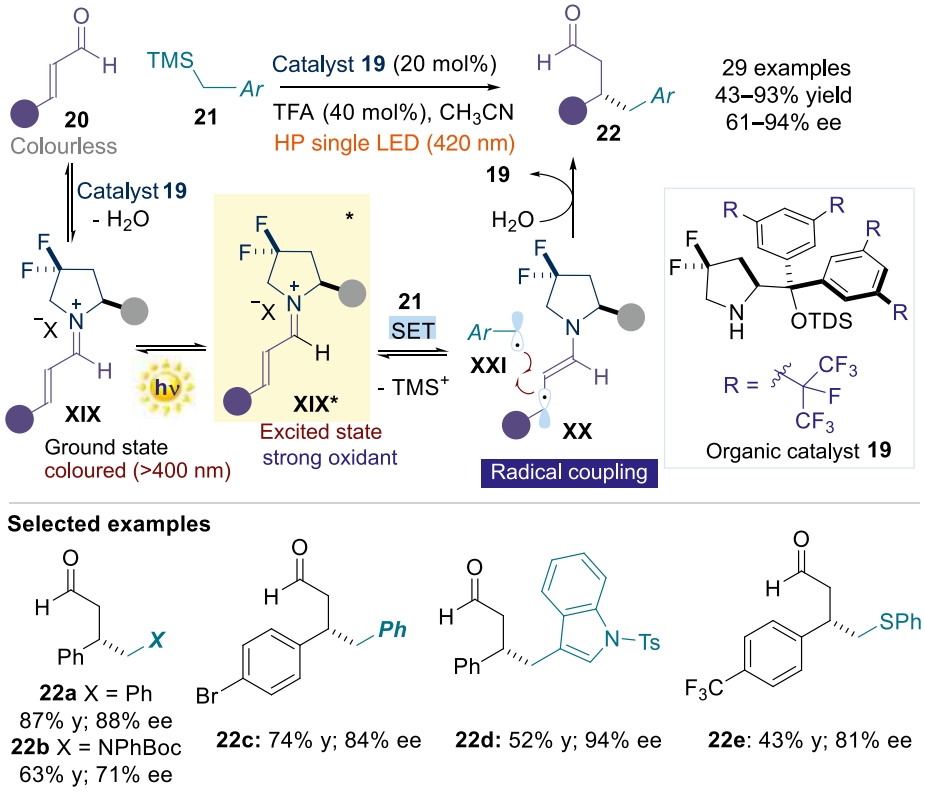

Scheme 9.6. The direct photoexcitation of catalytic chiral iminium ions **XIX** enables the stereocontrolled β-alkylation of enals **20** with non-nucleophilic alkyl silanes **21**; the chiral β-enaminyl radical **XX**, emerging from the SET reduction of the excited iminium ion **XIX***, which acts as a strong oxidant, governs the stereocontrolled radical coupling to afford products **22**. The filled gray circle represents a bulky substituent on the chiral amine catalyst **19**. TFA: trifluoroacetic acid; TMS: trimethylsilyl; TDS: thexyl-dimethylsilyl; Boc: *tert*-butyloxycarbonyl; Ts: 4-toluenesulfonyl.

Two factors were important for reaction development. First, the use of the fluorinated catalyst **19** enhanced stability toward oxidative conditions by increasing its oxidation potential, thus avoiding oxidative degradation pathways. Second, the presence of a trimethylsilyl (TMS) electro-auxiliary group within substrate **21** secured effective radical formation upon electron transfer [30]. Importantly, the organic trimethylsilane reagents **21** are non-nucleophilic substrates, which are recalcitrant to classical conjugate addition manifolds. Thus, the excitation of chiral iminium ions enables transformations that could not be realized within the framework of conventional catalytic asymmetric methodologies. A mechanistic departure from previous excited-state organocatalytic approaches is that the stereoselectivity is dictated by the chiral β-enaminyl radical intermediate **XX**, which governs the radical coupling event, and not by the ground-state organocatalytic intermediate.

The high oxidation potential of the excited iminium ion **XIX*** (E_{red}^{*} estimated as ≈+2.3 V vs Ag/Ag^{+} in CH_3CN on the basis of electrochemical and spectroscopic measurements) allowed this light-driven strategy to be used for the development of other unconventional and stereocontrolled enal β-functionalizations via radical pathways. For example, the use of 4-alkyl Hantzsch esters **23** as the radical precursors (Scheme 9.7) accounted for the stereocontrolled installation of simple alkyl fragments at the β-carbon of enals **20** [31]. An interesting example from this method was the preparation of saccharide-containing aldehyde **24d**; it was demonstrated that the diastereoselectivity of the reaction is controlled by the chiral catalyst and not by the inherent stereochemical information encoded within the chiral substrate. Mechanistically, the key step was the SET oxidation of **23** from the excited iminium ion to form a

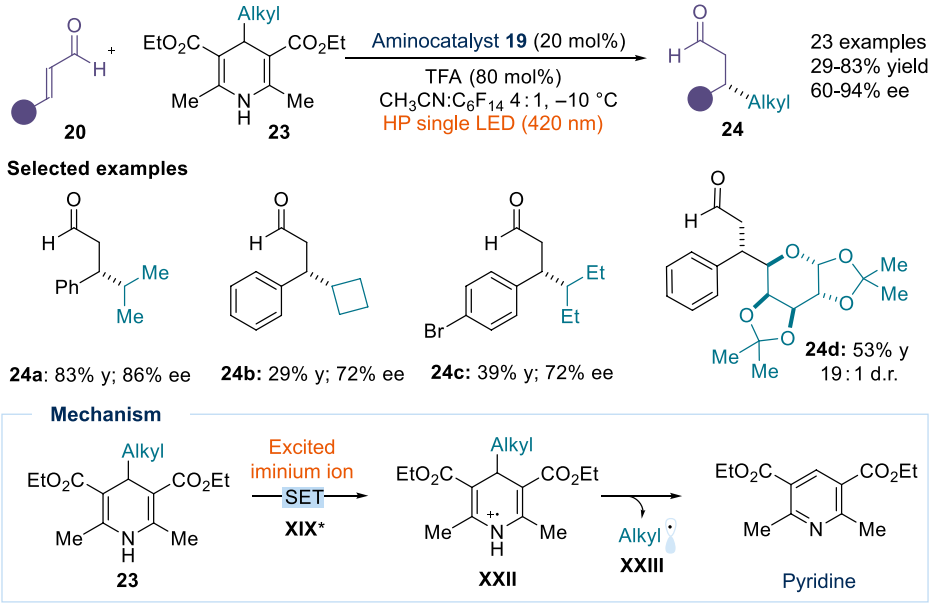

Scheme 9.7. Enantioselective photochemical organocatalytic β-alkylation of enals using Hantzsch esters **23** as radical precursors. TDS: thexyl-dimethylsilyl.

radical cation **XXII** that decomposes to pyridine and a carbon-centered radical **XXIII**, which was stereoselectively trapped to afford enantioenriched products **24**.

The oxidizing power of the excited-state iminium ion **XIX*** was also used to stereoselectively functionalize toluene and derivatives **25** (Scheme 9.8) [32]. SET oxidation of toluene increases the pk_a of the benzylic C_{sp3}–H bonds such that deprotonation can occur in the presence of a weak base. Mechanistically, the toluene oxidation from **XIX*** led to the radical cation **XXIV**, which is deprotonated by the counter anion of **XIX*** to form the benzyl radical **XXI**, which is eventually trapped to afford the β-benzylated products **26**. Mechanistic studies indicated that the generation of benzylic radicals is triggered by a sequential multisite proton-coupled electron transfer (MS-PCET) mechanism [33]. This protocol allows feedstock chemicals (e.g. toluene and xylene derivatives), which are generally used as solvents, to instead be used as substrates to make chiral molecules with high enantioselectivity. The functional group tolerance of this reaction includes functionalities that may not survive photoredox or transition metal catalysis conditions, such as redox-active esters **26d** or bromides **26e**.

The excited-state reactivity of chiral iminium ions has also been used to activate cyclopropanols [34] and olefins [35] via SET oxidation, while triggering asymmetric catalytic radical cascade processes leading to cyclic molecules with multiple stereocenters.

9.3. PHOTOEXCITATION OF METAL-BASED INTERMEDIATES

The possibility of using photoexcitation to expand the potential of generic modes of catalytic activation beyond their established ground-state reactivity is not limited to organocatalysis. Recent studies demonstrated that the field of metal-based asymmetric catalysis can also be combined with photochemical reactivity.

9.3.1. Use of Chiral Lewis Acids to Form Photoactive Intermediates

Chiral Lewis acids have been successfully used to trigger photochemical asymmetric radical processes upon formation of photoactive intermediates by coordination of carbonyl substrates. The bis-cyclometalated chiral-at-metal iridium and rhodium catalysts **28** introduced by Meggers proved particularly useful

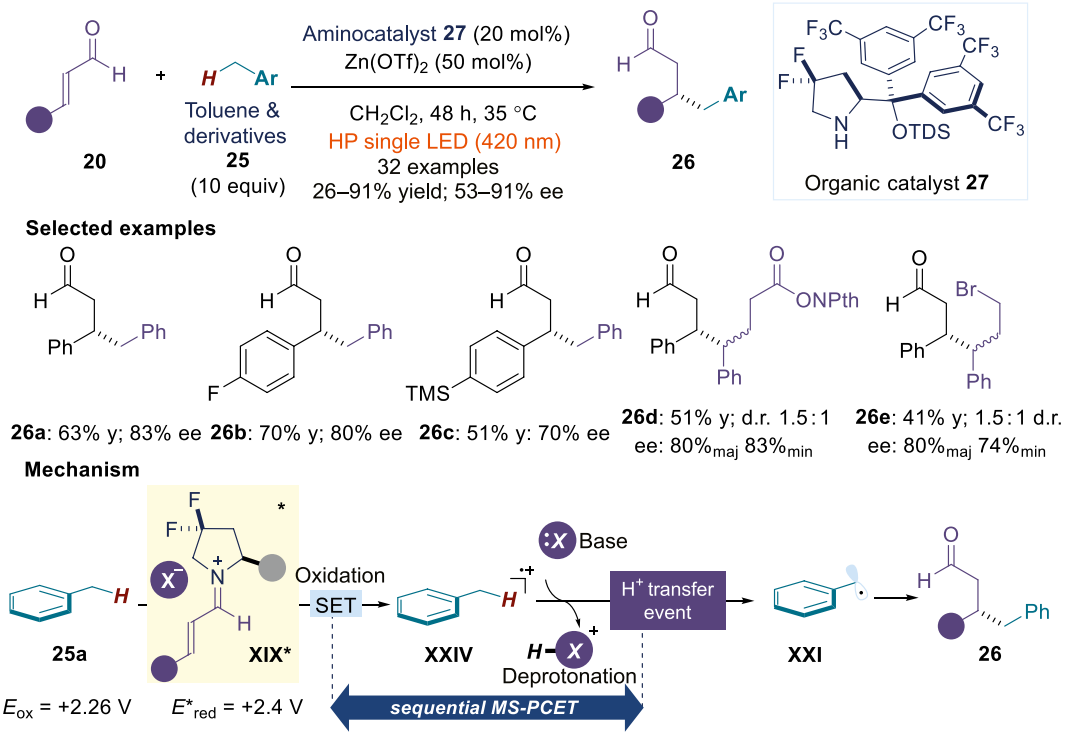

Scheme 9.8. Enantioselective photocatalytic C-H functionalization of toluene and derivatives. TDS: thexyl-dimethylsilyl; TMS: trimethylsilyl; NPth: *N*-phthalimide. Source: Adapted with permission from [32]/American Chemical Society.

(Figure 9.3). These propeller-type C_2-symmetrical catalysts, which are coordinated to two achiral 5-(*tert*-butyl)-2-phenyl benzoxazole or benzothiazole ligands and two labile acetonitrile ligands, can be further coordinated with carbonyl substrates with dual coordination ability. The resulting intermediates acquire useful photophysical properties, which upon excitation can promote SET events leading to stereocontrolled radical processes without the need for external photoredox catalysts [36].

The first application was reported in 2014 [37] with the development of an asymmetric photochemical α-alkylation of acyl imidazoles **29** with benzyl bromides and phenacyl bromides **2**, catalyzed by biscyclometalated chiral iridium complex Ir-**28** (Scheme 9.9). Coordination of substrates **29** by the iridium catalyst Ir-**28** led to the cationic complex **XXV**, which afforded the iridium enolate intermediate **XXVI** upon deprotonation at the α-position. In analogy to the photochemistry of enamines (see Section 9.2.4), the electron-rich enolate **XXVI** can absorb visible light to become an SET reductant (reduction potential of **XXVI*** estimated as = −1.74 V vs Ag/AgCl). SET activation of benzyl bromides or phenacyl bromides **2** yielded the electrophilic radical **XXVII**, which was stereoselectively intercepted by the chiral ground-state iridium enolate intermediate **XXVI** to generate the ketyl radical **XXVIII**. Subsequent SET oxidation by the oxidized form of **XXVI** afforded complex **XXIX**. Final ligand exchange yielded the chiral product **30** [39]. The photochemical process ensured high levels of stereocontrol for a variety of acyl imidazoles and electron-deficient alkyl bromides (see selected examples in Scheme 9.9).

The versatility of this photochemical system for the asymmetric radical α-functionalization of carbonyl substrates allowed for the asymmetric α-trichloromethylation, using $BrCCl_3$ as the radical precursor [40], and the α-perfluoroalkylation [41] of 2-acyl imidazoles. These studies also highlighted that, for specific α-functionalization processes, the chiral-at-rhodium complex Rh-**28** offered better results than the Ir-**28** catalyst, mainly due to faster substrate coordination rate and turnover frequency [42].

This catalytic photochemical platform also served to realize an unusual asymmetric β-functionalization of 2-acyl imidazoles and 2-acylpyridines **29** with 1,2-dicarbonyl compounds **31** catalyzed by the rhodium catalyst Rh-**28** (Scheme 9.10) [38].

Upon photoexcitation, the in-situ-generated chiral rhodium enolate **XXX**, acting as a reductant, promoted the SET activation of substrate **31**. This SET event, which generates the ketyl radical **XXXI**, is

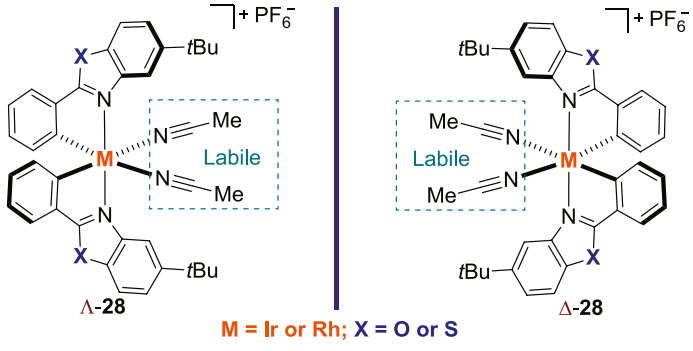

Figure 9.3. The two enantioisomers of octahedral chiral-at-metal catalysts.

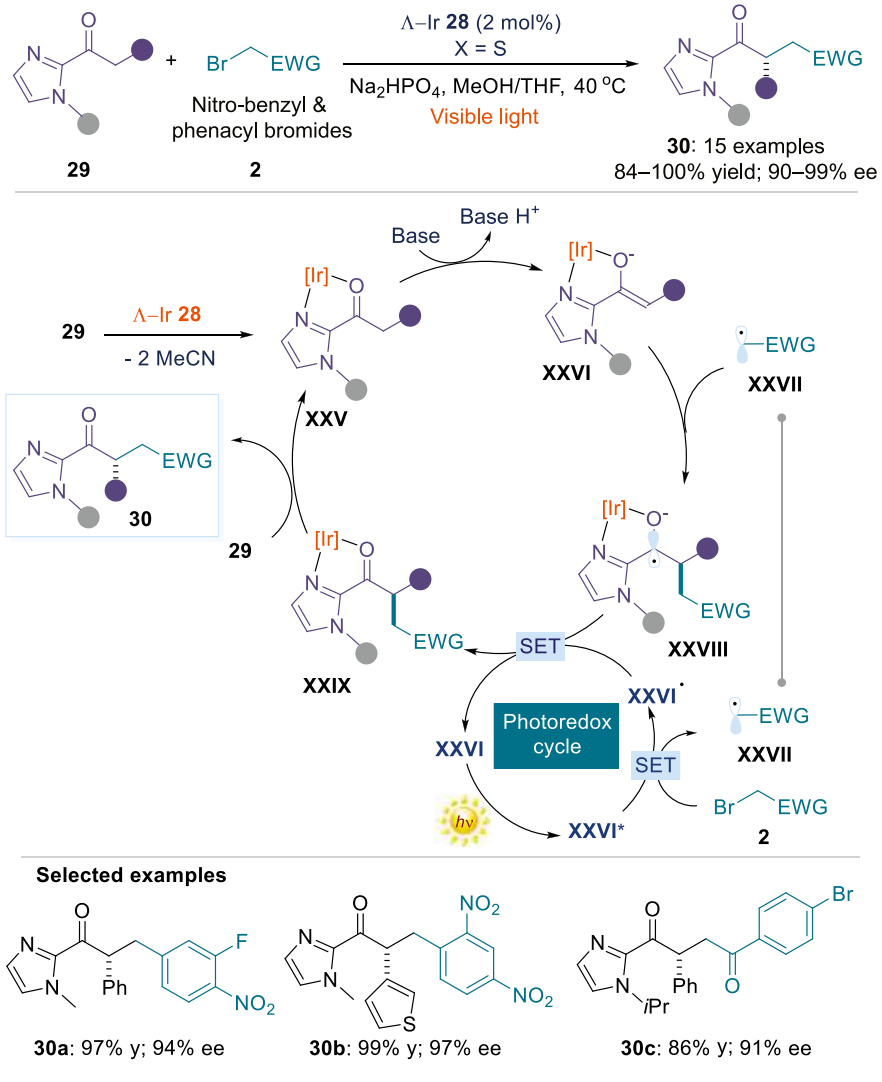

Scheme 9.9. Photochemical asymmetric α-alkylation of acyl imidazoles enabled by excitation of catalytic chiral iridium enolate complex **XXVI**. EWG: electron-withdrawing group. Source: Adapted with permission from [38]/American Chemical Society.

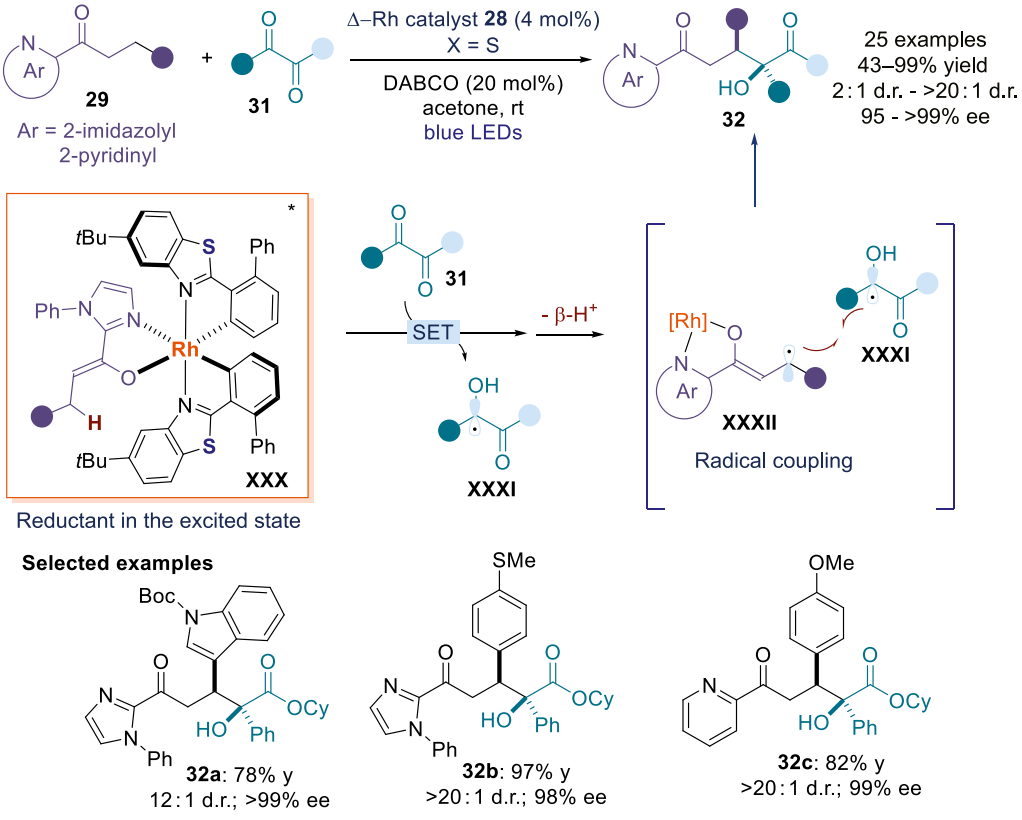

Scheme 9.10. Photochemical asymmetric β-C–H functionalization of 2-acyl azaarenes **29** with 1,2-dicarbonyl compounds **31** via excitation of in-situ-generated chiral rhodium enolate complex **XXX**. Rt, room temperature.

accompanied by a proton transfer (net hydrogen atom transfer [HAT]) affording the corresponding β-enolate carbon-centered radical **XXXII**. This sequence is favored by the low bond dissociation energy (BDE) of the C-H bond at the β-carbon within enolate intermediate **XXX**. A stereoselective radical coupling, followed by protonation and ligand exchange, yielded products **32** bearing two adjacent stereogenic centers with high fidelity.

The chemistry of the chiral-at-metal catalysts **28** discussed so far was used to generate in situ an electron-rich enolate, which acted as an SET reductant upon excitation. In 2016, Meggers demonstrated that also the cationic complex **XXXIII**, which is directly formed upon complexation of the iridium catalyst **28** with non-enolizable substrates, such as trifluoroacetyl imidazoles **33**, could absorb light (Scheme 9.11). The electron-poor intermediates **XXXIII** served as a mild SET oxidant upon photoexcitation [43]. SET oxidation of *N*,*N*-diaryl tertiary amines **34** afforded α-amino radicals **XXXIV** and the chiral ketyl radical **XXXV**. A stereocontrolled radical coupling was proposed to generate the chiral 1,2-amino alcohol products **35** with moderate to good yield, diastereoselectivity, and excellent enantiomeric excess (ee). The oxidizing ability of the chiral-at-metal coordinated cationic complex of type **XXXIII** was used to develop other asymmetric radical processes [44].

The Meggers' chiral-at-metal catalysts **28** also proved effective for the activation of electron-poor α,β-unsaturated carbonyl compounds. In analogy to the photochemistry of iminium ions (see Section 9.2.5), the coordination of α,β-unsaturated 2-acyl imidazoles **36** by the rhodium catalyst **28** afforded the electron-poor intermediate **XXXVI** (Scheme 9.12).

Photoexcitation turns this electrophilic intermediate into an SET oxidant, which can activate tetrahydroisoquinoline **37** to form the α-amino radical **XXXVII** [45]. Upon radical conjugate addition, governed by the chiral ground-state electrophilic intermediate **XXXVI**, the ensuing radical **XXXVIII** was reduced

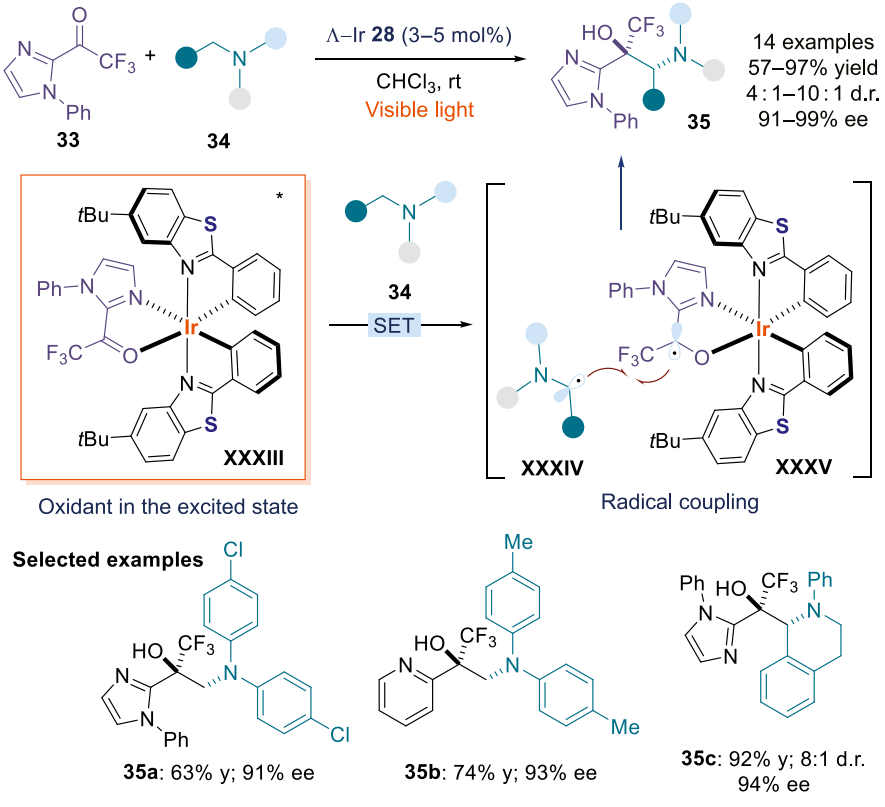

Scheme 9.11. Stereoselective synthesis of 1,2-amino alcohols with visible-light-excited chiral cationic complex **XXXIII** acting as an oxidant. Rt, room temperature.

to the enolate intermediate **XXXIX** by the reduced rhodium intermediate **XXXVI**$^{-}$ or by the substrate **37** itself. The latter pathway, which is consonant with a radical chain propagation, was supported by the measured quantum yield ($\Phi > 2$). Subsequent protonation, product release, and substrate re-coordination closed the catalytic cycle.

This photochemical strategy was successfully expanded to develop other asymmetric radical conjugate addition processes using a variety of easy-to-oxidize radical precursors [46]. Recently, it was demonstrated that chiral Lewis acids other than the Meggers' chiral-at-metal catalysts **28** could be used for the photochemical activation of unsaturated carbonyl substrates, such as a nickel catalyst coordinated by a chiral ligand [47].

9.3.2. Photoexcitation of Organometallic Intermediates

Recent examples demonstrated the ability of some transition metal complexes to absorb light and trigger synthetically useful catalytic processes [48]. The possibility of using photoexcitation to draw out new reactivity modes from chiral organometallic catalytic complexes has also been demonstrated in an asymmetric catalytic regime. As a notable example, Peters and Fu recently designed a copper-based catalytic system that, on excitation, can drive enantioselective C-N cross-coupling processes [49]. Specifically, they developed a photochemical enantioconvergent C-N bond-forming reaction between tertiary alkyl halides **39** and carbazole or indole nucleophilic substrates **40** catalyzed by a copper complex (Scheme 9.13). The overall process led to products **41** bearing a quaternary stereocenter in high stereoselectivity. Mechanistic studies revealed that the organocopper(I) complex **XL**, generated in situ from the copper catalyst, the

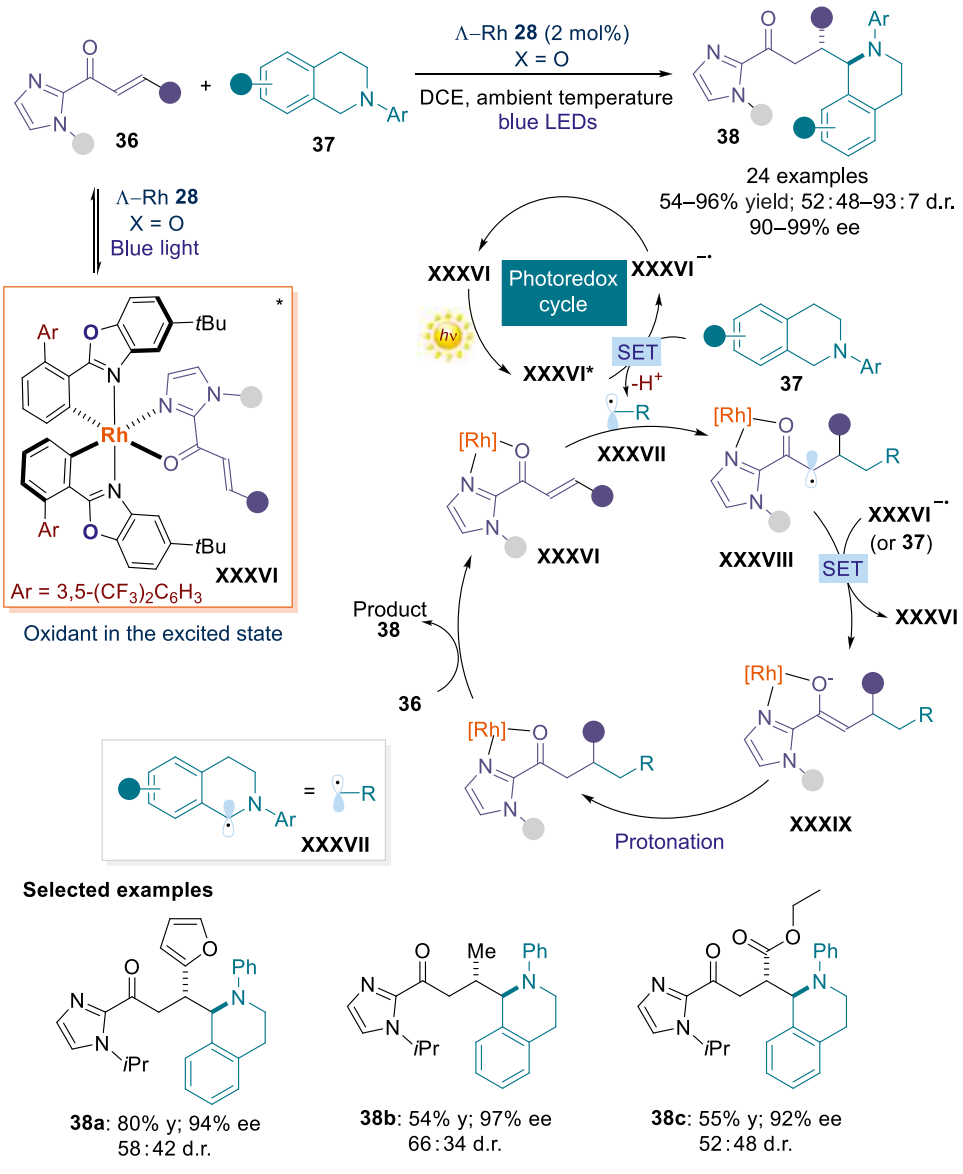

Scheme 9.12. Asymmetric conjugate addition of α-amino radicals to α,β-unsaturated 2-acyl imidazoles promoted by the photoexcitation of in-situ-generated complex **XXXVI**.

chiral phosphine ligand **42**, and the nucleophile **40**, could absorb visible light to become a reducing agent in the excited state (**XL***). Subsequent SET reduction of **39** generated the alkyl radical **XLI**, which was intercepted by the resulting chiral copper(II) intermediate **XLII**. Reductive elimination provided the enantioenriched chiral product **41** while regenerating the copper(I) catalyst. This study demonstrated that a single organometallic intermediate can be responsible for both the photochemistry and the enantioselective bond-forming process. Following this, other studies have used copper salts in combination with chiral ligands to develop photoinduced asymmetric radical processes [50].

Recently, photoexcitation was also exploited to upgrade the well-established ground-state reactivity of a chiral organometallic complex while switching on completely new catalytic functions, enabling

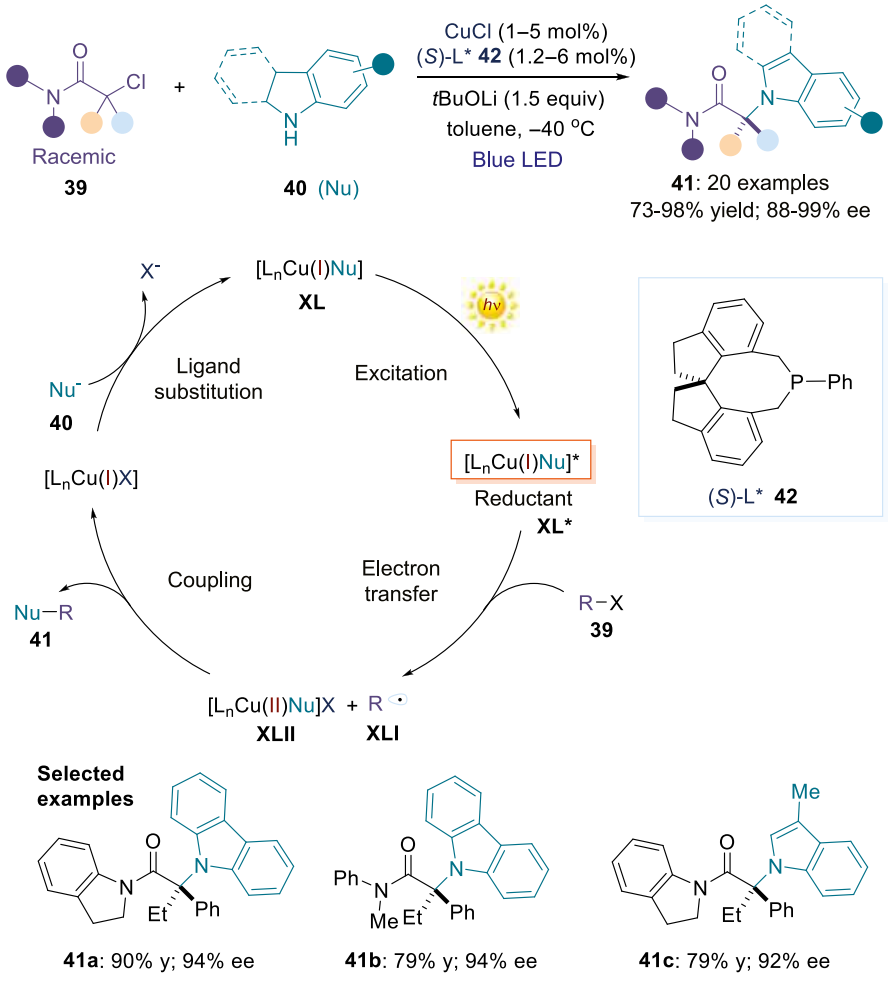

Scheme 9.13. Asymmetric copper-catalyzed C-N cross-couplings induced by visible light.

mechanistically unrelated radical-based enantioselective pathways [51]. Specifically, it was found that the chiral (η^3-allyl)iridium(III) complex (**XLIII**), which has a well-established electrophilic character in the ground state [52], acquires on excitation the ability to trigger SET pathways and empower cross-coupling mechanisms (Scheme 9.14). The organometallic complex **XLIII** is generated upon coordination of the iridium(I)-precatalyst $[Ir(cod)Cl]_2$ with the chiral phosphoramidite-olefin ligand **43** followed by oxidative addition into allylic alcohols **44** [53]. This complex **XLIII** is widely used in its ground state to promote enantioselective catalytic allylic substitution reactions with a variety of nucleophiles [52]. Its established polar reactivity could be completely diverted by simply using blue light (460 nm). This is because excitation provided **XLIII** with the ability to activate non-nucleophilic 1,4-dihydropyridine substrates **45** via an SET oxidation pathway.

The photoinduced SET unlocked an otherwise inaccessible cross-coupling mechanism, since the resulting iridium(II) center **XLV** could intercept the generated radicals **XLIV** to afford an iridium(III) complex **XLVI**, which promoted a reductive elimination to forge a stereogenic center within the final branched product **46**. This photochemical strategy enabled the enantioselective C(sp^3)-C(sp^3) cross-coupling of racemic allylic alcohols with stable radical precursors, which was not achievable under thermal activation.

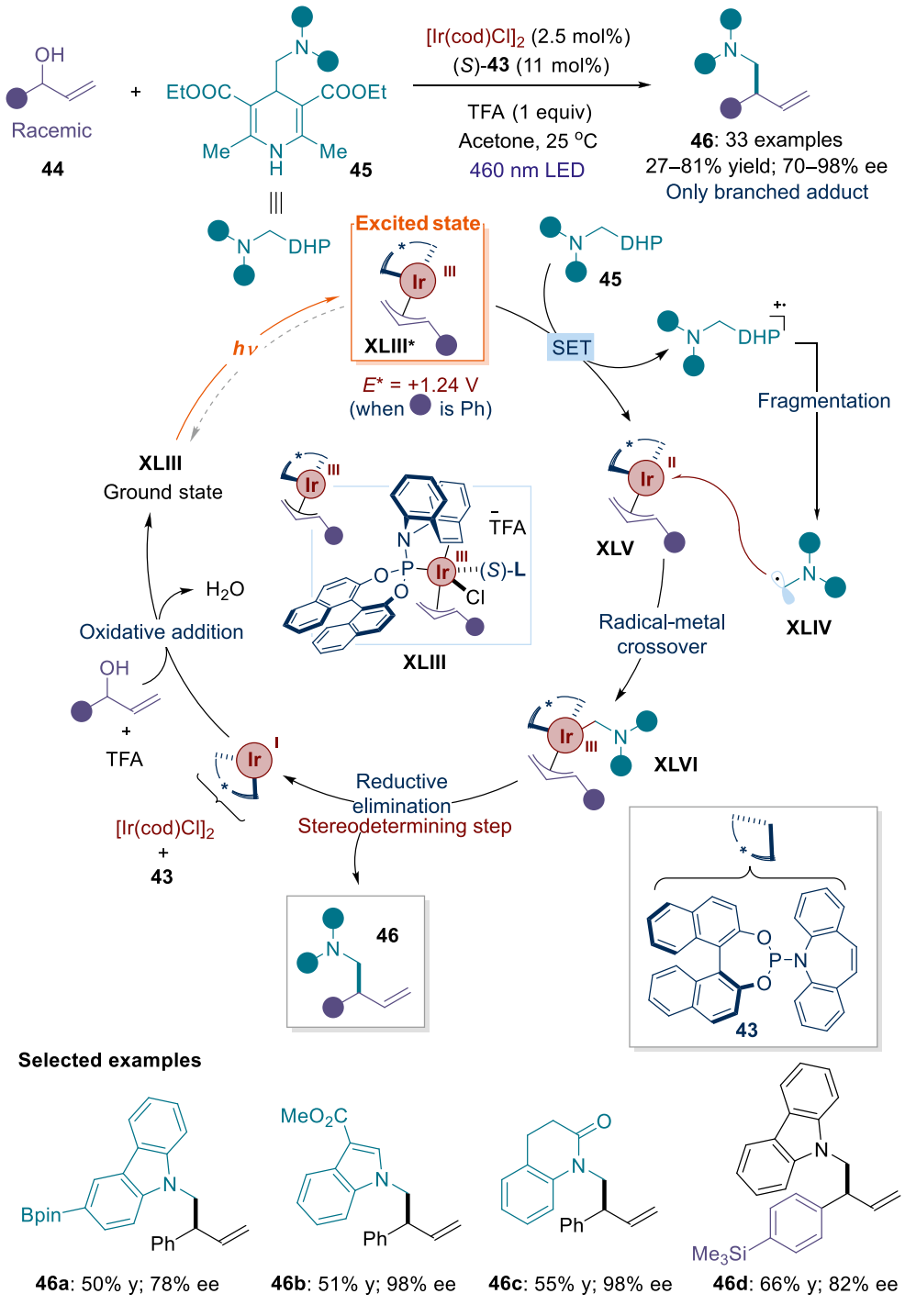

Scheme 9.14. Photoexcitation of the (η^3-allyl)iridium(III) complex **XLIII** promotes an asymmetric photochemical C-C cross-coupling process. DHP: 1,4-dihydropyridine; cod: cyclooctadiene.

9.4. PHOTOCHEMISTRY AND BIOCATALYSIS

Enzymes are excellent catalysts for asymmetric processes, and often their efficiencies and selectivities are unmatched by small molecular counterparts [54]. In addition, the selectivity of a natural enzyme can be opportunely enhanced and tuned by directed evolution [55]. Despite this potential, natural enzymes use only a relatively small section of "reaction space." This implies that it is possible to effectively promote only a limited number of stereocontrolled reaction classes, which are characterized by a similar reaction mechanism. This situation recently changed when biocatalysis was merged with photochemistry. Recent advances highlighted the ability of some enzymes to alter their native reactivity upon light excitation and to catalyze radical-based processes that are completely different than those for which they evolved [56].

9.4.1. EDA Complex Photochemistry and Enzymatic Catalysis

The seminal work by Hyster in 2016 was the first report of asymmetric photoenzymatic catalysis [57]. Specifically, it was demonstrated that the natural reactivity of nicotinamide-dependent ketoreductases (KREDs) can be altered upon light excitation of the photoresponsive nicotinamide adenine dinucleotide (NADH)/nicotinamide adenine dinucleotide phosphate (NADPH) cofactor, which is bound in the enzyme active site. KREDs are extensively used to prepare chiral alcohols upon reduction of ketones [58]. This native reactivity, which is based on classical polar two-electron mechanisms, is enabled by the ability of such enzymes to simultaneously bind a carbonyl compound and the cofactor via noncovalent weak interactions, and by the tendency of NADH (or NADPH) to serve as a hydride (H^-) source. Visible-light excitation of the cofactor, however, can switch on a completely distinct reactivity. This is because the NAD(P)H becomes a strong reducing agent [59] in the excited state, allowing access to radical manifolds (Scheme 9.15). This photochemical behavior was used to perform an enantioselective dehalogenation of racemic α-bromolactones **47**. These are substrates that can bind in the active site of KREDs but are not primed for carbonyl reduction. Once the NAD(P)H and the substrate **47** are brought in close proximity within the enzyme active site, they can form a visible-light-absorbing EDA complex **XLVII**. Photoinduced SET reduction of **47** triggers the mesolytic cleavage of the C-Br bond, leading to the prochiral radical intermediate **XLVIII**. The tendency of the cofactor radical cation **XLIX**, emerging from the SET, to act as a good hydrogen atom (H) donor for **XLVIII** drives the formation of the reduced chiral product **48**. Mechanistic insights indicated the last HAT step, which happens in the chiral environment provided by the enzyme, as being the enantio-determining event, since the binding of the racemic bromolactones **47** from the KRED enzyme is unselective. Variously substituted lactones of different ring sizes were suitable substrates in this photoenzymatic enantioconvergent debromination (see selected examples in Scheme 9.15).

In 2019, a photochemical asymmetric intramolecular addition of an electrophilic radical to a non-activated alkene was developed (Scheme 9.16). In this system, flavin hydroquinone (FMN_{hq}), a prosthetic group that is covalently anchored to the active site of "ene" reductase enzymes, behaved as a donor for charge transfer interactions with the substrate **49** [60]. The resulting EDA complex **L** could absorb cyan light to promote radical formation upon SET-induced mesolytic C-Cl cleavage. The enzyme exhibited excellent photochemical reactivity to afford cyclized products **50** with high stereocontrol.

Elevated reactivity was secured by a single point mutation (T36A), which altered an amino acid on the surface of the protein, far from the reaction site. Introducing a substituent to the alkene yielded a product with well-defined chirality at both stereocenters (product **50e**), revealing that both intramolecular radical addition and HAT steps are stereoselective. Formation of six- to eight-membered rings, or the opposite enantiomer, was also achieved using related enzymes, enabling access to diverse lactam ring scaffolds with good enantiocontrol. A similar photochemical enzymatic approach was recently used to elicit the generation of unstabilized nucleophilic radicals, which then participated in a stereocontrolled cyclization manifold [61].

Following this study, related asymmetric intermolecular processes were independently developed by Zhao [62] and Hyster [63]. Both methods used "ene" reductases to elicit the formation of an EDA complex within the enzyme's active site, which activated α-halo carbonyl substrate of type **51** toward SET-induced radical formation (Scheme 9.17). The resulting radical **LI** was then intercepted by a

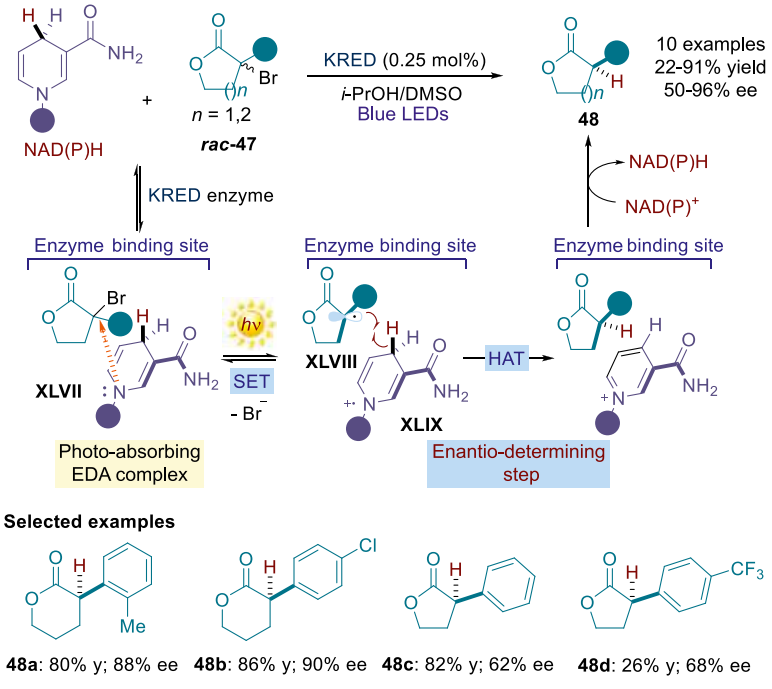

Scheme 9.15. Photoexcitation of a NAD(P)H-dependent enzyme enables a non-natural reactivity. When the carbonyl reductase KRED enzyme binds NAD(P)H and the substrate **47**, a photo-active EDA complex **XLVII** is formed. On excitation, an SET from NADH, eventually acting as a strong reductant, triggers the formation of the prochiral radical **XLVIII** upon reductive cleavage of the substrate C-Br bond. This photochemical strategy alters the native reactivity of the enzyme, which is now able to perform an enantioselective debromination of **47**. KRED: nicotinamide-dependent ketoreductase; HAT: hydrogen atom transfer.

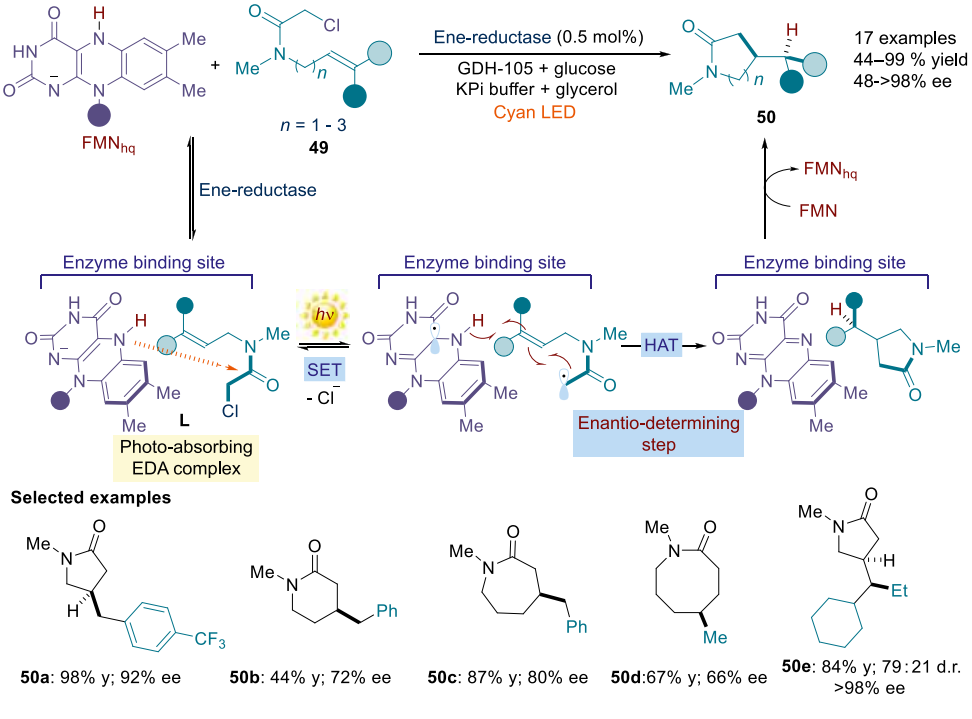

Scheme 9.16. Photoenzymatic radical cyclization: Flavin hydroquinone cofactor participates in an EDA interaction to promote the formation of radicals, which are primed for stereocontrolled cyclization. GDH: glucose dehydrogenase.

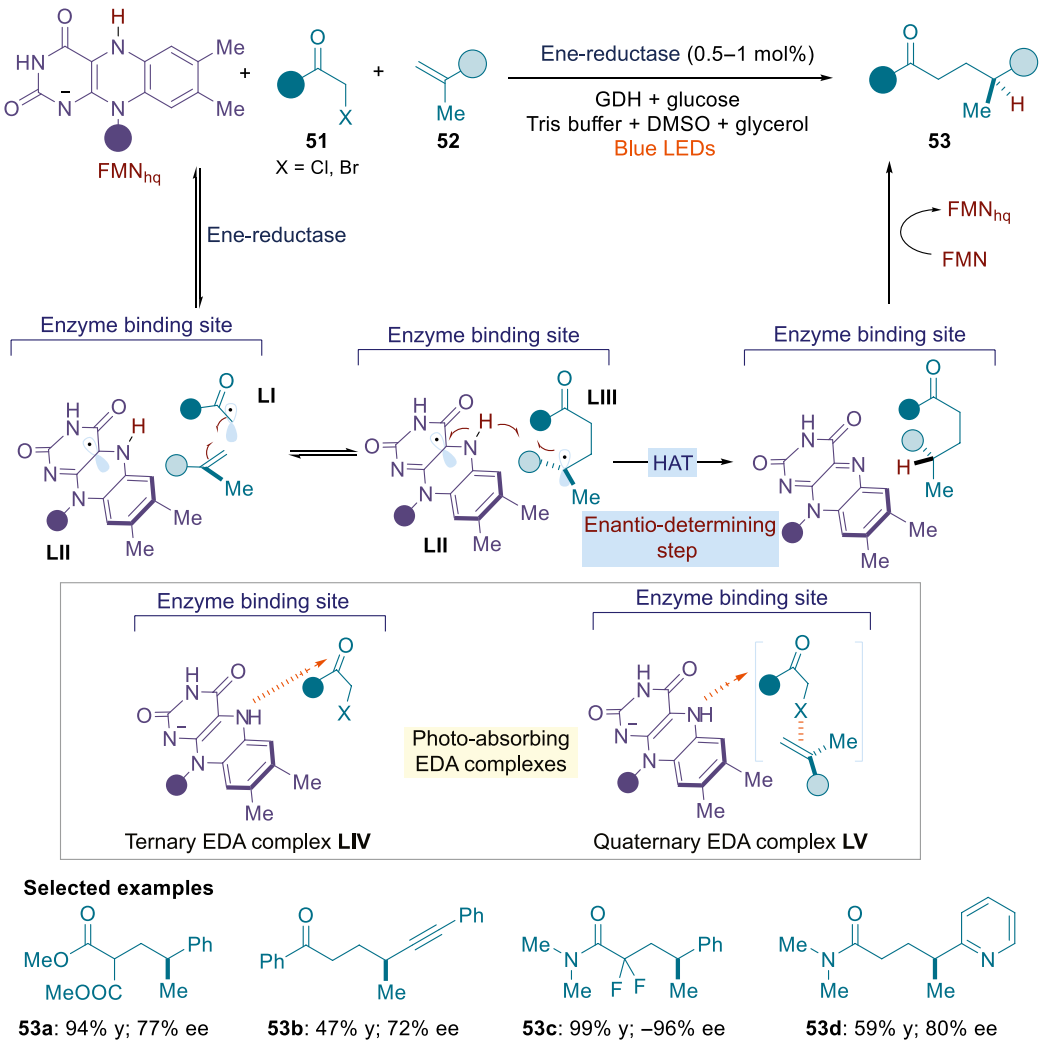

Scheme 9.17. Photoenzymatic enantioselective intermolecular radical coupling. GDH: glucose dehydrogenase.

1,1-disubstituted alkene **52**. The ensuing tertiary radical **LIII** was then quenched by a stereo-determining HAT step from flavin semiquinone **LII**.

Mechanistically, the two systems differ in that Zhao [62] proposed the photoactivity to arise from a ternary EDA complex **LIV** formed between substrate **51**, FMN_{hq}, and the ene-reductase. In contrast, Hyster's system was based on a quaternary EDA complex **LV** that also involved alkene **52**, as supported by spectroscopic studies [63].

9.4.2. Direct Photoexcitation Strategies in Enzymatic Catalysis

In analogy to photochemical strategies available to organocatalysis (discussed in Sections 9.2.4 and 9.2.5), it was found that the formation of an EDA complex in biocatalysis is not always needed to promote enantioselective photochemical processes. Recently, Hyster reported an enantioselective reduction enabled by direct photoexcitation of a flavin-dependent "ene"-reductase enzyme [64]. While acrylamides **54** are not suitable substrates for the ground-state reactivity of "ene" reductases, photoirradiation switched on a novel one-electron mechanism, leading to reduced chiral products **55** (Scheme 9.18).

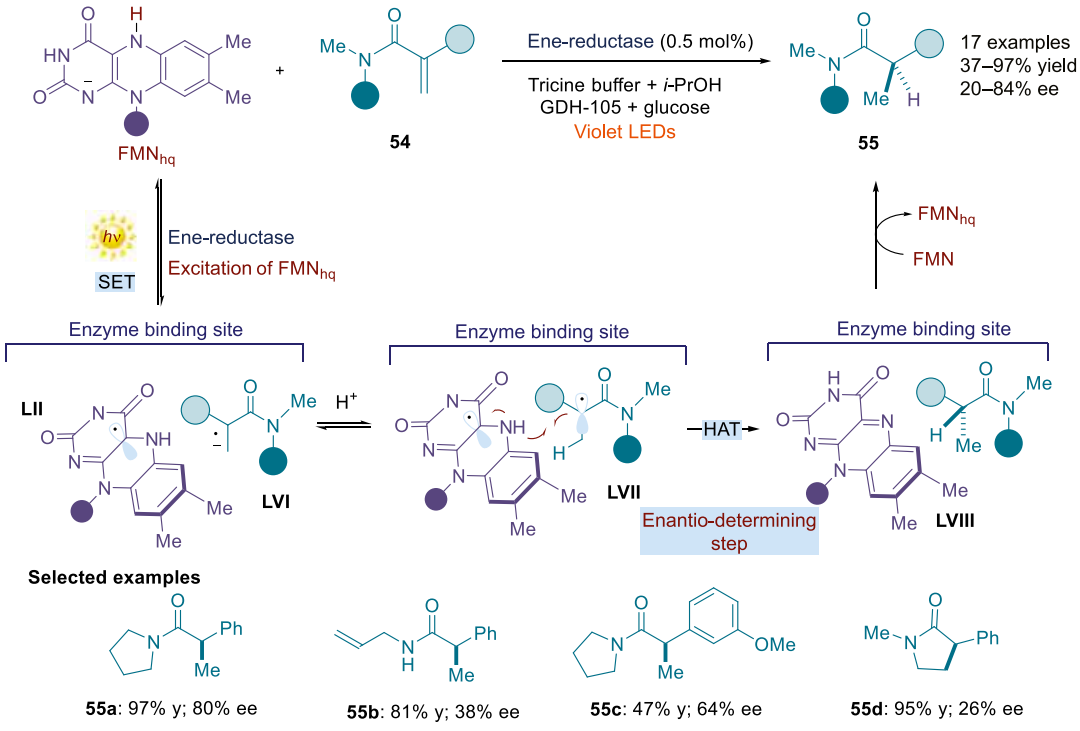

Scheme 9.18. Photoexcitation of flavin-dependent "ene"-reductases promotes the asymmetric reduction of acrylamides via an SET mechanism.

The FMN_{hq} cofactor present in "ene" reductases serves as the photochromic unit, which can directly absorb light. Indeed, its spectral characteristics remained unaltered when adding the substrate **54**, which implied that an EDA complex was not formed. Upon irradiation, the reaction proceeds by SET from the excited flavin cofactor, which acts as a reducing agent, to the alkene **54**. The ensuing radical anion intermediate **LVI** is protonated by solvent/acidic amino acids to afford **LVII**, which then proceeds to the rate-determining HAT step leading to product **55**.

9.5. METHODS BASED ON THE DIRECT EXCITATION OF SUBSTRATES

In addition to the photoexcitation of chiral catalytic intermediates, there is another strategy available to develop light-driven asymmetric radical processes, which relies on the direct excitation of light-responsive substrates. 1,4-Dihydropyridines **56**, also known as Hantzsch esters, proved particularly useful (Scheme 9.19). **56** is primarily understood as hydride (H^-) sources in its ground state [65]. In analogy to NAD(P)Hs [59], which are photoresponsive biological cofactors useful to develop photoenzymatic radical processes (see Section 9.4.1), also **56** can be excited with visible light to become a strong photo-reductant that can productively engage in SET manifolds [66]. This excited-state reactivity has been successfully used to develop an asymmetric radical allylation process (Scheme 9.19) [67].

Specifically, the photoexcited **56*** activated the chiral Rh(III)-substrate complex **LIX**, formed upon coordination of a chiral-at-rhodium complex **28** and the unsaturated substrate **57**. This SET reduction step provided the chiral β-enolate radical intermediate **LX**, which governed a stereoselective addition to allyl sulfones **58**. β-Scission within **LXI** yielded the allylation product **59**. Unexpectedly, product **60**, containing a β-sulfonyl group, was also formed. **60** arose from the trap of the sulfonyl radical **LXIII**, generated during the β-scission event, from the chiral Rh(III)-substrate complex **LIX**. Mechanistic studies revealed that the only photoactive species in this system was the Hantzsch ester **56**, which, on

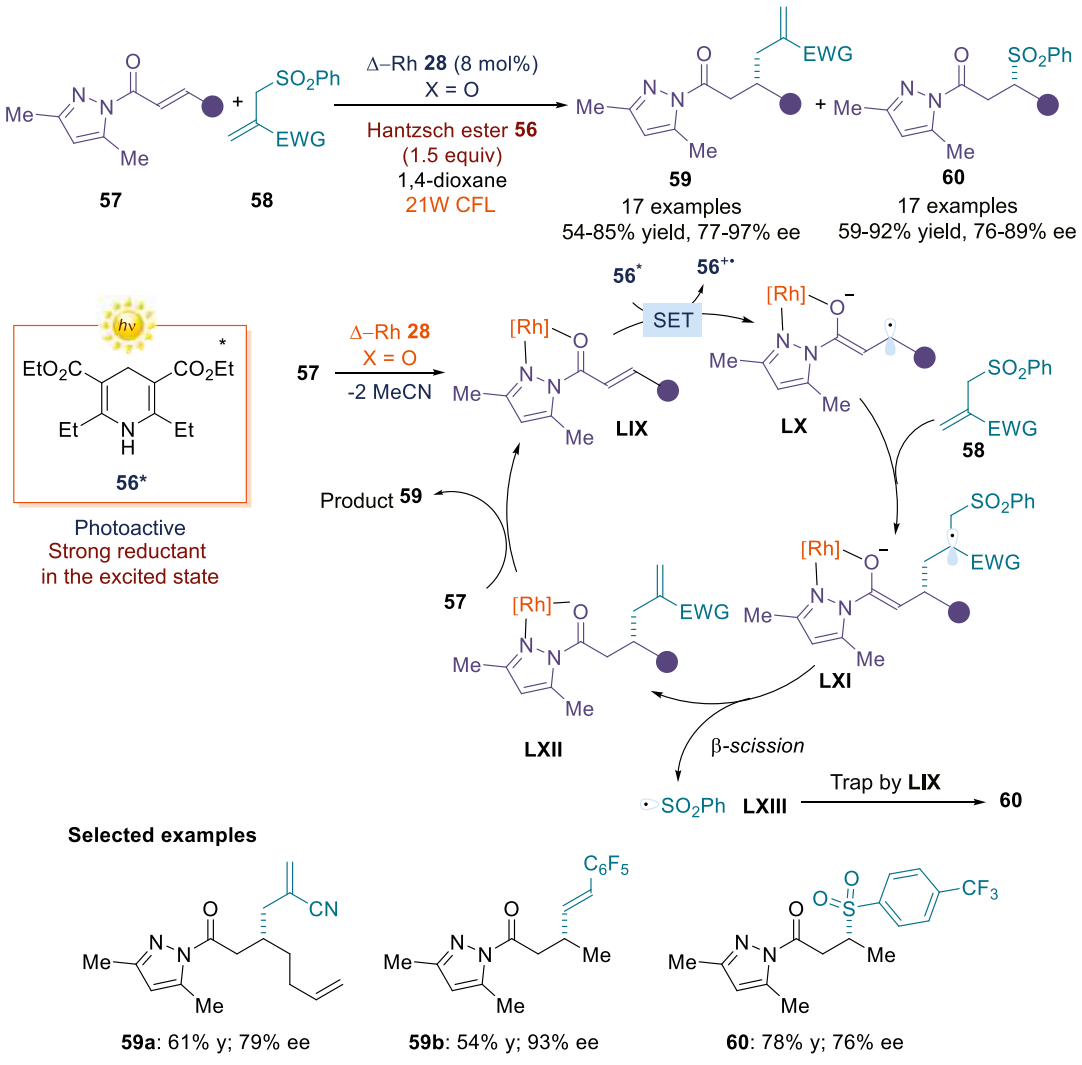

Scheme 9.19. Asymmetric β-allylation and β-sulfonylation of α,β-unsubstituted acyl pyrazoles triggered by the photoexcitation of Hantzsch ester **56**. CFL: compact fluorescent lamp.

excitation, triggered the whole process by promoting the SET step leading to the crucial chiral intermediate **LX**.

Recently, it was established that 4-substituted-1,4-dihydropyridines, which closely resemble the structure of Hantzsch ester **56**, can directly reach an electronically excited state upon light absorption, and trigger the generation of C-centered radicals without the need for an external photocatalyst [68]. This direct excitation strategy was also applied in asymmetric radical catalysis (Scheme 9.20). Specifically, an iminium-ion-based organocatalytic process was developed that accounts for the enantioselective acyl radical conjugate addition to enals **61**, affording valuable 1,4-dicarbonyl compounds **63** [69]. The process capitalizes upon the excited-state reactivity of 4-acyl-1,4-dihydropyridines **62** that, upon visible-light absorption, can trigger the generation of acyl radicals **LXIV**. By means of the chiral amine catalyst **27**, iminium ion activation of enals ensured a stereoselective radical trap. A moderate level of enantioselectivity was achieved with both aromatic- and aliphatic-substituted enals. Mechanistically, irradiance at 460 nm secured the selective excitation of the 4-acyl-1,4-dihydropyridine substrate **62**. The excitation of the transiently generated chiral iminium ion was not operative under these conditions, since this intermediate cannot absorb wavelengths longer than 430 nm.

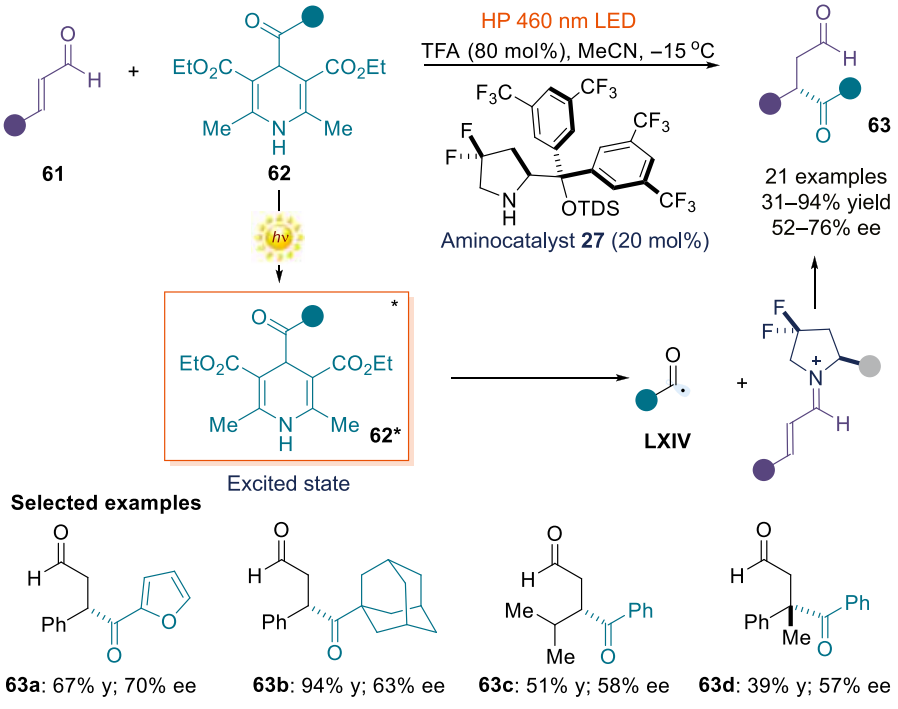

Scheme 9.20. Enantioselective acyl radical addition to enals to afford 1,4-dicarbonyl compounds **63** via photoexcitation of 4-acyl-1,4-dihydropyridines **62**. TDS: thexyl-dimethylsilyl.

A similar Lewis-acid-based catalytic system was recently developed that used a chiral octahedral cobalt(II) complex to activate α,β-unsubstituted acyl substrates and stereoselectively intercept acyl radicals, generated upon photoexcitation of 4-acyl-1,4-dihydropyridines **62** [70].

The excited-state reactivity of dihydropyridines was also used to develop an asymmetric nickel-catalyzed cross-coupling reaction [71]. Upon photoexcitation, the racemic 4-alkyl-1,4-dihydropyridines **64** can act simultaneously as a strong SET reductant, thus modulating the nickel oxidation state and securing catalyst turnover, and as a source of C-centered radicals **LXVII** (Scheme 9.21). The dual reactivity profile of the excited **64*** was used to implement an asymmetric cross-coupling process using symmetrical anhydrides **65** as electrophiles and bisoxazoline **67** as the chiral ligand. Mechanistically, the catalytically active Ni(0) intermediate **LXV** can readily undergo oxidative addition into the C(sp^2)-O bond of the anhydride **65**, generating a Ni(II)-acyl intermediate **LXVI** that captures the secondary alkyl radical **LXVII**. Formation of an electrophilic Ni(III) species **LXVIII** triggers a reductive elimination to afford the cross-coupling chiral ketone product **66**. The ensuing Ni(I) intermediate **LXIX** then undergoes SET reduction by the excited **64***, completing the nickel catalytic cycle while regenerating the C(sp^3) radical intermediate.

Few examples of symmetric catalytic transformations based on the photoexcitation of photochromic substrates other than 1,4-dihydropyridines have been recently reported [72]. It can be anticipated that other asymmetric catalytic methodologies will be developed based on the excited-state reactivity of photoactive compounds.

9.6. CONCLUSIONS

Over the last decade, the combination with light has created new opportunities to expand the synthetic applicability of asymmetric catalysis beyond conventional two-electron-pair reactivity patterns. These developments have been achieved by translating the generic mechanisms of activation, which govern the success of enantioselective polar catalysis, into the realm of excited-state reactivity and radical chemistry.

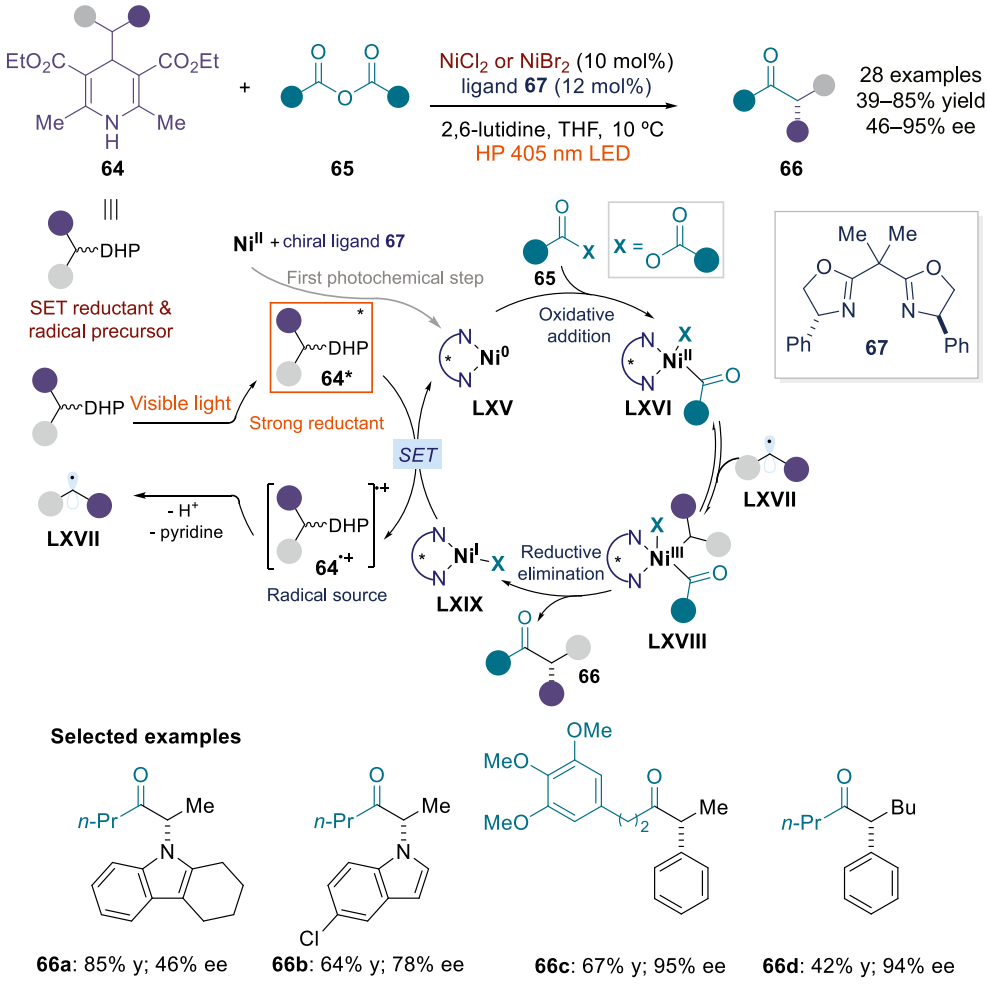

Scheme 9.21. Visible-light-driven asymmetric nickel-catalyzed acyl cross-coupling process.

The resulting photochemical methods provide new synthetic frameworks for making chiral molecules sustainably. But major developments are probably still to come. A force for innovation may arise by integrating the photochemical activity of chiral organocatalytic intermediates within metal-mediated catalytic cycles, which could enable unconventional mechanisms for stereocontrolled bond formation. This approach might also be useful for developing radical cascade processes, where the unique excited-state catalytic reactivities can be combined to provide powerful transformations for the one-step synthesis of complex chiral molecules. We also expect great strides in photochemical biocatalysis, which so far has been limited to a handful of applications based on the photoexcitation of specific cofactors in cofactor-dependent proteins to promote enantioselective radical processes. Given the many innovative reactivity concepts identified in the last decade thanks to the combination with light, the future of enantioselective catalysis looks bright.

ACKNOWLEDGMENTS

Research support from the European Research Council (ERC-2015-CoG 681840-CATA-LUX) and the Agencia Estatal de Investigación (PID2019-106278GB-I00) is gratefully acknowledged. D. Ma thanks the EU for a Horizon 2020 Marie Skłodowska-Curie Fellowship (IF-2019 894795).

REFERENCES

1. Noyori, R. Nat. Chem. **2009**, *1*, 5–6.
2. Walsh, P. J.; Kozlowski, M. C. Eds., Fundamental of Asymmetric Catalysis, University Science Books (**2009**).
3. Ojima, I. Ed. Catalytic Asymmetric Synthesis, 3; Wiley (**2010**).
4. Brimioulle, R.; Lenhart, D.; Maturi, M. M.; Bach, T. Angew. Chem., Int. Ed. **2015**, *54*, 3872–3890.
5. Turro, N. J.; Ramamurthy, V.; Scaiano, J. C. Eds., Modern Molecular Photochemistry of Organic Molecules, University Science Books (**2010**).
6. Foster, R. J. Phys. Chem. **1980**, *84*, 2135–2141.
7. Rosokha, S. V.; Kochi, J. K. Acc. Chem. Res. **2008**, *41*, 641–653.
8. Crisenza, G. E. M.; Mazzarella, D.; Melchiorre, P. J. Am. Chem. Soc. **2020**, *142*, 5461–5476.
9. MacMillan, D.W.C. Nature **2008**, *455*, 304–308.
10. List, B. Angew. Chem., Int. Ed. **2010**, *49*, 1730–1734.
11. Beeson, T. D.; Mastracchio, A.; Hong, J.-B.; Ashton, K.; MacMillan, D. W. C. Science **2007**, *316*, 582–585.
12. Nicewicz, D. A.; MacMillan, D. W. C. Science **2008**, *322*, 77–80.
13. Arceo, E.; Jurberg, I. D.; Álvarez-Fernández, A.; Melchiorre, P. Nat. Chem. **2013**, *5*, 750–756.
14. Bahamonde, A.; Melchiorre, P. J. Am. Chem. Soc. **2016**, *138*, 8019–8030.
15. Studer, A.; Curran, D. P. Angew. Chem., Int. Ed. **2016**, *55*, 58–102.
16. Silvi, M.; Melchiorre, P. Nature **2018**, *554*, 41–49.
17. Arceo, E.; Bahamonde, A.; Bergonzini, G.; Melchiorre, P. Chem. Sci. **2014**, *5*, 2438–2442.
18. Shirakawa, S.; Maruoka, K. Angew. Chem., Int. Ed. **2013**, *52*, 4312–4348.
19. Woźniak, Ł.; Murphy, J. J.; Melchiorre, P. J. Am. Chem. Soc. **2015**, *137*, 5678–5681.
20. Lelais, G.; MacMillan, D. W. C. Aldrichim. Acta **2006**, *39*, 79–87.
21. Cao, Z.-Y.; Ghosh, T.; Melchiorre, P. Nat. Commun. **2018**, *9*, 3274.
22. (a) Murphy, J. J.; Bastida, D.; Paria, S.; Fagnoni, M.; Melchiorre P. Nature **2016**, *532*, 218–222. (b) Bahamonde, A.; Murphy, J. J.; Savarese, M.; Bremond, E.; Cavalli, A.; Melchiorre, P. J. Am. Chem. Soc. **2017**, *139*, 4559–4567.
23. Quasdorf, K. W.; Overman, L. E. Nature **2014**, *516*, 181–191.
24. Morack, T.; Mück-Lichtenfeld, C.; Gilmour, R. Angew. Chem., Int. Ed. **2019**, *58*, 1208–1212.
25. Martínez-Gualda, A. M.; Domingo-Legarda, P.; Rigotti, R.; Díaz-Tendero, S.; Fraile, A.; Alemán, J. Chem. Commun. **2021**, *57*, 3046–3049.
26. Silvi, M.; Arceo, E.; Jurberg, I. D.; Cassani, C.; Melchiorre, P. J. Am. Chem. Soc. **2015**, *137*, 6120–6123.
27. (a) Cecere, G.; König, C. M.; Alleva, J. L.; MacMillan, D. W. C. J. Am. Chem. Soc. **2013**, *135*, 11521–11524. (b) Filippini, G.; Silvi, M.; Melchiorre, P. Angew. Chem., Int. Ed. **2017**, *56*, 4447–4451.
28. Silvi, M.; Verrier, C.; Rey, Y. P.; Buzzetti, L.; Melchiorre, P. Nat. Chem. **2017**, *9*, 868–873.
29. Mariano, P. S. Acc. Chem. Res. **1983**, *16*, 130–144.
30. Yoshida, J.; Kataoka, K.; Horcajada, R.; Nagaki, A. Chem. Rev. **2008**, *108*, 2265–2299.
31. Verrier, C.; Alandini, N.; Pezzetta, C.; Moliterno, M.; Buzzetti, L.; Hepburn, H. B.; Vega-Peñaloza, A.; Silvi, M.; Melchiorre, P. ACS Catal. **2018**, *8*, 1062–1066.
32. Mazzarella, D.; Crisenza, G. E. M.; Melchiorre, P. J. Am. Chem. Soc. **2018**, *140*, 8439–8443.
33. Miller, D. C.; Tarantino, K. T.; Knowles, R. R. Proton-coupled electron transfer in organic synthesis: fundamentals, applications and opportunities. In Topics in Current Chemistry. (Eds. Guillena, G., Ramón, D. J.), Vol. *374*. DOI: https://doi.org/10.1007/s41061-016-0030-6 Springer International Publishing, (**2016**).
34. Woźniak, Ł.; Magagnano, G.; Melchiorre, P. Angew. Chem., Int. Ed. **2018**, *57*, 1068–1072.
35. Bonilla, P.; Rey, Y. P.; Holden, C. M.; Melchiorre, P. Angew. Chem., Int. Ed. **2018**, *57*, 12819–12823.
36. (a) Zhang, L.; Meggers, E. Acc. Chem. Res. **2017**, *50*, 320–330. (b) Huang, X.; Meggers, E. Acc. Chem. Res. **2019**, *52*, 833–847.
37. Huo, H.; Shen, X.; Wang, C.; Zhang, L.; Röse, P.; Chen, L.-A.; Harms, K.; Marsch, M.; Hilt, G.; Meggers, E. Nature **2014**, *515*, 100–103.
38. Ma, J.; Rosales, A. R.; Huang, X.; Harms, K.; Riedel, R.; Wiest, O.; Meggers, E. J. Am. Chem. Soc. **2017**, *139*, 17245–17248.
39. Fernandez-Alvarez, V. M.; Maseras, F. Org. Biomol. Chem. **2017**, *15*, 8641–8647.
40. Huo, H.; Wang, C.; Harms, K.; Meggers, E. J. Am. Chem. Soc. **2015**, *137*, 9551–9554.
41. Huo, H.; Huang, X.; Shen, X.; Harms, K.; Meggers, E. Synlett **2016**, *27*, 749–753.
42. Shen, X.; Harms, K.; Marsch, M.; Meggers, E. Chem. Eur. J. **2016**, *22*, 9102–9105.
43. Wang, C.; Qin, J.; Shen, X.; Riedel, R.; Harms, K.; Meggers, E. Angew. Chem., Int. Ed. **2016**, *55*, 685–688.
44. (a) Huang, X.; Lin, J.; Shen, T.; Harms, K.; Marchini, M.; Ceroni, P.; Meggers, E. Angew. Chem., Int. Ed. **2018**, *57*, 5454–5458. (b) Zhou, Z.; Nie, X.; Harms, K.; Riedel, R.; Zhang, L.; Meggers, E. Sci. China: Chem. **2019**, *62*, 1512–1518.
45. Lin, S.-X.; Sun, G.-J.; Kang, Q. Chem. Commun. **2017**, *53*, 7665–7668.
46. (a) Ma, J.; Lin, J.; Zhao, L.; Harms, K.; Marsch, M.; Xie, X.; Meggers, E. Angew. Chem., Int. Ed. **2018**, *57*, 11193–11197. (b) De Assis, F. F.; Huang, X.; Akiyama, M.; Pilli, R. A.; Meggers, E. J. Org. Chem. **2018**, *83*, 10922–10932. (c) Chen, L.; Hu, L.; Du, Y.; Su, W.; Kang, Q. Chin. J. Org. Chem. **2020**, *40*, 3944–3952.

47. Shen, X.; Li, Y.; Wen, Z.; Cao, S.; Hou, X.; Gong, L. Chem. Sci. **2018**, *9*, 4562–4568.
48. Parasram, M.; Gevorgyan, V. Chem. Soc. Rev. **2017**, *46*, 6227–6240.
49. Kainz, Q. M.; Matier, C. D.; Bartoszewicz, A.; Zultanski, S. L.; Peters, J. C.; Fu, G. C. Science **2016**, *351*, 681–684.
50. (a) Li, Y.; Zhou, K.; Wen, Z.; Cao, S.; Shen, X.; Lei, M.; Gong, L. J. Am. Chem. Soc. **2018**, *140*, 15850–15858. (b) Han, B.; Li, Y.; Yu, Y.; Gong, L. Nat. Commun. **2019**, *10*, 3804–3812. (c) Xia, H. Li, Z.; Gu, Q.; Dong, X.; Fang, J.; Du, X.; Wang, L.; Liu, X. Angew. Chem., Int. Ed. **2020**, *59*, 16926–16932.
51. Crisenza, G. E. M.; Faraone, A.; Gandolfo, E.; Mazzarella, D.; Melchiorre, P. Nat. Chem. **2021**, *13*, 575–580.
52. Rössler, S. L.; Petrone, D. A.; Carreira, E. M. Acc. Chem. Res. **2019**, *52*, 2657–2672.
53. Rössler, S. L.; Krautwald, S.; Carreira, E. M. J. Am. Chem. Soc. **2017**, *139*, 3603–3606.
54. (a)Chen, K.; Arnold, F. H. Nat. Catal. **2020**, *3*, 203–213;(b) Hyster, T. K.; Ward, T. R. Angew. Chem., Int. Ed. **2016**, *55*, 7344–7357.
55. Arnold, F. H. Angew. Chem., Int. Ed. **2019**, *58*, 14420–14426.
56. Hyster, T. K. Synlett **2020**, 248–254.
57. Emmanuel, M. A.; Greenberg, N. R.; Oblinsky, D. G.; Hyster, T. K. Nature **2016**, *540*, 414–417.
58. Huisman, G. W.; Liang, J.; Krebber, A. Curr. Opin. Chem. Biol. **2009**, *14*, 1–8.
59. Fukuzumi, S.; Hironaka, K.; Tanaka, T. J. Am. Chem. Soc. **1983**, *105*, 4722–4727.
60. Biegasiewicz, K. F.; Cooper, S. J.; Gao, X.; Oblinsky, D. G.; Kim, J. H.; Garfinkle, S. E.; Joyce, L. A.; Sandoval, B. A.; Scholes, G. D.; Hyster, T. K. Science **2019**, *364*, 1166–1169.
61. Clayman, P. D.; Hyster, T. K. J. Am. Chem. Soc. **2020**, *142*, 15673–15677.
62. Huang, X.; Wang, B.; Wang, Y.; Jiang, G.; Feng, J.; Zhao, H. Nature **2020**, *584*, 69–74.
63. Page, C. G.; Cooper, S. J.; DeHovitz, J. S.; Oblinsky, D. G.; Biegasiewicz, K. F.; Antropow, A. H.; Armbrust, K. W.; Ellis, J. M.; Hamann, L. G.; Horn E. J.; Oberg, K. M.; Scholes, G. D.; Hyster T. K. J. Am. Chem. Soc. **2021**, *143*, 97–102.
64. Sandoval, B.A.; Clayman, P. D.; Oblinsky, D. G.; Oh, S.; Nakano, Y.; Bird, M.; Scholes, G. D.; Hyster, T. D. J. Am. Chem. Soc. **2021**, *143*, 1735–1739.
65. Zheng, C.; You, S.-L. Chem. Soc. Rev. **2012**, *41*, 2498–2518.
66. (a) Cheng, X.; Huang, W. Synlett **2017**, *28*, 148–158. (b) Panferova, L. I.; Tsymbal, A. V.; Levin, V. V.; Struchkova, M. I.; Dilman, A. D. Org. Lett. **2016**, *18*, 996–999.
67. Huang, X.; Luo, S.; Burghaus, O.; Webster, R. D.; Harms, K.; Meggers, E. Chem. Sci. **2017**, *8*, 7126–7131.
68. Buzzetti, L.; Prieto, A.; Raha Roy, S.; Melchiorre, P. Angew. Chem., Int. Ed. **2017**, *56*, 15039–15043.
69. Goti, G.; Bieszczad, B.; Vega-Peñaloza, A.; Melchiorre, P. Angew. Chem., Int. Ed. **2019**, *58*, 1213–1217.
70. Zhang, K.; Lu, L.-Q.; Jia, Y.; Wang, Y.; Lu, F.-D.; Pan, F.; Xiao, W.-J. Angew. Chem., Int. Ed. **2019**, *58*, 13375–13379.
71. Gandolfo, E.; Tang, X.; Raha Roy, S.; Melchiorre, P. Angew. Chem., Int. Ed. **2019**, *58*, 16854–16858.
72. Li, F.; Tian, D.; Fan, Y.; Lee, R.; Lu, G.; Yin, Y.; Qiao, B.; Zhao, X; Xiao, Z.; Jiang, Z. Nat. Commun. **2019**, *10*, 1774.

10

ENANTIOSELECTIVE PHOTOCHEMICAL [2+2] CYCLOADDITION REACTIONS

Freya M. Harvey and Thorsten Bach
School of Natural Sciences, Department Chemie and Catalysis Research Center (CRC), Technische Universität München, Garching, Germany

10.1. INTRODUCTION

Investigations into ground-state enantioselective reactions began in the early 1900s [1], and a variety of methods to access enantiopure chemicals using ground-state chemistry are available today. However, enantioselective photochemical reactions that afford products with >80% enantiomeric excess (ee) have only been reported in the past two decades [2]. *Catalytic* enantioselective photochemical reactions are an even more recent achievement [3–11]. These photochemical techniques have required more time to develop than their ground-state counterparts because photochemical reactions are inherently difficult to control. When an organic molecule absorbs a photon, highly reactive intermediates are generated, and channeling these intermediates into a selective reaction mode presents a considerable challenge.

Initial research into enantioselective photochemistry involved the use of circularly polarized light [12, 13], chiral sensitizers [14–17], or chiral solvents [18–20] to try to induce an ee in the product [21, 22]. Unfortunately, these attempts saw only limited success.

To achieve catalytic [2+2] photocycloadditions with a high ee, novel catalysts had to be designed, which could circumvent or even exploit the particularities of photochemical reactions. One of the most important features in a catalyst is that it must activate the bound substrate toward the reaction, so that the transformation takes place only within the chiral environment of the catalyst. It must also remain bound to the substrate for the duration of the reaction: if the catalyst detaches from the substrate once it has been activated, the photoproduct will form racemically. However, the catalyst must not bind so strongly that it cannot release the product.

A range of catalysts that meet these requirements have been developed recently. In this chapter, we have gathered examples of enantioselective, catalytic [2+2] photocycloaddition reactions that afford photoproducts with ees of over 80%. Photocycloaddition reactions to arenes, so-called *ortho*-photocycloaddition reactions, were excluded, as they are beyond the scope of the chapter (we refer the interested reader to some recent examples [23, 24] and reviews [25, 26]). The enantioselective catalytic [2+2] photocycloadditions have been organized by catalyst type, beginning with organocatalysts, followed by metal catalysts, then dual catalysis, and finally, an example of catalysis with a metal-organic cage (MOC).

Catalytic Asymmetric Synthesis, Fourth Edition. Edited by Takahiko Akiyama and Iwao Ojima.

10.2. CHIRAL ORGANOCATALYSTS

Organocatalysts for catalytic enantioselective reactions have enjoyed great success for many types of transformations over the past three decades [27]. They exploit reversible interactions with the substrate, ensuring that only the molecules bound to the catalyst can react. The transformation takes place within the chiral environment of the catalyst to afford enantioenriched products. Given the longstanding success of organocatalysis and the vast knowledge base on this subject, it is not surprising that the first example of an enantioselective [2+2] photocycloaddition was achieved using a chiral organocatalyst.

10.2.1. Xanthone and Thioxanthone

In previous work, chiral templates (+)–**1** and (−)-*ent*–**1** had been developed for the enantioselective [2+2] photocycloaddition of quinolones such as **2** (Figure 10.1) [28]. The templates can bind to the substrate via two hydrogen bonds, and they remain bound together throughout the reaction. This provides some much-needed control over the reactive photochemical intermediate: trapped within the chiral environment of the catalyst, upon irradiation with 366 nm light, photoproduct **3** was formed in good yield and 93% ee. The enantioselectivity arises from the bulky benzoxazole moiety of the template, which effectively blocks one face of the quinolone from reacting with the alkene [28].

Even though this system afforded the products with high ee, there was one drawback: superstoichiometric amounts of the template (2.6 eq.) were required to ensure that no unbound substrate was present in the reaction mixture. If (−)-*ent*–**1** was used in smaller amounts, unbound substrate molecules reacted to give the product in racemic form, diluting the ee of the final product [28].

It was hypothesized that, if the template also served as a photosensitizer, the cycloaddition would proceed only for the substrates that were bound to the template, because photosensitization is a distance-dependent phenomenon. Thus, the template could be used in catalytic amounts.

Based on this idea, xanthone catalysts (+)–**4** and (−)-*ent*–**4** were developed, and the first catalytic enantioselective [2+2] photocycloaddition of alkene-tethered quinolones **5** was reported in 2009 (Figure 10.2, r.r. = ratio of regioisomers) [29, 30]. The bulky xanthone backbone not only serves as a shield for

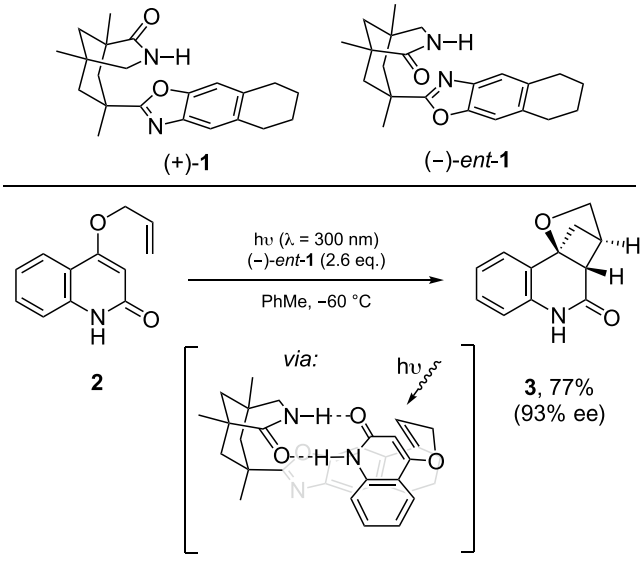

Figure 10.1. Stoichiometric amounts of template (−)-*ent*–**1** can bind to quinolone **2**, so that it reacts enantioselectively to form **3**. Source: [28].

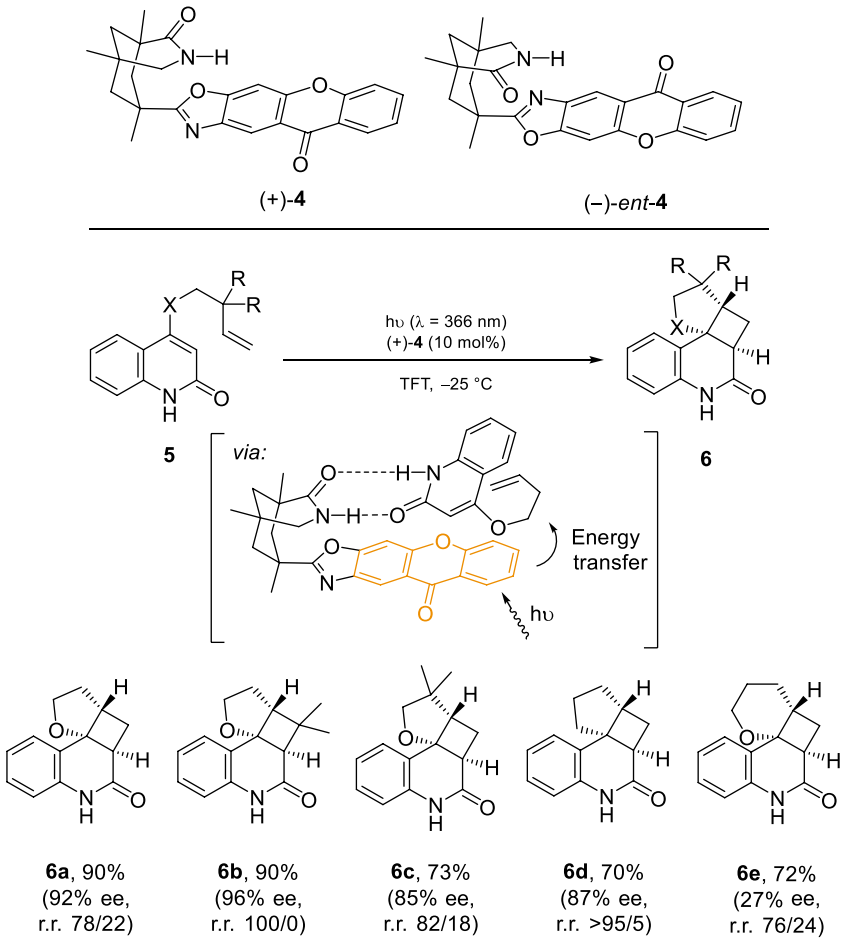

Figure 10.2. Catalyst (+)-**4** transfers triplet energy preferentially to the bound substrates, enabling a catalytic enantioselective reaction. Source: [29, 30].

enantioface differentiation, but also as a sensitizer, enabling triplet energy transfer to the bound substrate. Quinolones such as **5**, able to bind to (+)–**4** via hydrogen-bonding, reacted to give the cyclobutane products **6** in good to excellent yields with ees of up to 96% in the presence of 10 mol% of catalyst [29, 30].

Irradiation at 366 nm allows for selective excitation of the catalyst, which transfers its triplet energy (measured at 316 kJ mol^{-1} in pentane/isopentane) [31] to the bound quinolone substrate (triplet energy of over 270 kJ mol^{-1}) [32]. In most cases, small amounts of the crossed regioisomer are also formed. Trifluorotoluene (TFT) was found to be the ideal solvent, because reactions can be conducted at low temperature (unlike in benzene). The low temperature (–25 °C) and low polarity of TFT improved hydrogen-bonding to the catalyst, which was important for reaching high ees [33]. TFT is also compatible with the high triplet energy of **4**: indeed, **4** is very reactive, especially toward hydrogen abstraction. Solvents like toluene with abstractable benzylic hydrogen atoms were unsuitable. Even in TFT, prolonged reaction times led to lowered product yields and degradation of the catalyst due to hydrogen abstraction from the products themselves. It was important to stop the reaction once full conversion (or close to full conversion) was reached.

In further studies of quinolone substrates [30, 33], the impact of the cycloaddition rate constant on the ee became apparent. Although similar in structure, cyclobutane **6a** was obtained in much higher ee than **6e** (Figure 10.2). This substrate-dependent enantioselectivity can be explained by the slower cyclization

rate of the quinolone precursor of **6e** compared to that of **6a** (the rate constants were estimated at 4.5×10^7 s^{-1} [lower limit] for **6a** and 1.7×10^7 s^{-1} for **6e** using laser-flash photolysis experiments). Following energy transfer, an excited intermediate with biradical character localized over the reactive quinolone double bond is obtained. This triplet precursor to **6e** is so slow to cyclize that dissociation from the catalyst often occurs before the C–C bond can form. The biradical cyclizes to **6e** in a racemic fashion, away from the chiral environment of the catalyst. In contrast, the rapid cycloaddition to **6a** takes place while the triplet intermediate is still bound to the catalyst to afford the photoadduct in high ee.

It was also noted that changes in the structure of the quinolones could shift their absorption into the wavelength range used to irradiate the catalyst (366 nm). In these cases, lower ee was observed due to the racemic background reaction of the unbound substrate. This problem could be solved simply by reducing the number of fluorescent lamps used for the reaction (lowering the photon flux): catalyst **4** has a much larger molar absorption coefficient ($\varepsilon_{360} \geq 3000$ l mol^{-1} cm^{-1}) than the quinolones ($\varepsilon_{360} = 144$ l mol^{-1} cm^{-1}), allowing it to harvest all of the photons in the reaction medium before they can reach the unbound quinolone. Good enantioselectivities were obtained using a lower photon flux for quinolones with a racemic background reaction [30, 33].

To confirm the triplet mechanism, the catalytic [2+2] photocycloaddition was performed on isomeric compounds **7** and **8**, with an *E* or *Z* configuration at the double bond (Figure 10.3, d.r. = ratio of diastereoisomers) [30, 33].

Since triplet reactions proceed via a long-lived biradical intermediate **9**, which must undergo intersystem crossing (ISC) prior to ring closure, the geometric information in the double bond is lost over the course of the reaction. *E* and *Z* starting materials should provide the same cycloaddition product; in other words, the reaction for **7** and **8** should be stereoconvergent. Indeed, this is what was observed: **10a** was obtained as the major product starting from either **7** or **8** (d.r. of 85/15 for **7** and of 88/12 for **8**).

Despite the triplet state intermediates being generally considered as long-lived, their lifetime is only in the picosecond to nanosecond range. This renders bimolecular reactions difficult, because the intermediates usually relax to the ground state before they can encounter a reaction partner. For this reason, the literature was dominated by intramolecular reactions until recently.

The first intermolecular variant of a catalyzed enantioselective [2+2] photocycloaddition was achieved with 2-pyridones **11** and acetylenedicarboxylates (Figure 10.4) [34]. At –65 °C in a mixture of hexafluoro-*m*-xylene (HFX) and TFT, ees of up to 92% could be obtained with 2.5 or 5 mol% of catalyst loading [34].

For many years, it seemed that the short lifetimes of singlet intermediates were essential for reaching high enantioselectivities in intermolecular photochemical reactions. Triplet reactions, with their

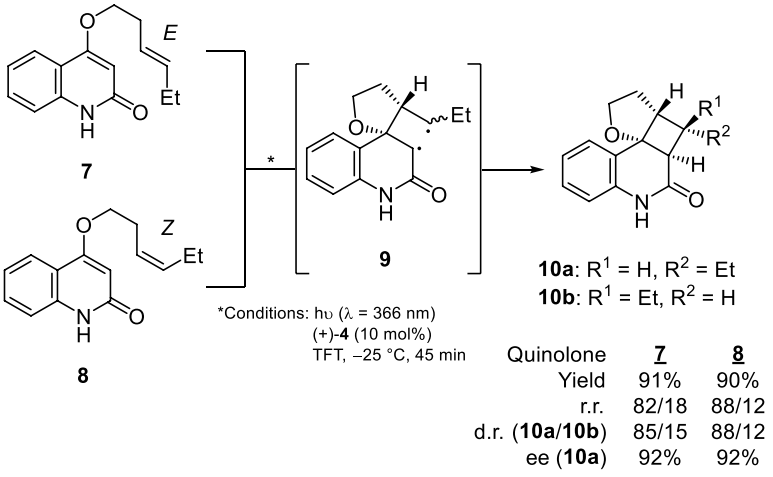

Figure 10.3. *E* and *Z* alkenes afford almost the same d.r. of cyclobutane product **10**, which supports a triplet mechanism via intermediate **9**. Source: [30, 33].

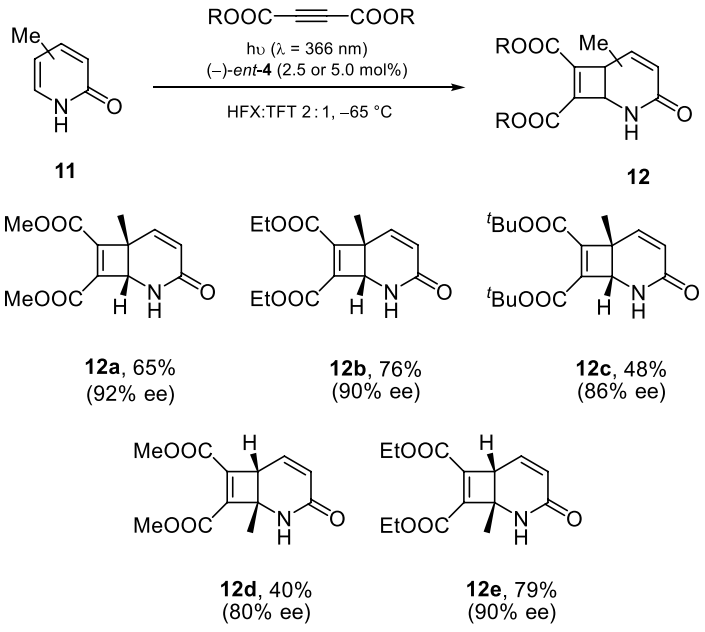

Figure 10.4. The first intermolecular catalytic enantioselective [2+2] photocycloaddition was developed with 2-pyridones **11** and acetylenedicarboxylates. Cyclobutanes **12a–e** were obtained in good yields and ees of up to 92%. Source: [34].

longer-lived biradical intermediates, were thought to react with little to no selectivity. However, with this work, it was shown that triplet reactions can in fact proceed with high enantioselectivities.

The requirements for obtaining high chemo- and enantioselectivities in organocatalyzed [2+2] photocycloadditions by triplet energy transfer can be summarized as follows:

(1) The triplet energy of the substrate must be lower than the triplet energy of the catalyst to ensure efficient triplet energy transfer.
(2) To avoid a racemic background reaction, the free substrate must not absorb at the same wavelength as the catalyst – there must be no spectral overlap between the substrate and catalyst at the irradiation wavelength.
(3) The catalyst must effectively block one face of the substrate from reacting with the alkene or alkyne partner.
(4) The rate constant of the intramolecular [2+2]-photocycloaddition must be higher than the rate constant of dissociation from the catalyst.
(5) The substrate must bind efficiently to the catalyst. Hydrogen-bonding is strongest at low temperatures in a non-polar solvent such as TFT (–25 °C) or in a mixture of TFT and HFX (–65 °C).

As mentioned above, in most cases, the reaction had to be monitored carefully and stopped as soon as full conversion was reached. This was necessary to limit decomposition of the products due to hydrogen abstraction by the catalyst. It was usually not possible to recover the catalyst in full.

This issue was overcome with the development of chiral thioxanthone catalysts (+)–**13** and (–)-*ent*–**13** (Figure 10.5) [35]. Compared to xanthone catalyst **4**, **13** has a lower triplet energy and absorbs visible light. It is much more photostable and less prone to decomposition by hydrogen abstraction.

In the presence of 10 mol% of thioxanthone (+)–**13** and upon irradiation with visible light, quinolones **14** underwent a clean intramolecular [2+2] photocycloaddition to afford the cycloadducts **15a–h** in excellent yields and up to 99% ee [32, 35].

The substrate scope included 3-alkylquinolones with 4-*O*-tethered alkenes to afford products **15e–h** [32]. It was previously assumed that the alkyl moiety in the α-position of these substrates would hinder coordination to the catalyst, and result in low ee of the products. However, it was found that the

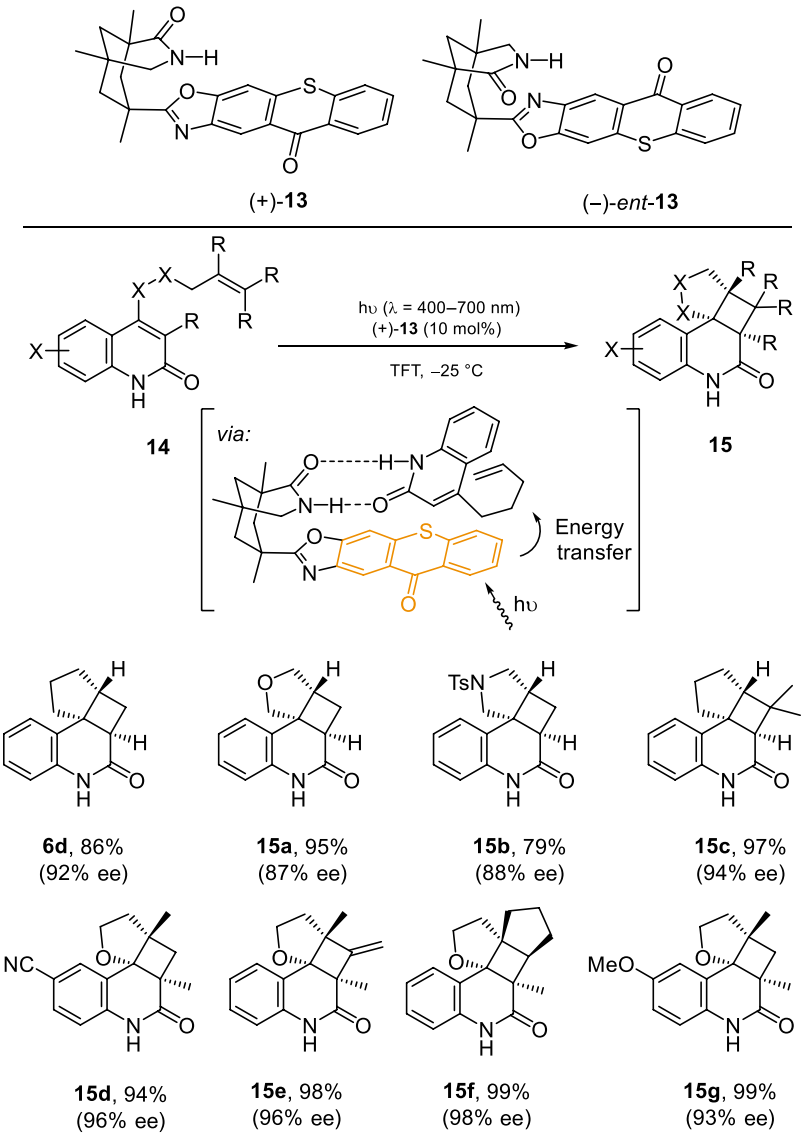

Figure 10.5. Thioxanthone catalyst (+)–**13** absorbs visible light and can be used to sensitize the intramolecular enantioselective [2+2] photocycloaddition of quinolones and 3-alkylquinolones. Source: [32, 35].

α-substituent does not impair binding to the catalyst, and instead lowers the triplet energy of the quinolones significantly: a difference of $\Delta E_T \approx 25$ kJ mol^{-1} was measured compared to the 3-unsubstituted 4-alkenyloxyquinolones. This allows the reaction to be carried out with catalyst **13**, whereas 3-unsubstituted 4-alkenyloxyquinolones required higher-energy catalyst **4** for the transformation. Notably, the reaction also took place with allenes to afford cyclobutanes such as **15f** with an exocyclic double bond.

The stereoconvergent reaction of quinolones bearing either *E* or *Z* alkenes supported a triplet mechanism. Detailed mechanistic studies by the groups of Yu [36] and Liao [37] confirmed this, and shed light on the individual bond-forming steps and the origin of the enantioselectivity.

An intermolecular variant of the reaction using thioxanthone catalyst (+)–**13** was developed with quinolones **16** and electron-deficient alkenes [38]. At an irradiation wavelength of 419 nm, photoadducts **17** could be obtained in high yields and with ees of up to 95% (Figure 10.6).

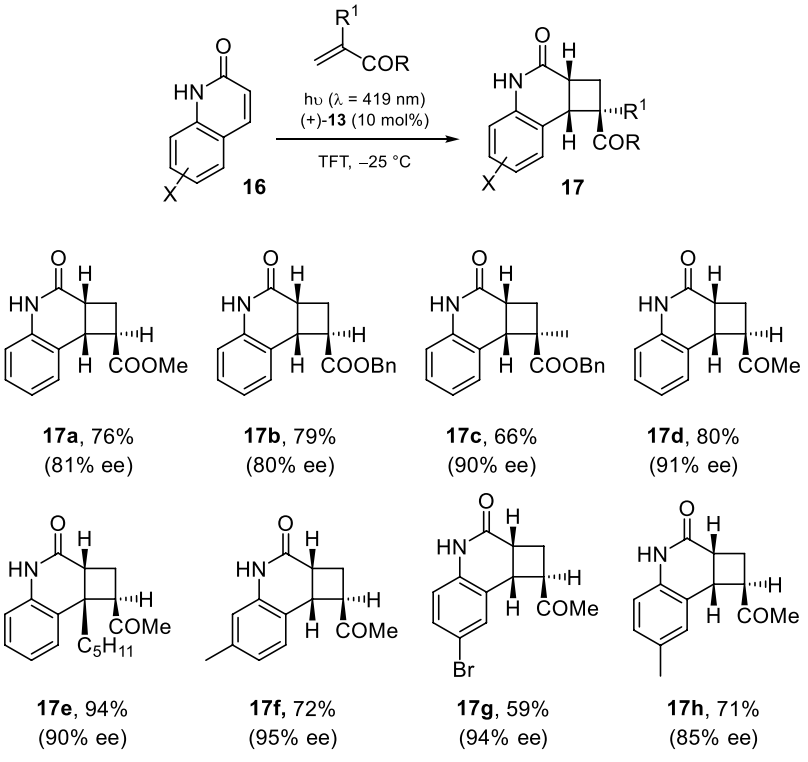

Figure 10.6. Catalyst (+)–**13** sensitizes the enantioselective intermolecular [2+2] photocycloaddition of quinolones and electron-deficient alkenes. Source: [38].

The reaction could also be conducted under solar irradiation with the use of an $Fe_2(SO_4)_3$ solution to filter ultraviolet (UV) light and suppress the racemic background reaction.

10.2.2. Thioureas

Another class of hydrogen-bonding organocatalysts that have found success in [2+2] photocycloadditions are thiourea catalysts such as **18** (Figure 10.7). Atropoisomeric thiourea **18**, developed by Sivaguru and co-workers, can hydrogen-bond efficiently to 4-alkenyl-substituted coumarins **19**. When irradiated with 350 nm light, [2+2] photocycloaddition takes place on the triplet energy surface to afford cyclobutanes **20** with high ees (88–94%) at low catalyst loadings (1–10 mol%) [39, 40].

In contrast to catalysts **4** and **13**, thiourea **18** works by forming an exciplex with the coumarin, rather than by energy transfer to the substrate. (The catalyst's excited-state energy is in fact lower than that of the coumarin substrates, which precludes an energy transfer mechanism.) At lower catalyst loading, when bound together, the catalyst–substrate complex absorbs at longer wavelengths than the catalyst or substrate alone. Thus, the complex can be excited preferentially by irradiating at a suitable wavelength (350 nm), and it reacts to give the enantioenriched photoproducts. The authors found that at higher catalyst loading, the reaction mechanism changes slightly: the unbound catalyst absorbs light first (because of its high optical density), and then binds to the substrate. The excited-state energy is then shared between the catalyst and the substrate to form the exciplex [39, 40].

In 2016, the intramolecular [2+2] photocycloaddition of 2,3-dihydropyridone-5-carboxylates was reported in the presence of a chiral bisthiourea catalyst [41]. However, catalyst loadings of 50 mol% were required to reach a modest ee of 56%. Interestingly, in the presence of 10 mol% of thioxanthone as the triplet sensitizer, the ee improved to 75%.

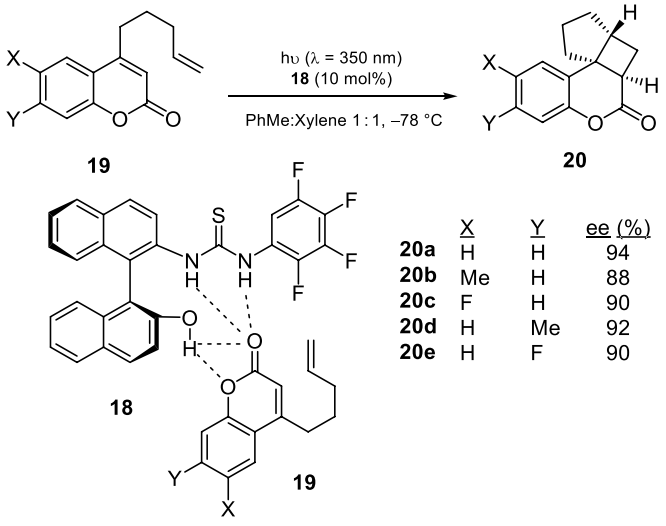

	X	Y	ee (%)
20a	H	H	94
20b	Me	H	88
20c	F	H	90
20d	H	Me	92
20e	H	F	90

Figure 10.7. Thiourea **18** binds to coumarins **19** and catalyzes their intramolecular enantioselective [2+2] photocycloaddition to afford cyclobutanes **20. Source:** [39, 40].

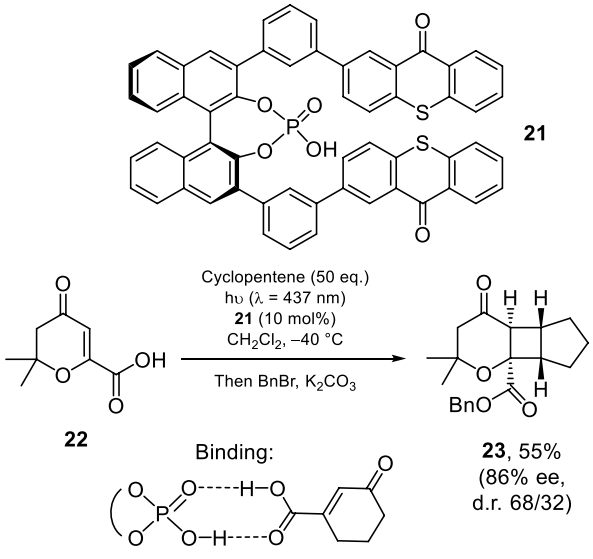

Figure 10.8. Chiral phosphoric acid **21** binds to β-carboxyl-substituted cyclic enone **22** and catalyzes its intermolecular enantioselective [2+2] photocycloaddition to afford cyclobutane **23.** Source: [42].

10.2.3. Brønsted Acids

A third class of catalysts which exploit hydrogen-bonding interactions with the substrate are chiral phosphoric acid catalysts. In 2020, catalyst **21** was prepared (Figure 10.8), which bears a 2,2′-binaphthol core and two thioxanthone moieties as light-harvesting antennas [42]. **21** is well-suited for binding with β-carboxyl-substituted cyclic enones such as **22**. Upon irradiation with visible light, cycloadduct **23** could be obtained in good yields and 86% ee with 10 mol% catalyst loading.

The carboxylic acid moiety of the substrate binds to **21** via two hydrogen bonds. Preliminary density functional theory (DFT) calculations showed that the enantioselectivity arises from shielding of one face of the substrate with one of the sensitizing thioxanthone units.

The catalyst's triplet energy was surprisingly low ($E_T = 235$ kJ mol^{-1}, 77 K, CH_2Cl_2), lower than the free carboxylic acid substrate's triplet energy. Thus, it was suspected that binding to the catalyst alters the substrate's triplet energy level, allowing for efficient energy transfer from **21** [42].

Catalyst **21** has recently been applied with great success to the enantioselective [2+2] photocycloaddition of eniminium ions in the triplet state, which is discussed in more detail in Section 10.4.2.2.

10.2.4. Iminium Ions

Amines have been used as organocatalysts with great success in ground-state chemistry: they can reversibly form iminium ions upon condensation with enones or α,β-unsaturated aldehydes to catalyze a variety of reactions. If a chiral amine is used, products can form with high ee [43, 44]. In 2001, Mariano's group carried out a [2+2] photocycloaddition with a pre-formed chiral eniminium ion (stoichiometric amounts of amine) obtained from a 3-alkenyloxy-2-cycloalkenone to afford a cycloadduct with up to 82% ee [45]. More recently, Melchiorre and co-workers reported the enantioselective photochemical β-alkylation of enals via a chiral iminium ion, using catalytic amounts of a pyrrolidine-based catalyst. They observed a bathochromic shift in the absorption spectrum of the iminium ion relative to the parent enal, which allowed them to irradiate it selectively using visible light [46]. Unfortunately, unlike enals, chiral iminium ions derived from enones cannot be excited selectively: enones have an n–π* transition at around the same wavelength as the π–π* transition of the iminium ion, and irradiating at this wavelength gives rise to a significant background reaction and diluted ees [47].

Alemán and co-workers found an innovative solution to this problem: they imagined that, if they used an electron-rich chiral amine to form the iminium ion, a charge-transfer complex would form with the electron-poor iminium moiety, generating with it a new absorption band at longer wavelengths. Thus, by irradiating at this wavelength, the charge-transfer complex could be excited selectively over the enone, enabling a catalytic enantioselective reaction.

Based on this idea, in 2020, Rigotti et al. reported the first aminocatalytic enantioselective [2+2] photocycloaddition of enones and alkenes using chiral diamine catalyst **24** [47]. The reaction takes place via an intermediate charge-transfer complex **27** to afford cyclobutane **26** in excellent yield and 80% ee (Figure 10.9).

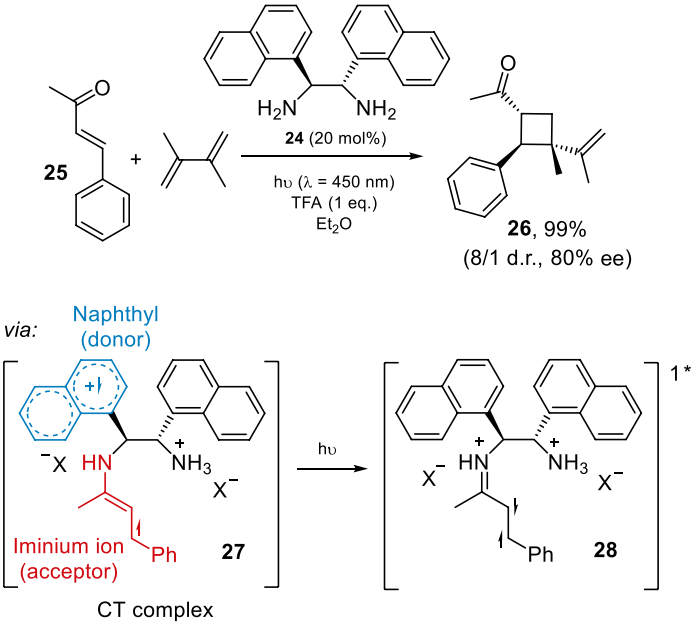

Figure 10.9. Chiral diamine **24** generates an intermediate charge-transfer complex **27** with enone **25**, which absorbs visible light and allows for the enantioselective synthesis of cyclobutane **26.** Source: [47].

When diamine **24** reacts with enone **25** to give an iminium ion, a charge-transfer interaction is generated between the electron-rich naphthyl ring and the electron-poor iminium moiety. The charge-transfer complex **27** absorbs in the visible light region, allowing for its selective excitation by irradiation with blue light-emitting diodes (LEDs). Once it reaches the singlet excited state, the complex equilibrates thermally on the singlet energy surface to give intermediate **28**, which undergoes a [2+2] cycloaddition with the diene. Hydrolysis of the iminium ion regenerates the diamine catalyst and liberates cyclobutane **26**. A range of enones and alkenes were tolerated, affording the cyclobutanes in high yields and good enantiomeric ratios [47].

In the presence of a triplet sensitizer, different diastereomeric ratios were observed in the product mixture, confirming that the reaction proceeds on the singlet energy surface. Indeed, ISC to the triplet state is known to be slow for iminium ions, and these species usually react via the singlet state unless sensitized. This concept is explained in more detail in Section 10.4.2.2.

10.3. CHIRAL METAL CATALYSTS

While organic molecules have certainly proven their worth as catalysts and triplet sensitizers, metallic photocatalysts have become increasingly popular in recent years [48, 49]. They present several advantages over organocatalysts: they are more photostable; their reactivity is easily optimized by modifying the ligands around the metal center; and the catalyst loadings required to obtain high ees tend to be lower than for organocatalysts [50]. These catalysts are composed of ligands and a metal atom, and both components can be used for binding to the substrate and for introducing chirality. The substrate can coordinate directly to the metal center, or to a ligand bearing a hydrogen-bonding moiety. Chirality can be introduced with a chiral-at-metal catalyst, or by using chiral ligands. This array of options for building catalytic systems has resulted in a variety of examples in the literature, all employing a unique method to afford cyclobutanes with high ees.

10.3.1. Transition Metals and Lanthanides

In 2017, Yoon and co-workers reported an enantioselective [2+2] photocycloaddition reaction using chiral-at-metal iridium complex **29** (Figure 10.10) [51]. The complex serves as a highly efficient enantioselective triplet sensitizer, and it bears a pyrazole ligand capable of hydrogen-bonding to a quinolone substrate.

In the presence of only 1 mol% of **29**, quinolone substrates **30** underwent a triplet-sensitized photocycloaddition to afford cyclobutanes **31** in high yields and ees of up to 91%. NMR studies and DFT calculations revealed that the catalyst binds to the substrate via a dual hydrogen-bonding interaction with the pyrazole ligand and an unexpected π–π interaction with the aromatic cyclometalating ligand. These interactions allow for efficient Dexter energy transfer to take place from the catalyst to the substrate. Since one face of the quinolone is blocked by the ligand, the stereocontrolled cycloaddition provides the enantioenriched products.

The Yoon group then sought to develop an intermolecular version of this reaction with 3-alkoxyquinolones and maleimides. They found that, in the presence of 1.5 mol% of chiral iridium catalyst **32**, the cycloaddition proceeded smoothly to afford photoproducts **34** in high yields and up to 99% ee (Figure 10.11) [50].

Like the previously developed iridium catalyst **29**, **32** bears a pyrazole ligand capable of hydrogen-bonding to the quinolone substrate. The catalyst acts as a triplet sensitizer through Dexter energy transfer. The O^{i}Pr moiety proved to be essential for the success of the reaction: if it was replaced with a hydrogen atom, no product formed; with an *n*-butoxy group, the product formed in 14% yield and only 7% ee. Notably, they found that the reaction also worked well with an *N*-methyl quinolone substrate, and cyclobutane **34g** was formed in 72% ee [50]. In the previously reported intramolecular reaction, *N*-methylated photoadduct **31f** was obtained in low ee (Figure 10.10), because the *N*-methyl disrupted the crucial hydrogen-bonding interaction with the ligand [51]. This unusual result indicated that there must be some differences in how the substrate binds to the pyrazole ligand. Mechanistic studies revealed that the N-H of the quinolone substrate is not involved in hydrogen-bonding, and, instead, the O^{i}Pr and carbonyl moieties are responsible for the interaction with the ligand. Moreover, they found that this new binding configuration inhibits Dexter energy transfer to the quinolone, and energy transfer takes place

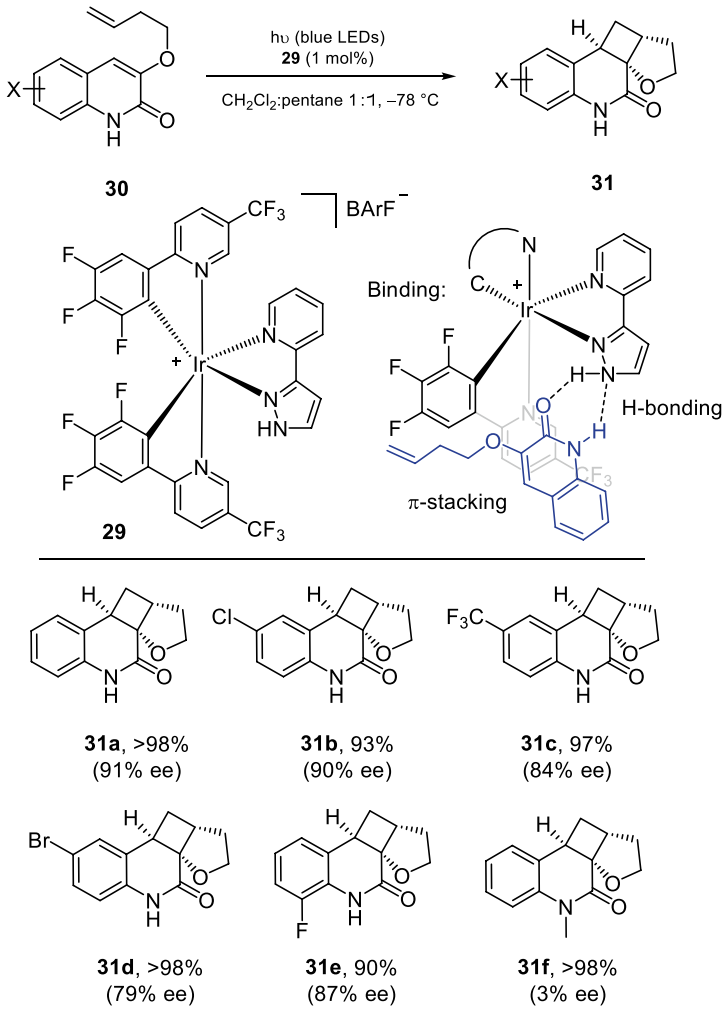

Figure 10.10. Iridium catalyst **29** catalyzes the enantioselective [2+2] photocycloaddition of **30** to **31** via triplet energy transfer. BArF = tetrakis(3,5-trifluoromethylphenyl)borate. Source: [51].

to maleimide instead. The sensitized maleimide then adds to quinolone within the chiral environment of the catalyst. This highly unusual mechanism represents the first example of a catalyzed, enantioselective photochemical reaction where the excited-state reactant is generated away from the sensitizer. Dexter energy transfer is strongly distance-dependent (and energy transfer to the bound quinolone was expected to be more likely than to maleimide), but it also relies on efficient overlap between the molecular orbitals. In this case, the hydrogen-bonding interaction with the quinolone positions it in such a way that its orbitals cannot overlap with those of the catalyst. Thus, energy transfer to maleimide is preferred [50].

Meggers and co-workers reported an enantioselective [2+2] photocycloaddition of alkenes to α,β-unsaturated imidazoles in the presence of rhodium complex **35** (Figure 10.12) [52]. Rather than acting as a triplet sensitizer, the catalyst behaves as a chiral Lewis acid, and coordinates to the imidazole handle of substrate **36**. Coordination to the catalyst induces a bathochromic absorption shift in the complex with a high extinction coefficient at 400 nm, so that it can be excited selectively upon irradiation at this wavelength. With 2–4 mol% of catalyst, cyclobutanes **37** were obtained in excellent yields and up to 99% ee. The reaction also proceeded smoothly with other coordinating moieties, including pyridines and pyrazoles. This method was extended to the asymmetric dearomatization of benzofurans by a [2+2]

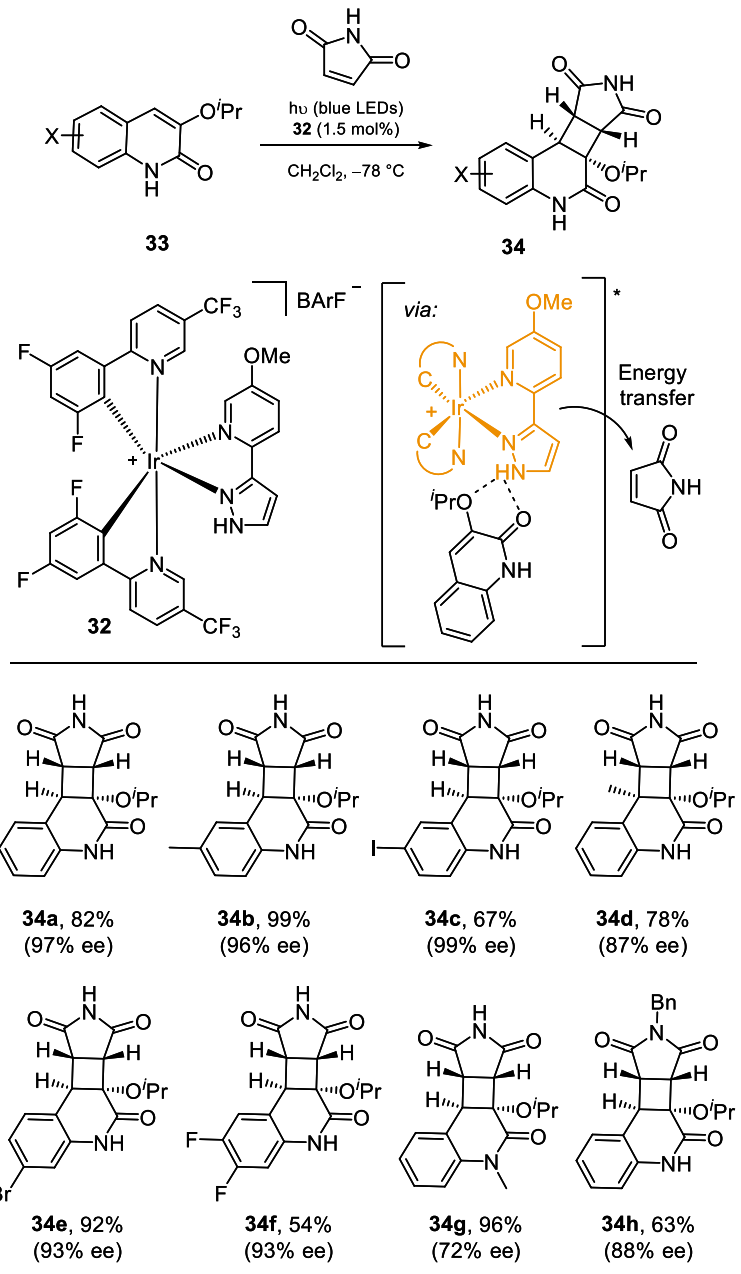

Figure 10.11. Iridium catalyst **32** catalyzes the intermolecular enantioselective [2+2] photocycloaddition of **33** with maleimide via triplet energy transfer to maleimide. BArF = tetrakis(3,5-trifluoromethylphenyl)borate. Source: [50].

photocycloaddition with a variety of styrenes. The cycloadducts were formed with excellent yields and enantioselectivities (98–99% ee) and with almost complete diastereo- and regioselectivities [24].

In 2018, the Feng group reported an enantioselective [2+2] photocycloaddition of 2-alkenoylpyridines **39** and alkenes with a terbium(III) catalyst bearing a chiral tetradentate *N,N′*-dioxide ligand **38** (Figure 10.13) [53]. The terbium(III) atom coordinates to the carbonyl oxygen atom and to the pyridine moiety, inducing a bathochromic shift in the substrate's absorption. The catalyst-bound substrate acts as a light-collecting antenna, and it can be excited selectively over the unbound substrate. The terbium(III)

atom also facilitates ISC of the catalyst–substrate complex from the S_1 to the T_1 energy surface, owing to its paramagnetic and heavy-atom effects. The chiral environment of the *N,N′*-dioxide ligand allows the reaction to take place with high enantioselectivity.

In the presence of 10 mol% of the catalyst, the cyclobutane products **40** were obtained in excellent yields and diastereomeric ratios, with up to 92% ee.

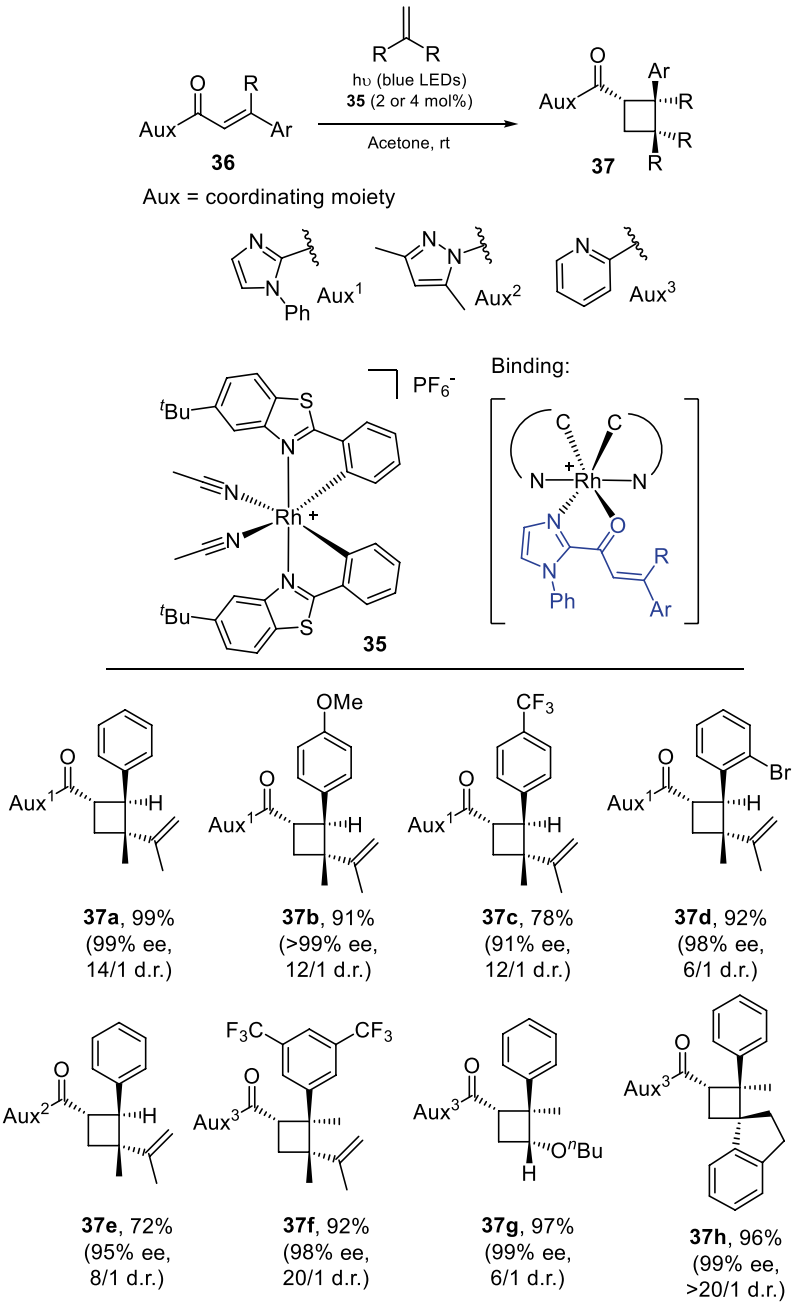

Figure 10.12. Rhodium complex **35** catalyzes the enantioselective [2+2] photocycloaddition of enones **36** bearing a coordinating moiety. Source: [52].

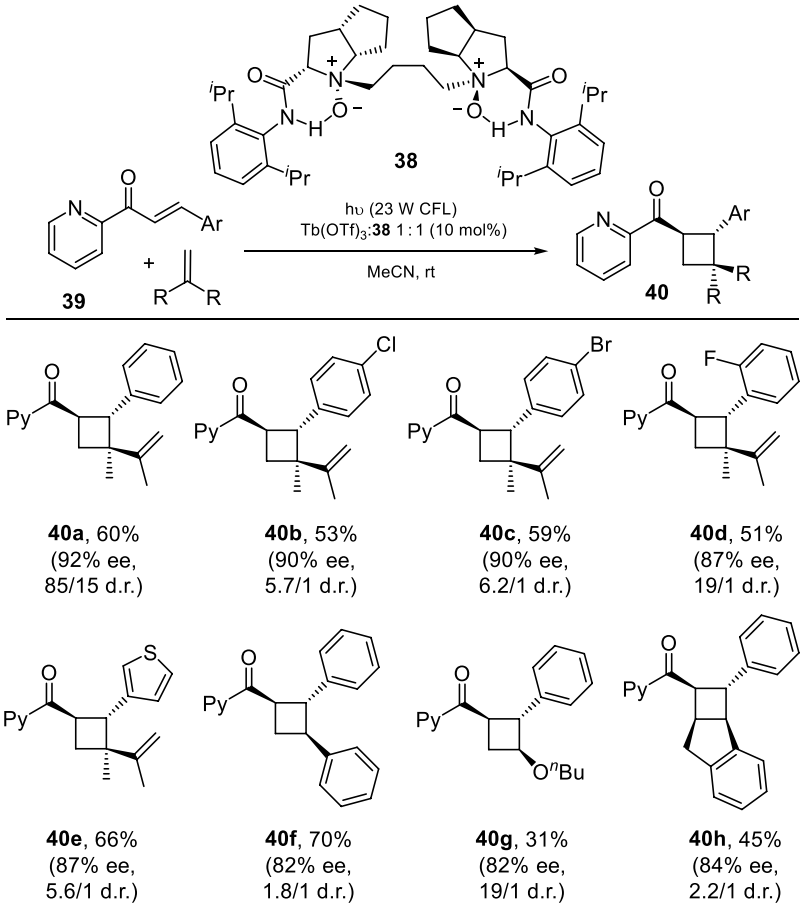

Figure 10.13. A terbium(III) catalyst with chiral *N,N*-dioxide ligand **38** catalyzes the [2+2] photocycloaddition of 2-alkenoylpyridines **39** and alkenes to afford cyclobutanes **40**. Source: [53].

10.3.2. $AlBr_3$-Activated Oxazaborolidines

The [2+2] photocycloaddition of coumarins (photodimerization or addition to alkenes upon direct irradiation) takes place slowly and in low yield from the short-lived S_1 ($^1\pi$–π^*) state. This is because the $^1\pi$–π^* and the ^{1}n–π^* excited states in coumarin are very close in energy, and the vibronic coupling of these states causes rapid, radiationless decay to the ground state (known as the proximity effect) [54–56]. However, when bound to a Lewis acid such as $BF_3{\cdot}OEt_2$, coumarins were found to undergo [2+2] photocycloaddition in higher yields [57]. The Lewis acid raises the energy of the ^{1}n–π^* state relative to the $^1\pi$–π^* state, preventing their vibronic coupling and suppressing the fast radiationless decay. The singlet state persists long enough for ISC onto the triplet energy surface to take place. The Lewis acid also slightly improves the spin-orbit coupling between the singlet and triplet energy surfaces (calculated at 0.8 cm^{-1} instead of 0.4 cm^{-1} for uncomplexed coumarin) [58], facilitating ISC onto T_1. Since the singlet and triplet states both have π–π^* character, transition between them is forbidden according to El-Sayed's rule [59], and ISC is very slow unless assisted by spin-orbit coupling. Thus, in the presence of a Lewis acid, the [2+2] photocycloaddition of coumarins proceeds efficiently on the triplet energy surface to afford the cyclobutane products in good yields.

It was theorized that, if a chiral Lewis acid was used, the [2+2] photocycloaddition of alkenes to coumarins could be performed enantioselectively. After screening a variety of Lewis acids, $AlBr_3$-activated oxazaborolidines such as **41**, **42**, and **43** were found to have the best activity (Figure 10.14).

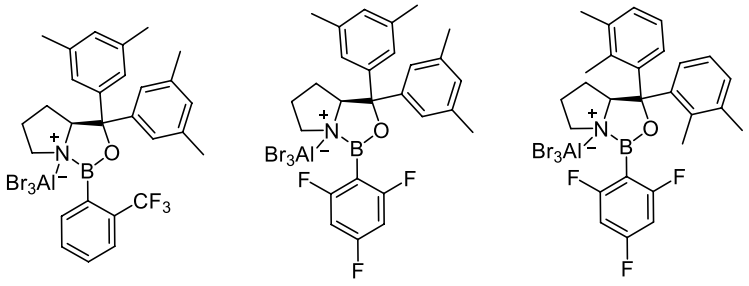

Figure 10.14. $AlBr_3$-activated oxazaborolidine catalysts **41**, **42**, and **43** were effective catalysts for the [2+2] photocycloaddition of a variety of coumarins and enones. Source: [60–64].

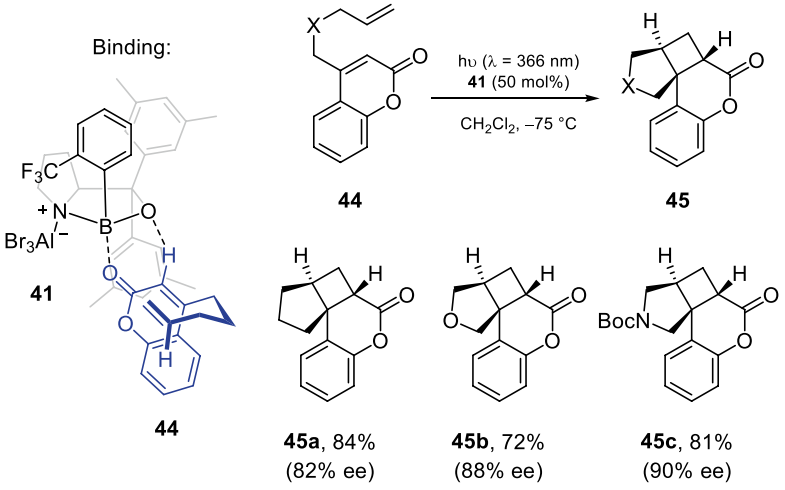

Figure 10.15. A variety of coumarins **44** underwent successful [2+2] photocycloaddition in the presence of catalyst **41** to afford cyclobutanes **45** in high yields and ees. Source: [60, 61].

Calculations by the Chen group revealed that the bromine atoms in the catalyst play an important role in improving the spin-orbit coupling between S_1 and T_1, allowing for even faster ISC compared to Lewis acids without heavy atoms [58]. Indeed, better experimental results were observed with $AlBr_3$ as a Lewis acid than with $BF_3{\cdot}OEt_2$. Using alkene-tethered coumarins **44** as substrates, photoadducts **45** were obtained in high yields and ees with 50 mol% of catalyst **41** (Figure 10.15) [60, 61].

The Lewis acid's mode of action is three-fold: first, upon coordination to a Lewis acid, the energy of the n–π* singlet state of coumarins increases, suppressing the aforementioned vibronic coupling with the π–π* singlet state and preventing radiationless decay to the ground state. Thus, the longer-lived singlet state can undergo ISC to the triplet state, from which the photocycloaddition takes place. Second, the heavy bromine atoms improve spin-orbit coupling between the singlet and triplet states, which further enhances ISC onto the triplet energy surface. Third, coordination to the Lewis acid induces a bathochromic shift in the absorption of the substrate. This boosts the absorption at the irradiation wavelength (366 nm), so that the catalyst–substrate complex is preferentially excited over the unbound substrate, suppressing the racemic background reaction [61].

The enantioselectivity can be explained by the two-point binding mode shown in Figure 10.15. Coumarin's carbonyl group coordinates to the boron atom, and the hydrogen atom at C3 also interacts electrostatically

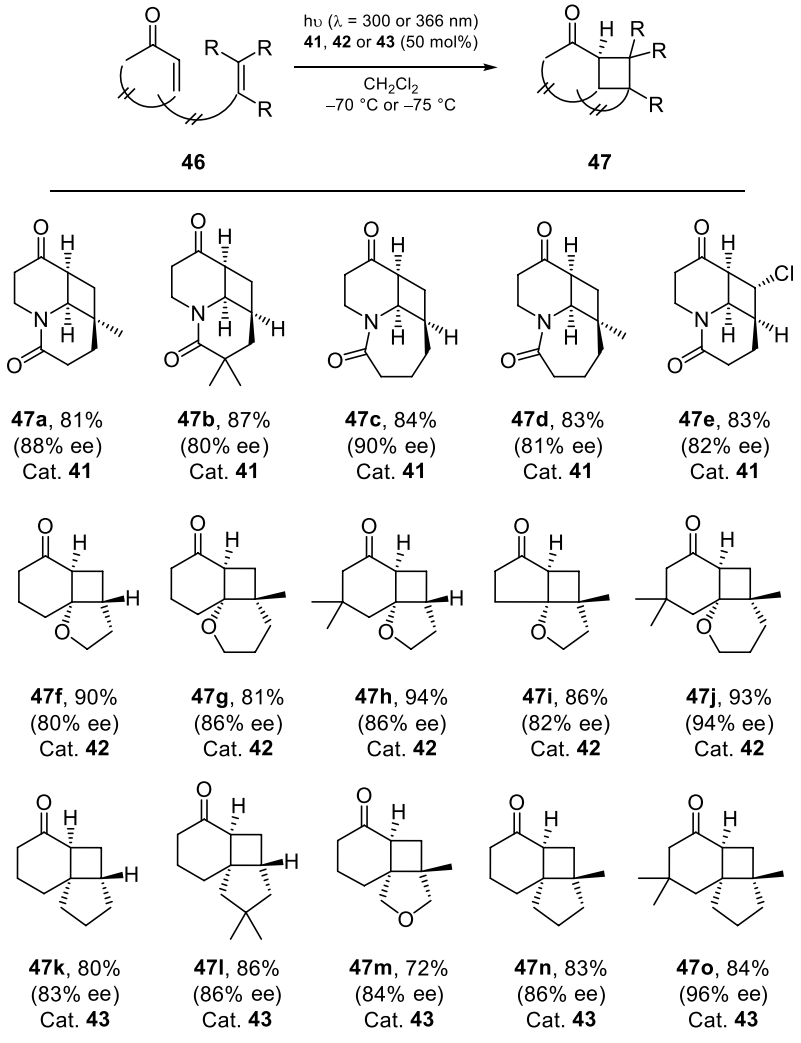

Figure 10.16. $AlBr_3$-activated oxazaborolidine catalysts **41**, **42**, and **43** were used successfully in the enantioselective [2+2] photocycloaddition of a variety of alkene-tethered enones **46**. Source: [62–64].

with the oxygen atom of the oxazaborolidine in a non-classical hydrogen bond. One of the two enantiotopic faces of coumarin is effectively shielded by the catalyst to afford the photoproduct with high ee [60].

When *E* or *Z* alkenes are used as the substrates, the reaction proceeds in a stereoconvergent fashion, which supports a triplet mechanism.

The [2+2] photocycloaddition with $AlBr_3$-activated chiral oxazaborolidine catalysts was also found to be generally applicable to enones, including dihydropyridones, 3-alkenyloxy-2-cycloalkenones, and 3-alkenyl-2-cycloalkenones (Figure 10.16) [62–64]. The choice of aryl substituents on the oxazaborolidine catalyst had a large influence on the enantioselectivity. For each substrate class, the catalyst could be readily reoptimized to afford the cycloadducts in high yields and ees. The positioning of the methyl groups on the two dimethylphenyl moieties was of particular importance: in some cases, decomposition of the catalyst and the products due to hydrogen abstraction from the methyl groups was observed. Moving these to the 2,3 positions (as in catalyst **43**) instead of the 3,5 positions (catalysts **41** and **42**) greatly improved the catalyst activity and stability in the photocycloaddition of 3-alkenyl-2-cycloalkenones.

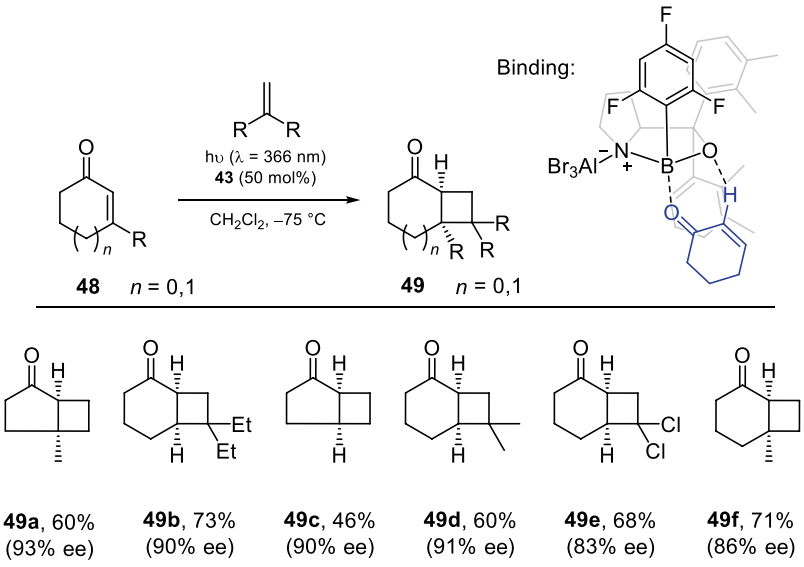

Figure 10.17. The enantioselective intermolecular [2+2] photocycloaddition of enones **48** to alkenes was catalyzed by $AlBr_3$-activated oxazaborolidine catalyst **43** [65].

As was observed with the coumarin substrates, enone substrates **46** bind to the catalyst via coordination of the carbonyl oxygen to the boron atom and a non-classical hydrogen bond between the hydrogen atom at C3 and the oxygen atom of the oxazaborolidine [62–64].

A challenging intermolecular variant was developed with cyclic enones **48** and olefin partners in the presence of catalyst **43** (50 mol%) (Figure 10.17). Photoproducts **49** were obtained in good yields and ees of up to 93% [65].

The value of these reactions was demonstrated with the enantioselective total synthesis of a variety of natural products, including (+)-Lupinine, (+)-Thermopsine, and (−)-Grandisol [62, 65].

Compared to coumarins, the Lewis acid-catalyzed photocycloaddition of enones shows some fundamental differences [11, 66]. First, while the addition of a Lewis acid accelerated the cycloaddition for coumarins, it slowed down the reaction for enones. This can be explained by changes in the n–π* energy levels upon coordination, which have been studied computationally [66, 67]. According to El-Sayed's rule, ISC between states with the same orbital type (for example, from ^{1}π–π* to ^{3}π–π*) is forbidden [59]. In uncomplexed enones (left, Figure 10.18a), the ^{1}n–π* and ^{3}π–π* states are very close in energy, allowing for an El-Sayed-type crossing onto the triplet energy surface. The spin-orbit coupling between ^{1}n–π* and ^{3}π–π* is large (calculated at 66.1 cm^{-1}) [67] and ISC is very efficient. However, upon coordination to a Lewis acid (right, Figure 10.18b), the energy of the ^{1}n–π* state is increased such that ^{1}π–π* is the lowest singlet state. Without any n–π* states to act as relays between ^{1}π–π* and ^{3}π–π*, ISC is forbidden and becomes extremely slow [11, 66].

Since ISC onto the triplet energy surface is slow in complexed enones, one would expect the reaction to take place from the singlet ^{1}π–π* state. Computational studies by Chen, Dolg, and co-workers [67] revealed why this is not the case: the relaxed ^{1}π–π* state of complexed enones is located in a deep, stable energy well, far below ^{1}n–π*. The ^{1}n–π* state has no opportunity to assist the relaxation onto S_0, and the depth of the energy well prevents any photochemical reaction from taking place. Once inside the ^{1}π–π* energy well, the only options for deactivation are fluorescence to the ground state, or ISC to ^{3}π–π*. The Chen group found that the local ^{1}π–π* minimum is very close in energy to the ^{3}π–π* energy surface, and spin-orbit coupling between the surfaces is large (37.4 cm^{-1}). This supports an anti-El-Sayed-type crossing between S_1 and T_1 for coordinated enones. The heavy bromine atoms in the catalyst play a crucial role in the anti-El-Sayed-type crossing: calculations with other Lewis acids without heavy atoms gave much

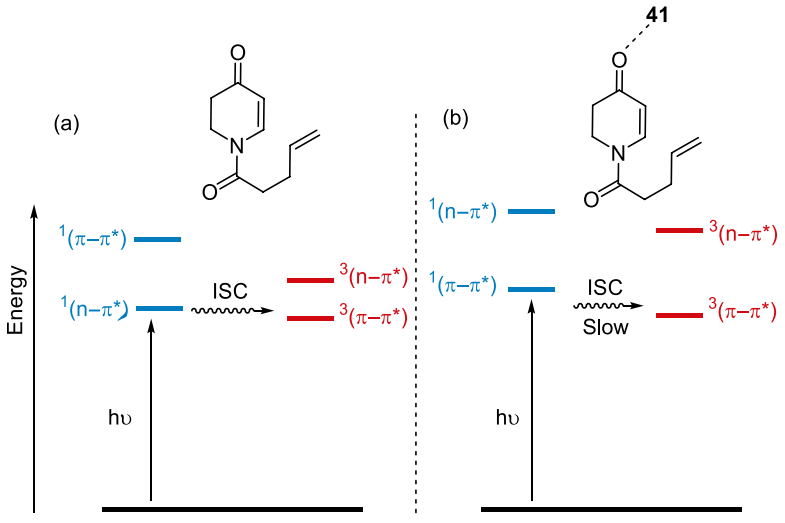

Figure 10.18. Coordination of a Lewis acid to enones induces changes in the excited-state energy levels, which impacts the reaction rate. (a) In a free enone, the proximity of the ^{1}n–π* and ^{3}π–π* states allows for efficient ISC from the singlet to the triplet energy surface. (b) In a Lewis acid-coordinated enone, the energy of ^{1}n–π* is raised, and transition from ^{1}π–π* to ^{3}π–π* is forbidden according to El-Sayed's rule [59]. For this reason, the [2+2] photocycloaddition of enones proceeds slowly in the presence of a Lewis acid. Source: [11, 66].

smaller spin-orbit coupling values and larger energy differences between S_1 and T_1. This explains why, experimentally, catalysts without heavy atoms give inferior results.

Another fundamental difference in the reactivity of enones and coumarins is the impact of the bathochromic shift upon binding to the Lewis acid. The shift is similar for both substrate classes (the wavelength difference is $\Delta\lambda = 43$ nm for coumarins and $\Delta\lambda = 52$ nm for dihydropyridones). For coumarins, the shift is not obvious in the absorption spectrum, because it overlaps with the relatively strong n–π* absorption of the uncomplexed substrate at $\lambda = 313$ nm. The shift has no real impact on the reaction, other than to enhance the absorption at the irradiation wavelength. For enones, the bathochromic shift of the π–π* transition is very obvious, as it is pushed into a region of the absorption spectrum where only a weak n–π* transition of the uncomplexed substrate is located (Figure 10.19) [11].

Despite the n–π* transition of the uncomplexed enone being a weak transition, ISC from this state onto the triplet energy surface is very efficient (unlike the complexed enone, as discussed in Figure 10.18). The quantum yield for product formation from the uncomplexed enone is much higher. Thus, even though the bathochromically shifted π–π* transition of the enone-catalyst complex has a much higher extinction coefficient, irradiation at this wavelength still gives rise to some degree of racemic background reaction due to absorption and efficient product formation from the uncomplexed n–π* transition. Thanks to the much larger extinction coefficient of the complexed π–π* transition, good enantioselectivities can still be reached by using a high-enough catalyst loading (typically up to 50 mol%) to outcompete the racemic background reaction. The enone-catalyst complex absorbs all the photons before they can reach the unbound substrate, affording the cyclobutanes with high ee.

10.4. DUAL CATALYSIS

In a dual-catalyzed [68] [2+2] photocycloaddition, two different catalysts are used to carry out the reaction: a photocatalyst to absorb and transfer light-energy, and a Lewis acid or an amine to activate the substrate. The main advantage of dual catalysis is that both catalysts can be tuned separately.

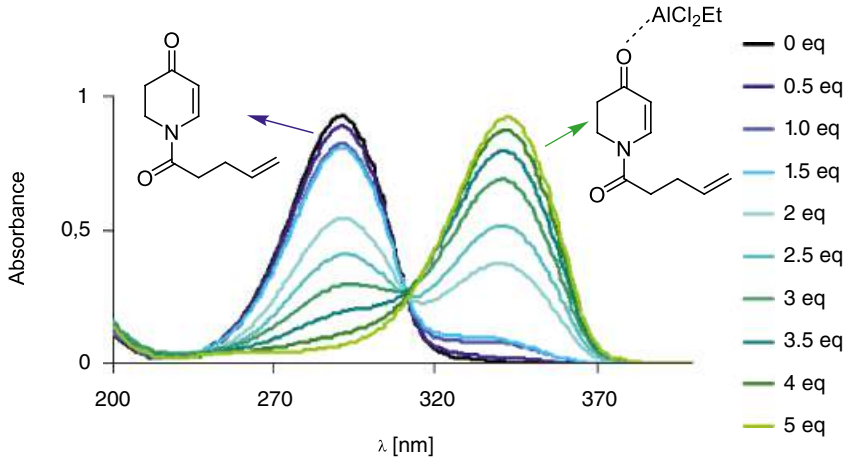

Figure 10.19. Upon coordination to a Lewis acid, there is a marked bathochromic shift in the absorption spectrum of enones. The shift overlays the weak n–π* transition after 320 nm. (The n–π* transition is so small that it is not visible in the above spectrum of the uncomplexed enone [11].) Source: Adapted from [66].

The enantioselectivity can be optimized without affecting the photophysical properties of the photocatalyst, and vice versa. In addition, chiral Lewis acid catalysis and iminium ion catalysis are well established in ground-state chemistry, and insights from these fields can be readily applied to the dual catalysis system [69].

10.4.1. Electron Transfer

To our knowledge, there is only a single example of a catalytic enantioselective [2+2] photocycloaddition which proceeds via an electron-transfer mechanism, and this was reported in 2014 by Yoon and co-workers [70].

The Yoon group has worked extensively on the [2+2] photocycloadditions of enones by one-electron reduction assisted by Lewis acids [71, 72]. The Lewis acid plays a key role of activating the enones toward reduction and stabilizing the resulting radical anion. Ruthenium catalysts like $[Ru(bpy)_3]Cl_2$, a powerful photoredox catalyst, were the catalysts of choice for reducing the activated enones.

They imagined that, by choosing a Lewis acid with chiral ligands to coordinate to the enone, the cycloaddition could be made enantioselective. Achiral background reactions in such a system would be suppressed for two reasons: first, the ruthenium catalyst absorbs light in the visible range, where the enone substrates do not absorb; and second, only the Lewis acid-bound enones can be reduced by the photocatalyst due to the Lewis acid-assisted modulation of their redox potential.

A screening of Lewis acids revealed that $Eu(OTf)_3$ (with chiral ligand **50**) and $[Ru(bpy)_3]Cl_2$ were the ideal catalyst partners. They allowed for an efficient cycloaddition using low catalyst loadings (5 mol% of Ru and 10 mol% of Eu) to give cyclobutane products **52** in good yields and ees of up to 93% (Figure 10.20) [70].

The aryl enones can be reduced by a Lewis acid-enabled single electron transfer from the photoredox catalyst, whereas the β-unsubstituted enones cannot. Thus, crossed cyclobutanes could be accessed with a variety of enone substrates. Once the reduced aryl enone has added to the β-unsubstituted enone, the electron must be transferred back to complete the catalytic cycle and afford neutral cyclobutane **52**. It can either be transferred to $^{i}Pr_2NEt^{\bullet+}$ to regenerate $^{i}Pr_2NEt$, or another molecule of starting aryl enone **51** can be reduced to give $\mathbf{51}^{\bullet-}$. The latter scenario corresponds to a radical chain mechanism, which has been confirmed in a similar system [73].

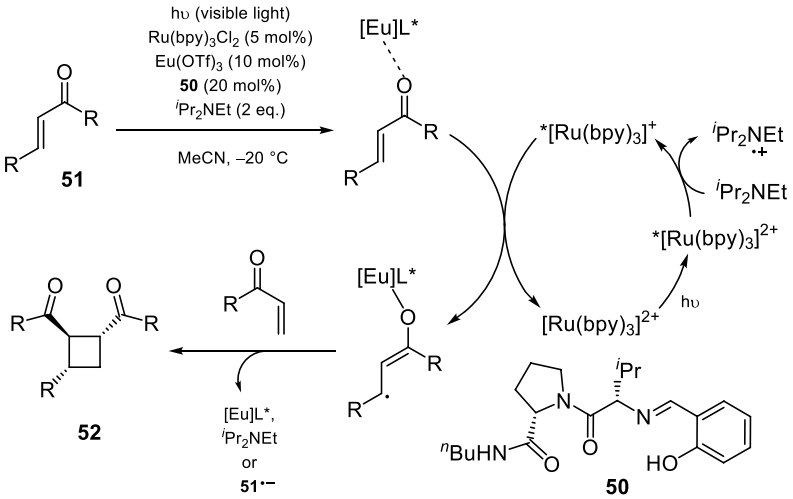

	R^1	R^2	R^3	Yield (%)	*ee* (%)	d.r.
52a	H	H	H	71	92	7/1
52b	Cl	H	H	65	90	7/1
52c	Br	H	H	69	90	5.5/1
52d	H	H	F	70	93	7/1
52e	OMe	H	H	54	86	6/1
52f	H	OMe	H	66	91	2.5/1

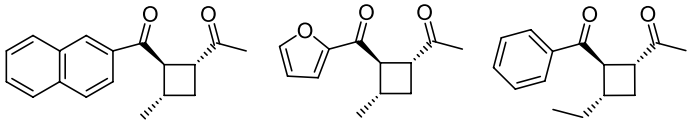

52g, 62% (89% ee, 3/1 d.r.) | **52g**, 72% (93% ee, 8/1 d.r.) | **52g**, 68% (91% ee, 4/1 d.r.)

Figure 10.20. The enantioselective [2+2] photocycloaddition of acyclic enones **51** was achieved with a dual-catalyst system consisting of a Lewis acid ($Eu(OTf)_3$) with chiral ligand **50**, and a photoredox catalyst ($[Ru(bpy)_3]Cl_2$). bpy = 2,2′-bipyridine. Source: [70].

10.4.2. Energy Transfer

10.4.2.1. Lewis Acid Catalysis As well as being excellent photoredox catalysts, ruthenium complexes such as $[Ru(bpy)_3](PF_6)_2$ are also known for their triplet-sensitization abilities [74]. Following the success of their electron-transfer [2+2] photocycloaddition, the Yoon group sought to develop a dual-catalyzed system based on energy transfer from a ruthenium catalyst. Indeed, electron transfer involves the creation of reactive radicals, which may limit the scope of the reaction, and energy transfer constitutes a milder approach.

2'-Hydroxychalcones **54** are able to coordinate in a bidentate fashion (via the phenolyl moiety and the carbonyl oxygen) to Lewis acids, and their photochemistry is well-documented in the literature [75–77]. Yoon and co-workers decided to investigate the ability of chalcones to undergo [2+2] photocycloadditions in the presence of Sc(III) salts. They found that, upon binding to Sc(III), there is an unexpectedly large energetic shift in the triplet state of the chalcone substrates (from 226 kJ mol^{-1} for unbound **54** to 134 kJ mol^{-1} upon binding to the Lewis acid; a difference of over 90 kJ mol^{-1}). This dramatic decrease in triplet energy makes the triplet state accessible to energy transfer from a $[Ru(bpy)_3](PF_6)_2$ sensitizer,

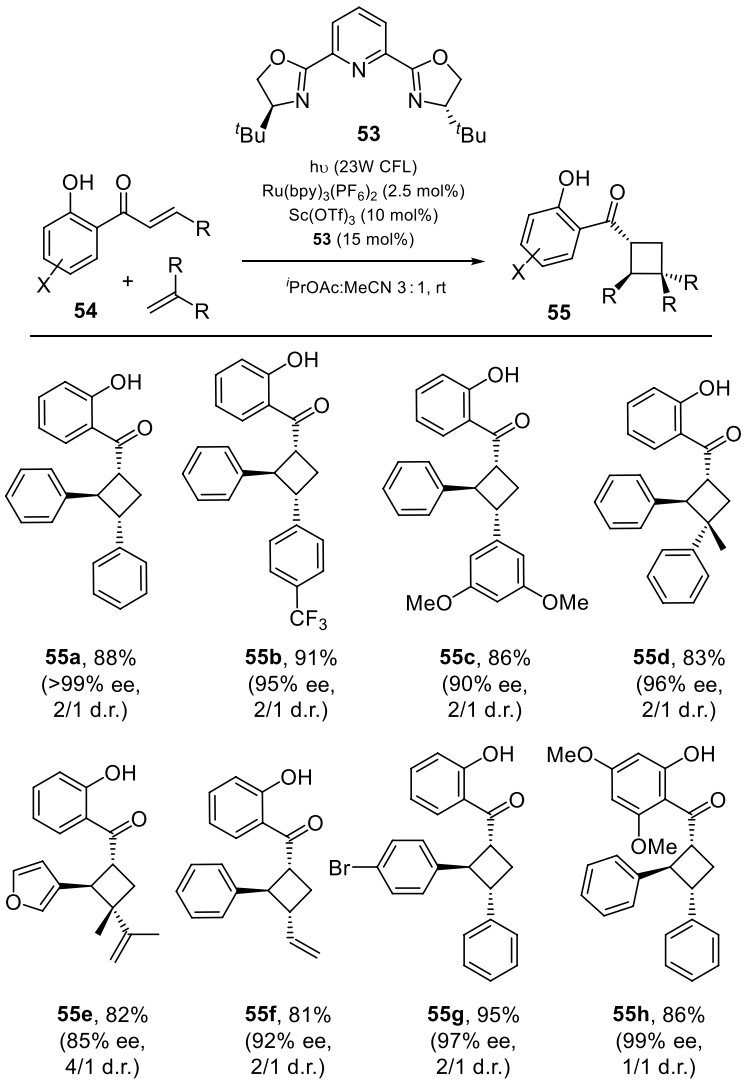

Figure 10.21. The enantioselective [2+2] photocycloaddition of 2′-hydroxychalcones **54** and alkenes was achieved with a dual-catalyst system consisting of a Lewis acid [$Sc(OTf)_3$] with chiral ligand **53**, and [$Ru(bpy)_3$](PF_6)$_2$ as a sensitizer. bpy = 2,2′-bipyridine. Source: [79, 80].

which has a triplet energy of 205 kJ mol^{-1} [78]. Thus, [$Ru(bpy)_3$](PF_6)$_2$ can transfer its triplet energy exclusively to the chiral Lewis acid-substrate complex, preventing any racemic background reactions.

Extensive screening of chiral ligands showed that $Sc(OTf)_3$ in the presence of PyBox-type ligand **53** gave the best results (Figure 10.21). The reaction takes place with a range of chalcones, dienes, and styrenes to afford vinyl and diaryl cyclobutanes in high yields and ees of >99% [79, 80].

Some electron-rich chalcones gave only low ee for the cyclobutane products, indicating the presence of a racemic, uncatalyzed background reaction. This is because electron-rich substrates absorb at the short wavelengths emitted by the compact fluorescent lamps bulbs. In these cases, the selectivity could be improved by irradiating the reaction mixture with a monochromatic blue LED.

Chalcones with different double-bond geometry (*E* or *Z*) afforded the same cyclobutane product, supporting a stepwise triplet mechanism. Yoon and co-workers could prove that the reaction takes place

via energy transfer and not electron transfer by using different catalysts: cyclobutane products were observed with an organic triplet sensitizer (benzil) and an electron-deficient ruthenium catalyst ($[Ru(deeb)_3](PF_6)_2$), both of which are unable to reduce the enone but can transfer their triplet energy. In addition, no reaction took place with chemical reductants (SmI_2, Cp_2Co, Li(naph), tetrakis(dimethylamino)ethylene) or oxidants (ceric ammonium nitrate, $K_3Fe(CN)_6$, $Fe(acac)_3$, $Mn(OAc)_3$). A detailed computational study of the mechanism has been published recently [81].

Using this dual catalyst system, the Yoon group synthesized an enantiopure naturally occurring norlignan in only five steps from alkene and chalcone partners. They could also access Artochamin and Lindleyanin scaffolds [80].

During their work on rare-earth-catalyzed enantioselective [2+2] photocycloadditions, the Feng group found that *N,N'*-dioxide ligands such as **56** are also well-suited for [2+2] photocycloadditions of chalcones using $Sc(OTf)_3$ and $[Ru(bpy)_3]Cl_2$ [53]. A variety of chalcones **54** reacted with dimethyl butadiene and styrene to afford vinyl cyclobutanes **55** in excellent yields and ees of up to 92% (Figure 10.22).

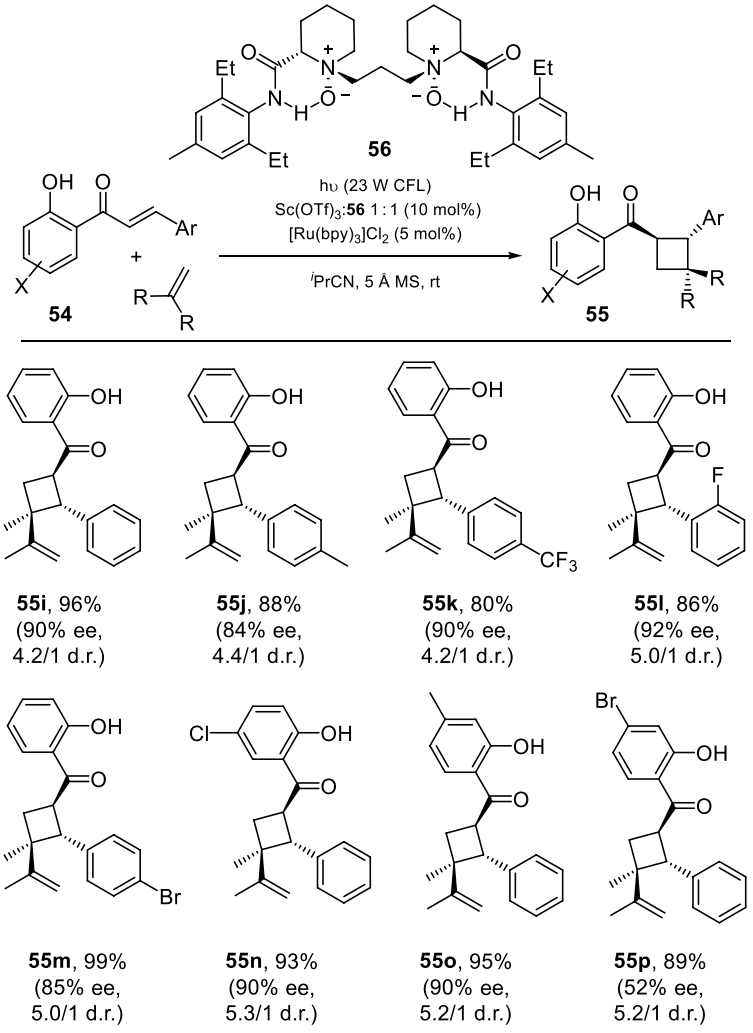

Figure 10.22. The enantioselective [2+2] photocycloaddition of 2′-hydroxychalcones **54** and alkenes was achieved with a dual-catalyst system consisting of a Lewis acid $[Sc(OTf)_3]$ with chiral ligand **56**, and $[Ru(bpy)_3]Cl_2$ as a sensitizer. bpy = 2,2′-bipyridine. Source: [53].

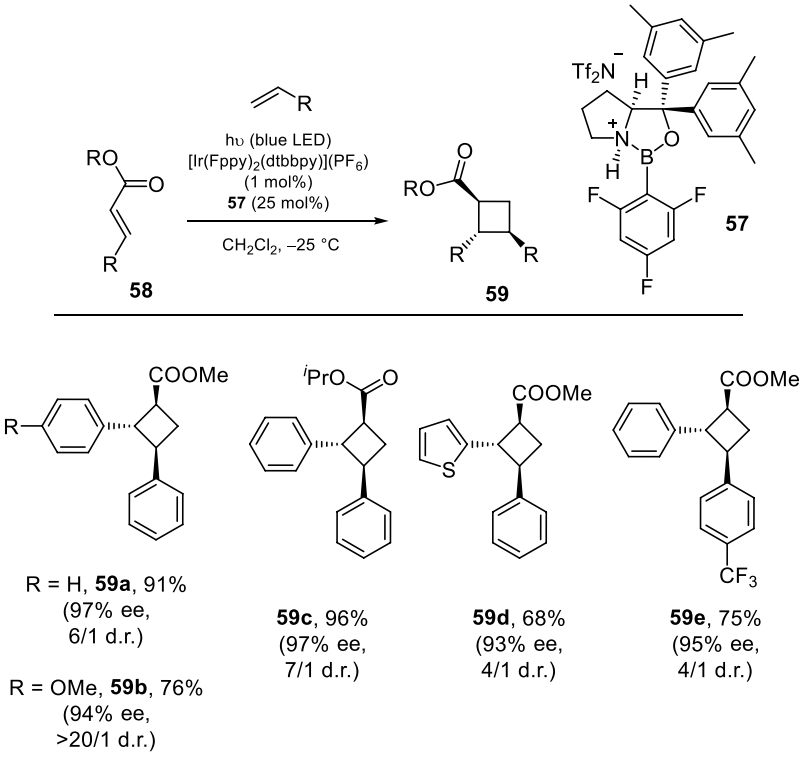

Figure 10.23. The enantioselective [2+2] photocycloaddition of cinnamates **58** and alkenes was achieved with a dual-catalyst system consisting of a Lewis acid (oxazaborolidine **57**) and $[Ir(Fppy)_2(dtbbpy)](PF_6)$ as the sensitizer. Fppy = 2-(2,4-difluorophenyl)pyridinate; dtbbpy = 4,4′-di-tert-butyl-2,2′-dipyridyl. Source: [82].

Although the value of this transformation is clear, the need for a coordinating handle was a serious drawback, which limited the scope and utility of the reaction. Indeed, for Yoon's five-step synthesis of the above-mentioned norlignan [80], three of these steps involved removing the coordinating phenolyl moiety.

To widen the scope of the dual catalysis system and make it more general, Yoon and co-workers sought to extend the reaction to the photocycloaddition of cinnamates **58**. They found that chiral oxazaborolidine catalyst **57** was the ideal Lewis acid for the transformation, accompanied by an iridium catalyst as the photosensitizer (Figure 10.23). The dual-catalyzed cycloaddition reaction gave cyclobutane carboxylates **59** in excellent yields and ees of up to 97% [82].

With this method, they could synthesize the previously mentioned norlignan in only two steps from cinnamate and styrene partners [82].

Next, they calculated the singlet-triplet energy gap of the free and coordinated esters. Surprisingly, and in contrast to previous work with 2′-hydroxychalcones, the ester's triplet energy is only lowered by ~30 kJ mol^{-1} when bound to **57**. Thus, the catalytic effect of the Lewis acid in this reaction cannot be explained solely by a lowering of the triplet energy. An analysis of the frontier molecular orbitals (FMOs) provided some clarity: calculations showed that the energies of the ester's FMOs decreased upon coordination to the Lewis acid, making them almost isoenergetic with the singly occupied molecular orbitals of the triplet photocatalyst. This improves the electronic coupling between the triplet sensitizer and the **57**-bound ester, facilitating triplet energy transfer to the ester.

With this work, Yoon and co-workers were able to shed light on a new functional role of Lewis acids in photocycloadditions: as well as lowering the singlet-triplet energy gap, Lewis acids can expedite triplet sensitization through changes in the FMO energies. The degree to which both of these effects influence the reaction appears to be substrate dependent.

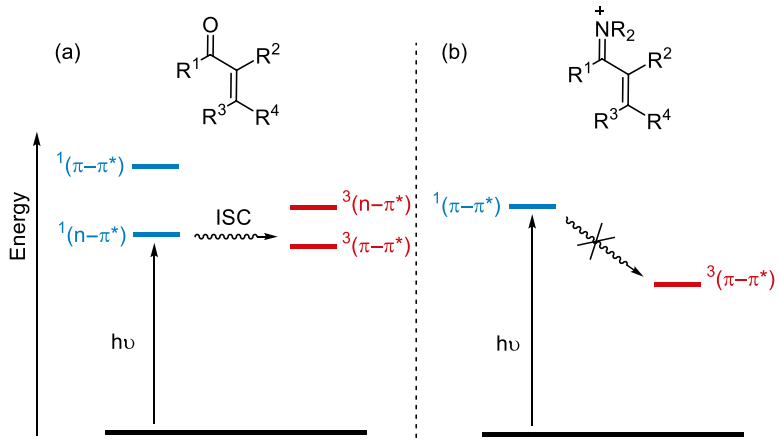

Figure 10.24. Formation of an eniminium ion induces changes in the excited-state energy levels. (a) In a free enone, the proximity of the ^{1}n–π* and ^{3}π–π* states allows for efficient ISC to the triplet energy surface. (b) In an eniminium ion, the ^{3}π–π* is difficult to reach by ISC from ^{1}π–π*. The [2+2] photocycloaddition of eniminium ions proceeds on the singlet energy surface unless sensitized. Source: [83].

10.4.2.2. Eniminium Ions Given the recent interest in triplet-sensitized photochemical reactions with visible light, it seemed desirable to explore the reactivity of triplet states of eniminium ions, as relatively little is known about their chemistry. Eniminium ions, compared to the parent enones, have a much lower energy triplet state T_1, and a higher energy singlet state S_1. In enones, the proximity of the ^{1}n–π* and ^{3}π–π* states makes ISC onto the triplet energy surface very efficient via an El-Sayed-type crossing [59], such that enones usually react from the triplet state upon direct irradiation (Figure 10.24 a; see also Figure 10.18a). In eniminium ions, the ^{1}π–π* state is shifted hypsochromically relative to the enone ^{1}n–π* and the ^{3}π–π* state is red-shifted [83]. This creates a large energy gap between ^{1}π–π* and ^{3}π–π*, and there is no nearby state of different orbital type (n–π*) to assist ISC between them. For these reasons, the triplet state of eniminium ions cannot easily be reached by direct irradiation (Figure 10.24b), and the cycloaddition usually takes place on the singlet energy surface. However, the triplet state can be accessed by energy transfer from an appropriate sensitizer. Since T_1 is relatively low in energy, sensitizers that absorb in the visible range are ideal.

The sensitized [2+2] photocycloaddition of eniminium ions (pre-formed with stoichiometric amounts of amine) and alkenes was studied as a starting point [83]. A chiral eniminium ion (made with a chiral amine) gave the cyclobutane product in high yield and ee using a ruthenium triplet sensitizer ($[Ru(bpy)_3](PF_6)_2$) and irradiation at $\lambda = 457$ nm. With this work, it was confirmed that the eniminium ion's triplet state energy is indeed much lower than that of the parent enone. Several chiral eniminium ions were successfully converted into enantioenriched cyclobutanecarbaldehydes (66–90% ee) in an intermolecular [2+2] photocycloaddition with various olefins.

It was theorized that, if catalytic amounts of a chiral amine were used, the eniminium ion formed in situ could be sensitized preferentially over the enone, owing to its much lower triplet energy.

Cinnamic aldehyde gives eniminium ion **61** with a triplet energy of ~200 kJ mol^{-1}, which is suitable for sensitization with a ruthenium catalyst such as $Ru(bpy)_3(PF_6)_2$ or $Ru(bpy)_3(BArF)_2$. In the presence of 50 mol% of chiral amine **60**, cyclobutanecarbaldehyde **62a** was obtained in modest yield and 92% ee (Figure 10.25) [84].

This was the first example of the preparation of a cyclobutanecarbaldehyde by an enantioselective [2+2] photocycloaddition.

Some important observations were made during the optimization of the reaction conditions: first, it was found that a proton source is crucial for establishing an equilibrium between the aldehyde and the eniminium ion. However, in acidic medium, some catalysts (like $[Ru(bpz)_3](PF_6)_2$) were protonated and became inactive; thus, the choice of catalyst was important. $[Ru(bpy)_3](PF_6)_2$ and $[Ru(bpy)_3](BArF)_2$

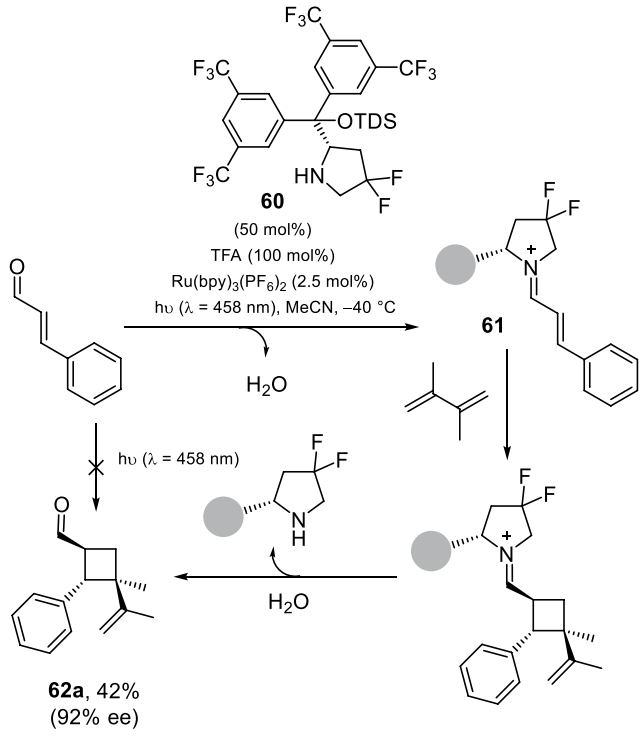

Figure 10.25. The eniminium ion **61** of cinnamic aldehyde, formed with catalytic amounts of chiral amine **60**, undergoes a [2+2] photocycloaddition on the triplet energy surface enabled by energy transfer from $[Ru(bpy)_3](PF_6)_2$, to afford cyclobutane **62a** in 92% ee. bpy = 2,2′-bipyridine; TDS = thexyldimethylsilyl. Source: [84].

were found to be ideal photosensitizers because they are not protonated under the reaction conditions, and they also do not catalyze any achiral background reactions. The choice of acid was also crucial. Trifluoroacetic acid (TFA) gave the best results. Secondly, the reaction conditions were quite narrow: above 0 °C, a substantial amount of the thermal Diels-Alder product was observed; but below –10 °C, the reaction was prohibitively slow. Lastly, amine **60** was found to be somewhat unstable under the reaction conditions and could not always be completely recovered.

It is well-known that ruthenium triplet sensitizers are also efficient photoredox catalysts. To confirm that the catalytic system does react via energy transfer, laser-flash photolysis experiments were carried out. It was found that both electron and energy transfer from the catalyst take place, but electron transfer is an unproductive pathway. Once formed, the one-electron-reduced eniminium ion does not add to the alkene; rather, it transfers the electron back to the ruthenium catalyst. Only the triplet-sensitized eniminium ion reacts with the alkene to form the cyclobutane product.

Since an acid was required for the reaction to proceed, it was hypothesized that combining eniminium ion photochemistry with a Brønsted acid catalyst such as **21** (see Section 10.2.3) could allow access to a range of cyclobutanecarbaldehydes in high yields.

Pre-formed *N,O*-acetals **63** were found to be ideal eniminium ion precursors for enantioselective [2+2] photocycloadditions using Brønsted acids. (Although the *N,O*-acetal is not formed catalytically, we have included this example in the current subsection for clarity.) In solution, the *N,O*-acetal exists as a mixture of the closed (**63**) and open (**64**) forms in a 2 : 1 ratio. In the presence of a Brønsted acid, the open protonated ion **65** is generated (Figure 10.26) [85].

Brønsted acid **21** is a chiral phosphoric acid catalyst bearing two thioxanthone chromophores that can capture long wavelength light ($\lambda_{max} = 394$ nm) and act as triplet photosensitizers (triplet energy $E_T = 235$ kJ mol^{-1}, 77 K, CH_2Cl_2) [42]. The triplet state of bound eniminium ion **65** (measured for a brominated

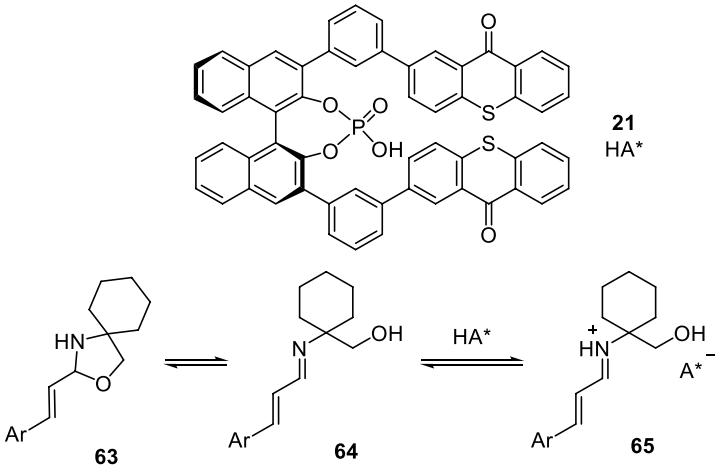

Figure 10.26. *N,O*-acetals **63** exist as a mixture of open and closed forms (**63–64**). In the presence of Brønsted acid **21**, eniminium ion **65** is generated. Source: [85].

derivative at $E_T = 213$ kJ mol^{-1}, 77 K, CH_3CN) is inaccessible upon direct irradiation, but it can be populated by energy transfer from the thioxanthone moieties on catalyst **21**. Thus, only the catalyst-bound substrate molecules reach the triplet excited state, and they react within the chiral environment of the catalyst. With 10 mol% of **21**, a variety of *N,O*-acetals **63** and alkenes **66** gave cyclobutanecarbaldehyde products **62** (Figure 10.27) in high yields and excellent enantioselectivities and diastereoselectivities [85]. A dual catalysis in which a chiral phosphoric acid activates the *N,O*-acetal and an achiral sensitizer initiates the reaction was also attempted but gave inferior results.

Several functional groups were tolerated, including boronate **62d**, which provides a useful handle for further synthetic transformations. Low-temperature NMR studies proved the existence of a 1 : 1 complex with **21** as a hydrogen-bond-assisted ion pair. The enantioselectivity of the reaction was tentatively explained as arising from a *Si* face attack in complex **65** [85–87].

10.5. CHIRAL METAL-ORGANIC CAGES

Chiral metal-organic cages (MOCs) have been studied extensively in recent years for their ability to preorganize molecules inside a confined space, acting as nanoreactors to catalyze reactions with high selectivity. However, there are relatively few examples of photochemical reactions using MOCs.

In 2020, Su and co-workers reported an unprecedented example of an enantioselective [2+2] photocycloaddition inside chiral MOCs Δ-MOC-**67** and Λ-MOC-**67** [88]. No binding interactions to a catalyst were required, and high ees were achieved solely from the encapsulation of the guests inside a portal of the cage.

Δ-MOC-**67** and Λ-MOC-**67** consist of a network of palladium and ruthenium atoms connected with metalloligands (Figure 10.28). The ruthenium-containing moieties allow for triplet energy transfer to a suitable substrate inside the cage. If another substrate molecule is present inside the cage, a stereocontrolled photodimerization can take place. With 1-bromoacenaphthylene as the substrate, Su and coworkers obtained photoadducts **68** with excellent regio- and stereoselectivities in up to 88% ee.

The *anti*-HH-dimer is obtained exclusively owing to the preorganization of the guests. There is an aromatic stacking interaction with the ligands and with the second substrate molecule inside the cage, and a dipolar interaction of the Br atom with a Ru^{2+} center. Guests are encapsulated via the hydrophobic effect. It is noteworthy that the MOC can be used in catalytic amounts: often, a consequence of the hydrophobic effect is that the products within the cage cannot be released easily to make way for new starting materials, and stoichiometric quantities of MOC are required. On the other hand, if the solvent is not hydrophobic enough, guest exchange can be too fast, resulting in low selectivity. In this example

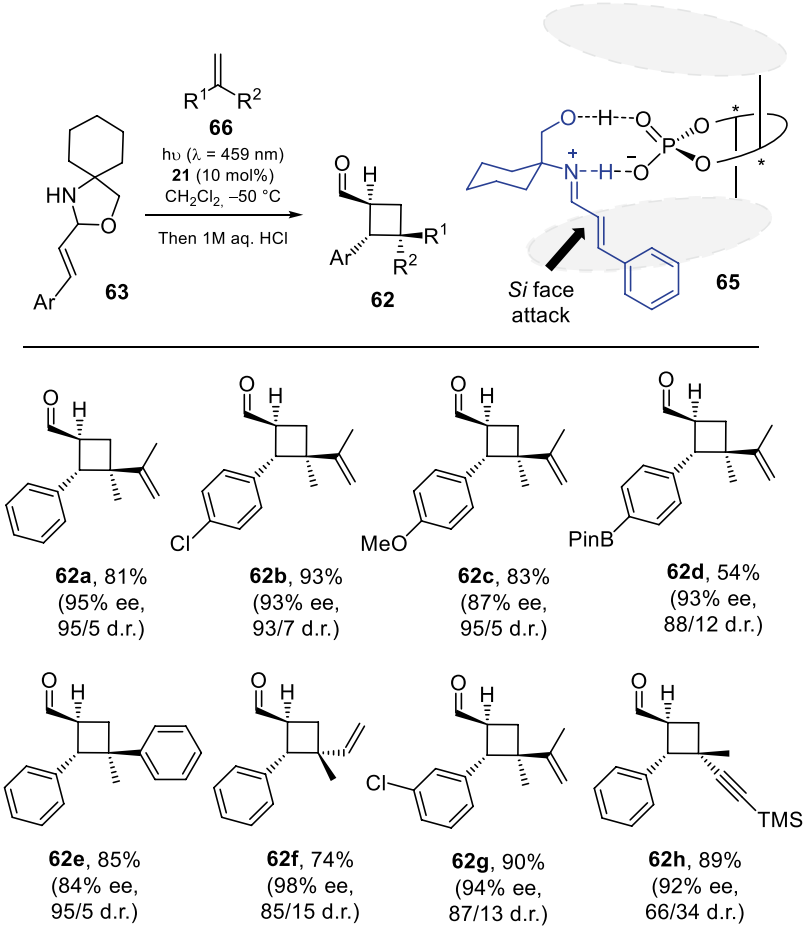

Figure 10.27. *N,O*-acetals **63** react enantioselectively with alkenes **66** in the presence of chiral phosphoric acid catalyst **21** to afford cyclobutanes **62**. Source: [85].

with 1-bromoacenaphthylene, the product can easily exit the cage once it has formed to make way for new starting materials. Product **68** interacts less favorably with the aromatic ligands than the starting material: loss of aromaticity in the bridge and protrusion of the Br atoms in **68** disrupt the host–guest interactions, so that the product is ejected from the cage and precipitates out of the reaction medium [88].

10.6. CONCLUDING REMARKS

Photochemical reactions are renowned for their ability to generate unusual high-energy products via reactive intermediates in the excited state. This has not only captured the imaginations of chemists for over a century, but has also made the development of enantioselective variants quite challenging. Recently, several examples of catalytic enantioselective [2+2] photocycloadditions have appeared in the literature, which we have organized and summarized in this chapter. We have seen that enantioselective [2+2] photocycloadditions can be achieved through a variety of catalytic systems, from hydrogen-bonding catalysts to transition metals to MOCs. Depending on the nature of the catalyst, different catalyst–substrate interactions have been exploited (for example, hydrogen-bonding, coordination to a metal center, and iminium ion formation) and there are many ways to activate the substrate once it is bound (for example, by sensitization, or by irradiation of a new shift in the absorption spectrum). Combined,

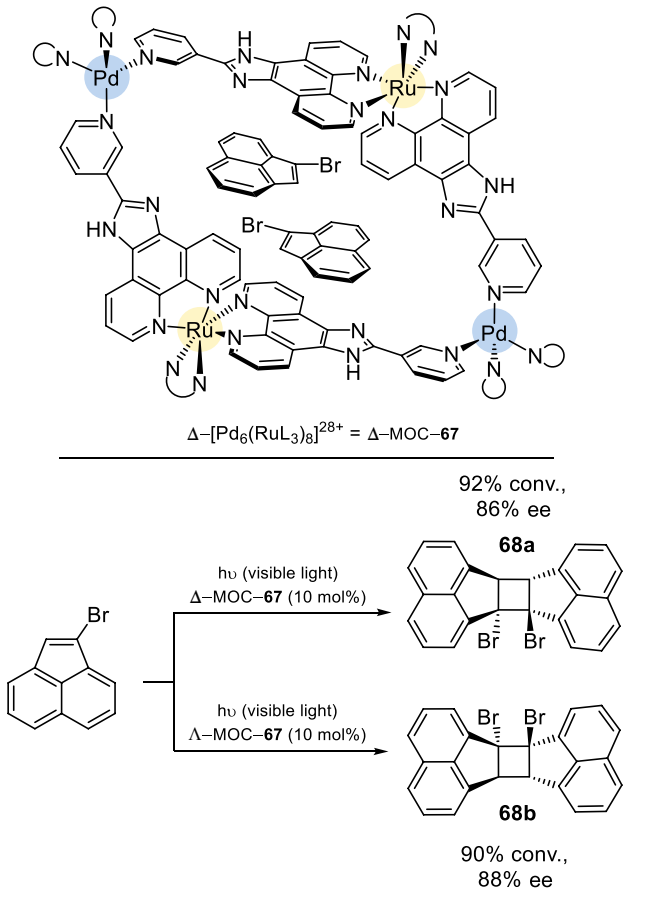

Figure 10.28. The enantioselective [2+2] photocycloaddition of 1-bromoacenaphthylene takes place with high yield and excellent regio-, diastereo-, and enantioselectivities inside chiral Δ-MOC-**67** and Λ-MOC-**67**. Source: [88].

these parameters offer an array of design possibilities. This is reflected in the diversity of the works we have presented here: each example is unique. Often, there are mechanistic surprises, where the reaction takes place through a totally different pathway than intended, revealing new and highly efficient reaction mechanisms.

We believe that there is still much to be explored in these reactions, and that many discoveries await concerning the properties and behavior of the excited state. Overall, great progress has already been made in the field of catalytic enantioselective [2+2] photocycloadditions, and we expect many more fascinating examples to appear in the future.

ACKNOWLEDGMENTS

Our research on asymmetric [2+2] photocycloadditions is generously supported by the Deutsche Forschungsgemeinschaft (DFG), the European Research Council (ERC), the Technical University of Munich, the Fonds der Chemischen Industrie, the Alexander von Humboldt Foundation, the Swiss National Science Foundation, the Studienstiftung des Deutschen Volkes, and the Elitenetzwerk Bayern. We thank Dr. Thomas Rigotti and Johannes Großkopf for proofreading the chapter and for helpful discussions. T.B. gratefully acknowledges all colleagues and co-workers who have worked on asymmetric [2+2] photocycloadditions. Their names can be found in the references.

REFERENCES

1. Kagan, H. B.; Gopalaiah, K. *New J. Chem.*, **2011**, *35*, **1933**.
2. Inoue, Y.; Ramamurthy, V. *Chiral Photochemistry* (Marcel Dekker, New York, **2004**).
3. Schwinger, D. P.; Bach, T. *Acc. Chem. Res.*, **2020**, *53*, 1933–1943.
4. Rigotti, T.; Alemán, J. *Chem. Commun.*, **2020**, *56*, 11169–11190.
5. Prentice, C.; Morrisson, J.; Smith, A. D.; Zysman-Colman, E. *Beilstein J. Org. Chem.*, **2020**, *16*, 2363–2441.
6. Yoon, T. P. *Acc. Chem. Res.*, **2016**, *49*, 2307–2315.
7. Brenninger, C.; Jolliffe, J. D.; Bach, T. *Angew. Chem. Int. Ed.*, **2018**, *57*, 14338–14349.
8. Silvi, M.; Melchiorre, P. *Nature*, **2018**, *554*, 41–49.
9. Huang, X.; Meggers, E. *Acc. Chem. Res.*, **2019**, *52*, 833–847.
10. Zou, Y.-Q.; Hörmann, F. M.; Bach, T. *Chem. Soc. Rev.*, **2018**, *47*, 278–290.
11. Brimioulle, R.; Bauer, A.; Bach, T. *J. Am. Chem. Soc.*, **2015**, *137*, 5170–5176.
12. Kagan, H.; Moradpour, A.; Nicoud, J. F.; Balavoine, G.; Tsoucaris, G. *J. Am. Chem. Soc.*, **1971**, *93*, 2353–2354.
13. Buchardt, O. *Angew. Chem. Int. Ed.*, **1974**, *13*, 179–185.
14. Murov, S. L.; Cole, R. S.; Hammond, G. S. *J. Am. Chem. Soc.*, **1968**, *90*, 2957–2958.
15. Hammond, G. S.; Cole, R. S. *J. Am. Chem. Soc.*, **1965**, *87*, 3256–3257.
16. Ouannes, C.; Beugelmans, R.; Roussi, G. *J. Am. Chem. Soc.*, **1973**, *95*, 8472–8474.
17. Horner, L. *Liebigs Ann. Chem.*, **1979**, *1979*, 1232–1257.
18. Seebach, D.; Daum, H. *J. Am. Chem. Soc.*, **1971**, *93*, 2795–2796.
19. Seebach, D.; Oei, H.-A.; Daum, H. *Chem. Ber.*, **1977**, *110*, 2316–2333.
20. Boyd, D. R.; Campbell, R. M.; Coulter, P. B.; Grimshaw, J.; Neill, D. C.; Jennings, W. B. *J. Chem. Soc., Perkin Trans. 1*, **1985**, 849.
21. Rau, H. *Chem. Rev.*, **1983**, *83*, 535–547.
22. Inoue, Y. *Chem. Rev.*, **1992**, *92*, 741–770.
23. Stegbauer, S.; Jandl, C.; Bach, T. *Angew. Chem. Int. Ed.*, **2018**, *57*, 14593–14596.
24. Hu, N.; Jung, H.; Zheng, Y.; Lee, J.; Zhang, L.; Ullah, Z.; Xie, X.; Harms, K.; Baik, M.-H.; Meggers, E. *Angew. Chem. Int. Ed.*, **2018**, *57*, 6242–6246.
25. Remy, R.; Bochet, C. G. *Chem. Rev.*, **2016**, *116*, 9816–9849.
26. Streit, U.; Bochet, C. G. *Beilstein J. Org. Chem.*, **2011**, *7*, 525–542.
27. Dondoni, A.; Massi, A. *Angew. Chem. Int. Ed.*, **2008**, *47*, 4638–4660.
28. Bach, T.; Bergmann, H.; Harms, K. *Angew. Chem. Int. Ed.*, **2000**, *39*, 2302–2304.
29. Müller, C.; Bauer, A.; Bach, T. *Angew. Chem. Int. Ed.*, **2009**, *48*, 6640–6642.
30. Müller, C.; Bauer, A.; Maturi, M. M.; Cuquerella, M. C.; Miranda, M. A.; Bach, T. *J. Am. Chem. Soc.*, **2011**, *133*, 16689–16697.
31. Burg, F.; Bach, T. *J. Org. Chem.*, **2019**, *84*, 8815–8836.
32. Li, X.; Jandl, C.; Bach, T. *Org. Lett.*, **2020**, *22*, 3618–3622.
33. Maturi, M. M.; Wenninger, M.; Alonso, R.; Bauer, A.; Pöthig, A.; Riedle, E.; Bach, T. *Chem. Eur. J.*, **2013**, *19*, 7461–7472.
34. Maturi, M. M.; Bach, T. *Angew. Chem. Int. Ed.*, **2014**, *53*, 7661–7664.
35. Alonso, R.; Bach, T. *Angew. Chem. Int. Ed.*, **2014**, *53*, 4368–4371.
36. Yang, Y.; Wen, Y.; Dang, Z.; Yu, H. *J. Phys. Chem. A*, **2017**, *121*, 4552–4559.
37. Zhou, T.-P.; Zhong, F.; Wu, Y.; Liao, R.-Z. *Org. Biomol. Chem.*, **2021**, *19*, 1532–1540.
38. Tröster, A.; Alonso, R.; Bauer, A.; Bach, T. *J. Am. Chem. Soc.*, **2016**, *138*, 7808–7811.
39. Vallavoju, N.; Selvakumar, S.; Jockusch, S.; Prabhakaran, M. T.; Sibi, M. P.; Sivaguru, J. *Adv. Synth. Catal.*, **2014**, *356*, 2763–2768.
40. Vallavoju, N.; Selvakumar, S.; Jockusch, S.; Sibi, M. P.; Sivaguru, J. *Angew. Chem. Int. Ed.*, **2014**, *53*, 5604–5608.
41. Mayr, F.; Brimioulle, R.; Bach, T. *J. Org. Chem.*, **2016**, *81*, 6965–6971.
42. Pecho, F.; Zou, Y.-Q.; Gramüller, J.; Mori, T.; Huber, S. M.; Bauer, A.; Gschwind, R. M.; Bach, T. *Chem. Eur. J.*, **2020**, *26*, 5190–5194.
43. Bertelsen, S.; Jørgensen, K. A. *Chem. Soc. Rev.*, **2009**, *38*, 2178–2189.
44. Donslund, B. S.; Johansen, T. K.; Poulsen, P. H.; Halskov, K. S.; Jørgensen, K. A. *Angew. Chem. Int. Ed.*, **2015**, *54*, 13860–13874.
45. Chen, C.; Chang, V.; Cai, X.; Duesler, E.; Mariano, P. S. *J. Am. Chem. Soc.*, **2001**, *123*, 6433–6434.
46. Silvi, M.; Verrier, C.; Rey, Y. P.; Buzzetti, L.; Melchiorre, P. *Nat. Chem.*, **2017**, *9*, 868–873.
47. Rigotti, T.; Mas-Ballesté, R.; Alemán, J. *ACS Catal.*, **2020**, *10*, 5335–5346.
48. Prier, C. K.; Rankic, D. A.; MacMillan, D. W. C. *Chem. Rev.*, **2013**, *113*, 5322–5363.
49. Shon, J.-H.; Teets, T. S. *Comments Inorg. Chem.*, **2020**, *40*, 53–85.
50. Zheng, J.; Swords, W. B.; Jung, H.; Skubi, K. L.; Kidd, J. B.; Meyer, G. J.; Baik, M.-H.; Yoon, T. P. *J. Am. Chem. Soc.*, **2019**, *141*, 13625–13634.

51. Skubi, K. L.; Kidd, J. B.; Jung, H.; Guzei, I. A.; Baik, M.-H.; Yoon, T. P. *J. Am. Chem. Soc.*, **2017**, *139*, 17186–17192.
52. Huang, X.; Quinn, T. R.; Harms, K.; Webster, R. D.; Zhang, L.; Wiest, O.; Meggers, E. *J. Am. Chem. Soc.*, **2017**, *139*, 9120–9123.
53. Yu, H.; Dong, S.; Yao, Q.; Chen, L.; Zhang, D.; Liu, X.; Feng, X. *Chem. Eur. J.*, **2018**, *24*, 19361–19367.
54. Lai, T. I.; Lim, E. C. *J. Am. Chem. Soc.*, **1985**, *107*, 1134–1137.
55. Lim, E. C. *J. Phys. Chem.*, **1986**, *90*, 6770–6777.
56. Krauter, C. M.; Möhring, J.; Buckup, T.; Pernpointner, M.; Motzkus, M. *Phys. Chem. Chem. Phys.*, **2013**, *15*, 17846–17861.
57. Lewis, F. D.; Barancyk, S. V. *J. Am. Chem. Soc.*, **1989**, *111*, 8653–8661.
58. Wang, H.; Fang, W.-H.; Chen, X. *J. Org. Chem.*, **2016**, *81*, 7093–7101.
59. El-Sayed, M. A. *Acc. Chem. Res.*, **1968**, *1*, 8–16.
60. Guo, H.; Herdtweck, E.; Bach, T. *Angew. Chem. Int. Ed.*, **2010**, *49*, 7782–7785.
61. Brimioulle, R.; Guo, H.; Bach, T. *Chem. Eur. J.*, **2012**, *18*, 7552–7560.
62. Brimioulle, R.; Bach, T. *Science*, **2013**, *342*, 840–843.
63. Brimioulle, R.; Bach, T. *Angew. Chem. Int. Ed.*, **2014**, *53*, 12921–12924.
64. Poplata, S.; Bauer, A.; Storch, G.; Bach, T. *Chem. Eur. J.*, **2019**, *25*, 8135–8148.
65. Poplata, S.; Bach, T. *J. Am. Chem. Soc.*, **2018**, *140*, 3228–3231.
66. Peschel, M. T.; Kabaciński, P.; Schwinger, D. P.; Thyrhaug, E.; Cerullo, G.; Bach, T.; Hauer, J.; de. Vivie-Riedle, R. *Angew. Chem. Int. Ed.*, **2021**, *60*, 10155–10163.
67. Wang, H.; Cao, X.; Chen, X.; Fang, W.; Dolg, M. *Angew. Chem. Int. Ed.*, **2015**, *54*, 14295–14298.
68. Skubi, K. L.; Blum, T. R.; Yoon, T. P. *Chem. Rev.*, **2016**, *116*, 10035–10074.
69. Yoon, T. P. *ChemPhotoChem*, **2019**, *3*, 1201–1202.
70. Du, J.; Skubi, K. L.; Schultz, D. M.; Yoon, T. P. *Science*, **2014**, *344*, 392–396.
71. Ischay, M. A.; Anzovino, M. E.; Du, J.; Yoon, T. P. *J. Am. Chem. Soc.*, **2008**, *130*, 12886–12887.
72. Du, J.; Yoon, T. P. *J. Am. Chem. Soc.*, **2009**, *131*, 14604–14605.
73. Amador, A. G.; Sherbrook, E. M.; Yoon, T. P. *J. Am. Chem. Soc.*, **2016**, *138*, 4722–4725.
74. Zhao, J.; Wu, W.; Sun, J.; Guo, S. *Chem. Soc. Rev.*, **2013**, *42*, 5323–5351.
75. Norikane, Y.; Itoh, H.; Arai, T. *J. Phys. Chem. A*, **2002**, *106*, 2766–2776.
76. Chou, P. T.; Martinez, M. L.; Cooper, W. C. *J. Am. Chem. Soc.*, **1992**, *114*, 4943–4944.
77. Sisa, M.; Bonnet, S. L.; Ferreira, D.; van der Westhuizen, J. H. *Molecules*, **2010**, *15*, 5196–5245.
78. Kalyanasundaram, K. *Coord. Chem. Rev.*, **1982**, *46*, 159–244.
79. Blum, T. R.; Miller, Z. D.; Bates, D. M.; Guzei, I. A.; Yoon, T. P. *Science*, **2016**, *354*, 1391–1395.
80. Miller, Z. D.; Lee, B. J.; Yoon, T. P. *Angew. Chem. Int. Ed.*, **2017**, *56*, 11891–11895.
81. Ma, L.; Fang, W.-H.; Shen, L.; Chen, X. *ACS Catal.*, **2019**, *9*, 3672–3684.
82. Daub, M. E.; Jung, H.; Lee, B. J.; Won, J.; Baik, M.-H.; Yoon, T. P. *J. Am. Chem. Soc.*, **2019**, *141*, 9543–9547.
83. Hörmann, F. M.; Chung, T. S.; Rodriguez, E.; Jakob, M.; Bach, T. *Angew. Chem. Int. Ed.*, **2018**, *57*, 827–831.
84. Hörmann, F. M.; Kerzig, C.; Chung, T. S.; Bauer, A.; Wenger, O. S.; Bach, T. *Angew. Chem. Int. Ed.*, **2020**, *59*, 9659–9668.
85. Pecho, F.; Sempere, Y.; Gramüller, J.; Hörmann, F. M.; Gschwind, R. M.; Bach, T. *J. Am. Chem. Soc.*, **2021**, *143*, 9350–9354.
86. Akiyama, T.; Itoh, J.; Yokota, K.; Fuchibe, K. *Angew. Chem. Int. Ed.*, **2004**, *43*, 1566–1568.
87. Yamanaka, M.; Itoh, J.; Fuchibe, K.; Akiyama, T. *J. Am. Chem. Soc.*, **2007**, *129*, 6756–6764.
88. Guo, J.; Fan, Y.-Z.; Lu, Y.-L.; Zheng, S.-P.; Su, C.-Y. *Angew. Chem. Int. Ed.*, **2020**, *59*, 8661–8669.

PART III

ASYMMETRIC SYNTHESIS THROUGH C–H BOND ACTIVATION

11

ASYMMETRIC C–H FUNCTIONALIZATION OF C(sp^2)–H BOND

UTTAM DHAWA[1], TOMASZ WDOWIK[1], AND LUTZ ACKERMANN[1,2]
[1]*Institut für Organische und Biomolekulare Chemie, Georg-August-Universität Göttingen, Göttingen, Germany*
[2]*Wöhler Research Institute for Sustainable Chemistry (WISCh), Georg-August-Universität Göttingen, Göttingen, Germany*

11.1. INTRODUCTION

Transition metal-catalyzed selective transformations of otherwise inert C–H bonds have been recognized as a powerful tool for the construction of complex molecular scaffolds [1], with notable applications to the synthesis of pharmaceutically relevant molecules [2], complex bioactive natural products [3], as well as in materials science [4]. Thus, the direct activation of inert C–H bonds represents a very attractive, atom- and step-economic approach for enabling novel transformations. Enantioselective C–H functionalization represents a valuable strategy for the assembly of complex chiral compounds from simple precursors. Thus, in recent years transition metal complexes have been identified as powerful catalysts for enantioselective C–H functionalization reactions [5], albeit until recently, full selectivity control relied heavily upon precious 4d and 5d transition metals, prominently featuring toxic or cost-intensive palladium, rhodium, and iridium complexes [6]. Recent focus has shifted toward Earth-abundant and cost-effective 3d transitions metals [7] for stereocontrolled organometallic C–H activations [8]. In addition, various strategies have evolved over the last decade for highly enantioselective transformations such as (i) the development of novel chiral ligands, (ii) use of chiral at-metal complexes, (iii) the transient directing group (TDG) approach, (iv) desymmetrization strategies, and (v) artificial metalloenzymes, among others. This review aims to provide the readers with a state-of-the-art summary in the bourgeoning area of inner-sphere enantioselective C(sp^2)–H bond functionalization until March 2021.

11.2. PALLADIUM CATALYSIS

Based on the pioneering studies by Sokolov and Reutov on stereoselective C–H activations [9], the combination of chiral ligands with palladium catalysts has been a dominant approach to achieve asymmetric induction in a variety of C–H activation reactions. The most commonly used ligands in this context include phosphorus-based ligands, such as $\alpha,\alpha,\alpha',\alpha'$-tetraaryl-2,2-disubstituted 1,3-dioxolane-4,5-dimethanol (TADDOL), 1,1′-bi-2-naphthol (BINOL), and 2,2′-bis(diphenylphosphino)-1,1′-binaphthyl (BINAP), as well as monoprotected amino acids (MPAAs) [10].

Catalytic Asymmetric Synthesis, Fourth Edition. Edited by Takahiko Akiyama and Iwao Ojima.

11.2.1. Phosphorus-Based Ligands

In 2009, Cramer presented an intramolecular desymmetrization of vinyl triflates **1** to deliver arylated chiral indane motifs **3** containing quaternary stereogenic centers (Scheme 11.1) [11]. TADDOL-derived ligand **2** was found to be the optimal choice to provide high enantioselectivity.

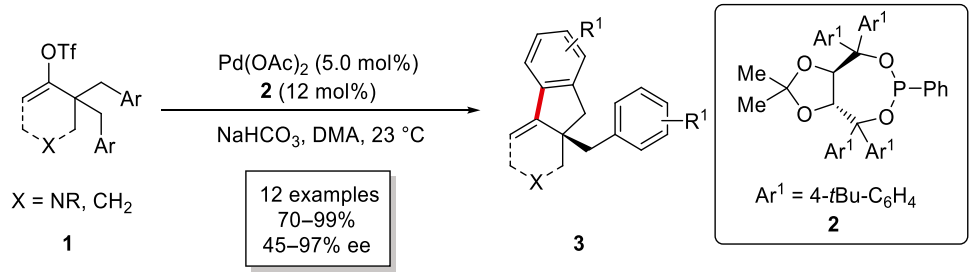

Scheme 11.1. Palladium-catalyzed arylation of vinyl triflates **1**. Source: [11]/John Wiley & Sons.

Later, a phosphoramidite ligand **5** was found to be crucial for the arylation of bromides **4** for the formation of dibenzazepinones **6** (Scheme 11.2) [12].

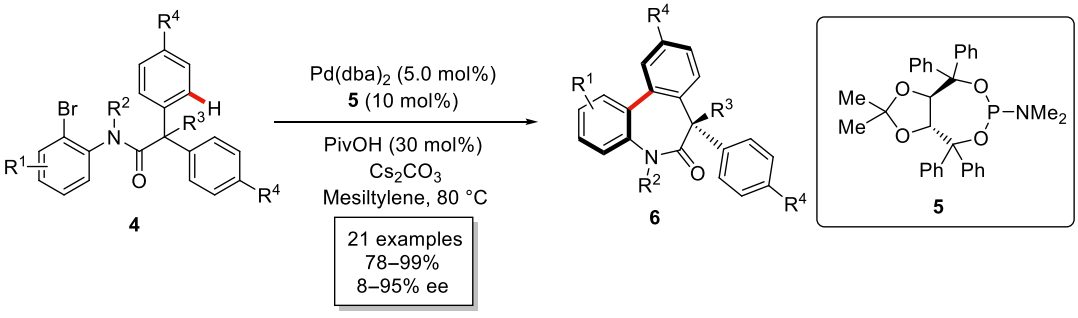

Scheme 11.2. Palladium-catalyzed asymmetric synthesis of dibenzazepinones **6**. Source: [12]/John Wiley & Sons.

In a related study, the same group reported an enantioselective C–H arylation strategy by the modification of the arene motifs to synthesize atropo-stable chiral dibenzazepinones [13]. TADDOL-based ligands were also applied to the formation of six-membered heterocycles containing a phosphorus stereogenic center, as reported independently by Duan [14] and Ma [15]. Another related example of TADDOL-ligand-facilitated asymmetric induction in an atroposelective cyclization was disclosed by Gu and coworkers in their C–H arylation of indole derivatives [16].

Planar chiral quinolinone-fused ferrocene derivatives have been successfully synthesized using TADDOL-derived phosphoramide ligands [17] but the majority of the contributions in this field focus on the use of BINAP as the chiral ligand [18].

In 2017, Zhu and You disclosed the enantioselective isocyanide insertion/desymmetrization C(sp²)–H bond activation reaction [19]. The key to success was represented by the use of 1,1′-spirobiindane-7,7′-diol (SPINOL)-derived ligand **9** to furnish the cyclized products **10** with high yields and enantioselectivities (Scheme 11.3).

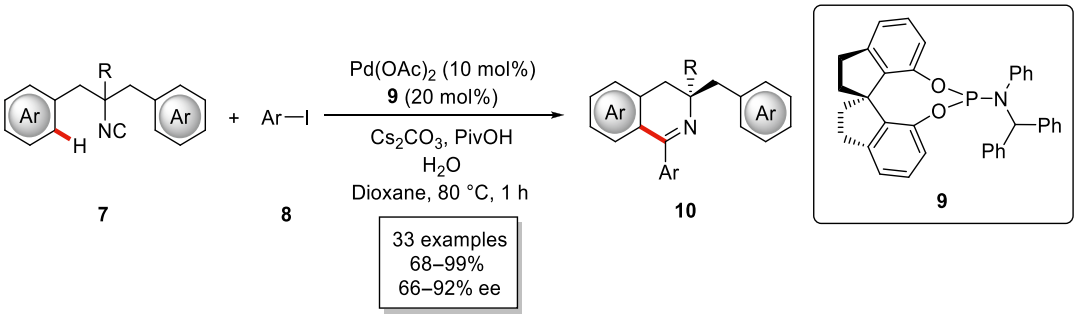

Scheme 11.3. Palladium-catalyzed desymmetrization toward 3,4-dihydroisoquinolines **10**.

SPINOL-derived chiral phosphoric acid **13** was also the best ligand in Shi's studies on the palladium-catalyzed atroposelective olefination of arenes **11** (Scheme 11.4) [20]. Later, the same group extended this approach to free amine (-NH_2) substrates [21].

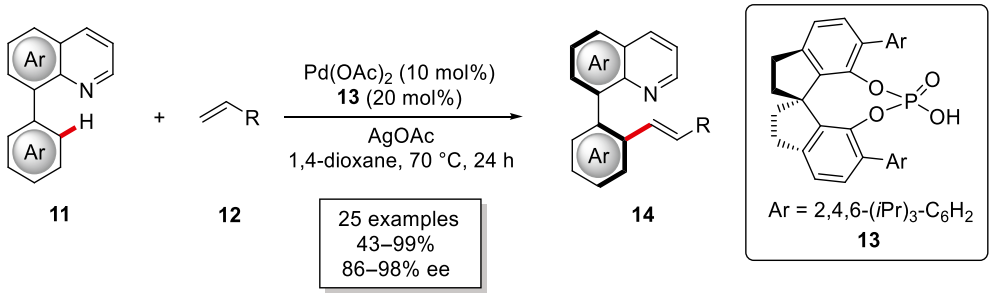

Scheme 11.4. Palladium-catalyzed atroposelective olefination of arene **11**. Source: [20]/John Wiley & Sons.

Atroposelective synthesis toward heterobiaryls [22] was disclosed by Baudoin and Cramer using another phosphorus-based ligand, namely H_8-BINAPO **17** (Scheme 11.5) [23]. Here, it was shown that for symmetrical bromides double C–H arylation leading to two stereogenic axes was possible.

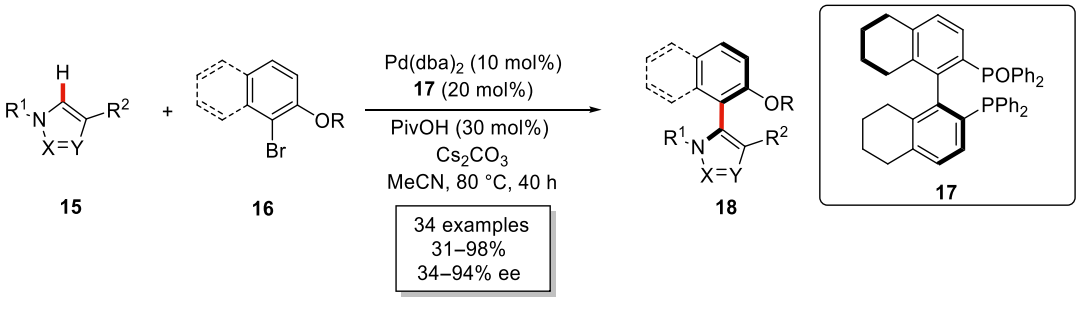

Scheme 11.5. Palladium-catalyzed atroposelective C–H arylation toward heterobiaryls **18**. Source: [23]/American Chemical Society.

In 2012, the intramolecular C–H arylation leading to five-membered rings containing a silicon-based stereogenic center **21** was demonstrated by Shintani and Hayashi with the aid of a Josiphos-type ligand

20 (Scheme 11.6) [24]. The authors proposed an oxidative addition of C–OTf bond into Pd(0), which subsequently undergoes base-assisted C–H metalation to form the palladacycle. Next, reductive elimination provides the desired silicon-based five-membered ring **21**.

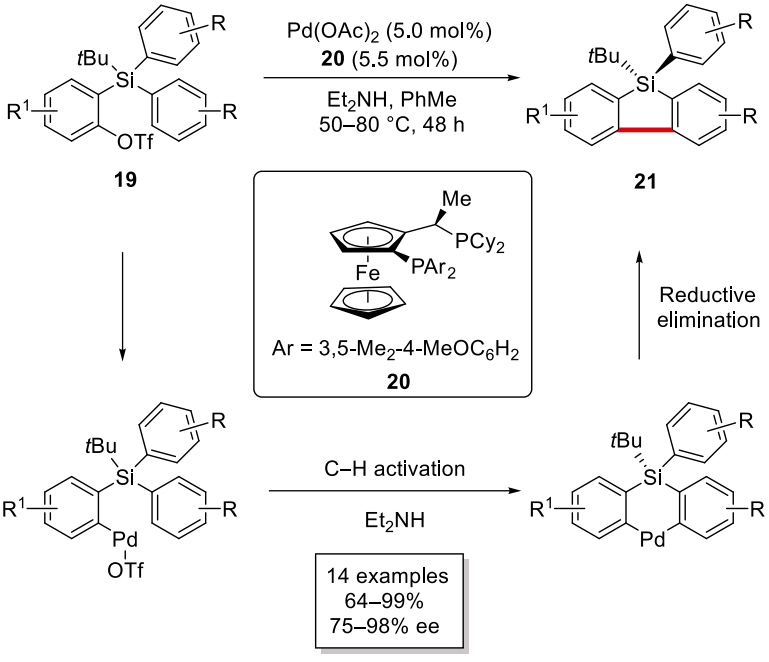

Scheme 11.6. Palladium-catalyzed desymmetrization of 2-(arylsilyl)aryl triflates **19**. Source: [24]/American Chemical Society.

Other noteworthy examples of the application of phosphorus ligands in enantioselective palladium catalysis include the intramolecular arylation toward 5,6-dihydrophenanthridines where a binaphthyl ligand containing both a phosphine and a carboxylate moiety was present [25], and the C–H alkenylation of ketene aminal phosphate with a phosphine ligand containing both point and axial chirality [26].

11.2.2. Monoprotected Amino Acids as Chiral Ligands

Based on a seminal study by Sokolov and Reutov [9], MPAAs have been identified as readily available sources of chirality and have been extensively employed in asymmetric C–H activation reactions [10a]. In an early report, Yu disclosed the bulky menthol-derived MPAA **23** enabled desymmetrization of diaryl(2-pyridyl)methane derivatives **22** with alkyl boronic acids **24** as coupling partners with high enantioselectivities (Scheme 11.7) [27].

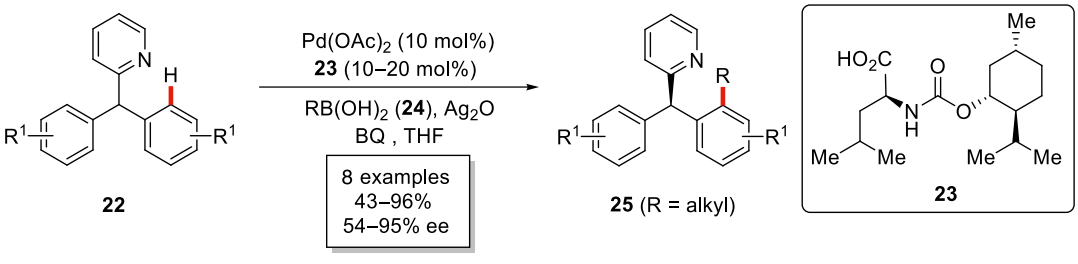

Scheme 11.7. Palladium-catalyzed desymmetrization using MPAA **23**. Source: [27]/John Wiley & Sons.

In subsequent studies on MPAA-induced enantioselective C–H activation, arylboronic acid pinacol esters were used as coupling partners for the desymmetrization of diarylmethylamines [28] and diarylphosphinamides [29].

In 2010, a combination of a palladium catalyst and the MPAA **27** was applied by Yu for the desymmetrization of *α,α*-diphenylacetates **26** with styrene derivatives **12** (Scheme 11.8) [30]. Later, a related protocol was established for the free acid, which underwent C–H activation/C–O cyclization [31].

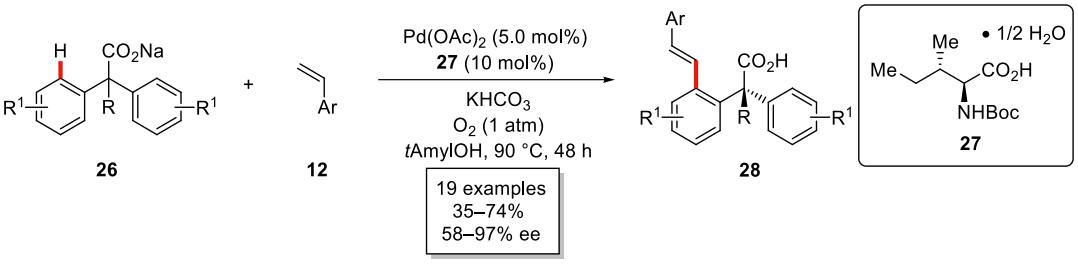

Scheme 11.8. Palladium-catalyzed olefination of *α,α*-diphenylacetates **26**. Source: [30]/American Chemical Society.

In 2013, Yu realized the desymmetrization of diarylmethylamines **29** using molecular iodine as both a reagent and an oxidant (Scheme 11.9) [32]. High enantioselectivity in this C–H iodination was achieved using protected leucine derivative **30**.

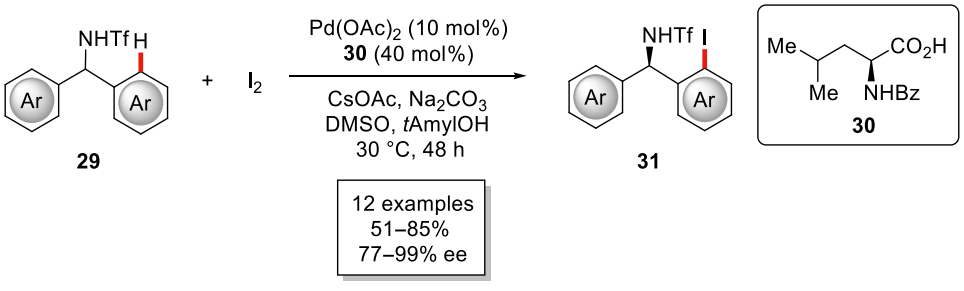

Scheme 11.9. Palladium-catalyzed C–H iodination of diarylmethylamines **29**. Source: [32]/American Chemical Society.

Asymmetric functionalizations of ferrocenes using MPAAs as chiral ligands are a subject of research by several groups (Scheme 11.10). In 2013, Gu and You reported the enantioselective arylation with arylboronic acids **32** using Boc-L-Val-OH (**33**) as the ligand [33]. In the same year, the olefination of ferrocenes [34] as well as dehydrogenative annulation with diarylethynes [35] under similar conditions were demonstrated. Later, further functionalizations were disclosed, including enantioselective biaryl couplings of ferrocenes **31** with heteroarenes **39** [36].

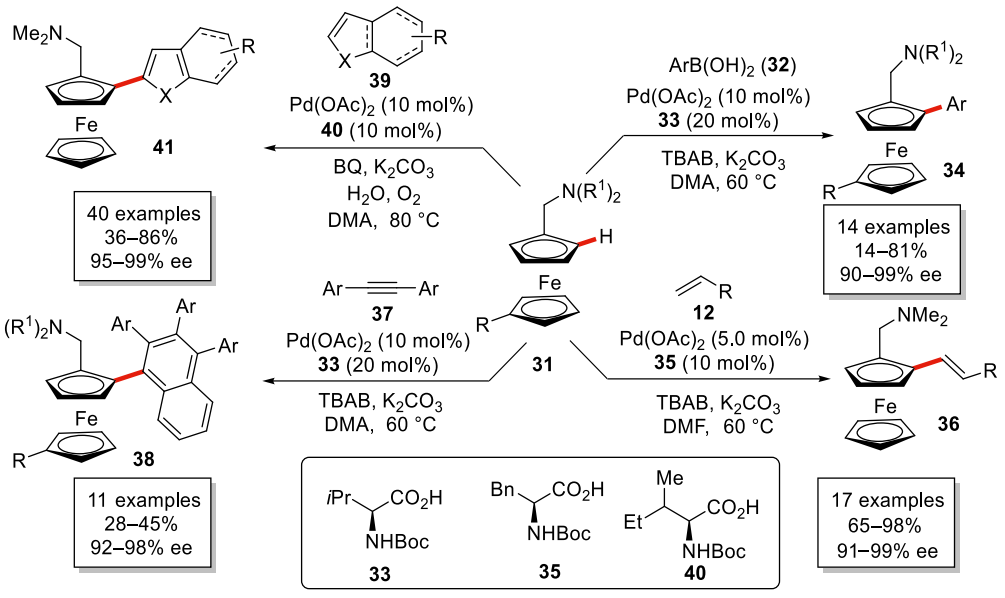

Scheme 11.10. Palladium-catalyzed asymmetric functionalization of ferrocenes **31**.

Yu employed MPAA ligands in the palladium-catalyzed iodination of chiral arylalkylamines as well as *β*-amino acid and *β*-amino alcohol derivatives [37]. As the starting materials were chiral themselves, the reaction proceeded via kinetic resolution with excellent levels of stereocontrol (Scheme 11.11). Later, olefins [38] and arylboronic acid pinacol esters [39] were also found as the efficient coupling partners

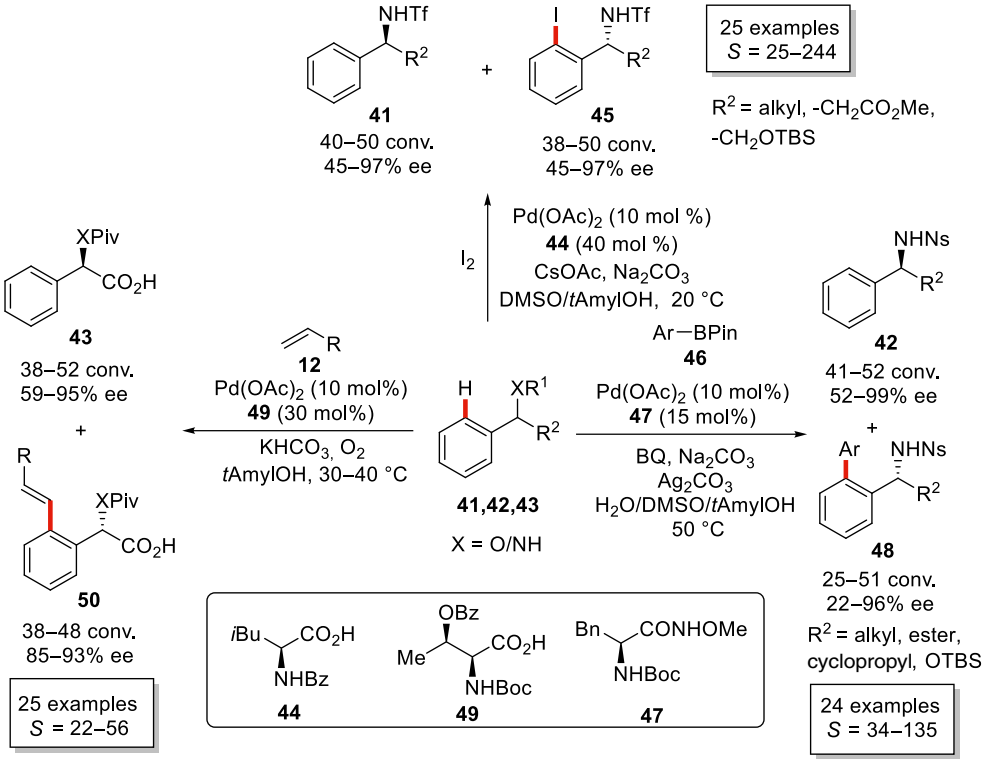

Scheme 11.11. Palladium-catalyzed enantioselective functionalization of arenes using MPAAs.

(Scheme 11.11). In the latter case, a mono-*N*-protected hydroxamic acid derivative was used instead of MPAA. Kinetic resolution for the atroposelective C–H iodination was also disclosed using MPAAs by You [40].

In 2017, Yang reported the atroposelective olefination of biaryls containing $P(O)Ph_2$ as the directing group [41]. A more recent example of atroposelective olefination was disclosed by Shi, employing L-pyroglutamic acid as the chiral ligand [42].

11.2.3. Other Ligands

In 2019, Cramer developed a protocol for the asymmetric synthesis of 1*H*-isoindole derivatives **53** (Scheme 11.12) [43]. For this reaction, diaminooxophosphine [44] ligand **52** provided the highest enantioselectivity.

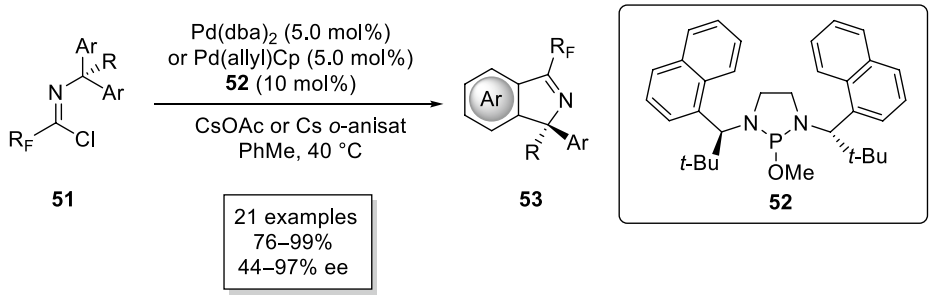

Scheme 11.12. Enantioselective C–H activation using phosphordiamidite ligand **52**.

In 2017, Han disclosed a C–H functionalization/intramolecular asymmetric allylation (Scheme 11.13) [45]. Crucial to this reaction was the use of ligands with sulfur stereogenic centers **56** as no reaction was observed when nitrogen or phosphorus ligands were tested.

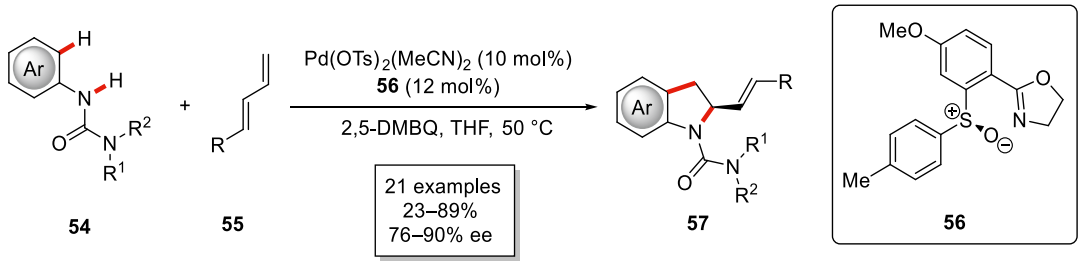

Scheme 11.13. Enantioselective C–H activation using sulfoxide-oxazoline ligand **56**. Source: [45]/John Wiley & Sons.

Ligands of this type were also applied to the atroposelective coupling of thiophene with napthylboronic acids by Itami [46], offering higher yields than the previously used chiral bisoxazoline ligand [47].

11.2.4. Chiral Transient Auxiliary

The introduction of chiral TDGs [1c] as a source of chirality [48] has become a rapidly growing field of research in C–H activation [49]. In 2017, Shi introduced this strategy for the atroposelective functionalizations of biaryl containing aldehydes **58** in the presence of commercially available L-*tert*-leucine, which forms a chiral imine that directs C–H activation and induces enantioselectivity [50]. This approach was

successfully extended to various coupling partners including olefins **12** [50], protected alkynyl bromides **60** [51], 7-oxabenzonorbornadiene derivatives **62** [52], 4-vinyl-1,1-dioxolan-2-one **64** [53], and allyl acetate derivatives **66** [53] by Shi (Scheme 11.14).

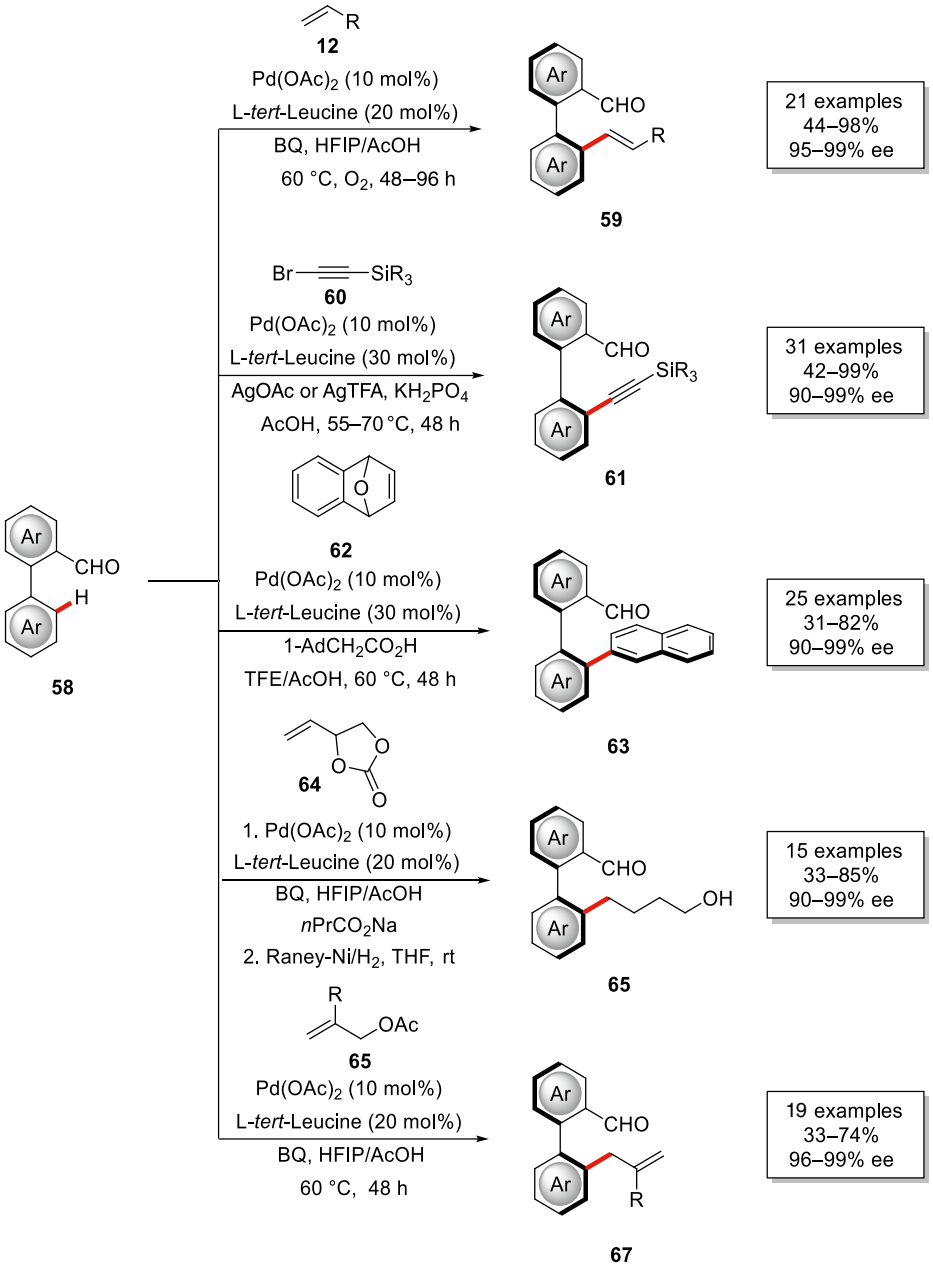

Scheme 11.14. Palladium-catalyzed atroposelective transformations of biaryls **58** using TDG strategy.

Subsequently, Shi's approach was further extended to the atroposelective synthesis of functionalized heterobiaryls as demonstrated by his group [54] as well as Xie [55]. In 2020, Shi disclosed bulky amino amide **69** as a chiral TDG, providing access to chiral styrenes **70**, via the atroposelective olefination of arenes **68**. (Scheme 11.15) [56].

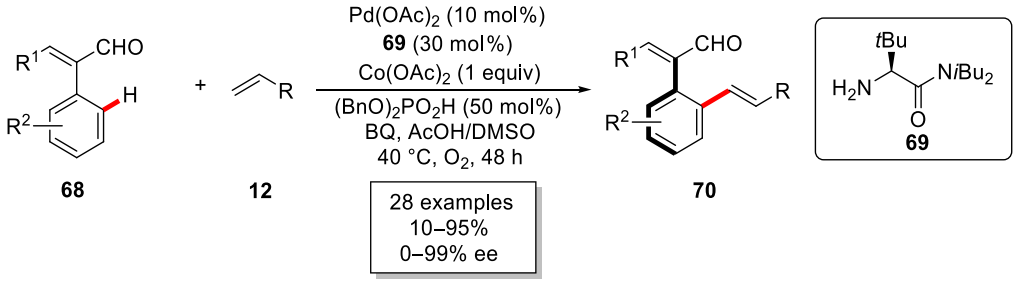

Scheme 11.15. Palladium-catalyzed atroposelective olefination of arenes **68**. Source: [56]/John Wiley & Sons.

11.2.5. Chiral Auxiliaries

Biaryls containing covalently attached chiral auxiliaries can induce diastereoselectivity in the functionalized products. This approach was explored by Colobert and Wencel-Delord for enantioenriched sulfoxides with sulfur as the stereogenic center **71** in olefination [57], acetoxylating and halogenation [58], as well as arylation [59] reactions (Scheme 11.16). With arene containing chiral auxiliary, the atroposelective olefination was possible via dynamic kinetic resolution [60].

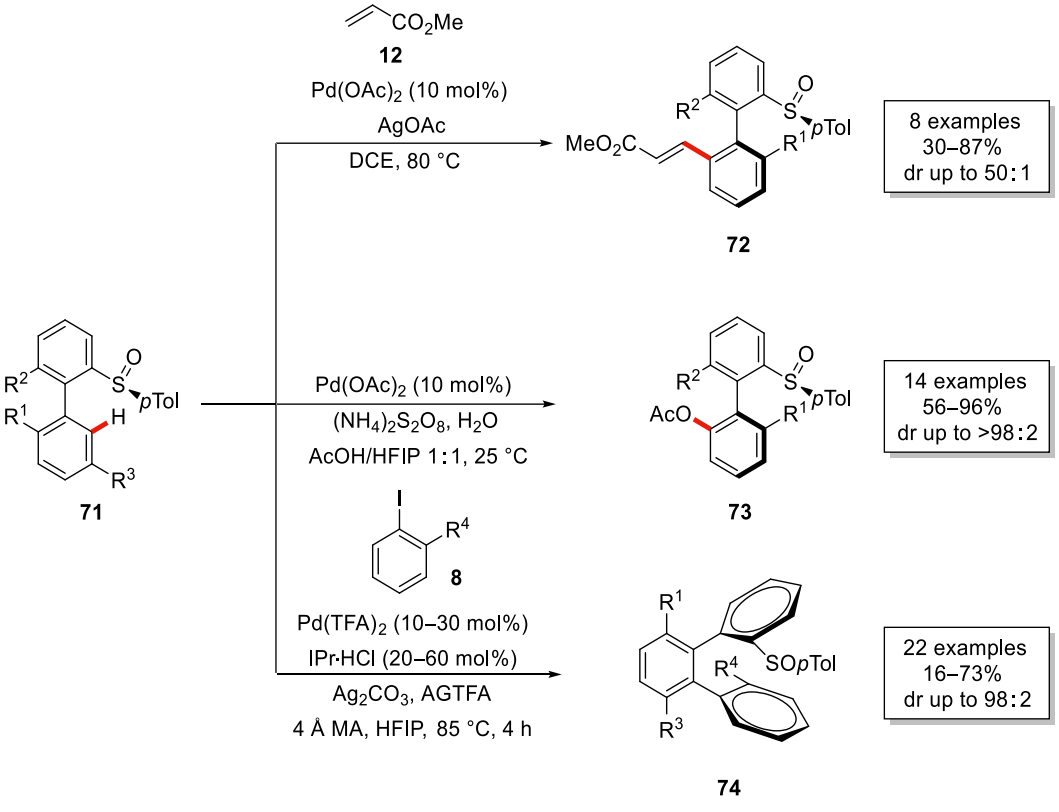

Scheme 11.16. Palladium-catalyzed diastereoselective C–H activation of biaryls **71**.

11.2.6. Cooperative Catalysis

In 2018, another approach toward asymmetric C–H activation was put into practice by Yu [61]. It involved the use of chiral norbornene derivative that inserts into the *ortho*-palladate intermediate and induces enantioselectivity. The use of norbornene derivative as a chiral mediator was demonstrated subsequently

in the three-component enantioselective reaction involving aryl iodides **8**, aryl bromides **75,** and variety of terminating reagents including olefins **12**, alkynes, cyanide, boronic acids, and ketones (Scheme 11.17) [62].

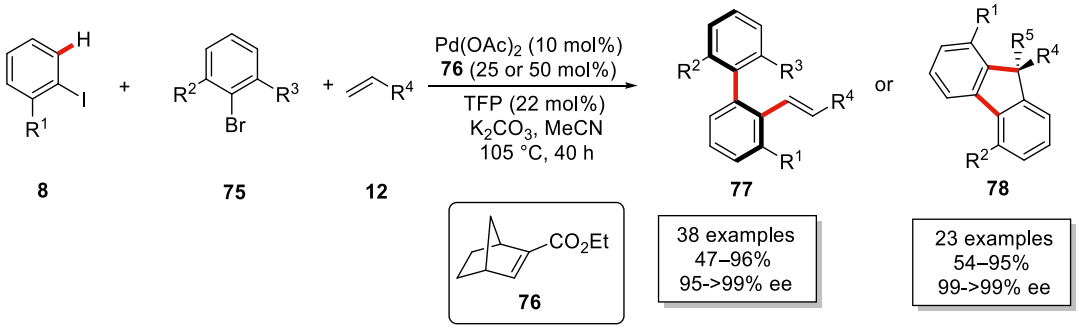

Scheme 11.17. Palladium/chiral norbornene cooperative catalysis. Source: [62]/Springer Nature.

11.2.7. Electrochemical C–H Activations

Despite significant advancement in palladium-catalyzed C–H activation, reports on enantioselective electrochemical transformations are scarce [63]. In 2020, Ackermann and coworkers reported on the first asymmetric metalla-electrocatalyzed [64] C–H activation (Scheme 11.18). The authors disclosed the unprecedented use of TDGs for the asymmetric pallada-electrocatalyzed C–H olefinations for the synthesis of enantiomerically enriched axially chiral biaryls **59** and heterobiaryl scaffolds **80** under mild conditions [65].

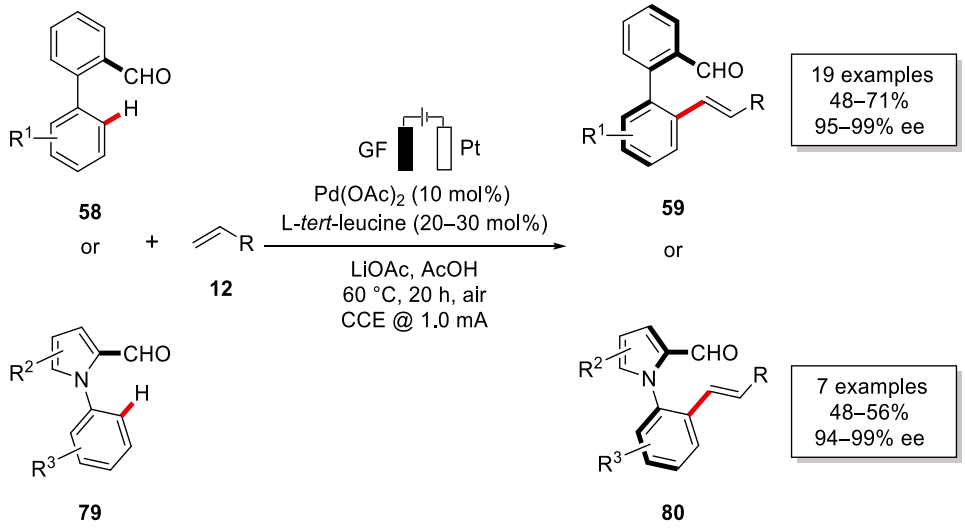

Scheme 11.18. Atroposelective pallada-electrocatalyzed C–H activation. Source: Based on [65].

11.3. RHODIUM CATALYSIS

11.3.1. Chiral Cp^x-Based Catalysts

During the past few years, chiral cyclopentadienyl-based catalysts have gained considerable momentum in enantioselective C–H activation reactions [66]. Key factors for the successful design of the chiral complexes were the C2 symmetry of the ligands, restricted rotation around the Cp ring, and a steric block perpendicular to the Cp plane. The utility of these complexes was first demonstrated by Cramer for the annulation of hydroxamic acid derivatives **81** with olefins **82** (Scheme 11.19) [67].

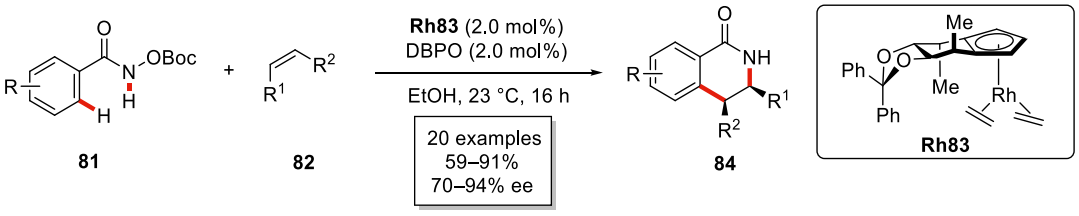

Scheme 11.19. Rhodium-catalyzed enantioselective C–H annulation. Source: [67]/American Association for the Advancement of Science.

The application of complex **Rh83** in the reaction of hydroxymates **85** with allenes **86** resulted in poor enantioselectivity and required a redesigned ligand having an axially chiral BINOL-derived biaryl moiety present [68]. The enantioselectivity of the reaction could be further tuned by changing the substitution pattern at the *ortho* positions of the arenes, with a bulky triisopropylsilyl (TIPS) substituent **Rh87** providing the optimal results (Scheme 11.20). The allene preferentially approaches from the vacant side of the ligand backbone in such a way where less substituted double bond co-ordinates with the cyclometalated intermediate and the substituent stays away from the bulky cyclopentadienyl ring.

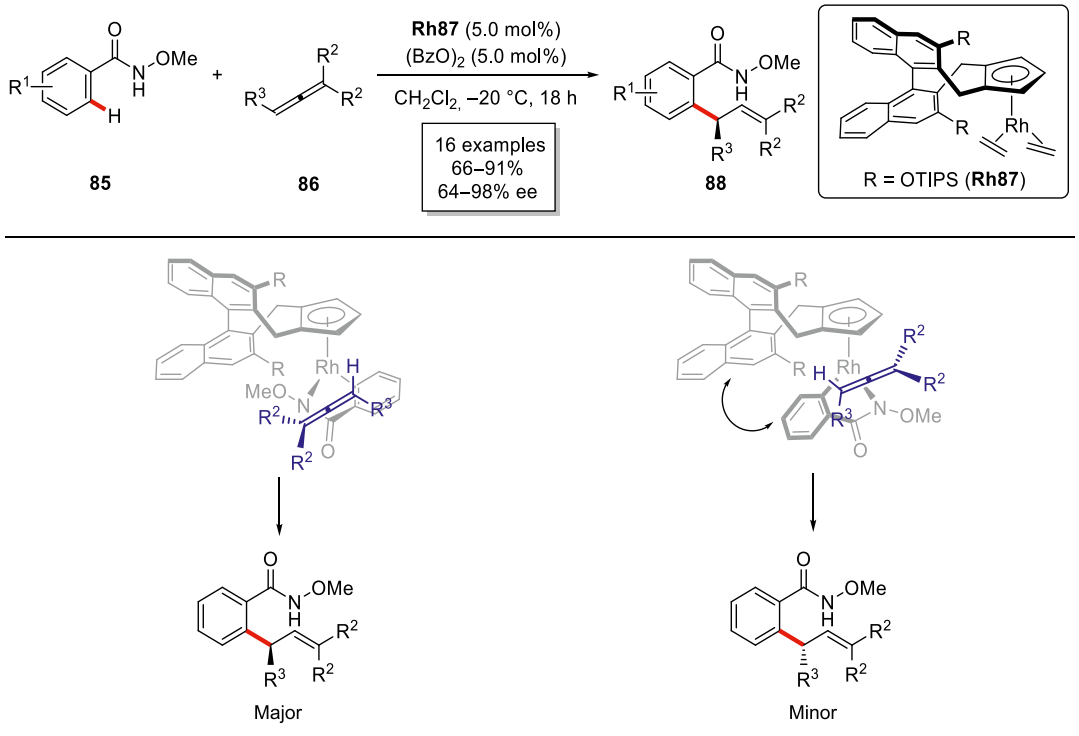

Scheme 11.20. Rhodium-catalyzed enantioselective C–H allylation.

In subsequent reports, a similar chiral Cp^x complex was efficiently used for several enantioselective intramolecular reactions to synthesize cyclized scaffold [69]. The application of diazo derivatives **90** as one-carbon components enabled the syntheses of isoindolone derivatives **92** via rhodium-catalyzed C–H activations using chiral Cp^x complex **Rh87** or **Rh91** (Scheme 11.21) [70].

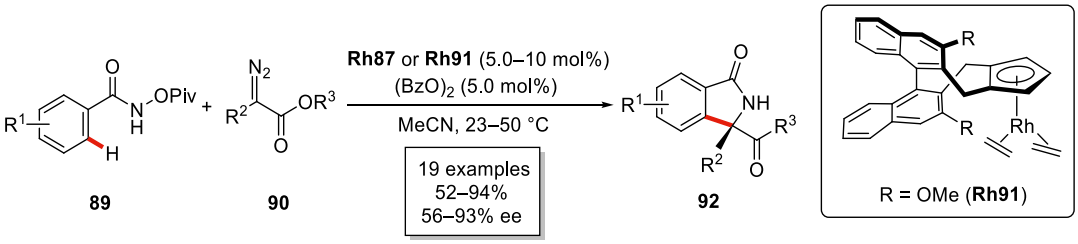

Scheme 11.21. Rhodium-catalyzed enantioselective synthesis of isoindolones. Source: [70]/John Wiley & Sons.

In 2015, You developed an asymmetric [3+2] spiroannulation to access quaternary stereogenic centers with the aid of Cramer's catalyst **Rh91** under oxidative conditions (Scheme 11.22) [71]. The reaction proceeds through an eight-membered rhodacycle **98** after the coordination with alkyne **37**, which is possibly in equilibrium with its six-membered isomer **99**. Subsequently, reductive elimination provides

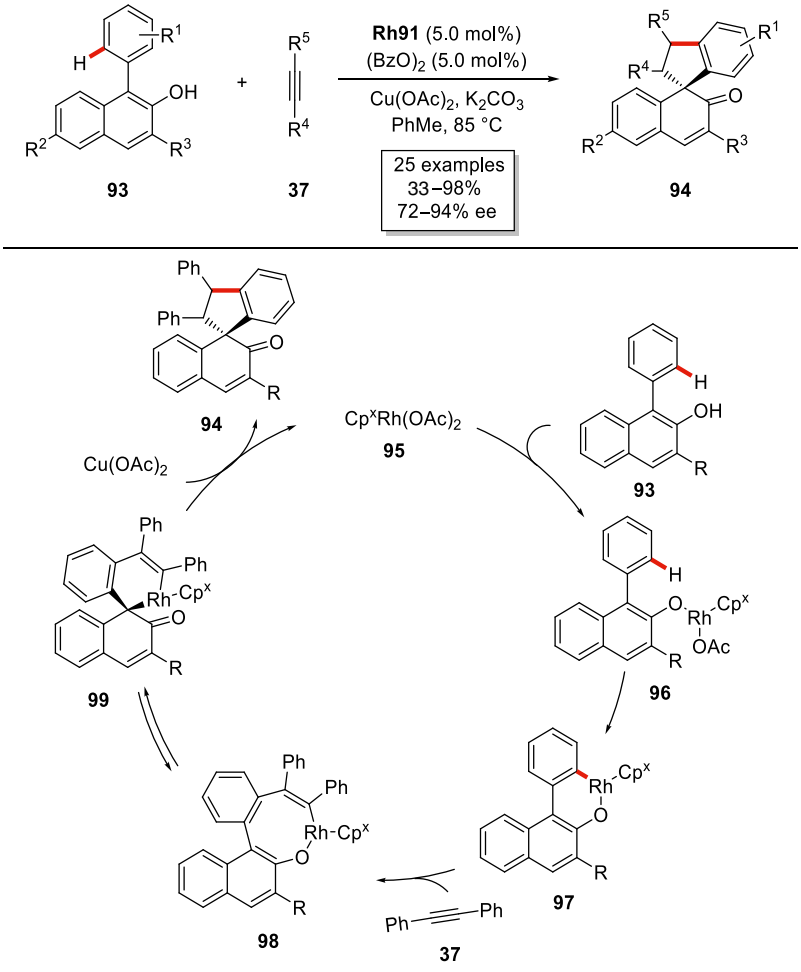

Scheme 11.22. Rhodium-catalyzed spiroannulation toward dearomatized naphthols **94**. Source: [71]/American Chemical Society.

the desired product **94** and Rh(III) is generated after oxidation by $Cu(OAc)_2$. Related studies were published around the same time and disclosed the synthesis of spiroindenes by coupling cyclic 1,3-dicarbonyl derivatives and internal alkynes [72].

Another class of spirocyclic compounds was obtained by combining 4-aryl-5-pyrazolone and alkynes using SPINOL-derived chiral rhodium complex [73].

In 2020, Li demonstrated chirality transfer from axial chirality to a stereogenic center toward spirocycles **103** (Scheme 11.23) [74]. The reaction proceeded via the atroposelective formation of a biaryl intermediate that transforms into the product via an intramolecular dearomative process.

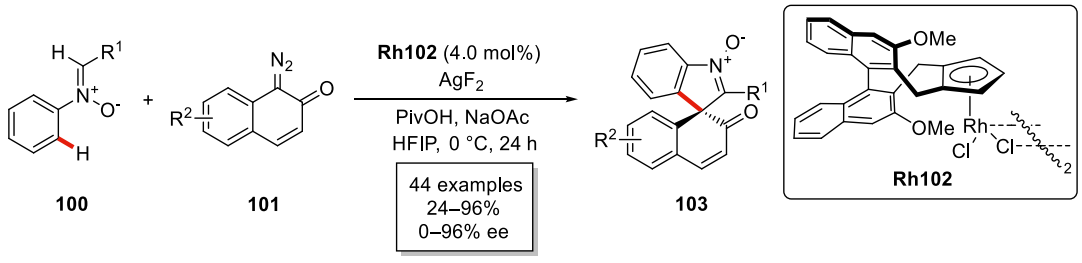

Scheme 11.23. Rhodium-catalyzed axial-to-central chirality transfer toward spirocycles **103**. Source: [74]/John Wiley & Sons.

In 2019, Cramer presented an enantioselective synthesis of cyclopentenylamines **108** or **109** from arenes **104** or **105** containing oxime ethers as the directing group and diazabicycle olefins **106** (Scheme 11.24) [75]. For this transformation, two ethylene groups needed to be replaced with cyclooctadiene **Rh107** in order to achieve high enantioselectivity.

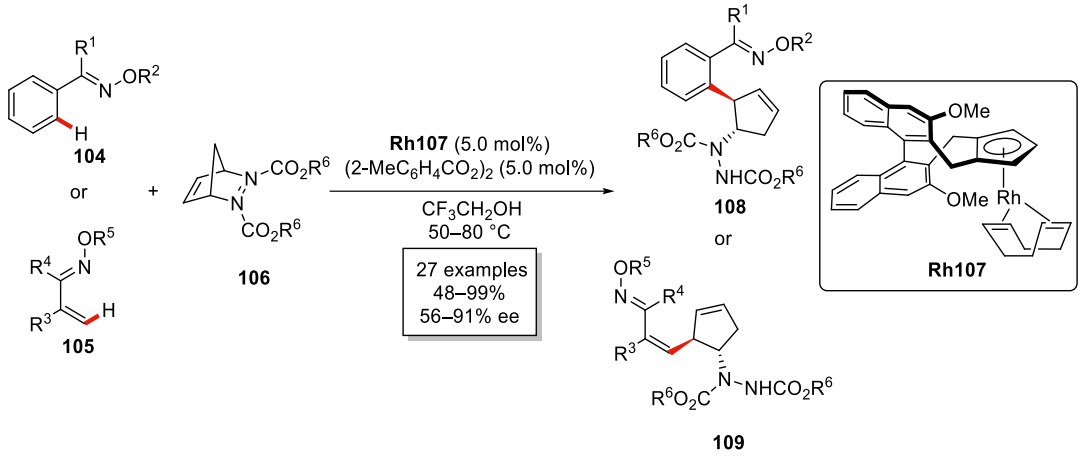

Scheme 11.24. Rhodium-catalyzed C–H activation toward cyclopentenylamines. Source: [75]/John Wiley & Sons.

7-Azabenzonorbornadienes were also applied to C2 functionalization of indoles by Li [76]. Subsequently, the same group developed an enantioselective [3+2] annulation of arene containing a flexible amide directing group **110** and 7-azabenzonorbornadiene derivatives **111** via twofold C–H activation pathway (Scheme 11.25) [77].

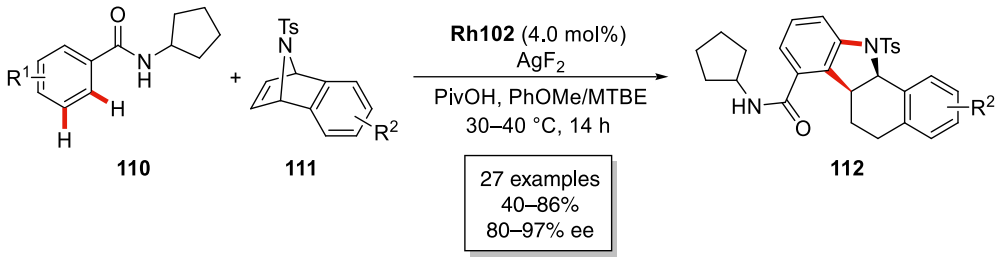

Scheme 11.25. Rhodium-catalyzed enantioselective dual C–H activation. Source: [77]/John Wiley & Sons.

A similar type of catalyst was also efficient in the addition of nitroalkenes **113** to aryl C–H bond as demonstrated for a few examples in studies by Ellman (Scheme 11.26) [78].

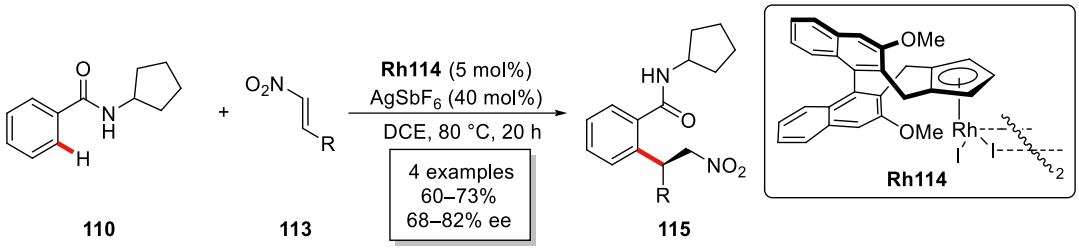

Scheme 11.26. Rhodium-catalyzed enantioselective addition of nitroalkenes **113**. Source: [78]/American Chemical Society.

Later, the same group showed the potential for the same rhodium complex in the three-component reaction involving arene **104**, ethylene, and aminating agent **116**, leading to the formation of α-methyl branched amines **117** (Scheme 11.27) [79].

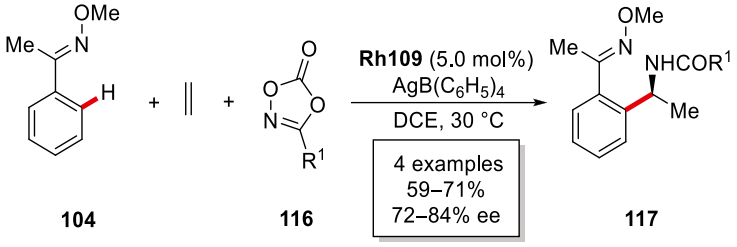

Scheme 11.27. Rhodium-catalyzed enantioselective three-component coupling. Source: [79]/Springer Nature.

While a majority of asymmetric C(sp²)–H activation reactions were studied for aryl C–H bonds, it was possible to activate alkenyl C–H bonds. It was demonstrated by Cramer for the [4+1] annulation between acrylamides derivatives and allenes [80].

In 2014, You demonstrated that chiral Cp^x rhodium complexes were also effective in atroposelective modification of biaryls **118** via olefination reactions with alkenes **12** (Scheme 11.28) [81]. In subsequent studies, it was found that decorating the complex with an SPINOL-type ligand led to improved enantioselectivities [82].

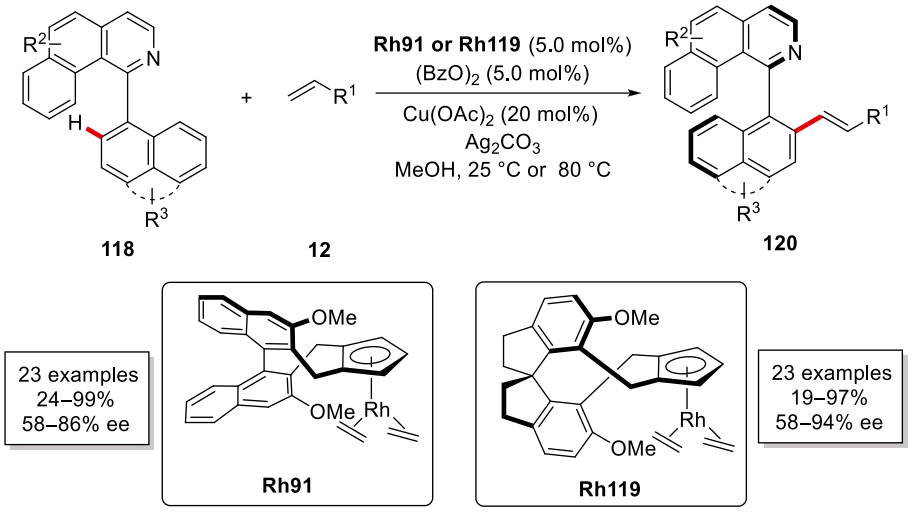

Scheme 11.28. Rhodium-catalyzed atroposelective C–H allylation. Source: [81]/John Wiley & Sons.

The same complex was employed in 2019 by Wang in their studies on the asymmetric version of the reaction developed by group of Satoh and Miura [83]. The reaction proceeds via dual C–H activation with the formation of additional arene producing atropo-stable indolinone derivative **122** with high levels of enantioselectivity (Scheme 11.29) [84].

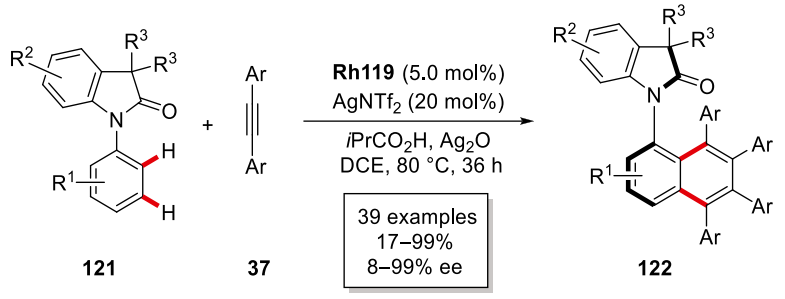

Scheme 11.29. Rhodium-catalyzed atroposelective synthesis of C–N axially chiral biaryls **122**. Source: [84]/John Wiley & Sons.

In addition to the aforementioned reports, successful approaches have been described for the atroposelective synthesis of biaryls using chiral Cp^x complex with notable contributions from Li [85], as well as Antonchick and Waldmann [86].

A different approach to the design of chiral rhodium Cp^x complex was proposed by Perekalin who developed a planar chiral catalyst $[(C_5H_2t\text{-}Bu_2CH_2t\text{-}Bu)RhI_2]_2$ and showed its application in the annulation of hydroxamic acids and alkenes [87].

Use of heteroarenes as coupling partners for atroposelective C–H arylation was also disclosed by You, but it required SPINOL-derived chiral rhodium complex together with chiral carboxylic acid [88].

As synthesis of chiral rhodium complexes is typically a complex multistep synthesis, Matsunaga investigated that mixing an achiral complex with a chiral organic anion can induce enantioselectivity as well. They developed a hybrid catalyst, namely a 1 : 1 mixture of Cp*Rh(III) and (*S*)-BINSate anion **124**, and successfully applied it to the enantioselective conjugate addition of 2-phenylpyridine **123** with α,β-unsaturated ketones **82** (Scheme 11.30) [89]. The scope of the reaction could be expanded to 6-arylpurines **126**, but it required the use of a redesigned catalyst based on (*R*)-SPISate spirocyclic anion **127**.

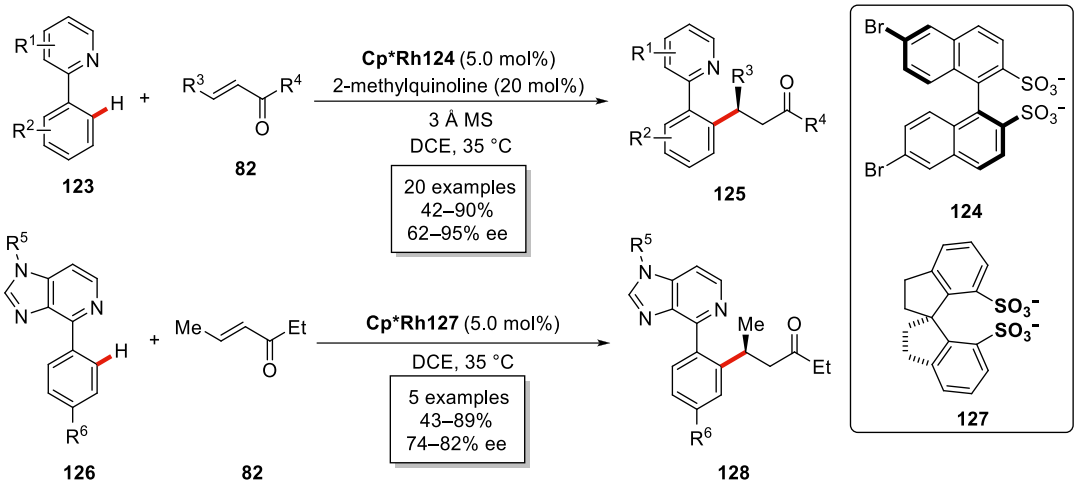

Scheme 11.30. Rhodium-catalyzed C–H activation using hybrid catalysts. Source: [89]/Springer Nature.

11.3.2. In-Situ Generated Chiral Complexes

Controlling enantioselectivity by the combination of exogenous chiral ligands with achiral rhodium complex, leading to the formation of in-situ chiral complexes, is another attractive approach to avoid the multistep challenging synthesis of chiral rhodium catalyst and was proven effective for several class of ligands.

11.3.2.1. Phosphine Ligand A pioneering elegant report by Murai disclosed rhodium(I)-catalyzed enantioselective hydroarylation with the aid of a homochiral monodentate phosphine ligand [90]. Later, Ellman/Bergman presented intramolecular imine-directed hydroarylations of ketimines **129** (Scheme 11.31). The use of BINOL-based chiral ligands **130** or **131** provided access to the indane scaffold **132** with high enantioselectivity [91].

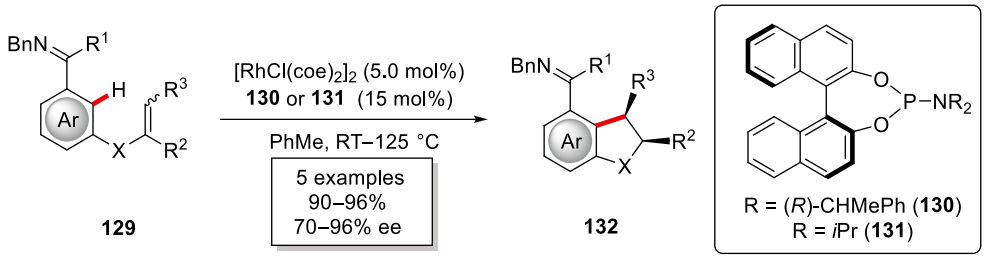

Scheme 11.31. Rhodium-catalyzed hydroarylation of ketimine **129**.

These early pioneering studies have set the stage for various enantioselective annulation reactions using alkynes and allenes as coupling partners by the aid of chiral biphosphine ligands [92].

Another asymmetric C–H activation relying on (*R*)-BINAP **134** was demonstrated by the group of Kuninobu for the synthesis of spirosilabifluorone derivatives (Scheme 11.32) [93]. Desymmetrization of bis(phenyl)silane **133** using a rhodium catalyst led to the formation of spirocyclic products **135** with a silicon-based stereogenic center.

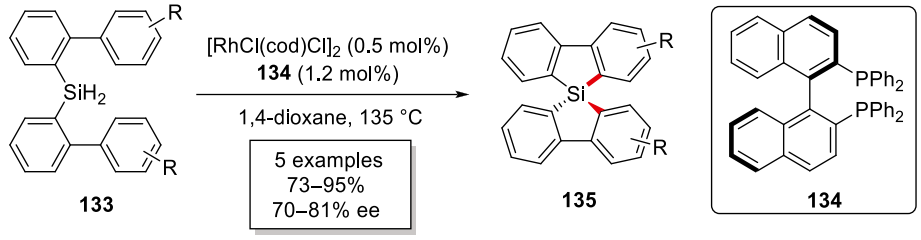

Scheme 11.32. Rhodium-catalyzed synthesis of spirosilabifluorone derivatives **135**. Source: [93]/John Wiley & Sons.

In 2018, Matsunaga disclosed a combination of chiral carboxylic acid **138** with Cp*Rh(III) complex to facilitate the formation of 1,4-dihydroisoquinolin-3(2*H*)-one derivatives **139** via desymmetrization of diarylmethylamines **136** (Scheme 11.33) [94].

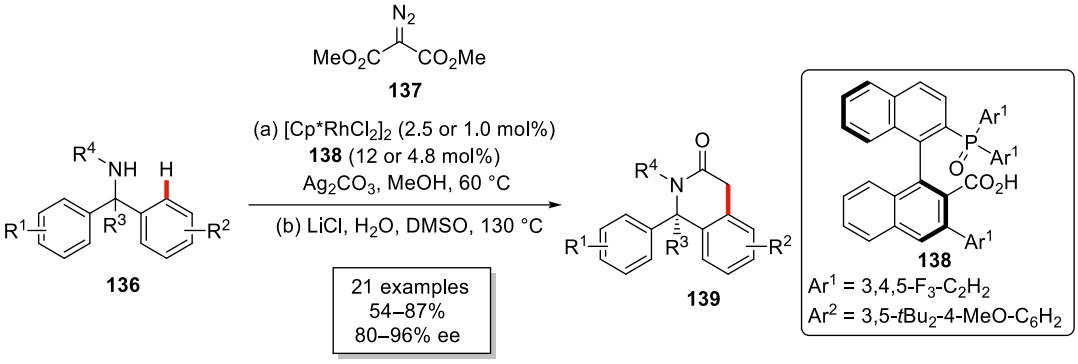

Scheme 11.33. Rhodium-catalyzed C–H activation using chiral carboxylic acid **138**. Source: [94]/John Wiley & Sons.

Enantioselective arylation toward five-membered ring containing silicon was also disclosed for the synthesis of chiral metallocenes with the aid of (*S*)-trimethylsilyl(TMS)-SEGPHOS [95] and (*R*)-3,5-di-*tert*-butyl-4-methoxyphenyl(DTBM)-SEGPHOS [96] ligands. In 2019, You demonstrated the arylation of ferrocenes **140** using TADDOL-based chiral ligand **141** facilitated by thioketone as the directing group (Scheme 11.34) [97].

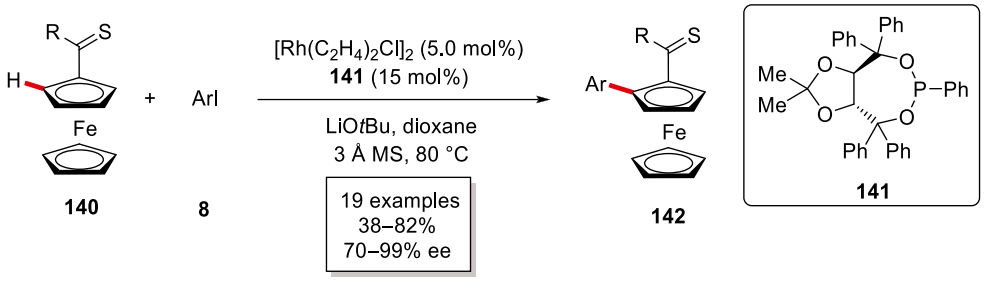

Scheme 11.34. Rhodium-catalyzed C–H arylation of ferrocenes **140**. Source: [97]/Springer Nature.

Later the same group applied similar reaction conditions with TADDOL-derived monodentate phosphonite for atroposelective C–H arylation to synthesize highly enantioenriched chiral biaryls [98].

11.3.3. Other Strategies

In 2012, Ward and Rovis devised a very different strategy for the enantioselective C–H activation using rhodium catalysis [99]. Here, Cp* ligand is linked with biotin derivative **143** that binds to streptavidin in a host-guest type of interaction typical for enzymes providing suitable environment for asymmetric induction. This system was initially investigated for enantioselective annulation of hydroxymates **89** and olefins **82** (Scheme 11.35).

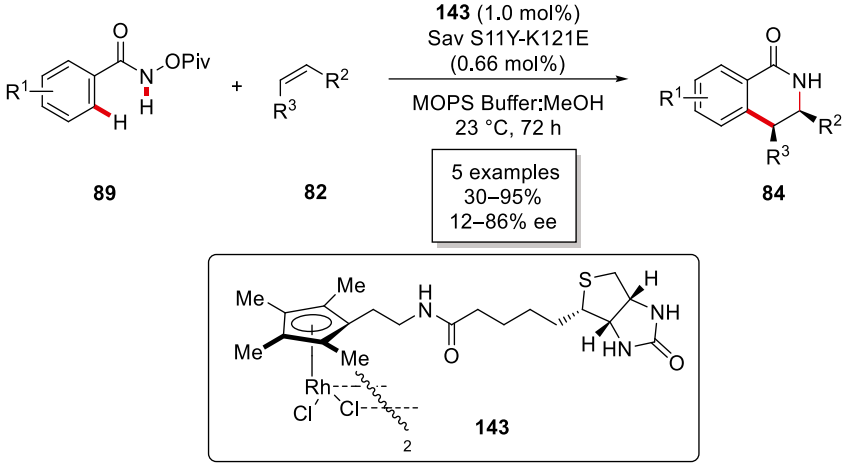

Scheme 11.35. Rhodium-catalyzed C–H activation with artificial metalloenzymes.

A few years later, the scope of this reaction was expanded to include acrylamide hydroxamate esters that reacted with styrenes to afford δ-lactams with high yields and enantioselectivity [100].

Using chiral TDG instead of chiral ligand, a strategy for enantioselective C–H activation was explored for multiple reactions catalyzed by palladium. In 2019, Wang introduced this concept to rhodium catalysis in their synthesis of chiral phathalides from simple aldehydes [101].

11.4. IRIDIUM CATALYSIS

Over the past years, iridium complexes have featured prominently in the activation of otherwise inert C–H bonds. Compared with rhodium and cobalt complexes, iridium catalysts often offer different selectivities due to their different electronegativities, ionization potentials, and high stabilities of organoiridium species [102]. Consequently, this has inspired the synthetic community for the development of novel enantioselective C–H transformations using iridium complexes [103].

11.4.1. C–C Bond Formations

11.4.1.1. Phosphorus-Based Ligands In 2000, Togni reported an early example of iridium-catalyzed enantioselective C–H hydroarylation of norbornene **145** with benzamide **144** to provide the alkylated product **147** in 94% ee, albeit with a low yield of 12% (Scheme 11.36) [104]. Later, in 2008, Shibata disclosed a single example of enantioselective C–H hydroarylation of 2'-methylacetophenone with norbornene in the presence of $[Ir(cod)_2]BF_4$ as the catalyst and (*R*)-MeO-2,2′-bis(diphenylphosphino) biphenyl (BIPHEP) as the chiral ligand [105].

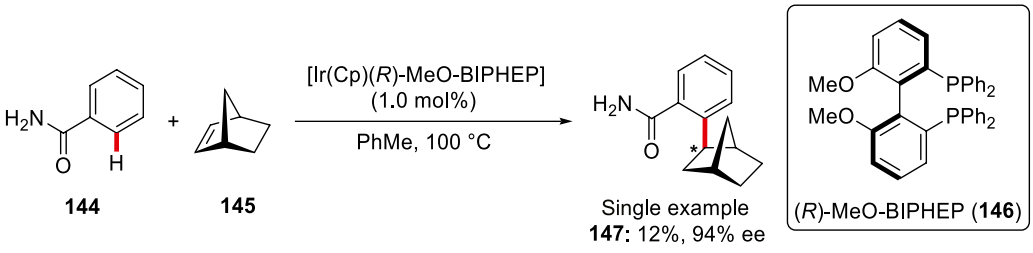

Scheme 11.36. Early example of the enantioselective hydroarylation of norbornene **145**. Source: [104]/Springer Nature.

In 2013, Hartwig and coworkers reported asymmetric C–H additions of heteroarenes **148** to bicycloalkenes **145** with the aid of (*S*)-DTBM-SEGPHOS **149** as the chiral ligand to provide the enantioenriched alkylated products **150** in good yields and excellent enantioselectivities (Scheme 11.37) [106]. It is noteworthy that various indoles, thiophenes, pyrroles, and furans were found as amenable substrates, selectively reacting at the C2 position, and even more strikingly, in the case of unprotected indoles, C2 alkylation was observed in contrast to typical reactivity at the C3 position. The authors proposed that the

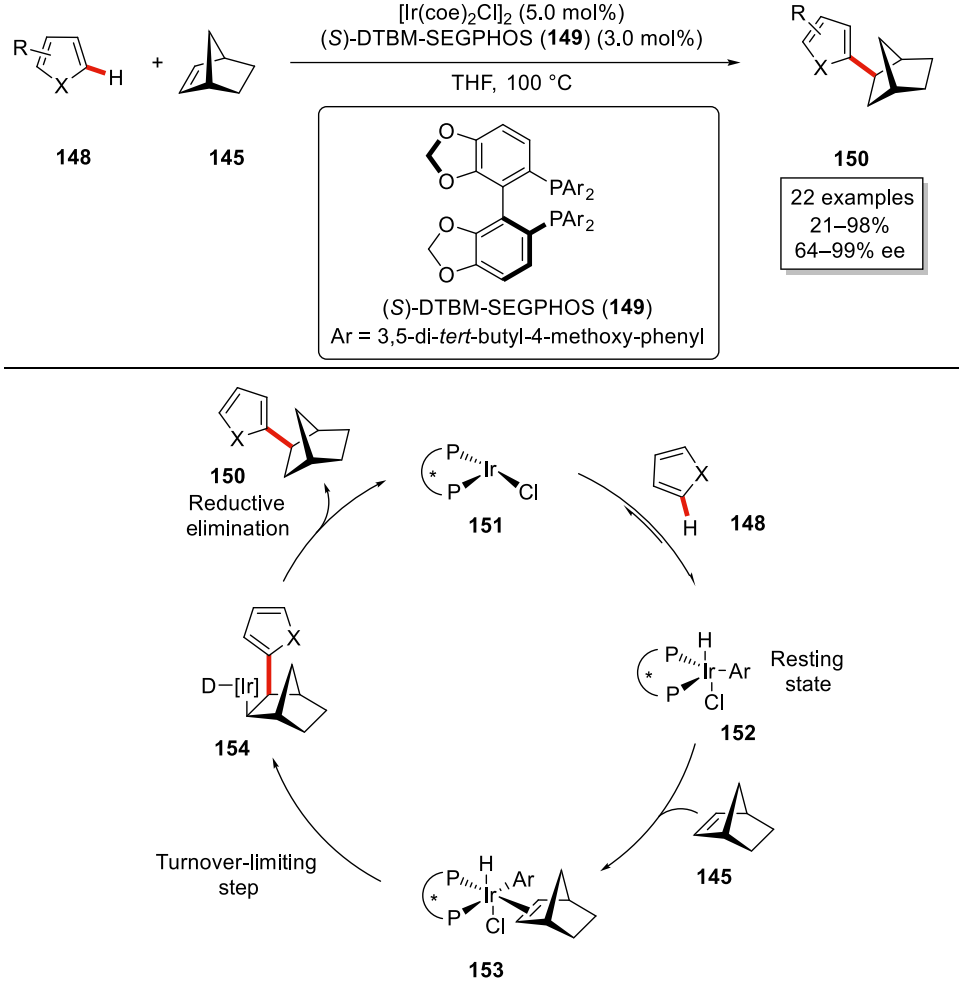

Scheme 11.37. Enantioselective hydroheteroarylation of bicycloalkanes **145**. Source: [106]/American Chemical Society.

turnover-limiting step is possibly the C–H cleavage step. Subsequently, C–H bond forming reductive elimination provide the chiral *exo*-product **150**.

Thereafter, Yamamoto demonstrated that amides and ketones directed highly enantioselective C–H hydroarylation of bicycloalkanes **145** using a cataionic iridium complex in the presence of the sulfur linked bis(phosphoramidite) ligand [(*R*,*R*)-S-Me-bidentate phosphoramidite(BIPAM)] **156** (Scheme 11.38) [107]. In addition, Nishimura reported an example showcasing a similar reactivity using (*R*,*R*)-QuinoxP* as the chiral ligand to enable the enantioselective C–H hydroarylation of norbornene with *N*-sulfonylbenzamide [108].

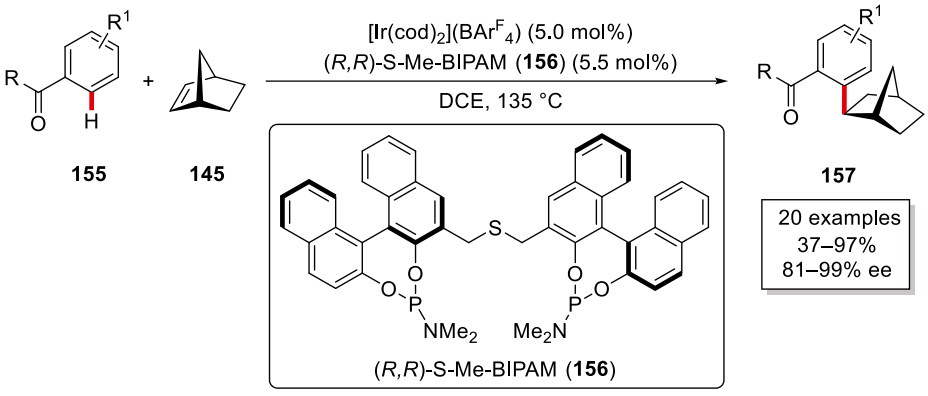

Scheme 11.38. Enantioselective hydroarylations of norbornenes **145**. Source: [107]/John Wiley & Sons.

In 2015, Shibata reported a highly enantioselective intramolecular C3-substituted ketone-directed C2 alkylation using a combination of iridium(I) catalyst and chiral diphosphine ligands (*S*)-SEGPHOS or (*S*)-Xyl-BINAP to synthesize highly enantioenriched annulated indole **159** (Scheme 11.39) [109].

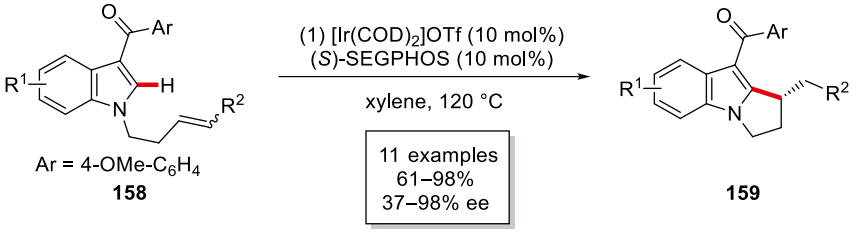

Scheme 11.39. Enantioselective C–H alkylation of indole derivatives **158**. Source: [109]/American Chemical Society.

In contrast, Bower demonstrated an efficient branch-selective, highly enantioselective iridium-catalyzed hydroarylation of styrenes **12** through anilide **160** directed *ortho*-C–H activation (Scheme 11.40) [110]. Key to success was the development of a chiral bisphosphite ligand **161** to generate tertiary benzylic stereocenters with high enantioselectivity. Tailoring the ligand structure led to ferrocene-based bisphosphonate **163**, which enabled the hydroheteroarylation of styrenes **12** with thiophene **148** in highly enantioselective fashion. Later, Nishimura employed a combination of cationic iridium catalyst and chiral phosphine ligand for highly enantioselective C–H hydroarylation of 2*H*-chromenes with aromatic ketones to provide access to highly enantioenriched 2-arylchromanes [111].

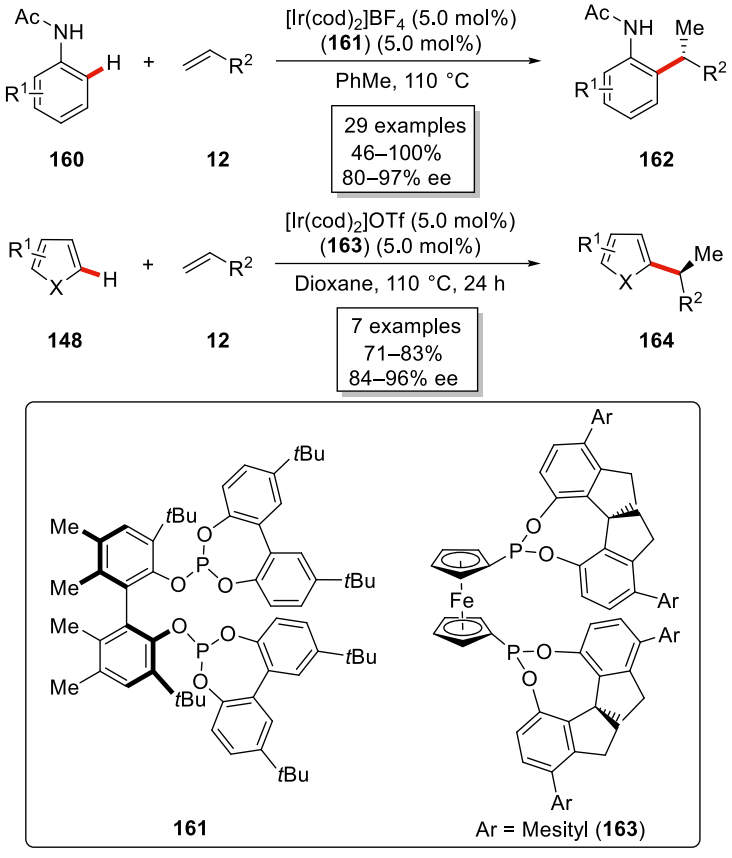

Scheme 11.40. Enantioselective hydroarylation of anilides **160** and thiophene **148**. Source: [110]/American Chemical Society.

In 2020, Rueping and Cavallo expanded the iridium-catalyzed intramolecular hydroarylation employing oxygen-tethered internal olefins through amide- and ketone-directed C–H activation [112]. The authors employed a combination of cationic iridium(I) and (*R,R*)-QuinoxP* as chiral ligand to achieve high enantioselectivities and enable versatile access to enantioenriched dihydrobenzofurans.

While significant advancement had been realized for C–H alkylations with neutral or electron-poor alkene partners, iridium complexes also have emerged as highly efficient catalysts for enantioselective hydroarylations of electron-rich olefins such as vinyl ethers [113]. In addition, Nishimura highlighted the great potential of iridium complexes for enantioselective [3+2] annulation reactions via C–H activation between ketimines and various acceptors including dienes, alkynes, or 1,3-enynes [114].

In addition to the aforementioned reports of C–H addition into carbon–carbon double bonds, in 2009, Shibata and coworkers reported iridium-catalyzed enantioselective addition to carbon–oxygen double bonds [115]. The authors employed a chiral bisphosphine ligand to achieve enantioenriched hydroxyindolines, albeit in moderate enantioselectivity of 72% ee. Later, Yamamoto was able to extend this approach to high enantioselectivity using a chiral bidentate bis-phosphoramidite ligand **166** with the aid of an amide directing group (Scheme 11.41) [116].

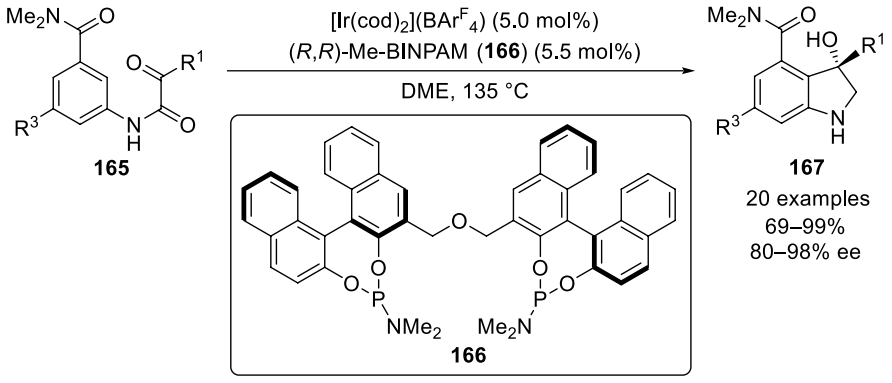

Scheme 11.41. Enantioselective C–H addition to α-ketoamides **165**. Source: [116]/John Wiley & Sons.

11.4.1.2. Chiral Diene Ligand Shibata and coworkers elegantly reported the first iridium-catalyzed enantioselective C(sp²)–H alkylation of ferrocene **168** using 1-isoquinolyl moiety as the directing group (Scheme 11.42) [117]. The authors utilized a combination of iridium(I) complex and an analogue of Carreira's diene ligand **169** to introduce planar chirality in ferrocene. Various olefin coupling partners **12** were tested to provide the alkylated products **170** in good yields and with excellent enantioselectivities.

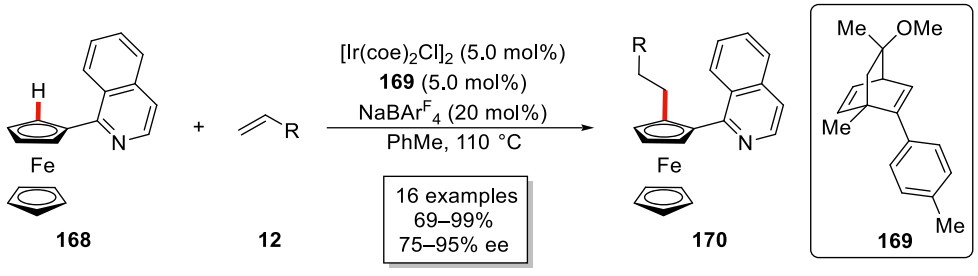

Scheme 11.42. Enantioselective C–H alkylation of ferrocenes **168**. Source: [117]/John Wiley & Sons.

11.4.2. C–H Borylations

In contrast, Hartwig and Shi achieved iridium-catalyzed enantioselective C–H borylation through a silyl directing group for the *ortho*-C–H activation of the adjacent aromatic ring (Scheme 11.43a) [118]. The key to success was the use of a chiral quinolyl oxazoline ligand **172** to form highly enantioenriched borylated products. Later, Xu and coworkers reported iridium-catalyzed enantioselective C–H

borylation of diarylmethylamines **174** with the aid of a free amine directing group (Scheme 11.43b) [119]. The authors employed a chiral bidentate boryl ligand **175** for achieving high enantioselectivity, although the amino directing group was primarily limited to *N*,*N*-dimethyl compounds **174**, otherwise slight changes in steric bulk significantly reduced the yield of the borylated product **177**. Also, the authors were able to achieve kinetic resolution of racemic diarylmethylamines **174** with slight modification in the chiral B,N-ligand **176**.

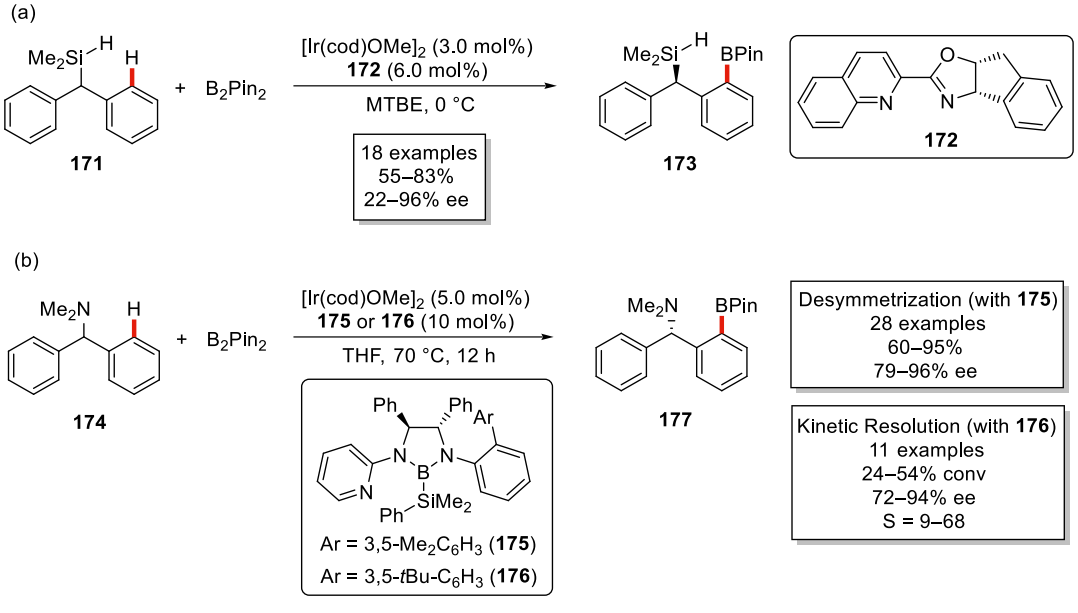

Scheme 11.43. Enantioselective C–H borylation with the aid of (a) silyl and (b) amine directing groups. (a) Source: [118]/John Wiley & Sons. (b) Source: [119]/American Chemical Society.

Very recently, a different approach was introduced by Phipps to achieve long-range enantioselective borylation [120]. The design of a sulfonate containing anionic bipyridine ligand **179**, along with a chiral cation derived from quinine, enabled the long-range asymmetric induction of prochiral geminal diaryl motif (Scheme 11.44). The sulfonate bearing bipyridine ligand was responsible for *meta*-selectivity due to hydrogen bond interaction between sulfonate and the substrate whereas the enantioselectivity was induced by the chiral cation. This new protocol allowed for the *meta*-borylation of benzhydrylamides **178** and diaryl phosphinamides **181,** which were further treated with H_2O_2 to provide the corresponding ***C***-chiral **180** and ***P***-chiral **182** phenol compounds in good yields and excellent enantioselectivities. It is noteworthy that this study presents a rare induction of enantioselectivity by chiral cations in transition metal catalysis [121].

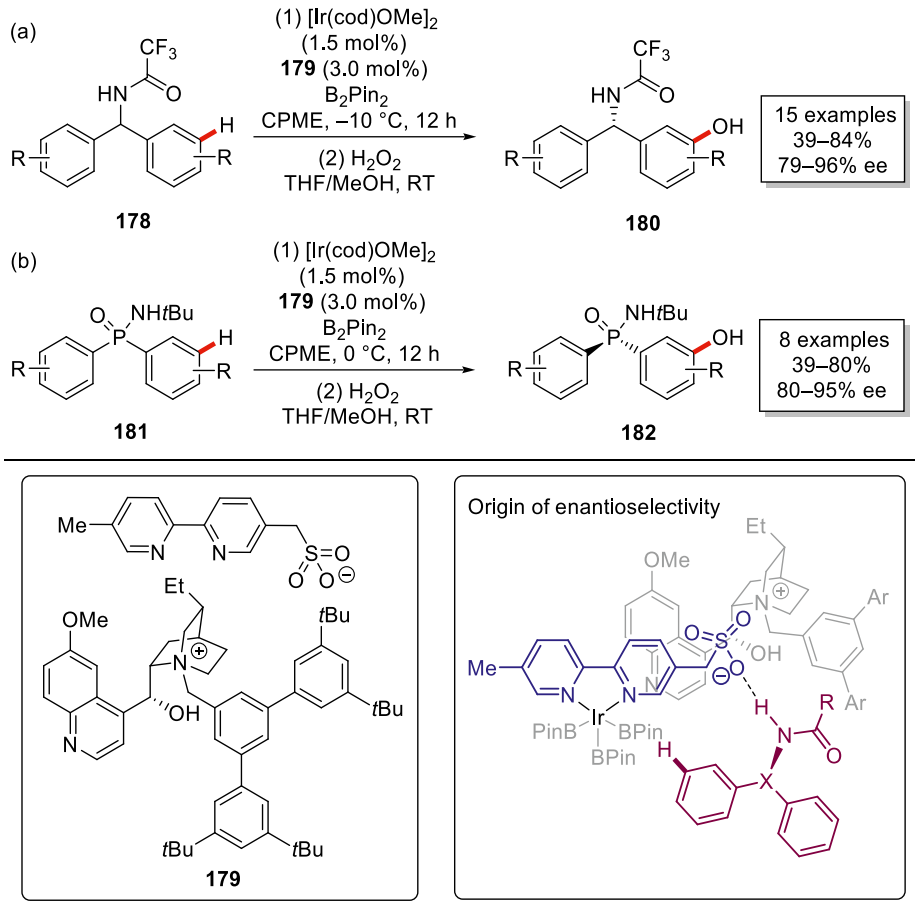

Scheme 11.44. Enantioselective remote C–H borylation of (a) benzhydrylamides and (b) diaryl phosphinamides.

11.4.3. C–H Silylations

In 2016, Shi and Hartwig reported a protocol for highly enantioselective iridium-catalyzed C–H silylation of hydridosilyl ethers **183** (Scheme 11.45) [122]. The key to success was the identification of the chiral pyridinyloxazoline-type ligand **184**, among various tested chiral dinitrogen ligands, which enabled the

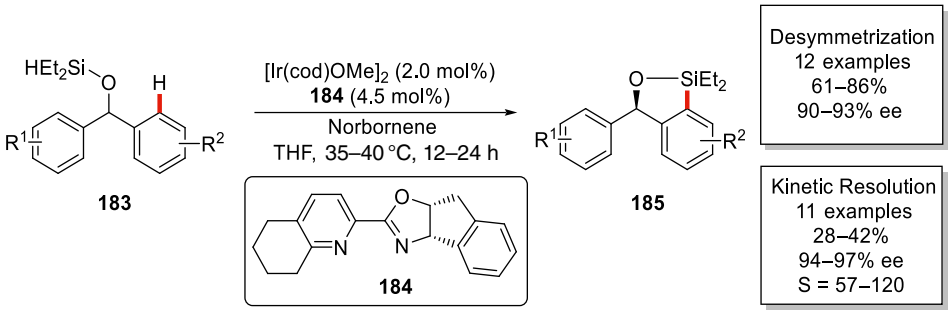

Scheme 11.45. Iridium-catalyzed enantioselective C–H silylation. Source: [122]/John Wiley & Sons

desymmetrization in a highly enantioselective fashion. Furthermore, the authors extended this protocol to the kinetic resolution of unsymmetrical *ortho*-substituted arenes to get access to highly enantioenriched diarylmethanols **185** with good selectivity factor.

11.5. RUTHENIUM CATALYSIS

Versatile and inexpensive ruthenium(II) arene complexes have been well investigated for the last few decades as powerful catalysts for various C–H activation reactions [123], but, surprisingly, enantioselective C–H transformations with well-established ruthenium catalysts remain considerably underdeveloped.

11.5.1. Chiral Amine as the TDG

Since the early contribution from Yu [48], the use of chiral TDG was primarily limited to palladium-catalyzed C–H activation reactions. However, Cui very recently developed ruthenium(II)-catalyzed intramolecular C–H hydroarylations of nitrogen-tethered olefin aldehydes **177** using commercially available α-methylamines **187** as chiral TDG for the synthesis of highly enantioenriched indoline derivatives **189** (Scheme 11.46a) [124]. The further addition of catalytic amounts of protected chiral carboxylic acid **188** was beneficial for the reactivity and enantiocontrol. Almost at the same time, Wang demonstrated similar reactivity using oxygen-tethered olefin aldehydes with the aid of an α-chiral amine **187** as the chiral TDG (Scheme 11.46b) [125]. This protocol provided access to **192** and **193**, containing all-carbon quaternary stereocenters in high yields and enantioselectivities.

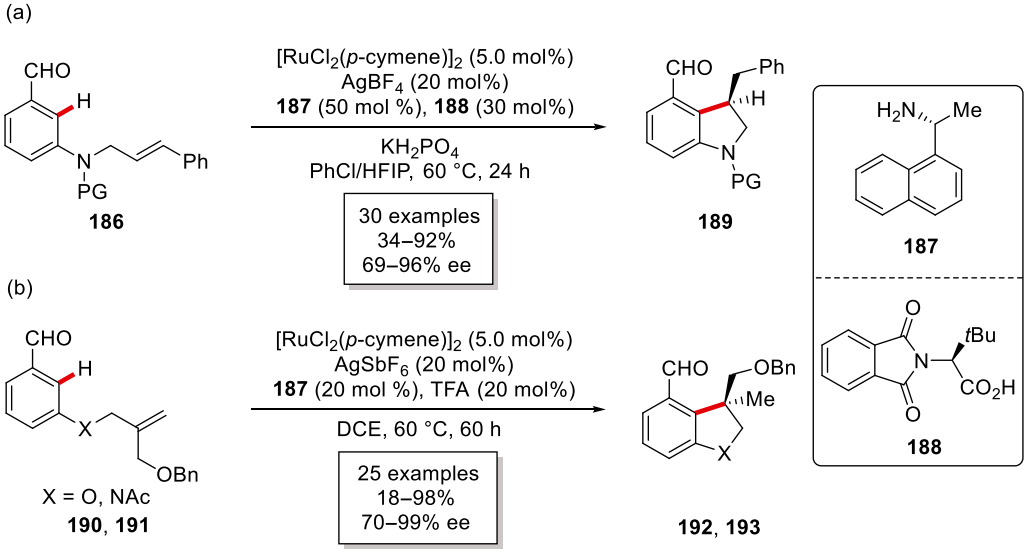

Scheme 11.46. Ruthenium(II)-catalyzed intramolecular C–H alkylation of (a) nitrogen-tethered and (b) oxygen-tethered olefin aldehydes. (a) Source: [124]/American Chemical Society. (b) Source: [125]/John Wiley & Sons.

11.5.2. Chiral Acid

In a recent study, Ackermann reported ruthenium-catalyzed enantioselective organometallic C–H alkylations by the cooperation of a C2 symmetrical chiral acid **196** via an enantio-determining proto-demetalation step (Scheme 11.47) [126]. This protocol set the stage for the assembly of chiral

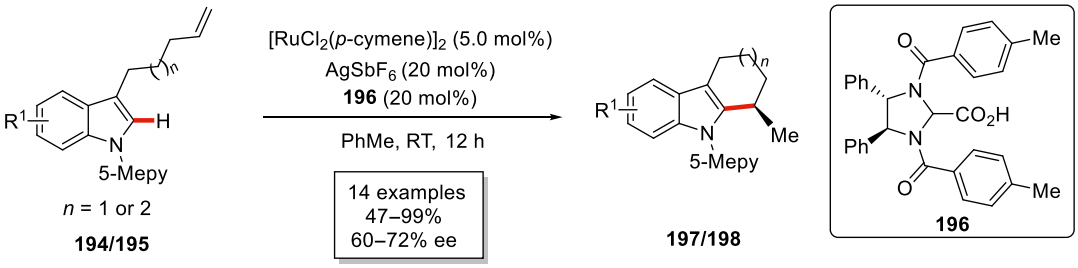

Scheme 11.47. Enantioselective ruthenium(II)-catalyzed C–H alkylation by chiral acid. Source: [126]/American Chemical Society.

tetrahydrocarbazoles and cyclohepta[*b*]indoles with high levels of enantioselectivity at room temperature. Density Functional Theory (DFT) studies supported for weak secondary dispersive interactions to be responsible for effective asymmetric induction.

11.6. SCANDIUM CATALYSIS

Scandium complexes have emerged as efficient catalysts in olefin polymerization [7, 127]. This has led to the development of novel catalytic C–H functionalization reactions by scandium catalysis including asymmetric transformations [128].

In 2014, Hou and coworkers reported on enantioselective C–H alkylations of pyridines, a rare example of enantioselective C–H functionalization of pyridines [129]. The authors achieved asymmetric version of their previously reported branched-selective *ortho*-alkylation of pyridines with unactivated alkenes [130]. A half-sandwich scandium complex **Sc200** bearing chiral cyclopentadienyl ligands (Cp^x), initially developed by Cramer [68, 131], enabled the highly enantioselective C–H alkylations of pyridines **199** (Scheme 11.48a) [129]. Diversely substituted 2-substituted pyridines **199** and unactivated alkenes **12** were efficiently converted to provide highly enantioenriched alkylated pyridines **201**.

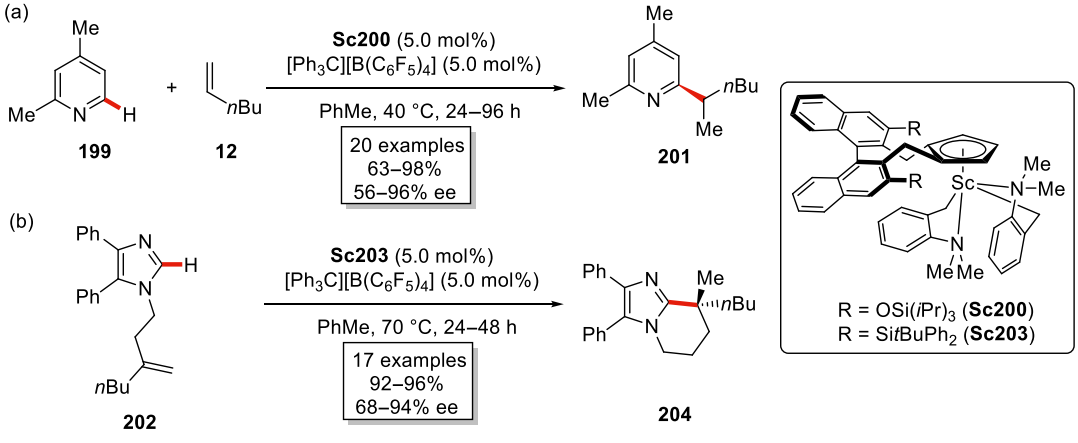

Scheme 11.48. Scandium-catalyzed enantioselective C–H activations: (a) intermolecular alkylations of pyridines, (b) intramolecular alkylations of imidazoles. (a) Source: [129]/American Chemical Society. (b) Source: [132]/American Chemical Society.

In 2020, the same group applied a similar half-sandwich scandium catalyst **Sc203** to achieve intramolecular *exo*-selective C–H cycloadditions of imidazoles to 1,1-disubstituted alkenes (Scheme 11.48b) [132]. Various aliphatic alkenes were *exo*-selectively converted to the polycyclic imidazole derivatives **204** having all β-carbon-substituted quaternary stereocenters with high level of enantiocontrol.

In a recent study, Luo and Hou employed a chiral half-sandwich scandium catalyst for the introduction of planar chirality into ferrocenes with internal alkynes. Enantioselective C–H alkenylation of ferrocenes proved viable with the aid of quinoline- and pyridine-based directing groups [133].

11.7. NICKEL CATALYSIS

Nickel catalysts have gained enormous attention for their versatile applications in C–H activation reactions [134]. In the last few years, the applications of nickel complexes have particularly increased to hydroarylations [135] type C–H activation reactions [136].

11.7.1. Formyl C–H Activation

Cramer and Donets applied chiral nickel/Lewis acid bimetallic catalysis for intramolecular hydrocarbamoylation of homoallylic formamides [137]. The development of air and bench-stable chiral diaminophopshine oxide allowed the activation of formamide C–H bonds for the synthesis of pyrrolidinone derivatives **207** with high yields and enantioselectivities (Scheme 11.49) [137]. From a mechanistic point of view, the heteroatom-substituted secondary phosphine oxide **206** (HASPO) [138] acted as bridging ligand between the nickel center and the aluminum Lewis acid, featuring a heterobimetallic activation mode for high efficacy.

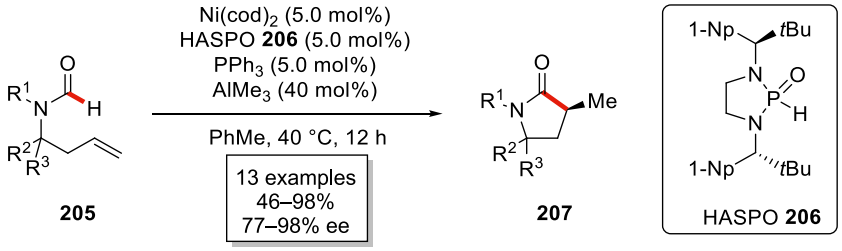

Scheme 11.49. Enantioselective nickel-catalyzed hydrocarbamoylations of alkenes **205**. Source: [137]/American Chemical Society.

11.7.2. Intramolecular Reactions

In 2009, Nakao and Hiyama devised a cooperative nickel/Lewis acid catalysis to achieve intramolecular C–H alkylation of pyridones with tethered olefins [139]. Intrigued by these findings, Cramer reported a regiodivergent annulation of alkene-tethered pyridines [140]. This protocol provided full control of regioselectivity by the judicious choice of the ligands. An *N*-heterocyclic carbene (NHC) ligand provided selectively the *endo*-product whereas the *exo*-cyclized product was obtained with cod as the ligand. Preliminary studies toward an enantioselective version of this protocol enabled the *endo*-cyclized pyridines **210** in 78.5 : 21.5 e.r. by using a chiral isoquinoline-based NHC [141] ligand **209** (Scheme 11.50a) [140]. Later, further improvement of this enantioselective protocol proved viable with a novel chiral NHC ligand **212,** which was developed based on previous ligand design by Gawley [142] (Scheme 11.50b) [143]. The modified acenaphthene backbone contained NHC ligand **212** provided the *endo*-cyclized products **213** in excellent enantioselectivities in the presence of MAD (methylaluminum bis(2,6-di-*tert*-butyl 4-methylphenoxide) as a Lewis acid.

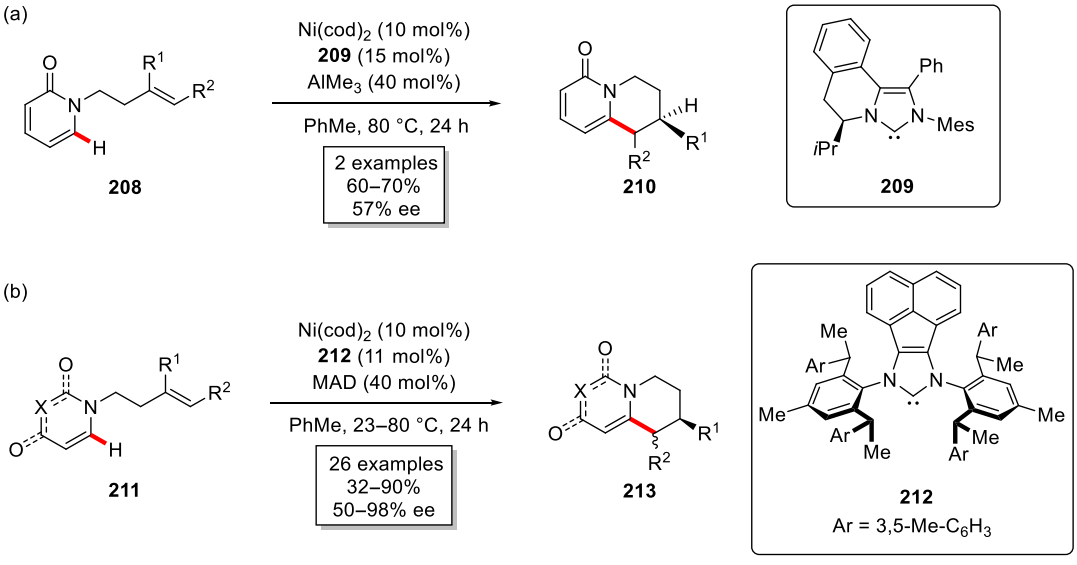

Scheme 11.50. Nickel-catalyzed asymmetric alkylation of pyridones: (a) early work, (b) improved conditions using acenaphthene-decorated ligand **212**. (a) Source: [140]/John Wiley & Sons. (b) Source: [143]/American Chemical Society.

In 2018, Ye achieved highly enantioselective *exo*-selective intramolecular C–H cyclization of imidazoles with various alkenes **214** for the assembly of diverse enantioenriched bi- or polycyclic imidazoles **216** with *β*-stereocenters (Scheme 11.51) [144]. Hence, TADDOL-based HASPOs **215** were the key to success to promote nickel-aluminum bimetallic catalysis.

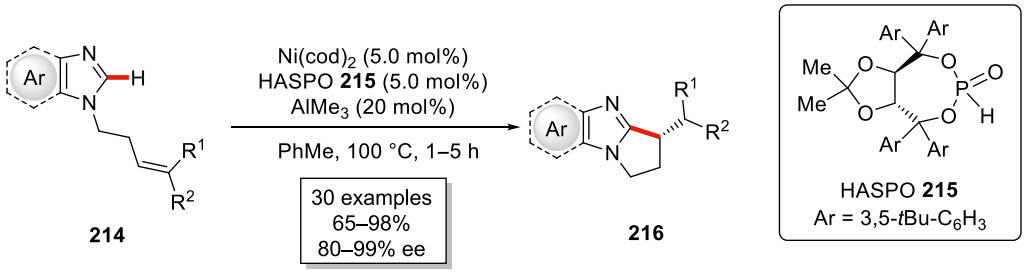

Scheme 11.51. Nickel-catalyzed *exo*-selective hydroarylation. Source: [144]/American Chemical Society.

All the beforementioned enantioselective cyclizations required pyrophoric organoaluminum reagents as additives [145], significantly jeopardizing the functional group tolerance. To overcome this drawback, Ackermann and coworkers reported aluminum-free nickel-catalyzed intramolecular *endo*-hydroarylations of unactivated alkenes (Scheme 11.52) [146]. Here, high levels of enantiocontrol were achieved by the unprecedented use of nickel/(1*R*)-1-[(*R*)-(1,1-dimethylethyl)phosphinyl]-2-[(1*R*)-1-(diphenylphosphino)ethyl]ferrocene (JoSPOphos) [147] manifold for the *endo*-cyclization of imidazoles with alkenes **217**. In addition to a broad substrate scope, the reaction was found to be highly chemoselective with respect to additional double bonds present in the tethered alkenes. The authors propose that the catalytic cycle initiates with organometallic nickel(II)-JoSPOphos complex **221**. In the next step it undergoes coordination with substrate **217**, followed by migratory insertion, to deliver

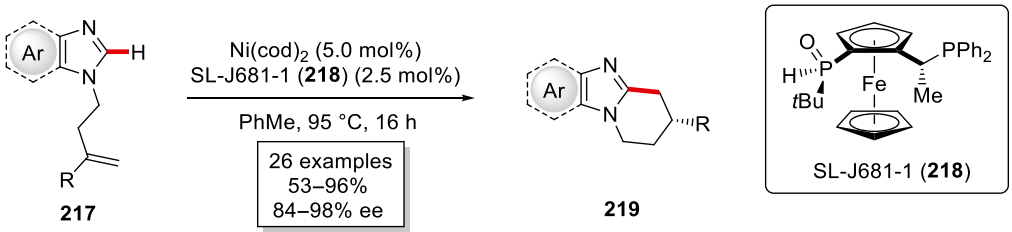

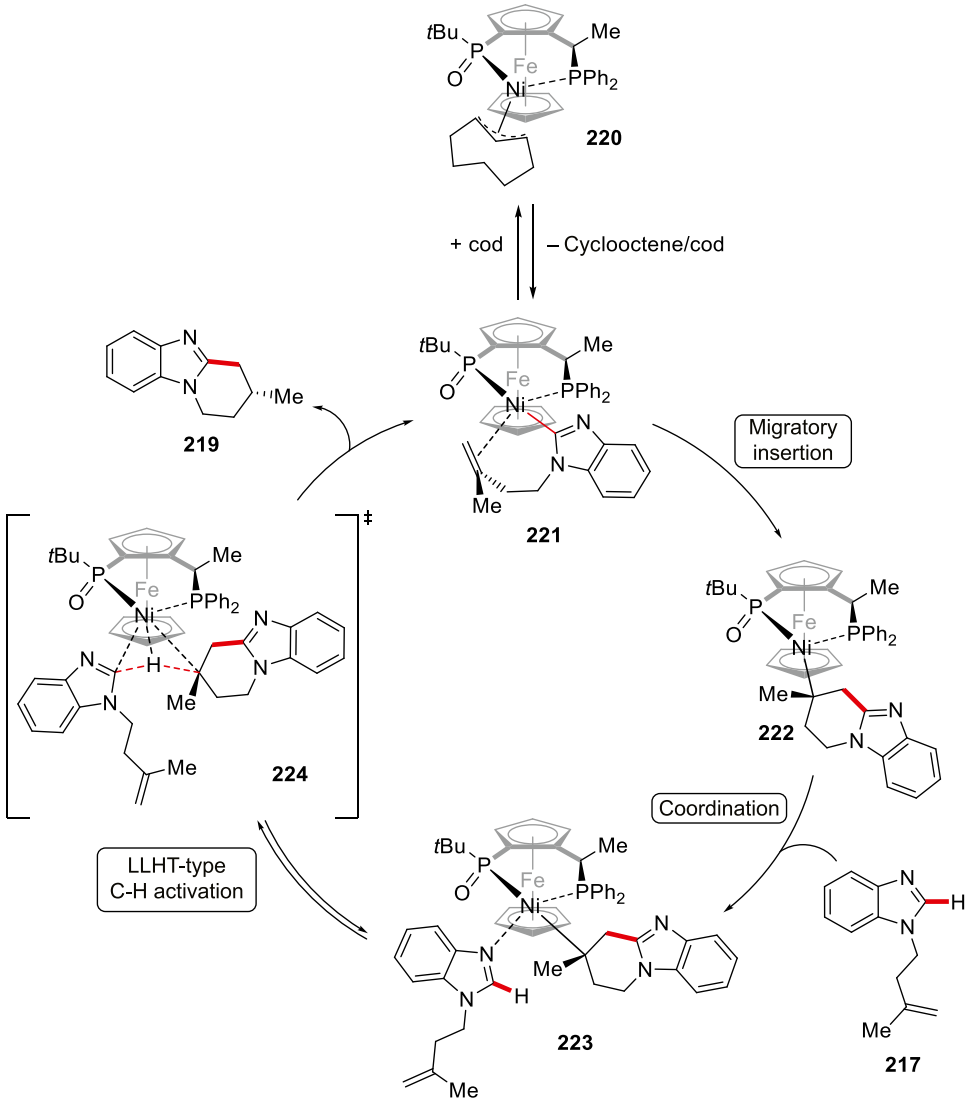

Scheme 11.52. Enantioselective nickel-catalyzed hydroarylation under aluminum-free conditions. Source: [146]/John Wiley & Sons.

the chiral cyclized intermediate **223**. In the subsequent step coordination with second molecule of substrate takes place, followed by LLHT (ligand-to-ligand hydrogen transfer) type C–H activation, which is proposed to occur.

Later, Cramer disclosed enantioselective nickel(0)-catalyzed C–H functionalization of indoles and pyrrole **225** in the absence of any Lewis basic directing group for the assembly of enantioenriched tetrahydropyridoindoles and tetrahydroindolizines under mild conditions (Scheme 11.53a) [148]. The key to success was represented by the use of a chiral 1,3-bis(2,6-diisopropylphenyl)imidazolidine (SIPR) ligand **226** with bulky flanking groups for highly enantioselective *endo*-cyclization process.

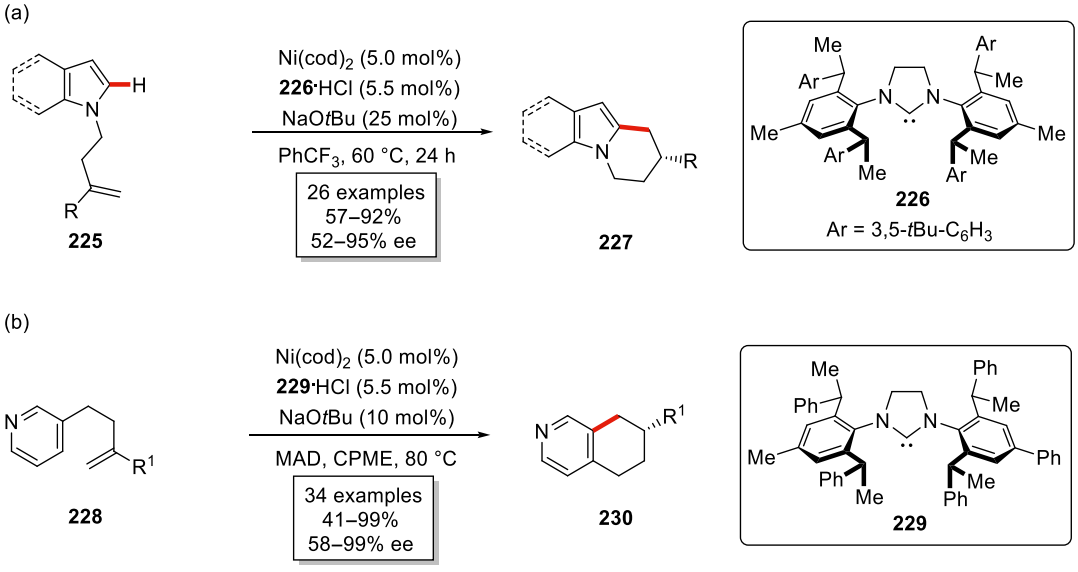

Scheme 11.53. Nickel-catalyzed enantioselective intramolecular C–H activations of: (a) indoles and pyrroles, (b) pyridines. (a) Source: [148]/John Wiley & Sons. (b) Source: [149]/American Chemical Society.

In 2019, Shi and coworkers extended this approach to pyridines. The authors reported enantioselective nickel-catalyzed intramolecular C–H alkylation at pyridyl 3- and 4-positions, utilizing a bulky chiral NHC ligand **229** in the presence of MAD as Lewis acid (Scheme 11.53b) [149]. This protocol provided access to chiral tetrahydroquinoline and tetrahydroisoquinoline derivatives in good yields and with excellent enantioselectivities. Shortly thereafter, the same group devised a similar strategy in the presence of a bulky chiral NHC ligand to synthesize enantioenriched fluorotetralins by achieving *endo*-selective C–H annulation of polyfluoroarenes [150].

11.7.3. Intermolecular Reactions

Despite significant progress on nickel-catalyzed intramolecular enantioselective hydroarylations, enantioselective intermolecular C–H activations remain extremely scarce in the literature. Inspired by the work on nickel/NHC-catalyzed three-component coupling by Ogata and Fukuzawa [151], enantioselective

version of this protocol was viable with a novel chiral NHC ligand (Scheme 11.54) [152]. The flanking *N*-aryl-substituted Grubbs-type chiral NHC **234** [153] was crucial to enable the highly enantioenriched synthesis of annulated indanols **235**.

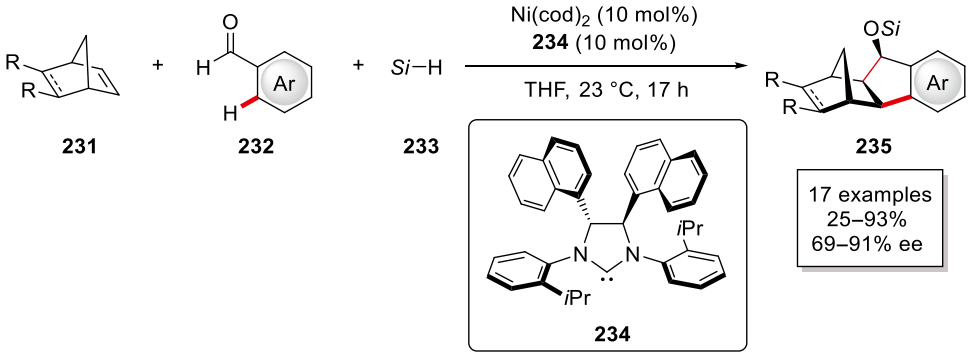

Scheme 11.54. Enantioselective nickel(0)-catalyzed reductive three-component coupling. Source: [152]/American Chemical Society.

11.8. COBALT CATALYSIS

During the last decades cobalt complexes have turned out to be among the most promising 3d metals with numerous application to the functionalization of inert C–H bonds [154]. In general, these reactions can be performed by two strategies, namely, by so-called low-valent cobalt catalysis [155], which is commonly done under reducing reaction conditions, and bench-stable high-valent cobalt(III) catalysis with cyclopentadienyl ligands [156].

11.8.1. Cobalt Catalysis under Reducing Conditions

Yoshikai and coworkers utilized a combination of $CoCl_2$ as the catalyst and (*R,R*)-2,4-bis(diphenylphosphino)pentane (BDPP) as the optimal chiral phosphine ligand for an intramolecular hydroacylation of 2-alkenylbenzaldehydes **236** to deliver highly enantioenriched indanones **238** (Scheme 11.55a) [157]. The authors further extended this strategy to 2-acylbenzaldehydes **239** using a catalytic system comprising of $CoBr_2$ and (*R,R*)-Ph-BPE **240** for the synthesis of phthalide building blocks **241** in high enantioselectivity (Scheme 11.55b). Later, the same group extended this approach to more challenging trisubstituted alkenes **242** for the synthesis of 2,3-disubstituted indanes **224** (Scheme 11.55c) [158]. The combination of a cobalt(II) salt and (*R,R*)-BDPP provided the corresponding chiral cyclic ketones **224** in high yields and enantioselectivities irrespective of the *E*/*Z* ratio of the starting olefin substrates. Shortly thereafter, Dong and coworkers presented a desymmetrization protocol for the intramolecular hydroacylation process to construct strained four-membered cyclobutanones **245** in preference to the five-membered regioisomers (Scheme 11.55d) [159]. The authors employed a cobalt catalyst derived from the chiral diphosphine ligand (*S,S*)-BDPP for the synthesis of cyclobutanones **245** with quaternary and tertiary stereogenic centers in high yields and high level of enantiocontrol.

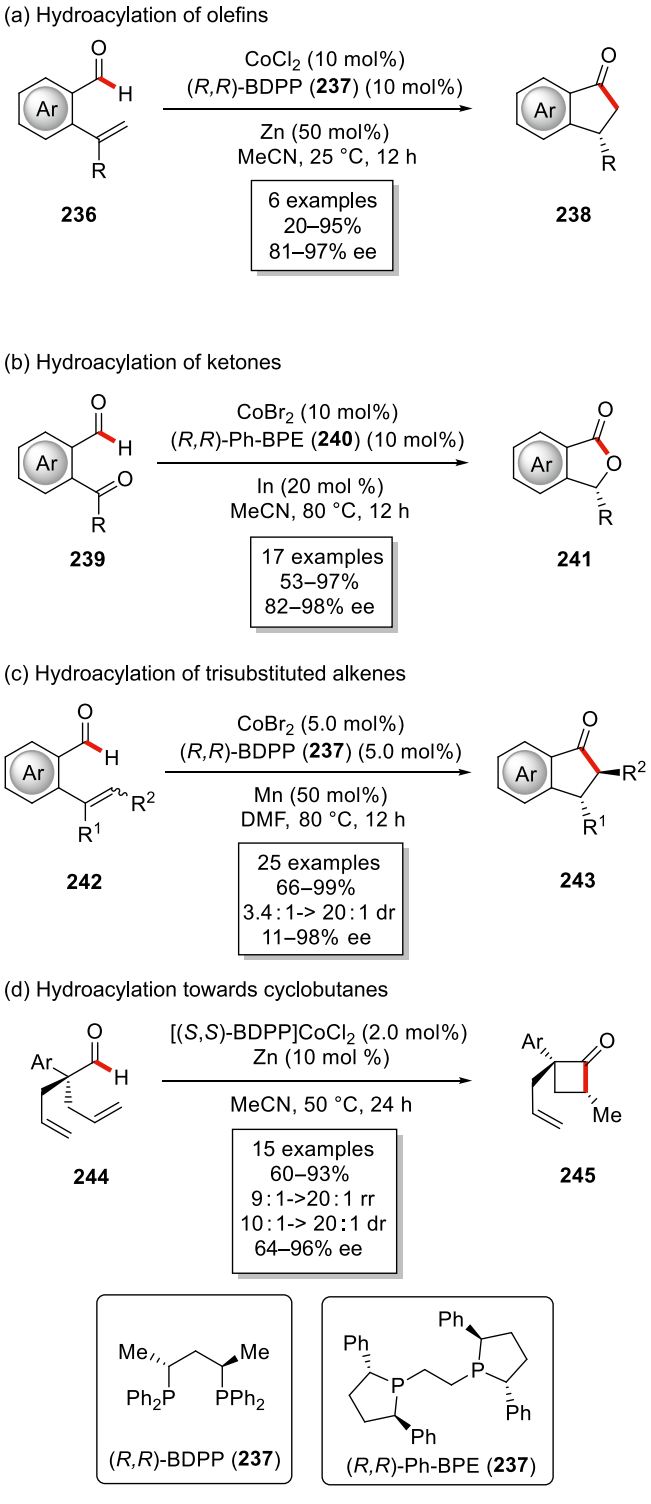

Scheme 11.55. Enantioselective cobalt-catalyzed intramolecular hydroacylations of (a) olefins, (b) ketones, (c) trisubstituted alkenes, and (d) olefins towards four-membered rings. (a) Source: [157]/American Chemical Society. (c) Source: [158]/John Wiley & Sons. (d) Source: [159]/American Chemical Society.

In 2016, Yoshikai unraveled the potential of cobalt catalysis for enantioselective C–H alkylation of indole derivatives [160]. Key to success was the use of BINOL-derived phosphoramidite **247** for the imine-directed C–H alkylation with styrenes **12** delivering enantioenriched 1,1-diarylethane derivatives **248** (Scheme 11.56) [160]. The alkylated products **248** were obtained in good yields and with high enantioselectivities.

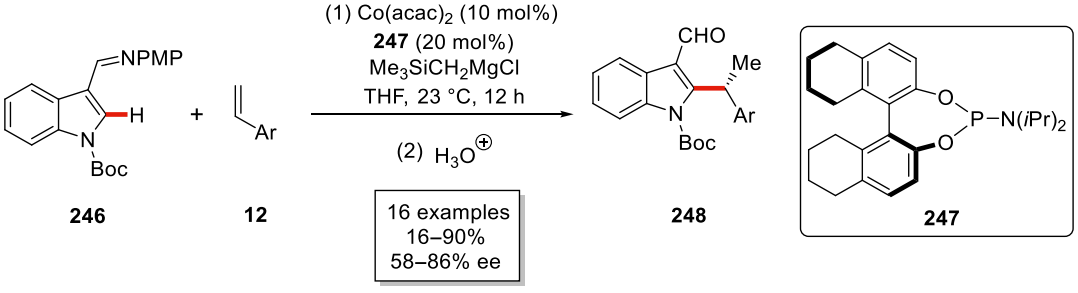

Scheme 11.56. Enantioselective cobalt-catalyzed hydroarylation of styrenes **12**. Source: [160]/American Chemical Society.

In contrast, the versatility of cobalt catalysis was recently represented by Lautens for the enantioselective hydroarylation of enynes with pyridyl indoles [161]. (*R*,*R*)-QuinoxP* was identified as the optimal chiral ligand for this highly enantioselective hydroarylative cyclization protocol.

11.8.2. Cobalt(III) Complexes

11.8.2.1. Chiral Acid Despite significant advances on low-valent cobalt catalysis, the use of superstoichiometric amounts of Grignard reagents significantly jeopardizes the atom economy of this approach. In this context, bench-stable Cp*Co(III) complexes provide new avenues for redox-neutral enantioselective transformations. In 2017, Ackermann reported branch-selective cobalt(III)-catalyzed C–H alkylation using stoichiometric amount of Brønsted acid [162]. Inspired by this result, in 2018, Ackermann and coworkers reported the enantioselective version of this challenging protocol (Scheme 11.57) [163]. The authors achieved the first highly enantioselective cobalt(III)-catalyzed C–H alkylation using a Cp*Co(III) complex and a chiral acid manifold [163]. The de-novo design of a novel C2-symmetric chiral carboxylic acid **250** enabled the pyridine-directed C–H alkylation of indoles **249** with unactivated alkenes **12** in good yields and high enantioselectivities. Detailed mechanistic studies revealed a considerable negative nonlinear effect in the absence of Amberlyst 15 that was rationalized by the formation of a hydrogen bond-stabilized dimeric resting state of the chiral ligand.

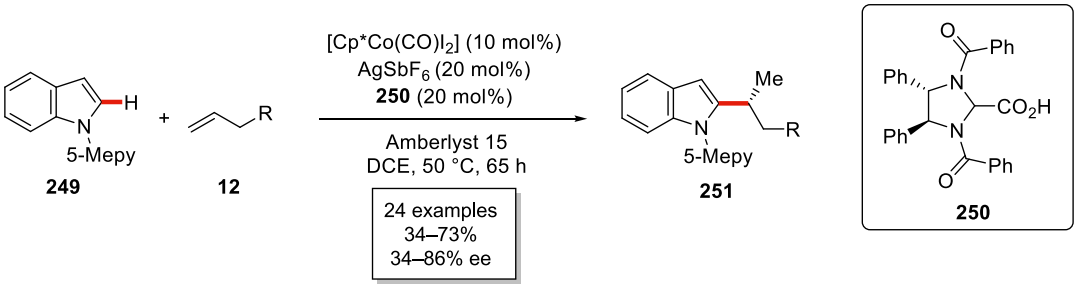

Scheme 11.57. Enantioselective cobalt(III)-catalyzed alkylation of indoles **249**. Source: [163]/John Wiley & Sons.

Later, inspired by the racemic amidation report of Dixon and Syaed [164], Yoshino and Matsunaga devised enantioselective cobalt(III)-catalyzed C(sp³)–H amidation of thioamides **252** with dioxazolones **116** utilizing a chiral carboxylic acid **254** (Scheme 11.58a) [165]. It is noteworthy to mention that it is one of the rare examples of enantioselective C(sp³)–H activations by 3d transition metal catalysts.

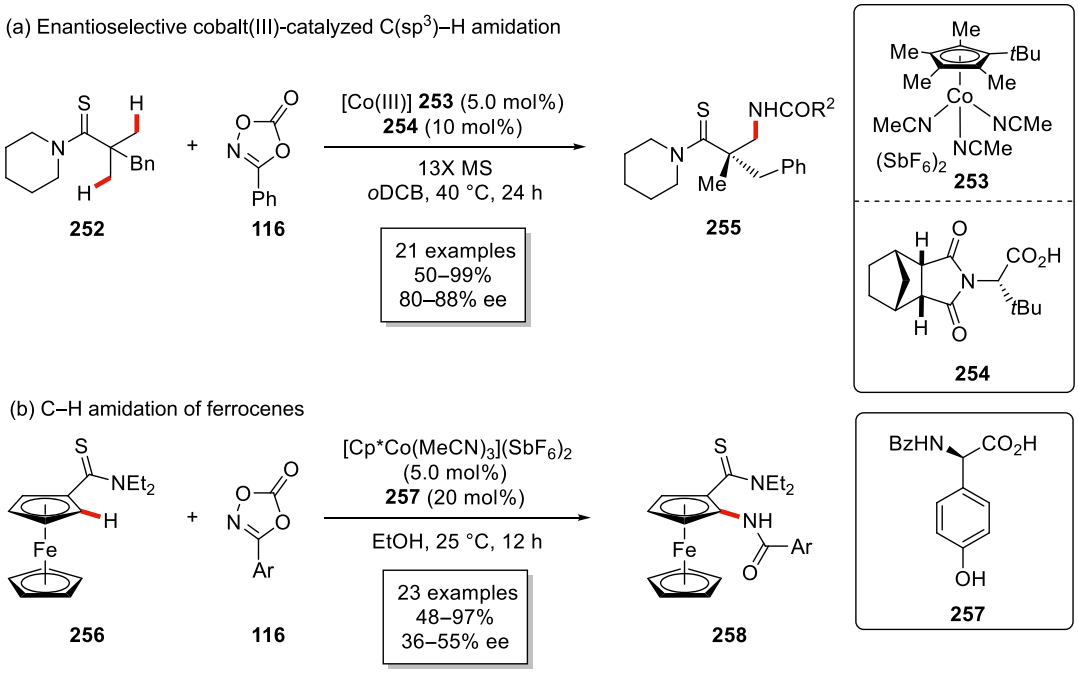

Scheme 11.58. Enantioselective amidation of (a) thioamides **252** and (b) ferrocenes **256**. (a) Source: [165]/John Wiley & Sons. (b) Source: [166]/American Chemical Society.

Recently, Shi reported on an enantioselective amidation of ferrocene thioamides **256** using a chiral MPAA ligand **257** (Scheme 11.58b) [166]. After detailed screening, *N*-benzoyl-protected D-*p*-hydroxyphenylglycine **257** was found to be the optimal ligand to achieve planar chiral amidated products **258** in high yields but with moderate enantiomeric excesses.

11.8.2.2. Chiral Cyclopentadienyl Cobalt Complex In addition to all the aforementioned reports that were based on the use of achiral Cp*Co-catalyst in combination with an external stereogenic carboxylic acid ligand, Cramer and coworkers very recently employed a different approach for highly enantioselective cobalt(III)-catalyzed C–H activation. The authors utilized a trisubstituted chiral cyclopentadienyl cobalt complex **241** for the synthesis of enantioenriched dihydroisoquinolones **84** (Scheme 11.59a) [167]. The introduction of a bulky *tert*-butyl group on the chiral Cp ligand proved to influence the dihedral angle of binaphthyl backbone to enable an excellent enantioselectivity up to 99.5 : 0.5 e.r. which even outperformed the rhodium(I)-based catalyst for this class of reaction.

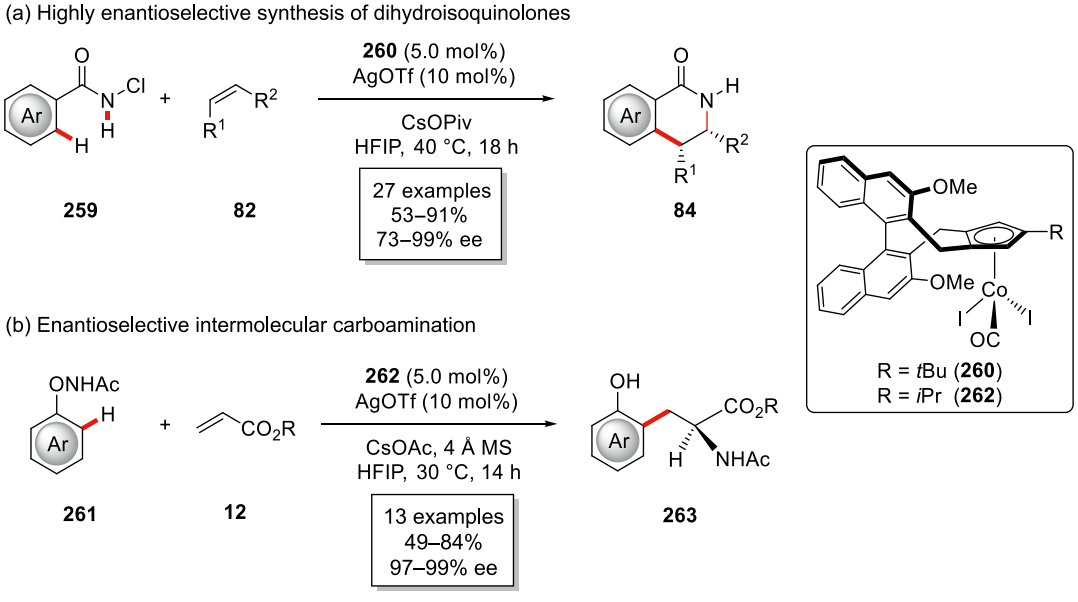

Scheme 11.59. Chiral cyclopentadienyl cobalt(III)-catalyzed C–H functionalizations: (a) synthesis of dihydroisoquinolones, (b) intermolecular carboamination of acrylates. (a) Source: [167]/American Chemical Society. (b) Source: [168]/John Wiley & Sons.

Very recently, a similar trisubstituted chiral cyclopentadienyl cobalt complex was utilized for the intermolecular carboamination of acrylates and bicyclic olefins for the synthesis of highly enantioenriched isotyrosine derivatives and amino-substituted bicyclic scaffolds (Scheme 11.59b) [168]. In contrast, analogous rhodium(III) complex failed to provide comparable reactivity, instead the corresponding Fujiwara-Moritani reactivity was observed.

11.9. COPPER CATALYSIS

Copper catalysis has witnessed significant momentum over the past years for various organic transformations [7] due to the high abundance of copper in the Earth's crust, its low toxicity, and cost-effectiveness [169]. However, many of the copper-catalyzed reactions are proposed to proceed via radical or outer-sphere mechanisms. Thus copper-catalyzed enantioselective transformations via organometallic C–H activation remain scarce in literature.

Based on their previous report on copper-catalyzed secondary alkylation of electron-deficient heterocycles [170], Ohmiya and Sawamura achieved the asymmetric synthesis of all-carbon quaternary stereocenters from azoles **264** and γ,γ-disubstituted primary allylic phosphates **265** (Scheme 11.60) [171]. The design of a novel naphthol-substituted bidentate NHC ligand **266** enabled excellent branch selectivity and high enantioselectivity for this enantioselective allylation protocol. Notably, *E*-alkenes were found to provide better enantiomeric excess compared to the corresponding *Z*-isomers. This protocol tolerated a wide variety of allyl phosphates **265** to give access to highly enantioenriched compounds **267** with quaternary stereocenters at the α-position to the heteroaromatic ring.

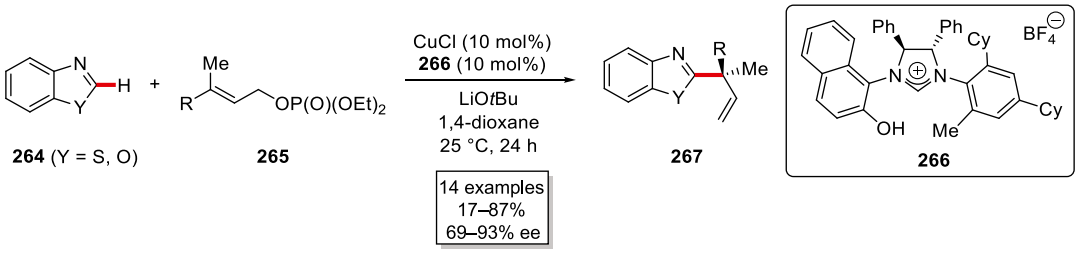

Scheme 11.60. Copper-catalyzed enantioselective allylation. Source: [171]/John Wiley & Sons.

11.10. IRON CATALYSIS

Iron is by far the most abundant transition metal on Earth. Low cost and toxicity have significantly promoted the use of iron catalysts in molecular syntheses, and pharmaceutical and agrochemical industries [172]. This has likewise recently set the stage for iron-catalyzed organometallic C–H functionalization processes [7, 173].

11.10.1. Phosphine-Based Ligands

In 2016, Ackermann and coworkers reported a novel strategy for the iron-catalyzed C–H allylation, alkylation, and benzylation of (hetero)arenes and alkenes using a combination of inexpensive iron salt and 1,2-bis(diphenylphosphino)ethane (dppe) as the ligand [174]. When the authors employed substituted allyl chlorides **269** in the presence of chiral diphosphine (*S*,*S*)-(ethane-1,2-diyl)bis[(2-methoxyphenyl)(phenyl)phosphane] (DIPAMP) **270** as the ligand in place of dppe, the branched product **271** was obtained with an unoptimized enantiomeric excess of 7% (Scheme 11.61a). Later, inspired by this report, Butenschön reported enantioselective arylation of ferrocenamides **272** using (*R*,*R*)-Chiralphos **273** as the chiral ligand (Scheme 11.61b) [175].

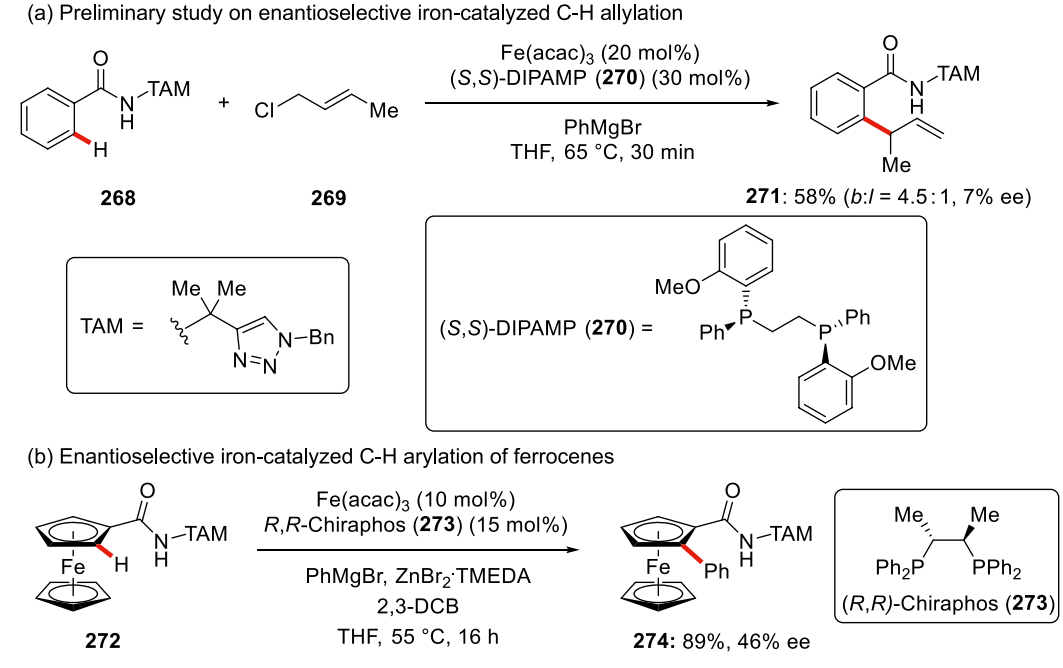

Scheme 11.61. Early example on enantioselective iron-catalyzed C–H activation. (a) Preliminary study on enantioselective iron-catalyzed C–H allylation. (b) Enantioselective iron-catalyzed C–H arylation of ferrocenes. TAM = Triazolyldimethyl. (b) Source: [175]/American Chemical Society.

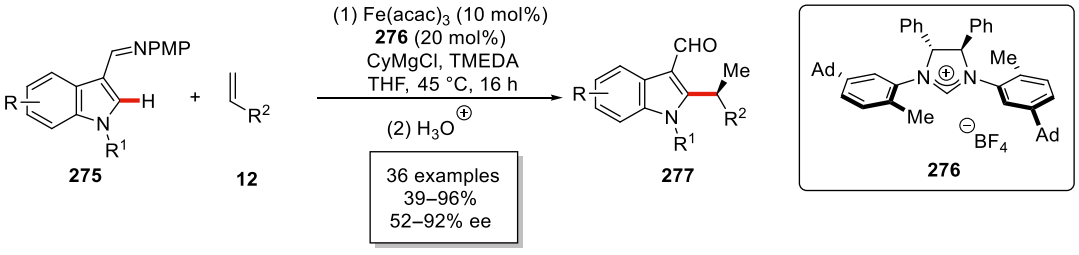

Scheme 11.62. Enantioselective iron-catalyzed C–H secondary alkylation. Source: [176]/John Wiley & Sons

11.10.2. N-Heterocyclic Carbene

In 2018, Ackermann and coworkers achieved the first highly enantioselective iron-catalyzed enantioselective C–H secondary alkylation of (aza)indoles (Scheme 11.62) [176]. The design of a novel *meta*-1-adamantyl-substituted NHC **276** was crucial for high level of enantiocontrol. A broad range of indoles and azaindoles **275** were tested with diversely substituted styrenes and vinylmetallocenes to afford the chiral C2-alkylated products **277** in excellent yields and enantioselectivities. The authors proposed an LLHT pathway for the C–H cleavage event. Later further investigations from the same group by Mössbauer spectroscopy and electrospray-ionization mass spectrometry provided support for an iron(II)–NHC species to be of key relevance during the asymmetric catalysis [177].

11.11. CONCLUSIONS

Direct C–H activations provide significant benefits for atom- and step-economic molecular syntheses. Consequently, over the past few decades, C–H activation has become a powerful strategy for the assembly of complex molecule. In stark contrast, enantioselective C(sp^2)–H functionalization continue to be underdeveloped. This research area demands further major attention to address the following key issues: (i) design of novel chiral ligands and catalyst systems, (ii) use of cost-effective Earth-abundant 3d transition metals, and (iii) the development of sustainable methods toward photo- and particularly electrochemical enantioselective transformations. Considering the key importance of chiral building blocks, more exciting developments are expected in this rapidly evolving research area.

ACKNOWLEDGMENTS

Generous support by the DAAD (fellowship to U.D.), the DFG (SPP1807 to L.A.), and Gottfried-Wilhelm-Leibniz award is gratefully acknowledged.

REFERENCES

1. (a) Rej, S.; Ano, Y.; Chatani, N., *Chem. Rev.* **2020**, *120*, 1788–1887. (b) Sambiagio, C.; Schönbauer, D.; Blieck, R.; Dao-Huy, T.; Pototschnig, G.; Schaaf, P.; Wiesinger, T.; Zia, M. F.; Wencel-Delord, J.; Besset, T.; Maes, B. U. W.; Schnürch, M., *Chem. Soc. Rev.* **2018**, *47*, 6603–6743. (c) Gandeepan, P.; Ackermann, L., *Chem* **2018**, *4*, 199–222. (d) Chu, J. C. K.; Rovis, T., *Angew. Chem. Int. Ed.* **2018**, *57*, 62–101. (e) Wei, Y.; Hu, P.; Zhang, M.; Su, W., *Chem. Rev.* **2017**, *117*, 8864–8907. (f) Park, Y.; Kim, Y.; Chang, S., *Chem. Rev.* **2017**, *117*, 9247–9301. (g) Daugulis, O.; Roane, J.; Tran, L. D., *Acc. Chem. Res.* **2015**, *48*, 1053–1064. (h) Wencel-Delord, J.; Glorius, F., *Nat. Chem.* **2013**, *5*, 369–375.
2. (a) Friis, S. D.; Johansson, M. J.; Ackermann, L., *Nat. Chem.* **2020**, *12*, 511–519. (b) Seki, M., *Org. Process Res. Dev.* **2016**, *20*, 867–877. (c) Ackermann, L., *Org. Process Res. Dev.* **2015**, *19*, 260–269.
3. (a) Lam, N. Y. S.; Wu, K.; Yu, J.-Q., *Angew. Chem. Int. Ed.* **2021**, *60*, 15767–15790. (b) Welin, E. R.; Ngamnithiporn, A.; Klatte, M.; Lapointe, G.; Pototschnig, G. M.; McDermott, M. S. J.; Conklin, D.; Gilmore, C. D.; Tadross, P. M.; Haley, C. K.; Negoro, K.; Glibstrup, E.; Grünanger, C. U.; Allan, K. M.; Virgil, S. C.; Slamon, D. J.; Stoltz, B. M., *Science* **2019**, *363*, 270–275. (c) Çapcı, A.; Lorion, M. M.; Wang, H.; Simon, N.; Leidenberger, M.; Borges Silva, M. C.; Moreira, D. R. M.; Zhu, Y.;

Meng, Y.; Chen, J. Y.; Lee, Y. M.; Friedrich, O.; Kappes, B.; Wang, J.; Ackermann, L.; Tsogoeva, S. B., *Angew. Chem. Int. Ed.* **2019**, *58*, 13066–13079.
4. Pouliot, J.-R.; Grenier, F.; Blaskovits, J. T.; Beaupré, S.; Leclerc, M., *Chem. Rev.* **2016**, *116*, 14225–14274.
5. Newton, C. G.; Wang, S.-G.; Oliveira, C. C.; Cramer, N., *Chem. Rev.* **2017**, *117*, 8908–8976.
6. (a) Yoshino, T.; Satake, S.; Matsunaga, S., *Chem. Eur. J.* **2020**, *26*, 7346–7357. (b) Achar, T. K.; Maiti, S.; Jana, S.; Maiti, D., *ACS Catal.* **2020**, *10*, 13748–13793. (c) Zheng, C.; You, S.-L., *RSC Adv.* **2014**, *4*, 6173–6214. (d) Wencel-Delord, J.; Colobert, F., *Chem. Eur. J.* **2013**, *19*, 14010–14017. (e) Giri, R.; Shi, B.-F.; Engle, K. M.; Maugel, N.; Yu, J.-Q., *Chem. Soc. Rev.* **2009**, *38*, 3242–3272.
7. Gandeepan, P.; Müller, T.; Zell, D.; Cera, G.; Warratz, S.; Ackermann, L., *Chem. Rev.* **2019**, *119*, 2192–2452.
8. (a) Woźniak, Ł.; Cramer, N., *Trends Chem.* **2019**, *1*, 471–484. (b) Loup, J.; Dhawa, U.; Pesciaioli, F.; Wencel-Delord, J.; Ackermann, L., *Angew. Chem. Int. Ed.* **2019**, *58*, 12803–12818.
9. Sokolov, V. I.; Troitskaya, L. L.; Reutov, O. A., *J. Organomet. Chem.* **1979**, *182*, 537–546.
10. (a) Shao, Q.; Wu, K.; Zhuang, Z.; Qian, S.; Yu, J.-Q., *Acc. Chem. Res.* **2020**, *53*, 833–851. (b) Engle, K. M.; Yu, J.-Q., *J. Org. Chem.* **2013**, *78*, 8927–8955.
11. Albicker, M. R.; Cramer, N., *Angew. Chem. Int. Ed.* **2009**, *48*, 9139–9142.
12. Saget, T.; Cramer, N., *Angew. Chem. Int. Ed.* **2013**, *52*, 7865–7868.
13. Newton, C. G.; Braconi, E.; Kuziola, J.; Wodrich, M. D.; Cramer, N., *Angew. Chem. Int. Ed.* **2018**, *57*, 11040–11044.
14. Lin, Z.-Q.; Wang, W.-Z.; Yan, S.-B.; Duan, W.-L., *Angew. Chem. Int. Ed.* **2015**, *54*, 6265–6269.
15. Liu, L.; Zhang, A.-A.; Wang, Y.; Zhang, F.; Zuo, Z.; Zhao, W.-X.; Feng, C.-L.; Ma, W., *Org. Lett.* **2015**, *17*, 2046–2049.
16. He, C.; Hou, M.; Zhu, Z.; Gu, Z., *ACS Catal.* **2017**, *7*, 5316–5320.
17. Liu, L.; Zhang, A.-A.; Zhao, R.-J.; Li, F.; Meng, T.-J.; Ishida, N.; Murakami, M.; Zhao, W.-X., *Org. Lett.* **2014**, *16*, 5336–5338.
18. (a) Deng, R.; Huang, Y.; Ma, X.; Li, G.; Zhu, R.; Wang, B.; Kang, Y.-B.; Gu, Z., *J. Am. Chem. Soc.* **2014**, *136*, 4472–4475. (b) Gao, D.-W.; Yin, Q.; Gu, Q.; You, S.-L., *J. Am. Chem. Soc.* **2014**, *136*, 4841–4844.
19. Wang, J.; Gao, D.-W.; Huang, J.; Tang, S.; Xiong, Z.; Hu, H.; You, S.-L.; Zhu, Q., *ACS Catal.* **2017**, *7*, 3832–3836.
20. Luo, J.; Zhang, T.; Wang, L.; Liao, G.; Yao, Q.-J.; Wu, Y.-J.; Zhan, B.-B.; Lan, Y.; Lin, X.-F.; Shi, B.-F., *Angew. Chem. Int. Ed.* **2019**, *58*, 6708–6712.
21. Zhan, B.-B.; Wang, L.; Luo, J.; Lin, X.-F.; Shi, B.-F., *Angew. Chem. Int. Ed.* **2020**, *59*, 3568–3572.
22. (a) Ackermann, L.; Althammer, A.; Fenner, S., *Angew. Chem. Int. Ed.* **2009**, *48*, 201–204. (b) Ackermann, L.; Vicente, R.; Born, R., *Adv. Synth. Catal.* **2008**, *350*, 741–748.
23. Nguyen, Q.-H.; Guo, S.-M.; Royal, T.; Baudoin, O.; Cramer, N., *J. Am. Chem. Soc.* **2020**, *142*, 2161–2167.
24. Shintani, R.; Otomo, H.; Ota, K.; Hayashi, T., *J. Am. Chem. Soc.* **2012**, *134*, 7305–7308.
25. Yang, L.; Neuburger, M.; Baudoin, O., *Angew. Chem. Int. Ed.* **2018**, *57*, 1394–1398.
26. Grosheva, D.; Cramer, N., *ACS Catal.* **2017**, *7*, 7417–7420.
27. Shi, B.-F.; Maugel, N.; Zhang, Y.-H.; Yu, J.-Q., *Angew. Chem. Int. Ed.* **2008**, *47*, 4882–4886.
28. Laforteza, B. N.; Chan, K. S. L.; Yu, J.-Q., *Angew. Chem. Int. Ed.* **2015**, *54*, 11143–11146.
29. Du, Z.-J.; Guan, J.; Wu, G.-J.; Xu, P.; Gao, L.-X.; Han, F.-S., *J. Am. Chem. Soc.* **2015**, *137*, 632–635.
30. Shi, B.-F.; Zhang, Y.-H.; Lam, J. K.; Wang, D.-H.; Yu, J.-Q., *J. Am. Chem. Soc.* **2010**, *132*, 460–461.
31. Cheng, X.-F.; Li, Y.; Su, Y.-M.; Yin, F.; Wang, J.-Y.; Sheng, J.; Vora, H. U.; Wang, X.-S.; Yu, J.-Q., *J. Am. Chem. Soc.* **2013**, *135*, 1236–1239.
32. Chu, L.; Wang, X.-C.; Moore, C. E.; Rheingold, A. L.; Yu, J.-Q., *J. Am. Chem. Soc.* **2013**, *135*, 16344–16347.
33. Gao, D.-W.; Shi, Y.-C.; Gu, Q.; Zhao, Z.-L.; You, S.-L., *J. Am. Chem. Soc.* **2013**, *135*, 86–89.
34. Pi, C.; Li, Y.; Cui, X.; Zhang, H.; Han, Y.; Wu, Y., *Chem. Sci.* **2013**, *4*, 2675–2679.
35. Shi, Y.-C.; Yang, R.-F.; Gao, D.-W.; You, S.-L., *Beilstein J. Org. Chem.* **2013**, *9*, 1891–1896.
36. Gao, D.-W.; Gu, Q.; You, S.-L., *J. Am. Chem. Soc.* **2016**, *138*, 2544.
37. Chu, L.; Xiao, K.-J.; Yu, J.-Q., *Science* **2014**, *346*, 451.
38. Xiao, K.-J.; Chu, L.; Yu, J.-Q., *Angew. Chem. Int. Ed.* **2016**, *55*, 2856–2860.
39. Xiao, K.-J.; Chu, L.; Chen, G.; Yu, J.-Q., *J. Am. Chem. Soc.* **2016**, *138*, 7796–7800.
40. Gao, D.-W.; Gu, Q.; You, S.-L., *ACS Catal.* **2014**, *4*, 2741–2745.
41. Li, S.-X.; Ma, Y.-N.; Yang, S.-D., *Org. Lett.* **2017**, *19*, 1842–1845.
42. Jin, L.; Yao, Q.-J.; Xie, P.-P.; Li, Y.; Zhan, B.-B.; Han, Y.-Q.; Hong, X.; Shi, B.-F., *Chem.* **2020**, *6*, 497–511.
43. Grosheva, D.; Cramer, N., *Angew. Chem. Int. Ed.* **2018**, *57*, 13644–13647.
44. Ackermann, L.; Born, R.; Spatz, J. H.; Meyer, D., *Angew. Chem. Int. Ed.* **2005**, *44*, 7216–7219.
45. Chen, S.-S.; Wu, M.-S.; Han, Z.-Y., *Angew. Chem. Int. Ed.* **2017**, *56*, 6641–6645.
46. Yamaguchi, K.; Kondo, H.; Yamaguchi, J.; Itami, K., *Chem. Sci.* **2013**, *4*, 3753–3757.
47. Yamaguchi, K.; Yamaguchi, J.; Studer, A.; Itami, K., *Chem. Sci.* **2012**, *3*, 2165–2169.
48. Zhang, F.-L.; Hong, K.; Li, T.-J.; Park, H.; Yu, J.-Q., *Science* **2016**, *351*, 252.
49. Liao, G.; Zhang, T.; Lin, Z.-K.; Shi, B.-F., *Angew. Chem. Int. Ed.* **2020**, *59*, 19773–19786.
50. Yao, Q.-J.; Zhang, S.; Zhan, B.-B.; Shi, B.-F., *Angew. Chem. Int. Ed.* **2017**, *56*, 6617–6621.

51. Liao, G.; Yao, Q.-J.; Zhang, Z.-Z.; Wu, Y.-J.; Huang, D.-Y.; Shi, B.-F., *Angew. Chem. Int. Ed.* **2018**, *57*, 3661–3665.
52. Liao, G.; Chen, H.-M.; Xia, Y.-N.; Li, B.; Yao, Q.-J.; Shi, B.-F., *Angew. Chem. Int. Ed.* **2019**, *58*, 11464–11468.
53. Liao, G.; Li, B.; Chen, H.-M.; Yao, Q.-J.; Xia, Y.-N.; Luo, J.; Shi, B.-F., *Angew. Chem. Int. Ed.* **2018**, *57*, 17151–17155.
54. (a) Zhang, S.; Yao, Q.-J.; Liao, G.; Li, X.; Li, H.; Chen, H.-M.; Hong, X.; Shi, B.-F., *ACS Catal.* **2019**, *9*, 1956–1961. (b) Chen, H.-M.; Zhang, S.; Liao, G.; Yao, Q.-J.; Xu, X.-T.; Zhang, K.; Shi, B.-F., *Organometallics* **2019**, *38*, 4022–4028.
55. Zhang, J.; Xu, Q.; Wu, J.; Fan, J.; Xie, M., *Org. Lett.* **2019**, *21*, 6361–6365.
56. Song, H.; Li, Y.; Yao, Q.-J.; Jin, L.; Liu, L.; Liu, Y.-H.; Shi, B.-F., *Angew. Chem. Int. Ed.* **2020**, *59*, 6576–6580.
57. Wesch, T.; Leroux, F. R.; Colobert, F., *Adv. Synth. Catal.* **2013**, *355*, 2139–2144.
58. Hazra, C. K.; Dherbassy, Q.; Wencel-Delord, J.; Colobert, F., *Angew. Chem. Int. Ed.* **2014**, *53*, 13871–13875.
59. (a) Dherbassy, Q.; Djukic, J. P.; Wencel-Delord, J.; Colobert, F., *Angew. Chem. Int. Ed.* **2018**, *57*, 4668–4672. (b) Dherbassy, Q.; Wencel-Delord, J.; Colobert, F., *Tetrahedron* **2018**, *74*, 6205–6212.
60. Ma, Y.-N.; Zhang, H.-Y.; Yang, S.-D., *Org. Lett.* **2015**, *17*, 2034–2037.
61. Shi, H.; Herron, A. N.; Shao, Y.; Shao, Q.; Yu, J.-Q., *Nature* **2018**, *558*, 581.
62. Liu, Z.-S.; Hua, Y.; Gao, Q.; Ma, Y.; Tang, H.; Shang, Y.; Cheng, H.-G.; Zhou, Q., *Nat. Catal.* **2020**, *3*, 727–733.
63. (a) Poremba, K. E.; Dibrell, S. E.; Reisman, S. E., *ACS Catal.* **2020**, *10*, 8237–8246. (b) Chang, X.; Zhang, Q.; Guo, C., *Angew. Chem. Int. Ed.* **2020**, *59*, 12612–12622. (c) Lin, Q.; Li, L.; Luo, S., *Chem. Eur. J.* **2019**, *25*, 10033–10044. (d) Ghosh, M.; Shinde, V. S.; Rueping, M., *Beilstein J. Org. Chem.* **2019**, *15*, 2710–2746.
64. (a) Meyer, T. H.; Choi, I.; Tian, C.; Ackermann, L., *Chem* **2020**, *6*, 2484–2496. (b) Ackermann, L., *Acc. Chem. Res.* **2020**, *53*, 84–104. (c) Meyer, T. H.; Finger, L. H.; Gandeepan, P.; Ackermann, L., *Trends Chem.* **2019**, *1*, 63–76.
65. Dhawa, U.; Tian, C.; Wdowik, T.; Oliveira, J. C. A.; Hao, J.; Ackermann, L., *Angew. Chem. Int. Ed.* **2020**, *59*, 13451–13457.
66. Mas-Roselló, J.; Herraiz, A. G.; Audic, B.; Laverny, A.; Cramer, N., *Angew. Chem. Int. Ed.* **2021**, *60*, 13198.
67. Ye, B.; Cramer, N., *Science* **2012**, *338*, 504.
68. Ye, B.; Cramer, N., *J. Am. Chem. Soc.* **2013**, *135*, 636–639.
69. (a) Ye, B.; Donets, P. A.; Cramer, N., *Angew. Chem. Int. Ed.* **2014**, *53*, 507–511. (b) Ye, B.; Cramer, N., *Synlett* **2015**, *26*, 1490–1495.
70. Ye, B.; Cramer, N., *Angew. Chem. Int. Ed.* **2014**, *53*, 7896–7899.
71. Zheng, J.; Wang, S.-B.; Zheng, C.; You, S.-L., *J. Am. Chem. Soc.* **2015**, *137*, 4880–4883.
72. Reddy Chidipudi, S.; Burns, D. J.; Khan, I.; Lam, H. W., *Angew. Chem. Int. Ed.* **2015**, *54*, 13975–13979.
73. Zheng, J.; Wang, S.-B.; Zheng, C.; You, S.-L., *Angew. Chem. Int. Ed.* **2017**, *56*, 4540–4544.
74. Kong, L.; Han, X.; Liu, S.; Zou, Y.; Lan, Y.; Li, X., *Angew. Chem. Int. Ed.* **2020**, *59*, 7188–7192.
75. Wang, S.-G.; Cramer, N., *Angew. Chem. Int. Ed.* **2019**, *58*, 2514–2518.
76. Yang, X.; Zheng, G.; Li, X., *Angew. Chem. Int. Ed.* **2019**, *58*, 322–326.
77. Mi, R.; Zheng, G.; Qi, Z.; Li, X., *Angew. Chem. Int. Ed.* **2019**, *58*, 17666–17670.
78. Potter, T. J.; Kamber, D. N.; Mercado, B. Q.; Ellman, J. A., *ACS Catal.* **2017**, *7*, 150–153.
79. Maity, S.; Potter, T. J.; Ellman, J. A., *Nat. Catal.* **2019**, *2*, 756.
80. Wang, S.-G.; Liu, Y.; Cramer, N., *Angew. Chem. Int. Ed.* **2019**, *58*, 18136–18140.
81. Zheng, J.; You, S.-L., *Angew. Chem. Int. Ed.* **2014**, *53*, 13244–13247.
82. Zheng, J.; Cui, W.-J.; Zheng, C.; You, S.-L., *J. Am. Chem. Soc.* **2016**, *138*, 5242–5245.
83. Umeda, N.; Tsurugi, H.; Satoh, T.; Miura, M., *Angew. Chem. Int. Ed.* **2008**, *47*, 4019–4022.
84. Li, H.; Yan, X.; Zhang, J.; Guo, W.; Jiang, J.; Wang, J., *Angew. Chem. Int. Ed.* **2019**, *58*, 6732–6736.
85. (a) Wang, F.; Qi, Z.; Zhao, Y.; Zhai, S.; Zheng, G.; Mi, R.; Huang, Z.; Zhu, X.; He, X.; Li, X., *Angew. Chem. Int. Ed.* **2020**, *59*, 13288–13294. (b) Tian, M.; Bai, D.; Zheng, G.; Chang, J.; Li, X., *J. Am. Chem. Soc.* **2019**, *141*, 9527–9532.
86. Jia, Z. J.; Merten, C.; Gontla, R.; Daniliuc, C. G.; Antonchick, A. P.; Waldmann, H., *Angew. Chem. Int. Ed.* **2017**, *56*, 2429–2434.
87. Trifonova, E. A.; Ankudinov, N. M.; Mikhaylov, A. A.; Chusov, D. A.; Nelyubina, Y. V.; Perekalin, D. S., *Angew. Chem. Int. Ed.* **2018**, *57*, 7714–7718.
88. Wang, Q.; Zhang, W.-W.; Song, H.; Wang, J.; Zheng, C.; Gu, Q.; You, S.-L., *J. Am. Chem. Soc.* **2020**, *142*, 15678–15685.
89. Satake, S.; Kurihara, T.; Nishikawa, K.; Mochizuki, T.; Hatano, M.; Ishihara, K.; Yoshino, T.; Matsunaga, S., *Nat. Catal.* **2018**, *1*, 585.
90. Fujii, N.; Kakiuchi, F.; Yamada, A.; Chatani, N.; Murai, S., *Chem. Lett.* **1997**, *26*, 425–426.
91. (a) Harada, H.; Thalji, R. K.; Bergman, R. G.; Ellman, J. A., *J. Org. Chem.* **2008**, *73*, 6772–6779. (b) Thalji, R. K.; Ellman, J. A.; Bergman, R. G., *J. Am. Chem. Soc.* **2004**, *126*, 7192–7193.
92. (a) Tran, D. N.; Cramer, N., *Angew. Chem. Int. Ed.* **2013**, *52*, 10630–10634. (b) Tran, D. N.; Cramer, N., *Angew. Chem. Int. Ed.* **2011**, *50*, 11098–11102.
93. Kuninobu, Y.; Yamauchi, K.; Tamura, N.; Seiki, T.; Takai, K., *Angew. Chem. Int. Ed.* **2013**, *52*, 1520–1522.
94. Lin, L.; Fukagawa, S.; Sekine, D.; Tomita, E.; Yoshino, T.; Matsunaga, S., *Angew. Chem. Int. Ed.* **2018**, *57*, 12048–12052.
95. Zhang, Q.-W.; An, K.; Liu, L.-C.; Yue, Y.; He, W., *Angew. Chem. Int. Ed.* **2015**, *54*, 6918–6921.
96. Murai, M.; Matsumoto, K.; Takeuchi, Y.; Takai, K., *Org. Lett.* **2015**, *17*, 3102–3105.
97. Cai, Z.-J.; Liu, C.-X.; Wang, Q.; Gu, Q.; You, S.-L., *Nat. Commun.* **2019**, *10*, 4168.

98. Wang, Q.; Cai, Z.-J.; Liu, C.-X.; Gu, Q.; You, S.-L., *J. Am. Chem. Soc.* **2019**, *141*, 9504–9510.
99. Hyster, T. K.; Knörr, L.; Ward, T. R.; Rovis, T., *Science* **2012**, *338*, 500–503.
100. Hassan, I. S.; Ta, A. N.; Danneman, M. W.; Semakul, N.; Burns, M.; Basch, C. H.; Dippon, V. N.; McNaughton, B. R.; Rovis, T., *J. Am. Chem. Soc.* **2019**, *141*, 4815–4819.
101. Li, G.; Jiang, J.; Xie, H.; Wang, J., *Chem. Eur. J.* **2019**, *25*, 4688–4694.
102. (a) Stoutland, P. O.; Bergman, R. G.; Nolan, S. P.; Hoff, C. D., *Polyhedron* **1988**, *7*, 1429–1440. (b) Ziegler, T.; Tschinke, V.; Becke, A., *J. Am. Chem. Soc.* **1987**, *109*, 1351–1358. (c) Janowicz, A. H.; Bergman, R. G., *J. Am. Chem. Soc.* **1983**, *105*, 3929–3939.
103. Woźniak, Ł.; Tan, J.-F.; Nguyen, Q.-H.; Madron du Vigné, A.; Smal, V.; Cao, Y.-X.; Cramer, N., *Chem. Rev.* **2020**, *120*, 10516–10543.
104. Aufdenblatten, R.; Diezi, S.; Togni, A., *Monatsh. Chem.* **2000**, *131*, 1345–1350.
105. Tsuchikama, K.; Kasagawa, M.; Hashimoto, Y.-K.; Endo, K.; Shibata, T., *J. Organomet. Chem.* **2008**, *693*, 3939–3942.
106. Sevov, C. S.; Hartwig, J. F., *J. Am. Chem. Soc.* **2013**, *135*, 2116–2119.
107. Shirai, T.; Yamamoto, Y., *Angew. Chem. Int. Ed.* **2015**, *54*, 9894–9897.
108. Nagamoto, M.; Fukuda, J.-I.; Hatano, M.; Yorimitsu, H.; Nishimura, T., *Org. Lett.* **2017**, *19*, 5952–5955.
109. Shibata, T.; Ryu, N.; Takano, H., *Adv. Synth. Catal.* **2015**, *357*, 1131–1135.
110. Grélaud, S.; Cooper, P.; Feron, L. J.; Bower, J. F., *J. Am. Chem. Soc.* **2018**, *140*, 9351–9356.
111. Sakamoto, K.; Nishimura, T., *Adv. Synth. Catal.* **2019**, *361*, 2124–2128.
112. Shinde, V. S.; Mane, M. V.; Cavallo, L.; Rueping, M., *Chem. Eur. J.* **2020**, *26*, 8308–8313.
113. (a) Romero-Arenas, A.; Hornillos, V.; Iglesias-Sigüenza, J.; Fernández, R.; López-Serrano, J.; Ros, A.; Lassaletta, J. M., *J. Am. Chem. Soc.* **2020**, *142*, 2628–2639. (b) Yamauchi, D.; Nishimura, T.; Yorimitsu, H., *Chem. Commun.* **2017**, *53*, 2760–2763. (c) Ebe, Y.; Onoda, M.; Nishimura, T.; Yorimitsu, H., *Angew. Chem. Int. Ed.* **2017**, *56*, 5607–5611. (d) Hatano, M.; Ebe, Y.; Nishimura, T.; Yorimitsu, H., *J. Am. Chem. Soc.* **2016**, *138*, 4010–4013. (e) Ebe, Y.; Nishimura, T., *J. Am. Chem. Soc.* **2015**, *137*, 5899–5902.
114. (a) Nagamoto, M.; Sakamoto, K.; Nishimura, T., *Adv. Synth. Catal.* **2018**, *360*, 791–795. (b) Nagamoto, M.; Yamauchi, D.; Nishimura, T., *Chem. Commun.* **2016**, *52*, 5876–5879. (c) Nishimura, T.; Nagamoto, M.; Ebe, Y.; Hayashi, T., *Chem. Sci.* **2013**, *4*, 4499–4504.
115. Tsuchikama, K.; Hashimoto, Y.-K.; Endo, K.; Shibata, T., *Adv. Synth. Catal.* **2009**, *351*, 2850–2854.
116. Shirai, T.; Ito, H.; Yamamoto, Y., *Angew Chem. Int. Ed.* **2014**, *53*, 2658–2661.
117. Shibata, T.; Shizuno, T., *Angew. Chem. Int. Ed.* **2014**, *53*, 5410–5413.
118. Su, B.; Zhou, T.-G.; Xu, P.-L.; Shi, Z.-J.; Hartwig, J. F., *Angew. Chem. Int. Ed.* **2017**, *56*, 7205–7208.
119. Zou, X.; Zhao, H.; Li, Y.; Gao, Q.; Ke, Z.; Senmiao, X., *J. Am. Chem. Soc.* **2019**, *141*, 5334–5342.
120. Genov, G. R.; Douthwaite, J. L.; Lahdenperä, A. S. K.; Gibson, D. C.; Phipps, R. J., *Science* **2020**, *367*, 1246–1251.
121. (a) Ye, X.; Moeljadi, A. M. P.; Chin, K. F.; Hirao, H.; Zong, L.; Tan, C.-H., *Angew. Chem. Int. Ed.* **2016**, *55*, 7101–7105. (b) Ohmatsu, K.; Imagawa, N.; Ooi, T., *Nat. Chem.* **2014**, *6*, 47–51.
122. Su, B.; Zhou, T.-G.; Li, X.-W.; Shao, X.-R.; Xu, P.-L.; Wu, W.-L.; Hartwig, J. F.; Shi, Z.-J., *Angew. Chem. Int. Ed.* **2017**, *56*, 1092–1096.
123. (a) Nareddy, P.; Jordan, F.; Szostak, M., *ACS Catal.* **2017**, *7*, 5721–5745. (b) De Sarkar, S.; Liu, W.; Kozhushkov, S. I.; Ackermann, L., *Adv. Synth. Catal.* **2014**, *356*, 1461–1479. (c) Ackermann, L., *Acc. Chem. Res.* **2014**, *47*, 281–295. (d) Arockiam, P. B.; Bruneau, C.; Dixneuf, P. H., *Chem. Rev.* **2012**, *112*, 5879–5918. (e) Ackermann, L., *Synlett* **2007**, *2007*, 0507–0526.
124. Li, Z.-Y.; Lakmal, H. H. C.; Qian, X.; Zhu, Z.; Donnadieu, B.; McClain, S. J.; Xu, X.; Cui, X., *J. Am. Chem. Soc.* **2019**, *141*, 15730–15736.
125. Li, G.; Liu, Q.; Vasamsetty, L.; Guo, W.; Wang, J., *Angew. Chem. Int. Ed.* **2020**, *59*, 3475–3479.
126. Dhawa, U.; Connon, R.; Oliveira, J. C. A.; Steinbock, R.; Ackermann, L., *Org. Lett.* **2021**, *23*, 2760–2765.
127. Nishiura, M.; Guo, F.; Hou, Z., *Acc. Chem. Res.* **2015**, *48*, 2209–2220.
128. (a) Pellissier, H., *Coord. Chem. Rev.* **2016**, *313*, 1–37. (b) Li, X.; Hou, Z., *Coord. Chem. Rev.* **2008**, *252*, 1842–1869.
129. Song, G.; Wylie W. N. O.; Hou, Z., *J. Am. Chem. Soc.* **2014**, *136*, 12209–12212.
130. Guan, B.-T.; Hou, Z., *J. Am. Chem. Soc.* **2011**, *133*, 18086–18089.
131. Newton, C. G.; Kossler, D.; Cramer, N., *J. Am. Chem. Soc.* **2016**, *138*, 3935–3941.
132. Lou, S.-J.; Mo, Z.; Nishiura, M.; Hou, Z., *J. Am. Chem. Soc.* **2020**, *142*, 1200–1205.
133. Lou, S.-J.; Zhuo, Q.; Nishiura, M.; Luo, G.; Hou, Z., *J. Am. Chem. Soc.* **2021**, *143*, 2470–2476.
134. (a) Tasker, S. Z.; Standley, E. A.; Jamison, T. F., *Nature* **2014**, *509*, 299–309. (b) Nakao, Y., *Chem. Rec.* **2011**, *11*, 242–251.

135. Ackermann, L.; Gunnoe, T. B.; Habgood, L. G., *Catalytic hydroarylation of carbon-carbon multiple bonds*. Wiley-VCH, Weinheim: **2018**.
136. Khake, S. M.; Chatani, N., *Trends Chem.* **2019**, *1*, 524–539.
137. Donets, P. A.; Cramer, N., *J. Am. Chem. Soc.* **2013**, *135*, 11772–11775.
138. (a) Ackermann, L., *Isr. J. Chem.* **2010**, *50*, 652–663. (b) Ackermann, L., *Synthesis* **2006**, 1557–1571.
139. Nakao, Y.; Idei, H.; Kanyiva, K. S.; Hiyama, T., *J. Am. Chem. Soc.* **2009**, *131*, 15996–15997.
140. Donets, P. A.; Cramer, N., *Angew. Chem. Int. Ed.* **2015**, *54*, 633–637.
141. Hirsch-Weil, D.; Abboud, K. A.; Hong, S., *Chem. Commun.* **2010**, *46*, 7525–7527.
142. (a) Albright, A.; Gawley, R. E., *J. Am. Chem. Soc.* **2011**, *133*, 19680–19683. (b) Albright, A.; Eddings, D.; Black, R.; Welch, C. J.; Gerasimchuk, N. N.; Gawley, R. E., *J. Org. Chem.* **2011**, *76*, 7341–7351.
143. Diesel, J.; Finogenova, A. M.; Cramer, N., *J. Am. Chem. Soc.* **2018**, *140*, 4489–4493.
144. Wang, Y.-X.; Qi, S.-L.; Luan, Y.-X.; Han, X.-W.; Wang, S.; Chen, H.; Ye, M., *J. Am. Chem. Soc.* **2018**, *140*, 5360–5364.
145. Wang, Y.-X.; Ye, M., *Sci. China Chem.* **2018**, *61*, 1004–1013.
146. Loup, J.; Müller, V.; Ghorai, D.; Ackermann, L., *Angew. Chem. Int. Ed.* **2019**, *58*, 1749–1753.
147. Landert, H.; Spindler, F.; Wyss, A.; Blaser, H.-U.; Pugin, B.; Ribourduoille, Y.; Gschwend, B.; Ramalingam, B.; Pfaltz, A., *Angew. Chem. Int. Ed.* **2010**, *49*, 6873–6876.
148. Diesel, J.; Grosheva, D.; Kodama, S.; Cramer, N., *Angew. Chem. Int. Ed.* **2019**, *58*, 11044–11048.
149. Zhang, W.-B.; Yang, X.-T.; Ma, J.-B.; Su, Z.-M.; Shi, S.-L., *J. Am. Chem. Soc.* **2019**, *141*, 5628–5634.
150. Cai, Y.; Ye, X.; Liu, S.; Shi, S.-L., *Angew. Chem. Int. Ed.* **2019**, *58*, 13433–13437.
151. Ogata, K.; Atsuumi, Y.; Shimada, D.; Fukuzawa, S.-I., *Angew. Chem. Int. Ed.* **2011**, *50*, 5896–5899.
152. Ahlin, J. S. E.; Cramer, N., *Org. Lett.* **2016**, *18*, 3242–3245.
153. Seiders, T. J.; Ward, D. W.; Grubbs, R. H., *Org. Lett.* **2001**, *3*, 3225–3228.
154. (a) Mei, R.; Dhawa, U.; Samanta, R. C.; Ma, W.; Wencel-Delord, J.; Ackermann, L., *ChemSusChem* **2020**, *13*, 3306–3356. (b) Moselage, M.; Li, J.; Ackermann, L., *ACS Catal.* **2016**, *6*, 498–525.
155. Gao, K.; Yoshikai, N., *Acc. Chem. Res.* **2014**, *47*, 1208–1219.
156. Yoshino, T.; Matsunaga, S., *Adv. Synth. Catal.* **2017**, *359*, 1245–1262.
157. Yang, J.; Yoshikai, N., *J. Am. Chem. Soc.* **2014**, *136*, 16748–16751.
158. Yang, J.; Rérat, A.; Lim, Y. J.; Gosmini, C.; Yoshikai, N., *Angew. Chem. Int. Ed.* **2017**, *56*, 2449–2453.
159. Kim, D. K.; Riedel, J.; Kim, R. S.; Dong, V. M., *J. Am. Chem. Soc.* **2017**, *139*, 10208–10211.
160. Lee, P.-S.; Yoshikai, N., *Org. Lett.* **2015**, *17*, 22–25.
161. Whyte, A.; Torelli, A.; Mirabi, B.; Prieto, L.; Rodríguez, J. F.; Lautens, M., *J. Am. Chem. Soc.* **2020**, *142*, 9510–9517.
162. Zell, D.; Bursch, M.; Müller, V.; Grimme, S.; Ackermann, L., *Angew. Chem. Int. Ed.* **2017**, *56*, 10378–10382.
163. Pesciaioli, F.; Dhawa, U.; Oliveira, J. C. A.; Yin, R.; John, M.; Ackermann, L., *Angew. Chem. Int. Ed.* **2018**, *57*, 15425–15429.
164. Tan, P. W.; Mak, A. M.; Sullivan, M. B.; Dixon, D. J.; Seayad, J., *Angew. Chem. Int. Ed.* **2017**, *56*, 16550–16554.
165. Fukagawa, S.; Kato, Y.; Tanaka, R.; Kojima, M.; Yoshino, T.; Matsunaga, S., *Angew. Chem. Int. Ed.* **2019**, *58*, 1153–1157.
166. Liu, Y.-H.; Li, P.-X.; Yao, Q.-J.; Zhang, Z.-Z.; Huang, D.-Y.; Le, M. D.; Song, H.; Liu, L.; Shi, B.-F., *Org. Lett.* **2019**, *21*, 1895–1899.
167. Ozols, K.; Jang, Y.-S.; Cramer, N., *J. Am. Chem. Soc.* **2019**, *141*, 5675–5680.
168. Ozols, K.; Onodera, S.; Woźniak, Ł.; Cramer, N., *Angew. Chem. Int. Ed.* **2020**, *60*, 655–659.
169. (a) Zhu, X.; Chiba, S., *Chem. Soc. Rev.* **2016**, *45*, 4504–4523. (b) McCann, S. D.; Stahl, S. S., *Acc. Chem. Res.* **2015**, *48*, 1756–1766. (c) Jerphagnon, T.; Pizzuti, M. G.; Minnaard, A. J.; Feringa, B. L., *Chem. Soc. Rev.* **2009**, *38*, 1039–1075.
170. Makida, Y.; Ohmiya, H.; Sawamura, M., *Angew. Chem. Int. Ed.* **2012**, *51*, 4122–4127.
171. Ohmiya, H.; Zhang, H.; Shibata, S.; Harada, A.; Sawamura, M., *Angew. Chem. Int. Ed.* **2016**, *55*, 4777–4780.
172. Fürstner, A., *ACS Cent. Sci.* **2016**, *2*, 778–789.
173. (a) Shang, R.; Ilies, L.; Nakamura, E., *Chem. Rev.* **2017**, *117*, 9086–9139. (b) Cera, G.; Ackermann, L., *Top. Curr. Chem.* **2016**, *374*, 57.
174. Cera, G.; Haven, T.; Ackermann, L., *Angew. Chem. Int. Ed.* **2016**, *55*, 1484–1488.
175. Schmiel, D.; Butenschön, H., *Organometallics* **2017**, *36*, 4979–4989.
176. Loup, J.; Zell, D.; Oliveira, J. C. A.; Keil, H.; Stalke, D.; Ackermann, L., *Angew. Chem. Int. Ed.* **2017**, *56*, 14197–14201.
177. Loup, J.; Parchomyk, T.; Lülf, S.; Demeshko, S.; Meyer, F.; Koszinowski, K.; Ackermann, L., *Dalton Trans.* **2019**, *48*, 5135–5139.

12

ASYMMETRIC C–H FUNCTIONALIZATION OF C(sp^3)–H BOND

Xiao Zhang, Yangyang Shen, Eva Bednářová, and Tomislav Rovis
Department of Chemistry, Columbia University, New York, NY, USA

12.1. INTRODUCTION

Catalytic C(sp^3)–H activation has revolutionized approaches in organic synthesis to access molecular complexity. Precise activation of targeted C(sp^3)–H bonds presents fundamental and practical challenges. The lack of reactivity and selectivity is attributed to their high bond dissociation energy (BDE, 90–100 kcal mol^{-1}), low acidity (pK_a 45–60), poor orbital interaction with metal catalyst, and non-distinguishable sites.

Given the ubiquitous presence of C–H bonds, the direct functionalization of those strong bonds has had a transformative impact on organic synthesis, material science, and drug discovery. Over the past few decades, complementary catalytic modes have been developed to selectively activate a C(sp^3)–H bond: (i) insertion of metal carbenoid or metal nitrenoid into C(sp^3)–H bonds; and (ii) direct C(sp^3)–H activation, involving concerted metalation deprotonation (CMD) via high valent metal species or oxidative addition via low valent metal catalyst (Scheme 12.1).

Despite the recent tremendous progress made in C(sp^3)–H activation, the development of asymmetric versions has lagged. Early examples focused on metal carbene or nitrene intermediates, while in recent years, the asymmetric C(sp^3)–H activation under other catalytic manifolds has received more attention.

This chapter will focus on the progress achieved mainly in the past decade and will be divided into three parts based on the working mechanism: (i) the update on carbene or nitrene insertion; (ii) the CMD mechanism; (iii) the direct oxidative addition.

12.2. C(sp^3)–H BOND INSERTION BY METAL CARBENOIDS AND METAL NITRENOIDS

Insertion of transition metal-coordinated carbenes and nitrenes into the C–H bond has been shown to be a generally practical and selective approach to C(sp^3)–H bond functionalization (Scheme 12.2). An overview of recent achievements in asymmetric metal carbene and metal nitrene insertions into C(sp^3)–H bonds will be given as an update from the Third Edition of this book [1].

Catalytic Asymmetric Synthesis, Fourth Edition. Edited by Takahiko Akiyama and Iwao Ojima.

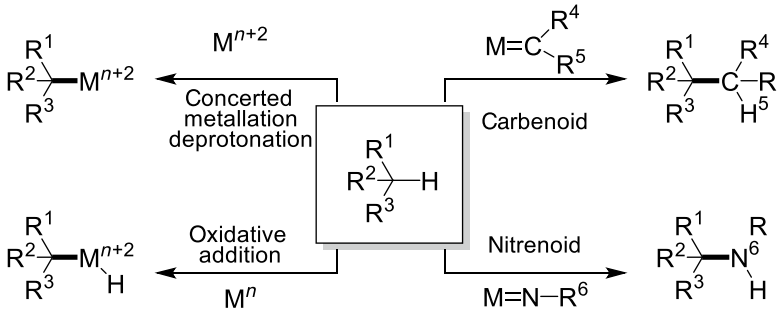

Scheme 12.1. Various modes of C(sp³)–H activation.

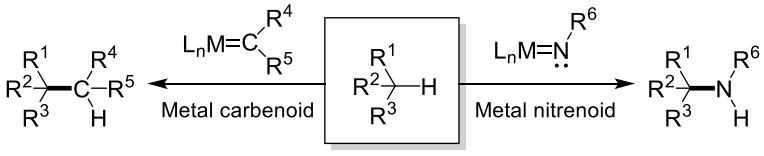

Scheme 12.2. C(sp³)–H bond insertion by metal carbenoids and metal nitrenoids.

12.2.1. C(sp³)–H Bond Insertion of Metal Carbenoids

12.2.1.1. Introduction Generation of metal carbenoids typically occurs through metal-catalyzed nitrogen extrusion from diazo compounds. Alternatively, ylide derivatives, hydrazones, and triazoles can also be employed as carbene precursors. A general catalytic cycle of C–H bond insertion of metal carbenoid is shown in Scheme 12.3, using a diazo compound as the carbene precursor for illustration. The diazo compound coordinates with the appropriate metal complex (ML_n) and generates a highly reactive transient metal carbenoid intermediate via extrusion of nitrogen. This electrophilic metal carbenoid complex then inserts into the C–H bond leading to the formation of a new C–C bond and regeneration of the metal complex to complete the catalytic cycle. Computational studies revealed that the C–H insertion process occurs via a concerted but asynchronous manner, with a transition state where a partial positive charge is built up at the carbon of the C–H bond, or via a considerable hydride transfer step and a subsequent C–C bond formation step for more activated C(sp³)–H bonds [2]. The critical intermediate proposed in Rh_2-catalyzed carbenoid C–H bond insertion was confirmed to be a genuine dirhodium carbene complex, according to recent experimental studies on the characterization of several reactive dirhodium carbene complexes reported by Davies and Berry [3], and Fürstner [4, 5].

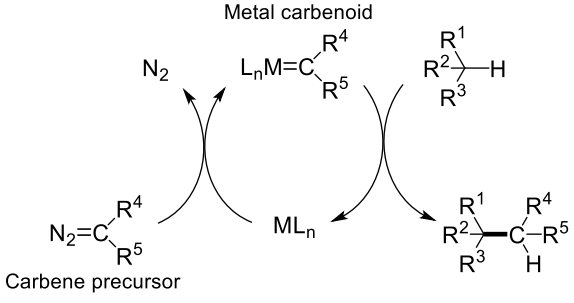

Scheme 12.3. General catalytic cycle of C(sp³)–H bond insertion by metal carbenoid.

Due to the significant reactivity of the metal carbenoid intermediates, they can react by many possible reaction pathways, such as cyclopropanations, cycloadditions, C–H insertions, and ylide formation.

Therefore, reactivity control over other reaction pathways has been crucial for developing synthetically practical methods of C–H activation. On the other hand, control of chemoselectivity of different C–H bonds is also critical for an efficient methodology, which is attributable to a balance between steric and electronic factors. In terms of electronics, the more reactive site is the more nucleophilic site, such as allylic, benzylic, tertiary, or α to a heteroatom, since they can best stabilize a build-up of positive charge in the transition state for the C–H insertion process. Meanwhile, if the most electron-rich site is comparatively congested and the metal complex is sterically hindered, and/or the substituents on the carbenoid are bulky, the steric effect will play a role, and insertion will happen at the sterically less hindered C–H bond.

In order to afford metal carbenoid intermediates with appropriate steric and electronic properties, efforts have been made on modulation of the metal complex, the ligands, and the substituents on the carbenoid carbon. In the past two decades, a series of chiral metal catalysts and carbene precursors have been developed. According to the substituents on the carbenoid carbon, the carbenoid complexes are generally classified into three classes (Figure 12.1): acceptor carbenoids, acceptor/acceptor carbenoids, and donor/acceptor carbenoids. The terms "acceptor" and "donor" represent the electron-withdrawing and electron-donating property of the substituent groups. An electron-withdrawing group makes the metal carbenoid complex highly electrophilic and reactive, while an electron-donating group stabilizes the metal carbenoid. Due to their high reactivity, acceptor and acceptor/acceptor carbenoids have limited site selectivity and are susceptible to other competing reaction pathways, making them a better fit for intramolecular C(sp³)–H bond insertion. The donor/acceptor carbenoids that have increased stability imparted by the donor group arrived later in the field and demonstrated superior selectivity for intermolecular C(sp³)–H bond functionalization.

Among a variety of metal catalysts for carbene C–H insertions, dirhodium(II) complexes are the earliest and the most widely researched chiral catalysts, of which the major classes are Rh(II) carboxylates, Rh(II) carboxamidates, Rh(II) phosphonates, and *ortho*-metallated arylphosphine Rh(II) complexes. In recent years, attention has also been drawn to efficient and selective chiral catalysts based on copper, iridium, ruthenium, and iron, with some of these embedded in enzymes.

Since asymmetric C–H functionalization via carbenoid insertion is a well-developed methodology and intramolecular reactions have mostly been covered in the Third Edition of this book [1], this section will discuss the recent progress of asymmetric carbenoid C–H insertion with an emphasis on intermolecular reactions.

12.2.1.2. Intermolecular C(sp³)–H Functionalization Intermolecular carbenoid C(sp³)–H insertion has been a long-standing challenge due to the poor chemoselectivity and tendency to dimerize. The breakthrough in this area has been made by the introduction of donor/acceptor carbenoid complexes that have higher stability and selectivity, which has enabled vast developments in asymmetric intermolecular carbenoid C(sp³)–H insertion. The examples demonstrated here are classified according to the type of the C–H bond being functionalized via carbene insertion.

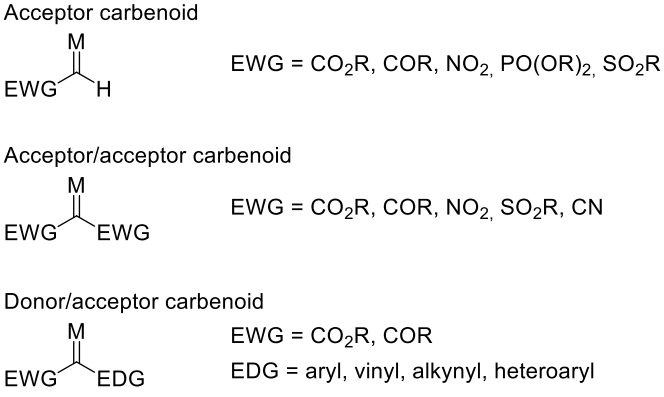

Figure 12.1. Classification of metal carbenoids.

12.2.1.2.1. Insertion into Unactivated C(sp³)–H Bonds The first practical and enantioselective intermolecular carbenoid C–H insertion was realized by Davies and Hansen in 1997 [6]. Utilizing aryldiazoacetates **2** as donor/acceptor carbenoid precursors and Rh_2(*S*-DOSP)$_4$ as a catalyst, intermolecular carbenoid C–H insertions of cycloalkanes were achieved in 55–96% yield with 60–93% enantiomeric excess (ee) under refluxing conditions when the cycloalkanes were employed as solvents. Further improvements in enantioselectivity (88–96% ee) without an appreciable drop in yield (23–81%) were achieved when the reaction was carried out at 10 °C in degassed solvent (Scheme 12.4a) [7]. The selectivity of the C–H bond insertion by this catalytic system is a good illustration of the general trend described before. Tertiary C–H bond is the most reactive site compared to secondary and primary C–H bonds. For example, the tertiary functionalized product **6** is the only product from C–H insertion into 2-methylbutane **4**, formed in 60% yield and 68% ee (Scheme 12.4b). The steric effect can be demonstrated with 2-methylpentane **7** as substrate, where C–H insertion happens at both the tertiary site (44% yield and 26% ee) and the secondary site that has less steric hindrance (31% yield and 86% ee) (Scheme 12.4c).

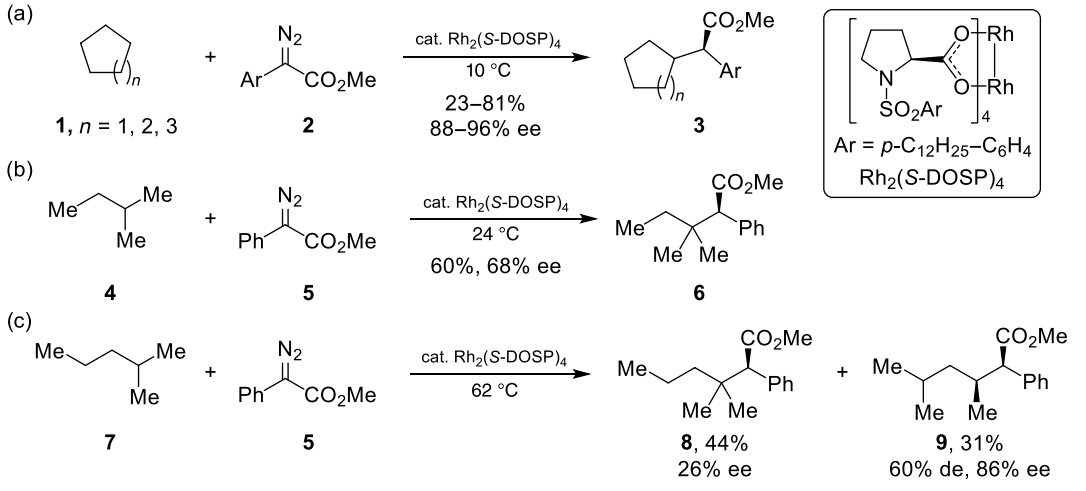

Scheme 12.4. C–H insertion of alkanes with aryldiazoacetates. (a) C–H insertions of cycloalkanes. Source: [7]/American Chemical Society. (b) C–H insertion of 2-methylbutane. (c) C–H insertion of 2-methylpentane.

In 2011, the Fokin group employed azavinyl carbenoids generated from 1-sulfonyl triazoles **11** as carbene precursors in the presence of Rh carboxylates Rh_2(*S*-NTTL)$_4$ or Rh_2(*S*-PTAD)$_4$ and realized asymmetric C–H functionalization of secondary and tertiary C–H bonds of alkanes to afford β-chiral sulfonamides after subsequent reduction (Scheme 12.5) [8]. Higher chemoselectivity toward the insertion into tertiary over secondary C–H bonds was achieved compared to the previous report from the Davies group, as shown in Scheme 12.4 [7], affording tertiary C–H functionalized product **12c** from C–H insertion of 2-methylbutane **4** with 87% yield and 92% ee, as well as **12d** from 2-methylpentane **7** with 63% yield and 91% ee. The dramatic increase in the selectivity toward tertiary C–H bonds for azavinyl carbenes was attributed to the lower steric demand of the aldimine group compared to the ester group in diazoacetates.

Besides the modulation of carbenoid precursor, the site selectivity of C–H insertion can also be improved by altering the steric nature of the catalyst. By employing a robust sterically encumbered rhodium porphyrin catalyst Rh(D_4-por*)(Me)(MeOH), the Che group demonstrated selective primary C–H bond insertion with methyl phenyldiazoacetate **5** in 2008 [9], providing primary functionalized hexane product **14** selectively over secondary functionalized product **15** (Scheme 12.6). Without the presence of primary C–H bonds, highly enantioselective secondary C–H functionalization could also be achieved, as shown with cyclohexane **16** as substrate. To further improve site- and enantioselectivity of primary C–H bond functionalization, in 2018, the Davies group described a new sterically demanding C_2-symmetric dirhodium catalyst Rh_2[*R*-tris(*p*-*t*-Bu-C_6H_4)TPCP]$_4$ and achieved highly selective

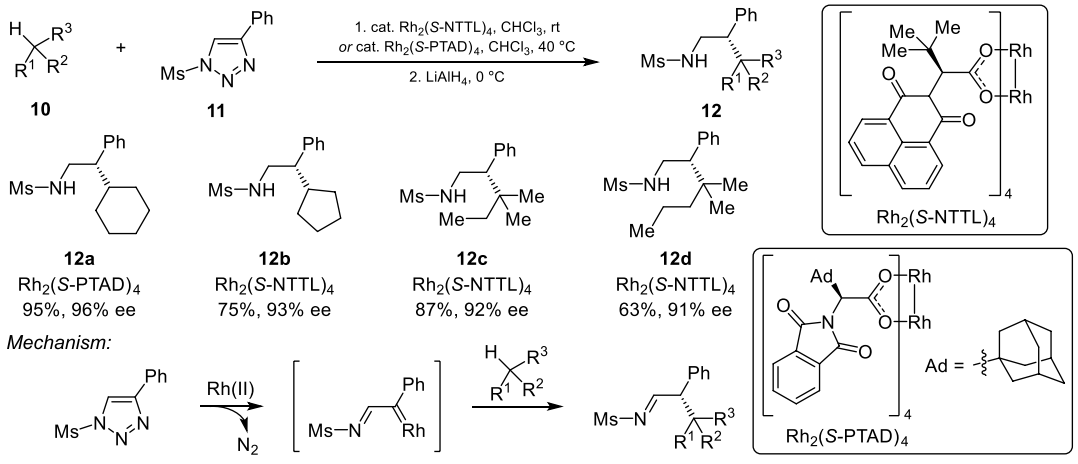

Scheme 12.5. C–H insertion of alkanes with azavinyl carbenoids. Source: [8]/American Chemical Society.

functionalization of non-activated primary C–H bonds in 40–93% yield with 90–>99% ee using tribromoethyl aryldiazoacetate **19** (Scheme 12.7) [10]. The sterically demanding triphenylcyclopropanecarboxylate (TPCP) ligands, first synthesized to serve as ligands for Rh complexes by the Davies group in 2011 [11], can cause the insertion reaction to favor more sterically accessible C–H bonds.

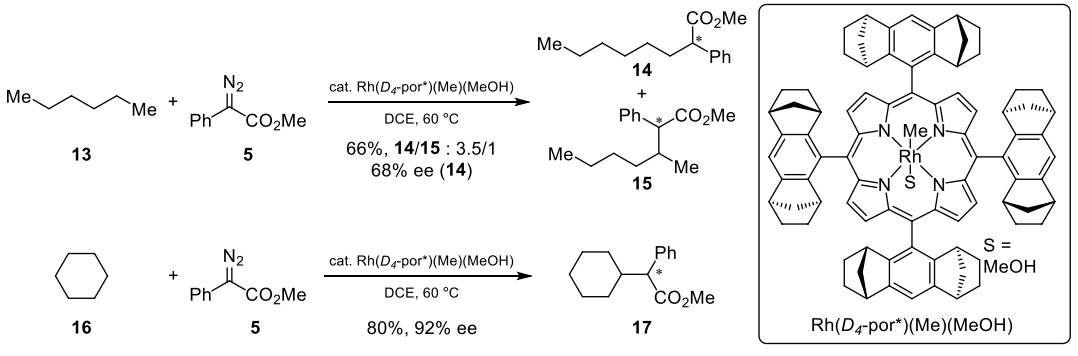

Scheme 12.6. C–H insertion of primary and secondary C–H bonds with Rh porphyrin. Source: [9]/John Wiley & Sons.

For selective functionalization of unactivated secondary C–H bonds, Davies developed a D_2-symmetric dirhodium catalyst Rh_2[*R*-3,5-di(*p*-*t*-Bu-C_6H_4)TPCP]$_4$ in 2016 and achieved highly regio-, diastereo-, and enantioselective C–H functionalization with tribromoethyl aryldiazoacetate **19** or trichloroethyl aryldiazoacetate **22** at the most accessible C2 position of *n*-alkanes and terminally substituted *n*-alkyl compounds (Scheme 12.8) [12]. Unactivated tertiary C–H bonds were later functionalized with excellent site- and enantioselectivity using a less sterically demanding C_4-symmetric dirhodium catalyst Rh_2(*S*-TCPTAD)$_4$ (Scheme 12.9) [13].

12.2.1.2.2. Insertion into Allylic and Benzylic C(sp³)–H Bonds Allylic C–H bonds are activated toward C–H bond insertion due to the ability of the adjacent double bond to stabilize the build-up of positive charge in the transition state of the C–H carbenoid insertion process. However, the use of such substrate is associated with the chemoselectivity issues as cyclopropanation of the double bond of allyl moiety is a common competing reaction pathway. The chemoselectivity between the intermolecular allylic C–H insertion vs cyclopropanation was first tuned by Müller and Tohill in 2000 by employing donor/acceptor carbenoids derived from aryldiazoacetates [14]. On the contrary to acceptor and acceptor/acceptor carbenoids that favor the cyclopropanation process, donor/acceptor carbenoids are far more prone

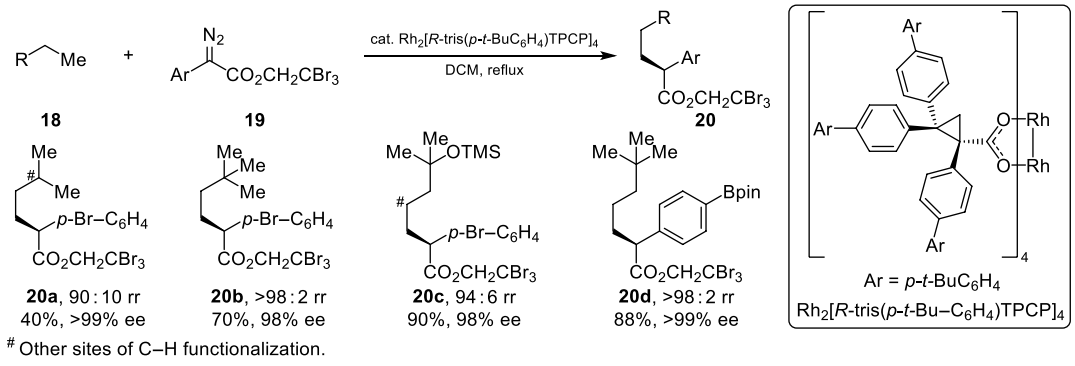

Scheme 12.7. Highly selective C–H insertion of primary C–H bonds. Source: [10]/Springer Nature.

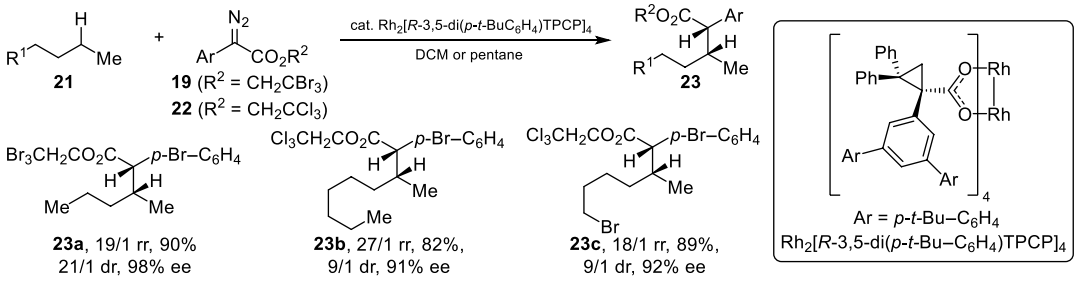

Scheme 12.8. Highly selective carbenoid insertion into secondary C–H bonds. Source: [12]/Springer Nature.

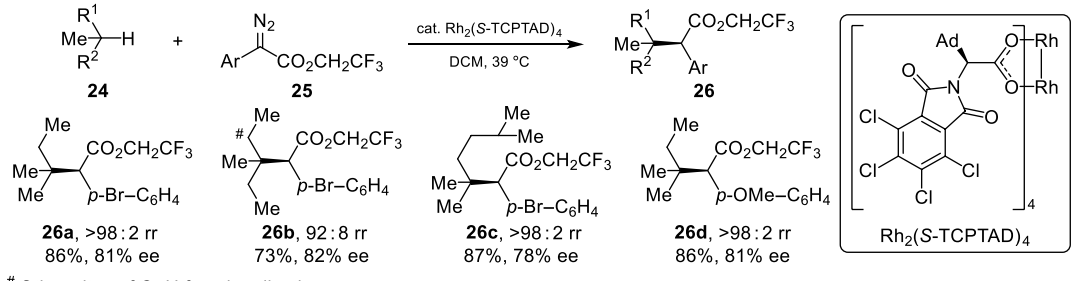

Scheme 12.9. Highly selective carbenoid insertion into tertiary C–H bonds. Source: [13]/Springer Nature.

toward C–H bond insertion and thus have been utilized extensively in allylic C–H functionalization, with the substrate scope of cyclic and acyclic olefins [14], cyclic vinylsilane [15], cyclic and acyclic silyl enol ethers [15], and cyclohexadienes [14, 16].

C–H bond insertion into doubly allylic sites is a very favorable process, and various chiral metal complexes have been reported for the intermolecular C–H insertion of 1,4-cyclohexadiene **27** (Table 12.1). Davies and coworkers first reported C–H insertion into 1,4-cyclohexadiene **27** with methyl phenyldiazoacetate and $Rh_2(S\text{-DOSP})_4$ in 1999 [14, 16] and later improved the reaction to afford product **29** with up to 95% ee and 84% yield (Table 12.1, Entry 1) [17]. In 2009, the Davies group employed donor/acceptor carbenoids derived from α-aryl-α-diazoketones and a chiral dirhodium complex $Rh_2(S\text{-PTAD})_4$, providing C–H insertion product **29** in up to 89% ee with 88% yield in 2,2-dimethylbutane (DMB) (Table 12.1, Entry 2) [18]. In 2012, the Hashimoto group reported the first example using α-alkyl-α-diazoester for asymmetric intermolecular carbenoid C–H insertion with rhodium carboxylate

TABLE 12.1. C–H insertion into doubly allylic sites.

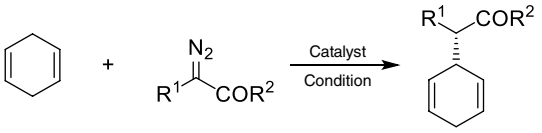

27 **28** **29**

Entry	R^1	R^2	Catalyst	Conditions	Yield (%)	ee (%)	Ref.
1	*p*-Cl–C_6H_4	OMe	Rh_2(*S*-DOSP)$_4$	Hexane, 23 °C	84	95	[17]
2	*p*-Br–C_6H_4	Me	Rh_2(*S*-PTAD)$_4$	DMB (2,2-dimethylbutane)	88	89	[18]
3	Me	OCH*i*-Pr_2	Rh_2(*S*-TFPTTL)$_4$	DMB, 23 °C	66	80(S)	[19]
4	Ph	OMe	Ir(III)-salen **30**	4 Å MS, 0 °C	91	94	[20]
5	Ph	OMe	Ir((−)-D_4Por*) (Me)(EtOH) **31**	DCM, −40 °C	90	95	[21]
6	Ph	OMe	Ir(III)-bis(oxz) **32**	rt	93	97	[22]
7	Ph	OMe	Ru(D_4-Por)$(IMe)_2$ **33**	DCM, 40 °C	80	92	[23]

Rh_2(*S*-TFPTTL)$_4$ (Table 12.1, Entry 3) [19], which was utilized for asymmetric cyclopropenation of alkyne in a previous report [17]. Several chiral iridium and ruthenium complexes have also been reported for asymmetric C–H insertion of 1,4-cyclohexadienes using aryl diazo ester (Table 12.1, Entry 4–7), among which are Ir(III)-salen **30** by Katsuki [20], Ir(III)-porphyrin complex Ir((−)-D_4-Por*)(Me)(EtOH) **31** by Che [21], Ir(III)-bis(oxazolinyl)phenyl complex **32** by Musaev, Davies, and Blakey [22], and bis(NHC)Ru(II)-porphyrin complex Ru(D_4-Por)$(IMe)_2$ **33** by Che [23] (Figure 12.2).

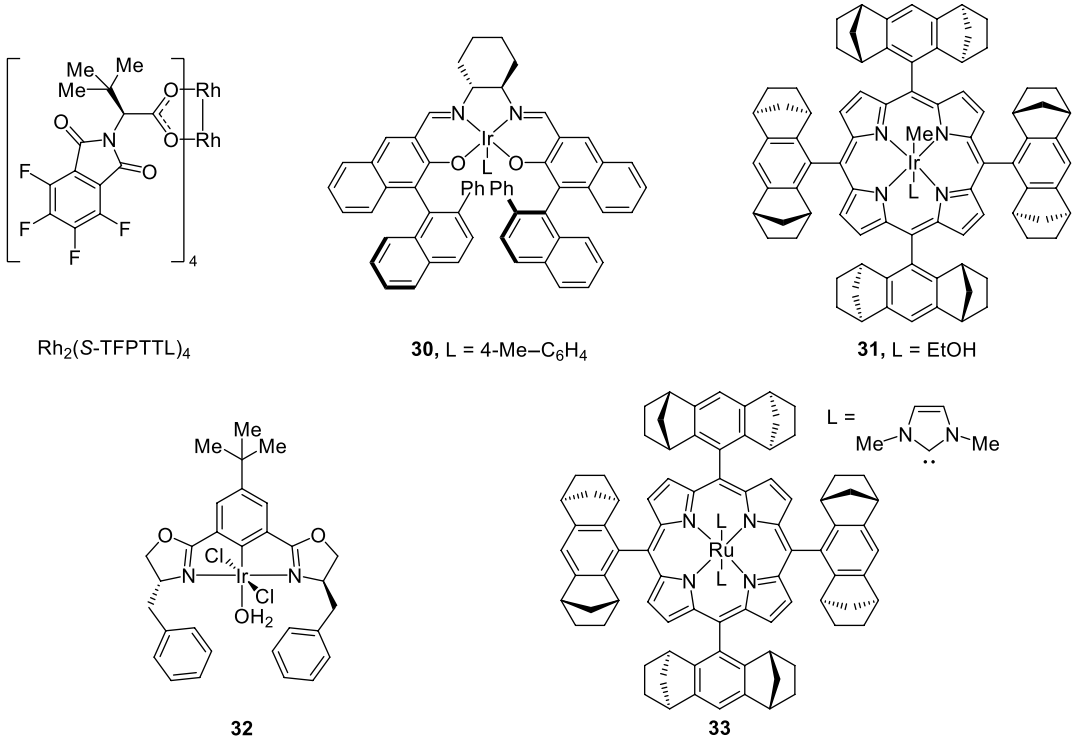

Figure 12.2. Chiral metal complexes for asymmetric C–H insertion of 1,4-cyclohexadiene.

Other than electron-rich allylic positions that are activated toward carbene insertion, relatively electron-deficient methyl sites, such as ethyl crotonate and more highly conjugated substrates, were employed in enantioselective C–H functionalization by the Davies group in 2016. This was achieved with the combination of 2,2,2-trichloroethyl (TCE) aryldiazoacetates **22** and tetrakis(triarylcyclopropanecarboxylate) dirhodium catalysts $Rh_2(R\text{-}p\text{-PhTPCP})_4$ (Scheme 12.10) [24]. 1,6-dicarbonyl compounds (**35a** and **35b**) are provided from crotonate derivatives, which is a valuable strategy for further diversification.

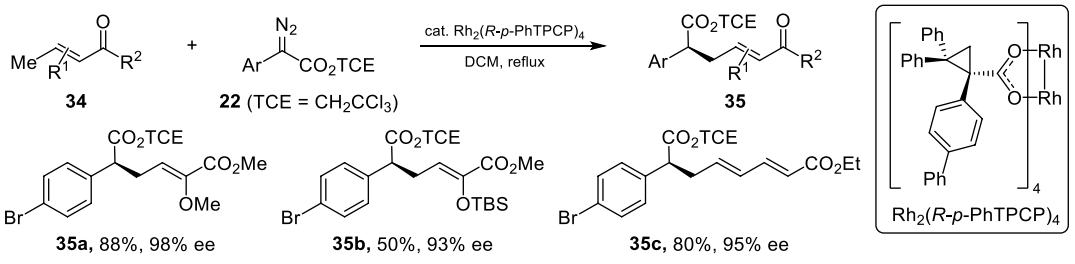

Scheme 12.10. C–H insertion of electron-deficient methyl sites. Source: [24]/American Chemical Society.

In addition to donor/acceptor carbenoids derived from diazo compounds, triazoles have been utilized as carbene precursors for allylic C–H functionalization. In 2016, the Davies group employed *N*-sulfonyltriazoles **11** as carbene precursor and Rh carboxylate $Rh_2(S\text{-NTTL})_4$ as a catalyst to achieve enantioselective intermolecular C–H functionalization at the allylic and benzylic positions

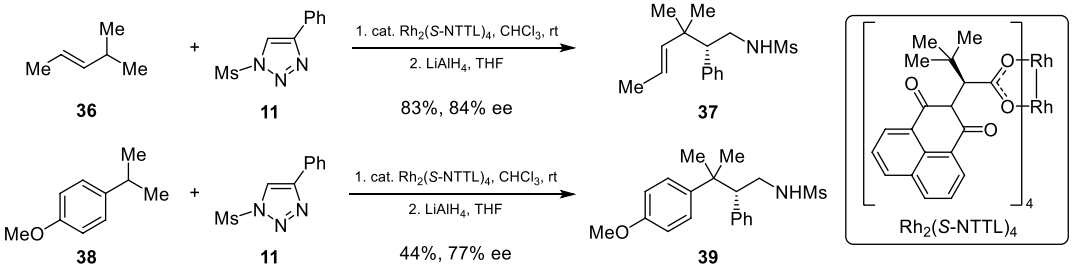

Scheme 12.11. C–H insertion of allylic and benzylic C–H bonds with triazoles. Source: [25]/American Chemical Society.

(Scheme 12.11) [25]. The synthetic application of the allylic C–H functionalization was further demonstrated by Davies in 2018 with the highly diastereo- and enantioselective synthesis of β-arylpyrrolidines **40**, which was achieved via an enantioselective intermolecular allylic C–H carbenoid insertion of trans-alkenes followed by immediate reduction, ozonolysis, and then in situ diversification of the resulting cyclic hemiaminal (Scheme 12.12) [26].

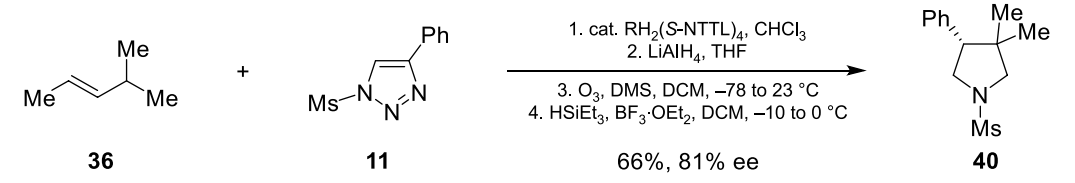

Scheme 12.12. Synthesis of β-arylpyrrolidines. Source: [26]/American Chemical Society.

Similar to allylic positions, benzylic positions are also activated toward carbenoid C–H insertion due to the stabilization of the positive charge built up in the transition state by the aromatic ring. The competing double cyclopropanation of the benzene ring can be suppressed completely in the presence of a *para*-substituent on the phenyl group. Asymmetric benzylic C–H activation of substituted ethylbenzenes **41** was achieved with good regio- and enantioselectivity with $Rh_2(S\text{-DOSP})_4$ (Scheme 12.13) [27]. Benzylic C–H functionalization of benzyl silyl ethers **45** affords low enantioselectivity with $Rh_2(S\text{-DOSP})_4$, but Hashimoto's $Rh_2(S\text{-PTTL})_4$ catalyst delivers high diastereo- and enantioselectivity (up to >95% de and 98% ee), as described by Davies in 2005 (Scheme 12.14) [28]. This transformation was later followed by the removal of the TBS group and Yu's Pd-catalyzed C–H functionalization/C–O cyclization [29] to construct complex 2,3-dihydrobenzofurans **51** in a highly regio-, diastereo-, and enantioselective manner (Scheme 12.15) [30] It demonstrates the potential application of selective C–H bond functionalization methodologies in the synthesis of complex targets.

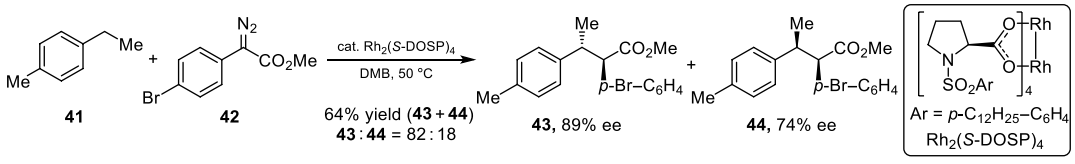

Scheme 12.13. Carbenoid insertion into benzylic C–H bonds of substituted ethylbenzenes. Source: [27]/American Chemical Society.

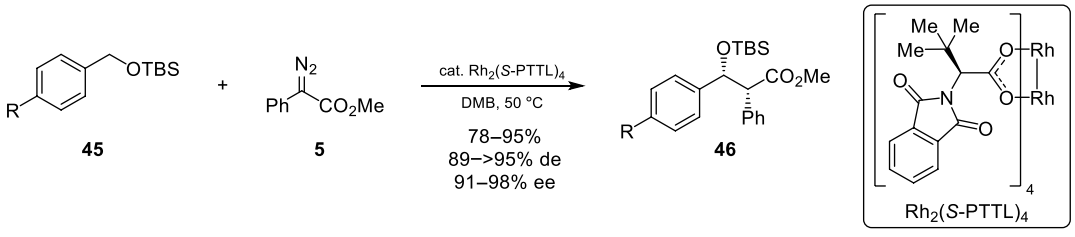

Scheme 12.14. Carbenoid insertion into benzylic C–H bonds of benzyl silyl ethers. Source: [28]/American Chemical Society.

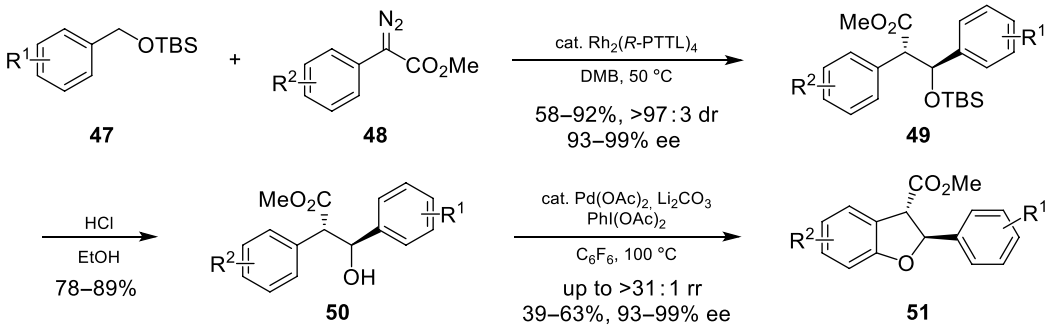

Scheme 12.15. Synthesis of 2,3-dihydrobenzofurans by sequential C–H functionalization. Source: [30]/American Chemical Society.

In 2019, the Arnold group introduced a new enzymatic strategy for the alkylation of benzylic, allylic, or α-amino C–H bonds with high enantio-, regio-, and chemoselectivity (Scheme 12.16) [31]. The iron-based catalysts employed are derived from a cytochrome P450 enzyme in which the native cysteine axial ligand is substituted for serine (cytochrome P411) and have been tuned by directed evolution for enhanced selectivity and activity. These proteins activate iron, the most abundant transition metal, to perform C–H functionalization via carbene insertion.

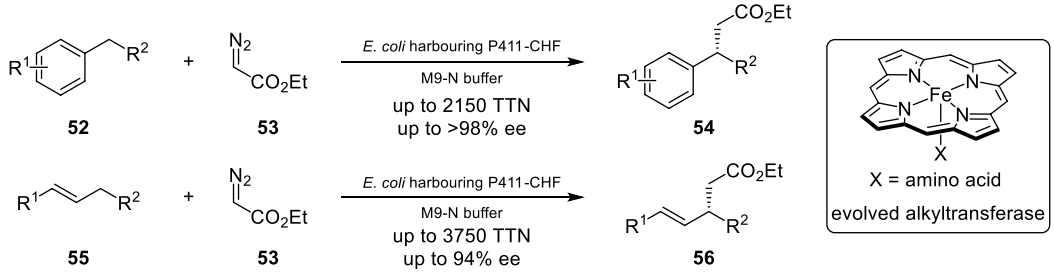

Scheme 12.16. Synthesis of 2,3-dihydrobenzofurans by sequential C–H functionalization. Source: [31]/Springer Nature.

12.2.1.2.3. Insertion into C(sp³)–H Bonds α *to Heteroatoms* C–H bonds α to a heteroatom (oxygen or nitrogen) are highly reactive toward carbenoid insertion due to the ability of lone-pair electrons on the adjacent heteroatom to stabilize the built-up positive charge in the transition state. Tetrahydrofuran **57** is a generally used substrate for this transformation, and the first catalyst utilized for its asymmetric C–H functionalization was Rh_2(*S*-DOSP)$_4$ (Table 12.2, Entry 1), affording moderate yield (67%) and diastereoselectivity (2.8 : 1 dr), but high enantioselectivity (97% ee) when phenyldiazoacetate **5** is employed as carbene precursor [7]. In the past decade, chiral iridium complexes have been reported to realize the same functionalization, with Ir(III)-salen **30** by Katsuki [20] in 2009 and Ir(III)-porphyrin complex Ir((−)-D_4-Por*)(Me)(EtOH) **31** by Che [21] in 2012 (Table 12.2, Entry 2, 3), both achieving higher yield (75 and 82%), higher diastereoselectivity (13 : 1 and 1 : 10), and good enantioselectivity (95% and 90%). Copper complexes with bis(oxazoline) (BOX) ligands were reported by Fraile and Mayoral as efficient catalysts for this type of transformation when they are immobilized onto a cheap support (**60**) (Figure 12.3), achieving good enantioselectivity (up to 88% ee) (Table 12.2, Entry 4) [32]. They later determined the absolute configuration of the conformationally flexible products **58** and **59** by using the combination of chiral preparative HPLC separation, VCD measurements, and vigorous quantum mechanics calculations in collaboration with the Jiménez-Osés group [33].

TABLE 12.2. C–H insertion of THF.

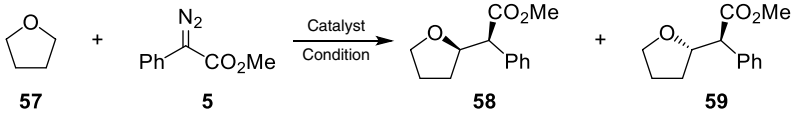

57 **5** **58** **59**

Entry	Catalyst	Conditions	Yield (%) **58** + **59**	*syn*/*anti* **58**/**59**	ee (%) **58**	ee (%) **59**	Ref.
1	Rh_2(*S*-DOSP)$_4$	Hexane, –50 °C	67	2.8 : 1	97	—	[7]
2	Ir(III)-salen **30**	THF, –50 °C	75	13 : 1	95	—	[20]
3	Ir((−)-D_4Por*)(Me)(EtOH) **31**	DCM, –40 °C	82	1 : 10	90	—	[21]
4	Immobilized Cu(box) **60**	THF, reflux	59	78 : 22	88	46	[32]

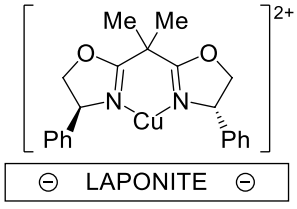

60

Figure 12.3. Immobilized Cu(box) complex. Source: [32]/American Chemical Society.

TABLE 12.3. C–H insertion of 1-methoxybutane.

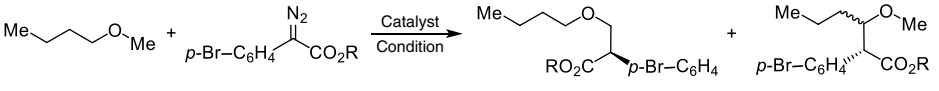

61 **62** **63** **64**

Entry	R	Catalyst	Conditions	Ratio **63**/**64**	Yield (%)	ee (%) **63**	Ref.
1	Me	Rh_2(*R*-DOSP)$_4$	DCM, reflux	3/2	77	61	[34]
2	Me	Rh_2(*R*-*p*-PhTPCP)$_4$	DCM, reflux	>20/1	86	64	[34]
3	CH_2CCl_3	Rh_2(*R*-*p*-PhTPCP)$_4$	DCM, 0 °C	>20/1	78	88	[35]

The site selectivity of functionalization of C–H bonds α to oxygen can be tuned by Rh catalysts. In contrast to Rh_2(*R*-DOSP)$_4$ that prefers C–H carbene insertion of secondary C–H bonds (Table 12.3, Entry 1), in 2014 Davies showed that a sterically more demanding dirhodium tetrakis(triarylcyclopropanecarboxylate) catalyst Rh_2(*R*-*p*-PhTPCP)$_4$ [24] changed the site selectivity to favor primary C–H bonds (Table 12.3, Entry 2) [34]. The primary C–H bond adjacent to oxygen in 1-methoxybutane **61** is selectively functionalized and affords product **63** with high regioselectivity (>20 : 1), high yield (86%), and good enantioselectivity (64% ee). Selective primary C–H functionalization is also achieved with various substrates containing primary benzylic C–H bonds and allylic C–H bonds, with high levels of asymmetric induction (up to 97% ee). Later that year, with the same catalyst Rh_2(*R*-*p*-PhTPCP)$_4$, also called Rh_2(*R*-BPCP)$_4$, Davies developed a new class of reagents, 2,2,2-trichloroethyl (TCE) aryldiazoacetates, and achieved enantioselective intermolecular C–H functionalization of methyl ethers with better site selectivity and enantioselectivity, affording primary functionalized product **63** with 78% yield and 88% ee (Table 12.3, Entry 3) [35].

In addition to the donor-acceptor metallocarbenes, acceptor-only metallocarbenes were also employed in the intermolecular enantioselective C–H functionalization by Musaev, Davies, and Blakey in 2016 (Scheme 12.17) [36]. A new family of Ir(III)-bis(imidazolinyl)phenyl catalysts was developed based on the combination of experimental and computational studies. With diazoacetate **53** as carbene

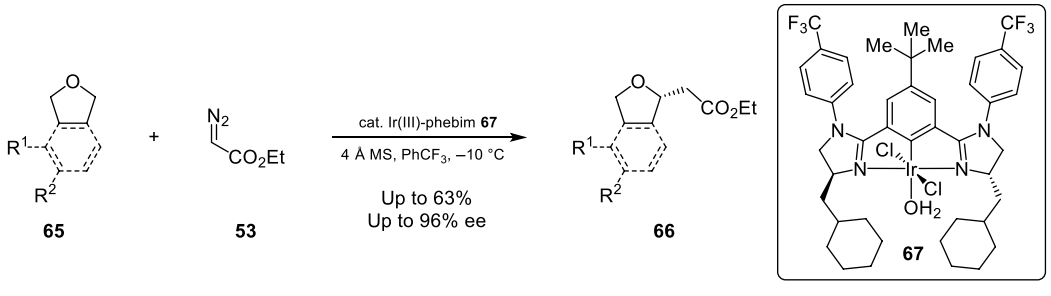

65 **53** **66** **67**

Scheme 12.17. C–H insertion of phthalan and dihydrofuran derivatives. Source: [36]/Royal Society of Chemistry.

precursor, phthalan and dihydrofuran derivatives **65** are functionalized in good yields (up to 63% yield) and excellent enantioselectivities (up to 96% ee).

Similar to C–H activation α to oxygen mentioned above, C–H activation α to nitrogen is also a very favorable process. Both cyclic [37–40] and acyclic [41–43] *N*-protected amines have been functionalized via asymmetric Rh carbenoid insertion with donor/acceptor diazo compounds as precursors, which have been demonstrated in the Third Edition of this book [1].

12.2.1.2.4. Insertion into C(sp³)–H Bonds β to Silicon Harnessing the β-silicon effect and demonstrating the role of hyperconjugation toward enhancing C–H bond lability, the Davies group realized regioselective and stereoselective Rh carbenoid insertion into the β position of silicon in recent years. Utilizing 1-sulfonyl-1,2,3-triazoles **69** as carbene precursor, in 2018, Davies reported the first enantioselective C–H functionalization of silicon-substituted alkanes **68** with Rh_2(S-NTTL)$_4$ (Scheme 12.18) [44]. In 2019, aryl diazoacetates **71** were employed as carbene precursors for the regioselective and enantioselective intermolecular sp³ C–H functionalization of silicon-substituted alkanes **68** using the recently developed dirhodium catalyst Rh_2(*S*-TPPTTL)$_4$ (Scheme 12.19), allowing the expansion of the substrate scope by changing the donor group on the donor/acceptor carbene [45].

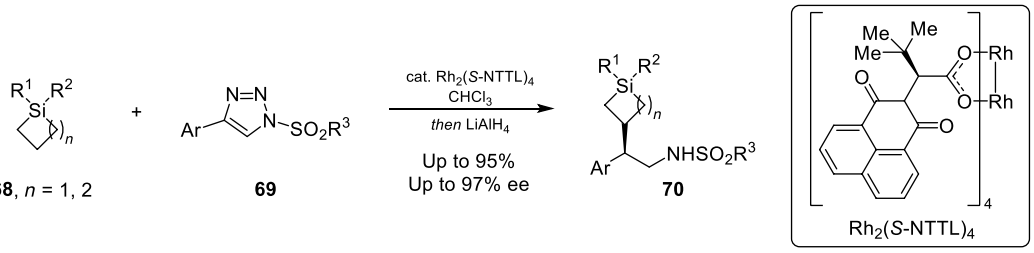

Scheme 12.18. C–H insertion of silicon-substituted alkanes with 1-sulfonyl-1,2,3-triazoles. Source: [44]/American Chemical Society.

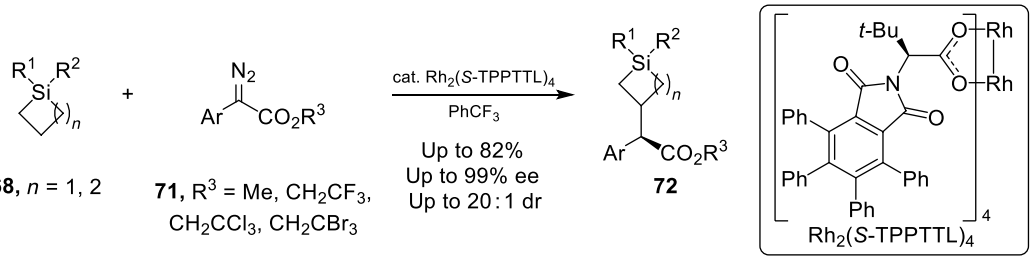

Scheme 12.19. C–H insertion of silicon-substituted alkanes with aryl diazoacetates. Source: [45]/American Chemical Society.

12.2.1.2.5. Combined C(sp³)–H Functionalization/Cope Rearrangement The combined C–H functionalization/Cope rearrangement (CHCR), a reaction that occurs between allylic C–H bonds and Rh-stabilized vinylcarbenoids, has been developed into a reliable methodology and has shown broad applications in organic synthesis [46]. The CHCR reaction can be applied as a surrogate to the vinylogous Mukaiyama aldol reaction [47], the tandem Claisen rearrangement/Cope rearrangement [48], the tandem aldol reaction/siloxy-Cope rearrangement [49], and the Michael reaction[50] (Scheme 12.20). With chiral dirhodium catalyst Rh_2(*S*-DOSP)$_4$ or Rh_2(*S*-PTAD)$_4$ employed, the products are generated with very high diastereo- and enantioselectivity in all these cases. Furthermore, the CHCR reaction has been exploited in the total synthesis of several natural products such as (+)-sertraline [16], (+)-erogorgiaene [51], (−)-colombiasin A, and (−)-elisapterosin B [52].

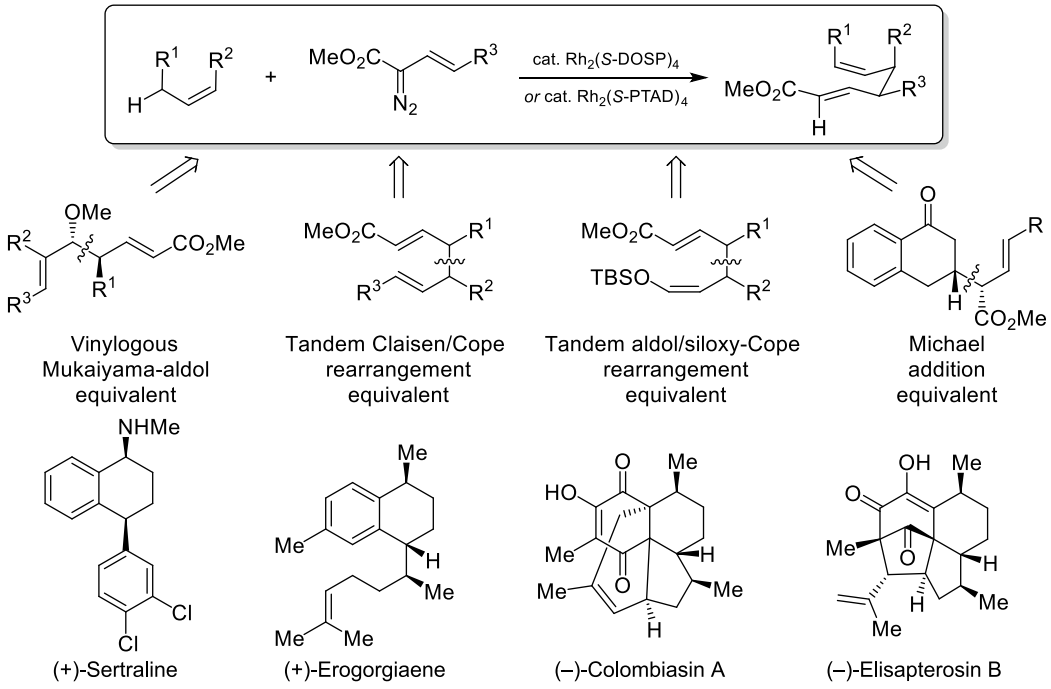

Scheme 12.20. Application of the combined C–H functionalization/Cope rearrangement (CHCR).

A detailed computational study of the CHCR reaction was conducted in 2011 and showed that the reaction proceeds through a concerted but highly asynchronous process involving an initial hydride transfer from the allyl site to the Rh carbenoid, followed by vinylogous C–C bond formation [53]. The early examples of the CHCR reaction were highly diastereoselective, consistent with a reaction proceeding through a chair-like transition state with the Rh vinylcarbenoid adopting an *s-cis* orientation. However, the calculations revealed that other transition-states and stereochemical outcomes are possible by modifying the reagents, and these results have directed toward switching the diastereoselectivity of the CHCR reactions by forcing the reaction to proceed through the *s-cis* boat transition state instead of the *s-cis* chair transition state [46, 53].

12.2.1.3. Intramolecular C(sp³)–H Functionalization Intramolecular C–H insertions of diazocarbonyl compounds have been well-developed, and usually proceed with high selectivity compared to the intermolecular process. As demonstrated in the Third Edition of this book [1], a variety of carbocyclic and heterocyclic structures can be formed with high regio- and stereocontrol. The typical ones are cyclopentanones, lactones, lactams, furans, and pyrans. Herein, we provide some updates from the past decade.

After the first example of asymmetric C–H insertion employing α-diazosulfones was achieved with 12% ee catalyzed by rhodium(II) (*S*)-mandelate prolinate catalyst [54], in 2010, Maguire and coworkers reported the first application of Cu catalysts for C–H bond insertion reactions with α-diazosulfones (Scheme 12.21a) [55]. Use of CuCl with the chiral bis-oxazoline ligand (*R*,*R*)-**L-1** afforded the formation of six-membered ring thiopyrans **74** with excellent enantioselectivity (up to 98% ee), and five-membered ring sulfolanes **75** with up to 60% ee when six-membered ring formation was not possible. Subsequently, the Maguire group continued their investigations with copper-catalyzed diazocarbonyl chemistry, and in 2011 they reported enantioselective intramolecular C–H insertion of α-diazo-β-keto sulfones **76** to yield α-sulfonyl cyclopentanones **77** with up to 82% ee (Scheme 12.21b) [56].

Intramolecular C–H insertion has been an attractive strategy for generating lactones. In 2013, Che reported enantioselective intramolecular carbene insertion into methylene C–H bonds of α-diazoesters

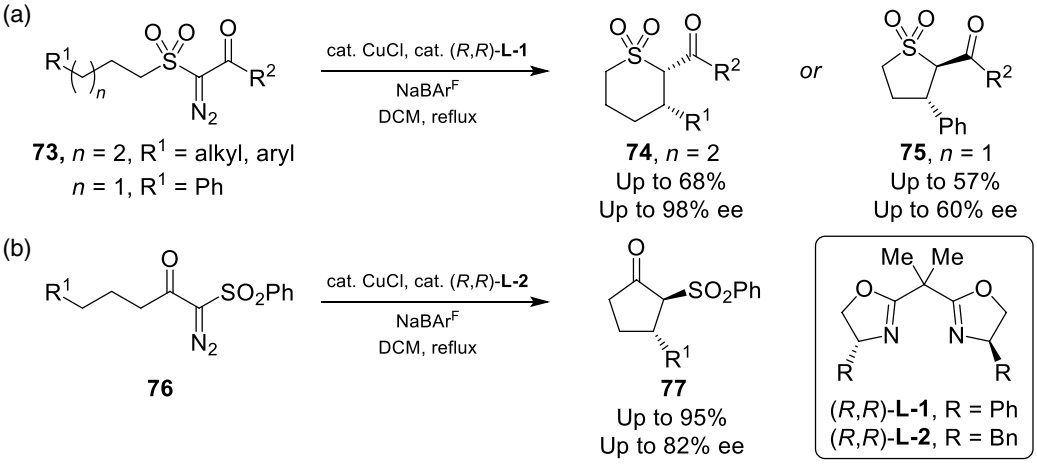

Scheme 12.21. Intramolecular C–H insertion with α-diazosulfones. (a) Synthesis of thiopyrans and sulfolanes. (b) Synthesis of cyclopentanones. Source: (a) [55]/American Chemical Society. (b) [56]/Royal Society of Chemistry.

78 by using iridium(III) porphyrin complex [Ir((+)-*D*4-Por)Me(L)] (L = H_2O or solvent), affording cis-β-lactones **79** in good yields (up to 87%) and good enantioselectivities (up to 78% ee) (Figure 12.4) (Table 12.4, Entry 1, 2) [57]. In 2014, the Davies group employed rhodium catalyst Rh_2(*S*-TCPTTL)$_4$ for the asymmetric synthesis of β-lactones **79** via intramolecular carbene insertion into aryldiazoacetates, with high yields (up to 95%) and high enantioselectivities (up to 99% ee) [58]. The introduction of halo and trifluoromethyl substituents at the ortho position of the aryldiazoacetates enhances intramolecular over intermolecular C–H insertion, allowing C–H insertion into not only methylene and methine C–H bonds, but also methyl C–H bonds (Table 12.4, Entry 3–5).

In recent years, carbene-transfer reactions by non-diazo approaches have received much attention in response to the challenges of safety (gas emission) and practicality (slow addition) inherent to the diazo chemistry. Using enynones as the carbene source, in 2016, Zhang and Zhu reported the first enantioselective intramolecular C–H insertion and cyclopropanation reactions of donor- and donor/donor-carbenes by a non-diazo approach (Scheme 12.22) [59]. Dihydroindoles **81**, dihydrobenzofurans, or tetrahydrofurans **83** were synthesized with up to 99% ee and up to 99% yield via C–H insertion reactions of 2-furyl rhodium carbenoids generated from the cyclization of enynones **80** or **82** (Scheme 12.22a,b). With *N*-allylic enynone substrates **84**, however, cyclopropanation occurs selectively. Later, the Zhu group

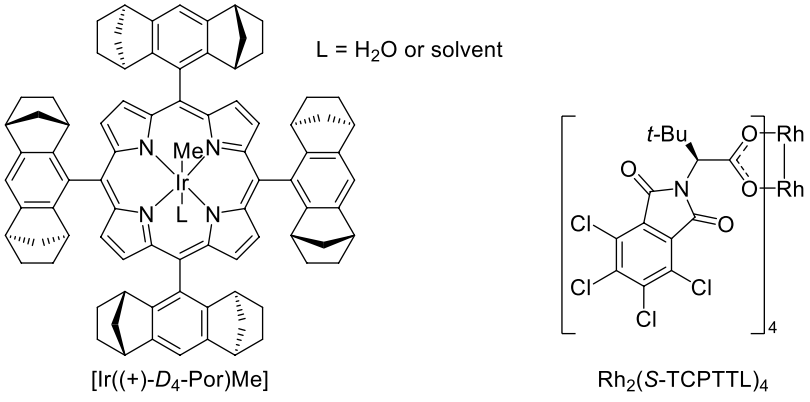

Figure 12.4. Chiral metal catalysts used for synthesis of β-lactones.

TABLE 12.4. Synthesis of β-lactones.

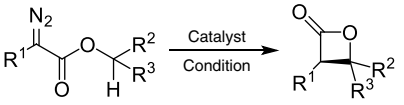

78 79

Entry	R^1	R^2	R^3	Catalyst	Conditions	Yield (%)	ee (%)	Ref.
1	Ph	Ph	H	[Ir((+)-*D*4-Por)Me]	DCM, 25 °C	90	76	[57]
2	4-F–C_6H_4	Ph	H	[Ir((+)-*D*4-Por)Me]	DCM, 25 °C	85	76	[57]
3	2-CF_3–C_6H_4	Ph	H	Rh_2(*S*-TCPTTL)$_4$	DCM, 40 °C	60	99	[58]
4	2-Br–6-OMe–C_6H_3	Me	Me	Rh_2(*S*-TCPTTL)$_4$	DCM, 40 °C	95	93	[58]
5	2-I–6-OMe–C_6H_3	H	H	Rh_2(*S*-TCPTTL)$_4$	DCM, 40 °C	67	92	[58]

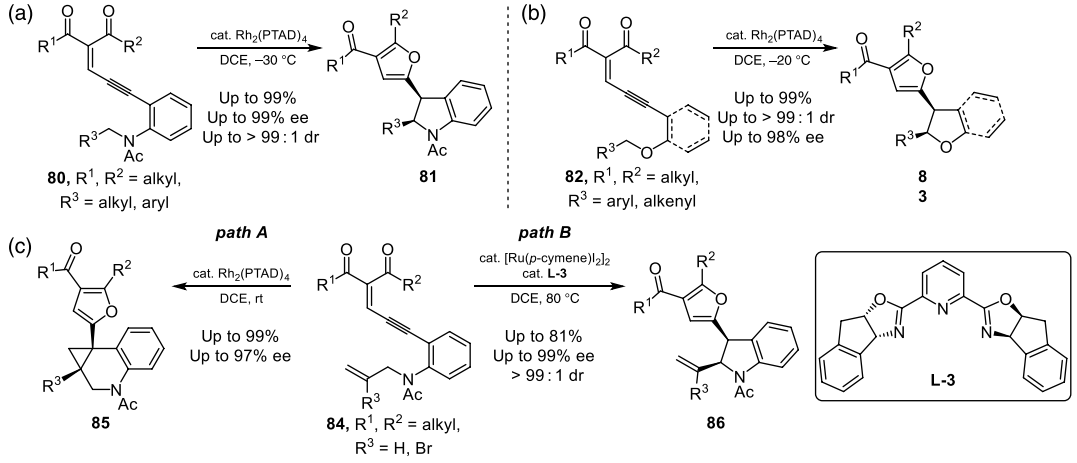

Scheme 12.22. Intramolecular C–H insertion by non-diazo approaches. (a) Synthesis of dihydroindoles. (b) Synthesis of dihydrobenzofurans or tetrahydrofurans. (c) Chemo- and stereoselective catalyst-controlled allylic C–H Insertion and cyclopropanation. Source: (a) and (b) [59]/John Wiley & Sons. (c) [60]/John Wiley & Sons.

realized chemoselective intramolecular C–H insertion of *N*-allylic enynones **84** by using Ru(II)/Pybox complex, providing vinyl-substituted dihydroindoles **86** with up to 99% ee and up to 81% yield (Scheme 12.22c, path B), while cyclopropanation is promoted with $Rh_2(PTAD)_4$ to afford cyclopropane-fused tetrahydroquinoline derivatives **85** in excellent yield (up to 99%) and up to 97% ee (Scheme 12.22c, path A) [60].

In 2018, Doyle and Xu provided a general access to chiral dihydroindole derivatives by C–H functionalization in a highly site- and enantioselective cascade reaction of propargyl diazoacetates **87** (Scheme 12.23) [61]. Highly site-selective intramolecular C–H bond insertions are achieved by catalyst control: sterically demanding dirhodium carboxylate Rh_2(*S*-BTPCP)$_4$ favors C–H insertion into 1° C–H bonds with regioselectivities reaching >95 : 5 (1°>2° benzylic) and >90% ee, while Rh_2(*S*-TBPTTL)$_4$ prefers 2° and 3° C–H bond insertion (up to 92% yield and 99% ee) due to the configuration of catalyst and electronic effects. The chiral dirhodium catalyst not only promotes carbene/alkyne metathesis (CAM) to generate the donor/donor carbene intermediate **90**, but also contributes to asymmetric induction in the terminating C–H insertion process.

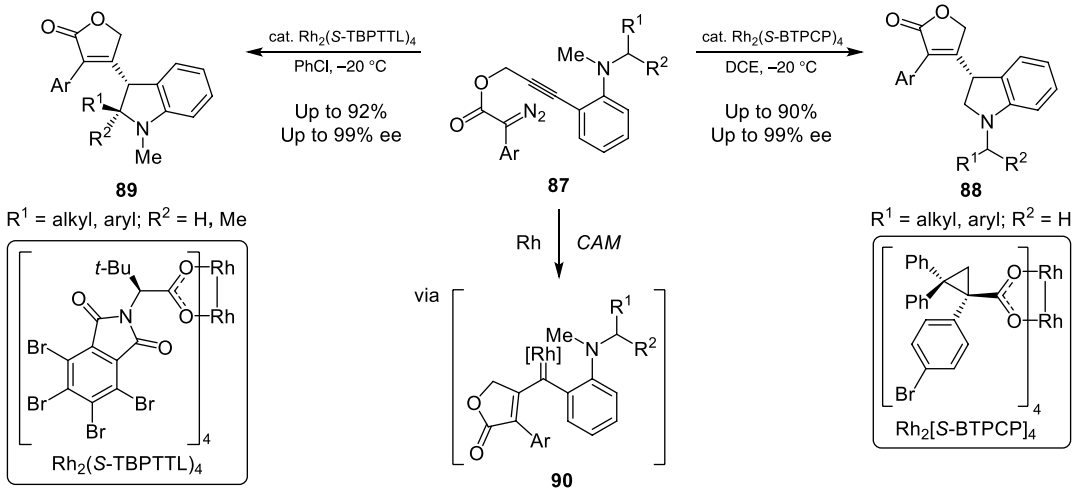

Scheme 12.23. C–H insertion in carbene/alkyne metathesis (CAM). Source: [61]/John Wiley & Sons.

12.2.2. C(sp³)–H Bond Insertion of Metal Nitrenoids

12.2.2.1. Introduction The installation of the amine functional group by C–H functionalization has emerged as an efficient strategy to afford molecules of relevance to many chemical areas, including the synthesis of biologically active compounds in the pharmaceutical industry. The development of metal-catalyzed C–H amination via nitrene insertion greatly enhances the synthetic potential of such transformations due to its advantages of mild reaction conditions and high chemo- and stereoselectivities.

As illustrated in Scheme 12.24, catalytic C–H amination reactions via nitrene insertion involve the metal nitrenoid species as the key intermediates, which are generated by the reaction of the metal complex (ML_n) with nitrene precursors. The most widely used ones are iminoiodinanes, azides, or *N*-(sulfonyloxy)carbamates, from which iodobenzene, dinitrogen, or sulfonic acid is extruded as byproduct of metal nitrenoid formation. Dioxazolones and hydroxylamine derivatives have also been utilized as nitrogen sources in recent years. Subsequently, the metal nitrenoid intermediate undergoes C–H insertion to form the amination product. It has been proposed that the C–H insertion step could proceed through a concerted asynchronous pathway via a hydride transfer/C–N bond formation transition state [62–65], or a stepwise process of hydrogen atom abstraction followed by radical recombination [66, 67].

Of the metal complexes that can catalyze C–H insertion of nitrenes, the most studied ones are dirhodium(II) complexes, Ru(II) and Mn(III) porphyrin complexes, and Ru(II) and Mn(III) salen complexes. In recent years, efforts have also been made to develop other chiral catalysts based on iridium, ruthenium, iron, and silver.

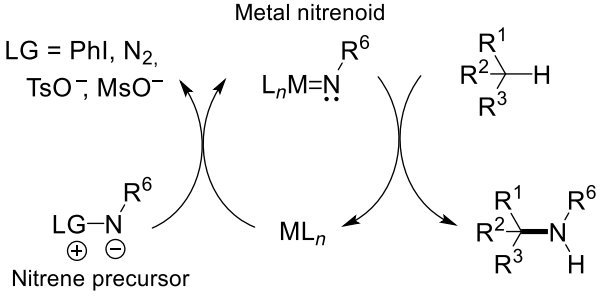

Scheme 12.24. General catalytic cycle of C(sp³)–H bond insertion of metal nitrenoid.

In the past two decades, remarkable progress has been made in the area of asymmetric C–H amination via nitrenoid insertion. As an update from the Third Edition of this book [1], this section will present the recent progress according to the type of nitrene precursors for intramolecular and intermolecular C–H aminations.

12.2.2.2. C(sp³)–H Functionalization with Iminoiodinanes

12.2.2.2.1. Intermolecular C(sp³)–H Amination with Iminoiodinanes The first enantioselective C–H bond insertion of Rh nitrenoids was reported by Müller and coworkers in 1997 [68], utilizing iminoiodinane PhI=NNs **94** as nitrene precursor. Preliminary experiments showed that enantioselective amidation of indane could be realized with 31% ee when using a chiral dirhodium(II) phosphate complex Rh_2(*R*-BNP)$_4$ (Figure 12.5) (Table 12.5, Entry 1). Later, Hashimoto achieved higher enantioinduction of the intermolecular C–H amidation with PhI=NNs **94** and a dirhodium(II) carboxylate complex Rh_2(*S*-TCPTTL)$_4$, affording an aminated indane compound with 70% ee and an aminated tetraline compound with 76% ee (Table 12.5, Entry 2, 3) [69]. In 2001, Mn(III) salen complexes were introduced by Katsuki and coworkers [70]. Under the catalysis of Mn(III)-salen **98**, an aminated tetraline compound is generated in 67% yield and 77% ee using PhI=NTs **95** as the nitrene source (Table 12.5, Entry 4).

Besides using iminoiodinane reagents directly as nitrene precursors, iminoiodinanes can be generated in situ from various nitrogen functions such as sulfamates and carbamates with iodine(III) oxidants. In 2006, Müller, Dodd, and Dauban utilized chiral sulfonimidamide **100** as the nitrene source and designed an efficient diastereoselective intermolecular C–H amination with a chiral rhodium catalyst, affording aminated indane product **101** with >99% de with Rh_2(*S*-NTTL)$_4$ as catalyst (Scheme 12.25) [71]. With the same approach, the Dauban group further explored the chemoselective functionalization of more complex molecules and reported the site-selective C–H amination of complex substrates including terpenes, enol ethers, and alkanes in 2012 [72], giving access to enantiopure aminated derivatives that are not easily obtained by classical organic synthesis. In 2014, they applied this strategy to synthesize a series of octahydroindole derivatives with high efficiency [73].

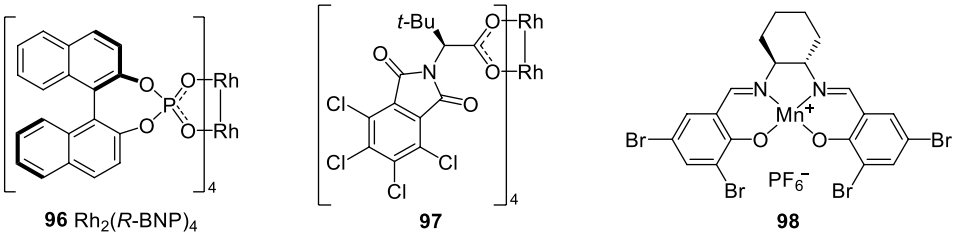

Figure 12.5. Chiral metal catalysts used for C–H amination of indane.

TABLE 12.5. C–H amidation of indane and tetraline.

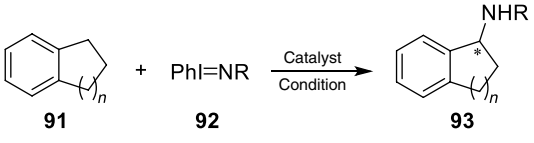

Entry	R	*n*	Catalyst	Conditions	Yield (%)	ee (%)	Config.	Ref.
1	Ns (**94**)	1	Rh_2(*R*-BNP)$_4$	DCM, 20 °C	71	31	*S*	[68]
2	Ns (**94**)	1	Rh_2(*S*-TCPTTL)$_4$ **97**	DCM, –23 °C	82	70	*R*	[69]
3	Ns (**94**)	2	Rh_2(*S*-TCPTTL)$_4$ **97**	DCM, –23 °C	88	76	*R*	[69]
4	Ts (**95**)	2	Mn(III)-salen **98**	DCM, 4 Å MS, –40 °C	67	77	*S*	[70]

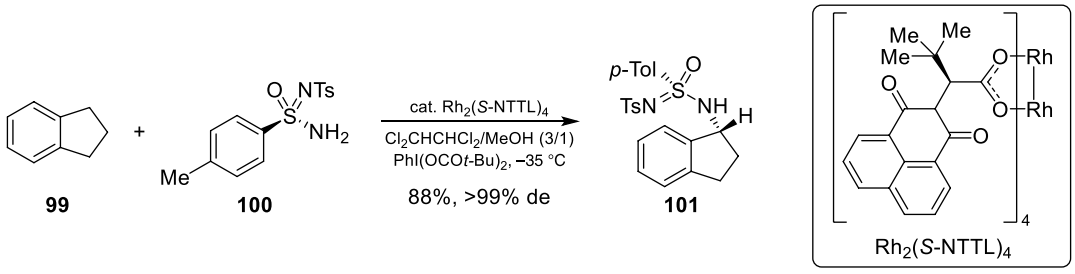

Scheme 12.25. Diastereoselective C–H amination of indane with chiral sulfonimidamide. Source: [71]/John Wiley & Sons.

In 2019, Dauban and coworkers developed a practical general method for asymmetric intermolecular benzylic C–H amination with the combination of the pentafluorobenzyl sulfamate $PfbsNH_2$ **103** and the chiral rhodium(II) catalyst Rh_2(*S*-TFPTAD)$_4$ (Scheme 12.26) [74]. Excellent yields of up to 99% and enantioselectivities of up to 89% have been achieved, showing the high reactivity of benzylic sulfamates as nitrene precursors. Additional key features are the low catalyst loading (0.1 mol%) and the ability to remove the Pfbs protecting group under mild conditions to afford free benzylic amines.

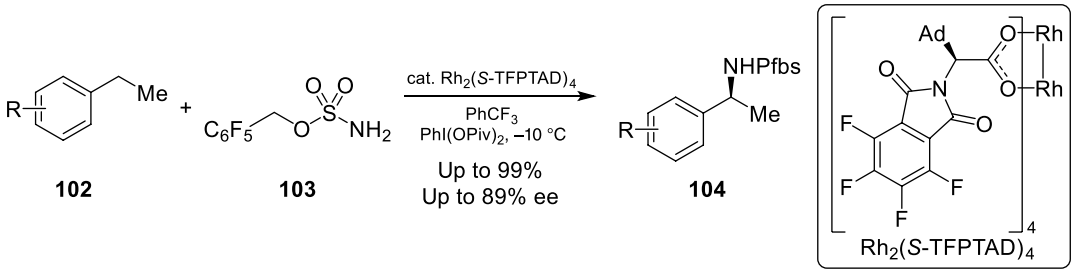

Scheme 12.26. Enantioselective intermolecular benzylic C–H amination with sulfamates. Source: [74]/John Wiley & Sons.

Recently, Bach and coworkers developed silver-catalyzed amination of aliphatic methylene groups in pyridines and quinolones with high site- and enantioselectivity (Scheme 12.27) [75]. Pivotal to the selectivity is the use of a chiral phenanthroline ligand that is attached to an octahydro-1*H*-4,7-methanoisoindo-1-one, which binds to the substrate through hydrogen-bonding. Utilizing $AgPF_6$ as the silver source, PhI=NNs as the nitrene precursor, and 1,10-phenanthroline as the coligand, nitrene C–H insertion happened within a hydrogen-bonded silver complex in which only one enantiotopic C–H bond is exposed to the catalytic reaction center.

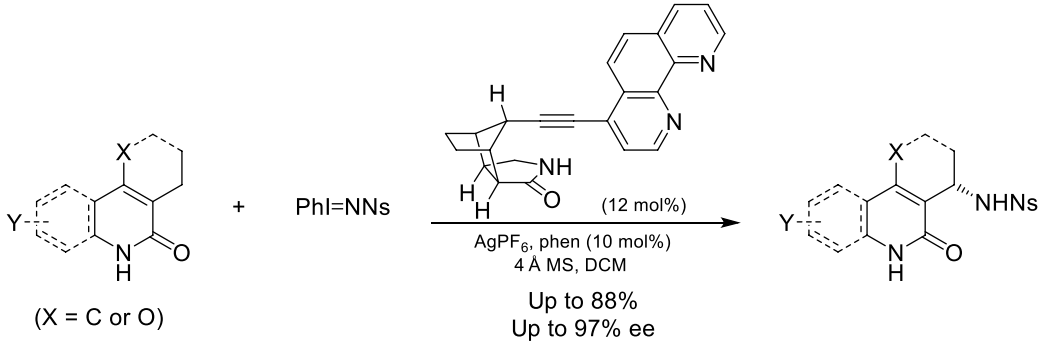

Scheme 12.27. Enantioselective intermolecular benzylic C–H amination with sulfamates. Source: [75]/American Chemical Society.

12.2.2.2.2. Intramolecular C(sp³)–H Amination with Iminoiodinanes By employing the in situ generated iminoiodinanes, the first enantioselective intramolecular C–H amination of prochiral RNH_2 substrates was realized by Che and coworkers in 2002 [76]. Using chiral Ru(II) porphyrin complex Ru(Por*)(CO) **107** (Figure 12.6), a variety of sulfamidates of five- and six-membered rings were produced with 77–88% ee from sulfamate ester substrates **105** (Table 12.6, Entry 1, 2). Chiral manganese Schiff base complex Mn(III)-salen **108** was employed for the enantioselective cyclizations of sulfamate esters by Che in 2005 (Table 12.6, Entry 3, 4) [77]. Efficient Rh-catalyzed intramolecular amination of benzylic and allylic C–H bonds was realized by Du Bois and coworkers in 2008 [78], with high enantioselectivity achieved by a new chiral dirhodium catalyst Rh_2(*S*-NAP)$_4$ containing a hydrogen bond between the N–H and the carbonyl oxygen of the amide (Table 12.6, Entry 5, 6). Subsequently, Blakey designed a cationic Ru(II)-pybox catalyst via halide abstraction from the parent complex **109** for the development of effective asymmetric intramolecular amination of benzylic and allylic C–H bonds (Table 12.6, Entry 7, 8) [79].

Recently, Schomaker reported the first general silver catalyst for intramolecular, enantioselective propargylic C–H amination via a nitrene transfer (NT) pathway (Scheme 12.28) [80]. The design of a new bis(oxazoline) ligand Min-BOX enabled the intramolecular amination of carbamate esters bearing γ-propargylic C–H bonds and furnished γ-aminoalcohol motifs in good yields and enantioselectivities. Computational studies indicated that the design of Min-BOX ligand promotes the putative Ag-nitrene species to undergo enantiodetermining hydrogen-atom-transfer (HAT) during the C–H amination event.

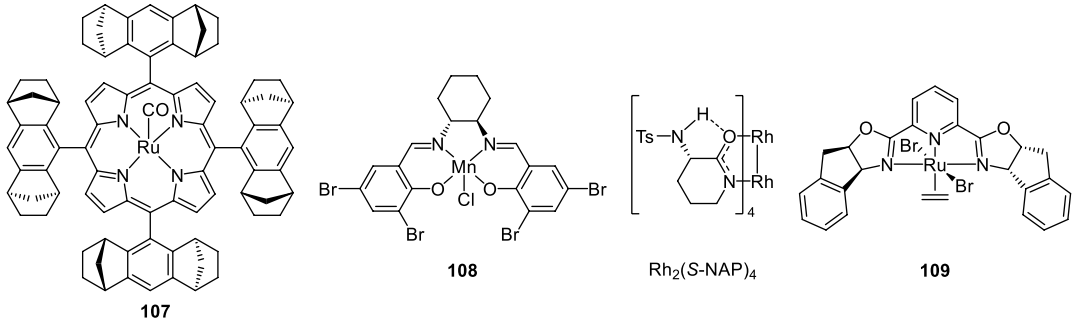

Figure 12.6. Chiral metal catalysts used for the synthesis of cyclic sulfamidates with iminoiodinane.

TABLE 12.6. Synthesis of cyclic sulfamidates with iminoiodinane.

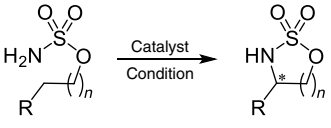

Entry	*n*	R	Catalyst	Conditions	Yield (%)	ee (%)	Ref.
1	1	Ph	Ru(Por*)(CO) **107**	$PhI(OAc)_2$, Al_2O_3, PhH, 5 °C	35	87	[76]
2	2	Ph	Ru(Por*)(CO) **107**	$PhI(OAc)_2$, Al_2O_3, PhH, 5 °C	48	84	[76]
3	1	Ph	Mn(III)-salen **108**	$PhI(OAc)_2$, Al_2O_3, PhH, 5 °C	57	54	[77]
4	2	*p*-F–C_6H_4	Mn(III)-salen **108**	$PhI(OAc)_2$, Al_2O_3, PhH, 5 °C	68	47	[77]
5	2	Ph	Rh_2(*S*-NAP)$_4$	PhI=O, 3 Å MS, DCM	85	92	[78]
6	2	PhCH=CH	Rh_2(*S*-NAP)$_4$	PhI=O, 3 Å MS, DCM	55	84	[78]
7	2	*p*-OMe–C_6H_4	Ru(II)-pybox **109**	$PhI(O_2Ct\text{-}Bu)_2$, AgOTf, MgO, PhH, 22 °C	68	90	[79]
8	2	MeCH=CH	Ru(II)-pybox **109**	$PhI(O_2Ct\text{-}Bu)_2$, AgOTf, MgO, PhH, 22 °C	60	89	[79]

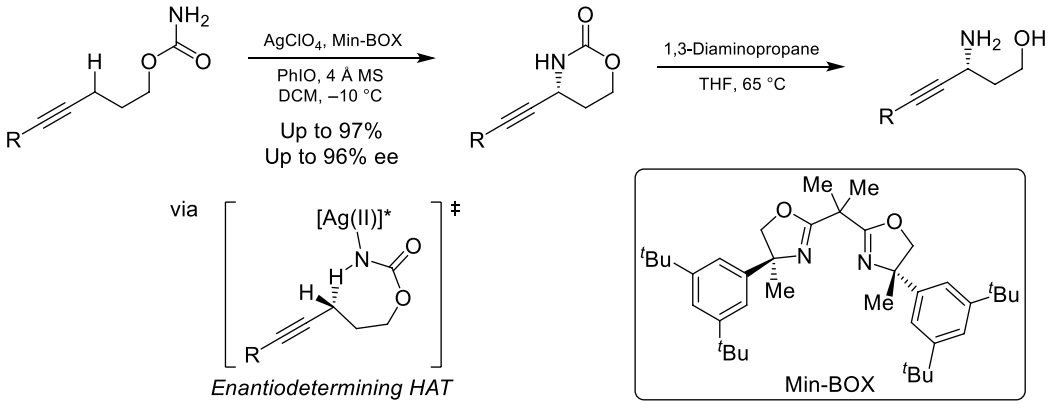

Scheme 12.28. Enantioselective intermolecular benzylic C–H amination with sulfamates. Source: [80]/American Chemical Society.

12.2.2.3. C(sp³)–H Functionalization with Azides

12.2.2.3.1. Intermolecular C(sp³)–H Amination with Azides Organic azides are important nitrene precursors for C–H amination reactions, producing linear or cyclic amines and only N_2 as a side product. The past decade witnessed the utility of azide in asymmetric C(sp³)–H amination. The first efficient asymmetric intermolecular C–H amination using azides was reported by Katsuki and coworkers in 2013 with the design and development of a highly efficient new Ru(CO)-salen complex **121**, which bears a durable 2,6-difluorophenyl group at the C2″ position of the BINOL moiety. Using [2-(trimethylsilyl) ethanesulfonyl] azide $SESN_3$ as the nitrene precursor, they realized a highly enantio- and regioselective intermolecular benzylic and allylic C–H amination (Table 12.7, Entry 1, 2) [81]. The use of the easily cleavable SES protecting group provides the opportunity to isolate the free amines by reaction with a fluoride source. In 2017, enzyme-catalyzed enantioselective intermolecular benzylic C–H amination was achieved by Arnold with tosylazide [82]. The iron-containing cytochrome $P411_{CHA}$, developed by directed evolution based on a cytochrome P450 monooxygenase, turned out to be highly active and exhibits high enantioselectivities (up to >99% ee and up to 1300 turnovers) (Table 12.7, Entry 3). The enzyme's protein framework not only contributes to the excellent enantiocontrol, but also promotes reactivity for C–H amination on an otherwise unreactive iron-heme cofactor.

12.2.2.3.2. Intramolecular C(sp³)–H Amination with Azides Pioneering work in intramolecular C–H amination with azide compounds was carried out by Katsuki and coworkers in 2011 [83], and it was the first time the highly enantioselective intramolecular C–H amination using azides as nitrene precursors was achieved. They synthesized a series of Ir-salen complexes and found that the introduction of a bulky *tert*-butyldiphenylsilyl group at the para position of the C2″-phenyl rings provides Ir(III)(salen) complex

TABLE 12.7. Intermolecular C–H amination with azides.

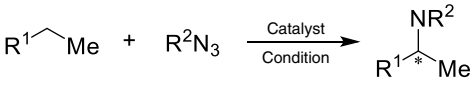

18 **110** **111**

Entry	R^1	R^2	Catalyst	Conditions	Yield (%)	ee (%)	Ref.
1	*p*-OMe–C_6H_4	SES	Ru(CO)-salen **121**	4 Å MS, –10 °C	97	94	[81]
2	PhCH=CH	SES	Ru(CO)-salen **121**	DCM, 4 Å MS, –10 °C	99	93	[81]
3	*p*-OMe–C_6H_4	Ts	Fe^{2+}-$P411_{CHA}$	KPi buffer (pH 8.0)	86	>99	[82]

122 (Figure 12.7) as the best catalyst for the intramolecular C–H amination of arylsulfonyl azides **112** via nitrenoid insertion. The cyclization of 2-ethylbenzenesulfonyl azides proceeds only at the benzylic position and provides five-membered arylsulfonamide **113** with 85% yield and high enantioselectivity of 91% (Table 12.8, Entry 1). Surprisingly, the cyclization of substrates with a homobenzylic methylene carbon atom occurs at the homobenzylic position, producing six-membered sultams **114** (Table 12.8, Entry 2). This switch in regioselectivity would result from the combination of steric and stereoelectronic effects depending on the catalyst and the substrate used.

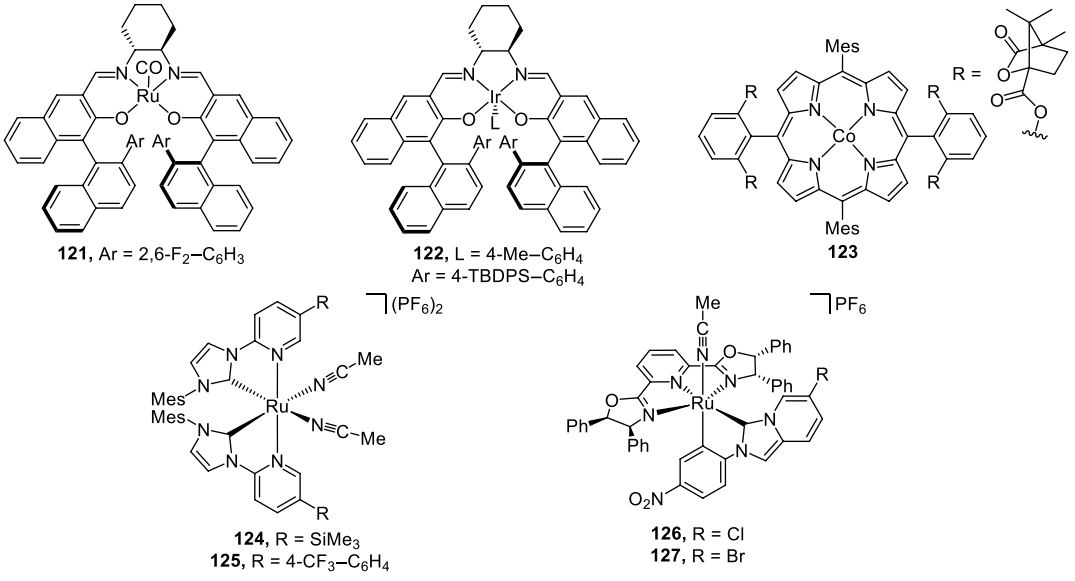

Figure 12.7. Chiral metal catalysts used for C–H amination with azides.

TABLE 12.8. Synthesis of arylsulfonamides.

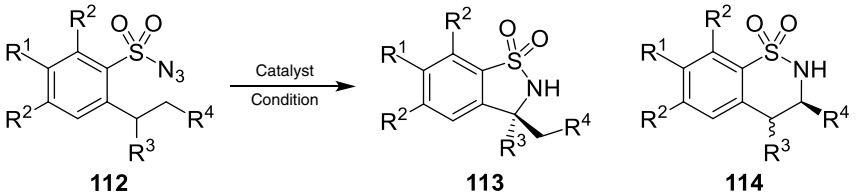

Entry	R^1	R^2	R^3	R^4	Catalyst	Conditions	Ratio **113** : **114**	Yield (%)	ee (%)	Ref.
1	Et	H	H	H	Ir(II)-salen **122**	tol, 25 °C	1:0	85	91	[83]
2	Cy	H	*c*-C_4H_8		Ir(II)-salen **122**	tol, 25 °C	1:9	89	82	[83]
3	H	Et	H	H	Fe^{2+}-$P411_{BM3}$CIS-T438S	NADPH; KPi buffer (pH 8.0)	1:0	58% 430 TTN	87	[84]
4	H	Et	H	H	Fe^{2+}-$P450_{BM3}$FL#62	$Na_2S_2O_4$; KPi buffer (pH 8.0)	1:0	47 TTN	50	[85]
5	Pr	H	H	Me	Fe^{2+}-$P411_{BM3}$CIS-T438S-I263F	25 °C	3:97	361 TTN	99	[86]
6	Bu	H	H	Et	Fe^{2+}-$P411_{BM3}$-T268A-F87A	25 °C	97:3	128 TTN	99	[86]
7	H	H	H	H	Ir(Me)-CYP119 C317G, T213G, V254L	NaCl, NaPi buffer (pH 6.0)	1:25	84% 255 TTN	80	[87]

Whereas enzymes are known for their capability of inserting oxygen atoms into even unactivated C–H bonds, the sites into which nitrogen atoms can be introduced are more constrained. Not until the past decade had enzymes been developed to catalyze C–H amination, benefiting from the engineering of cytochrome P450. The groups of Arnold [84] and Fasan [85] achieved intramolecular benzylic C–H amination of ortho-substituted benzenesulfonyl azides with engineered P450 enzymes that include a reduced Fe(II) center, affording five-membered arylsulfonamide **113** with good yield and good enantioselectivity (Table 12.8, Entry 3, 4). Additionally, expression of the catalyst in *Escherichia coli* allows the reaction to proceed smoothly on a preparative 50 mg scale with high enantioselectivity. Soon after, Arnold developed two engineered variants of $P450_{BM3}$ that enable regiodivergent C–H amination reactions [86]. With the employment of different types of enzyme variants, either α- or β-amination of 2,5-disubstituted benzenesulfonyl azides occurs, providing five-membered arylsulfonamides **113** or six-membered sultams **114**, respectively (Table 12.8, Entry 5, 6). Then in 2017, the Hartwig group designed a new mutant, Ir(Me)-PIX CYP119, derived from P450 enzymes, which contains an iridium porphyrin cofactor, and achieved asymmetric intramolecular C–H amination of arylsulfonyl azides, furnishing six-membered sultams **114** with up to 98% yield and up to 99% ee (Table 12.8, Entry 7) [87].

Concerning non-activated aliphatic azides, the first enantioselective intramolecular C–H amination was developed by de Bruin with a new chiral cobalt(II) porphyrin catalyst **123** equipped with four (1*S*)-(−)-camphanic-ester groups [88]. Ring-closing of (4-azidobutyl)benzene enables the direct synthesis of Boc-protected pyrrolidine product **116** with 46% ee and 22% yield at 80 °C (Table 12.9, Entry 1). Kinetic studies and density-functional theory (DFT) calculations reveal a metallo-radical-type mechanism involving rate-limiting azide activation to generate the critical cobalt(III)-nitrene radical intermediate. Subsequent low-barrier intramolecular hydrogen-atom transfer (HAT) from a benzylic C–H bond to the nitrene-radical intermediate, followed by a radical rebound step, leads to the production of the desired *N*-heterocycles.

The first highly enantioselective C–H amination with aliphatic azides was reported by Houk and Meggers in 2019 [90]. With a "chiral-at-metal" bis(pyridyl-NHC) ruthenium complex Λ-Ru **125** that contains merely achiral ligands and acquires its chirality entirely from octahedral centrochirality, a class of ruthenium catalysts first introduced by Meggers in 2017 [91], an enantioselective ring-closing C–H amination of 2-azidoacetamides **117** is achieved and provides chiral imidazolidin-4-ones **118** in 31–95% yield, with up to 95% ee and up to 740 TON (Scheme 12.29). Mechanistic studies showed the importance of the amide group on 2-azidoacetamides **117**, which presumably enables the initiation of the reaction by

TABLE 12.9. Synthesis of pyrrolidines.

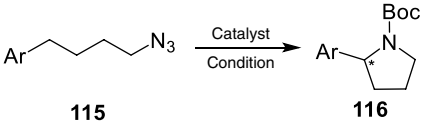

115 **116**

Entry	Ar	Catalyst	Conditions	Yield (%)	ee (%)	Ref.
1	Ph	Co(Por*) **123**	Boc_2O, tol, 80 °C	22	46	[88]
2	Ph	Λ-Ru-cat. **124**	Boc_2O, P(4-F–C_6H_4)$_3$, 1,2-dichlorobenzene, 95 °C	54	95	[89]
3	*p*-OMe–C_6H_4	Λ-Ru-cat. **124**	Boc_2O, P(4-F–C_6H_4)$_3$, 1,2-dichlorobenzene, 95 °C	53	99	[89]

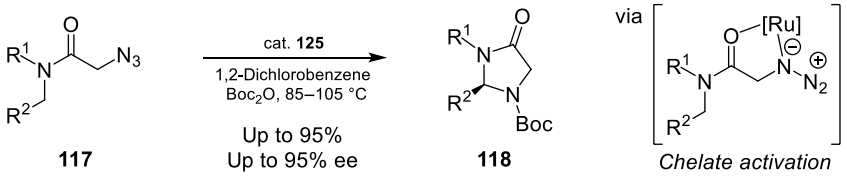

117 **118**

Scheme 12.29. Diastereoselective C–H amination of indane with chiral sulfonimidamide. Source: [90]/John Wiley & Sons.

bidentate coordination of ruthenium to the substrate through the amide carbonyl group and the α-nitrogen atom of the azide. To improve the restricted structure, Meggers developed a dual catalytic system combining chiral-at-metal ruthenium complex Λ-Ru **124** and nucleophilic phosphine, which facilitates the cyclization of unactivated aliphatic azides **115** to produce chiral α-aryl pyrrolidines with up to 99% ee (Table 12.9, Entry 2, 3) [89]. Mechanistically, the phosphine activates the organic azide to form an iminophosphorane through the Staudinger reaction and then transfers the nitrene to the ruthenium to provide a ruthenium imido complex, followed by a stereo-controlled δ-C–H insertion of the nitrene moiety.

As exemplified by the pioneering work of de Bruin as described before [88], the emergence of metalloradical catalysis (MRC) has provided a conceptually new strategy for addressing the challenge of enantioselectivity control in radical chemistry. With the employment of *D2*-symmetric chiral amidoporphyrins as the supporting ligands, Zhang and coworkers applied Co(II)-based metalloradical catalysis (MRC) systems into the enantioselective C–H amination of sulfamyl azides [92] and aryl/alkyl sulfonyl azides [93], producing five-membered cyclic sulfamides and sulfonamides with excellent enantioselectivities (Table 12.10, Entry 1–3). As an alternative to the synthetically complicated chiral cobalt systems, Meggers combined a ruthenium(II) pybox fragment with a cyclometalated NHC ligand to generate catalysts **126** and **127** for enantioselective nitrenoid insertion and achieved asymmetric C–H amination of a sulfamyl azide and sulfonyl azide with up to 97% ee (Table 12.10, Entry 4, 5) [94]. The cyclometalated ligand strongly modulates the catalytic activity of the ruthenium center and exerts a vital role in the asymmetric induction.

12.2.2.4. C(sp³)–H Functionalization with N-(Sulfonyloxy)Carbamates *N*-(sulfonyloxy)carbamate as a nitrene precursor was first utilized for asymmetric C–H amination reactions in 2006 by the Davies group [95]. With bulky catalyst Rh_2(*S*-TCPTAD)$_4$ (Scheme 12.9), intramolecular C–H amination of *N*-tosyloxycarbamate affords oxazolidinones with enantioselectivities of 43–82%. In 2011, a novel chiral nitrene precursor *N*-tosyloxycarbamate **128** was introduced by the Lebel group [96]. With rhodium catalyst Rh_2(*S*-Br-NTTL)$_4$, monosubstituted alkenes can produce aziridinated products, while di- or trisubstituted alkenes afford carbamate-protected allylic amine products with good diastereoselectivities (Table 12.11, Entry 1). Later, Lebel expanded the scope of this intermolecular C–H amination process from allylic sites to benzylic and propargylic positions with excellent diastereoselectivities by using *N*-mesyloxycarbamate **128** (Table 12.11, Entry 2, 3) [97]. The corresponding free amines can be obtained by easy cleavage of the Ph-Troc protecting group.

12.2.2.5. C(sp³)–H Functionalization with Dioxazolones As described above, in the past two decades, various research groups have realized the synthesis of chiral azacyclic compounds such as sulfamidates, sulfonamides, and carbamates through C–H amidation reactions by utilizing easily accessible and robust nitrene precursors such as iminoiodinanes and organic azides. In contrast, the synthesis of lactams through nitrene C–H insertion has been hindered by competing isocyanate formation via Curtius-type rearrangement until the introduction of 1,4,2-dioxazol-5-one compounds **130** as robust nitrene precursors in combination with electron-rich pentamethylcyclopentadienyl iridium(III) catalysts by the Chang group in 2018 [98]. DFT calculations suggested more electron-rich auxiliary ligands

TABLE 12.10. Synthesis of sulfamides and sulfonamides.

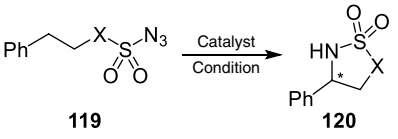

119 **120**

Entry	X	Catalyst	Conditions	Yield (%)	ee (%)	Config.	Ref.
1	NBn	Co(2,6-DiMeO-Hu(C_6)Phyrin)	MTBE, 40 °C	75	88	*S*	[92]
2	NBn	Co(3,5-Di*t*-Bu-Hu(C_8)Phyrin)	MTBE, 40 °C	98	94	*R*	[92]
3	CH_2	Co(2,6-DiMeO-Qing(4′-Me)Phyrin)	PhH, 40 °C	92	94	*S*	[93]
4	NBn	Ru-Pybox **126**	DCE, 50 °C	93	95	*S*	[94]
5	CH_2	Ru-Pybox **127**	DCE, 40 °C	99	97	*R*	[94]

TABLE 12.11. Stereoselective C–H amination with *N*-(sulfonyloxy)carbamates.

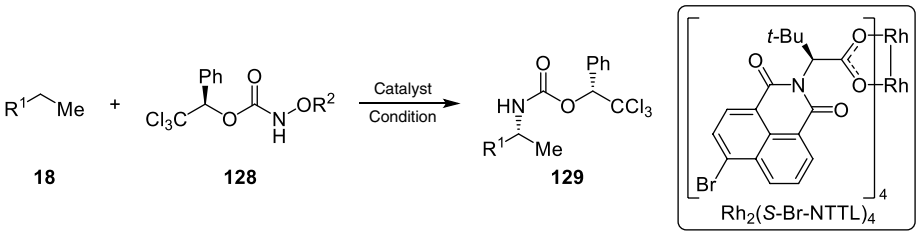

Entry	R^1	R^2	Catalyst	Conditions	Yield (%)	dr	Ref.
1	*o*-Cl–C_6H_4CH=CH	Ts	Rh_2(*S*-Br-NTTL)$_4$	K_2CO_3, $PhCF_3$	43	>50 : 1	[96]
2	*p*-Br–C_6H_4	Ms	Rh_2(*S*-Br-NTTL)$_4$	KOAc, EtOAc	74	>99 : 1	[97]
3	*p*-MeO–C_6H_4C≡C	Ms	Rh_2(*S*-Br-NTTL)$_4$	KOAc, EtOAc	50	>99 : 1	[97]

to lower the nitrene C–H insertion barrier favoring the desired reaction: Remarkable reduction of the positive partial charge of the iridium center in the transition state is seen for the Curtius-type rearrangement, while C–H insertion is not accompanied by any notable change of partial charge, thereby indicating that electron-donating ligands may increase the Curtius-rearrangement barrier to a larger extent than the C–H insertion barrier. Subsequently, several groups achieved asymmetric variants of this intramolecular C–H amidation process by utilizing chiral iridium and ruthenium complexes (Figure 12.8), affording chiral γ-lactams **131**.

In 2019, Chang developed a new Cp*Ir-based catalyst **132** utilizing hydrogen-bond-donor ligand and displayed excellent reactivity and enantioselectivity toward direct C–H amidation with 1,4,2-dioxazol-5-ones **130** (Table 12.12, Entry 1, 2) [99]. Computational studies and spectroscopic analysis indicate that the excellent stereoselectivity is attributed to a transient intramolecular hydrogen bonding between the carbonyl of the substrate amide moiety and the NH_2 group of the diamine ligand that stabilizes the key intermediates and transition states selectively (Scheme 12.30). The same reaction was also achieved by Yu using Ru complex **133** with diphenyl-1,2-diamine (dpen) ligand that bears electron-withdrawing arylsulfonyl substituents, furnishing γ-lactams **131** in up to 97% yield and 98% ee [100]. Besides benzylic C–H amidation, allylic/propargylic C–H amidation was also achieved with excellent tolerance to the C=C and C≡C bonds (Table 12.12, Entry 3–5).

To achieve asymmetric reaction of more demanding unactivated alkyl-substituted dioxazolone substrates, Park, Chang, and Chen developed a novel Cp*Ir-based catalyst **134** that has a newly designed *α*-amino-acid-based chiral ligand [101]. This iridium-catalyzed reaction proceeds with excellent efficiency and outstanding enantioselectivity (up to 99.6% ee) for both activated and unactivated alkyl C–H bonds under mild conditions (Table 12.12, Entry 6–8). It provided the first general route for the asymmetric synthesis of *γ*-alkyl *γ*-lactams. Mechanistic studies elucidated that the Cp*, AQ, and Phth moieties

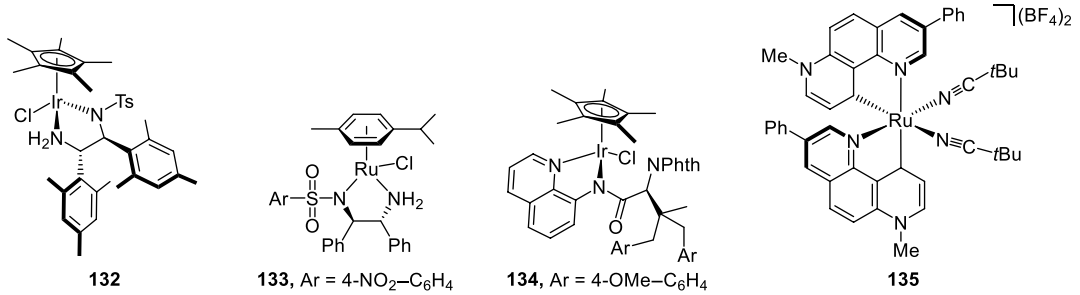

Figure 12.8. Chiral metal catalysts used for C–H amination with dioxazolones.

TABLE 12.12. Synthesis of γ-lactams.

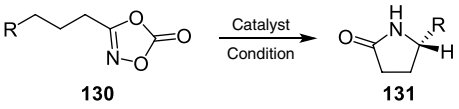

130 131

Entry	R	Catalyst	Conditions	Yield (%)	ee (%)	Ref.
1	Ph	Cp*IrCl **132**	$NaBAr^F_4$, TCE, 35 °C	96	>98	[99]
2	Bn	Cp*IrCl **132**	$NaBAr^F_4$, TCE, 35 °C	86	92	[99]
3	Ph	[RuCl(*p*-cymene)(*R*,*R*)-dpen] **133**	$AgSbF_6$, DCE, 40 °C	92	94	[100]
4	CH_2=CH	[RuCl(*p*-cymene)(*R*,*R*)-dpen] **133**	$AgSbF_6$, DCE, 40 °C	80	77	[100]
5	PhC≡C	[RuCl(*p*-cymene)(*R*,*R*)-dpen] **133**	$AgSbF_6$, DCE, 40 °C	90	41	[100]
6	Ph	Cp*IrCl **134**	HFIP/H_2O (1 : 2), 20 °C	98	98	[101]
7	CH_2=CH	Cp*IrCl **134**	HFIP/H_2O (1 : 2), 20 °C	90	98	[101]
8	Et	Cp*IrCl **134**	HFIP, 20 °C	89	98	[101]
9	Ph	Λ-rNHCRu **135**	1,2-dichlorobenzene, 4 °C	95	92	[102]
10	CH_2=CH	Λ-rNHCRu **135**	1,2-dichlorobenzene, 4 °C	61	86	[102]
11	Et	Λ-rNHCRu **135**	1,2-dichlorobenzene, 4 °C	42	60	[102]

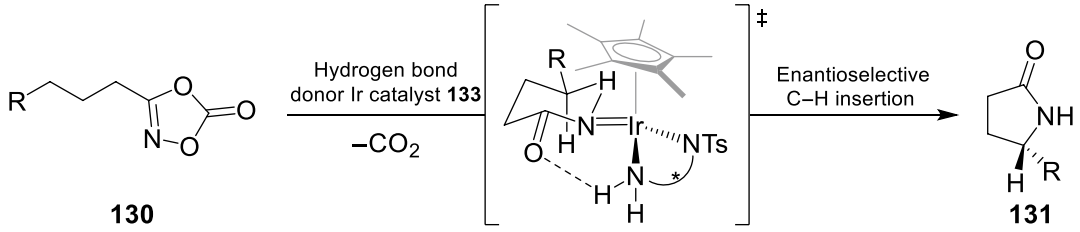

130 131

Scheme 12.30. Asymmetric synthesis of γ-lactams via C–H amidation enabled by hydrogen-bond-donor catalysts. Source: [99]/Springer Nature.

of the ligand form a well-defined groove-type chiral pocket around the Ir center. The hydrophobic effect of this pocket allows facile stereocontrolled binding of substrates in polar or aqueous media. Unlike conventional approaches that capitalize on steric repulsions, this new enzyme-like Ir catalyst **134** operates through an unprecedented enantiocontrol mechanism for C–H functionalization featuring multiple noncovalent interactions.

Later in 2019, Houk and Meggers introduced a new class of chiral-at-ruthenium catalyst **135** containing two strongly electron-donating remote *N*-heterocyclic carbene (rNHC) ligands 7-methyl-1,7-phenanthrolinium heterocycles coordinated in a non-C_2-symmetric fashion [102]. This catalyst displays unprecedented catalytic activity for the intramolecular C–H amidation of 1,4,2-dioxazol-5-ones **130** to afford chiral γ-lactams **131** with up to 98% ee and catalyst loadings down to 0.005 mol% (up to 11 200 ton) (Table 12.12, Entry 9–11). DFT calculations suggested that the combination of strongly electron-donating remote NHC ligands with the non-C_2-symmetric arrangement of these ligands in the coordination sphere leads to an especially electron-rich Ru nitrene intermediate favorable for efficient C–H amidation step.

12.2.2.6. C(sp³)–H Functionalization with Hydroxylamine Derivatives Employing a readily available hydroxylamine ester as the nitrogen precursor, in 2020, Arnold realized the first example of direct primary amination of C(sp³)–H bonds catalyzed by a set of new-to-nature enzymes with excellent chemo-, regio-, and enantioselectivity (Scheme 12.31) [103]. Directed evolution of genetically encoded cytochrome P411 enzymes (derived from P450s in which Cys axial ligand to the heme iron are replaced with Ser) generated variants that selectively functionalize benzylic and allylic C–H bonds, affording a broad scope of primary amines with high up to 3930 TTN and 96% ee.

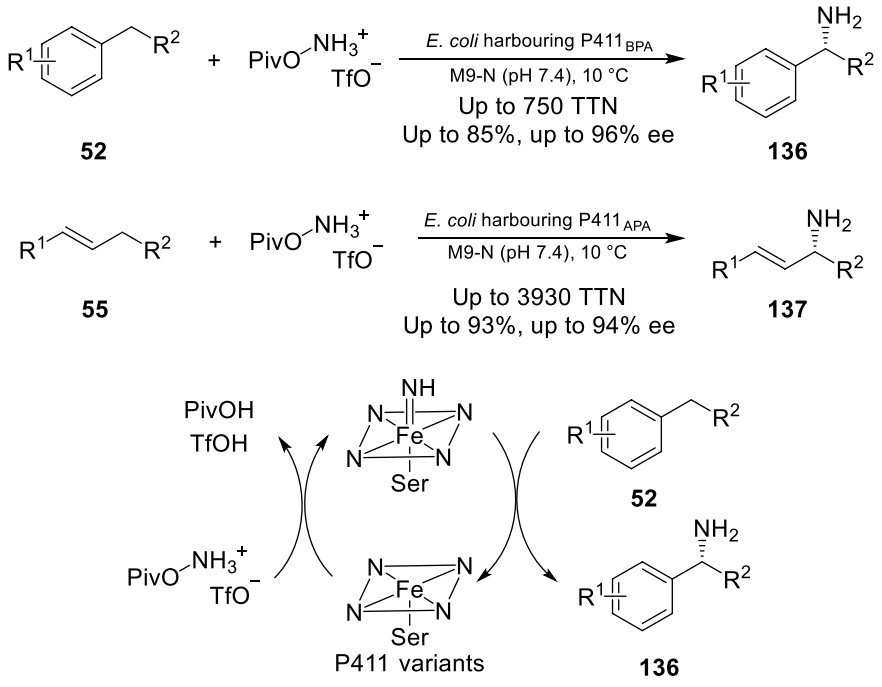

Scheme 12.31. Asymmetric enzymatic C–H primary amination. Source: [103]/American Chemical Society.

12.3. CONCERTED METALATION-DEPROTONATION FOR ASYMMETRIC C(sp³)–H ACTIVATION

Last few decades have experienced the exponential growth of strategies toward site-selective C(sp³)–H activation. One of the most popular and powerful ways to break C(sp³)–H bond is concerted metalation-deprotonation (CMD) (Scheme 12.32). In general, a high-valent transition metal catalyst is brought close enough to the targeted C(sp³)–H bond, followed by deprotonation with carboxylate or carbonate base and C–M bond formation in a concerted pathway. In this catalytic regime, palladium has played a significant role in asymmetric C(sp³)–H activation arena [104].

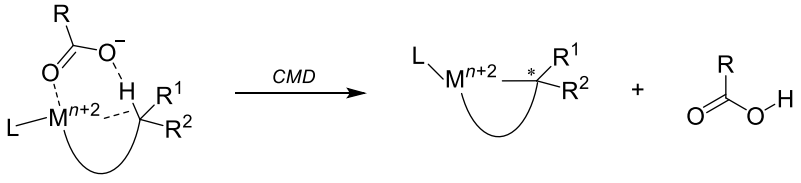

Scheme 12.32. Concerted metalation-deprotonation (CMD).

12.3.1. Pd(0)-catalyzed C(sp³)–H Activation

Pioneering work in 1992 from Dyker disclosed the possibility to activate C(sp³)–H bond with Pd(II) salt (Scheme 12.33) [105]. The reaction was proposed through a sophisticated sequence involving a number of Pd-complexes as intermediates. First, oxidative addition of aryl iodide to an in situ generated Pd(0) occurs, followed by an intramolecular C(sp³)–H activation. Subsequently, the five-membered palladacycle **140** undergoes another oxidative addition event to **138** to a Pd(IV) intermediate, forming the biaryl species **142** via reductive elimination. Followed by an intramolecular C(sp²)–H activation and oxidative addition to another aryl iodide, **143** is obtained. Then a rare seven-membered palladacycle **144** is formed.

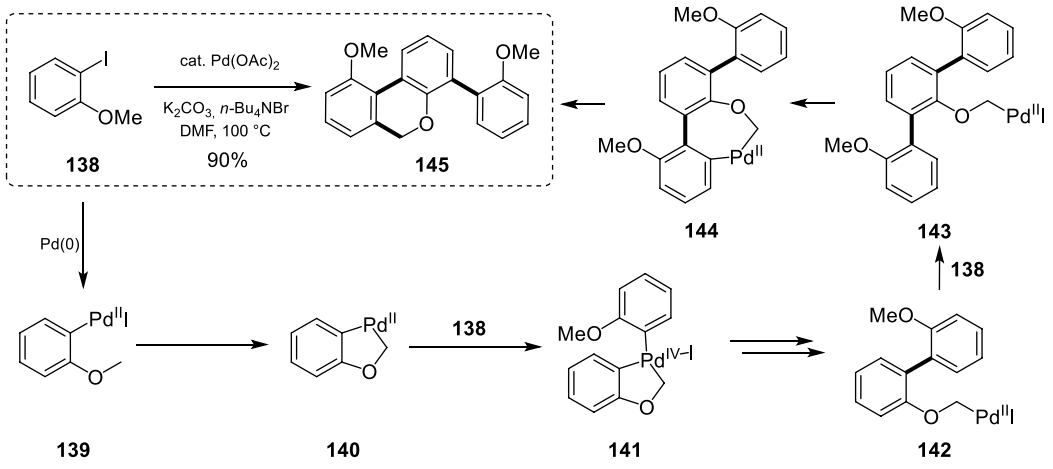

Scheme 12.33. Early discovery of C(sp³)–H activation.

Last, an ending event of reductive elimination gives rise to the product **145** with the construction of multiple C–C bonds.

The activation of a methyl group via similar reaction pathway was presented by the same group in 1994 [106]. In this case, the benzocyclobutane was obtained (Scheme 12.34).

Based on these reports, Baudoin contributed the first example of Pd(0)/PAr_3 catalyzed synthesis of benzocyclobutanes in 2003 (Scheme 12.35) [107]. Perhaps the most salient feature of Baudoin's work is the introduction of ligand into this type of transformation, leaving ample space for the development of asymmetric versions by using a chiral ligand. Later, the reaction pattern was extended to the synthesis of benzofused five-membered cyclic structures, even in an asymmetric manner.

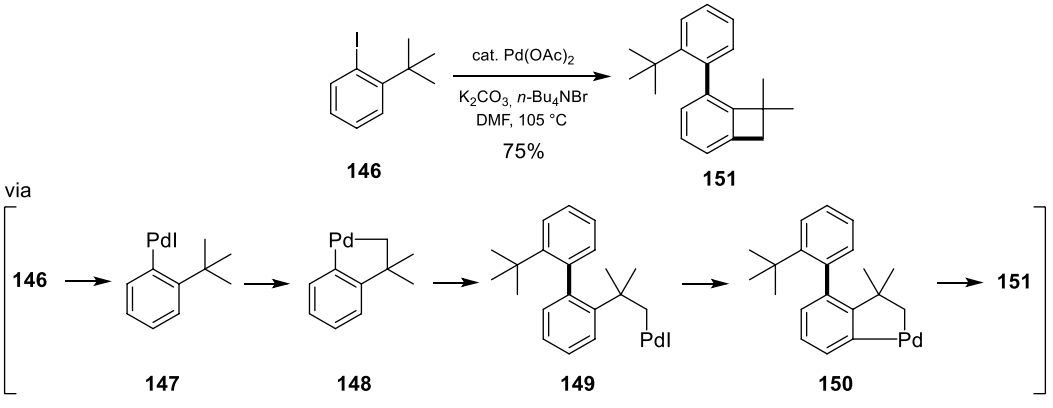

Scheme 12.34. Dyker's synthesis of benzocyclobutane.

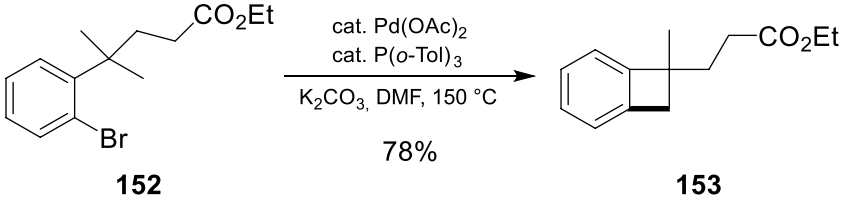

Scheme 12.35. Pd(0)/PAr_3-catalyzed intramolecular arylation. Source: [107]/John Wiley & Sons.

12.3.1.1. Pd(0)-catalyzed Enantioselective C(sp³)–C(sp²) Bond Formation Recently, Kündig utilized chiral NHC ligands **L-4** for the synthesis of highly enantioenriched indolines **155** by Pd(0)-catalyzed intramolecular C(sp³)–H activation of cycloalkanes (Scheme 12.36) [108]. Despite the high temperature that is required for the reactivity, the excellent recognition of two enantiotopic C(sp³)–H bonds in unactivated methylene unit holds potential for the NHC ligand system. Shortly after Kündig's work, Kagan reported the desymmetrization of isopropyl group in **156** using the commercially available **L-5** ((*R,R*)-Me-DUPHOS) as the ligand [109]. High yield and ee values could be obtained under the reaction conditions. While this system is effective for a methyl group, methylenes perform poorly as can be seen from the low ee in product **159**. Further optimization of this transformation was reported by Cramer who described the catalytic combination of a newly designed monodentate phosphine ligand (**L-6)** and a diaryl acetic acid (**Acid-1**) for the intramolecular arylation of both methyl and methylene with high level of enantioselectivity [110].

In 2012, Baudoin reported preliminary result to the synthesis of chiral indanes with moderate to good ee values using binepine-type ligand **L-7** (Scheme 12.37) [111]. As continued interest in Pd(0)-catalyzed asymmetric C(sp³)–H arylation reaction, the same group disclosed a refined system by synthesizing a series of new binepine-type ligands (**L-8** and **L-9**) in 2015, in which excellent ee values could be obtained with broad substrate scope [112].

As can be seen from previous reports, all the transformations deal with methyl or cyclic methylene. However, differentiation of enantiotopic unactivated acyclic methylene remains largely underexplored. Five years later, with extensive screening of different ligands in 2020, Baudoin successfully identified the

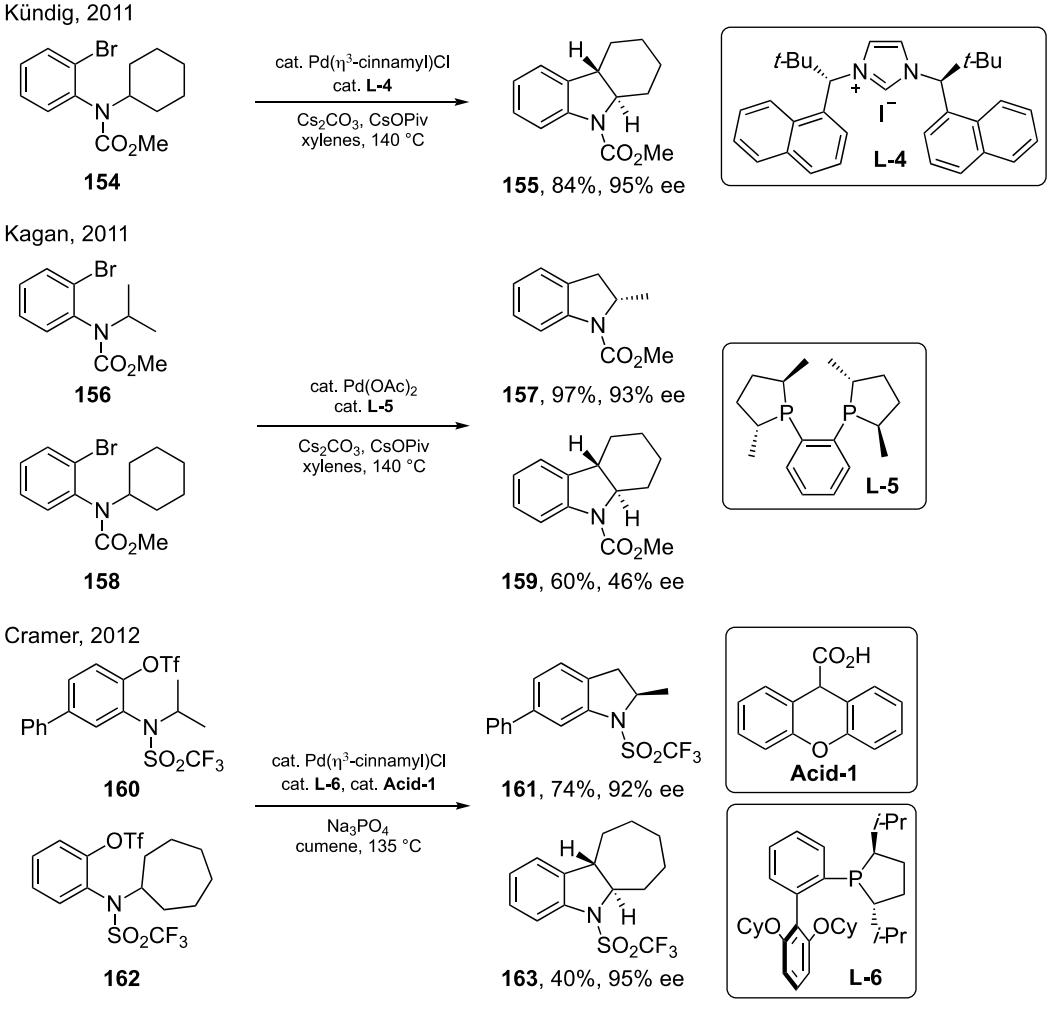

Scheme 12.36. Pd(0)-catalyzed enantioselective intramolecular arylation.

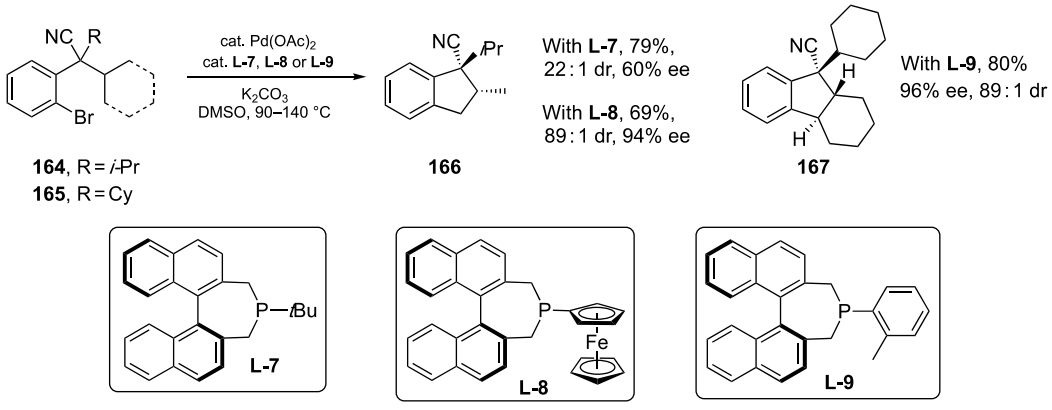

Scheme 12.37. Baudoin's asymmetric synthesis of indanes.

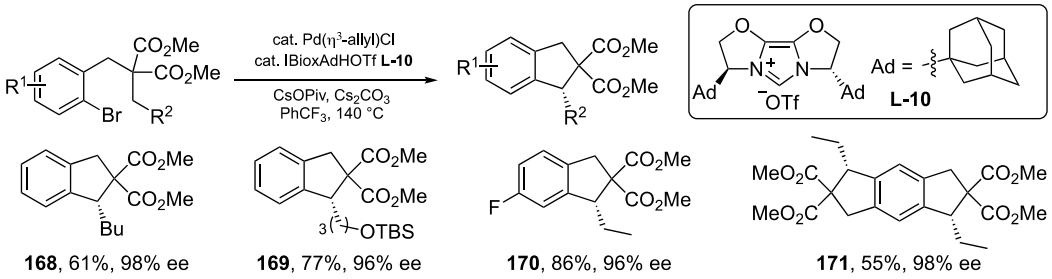

Scheme 12.38. Pd(0)-catalyzed arylation of unactivated acylic methylenes.

enabling chiral bioxazoline-derived NHC ligand (IBiox), derived from an achiral scaffold initially designed by Glorius [113], to differentiate remote enantiotopic H atoms [114]. The IBioxAd (**L-10**) proved to be a privileged ligand for a broad range of indanes delivering excellent enantioselectivity (Scheme 12.38).

Since Kündig, Kagan, and Cramer's work, these types of substrates have become a classic test for different enantioselective conditions. While previous work focused on the development of chiral ligands, the use of chiral acid as catalyst to induce enantioselectivity is less developed. In 2016, Duan reported a combination of PPh_3 and simple BINOL-based chiral phosphoric acids promoted intramolecular arylation to form **157** (47, 50% ee) (Scheme 12.39) [115]. Inspired by this work, Baudoin reported that high levels of enantioselectivity could be obtained by the optimization of the chiral acid catalysts [116].

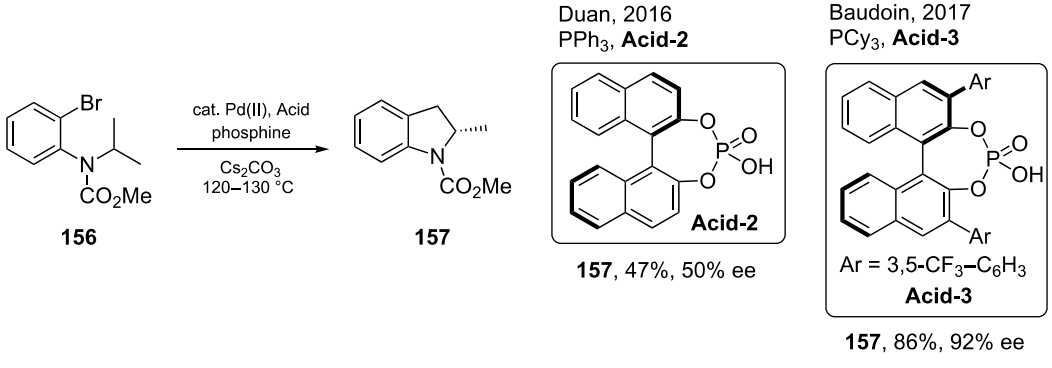

Scheme 12.39. Chiral phosphoric acid catalyst promoted intramolecular arylation.

A variety of chiral indoline and indane derivatives could be accessed via C–H activations, however, synthesis of chiral tetrahydroquinoline units remains elusive when using similar strategies. Due to the geometry of the cyclopropane ring, the rehybridized orbital of cyclopropane C–H bonds displays enhanced acidity, thus leading to a facile C–H activation event. In 2012, using monodentate TADDOL-derived phosphoramidite as chiral ligand, Cramer developed a Pd(0)-catalyzed enantioselective synthesis of cyclopropane fused tetrahydroquinolines via a rare seven-membered palladacyle intermediate **172** (Scheme 12.40) [117]. The catalytic amount of pivalic acid proved to be essential for increasing both

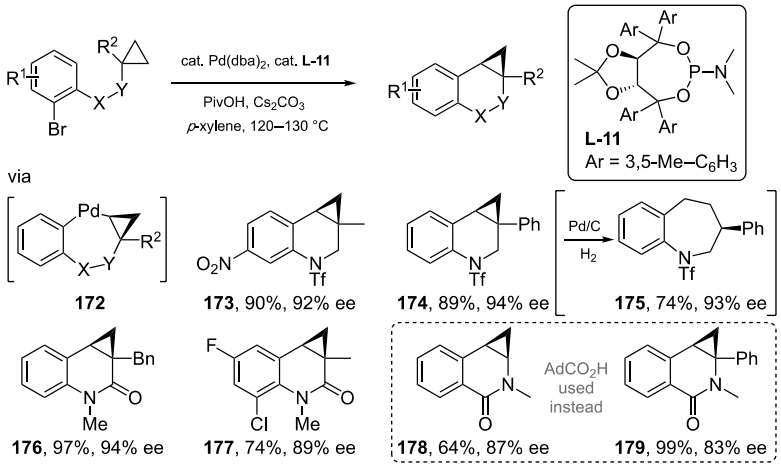

Scheme 12.40. Enantioselective intramolecular arylation of cyclopropanes.

reactivity and enantioselectivity. The catalytic system enabled a broad substrate scope and facile synthesis of chiral benzoazepine **175** upon simple treatment with Pd/C hydrogenation condition. Interestingly, the same group showed that the simple change of starting material from aniline derivative to amide derivative under similar reaction conditions leads to the rapid synthesis of chiral cyclopropane-fused dihydroquinolones and dihydroisoquinolones under similar reaction conditions [118].

As a continued interest to make complex chiral *N*-heterocyclic architectures, Cramer designed a new enantioselective intramolecular trifluoroacetimidoylation (Scheme 12.41) [119]. The chiral cyclized imine products could be easily transformed into other chiral secondary amine structures in the presence of nucleophiles (**183**). Intriguingly, the authors showed that the phosphine ligand can further tune the regioselectivity profile. When electron-rich PPh_3 is used instead of **L-12**, activation of phenyl ring is observed as a major product (**181**).

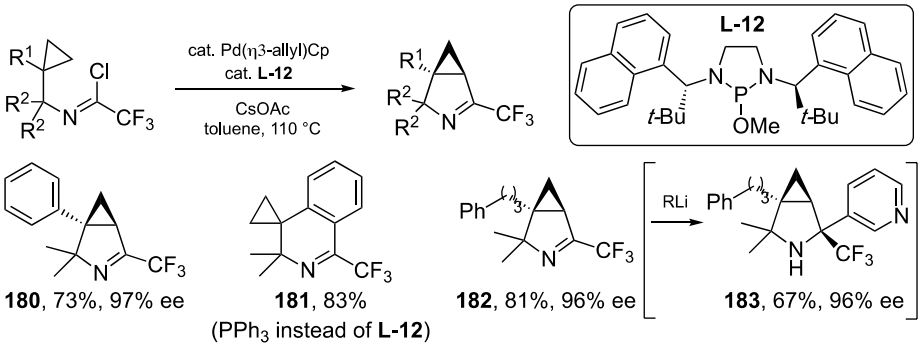

Scheme 12.41. Enantioselective trifluoroacetimidoylation of cyclopropane.

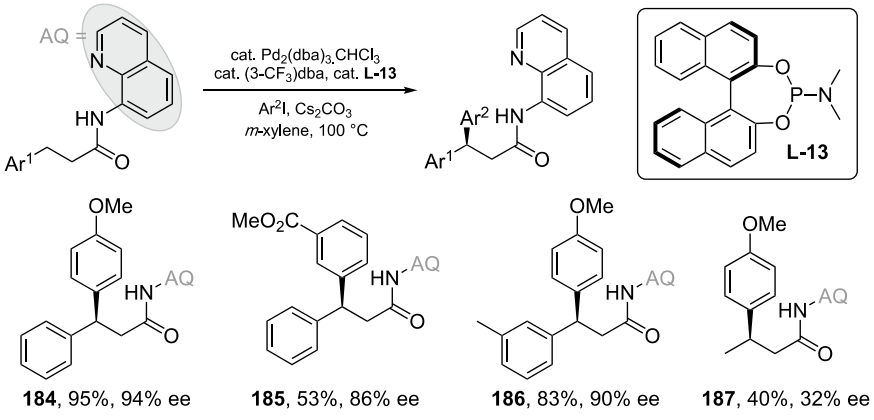

Scheme 12.42. Pd(0)-catalyzed directed intermolecular arylation.

While most of the Pd(0)-catalyzed C(sp³)–H arylations are intramolecular, Chen showed the posibility to perform aminoquinoline-directed intermolecular arylation of benzylic C(sp³)–H bond by using phosphoramidite ligand via Pd(0) catalysis (Scheme 12.42) [120]. The inclusion of catalytic ammount of electron-deficient dba ligand slightly improves the yield and ee values. However, the reactivity and selectivty are not transferable to unactivated methylene (**187**).

12.3.1.2. Pd(0)-catalyzed C(sp³)–C(sp³) Bond Formation In contrast to the increasing progress of Pd(0)-catalyzed C–H activation for C(sp³)–C(sp²) coupling, related transformations involving the formation of C(sp³)–C(sp³) bonds remain elusive. One of the difficulties for Pd-complexes to perform C(sp³)–C(sp³) cross coupling is the parasitic β-hydride elimination of alkyl palladium species. However, such problem could be circumvented with engineered substrates or directing groups. In 2014, Cramer reported a challenging C(sp³)–C(sp³) bond formation via C(sp³)–H activation (Scheme 12.43) [121]. The enabling catalytic conditions consist of a bulky TADDOL-phosphoramidite ligand and adamantyl carboxylic acid.

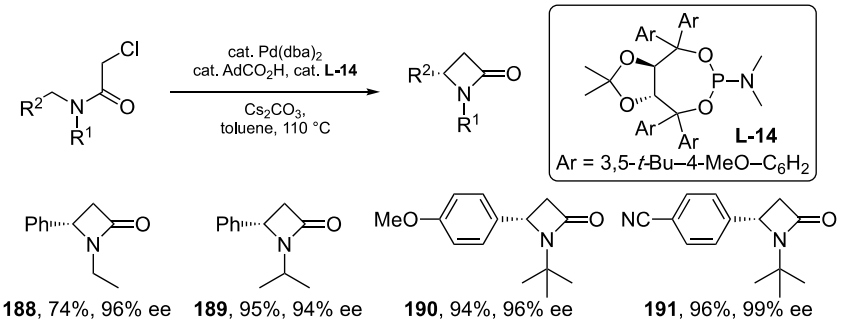

Scheme 12.43. Cramer's synthesis of chiral β-lactams.

A variety of readily accessible chloroacetamides are transformed into valuable chiral β-lactams in high yields with excellent enantioselectivity.

In line with this protocol, the same group realized an efficient synthesis of chiral γ-lactams fused with cyclopropane (Scheme 12.44) [122]. In this case, the activation site of C(sp³)–H is dictated by the cyclopropane in the presence of C(sp³)–H bond α to nitrogen. Again, bulky TADDOL-phosphoramidite ligand (**L-15**) and adamantyl carboxylic acid guaranteed the reaction efficiency.

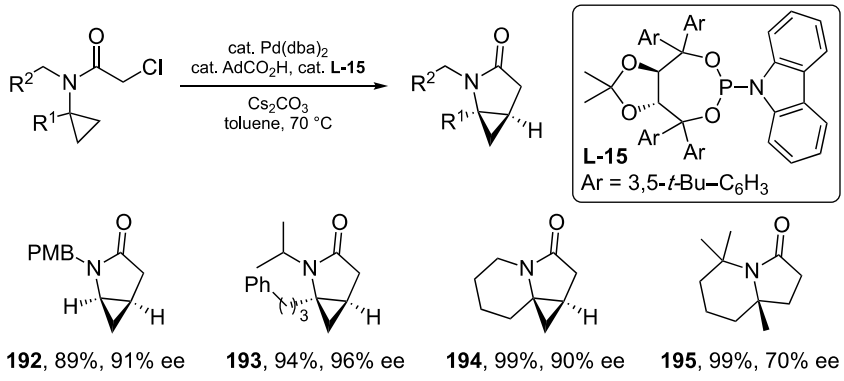

Scheme 12.44. Cramer's synthesis of chiral γ-lactams.

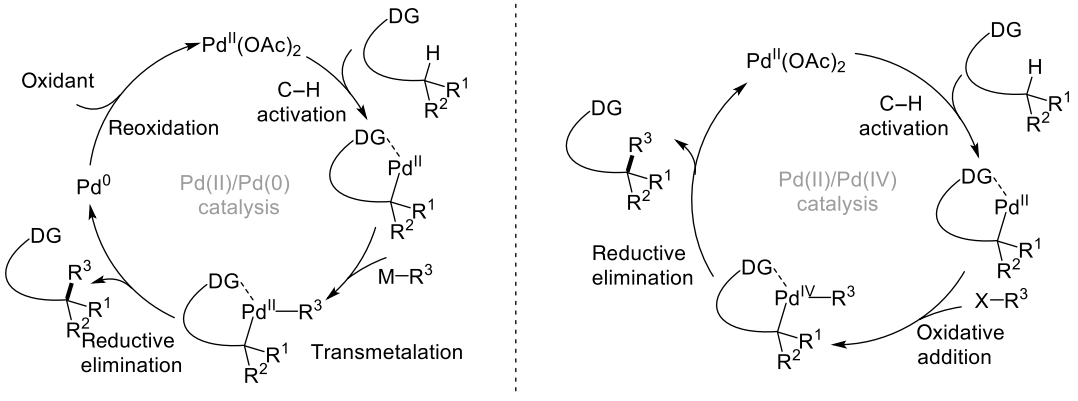

Scheme 12.45. Pd(II) catalysis for C(sp³)–H activation.

12.3.2. Pd(II)-catalyzed C(sp³)–H Activation

Different from Pd(0)/Pd(II) catalysis, the use of Pd(II) as the catalyst for C(sp³)–H activation also proves to be versatile and has grown tremendously (Scheme 12.45). In general, two catalytic manifolds could be involved in the C–H activation. One of them is oxidative cross coupling catalyzed by Pd(II)/Pd(0), and the other is redox neutral mechanism promoted by a Pd(II)/Pd(IV) catalytic cycle. As for Pd(II)/Pd(0) catalysis, in which a nucleophilic coupling partner is applied, the design of using a Pd(II)/Pd(IV) catalytic regime, in which an electrophilic coupling partner is applied, enables a mild reaction condition and wider substrate scope without using external oxidant.

12.3.2.1. Pd(II)/Pd(0)-catalyzed C(sp³)–H Activation

In 2008, Yu first introduced mono-*N*-protected amino acids (MPAAs) as bidentate ligands for Pd-catalyzed C(sp²)–H activation (Scheme 12.46) [123]. Silver oxide and benzoquinone function as oxidant. The ligand (**Acid-4**) shows moderate enantioselectivity for a C(sp³)–H alkylation event. Later, CMD pathway-promoted enantioselective C(sp³)–H activation has witnessed exponential progress as judged by the wealth of reported publications [124].

The first example of Pd(II)-catalyzed enantioselective cyclopropyl C(sp³)–H activation with organoboron reagents was reported in 2011 (Scheme 12.47)[125]. Systematic ligand engineering has led to the discovery of a platform that enables synthetically interesting stereoinduction under mild conditions. A variety of aryl-, vinyl-, and alkylboronic esters are coupled under the reaction conditions. Following the same research line, the Yu group developed an enantioselective arylation of cyclobutane scaffolds using

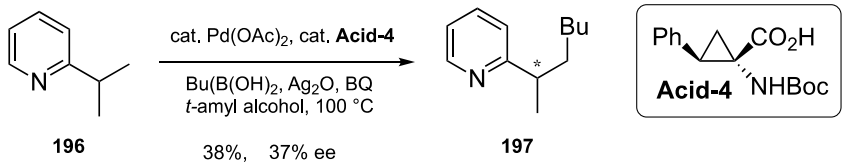

Scheme 12.46. Yu's preliminary asymmetric C(sp³)–H activation.

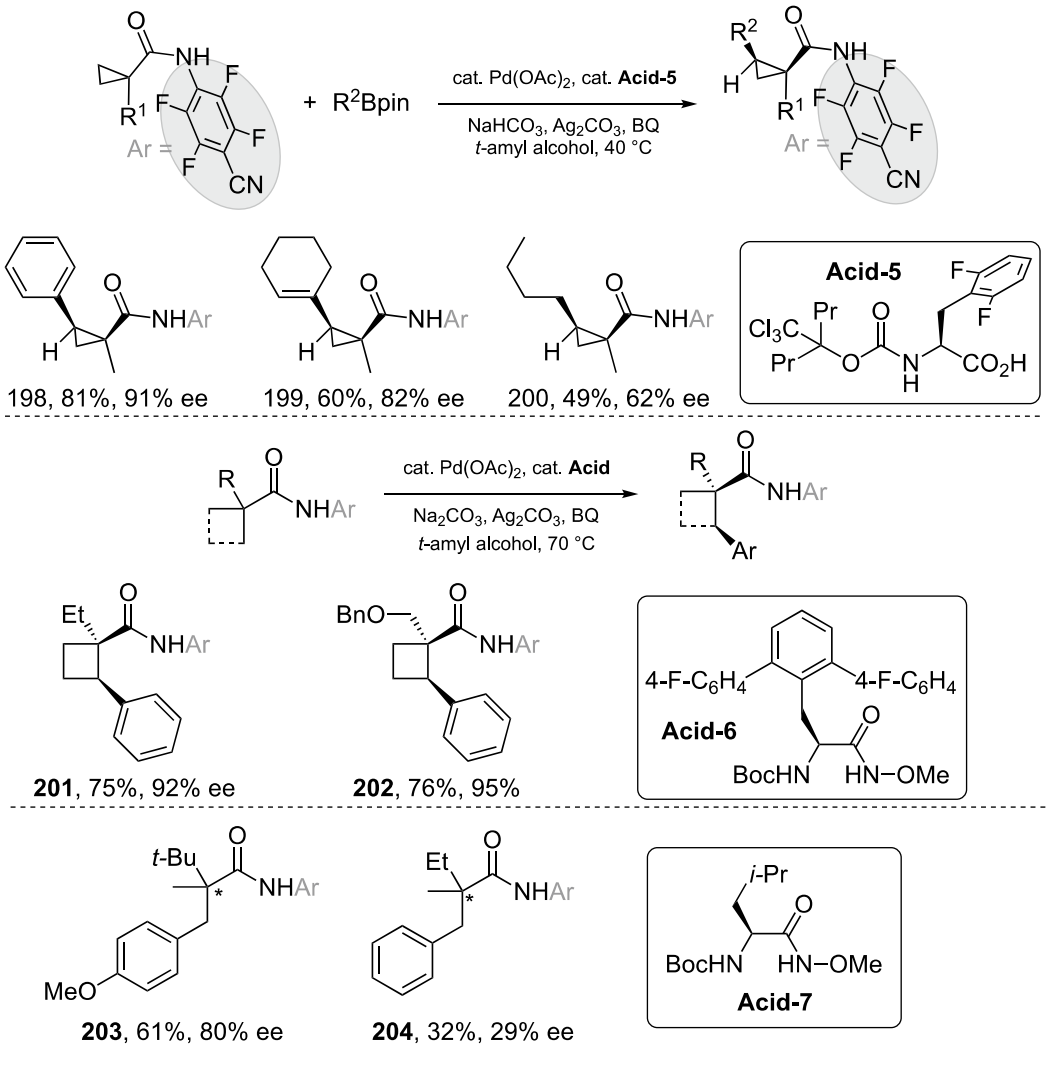

Scheme 12.47. Oxidative arylation of α-tertiary amide.

the same directing group in the presence of chiral hydroxamic acid derivative as ligand [126]. The key to success of this method was the employment of an electron-deficient amide as a weakly coordinating directing group. While arylation of cyclobutane gives excellent ees, arylation of the acyclic system only showed moderate to good enantioselectivity (**203** and **204**), highlighting the challenge to perform asymmetric C(sp³)–H activation of an unbiased system.

Saturated *N*-heterocycles are highly prevalent in bioactive molecules. The direct C(sp³)–H activation in these motifs would accelerate drug discovery. In 2017, Yu reported an enantioselective arylation event of cyclic amine derivatives [127]. Thiocarbonyl is employed as the directing group and chiral BINOL-based phosphoric acid as ligand. A number of thioamides undergo the targeted arylation in good yields with high ee values. A salient feature of the protocol is the ability to differentiate two nearly identical methylenes (**210**). This seminal report engendered several follow-up studies. Two years later, Zhang and Gong also contributed to the arylation of cyclic thioamide [128]. The catalytic combination of two chiral species synergistically controls the reactivity and selectivity. Although no acyclic susbtrates were tested, the novel system indeed showed excellent enantiocontrol, highlighting the potential of **L-18** as chiral ligand or base in Pd(II)-catalyzed asymmetric C–H activation via CMD-pathway (Scheme 12.48).

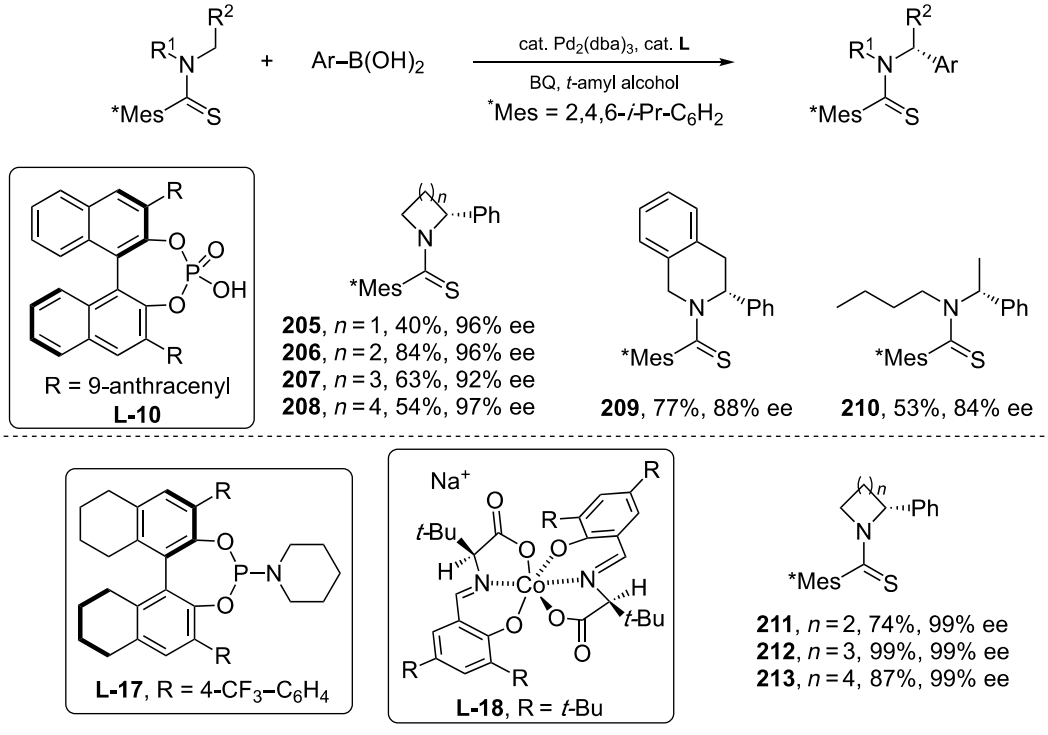

Scheme 12.48. Oxidative arylation with aryl boronic acid.

While thioamide has been a priviliged directing group to activate α-C(sp³)–H of amines, less attention has been paid to activating the thiocarbonyl part. In 2020, Zhang and Gong showed that Yu's conditions could be applied for this transformation [129]. Density-functional theory (DFT) calculations suggested that increasing the sterics of amine part can swith the site-selectivity of C–H activation. Based on these theoretical predictions, the *N*,*N*-diisopropyl amine group was incorporated. As a result, Pd(II)-catalyzed β-C(sp³)–H arylation was disclosed to achieve highly enantioselective desymmetrization of the isopropyl group (Scheme 12.49).

Previous amine C(sp³)–H activations are focused on proximal position; the activation of remote sites would expand the synthetic toolbox. In general, the kinetically favored activation of proximal sites poses the challenge to design a new ligand to enable remote C(sp³)–H cleavage via a fluxional transition state (large membered-palladacycle involved). Indeed, the amino oxazoline ligands (**L-20**, **L-21**) are quite efficient for γ-C(sp³)–H arylation/vinylation reactions of an α-secondary triflamides (Scheme 12.50) [130].

However, starting materials in these transformations require preinstalled directing groups that need to be removed after C–H activation. It would be more synthetically meaningful to use innate functionality

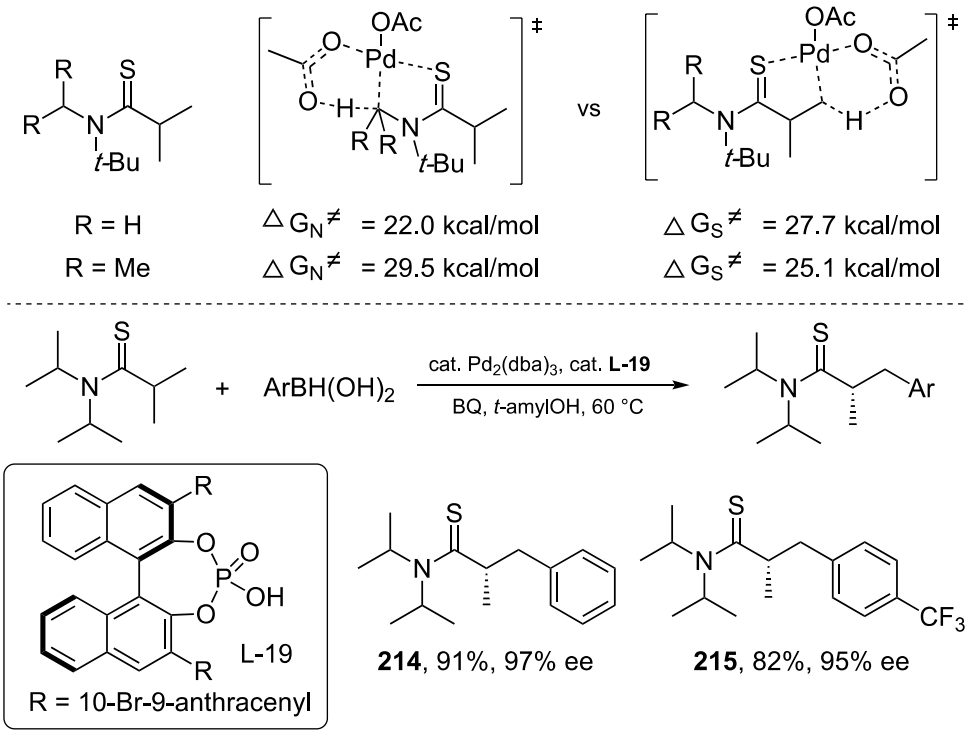

Scheme 12.49. Enantioselective desymmetrization of thioamide.

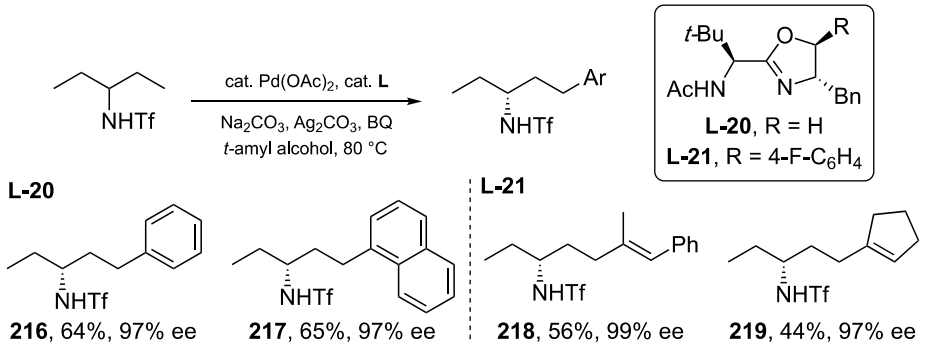

Scheme 12.50. Enantioselective desymmetrization of triflamide.

as the directing group in C(sp³)–H activation. In 2019, Yu developed an oxidative cross coupling between the cyclic C(sp³)–H bond and the organoboron reagent, in which the free carboxylic acid serves as the directing group [131]. Interestingly, the arylation of cyclopropane and cyclobutane required completely different ligand scaffolds (Scheme 12.51).

Complex amines are privileged scaffolds widely found in natural products and pharmaceuticals. The catalytic construction of complex amines is a longstanding challenge in chemical synthesis. One of the appealing strategies is C–H activation of simple amines. In 2014, Gaunt reported a Pd(II)-catalyzed intramolecular amination of cyclic secondary amines via a strained four-membered palladacycle in which the amine functionality serves as a directing group (Scheme 12.52a) [132]. To expand the reactivity of four-membered palladacycle, the same group disclosed an arylation event. While the racemic

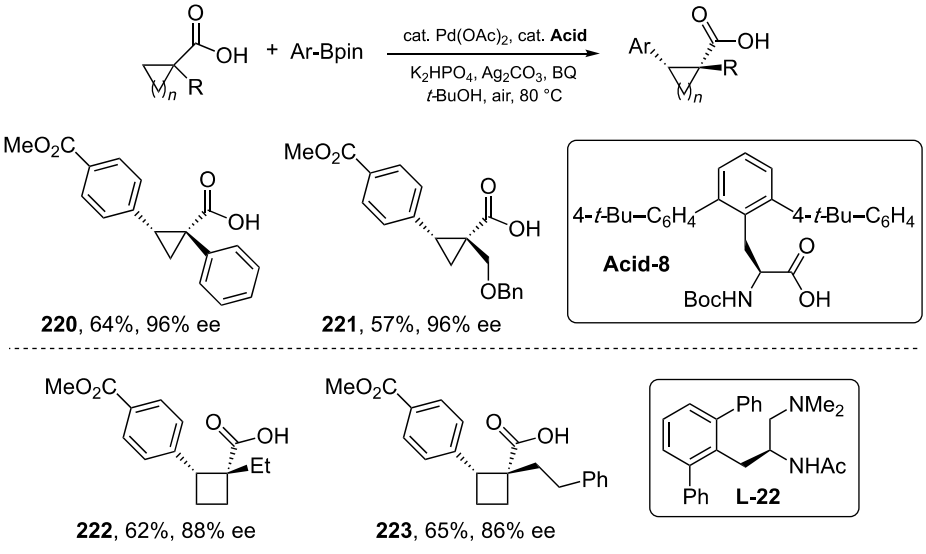

Scheme 12.51. Arylation of cyclic α-tertiary carboxylic acids.

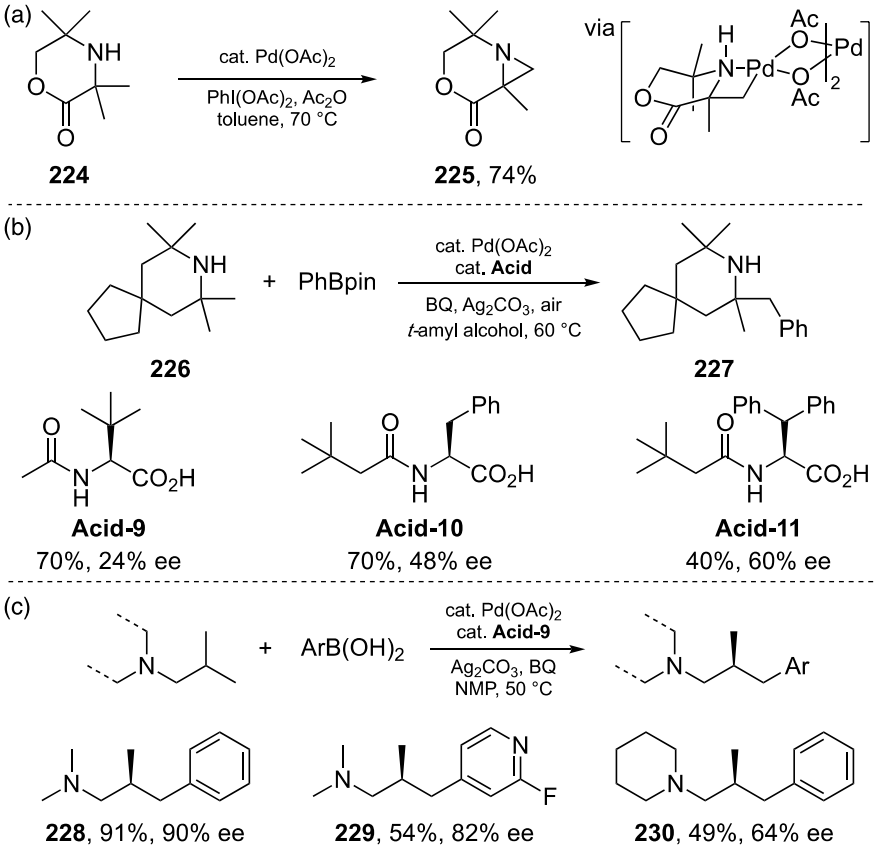

Scheme 12.52. Arylation of aliphatic amines. (a) β-C(sp³)–H amination. (b) β-C(sp³)–H arylation. (c) γ-C(sp³)–H arylation. Source: (a) [132]/Springer Nature. (b) [133]/John Wiley & Sons. (c) [134]/Springer Nature.

arylation works quite well, the asymmetric version remained a challenge, as only moderate ee is obtained in the presence of various protected amino acid ligands (Scheme 12.52b) [133]. In 2020, Gaunt showed that tertiary amine can also direct remote metalation in the presence of the Pd(II) catalyst via a five-membered palladacyle, followed by an oxidative arylation event with boronic acid (Scheme 12.52c) [134]. The protocol shows broad substrate scope with good-to-excellent yield and enantioselectivity.

12.3.2.2. Pd(II)/Pd(IV)-catalyzed C(sp³)–H Activation

Pd(II)/Pd(IV) catalysis for C–H activation (Scheme 12.45) has been one of the most extensively studied processes since the 1990s. Despite the exponential progress in this field, the highly enantioselective C(sp³)–H activation via Pd(II)/Pd(IV) catalysis remained elusive until 2015. Yu disclosed a Pd(II)-catalyzed highly enantioselective arylation of cyclopropyl C–H bonds with aryl iodides using mono-*N*-protected amino acid ligands, providing a redox neutral pathway for the preparation of chiral amines with small rings (Scheme 12.53) [135]. The dual role of silver salts in Pd(II)-catalyzed C–H activation is as either oxidant in the Pd(II)/Pd(0) catalytic system or halide scavenger in the Pd(II)Pd(IV) catalytic system. Later, the scope of C(sp³)–H coupling partner was extended to cyclobutanes with amino oxazoline (**L-23**) as chiral ligand [136]. Both transformations show excellent enantioselectivity and broad substrate scope.

The strategies developed for enantioselective C–H activation of cyclopropanes and cyclobutanes via Pd(II)/Pd(IV) catalysis are not applicable for acyclic sytems. Duan reported Pd(II)-catalyzed aminoquinoline-directed benzylic C–H arylation protocols by using chiral phosphoric acid and amide as ligand (Scheme 12.54) [137]. While in this study, most benzylic C(sp³)–H arylations show synthetically interesting level of ee, only moderate enantioselectivity is obtained with unactivated methylenes. Encouraged by Duan's work, Chen applied chiral phosphoric acid to picolinamide-directed γ-C(sp³)–H

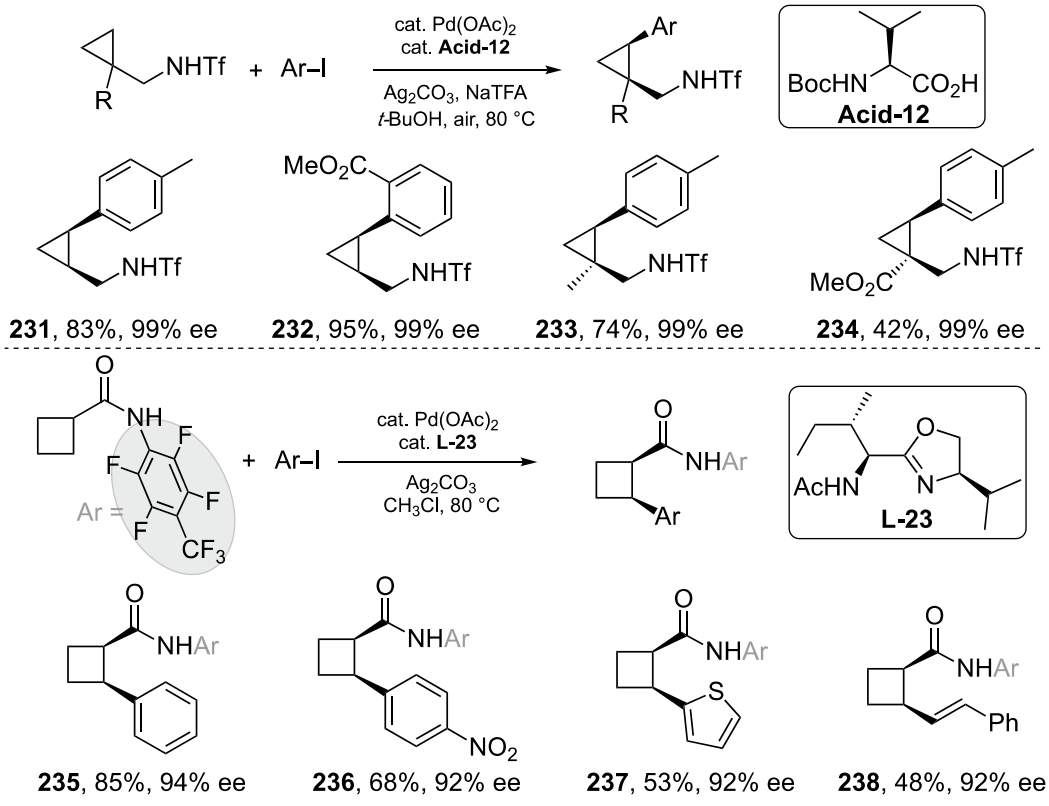

Scheme 12.53. Redox-neutral arylation of C(sp³)–H bond in small rings.

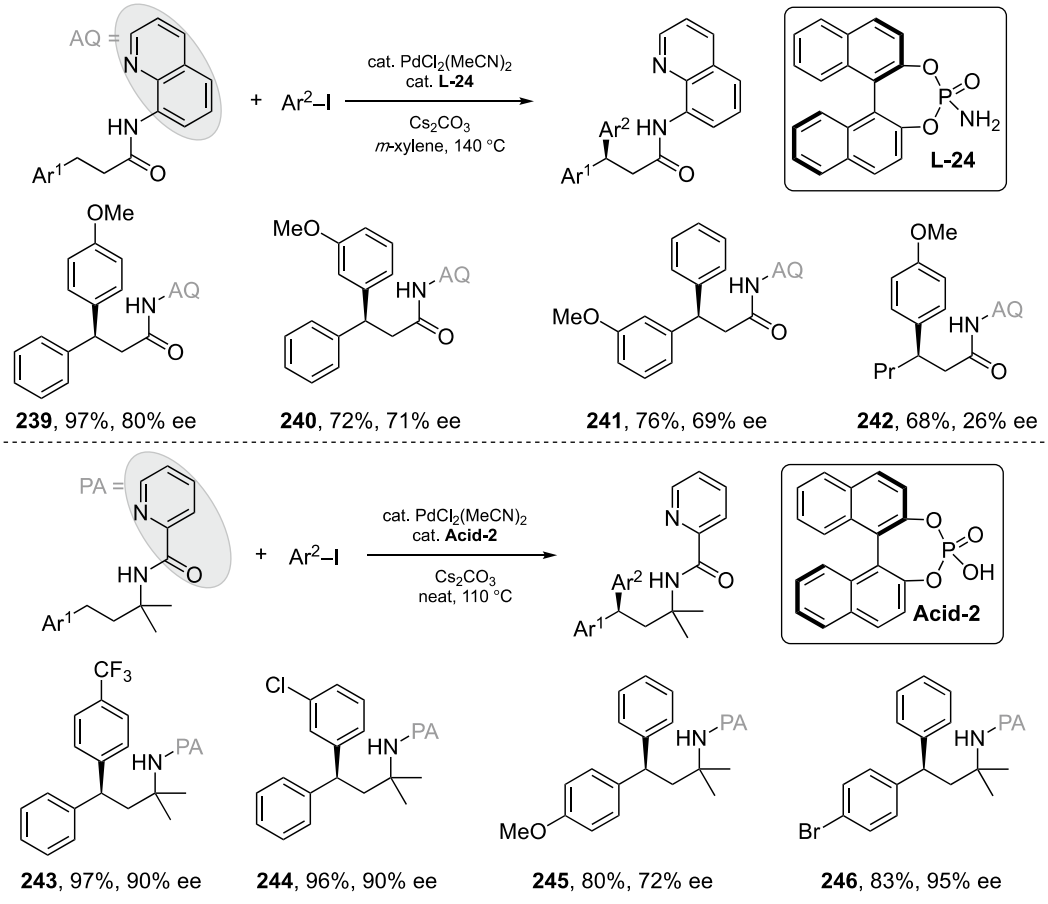

Scheme 12.54. Directed arylation of benzylic positions.

(benzylic) arylation. Interestingly, solvents show detrimental effect to the ee values, as low enantioselectivities are obtained in organic solvents [138].

As evident, a preinstalled directing group is crucial for the reactivity and selectivity. Yu successfully introduced transient directing group (TDG) tactics into the Pd(II)/Pd(IV)-catalyzed C(sp³)–H activation arena, dislosing a new strategy for the enantioselective activation of benzylic C–H bonds (Scheme 12.55). Taking advantage of reversible imine condensation, the simple addition of L-*tert*-leucine (20 mol%) into the reaction allowed arylation with excellent ee for various types of substituted benzaldehydes [139]. The TDG strategy was later successfully applied in the enantioselective arylation of cyclobutylketone substrates by the Yu group. They found that a dual ligand system and a silver salt are crucial for the reactivity and selectivity. However, the chemistry is not transferrable to linear ketone substrates, leaving ample space for further optimizations [140].

Despite the fruitful progress in the asymmetric C(sp³)–H activation arena, the enantioselective differentiation of enantiotopic C–H bonds of unactivated methylene group remains an elusive challenge. In 2016, the Yu group made such long-standing challenge possible by designing a novel chiral acetyl-protected aminoethyl quinoline (APAQ) ligands (**L-26**) in presence of a Pd(II) catalyst (Scheme 12.56, top) [141]. Having successfully solved the challenge of enantiodescrimination of the unactivated methylene group, the Yu group continued their efforts toward a more challenging problem-desymmetrizing the isopropyl group one year later. The distal steric interaction in the transition state requires a more sublte ligand system to maximize the remote steric repulsion. The mono-protected aminomethyl oxazoline ligands turned out to be quite efficient for this task [142]. Asymmetric arylation, alkenylation, and even

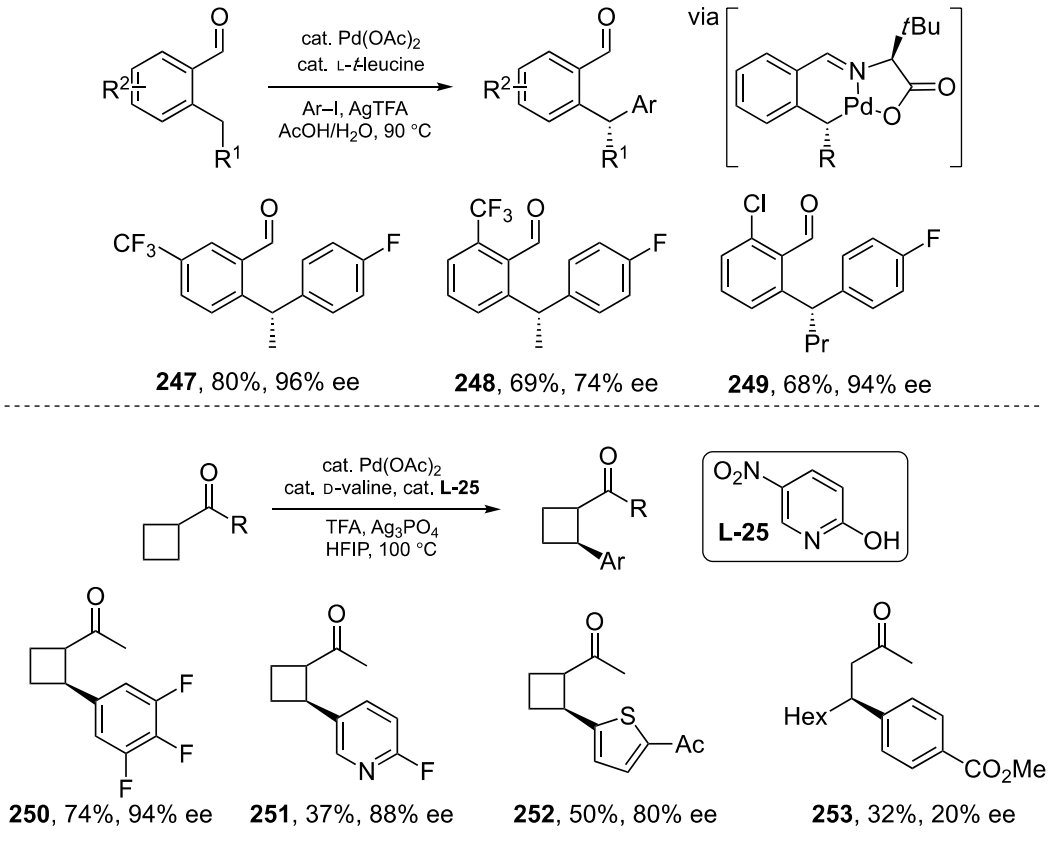

Scheme 12.55. Arylation of aldehyde/ketone via transient directing group strategy.

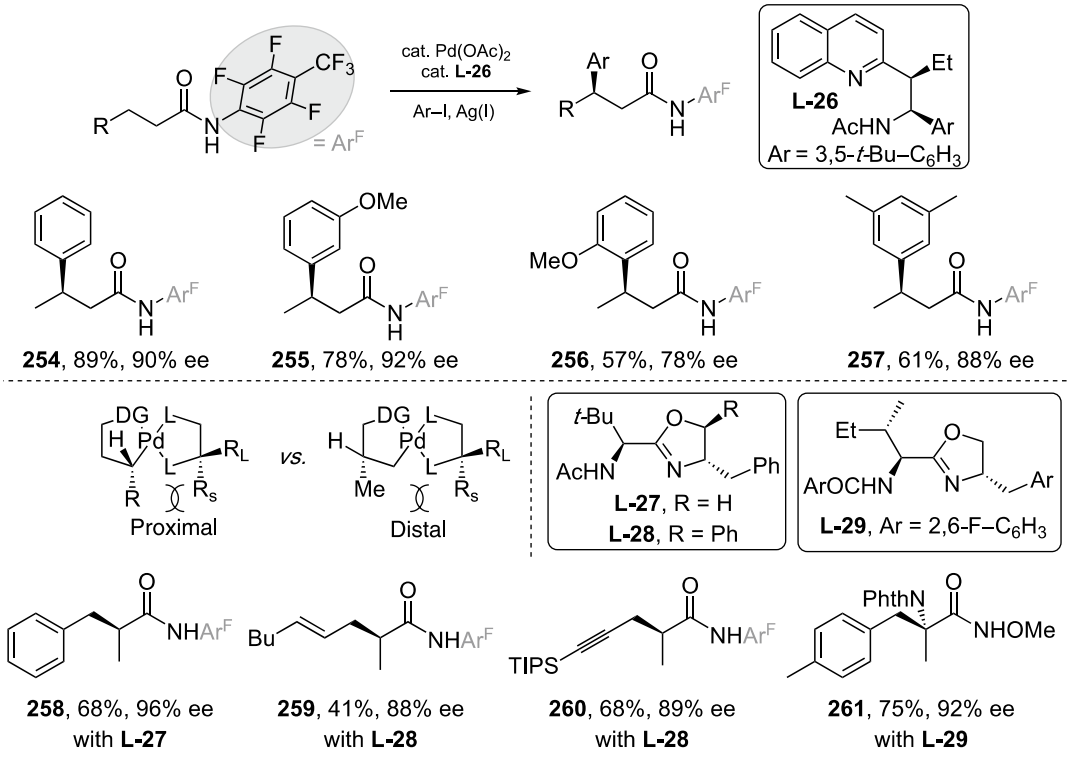

Scheme 12.56. (Top and bottom) Bidentate-ligand-enabled arylation of unactivated methylenes and methyl group. (Top) Source: [141]/American Association for the Advancement of Science.

alkynylation of the isopropyl group were all accommodated in good yield with excellent enantioselectivity. Both transformations showed broad substrate scope and functional group tolerance.

So far, most of the Pd(II)/Pd(IV)-catalyzed asymmetric arylation reactions utilize relatively more expensive and less available aryl iodides as aryl sources. Shi presented the first Pd(II)-catalyzed enantioselective arylation with less reactive and more available aryl bromides with 2-pyridinylisopropyl (PIP) group as a directing group (Scheme 12.57) [143]. The PIP directing group proved to be effective for

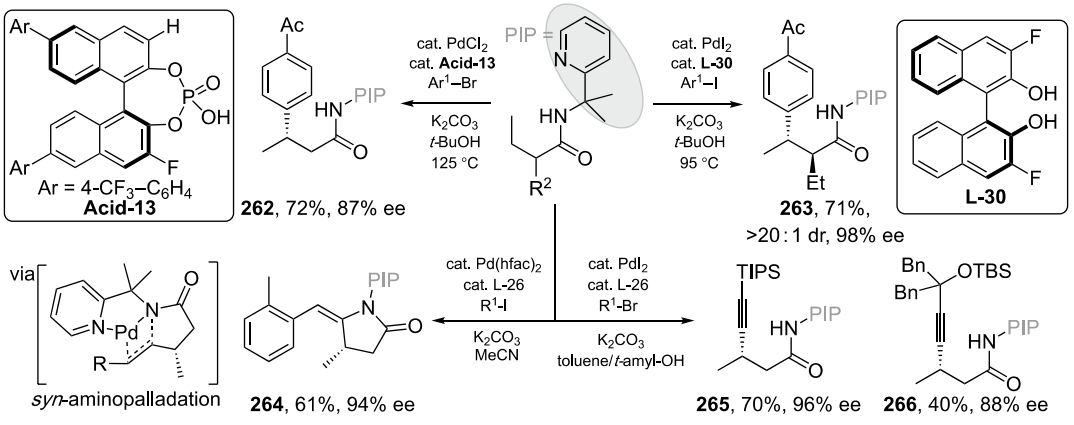

Scheme 12.57. Phosphoric acid enabled arylation of unactivated methylenes.

desymmetrizing the 3-pentyl group, leading to two contiguous stereogenic centers in the presence of a BINOL-type chiral ligand (**L-30**) [144]. The combination of the PIP directing group and the chiral BINOL ligand turned out to be highly efficient to enable asymmetric vinylation/aza-Wacker cyclization [145] and alkynylation [146] events (**264**).

As previously mentioned in the Pd(II)/Pd(0) catalysis session, the use of native functionality as a directing group would largely improve synthetic efficiency. In line with this notion, Yu found that ethylenediamine-derived chiral ligand (**L-31**) is quite useful for enantioselective arylation of free carboxylic acids [147]. While the conformation of metal carboxylate complex is more flexible, the metal bisamine bonding complex could be very strong and unreactive. The same group developed chiral β-aminothio ether as a ligand to the free-primary-amine directed arylation (Scheme 12.58) [148]. Interestingly, carbonylation could be accessed in moderate yield with good ee. The thioether motif was believed to facilitate the dissociation of bis(amine) Pd(II) complex.

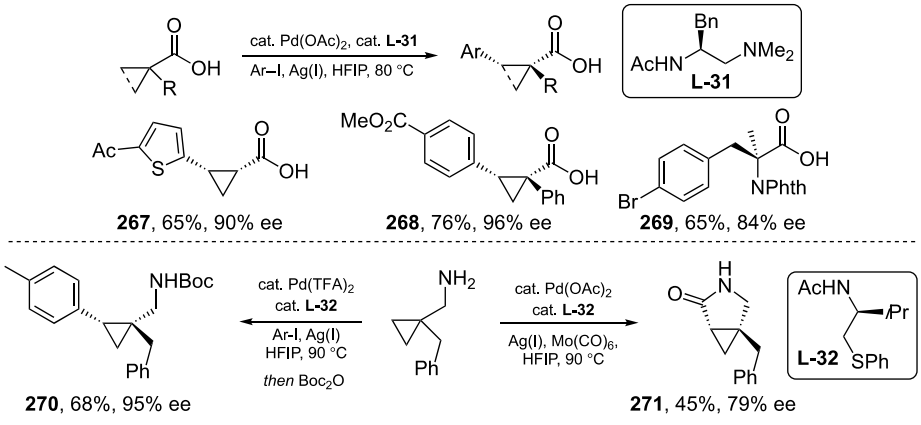

Scheme 12.58. Arylation of cyclopropane-containing acids/amines.

C–C bond formation via asymmetric C(sp³)–H activation has greatly expanded the toolbox to the synthesis of chiral molecules. The construction of C–X bond via asymmetric C(sp³)–H activation remains less explored, probably due to the difficult C–X bond reductive elimination and other competitive bond forming pathways.

Yu disclosed several important transformations during their long pursuit of C–H activation. They first reported a direct asymmetric borylation event (Scheme 12.59) [149]. The use of acetyl protected amino oxazoline ligand (**L-33**) guaranteed the excellent enantioselectivity. The chiral boronic ester products can be easily derivatized to many other functionalities.

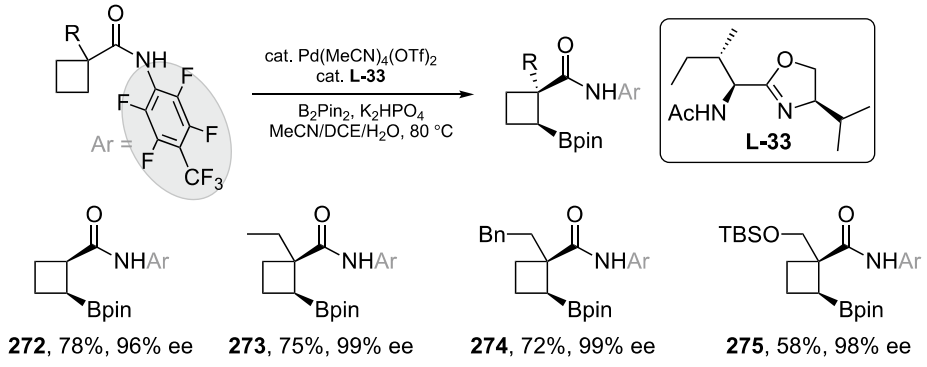

Scheme 12.59. Directed enantioselective borylation of cyclobutane.

Perhaps one of the most challenging transformations is an enantioselective C(sp³)–F bond construction via C(sp³)–H activation. In 2018, Yu applied the transient directing group strategy to solve this problem (Scheme 12.60) [150]. The stereochemical analysis of a preformed palladacycle suggested that while the targeted C(sp³)–F formation undergoes via an inner-sphere reductive elimination pathway, the undesired C(sp³)–O formation occurs through an S_N2-type mechanism with inversion of the configuration of

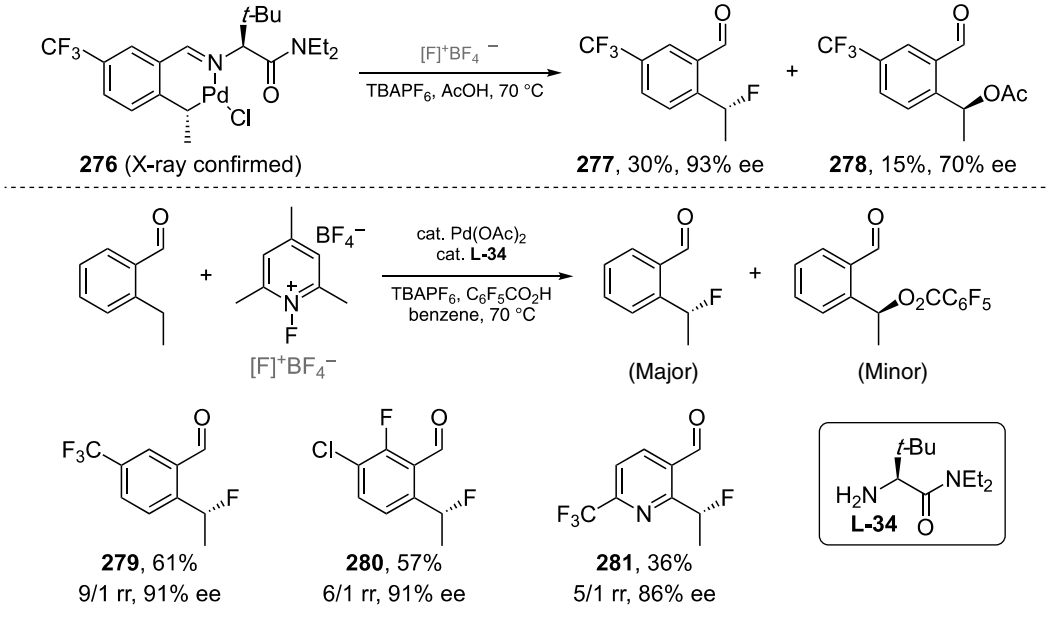

Scheme 12.60. Enantioselective fluorination of benzylic position.

Pd–C bond (**276–278**). This finding allowed the selectivity to be further optimized by using an electron-deficient aromatic acid as an additive in benzene. The reaction delivers good yields with high ee values.

Amination via asymmetric C(sp³)–H activation provides an efficient way to access chiral *N*-containing molecules, which are widely found in pharmaceuticals, agrochemicals, and natural products. Unlike other C–X bond formations, there are a handful of seminal reports regarding asymmetric intramolecular C(sp³)–H amination events.

In 2017, Gaunt developed an enantioselective intramolecular amination by using a commercially available phosphoric acid ligand (**Acid-14**) [151]. The protocol enables the conversion of secondary amines to synthetically useful chiral aziridines (Scheme 12.61).

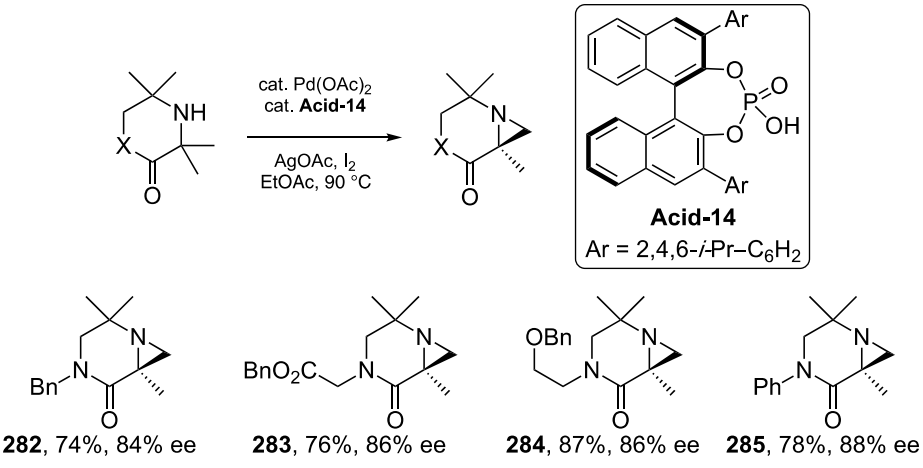

Scheme 12.61. Synthesis of chiral aziridines.

Amide served as a directing group for C–C bond formation in a number of C(sp³)–H activation reactions until 2014, when Wu disclosed that by using an electron-deficient aryl iodide, the amide directing group can also serve as an intramolecular aminating source *en route* to β-lactams. The aryl iodide functions as an oxidant as well as tuning the reductive elimination from the Pd(IV) center [152]. This seminal work inspired two other groups to develop an enantioselective version. Chen reported an enantioselective intramolecular amination in the presence of Pd(II), BINOL-type ligand and aryl iodide [153]. Concurrently, Shi presented a similar catalytic system to form chiral β-lactams. While Chen's work was limited to benzylic position, Shi could aminate unbiased methylene in good yields with high ee (Scheme 12.62) [154].

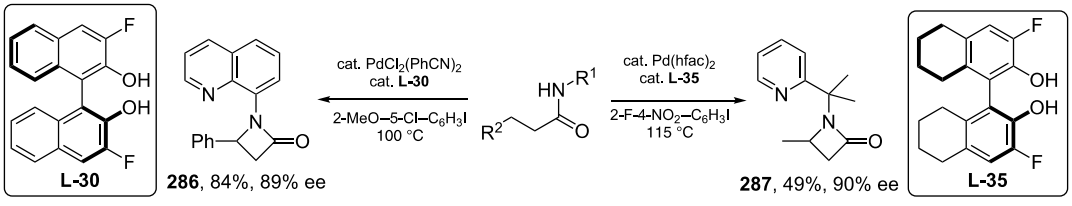

Scheme 12.62. Synthesis of chiral β-lactams.

12.3.3. Pd(II)-catalyzed Allylic C(sp³)–H Activation

Allylic substitution via direct allylic C(sp³)–H activation is an important chemical transformation in organic synthesis. When sulfoxide or nitrogen ligands are employed, the generally accepted C–H cleavage

mechanism is acetate-base-assisted CMD pathway like many other C(sp³)–H activation reactions. However, experimental and computational studies showed that when quinone is utilized as oxidant, the allylic C–H is cleaved via quinone/Pd(0)-mediated redox pathway (Scheme 12.63) [155].

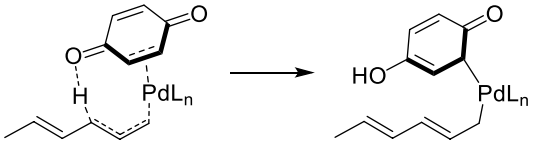

Scheme 12.63. Benzoquinone-assisted Pd(0)-catalyzed allylic C(sp³)–H activation.

The first enantioselective allylation of β-diketone substrates via allylic C(sp³)–H activation was realized by Trost in 2013 [156]. They designed a novel phosphoramidite ligand (**L-36**) which enabled allylic alkylation with activated carbon nucleophile in excellent yields with good ee values. One year later, Gong disclosed a synergy of chiral counteranion and enamine catalysis in the context of Pd(II)-catalyzed allylic C(sp³)–H alkylation event (Scheme 12.64) [157]. The less reactive aldehyde forms reactive enamine with **Amine-1** catalyst in situ, while the chiral phosphoric acid provides a chiral platform to bring together the Pd(II)-allyl intermediate and the enamine. In both cases, 2,6-dimethyl benzoquinone (2,6-DMBQ) proved to be a compatible terminal oxidant to turn over the palladium catalyst. Later, this type of reactivity for both nucleophiles and alkenes was largely expanded by Gong and White [155, 158].

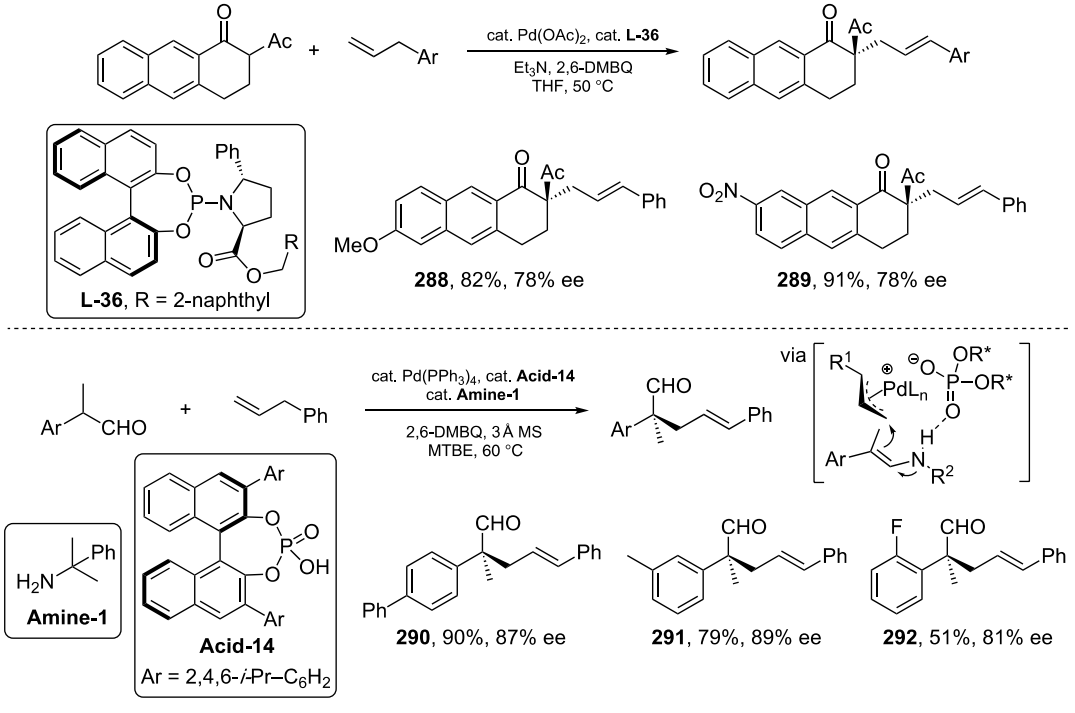

Scheme 12.64. Enantioselective allylic C(sp³)–H alkylation.

As a pioneer in Pd(II)-catalyzed allylic C–H oxidation arena, White in 2008 disclosed a combination of Pd(II)/bis(sulfoxide) and chiral Cr(III)(salen) Lewis acid, which enabled asymmetric allylic

C–H oxidation in moderate enantioselectivity (Scheme 12.65) [159]. The Cr(III) Lewis acid catalyst was proposed to coordinate with benzoquinone (BQ) in the transition state. Although preliminary, these results may pave the base for other asymmetric allylic C–H activation reactions.

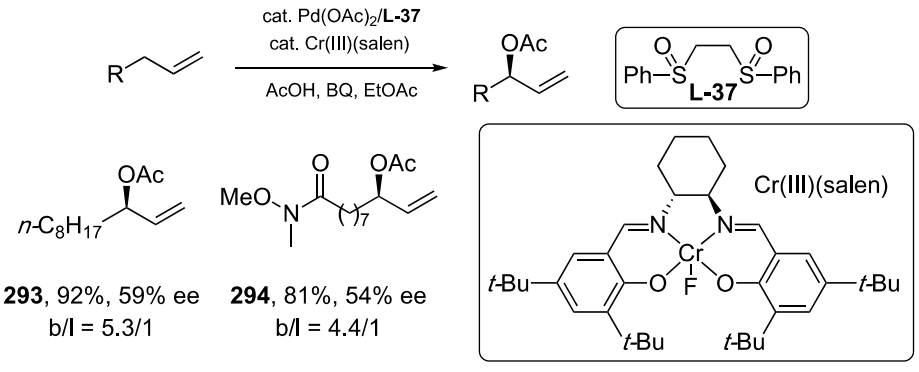

Scheme 12.65. Enantioselective allylic C(sp³)–H acetoxylation. Source: [159]/John Wiley & Sons.

While the intermolecular asymmetric allylic C–H oxidation remains synthetically elusive, the intramolecular version was realized by Gong [160]. The key to success was the use of bulky chiral phosphoramidite ligand (**L-38**) and achiral Brønsted acid catalyst in the presence of $Pd(dba)_2$. The reaction shows broad substrate scope for the synthesis of bioactive chiral chromans. Mechanistic experiments revealed a C–H activation pathway rather than a Wacker type reaction (Scheme 12.66). Interestingly, White developed a similar transformation using chiral sulfoxide/oxazoline ligand scaffold (**L-39**) in 2016, in which a number of chiral isochromans could be accessed in good yields with excellent enantioselectivities [161].

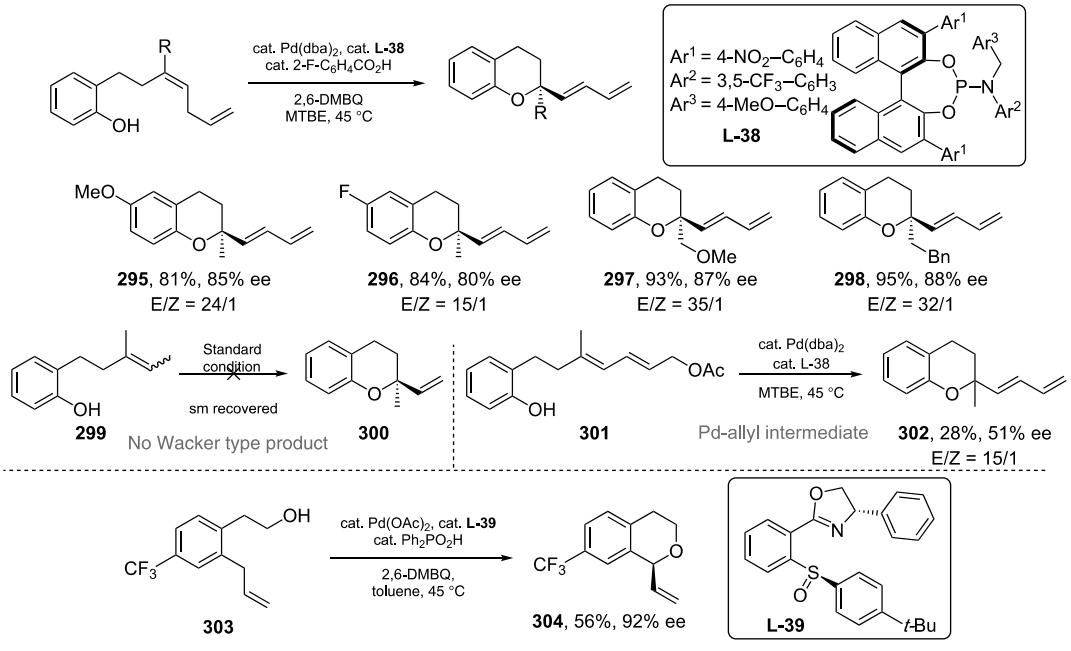

Scheme 12.66. Asymmetric intramolecular oxidation of allylic C(sp³)–H bond.

12.3.4. Other Transition Metal Catalyzed Asymmetric C(sp³)–H Activation

As can be seen from the vast majority of publications, the field of asymmetric C(sp³)–H activation is dominated by Pd-catalysis. However, this is not to say other transition metals do not play a role in this important field. The catalytic modes/strategies developed are very similar to those of palladium catalysis.

In 2017, although preliminary, the Cramer group showed the potential to use chiral Ir-Cp* complex to control enantioselective C(sp³)–H transformation (Scheme 12.67) [162].

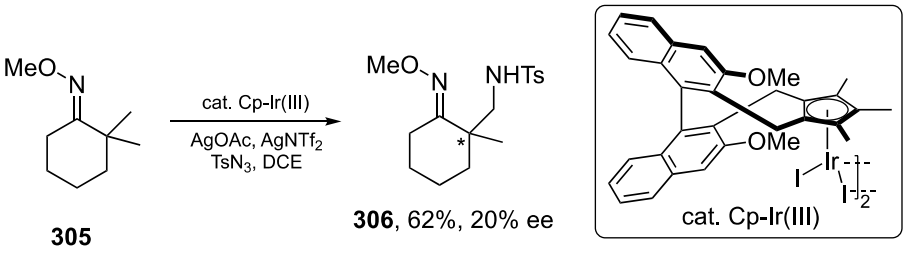

Scheme 12.67. Chiral-Ir(III) catalyzed amination of methyl group.

Matsunaga's group contributed to this field with several works. They found out that a catalytic combination of CpM(III) and a chiral acid could enable enantioselective amination of unactivated C(sp³)–H bonds (Scheme 12.68) [163, 164].

Group IX transition metal catalysts have proven quite efficient for asymmetric C(sp³)–H activation. Blakey and Glorius, respectively, showed that enantioselective amination (with Ir) and arylation (with Rh) could be achieved by using chiral ligands as modifiers (Scheme 12.69) [165, 166].

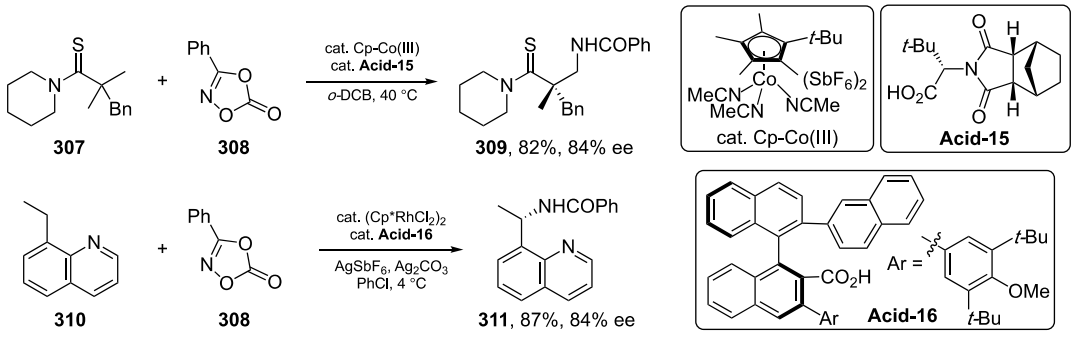

Scheme 12.68. Co(III) and Rh(III)-catalyzed asymmetric amination reactions. Source: Based on [163] and [164].

12.4. C(sp³)–H ACTIVATION VIA OXIDATIVE ADDITION MECHANISM

12.4.1. Introduction

Asymmetric reactions involving C(sp³)–H activation, which proceed via oxidative addition mechanism, are almost exclusively limited to iridium and rhodium catalysts. The mechanism of the C–H activation step depends on the oxidation state of the preformed catalyst. Low-valent Ir(I) or Rh(I) complexes can either insert directly into C–H bond to form Ir(III) hydride species or can be prefunctionalized to form

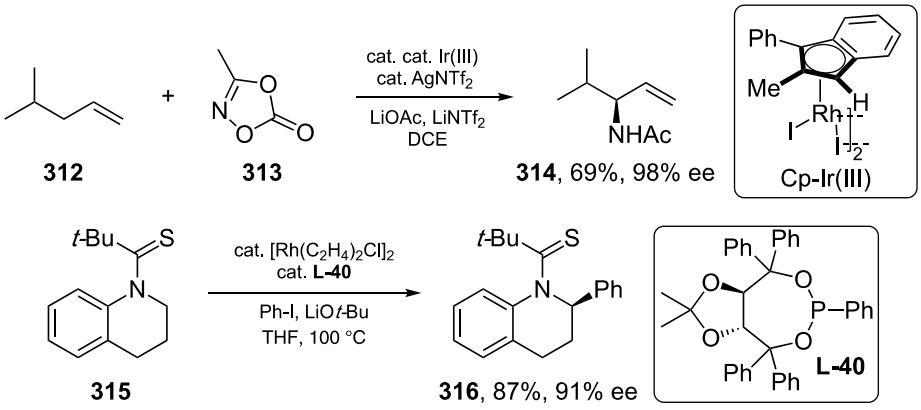

Scheme 12.69. Ir(III) and Rh(III)-catalyzed asymmetric C(sp³)–H activation.

Ir(III) or Rh(III) complexes, which are then oxidatively added into C–H bond to form Ir(V) or Rh(V) species, respectively (Scheme 12.70). While the first type of the mechanism is typical for C–C bond forming reactions [167], the latter was proposed for C–H borylations [168] and silylations [169, 170]. It should be noted that some of the original reports dealing with C–H silylation reactions proposed M(I)/M(III)-type mechanism [171, 172].

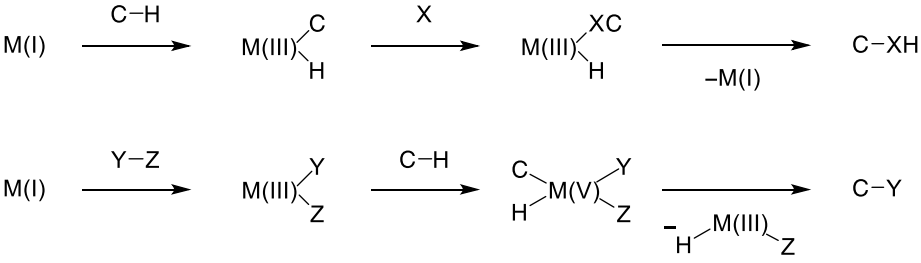

Scheme 12.70. General mechanism of C–H activation via oxidative addition.

12.4.2. C–C Bond Forming Reaction

12.4.2.1. Allylic and Benzylic C–H Bond Activation A way toward the development of the first enantioselective C(sp³)–H activation/C–C bond forming reaction via oxidative addition mechanism started in the Yu group in 2011 during their attempts to develop Rh-catalyzed intramolecular Diels-Alder reaction [173]. Starting from triene **317**, they observed a formation of tetrahydropyrazole derivative **318** instead of sterically hindered product of [4+2] cycloaddition (Scheme 12.71). The reaction was proposed to proceed via a coordination of all three double bonds to Rh-complex, diene-assisted oxidative addition of Rh-complex to allylic

Scheme 12.71. Achiral allylic C–H activation/C–C bond formation by Yu.

C–H bond to form intermediate **319**, alkene insertion to the Rh–H bond, and di-π-allyl assisted C(sp³)–Rh–C(sp³) reductive elimination, which was later supported by the DFT calculations [167].

The asymmetric version of this C–H activation reaction was introduced only one year later [174]. The key for the development of highly enantioselective reaction was the observation that bidentate phosphine ligands inhibit the reaction; therefore, Yu decided to test monodentate phosphoramidite ligands. All screened substrates provided *cis*-derivatives of tetrahydropyrroles, tetrahydrofurans, and cyclopentanes with two adjacent sp³ carbon centers using $[RhCl(coe)_2]_2$ as a catalyst and phosphoramidite **L-41** as a chiral ligand in high ees (Scheme 12.72).

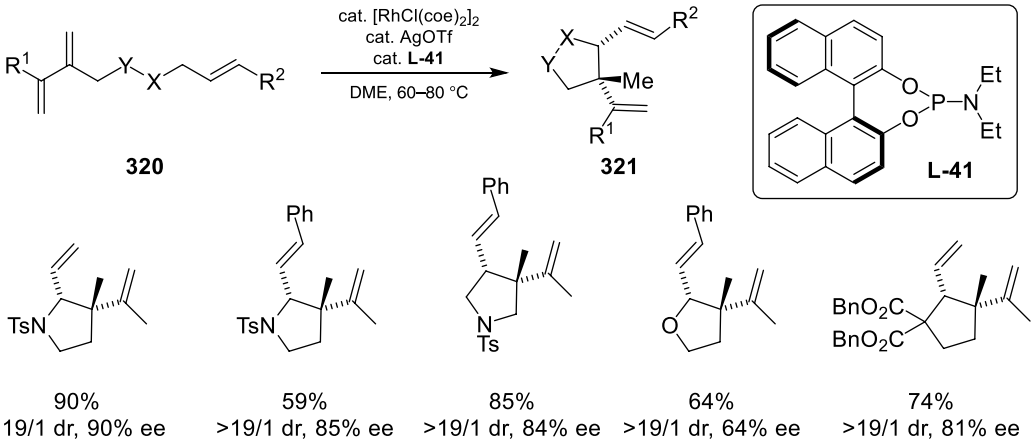

Scheme 12.72. Asymmetric allylic C–H activation/C–C bond formation by Yu.

In 2017, Mita and Sato developed Co-catalyzed carbonyl insertion into C(sp³)–H bond [175]. Although the study mainly focused on the achiral version of this reaction, the enantioselective variant was also investigated. After short screening of potential chiral ligands for asymmetric addition of allylic-benzylic bond to acetone, (*R*)-DIFLUORPHOS was found to provide homoallylic alcohol **322** in the best 81% ee (Scheme 12.73). Although the product was isolated in only low 21% yield, the reaction proceeds with excellent chemoselectivity as the other potential isomers of the product (linear product, etc.) were not observed.

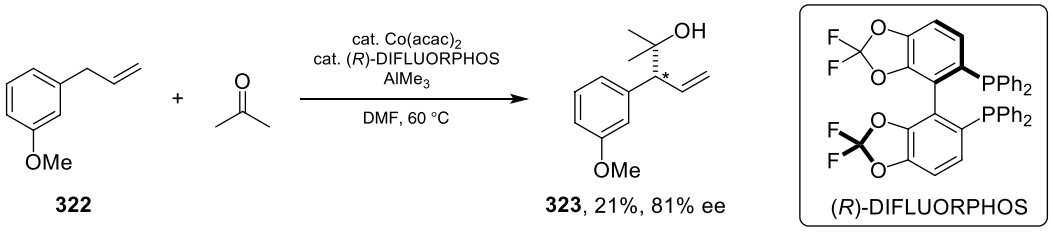

Scheme 12.73. Enantioselective alkylation of allyl benzene by Mita and Sato.

12.4.2.2. α-Heteroatom C–H Bond Activation During their previous study on aromatic C(sp²)–H activation/alkenylation, Shibata observed that the reaction of *N*,*N*-dimethylbenzamide catalyzed by cationic Ir(I)–BINAP complex causes a formation of an unexpected product of C(sp³)–H activation [176, 177]. Authors thus decided to study the effect of the same catalytic system on C(sp³)–H activation/alkylation of 2-(alkylamino)pyridines, which encouraged the development of the asymmetric process [178]. The key for

its success was the identification of the optimal ligand. The change from (*S*)-BINAP to (*S*)-Tol-BINAP showed to have a large influence on the reactivity of the system and most of the tested substrates react in high yields and enantioselectivities (Scheme 12.74) [179].

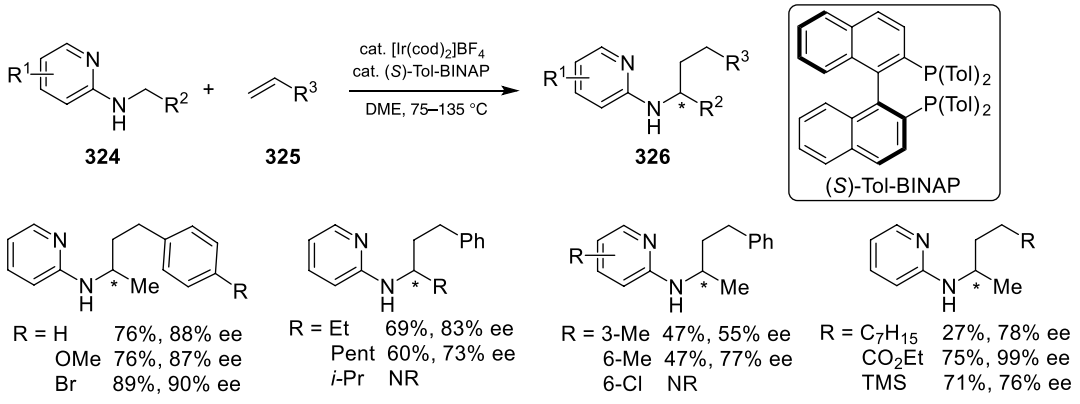

Scheme 12.74. α-Nitrogen C(sp³)–H alkylation of linear amines by Shibata. Source: [179]/Elsevier.

Later on, Shibata applied the developed system on C–H activation of *N*-(2-pyridyl)-γ-butyrolactam **327**, potential precursors of chiral derivatives of γ-aminobutyric acid (GABA) [180]. The formed C–H activated intermediate underwent reaction with various alkenes as styrenes and electron-deficient olefins with high enantioselectivities (Scheme 12.75).

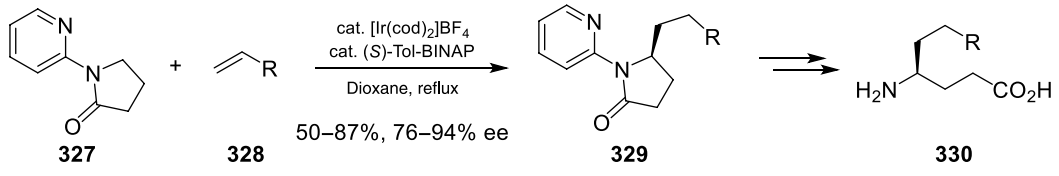

Scheme 12.75. α-Nitrogen C(sp³)–H alkylation of cyclic amines by Shibata.

In 2018, Nishimura reported Ir(I)-catalyzed sequential two-fold C(sp³)–H activation/alkylation sequence of *N*-methyl amines **331** [181]. They used 3-(pyrrolidine-1-carbonyl)pyridin-2-yl as a directing group for this transformation (Scheme 12.76), which was developed by the same group for a related reaction one year earlier [182]. While pyridine moiety represents a real directing group and coordinates the iridium(I) complex, the carbonyl group on the pyridine core is proposed to form a hydrogen bond with

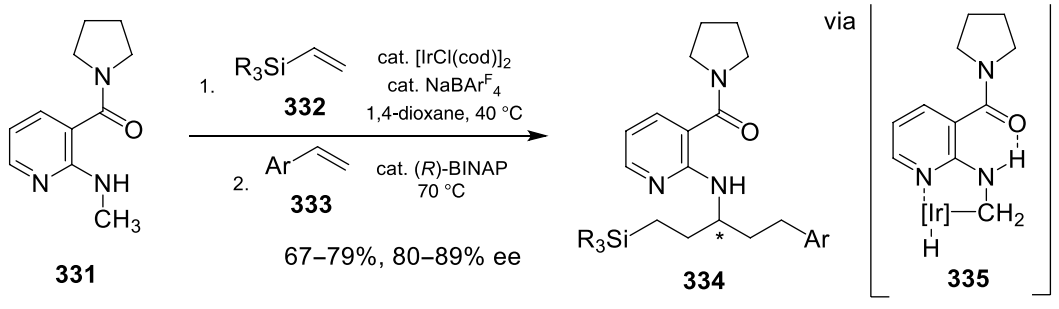

Scheme 12.76. Two-fold C(sp³)–H alkylation of *N*-methyl amines by Nishimura.

the amino group. This interaction stabilizes the whole complex and also brings the reacting methyl C–H bond closer to the iridium center, which facilitates the C–H activation step. After the successful C–H activation, the intermediate **335** reacts with the first molecule of alkene under achiral conditions forming a monoalkylated product. The subsequent addition of the chiral phosphine ligands causes the formation of the chiral iridium complex, which undergoes the second C–H activation followed by the enantioselective alkylation with the second molecule of alkene. The major issue of this reaction is a formation of a symmetrically dialkylated product. This can be overcome by using vinylsilane as a first alkylating agent, which selectively forms a monoalkylated product.

The intramolecular variant of *N*-methyl C(sp³)–H alkylation reaction of methyl amines with alkenes was published in 2017 by Ohmura and Suginome (Scheme 12.77a) [183]. Compared to the previously discussed intermolecular variants, this reaction does not require any other type of activation of the C–H bond (e.g. directing group, allylic or benzylic position). The Ir(I)-(*S*)-DTBM-SEGPHOS complex was identified as an optimal catalytic system and provides indoline derivatives **337** in excellent ees despite the high reaction temperature, which is required for sufficient reactivity of the substrates. The performed mechanistic studies suggest that oxidative addition of the C–H bond to the iridium complex is the rate-limiting step. The formed intermediate **338**, which is probably stabilized by coordination to the nearby double bond, undergoes 5-*exo*-trig cyclization to form **339**, which is then turned into the reaction product **337** by reductive elimination. Subsequently, they also showed that the same type of activation can be conducted α to the oxygen atom of aromatic methyl ethers **340** (Scheme 12.77b) [184].

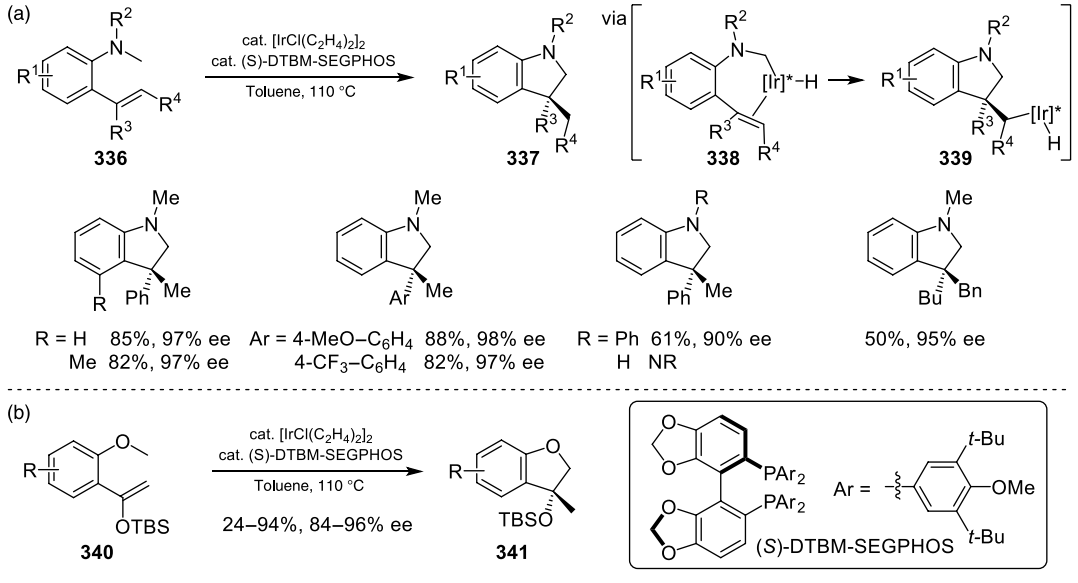

Scheme 12.77. C(sp³)–H alkylation of methyl amines and ethers by Ohmura and Suginome. (a) C(sp³)–H alkylation of methyl amines. (b) C(sp³)–H alkylation of methyl ethers. Source: (a) [183]/John Wiley & Sons. (b) [184]/John Wiley & Sons.

In 2020, Ohmura and Suginome developed a new tandem single-iridium complex-catalyzed dehydrogenation/α to nitrogen C(sp³)–H bond addition to alkene/dehydrogenation method for synthesis of indoles (Scheme 12.78, **344** R = H) [185]. Starting from branched starting material **342** (R = aryl or benzyl), and thus preventing the final dehydrogenation step, the reaction provides chiral indolines **343** in high yields and enantioselectivities using chiral SEGPHOS or GARPHOS-type ligands.

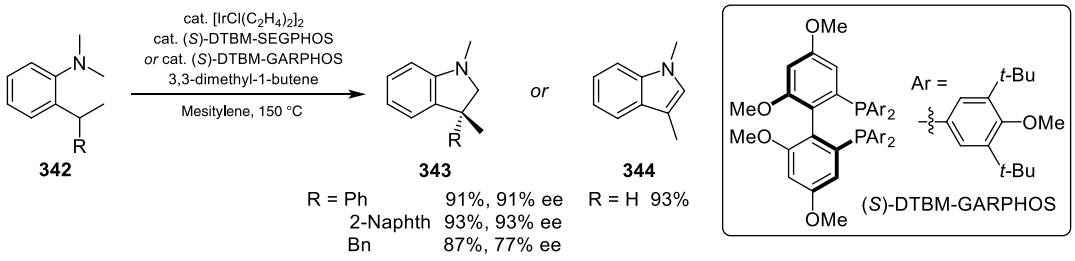

Scheme 12.78. Tandem dehydrogenation/C–H alkylation by Suginome.

12.4.3. C(sp³)–H Borylation

Organoboronates are key building blocks in organic synthesis as they can be easily transformed to other molecules by well-studied transformations such as Suzuki-Miyaura cross-coupling, oxidation, boron-halogen exchange reactions, amidation, amination, etc. The most straightforward and atom-economic way of their preparation is C–H borylation. Besides the general issues associated with any C–H activation reaction, and especially C(sp³)–H activation, the selectivity of C–H borylation is complicated due to its own unique mechanism. The reacting species of transition metal-catalyzed C–H borylation is a 16-electron trisboryl complex, which has no vacant orbital available for coordination of a directing group (Scheme 12.79a) [168]. This impedes the overall chemoselectivity of C–H activation. In recent years, two different solutions to this obstacle were developed: (i) the use of monodentate ligands (e.g. phosphoramidite and phosphite used by the Sawamura group) to form a 14-electron trisboryl complex (Scheme 12.79b); or (ii) the use of LX-type ligands to form a 14-electron bisboryl complex (Scheme 12.79c, e.g. *N*,*B*-anionic ligand developed by the Li group [186]).

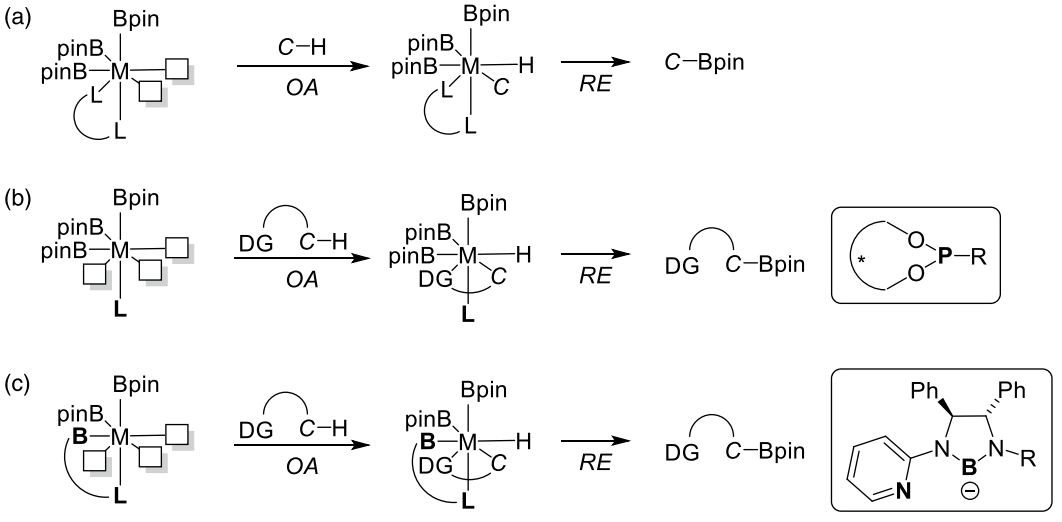

Scheme 12.79. Modification of C(sp³)–H borylation mechanisms based on used ligand. (a) C–H activation via 16-electron trisboryl complex. (b) C–H activation via 14-electron trisboryl complex. (c) C–H activation via 14-electron bisboryl complex.

The first successful asymmetric C(sp³)–H borylation was developed by Sawamura in 2017 [187]. Their first study attempted to use Rh(I) or Ir(I) catalyst and chiral phosphoramidite **L-42** as a catalyst–ligand system and bis(pinacolato)diboron as a borylation agent for borylation of 2-substituted pyridines **345**

(Scheme 12.80). This system allowed selective desymmetrization of unactivated methylene C(sp³)–H bonds located γ to the nitrogen atom of the pyridine directing group albeit with only moderate enantioselectivity. A significant improvement regarding enantioselectivity of the reaction was achieved by the same group in 2019 [188]. The introduction of chiral phosphite **L-43** bearing two BINOL moieties, together with an addition of catalytic amount of 2,6-lutidine, increased both yields and enantioselectivity of the reaction (up to 99% ee, the enantioselectivity was determined after oxidation of alkylboronates to appropriate alcohols). The authors also studied the reaction mechanism using experimental kinetic studies and DFT calculations. The results suggested that the cleavage of the C(sp³)–H bond is a turnover-limiting step and that this step proceeds via concerned C(sp³)–H oxidative addition to the Ir(III) center forming intermediate **348** (Scheme 12.80). Furthermore, the studies showed that the **L-43**–Ir(III)$(Bpin)_3$ complex provides a narrow chiral reaction pocket analogous to the enzyme active site with several interactions between the substrate and the complex including metal-centered coordination, π/π, C–H/π, and C–H·O interactions. Further computations showed that the *S*-producing transition state is 2.8 kcal mol^{-1} lower in energy that the *R*–producing transition state, which explains the exclusive formation of the *S* enantiomer.

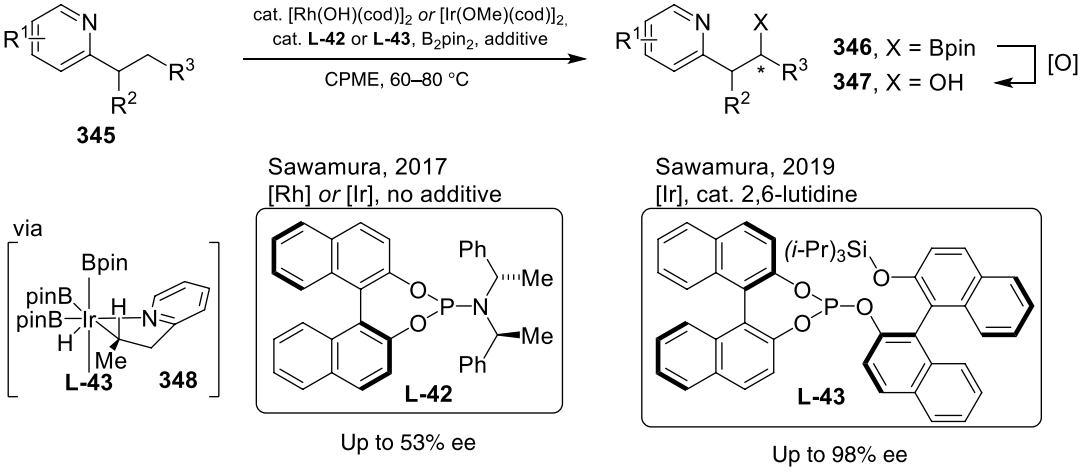

Scheme 12.80. C(sp³)–H borylation directed by pyridine by Sawamura.

Recently, Sawamura extended their study of C(sp³)–H borylation by an application of various *N*-heteroarene substrates, but more importantly amide substrates **349** forming α-aminoboronates **350** (Scheme 12.81), an interesting class of studied enzyme inhibitors [189]. They found that amide substrates

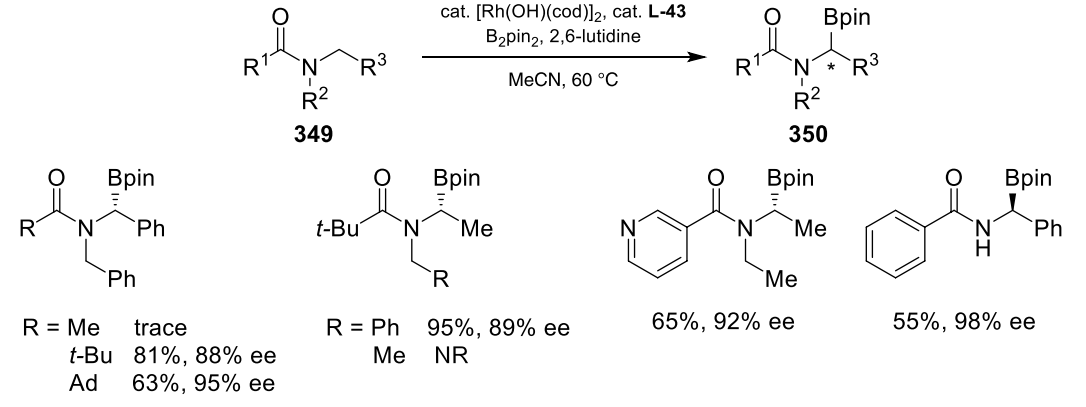

Scheme 12.81. Carbonyl directed C(sp³)–H borylation by Sawamura.

with simple and sterically less demanding *N*-alkanoyl groups result in poor reactivity. On the contrary, bulkier *N*-alkanoyl groups such as pivaloyl or adamantoyl give boronates in both high yields and enantioselectivities. The reaction proved to be site-selective as the borylation exclusively occurs on the *N*-ethyl rather than on the *N*-benzyl chain. On the other hand, the reaction is completely suppressed with *N*,*N*-diethyl amide substrates. The authors suggested that this induced reactivity generated by the *N*-benzyl group is caused by the noncovalent substrate-ligand interactions (e.g. π/π). In the same fashion, the π/π substrate/ligand interactions are presumably causing the increased reactivity and enantioselectivity of the *N*-aroyl tertiary and secondary amides. Surprisingly, all the studied secondary amides provide *S*-configured products, while tertiary amides give *R*-enantiomers.

Sawamura subsequently achieved a unique remote γ-C(sp³)–H activation/borylation of aliphatic esters and amides. They introduced a urea-containing pyridine **L-44** as a second ligand with ability to interact with the substrate by hydrogen bonding, and thus deliver it to the Ir(I) complex and the chiral phosphite **L-43** (for structure, see Scheme 12.80) [190]. The reaction was tested on various substrates and showed exclusive site- and enantioselectivity with tertiary and secondary carboxamides and esters (Scheme 12.82). The application of carboxamide with a different aliphatic chain showed tolerance of this method toward steric hindrance, while the sense of enantioselectivity is opposite when the reaction proceeded in the benzyl position of the phenyl substituted amide chain.

DFT calculations of various conformers of the C(sp³)–H cleavage transition state **354** showed the stabilization of the productive transition state by various interactions. The carbonyl group of the substrate is bound to the urea moiety of the receptor ligand, which is stabilized by π/π interactions between both phenyl and pyridine moieties and one of the naphthalene rings of the phosphite ligand. Furthermore, the whole complex is stabilized by noncovalent C(sp³)–H·O interactions between the substrate's hydrogens and oxygens of the phosphite ligand and one of the boronate groups.

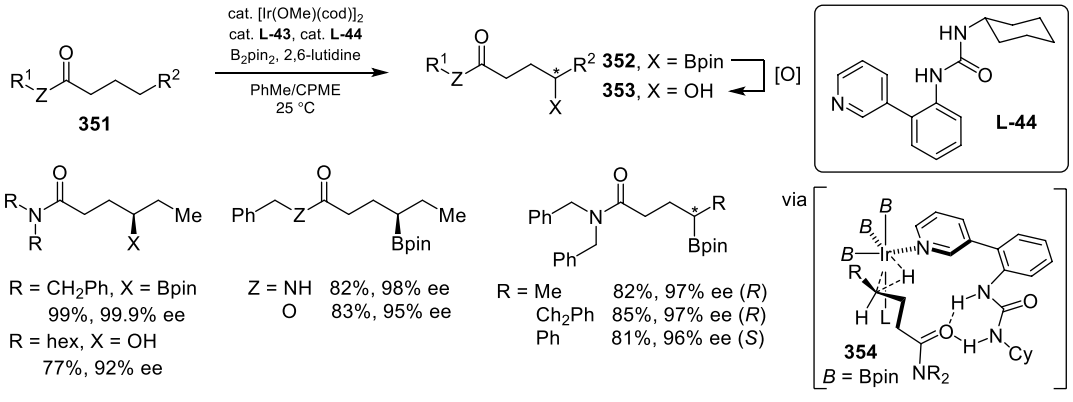

Scheme 12.82. Carbonyl directed C(sp³)–H γ-borylation by Sawamura.

In 2019, Xu published C(sp³)–H borylation of a cyclopropane ring, which was directed by a carboxamide moiety to the β-position [191]. The reaction was catalyzed by an Ir(I)-dimer complex and a bidentate boryl ligand **L-45** and showed a wide compatibility of the reaction conditions with a variety of substrates including substituted α-aryl, as well as α-alkyl carboxamides **355** (Scheme 12.83). Notably, *p*-bromo and *p*-Bpin substituted α-phenyl carboxamides react cleanly to give target products in excellent ees (94 and 93% ee, respectively). These functional groups proved to be incompatible with classical C–H activation conditions using Pd-catalysts [130]. Xu later extended the application of the catalytic system on borylation of a cyclobutane ring [192]. The benzoxazole moiety serves as a directing group in this system and products are isolated in slightly lower enantioselectivities (up to 92% ee) using related boryl ligands **L-46** and **L-47** (Scheme 12.84).

Another example of asymmetric C(sp³)–H borylation using a chiral boryl ligand was published by the Xu group in 2020 [193]. The β-selectivity was in this case directed by a pyrazole moiety

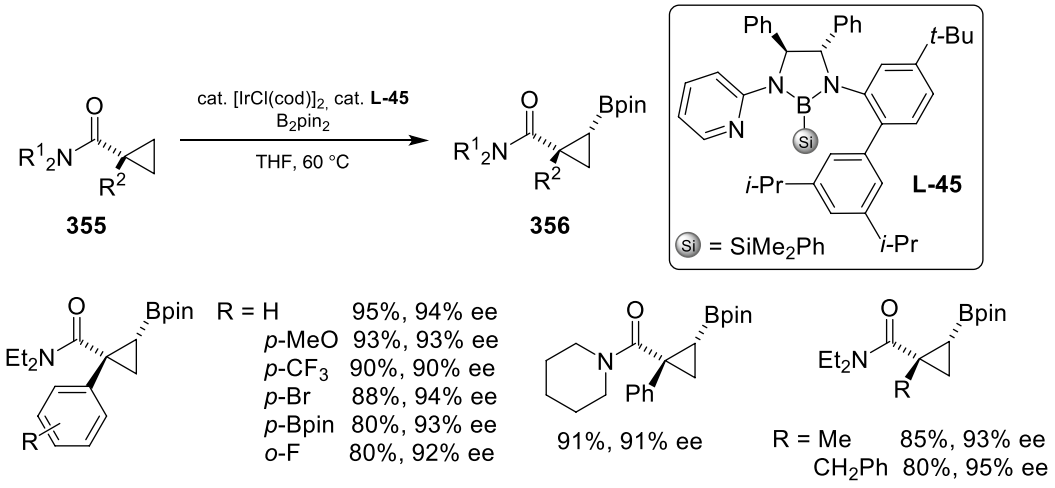

Scheme 12.83. C(sp³)–H borylation of cyclopropanes by Xu.

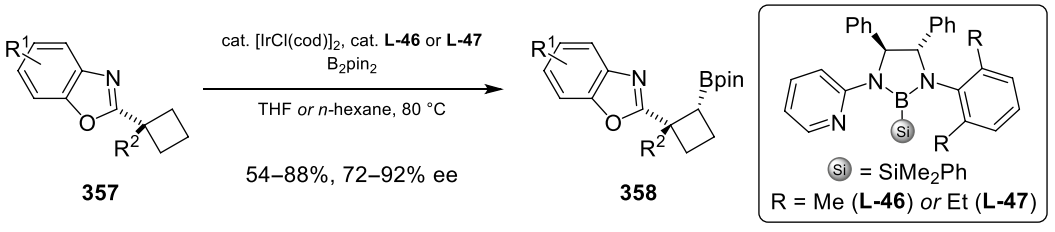

Scheme 12.84. C(sp³)–H borylation of cyclobutanes by Xu.

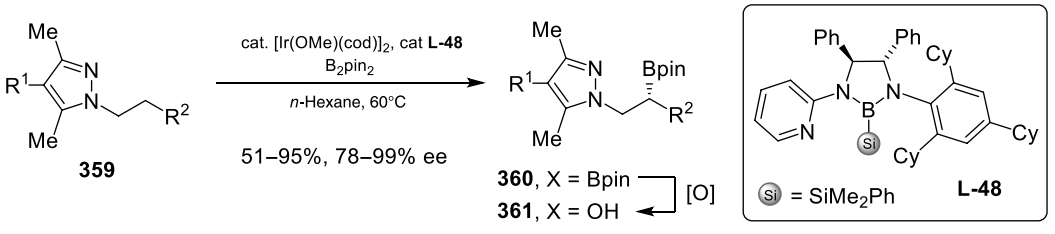

Scheme 12.85. Pyrazole-directed C(sp³)–H borylation by Xu.

(Scheme 12.85), which is furthermore synthetically useful as it can be easily converted into an amide moiety by simple ozonolysis.

In 2020, the same group published a study of enantioselective α-C(sp³)–H borylation of azaheterocycles (α with respect to the nitrogen heteroatom) [194]. The studied scope of tetrahydroisoquinolines showed excellent chemoselectivity for reaction in the benzylic position α to the nitrogen atom with variously substituted substrates (Scheme 12.86). One of the few limitations of the reaction is C–H activation of C8 substituted tetrahydroisoquinolines, which showed low reactivity probably because of the induced steric hindrance. The reaction was also successfully applied to other azaheterocycles with a different ring size.

Recently, Xu studied enantioselective β-selective C(sp³)–H borylation of acyclic amides using the already-mentioned system of the Ir(I)-dimer complex and the chiral bidentate boryl ligand [195]. The study showed excellent enantioselectivity for substrates with a various length of the alkyl chain including derivatives of

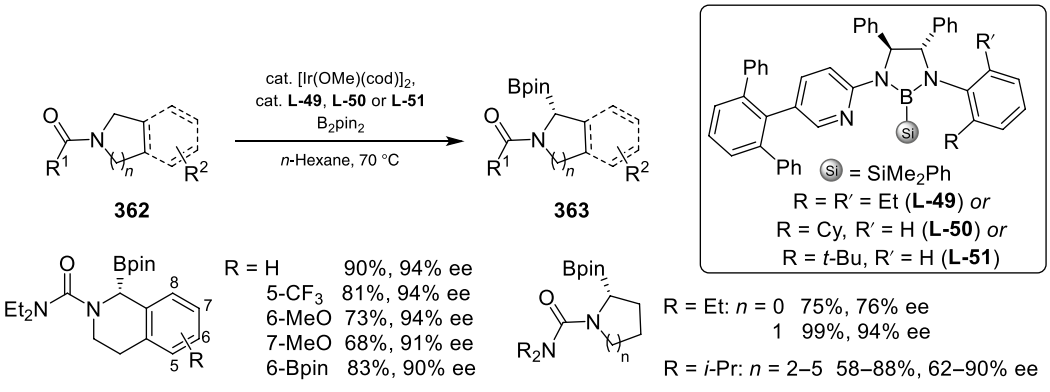

Scheme 12.86. C(sp³)–H borylation of tetrahydroisoquinolines and other azaheterocycles by Xu.

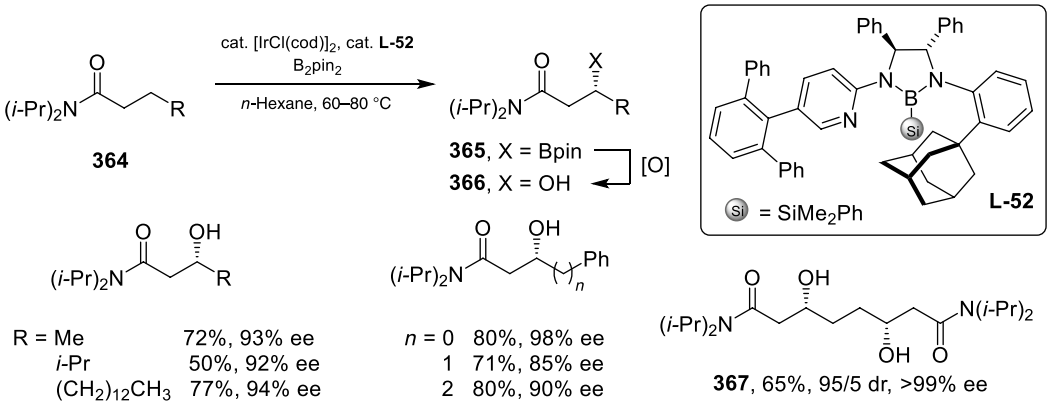

Scheme 12.87. Carbonyl directed C(sp³)–H borylation by Xu.

fatty acids (Scheme 12.87). The reaction also proceeds smoothly on phenyl-substituted amides and showed tolerance of various functionalities on the aromatic ring. Interestingly, the reaction with diamide provides a product of double borylation **367** as a single enantiomer in an excellent diastereomeric ratio.

12.4.4. C(sp³)–H Silylation

Chiral organosilanes are not only valuable compounds by themselves, but are also important intermediates in organic synthesis. Particularly valuable is their oxidation producing chiral alcohols. The two-step process of transition metal-catalyzed C(sp³)–H silylation-oxidation generally tends to proceed on the primary over the secondary C–H bond, and so it can lead to products distinct from those formed by direct oxidation of the C–H bond, which preferentially proceeds on a weaker and/or more electron-rich secondary or tertiary C–H bond.

The mechanism of dehydrogenative C–H silylation is a matter of debate. While the original reports proposed a catalytic cycle based on only M(I) and M(III) intermediates and were mostly focused on Rh-catalyzed C–H silylations [171, 196, 197], the recent DFT calculations performed by Li and Huang on the Ir-catalyzed reaction suggested the operation of M(III) and M(V) species (Scheme 12.88) [169, 170].

12.4.4.1. Rhodium-catalyzed Silylation In 2013, Kuninobu and Takai found that a system of a rhodium catalyst ($[RhCl(cod)]_2$) and a bidentate phosphine ligand (dppp) is able to catalyze intramolecular

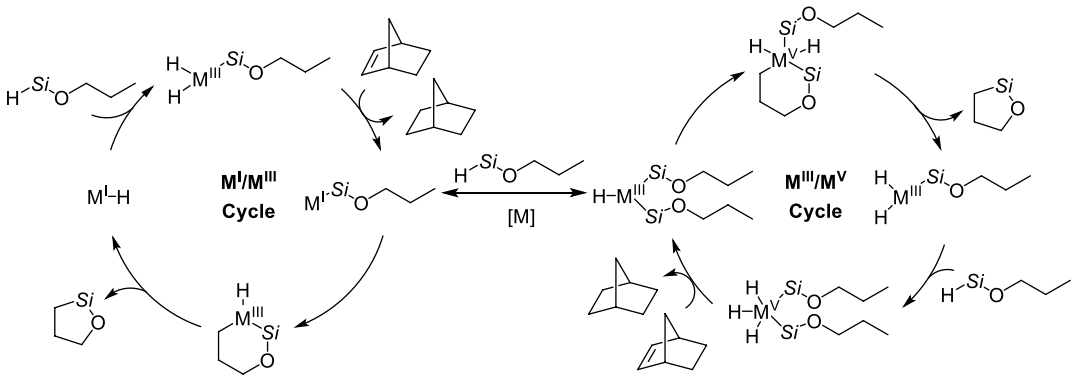

Scheme 12.88. The proposed catalytic cycles for transition metal-catalyzed C(sp³)–H silylations. Source: Based on [169] and [170].

dehydrogenative silylation of 2-alkylphenylsilanes to form 2,3-dihydrobenzo[*b*]siloles [198]. Even though the reaction selectively constructs five-membered silicon heterocycles, it requires harsh reaction conditions (180 °C) to overcome the low reactivity of C(sp³)–H bonds, and thus it lacks synthetic utility. Encouraged by the studies of other groups, which showed that the C_2-symmetric bidentate phosphine ligands with a combination of the Rh- or Ir-catalysts can be used for similar reactions using milder conditions, Murai and Takai re-examined the reaction in order to develop a more efficient system [171]. They aptly showed that the electron-rich and wide bidentate phosphine ligands are the most effective when 3,3-dimethyl-1-butene is used as a hydrogen acceptor leading to a decreased reaction temperature without loss of reactivity (Scheme 12.89).

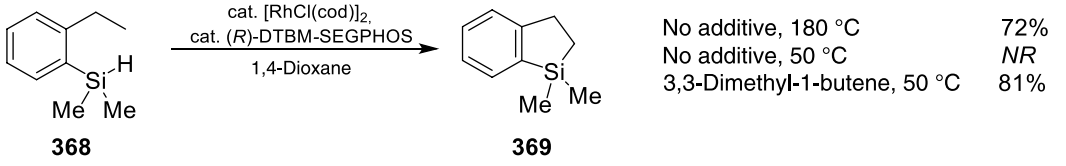

Scheme 12.89. Achiral C(sp³)–H dehydrogenative silylations.

They also examined an unprecedented desymmetrization of C(sp³)–H bonds via dehydrogenative silylation. The axially chiral diphosphine ligands showed a great potential to provide enantioenriched product **371**, even if ees do not exceed 37% (Scheme 12.90a). In addition, the catalytic system was also used for two-fold intramolecular dehydrogenative silylation of C(sp³)–H bonds to provide spirosilabiindane **373** with rare tetraorganisilicon stereocenter in 40% ee (Scheme 12.90b).

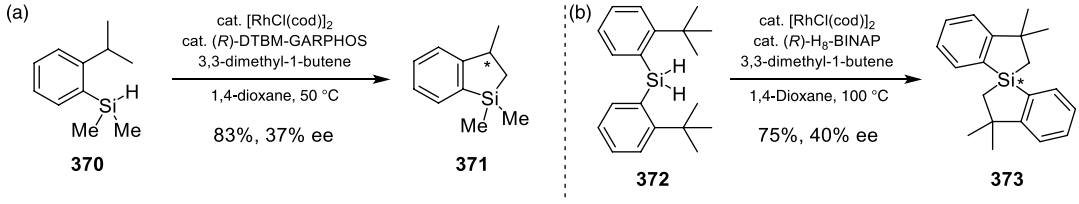

Scheme 12.90. First enantioselective C(sp³)–H dehydrogenative silylations.

Later, Hartwig reported the first enantioselective silylation via the activation of enantiotopic methylene C(sp³)–H bonds [199]. To achieve that, they took advantage of the higher reactivity of C–H bonds of the strained cyclopropane ring (Scheme 12.91). The meticulous optimization of the reaction condition resulted in not only a high enantioselectivity of the reaction, but also in a suppression of all the competing side processes (silylation of an aromatic C–H bond, ring opening of a cyclopropane ring, etc.).

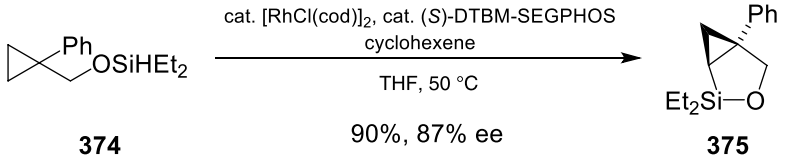

Scheme 12.91. Enantioselective C(sp³)–H silylation of cyclopropanes by Hartwig.

As part of the same publication, they also reported a two-step protocol to form the silylcyclopropane products **377** starting from cyclopropylmethanols **376**, which consisted of Ru-catalyzed dehydrogenative coupling of alcohols with diethylsilane followed by the studied intramolecular enantioselective C(sp³)–H silylation (Scheme 12.92). The scope of the reaction revealed that the high enantioselectivity is limited to only aryl-substituted cyclopropanes as it dramatically drops with cyclopropanes substituted by alkyl groups. This was attributed to the secondary π/π interactions between the aromatic rings of the substrate and the catalyst. In addition, the performed kinetic studies suggested that the C(sp³)–H bond cleavage is not only a turnover-limiting step, but also an enantio-determining step of the reaction.

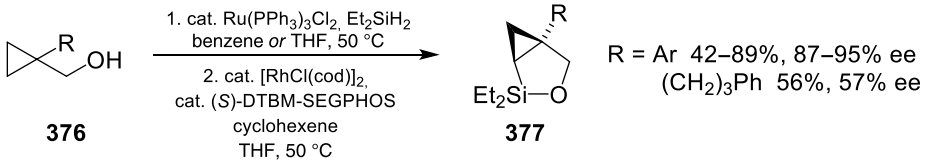

Scheme 12.92. The two-step protocol for C(sp³)–H silylation by Hartwig.

Recently, He used the enantioselective dehydrogenative silylation reaction for the construction of dihydrobenzosiloles with a tetrasubstituted silicon stereogenic center [200]. The reaction proceeds via a tandem reaction sequence, where the starting dihydrosilanes **378** undergo enantioselective C(sp³)–H activation/intramolecular dehydrogenative silylation leading to the chiral hydrosilanes **381**. Because of the low stability of the hydrosilane products, which would lead to their decomposition or racemization, the monohydrosilane products are in situ stereoselectively trapped with alkenes, leading to the target products **380**. The optimization of the reaction conditions showed that an Rh(I)-dimer complex in combination with a Josiphos type ligand **L-53** catalyzes the reaction in high yields and enantioselectivities (albeit in low diastereoselectvities) with a wide substrate scope (Scheme 12.93). The mechanistic studies then supported the proposed pathway, where the chirality of the silicon center is induced in the first C–H silylation step.

12.4.4.2. Iridium-catalyzed Silylation

The first example of enantioselective C(sp³)–H activation/silylation catalyzed by an iridium complex was published by the Hartwig group in 2017 [201]. They achieved high reactivities and enantioselectivities by utilizing an Ir(I)-dimer complex together with a chiral pyridine–oxazoline type ligand **L-54** and norbornene as a hydrogen acceptor (Scheme 12.94), the system developed for their enantioselective silylation of aromatic C(sp²)–H bonds [172]. The mechanistic studies performed by Huang suggest that a rate-limiting step of the overall reaction is C(sp³)–H oxidative addition to the iridium complex, which is at the same time an enantio-determining step [170].

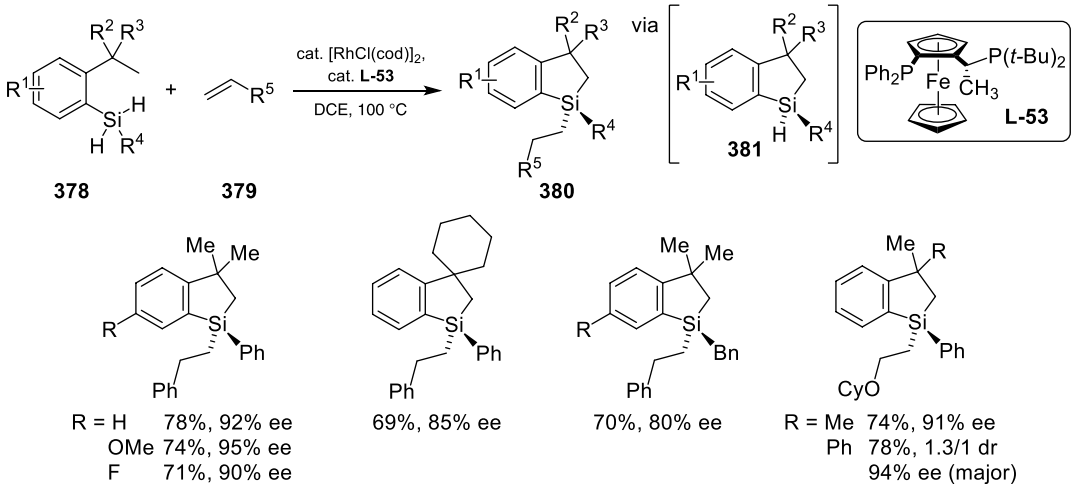

Scheme 12.93. Enantioselective C(sp^3)–H silylation by He.

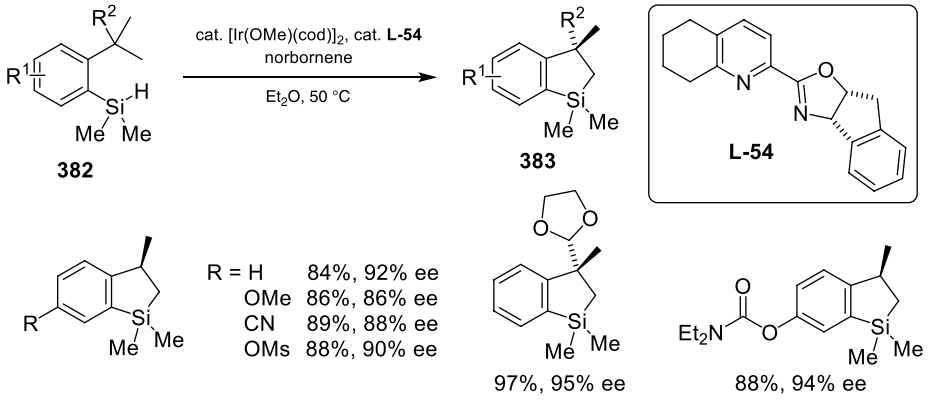

Scheme 12.94. Ir-catalyzed C(sp^3)–H activation/silylation by Hartwig.

A year later, the same group published Ir-catalyzed intramolecular β-selective C(sp^3)–H silylation of aliphatic amines [202]. Generally, β-selective C(sp^3)–H activation of amines is very challenging as the C–H bond β to the nitrogen is stronger than the C–H bond in the α position. In addition, the common catalysts are directed by the nitrogen atom of the amine to react in position γ or δ as they form a five- or six-membered metallacyclic intermediate. Nevertheless, the reaction was enabled to proceed in the β-position by a meticulously designed, but easy to prepare substrate, which consists of a methylene linker between the hydrosilane moiety and the nitrogen of the aliphatic amine. While a combination of an Ir(I)-dimer and phenanthroline-type ligands showed to be optimal for an achiral reaction, the asymmetric variant was conducted with more electron-donating pyridyl–imidazoline-type ligand **L-55** (Scheme 12.95). The reaction showed high site-selectivity and decent enantioselectivity, unfortunately with a limited substrate scope.

12.5. CONCLUSION

In recent years, the design of novel ligand scaffolds and discovery of new catalytic paradigms have created an avalanche of opportunities for performing asymmetric C(sp^3)–H activation. The catalytic conversion of C(sp^3)–H bonds into value-added enantiopure organic settings has gained enormous progress. As

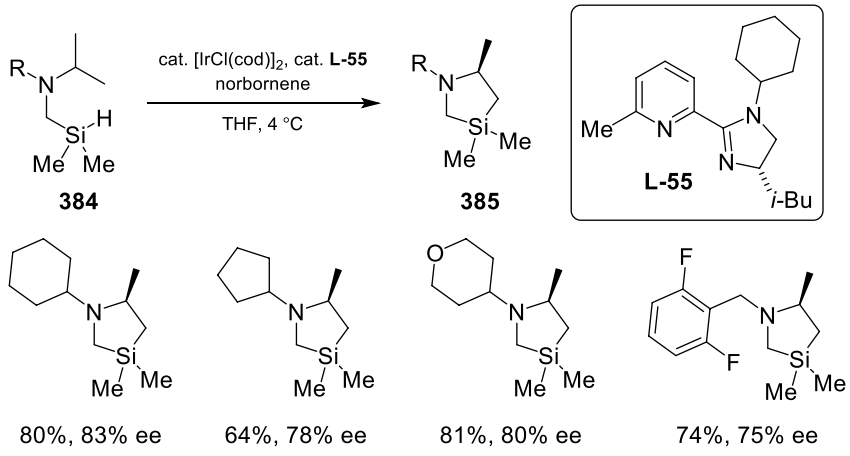

Scheme 12.95. Ir-catalyzed C(sp³)–H activation/silylation of amines by Hartwig.

evident from the results compiled in this chapter, the vast majority of literature focuses on the intramolecular reactivity or intermolecular reactivity with biased substrates or using a directing group strategy. In view of current asymmetric C(sp³)–H activation portfolio [203–206], a general intermolecular version targeting unactivated C(sp³)–H bonds with improved chemofidelity is most daunting, only with a few exceptions developed by Davies. It is therefore safe to note that catalytic asymmetric C(sp³)–H activation has not reached full potential and spectacular reports are anticipated in the near future.

REFERENCES

1. H. M. L. Davies, J. Hansen, Asymmetric synthesis through C-H activation. in *Catalytic Asymmetric Synthesis* (Ed.: I. Ojima), John Wiley & Sons, Inc., Hoboken, NJ, **2010**, pp. 163–226.
2. J. Hansen, J. Autschbach, H. M. L. Davies, *J. Org. Chem.* **2009**, *74*, 6555–6563.
3. K. P. Kornecki, J. F. Briones, V. Boyarskikh, F. Fullilove, J. Autschbach, K. E. Schrote, K. M. Lancaster, H. M. L. Davies, J. F. Berry, *Science* **2013**, *342*, 351–354.
4. C. Werlé, R. Goddard, A. Fürstner, *Angew. Chem. Int. Ed.* **2015**, *54*, 15452–15456.
5. C. Werlé, R. Goddard, P. Philipps, C. Farès, A. Fürstner, *J. Am. Chem. Soc.* **2016**, *138*, 3797–3805.
6. H. M. L. Davies, T. Hansen, *J. Am. Chem. Soc.* **1997**, *119*, 9075–9076.
7. H. M. L. Davies, T. Hansen, M. R. Churchill, *J. Am. Chem. Soc.* **2000**, *122*, 3063–3070.
8. S. Chuprakov, J. A. Malik, M. Zibinsky, V. V. Fokin, *J. Am. Chem. Soc.* **2011**, *133*, 10352–10355.
9. H.-Y. Thu, G. S.-M. Tong, J.-S. Huang, S. L.-F. Chan, Q.-H. Deng, C.-M. Che, *Angew. Chem. Int. Ed.* **2008**, *47*, 9747–9751.
10. K. Liao, Y.-F. Yang, Y. Li, J. N. Sanders, K. N. Houk, D. G. Musaev, H. M. L. Davies, *Nat. Chem.* **2018**, *10*, 1048–1055.
11. C. Qin, V. Boyarskikh, J. H. Hansen, K. I. Hardcastle, D. G. Musaev, H. M. L. Davies, *J. Am. Chem. Soc.* **2011**, *133*, 19198–19204.
12. K. Liao, S. Negretti, D. G. Musaev, J. Bacsa, H. M. L. Davies, *Nature* **2016**, *533*, 230–234.
13. K. Liao, T. C. Pickel, V. Boyarskikh, J. Bacsa, D. G. Musaev, H. M. L. Davies, *Nature* **2017**, *551*, 609–613.
14. P. Müller, S. Tohill, *Tetrahedron* **2000**, *56*, 1725–1731.
15. H. M. L. Davies, P. Ren, *J. Am. Chem. Soc.* **2001**, *123*, 2070–2071.
16. H. M. L. Davies, D. G. Stafford, T. Hansen, *Org. Lett.* **1999**, *1*, 233–236.
17. T. Goto, K. Takeda, N. Shimada, H. Nambu, M. Anada, M. Shiro, K. Ando, S. Hashimoto, *Angew. Chem. Int. Ed.* **2011**, *50*, 6803–6808.
18. J. R. Denton, H. M. L. Davies, *Org. Lett.* **2009**, *11*, 787–790.
19. S. Hashimoto, T. Goto, T. Onozuka, Y. Kosaka, M. Anada, K. Takeda, *Heterocycles* **2012**, *86*, 1647.
20. H. Suematsu, T. Katsuki, *J. Am. Chem. Soc.* **2009**, *131*, 14218–14219.
21. J.-C. Wang, Z.-J. Xu, Z. Guo, Q.-H. Deng, C.-Y. Zhou, X.-L. Wan, C.-M. Che, *Chem. Commun.* **2012**, *48*, 4299–4301.
22. C. P. Owens, A. Varela-Álvarez, V. Boyarskikh, D. G. Musaev, H. M. L. Davies, S. B. Blakey, *Chem. Sci.* **2013**, *4*, 2590–2596.
23. K.-H. Chan, X. Guan, V. K.-Y. Lo, C.-M. Che, *Angew. Chem. Int. Ed.* **2014**, *53*, 2982–2987.

24. L. Fu, D. M. Guptill, H. M. L. Davies, *J. Am. Chem. Soc.* **2016**, *138*, 5761–5764.
25. R. W. Kubiak, J. D. Mighion, S. M. Wilkerson-Hill, J. S. Alford, T. Yoshidomi, H. M. L. Davies, *Org. Lett.* **2016**, *18*, 3118–3121.
26. R. W. Kubiak, H. M. L. Davies, *Org. Lett.* **2018**, *20*, 3771–3775.
27. H. M. L. Davies, Q. Jin, P. Ren, A. Yu. Kovalevsky, *J. Org. Chem.* **2002**, *67*, 4165–4169.
28. H. M. L. Davies, S. J. Hedley, B. R. Bohall, *J. Org. Chem.* **2005**, *70*, 10737–10742.
29. X. Wang, Y. Lu, H.-X. Dai, J.-Q. Yu, *J. Am. Chem. Soc.* **2010**, *132*, 12203–12205.
30. H. Wang, G. Li, K. M. Engle, J.-Q. Yu, H. M. L. Davies, *J. Am. Chem. Soc.* **2013**, *135*, 6774–6777.
31. R. K. Zhang, K. Chen, X. Huang, L. Wohlschlager, H. Renata, F. H. Arnold, *Nature* **2019**, *565*, 67–72.
32. J. M. Fraile, J. I. García, J. A. Mayoral, M. Roldán, *Org. Lett.* **2007**, *9*, 731–733.
33. G. Jiménez-Osés, E. Vispe, M. Roldán, S. Rodríguez-Rodríguez, P. López-Ram-de-Viu, L. Salvatella, J. A. Mayoral, J. M. Fraile, *J. Org. Chem.* **2013**, *78*, 5851–5857.
34. C. Qin, H. M. L. Davies, *J. Am. Chem. Soc.* **2014**, *136*, 9792–9796.
35. D. M. Guptill, H. M. L. Davies, *J. Am. Chem. Soc.* **2014**, *136*, 17718–17721.
36. N. M. Weldy, A. G. Schafer, C. P. Owens, C. J. Herting, A. Varela-Alvarez, S. Chen, Z. Niemeyer, D. G. Musaev, M. S. Sigman, H. M. L. Davies, S. B. Blakey, *Chem. Sci.* **2016**, *7*, 3142–3146.
37. H. M. L. Davies, A. M. Walji, R. J. Townsend, *Tetrahedron Lett.* **2002**, *43*, 4981–4983.
38. J. M. Axten, R. Ivy, L. Krim, J. D. Winkler, *J. Am. Chem. Soc.* **1999**, *121*, 6511–6512.
39. H. M. L. Davies, T. Hansen, D. W. Hopper, S. A. Panaro, *J. Am. Chem. Soc.* **1999**, *121*, 6509–6510.
40. H. M. L. Davies, C. Venkataramani, *Org. Lett.* **2001**, *3*, 1773–1775.
41. H. M. L. Davies, C. Venkataramani, *Angew. Chem. Int. Ed.* **2002**, *41*, 2197–2199.
42. H. M. L. Davies, Q. Jin, *Org. Lett.* **2004**, *6*, 1769–1772.
43. H. M. L. Davies, A. Ni, *Chem. Commun.* **2006**, 3110–3112.
44. Z. J. Garlets, H. M. L. Davies, *Org. Lett.* **2018**, *20*, 2168–2171.
45. Z. J. Garlets, E. F. Hicks, J. Fu, E. A. Voight, H. M. L. Davies, *Org. Lett.* **2019**, *21*, 4910–4914.
46. H. M. L. Davies, Y. Lian, *Acc. Chem. Res.* **2012**, *45*, 923–935.
47. Y. Lian, H. M. L. Davies, *J. Am. Chem. Soc.* **2011**, *133*, 11940–11943.
48. H. M. L. Davies, Q. Jin, *Proc. Natl. Acad. Sci.* **2004**, *101*, 5472–5475.
49. H. M. L. Davies, R. E. J. Beckwith, *J. Org. Chem.* **2004**, *69*, 9241–9247.
50. H. M. L. Davies, Q. Jin, *J. Am. Chem. Soc.* **2004**, *126*, 10862–10863.
51. H. M. L. Davies, A. M. Walji, *Angew. Chem. Int. Ed.* **2005**, *44*, 1733–1735.
52. H. M. L. Davies, X. Dai, M. S. Long, *J. Am. Chem. Soc.* **2006**, *128*, 2485–2490.
53. J. H. Hansen, T. M. Gregg, S. R. Ovalles, Y. Lian, J. Autschbach, H. M. L. Davies, *J. Am. Chem. Soc.* **2011**, *133*, 5076–5085.
54. M. Kennedy, M. A. McKervey, A. R. Maguire, G. H. P. Roos, *J. Chem. Soc. Chem. Commun.* **1990**, 361–362.
55. C. J. Flynn, C. J. Elcoate, S. E. Lawrence, A. R. Maguire, *J. Am. Chem. Soc.* **2010**, *132*, 1184–1185.
56. C. N. Slattery, A. R. Maguire, *Org. Biomol. Chem.* **2011**, *9*, 667–669.
57. J.-C. Wang, Y. Zhang, Z.-J. Xu, V. K.-Y. Lo, C.-M. Che, *ACS Catal.* **2013**, *3*, 1144–1148.
58. L. Fu, H. Wang, H. M. L. Davies, *Org. Lett.* **2014**, *16*, 3036–3039.
59. D. Zhu, J. Ma, K. Luo, H. Fu, L. Zhang, S. Zhu, *Angew. Chem. Int. Ed.* **2016**, *55*, 8452–8456.
60. D. Zhu, L. Chen, H. Zhang, Z. Ma, H. Jiang, S. Zhu, *Angew. Chem. Int. Ed.* **2018**, *57*, 12405–12409.
61. K. Dong, C. Pei, Q. Zeng, H. Wei, M. P. Doyle, X. Xu, *ACS Catal.* **2018**, *8*, 9543–9549.
62. E. Azek, M. Khalifa, J. Bartholoméüs, M. Ernzerhof, H. Lebel, *Chem. Sci.* **2019**, *10*, 718–729.
63. X. Lin, C. Zhao, C.-M. Che, Z. Ke, D. L. Phillips, *Chem. Asian J.* **2007**, *2*, 1101–1108.
64. X. Zhang, Z. Ke, N. J. DeYonker, H. Xu, Z.-F. Li, X. Xu, X. Zhang, C.-Y. Su, D. L. Phillips, C. Zhao, *J. Org. Chem.* **2013**, *78*, 12460–12468.
65. X. Zhang, H. Xu, C. Zhao, *J. Org. Chem.* **2014**, *79*, 9799–9811.
66. J. L. Roizen, D. N. Zalatan, J. Du Bois, *Angew. Chem. Int. Ed.* **2013**, *52*, 11343–11346.
67. A. Nörder, S. A. Warren, E. Herdtweck, S. M. Huber, T. Bach, *J. Am. Chem. Soc.* **2012**, *134*, 13524–13531.
68. I. Nägeli, C. Baud, G. Bernardinelli, Y. Jacquier, M. Moraon, P. Müller, *Helv. Chim. Acta* **1997**, *80*, 1087–1105.
69. M. Yamawaki, H. Tsutsui, S. Kitagaki, M. Anada, S. Hashimoto, *Tetrahedron Lett.* **2002**, *43*, 9561–9564.
70. Y. Kohmura, T. Katsuki, *Tetrahedron Lett.* **2001**, *42*, 3339–3342.
71. C. Liang, F. Robert-Peillard, C. Fruit, P. Müller, R. H. Dodd, P. Dauban, *Angew. Chem. Int. Ed.* **2006**, *45*, 4641–4644.
72. C. Lescot, B. Darses, F. Collet, P. Retailleau, P. Dauban, *J. Org. Chem.* **2012**, *77*, 7232–7240.
73. M. Mazurais, C. Lescot, P. Retailleau, P. Dauban, *Eur. J. Org. Chem.* **2014**, *2014*, 66–79.
74. A. Nasrallah, V. Boquet, A. Hecker, P. Retailleau, B. Darses, P. Dauban, *Angew. Chem. Int. Ed.* **2019**, *58*, 8192–8196.
75. R. R. Annapureddy, C. Jandl, T. Bach, *J. Am. Chem. Soc.* **2020**, *142*, 7374–7378.
76. J.-L. Liang, S.-X. Yuan, J.-S. Huang, W.-Y. Yu, C.-M. Che, *Angew. Chem. Int. Ed.* **2002**, *41*, 3465–3468.
77. J. Zhang, P. W. Hong Chan, C.-M. Che, *Tetrahedron Lett.* **2005**, *46*, 5403–5408.
78. D. N. Zalatan, J. Du Bois, *J. Am. Chem. Soc.* **2008**, *130*, 9220–9221.

79. E. Milczek, N. Boudet, S. Blakey, *Angew. Chem. Int. Ed.* **2008**, *47*, 6825–6828.
80. M. Ju, E. E. Zerull, J. M. Roberts, M. Huang, I. A. Guzei, J. M. Schomaker, *J. Am. Chem. Soc.* **2020**, *142*, 12930–12936.
81. Y. Nishioka, T. Uchida, T. Katsuki, *Angew. Chem. Int. Ed.* **2013**, *52*, 1739–1742.
82. C. K. Prier, R. K. Zhang, A. R. Buller, S. Brinkmann-Chen, F. H. Arnold, *Nat. Chem.* **2017**, *9*, 629–634.
83. M. Ichinose, H. Suematsu, Y. Yasutomi, Y. Nishioka, T. Uchida, T. Katsuki, *Angew. Chem. Int. Ed.* **2011**, *50*, 9884–9887.
84. J. A. McIntosh, P. S. Coelho, C. C. Farwell, Z. J. Wang, J. C. Lewis, T. R. Brown, F. H. Arnold, *Angew. Chem. Int. Ed.* **2013**, *52*, 9309–9312.
85. R. Singh, M. Bordeaux, R. Fasan, *ACS Catal.* **2014**, *4*, 546–552.
86. T. K. Hyster, C. C. Farwell, A. R. Buller, J. A. McIntosh, F. H. Arnold, *J. Am. Chem. Soc.* **2014**, *136*, 15505–15508.
87. P. Dydio, H. M. Key, H. Hayashi, D. S. Clark, J. F. Hartwig, *J. Am. Chem. Soc.* **2017**, *139*, 1750–1753.
88. P. F. Kuijpers, M. J. Tiekink, W. B. Breukelaar, D. L. J. Broere, N. P. van Leest, J. I. van der Vlugt, J. N. H. Reek, B. de Bruin, *Chem. – Eur. J.* **2017**, *23*, 7945–7952.
89. J. Qin, Z. Zhou, T. Cui, M. Hemming, E. Meggers, *Chem. Sci.* **2019**, *10*, 3202–3207.
90. Z. Zhou, S. Chen, J. Qin, X. Nie, X. Zheng, K. Harms, R. Riedel, K. N. Houk, E. Meggers, *Angew. Chem. Int. Ed.* **2019**, *58*, 1088–1093.
91. Y. Zheng, Y. Tan, K. Harms, M. Marsch, R. Riedel, L. Zhang, E. Meggers, *J. Am. Chem. Soc.* **2017**, *139*, 4322–4325.
92. K. Lang, S. Torker, L. Wojtas, X. P. Zhang, *J. Am. Chem. Soc.* **2019**, *141*, 12388–12396.
93. Y. Hu, K. Lang, C. Li, J. B. Gill, I. Kim, H. Lu, K. B. Fields, M. Marshall, Q. Cheng, X. Cui, L. Wojtas, X. P. Zhang, *J. Am. Chem. Soc.* **2019**, *141*, 18160–18169.
94. L. Li, F. Han, X. Nie, Y. Hong, S. Ivlev, E. Meggers, *Angew. Chem. Int. Ed.* **2020**, *59*, 12392–12395.
95. R. P. Reddy, H. M. L. Davies, *Org. Lett.* **2006**, *8*, 5013–5016.
96. H. Lebel, C. Spitz, O. Leogane, C. Trudel, M. Parmentier, *Org. Lett.* **2011**, *13*, 5460–5463.
97. H. Lebel, C. Trudel, C. Spitz, *Chem. Commun.* **2012**, *48*, 7799–7801.
98. S. Y. Hong, Y. Park, Y. Hwang, Y. B. Kim, M.-H. Baik, S. Chang, *Science* **2018**, *359*, 1016–1021.
99. Y. Park, S. Chang, *Nat. Catal.* **2019**, *2*, 219–227.
100. Q. Xing, C.-M. Chan, Y.-W. Yeung, W.-Y. Yu, *J. Am. Chem. Soc.* **2019**, *141*, 3849–3853.
101. H. Wang, Y. Park, Z. Bai, S. Chang, G. He, G. Chen, *J. Am. Chem. Soc.* **2019**, *141*, 7194–7201.
102. Z. Zhou, S. Chen, Y. Hong, E. Winterling, Y. Tan, M. Hemming, K. Harms, K. N. Houk, E. Meggers, *J. Am. Chem. Soc.* **2019**, *141*, 19048–19057.
103. Z.-J. Jia, S. Gao, F. H. Arnold, *J. Am. Chem. Soc.* **2020**, *142*, 10279–10283.
104. J. He, M. Wasa, K. S. L. Chan, Q. Shao, J.-Q. Yu, *Chem. Rev.* **2017**, *117*, 8754–8786.
105. G. Dyker, *Angew. Chem. Int. Ed. Engl.* **1992**, *31*, 1023–1025.
106. G. Dyker, *Angew. Chem. Int. Ed. Engl.* **1994**, *33*, 103–105.
107. O. Baudoin, A. Herrbach, F. Guéritte, *Angew. Chem. Int. Ed.* **2003**, *42*, 5736–5740.
108. M. Nakanishi, D. Katayev, C. Besnard, E. P. Kündig, *Angew Chem Int Ed* **2011**, *50*, 7438–7441.
109. S. Anas, *Comm Chem* **2011**, *47*, 11483–11485.
110. T. Saget, S. J. Lemouzy, N. Cramer, *Angew. Chem. Int. Ed.* **2012**, *51*, 2238–2242.
111. N. Martin, C. Pierre, M. Davi, R. Jazzar, O. Baudoin, *Chem. Eur. J.* **2012**, *18*, 4480–4484.
112. P. M. Holstein, M. Vogler, P. Larini, G. Pilet, E. Clot, O. Baudoin, *ACS Catal.* **2015**, *5*, 4300–4308.
113. G. Altenhoff, R. Goddard, C. W. Lehmann, F. Glorius, *J. Am. Chem. Soc.* **2004**, *126*, 15195–15201.
114. R. Melot, M. Zuccarello, D. Cavalli, N. Niggli, M. Devereux, T. Bürgi, O. Baudoin, *Angew. Chem. Int. Ed.* **2021**, *60*, 7245–7250.
115. Zhang S., Lu J., Ye J., Duan W., *Chin. J. Org. Chem.* **2016**, *36*, 752.
116. L. Yang, R. Melot, M. Neuburger, O. Baudoin, *Chem. Sci.* **2017**, *8*, 1344–1349.
117. T. Saget, N. Cramer, *Angew. Chem. Int. Ed.* **2012**, *51*, 12842–12845.
118. J. Pedroni, T. Saget, P. A. Donets, N. Cramer, *Chem. Sci.* **2015**, *6*, 5164–5171.
119. J. Pedroni, N. Cramer, *J. Am. Chem. Soc.* **2017**, *139*, 12398–12401.
120. H.-R. Tong, S. Zheng, X. Li, Z. Deng, H. Wang, G. He, Q. Peng, G. Chen, *ACS Catal.* **2018**, *8*, 11502–11512.
121. J. Pedroni, M. Boghi, T. Saget, N. Cramer, *Angew. Chem. Int. Ed.* **2014**, *53*, 9064–9067.
122. J. Pedroni, N. Cramer, *Angew. Chem. Int. Ed.* **2015**, *54*, 11826–11829.
123. B.-F. Shi, N. Maugel, Y.-H. Zhang, J.-Q. Yu, *Angew Chem Int Ed* **2008**, *47*, 4882–4886.
124. Q. Shao, K. Wu, Z. Zhuang, S. Qian, J.-Q. Yu, *Acc. Chem. Res.* **2020**, *53*, 833–851.
125. M. Wasa, K. M. Engle, D. W. Lin, E. J. Yoo, J.-Q. Yu, *J. Am. Chem. Soc.* **2011**, *133*, 19598–19601.
126. K.-J. Xiao, D. W. Lin, M. Miura, R.-Y. Zhu, W. Gong, M. Wasa, J.-Q. Yu, *J. Am. Chem. Soc.* **2014**, *136*, 8138–8142.
127. P. Jain, P. Verma, G. Xia, J.-Q. Yu, *Nat. Chem.* **2017**, *9*, 140–144.
128. H.-J. Jiang, X.-M. Zhong, J. Yu, Y. Zhang, X. Zhang, Y.-D. Wu, L.-Z. Gong, *Angew. Chem. Int. Ed.* **2019**, *58*, 1803–1807.
129. H. Jiang, X. Zhong, Z. Liu, R. Geng, Y. Li, Y. Wu, X. Zhang, L. Gong, *Angew. Chem. Int. Ed.* **2020**, *59*, 12774–12778.
130. Q. Shao, Q.-F. Wu, J. He, J.-Q. Yu, *J. Am. Chem. Soc.* **2018**, *140*, 5322–5325.
131. L. Hu, P. Shen, Q. Shao, K. Hong, J. X. Qiao, J. Yu, *Angew. Chem. Int. Ed.* **2019**, *58*, 2134–2138.

132. A. McNally, B. Haffemayer, B. S. L. Collins, M. J. Gaunt, *Nature* **2014**, *510*, 129–133.
133. C. He, M. J. Gaunt, *Angew Chem Int Ed* **2015**, *54*, 15840–15844.
134. J. Rodrigalvarez, M. Nappi, H. Azuma, N. J. Flodén, M. E. Burns, M. J. Gaunt, *Nat. Chem.* **2020**, *12*, 76–81.
135. K. S. L. Chan, H.-Y. Fu, J.-Q. Yu, *J. Am. Chem. Soc.* **2015**, *137*, 2042–2046.
136. Q.-F. Wu, X.-B. Wang, P.-X. Shen, J.-Q. Yu, *ACS Catal.* **2018**, *8*, 2577–2581.
137. S.-B. Yan, S. Zhang, W.-L. Duan, *Org. Lett.* **2015**, *17*, 2458–2461.
138. H. Wang, H.-R. Tong, G. He, G. Chen, *Angew. Chem. Int. Ed.* **2016**, *55*, 15387–15391.
139. F.-L. Zhang, K. Hong, T.-J. Li, H. Park, J.-Q. Yu, *Science* **2016**, *351*, 252–256.
140. L. Xiao, K. Hong, F. Luo, L. Hu, W. R. Ewing, K. Yeung, J. Yu, *Angew. Chem. Int. Ed.* **2020**, *59*, 9594–9600.
141. G. Chen, W. Gong, Z. Zhuang, M. S. Andrä, Y.-Q. Chen, X. Hong, Y.-F. Yang, T. Liu, K. N. Houk, J.-Q. Yu, *Science* **2016**, *353*, 1023–1027.
142. Q.-F. Wu, P.-X. Shen, J. He, X.-B. Wang, F. Zhang, Q. Shao, R.-Y. Zhu, C. Mapelli, J. X. Qiao, M. A. Poss, J.-Q. Yu, *Science* **2017**, *355*, 499–503.
143. S.-Y. Yan, Y.-Q. Han, Q.-J. Yao, X.-L. Nie, L. Liu, B.-F. Shi, *Angew. Chem. Int. Ed.* **2018**, *57*, 9093–9097.
144. Y. Han, X. Yang, K. Kong, Y. Deng, L. Wu, Y. Ding, B. Shi, *Angew. Chem. Int. Ed.* **2020**, *59*, 20455–20458.
145. Y. Ding, Y. Han, L. Wu, T. Zhou, Q. Yao, Y. Feng, Y. Li, K. Kong, B. Shi, *Angew. Chem. Int. Ed.* **2020**, *59*, 14060–14064.
146. Y.-Q. Han, Y. Ding, T. Zhou, S.-Y. Yan, H. Song, B.-F. Shi, *J. Am. Chem. Soc.* **2019**, *141*, 4558–4563.
147. P.-X. Shen, L. Hu, Q. Shao, K. Hong, J.-Q. Yu, *J. Am. Chem. Soc.* **2018**, *140*, 6545–6549.
148. Z. Zhuang, J.-Q. Yu, *J. Am. Chem. Soc.* **2020**, *142*, 12015–12019.
149. J. He, Q. Shao, Q. Wu, J.-Q. Yu, *J. Am. Chem. Soc.* **2017**, *139*, 3344–3347.
150. H. Park, P. Verma, K. Hong, J.-Q. Yu, *Nat. Chem.* **2018**, *10*, 755–762.
151. A. P. Smalley, J. D. Cuthbertson, M. J. Gaunt, *J. Am. Chem. Soc.* **2017**, *139*, 1412–1415.
152. W.-W. Sun, P. Cao, R.-Q. Mei, Y. Li, Y.-L. Ma, B. Wu, *Org. Lett.* **2014**, *16*, 480–483.
153. H.-R. Tong, W. Zheng, X. Lv, G. He, P. Liu, G. Chen, *ACS Catal.* **2020**, *10*, 114–120.
154. T. Zhou, M. Jiang, X. Yang, Q. Yue, Y. Han, Y. Ding, B. Shi, *Chin. J. Chem.* **2020**, *38*, 242–246.
155. P.-S. Wang, L.-Z. Gong, *Acc. Chem. Res.* **2020**, *53*, 2841–2854.
156. B. M. Trost, D. A. Thaisrivongs, E. J. Donckele, *Angew. Chem. Int. Ed.* **2013**, *52*, 1523–1526.
157. P.-S. Wang, H.-C. Lin, Y.-J. Zhai, Z.-Y. Han, L.-Z. Gong, *Angew. Chem. Int. Ed.* **2014**, *53*, 12218–12221.
158. W. Liu, S. Z. Ali, S. E. Ammann, M. C. White, *J. Am. Chem. Soc.* **2018**, *140*, 10658–10662.
159. D. J. Covell, M. C. White, *Angew. Chem. Int. Ed.* **2008**, *47*, 6448–6451.
160. P.-S. Wang, P. Liu, Y.-J. Zhai, H.-C. Lin, Z.-Y. Han, L.-Z. Gong, *J. Am. Chem. Soc.* **2015**, *137*, 12732–12735.
161. S. E. Ammann, W. Liu, M. C. White, *Angew. Chem. Int. Ed.* **2016**, *55*, 9571–9575.
162. G. Smits, B. Audic, M. D. Wodrich, C. Corminboeuf, N. Cramer, *Chem. Sci.* **2017**, *8*, 7174–7179.
163. S. Fukagawa, Y. Kato, R. Tanaka, M. Kojima, T. Yoshino, S. Matsunaga, *Angew. Chem. Int. Ed.* **2019**, *58*, 1153–1157.
164. S. Fukagawa, M. Kojima, T. Yoshino, S. Matsunaga, *Angew. Chem. Int. Ed.* **2019**, *58*, 18154–18158.
165. C. M. B. Farr, A. M. Kazerouni, B. Park, C. D. Poff, J. Won, K. R. Sharp, M.-H. Baik, S. B. Blakey, *J. Am. Chem. Soc.* **2020**, *142*, 13996–14004.
166. S. Greßies, F. J. R. Klauck, J. H. Kim, C. G. Daniliuc, F. Glorius, *Angew. Chem. Int. Ed.* **2018**, *57*, 9950–9954.
167. Q. Li, Z.-X. Yu, *Organometallics* **2012**, *31*, 5185–5195.
168. H. Tamura, H. Yamazaki, H. Sato, S. Sakaki, *J. Am. Chem. Soc.* **2003**, *125*, 16114–16126.
169. Z. Li, M. Xia, R. J. Boyd, *Can. J. Chem.* **2016**, *94*, 1028–1037.
170. M. Zhang, J. Liang, G. Huang, *J. Org. Chem.* **2019**, *84*, 2372–2376.
171. M. Murai, H. Takeshima, H. Morita, Y. Kuninobu, K. Takai, *J. Org. Chem.* **2015**, *80*, 5407–5414.
172. B. Su, T.-G. Zhou, X.-W. Li, X.-R. Shao, P.-L. Xu, W.-L. Wu, J. F. Hartwig, Z.-J. Shi, *Angew. Chem. Int. Ed.* **2017**, *56*, 1092–1096.
173. Q. Li, Z.-X. Yu, *J. Am. Chem. Soc.* **2010**, *132*, 4542–4543.
174. Q. Li, Z.-X. Yu, *Angew. Chem. Int. Ed.* **2011**, *50*, 2144–2147.
175. T. Mita, S. Hanagata, K. Michigami, Y. Sato, *Org. Lett.* **2017**, *19*, 5876–5879.
176. K. Tsuchikama, M. Kasagawa, Y.-K. Hashimoto, K. Endo, T. Shibata, *J. Organomet. Chem.* **2008**, *693*, 3939–3942.
177. K. Tsuchikama, M. Kasagawa, K. Endo, T. Shibata, *Org. Lett.* **2009**, *11*, 1821–1823.
178. S. Pan, K. Endo, T. Shibata, *Org. Lett.* **2011**, *13*, 4692–4695.
179. S. Pan, Y. Matsuo, K. Endo, T. Shibata, *Tetrahedron* **2012**, *68*, 9009–9015.
180. Y. Tahara, M. Michino, M. Ito, K. S. Kanyiva, T. Shibata, *Chem. Commun.* **2015**, *51*, 16660–16663.
181. H. Hattori, T. Nishimura, *Adv. Synth. Catal.* **2018**, *360*, 4827–4831.
182. M. Nagai, M. Nagamoto, T. Nishimura, H. Yorimitsu, *Chem. Lett.* **2017**, *46*, 1176–1178.
183. T. Torigoe, T. Ohmura, M. Suginome, *Angew. Chem. Int. Ed.* **2017**, *56*, 14272–14276.
184. T. Ohmura, S. Kusaka, T. Torigoe, M. Suginome, *Adv. Synth. Catal.* **2019**, *361*, 4448–4453.
185. T. Ohmura, K. Yagi, S. Kusaka, M. Suginome, *ACS Catal.* **2020**, *10*, 3152–3157.
186. G. Wang, L. Liu, H. Wang, Y.-S. Ding, J. Zhou, S. Mao, P. Li, *J. Am. Chem. Soc.* **2017**, *139*, 91–94.

187. R. L. Reyes, T. Harada, T. Taniguchi, K. Monde, T. Iwai, M. Sawamura, *Chem. Lett.* **2017**, *46*, 1747–1750.
188. R. L. Reyes, T. Iwai, S. Maeda, M. Sawamura, *J. Am. Chem. Soc.* **2019**, *141*, 6817–6821.
189. R. L. Reyes, M. Sato, T. Iwai, M. Sawamura, *J. Am. Chem. Soc.* **2020**, *142*, 589–597.
190. R. L. Reyes, M. Sato, T. Iwai, K. Suzuki, S. Maeda, M. Sawamura, *Science* **2020**, *369*, 970–974.
191. Y. Shi, Q. Gao, S. Xu, *J. Am. Chem. Soc.* **2019**, *141*, 10599–10604.
192. X. Chen, L. Chen, H. Zhao, Q. Gao, Z. Shen, S. Xu, *Chin. J. Chem.* **2020**, *38*, 1533–1537.
193. R. Du, L. Liu, S. Xu, *Angew. Chem. Int. Ed.* **2021**, *60*, 5843–5847.
194. L. Chen, Y. Yang, L. Liu, Q. Gao, S. Xu, *J. Am. Chem. Soc.* **2020**, *142*, 12062–12068.
195. Y. Yang, L. Chen, S. Xu, *Angew. Chem. Int. Ed.* **2021**, *60*, 3524–3528.
196. C. Karmel, B. Li, J. F. Hartwig, *J. Am. Chem. Soc.* **2018**, *140*, 1460–1470.
197. A. Parija, R. B. Sunoj, *Org. Lett.* **2013**, *15*, 4066–4069.
198. Y. Kuninobu, T. Nakahara, H. Takeshima, K. Takai, *Org. Lett.* **2013**, *15*, 426–428.
199. T. Lee, J. F. Hartwig, *Angew. Chem. Int. Ed.* **2016**, *55*, 8723–8727.
200. B. Yang, W. Yang, Y. Guo, L. You, C. He, *Angew. Chem. Int. Ed.* **2020**, *59*, 22217–22222.
201. B. Su, J. F. Hartwig, *J. Am. Chem. Soc.* **2017**, *139*, 12137–12140.
202. B. Su, T. Lee, J. F. Hartwig, *J. Am. Chem. Soc.* **2018**, *140*, 18032–18038.
203. C. G. Newton, S.-G. Wang, C. C. Oliveira, N. Cramer, *Chem. Rev.* **2017**, *117*, 8908–8976.
204. T. G. Saint-Denis, R.-Y. Zhu, G. Chen, Q.-F. Wu, J.-Q. Yu, *Science* **2018**, *359*, eaao4798.
205. G. Liao, T. Zhang, Z. Lin, B. Shi, *Angew. Chem. Int. Ed.* **2020**, *59*, 19773–19786.
206. C. Zhang, Z.-L. Li, Q.-S. Gu, X.-Y. Liu, *Nat. Commun.* **2021**, *12*, 475.

PART IV

ASYMMETRIC SYNTHESIS THROUGH CARBON–HALOGEN BOND FORMATION AND ENZYME CATALYSIS

13

ASYMMETRIC CARBON–HALOGEN BOND FORMING REACTIONS (EXCLUDING C–H ACTIVATION PROCESSES)

Santos Fustero[1], Attila M. Remete[2,3], Loránd Kiss[4], Mercedes Medio-Simón[1], Jorge Escorihuela[1], and Daniel M. Sedgwick[1]
[1]*Department of Organic Chemistry, Pharmacy Faculty, University of Valencia, Valencia, Spain*
[2]*Institute of Pharmaceutical Chemistry, University of Szeged, Szeged, Hungary*
[3]*Interdisciplinary Excellence Centre, Institute of Pharmaceutical Chemistry, University of Szeged, Szeged, Hungary*
[4]*Institute of Organic Chemistry, Research Centre for Natural Sciences, Budapest, Hungary*

13.1. INTRODUCTION

Asymmetric carbon–halogen bond forming reactions have gained traction in recent years, with considerable developments related to new reaction discoveries and mechanistic understanding. These continuous efforts have led to the synthesis of a growing number of complex natural or synthetic products bearing halogen atoms at stereogenic centers, which can have great importance in medicinal chemistry or material science. Examples of all halogens are covered in the literature. The following chapter covers the main contributions made along the last 10 years, involving procedures devoted to the generation of C–F, C–Cl, C–Br, and C–I stereogenic centers.

13.2. ASYMMETRIC C–F BOND FORMATION WITH METAL CATALYSTS

Organic fluorine compounds are of great importance in medicinal chemistry, materials science, and also as agrochemicals. In this context, the study of the synthesis, properties, and reactivity of *monofluorinated* derivatives has blossomed in the last two decades. In fact, nowadays the asymmetric construction of enantioenriched carbon–fluorine bonds represents an important challenge in medicinal chemistry and organic synthesis. In this section, the most significant advances in the last decade (2010–2020) related to the synthesis of enantioenriched monofluorinated derivatives are highlighted. Certain previous papers are also cited due to their importance in this kind of chemistry. Recent reviews discussing the state-of-the-art in this period of time have also emphasized the importance and utility of this kind of fluorinated derivatives [1–5].

Catalytic Asymmetric Synthesis, Fourth Edition. Edited by Takahiko Akiyama and Iwao Ojima.

13.2.1. Allylic Substitution

Chiral allylic fluorides belong to a class of building blocks of great interest for the preparation of new bioactive molecules. Among the different strategies for synthesizing chiral allylic fluorides, transition metal complexes, particularly of palladium and iridium, and chiral small organic molecules have been found to be efficient catalysts for obtaining these derivatives with high enantioselectivity.

One of the first studies related to the synthesis of enantioenriched allylic fluorides was reported by Gouverneur et al. in 2005 in a noncatalyzed metal-free process, consisting in the electrophilic fluorodesilylation of acyclic chiral allylsilanes. The fluorodesilylation of enantiopure allylsilanes was carried out with Selectfluor in acetonitrile at room temperature, affording fluorinated alcohols after reduction of the formed carboxylic acid with $LiAlH_4$ in tetrahydrofuran (THF) at room temperature [6].

The asymmetric synthesis of allylic fluorides involving palladium fluoride intermediates was first described by Doyle and coworkers in 2010 [7], who reported a simple and novel strategy for the enantioselective synthesis of cyclic allylic fluorides in a Pd(0)-catalyzed process, using Trost's commercially available chiral bisphosphine ligands in conjunction with AgF as the fluorine source (Scheme 13.1). The authors suggest a mechanism that implies a nucleophilic attack of the fluoride on an electrophilic Pd(II)-allyl intermediate, resulting in the desired chiral cyclic allylic fluorides. The selective formation of the trans stereoisomer indicates that the reductive elimination takes place with inversion of the configuration due to the preferential nucleophilic attack of fluoride on the allyl ligand of **I**. While allylic acetates and carbonates were unreactive in the presence of a Pd(0) catalyst and AgF, the use of cyclic allylic chlorides and Trost ligand **L1** provided the best results in terms of yield, and diastereo- and enantioselectivities. The driving force for the C–F bond formation was, apparently, the precipitation of AgCl.

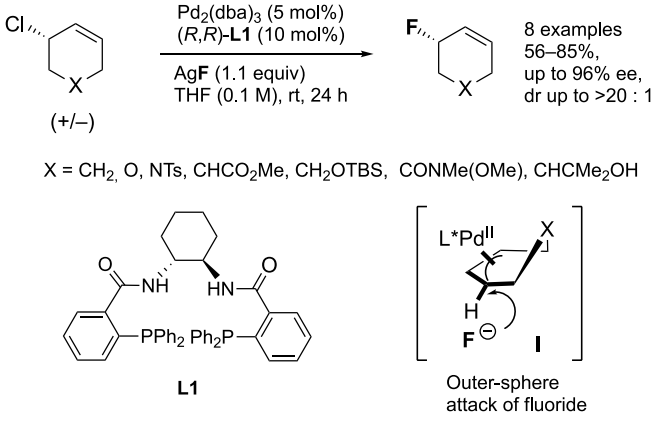

Scheme 13.1. Pd-catalyzed asymmetric synthesis of allylic fluorides.

One year later, the same group reported the Pd(0)-catalyzed fluorination of linear allylic chlorides affording various branched allylic fluorides in high selectivity [8]. The authors indicated that many of the synthetic limitations associated with the synthesis of these products such as formation of regio- and stereoisomeric mixtures and limited scope can be overcome by this catalytic method. The allylic fluorination of simple acyclic chlorides was carried out with silver fluoride in the presence of $Pd_2(dba)_3$, chiral ligands, and the nonpolar solvent toluene in a Pd(0)/Pd(II) redox cycle. Commercial Trost naphthyl ligand **L2** provided the best results and the final fluorinated allylic product was obtained in an excellent branched : linear ratio (b : l > 20.1) and good yield but moderate to low enantioselectivity (up to 71% ee) (Scheme 13.2).

Concerning the same topic, and using relatively similar reaction conditions as Doyle's group, Wu and Lauer reported the regioselective Pd-catalyzed allylic fluorination of phosphorothioate esters in 2012 [9].

In 2015, Nguyen et al. reported a mild and efficient route for obtaining enantioenriched allylic fluorides in an interesting study of the asymmetric fluorination of racemic secondary allylic trichloroacetimidates with

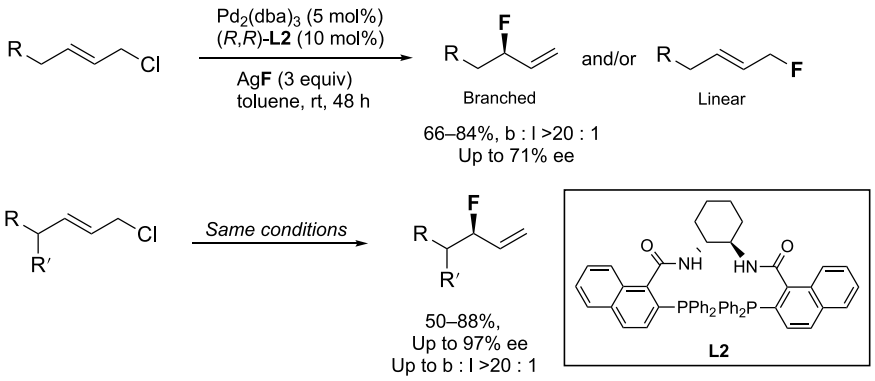

Scheme 13.2. Pd-catalyzed enantioselective fluorination of acyclic allylic chlorides.

Et_3N 3HF as the fluorine source [10]. The global process took place in the presence of a chiral-diene-ligated iridium complex. The process occurred in good yields and excellent asymmetric induction (up to 99% ee) (Scheme 13.3). The best result in terms of efficiency was obtained in just 1 hour using the $[IrCl(L3)]_2$ complex in methyl *tert*-butyl ether (MTBE) at room temperature. The reaction tolerates a wide range of functional groups including trichloroacetimidates bearing heteroatoms and, particularly, α-linear substituents.

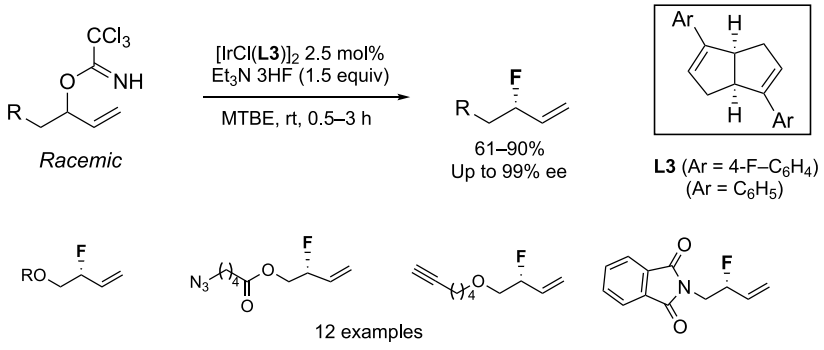

Scheme 13.3. Ir-catalyzed enantioselective fluorination of allylic trichloroacetimidates.

13.2.2. Addition to Alkenes

On the other hand, Toste and coworkers described an asymmetric palladium-catalyzed 1,2-fluoroarylation of styrenes with aryl boronic acids in the presence of Selectfluor, generating secondary benzyl fluorides in good yields and good selectivities [11]. *N*,*N*-Bipyridine-type ligands, in particular pyridyl-oxazolidine ligand (**L4**), $Pd(OAc)_2$ as palladium source, and DCM/water (5 : 1 :v/v) as solvent were vital to achieving the fluorinative reaction in an enantioselective and effective manner (Scheme 13.4). The authors claim the reaction is directed by the *ortho*-amide group, which can be removed in subsequent steps.

In 2015, Toste's group published an enantioselective palladium-catalyzed 1,1-fluoroarylation of unactivated allyl amines (Scheme 13.5), showcasing the feasibility of 1,1-difunctionalization [12]. Similar to the previously reported 1,2-fluoroarylation reaction, chiral bidentate diimine BOX-type ligands **L5** were used to render the process enantioselective. Once again, the presence of a directing nosyl group was critical to carry out the insertion. The reaction worked well with different substituents in the aromatic group of the boronic acid coupling partner, as well as the nitrogen atom, producing the final fluoroamines with high enantioselectivities. The potential application of this methodology was studied by removal of the nosyl group.

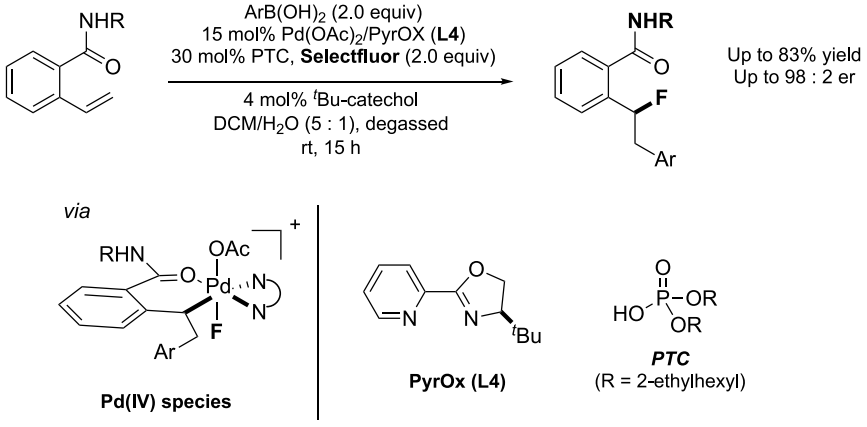

Scheme 13.4. Pd-catalyzed oxidative 1,2-fluoroarylation of styrenes.

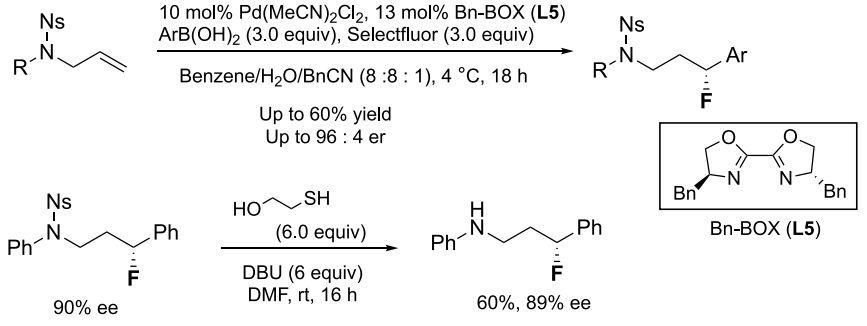

Scheme 13.5. 1,1-Fluoarylation of allyl amines.

On the other hand, while great progress has been made in the assembly of C–F bonds adjacent to an electron-withdrawing group, very few protocols that incorporate fluorine at the β-position of a carbonyl derivative have been reported, and most of them racemic. Considering the few reports of oxidative transition-metal-catalyzed fluorinations, and inspired by previous examples of palladium-catalyzed 1,1-difunctionalizations, Fustero, Toste et al. envisioned accessing β-fluorinated carbonyl derivatives via a single-step three-component Heck arylation-oxidative fluorination cascade (Scheme 13.6) [13].

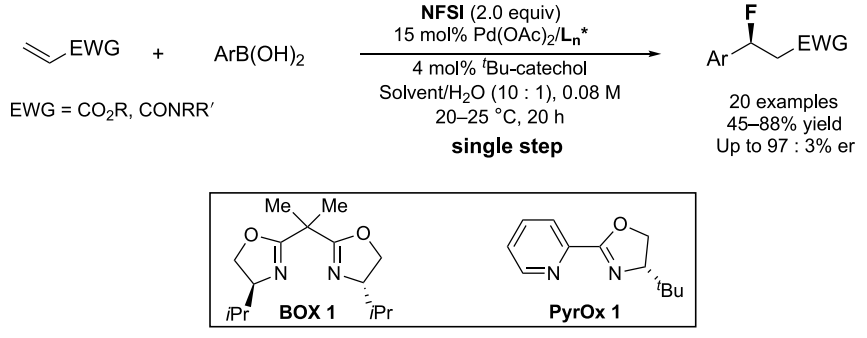

Scheme 13.6. Heck arylation-oxidative fluorination. Source: Miró et al. [13]/John Wiley & Sons.

After checking different reaction conditions, they observed that the presence of both bipyridine-type ligand (i.e. 1,10-phenantroline) and a radical scavenger (*t*-Bu-catechol) to preclude alternative radical pathways involving the arylboronic acid was critical to the formation of the final product. A range of bidentate chiral ligands was evaluated, with **BOX 1** and **PyrOX 1** being the most efficient ligands for acrylates and acrylamides, respectively. Solvents such as AcOEt and acetone were the most efficient in terms of enantioselectivity. A wide range of boronic acids was tested, and the final β-fluoroesters and β-fluoroamides were obtained in good yields and enantioselectivity.

13.2.3. Lewis Acid Catalysis

In the context of the monofluorination of dicarbonyl compounds, Sodeoka's group reported in 2002 an efficient catalytic enantioselective monofluorination of β-ketoesters using chiral palladium complexes (Scheme 13.7) [14a]. The reaction proceeded with high enantioselectivity (up to 94% ee) when using *N*-fluorobenzenesulfonimide (NFSI) as the fluorine source and polar solvents such as acetone, ethanol, or *i*-PrOH. The use of Pd(II) μ-hydroxo complexes and chiral phosphine ligands such as (*R*)-DM-2,2′-bis(diphenylphosphino)-1,1′-binaphthyl) (BINAP) and, particularly, (*R*)-DTBM-SEGPHOS **L6** (DTB M = 3,5-di-*tert*-butyl-4-methoxypheny) provided the best results in terms of efficiency and selectivity. Ten years later, the same group extended this study to α-ketoesters and developed the first example of their catalytic enantioselective monofluorination, using similar chiral palladium μ-hydroxo complexes (Scheme 13.7) [14b]. The obtained products were also successfully transformed into chiral β-fluoro α-hydroxy esters and β-fluoro α-amino esters. The reaction conditions were similar to those used for 1,3-dicarbonyl compounds, but in this case cyclopentyl methyl ether (CPME) was the solvent of choice. Among the catalysts studied, (*R*)-DM-SEGPHOS was found to be the best.

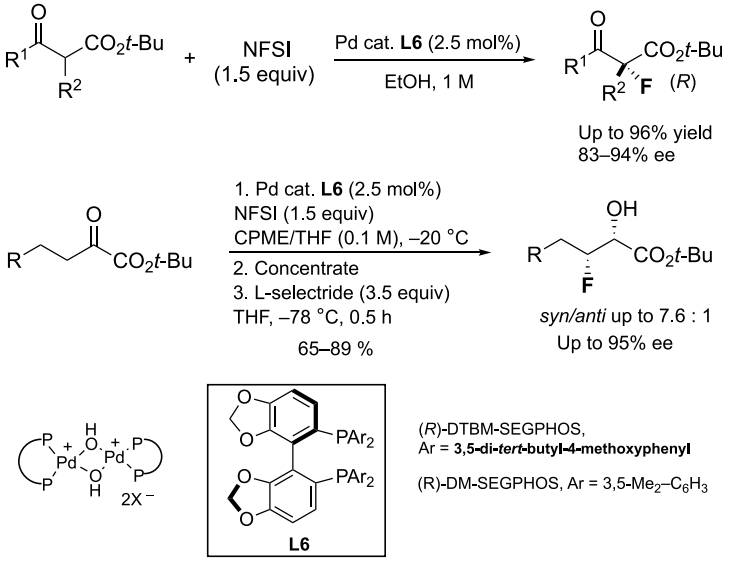

Scheme 13.7. Catalytic enantioselective fluorination of β- and α-ketoesters.

In 2015, Zhao et al. reported a new strategy for preparing monofluorinated allylic compounds through the initial design and synthesis of representative chiral *S*,*N*-ligands derived from Ellman *tert*-butanesulfinamides and 2,6-pyridinedicarboxylic acid [15]. These ligands were later used in a Pd-catalyzed asymmetric allylic substitution of allylic acetates with dimethyl 2-fluoromalonate.

Using a quite different strategy Zhou, Hartwig et al. [16] described in 2016 an interesting methodology for preparing a variety of enantioenriched α-aryl-α-fluoroketones in good yield and enantioselectivity

(Scheme 13.8). They studied a practical method for the enantioselective coupling of aryl and heteroaryl halides and triflates with α-fluoroindanones and α-fluorotetralones in the presence of different chiral ligands and palladium complexes as catalysts. In the case of α-fluoroindanones, the enolates were directly generated using potassium phosphate as base and a chiral complex Pd-(*R*)-ligand **L7**. The reactions with α-fluorotetralones were conducted with enolates generated by elimination of trifluoroacetate from trifluoromethyl β-diketone hydrates and Pd-(*S*)-difluorphos as chiral complex. Recently, these kinds of processes have also been studied by other research groups such as the Toste group, through an asymmetric fluorination of substituted cyclohexanones using enamine activation of the ketone and chiral anion phase transfer activation of Selectfluor [17], and in the case of Fu's group employing Negishi reactions of racemic α-halo-α-fluoroketones [18].

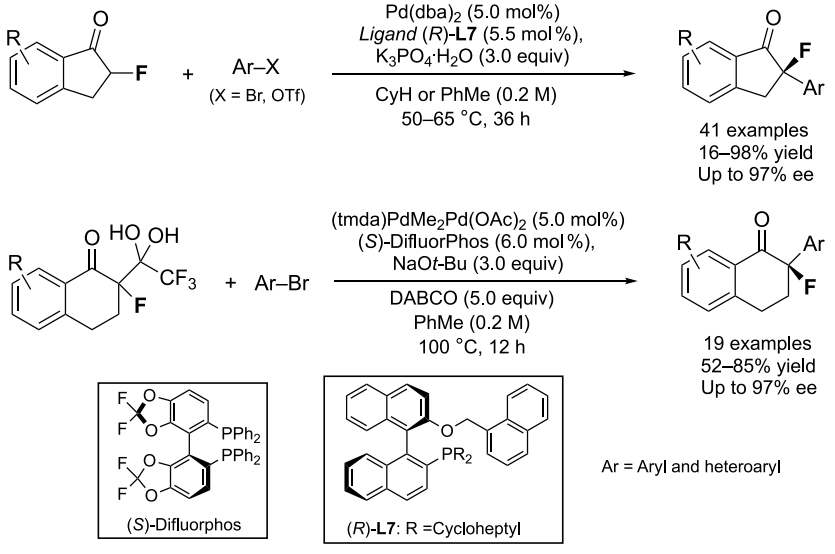

Scheme 13.8. Pd-catalyzed enantioselective α-arylation of α-fluoroketones.

In the context of palladium-catalyzed asymmetric allylic alkylations, Han, Soloshonok, and Hayashi reported in 2018 a methodology for preparing 3-fluorooxoindole derivatives, by reaction of Colby-type pro-enotates with Morita-Baylis-Hillman (MBH) carbonates in the presence of a Pd-chiral ligand catalyst (Scheme 13.9) [19]. The authors carried out an exhaustive study to find the best conditions for obtaining high levels of enantioselectivity, and finally they found that Ding-SKP chiral C_2-symmetric ligand **L8** was the best option.

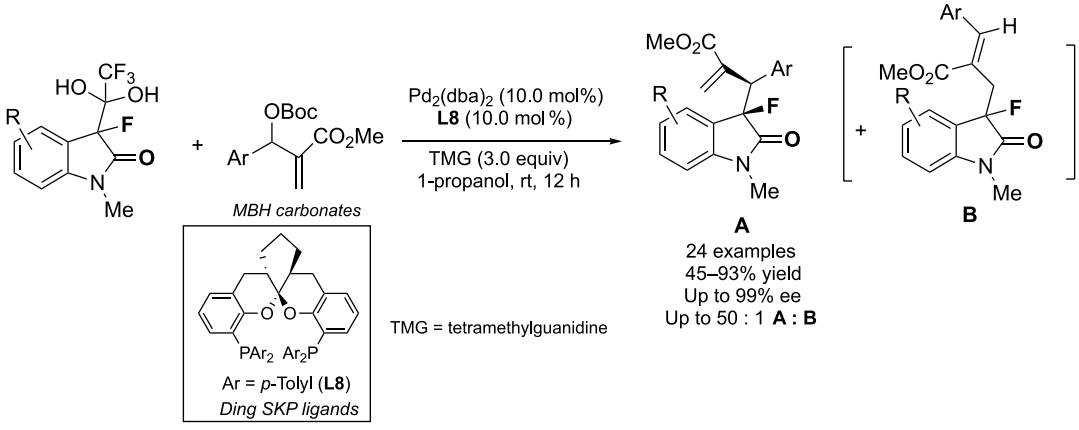

Scheme 13.9. S_N2 reactivity of the Colby pro-enolates with MBH carbonates. Source: Zhu et al. [19]/John Wiley & Sons.

A small number of examples concerning the asymmetric construction of C–F bonds in processes catalyzed by copper complexes has recently appeared in the literature. In this context, Wang et al. reported in 2015 a simple strategy for preparing enantioenriched monofluorinated 3-substituted 3-amino-2-oxindoles. This reaction implies an asymmetric detrifluoroacetylative Mannich reaction of 2-fluoro-1,3-diketones/hydrates with isatin-derived ketimines in a process catalyzed by chiral Cu(II)-diamine complexes (Scheme 13.10) [20]. The authors found that the best reaction conditions, in terms of efficiency and enantioselectivity, were obtained when using the $Cu(OTf)_2$-**L9** complex,

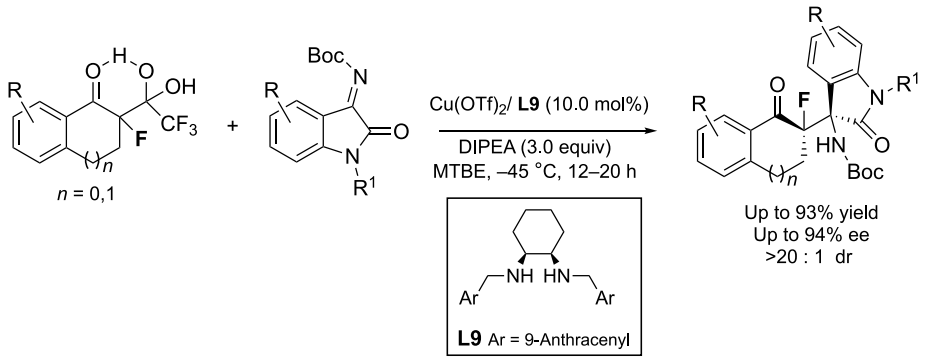

Scheme 13.10. Mannich reactions of 2-fluoro-1,3-diketones/hydrates and isatin derivatives. Source: Liu et al. [20]/American Chemical Society.

N,*N*-diisopropylethylamine (DIPEA) as base, ethereal solvents such as MTBE, and low temperatures (–45 °C). Excellent yields (up to 99%), diastereoselectivity (>20 : 1), and enantioselectivity (up to 94% ee) were obtained. They also studied the reaction of a simple α-fluorinated ketone with isatin-derived ketimines but they found that no reaction occurred, indicating that the in situ formation of enolates from precursors is a crucial step for the success of the Mannich reaction.

Another interesting example of a process catalyzed by copper complexes was reported by Lou, Deng, and coworkers in 2017, who studied the asymmetric synthesis of monofluorinated chiral densely substituted pyrrolidines with four contiguous stereocenters through a 1,3-dipolar cycloaddition of azomethine ylides with β,β-disubstituted β-fluoroacrylates, which took place in the presence of a chiral *N*,*O*-ligand **L10**/$Cu(CH_3CN)_4BF_4$ system (Scheme 13.11) [21]. The process provided excellent chemical yields as well as enantioselectivities (up to 99% ee) and diastereoselectivities (>20 : 1). The authors rationalized the obtained stereoselectivity with a transition state favoring the *endo* cycloadduct.

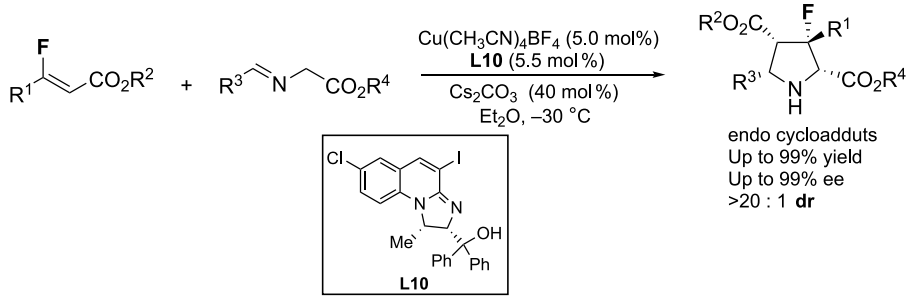

Scheme 13.11. 1,3-Dipolar cycloaddition of azomethine ylides with β-fluoroacrylates. Source: Liu et al. [21]/American Chemical Society.

In 2013, Huang, Weng et al. also reported the preparation of Cu(I) complexes **L11** and their use in the fluorination of primary and, particularly, secondary alkyl bromides [22]. The authors suggest that the fluorination takes place through an S_N2-type displacement of the leaving group with the copper fluoride complex (Scheme 13.12).

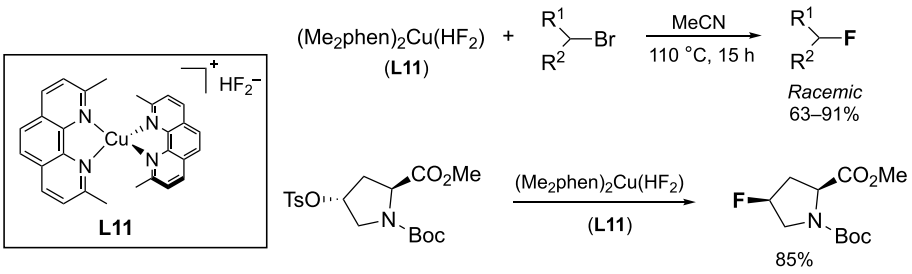

Scheme 13.12. S_N2 fluorination of alkyl bromides by copper(I) fluoride complexes.

13.3. ASYMMETRIC C–F BOND FORMING REACTIONS USING CHIRAL PHASE TRANSFER CATALYSIS

Chiral phase transfer catalysis has received a great deal of attention in recent decades. Important advantages of these processes are mild reaction conditions, inexpensive and environmentally benign solvents, and good scalability. The mechanism behind the enantioselectivity provided by chiral phase transfer catalysts in fluorination reactions is charge dependent. Cationic catalysts usually form an ion pair with the deprotonated substrate (deprotonation usually happens at the interphase of the organic and aqueous phases) [5]. The reaction of this chiral ion pair with the achiral electrophilic fluorinating agent is diastereoselective [23]. Anionic catalysts, on the other hand, are usually applied to solubilize Selectfluor, a dicationic reagent capable of electrophilic fluorination. The resulting chiral fluorinating agent performs the asymmetric fluorination of the substrate [24]. The use of neutral phase transfer catalysts is a recent development. Hydrogen bonding is used to solubilize the nucleophilic fluoride ion, resulting in a chiral nucleophilic fluorinating agent, which transforms the substrate enantioselectively [25].

The reactions discussed in this part will be grouped mainly according to the substrate. Note that chiral phase transfer catalysis is a well-defined subtype of organocatalysis, which will be discussed in the following subsection.

13.3.1. α-Fluorination of Simple Oxo Compounds and Their Derivatives

There is no report on chiral phase transfer fluorination of aldehydes, but there are some examples concerning ketones and their derivatives [17, 26]. Toste and coworkers developed a dual catalyst system [organocatalysts D-CAT1a–c and chiral phosphoric acid phase transfer catalyst (*R*)-CAT2] for enantioselective fluorination of α-aryl cyclohexanones (Scheme 13.13). Yields were calculated based on

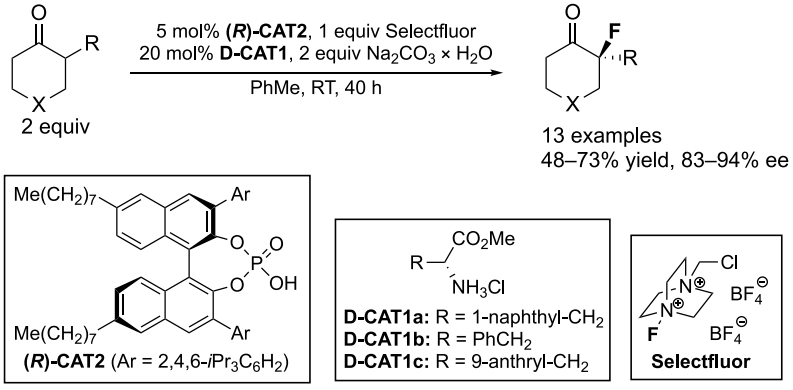

Scheme 13.13. Enantioselective fluorination of α-aryl cyclohexanones.

Selectfluor as the limiting reactant. Both catalysts were used to obtain high enantioselectivity, and pronounced matched/mismatched effects were observed [17].

Toste and coworkers also reported the asymmetric fluorination of *N*-benzoylenamines of cyclic ketones using an axially chiral phosphoric acid catalyst. After F^+ transfer, *N*-deprotonation yielded stable, isolable α-fluorinated *N*-benzoylimines [27]. Under similar conditions, *N*-benzoylenamines of open-chain ketones underwent a tandem oxyfluorination instead [28].

13.3.2. α-Fluorination of β-Ketoesters

Asymmetric fluorinations of β-ketoesters under phase transfer conditions have some common properties: the catalysts are quaternary ammonium salts (often derived from cinchona alkaloids), and the substrates are indane-1-one-2-carboxylates and related compounds [29].

The most efficient method, reported by Maruoka and coworkers, used bifunctional catalysts **(*S*)-CAT3a,b**, bulky *tert*-butyl β-ketoesters, and NFSI [$FN(SO_2Ph)_2$] as fluorinating agent. From cyclic substrates, products were obtained almost quantitatively with excellent ee values (Scheme 13.14) [29a].

Shi and coworkers described a notable example from the green chemistry perspective, in which a urea-containing quaternary ammonium salt was covalently bound to PEG8000 and used as the catalyst. This catalyst is soluble in many organic solvents but can be precipitated in diethyl ether and reused. Yields of 69–96% and ees of 70–85% were achieved for the fluorination of *tert*-butyl indane-1-one-2-carboxylates using this system [29f].

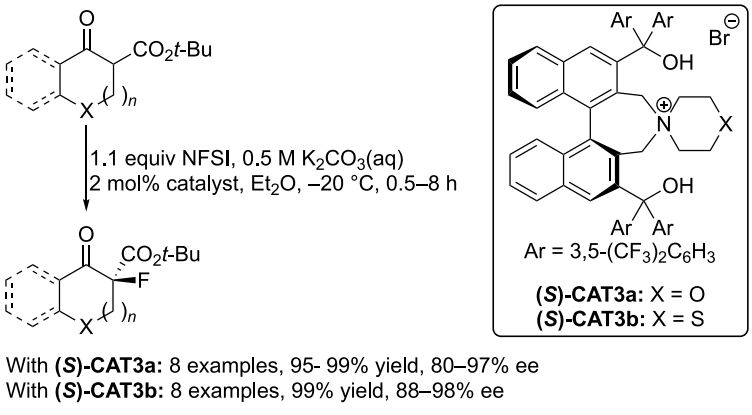

With **(*S*)-CAT3a:** 8 examples, 95- 99% yield, 80–97% ee
With **(*S*)-CAT3b:** 8 examples, 99% yield, 88–98% ee

Scheme 13.14. α-Fluorination of β-ketoesters. Source: Wang et al. [29a]/Royal Society of Chemistry.

13.3.3. Transformations of Olefin Bonds

In many cases, the electrophilic fluorination of olefins requires a directing group to achieve sufficient enantiocontrol. In addition, the initial carbocationic intermediates have to undergo further reactions to yield the final products.

The behavior of *N*-acylated allylic amines in phase transfer electrophilic fluorination reactions is highly dependent on the structure of the substrate. Some representative examples are: (i) fluorination accompanied by C=C bond migration [30], (ii) fluorocyclization via attack of the amide oxygen (with formation of six- [31] or five-membered [32] rings), and (iii) 1,4-fluoroaminations [33]. Of these reactions, only fluorocyclization to 4,5-dihydrooxazoles is discussed in detail, as this was the first reported asymmetric C–F bond forming reaction that used an anionic chiral phase transfer catalyst. The method uses Selectfluor in the presence of **(*R*)-CAT2** and a suitable base. In the case of dihydropyran-derived substrates, the use of 1,8-bis(dimethylamino)naphthalene ("proton sponge," PS) was optimal, while the reaction of

substrates with a less electron-rich olefin bond (chromenes and dihydronaphthalenes) performed better with Na_2CO_3 as the base (Scheme 13.15). With slight changes, fluorocyclization of some benzotiophene substrates and an open-chain allylic amine was also accomplished [32].

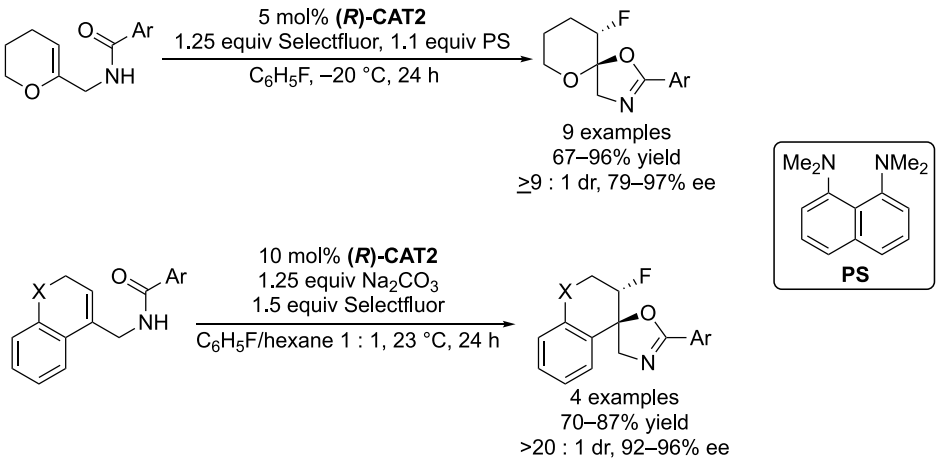

Scheme 13.15. Asymmetric fluorocyclization of allylic amines.

Hamashima and coworkers reported the asymmetric fluorolactonization of *ortho*-vinyl-substituted benzoic acids using a bifunctional phase transfer catalyst [34].

The initial carbocationic intermediates can also undergo deprotonation, recreating a double bond. In this context, Toste and coworkers described a method, using allylic alcohol substrates, phase transfer catalyst **(*S*)-CAT4**, and an arylboronic acid additive (Scheme 13.16) [35]. Boronic acid monoesters form and hydrolyze easily, and act as powerful in situ directing groups. The enantioselectivity strongly depended on the achiral boronic acid additive, and even its complete reversal was possible [36]. The method was also extended to homoallylic alcohols [37].

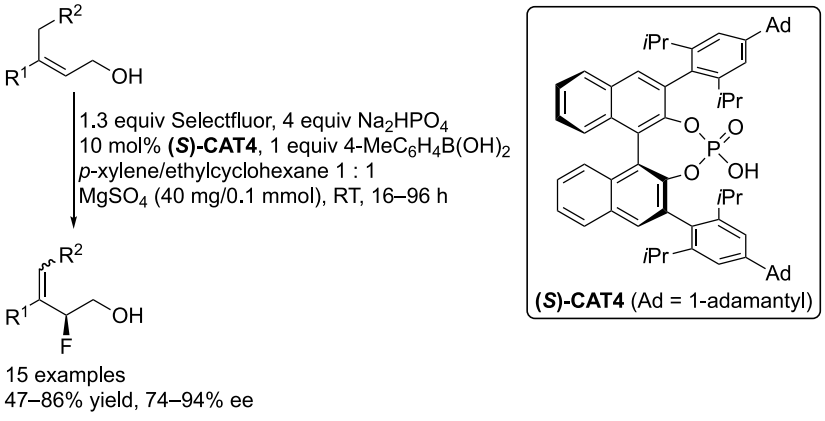

Scheme 13.16. Electrophilic fluorination of allylic alcohol substrates. Source: Zi et al. [35]/American Chemical Society.

Carbocationic intermediates can also undergo alkyl migration. Alexakis and coworkers reported asymmetric fluorination-induced semipinacol [38] and aza-semipinacol rearrangements [39] under phase transfer conditions using axially chiral phosphoric acid catalysts.

13.3.4. Dearomative Fluorination of Arenes

The generation of a chiral C–F unit by electrophilic fluorination of an arene requires the loss of aromaticity. One possibility is the deprotonation of the OH group of σ-complexes formed from phenol-based substrates. Hamashima and coworkers reported such a process involving 1-substituted 2-naphthols using a dicarboxylic acid catalyst [40]. A similar process applied to phenols used an axially chiral phosphoric acid catalyst [41]. Another possibility is the intramolecular nucleophilic addition to the σ-complex [42]. You and coworkers fluorocyclized *N*-protected tryptamines in the presence of Selectfluor, an axially chiral phosphoric acid catalyst **(*S*)-CAT5**, and 1,8-bis(dimethylamino)naphthalene (**PS**) as a strong base (Scheme 13.17) [42a]. A modified version of this method was extended to tryptophol substrates [42b].

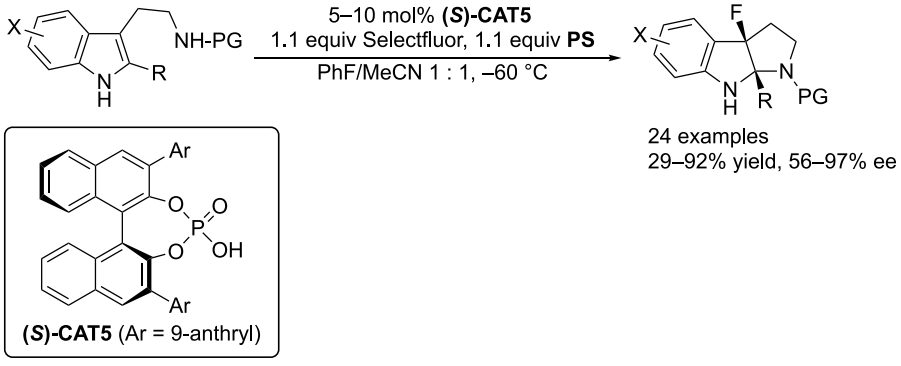

Scheme 13.17. Fluorocyclization of tryptamines. Source: Liang et al. [42a]/American Chemical Society.

13.3.5. Application of Neutral Phase Transfer Catalysts

The use of neutral phase transfer catalysts for asymmetric fluorinations is a relatively new method, pioneered by Gouverneur and coworkers. First, the synthesis of enantiopure β-fluorosulfides from β-bromosulfides was reported in 2018 including the generation of a *meso* thiiranium ion followed by its enantioselective desymmetrization by the chiral fluoride adduct [25a]. In 2019, the method was extended to the asymmetric β-fluoroamine synthesis from β-haloamines via *meso* aziridinium ions, using cheap KF (or more expensive CsF) as the fluoride source and chiral urea catalyst **(*S*)-CAT6** (Scheme 13.18). Note that β-fluoroamines have attracted considerable interest in medicinal chemistry [25b]. In 2020, enantioselective desymmetrization of achiral 3-substituted azetidinium ions was also reported by the same group [25c].

13.4. ASYMMETRIC ORGANOCATALYTIC FORMATION OF C–F BONDS

Organocatalysis uses small organic molecules to induce organic transformations. The rapid development of this field of chemistry started in the late 1990s, and quickly established itself as one of the main branches of enantioselective synthesis [43]. The first enantioselective fluorinations involving organocatalysts used chiral *N*-fluoroammonium salts prepared from stoichiometric amounts of cinchona alkaloid and Selectfluor (sometimes in situ) [44]. This noncatalytic strategy is still in use [45, 46], but will not be discussed here in detail. Since then, a wide variety of organocatalysts has been successfully applied to enantioselective fluorinations (mostly in electrophilic fluorination reactions). These transformations will be discussed here, grouped mainly according to the substrate. Chiral phase transfer catalysis, an important subtype of organocatalysis, was dealt with in the previous subsection.

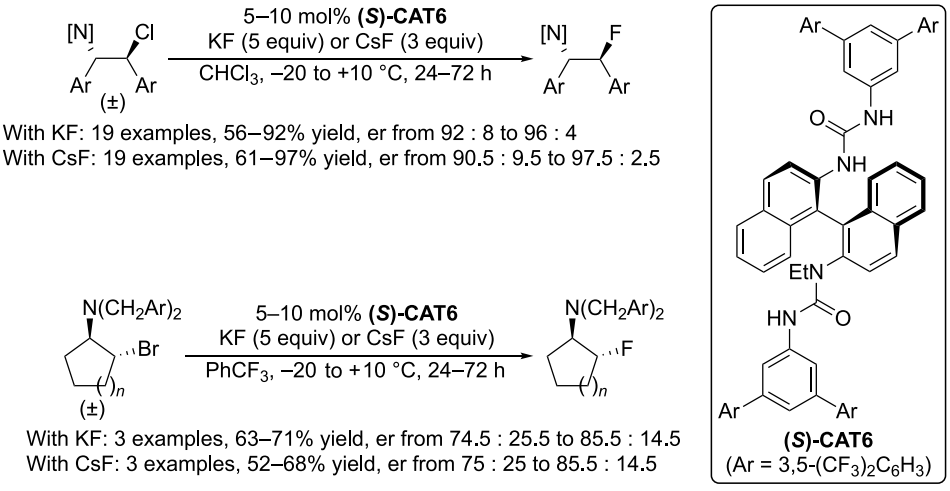

Scheme 13.18. Asymmetric β-fluoroamine synthesis from β-haloamines.

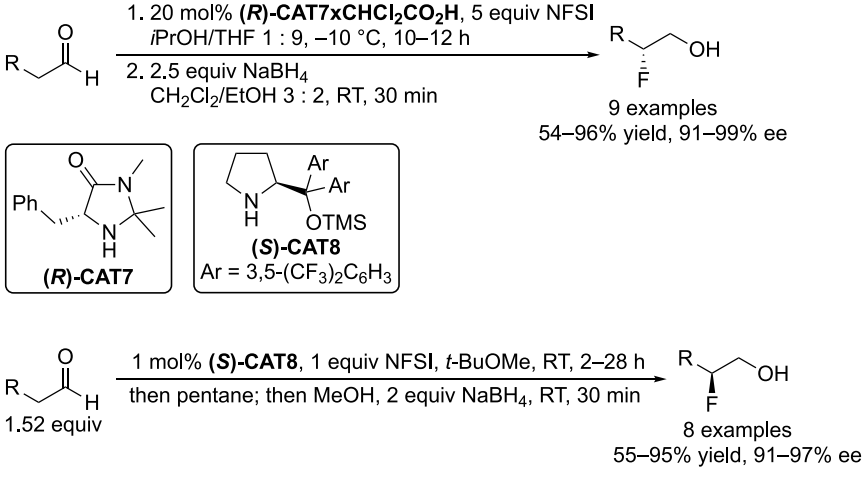

Scheme 13.19. Asymmetric α-fluorination of aldehydes.

13.4.1. α-Fluorination of Aldehydes

In the case of enantioselective α-fluorination of aldehydes, mostly secondary amine organocatalysts (enamine catalysis) are used. Among the first methods reported in 2005 [47], the methods of MacMillan's [47a] and Jørgensen's groups [47b] had the greatest impact (Scheme 13.19). Both worked efficiently only on aldehydes without α-branching, and both reduced the fluoroaldehyde products to β-fluoroalcohols without isolation. MacMillan et al. used NFSI as fluorinating agent, the dichloroacetate of imidazolidinone **(*R*)-CAT7** as catalyst, and THF/*i*PrOH 9 : 1 as solvent (54–96% isolated yield, 91–99% ee) [47a]. The **(*R*)-CAT7 × $CHCl_2CO_2H$** salt and similar α-amino-acid-derived imidazolidinones became known as MacMillan catalysts. Jørgensen et al. used NFSI [$(PhSO_2)_2NF$] as fluorinating agent in the presence of the proline-derived catalyst **(*S*)-CAT8** (aldehydes without α-branching: 55–95% yield, 91–97% ee) [47b].

Notably, MacMillan's and Jørgensen's catalysts differentiate the α-fluorinated aldehyde products and the nonfluorinated aldehyde substrates efficiently [47]. These catalysts have been used in most asymmetric aldehyde fluorination reactions [48]. The primary α-fluoroaldehyde products were often transformed further, yielding β-fluoroalcohols [48a, b], β-fluoroamines [48c, d], or β-hydroxy-γ-fluoroketones [48e].

The organocatalytic asymmetric fluorination of α-branched aldehydes with secondary amine catalysts is often prone to failure, although some successful examples are known [48f, 49], including a D-proline-catalyzed reaction on a 650 g scale [49]. The use of primary amine catalysts is generally much more successful [50]. A reagent-controlled enantiodivergent method is highlighted. Diamine catalysts **CAT9a,b** were used here, with their tertiary amino group in a protonated state due to the acid additive. The resulting ammonium ion can form attractive hydrogen bonds with NFSI, but repels the positively charged 2,4,6-trimethyl-*N*-fluoropyridinium cation (**NFCO+**) electrostatically, resulting in opposite enantioinduction with the two reagents. Good ee values were achieved on α-aryl aldehyde substrates (Scheme 13.20) [50c].

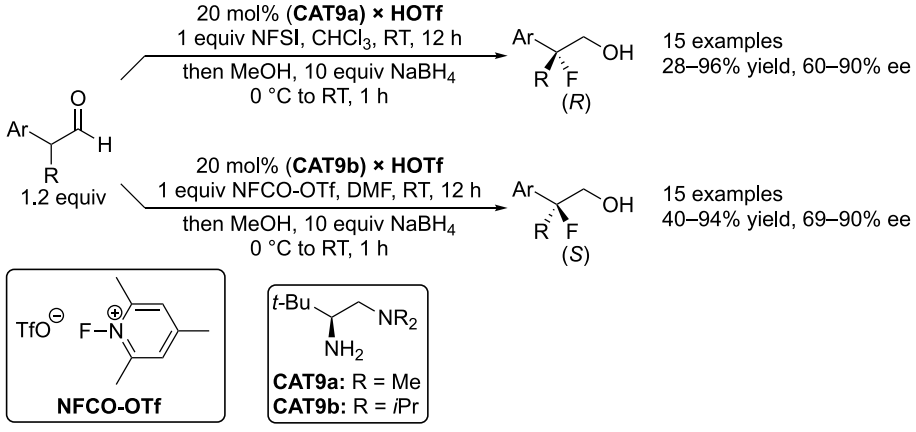

Scheme 13.20. Asymmetric α-fluorination of α-substituted aldehydes. Source: Witten et al. [50c]/American Chemical Society.

Thanks to their conjugated C=C and C=O bonds, enals are versatile substrates. Appayee and Brenner-Moyer used a prolinol catalyst for aminofluorination of enals. Stereoinduction of the second step was controlled by the catalyst, rather than the chiral β-carbon [51]. On the other hand, Arimitsu et al. accomplished enantioselective α-fluorination of enals accompanied by C=C bond migration via dienamine intermediates. In this case, a chiral primary amine and an axially chiral phosphoric acid were both used as catalysts, although the enantioinduction was mainly controlled by the former [52].

13.4.2. α-Fluorination of Ketones

In comparison to aldehydes, the efficient asymmetric organocatalytic fluorination of ketones is more difficult. Firstly, the condensation of ketones with secondary amine catalysts is slower and the equilibrium is shifted toward the ketone, decreasing overall efficiency. Secondly, the ratio of the two *N*-olefin rotational isomers in ketone-derived enamines is more balanced, making the enamine less organized and decreasing enantiocontrol [53].

Tertiary amines, however, have shown promising stereoinduction in fluorinations of preformed enol equivalents. A good example is the application of a catalytic amount of cinchona alkaloids with stoichiometric Selectfluor, which fluorinates the alkaloid into a chiral *N*-fluoroammonium salt. In CH_2Cl_2, the dicationic Selectfluor is insoluble, while the alkaloid *N*-fluoroammonium salt is soluble. As a result, this chiral reagent is the only species available for substrate fluorination, after which the alkaloid salt is regenerated. Use of the sterically demanding NFSI analog improves the enantioselectivity but reduces the yield [54]. These reactions take place under homogenous conditions, given that the neutral NFSI is soluble in most organic solvents.

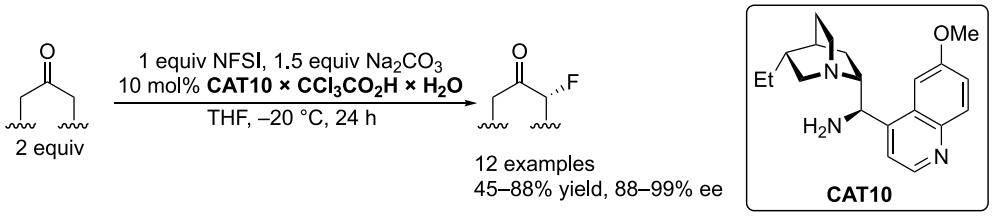

Scheme 13.21. Selective α-fluorination of ketones. Source: Kwiatkowski et al. [53] and Lam et al. [55].

In fact, the introduction of primary amine catalysis was the true breakthrough in the enantioselective organocatalytic fluorination of ketones. MacMillan et al. reported the highly enantioselective, efficient, and regioselective fluorination of cyclic ketones using primary amine catalyst **CAT10** (a cinchona alkaloid derivative). The sterically less hindered α-position of the ketone is fluorinated (Scheme 13.21) [53, 55]. Commercially available cheap chiral primary amines (e.g. α-methoxymethylbenzylamine) are also viable catalysts, although they result in lower enantioselectivity [56].

13.4.3. α-Fluorination of β-Oxo Carbonyl Compounds

Organocatalytic asymmetric fluorinations of β-oxo carbonyl compounds were successfully carried out with a wide variety of catalysts. Luo et al. reported the organocatalytic fluorination of β-ketoesters with reagent-controlled enantioselectivity (Scheme 13.22) [57]. The (*S*)-selective process,

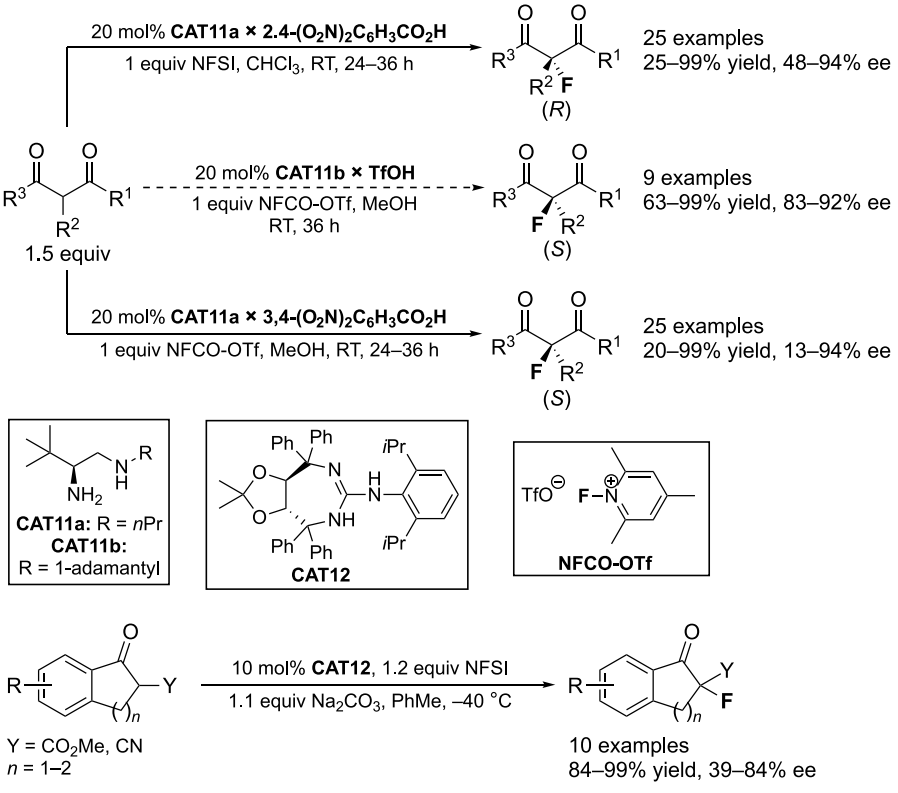

Scheme 13.22. Asymmetric fluorination of 1,3-dicarbonyl compounds. Source: You et al. [57]/Royal Society of Chemistry and Wang et al. [60b]/Royal Australian Chemical Institute.

using **CAT11a** ×3,4-dinitrobenzoic acid with NFCO-OTf as the fluorinating reagent, took place efficiently with β-ketoamides and open-chain 1,3-diketones. In some cases, however, catalyst **CAT11b** ×TfOH was superior. The (*R*)-selective process, using **CAT11a** ×2,4-dinitrobenzoic acid with NFSI instead, was mostly limited to acetoacetates and some acetoacetamides. The reagent-dependent enantioinduction is based on protonation of one of the amine moieties by the acid, in a similar manner to that seen in the previous sections. The resulting ammonium cation electrostatically repels NFCO, but attracts NFSI through hydrogen bonds. With some modifications, this method allowed the enantiodivergent fluorination of α-branched aldehydes. Yi et al. fluorinated mostly benzoylacetates using a tertiary amine catalyst (a fluorous cinchona alkaloid derivative) that can be recovered easily via fluorous solid-phase extraction and reused at least four times without serious degradation of enantioselectivity [58].

Other processes performed better with cyclic structures. The methods of Akiyama et al. (using an axially chiral phosphate catalyst) [59] and Hu et al. (using a cinchona-alkaloid-derived tertiary amine with a thiourea moiety) [60a] displayed good enantioselectivity but a relatively narrow substrate scope. The protocol of Wang et al. (using an L-tartaric-acid-based guanidine **CAT12**) had a slightly broader substrate scope; apart from indane-1-one-2-carboxylates, 1-tetralone-2-carboxylates and 1-tetralone-2-carbonitrile were also fluorinated successfully [60b] (Scheme 13.22).

13.4.4. α-Fluorination of Simple Carboxylic Acid Derivatives

Asymmetric organocatalytic α-fluorination of simple carboxylic acid derivatives was accomplished mainly with tertiary amine catalysts [61, 62]. Oxindoles were particularly popular substrates [61]. An interesting method transforms ketenes into α-fluoroesters [62].

13.4.5. Fluorinative Transformations of Carbon–Carbon Double Bonds

The asymmetric electrophilic fluorination of alkenes (or arenes) generates a carbocationic intermediate, which undergoes further reactions (depending on the type of substrate) to form a stable, neutral product. From allyl silanes, chiral allyl fluorides are formed (desilylation regenerates the C=C bond) [61b]. The enantioselective electrophilic fluorination of α-alkyl(aryl) allylic alcohols by catalytic methods [63] can trigger a semipinacol rearrangement, in this case the asymmetric fluorination step is followed by diastereoselective alkyl migration.

The electrophilic fluorination of tryptamines and tryptophols results in fluorinative dearomatization (F^+ transfer, then cyclization via S_Ni) [46, 64]. Gouverneur and coworkers compared two protocols using Selectfluor and a bis-cinchona alkaloid. The stoichiometric method usually produced better ees, while the catalytic method produced higher yields [46]. Jiang et al. synthesized phthalazines from pipecolinic acids, whose enantiomers are both cheap and commercially available. Fluorocyclization of tryptamines and tryptophols catalyzed by these phthalazines proceeded with good yields and excellent ees [64].

13.5. ASYMMETRIC FORMATION OF C–F BONDS VIA MISCELLANEOUS REACTIONS

13.5.1. Fluorination Using *N*-Heterocyclic Carbene Catalysis

The fluorination of aldehydes can be catalyzed by *N*-heterocyclic carbenes (NHCs). Usually, the primary aldehyde–NHC adduct is oxidized into a ketone, which undergoes electrophilic fluorination followed by nucleophilic displacement of the NHC group. The electrophilic fluorinating agent is both the oxidant and the fluorine source. Wang et al. reported such a process with **CAT13** as a precatalyst and alcohols as nucleophiles (Scheme 13.23), however the reaction failed with MeOH, EtOH, or *t*-BuOH [65]. From α-chloroaldehydes, the enolate intermediate is formed without external oxidant. Sun et al. reported such reactions using alcohols (including MeOH), amines, and thiols as nucleophiles [66].

NHC-catalyzed hydrofluorination of enals yields α-fluorinated esters. Depending on the β-substitution, different additives were required for efficient transformation [67]. NHC catalysis also

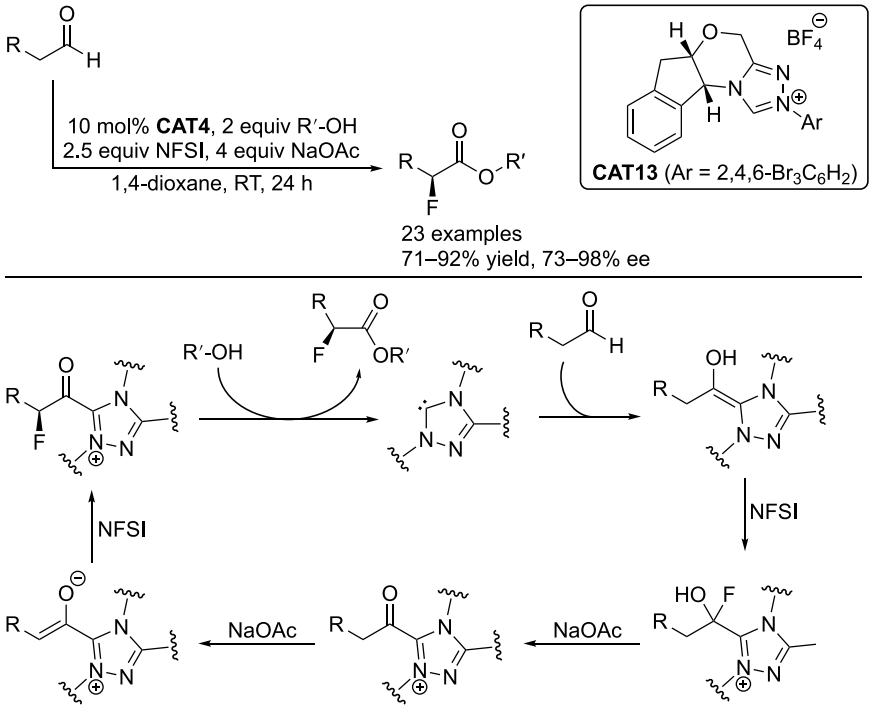

Scheme 13.23. NHC-catalyzed oxidative α-fluorination of aldehydes.

enables the transformation of enals with a leaving group in the γ-position into enantiopure α-fluorinated β,γ-unsaturated esters [68].

13.5.2. Fluorination Using Chiral Iodoarene Difluorides

A recent development is the use of chiral iodoarene difluorides (Ar^*IF_2) (Ar* = aryl group with chiral substituents) for various fluorination reactions. These compounds act as sources of electrophilic iodine(III) and nucleophilic F^- [69, 70]. During fluorination, Ar^*IF_2 reagents are transformed into Ar*I. If stoichiometric amounts of a fluorine source and an oxidant are present, Ar*I is transformed back into Ar^*IF_2 and only a catalytic amount of Ar*I is required. Jacobsen and coworkers described such a fluorolactonization (*ortho*-alkenylbenzoate substrates, Ar^*IF_2 regeneration with pyridine × 9HF and *m*-chloroperbenzoic acid [MCPBA]). Most products were obtained in moderate to good yields and excellent ees [69].

Asymmetric intramolecular aminofluorination reactions were reported with an isolated Ar^*IF_2 reagent [71] and MCPBA/pyridine × *n*HF/catalytic Ar*I systems [72]. Jacobsen et al. successfully fluorocyclized *N*-sulfonylated 3-arylallylamine derivatives into aziridines using **(*R*,*R*)-CAT14**. The reaction proceeded well when the aryl group was sufficiently electron deficient (Scheme 13.24). If not, aryl migration took place leading to difluoromethylated sulfonamides. *N*-Cbz-protected 3-arylallylamines and 3-arylallylalcohol derivatives underwent selective 1,2-oxyfluorination instead [72]. Chiral iodoarene difluorides can also difluorinate olefins enantio- and diastereoselectively [70, 73, 74]. Jacobsen and coworkers difluorinated 2-substituted (*E*)-cinnamamides using **(*R*,*R*)-CAT14** (Scheme 13.24). Anchimeric assistance of the amide oxygen is responsible for the *trans* selectivity, and aryl group migration (a common side reaction) can be suppressed by reducing the acidity of the mixture [73, 74].

Gilmour and coworkers reported the enantioselective difluorination of vinyl-substituted arenes using a chiral aryl iodide catalyst, Selectfluor, and pyridine × 4.5HF [75]. Finally, chiral iodoarene difluorides were also used for the enantioselective fluorination of β-ketoesters [76]. Rueping et al. achieved 18–68%

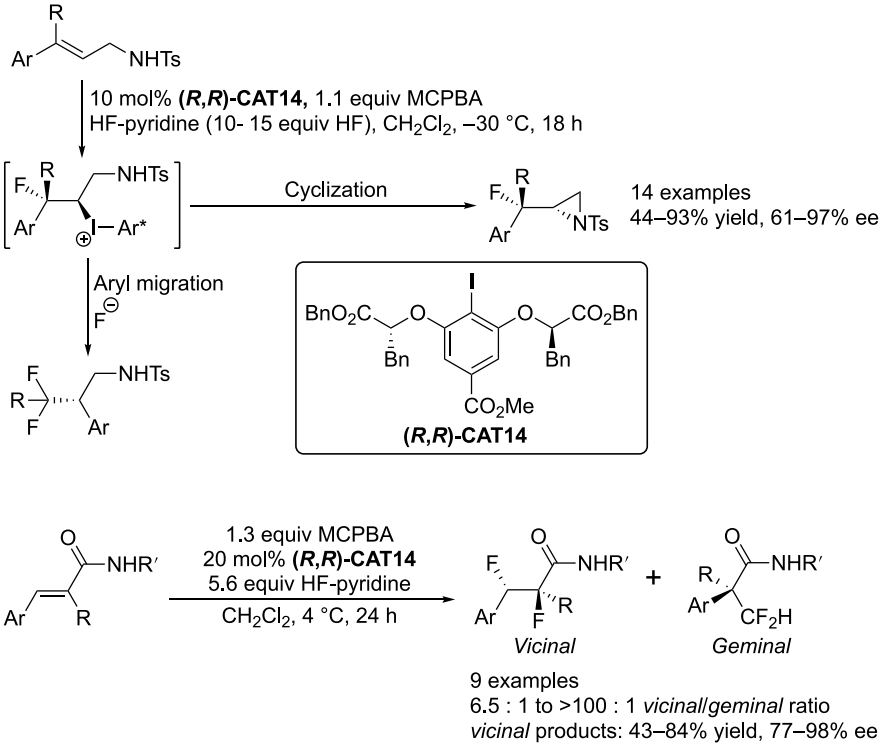

Scheme 13.24. Fluorination of 2-substituted (*E*)-cinnamamides.

yields and 91 : 9 or higher enantiomeric ratios in the fluorination of indane-1-one-2-carboxylates using a iodobiphenyl catalyst, MCPBA, and $Et_3N \times 5HF$ [76b].

13.6. ENANTIOSELECTIVE CHLORINATION

The stereoselective synthesis of molecules with chlorine atoms at their stereogenic centers constitutes a challenging objective. In spite of the intrinsic difficulties, continuous efforts have been made to achieve this goal, as this structural element is present in many compounds of great interest. Hence, several strategies have been developed mainly based on the use of organocatalytic methods and chiral metal complexes.

13.6.1. Organocatalysis

13.6.1.1. Chlorination of Carbonyl Compounds Carbonyl compounds represent classical substrates for the introduction of chlorine atoms into their structure in an asymmetric manner. Since chiral α-chlorocarbonyl compounds can easily be transformed into interesting building blocks, their preparation has been achieved, frequently following organocatalytic procedures. A review by Maruoka [77] compiled the contributions made in this field until 2009.

Thereafter, in 2010, the organocatalytic asymmetric chlorination of enals through the asymmetric copper-catalyzed Michael addition of dimethyl zinc followed by chlorination with *N*-chlorosuccinimide (NCS) of the resulting enolate using aminal-pyrrolidine (**CAT15**) catalysis was described (Scheme 13.25) [78]. In this manner, α-chloroaldehydes were obtained in high yields with good *anti/syn* selectivity and high ee.

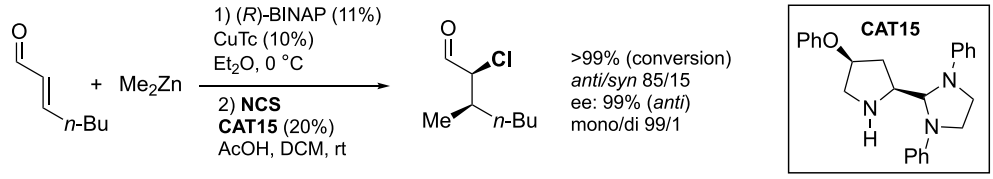

Scheme 13.25. Preparation of chiral α-chloroaldehydes from enals. Source: Quintard and Alexakis [78]/John Wiley & Sons.

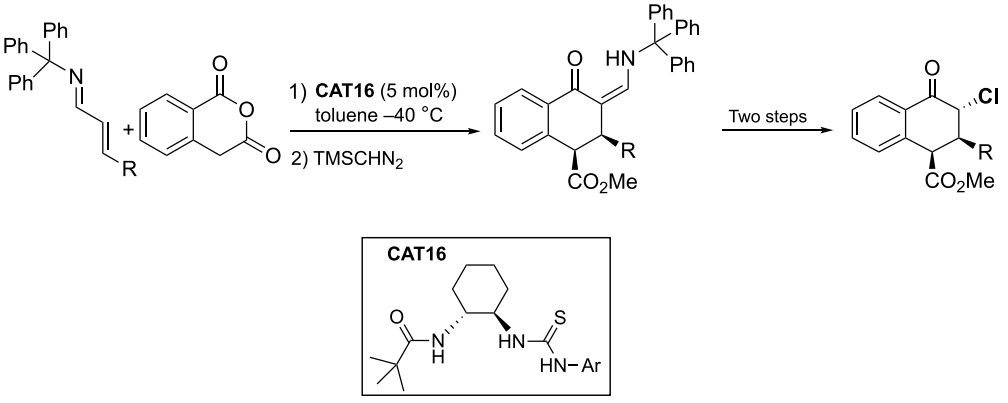

Scheme 13.26. Three-step synthesis of chiral α-chloroketones from enaminones. Source: Gutierrez Collar et al. [79]/John Wiley & Sons.

More recently, the transformation of enaminones, resulting from the Tamura reaction of imines and homophthalic anhydride, under chiral thiourea catalyst (**CAT16**) in asymmetric chloroketones through a two-step sequence has been accomplished (Scheme 13.26) [79]. Treatment of the vinylogous amide with NCS led to the corresponding α-chloroimine, which, after being treated with neutral alumina and chloroform, underwent a hydrolysis–oxidation–decarboxylation sequence, leading to the corresponding chiral α-chloroketone in 96% ee as a single diastereomer.

13.6.1.2. Dichlorination of Alkenes The vicinal dihalogenation of unactivated alkenes following organocatalytic-based strategies enables the preparation of chiral compounds bearing the 1,2-dichloro motif that is present in a variety of natural products. However, asymmetric dichlorination of unactivated alkenes is a challenging transformation, and, consequently, only few examples have been described.

Recently, the efficient enantioselective dichlorination of 1,2-dihydronaphthalene using unsymmetrical cinchona-alkaloid-based phthalazines (**CAT17**) has been reported, reaching enantioselectivities of up to 94 : 6 er, while $(DHQD)_2PHAL$ (**CAT18**) as catalyst provided the dichloroderivative with low enantioselectivity (35 : 65 er) (Scheme 13.27) [80].

Allylic alcohols are also suitable substrates for enantioselective dichlorination reactions, first described by Nicolaou [81]. The transformation can be extended to allylic amides that have undergone enantioselective dichlorination reactions using $(DHQD)_2PHAL$ (CAT18) as catalyst in combination with 1,3-dichloro-5,5-dimethylhydantoin (DCDMH) and a large excess of LiCl (100 equiv.) (Scheme 13.27) [82].

13.6.1.3. Chlorofunctionalization of Alkenes Enantioselective chloro-oxygenation reactions constitute a complementary approach to enantioselective electrophilic chlorination reactions. Both, inter- and intramolecular versions, the latter involving a chlorocyclization reaction, have been reported. Simple selection of the nucleophile used for intercepting the putative intermediate allows a rapid increase in the molecular complexity of the products obtained. Face selectivity in double-bond halogenation together with the excellent control of regioselectivity by the catalyst, instead of the substrate, are imperative aspects to be controlled (Scheme 13.28) [83].

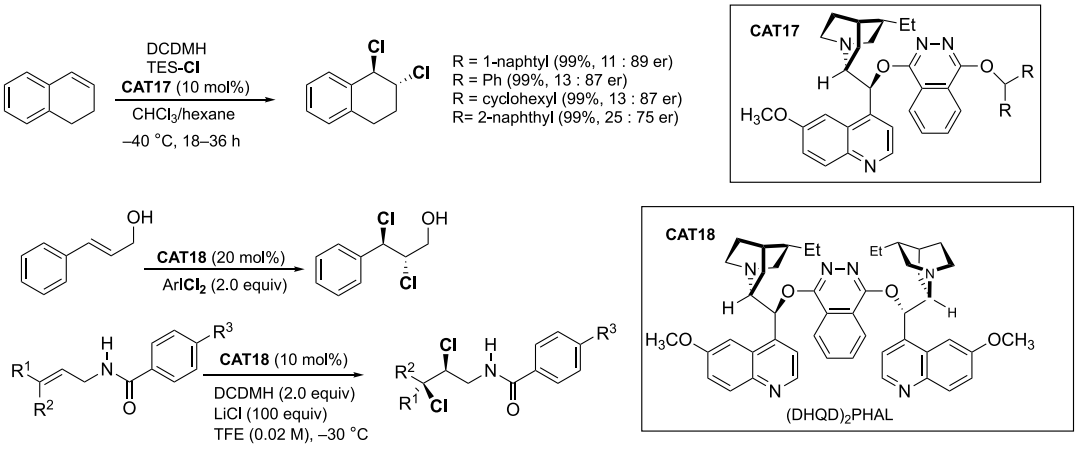

Scheme 13.27. Asymmetric vicinal dichlorination of styrenes, allylic alcohols, and amides.

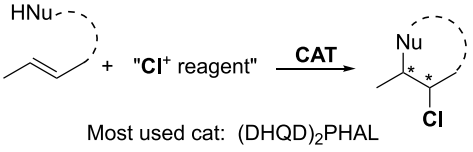

Scheme 13.28. Asymmetric chlorocyclization reactions. Source: Soltanzadeh et al. [82]/American Chemical Society.

The pioneering examples in this strategy were achieved by Borhan and coworkers [84], who described the chloroetherification and chloroesterification of unsaturated acids and amides using cinchona-alkaloid-based organocatalysts.

Although cinchona-alkaloid-based organocatalysts vastly dominate asymmetric electrophilic chlorination reactions, their relative strong basicity is occasionally apt to reduce the scope of the substrates. Alternatively, Lewis-basic organochalcogen catalysts are not only less basic and more compatible with neutral or acidic conditions but also readily available. These catalysts can form a complex with either ArS^+, Br^+, or CF_3S^+, which then reacts with alkenes forming chiral iranium ions, and subsequently reacts with nucleophiles to give the corresponding products. However, the organochalcogen-catalyzed enantioselective electrophilic chlorination of alkenes poses certain difficulties. Consequently, successful examples leading to good enantioselectivities in the asymmetric chlorination were elusive until very recently, when a bifunctional catalyst was described that due to the stabilization of the chloriranium ion is able to prevent its decomposition. Thus, using a bifunctional chiral sulfide (**CAT19**), a desymmetrizing chlorination of aryl-tethered diolefins to give chiral chlorinated tetralines bearing an all-carbon quaternary stereocenter was described (Scheme 13.29) [85].

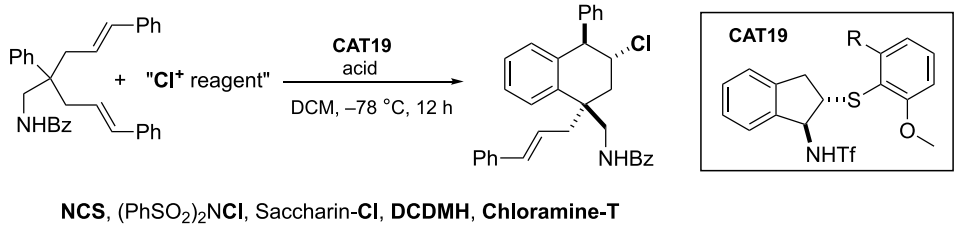

Scheme 13.29. Desymmetrizing chlorination of diolefins using chiral sulfide organocatalysts. Source: Cao et al. [85]/John Wiley & Sons.

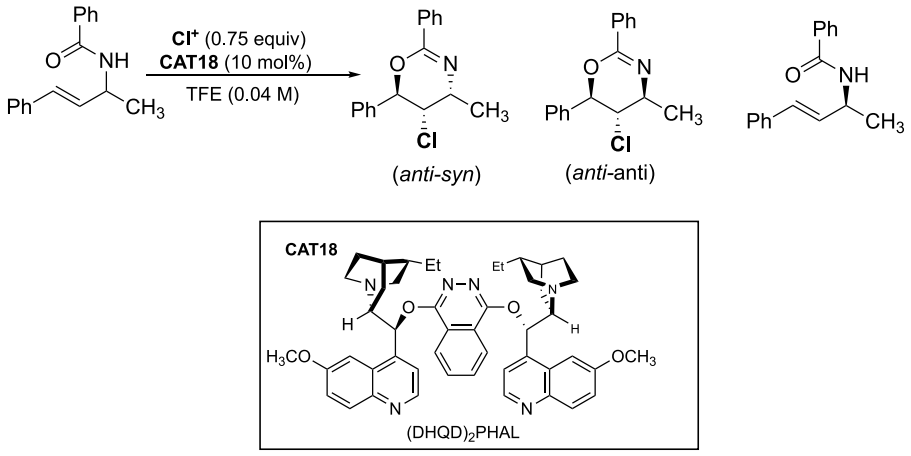

Scheme 13.30. Kinetic resolution of allylic amides through an intramolecular asymmetric chloro-oxygenation reaction. Source: Jaganathan et al. [86]/American Chemical Society.

A complementary approach for the preparation of optically active chlorinated derivatives is the kinetic resolution of racemic precursors instead of the asymmetric chlorination of prochiral alkenes described above. In this sense, the first example of kinetic resolution of allylic amides by means of an asymmetric chlorocyclization reaction using $(DHQD)_2PHAL$ (**CAT18**) as catalyst was described by Borhan in 2013 (Scheme 13.30) [86].

13.6.2. Strategies Based on Chiral Metal Complexes

13.6.2.1. Chlorination of β-Ketoesters Acyclic and cyclic β-ketoesters and α,β-diketones can be converted into α-chlorinated derivatives with excellent yields and moderate to good enantioselectivities by using chiral bisoxazoline **L11** and **L12** copper(II) complexes as catalyst and NCS as chlorine source (Scheme 13.31) [87].

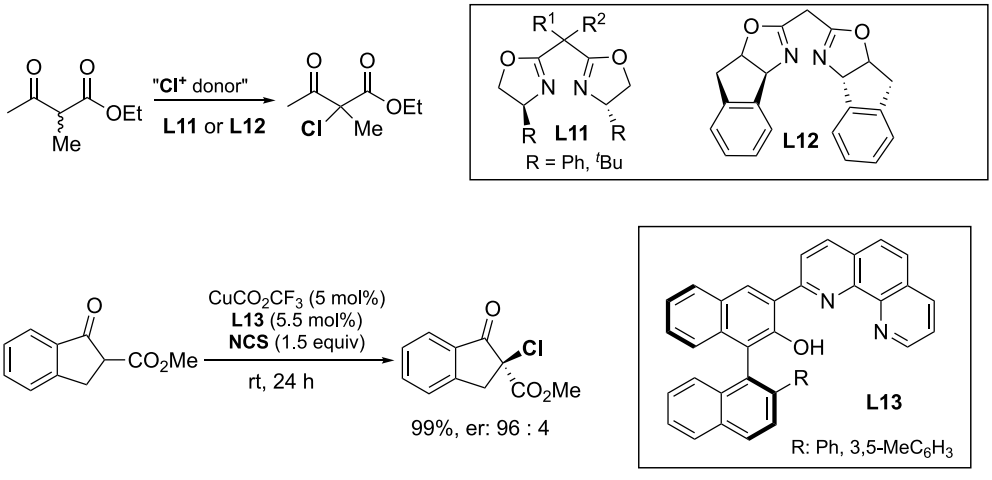

Scheme 13.31. Asymmetric chlorination of α-substituted β-ketoesters. Source: Marigo et al. [87]/John Wiley & Sons.

The complex of *N*,*N*,*O*-tridentate chiral phenanthroline ligand **L13** together with copper(II) trifluoroacetate also turned out to be effective for the asymmetric chlorination of cyclic β-ketoesters (Scheme 13.31) [88].

13.6.2.2. Chlorination of Alkenes The methods of dihalogenation of olefins catalyzed by chiral Lewis acid complexes to afford enantioenriched vicinal dihalide products were revised and analyzed in depth in an extensive review by Denmark in 2015 [89], who also provided a detailed list of the main group of halides and transition metal halides in high-oxidation states used in this context. Since metal also acts as oxidant, stoichiometric amounts of the metal halides are usually required, although titanium and molybdenum have also been used in substoichiometric amounts coupled with a stoichiometric oxidant.

Catalysis with chiral metal complexes directed at the halofunctionalization of both electron-rich and electron-deficient alkenes has been extensively used. Electrophilic dichlorination, halo-oxygenation, and aminohalogenation reactions are also known. Intramolecular versions constitute a simple way to prepare enantioenriched oxa- and aza-heterocycles that are common motifs in natural products. Five- and six-membered rings are the most frequently accessed cycles, while the preparation of larger heterocycles remains a challenge due to both entropic and enthalpic barriers.

Asymmetric intramolecular chloroetherification of enones catalyzed by an Fe(II) complex with a chiral *N*,*N*-dioxide **L14** provides the chlorocyclization products with good yields (70–90%) and high dr (>99%). The intermolecular haloetherification of enones is a more challenging transformation, requiring the catalysis of the $Sc(OTf)_3$ complex (**L15**) and a large excess of alcohol to provide the product with only acceptable yield and enantioselectivity (Scheme 13.32) [90].

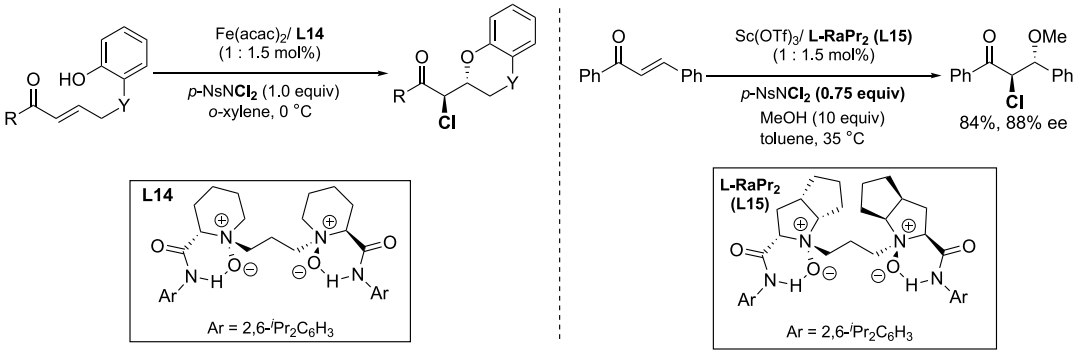

Scheme 13.32. Asymmetric chloroetherification of enones catalyzed by chiral *N*,*N*′-dioxide-metal complexes. Source: Zhou et al. [90]/American Chemical Society.

Vicinal aminochloride compounds are valuable chiral building blocks, while examples of aminochlorination reactions are rather scarce.

Chiral Lewis (**L16**) acid-catalyzed aminochlorination reactions of α,β-unsaturated olefins [91], and particularly chalconic olefins, were first described by Feng (Scheme 13.33a) [92]. On the other hand, the aminochlorination of terminal olefins with a radical chlorine donor in the presence of MnO_2 was described by Chemler (Scheme 13.33b) [93].

Chiral Fe(II) complexes (**L17**) efficiently catalyze the intramolecular aminochlorination of internal nonchalconic olefins, giving the corresponding aminochlorides with two contiguous stereogenic centers with high yields and enantioselectivities (Scheme 13.33c) [94].

Preparation of chiral allyl chlorides is particularly challenging as they are prone to isomerization and racemization. Despite the difficulties, the preparation of enantiomerically enriched tetrahydropyridine allyl chlorides by kinetic resolution using Zr-nucleophiles and copper catalysis (**L18**) has recently been described (Scheme 13.34) [95].

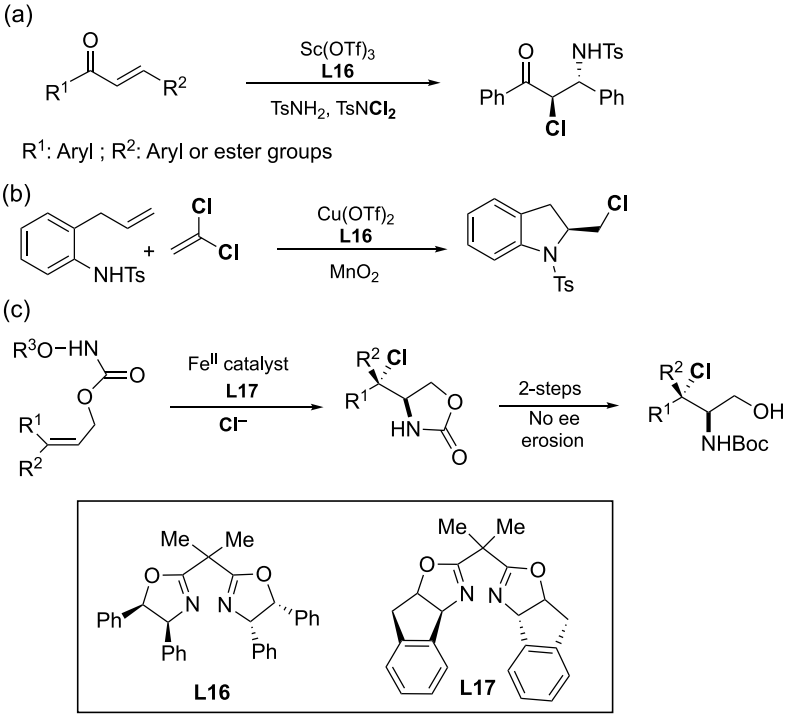

Scheme 13.33. Asymmetric chloroamination of unsaturated olefins catalyzed by chiral metal complexes. (a) Chlororoamination reaction of activated olefins. (b) Chloroamination reaction of terminal olefins. (c) Chloroamination reaction of internal olefins. Source: [93]/John Wiley & Sons.

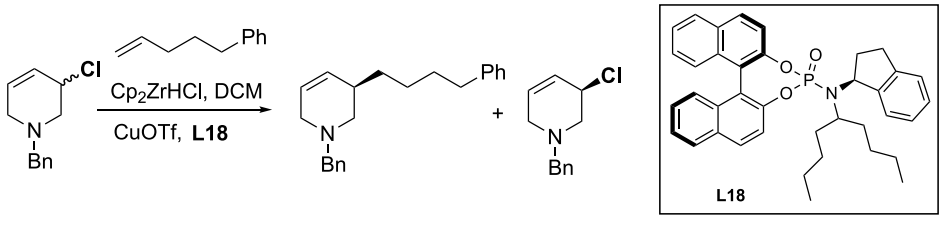

Scheme 13.34. Kinetic resolution of tetrahydropyridine allyl chlorides. Source: [95]/Royal Society of Chemistry.

13.7. ENANTIOSELECTIVE BROMINATION

Bromine is present in a wide range of bromo-organic compounds. The incorporation of bromine through natural methods has been described, applying photochemical reactions, geothermal events, and enzymatic pathways [96]. The use of molecular bromine as brominating agent is limited due to its high volatility, reactivity, and corrosiveness. Other alternative bromine sources such as *N*-bromoamide reagents, e.g. *N*-bromosuccinimide (NBS), are commonly used due to their high stability and easy handling.

13.7.1. Strategies Based on Chiral Metal Complexes

Among the different strategies for generating chiral C–Br, transition metal complexes, particularly that of Sc(III) and Fe(III), have been found to be efficient catalysts for obtaining these derivatives with high enantioselectivity.

13.7.1.1. Bromination of Alkenes Asymmetric bromoamination of chalcones allows the obtention of chiral α-bromo-β-amino ketone derivatives. Since the first catalytic asymmetric bromoamination of chalcones with sulfonamide and NBS reported by Feng and coworkers, this reaction has experienced rapid growth [97]. In their work, the authors used a chiral *N*,*N*′-dioxide catalyst and Sc(III), which, under mild conditions, yielded the corresponding α-bromo-β-amino ketones with excellent regio-, diastereo-, and enantioselectivities. Later, Feng and coworkers reported a catalytic asymmetric bromoamination of chalcones with NBS using a chiral *N*,*N*′-dioxide-Sc(NTf$_2$)$_3$ catalyst. The corresponding chiral *anti*-α-amino-β-bromo ketones were obtained in high yields with high dr and good ee (up to 92% yield, 93 : 7 dr, and 97% ee). Further optimization of the chiral ligand **L-RaPr2** (**L15**) led to higher yields and enantioselectivities (Scheme 13.35) [98]. The catalytic asymmetric halohydroxylation of α,β-unsaturated ketones with water as

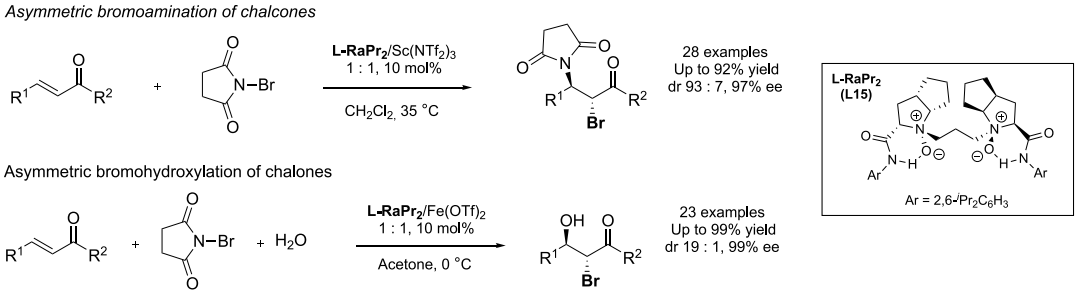

Scheme 13.35. Asymmetric bromoamination of chalcones with NBS catalyzed by chiral *N*,*N*′-dioxide-Sc(NTf$_2$)$_3$ complexes.

nucleophile was achieved in good yields and high dr and ee values, applying the same chiral complex [99]. Other bromofunctionalization reactions of α,β-unsaturated carbonyl compounds have also been described with other *N*,*N*′-dioxide ligands [100].

Feng's group also described an asymmetric intramolecular haloetherification of alkenes in the presence of Fe(III) complexes [101]. Using BsNMeBr (Bs = benzenesulfonyl) as the brominating reagent, the Fe(III) complexes afforded bromocyclization of electron-deficient alkenes yielding tetrahydrobenzopyran derivatives in high enantioselectivities (77–97% ee). They also extended the scope to the bromoazidation of α,β-unsaturated ketones [102] and α,β-unsaturated amides [103].

Other chiral ligands able to form efficient metal catalysts for the bromoazidation of unsaturated compounds have also been described. In this sense, Burns and coworkers reported a highly regio- and stereoselective haloazidation of allylic alcohols using a chiral tridentate Schiff base ((1*S*,2*R*)-(−)-2-[*N*-(3′,5′-di-*tert*-butylsalicylidene)amino]-1,2-diphenylethanol) (**L19**), Ti(O*i*-Pr)$_4$, and NBS as bromine source [104]. The chiral titanium-based catalysts turned out to be very efficient in this process, providing the haloazide product in good yields (44–92%) and enantioselectivity (86–96% ee) (Scheme 13.36).

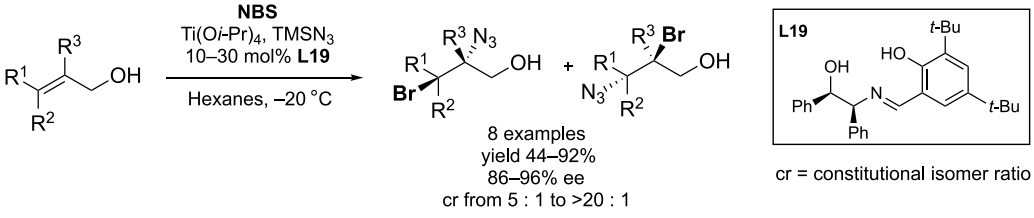

Scheme 13.36. Asymmetric haloazidation of allylic alcohols.

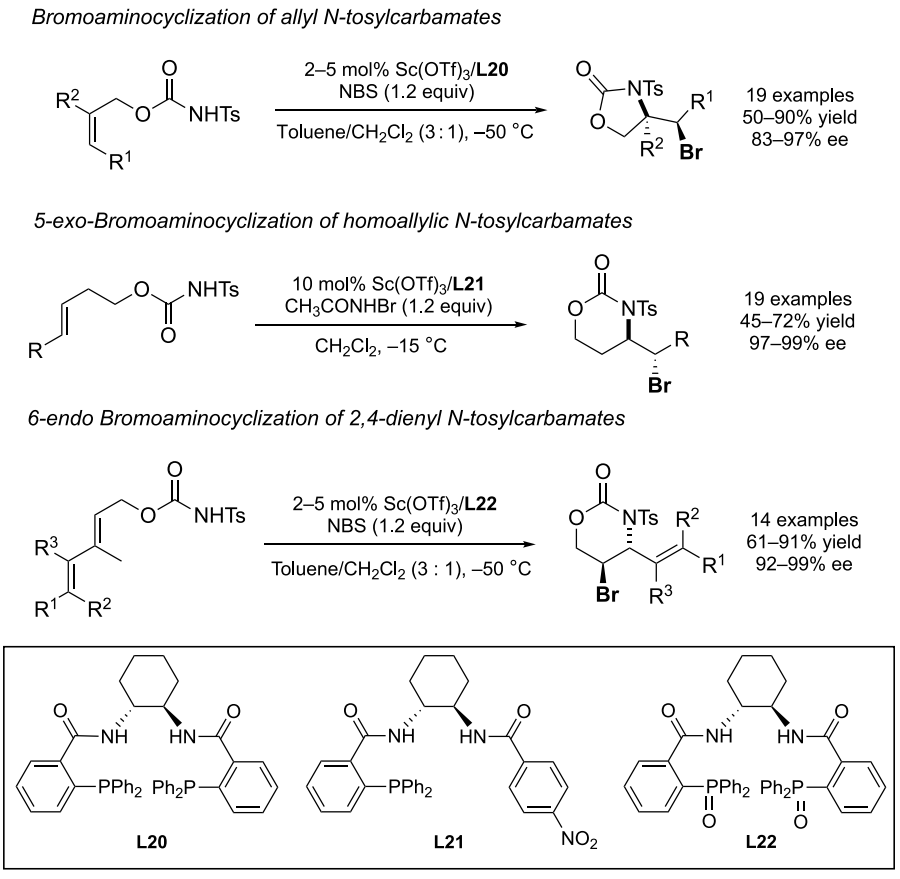

Scheme 13.37. Asymmetric haloazidation of allylic alcohols.

13.7.1.2. Bromoaminocyclization Reactions The asymmetric electrophilic halogenation of olefinic substrates catalyzed by phosphine oxides has recently gained a great deal of attention (Scheme 13.37). Thus, in 2013, the intramolecular asymmetric Sc(III)-catalyzed bromoaminocyclization of allyl *N*-tosylcarbamates was reported by Shi and coworkers [105]. The reaction was promoted by a chiral catalyst generated in situ from $Sc(OTf)_3$ and Trost chiral phosphine ligand **L20**, providing a variety of these products in moderate to high yields (50–90%) and enantioselectivities (83–97% ee). In 2015, the same authors described the synthesis of a novel chiral monophosphine based on Trost ligand **L21** [106]. The $Sc(OTf)_3$ catalyst generated in situ efficiently catalyzed the 6-*exo*-bromoaminocyclization of (*E*)-homoallylic *N*-tosylcarbamates. In that case, *N*-bromoacetamide was used as the bromine source, and chiral oxazinanones were obtained in moderate to good yields (45–72%) and excellent enantioselectivities (97–99% ee). An extension of this work revealed that the addition of NaCl was crucial for the reaction process and the chiral phosphine oxide **L22**-$Sc(OTf)_3$ catalyst promoted the enantioselective 6-*endo* bromoaminocyclization of 2,4-dienyl *N*-tosylcarbamates containing various functional groups, yielding 5-bromo-1,3-oxazinan-2-ones in 61–91% yield and 92–99% ee [107].

The same group also reported the use of metallic complexes of $Sc(OTf)_3$ with chiral Trost phosphine oxide **L22** in the asymmetric bromoaminocyclization of 2-benzofuranylmethyl *N*-tosylcarbamates containing various electron-rich or electron-deficient substituents at the C4, C5, and C6 positions [108]. The optimal reaction conditions required the use of 1,3-dibromo-5,5-dimethylhydantoin (DBDMH) as the bromine source and Na_2CO_3 as additive. Under these conditions, a wide variety of optically active spirobenzofuran oxazolidinones was isolated in good yields (62–97%) and enantioselectivities (91–97% ee). Later, Shi's group extended the catalytic activity of $Sc(OTf)_3$ and Trost phosphine ligand **L22**, using NaCl

as an additive to the enantioselective bromoaminocyclization of (*E*)-cinnamyl tosylcarbamates [109]. A wide variety of optically active aryl 5-bromo-1,3-oxazinan-2-onesin derivatives was synthesized in high yields (65–96%) and enantioselectivity (87–99% ee). Subsequently, the study was extended to the enantioselective bromoaminocyclization of trisubstituted allyl *N*-tosylcarbamates resulting in a wide variety of chiral tertiary 5-bromo-1,3-oxazinan-2-ones with high regio- and enantioselectivities (up to 98% ee) [110]. KBr was found to be the best additive for that reaction (Scheme 13.38).

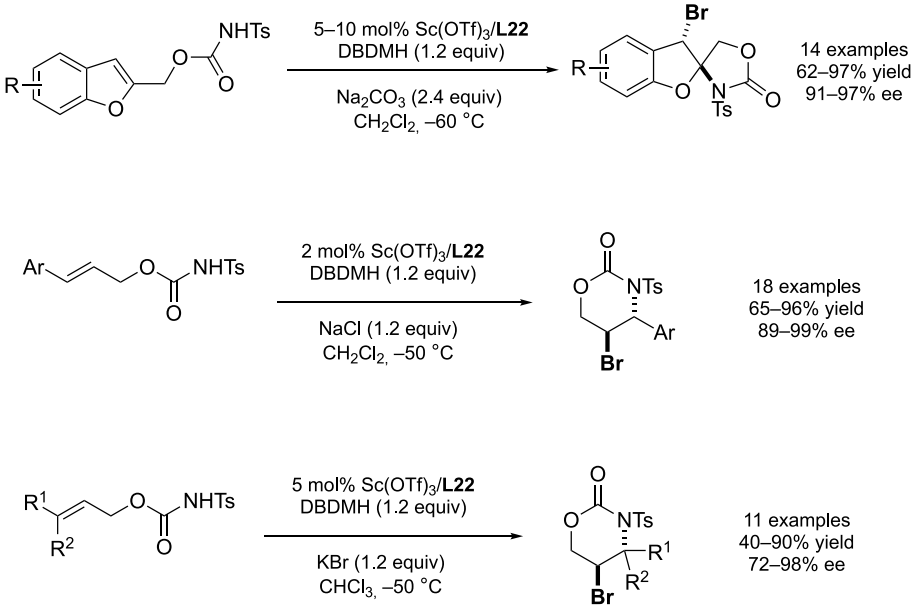

Scheme 13.38. Enantioselective bromoaminocyclization of tosylcarbamate derivatives catalyzed by phosphine oxide–$Sc(OTf)_3$. (a) Bromoaminocyclization of 2-benzofuranylmethyl *N*-tosylcarbamates. (b) Bromoaminocyclization of (*E*)-cinnamyl tosylcarbamates. (c) Bromoaminocyclization of tri-substituted allyl *N*-tosylcarbamates.

13.7.2. Strategies Based on the Use of Chiral Auxiliaries

13.7.2.1. Bromolactonization Reactions Since Martin and coworkers documented the first example of an asymmetric bromolactonization using a 1,1′-bi-2-naphthol (BINOL)-derived bifunctional catalyst [111], several organocatalytic bromocyclization reactions have been developed. An interesting asymmetric bromolactonization of prochiral cyclohexadiene compounds with NBS was also described using $(DHQD)_2PHAL$ as a chiral catalyst, which yielded the corresponding bromolactones in moderate yields and enantioselectivities of up to 93% [112]. An enantioselective bromolactonization to give α-*exo*-methylene-γ-butyrolactones using NBS as bromine source catalyzed by a $(DHQD)_2PHAL$ derivative (**CAT20**) turned out to be very effective in terms of yield and enantioselectivity (Scheme 13.39) [113]. In that transformation, a biscinchonine $(DHQD)_2PHAL$ catalyst derived from the amino acid (*L*)-proline was synthesized. Jiang and coworkers extended the use of the C_2-symmetrical amino-acid-derived phthalazine catalyst to the enantioselective halolactonization of prochiral dienoic acids yielding α-*exo*-methylene-halolactones with enantioselectivities of up to 99.8% [114].

Other phthalazine catalysts, in particular hydroquinidine 1,4-phthalazinediyl diether, were efficiently used in the stereoselective intermolecular bromofunctionalization of allyl amides [115]. Extending the use of phthalazine catalysts, Shi and coworkers described an organocatalytic enantioselective bromination of unfunctionalized olefins catalyzed by a dimeric cinchona alkaloid $(DHQD)_2PHAL$ (**CAT18**), using water as a nucleophile and *N*-bromobenzamide as a bromine source, giving a variety of optically active bromohydrins with good yields and moderate enantioselectivities (39–88% ee) [116]. The same

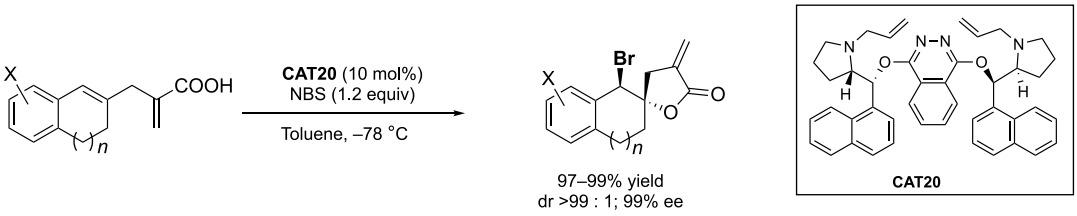

Scheme 13.39. Asymmetric organocatalytic bromolactonization of α-*exo*-methylene-γ-butyrolactones. Source: [113]/John Wiley & Sons.

group extended the use of the asymmetric organocatalytic bromohydroxylation of aryl olefins with **CAT18** as the organocatalyst in the presence of a catalytic amount of (+)-camphor sulfonic acid and *N*-bromobenzamide as a bromine source and water as a nucleophile [117]. Bromohydroxylation of 2-aryl allylic alcohols proceeded in high yields (65–95%) providing a variety of optically active bromohydrins with up to 98% ee. In general, monosubstituted substrates gave higher enantioselectivities than di- and trisubstituted phenyl allylic alcohols (Scheme 13.40).

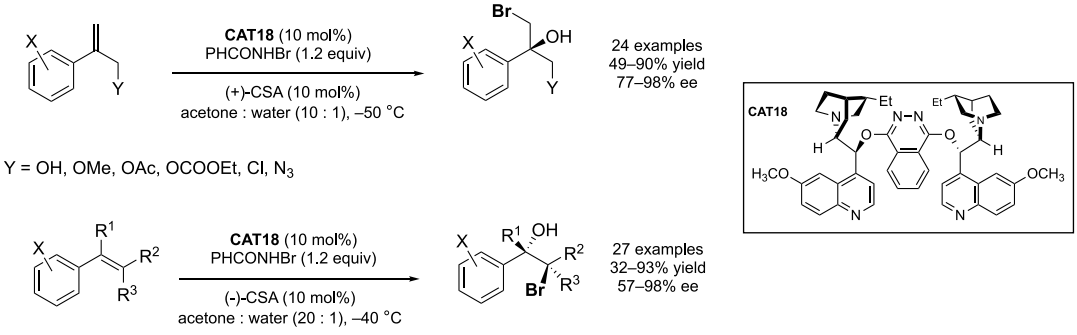

Scheme 13.40. Asymmetric organocatalytic bromohydroxylation of aryl olefins and styrenes.

Considering the intermolecular halofunctionalization of olefins, an asymmetric intermolecular bromoesterification of alkenes was reported by Tang and coworkers using cinchona alkaloid derivatives, structurally related to $(DHQD)_2PHAL$ [118]. Using these catalysts, chiral building blocks with stereogenic C–O and C–Br bonds were prepared in good yields and high enantioselectivity (up to 90% ee). Another asymmetric intermolecular bromoesterification catalyzed by 9-phenanthryl-substituted chiral phosphoric acid catalyst was described by Zhang, Tang, and coworkers [119]. The use of this chiral Brønsted acid yielded bromoesterification products in low yields and enantioselectivities of up to 70% ee.

Other examples of bromolactonizations include a 5-*exo* and 6-*endo*-bromolactonization of substituted olefinic acids, providing chiral lactones with two contiguous asymmetric centers and NBS as a bromine source [120]. A chiral BINOL-derived pyridyl phosphoramide catalyst was developed for this reaction and promoted two different modes of cyclization, giving access to a large variety of bromolactones with high yields and excellent enantioselectivities. Christmann and coworkers described the catalytic activity of chiral BINOL-based phosphoric acid **CAT21** in a bromocyclization followed by a regiodivergent reaction of a racemic mixture of cinnamyl esters and homoallylic esters using NBS and water in high yields and enantioselectivities [121]. Another chiral BINOL derivative was used in the catalytic asymmetric bromocyclization of homogeranylbenzene derivatives applying DBDMH as bromine source [122]. For this bromocyclization, a chiral BINOL-derived thiophosphoramide catalyst was synthesized and bromocyclization products were obtained in high yields, with good enantiomeric ratios and high diastereoselectivity (Scheme 13.41). Ishihara and Sakakura's group also developed phosphite-urea bifunctional catalysts

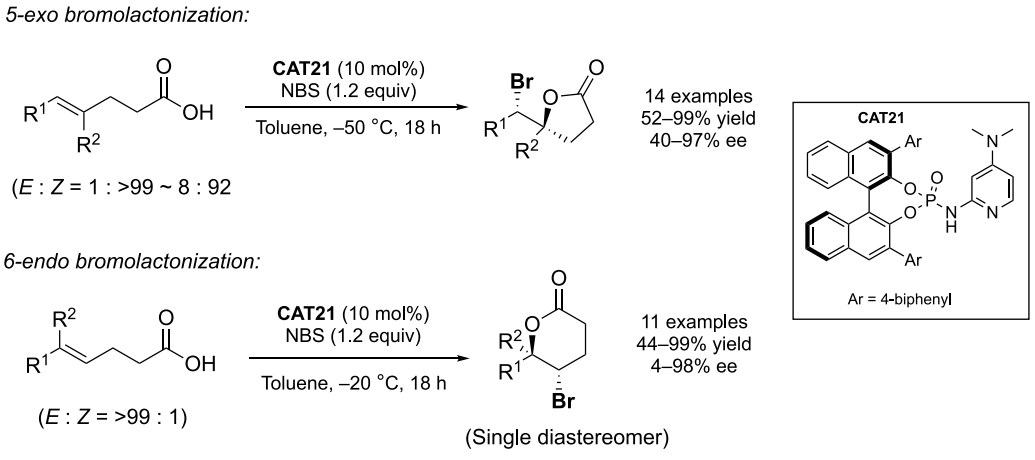

Scheme 13.41. Asymmetric organocatalytic 5-*exo* and 6-*endo*-bromolactonization of α-substituted olefinic acids.

for the bromocyclization of 2-geranylphenols [123]. An interesting enantioselective halocyclization of 2-alkenylphenols and enamides was also reported by Ishihara and coworkers using chiral BINOL amidophosphate catalysts and halo-Lewis acids, affording chiral chromans and pyrrolidines in high yields and enantioselectivities of up to 97%. BINOL-derived amidophosphates were demonstrated to be efficient catalysts for highly enantioselective halo-oxy- and halo-azacyclizations of 2-alkenylphenols [124]. Very recently, Yeung and coworkers reported an interesting tandem bromo-spiroketalization reaction of olefinic ketoacids using electron-rich thiourea catalysts [125]. Applying this approach, bromocyclized products could be obtained in good to excellent yields and excellent stereoselectivities, and in some cases as the only enantiopure compounds. The iodo-spiroketalization of ketoacids was also evaluated, affording the corresponding iodocyclized products in good yields and high enantioselectivities.

Other BINAP derivatives have been efficiently used as catalysts in bromofunctionalization reactions (Figure 13.1). For example, using a chiral P/P=S double-site Lewis base BINAP monosulfide ligand, the enantioselective intramolecular bromoaminocyclization of allyl anilines with NBS as bromine source was described by Deng and coworkers in 2017 [126]. Their methodology provided a series of chiral 2-bromomethyl indolines (26 examples), which were obtained in good to excellent yields (33–91%) with enantioselectivities of up to 87%. Similarly, Hamashima and coworkers reported the enantioselective bromocyclization of allylic amides using DTBM-BINAP and NBS as bromine source [127]. The DTBM-BINAP ligand (10 mol%) afforded chiral oxazolines with a tetrasubstituted carbon center in high yields and enantioselectivities of up to 99% [128]. Later, the same authors used a P/P=O double-site Lewis base monophosphine oxide based on DTBM-BINAP for the same reaction but lowering the catalyst loading (1 mol%), affording enantioenriched oxazolines with enantioselectivities of up to 99.5%.

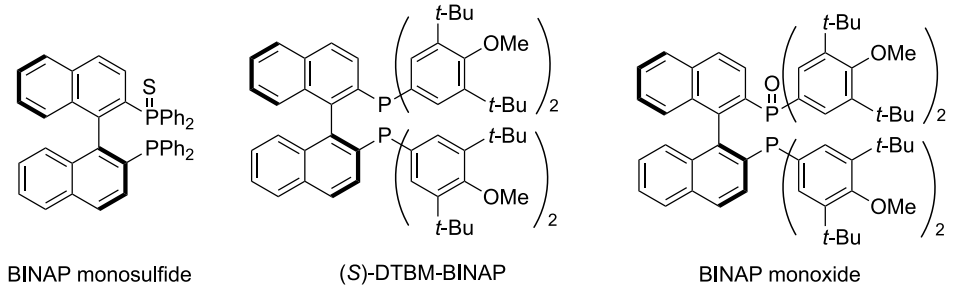

Figure 13.1. BINAP ligands used in bromofunctionalization reactions.

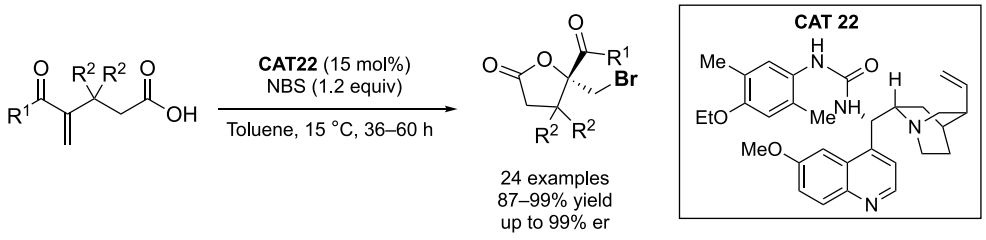

Scheme 13.42. Enantioselective bromolactonization of deactivated olefinic acids. Source: [129]/American Chemical Society.

A novel enantioselective bromolactonization of α,β-unsaturated ketones using a chiral bifunctional amino-urea catalyst (**CAT22**) was studied by Jiang et al. [129]. The scope of the reaction was evidenced by more than 20 examples of halolactones with different functionalities with yields of up to 99% and 99% ee (Scheme 13.42) [129].

13.7.3. Strategies Based on the Use of Organocatalysts

13.7.3.1. Bromocyclization Reactions In 2010, several important examples of organocatalytic asymmetric bromolactonization of simple alkenes were reported by different authors. Fujioka and coworkers reported an enantioselective bromolactonization of 5-substituted 5-hexenoic acids catalyzed by a trisimidazoline catalyst in the presence of DBDMH as the bromine source [130]. A bifunctional cinchonidine catalyst was described by Tang and coworkers, affording high enantioselective bromolactonization of (*Z*)-enynes, using NBS [131]. A bromolactonization of unsaturated carboxylic acid was reported by Yeung and coworkers using an amino-thiocarbamate catalyst and NBS as the bromine source, yielding chiral γ-lactones with almost quantitative yield and high enantioselectivity [132]. A unique synthesis of axially chiral compounds was reported by Miller and coworkers by means of a catalytic bromination using a tripeptide-derived catalyst. The reaction proceeded through an atropisomer-selective electrophilic aromatic substitution reaction using NBS and *N*-bromophthalimide (NBP) as bromine sources [133].

The organocatalytic enantioselective bromoamination reaction of allylic alcohols using newly designed cinchona-derived thiourea as catalyst and *N*,*N*-dibromo-4-nitrobenzenesulfonamide as bromine and amine source led to the formation of enantioenriched vicinal bromoamines with good yields and high to excellent enantioselectivities [134]. The scope of the catalyst revealed that the presence of strongly electron-rich substituents was detrimental to the enantioselectivity. The steric bulk at the *para* position of the phenyl thiourea and the interaction between the substrate OH group and the catalyst played an important role in the enantioinduction.

Several organocatalytic bromocyclization reactions have recently been developed. The following two studies based on halogenation-induced carbocyclization are important, although it is noteworthy that they are not enantioselective. The bromocyclization of geranyl derivatives catalyzed by electron-deficient thioureas using NBS afforded a 1 : 1 mixture of *endo*- and *exo*-isomers [135]. The reactivity of the bromocyclization was found to be highly dependent on the solvent and the protecting group of the hydroxy group. In this sense, a geranyl *tert*-butyldimethylsilyl (TBS) ether was rapidly converted into the corresponding product, while the analogous geranyl acetate did not undergo bromocyclization under the same conditions. A halogen bond catalyzed the bromo-carbocyclization of *N*-cinnamyl sulfonamides and *O*-cinnamyl phenyl ethers catalyzed by *N*-methyl 4-iodopyridinium triflate was reported using DBDMH as the halogen source with good yields and excellent diastereoselectivities (dr > 99 : 1) [136].

13.7.3.2. Bromofunctinalization of Carbonyl Compounds Enantioselective α-bromination of aldehydes has been reported using chiral secondary amines as organocatalyst (Scheme 13.43). The first organocatalytic enantioselective α-bromination of aldehydes and ketones was reported by Jørgensen and coworkers in 2005, using C_2-symmetric chiral secondary amine catalysts [137]. The α-bromination of aldehydes was performed in the presence of (2*R*,5*R*)-diphenylpyrrolidine (**CAT23**), using 4,4-dibromo-2,6-di-*tert*-butyl-cyclohexa-2,5-dienone as the bromine source, yielding α-brominated aldehydes in high yields and

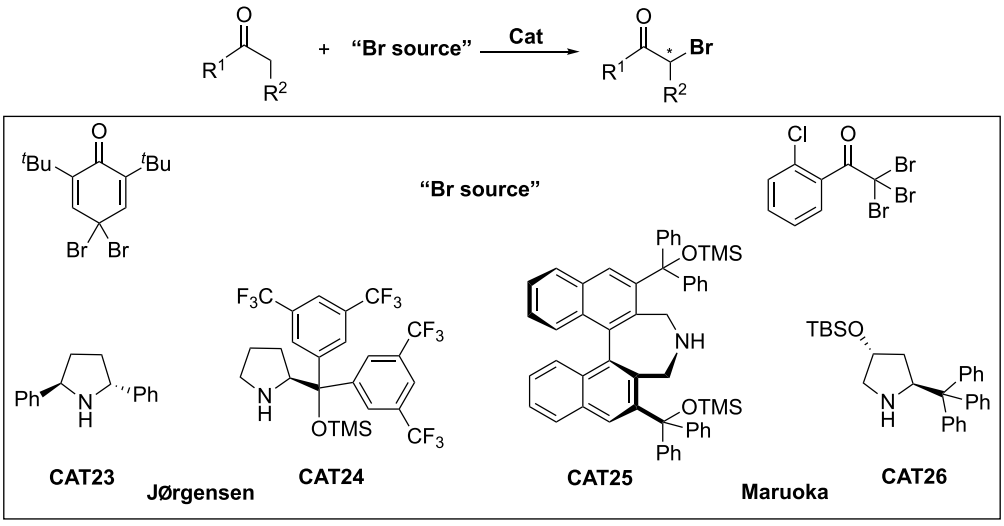

Scheme 13.43. Organocatalysts used in the asymmetric α-bromination of aldehydes.

enantioselectivities (92–95% ee), while ketones were α-brominated by a C_2-symmetric imidazolidine in good yields (72–95%) and up to 94% ee. Jørgensen and coworkers also synthesized a trifluoro pyrrolidine-based organocatalyst (**CAT24**) for the α-functionalization of aldehydes for the stereogenic formation of C–C, C–N, C–F, C–Br, and C–S bonds in good to high yields, and *S*-enantiomers were obtained with excellent enantioselectivities [138]. Maruoka and coworkers reported the use of a binaphthyl-based catalyst (**CAT25**) for the α-bromination of aldehydes using the same bromine source in good yields (71–94%) and high enantioselectivities for the *R*-enantiomer (92–99% ee) [139]. Recently, Maruoka's group reported the α-bromination of aldehydes catalyzed by a pyrrolidine-based amine (**CAT26**) catalyst in combination with a ketone-based brominating agent (2,2,2-tribromoacetophenone) bearing a chlorine atom at the *ortho*-position [140]. α-Bromination of aldehydes was accomplished in good yields (84–99%) and high enantioselectivities (83–97% ee) using a low catalyst loading in toluene.

13.8. ASYMMETRIC CARBON–IODINE BOND FORMATION

Much like previous examples with other halogen atoms, reports detailing the controlled formation of chiral carbon–iodine bonds are mainly based on the addition of an electrophilic iodine species across a double bond with concomitant trapping or stabilizing of the transient addition product. Despite Ishihara and coworkers' seminal contribution in 2007 in which the electrophilic halogen was trapped in a cascade of carbon-based nucleophiles [141], the trapping agent is often a pendent nucleophilic nitrogen or oxygen-based group, and as such iodoaminations or iodolactonizations are common in this field of study. As a side note, it should be mentioned that several reports compiled in this section include the formation of products bearing a chiral R*CH_2I group rather than a chiral R*I bond, due to the intertwined mechanism of formation of the two products when discussing intramolecular iodoamination/lactonization reactions (Scheme 13.44).

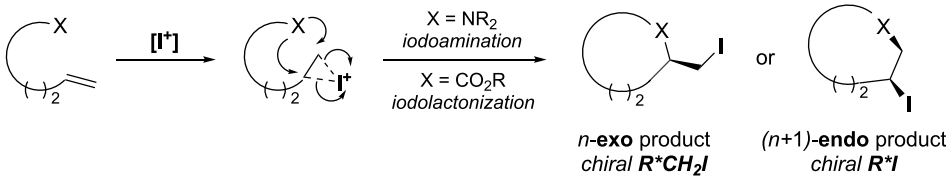

Scheme 13.44. Mechanism of cyclization by iodoamination or iodolactonization; formation of either chiral R*I or R*CH_2I groups.

13.8.1. Iodoaminations

In 2013, Jacobsen's group reported an elegant synthesis of chiral β-iodoamines through iodocyclization of trichloroacetamides catalyzed by chiral ureas (**CAT27** and **CAT28**) (Scheme 13.45) [142], based on the group's past experience with iodolactonizations [143]. In that case, *N*-iodosuccinimide was found to be the optimal electrophilic iodine donor, and the best catalyst was found to be **CAT27**. The reaction was suitable for substrates bearing a range of functional groups, although the scope was mainly restricted to α-styrenyl double bonds.

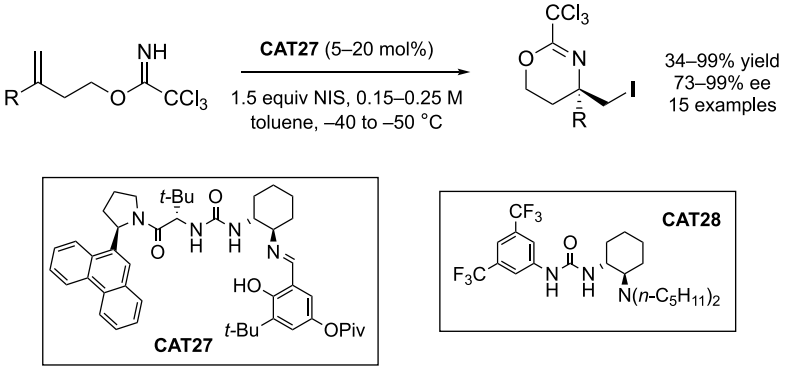

Scheme 13.45. Asymmetric iodoamination reaction developed by Jacobsen's group. Source: [142]/Royal Society of Chemistry.

Interestingly, catalyst **CAT28** that had previously been optimized for similar iodolactonization reactions induced little enantioselectivity here, and the salicylaldimine moiety bearing a free OH group was found to play an important role. The group speculated that this could be due to two things: (i) restriction of catalyst conformation through an intramolecular hydrogen bond, and (ii) an interaction with the basic imidate formed during the cyclization. Furthermore, **CAT27** was shown to be a phase transfer catalyst, shifting the insoluble *N*-iodosuccinimide (NIS) into the reaction media as well as promoting the reaction with the trichloroacetimide substrate.

Tripathi and Mukherjee documented a novel organocatalytic iodoaminocyclization using β,γ-unsaturated hydrazones [144], building on their past experience with oximes [145]. The combination of nonsymmetrical *N*-iodopyrrolidinone (NIP) and *trans*-1,2-diaminocyclohexane-derived thiourea **CAT29** as the catalyst provided the best conditions in terms of yield and enantioselectivity (Scheme 13.46).

Thus, they were able to achieve both high yields and enantioselectivities under the optimum conditions, which were found to be –80 °C in a 1 : 1 mixture of dichloromethane and toluene and in the presence

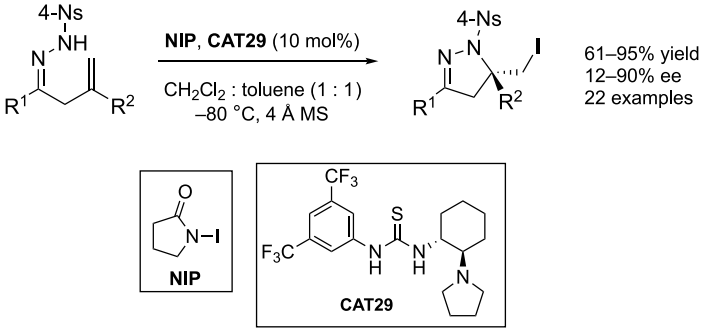

Scheme 13.46. Iodoaminocyclization procedure developed by Tripathi and Mukherjee.

of molecular sieves. Despite a favorable outcome with a variety of aromatic substrates, three distinct cases were identified as dramatically lowering the enantioselectivity of the process: (i) an electron-rich group such as *para*-methoxyphenyl on the double bond; (ii) a sterically hindered 2-chlorophenyl group on the hydrazone moiety, although the similarly positioned 2-naphthyl group resulted in a high 90% ee; and (iii) aliphatic substituents in either position. Furthermore, the protecting group of the hydrazone was also found to affect the reaction, the most effective being the 4-nitrobenzenesulfonyl (4-Ns) group.

Mizar and coworkers also reported a simple and efficient enantioselective iodoaminocyclization procedure in 2014, in which they explored the interaction between their novel cyclic thiourea-based catalyst **CAT30**, NIS, and certain additives (Scheme 13.47) [146]. Intriguingly, they found that the addition of KBr to the reaction mixture changed the regioselectivity of the reaction and led exclusively to the

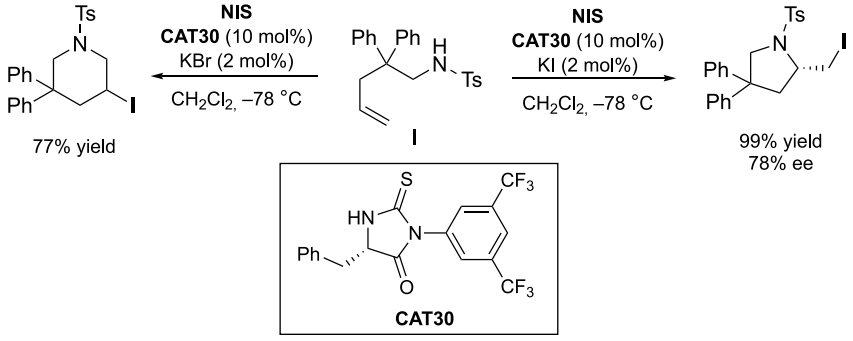

Scheme 13.47. Effects of KBr vs KI additive in the iodoaminocyclization reaction of **I**.

tetrahydropyridine derivative. However, when KI or I_2 was used as the additive, the chiral five-membered ring turned out to be product. Furthermore, the authors were able to achieve similarly high enantioselectivities when a substituted olefin was used as the substrate, resulting in a chiral tetrasubstituted center.

In 2016, Lebée, Blanchard, and Masson reported the TRIP-catalyzed addition of NIS to the double bond of enecarbamates (Scheme 13.48) [147]. This was compared with the analogous addition of NCS to

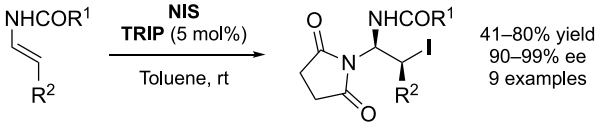

Scheme 13.48. TRIP-catalyzed enantioselective addition of NIS to enecarbamates. Source: [147]/Georg Thieme Verlag Stuttgart.

the same substrates, and the authors found that in the latter case, the calcium salt of TRIP had to be used. This meant that while the enantioselectivity of the addition of NIS was dependent on the TRIP catalyst, the addition of NCS was more greatly affected by the substrate in question. Therefore, the addition of NIS resulted in higher enantioselectivities than its chlorine analog, tolerating a range of substitutions at both the nitrogen in the carbamate and the double bond. This reaction stands out for its simplicity; the reagents and catalyst were stirred in anhydrous toluene at room temperature for 2 hours for the reaction to complete.

More recently, Struble and coworkers described the synthesis of chiral ureas starting from allylic amines via an amine-isocyanate capture/iodoaminocyclization mechanism (Scheme 13.49) [148]. This work comes from a long line of research within the Johnston group, starting with the first seminal iodolactonization reaction with the same class of BAM catalysts in 2012 [149] and followed by a carbon dioxide trapping iodolactonization in 2015 [150]. Seeking to exploit this reaction in the formation of the analogous

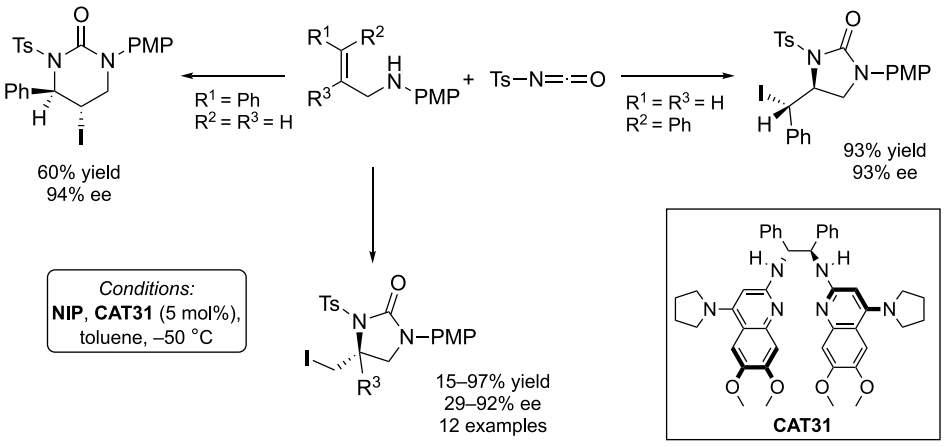

Scheme 13.49. Formation of chiral cyclic ureas described by Struble and coworkers. Source: [148]/American Chemical Society.

six-membered cyclic urea, the group then explored different *E* and *Z*-1,2-disubstituted double bonds, and found that the *Z* isomer favored the 5-*exo* cyclization, whereas the analogous *E* isomer favored the six-membered product resulting from the 6-*endo* cyclization. A small series of the six-membered cyclic ureas was synthesized, with respectable ee as long as the R^1 substituent was larger than R^2. The value of this reaction was then demonstrated in the synthesis of an imidazolidinone NK_1 antagonist.

A year later, in 2019, the group combined this methodology with their knowledge of CO_2 trapping [151]. In this case, however, the catalyst performed better in the form of a triflimidate salt due to the reduced reactivity of the intermediate carbamic acid when compared to the carbonic acid in the related iodolactonization. Under these conditions, the group was able to perform the reaction to form an array of iodinated chiral cyclic carbamates with high yields and enantioselectivities across the board (Scheme 13.50).

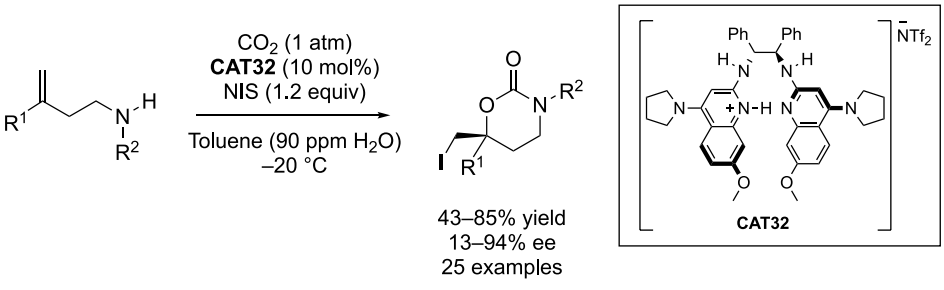

Scheme 13.50. Iodoamination with concomitant trapping of CO_2.

13.8.2. Iodolactonizations

First, it should be mentioned that an excellent review was published specifically on the topic of iodolactonizations in 2019 by Kristianlund et al. [152]. Therefore, this section will only cover more recent research not described therein.

Arai and coworkers reported an interesting enantioselective iodolactonization reaction catalyzed by BINOL-based ligands coordinated to three zinc centers [153]. The authors studied a range of ligands to optimize the reaction and found that the best results were obtained with catalyst **L23**-$Zn(OAc)_2$ complex (**tri-Zn**), a chiral ligand of Zn acetate, in which three zinc centers could be coordinated to the ligand at

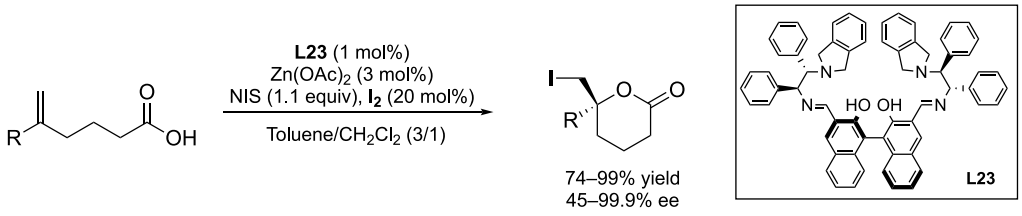

Scheme 13.51. Enantioselective iodolactonizations catalyzed by tri-Zn complexes.

the same time. The group used these optimal conditions to study the scope of the reaction to form a series of six-membered lactones (Scheme 13.51). Although the scope was limited to substrates bearing an aromatic or heteroaromatic group on the double bond, the yields were generally excellent and the enantioselectivity was high in most cases. Electron-neutral and electron-poor aromatic rings were well tolerated, although the electron-rich *para*-methoxyphenyl substituent resulted in lower enantioselectivity.

The authors also carried out elegant desymmetrization reactions, successfully cyclizing a variety of diallyl acetic acid derivatives with high diastereo- and enantioselectivities across the board (Scheme 13.52). The reaction only faltered slightly when a substrate bore an *ortho*-tolyl substituent at the double bond, although the system still achieved a respectable 79% ee even in this case.

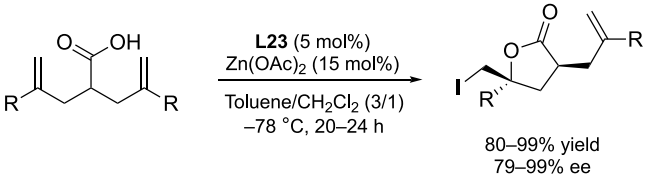

Scheme 13.52. Desymmetrization of diallylacetic acid derivatives catalyzed by tri-Zn complexes.

The Johnston group also published an elegant desymmetrization reaction by iodolactonization of cyclic carboxylic acids in 2018 [154]. Once again, the group utilized a BAM-based catalyst **CAT33** to achieve the best yields and enantioselectivities of the desired bridged bicyclic lactones (Scheme 13.53). These iodine-bearing products could also be further transformed into useful compounds such as diols.

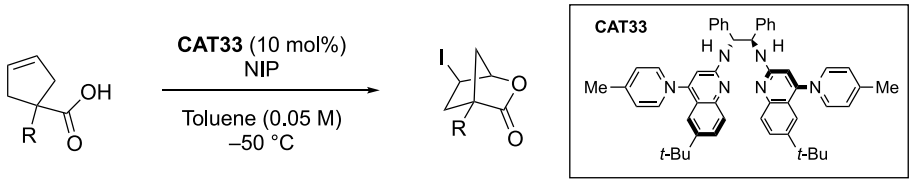

Scheme 13.53. Desymmetrization reaction described by the Johnston group.

13.9. CONCLUSIONS

The chapter covers the methods reported in the last 10 years concerning the generation of chiral carbons bonded to the four common halogens. Among the strategies described, the halofunctionalization of double bonds is the most general, having been applied from fluorine to iodine. Overall, procedures related to the incorporation of fluorine atoms are quantitatively more common, probably due to the significance of organofluorine compounds as drugs or agrochemicals.

ACKNOWLEDGMENTS

The authors thank the Spanish Ministerio de Ciencia, Innovación y Universidades (MICINN) and Agencia Estatal de Investigación (AEI) for their financial support (CTQ2017-84249-P). The authors are also grateful to the Hungarian Research Foundation (NKFIH No K 119282) for its financial support. The financial support of the GINOP-2.3.2-15-2016-00038 project is also acknowledged. This research was supported by the EU-funded Hungarian grant EFOP-3.6.1-16-2016-00008. Ministry of Human Capacities, Hungary (grant 20391-3/2018/FEKUSTRAT), is also acknowledged.

REFERENCES

1. Y. Zhu, J. Han, J. Wang, N. Shibata, M. Sodeoka, V. A. Soloshonok, J. A. S. Coelho, F. D. Toste, *Chem. Rev.* **2018**, *118*, 3887–3964.
2. P. A. Champagne, J. Desroches, J.-D. Hamel, M. Vandamme, J.-F. Paquin, *Chem. Rev.* **2015**, *115*, 9073–9174.
3. Ch. Chen, L. Fu, P. Chen, G. Liu, *Chin. J. Chem.* **2017**, *35*, 1781–1788.
4. X. Yang, T. Wu, R. J. Phipps, F. D. Toste, *Chem. Rev.* **2015**, *115*, 826–870.
5. S. E. Brenner-Moyer, Stereoselective Organocatalysis: Bond Formation Methodologies and Activation Modes, First Edition. Edited by R. Rios Torres, **2013**, John Wiley & Sons, Inc., Hoboken, NJ, pp. 465–492.
6. M. Tredwell, K. Tenza, M. C. Pacheco, V. Gouverneur, *Org. Lett.* **2005**, *7*, 4495–4497.
7. M. H. Katcher, A. G. Doyle, *J. Am. Chem. Soc.* **2010**, *132*, 17402–17404.
8. M. H. Katcher, A. Sha, A. G. Doyle, *J. Am. Chem. Soc.* **2011**, *133*, 15902–15905.
9. A. M. Lauer, J. Wu, *Org. Lett.* **2012**, *14*, 5138–5141.
10. Q. Zhang, D. P. Stockdale, J. C. Mixdorf, J. J. Topczewski, H. M. Nguyen, *J. Am. Chem. Soc.* **2015**, *137*, 11912–11915.
11. E. P. A. Talbot, T. A. Fernandes, J. M. McKenna, F. D. Toste, *J. Am. Chem. Soc.* **2014**, *136*, 4101–4104.
12. Y. He, Zh. Yang, R. T. Thornbury, F. D. Toste, *J. Am. Chem. Soc.* **2015**, *137*, 12207–12210.
13. J. Miró, C. del Pozo, F. D. Toste, S. Fustero, *Angew. Chem. Int. Ed.* **2016**, *55*, 9045–9049.
14. (a) Y. Hamashima, K. Yagi, H. Takano, L. Tamás, M. Sodeoka, *J. Am. Chem. Soc.* **2002**, *124*, 14530–14531. (b) Sh. Suzuki, Y. Kitamura, S. Lectard, Y. Hamashima, M. Sodeoka, *Angew. Chem. Int. Ed.* **2012**, *51*, 4581–4585.
15. N. Gao, X.-M. Zhao, Ch-S. Cai, J.-W. Cai, *Org. Biomol. Chem.* **2015**, *13*, 9551–9558.
16. Zh. Jiao, J. J. Beiger, Y. Jin, Sh. Ge, J. S. Zhou, J. F. Hartwig, *J. Am. Chem. Soc.* **2016**, *138*, 15980–15986.
17. X. Yang, R. J. Phipps, F. D. Toste, *J. Am. Chem. Soc.* **2014**, *136*, 5225–5228.
18. Y. Liang, G. C. Fu, *J. Am. Chem. Soc.* **2014**, *136*, 5520–5524.
19. Y. Zhu, Y. Mao, H. Mei, Y. Pan, J. Han, V. A. Soloshonok, T. Hayashi, *Chem. Eur. J.* **2018**, *24*, 8994–8998.
20. X. Liu, J. Zhang, L. Zhao, Sh. Ma, D. Yang, W. Yan, R. Wang, *J. Org. Chem.* **2015**, *80*, 12651–12658.
21. Y-Z. Liu, S.-J. Shang, W.-L. Yang, X. Luo, W.-P. Deng, *J. Org. Chem.* **2017**, *82*, 11141–11149.
22. Y. Liu, Ch. Chen, H. Li, K.-W. Huang, J. Tan, Zh. Weng, *Organometallics* **2013**, *32*, 6587–6592.
23. T. Hashimoto, K. Maruoka, *Chem. Rev.* **2007**, *107*, 5656–5682.
24. J. Schörgenhumer, M. Tiffner, M. Waser, *Beilstein J. Org. Chem.* **2017**, *13*, 1753–1769.
25. (a) G. Pupo, F. Ibba, D. M. H. Ascough, A. C. Vicini, P. Ricci, K. E. Christensen, L. Pfeifer, J. R. Morphy, J. M. Brown, R. S. Paton, V. Gouverneur, *Science* **2018**, *360*, 638–642. (b) G. Pupo, A. C. Vicini, D. M. H. Ascough, F. Ibba, K. E. Christensen, A. L. Thompson, J. M. Brown, R. S. Paton, V. Gouverneur, *J. Am. Chem. Soc.* **2019**, *141*, 2878–2883. (c) G. Roagna, D. M. H. Ascough, F. Ibba, A. C. Vicini, A. Fontana, K. E. Christensen, A. Peschiulli, D. Oehlrich, A. Misale, A. A. Trabanco, R. S. Paton, G. Pupo, V. Gouverneur, *J. Am. Chem. Soc.* **2020**, *142*, 14045–14051.
26. S. Peng, Z. Wang, L. Zhang, X. Zhang, Y. Huang, *Nat. Commun.* **2018**, *9*, 375.
27. R.J. Phipps, K. Hiramatsu, F. D. Toste, *J. Am. Chem. Soc.* **2012**, *134*, 8376–8379.
28. T. Honjo, R. J. Phipps, V. Rauniyar, F. D. Toste, *Angew. Chem. Int. Ed.* **2012**, *51*, 9684–9688.
29. (a) X. Wang, Q. Lan, S. Shirakawa, K. Maruoka, *Chem. Commun.* **2010**, *46*, 321–323. (b) E.-M. Tanzer, W. B. Schweizer, M.-O. Ebert, R. Gilmour, *Chem. Eur. J.* **2012**, *18*, 2006–2013. (c) J. Luo, W. Wu, L.-W. Xu, Y. Meng, Y. Lu, *Tetrahedron Lett.* **2013**, *54*, 2623–2626. (d) J. Novacek, M. Waser, *Eur. J. Org. Chem.* **2014**, 802–809. (e) B. Wang, Y. He, X. Fu, Z. Wei, Y. Lin, H. Duan, *Synlett* **2015**, *26*, 2588–2592. (f) B. Zhang, L. Shi, R. Guo, S. Liu, *ARKIVOC* **2016**, 363–370.
30. T. Niwa, K. Ujiie, H. Sato, H. Egami, Y. Hamashima, *Chem. Pharm. Bull.* **2018**, *66*, 920–922.
31. H. Egami, T. Niwa, H. Sato, R. Hotta, D. Rouno, Y. Kawato, Y. Hamashima, *J. Am. Chem. Soc.* **2018**, *140*, 2785–2788.
32. V. Rauniyar, A. D. Lackner, G. L. Hamilton, F. D. Toste, *Science* **2011**, *334*, 1681–1684.
33. H. P. Shunatona, N. Früh, Y.-M. Wang, V. Rauniyar, F. D. Toste, *Angew. Chem. Int. Ed.* **2013**, *52*, 7724–7727.
34. H. Egami, J. Asada, K. Sato, D. Hashizume, Y. Kawato, Y. Hamashima, *J. Am. Chem. Soc.* **2015**, *137*, 10132–10135.
35. W. Zi, Y.-M. Wang, F. D. Toste, *J. Am. Chem. Soc.* **2014**, *136*, 12864–12867.
36. A. J. Neel, A. Milo, M. S. Sigman, F. D. Toste, *J. Am. Chem. Soc.* **2016**, *138*, 3863–3875.

37. J. A. S. Coelho, A. Matsumoto, M. Orlandi, M. J. Hilton, M. S. Sigman, F. D. Toste, *Chem. Sci.* **2018**, *9*, 7153–7158.
38. (a) F. Romanov-Michailidis, L. Guénée, A. Alexakis, *Angew. Chem. Int. Ed.* **2013**, *52*, 9266–9270. (b) F. Romanov-Michailidis, M. Pupier, L. Guénée, A. Alexakis, *Chem. Commun.* **2014**, *50*, 13461–13464.
39. F. Romanov-Michailidis, M. Pupier, C. Besnard, T. Bürgi, A. Alexakis, *Org. Lett.* **2014**, *16*, 4988–4991.
40. H. Egami, T. Rouno, T. Niwa, K. Masuda, K. Yamashita, Y. Hamashima, *Angew. Chem. Int. Ed.* **2020**, *59*, 14101–14105.
41. R. J. Phipps, F. D. Toste, *J. Am. Chem. Soc.* **2013**, *135*, 1268–1271.
42. (a) X.-W. Liang, C. Liu, W. Zhang, S.-L. You, *Chem. Commun.* **2017**, *53*, 5531–5534. (b) X.-W. Liang, Y. Cai, S.-L. You, *Chin. J. Chem.* **2018**, *36*, 925–928. (c) H. Egami, R. Hotta, M. Otsubo, T. Rouno, T. Niwa, K. Yamashita, Y. Hamashima, *Org. Lett.* **2020**, *22*, 5656–5660.
43. D. W. C. MacMillan, *Nature* **2008**, *455*, 304–308.
44. (a) N. Shibata, E. Suzuki, Y. Takeuchi, *J. Am. Chem. Soc.* **2000**, *122*, 10728–10729. (b) D. Cahard, C. Audouard, J.-C. Plaquevent, N. Roques, *Org. Lett.* **2000**, *2*, 3699–3701.
45. T. Yamamoto, Y. Suzuki, E. Ito, E. Tokunaga, N. Shibata, *Org. Lett.* **2011**, *13*, 470–473.
46. O. Lozano, G. Blessley, T. M. del Campo, A. L. Thompson, G. T. Giuffredi, M. Bettati, M. Walker, R. Borman, V. Gouverneur, *Angew. Chem. Int. Ed.* **2011**, *50*, 8105–8109.
47. (a) T. D. Beeson, D. W. C. MacMillan, *J. Am. Chem. Soc.* **2005**, *127*, 8826–8828. (b) M. Marigo, D. Fielenbach, A. Braunton, A. Kjærsgaard, K. A. Jørgensen, *Angew. Chem. Int. Ed.* **2005**, *44*, 3703–3706.
48. (a) N. Kojima, H. Hayashi, H. Iwasaki, M. Yamashita, *Chem. Pharm. Bull.* **2020**, *68*, 675–678. (b) X.-G. Hu, A. Lawer, M. B. Peterson, H. Iranmanesh, G. E. Ball, L. Hunter, *Org. Lett.* **2016**, *18*, 662–665. (c) M. L. Schulte, C. W. Lindsley, *Org. Lett.* **2011**, *13*, 5684–5687. (d) P. J. Chevis, S. Wangngae, T. Thaima, A. W. Carroll, A. C. Willis, M Pattarawarapan, S. G. Pyne, *Chem. Commun.* **2019**, *55*, 6050–6053. (e) A. Quintard, J. Rodriguez, *ACS Catal.* **2017**, *7*, 5513–5517. (f) K. Fjelbye, M. Marigo, R. P. Clausen, K. Juhl, *Org. Lett.* **2016**, *18*, 1170–1173.
49. P. Garcia-Losada, M. Barberis, Y. Shi, E. Hembre, C. A. Jimenez, L. L. Winneroski, B. M. Watson, C. Jones, A.C. DeBaillie, F. Martínez-Olid, D. J. Mergott, *Org. Process Res. Dev.* **2018**, *22*, 650–654.
50. (a) M. R. Witten, E. N. Jacobsen, *Org. Lett.* **2015**, *17*, 2772–2775. (b) K. Shibatomi, K. Kitahara, T. Okimi, Y. Abe, S. Iwasa, *Chem. Sci.* **2016**, *7*, 1388–1392. (c) L. Cui, Y. You, X. Mi, S. Luo, *J. Org. Chem.* **2018**, *83*, 4250–4256.
51. C. Appayee, S. E. Brenner-Moyer, *Org. Lett.* **2010**, *12*, 3356–3359.
52. S. Arimitsu, T. Yonamine, M. Higashi, *ACS Catal.* **2017**, *7*, 4736–4740.
53. P. Kwiatkowski, T. D. Beeson, J. C. Conrad, D. W. C. MacMillan, *J. Am. Chem. Soc.* **2011**, *133*, 1738–1741.
54. H. Yasui, T. Yamamoto, T. Ishimaru, T. Fukuzumi, E. Tokunaga, K. Akikazu, M. Shiro, N. Shibata, *J. Fluorine Chem.* **2011**, *132*, 222–225.
55. Y.-h. Lam, K. N. Houk, *J. Am. Chem. Soc.* **2014**, *136*, 9556–9559.
56. S. J. Shaw, D. A. Goff, L. A. Boralsky, M. Irving, R. Singh, *J. Org. Chem.* **2013**, *78*, 8892–8897.
57. Y. You, L. Zhang, S. Luo, *Chem. Sci.* **2017**, *8*, 621–626.
58. W.-B. Yi, X. Huang, Z. Zhang, D.-R. Zhu, C. Cai, W. Zhang, *Beilstein J. Org. Chem.* **2012**, *8*, 1233–1240
59. K. Mori, A. Miyake, T. Akiyama, *Chem. Lett.* **2014**, *43*, 137–139.
60. (a) J. Xu, Y. Hu, D. Huang, K.-H. Wang, C. Xu, T. Niu, *Adv. Synth. Catal.* **2012**, *354*, 515–526. (b) L. Zou, X. Bao, H. Zhang, Y. Song, J. Qu, B. Wang, *Aust. J. Chem.* **2014**, *67*, 1115–1118.
61. (a) X. Jiang, H. Wang, H. He, W. Wang, Y. Wang, Z. Ke, Y.-Y. Yeung, *Adv. Synth. Catal.* **2018**, *360*, 4710–4714. (b) T. Ishimaru, N. Shibata, T. Horikawa, N. Yasuda, S. Nakamura, T. Toru, M. Shiro, *Angew. Chem. Int. Ed.* **2008**, *47*, 4157–4161. (c) Y. Zhang, X.-J. Yang, T. Xie, G.-L. Chen, W.-H. Zhu, X.-Q. Zhang, X.-Y. Yang, X.-Y. Wu, X.-P. He, H.-M. He, *Tetrahedron* **2013**, *69*, 4933–4937.
62. S. Y. Lee, S. Neufeind, G. C. Fu, *J. Am. Chem. Soc.* **2014**, *136*, 8899–8902.
63. Z.-M. Chen, B.-M. Yang, Z.-H. Chen, Q.-W. Zhang, M. Wang, Y.-Q. Tu, *Chem. Eur. J.* **2012**, *18*, 12950–12954.
64. H. Wang, Y. Wang, S. Liu, Y. Mai, X. Zong, H. Gao, R. Hu, X. Jiang, Y.-Y. Yeung, *Adv. Synth. Catal.* **2019**, *361*, 5334–5339
65. F. Li, Z. Wu, J. Wang, *Angew. Chem. Int. Ed.* **2015**, *54*, 656–659.
66. X. Dong, W. Yang, W. Hu, J. Sun, *Angew. Chem. Int. Ed.* **2015**, *54*, 660–663.
67. L. Wang, X. Jiang, J. Chen, Y. Huang, *Angew. Chem. Int. Ed.* **2019**, *58*, 7410–7414.
68. Y.-M. Zhao, M. Sing Cheung, Z. Lin, J. Sun, *Angew. Chem. Int. Ed.* **2012**, *51*, 10359–10363.
69. E. M. Woerly, S. M. Banik, E. N. Jacobsen, *J. Am. Chem. Soc.* **2016**, *138*, 13858–13861.
70. I. G. Molnár, R. Gilmour, *J. Am. Chem. Soc.* **2016**, *138*, 5004–5007.
71. W. Kong, P. Feige, T. de Haro, C. Nevado, *Angew. Chem. Int. Ed.* **2013**, *52*, 2469–2473.
72. K. M. Mennie, S. M. Banik, E. C. Reichert, E. N. Jacobsen, *J. Am. Chem. Soc.* **2018**, *140*, 4797–4802.
73. S. M. Banik, J. W. Medley, E. N. Jacobsen, *J. Am. Chem. Soc.* **2016**, *138*, 5000–5003.
74. M. K. Haj, S. M. Banik, E. N. Jacobsen, *Org. Lett.* **2019**, *21*, 4919–4923.
75. F. Scheidt, M. Schäfer, J. C. Sarie, C. G. Daniliuc, J. J. Molloy, R. Gilmour, *Angew. Chem. Int. Ed.* **2018**, *57*, 16431–16435.
76. (a) S. Suzuki, T. Kamo, K. Fukushi, T. Hiramatsu, E. Tokunaga, T. Dohi, Y. Kita, N. Shibata, *Chem. Sci.* **2014**, *5*, 2754–2760. (b) R. Pluta, P. E. Krach, L. Cavallo, L. Falivene, M. Rueping, *ACS Catal.* **2018**, *8*, 2582–2588. (c) Y. Wang, H. Yuan, H. Lu, W.-H. Zheng, *Org. Lett.* **2018**, *20*, 2555–2558.

77. M. Ueda, T. Kano, K. Maruoka, *Org. Biomol. Chem.* **2009**, *7*, 2005–2012.
78. A. Quintard, A. Alexakis, *Adv. Synth. Catal.* **2010**, *352*, 1856–1860.
79. A. Gutierrez Collar, C. Trujillo, S. J. Connon, *Chem. Eur. J.* **2019**, *25*, 7270–7274.
80. V. Wedek, R. Van Lommel, C. G. Daniliuc, F. De Proft, U. Hennecke, *Angew. Chem. Int. Ed.* **2019**, *58*, 9239–9243.
81. K. C. Nicolaou, N. L. Simmons, Y. Ying, P. M. Heretsch, J. S. Chen, *J. Am. Chem. Soc.* **2011**, *133*, 8134–8137.
82. B. Soltanzadeh, A. Jaganathan, Y. Yi, H. Yi, R. J. Staples, B. Borhan, *J. Am. Chem. Soc.* **2017**, *139*, 2132–2135.
83. U. Hennecke, *Chem. Asian J.* **2012**, *7*, 456–465.
84. A. Jaganathan, A. Garzan, D. C. Whitehead, R. J. Staples, B. Borhan, *Angew. Chem. Int. Ed.* **2011**, *50*, 2593–2596.
85. Q. Cao, J. Luo, X. Zhao, *Angew. Chem. Int. Ed.* **2019**, *58*, 1315–1319.
86. A. Jaganathan, R. J. Staples, B. Borhan, *J. Am. Chem. Soc.* **2013**, *135*, 14806–14813.
87. M. Marigo, N. Kumaragurubaran, K. A. Jögensen, *Chem. Eur. J.* **2004**, *10*, 2133–2137.
88. Y. Naganawa, T. Aoyama, K. Kato, H. Nishiyama, *ChemistrySelect* **2016**, *1*, 1938–1942.
89. A. J. Cresswell, S. T.-C. Eey, S. E. Denmark, *Angew. Chem. Int. Ed.* **2015**, *54*, 15642–15682.
90. P. Zhou, Y. Cai, X. Zhong, W. Luo, T. Kang, J. Li, X. Liu, L. Lin, X. Feng, *ACS Catal.* **2016**, *6*, 7778–7783.
91. C. B. Tripathi, S. Mukherjee, *Synlett* **2014**, *25*, 163–169.
92. (a) Y. F. Cai, X. H. Liu, J. Jiang, W. L. Chen, L. L. Lin, X. M. Feng, *J. Am. Chem. Soc.* **2011**, *133*, 5636–5639. (b) Y. Cai, X. Liu, P. Zhou, Y. Kuang, L. Lin, X. M. Feng, *Chem. Commun.* **2013**, *49*, 8054–8056.
93. M. T. Bovino, S. R. Chemler, *Angew. Chem. Int. Ed.* **2012**, *51*, 3923–3927.
94. C.-L. Zhu, J.-S. Tian, Z.-Y. Gu, G.-W. Xing, H. Xu, *Chem. Sci.* **2015**, *6*, 3044–3050.
95. S. Karabiyikoglu, A. V. Brethom´e, T. Palacin, R. S. Paton, S. P. Fletcher, *Chem. Sci.* **2020**, *11*, 4125–4130.
96. I. Saikia, A. J. Borah, P. Phukan, *Chem. Rev.* **2016**, *116*, 6837–7042.
97. Y. F. Cai, X. H. Liu, Y. H. Hui, J. Jiang, W. T. Wang, W. L. Chen, L. L. Lin, X. M. Feng, *Angew. Chem. Int. Ed.* **2010**, *49*, 6160–6164.
98. Z. Wang, L. Lin, P. Zhou, X. Liua, X. M. Feng, *Chem. Commun.* **2017**, *53*, 3462–3465.
99. W. Li, P. Zhou, G. Li, L. Lin, X. M. Feng, *Adv. Synth. Catal.* **2020**, *362*, 1982–1987.
100. Y. Cai, X. Liu, P. Zhou, X. M. Feng. *J. Org. Chem.* **2019**, *84*, 1–13.
101. (a) See, Ref. 91. (b) X. Liu, L. Lin, X. M Feng, *Org. Chem. Front.* **2014**, *1*, 298–302.
102. P. Zhou, L. Lin, L. Chen, X. Zhong, X. Liu, X. M. Feng, *J. Am. Chem. Soc.* **2017**, *139*, 13414–13419.
103. P. Zhou, X. Liu, W. Wu, C. Xu, X. M. Feng, *Org. Lett.* **2019**, *21*, 1170–1175.
104. F. J. Seidl, C. Min, J. A. Lopez, N. Z. Burns, *J. Am. Chem. Soc.* **2018**, *140*, 15646–15650.
105. D. Huang, X. Liu, L. Li, Y. Cai, W. Liu, Y. Shi, *J. Am. Chem. Soc.* **2013**, *135*, 22, 8101–8104.
106. W. Liu, H. Pan, H. Tian, Y. Shi, *Org. Lett.* **2015**, *17*, 3956–3959.
107. H. Huang, H. Pan, Y. Cai, M. Liu, H. Tian, Y. Shi, *Org. Biomol. Chem.* **2015**, *13*, 3566–3570.
108. Z. Li, Y. Shi, *Org. Lett.* **2015**, *17*, 5752–5755.
109. H. Pan, H. Huang, W. Liu, H. Tian, Y. Shi, *Org. Lett.* **2016**, *18*, 896–899.
110. X. Tan, H. Pan, H. Tian, Y. Shi, *Sci. China Chem.* **2018**, *61*, 656–659.
111. D. H. Paull, C. Fang, J. R. Donald, A. D. Pansick, S. F. Martin, *J. Am. Chem. Soc.* **2012**, *134*, 27, 11128–11131.
112. K. Ikeuchi, S. Ido, S. Yoshimura, T. Asakawa, M. Inai, Y. Hamashima, T. Kan, *Org. Lett.* **2012**, *14*, 6016–6019.
113. W. Wang, H. He, M. Gan, H. Wang, Y. Wang, X. Jiang, *Adv. Synth. Catal.* **2019**, *361*, 4797–4804.
114. M. Gan, W. Wang, H. Wang, Y. Wang, X. Jiang, *Org. Lett.* **2019**, *21*, 8275–8279.
115. B. Soltanzadeh, A. Jaganathan, R. J. Staples, B. Borhan, *Angew. Chem. Int. Ed.* **2015**, *54*, 9517–9522.
116. X. Zhang, J. Li, H. Tian, Y. Shi, *Chem. Eur. J.* **2015**, *21*, 11658–11663.
117. J. Li, Z. Li, X. Zhang, B. Xua, Y. Shi, *Org. Chem. Front.* **2017**, *4*, 1084–1090.
118. W. Zhang, N. Liu, C. M. Schienebeck, X. Zhou, I. I. Izhar, I. A. Guzeib, W. Tang, *Chem. Sci.* **2013**, *4*, 2652–2656.
119. G.-X. Li, Q.-Q. Fu, X.-M. Zhang, J. Jiang, Z. Tang, *Tetrahedron: Asymmetry* **2012**, *23*, 245–251.
120. Y. Nishikawa, Y. Hamamoto, R. Satoh, N. Akada, S. Kajita, M. Nomoto, M. Miyata, M. Nakamura, C. Matsubara, O. Hará, *Chem. Eur. J.* **2018**, *24*, 18880–18885.
121. Y.-M. Cao, D. Lentz, M. Christmann, *J. Am. Chem. Soc.* **2018**, *140*, 10677–10681.
122. R. C. Samanta, H. Yamamoto, *J. Am. Chem. Soc.* **2017**, *139*, 1460–1463.
123. Y. Sawamura, Y. Ogura, H. Nakatsuji, A. Sakakura, K. Ishihara, *Chem. Commun.* **2016**, *52*, 6068–6071.
124. Y. Lu, H. Nakatsuji, Y. Okumura, L. Yao, K. Ishihara, *J. Am. Chem. Soc.* **2018**, *140*, 6039–6043.
125. T. Zheng, X. Wang, W.-H. Ng, Y.-L. Steve Tse, Y.-Y. Yeung, *Nat. Catal.* **2020**, *3*, 993–1001.
126. S.-N. Yu, Y.-L. Li, J. Deng, *Adv. Synth. Catal.* **2017**, *359*, 2499–2508.
127. Y. Kawato, A. Kubota, H. Ono, H. Egami, Y. Hamashima, *Org. Lett.* **2015**, *17*, 1244–1247.
128. Y. Kawato, H. Ono, A. Kubota, Y. Nagao, N. Morita, H. Egami, Y. Hamashima, *Chem. Eur. J.* **2016**, *22*, 2127–2133.
129. X. Jiang, S. Liu, S. Yang, M. Jing, L. Xu, P. Yu, Y. Wang, Y.-Y. Yeung, *Org. Lett.* **2018**, *20*, 3259–3262.
130. K. Murai, T. Matsushita, A. Nakamura, S. Fukushima, M. Shimura, H. Fujioka, *Angew. Chem. Int. Ed.* **2010**, *49*, 9174–9177.
131. W. Zhang, S. Zheng, N. Liu, J. B. Werness, I. A. Guzei, W. Tang, *J. Am. Chem. Soc.* **2010**, *132*, 3664–3665.

132. L. Zhou, C. K. Tan, X. Jiang, F. Chen, Y.-Y. Yeung, *J. Am. Chem. Soc.* **2010**, *132*, 15474–15476.
133. J. L. Gustafson, D. Lim, S. J. Miller, *Science* **2010**, *328*, 1251–1255.
134. J. Qi, G.-T. Fan, J. Chen, M.-H. Sun, Y.-T. Dong, L. Zhou, *Chem. Commun.* **2014**, *50*, 13841–13844.
135. M. Terazaki, K. Shiomoto, H. Mizoguchi, A. Sakakura, *Org. Lett.* **2019**, *21*, 2073–2076.
136. Y.-C. Chan, Y.-Y. Yeung, *Angew. Chem. Int. Ed.* **2018**, *57*, 3483–3487.
137. S. Bertelsen, N. Halland, S. Bachmann, M. Marigo, A. Braunton, K. A. Jørgensen, *Chem. Commun.* **2005**, 4821–4823.
138. J. Franzén, M. Marigo, D. Fielenbach, T. C. Wabnitz, A. Kjærsgaard, K. A. Jørgensen, *J. Am. Chem. Soc.* **2005**, *127*, 18296–18304.
139. T. Kano, F. Shirozu, K. Maruoka, *Chem. Commun.* **2010**, *46*, 7590–7592.
140. A. Takeshima, M. Shimogaki, T. Kano, K. Maruoka, *ACS Catal.* **2020**, *10*, 5959–5963.
141. A. Sakakura, A. Ukai, K. Ishihara, *Nature* **2007**, *445*, 900
142. C. S. Brindle, C. S. Yeung, E. N. Jacobsen, *Chem. Sci.* **2013**, *4*, 2100–2104.
143. G. E. Veitch, E. N. Jacobsen, *Angew. Chem. Int. Ed.* **2010**, *49*, 7332–7335.
144. C. B. Tripathi, S. Mukherjee, *Org. Lett.* **2014**, *16*, 3368–3371.
145. C. B. Tripathi, S. Mukherjee, *Angew. Chem. Int. Ed.* **2013**, *52*, 8450–8453.
146. P. Mizar, A. Burrelli, E. Günther, M. Söftje, U. Farooq, T. Wirth, *Chem. Eur. J.* **2014**, *20*, 13113–13116.
147. C. Lebée, F. Blanchard, G. Masson, *Synlett.* **2016**, *27*, 559–563.
148. T. J. Struble, H. M. Lankswert, M. Pink, J. N. Johnston, *ACS Catal.* **2018**, *8*, 11926–11931.
149. M. C. Dobish, J. N. Johnston, *J. Am. Chem. Soc.* **2012**, *134*, 6068–6071.
150. B. A. Vara, T. J. Struble, W. Wang, M. C. Dobish, J. N. Johnston, *J. Am. Chem. Soc.* **2015**, *137*, 7302–7305.
151. R. Yousefi, T. J. Struble, J. L. Payne, M. Vishe, N. D. Schley, J. N. Johnston, *J. Am. Chem. Soc.* **2019**, *141*, 618–625.
152. R. Kristianlund, J. E. Tungen, T. V. Hansen, *Org. Biomol. Chem.* **2019**, *17*, 3079–3092.
153. (a) T. Arai, N. Sugiyama, H. Masu, S. Kado, Sh. Yabe, M. Yamanaka, *Chem. Commun.* **2014**, *50*, 8227–8290. (b) T. Arai, K. Horigane, O. Watanabe, J. Kakino, N. Sugiyama, H. Makino, Y. Kamei, S. Yabe, M. Yamanaka, *iScience* **2019**, *12*, 280–292. (c) T. Arai, K. Horigane, T. K. Suzuki, R. Itoh, M. Yamanaka, *Angew. Chem. Int. Ed.* **2020**, *59*, 12680–12683.
154. M. T. Knowe, M. W. Danneman, S. Sun, M. Pink, J. N. Johnston, *J. Am. Chem. Soc.* **2018**, *140*, 1998–2001.

14

ENZYME-CATALYZED ASYMMETRIC SYNTHESIS

Gonzalo de Gonzalo[1] and Andrés R. Alcántara[2]
[1] *Department of Organic Chemistry, University of Seville, Seville, Spain*
[2] *Department of Chemistry in Pharmaceutical Sciences, Section of Organic and Pharmaceutical Chemistry, Faculty of Pharmacy, Complutense University of Madrid, Madrid, Spain*

14.1. TYPES OF BIOCATALYZED PROCESSES

The application of biological systems (whole cells, cell-free extracts, or isolated enzymes) as catalysts in the preparation of optically active compounds has experienced a great development since the beginning of the 1980s, with the seminal work from Zaks and Klibanov [1]. Biocatalysis offers some advantages over other catalytic methodologies, in terms of exquisite enzymatic precision upon chirality recognition, while working under mild and environmentally friendly conditions, and has been widely employed in asymmetric synthesis [2–6]. By this reason, the focus of the current chapter is to illustrate some recently developed stereoselective enzymatic procedures leading to useful products, both at lab and industrial scales.

Several enzymatic procedures use racemic compounds as starting materials. One way to perform the resolution of a racemic substrate to furnish pure enantiomers is through a kinetic resolution (KR), a process based on the different rates at which both enantiomers of the racemic mixture react in presence of the biocatalyst, as shown in Scheme 14.1.

Using this strategy, under ideal conditions, the KR would provide a mixture of two enantiopure compounds, namely, the product ($\mathbf{P}_R$) resulting from the conversion of the fast-reacting enantiomer of the substrate ($\mathbf{S}_R$), and the remnant not-converted substrate $\mathbf{S}_S$; as $\mathbf{P}_R$ and $\mathbf{S}_S$ are chemically different, they can be easily separated. In these processes, the enantiomeric ratio or enantioselectivity (E) is an adimen-

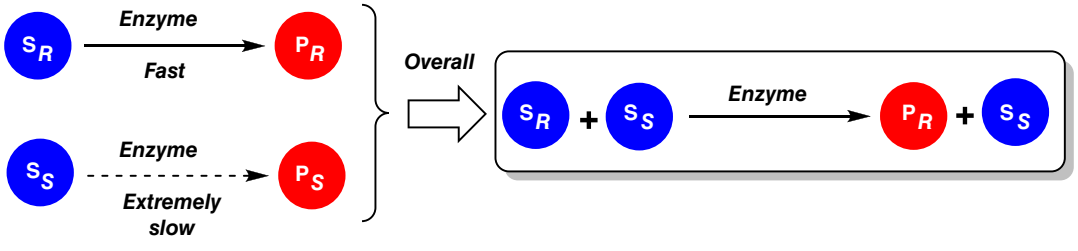

Scheme 14.1. Enzymatic kinetic resolution (*R* isomer is considered the fast-reacting one).

Catalytic Asymmetric Synthesis, Fourth Edition. Edited by Takahiko Akiyama and Iwao Ojima.

sional parameter (ratio of the relative second-order rate constants for both enantiomers) generally used to describe the quality of the KRs [7]. *E* can be calculated from reaction parameters such as the time, the conversion, and enantiomeric excesses of both the substrate and/or the product [8]. Due to the formula used to calculate *E*, the interpretation of this parameter is not that straightforward; thus, as a rule of thumb, *E* values below 15 are inacceptable for practical purposes, being moderate to good in the range of 15–30, and excellent above this value. For a detailed description of this parameter, and how to calculate it in different scenarios (reversible or irreversible reactions), please see Faber's book [9] or Diaz-Rodriguez and Lavandera [10].

In any case, the main drawback of a KR comes from the fact that the maximum theoretical yield for each one of the desired enantiomers (either $\mathbf{P}_R$ or $\mathbf{S}_S$) is limited to 50%. If $\mathbf{P}_R$ is the target compound, the KRs demand the racemization of non-converted $\mathbf{S}_S$ and its subsequent addition to the reaction mixture, in what is sometimes termed as repeated KR (Scheme 14.2). This sequential procedure, not generally applicable on a small scale, can be useful at industrial scale for continuous processes, so that the racemized material can be re-fed into the reaction batch.

A parallel kinetic resolution (PKR) is performed when both enantiomers of the racemic substrate react leading to two different products, which are not optical antipodes (Scheme 14.3).

PKRs avoid the limitation of KRs related to the enrichment of the non-reacting isomer of the racemic compound over time by removing the slow-reacting enantiomer in a different reaction. These PKRs can be classified as chemo-, regio-, or stereodivergent, depending on the enzymatic behavior [10]. Anyhow, the limitation of a maximal theoretical yield of 50% for both products ($\mathbf{P}_R$ and $\mathbf{Q}_S$) is still present.

Then, a logical step for allowing theoretical conversion values up to 100% is to transform KRs into dynamic kinetic resolutions (DKRs). In these systems, both substrate enantiomers are dynamically interconverting through an in situ racemization, so that the enzymatic transformation of the fast-reacting enantiomer can reach completion, as the equilibrium is continuously adjusted because of the permanent racemization of the slow-reacting antipode (Scheme 14.4).

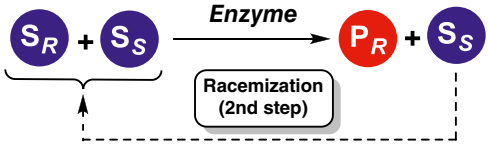

Scheme 14.2. Enzymatic repeated kinetic resolution.

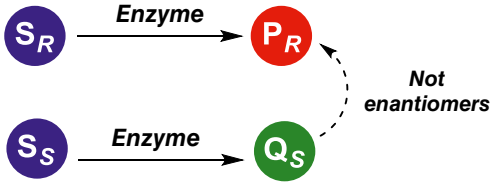

Scheme 14.3. Parallel kinetic resolution (PKR).

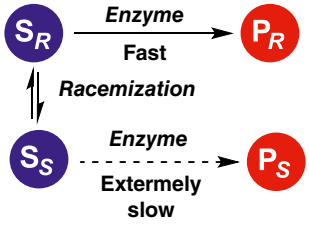

Scheme 14.4. Dynamic kinetic resolution (DKR) general scheme.

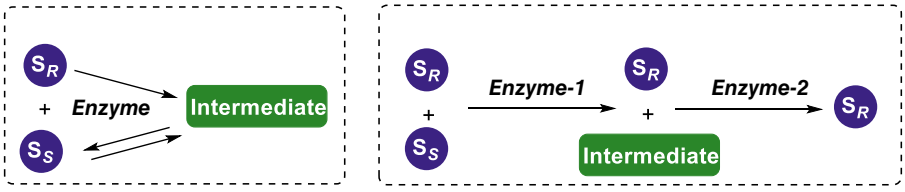

Scheme 14.5. Deracemization procedures for obtaining optically active compounds.

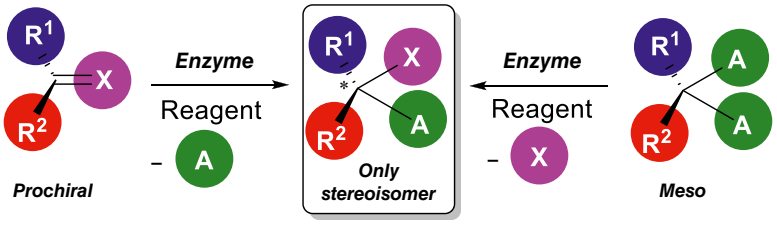

Scheme 14.6. Desymmetrization of prochiral or *meso*-compounds.

Another way to obtain chiral compounds starting from a racemic mixture consists in performing deracemization procedures, in which it is possible to obtain one single enantiomer of a compound starting from the same racemic compound (Scheme 14.5). Deracemizations are very efficient processes, as the desired chiral material is achieved in a single step with high atom economy [11–13]. These processes involve two half-reactions that are opposite in reacting direction; by this reason, redox processes are generally used in deracemizations. One of these half-reactions must be at least enantioselective to ensure an efficient process. Different approaches can be performed to obtain deracemizations, including the stereoinversion, the linear or the cyclic deracemization, and the enantioconvergent processes.

Apart from racemic mixtures, biocatalyzed methodologies have been widely employed in the preparation of enantiomerically enriched compounds starting from prochiral or *meso*-molecules, the so-called desymmetrizations (Scheme 14.6). The chiral products can be obtained with a maximum theoretical yield of 100% in a desymmetrization process, whose selectivity is determined by the relative constants of the conversion of the starting material in each of the enantiomers of the final product.

14.2. KINETIC RESOLUTION

As previously commented, KRs (Scheme 14.1) were the first type of enzymatic procedures employed for the preparation of enantiopure compounds [14–16]. Therefore, there is a plethora of enzymatic KRs reported in literature. As also mentioned before, the limitation of a maximal theoretical yield of 50% has made these KRs to be implemented in pharma industry, as the urgent requirement for obtaining the desired active pharmaceutical ingredient (API) generally outweighs the generation and posterior removal of the waste (the non-converted enantiomer). In fact, it has been reported that pharma industry generates a huge amount of waste [17–19], with Environmental Factor (E, mass of waste/mass of product, usually expressed as kg/kg [20, 21]) values up to 200 in preclinical phases.

The most classical examples are those in which hydrolases (lipases, mainly) catalyze a transacylation between an acyl donor (acid, anhydride, ester) and a nucleophile (water, alcohol, amine) [22, 23]. These reversible reactions can occur in aqueous media (hydrolysis of esters, amides, thioesters, etc.) [23] or in low-water-containing environments (esterification, transesterification, interesterification, acidolysis, alcoholysis, or aminolysis) [24, 25], and have been thoroughly revised in several papers [22, 23, 26–34] and books [35–47]. The stereochemical course of the reaction is shown in Scheme 14.7.

As can be see, there is a marked stereopreference in the chiral recognition of both enantiomers of the substrates Type III (stereocenter in the alcohol moiety, according to Faber's classification [9])

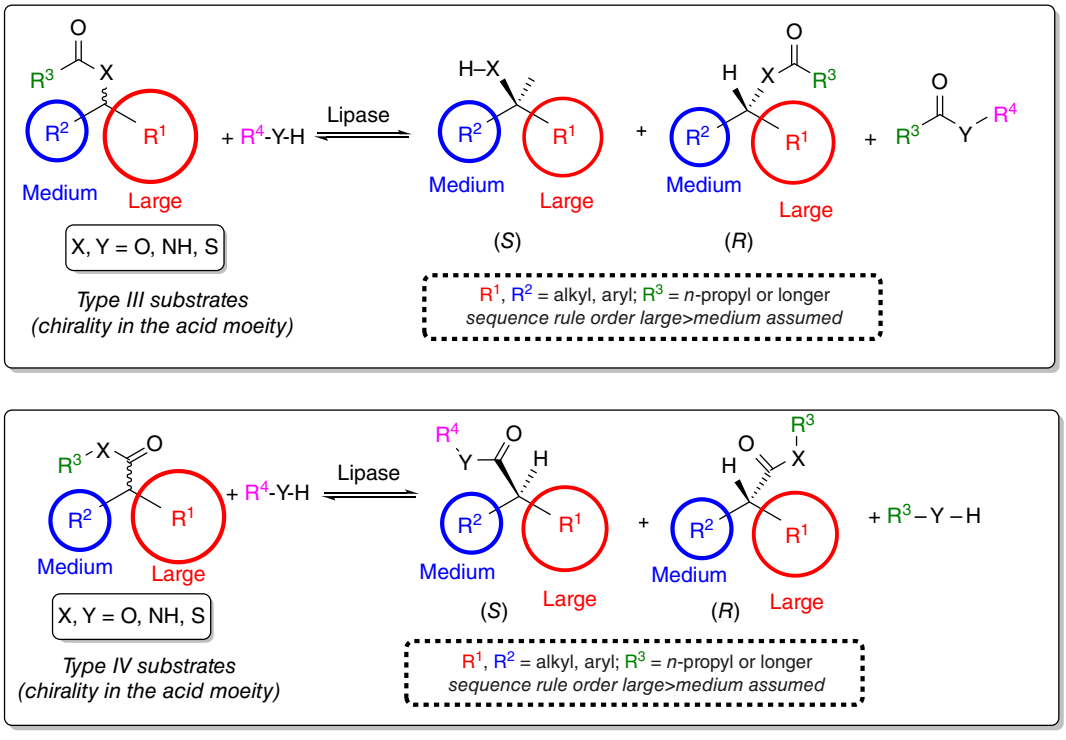

Scheme 14.7. Schematic stereopreference of lipases.

and Type IV (stereocenter in the acid moiety). This assumption follows the well-known empirical Kazlauskas' rule [48], based on the different size of the "medium" and "large" substituents directly attached to the asymmetric carbon atom. Assuming that the sequence rule order of substituents R^1 and R^2 is large > medium, the preferably accepted enantiomer lipase substrate of Type III should possess an (*R*)-configuration at the alcoholic center (accuracy ≥ 90), while for the corresponding α-chiral acids (Type IV) the prediction for (*S*)-stereopreference is less reliable. This rule has been explained by X-ray and modeling studies [49], showing the recognition areas for substrates in the active site of lipases.

Some examples of KR of different substrates by lipase-catalyzed hydrolytic procedures are shown in Scheme 14.8. These examples derive from patents granted in the pharma industry in the last years, as recently covered [50]. Thus, an enzymatic hydrolysis of racemic Type III substrates, useful for synthesizing drug precursors, was patented by Beijing University of Chemical Technology [51] and granted in 2017; the stereoselective hydrolysis of a racemic mixture of *N*-protected *cis*-4-amino-cyclopent-2-en-1-ol (*cis*-**1**, 20 g l^{-1}, Scheme 14.8a.) was carried out using lipase B from *Candida antarctica* (CAL-B) at pH 5.0 and 60 °C in 4 hours, to furnish the desired alcohol (1*S*,4*R*)-**2** (conversion 45%, 99% ee). This enantiopure alcohol is a building block for the preparation of Ticagrelor (Brilinta®, Brilique®, Possia®) a platelet aggregation inhibitor originally produced by AstraZeneca [52, 53]. In another example, developed by Daiichi Sankyo Co. Ltd., and granted in 2019 [54], the KR of (±)-1-((((1,1,1,3,3,3-hexafluoropropan-2-yl) oxy)carbonyl)oxy)ethyl isobutyrate, (±)-**4** was carried out by a lipase-catalyzed hydrolysis in a buffer/organic solvent biphasic system to discard the corresponding alcohol (*S*)-**5** from the desired ester (*R*)-**4** (Scheme 14.8b). In order to catalyze this enzymatic hydrolysis, different commercial lipases (from *C. antarctica*, *Candida rugose*, and *Thermomyces lanuginosus*), organic cosolvents (acetonitrile, ethers, saturated and aromatic hydrocarbons, alcohols), and reaction conditions (temperature from 0 to 80 °C, reaction times ranging from 1 to 120 hours) were tested. The best conditions were obtained with Chirazyme L2, C4 (commercial preparation of *C. antarctica* lipase) and buffer pH 7.0/methyl *tert*-butyl ether (MTBE)

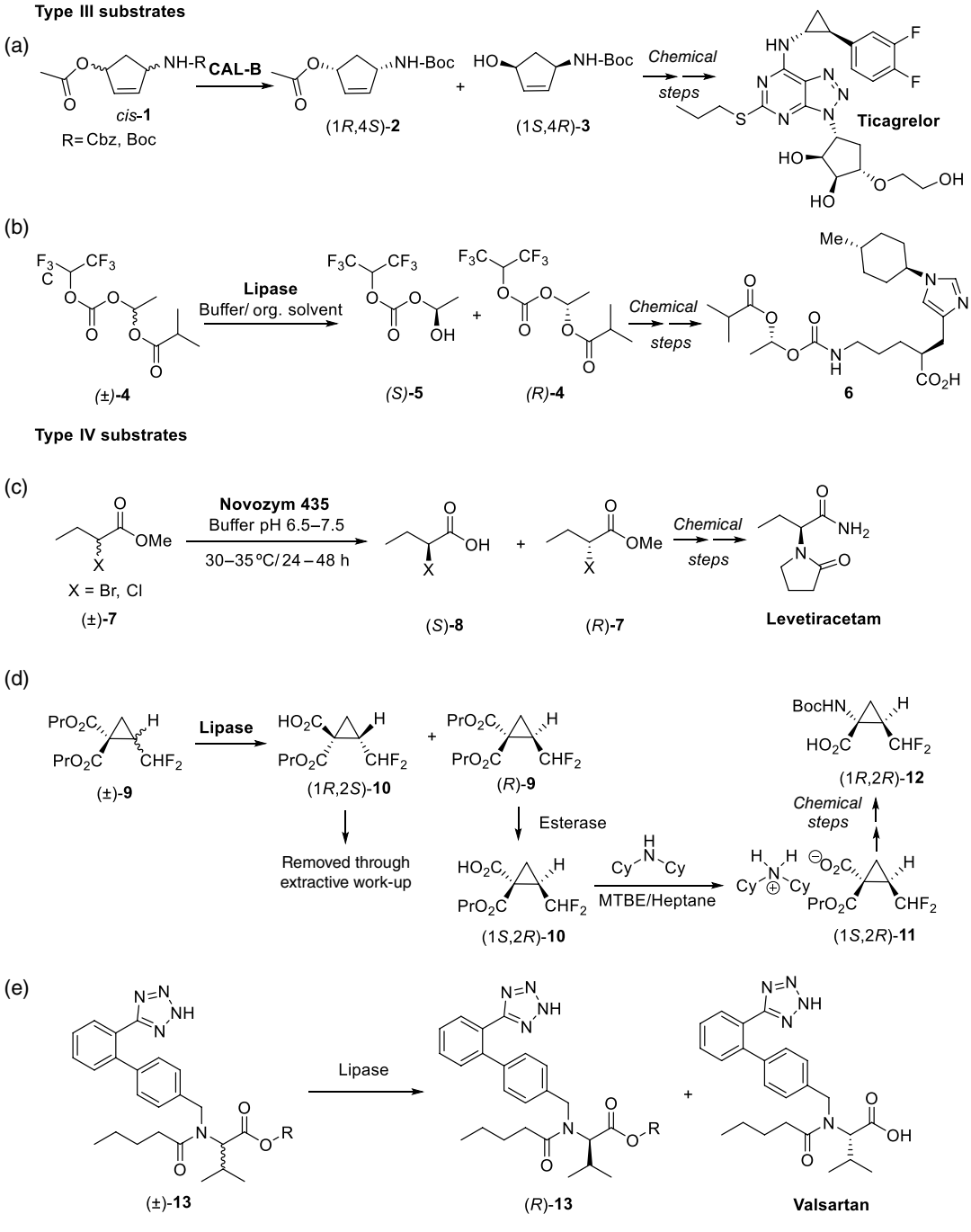

Scheme 14.8. Examples of hydrolytic KRs catalyzed by lipases. (a) Stereoselective hydrolysis of racemic *N*-protected *cis*-4-amino-cyclopent-2-en-1-ol; (b) KR of (±)-1-((((1,1,1,3,3,3-hexafluoropropan-2-yl)oxy)carbonyl)oxy)ethyl isobutyrate; (c) KR of racemic 2-haloester **7** catalyzed by Novozym 435; (d) Lipase-catalyzed KR of (±)-dipropyl 2-(difluoromethyl) cyclopropane-1,1-dicarboxylate; (e) Lipase-catalyzed synthesis of Valsartan by KR.

at 5 : 1 v/v ratio and 20 °C, reporting conversions around 40% and ee values higher than 99%. Subsequently, (*R*)-**4** was used to furnish a carbamate **6**, a promising prodrug useful as inhibitor of carboxypeptidase U (also known as activated thrombin-activatable fibrinolysis inhibitor, TAFIa), for treating thromboembolic disorders [55–57].

Some examples of hydrolytic KRs on Type IV substrates are also depicted in Scheme 14.8. For instance, a patent from Zhejiang Changming Pharmaceutical Co., Ltd. [58], granted in 2018, describes the preparation of anti-epileptic Levetiracetam (Keppra®, Elepsia®) starting from racemic methyl 2-bromo(chloro)butanoate, using Novozym 435, a commercially available preparation of lipase B from *C. antarctica* immobilized on Lewatit VP OC 1600, a macroporous acrylic polymer resin [59] (Scheme 14.8c). The key step, a KR of a racemic 2-haloester **7**, leads to the (*S*)-acid and the desired ester (*R*)-**7**, which is extracted using ethyl acetate and converted into Levetiracetam via transformation of the (*R*)-ester into an α-aminoamide and a further cyclization with 4-chlorobutanoyl chloride. In another example of KR on Type IV substrates (Scheme 14.8d), patented by AbbVie Inc. (granted in 2019) for the preparation of (1*R*,2*R*)-**12** (an intermediate in the synthesis of viral protease inhibitors [60]), a double enzymatic procedure is followed: thus, starting from (±)-dipropyl 2-(difluoromethyl)cyclopropane-1,1-dicarboxylate (±)-**9**, and employing primarily a lipase (from *T. lanuginosus* or *Rhizomucor miehei*) in a biphasic media (phosphate buffer with 10% DMF [dimethylformamide], 30 °C, 95 hours) to separate the undesired monoacid (1*R*,2*S*)-**10** (extracted from the reaction media using MTBE) from the chiral diester (*R*)-**9** (64% yield, 97% ee). In a second step, an esterase from *Bacillus subtilis* cloned and expressed in cells from *Escherichia coli* was employed for the desymmetrization of the stereocenter at C1 of (*R*)-**9** to yield (1*S*,2*R*)-**10** (84% yield, 99% ee) in an aqueous solution at 30 °C in 68 hours. Finally, (1*S*,2*R*)-**10** was chemically converted into the target intermediate (1*R*,2*R*)-**12**.

All the examples mentioned up to this point apply the enzymatic asymmetric hydrolysis in an initial stage of the synthetic scheme leading to the desired API, as it is generally assumed that the asymmetric step should be introduced at the first stages of a synthetic scheme [61]. Less commonly, the enzymatic biotransformation is carried out once the structure of the API is almost complete. For instance, a patent from Tiantai Yisheng Biochemical Technology Co., Ltd. (granted in 2019) describes the enantioselective hydrolysis of racemic esters of Valsartan (Diovan®, an angiotensin II receptor blocker [ARBs or sartans], a drug that modulates the renin–angiotensin system, used in the treatment of hypertension, diabetic nephropathy, and congestive heart failure [62]) catalyzed by lipases [63]. Thus, different commercial immobilized lipases (Lipozyme TL IM [*T. lanuginosus*], Lipozyme RM IM [*R. miehei*], Novozym 435 from Novozymes; lipases PS IM [*Burkholderia cepacia*], Lipase AK [*Pseudomonas fluorescens*], and Lipase AS [*Aspergillus niger*] from Amano) were used for the hydrolysis of racemic esters ((±)-**13**, R = ethyl, methyl, or isopropyl) in a buffer solution (pH 4.0~9.0) with different amounts of organic cosolvents (acetone, isopropanol, or ethyl acetate). The desired Valsartan ((*S*) absolute configuration) was recovered in good yields (up to 90–95% after work-up) and enantiopurity (up to 99.5%), as shown in Scheme 14.8e.

Lipases are perfectly capable to work in low-water-containing reaction media, therefore catalyzing acyl transfer processes (esterifications, transesterifications, amidations, etc.) with excellent precision [24, 31, 64–68]. Some examples are shown in Scheme 14.9. For instance, a patent from Everlight Chemical Industrial Corporation (granted in 2016) reported the stereo- and regioselective acylation of diol **14** with vinyl acetate, performed in *n*-hexane at 22 °C with lipase AK from Amano. This process leads to the regioselective acylation of the hydroxyl group in the cyclic moiety of **14** without acylating that one on the exocyclic chain, and thus conducting to the desired stereochemistry of **15** (neither yields nor *ee*s reported). Enantiopure **15** is required as an intermediate for Treprostinil (Remodulin®, Orenitram®, Tyvaso®, Scheme 14.9a), a synthetic analog of prostacyclin (PGI2) acting as a vasodilator in the treatment of pulmonary arterial hypertension [69]. In another patent from Wuxi Fortune Pharmaceutical Co., Ltd., granted in 2018 [70], the gram-scale KR of racemic hydroxynitrile (±)-**17**, obtained from racemic epyclorhydrine (±)-**16**, was reported using an enzymatic transesterification with perchlorophenyl acetate and CAL-B, supported on an acid resin (Scheme 14.9b), to obtain acetate (*R*)-**18**, the hydrolysis of which leads to L-carnitine, an essential cofactor in the metabolism of lipids involved in the generation of cellular energy [71, 72]. The use of biotransformations in the synthesis of statins, inhibitors of 3-hydroxy-3-methylglutaryl coenzyme A (HMG-CoA) reductase, widely prescribed for the pharmacological treatment of hypercholesterolemia and dyslipidemia, has been recently reviewed [73, 74]. In this

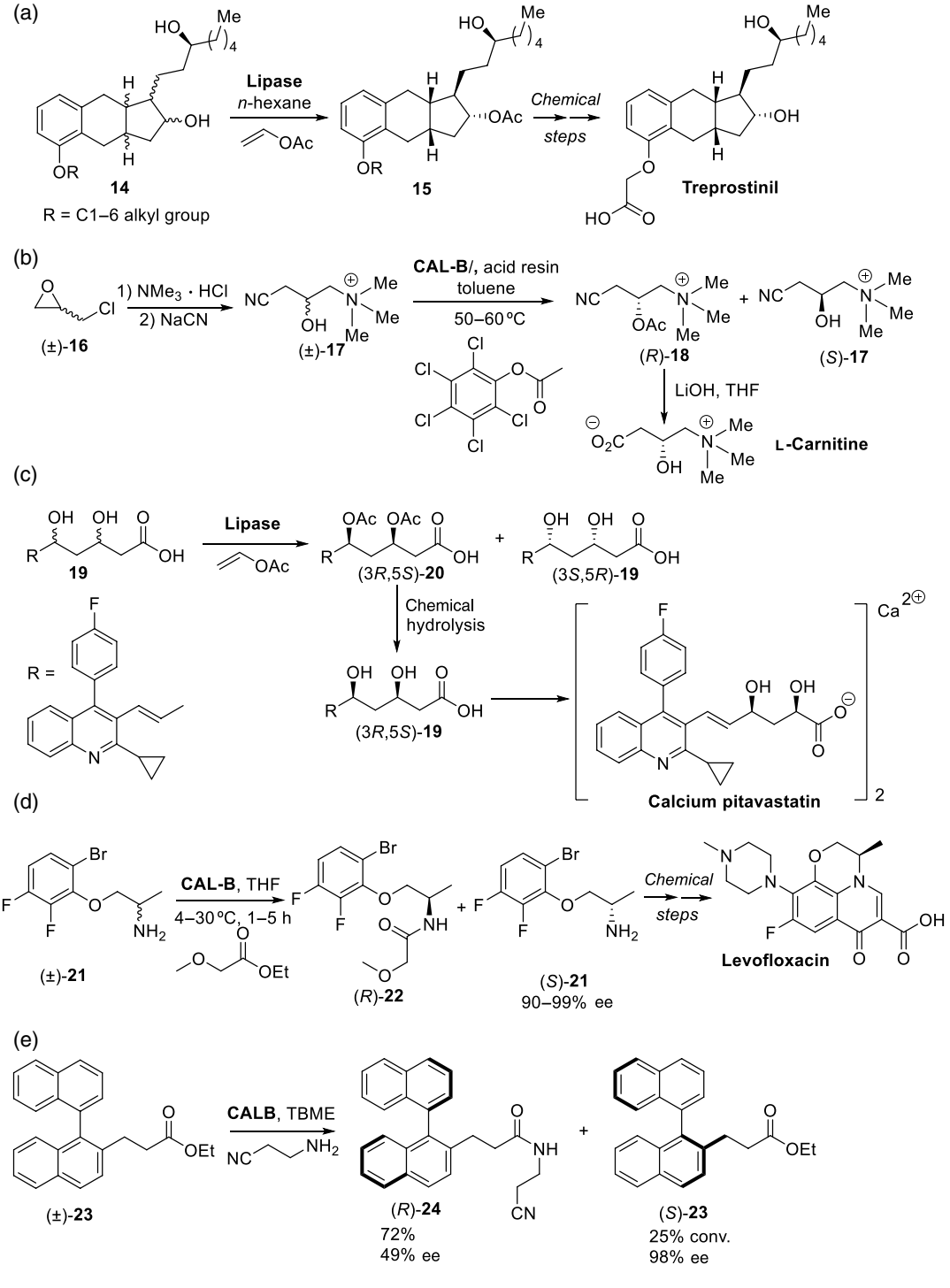

Scheme 14.9. Some examples of lipase-catalyzed KRs via *O*- and *N*-acylations. (a) Lipase-catalyzed *O*-acylation of a Treprostinil precursor; (b) CAL-B catalyzed synthesis of a L-carnitine precursor; (c) Biocatalyzed synthesis of Pitavastatin employing lipases; (d) Cal-B catalyzed *N*-acylation in the synthesis of Levofloxacin; (e) CAL-B catalyzed KR of biaryl esters by aminolysis.

context, Shandong Qidu Pharmaceutical Co., Ltd. patented a transesterification protocol, granted in 2016 [75], depicted in Scheme 14.9c, for the preparation of Pitavastatin (Livalo®, Livazo®, among other trade names), a member of the superstatin family [73]. Hence, the biocatalyst (commercial lipases from different origins, best results obtained with lipase from *B. cepacia*) is able to discriminate between the stereoisomers of starting diol **19** (it is not specified in the patent if **19** is a mixture of the four possible stereoisomers, although according to the reported results, it must be a racemic mixture of *syn* enantiomers).

The acylation is carried out in a biphasic medium phosphate buffer/organic solvent (dichloromethane, ethyl acetate, tetrahydrofuran, MTBE, cyclohexane, toluene, or xylene) in different ratios (from 1/2 to 1/5 v/v) at temperatures ranging from 0 to 40 °C, and different reaction times (up to 72 hours). Reaction yields varied between 43 and 47%, with excellent enantiopurity of the diacetate (3*R*,5*S*)-**20** (97–99% ee), which is separated (through ethanol precipitation) from the non-converted diol (3*S*,5*R*)-**19**, and subsequently hydrolyzed chemically (EtOH/NaOH) and stirred with a $CaCl_2$ solution to finally furnish the calcium salt of Pitavastatin.

The resolution of chiral amines is a very attractive research area, because of the plethora of applications described for such enantiopure compounds [76, 77], which can be obtained by using oxidoreductases [78], transaminases (TAs) [79], and also by lipase-catalyzed acylations [30, 80–82], as also depicted in Scheme 14.9. For instance, the synthesis of enantiopure amine (*S*)-**21**, an intermediate in the preparation of antimicrobial Levofloxacin, was reported by Mourelle-Insua et al. [83] starting from the corresponding racemic secondary amine (±)-**21** via CAL-B-catalyzed aminolysis using ethyl methoxyacetate as the acyl donor, leading to the desired (*S*)-**21** with 90–99% enantiomeric excess [(*R*)-**22**-amide with 88–99%]. This example would be similar to those previously commented reporting the *O*-acylation of Type III substrates, as in this case the chirality is present in the amine moiety; similarly, it is possible to use this enzyme in the stereorecognition of *N*-Type IV substrates. As an interesting example, illustrating the capability of recognizing axial chirality, CAL-B-catalyzed aminolysis was tested on the resolution of chiral biaryl esters **23**, useful as chiral ligands in transition metal catalysis; using 3-aminopropionitrile as the amine donor, **23** was successfully converted into amide (*R*)-**24** in 72% yield and with 49% ee, leaving he residual (*S*)-**23** ester in 25% yield and with 98% ee. Many other examples can be found in the recent reviews of Petchey and Grogan [82] and Lima et al. [81].

Another interesting methodology in which KRs are very attractive is the insertion of oxygen into Csp^3–H using oxidizing enzymes, as shown in Scheme 14.10 [84]. For instance, the use of flavin-dependent Baeyer-Villiger monooxigenases (BVMOs) on ketones having a stereocenter close to the carbonyl moiety would mediate the oxygen insertion (normally forming the product resulting from the migration of the more substituted bond of the substrate) leading to an enantiopure ester, leaving a remnant enantioenriched ketone, as shown in Scheme 14.10a, using 2-substitued cyclohexanone (±)-**25** as substrate. The absolute configuration of the lactone product **26** and the remaining ketone **25** would depend on the nature of the "*R*" substituent, and the enantiopurity is dependent on the type of BVMO used (cyclohexanone monooxygenase, CHMO [85]; phenylacetone monooxygenase, PAMO [86]; camphor monooxygenase; CAMO [87]; cyclopentadecanone monooxygenase, CPDMO [88]; or 2-oxo-Δ3–4,5,5-trimethylcyclopentenyl-acetyl-coenzyme A monooxygenase, OTEMO [87]). Interestingly, Oberleitner et al. reported a smart whole-cell biocatalytic cascade including the BVMO-catalyzed KR of racemic 2-methyl cyclohexanone (±)-**25** [89]; thus, by expressing the sequences of an alcohol dehydrogenase (ADH), an enoate reductase (ERED), and BVMO in *E. coli*, it was possible to convert racemic alcohol (±)-**27** into the corresponding caprolactone (*S*)-**26a** in 62% overall yield and >99% ee. Furthermore, by creating a fusion protein of the ERED and BVMO, it became possible to obtain a 40% increase in lactone production compared to that obtained using the separate enzymes (Scheme 14.10b) [90].

Some other examples of these BVMO-catalyzed KRs of racemic ketones can be found in the recent review from Harwood et al. [84], in which these authors also cover other oxidative KRs. In fact, epoxidation of alkene double bonds is mediated by styrene monooxygenases (SMOs) [91]; using this methodology, Lin et al. [92] reported the use of SMO StyAB2 for the transformation of different racemic allylic alcohols (±)-**28** into enantiopure epoxides **29** through the insertion of oxygen in Csp^2–H bonds (Scheme 14.10c). Very recently this same group has reported [93] the use of a new monooxygenase from *Herbaspirillum huttiense*, leading also to excellent results in shorter reaction times.

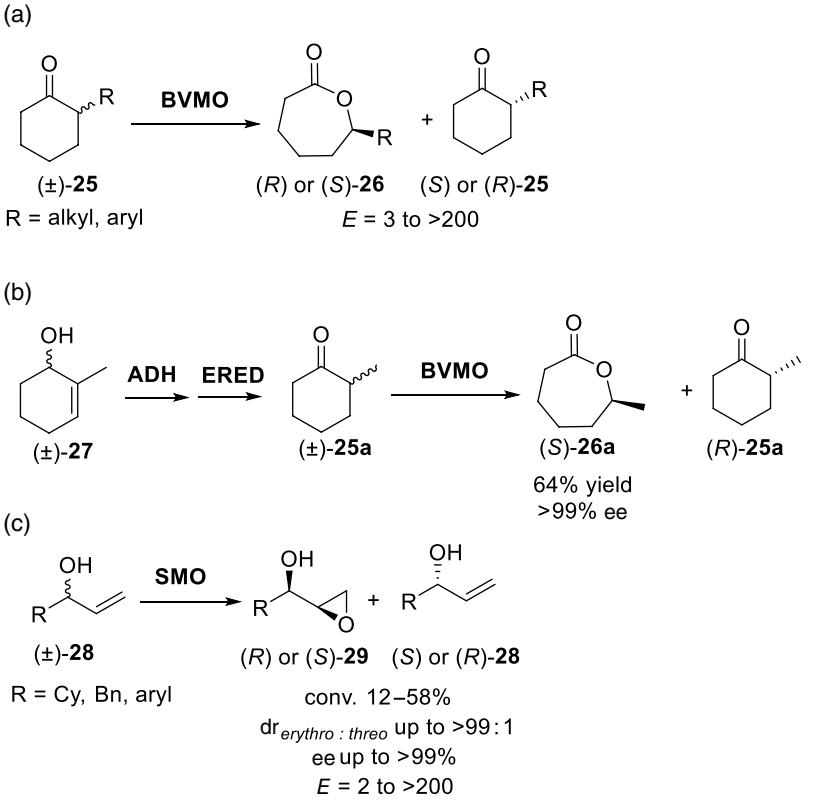

Scheme 14.10. KRs via oxygen insertion in C–H bonds employing oxidoreductases. (a) BVMO-catalyzed kinetic resolution of cyclic ketones; (b) Whole-cell biocatalytic cascade with the BVMO- catalyzed KR of racemic 2-methyl cyclohexanone as final step; (c) KR of racemic allylic alcohols by epoxidation catalyzed by SMO.

14.3. DYNAMIC PROCESSES IN BIOCATALYZED ASYMMETRIC SYNTHESIS

Chemoenzymatic DKRs are very well established in the resolution of racemic alcohols and amines by combining the lipase-catalyzed KR of the starting material with the racemization of the non-converted enantiomer using different metal-catalysts [94–98]. Thus, in 2020 the DKR of 1-methyl-1-tetralol (**29**) was reported (Scheme 14.11a) [99]; this is an interesting example as, until now, very few examples of the DKR of tertiary alcohols have been shown. Initially, different vanadium-based racemization catalysts were tested, obtaining the highest racemization rates with V-MPS4, a vanadium catalyst immobilized onto mesoporous silica of 4.0 nm. Temperatures lower than 15 °C were required in order to reduce the formation of side products. Reactions were performed in diisopropyl ether (DIPE), as in this solvent good racemization rates were measured with side-product formation suppressed. The KR of racemic 1-methyl-1-tetralol was catalyzed by *C. antarctica* lipase A (CAL-A) with excellent selectivity, leading to (*R*)-1-methyl-1-tetralol acetate (**30**) with excellent optical purity and 32% conversion after 48 hours. When the biocatalyst was combined with V-MPS4, enantiopure (*R*)-**30** was obtained with only 29% conversion, indicating a partial deactivation of the lipase by the metal catalyst. By this reason, the continuous addition of fresh active CAL-A is required in order to ensure a proper DKR, leading to enantiopure final product with 77% conversion after 312 hours.

The DKR of racemic amines (**31**) has been recently performed using a hybrid biocatalyst composed of palladium nanoparticles supported onto cross-linking enzyme aggregates of the *C. antarctica* B lipase (CAL-B-CLEAs), as shown in Scheme 14.11b [100]. The use of coimmobilized catalysts presents a great advance in terms of process efficiency, as one of the main drawbacks of using immobilized catalysts is the

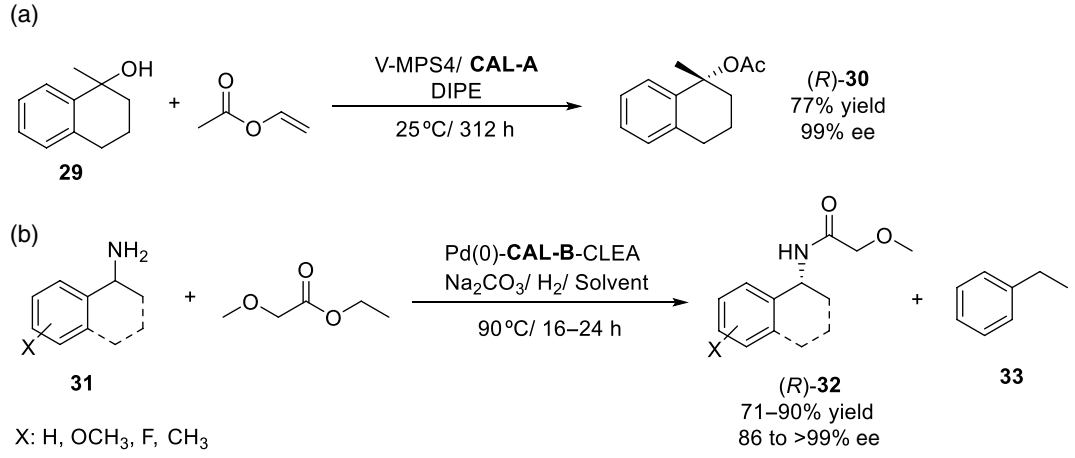

Scheme 14.11. DKRs employing metal catalysts for the substrate racemization. (a) DKR of KR of 1-methyl-1-tetralol combining a metal catalyst and lipase CAL-A; (b) DKR of racemic amines employing an hybrid catalyst Pd(0)-CAL-B-CLEA.

presence of high percentages of inert material, something that in this system does not occur [101]. CAL-B-CLEAs were able to catalyze the selective acylation of the racemic amines employing ethyl methoxyacetate as acyl donor, whereas the Pd(0) nanoparticles were able to efficiently racemize the unreacted enantiomer at high temperature in hydrogen atmosphere and in presence of a base as Na_2CO_3, but with the concomitant formation of ethyl benzene (**33**) as by-product of this reaction. Process optimization of the DKRs catalyzed by Pd(0)-CAL-B-CLEAs showed that reactions carried out in 1,4-dioxane at 90 °C afforded the chiral (*R*)-amides (**32**) with high conversions and optical purities after 18 hours, but with amounts of the undesired by-product around 10%. The use of tetrahidrofuran (THF) at 90 °C led to lower conversions at the same time, but the formation of **33** is almost suppressed.

The racemization of the starting material on different proposed DKRs can be also performed by other methodologies different to metal-based catalysts, using for this purpose a chemocatalyst or a second enzymatic system [102–105]. Some examples are following, for instance, on the synthesis of Brivaracetam and Pregabalin, valuable drugs for the treatment of neurological diseases. The preparation of the key intermediates for the synthesis of these compounds has been developed employing TAs, biocatalysts that catalyze the amine transfer from an amine donor (most commonly L- or D-alanine) to a carbonyl compound acceptor, employing pyridoxal-5′-phosphate (PLP) as cofactor [106, 107]. Thus, different racemic aldehydes bearing aliphatic residues at a chiral center in α-position to the aldehyde moiety have been used as starting materials in the amination reactions (Scheme 14.12a) [108]. The amine donors presented in the reaction medium are responsible for the racemization of the aldehyde chiral center, so a DKR process was achieved, making it possible to obtain the final amines with theoretical yields up to 100%. A set of racemic oxoesters (±)-**34** was tested in amination reactions catalyzed by different available TAs, modifying the ester structure as well as the reaction conditions in order to achieve the best results. Both enantiomers of amine **35** can be achieved depending on the TAs employed, making it possible to obtain enantiomeric excesses from 92% (*R*) to 80% (*S*) in the case of the Brivaracetam precursor, and from 94% (*R*) to 80% (*S*) for the Pregabalin intermediate. The TA-catalyzed bioamination of the aldehyde precursors of both drugs was performed on preparative scale (200 mg, 20 ml). Thus *E. coli* cells expressing the *Paracoccus dentrificans* TA were employed for the amination of the Brivaracetam precursor in phosphate buffer pH 7.0 containing 1,2-dimethoxyethane as cosolvent, achieving the (*R*)-amine in 65% isolated yield and 90% ee after 24 hours at 30 °C. For the Pregabalin precursor synthesis, *E. coli* cells expressing the *Vibrio fluvialis*-TA (*Vb*TA) led to a 55% yield of the (*R*)-amine at the same reaction conditions, but in this case with 60% ee.

Imine reductases (IREDs) are biocatalysts able to catalyze the hydrogenation of imines to the corresponding amines in presence of NAD(P)H as cofactor [109–111]. IRED from *Streptomyces ipomoeae*

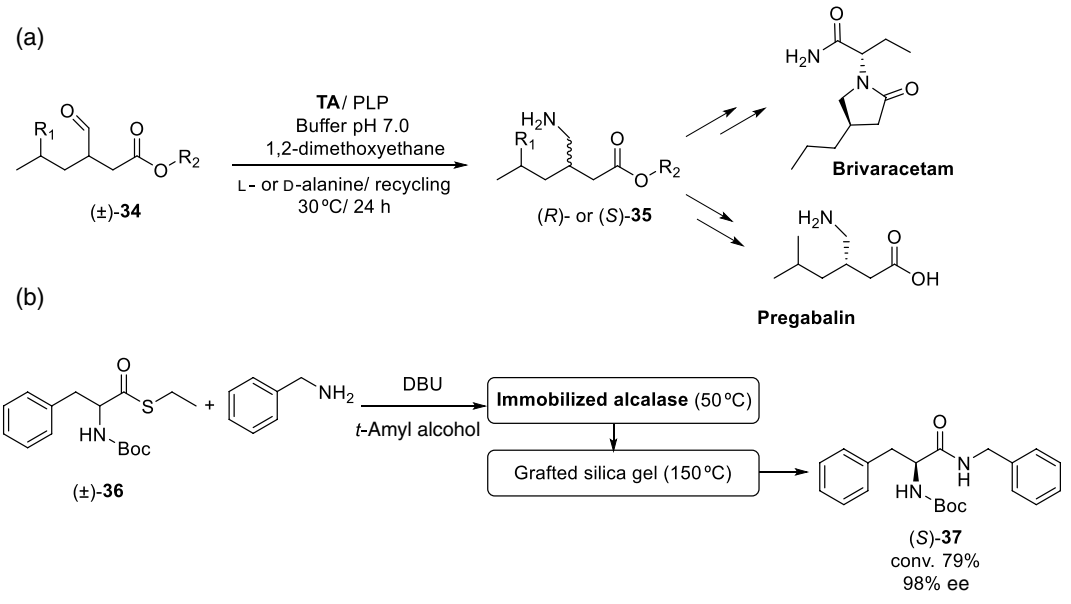

Scheme 14.12. Biocatalyzed DKRs employing transaminases and alcalases. (a) DKR of racemic aldehydes catalyzed by TAs for the synthesis of Brivaracetam and Pregabalin; (b) DKR of racemic amides employing alcalase in continuous-flow mode using a multicolumn reactor system.

is an effective biocatalyst for the reductive amination of aliphatic β-branched aldehydes into the corresponding secondary β-chiral amines [112]. Several aliphatic aldehydes were employed as substrates in presence of different nitrogen sources, including ammonia, methylamine, ethylamine, dimethylamine, and pyrrolidine. Reactions were conducted at pH 9.5, optimal for the substrate racemization in a DKR. In general, the chiral amines are obtained with high conversions and moderate to good optical purities.

Amides are valuable functional groups present in a wide set of naturally occurring and synthetic compounds. These compounds can be prepared through enzymatic KRs, but some DKR-procedures have been further developed for their preparation. Thus, alcalase (subtilisin A) has been recently immobilized by adsorption onto 24 different supports and tested in the selective amidation of *N*-Boc-Phe thioethyl ester (±)-**36** with benzylamine (Scheme 14.12b) [113]. The best results for the KR were obtained with Alc-Dv250-Et (alcalase adsorbed on ethyl-grafted macroporous silica gel), a process with excellent selectivity ($E > 200$) and 41% conversion after 24 hours. The KR of racemic starting material was also performed in continuous-flow mode using a multicolumn reactor system, with the aim of developing the DKR of this compound in these conditions. Racemization of the starting material was performed employing 1,8-diazabicyclo[5.4.0]undec-7-ene (DBU) as base at 150 °C, which proved to be the optimal temperature for this process. The DKR of racemic starting material in continuous-flow mode was carried out in a system with two multicolumn reactors where packed-bed columns were placed. Six of the columns were employed for the KR at 50 °C and five columns were used for the racemization at 150 °C. The DKR of the racemic thioester with benzylamine in *tert*-amyl alcohol and using DBU as base took place with 79% conversion and 8.17 $g\,l^{-1}\,h^{-1}$ of volumetric productivity after 3 hours. (*S*)-amide **37** was recovered with 98% enantiomeric excess.

Alcohol dehydrogenases (ADHs) or ketoreductases (KREDs) are enzymes that catalyze the reversible reduction of carbonyl compounds into the corresponding alcohols in presence of nicotinamide cofactors [NAD(P)H]. These enzymes have been tested in dynamic processes for the synthesis of chiral alcohols with more than one chiral centers. When the epimerizable chiral center is located in an adjacent position to the carbonyl moiety, the racemization is facilitated due to the acidic character of this position, leading to a dynamic reductive kinetic resolution (DYRKR), in which one single diastereomer can be obtained from the starting material [114]. In this sense, a DYRKR has been described for the preparation

of biologically active chiral 3,4-dihydroisocoumarins (**38**), present in many natural products, starting from racemic 2-(3-oxoalkyl)benzonitriles (**40**, Scheme 14.13a) [115]. Thus, 2-(3-oxobutan-2-yl)benzonitrile (**40a**) was reduced by the ADH from *Rhodococcus ruber* (ADH-A) overexpressed in *E. coli* employing Tris-HCl buffer containing 5% v/v isopropanol (isopropyl alcohol, IPA) as cosubstrate and 5% v/v hexane cosolvent. After 24 hours, chiral (*S*,*S*)-alcohol **39a** was recovered with 56% conversion and excellent selectivity. Triethylamine was studied as racemization agent, allowing to obtain enantiopure (*S*,*S*)-**39a** with 86% conversion after 72 hours. Acid-catalyzed cyclization of the chiral alcohol leads to the desired (*S*,*S*)-3,4-dimethyl-3,4-dihydroisocoumarin (**40a)** with 86% yield and excellent enantio- and diastereoselectivities. This methodology was extended to the preparation of a set of (*S*,*S*)-3,4-dihydroisocoumarins starting from 0.3 mmol of different 2-(3-oxoalkyl)benzonitriles, achieving in all cases moderate to good yields (24–68%) and complete selectivity in the preparation of the desired diastereomer.

DYRKR has been also applied to the synthesis of α-fluoro-β-hydroxy esters (**41**) starting from racemic α-fluoro-β-keto esters (**42**) through a bioreduction process catalyzed by commercially available ADHs (Scheme 14.13b) [116]. As the starting material presents an epimerizable carbon, it is racemized at the reaction conditions, so it is possible to obtain one of the possible diastereomers as the sole product. Bioreductions were fast processes, achieving completion for almost all the substrates after short times. When employing KRED 130 as biocatalyst, enantiopure (2*S*,3*S*)-**41** are recovered, whereas the application of KREDs P1-B02 and P2-C02 leads to (2*R*,3*S*)-**41** esters with complete selectivity.

Optically active α-alkyl-β-hydroxy amides (**43**) are building blocks of different valuable biologically active compounds, including oxazolines, oxazoles, pyrrolidines, or 1,3-amino alcohols. In 2019, a biocatalytic approach to prepare these compounds has been developed starting from racemic α-alkyl-β-keto amides (**44**) in a DYRKR procedure catalyzed by different ADHs expressed in *E. coli* (Scheme 14.13c) [117]. The high acidity of the α-proton ensured a fast racemization of the starting material at the reaction conditions (buffer pH 7.5). Best activity and selectivity were achieved with ADH-A from *Rhodococcus ruber*,

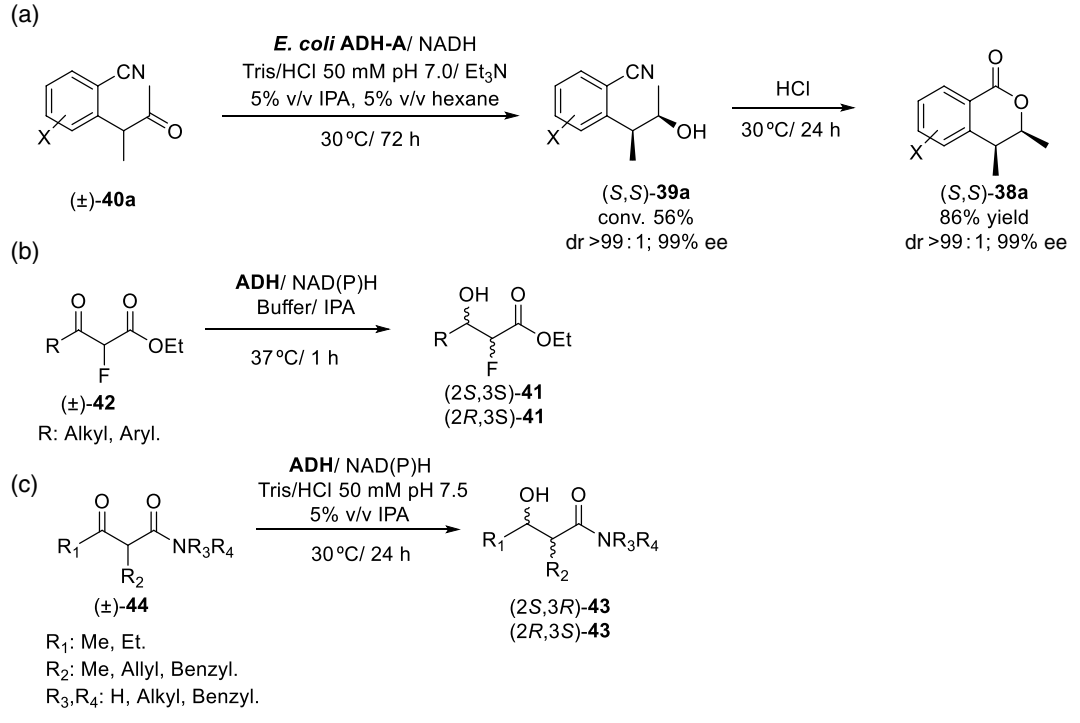

Scheme 14.13. Some examples of DYRKR for the synthesis of optically active compounds. (a) DYRKR for the preparation of chiral 3,4-dihydroisocoumarins employing ADHs; (b) Synthesis of α-fluoro-β-hydroxy esters catalyzed by ADHs; (c) Preparation of optically active α-alkyl-β-hydroxy amides using ADHs in a DYRKR procedure.

making it possible to obtain (2*R*,3*S*)-**43** diastereomer with excellent conversions and high enantiomeric excesses, whereas the use of evo-1.1.200 allowed the formation of the diastereomer (2*S*,3*R*)-**43** with good results. Reactions catalyzed by ADH-A were scaled up to 100 mg of starting material, carrying the bioreductions in Tri/HCl 50 mM pH 7.5 with NADH (1 mM) as cofactor and 5% v/v IPA as cosolvent and cofactor recycling system. After 24 hours, the *syn*-(2*R*,3*S*)-diastereomers were recovered with moderate to high yields (52–94%) and excellent selectivity.

14.4. DERACEMIZATIONS

In the last years, several biocatalytic procedures have been developed for the conversion of one racemic compound into one of its enantiomers [11–12, 118]. In most cases, redox deracemizations are performed to synthesize chiral alcohols and amines, as these compounds present stable oxidized intermediates as ketones and imines, respectively. One example is the deracemization of profenol (2-phenyl-1-propanol **45**), key core of non-steroidal anti-inflammatory drugs (NSAIDs), as shown in Scheme 14.14a. This compound was obtained applying a bienzymatic system in a linear deracemization procedure. Thus, the laccase from *Trametes versicolor* in presence of (2,2,6,6-Tetramethylpiperidin-1-yl)oxyl (TEMPO) was employed for the oxidation of the alcohol **45** to the racemic aldehyde **46**, which is then selectively reduced by ADHs [119]. Racemic **45** (90 mM) was oxidized with 85% conversion after 2 hours. Aldehyde was subjected, without any purification, to bioreduction catalyzed by the ADHs from *E. coli* (ADH-P) or horse liver ADH (HLADH) to obtain (*S*)-**45**, whereas the (*R*)-enantiomer was achieved in presence of evo.-1.1.200. Deracemization was performed in a stepwise process, obtaining conversions higher than 95% and good enantioselectivity (86–87% ee) for all the ADHs studied. The process was also studied in a one-pot procedure starting from

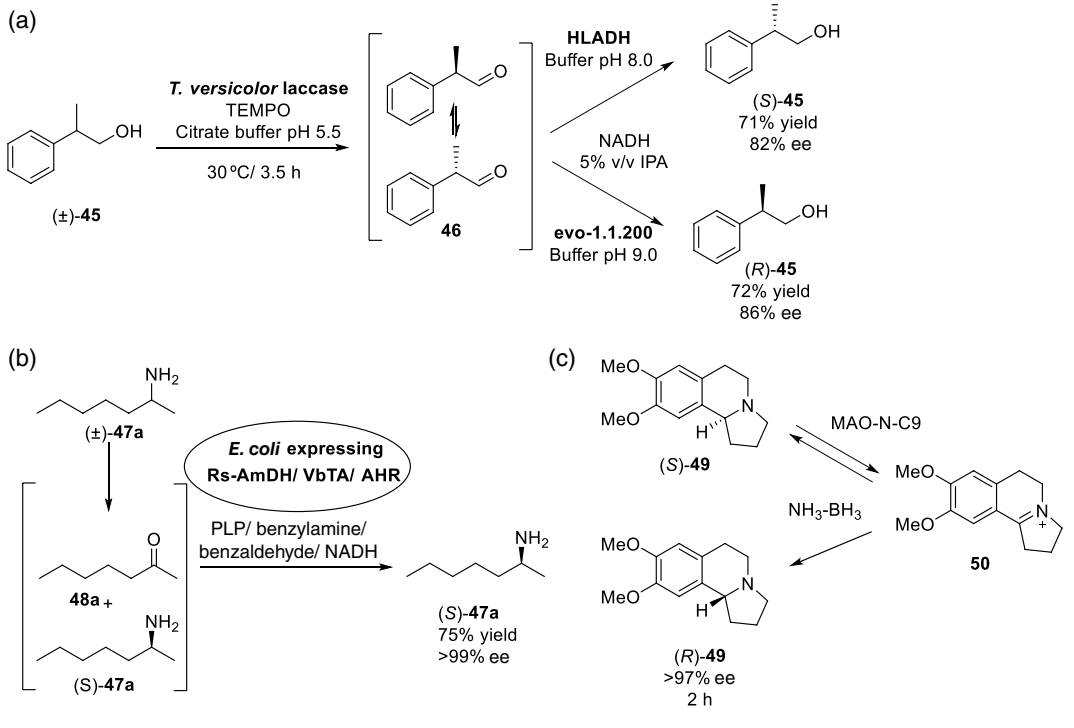

Scheme 14.14. Some examples of deracemizations catalyzed by enzymes for the synthesis of chiral compounds. (a) Deracemization of profenol employing the laccase from *Trametes versicolor* and ADHs; (b) Deracemization of(±)-heptan-2-amine using *E. coli* cells expressing amine dehydrogenase, transaminase and aldehyde reductase; (c) Deracemisation of Crispine A employing MAO-N5 and ammonia-borane complex.

150 mg of racemic alcohol. After the oxidation step for 3.5 hours in presence of the laccase/TEMPO system in buffer pH 5.5, the reaction was diluted with phosphate buffer and pH was adjusted to 8.0 for HLADH or 9.0 for evo-1.1.200, to inactivate the laccase. Then, NADH and 5% v/v IPA were added to the reaction medium, recovering (*S*)- or (*R*)-**45** with yields around 70% and 82–86% ees, respectively.

Deracemizations have been also described for the synthesis of optically active amines. Thus, the deracemization of different aliphatic and aromatic racemic amines (**47**) to the (*R*)- or (*S*)-enantiomers was described in 2019 by combining ω-TAs and amine dehydrogenases (AmDHs), biocatalysts that catalyze the reductive amination of ketones in presence of a catalytic amount of nicotinamides [120]. First experiments were devoted to the preparation of the (*R*)-amines. The deamination of the racemic amines was catalyzed by the (*S*)-selective TA from *Polaromonas* sp. JS666 in order to obtain the (*R*)-amines and the corresponding carbonyl compounds (**48**). The second step was the amination of the ketones achieved in the initial step by a (*R*)-selective L-phenylalanine dehydrogenase from *Rhodococcus* sp. (*Rs*AmDH) or by a chimeric AmDH (Chi-AmDH). After process optimization in presence of 15% v/v dimethylsufoxide (DMSO) as cosolvent and using glucose dehydrogenase (GDH) from *B. subtilis* for NADH regeneration, all the (*R*)-amines tested were obtained with high to excellent conversions (80–99%) and complete enantioselectivity. A similar procedure was followed for the synthesis of the (*S*)-enantiomers of the different amines. In this case, the first step was the racemic amines' deamination catalyzed by the (*R*)-selective *Rs*-AmDH. Once obtained, the chiral amine and the ketone, this last compound was aminated in a process catalyzed by the (*S*)-selective TA from *Vb*TA. Unfortunately, the preparation of the (*S*)-amines presents as drawback in that the equilibrium of both reactions is unfavorable, so benzylamine was employed as amine donor in the amination of the ketone. This amine donor produces benzaldehyde as product, which is reduced to benzyl alcohol by the aldehyde reductase (AHR) from *Synechocystis* sp. in a process that regenerates the NAD^+ cofactor that *Rs*AmDH requires for its activity. Once this modification was performed, the conversion of the system was improved. The deracemizations were tested using a whole-cell system expressing the AmDH, the AHR, and the TA. All the (*S*)-amines were obtained with excellent conversions and enantioselectivities after 24 hours. Both systems were scaled up in the deracemization of (±)-heptan-2-amine (**47a**) (Scheme 14.14b). Both (*R*)- and (*S*)-**47a** were recovered as enantiopure compounds with 53 and 75% yields, respectively, after 24 hours at 37 °C.

Crispine A (**49**) is an alkaloid isolated from *Carduus crispus*. Several syntheses have been reported for this optically active compound. One of these approaches consists in the deracemization of racemic Crispine A employing a monoamine oxidase variant (MAO-N5) in combination with amine-borane complex, leading to the chiral compound in 48% yield and >97% ee after 40 hours (Scheme 14.14c) [121]. In this process, MAO is responsible for the selective oxidation of the starting amine to the corresponding imine **50**, which is non-selectively reduced by the ammonia-borane complex. After several redox cycles, it is possible to obtain the enantioenriched starting material in a so-called cyclic deracemization, from which several examples have been described in the bibliography. A similar compound to Crispine A without the two methoxy groups led to a similar result but in a much shorter reaction time (6 hours). In view of this result, the biocatalyst MAO-N5 was subjected to rational design in order to fit in a better way a substrate like Crispine A. After several rounds of biocatalyst optimization, MAO-N-9C was obtained, presenting a 990-fold increase in the specific activity regarding MAO-N5 (DOI: 10.1002/cctc201200202). The use of the novel variant in combination with the ammonia-borane complex led to optically active (*R*)-Crispine A (ee > 97%) in 2 hours.

14.5. PARALLEL KINETIC RESOLUTIONS

Asymmetric PKRs are not so common processes when employing biocatalysts, but in the last years, some examples have been developed employing hydrolases and oxidoreductases.

Non-natural β-L-nucleosides present valuable properties as antiviral and anticancer reagents [122]. When mixtures of β-D/L-nucleosides were selectively acylated with acetonoxime levulinate in presence of *Pseudomonas cepacia* lipase (PSC) using THF as solvent at 30 °C, a mixture of two enantiopure esters (the β-D-3′-*O*-levulinyl ester and the β-L-5′-*O*-levulinyl derivative) was obtained in a PKR process [123]. PSC was able to catalyze with complete regioselectivity the acylation of the 3′-hydroxyl group of β-D-nucleosides, whereas the same biocatalyst showed an opposite selectivity for the β-L-isomer, acylating exclusively the 5′-hydroxyl group.

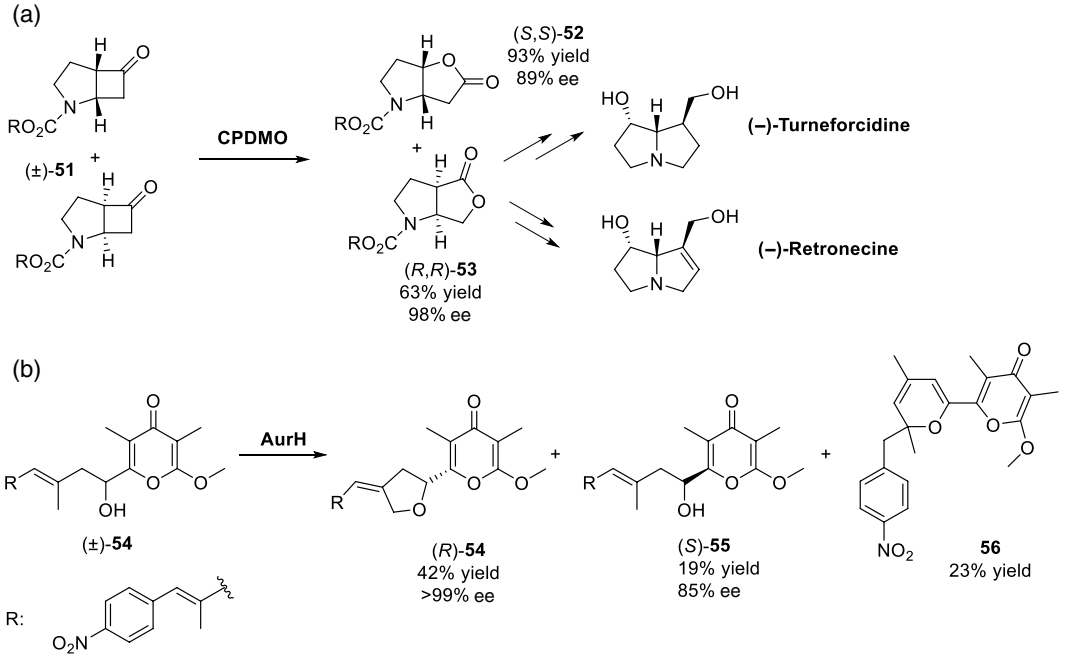

Scheme 14.15. Parallel kinetic resolutions catalyzed by oxidative biocatalysts. (a) Regiodivergent oxidation of bicyclic ketones catalyzed by CPDMO; (b) Regiodivergent PKR for the preparation of (+)-aureothin in presence of CYP450.

The regiodivergent oxidation of bicyclic ketones employing CPDMO from *Pseudomonas* sp. as catalyst was reported [88] (see Section 14.3 for examples on KRs using this enzyme). When the *N*-heterocyclic bicyclic ketone (±)-**51** was oxidized in presence of CPDMO, a 1 : 1 mixture of both lactone **52** and the Geissman-Waiss lactone **53**, a valuable precursor of the necine bases (+)-retronecine and (–)-turneforcidine, was achieved (Scheme 14.15a). When the biooxidation was carried out at 100 mg scale, (*S*,*S*)-**52** was obtained with 93% yield (89% ee), whereas compound (*R*,*R*)-**53** was recovered in 63% yield (98% ee).

A regiodivergent PKR was also described in the preparation of (+)-aureothin (**54**) [124], a polyketide with valuable antitumor, antifungal, and antiparasitic properties, employing a multifunctional cytochrome P450 monooxygenase (AurH) [125]). Cytochrome P450 monooxygenases (CYPs) are widely spread enzymes able to perform the insertion of one atom of oxygen in a wide variety of organic substrates [126, 127]. This CYP is responsible for one of the synthetic steps involving the formation of a homochiral tetrahydrofuran ring in the molecule starting from racemic precursor **54** (Scheme 14.15b). Thus, the treatment of **54** with AurH led to (*R*)-**54** with 42% yield and 99% ee, with 19% of enantioenriched (*S*)-precursor **55** (85% ee) being recovered in a KR step while 23% of a racemic-2*H*-pyran **56** recovered as side product. Studies performed to analyze this result showed that AurH catalyzes the PKR of racemic starting material **54**, leading to (*R*)-**54** with complete selectivity by oxidation of the methyl group in the (*R*)-enantiomer of the substrate. In a parallel way, the (*S*)-enantiomer was partially converted into an enol intermediate in a process catalyzed by AurH, which is then transformed into the pyran **56** in a two-step process involving an isomerization and an electrocyclization.

14.6. DESYMMETRIZATION

Different classes of biocatalysts have been utilized for the desymmetrization of prochiral or *meso*-compounds in order to obtain one enantiomerically enriched product [128]. One example is the preparation of the chiral 2-arylpropionic acid (profen) moiety, a group present in several valuable structures, as for instance the NSAIDs ibuprofen, naproxen, and ketoprofen, or the anti-Alzheimer drug flurbiprofen.

Ene reductase enzymes (EREDs) are flavin-dependent enzymes that catalyze the reduction of activated alkenes employing NAD(P)H as cofactor [129, 130]. These biocatalysts have been employed in the preparation of chiral 2-arylpropionic acids by catalyzing the hydrogenation of the starting α,β-unsaturated ketones (Scheme 14.16a) [131]. Thus, after process optimization using phosphate buffer 20 mM and 2-methyltetrahydrofuran as cosolvent, YqjM from *B. subtilis* was able to catalyze the hydrogenation of methyl 2-phenylacrylate to enantiopure (*R*)-profen with 97% conversion using GDH for cofactor regeneration. This enzyme was employed in the chemoenzymatic synthesis of flurbiprofen methyl ester. The first step of this synthesis is the enzymatic reduction of methyl 2-(3-fluoro-4-hydroxyphenyl)acrylate **57** to (*R*)-**58** with 68% yield and excellent selectivity.

Tetrahydroisoquinolines (THIQs) are valuable building blocks in bioactive and pharmaceutical compounds. Among them, 1-substituted THIQs are presented in several valuable drugs. These molecules can be selectively prepared employing IREDs, but in general these biocatalysts cannot be used for preparative synthesis due to their low activity at high concentrations. In 2017, the application of the (*S*)-selective IRED from *Stackebrandtia nassauensis* (*Sn*IR) was reported for the preparation of (*S*)-1-alkyltetrahydroisoquinolines (**59**) from the starting imines **60** at preparative scale (1.0 mmol) with a substrate concentration of 100 mM (Scheme 14.16b) [132]. After optimizing the amount of reaction cosolvent to 1% v/v DMSO, the bioreductions of THIQs presenting relatively small size alkyl substituents led to the formation of the (*S*)-amines with good yields (72–81%) and high optical purities (91–99%) after

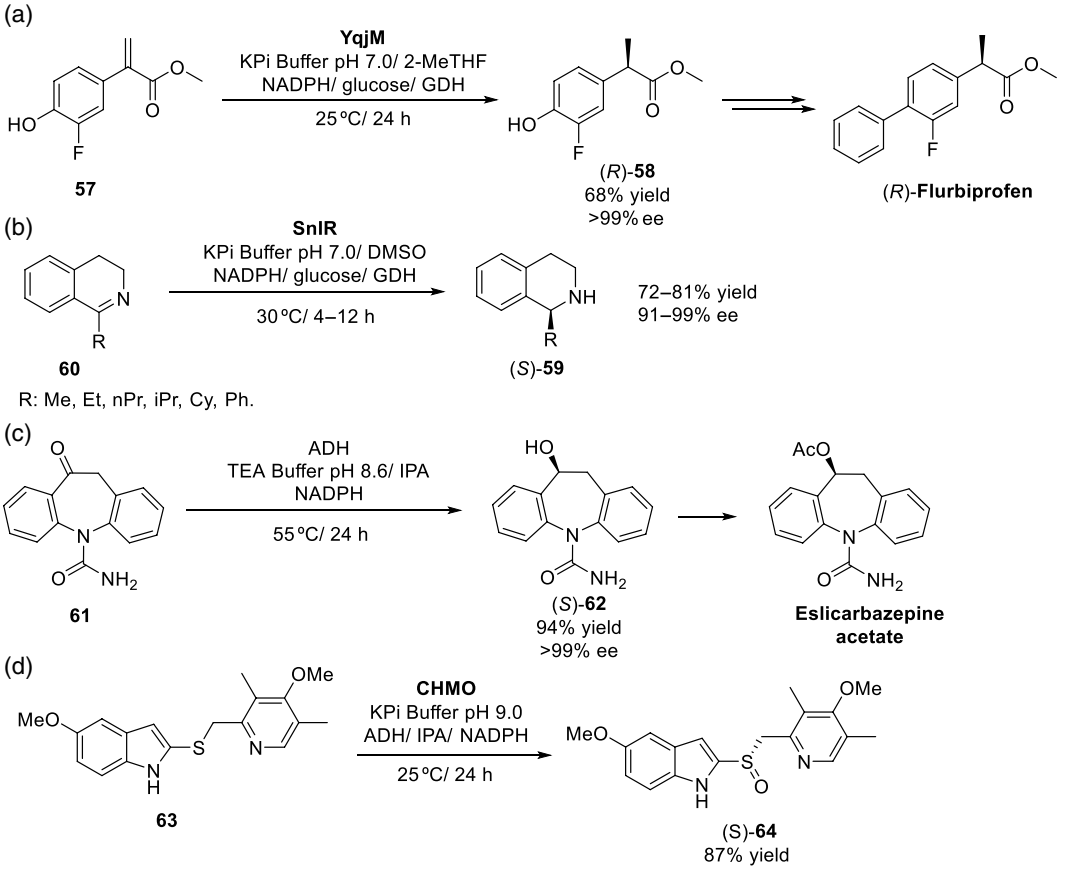

Scheme 14.16. Desymmetrization of prochiral compounds catalyzed by different types of biocatalysts. (a) ERED-catalyzed hydrogenation of methyl 2-(3-fluoro-4-hydroxyphenyl)acrylate as key-step for obtaining flurbiprofen; (b) Synthesis of (*S*)-1-alkyltetrahydroisoquinolines catalyzed by SnIR; (c) Synthesis of (*S*)-licarbazepine catalyzed by *Lk*ADH; (d) CHMO-catalyzed preparation of esomeprazole.

short reaction times (2–4 hours). Bulkier substrates required lower concentrations (5–50 mM) and longer reaction times (3–12 hours) to achieve complete conversions.

ADHs have been widely exploited in desymmetrization procedures for the preparation of optically active alcohols. One interesting example was shown in 2014, regarding the enzymatic synthesis of (*S*)-licarbazepine **61**, precursor of eslicarbazepine acetate, used for the treatment of epileptic seizures. (*S*)-**61** is obtained by enzymatic reduction of oxcarbazepine **62** employing the ADH from *Lactobacillus kefir* (*Lk*ADH) [133], as shown in Scheme 14.16c. Different mutants of this biocatalyst were employed in this procedure, achieving excellent selectivities. One of the tested variants was further improved in order to develop a biocatalyzed process with low cofactor loading, high IPA concentrations, and high temperatures. Thus, when the bioreduction of **62** was scaled up at 500 ml using 100 $g\,l^{-1}$ of ketone, 0.1 $g\,l^{-1}$ of $NADP^+$, 60% v/v of IPA, and 55 °C in tris/acetic acid/ EDTA (TEA) buffer, (*S*)-licarbazepine was recovered in 96% yield, with a 99% purity and complete enantioselectivity.

In Section 14.3, the use of flavin-dependent BVMOs in KR was commented. These enzymes are also capable to catalyze the oxygenation of heteroatoms, requiring nicotinamides as electron source for performing their activity [134, 135], and have been widely employed, as well as other oxidative biocatalysts, in the preparation of optically active sulfoxides [136], valuable ligands in asymmetric synthesis as well as bioactive compounds [137]. One of the most applied BVMOs is CHMO from *Acinetobacter* sp. *strain NCIB 9871*, but this biocatalyst presents a low stability. In 2018, CHMO was improved by direct evolution, in order to perform the oxidation of pyrmetazole (**63**) to esomeprazole (**64**), the (*S*)-enantiomer of omeprazole (Scheme 14.16d) [138]. After finding a suitable mutant of CHMO able to catalyze this reaction, the process was further optimized. When employing 50 $mg\,ml^{-1}$ of starting material, 1 $g\,l^{-1}$ of the BVMO variant, 0.5 $g\,l^{-1}$ of the ADH responsible for the $NADP^+$ regeneration, 4% v/v of IPA as cosubstrate, 0.1 $g\,l^{-1}$ $NADP^+$, and 0.2% v/v of catalase in phosphate buffer pH 9.0, enantiopure esomeprazole was obtained in 87% yield, with 99% purity.

Microbial whole-cells of *Rhodococcus erythropolis* AJ270 containing an amidase have been recently employed in the desymmetrization of a set of prochiral 3-aryl and 3-arylmethyl glutaramides [139]. In presence of this biocatalyst, it was possible to perform the selective hydrolysis of the starting materials in phosphate buffer pH 7.0 at 30 °C, leading to the optically active 3-substituted glutaric acid monoamides with yields up to 95% and enantiomeric excesses higher than 99.5%.

The Pictet-Spengler reaction consists in the condensation of β-arylethylamines with an aldehyde or a ketone, representing a valuable method for the preparation of nitrogen heterocycles. This reaction can be catalyzed enzymatically by strictoside synthases (STRs), members of the Pictet-Spenglerases group [140]. This process has been recently studied for the condensation of tryptamine (**65**) with different low-molecular-weight aldehydes employing various STRs. The synthetic applicability of this process was demonstrated in the preparation of the natural alkaloid (*R*)-harmacine starting from tryptamine and 4-oxobutanoate in a reaction catalyzed by the STR from *Rauvolfia serpentine* (*Rs*STR) [141], as shown in Scheme 14.17a. After 48 hours at 35 °C in piperazine-*N*,*N*′-bis(2-ethanesulfonic acid) (PIPES) buffer pH 6.1, the condensation product **66** suffers spontaneous ring closure to afford the enantiopure (*R*)-lactam **67** with 95% conversion (67% isolated yield). This compound was then chemically reduced with lithium aluminum hydride, affording enantiopure (*R*)-harmacine in a process with 62% overall yield.

MAOs can be also used for desymmetrization purposes. In fact, by using engineered MAO-ND5 from *Aspergillus niger*, Turner and coworkers [142] developed the enantioselective oxidative desymmetrization of a prochiral bicyclic amine **68** to furnish key chiral imine **69** (in equilibrium with its trimeric form); a chemical diastereoselective addition of cyanide to **69** and subsequent hydrolysis of the amino-nitrile intermediate **70** with aqueous HCl yielded cyclic amino acid **71** with good optical purity after a single recrystallization (Scheme 14.17b). This **71** is one of the components of peptidomimetic Telaprevir, an NS3.4A serine protease inhibitor used for the treatment of hepatitis C. Following a similar strategy on amine **72**, Li et al. [143] reported the use of different genetically modified MAOs for the generation of enantiopure nitrile **73**, a key intermediate for the preparation of anti-HIV drug Boceprevir (Scheme 14.17c).

TAs can be also used for desymmetrization purposes. For instance, the preparation of Filorexant (code name MK-6096, an orexin dual antagonist of the OX1 and OX2 receptors initially tested by Merck for the treatment of insomnia and migraine prophylaxis or as antidepressant, although not found effective and retired from development pipeline) was reported by Girardin et al. [144] via transamination of

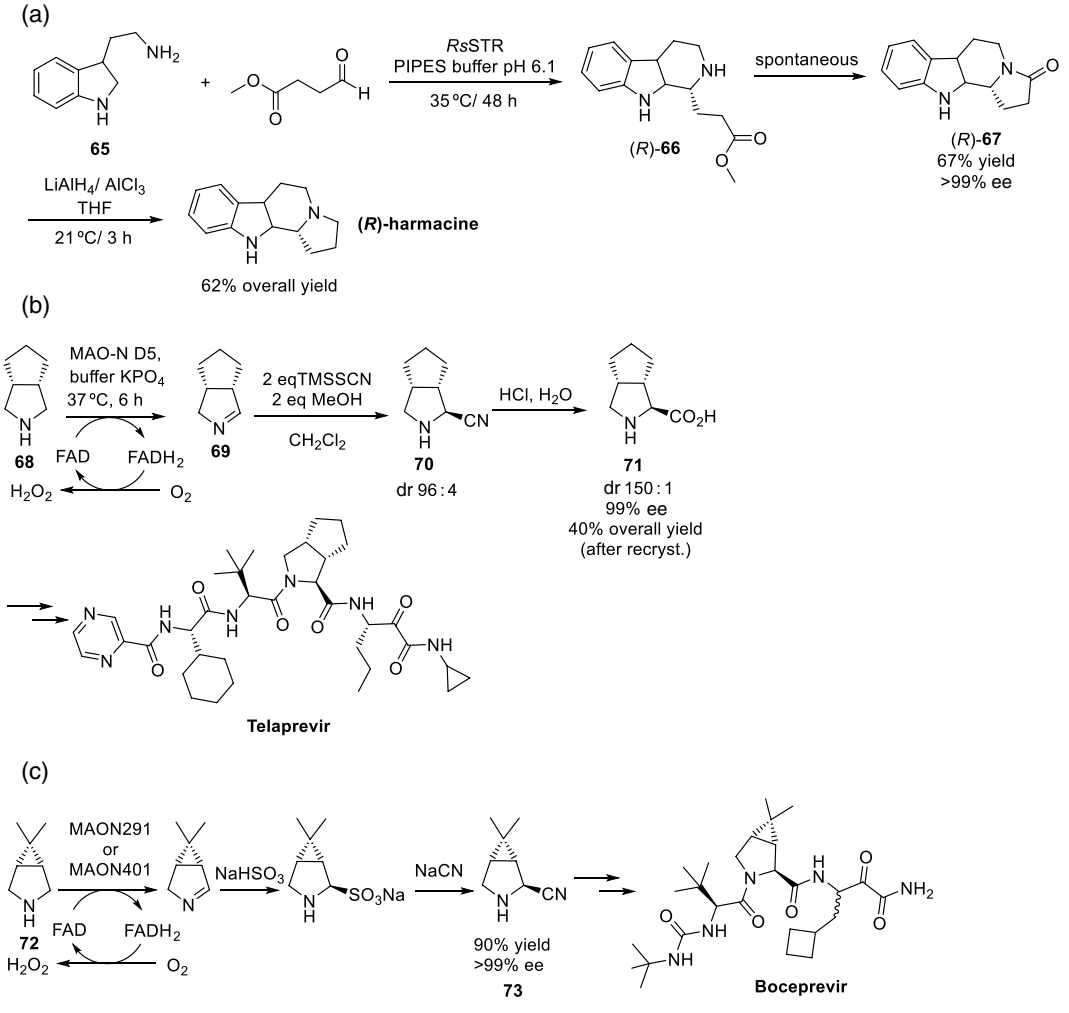

Scheme 14.17. Synthesis of valuable compounds in enzymatic desymmetrizations employing STR and MAO. (a) Synthesis of (*R*)-harmacine catalyzed by RsSTR; (b) Application of MAO-ND5 for the preparation of the cyclic amino acid **71**; (c) MAO-catalyzed synthesis of boceprevir.

prochiral oxodiester **74**, using ATA117 and D-alanine as sacrificial amine, by coupling to an enzymatic cascade involving lactate dehydrogenase (LDH) and GDH in order to shift the equilibrium (Scheme 14.18a). Thus, the resulting aminodiester (*R*)**-75** spontaneously cyclized to the desired piperidone (*R*)**-76** in an overall reaction performed in water with NaH_2PO_4, with a continuous addition of 5.0 N NaOH necessary to maintain the optimal pH at 7.4, which was found to be optimal. The reaction could be successfully conducted in a concentration range of 50–75 g l^{-1} of **74** and best conditions required D-alanine to be close to its solubility limit, using glucose levels limited to 1.1–1.3 equivalents.

It is worth to mention the use of symmetric *ortho*-xylylenediamine **77** as a highly effective amine donor for TA-catalyzed reactions on prochiral ketones [145]. The use of stoichiometric quantities of this reagent leads to quantitative conversions to the desired chiral amine, without any by-product removal systems; this fact is caused by the spontaneous aromatization of the cyclic imine by-product **79** to the more stable aromatic isoindole **80**, therefore removing this component from the system. Remarkably, this electron-rich **80** is consequently oxidized spontaneously into an intensely colored polymeric derivative; this provides an operationally simple and sensitive method to detect TA activity. These colored

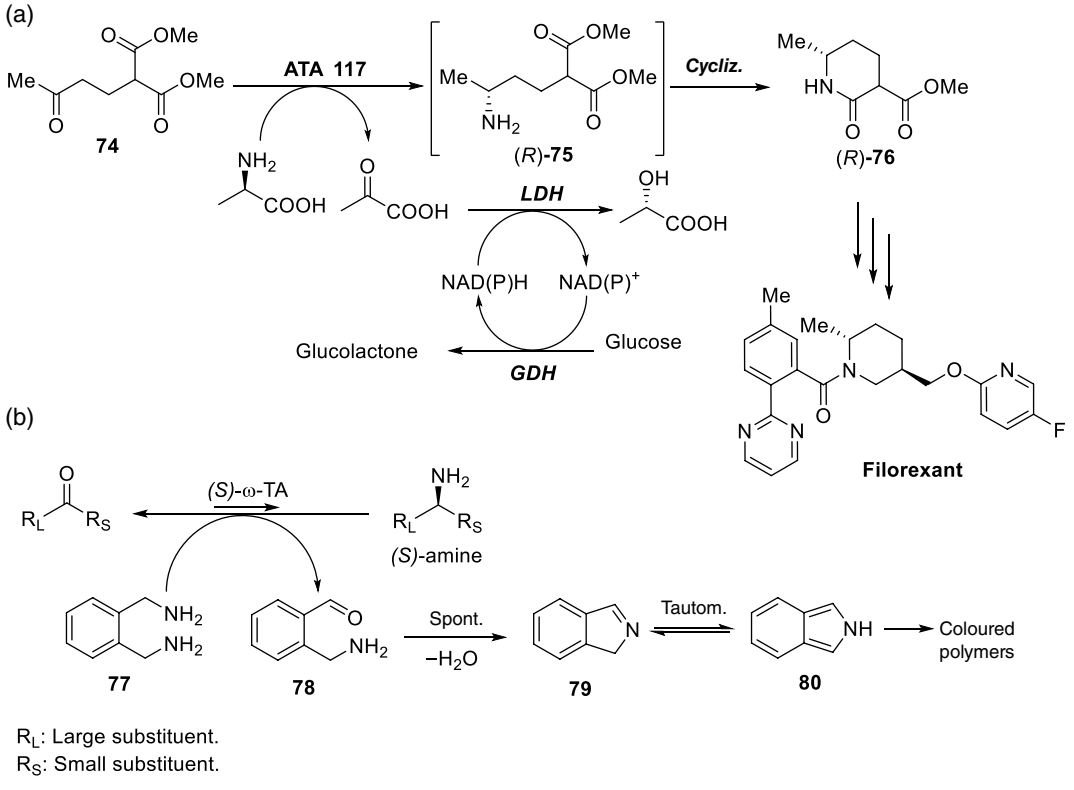

Scheme 14.18. Transaminase-catalyzed desymmetrization procedures. (a) Synthesis of a Filorexant precursor employing ATA117; (b) Use of *o*-xylylenediamine as amine donor for detecting TA activity.

structures can be easily detected in liquid phase transformations or directly in *E. coli* colonies expressing TA genes, therefore being extremely useful in high-throughput assays for the identification of new TAs (Scheme 14.18b).

14.7. MULTI(CHEMO)ENZYMATIC REACTIONS

The coupling of different (chemo)enzymatic steps into one-pot processes presents several advantages respecting other synthetic approaches. When carrying out this type of processes, it is possible to avoid work-up, purification steps, or isolation of intermediates in order to develop sustainable and economically feasible procedures. Biocatalytic processes have been combined with other reactions catalyzed by other enzymes, metal catalysts, or organocatalysts, in multistep processes, which has been described in several reviews [146–150]. For these procedures, it has to be taken into account that all the catalysts involved in these reactions have to be compatible with each other in order to avoid inhibition or deactivation effects and that different reaction conditions are required for each step.

Methoxamine is a valuable chiral 1,2-aminoalcohol used for the treatment of hypotension and incontinence. In 2019, a multienzymatic procedure was described for the synthesis of the four stereoisomers of this compound with high conversions and selectivities in a sequential two-step process without intermediate purification [151]. Using 2,5-dimethoxybenzaldehyde (**81**) and pyruvate as starting substrates, the use of a mutant of the pyruvate decarboxylase from *Acetobacter pasteurianus* (ApPDC-E469GI468A-W543F) afforded (*S*)-1-hydroxy-1-(2,5-dimethoxyphenyl)propan-2-one **82** in a carboligation step with 98% *ee*, whereas the reaction catalyzed by acetohydroxyacid synthase I from *E. coli* (EcAHAS-I) was selected for the preparation of the (*R*)-enantiomer with 96% ee. Amination of the resulting hydroxyl

ketones was catalyzed by the (*S*)-selective TA from *Bacillus megaterium* or by the (*R*)-TA from *Arthrobacter* sp., leading to the optically active final compounds with excellent selectivity. Both biocatalysts use isopropylamine as amine donor. The four methoxamine stereoisomers were achieved with selectivities between 94 and 99% and total conversions between 59 and 80%. The development of the synthesis in a one-pot two-step procedure at 75 ml scale afforded (1*S*,2*R*)-methoxamine hydrochloride with 98% ee and 46% isolated yield (94% purity), as shown in Scheme 14.19a.

The preparation of optically active 1,3,4-trisubstituted THIQs has been developed in a three-step cascade starting from inexpensive 3-hydroxybenzaldehyde (**83**) and pyruvate (Scheme 14.19b) [152]. The carboligation of these two compounds catalyzed by acetohydroxy acid synthase I from *E. coli* (EcAHAS-I) led to (*R*)-**84**, which was converted into the (1*R*,2*S*)-aminoalcohol **85** in a reaction catalyzed by TAs from *Chromobacterium violaceum* using isopropylamine as amine donor. The chiral 1,2-aminoalcohol was then subjected to a Pictec-Spengler reaction with phenylacetaldehyde using the Pictet-Spenglerase variant A79I from *Coptis japonica* as biocatalyst. The desired (1*S*,3*S*,4*R*)-THIQ **86** was recovered with an overall 88% yield and excellent optical purity. The last step of the cascade can be also carried out in presence of a chemical catalyst as potassium phosphate employing 2-bromobenzaldehyde as carbonyl donor. Once the chiral aminoalcohol is obtained, enzymes are removed by ultrafiltration and phosphate buffer and the aldehyde is added in order to obtain (1*S*,3*S*,4*R*)-**86** with excellent selectivity and a good global yield (77%). Thus, it was possible to obtain both enantiomers of position 1 by modifying the catalyst of the last step of the process.

Pd(0)-CAL-B-CLEAs have been also employed as bifunctional biohybrid catalyst for the KR of racemic alcohols. The Pd-catalyzed cycloisomerization of 4-pentynoic acid led to a lactone, which can be employed as acyl donor for the KR of different secondary racemic alcohols [153]. After the optimization of both processes, it was observed that the best results were obtained when carrying the processes in one-pot at 60 °C, using trimethylamine as base for the isomerization and toluene as solvent. In these conditions, a set of 1-phenylethanol derivatives was obtained with yields around 50% and excellent selectivity.

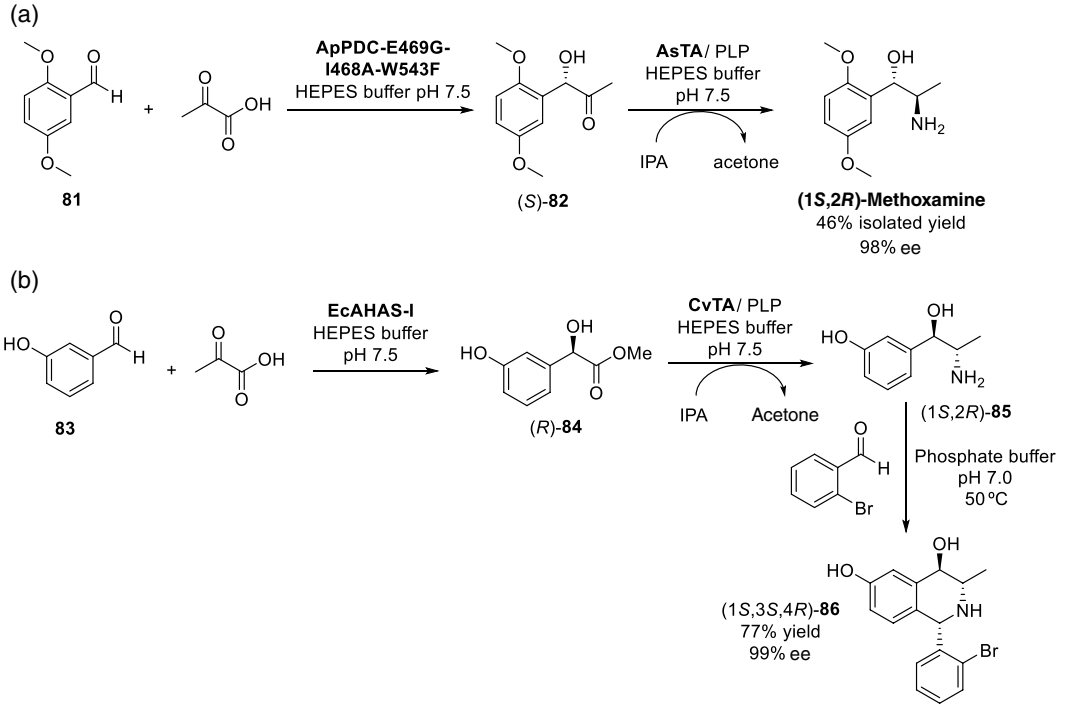

Scheme 14.19. Multienzymatic systems for the preparation of valuable chiral compounds. (a) Synthesis of (1*S*,2*R*)-methoxamine hydrochloride combining a pyruvate decarboxylase and a TA in a one-pot two-steps procedure; (b) Synthesis of 1,3,4-trisubstituted THIQs in a three-step process combining acetohydroxy acid synthase and TAs.

Catalyst was recycled for six cycles in the KR of 1-phenylethanol, without loss in its catalytic properties, making it possible to obtain the enantiopure chiral alcohol with yields around 42–45%.

Biocatalysts can be also combined with organocatalysts in order to perform multicatalytic procedures [146, 154]. The application of small organic molecules as asymmetric catalysts has gained a great interest since the beginning of this century and is widely employed in asymmetric synthesis [155, 156]. By this reason, some examples have been recently described employing enzymes in presence of organocatalysts. Thus, the preparation of 3-substituted 2,3-dihidrobenzofuran-2,5-diols (**87**) in moderate to good yields and moderate to excellent selectivities was described in 2015 by combining a laccase-catalyzed oxidation of a set of 1,4-dihydroxybenzenes (**88**) with the α-arylation of different aldehydes with the 1,4-hydroquinones formed in the first step, catalyzed by a proline-based catalyst [157], as depicted in Scheme 14.20a. Reaction optimization was performed in the reaction between 3-methylbutanal and 1,4-dihydroxybenzene in the presence of (*S*)-2-[diphenyl(trimethylsilyloxy)methyl]pyrrolidine (Cat. **I**) as organocatalyst and the laccase from *Agaricus bisporus*. The process was carried out with 0.25 mmol of 1,4-dihydroxybenzene in 0.5 ml buffer/acetonitrile pH 6.0 containing 10 mol% of (*S*)-**I**, 15 units of laccase, and 5 equivalents of aldehyde per equivalent of 1,4-dihydroxybenzene, recovering the final product with 76% yield and 87% ee after 72 hours at room temperature. The reaction was scaled up to 2 mmol of 1,4-dihydroxybenzene using 45 units of laccase with an 84% yield of the final hemiacetal after 72 hours with an optical purity of 92%. The multicatalytic system was extended to other aldehydes. For β-branched aldehydes such as 2-cyclohexylacetaldehyde excellent results are obtained (91% yield and 92% ee), whereas unbranched aldehydes led to moderate to good yields (51–90%) and lower optical purities.

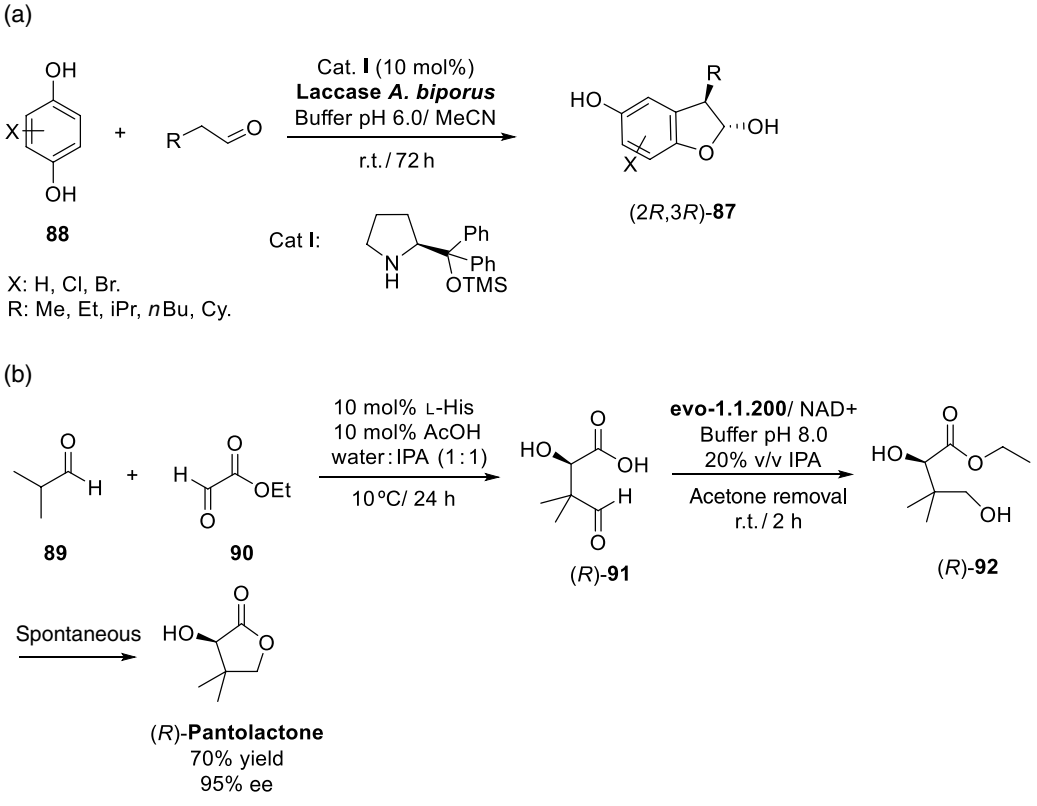

Scheme 14.20. Multicatalytic systems combining enzymes and organocatalysts for the preparation of chiral compounds. (a) Preparation of 3-substituted 2,3-dihidrobenzofuran-2,5-diols combining a laccase-catalyzed oxidation with a proline-catalyzed arylation; (b) Synthesis of (*R*)-pantolactone by using ADHs and L-histidide.

The synthesis of (*R*)-pantolactone, a valuable vitamin-B5 intermediate, has been recently described combining ADHs and L-histidine as organocatalyst, as shown in Scheme 14.20b [158]. In a first step, the aminoacid was able to catalyze the aldol reaction between isobutanal (**89**) and ethyl glyoxylate (**90**) with good activity and selectivity. This process was carried out in presence of acetic acid as co-catalyst, as this acid is able to increase the process yield by facilitating the hydrolysis of iminium ion intermediate that is formed in the catalytic cycle. After 24 hours at 10 °C in presence of 10 mol% of L-histidine and acetic acid in a 1 : 1 mixture of water : IPA, the final adduct (*R*)-**91** was recovered with 85% yield and 79% ee. The aldol obtained was selectively reduced by the ADH evo-1.1.200 from Evocatal at pH 8.0 in a mixture buffer pH 8.0 containing 20% IPA as cosubstrate. It was observed that the removal of the acetone formed as coproduct has a beneficial effect in the process conversion in an in situ product removal (ISPR) [159] employing a flow of air saturated with water containing 5% v/v IPA. After 2 hours, the diol (*R*)-**92** was obtained with 86% conversion and 95% ee, spontaneously forming (*R*)-pantolactone in a lactonization process.

14.8. CONCLUSIONS AND OUTLOOK

Biocatalysis has already proven to be an outstanding and useful tool for the preparation of valuable optically active compounds. It has been far from our intention to be exhaustive in this chapter, but, as can be inferred from the examples so far presented, biocatalysis represents an excellent and greener alternative to classical organic synthesis in the preparation of chiral entities. For this purpose, and by employing the different strategies commented herein (KR, DKR, deracemization, PKR, or desymmetrization), it has been shown how it is possible to use different families of biocatalysts (hydrolases, oxidoreductases, lyases, etc.), and, remarkably, in a smart combination with classical chemical processes, in order to furnish the target optically active products.

Therefore, we foresee a growing increase in the use of biotransformations for the preparation of enantiopure drugs, bioactive compounds, or fine chemicals, largely promoted by the enhancement of biocatalyst performance through chemical modification and genetic engineering, as recent Nobel Prize awarded to Frances Arnold has shown. In fact, Directed Evolution has opened the possibility of designing tailor-made enzymes for catalyzing biotransformations on non-natural substrates, thus increasing the catalytic promiscuity that some enzymes (e.g. lipases) do intrinsically display. Finally, yet importantly, the intrinsic sustainability gained by using biocatalysts is a green motor to promote the gradual replacement of some non-eco-friendly chemical catalysts by this more sustainable alternative.

REFERENCES

1. Zaks, A.; Klibanov, A. M., Enzyme-catalyzed processes in organic-solvents. *Proc. Natl. Acad. Sci. U. S. A.* **1985**, *82* (10), 3192–3196.
2. Sheldon, R. A.; Brady, D., Broadening the scope of biocatalysis in sustainable organic synthesis. *ChemSusChem* **2019**, *12* (13), 2859–2881.
3. Patel, R. N., Biocatalysis for synthesis of pharmaceuticals. *Bioorg. Med. Chem.* **2018**, *26* (7), 1252–1274.
4. Sheldon, R. A. A.; Brady, D.; Bode, M. L. L., The Hitchhiker's guide to biocatalysis: recent advances in the use of enzymes in organic synthesis. *Chem. Sci.* **2020**, *11* (10), 2587–2605.
5. Gröger, H., Enzyme-catalyzed asymmetric synthesis. In *Catalytic Asymmetric Synthesis*, 3rd edition, Ojima, I., Ed. John Wiley & Sons: Hoboken, NJ, **2010**; pp. 269–341.
6. Bornscheuer, U. T., The fourth wave of biocatalysis is approaching. *Philos. Trans. R. Soc. A-Math. Phys. Eng. Sci.* **2018**, *376* (2110), 7.
7. Chen, C. S.; Fujimoto, Y.; Girdaukas, G.; Sih, C. J., Quantitative-analyses of biochemical kinetic resolutions of enantiomers. *J. Am. Chem. Soc.* **1982**, *104* (25), 7294–7299.
8. Straathof, A. J. J.; Jongejan, J. A., The enantiomeric ratio: origin, determination and prediction. *Enzyme Microb. Technol.* **1997**, *21* (8), 559–571.
9. Faber, K., *Biotransformations in Organic Chemistry: A Textbook*, 7th extended and corrected edition. Springer International Publishing AG: Cham, Switzerland, **2018**; pp. 31–313.
10. Díaz-Rodríguez, A.; Lavandera, I., Strategies and methods in biocatalysis. In *Biocatalysis in Organic Synthesis 1*, Faber, K.; Fessner, W. D.; Turner, N. J., Eds. Georg Thieme Verlag: Stuttgart, Germany, **2015**; Vol. 1, pp. 95–128.

11. Aranda, C.; Oksdath-Mansilla, G.; Bisogno, F. R.; de Gonzalo, G., Deracemisation processes employing organocatalysis and enzyme catalysis. *Adv. Synth. Catal.* **2020**, *362* (6), 1233–1257.
12. Rachwalski, M.; Vermue, N.; Rutjes, F., Recent advances in enzymatic and chemical deracemisation of racemic compounds. *Chem. Soc. Rev.* **2013**, *42* (24), 9268–9282.
13. Moberg, C., Recycling in asymmetric catalysis. *Accounts Chem. Res.* **2016**, *49* (12), 2736–2745.
14. Williams, J. M. J.; Parker, R. J.; Neri, C., Enzymatic kinetic resolution. In *Enzyme Catalysis in Organic Synthesis*, Drauz, K.; Waldman, H., Eds. Wiley-VCH Verlag GmbH: Weinheim, Germany, **2002**; pp. 287–312.
15. Nakamura, K.; Matsuda, T., Enzymatic kinetic resolution. In *Enantiomer Separation*, Toda, F., Ed. Springer: Dordrecht, The Netherlands, **2004**, pp. 231–260.
16. Straathof, A. J. J.; Rakels, J. L. L.; Heijnen, J. J., Evaluation of process options for enzymatic kinetic resolution. *Ann. N. Y. Acad. Sci.* **1992**, *672*, 497–501.
17. Alcántara, A. R., Biotransformations in drug synthesis: a green and powerful tool for medicinal chemistry. *J. Med. Chem. Drug Des.* **2018**, *1* (1), 1–7.
18. Hoyos, P.; Hernáiz, M. J.; Alcántara, A. R., Biocatalyzed production of fine chemicals. In *Reference Module in Life Sciences*, Moo-Young, M., Ed. Pergamon: Oxford, **2017**, pp. 334–373.
19. Hoyos, P.; Pace, V.; Hernáiz, M. J.; Alcántara, A. R., Biocatalysis in the pharmaceutical industry. A greener future. *Curr. Green Chem.* **2014**, *1* (2), 155–181.
20. Roschangar, F.; Colberg, J.; Dunn, P. J.; Gallou, F.; Hayler, J. D.; Koenig, S. G.; Kopach, M. E.; Leahy, D. K.; Mergelsberg, I.; Tucker, J. L.; Sheldon, R. A.; Senanayake, C. H., A deeper shade of green: inspiring sustainable drug manufacturing. *Green Chem.* **2017**, *19* (1), 281–285.
21. Sheldon, R. A., The E factor 25 years on: the rise of green chemistry and sustainability. *Green Chem.* **2017**, *19* (1), 18–43.
22. Tarczykowska, A.; Sikora, A.; Marszall, M. P., Lipases – valuable biocatalysts in kinetic resolution of racemates. *Mini-Rev. Org. Chem.* **2018**, *15* (5), 374–381.
23. Bertau, M.; Jeromin, G. E., Hydrolysis and transacylation: esterases, lipases, phosphatases, and phosphoryl transferases. In *Biocatalysis in Organic Synthesis 1*, Faber, K.; Fessner, W. D.; Turner, N. J., Eds. Georg Thieme Verlag: Stuttgart, Germany, **2015**; Vol. 1, pp. 129–187.
24. Busto, E.; Gotor-Fernandez, V.; Gotor, V., Hydrolases: catalytically promiscuous enzymes for non-conventional reactions in organic synthesis. *Chem. Soc. Rev.* **2010**, *39* (11), 4504–4523.
25. Rodríguez-Mata, M.; Gotor-Fernández, V., Resolution of alcohols, amines, acids, and esters by nonhydrolytic processes. In *Biocatalysis in Organic Synthesis 1*, Faber, K.; Fessner, W. D.; Turner, N. J., Eds. Georg Thieme Verlag: Stuttgart, Germany, **2015**; Vol. 1, pp. 189–232.
26. Chandra, P.; Enespa; Singh, R.; Arora, P. K., Microbial lipases and their industrial applications: a comprehensive review. *Microb. Cell Fact.* **2020**, *19* (1), 169.
27. Filho, D. G.; Silva, A. G.; Guidini, C. Z., Lipases: sources, immobilization methods, and industrial applications. *Appl. Microbiol. Biotechnol.* **2019**, *103* (18), 7399–7423.
28. Dwivedee, B. P.; Soni, S.; Sharma, M.; Bhaumik, J.; Laha, J. K.; Banerjee, U. C., Promiscuity of lipase-catalyzed reactions for organic synthesis: a recent update. *Chemistryselect* **2018**, *3* (9), 2441–2466.
29. Seddigi, Z. S.; Malik, M. S.; Ahmed, S. A.; Babalghith, A. O.; Kamal, A., Lipases in asymmetric transformations: recent advances in classical kinetic resolution and lipase–metal combinations for dynamic processes. *Coord. Chem. Rev.* **2017**, *348*, 54–70.
30. Bhardwaj, K. K.; Gupta, R., Synthesis of chirally pure enantiomers by lipase. *J. Oleo Sci.* **2017**, *66* (10), 1073–1084.
31. Kumar, A.; Dhar, K.; Kanwar, S. S.; Arora, P. K., Lipase catalysis in organic solvents: advantages and applications. *Biol. Proced. Online* **2016**, *18*.
32. de Miranda, A. S.; Miranda, L. S. M.; de Souza, R., Lipases: valuable catalysts for dynamic kinetic resolutions. *Biotechnol. Adv.* **2015**, *33* (5), 372–393.
33. Daiha, K. D.; Angeli, R.; de Oliveira, S. D.; Almeida, R. V., Are lipases still important biocatalysts? A study of scientific publications and patents for technological forecasting. *PLoS One* **2015**, *10* (6), 20.
34. Carvalho, A.; Fonseca, T. D.; de Mattos, M. C.; de Oliveira, M. D. F.; de Lemos, T. L. G.; Molinari, F.; Romano, D.; Serra, I., Recent advances in lipase-mediated preparation of pharmaceuticals and their intermediates. *Int. J. Mol. Sci.* **2015**, *16* (12), 29682–29716.
35. Arroyo, M.; de la Mata, I.; Garcia, J. L.; Barredo, J. L., *Biocatalysis for Industrial Production of Active Pharmaceutical Ingredients (APIs)*. Academic Press Ltd-Elsevier Science Ltd: London, **2017**; pp. 451–473.
36. Bornscheuer, U.; Kazlauskas, R. J., *Hydrolases in Organic Synthesis. Regio- and Stereoselective Biotransformations*, 2nd edition. WILEY-VCH Verlag: Weinheim, Germany, **2006**.
37. Fessner, W. D.; Anthonsen, T., *Modern Biocatalysis: Stereoselective and Environmentally Friendly Reactions*. Wiley-VCH: Weinheim, Germany, **2009**.
38. Gröger, H.; Hummel, W., *Science of Synthesis: Biocatalysis in Organic Synthesis. Thieme Chemistry*. Georg Thieme Verlag: Stuttgart, Germany, **2015**; Vol. 3, p. 505.
39. Grunwald, P., *Biocatalysis: Biochemical Fundamentals and Applications*. Imperial College Press: London, **2009**.

40. Liese, A.; Seelbach, K.; Wandrey, C., *Industrial Biotransformations*, 2nd edition. John Wiley & Sons, Inc. Verlag GmbH & Co, kGaA.: Weinheim, Germany, **2006**.
41. Matsuda, T., *Future Directions in Biocatalysis*. Elsevier Science: Amsterdam, the Netherlands, **2011**.
42. Meyer, H.-P.; Ghisalba, O.; Leresche, J. E., *Biotransformations and the Pharma Industry*. Wiley-VCH Verlag GmbH & Co. KGaA: Weinheim, Germany, **2010**.
43. Patel, R. N., *Stereoselective Biocatalysis*. M. Dekker: New York, **2000**.
44. Patel, R. N., *Biocatalysis in the Pharmaceutical and Biotechnology Industries*. CRC Press: Boca Raton, FL, **2006**.
45. Patel, R. N., *Green Biocatalysis*. John Wiley & Sons, Inc: Hoboken, NJ, **2016**.
46. Tao, J.; Lin, G. Q.; Liese, A., *Biocatalysis for the Pharmaceutical Industry: Discovery, Development, and Manufacturing*. John Wiley & Sons Asia: Singapore, **2009**.
47. Tao, J. A.; Kazlauskas, R. J., *Biocatalysis for Green Chemistry and Chemical Process Development*. John Wiley & Sons: Hoboken, NJ, **2011**.
48. Kazlauskas, R. J.; Weissfloch, A. N. E.; Rappaport, A. T.; Cuccia, L. A., A rule to predict which enantiomer of a secondary alcohol reacts faster in reactions catalyzed by cholesterol esterase, lipase from *Pseudomonas cepacia*, and lipase from *Candida rugosa*. *J. Org. Chem.* **1991**, *56* (8), 2656–2665.
49. Chen, H.; Meng, X.; Xu, X. Q.; Liu, W. B.; Li, S. Y., The molecular basis for lipase stereoselectivity. *Appl. Microbiol. Biotechnol.* **2018**, *102* (8), 3487–3495.
50. Domínguez de María, P.; de Gonzalo, G.; Alcántara, A. R., Biocatalysis as useful tool in asymmetric synthesis: an assessment of recently granted patents (2014–2019). *Catalysts* **2019**, *9* (10), 802.
51. Zheng, G.; Chen, Q. Method for producing ticagrelor chiral drug intermediates by using *Candida antarctica* lipase B. CN104164469A, **2014**.
52. Husted, S.; van Giezen, J. J. J., Ticagrelor: the first reversibly binding oral P2Y(12) receptor antagonist. *Cardiovasc. Ther.* **2009**, *27* (4), 259–274.
53. Danielak, D.; Karazniewicz-Lada, M.; Glowka, F., Ticagrelor in modern cardiology – an up-to-date review of most important aspects of ticagrelor pharmacotherapy. *Expert Opin. Pharmacother.* **2018**, *19* (2), 103–112.
54. Ueda, T.; Abe, Y. Novel method for producing 1-(acyloxy)alkyl carbamate derivatives. WO2016208709A1, **2016**.
55. Boffa, M. B.; Koschinsky, M. L., Curiouser and curiouser: recent advances in measurement of thrombin-activatable fibirinolysis inhibitor (TAFI) and in understanding its molecular genetics, gene regulation, and biological roles. *Clin. Biochem.* **2007**, *40* (7), 431–442.
56. Leurs, J.; Hendriks, D., Carboxypeptidase U (TAFIa): a metallocarboxypeptidase with a distinct role in haemostasis and a possible risk factor for thrombotic disease. *Thromb. Haemost.* **2005**, *94* (3), 471–487.
57. Colucci, M.; Semeraro, N., Thrombin activatable fibrinolysis inhibitor: at the nexus of fibrinolysis and inflammation. *Thromb. Res.* **2012**, *129* (3), 314–319.
58. Ji, Y.; Chen, B.; Qian, F.; He, Y.; Gao, X.; Hong, X., A method for preparing levetiracetam. CN105063120A, **2015**.
59. Ortiz, C.; Ferreira, M. L.; Barbosa, O.; dos Santos, J. C. S.; Rodrigues, R. C.; Berenguer-Murcia, A.; Briand, L. E.; Fernandez-Lafuente, R., Novozym 435: the "perfect" lipase immobilized biocatalyst? *Catal. Sci. Technol.* **2019**, *9* (10), 2380–2420.
60. Abrahamson, M. J.; Kielbus, A. B.; Riordan, W. T.; Hill, D. R.; Chemburkar, S. R.; Reddy, R. E.; Towne, T. B.; Mei, J.; Brown, G. J.; Mix, S., Enzymatic process for the preparation of (1S,2R)-2-(difluoromethyl)-1-(propoxycarbonyl)cyclopropanecarboxylic acid. US10316338B1, **2019**.
61. Gawley, R.; Aubé, J., *Principles of Asymmetric Synthesis*. Elsevier Ltd: Oxford, **2012**.
62. Markham, A.; Goa, K. L., Valsartan – a review of its pharmacology and therapeutic use in essential hypertension. *Drugs* **1997**, *54* (2), 299–311.
63. Xia, J.; Chen, D., Method for preparing l-valsartan by separating dl-valsartan ester with lipase. CN105420338A, **2016**.
64. Adlercreutz, P., Immobilisation and application of lipases in organic media. *Chem. Soc. Rev.* **2013**, *42* (15), 6406–6436.
65. Bornscheuer, U. T.; Flickinger, M. C., Lipases, synthesis of chiral compounds, aqueous and organic solvents. In *Encyclopedia of Industrial Biotechnology*, Fickinger, M. C. Ed. John Wiley & Sons, Inc.: Hoboken, NJ, **2010**; pp. 1–16. doi:https://doi.org/10.1002/9780470054581.eib648.
66. Roy, I.; Mukherjee, J.; Gupta, M. N., High activity preparations of lipases and proteases for catalysis in low water containing organic solvents and ionic liquids. In *Immobilization of Enzymes and Cells*, 3rd edition, Guisan, J. M., Ed. Humana Press: Totowa, NJ, **2013**; Vol. 1051, pp. 275–284.
67. Priyanka, P.; Tan, Y. Q.; Kinsella, G. K.; Henehan, G. T.; Ryan, B. J., Solvent stable microbial lipases: current understanding and biotechnological applications. *Biotechnol. Lett.* **2019**, *41* (2), 203–220.
68. Chakravorty, D.; Parameswaran, S.; Dubey, V. K.; Patra, S., Unraveling the rationale behind organic solvent stability of lipases. *Appl. Biochem. Biotechnol.* **2012**, *167* (3), 439–461.
69. Torres, F.; Rubin, L. J., Treprostinil for the treatment of pulmonary arterial hypertension. *Expert Rev. Cardiovasc. Ther.* **2013**, *11* (1), 13–25.
70. Wang, Q.; Wang, T.; Sun, Y.; Wang, B.; You, B.; Pu, J.; Li, X.; Jiang, Y., Preparation of levocarnitine. CN106748843A, **2017**.
71. Kraemer, W. J.; Volek, J. S.; Dunn-Lewis, C., l-Carnitine supplementation: Influence upon physiological function. *Curr. Sport. Med. Rep.* **2008**, *7* (4), 218–223.

72. Bloomer, R. J.; Butawan, M.; Farney, T. M.; McAllister, M. J., *An Overview of the Dietary Ingredient Carnitine*. Academic Press Ltd-Elsevier Science Ltd: London, **2019**; pp. 605–617.
73. Hoyos, P.; Pace, V.; Alcántara, A. R., Chiral building blocks for drugs synthesis via biotransformations. In *Asymmetric Synthesis of Drugs and Natural Products*, Nag, A., Ed. CRC Press: Boca Raton, FL, **2018**; pp. 346–448.
74. Hoyos, P.; Pace, V.; Alcántara, A. R., Biocatalyzed synthesis of statins: a sustainable strategy for the preparation of valuable drugs. *Catalysts* **2019**, *9* (3), 260.
75. Yu, C.; Zhai, M.; Wang, M.; Gong, X.; Zhang, T.; Zhai, H., Preparation method of high-purity pitavastatin calcium for treating hypercholesterolemia. CN103834705A, **2014**.
76. Gröger, H. J. A. M., Biocatalytic concepts for synthesizing amine bulk chemicals: recent approaches towards linear and cyclic aliphatic primary amines and ω-substituted derivatives thereof. *Appl. Microbiol. Biotechnol.* **2019**, *103* (1), 83–95.
77. Kohls, H.; Steffen-Munsberg, F.; Höhne, M., Recent achievements in developing the biocatalytic toolbox for chiral amine synthesis. *Curr. Opin. Chem. Biol.* **2014**, *19*, 180–192.
78. Grogan, G., Synthesis of chiral amines using redox biocatalysis. *Curr. Opin. Chem. Biol.* **2018**, *43*, 15–22.
79. Gomm, A.; O'Reilly, E., Transaminases for chiral amine synthesis. *Curr. Opin. Chem. Biol.* **2018**, *43*, 106–112.
80. Ismail, H.; Lau, R. M.; van Rantwijk, F.; Sheldon, R. A., Fully enzymatic resolution of chiral amines: acylation and deacylation in the presence of *Candida antarctica* lipase B. *Adv. Synth. Catal.* **2008**, *350* (10), 1511–1516.
81. Lima, R. N.; dos Anjos, C. S.; Orozco, E. V. M.; Porto, A. L. M., Versatility of *Candida antarctica* lipase in the amide bond formation applied in organic synthesis and biotechnological processes. *Mol. Catal.* **2019**, *466*, 75–105.
82. Petchey, M. R.; Grogan, G., Enzyme-catalysed synthesis of secondary and tertiary amides. *Adv. Synth. Catal.* **2019**, *361* (17), 3895–3914.
83. Mourelle-Insua, A.; Lopez-Iglesias, M.; Gotor, V.; Gotor-Fernandez, V., Stereoselective access to 1-2-bromo(het)aryloxy propan-2-amines using transaminases and lipases; development of a chemoenzymatic strategy toward a levofloxacin precursor. *J. Org. Chem.* **2016**, *81* (20), 9765–9774.
84. Harwood, L. A.; Wong, L. L.; Robertson, J., Enzymatic kinetic resolution by addition of oxygen. *Angew. Chem. Int. Ed.* **2020**, *59*, 2–16.
85. Opperman, D. J.; Reetz, M. T., Towards practical Baeyer-Villiger-monooxygenases: design of cyclohexanone monooxygenase mutants with enhanced oxidative stability. *ChemBiochem* **2010**, *11* (18), 2589–2596.
86. Wu, S.; Acevedo, J. P.; Reetz, M. T., Induced allostery in the directed evolution of an enantioselective Baeyer-Villiger monooxygenase. *Proc. Natl. Acad. Sci. U. S. A.* **2010**, *107* (7), 2775–2780.
87. Rudroff, F.; Fink, M. J.; Pydi, R.; Bornscheuer, U. T.; Mihovilovic, M. D., First chemo-enzymatic synthesis of the (*R*)-Taniguchi lactone and substrate profiles of CAMO and OTEMO, two new Baeyer-Villiger monooxygenases. *Monatsh. Chem.* **2017**, *148* (1), 157–165.
88. Fink, M. J.; Fischer, T. C.; Rudroff, F.; Dudek, H.; Fraaije, M. W.; Mihovilovic, M. D., Extensive substrate profiling of cyclopentadecanone monooxygenase as Baeyer-Villiger biocatalyst reveals novel regiodivergent oxidations. *J. Mol. Catal. B Enzym.* **2011**, *73* (1–4), 9–16.
89. Oberleitner, N.; Peters, C.; Muschiol, J.; Kadow, M.; Sass, S.; Bayer, T.; Schaaf, P.; Iqbal, N.; Rudroff, F.; Mihovilovic, M. D.; Bornscheuer, U. T., An enzymatic toolbox for cascade reactions: a showcase for an in vivo redox sequence in asymmetric synthesis. *ChemCatChem* **2013**, *5* (12), 3524–3528.
90. Peters, C.; Rudroff, F.; Mihovilovic, M. D.; Bornscheuer, U. T., Fusion proteins of an enoate reductase and a Baeyer-Villiger monooxygenase facilitate the synthesis of chiral lactones. *Biol. Chem.* **2017**, *398* (1), 31–37.
91. Toda, H.; Imae, R.; Itoh, N., Bioproduction of chiral epoxyalkanes using styrene monooxygenase from *Rhodococcus* sp. ST-10 (RhSMO). *Adv. Synth. Catal.* **2014**, *356* (16), 3443–3450.
92. Lin, H.; Liu, Y.; Wu, Z.-L., Highly diastereo- and enantio-selective epoxidation of secondary allylic alcohols catalyzed by styrene monooxygenase. *Chem. Commun.* **2011**, *47* (9), 2610–2612.
93. Lin, H.; Tang, Y. H.; Dong, S.; Lang, R. B.; Chen, H. G., A new monooxygenase from *Herbaspirillum huttiense* catalyzed highly enantioselective epoxidation of allylbenzenes and allylic alcohols. *Catal. Sci. Technol.* **2020**, *10* (7), 2145–2151.
94. Kim, Y.; Park, J.; Kim, M. J., Dynamic kinetic resolution of amines and amino acids by enzyme-metal cocatalysis. *ChemCatChem* **2011**, *3* (2), 271–277.
95. Lee, J. H.; Han, K.; Kim, M. J.; Park, J., Chemoenzymatic dynamic kinetic resolution of alcohols and amines. *Eur. J. Org. Chem.* **2010**, *2010* (6), 999–1015.
96. Hoyos, P.; Pace, V.; Alcantara, A. R., Dynamic kinetic resolution via hydrolase-metal combo catalysis in stereoselective synthesis of bioactive compounds. *Adv. Synth. Catal.* **2012**, *354* (14–15), 2585–2611.
97. Verho, O.; Backvall, J. E., Chemoenzymatic dynamic kinetic resolution: a powerful tool for the preparation of enantiomerically pure alcohols and amines. *J. Am. Chem. Soc.* **2015**, *137* (12), 3996–4009.
98. Hoyos, P.; Pace, V.; Hernáiz, M. J.; Alcántara, A. R., Dynamic kinetic resolution via hydrolase–metal combo catalysis. In *Green Biocatalysis*, Patel, R. N. Ed. John Wiley & Sons, Inc.: New York, **2016**; pp. 373–396.
99. Kuhn, F.; Katsuragi, S.; Oki, Y.; Scholz, C.; Akai, S.; Groger, H., Dynamic kinetic resolution of a tertiary alcohol. *Chem. Commun.* **2020**, *56* (19), 2885–2888.

100. Gustafson, K. P. J.; Gorbe, T.; De Gonzalo, G.; Yuan, N.; Schreiber, C. L.; Shchukarev, A.; Tai, C. W.; Persson, I.; Zou, X. D.; Backvall, J. E., Chemoenzymatic dynamic kinetic resolution of primary benzylic amines using Pd-0-CalB CLEA as a biohybrid catalyst. *Chem.-Eur. J.* **2019**, *25* (39), 9174–9179.
101. Filice, M.; Marciello, M.; Morales, M. D.; Palomo, J. M., Synthesis of heterogeneous enzyme-metal nanoparticle biohybrids in aqueous media and their applications in C–C bond formation and tandem catalysis. *Chem. Commun.* **2013**, *49* (61), 6876–6878.
102. Tanner, M. E., Understanding nature's strategies for enzyme-catalyzed racemization and epimerization. *Acc. Chem. Res.* **2002**, *35* (4), 237–246.
103. Musa, M. M., Enzymatic racemization of alcohols and amines: an approach for bi-enzymatic dynamic kinetic resolution. *Chirality* **2020**, *32* (2), 147–157.
104. Ahn, Y.; Ko, S. B.; Kim, M. J.; Park, J., Racemization catalysts for the dynamic kinetic resolution of alcohols and amines. *Coord. Chem. Rev.* **2008**, *252* (5–7), 647–658.
105. Parvulescu, A.; Janssens, J.; Vanderleyden, J.; De Vos, D., Heterogeneous catalysts for racemization and dynamic kinetic resolution of amines and secondary alcohols. *Top. Catal.* **2010**, *53* (13–14), 931–941.
106. Slabu, I.; Galman, J. L.; Lloyd, R. C.; Turner, N. J., Discovery, engineering, and synthetic application of transaminase biocatalysts. *ACS Catal.* **2017**, *7* (12), 8263–8284.
107. Guo, F.; Berglund, P., Transaminase biocatalysis: optimization and application. *Green Chem.* **2017**, *19* (2), 333–360.
108. Fuchs, C. S.; Farnberger, J. E.; Steinkellner, G.; Sattler, J. H.; Pickl, M.; Simon, R. C.; Zepeck, F.; Gruber, K.; Kroutil, W., Asymmetric amination of alpha-chiral aliphatic aldehydes via dynamic kinetic resolution to access stereocomplementary brivaracetam and pregabalin precursors. *Adv. Synth. Catal.* **2018**, *360* (4), 768–778.
109. Mangas-Sanchez, J.; France, S. P.; Montgomery, S. L.; Aleku, G. A.; Man, H.; Sharma, M.; Ramsden, J. I.; Grogan, G.; Turner, N. J., Imine reductases (IREDs). *Curr. Opin. Chem. Biol.* **2017**, *37*, 19–25.
110. Stockinger, P.; Roth, S.; Muller, M.; Pleiss, J., Systematic evaluation of imine-reducing enzymes: common principles in imine reductases, beta-hydroxy acid dehydrogenases, and short-chain dehydrogenases/reductases. *ChemBiochem* **2020**, *21* (18), 2689–2695.
111. Montgomery, S. L.; Pushpanath, A.; Heath, R. S.; Marshall, J. R.; Klemstein, U.; Galman, J. L.; Woodlock, D.; Bisagni, S.; Taylor, C. J.; Mangas-Sanchez, J.; Ramsden, J. I.; Dominguez, B.; Turner, N. J., Characterization of imine reductases in reductive amination for the exploration of structure-activity relationships. *Sci. Adv.* **2020**, *6* (21), 12.
112. Matzel, P.; Wenske, S.; Merdivan, S.; Gunther, S.; Hohne, M., Synthesis of beta-chiral amines by dynamic kinetic resolution of alpha-branched aldehydes applying imine reductases. *ChemCatChem* **2019**, *11* (17), 4281–4285.
113. Falus, P.; Cerioli, L.; Bajnoczi, G.; Boros, Z.; Weiser, D.; Nagy, J.; Tessaro, D.; Servi, S.; Poppe, L., A continuous-flow cascade reactor system for subtilisin a-catalyzed dynamic kinetic resolution of *N-tert*-butyloxy-carbonylphenylalanine ethyl thioester with benzylamine. *Adv. Synth. Catal.* **2016**, *358* (10), 1608–1617.
114. Applegate, G. A.; Berkowitz, D. B., Exploiting enzymatic dynamic reductive kinetic resolution (DYRKR) in stereocontrolled synthesis. *Adv. Synth. Catal.* **2015**, *357* (8), 1619–1632.
115. Mangas-Sanchez, J.; Busto, E.; Gotor, V.; Gotor-Fernandez, V., One-pot synthesis of enantiopure 3,4-dihydroisocoumarins through dynamic reductive kinetic resolution processes. *Org. Lett.* **2013**, *15* (15), 3872–3875.
116. Green, T. K.; Damarancha, A.; Vanagel, M.; Showalter, B.; Kolberg, S.; Thompson, A., Stereoselective reduction of alpha-fluoro-beta-keto esters by NADH and NADPH-dependent ketoreductases. *Eur. J. Org. Chem.* **2019**, *2019* (25), 4080–4084.
117. Mendez-Sanchez, D.; Mourelle-Insua, A.; Gotor-Fernandez, V.; Lavandera, I., Synthesis of alpha-alkyl-beta-hydroxy amides through biocatalytic dynamic kinetic resolution employing alcohol dehydrogenases. *Adv. Synth. Catal.* **2019**, *361* (11), 2706–2712.
118. Gruber, C. C.; Lavandera, I.; Faber, K.; Kroutil, W., From a racemate to a single enantiomer: deracemization by stereoinversion. *Adv. Synth. Catal.* **2006**, *348* (14), 1789–1805.
119. Diaz-Rodriguez, A.; Rios-Lombardia, N.; Sattler, J. H.; Lavandera, I.; Gotor-Fernandez, V.; Kroutil, W.; Gotor, V., Deracemisation of profenol core by combining laccase/TEMPO-mediated oxidation and alcohol dehydrogenase-catalysed dynamic kinetic resolution. *Catal. Sci. Technol.* **2015**, *5* (3), 1443–1446.
120. Yoon, S.; Patil, M. D.; Sarak, S.; Jeon, H.; Kim, G. H.; Khobragade, T. P.; Sung, S.; Yun, H., Deracemization of racemic amines to enantiopure (*R*)- and (*S*)-amines by biocatalytic cascade employing omega-transaminase and amine dehydrogenase. *ChemCatChem* **2019**, *11* (7), 1898–1902.
121. Bailey, K. R.; Ellis, A. J.; Reiss, R.; Snape, T. J.; Turner, N. J., A template-based mnemonic for monoamine oxidase (MAO-N) catalyzed reactions and its application to the chemo-enzymatic deracemisation of the alkaloid (+/–)-crispine A. *Chem. Commun.* **2007**, (35), 3640–3642.

122. Mathe, C.; Gosselin, G., l-Nucleoside enantiomers as antivirals drugs: a mini-review. *Antiviral Res.* **2006**, *71* (2–3), 276–281.
123. Martinez-Montero, S.; Fernandez, S.; Sanghvi, Y. S.; Gotor, V.; Ferrero, M., Enzymatic parallel kinetic resolution of mixtures of d/l 2′-deoxy and ribonucleosides: an approach for the isolation of beta-l-nucleosides. *J. Org. Chem.* **2010**, *75* (19), 6605–6613.
124. Henrot, M.; Richter, M. E. A.; Maddaluno, J.; Hertweck, C.; De Paolis, M., Convergent asymmetric synthesis of (+)-aureothin employing an oxygenase-mediated resolution step. *Angew. Chem. Int. Ed.* **2012**, *51* (38), 9587–9591.
125. Richter, M. E. A.; Traitcheva, N.; Knupfer, U.; Hertweck, C., Sequential asymmetric polyketide heterocyclization catalyzed by a single cytochrome P450 monooxygenase (AurH). *Angew. Chem. Int. Ed.* **2008**, *47* (46), 8872–8875.
126. Weis, R.; Winkler, M.; Schittmayer, M.; Kambourakis, S.; Vink, M.; Rozzell, J. D.; Glieder, A., A diversified library of bacterial and fungal bifunctional cytochrome P450 enzymes for drug metabolite synthesis. *Adv. Synth. Catal.* **2009**, *351* (13), 2140–2146.
127. Fasan, R., Tuning P450 enzymes as oxidation catalysts. *ACS Catal.* **2012**, *2* (4), 647–666.
128. Garcia-Urdiales, E.; Alfonso, I.; Gotor, V., Update 1 of: enantioselective enzymatic desymmetrizations in organic synthesis. *Chem. Rev.* **2011**, *111*, PR110–PR180.
129. Toogood, H. S.; Scrutton, N. S., Correction to "discovery, characterization, engineering and applications of ene-reductases for industrial biocatalysis". *ACS Catal.* **2018**, *8* (5), 4333–4333.
130. Winkler, C. K.; Faber, K.; Hall, M., Biocatalytic reduction of activated C–C-bonds and beyond: emerging trends. *Curr. Opin. Chem. Biol.* **2018**, *43*, 97–105.
131. Pietruszka, J.; Scholzel, M., Ene reductase-catalysed synthesis of (*R*)-profen derivatives. *Adv. Synth. Catal.* **2012**, *354* (4), 751–756.
132. Li, H.; Tian, P.; Xu, J. H.; Zheng, G. W., Identification of an imine reductase for asymmetric reduction of bulky dihydroisoquinolines. *Org. Lett.* **2017**, *19* (12), 3151–3154.
133. Modukuru, N. K.; Sukumaran, J.; Collier, S. J.; Chan, A. S.; Gohel, A.; Huisman, G. W.; Keledjian, R.; Narayanaswamy, K.; Novick, S. J.; Palanivel, S. M.; Smith, D.; Wei, Z.; Wong, B.; Yeo, W. L.; Entwistle, D. A., Development of a practical, biocatalytic reduction for the manufacture of (*S*)-licarbazepine using an evolved ketoreductase. *Org. Process Res. Dev.* **2014**, *18* (6), 810–815.
134. de Gonzalo, G.; Mihovilovic, M. D.; Fraaije, M. W., Recent developments in the application of Baeyer-Villiger monooxygenases as biocatalysts. *ChemBiochem* **2010**, *11* (16), 2208–2231.
135. Bucko, M.; Gemeiner, P.; Schenkmayerova, A.; Krajcovic, T.; Rudroff, F.; Mihovilovic, M. D., Baeyer-Villiger oxidations: biotechnological approach. *Appl. Microbiol. Biotechnol.* **2016**, *100* (15), 6585–6599.
136. Matsui, T.; Dekishima, Y.; Ueda, M., Biotechnological production of chiral organic sulfoxides: current state and perspectives. *Appl. Microbiol. Biotechnol.* **2014**, *98* (18), 7699–7706.
137. Carreno, M. C.; Hernandez-Torres, G.; Ribagorda, M.; Urbano, A., Enantiopure sulfoxides: recent applications in asymmetric synthesis. *Chem. Commun.* **2009**, (41), 6129–6144.
138. Bong, Y. K.; Song, S. W.; Nazor, J.; Vogel, M.; Widegren, M.; Smith, D.; Collier, S. J.; Wilson, R.; Palanivel, S. M.; Narayauaswamy, K.; Mijts, B.; Clay, M. D.; Fong, R.; Colbeck, J.; Appaswami, A.; Muley, S.; Zhu, J.; Zhang, X. Y.; Liang, J.; Entwistle, D., Baeyer-Villiger monooxygenase-mediated synthesis of esomeprazole as an alternative for kagan sulfoxidation. *J. Org. Chem.* **2018**, *83* (14), 7453–7458.
139. Ao, Y. F.; Zhang, L. B.; Wang, Q. Q.; Wang, D. X.; Wang, M. X., Biocatalytic desymmetrization of prochiral 3-aryl and 3-arylmethyl glutaramides: different remote substituent effect on catalytic efficiency and enantioselectivity. *Adv. Synth. Catal.* **2018**, *360* (23), 4594–4603.
140. Fischereder, E. M.; Pressnitz, D.; Kroutil, W., Stereoselective cascade to C3-methylated strictosidine derivatives employing transaminases and strictosidine synthases. *ACS Catal.* **2016**, *6* (1), 23–30.
141. Pressnitz, D.; Fischereder, E. M.; Pletz, J.; Kofler, C.; Hammerer, L.; Hiebler, K.; Lechner, H.; Richter, N.; Eger, E.; Kroutil, W., Asymmetric synthesis of (*R*)-1-alkyl-substituted tetrahydro-beta-carbolines catalyzed by strictosidine synthases. *Angew. Chem. Int. Ed.* **2018**, *57* (33), 10683–10687.
142. Kohler, V.; Bailey, K. R.; Znabet, A.; Raftery, J.; Helliwell, M.; Turner, N. J., Enantioselective biocatalytic oxidative desymmetrization of substituted pyrrolidines. *Angew. Chem. Int. Ed.* **2010**, *49* (12), 2182–2184.
143. Li, T.; Liang, J.; Ambrogelly, A.; Brennan, T.; Gloor, G.; Huisman, G.; Lalonde, J.; Lekhal, A.; Mijts, B.; Muley, S.; Newman, L.; Tobin, M.; Wong, G.; Zaks, A.; Zhang, X., Efficient, chemoenzymatic process for manufacture of the Boceprevir bicyclic [3.1.0]proline intermediate based on amine oxidase-catalyzed desymmetrization. *J. Am. Chem. Soc.* **2012**, *134* (14), 6467–6472.
144. Girardin, M.; Ouellet, S. G.; Gauvreau, D.; Moore, J. C.; Hughes, G.; Devine, P. N.; O'Shea, P. D.; Campeau, L. C., Convergent kilogram-scale synthesis of dual orexin receptor antagonist. *Org. Process Res. Dev.* **2013**, *17* (1), 61–68.

145. Green, A. P.; Turner, N. J., Biocatalytic retrosynthesis: redesigning synthetic routes to high-value chemicals. *Perspect. Sci.* **2016**, *9*, 42–48.
146. Groger, H.; Hummel, W., Combining the "two worlds" of chemocatalysis and biocatalysis towards multi-step one-pot processes in aqueous media. *Curr. Opin. Chem. Biol.* **2014**, *19*, 171–179.
147. Denard, C. A.; Hartwig, J. F.; Zhao, H. M., Multistep one-pot reactions combining biocatalysts and chemical catalysts for asymmetric synthesis. *ACS Catal.* **2013**, *3* (12), 2856–2864.
148. Muschiol, J.; Peters, C.; Oberleitner, N.; Mihovilovic, M. D.; Bornscheuer, U. T.; Rudroff, F., Cascade catalysis – strategies and challenges en route to preparative synthetic biology. *Chem. Commun.* **2015**, *51* (27), 5798–5811.
149. Schrittwieser, J. H.; Velikogne, S.; Hall, M.; Kroutil, W., Artificial biocatalytic linear cascades for preparation of organic molecules. *Chem. Rev.* **2018**, *118* (1), 270–348.
150. France, S. P.; Hepworth, L. J.; Turner, N. J.; Flitsch, S. L., Constructing biocatalytic cascades: in vitro and in vivo approaches to de novo multi-enzyme pathways. *ACS Catal.* **2017**, *7* (1), 710–724.
151. Erdmann, V.; Sehl, T.; Frindi-Wosch, I.; Simon, R. C.; Kroutil, W.; Rother, D., Methoxamine synthesis in a biocatalytic 1-pot 2-step cascade approach. *ACS Catal.* **2019**, *9* (8), 7380–7388.
152. Erdmann, V.; Lichman, B. R.; Zhao, J. X.; Simon, R. C.; Kroutil, W.; Ward, J. M.; Hailes, H. C.; Rother, D., Enzymatic and chemoenzymatic three-step cascades for the synthesis of stereochemically complementary trisubstituted tetrahydroisoquinolines. *Angew. Chem. Int. Ed.* **2017**, *56* (41), 12503–12507.
153. Gorbe, T.; Gustafson, K. P. J.; Verho, O.; Kervefors, G.; Zheng, H. Q.; Zou, X. D.; Johnston, E. V.; Backvall, J. E., Design of a Pd(0)-CalB CLEA biohybrid catalyst and its application in a one-pot cascade reaction. *ACS Catal.* **2017**, *7* (3), 1601–1605.
154. Bisogno, F. R.; Lopez-Vidal, M. G.; de Gonzalo, G., Organocatalysis and biocatalysis hand in hand: combining catalysts in one-pot procedures. *Adv. Synth. Catal.* **2017**, *359* (12), 2026–2049.
155. Grondal, C.; Jeanty, M.; Enders, D., Organocatalytic cascade reactions as a new tool in total synthesis. *Nat. Chem.* **2010**, *2* (3), 167–178.
156. Oliveira, V. D.; Cardoso, M. F. D.; Forezi, L. D. M., Organocatalysis: a brief overview on its evolution and applications. *Catalysts* **2018**, *8* (12), 29.
157. Suljic, S.; Pietruszka, J.; Worgull, D., Asymmetric bio- and organocatalytic cascade reaction – laccase and secondary amine-catalyzed alpha-arylation of aldehydes. *Adv. Synth. Catal.* **2015**, *357* (8), 1822–1830.
158. Heidlindemann, M.; Hammel, M.; Scheffler, U.; Mahrwald, R.; Hummel, W.; Berkessel, A.; Groger, H., Chemoenzymatic synthesis of vitamin B5-intermediate (*R*)-pantolactone via combined asymmetric organo- and biocatalysis. *J. Org. Chem.* **2015**, *80* (7), 3387–3396.
159. Wohlgemuth, R., The locks and keys to industrial biotechnology. *New Biotechnol.* **2009**, *25* (4), 204–213.

PART V

ASYMMETRIC HYDROGENATION

15

ASYMMETRIC HYDROGENATION

Anton Vidal-Ferran[1,2,3], Arnald Grabulosa[1,3], Xavier Verdaguer[1,4], and Antoni Riera[1,4]
[1]*Departament de Química Inorgànica i Orgànica, Facultat de Química, Universitat de Barcelona, Barcelona, Spain*
[2]*Catalan Institution for Research and Advanced Studies (ICREA), Barcelona, Spain*
[3]*Institut de Nanociència i Nanotecnologia (IN$_2$UB), Universitat de Barcelona, Barcelona, Spain*
[4]*Institute for Research in Biomedicine (IRB Barcelona), The Barcelona Institute of Science and Technology (BIST), Barcelona, Spain*

15.1. INTRODUCTION

The development of active and enantioselective catalysts for the asymmetric hydrogenation (AH) has progressed in parallel with the research field of enantioselective catalysis. Since the first examples of use of enantiopure monodentate phosphines by Hörner [1] and Knowles [2], and the chelating C_2-symmetric-diphosphine 2,3-*O*-isopropylidene-2,3-dihydroxy-1,4-bis(diphenylphosphino)butane (DIOP) by Kagan [3], a myriad of enantiopure ligands has been developed and tested in AHs. The carbon backbones of the ligands for AH are nowadays almost unlimited and every conceivable type of stereogenic element has been incorporated to the ligands, which have been functionalized with numerous coordinating groups for catalytically active metals in this chemistry [4]. Overall, the transition-metal-catalyzed AH of prochiral unsaturated compounds is now among the most efficient and reliable methodologies in catalytic asymmetric synthesis.

Due to the large number of publications from 2010 to 2020 in the area of AH, this text does not intend to be a comprehensive summary of all articles published in the literature on AH. The aim of this text is to present significant results to the reader, by prioritizing transition-metal-based catalysts that are highly enantioselective for the highest possible number of substrate classes or for large arrays of structurally diverse substrates belonging to a specific substrate class. For exhaustive summaries in this area of research, the reader is referred to the general reviews [5] already published or to the relevant publications indicated in this text.

We have structured the results in this area of research in four main categories: (i) AH of functionalized olefins (Section 15.2), (ii) AH of unfunctionalized olefins (Section 15.3), (iii) AH of ketones (Section 15.4), and (iv) AH of imines (Section 15.5).

Catalytic Asymmetric Synthesis, Fourth Edition. Edited by Takahiko Akiyama and Iwao Ojima.

15.2. ASYMMETRIC HYDROGENATION OF FUNCTIONALIZED OLEFINS

15.2.1. Introduction

Hydrogenation reactions of functionalized alkenes can be divided into two categories, based on the mode of interaction between the alkene and the metal center: (i) hydrogenations of alkenes that coordinate to the metal through both a C═C double bond and a functional group attached to the alkene motif, and (ii) hydrogenations of alkenes that during the hydrogenation process mainly interact with the catalyst through the C═C bond (even if functional groups are attached to it). While the first type involves generally rhodium or ruthenium catalysts, the second category of hydrogenations mainly involves iridium-based catalysts. The successful application of rhodium complexes in AH relies on the ability of the substrate to form a metal chelate involving the C═C double bond and a donor atom, which is generally placed at the γ-position of a substituent attached to the C═C double bond. Chelating assistance of an *N*-acyl group directly bonded to the C═C double bond, with the carbonyl oxygen coordinating to the metal (generally rhodium) center, is the classic paradigm for achieving high enantioselectivities in this chemistry.

15.2.2. Rhodium Catalysts

Since the early days of asymmetric catalysis, intensive research activities on rhodium-catalyzed AHs have been carried out by both academia and industry. This research has provided a deep mechanistic understanding of this transformation and has facilitated the development of a myriad of Rh-coordination complexes capable of mediating the hydrogenation of prochiral functionalized C═C bonds with very high enantioselectivities. As a result of these research efforts, this chemistry has become among the most efficient and reliable methodologies in asymmetric catalysis.

Despite the remarkably advanced state of the field, many research groups are still actively pursuing new catalysts that show higher activity and/or improved enantioselectivity for poorly explored substrate classes or for recently discovered pharmaceutically relevant compounds. In other cases, research is directed toward the development of catalysts with an attractive industrial profile (i.e. high reaction rates with minimal amounts of catalyst, high enantioselectivities, robustness of the catalyst, and convenient preparation, among other aspects) and amenability to industrial manufacturing conditions. Thus, the design, development, screening, and optimization of new rhodium catalysts for AH have remained an appealing challenge for the last 10 years.

Providing a detailed summary of all the results in the AH of functionalized alkenes (**S1**) employing rhodium catalysts that have been published in the last 10 years is not possible due to space limitations. The discussion that follows summarizes the performance of asymmetric rhodium-based catalysts that have been applied to an array of structurally diverse substrates belonging to the following substrate classes: (i) α-(acylamino)acrylates (**S2**), (ii) itaconic acid derivatives and analogues (**S3**), (iii) α-alkyl- or aryl-substituted enamides (**S4**), (iv) α-alkyl- or aryl-substituted enol ester derivatives (**S5**), and (v) β-(acylamino)acrylates (**S6**) (see Scheme 15.1 for the benchmark example of each substrate class).

The ligands selected for the following discussion (see Scheme 15.1 for the structures) have been developed by X. Zhang (**L1**) [6], Stephan and Mohar (**L2** and **L2′**) [7], X. Zhang (**L3**) [8], Tang (**L4**) [9], Riera and Verdaguer (**L5**) [10], Vidal-Ferran (**L6** [11] and **L7** [12]), Imamoto and Gridnev (**L8**) [13], and Imamoto (**L9**) [14]. Most of the selected structures incorporate *P*-stereogenic groups in their framework (**L1**–**L5** and **L8**–**L9**). Though the presence of *P*-stereogenic groups in a ligand is not a prerequisite for achieving high enantioselectivities in this chemistry (for instance, see ligands **L6**–**L7** and many other structures not highlighted in this text) [5], the design principle in enantioselective catalysis "the closer the stereogenic element to the metal center, the better" appears to have influenced to a great extent the design of new ligands for rhodium-catalyzed AHs. The C_2-symmetry of seminal ligands in this chemistry [3] is still influencing the design of new catalysts, with some of the selected ligands preserving the C_2-symmetry features (**L1**, **L2**, **L4**, and **L8**). C_2-ligands might aid in reducing the number of possible catalyst-substrate adducts (and transition states), and this was believed to have favorable effects on the asymmetric bias of the transformation. Later advancements in the field of asymmetric catalysis have

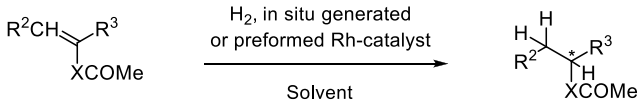

S1 (X = CH_2, NH, O) **P1** (X = CH_2, NH, O)

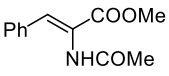

S2

L1	>99% ee (*S*)
L2	99.9% ee (*S*)
L3	>99% ee (*S*)
L4	97% ee (*R*)[a]
L5	99% ee (*S*)
L6	99% ee (*R*)
L7	99% ee (*R*)
L8	99.9% ee (*R*)
L9	99.1% ee (*R*)

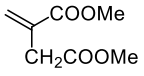

S3

L1	>99% ee (*R*)
L2	99.3% ee (*R*)
L3	98% ee (*R*)
L4	94% ee (*S*)
L5	95% ee (*R*)
L6	99% ee (*R*)
L7	99% ee (*R*)
L9	99% ee (*S*)

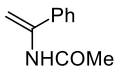

S4

L1	>99% ee (*S*)
L2	99.9% ee (*S*)
L4	99% ee (*R*)
L5	97% ee (*S*)
L6	98% ee (*R*)
L7	99% ee (*R*)
L8	99.4% ee (*R*)
L9	96.9% ee (*R*)

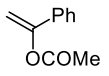

S5

L1	97% ee (*S*)
L2	97% ee (*S*)
L6	96% ee (*R*)
L7	99% ee (*R*)

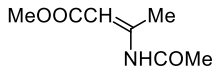

(*Z*)-**S6** (*E*)-**S6**

L1	97% ee (*S*)	>99% ee (*S*)
L2	88.2% ee (*S*)	97.8% ee (*S*)
L3	97% ee (*S*)	98% ee (*S*)
L4	99% ee (*R*)	99% ee (*R*)
L5	89% ee (*S*)	99% ee (*S*)
L8	99% ee (*R*)	99.9% ee (*R*)
L9	96.5% ee (*R*)	99.9% ee (*R*)

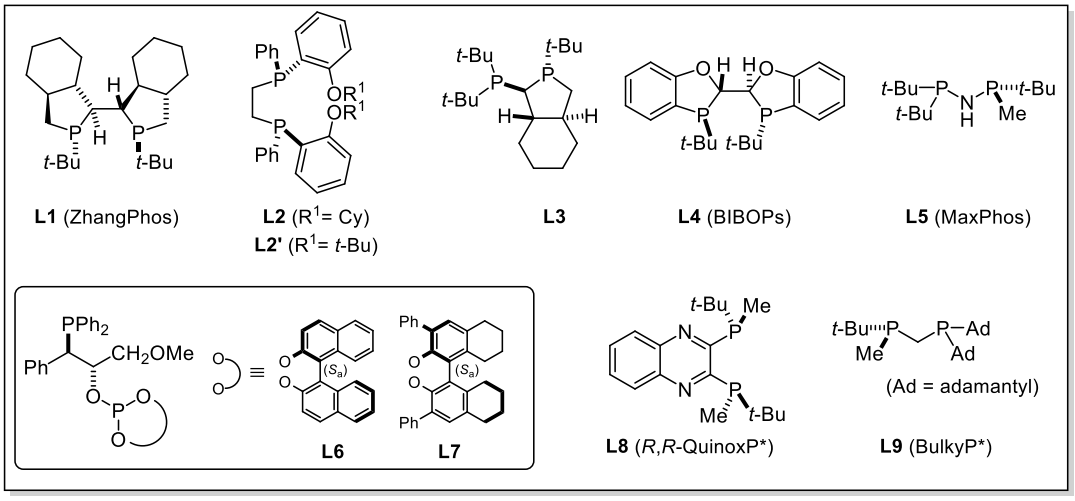

Scheme 15.1. Rhodium-catalyzed AH of functionalized alkenes with the general formula **S1**. [a]Results for the NHCO*t*-Bu analogue.

demonstrated that, in terms of enantioselectivities, C_2-symmetric ligands are not intrinsically better than their analogs lacking any symmetry element, as demonstrated by the remarkable stereoselectivities achieved in rhodium-catalyzed AHs with C_1-ligands **L3**, **L5**, **L6**, **L7**, and **L9**.

Experimental conditions for achieving high activities and enantioselectivities in this chemistry are low demanding and versatile, as generally: (i) no temperature control is required; (ii) low hydrogen pressures (ranging from 1 to 10 bars) are required; (iii) rhodium catalysts (including those derived from **L1**–**L9**) are active at low concentrations (substrate-to-catalyst [S/C] ratios range from 100–1000 in catalytic tests to up to 30000 for certain substrates and ligands under optimized hydrogenation reaction conditions); and (iv) catalytically active species can be indistinctly generated in situ (by mixing in the reaction cationic rhodium(I) precursors and the corresponding ligand) or from preformed rhodium coordination complexes of the type [Rh(diene)(ligand)]counterion. These are general observations that refer to the majority of published results for rhodium catalysts derived from **L1**–**L9** (and other

ligands not highlighted in this text). However, there may be exceptions to the ranges provided in the text and the reader is referred to the original publications for exact details of each example.

The great importance of enantiopure α-amino acids and their derivatives in the life-science sectors has made their stereoselective synthesis a central subject in organic synthesis. The AH of α-(acylamino) acrylates has proven to be a highly successful synthetic approach toward amino acid derivatives, with numerous efficient examples of AH of this substrate class having been published [5]. Interestingly, hydrogenations of β-aryl-substituted α-(acylamino)acrylates are widely studied and serve as a typical reaction to evaluate the efficiency of a new enantiopure ligand. As indicated in Scheme 15.1, the hydrogenation of methyl (*Z*)-methyl 2-acetamido-3-phenylacrylate **S2** (commonly referred to as Z-MAC in the literature) has been studied employing ligands **L1**–**L9**, with perfect enantioselectivities having been obtained in most cases. As for the activity of the catalysts, the highest catalytic activities in the hydrogenation of **S1** (or analogues) are reported for rhodium catalysts derived from **L1** [6], **L3** [8], and **L5** [10] (full conversion with S/C of 50 000, 10 000, and 10 000 at 1.4, 3.4, and 5 bar of hydrogen pressure, respectively).

Rhodium catalysts derived from **L1**–**L9** also led to perfect enantioselectivities in the hydrogenation of aryl-substituted analogues of **S2**, regardless of the positional and electronic nature of the substituents on the aromatic ring. Substitution patterns at the nitrogen atom that differ in the acetyl group are also tolerated, if the carbonyl group bonded to nitrogen is maintained (as for instance in the *N*-protecting Cbz, Boc, or Fmoc groups) [7, 10, 11, 13, 14]. β-Monoalkyl-substituted dehydro-α-amino acid derivatives are often synthesized as mixtures of *E/Z* isomers, which has prevented this synthetic approach to be as widely applied as that for the aryl-substituted analogues (hydrogenation of *E*-isomers [5] is often slower and less selective than that of *Z*-isomers). Examples of hydrogenation of β-dialkyl-substituted or β-alkyl, aryl-substituted dehydro-α-amino acid derivatives (**S7** and **S8**) are scarce, with ligands **L2′** [7] and **L9** [14] showing high activities (full conversion with S/C = 1000) and providing enantioselectivities higher than 99% ee (see selected examples in Figure 15.1). Heteroaryl-substituted substrates **S9** and **S10** have also been hydrogenated employing ligands **L2′** [7b] and **L5** [10] with excellent enantioselectivities toward the corresponding non-natural amino acids (Figure 15.1). The hydrogenation of the interesting substrates **S11** and **S12** with rhodium catalysts derived from ligands **L6** [11b] and **L7** [12] is also highlighted in Figure 15.1.

Research efforts have also been directed to the development of enantioselective catalysts for specific substrate classes. It is interesting to highlight the highly enantioselective hydrogenation developed by W. Zhang for cyclic α-dehydroamino ketones **S13** employing trichickenfootphos-based catalysts **C1**, with ees ranging from 97 to 99% for 16 examples (Scheme 15.2) [15]. Molinaro, Scott, Shevlin have used rhodium catalysts derived from the JosiPHOS family of ligands **L10** or **L11** to hydrogenate β-diaryl-substituted dehydro-α-amino acid derivatives **S14** with high enantioselectivities (23 examples with ees ≥92%, Scheme 15.2), though an S/C ratio of 10 had to be used for some of these challenging substrates [16]. W. Zhang has developed an elegant method for selectively hydrogenating α-formyl enamides **S15** to the corresponding enantiopure (or highly enantioenriched) α-amido aldehydes **P15** (27 examples with ees ranging from 92 to 99%, Scheme 15.3) [17]. The authors used rhodium catalysts derived from the (*R*,*R*)-BenzP* ligand **L12**, which turned out to be selective for the reduction of the C=C bond in the presence of an aldehyde group at a pressure of 10.1 bar of hydrogen. Interestingly, the C=C and C=O groups were both hydrogenated at 30.3 bar, with the high enantioselectivities in the final β-amido alcohols **P15′** being maintained [17]. The last example of hydrogenation of a particular substrate class is highlighted in Scheme 15.3. X. Zhang described the efficient synthesis of γ,δ-unsaturated amido esters **P16** by the enantioselective hydrogenation of conjugated enamides **S16** employing rhodium catalysts derived from TangPhos ligand **L13** [18]. High enantioselectivities were obtained (99% ee for 13

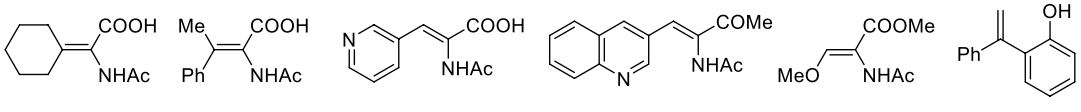

S7 >99% ee (*S*) with **L2′**

S8 98% ee (2*R*,3*S*) with **L9**

S9 99.8% ee (*S*) with **L2′**

S10 99% ee (*S*) with **L5**

S11 97% ee (*R*) with **L6**

S12 99% ee (*R*) with **L7**

Figure 15.1. Rhodium-catalyzed AH of some less common substrates.

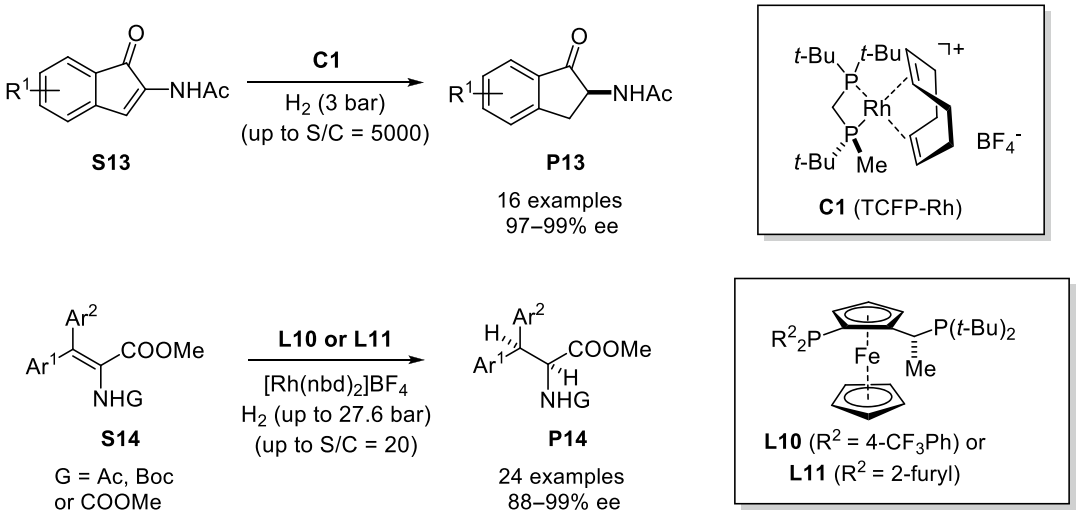

Scheme 15.2. AH of cyclic α-dehydro ketones and synthesis of β,β-diaryl-α-amino acids. Source: [15].

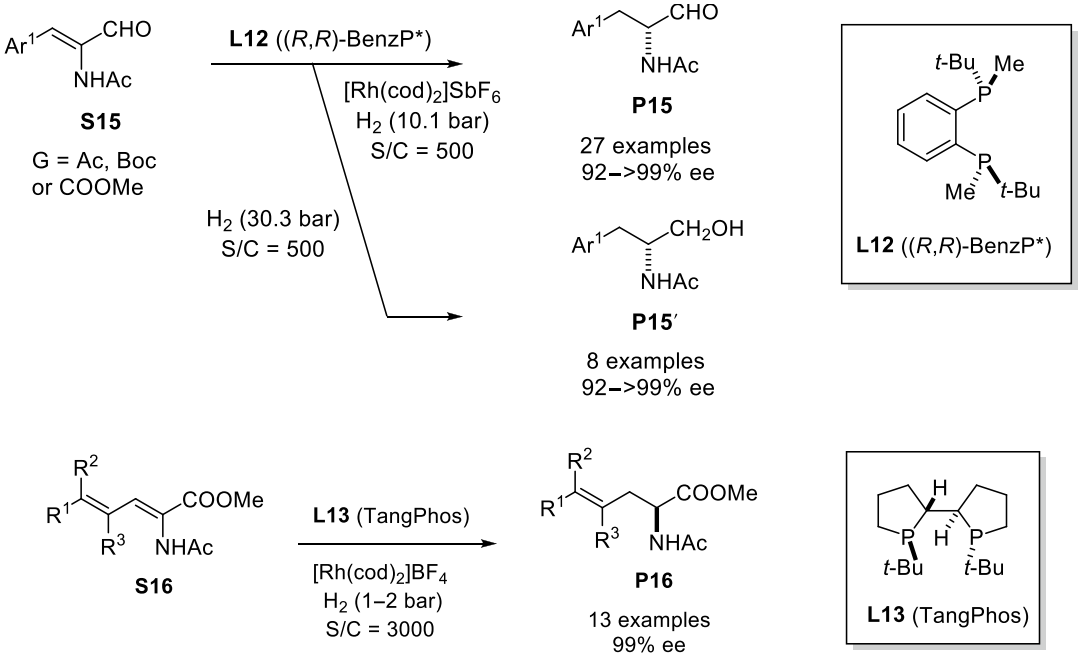

Scheme 15.3. AH of α-formyl and conjugated enamides. Source: [17]/John Wiley & Sons.

substrates with an S/C ratio of 3000). It is interesting to highlight that only the *N*-acetyl-substituted double bond was hydrogenated. The origin of this selectivity arises from the fact that rhodium-catalyzed hydrogenations only take place when the substrate is capable of forming a rhodium chelate involving the C=C double bond and the oxygen donor atom of the acetyl group, with the chelated C=C double bond being hydrogenated.

The products derived from the AH of **S3** and other itaconic acid derivatives have been well studied, with plenty of highly enantioselective hydrogenation catalysts having been reported [5]. Interestingly, the AH of substrate **S3** still attracts the interest of researchers because its hydrogenation is generally used to evaluate the efficiency in the AH of a new enantiopure ligand. Rhodium catalysts derived from **L1**–**L9** mediated the AH with high activities, and with enantioselectivities ranging from 94 to >99% (Scheme 15.1). The hydrogenation of **S3** has been reported to proceed with full conversion and 99% ee employing catalysts derived from **L6** with an S/C ratio of 10 000 [11a]. Moreover, the catalyst was recovered and reused five times without any loss of activity or enantioselectivity [11a]. The hydrogenation of analogues of **S3** with $CONH_2$ or COOH groups instead of the COOMe group has also been accomplished with high enantioselectivities employing ligands **L3** and **L6**. The performance of rhodium-based catalysts with itaconic acid analogues incorporating a substituent at the terminal methylene position has been scarcely studied. The most comprehensive report has been published by Stephan and Mohar, who reported the use of ligand **L14** (Scheme 15.4) in the hydrogenation of a large array of itaconic acid analogues **S17** with enantioselectivities ranging from 90 to >99% ee [19].

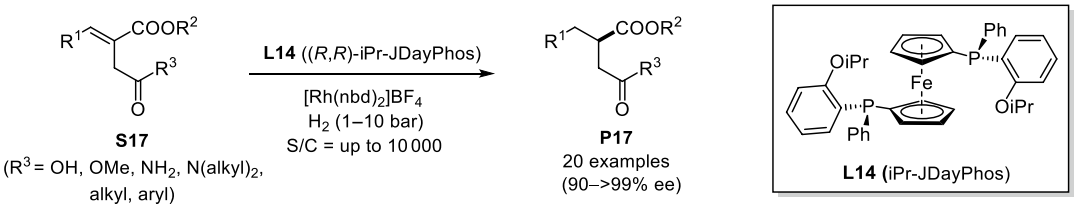

Scheme 15.4. Hydrogenation of itaconic acid analogues.

Enantiopure amines are important intermediates in organic synthesis that can be synthesized by several methods, as for instance chemical resolution or asymmetric synthesis employing chiral auxiliaries or biocatalysts. The catalytic AH of *N*-acyl enamides constitutes an efficient and convenient method for the preparation of enantiopure (or highly enantioenriched) amines and their derivatives [5aa]. Rhodium catalysts derived from **L1**–**L9** lead to perfect enantioselectivities (from 97 to >99% ee) in the hydrogenation of the benchmark substrate for this substrate class (**S4**). Rhodium catalysts derived from both **L1** and **L2′** are highly active, as an S/C ratio of 10 000 was enough to efficiently hydrogenate the corresponding substrates. It is difficult to make comparisons between ligands **L1**–**L9** in terms of the broadness of the substrate scope that they tolerate, as the set of studied enamides differs from one ligand to the other. While **L1**, **L2**, **L4**, **L5**–**L7**, and **L9** tolerate substituents in the *meta* and *para* positions of the aryl group in *N*-(1-arylvinyl)acetamides without significant losses in the enantioselectivity, the effects of *ortho* substituents in the enantioselectivity of the reaction appear to be detrimental (for instance, 82% and 99.9% ee for the *ortho*-CF_3- and *para*-CF_3-substituted *N*-(1-((trifluoromethyl)phenyl)vinyl)-acetamide, respectively, with **L2′**). Catalytic systems derived from **L1** and **L2′** tolerate *E/Z* mixtures of isomers in the AH of substrates incorporating a substituent at the terminal position of the methylene group (**S18**, Figure 15.2). Several challenging substrates have been identified in this chemistry with good results in terms of enantiose-

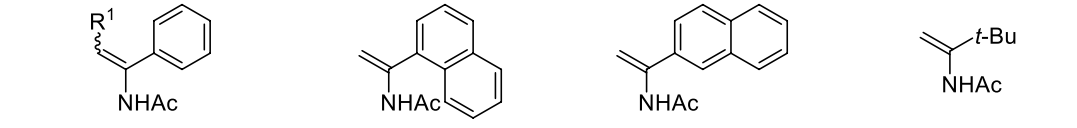

Figure 15.2. Rhodium-catalyzed AH of less conventional enamides.

lectivity being only obtained with particular ligands (93% ee for **S19** with **L7**; [12] >99% ee for **S20** with **L1** [6] and **L2′**; [7] and 99% ee for **S21** with **L8** [13].).

The AH of specific types of enamides (**S22**–**S24**, Scheme 15.5) deserves mention. X. Zhang and coworkers developed the synthesis of allyl amines by AH of *E*-(*N*)-(buta-1,3-dien-2-yl)acetamides (**S22**, Scheme 15.5) [20]. In these dienamides, only the double bond bearing the acetamido group is hydrogenated while the other one remains unaltered. Notably, full conversions and enantioselectivities ranging from 98 to >99% were obtained with rhodium catalysts derived from DuanPhos ligand **L15**. Efficient AHs for substrates structurally related to **S22** have also been developed by the same authors employing **L15** [21]. The hydrogenation of β-aryl bicyclic enamides **S23** has proven to be very challenging, with many high-performing ligands failing to provide good enantioselectivities for these substrates. Interestingly, Tang developed the WingPhos ligand **L16** that incorporates a deep chiral pocket provided by two 9-anthryl substituents and leads to the AH products **P23** with enantioselectivities ranging from 94 to 98% ee [22]. Cyclic tetrasubstituted enamides have also proven to be challenging substrates toward hydrogenation. Tang, Yu, and McWilliams reported the highly enantioselective hydrogenation of this type of substrates employing ligand **L17** that also incorporates a deep chiral pocket (Scheme 15.5). With rhodium catalysts derived from ligand **L17**, excellent enantioselectivities with high S/C ratios were described in the AH of carbocyclic and heterocyclic tetrasubstituted enamides **S24**, with the highest enantioselectivities being obtained with six-membered compounds (93% average ee value, 13 examples) and the lowest with the seven-membered analogue (22% ee, one example) [23].

The AH of enol esters is a convenient strategy for obtaining enantiopure (or highly enantioenriched) alcohols after hydrolysis of the ester groups. Rhodium complexes of phosphorus ligands are known to catalyze this transformation with high enantioselectivities for acyclic derivatives and less efficient outcomes for cyclic enol ethers. In terms of the progress in the AH of enol derivatives from 2010 to 2020, not many reports exist in which the highly enantioselective hydrogenation of such substrates is described.

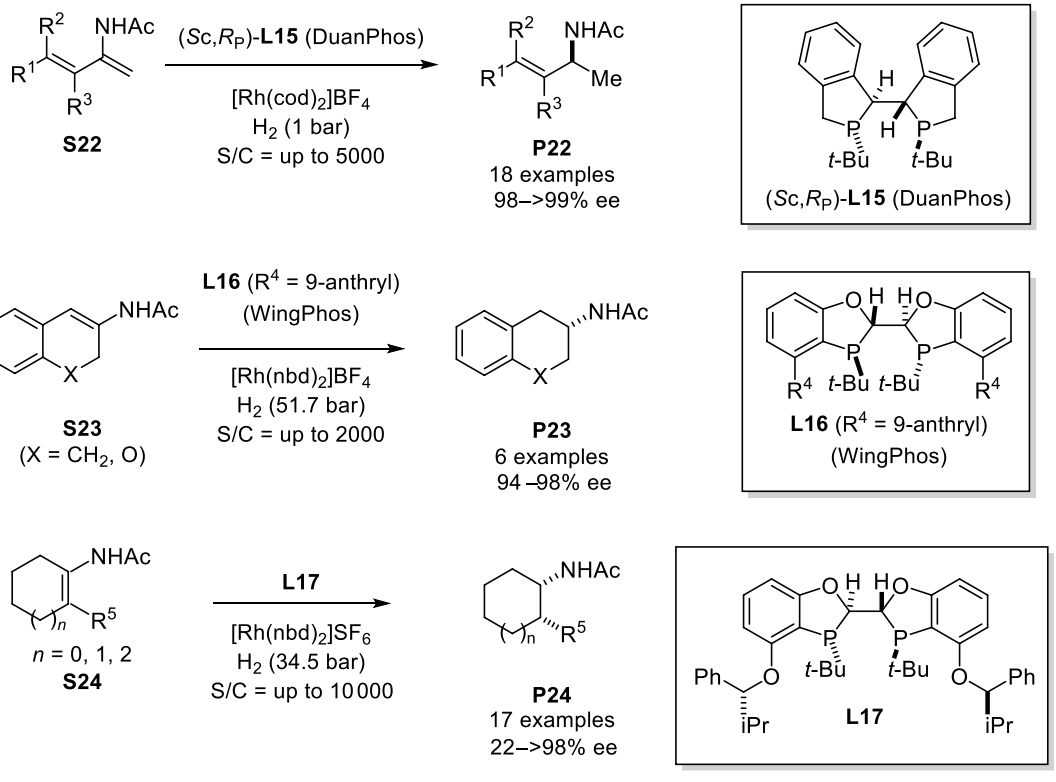

Scheme 15.5. AH of other enamides: conjugated, β-aryl bicyclic, and tetrasubstituted. Source: [20]/John Wiley & Sons.

Vidal-Ferran described the preparation of advanced synthetic intermediates of pharmaceutical ingredients by hydrogenation of enol esters employing rhodium catalysts derived from **L6** [11b], as well as the hydrogenation of model enol esters (**S5** and other substrates, 90–98% ee, 10 examples) [11c]. Remarkable examples of AH of two arrays of structurally diverse enol ester derivatives **S25** and **S26** (Scheme 15.6) have been published by Leitner and Franciò [24] and Pizzano and Cadierno [25], respectively. Enol esters **S25** (16 examples) were hydrogenated with rhodium-complexes of phosphine-phosphoramidite ligand **L18** toward secondary alkan-2-ols **P25**, which were obtained with enantioselectivities up to 99% [24]. Variation of the ester group or substitution at the 1-position of the vinyl fragment in **S25** was tolerated. Pizzano and Cadierno described an efficient synthesis of (*Z*)-1-alkyl-2-arylvinyl acetates **S26** followed by the efficient AH of these substrates. Rhodium catalysts of phosphine-phosphite (P-OP) ligand **L19** led to the hydrogenated products in up to 99% ee. The scope of the final products is broad, including valuable optically active homobenzylic esters. For instance, substrates with the R^3 substituents being a linear C3–C6 alkyl substituent (Scheme 15.6) were hydrogenated with full conversion and enantioselectivities ranging from 94 to 98% ee. The rhodium catalysts also tolerate *meta*- and *para*-functionalized aryl substituents in **S26** [25].

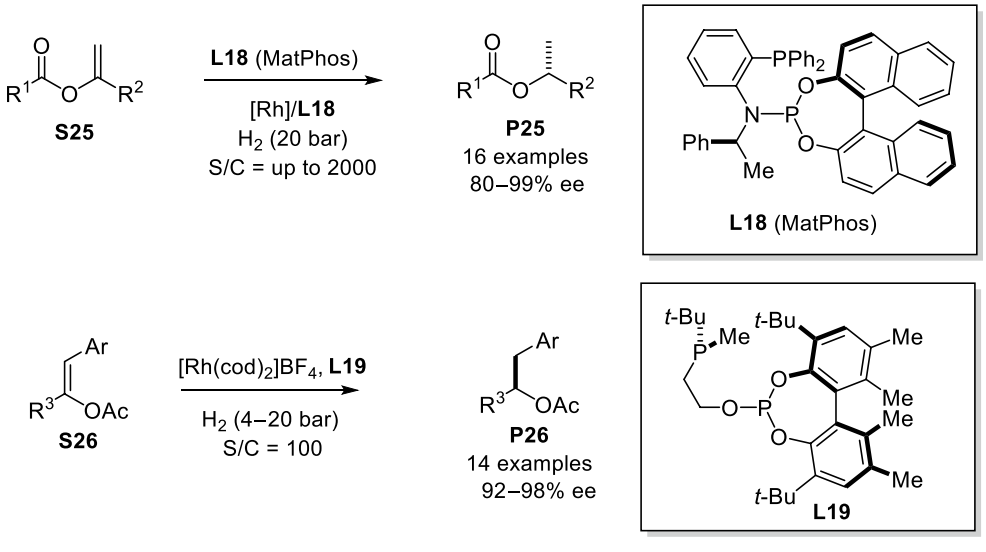

Scheme 15.6. AH of enol ester derivatives: 1-alkyl vinyl esters and aryl vinyl acetates.

The synthesis of β-amino acids by AH of the corresponding dehydro-β-amino acid derivatives has benefited from the successes achieved in the preparation of other substrate classes by AH and the operational simplicity of this synthetic methodology. Despite the fact that, frequently, dehydro-β-amino acid derivatives are synthesized as a mixture of *E*- and *Z*-isomers, efficient methods to synthesize new β-amino acids and derivatives have been discovered. Ligands **L1** [6], **L2′** [7b], **L3** [8], **L4** [9], **L8** [13], and **L9** [14] mediate the AH of benchmark substrate **S6** with high enantioselectivities and tolerate mixtures of the *E*/*Z* isomers as starting materials without a notable decrease in the enantioselectivity (Scheme 15.1). Moreover, rhodium catalysts derived from these ligands have been employed in the AH of an array of structurally diverse analogues of **S6**. Ligands **L3**, **L8**, and **L9** deserve special mention since they have provided high enantioselectivities in the hydrogenation of an array of 3-alkyl- and 3-aryl-substituted 3-amino-acrylic acid derivatives.

Apart from β-amino acids, other optically active 1,2-difunctional products have been efficiently obtained by AH. For instance, X. Zhang has reported the catalytic enantioselective synthesis of β-amino ketones **P27** by AH (Scheme 15.7) [26]. Readily prepared β-keto enamides **S27** were hydrogenated by rhodium complexes derived from the ligand DuanPhos (**L15**) leading to the corresponding β-amino ketones with enantioselectivities ranging from 81 to >99% (15 examples). The highest enantioselectivity was obtained with substrate **S27** with $R^1 = R^2 = Me$ (>99% ee), though ees were also high with $R^1 = Ar$ or

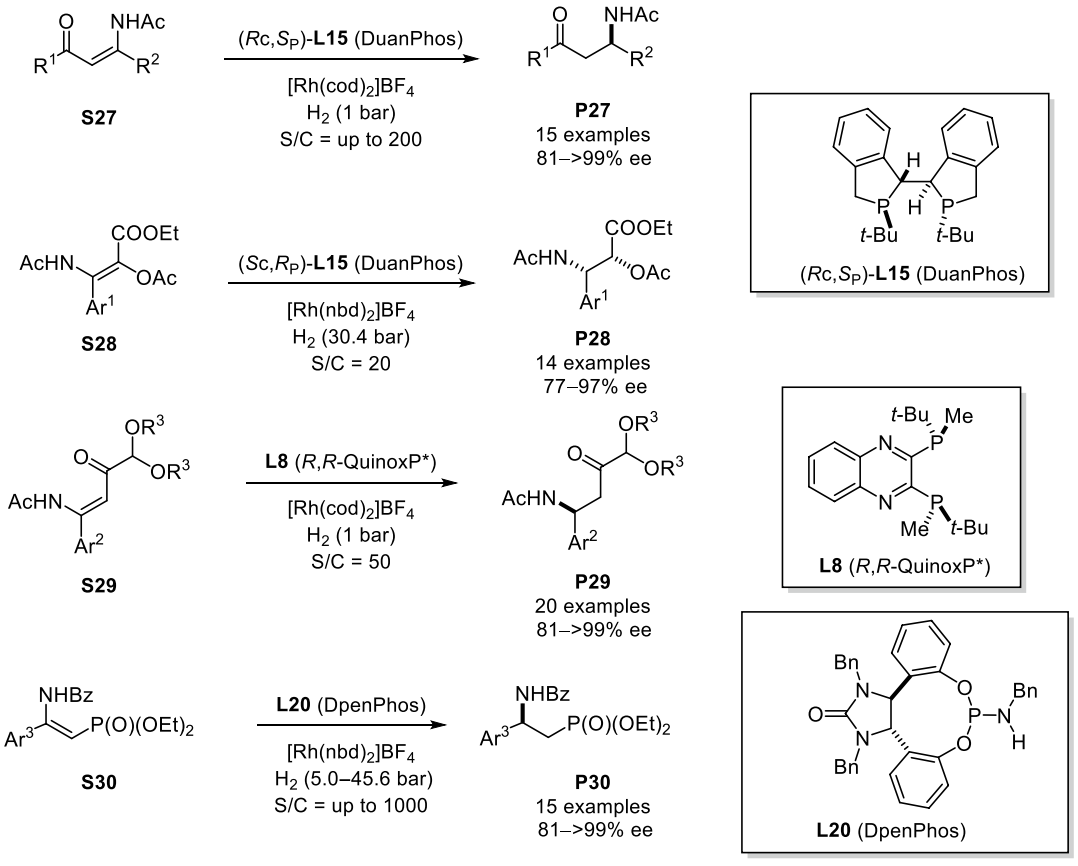

Scheme 15.7. Preparation of 1,2-difunctional products by rhodium-catalyzed AH.

heteroaryl and R^2 = Me, regardless of the positional or electronic nature of the substituents on the aryl or heteroaryl substituents (95–99% ee, 12 examples). Similar results in terms of enantioselectivity of the hydrogenation products of **S27** were obtained with ligand **L1** [27]. The incorporation of an additional acetoxy substituent in the β-keto enamide framework (substrates **S28**, Scheme 15.7) was tolerated by the rhodium catalyst derived from the ligand **L15** [28]. This synthetic strategy provided a concise route to *syn*-α-hydroxy-β-amino acid derivatives with enantioselectivities ranging from 77 to 97% (14 examples). Ratovelomanana-Vidal and coworkers have recently reported an efficient AH method toward α-acetal-β′-amino ketone derivatives **P29** (Scheme 15.7) employing (*R*,*R*)-QuinoxP* ligand **L8** [29]. High enantioselectivities (89–99% ee, 20 examples) have been reported by the authors. The rhodium catalyst derived from **L8** tolerates acyclic, five- and six-membered cyclic acetal groups, as well as structural variation in the substitution pattern on the aromatic ring (the lowest enantioselectivity in the study was observed for the substituent Ar^2 = *ortho*-Me–C_6H_4).

Analogues of β-amino acid derivatives with another functional group instead of the carboxylic acid motif have been efficiently prepared by AH. For instance, Ding has reported the efficient AH of β-enamido phosphonates toward products **P30** (Scheme 15.7) [30]. Phosphoramidite **L20** was found to be a highly efficient ligand in the hydrogenation of structurally diverse β-enamido phosphonates **S30**. Enantioselectivity values ranged from 81 to >99% ee (15 examples). Higher enantioselectivities were obtained from the *Z*-isomer of the starting material, with a slight erosion in the enantioselectivity being observed when the hydrogenation was carried out from a *E*/*Z* mixture of isomers. In terms of the structural diversity of the aryl substituents, the catalyst tolerates *ortho*-, *meta*-, and *para*-substituted aryl groups, heteroaryl fragments, and the 2-naphthyl substituent.

Non-covalent interactions such as hydrogen bonding or ion pairing have also been used to facilitate the AH of atypical substrates employing rhodium catalysts. X. Zhang and coworkers developed new diphosphine-thiourea ligands that have been applied to the highly enantioselective AH of a number of substrates, including β,β-disubstituted nitroalkenes [31] (seminal work) and dehydro-lactams [32], among other substrate classes [5z]. The designed ligand **L21**, also referred to as ZhaoPhos, incorporated a diphosphine motif derived from Ugi's amine for rhodium-based catalysis and a thiourea group as an activating and directing group in AHs (Scheme 15.8). The authors envisioned that the incorporation of a thiourea group could activate substrates toward AH and also provide an adequate chiral environment for catalysis. Remarkable results were obtained with this strategy in the AH of dehydro-lactams **S31** and **S32**. The authors identified a straightforward AH approach toward 3-substituted succinimides **P31** and γ-lactams **P32** with a high-performing profile of ZhaoPhos (**L21)**, especially for dehydro-lactams with the free NH group. Enantioselectivities ranged from 91 to >99% ee for 34 examples with S/C ratios up to 2000. The same research group also developed the secondary phosphine oxide (SPO)-Wudaphos ligand **L22** operating under the same principles as the ZhaoPhos, but with an SPO group as activator instead of a thiourea motif (Scheme 15.8) [33]. The authors demonstrated that ion pair and hydrogen bonding interactions between the carboxylic acid group of the substrate and the amino fragment from the ligand were

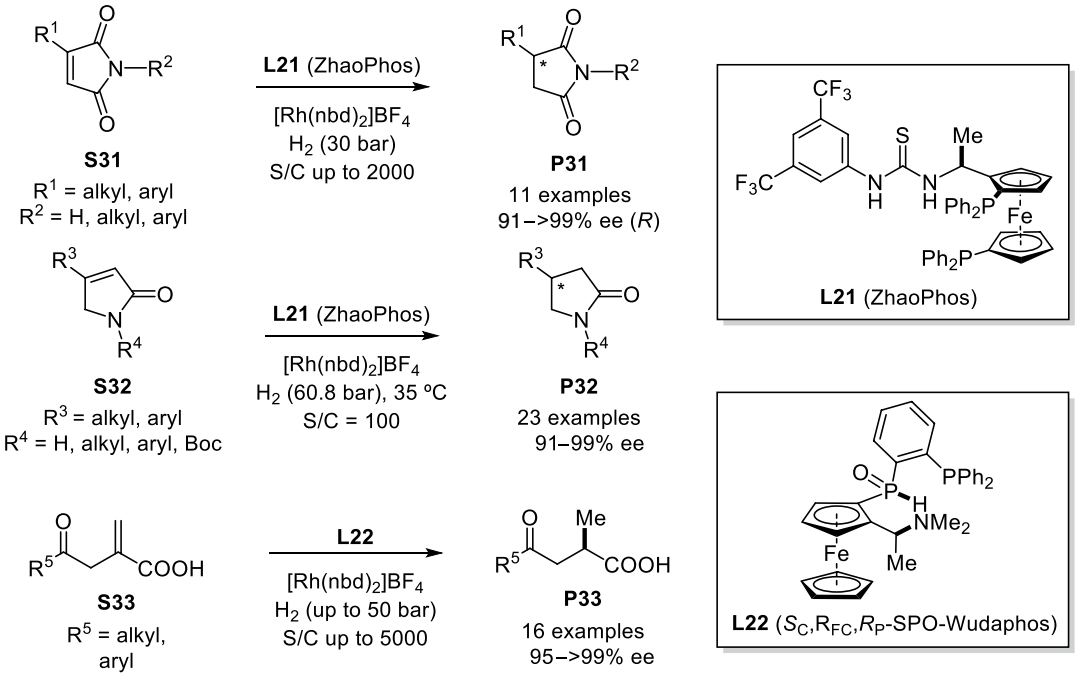

Scheme 15.8. AH involving supramolecular interactions between the catalyst and substrate. AH of dehydro-lactams and α-methylene-γ-keto carboxylic acids. Source: [33]/John Wiley & Sons.

very strong and not influenced to a great extent by the nature of the solvent. The authors also demonstrated that these non-covalent interactions were crucial for achieving high enantioselectivities. Overall, the ees were very high (from 95 to >99%) for an array of substrates irrespective of their substitution pattern with alkyl or (substituted) aryl groups. The S/C ratio could be increased up to 5000, which demonstrates the high catalytic activity of the rhodium catalysts derived from **L22**.

The catalysts for AH summarized thus far in this section have been used on prochiral substrates, with overall creation of one (or more) stereocenters. Catalyst discovery for AH in the last decade has also witnessed the development of catalytic methods for hydrogenative transformations on achiral substrates

(by hydrogenative desymmetrizations) or on chiral substrates (by kinetic resolutions via hydrogenation reactions). Vidal-Ferran described efficient stereoselective hydrogenative desymmetrization reactions mediated by rhodium complexes derived from enantiopure *P,OP*- ligand **L23** [34], which presented excellent catalytic properties for the desymmetrization of a set of 1,4-dienes **S34** (Scheme 15.9). This synthetic methodology provided access to the selective formation of a set of enantioenriched secondary and tertiary alcohols **P34** (six examples, up to 92% ee). Vidal-Ferran also developed an efficient and highly stereoselective hydrogenation method for the preparation of structurally diverse *S*- and *P*-stereogenic oxides [35]. The approach relies on the ability of rhodium complexes derived from ligand **L7** to kinetically resolve racemic α,β-unsaturated sulfoxides and P=O-derivatives by hydrogenation of the C=C motif and formation of highly enantioenriched (or even enantiopure) *S*- and *P*-stereogenic oxides. The practicality of the methodology was demonstrated by the resolution of an array of structurally diverse sulfur- and phosphorus-containing substrates and by preparing advanced synthetic intermediates of biologically active molecules and potentially functional molecules for catalytic enantioselective synthesis. Regarding hydrogenated products **P35**, enantiomers of the starting material with an *R* configuration at the sulfur or phosphorus atom were those being hydrogenated. In the only studied example in which more than one stereogenic center was created during the kinetic resolution, the diastereoselectivity of the process was very high (≥99 : 1 in favor of one of the diastereoisomers) [35c]. The rhodium catalysts derived from **L7** tolerated different substitution patterns at the sulfur or phosphorus atoms (alkyl, aryl, or methoxy groups), as well as at the C=C motif (alkyl and aryl substituents at the α- and β-positions of the alkene group), and led to the unreacted and hydrogenated enantiomers of the starting material with high selectivity factors (up to ca. 230).

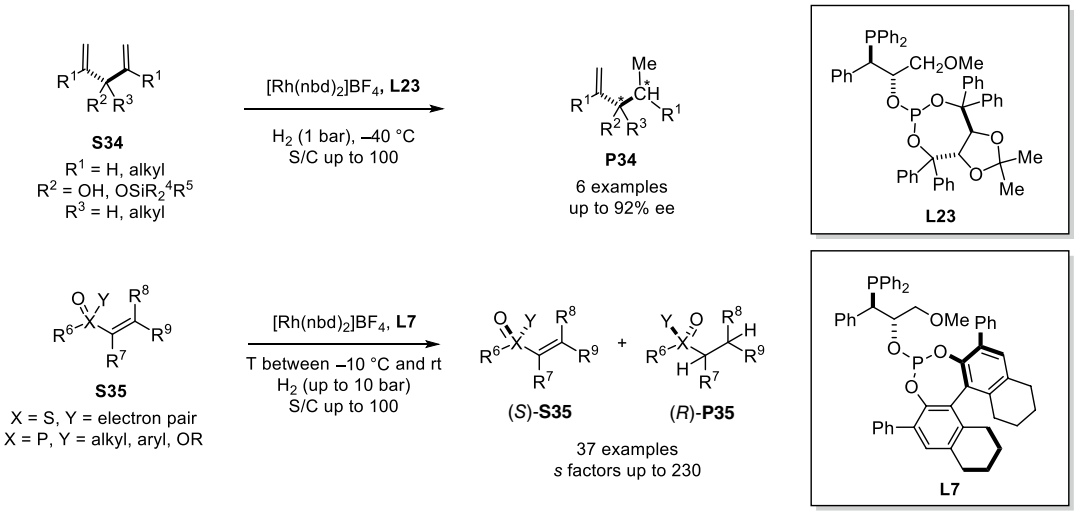

Scheme 15.9. Hydrogenative desymmetrization reactions and kinetic resolutions using rhodium catalysts.

Although rhodium catalysts usually give poor results in the hydrogenation of non-coordinating substrates, there are some relevant examples of enantioselective catalysts for specific classes of poorly functionalized compounds. Ding reported [36] the highly enantioselective AH of an array of structurally diverse α- or β-trifluoromethyl-substituted acrylic acids (35 examples), using a rhodium catalyst generated in situ from a mixture of an enantiopure SPO (**L24**) and an achiral triaryl phosphine ligand. The screening of the achiral phosphine ligand, the optimization of the rhodium(I) precursor, and the variation of the molar ratios of SPO/achiral phosphine resulted in optimized reaction conditions for AH, including 10 mol% of morpholine as additive. High yields and enantioselectivities (ranging from 90 to >99% ee) were thus observed in the hydrogenation of **S36a** and **S36b** (Scheme 15.10).

Hou reported the use of rhodium catalysts derived from ligand **L25** for the highly stereoselective AH of prochiral sulfones **S37**–**S39** [37]. Although the chelating assistance of the sulfone group during the AH

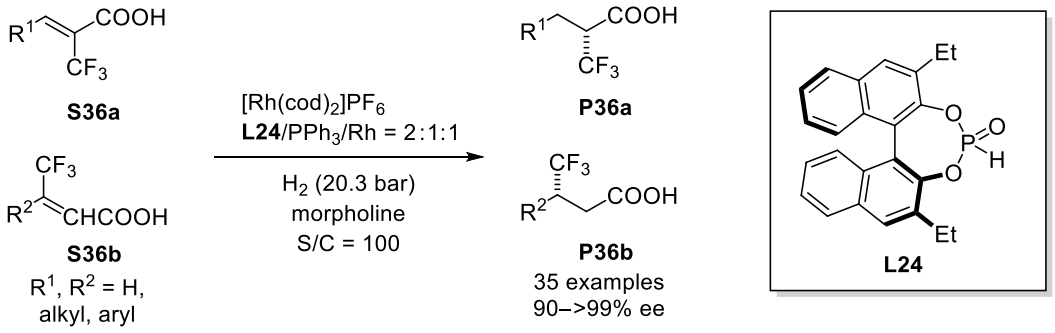

Scheme 15.10. Rhodium-catalyzed AH of α- or β-trifluoromethyl-substituted acrylic acids.

process was established, catalysts derived from **L25** hydrogenate 3,3-diaryl α,β-unsaturated sulfones **S37** with ees higher than 99% ee (15 examples; Scheme 15.11). These rhodium catalysts were also proficient in the AH of bicyclic- and benzo[*b*]thiophene-1,1-dioxides (**S38** and **S39**, respectively) with excellent enantioselectivities (up to >99% ee) regardless of the positional and electronic nature of the substituents. The authors demonstrated the usefulness of this synthetic methodology by synthesizing (*S*)-(+)-*ar*-turmerone.

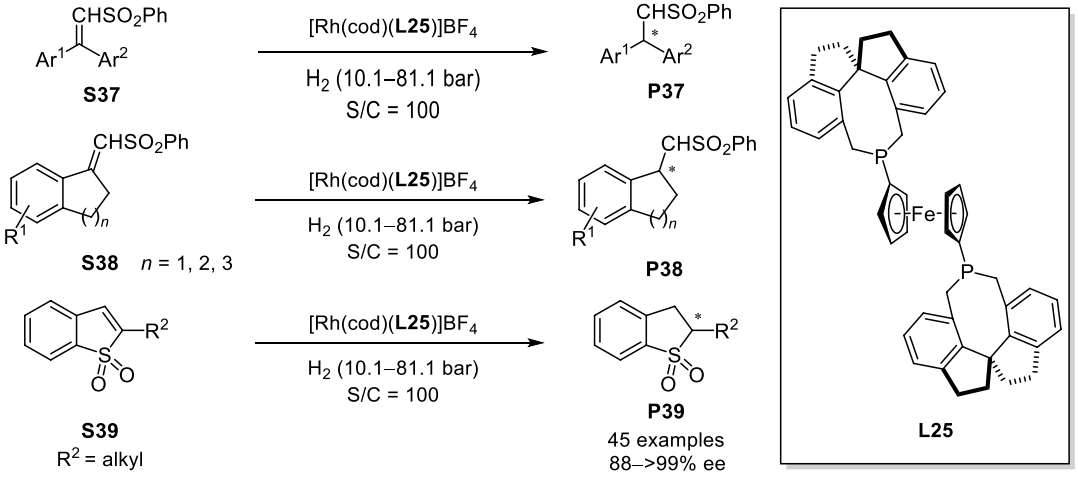

Scheme 15.11. Preparation of acyclic and cyclic sulfones by rhodium-catalyzed AH.

15.2.3. Cobalt and Nickel Catalysts

Catalysts based on noble metal complexes have played a central role in the homogeneous AH of C–C double bonds. However, earth-abundant metal catalysis would have the advantages of low cost, low toxicity, and minimal environmental impact. As a result, in the last decade, this field has grown and matured developing efficient AH catalysts based mainly on cobalt and nickel.

Following the seminal work from Ohgo in 1981 on the AH of α-acyl acrylates catalyzed by cobalt complexes [38], several research groups have made relevant contributions in this area. Most of the early works on cobalt-catalyzed AH failed to provide synthetically useful activities and (stereo)selectivities. An important breakthrough in cobalt-catalyzed hydrogenations came from the discovery of cobalt complexes derived from achiral bis(imino)pyridines [39] or bis(phosphino)amines [40], which exhibited highly improved catalytic activities in the achiral hydrogenation of simple alkenes. Chirik developed bis(imino) pyridine-based enantioselective catalysts for the hydrogenation of unfunctionalized geminal disubstituted

alkenes with high activity and enantioselectivity [41]. Further developments in this area of research were made in 2013 by Chirik and coworkers [42], who discovered cobalt catalysts derived from the iPr-DuPhos ligands **L26** and **L27** that were highly efficient and enantioselective in the AH of α-acylacrylates and enamides (Scheme 15.12). The authors described that the diphosphine favorably coordinated to both hydrated and anhydrous cobalt(II) precursors and led to active and selective catalysts after activation with $LiCH_2SiMe_3$ or $ClMgCH_2SiMe_3$ [42]. It is interesting to highlight that neutral cobalt-catalysts derived from the DuPhos-ligand (catalysts [$Co(CH_2SiMe_3)_2$(**L26** or **L27**)], Scheme 15.12) led to high catalytic activities (full conversion with an S/C ratio of 20) and high enantioselectivities in the AH of **S2** and **S4** (93 and 82% ees in favor of the *S* enantiomers of **P2** and **P4**, respectively). Overall, these results paved the way to the use of earth-abundant metals in AH. Chirik and coworkers studied in great detail the structure, stability, and utility of cobalt complexes derived from diphosphine ligands in the AH of functionalized alkenes. Interestingly, the authors discovered that zinc metal can be used as an activator of cobalt-diphosphine complexes toward hydrogenation rather than $LiCH_2SiMe_3$ or $ClMgCH_2SiMe_3$, which are air-sensitive and incompatible with protic solvents. Cobalt(I) complex **C2** [43a] exhibited high activity and enantioselectivity in protic media and enabled the catalytic asymmetric synthesis of the antiepileptic drug levetiracetam (**P40**, 97% isolated yield, 98% ee, 200-gram scale synthesis; Scheme 15.12) [43a].

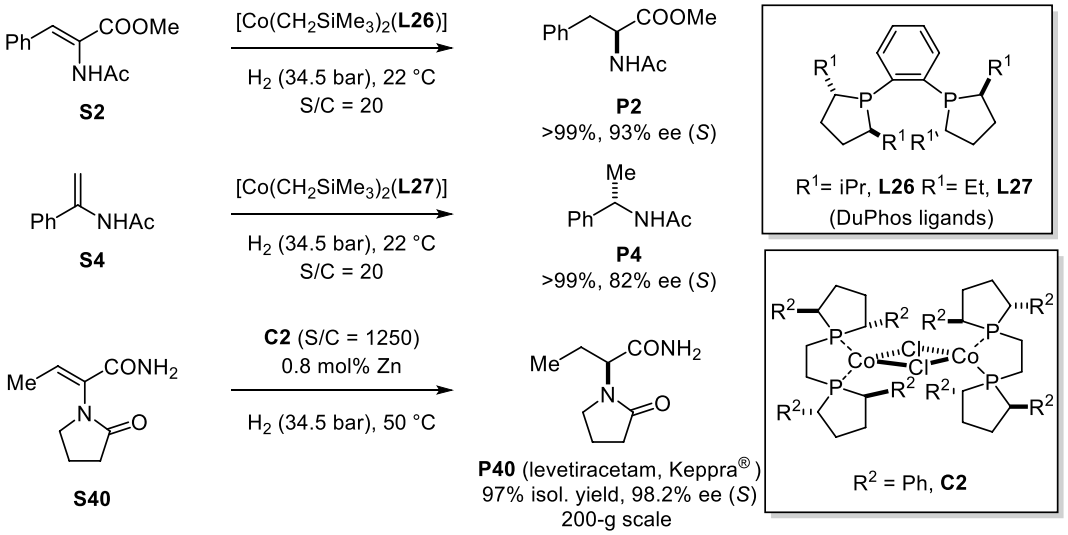

Scheme 15.12. Cobalt-catalyzed AH of α-*N*-acyl acrylates and enamides with neutral cobalt(II) complexes as catalysts. Example of the preparation of an active pharmaceutical ingredient (API) (levetiracetam) by co-catalyzed AH. Source: [43a]/ American Association for the Advancement of Science.

Chirik and coworkers deeply studied the modification of the coordination spheres of cobalt-diphosphine complexes. For instance, analogues of complex **C2** with the DuPhos ligand were efficiently transformed into the corresponding cationic complexes **C3** or **C4**, which catalyzed the AH of substrate **S2** with improved enantioselectivities with respect to the neutral cobalt(I) complexes (99% ee for **C3** or **C4**, Scheme 15.13) [43b]. As for cobalt(0) complexes **C5** [44], these precatalysts were efficiently used in the AH of di-, tri-, and tetrasubstituted acrylic acid derivatives **S41** (Scheme 15.13) with high yields and enantioselectivities ranging from 30% (for β-methylcinnamic acid) to 99% ee (for 1,1-di- and trisubstituted α,β-unsaturated carboxylic acids) [44]. Turnover numbers of up to 200 were routinely observed for substrates **S41** that should be considered poorly coordinating olefins. It is interesting to note that APIs (or advanced synthetic intermediates of these compounds) were efficiently obtained with this synthetic methodology.

Other cobalt complexes derived from enantiopure ligands have been used as catalysts for the enantioselective sequential hydroboration/hydrogenation of internal alkenes [45], regio- and enantioselective cobalt-catalyzed sequential hydrosilylation/hydrogenation of terminal alkynes [46], and enantioselective hydrogenation of diboron-substituted olefins [47].

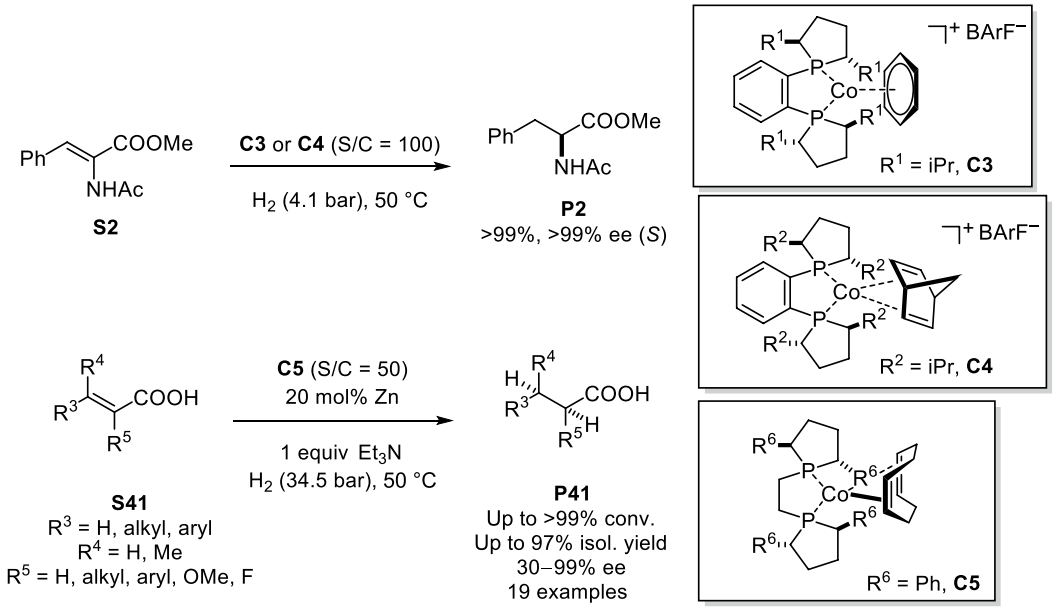

Scheme 15.13. AH of α-*N*-acyl acrylates and enamides with cationic cobalt(I) complexes. Cobalt-catalyzed AH of α,β-unsaturated acids.

Nickel is another first-row element with interesting properties in hydrogenation. While the use of heterogeneous nickel catalysts in the hydrogenation of C=C bonds has played, and still plays, an important role in synthetic chemistry [48], the use of homogeneous nickel hydrogenation catalysts remains largely underexplored. One of the reasons of the very few applications of homogeneous nickel catalysts in AH was that significant research efforts in catalyst development were required before nickel-catalysts could rival the reactivity and ease of handling associated with noble metal-based hydrogenation catalysts. Two recent publications in the area of nickel-catalyzed AHs deserve mention. Chirik reported the discovery of a Duphos-derived nickel catalysts for the AH of α,β-unsaturated esters **S42** (Scheme 15.14) [49].

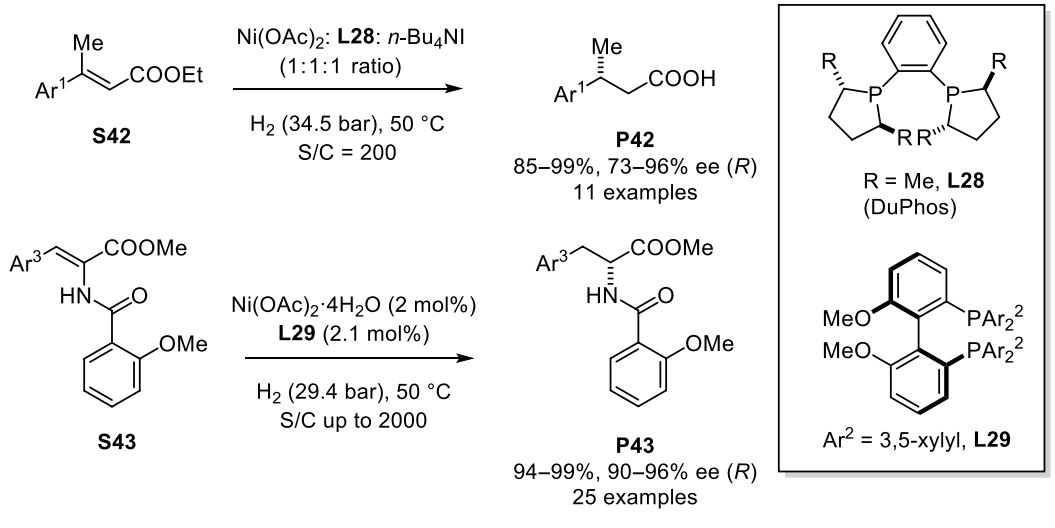

Scheme 15.14. Nickel-catalyzed AH of α,β-unsaturated esters and α-*N*-acyl acrylates. Source: [49]/American Chemical Society.

The combination of ligand **L28** and a number of nickel precursors were tested and their catalytic performances were assessed. Optimal reaction conditions involved the use of nickel acetate, the ligand, and tetrabutylammonium iodide in equimolar amounts. Mechanistic studies revealed that a trinuclear nickel complex activated molecular hydrogen, with this process being the rate-determining step. Subsequent conjugate addition of a nickel hydride to the substrate followed by protonation led to the hydrogenated products with high yields and enantioselectivities ranging from 73 to 96% ee (11 examples, Scheme 15.14) [49]. Nickel complexes derived from the conformationally stable 2,2′-bis(phosphaneyl)-1,1′-biphenyl ligand **L29** were discovered by W. Zhang as efficient enantioselective catalysts for the AH of an array of structurally diverse α-*N*-acylacrylates **S43** (25 examples, Scheme 15.14) [50]. The hydrogenated products were obtained in quantitative yields and enantioselectivities ranging from 93 to 96%. It is interesting to note that a 2-methoxybenzoyl substituent at the nitrogen was necessary to achieve high levels of stereoinduction in the final products (the ee of the hydrogenation product with an acetyl substituent was 40% ee with respect to a 96% ee with the 2-methoxybenzoyl substituent). In particular cases, an S/C ratio up to 2000 was used, with excellent final enantioselectivities being obtained. Other nickel complexes derived from enantiopure ligands have been used as catalysts for the AH of enantioselective β-acylamino nitroolefins[51] and the diastereo- and enantio-selective hydrogenation of tetrasubstituted fluorinated enamides [52].

15.2.4. Iridium Catalysts

With unfunctionalized olefins and olefins lacking adequate substituents, rhodium catalysts may fail to provide good enantioselectivities since, in general, they require the presence of coordinating groups, such as an *N*-acyl group next to the C=C double bond. However, in 1998, Pfaltz discovered a new class of AH catalysts based on iridium complexes incorporating *P*,*N*-ligands [53], which overcame this limitation. Pfaltz's catalysts showed very high activity and stereoselectivity in the hydrogenation of tri- or even tetrasubstituted olefins. The catalysts developed by Pfaltz were inspired in Crabtree's catalyst [54] (i.e. [Ir(cod)(pyridine)(Cy_3P)]PF_6). These seminal results on AH of unfunctionalized alkenes from Pfaltz provided the stimulus for further research in this area and paved the way to the discovery of numerous catalysts for the AH of olefins based on cationic iridium(I) complexes, mainly incorporating *P*,*N*-ligands.

These AH catalysts have been applied to the following substrate classes: (i) α,β-unsaturated esters (**S44–45**) and acids (**S46**), (ii) allyl alcohols (**S47–48**), (iii) diboron derivatives (**S49**), (iv) cyclic 2-alkylydene carbonyl compounds (**S50**), (v) P-containing α,β-unsaturated esters (**S51**), and (vi) Si-containing substrates (**S52**), (Scheme 15.15).

As summarized in Scheme 15.15, the selected ligands **L30–L33** have mediated the AH of substrates **S44–52** with high yields and enantioselectivities. These ligands have been developed by Pfaltz (**L30**) [55], Norrby, Andersson, and Diéguez (**L31**) [56], Zhou (**L32**) [57], and Andersson, Diéguez, and Pàmies (**L33**) [58]. All the selected ligand structures **L30–L33** correspond to *P*,*N*-ligands for iridium(I) metal centers and lead to highly stereoselective AH catalysts for an array of structurally diverse substrates **S44–S52**. It is difficult to make comparisons between ligands **L30–L33** in terms of the broadness of the substrate scope that they tolerate, as the set of studied functionalized olefins differs from one ligand to the other. However, the following general considerations can be made: (i) Ligands **L30–L33** led to high enantioselectivities in the AH of 3-phenylacryloyl derivatives **S44** and **S45** (ees ranging from 89 to >99%); (ii) examples on the AH of 2-phenylacrylic acid derivatives are scarce in the literature, but very good enantioselectivities were obtained with AH catalysts derived from **L32**; and (iii) the most general AH catalyst in terms of broadness of the substrate scope came from ligand **L33**, with C-, P-, Si-, and B-substituted olefins being efficiently hydrogenated. Moreover, four out of seven substrates highlighted in Scheme 15.15 were hydrogenated with ees higher than 94%.

Experimental conditions for achieving high activities and enantioselectivities in this chemistry are low demanding and versatile, as generally: (i) no temperature control is required, though in some cases hydrogenations are performed at temperatures higher than 25 °C; (ii) relatively low hydrogen pressures (up to 50 bar) are required; (iii) iridium catalysts derived from **L30–L33** are active at low concentrations (S/C ratios range from 50 to 1000 in catalytic tests); and (iv) catalytically active species are normally generated from preformed iridium complexes [Ir(diene)(ligand)]BArF (BArF = [B(3,5-$(CF_3)_2C_6H_3)_4$]). These are general

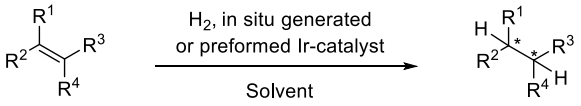

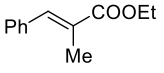

S44

L30 97% ee (*S*)
L31 89% ee (*S*)[b]
L32 99% ee (*S*)[c]
L33 98% ee (*S*)[d]

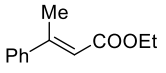

S45

L30 94% ee (*R*)[a]
L31 99% ee (*R*)

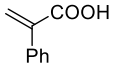

S46

L32 98% ee (*R*)

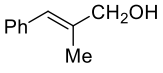

S47

L30 72% ee (*R*)
L31 88% ee (*R*)
L33 98% ee (*R*)

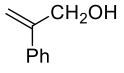

S48

L31 41% ee (*R*)
L33 87% ee (*R*)

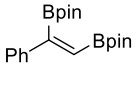

S49

L30 94% ee (*R*)
L33 85% ee (*R*)

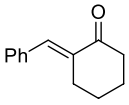

S50

L33 94% ee (*S*)

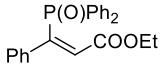

S51

L33 81% ee (*R*)

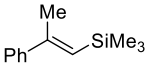

S52

L31 97% ee (*R*)
L33 98% ee (*R*)

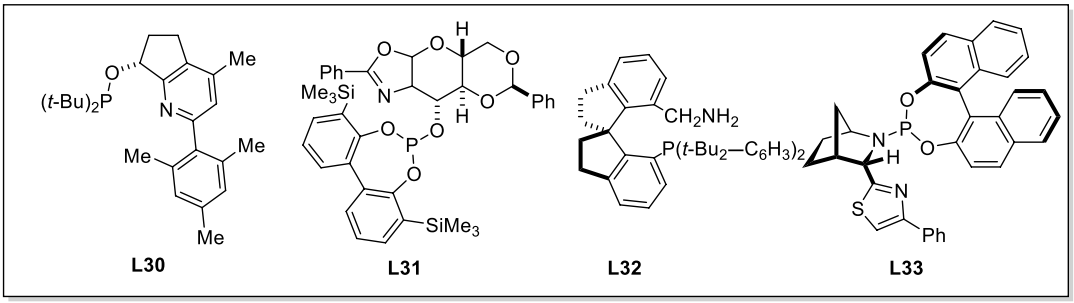

L30 **L31** **L32** **L33**

Scheme 15.15. AH of alkenes without any specific requirement in terms of the nature of the substituents. [a] For the $PhCH_2CH_2$ substituent instead of Ph. [b] For the COMe substituent instead of COOEt. [c] For the COOH substituent instead of COOEt. [d] For the COMe substituent instead of COOEt. Source: [61]/John Wiley & Sons.

observations that refer to the majority of published results for iridium-catalysts derived from **L30**–**L33** (and other ligands not highlighted in this text). However, there may be exceptions to the ranges provided in the text and the reader is referred to the original publications for the exact details of each example.

In 2014, Pfaltz developed pyridine-phosphinite ligand **L34** for the AH of maleic and fumaric acid derivatives enabling the conversion of substrates **S53** into the corresponding 2-alkyl or 2-aryl-substituted succinic acid diesters in high enantiomeric purity (91–99% ee, 18 examples, Scheme 15.16) [59]. Interestingly, mixtures of *Z*/*E* isomers of the substrates were hydrogenated in an enantioconvergent fashion without any loss of enantioselectivity with respect to the pure geometric isomers. Zhu and Zhou have recently discovered neutral iridium(I) catalysts incorporating phosphine-carboxy ligands (**L35**) and used them for the AH hydrogenation of unsaturated carboxylic acids **S54** and **S55** (Scheme 15.16) [60]. The neutral iridium catalysts developed by the authors were highly stable with a long lifetime under air. These iridium catalysts exhibited an unprecedented high enantioselectivity (>99% ee) in the AH of an array of structurally diverse α,β-unsaturated acids (18 examples). The hydrogenation of substrates **S54** is challenging and it is interesting to highlight the high performance of iridium(I) catalyst [Ir(**L35**)(cod)] BArF (86–98% ee, 10 examples, Scheme 15.16). Andersson and coworkers have also developed an

interesting synthetic method for the preparation of highly enantioenriched fluorine-containing ketones by AH of substrates **S56** (Scheme 15.16) [61]. The AH of these substrates with iridium(I) catalysts derived from ligand **L36** enabled the synthesis of various aromatic, aliphatic, and heterocyclic systems, with a variety of functional groups (for instance, carbonyl, fluorine, and trifluoromethyl substituents) in good yields and high enantioselectivities (27 examples, 90–96% ee).

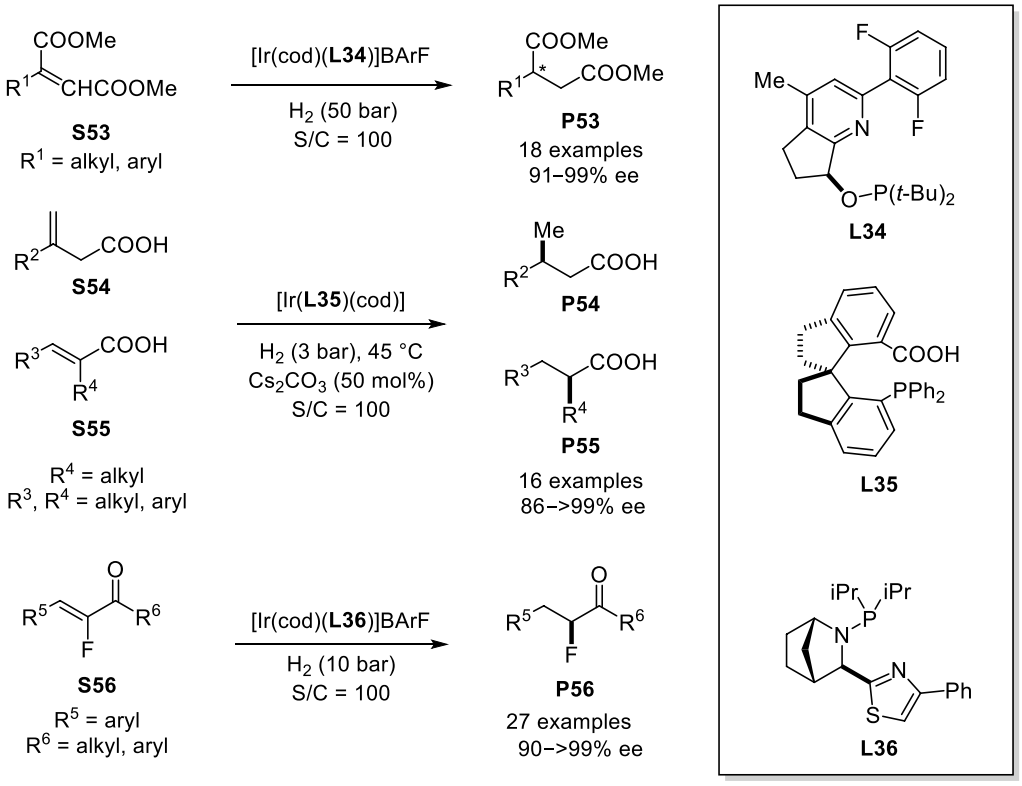

Scheme 15.16. Iridium-catalyzed AH of α,β-unsaturated acid derivatives: maleic and fumaric acid diesters, unsaturated carboxylic acids, and fluorinated α,β-unsaturated ketones.

In addition to the AH methods for the acyclic derivatives previously summarized in Scheme 15.16, numerous iridium-based catalysts for the highly efficient AH of cyclic compounds have been developed. For instance, W. Zhang discovered iridium(I) catalysts derived from ligand **L37**, which efficiently led to succinimide derivatives **P57** (Scheme 15.17) [62]. It should be noted that the substituent on the oxazoline group strongly influenced the outcome of the reaction, with the isopropyl group being the optimal substituent. The hydrogenation of α-alkylidene succinamides under optimized reaction conditions (20 bar hydrogen, room temperature S/C = 100, preformed catalyst) led to the products in quantitative yield with excellent enantioselectivities (up to 99% ee, 24 examples). Though a hydrogen pressure of 20 bar was used in catalyst screening assays, the authors demonstrated for certain substrates that the hydrogenations were also successful at a reduced catalyst loading (S/C = 2000) and using 1 bar of hydrogen.

Ding has developed an efficient synthetic method toward medium-sized cyclic carbonyl compounds based on the AH of α-alkylidene carbonyl compounds. The catalysts employed were derived from iridium(I) complexes of spirophosphine oxazoline ligand **L38** (Scheme 15.17) [63]. The catalysts were demonstrated to be highly enantioselective in the AH of exocyclic α,β-unsaturated seven-membered lactams and carbonyl compounds (**S58**). In general, excellent enantioselectivities were obtained (up to 98% ee) for a set of 18 compounds containing a stereogenic center adjacent to the carbonyl group. It is interesting to highlight that the AHs were quite general and not influenced by the electronic nature or the steric bulk of the aryl substituents in the substrates.

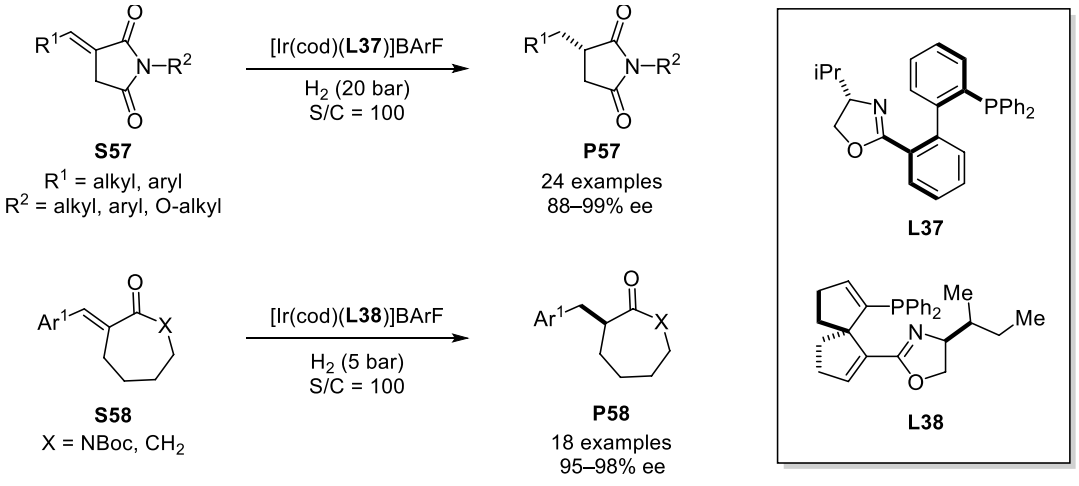

Scheme 15.17. Iridium-catalyzed AH of exocyclic compounds. Source: [63]/John Wiley & Sons.

Zhou and coworkers developed a highly efficient AH method for unsaturated heterocyclic acids (Scheme 15.18) [64]. The authors used cationic iridium(I) complexes derived from spirophosphine oxazoline ligand **L39** as AH catalyst. The AH method provided a direct and efficient synthetic method to the synthesis of enantiopure (or highly enantioenriched) *N*- or *O*-containing heterocyclic acids encompassing five-, six-, and seven-membered monocyclic structures and bicyclic compounds (for the structures, see Scheme 15.18). The synthesis of several natural products (e.g. (*R*)-nipecotic acid and (*R*)-tiagabine) with the developed methodology illustrates the practicality of this AH method.

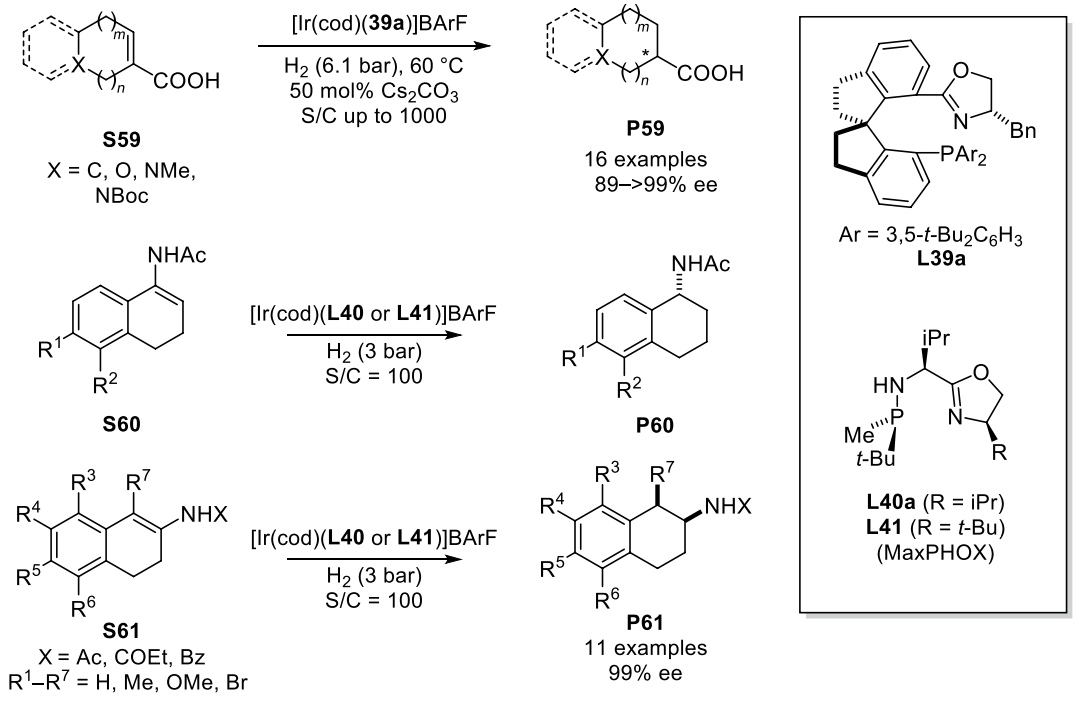

Scheme 15.18. Iridium-catalyzed AH of (poly)cyclic compounds. Source: [66]/John Wiley & Sons.

Ligand **L39** or a diastereomeric analogue proved to be useful in the AH of the five- and six-membered analogues of substrates **S59** (22 examples, ees ranging from 79 to 97%) [63]. The authors have also published the AH of 3-ylidenephthalides (i.e. *O*-containing five-membered cyclic analogues of **S59**) with iridium(I) complexes of spirophosphine oxazoline ligands. The synthetic utility of this AH method was demonstrated by preparing loxoprofen, biologically relevant ε-aminocaproic acid derivatives, (*R*)-chuangxinol, and (*R*)-typhaphtalide [63, 65]. Riera and Verdaguer discovered iridium(I) catalysts derived from phosphino-oxazoline (PHOX) ligands **L40a** and **L41**, which incorporate a *P*-stereogenic group. These catalysts provided the highest selectivity ever reported in the hydrogenation of *N*-(3,4-dihydronaphthalen)-1-yl and *N*-(3,4-dihydronaphthalen)-2-yl acetamides **S60** and **S61**, respectively, and related compounds (99% ee for an array of structurally diverse compounds, Scheme 15.18) [66]. Ligands **L40a** and **L41** from the MaxPHOX family contain three stereogenic centers, and the matched combination for achieving high enantioselectivities in this chemistry is indicated in Scheme 15.18. The enantioselectivity of the hydrogenations was pressure dependent, with a lowering of the pressure down to 3 bar resulting in an increase in the enantioselectivities. This result indicates that iridium catalysts can also be used in the AH of alkenes with coordinating groups, although the reaction mechanism, in this particular case, has not been established. The authors demonstrated the usefulness of the methodology by synthesizing a precursor of rotigotine.

Wang and Ding have reported an elegant strategy toward functionalized spiroketals **P62** by AH (Scheme 15.19) [67]. The authors described that iridium complex **C6** was highly efficient in the enantioselective hydrogenation of α,α′-bis(2-hydroxyarylidene) ketones **S62** to afford the corresponding aromatic spiroketals with excellent diastereo- and enantioselectivities. The complex plays a dual role in the reaction, acting as catalyst for both the hydrogenation of C=C bonds and the subsequent spiroketalization reaction. Zhou and Ding have discovered an iridium complex analogous to **C6** that mediates this spirocyclization process with higher enantioselectivities [68].

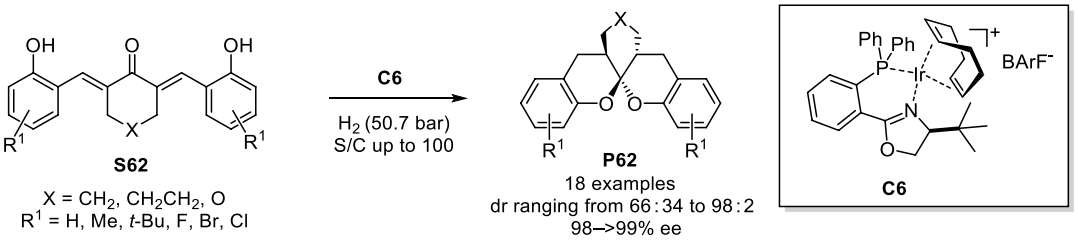

Scheme 15.19. Iridium-catalyzed hydrogenation and spiroketalization of bis(2-hydroxyarylidene) ketones. Source: [67]/John Wiley & Sons.

Several efficient catalysts have been discovered for the hydrogenation of large arrays of olefins incorporating boron-, silicon-, phosphorus-, and sulfur-containing functional groups [4, 5]. Some examples have already been highlighted in this section. Regarding boron-substituted olefins, Pfaltz has developed efficient AH catalysts based on iridium complexes of *P*,*N*-ligands **L42** and **L43** for the hydrogenation of alkenyl boronic esters [69]. Geminally substituted boronates **S63** were efficiently hydrogenated in high enantioselectivities with [Ir(cod)(**L42**)]BArF as the catalyst (Scheme 15.20). Substrates having a CH_2 group or a phenyl substituent next to C=C bond were well tolerated, as well as additional functional groups in the R^1 fragment. *trans*-Disubstituted boronates **S64** were efficiently hydrogenated with another iridium catalyst from the Pfaltz group ([Ir(cod)(**L43**)]BArF). It is interesting to note that bisboronic esters (i.e. substrates **S64** with R^3 = Bpin) were stereoselectively obtained (three examples, ees ranging from 85 to 98%). Moreover, various groups at the C=C bond (R^2, R^3 = cyclohexyl, *n*-hexyl, *t*-butyl, phenyl-substituted) were tolerated, giving high conversions and enantioselectivities.

Časar has developed chemoselective and enantioselective iridium-based catalysts for the hydrogenation of chloro-substituted alkenyl boronic esters (Scheme 15.20) [70]. The AH of chloro-substituted alkenyl boronic esters was an unprecedented transformation and led to highly enantioenriched

(α-chloroalkyl) boronic esters **P65**, which are highly versatile building blocks in asymmetric synthesis. Catalyst [Ir(cod)(**L44**)]BArF reduced an array of diverse substrates very efficiently (10 examples, up to 94% ee), with the dechlorinating process ranging from 3 to 19%.

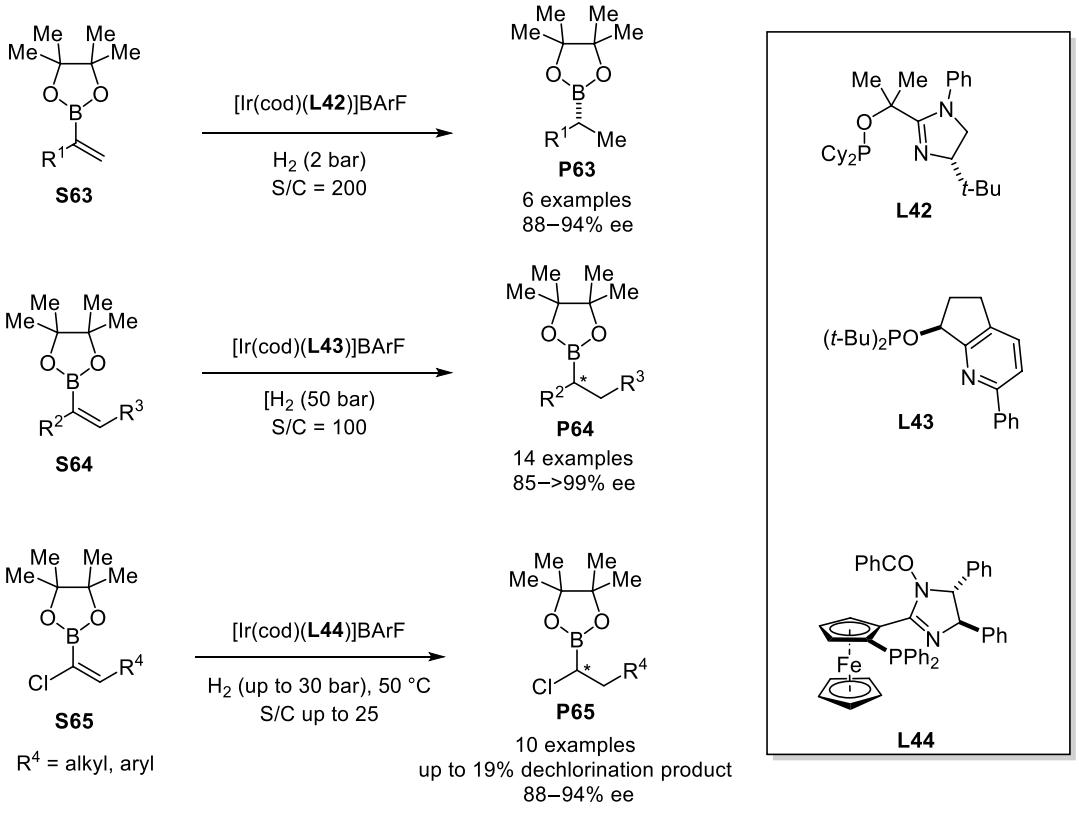

Scheme 15.20. AH of alkenylboronic esters and chloro alkenyl boronic esters. Source: [70]/John Wiley & Sons.

Regarding the hydrogenation of sulfur-containing olefins, Andersson described the enantioselective preparation of sulfonyl compounds (**P66–68**) employing cationic iridium(I) catalysts derived from ligand **L45a** [71]. High enantioselectivities (84–99%, 35 examples) were obtained regardless of the location of the olefin with respect to the sulfone group (Scheme 15.21). The high stereoselectivities obtained for dialkyl-substituted olefins should be highlighted, as these substrates are typically challenging in AH. The geometry of the olefin greatly influenced the outcome of the reaction, with *E*- and *Z*-isomers providing hydrogenated products with opposite configurations. Moreover, the bulkier *Z*-substrates were hydrogenated slower than the corresponding *E*-isomers and in slightly lower enantioselectivities.

The same group developed the enantioselective hydrogenation of several fluorinated olefins (Scheme 15.21) [61, 72]. Good yields and enantioselectivities were found for trisubstituted substrates with ligands such as **L45b** [61]. Selectivities of up to 98% ee were found for other substrates and very little defluorination was observed. In a subsequent study [72], the authors reported the hydrogenation of a tetrasubstituted alkenyl fluoride (R^4 = Me, **S69b**) with ligand **L45c** also with good selectivity, although in modest yield.

15.2.5. Ruthenium Catalysts

Highly stereoselective AH methods of C=C double bonds in cyclic compounds have not been restricted to rhodium- or iridium-based catalysts derived from phosphorus ligands. For instance, Li and Glorius have discovered highly interesting ruthenium catalysts based on enantiopure *N*-heterocyclic carbenes (NHCs) and 1,2-diamines (structure **C7**, Scheme 15.22) and applied them to the enantioselective AH of

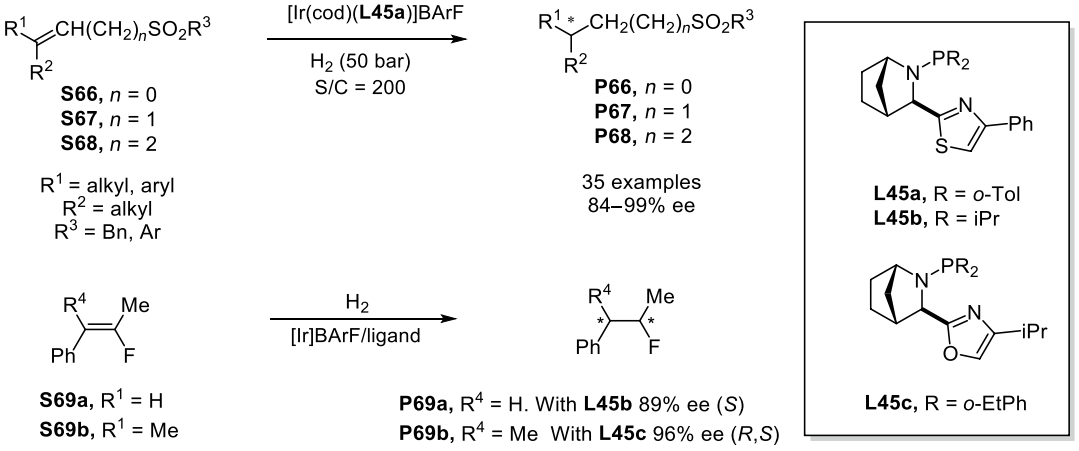

Scheme 15.21. Iridium-catalyzed AH of sulfones and fluorine-substituted olefins. Source: Based on [61] and [72].

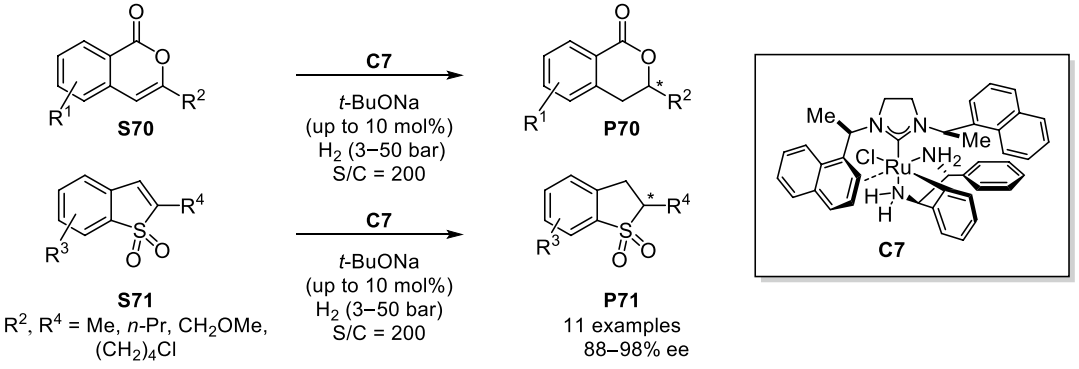

Scheme 15.22. Ruthenium-catalyzed AH of isocoumarines and benzothiophene dioxides.

functionalized unsaturated compounds, such as isocoumarines **S70** and benzothiophene dioxides **S71** [73]. The air- and moisture-stable precatalyst **C7** was isolated and activated toward AH with a strong base. Varieties of highly enantioenriched 3-substituted 3,4-dihydroisocoumarins **P70** and 2-substituted 2,3-dihydrobenzo[*b*]thiophene 1,1-dioxides **P71** were obtained in excellent enantioselectivities (up to 98% ee). Instead of using precatalyst **C7**, Glorius also described the in situ generation of the corresponding catalytic species with excellent results in terms of enantioselectivity in the AH of substrates **S70** [74].

15.3. ASYMMETRIC HYDROGENATION OF UNFUNCTIONALIZED OLEFINS

Despite lagging far behind the hydrogenation of functionalized olefins, the AH of unfunctionalized olefins (i.e. those lacking any functionality adjacent to the C=C bond) has matured considerably during the last decade. A considerable number of catalytic systems that effectively hydrogenate a growing variety of substrates has been reported. A proof of this activity is that numbers of reviews have recently appeared on this topic [75].

15.3.1. Iridium-Catalyzed Hydrogenations

The most successful type of catalytic precursors continues to be Ir(I) cationic complexes, which trace their origins to the Crabtree's catalyst [54]. Almost invariably, they have general formulae [Ir(cod)(*P*,*N*-ligand)]BArF [76] although they are often prepared in situ and were developed after the excellent results

of Pfaltz's PHOXs in the previous decade [77]. Since then, there has been a considerable development of new ligand types allowing the reduction of difficult substrates, including some tetrasubstituted olefins, in full conversions and high enantioselectivities.

Ir-catalyzed hydrogenation of unfunctionalized olefins has finally become a useful synthetic method because it has already been used in the synthesis of natural products [78] and molecules with pharmacological activity [79]. In addition, attempts to recycle the catalyst [80] and perform the hydrogenation in environmentally benign solvents [81, 82] have also been reported. In parallel, the mechanism of the transformation has been investigated in detail [54, 83].

15.3.1.1. Model Substrate: (E)-2-Methyl-2-Stilbene (*E*)-2-methyl-2-stilbene ((*E*)-α-methylstilbene) (**S72**) is probably the most widely used substrate to test the AH of unfunctionalized olefins. In order to show the diversity of ligand structures and for comparison purposes, the results obtained in the last decade on the AH of this model substrate with iridium catalysts will be first discussed. Following Pfaltz's footsteps, Hou developed phosphinobenzyl oxazolines **L46** [84] that provided good asymmetric induction in the iridium-catalyzed AH of unfunctionalized alkenes, as well as other functionalities. Pfaltz developed other PHOXs such as **L47** [85], **L48**[86], and **L49** [87] and tested in this benchmark reaction (Scheme 15.23).

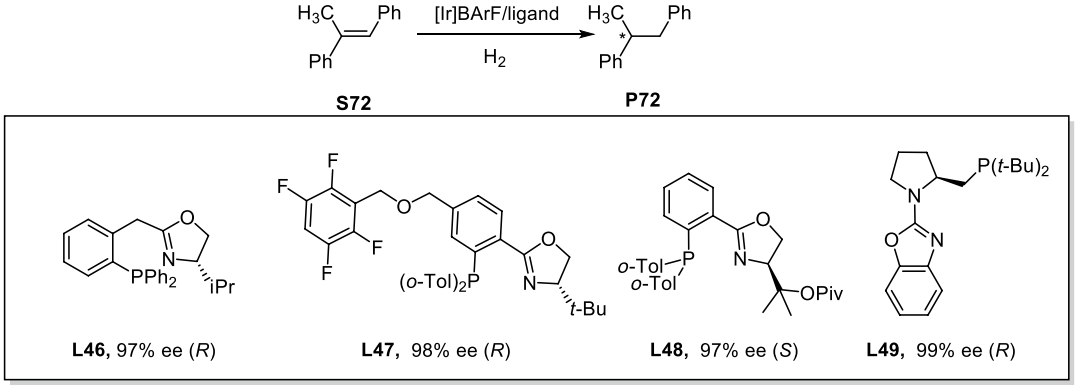

Scheme 15.23. Asymmetric hydrogenation of (*E*)-2-methyl-2-stilbene (**S72**) using iridium catalysts derived from phosphinooxazoline ligands.

The nitrogen coordination of the oxazoline ring can be substituted by other nitrogenated heterocycles such as quinolines (**L50**) [88], triazoles (**L51**) [89], imidazolines (**L52**) [90], or pyridines (**L53**)[91] (Figure 15.3). The Boehringer-Ingelheim phosphinoimidazoline (BIPI) ligand (**L52**) developed in Boehringer-Ingelheim Pharmaceuticals and the simple phosphino pyridine **L53** developed by Andersson gave the best results on **S72.** This substrate was typically hydrogenated quantitatively at room temperature

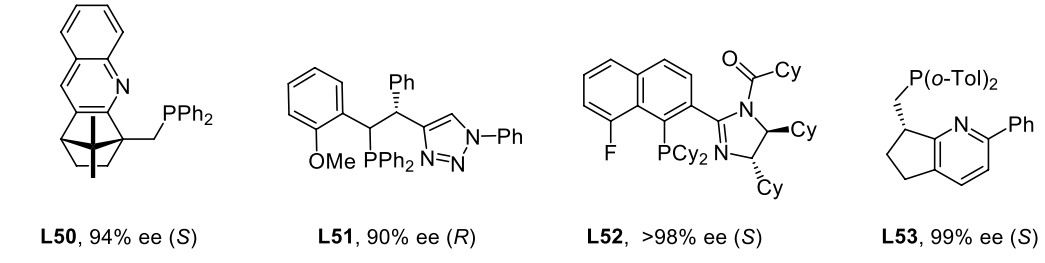

Figure 15.3. Chiral *P*,*N*-ligands bearing heterocycles other than oxazolines used in the iridium-catalyzed asymmetric hydrogenation of (*E*)-2-methyl-2-stilbene (**S72**).

in dichloromethane at 50 bar of hydrogen pressure, although with two optimally designed ligands (**L50** and **L52**) reductions were performed at low pressure (10 and 1 bar, respectively).

The attachment of the phosphorus fragment to the nitrogenated counterpart in *P*,*N*-ligands can be facilitated using nitrogen or oxygen atoms as linkers. Andersson pioneered this field developing several phosphinoamines (**L54** [92], **L55** [93], **L56** [94]) anchored to a nitrogenated heterocycle (Figure 15.4). More recently, Fan described pyridine-aminophosphine ligands such as **L57** [95] that provided complete enantioselectivity in the hydrogenation of **S72** (Figure 15.4). Chiral phosphinites such as **L58** developed by Diéguez [96] or **L59** developed by Pfaltz [55] also gave good to excellent enantioselectivities.

P,*N*-Phosphinoferrocenyl ligands have also been tested in the iridium-catalyzed hydrogenation of unfunctionalized alkenes (Figure 15.5). A family of enantiopure 2-phosphino-1-aminoferrocene ligands was described by Metallinos in 2011. The dimethylamino ligand **L60** [97], gave moderate enantioselectivity. Better results were obtained by Van der Eycken [98] with ligand **L61.** On the other hand, *P*-stereogenic ligands have been scarcely used. Qu developed a family of air-stable chiral pyridyl-dihydrobenzooxaphosphole ligands (BoQPhos) [99]. Among them, **L62** gave good enantioselectivities with unfunctionalized alkenes (Figure 15.5).

In ligand design, the use of phosphites as phosphorus donors has several advantages. Their preparation is convenient, and the modular approach allows the easy introduction of bulky substituents. Pàmies, Diéguez, and Andersson followed this approach in the design of ligands **L63** [100], **L64** [56], and **L65** [101] (Figure 15.6). An additional benefit of the use of phosphites is the possibility to introduce a new stereogenic fragment with axial chirality. This approach has been thoroughly studied by Pàmies and Diéguez

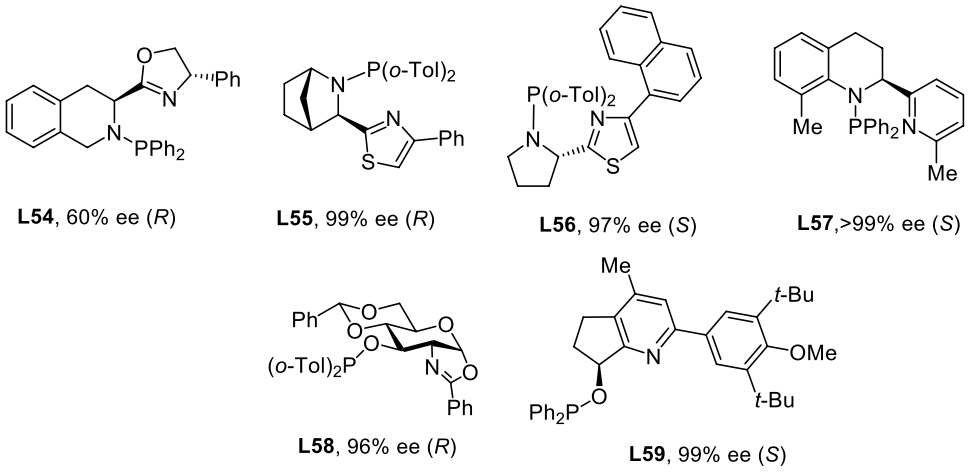

L54, 60% ee (*R*) **L55**, 99% ee (*R*) **L56**, 97% ee (*S*) **L57**,>99% ee (*S*)

L58, 96% ee (*R*) **L59**, 99% ee (*S*)

Figure 15.4. Chiral phosphinoamines and phosphinites as *P*,*N*-ligands used in the iridium-catalyzed asymmetric hydrogenation of (*E*)-2-methyl-2-stilbene (**S72**).

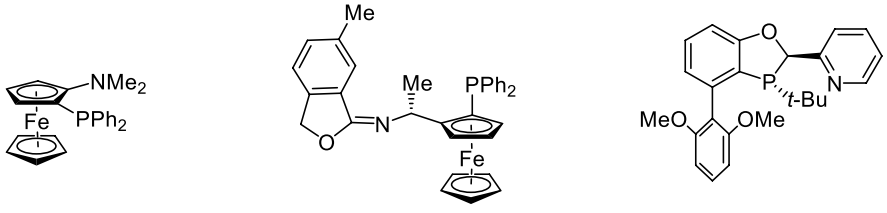

L60, 84% ee (*R*) **L61,** 91% ee (*R*) **L62,** 90% ee

Figure 15.5. Phosphinoferrocenyl ligands and a *P*-stereogenic pyridyl-dihydrobenzooxaphosphole ligand used in the iridium-catalyzed asymmetric hydrogenation of (*E*)-2-methyl-2-stilbene (**S72**).

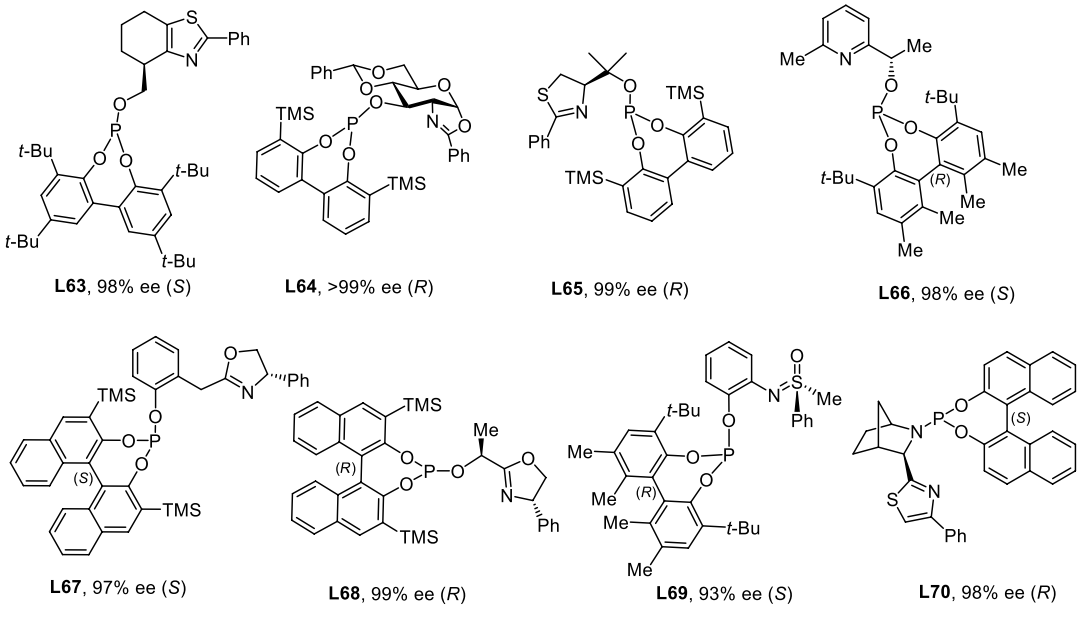

Figure 15.6. Phosphites as phosphorus donors in *P*,*N*-ligands for the iridium-catalyzed asymmetric hydrogenation of (*E*)-2-methyl-2-stilbene (**S72**).

reporting several families of *P*,*N*-ligands (**L66** [102], **L67** [103], **L68** [104], and **L69** [105]) with chiral phosphites. The fine tuning of the bulkiness and the stereochemistry of the fragment allowed obtaining excellent results in many substrates such as (*E*)-2-methyl-2-stilbene (**S72**). In collaboration with Andersson, they developed phosphoramidite **L70** [58] (Figure 15.6).

Although the vast majority of catalysts bear *P*,*N*-donor ligands (ligands **L46**–**L70**), which judiciously exploit all kinds of stereogenic elements to afford excellent enantioselectivities, there are relevant examples of *P*,*O*- and *P*,*S*-ligands. In 2011, Pfaltz described a family of proline-derived phosphines bearing a bulky amide or urea groups at the pyrrolidine nitrogen atom [106]. Compound **L71** (Figure 15.7)

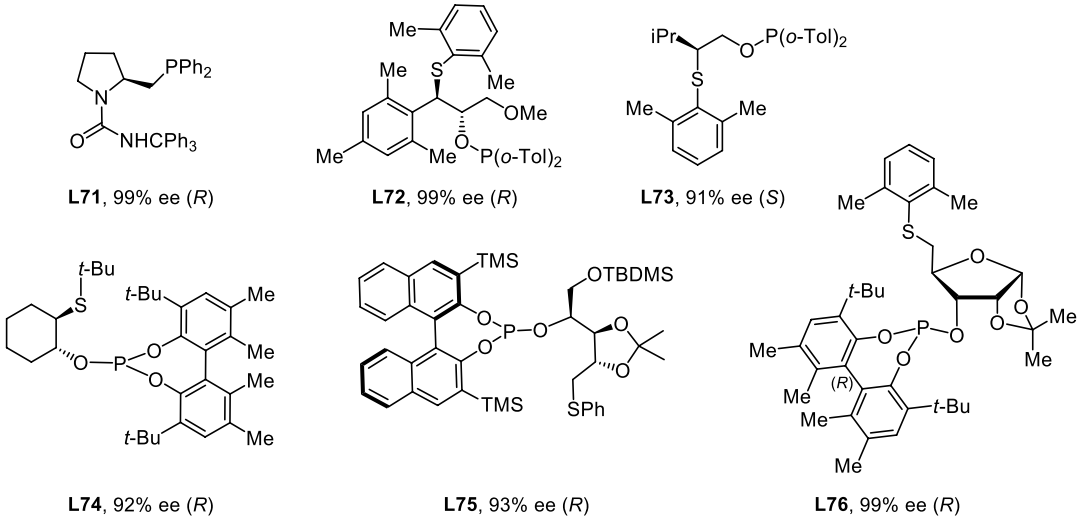

Figure 15.7. Chiral *P*,*O*- and *P*,*S*-ligands used in the iridium-catalyzed asymmetric hydrogenation of (*E*)-2-methyl-2-stilbene (**S72**).

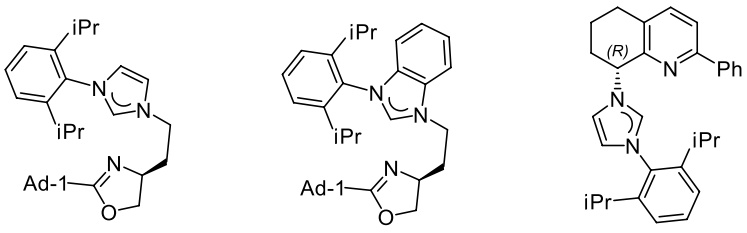

L77a, 99% ee, (*S*) **L77b,** 95% ee, (*S*) **L78,** 97% ee, (*R*)

Figure 15.8. Chiral *C*,*N*-ligands with *N*-heterocyclic carbenes reported for the iridium-catalyzed asymmetric hydrogenation of (*E*)-2-methyl-2-stilbene.

performed as a *P*,*O*-ligand when complexed with iridium and gave excellent enantioselectivities in the hydrogenation of trisubstituted alkenes and α,β-unsaturated esters and ketones. On the other hand, Pàmies and Diéguez explored several families of modular *P*,*S*-ligands (**L72** [82], **L73** [107], **L74** [83e], **L75** [108], and **L76** [109]) with good to excellent results (Figure 15.7).

The replacement of a phosphorus coordination fragment by a carbene is a well-established strategy to gain stability of organometallic complexes. Thus, several iridium complexes of NHCs have been described as *C*,*N*-ligands and applied to AH. Oxazoline-imidazolylidine ligand **L77a** [110] gave good to excellent results with several poorly functionalized olefins. This ligand gave slightly better results than the related benzimidazolylidene ligand **L77b** (Figure 15.8). In 2013, Pfaltz developed several ligands with an NHC moiety for the iridium-catalyzed hydrogenation of olefins. Ligand **L78** [111] gave results similar to the analogous phosphinite ligand and was better suited for acid-sensitive substrates. Recently, an NHC-donor, *C*,*S*-ligand has been described by Pàmies and Diéguez [107].

15.3.1.2. Trisubstituted Alkenes and Dienes Apart from the model substrate, (*E*)-α-methylstilbene (**S72**), many other trisubstituted olefins have been successfully hydrogenated, including several that until recently were considered very difficult substrates. The *E*- and *Z*-isomers of the same alkene are usually hydrogenated to products of opposite configurations and usually it is found that (*Z*)-configured olefins are more difficult to reduce in high enantioselectivity [102]. Examples of hydrogenation of (*Z*)-configured olefins are *p*-anisylbutene (**S73**) and the 7-methoxy-4-methyl-1,2-dihydronaphthalene (**S74**) (Scheme 15.24), which have been hydrogenated in excellent enantioselectivity by the groups of Pfaltz [53, 111], Andersson [56, 101], and Pàmies and Diéguez [56, 102, 104, 109b]. Other substituted-dihydronaphthalenes (dialins) have been also hydrogenated in high ee by the groups of Busacca [90], Diéguez and Pàmies [56, 102], and Qu [112], giving valuable optically enriched 1-substituted tetralins. Another class of interesting substrates is those olefins with exocyclic double bonds, such as (*E*)-1-benzyldiene-2,3-dihydro-1*H*-indene (**S75**). A report by Zhang [113] described its hydrogenation with 93% ee at 40 bar of H_2 pressure at room temperature with 1% of Ir catalyst containing ligand **L79**. This result was extended to other substrates bearing exocyclic double bonds. Similar results have been obtained more recently by Diéguez, Pàmies with phosphite-oxazoline ligands [102, 104]. Even more difficult is to reduce purely alkyl-substituted olefins. This has been achieved by Pfaltz [78b] for a few substrates with ligand **L79** (Scheme 15.24). Very good enantioselectivity was found for cyclohexylbutene (**S76**) at 50 bar of H_2 and it only decreased to 95% ee at 1 bar and 0.1% of catalyst loading. The hydrogenation of (*E*)- and (*Z*)-3,4-dimethyl-2-pentene (**S77**) also provided good enantioselectivities and as expected the isomeric alkenes gave opposite configurations in the product.

The AH of unfunctionalized dienes is rare, but the group of Andersson [114] pioneered the use of substituted cyclohexadienes, obtainable from the Birch reaction, as substrates for AH with Ir catalysts with *P*,*N*-ligand **L81** (Scheme 15.24).

More recently, this chemistry has been expanded to other cyclohexadienes and related substrates such as tetrahydronaphthalenes [115]. In addition, the asymmetric monohydrogenation of substituted 1,4-ciclohexadienes under mild conditions has also been reported [116].

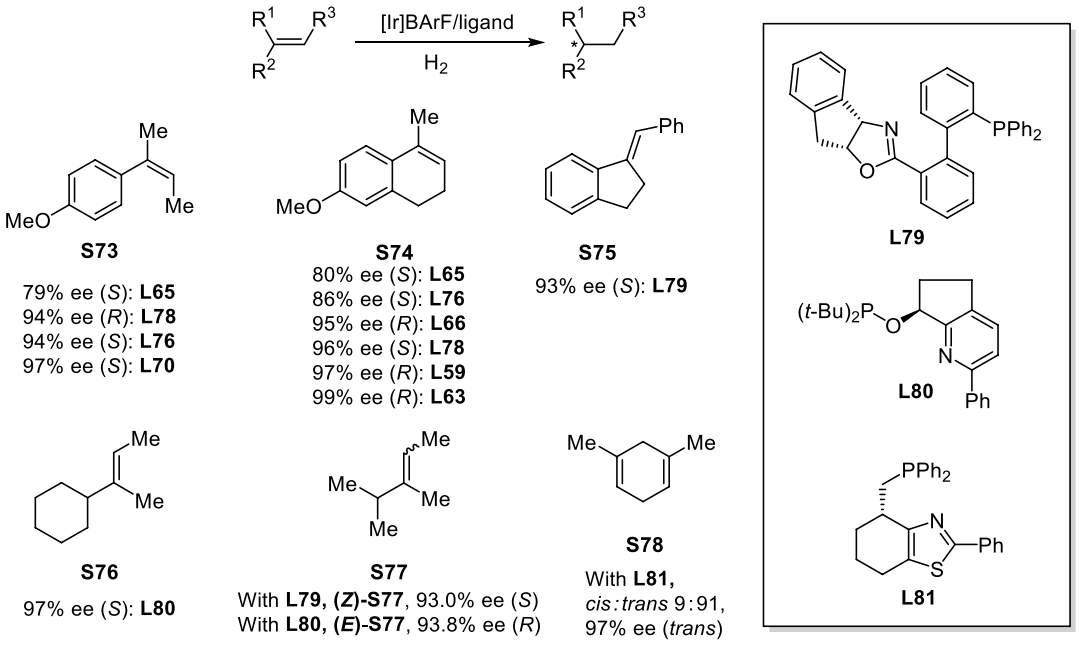

Scheme 15.24. Hydrogenation of trisubstituted unfunctionalized alkenes and dienes.

15.3.1.3. Terminal (1,1,-Disubstituted) Alkenes Enantioselectivity is more difficult to control in 1,1-disubstituted terminal olefins than in trisubstituted olefins because in the former the two substituents can interchange their positions easily, reversing the coordinated face, and in addition the terminal double bond is prone to isomerize to the more stable internal alkene, which often leads to the opposite enantiomer [117]. Despite this, some Ir-based systems have given very good results with several terminal olefins (Scheme 15.25).

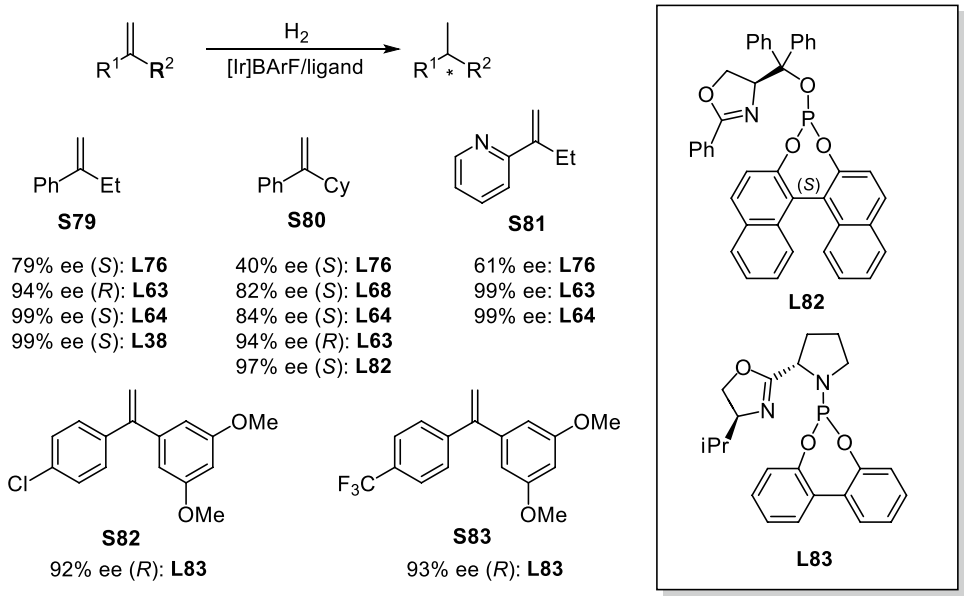

Scheme 15.25. Examples of asymmetric hydrogenation of 1,1-disubstituted alkenes.

For the simple substrate 2-phenyl-1-butene (**S79**, Scheme 15.25), full conversions and excellent enantioselectivities have been obtained by the groups of Andersson, Diéguez, and Pàmies [54, 100, 103, 104, 109b] and by Van der Eycken [98], usually at 1 bar of hydrogen pressure since for this kind of substrates higher hydrogen pressures are deleterious for the enantioselectivity. Equally good results have been obtained with many other 1,1-disubstituted alkyl-aryl olefins including those with an heteroaromatic substituent group such as **S81** [53, 56, 82, 83e, 102, 103, 104, 107]. In contrast, 1,1-diarylalkenes are more difficult to reduce in high enantioselectivity [117b, 118]. In this area, Sigman [119] developed an Ir system with ligand **L83** capable of hydrogenating in high selectivity substrates such as **S82** or **S83**, although it was limited to substrates with a 3,5-dimethoxyphenyl group (Scheme 15.25).

15.3.1.4. Tetrasubstituted Alkenes Tetrasubstituted olefins are interesting substrates because they can generate two vicinal stereocenters, but their enantioselective hydrogenation is still difficult. The high modularity of some of the ligands developed for Ir-catalyzed hydrogenation has allowed, however, to find a few systems leading to good results for some tetrasubstituted alkenes (Scheme 15.26).

The hydrogenation of 2,3-dimethylindene (**S84**) has been explored by several groups to test their ligands. Busacca [90] found full conversions and high enantioselectivities for some of their BIPI ligands such as **L52** (Scheme 15.26). The results were also relatively good for the more challenging substrate 3,4-dimethyldihydronaphthalene (**S85**), at 1 bar of hydrogen pressure. In all cases, full *cis* selectivity is observed. Interestingly, very similar results have been obtained by Pàmies and Diéguez [104] with very different oxazoline *P,N*-ligands (**L68** and **L84**), albeit at higher hydrogen pressures (Scheme 15.26). The same group, in collaboration with the group of Riera and Verdaguer [120], used *P*-stereogenic *N,P*-donor ligands MaxPHOX (**L40**) to improve the results for several disubstituted indenes and also for tetrasubstituted acyclic olefins (Scheme 15.26). The latter type of substrates is considered to be the most challenging substrate class in AH [75c, d]. Recently, Bigler, Zhang, and Gosselin [121] expanded the substrate scope to include olefins giving two stereocenters upon hydrogenation, such as (*E*)-2,3-diphenyl-2-butene (**S87**) with PHOX ligands such as **L85**. Good results were obtained for other diarylbutenes and related substrates (Scheme 15.26).

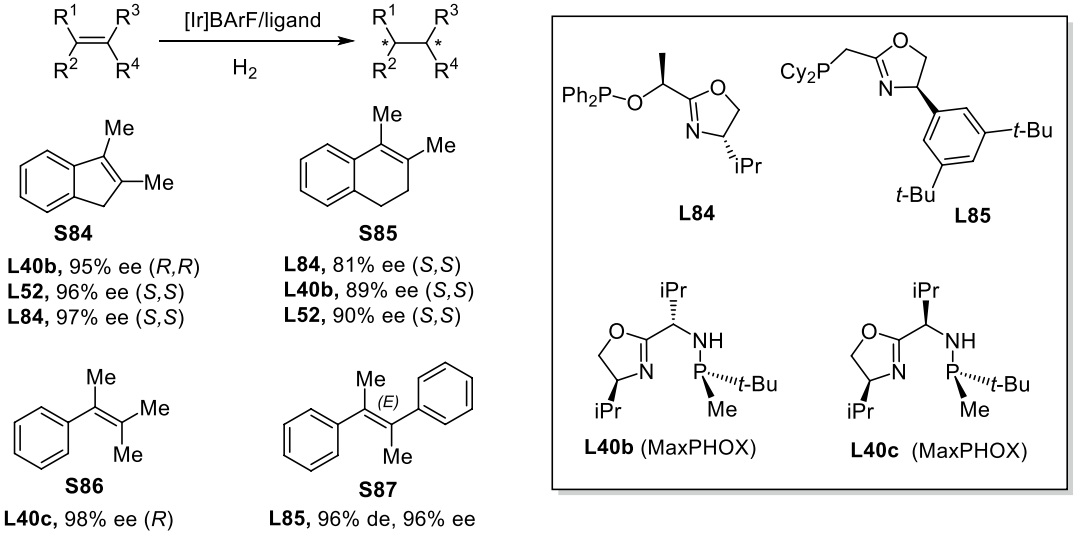

Scheme 15.26. Examples of asymmetric hydrogenation of tetrasubstituted olefins.

15.3.2. Rhodium-Catalyzed Hydrogenations

The extended belief that Rh-based catalysts are not suitable to hydrogenate unfunctionalized olefins enantioselectively has been challenged by a few recent publications (Scheme 15.27). Instead of the typical Rh(I) precursors employed in the hydrogenation of functionalized olefins, Mashima [122] developed cationic

triply chloride-bridged dinuclear Rh(III) hydride complexes (**C8**) with 2,2′-bis(diphenylphosphino)-1,1′-binaphthyl (BINAP)-type ligands that were able to hydrogenate (*E*)-2-methyl-2-stilbene (**S72**) in very good yield and enantioselectivity with the 5,5′-bis[di(3,5-di-*tert*-butyl-4-methoxyphenyl)phosphino]-4,4′-bi-1,3-benzodioxole (DTBM-SegPHOS) (**L86**). Other substituted stilbenes were also hydrogenated efficiently. More recently, an extension of this work [123] has uncovered a mononuclear Rh(III) complex (**C9**) with the same ligand as an improved catalyst for the same substrate but that also efficiently hydrogenated (*E*)-1-benzyldiene-2,3-dihydro-1*H*-indene (**S75**) and related substrates in high ee. Shen, Li, and Zhang [124] used classical Rh(I) precursors of the type [Rh(bisphosphine)(nbd)]BF_4 for the hydrogenation of the substituted indene **S88** of and were able to obtain good enantioselectivity with the bisdihydrobenzooxaphosphole (BIBOP) ligand **L87**. This was extended to several other indenes with good results, including a precursor of the alkaloid delavatine A. In a related work, Strotman [125] found that Rh-DTBM-SegPHOS outperformed Ir in the reduction of an indene while preparing a precursor of a γ-secretase modulator (Scheme 15.27).

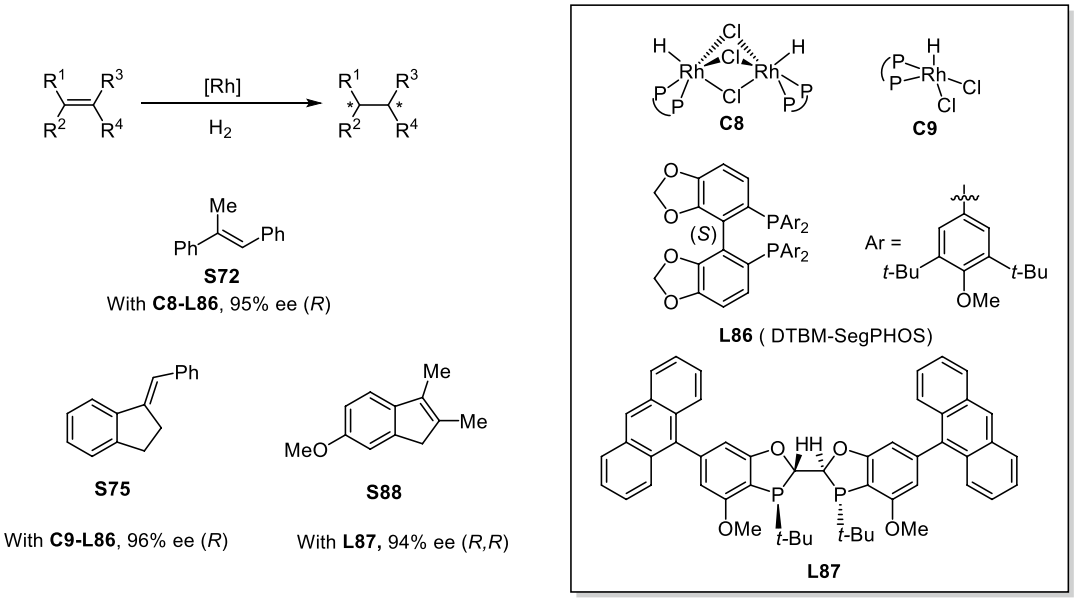

Scheme 15.27. Rh-catalyzed hydrogenation of unfunctionalized olefins.

15.3.3. Cobalt-Catalyzed Hydrogenations

The tendency of transition metal catalysis to move toward catalysts based on earth-abundant, first-row transition metals has reached the hydrogenation of unfunctionalized alkenes. In this respect, cobalt appears to be a very promising metal (Scheme 15.28). Chirik and coworkers [41]. described Co(I) complexes with a chiral, C_1-symmetric bis(imino)pyridine ligand (**C10**) that hydrogenated several terminal olefins in good yields and enantioselectivities with a 5% of catalyst loading. The substrate scope was subsequently expanded by the same group [126] to include other terminal olefins as well as cyclic olefins including indenes and dialins, generally obtaining with good results. Mechanistic studies have been published [127]. In a related research, Lu [128] presented bench-stable Co(II) precursors featuring a chiral oxazoline-iminopyridine (**C11**), which in the presence of sodium triethylborohydride as reductant was able to perform the hydrogenation of several 1,1-diarylethenes in good yields and enantioselectivities, under mild conditions (Scheme 15.28).

Finally, Chirik and coworkers [42] also carried out an impressive catalyst screening with simple Co(II) precursors (10%) and 192 typical chiral C_2-symmetric diphosphines and found that some combinations generated systems such as **C12** competent to hydrogenate (*E*)-2-methyl-2-stilbene (**S72**) with good enantioselectivities, with a Biphep derivative ligand **L88**. A Co(0)-Co(II) catalytic cycle has been proposed to operate in this chemistry (Scheme 15.28) [42].

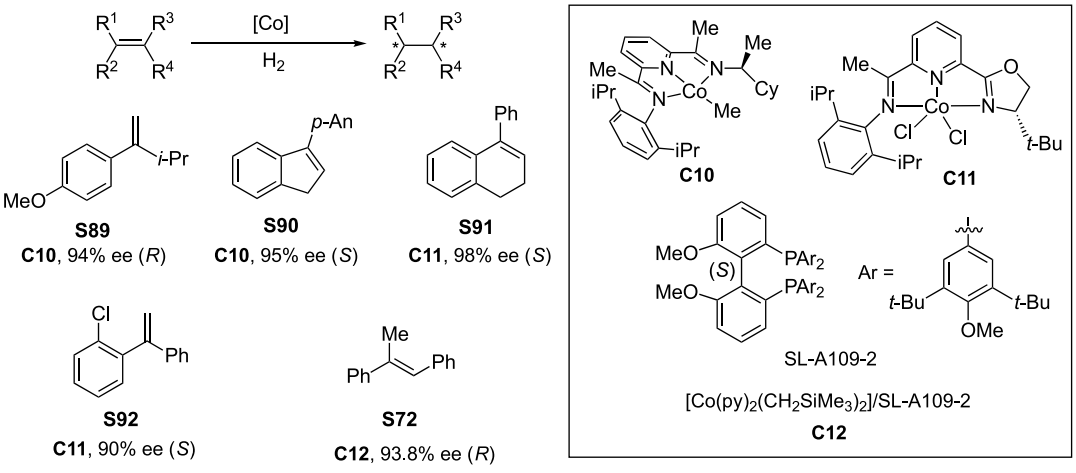

Scheme 15.28. Co-catalyzed hydrogenation of unfunctionalized olefins.

15.4. ASYMMETRIC HYDROGENATION OF KETONES

The reduction of ketones to secondary alcohols is a fundamental transformation in organic synthesis. The process can be enantioselective when the groups attached to the carbonyl are different. This transformation can be performed stoichiometrically using metal hydrides that are hydrolyzed at the end of the reaction. However, enantioselective catalytic hydrogenation processes are, arguably, the best processes since they are environmentally clean, offer a perfect atom economy, and they are industrially scalable. The source of hydrogen can be hydrogen gas (AH) or alternative reagents such as isopropanol or formic acid (asymmetric transfer hydrogenation, ATH). We will not cover enzymatic, heterogeneous hydrogenation nor the reductions based on metal hydride nucleophilic attack followed by a reductive step. We will focus on AH, although to understand the evolution of the catalysts, which on many occasions started in ATH, we will comment on the main ATH catalytic systems as well.

Noyori pioneered the field in 1987, with the ruthenium-catalyzed hydrogenation of β-keto esters [129]. Few years later two major breakthroughs by the same author introduced two important catalytic systems based on the outer sphere participation of the ligand in the catalytic cycle [131–133]. In both cases, the NH of the ligand had a crucial role activating the ketone toward hydride attack. Therefore, the H–N–Ru–H was the essential fragment of the catalyst for the bifunctional mechanism, which was thoroughly studied both theoretically [134] and experimentally [135]. Since then, many other ruthenium catalysts were developed. In parallel, other precious metal-catalysts were discovered using mainly Ir and Rh. More recently, the effort finding catalysts using inexpensive metals such as Fe, Co, Mn, and Ni has started to give fruits.

15.4.1. Ruthenium Catalysts

15.4.1.1. Diphosphine-Diamine Catalytic Systems

The catalytic system formed by $RuCl_2$, a chiral diphosphine, chiral diamine, and KOH, discovered by Noyori and Ohkuma, is considered the starting point on this field [130, 131]. After a first optimization of the ligands, the complex Ru[Cl_2(Xylbinap)(*S*)-daipen] afforded 97% yield and 99% ee in the hydrogenation of acetophenone [136]. This extraordinary result was even improved with the use of catalyst Ru[H(η^1-BH_4)(*S*)-Xylbinap,(*S,S*)-dpen] [137]. These catalysts were more robust than the standard $RuCl_2$ complexes, could be used under base-free conditions, and expanded the scope of ketones. Ohkuma reviewed the numerous modifications and optimizations of this catalytic system in 2010 [133, 138].

Further modifications of this catalytic system involved the replacement of either the chiral diphosphine or the diamine. Many of these catalysts were developed in the first decade of the century [139]. In 2003, Zhou and coworkers replaced the BINAP by a new type of axially chiral diphosphines named spirodiphosphines (SDP) [140]. These catalysts are very active in ATH and AH of ketones. In 2016, the same group used Ru-(*R*)-Xyl-SDP/(*S,S*)-DPEN (**C13**) in the synthesis of hepaindole alkaloids by AH of the ketone intermediate **S93** (Scheme 15.29) [141].

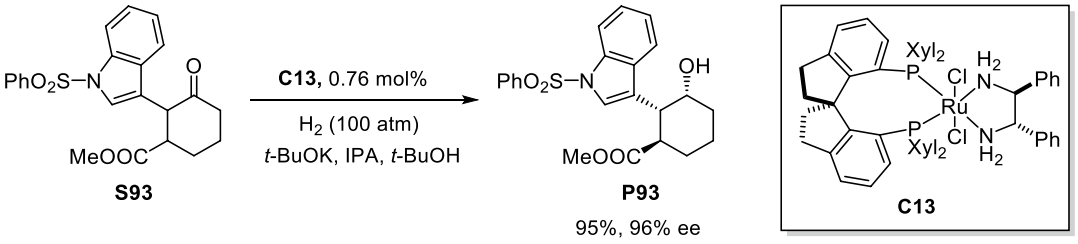

Scheme 15.29. Synthesis of an intermediate (**P93**) of hepaindole alkaloids by AH. Source: [141]/Royal Society of Chemistry.

A more recent modification of the diphosphine fragment was developed in the company Boehringer-Ingelheim Pharmaceuticals [142]. Using BIBOP in the preparation of the corresponding diamine-ruthenium complexes such as **C14**, the enantioselective hydrogenation of several challenging ketones took place with S/C ratios as high as 100000. The diamine fragment was fine-tuned to optimize the results and even to reverse the sense of the enantioselectivity (Scheme 15.30). These catalysts gave particularly good results in the reduction of bicyclic ketones and were applied to the preparation of intermediates of the synthesis of cholesteryl ester transfer protein (CETP) inhibitors.

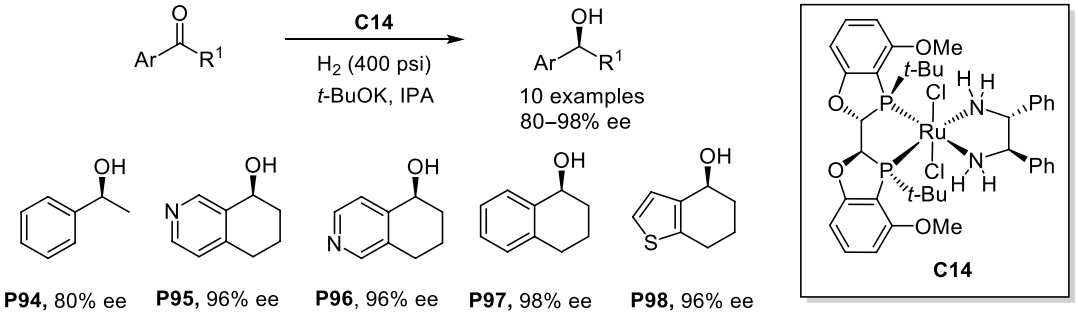

Scheme 15.30. Selected examples of AH of bicyclic ketones by Boehringer-Ingelheim catalyst **C14.**

A significant modification of the original catalytic system was the development of rutenabicyclic complexes (**C15,** Scheme 15.31) by Ohkuma [143]. These precatalysts (activated with *t*-BuOK) showed a superior efficiency, enantioselectivity, and scope than the initial Noyori's diphosphine-diamine catalysts. The hydrogenation of acetophenone, for instance, afforded 1-phenylethanol in >99% ee with a turnover frequency of 35000 min^{-1}.

15.4.1.2. Arene-Diamine Catalytic Systems Back in 1995, Noyori and Ikariya discovered a new catalytic system based on (η^6-arene)/*N*-Ts-diamine ruthenium complexes for the ATH of aromatic ketones (Scheme 15.32). Many catalysts of this type were subsequently developed, although the initial catalyst with *N*-tosyl-1,2-diphenylethylene-1,2-diamine (TsDPEN) and *p*-cymene (**C16a**) was widely used in ATH [132, 133]. In 2013, Ohkuma described the hydrogenation of alkynyl ketones using precatalyst **C16b** affording the

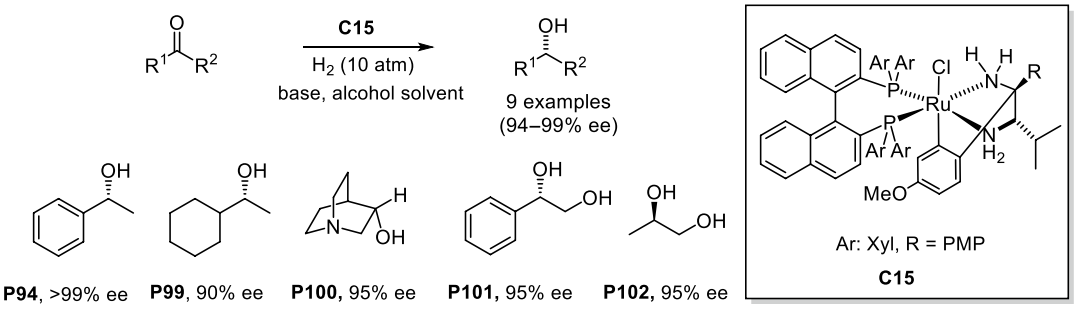

Scheme 15.31. Selected examples of AH by Ohkuma's rutenabicyclic catalysts **C15**.

chiral propargylic alcohols in up to 97% ee. The reaction was conducted with an S/C ratio of 5000 under moderate hydrogen pressure (10 atm) [144].

The most relevant improvement to the initial Ikariya-Noyori's catalysts was to introduce a tether between the η^6-arene and the ligand. The restriction of the arene rotation allowed the design of much more stable and efficient catalysts that outperformed the first generation of Ikariya-Noyori's reagents. Wills and coworkers pioneered the field [145]. In 2005, their group reported complex **C17** [146], which is one of the most successful catalyst of this type in transfer hydrogenation. Johnson Matthey developed an industrial multi-kg scale synthesis of this and related catalysts. A large family of tethered catalysts has been reported since then. An important step forward in the design of new tethered catalysts was to include heteroatoms in the tethering chain. Ikariya, in collaboration with Takasago, developed chloro [(*R*,*R*)-*N*-[2-[2-(4-methylbenzyloxy)ethyl] amino-1,2-diphenylethyl]-*p*-toluenesulfonamide]ruthenium(II) (Ts-DENEB) (**C18a**) [147]. Independently, at the same time, Wills, in collaboration with Dr. Reddys, developed an alternative route to the same compound [148]. Using **C18a,** unsymmetrical benzophenones were reduced in a mixture of formic acid and trimethylamine with outstanding enantioselectivities (up to 99% ee) [149]. Although initially developed for ATH, **C17** and **C18** have found widespread application in AH reactions as well [150]. In 2013, Wills reported the "arene approach" to synthetize tethered complexes with electron-rich arenes such as **C19** [151]. All these catalysts were used in the AH of ketones with similar results (Scheme 15.32).

On the other hand, the group of Mohar has developed several families of tethered η^6-arene-ruthenium catalysts for ATH (Figure 15.9). The initial approach involved the linkage between the sulfonamide group and the arene (**C20**) and was applied to the ATH of naphthyl ketones [152]. The last generations of catalysts are ansa-ruthenium hydrides generated in situ (**C21** and **C22**, Figure 15.9). **C21** was applied to the dynamic kinetic resolution (DKR) of CF_3-substituted diketones [153] whereas **C22** gave excellent results in the ATH of α-acetamido benzocyclic ketones [154].

15.4.1.3. Other Ruthenium Catalytic Systems Besides the two main catalytic systems discovered by Noyori and coworkers, several other complexes, some of them lacking the Ru–NH functionality, were found to be active in the AH of ketones (Figure 15.10). W. Zhang developed phosphine-oxazoline-ruthenium ligands. The bimetallic ruthenium complex of RuPHOX–Ru (**C23**) gave excellent enantiomeric excesses in the AH of aromatic ketones, aromatic β-amino ketones [155], and α,β-unsaturated pentanones [156].

Cyclometallated ruthenium complexes derived from primary and secondary amines were found to be active in the ATH of ketones. Complex **C24** derived from (2*R*,5*R*)-2,5-diphenylpyrrolidine ligand gave excellent results in the reduction of aryl alkyl ketones (up to 97% ee) whereas the reduction of aryl *tert*-alkyl ketones was best performed with **C25**, derived from bis[(*R*)-1-phenylethyl]amine [157].

Catalytic systems using ruthenium and *P*,*N*,*N* or *P*,*N*,*O*-ligands have been investigated [158]. Although the performance of the catalysts was generally poorer than those from Noyori, the studies of the catalytic systems helped to shed light into the mechanism paving the way for the design of new catalysts.

Z. Yu's group described a new ruthenium catalytic system, using chiral *N*,*N*,*N* ligands (**C26–28**) [159]. These Ru(II) complexes were exceptionally active in ATH of ketones (turnover frequency [TOF] up to 15 000 h^{-1}) affording the corresponding alcohols in excellent yields and enantiomeric excesses up to 99.9% ee (Figure 15.10).

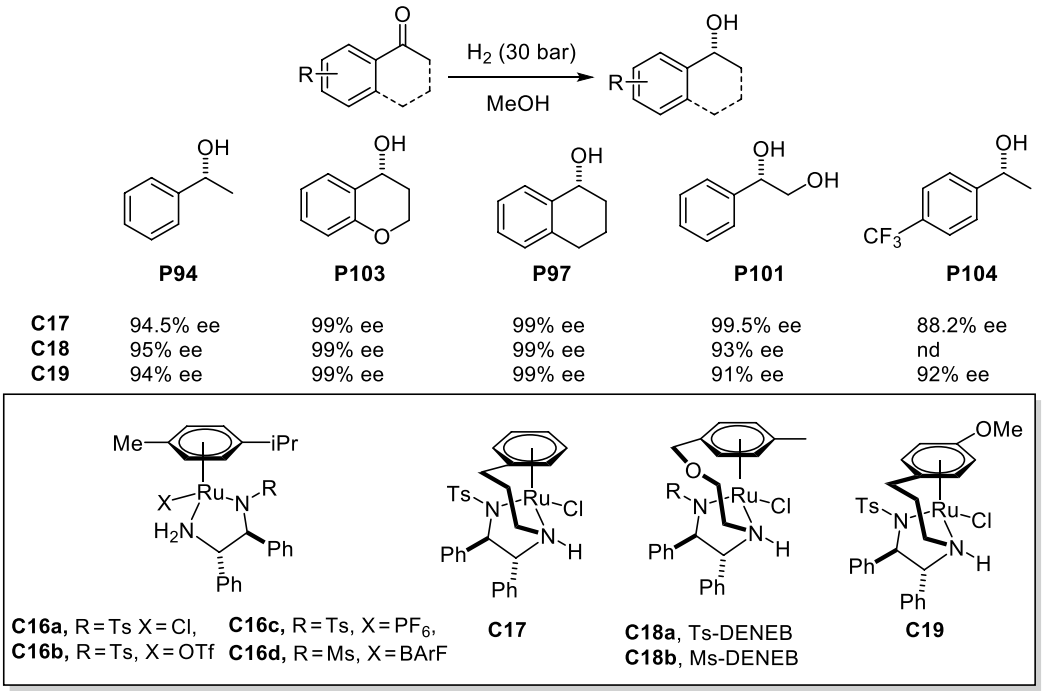

Scheme 15.32. Initial (η^6-Arene)/*N*-Ts-diamine ruthenium catalysts (**C16**). Selected results of AH of ketones using tethered η^6-arene)/*N*-sulfonyl-diamine ruthenium catalyst (**C17–19**).

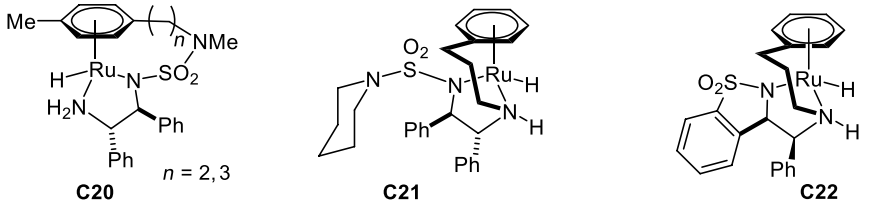

Figure 15.9. Mohar's catalyst for ATH.

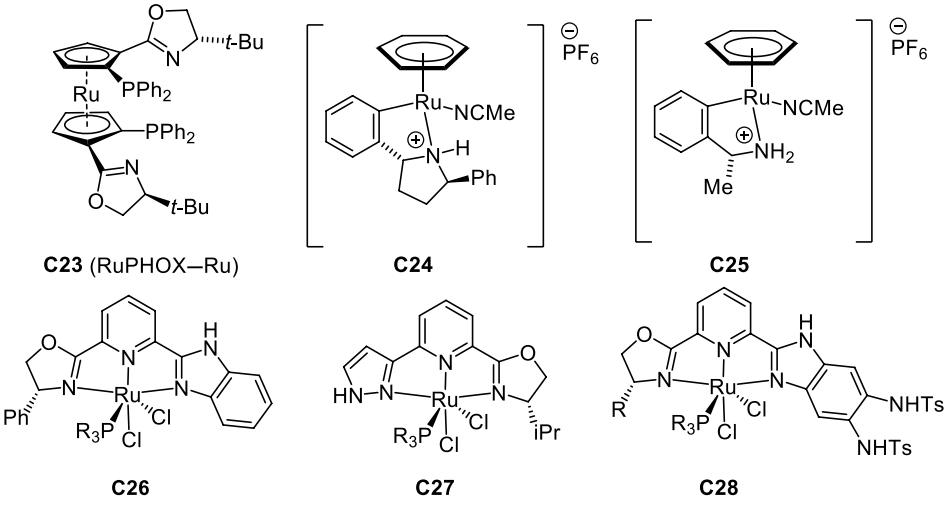

Figure 15.10. Other ruthenium catalysts: bimetallic, cyclometallated, and with chiral *N*,*N*,*N*-ligands.

15.4.2. Rhodium Catalysts

The success of the Ru(η^6-arene,TsDPEN) catalysts in the ATH of ketones prompted Noyori and Ikariya in the preparation of analogous Rh and Ir catalysts. **C29** was designed to have an isoelectronic structure with the ruthenium catalyst by replacing the η^6-arene ligand with the η^5-C_5Me_5 (Cp*) group (Figure 15.11). The reduction of acetophenone by isopropanol and *t*-BuOK in the presence of **C29** afforded (*R*)-1-phenylethanol with 97% ee in 85% yield after 12 hours at 30 °C [160]. The high cost of rhodium fostered the work in the preparation of heterogeneous catalyst that could be recycled. The cationic rhodium catalysts derived from **C29** were successfully encapsulated or immobilized in several solid phases. These heterogeneous catalysts presented excellent catalytic activities and high enantioselectivities in ATH of aromatic ketones [161–165].

The cyclometallated rhodium derivatives of the (2*R*,5*R*)-2,5-diphenylpyrrolidine ligand (**C30**, Figure 15.11) reduced aryl alkyl ketones by ATH in good enantiomeric excess (up to 89% ee). However, they displayed, in general, slightly worse enantioselectivities than the isoelectronic ruthenium catalyst **C24** [157]. Amides and hydroxamic acids derived from α-amino acids were used as ligands in combination with rhodium and iridium half-sandwich complexes in ATH of ketones with good to moderate *ee*s (76% ee in the reduction of acetophenone) [166]. A theoretical study of the mechanism using density-functional theory (DFT) calculation was reported [167].

Rhodium complexes of *P*-stereogenic bis-phosphines such as BenzP* (**L12**) and 3H-QuinoxP* (**L89**) developed by Imamoto [13, 14], were well established as excellent catalysts for the hydrogenation of enamides and other functionalized olefins. W. Zhang and coworkers in 2015 explored the use of such complexes in the hydrogenation of ketones with coordinating amino groups. They found that, in combination with $ZnCl_2$, the rhodium complexes of BenzP* hydrogenated β-secondary-amino ketones with excellent enantioselectivities (90–99% ee) with turnover numbers up to 2000 S/C (Scheme 15.33). This

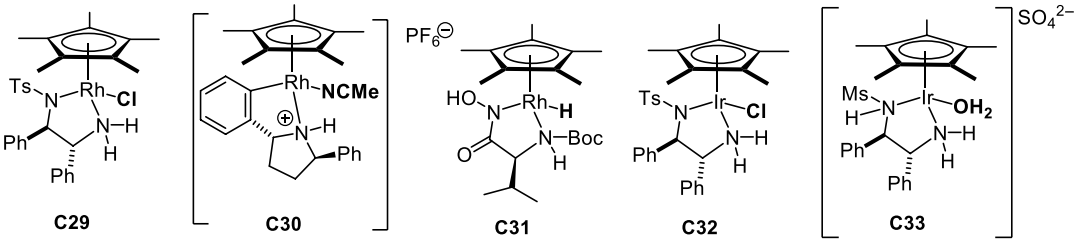

Figure 15.11. Chiral η^5 C_5Me_5 (Cp*)-rhodium and iridium complexes.

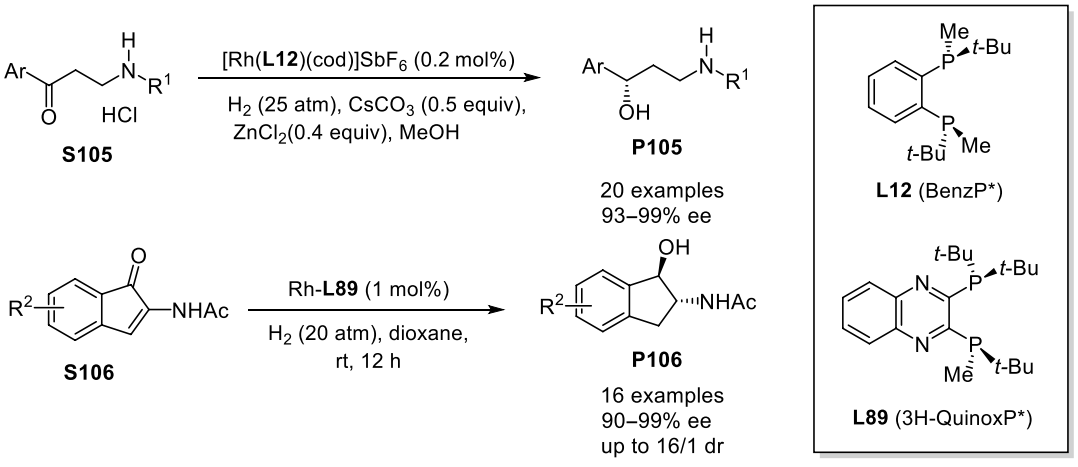

Scheme 15.33. Rhodium-catalyzed AHs of ketones with *P*-stereogenic bisphosphines. Source: [169]/American Chemical Society.

method was successfully applied to the asymmetric syntheses of three important drugs such as (*S*)-duloxetine, (*R*)-fluoxetine, and (*R*)-atomoxetine, in high yields and with excellent enantioselectivities [168]. Another *P*-stereogenic bis-phosphine (3H-QuinoxP*, **L89**) was utilized by the same authors in the hydrogenation of α-dehydroamino ketones (Scheme 15.33) [169].

Other catalysts based on rhodium complexes of electron-rich *P*-stereogenic bis-phosphines have been developed. Direct AH of 2-pyridine ketones was difficult due to the coordination effect of pyridines. X. Zhang found that the use of a rhodium complex derived from the bulky, electron-rich ligand binapine (**L90**) solved the problem. Using [Rh(cod)Binapine]BF_4 as catalyst, the corresponding 2-pyridine alkyl and aryl alcohols were obtained with excellent yields and enantioselectivities without the need of an *ortho* substituent in the aromatic group (Scheme 15.34) [170].

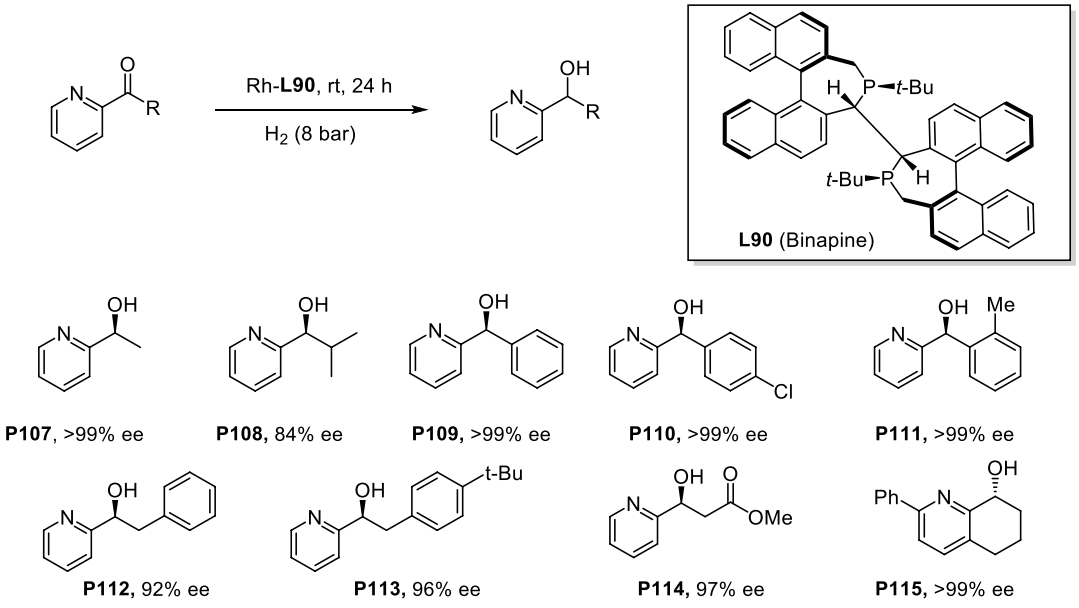

Scheme 15.34. Rhodium-catalyzed AH of 2-pyridine ketones. Source: [170]/American Chemical Society.

Another challenging substrate for AH is the reduction of aryl perfluoroalkyl ketones. In this case, A. Togni could solve the problem using rhodium catalysts with the chiral ferrocenyl bis-phosphine **L91** of the JosiPHOS family (Scheme 15.35) [171].

15.4.3. Iridium Catalysts

In 2003, Ogo and Fukuzumi pioneered the use of iridium complexes for the reduction of carbonyl compounds, describing the preparation of a water soluble hydride complex bearing 2,2′-bipyridine (Bpy) and η^5-C_5Me_5 (Cp*) as ligands. [Cp*Ir^{III}(bpy)H]PF_6 showed a good catalytic activity in the racemic transfer hydrogenation of carbonyl compounds [172]. Although Ikariya and Noyori reported in 1999 that **C32**, isoelectronic with the ruthenium Ru(II)/TsDPEN complexes (Figure 15.11), was not very active, yielding high ees but low conversions [160], numerous related chiral iridium complexes using a η^5-cyclopentadienyl ligands were described by several groups. Carreira, for instance, reported **C33** (Figure 15.11) as a pH independent transfer hydrogenation catalyst for the asymmetric reduction of β-keto esters with excellent *ee*s [173].

In a completely different approach, Kempe found that iridium complexes of some chiral diamines could be used in the AH of simple aryl alkyl ketones. The phosphorus-free *N*,*N*-ligands **C34** gave excellent ees (>99%) in the hydrogenation of propiophenone and other aromatic ketones (**P122–129**) (Scheme 15.36) [174].

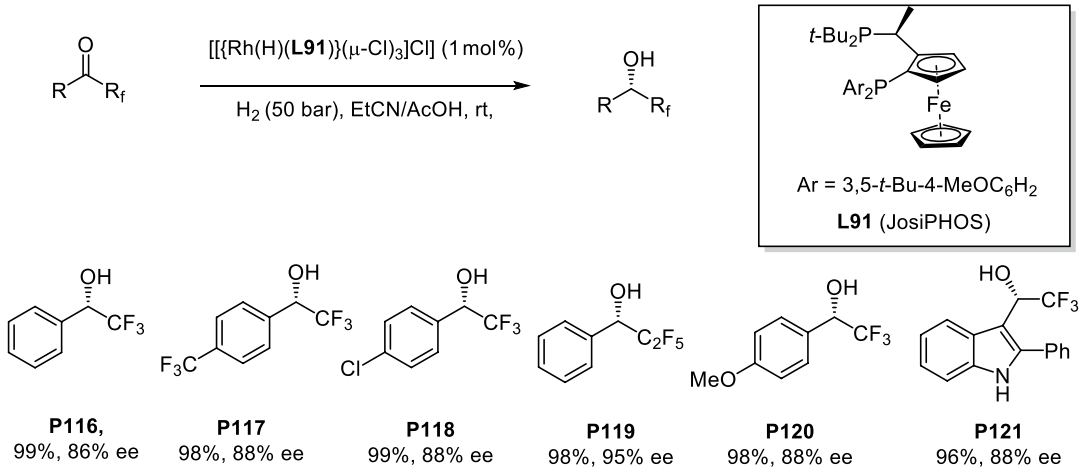

Scheme 15.35. Rhodium-catalyzed AH of aryl perfluoroalkyl ketones and trifluoroacetyl indoles. Source: [171]/John Wiley & Sons.

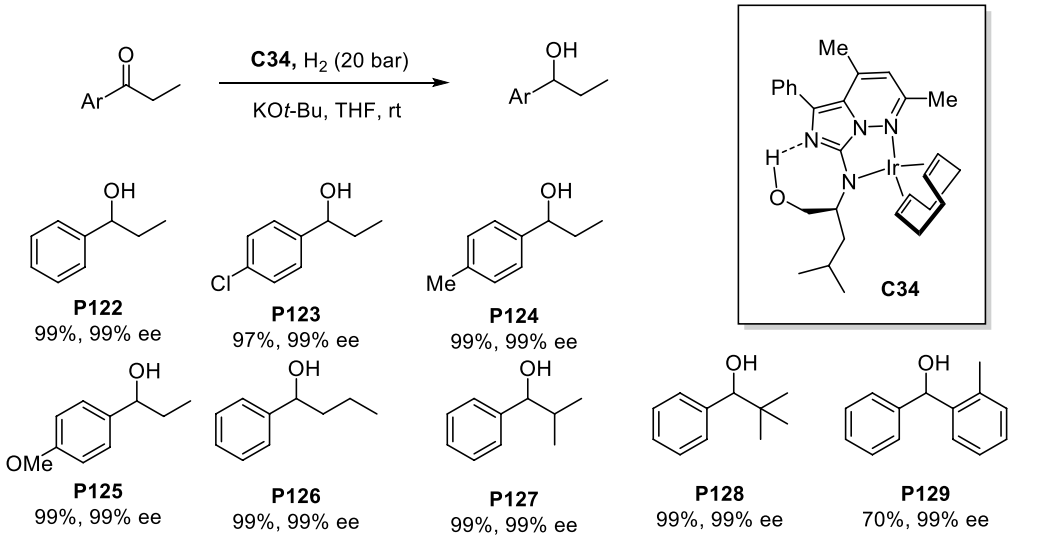

Scheme 15.36. Selected examples of AH of alkyl aryl ketones by the iridium catalyst **C34** with a phosphorus-free *N*,*N*-ligand. Source: [174]/John Wiley & Sons.

Looking for more robust complexes, Zhou described iridium complexes of chiral aminophosphines with a spiranic core. They found that the iridium complexes of the spiranic aminophosphine SpiroAP were very active in AH of enones. The in situ prepared iridium complex of this ligand afforded excellent results in the AH of *exo*-cyclic α,β-unsaturated enones [175]. However, the iridium-SpiroAP complexes tend to lose activity due to the formation of bis-SpiroAP complexes. By adding an additional coordination fragment, Xie and Zhou avoided deactivation of the catalyst. The iridium complexes with Spiro *P*,*N*,*N*-ligands (**L92**), so-called Spiro Pyridine-AminoPhosphine (Spiro PAP), with a coordinative pyridine ring, showed an unprecedented performance in the hydrogenation of simple ketones with ees ranging from 96 to 99.9% and turnover number (TON) up to 4550000 (Scheme 15.37) [176]. These catalysts were, subsequently, applied to the AH of β-aryl-β-ketoesters [177] and to the synthesis of chiral 1,5-diols [178].

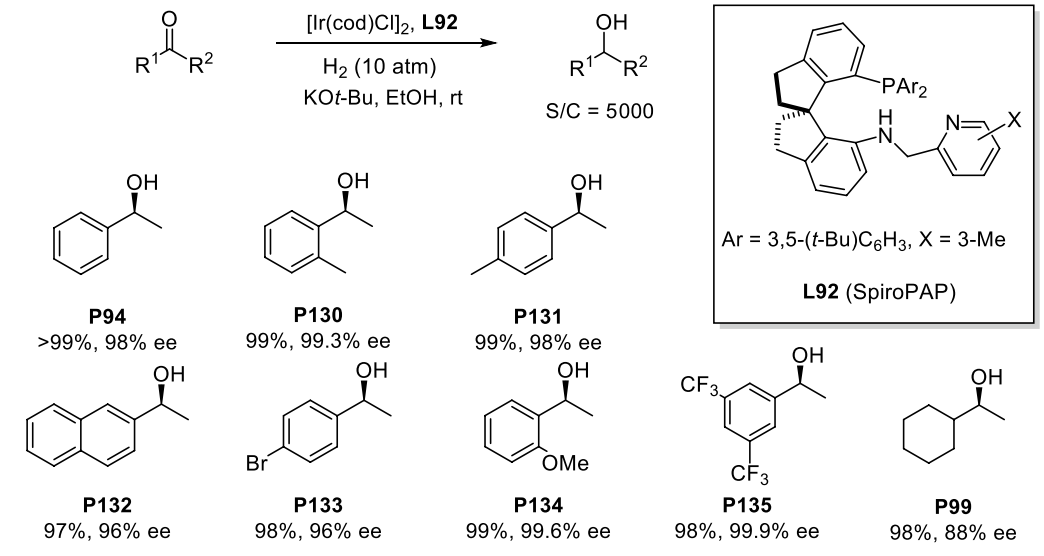

Scheme 15.37. AH of aryl ketones by iridium-SpiroPAP complexes. Source: [176]/John Wiley & Sons.

The much more challenging hydrogenation of dialkyl ketones required the replacement of the pyridyl ring by a very bulky aryl phosphine. The iridium complexes of these *P*,*N*,*P*-ligands, under hydrogen, afforded hydride complexes such as **C35**. These complexes, due to the huge steric protection, were enough stable to be stored in air for a month without losing its catalytic activity. Remarkably, **C35** hydrogenated a wide range of dialkyl ketones (selected examples: **P136–143**) with high enantioselectivity (Scheme 15.38) [179].

In 2016, Lan, Dong, and X. Zhang introduced the chiral ferrocenylphosphine motif in the *P*,*N*,*N* ligands. They developed the f-amphox family of ligands (**L93**) with an ozaxolidine ring and a chiral ferrocenylphosphine fragment (Scheme 15.39) [180]. The iridium complexes of these ligands were used in the AH of simple ketones, showing outstanding enantioselectivities (>99% ee) and extremely high

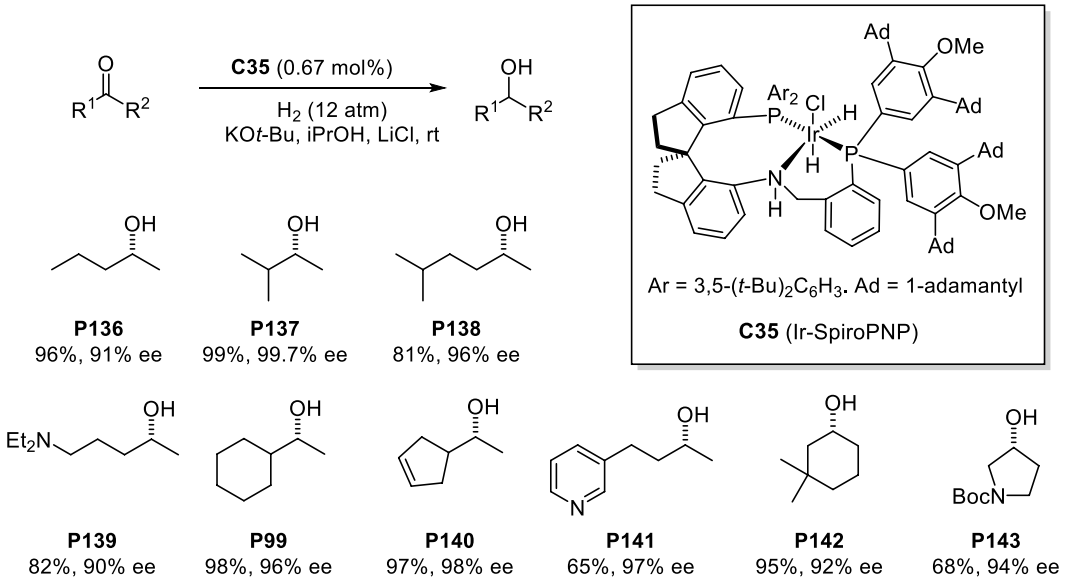

Scheme 15.38. AH of alkyl ketones by iridium-SpiroPNP complexes. Source: [179]/Springer Nature.

activities (up to 1 M TON). The same ligand (**L93**) was used in the AH of α-hydroxy ketones affording 1,2-diols in >99% ee in most cases and TON up to 1 000 000 [181]. These results opened the way to other ferrocenyl phosphine ligands developed by the same authors leading also to excellent results. The readily available *P*,*N*,*O*-ligand f-amphol (**L94**) [182], was used in the iridium-catalyzed AH of simple ketones giving excellent enantioselectivities (up to 99.9% ee) and TON up to 200 000) (Scheme 15.39). The same ligand (**L94**) gave outstanding results in the hydrogenation of benzo-fused five- to seven-membered cyclic ketones [183]. This methodology was applied to the formal asymmetric synthesis of anticonvulsant drug eslicarbazepine acetate (BIA 2-093). More recently, the same catalyst was applied to the hydrogenation of α-fluoroketones via DKR with excellent results [184]. The same group also developed another tridentate ferrocene-based ligand, the so-called f-ampha (**L95**). This is an extremely air-stable *P*,*N*,*O*-ligand derived from *tert*-leucine. It showed extraordinary performance in the Ir-catalyzed AH of ketones with enantioselectivities of 99% ee in a wide variety of aromatic methyl ketones (Scheme 15.39) [185]. The mechanism was studied in depth, revealing the crucial role of the carboxyl group.

On the other hand, Xie and W. Zhang developed a ferrocenyl ligand without an NH-bridge (**L96**), attesting that the NH-hydrogen assistance was not necessary in this type of catalysts [186]. The corresponding BArF iridium-complex was air stable and showed excellent performance in the AH of simple ketones (up to 99% ee) (Scheme 15.39). The catalyst was also efficient in the AH of α,β-unsaturated cyclic ketones.

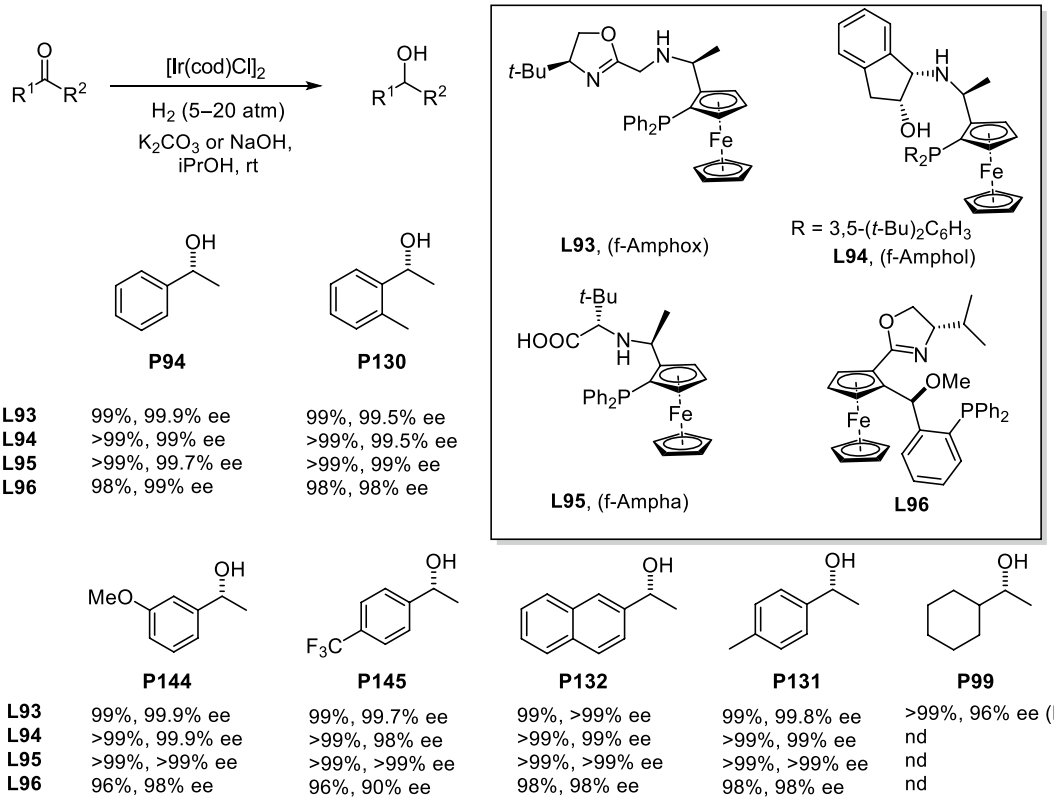

	P94	P130	P144	P145	P132	P131	P99
L93	99%, 99.9% ee	99%, 99.5% ee	99%, 99.9% ee	99%, 99.7% ee	99%, >99% ee	99%, 99.8% ee	>99%, 96% ee (R)
L94	>99%, 99% ee	>99%, 99.5% ee	>99%, 99.9% ee	>99%, 98% ee	>99%, 99% ee	>99%, 99% ee	nd
L95	>99%, 99.7% ee	>99%, 99% ee	>99%, >99% ee	>99%, >99% ee	>99%, >99% ee	>99%, >99% ee	nd
L96	98%, 99% ee	98%, 98% ee	96%, 98% ee	96%, 90% ee	98%, 98% ee	98%, 98% ee	nd

Scheme 15.39. Selected examples of the AH of simple ketones by iridium complexes derived from ferrocenyl ligands. Source: [180]/American Chemical Society.

Another type of ferrocene-based *P*,*N*,*N*-ligands (**L97**) named f-diaphos was developed by Zhong for the iridium-catalyzed AH of ketones [187]. These ligands afforded excellent enantioselectivities for aryl alkyl ketones (up to 99.4% ee) and diaryl ketones (up to 98.2% ee). Later, this catalytic system was

successfully applied to AH of non-*ortho*-substituted 2-pyridyl aryl ketones **S146** (Scheme 15.40) [188]. Recently, the iridium complex **C36**, based on the *P*-stereogenic *P*,*N*,*P*-ligand (Heng-PNP) developed by Wen and X. Zhang, has been successfully applied to the AH of *ortho*-substituted diaryl ketones **S147** with excellent ees and up to 500 TON (Scheme 15.40) [189].

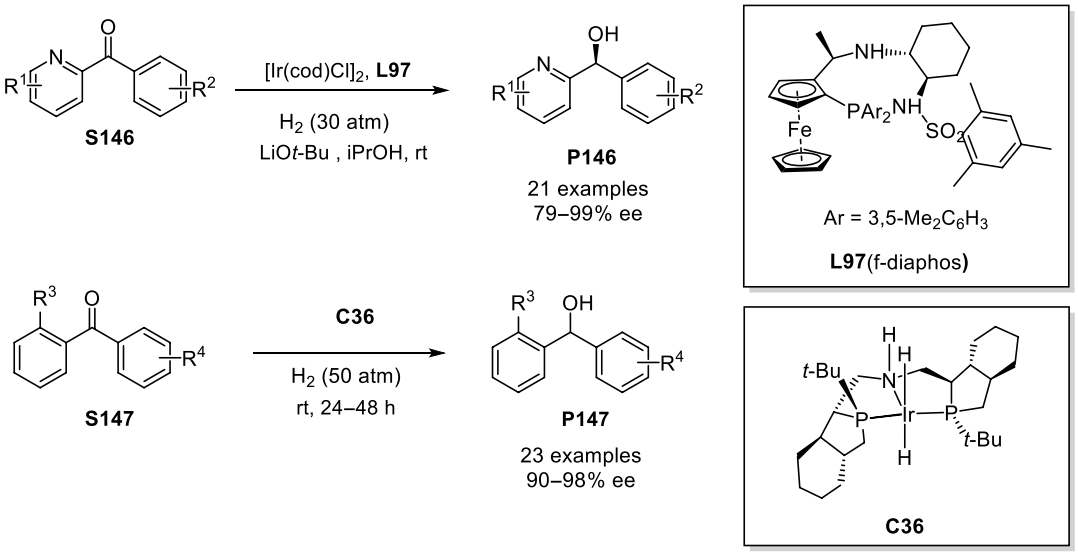

Scheme 15.40. Iridium-catalyzed AH of diaryl ketones. Source: [189]/American Chemical Society.

Replacement of phosphines by NHCs is a usual strategy to increase the stability of transition-metal complexes due to their stronger σ-donating capacity. Until very recently, very few examples of AH of aryl ketones catalyzed by NHC-complexes were described [190]. Yoshida and Yanagisawa reported excellent performance (up to 97% ee) of a chiral bicyclic NHC–Iridium complex (**C37**) in the ATH of aromatic ketones [191]. G. Ruiter described the first Ir-NHC-oxazoline catalyst that was able to hydrogenate aromatic ketones with excellent yields and moderate enantioselectivities (Figure 15.12) [192]. Acetophenone was hydrogenated under 6 bar hydrogen at 0 °C temperature in the presence of **C38** and KO*t*-Bu, affording the enantioenriched alcohol in 88% ee. Moreover, racemic α-substituted ketones were reduced with excellent diastereoselectivities (dr 99 : 1) by DKR but with modest enantioselectivity. In 2020, Andersson described the cationic iridium NHC–phosphine complex **C39** [193]. This ligand exhibited extremely high reactivity and good enantioselectivity under base-free and mild conditions. Acetophenone was hydrogenated under 1 bar hydrogen at room temperature in the presence of **C39** affording the enantioenriched alcohol in 94% ee.

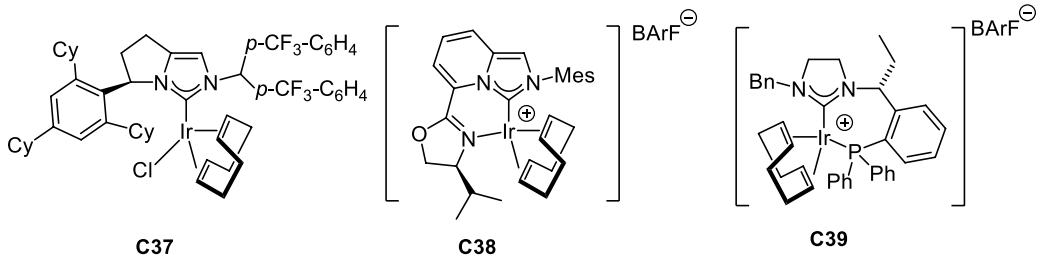

Figure 15.12. Structures of Iridium complexes with chiral NHC employed in the ATH or AH of ketones. Source: [192]/John Wiley & Sons.

15.4.4. Iron Catalysts

The unbeatable performance of the Ru and Ir catalysts drove the research toward the replacement of precious metals with cheaper and more sustainable metals such as Fe, Mn, Ni, or Co [194]. Among them, iron is the most abundant and environmentally friendly. Therefore, iron catalysts are especially attractive for industrial processes. The first well-defined Fe(II) complex for the ATH of ketones was developed by Morris and coworkers [195]. Using a *P*,*N*,*N*,*P*-ligand **L-98** (Figure 15.13) derived from *trans*-cyclohexanediamine, they described good conversion but low to moderate ees in the ATH of ketones as well as in the AH of acetophenone [196]. Interestingly, in 2014, Gao and coworkers found very high enantioselectivities in the AH of a wide variety of ketones using a related 22-membered P_2N_4 macrocycle **L99** also derived from cyclohexandiamine (Figure 15.13). The reaction was catalyzed by a combination of the macrocycle **L99** with $Fe_3(CO)_{12}$. The mechanism of the AH is not clearly understood, but the authors proposed that iron nanoparticles coordinated to the macrocycle were the actual catalyst [197]. An analogous rhodium complex has been recently described for the ATH of ketones that could be conducted in air [198]. Related macrocycles with a smaller ring were introduced by Mezzetti to ensure proper binding with the iron metal to afford definite complexes. N_2P_2-Ligand **L100** produced stable diamagnetic iron complexes that reduced aromatic ketones with good enantioselectivity under ATH conditions [199]. The system was improved by the reduction of the imines of the ligand and the preparation of iron complexes with bulky bis-isonitrile ligands. These catalysts gave excellent enantioselectivities in a broad scope of ketones [200]. Further improvements[201] involved the preparation of catalysts such as **C40** for ATH that do not require the activation by base (Figure 15.13).

In parallel to this work, other researchers worked in well-defined iron complexes. Milstein developed an iron complex of a pincer *P*,*N*,*P*-ligand (**C41**) that was very active in the racemic hydrogenation of ketones (Figure 15.14) [202]. An important breakthrough was the discovery of iron complexes **C42**, with partially reduced *P-NH*,*N-P*- ligands. This catalytic system afforded, for the first time, enantiomeric excesses in the ATH of ketones and imines close to the ones obtained by ruthenium catalysts [203]. However, the enantiomeric excess dropped when the reaction reached the equilibrium. Based on Milstein pincer catalysts, Morris developed iron complex **C43** that gave excellent results in the AH of ketones and imines [204]. This precatalysts had to be activated by reduction with $LiAlH_4$ and adding an alcohol to

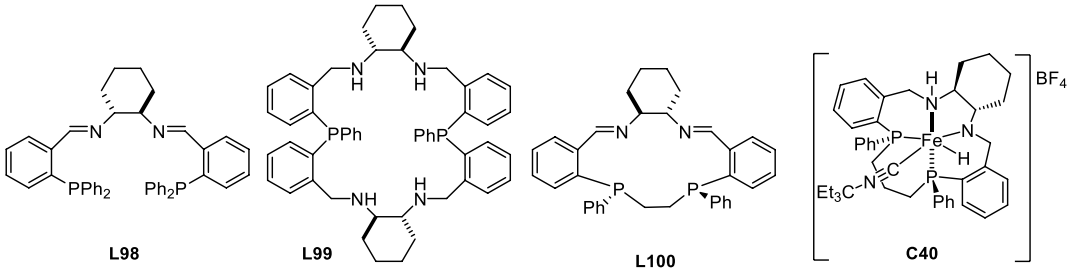

Figure 15.13. Open-chain N_2P_2-ligand and macrocyclic ligands used in the preparation of iron catalysts for ATH and/or AH.

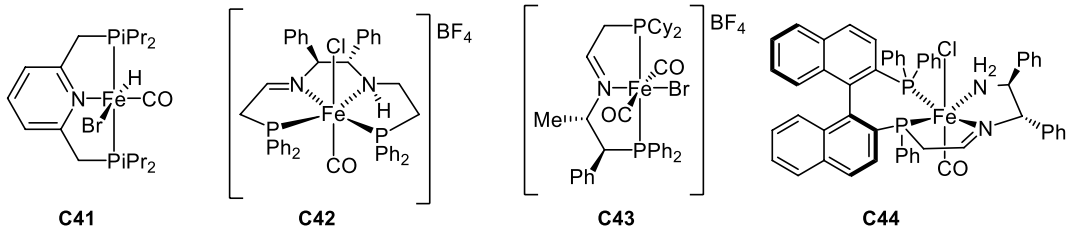

Figure 15.14. Iron catalysts for the ATH or AH of ketones. Source: [202]/John Wiley & Sons.

form the required NH functionality [205]. This problem was solved with the preparation of complexes **C45** from pincer *P-NH-P* ligands, which gave good to excellent results in the AH of aromatic ketones (Scheme 15.41) [206]. In 2020, Zuo described a new iron catalyst (**C44**) for ATH combining a binaphthyl fragment with the amine-imine group [207].

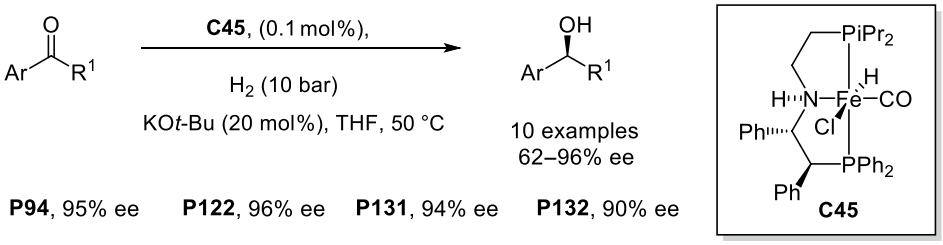

Scheme 15.41. AH of aromatic ketones using iron complex **C45**. Source: [206]/Royal Society of Chemistry.

15.4.5. Manganese and Cobalt Catalysts

As iron compounds, manganese complexes have the advantage over precious-metal complexes of their low price and toxicity. The development of Mn-catalysts for AH of ketones took place some years later than iron catalysts but very quickly attained excellent results. The seminal work of Beller and Kempe in the field began with the report of achiral complexes able to perform the hydrogenation of simple ketones in good yields [208]. In 2017, Clarke described the first efficient catalyst for the AH of ketones. Manganese complex **C46**, with a ferrocenyl *P*,*N*,*N*-ligand (Figure 15.15), afforded good to excellent enantioselectivities (up to 97% ee) in the hydrogenation of bulky aryl ketones [209]. Almost at the same time, Beller described **C47**, which gave good results in the hydrogenation of aliphatic ketones [210]. Interestingly, **C47** showed poor enantioselectivity with aromatic ketones. At the same time, Kirchner described a manganese complex with a ferrocenyl *P*,*N*,*P*-ligand (**C48**, Figure 15.15) that was the first to afford excellent enantioselectivities (up to 86% ee) in ATH of aromatic ketones [211]. Very recently, several other catalytic systems have been developed for the ATH of ketones [212] including the Gao's macrocyclic P_2N_4-ligand similar to the one reported for the iron-catalyzed AH [213]. In 2019, Han and Ding reported the first manganese complex (**C49)** with high activity, wide scope, and excellent enantioselectivities (Scheme 15.42) [214].

The research on AH using other metals has been much less abundant and successful [215]. The first AH using a Co-complex that afforded good enantioselectivity was described by Li and Gao [216]. More recently, Tang described the in situ preparation of a chiral cobalt pincer complex that, in combination with tris-(5-ethylfuryl)phosphine, gave moderate enantioselectivities in the AH of aromatic ketones [217].

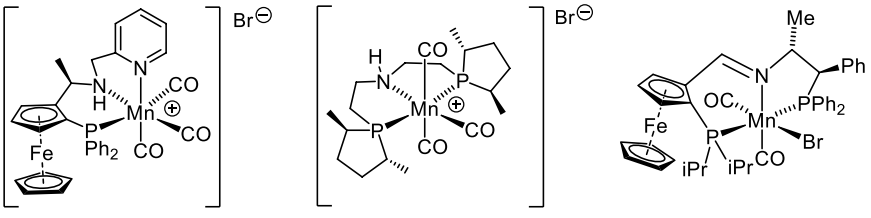

Figure 15.15. Initial manganese complexes for AH and ATH.

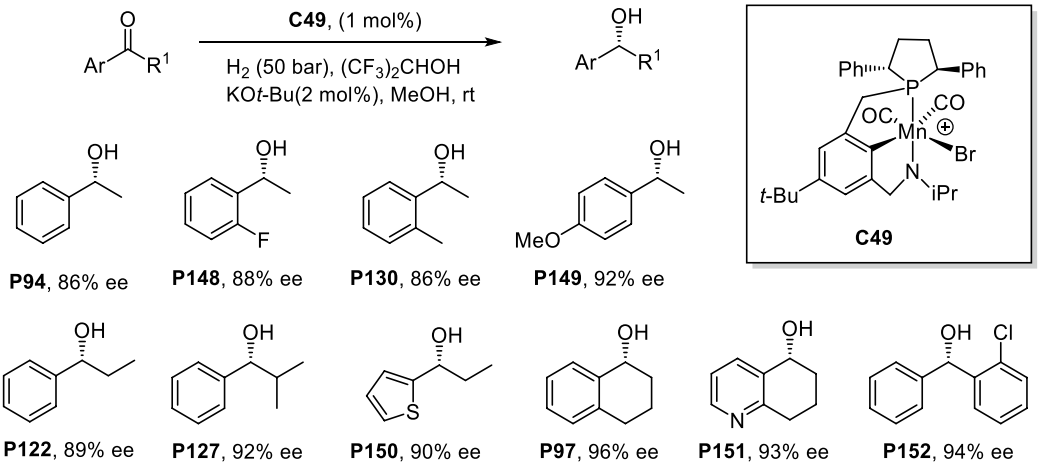

Scheme 15.42. AH catalyzed by a manganese complex. Source: [214]/John Wiley & Sons.

15.5. ASYMMETRIC HYDROGENATION OF IMINES

Imines offer additional challenges as substrates for AH with respect to ketones and olefins. Acyclic imines are prone to hydrolysis under acidic condition to yield the initial ketone and amine constituents. They usually exist as a mixture of *E*/*Z* stereoisomers. This obviously is a big hurdle for their reduction in a stereocontrolled manner. Moreover, the resulting amine products are more basic and nucleophilic than the starting material, which can lead to catalyst deactivation and poisoning. For these reasons, asymmetric imine hydrogenation is somehow underdeveloped when compared to the substrates in the previous sections.

AH of imines is dominated by iridium followed by ruthenium since they provide the most active catalysts. However, within the last 10 years, non-noble metals like iron, nickel, or cobalt have entered the arena and with the help of special and dedicated ligands have showed encouraging results. Recently, the AH of imines and heteroaromatic compounds has been reviewed [5s, 5aa, 218]. In the following sections, there is a representative selection of the advances in the field for the last decade. The topic is mainly focused on direct AH; however, selected examples of ATH are also included.

15.5.1. Heterocyclic Imines and Nitrogenated Heteroaromatics

Within the last 10 years, an enormous advancement has been attained in the reduction of nitrogen-containing heterocycles. Traditional cyclic imine substrates like 3,4-dihydroisoquinolines have somewhat been put aside and chemists have focused on their aromatic parent compounds like quinolines, isoquinolines, quinoxalines, or even pyridines. Because in this case it is compulsory to surmount the extra stabilization of aromaticity, these substrates are harder to hydrogenate. However, they offer some intrinsic benefits; they are easier to synthesize, they are more stable, and as any cyclic compound we benefit from a fixed stereochemistry around the C=N bond. Mostly traditional catalytic systems (iridium-*P*,*P*- and *P*,*N*-ligands or ruthenium-*N*,*N*-ligands) have been used to tackle the hydrogenation of these substrates; however, activation through protonation or alkylation is often needed for the hydrogenation to take place [219].

Alkylated or simply protonated isoquinolines were efficiently reduced by a combination of [Ir(cod)Cl]$_2$ precursor and a biaryl ligand (Scheme 15.43). TunePHOS (**L101**) was successful in the hydrogenation of 1-subtituted *N*-benzyl isoquinolinium salts (**S153**). In certain cases, changing the plain benzyl group for a bulkier benzyl group increased the selectivity [220]. From the same laboratory, it was also shown that 3,4-disubstituted isoquinolines (**S154**) could be also reduced when using the right halogen additive and diphosphine ligand **L102**. It is known that iodine can significantly improve the performance of iridium catalysts in AH. Here, Zhou employed 1-bromo-3-chloro-5,5-dimethyl-hydantoin (BCDMH) to reach 93% ee with a low H_2 pressure [221].

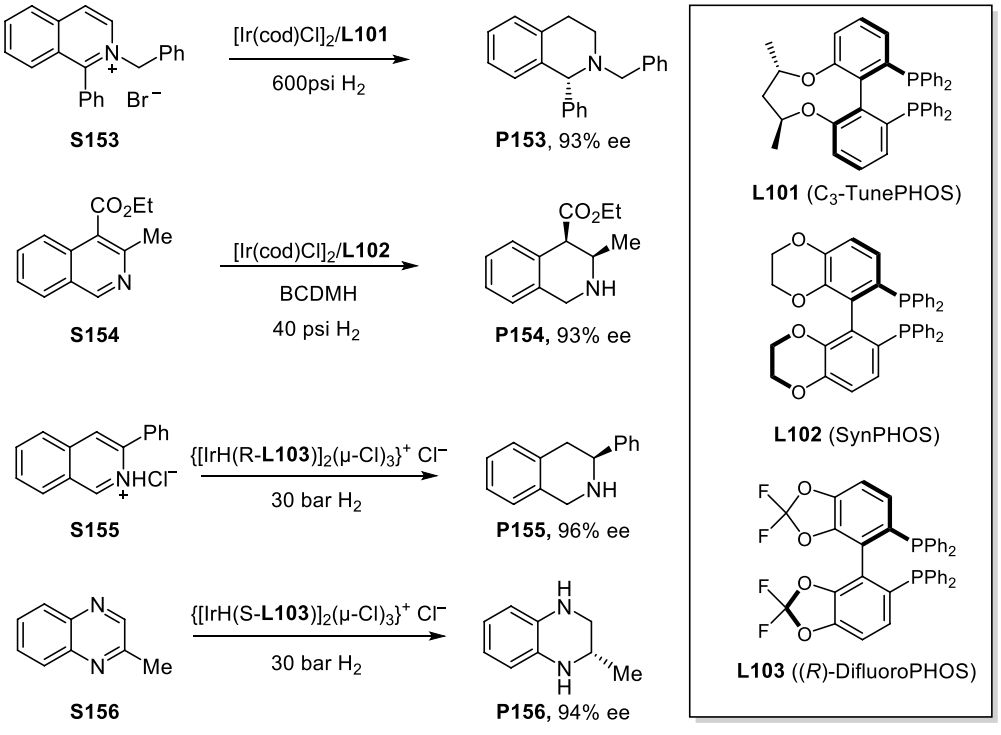

Scheme 15.43. Selected examples of asymmetric hydrogenation of isoquinolines and quinoxalines with Ir-*P*,*P*-ligand catalysts.

Halogen-bridged dinuclear iridium(III) complexes of ligand **L103**, developed by Mashima, are also effective in the AH of 3-substituted isoquinolines. Using the hydrochloric salt of the substrate (**S155**) was the key to success; the neutral heterocycle could be reduced with lower conversion and selectivity [222]. Using the same catalytic system, 2-alkyl quinoxalines (**S156**) were reduced with no need for substrate activation [223].

In 2015, Kuwano reported the hydrogenation of 2,4-disubstituted pyrimidines (**S157**) to the corresponding chiral amidines using $[Ir(cod)Cl]_2$ and a JosiPHOS ligand (**L104**) (Scheme 15.44). Iodine is used as additive. Also, addition of a lanthanide triflate (50 mol%) is crucial to achieve high enantioselectivity and activate the heteroarene substrate [224]. Later on, 4,6-disubstituted 2-hydroxypyrimidines (**S158**) were also effectively reduced using ligand **L105** to yield chiral cyclic ureas. Here, 1,3,5-trichloroisocyanuric acid (TCCA) was used as additive (10 mol%), the HCl generated in situ from the TCCA, and H_2 is key to shift the equilibrium toward the oxo-tautomer, which is more easily reduced [225]. Vidal-Ferran showed that various six- and seven-membered N=C containing heterocycles could be reduced with iridium catalysts containing *P*-*OP*- ligands **L106a** and **L106b** [226]. As shown in Scheme 15.44, phenylbenzoxazinone (**S160**) could be reduced up to 95% ee using 80 bar of H_2. More recently, Zhang and coworkers have shown that activation of **S160** with 1 equivalent of HCl and the use of the *N*-methylated ZhaoPHOS ligand (**L107**) provides a very active catalytic system. They report 15 examples with selectivities from 91 to 99% ee and TONs up to 40000 [227].

Iridium in conjunction with a chiral SpiroPhox ligand (**L39b**) was reported to accomplish the reduction of 2-pyridylpyrrolines (**S161**, Scheme 15.45). Because of the coordination ability of pyridine, it is difficult to reduce substrates containing this moiety. Zhou succeeded in this challenge by introducing a halogen adjacent to the pyridyl nitrogen, thus reducing the coordination ability of the pyridine [228]. Remarkably, the chemists from Boehringer-Ingelheim accomplished the reduction of pyridine itself by using a *P*-stereogenic phosphino-pyridine ligand (**L108**) developed in-house. The pyridine had to be previously activated by alkylation with benzylbromide to give **S162** and iodine was used to oxidize the metal to the active Ir(III) species [229]. Using the same $[Ir(cod)Cl_2]$-MeO-BoQPhos catalyst system, a

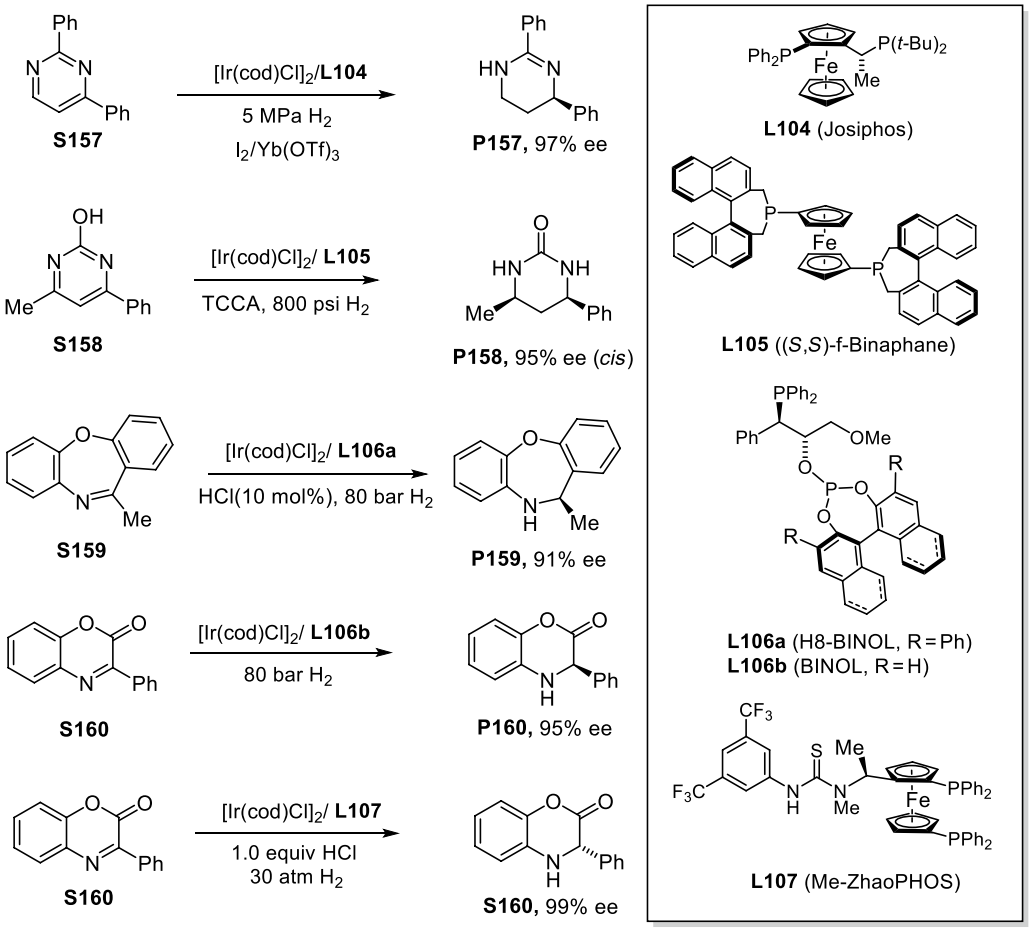

Scheme 15.44. Hydrogenation of pyrimidines and benzoxazinones with Ir-*P*,*P* catalysts.

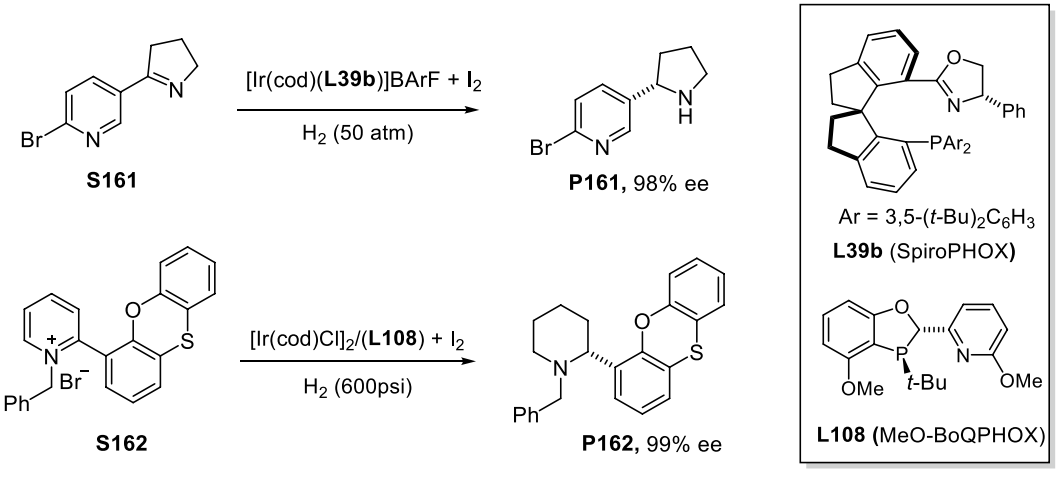

Scheme 15.45. Hydrogenation of 1-pyrrolines and pyridinium salts with Ir-*P*,*N* catalysts.

pyridinium intermediate was reduced in a 1.5 kg scale in the total synthesis of an 11β-hydroxysteroid dehydrogenase type 1 inhibitor [230].

The laboratory of Fan has actively used cationic Ru-arene-diamine catalysts for the hydrogenation of novel heteroaromatic substrates (Scheme 15.46). In this regard, 2-substituted quinolines (**S163**) were efficiently reduced by cationic arene-diamine Ru catalyst **C50** with up to 99% ee [231]. Theoretical calculations pointed out that enantioselectivity originated from the CH/π attraction between the η^6-arene ligand in the Ru-complex and the fused phenyl ring of dihydroquinoline with the participation of triflate anion. They have also reported the hydrogenation of 2,2′-bisquinolines (**S164**) with complete selectivity using catalyst **C51** [232]. 1*H*-Indoles (**S165**) could be reduced with the same catalytic system. While 2-subtituted indoles were hydrogenated at ambient temperature and pressure, 2,3-disubstituted indoles required 50 atm of hydrogen pressure [233].

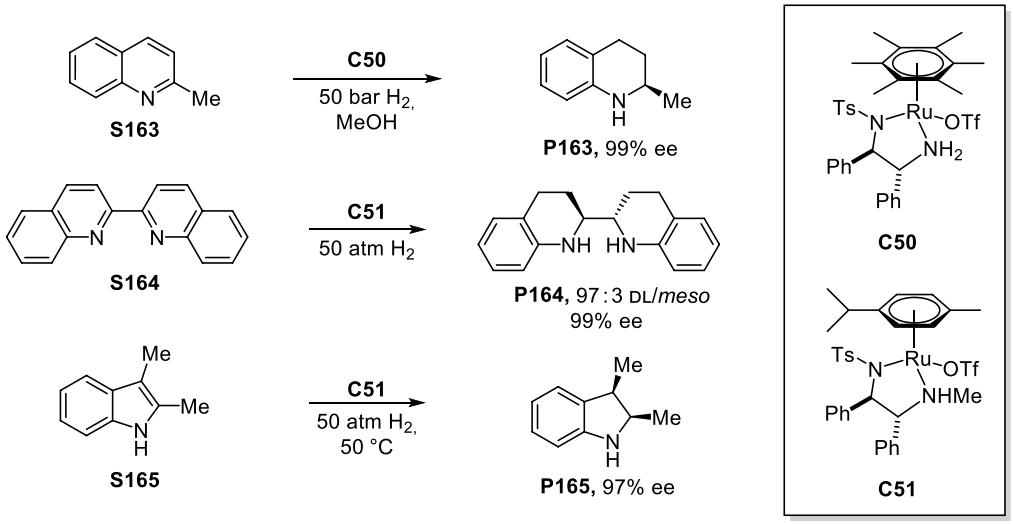

Scheme 15.46. AH of various *N*-aromatic heterocycles with ruthenium arene-diamine catalysts.

F. Glorius using a ruthenium complex derived from the chiral ligand **L109** has reported the chemoselective AH of quinoxalines (**S166**) (Scheme 15.47). Remarkably, depending on NHC ligand employed, either the 1,2,3,4-tetrahydroquinoxaline or the 5,6,7,8-tetrahydroquinoxaline was obtained exclusively [234].

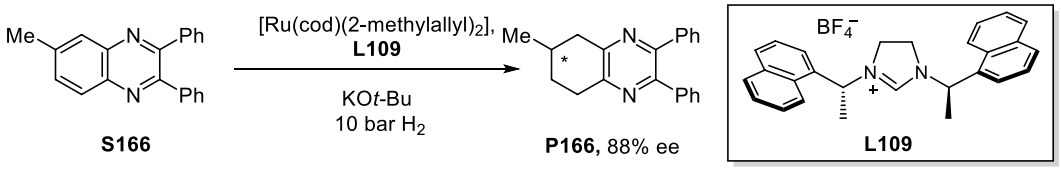

Scheme 15.47. Ruthenium-catalyzed AH of quinoxalines with an NHC ligand.

Recently it has been shown that heteroaromatics can undergo AH with an achiral transition-metal catalyst in combination with a chiral organocatalyst using hydrogen gas as the terminal reductant (Scheme 15.48). The laboratory of Zhou has shown that dihydrophenanthridine (DHPD) is a mimic of the biological reducing agent dihydro-nicotinamide-adenine-dinucleotide phosphate (NADPH). Taking advantage of this, they set up a catalytic system in which a Ru-catalyzed hydrogenation of phenanthridine (PD) produces in situ DHPD. Biaryl chiral phosphoric acid acts then as a template bringing together the substrate benzoxazinone **S160** and reducing agent DHPD [235]. Later on, the laboratory of Beller showed that a non-noble metal could be used in a similar catalytic system [236].

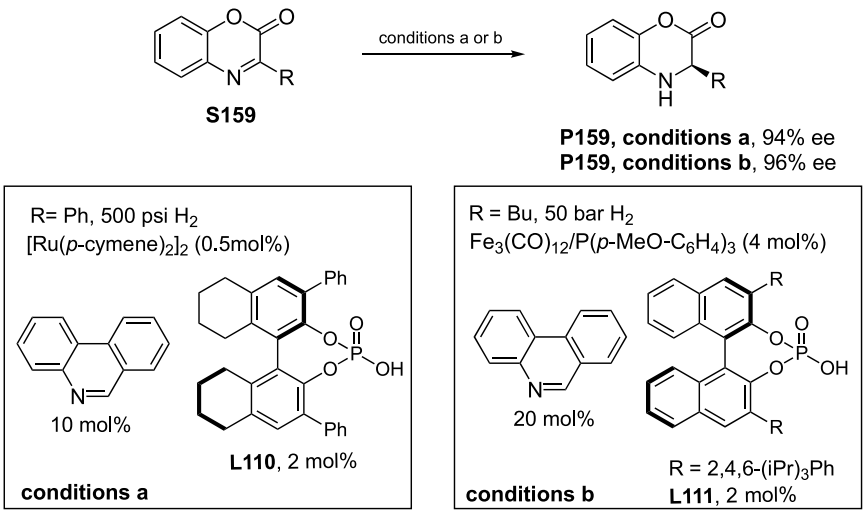

Scheme 15.48. Biomimetic asymmetric hydrogenation of benzoxazinones.

15.5.2. Acyclic Imines

Within the last decade, major advances have been reported for catalytic systems that rely on non-noble metals like Fe, Co, or Ni. The tradeoff for using such metals is often the need for activated imines like phosphinyl or sulfonyl imines. Thus, the group of W. Zhang has reported the hydrogenation of *tert*-butylsulfonyl ketimines such as **S167–170**, using the $Ni(OAc)_2$ as a metal source and the QuinoxP* ligand (**L8,** Scheme 15.49). This showed to be a highly active system since S/C of 10 500 were achieved for a cyclic substrate [237]. The same group recently described the AH of benzoylhydrazones such as **S171–173** using the diphosphine/CoX_2/Zn catalytic system. Interestingly enough, only 1,2-bis (2,5-diphenylphospholano)ethane (Ph-BPE) ligand (**L112**) provided positive results while the similar 1,2-bis(2,5-dimethylphospholano)ethane (Me-BPE) did not produce any product. The authors claim that the coordination of the NHBz group to the metal and the non-bonding interaction between the ligand and substrate are crucial to attain catalytic activity (Scheme 15.49) [238].

The groups of Morris and Beller have pioneered the enantioselective Fe-catalyzed reduction of activated imines. Beller showed that the same Fe-*P*,*N*,*N*,*P* system from **L98**, initially developed by Morris in the ATH of ketones, was active in the ATH of phosphinyl imines, which could be reduced with high selectivity and low catalyst loading (Scheme 15.50) [239]. Later on, Morris unveiled that during the reaction one N=C linkage of the ligand was reduced to produce an NH-FeH complex and lead to the development of cationic amine(imine)diphosphine iron catalysts (**C42**) with improved catalytic activity as happened with ketones. Complete conversion and selectivity was achieved within 10 seconds under ATH conditions [203]. Finally, the Morris group also developed an unsymmetrical *P*,*N*,*P*′-Fe system (**C45**), which catalyzed the direct AH of phosphinyl imines (Scheme 15.50) [204].

Beller also showed that a 1 : 1 mixture of the iron Knölker complex with a chiral Brønsted acid works in a cooperative manner (**C52**) to achieve the AH of *N*-aryl imines with molecular hydrogen (Scheme 15.51). The Knölker complex on its own does not reduce the imine but coordination of the phosphoric acid activates the reduction [240].

With respect to noble metal catalysis, some new catalytic systems have been reported that either produced very high selectivity or allowed the direct hydrogenation of unprecedented substrates. For instance, Gamasa and Pizzano reported a phosphite-PyBOX-Ru catalyst (**C53**) that produced complete selectivity in the hydrogenation of acetophenone *N*-phenyl imine (Scheme 15.52) [241]. Verdaguer and Riera showed that *N*-methyl imines could be hydrogenated under very mild conditions with an iridium (III) catalyst. The Ir(III) hydride **C54** contained a *P*-stereogenic *P*,*N* ligand (MaxPHOX) an a cyclometallated imine and could be isolated and used directly in hydrogenation reactions [242].

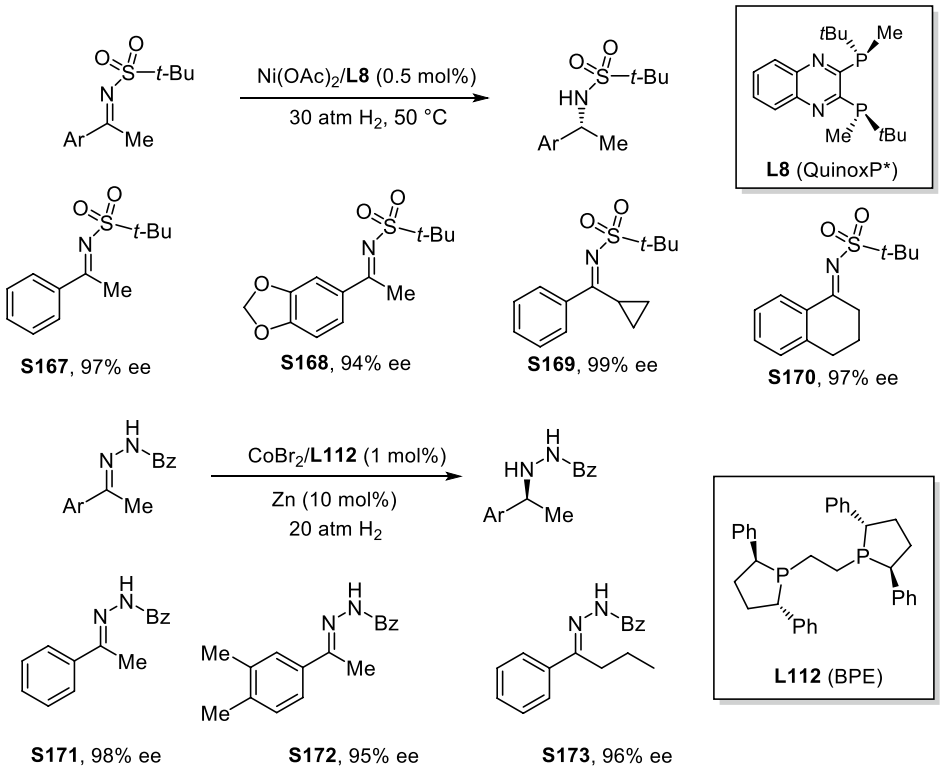

Scheme 15.49. Cobalt- and nickel-catalyzed AH of sulfonyl ketimines and benzoyl hydrazones.

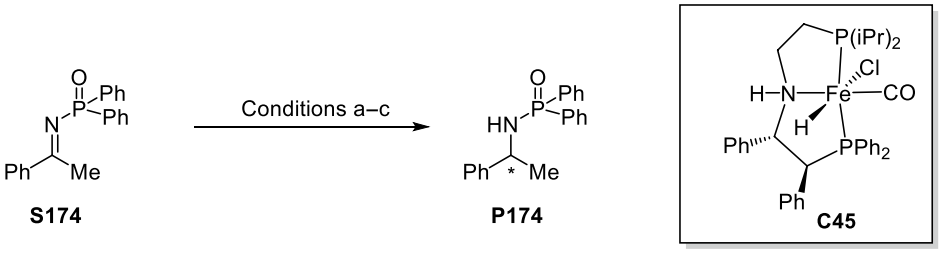

Conditions a. L98, $(Et_3NH)[HFe_3(CO)_{11}]$, KOH (5 mol%), 45 °C, iPrOH — 96% ee

Conditions b. C42, KO*t*-Bu (8 mol%), iPrOH — 99% ee

Conditions c. C45, KO*t*-Bu (10 mol%), 30 bar H_2, 80 °C, toluene — 98% ee

Scheme 15.50. Iron-catalyzed ATH and AH of phosphinyl imines.

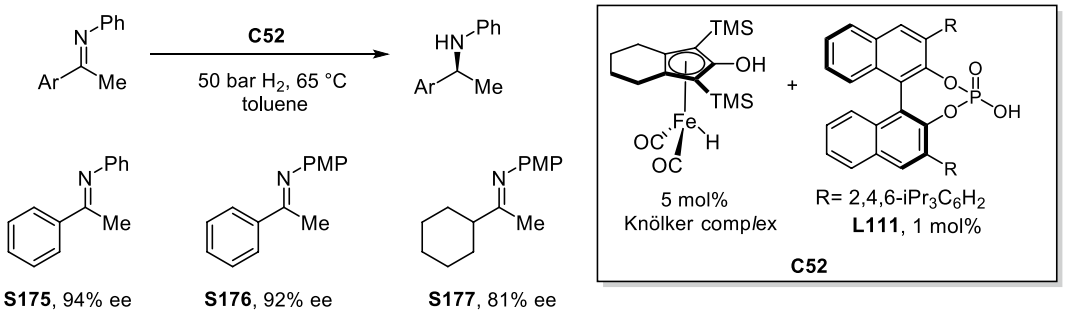

Scheme 15.51. Cooperative iron-catalyzed asymmetric hydrogenation of *N*-phenyl imines.

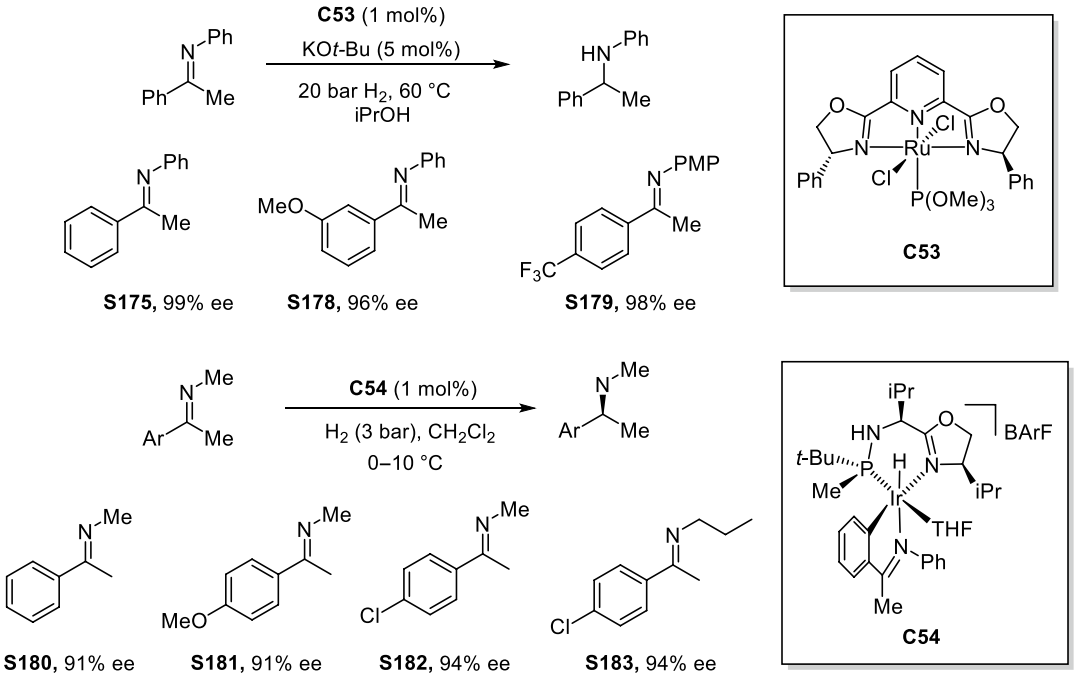

S175, 99% ee **S178,** 96% ee **S179,** 98% ee

S180, 91% ee **S181,** 91% ee **S182,** 94% ee **S183,** 94% ee

Scheme 15.52. Asymmetric hydrogenation of *N*-aryl and *N*-alkyl imines. Source: [241]/John Wiley & Sons.

Very recently, Cramer and coworkers described the hydrogenation of *O*-alkyl oximes to the corresponding hydroxyl amine derivatives (Scheme 15.53). The authors use a half-sandwich Ir(III) catalyst (**C55**) containing a chiral cyclopentadienyl ligand and an achiral arylimine C,N-chelate. The reaction is performed under highly acidic conditions in order to activate the unreactive oxime through protonation [243].

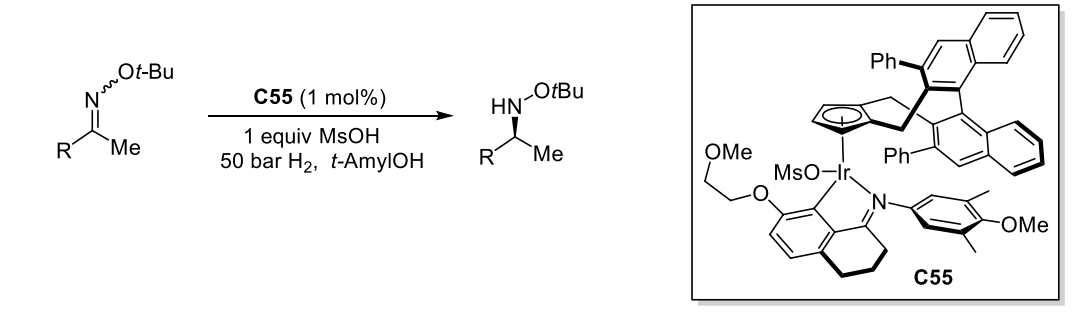

(*E*)-S184, 95% ee **(*E*)-S185,** 56% ee **(*E*)-S186,** 0% ee **(*E*/*Z*)-S187** (1 : 1), 86% ee

Scheme 15.53. Asymmetric hydrogenation of *O*-alkyl oximes.

15.5.3. Reductive Amination

Exciting and great advances have been reported with respect to the asymmetric reductive amination (ARA) processes, either in an intramolecular or intermolecular fashion. Even ammonia has been used in ARA of acetophenone! Most often, however, when a primary nucleophilic amine is used, an equimolar amount of acid is used to neutralize the amine functionality. Strotman et al. at Merck have reported an intramolecular ARA of **S188** that yields a diazepane intermediate en route to Suvorexant, an Orexin antagonist used for treatment of sleep disorders (Scheme 15.54) [244]. The reaction takes place under ATH conditions and was scaled up to 100 kg. A detailed mechanistic study revealed that the Ruthenium Noyori-type catalyst (**C56**) reacted with the evolved CO_2 and was trapped as Ru-formate. A simple purge of CO_2 led to an increase in the rate of reaction and allowed for a nearly quantitative yield.

Chang reported the ARA of Boc-aminoketones **S189** to furnish tetrahydroisoquinolines in excellent selectivity (Scheme 15.54). The protecting group is first removed with trifluoroacetic acid (TFA) and the resulting salt is submitted to hydrogenation. An iodide-bridged dimeric-Ir complex was used along with

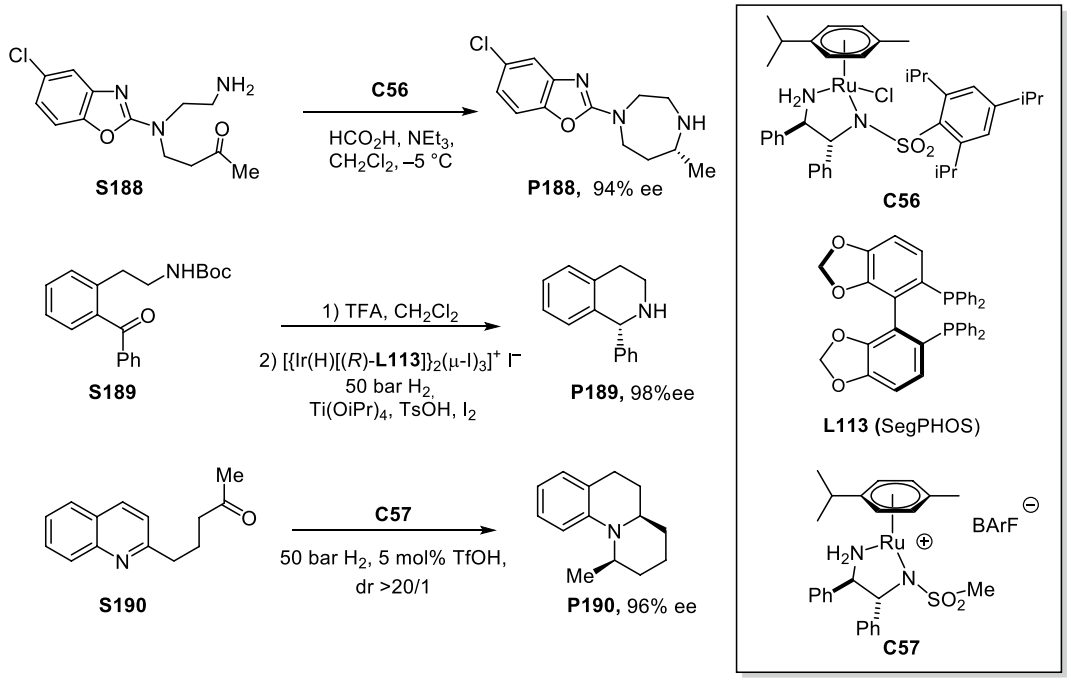

Scheme 15.54. Intramolecular asymmetric reductive amination (ARA). Source: [244].

$Ti(OiPr)_4$, TsOH, and iodine as additives [245]. Fan recently reported the tandem AH/reductive amination of quinolines bearing a ketone group (**S190**) to yield optically active quinolizidines. A cationic Noyori-type catalyst (**C57**) was used in this case. It was found that the configuration of the second chiral center was substrate controlled. Thus, the initial reduction of the quinoline ring dictates the stereochemical outcome of the whole process [246].

The challenging intermolecular reductive amination of benzyl methyl ketones (**S191**) was described by the laboratory of M. Chang with benzhydryl amine (Scheme 15.55). Excellent selectivities were achieved with an iridium catalyst containing 1 equivalent of a MonoPHOS derivative (**L114**). A combination of three different additives (molecular sieves, TFA, and $Ti(OiPr)_4$) was necessary to achieve good conversions of the desired amine. Unfortunately, no details are given on the nature of the active catalytic species in this process [247].

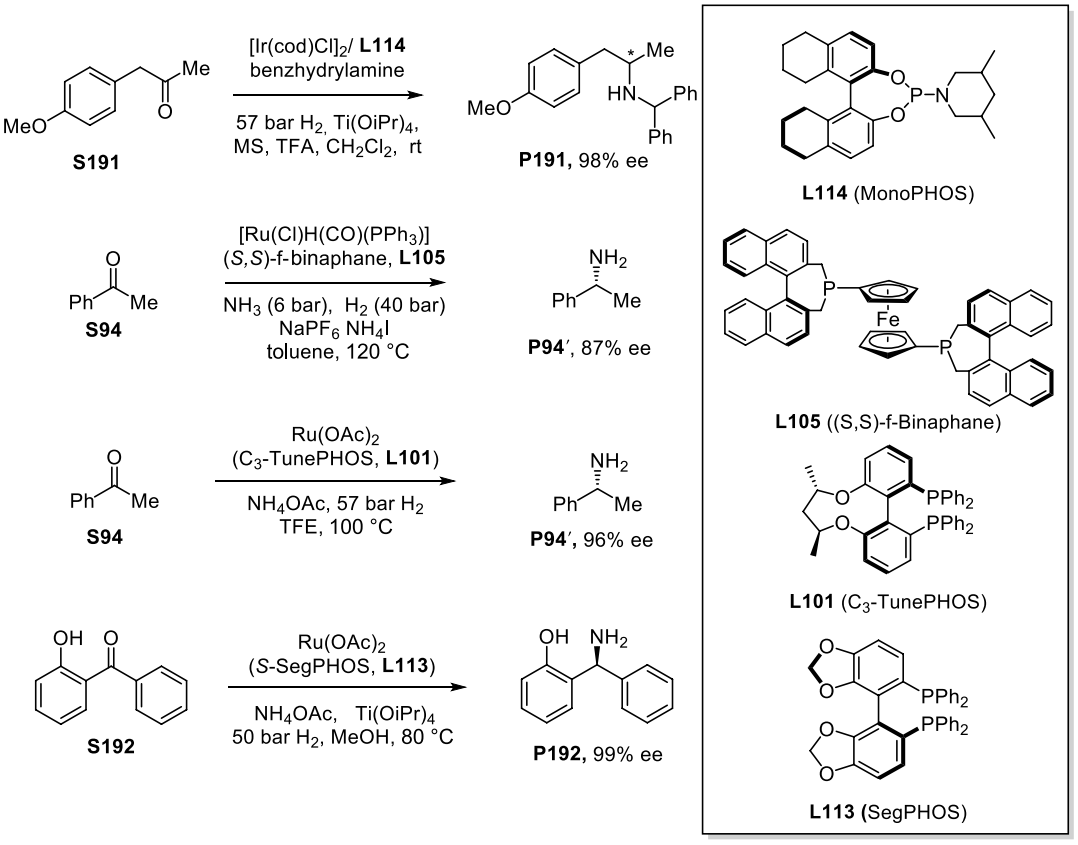

Scheme 15.55. Intermolecular asymmetric reductive amination (ARA). Source: [250]/John Wiley & Sons.

In 2018, two laboratories reported the direct reductive amination of methyl aryl ketones to yield primary amines (Scheme 15.55). Schaub employed ammonia (6 bar) and a ruthenium/(*S,S*)-f-binaphane (**L105**) catalyst with iodine as additive [248]. X-ray and detailed mechanistic studies showed that iodide is coordinated to the metal center and that the reaction operates through an inner sphere mechanism in which the rate-determining step is the protonation of the nitrogen attached to the Ru-center. X. Zhang used ammonium acetate as NH_3 source instead. By using a protic solvent to solubilize the NH_4OAc and an Ru/C_3-TunePHOS (**L101**) catalyst, they managed to obtain the product amine with improved selectivity [249]. Later on, the same laboratory, using a similar catalytic system, reported the ARA of 2-hydroxybenzophenones (Scheme 15.55) [250]. This time, 1 equivalent of $Ti(OiPr)_4$ was necessary to ensure good conversions. The authors argue that the additive is essential in the imine reduction step.

15.6. CONCLUSIONS

AH was one of the first methodologies to attain useful enantioselectivities and to reach industrial applications more than 30 years ago. Nevertheless, the research on this area has not stopped its growth. During the last decade, hundreds of new catalysts have been developed and myriads of new substrates have been reduced with high yields and enantiomeric excesses.

In the area of AH of functionalized alkenes, research activities have been directed not only to expand the structural diversity of typical substrates in this chemistry but also to develop highly enantioselective catalysts for new substrate classes and/or new hydrogenative transformations. As for the AH of poorly

functionalized olefins, iridium-based AH has allowed for the hydrogenation of many new substrate classes that could otherwise not be hydrogenated with high enantioselectivities with previously existing catalysts.

In the case of ketone reduction, the ruthenium complexes have shared its dominant position with iridium complexes. Moreover, complexes of earth-abundant metals have started to be competitive.

With respect to the reduction of carbon–nitrogen double bonds, in the last 10 years we have witnessed incredible advances on the reduction of nitrogen-containing heteroaromatics, on the use of non-precious metals as catalyst, and on the development of ARA processes. In the years to come, we might expect further development in these areas. For these challenges, novel catalytic systems that are active and resistant to basic conditions, catalyst deactivation, and poisoning by amines are much needed.

REFERENCES

1. Hörner, L.; Siegel, H.; Büthe, H. *Angew. Chem. Int. Ed. Engl.* **1968**, *7*, 942.
2. Knowles, W. S.; Sabacky, M. J. *Chem. Commun.* **1968**, 1445–1446.
3. Kang, T. P.; Kagan, H. B. *Chem. Commun.* **1971**, 481–481.
4. (a) Ojima, I., Ed. *Catalytic Asymmetric Synthesis*. VCH: New York, **1993**; pp. 1–39. (b) Ojima, I., Ed. *Catalytic Asymmetric Synthesis*, Second Edition. Wiley: New York, **2000**; pp. 1–110. (c) Ojima, I., Ed. *Catalytic Asymmetric Synthesis*, Third Edition. John Wiley & Sons, Inc.: Hoboken, NJ, **2010**; pp. 343–436.
5. For reviews from the period 2010–2020, see: (a) Li, W.; Hou, G.; Sun, X.; Shang, G.; Zhang, W.; Zhang, X. *Pure Appl. Chem.* **2010**, *82*, 1429–1441. (b) Fernández-Pérez, H.; Etayo, P.; Panossian, A.; Vidal-Ferran, A. *Chem. Rev.* **2011**, *111*, 2119. (c) Ager, D. J.; de Vries, A. H. M.; de Vries, J. G. *Chem. Soc. Rev.* **2012**, *41*, 3340–3380. (d) Cadu, A.; Andersson, P. G. *J. Organomet. Chem.* **2012**, *714*, 3–11. (e) Ganic, A.; Rageot, D.; Trondlin, L.; Pfaltz, A. *Chimia* **2012**, *66*, 187–191. (f) Cadu, A.; Andersson, P. G. *Dalton Trans.* **2013**, *42*, 14345–14356. (g) Chen, Q.-A.; Ye, Z.-S.; Duan, Y.; Zhou, Y.-G. *Chem. Soc. Rev.* **2013**, *42*, 497–511. (h) Etayo, P.; Vidal-Ferran, A. *Chem. Soc. Rev.* **2013**, *42*, 728. (i) de Vries, J. G.; Lefort, L. *Oil Gas Sci. Technol* **2013**, *68*, 519–528. (j) Khumsubdee, S.; Burgess, K. *ACS Catal.* **2013**, *3*, 237–249. (k) Carroll, M. P.; Guiry, P. J. *Chem. Soc. Rev.* **2014**, *43*, 819–833. (l) He, Y.-M.; Feng, Y.; Fan, Q.-H. *Acc. Chem. Res.* **2014**, *47*, 2894–2906. (m) Verendel, J. J.; Pàmies, O.; Diéguez, M.; Andersson, P. G. *Chem. Rev.* **2014**, *114*, 2130–2169. (n) Kleman, P.; Pizzano, A. *Tetrahedron Lett.* **2015**, *56*, 6944–6963. (o) Zhao, D.; Candish, L.; Paul, D.; Glorius, F. *ACS Catal.* **2016**, *6*, 5978–5988. (p) Kraft, S.; Ryan, K.; Kargbo, R. B. *J. Am. Chem. Soc.* **2017**, *139*, 11630–11641. (q) Zhu, S.-F.; Zhou, Q.-L. *Acc. Chem. Res.* **2017**, *50*, 988–1001. (r) Zhang, Z.; Butt, N. A.; Zhou, M.; Liu, D.; Zhang, W. *Chin. J. Chem.* **2018**, *36*, 443–454. (s) Seo, C. S. G.; Morris, R. H. *Organometallics* **2019**, *38*, 47–65. (t) Biosca, M.; Pàmies, O.; Diéguez, M. *Catal. Sci. Technol.* **2020**, *10*, 613–624. (u) Cabré, A.; Riera, A.; Verdaguer, X. *Acc. Chem. Res.* **2020**, *53*, 676–689. (v) Cunningham, L.; Benson, A.; Guiry, P. J. *Org. Biomol. Chem.* **2020**, *18*, 9329–9370. (w) Fanourakis, A.; Docherty, P. J.; Chuentragool, P.; Phipps, R. J. *ACS Catal.* **2020**, *10*, 10672–10714. (x) Massaro, L.; Zheng, J.; Margarita, C.; Andersson, P. G. *Chem. Soc. Rev.* **2020**, *49*, 2504–2522. (y) Noda, H.; Shibasaki, M. *Eur. J. Org. Chem.* **2020**, *2020*, 2350–2361. (z) Zhao, Q.; Chen, C.; Wen, J.; Dong, X.-Q.; Zhang, X. *Acc. Chem. Res.* **2020**, *53*, 1905–1921. (aa) Cabré, A.; Verdaguer, X.; Riera, A. *Chem. Rev.* **2022**, *122*, 269–339.
6. Zhang, X.; Huang, K.; Hou, G.; Cao, B.; Zhang, X. *Angew. Chem. Int. Ed.* **2010**, *49*, 6421–6424.
7. (a) Zupančić, B.; Mohar, B.; Stephan, M. *Org. Lett.* **2010**, *12*, 3022–3025. (b) Mohar, B.; Stephan, M. *Adv. Synth. Catal.* **2013**, *355*, 594–600.
8. Huang, K.; Zhang, X.; Emge, T. J.; Hou, G.; Cao, B.; Zhang, X. *Chem. Commun.* **2010**, *46*, 8555–8557.
9. Tang, W.; Qu, B.; Capacci, A. G.; Rodriguez, S.; Wei, X.; Haddad, N.; Narayanan, B.; Ma, S.; Grinberg, N.; Yee, N. K.; Krishnamurthy, D.; Senanayake, C. H. *Org. Lett.* **2010**, *12*, 176–179.
10. (a) Revés, M.; Ferrer, C.; León, T.; Doran, S.; Etayo, P.; Vidal-Ferran, A.; Riera, A.; Verdaguer, X. *Angew. Chem. Int. Ed.* **2010**, *49*, 9452–9455. (b) Cristobal-Lecina, E.; Etayo, P.; Dorán, S.; Revés, M.; Martín-Gago, P.; Grabulosa, A.; Costantino, A. R.; Vidal-Ferran, A.; Riera, A.; Verdaguer, X. *Adv. Synth. Catal.* **2014**, *356*, 795–804.
11. (a) Fernández-Pérez, H.; Donald, S. M. A.; Munslow, I. J.; Benet-Buchholz, J.; Maseras, F.; Vidal-Ferran, A. *Chem. Eur. J.* **2010**, *16*, 6495–6508. (b) Etayo, P.; Núñez-Rico, J. L.; Fernández-Pérez, H.; Vidal-Ferran, A. *Chem. Eur. J.* **2011**, *17*, 13978–13982. (c) Núñez-Rico, J. L.; Etayo, P.; Fernández-Pérez, H.; Vidal-Ferran, A. *Adv. Synth. Catal.* **2012**, *354*, 3025–3035.
12. Fernández-Pérez, H.; Balakrishna, B.; Vidal-Ferran, A. *Eur. J. Org. Chem.* **2018**, *2018*, 1525–1532.
13. Imamoto, T.; Tamura, K.; Zhang, Z.; Horiuchi, Y.; Sugiya, M.; Yoshida, K.; Yanagisawa, A.; Gridnev, I. D. *J. Am. Chem. Soc.* **2012**, *134*, 1754–1769.
14. Sawatsugawa, Y.; Tamura, K.; Sano, N.; Imamoto, T. *Org. Lett.* **2019**, *21*, 8874–8878.
15. Zhang, Z.; Hu, Q.; Wang, Y.; Chen, J.; Zhang, W. *Org. Lett.* **2015**, *17*, 5380–5383.
16. Molinaro, C.; Scott, J. P.; Shevlin, M.; Wise, C.; Menard, A.; Gibb, A.; Junker, E. M.; Lieberman, D. *J. Am. Chem. Soc.* **2015**, *137*, 999–1006.
17. Zhang, J.; Jia, J.; Zeng, X.; Wang, Y.; Zhang, Z.; Gridnev, I. D.; Zhang, W. *Angew. Chem. Int. Ed.* **2019**, *58*, 11505–11512.
18. Gao, M.; Meng, J.-J.; Lv, H.; Zhang, X. *Angew. Chem. Int. Ed.* **2015**, *54*, 1885–1887.

19. Poklukar, G.; Stephan, M.; Mohar, B. *Adv. Synth. Catal.* **2018**, *360*, 2566–2570.
20. Liu, T.-L.; Wang, C.-J.; Zhang, X. *Angew. Chem. Int. Ed.* **2013**, *52*, 8416–8419.
21. (a) Zhou, M.; Liu, T.-L.; Cao, M.; Xue, Z.; Lv, H.; Zhang, X. *Org. Lett.* **2014**, *16*, 3484–3487. (b) Wang, Q.; Gao, W.; Lv, H.; Zhang, X. *Chem. Commun.* **2016**, *52*, 11850–11853.
22. Liu, G.; Liu, X.; Cai, Z.; Jiao, G.; Xu, G.; Tang, W. *Angew. Chem. Int. Ed.* **2013**, *52*, 4235–4238.
23. Li, C.; Wan, F.; Chen, Y.; Peng, H.; Tang, W.; Yu, S.; McWilliams, J. C.; Mustakis, J.; Samp, L.; Maguire, R. J. *Angew. Chem. Int. Ed.* **2019**, *58*, 13573–13583.
24. Konrad, T. M.; Schmitz, P.; Leitner, W.; Franciò, G. *Chem. Eur. J.* **2013**, *19*, 13299–13303.
25. González-Liste, P. J.; León, F.; Arribas, I.; Rubio, M.; García-Garrido, S. E.; Cadierno, V.; Pizzano, A. *ACS Catal.* **2016**, *6*, 3056–3060.
26. Geng, H.; Huang, K.; Sun, T.; Li, W.; Zhang, X.; Zhou, L.; Wu, W.; Zhang, X. *J. Org. Chem.* **2011**, *76*, 332–334.
27. Huang, K.; Zhang, X.; Geng, H.; Li, S.-K.; Zhang, X. *ACS Catal.* **2012**, *2*, 1343–1345.
28. Wang, Q.; Huang, W.; Yuan, H.; Cai, Q.; Chen, L.; Lv, H.; Zhang, X. *J. Am. Chem. Soc.* **2014**, *136*, 16120–16123.
29. Llopis, Q.; Guillamot, G.; Phansavath, P.; Ratovelomanana-Vidal, V. *Org. Lett.* **2017**, *19*, 6428–6431.
30. Zhang, J.; Li, Y.; Wang, Z.; Ding, K. *Angew. Chem. Int. Ed.* **2011**, *50*, 11743–11747.
31. Zhao, Q.; Li, S.; Huang, K.; Wang, R.; Zhang, X. *Org. Lett.* **2013**, *15*, 4014–4017.
32. (a) Han, Z.; Li, P.; Zhang, Z.; Chen, C.; Wang, Q.; Dong, X.-Q.; Zhang, X. *ACS Catal.* **2016**, *6*, 6214–6218. (b) Lang, Q.; Gu, G.; Cheng, Y.; Yin, Q.; Zhang, X. *ACS Catal.* **2018**, *8*, 4824–4828.
33. Chen, C.; Zhang, Z.; Jin, S.; Fan, X.; Geng, M.; Zhou, Y.; Wen, S.; Wang, X.; Chung, L. W.; Dong, X.-Q.; Zhang, X. *Angew. Chem. Int. Ed.* **2017**, *56*, 6808–6812.
34. Fernández-Pérez, H.; Lao, J. R.; Vidal-Ferran, A. *Org. Lett.* **2016**, *18*, 2836–2839.
35. (a) Lao, J. R.; Fernández-Pérez, H.; Vidal-Ferran, A. *Org. Lett.* **2015**, *17*, 4114–4117. (b) Fernández-Pérez, H.; Vidal-Ferran, A. *Org. Lett.* **2019**, *21*, 7019–7023. (c) Fernández-Pérez, H.; Lao, J. R.; Grabulosa, A.; Vidal-Ferran, A. *Eur. J. Org. Chem.* **2020**, 4331–4338.
36. Dong, K.; Li, Y.; Wang, Z.; Ding, K. *Angew. Chem. Int. Ed.* **2013**, *52*, 14191–14195.
37. Yan, Q.; Xiao, G.; Wang, Y.; Zi, G.; Zhang, Z.; Hou, G. *J. Am. Chem. Soc.* **2019**, *141*, 1749–1756.
38. Ohgo, Y.; Takeuchi, S.; Natori, Y.; Yoshimura, J. *Bull. Chem. Soc. Jpn.* **1981**, *54*, 2124–2135
39. Knijnenburg, Q.; Horton, A. D.; van der Heijden, H.; Kooistra, T. M.; Hetterscheid, D. G. H.; Smits, J. M. M.; de Bruin, B.; Budzelaar, P. H. M.; Gal, A. W. *J. Mol. Catal. A: Chem.* **2005**, *232*, 151–159.
40. (a) Zhang, G.; Scott, B. L.; Hanson, S. K. *Angew. Chem. Int. Ed.* **2012**, *51*, 12102–12106. (b) Zhang, G.; Vasudevan, K. V.; Scott, B. L.; Hanson, S. K. *J. Am. Chem. Soc.* **2013**, *135*, 8668–8681.
41. Monfette, S.; Turner, Z. R.; Semproni, S. P.; Chirik, P. J. *J. Am. Chem. Soc.* **2012**, *134*, 4561–4564.
42. Friedfeld, M. R.; Shevlin, M.; Hoyt, J. M.; Krska, S. W.; Tudge, M. T.; Chirik, P. J. *Science* **2013**, *342*, 1076–1080.
43. (a) Friedfeld, M. R.; Zhong, H.; Ruck, R. T.; Shevlin, M.; Chirik, P. J. *Science* **2018**, *360*, 888–893. (b) Zhong, H.; Friedfeld, M. R.; Chirik, P. J. *Angew. Chem. Int. Ed.* **2019**, *58*, 9194–9198.
44. Zhong, H.; Shevlin, M.; Chirik, P. J. *J. Am. Chem. Soc.* **2020**, *142*, 5272–5281.
45. Guo, J.; Cheng, B.; Shen, X.; Lu, Z. *J. Am. Chem. Soc.* **2017**, *139*, 15316–15319.
46. Guo, J.; Shen, X.; Lu, Z. *Angew. Chem. Int. Ed.* **2017**, *56*, 615–618.
47. Viereck, P.; Krautwald, S.; Pabst, T. P.; Chirik, P. J. *J. Am. Chem. Soc.* **2020**, *142*, 3923–3930.
48. de Vries, J. G., Ed. Science of Synthesis: Catalytic Reduction in Organic Synthesis (two volumes). Georg Thieme Verlag: Stuttgart, Germany, **2018**.
49. Shevlin, M.; Friedfeld, M. R.; Sheng, H.; Pierson, N. A.; Hoyt, J. M.; Campeau, L.-C.; Chirik, P. J. *J. Am. Chem. Soc.* **2016**, *138*, 3562–3569.
50. Hu, Y.; Chen, J.; Li, B.; Zhang, Z.; Gridnev, I. D.; Zhang, W. *Angew. Chem. Int. Ed.* **2020**, *59*, 5371–5375.
51. Gao, W.; Lv, H.; Zhang, T.; Yang, Y.; Chung, L. W.; Wu, Y.-D.; Zhang, X. *Chem. Sci.* **2017**, *8*, 6419–6422.
52. Guan, Y.-Q.; Han, Z.; Li, X.; You, C.; Tan, X.; Lv, H.; Zhang, X. *Chem. Sci.* **2019**, *10*, 252–256.
53. Lightfoot, A.; Schnider, P.; Pfaltz, A. *Angew. Chem. Int. Ed.* **1998**, *37*, 2897–2899.
54. Crabtree, R. *Acc. Chem. Res.* **1979**, *12*, 331–337.
55. Woodmansee, D. H.; Müller, M.-A.; Neuburger, M.; Pfaltz, A. *Chem. Sci.* **2010**, *1*, 72–78.
56. Mazuela, J.; Norrby, P.-O.; Andersson, P. G.; Pàmies, O.; Diéguez, M. *J. Am. Chem. Soc.* **2011**, *133*, 13634–13645.
57. Zhu, S.-F.; Yu, Y.-B.; Li, S.; Wang, L.-X.; Zhou, Q.-L. *Angew. Chem. Int. Ed.* **2012**, *51*, 8872–8875.
58. Biosca, M.; Paptchikhine, A.; Pàmies, O.; Andersson, P. G.; Diéguez, M. *Chem. Eur. J.* **2015**, *21*, 3455–3464.
59. Bernasconi, M.; Müller, M.-A.; Pfaltz, A. *Angew. Chem. Int. Ed.* **2014**, *53*, 5385–5388.
60. Yang, S.; Che, W.; Wu, H.-L.; Zhu, S.-F.; Zhou, Q.-L. *Chem. Sci.* **2017**, *8*, 1977–1980.
61. Ponra, S.; Yang, J.; Kerdphon, S.; Andersson, P. G. *Angew. Chem. Int. Ed.* **2019**, *58*, 9282–9287.
62. Liu, Y.; Zhang, W. *Angew. Chem. Int. Ed.* **2013**, *52*, 2203–2206.
63. Liu, X.; Han, Z.; Wang, Z.; Ding, K. *Angew. Chem. Int. Ed.* **2014**, *53*, 1978–1982.
64. Song, S.; Zhu, S.-F.; Pu, L.-Y.; Zhou, Q.-L. *Angew. Chem. Int. Ed.* **2013**, *52*, 6072–6075.
65. Ge, Y.; Han, Z.; Wang, Z.; Feng, C.-G.; Zhao, Q.; Lin, G.-Q.; Ding, K. *Angew. Chem. Int. Ed.* **2018**, *57*, 13140–13144.

66. Salomó, E.; Orgue, S.; Riera, A.; Verdaguer, X. *Angew. Chem. Int. Ed.* **2016**, *55*, 7988–7992.
67. Wang, X.; Han, Z.; Wang, Z.; Ding, K. *Angew. Chem. Int. Ed.* **2012**, *51*, 936–940.
68. Zheng, Z.; Cao, Y.; Chong, Q.; Han, Z.; Ding, J.; Luo, C.; Wang, Z.; Zhu, D.; Zhou, Q.-L.; Ding, K. *J. Am. Chem. Soc.* **2018**, *140*, 10374–10381.
69. Ganic, A.; Pfaltz, A. *Chem. Eur. J.* **2012**, *18*, 6724–6728.
70. Gazić Smilović, I.; Casas-Arcé, E.; Roseblade, S. J.; Nettekoven, U.; Zanotti-Gerosa, A.; Kovačevič, M.; Časar, Z. *Angew. Chem. Int. Ed.* **2012**, *51*, 1014–1018.
71. Peters, B. K.; Zhou, T.; Rujirawanich, J.; Cadu, A.; Singh, T.; Rabten, W.; Kerdphon, S.; Andersson, P. G. *J. Am. Chem. Soc.* **2014**, *136*, 16557–1656.
72. (a) Ponra, S.; Rabten, W.; Yang, J.; Wu, H.; Kerdphon, S.; Andersson, P. G. *J. Am. Chem. Soc.* **2018**, *140*, 13878–13883. (b) Ponra, S.; Yang, J.; Wu, H.; Rabten, W.; Andersson, P. G. *Chem. Sci.* **2020**, *11*, 11189–11194.
73. Li, W.; Wagener, T.; Hellmann, L.; Daniliuc, C. G.; Mück-Lichtenfeld, C.; Neugebauer, J.; Glorius, F. *J. Am. Chem. Soc.* **2020**, *142*, 7100–7107.
74. Li, W.; Wiesenfeldt, M. P.; Glorius, F. *J. Am. Chem. Soc.* **2017**, *139*, 2585–2588.
75. (a) Verendel, J. J.; Pàmies, O.; Diéguez, M.; Andersson, P. G. *Chem. Rev.* **2014**, *114*, 2130–2169. (b) Pàmies, O.; Magre, M.; Diéguez, M. *Chem. Rec.* **2016**, *16*, 1578–1590. (c) Kraft, S.; Ryan, K.; Kargbo, R. B. *J. Am. Chem. Soc.* **2017**, *139*, 11630–11641. (d) Margarita, C.; Andersson, P. G. *J. Am. Chem. Soc.* **2017**, *139*, 1346–1356. (e) Chen, J.; Lu, Z. *Org. Chem. Front.* **2018**, *5*, 260–272.
76. Carroll, M. P.; Guiry, P. J. *Chem. Soc. Rev.* **2014**, *43*, 819–833.
77. (a) Bell, S.; Wüstenberg, B.; Kaiser, S.; Menges, F.; Netscher, T.; Pfaltz, A. *Science* **2006**, *311*, 642–644. (b) Roseblade, S. J.; Pfaltz, A. *Acc. Chem. Res.* **2007**, *40*, 1402–1411.
78. (a) Yoshinari, T.; Ohmori, K.; Schrems, M. G.; Pfaltz, A.; Suzuki, K. *Angew. Chem. Int. Ed.* **2010**, *49*, 881–885. (b) Wang, A.; Fraga, R. P. A.; Hörmann, E.; Pfaltz, A. *Chem. Asian J.* **2011**, *6*, 599–606.
79. Zanotti-Gerosa, A.; Gazić Smilović, I.; Časar, Z. *Org. Chem. Front.* **2017**, *4*, 2311–2322.
80. Pfaltz, A.; Müller, M.-A.; Gruber, S. *Adv. Synth. Catal.* **2018**, *360*, 1340–1345.
81. Verevkin, S. P.; Emel'yanenko, V. N.; Bayardon, J.; Schäffner, B.; Baumann, W.; Börner, A. *Ind. Eng. Chem. Res.* **2012**, *51*, 126–132.
82. Margalef, J.; Caldentey, X.; Karlsson, E. A.; Coll, M.; Mazuela, J.; Pàmies, O.; Diéguez, M.; Pericàs, M. A. *Chem. Eur. J.* **2014**, *20*, 12201–12214.
83. (a) Church, T. L.; Rasmussen, T.; Andersson, P. G. *Organometallics* **2010**, *29*, 6769–6781. (b) Hopmann, K. H.; Bayer, A. *Organometallics* **2011**, *30*, 2483–2497. (b) Gruber, S.; Pfaltz, A. *Angew. Chem. Int. Ed.* **2014**, *53*, 1896–1900. (c) Hopmann, K. H.; Frediani, L.; Bayer, A. *Organometallics* **2014**, *33*, 2790–2797. (d) Sparta, M.; Riplinger, C.; Neese, F. *J. Chem. Theory Comput.* **2014**, *10*, 1099–1108. (e) Borràs, C.; Biosca, M.; Pàmies, O.; Diéguez, M. *Organometallics* **2015**, *34*, 5321–5334.
84. Lu, W.-J.; Chen, Y.-W.; Hou, X.-L. *Adv. Synth. Catal.* **2010**, *352*, 103–107.
85. Franzke, A.; Pfaltz, A. *Chem. Eur. J.* **2011**, *17*, 4131–4144.
86. Franzke, A.; Voss, F.; Pfaltz, A. *Tetrahedron* **2011**, *67*, 4358–4363.
87. Rageot, D.; Pfaltz, A. *Helv. Chim. Acta* **2012**, *95*, 2176–2193.
88. Chelucci, G.; Marchetti, M.; Malkov, A. V.; Friscourt, F.; Swarbrick, M. E.; Kočovský, P. *Tetrahedron* **2011**, *67*, 5421–5431.
89. Wassenaar, J.; Detz, R. J.; de Boer, S. Y.; Lutz, M.; van Maarseveen, J. H.; Hiemstra, H.; Reek, J. N. H. *J. Org. Chem.* **2015**, *80*, 3634–3642.
90. Busacca, C. A.; Qu, B.; Grět, N.; Fandrick, K. R.; Saha, A. K.; Marsini, M.; Reeves, D.; Haddad, N.; Eriksson, M.; Wu, J. P.; Grinberg, N.; Lee, H.; Li, Z.; Lu, B.; Chen, D.; Hong, Y.; Ma, S.; Senanayake, C. H. *Adv. Synth. Catal.* **2013**, *355*, 1455–1463.
91. Quan, X.; Parihar, V. S.; Bera, M.; Andersson, P. G. *Eur. J. Org. Chem.* **2014**, 140–146.
92. Chakka, S. K.; Peters, B. K.; Andersson, P. G.; Maguire, G. E. M.; Kruger, H. G.; Govender, T. *Tetrahedron Asymmetry* **2010**, *21*, 2295–2301.
93. Li, J.-Q.; Paptchikhine, A.; Govender, T.; Andersson, P. G. *Tetrahedron Asymmetry* **2010**, *21*, 1328–1333.
94. Yotapan, N.; Paptchikhine, A.; Bera, M.; Avula, S. K.; Vilaivan, T.; Andersson, P. G. *Asian J. Org. Chem.* **2013**, *2*, 674–680.
95. Liu, Y.; Chen, F.; He, Y.-M.; Li, C.; Fan, Q.-H. *Org. Biomol. Chem.* **2019**, *17*, 5099–5105.
96. Mazuela, J.; Pàmies, O.; Diéguez, M. *Eur. J. Inorg. Chem.* **2013**, 2139–2145.
97. Metallinos, C.; Van Belle, L. *J. Organomet. Chem.* **2011**, *696*, 141–149.
98. Bert, K.; Noël, T.; Kimpe, W.; Goeman, J. L.; Van der Eycken, J. *Org. Biomol. Chem.* **2012**, *10*, 8539–8550.
99. Qu, B.; Samankumara, L. P.; Savoie, J.; Fandrick, D. R.; Haddad, N.; Wei, X.; Ma, S.; Lee, H.; Rodriguez, S.; Busacca, C. A.; Yee, N. K.; Song, J. J.; Senanayake, C. H. *J. Org. Chem.* **2014**, *79*, 993–1000.
100. Mazuela, J.; Paptchikhine, A.; Pàmies, O.; Andersson, P. G.; Diéguez, M. *Chem. Eur. J.* **2010**, *16*, 4567–4576.
101. Mazuela, J.; Pàmies, O.; Diéguez, M. *ChemCatChem* **2013**, *5*, 2410–2417.
102. Mazuela, J.; Pàmies, O.; Diéguez, M. *Adv. Synth. Catal.* **2013**, *355*, 2569–2583.
103. Biosca, M.; Magre, M.; Coll, M.; Pàmies, O.; Diéguez, M. *Adv. Synth. Catal.* **2017**, *359*, 2801–2814.
104. Biosca, M.; Magre, M.; Pàmies, O.; Diéguez, M. *ACS Catal.* **2018**, *8*, 10316–10320.

105. Biosca, M.; Pàmies, O.; Diéguez, M. *J. Org. Chem.* **2019**, *84*, 8259–8266.
106. Rageot, D.; Woodmansee, D. H.; Pugin, B.; Pfaltz, A. *Angew. Chem. Int. Ed.* **2011**, *50*, 9598–9601.
107. de la Cruz-Sánchez, P.; Faiges, J.; Mazloomi, Z.; Borràs, C.; Biosca, M.; Pàmies, O.; Diéguez, M. *Organometallics* **2019**, *38*, 4193–4205.
108. Diéguez, M.; Margalef, J.; Borràs, C.; Alegre, S.; Alberico, E.; Pàmies, O. *ChemCatChem* **2019**, *11*, 2142–2168.
109. (a) Coll, M.; Pàmies, O.; Diéguez, M. *Chem. Commun.* **2011**, *47*, 9215–9217. (b) Coll, M.; Pàmies, O.; Diéguez, M. *Adv. Synth. Catal.* **2013**, *355*, 143–160.
110. Khumsubdee, S.; Fan, Y.; Burgess, K. *J. Org. Chem.* **2013**, *78*, 9969–9974.
111. Schumacher, A.; Bernasconi, M.; Pfaltz, A. *Angew. Chem. Int. Ed.* **2013**, *52*, 7422–7425.
112. Qu, B.; Samankumara, L. P.; Ma, S.; Fandrick, K. R.; Desrosiers, J.-N.; Rodriguez, S.; Li, Z.; Haddad, N.; Han, Z. S.; McKellop, K.; Pennino, S.; Grinberg, N.; Gonnella, N. C.; Song, J. J.; Senanayake, C. H. *Angew. Chem. Int. Ed.* **2014**, *53*, 14428–14432.
113. Xia, J.; Yang, G.; Zhuge, R.; Liu, Y.; Zhang, W. *Chem. Eur. J.* **2016**, *22*, 18354–18357.
114. Paptchikhine, A.; Itto, K.; Andersson, P. G. *Chem. Commun.* **2011**, *47*, 3989–3991.
115. Peters, B. K.; Liu, J.; Margarita, C.; Rabten, W.; Kerdphon, S.; Orebom, A.; Morsch, T.; Andersson, P. G. *J. Am. Chem. Soc.* **2016**, *138*, 11930–11935.
116. Liu, J.; Krajangsri, S.; Singh, T.; De Seriis, G.; Chumnanvej, N.; Wu, H.; Andersson, P. G. *J. Am. Chem. Soc.* **2017**, *139*, 14470–14475.
117. (a) Cui, X.; Burgess, K. *Chem. Rev.* **2005**, *105*, 3272–3296. (b) Pàmies, O.; Andersson, P. G.; Diéguez, M. *Chem. Eur. J.* **2010**, *16*, 14232–14240.
118. Mazuela, J.; Verendel, J. J.; Coll, M.; Schäffner, B.; Börner, A.; Andersson, P. G.; Pàmies, O.; Diéguez, M. *J. Am. Chem. Soc.* **2009**, *131*, 12344–12353.
119. Bess, E. N.; Sigman, M. S. *Org. Lett.* **2013**, *15*, 646–649.
120. Biosca, M.; Salomó, E.; de la Cruz-Sánchez, P.; Riera, A.; Verdaguer, X.; Pàmies, O.; Diéguez, M. *Org. Lett.* **2019**, *21*, 807–811.
121. Bigler, R.; Mack, K. A.; Shen, J.; Tosatti, P.; Han, C.; Bachmann, S.; Zhang, H.; Scalone, M.; Pfaltz, A.; Denmark, S. E.; Hildbrand, S.; Gosselin, F. *Angew. Chem. Int. Ed.* **2020**, *59*, 2844–2849.
122. Kita, Y.; Hida, S.; Higashihara, K.; Jena, H. S.; Higashida, K.; Mashima, K. *Angew. Chem. Int. Ed.* **2016**, *55*, 8299–8303.
123. Higashida, K.; Brüning, F.; Tsujimoto, N.; Higashihara, K.; Nagae, H.; Togni, A.; Mashima, K. *Chem. Eur. J.* **2020**, *26*, 8749–8759.
124. Zhang, Z.; Wang, J.; Li, J.; Yang, F.; Liu, G.; Tang, W.; He, W.; Fu, J.-J.; Shen, Y.-H.; Li, A.; Zhang, W.-D. *J. Am. Chem. Soc.* **2017**, *139*, 5558–5567.
125. Strotman, N. A.; Ramirez, A.; Simmons, E. M.; Soltani, O.; Parsons, A. T.; Fan, Y.; Sawyer, J. R.; Rosner, T.; Janey, J. M.; Tran, K.; Li, J.; La Cruz, T. E.; Pathirana, C.; Ng, A. T.; Deerberg, J. *J. Org. Chem.* **2018**, *83*, 11133–11144.
126. Friedfeld, M. R.; Shevlin, M.; Margulieux, G. W.; Campeau, L.-C.; Chirik, P. J. *J. Am. Chem. Soc.* **2016**, *138*, 3314–3324.
127. Hopmann, K. H. *Organometallics* **2013**, *32*, 6388–6399.
128. Chen, J.; Chen, C.; Ji, C.; Lu, Z. *Org. Lett.* **2016**, *18*, 1594–1597.
129. (a) Noyori, R.; Ohkuma, T.; Kitamura, M.; Takaya, H.; Sayo, N.; Kumobayashi, H.; Akutagawa, S. *J. Am. Chem. Soc.* **1987**, *109*, 5856–5858. (b) Kitamura, M.; Ohkuma, T.; Inoue, S.; Sayo, N.; Kumobayashi, H.; Akutagawa, S.; Ohta, T.; Takaya, H.; Noyori, R. *J. Am. Chem. Soc.* **1988**, *110*, 629–631.
130. Ohkuma, T.; Ooka, H.; Hashiguchi, S.; Ikariya, T.; Noyori, R. *J. Am. Chem. Soc.* **1995**, *117*, 2675–2676.
131. Ohkuma, T.; Ooka, H.; Yamakawa, M.; Ikariya, T.; Noyori, R. *J. Org. Chem.* **1996**, *61*, 4872–4873
132. (a) Fujii, A.; Hashiguchi, S.; Uematsu, N.; Ikariya, T.; Noyori, R. *J. Am. Chem. Soc.* **1996**, *118*, 2521–2522. (b) Matsumura, K.; Hashiguchi, S.; Ikariya, T.; Noyori, R. *J. Am. Chem. Soc.* **1997**, *119*, 8738–8739.
133. Noyori, R.; Ohkuma, T. *Angew. Chem. Int. Ed. Engl.* **2001**, *40*, 40–73.
134. Dub, P. A.; Gordon, J. C. *Dalt. Trans.* **2016**, *45*, 6756–6781.
135. Ikariya, T.; Blacker, A. J. *Acc. Chem. Res.* **2007**, *40*, 1300–1308.
136. Ohkuma, T.; Koizumi, M.; Doucet, H.; Pham, T.; Kozawa, M.; Murata, K.; Katayama, E.; Yokozawa, T.; Ikariya, T.; Noyori, R. *J. Am. Chem. Soc.* **1998**, *120*, 13529–13530.
137. Ohkuma, T.; Koizumi, M.; Mun, K.; Hilt, G.; Kabuto, C.; Noyori, R. *J. Am. Chem. Soc.* **2002**, *124*, 6508–6509.
138. Ohkuma, T. *Proc. Jpn. Acad. Ser. B Phys. Biol. Sci.* **2010**, *86*, 202–219.
139. See, for instance: Xie, J. H.; Bao, D. H.; Zhou, Q. L. *Synthesis* **2015**, *47*, 460–471.
140. Xie, J. H.; Wang, L. X.; Fu, Y.; Zhu, S. F.; Fan, B. M.; Duan, H. F.; Zhou, Q. L. *J. Am. Chem. Soc.* **2003**, *125*, 4404–4405.
141. Liu, Y.; Cheng, L. J.; Yue, H. T.; Che, W.; Xie, J. H.; Zhou, Q. L. *Chem. Sci.* **2016**, *7*, 4725–4729.
142. Rodríguez, S.; Qu, B.; Fandrick, K. R.; Buono, F.; Haddad, N.; Xu, Y.; Herbage, M. A.; Zeng, X.; Ma, S.; Grinberg, N.; Lee, H.; Han, Z. S.; Yee, N. K.; Senanayake, C. H. *Adv. Synth. Catal.* **2014**, *356*, 301–307.
143. Matsumura, K.; Arai, N.; Hori, K.; Saito, T.; Sayo, N.; Ohkuma, T. *J. Am. Chem. Soc.* **2011**, *133*, 10696–10699.
144. Arai, N.; Satoh, H.; Utsumi, N.; Murata, K.; Tsutsumi, K.; Ohkuma, T. *Org. Lett.* **2013**, *15*, 3030–3033.
145. Palmer, M.; Walsgrove, T.; Wills, M. *J. Org. Chem.* **1997**, *62*, 5226

146. (a) Hayes, A. M.; Morris, D. J.; Clarkson, G. J.; Wills, M. A. *J. Am. Chem. Soc.* **2005**, *127*, 7318–7319. (b) Morris, D. J.; Hayes, A. M.; Wills, M. *J. Org. Chem.* **2006**, *71*, 7035–7044.
147. (a) Touge, T.; Hakamata, T.; Nara, H.; Kobayashi, T.; Sayo, N.; Saito, T.; Kayaki, Y.; Ikariya, T. *J. Am. Chem. Soc.* **2011**, *133*, 14960–14963. (b) Takasago, WO2012026201, **2012**.
148. Parekh, V.; Ramsden, J. A.; Wills, M. *Catal. Sci. Technol.* **2012**, *2*, 406–414.
149. Touge, T.; Nara, H.; Fujiwhara, M.; Kayaki, Y.; Ikariya, T. *J. Am. Chem. Soc.* **2016**, *138*, 10084–10087.
150. Jolley, K. E.; Zanotti-Gerosa, A.; Hancock, F.; Dyke, A.; Grainger, D. M.; Medlock, J. A.; Nedden, H. G.; Le Paih, J. J. M.; Roseblade, S. J.; Seger, A.; Sivakumar, V.; Prokes, I.; Morris, D. J.; Wills, M. *Adv. Synth. Catal.* **2012**, *354*, 2545–2555.
151. Soni, R.; Jolley, K. E.; Clarkson, G. J.; Wills, M. *Org. Lett.* **2013**, *15*, 5110–5113.
152. Kišić, A.; Stephan, M.; Mohar, B. *Org. Lett.* **2013**, *15*, 1614–1617.
153. Cotman, A. E.; Cahard, D.; Mohar, B. *Angew. Chem. Int. Ed.* **2016**, *55*, 5294–5298.
154. Cotman, A. E.; Lozinšek, M.; Wang, B.; Stephan, M.; Mohar, B. *Org. Lett.* **2019**, *21*, 3644–3648.
155. Wang, J.; Liu, D.; Liu, Y.; Zhang, W. *Org. Biomol. Chem.* **2013**, *11*, 3855–3861.
156. Li, J.; Zhu, Y.; Lu, Y.; Wang, Y.; Liu, Y.; Liu, D.; Zhang, W. *Organometallics* **2019**, *38*, 3970–3978.
157. Pannetier, N.; Sortais, J. B.; Issenhuth, J. T.; Barloy, L.; Sirlin, C.; Holuigue, A.; Lefort, L.; Panella, L.; De Vries, J. G.; Pfeffer, M. *Adv. Synth. Catal.* **2011**, *353*, 2844–2852.
158. Phillips, S. D.; Fuentes, J. A.; Clarke, M. L. *Chem. Eur. J.* **2010**, *16*, 8002–8005.
159. (a) Ye, W.; Zhao, M.; Du, W.; Jiang, Q.; Wu, K.; Wu, P.; Yu, Z. *Chem. Eur. J.* **2011**, *17*, 4737–4741. (b) Ye, W.; Zhao, M.; Yu, Z. *Chem. Eur. J.* **2012**, *18*, 10843–10846. (c) Chai, H.; Liu, T.; Yu, Z. *Organometallics* **2017**, *36*, 4136–4144.
160. Murata, K.; Ikariya, T.; Noyori, R. *J. Org. Chem.* **1999**, *64*, 2186–2187.
161. Xu, Y.; Cheng, T.; Long, J.; Liu, K.; Qian, Q.; Gao, F.; Liu, G.; Li, H. *Adv. Synth. Catal.* **2012**, *354*, 3250–3258.
162. Tang, S.; Jin, R.; Zhang, H.; Yao, H.; Zhuang, J.; Liu, G.; Li, H. *Chem. Commun.* **2012**, *48*, 6286–6288.
163. Zhang, H.; Jin, R.; Yao, H.; Tang, S.; Zhuang, J.; Liu, G.; Li, H. *Chem. Commun.* **2012**, *48*, 7874–7876.
164. Gao, F.; Jin, R.; Zhang, D.; Liang, Q.; Ye, Q.; Liu, G. *Green Chem.* **2013**, *15*, 2208–2214.
165. Liu, R.; Jin, R.; Kong, L.; Wang, J.; Chen, C.; Cheng, T.; Liu, G. *Chem. Asian J.* **2013**, *8*, 3108–3115.
166. Ahlford, K.; Adolfsson, H. *Catal. Commun.* **2011**, *12*, 1118–1121.
167. Nordin, M.; Liao, R. Z.; Ahlford, K.; Adolfsson, H.; Himo, F. *ChemCatChem* **2012**, *4*, 1095–1104.
168. Hu, Q.; Zhang, Z.; Liu, Y.; Imamoto, T.; Zhang, W. *Angew. Chem. Int. Ed.* **2015**, *54*, 2260–2264.
169. Hu, Q.; Chen, J.; Zhang, Z.; Liu, Y.; Zhang, W. *Org. Lett.* **2016**, *18*, 1290–1293.
170. Yang, H.; Huo, N.; Yang, P.; Pei, H.; Lv, H.; Zhang, X. *Org. Lett.* **2015**, *17*, 4144–4147.
171. Brüning, F.; Nagae, H.; Käch, D.; Mashima, K.; Togni, A. *Chem. Eur. J.* **2019**, *25*, 10818–10822.
172. Abura, T.; Ogo, S.; Watanabe, Y.; Fukuzumi, S. *J. Am. Chem. Soc.* **2003**, *125*, 4149–4154.
173. Ariger, M. A.; Carreira, E. M. *Org. Lett.* **2012**, *14*, 4522–4524.
174. Irrgang, T.; Friedrich, D.; Kempe, R. *Angew. Chem. Int. Ed.* **2011**, *50*, 2183–2186.
175. Xie, J. B.; Xie, J. H.; Liu, X. Y.; Kong, W. L.; Li, S.; Zhou, Q. L. *J. Am. Chem. Soc.* **2010**, *132*, 4538–4539.
176. Xie, J. H.; Liu, X. Y.; Xie, J. B.; Wang, L. X.; Zhou, Q. L. *Angew. Chem. Int. Ed.* **2011**, *50*, 7329–7332.
177. Xie, J. H.; Liu, X. Y.; Yang, X. H.; Xie, J. B.; Wang, L. X.; Zhou, Q. L. *Angew. Chem. Int. Ed.* **2012**, *51*, 201–203.
178. Yang, X. H.; Xie, J. H.; Liu, W. P.; Zhou, Q. L. *Angew. Chem. Int. Ed.* **2013**, *52*, 7833–7836.
179. Zhang, F. H.; Zhang, F. J.; Li, M. L.; Xie, J. H.; Zhou, Q. L. *Nat. Catal.* **2020**, *3*, 621–627.
180. Wu, W.; Liu, S.; Duan, M.; Tan, X.; Chen, C.; Xie, Y.; Lan, Y.; Dong, X. Q.; Zhang, X. *Org. Lett.* **2016**, *18*, 2938–2941.
181. Wu, W.; Xie, Y.; Li, P.; Li, X.; Liu, Y.; Dong, X. Q.; Zhang, X. *Org. Chem. Front.* **2017**, *4*, 555–559.
182. Yu, J.; Duan, M.; Wu, W.; Qi, X.; Xue, P.; Lan, Y.; Dong, X. Q.; Zhang, X. *Chem. Eur. J.* **2017**, *23*, 970–975.
183. Yin, C.; Dong, X. Q.; Zhang, X. *Adv. Synth. Catal.* **2018**, *360*, 4319–4324.
184. Tan, X.; Zeng, W.; Wen, J.; Zhang, X. *Org. Lett.* **2020**, *22*, 7230–7233.
185. Yu, J.; Long, J.; Yang, Y.; Wu, W.; Xue, P.; Chung, L. W.; Dong, X. Q.; Zhang, X. *Org. Lett.* **2017**, *19*, 690–693.
186. Wang, Y.; Yang, G.; Xie, F.; Zhang, W. *Org. Lett.* **2018**, *20*, 6135–6139.
187. Ling, F.; Nian, S.; Chen, J.; Luo, W.; Wang, Z.; Lv, Y.; Zhong, W. *J. Org. Chem.* **2018**, *83*, 10749–10761.
188. Nian, S.; Ling, F.; Chen, J.; Wang, Z.; Shen, H.; Yi, X.; Yang, Y. F.; She, Y.; Zhong, W. *Org. Lett.* **2019**, *21*, 5392–5396.
189. Wang, H.; Zhang, Y.; Yang, T.; Guo, X.; Gong, Q.; Wen, J.; Zhang, X. *Org. Lett.* **2020**, *22*, 8796–8801.
190. Janssen-Müller, D.; Schlepphorst, C.; Glorius, F. *Chem. Soc. Rev.* **2017**, *46*, 4845–4854.
191. Yoshida, K.; Kamimura, T.; Kuwabara, H.; Yanagisawa, A. *Chem. Commun.* **2015**, *51*, 15442–15445.
192. Ayya Swamy, P. C.; Varenikov, A.; de Ruiter, G. *Chem. Eur. J.* **2020**, *26*, 2333–2337.
193. Quan, X.; Kerdphon, S.; Peters, B. B. C.; Rujirawanich, J.; Krajangsri, S.; Jongcharoenkamol, J.; Andersson, P. G. *Chem. Eur. J.* **2020**, *26*, 13311–13316.
194. Filonenko, G. A.; Van Putten, R.; Hensen, E. J. M.; Pidko, E. A. *Chem. Soc. Rev.* **2018**, *47*, 1459–1483.
195. Sui-Seng, C.; Freutel, F.; Lough, A. J.; Morris, R. H. *Angew. Chem. Int. Ed.* **2008**, *47*, 940–943.
196. Sui-Seng, C.; Haque, F. N.; Hadzovic, A.; Pütz, A. M.; Reuss, V.; Meyer, N.; Lough, A. J.; Luliis, M. Z.-D. Morris, R. H. *Inorg. Chem.* **2009**, *48*, 735–743.
197. Li, Y.; Yu, S.; Wu, X.; Xiao, J.; Shen, W.; Dong, Z.; Gao, J. *J. Am. Chem. Soc.* **2014**, *136*, 4031–4039.

198. Zhang, W. J.; Ruan, S. H.; Shen, W. Y.; Wang, Z.; An, D. L.; Li, Y. Y.; Gao, J. X. *Catal. Commun.* **2019**, *119*, 153–158.
199. Bigler, R.; Mezzetti, A. *Org. Lett.* **2014**, *16*, 6460–6463.
200. Bigler, R.; Huber, R.; Mezzetti, A. *Angew. Chem. Int. Ed.* **2015**, *54*, 5171–5174.
201. (a) De Luca, L.; Mezzetti, A. *Angew. Chem. Int. Ed.* **2017**, *56*, 11949–11953. (b) De Luca, L.; Passera, A.; Mezzetti, A. *J. Am. Chem. Soc.* **2019**, *141*, 2545–2556.
202. Langer, R.; Leitus, G.; Ben-David, Y.; Milstein, D. *Angew. Chem. Int. Ed.* **2011**, *50*, 2120–2124.
203. Zuo, W.; Lough, A. J.; Li, Y. F.; Morris, R. H. *Science* **2013**, *342*, 1080–1084.
204. Lagaditis, P. O.; Sues, P. E.; Sonnenberg, J. F.; Wan, K. Y.; Lough, A. J.; Morris, R. H. *J. Am. Chem. Soc.* **2014**, *136*, 1367–1380.
205. Sonnenberg, J. F.; Wan, K. Y.; Sues, P. E.; Morris, R. H. *ACS Catal.* **2017**, *7*, 316–326.
206. Smith, S. A. M.; Lagaditis, P. O.; Lüpke, A.; Lough, A. J.; Morris, R. H. *Chem. Eur. J.* **2017**, *23*, 7212–7216.
207. Huo, S.; Wang, Q.; Zuo, W. *Dalt. Trans.* **2020**, *49*, 7959–7967.
208. (a) Elangovan, S.; Topf, C.; Fischer, S.; Jiao, H.; Spannenberg, A.; Baumann, W.; Ludwig, R.; Junge, K.; Beller, M. *J. Am. Chem. Soc.* **2016**, *138*, 8809–8814. (b) Elangovan, S.; Garbe, M.; Jiao, H.; Spannenberg, A.; Junge, K.; Beller, M. *Angew. Chem. Int. Ed.* **2016**, *55*, 15364–15368. (c) Kallmeier, F.; Irrgang, T.; Dietel, T.; Kempe, R. *Angew. Chem. Int. Ed.* **2016**, *55*, 11806–11809.
209. Widegren, M. B.; Harkness, G. J.; Slawin, A. M. Z.; Cordes, D. B.; Clarke, M. L. *Angew. Chem. Int. Ed.* **2017**, *56*, 5825–5828.
210. Garbe, M.; Junge, K.; Walker, S.; Wei, Z.; Jiao, H.; Spannenberg, A.; Bachmann, S.; Scalone, M.; Beller, M. *Angew. Chem. Int. Ed.* **2017**, *56*, 11237–11241.
211. Zirakzadeh, A.; de Aguiar, S. R. M. M.; Stöger, B.; Widhalm, M.; Kirchner, K. *ChemCatChem* **2017**, *9*, 1744–1748.
212. (a) Azouzi, K.; Bruneau-Voisine, A.; Vendier, L.; Sortais, J. B.; Bastin, S. *Catal. Commun.* **2020**, *142*, 106040. (b) Schneekönig, J.; Junge, K.; Beller, M. *Synlett* **2019**, *30*, 503–507.
213. Zhang, G. Y.; Ruan, S. H.; Li, Y. Y.; Gao, J. X. *Chin. Chem. Lett.* **2020**, *4*, 2–5.
214. Zhang, L.; Tang, Y.; Han, Z.; Ding, K. *Angew. Chem. Int. Ed.* **2019**, *58*, 4973–4977.
215. Wen, J.; Wang, F.; Zhang, X. *Chem. Soc. Rev.* **2021**, *50*, 3211–3237.
216. Li, Y. Y.; Yu, S. L.; Shen, W. Y.; Gao, J. X. *Acc. Chem. Res.* **2015**, *48*, 2587–2598.
217. Du, T.; Wang, B.; Wang, C.; Xiao, J.; Tang, W. *Chin. Chem. Lett.* **2020**, *32*, 1241–1244.
218. (a) Kim, A. N.; Stoltz, B. M. *ACS Catal.* **2020**, *10*, 13834–13851. (b) Barrios-Rivera, J.; Xu, Y.; Wills, M.; Vyas, V. K. *Org. Chem. Front.* **2020**, *7*, 3312–3342. (c) Abdine, R. A. A.; Hedouin, G.; Colobert, F.; Wencel-Delord, J. *ACS Catal.* **2021**, *11*, 215–247.
219. (a) Balakrishna, B.; Nunez-Rico, J. L.; Vidal-Ferran, A. *Eur. J. Org. Chem.* **2015**, *36*, 5293–5303. (b) Núñez-Rico, J. L.; Fernández-Pérez, H.; Vidal-Ferran, A. *Green Chem.* **2014**, *16*, 1153–1157. (c) Núñez-Rico, J. L.; Fernández-Pérez, H.; Benet-Buchholz, J.; Vidal-Ferran, A. *Organometallics* **2010**, *29*, 6627–6631.
220. Ye, Z.-S.; Guo, R.-N.; Cai, X.-F.; Chen, M.-W.; Shi, L.; Zhou, Y.-G. *Angew. Chem. Int. Ed.* **2013**, *52*, 3685–3689.
221. Shi, L.; Ye, Z. S.; Cao, L. L.; Guo, R. N.; Hu, Y.; Zhou, Y. G. *Angew. Chem. Int. Ed.* **2012**, *51*, 8286–8289.
222. Iimuro, A.; Yamaji, K.; Kandula, S.; Nagano, T.; Kita, Y.; Mashima, K. *Angew. Chem. Int. Ed.* **2013**, *52*, 2046–2050.
223. Cartigny, D.; Berhal, F.; Nagano, T.; Phansavath, P.; Ayad, T.; Genêt, J. P.; Ohshima, T.; Mashima, K.; Ratovelomanana-Vidal, V. *J. Org. Chem.* **2012**, *77*, 4544–4556.
224. Kuwano, R.; Hashiguchi, Y.; Ikeda, R.; Ishizuka, K. *Angew. Chem. Int. Ed.* **2015**, *54*, 2393–2396.
225. Feng, G.-S.; Shi, L.; Meng, F.-J.; Chen, M.-W.; Zhou, Y.-G. *Org. Lett.* **2018**, *20*, 6415–6419.
226. (a) Núñez-Rico, J. L.; Vidal-Ferran, A. *Org. Lett.* **2013**, *15*, 2066–2069. (b) Balakrishna, B.; Bauzá, A.; Frontera, A.; Vidal-Ferran, A. *Chem. Eur. J.* **2016**, *22*, 10607–10613.
227. Han, Z.; Liu, G.; Wang, R.; Dong, X.-Q.; Zhang, X. *Chem. Sci.* **2019**, *10*, 4328–4333.
228. Guo, C.; Sun, D.-W.; Yang, S.; Mao, S.-J.; Xu, X.-H.; Zhu, S.-F.; Zhou, Q.-L. *J. Am. Chem. Soc.* **2015**, *137*, 90–93.
229. Qu, B.; Mangunuru, H. P. R.; Tcyrulnikov, S.; Rivalti, D.; Zatolochnaya, O. V.; Kurouski, D.; Radomkit, S.; Biswas, S.; Karyakarte, S.; Fandrick, K. R.; Sieber, J. D.; Rodriguez, S.; Desrosiers, J.-N.; Haddad, N.; McKellop, K.; Pennino, S.; Lee, H.; Yee, N. K.; Song, J. J.; Kozlowski, M. C.; Senanayake, C. H. *Org. Lett.* **2018**, *20*, 1333–1337.
230. Wei, X.; Qu, B.; Zeng, X.; Savoie, J.; Fandrick, K. R.; Desrosiers, J. N.; Tcyrulnikov, S.; Marsini, M. A.; Buono, F. G.; Li, Z.; Yang, B. S.; Tang, W.; Haddad, N.; Gutierrez, O.; Wang, J.; Lee, H.; Ma, S.; Campbell, S.; Lorenz, J. C.; Eckhardt, M.; Himmelsbach, F.; Peters, S.; Patel, N. D.; Tan, Z.; Yee, N. K.; Song, J. J.; Roschangar, F.; Kozlowski, M. C.; Senanayake, C. H. *J. Am. Chem. Soc.* **2016**, *138*, 15473–15481.
231. Wang, T.; Zhuo, L.-G.; Li, Z.; Chen, F.; Ding, Z.; He, Y.; Fan, Q.-H.; Xiang, J.; Yu, Z.-X.; Chan, A. S. C. *J. Am. Chem. Soc.* **2011**, *133*, 9878–9891.
232. Ma, W.; Zhang, J.; Xu, C.; Chen, F.; He, Y. M.; Fan, Q. H. *Angew. Chem. Int. Ed.* **2016**, *55*, 12891–12894.
233. Yang, Z.; Chen, F.; He, Y.; Yang, N.; Fan, Q. H. *Angew. Chem. Int. Ed.* **2016**, *55*, 13863–13866.
234. Urban, S.; Ortega, N.; Glorius, F. *Angew. Chem. Int. Ed.* **2011**, *50*, 3803–3806.
235. Chen, Q.-A.; Gao, K.; Duan, Y.; Ye, Z.-S.; Shi, L.; Yang, Y.; Zhou, Y.-G. *J. Am. Chem. Soc.* **2012**, *134*, 2442–2448.
236. Lu, L.-Q.; Li, Y.; Junge, K.; Beller, M. *J. Am. Chem. Soc.* **2015**, *137*, 2763–2768.

237. Li, B.; Chen, J.; Zhang, Z.; Gridnev, I. D.; Zhang, W. *Angew. Chem. Int. Ed.* **2019**, *58*, 7329–7334.
238. Hu, Y.; Zhang, Z.; Zhang, J.; Liu, Y.; Gridnev, I. D.; Zhang, W. *Angew. Chem. Int. Ed.* **2019**, *58*, 15767–15771.
239. Zhou, S.; Fleischer, S.; Junge, K.; Das, S.; Addis, D.; Beller, M. *Angew. Chem. Int. Ed.* **2010**, *49*, 8121–8125.
240. Zhou, S.; Fleischer, S.; Junge, K.; Beller, M. *Angew. Chem. Int. Ed.* **2011**, *50*, 5120–5124.
241. Menéndez-Pedregal, E.; Vaquero, M.; Lastra, E.; Gamasa, P.; Pizzano, A. *Chem. Eur. J.* **2015**, *21*, 549–553.
242. Salomó, E.; Gallen, A.; Sciortino, G.; Ujaque, G.; Grabulosa, A.; Lledós, A.; Riera, A.; Verdaguer, X. *J. Am. Chem. Soc.* **2018**, *140*, 16967–16970.
243. Mas-Roselló, J.; Smejkal, T.; Cramer, N. *Science*, **2020**, *368*, 1098–1102.
244. Strotman, N. A.; Baxter, C. A.; Brands, K. M. J.; Cleator, E.; Krska, S. W.; Reamer, R. A.; Wallace, D. J.; Wright, T. J. *J. Am. Chem. Soc.* **2011**, *133*, 8362–8371.
245. Zhou, H.; Liu, Y.; Yang, S.; Zhou, L.; Chang, M. *Angew. Chem. Int. Ed.* **2017**, *56*, 2725–2729.
246. Chen, Y.; He, Y.; Zhang, S.; Miao, T.; Fan, Q. *Angew. Chem. Int. Ed.* **2019**, *58*, 3809–3813.
247. Huang, H.; Liu, X.; Zhou, L.; Chang, M.; Zhang, X. *Angew. Chem. Int. Ed.* **2016**, *55*, 5309–5312.
248. Gallardo-Donaire, J.; Hermsen, M.; Wysocki, J.; Ernst, M.; Rominger, F.; Trapp, O.; Hashmi, A. S. K.; Schäfer, A.; Comba, P.; Schaub, T. *J. Am. Chem. Soc.* **2018**, *140*, 355–361.
249. Tan, X.; Gao, S.; Zeng, W.; Xin, S.; Yin, Q.; Zhang, X. *J. Am. Chem. Soc.* **2018**, *140*, 2024–2027.
250. Hu, L.; Zhang, Y.; Zhang, Q.; Yin, Q.; Zhang, X. *Angew. Chem. Int. Ed.* **2020**, *59*, 5321–5325.

PART VI

ASYMMETRIC CARBON–CARBON BOND FORMING REACTIONS CHAPTER

16

ASYMMETRIC NUCLEOPHILIC ADDITION TO KETONES AND KETIMINES AND CONJUGATE ADDITION REACTIONS

Luo Ge and Syuzanna R. Harutyunyan
Stratingh Institute for Chemistry, University of Groningen, Groningen, The Netherlands

16.1. INTRODUCTION

Catalytic carbon–carbon (C–C) bond-forming reactions are essential transformations in organic chemistry, allowing the building up of molecular complexity, often with concomitant generation of carbon stereocenters. Some of the representative transformations in this regard are catalytic asymmetric nucleophilic additions to carbonyls and imines, and conjugate additions to Michael acceptors. These transformations often enjoy similar reaction conditions and chiral catalyst structures for a given class of nucleophiles. In this chapter, recent advances in three categories of reactions are described: (i) asymmetric nucleophilic addition to ketones, (ii) asymmetric nucleophilic addition to ketimines, and (iii) asymmetric conjugate addition (ACA) reactions. While the field is much broader and many great contributions have been reported since the last edition of this book, space constraints prevent all relevant literature to be covered. Instead, we limit our discussion to a selection of the most recent developments with a particular focus on works using non-stabilized nucleophiles, such as organomagnesium (Grignard), organozinc, organoboron, organozirconium, and organotitanium reagents, published since 2015 and providing references to the important reviews covering preceding period.

16.2. ASYMMETRIC NUCLEOPHILIC ADDITION TO KETONES

Chiral tertiary alcohols are an important class of building blocks, due to their widespread occurrence in bioactive natural products and pharmaceuticals, as well as their application as chiral building blocks in organic synthesis (Figure 16.1) [1–5]. Catalytic asymmetric C–C bond formation is one of the most direct methods to access single enantiomers of chiral alcohols, but generating chiral tertiary alcohols is particularly difficult.

Catalytic asymmetric hydrogenation is often used for the synthesis of chiral secondary alcohols, but cannot be applied to the formation of chiral tertiary alcohols. The main problem of generating chiral tertiary alcohols from ketones rests in their low reactivity toward nucleophilic attack (contrary to aldehydes) as well as in the challenge presented to chiral catalysts in differentiating between the two prochiral faces when the substituents on the ketone moiety are similar. Until now various methods for the synthesis of chiral tertiary alcohols have been attempted and highly successful strategies have been reported [6, 7].

Catalytic Asymmetric Synthesis, Fourth Edition. Edited by Takahiko Akiyama and Iwao Ojima.

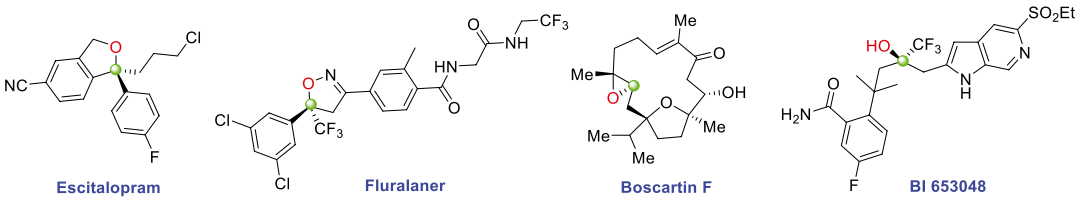

Figure 16.1. Selection of bioactive and pharmaceutically active compounds containing a chiral tertiary alcohol moiety in their structure.

Among them, the catalytic enantioselective addition of non-stabilized nucleophiles to ketones is one of the most straightforward and efficient routes. In this section, the selection of non-stabilized nucleophiles, such as Grignard reagents, organoboranes, and organotitanium reagents, is discussed.

16.2.1. Asymmetric Nucleophilic Addition of Grignard Reagents to Ketones

Organomagnesium reagents (Grignard reagents) are the most desirable organometallics in terms of cost, availability, and atom efficiency, as well as due to their high reactivity that, if well controlled, can reduce the reaction times. However, although the first publication of a Grignard reaction, for which Viktor Grignard received the Nobel Prize in Chemistry (1912), dates back to 1900, and many successful racemic and stereoselective applications were developed in the following years [8, 9], it took more than 100 years before the first catalytic asymmetric additions to both aldehydes and ketones were realized. The long delay between the discovery of these extremely useful organometallics and their first successful applications in catalytic asymmetric reactions can be attributed to the challenges of controlling (i) the extreme reactivity profiles of these reagents that result in uncatalyzed reactions; (ii) the basicity that leads to enolization; and (iii) competitive reduction through β-hydride transfer when possible. Catalytic non-asymmetric addition of Grignard reagents to ketones was reported by Ishihara and co-workers [10], using Zinc(II) salts as catalysts. However, the first step toward catalytic asymmetric Grignard reactions was taken in 2008 when the group of Harada [11] reported that highly enantioselective catalytic addition of Grignard reagents to aldehydes is possible in the presence of superstoichiometric amounts of titanium tetraisopropoxide (Scheme 16.1a). Subsequently, the group of Yus and Macia [13, 14] and the group of

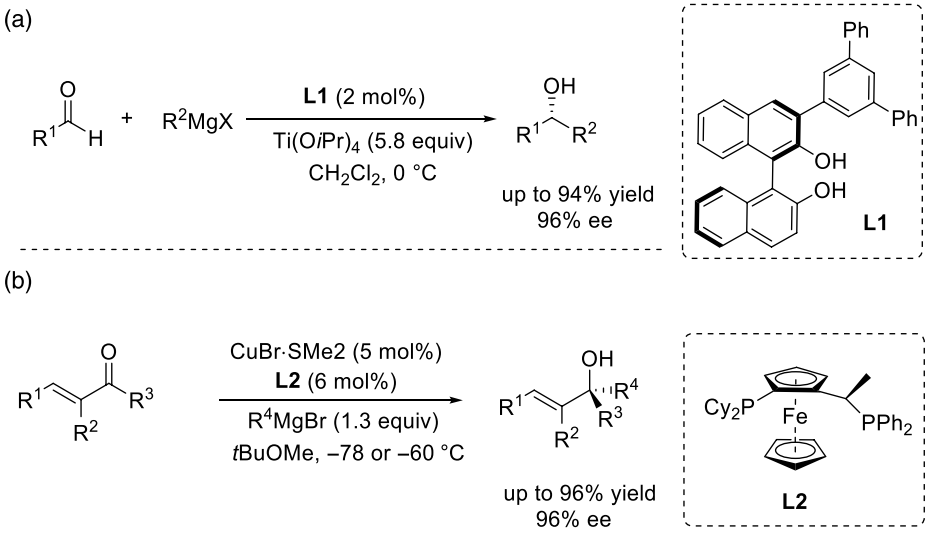

Scheme 16.1. Enantioselective addition of Grignard reagents to aldehydes catalyzed by Ti/Binol-based catalyst system (a) [11] and to α-substituted α, β-unsaturated ketones catalyzed by Cu(I)/diphosphine (b) [12].

Da [15, 16] reported additional examples and improvements for catalytic asymmetric additions of Grignard reagents to aldehydes in the presence of superstoichiometric amounts of additives.

However, the application of readily available Grignard reagents in catalytic asymmetric addition to carbonyls in the absence of additives (Grignard reaction) remained a challenge until Harutyunyan, Minnaard, and co-workers [12] reported, in 2011, the first example, namely catalytic asymmetric addition of Grignard reagents to ketones. They demonstrated that Grignard reagents could be used in the enantioselective addition to α-methyl-substituted α,β-unsaturated ketones, efficiently catalyzed by chiral copper(I)-diphosphine complexes. These reactions provide access to highly valuable chiral tertiary allylic alcohols in good yields and with moderate to excellent enantioselectivities (Scheme 16.1b). Later, this methodology was extended to α-bromo-substituted α,β-unsaturated ketones [17]. The presence of a bromo substituent constitutes an important advantage, since it can be easily transformed into a hydrogen or any other functionality with retention of the configuration, thus allowing quick building up of the structural complexity.

Importantly, the later work demonstrated that simple aryl alkyl ketones can also be subjected to Cu-catalyzed Grignard reactions, providing excellent enantioselectivities and product yields in just a few hours (Scheme 16.2a) [18]. The scope of this transformation is quite broad, both in substrates and in branched Grignard reagents, which provide the products with good enantioselectivities. On the contrary, the use of linear Grignard reagents affords the products with lower enantiomeric excesses, while MeMgBr proved completely inactive. In the same year, Harutyunyan and co-workers proved that the catalytic enantioselective alkylation of diaryl ketones is also possible, although enantioselectivities are lower and a mixture of Lewis acids is required to avoid Grignard-reagent-induced reduction of the ketones [19]. In 2015, Harutyunyan and co-workers [20] applied the copper(I)-based catalytic system in addition reactions of alkyl Grignard reagents to acylsilanes, thus allowing the first general synthesis of chiral tertiary α-silyl alcohols. This method provides access to a range of aryl- and vinyl-substituted α-hydroxysilanes bearing a tetrasubstituted chiral carbon atom, with yields of up to 97% and enantioselectivities of up to 96% (Scheme 16.2b). It should be noted that mixtures of Lewis acids were required to prevent the side reactions resulting from reduction of the carbonyl group. The main drawbacks of copper-catalyzed asymmetric Grignard reactions are the poor yields and nearly racemic products when using MeMgBr and the racemic products obtained with arylmagnesium reagents.

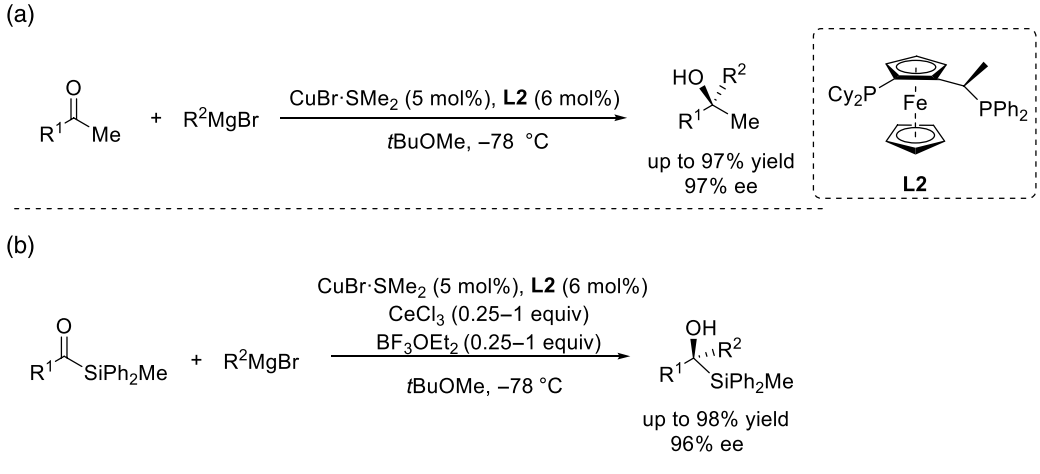

Scheme 16.2. Cu(I)-catalyzed enantioselective addition of Grignard reagent to ketones (a) [18] and acyl silanes (b) [20].

Catalytic asymmetric arylations of ketones with Grignard reagents remained unsolved until 2014, when Yus, Maciá, and co-workers [21] reported a new catalytic system based on 1,1'-Bi-2-naphthol (BINOL) derivative (**L5**) (Scheme 16.3a). They showed that arylation of various ketones with Grignard reagents in the presence of 10 equivalent of $Ti(OiPr)_4$ can be promoted by 20 mol% of **L5**, affording the

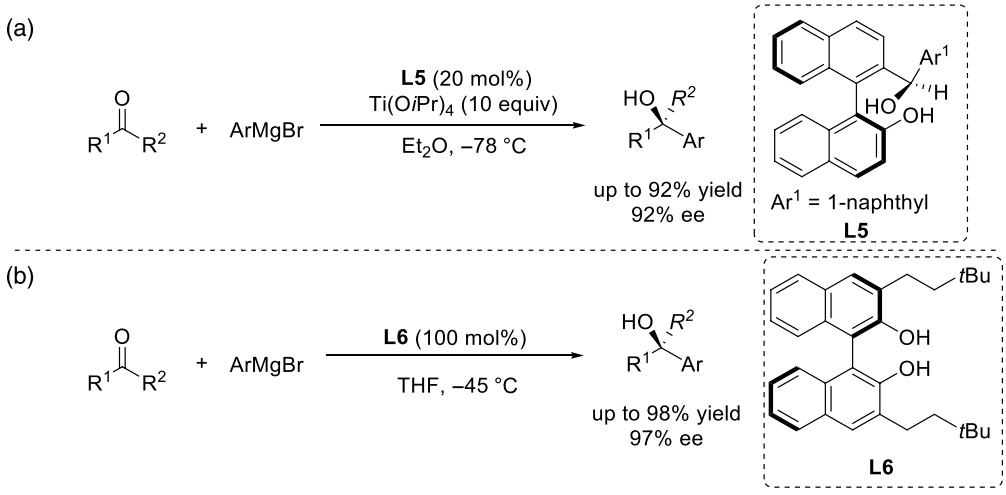

Scheme 16.3. Arylation of ketones catalyzed by Ti/Binol (a) [21] and Mg/Binol (b) based catalyst systems [22].

corresponding tertiary alcohols with up to 92% yields and 92% ees. The main drawback of this methodology is the large amount of $Ti(OiPr)_4$ required to achieve high yields.

Finally, in 2016, Nakajima and co-workers [22] found that arylation of ketones with Grignard reagents can be achieved without the need of additives in the presence of catalytic amounts of BINOL derivative (**L6**). The products were obtained with good yields and high ees (Scheme 16.3b). It should be mentioned that aliphatic ketones were not well tolerated in both cases.

16.2.2. Asymmetric Nucleophilic Addition of Organoboron Reagents to Ketones

Organoboron compounds constitute one of the most diverse classes of reagents in organic synthesis, providing access to a wide range of transformations. These reagents are considered very good nucleophiles due to their wide availability, stability, non-toxicity, and broad functional group tolerance. Furthermore, their susceptibility to transmetallation reactions with various transition metals renders them useful for transition-metal-catalyzed catalytic carbon–carbon bond-forming reactions [7, 23, 24]. In contrast to Grignard reagents, which typically require temperatures below 0 °C to avoid background non-catalyzed reactions, organoboron reagents' much lower reactivities demand temperatures above ambient to allow even the catalytic reactions. Thanks to these features, organoboron reagents have been successfully applied in catalytic asymmetric synthesis of chiral tertiary alcohols [25–29]. In this section, a selection of the recent developments in this area since 2015 is discussed, divided into three categories: arylations, allylations, and propargylation reactions.

16.2.2.1. Arylation Reactions In 2016, Tang and co-workers [30] reported that an [Rh]/**L7**-complex-catalyzed addition of arylboroxines to aryl ketones provided the corresponding chiral alcohols with up to 97% yield and 99% ee. This methodology enjoys a broad substrate scope and good functional group compatibility and it was in the synthesis of a natural product *Escitalopram* (Scheme 16.4).

Apart from simple aryl alkyl ketones, β-branched keto esters have also been employed as carbonyl substrates in arylations with organoboron reagents. In 2017, Johnson and co-workers [31] presented an enantioconvergent arylation of racemic β-alkyl-substituted α-keto esters catalyzed by a chiral rhodium-diene complex [Rh]/**L8**. A wide range of complex aryl glycolate derivatives could be obtained in good yields with excellent enantiomeric purities and diastereoselectivities (Scheme 16.5a). This is an example of a dynamic kinetic arylation and it was found that the nature of the amine base additive has a significant influence on the rate of substrate racemization. Interestingly, as the authors noted, despite the long-standing use of transition metal catalysts in dynamic kinetic hydrogenations, the title reaction is a rare case of installing C–C bonds in dynamic kinetic additions to carbonyl electrophiles.

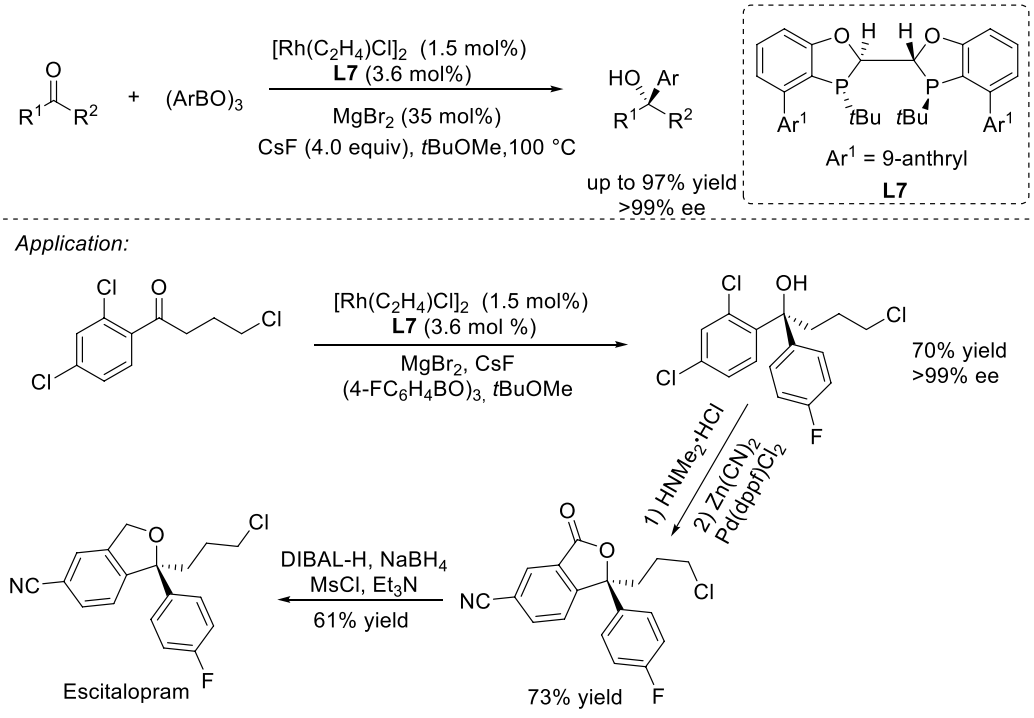

Scheme 16.4. Rh(I)-catalyzed enantioselective addition of arylboroxines to ketones [30].

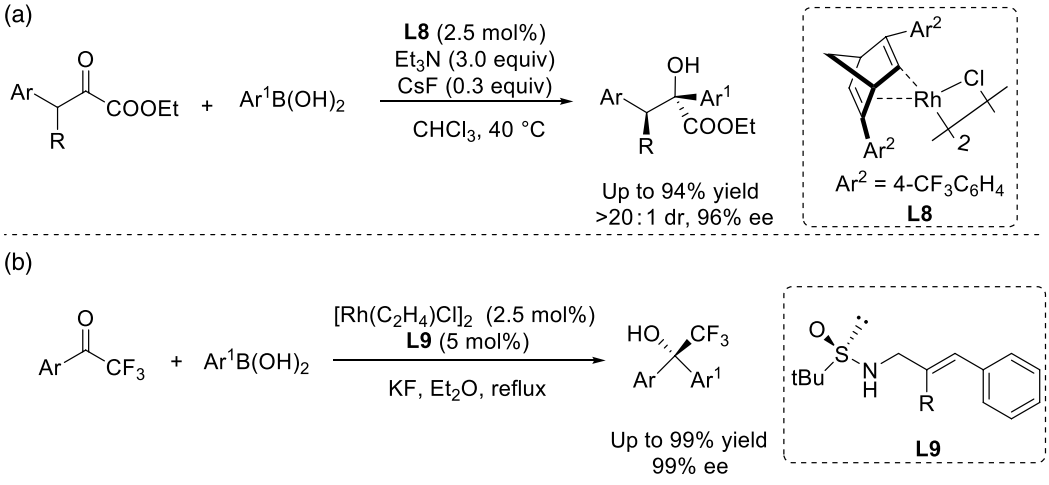

Scheme 16.5. Rh-catalyzed enantioselective arylation of keto esters (a) [31] and trifluoromethyl ketones (b) with arylboronic acids [32].

In 2018, Fernandez and co-workers [32] reported an air and moisture stable sulfinamide/olefin-based chiral ligand (**L9**), allowing the enantioselective rhodium-catalyzed addition of aryl-boronic acids to trifluoromethyl ketones. The new synthesized ligand allows the use of hindered boronic acids and leads to the formation of various chiral trifluoromethyl-substituted tertiary alcohols (Scheme 16.5b).

In the past years, there have been several reports using noble metal (e.g. rhodium) based chiral catalysts for asymmetric arylboration of simple ketones [30–32]. However, the use of earth-abundant metal-based

catalysts, such as Ni and Cu, for the synthesis of chiral tertiary alcohols remains to be established further. Very recently, Shi's group [33] reported an [Ni]/**L10** complex that catalyzes the arylboration of ketones, affording the corresponding chiral tertiary alcohols in up to 99% yield and 98% ee (Scheme 16.6). This reaction has a broad substrate scope (more than 70 examples) and good functional group compatibility. Also, various densely functionalized medicinally relevant substrates were tolerated.

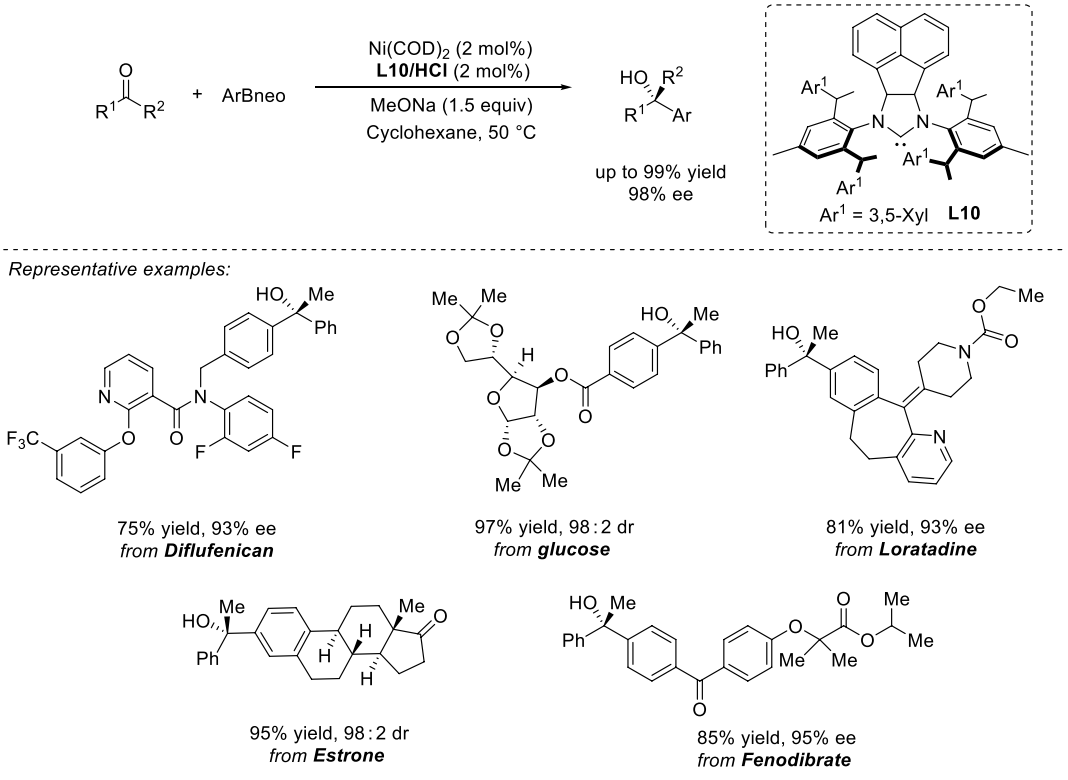

Scheme 16.6. Ni-catalyzed enantioselective arylation of ketones with organoboronic esters [33].

In the same year, Fang and co-workers [34] disclosed that a [Cu]/**L11** complex could be used in enantioselective intramolecular addition of aryl pinacol boronic esters to ketones. This methodology provides a facile method to access various chiral 2,3-dihydrobenzofuran-3-ol derivatives in good yields with excellent enantioselectivities (Scheme 16.7).

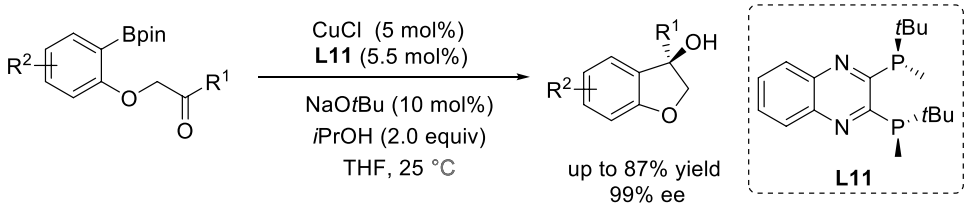

Scheme 16.7. Cu(I)-catalyzed enantioselective intramolecular addition of aryl pinacol boronic esters to ketones [34].

16.2.2.2. Allylation Reactions Chiral tertiary alcohols bearing an allylic group are very important building blocks in organic synthesis, which has prompted significant development in this area [35, 36]. In 2015, Szabo and co-workers [37] reported that chiral BINOL derivatives can catalyze allylboration of ketones with γ-disubstituted allylboronic acids. Varieties of ketones were suitable for this transformation, providing the corresponding products in high yields (up to 98%) and excellent enantio- and diastereoselectivities (Scheme 16.8). Significantly, this method allowed access to all four possible product stereoisomers with excellent results via an appropriate choice of the chiral catalyst and the stereoisomeric phenyl substrate.

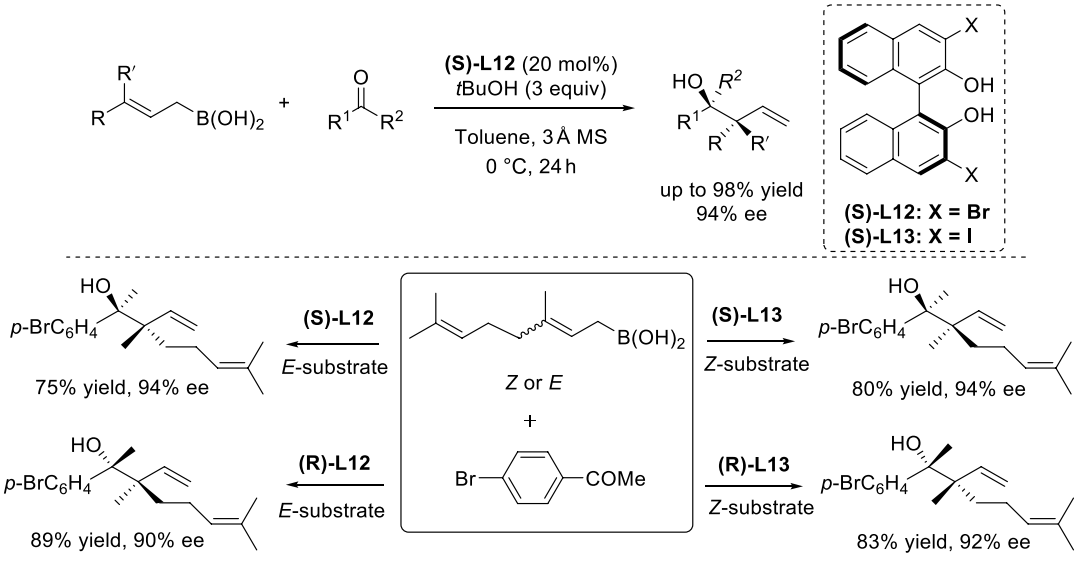

Scheme 16.8. Catalytic enantio- and diastereoselective synthesis of adjacent quaternary stereocenters by asymmetric allylboration [37].

In 2016, the aminophenol-based catalyst (**L14**) catalyzed addition of allyl and allenyl organoboron reagents to fluorine-substituted ketones was reported by Hoveyda and co-workers (Scheme 16.9a) [38]. The authors showed that various tertiary homoallylic alcohols can be obtained with up to 98% yield and >99% enantiomeric purity. To highlight the efficiency of the proposed strategy, the authors applied the methodology to a concise enantioselective synthesis of the antiparasitic drug *fluralaner* (*Bravecto*) (Scheme 16.9e). They also found that ammonium–organofluorine interactions play a key role in controlling the enantioselectivity of the reaction. Later, this protocol was extended to the synthesis of fluoroalkylated *Z*-homoallylic tertiary alcohols via enantioselective addition of *Z*- or *E*-γ-substituted boronic acid pinacol esters to fluoroalkyl-substituted ketones (Scheme 16.9b) [39]. In this approach, both *Z*- and *E*-γ-substituted boronates were well tolerated. With a *Z*-organoboron reagent, additions to ketones proceeded in high yields, 97 : 3 α : γ selectivity, >95 : 5 *Z : E* selectivity, and ees up to 98%. Transformations were similarly efficient and α- and *Z*-selective when an *E*-allylboronate compound was used, although the enantioselectivities were lower.

Recently, this strategy was applied in additions to simple ketones and α-keto esters [40]. For ketone substrates, a bulkier ligand (**L15**) was used (Scheme 16.9c), while for α-keto ester a less bulky ligand (**L16**) was required (Scheme 16.9d). Both substrates were well tolerated. Using this method, asymmetric synthesis of a lactone derivative, a key intermediate that has been converted to antiviral nucleoside analogues has been synthesized (Scheme 16.9f). Very recently, the substrate scope was expanded to ketones containing a tri-, di-, or mono-halomethyl moiety [41]. The reactions require only 0.5–5.0 mol% of chiral

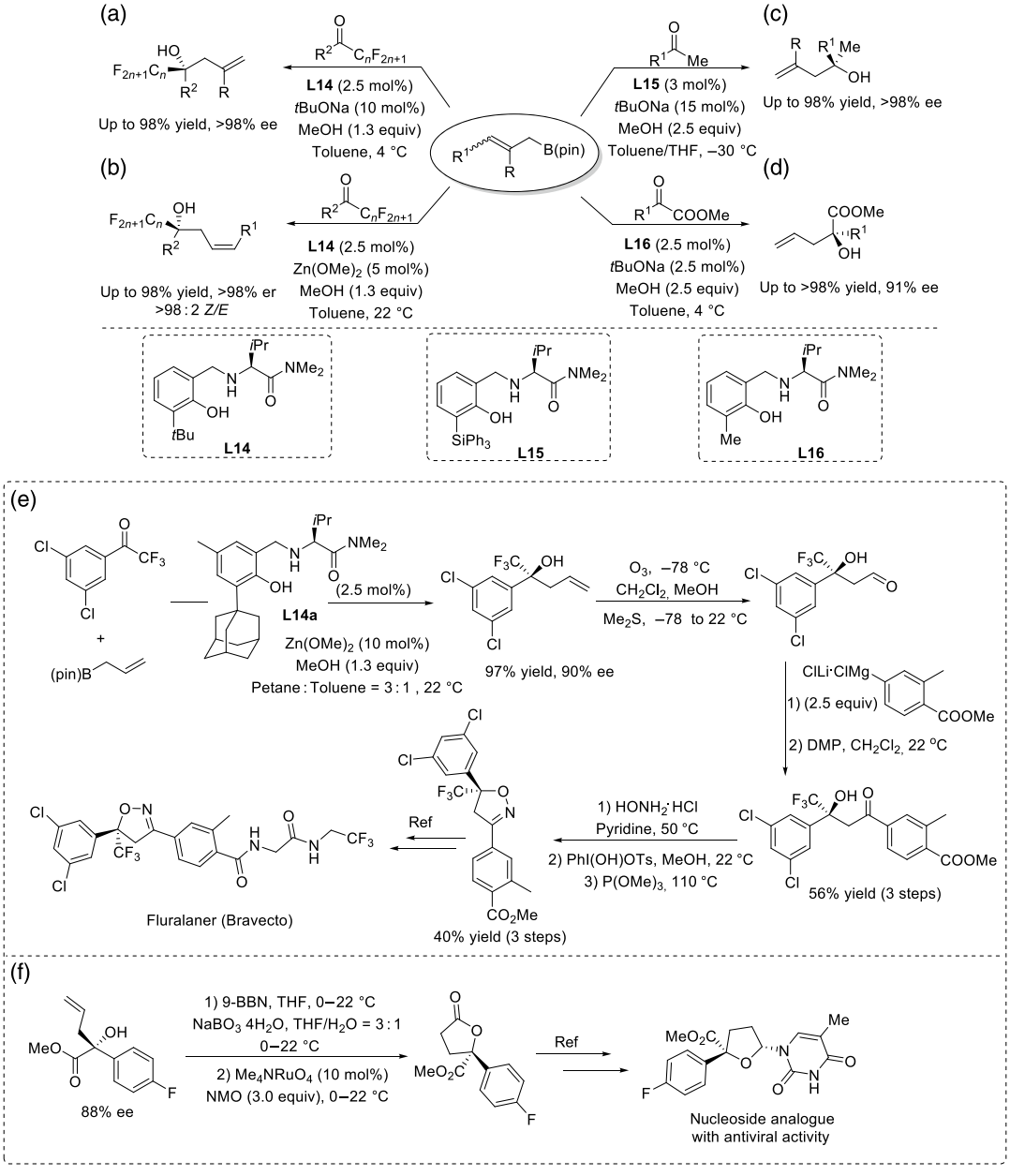

Scheme 16.9. Addition of allyl and allenyl organoboron reagents to ketones, catalyzed by chiral aminophenol derivatives [38–40].

ligand and afford products in high yields and up to 98% enantiomeric excess (Scheme 16.10). Importantly, this approach offers an expeditious route to the enantioselective synthesis of versatile 2,2-disubstituted epoxides that contain an easily modifiable alkene. This methodology was successfully applied to the synthesis of a chiral 2,2-disubstituted epoxide, a key intermediate in the synthesis of *Boscartin F*.

In 2019, a newly designed C_2-symmetric chiral-substituted 1,16-dihedroxytetraphenylene (**L17**) was reported by Chang and co-workers [42]. This chiral ligand was successfully used in the asymmetric allylboration of a variety of ketones, generating several tertiary alcohols in moderate to good yields and up to 99% ee (Scheme 16.11).

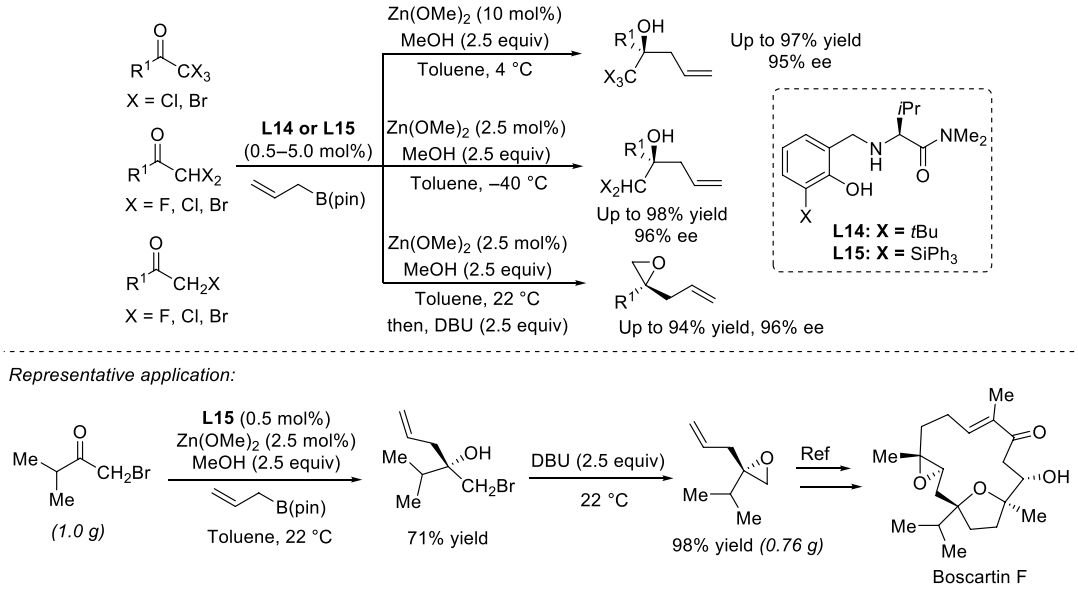

Scheme 16.10. Enantioselective allylation of ketones containing a tri-, a di-, or a monohalomethyl moiety [41].

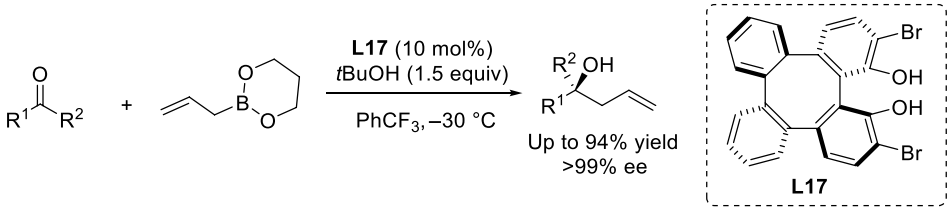

Scheme 16.11. Enantioselective allylboration of ketones catalyzed by 1,16-dihedroxytetraphenylene [42].

16.2.2.3. Propargylation Reactions The catalytic asymmetric synthesis of homopropargylic tertiary alcohols is typically achieved via propargylation of ketones. However, the developments in this direction are still limited. Apart from the reactivity issue, the isomerization of propargyl- and allenylmetal species poses additional hurdles for the regioselectivity and enantioselectivity. Since the first report by Shibasaki and co-workers [43] in 2010 on catalytic enantioselective propargylation of ketones, several methods have been developed and efforts in this area are continuing.

In 2015, Kobayashi and co-workers [44] reported a regioselective propargylation of ketones using boronate derivatives as the nucleophiles. In the presence of $Zn(HMDS)_2$ and a chiral ligand (**L18**), the propargylation product was obtained with 92% yield and 90% ee (Scheme 16.12).

Hoveyda and co-workers [45] recently presented a method for the synthesis of chiral tertiary alcohols utilizing a combination of Lewis acid, $Zn(OMe)_2$, and activated chiral aminophenol-based ligand (**L19**). This method was applicable to aryl-, heteroaryl-, alkyl-, alkynyl-, and alkenyl-substituted trifluoromethyl

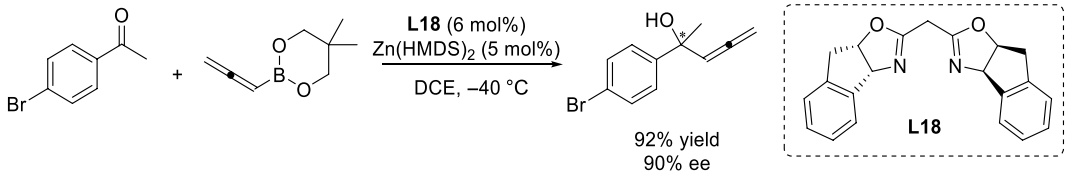

Scheme 16.12. Zn(II)-catalyzed enantioselective allenylation of ketones [44].

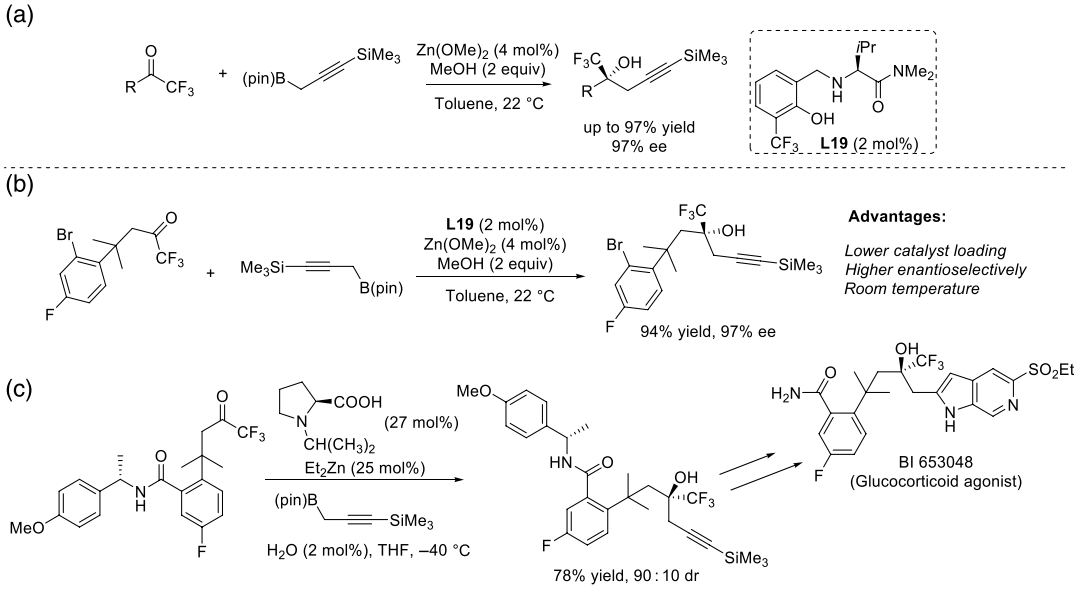

Scheme 16.13. Catalytic enantioselective propargylation of trifluoromethyl ketones [45, 46].

ketones (Scheme 16.13a). In particular, the use of a complex ketone substrate was also tolerated, providing the desired homopropargyl alcohol (Scheme 16.13b), a key precursor for the synthesis of glucocorticoid agonist *BI 653048* (Scheme 16.13c) [46]. Compared with the previous work, this approach was more efficient, namely higher asymmetric induction at room temperature using lower catalyst loading was obtained.

The use of sterically encumbered tri- and tetrasubstituted allenylboronic acids for the synthesis of highly enantioenriched tertiary homopropargyl alcohols was developed by Szabo and co-workers [47]. This methodology provides a facile route to various chiral enantioenriched alcohols in good yields (Scheme 16.14).

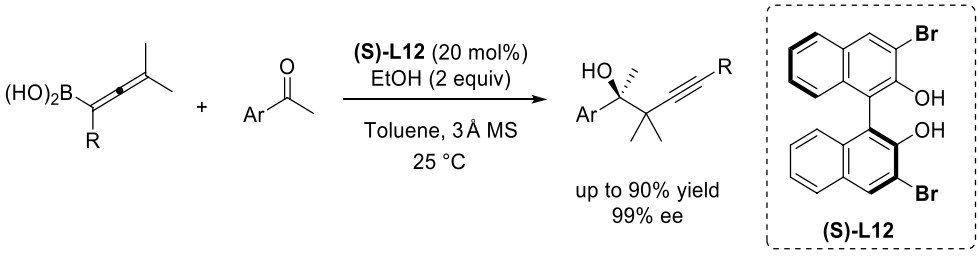

Scheme 16.14. Catalytic enantioselective propargylation of aryl ketones [47].

16.2.3. Asymmetric Nucleophilic Addition of Organotitanium Reagents to Ketones

In 2015, Gau and co-workers [48] reported the enantioselective arylation of ketones using organotitanium reagents. For this transformation, **L20** was used as a chiral ligand and $MgBr_2$ as an additive, both in substoichiometric amounts (Scheme 16.15a). Interestingly, aliphatic ketones, which are commonly more difficult substrates than their aromatic analogues, showed substantially improved reactivity in this case, albeit with relatively low enantioselectivity. In 2017, on the other hand, Harada and co-workers [49] developed a straightforward method for the catalytic asymmetric arylation and heteroarylation of ketones with organotitanium reagents generated in situ from $ClTi(OiPr)_3$ and aryl- and heteroaryllithium

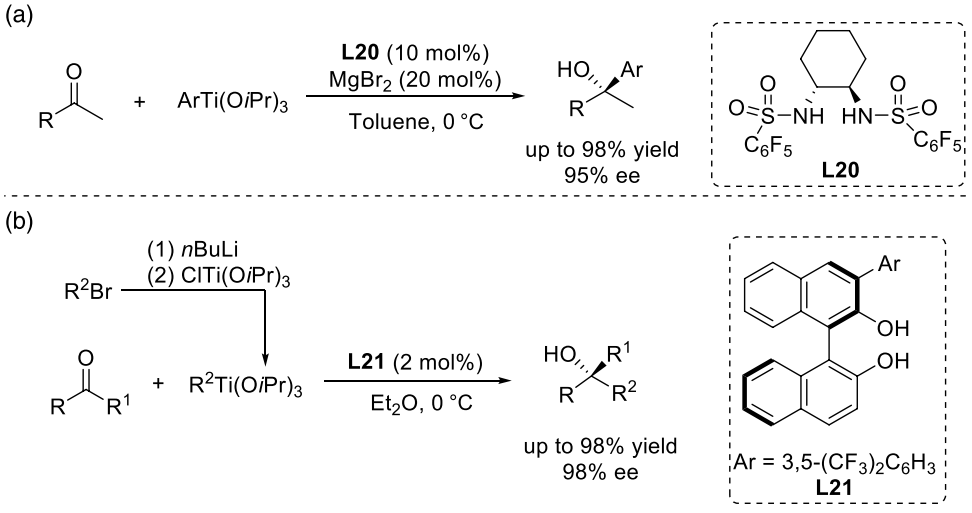

Scheme 16.15. Catalytic enantioselective arylation of ketones with organotitanium reagents using chiral derivatives of sulfonamides (a) [48] and binols (b) as chiral ligands [49].

reagents (Scheme 16.15b). With this method, various enantioenriched tertiary homopropargylic alcohols were obtained with good enantioselectivities. A number of enantioenriched tertiary alcohols could be synthesized on a gram scale using this one-pot procedure, and ligand **L21** could be recovered and reused.

16.3. ASYMMETRIC NUCLEOPHILIC ADDITION TO KETIMINES

Chiral C-tertiary amines are an important motif present in many pharmaceuticals, alkaloids, agrochemicals, and functional organic molecules (Figure 16.2) [50]. The asymmetric addition of organometallic reagents to C=N double bonds is a fundamentally important transformation that can provide direct access to these enantiomerically enriched α-chiral amines. In particular, such additions to ketimines are the most straightforward strategy for the synthesis of chiral C-tertiary amines, which are difficult to access otherwise, due to the simultaneous construction of the carbon skeleton and the stereocenters.

The first catalytic asymmetric addition of non-stabilized organometallics to aldimines via Lewis base activation reported by Soai and co-workers [51] and the Lewis acid activated copper-catalyzed organozinc additions to aldimines by Tomioka and co-workers [52] were important steps. These initial reports triggered intensive research efforts in this area, leading to the development of a number of successful catalytic asymmetric methodologies for the addition to aldimines [35, 53–59]. In contrast, the progress in the catalytic asymmetric addition of organometallics to ketimines, leading to α-tertiary chiral amines, has been much slower, owing to the poorer electrophilicity of the ketimines and the more difficult enantiodiscrimination

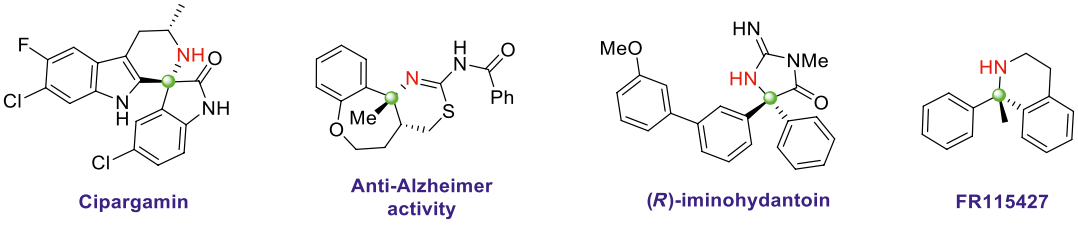

Figure 16.2. Selection of bioactive and pharmaceutically active compounds containing a chiral carbon tertiary (C-tertiary) amine moiety in their structure.

between the two substituents on the prochiral azomethine carbon [7, 60]. Although several elegant examples of arylation, alkynylation, and allylation of ketimines have been reported recently [61–67], the reactivity and selectivity issues described above remain challenging, particularly for alkylation, which even now is restricted to methylation and ethylation of a small set of activated ketimines [68–70].

In this section, examples of catalytic asymmetric additions to ketimines using Grignard and organoboron reagents reported since 2015 are presented.

16.3.1. Asymmetric Nucleophilic Addition of Grignard Reagents to Ketimines

Strong nucleophiles could compensate for the lower electrophilicity of ketimines, which is one of the major problems in this type of chemistry. Highly reactive organomagnesium reagents are the most commonly used organometallics both in the laboratory and in industry [71] and would be ideal for tackling the low reactivity of the ketimines, but to date Grignard reagents have been used solely in combination with chiral ketimines derived from Ellman's auxiliary [72]. Given the fact that the uncatalyzed addition of the Grignard reagent is a formidable competitor, this may not be surprising. Also, the increased basicity implied by the higher nucleophilicity can cause deprotonation and therefore enamide formation when enolizable ketimines are used [73]. As a result, catalytic asymmetric additions of Grignard reagents to enolizable ketimines have so far remained elusive.

In 2016, Harutyunyan and co-workers [74] reported the use of Grignard reagents as suitable nucleophiles in the catalyzed and highly enantioselective addition to silylated ketimines leading to a wide variety of *N*-protected α-chiral silyl amines with tetrasubstituted carbon stereocenters (Scheme 16.16a). While aryl sulfonyl protecting groups provided the best results, this protocol was compatible with a variety of functional groups. The enantioselection of the methodology was conditioned to the substituents at the silyl group, with $SiPh_2Me$ affording the highest ee. In contrast to the results with ketones, this chemistry also works with the less reactive MeMgBr, providing the corresponding product with good enantiomeric purity. Following this initial report, the methodology was further extended to the more challenging enolizable ketimines (Scheme 16.16b) [75]. The use of copper(I) salt in combination with chiral ligand (**L2**) led to a robust methodology that tolerates both linear and branched Grignard reagents. Remarkably, excellent chemoselectivity was observed with ketimine substrates bearing vinyl, ester, and cyano moieties in the aromatic ring, known for their reactivity toward Grignard reagents.

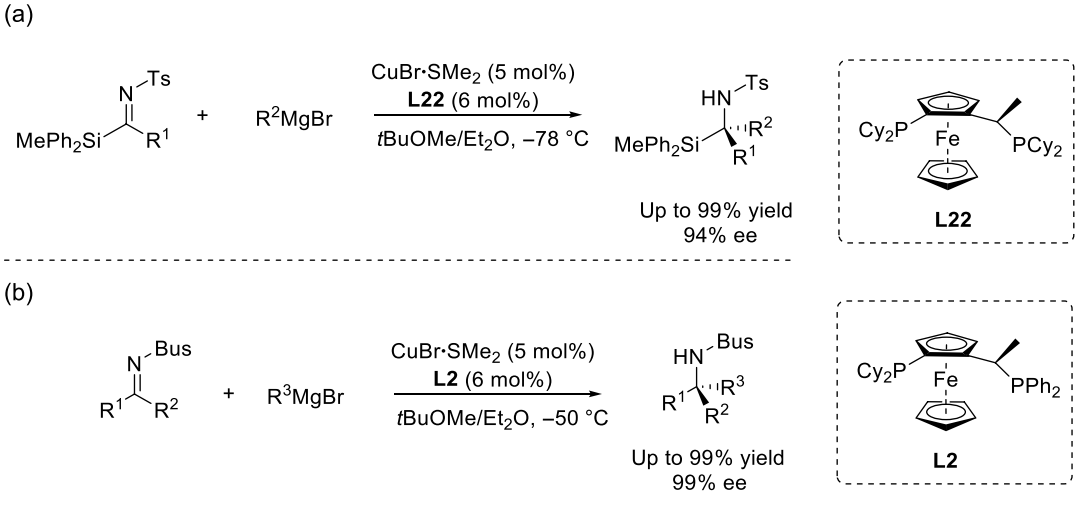

Scheme 16.16. Cu(I)-catalyzed enantioselective alkylation of silyl/aryl (a) [74] and alky/aryl (b) sulfonyl protected ketimines [75].

16.3.2. Asymmetric Nucleophilic Addition of Organoboron Reagents to Ketimines

Transition-metal-catalyzed enantioselective addition of organoboron reagents to ketimines has seen much progress over the past few years. Rhodium is the most commonly used among these metals, but recently catalysts derived from other transition metals, such as palladium, nickel, copper, and cobalt, were also reported to catalyze asymmetric addition of organoboron reagents to ketimines. In this section, the development of additions to ketimines catalyzed by these five metals is described.

16.3.2.1. Rh-Catalyzed Enantioselective Additions of Organoboron Reagents to Ketimines Since Shintani and Hayashi [62] reported their pioneering work on the asymmetric addition of organoboron reagents to *N*-tosyl ketimines with chiral Rh catalysts in 2010 (Scheme 16.17a), several new developments in this area have emerged. However, achieving excellent enantiocontrol with a broad substrate scope still represents a challenging task [64, 76, 79, 80]. In 2015, Xu and co-workers [77] reported an efficient Rh-catalyzed asymmetric arylation. Various cyclic *N*-sulfonyl ketimines reacted smoothly with organoboron reagents in the presence of a simple chiral Rh/**L24** complex to give α-arylalkyl-substituted benzosultams and benzosulfamidates with excellent enantioselectivities (Scheme 16.17b). Importantly, the methodology was applied to the synthesis of an *N*-Methyl-D-aspartate (NMDA) antagonist-*FR115427* and

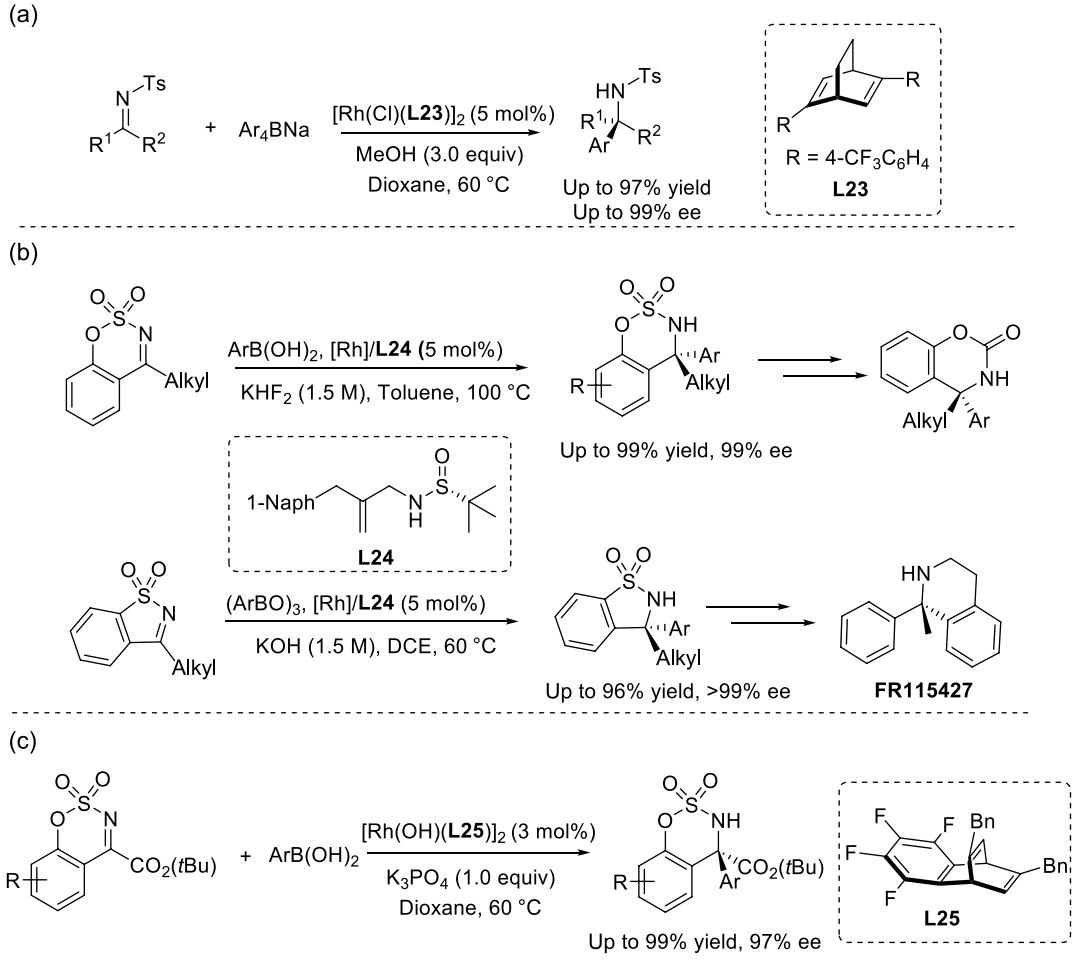

Scheme 16.17. Rh(I)-catalyzed enantioselective arylation of acyclic (a) [62], cyclic (b) [77], and α-ester substituted (c) sulfonyl protected ketimines with organoboron reagents [78].

a chiral benzoxazinone derivative. Later, Nishimura and co-workers [78] developed an Rh/**L25**-based catalytic system to promote the asymmetric addition of arylboronic acids to cyclic aromatic ketiminoesters, providing the corresponding products in high yields and enantiopurities (Scheme 16.17c). Notably, the product could be transformed into a linear α,α-diaryl-α-*N*-methylamino acid ester by reductive cleavage of a carbon–oxygen bond of the cyclic structure.

Also in 2015, Mondschein and co-workers [81] described an [Rh]/**L26-**complex-catalyzed enantioselective arylation of cyclic ketimines for the synthesis of chiral α-tertiary amines. The utility of this protocol was demonstrated by converting one of the addition products into an enantiopure α,α-diaryl-substituted amino acid (Scheme 16.18a).

Later, Xu and co-workers [82] reported that chiral phosphite-based olefin ligand (**L27**) can be successfully applied in Rh-catalyzed asymmetric arylation of 4-aryl 3-oxo-1,2,5-thiadiazol 1,1-dioxides, providing quick access to gem-diaryl-substituted sulfahydantoins with excellent enantioselectivities (Scheme 16.18b). The products resulting from this approach could be easily converted to α,α-diaryl-α-amino acid derivatives as well. An enantioselective synthesis of (*R*)-iminohydantoin, a promising beta-site APP cleaving enzyme 1 (BACE1) inhibitor for treating Alzheimer's disease, was performed using this strategy. This methodology was subsequently expanded by Xu and co-workers [83] to non-benzofused five-membered *N*-sulfonyl alkylketimines utilizing a simple branched chiral sulfur-olefin (**L24**) as the ligand, obtaining good yields and enantioselectivities (Scheme 16.18c).

In 2019, Xu and co-workers [84] reported rhodium-catalyzed asymmetric arylation of isatin-derived *N*-Boc ketimines utilizing **L28** as ligand (Scheme 16.19a). The method has a broad substrate scope, providing access to various valuable 3-aryl-3-aminooxindoles bearing a stereodefined quaternary carbon center in moderate to good yields (up to 98%) with excellent enantioselectivities (up to 98%). It should be pointed out that a range of biologically interesting complex molecules could be synthesized via this methodology. In the same year, the use of *N*-unprotected ketimines as the electrophilic acceptors for the enantioselective arylation reactions was first developed by Tang and co-workers [85]. This method provides a direct way to synthesize *C*-tertiary amines and also enables an efficient enantioselective synthesis of the antimalarial agent *Cipargamin* (Scheme 16.19b).

16.3.2.2. Pd-Catalyzed Enantioselective Additions of Organoboron Reagents to Ketimines After a few Pd-catalyzed enantioselective additions of organoboron reagents to ketimines had been developed [65, 86], Zhang and co-workers [87] reported in 2015 an addition reaction to cyclic *N*-sulfonyl ketimine esters (Scheme 16.20a). A series of α-tertiary amino esters was synthesized in excellent yields (up to 99%) and enantioselectivities (up to 99%) under mild reaction condition via this method. A year later, Zhou and co-workers [88] extended the Pd-catalyzed arylation reactions to cyclic α-ketiminophosphonates (Scheme 16.20b). They used a chiral palladium phosphino-oxazoline catalyst ([Pd]/**L31**), providing an efficient and facile route to enantioenriched quaternary α-aminophosphonates.

In 2015, Lassaletta and co-workers [89] developed a chiral pyridine–hydrazone ligand (**L32**) that allowed palladium-catalyzed addition of boronic acids to cyclic sulfonylketimines (Scheme 16.21). Apart from saccharin-derived cyclic ketimines, the catalytic system was also applied to more challenging 3,4-disubstituted 1,2,5-thiadiazole 1,1-dioxides, furnishing high yields (up to 99%) and enantioselectivities (up to 98%) along with high regioselectivities for unsymmetrically substituted derivatives.

Cyclic ketimines bearing fluoroalkyl groups, such as trifluoromethyl and perfluoroalkyl, have captured significant attention from synthetic chemists, due to their prominence in medicinal chemistry. In 2016, Lu, Hayashi, and co-workers [90] described palladium-catalyzed asymmetric arylation of 2-quinazolinone derivatives bearing fluoroalkyl groups, offering the corresponding products with high enantiopurity (Scheme 16.22). This method provides an efficient route for enantioselective synthesis of chiral trifluoromethylated and perfluoroalkylated 2-quinazolinones.

In 2016, Zhang and co-workers [91] reported the enantioselective arylation of 3-ketimino oxindoles utilizing a [Pd]/**L34** complex, providing various chiral 3-amino-2-oxindoles with a quaternary stereocenter (Scheme 16.23a). Asymmetric addition of arylboronic acids to isatin-derived *N*-Boc ketimines was reported by Jiang and co-workers [92] using a chiral catalyst based on palladium combined with chiral

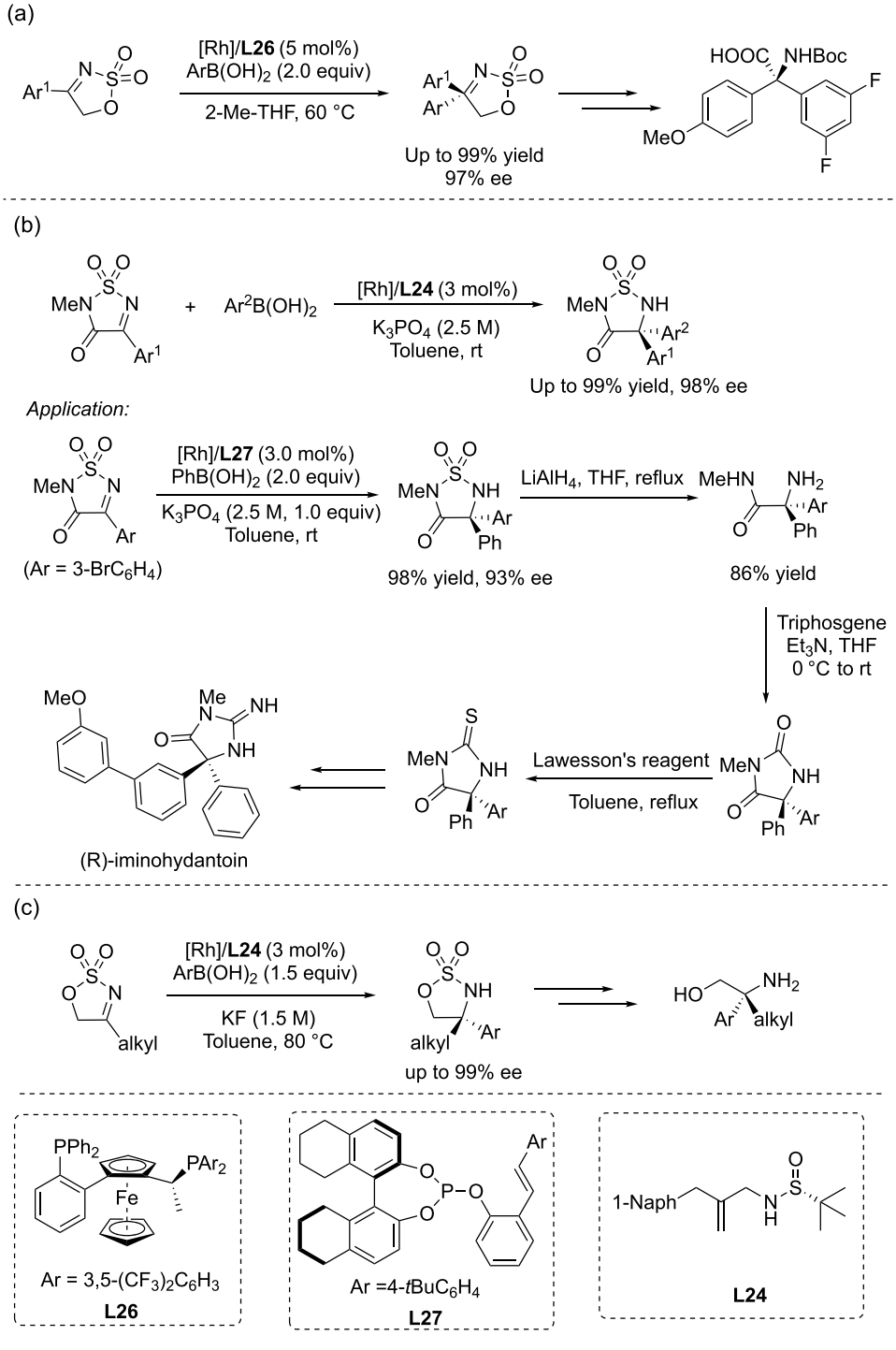

Scheme 16.18. Rh(I)-catalyzed enantioselective additions of arylboronic acids to cyclic ketimines [81–83].

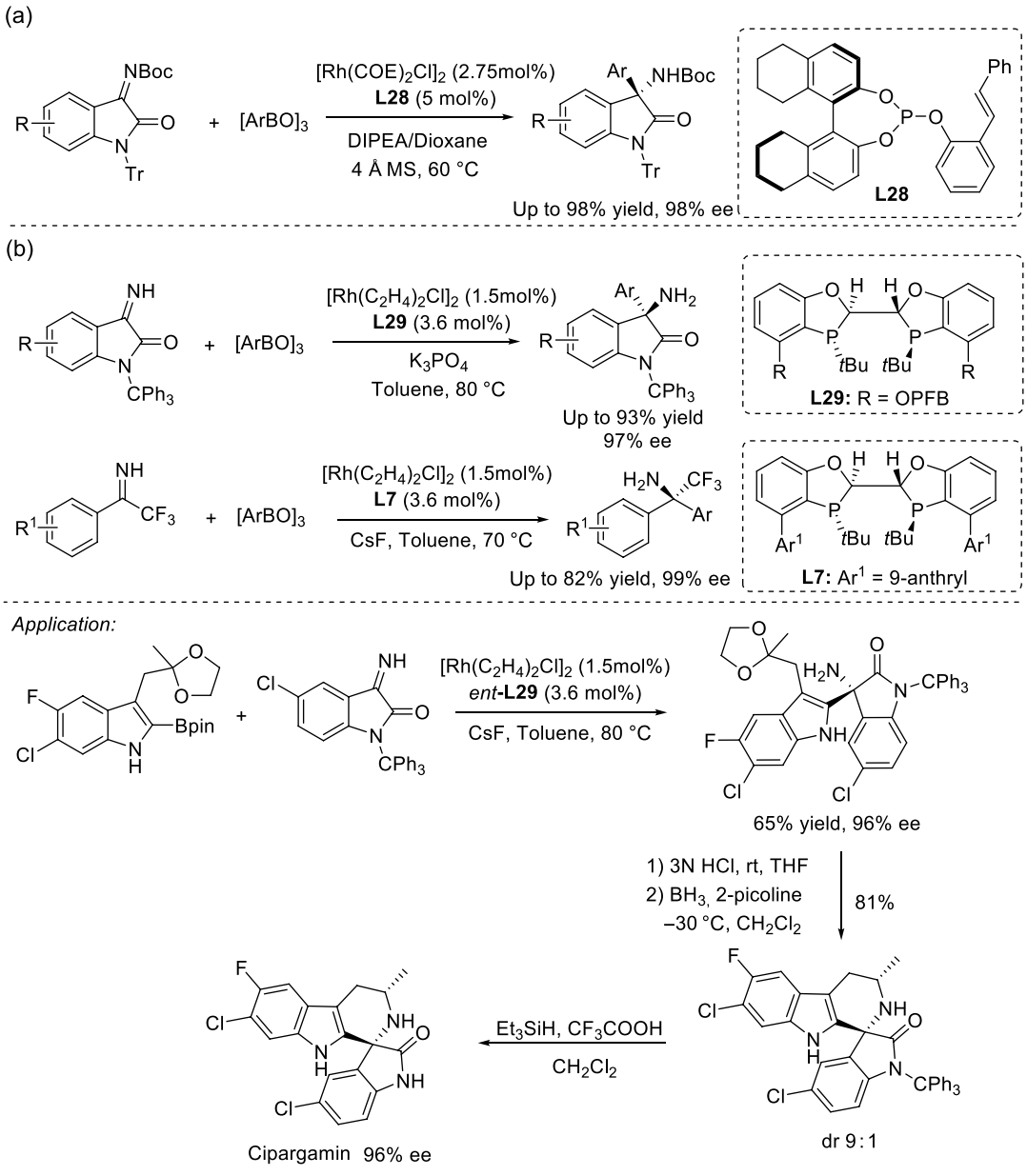

Scheme 16.19. Rh(I)-catalyzed enantioselective arylation of isatin-derived N-Boc protected (a) [84] and N-unprotected (b) ketimines [85].

N-sulfonyl bisimidazoline (Bim) ligand **L35** (Scheme 16.23b). This air stable [Pd]/**L35** catalytic system enables highly enantioselective synthesis of corresponding *C*-tertiary amines with generally good to high yields and excellent enantioselectivities.

Recently, Zhou and co-workers [93] described a method for the synthesis of chiral seven-membered cyclic sulfonamides via Pd-catalyzed asymmetric addition of arylboronic acids to seven-membered *N*-sulfonyl ketimines (Scheme 16.24). The products accessed with this method are important building blocks for the synthesis of biologically active molecules.

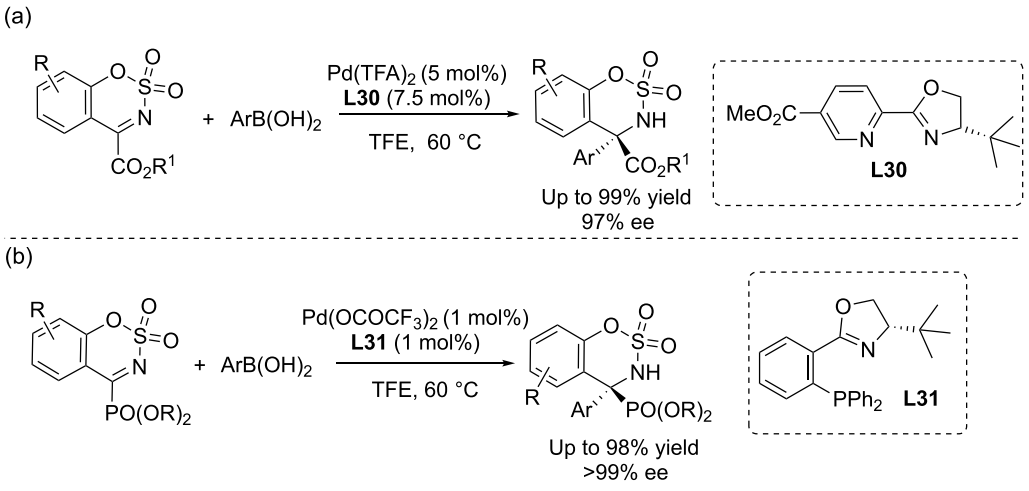

Scheme 16.20. Pd(II)-catalyzed enantioselective arylation of cyclic α-ketiminoesters (a) [87] and α-ketiminophosphonates (b) [88].

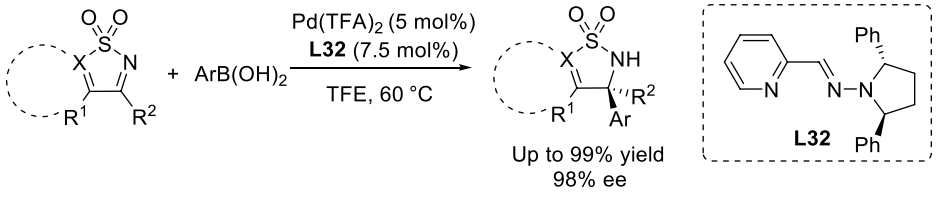

Scheme 16.21. Pd(II)-catalyzed enantioselective arylation cyclic ketimines [89].

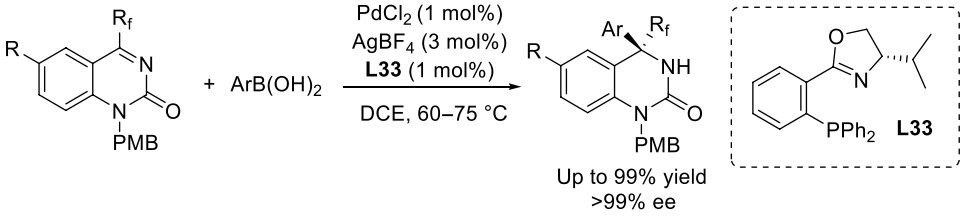

Scheme 16.22. Pd(II)-catalyzed enantioselective arylation of trifluoromethylated/perfluoroalkylated 2-quinazolinones [90].

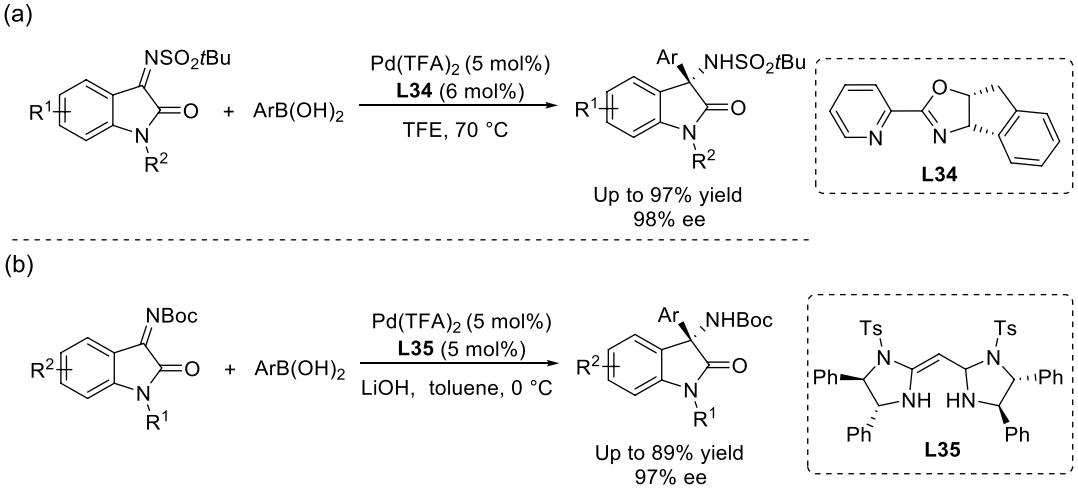

Scheme 16.23. Pd(II)-catalyzed enantioselective arylation of isatin-derived N-sulfonyl (a) [91] and N-Boc (b) protected ketimines [92].

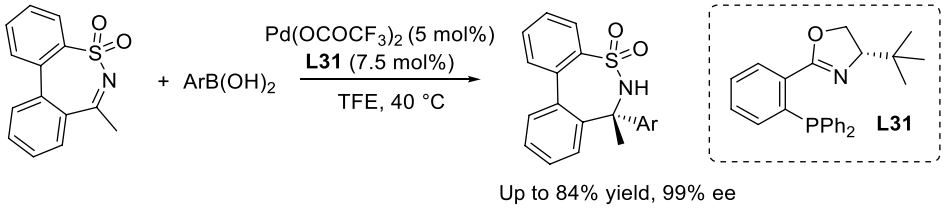

Scheme 16.24. Pd(II)-catalyzed enantioselective arylation of cyclic seven-membered N-sulfonyl protected ketimines [93].

16.3.2.3. Other Transition-Metal-Catalyzed Enantioselective Additions of Organoboron Reagents to Ketimines

The use of earth-abundant first-row transition metals such as Ni, Co, and Cu for the asymmetric addition of organoboron reagents to ketimines has gained momentum in recent years. Ni-catalyzed asymmetric addition of arylboronic acids to cyclic imines was reported in 2017 by the group of Zhang (Scheme 16.25a) [94]. The corresponding chiral amine products were obtained with high

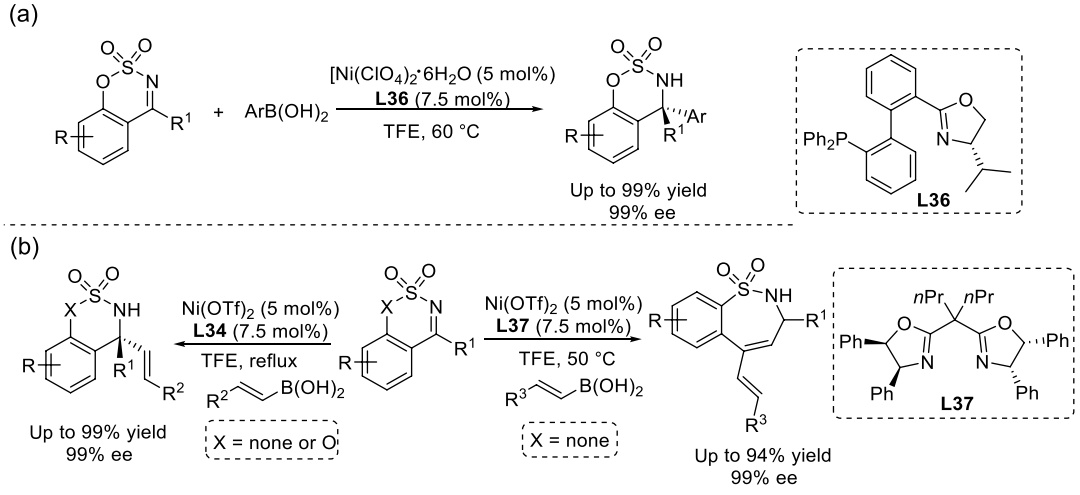

Scheme 16.25. Ni(II)-catalyzed enantioselective arylations (a) [94] and alkenylations (b) of cyclic ketimines [95].

yields (up to 99%) and enantiopurities (up to 99.8%) under mild reaction conditions. The same group [95] extended this methodology to alkenylboronic acids (Scheme 16.25b). Interestingly, when applied to ketimines bearing alkyl or alkoxycarbonyl groups, the alkenylation affords five- and six-membered cyclic α-tertiary allylic amine products. On the other hand, for alkenyl five-membered ketimine substrates, an alkenylation/rearrangement reaction occurs, leading to seven-membered chiral sulfamide products bearing a conjugated diene skeleton. Mechanistic studies supported an acid-catalyzed ring expansion step that was found to be a stereospecific, site-selective process.

Enantioselective vinylation of imines enabled by a chiral cobalt complex was reported by Zhao and co-workers [96] in 2016. Subsequently, Zhang and co-workers [97] extended this method to the allylation of alkoxycarbonyl- and alkyl-substituted saccharin-derived ketimines (Scheme 16.26). This methodology was successfully applied to the synthesis of the kinesin spindle protein inhibitor *MK-0371*.

The first example of a Cu-catalyzed asymmetric addition of organoboron reagents to ketimines was reported by Shibasaki and co-workers [61] already in 2006, prompting further research in this direction. Recently, Cho and co-workers [98] reported a copper-catalyzed 1,2-addition of 1,1-diborylalkanes to cyclic ketimines and α-imino esters that affords the corresponding β-aminoboronate esters with high

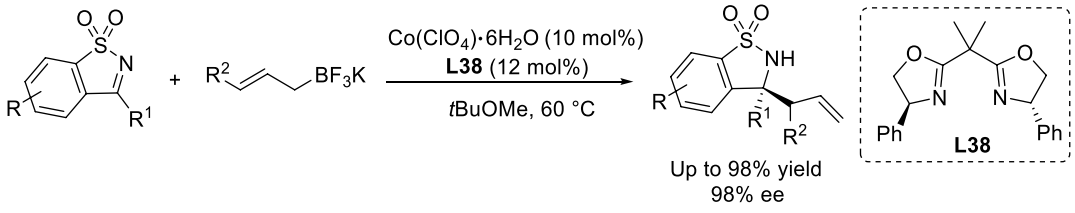

Scheme 16.26. Co-catalyzed enantioselective allylation of cyclic ketimines [97].

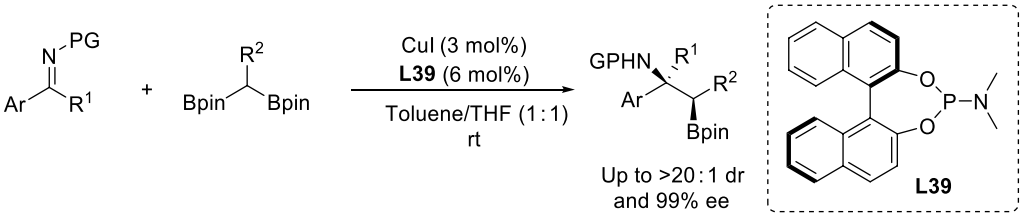

Scheme 16.27. Cu(I)-catalyzed diastereoselective and enantioselective addition of 1,1-diborylalkanes to ketimines [98].

diastereoselectivity and enantioselectivity (Scheme 16.27). Further transformations of these β-aminoboronate esters allow access to various synthetically useful chiral building blocks.

Finally, an interesting example of copper-catalyzed asymmetric synthesis of chiral C-tertiary amines was reported by Hoveyda and co-workers [99] in 2017. The reported method is rather unusual as it goes against the general trend observed in addition reactions to ketimines: all the ketimines used require either an electron-withdrawing substituent at the imino group, or an activating/protecting group on the nitrogen atom and thus subsequent unmasking of the amino group of the product. Hoveyda's group has demonstrated that non-protected ketimines, obtained via addition of organolithium reagents to the corresponding nitriles, undergo highly diastereo- and enantioselective reactions with monosubstituted allene and $B_2(pin)_2$ in the presence of catalytic amounts of Cu(I)-*N*-heterocyclic carbene (NHC) complexes (Scheme 16.28). The importance of these results lies in the fact that the ketimines used in the majority of methods require sulfonyl protecting groups for reactions to proceed efficiently. However, the deprotection step necessary to unmask the amino group often requires harsh conditions and is not always successful. This report by Hoveyda and co-workers is the first step toward the development of a series of catalytic enantioselective reactions involving unactivated N–H ketimines. In addition, this methodology was successfully applied in the synthesis of an anti-Alzheimer compound.

16.4. CATALYTIC ASYMMETRIC CONJUGATE ADDITION

The catalytic enantioselective conjugate addition of organometallic nucleophiles to α,β-unsaturated compounds represents one of the most useful synthetic tools for the construction of carbon–carbon bonds [100, 101]. This methodology has been used as a key step in the synthesis of various natural products and biologically active molecules and still remains an active field of research, despite hundreds of methodologies having been developed to date. Many reviews have covered the major developments in this field [102–105]. Here, we focus on the progress in the catalytic enantioselective conjugate addition reactions of non-stabilized nucleophiles to activated olefins in the last five years.

16.4.1. Asymmetric Conjugate Addition (ACA) of Grignard Reagents

As Grignard reagents are highly reactive nucleophiles, they pose a challenge in addition reactions to activated olefins (Michael acceptors), not only due to non-catalyzed background reactions but also due to regioselectivity issues. The development of methodologies for the addition of Grignard reagents to

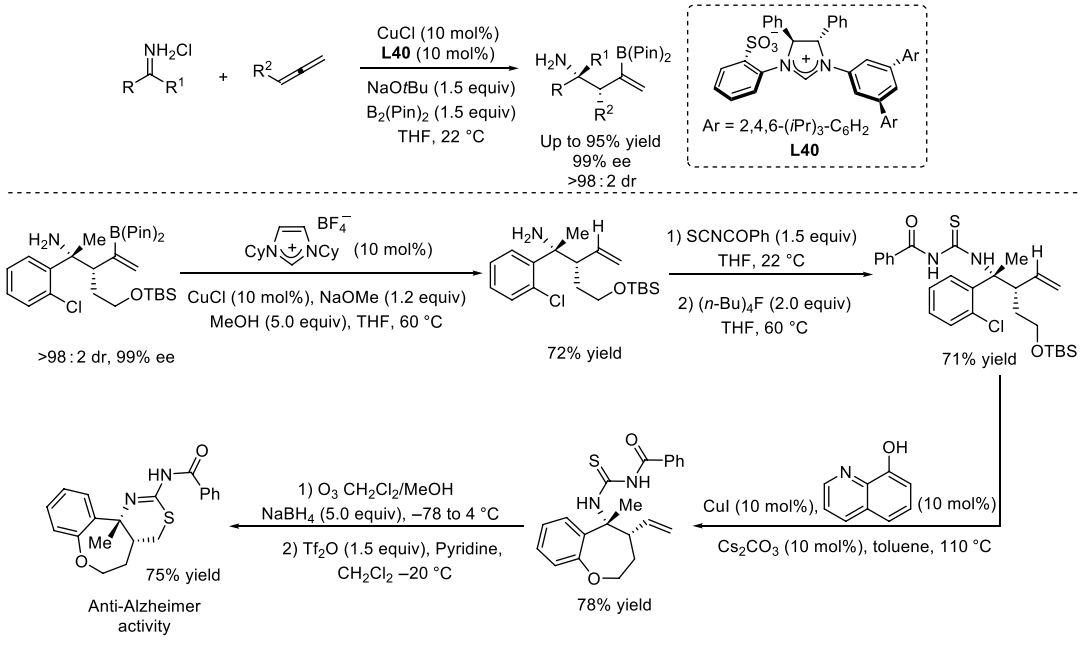

Scheme 16.28. Catalytic Cu(I)-catalyzed synthesis of C-tertiary amine from unactivated NH-ketimines [99].

Michael acceptors has focused on promotion by Cu(I) salts, which allows overcoming of the key challenge of regioselectivity, that is, 1,4-addition (conjugate addition) versus 1,2-addition (direct addition). In the absence of any catalyst, hard organometallics tend to give a racemic mixture of 1,2- and 1,4-addition products with a preference for the former. The first example of regioselective conjugate addition of Grignard reagents to α,β-unsaturated systems was reported by Kharash and Tawney [106]. These authors discovered that traces of copper(I) salts in the reaction mixture promote conjugate addition with good regioselectivity. In the 70 years following this discovery, Cu(I)-based catalysts have become a mainstay in direct 1,4-additions (conjugate additions), which led to the development of many catalytic asymmetric 1,4-addition methodologies using organometallic reagents. However, it took almost 50 years for the first example of catalytic ACA of Grignard reagents to be reported. In 1988, copper-catalyzed asymmetric addition to enones was reported by Lippard and co-workers, [107, 108] providing the corresponding conjugate addition products with moderate enantioselectivity. Many reports of ACA of Grignard reagents have been published since. The first highly enantioselective example of ACA to Michael acceptors was reported by Feringa and co-workers [109] in 2003 for the addition of alkyl Grignard reagents to cyclic enones catalyzed by chiral Cu(I)-ferrocenyl diphosphine complex. Following this work, many more successful examples that make use of the same catalytic system have been reported for other common Michael acceptors [102, 103, 105, 110]. The focus of this section will be on catalytic ACAs of Grignard reagents to less conventional Michael acceptors with diminished electrophilic reactivity.

16.4.1.1. ACA to Alkenyl-Heteroarenes

Conjugate addition of nucleophiles to alkenyl-heteroaromatic compounds would allow direct access to single enantiomers of valuable *N*-containing aromatic heterocycles. However, as of 2016, the only known examples of additions to alkenyl-heteroaromatic compounds were Rh-catalyzed arylations using organoboron reagents [111–113], despite the numerous efficient methods for catalytic ACA of common Michael acceptors. This lack of methodologies for nucleophilic additions to β-substituted alkenyl-heteroarenes is the result of the intrinsically lower reactivity of these molecules compared to common Michael acceptors. The activation provided by the heteroaromatic moiety is far weaker than that provided by the electron-withdrawing groups. In 2016, Harutyunyan and co-workers [114] reported an

operationally simple, chemoselective, and highly enantioselective addition of Grignard reagents to these relatively unreactive alkenyl-heteroaromatics leading to the corresponding chiral *N*-containing aromatic heterocycles (Scheme 16.29a). The key to this success was a combination of several critical elements: (i) enhancing the reactivity of alkenyl-heteroaromatics via Lewis acid activation, (ii) harnessing the high reactivity of readily available and atom-efficient Grignard reagents, and (iii) using inexpensive, chiral Cu-complex as the catalytically active structure. Later, the same authors [115] also employed this strategy for conjugate additions to β-substituted alkenyl pyridines, which afforded the chiral pyridine derivatives in both high yields and ees for a broad range of products (Scheme 16.29b).

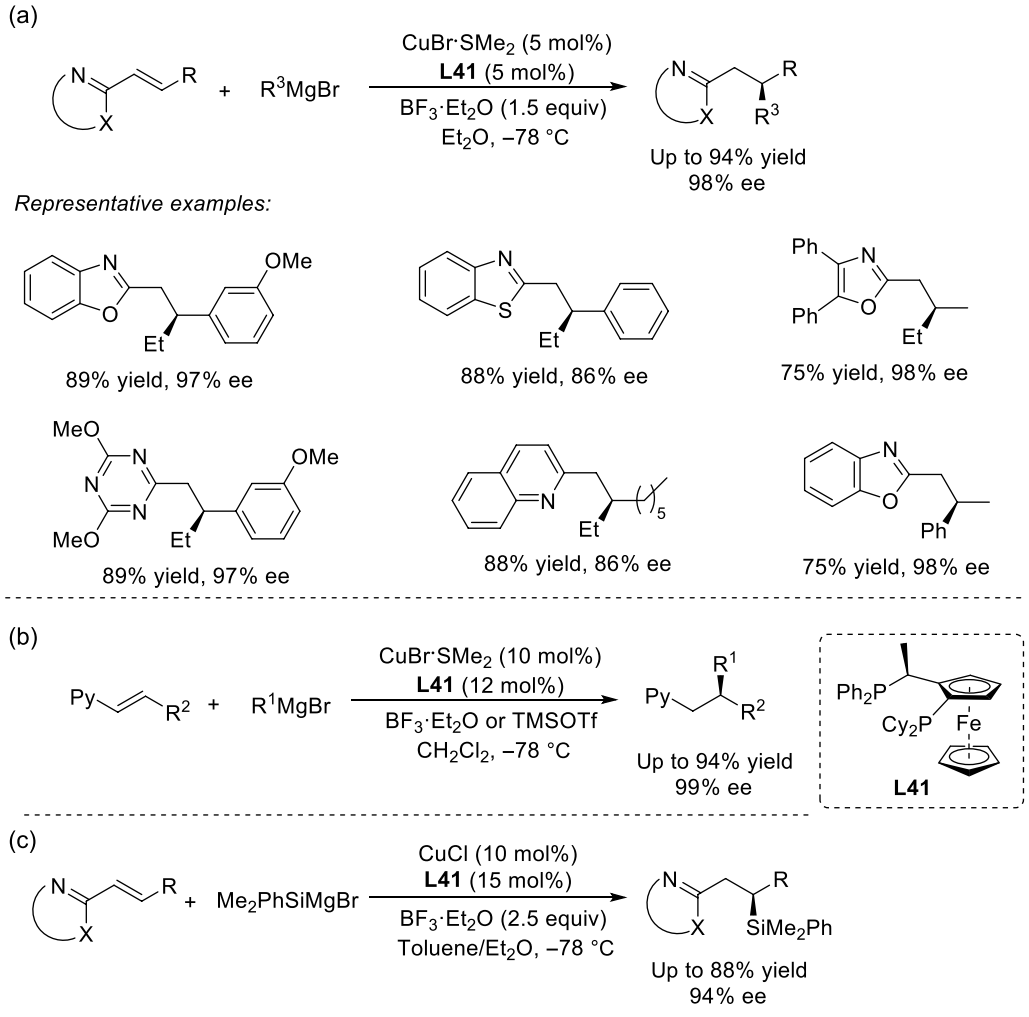

Scheme 16.29. Alkenyl-substituted N-heteroaromatics as Michael acceptors in Cu(I)-catalyzed conjugate additions of alkyl (a and b) [114, 115] and silicon (c) Grignard reagents [117].

In early 2019, a one-pot procedure for the ACA of alkenyl-heteroarenes with subsequent trapping of the resulting aza-enolate with Michael acceptors was developed by the Harutyunyan group [116]. While the process shows high stereoselectivity, the high specificity for oxazole and benzoxazole derivatives, as well as for α,β-unsaturated esters, limits the scope of its application. More recently, the group of Oestreich [117] revealed a copper-catalyzed, highly β-selective addition of silicon Grignard reagents to alkenyl-heteroarenes (Scheme 16.29c). Moderate to good yields with up to 94% ee were obtained for most substrates.

16.4.1.2. ACA to α,β-Unsaturated Carboxamides and Carboxylic Acids Despite the advances made in ACA of organometallics, the conjugate alkylation of unactivated α,β-unsaturated carboxamides remained unsolved for a long time [118]. In 2017, Harutyunyan and co-workers [119] reported that readily available silyl- and boron-based Lewis acids in combination with chiral copper catalysts are able to catalyze the ACA of Grignard reagents to unactivated carboxamides (Scheme 16.30a), delivering various chiral β-substituted amides in moderate to high yields with 91–99% ee. It is worth noting that the corresponding products could easily be transformed into a number of useful molecules. The same catalytic system was applied to addition reactions of Grignard reagents to dienyl caroboxamides [120], yielding the products preferentially with 1,6-selectivity for linear aliphatic systems and with 1,4-selectivity for aromatic or branched aliphatic systems (Scheme 16.30b).

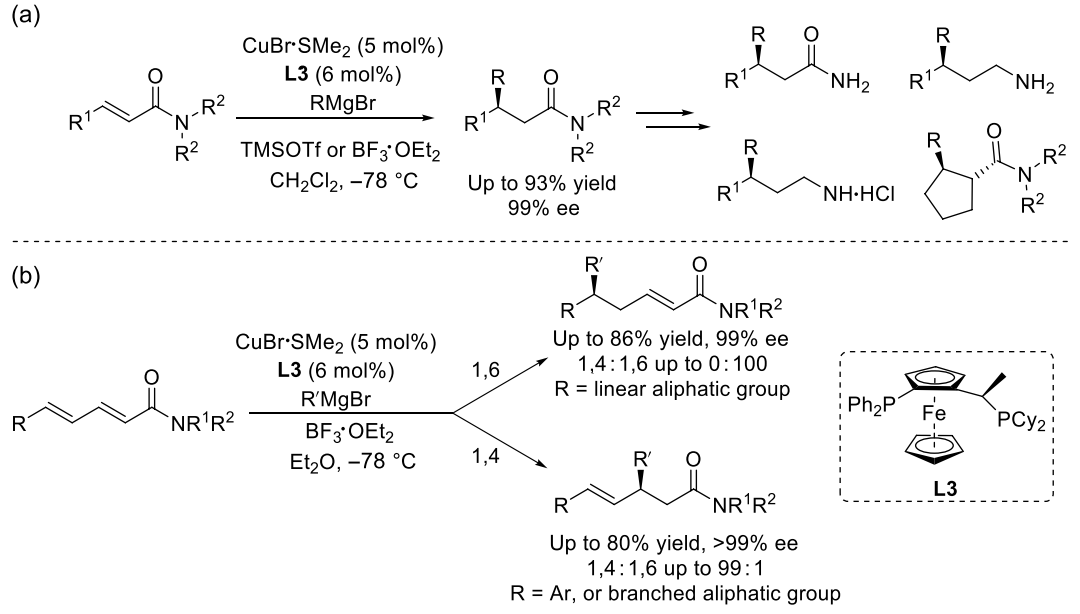

Scheme 16.30. Lewis acid enabled Cu(I)-catalyzed conjugate additions to unactivated α,β-unsaturated (a) [119] and α,β,γ, δ-unsaturated carboxamides (b) [120].

As highlighted earlier, over the past four decades, ACA of organometallics to Michael acceptors has resulted in applications to many types of carbonyl-based Michael acceptors, including derivatives of carboxylic acids. However, readily available, simple unsaturated unprotected α,β-unsaturated carboxylic acids defied this type of reaction until recently. For these substrates this transformation is inhibited for a fundamental reason, namely that the high basicity of organometallics and the acidity of unsaturated carboxylic acids overpowers any type of reactivity and leads invariably to acid-base reactions. The resulting carboxylate salts are insoluble in organic solvents and unreactive toward further nucleophilic additions. Recently, the group of Harutyunyan [121] described a transient protecting group strategy that allowed catalytic ACA of Grignard reagents to unprotected α,β-unsaturated carboxylic acids under mild conditions with high yields and enantioselectivities (Scheme 16.31). This strategy is based on activation of carboxylic acids via the formation of reactive labile silyl or boron intermediates allowing the fundamental problem of carboxylate salt formation during the conjugate addition step to be overcome. Thus, this new approach allowed highly enantioselective catalytic C–C bond-forming reactions between organometallics and carboxylic acids without the use of separate protection/deprotection steps. To showcase the potential of this catalytic protocol, β-chiral-substituted carboxylic acids were transformed into a variety of valuable molecules via stereoselective decarboxylative cross-coupling reactions.

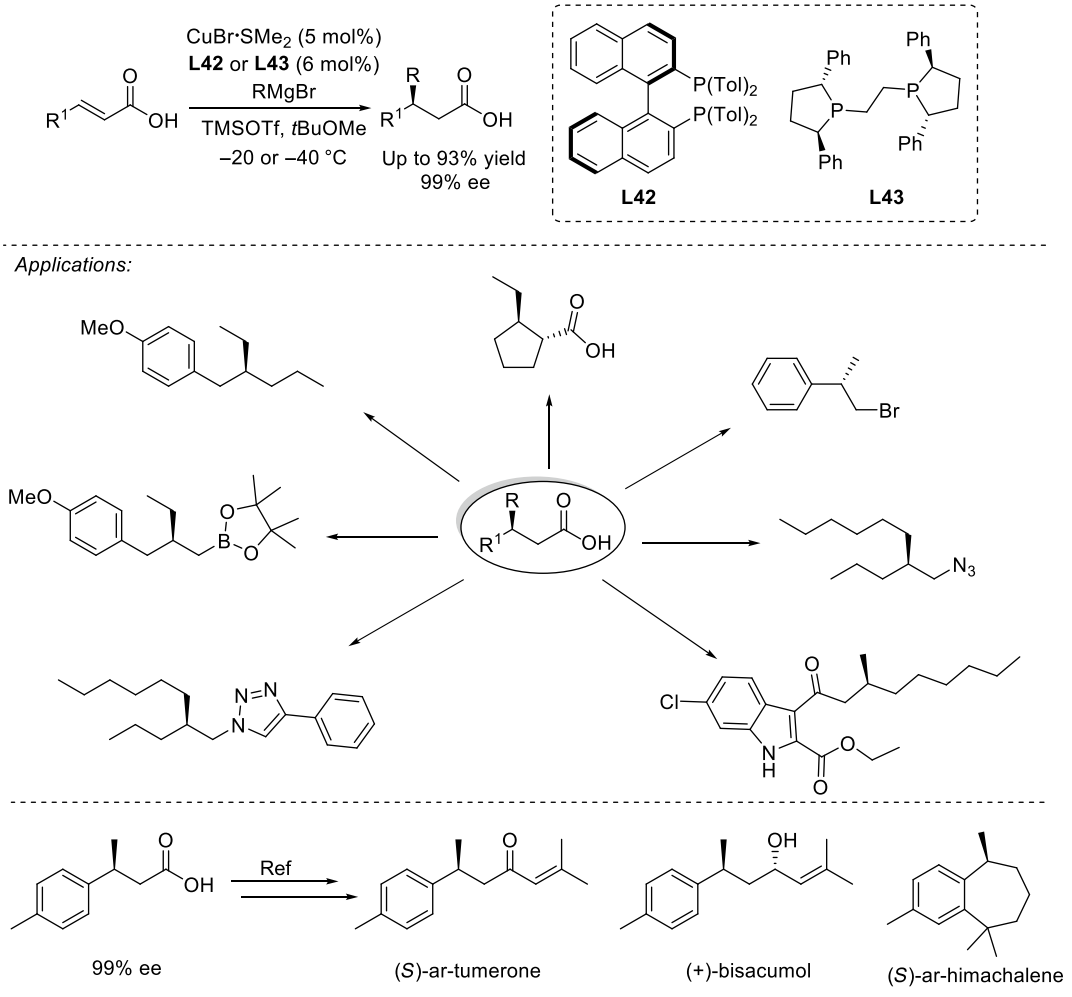

Scheme 16.31. Cu(I)-catalyzed enantioselective addition of Grignard reagents to unprotected carboxylic acids [121].

16.4.1.3. ACA to Heterocyclic Michael Acceptors Among the various acceptors employed in ACA reactions, those with a heterocyclic scaffold are of special importance due to the frequent occurrence of heterocyclic structures in natural products and bioactive molecules [110]. As a result, significant effort has been invested in establishing catalytic enantioselective methods for the synthesis of chiral heterocyclic cores.

A highly regio- and enantioselective method for copper-catalyzed ACA of Grignard reagents to chromones was developed by the Feringa group [122] in 2013, providing an efficient route for the synthesis of chiral 2-alkylchromanones and coumarins (Scheme 16.32). The resulting products are valuable intermediates for the synthesis of versatile, optically active building blocks.

The first general protocol for the alkylation of various classes of *N*-heterocyclic acceptors with Grignard reagents using a Cu(I) complex with **L43** was reported by Harutyunyan and co-workers [123], providing an efficient catalytic system for the synthesis of chiral 2- and 4-substituted tetrahydroquinolones and dihydro-4-pyridones (Scheme 16.33). The addition reactions to *N*-substituted-4-quinolones can be carried out at room temperature, while consecutive alkylation of pyridone and the resulting 2,3-dihydro-4-pyridones allows convenient catalytic access to 2,6-substituted diastereomerically and enantiomerically pure piperidones.

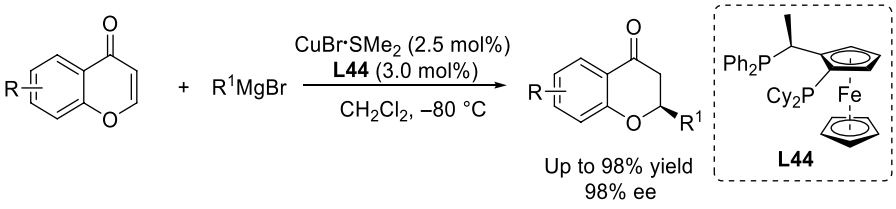

Scheme 16.32. Cu(I)-catalyzed enantioselective addition of Grignard reagents to chromones [122].

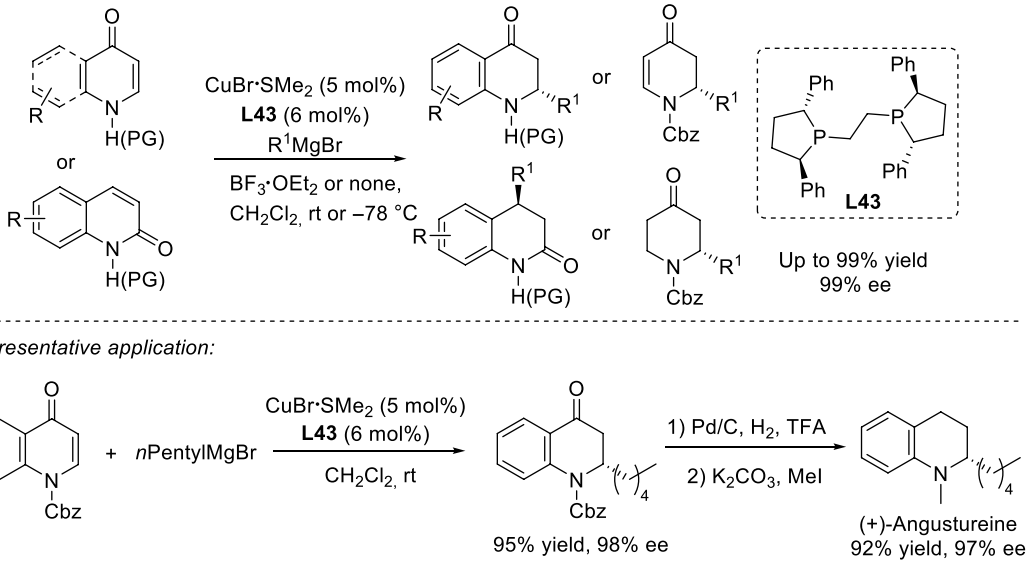

Scheme 16.33. Cu(I)-catalyzed enantioselective addition of Grignard reagents to N-heterocyclic acceptors [123].

Another interesting example of catalytic ACA that allows access to chiral *N*-containing heterocycles is the reaction of Grignard reagent to quinolines. Direct nucleophilic addition to quinolines is challenging because of issues with reactivity (addition to quinolines is only possible at the cost of loss of aromaticity) and regioselectivity (two electrophilic positions, C-2 and C-4, can undergo nucleophilic attack). Nevertheless, the first catalytic system that allows highly enantioselective nucleophilic dearomatization of quinolines via C4-functionalization using Grignard reagents and copper catalysis was reported very recently (Scheme 16.34a) [124]. The key to this success was the use of chiral copper catalysis in combination with suitable Lewis acids for transient activation of the quinoline aromatic ring toward nucleophilic addition. The products accessed with this method are important building blocks for the synthesis of alkaloids.

Even though enantioselective ACA to conventional Michael acceptors had experienced substantial development, it was not until 2020 that the enantioselective addition of Grignard reagents to indole derivatives was first tackled by the Harutyunyan group [125]. The strategy they used transforms the indole derivatives into a Michael acceptor via an initial elimination reaction promoted with the very same Grignard reagents. Using copper catalysis in combination with phosphoramidite ligand (**L45**) led to efficient enantioselective synthesis of 3-sec-alkyl-substituted indoles (Scheme 16.34b).

16.4.2. Asymmetric Conjugate Addition of Organozinc Reagents

The first example of catalytic ACA of organozinc reagents to α,β-unsaturated compounds was reported by Soai and co-workers [126]. A complex prepared in situ from $Ni(acac)_2$ and **L46** in the presence of 2,2′-bipyridyl as additive catalyzed the formation of conjugate addition product in 44% yield with 87% ee (Scheme 16.35a).

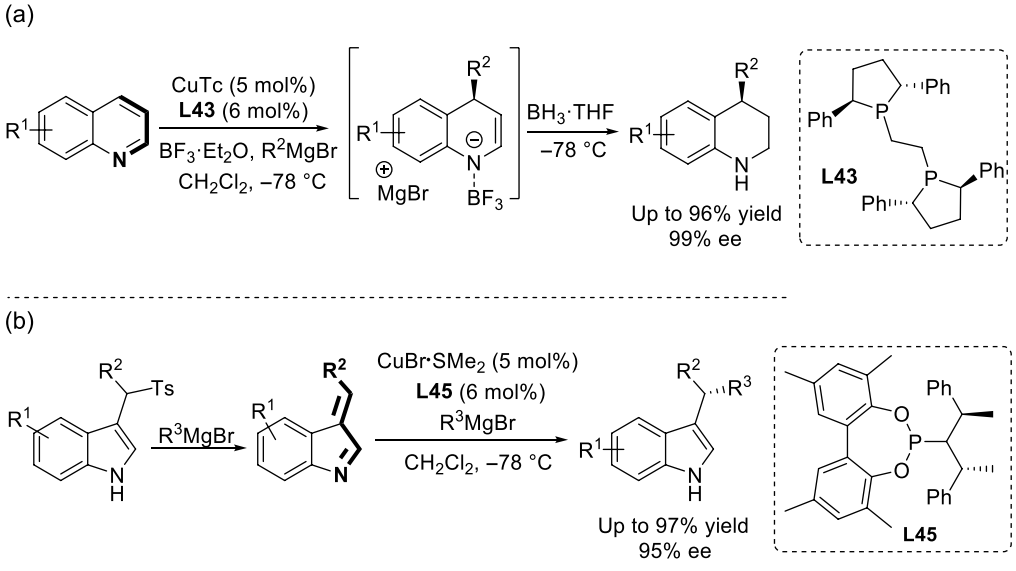

Scheme 16.34. Cu(I)-catalyzed enantioselective reactions with N-heteroaromatics: C4-selective dearomatization of quinolines promoted by Lewis acids (a) [124] and additions to in situ generated indole-derived vinylogous imines (b) [125].

Later, various reports focused on asymmetric 1,4-addition of cyclic and acyclic enones with dialkylzincs in the presence of chiral copper complexes. A remarkable improvement was introduced by Feringa [127, 128] in 1997: the combination of Cu(II) salt and chiral phosphoramidite (**L47**) allowed conjugate additions of organozinc reagents to enones with excellent yields and enantioselectivities (Scheme 16.35b).

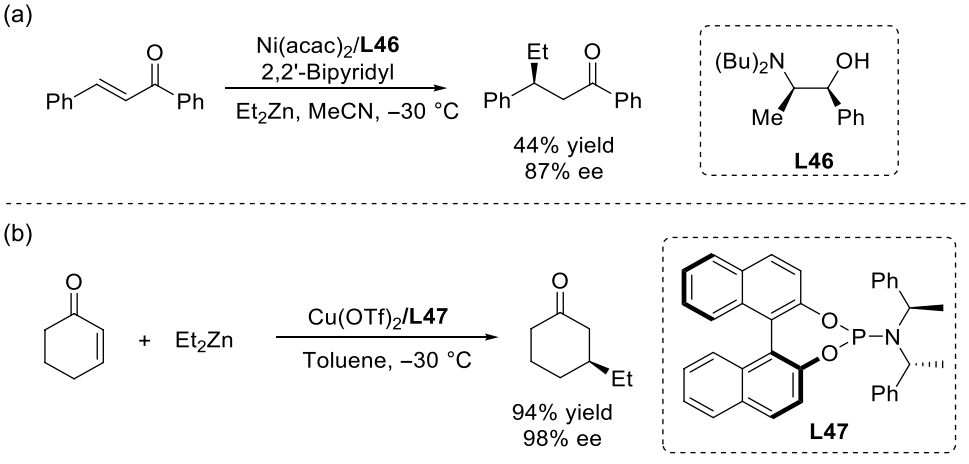

Scheme 16.35. Catalytic enantioselective conjugate additions of organozinc reagents to enones catalyzed by Ni(II) (a) [126] and Cu(I) (b) chiral complexes [127, 128].

16.4.2.1. ACA to Cyclic Enones Following initial progress in ACA of organozinc reagents to cyclic enones using chiral catalysts based on copper and phosphoramidite ligands, continuous efforts were directed toward the development of new chiral ligands to further improve yields and enantioselectivities, a selection of which is presented in Scheme 16.36 [129–133].

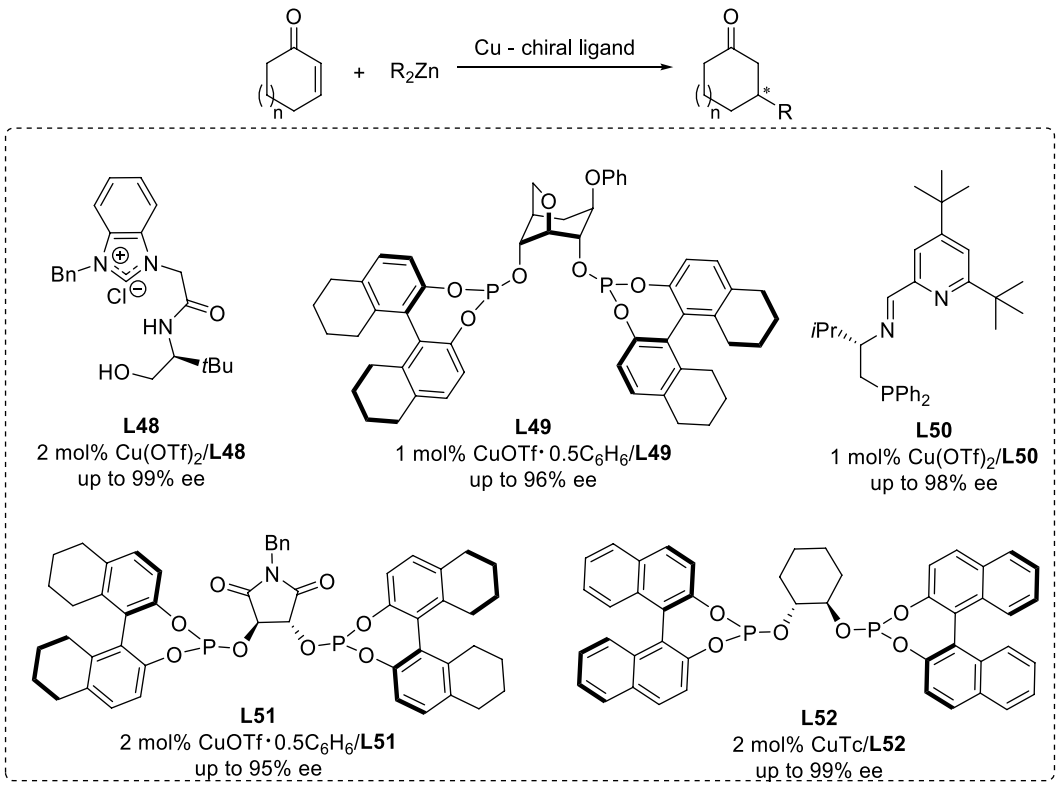

Scheme 16.36. Selection of successful chiral ligands developed for catalytic enantioselective conjugate additions of organozinc reagents to cyclic enones [129–133].

In 2015, Mauduit and co-workers [134] developed a chiral NHC-Cu(I)-based catalyst system ([Cu]/**L53**) for the enantioselective conjugate alkylation of β-substituted cyclohexenones to furnish the corresponding products with quaternary carbon centers, in up to 98% ee (Scheme 16.37).

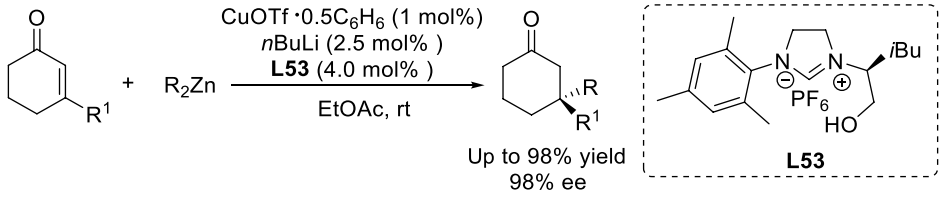

Scheme 16.37. Cu(I)-catalyzed conjugate additions of organozinc reagents to β-substituted cyclohexenone [134].

Most recently, a highly enantioselective copper-catalyzed 1,4-addition/trapping sequence starting from cyclobutenones was reported by Liu and co-workers [135]. A series of cyclobutenones was tolerated, providing the corresponding adducts in high ees (Scheme 16.38).

16.4.2.2. ACA to Acyclic Enones ACA to acyclic enones is more demanding in terms of regio- and enantioselectivities due to their less rigid structure. Recent work aimed at improved methods for ACA of these compounds has resulted in the development of many new efficient chiral ligands, **L55–L67** (Scheme 16.39), such as BINOL-type ligands, [136–138] phosphoramidite ligands [139, 140], chiral NHC ligands [141, 142], axially chiral 1,1'-spirobiindane-7,7'-diol- phosphorus (SPINOL-PHOS) ligands [143], and others [144–148].

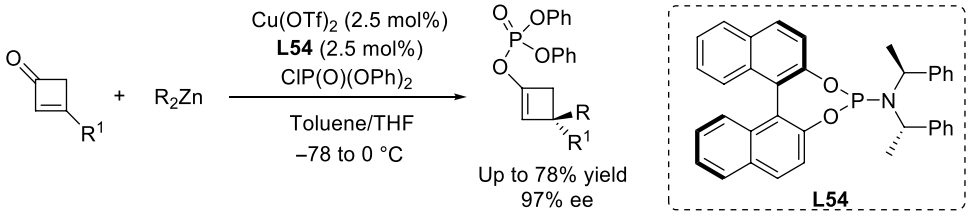

Scheme 16.38. Cu(I)-catalyzed conjugate additions of organozinc reagents to cyclobutenone [135].

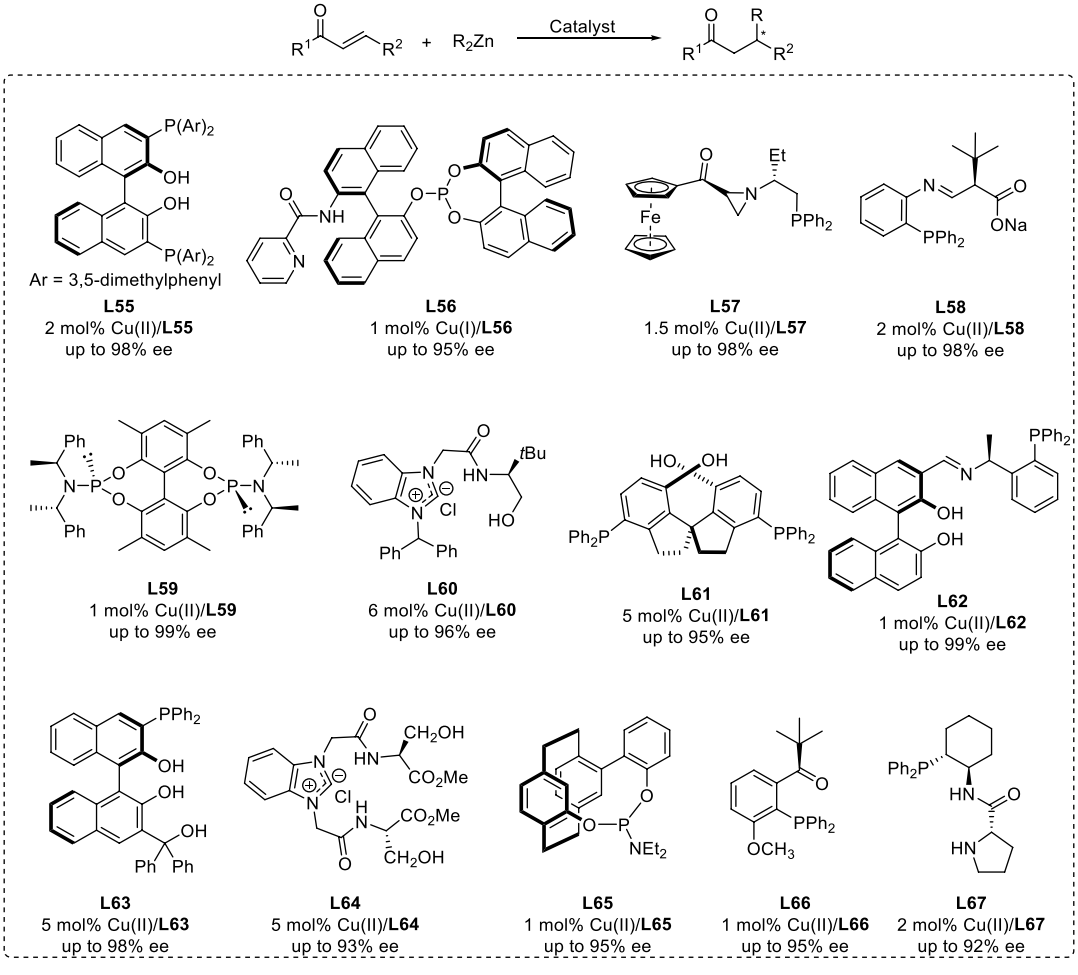

Scheme 16.39. Selection of successful chiral ligands developed for catalytic enantioselective conjugate additions of organozinc reagents to acyclic enones [136–148].

16.4.2.3. ACA to Nitroalkenes Nitroalkenes are important synthetic building blocks for both natural product synthesis and drug discovery. As excellent Michael acceptors, nitroalkenes react with a broad range of functionalized nucleophiles. Zhang and co-workers [149] successfully developed **L59**-Cu(II)-promoted ACA of nitroalkenes with organozinc reagents, achieving chiral β-substituted nitroalkanes with good ees (Scheme 16.40). Recently, a new phosphino-oxazoline ligand (**L68**) was synthesized and used in the enantioselective addition of nitroalkenes [150]. In the same year, the

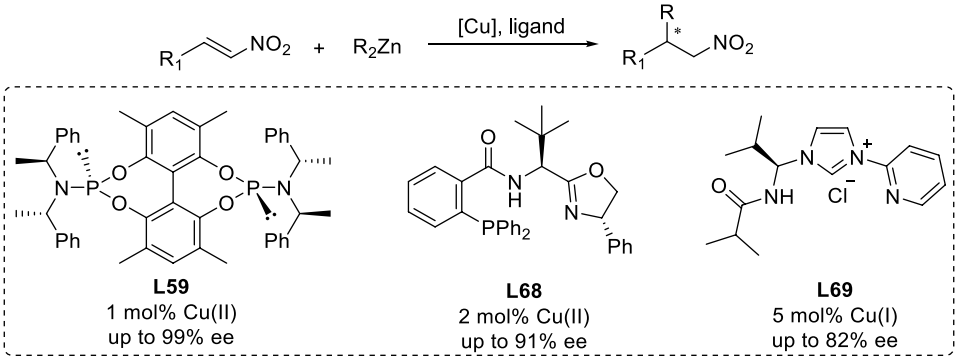

Scheme 16.40. Selection of successful chiral ligands developed for catalytic enantioselective conjugate additions of organozinc reagents to nitroolefins [149–151].

group of Ukaji [151] reported that a combination of Cu(I) salts with chiral NHC (**L69**) catalyzes the ACA of nitroalkenes (Scheme 16.40).

16.4.3. Asymmetric Conjugate Addition of Organozirconium Reagents

The organomagnesium and organozinc reagents discussed so far are prepared from the corresponding halide and are often limited in their functional group compatibility and commonly require operating temperatures below ambient. Aiming to address these limitations of premade organometallic reagents, in 2012 Fletcher and co-workers [152] developed conjugate addition chemistry with organozirconium reagents formed in situ by hydrometallation of simple alkenes with Schwartz reagent (Schemes 16.41).

By combining alkylzirconium reagents and Michael acceptors with a catalytic amount of chiral phosphoramidite ligand (**L70**) and copper salt, the authors were able to demonstrate for the first time highly

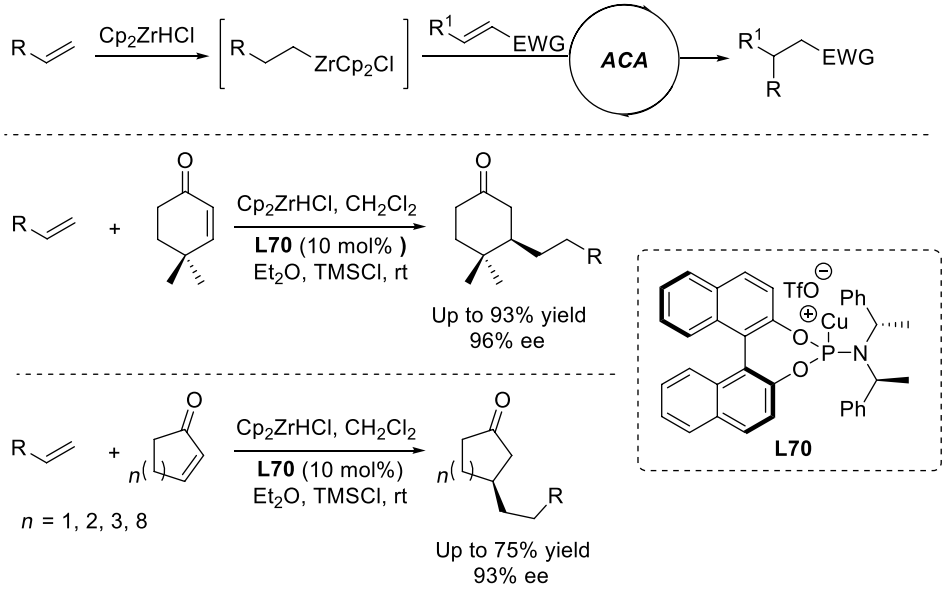

Scheme 16.41. Cu(I)-catalyzed conjugate additions of organozirconium reagents to cyclic enones [152].

efficient catalytic ACA reactions with alkylmetal species generated in situ from alkenes. They initially applied this strategy to ACA reactions with cyclic-enone-derived Michael acceptors [153] and found that excellent yields (up to 93%) and excellent enantioselectivities (up to 96% ee) can be obtained at room temperature in a range of solvents, and that the reaction tolerates a variety of functional groups.

To show the potential of this methodology for synthetic applications, the authors applied it in the synthesis of a natural product isolated from the New Zealand liverwort *Balantiopsis rosea* and its enantiomer [154].

After these preliminary reports, this chemistry was extended to various types of Michael acceptors and applied in the synthesis of several natural products and was recently reviewed by Pinheiro and co-workers [155]. The methodology was successful not only with enones [156–158], α,β-unsaturated lactones [159], thioesters [160], and *N*-heterocyclic Michael acceptors [161] but was also found to be useful for generating challenging quaternary stereocenters when combined with enones [162–167] (Scheme 16.42).

Finally, Fletcher and co-workers [168] performed extensive experimental and computational studies that allowed them to establish the stereochemical role of the phosphoramidite ligand in the ACA of alkylzirconium reagents to cyclic enones. These studies prove useful for the rational modification of chiral ligands to achieve enhanced levels of selectivity.

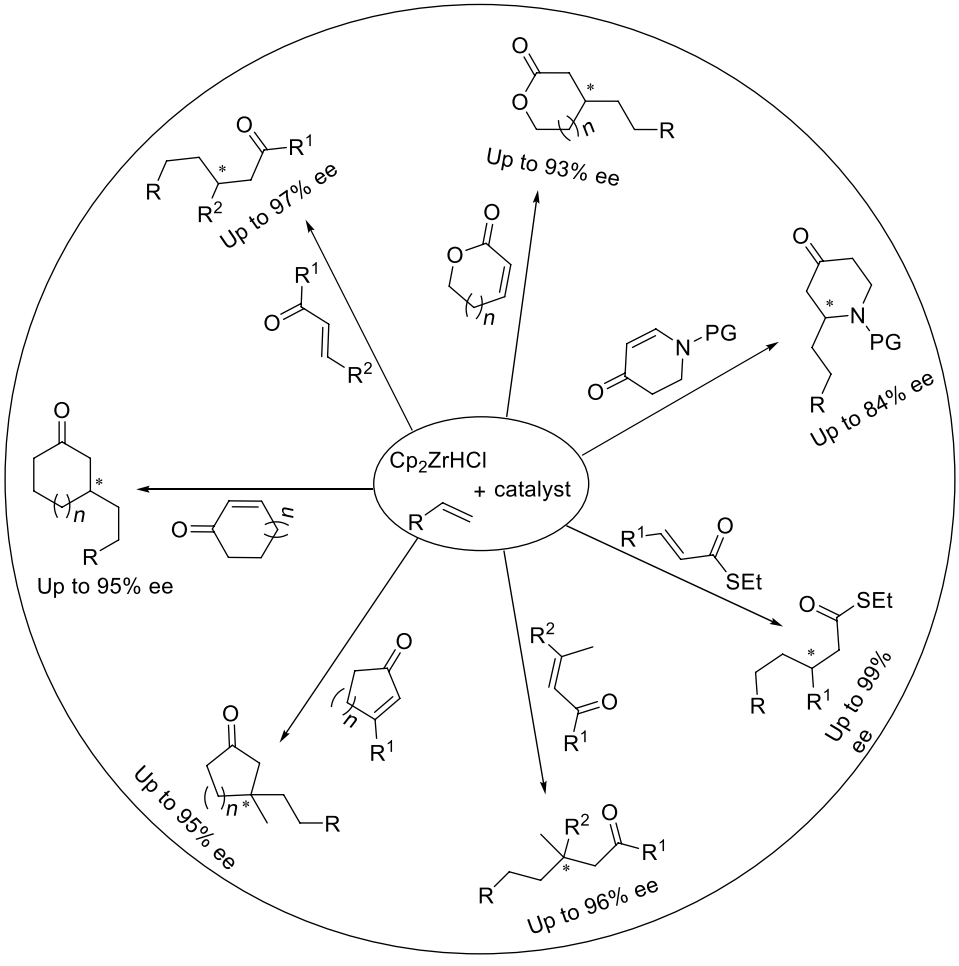

Scheme 16.42. Cu(I)-catalyzed conjugate additions of organozirconium reagents to various Michael acceptors [156–168].

16.4.4. Asymmetric Conjugate Addition of Organoborane Reagents

ACAs using organoboron reagents is a major area in conjugate additions that has been researched extensively over the last 24 years. Originally described by Hayashi and Miyaura (Scheme 16.43) [169], conjugate additions of organoboron reagents have not only become a versatile tool for asymmetric synthesis but also found applications in industrial chemistry due to the availability, low reactivity, and ease of handling of many organoboron reagents. Large numbers of examples have been mentioned in several reviews on this topic [170–172] before 2015. Therefore, we fill focus in this review on representative examples that have appeared after 2015.

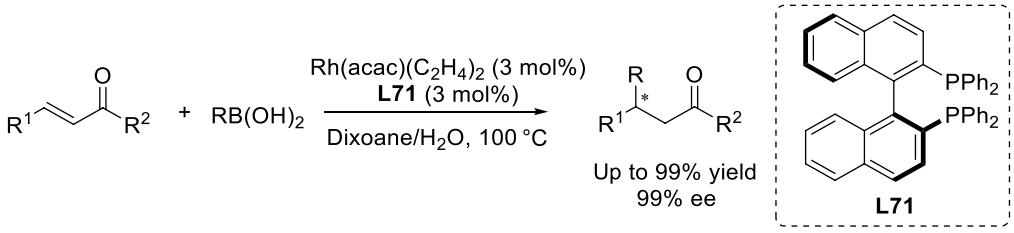

Scheme 16.43. Rh(I)-catalyzed conjugate additions of organoboron reagents to acyclic enones [169].

16.4.4.1. ACA to α,β-Unsaturated Ketimines ACA to α,β-unsaturated imino esters is a convenient strategy to obtain chiral unnatural dehydroaminoacids or amino esters. Kim and co-workers [173, 174] reported bicyclic bridgehead phosphoramidites (**L72**) as a new type of ligand for Rh(I)-catalyzed asymmetric 1,4-addition of boronic acids to α,β-unsaturated imino esters (Scheme 16.44a). In the presence of complex Rh(I)/**L72** and at room temperature, up to 99% yield and 96% ee was obtained for the conjugate addition products. Later, this work was extended to ACA of boronic acids to α,β-unsaturated *N*-tosyl ketimines [175], allowing the synthesis of chiral *N*-tosyl enamines with high yields and stereoselectivities (Scheme 16.44b).

In 2016, the group of Xu [176] demonstrated that the addition of arylboronic acids to α,β-unsaturated cyclic *N*-sulfonyl ketimines can also be accomplished with good results (up to 99% yield and 99% ee) in the presence of Rh(I)/**L73** complex (Scheme 16.45a). Follow-up research revealed that the similar catalyst system Rh(I)/**L74** is successful in ACA reactions to α,β-unsaturated cyclic ketimines

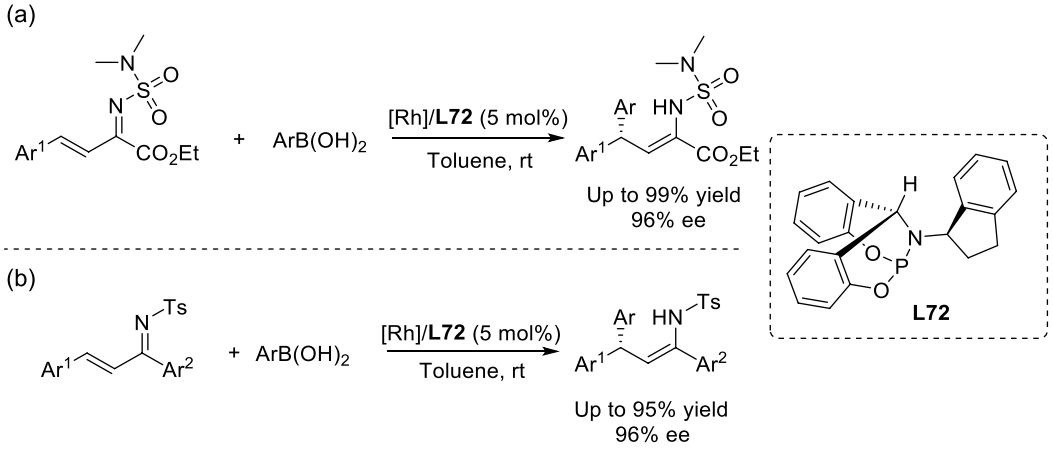

Scheme 16.44. Rh(I)-catalyzed conjugate additions of boronic acids to α,β-unsaturated N-protected imino esters (a) [173] and α,β-unsaturated N-tosyl ketimines (b) [174].

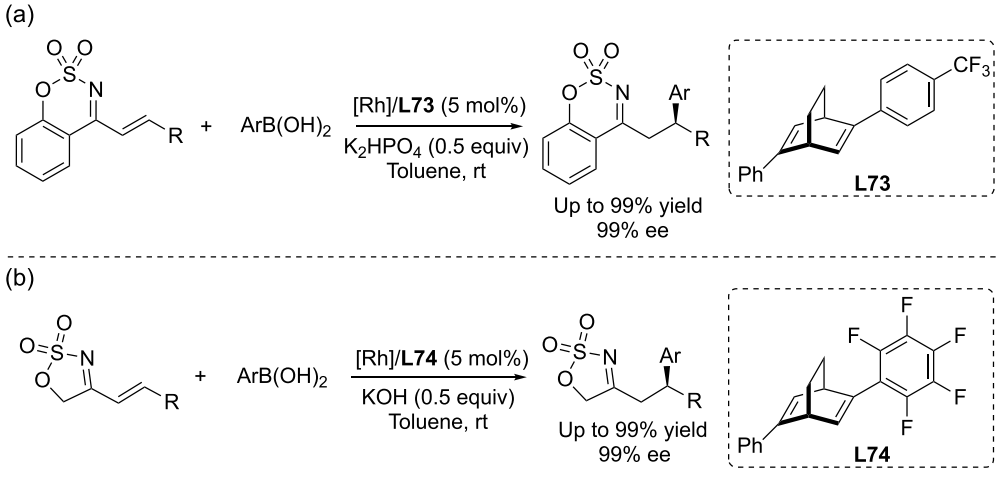

Scheme 16.45. Rh(I)-catalyzed conjugate addition of boronic acids to cyclic N-protected conjugated imines (a and b) [176, 177].

(Scheme 16.45b) [177]. This protocol provides a simple route for the synthesis of various chiral amine derivatives bearing multifunctional groups.

16.4.4.2. ACA to α,β-Unsaturated Enones In 2015, Hayashi and co-workers [178] developed a new strategy for the synthesis of chiral triarylmethanes, which is realized by an Rh(I)/**L75**-catalyzed asymmetric addition of arylboron reagents to diarylmethylamines (Scheme 16.46a). This reaction is assumed to proceed through *o*-quinone methide intermediates generated from diarylmethylamine derivatives, and provides generally high enantioselectivities and yields. Later, the same group [179] reported an example of asymmetric conjugate arylation of various α,β-unsaturated carbonyl compounds with potassium aryloxymethyltrifluoroborates in the presence of a chiral Rh(I)/**L76** catalyst. This approach allowed the introduction of *o*-methoxyaryl groups at the β-position of the newly formed C–C bond in high enantioselectivity. It was proposed that the reaction proceeds through 1,4-Rh shift from the aryloxymethyl-Rh intermediate to 2-methoxyaryl-Rh (Scheme 16.46b).

In 2016, Zhou and co-workers [180] developed the copper-catalyzed ACA of arylboron reagents to acyclic enones. Importantly, a new mechanism was demonstrated in this work that led directly to *O*-bound copper enolates, namely an unusual 1,4-insertion of an arylcopper(I) species (Scheme 16.47). This 1,4-insertion pathway is fundamentally different from the classical oxidative addition/reductive elimination of organocopper(I) on enones and was used to rationalize the lack of reactivity with cyclic enones, since 1,4-insertion would require s-cisoid reactive conformation not possible with cyclic enones.

In 2016, the Hayashi group [181] demonstrated that the chiral complex Rh(I)/**L78** was capable of promoting asymmetric arylation of cyclopent-4-ene-1,3-diones in high yields and selectivities (Scheme 16.48). Significantly, the reaction does not require the use of a base. The application of this catalyst system was further extended to the reaction with γ,δ-unsaturated β-dicarbonyl compounds [182] and γ,δ-unsaturated β-ketophosphonates [183], providing a range of 1,4-adducts in high yields with up to 99% ee (Scheme 16.48). The Rh-catalyzed ACA of cyclic enones using different ligands such as **L79** [184], **L80** [185], **L76** [186], and **L82** [187], was also reported. Recently, a novel approach for the synthesis of a variety of chiral phenols was developed by Dou and co-workers [188] using the recyclable complex Rh(I)/**L81** as the chiral catalyst. Later, they applied another catalyst based on (*R*)-DM-Segphos Ligand **L82** and Rh(I) to the highly enantioselective ACA of organoboronic acids to carbonyl-activated alkenyl-azaarenes [189].

Finally, Hayashi and co-workers [190] provided an efficient method for the synthesis of a series of C2-symmetric 3,3′-diarylated 1,1′-spirobiindane-7,7′-diols (3,3′-diaryl-SPINOLs) in the presence of complex Rh(I)/**L76** (Scheme 16.49). More importantly, the application of this methodology was demonstrated in the synthesis of 3,3′-diaryl-SPINOL-based phosphoramidite ligands, which was found to be an

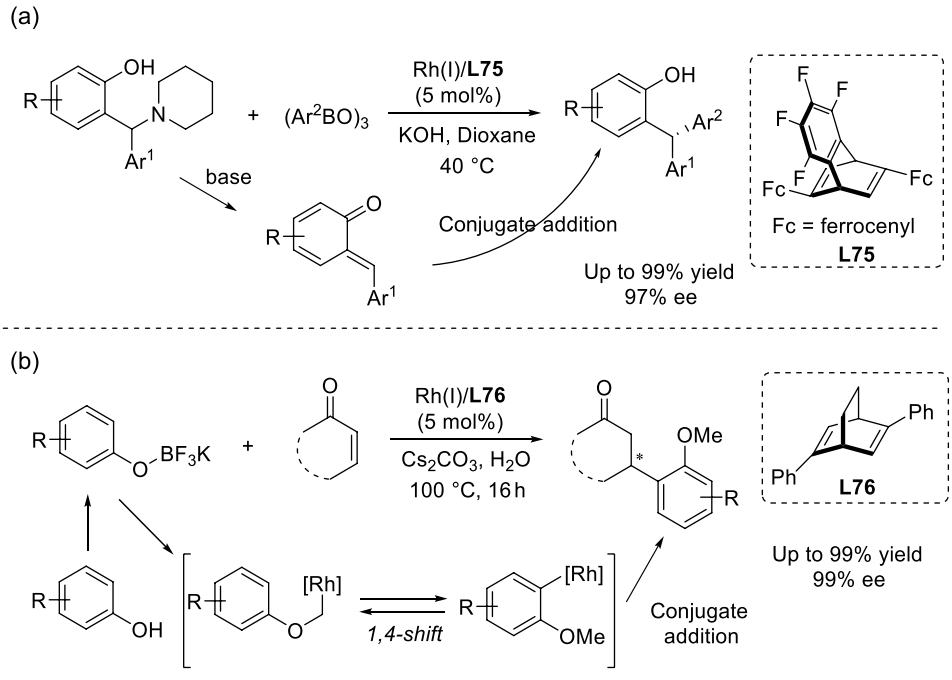

Scheme 16.46. Rh(I)-catalyzed conjugate addition of organoboron reagent to an in situ generated Michael acceptor (a) [178] and cycloalkenone (b) [179].

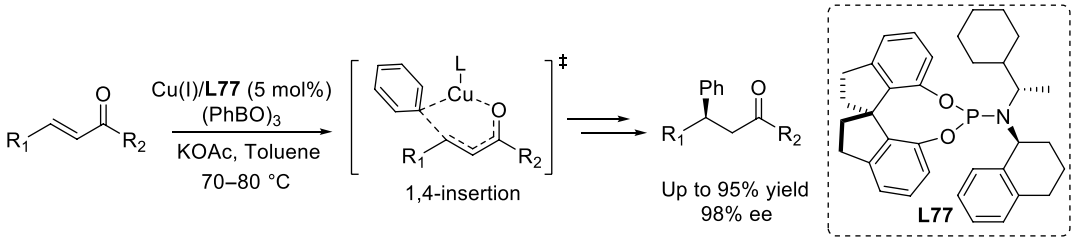

Scheme 16.47. Copper(I)-catalyzed conjugate addition of arylboron reagents to acyclic enones [180].

excellent chiral ligand comparable to or even outperforming the privileged SPINOL-based ligands in various types of transformations [191, 192].

16.4.4.3. ACA to Nitroalkenes Catalytic ACA to nitroalkenes leads to products that give straightforward access to β-chiral amines. In this context the asymmetric conjugate arylation of nitrostyrenes using aryl boronic acids allows access to β-chiral benzhydryl amines, which are important precursors for the synthesis of biologically relevant compounds. The potential for applications of these reaction products has triggered significant research efforts in this area, resulting in an expanded scope of metals and chiral ligands that catalyze this reaction.

In 2015, the Zhang group [193] described enantioselective conjugate borylation of nitroalkenes with arylboronic acids, catalyzed by the complex Pd(II)/**L83** (Scheme 16.50).

Later, the synthesis of isopavine alkaloids was achieved, utilizing this method in the key step [199]. A structurally similar catalyst complex (IsoQuinox, Pd(II)/**L87**) was developed by Li and co-workers [194].

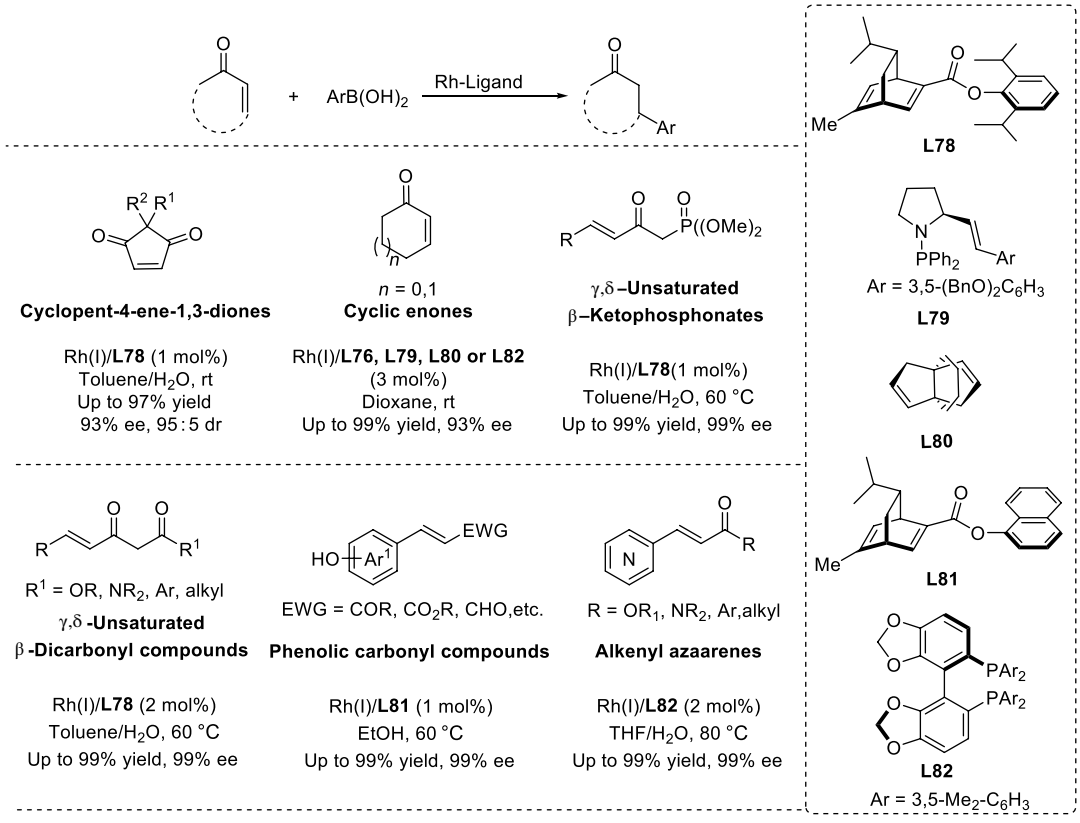

Scheme 16.48. Rh(I)-catalyzed conjugate addition of arylboronic acids to various Michael acceptors [181–189].

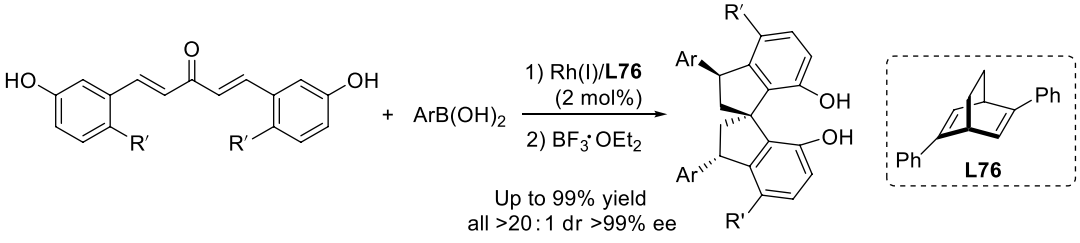

Scheme 16.49. Rh(I)-catalyzed enantioselective synthesis of 3,3-diaryl-SPINOLs [190].

Senanayake and co-workers [195] reported Rh-catalyzed ACA of aryl boronic acids to β-substituted nitroalkenes employing a P,π-hybrid bidentate ligand **L84** (Scheme 16.50). The corresponding products were obtained with moderate to good yields and up to 88% ee.

Later studies of ACA to nitroalkenes were focused on the development of Rh- complexes with various ligands, including chiral dienes **L85** [196] and **L86** [197], and chiral olefin–sulfoxide **L24** [198] (Scheme 16.50).

16.4.4.4. ACA to α,β-Unsaturated Esters α,β-Unsaturated esters form another common class of Michael acceptors extensively explored in ACA of organoboron reagents. An Rh(I)/**L88-**complex-catalyzed asymmetric 1,4-addition of arylboronic acids to indole-derived α,β-unsaturated esters was developed by the Xu group [200] (Scheme 16.51a). This method is also applicable to α,β-unsaturated benzofuran, *N*-protected 3-indolyl acrylates and benzothiophene-derived acrylates. In 2019, Wu and

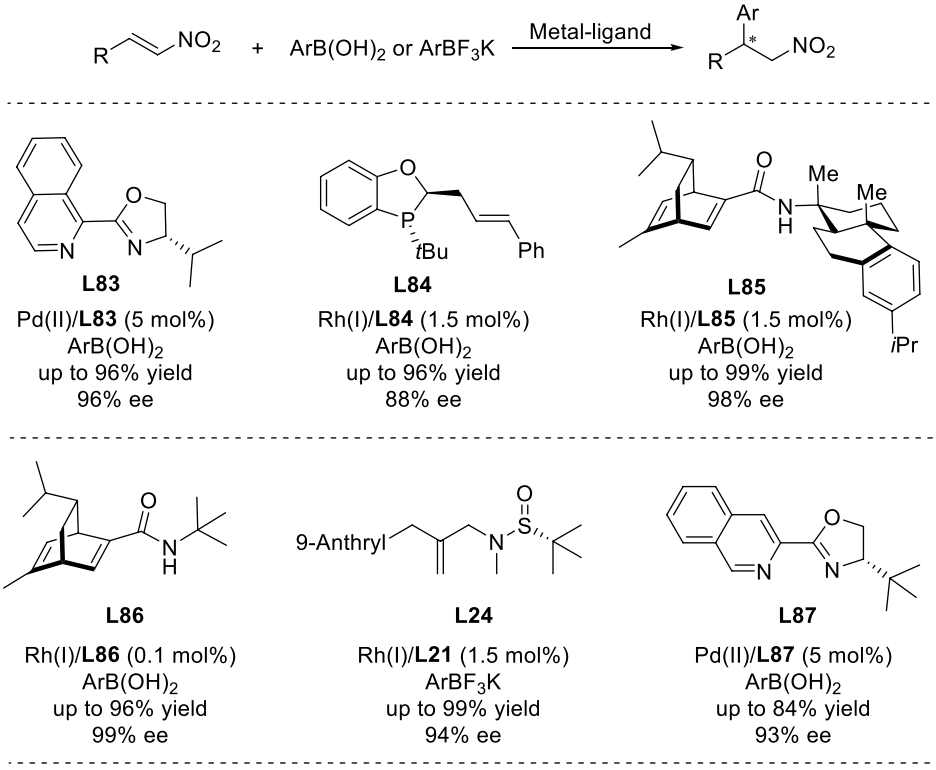

Scheme 16.50. Selection of successful chiral ligands developed for catalytic enantioselective conjugate addition of organoboron reagents to nitroalkenes [193–198].

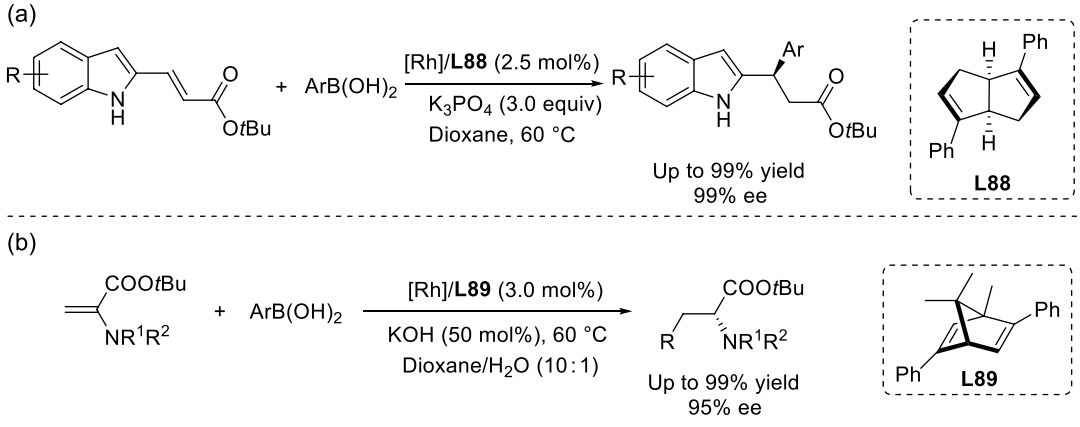

Scheme 16.51. Rh(I)-catalyzed enantioselective synthesis of chiral indole (a) [200] and phenylalanine (b) derivatives [201].

co-workers [201] reported that Rh(I)/**L89** promoted ACA of boronic acids to substituted dehydroalanines, opening a convenient route for the synthesis of functionalized phenylalanine derivatives with good enantioselectivity (up to 95%) (Scheme 16.51b).

Meng and co-workers [202, 203] revealed that the NHC ([Cu]/**L53**) complex acts as an excellent chiral catalyst for enantioselective conjugate addition of easily accessible alkenylboronic and allenylboronic acid pinacol esters to α,β-unsaturated diesters with good yields and ees (Scheme 16.52a, b).

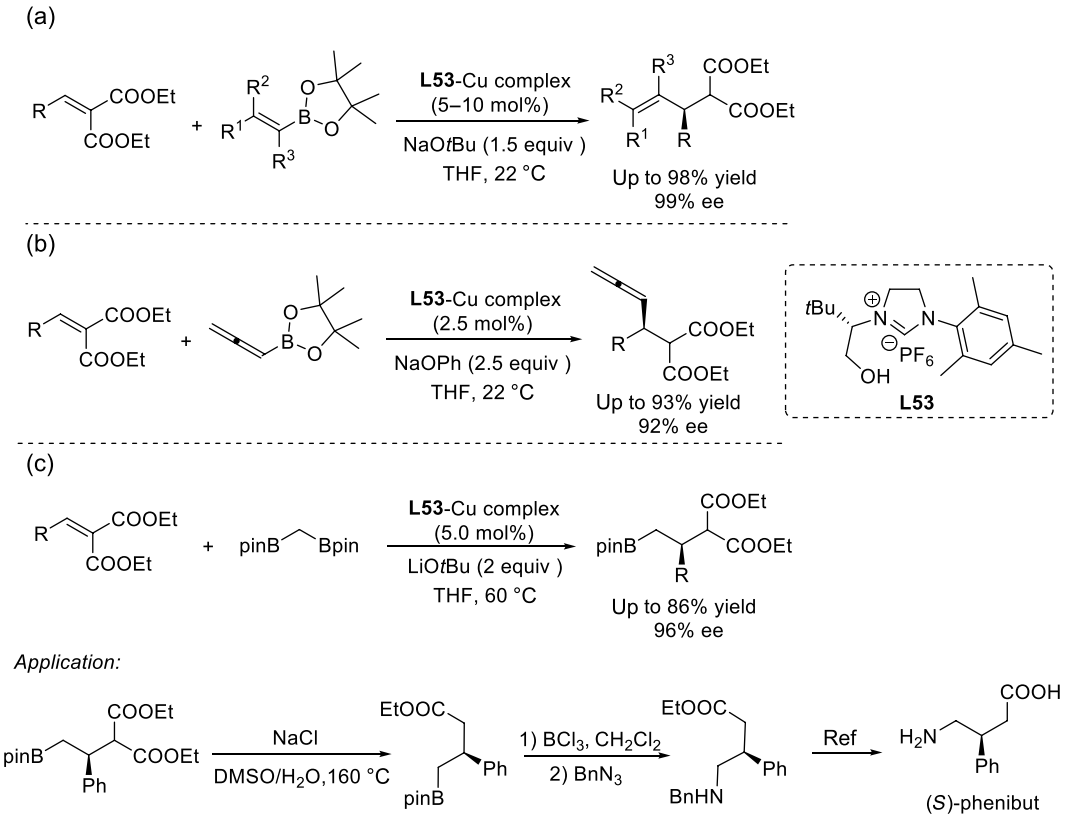

Scheme 16.52. Cu(I)-carbene catalyzed conjugate additions to α,β-unsaturated diesters (a–c) [202–204].

Analysis of ACA of organoboron reagents to Michael acceptors reveals that these boron reagents are mostly limited to aryl, alkenyl, and allenylboron functionalities, while the use of alkylboron reagents in ACA is extremely rare. Importantly, Yun and co-workers [204] reported in 2019 that α,β-unsaturated diesters undergo Cu(I)-NHC (**L53**)-catalyzed ACA of a borylalkyl nucleophile generated in situ from a 1,1-diborylmethane derivative (Scheme 16.52c). This method yielded β-chiral alkyl boronates in up to 86% yield with high enantioselectivity. The alkylboron moiety in the resulting chiral diester products was converted into various functional groups by C–B bond transformations. Significantly, the versatility of this methodology was demonstrated by stereospecific transformation of the resulting chiral organoboron compounds into various organic molecules. Moreover, this approach was successfully applied to the enantioselective synthesis of the benzyl-protected amine, which is a key intermediate in the synthesis of antianxiety drug *(S)-phenibut* (Scheme 16.52c).

16.4.4.5. ACA to Other Michael Acceptors In 2015, Hayashi and co-workers [205] developed a new type of rhodium-catalyzed asymmetric arylation, where 3-sulfolene is in equilibrium with 2-sulfolene via a base-catalyzed isomerization under the conditions of rhodium-catalyzed arylation. The chiral rhodium complex Rh/**L75** catalyzed the arylation of 2-sulfolene under the isomerization condition to finally consume all the 3-sulfolene, providing the corresponding products in high yields (up to 97%) and enantiopurities (up to 99%) (Scheme 16.53a). Two years later, the same authors [206] reported an interesting case of dynamic kinetic resolution in Rh-catalyzed asymmetric arylation of phospholene oxides with ArB(pin) that gives the hydroarylation products with high diastereo- and enantioselectivities (Scheme 16.53b). The reaction opened a new synthetic route to chiral organophosphorus compounds containing two stereogenic centers: one on phosphorus and the other on carbon. The corresponding adducts were obtained with high diastereoselectivity as well as high enantioselectivity.

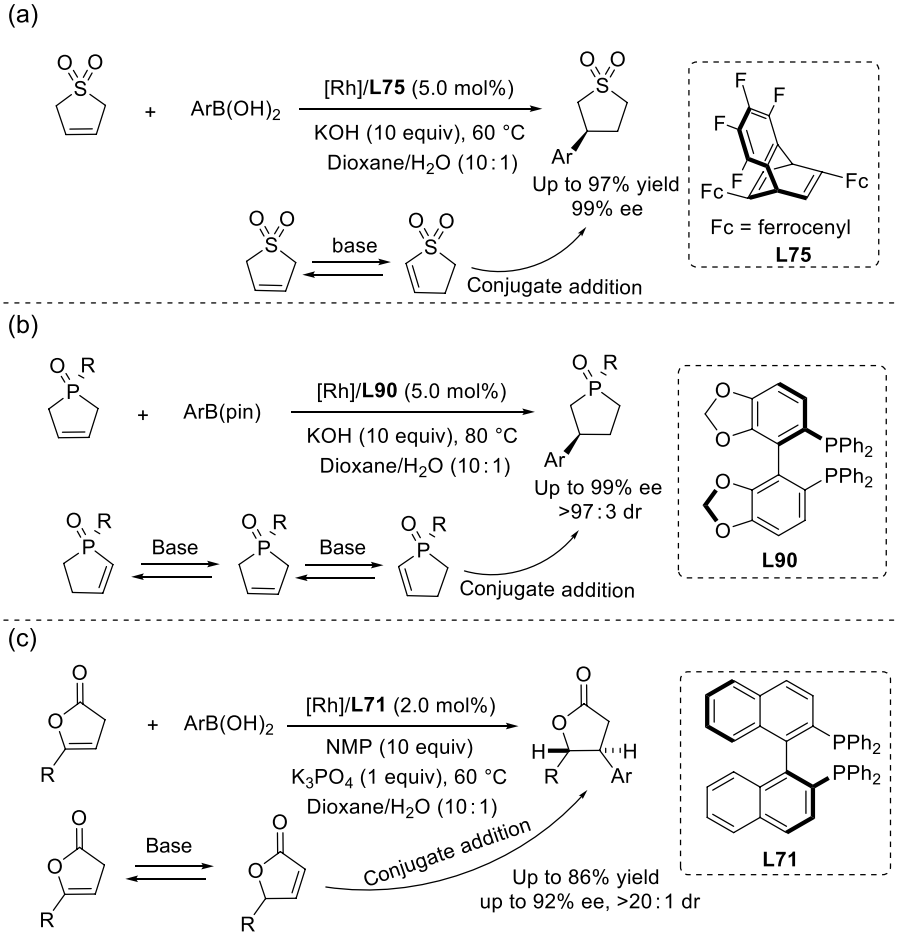

Scheme 16.53. Rh(I)-catalyzed enantioselective arylation of sulfolene (a) [205], phospholene (b) [206], and α-angelica lactone (c) derivatives [207].

Recently, the group of Johnson [207] reported enantioconvergent 1,4-arylation of γ-substituted α,β-unsaturated butenolides using rhodium- 2,2'-bis(diphenylphosphino)-1,1'-binaphthyl (Rh-BINAP)-catalyzed conjugate addition of aryl boronic acids (Scheme 16.53c). This reaction is an example of a dynamic kinetic resolution that takes advantage of racemization of a γ-stereocenter through formation of a dienolate. A wide range of β-aryl, γ-substituted γ-butyrolactones can be accessed in good yields, excellent enantioselectivities, and as a single diastereomer.

In 2019, the group of Qin [208] demonstrated that a chiral [Rh]/**L91** complex is an efficient catalyst for the ACA of arylboronic acids to α,β-ethene sulfonyl fluorides, affording various aryl-substituted chiral sulfonylfluorides, which are otherwise extremely difficult to access (Scheme 16.54a). Later, this catalyst system was also employed in ACA of arylboronic acids to α,β,γ,δ-dienesulfonyl fluorides [209]. This method provides access to a new class of chiral (*E*)-2-aryl-4-(alkyl or aryl) but-3-ene-1-sulfonyl fluorides with perfect 1,4-selectivity and high enantioselectivity (Scheme 16.54b).

16.5. CONCLUSIONS

We have summarized the recent progress in catalytic asymmetric nucleophilic additions to ketones and ketimines and Michael acceptors with special focus on non-stabilized nucleophiles. The amount of methodologies available to synthetic chemists for asymmetric carbon–carbon bond-forming reactions using

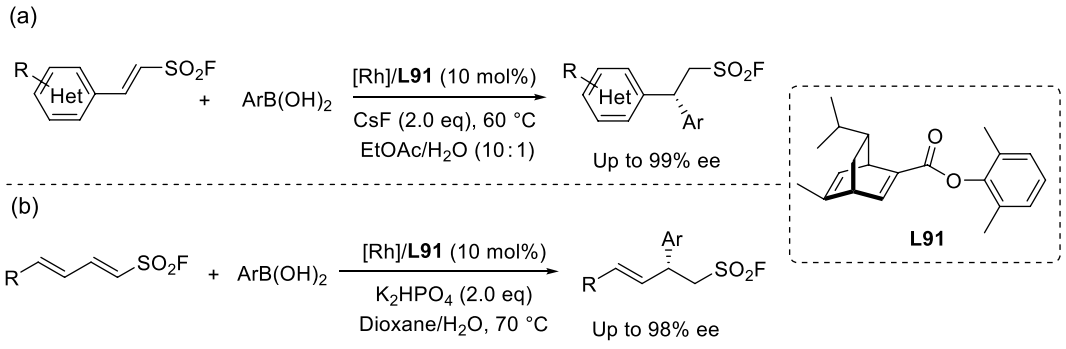

Scheme 16.54. Rh(I)-catalyzed enantioselective arylation of α,β-unsaturated (a) [208] and α,β,γ,δ-unsaturated (b) sulfonyl fluorides [209].

these classes of organic substrates has substantially increased in the past decade. Efficient catalytic systems have been developed with various metals and many classes of novel chiral ligands have been developed. Novel developments using catalytic systems based on earth-abundant metals are of special note. These developments allowed introduction of more sustainable methods and led to substantial broadening of substrate scope.

However, despite the remarkable progress the field witnessed in recent years, the current state is certainly incomplete. Future developments that would allow broader substrate and nucleophile scope, lower catalyst loading, as well as more efficient methods for generating quaternary stereocenters in conjugate additions can be expected in the years to come.

ACKNOWLEDGMENTS

Financial support from the European Research Council (S.R.H. Grant No. 773264, LACOPAROM), The Netherlands Organization for Scientific Research (S.R.H. NWO-VICI), and the China Scholarship Council (CSC, to L.G.) is acknowledged.

REFERENCES

1. Naredla, R. R.; Klumpp, D. A. *Chem. Rev.* **2013**, *113*, 6905–6948.
2. Chen, L.; Yin, X. P.; Wang, C. H.; Zhou, J. *Org. Biomol. Chem.* **2014**, *12*, 6033–6048.
3. Garcia, C.; Martin, V. *Curr. Org. Chem.* **2006**, *10*, 1849–1889.
4. Jacobsen, E.; Pfaltz, A.; Yamamoto, H. *Comprehensive Asymmetric Catalysis: Supplement 1*; Springer Science & Business Media: New York, **2003**.
5. Blaser, H. U.; Federsel, H. J. *Asymmetric Catalysis on Industrial Scale: Challenges, Approaches and Solutions*, *Second Edition*; WILEY-VCH Verlag GmbH & Co. KGaA: Weinheim, Germany **2010**.
6. Liu, Y. L.; Lin, X. T. *Adv. Synth. Catal.* **2019**, *361*, 876–918.
7. Shibasaki, M.; Kanai, M. *Chem. Rev.* **2008**, *108*, 2853–2873.
8. Rakita, P. E. Grignard reactions. In *Kirk-Othmer Encyclopedia of Chemical Technology*; John Wiley & Sons, Inc.: Hoboken, NJ, **2005**.
9. Knochel, P.; Sapountzis, I.; Gommermann, N. *Metal-Catalyzed Cross-Coupling Reactions*; Wiley-VCH Verlag GmbH: Weinheim, Germany, **2008**; pp. 671–698.
10. Hatano, M.; Suzuki, S.; Ishihara, K. *J. Am. Chem. Soc.* **2006**, *128*, 9998–9999.
11. Muramatsu, Y.; Harada, T. *Angew. Chem. Int. Ed.* **2008**, *47*, 1088–1090.
12. Madduri, A. V. R.; Minnaard, A. J.; Harutyunyan, S. R. *Chem. Commun.* **2012**, *48*, 1478–1480.
13. Fernández-Mateos, E.; Maciá, B.; Ramón, D. J.; Yus, M. *Eur. J. Org. Chem.*, **2011**, *2011*, 6851–6855.
14. Fernández-Mateos, E.; Maciá, B.; Ramón, D. J.; Yus, M. *Adv. Synth. Catal.* **2013**, *335*, 1249–1254
15. Liu, Y.; Da, C. S.; Yu, S. L.; Yin, X. G.; Wang, J. R.; Fan, X. Y.; Li, W. P.; Wang, R. *J. Org. Chem.* **2010**, *75*, 6869–6878
16. Da, C. S.; Wang, J. R.; Yin, X. G.; Fan, X. Y.; Liu, Y.; Yu, S. L. *Org. Lett.* **2009**, *11*, 5578–5581
17. Madduri, A. V. R.; Minnaard, A. J.; Harutyunyan, S. R. *Org. Biomol. Chem.* **2012**, *10*, 2878.

18. Madduri, A. V. R.; Harutyunyan, S. R.; Minnaard, A. J. *Angew. Chem., Int. Ed.* **2012**, *51*, 3164–3167.
19. Ortiz, P.; Del Hoyo, A. M.; Harutyunyan, S. R. *Eur. J. Org. Chem.* **2015**, *2015*, 72–76.
20. Rong, J.; Oost, R.; Desmarchelier, A.; Minnaard, A. J.; Harutyunyan, S. R. *Angew. Chem. Int. Ed.* **2015**, *54*, 3038–3042.
21. Fernández-Mateos, E.; Maciá, B.; Yus, M. *Eur. J. Org. Chem.* **2014**, *2014*, 6519–6526.
22. Osakama, K.; Nakajima, M. *Org. Lett.* **2016**, *18*, 236–239.
23. Hatano, M.; Ishihara, K. *Synthesis* **2008**, *2008*, 1647–1675.
24. Kalita, S. J.; Cheng, F.; Huang, Y. *Adv. Synth. Catal.* **2020**, *362*, 2778–2800.
25. Shintani, R.; Inoue, M.; Hayashi, T. *Angew. Chem. Int. Ed.* **2006**, *45*, 3353–3356.
26. Duan, H. F.; Xie, J. H.; Qiao, X. C.; Wang, L. X.; Zhou, Q. L. *Angew. Chem. Int. Ed.* **2008**, *47*, 4351–4353.
27. Cai, F.; Pu, X.; Qi, X.; Lynch, V.; Radha, A.; Ready, J. M. *J. Am. Chem. Soc.* **2011**, *133*, 18066–18069.
28. Zhu, T. S.; Jin, S. S.; Xu, M. H. *Angew. Chem. Int. Ed.* **2012**, *51*, 780–783.
29. Low, D. W.; Pattison, G.; Wieczysty, M. D.; Churchill, G. H.; Lam, H. W. *Org. Lett.* **2012**, *14*, 2548–2551.
30. Huang, L.; Zhu, J.; Jiao, G.; Wang, Z.; Yu, X.; Deng, W. P.; Tang, W. *Angew. Chem. Int. Ed.* **2016**, *55*, 4527–4531.
31. Bartlett, S. L.; Keiter, K. M.; Johnson, J. S. *J. Am. Chem. Soc.* **2017**, *139*, 3911–3916.
32. Borrego, L. G.; Recio, R.; Alcarranza, M.; Khiar, N.; Fernández, I. *Adv. Synth. Catal.* **2018**, *360*, 1273–1279.
33. Cai, Y.; Ruan, L. X.; Rahman, A.; Shi, S. L. *Angew. Chem. Int. Ed.* **2021**, *60*, 5262–5267.
34. Ni, C.; Gao, J.; Fang, X. *Chem. Commun.* **2020**, *56*, 2654–2657.
35. Yus, M.; González-Gómez, J. C.; Foubelo, F. *Chem. Rev.* **2011**, *111*, 7774–7854.
36. Luo, H. X.; Duvall, J. R.; Huang, M. Y.; Hong, R. *Org. Chem. Front.* **2014**, *1*, 303–320.
37. Alam, R.; Vollgraff, T.; Eriksson, L.; Szabó, K. J. *J. Am. Chem. Soc.* **2015**, *137*, 11262–11265.
38. Lee, K.; Silverio, D. L.; Torker, S.; Robbins, D. W.; Haeffner, F.; Van Der Mei, F. W.; Hoveyda, A. H. *Nat. Chem.* **2016**, *8*, 768–777
39. Van Der Mei, F. W.; Qin, C.; Morrison, R. J.; Hoveyda, A. H. *J. Am. Chem. Soc.* **2017**, *139*, 9053–9065.
40. Robbins, D. W.; Lee, K.; Silverio, D. L.; Volkov, A.; Torker, S.; Hoveyda, A. H. *Angew. Chem., Int. Ed.* **2016**, *55*, 9610–9614.
41. Fager, D. C.; Lee, K.; Hoveyda, A. H. *J. Am. Chem. Soc.* **2019**, *141*, 16125–16138.
42. Chai, G. L.; Zhu, B.; Chang, J. *J. Org. Chem.* **2019**, *84*, 120–127.
43. Shi, S. L.; Xu, L. W.; Oisaki, K.; Kanai, M.; Shibasaki, M. *J. Am. Chem. Soc.* **2010**, *132*, 6638–6639.
44. Yamashita, Y.; Cui, Y.; Xie, P.; Kobayashi, S. *Org. Lett.* **2015**, *17*, 6042–6045.
45. Mszar, N. W.; Mikus, M. S.; Torker, S.; Haeffner, F.; Hoveyda, A. H. *Angew. Chem. Int. Ed.* **2017**, *56*, 8736–8741.
46. Fandrick, D. R.; Reeves, J. T.; Bakonyi, J. M.; Nyalapatla, P. R.; Tan, Z.; Niemeier, O.; Akalay, D.; Fandrick, K. R.; Wohlleben, W.; Ollenberger, S.; Song, J. J.; Sun, X.; Qu, B.; Haddad, N.; Sanyal, S.; Shen, S.; Ma, S.; Byrne, D.; Chitroda, A.; Fuchs, V.; Narayanan, B. A.; Grinberg, N.; Lee, H.; Yee, N.; Brenner, M.; Senanayake, C. H.; *J. Org. Chem.* **2013**, *78*, 3592–3615.
47. Zhao, J.; Jonker, S. J. T.; Meyer, D. N.; Schulz, G.; Tran, C. D.; Eriksson, L.; Szabó, K. *J. Chem. Sci.* **2018**, *9*, 3305–3312.
48. Shu, C. C.; Zhou, S.; Gau, H. M. *RSC Adv.* **2015**, *5*, 98391–98398.
49. Matsuda, A.; Ushimaru, T.; Kobayashi, Y.; Harada, T. *Chem. Eur. J.* **2017**, *23*, 8605–8609.
50. Mailyan, A. K.; Eickhoff, J. A.; Minakova, A. S.; Gu, Z.; Lu, P.; Zakarian, A. *Chem. Rev.* **2016**, *116*, 4441–4557.
51. Soai, K.; Hatanaka, T.; Miyazawa, T. *J. Chem. Soc. Chem. Commun.* **1992**, *16*, 1097–1098.
52. Fujihara, H.; Nagai, K.; Tomioka, K. *J. Am. Chem. Soc.* **2000**, *122*, 12055–12056.
53. Côté, A.; Boezio, A. A.; Charette, A. B. *Proc. Natl. Acad. Sci. U. S. A.* **2004**, *101*, 5405–5410.
54. Zhang, H. L.; Liu, H.; Cui, X.; Mi, A. Q.; Jiang, Y. Z.; Gong, L. Z. *Synlett* **2005**, *2005*, 615–618.
55. Nakamura, S.; Nakashima, H.; Sugimoto, H.; Sano, H.; Hattori, M.; Shibata, N.; Toru, T. *Chem. Eur. J.* **2008**, *14*, 2145–2152.
56. Perron, Q.; Alexakis, A. *Tetrahedron: Asymmetry.* **2008**, *19*, 1871–1874.
57. Lindsay, V. N. G.; Charette, A. B. *Comprehensive Organic Synthesis II: Additions to and substitutions at CC [pi]-bonds*, Second Edition (Eds. Knochel, P. G.; Molander, A.); Elsevier: Oxford, **2014**; pp. 365–394.
58. Yamada, K.; Tomioka, K. *Chem. Rev.* **2008**, *108*, 2874–2886.
59. Kobayashi, S.; Mori, Y.; Fossey, J. S.; Salter, M. M. *Chem. Rev.* **2011**, *111*, 2626–2704.
60. Marques, C. S.; Burke, A. J. *ChemCatChem.* **2011**, *3*, 635–645.
61. Wada, R.; Shibuguchi, T.; Makino, S.; Oisaki, K.; Kanai, M.; Shibasaki, M. *J. Am. Chem. Soc.* **2006**, *128*, 7687–7691.
62. Shintani, R.; Takeda, M.; Tsuji, T.; Hayashi, T. *J. Am. Chem. Soc.* **2010**, *132*, 13168–13169.
63. Huang, G.; Yang, J.; Zhang, X. *Chem. Commun.* **2011**, *47*, 5587–5589.
64. Nishimura, T.; Noishiki, A.; Chit Tsui, G.; Hayashi, T. *J. Am. Chem. Soc.* **2012**, *134*, 5056–5059.
65. Yang, G.; Zhang, W. *Angew. Chem. Int. Ed.* **2013**, *52*, 7540–7544.
66. Yin, L.; Otsuka, Y.; Takada, H.; Mouri, S.; Yazaki, R.; Kumagai, N.; Shibasaki, M. *Org. Lett.* **2013**, *15*, 698–701.
67. Nakamura, S.; Hyodo, K.; Nakamura, M.; Nakane, D.; Masuda, H. *Chem. Eur. J.* **2013**, *19*, 7304–7309.
68. Lauzon, C.; Charette, A. B. *Org. Lett.* **2006**, *8*, 2743–2745.
69. Fu, P.; Snapper, M. L.; Hoveyda, A. H. *J. Am. Chem. Soc.* **2008**, *130*, 5530–5541.
70. Hirner, S.; Kolb, A.; Westmeier, J.; Gebhardt, S.; Middel, S.; Harms, K.; Zezschwitz, P. *Org. Lett.* **2014**, *16*, 3162–3165.

71. Richey, H. G., Ed. *Grignard Reagents—New Developments*; Wiley: Chichester, **2000**.
72. Ellman, J. A.; Owens, T. D.; Tang, T. P. *Acc. Chem. Res.* **2002**, *35*, 984–995.
73. Gandon, V.; Bertus, P.; Szymoniak, J. *Eur. J. Org. Chem.* **2001**, 3677–3681.
74. Rong, J.; Collados, J. F.; Ortiz, P.; Jumde, R. P.; Otten, E.; Harutyunyan, S. R. *Nat. Commun.* **2016**, *7*, 1–7.
75. Ortiz, P.; Collados, J. F.; Jumde, R. P.; Otten, E.; Harutyunyan, S. R. *Angew. Chem. Int. Ed.* **2017**, *56*, 3041–3044.
76. Nishimura, T.; Noishiki, A.; Ebe, Y.; Hayashi, T. *Angew. Chem. Int. Ed.* **2013**, *52*, 1777–1780.
77. Jiang, T.; Wang, Z.; Xu, M. H. *Org. Lett.* **2015**, *17*, 528–531.
78. Takechi, R.; Nishimura, T. *Org. Biomol. Chem.* **2015**, *12*, 4918–4924.
79. Cui, Z.; Yu, H. J.; Yang, R. F.; Gao, W. Y.; Feng, C. G.; Lin, G. Q. *J. Am. Chem. Soc.* **2011**, *133*, 12394–12397.
80. Wang, H.; Jiang, T.; Xu, M. H. *J. Am. Chem. Soc.* **2013**, *135*, 971–974.
81. Kong, J.; McLaughlin, M.; Belyk, K.; Mondschein, R. *Org. Lett.* **2015**, *17*, 5520–5523.
82. Li, Y.; Yu, Y. N.; Xu, M. H. *ACS Catal.* **2016**, *6*, 661–665.
83. Liu, M. Q.; Jiang, T.; Chen, W. W.; Xu, M. H. *Org. Chem. Front.* **2017**, *4*, 2159–2162.
84. Yu, Y. N.; Qi, W. Y.; Wu, C. Y.; Xu, M. H. *Org. Lett.* **2019**, *21*, 7493–7497.
85. Zhu, J.; Huang, L.; Dong, W.; Li, N.; Yu, X.; Deng, W. P.; Tang, W. *Angew. Chem. Int. Ed.* **2019**, *58*, 16119–16123.
86. Jiang, C.; Lu, Y.; Hayashi, T. *Angew. Chem. Int. Ed.* **2014**, *53*, 9936–9939.
87. Quan, M.; Yang, G.; Xie, F.; Gridnev, I. D.; Zhang, W. *Org. Chem. Front.* **2015**, *2*, 398–402.
88. Yan, Z.; Wu, B.; Gao, X.; Zhou, Y. G. *Chem. Commun.* **2016**, *52*, 10882–10885.
89. Álvarez-Casao, Y.; Monge, D.; Álvarez, E.; Fernández, R.; Lassaletta, J. M. *Org. Lett.* **2015**, *17*, 5104–5107.
90. Zhou, B.; Jiang, C.; Gandi, V. R.; Lu, Y.; Hayashi, T. *Chem. Eur. J.* **2016**, *22*, 13068–13071.
91. He, Q.; Wu, L.; Kou, X.; Butt, N.; Yang, G.; Zhang, W. *Org. Lett.* **2016**, *18*, 288–291.
92. Wang, J. Y.; Li, M.-W.; Li, M.-F.; Hao, W. J.; Li, G.; Tu, S. J.; Jiang, B. *Org. Lett.* **2018**, *20*, 6616–6621.
93. Zhao, Z. B.; Shi, L.; Meng, F. J.; Li, Y.; Zhou, Y. G. *Org. Chem. Front.* **2019**, *6*, 1572–1576.
94. Quan, M.; Tang, L.; Shen, J.; Yang, G.; Zhang, W. *Chem. Commun.* **2017**, *53*, 609–612.
95. Quan, M.; Wang, X.; Wu, L.; Gridnev, I. D.; Yang, G.; Zhang, W. *Nat. Commun.* **2018**, *9*, 1–11.
96. Huang, Y.; Huang, R. Z.; Zhao, Y. *J. Am. Chem. Soc.* **2016**, *138*, 6571–6576.
97. Wu, L.; Shao, Q.; Yang, G.; Zhang, W. *Chem. Eur. J.* **2018**, *24*, 1241–1245.
98. Kim, J.; Shin, M.; Cho, S. H. *ACS Catal.* **2019**, *9*, 8503–8508.
99. Jang, H.; Romiti, F.; Torker, S.; Hoveyda, A. H. *Nat. Chem.* **2017**, *9*, 1269–1275.
100. Alexakis, A.; Krause, N.; Woodward, S. *Copper-Catalyzed Asymmetric Synthesis*; Wiley-VCH: Weinheim, Germany, **2014**.
101. Harutyunyan, S. R. *Progress in Enantioselective Cu(I)-Catalyzed Formation of Stereogenic Centers*; Springer: Heidelberg, Germany, **2015**.
102. Alexakis, A.; Backvall, J. E.; Krause, N.; Pamies, O.; Dieguez, M. *Chem. Rev.* **2008**, *108*, 2796–2823.
103. Harutyunyan, S. R.; den Hartog, T.; Geurts, K.; Minnaard, A. J.; Feringa, B. L. *Chem. Rev.* **2008**, *108*, 2824–2852.
104. Jerphagnon, T.; Pizzuti, M. G.; Minnaard, A. J.; Feringa, B. L. *Chem. Soc. Rev.* **2009**, *38*, 1039–1075.
105. Schmid, T. E.; Drissi-Amraoui, S.; Crevisy, C.; Basle, O.; Mauduit, M. *Beilstein J. Org. Chem.* **2015**, *11*, 2418–2434.
106. Kharasch, M. S.; Tawney, P. O. *J. Am. Chem. Soc.* **1941**, *63*, 2308–2316.
107. Villacorta, G. M.; Rao, C. P.; Lippard, S. J. *J. Am. Chem. Soc.* **1988**, *110*, 3175–3182.
108. Ahn, K. H.; Bryan Klassen, R.; Lippard, S. J. *Organometallics* **1990**, *9*, 3178–3181.
109. Feringa, B. L.; Badorrey, R.; Pena, D.; Harutyunyan, S. R.; Minnaard, A. J. *Proc. Natl. Acad. Sci. U. S. A.* **2004**, *101*, 5834–5838.
110. Guo, Y.; Harutyunyan, S. R. *Beilstein J. Org. Chem.* **2020**, *16*, 1006–1021.
111. Rupnicki, L.; Saxena, A.; Lam, H. W. *J. Am. Chem. Soc.* **2009**, *131*, 10386–10387.
112. Pattison, G.; Piraux, G.; Lam, H. W. *J. Am. Chem. Soc.* **2010**, *132*, 14373–14375.
113. Saxena, A.; Lam, H. W. *Chem. Sci.* **2011**, *2*, 2326–2331.
114. Jumde, R. P.; Lanza, F.; Veenstra, M. J.; Harutyunyan, S. R. *Science* **2016**, *352*, 433–437.
115. Jumde, R. P.; Lanza, F.; Pellegrini, T.; Harutyunyan, S. R. *Nat. Commun.* **2017**, *8*, 1–10.
116. Lanza, F.; Pérez, J. M.; Jumde, R. P.; Harutyunyan, S. R. *Synthesis* **2019**, *51*, 1253–1262.
117. Mao, W.; Xue, W.; Irran, E.; Oestreich, M. *Angew. Chem. Int. Ed.* **2019**, *58*, 10723–10726.
118. Byrd Review, K. M. *Beilstein J. Org. Chem* **2015**, *11*, 530–562.
119. Rodríguez-Fernández, M.; Yan, X.; Collados, J. F.; White, P. B.; Harutyunyan, S. R. *J. Am. Chem. Soc.* **2017**, *139*, 14224–14231.
120. Guo, Y.; Kootstra, J.; Harutyunyan, S. R. *Angew. Chem. Int. Ed.* **2018**, *57*, 13547–13550.
121. Yan, X.; Harutyunyan, S. R. *Nat. Commun.* **2019**, *10*, 1–10.
122. Vila, C.; Hornillos, V.; Fañanás-Mastral, M.; Feringa, B. L. *Chem. Commun.* **2013**, *49*, 5933–5935.
123. Guo, Y.; Harutyunyan, S. R. *Angew. Chem. Int. Ed.* **2019**, *58*, 12950–12954.
124. Yan, X.; Ge, L.; Castiñeira Reis, M.; Harutyunyan, S. R. *J. Am. Chem. Soc.* **2020**, *142*, 20247–20256.
125. Ge, L.; Zurro, M.; Harutyunyan, S. R. *Chem. Eur. J.* **2020**, *26*, 16277–16280.
126. Soai, K.; Hayasaka, T.; Ugajin, S. *J. Chem. Soc. Chem. Commun.* **1989**, *8*, 516–517.

127. De Vries, A. H. M.; Meetsma, A.; Feringa, B. L. *Angew. Chem. Int. Ed.* **1996**, *35*, 2374–2376.
128. Feringa, B. L.; Pineschi, M.; Arnold, L. A.; Imbos, R.; De Vries, A. H. M. *Angew. Chem. Int. Ed.* **1997**, *36*, 2620–2623.
129. Shibata, N.; Okamoto, M.; Yamamoto, Y.; Sakaguchi, S. *J. Org. Chem.* **2010**, *75*, 5707–5715.
130. Zhao, Q. L.; Tse, M. K.; Wang, L. L.; Xing, A. P.; Jiang, X. *Tetrahedron Asymmetry.* **2010**, *21*, 2788–2793.
131. Xing, A. P.; Bai, C. B.; Wang, L. L. *Tetrahedron* **2013**, *69*, 455–459.
132. Pang, Z. B.; Li, H. F.; Wang, L. L. *Chin. Chem. Lett.* **2016**, *27*, 271–276.
133. Ebisu, Y.; Kawamura, K.; Hayashi, M. *Tetrahedron Asymmetry.* **2012**, *23*, 959–964.
134. Jahier-Diallo, C.; Morin, M. S. T.; Queval, P.; Rouen, M.; Artur, I.; Querard, P.; Toupet, L.; Crévisy, C.; Baslé, O.; Mauduit, M. *Chem. Eur. J.* **2015**, *21*, 993–997.
135. Zhong, C.; Huang, Y.; Zhang, H.; Zhou, Q.; Liu, Y.; Lu, P. *Angew. Chem. Int. Ed.* **2020**, *59*, 2750–2754.
136. Endo, K.; Ogawa, M.; Shibata, T. *Angew. Chem. Int. Ed.* **2010**, *49*, 2410–2413.
137. Endo, K.; Yakeishi, S.; Hamada, D.; Shibata, T. *Chem. Lett.* **2013**, *42*, 547–549.
138. Ye, F.; Zheng, Z. J.; Deng, W. H.; Zheng, L. S.; Deng, Y.; Xia, C. G.; Xu, L. W. *Chem. Asian J.* **2013**, *8*, 2242–2253.
139. Yu, H.; Xie, F.; Ma, Z.; Liu, Y.; Zhang, W. *Org. Biomol. Chem.* **2012**, *10*, 5137–5142.
140. Han, L.; Lei, Y.; Xing, P.; Zhao, X. L.; Jiang, B. *J. Org. Chem.* **2015**, *80*, 3752–3757.
141. Kondo, J.; Harano, A.; Dohi, K.; Sakaguchi, S. *J. Mol. Catal. A Chem.* **2014**, *395*, 66–71.
142. Dohi, K.; Kondo, J.; Yamada, H.; Arakawa, R.; Sakaguchi, S. *Eur. J. Org. Chem.* **2012**, *36*, 7143–7152.
143. Endo, K.; Hamada, D.; Yakeishi, S.; Ogawa, M.; Shibata, T. *Org. Lett.* **2012**, *14*, 2342–2345.
144. Guo, S.; Xie, Y.; Hu, X.; Xia, C.; Huang, H. *Angew. Chem. Int. Ed.* **2010**, *49*, 2728–2731.
145. Dogan, Ö.; Bulut, A.; Polat, S.; Ali Tecimer, M. *Tetrahedron Asymmetry* **2011**, *22*, 1601–1604.
146. Magrez, M.; Wencel-Delord, J.; Crévisy, C.; Mauduit, M. *Tetrahedron* **2012**, *68*, 3507–3511.
147. Yang, T.; Zhang, Y.; Cao, P.; Wang, M.; Li, L.; Li, D.; Liao, J. *Tetrahedron* **2016**, *72*, 2707–2711.
148. Rexiti, R.; Lu, J.; Sha, F.; Wu, X. Y. *Tetrahedron* **2019**, *75*, 3596–3604.
149. Zhang, H.; Fang, F.; Xie, F.; Yu, H.; Yang, G.; Zhang, W. *Tetrahedron Lett.* **2010**, *51*, 3119–3122.
150. Shin, M.; Gu, M.; Lim, S. S.; Kim, M. J.; Lee, J. H.; Jin, H. G.; Jang, Y. H.; Jung, B. *Eur. J. Org. Chem.* **2018**, *2018*, 3122–3130.
151. Soeta, T.; Hatanaka, Y.; Ishizaka, T.; Ukaji, Y. *Tetrahedron* **2018**, *74*, 4601–4605.
152. Maksymowicz, R. M.; Roth, P. M. C.; Fletcher, S. P. *Nat. Chem.* **2012**, *4*, 649–654.
153. Maksymowicz, R. M.; Sidera, M.; Roth, P. M. C.; Fletcher, S. P. *Synthesis* **2013**, *45*, 2662–2668.
154. Maksymowicz, R. M.; Roth, P. M. C.; Thompson, A. L.; Fletcher, S. P. *Chem. Commun.* **2013**, *49*, 4211–4213.
155. Pinheiro, D. L. J.; de Castro, P. P.; Amarante, G. W. *Eur. J. Org. Chem.* **2018**, *2018*, 4828–4844.
156. Roth, P. M. C.; Fletcher, S. P. *Org. Lett.* **2015**, *17*, 912–915.
157. Gao, Z.; Fletcher, S. P. *Chem. Commun.* **2018**, *54*, 3601–3604.
158. Brethomé, A. V.; Paton, R. S.; Fletcher, S. P. *ACS Catal.* **2019**, *9*, 7179–7187.
159. Maciver, E. E.; Maksymowicz, R. M.; Wilkinson, N.; Roth, P. M. C.; Fletcher, S. P. *Org. Lett.* **2014**, *16*, 3288–3291.
160. Gao, Z.; Fletcher, S. P. *Chem. Commun.* **2017**, *53*, 10216–10219.
161. Némethová, I.; Bilka, S.; Šebesta, R. *J. Organomet. Chem.* **2018**, *856*, 100–108.
162. Sidera, M.; Roth, P. M. C.; Maksymowicz, R. M.; Fletcher, S. P. *Angew. Chem. Int. Ed.* **2013**, *52*, 7995–7999.
163. Roth, P. M. C.; Sidera, M.; Maksymowicz, R. M.; Fletcher, S. P. *Nat. Protoc.* **2014**, *9*, 104–111.
164. Mola, L.; Sidera, M.; Fletcher, S. P. *Aust. J. Chem.* **2015**, *68*, 401–403.
165. Garrec, K.; Fletcher, S. P. *Org. Lett.* **2016**, *18*, 3814–3817.
166. Ardkhean, R.; Mortimore, M.; Paton, R. S.; Fletcher, S. P. *Chem. Sci.* **2018**, *9*, 2628–2632.
167. Wang, J. Y. J.; Palacin, T.; Fletcher, S. P. *Org. Lett.* **2019**, *21*, 378–381.
168. Ardkhean, R.; Roth, P. M. C.; Maksymowicz, R. M.; Curran, A.; Peng, Q.; Paton, R. S.; Fletcher, S. P. *ACS Catal.* **2017**, *7*, 6729–6737.
169. Takaya, Y.; Ogasawara, M.; Hayashi, T.; Sakai, M.; Miyaura, N. *J. Am. Chem. Soc.* **1998**, *120*, 5579–5580.
170. Hayashi, T.; Yamasaki, K. *Chem. Rev.* **2003**, *103*, 2829–2844.
171. Fagnou, K.; Lautens, M. *Chem. Rev.* **2003**, *103*, 169–196.
172. Heravi, M. M.; Dehghani, M.; Zadsirjan, V. *Tetrahedron Asymmetry* **2016**, *27*, 513–588.
173. Lee, A.; Ahn, S.; Kang, K.; Seo, M. S.; Kim, Y.; Kim, W. Y.; Kim, H. *Org. Lett.* **2014**, *16*, 5490–5493.
174. Lee, A.; Kim, H. *J. Am. Chem. Soc.* **2015**, *137*, 11250–11253.
175. Lee, A.; Kim, H. *J. Org. Chem.* **2016**, *81*, 3520–3527.
176. Zhang, Y. F.; Chen, D.; Chen, W. W.; Xu, M. H. *Org. Lett.* **2016**, *18*, 2726–2729.
177. Wu, C. Y.; Zhang, Y. F.; Xu, M. H. *Org. Lett.* **2018**, *20*, 1789–1793.
178. Huang, Y.; Hayashi, T. *J. Am. Chem. Soc.* **2015**, *137*, 7556–7559.
179. Ming, J.; Hayashi, T. *Org. Lett.* **2016**, *18*, 6452–6455.
180. Wu, C.; Yue, G.; Nielsen, C. D. T.; Xu, K.; Hirao, H.; Zhou, J. *J. Am. Chem. Soc.* **2016**, *138*, 742–745.
181. Dou, X.; Lu, Y.; Hayashi, T. *Angew. Chem. Int. Ed.* **2016**, *55*, 6739–6743.
182. Yao, J.; Yin, L.; Shen, Y.; Lu, T.; Hayashi, T.; Dou, X. *Org. Lett.* **2018**, *20*, 6882–6885.

183. Yin, L.; Zhang, D.; Xing, J.; Wang, Y.; Wu, C.; Lu, T.; Chen, Y.; Hayashi, T.; Dou, X. *J. Org. Chem.* **2018**, *83*, 5869–5875.
184. Chen, Q.; Li, L.; Zhou, G.; Ma, X.; Zhang, L.; Guo, F.; Luo, Y.; Xia, W. *Chem. Asian J.* **2016**, *11*, 1518–1522.
185. Pecchioli, T.; Christmann, M. *Org. Lett.* **2018**, *20*, 5256–5259.
186. Fan, C.; Wu, Q.; Zhu, C.; Wu, X.; Li, Y.; Luo, Y.; He, J. B. *Org. Lett.* **2019**, *21*, 8888–8892.
187. Zhang, S. S.; Hu, T. J.; Li, M. Y.; Song, Y. K.; Yang, X. D.; Feng, C. G.; Lin, G. Q. *Angew. Chem. Int. Ed.* **2019**, *58*, 3387–3391.
188. Yao, J.; Liu, N.; Yin, L.; Xing, J.; Lu, T.; Dou, X. *Green Chem.* **2019**, *21*, 4946–4950.
189. Zhu, H.; Yin, L.; Chang, Z.; Wang, Y.; Dou, X. *Adv. Synth. Catal.* **2020**. *362*, 3142–3147.
190. Yin, L.; Xing, J.; Wang, Y.; Shen, Y.; Lu, T.; Hayashi, T.; Dou, X. *Angew. Chem. Int. Ed.* **2019**, *58*, 2474–2478.
191. Xie, J.-H.; Zhou, Q. L. *Acc. Chem. Res.* **2008**, *41*, 581–593.
192. Zhu, S.-F.; Zhou, Q. L. *Acc. Chem. Res.* **2012**, *45*, 1365–1377.
193. He, Q.; Xie, F.; Fu, G.; Quan, M.; Shen, C.; Yang, G.; Gridnev, I. D.; Zhang, W. *Org. Lett.* **2015**, *17*, 2250–2253.
194. Li, W.; Wang, G.; Lai, J.; Li, S. *Chem. Commun.* **2019**, *55*, 5902–5905.
195. Sieber, J. D.; Rivalti, D.; Herbage, M. A.; Masters, J. T.; Fandrick, K. R.; Fandrick, D. R.; Haddad, N.; Lee, H.; Yee, N. K.; Gupton, B. F.; Senanayake, C. H. *Org. Chem. Front.* **2016**, *3*, 1149–1153.
196. Li, R.; Wen, Z.; Wu, N. A. *Org. Biomol. Chem.* **2016**, *14*, 11080–11084.
197. Miyamura, H.; Nishino, K.; Yasukawa, T.; Kobayashi, S. *Chem. Sci.* **2017**, *8*, 8362–8372.
198. Wang, Z.; Chen, W. W.; Xu, M. H. *J. Chin. Chem. Soc.* **2018**, *65*, 331–336.
199. Sun, L.; Li, D.; Zhou, X.; Zhang, D.; Wang, J.; He, Z.; Jiang, R.; Chen, W. *J. Org. Chem.* **2017**, *82*, 12899–12907.
200. Wu, C.; Yu, Y.; Xu, M. *Org. Lett.* **2017**, *19*, 384–387.
201. Jian, J. H.; Zeng, H. W.; Kuo, T. S.; Wu, P. Y.; Wu, H. L. *Org. Lett.* **2019**, *21*, 9468–9472.
202. Chong, Q.; Yue, Z.; Zhang, S.; Ji, C.; Cheng, F.; Zhang, H.; Hong, X.; Meng, F. *ACS Catal.* **2017**, *7*, 5693–5698.
203. Chong, Q.; Zhang, S.; Cheng, F.; Wang, J.; Hong, X.; Meng, F. *Org. Lett.* **2018**, *20*, 6896–6900.
204. Jang, W. J.; Yun, J. *Angew. Chem. Int. Ed.* **2019**, *58*, 18131–18135.
205. Lim, K. M.-H.; Hayashi, T. *J. Am. Chem. Soc.* **2015**, *137*, 3201–3204.
206. Lim, K. M. H.; Hayashi, T. *J. Am. Chem. Soc.* **2017**, *139*, 8122–8125.
207. Griswold, J. A.; Johnson, J. S. *ACS Catal.* **2019**, *9*, 11614–11618.
208. Moku, B.; Fang, W. Y.; Leng, J.; Li, L.; Zha, G. F.; Rakesh, K. P.; Qin, H. L. *iScience* **2019**, *21*, 695–705.
209. Moku, B.; Fang, W. Y.; Leng, J.; Kantchev, E. A. B.; Qin, H. L. *ACS Catal.* **2019**, *9*, 10477–10488.

17

ASYMMETRIC ALLYLIC ALKYLATION, ALLYLATION, AND RELATED REACTIONS

Tyler J. Fulton, Yun E. Du, and Brian M. Stoltz
California Institute of Technology, Pasadena, CA, USA

17.1. INTRODUCTION AND SCOPE

The metal-catalyzed asymmetric substitution reaction has been a mainstay in the toolbox of organic chemists for decades. Indeed, the continued development of this transformation has rendered a broad scope of metals, nucleophiles, and electrophilic moieties compatible with this transformation. In the present series of books, the field of metal-catalyzed allylic alkylation was last reviewed by Helmchen et al. [1]. Since that time, enormous accomplishments have been achieved in the field of asymmetric allylic alkylation, particularly with respect to the fundamental development of non-palladium-mediated reactions. This chapter highlights some of the most significant advances from c. 2010 to 2020 in the understanding and application of metal-catalyzed asymmetric allylic alkylation and related processes organized by transition metal. The focus of this chapter will be on the diversity of catalytic metals and therefore this is not meant to serve as a comprehensive review of metals such as Pd, Ir, and Cu, which are among the most broadly developed. Stereospecific, non-dynamic kinetic resolutions, and hydroalkylation reactions will not be discussed in detail.

17.2. PALLADIUM-CATALYZED ENANTIOSELECTIVE ALLYLIC ALKYLATIONS

Palladium is by far the most developed transition-metal catalyst for asymmetric allylic substitution chemistry. Pd-catalysts typically provide linear alkylation products, although this selectivity can be overturned. A tremendous effort has been made from 2010 to 2020 in the development of novel chiral Pd/L catalyst systems for asymmetric allylic substitution, largely focused on generating new catalysts that are broadly amenable to many substrate classes. Within this context, a vast array of new heterodonor ligands that perform well in cases of both hindered and non-hindered electrophiles has been developed. Mechanistic understanding, aided by new experimental evidence and computational modeling, as well as development of novel strategies such as C–H allylic alkylation have greatly benefitted the substrate scope and complexity tolerated in Pd-catalyzed allylic alkylation. While several examples of kinetic resolutions have been developed, these will not be discussed here. Asymmetric oxidative allylic C–H alkylations will not be discussed in detail.

Catalytic Asymmetric Synthesis, Fourth Edition. Edited by Takahiko Akiyama and Iwao Ojima.

17.2.1. Pd-Catalyzed Asymmetric Allylic and Benzylic Substitution with Stabilized Carbon and Heteroaromatic Nucleophiles

Stabilized carbon nucleophiles are broadly utilized in the Pd-catalyzed allylic substitution for the construction of C–C bonds. Among the nucleophiles and electrophiles utilized in this transformation, the Pd-catalyzed allylic alkylation of *rac*-1,3-diphenylallyl acetate with dimethyl malonate has long served as the benchmark for examining novel ligand scaffolds. Within this context, vast arrays of novel ligands were developed from 2010 to 2020, precluding a comprehensive review here. The ligands successfully applied to these transformations include: monodentate P-donor, bidentate homodonor *P-P*, bidentate heterodonor *P-P′*, bidentate heterodonor *P-N*(sp^2), bidentate heterodonor *P-N*(sp^3), bidentate heterodonor *P-S*, bidentate heterodonor P-olefin, bidentate homodonor *N-N* ligands, bidentate heterodonor *N-N′*, bidentate heterodonor *N-S* and *N-Se*, bidentate homodonor biscarbene, and other ligand scaffolds. The discussion here will be limited to examples of more challenging substrates and novel substrate classes, utilizing both novel and well-established ligands. This section is generally organized by the type of ligand scaffold utilized.

17.2.1.1. Monodentate P-ligands Ooi reported a novel chiral binaptholate ligand with an achiral ammonium-phosphine cation, which provided excellent enantioinduction in the allylic alkylation of cinnamyl carbonates with prochiral acyclic α-nitro esters (Scheme 17.1) [2]. While a variety of cinnamyl electrophiles were tolerated, utilization of allyl methyl carbonate resulted in no enantioinduction. This modular ion-paired ligand scaffold has proven extremely versatile for ligand tailoring; replacement of the binaptholate with a phosphate-based anion enabled highly stereoselective allylic alkylation of prochiral benzofuranones [3], benzothiophenones [4], and α-nitro esters [5].

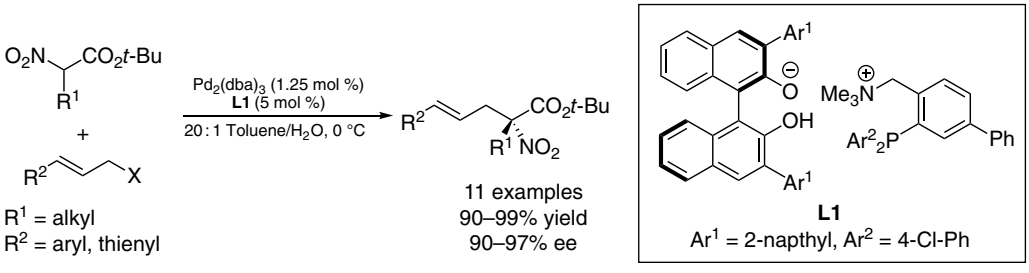

Scheme 17.1. Pd-catalyzed asymmetric allylic alkylation of α-nitro esters with a binaptholate ammonium-phosphine ligand. Source: Ooi [2].

Maulide and coworkers reported the deracemization of strained *cis*-2-oxabicyclo[2.2.0]hex-5-en-3-one with malonate nucleophiles utilizing α,α,α,α-tetraaryl-1,3-dioxolane-4,5-dimethanol (TADDOL)-derived phosphoramidite ligand **L2** (Scheme 17.2a) to afford *cis*-products with high enantio- and diastereoselectivities [6]. In addition to malonate nucleophiles, prochiral azlactones bearing a 4-NO_2–C_6H_4 moiety were also compatible with this electrophile utilizing phosphoramidite ligand **L3**, affording *cis*-products in high enantio- and diastereoselectivities (not shown). This reaction could be rendered *trans*-selective while maintaining excellent enantioselectivity by utilizing phosphinooxazoline (PHOX) ligand **L4** instead of phosphoramidite ligands **L2** or **L3**. Later, Maulide and coworkers reported Feringa phosphoramidite ligand **L3** enabled deracemization of both *cis*- and *trans*-4-chlorocyclobut-2-ene carboxylic acids with malonate nucleophiles in high *cis*-diastereoselectivity and enantioselectivity (Scheme 17.2b) [7]. Interestingly, the use of *trans*-4-chlorocyclobut-2-ene carboxylate esters reversed the selectivity observed in this transformation with *trans*-acids, favoring formation of the *trans*-alkylation product. Maulide further demonstrated the diastereoselectivities shown could be reversed in every case when PHOX ligand **L4** was utilized (not shown).

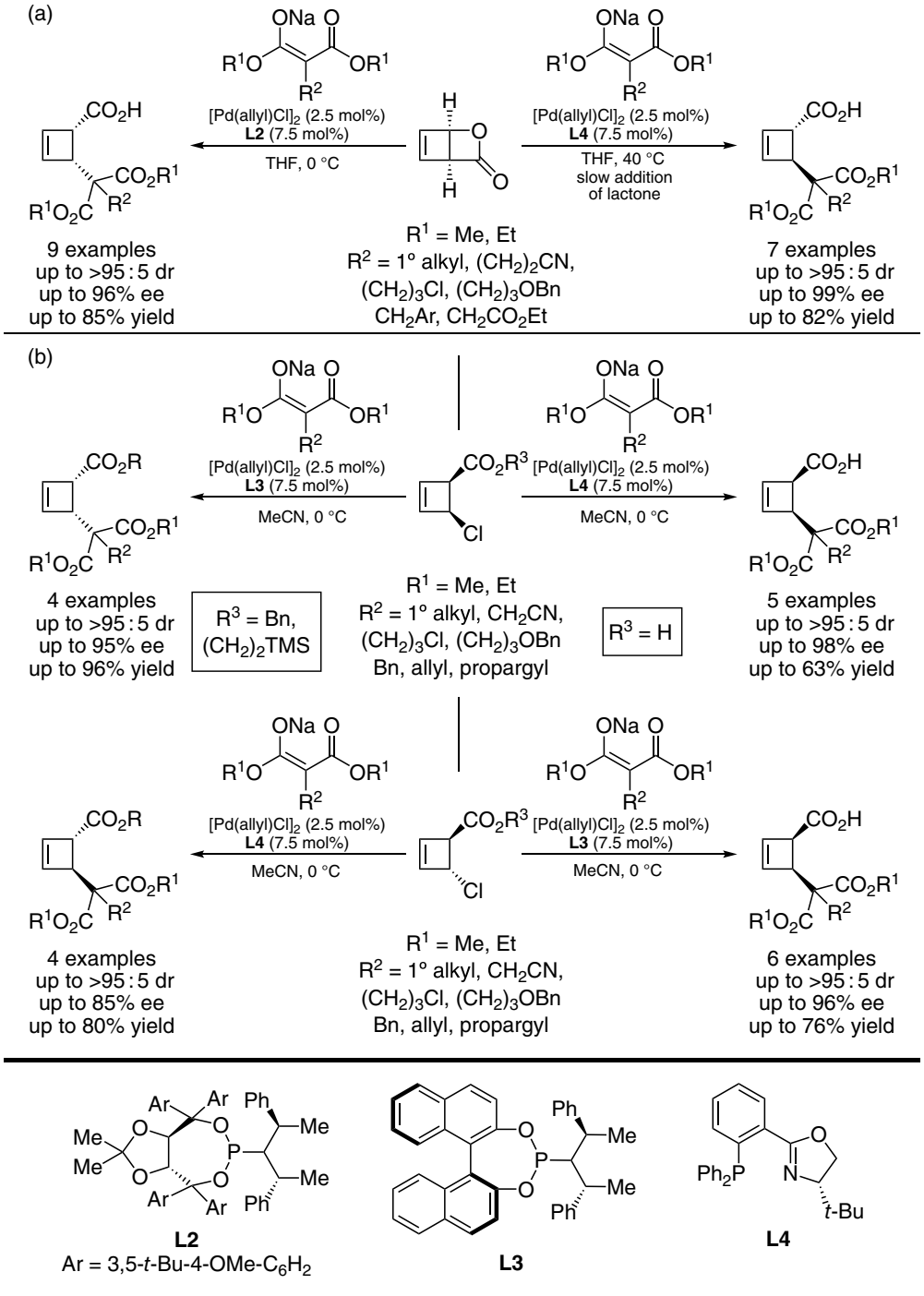

Scheme 17.2. (a) Enantio- and diastereoselective deracemization of *cis*-2-oxabicyclo[2.2.0]hex-5-en-3-one with malonate nucleophiles. Source: Maulide [6]. (b) Enantio- and diastereoselective deracemization of *cis*- and *trans*-4-chlorocyclobut-2-ene carboxylic acids with malonate nucleophiles. Source: Maulide [7].

Trost and coworkers developed a novel non-C_2-symmetric pyroglutamic acid-derived phosphoramidite ligand for the enantioselective allylic alkylation of 1,3-diketone nucleophiles (Scheme 17.3) [8, 9]. Notably, this ligand enables allylic alkylation via oxidative C–H activation of allyl arenes or with a traditional electrophile such as allyl acetate. In all examples reported, however, the allylic alkylation with cinnamyl acetates proceeded in 7–20% higher ee than the corresponding allyl arene electrophile.

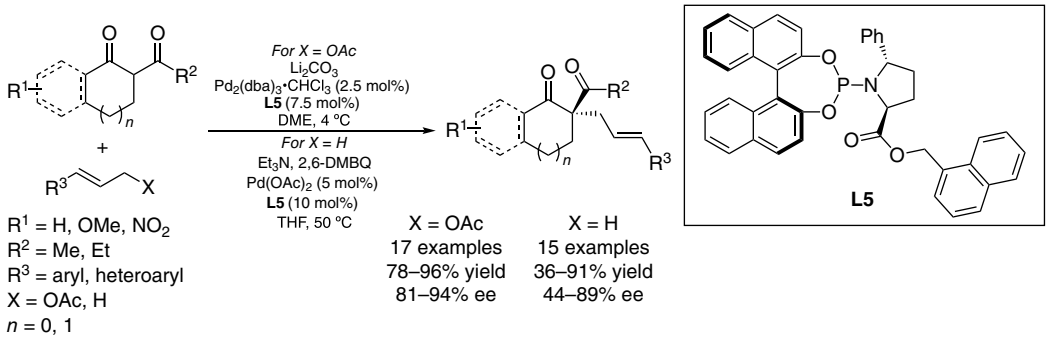

Scheme 17.3. Oxidative and redox neutral Pd-catalyzed allylic arylation with a non-C_2-symmetric phosphoramidite ligand. Source: Trost [8, 9].

17.2.1.2. C_2-Symmetric P,P-ligands The most widely utilized *P*,*P*-ligands in Pd-catalyzed allylic alkylations are the Trost diphosphine ligands. In 2018, Trost reported the utilization of stilbene-derived ligand **L6** in the allylic alkylation of indole and tryptophan derivatives with vinyl cyclopropane electrophiles (Scheme 17.4) [10]. In this methodology vinyl cyclopropanes were leveraged as electrophilic species whereas these compounds typically serve as initiating 1,3-dipole nucleophiles with Pd-catalysts. Generally excellent yields and enantioselectivities were obtained in both substrate classes explored.

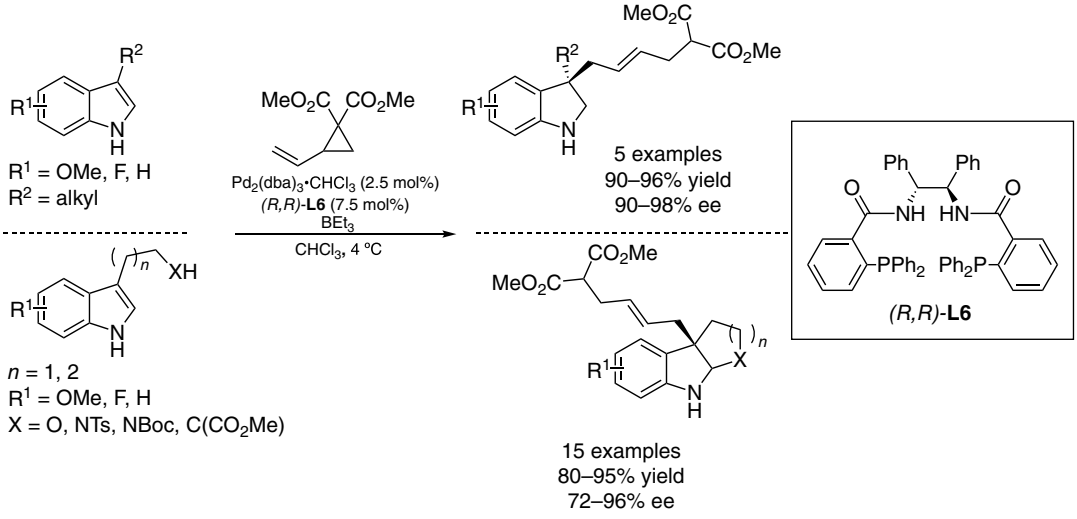

Scheme 17.4. Pd-catalyzed asymmetric allylic alkylation with vinylcyclopropane electrophiles. Source: Trost [10].

Hossain demonstrated the first example of hydroxyacrylates as nucleophiles with Pd/*trans*-1,2-diaminocyclohexane (DACH)-naphthyl ligand **L7**, affording enantioenriched α-quaternary aldehydes with generally high enantioselectivity (Scheme 17.5) [11]. Hossain further expanded the scope of this transformation to intramolecular examples via allyl enol carbonates, affording α-aryl quaternary stereogenic aldehydes in high ee [12].

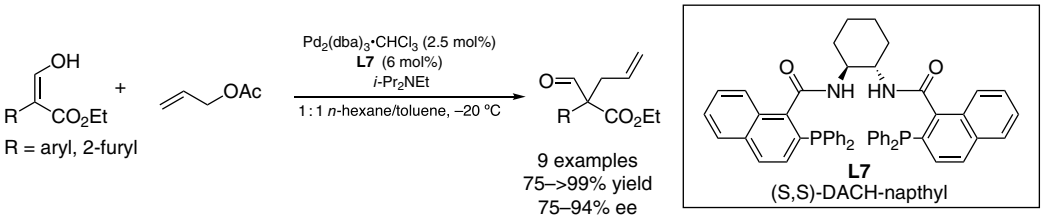

Scheme 17.5. Hydroxyacrylate nucleophiles in the Pd-catalyzed asymmetric allylic alkylation. Source: Hossain [11].

While the Trost bisphosphine ligands have been widely applied to a variety of new substrate classes, many other *P*,*P*-ligands have been utilized in powerful new Pd-catalyzed allylic and benzylic alkylations. In 2016, Hirano and Miura reported the asymmetric benzylic alkylation of diarylmethyl carbonates with (*R*)-H_8-2,2′-bis(diphenylphosphino)-1,1′-binaphthyl (BINAP) ligand **L8** (Scheme 17.6) [13]. These racemic diarenes effectively undergo a dynamic kinetic asymmetric transformation (DYKAT) to afford tertiary stereogenic diarylmethanes in generally excellent enantioselectivity with a broad range of stabilized nucleophiles.

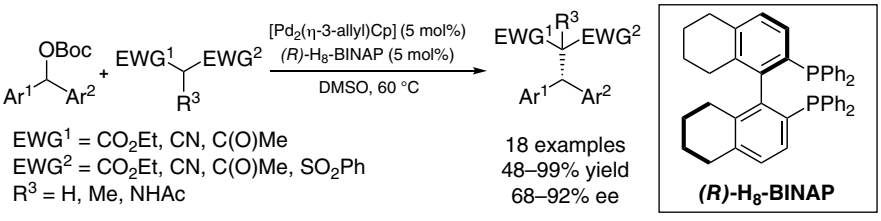

Scheme 17.6. Pd-catalyzed DYKAT of benzylic diarylmethyl carbonates. Source: Hirano and Miura [13].

In 2017, Wang and Ding reported an enantio- and diastereoselective allylic alkylation of β-ketocarbonyls with Mortia–Baylis–Hillman adducts with spiroketal-based diphosphine (SKP) ligand (**L9**) (Scheme 17.7) [14]. These powerful new SKP ligands enable excellent control over both enantio- and diastereoselectivities and for branched allylic alkylation products with Pd for a variety of nucleophiles [15]. In this example, generally excellent diastereoselectivity is observed in the formation of *vic*-quaternary and tertiary stereogenic centers.

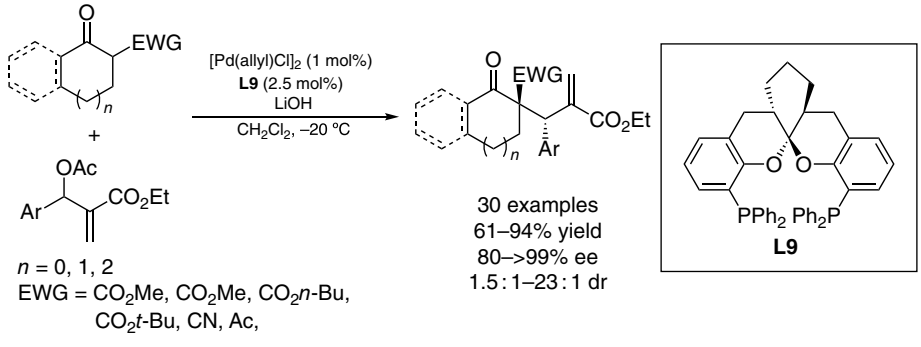

Scheme 17.7. Asymmetric allylic alkylation with Mortia–Baylis–Hillman adducts enabled by a spiroketal-based diphosphine. Source: Wang and Ding [14].

In 2019, Trost reported the synthesis of enantioenriched polyfluorinated products via the Pd-catalyzed asymmetric allylic alkylation of cyclic allylic fluorides (Scheme 17.8) [16]. A broad scope of fluorinated nucleophiles were tolerated in this transformation. In optimization studies, diamidophosphite ligands such as **L10** were uniquely effective for promoting the desired reactivity with other ligands, including DACH-Ph providing ≤20% yield.

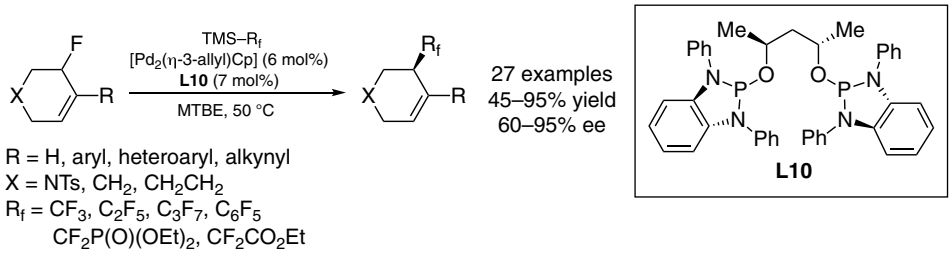

Scheme 17.8. Pd-catalyzed asymmetric allylic fluoroalkylation of cyclic allylic fluorides. Source: Trost [16].

Dearomative allylic alkylation has provided valuable access to heterocyclic motifs with high enantioinduction. A recent example from the You lab demonstrated the dearomative alkylation of pyrroles with high C2-selectivity with *(R)*-SEGPHOS (**L11**) (Scheme 17.9) [17]. Computational studies suggest that enantioinduction in this transformation is predominately controlled via secondary orbital interactions between the allyl electrophile and the pyrroles and not the chiral ligand interacting with the pyrrole [18].

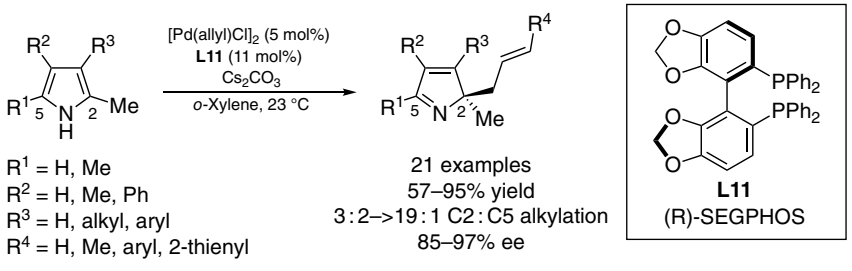

Scheme 17.9. Dearomative C_2 selective allylic alkylation of pyrrole nucleophiles. Source: You [17].

17.2.1.3. Bidentate P,N(sp²)-ligands PHOX ligand scaffolds have long dominated the *P*,*N*(sp²) ligand class for their compatibility with hindered, disubstituted electrophiles. Malcolmson has recently pioneered new methodologies for the enantioselective hydroalkylation of terminal [19] and internal [20] diene electrophiles with excellent enantioinduction. Other recent applications of PHOX ligands in complex systems include Maulide's deracemization of strained *cis*-2-oxabicyclo[2.2.0]hex-5-en-3-one electrophiles (Scheme 17.2a, vide supra). Recently, Liu and Zhang accessed various piperidine amino acids with ferrocenyl ligand **L12** (Scheme 17.10) [21]. Generally high enantioselectivities were observed with the in situ generated pyridinium species. In general, Hou and Dai's SIOCPHOX ligand (not shown) remains the optimal ligand choice in the allylic alkylation of monosubstituted allyl electrophiles; however, Ir/phosphoramidite systems have become the catalysts of choice in this regard (vide infra) [22].

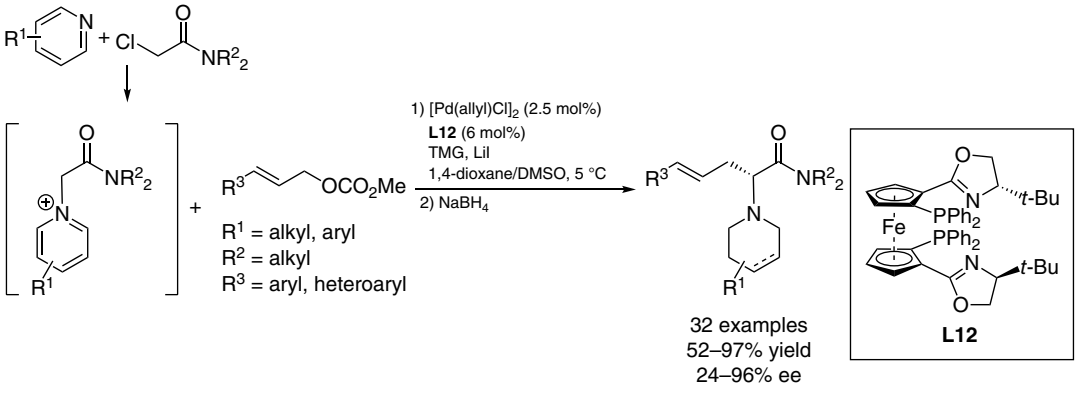

Scheme 17.10. Pd-catalyzed asymmetric allylic alkylation of in situ generated α-pyridinium acetamides. Source: Liu and Zhang [21].

17.2.2. Pd-Catalyzed Asymmetric Allylic Substitution with Non-Stabilized C-nucleophiles

Simple ketone-derived enolates are generally challenging nucleophiles for Pd-catalyzed asymmetric allylic alkylation due to side reactions such as aldol condensation and, in the case of non-symmetric ketones, regioselective enolization. In acyclic settings, control of enolate geometry is often critical to the stereochemical outcome. Strategies to circumvent these challenges include the use of symmetrical ketones and the use of ketones bearing only one enolizable position. In 2016, List and coworkers developed an allylation of ketones utilizing CO_2 for the in situ activation of allylic alcohol electrophiles as the corresponding carbonic acid (Scheme 17.11) [23]. Notably, the only byproduct generated under these mild conditions is water. A thermodynamic formation of the more substituted enol mediated by (*S*)-H_8-3,3′-bis(2,4,6-triisopropylphenyl)-1,1′-binaphthyl-2,2′-diyl hydrogen phosphate (TRIP) (**L13**) is responsible for the highly regioselective allylic alkylation observed. In addition to ketones, many other carbonyl-derived carbon nucleophiles have been employed in Pd-catalyzed allylic alkylation, including aryl pyrrolidyl ketones and 2-monosubstituted indolin-3-ones; [24], β-naphthols (via dearomatization); [25], enamines derived from ketones [26], aldehydes [27], and β-ketoesters; [28], silyl enol ethers; [29, 30], bis-silylketene acetals; [31], ester and lactone enolates; [32], and enol acetates [33].

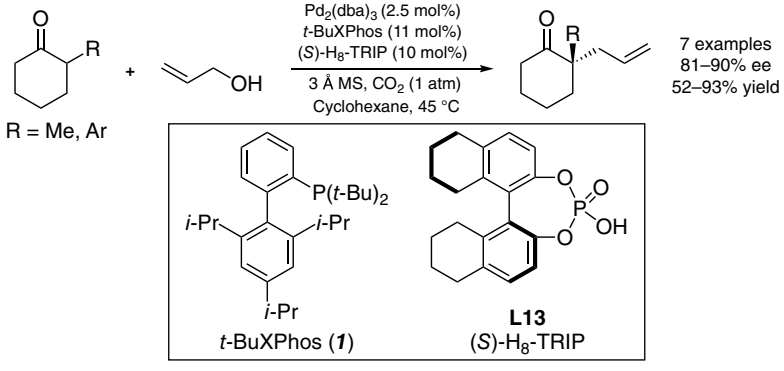

Scheme 17.11. Allylic alkylation of enols with allyl alcohol via CO_2 activation. Source: List [23].

Dual-catalytic processes have also emerged as important strategies for enabling new nucleophile classes. Kumagai and Shibasaki were among the first to utilize Cu/Pd dual catalysis to accomplish highly enantioselective transformations (Scheme 17.12) [34]. In this example, chiral Cu-enolate is formed via chelation to *N*-acyl azaindolines for Pd-catalyzed allylic alkylation of α-trifluoromethyl amides. Pd/Cu dual catalysis has additionally been developed for the enantio- and diastereoselective allylic alkylation of aldimine esters and peptides [35], enantioselective allylic alkylation of aldimine esters [36], and the stereodivergent coupling of 1,3-dienes with aldimine esters [37]. In 2020, Liao and Zhang accomplished the first DYKAT of racemic and non-symmetric 1,3-disubstituted allylic electrophiles in the synthesis of α-tetrasubstituted,β-trisubstituted amino acid derivatives (Scheme 17.13) [38].

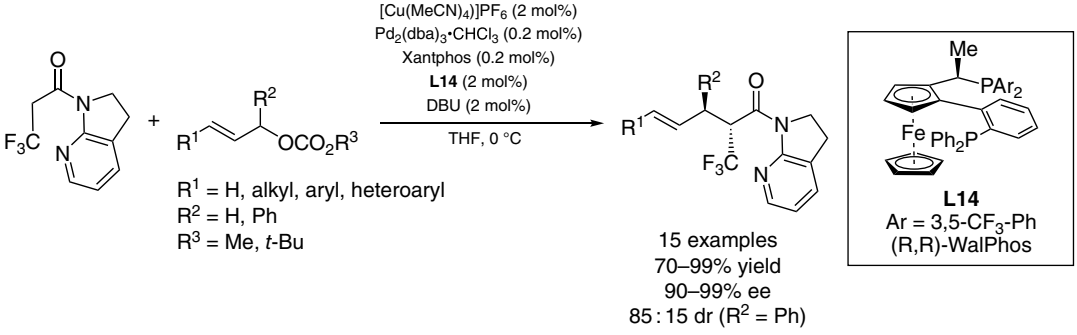

Scheme 17.12. Cu/Pd dual catalysis for the asymmetric allylic alkylation of α-trifluoromethyl *N*-acyl azaindolines. Source: Kumagai and Shibasaki [34].

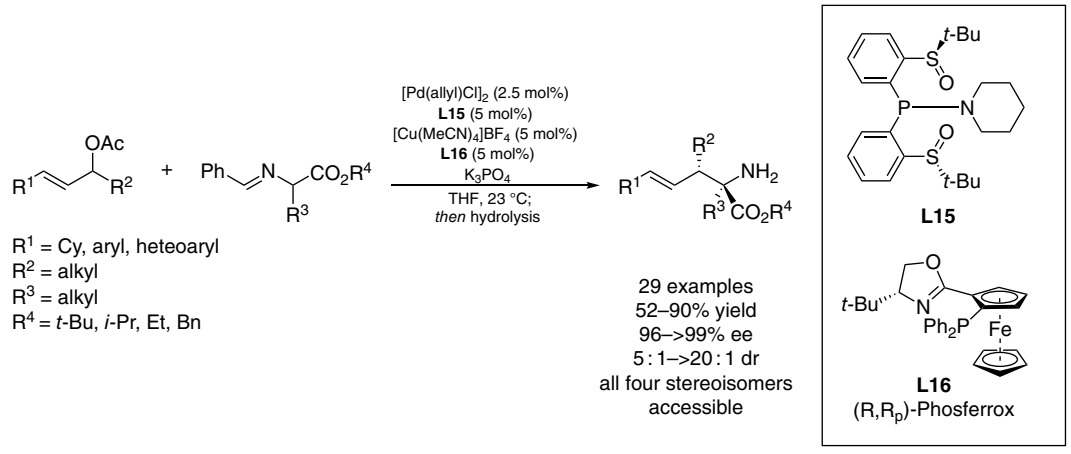

Scheme 17.13. Pd/Cu dual catalysis for enantio- and diastereodivergent allylic alkylation of aldimine bases. Source: Liao and Zhang [38].

Photoredox catalysis has also been utilized by Yu and coworkers as an effective strategy for the coupling of alkyl radicals with chiral Pd-π-allyl species (Scheme 17.14) [39]. A broad substrate scope was demonstrated in this methodology, affording branched allylic alkylation products with (*R*)-GarPhos (**17**) in generally excellent enantioselectivity. This novel strategy greatly expands the portfolio of non-stabilized nucleophiles compatible with Pd-catalyzed allylic alkylations.

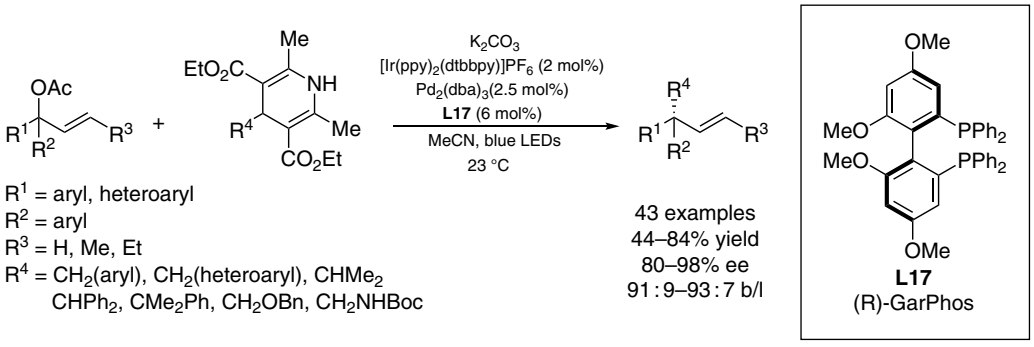

Scheme 17.14. Merger of photoredox catalysis and Pd-catalyzed enantioselective allylic alkylation. Source: Yu [39].

Other nucleophilic partners recently developed for asymmetric allylic alkylation include acyclic 1,3-dioxaboroles [40], diorganozinc reagents [41], Cu-alkenylborates [42], metallated pyridines [43] and other *N*-heterocycles [44], toluene–chromium complexes [45], 1,3-dithianes as acyl anion equivalents [46], and carboxylic acid dianions [47], among many others. A recent example from Shimizu and Kanai demonstrates Pd-catalyzed ionization of *O*-allyl carboxylate esters wherein the resultant carboxylate can undergo enolization with a chiral boron complex to react with the generated chiral Pd-π-allyl species [48].

17.2.3. Pd-Catalyzed Decarboxylative Allylic Substitution

From 2010 to 2020, the scope of substrates developed in the Pd-catalyzed decarboxylative asymmetric allylic alkylation has greatly expanded. Generally, these reactions are dominated by the utilization of Trost bisphosphine ligands and PHOX ligands. Mechanistically, the Trost ligand scaffolds are thought to operate through an outer-sphere mechanism and thus provide optimal selectivity with more stabilized enolates [49]. PHOX ligand scaffolds are believed to proceed through inner-sphere pathways and thus perform best in the case of non-stabilized enolates. Recent mechanistic investigations have provided valuable insight into the unusual inner-sphere pathways proposed for Stoltz-type reactions involving PHOX ligands [50]. Because of the large number of recent contributions to this field, select examples are highlighted with references provided for other substrate classes not shown [51].

From 2010 to 2020, Stoltz and coworkers have developed numerous methodologies for accessing cyclic enantioenriched tertiary and quaternary stereogenic centers with PHOX ligands, in particular electron-deficient variants such as (*S*)-$(CF_3)_3$-*t*-BuPHOX (**L19**). The cyclic structural motifs accessed by Stoltz and coworkers include cyclobutanones [52], cyclopentanones [53], α-quaternary lactams [54], α-tertiary lactams [55], α-tertiary- and quaternary-substituted piperazin-2-ones [56, 57], 1,4-diazepan-5-ones [58], *N*,*S*- and *N*,*O*-containing heterocycles [59], thiopyranone [60], (poly)fluorinated building blocks [61], α-quaternary carbonyls bearing masked methyl vinyl ketones [62], an α-silyl-substituted carbonyl [63], α-quaternary cyclic siloxanes [64], α-quaternary α′-enaminones [65], and α-quaternary Mannich adducts (Figure 17.1) [66].

Trost diphosphine ligands have also been instrumental in the continued expansion of decarboxylative allylic alkylation into new substrate classes. Recent examples include tetrasubstituted α2,2-amino acids via oxazol-5-ones [67], α-allyl-α-aryl cyclopentanones [68], α-quaternary oxindoles, [69] α-allyl-α-aryl-oxindoles [70], α-tetrasubstituted azido and α-quaternary cyano indanones [71], α-alkynyl indanones [72], δ-valerolactams [73], γ-butenolides [74], α-aryl nitroalkanes [75], α-trifluoromethoxy ketones [76], α-quaternary γ-butyrolactones [77], α-aryl, α-allyl γ-butyrolactones [78], α-difluoromethylthio, α-allyl- and α-trifluoromethylthio, α-allyl ketones [79], allyl 2,2-diarylglycinate aryl imines [80], and isoxazolidin-5-ones (Figure 17.2) [81].

While the decarboxylative allylation has been highly developed, the corresponding propargylation remains heavily underdeveloped. In 2019, Guiry disclosed the enantioselective decarboxylative asymmetric propargylation of α-aryl indanones with *N*-1-(2′-diphenylphosphino-3′,6′-dimethyloxyphenyl) phthalazine (PINAP) ligand **L18** (Scheme 17.15) [82]. This is the most successful methodology reported to date, with only one previous report from Stoltz and coworkers achieving a modest 44% ee [50a].

Cyclobutanones (ref 52)

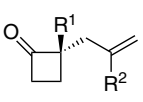

15 examples
62–95% yield
86–99% ee

Cyclopentanones (ref 53)

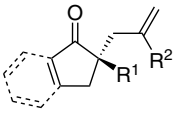

19 examples
62–>99% yield
84–94% ee

α-Quaternary lactams (ref 54)

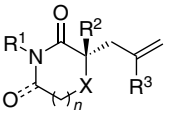

22 examples
60–97% yield
88–99% ee

α-Tertiary lactams (ref 55)

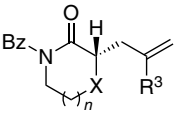

6 examples
42–90% yield
59–99% ee

α-Tertiary and -quaternary piperazin-2-ones (refs 56,57)

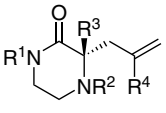

29 examples
56–93% yield
52–99% ee

1,4-Diazepan-5-ones (ref 58)

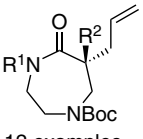

12 examples
44–>99% yield
83–95% ee

Hydroxamates (ref 59)

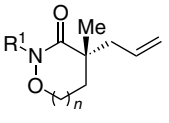

9 examples
29–98% yield
72–93% ee

N,X-Heterocycles (ref 59)

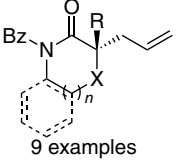

9 examples
29–98% yield
72–92% ee

Thiopyranones (ref 60)

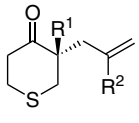

12 examples
29–92% yield
50–94% ee

(Poly)fluorinated building blocks (ref 61)

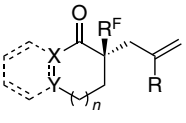

13 examples
82–99% yield
64–97% ee

Masked methyl vinyl ketone bearing substrates (ref 62)

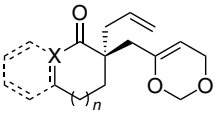

3 examples
91–95% yield
82–99% ee

α-Silyl carbonyl (ref 63)

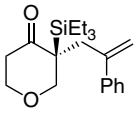

1 example
75% yield
81% ee

Cyclic siloxanes (ref 64)

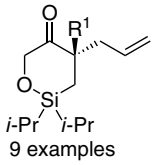

9 examples
63–93% yield
89–94% ee

Enaminones (ref 65)

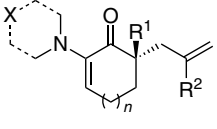

16 examples
52–99% yield
72–99%

Mannich adducts (ref 66)

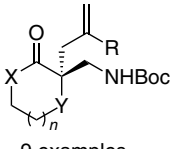

9 examples
51–99% yield
82–99% ee

Figure 17.1. Enantioenriched motifs accessed by Stoltz via decarboxylative allylic alkylation. Source: Stoltz [52–66].

Oxazol-5-ones
(Serra and Colombo, ref 67)

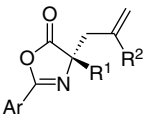

7 examples
83–96% yield
30–85% ee

α-Aryl cyclopentanones
(Guiry, ref 68)

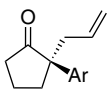

13 examples
85–97% yield
83–>99% ee

α-Quaternary oxindoles
(Taylor, ref 69)

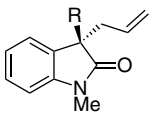

11 examples
65–>99% yield
68–95% ee

α-Aryl quaternary oxindoles
(Guiry, ref 70)

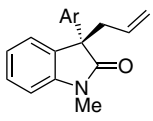

12 examples
91–98% yield
56–99% ee

α-Azide and α-nitrile indanones
(Waser, ref 71)

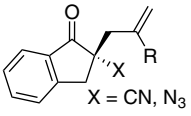

20 examples
46–98% yield
75–97% ee

α-Alkynyl indanones
(Waser, ref 72)

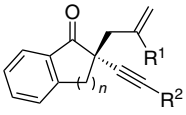

15 examples
41–>99% yield
73–97% ee

δ-Valerolactams
(Trost, ref 73)

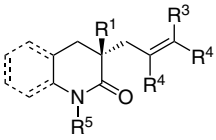

19 examples
32–99% yield
77–99% ee

γ-Butenolides
(Arseniyadis and Cossy, ref 74)

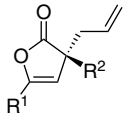

19 examples
32–99% yield
77–99% ee

α-Aryl nitroalkanes
(Trost, ref 75)

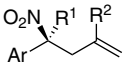

22 examples
46–98% yield
62–98% ee

α-Trifluoromethoxy ketones
(Shibata, ref 76)

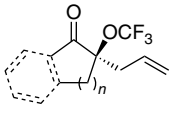

22 examples
40–94% yield
32–91% ee

γ-Butyrolactones
(Arseniyadis and Cossy, ref 77)

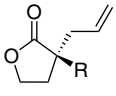

14 examples
69–98% yield
77–99% ee

α-Aryl-γ-butyrolactones
(Guiry, ref 78)

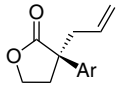

19 examples
32–99% yield
77–99% ee

α-SCF_3 ketones
(Shibata, ref 79)

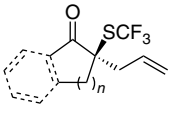

15 examples
58–96% yield
29–95% ee

Diarylglycinate imines
(Chruma, ref 80)

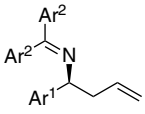

11 examples
71–98% yield
46–97% ee

Isoxazolidin-5-ones
(Shibasaki, ref 81)

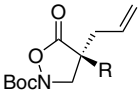

14 examples
58–96% yield
90–94% ee

Figure 17.2. Substrate classes prepared via Pd-catalyzed decarboxylative allylic alkylation with Trost diphosphine ligands (2010–2020).

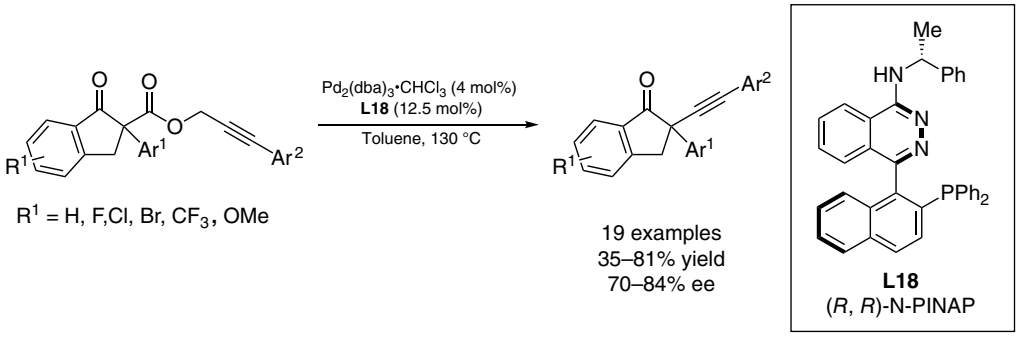

Scheme 17.15. Asymmetric decarboxylative propargylation of α-aryl indanones. Source: Guiry [82].

Within optimization studies by Guiry, terminal substitution of the propargyl group with an arene was found to be necessary to avoid undesired protonation. Despite the harsh conditions required for reactivity, good enantioselectivities (up to 84% ee) were obtained.

Aside from traditional allylation products, Stoltz and coworkers demonstrated that intermediate chiral Pd-enolates generated in the decarboxylative asymmetric allylic alkylation could be intercepted by conjugate acceptors with subsequent allylation (Scheme 17.16) [83]. Generally good levels of diastereo- and enantioselectivities are observed in this transformation; however, alkyl substitution for *R*2 did not achieve the desired reactivity. In addition to the intermolecular conjugate acceptor interrupted allylation, Stoltz and coworkers further demonstrated alkylation interruption via intramolecular aldol reactions with phenol additive *O*-alkylation to complete the catalytic cycle [84].

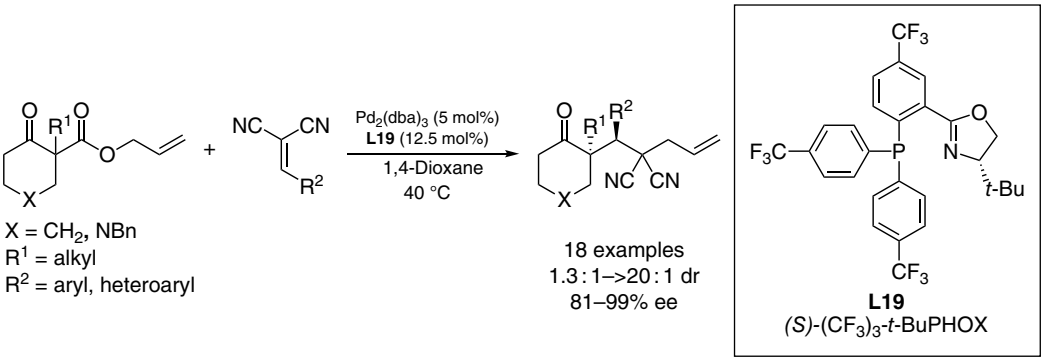

Scheme 17.16. Michael acceptor interrupted Pd-catalyzed allylic alkylation. Source: Stoltz [83].

Several important methods for acyclic stereocontrol have been developed within the decarboxylative asymmetric allylic alkylation [85]. These developments have lagged behind cyclic systems due to their increased conformational flexibility. A stereodefined enolate is generally required for high enantioselectivity, a challenge exacerbated in fully substituted systems. In 2010, Trost demonstrated 2-imidazole-substituted enol carbonates as ester enolate surrogates in the Pd-catalyzed decarboxylative asymmetric allylic alkylation [86]. While this and non-decarboxylative methods [87, 88] have enabled access to allylic alkylation products of carboxylic acid derivatives, the synthesis and utilization of these substrates are not straightforward. An improvement was reported by Trost in 2012 with the implementation of benzoxazolinone-based allyl enol carbonates as ester equivalents (Scheme 17.17) [89]. These products are readily converted to various carboxylic acid derivatives without erosion of ee. The Trost benzoxazolinone-based allyl enol carbonates are limited to the synthesis of tertiary stereocenters. Tunge later investigated β-keto-*N*-acyl pyrrole substrates for the synthesis of acyclic quaternary stereocenters; however, poor enantioinduction was obtained due to the inability to control enolate geometry [90].

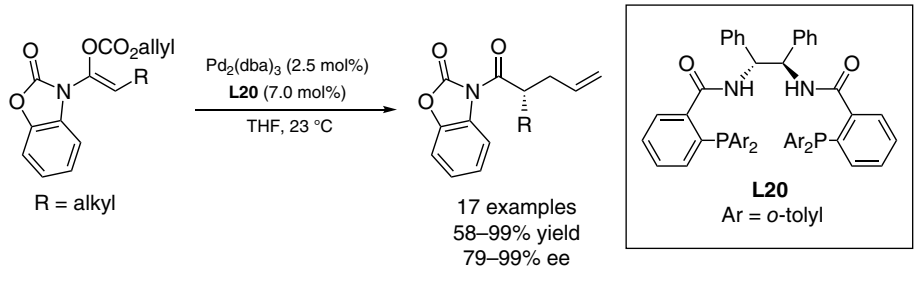

Scheme 17.17. Decarboxylative allylic alkylation of benzoxazolinone-derived allyl enol carbonates as acyclic ester enolate equivalents. Source: Trost [89].

In 2017, Stoltz and Marek developed a highly selective route to stereodefined tetrasubstituted amide enolates for highly enantioselective decarboxylative allylic alkylation with novel electron-deficient Trost ligand derivative **21** (Scheme 17.18a) [91]. Notably, opposite enolate geometries lead to opposite enantiomers of product in this transformation, thus the highly selective enolization is required for high ee. Stoltz and Zhang later employed a highly selective enolization procedure [92] for the synthesis and decarboxylative allylic alkylation of α-aryl aryl ketones with PHOX ligand **19** (Scheme 17.18b) [93]. Previous access to acyclic ketones was limited to α-tertiary center formation [94], required tin-enolates and provided products in moderate ee [95], or utilized cyclic substrates indirectly [60]. Surprisingly, starting enolate geometry was found to be inconsequential in this transformation, leading the authors to propose a possible dynamic kinetic resolution in situ of the enolate geometries. Further expanding the scope of this selective enolization/decarboxylative allylic alkylation, Stoltz and Zhang examined *N*-acyl indole and pyrrole ester enolate equivalents with modified PHOX ligand TyPHOX (**L22**) (Scheme 17.18c) [96]. While α-aryl esters could be enolized with high geometry-selectivity, the corresponding enol carbonates proved poor substrates for the allylic alkylation, leading Stoltz and Zhang to explore *N*-acyl groups inspired by Trost [86, 89] and Tunge [90]. Here, selective enolization is required for high ee; however, control experiments demonstrate an appreciable level of enolate equilibration.

The α-aryl examples reported by Stoltz and Zhang are unusual for their high enantioselectivity with PHOX ligands that typically give poor ee with α-aryl stabilized enolates. The authors thus propose this

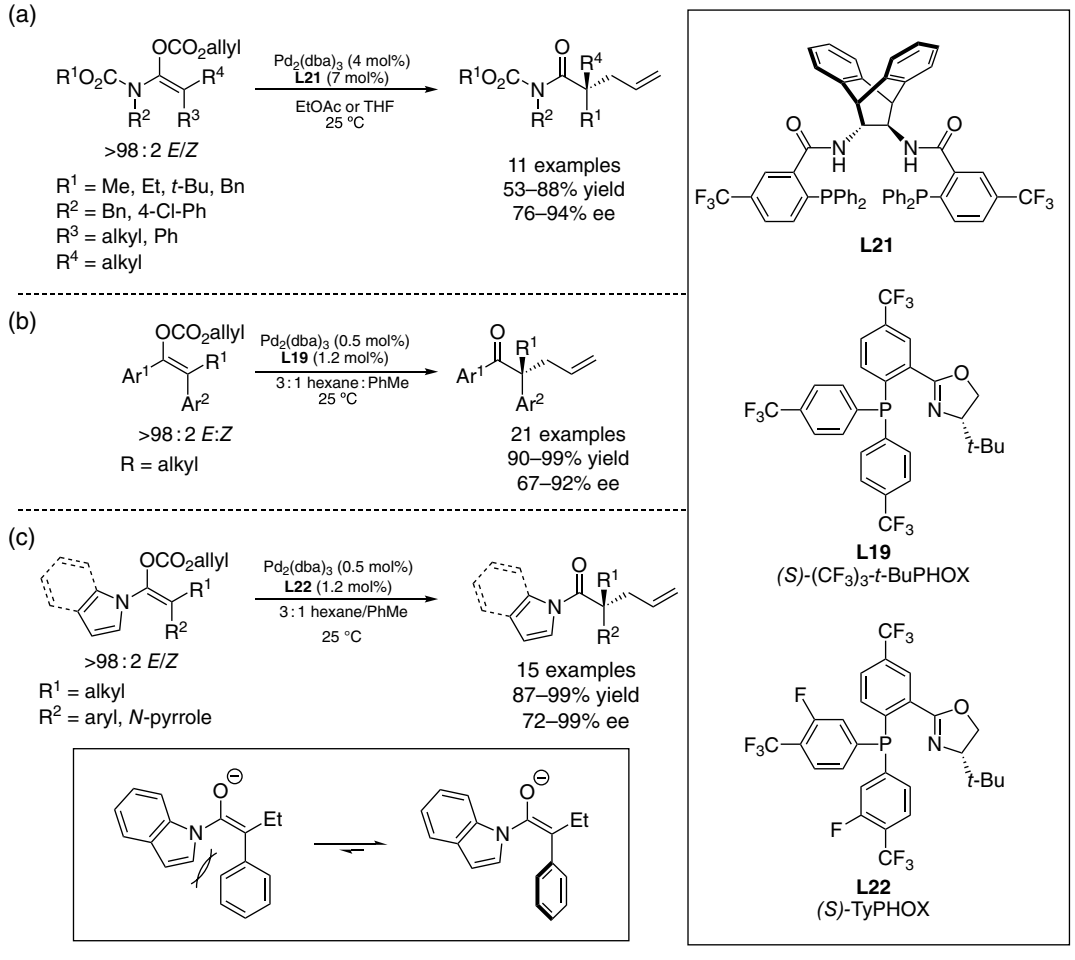

Scheme 17.18. (a) Acyclic stereocontrol in amides. Source: Stoltz and Marek [91]. (b) Acyclic stereocontrol in α-aryl,α-alkyl aryl ketones. Source: Zhang and Stoltz [93]. (c) Acyclic stereocontrol in α-aryl,α-alkyl *N*-acyl indole and pyrrole ester equivalents. Source: Zhang and Stoltz [96].

effect is due to twisting of the α-aryl ring of plane with the enolate, diminishing its resonance stabilization of the enolate (Scheme 17.18c). Stoltz and Zhang further expanded this enolization and allylic alkylation strategy to acyclic benzoin-derived enol carbonates [97] and α-pyrrolyl/indolyl ketones [98].

17.2.4. Pd-Catalyzed Asymmetric Oxidative Allylic Alkylation

The seminal examples of oxidative C–H allylic alkylation were developed by Shi [99] and White [100] in 2008. Since these reports, enantioselective allylic C–H alkylations have continued to emerge as powerful complements to traditional functionalized electrophiles. In 2013, Trost and coworkers developed a novel phosphoramidite ligand that enabled C–H allylic alkylation of tetralone substrates (Scheme 17.3, vide supra) [8, 9]. Gong and coworkers developed oxidative C–H alkylation for the synthesis of α-aryl quaternary aldehydes [101] and α-quaternary pyrazol-5-ones [102]. White recently developed air-stable aryl sulfoxide oxazoline ligands for terminal olefin allylic C–H alkylation with α-nitrotetralones and β-ketoester nucleophiles [103] while Gong demonstrated monodentate phosphorus ligands with pyrazol-5-one nucleophiles [104]. Phosphonium-based phase-transfer catalysts have also been demonstrated as effective catalysts by Du and Chen for the synthesis of α-quaternary oxindoles [105]. In the preceding examples, stereogenic centers were formed at the nucleophile with the exception of a single example by Gong [101]. Building on these examples, Gong further pioneered the synthesis of vicinal stereogenic centers wherein stereogenic centers are formed on both the electrophilic olefin partner and nucleophilic partner in the allylic alkylation of azlactones [106] and 2-acylimidazoles [107, 108].

17.3. NICKEL- AND PLATINUM-CATALYZED ALLYLIC ALKYLATION

17.3.1. Ni-Catalyzed Allylic Alkylation

Compared with palladium, the asymmetric nickel-catalyzed allylic substitution reaction remains significant. Historically, Ni-catalyzed allylic substitution has been dominated by the use of hard nucleophiles such as organometallic and organoboron compounds with few examples of soft nucleophiles [109]. In 2016, Walsh and Mashima concurrently reported the first examples of asymmetric allylic alkylation of soft nucleophiles with nickel. Walsh found that the allylic alkylation of cyclic allyl carbonates with diarylmethanes provided allylic alkylation products in excellent yield, with two examples showing promising excellent levels of enantioinduction with Josiphos derivative **L23** (Scheme 17.19) [110]. No updated scope of this transformation with respect to enantioselective reactions has been disclosed.

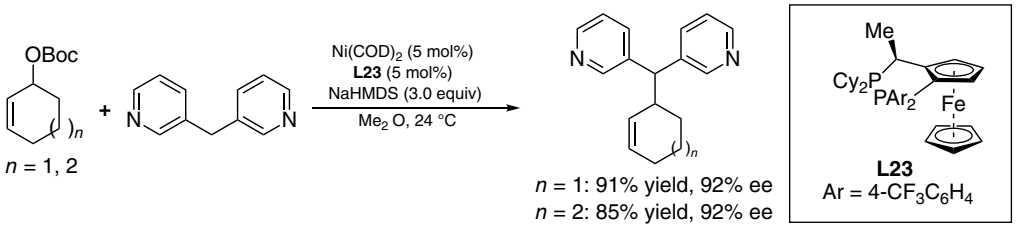

Scheme 17.19. Ni-catalyzed asymmetric allylic alkylation of diarylmethanes as soft nucleophiles. Source: Walsh [110].

Mashima and coworkers demonstrated the asymmetric allylic alkylation of cyclic β-ketoesters with linear and branched allylic alcohol electrophiles (Scheme 17.20) [111]. Utilizing the H8-BINAP ligand **L24**, quaternary carbon stereogenic centers were generated in generally excellent yields and enantioselectivities. A broad scope of β-ketoesters was well tolerated; however, lower enantioselectivity was obtained with cyclic seven-membered carbocycles and poor enantioinduction was observed in acyclic substrates (not shown).

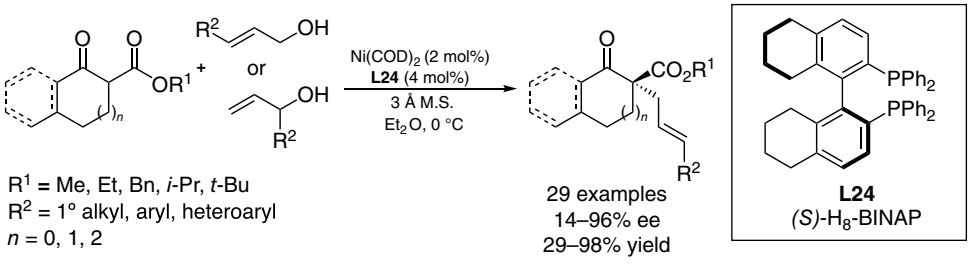

Scheme 17.20. Ni-catalyzed allylic alkylation of cyclic β-ketoesters with unactivated allylic alcohols. Source: Mashima [111].

In 2018, Stoltz and coworkers demonstrated the use of α-acyl lactones and lactams as prochiral nucleophiles with linear or branched allylic alcohol electrophiles (Scheme 17.21) [112]. The use of bisphosphine ligand P-Phos (**L25**) was found to be the optimal ligand in this transformation, enabling access to cyclic α-quaternary stereogenic centers in good yield and enantiomeric excess. Importantly, the transformations developed by Mashima and Stoltz allow the use of ubiquitous allylic alcohols that do not require prior activation as electrophiles.

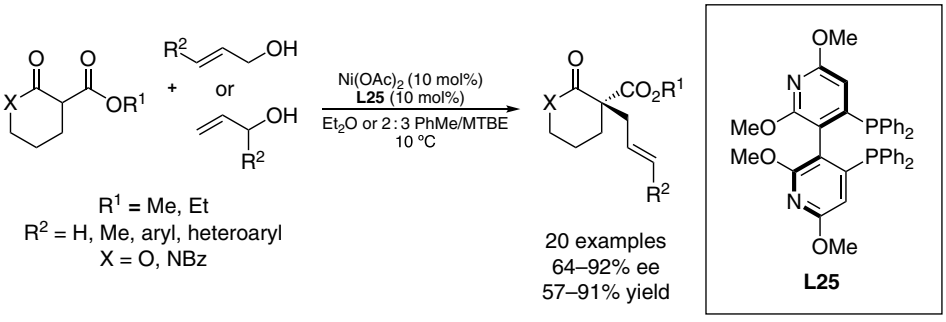

Scheme 17.21. Ni-catalyzed allylic alkylation of α-acyl lactones with unactivated allylic alcohols. Source: Stoltz [112].

Most recently, Zhang, Carpentier, Mashima, and coworkers found that *N*-allyl-*N*-methylanilines could serve as allyl fragments in the Ni-catalyzed allylic alkylation of prochiral β-ketoesters via C–N bond cleavage (Scheme 17.22) [113]. Bisphosphine ligand (*S*)-Tol-MeO-2,2′-bis(di-p-tolylphosphino)-6,6′-dimethoxy-1,1′-biphenyl (BIPHEP) (**L26**) provided optimal levels of enantioselectivity for six- and seven-membered β-ketoesters; however, H8-BINAP (**L24**) provided higher enantioinduction with five-membered and benzo-fused β-ketoesters. In addition to β-ketoesters, a β-ketonitrile substrate provided the corresponding allylic alkylation product in 94% yield and >99% ee; however, β-ketoamides were unreactive and β-diketones provided products in low enantiomeric excess. On the basis of density functional theory (DFT) calculations, the authors propose this transformation may proceed through an outer-sphere mechanism wherein an unbound enolate anion attacks the nickel(II) π-allyl species to generate the C–C bond.

In 2017, Yang and Wang developed a method for the enantio- and diastereoselective allylic alkylation of acylimidazoles with nitroallylic acetates to generate acyclic γ-nitro carboxylate ester derivatives

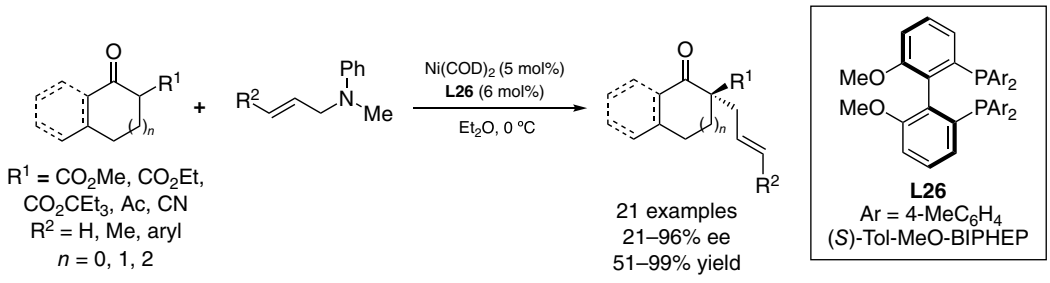

Scheme 17.22. Ni-catalyzed allylic alkylation of cyclic β-ketoesters with *N*-methyl-*N*-allylanilines via C–N bond cleavage. Source: Zhang, Carpentier, and Mashima [113].

(Scheme 17.23) [114]. Here, a simple chiral diamine ligand **L27** affords acyclic stereodyads with excellent enantioselectivity and good to excellent diastereoselectivity. The allylic alkylation product is readily transformed into the corresponding γ-nitro methyl ester (not shown).

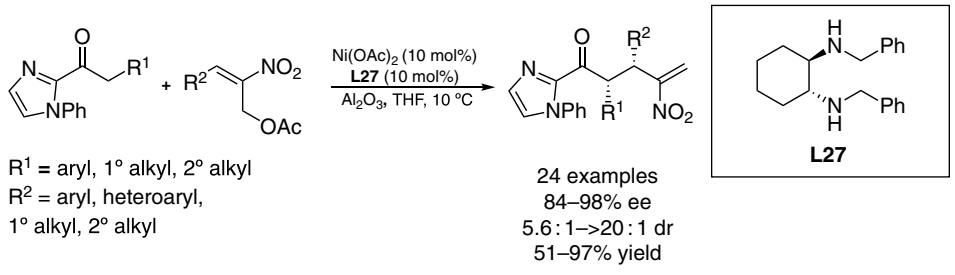

Scheme 17.23. Ni-catalyzed allylic alkylation of acyclic acyl imidazoles with nitroallylic acetates. Source: Yang and Wang [114].

Doyle and coworkers reported the Ni-catalyzed Suzuki-type cross-coupling of aryl boronates with pro-quinolinium electrophiles utilizing phosphite ligand **L28** (Scheme 17.24) [115]. The authors proposed that an active π-allyl Ni–quinolinium species is generated by boronate-assisted ionization. Slow addition of the boronate and the use of $NaOPh{\cdot}3H_2O$ as a reductant for the in situ generation of Ni(0) were found to be optimal for maintaining high yields in this transformation. Doyle has also demonstrated the enantioselective Ni-catalyzed Negishi-type arylation of in situ generated *N*-acyl pyridinium ion electrophiles with chiral phosphoramidite ligands (not shown) [116].

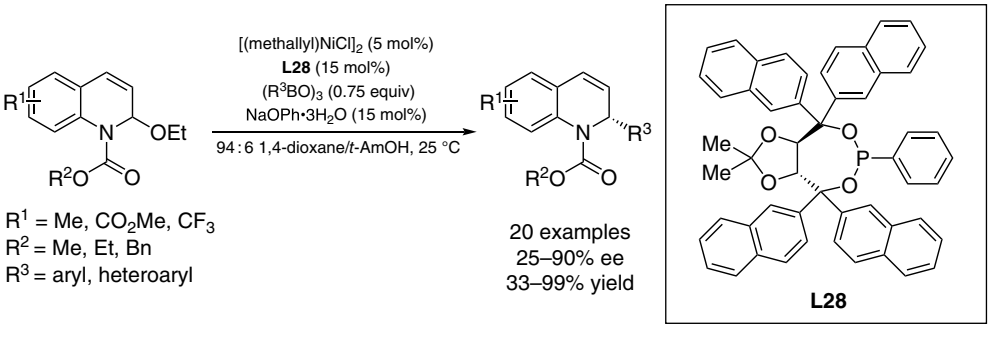

Scheme 17.24. Ni-catalyzed Suzuki-type cross-coupling of pro-quinolinium electrophiles and aryl boronates. Source: Doyle [115].

17.3.2. Pt-Catalyzed Allylic Alkylation

Platinum catalysis remains extremely rare in asymmetric allylic alkylation chemistry. Just one example of Pt-catalyzed allylic alkylation was reported from 2010 to 2020, wherein cyclic allyl fluorides were reported as superior electrophiles in stereoretentive allylic alkylation with malonate nucleophiles compared with the corresponding carbonates, benzoates, and acetates (not shown) [117]. No enantioselective variant has been reported.

17.4. MOLYBDENUM- AND TUNGSTEN-CATALYZED ENANTIOSELECTIVE ALLYLIC ALKYLATION

17.4.1. Mb-Catalyzed Allylic Alkylation

In the context of metal-catalyzed allylic substitution reactions, molybdenum was one of the first metal catalysts to display branched regioselectivity complimentary to the linear selectivity afforded by palladium [1, 118]. Asymmetric Mo-catalyzed allylic alkylation is largely dominated by the use of σ-donor nitrogen ligands, namely pyridylamide and bisoxazoline ligands. Mo-catalyzed allylic substitution is characterized by a rapid equilibration of intermediate allyl complexes; thus, identical results are often obtained from both linear and branched electrophiles with high regio- and enantioselectivities. The major limitation of Mo-catalyzed allylic alkylation for C–C bond construction is the narrow scope of stabilized prochiral nucleophilic partners tolerated. Like Pd- and Ir-catalysts, Mo-catalysts provide allylic substitution products with a net retention of configuration; however, in contrast to Pd- and Ir-catalysts, this is the result of a double-retention mechanism and not a double-inversion process [119].

In 2011, Trost and coworkers described the highly enantio-, regio-, and diastereoselective Mo-catalyzed allylic alkylation of prochiral α-cyanoester nucleophiles (Scheme 17.25) [120]. Here, the authors propose that electron-rich pyridylamide ligand **L29** is critical for establishing a Curtin–Hammet equilibrium between the diastereomeric molybdenum enolates due to the slow reductive elimination of an electron-rich Mo center, thus rendering enolization selectivity inconsequential to the stereochemical outcome. The authors found that the highest levels of stereoselectivity were obtained with more sterically encumbered *R*1 substitution of the cyanoester.

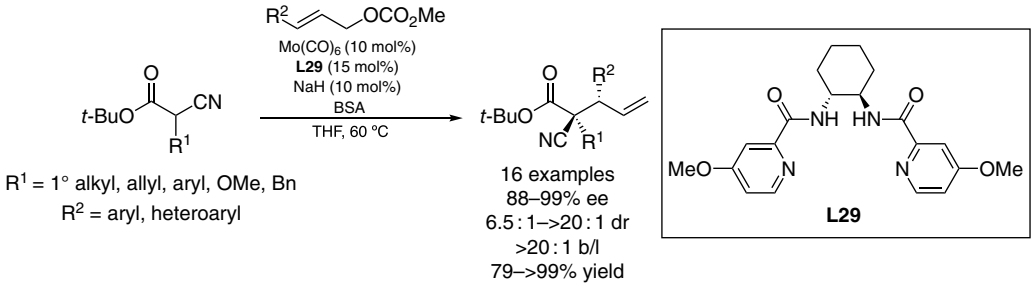

Scheme 17.25. Mo-catalyzed allylic alkylation of acyclic α-cyanoesters. Source: Trost [120].

17.4.2. W-Catalyzed Allylic Alkylation

Tungsten-catalyzed allylic alkylation has been successfully applied with PHOX ligands and linear allylic substrates, although poor selectivity is observed relative to Mo-catalyzed reactions [121]. W-catalyzed reactions are largely stereospecific reactions with stabilized carbon nucleophiles, therefore no enantioinduction has been observed in cases of branched racemic electrophiles [122]. Additionally, only a single example of a heteroatom nucleophile has been disclosed with Khan's 2020 study of sodium sulfinate as a nucleophilic partner in W-catalyzed allylic substitution [123].

17.5. IRON- AND RUTHENIUM-CATALYZED ALLYLIC ALKYLATION

17.5.1. Fe-Catalyzed Allylic Alkylation

While iron is one of the cheapest and least toxic transition metals, it remains heavily underdeveloped in allylic substitution chemistry. Fe-catalysts are characterized by extremely slow isomerization, thus allylic substitution proceeds with exceptional stereo- and regiochemical retention. To date, enantioinduction has not been achieved with an Fe-catalyst. Regioselective examples of iron-catalyzed-allylic alkylation are covered in detail in the previous edition of this series [1].

17.5.2. Ru-Catalyzed Allylic Alkylation

Ruthenium complexes preferentially generate branched products from both linear and branched allylic electrophiles. Ruthenium has recently shown promise in enantioselective allylic alkylation reactions. In 2015, Onitsuka and coworkers reported cyclopentadienyl ruthenium catalyst (**C1**) as an effective catalyst for the enantio- and diastereoselective allylic alkylation of prochiral 1,3-diketones with cinnamyl chlorides to provide acyclic stereodiads in good diastereoselectivity and excellent enantioselectivity (Scheme 17.26a) [124]. Importantly, $NaHCO_3$ is essential for limiting epimerization of the allylic alkylation products. Onitsuka and coworkers further demonstrated that acyclic silyl ketene acetals are competent pronucleophiles for the allylic alkylation of cinnamyl chlorides catalyzed by complex **C1** (Scheme 17.26b) [125].

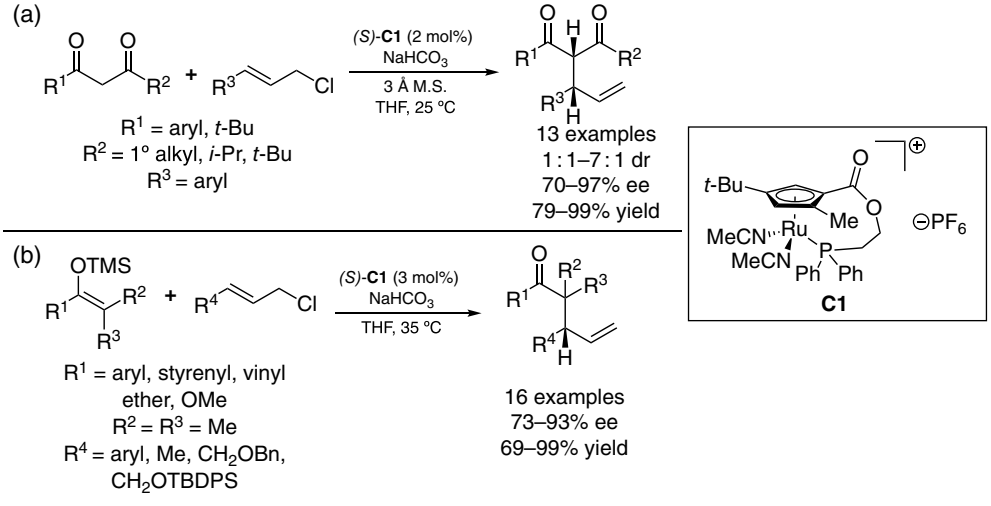

Scheme 17.26. (a) Cyclopentadienyl ruthenium complex catalyzed allylic alkylation of 1,3-diketones. Source: Onitsuka [124]. (b) Cyclopentadienyl ruthenium complex catalyzed allylic alkylation of acyclic silyl enol ethers. Source: Onitsuka [125].

17.6. RHODIUM-CATALYZED ENANTIOSELECTIVE ALLYLIC ALKYLATION

Rhodium has been a popular transition-metal catalyst for the stereoretentive allylic alkylation of enantioenriched branched allylic alcohol derivatives via a double-inversion pathway. On the other hand, methods for the Rh-catalyzed asymmetric and enantioconvergent allylic substitution have lagged behind other metals in the field, presumably as a consequence of the slow π–σ–π isomerization and poor regioselectivity observed with linear allylic electrophiles in Rh-mediated reactions [126]. While the hydrometallation of allene and alkyne proelectrophiles has emerged as powerful methods for inter- and intramolecular coupling reactions, this section is limited to reaction manifolds that proceed via Rh-allyl species derived from allylic alcohol derivatives.

In 2016, Fletcher and coworkers reported the enantioselective allylic arylation of cyclic allyl bromides and chlorides with aryl boronic acids utilizing bisphosphine ligand **L30** (Scheme 17.27a) [127]. Experimental

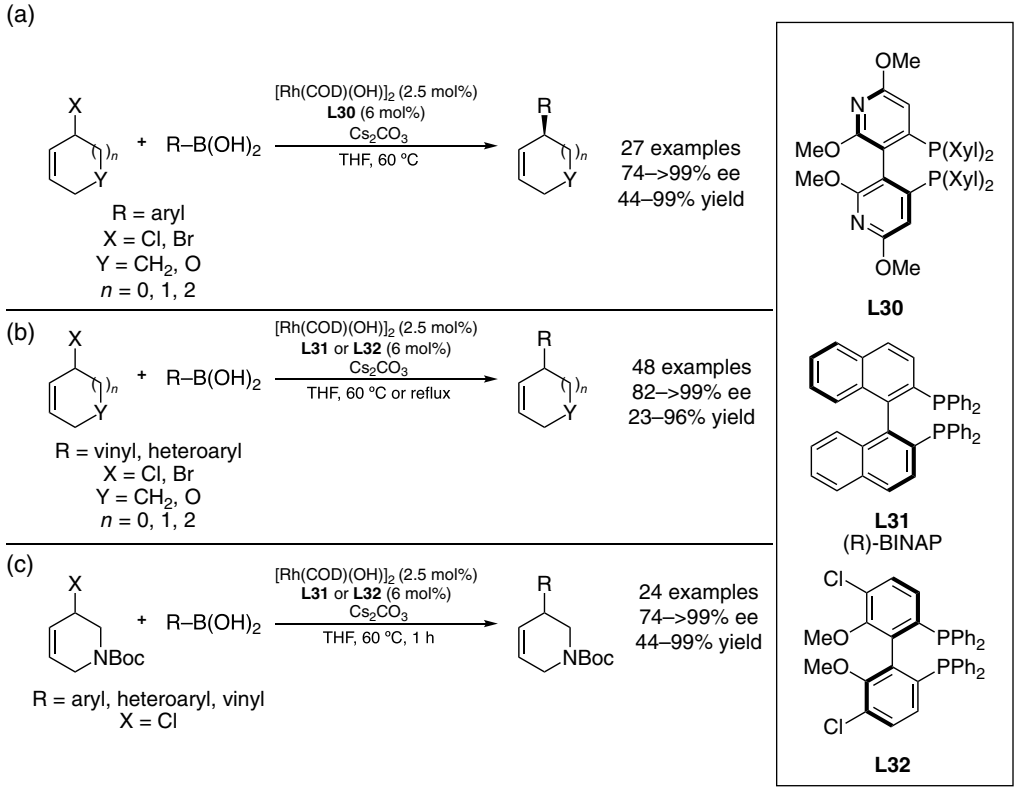

Scheme 17.27. (a) Rh-catalyzed DYKAT of cyclic allylic bromides and chlorides with sp^2 boronic acid nucleophiles. Source: Fletcher [127]. (b) Utilization of vinyl and heteroaryl sp^2 boronic acid nucleophiles. Source: Fletcher [128]. (c) Utilization of piperidine-based electrophiles enabled by BIPHEP ligand **L32**.

observations are consistent with a DYKAT process wherein the racemic electrophiles are converted selectively to one enantiomer of product by the chiral Rh catalyst. Notably, the use of non-stabilized carbon nucleophiles in Rh-catalyzed allylic alkylation remains limited to examples with cyclic allyl electrophiles. Fletcher and coworkers further expanded this technology to enable the Suzuki–Miyaura-type cross-coupling of heteroaryl and vinyl boronic acids with (*R*)-BINAP (**L31**); however, in some cases **L32** provided optimal yield and enantioinduction (Scheme 17.27b) [128]. Pyridine-derived boronic acids were found to inhibit the Rh-catalyzed transformation, whereas 2-Cl pyridines were well tolerated. Furthermore, BIPHEP ligand **L32** enables the use of piperidine-based electrophiles in this transformation (Scheme 17.27c).

Evans and coworkers developed the first examples of Rh-catalyzed allylic alkylation of prochiral nucleophiles. In 2016, Evans reported the synthesis of acyclic quaternary stereogenic centers via the Rh-catalyzed allylic alkylation of benzylnitriles with (*R*)-1,1′-bi-2-napthol methoxy phosphite (BINOL-MeOP) ligand **L33** (Scheme 17.28a) [129]. This example also constitutes the first use of a nitrile anion in an allylic alkylation reaction that enables rapid access to α-quaternary aldehyde, ketone, amide, and β-quaternary amino motifs. This catalyst system was further demonstrated in the direct synthesis of acyclic α-quaternary aldehydes in 2016 (Scheme 17.28b) [130]. Interestingly, control experiments demonstrated that both *E*- and *Z*-enolate geometries of the aldehyde enolate converge to the same major enantiomer of product in this reaction manifold, obviating the requirement of a selective enolization that is often required for good enantioinduction in acyclic systems. Thus, either enantiomeric series of alkylation products can be accessed via *catalyst control* without additional control of enolization geometry, which remains difficult, especially with respect to fully substituted acyclic enolates. Most recently, Evans utilized the Rh/**L33** catalyst system to generate acyclic tertiary stereogenic centers with β,γ-unsaturated α-amino nitriles as homoenolate

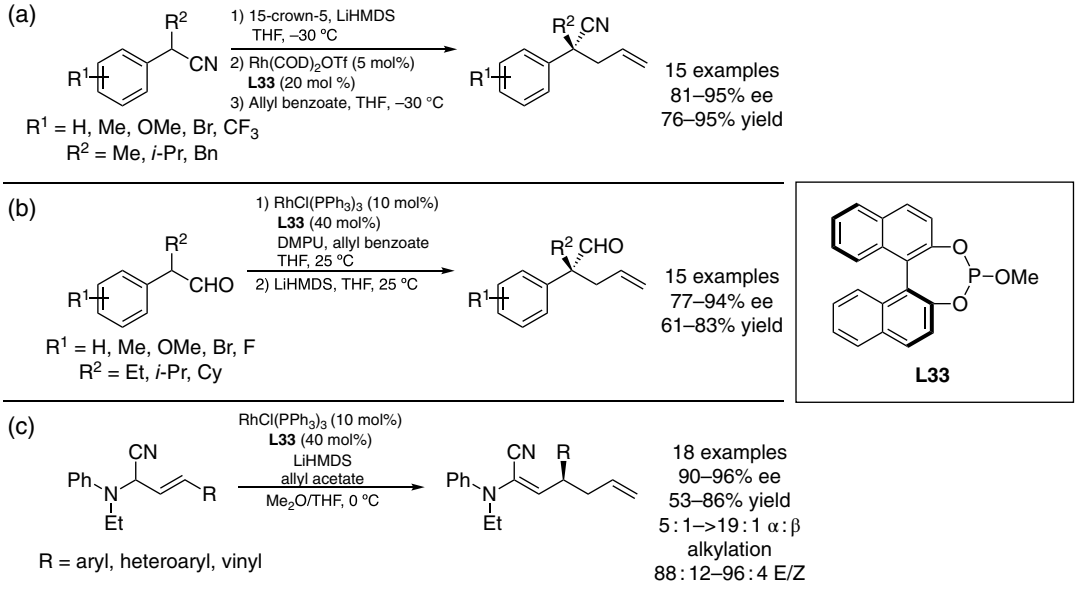

Scheme 17.28. (a) Enantioselective Rh-catalyzed allylic alkylation of acyclic benzylnitriles. Source: Evans [129]. (b) Enantioselective Rh-catalyzed allylic alkylation of acyclic aldehydes. Source: Evans [130]. (c) Enantioselective Rh-catalyzed allylic alkylation of acyclic β,γ-unsaturated α-amino nitriles. Source: Evans [131].

equivalents (Scheme 17.28c) [131]. While *E*-olefin geometry products were generated with excellent enantioselectivity, the corresponding *Z*-olefin products were generated in significantly lower 20–25% ee. Thus, the high degree of *E*-selectivity observed is critical as the hydrolysis of the *E*/*Z* product mixture to the β-stereogenic carboxylic acid would otherwise result in low ee of the carboxylic acid.

You and coworkers recently found that the use of Carreira (*P*,olefin)-ligand **L34** enabled the utilization of readily available branched racemic allylic alcohols in Rh-catalyzed allylic alkylations under acidic conditions. In 2018, You reported the use of 1,3-diketones as nucleophiles with branched allylic alcohols to afford branched acyclic tertiary stereogenic centers with excellent enantioinduction (Scheme 17.29a) [132]. Recovery of enantioenriched allylic alcohol at incomplete conversion revealed

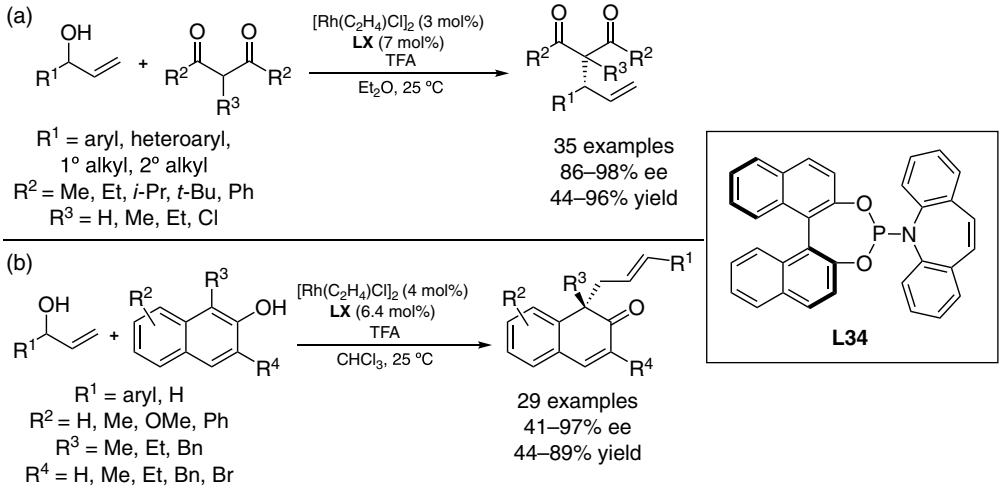

Scheme 17.29. (a) Rh-catalyzed allylic alkylation of 1,3-diketones with allyl alcohols. Source: You [132]. (b) Rh-catalyzed dearomative allylic alkylation of β-naphthol nucleophiles. Source: You [133].

the reaction was proceeding via a dynamic kinetic resolution. In 2019, You reported the first dearomative Rh-catalyzed allylic alkylation of prochiral β-naphthol nucleophiles with the Carreira (*P*,olefin)-ligand (Scheme 17.29b) [133]. In this transformation, linear alkylation products are generated with generally excellent enantioselectivity. A broad range of substitution patterns are tolerated; however, phenyl substitution at *R*3 or *R*4 results in no reaction, allyl alcohol provides moderate yield (58%) and poor ee (41% ee), and buten-3-ol is unreactive with these conditions.

17.7. IRIDIUM-CATALYZED ENANTIOSELECTIVE ALLYLIC ALKYLATION

Iridium-catalyzed allylic substitution is largely characterized by its complimentary regioselectivity to Pd for branched substitution products from both linear and branched allylic electrophiles. While Ir-catalyzed allylic substitution with branched electrophiles tends to proceed in lower enantioselectivity due to a slow π–σ–π interconversion relative to nucleophilic attack, this memory effect is highly dependent on the ligand utilized and can also be circumvented via sequential Pd-catalyzed isomerization/Ir-catalyzed allylic substitution as demonstrated by Hartwig [134]. Phosphoramidite ligands dominate the field of Ir-catalyzed allylic substitution, although other ligand types have also been effective. Although no general method for the stereoselective union of prochiral nucleophiles and electrophiles has been developed, several examples of diastereoselective transformations with prochiral nucleophiles have been reported. Several reviews have been published on Ir-catalyzed allylic alkylation and its applications [135].

Mechanistic understanding of Ir-catalyzed allylic substitution has been significantly advanced from 2010 to 2020, especially with respect to the origin of enantioselectivity; however, these studies will not be discussed here. Ir-catalyzed allylic alkylation reactions can generally be divided into type I and type II based on the electrophile and reaction conditions [135d]. In type I reactions, a linear allylic electrophile is utilized under basic reaction conditions. These reactions are largely catalyzed by Ir/phosphoramidite systems wherein basic conditions promote the in situ generation of cyclometallated Ir-complexes via C(sp^3)–H activation or C(sp^2)–H activation of the ligand scaffold. Type II reactions, first pioneered by Carreira [136], utilize branched allylic alcohol electrophiles with Ir/(*P*,olefin) ligands. Both type I and II reactions typically favor the formation of branched products; however, type II allyl complexes are generally more electrophilic than their type I counterparts, enabling the use of weak nucleophiles such as olefins.

17.7.1. Ir-Catalyzed Allylic Alkylation with Stabilized Nucleophiles

Stabilized malonic ester nucleophiles were the first nucleophiles demonstrated in an enantioselective Ir-catalyzed allylic alkylation [137]. Since this initial report, the scope of electrophilic partners has been greatly expanded. One recent notable example from Hartwig is the allylic alkylation of 3-fluorosubstituted allyl electrophiles with complex **C2·BF$_4$** (Scheme 17.30a) [138]. Here, the utilization of phosphonate or trifluoroacetate

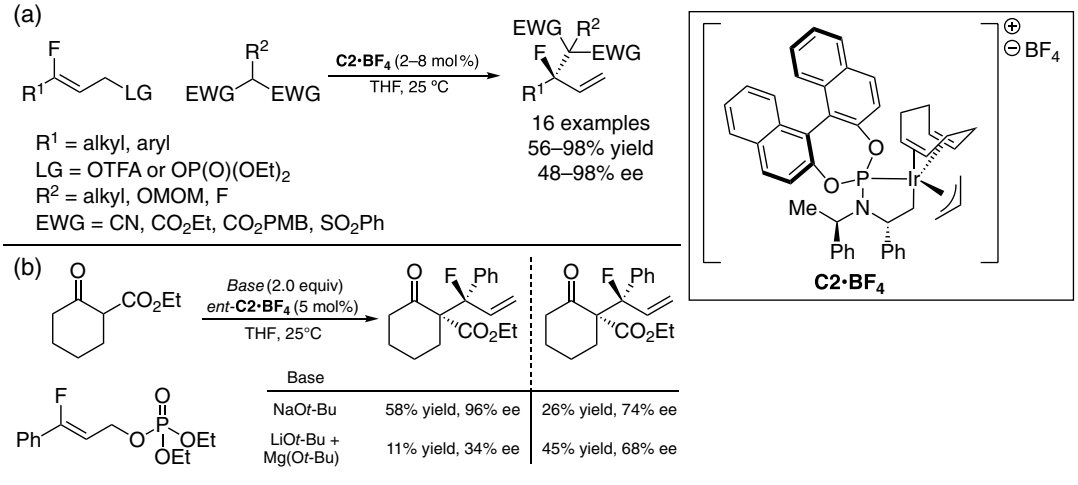

Scheme 17.30. (a) Ir-catalyzed allylic alkylation of 3-fluorosubstituted electrophiles. Source: Hartwig [138]. (b) Diastereodivergent Ir-catalyzed allylic alkylation of 3-fluorosubstituted phosphonates with prochiral nucleophiles. Source: Hartwig [138].

leaving groups were required for efficient reactivity and the utilization of substituted malonates avoided problematic E1cB of fluoride. Hartwig further demonstrated that prochiral nucleophiles could be utilized and either diastereomer of product could be favored depending on the base utilized (Scheme 17.30b).

In 2017, Stoltz and coworkers introduced a masked acyl cyanide (MAC) nucleophile as an acyl anion equivalent in the Ir-catalyzed allylic alkylation with **L35** (Scheme 17.31a) [139]. The choice of the methoxymethyl acetal protecting group was critical to the success of the transformation. This MAC nucleophile was further applied to the synthesis of acyclic α-quaternary carboxylic acids with Carreira ligand **L34** (Scheme 17.31b) [140]. In this example, replacement of LiBr with BEt_3 was required to facilitate ionization of the trisubstituted allylic electrophiles. In 2018, Stoltz and coworkers reported the synthesis of acyclic vicinal all-carbon quaternary centers via the Ir-catalyzed allylic alkylation with methylmalononitrile as a similarly acidic isostere of the MAC nucleophile previously utilized (Scheme 17.31c) [141]. In this example, 1,4-diazabicyclo[2.2.2]octane (DABCO) was critical to achieve high levels of enantiomeric excess. Although the role of DABCO is unknown, the authors hypothesize this additive facilitates equilibration of diastereomeric Ir-π-allyl complexes by slowing the rate of nucleophilic attack.

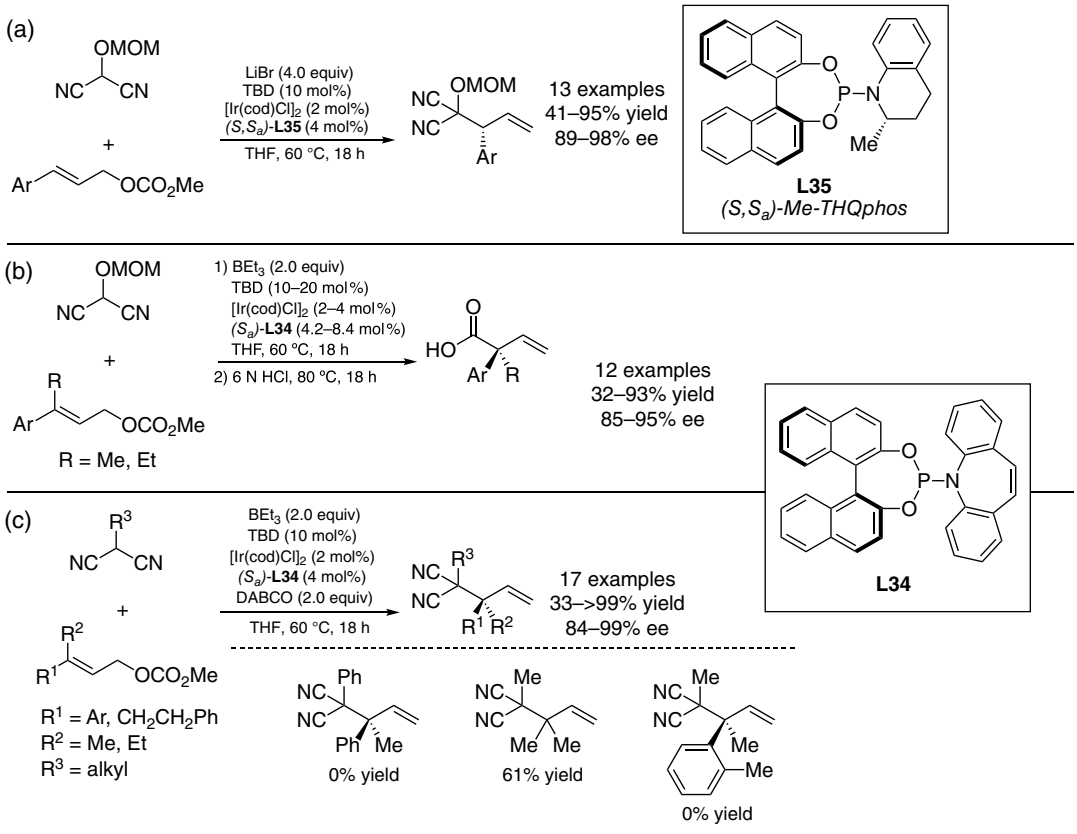

Scheme 17.31. (a) First report of an MAC nucleophile in the Ir-catalyzed allylic alkylation. Source: Stoltz [139]. (b) Synthesis of acyclic α-quaternary carboxylic acids with an MAC nucleophile. Source: Stoltz [140]. (c) Synthesis of vicinal quaternary centers with methylmalononitrile. Source: Stoltz [141].

Although no general strategies for the diastereoselective union of prochiral nucleophiles and electrophiles have been developed, several examples of diastereoselective transformations have been accomplished. Hartwig demonstrated the first diastereoselective Ir-catalyzed allylic alkylation wherein azlactone nucleophiles could be alkylated with generally high diastereocontrol induced by counterion effects from silver salts (Scheme 17.32) [142]. Control experiments delineated that the identity of the leaving group and counterion were critical for achieving high diastereoselectivity.

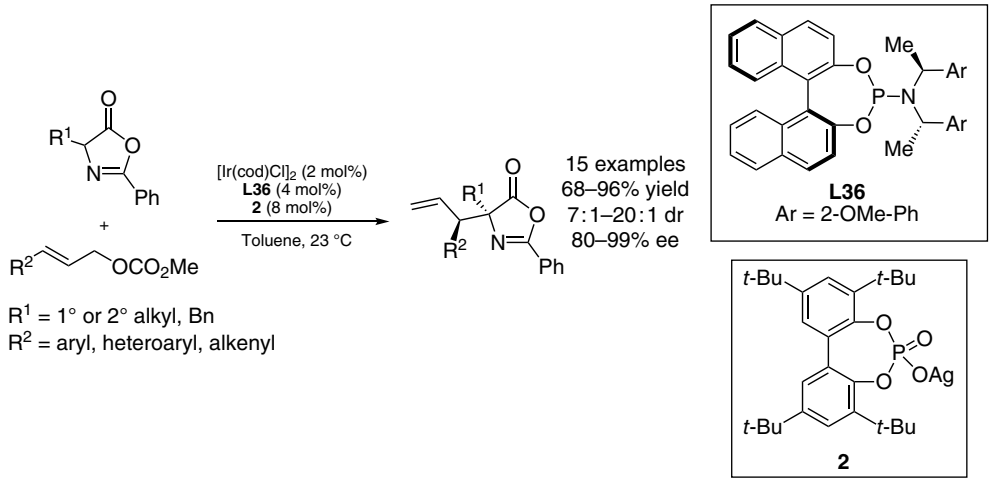

Scheme 17.32. Counterion-controlled diastereoselective Ir-catalyzed allylic alkylation. Source: Hartwig [142].

Hartwig further reported the diastereoselective allylic alkylation of prochiral 5*H*-oxazol-4-ones (Scheme 17.33a) and 5*H*-thiazol-4-ones (Scheme 17.33b); however, the direct adaptation of the counterion strategy utilized in azlactones (vide supra) failed to impart efficient diastereocontrol [143]. Instead, neutral iridacycle **C3** with Et_2Zn base for 5*H*-oxazol-4-ones or $Mg(Ni\text{-}Pr_2)_2$ base for 5*H*-thiazol-4-ones provided optimal diastereoselectivity.

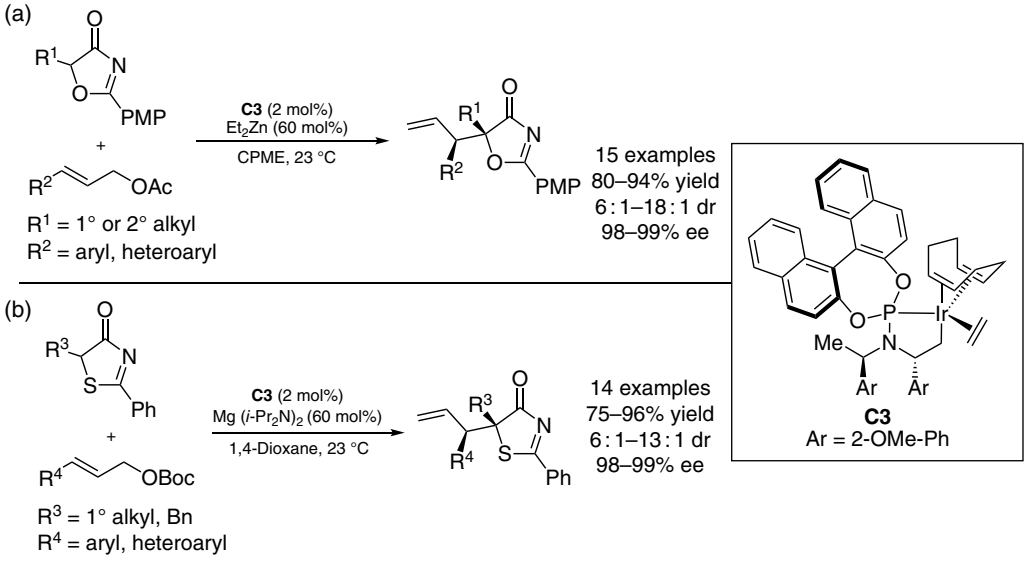

Scheme 17.33. (a) Diastereo- and enantioselective allylic alkylation of 5*H*-oxazol-4-ones. Source: Hartwig [143]. (b) Diastereo- and enantioselective allylic alkylation of 5*H*-thiazol-4-ones. Source: Hartwig [143].

Stoltz achieved a direct ligand-controlled diastereoselective Ir-catalyzed allylic alkylation in 2013 with prochiral cyclic β-ketoester nucleophiles utilizing ***ent*-L35** with in situ activation of the Ir-complex by 1,5,7-triazabicyclo[4.4.0]dec-5-ene (TBD) (Scheme 17.34a) [144]. Stoltz demonstrated that 2-(trimethylsilyl)

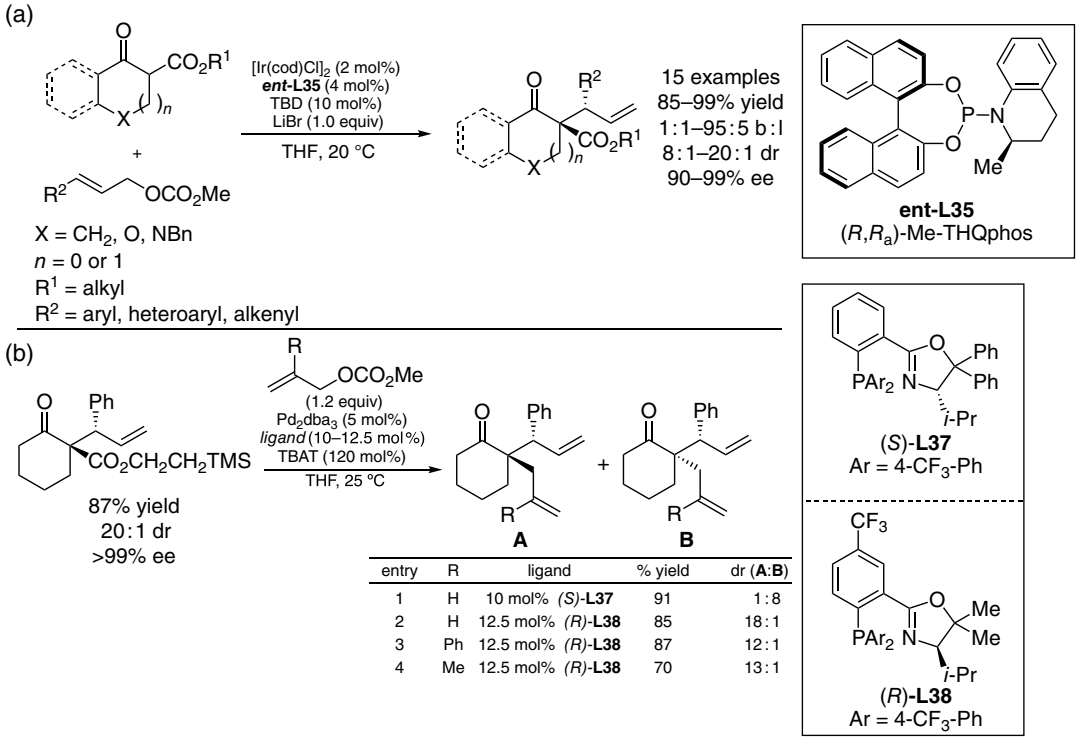

entry	R	ligand	% yield	dr (**A**:**B**)
1	H	10 mol% *(S)*-**L37**	91	1:8
2	H	12.5 mol% *(R)*-**L38**	85	18:1
3	Ph	12.5 mol% *(R)*-**L38**	87	12:1
4	Me	12.5 mol% *(R)*-**L38**	70	13:1

Scheme 17.34. (a) Ir-catalyzed allylic alkylation of cyclic β-ketoesters. (b) Pd-catalyzed diastereoselective allylic alkylation of Ir-catalyzed allylic alkylation products. Source: Stoltz [144].

ethyl β-ketoester products could be further elaborated via Pd-catalyzed allylic alkylation, granting access to either diastereomeric series of **A** or **B** selectively depending on the PHOX catalyst used (Scheme 17.34b). Later in 2013, Stoltz applied this methodology to the synthesis of *vic*-tertiary and quaternary centers in acyclic β-ketoesters with ***ent*-L35** and LiO*t*-Bu as a base (Scheme 17.35) [145]. Despite the increased conformational complexity of these acyclic systems, generally excellent enantio-, diastereo-, and regioselectivities were achieved. The substitution of the cinnamyl electrophile led to poorer levels of regioselection, found to correlate linearly with a negative ρ value when plotted vs. Brown σ+ values.

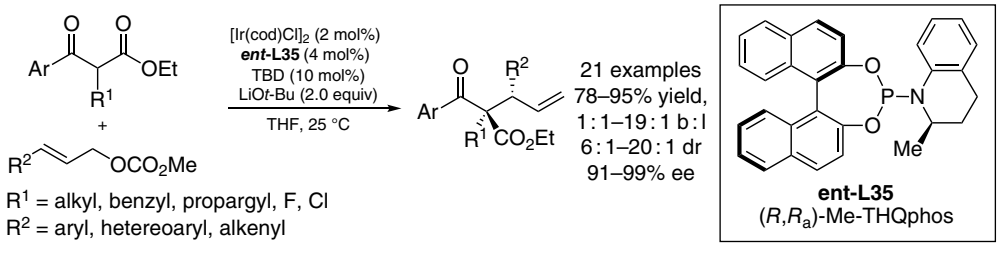

Scheme 17.35. Ir-catalyzed regio-, diastereo-, and enantioselective allylic alkylation of acyclic β-ketoesters. Source: Stoltz [145].

In 2016, Stoltz further expanded the substrate scope of the Ir-catalyzed allylic alkylation to α,β-unsaturated malonates and β-ketoester pro-enolates (Scheme 17.36) [146]. In the case of exocyclic pronucleophiles, the Ir-catalyzed allylic alkylation proceeded with a high degree of stereoselectivity and underwent subsequent Cope rearrangement with excellent transfer of chirality (Scheme 17.36a).

Endocyclic pronucleophiles performed well in the Ir-catalyzed allylic alkylation (Scheme 17.36b); however, efficient Cope rearrangement required the separation of diastereomers (not shown).

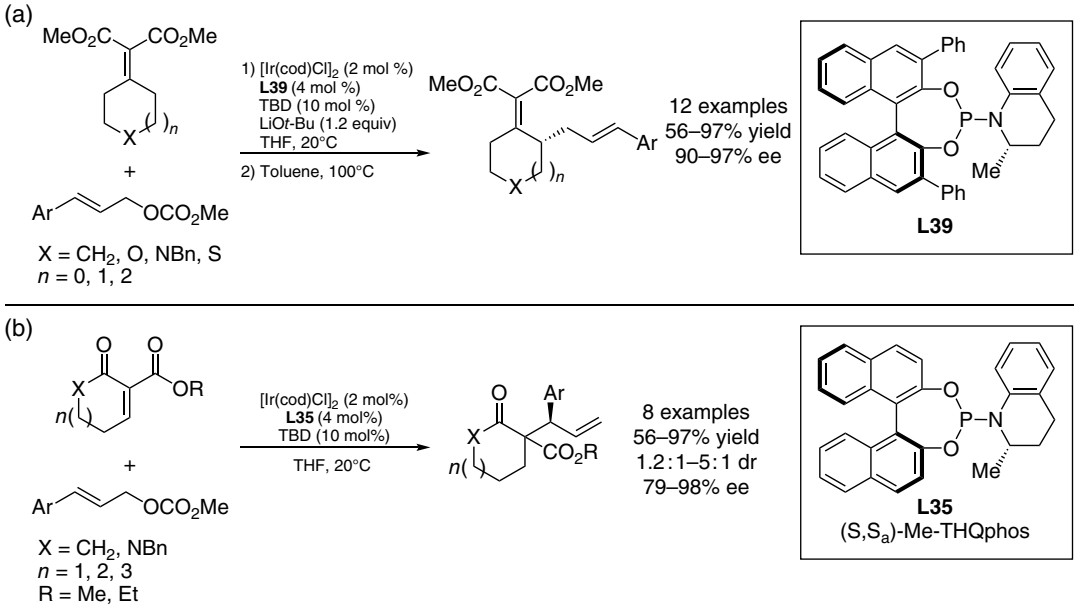

Scheme 17.36. (a) Tandem Ir-catalyzed allylic alkylation/Cope rearrangement. (b) Ir-catalyzed allylic alkylation of endocyclic enolate nucleophiles. Source: Stoltz [146].

Alkyl-substituted allylic electrophiles are difficult substrates for enantioselective Ir-catalyzed allylic alkylation. In 2016, Stoltz reported the regio-, enantio-, and diastereoselective allylic alkylation of tetralone β-ketoesters (Scheme 17.37) [147]. Products bearing vicinal quaternary and tertiary stereogenic could be generated in fair to excellent yield and good to excellent stereoselectivities under carefully optimized reaction conditions. In this reaction, chloride plays a pivotal role: excess LiCl and the utilization of crotyl chloride instead of crotyl carbonate were necessary for higher regio- and stereoselectivities. Proton sponge base provided optimal levels of enantio- and diastereoselectivities.

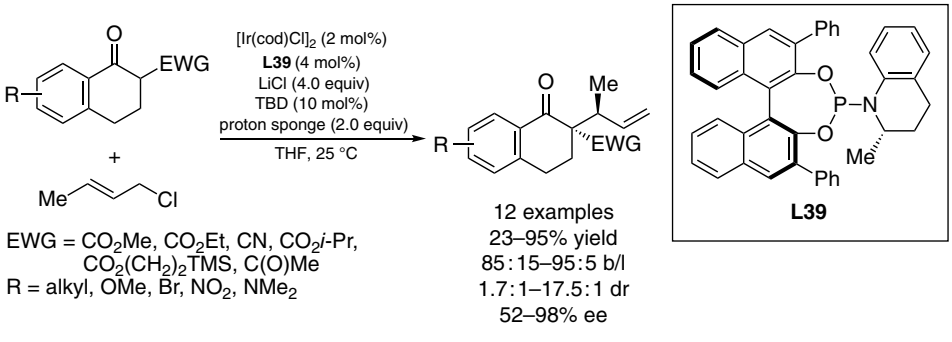

Scheme 17.37. Ir-catalyzed enantioselective allylic alkylation with crotyl chloride. Source: Stoltz [147].

Dual stereodivergent catalysis has become an important method for the enantio- and diastereoselective Ir-catalyzed allylic alkylation, first pioneered by Carreira [148]. In 2018, Hartwig reported the diastereodivergent Ir-catalyzed allylic alkylation via synergistic Ir/Cu catalysis utilizing Ir complex **C2•BF$_4$** in

concert with Cu/**L14** (Scheme 17.38a) [149]. Here, stereocontrol of the nucleophilic partner is controlled via chelation to the Cu-complex whereas stereocontrol of the electrophilic partner is controlled via the Ir-complex. Thus, switching the enantiomeric series of the catalyst complex enables access to all four possible stereoisomers in exceptional diastereo- and enantioselectivities (Scheme 17.38b). Other chiral bisphosphine ligands led to decreased levels of diastereoselectivity compared with Walphos (**L14**). This technology has also recently been applied to the synthesis of tertiary fluoride containing vicinal stereogenic centers [150, 151]. In addition, Wang and coworkers demonstrated a similar strategy for Cu/Ir dual catalysis to synthesize α,α-disubstituted amino acid derivatives with aldimine ester nucleophiles [152].

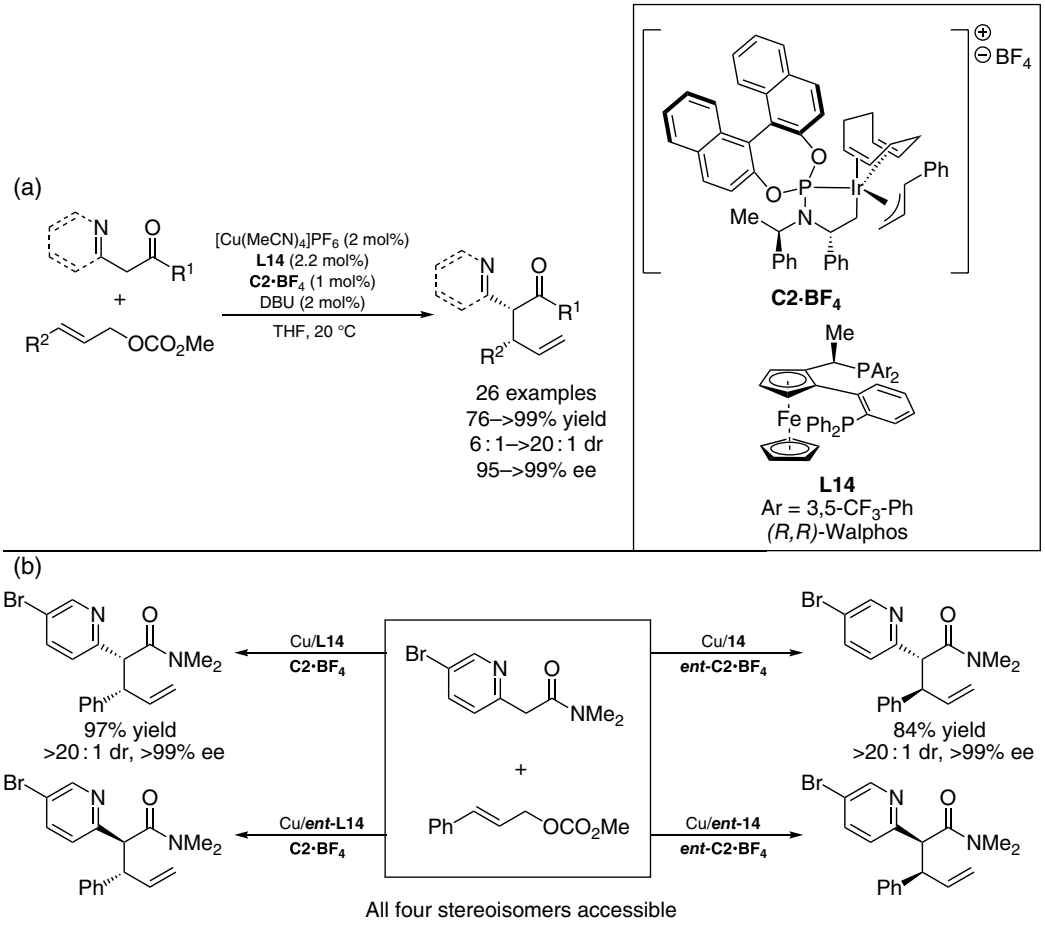

Scheme 17.38. Stereodivergent Ir-catalyzed catalyzed allylic alkylation via dual Ir/Cu synergistic catalysis. (a) Diastereoselective dual Ir/Cu-catalyzed allylic alkylation. Source: Hartwig [149]. (b) Synergistic Ir/Cu-catalyzed allylic alkylation enables access to all four stereoisomers of products. Source: Hartwig [149].

17.7.2. Ir-Catalyzed Allylic Alkylation with Non-Stabilized Nucleophiles

The seminal example of an Ir-catalyzed allylic alkylation with a non-stabilized ester enolate was reported by Hartwig in 2012 with trimethylsiloxy furan, activated in situ by ZnF_2 (Scheme 17.39) [153]. In this study, Hartwig achieved excellent 3-position selectivity for branched allylic alkylation products. Olefin migration provided α,β-unsaturated lactones of type **A** as the major products bearing a single stereogenic center in exceptional enantiomeric excess. Minor side products **B** and **C** were observed due to 5-position alkylation and 5-position alkylation with subsequent Cope rearrangement and tautomerization, respectively. Hartwig also demonstrated 4- and 5-methyl-substituted trimethylsiloxy furan nucleophiles, although these gave more complex mixtures that required further manipulation to simplify reaction mixtures (not shown).

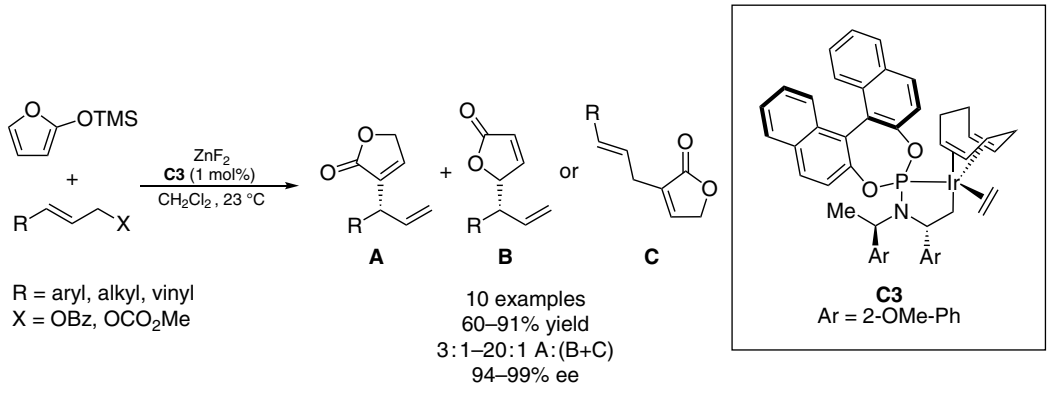

Scheme 17.39. Ir-catalyzed allylic alkylation of trimethylsiloxy furan. Source: Hartwig [153].

In 2014, Hartwig expanded the nucleophile scope of the Ir-catalyzed allylic alkylation to acyclic trimethylsilyl enol ethers derived from α,β-unsaturated ketones [154]. With these sensitive substrates, the combination of KF and 18-crown-6 was critical for achieving the desired reactivity. This methodology was further extended to dioxinone-derived silyl dienolates [154] and acyclic vinylogous ester and amide-derived trimethylsilyl enol ethers [155]. With respect to dioxinone-derived silyl dienolate nucleophiles, Hartwig also reported the first example of trisubstituted allylic electrophiles by utilizing allylic phosphate electrophiles [156]. In 2017, Hartwig developed silyl ketene acetal nucleophiles to generate acyclic esters bearing α-quaternary centers with β-stereogenic tertiary centers [157]. Although these products could be obtained with excellent enantioinduction, an enantio- and diastereoselective reaction could not be achieved. While Hartwig's development of the Ir-catalyzed allylic alkylation in silyl ketene acetals and silyl enol ethers utilized type I reactivity with a fluoride additive, Liang and Yang developed a type II variant of aryl ketone-derived silyl enol ethers with the Carreira ligand **L34** and branched allylic alcohol electrophiles with $Sc(OTf)_3$ as a Lewis acid activator in absence of fluoride [158].

The development of diastereoselective Ir-catalyzed allylic alkylation with non-stabilized enolates has proven challenging compared with their stabilized counterparts. Hartwig and coworkers developed an approach to non-stabilized ketone enolate nucleophiles utilizing the counterion effect previously harnessed by their group in stabilized enolates [142, 143]. In this regard, diastereoselectivity of prochiral ketone enolates was achieved by use of the barium enolate (Scheme 17.40) [159]. Good to excellent diastereoselectivity and excellent enantioselectivity were achieved with **C4·BF$_4$**. In acyclic systems, increased conformational flexibility and enolate geometry control bring additional challenges to non-stabilized ketone nucleophiles. In this regard, Hartwig utilized Cu(I)-chelation-controlled enolization of α-alkoxy ketones to perform an enantio- and diastereoselective Ir-catalyzed allylic alkylation of acyclic ketone enolates [160].

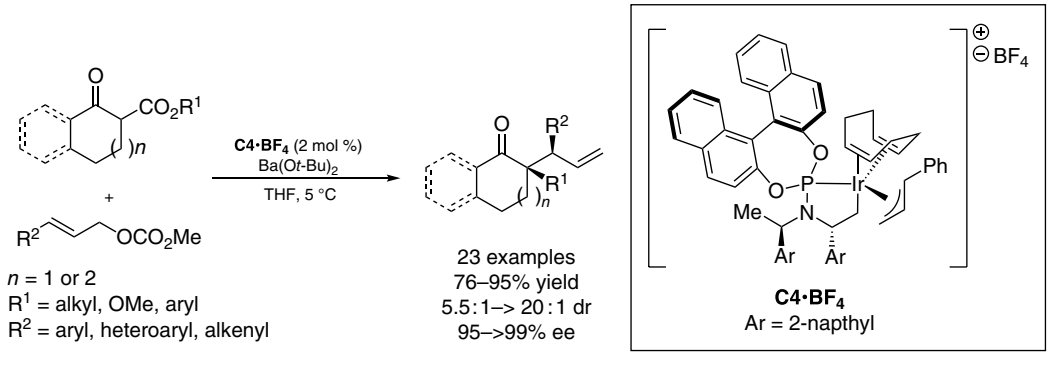

Scheme 17.40. Diastereo- and enantioselective allylic alkylation of non-stabilized ketone enolates. Source: Hartwig [159].

In an alternative strategy, Zhang utilized dual-catalytic Ir/Zn systems to achieve stereodivergent access to all four stereoisomers of product with unprotected α-hydroxy ketone nucleophiles [161]. In this strategy, a chiral Zn Lewis acid complex provides well-defined enolization geometry selectivity. This stereodivergent reactivity was further developed in unprotected α-hydroxyindanones by Zhang [162]. In addition to chiral Lewis acid geometry control, Hartwig has demonstrated that chiral Lewis bases can control enolization geometry in activated acyclic pentafluorophenyl ester enolate nucleophiles, enabling stereodivergent access to vicinal tertiary stereogenic centers [163]. In addition to ketone and ester enolate nucleophiles, trimethyl orthoacetate and ethylene glycol monovinyl ether have been developed as an acetate enolate and silyl enol ether nucleophile equivalent, respectively, by Carreira and coworkers [164].

17.7.3. Ir-Catalyzed Allylic Alkylation with Enamine Catalysis

In 2013, Carreira reported the first dual-catalytic stereodivergent approach to accessing all possible stereoisomeric products in an enantio- and diastereoselective allylic alkylation [148]. This powerful new strategy utilizes a chiral cinchona alkaloid to control the stereogenic center derived from aldehyde pronucleophiles with control of the branched allyl alcohol electrophile-derived stereogenic center via the Ir-catalyst (Scheme 17.41). Importantly, all four stereoisomeric products bearing vicinal α-quaternary β-tertiary stereogenic centers are obtained under identical reaction conditions, with absolute stereochemical control achieved via the choice of amine pseudoenantiomer and phosphoramidite ligand enantiomeric series. DFT calculations by Sunoj and coworkers revealed that weak interactions in the C–C bond formation transition states were responsible for the stereodivergent reactivity [165]. Carreira later addressed the challenges of epimerization and self-aldol side reactions with products bearing α-tertiary stereogenic centers reactions by utilizing dimethyl hydrogen phosphate as an activator in concert with a proline-derived chiral amine catalyst [166]. The scope of this stereodivergent transformation was additionally expanded to protected α-amino and α-hydroxy acetaldehyde pronucleophiles [167], as well as to the synthesis of all stereoisomers of Δ9-tetrahydrocannabinol natural products [168]. Jørgensen utilized a related proline-derived catalyst in the remote functionalization of α,β-unsaturated aldehydes to generate remote stereocenters [169]. In addition to these intermolecular examples, Carreira and coworkers developed an

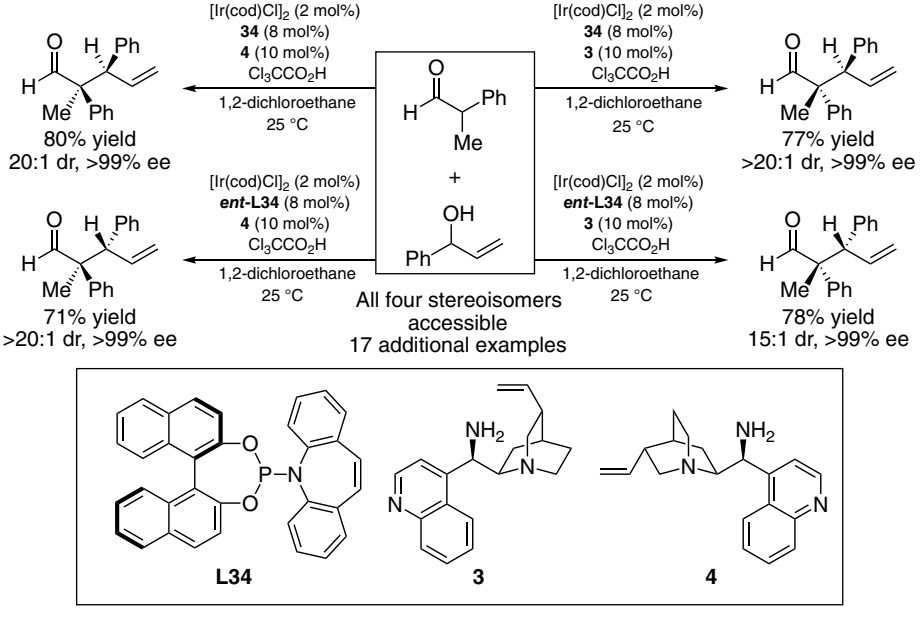

Scheme 17.41. Dual-catalytic stereodivergence in the Ir-catalyzed allylic alkylation. Source: Carreira [148].

intramolecular example wherein the allylic alcohol electrophile contained amine moiety, enabling access to chiral piperidines following facile intramolecular reductive amination [170].

17.7.4. Ir-Catalyzed Allylic Alkylation with Arene Nucleophiles

Electron-rich arene and heteroarene nucleophiles have been developed as nucleophiles both in Friedel–Crafts-type alkylations and in catalytic asymmetric dearomative (CADA) reactions with Ir. An exhaustive review of recent developments in Friedel–Crafts-type alkylations and CADA reactions is outside the scope of this section [135e], hence references are provided for recently developed substrates in these transformations for C–C bond formation. Nucleophiles recently investigated in CADA reactions include indole derivatives [171], pyrroles [171c, 172], phenols [173], and naphthols [174], while the Ir-catalyzed allylic Friedel–Crafts reaction has been explored in indoles [171d, 175], 10-allylanthrones [176], and anilines (via C-alkylation) [177].

A noteworthy recent example is the desymmetrizing CADA of bisphenol derivatives (Scheme 17.42) [178]. This reaction is impressive for several reasons: short reaction times (c. 30 min), ability to generate up to three contiguous stereogenic centers in high yield and ee (up to 90% yield and 99% ee), and the reaction can be utilized in gram-scale reactions with unusually low catalyst loadings (down to 0.20 mol%). The utility of this method was further showcased, albeit in a diastereoselective manner, in the total synthesis of (+)-tatanan B and (+)-tatanan C (not shown).

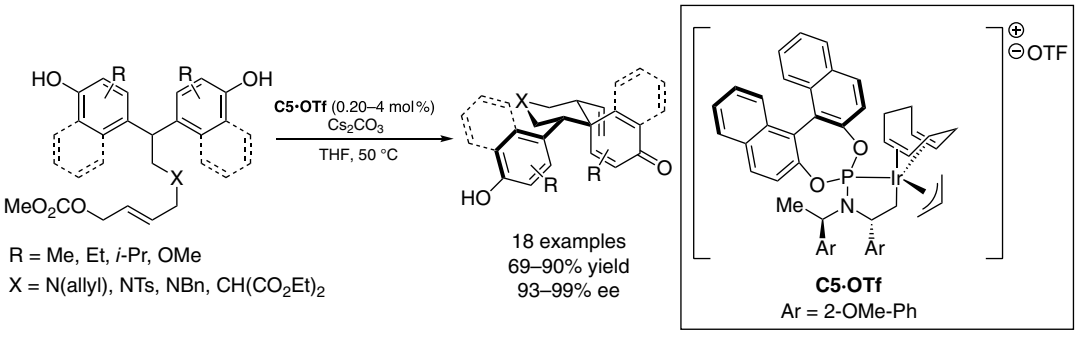

Scheme 17.42. Desymmetrizing CADA of bisphenol derivatives. Source: You [178].

17.7.5. Ir-Catalyzed Allylic Alkylation with Olefin Nucleophiles

Olefins have been utilized as nucleophilic partners in Ir-catalyzed allylic substitution via C–H activation and direct allyl–olefin coupling. With respect to C–H activation, You and coworkers discovered that 2-vinylanilines afforded Heck-type vinylation with allylic carbonate electrophiles via aniline directed C–H insertion [179]. Carreira and coworkers have pioneered the direct utilization of olefin nucleophiles in Ir-catalyzed allylic substitution under type II reactivity (vide supra). In 2014, Carreira reported the intermolecular coupling of olefins with branched allylic alcohol electrophiles (Scheme 17.43) [180]. Under these

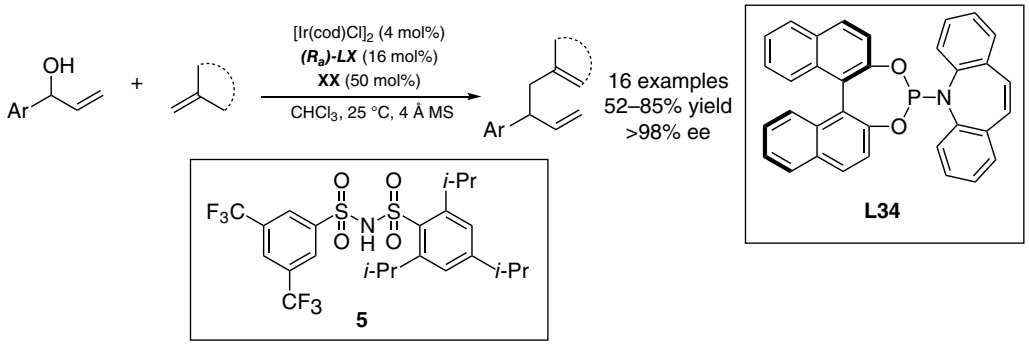

Scheme 17.43. Allyl–olefin coupling via Ir-catalyzed allylic substitution. Source: Carreira [180].

reaction conditions, mono- 1,2-di- and trisubstituted alkenes are generally unreactive. Additionally, unsymmetrical olefin nucleophiles led to the formation of constitutional isomers. These challenges were later addressed via the utilization of allyl silane nucleophiles [180]. Unsymmetrical sulfonimide acid **5** was found to be optimal for promoting the desired reactivity. Carreira has also demonstrated Ir-catalyzed allylic substitution in promoting intramolecular polyene cyclizations [181], culminating in the total synthesis of asperolide C [182].

17.7.6. Ir-Catalyzed Allylic Alkylation with Organometallic Nucleophiles

Strongly basic organometallic compounds are relatively rare in Ir-catalyzed allylic alkylation reactions. Carreira reported the first examples of functionalized mono-organozinc bromide nucleophiles in Ir-catalyzed allylic alkylations with (*P*,olefin)-ligand ***ent*-L34** (Scheme 17.44) [183]. This methodology enabled access to many enantioenriched functionalized products that were previously inaccessible via Ir-catalyzed allylic alkylation. Carreira later utilized functionalized organozinc nucleophiles with allenylic carbonate electrophiles [184]. Recent developments in the advancement of organometallic nucleophiles include 2-methylpyridines [185], allyl silanes [180], bis(pinacolatoboryl)-methane [186], and (gem-diborylalkyl)zinc(II) species [187].

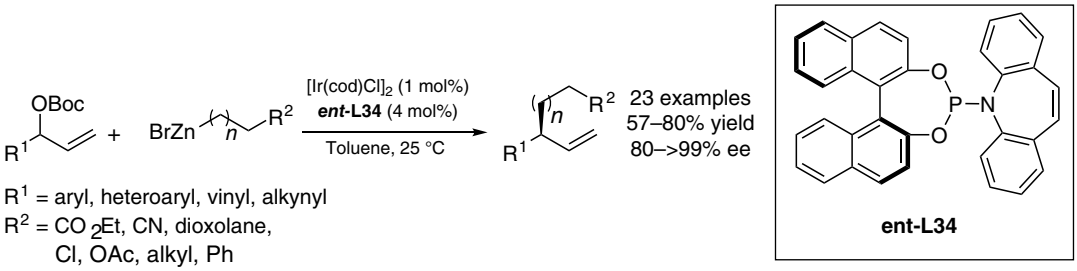

Scheme 17.44. Ir-catalyzed allylic alkylation with functionalized organozinc bromides. Source: Carreira [183].

17.7.7. Ir-Catalyzed Allylic Alkylation with Umpolung Reactivity of Imines

The umpolung reaction of imines in Ir-catalyzed allylic alkylations enables access to valuable amino functionalized products. In 2016, Niu developed the formal umpolung allylation of *N*-fluorenyl imines via tandem regioselective allylation of the fluorenyl moiety followed by a 2-aza Cope-rearrangement (Scheme 17.45) [188]. Products could be isolated either as hydrochloride salts or as Boc carbamates. Stronger bases than 1,8-diazabicyclo[5.4.0]undec-7-ene (DBU) (e.g. lithium hexamethyl bis(trimethylsilyl)

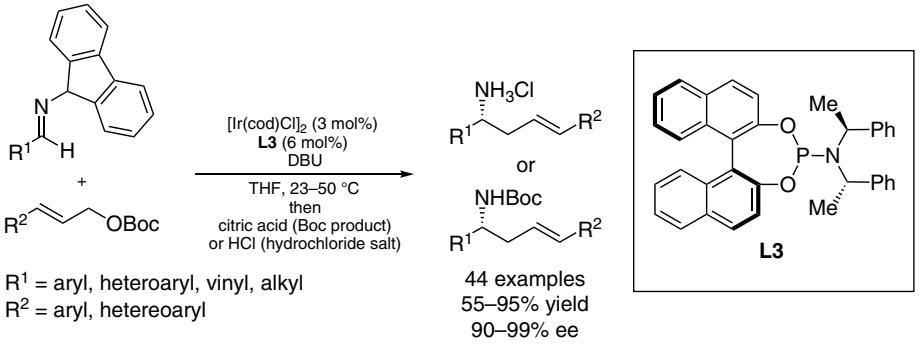

Scheme 17.45. Formal umpolung allylation of *N*-fluorenyl imines. Source: Niu [188].

amide [LiHMDS]) generally provided lower ee, possibly due to racemization of the C-allylated fluorenyl imine while weaker bases (e.g. Et_3N) provided low yields. Interestingly, the intermediate C-allylated fluorenyl imine can be isolated and subjected to thermal 2-aza-Cope rearrangement, providing evidence for the proposed mechanism. Umpolung reactivity of imines has also been harnessed by Han in a diastereo- and enantioselective Ir/phase transfer catalyst (PTC) allylic alkylation of α-imino esters to generate tetrasubstituted α-amino acids bearing vicinal tertiary stereogenic centers [189].

17.8. COPPER-CATALYZED ENANTIOSELECTIVE ALLYLIC ALKYLATION

Cu-catalyzed asymmetric allylic substitution is a powerful tool for the introduction of new C–C bonds with branched regioselectivity, especially for organometallic and hard, non-stabilized carbon nucleophiles. These reactions typically proceed via a regiospecific S_N2' mechanism wherein nucleophile transmetallation generates a Cu(I) complex that undergoes subsequent enantiodetermining oxidative addition to a Cu(III) σ-allyl complex. In this way Cu serves as an important complimentary catalyst to Pd and Ir for the introduction of allylic C–C bonds. Many advances have been made in the field of Cu-catalyzed allylic substitution from 2010 to 2020 with phosphoramidite, diphosphine, phosphine–phosphite, and *N*-heterocyclic carbene (NHC) ligand complexes. Our discussion here is limited to Cu-catalyzed reactions wherein stereoselectivity is imparted by catalyst control.

17.8.1. Allylic Alkylation of Grignard Reagents

Since the initial studies of Bäckvall and Koten [190], widely available Grignard reagents have been harnessed as nucleophilic partners with a broad scope of allyl electrophiles in Cu-catalyzed allylic substitution reactions. Recently, Cu-catalyzed asymmetric allylic alkylation with Grignard reagents has been successfully developed for the allylic alkylation of *ortho*-substituted cinnamyl halides [191, 192], diene bromides [193], halocrotonates [194], allyl phosphates [195], phosphonates and phosphine oxides [196], and enyne chlorides [197]. Various enantioenriched cyclic carbocycles and heterocycles have been prepared via tandem Cu-catalyzed asymmetric allylic alkylation/ring-closing metathesis [198]. Recently, *P*-chiral monophosphorus ligands have been demonstrated as a new ligand scaffold amenable to asymmetric allylic alkylation with copper [199]. Alexakis and coworkers have identified direct enantioselective transformations of cyclic allylic bromides [200] and a stereodivergent kinetic resolution in the accompanying cyclic systems [201] with Cu/phosphoramidite catalysts.

17.8.2. Allylic Alkylation of Organolithium Reagents

A longstanding challenge in transition-metal-mediated C–C bond forming reactions has been the utilization of broadly available and highly reactive organolithium reagents. In 2011, Feringa and coworkers reported the first general Cu-catalyzed asymmetric allylic substitution of allylic bromides with alkyllithium reagents utilizing TaniaPhos (**L40**) as a chiral ligand (Scheme 17.46) [202]. While generally

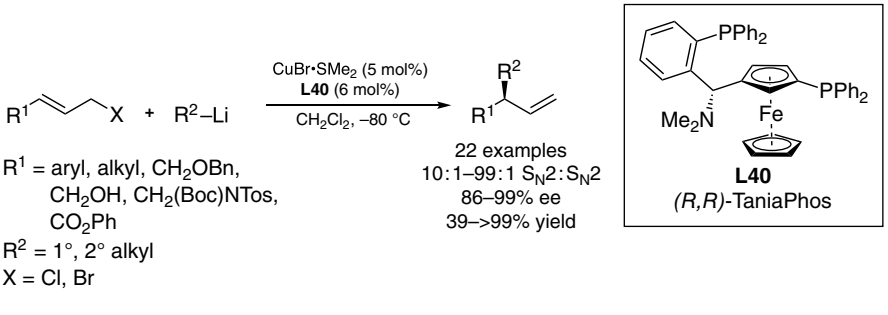

Scheme 17.46. Cu-catalyzed allylic alkylation of organolithium reagents. Source: Feringa [202].

excellent regio- and enantioselectivities were observed for allylic bromides with TaniaPhos, allylic chlorides performed poorly. Preliminary results demonstrated that high regio- and enantioselectivities could be achieved with allylic chlorides (X = Cl) if phosphoramidite ligands were utilized.

In 2012, Feringa expanded on these results and demonstrated that phosphoramidite ligand **L36** enabled access to acyclic tertiary stereogenic centers in high selectivities from both allylic chlorides and bromides (Scheme 17.47a) [203]. Furthermore, the use of phosphoramidite ligand **L3** enabled the use of *sec*-alkyllithium reagents, albeit with no diastereoselectivity (Scheme 17.47b). Access to acyclic quaternary centers was achieved from allylic bromides utilizing phosphoramidite ligand **L41** (Scheme 17.47c). Interestingly, *ortho*-bromo and *ortho*-methoxy substitution of the cinnamyl bromides led to highly sterically encumbered quaternary centers in excellent regio- and enantioselectivities; however, *ortho*-methyl substitution led to nearly racemic products in high S_N2' selectivity. The scope of electrophiles compatible with this transformation has been further expanded to include allylic ethers [204], *Z*-trisubstituted allylic bromides [205], oxabicyclic alkenes [206], and a one-pot synthesis of optically active β- and γ-alkyl alcohols [207].

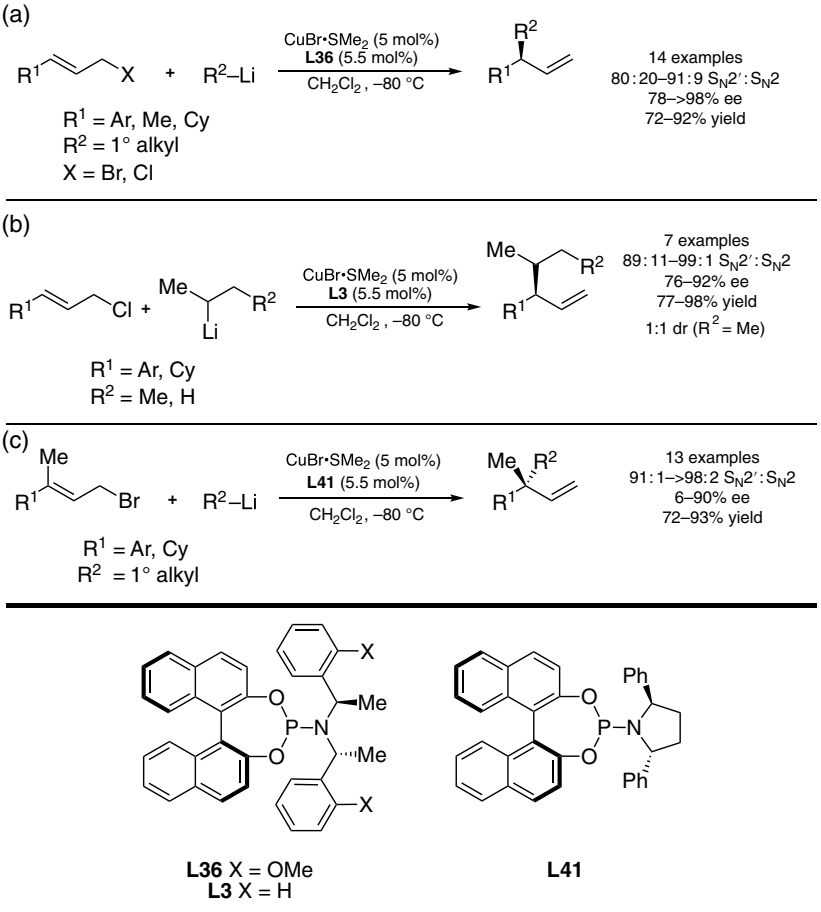

Scheme 17.47. (a) Cu-catalyzed asymmetric allylic alkylation of allylic chlorides and bromides to generate tertiary stereogenic centers with primary organolithium reagents. Source: Feringa [203]. (b) Cu-catalyzed asymmetric allylic alkylation of allylic chlorides with 2° organolithium reagents. Source: Feringa [203]. (c) Cu-catalyzed asymmetric allylic alkylation of cinnamyl bromides to generate quaternary stereogenic centers. Source: Feringa [203].

Feringa and coworkers further expanded the asymmetric Cu-catalyzed allylic substitution to readily accessible aryllithium nucleophiles. In 2016, Feringa disclosed the use of chiral NHC complex CuCl·**L42** as a catalyst for the allylic arylation of a variety of allyl bromides with aryllithium reagents to generate

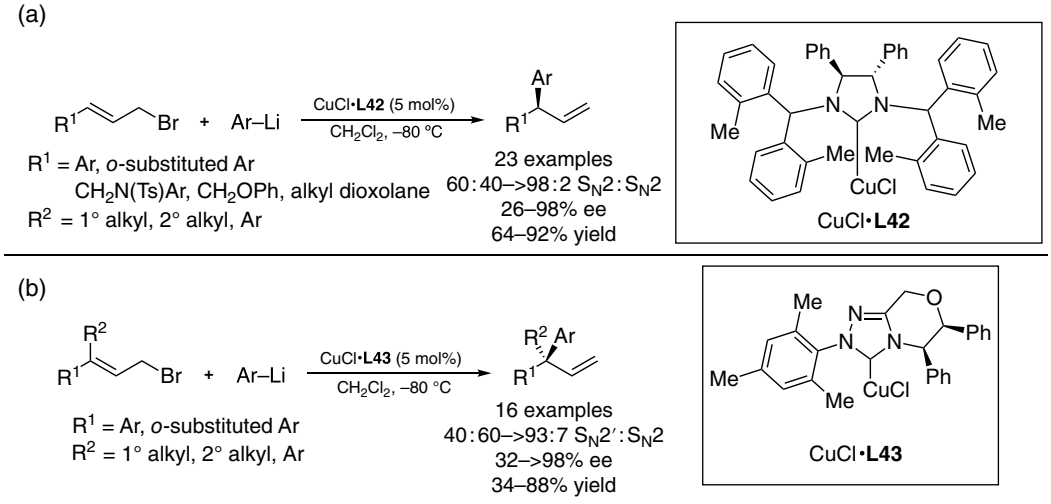

Scheme 17.48. (a) Enantioselective allylic arylation of allylic bromides to form acyclic tertiary stereogenic centers. Source: Feringa [208]. (b) Enantioselective allylic arylation of allylic bromides to form acyclic quaternary stereogenic centers. Source: Feringa [209].

diaryl methane motifs in high regio- and enantioselectivities (Scheme 17.48a) [208]. Later that year, catalyst CuCl·**L43** enabled access to di- and triaryl acyclic quaternary stereogenic centers (Scheme 17.48b) [209].

17.8.3. Allylic Alkylation of Organoaluminum Reagents

Hoveyda and coworkers have pioneered the use of organoaluminum reagents in Cu-catalyzed asymmetric allylic substitution with chiral NHC complexes. The first successful asymmetric alkylation of organoaluminum reagents utilized Me_3Al [210] and vinylaluminum reagents [211]. Subsequently, Hoveyda demonstrated the synthesis of acyclic quaternary stereogenic centers with arylaluminum reagents [212]. Most recently, Hoveyda harnessed alkynylaluminum reagents for the synthesis of acyclic quaternary [213] and tertiary [214] stereogenic centers (Scheme 17.49). The Hoveyda Cu/NHC complexes are quite general

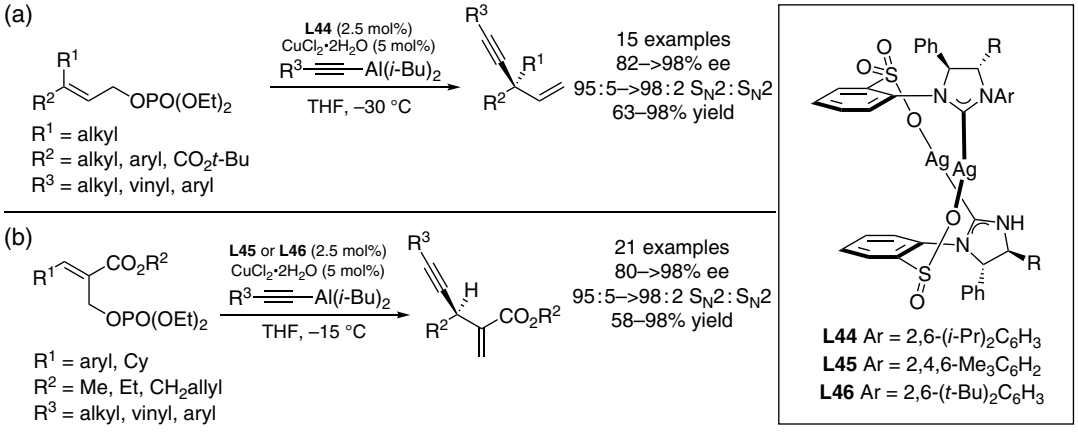

Scheme 17.49. (a) Enantioselective allylic alkylation of alkynylaluminum for the synthesis of acyclic quaternary stereogenic centers. Source: Hoveyda [213]. (b) Enantioselective allylic alkylation of alkynylaluminum for the synthesis of acyclic tertiary stereogenic centers. Source: Hoveyda [214].

for the asymmetric allylic substitution of organoaluminum nucleophiles with variation of the Ar used to fine-tune selectivity between different substrate classes. Organoaluminum reagents offer an advantage over the corresponding diorganozinc reagents in that they are relatively easier to prepare in high purity. Additionally, diorganozinc reagents typically only transfer one of their organic units.

17.8.4. Allylic Alkylation of Organoboron Reagents

The first examples of organoboron nucleophiles in Cu-catalyzed allylic alkylations were reported by Ohmiya and Sawamura [215] and Lalic [216] in 2010. The first enantioselective example emerged in 2011 from Shintani and Hayashi with aryl and alkenyl boronate nucleophiles and allyl phosphates (Scheme 17.50) [217]. A Mauduit-type chiral alkoxy NHC (**L47·PF$_6$**) ligand paired with NaOMe provided products in generally excellent regio- and enantioselectivities. The use of a sodium base in combination with a neopentylglycol boronate ester was critical for high enantioinduction.

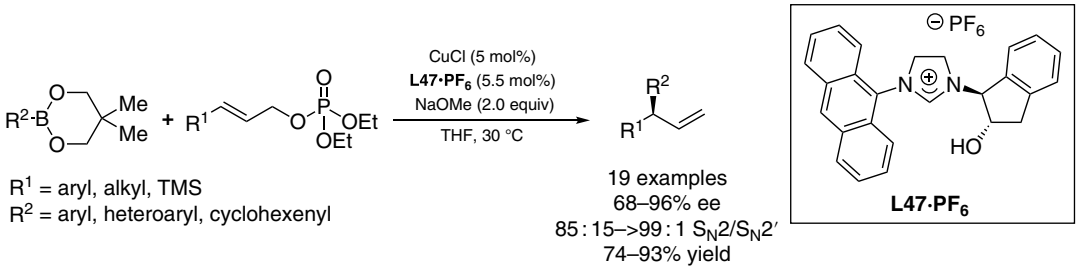

Scheme 17.50. Cu-catalyzed enantioselective allylic alkylation with organoboronate nucleophiles. Source: Shintani and Hayashi [217].

In 2012, Hoveyda demonstrated the synthesis of allene-substituted acyclic tertiary and all-carbon quaternary stereogenic centers via the Cu-catalyzed allylic alkylation of allyl phosphates with commercially available and air-stable allenylboronic acid pinacol esters (Scheme 17.51) [218]. In the synthesis of tertiary center formation, ligand **L48** provided optimal levels of regio- and enantioselectivities, while ligand **L49** provided optimal selectivities in the synthesis of quaternary stereogenic centers. The allylic propargylation (not shown) was observed to be <2% in all examples. This technology was later adapted for S_N2'' allylic alkylations with allenylboronic acid pinacol ester and dialkenyl phosphates by Torker and Hoveyda [219].

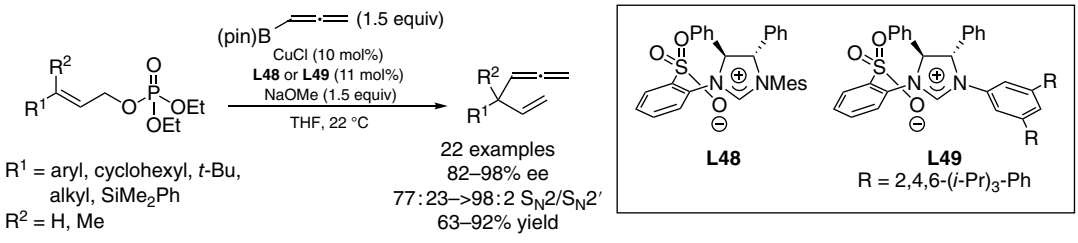

Scheme 17.51. Cu-catalyzed asymmetric allylic allenylation with bench-stable allenylboronic acid pinacol ester. Source: Hoveyda [218].

Alkylborane nucleophiles generated by the in situ hydroboration of terminal olefins with 9-borabicyclo[3.3.1]nonane (BBN) with *Z*-allylic chloride electrophiles were reported by Ohmiya and Sawamura in 2012 (Scheme 17.52) [220]. Here, bisphosphine ligand (*R*)-DTBM-SEGPHOS (**L50**) provided the highest levels of enantioselectivity. The corresponding *E*-allylic chlorides provided lower levels of enantioinduction. Sawamura later extended this methodology to the enantioselective synthesis of acyclic all-carbon quaternary stereogenic centers with *E*-allylic chlorides [221]. Most recently, Ohmiya

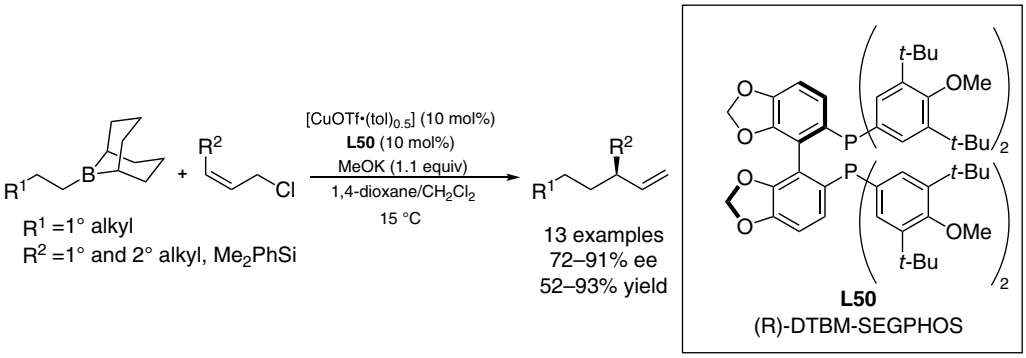

Scheme 17.52. Cu-catalyzed allylic alkylation of alkyl boranes with *Z*-allylic chlorides. Source: Ohmiya and Sawamura [220].

and Sawamura reported an intramolecular variant to generate tertiary and all-carbon quaternary stereogenic centers [222].

17.8.5. Allylic Alkylation of Organozirconium Reagents

One attractive feature of Pd-catalyzed allylic alkylations is the ability to utilize racemic starting materials in DYKAT processes. The generally accepted mechanism of oxidative addition with racemic chiral substrates in Cu-catalyzed processes is a substrate-controlled enantiodetermining oxidative addition. Because Cu-complexes generally undergo a significantly slower π–σ–π interconversion compared with Pd, utilization of racemic starting materials in a highly stereoconvergent process has been challenging. In 2015, Fletcher and coworkers found that in situ generated alkylzirconium reagents allowed for efficient DYKAT of cyclic racemic allyl chlorides with Cu, presumably due to their lower reactivity compared with other organometallic reagents (Scheme 17.53) [223]. Mechanistic studies by Fletcher demonstrate this DYKAT process is likely mediated by oligomeric copper complexes that, over the course of the reaction, become more enantioselective and lead to faster reaction [224]. This methodology has been further expanded to 3,6-dihydro-2*H*-pyran electrophiles [225].

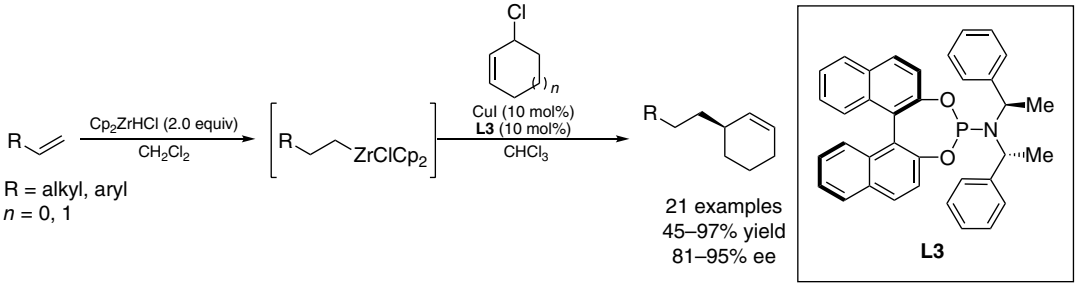

Scheme 17.53. Dynamic kinetic asymmetric allylic alkylation of alkylzirconium reagents. Source: Fletcher [223].

17.8.6. Other Carbon Nucleophiles

Following an initial report of stereospecific allylic alkylation [226], Ohmiya and Sawamura disclosed the enantioselective allylic alkylation of terminal alkynes with *Z*-allylic phosphates with NHC ligand **L51·BF$_4$** (Scheme 17.54) [227]. The use of *Z*-allylic phosphates was critical as the use of the corresponding *E*-allyl phosphates led to poor enantioinduction and low yield. Enantioenriched chiral alkynes provided similar levels of diastereoselectivity with a slight matched/mismatched effect (not shown).

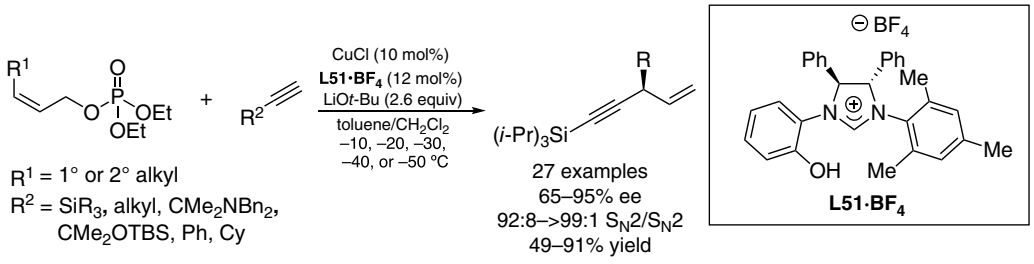

Scheme 17.54. Cu-catalyzed allylic alkylation with terminal alkyne nucleophiles. Source: Ohmiya and Sawamura [227].

Internal alkynes have also been utilized as nucleophiles with Cu/NHC catalysts via in situ hydrometallation [228].

In 2017, Ohmiya and Sawamura developed a Cu-catalyzed three-component allylic alkylation via in situ formation of a formidyl cuprate (Scheme 17.55) [229]. Naphthol NHC ligand **L52·BF$_4$** provided

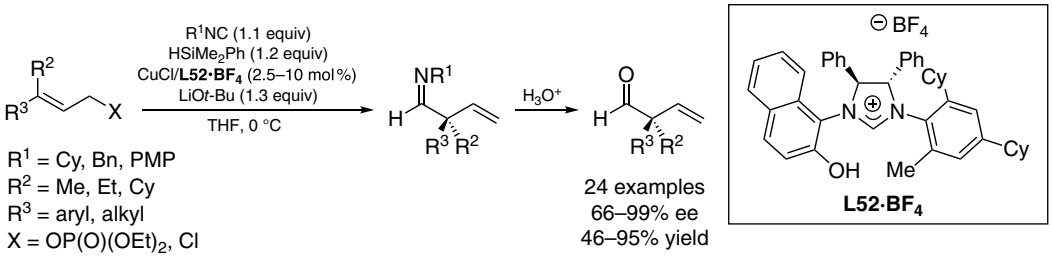

Scheme 17.55. Cu-catalyzed allylic alkylation of formidyl cuprates. Source: Ohmiya and Sawamura [229].

exceptional regioselectivity and generally high enantioinduction in this transformation with isocyanides functioning as umpolung C1 synthons.

In 2020, Stoltz and coworkers reported the first example of a Cu-catalyzed allylic alkylation with a prochiral γ-butyrolactone-derived silyl ketene acetal nucleophile (Scheme 17.56) [230]. Critical to the success of this transformation was the utilization of monopicolinimide ligand **L53**. Preliminary mechanistic investigations via continuous-wave (CW) X-band electron paramagnetic resonance (EPR), UV-Vis spectroscopy, and DFT calculations in concert with experimental observations indicate that the active catalytic species is CuI and the catalytic cycle may proceed through a CuIII[σ + π] intermediate. DFT calculations support monopicolinimide ligand **L53** binding to copper in a tridentate fashion via the N_{pyridine}, $N_{\text{picolinamide}}$, and $O_{\text{benzamide}}$ atoms.

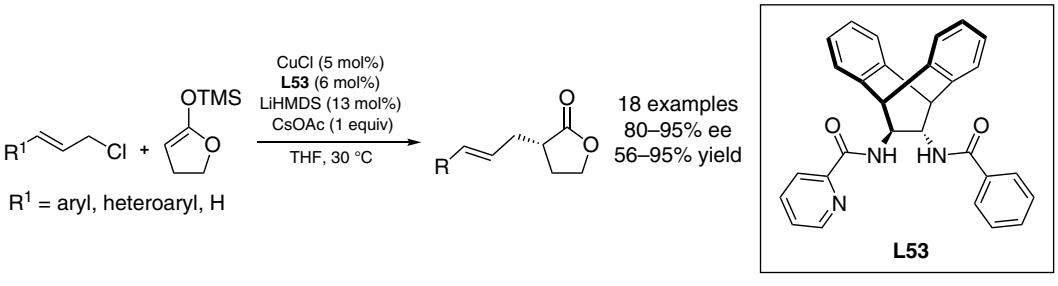

Scheme 17.56. Cu-catalyzed enantioselective allylic alkylation of γ-butyrolactone-derived silyl ketene acetal.

17.9. COBALT-CATALYZED ENANTIOSELECTIVE ALLYLIC ALKYLATION

Compared with other metals, cobalt-catalysts have been much less explored in asymmetric allylic substitution chemistry. Only recently examples of highly regio- and enantioselective cobalt-catalyzed allylic alkylations have been reported; however, these studies are limited to the use of soft nucleophiles. In 2019, Li and coworkers reported the first highly enantioselective Co-catalyzed allylic alkylation with benzo-fused cyclic β-ketoesters and allylic carbonates to generate vicinal quaternary stereogenic centers in exceptional branched selectivity and good enantioselectivity. The use of more hindered *t*-Bu β-ketoesters as well as (*S,S*)-2,5-diphenylphospholano ethane (Ph-BPE) ligand **L54** provided the optimal selectivity (Scheme 17.57) [231]. Two examples of vicinal quaternary stereogenic centers are reported; however, a maximum diastereomeric ratio of 4 : 1 is observed.

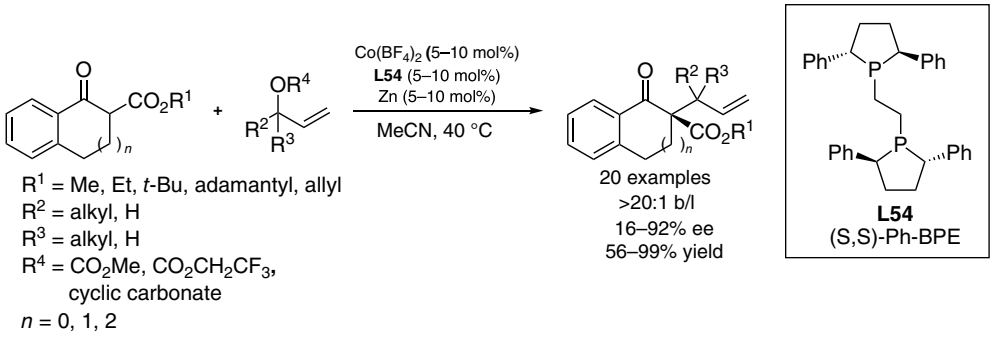

Scheme 17.57. First example of a highly enantio- and regioselective Co-catalyzed allylic alkylation. Source: Li [231].

In 2020, Li and coworkers reported that a Co(II) catalyst with bisoxazolinephosphine ligand **L55**, previously utilized for Co-catalyzed allylic amination [232], provided excellent branched selectivity and enantioselectivity in the allylic alkylation of malononitriles to generate acyclic tertiary stereogenic centers (Scheme 17.58) [233]. A single example of vicinal tertiary stereogenic centers was achieved, albeit in poor diastereoselectivity (1.5 : 1 dr).

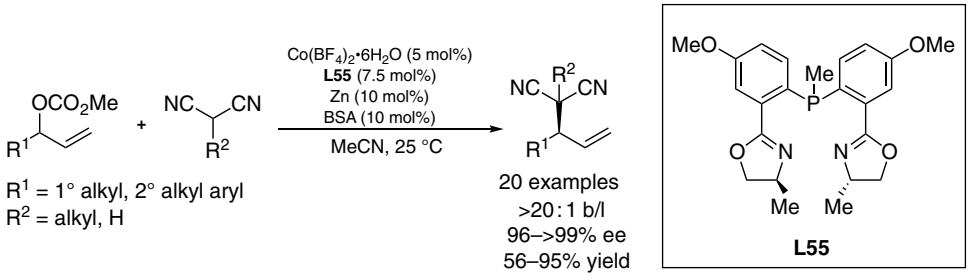

Scheme 17.58. Enantio- and regioselective Co-catalyzed allylic alkylation of malononitriles. Source: Li [233].

To date, these two studies from Li and coworkers constitute the only general examples of Co-catalyzed allylic alkylation with high levels of enantioinduction. Kojima and Matsunaga developed an organophotoredox approach to regioselective Co-catalyzed allylic substitution of allylic carbonates with malonate nucleophiles; however, only a single preliminary example with promising enantioinduction has been

reported (Scheme 17.59) [234]. These examples demonstrate the promising reactivity of Co-catalysts in allylic alkylation chemistry, warranting further investigation into Co as an earth-abundant catalyst.

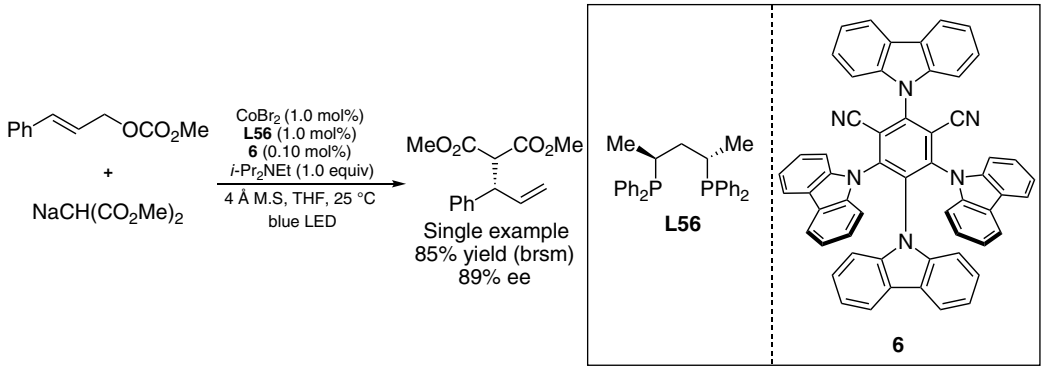

Scheme 17.59. Organophotoredox approach to Co-catalyzed enantioselective allylic alkylation. Source: Kojima and Matsunaga [234].

17.10. CONCLUDING REMARKS

A vast array of new technologies for the transition-metal-catalyzed enantioselective allylic alkylation and related reactions have been developed since the previous edition of this book series [1]. These new technologies provide reliable access to a diverse suite of substrate classes with broad applications across synthetic chemistry. While palladium catalysts remain the most highly developed, a surge of contributions to the development of other metals, particularly Ir, Cu, and Rh, have significantly expanded and diversified capabilities for enantioselective C–C bond construction. Industrial adoption of this technology has remained slow due to the relatively high catalyst loadings required, which necessitate the further development of greener methodologies that employ lower catalyst loadings and earth-abundant metals. We hope this entry will be a valuable reference for general developments from c. 2010 to 2020 and serve to inspire further development of novel catalytic systems, particularly for undeveloped metals.

REFERENCES

1. G. Helmchen, U. Kazmaier, S. Förster. Enantioselective allylic substitutions with carbon nucleophiles. In *Catalytic Asymmetric Synthesis*, 3rd ed. (Ed. Ojima, I.). Weinheim, Germany: Wiley-VCH, **2010**; pp. 497–641.
2. K. Ohmatsu, M. Ito, T. Kunieda, T. Ooi. *Nat. Chem.* **2012**, *4*, 473–477.
3. (a) K. Ohmatsu, M. Ito, T. Kunieda, T. Ooi. *J. Am. Chem. Soc.* **2013**, *135*, 590–593. (b) K. Ohmatsu, M. Ito, T. Ooi. *Chem. Commun.* **2014**, *50*, 4554–4557.
4. K. Ohmatsu, Y. Hara, T. Ooi. *Chem. Sci.* **2014**, *5*, 3645–3650.
5. K. Ohmatsu, Y. Hara, Y. Kusano, T. Ooi. *Synlett.* **2016**, *27*, 1047–1050.
6. M. Luparia, M. T. Oliveira, D. Audisio, F. Frébault, R. Goddard, N. Maulide. *Angew. Chem. Int. Ed.* **2011**, *50*, 12631–12635.
7. D. Audisio, M. Luparia, M. T. Oliveira, D. Klütt, N. Maulide. *Angew. Chem. Int. Ed.* **2012**, *51*, 7314–7317.
8. B. M. Trost, D. A. Thaisrivongs, E. J. Donckele. *Angew. Chem. Int. Ed.* **2013**, *52*, 1523–1526.
9. B. M. Trost, E. J. Donckele, D. A. Thaisrivongs, M. Osipov, J. T. Masters. *J. Am. Chem. Soc.* **2015**, *137*, 2776–2784.
10. B. M. Trost, W.-J. Bai, C. Hohn, Y. Bai, J. J. Cregg. *J. Am. Chem. Soc.* **2018**, *140*, 6710–6717.
11. S. A. Asad, J. Ulicki, M. Shevyrev, N. Uddin, E. Alberch, M. M. Hossain. *Eur. J. Org. Chem.* **2014**, 5695–5699.
12. N. Uddin, M. Rahaman, E. Alberch, S. A. Asad, M. M. Hossain. *Tetrahedron Lett.* **2018**, *59*, 3401–3404.
13. S. Tabuchi, K. Hirano, M. Miura. *Angew. Chem. Int. Ed.* **2016**, *55*, 6973–6977.
14. J. Liu, Z. Han, X. Wang, F. Meng, Z. Wang, K. Ding. *Angew. Chem. Int. Ed.* **2017**, *56*, 5050–5054.

15. (a) X. Wang, F. Meng, Y. Wang, Z. Han, Y.-J. Chen, L. Liu, Z. Wang, K. Ding. *Angew. Chem. Int. Ed.* **2012**, *51*, 9276–9282. (b) X. Wang, P. Guo, Z. Han, X. Wang, Z. Wang, K. Ding. *J. Am. Chem. Soc.* **2014**, *136*, 405–411. (c) J. Liu, Z. Han, X. Wang, Z. Wng, K. Ding. *J. Am. Chem. Soc.* **2015**, *137*, 15346–15349. (d) X. Wang, X. Wang, Z. Han, Z. Wang, K. Ding. *Angew. Chem. Int. Ed.* **2017**, *56*, 1116–1119. (e) X. Wang, X. Wang, Z. Han, Z. Wang, K. Ding. *Org. Chem. Front.* **2017**, *4*, 271–276.
16. B. M. Trost, H. Gholami, D. Zell. *J. Am. Chem. Soc.* **2019**, *141*, 11446–11451.
17. C.-X. Zhuo, Y. Zhou, S.-L. You. *J. Am. Chem. Soc.* **2014**, *136*, 6590–6593.
18. C. Zheng, C.-X. Zhuo, S.-L. You. *J. Am. Chem. Soc.* **2014**, *136*, 16251–16259.
19. N. J. Adamson, K. C. E. Wilbur, S. J. Malcolmson. *J. Am. Chem. Soc.* **2018**, *140*, 2761–2764.
20. S. Park, N. J. Adamson, S. J. Malcolmson. *Chem. Sci.* **2019**, *10*, 5176–5182.
21. K. Yao, Q. Yuan, X. Qu, Y. Liu, D. Liu, W. Zhang. *Chem. Sci.* **2019**, *10*, 1767–1772.
22. S.-L. You, X.-Z. Zhu, Y.-M. Luo, X.-L. Hou, L.-X. Dai. *J. Am. Chem. Soc.* **2001**, *123*, 7471–7472.
23. G. Pupo, R. Properzi, B. List. *Angew. Chem. Int. Ed.* **2016**, *55*, 6099–6102.
24. (a) W.-F. Lian, C.-C. Wang, H.-P. Kang, H.-L. Li, J. Feng, S. Liu, Z.-W. Zhang. *Tetrahedron Lett.* **2017**, *58*, 1399–1402. (b) T.-G. Chen, P. Fang, X.-L. Hou, L.-X. Dai. *Synthesis* **2015**, *47*, 134–140.
25. C.-X. Zhou, S.-L. You. *Angew. Chem. Int. Ed.* **2013**, *52*, 10056–10059.
26. (a) X. Zhao, D. Liu, F. Xie, W. Zhang. *Tetrahedron* **2009**, *65*, 512–517. (b) X. Zhao, D. Liu, H. Guo, Y. Liu, W. Zhang. *J. Am. Chem. Soc.* **2011**, *133*, 19354–19357.c X. Zhao, D. Liu, F. Xie, Y. Liu, W. Zhang. *Org. Biomol. Chem.* **2011**, *9*, 1871–1875. (d) X. Huo, G. Yang, D. Liu, Y. Liu, I. D. Gridnev, W. Zhang. *Angew. Chem. Int. Ed.* **2014**, *53*, 6776–6780. (e) X. Huo, M. Quan, G. Yang, X. Zhao, D. Liu, Y. Liu, W. Zhang. *Org. Lett.* **2014**, *16*, 1570–1573.
27. G. Jiang, B. List. *Angew. Chem. Int. Ed.* **2011**, *50*, 9471–9474.
28. Y. Wang, J. Chai, C. You, J. Zhang, X. Mi, L. Zhang, S. Lou. *J. Am. Chem. Soc.* **2020**, *142*, 3184–3195.
29. R. A. Craig, J. L. Roizen, R. C. Smith, A. C. Jones, B. M. Stoltz. *Org. Lett.* **2012**, *14*, 5716–5719.
30. F. Nahra, Y. Macé, A. Boreux, F. Billard, O. Riant. *Chem. Eur. J.* **2014**, *20*, 10970–10981.
31. I. Alvarado-Beltra, E. Maerten, R. A. Toscano, J. G. Lopez-Cortes, A. Baceiredo, C. Alvarez-Toledano. *Tetrahedron Asymmetry* **2015**, *26*, 802–809.
32. (a) X.-H. Li, S.-L. Wan, D. Chen, Q.-R. Liu, C.-H. Ding, P. Fang, X.-L. Hou. *Synthesis* **2016**, *48*, 1568–1572. (b) R. Visse, M.-A. Mollemann, M. Braun. *Eur. J. Org. Chem.* **2019**, *2019*, 4604–4608.
33. J. Liu, S. Mishra, A. Aponick. *J. Am. Chem. Soc.* **2018**, *140*, 16152–16158.
34. A. Saito, N. Kumagai, M. Shibasaki. *Angew. Chem. Int. Ed.* **2017**. *56*, 5551–5555.
35. X. Huo, R. He, J. Fu, J. Zhang, G. Yang, W. Zhang. *J. Am. Chem. Soc.* **2017**, *139*, 9819–9822.
36. L. Wei, S.-M. Xu, Q. Zhu, C. Che, C.-J. Wang. *Angew. Chem. Int. Ed.* **2017**, *56*, 12312–12316.
37. Q. Zhang, H. Yu, L. Shen, T. Tang, D. Dong, W. Chai, W. Zi. *J. Am. Chem. Soc.* **2019**, *141*, 14554–14559.
38. R. He, X. Huo, L. Zhao, F. Wang, L. Jiang, J. Liao, W. Zhang. *J. Am. Chem. Soc.* **2020**, *142*, 8097–8103.
39. (a) H.-H. Zhang, J.-J. Zhao, S. Yu. *J. Am Chem. Soc.* **2018**, *140*, 16914–16919.For a related amination see: (b) H.-H. Zhang, J.-J. Zhao, S. Yu. *ACS Catal.* **2020**, *10*, 4710–4716.
40. B. M. Trost, J. E. Schultz, T. Chang, M. R. Maduabum *J. Am. Chem. Soc.* **2019**, *141*, 9521–9526.
41. A. Misale, S. Niyomchon, M. Luparia, N. Maulide. *Angew. Chem. Int. Ed.* **2014**, *53*, 7068–7073.
42. J. Mateos, N. Fuentas-Vara, L Fra, E. Rivera-Chao, N. Vázquez-Galiñanes, A. Chaves-Pouso, M. Fañanás-Mastral. *Organometallics* **2020**, *39*, 740–745.
43. (a) F. Giacomina, D. Riat, A. Alexakis. *Org. Lett.* **2010**, *12*, 1156–1159. (b) J. F. Teichert, S. Zhang, A. W. van Zijl, J. W. Slaa, A. J. Minnaard, B. L. Feringa. *Org. Lett.* **2010**, *12*, 4658–4660. (c) B. Mao, K. Geurts, M. Fañanas-Mastral, A. W. van Zijl, S. P. Fletcher, A. J. Minnaard, B. L. Feringa. *Org. Lett.* **2011**, *13*, 948–951. (d) Giacomina, F.; Alexakis, A. *Eur. J. Org. Chem.* **2013**, 6710–6721. (e) W. Xiong, G. Xu, X. Yu, W. Tang. *Organometallics.* **2019**, *38*, 4003–4013.
44. B. M. Trost, D. A. Thaisrivongs, J. Hartwig. *J. Am. Chem. Soc.* **2011**, *133*, 12439–12441.
45. J. Mao, J. Zhang, H. Jiang, A. Bellomo, M. Zhang, Z. Gao, S. D. Dreher, P. J. Walsh. *Angew. Chem. Int. Ed.* **2016**, *55*, 2526–2530.
46. K. Yao, D. Liu, Q. Yuan, T. Imamoto, Y. Liu, W. Zhang. *Org. Lett.* **2016**, *18*, 6296–6299.
47. M. Braun, P. Meletis, R. Visse. *Adv. Synth. Catal.* **2011**, *353*, 3380–3384.
48. Fujita, T.; Yamamoto, T.; Morita, Y.; Chen, H.; Shimizu, Y.; Kanai, M. *J. Am. Chem. Soc.* **2018**, *140*, 5899–5903.
49. B. M. Trost, J. Xu, T. Schmidt. *J. Am. Chem. Soc.* **2009**, *131*, 18343–18357.
50. For mechanistic and computational studies see: (a) D. C. Behenna, J. T. Mohr, N. H. Sherdan, S. C. Marinescu, A. M. Harned, K. Tani, M. Seto, S. Ma, Z. Novák, M. R. Krout, R. M. McFadden, J. L. Roizen, J. A. Enquist, D. E. White, S. R. Levine, K. V. Petrova, A. Iwashita, S. C. Virgil, B. M. Stoltz. *Chem. Eur. J.* **2011**, *17*, 14199–14223. (b) A. Q. Cusumano, W. A. Goddard, III, B. M. Stoltz. *J. Am. Chem. Soc.* **2020**, *142*, 19033–19039. (c) A. Q. Cusumano, B. M. Stoltz, W. A. Goddard, III. *J. Am. Chem. Soc.* **2020**, *142*, 13917–13933. (d) J. A. Keith, D. C. Behenna, N. Sherden, J. T. Mohr, S. Ma, S. C. Marinescu, R. J. Nielsen, J. Oxgaard, B. M. Stoltz, W. A. Goddard, III. *J. Am. Chem. Soc.* **2012**, *134*, 19050–19060. (e) J. A. Keith, D. C. Behenna, N. Sherden, J. T. Mohr, S. Ma, S. C. Marinescu, R. J. Nielsen, J. Oxgaard, B. M. Stoltz, W. A. Goddard, III. *J. Am. Chem. Soc.* **2007**, *129*, 11876–11877. (f) K. E. McPherson, M. P. Croatt, A. T. Morehead, Jr., A. L. Sargent. *Organometallics* **2018**, *37*, 3791–3802.

51. For a recent review, see: J. James, M. Jackson, P. J. Guiry. *Adv. Synth. Catal.* **2019**, *361*, 3016–3049.
52. C. M. Reeves, C. Eidamshaus, J. Kim, B. M. Stoltz. *Angew. Chem. Int. Ed.* **2013**, *52*, 6718–6721.
53. R. A. Craig, S. A. Loskot, J. T. Mohr, D. C. Behenna, A. M. Harned, B. M. Stoltz. *Org. Lett.* **2015**, *17* 5160–5163.
54. D. C. Behenna, Y. Liu, T. Yurino, J. Kim, D. E. White, S. C. Virgil, B. M. Stoltz. *Nat. Chem.* **2012**, *4*, 130–133.
55. Y. Kita, Y. Numajiri, N. Okamoto, B. M. Stoltz. *Tetrahedron* **2015**, *71*, 6349–6354.
56. K. M. Korch, C. Eidamhaus, D. C. Behenna, S. Nam, D. Horne, B. M. Stoltz. *Angew. Chem. Int. Ed.* **2015**, *54*, 179–183.
57. A. W. Sun, S. N. Hess, B. M. Stoltz. *Chem. Sci.* **2019**, *10*, 788–792.
58. Z. P. Sercel, A. W. Sun, B. M. Stoltz. *Org. Lett.* **2019**, *21*, 9158–9161.
59. Y. Numajiri, G. Jiménez-Osés, B. Wang, K. N. Houk, B. M. Stoltz. *Org. Lett.* **2015**, *17*, 1082–1085.
60. E. J. Alexy, S. C. Virgil, M. D. Bartberger, B. M. Stoltz. *Org. Lett.* **2017**, *19*, 5007–5009.
61. Y. Lu, E. L. Goldstein, B. M. Stoltz. *Org. Lett.* **2018**, *20*, 5657–5660.
62. S. E. Shockley, J. C. Hethcox, B. M. Stoltz. *Tetrahedron Lett.* **2017**, *58*, 3341–3343.
63. M. M. Yamano, R. R. Knapp, A. Ngamnithiporn, M. Ramirez, K. N. Houk, B. M. Stoltz, N. K. Garg. *Angew. Chem. Int. Ed.* **2019**, *58*, 5653–5657.
64. A. Ngamnithiporn, T. Iwayama, M. D. Bartberger, B. M. Stoltz. *Chem. Sci.* **2020**, *11*, 11068–11071.
65. D. C. Duquette, A. Q. Cusumano, L. Lefoulon, J. T. Moore, B. M. Stoltz. *Org. Lett.* **2020**, *22*, 4966–4969.
66. Y. Numajiri, B. P. Pritchett, K. Chiyoda, B. M. Stoltz. *J. Am. Chem. Soc.* **2015**, *137*, 1040–1043.
67. M. Serra, E. Bernardi, G. Marrubini, E. De Lorenzi, L. Colombo. *Eur. J. Org. Chem.* **2019**, *2019*, 732–741.
68. R. Akula, R. Doran, P. J. Guiry, *Chem. Eur. J.* **2016**, *22*, 9938–9942.
69. V. Franckevičius, J. D. Cuthbertson, M. Pickworth, D. S. Pugh, R. J. K. Taylor. *Org. Lett.* **2011**, *13*, 4264–4267.
70. M. Jackson, C. Q. O'Broin, H. Müller-Bunz, P. J. Guiry. *Org. Biomol. Chem.* **2017**, *15*, 8166–8178.
71. M. V. Vita, P. Caramenti, J. Waser. *Org. Lett.* **2015**, *17*, 5832–5835.
72. M. V. Vita, P. Mieville, J. Waser. *Org. Lett.* **2014**, *16*, 5768–5771.
73. B. M. Trost, A. Nagaraju, F. Wang, Z. Zuo, J. Xu, K. L. Hull. *Org. Lett.* **2019**, *21*, 1784–1788.
74. J. Fournier, O. Lozano, C. Menozzi, S. Arseniyadis, J. Cossy. *Angew. Chem. Int. Ed.* **2013**, *52*, 1257–1261.
75. B. M. Trost, J. E. Schultz, Y. Bai. *Angew. Chem. Int. Ed.* **2019**, *58*, 11820–11825.
76. H. Kondo, M. Maeno, K. Hirano, N. Shibata. *Chem. Commun.* **2018**, *54*, 5522–5525.
77. M. Nascimento de Oliveira, J. Fournier, S. Arseniyadis, J. Cossy. *Org. Lett.* **2017**, *19*, 14–17.
78. J. James, P. J. Guiry. *ACS Catal.* **2017**, *7*, 1397–1402.
79. H. Kondo, M. Maeno, K. Sasaki, M. Guo, M. Hashimoto, M. Shiro, N. Shibata. *Org. Lett.* **2018**, *20*, 7044–7048.
80. S. Wang, X. Qian, Y. Chang, J. Sun, X. Xing, W. F. Ballard, J. J. Chruma. *J. Org. Chem.* **2018**, *83*, 4054–4069.
81. J. S. Yu, H. Noda, M. Shibasaki. *Angew. Chem. Int. Ed.* **2018**, *57*, 818–822.
82. C. Q. O'Broin, P. J. Guiry. *Org. Lett.* **2019**, *21*, 5402–5406.
83. J. Streff, D. E. White, S. C. Virgil, B. M. Stoltz. *Nat. Chem.* **2010**, *2*, 192–196.
84. K. Inanaga, M. Wollenburg, S. Bachman, N. J Hafeman, B. M. Stoltz. *Chem. Sci.* **2020**, *11*, 7390–7395.
85. For a recent review on acyclic quaternary center stereocontrol via transition metal catalysis see: J. Feng, M. Holmes, M. J. Kriche. *Chem. Rev.* **2017**, *117*, 12564–12580.
86. B. M. Trost, K. Lehr, D. J. Michaelis, J. Xu, A. K. Buckl. *J. Am. Chem. Soc.* **2010**, *132*, 8915–8917.
87. K. Zhang, Q. Peng, X.-L. Hou, Y.-D. Wu. *Angew. Chem. Int. Ed.* **2008**, *47*, 1741–1744.
88. J.-P. Chen, C.-H. Ding, W. Liu, X.-L. Hou, L.-X. Dai. *J. Am. Chem. Soc.* **2010**, *132*, 15493–15495.
89. B. M. Trost, D. J. Michaelis, J. Charpentier, J. Xu. *Angew. Chem. Int. Ed.* **2012**, *51*, 204–208.
90. Y. Ariyarathna, J. A. Tunge. *Org. Biomol. Chem.* **2014**, *12*, 8386–8389.
91. P. Starkov, J. T. Moore, D. C. Duquette, B. M. Stoltz, I. Marek. *J. Am. Chem. Soc.* **2017**, *139*, 9615–9620.
92. (a) K. A. Mack, A. McClory, H. Zhang, F. Gosselin, D. B. Collum. *J. Am. Chem. Soc.* **2017**, *139*, 12182–12189. (b) B. X. Li, D. N. Le, K. A. Mack, A. McClory, N. K. Lim, T. Cravillion, S. Savage, C. Han, D. B. Collum, H. Zhang, F. J. Gosselin. *J. Am. Chem. Soc.* **2017**, *139*, 10777–10783.
93. E. J. Alexy, H. Zhang, B. M. Stoltz. *J. Am. Chem. Soc.* **2018**, *140*, 10109–10112.
94. B. M. Trost, J. Xu. *J. Am. Chem. Soc.* **2005**, *127*, 17180–17181.
95. A. G. Doyle, E. N. Jacobsen. *Angew. Chem. Int. Ed.* **2007**, *46*, 3701–3705.
96. E. J. Alexy, T. J. Fulton, H. Zhang, B. M. Stoltz. *Chem. Sci.* **2019**, *10*, 5996–600.
97. R. Lavernhe, E. J. Alexy, H. Zhang, B. M. Stoltz. *Adv. Synth. Catal.* **2020**, *362*, 344–347.
98. R. Lavernhe, E. J. Alexy, H. Zhang, B. M. Stoltz. *Org. Lett.* **2020**, *22*, 4272–4275.
99. S. Lin, C.-X. Song, G.-X. Cai, W.-H. Wang, Z.-J. Shi. *J. Am. Chem. Soc.* **2008**, *130*, 12901–12903.
100. A. J. Young, M. C. White. *J. Am. Chem. Soc.* **2008**, *130*, 14090–14091.
101. P.-S. Wang, H.-C. Lin, Y.-J. Zhai, Z.-Y. Han, L.-Z. Gong. *Angew. Chem. Int. Ed.* **2014**, *53*, 12218–12221.
102. H.-C. Lin, P.-S. Wang, Z.-L. Tao, Y.-G. Chen, Z.-Y. Han, L.-Z. Gong. *J. Am. Chem. Soc.* **2016**, *138*, 14354–14351.
103. W. Liu, S. Z. Ali, S. E. Ammann, M. C. White. *J. Am. Chem. Soc.* **2018**, *140*, 10658–10662.
104. L.-F. Fan, P.-S. Wang, L.-Z. Gong. *Org. Lett.* **2019**, *21*, 6720–6725.

105. G.-Y. Ran, X.-X. Yang, J.-F. Yue, W. Du, Y.-C. Chen. *Angew. Chem. Int. Ed.* **2019**, *58*, 9210–9214.
106. H.-C. Lin, P.-P. Xie, Z.-Y. Dai, S.-Q. Zhang, P.-S. Wang, Y.-G. Chen, T.-C. Wang, X. Hong, L.-Z. Gong. *J. Am. Chem. Soc.* **2019**, *141*, 5824–5834.
107. T.-C. Wang, L.-F. Fan, Y. Shen, P.-S. Wang, L.-Z. Gong. *J. Am. Chem. Soc.* **2019**, *141*, 10616–10620.
108. L.-F. Fan, S.-W. Lo, S.-S. Chen, T.-C. Wang, P.-S. Wang, L.-Z. Gong. *Angew. Chem. Int. Ed.* **2019**, *58*, 16806–16810.
109. For a review see: Z. Huijuna, G. Qing, S.-L. You. *Chin. J. Org. Chem.* **2019**, *39*, 15–27.
110. S.-C. Sha, H. Jiang, J. Mao; A. Bellomo; S. A. Jeong, P. J. Walsh. *Angew. Chem. Int. Ed.* **2016**, *55*, 1070–1074.
111. Y. Kita, R. D. Kavthe, H. Oda; K. Mashida. *Angew. Chem. Int. Ed.* **2016**, *55*, 1098–1101.
112. A. Ngamnithiporn, C. I. Jette, S. Bachman, S. C. Virgil, B. M. Stoltz. *Chem. Sci.* **2018**, *9*, 2547–2551.
113. H. Nagae, J. Xia; E. Kirillov, K. Higashida, K. Shoji, V. Boiteau,W. Zhang, J.-F. Carpentier, K. Mashima. *ACS Catal.* **2020**, *10*, 5828–5839.
114. J. Wang, P. Wang, L. Wang, D. Li, K. Wang, Y. Wang, H. Zhu, D. Yang, R. Wang. *Org. Lett.* **2017**, *19*, 4826–4829.
115. J. D. Shields, D. T. Ahneman, T. J. A. Graham, A. G. Doyle. *Org. Lett.* **2014**, *16*, 142–145.
116. (a) J. P. Lutz, S. T. Chau, A. G. Doyle. *Chem. Sci.* **2016**, *7*, 4105–4109. (b) S. T. Chau, J. P. Lutz, K. Wu, A. G. Doyle. *Angew. Chem. Int. Ed.* **2013**, *52*, 9153–9156.
117. E. Benedetto, M. Keita, M. Tredwell, C. Hollingworth, J. M. Brown, V. Gouverneur. *Organometallics* **2012**, *31*, 1408–1416.
118. C. Moberg. Scott E. Denmark et al. Molybdenum-catalyzed asymmetric allylic alkylations. In *Organic Reactions*. Hoboken, NJ: John Wiley & Sons, Inc., **2014**; pp. 1–74. https://doi.org/10.1002/0471264180.or084.01.
119. G. C. Lloyd-Jones, S. W. Krska, D. L. Huges, L. Gouriou, V. D. Bonnet, K. Jack, Y. Sun, R. A. Reamer. *J. Am. Chem. Soc.* **2004**, *126*, 702–703.
120. B. M. Trost. J. R. Miller. C. M. Hoffman, Jr. *J. Am. Chem. Soc.* **2011**, *133*, 8165–8167.
121. C. Moberg. *Top. Organomet. Chem.* **2012**, *38*, 209–234.
122. (a) B. M. Trost, M.-H. Hung. *J. Am. Chem. Soc.* **1983**, *105*, 7757–7759. (b) G. C. Lloyd-Jones, A. Pfaltz. *Angew. Chem.* **1995**, *34*, 462–464. (c) F. Glorius, M. Neuburger, A. Pfaltz. *Helv. Chim. Acta.* **2001**, *84*, 3178–3196. (d) J. Lehmann, G. C. Lloyd-Jones. *Tetrahedron* **1995**, *51*, 8863–8874.
123. Y. Xu, M. Salman, S. Khan, J. Zhang, A. Khan. *J. Org. Chem.* **2020**, *85*, 11501–11510.
124. This complex has been previously employed in the asymmetric allylic alkylation to generate C–O and C–N bonds. For C–O bond forming reactions, see: (a) K. Onitsuka, H. Okuda, H. Sasai. *Angew. Chem. Int. Ed.* **2008**, *47*, 1454–1457. (b) N. Kanbayashi, K. Onitsuka. *J. Am. Chem. Soc.* **2010**, *132*, 1206–1207. (c) N. Kanbayashi, K. Onitsuka. *Angew. Chem. Int. Ed.* **2011**, *50*, 5197–5199. (d) K. Takii, N. Kanbayashi, K. Onitsuka. *Chem. Commun.* **2012**, *48*, 3872–3874.For C–N bond forming reactions, see: e N. Kanbayashi, K. Takenaka, T. Okamura, K. Onitsuka. *Angew. Chem. Int. Ed.* **2013**, *52*, 4897–4901.f N. Kanbayashi, T.-A. Okamura, K. Onitsuka. *Macromolecules* **2014**, *47*, 4178–4185.
125. N. Kanbayashi, A. Yamazawa, K. Takii, T. Okamura, K. Onitsuka. *Adv. Synth. Catal.* **2016**, *358*, 555–560.
126. For reviews, see: For selected reviews, see: (a) J.-M. Begouin, J. Klein, D. Weickmann, B. Plietker. *Top. Organomet. Chem.* **2011**, *38*, 269–320. (b) S. Oliver, P. A. Evans. *Synthesis* **2013**, *45*, 3179–3198. (c) P. Koschker, B. Breit. *Acc. Chem. Res.* **2016**, *49*, 1524–1536. (d) A. M. Haydl, B. Breit, T. Liang, M. J. Krische. Alkynes as electrophilic or nucleophilic allylmetal precursors in transition-metal catalysis. *Angew. Chem. Int. Ed.* **2017**, *56*, 11312–11325. (e) B. W. H. Turnbull, P. A. Evans. *J. Org. Chem.* **2018**, *83*, 11463–11479.
127. M. Sidera, S. P. Fletcher. *Nat. Chem.* **2015**, *7*, 935–939.
128. P. Schäffer, T. Palacin, M. Sidera, S. P. Fletcher. *Nat. Commun.* **2017**, *8*, 15762–15769.
129. B. W. H. Turnbull, P. A. Evans. *J. Am. Chem. Soc.* **2015**, *137*, 6156–6159.
130. T. B. Wright, P. A. Evans. *J. Am. Chem. Soc.* **2016**, *138*, 15303–15306.
131. T. B. Wright, B. W. H. Turnbull, P. A. Evans. *Angew. Chem. Int. Ed.* **2019**, *58*, 9886–9890.
132. S.-B. Tang, X. Zhang, H.-F. Tu, S.-L. You. *J. Am. Chem. Soc.* **2018**, *140*, 7737–7742.
133. S.-B. Tang, H.-F. Tu, X. Zhang, S.-L. You. *Org. Lett.* **2019**, *21*, 6130–6134.
134. S. Shekhar, B. Trantow, A. Leitner, J. F. Hartwig. *J. Am. Chem. Soc.* **2006**, *128*, 11770–11771.
135. (a) J. F. Hartwig, L. M. Stanley. *Acc. Chem. Res.* **2010**, *43*, 1461–1475. (b) J. C. Hethcox, S. E. Shockley, B. M. Stoltz. *ACS Catal.* **2016**, *6*, 6207–6213. (c) S. E. Shockley, J. C. Hethcox, B. M. Stoltz. *Synlett* **2018**, *29*, 2481–2492. (d) J. Qu, G. Helmchen. *Acc. Chem. Res.* **2017**, *50*, 2539–2555. (e) Q. Cheng, H.-F. Tu, C. Zheng, J.-P. Qu, G. Helmchen, S.-L. You. *Chem. Rev.* **2019**, *119*, 1855–1969. (f) S. L. Rössler, D. A. Petrone, E. M. Carreira. *Acc. Chem. Res.* **2019**, *52*, 2657–2672.
136. Defieber, C.; Ariger, M. A.; Moriel, P.; Carreira, E. M. *Angew. Chem. Int. Ed.* **2007**, *46*, 3139–3143.
137. Janssen, J. P.; Helmchen, G. *Tetrahedron Lett.* **1997**, *38*, 8025–8026.
138. T. W. Butcher, J. F. Hartwig. *Angew. Chem. Int. Ed.* **2018**, *57*, 13125–13129.
139. J. C. Hethcox, S.E. Shockley, B. M. Stoltz. *Org. Lett.* **2017**, *19*, 1527–1529.
140. S. E. Shockley, J. C. Hethcox, B. M. Stoltz. *Angew. Chem. Int. Ed.* **2017**, *56*, 11545–11548.
141. J. C. Hethcox, S. E. Shockley, B. M. Stoltz. *Angew. Chem. Int. Ed.* **2018**, *57*, 8664– 8667.
142. W. Chen, J. F. Hartwig. *J. Am. Chem. Soc.* **2013**, *135*, 2068–2071.

143. W. Chen, J. F. Hartwig. *J. Am. Chem. Soc.* **2014**, *136*, 377–382.
144. W.-B. Liu, C. M. Reeves, S. C. Virgil, B. M. Stoltz. *J. Am. Chem. Soc.* **2013**. *135*, 10626–10629.
145. W.-B. Liu, C. M Reeves, B. M. Stoltz. *J. Am. Chem. Soc.* **2013**, *135*, 17298–17301.
146. W.-B. Liu, N. Okamoto, E. J. Alexy, A. Y. Hong, K. Tran, B. M. Stoltz. *J. Am. Chem. Soc.* **2016**, *138*, 5234–5237.
147. J. C. Hethcox, S. E. Shockley, B. M. Stoltz. *Angew. Chem. Int. Ed.* **2016**, *55*, 16092–16095.
148. S. Krautwald, D. Sarlah, M. A. Schafroth, E. M. Carreira. *Science* **2013**, *340*, 1065–1068.
149. X. Jiang, P. Boehm, J. F. Hartwig. *J. Am. Chem. Soc.* **2018**, *140*, 1239–1242.
150. Z. T. He, X. Jiang, J. F. Hartwig. *J. Am. Chem. Soc.* **2019**, *141*, 13066–13073.
151. A related single catalyst report by You and coworkers was reported shortly after, see: X.-J. Liu, S. Jin, W.-Y. Zhang, Q.-Q. Liu, C. Zhang, S.-L. You. *Angew. Chem. Int. Ed.* **2020**, *59*, 2039–2043.
152. L. Wei, Q. Zhu, S.-M. Xu, X. Chang, C.-J. Wang. *J. Am. Chem. Soc.* **2018**, *140*, 1508–1513.
153. W. Chen, J. F. Hartwig. *J. Am. Chem. Soc.* **2012**, *134*, 15249–15252.
154. M. Chen, J. F. Hartwig. *Angew. Chem. Int. Ed.* **2014**, *53*, 8691–8695.
155. M. Chen, J. F. Hartwig. *J. Am. Chem. Soc.* **2015**, *137*, 13972–13979.
156. M. Chen, J. F. Hartwig. *Angew. Chem. Int. Ed.* **2016**, *55*, 11651–11655.
157. X. Jiang, J. F. Hartwig. *Angew. Chem. Int. Ed.* **2017**, *56*, 8887–8891.
158. X. Liang, K. Wei, Y.-R. Yang. *Chem. Commun.* **2015**, *51*, 17471–17474.
159. W. Chen, M. Chen, J. F. Hartwig. *J. Am. Chem. Soc.* **2014**, *136*, 15825–15828.
160. X. Jiang, W. Chen, J. F. Hartwig. *J. Am. Chem. Soc.* **2016**, *55*, 5819–5823.
161. X. Huo, R. He, X. Zhang, W. Zhang. *J. Am. Chem. Soc.* **2016**, *138*, 11093–11096.
162. R. He, P. Liu, X. Huo, W. Zhang. *Org. Lett.* **2017**, *19*, 5513–5516.
163. X. Jiang, J. J. Beiger, J. F. Hartwig. *J. Am. Chem. Soc.* **2017**, *139*, 87–90.
164. Y. Sempere, E. M Carreira. *Angew. Chem. Int. Ed.* **2018**, *57*, 7654–7658.
165. B. Bhaskararao, R. Sunoj. *J. Am. Chem. Soc.* **2015**, *137*, 15712–15722.
166. S. Krautwald, M. A. Schafroth, D. Sarlah, E. M. Carreira. *J. Am. Chem. Soc.* **2014**, *136*, 3020–3023.
167. T. Sandmeier, S. Krautwald, H. F. Zipfel, E. M. Carreira. *Angew. Chem. Int. Ed.* **2015**, *54*, 14363–14367.
168. M. A. Schafroth, G. Zuccarello, S. Krautwald, D. Sarlah, E. M. Carreira. *Angew. Chem. Int. Ed.* **2014**, *53*, 13898–13901.
169. L. Næsborg, K. S. Halskov, F. Tur, S. M. N. Mønsted, K. A. Jørgensen. *Angew. Chem. Int. Ed.* **2015**, *54*, 10193–10197.
170. T. Sandmeier, S. Krautwald, E. M. Carreira. *Angew. Chem. Int. Ed.* **2017**, *56*, 11515–11519.
171. (a) Q.-F. Wu, H. He, W.-B. Liu, S.-L. You. *J. Am. Chem. Soc* **2010**, *132*, 11418–11419. (b) Q.-F. Wu, C. Zheng, S.-L. You. *Angew. Chem. Int. Ed.* **2012**, *51*, 1680–1683. (c) C.-X. Zhuo, Q.-F. Wu, Q. Zhao, Q.-L. Xu, S.-L. You. *J. Am. Chem. Soc.* **2013**, *135*, 8169–8172. (d) Q.-L. Xu, C.-X. Zhuo, L.-X. Dai, S.-L. You. *Org. Lett.* **2013**, *15*, 5909–5911. (e) X. Zhang, L. Han, S.-L. You. *Chem. Sci.* **2014**, *5*, 1059–1063. (f) C.-X. Zhuo, Y. Zhou, Q. Cheng, L. Huang, S.-L. You. *Angew. Chem. Int. Ed.* **2015**, *54*, 14146–14149. (g) X. Zhang, W.-B. Liu, H.-F. Tu, S.-L. You. *Chem. Sci.* **2015**, *6*, 4525–4529. (h) Q.-F. Wu, C. Zheng, C.-X. Zhuo, S.-L. You. *Chem. Sci.* **2016**, *7*, 4453–4459. (i) L. Huang, L.-X. Dai, S.-L. You. *J. Am. Chem. Soc.* **2016**, *138*, 5793–5796. (j) Y. Wang, C. Zhen, S.-L. You. *Angew. Chem. Int. Ed.* **2017**, *56*, 15093–15097.
172. (a) C.-X. Zhuo, W.-B. Liu, Q.-F. Wu, S.-L. You. *Chem. Sci.* **2012**, *3*, 205–208. (b) C.-X. Zhuo, Q. Cheng, W.-B. Liu, Q. Zhao, S.-L. You. *Angew. Chem. Int. Ed.* **2015**, *54*, 8475–8479. (c) L. Huang, Y. Cai, C. Zheng, L.-X. Dai, S.-L. You. *Angew. Chem. Int. Ed.* **2017**, *56*, 10545–10548.
173. (a) Q.-F. Wu, W.-B. Liu, C.-X. Zhuo, Z.-Q. Rong, K.-Y. Ye, S.-L. You. *Angew. Chem. Int. Ed.* **2011**, *50*, 4455–4458. (b) T. Nemoto, Y. Ishige, M. Yoshida, Y. Kohno, M. Kanematsu, Y. Hamada. *Org. Lett.* **2010**, *12*, 5020–5023. (c) M. Yoshida, T. Nemoto, Z. Zhao, Y. Ishige, Y. Hamada. *Tetrahedron Asymmetry* **2012**, *23*, 859–866. (d) Q.-L. Xu, L.-X. Dai, S.-L. You. *Org. Lett.* **2012**, *14*, 2579–2581.
174. (a) Q. Cheng, Y. Wang, S.-L. You. *Angew. Chem. Int. Ed.* **2016**, *55*, 3496–3499. (b) H. F. Tu, C. Zheng, R.-Q. Xu, X.-J. Liu, S.-L. You. *Angew. Chem. Int. Ed.* **2017**, *56*, 3237–3241. (c) D. Chen, Q. L. Chen, P.-P. Yan, X.-F. Zeng, G.-F. Zhong. *Angew. Chem. Int. Ed.* **2017**, *56*, 3242–3246.
175. Q.-L. Xu, C.-X. Zhuo, L.-X. Dai, S.-L. You. *Org. Lett.* **2013**, *15*, 5909–5911.
176. Z.-L. Zhao, Q. Gu, X.-Y. Wu, S.-L. You. *Chin. Chem. Lett.* **2016**, *27*, 619–622.
177. Z.-L. Zhao, Q. Gu, X.-Y. Wu, S.-L. You. *Chem. Asian J.* **2017**, *12*, 2680–2683.
178. Y. Wang, W.-Y. Zhang, J.-H. Xie, Z.-L. Yu, J.-H. Tan, C. Zheng, X.-L. Hou, S.-L. You. *J. Am. Chem. Soc.* **2020**, *142*, 19354–19359.
179. (a) H. He, W.-B. Liu, L.-X. Dai, S.-L. You. *J. Am. Chem. Soc.* **2009**, *131*, 8346–8347. (b) K.-Y. Ye, H. He, W.-B. Liu, L.-X. Dai, G. Helmchen, S.-L. You. *J. Am. Chem. Soc.* **2011**, *133*, 19006–19014. (c) H. He, W.-B. Liu, L.-X. Dai, S.-L. You. *Angew. Chem. Int. Ed.* **2010**, *49*, 1496–1499. (d) K.-Y. Ye, L.-X. Dai, S.-L. You. *Asian J. Org. Chem.* **2013**, *2*, 244–249.
180. J. Y. Hamilton, D. Sarlah, E. M. Carreira. *J. Am. Chem. Soc*, **2014**, *136*, 3006–3009.
181. M. A. Schafroth, D. Sarlah, S. Krautwald, E. M. Carreira. *J. Am. Chem. Soc.* **2012**, *134*, 20276–20278.
182. O. F. Jeker, A. G. Kravina, E. M. Carreira. *J. Am. Chem. Soc.* **2012**, *134*, 20276–20278.
183. J. Y. Hamilton, D. Sarlah, E. M. Carreira. *Angew. Chem. Int. Ed.* **2015**, *54*, 7644–7647.

184. D. A. Petrone, M. Isomura, I. Franzoni, S. L. Rössler, E. M. Carreira. *J. Am. Chem. Soc.* **2018**, *140*, 4697–4704.
185. X.-J. Liu, S.-L. You. *J. Am. Chem. Soc.* **2014**, *136*, 3006–3009.
186. M. Zhan, R.-Z. Li, Z.-D. Mou, C.-G. Cao, J. Liu, Y.-W. Chen, D. Niu. *ACS Catal.* **2016**, *6*, 3381–3386.
187. Y. Lee, J. Park, S. H. Cho. *Angew. Chem. Int. Ed.* **2018**, *57*, 12930–12934.
188. J. Liu, C.-G. Cao, H.-B. Sun, X. Zhang, D. Niu. *J. Am. Chem. Soc.* **2016**, *138*, 13103–13106.
189. Y.-L. Su, Y.-H. Li, Y.-G. Chen, Z.-Y. Han. *Chem. Commun.* **2017**, *53*, 1985–1988.
190. M. van Klaveren, E. S. M. Persson, A. del Villar, D. M. Grove, J.-E. Bäckvall, G. van Koten. *Tetrahedron Lett.* **1995**, *36*, 3059–3062.
191. N. C. van der Molen, T. D. Tiemersma-Wegman, M. Fañanás-Mastral, B. L Feringa. *J. Org. Chem.* **2015**, *80*, 4981–4984.
192. Cu-catalyzed allylic alkylation of *ortho*-substituted cinnamyl bromides with Grignard reagents was further applied to the synthesis of chromenes and tetrahdyroquinolines via sequential asymmetric allylic alkylation/intramolecular Heck reactions: V. Hornillos, A. W. van Zijl, B. L. Feringa. *Chem. Commun.* **2012**, *48*, 3712–3714.
193. Y. Huang, M. Fañanás-Mastral, A. J. Minnaard, B. L. Feringa. *Chem. Commun.* **2013**, *49*, 3309–3311.
194. T. den Hartog, B. Marciá, A. Minnaard, B. L. Feringa. *Adv. Synth. Catal.* **2010**, *352*, 999–1013.
195. M. Magrez, Y. Le Guen, O. Baslé, C. Crévisy, M. Mauduit. *Chem. Eur. J.* **2013**, *19*, 1199–1203.
196. V. Hornillos, M. Pérez, M. Fañanás-Mastral, B. L. Feringa. *Chem. Eur. J.* **2013**, *19*, 5432–5441.
197. H. Li, A. Alexakis. *Angew. Chem. Int. Ed.* **2012**, *51*, 1055–1058.
198. (a) F. Giacomina, D. Riat, A. Alexakis. *Org. Lett.* **2010**, *12*, 1156–1159. (b) J. F. Teichert, S. Zhang, A. W. van Zijl, J. W. Slaa, A. J. Minnaard, B. L. Feringa. *Org. Lett.* **2010**, *12*, 4658–4660. (c) B. Mao, K. Geurts, M. Fañanas-Mastral, A. W. van Zijl, S. P. Fletcher, A. J. Minnaard, B. L. Feringa. *Org. Lett.* **2011**, *13*, 948–951. (d) Giacomina, F.; Alexakis, A. *Eur. J. Org. Chem.* **2013**, 6710–6721.
199. W. Xiong, G. Xu, X. Yu, W. Tang. *Organometallics.* **2019**, *38*, 4003–4013.
200. (a) J.-B. Langlois, A. Alexakis. *Chem. Commun.* **2009**, 3868–3870. (b) J.-B. Langlois, A. Alexakis. *Adv. Synth. Catal.* **2010**, *352*, 447–457. (c) J.-B. Langlois, D. Emery, J. Mareda, A. Alexakis. *Chem. Sci.* **2012**, *3*, 1062–1069.
201. J.-B. Langlois, A. Alexakis. *Angew. Chem. Int. Ed.* **2011**, *50*, 1877–1881.
202. M. Pérez, M. Fañanás-Mastral, P. H. Bos, A. Rudolph, S. R. Harutyunyan, B. L. Feringa. *Nat. Chem.* **2011**, *3*, 377–381.
203. M. Fañanás-Mastral, M. Pérez, P. H. Bos, A. Rudolph, S. R. Harutyunyan, B. L. Feringa. *Angew. Chem. Int. Ed.* **2012**, *51*, 1922–1925.
204. M. Pérez, M. Fañanás-Mastral, V. Hornillos, A. Rudolph, P. H. Bos, S. R. Harutyunyan, B. L. Feringa. *Chem. Eur. J.* **2012**, *18*, 11880–11883.
205. M. Fañanás-Mastral, R. Vitale, M. Pérez, B. L. Feringa. *Chem. Eur. J.* **2015**, *21*, 4209–4212.
206. P. H. Bos, A. Rudolph, M. Pérez, M. Fañanás-Mastral, S. R. Harutyunyan, B. L. Feringa. *Chem. Commun.* **2012**, *48*, 1748–1750.
207. S. Guduguntla, M. Fañanás-Mastral, B. L. Feringa. *J. Org. Chem.* **2013**, *78*, 8274–8280.
208. S. Guduguntla, V. Hornillos, R. Tessier, M. Fañanás-Mastral, B. L. Feringa. *Org. Lett.* **2016**, *18*, 252–255.
209. S. Guduguntla, J.-B. Gualtierotti, S. S. Goh, B. L. Feringa. *ACS Catal.* **2016**, *6*, 6591–6595.
210. D. G. Gillingham, A. H. Hoveyda. *Angew. Chem. Int. Ed.* **2007**, *46*, 3860–3864.
211. F. Gao, K. P. McGrath, Y. Lee, A. H. Hoveyda. *J. Am. Chem. Soc.* **2010**, *132*, 14315–14320.
212. F. Gao, Y. Lee, K. Mandai, A. H. Hoveyda. *Angew. Chem. Int. Ed.* **2010**, *49*, 8370–8374.
213. J. A. Dabrowski, F. Gao, A. H. Hoveyda. *J. Am. Chem. Soc.* **2011**, *133*, 4778–4781.
214. J. A. Dabrowski, F. Haeffner, A. H. Hoveyda. *Angew. Chem. Int. Ed.* **2013**, *52*, 7694–7699.
215. (a) H. Ohmiya, U. Yokobori, Y. Makida, M. Sawamura. *J. Am. Chem. Soc.* **2010**, *132*, 2895–2897. (b) H. Ohmiya, N. Yokokawa, M. Sawamura. *Org. Lett.* **2010**, *12*, 2438–2440.
216. A. M. Whittaker, R. P. Rucker, G. Lalic. *Org. Lett.* **2010**, *12*, 3216–3218.
217. R. Shitani, K. Takatsu, M. Takeda, T. Hayashi. *Angew. Chem. Int. Ed.* **2011**, *50*, 8656–8659.
218. B. Jung, A. H. Hoveyda. *J. Am. Chem. Soc.* **2012**, *134*, 1490–1493.
219. Y. Zhou, Y. Shi, S. Torker, A. H. Hoveyda. *J. Am. Chem. Soc.* **2018**, *140*, 16842–16854.
220. Y. Shido, M. Yoshida, M. Tanabe, H. Ohmiya, M. Sawamura. *J. Am. Chem. Soc.* **2012**, *134*, 18573–18576.
221. K. Hojoh, Y. Shido, H. Ohmiya, M. Sawamura. *Angew. Chem. Int. Ed.* **2014**, *53*, 4954–4958.
222. K. Hojoh, Y. Shido, H. Ohmiya, M. Sawamura. *Chem. Lett.* **2018**. *47*, 632–635.
223. H. You, E. Rideau, M. Sidera, S. P. Fletcher. *Nature* **2015**, *517*, 351–355.
224. E. Rideau, H. You, M. Sidera, T. D. W. Claridge, S. P. Fletcher. *J. Am. Chem. Soc.* **2017**, *139*, 5614–5624.
225. E. Rideau, S. P. Fletcher. *Beilstein J. Org. Chem.* **2015**, *11*, 2435–2443.
226. Y. Makida, Y. Takayama, H. Ohmiya, M. Sawamura. *Angew. Chem. Int. Ed.* **2013**, *52*, 5350–5354.
227. A. Harada, Y. Makida, T. Sato, H. Ohmiya, M. Sawamura. Copper-catalyzed enantioselective allylic alkylation of terminal alkyne pronucleophiles. *J. Am. Chem. Soc.* **2014**, *136*, 13932–13939.
228. G. Xu, H. Zhao, B. Fu, A. Cang, G. Zhang, Q. Zhang, T. Xiong, Q. Zhang. *Angew. Chem. Int. Ed.* **2017**, *56*, 13130–13134.
229. K. Hojoh, H. Ohmiya, M. Sawamura. *J. Am. Chem. Soc.* **2017**, *139*, 2184–2187.

230. C. I. Jette. Z. J. Tong, R. G. Hadt, B. M. Stoltz. *Angew. Chem. Int. Ed.* **2020**, *59*, 2033–2038.
231. M. Sun, J.-F. Chen, S. Chen, C. Li. *Org. Lett.* **2019**, *21*, 1278–1282.
232. S. Ghorai, S. S. Chirke, W.-B. Xu, J.-F. Chen. C. Li. Cobalt-catalyzed regio- and enantioselective allylic amination. *J. Am. Chem. Soc.* **2019**, *141*, 11430–11434.
233. S. Ghorai, S. U. Rehman, W.-B. Xu, W.-Y. Huang, C. Li. *Org. Lett.* **2020**, *22*, 3519–3523.
234. Sekino, T.; Sato, S.; Yoshino, T.; Kojima, M.; Matsunaga, S. *Angew. Chem. Int. Ed.* **2019**, *58*, 9199–9203.

18

ASYMMETRIC CARBOMETALLATIONS INCLUDING CARBOCYCLIZATIONS

Ken Tanaka
Department of Chemical Science and Engineering, Tokyo Institute of Technology, Tokyo, Japan

18.1. INTRODUCTION

Organometallic compounds ($R–ML_n$) react with carbon–carbon π-bonds, such as alkynes and alkenes, to form new organometallic compounds through the formation of new carbon–carbon and carbon–metal σ-bonds (Scheme 18.1) [1]. These reactions are classified as "carbometallation reactions." A full discussion of the mechanism and historical background can be found in the second edition of this book [2].

Importantly, a chiral center will be generated in the carbometallation reactions of substituted alkenes, and various electrophiles (E^+) can react with the thus generated carbon–metal σ-bond (Scheme 18.2) [1, 2]. Therefore, the development of asymmetric carbometallation reactions is an important target in catalytic asymmetric synthesis.

This chapter describes the advances in the field of asymmetric carbometallation reactions since 2010. The reactions developed until 2010 can be found in the third edition of this book [3]. The asymmetric carbometallation reactions with typical metals (carboalumination, carbomagnesiation, and carbozincation) and transition metals (carbopalladation, carbonickelation, carborhodation, and carbocobaltation) will be highlighted. In addition, the carbometallation reactions can construct carbocycles, and so the asymmetric carbocyclization reactions involving the carbometallation process will also be described. The asymmetric carbometallation reactions via the C–H bond activation and the conjugate/nucleophilic addition are excluded because these reactions are described in Chapters 11 and 16, respectively. Additionally, the asymmetric carbometallation reactions of allylmetal compounds, described in Chapter 17, are also excluded.

18.2. CARBOMETALLATIONS WITH MAIN GROUP METALS

The catalytic asymmetric carbometallation of alkenes with typical metals is a useful method in synthetic organic chemistry because the thus generated organometallic compounds can react with various electrophiles (E^+) to give further functionalized products as shown in Scheme 18.2. In this section, catalytic asymmetric carboalumination, carbomagnesiation, and carbozincation reactions of unactivated alkenes using various chiral transition metal complexes as catalysts will be disclosed.

Catalytic Asymmetric Synthesis, Fourth Edition. Edited by Takahiko Akiyama and Iwao Ojima.

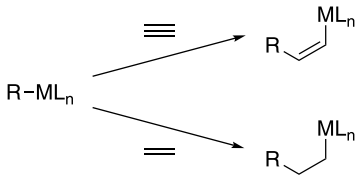

Scheme 18.1. Carbometallation of alkynes and alkenes.

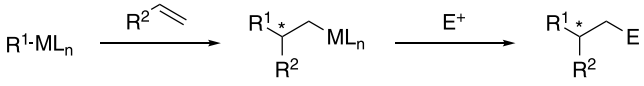

Scheme 18.2. Asymmetric carbometallation of alkenes.

18.2.1. Carboaluminations

Among the methods for the catalytic asymmetric carbometallation of unfunctionalized alkenes with typical metals, the zirconium-catalyzed asymmetric carboalumination of alkenes (ZACA) is one of the most reliable and practical methods [4]. The use of a chiral zirconium complex bearing a (1-neomenthyl) indenyl ligand enables the asymmetric functionalization of unactivated alkenes. This carboalumination generally proceeds with high regioselectivity as well as high enantioselectivity, and the aluminum functionality occupies the position with less steric hindrance. Although the enantioselectivity of the ZACA reaction is not perfect, enantiopure compounds can be readily synthesized by a combination of the ZACA reaction and the lipase-catalyzed acylative optical kinetic resolution.

Various chiral 2,3-disubstituted-1-alkanols were synthesized by the ZACA reactions using (–)-(NMI [neomenthylindenyl])$_2$ZrCl$_2$ as a chiral transition metal catalyst (Scheme 18.3) [5]. The ZACA reactions of allyl alcohol afforded carboalumination products **A** and the subsequent iodination afforded chiral 3-iodo-2-alkyl-1-alkanols **1** with good yields and ee values. Enantiopure **1** (>99% ee) could be readily obtained by the lipase-catalyzed acylative optical kinetic resolution of

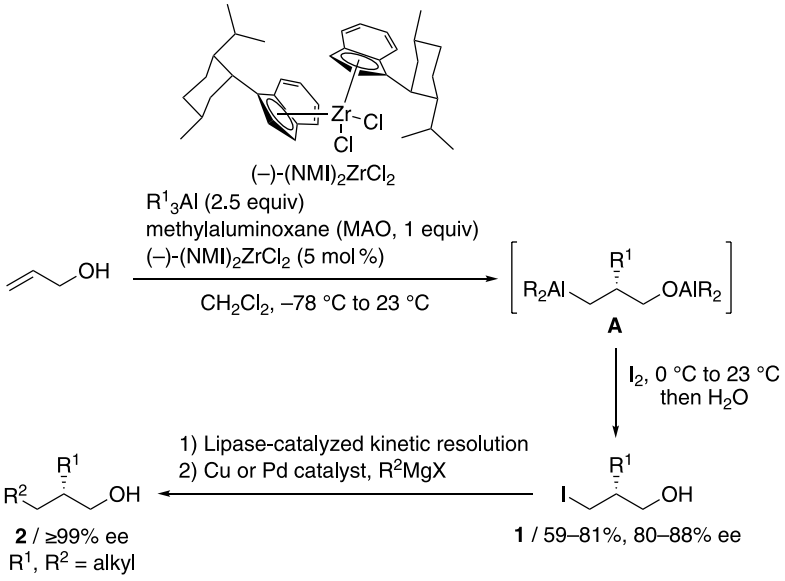

Scheme 18.3. ZACA reactions of allyl alcohols.

enantioenriched **1**. The subsequent palladium- or copper-catalyzed cross-coupling reactions of **1**-acetate afforded enantiopure 2,3-disubstituted-1-alkanols **2**.

The ZACA reactions followed by oxidation with O_2 of *tert*-butyldimethylsilyl-protected terminal alkenyl alcohols **3** and the subsequent lipase-catalyzed acylative optical kinetic resolution afforded enantiopure mono-*tert*-butyldimethylsilyl-protected diols **4**. Iodination followed by the copper-catalyzed cross-coupling reaction of **4** with organomagnesium compounds afforded enantiopure 2,3-disubstituted-1-alkanols **5** (Scheme 18.4) [6]. This process was successfully applied to the asymmetric synthesis of various enantiopure chiral 1-alkanol isotopomers **5**-D_5 with the introduction of the deuterium-labeled groups by the copper-catalyzed cross-coupling reactions.

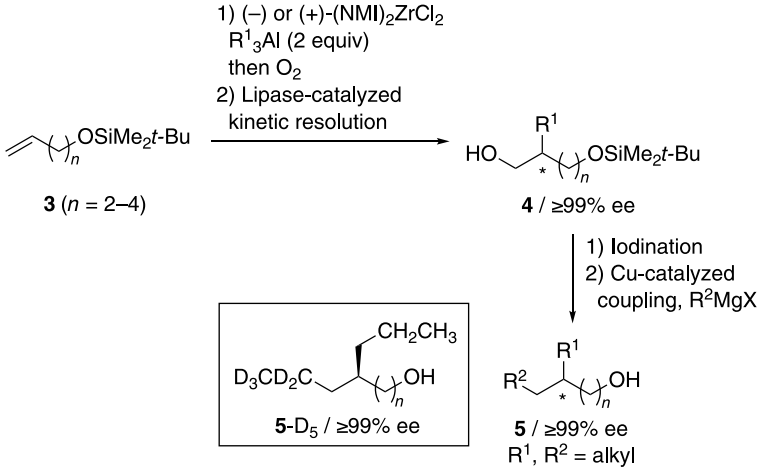

Scheme 18.4. ZACA reactions of *tert*-butyldimethylsilyl-protected terminal alkenyl alcohols.

A combination of the ZACA reaction, the palladium-catalyzed vinylation reaction, and the ZACA-oxidation reaction enables the asymmetric homologation of unfunctionalized alkenes leading to chiral primary alcohols with controlling multiple unfunctionalized stereogenic centers. The ZACA reaction of unfunctionalized alkene **6** afforded chiral organoaluminum compound **B** bearing a single stereogenic center, which was subjected to the palladium-catalyzed vinylation giving chiral alkene **7**. This alkene **7** was subjected to the ZACA reaction followed by the palladium-catalyzed vinylation, which gave alkene **8** bearing two stereogenic centers. The subsequent ZACA-oxidation of **8** afforded alkene **9** bearing three stereogenic centers with high diastereo- and enantioselectivities (Scheme 18.5) [7].

A combination of the zirconium-catalyzed inter- and intramolecular double carboalumination of dienes enables the diastereo- and enantioselective synthesis of chiral cyclopentanes (Scheme 18.6) [8]. The zirconium-catalyzed double carboalumination of unactivated 2-substituted 1,5-dienes **10** afforded chiral aluminocyclopentanes **D** with two stereocenters including one quaternary stereocenter, through chemo- and regioselective formation of acyclic organoaluminum compound **C**. Oxidation or hydrolysis of **C** gave chiral cyclopentanes **11** or **12**, respectively, with high diastereo- and enantioselectivities.

A general procedure for the enantioselective tandem hydroalumination–vinylmetallation reaction was reported. The reaction of cyclopropenes **13** with vinylaluminum reagents **14**, generated from the corresponding terminal alkynes and $HAl(iBu)_2$, in the presence of a copper(I)-thiophene-2-carboxylate (CuTC)/(*R*)-DTBM (5,5'-bis[di(3,5-di-*t*-butyl)-Segphos or SchmalzPhos catalyst and stoichiometric amount of Et_2Zn followed by treatment with aqueous HCl gave chiral vinylcyclopropanes **15** in good yields with good diastereo- and enantioselectivities (Scheme 18.7) [9]. In these reactions, the use of Et_2Zn as a Lewis acid is necessary to obtain 1 : 1 coupling products. In the absence of Et_2Zn, the desired products **15** were not observed after hydrolysis, and higher molecular weight materials were generated.

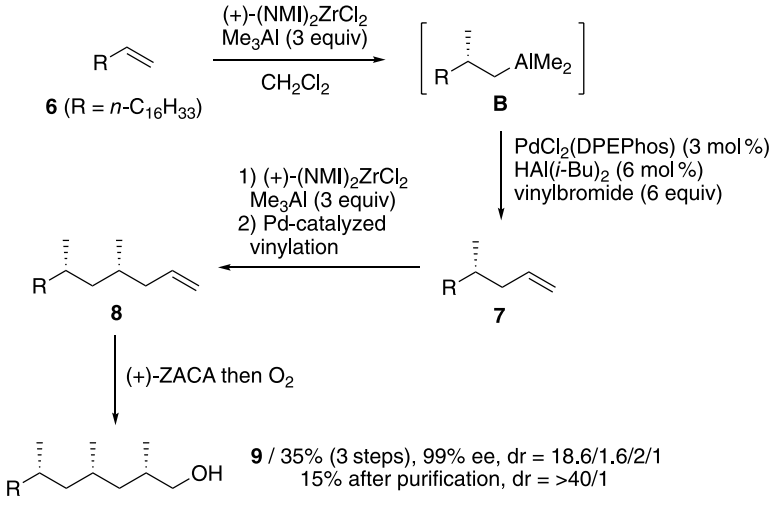

Scheme 18.5. ZACA reactions of unfunctionalized alkenes.

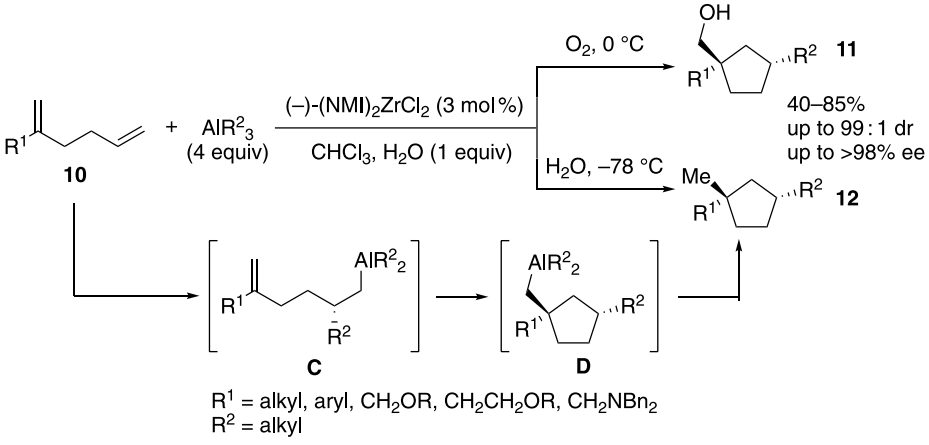

Scheme 18.6. Zirconium-catalyzed inter- and intramolecular double carboalumination.

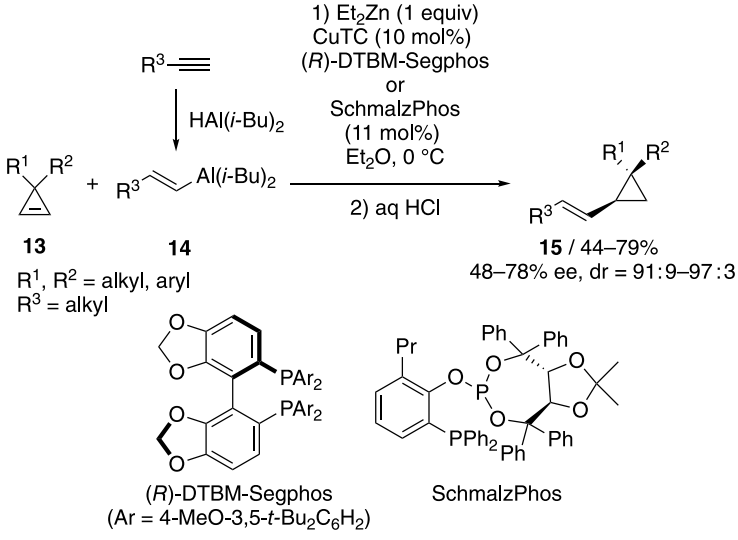

Scheme 18.7. Copper-catalyzed carbometallation of cyclopropenes with vinylaluminum reagents generated by hydroalumination of alkynes.

18.2.2. Carbomagnesiations and Carbozincations

Carbomagnesiation and carbozincation reactions are valuable methods for the synthesis of complex organomagnesium and organozinc compounds, which can further react with various electrophiles, from readily available organomagnesium and organozinc reagents [10]. Although unbiased carbon–carbon double bonds are generally unreactive toward organomagnesium and organozinc reagents, the use of transition metal complexes enables the catalytic carbomagnesiation and carbozincation of unfunctionalized alkenes. Furthermore, the enantioselective reactions have been developed by using chiral transition metal complexes as catalysts.

The palladium-catalyzed enantio- and diastereoselective carbozincation of achiral 3,3-disubstituted cyclopropenes **16** and **19** with Et_2Zn in the presence of (*R*)-tol-BINAP and $Zn(OTf)_2$ in CH_2Cl_2 proceeded at low temperatures to give organozinc products **17** and **20**, respectively (Schemes 18.8 and 18.9) [11]. In these reactions, the solvent effect is crucial, and more coordinating solvents such as

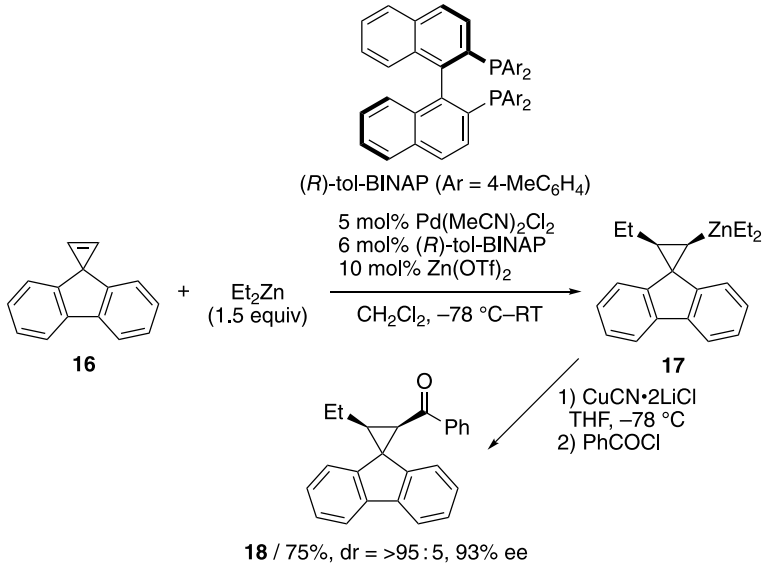

Scheme 18.8. Palladium-catalyzed carbozincation of spirocyclopropenes.

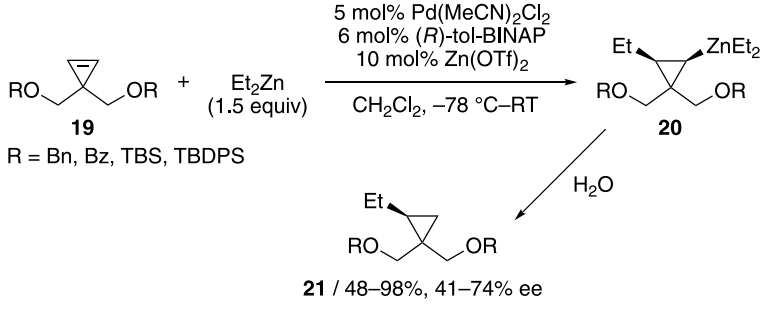

Scheme 18.9. Palladium-catalyzed carbozincation of 3,3-disubstituted cyclopropenes.

tetrahydrofuran (THF) or *N*-methyl-2-pyrrolidone inhibited the catalysis. The addition of $Zn(OTf)_2$ increases the reaction rate. The subsequent copper-mediated benzoylation of **17** gave chiral spiro compound **18** in good yield with high diastereo- and enantioselectivities. On the other hand, hydrolysis of **20** gave chiral cyclopropane **21** with moderate ee values.

Copper(I) complexes can also catalyze the asymmetric carbozincation of achiral 3,3-disubstituted cyclopropenes **22** with diorganozinc reagents (Scheme 18.10) [12]. A combination of a highly encumbered phosphine ligand, (*R*)-DTBM-Segphos, with $Cu(CH_3CN)_4PF_6$ (condition **A**) or CuTC (condition **B**) completely suppressed dimeric side products and afforded highly enantioenriched polysubstituted cyclopropanes **24** with excellent diastereoselectivity and enantioselectivity via configurationally stable cyclopropylzinc **23**.

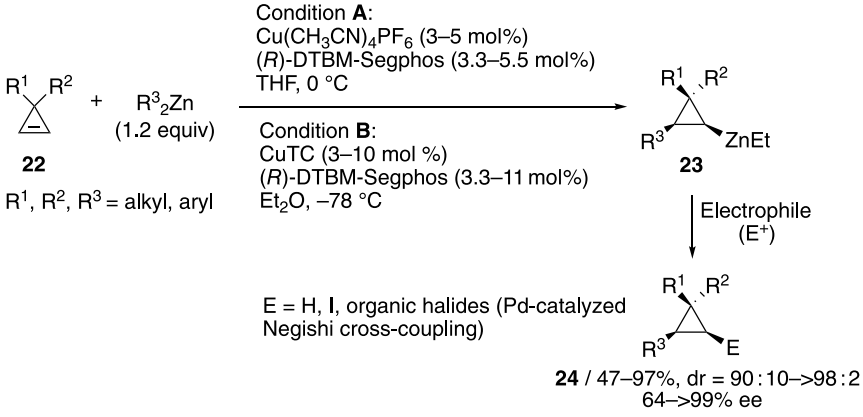

Scheme 18.10. Copper-catalyzed carbozincation of 3,3-disubstituted cyclopropenes.

Copper(I) complexes can also catalyze the asymmetric carbomagnesiation of achiral 3,3-disubstituted cyclopropenes **25** with organomagnesium reagents (Scheme 18.11) [13]. The copper(I)/(*R,S*)-Josiphos **L1** complex-catalyzed asymmetric carbomagnesiation reaction of unfunctionalized 3,3-disubstituted cyclopropene derivatives **25** afforded the corresponding organomagnesium species, which readily underwent the C–C and C–X bond-forming reactions with various electrophiles to give highly enantioenriched polysubstituted cyclopropanes **26** with complete retention of configuration.

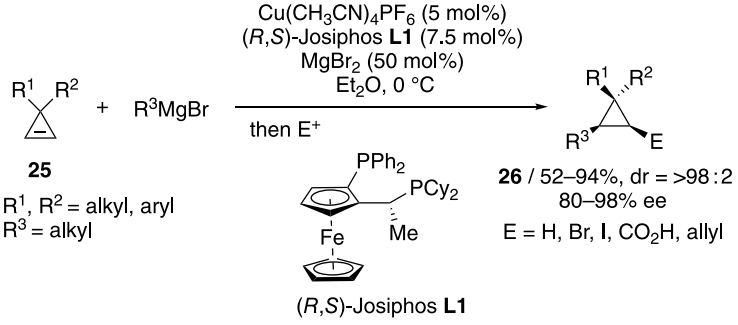

Scheme 18.11. Copper-catalyzed carbomagnesiation of 3,3-disubstituted cyclopropenes.

The copper(I)/(*R,S*)-Josiphos **L1** complex-catalyzed asymmetric carbometallation of achiral 3,3-disubstituted cyclopropenes **27** with organomagnesium reagents giving organomagnesium compounds **E** followed by either the electrophilic oxidation or amination reaction provides a unique approach to the formation of diastereomerically pure and enantiomerically enriched cyclopropanol derivatives **28** and cyclopropylamine derivatives **29**, respectively (Scheme 18.12) [14].

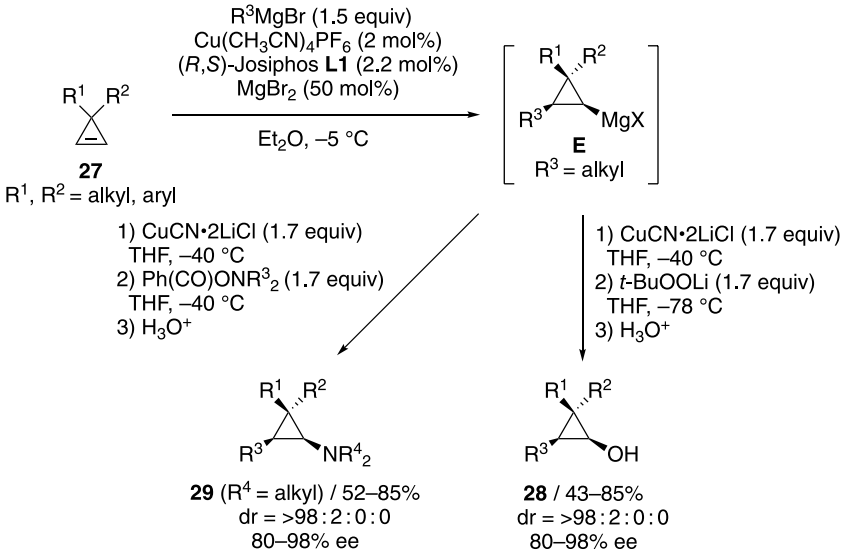

Scheme 18.12. Copper-catalyzed carbomagnesiation of 3,3-disubstituted cyclopropenes followed by oxidation or amination.

18.3. CARBOMETALLATIONS WITH TRANSITION METALS

Carbometallations with transition metals are also valuable methods for the difunctionalization of alkenes. The transition metal–carbon bonds, generated through the oxidative addition or the transmetallation process, react with alkenes to give transition metal alkyl complexes. β-hydrogen elimination, reductive elimination, or the reaction with nucleophiles affords the corresponding coupling products. As with the carbometallations with typical metals, the enantioselective reactions have been developed by using chiral transition metal complexes as catalysts.

18.3.1. Carbopalladations

For the carbometallation reactions with transition metals, the carbopalladation-initiated domino transformations are useful methods for the construction of quaternary stereocenters. For example, the palladium-catalyzed and carbopalladation-initiated carbocyclization reactions giving various bicyclic compounds have been reported [15]. As shown in Scheme 18.13, the reactions use alkenyl aryl halides **30** as starting substrates. The oxidative addition of a palladium(0) complex into the C–X bond of **30** followed by the intramolecular carbopalladation of the pendant alkene affords alkyl palladium(II) intermediate **F**. β-hydrogen elimination (classical Heck reaction), reductive elimination, or the reaction with nucleophiles affords the corresponding cyclization products **31**, **32**, or **33**, respectively. In this section, enantioselective variants of these cyclization reactions, that can provide enantiomerically enriched bicyclic compounds bearing quaternary stereocenters, are disclosed.

After the discovery of the palladium-catalyzed carboiodination reaction involving unprecedented reductive elimination of the σ-alkylpalladium iodide complex [16], the enantioselective domino Heck cyclization of aryl bromide **34** and halogen exchange (from **G** to **H**) with potassium iodide leading to cyclic alkyl iodide **35** was developed by using palladium(0)/(*R,S*)-Josiphos **L2** complex as a catalyst with high enantioselectivity of 94% ee, albeit in low yield (Scheme 18.14) [17].

The asymmetric intramolecular reductive Heck reaction of (*E*)-*ortho*-bromochalcones **36** afforded 3-substituted indanones **37** with high enantioselectivity (Scheme 18.15) [18]. The spiro-di(1,1′-indanyl)bisphosphine (SDP) derivatives were superior ligands compared to the 2,2′-bis(diphenylphosphino)-1,1′-bina phthyl (BINAP) derivatives, and tol-SDP was selected as the best ligand. The use of the hydrogen-bond

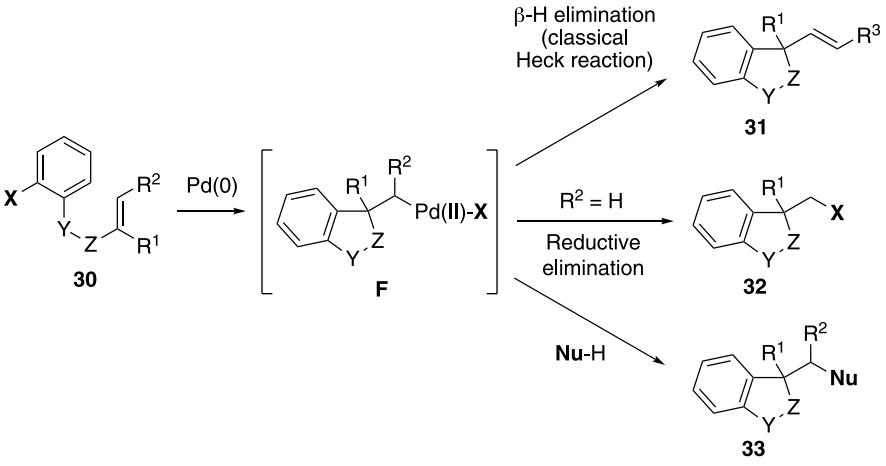

Scheme 18.13. Palladium-catalyzed and carbopalladation-initiated carbocyclization.

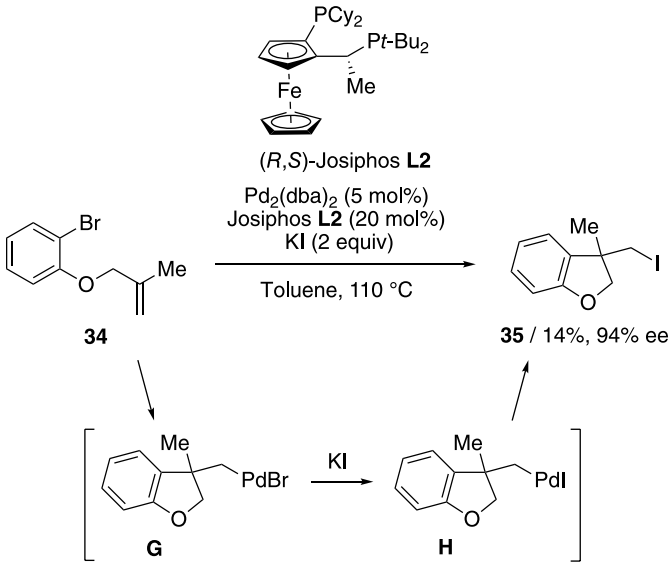

Scheme 18.14. Palladium-catalyzed intramolecular carboiodination.

donors, trialkylammonium salts, in a glycol solvent is important to promote halide dissociation from neutral aryl palladium complexes. Subsequently, the asymmetric intramolecular reductive Heck reaction of (*E*)-*ortho*-iodochalcones **38** leading to 3-aryl-indanones **39** was achieved with high enantioselectivity by using α,α,α′,α′-tetraaryl-2,2-disubstituted 1,3-dioxolane-4,5-dimethanol (TADDOL)-based monodentate phosphoramidite **L3** as a chiral ligand (Scheme 18.15) [19].

The asymmetric arylative dearomatization of indoles was achieved by the palladium-catalyzed reductive Heck reaction. Thus, enantiomerically enriched chiral tetracyclic indolines **40** bearing quaternary stereocenters were generated from indoles **41** in moderate to good yields with high enantioselectivity (up to 99% ee) by using HCOONa as a hydride donor and (*R*)-BINAP as a chiral ligand (Scheme 18.16) [20].

Isocyanides are valuable C1 building blocks in the palladium-catalyzed coupling reactions, but the development of isocyanide-based enantioselective transformations is difficult due to the high coordinating ability of isocyanide to transition metals. However, the combined use of an electron-rich bis(phospholane)

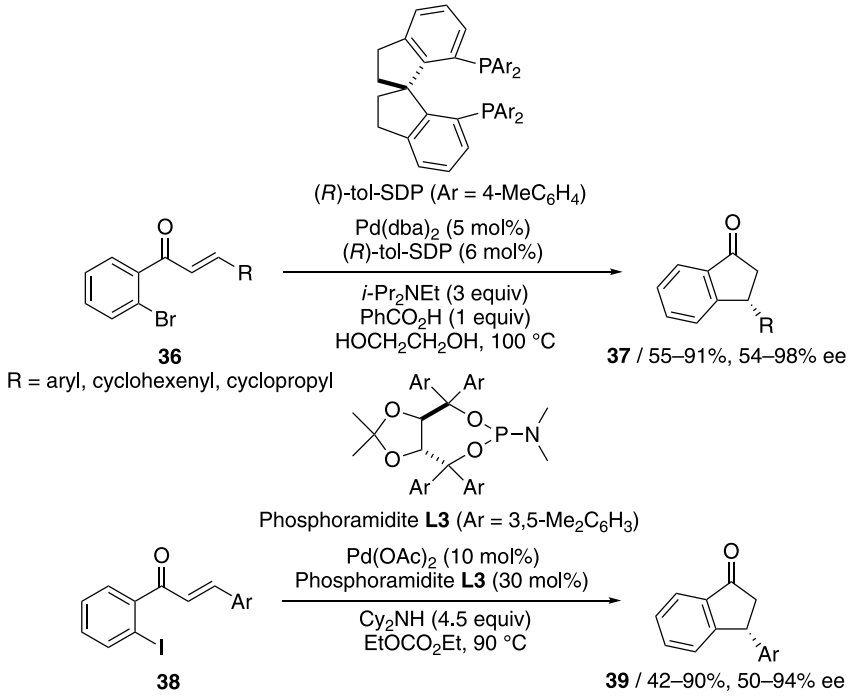

Scheme 18.15. Palladium-catalyzed intramolecular reductive Heck reactions.

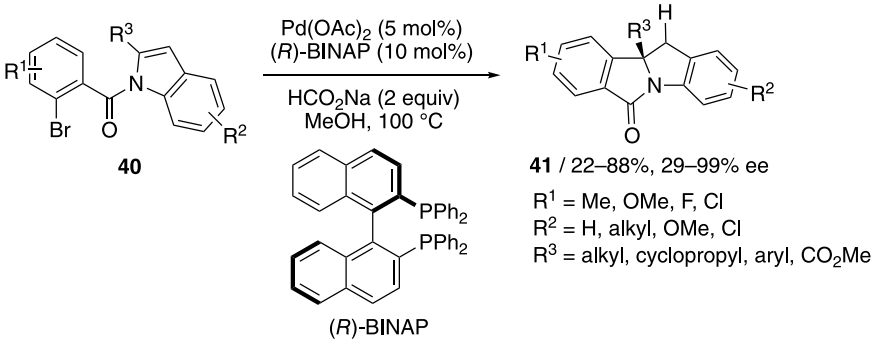

Scheme 18.16. Palladium-catalyzed intramolecular arylative dearomatization of indoles.

ligand, (1*R*,1′*R*,2*S*,2′*S*)-DuanPhos, and bulky less nucleophilic aryl isocyanide **43** realized this enantioselective transformation. Thus, enantiomerically enriched chiral imidate **44** was obtained in high yield with a good ee value of 75% from aryl iodide **42** through imidoyl palladium intermediate **I** (Scheme 18.17) [21].

Diboron–H_2O could also be used as a hydride donor in the palladium-catalyzed asymmetric reductive Heck reaction. By using heavy water as a D-atom donor and bis(catecholato)diboron (Cat_2B_2), *N*-aryl acrylamides **45** were converted to 3,3-disubstituted oxindoles **46** with a high level of D-incorporation in high yields with excellent enantioselectivity (up to 94% ee, Scheme 18.18) [22]. Mechanistically, transmetallation of the palladium(II) hydroxo complex **J** with Cat_2B_2 affords σ-alkyl palladium(II) boron complex **K**, which will furnish intermediate **L** upon reaction with D_2O. The reductive elimination from **L** delivers D-labeled oxindoles **46** (Scheme 18.18) [22].

The highly enantioselective construction of 3,3-disubstituted tetrahydropyridines **48** was accomplished by the palladium(0)/(*S*)-CF_3-*t*-BuPHOX (phosphinooxazoline) complex-catalyzed asymmetric

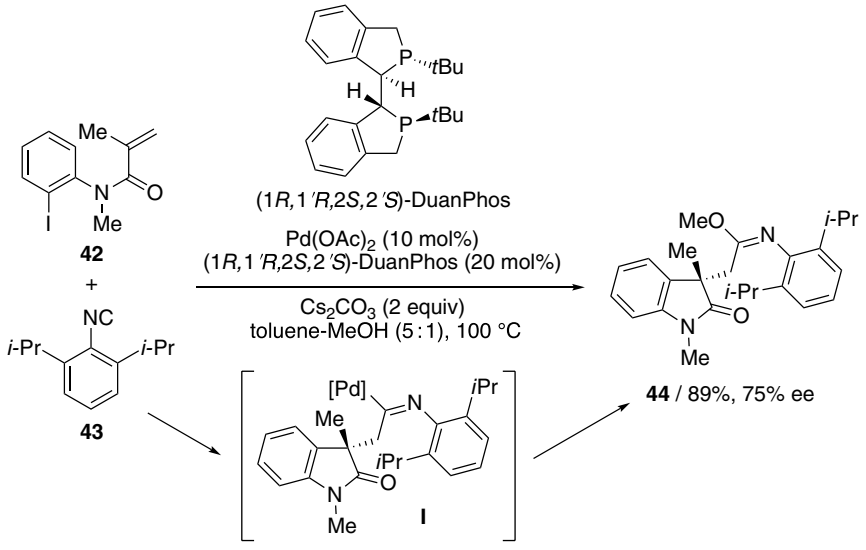

Scheme 18.17. Palladium-catalyzed intramolecular carboiodination-isocyanide insertion-methoxylation cascade.

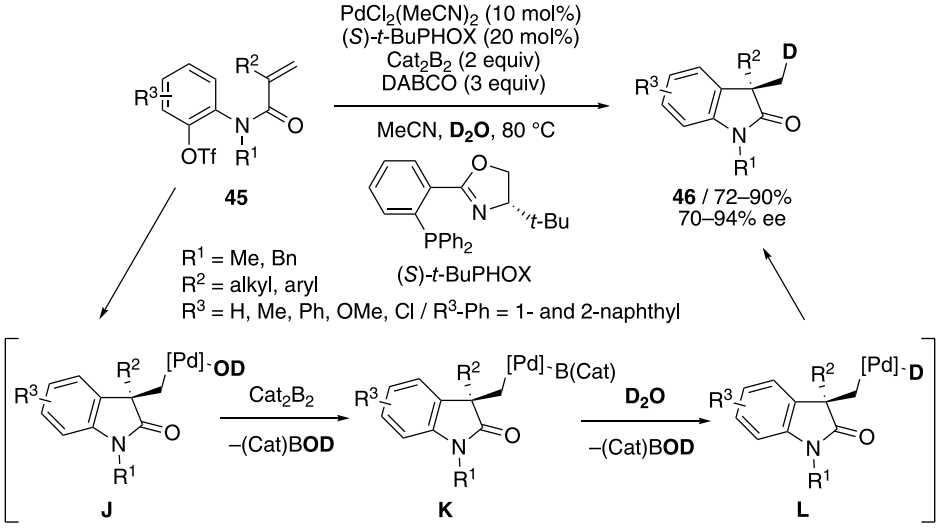

Scheme 18.18. Palladium-catalyzed intramolecular reductive Heck reactions using Diboron–H_2O as a hydride donor.

vinylborylation of (*Z*)-1-iododienes **47** (Scheme 18.19) [23]. This transformation would proceed via the following sequence: (i) the oxidative addition of palladium(0) to vinyl iodide, (ii) the Ag_2CO_3-mediated transmetallation with bis(pinacolato)diboron (B_2Pin_2) to form vinylpalladium(II)–BPin intermediate, (iii) the intramolecular enantioselective carbopalladation, and (iv) reductive elimination.

Following the palladium-catalyzed asymmetric reductive Heck cyclization of indoles, the palladium-catalyzed asymmetric arylalkynylation of indoles **49** by a sequence of Heck cyclization and intermolecular capture of a secondary σ-alkyl palladium species by terminal alkynes **50** was developed (Scheme 18.20) [24]. This process afforded a series of 2,3-disubstituted indolines **51** bearing vicinal quaternary and tertiary stereocenters in good yields with excellent enantioselectivity (up to 97% ee) and diastereoselectivities (dr = >20 : 1) by using chiral phosphoramidite ligand **L4**.

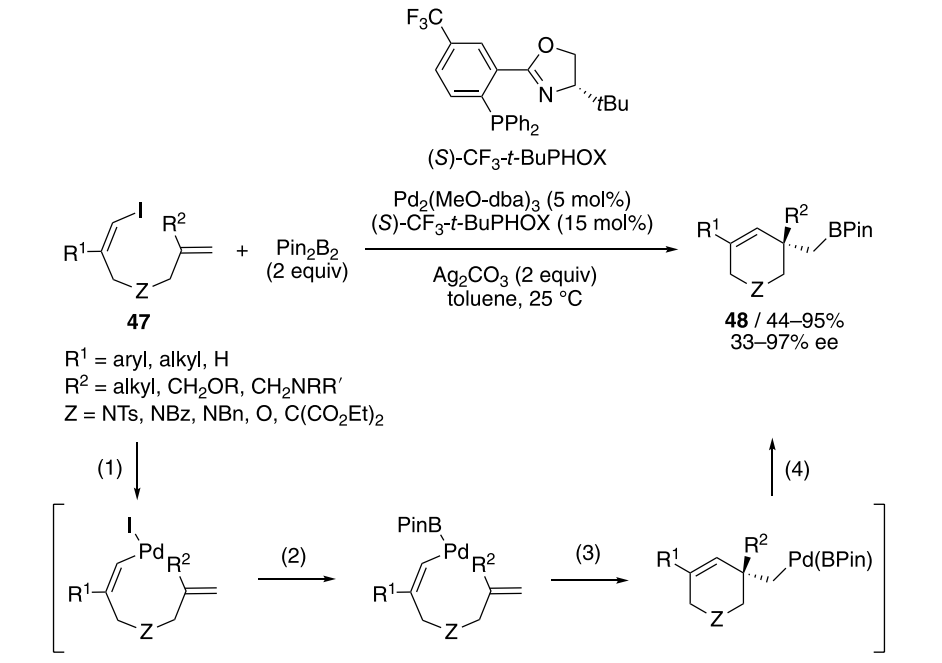

Scheme 18.19. Palladium-catalyzed vinylborylation of (*Z*)-1-iododienes with bis(pinacolato)diboron.

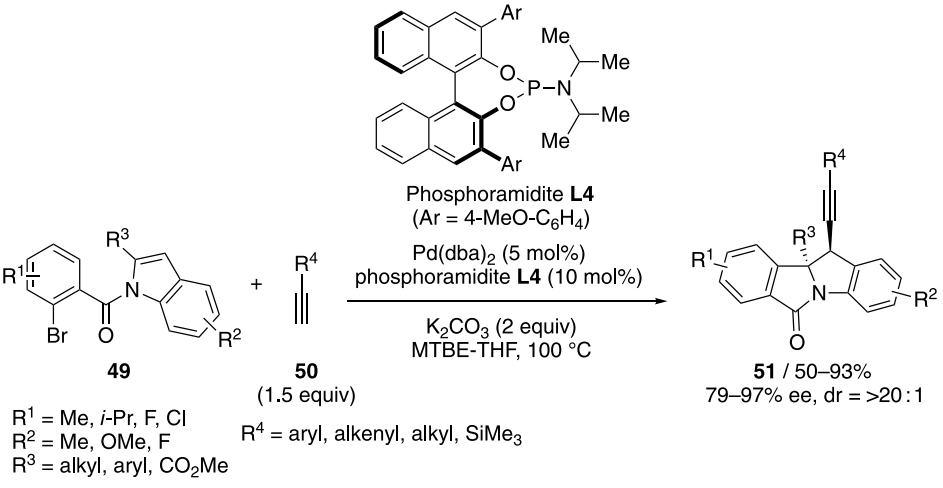

Scheme 18.20. Palladium-catalyzed arylalkynylation of indoles.

A palladium(0)/chiral phosphoramidite **L5** complex-catalyzed asymmetric dearomative arylborylation of indoles **52** with sp^2–sp^3 mixed-boron reagent **53** was also reported, which provides facile access to structurally diverse chiral indolines **54** bearing vicinal tetrasubstituted and borylated trisubstituted stereocenters (Scheme 18.21) [25].

The enantioselective synthesis of 3,4-dihydroisoquinolines **57** bearing an all-carbon quaternary stereocenter was achieved by the palladium/(*S*)-Segphos complex-catalyzed enantioselective intramolecular carbonylative Heck reaction of alkenyl-aryliodide **55** by using formates **56** as the source of CO (Scheme 18.22) [26]. This asymmetric reaction has been successfully applied to the first asymmetric synthesis of pharmaceutically privileged Minalrestat (aldose reductase inhibitors) analogs.

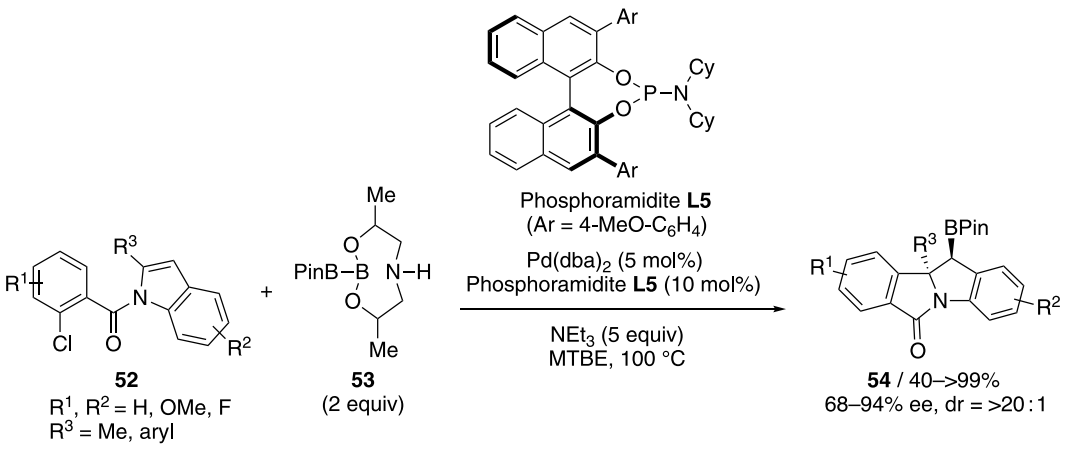

Scheme 18.21. Palladium-catalyzed dearomative arylborylation of indoles.

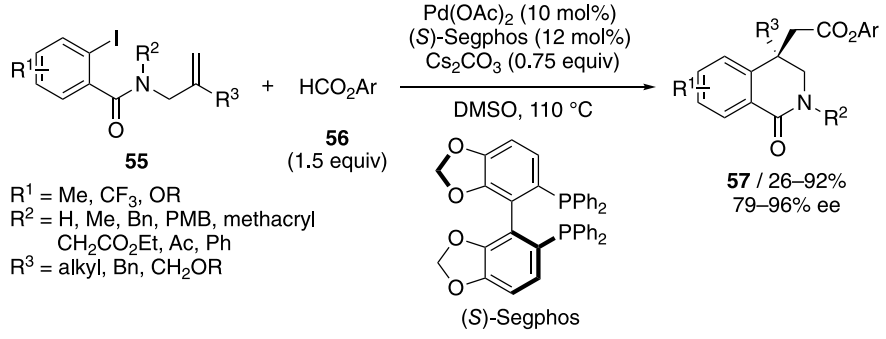

Scheme 18.22. Palladium-catalyzed intramolecular carbonylative Heck reactions of alkenyl-aryliodide.

The palladium-catalyzed enantioselective coupling of 2,5-cyclohexadienyl-substituted aryl iodides **58** and carbon or heteroatom nucleophiles proceeded via the tandem asymmetric Heck insertion and the Tsuji–Trost allylation to give chiral tetrahydrofluorenes **59** with high ee values by using a chiral H_8-BINOL (1,1'-bi-2-naphtol)-based phosphoramidite ligand **L6** (Scheme 18.23) [27].

The enantioselective construction of tetrasubstituted fluorine stereogenic centers is a challenging target in synthetic organic chemistry due to the importance in pharmaceutical industry. The palladium-catalyzed enantioselective Heck reaction of acyclic alkenyl fluorides **60** with aryl boronic acids **61** proceeded via alkyl palladium(II) intermediate **M** to give aldehydes **62** bearing C–F tertiary benzylic stereocenters (Scheme 18.24) [28]. Unstable aldehydes **62** were reduced by $NaBH_4$ and isolated as stable alcohols **63** with high ee values. It is worthy of note that this method can install the tetrasubstituted fluorine stereogenic centers remotely from pre-existing functional groups.

The asymmetric Heck insertion and Sonogashira coupling reaction of CF_3-substituted *o*-iodoacrylanilides **64** with terminal alkynes **65** were accomplished by the combined use of palladium and copper complexes as co-catalysts and Josiphos **L7** as a ligand (Scheme 18.25) [29]. The corresponding chiral oxindoles **66** containing trifluoromethylated quaternary stereogenic centers were obtained in high yields with excellent enantioselectivity.

The simple asymmetric hydroalkynylation reaction of alkenes with terminal alkynes was also achieved by using a chiral palladium complex as a catalyst. Thus, a palladium/(*R*)-xyl-BINAP complex catalyzed the enantioselective hydroalkynylation reaction of achiral 3,3-disubstituted cyclopropenes **67** with terminal alkynes **68** at room temperature to give the corresponding enantiomerically enriched alkynylated cyclopropanes **69** with excellent diastereo- and enantioselectivities (Scheme 18.26) [30].

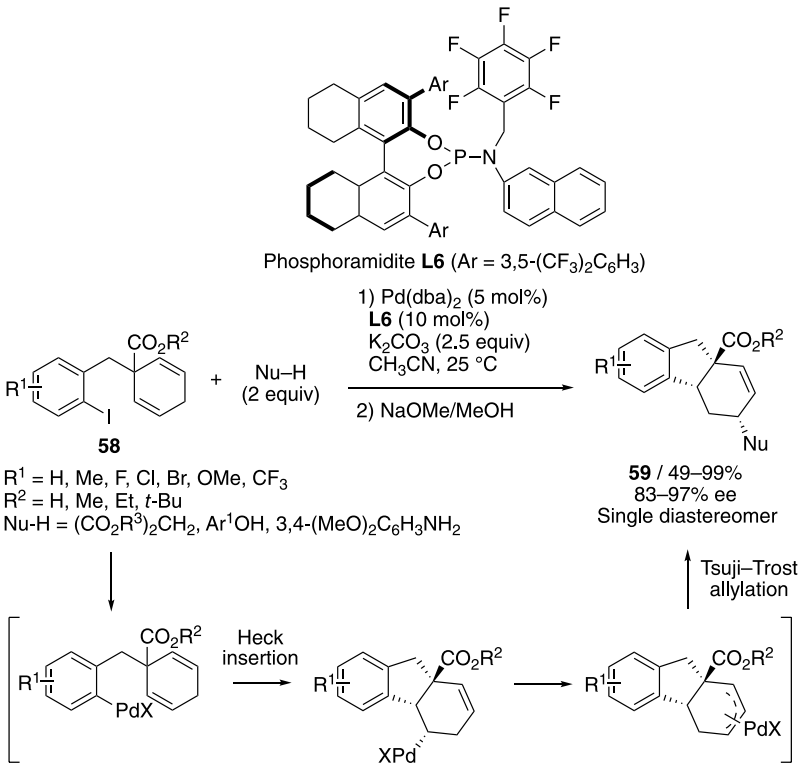

Scheme 18.23. Palladium-catalyzed tandem intramolecular Heck insertion and Tsuji–Trost allylation.

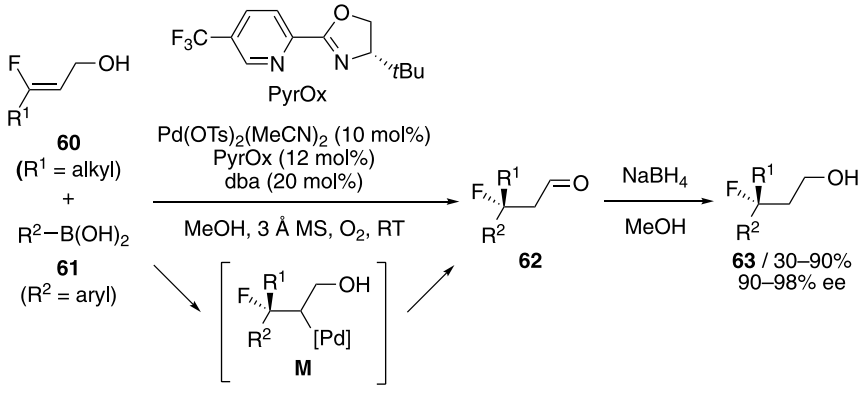

Scheme 18.24. Palladium-catalyzed Heck reactions of acyclic alkenyl fluorides with aryl boronic acids.

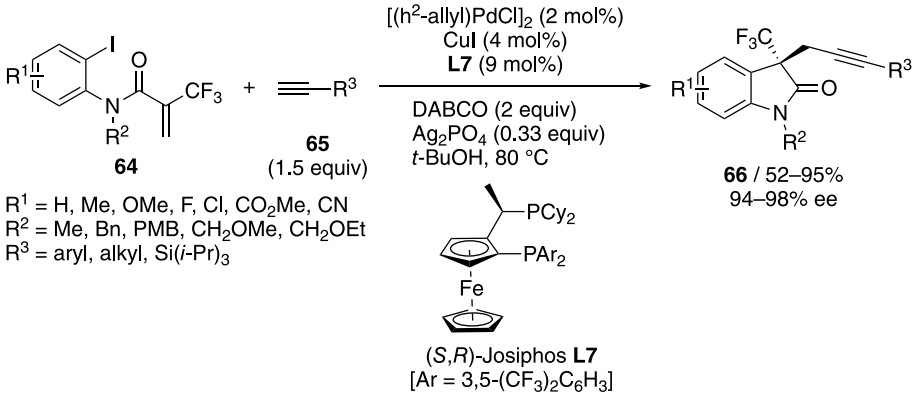

Scheme 18.25. Palladium-catalyzed tandem Heck insertion and Sonogashira coupling of CF_3-substituted *o*-iodoacrylanilides.

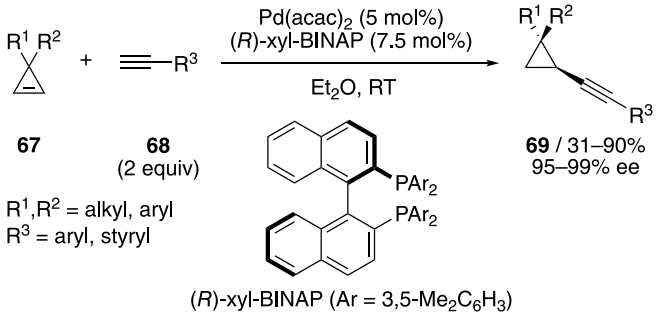

Scheme 18.26. Palladium-catalyzed hydroalkynylation of 3,3-disubstituted cyclopropenes.

18.3.2. Carbonickelations

The use of nickel complexes is advantageous than the use of palladium complexes because nickel is one of the most abundant and cheap transition metals. The intramolecular asymmetric carboiodination of aryliodides **70** proceeded via carbonickelation by using NiI_2, Mn, and a 9 : 1 mixture of (*S*)-tol-BINAP/(*S*)-BINAP oxide to give the corresponding chiral oxindoles **71** containing quaternary stereogenic centers with good yields and ee values (Scheme 18.27) [31]. Interestingly, the use of a dual ligand system was essential in achieving higher enantioselectivity.

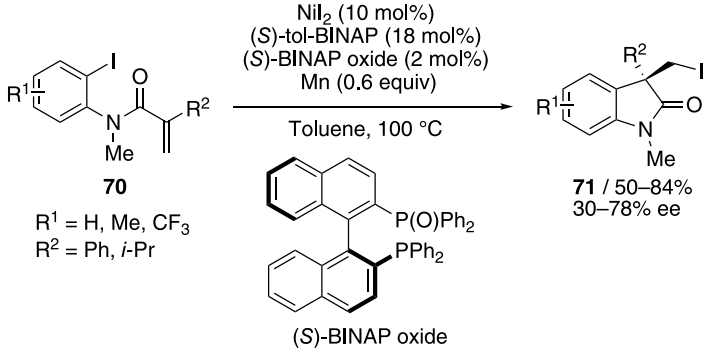

Scheme 18.27. Nickel-catalyzed intramolecular carboiodination of alkenes with aryliodides.

The nickel-catalyzed enantioselective intramolecular Mizoroki–Heck coupling of arylbromidides **72** was achieved by using *R*,*R*-QuinoxP* as a chiral ligand to give oxindoles **73** containing quaternary stereocenters with good reactivity and selectivity in the presence of various functional groups (Scheme 18.28) [32].

A nickel-catalyzed asymmetric dearomative and reductive Heck reaction of indoles **74** was achieved by using chiral Pfaltz's semicorrin **L8** as the ligand and manganese powder as the terminal reductant to give substituted indolines **75** in moderate to high yields with high enantioselectivity (Scheme 18.29) [33].

Alternatively, similar enantiomerically enriched 3,3-disubstituted oxindoles **77** were synthesized with good yields and ee values by the intramolecular asymmetric carboiodination of carbamoyl chloride **76** (Scheme 18.30) [34]. This transformation proceeded via halogen exchange with KI followed by carbonickelation by using (*S*)-*t*BuPHOX as a chiral ligand.

The enantioselective nickel-catalyzed carbocyclization reaction of tethered allene–ketone **78** with arylboronic acid **79** proceeded by using (*S*)-*t*-BuPHOX as a chiral ligand to give chiral tertiary-alcohol-containing lactam **80** with high diastereo- and enantioselectivities (Scheme 18.31) [35]. This carbocyclization reaction proceeds via carbonickelation of the allene giving allylnickel species followed by cyclization.

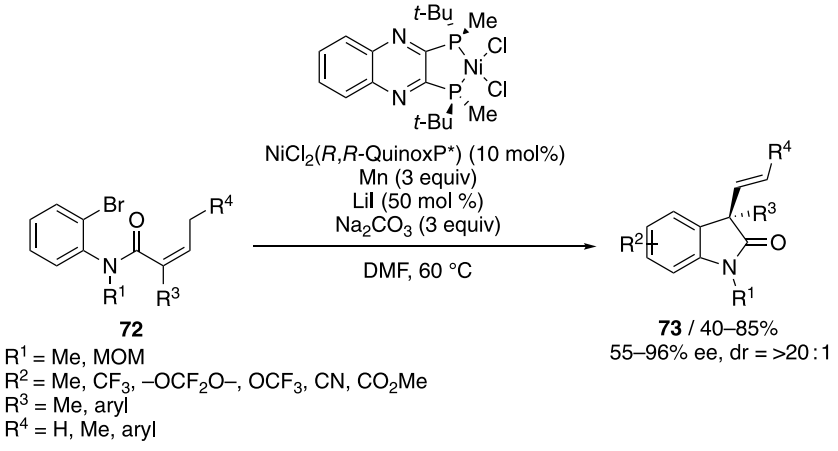

Scheme 18.28. Nickel-catalyzed intramolecular intramolecular Mizoroki–Heck coupling of alkenes with arylbromides.

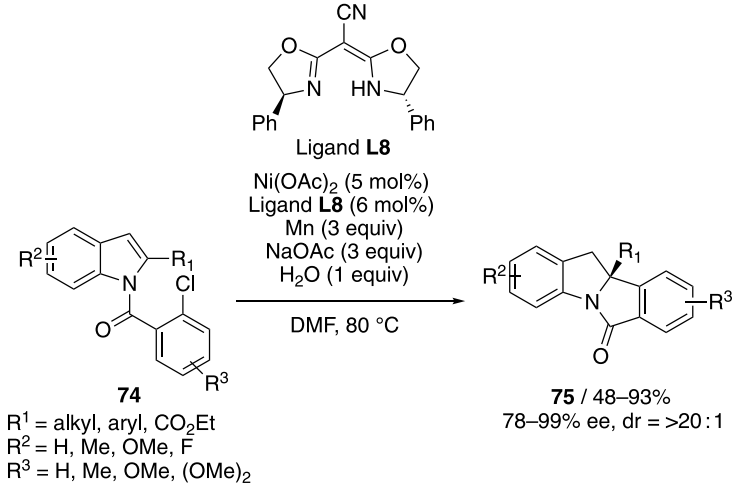

Scheme 18.29. Nickel-catalyzed intramolecular dearomative and reductive Heck reactions of indoles with arylchlorides.

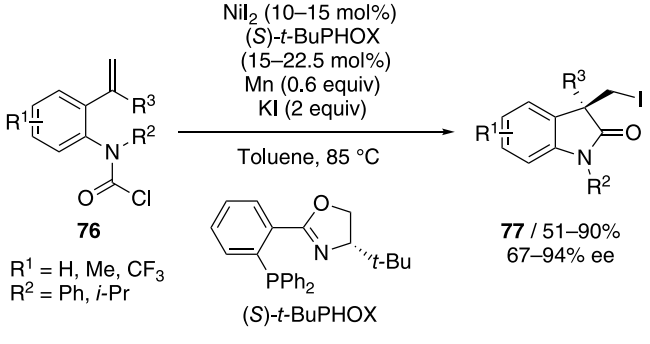

Scheme 18.30. Nickel-catalyzed intramolecular carboiodination of alkenes with carbamoyl chlorides.

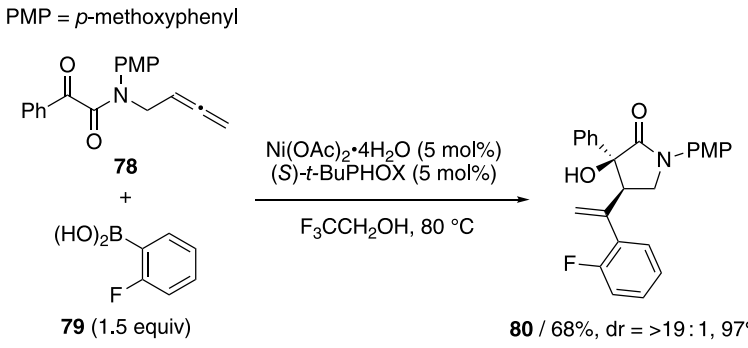

Scheme 18.31. Nickel-catalyzed carbocyclization of tethered allene–ketone with arylboronic acid.

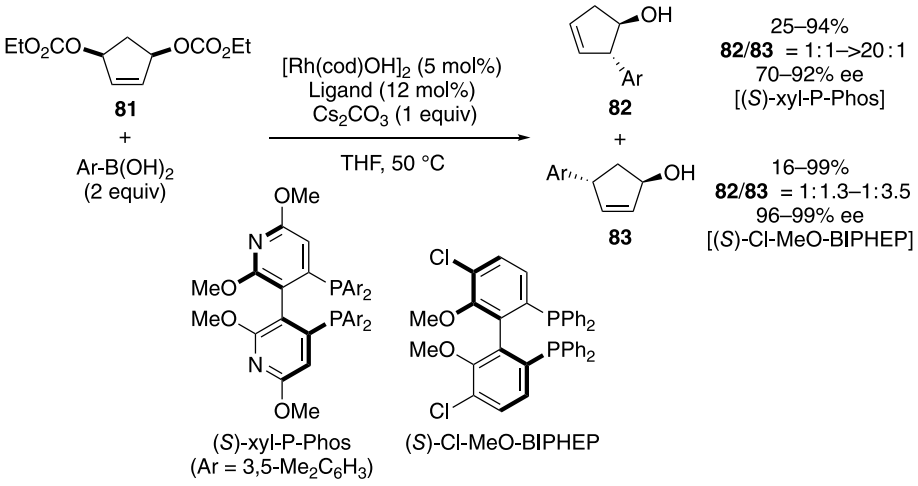

Scheme 18.32. Rhodium-catalyzed carborhodation of cyclopent-2-ene-1,4-diethyl decarbonates with arylboronic acids.

18.3.3. Carborhodations

The enantioselective desymmetrization of meso-cyclopent-2-ene-1,4-diethyl decarbonates **81** was accomplished in good yields with excellent enantioselectivity by the rhodium(I)-catalyzed asymmetric carborhodation with arylboronic acids (Scheme 18.32) [36]. Interestingly, the use of (*S*)-xyl-P-Phos as a chiral ligand afforded *trans*-1,2-arylcyclopentenols **82** as the major product, whereas the use of (*S*)-Cl-MeO-BIPHEP (2,2'-bis(diphenylphosphino)biphenyl) as a chiral ligand afforded *trans*-1,4-arylcyclopentenols **83** as the major product.

The rhodium(I)-catalyzed asymmetric arylation of azabicycles **84** proceeded with high enantioselectivity by using IBiox[(−)-menthyl] as a chiral ligand to give the corresponding arylative diazacycles **85** with high ee values (Scheme 18.33) [37]. This method was successfully applied to the asymmetric synthesis of the *N*-Boc-protected alkaloid epibatidine.

The rhodium(I)-catalyzed enantioselective arylation of β-substituted alkenyl-*para*-nitroarenes **86** with arylboronic acids proceeded at 80 °C to give the corresponding arylated products **87** with good yields and ee values by using dibenzylamide-containing chiral diene **L9** as a ligand (Scheme 18.34) [38]. The enantioselective arylation of an alkenyl-*p*-cyano-*m*-(trifluoromethyl)benzene **86** also proceeded under the same reaction conditions with good ee value, although the product yield was moderate.

Chiral dihydrobenzofuran framework **90** could be constructed with high enantioselectivity by the one-pot rhodium(I)/(*S,R*)-Josiphos **L10** complex-catalyzed asymmetric ring-opening and palladium/X-Phos complex-catalyzed intramolecular C–O coupling reactions of dihydro-1,4-epoxynaphthalene **88** and aryl

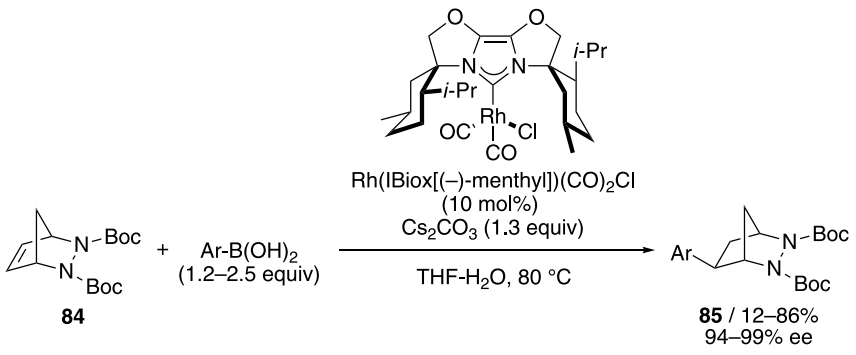

Scheme 18.33. Rhodium-catalyzed arylation of azabicyclic alkene with arylboronic acids.

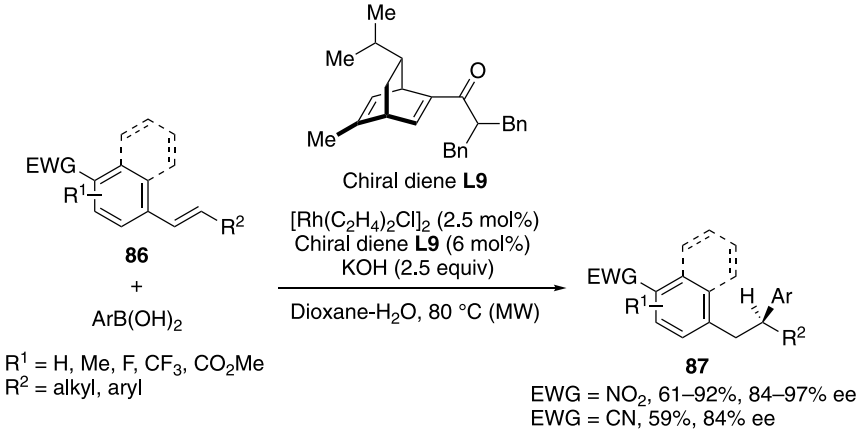

Scheme 18.34. Rhodium-catalyzed arylation of β-Substituted alkenyl-*para*-nitroarenes with arylboronic acids.

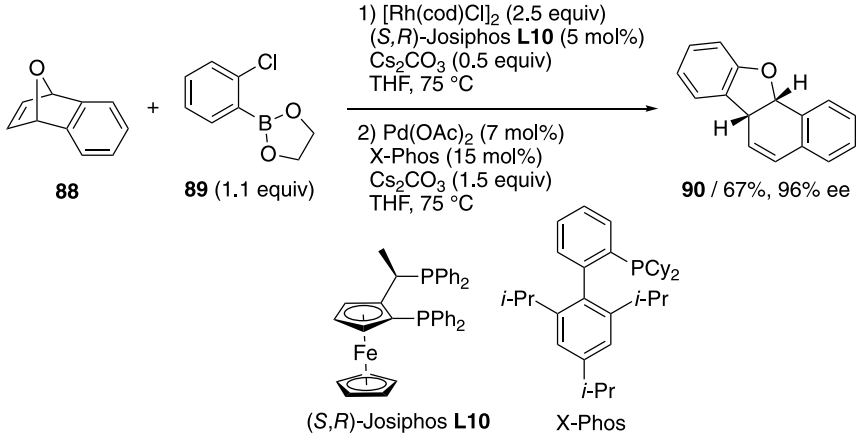

Scheme 18.35. Rhodium-catalyzed tandem ring-opening and intramolecular C–O coupling of dihydro-1,4-epoxynaphthalene with aryl boronate.

boronate **89** (Scheme 18.35) [39]. Importantly, this protocol does not require any workup or isolation of the intermediate.

A rhodium(I)/chiral bisphosphine complex is a suitable catalyst for the asymmetric arylation of achiral 3,3-disubstituted cyclopropenes with aryl boronic acids. Thus, a variety of highly diastereo- and

enantiomerically enriched arylcyclopropanes **92** was synthesized by the rhodium(I)/(*R,S*)-Josiphos **L1** complex-catalyzed enantioselective arylation of achiral 3,3-disubstituted cyclopropenes **91** with commercially available aryl boronic acids (Scheme 18.36) [40].

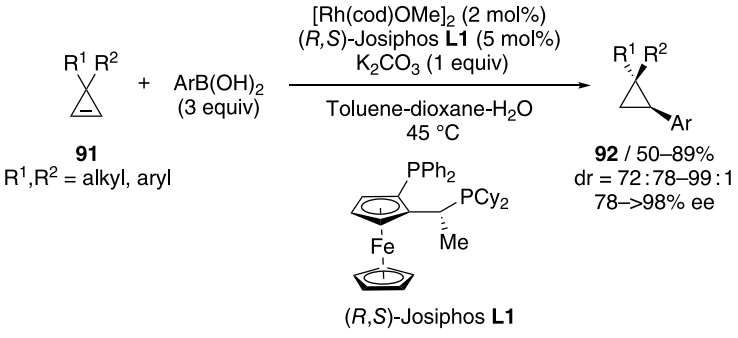

Scheme 18.36. Rhodium-catalyzed arylation of 3,3-disubstituted cyclopropenes with aryl boronic acids.

The asymmetric arylation of 2*H*-chromenes **93** with aryl boronic acids also proceeded by using a hydroxorhodium(I)/chiral diene **L11** complex as a catalyst to give chiral 3-arylchromanes **94** in good yields with high enantioselectivity (Scheme 18.37) [41]. This reaction proceeds via carborhodation giving intermediate **N**, 1,4-Rh shift giving intermediate **O**, and protodemetallation.

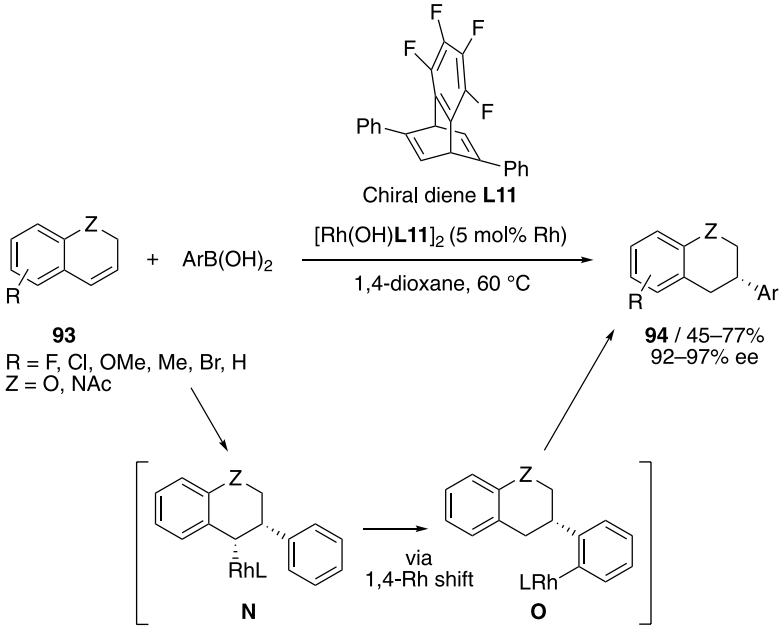

Scheme 18.37. Rhodium-catalyzed arylation of 2*H*-chromenes with aryl boronic acids.

Chiral diene-rhodium(I) complex **96** catalyzed the carbozincation of 1,6-enynes **95** with ArZnCl to give 2-(alkylidene)cyclopentylmethylzincs **P** with high yields and high enantioselectivity. The obtained enantioenriched alkylzincs were readily converted into a wide variety of functionalized products **97** in a one-pot approach by taking advantage of their unique reactivity (Scheme 18.38) [42].

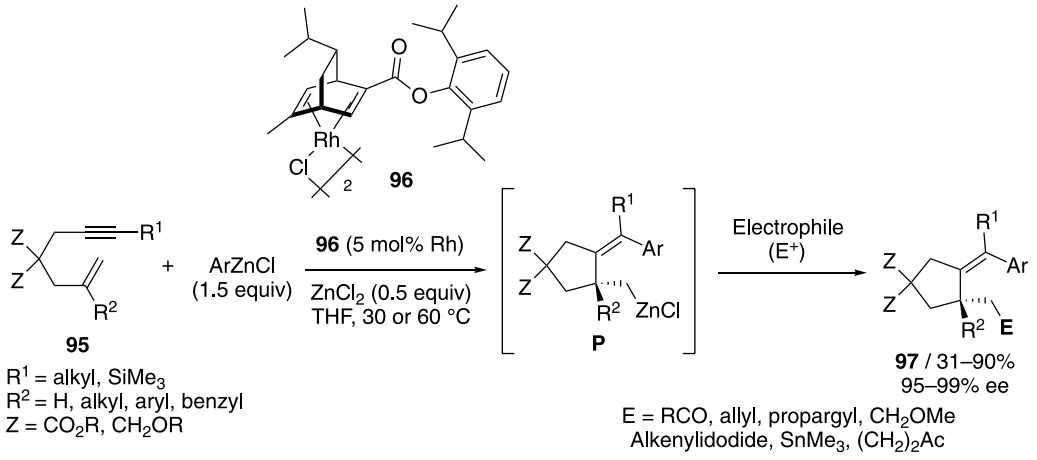

Scheme 18.38. Rhodium-catalyzed carbozincation of 1,6-enynes with ArZnCl.

18.3.4. Carbocobaltations

The asymmetric alkynylation of 1,1-disubstituted allenes **99** with silylacetylenes **98** proceeded in the presence of catalytic amounts of $Co(OAc)_2$, (*R,S*)-Josiphos **L12**, and Zn to give the corresponding enynes **100** with high yields and enantioselectivity, although isomers **101** were also generated as minor products (Scheme 18.39) [43]. The mechanistic studies revealed that this reaction proceeds via π-allylcobalt(I) intermediates generated through carbocobaltation of allenes with alkynyl cobalt(I) complexes.

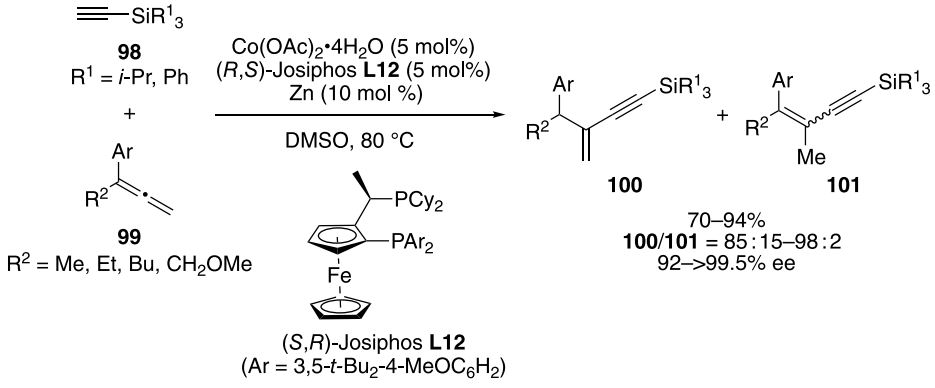

Scheme 18.39. Cobalt-catalyzed alkynylation of 1,1-disubstituted allenes with silylacetylenes.

The asymmetric synthesis of chiral boryl-functionalized γ-lactams **103** containing all-carbon quaternary stereocenters was achieved by the cobalt-catalyzed enantioselective hydroborative cyclization of amide-tethered 1,6-enynes **102** with pinacolborane (HBpin, Scheme 18.40) [44]. This tandem reaction proceeds via intermolecular hydrocobaltation of the alkyne giving vinyl cobalt(I) intermediate **Q**, intramolecular carbocobaltation of the alkene giving alkyl cobalt(I) intermediate **R**, and the reaction with HBpin giving product **103** and cobalt(I) hydride.

Not only 1,6-enynes but also 1,7-enynes could be employed in the cobalt-catalyzed asymmetric hydroborative cyclization. Thus, chiral boryl-functionalized quinoline derivatives **105** were synthesized in high yields with high enantioselectivity from a variety of aniline-tethered 1,7-enynes **104** and HBpin (Scheme 18.41) [45]. This process provides a general approach to access a series of chiral quinoline derivatives containing quaternary stereocenters.

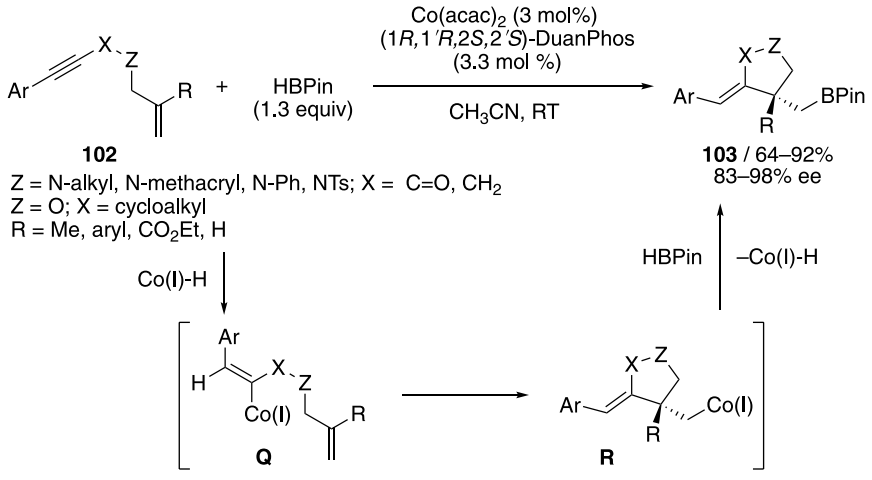

Scheme 18.40. Cobalt-catalyzed hydroborative cyclization of amide-tethered 1,6-enynes with pinacolborane.

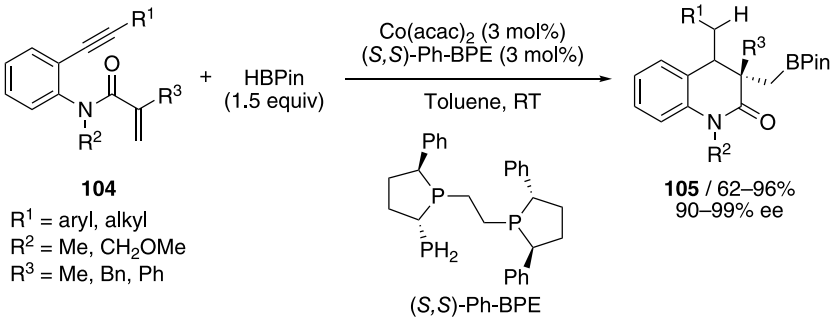

Scheme 18.41. Cobalt-catalyzed hydroborative cyclization of anilide-tethered 1,7-enynes with pinacolborane.

The cobalt-catalyzed enantioselective and chemodivergent reactions between cyclopropanols **106** and oxabicyclic alkenes **107** via a cobalt homoenolate afforded either alkylative ring-opening products **108** or hydroalkylation products **109**, with the counterion of the cobalt catalyst being a major chemoselectivity-controlling factor (Scheme 18.42) [46]. A catalyst generated from $CoCl_2$ and chiral diphosphine ligand [(*R,R*)-BDPP] promotes alkylative ring-opening to afford 1,2-dihydronaphthalen-1-ol derivatives **108** in

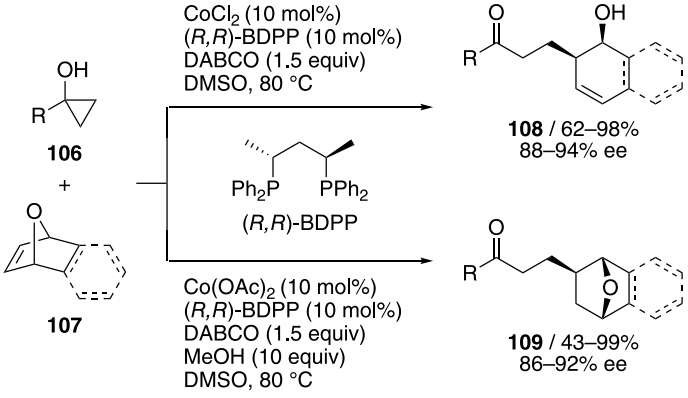

Scheme 18.42. Cobalt-catalyzed hydroalkylation of oxabicyclic alkenes with cyclopropanols.

good yields with high enantioselectivity. By contrast, a catalyst generated from $Co(OAc)_2$ and BDPP (2,4-bis(diphenylphosphino)pentane), with the assistance of methanol, selectively affords hydroalkylation products **109** with retention of the bicyclic structure at a comparable level of enantioselectivity.

18.4. CONCLUSION

As described in this chapter, catalytic asymmetric carbometallation reactions are valuable methods for the functionalization of unactivated alkenes. The enantiomerically enriched carbon–carbon bond-forming products including carbocyclization products bearing a chiral center are readily obtained from substituted alkenes. Thus, the catalytic asymmetric carbometallation reactions have been widely employed for the synthesis of complex organic molecules. Recently, the reactions using inexpensive and abundant transition metals such as copper, nickel, and cobalt have been developed, and catalytic asymmetric carbometallation reactions are becoming a practical method. Further development of inexpensive, efficient, and powerful catalytic asymmetric carbometallation reactions is expected to realize the simpler, more practical, and diverse synthesis of complex organic molecules.

REFERENCES

1. Olah, G. A.; Molnár, A. *Hydrocarbon Chemistry*. Toronto: J.P. Wiley, **1995**.
2. Negishi, E.-I. Asymmetric carbometallations. In *Catalytic Asymmetric Synthesis*, 2nd Edition (Ed. Ojima, I.) New York: Wiley-VCH, **2000**; pp. 165–189.
3. Ojima, I.; Kaloko, J. J.; Chaterpaul, S. J.; Teng, Y.-H. G.; Lin, C.-F. Asymmetric Carbometallation and Carbocyclizations. In *Catalytic Asymmetric Synthesis*, 3rd Edition (Ed. Ojima, I.). New York: Wiley-VCH, **2010**; pp. 643–682.
4. Xu, S.; Negishi, E.-I. *Acc. Chem. Res.* **2016**, *49*, 2158–2168.
5. Xu, S.; Lee, C.-T.; Wang, G.; Negishi, E.-I. *Chem. Asian J.* **2013**, *8*, 1829–1835.
6. Xu, S.; Oda, A.; Negishi, E.-I. *Chem. Eur. J.* **2014**, *20*, 16060–16064.
7. Xu, S.; Li, H.; Komiyama, M.; Oda, A.; Negishi, E.-I. *Chem. Eur. J.* **2017**, *23*, 149–156.
8. Xu, S.; Wang, C.; Komiyama, M.; Tomonari, Y.; Negishi, E.-I. *Angew. Chem. Int. Ed.* **2017**, *56*, 11502–11505.
9. Müller, D. S.; Werner, V.; Akyol, S.; Schmalz, H.-G.; Marek, I. *Org. Lett.* **2017**, *19*, 3970–3973.
10. Murakami, K.; Yorimitsu, H. *Beilstein J. Org. Chem.* **2013**, *9*, 278–302.
11. Krämer, K.; Leong, P.; Lautens, M. *Org. Lett.* **2011**, *13*, 819–821.
12. Müller, D. S.; Marek, I. *J. Am. Chem. Soc.* **2015**, *137*, 15414–15417.
13. Dian, L.; Mueller, D. S.; Marek, I. *Angew. Chem. Int. Ed.* **2017**, *56*, 6783–6787.
14. Simaan, M.; Marek, I. *Angew. Chem. Int. Ed.* **2018**, *57*, 1543–1546.
15. Ping, Y.; Li, Y.; Zhu, J.; Kong, W. *Angew. Chem. Int. Ed.* **2019**, *58*, 1562–1573.
16. Newman, S. G.; Lautens, M. *J. Am. Chem. Soc.* **2011**, *133*, 1778–1780.
17. Newman, S. G.; Howell, J. K.; Nicolaus, N.; Lautens, M. *J. Am. Chem. Soc.* **2011**, *133*, 14916–14919.
18. Yue, G.; Lei, K.; Hirao, H.; Zhou, J. *Angew. Chem. Int. Ed.* **2015**, *54*, 6531–6535.
19. Mannathan, S.; Raoufmoghaddam, S.; Reek, J. N. H.; Vries, J. G.; Minnaard, A. J. *ChemCatChem* **2017**, *9*, 551–554.
20. Shen, C.; Liu, R.; Fan, R.; Li, Y.; Xu, T.; Gao, J.; Jia, Y.-X. *J. Am. Chem. Soc.* **2015**, *137*, 4936–4939.
21. Kong, W.; Wang, Q.; Zhu, J. *Angew. Chem. Int. Ed.* **2016**, *55*, 9714–9718.
22. Kong, W.; Wang, Q.; Zhu, J. *Angew. Chem. Int. Ed.* **2017**, *56*, 3987–3991.
23. Jiang, Z.; Hou, L.; Ni, C.; Chen, J.; Wang, D.; Tong, X. *Chem. Commun.* **2017**, *53*, 4270–4273.
24. Liu, R.; Wang, Y.; Li, Y.; Huang, B.; Liang, R.; Jia, Y.-X. *Angew. Chem. Int. Ed.* **2017**, *56*, 7475–7478.
25. Shen, C.; Zeidan, N.; Wu, Q.; Breuers, C. B. J.; Liu, R.-R.; Jia, Y.-X.; Lautens, M. *Chem. Sci.* **2019**, *10*, 3118–3122.
26. Cheng, C.; Wan, B.; Zhou, B.; Gu, Y.; Zhang, Y. *Chem. Sci.* **2019**, *10*, 9853–9858.
27. Zhang, Y.; Shen, H.-C.; Li, Y.-Y.; Huang, Y.-S.; Han, Z.-Y.; Wu, X. *Chem. Commun.* **2019**, *55*, 3769–3771.
28. Liu, J.; Yuan, Q.; Toste, F. D.; Sigman, M. S. *Nat. Chem.* **2019**, *11*, 710–715.
29. Bai, X.; Wu, C.; Ge, S.; Lu, Y. *Angew. Chem. Int. Ed.* **2020**, *59*, 2764–276.
30. Dian, L.; Marek, I. *ACS Catal.* **2020**, *10*, 1289–1293.
31. Yoon, H.; Marchese, A. D.; Lautens, M. *J. Am. Chem. Soc.* **2018**, *140*, 10950–10954.
32. Desrosiers, J.-N.; Wen, J.; Tcyrulnikov, S.; Biswas, S.; Qu, B.; Hie, L.; Kurouski, D.; Wu, L.; Grinberg, N.; Haddad, N.; Busacca, C. A.; Yee, N. K.; Song, J. J.; Garg, N. K.; Zhang, X.; Kozlowski, M. C.; Senanayake, C. H. *Org. Lett.* **2017**, *19*, 3338–3341.
33. Qin, X. R.; Lee, M. W. Y.; Zhou, J. R. S. *Angew. Chem. Int. Ed.* **2017**, *56*, 12723–12726.
34. Marchese, A. D.; Wollenburg, M.; Mirabi, B.; Abel-Snape, X.; Whyte, A.; Glorius, F.; Lautens, M. *ACS Catal.* **2020**, *10*, 4780–4785.

35. Sanza, R. D.; Nguyen, T. L. N.; Iqbal, N.; Argent, S. P.; Lewis, W.; Lam, H. W. *Chem. Sci.* **2020**, *11*, 2401–2406.
36. Menard, F.; Perez, D.; Roman, D. S.; Chapman, T. M.; Lautens, M. *J. Org. Chem.* **2010**, *75*, 4056–4068.
37. Bexrud, J.; Lautens, M. *Org. Lett.* **2010**, *12*, 3160–3163.
38. Saxena, A.; Lam, H. W. *Chem. Sci.* **2011**, *2*, 2326–2331.
39. Tsui, G. C.; Tsoung, J.; Dougan, P.; Lautens, M. *Org. Lett.* **2012**, *14*, 5542–5545.
40. Dian, L.; Marek, I. *Angew. Chem. Int. Ed.* **2018**, *57*, 3682–3686.
41. Umeda, M.; Sakamoto, K.; Nagai, T.; Nagamoto, M.; Ebe, Y.; Nishimura, T. *Chem. Commun.* **2019**, *55*, 11876–11879.
42. Chen, J.; Hayashi, T. *Angew. Chem. Int. Ed.* **2020**, *59*, 18510–18514.
43. Sawano, T.; Ou, K.; Nishimura, T.; Hayashi, T. *J. Org. Chem.* **2013**, *78*, 8986–8993.
44. Wang, C.; Ge, S. *J. Am. Chem. Soc.* **2018**, *140*, 10687–10690.
45. Wu, C.; Liao, J.; Ge, S. *Angew. Chem. Int. Ed.* **2019**, *58*, 8882–8886.
46. Yang, J.; Sekiguchi, Y.; Yoshikai, N. *ACS Catal.* **2019**, *9*, 5638–5644.

PART VII

ASYMMETRIC SYNTHESIS OF NON-CENTRO-CHIRAL COMPOUNDS

19

ASYMMETRIC SYNTHESIS OF AXIALLY CHIRAL COMPOUNDS

Shaohua Xiang, Jun Kee Cheng, and Bin Tan
Department of Chemistry, Southern University of Science and Technology, Shenzhen, China

19.1. INTRODUCTION

Axially chiral compounds derive optical activity from the existence of one or more stereogenic axis, namely a rotationally restricted sigma bond. The occurrence and utilization potentials of atropisomers are increasingly recognized in natural product chemistry [1], medicinal chemistry [2], asymmetric synthesis [3], and material science [4]. In particular, the progression of asymmetric catalysis is tied to the efficiency with which axially chiral skeletons could be constructed as the scaffolds enable precise spatial positioning of catalytic functionalities. 1,1′-Bi-2-naphthol (BINOL), 2′-amino-1,1′-binaphthalen-2-ol (NOBIN), 1,1′-binaphthyl-2,2′-diamine (BINAM), and BINOL-derived chiral phosphoric acids (CPAs) are among the highly prized ligands or organocatalysts that embody axially chiral skeleton. Consequently, catalytic preparations of atropisomers become important and have advanced exponentially in the past decade [5–15]. This chapter offers an overview of different disconnections that have been designed to construct atropisomers under catalyst control. The content will be categorized into metal catalysis, organocatalysis, and enzymatic catalysis, the three main pillars of asymmetric catalysis. For more lucid presentation, each catalysis domain is presented with the preparation methods of structural class (biaryls, heterobiaryls, and nonbiaryls). Each strategy is illustrated with selected recent report(s).

19.2. METAL CATALYSIS

19.2.1. Biaryl Atropisomers

19.2.1.1. Formation of C(aryl)-C(aryl) Bond

19.2.1.1.1. Transition Metal-Catalyzed Cross-Coupling Although transition metal-catalyzed synthesis of biaryl atropisomers could benefit from the well-studied non-asymmetric versions, the substitution requirement to ensure conformational stability has always challenged the potency of a catalytic system [16]. In 2019, the Shi group realized a highly enabling Suzuki-Miyaura protocol that furnished diverse challenging biaryl atropisomers **3** of different axial stability from arylboronic acids **1** and aryl halides **2** (Scheme 19.1) [17]. The experimental results clearly demonstrated that the bulky substituent on *N*-heterocyclic-carbene (NHC) (**L1**) is crucial to implement an effective stereodiscrimination and

Catalytic Asymmetric Synthesis, Fourth Edition. Edited by Takahiko Akiyama and Iwao Ojima.

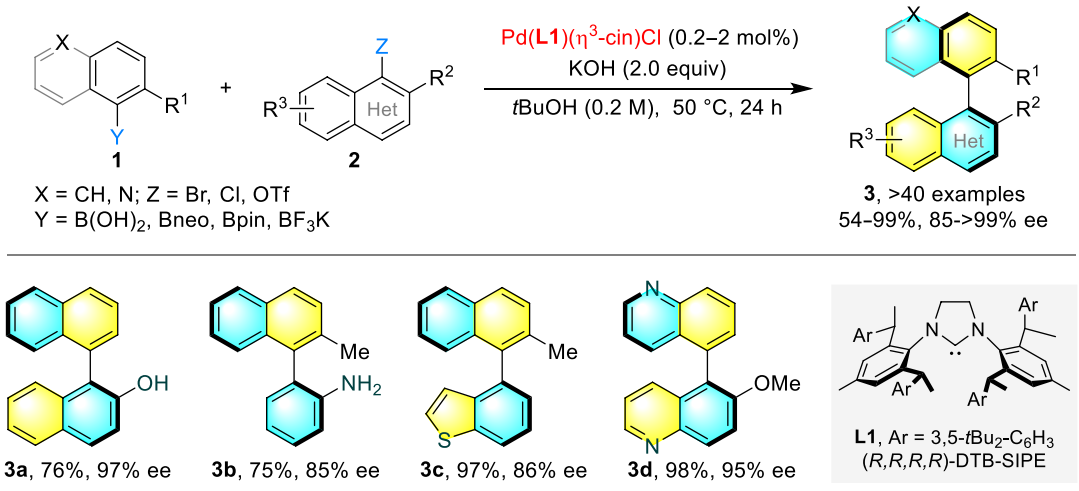

Scheme 19.1. Pd/DTB-SIPE-catalyzed asymmetric Suzuki-Miyaura coupling. Source: [17]/American Chemical Society.

facilitate the key reductive elimination step. Meanwhile, the electron-dense property of NHC ligand is helpful to suppress substrate coordination and promote oxidative addition.

The utilization of bulky *P*-chiral BaryPhos **L2** by Tang provided a unified access to axially chiral tetra-*ortho*-substituted biaryls, including phenyl-naphthyls (**6a-b**), binaphthyls (**6c**), and biphenyls (**6d**), through asymmetric Suzuki-Miyaura coupling reactions (Scheme 19.2) [18]. While sterics primarily dictates atroposelection in biaryl couplings of **6**, formation of **6d** is further mediated by unique interactions between the two formyl moieties with ligand. Weak O•••H interaction with aliphatic H atom of cyclopentyl ring and H-bonding with tertiary alcohol on **L2** have respectively determined the orientations of two coupling phenyl rings.

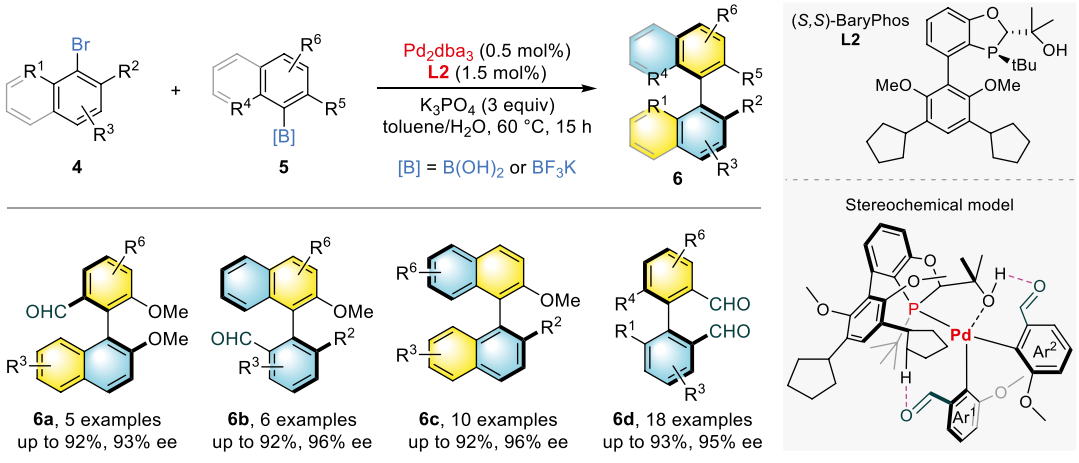

Scheme 19.2. Pd/BaryPhos-catalyzed asymmetric Suzuki-Miyaura cross-coupling. Source: [18]/American Chemical Society.

Mei and coworkers included electrochemistry for nickel-catalyzed reductive homo-coupling of aryl bromides **7** using pyridine oxazoline ligands (**L3**, **L4**) (Scheme 19.3) [19]. Aside from providing improved reaction efficiency and enantiocontrol than manganese reductant, this set of conditions assembled diverse BINOL derivatives **8** at gram scale.

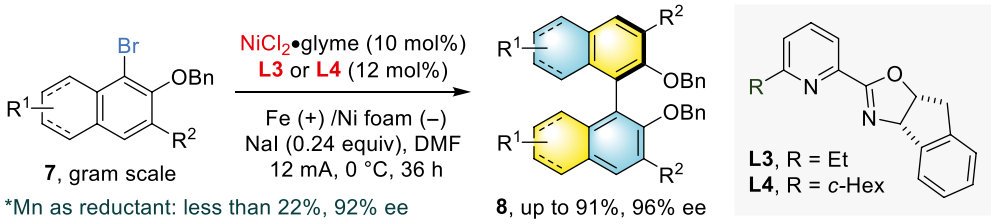

Scheme 19.3. Electrochemical-mediated Ni-catalyzed reductive homo-coupling. Source: [19]/American Chemical Society.

A three-component cross-coupling of aryl iodides, *ortho*-aldehyde-substituted boronic acids, and chloromethyl benzoate was developed by the Gu group through a sequence of Catellani reaction and Suzuki-Miyaura coupling to afford aldehyde-substituted biaryls using a *P*,*C*-type ligand that displays axial and *P*-center chirality [20]. More recently, Zhou and coworkers have improved this three-component coupling manifold using Pd/chiral norbornene co-catalytic system [21]. From aryl iodides **9**, 2,6-disubstituted aryl bromides **10**, and chiral norbornene **NBE*-1** ligand, versatile axially chiral Pd-complex was generated (Scheme 19.4). Various kinds of compounds, including olefins, alkynes, boronic acids, cyanide, and ketone, could be effectively employed as terminating agents for this reaction to give the structurally diverse axially chiral molecules **11** in moderate to good yields with excellent enantiocontrol.

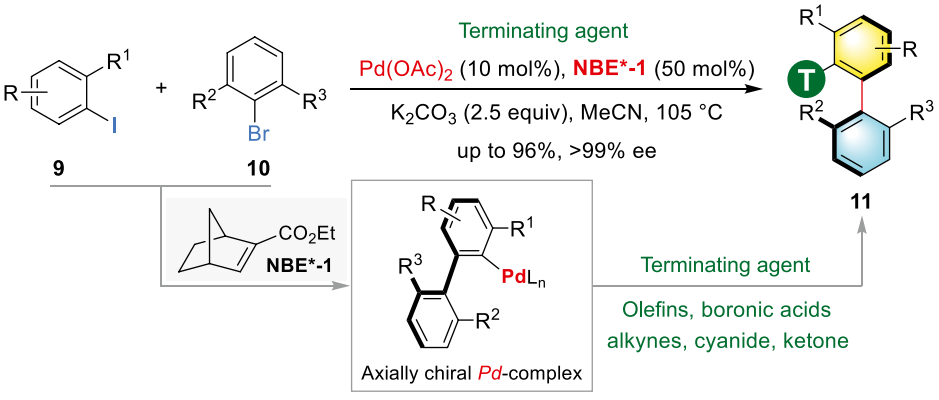

Scheme 19.4. Pd/chiral norbornene-catalyzed three-component coupling with varied terminating groups.

19.2.1.1.2. Direct C-H Arylation Through palladium catalysis incorporating TADDOL-derived phosphoramidite **L5**, Cramer constructed dibenzazepinones **13** from intramolecular C-H arylation of amide compounds **12** [22]. The installation of a steric substituent (R^2) adjacent to chiral axis crucially bestowed the atropostability as well as enantioselectivity (**13a** vs. **13b**). Given that the isomerization barrier of the eight-membered palladacycle **14** ($\mathbf{TS_{iso}}$) was higher than respective barriers of reductive elimination (5.2–5.9 kcal/mol), ligand **L5** was believed to first selectively mediate concerted metalation deprotonation (CMD) and then gives one isomer of **14** (Scheme 19.5).

Enantioselective C-H arylation of *o*-quinone diazide **15** by phosphine oxides **16** with chiral iridium(III) complex **17** and phthaloyl *tert*-leucine as the co-catalyst generated axially and *P*-chiral biaryl phosphine oxides (**18**) or axially chiral MOP-type phosphine oxides **19** (Scheme 19.6) [23]. Whereas bulky substituent (R^1) in **16** contributed to high diastereoselectivity of product **18**, arylation occurred preferentially in 3,5-dimethoxyphenyl ring to afford **19**.

Tan and coworkers have devised the oxidant-free copper-catalyzed Michael-type addition of azonaphthalenes **20** by arylboronic acids **21** to form atropisomerically enriched biaryls **22** with BINOL-derived

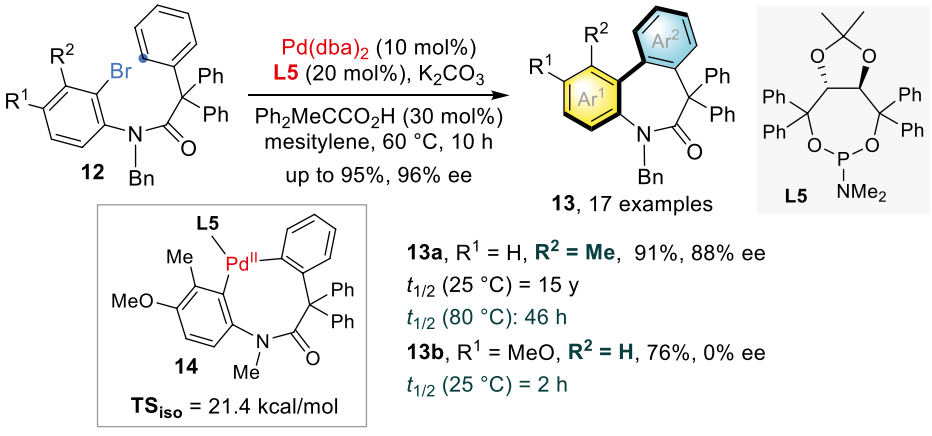

Scheme 19.5. Pd-catalyzed asymmetric intramolecular C-H arylation.

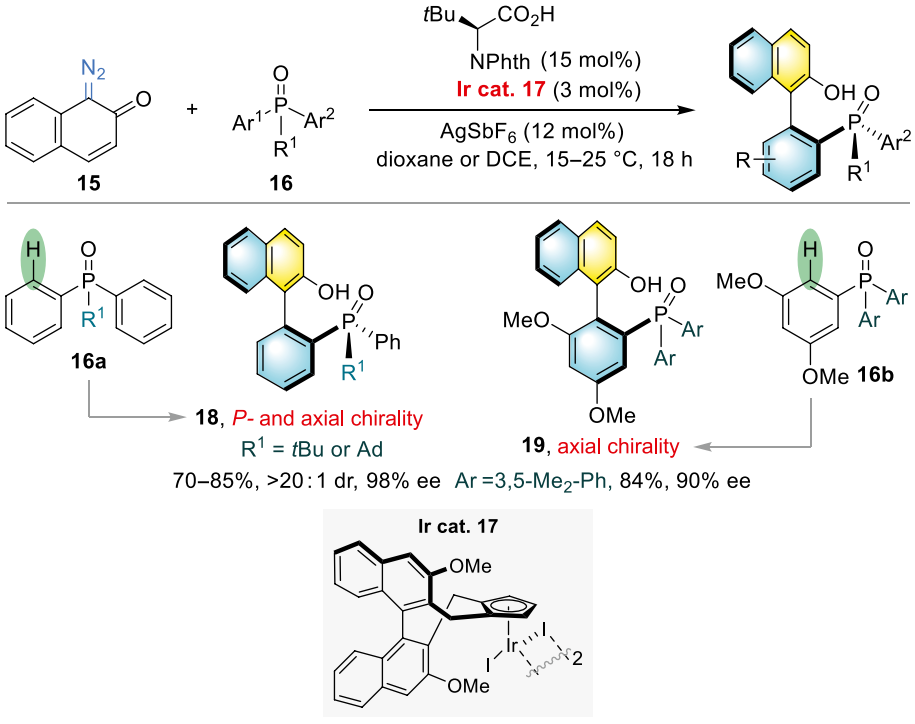

Scheme 19.6. Iridium-catalyzed asymmetric intermolecular C-H arylation. Source: [23]/John Wiley & Sons.

phosphoramidite ligands (**L6**, **L7**) [24]. The transmetallated chiral Cu species will coordinate and activate azonaphthalene substrate for enantioselective 1,4-addition. Aromatization of **A** with chirality transfer furnishes **22** (Scheme 19.7).

19.2.1.1.3. Dehydrogenative Cross-Coupling Direct oxidative homo-coupling of naphthols **23** has proven efficiency to produce optically active BINOLs with C_2-symmetry under catalytic frameworks of copper, vanadium, iron, and ruthenium [25]. Conversely, the chemoselectivity for non-C_2-symmetric BINOL analogues is generally low and thus the overall reaction is lower-yielding. Katsuki and

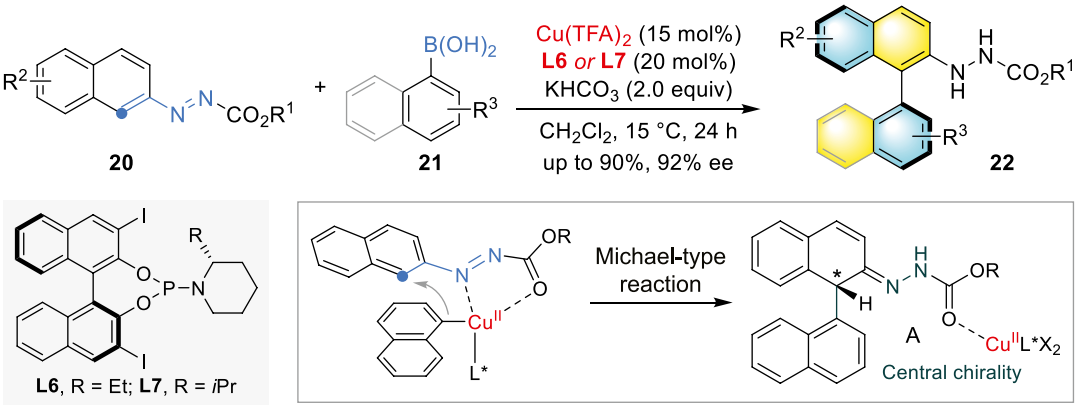

Scheme 19.7. Copper-catalyzed asymmetric Michael-type addition.

coworkers devised iron(salan) complex to realize cross-coupling of 3-substituted-2-naphthols and 6-substituted-2-naphthols in moderate yields (**24A**) [26]. The Tu group pursed the formation of 3,3′-disubstituted BINOLs (**24B**) with chiral copper complex of 1,5-*N,N*-bidentate ligand spirocyclic pyrrolidine oxazoline (SPDO) **L8** [27]. These strategies capitalized on using electronically complementary 2-napthols **23** for optimal efficiencies and selectivities. Pappo, Toste, and coworkers derived iron complex from CPA (*R*)-**C1** to promote oxidative radical-anion coupling of 2-naphthols employing di-*tert*-butylperoxide (DTBP) as oxidant toward C_2-symmetric (**25A-B**) and non-C_2-symmetric (**24C-D**) BINOLs [28]. They have notably disclosed that enantioenriched BINOLs formed from radical-anion coupling could racemize via metal-promoted reversible single electron transfer (SET) (Scheme 19.8).

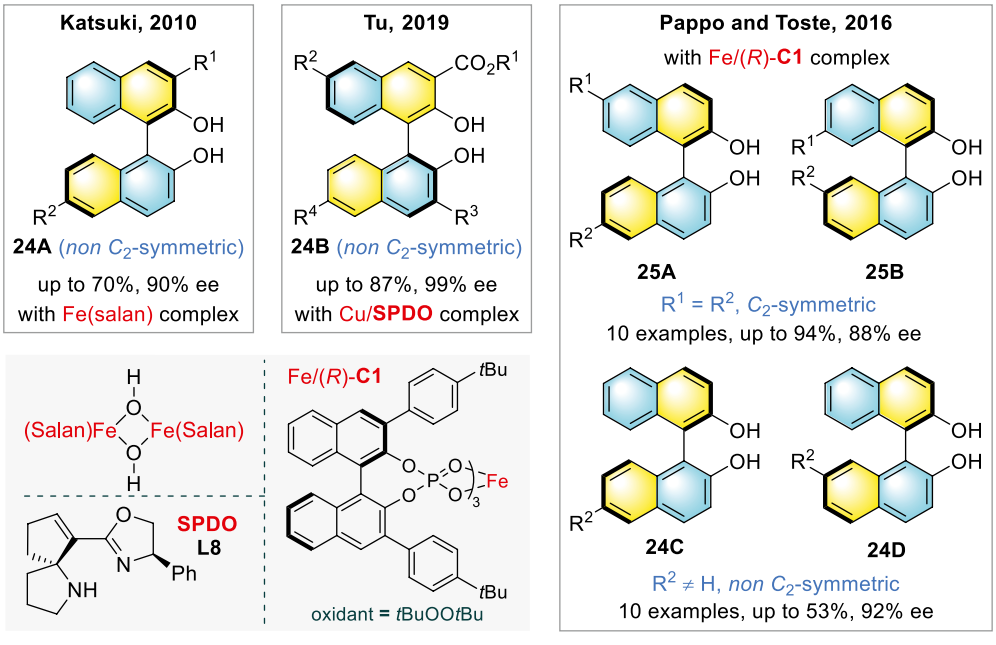

Scheme 19.8. Recent achievements in direct asymmetric oxidative coupling of naphthols.

Tan and coworkers introduced azonaphthalenes (**20**) as electrophiles in redox-neutral cross-coupling with aromatic alcohols **23** to form NOBIN analogues **26** (Scheme 19.9). The actual catalyst was produced from pretreated Lewis acidic $Zn(BArF)_2(CH_3CN)_6$ and (*S*)-**C2-Ca**. The BINAM derivatives **28** were formed from 2-naphthylamines **27** by applying $Ni(OTf)_2$ and sidearm-modified bis(oxazoline) (SaBOX) ligand **L10**. The modified Ni/BOX system (conditions B) could improve the synthesis of certain NOBIN derivatives and enabled gateway to more NOBIN analogues [29].

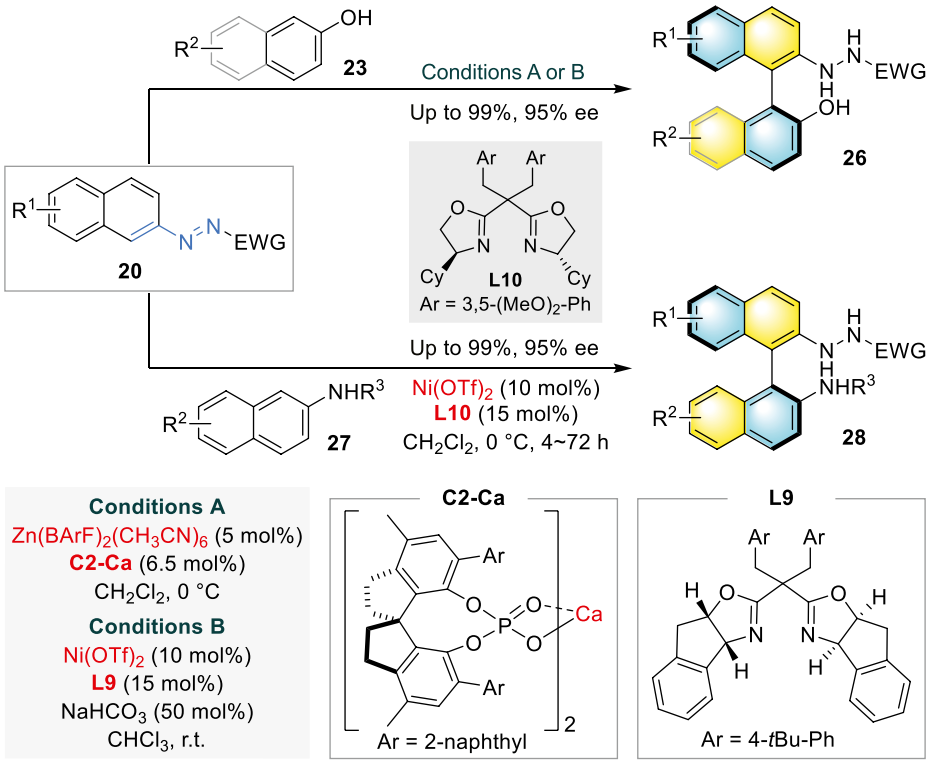

Scheme 19.9. Redox-neutral coupling of azonaphthalenes with aryl alcohols or amines.

19.2.1.2. De Novo Arene Formation Shibata's group achieved rhodium catalytic enantioselective formation of sulfur-containing biaryl atropisomers through a series of cycloisomerization protocols [30]. They envisioned the transformation of aromatic tetraynes **29** into bis(dibenzothiophene) derivatives **30** via successive dehydro-Diels-Alder (DDA) reactions where the thermal variant was incorporated to first yield monocyclized diyne before chiral Rh complex promotes the second asymmetric DDA (Scheme 19.10a) [31]. Axially chiral benzo[b]fluoranthene-based polycyclic aromatic hydrocarbons (PAHs) (**32**) possessing promising photophysical properties were prepared with (*R*,*R*)-Ph-bod diene ligand (**L12**) (Scheme 19.10b) [32]. Site-selective C-C bond scission to form key dibenzometallacyclopentadiene complex **A** is induced by high strain energy of four-membered ring and alkyne association. Tanaka and coworkers studied using palladium or gold(I) complex to achieve biaryl synthesis through intramolecular hydroarylation of alkynones or *N*-aryl alkynylamides-benzenoid [33, 34].

19.2.1.3. Atroposelective Functionalization of Prochiral/Racemic Biaryls

19.2.1.3.1. Asymmetric Ring-Opening Transformation Atroposelective functionalization of preformed biaryls is another major reaction mode explored. This could embody dynamic kinetic resolution (DKR) and kinetic resolution (KR) for racemic substrates or desymmetrization for prochiral biaryls.

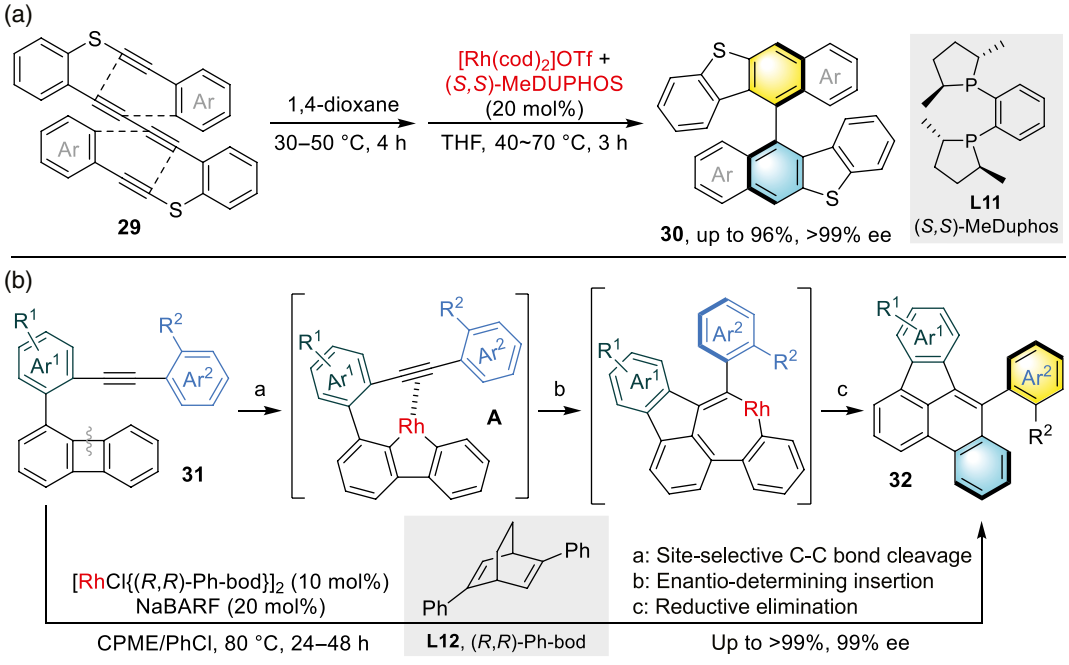

Scheme 19.10. Rh-catalyzed cycloisomerization reactions. (a) Access of axially chiral bis(dibenzothiophene) derivatives via sequential thermal and metal-catalyzed dehydro-Diels–Alder (DDA) reactions. Source: [31]/John Wiley & Sons. (b) Access of PAHs via C–C bond activation of biphenylenes. Source: [32]/American Chemical Society.

Atroposelective ring-opening reaction of five- or six-membered-ring-fused biaryls, which isomerize rapidly via ring-opening/closing, is a notable DKR concept founded by Bringmann [35]. Zhang et al. developed *O*-SpiroPAP ligand **L13** to reduce bridged biaryl lactones **33** asymmetrically with molecular hydrogen in the presence of iridium catalyst in excellent yield and enantiomeric excess (Scheme 19.11) [36]. The DKR could occur during reduction of biaryl lactone or both biaryl lactone and lactol, depending on the stability of the constituted chiral axis (substrate dependent).

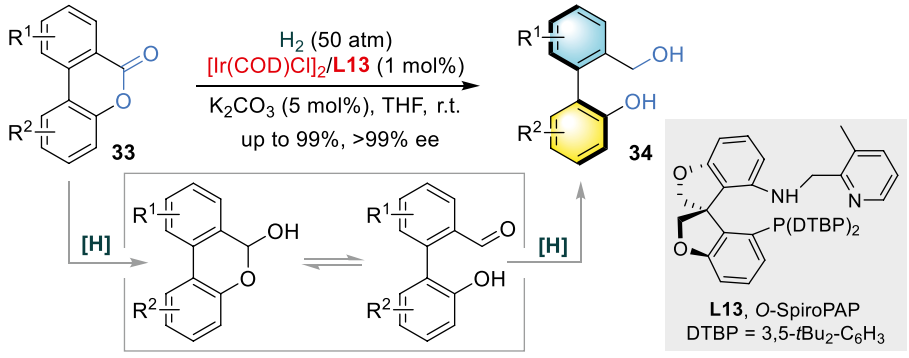

Scheme 19.11. Ir-catalyzed asymmetric hydrogenation of bridged biaryl lactones. Source: [36]/American Chemical Society.

Gu's group accomplished Cu-catalyzed highly atropoenantioselective ring-opening amination [37–39], thiolation [40], and oxygenation [41] reactions to form biaryliodides **36** from cyclic diaryliodoniums

35 that possess two *ortho*-substituents neighboring the biaryl linkage. This structural feature promotes ring-opening to release the torsional strain and enhances axial stability in atropisomerically enriched products (**36A-D**). Nucleophile adds selectively at the less sterically hindered site for unsymmetrical substrates (Scheme 19.12).

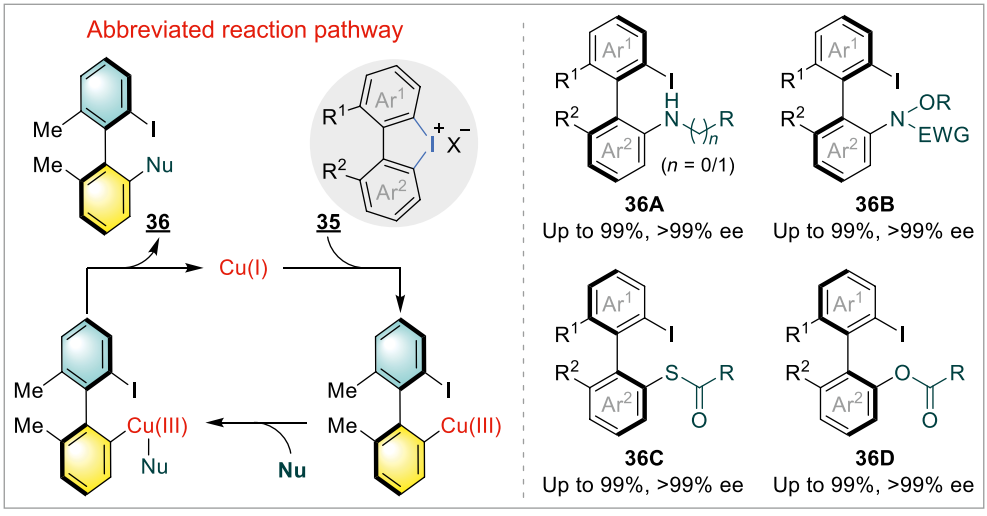

Scheme 19.12. Atroposelective ring-opening reactions of cyclic diaryliodoniums.

19.2.1.3.2. Ortho-*C-H Functionalization* The design logic of *ortho*-C-H functionalization or functionalization of *ortho*-substituent lies in congesting the chiral axis by substituting the hydrogen or small substituent with larger group, which will rigidify the originally labile axis. Shi and coworkers united *ortho*-C-H functionalization and transient directing group chemistry to access a suite of atroposelective C-H functionalization reactions for biaryl aldehydes **37** (Scheme 19.13). The amino acid first condenses reversibly with aldehyde, giving equilibrating imine mixtures of **int-1** and **int-2.** Steric factor governs C-H cleavage in one diastereomer to form atropo-enantioenriched biaryl palladacycle **int-3** as key intermediate. Under this strategy, atroposelective alkenylation (**38A**) [42], allylation (**38B**) [43], alkynylation (**38C**) [44], and naphthylation (**38D**) [45] have been realized through KR, DKR, or desymmetrization, depending on substrates applied. Extension of this chemistry delivered alkynylated heteroatropisomers (**39**) [46] and axially chiral styrenes (**40**) [47]. By means of electrocatalysis, this chemistry was utilized by Ackermann's group to procure biaryl aldehydes (**38A**) without an organic oxidant [48].

19.2.1.3.3. Functionalization of Ortho-*Substituents* Wang's work detailed the co-catalysis of iridium complex **43** and pentafluorobenzoic acid to mediate redox-neutral atroposelective amination of phenol-benzyl alcohol **41** with aniline via "borrowing hydrogen" chemistry (Scheme 19.14) [49]. The aldehyde intermediate forms interconverting imines through lactol, from where selective reduction proceeds.

19.2.2. Heterobiaryl Atropisomers

19.2.2.1. Stereoselective Formation of Aryl-Heteroaryl Bond By utilizing Pd(0) and H_8-BINAPO ligand **L14**, Cramer, Baudoin, and coworkers reported on highly enantioselective C-H arylation of 1,2,3-triazoles **45** with 1-bromo-2-alkoxyarene **44** (Scheme 19.15) [50]. A correspondence between reaction enantioselectivity and biaryl dihedral angle of ligand led to proposal of a stereodetermining reductive elimination step.

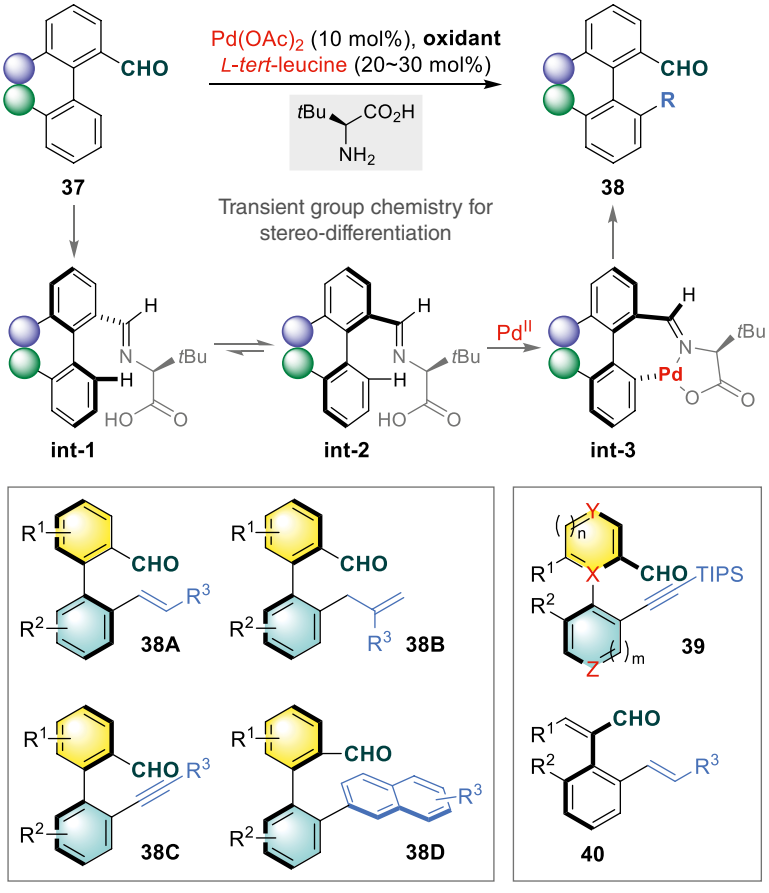

Scheme 19.13. Atroposelective C-H functionalization with transient directing group strategy.

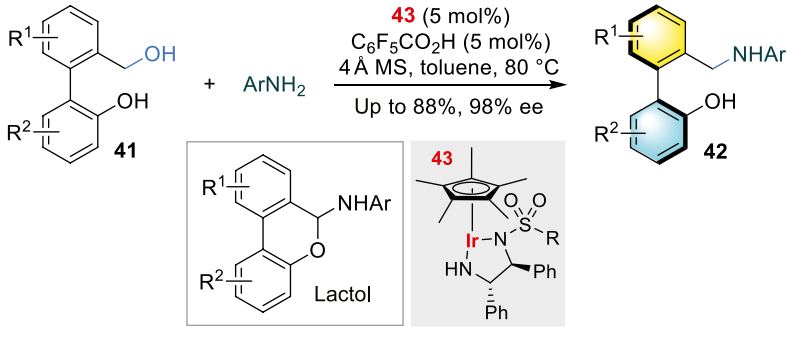

Scheme 19.14. Redox-neutral amination of phenol-benzyl alcohols. Source: [49]/John Wiley & Sons.

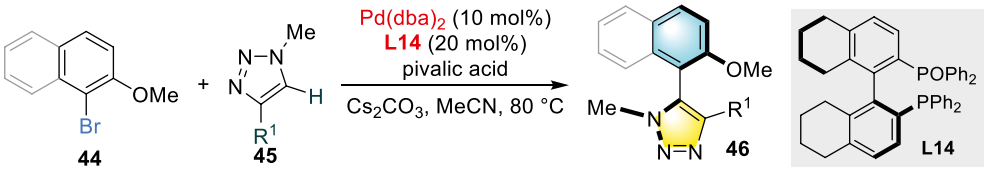

R1 = Ph, **46a**, 93%, 90% ee
R1 = *i*Pr, **46b**, 77%, 65% ee
R1 = 2-Me-Ph, **46c**, 91%, 45% ee
R1 = 4-Me-Ph, **46d**, 98%, 90% ee

Scheme 19.15. Atroposelective C-H arylation of 1,2,3-triazoles. Source: [50]/American Chemical Society.

19.2.2.2. De Novo Heteroarene Formation Combining acidic $Fe(OTf)_3$ and (*S*)-**C3,** Paal-Knorr reaction of 1,4-diones **47** and *ortho*-substituted anilines **48** was achieved asymmetrically by the Tan group to afford arylpyrroles **49** with *N*-aryl chiral axis (Scheme 19.16) [51]. A solvent swap of cyclohexane to ethanol intriguingly provided enantiomeric products (*ent*-**49**) in modest enantioselectivity. Product **49** is formed from enantiodetermining dehydrative cyclization of isolable enamine intermediate **50**.

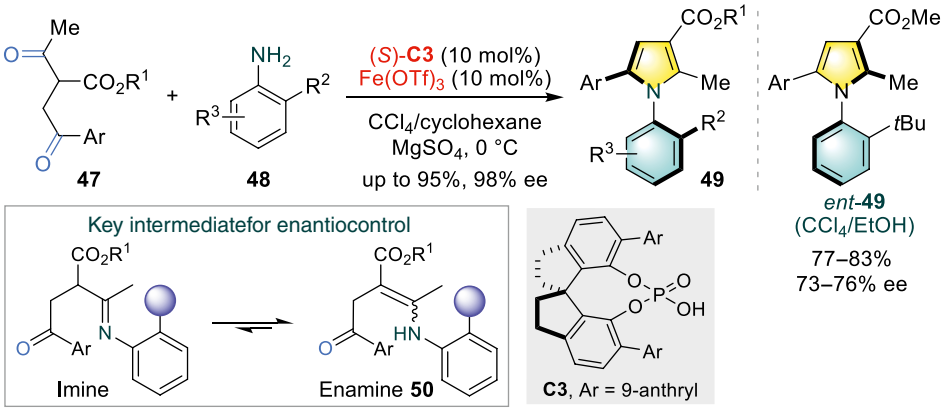

Scheme 19.16. Asymmetric Paal-Knorr reaction toward arylpyrrole atropisomers. Source: [51]/American Chemical Society.

Zhu and coworkers included silver oxide and cinchona alkaloid-derived phosphine ligand (**L15**) for heteroannulation of α-isocyanoacetates **52** with β-aryl-α,β-alkynic ketones **51** that yielded 3-arylpyrrole atropisomers **53** (Scheme 19.17a) [52]. Electron-rich carbonyl substituent minimized competitive 1,2-addition, thus improving reaction efficiency. They prepared 2,3-disubstituted indoles **55** with C2-aryl stereogenic axis via asymmetric Cacchi reaction between *N*-aryl(alkyl)sulfonyl-2-alkynyl anilides **54** and arylboronic acids (Scheme 19.17b) [53]. *anti*-Aminopalladation and reductive elimination proceeds from **int-A** with minimal repulsion between the bulkier aryl substituent and ligand.

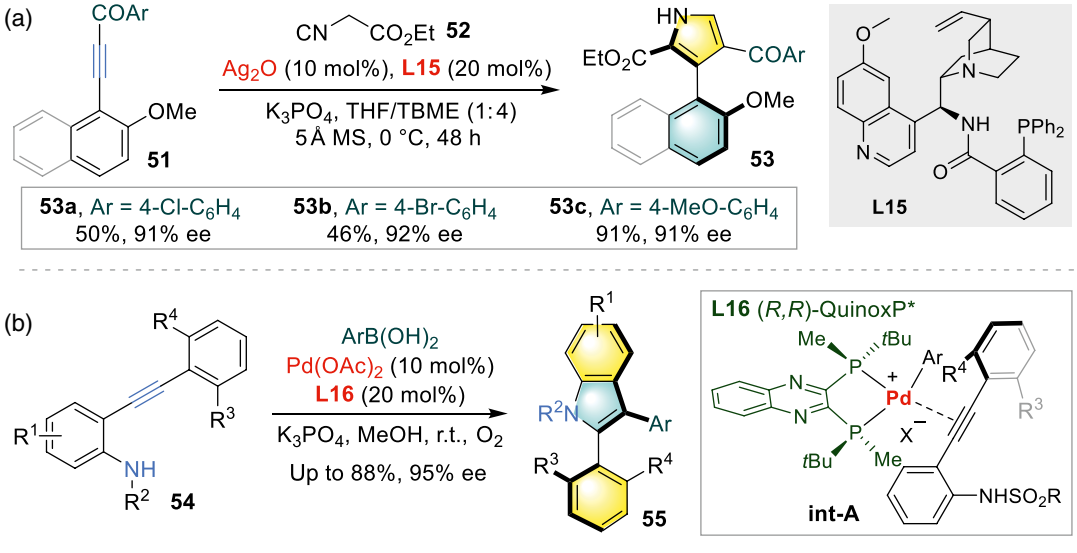

Scheme 19.17. Asymmetric heteroannulation toward atropisomeric pyrrole derivatives. (a) Silver-catalyzed asymmetric heteroannulation toward 3-arylpyrroles. Source: [52]/John Wiley & Sons. (b) Palladium-catalyzed Cacchi reaction toward 2-arylindoles. Source: [53]/John Wiley & Sons.

An exceedingly powerful Rh(III) catalytic system (**59**) was invented by Li and coworkers to synthesize highly enantioenriched but also highly stereolabile 2,3′-biindolyl atropisomers **58** via C-H activation and nucleophilic cyclization from indoles **56** and *o*-alkynylanilines **57** (Scheme 19.18) [54].

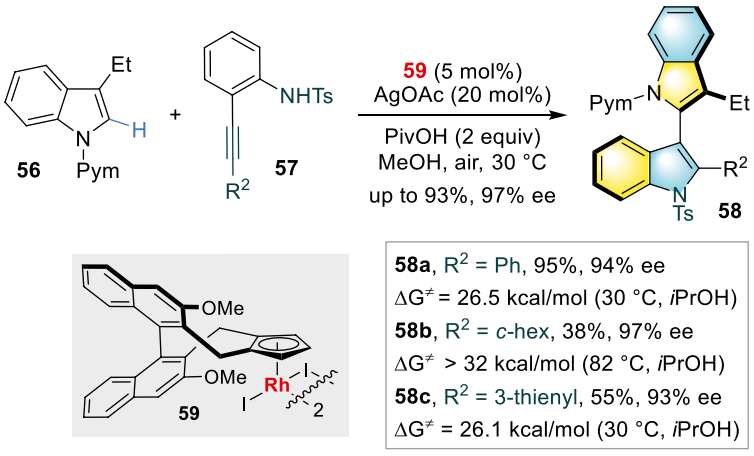

Scheme 19.18. Rh-catalyzed synthesis of 2,3′-biindolyls. Source: [54]/American Chemical Society.

Kato and coworkers illustrated using Pd(II)/chiral bisoxazoline (**L17**) complex to synthesize bisbenzothiophenes **61** from precursor **60** through the formation of benzothiophene in tandem before dimerization (Scheme 19.19) [55]. The chiral box ligand increases alkynophilicity of benzothienyl Pd(II) intermediate for coordination of another alkyne reactant.

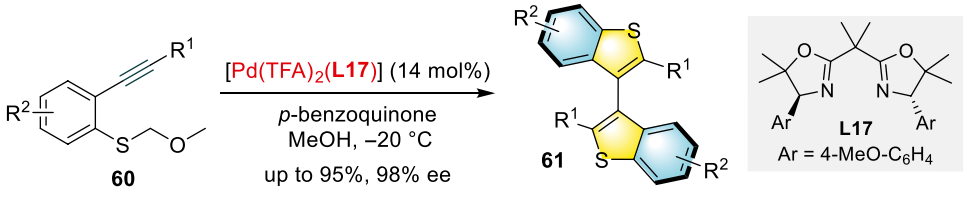

Scheme 19.19. Pd-catalyzed cyclizative dimerization to form bisbenzothiophenes. Source: [55]/John Wiley & Sons.

19.2.2.3. Atroposelective Functionalization of Prochiral/Racemic Heterobiaryls

19.2.2.3.1. C-H Functionalization You and coworkers described the application of Cramer Cp^{x}Rh catalysts (*R*)-**64-1** and (*S*)-**64-2** to perform asymmetric oxidative coupling of benzo[h]isoquinolines **62** with olefins (Scheme 19.20) [56]. (*S*)-**64-2** could improve reaction stereoselectivity at reduced temperature (**63a**) [57]. Going further, they realized atroposelective C-H arylation of *N*-heterocycles containing 2-pyridine derivatives with bromide partners [58] as well as oxidative C-H/C-H cross-coupling between 1-aryl isoquinoline derivatives and electron-rich heteroaromatics [59].

On the other hand, axially chiral *N*-arylpyrroles were efficiently acquired by Meggers, Houk, and coworkers through chiral-at-metal rhodium Lewis acid catalyzed atroposelective C-H functionalization. The acylpyrazole moiety was essential to the success of transformation [60].

19.2.2.3.2. Functionalization of Ortho-*Substituent* Lewis acid-base interaction between heterocyclic *N* atom and carbonyl carbon in ketone precursors **65** could induce rapid racemization (**int-1**). This was demonstrated in Lassaletta's synthesis of heterobiaryl carbinols **66** with point and axial chirality through zinc-catalyzed asymmetric hydrosilylation via DKR (Scheme 19.21) [61].

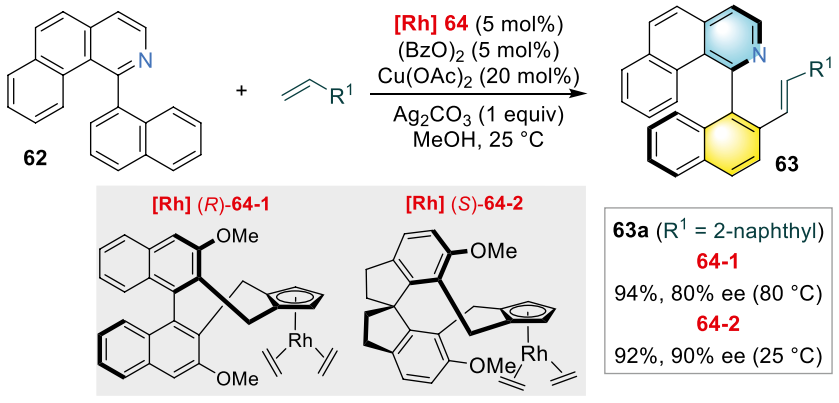

Scheme 19.20. Rh-catalyzed oxidative olefination of benzo[h]isoquinolines. Source: [56]/John Wiley & Sons.

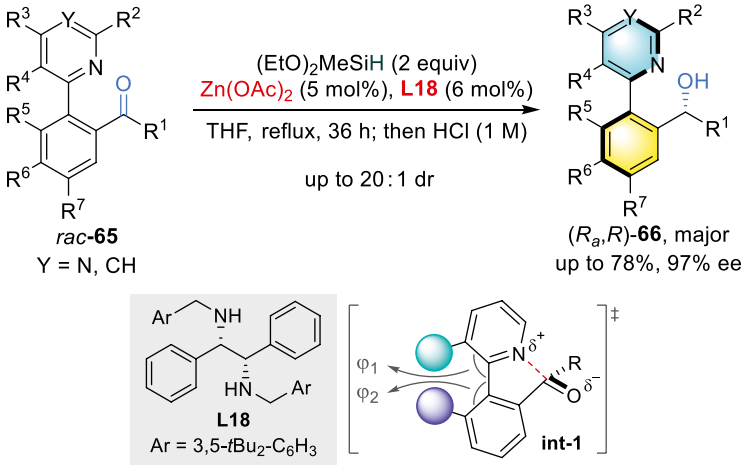

Scheme 19.21. Asymmetric hydrosilylation of heterobiaryl ketones. Source: [61]/John Wiley & Sons.

19.2.2.3.3. Dynamic Kinetic Asymmetric Transformation (DYKAT) Lassaletta and coworkers also exemplified dynamic kinetic asymmetric transformation (DYKAT) to procure enantioenriched heterobiaryls from conformationally stable isoquinoline triflate derivatives **67a** (Scheme 19.22). The widening of Ψ_1 and Ψ_2 in the five-membered cyclic cationic oxidative addition complex (**OAI**, **OAI'**) promotes rotation of the otherwise rigid chiral axis, thus inducing facile axial interconversion. This reactivity principle underlies that Suzuki-Miyaura coupling (**68**) [62], C-P bond formation (**69**) [63, 64], Buchwald-Hartwig amination (**70**) [65], alkynylation (**71**) [66], and Heck reaction (**72A-B**) [67] successfully worked on heterobiaryl triflates or their analogues **67**.

19.2.3. Nonbiaryl Atropisomers

19.2.3.1. Stereogenic C-N Axis

19.2.3.1.1. Stereoselective Formation of C-N Bond Wencel-Delord et al. deployed mild Cu-catalyzed Ullmann-type $C_{(aryl)}$-N coupling conditions to form nonbiaryl C-N atropisomers **75** with highly reactive hypervalent iodine reagents **73** (Scheme 19.23) [68]. Strong nonlinear amplification was observed, pointing to existence of (Cu-**L19**)$_n$ metallic species that is much more reactive.

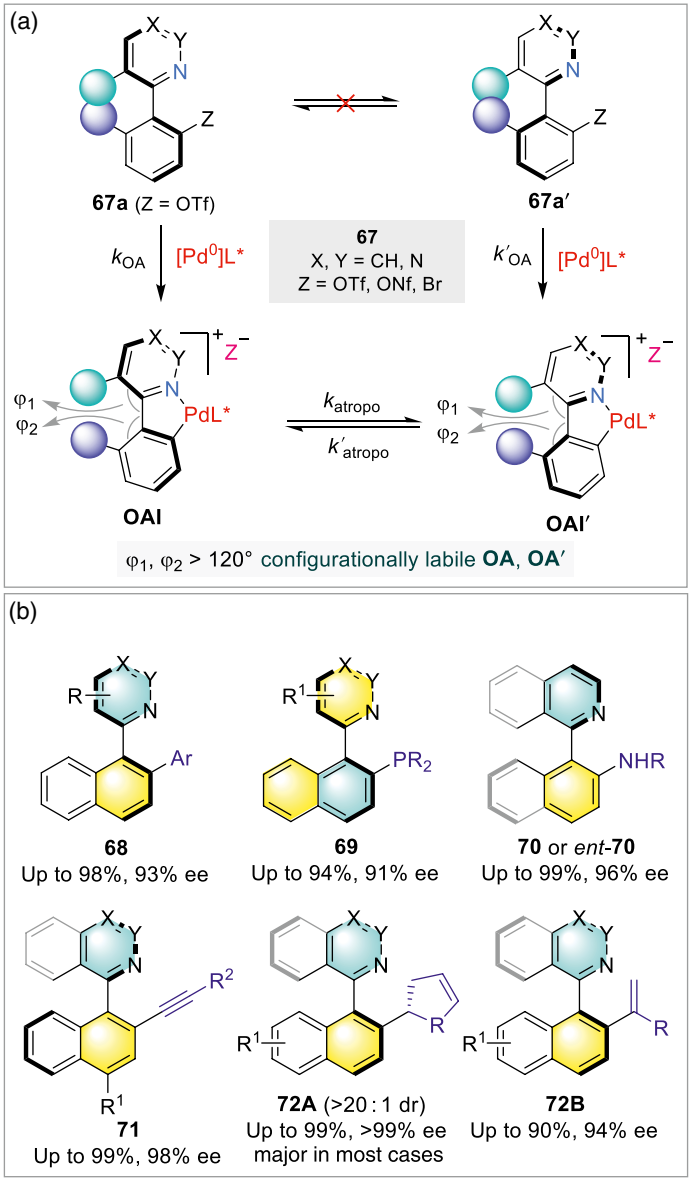

Scheme 19.22. DYKAT of stable heterobiaryl atropisomers. (a) General mechanistic pathway. (b) Heterobiaryl atropisomers derived from DYKAT of **67**.

In the same year, N-C stereogenic axis of axially chiral enamides was efficiently synthesized by He, Liu, and coworkers via iridium/chiral ligand catalyzed asymmetric allylic substitution and hydrogen-bonding-directed central-to-axial chirality conversion [69].

19.2.3.1.2. Atroposelective Functionalization on Preformed Nonbiaryl C-N Scaffold Aside from atroposelective *N*-functionalization commonly encountered in anilide synthesis, Wang and coworkers conducted atroposelective Satoh-Miura-type reaction with spiro-CpRh catalyst (*R*)-**64-2** on *N*-aryloxindoles **76** and alkynes **77** via dual C-H activation (Scheme 19.24) [70].

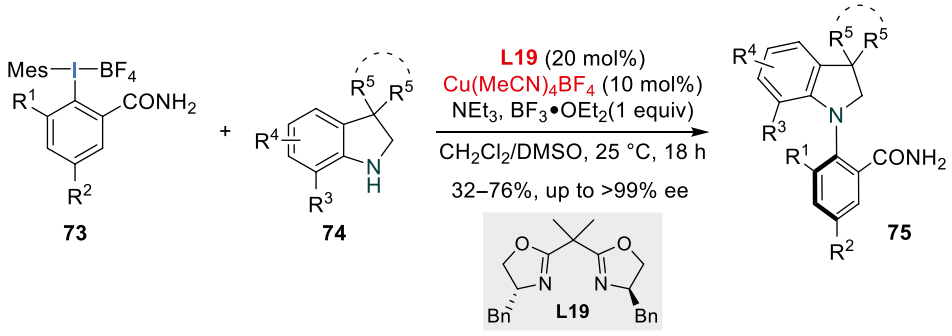

Scheme 19.23. Copper-catalyzed asymmetric aryl amination. Source: [68]/John Wiley & Sons.

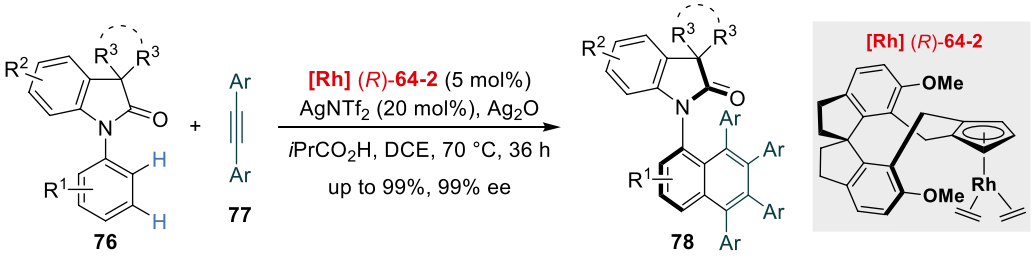

Scheme 19.24. Atroposelective Satoh-Miura-type reaction. Source: [70]/John Wiley & Sons.

Shi and Hong conceived Pd(II)-catalyzed atroposelective *ortho* C-H olefination for anilides **79** by using *L*-pyroglutamic acid ligand (Scheme 19.25) [71]. Distortion of chiral amino acid accounts for stereoselectivity during C-H activation.

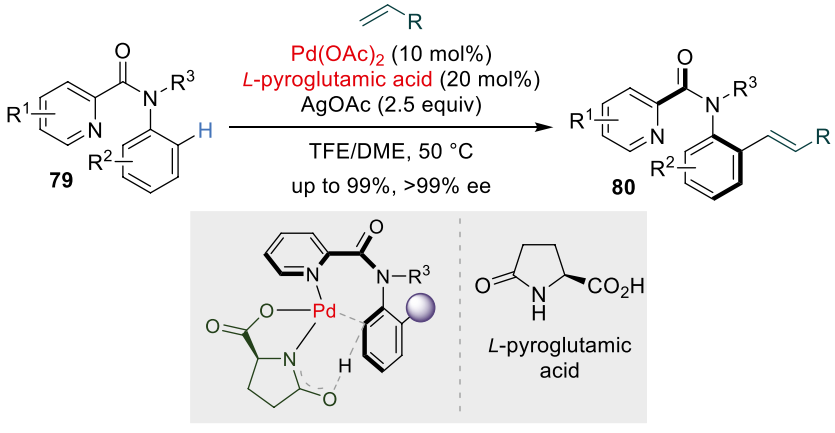

Scheme 19.25. Axially chiral anilides generated from asymmetric C-H olefination. Source: [71]/American Chemical Society.

19.2.3.1.3. Atroposelective N*-Annulation* Phenanthridin-6-one derivatives **82** with nitrogen connected to *ortho*-substituted arene were generated through asymmetric intramolecular Buchwald-Hartwig or Ullmann-type amination of **81** (Scheme 19.26) [72, 73].

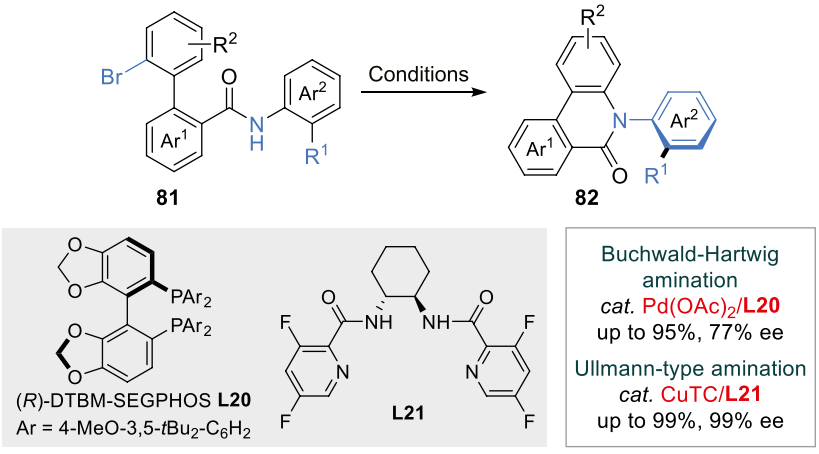

Scheme 19.26. Atroposelective intramolecular amination. Source: Based on [72] and [73].

19.2.3.2. Stereogenic C-C Axis

19.2.3.2.1. Atroposelective $C_{(aryl)}$-$C_{(alkenyl)}$ Bond Formation The combination of palladium catalyst and BoPhoz-type ligand **L22** allowed coupling of 2-iodo-3-methylcyclohex-2-enone (**83**) and naphthalene boronic acids (**84**) to form 2-aryl cyclohex-2-enone atropisomers **85** (Scheme 19.27) [74]. The enone entity could undertake a wealth of follow-up chemistry. Other $C_{(aryl)}$-$C_{(alkenyl)}$ bond formation methods to synthesize chiral styrenes involve palladium-catalyzed asymmetric coupling of aryl bromides and hydrazones [75].

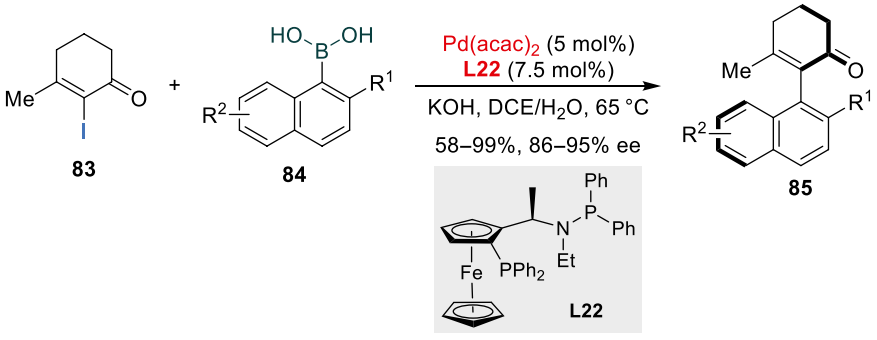

Scheme 19.27. Asymmetric synthesis of 2-aryl cyclohex-2-enone atropisomers. Source: [74]/John Wiley & Sons.

19.2.3.2.2. Alkyne Annulation Ni(0)-catalyzed denitrogenative transannulation of 1,2,3-benzotriazin-4(3*H*)-ones **86** with bulky internal alkynes afforded 3-arylisoquinolones **87** with chiral *N*-$C_{(aryl)}$ axis, as reported by Liu, Tan, and coworkers (Scheme 19.28a) [76]. The differing substituent size on alkyne allows regioselective nickel-carbon bond insertion whereas steric effect between chiral ligand and large substituent (R_L) determines the axis disposition (**int-B**). Waldmann's group derived 4-arylisoquinolones **89** by rhodium(III)-catalyzed C-H bond activation and intramolecular annulation of **88** (Scheme 19.28b) [77].

19.2.3.2.3. Atroposelective Functionalization of Aryl-Alkene scaffold The ketoxime directing group in 2-aryl cyclohex-2-enone **91** with preformed aryl-alkene scaffold enabled atroposelective olefination to introduce axial chirality in **92** by the way of palladium-catalyzed C-H olefination (Scheme 19.29a) [78].

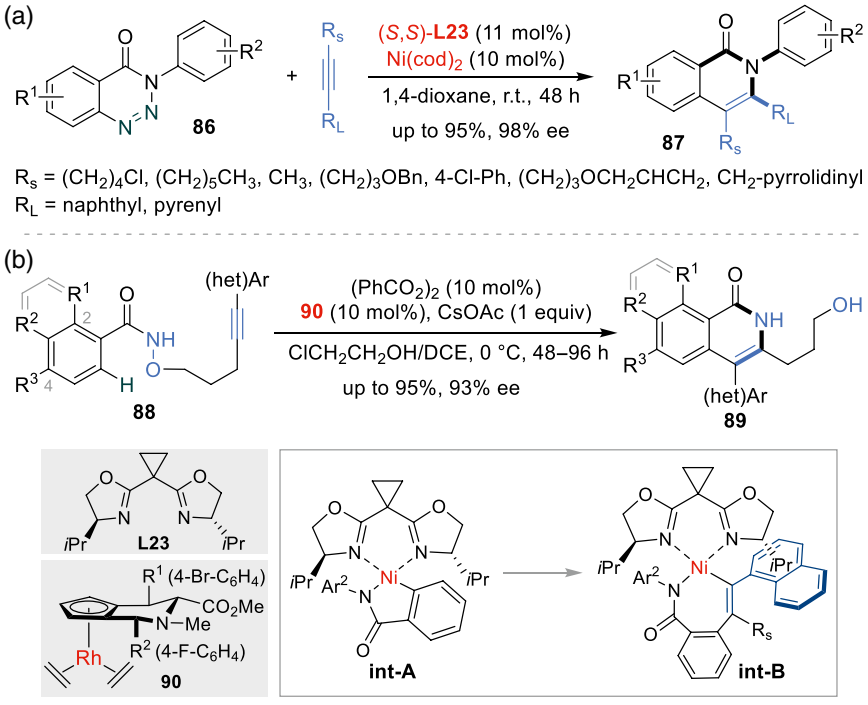

Scheme 19.28. Alkyne annulation in synthesis of axially chiral isoquinolones. (a) Ni-catalyzed denitrogenative transannulation. Source: [76]/John Wiley & Sons. (b) Rh-catalyzed C–H activation and intramolecular [4+2] annulation. Source: [77]/John Wiley & Sons.

The Shi group installed pyridine directing group (**93**) and used *L*-pyroglutamic acid ligand to establish C-H alkenylation and alkynylation for accessing **94** and **95** (Scheme 19.29b) [79]. More recently, Wang et al. reported the construction of axially chiral styrenes-type carboxylic acids through palladium-catalyzed atroposelective C-H arylation or olefination reactions with amino acid derivative as the chirality source [80].

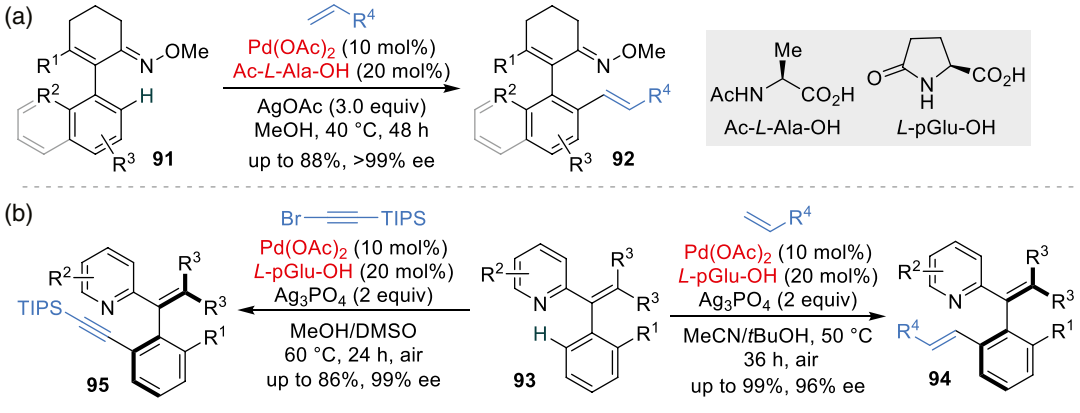

Scheme 19.29. Atroposelective C–H functionalization of aryl alkenes. (a) Palladium-catalyzed ketoxime-directed C–H olefination. Source: [78]/Royal Society of Chemistry. (b) Palladium-catalyzed C-H alkenylation and alkynylation of aryl alkenes with pyridine directing group. Source: [79]/ELSEVIER.

19.3. ORGANOCATALYSIS

19.3.1. Biaryl Atropisomers

19.3.1.1. Formation of C(aryl)-C(aryl) Bond An explosion of interest has been observed in metal-free catalytic atroposelective synthesis of axially chiral scaffolds following Kürti's and List's contemporaneous disclosures on CPA catalytic formation of BINAM in 2013 [81, 82]. Organocatalytic arylation generally exploits the nucleophilicity of aromatic nucleophiles (alcohols, amines, heteroarenes) for the addition with elaborated electrophiles (quinones, azonaphthalenes, etc.). After stereoselective addition, intermediate with defined point chirality aromatizes with central-to-axial chirality conversion. On (*R*)-**C4**-catalyzed arylation of ester quinones **96** with 2-naphthols **23**, Tan and coworkers illustrated the synthesis of non-symmetric biaryldiol **97** in good efficiency with excellent enantioselectivities (Scheme 19.30) [83]. Salvio and Bella complemented this reaction with organo-quinine catalyst [84] while Miller's method enlisted Lewis basic tetrameric peptide catalyst [85].

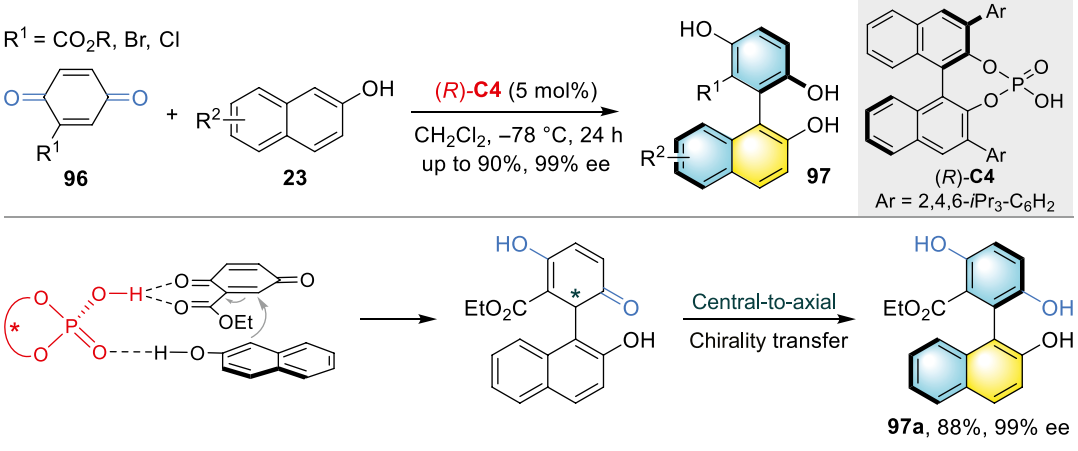

Scheme 19.30. CPA-catalyzed direct arylation of 2-naphthols with quinones. Source: [83]/American Chemical Society.

Xu and Kürti examined the asymmetric addition of different aromatic alcohols **23** with *N*-sulfonyl iminoquinones **98** to obtain biaryldiols **99** using (*S*)-**C4** (Scheme 19.31) [86]. In contrast to 1,4-addition pathway proposed by Tan and coworkers (Scheme 19.30), hydroxy addition onto iminoquinone to form

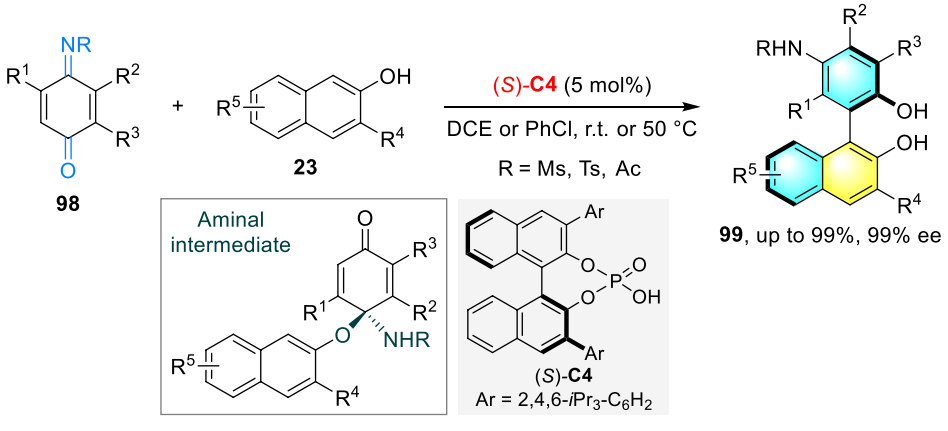

Scheme 19.31. CPA-catalyzed arylation of hydroxyarenes with *N*-sulfonyl iminoquinones. Source: [86]/American Chemical Society.

chiral aminal intermediate before [3,3]-rearrangement and aromatization was envisioned due to the low enantioselectivity observed in products that arose from symmetric or pseudosymmetric aminal intermediate.

19.3.1.2. De Novo Arene Formation Sparr's group developed organocatalyzed atroposelective arene-forming aldol reaction that patterned after aromatic polyketide biosynthesis [89]. Amine catalyst forms dienamine with aldehyde **100**, which is poised to perform stereoselective intramolecular aldol addition with tethered ketone. Dehydration-aromatization ensues with chirality conversion to provide 1,1′-binap hthalene-2-carbaldehyde **101** (Scheme 19.32a). Treatment of ketoaldehyde **102** with *L*-isoleucine yielded enantioenriched 1,2-ternaphthalene carbaldehyde (*aS*)-**103** containing two stereogenic axes (Scheme 19.32b) [87]. Access to highly encumbered tetra-*ortho*-substituted binaphthalenes **105** from non-canonical hexacarbonyl substrates **104** via two arene ring formation was granted by aminoethanol-derived proline-based catalyst (Scheme 19.32c) [88]. A process with twofold aldol additions followed by a double dehydration was proposed based on the in situ nuclear magnetic resonance (NMR) results analysis.

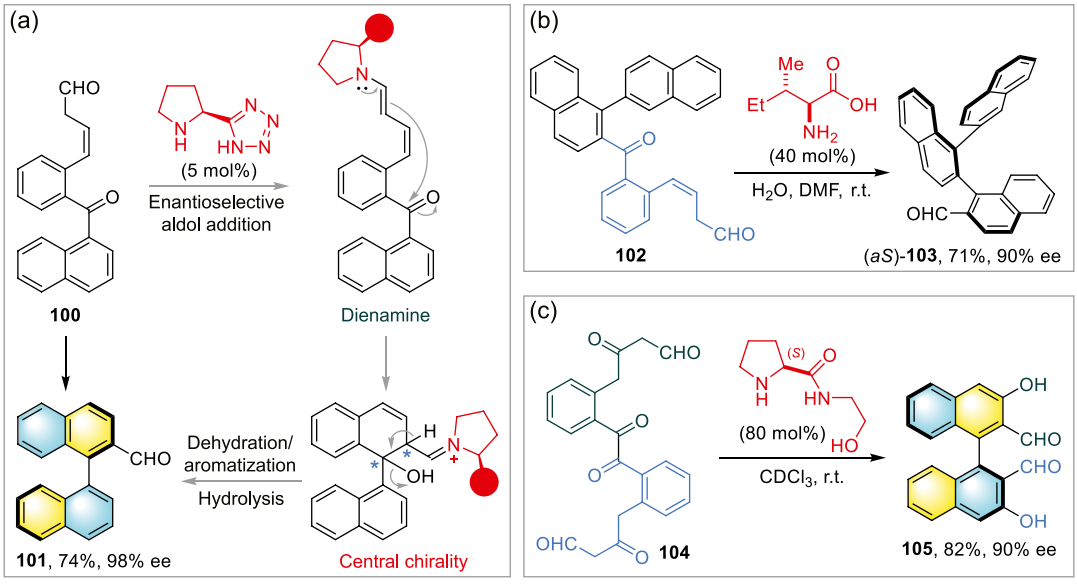

Scheme 19.32. Aminocatalytic atroposelective arene-forming aldol condensation. (a) Application in the synthesis of 1,1'-bin aphthalene-2-carbaldehyde **101**. (b) Application in the synthesis of 1,2-ternaphthalene carbaldehyde **103**. Source: [87]/John Wiley & Sons. (c) Application in the synthesis of tetra-*ortho*-substituted binaphthalenes **105**. Source: [88]/Springer Nature.

The Yan group forged carbo [6] helicenes **107** displaying helical and axial chirality from 2-ethynylnaphthols **106** with bisquinine squaramide catalyst **108** (Scheme 19.33) [90]. After tautomerization to vinylidene *ortho*-quinone methide (VQM) intermediate **A** and nucleophilic cyclization, the generated int-**B** possesses stable stereogenic axis **I** but the barriers to helix inversion and rotation of axis **III** are low. Int-**B** cyclizes diastereoselectively via DKR under catalyst control and generates helical compound with two locked chiral axes **107**.

Tong et al. invented a phosphine-catalyzed atroposelective (4+2) annulation of δ-acetoxy allenoates **109** and 2-hydroxyquinones **110** to forge chiral aryl-naphthaquinones **111** (Scheme 19.34) [91]. Catalyst **112** generates phosphonium diene from **110** and orients it together with allenoate for pseudo-intramolecular [4+2] cycloaddition.

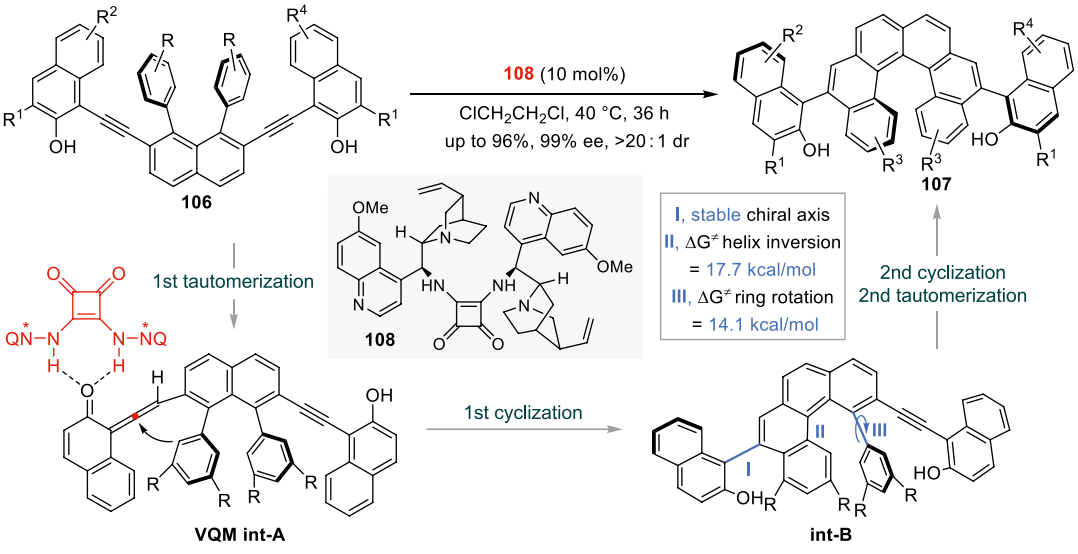

Scheme 19.33. Organocatalytic construction of compounds with helical and axial chirality. Source: [90]/American Chemical Society.

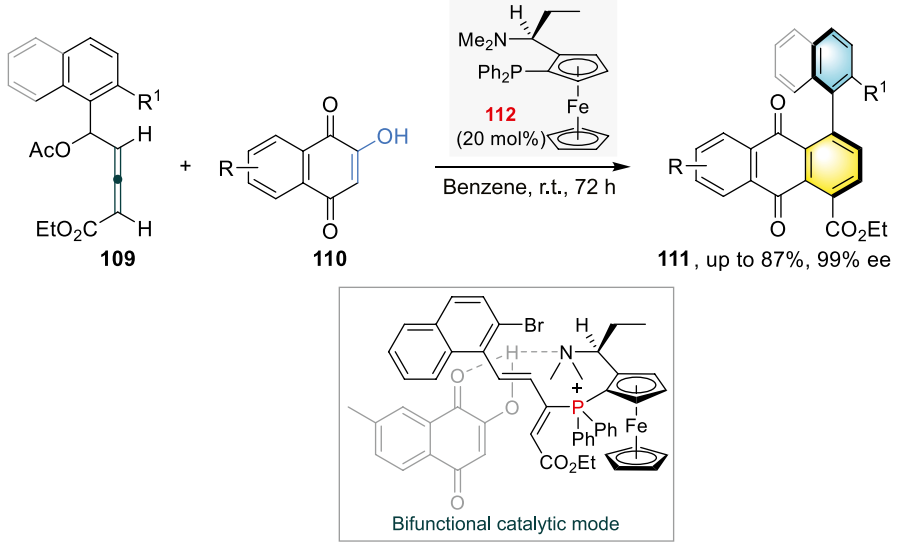

Scheme 19.34. Asymmetric (4+2) annulation of δ-acetoxy allenoates and 2-hydroxyquinones. Source: [91]/Springer Nature.

19.3.1.3. Atroposelective Functionalization of Prochiral/Racemic Biaryls

19.3.1.3.1. DKR By using amine thiourea catalyst **115**, Wang realized the atroposelective transesterification of Bringmann's lactones **113** with benzyl, aliphatic alcohols, and phenols (Scheme 19.35) [92]. The exceptional efficiency and enantioselectivity arose from concurrent activation of tensioned lactone ring and alcohol by thiourea and amine, respectively, for the nucleophilic attack.

Akiyama detailed atropodivergent CPA-catalyzed reductive amination of biaryl lactols **116**, which was achieved through employing regioisomeric hydroxyl anilines **117** (Scheme 19.36) [93]. This chemistry observed effective KR in asymmetric transfer hydrogenation of imine and appropriate rate difference between imine isomerization and the transfer hydrogenation.

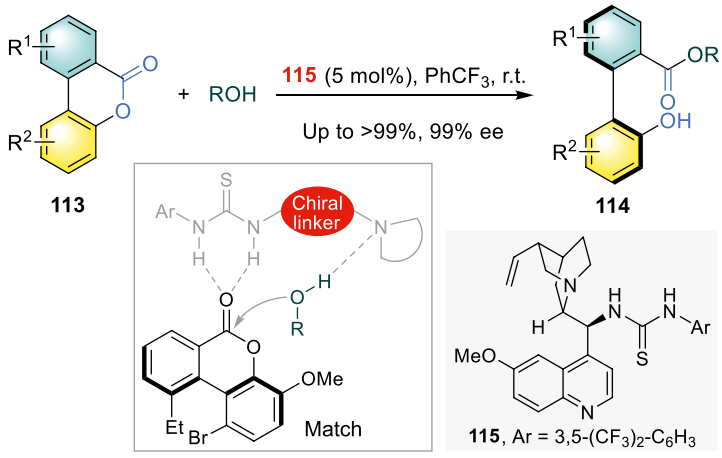

Scheme 19.35. Organocatalytic transesterification of Bringmann's lactones. Source: [92]/Springer Nature.

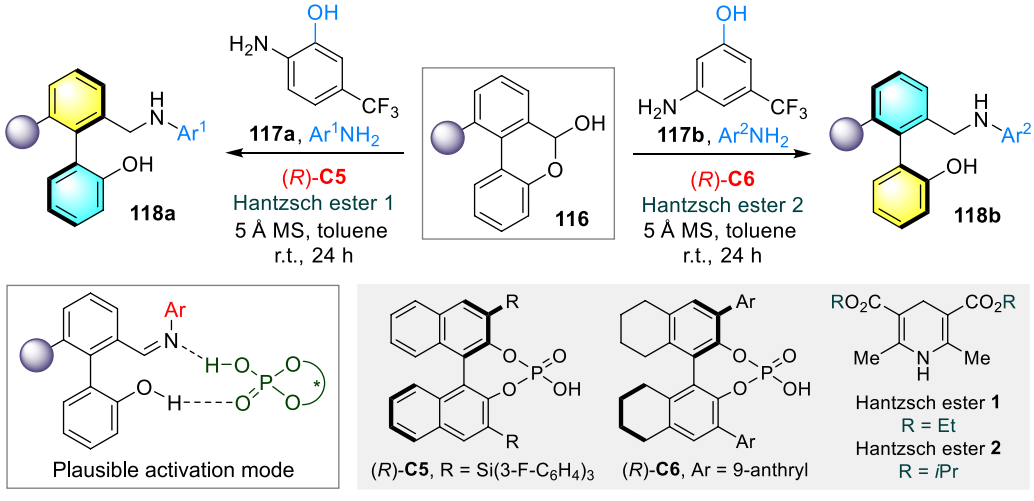

Scheme 19.36. Atropodivergent reductive amination of biaryl lactols. Source: [93]/John Wiley & Sons.

Miller, Toste, and coworkers orchestrated twofold DKR via disparate chemical processes to fabricate two-axis terphenyl atropisomers **121** (Scheme 19.37) [94]. Ring-opening/transesterification of lactones **119** is first aided by strongly basic guanidine peptide catalyst **P1**. Thus-revealed phenol group then facilitates **P2**-catalyzed C-H halogenation at *para*-carbon to form the second chiral axis.

19.3.1.3.2. Desymmetrization Wang and coworkers exemplified NHC-catalyzed acylation of prochiral amino biphenols **122** to derive enantiopure biaryl amino-alcohols **123** (Scheme 19.38) [95]. As corroborated by the control experiments, the desymmetrized atropisomers (**123** and *ent*-**123**) underwent second acylation as KR that further improved the optical purity. The Zhao group reported similar approach [96] while Cheong and Smith utilized isothiourea catalysis for acylation of tri- and tetra-*ortho*-substituted biaryl diols [97].

19.3.1.3.3. KR The application of hydroquinidine (anthraquinone-1,4-diyl) diether ($(DHDQ)_2AQN$) catalyst and Morita–Baylis–Hillman (MBH) carbonate on racemic NOBINs (*rac*)-**125** by Zhao and coworkers has effected *N*-allylative KR that returned stereoisomerically enriched NOBIN analogues (*R*)-**125** and **126** (Scheme 19.39) [98]. The Yang group applied CPA for KR of protecting group-free BINAMs or NOBINs via the formation of triazanes (**128**) with diazocarboxylate [99].

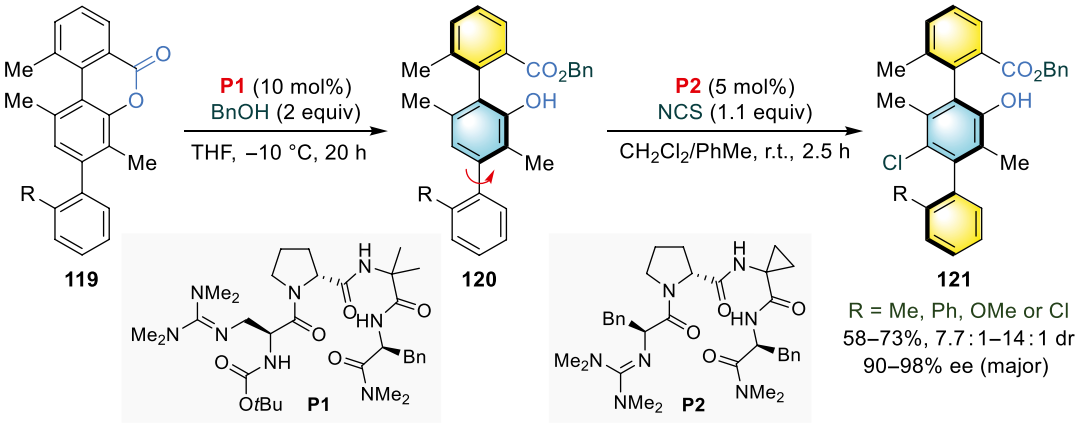

Scheme 19.37. Sequential DKR events catalyzed by peptide catalysts. Source: [94]/American Chemical Society.

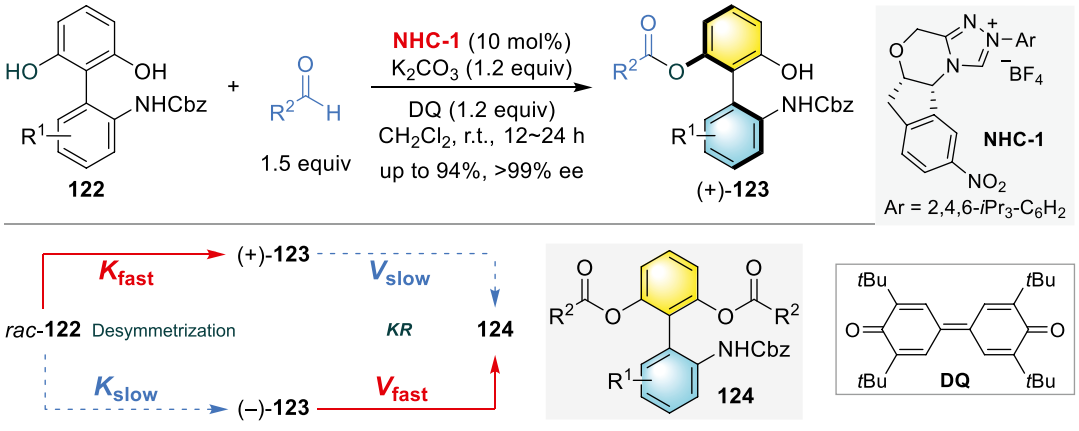

Scheme 19.38. Desymmetrization and secondary kinetic resolution of biaryl amino alcohols. Source: [95]/Springer Nature.

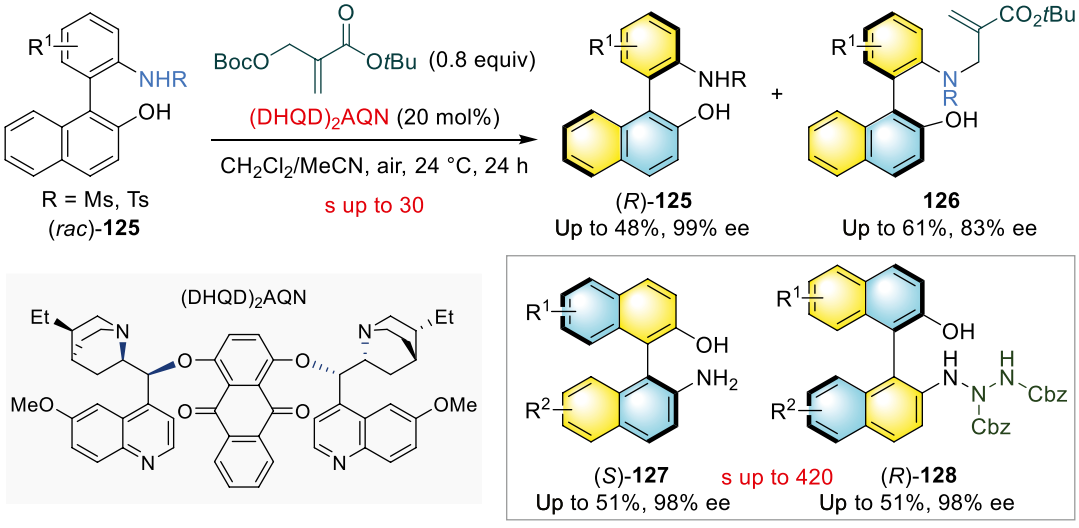

Scheme 19.39. Organocatalyzed KR via *N*-functionalization. Source: [98]/Springer Nature.

Acylative KR of unprotected biaryl diols and amino alcohol **129** was conducted in gram scale with 1 mol% of isothiourea organocatalyst (*R*)-BTM (benzotetramisole) **131** by Smith and coworkers where the unsymmetrical anhydride established only mono-acylation (Scheme 19.40a) [100]. Another group implemented KR/*O*-benzylation using ammonium counterion **134** on mono-protected BINOLs **132** where OH group is reversibly deprotonated to form diastereomeric BINOLate ammonium salts (Scheme 19.40b) [101]. Benzylation occurs at different rates and thus provides enantioenriched **132** and **133**. Distinctively, the Zhou group demonstrated that 5- or 8-substituted quinolines could be resolved through CPA-catalyzed asymmetric transfer hydrogenation of the heteroaromatic ring [102].

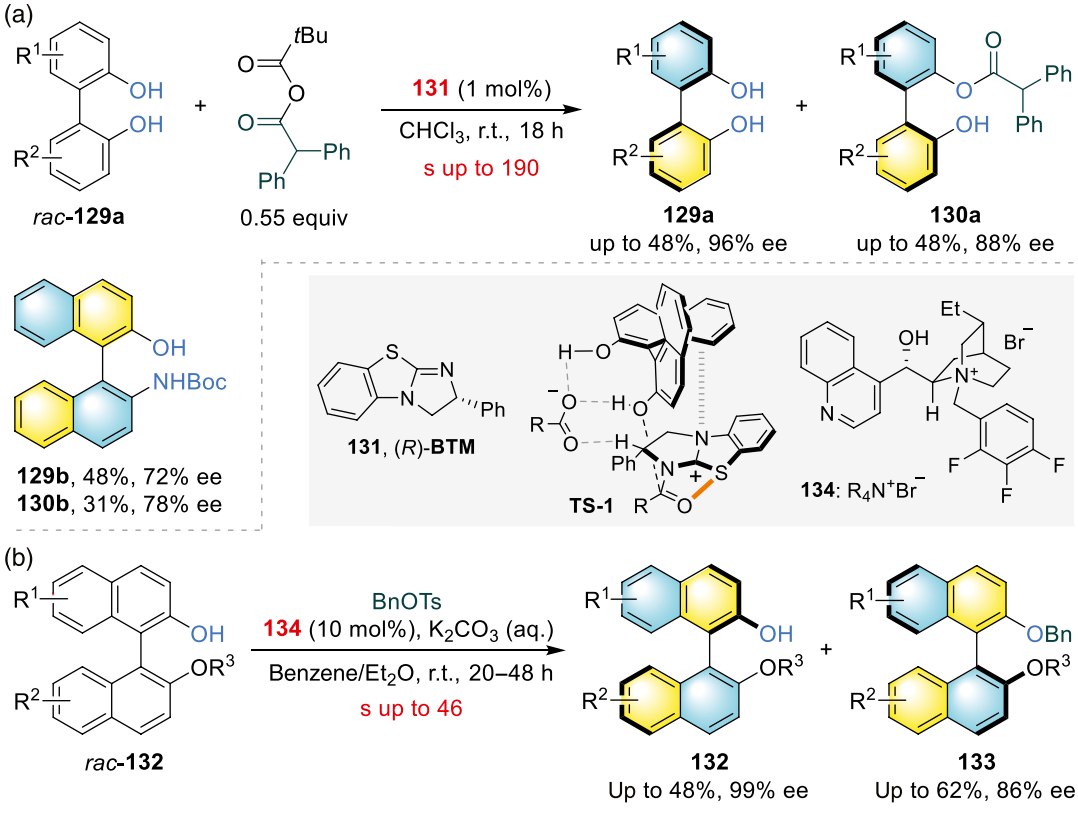

Scheme 19.40. Organocatalyzed KR of BINOLs via *O*-functionalization. (a) Isothiourea-catalyzed *O*-acylation. Source: [100]/John Wiley & Sons. (b) Chiral counterion-mediated *O*-benzylation. Source: [101]/John Wiley & Sons.

19.3.2. Heterobiaryl Atropisomers

19.3.2.1. Stereoselective Formation of Aryl-Heteroaryl Bond As with the case of biaryl atropisomers (19.2.1.1), organocatalyst-derived enantioselective (hetero)aryl-heteroaryl bond formation generally evolves through similar reaction pathway. Varied heteroatropisomers that were synthesized from heteroaromatics taking on the role as nucleophiles while azonaphthalenes and quinones serve as electrophiles were summarized in Scheme 19.41. Tan's group pursued coupling of azonaphthalenes with indoles and carbazoles where the specific substrates and tailored conditions led to partitioned pathways. Under CPA catalysis, azonaphthalenes **20** reacted with indoles **135** through formal nucleophilic aromatic substitution to give atropochiral naphthyl-indoles **136** and aniline-indoles **137** [103]. Pathway divergence was governed by substituent R^3 on **135** where a smaller group promoted another intramolecular attack.

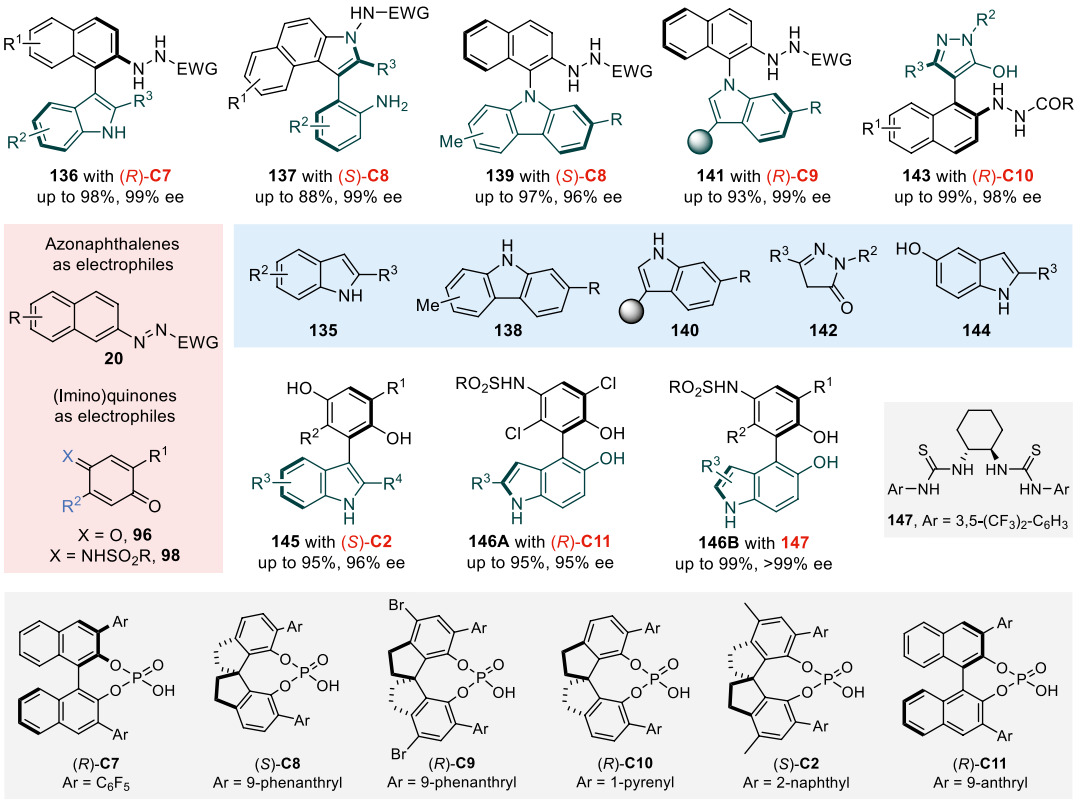

Scheme 19.41. Heteroatropisomers formed from organocatalytic arylation.

On subjection to different conditions with **C8** and **C9** chemoselectivity switched where carbazoles **138** and indoles **140** coupled onto azonaphthalenes **20** through nucleophilic nitrogen sites [104]. Li and coworkers incorporated nucleophilic pyrazolones **142** to furnish pyrazole atropisomers **143** displaying chiral C4-naphthyl axis as catalyzed by **C10** [105].

Li's group demonstrated that by modulating the sterics of substituent (**135**) or ring electronics (**144**), indoles could react from heterocyclic ring (**145**, C3 site) or carbocyclic ring (**146A**, C4 site) when treated, respectively, with quinone and iminoquinone under CPA catalysis [106]. Xu achieved synthesis of **146B** with a chiral hydrogen bond donor **147** instead [107].

While indoles are the usual nucleophiles, the Shi group exemplified using C3-electrophilic 2-indolylmethanols **148** for CPA-catalyzed atroposelective arylation with aromatic alcohols **23** to generate 3-aryl-indoles **149** (Scheme 19.42) [108]. The *gem*-diaryl groups in **148** stabilize the chiral axis and cation intermediate aside from directing regioselectivity.

19.3.2.2. De Novo Arene Formation

19.3.2.2.1. N-*Heteroatropisomers* Many organocatalytic de novo heteroarene formation approaches feature central-to-axial chirality conversion events, leveraging the abundant methods that exist to form partially saturated heterocycles organocatalytically. With this strategy, Bressy, Bugaut, and Rodriguez approached the Hantzsch-type synthesis of axially chiral 4-arylpyridine (*aS*)-**154a** through thiourea-catalyzed Michael addition and MnO_2-mediated oxidative aromatization of chiral 4-aryl-1,4-dihydropyridine intermediate (*S*)-**153a** (Scheme 19.43) [109]. The more accessible hydride in minor conformer *ap*-(*S*)-**153a** is more readily captured by MnO_2.

In similar vein, Bertuzzi, Corti, and coworkers prepared indole-quinoline **155** through Povarov cycloaddition of 3-alkenylindols and *N*-arylimines followed by 2,3-dichloro-5,6-dicyano-*p*-benzoquinone

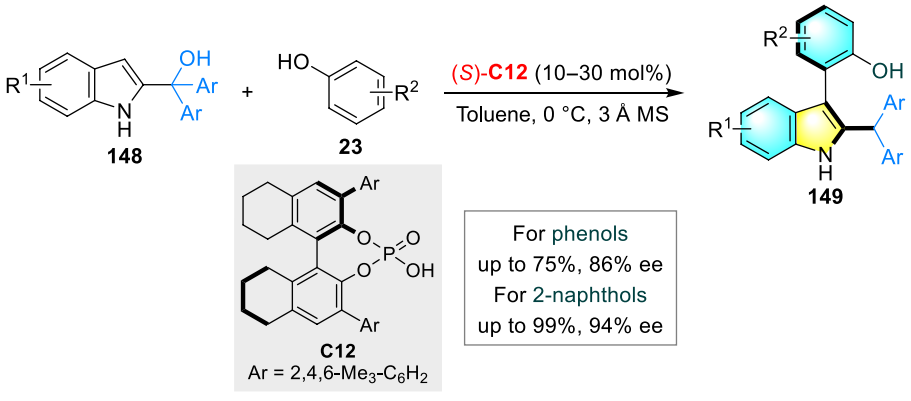

Scheme 19.42. Coupling of aromatic alcohols and electrophilic 2-indolylmethanols. Source: [108]/John Wiley & Sons.

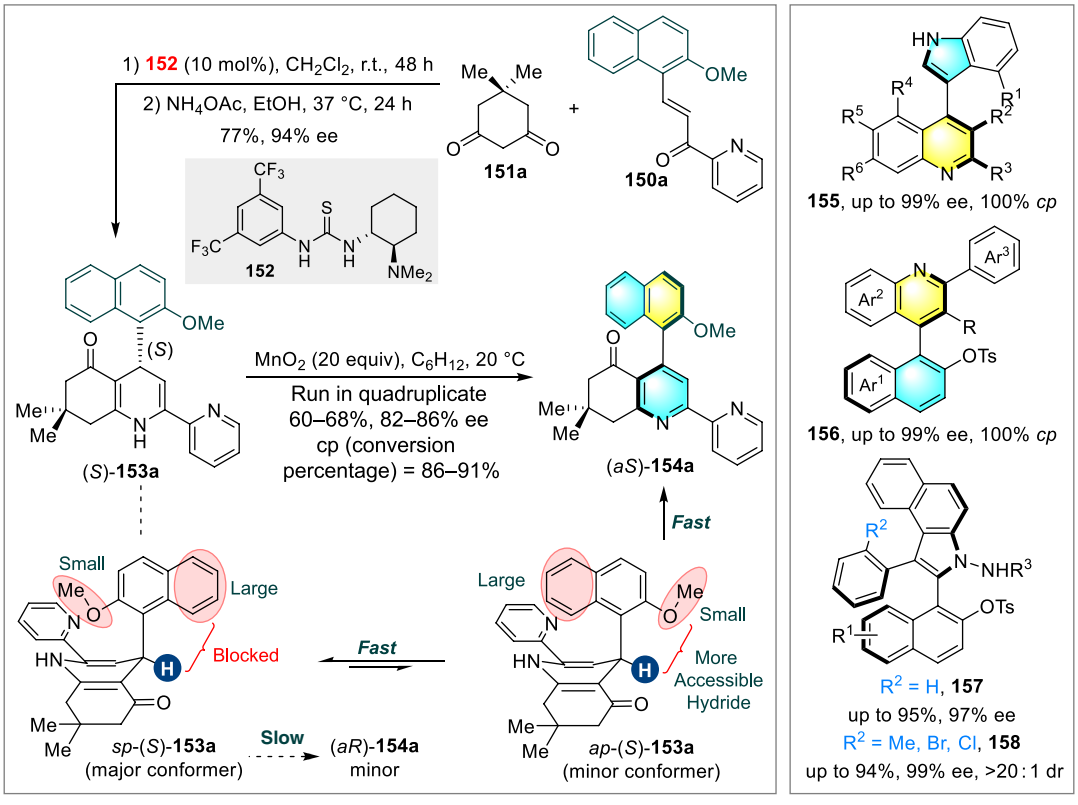

Scheme 19.43. *N*-heterobiaryl atropisomers formed from annulation-oxidative aromatization sequence with central-to-axial chirality conversion. Source: [109]/John Wiley & Sons.

(DDQ)-mediated oxidation [110]. Zhou and Chen deployed Povarov reaction-DDQ oxidation sequence of 1-styryl naphthols, anilines, and benzaldehydes to target quinoline-naphthalene atropisomers **156** [111]. 2,3-Diarylbenzoindoles containing one (**157**) or two (**158**) chiral axes were generated from [3+2] formal cycloaddition between 1-styrylnaphthols and azonaphthalenes followed by oxidative conversion of two stereocenters to one or two chiral axes [112].

Chen performed asymmetric Barton-Zard reaction to access moderately atropostable 3-aryl or 3-heteroaryl pyrroles **162** through union of nitroolefins **159** and α-isocyano substrates **160** with varied electron-withdrawing groups followed by central-to-axial chirality transfer (Scheme 19.44a) [113]. Interestingly, enantioenriched 3-arylpyrroles **164** could arise from KR of racemic 3,4-dihydro-2*H*-pyrroles **163** through sequential *syn* elimination of HNO_2 and aromatization of 2*H*-pyrrole where thiourea unit of **115** associates with nitro moiety while tertiary amine group performs C-H abstraction (Scheme 19.44b) [114].

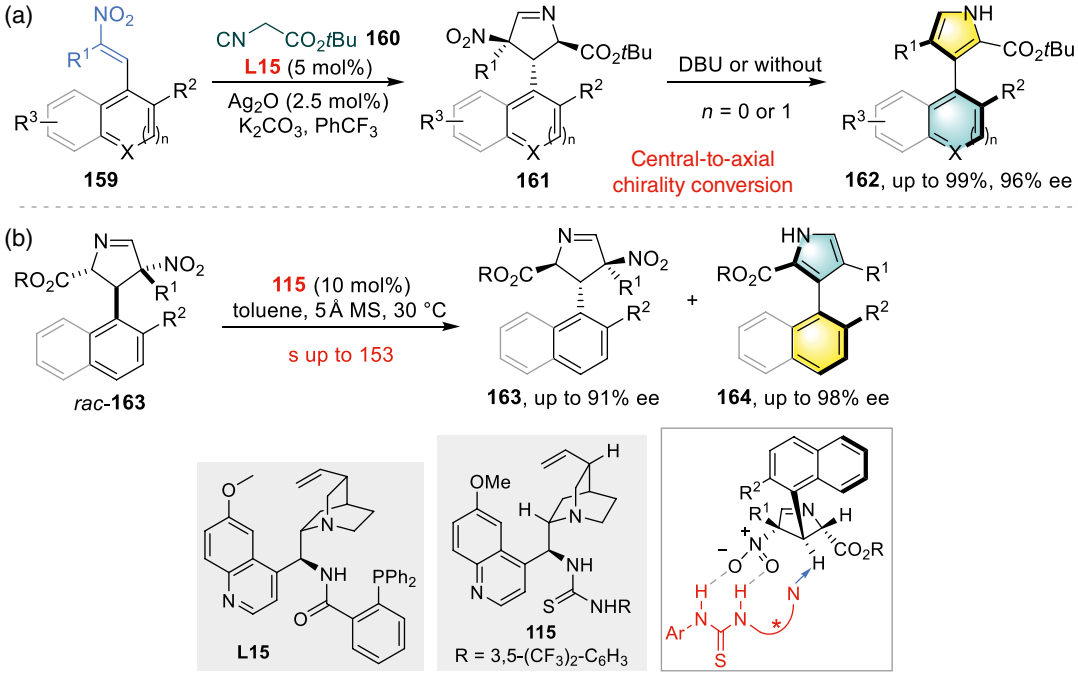

Scheme 19.44. Asymmetric construction of 3-arylpyrroles. (a) Asymmetric Barton-Zard reaction. Source: [113]/American Chemical Society. (b) KR of 3,4-dihydro-2H-pyrroles via enantioselective aromatization. Source: [114]/John Wiley & Sons.

Lin and coworkers presented three-component heteroannulation of 2,3-diketoesters **165**, aromatic amines **48**, and 1,3-cyclohexanediones **166** to construct *N*-arylindoles **167** with spirocyclic (*R*)-**C13** (Scheme 19.45) [115]. Aldol product of enamine (from amine and dione) and dehydrated 2,3-diketoester

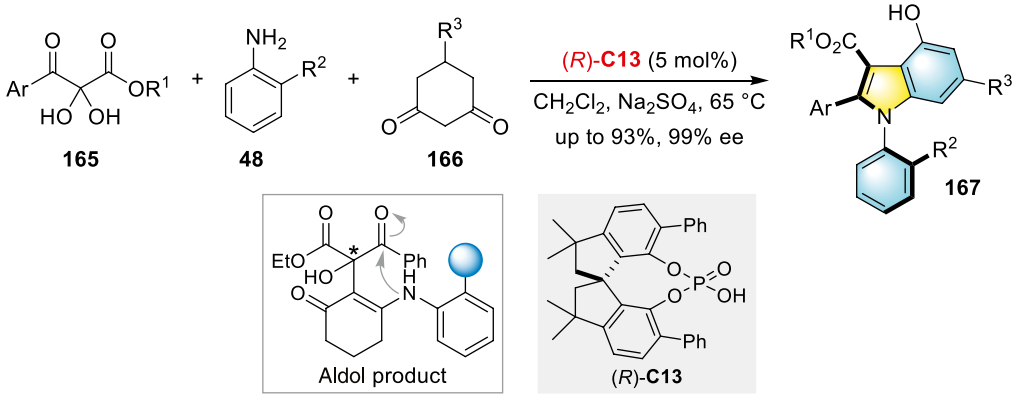

Scheme 19.45. CPA-catalyzed three-component heteroannulation. Source: [115]/John Wiley & Sons.

is stereodefined, which converts to axial chirality during dehydrative cyclization/aromatization process. Asymmetric Friedländer heteroannulation between 2-aminoaryl ketones with α-methylene carbonyl derivatives was catalyzed by CPA to form atropochiral 4-arylquinoline [116, 117].

The Miller group synthesized *N*-aryl benzimidazole **169a** stereoselectively via intramolecular cyclodehydration of **168a** in comparable efficiency using either C_2-symmetric CPA (*R*)-**C4** or phosphothreonine-derived phosphoric acid (***p*Thr1**) (Scheme 19.46) [118].

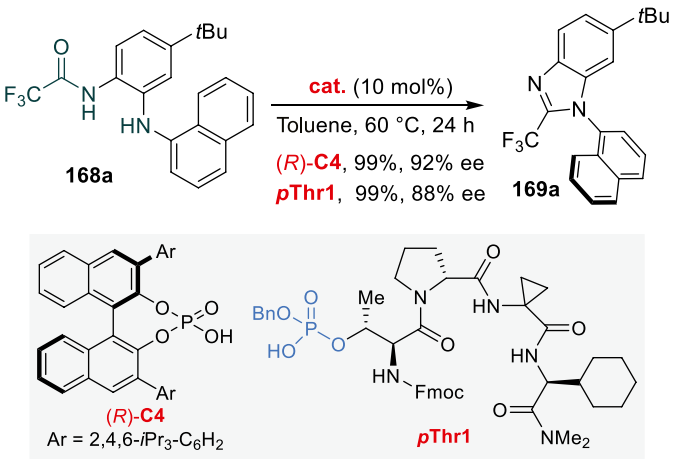

Scheme 19.46. Atroposelective synthesis of *N*-aryl benzimidazoles. Source: [118]/John Wiley & Sons.

19.3.2.2.2. O-Heteroatropisomers In analogy to pyridine synthesis, Bonne and Rodriguez constructed furan atropisomers (**174**, **175**) from nitroolefins **170** and 1,3-dicarbonyls **171** or naphthols **23** as C/O-bisnucleophiles via dihydrofuran intermediates **173** (Scheme 19.47) [119].

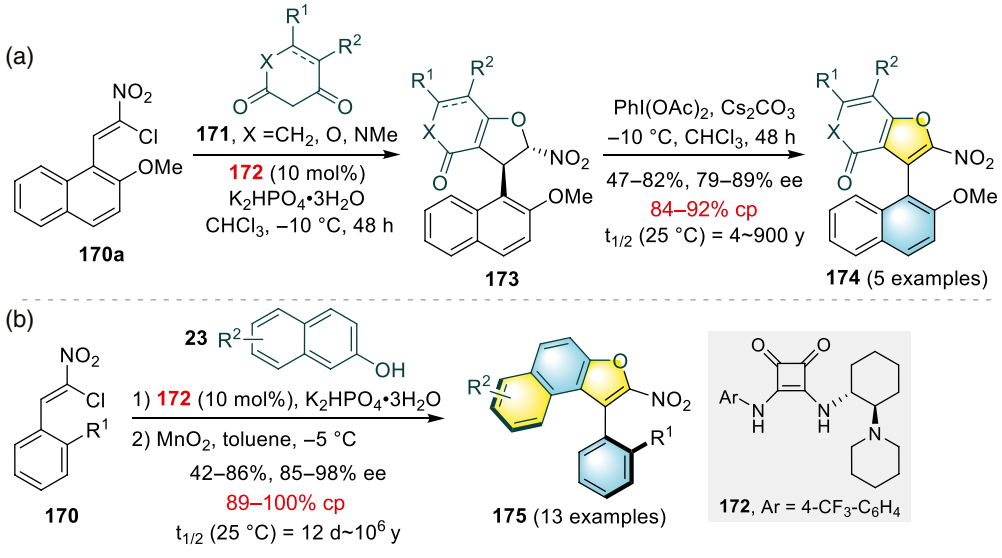

Scheme 19.47. Furan atropisomers from *β*-naphthyl nitroolefin and C/O-bisnucleophiles. (a) 1,3-Dicarbonyls C/O-bisnucleophiles. (b) Naphthols as C/O-bisnucleophiles. Source: [119]/American Chemical Society.

Zhao and coworkers provided benzofuran-derived biaryls bridged with eight-membered lactones **178** in an NHC catalytic protocol from α,β-unsaturated aldehydes **177** and symmetrical triols **176** (Scheme 19.48) [120]. The reaction pathway involves propargylic substitution of azolium enolates and a two-directional cyclization sequence. Amino phenols were also well suited and yielded indole-bridged biaryls **179** in tetrahydrofuran (THF). Tong and Wang utilized phosphine catalyst to develop (3+2) annulation of δ-acetoxy allenoates with 2-naphthol toward 3-aryl furan atropisomers [121].

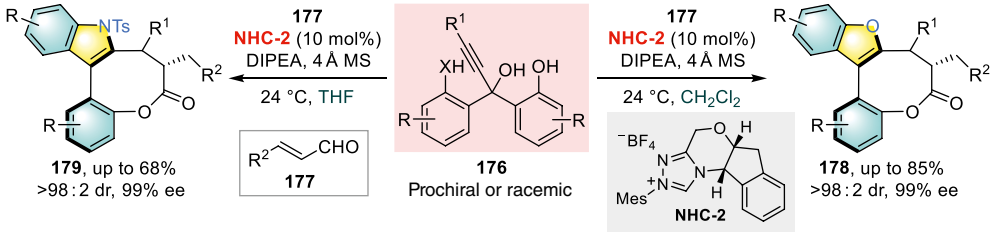

Scheme 19.48. NHC-catalyzed synthesis of benzofuran- and indole-derived bridged biaryls. Source:[120]/American Chemical Society.

19.3.2.3. Atroposelective Functionalization of Prochiral/Racemic Heterobiaryls The Shi group designed the synthesis of 2,2′-substituted 3,3′-bisindoles **182** through CPA-catalyzed addition of 2-substituted 3,3′-bisindoles **180** with bulky electrophilic isatin-derived 3-indolylmethanol **181** to sterically hinder the rotation of the heterobiaryl linkage in **182** (Scheme 19.49) [122]. Stable naphthyl-indole atropisomers were formed from C2-addition of bulky electrophiles [123].

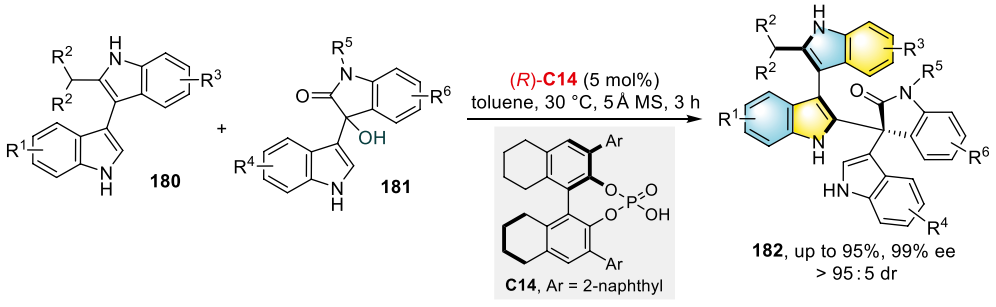

Scheme 19.49. Asymmetric addition to form axially chiral 3,3′-bisindoles. Source: [122]/John Wiley & Sons.

The Matsubara group incorporated quinidine-derived catalyst **184** in atroposelective aromatic electrophilic bromination of isoquinoline *N*-oxides [124] and 3-(quinolin-8-yl)phenols **183** (Scheme 19.50) [125]. In latter case, the aryl-aryl linkage becomes configurationally stable on halogenation of two *ortho* sites. This allowed procurement of aryl-quinoline atropisomers with two halogen groups (**185-1**, **185-2**).

Tan and coworkers demonstrated that 2,5-disubstituted phenylpyrroles **186** could be rendered atropochiral through desymmetrization ($R = R^1$, Scheme 19.51) or KR ($R \neq R^1$, $R^3 = t$Bu, not shown) with efficient remote stereocontrol upon asymmetric addition with ketomalonates **187** at C3-site [126].

19.3.3. Nonbiaryl Atropisomers

19.3.3.1. Stereogenic C-N Axis

19.3.3.1.1. Stereoselective Formation of C-N Bond Motivated by the pioneering work of Jørgensen, Bella, and coworkers [127], Zhang et al. prepared nonbiaryl N-C atropisomers, naphthalene-1,2-diamines

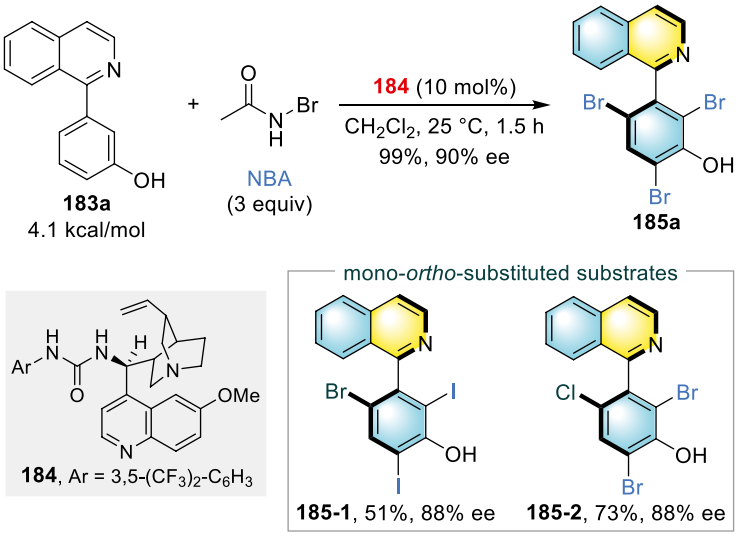

Scheme 19.50. Atroposelective halogenation of 8-arylquinolines. Source: [125]/John Wiley & Sons.

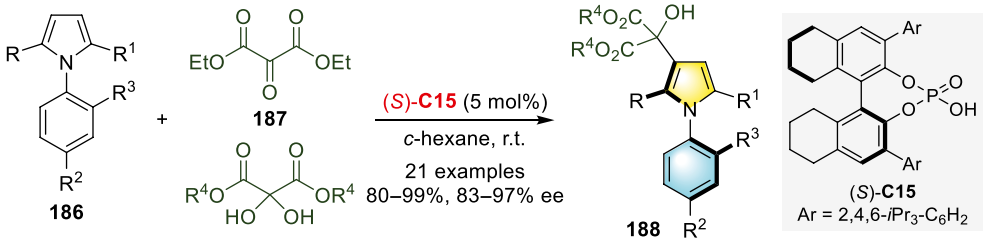

Scheme 19.51. CPA-catalyzed desymmetrization of *N*-phenylpyrroles.

190, via C-H amination of *N*-aryl-2-naphthylamines **189** with bulky azodicarboxylate (Scheme 19.52) [128]. The *N*-aryl entity in **189** establishes π–π interactions with (*R*)-**C16** besides dual H-bonding interactions for stereocontrol. An intramolecular H-bonding was operable in **190** to stabilize axial conformation.

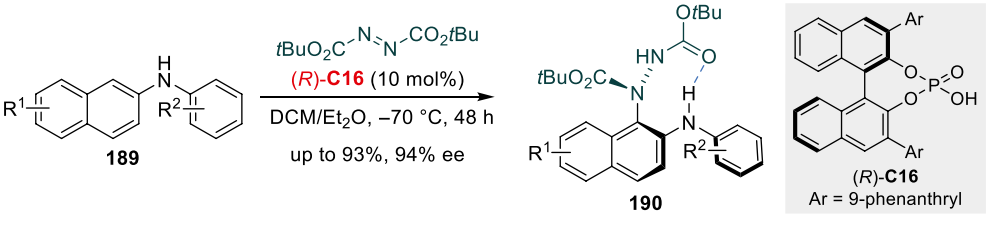

Scheme 19.52. Atroposelective C-H amination of *N*-aryl-2-naphthylamines. Source: [128]/Springer Nature.

19.3.3.1.2. Atroposelective N*-Annulation* CPA-catalyzed two-component annulation reaction between *N*-aryl anthranilamides **191** and aldehydes or 4-methoxypentenone generated *N*-arylquinazolinone atropisomers (**192a**, **192b**) via stereoselective *N*,*N*-aminal formation of imine (from aldehyde) or enamine (from 4-methoxypentenone) intermediate (Scheme 19.53) [129]. The more acidic (*R*)-**C17** catalyzes C-C bond cleavage in dihydroquinazolinone **B** whereas dihydroquinazolinone **A** undergoes oxidation.

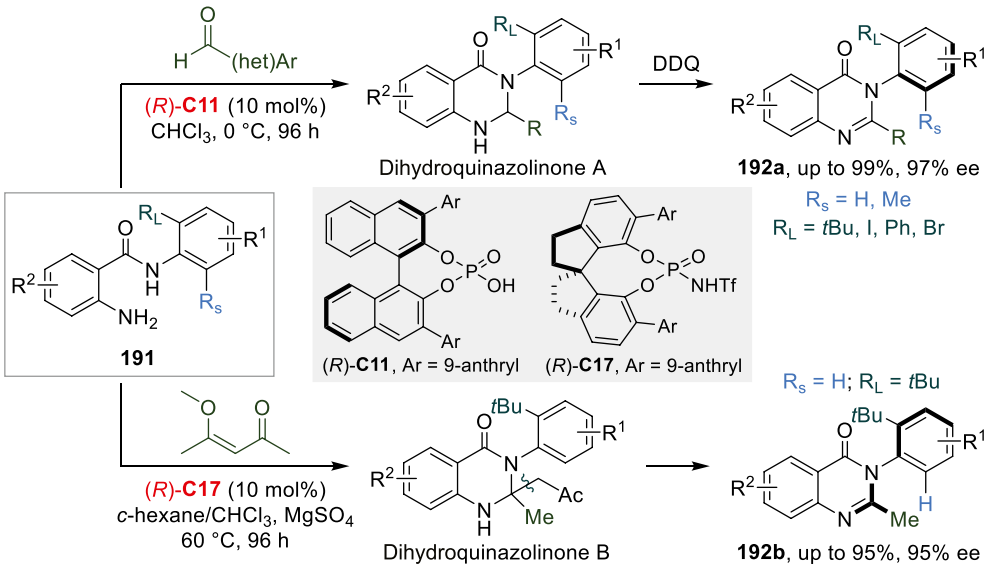

Scheme 19.53. CPA-catalyzed asymmetric synthesis of *N*-arylquinazolinones. Source: [129]/Springer Nature.

On the other hand, spirobenzazepinones **195** were asymmetrically assembled in an NHC-promoted formal [3+4] cycloaddition of isatin-derived enals **193** and aza-*o*-quinone methides formed in situ from *N*-(*ortho*-chloromethyl)aryl amides **194** (Scheme 19.54) [130].

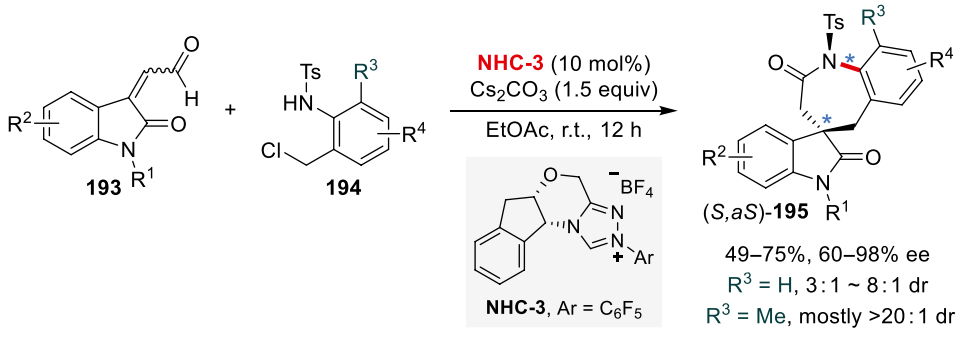

Scheme 19.54. Atroposelective synthesis of spirobenzazepinones. Source: [130]/John Wiley & Sons.

19.3.3.1.3. Atroposelective Functionalization on Preformed Nonbiaryl C-N Scaffold Cheng and coworkers employed a biscinchona alkaloid catalyst, hydroquinine 2,5-diphenyl-4,6-pyrimidinediyl diether ($(DHQ)_2PYR$) to conduct *N*-allylation of anilides **196** where the acyl substituents could depart from common nucleophilic alkyl and styryl-substituted derivatives (Scheme 19.55) [131]. Similar synthetic operations introduced atropisomerically enriched $C_{(aryl)}$-N axis in phosphonamides [132] and *N*-sulfonyl anilides [133].

Beyond the biaryl [134] and tertiary benzamide [135] systems, Miller's exemplary peptide catalysis enabled atroposelective bromination of 3-arylquinazolin-4(3*H*)-one **198a** (Scheme 19.56) [136]. The chiral axis was set on introduction of first *ortho*-bromo substituent (**200a**).

Gustafson et al. judiciously designed *N*-aryl naphthoquinoide substrates **201** with a locked quinoid-nitrogen axis in intramolecular hydrogen bond network, and thus simplified the two-axis system into

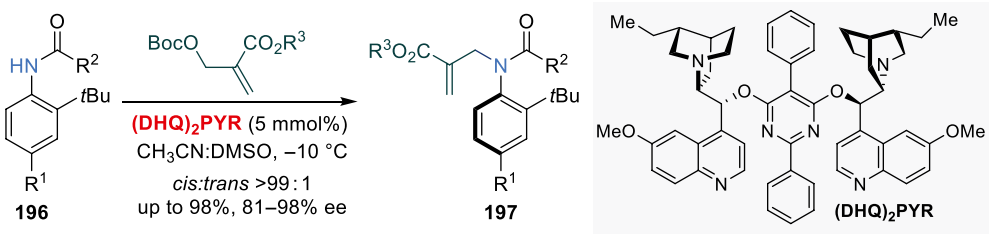

Scheme 19.55. Asymmetric allylic alkylation of anilides. Source: [131]/American Chemical Society.

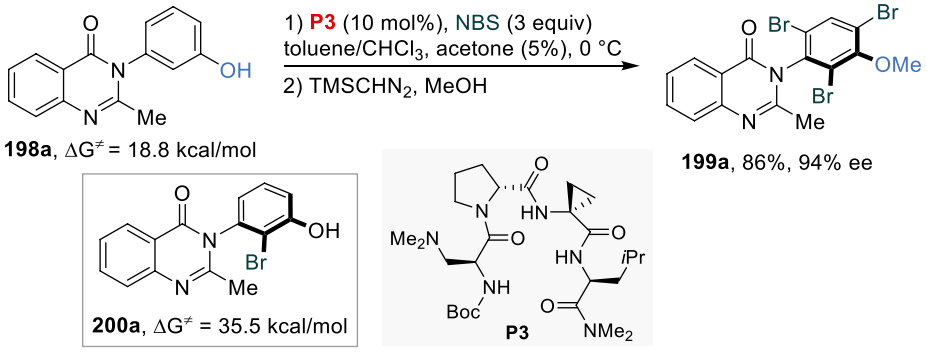

Scheme 19.56. Peptide-catalyzed asymmetric bromination of quinazolinones. Source: [136]/American Chemical Society.

single axis for atroposelective C-H halogenation (Scheme 19.57) [137]. *N*-Aryl quinoids **202** are diarylamine mimics and are stable in protic solvents, holding promises for incorporation in medicinal chemistry.

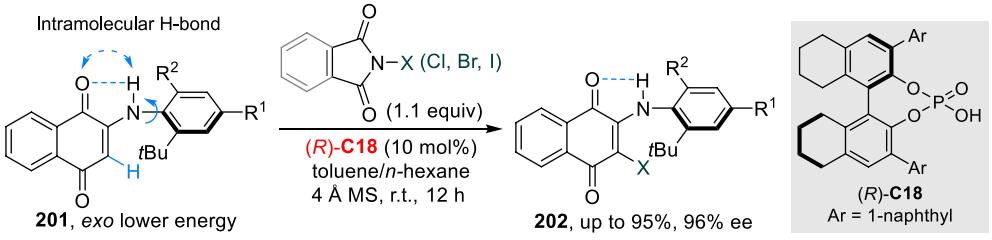

Scheme 19.57. Atroposelective halogenation of *N*-aryl quinoids. Source: [137]/American Chemical Society.

Bencivenni's group has studied organocatalytic nucleophilic desymmetrization of *N*-(2-*tert*-butylphenyl)maleimide (**203**) (and derivatives) extensively through Michael reactions with various carbon nucleophiles or Diels-Alder reaction (Scheme 19.58a) [138]. As *t*Bu group freezes rotation of N–C_{aryl} axis, catalyst distinguishes between *Re* and *Si* atropotopic face and controls a facial selective nucleophilic attack from opposite side of *t*Bu group. As maleimide is desymmetrized upon nucleophilic attack, the distant C_{aryl}–N axis becomes chiral.

Tan's group performed desymmetrization of 4-aryl-1,2,4-triazole-3,5-diones (ATAD) **204** via tyrosine click reaction with nucleophilic aromatic alcohols or 2-substituted indoles (Scheme 19.58b) [139]. Moreover, electrophilicity and a weak N=N π-bond made tandem Diels-Alder and ene reactions of ATAD with 3-vinylindoles and methyleneindolinone feasible [140].

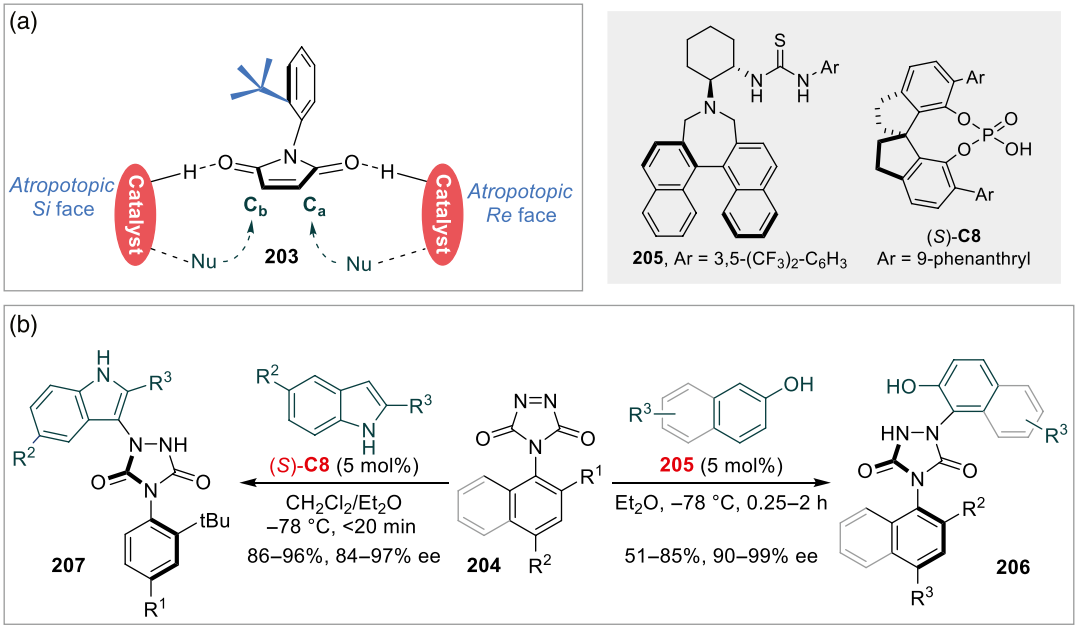

Scheme 19.58. Desymmetrization of *N*-(2-*tert*-butylphenyl)maleimides and ATADs. (a) Desymmetrization of *N*-(2-*tert*-butylphenyl)maleimides **203**. Source: [138]/John Wiley & Sons. (b) Desymmetrization of 4-aryl-1,2,4-triazole-3,5-diones (ATAD) **204**. Source: [139]/Springer Nature.

19.3.3.2. Stereogenic C-C Axis: Aromatic Amides

19.3.3.2.1. De Novo Arene Formation Sparr and coworkers applied aminocatalytic atroposelective aldol condensation strategy to *ortho*-substituted arylglyoxylic amides **208** to yield chiral aromatic amides **209A** (Scheme 19.59) [141]. The formyl products (**209B**) were reduced in situ into the more stable *ortho*-hydroxymethyl aromatic amides **209A**, hence expanding the product scope.

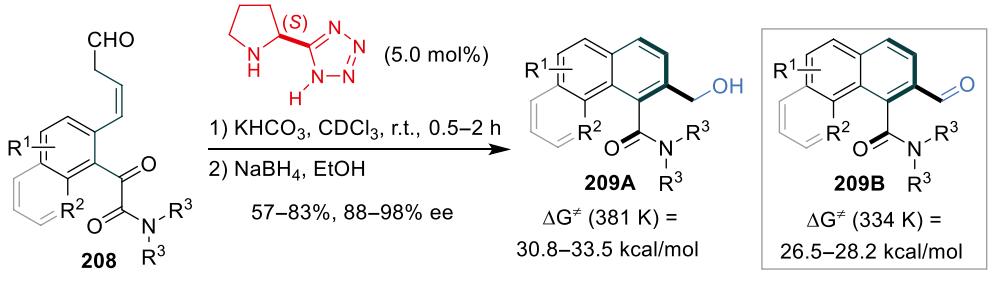

Scheme 19.59. Aromatic amides from arene-forming aldol condensation. Source: [141]/John Wiley & Sons.

19.3.3.2.2. Atroposelective Functionalization of Aromatic Amides Pioneering work from the Clayden group demonstrated that the functionalization of aromatic amides could install axial chirality [142]. Smith and coworkers have prepared non-racemizing aromatic amides **211** via counterion-mediated benzylation of the *ortho*-hydroxy group in amide naphthols **210** (Scheme 19.60) [143]. Substrate racemization for DKR was facilitated by intramolecular hydrogen bond between O-H and N(CO). Conversely, hydroquinine catalyst processed *O*-allylic alkylation of amide naphthols without *peri*-substitution in Cheng's protocol [144].

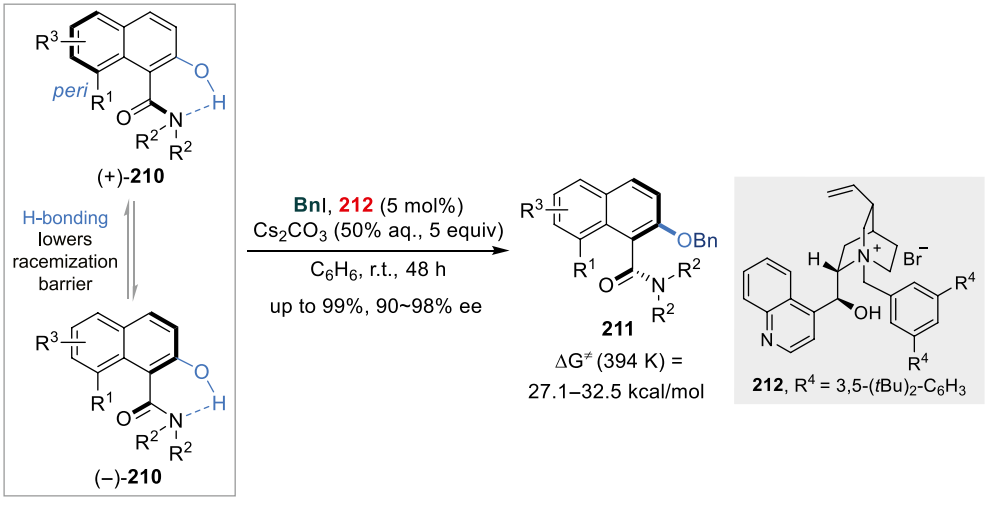

Scheme 19.60. DKR of atropisomeric amides enabled by transition-state hydrogen bond. Source: [143]/John Wiley & Sons.

19.3.3.3. Stereogenic C-C Axis: Aryl Alkenes

19.3.3.3.1. Atroposelective $C_{(aryl)}$-$C_{(alkenyl)}$ Bond Formation The Tan group studied arylation of *o*-naphthoquinones **213** with different arene nucleophiles that gave arylquinones **214** harboring chiral $C_{(olefinic)}$-$C_{(aryl)}$ axis (Scheme 19.61) [145]. After enantioselective 1,4-addition and aromatization, oxidation of **Int-2** by the excess *o*-naphthoquinone substrate (used in 2–2.2 equivalent) yields **214**. Atroposelective arylation of monocyclic 1,4-benzoquinones with 2-naphthols **23** yielded stable aryl-*p*-quinone atropisomers that were readily diversifiable [146].

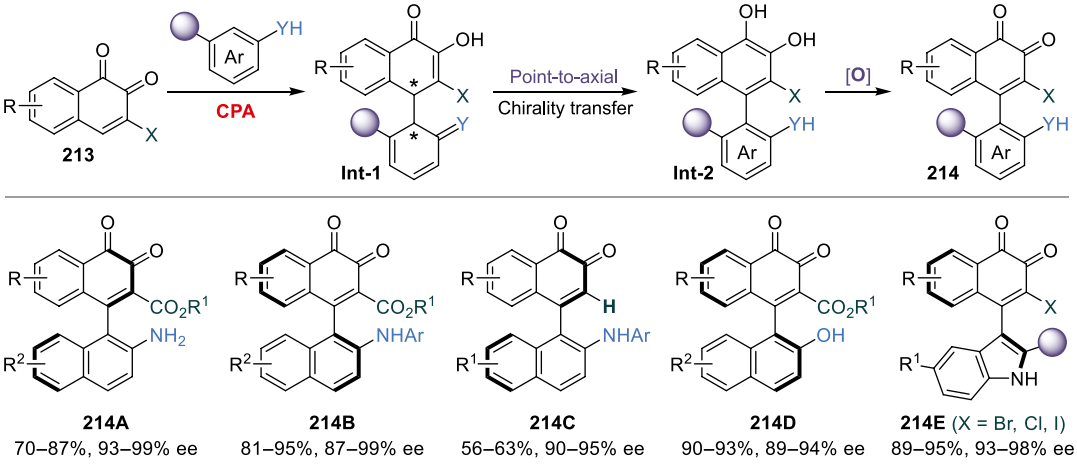

Scheme 19.61. Atroposelective synthesis of axially chiral arylquinones.Source: [145]/Springer Nature.

19.3.3.3.2. Alkyne Annulation Wang's group conceived NHC-catalyzed annulation of ynals **215** with cyclic 1,3-diones **216** to provide axially chiral α-pyrone-aryls **217** with **NHC-4** (Scheme 19.62) [147]. The [3+3] annulation between alkynyl acyl azolium intermediate and **216** involves stereoselective Michael

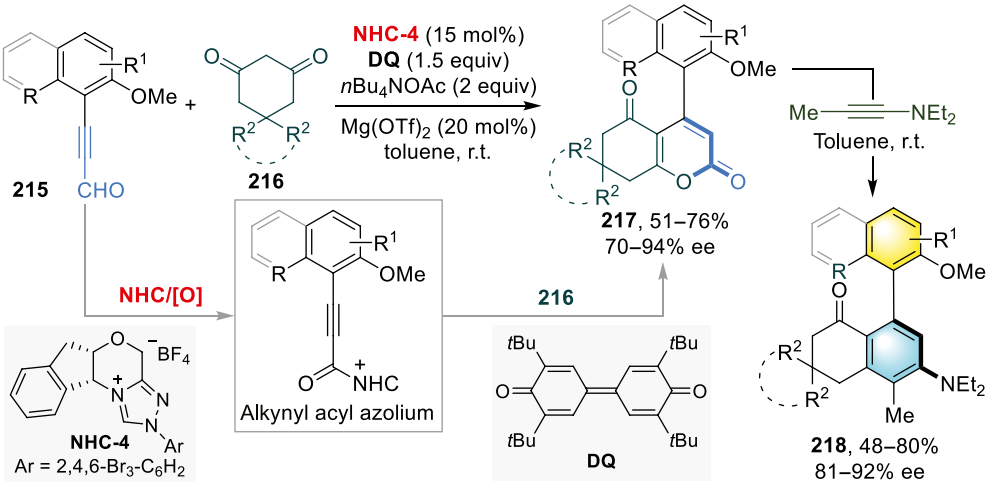

Scheme 19.62. NHC-catalyzed asymmetric [3+3]-annulation. Source: [147]/Springer Nature.

addition of ketoenolate to the alkynyl azolium moiety. **217** could transform into naphthyl-phenyl atropisomers **218** on Diels-Alder reaction.

In Zhao's method, bifunctional sulfide catalyst **222** enabled carbothiolation of *ortho*-alkynylaryl amines **219** with electrophilic thiolating reagent **220** to form vinyl-aryl amino sulfides **221** (Scheme 19.63) [148]. The selected amine protecting groups on **219** and catalyst crucially establish

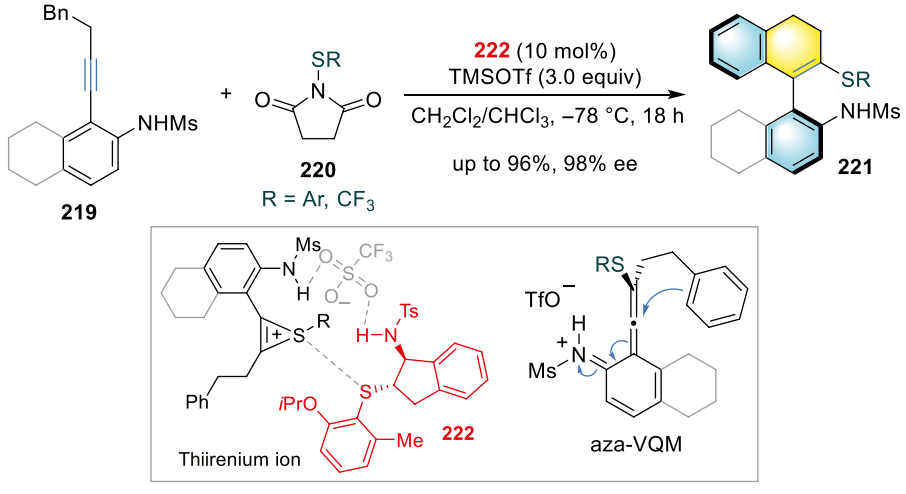

Scheme 19.63. Chiral sulfide-catalyzed electrophilic carbothiolation of alkynes. Source: [148]/John Wiley & Sons.

H-bond interactions for stereocontrol. After the conversion of thiirenium ions into aza-VQM intermediate, intramolecular hydroarylation releases **221**.

19.3.3.3.3. Addition reaction of alkynes Atroposelective synthesis of alkenes observes rising utilizations of alkyne functionalization pathway through nucleophilic addition on electron-deficient alkynes. Tan's work in 2017 raises the exciting prospect of this chemistry: organocatalytic atroposelective synthesis of axially chiral alkenes **225** arises through an enantioselective nucleophilic addition of 1,3-dicarbonyls **224**

or malononitriles to alkynals **223** (Scheme 19.64) [149]. Axial chirality is converted from the chiral allenamine intermediate, the Michael adduct of iminium ion.

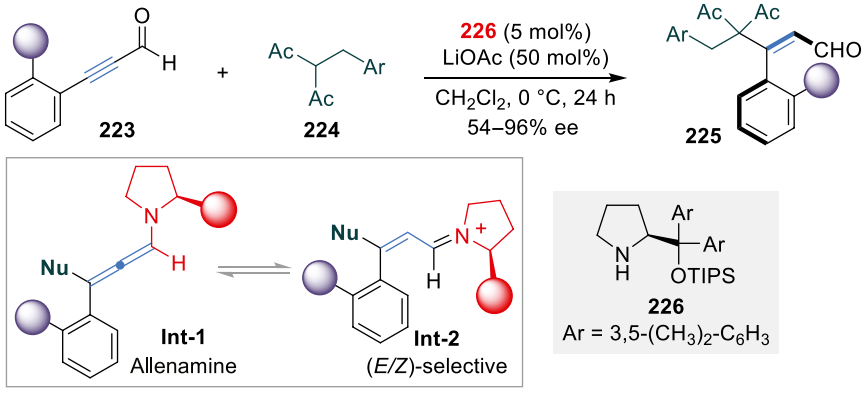

Scheme 19.64. Organocatalytic Michael addition of alkynals. Source:[149]/Springer Nature.

Shi and coworkers uniquely merged 3-alkynyl-2-indolylmethanols **227** (1,4-dielectrophiles) with 2-naphthols or phenols **23** (1,3-dinucleophiles) to forge aryl alkene-indoles fused with seven-membered ring **228** via a formal (4+3) cyclization (Scheme 19.65) [150].

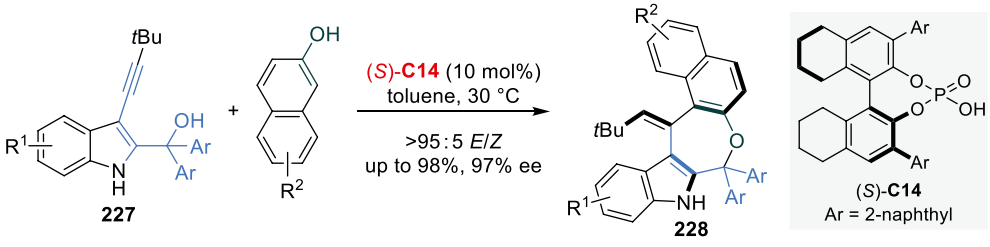

Scheme 19.65. Asymmetric synthesis of aryl-alkene-indoles. Source: [150]/John Wiley & Sons.

ortho-Ethynylphenols or *ortho*-ethynylanilines are frequently invoked for addition reaction as catalyst readily aided their stereoselective tautomerizations to stereodefined VQMs, which are primed for nucleophilic additions (Scheme 19.66a). Yan et al. tactically designed reacting systems to access skeletally diverse styrene atropisomers. From 1-(arylethynyl)naphthalen-2-ols **229** and sodium sulfinates, sulfone-containing styrenes **230** were obtained with the use of thiourea catalyst **115** (Scheme 19.66b) [151]. This chemistry underlies the synthesis of 1,4-distyrene 2,3-naphthalene diols **231** [152], 1,2-diaxial styrenes **232** [153], and atropisomeric styrenes containing 5*H*-oxazol-4-one subunit **233** [154]. In Zhang's conditions, CPA-catalyzed atroposelective addition of indoles (**234**) or 4-hydroxycoumarins (**235**) on *ortho*-alkynylnaphthylamines was described [155]. Tan and Houk disclosed new disubstituted 1,1′-(ethene-1,1-diyl)binaphthol (EBINOL) scaffolds (**236**) when 2-naphthols or 3,5-dimethoxyphenol were combined with various alkynes [156] (Scheme 19.66c).

19.3.3.3.4. Atroposelective Functionalization of Aryl-Alkene Scaffold Smith executed *O*-benzylation of racemic 1-aryl-2-tetralones **237** by quinidine-derived ammonium salt **239** for enantiomeric enrichment [157]. The diastereoisomeric ion pairs are alkylated at different rates to gain atropo-enantioenrichment. Enol ethers **238** are immediate precursors to BINOLs on oxidation (Scheme 19.67a). Other structures produced from this disconnection encompass enamine-like alkenes **240** [159] and oxindole-derived styrenes (**241**, **242**) from a CPA-catalyzed KR process (Scheme 19.67b) [158].

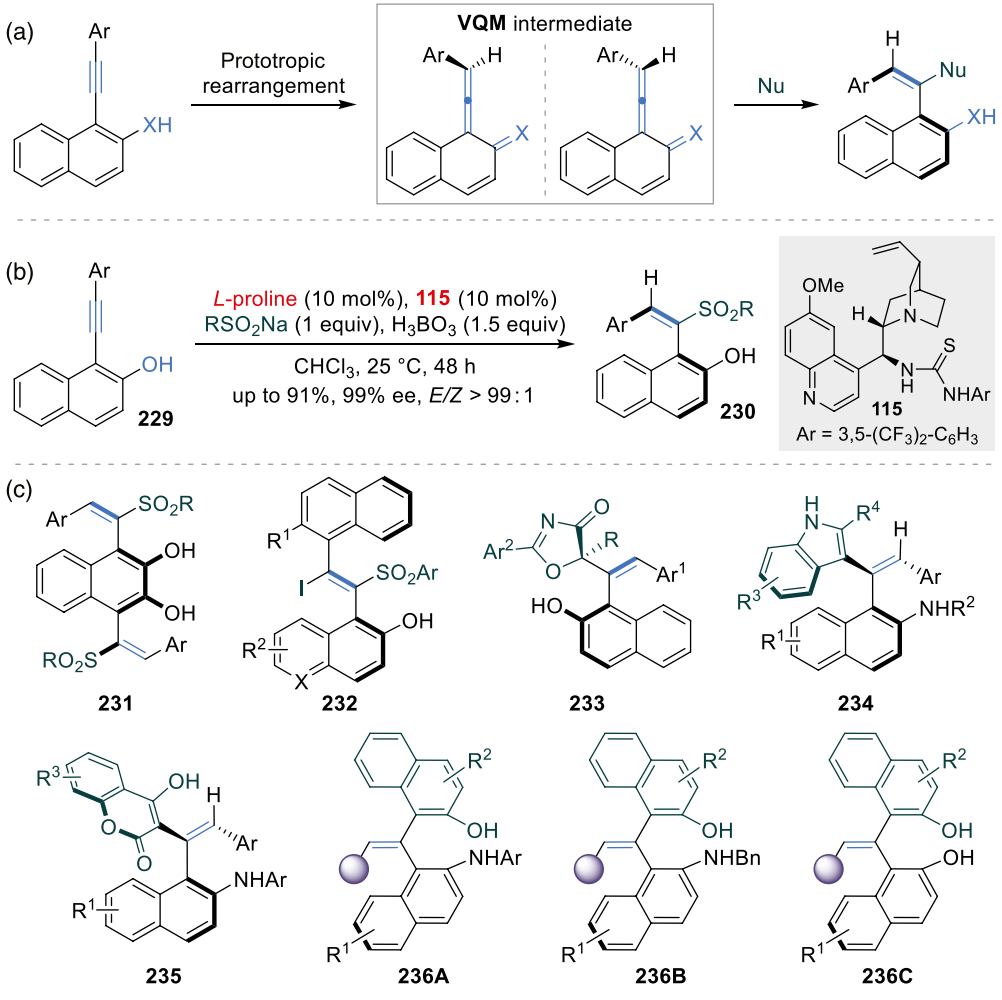

Scheme 19.66. Synthesis of atropochiral styrenes via VQM intermediate. (a) General mechanistic pathway. (b) Synthesis of sulfone-containing styrenes. Source: [151]/American Chemical Society. (c) Various styrene-type atropisomers derived from VQM intermediate.

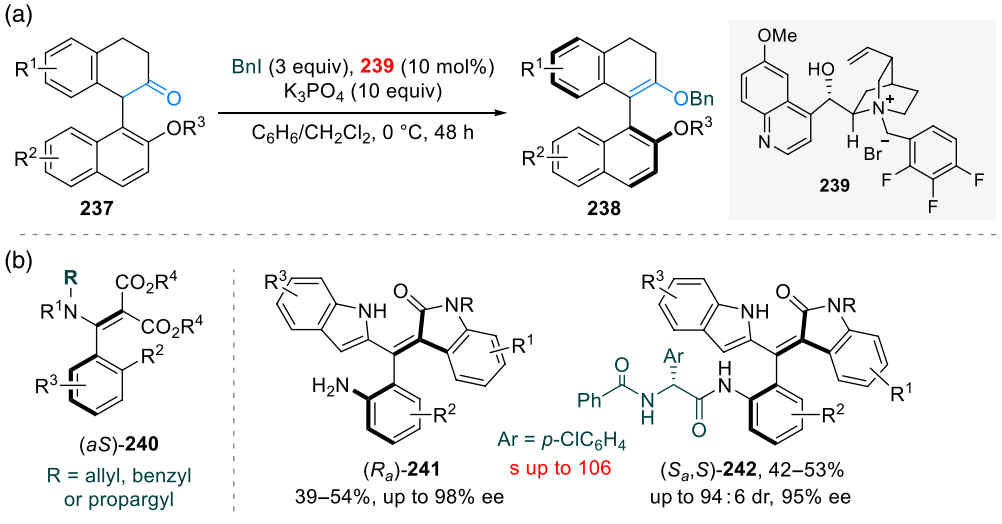

Scheme 19.67. Enantioenriched alkene atropisomers from atroposelective functionalization. (a) Chiral cation-mediated *O*-benzylation. (b) Asymmetric *N*-alkylation toward atropisomeric enamine-like alkenes and *N*-functionalization of oxindole-based styrenes. Source: [158]/American Chemical Society.

19.4. ENZYMATIC CATALYSIS

19.4.1. Biaryl Atropisomers

Akai and coworkers recruited immobilized *Pseudomonas* sp. lipoprotein lipase (Toyobo LIP301) in a chemoenzymatic DKR reaction to promote KR of unprotected biaryldiols **243** (Scheme 19.68) [160]. Interestingly, the interconversion of atropostable reactants was catalyzed by ruthenium catalyst via otherwise undesired SET-mediated racemization.

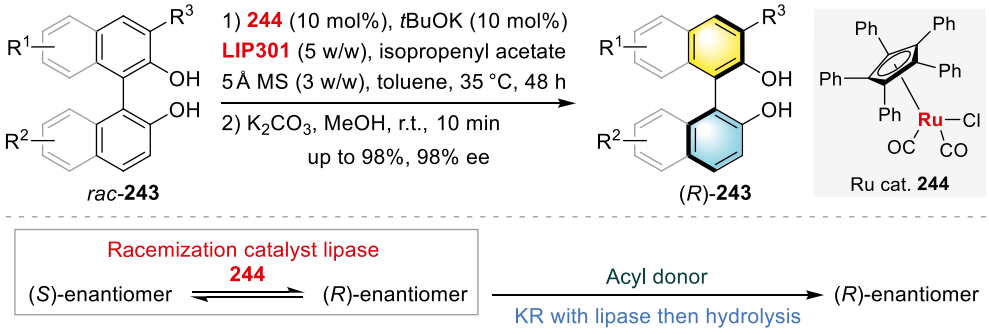

Scheme 19.68. Ru-complex and lipase co-mediated DKR of biaryls. Source: [160]/John Wiley & Sons.

19.4.2. Heteorobiaryl Atropisomers

As reported by Clayden and Turner, aldehyde-bearing biaryl isoquinolines and pyridine *N*-oxides **245** could be reduced to both enantiomers of **246** on using suitable ketoreductase enzyme (KRED) and nicotinamide adenine dinucleotide phosphate (NADPH) as reductant (Scheme 19.69) [161]. The ablation of interaction between *N*-oxide and carbonyl carbon that promotes axial rotation in **245** would stabilize the axis in alcohols **246**.

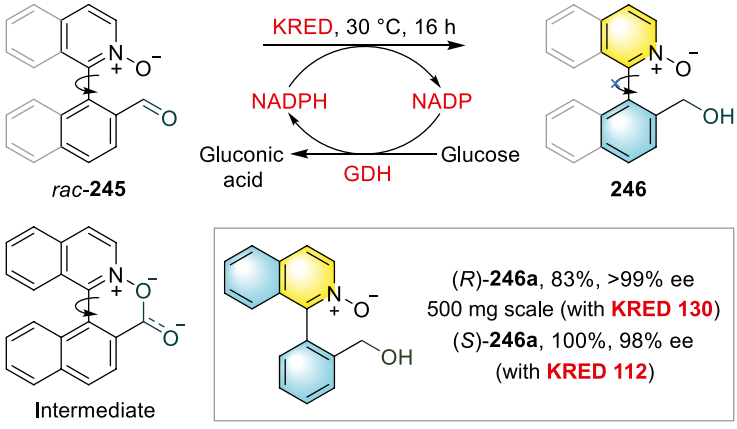

Scheme 19.69. Biocatalytic aldehyde reduction. Source: [161]/John Wiley & Sons.

19.5. CONCLUSION

Various chemistry disciplines have shown growing interests in the unique three-dimensional framework of atropisomers, requesting for more efficient and modular preparation methods. This chapter disclosed contemporary metal-based, organocatalyst-based, and enzymatic approaches to access three major

families of atropisomers asymmetrically and catalytically. As could be recognized from preceding sections, certain strategies are explored more regularly than others, confining the structural diversity of atropisomers. To fully appreciate atropisomerism for mere scientific curiosities or for utilization potential in interdisciplinary research, highly selective and efficient protocols that allow rapid expansion of chemical space are still in demand. We hope this chapter provides insights and inspiration for those who aspire to pursue research in this area.

REFERENCES

1. Smyth, J. E.; Butler, N. M.; Keller, P. A. *Nat. Prod. Rep.* **2015**, *32*, 1562–1583.
2. LaPlante, S. R.; Edwards, P. J.; Fader, L. D.; Jakalian, A.; Hucke, O. *ChemMedChem* **2011**, *6*, 505–513.
3. Privileged Chiral Ligands and Catalysts; Zhou, Q.-L., Ed.; WileyVCH: Weinheim, Germany, **2011**.
4. Zhang, D.-W.; Li, M.; Chen, C.-F. *Chem. Soc. Rev.* **2020**, *49*, 1331–1343.
5. Kumarasamy, E.; Raghunathan, R.; Sibi, M. K.; Sivaguru, J. *Chem. Rev.* **2015**, *115*, 11239–11300.
6. Wencel-Delord, J.; Panossian, A.; Leroux, F. R.; Colobert, F. *Chem. Soc. Rev.* **2015**, *44*, 3418–3430.
7. Wang, Y.-B.; Tan, B. *Acc. Chem. Res.* **2018**, *51*, 534–547.
8. Bonne, D.; Rodriguez, J. *Eur. J. Org. Chem.* **2018**, *2018*, 2417–2431.
9. Liao, G.; Zhou, T.; Yao, Q.-J.; Shi, B.-F. *Chem. Commun.* **2019**, *55*, 8514–8523.
10. Corti, V.; Bertuzzi, G. *Synthesis* **2020**, *52*, 2450–2468.
11. Yang, H.; Chen, J.; Zhou, L. *Chem. Asian J.* **2020**, *15*, 2939–2951.
12. Cheng D.-J.; Shao, Y.-D. *Adv. Synth. Catal.* **2020**, *362*, 3081–3099.
13. Li, T.-Z.; Liu, S.-J.; Tan, W.; Shi, F. *Chem. Eur. J.* **2020**, *26*, 15779–15792.
14. Wencel-Delord, J.; Colobert, F. *SynOpen* **2020**, *4*, 107–115.
15. Carmona, J. A.; Rodríguez-Franco, C.; Fernández, R.; Hornillos, V.; Lassaletta, J. M. *Chem. Soc. Rev.* **2021**, *50*, 2968–2983.
16. Loxq, P.; Manoury, E.; Poli, R.; Deydier, E.; Labande, A. *Coord. Chem.* **2016**, *308*, 131–190.
17. Shen, D.; Xu, Y.; Shi, S.-L. *J. Am. Chem. Soc.* **2019**, *141*, 14938–14945.
18. Yang, H.; Sun, J.; Gu, W.; Tang, W. *J. Am. Chem. Soc.* **2020**, *142*, 8036–8043.
19. Qiu, H.; Shuai, B.; Wang, Y.-Z.; Liu, D.; Chen, Y.-G.; Gao, P.-S.; Ma, H.-X.; Chen, S.; Mei, T.-S. *J. Am. Chem. Soc.* **2020**, *142*, 9872–9878.
20. Ding, L.; Sui, X.; Gu, Z. *ACS Catal.* **2018**, *8*, 5630–5635.
21. Liu, Z.-S.; Hua, Y.; Gao, Q.; Ma, Y.; Tang, H.; Shang, Y.; Cheng, H.-G.; Zhou, Q. *Nat. Catal.* **2020**, *3*, 727–733.
22. Newton, C. G.; Braconi, E.; Kuziola, J.; Wodrich, M. D.; Cramer, N. *Angew. Chem. Int. Ed.* **2018**, *57*, 11040–11044.
23. Jang, Y.-S.; Woźniak, Ł.; Pedroni, J.; Cramer, N. *Angew. Chem. Int. Ed.* **2018**, *57*, 12901–12905.
24. Yan, S.; Xia, W.; Li, S.; Song, Q.; Xiang, S.-H.; Tan, B. *J. Am. Chem. Soc.* **2020**, *142*, 7322–7327.
25. Wang, H. *Chirality* **2010**, *22*, 827–837.
26. Egami, H.; Katsuki, T. *J. Am. Chem. Soc.* **2009**, *131*, 6082–6083.
27. Tian, J.-M.; Wang, A.-F.; Yang, J.-S.; Zhao, X.-J.; Tu, Y.-Q.; Zhang, S.-Y.; Chen, Z.-M. *Angew. Chem. Int. Ed.* **2019**, *58*, 11023–11027.
28. Narute, S.; Parnes, R.; Toste, F. D.; Pappo, D. *J. Am. Chem. Soc.* **2016**, *138*, 16553–16560.
29. Qi, L.-W.; Li, S.; Xiang, S.-H.; Wang, J.; Tan, B. *Nat. Catal.* **2019**, *2*, 314–323.
30. Mitake, A.; Fusamae, T.; Kanyiva, K. S.; Shibata, T. *Eur. J. Org. Chem.* **2017**, *2017*, 7266–7270.
31. Shibata, T.; Sekine, A.; Mitake, A.; Kanyiva, K. S. *Angew. Chem. Int. Ed.* **2018**, *57*, 15862–15865.
32. Takano, H.; Shiozawa, N.; Imai, Y.; Kanyiva, K. S.; Shibata, T. *J. Am. Chem. Soc.* **2020**, *142*, 4714–4722.
33. Satoh, M.; Shibata, Y.; Kimura, Y.; Tanaka, K. *Eur. J. Org. Chem.* **2016**, *2016*, 4465–4469.
34. Shibuya, T.; Shibata, Y.; Noguchi, K.; Tanaka, K. *Angew. Chem. Int. Ed.* **2011**, *50*, 3963–3967.
35. Bringmann, G.; Breuning, M.; Tasler, S. *Synthesis* **1999**, *1999*, 525–558.
36. Chen, G.-Q.; Lin, B.-J.; Huang, J.-M.; Zhao, L.-Y.; Chen, Q.-S.; Jia, S.-P.; Yin, Q.; Zhang, X. *J. Am. Chem. Soc.* **2018**, *140*, 8064–8068.
37. Zhao, K.; Duan, L.; Xu, S.; Jiang, J.; Fu, Y.; Gu, Z. *Chem* **2018**, *4*, 599–612.
38. Zhang, X.; Zhao, K.; Li, N.; Yu, J.; Gong, L.-Z.; Gu, Z. *Angew. Chem. Int. Ed.* **2020**, *59*, 19899–19904.
39. Li, Q.; Zhang, M.; Zhan, S.; Gu, Z. *Org. Lett.* **2019**, *21*, 6374–6377.
40. Hou, M.; Deng, R.; Gu, Z. *Org. Lett.* **2018**, *20*, 5779–5783.
41. Xue, X.; Gu, Z. *Org. Lett.* **2019**, *21*, 3942–3945.
42. Yao, Q.-J.; Zhang, S.; Zhan, B.-B.; Shi, B.-F. *Angew. Chem. Int. Ed.* **2017**, *56*, 6617–6621.
43. Liao, G.; Li, B.; Chen, H.-M.; Yao, Q.-J.; Xia, Y.-N.; Luo, J.; Shi, B.-F. *Angew. Chem. Int. Ed.* **2018**, *57*, 17151–17155.
44. Liao, G.; Yao, Q.-J.; Zhang, Z.-Z.; Wu, Y.-J.; Huang, D.-Y.; Shi, B.-F. *Angew. Chem. Int. Ed.* **2018**, *57*, 3661–3665.
45. Liao, G.; Chen, H.-M.; Xia, Y.-N.; Li, B.; Yao, Q.-J.; Shi, B.-F. *Angew. Chem. Int. Ed.* **2019**, *58*, 11464–11468.

46. Zhang, S.; Yao, Q.-J.; Liao, G.; Li, X.; Li, H.; Chen, H.-M.; Hong, X.; Shi, B.-F. *ACS Catal.* **2019**, *9*, 1956–1961.
47. Song, H.; Li, Y.; Yao, Q.-J.; Jin, L.; Liu, L.; Liu, Y.-H.; Shi, B.-F. *Angew. Chem. Int. Ed.* **2020**, *59*, 6576–6580.
48. Dhawa, U.; Tian, C.; Wdowik, T.; Oliveira, J. C. A.; Hao, J.; Ackermann, L. *Angew. Chem. Int. Ed.* **2020**, *59*, 13451–13457.
49. Zhang, J.; Wang, J. *Angew. Chem. Int. Ed.* **2018**, *57*, 465–469.
50. Nguyen, Q.-H.; Guo, S.-M.; Royal, T.; Baudoin, O.; Cramer, N. *J. Am. Chem. Soc.* **2020**, *142*, 2161–2167.
51. Zhang, L.; Zhang, J.; Ma, J.; Cheng, D.-J.; Tan, B. *J. Am. Chem. Soc.* **2017**, *139*, 1714–1717.
52. Zheng, S.-C.; Wang, Q.; Zhu, J. *Angew. Chem. Int. Ed.* **2019**, *58*, 1494–1498.
53. He, Y.-P.; Wu, H.; Wang, Q.; Zhu, J. *Angew. Chem. Int. Ed.* **2020**, *59*, 2105–2109.
54. Tian, M.; Bai, D.; Zheng, G.; Chang, J.; Li, X. *J. Am. Chem. Soc.* **2019**, *141*, 9527–9532.
55. Peng, C.; Kusakabe, T.; Kikkawa, S.; Mochida, T.; Azumaya, I.; Dhage, Y. D.; Takahashi, K.; Sasai, H.; Kato, K. *Chem. Eur. J.* **2019**, *25*, 733–737.
56. Zheng, J.; You, S.-L. *Angew. Chem. Int. Ed.* **2014**, *53*, 13244–13247.
57. Zheng, J.; Cui, W.-J.; Zheng, C.; You, S.-L. *J. Am. Chem. Soc.* **2016**, *138*, 5242–5245.
58. Wang, Q.; Cai, Z.-J.; Liu, C.-X.; Gu, Q.; You, S.-L. *J. Am. Chem. Soc.* **2019**, *141*, 9504–9510.
59. Wang, Q.; Zhang, W.-W.; Song, H.; Wang, J.; Zheng, C.; Gu, Q.; You, S.-L. *J. Am. Chem. Soc.* **2020**, *142*, 15678–15685.
60. Ye, C.-X.; Chen, S.; Han, F.; Xie, X.; Ivlev, S.; Houk, K. N.; Meggers, E. *Angew. Chem. Int. Ed.* **2020**, *59*, 13552–13556.
61. Hornillos, V.; Carmona, J. A.; Ros, A.; Iglesias-Sigüenza, J.; López-Serrano, J.; Fernández, R.; Lassaletta, J. M. *Angew. Chem. Int. Ed.* **2018**, *57*, 3777–3781.
62. Ros, A.; Estepa, B.; Ramírez-López, P.; Álvarez, E.; FernÁndez, R.; Lassaletta, J. M. *J. Am. Chem. Soc.* **2013**, *135*, 15730–15733.
63. Ramírez-López, P.; Ros, A.; Estepa, B.; FernÁndez, R.; Fiser, B.; Gómez-Bengoa, E.; Lassaletta, J. M. *ACS Catal.* **2016**, *6*, 3955–3964.
64. Bhat, V.; Wang, S.; Stoltz, B. M.; Virgil, S. C. *J. Am. Chem. Soc.* **2013**, *135*, 16829–16832.
65. Ramírez-López, P.; Ros, A.; Romero-Arenas, A.; Iglesias-Sigüenza, J.; FernÁndez, R.; Lassaletta, J. M. *J. Am. Chem. Soc.* **2016**, *138*, 12053–12056.
66. Hornillos, V.; Ros, A.; Ramírez-López, P.; Iglesias-Sigüenza, J.; FernÁndez, R.; Lassaletta, J. M. *Chem. Commun.* **2016**, *52*, 14121–14124.
67. Carmona, J. A.; Hornillos, V.; Ramírez-López, P.; Ros, A.; Iglesias-Sigüenza, J.; Gómez-Bengoa, E.; Fernández, R.; Lassaletta, J. M. *J. Am. Chem. Soc.* **2018**, *140*, 11067–11075.
68. Frey, J.; Malekafzali, A.; Delso, I.; Choppin, S.; Colobert, F.; Wencel-Delord, J. *Angew. Chem. Int. Ed.* **2020**, *59*, 8844–8848.
69. Sun, C.; Qi, X.; Min, X.-L.; Bai, X.-D.; Liu, P.; He, Y. *Chem. Sci.* **2020**, *11*, 10119–10126.
70. Li, H.; Yan, X.; Zhang, J.; Guo, W.; Jiang, J.; Wang, J. *Angew. Chem. Int. Ed.* **2019**, *58*, 6732–6736.
71. Yao, Q.-J.; Xie, P.-P.; Wu, Y.-J.; Feng, Y.-L.; Teng, M.-Y.; Hong, X.; Shi, B.-F. *J. Am. Chem. Soc.* **2020**, *142*, 18266–18276.
72. Hirata, T.; Takahashi, I.; Suzuki, Y.; Yoshida, H.; Hasegawa, H.; Kitagawa, O. *J. Org. Chem.* **2016**, *81*, 318–323.
73. Fan, X.; Zhang, X.; Li, C.; Gu, Z. *ACS Catal.* **2019**, *9*, 2286–2291.
74. Pan, C.; Zhu, Z.; Zhang, M.; Gu, Z. *Angew. Chem. Int. Ed.* **2017**, *56*, 4777–4781.
75. Feng, J.; Li, B.; He, Y. Gu, Z. *Angew. Chem. Int. Ed.* **2016**, *55*, 2186–2190.
76. Fang, Z.-J.; Zheng, S.-C.; Guo, Z.; Guo, J.-Y.; Tan, B.; Liu, X.-Y. *Angew. Chem. Int. Ed.* **2015**, *54*, 9528–9532.
77. Shan, G.; Flegel, J.; Li, H.; Merten, C.; Ziegler, S.; Antonchick, A. P.; Waldmann, H. *Angew. Chem. Int. Ed.* **2018**, *57*, 14250–14254.
78. Sun, Q.-Y.; Ma, W.-Y.; Yang, K.-F.; Cao, J.; Zheng, Z.-J.; Xu, Z.; Cui, Y.-M.; Xu, L.-W. *Chem. Commun.* **2018**, *54*, 10706–10709.
79. Jin, L.; Yao, Q.-J.; Xie, P.-P.; Li, Y.; Zhan, B.-B.; Han, Y.-Q.; Hong, X.; Shi, B.-F. *Chem.* **2020**, *6*, 497–511.
80. Yang, C.; Wu, T.-R.; Li, Y.; Wu, B.-B.; Jin, R.-X.; Hu, D.-D.; Li, Y.-B.; Bian, K.-J.; Wang, X.-S. *Chem. Sci.* **2021**, *12*, 3726–3732.
81. Li, G.-Q.; Gao, H.; Keene, C.; Devonas, M.; Ess, D. H.; Kürti, L. *J. Am. Chem. Soc.* **2013**, *135*, 7414–7417.
82. De, C. K.; Pesciaioli F.; List, B. *Angew. Chem. Int. Ed.* **2013**, *52*, 9293–9295.
83. Chen, Y.-H.; Cheng, D.-J.; Zhang, J.; Wang, Y.; Liu, X.-Y.; Tan, B. *J. Am. Chem. Soc.* **2015**, *137*, 15062–15065.
84. Moliterno, M.; Cari, R.; Puglisi, A.; Antenucci, A.; Sperandio, C.; Moretti, E.; Sabato, A. D.; Salvio, R.; Bella, M. *Angew. Chem. Int. Ed.* **2016**, *55*, 6525–6529.
85. Coombs, G.; Sak, M. H.; Miller, S. J. *Angew. Chem. Int. Ed.* **2020**, *59*, 2875–2880.
86. Wang, J.-Z.; Zhou, J.; Xu, C.; Sun, H.; Kürti, L.; Xu, Q.-L. *J. Am. Chem. Soc.* **2016**, *138*, 5202–5205.
87. Lotter, D.; Neuburger, M.; Rickhaus, M.; Häussinger, D.; Sparr, C. *Angew. Chem. Int. Ed.* **2016**, *55*, 2920–2923.
88. Witzig, R. M.; Fäseke, V. C.; Häussinger, D.; Sparr, C. *Nat. Catal.* **2019**, *2*, 925–930.
89. Link, A.; Sparr, C. *Angew. Chem. Int. Ed.* **2014**, *53*, 5458–5461.
90. Jia, S.; Li, S.; Liu, Y.; Qin, W.; Yan, H. *Angew. Chem. Int. Ed.* **2019**, *58*, 18496–18501.
91. Chen, X.; Gao, D.; Wang, D.; Xu, T.; Liu, W.; Tian, P.; Tong, X. *Angew. Chem. Int. Ed.* **2019**, *58*, 15334–15338.
92. Yu, C.; Huang, H.; Li, X.; Zhang, Y.; Wang, W. *J. Am. Chem. Soc.* **2016**, *138*, 6956–6959.

93. Mori, K.; Itakura, T.; Akiyama, T. *Angew. Chem. Int. Ed.* **2016**, *55*, 11642–11646.
94. Beleh, O. M.; Miller, E.; Toste, F. D.; Miller, S. J. *J. Am. Chem. Soc.* **2020**, *142*, 16461–16470.
95. Yang, G.; Guo, D.; Meng, D.; Wang, J. *Nat. Commun.* **2019**, *10*, 3062.
96. Lu, S.; Poh, S. B.; Rong, Z.-Q.; Zhao, Y. *Org. Lett.* **2019**, *21*, 6169–6172.
97. Munday, E. S.; Grove, M. A.; Feoktistova, T.; Brueckner, A. C.; Walden, D. M.; Young, C. M.; Slawin, A. M. Z.; Campbell, A. D.; Cheong, P. H.-Y.; Smith, A. D. *Angew. Chem. Int. Ed.* **2020**, *59*, 7897–7905.
98. Lu, S.; Ng, S. V. H.; Lovato, K.; Ong, J.-Y.; Poh, S.-B.; Ng, X. Q.; Kürti, L.; Zhao, Y. *Nat. Commun.* **2019**, *10*, 3061.
99. Liu, W.; Jiang, Q.; Yang, X. *Angew. Chem. Int. Ed.* **2020**, *59*, 23598–23602.
100. Qu, S.; Greenhalgh, M. D.; Smith, A. D. *Chem. Eur. J.* **2019**, *25*, 2816–2823.
101. Jones, B. A.; Balan, T.; Jolliffe, J. D.; Campbell, C. D.; Smith, M. D. *Angew. Chem. Int. Ed.* **2019**, *58*, 4596–4600.
102. Wang, J.; Chen, M.-W.; Ji, Y.; Hu, S.-B.; Zhou, Y.-G. *J. Am. Chem. Soc.* **2016**, *138*, 10413–10416.
103. Qi, L.-W.; Mao, J.-H.; Zhang, J.; Tan, B. *Nat. Chem.* **2018**, *10*, 58–64.
104. Xia, W.; An, Q.-J.; Xiang, S.-H.; Li, S.; Wang, Y.-B.; Tan, B. *Angew. Chem. Int. Ed.* **2020**, *59*, 6775–6779.
105. Yuan, H.; Li, Y.; Zhao, H.; Yang, Z.; Li, X.; Li, W. *Chem. Commun.* **2019**, *55*, 12715–12718.
106. Lu, D.-L.; Chen, Y.-H.; Xiang, S.-H.; Yu, P.; Tan, B.; Li, S. *Org. Lett.* **2019**, *21*, 6000–6004.
107. Liu, J.-Y.; Yang, X.-C.; Liu, Z.; Luo, Y.-C.; Lu, H.; Gu, Y.-C.; Fang, R.; Xu, P.-F. *Org. Lett.* **2019**, *21*, 5219–5224.
108. Zhang, H.-H.; Wang, C.-S.; Li, C.; Mei, G.-J.; Li, Y.; Shi, F. *Angew. Chem. Int. Ed.* **2017**, *56*, 116–121.
109. Quinonero, O.; Jean, M.; Vanthuyne, N.; Roussel, C.; Bonne, D.; Constantieux, T.; Bressy, C.; Bugaut, X.; Rodriguez, J. *Angew. Chem. Int. Ed.* **2016**, *55*, 1401–1405.
110. Bisag, G. D.; Pecorari, D.; Mazzanti, A.; Bernardi, L.; Fochi, M.; Bencivenni, G.; Bertuzzi, G.; Corti, V. *Chem. Eur. J.* **2019**, *25*, 15694–15701.
111. Wang, S.-J.; Wang, Z.; Tang, Y.; Chen, J.; Zhou, L. *Org. Lett.* **2020**, *22*, 8894–8898.
112. Hu, Y.-L.; Wang, Z.; Yang, H.; Chen, J.; Wu, Z.-B.; Lei, Y.; Zhou, L. *Chem. Sci.* **2019**, *10*, 6777–6784.
113. He, X.-L.; Zhao, H.-R.; Song, X.; Jiang, B.; Du, W.; Chen, Y.-C. *ACS Catal.* **2019**, *9*, 4374–4381.
114. Zheng, S.-C.; Wang, Q.; Zhu, J. *Angew. Chem. Int. Ed.* **2019**, *58*, 9215–9219.
115. Wang, L.; Zhong, J.; Lin, X. *Angew. Chem. Int. Ed.* **2019**, *58*, 15824–15828.
116. Shao, Y.-D.; Dong, M.-M.; Wang, Y.-A.; Cheng, P.-M.; Wang, T.; Cheng, D.-J. *Org. Lett.* **2019**, *21*, 4831–4836.
117. Wan, J.; Liu, H.; Lan, Y.; Li, X.; Hu, X.; Li, J.; Xiao, H.-P.; Jiang, J. *Synlett* **2019**, *30*, 2198–2202.
118. Kwon, Y.; Chinn, A. J.; Kim, B.; Miller, S. J. *Angew. Chem. Int. Ed.* **2018**, *57*, 6251–6255.
119. Raut, V. S.; Jean, M.; Vanthuyne, N.; Roussel, C.; Constantieux, T.; Bressy, C.; Bugaut, X.; Bonne, D.; Rodriguez, J. *J. Am. Chem. Soc.* **2017**, *139*, 2140–2143.
120. Lu, S.; Ong, J.-Y.; Yang, H.; Poh, S. B.; Liew, X.; Seow, C. S. D.; Wong, M. W.; Zhao, Y. *J. Am. Chem. Soc.* **2019**, *141*, 17062–17067.
121. Wang, D.; Tong, X. *Org. Lett.* **2017**, *19*, 6392–6395.
122. Ma, C.; Jiang, F.; Sheng, F.-T.; Jiao, Y.; Mei, G.-J.; Shi, F. *Angew. Chem. Int. Ed.* **2019**, *58*, 3014–3020.
123. Jiang, F.; Chen, K.-W.; Wu, P.; Zhang, Y.-C.; Jiao, Y.; Shi, F. *Angew. Chem. Int. Ed.* **2019**, *58*, 15104–15110.
124. Miyaji, R.; Asano, K.; Matsubara, S. *J. Am. Chem. Soc.* **2015**, *137*, 6766–6769.
125. Miyaji, R.; Asano, K.; Matsubara, S. *Chem. Eur. J.* **2017**, *23*, 9996–10000.
126. Zhang, L.; Xiang, S.-H.; Wang, J.; Xiao, J.; Wang, J.-Q.; Tan, B. *Nat. Commun.* **2019**, *10*, 566.
127. Brandes, S.; Bella, M.; Kjærsgaard, A.; Jørgensen, K. A. *Angew. Chem. Int. Ed.* **2006**, *45*, 1147–1151.
128. Bai, H.-Y.; Tan, F.-X.; Liu, T.-Q.; Zhu, G.-D.; Tian, J.-M.; Ding, T.-M.; Chen, Z.-M.; Zhang, S.-Y. *Nat. Commun.* **2019**, *10*, 3063.
129. Wang, Y.-B.; Zheng, S.-C.; Hu, Y.-M.; Tan, B. *Nat. Commun.* **2017**, *8*, 15489.
130. Wang, L.; Li, S.; Blümel, M.; Philipps, A. R.; Wang, A.; Puttreddy, R.; Rissanen, K.; Enders, D. *Angew. Chem. Int. Ed.* **2016**, *55*, 11110–11114.
131. Li, S.-L.; Yang, C.; Wu, Q.; Zheng, H.-L.; Li, X.; Cheng, J.-P. *J. Am. Chem. Soc.* **2018**, *140*, 12836–12843.
132. Yang, G.-H.; Zheng, H.; Li, X.; Cheng, J.-P. *ACS Catal.* **2020**, *10*, 2324–2333.
133. Ong, J.-Y.; Ng, X. Q.; Lu, S.; Zhao, Y. *Org. Lett.* **2020**, *22*, 6447–6451.
134. Gustafson, J. L.; Lim, D.; Miller, S. J. *Science* **2010**, *328*, 1251–1255.
135. Barrett, K. T.; Miller, S. J. *J. Am. Chem. Soc.* **2013**, *135*, 2963–2966.
136. Diener, M. E.; Metrano, A. J.; Kusano, S.; Miller, S. J. *J. Am. Chem. Soc.* **2015**, *137*, 12369–12377.
137. Vaidya, S. D.; Toenjes, S. T.; Yamamoto, N.; Maddox, S. M.; Gustafson, J. L. *J. Am. Chem. Soc.* **2020**, *142*, 2198–2203.
138. Iorio, N. D.; Crotti, S.; Bencivenni, G. *Chem. Rec.* **2019**, *19*, 2095–2104.
139. Zhang, J.-W.; Xu, J.-H.; Cheng, D.-J.; Shi, C.; Liu, X.-Y.; Tan, B. *Nat. Commun.* **2016**, *7*, 10677.
140. Zhang, L.-L.; Zhang, J.-W.; Xiang, S.-H.; Guo, Z.; Tan, B. *Org. Lett.* **2018**, *20*, 6022–6026.
141. Fäseke, V. C.; Sparr, C. *Angew. Chem. Int. Ed.* **2016**, *55*, 7261–7264.
142. Clayden, J. *Chem. Commun.* **2004**, 127–135.
143. Fugard, A. J.; Lahdenperä, A. S. K.; Tan, J. S. J.; Mekareeya, A.; Paton, R. S.; Smith, M. D. *Angew. Chem. Int. Ed.* **2019**, *58*, 2795–2798.

144. Li, S.-L.; Wu, Q.; Yang, C.; Li, X.; Cheng, J.-P. *Org. Lett.* **2019**, *21*, 5495–5499.
145. Zhu, S.; Chen, Y.-H.; Wang, Y.-B.; Yu, P.; Li, S.-Y.; Xiang, S.-H.; Wang, J.-Q.; Xiao, J.; Tan, B. *Nat. Commun.* **2019**, *10*, 4268.
146. Chen, Y.-H.; Li, H.-H.; Zhang, X.; Xiang, S.-H.; Li, S.; Tan, B. *Angew. Chem. Int. Ed.* **2020**, *59*, 11374–11378.
147. Zhao, C.; Guo, D.; Munkerup, K.; Huang, K.-W.; Li, F.; Wang, J. *Nat. Commun.* **2018**, *9*, 611.
148. Liang, Y.; Ji, J.; Zhang, X.; Jiang, Q.; Luo, J.; Zhao, X. *Angew. Chem. Int. Ed.* **2020**, *59*, 4959–4964.
149. Zheng, S.-C.; Wu, S.; Zhou, Q.; Chung, L. W.; Ye, L.; Tan, B. *Nat. Commun.* **2017**, *8*, 15238.
150. Wang, C.-S.; Li, T.-Z.; Liu, S.-J.; Zhang, Y.-C.; Deng, S.; Jiao, Y.; Shi, F. *Chin. J. Chem.* **2020**, *38*, 543–552.
151. Jia, S.; Chen, Z.; Zhang, N.; Tan, Y.; Liu, Y.; Deng, J.; Yan, H. *J. Am. Chem. Soc.* **2018**, *140*, 7056–7060.
152. Li, S.; Xu, D.; Hu, F.; Li, D.; Qin, W.; Yan, H. *Org. Lett.* **2018**, *20*, 7665–7669.
153. Tan, Y.; Jia, S.; Hu, F.; Liu, Y.; Peng, L.; Li, D.; Yan, H. *J. Am. Chem. Soc.* **2018**, *140*, 16893–16898.
154. Huang, A.; Zhang, L.; Li, D.; Liu, Y.; Yan, H.; Li, W. *Org. Lett.* **2019**, *21*, 95–99.
155. Li, Q.-Z.; Lian, P.-F.; Tan, F.-X.; Zhu, G.-D.; Chen, C.; Hao, Y.; Jiang, W.; Wang, X.-H.; Zhou, J.; Zhang, S.-Y. *Org. Lett.* **2020**, *22*, 2448–2453.
156. Wang, Y.-B.; Yu, P.; Zhou, Z.-P.; Zhang, J.; Wang, J.; Luo, S.-H.; Gu, Q.-S.; Houk, K. N.; Tan, B. *Nat. Catal.* **2019**, *2*, 504–513.
157. Jolliffe, J. D.; Armstrong, R. J.; Smith, M. D. *Nat. Chem.* **2017**, *9*, 558–562.
158. Ma, C.; Sheng, F.-T.; Wang, H.-Q.; Deng, S.; Zhang, Y.-C.; Jiao, Y.; Tan, W.; Shi, F. *J. Am. Chem. Soc.* **2020**, *142*, 15686–15696.
159. Wang, Y.-B.; Wu, Q.-H.; Zhou, Z.-P.; Xiang, S.-H.; Cui, Y.; Yu, P.; Tan, B. *Angew. Chem. Int. Ed.* **2019**, *58*, 13443–13447.
160. Moustafa, G. A. I.; Oki, Y.; Akai, S. *Angew. Chem. Int. Ed.* **2018**, *57*, 10278–10282.
161. Staniland, S.; Adams, R. W.; McDouall, J. J. W.; Maffucci, I.; Contini, A.; Grainger, D. M.; Turner, N. J.; Clayden, J. *Angew. Chem. Int. Ed.* **2016**, *55*, 10755–10759.

20

ASYMMETRIC SYNTHESIS OF PLANAR CHIRAL AND HELICALLY CHIRAL COMPOUNDS

Takanori Shibata
Department of Chemistry and Biochemistry, Faculty of Science and Engineering, Waseda University, Tokyo, Japan

20.1. INTRODUCTION

As a family of non-centro-chiral compounds, this chapter describes various approaches to the asymmetric synthesis of chiral compounds with planar or helical chirality. I focus on catalytic and enantioselective syntheses and do not mention asymmetric synthesis via a stoichiometric protocol or kinetic resolution.

Five classes of compound are listed as representatives of planar chiral molecules (Scheme 20.1). The simplest are *trans*-cyclic alkenes, where the tether moiety is difficult to flip. *Meta*- and *para*-cyclophanes are also conventional planar chiral compounds. Among them, substituted [2.2]paracyclophane is often used as a chiral scaffold. Metallocene with different substituents possesses planar chirality. In particular, asymmetric synthesis of planar chiral ferrocenes (M = Fe) is important due to their versatility as chiral ligands. Substituted arene and 1,3-diene complexes also have planar chirality, but the examples of their catalytic and enantioselective syntheses are limited compared with ferrocenes.

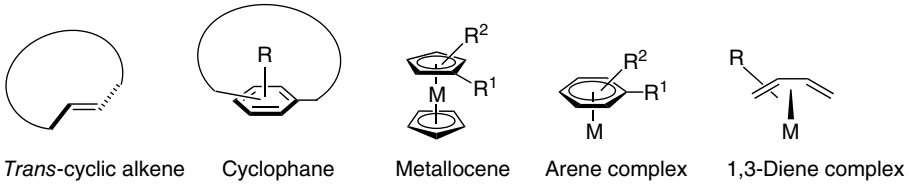

Scheme 20.1. Representatives of planar chiral molecules.

Helicene is an *ortho*-fused polycyclic aromatic compound with angularly annulated aromatic moieties. It is probably the most famous helically chiral molecule among synthetic compounds. Although the enantiomers of carbo[5]helicene freely interconvert at room temperature, more than five carbohelicenes are conformationally stable at room temperature [1]. The characteristics of helicenes are their extremely high optical rotation values (Scheme 20.2) [2].

Catalytic Asymmetric Synthesis, Fourth Edition. Edited by Takahiko Akiyama and Iwao Ojima.

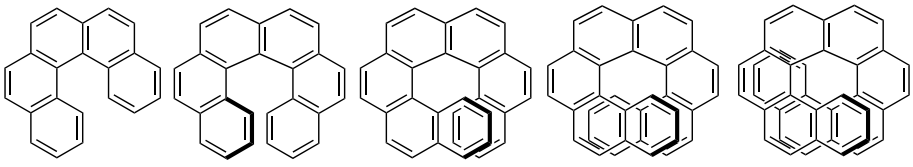

	[5]helicene	(*P*)-[6]helicene	(*P*)-[7]helicene	(*P*)-[8]helicene	(*P*)-[9]helicene
$\Delta G^{\neq}$ (kcal/mol)	24.1	37.0	~40	~40	~40
$[\alpha]_D^{25}$		+3640	+5900	+7170	+8100

Scheme 20.2. Characteristics of carbohelicenes. Source: Based on [2].

Recently, the chiroptical properties of helicenes have attracted much attention in the material sciences due to their circularly polarized luminescence (CPL), which has potential applications in quantum computer, 3D display, and organic electro luminescence diode (OLED) screen. Therefore, the facile asymmetric synthesis of helicenes, including heterohelicene, which has one or more heteroatoms in the π-system, is an important topic in organic chemistry.

20.2. ENANTIOSELECTIVE SYNTHESIS OF PLANAR CHIRAL COMPOUNDS

I have divided this chapter into four sections dependent on the type of planar chirality. The enantioselective synthesis of planar chiral ferrocenes is a major focus of this section because of its variety and usefulness in organic synthesis [3].

20.2.1. Enantioselective Synthesis of Planar Chiral Ferrocenes

20.2.1.1. Pioneering Works The direct C-H functionalization of ferrocene is a straightforward strategy for the generation of planar chirality in ferrocenes. A pioneering achievement was the enantioselective lithiation using a directing group (DG) in the presence of a stoichiometric amount of chiral amines (Scheme 20.3) [4a–c]. Phosphinyl, aminomethyl, and amide groups work as efficient DGs, and various types of functionalized ferrocenes can be prepared through the choice of electrophiles. Among them, sparteine can exhibit high to excellent enantioselectivity and catalytic reactions can also be achieved along with a slight decrease in ee [4d].

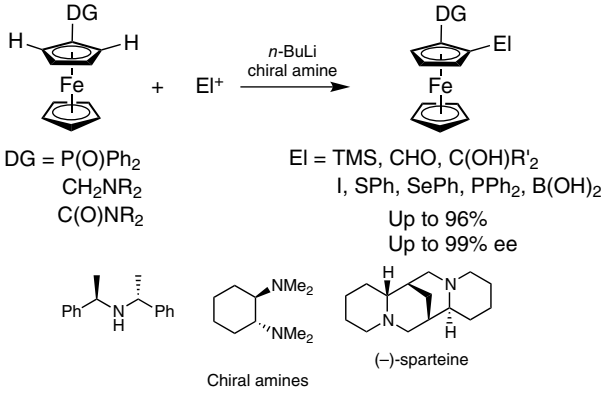

Scheme 20.3. Enantioselective lithiation of ferrocenes using chiral amines. Source: Based on [4a–c].

Another pioneering work regarding transition-metal-catalyzed reactions was the intramolecular C-H activation using α-keto diazo compounds (Scheme 20.4), where a chiral Cu(I)-catalyzed reaction provides cyclic ketone-fused ferrocenes in good ee [5].

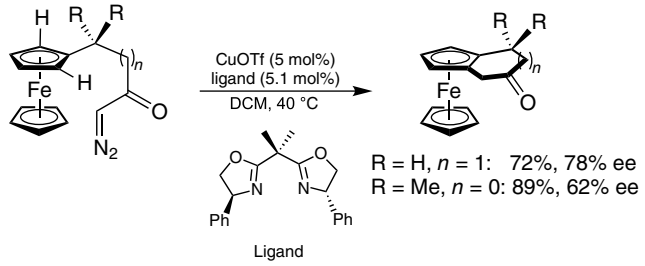

Scheme 20.4. Intramolecular reaction of diazo compounds. Source: [5]/John Wiley & Sons.

20.2.1.2. Pd-Catalyzed Intermolecular Reactions Using Amino Acid-Derived Ligands A crucial advance was the Pd(II)-catalyzed enantioselective C-H activation of ferrocenes using a mono-protected amino acid as a chiral ligand [6]. In this context, dimethylaminomethyl was an efficient DG, and its reaction with arylboronic acids under the aerobic conditions provides C-H arylated product in excellent ee (Scheme 20.5).

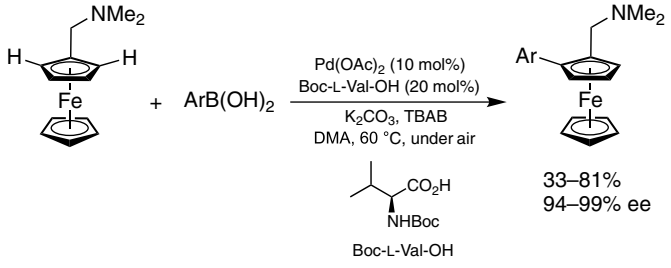

Scheme 20.5. C–H arylation using aryl boronic acids directed by an aminomethyl group.

The combination of $Pd(OAc)_2$ and a mono-protected amino acid was consecutively used in the enantioselective C-H activation of ferrocenes that possess an aminomethyl group as a DG. A Heck-type reaction with mono-substituted alkenes proceeded to give alkenylated products in *E*-form (Scheme 20.6) [7]. The reaction of aminomethylferrocene with two molecules of diarylethyne produced 2,3,4-triarylnaphthan-1-yl-substituted ferrocenes as annulated products (Scheme 20.7) [8]. In the presence of *tert*-butyl peroxide, the introduction of an aryloyl group was achieved initiated by the C-C bond cleavage of 1,2-diketone (Scheme 20.8) [9]. *N*-Protected phenylalanine induced high to excellent enantioselectivity in these transformations.

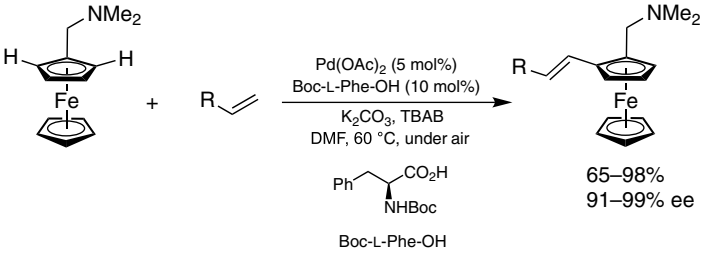

Scheme 20.6. C–H alkenylation using alkenes directed by an aminomethyl group. Source: [7]/Royal Society of Chemistry.

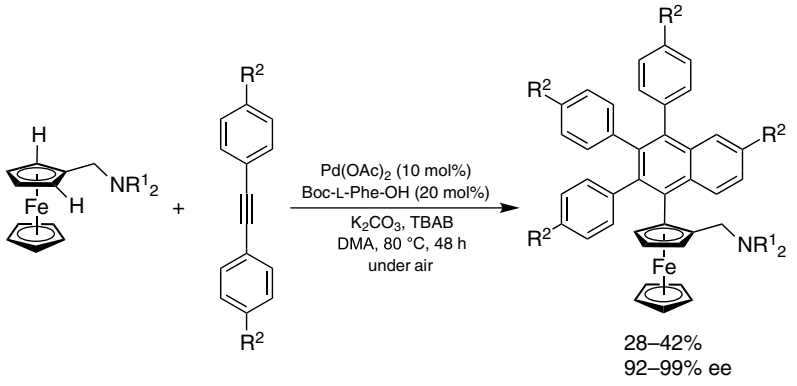

Scheme 20.7. C–H annulation using diaryl alkynes directed by an aminomethyl group. Source: [8]/Beilstein Institute for the Advancement of Chemical Sciences.

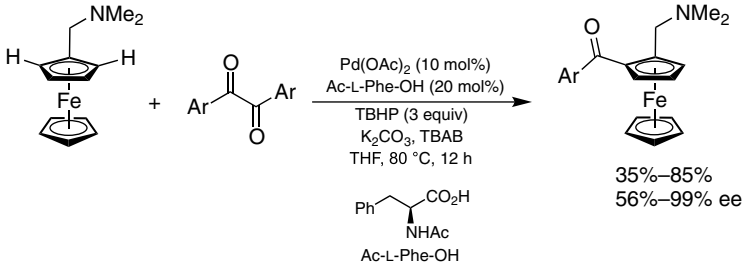

Scheme 20.8. C–H acylation using 1,2-diketones directed by an aminomethyl group. Source: [9]/American Chemical Society.

The dehydrogenative coupling of relatively reactive C-H bonds was also possible. The C2-position of (benzo)heteroles (Scheme 20.9) and the C5-position of azoles (Scheme 20.10) reacted with aminomethylferrocenes in the presence of 1,4-benzoquinone (BQ) to provide planar chiral heteroaryl-substituted ferrocenes [10, 11].

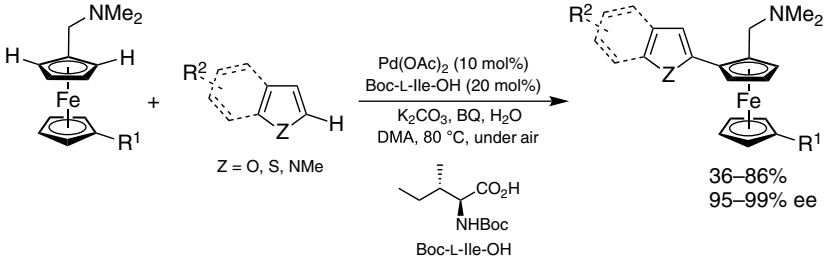

Scheme 20.9. C–H/C–H coupling using (benzo)heteroles directed by an aminomethyl group.

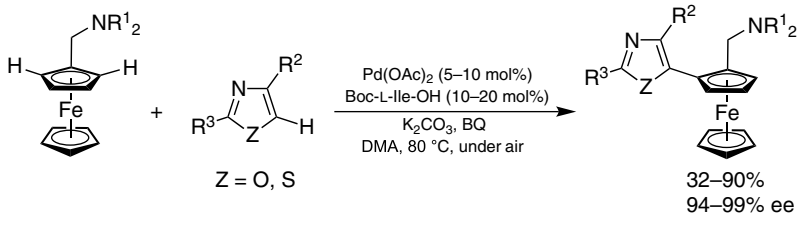

Scheme 20.10. C–H/C–H coupling using heteroles directed by an aminomethyl group.

The chiral Pd catalysts with a mono-protected amino acid were also available for the other DGs. In a carbonyl-directed reaction, C-H arylation proceeded using various iodoarenes (Scheme 20.11) [12]. The carboxylate-directed transformation using mono-substituted alkenes, such as styrenes and functionalized alkenes, produced 2-alkenylated ferrocene carboxylic acids (Scheme 20.12) [13].

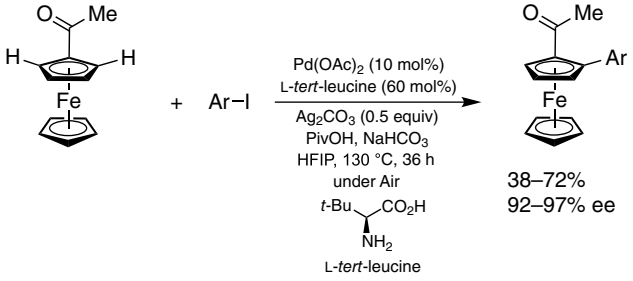

Scheme 20.11. C–H arylation using iodoarenes directed by a carbonyl group. Source: [12]/Royal Society of Chemistry.

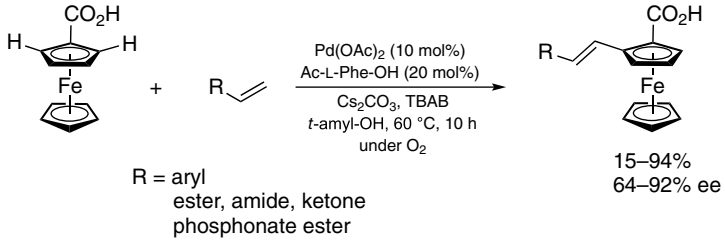

Scheme 20.12. C–H alkenylation using alkenes directed by a carboxyl group. Source: [13]/ELSEVIER.

20.2.1.3. Intermolecular Reactions Using Other Metal Catalysts Besides Pd-amino acid derivative catalysts, an Ir-chiral diene complex can accelerate an enantioselective C-H alkylation using various alkenes. An isoquinolyl group was critical as a DG in achieving high enantioselectivity and selective mono-alkylation (Scheme 20.13) [14]. Regarding C-H alkenylation by alkynes, an Sc-chiral Cp catalyst realized high to excellent ee by using a quinolyl group as a DG (Scheme 20.14) [15].

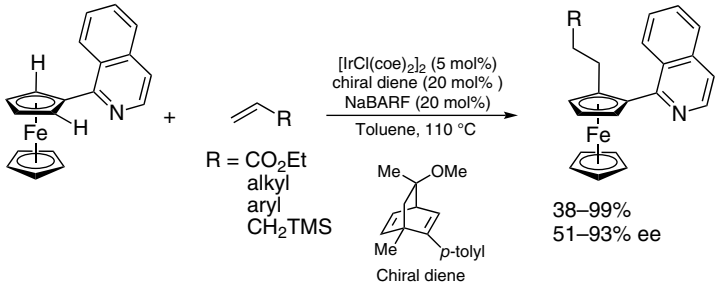

Scheme 20.13. C–H alkylation using alkenes directed by an isoquinolyl group. Source: [14]/John Wiley & Sons.

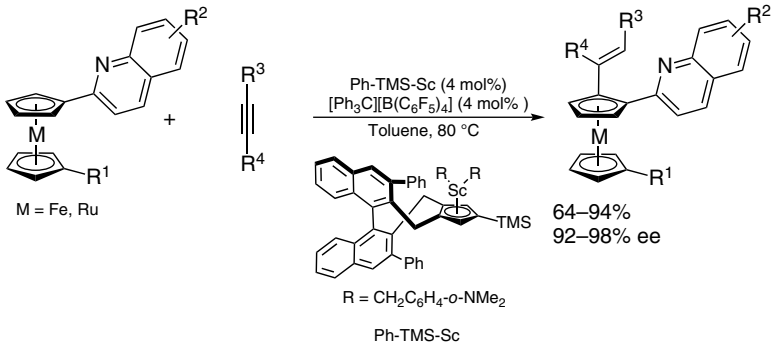

Scheme 20.14. C–H alkenylation using alkynes by a quinolyl group. Source: [15]/American Chemical Society.

1,4,2-Dioxazol-5-ones is often used for C-H amidation. Pyridyl group worked well in Cp*Rh(III)-catalyzed C-H amidation of ferrocene and Cramer's chiral CpRh catalyst induced moderate enantioselectivity (Scheme 20.15) [16]. Thioamide group was effective in Cp*Co(III)-catalyzed C-H amidation and phenylglycine derivative was an optimal chiral ligand, but the ee was moderate (Scheme 20.16) [17]. The combination of Cp*Ir(III) and chiral carboxylic acid derived from *tert*-leucine realized good enantioselectivity, where an amide group was used as a DG (Scheme 20.17) [18].

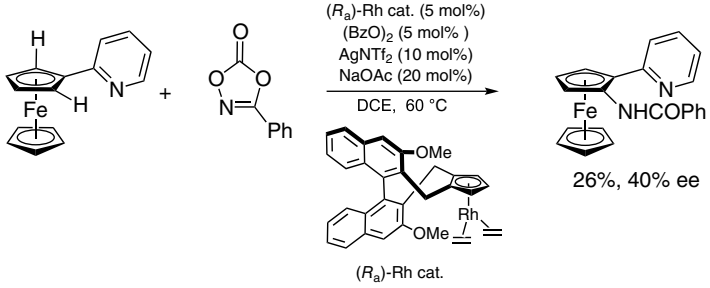

Scheme 20.15. C–H amidation using 1,4,2-dioxazol-5-ones directed by a pyridyl group. Source: [16]/American Chemical Society.

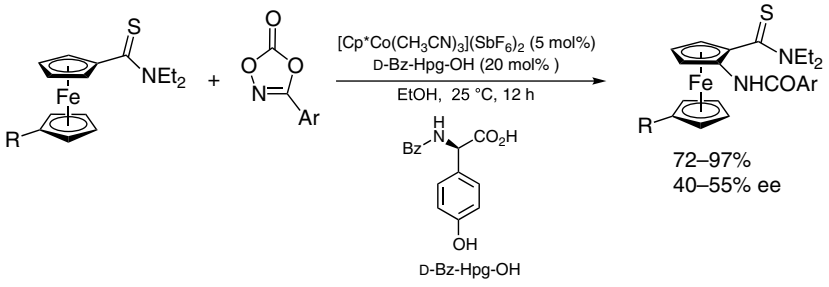

Scheme 20.16. C–H amidation using 1,4,2-dioxazol-5-ones directed by a thioamide group. Source: [17]/American Chemical Society.

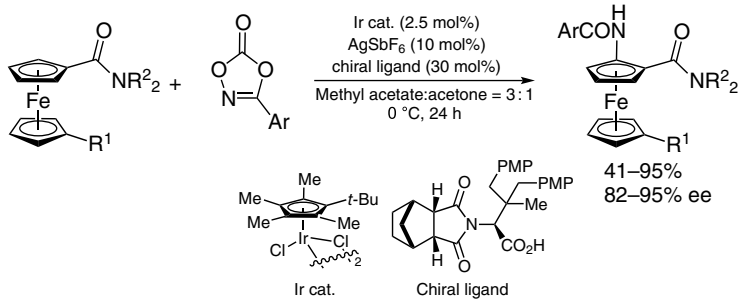

Scheme 20.17. C–H amidation using 1,4,2-dioxazol-5-ones directed by an amide group. Source: [18]/American Chemical Society.

Pyridylferrocenes were good substrates for C-H arylation using haloarenes. A Rh(I) complex with a α,α,α′,α′-tetraaryl-2,2-disubstituted 1,3-dioxolane-4,5-dimethanol (TADDOL)-derived phosphonite was an efficient chiral catalyst, and a wide variety of arenes, including heteroarenes, could be introduced in a highly enantioselective manner (Scheme 20.18) [19].

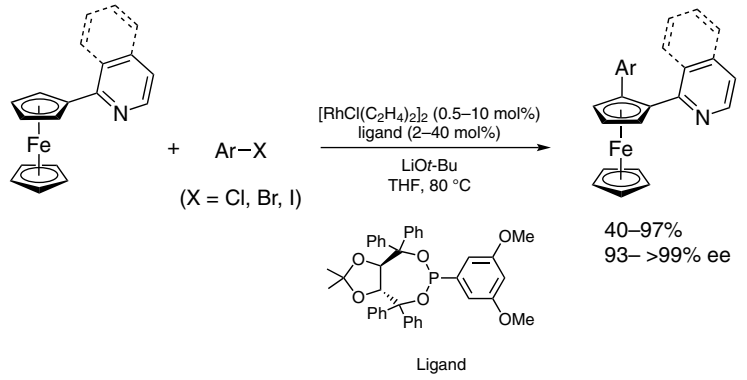

Scheme 20.18. C–H arylation using haloarenes directed by a pyridyl group. Source: [19]/Chinese Chemical Society.

Thioketone-directed C-H arylation proceeded using iodoarene under almost the same conditions as above (Scheme 20.19) [20]. While the thiocarbonyl group was critical for the C-H activation of ferrocene, no reaction proceeded using a carbonyl counterpart.

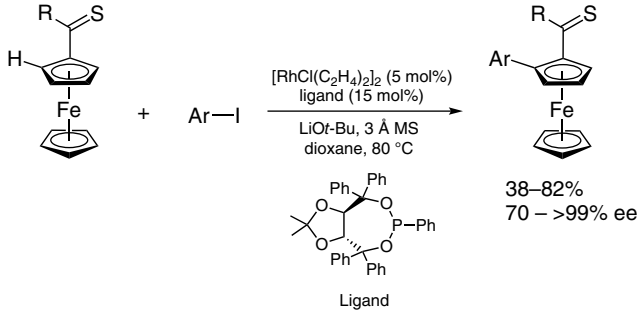

Scheme 20.19. C–H arylation using iodoarenes directed by a thiocarbonyl group. Source: [20]/Springer Nature.

20.2.1.4. Pd-Catalyzed Intramolecular Cross-Coupling The Pd-catalyzed intramolecular reaction of ferrocene with a haloarene moiety is a general protocol for the preparation of planar chiral bicyclic-fused ferrocene. Two groups have independently reported a Pd-2,2′-bis(diphenylphosphino)-1,1′-binaphthyl (BINAP)-complex-catalyzed reaction of 2-halobenzoyl-substituted metallocenes under almost identical conditions (Scheme 20.20) [21]. Indenone-fused ferrocenes were obtained in high yields with high to excellent ee.

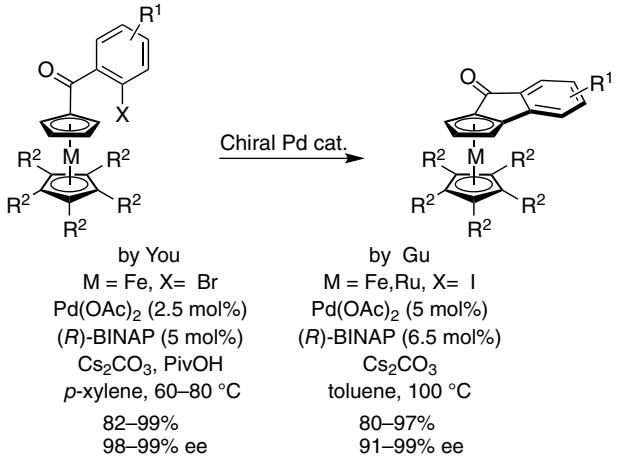

Scheme 20.20. Intramolecular C–H arylation using carbonyl-tethered haloarenes. Source: Based on [21].

Ferrocenyl pyridyl ketones were also transformed into cyclic ketone-fused ferrocenes using ketone-tethered substrates under almost the same reaction conditions (Scheme 20.21) [22].

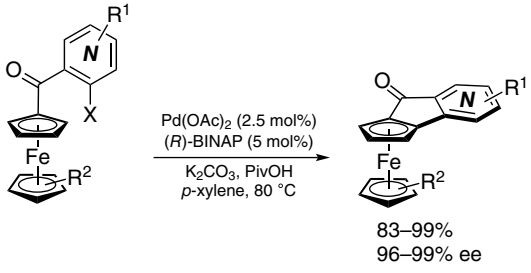

Scheme 20.21. Intramolecular C–H arylation using carbonyl-tethered halopyridines. Source: [22]/American Chemical Society.

In place of ketone, amide-tethered substrates were derived into ferrocene-fused δ-lactams. The Pd-catalyzed intramolecular reaction of *N*-2-halophenylferrocenylamide gave quinolinone-fused ferrocenes (Scheme 20.22), and *P*,*N*-ligand possessing both axial and central chiralities and a TADDOL-based phosphoramidite ligand were reported to be efficient [23]. In contrast, the reaction of *N*-ferrocenyl-2-bromobenzamides provided isoquinolinone-fused ferrocenes, where a *P*,*O*-ligand possessing both carbon and phosphorus chiralities was used (Scheme 20.23) [24].

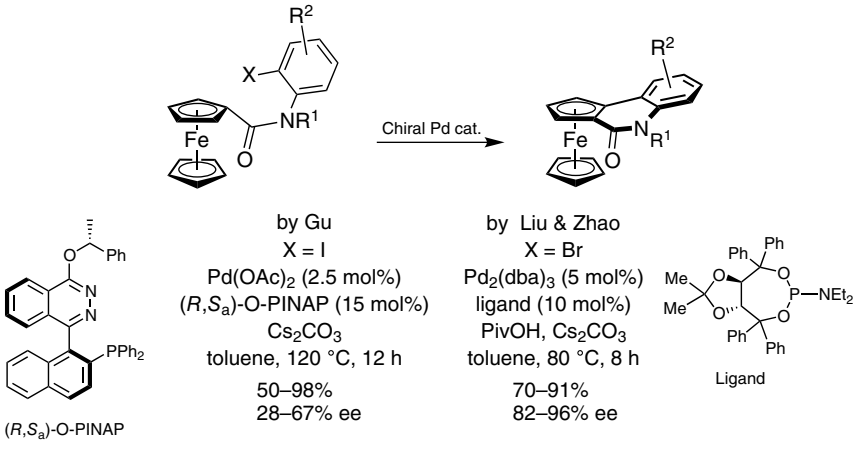

Scheme 20.22. Intramolecular C–H arylation using amide-tethered haloarenes.

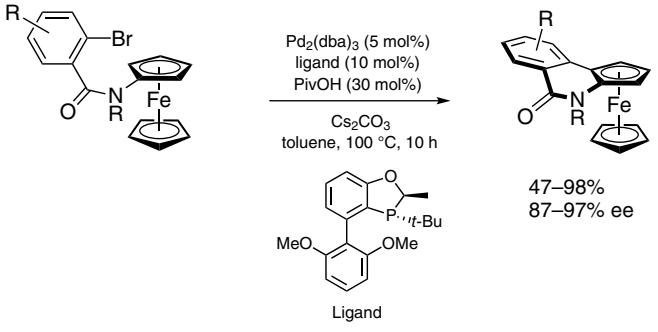

Scheme 20.23. Intramolecular C–H arylation using amide-tethered bromoarenes. Source: [24]/ELSEVIER.

An intramolecular reaction of 2-bromoaryl ferrocenyl sulfides proceeded to afford benzothiophene-fused ferrocenes, where a Pd-BINAP derivative catalyst realized excellent enantioselectivity. Notably, 1,1′-bis(2-bromoarylthio)ferrocenes could be transformed into *C2*-symmetric compounds fused with two benzothiophenes to each Cp ring in an excellent diastereo- and enantioselective manner (Scheme 20.24) [25].

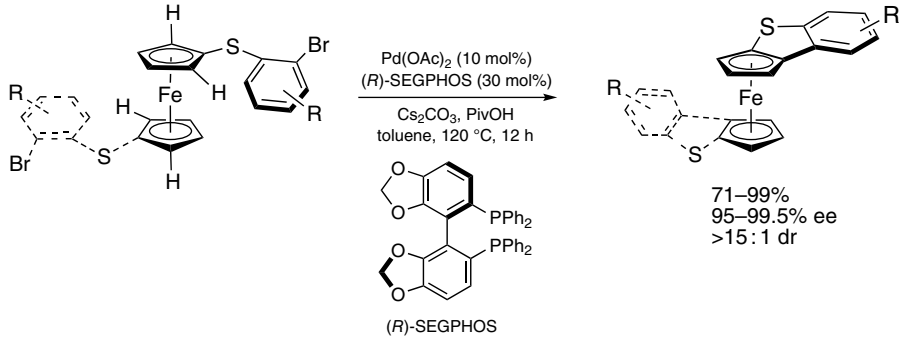

Scheme 20.24. Intramolecular C–H arylation using sulfide-tethered bromoarenes. Source: [25]/American Chemical Society.

Annulation initiated by oxidative addition of haloarene is another strategy for the preparation of ring-fused ferrocenes. For example, isocyanide moiety inserted into arylpalladium halide, and subsequent annulation along with C-H activation gave pyridine-fused ferrocene (Scheme 20.25) [26]. A 7,7′-dihydroxy-1,1′-spirobiindane (SPINOL)-derived phosphoramidite ligand induced high enantioselectivity.

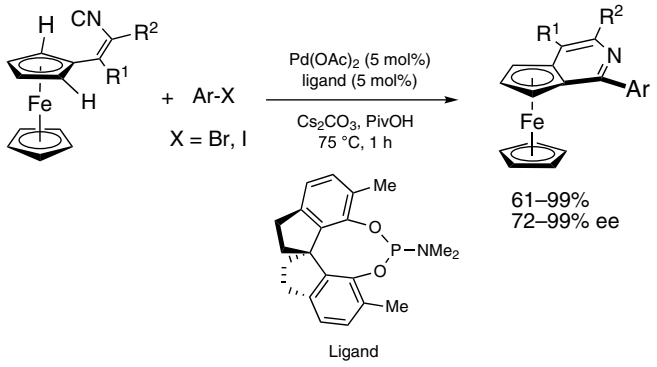

Scheme 20.25. C–H annulation of isocyanides using haloarenes. Source: [26]/American Chemical Society.

When an amide-tethered alkyne moiety was regioselectively inserted into arylpalladium species along with C-H cleaved annulation, planar chiral γ-lactam-fused ferrocenes were provided in good to excellent ee using BINOL-based phosphoramidite ligand (Scheme 20.26) [27].

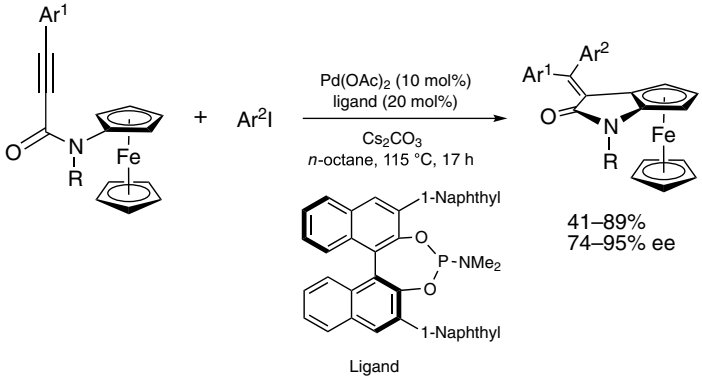

Scheme 20.26. C–H annulation of alkynyl amides using iodoarenes. Source: [27]/Royal Society of Chemistry.

20.2.1.5. Rh- and Ni-Catalyzed Dehydrogenative Couplings Dehydrogenative coupling is generally atom-economical, where hydrogen is the only waste. The Rh-catalyzed intramolecular dehydrogenative coupling of silane and metallocene has been reported from three groups (Scheme 20.27). When chiral diene ligand was used, bulky alkene was needed as a hydrogen acceptor for high conversion [28a]. BINAP derivatives also achieved high yield and enantioselectivity without the use of a hydrogen acceptor, and planar chiral benzosilole-fused ferrocenes were obtained [28b, c].

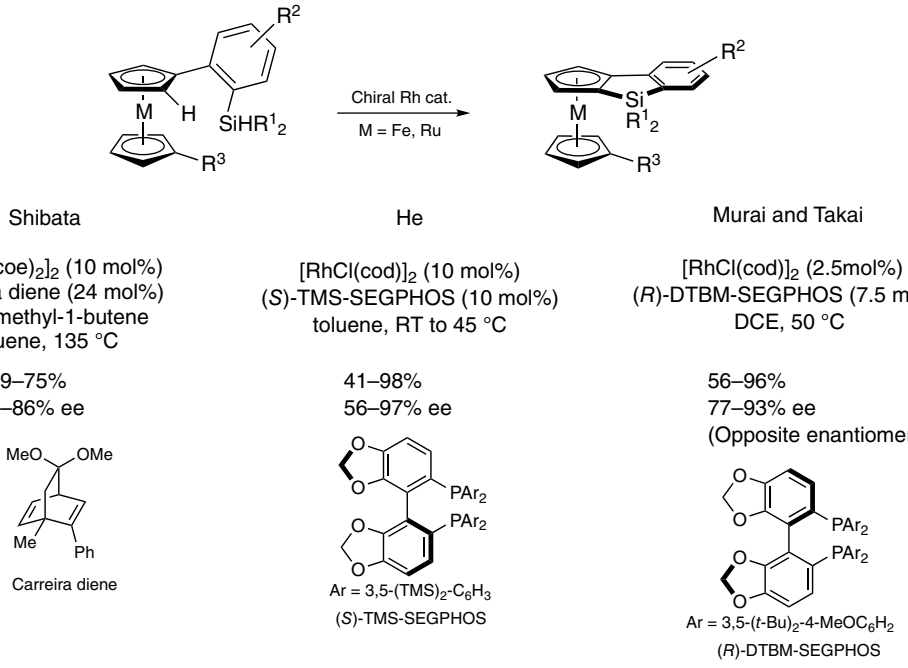

Scheme 20.27. Intramolecular C–H/Si–H coupling.

The consecutive intermolecular and intramolecular dehydrogenative coupling of diethylsilane offered a new access to benzooxasiline-fused ferrocenes (Scheme 20.28). The first step was catalyzed by an Ir(I) complex and the second enantioinductive step was catalyzed by a Rh(I)-ferrocene-based diphosphine complex, and six-membered silacyclized products were obtained in excellent ee [29].

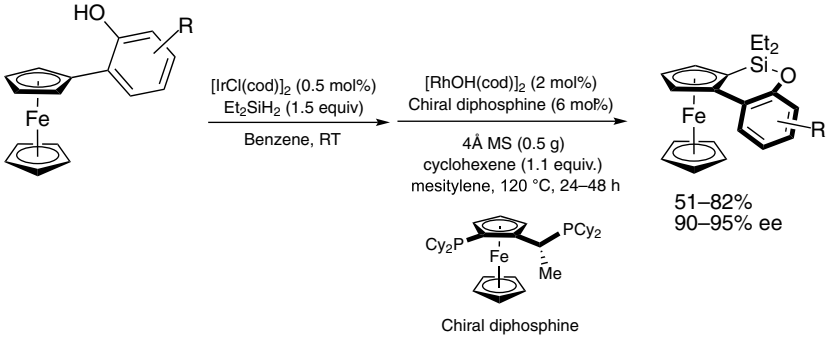

Scheme 20.28. Inter- and intramolecular dehydrogenative couplings of diethylsilane.

The Cp*Rh(III)-catalyzed annulation of ferrocene carboxamides with internal alkynes proceeded to give pyridinone-fused ferrocenes [30]. One example of enantioselective reaction was reported by using Cramer's chiral CpRh catalyst (Scheme 20.29).

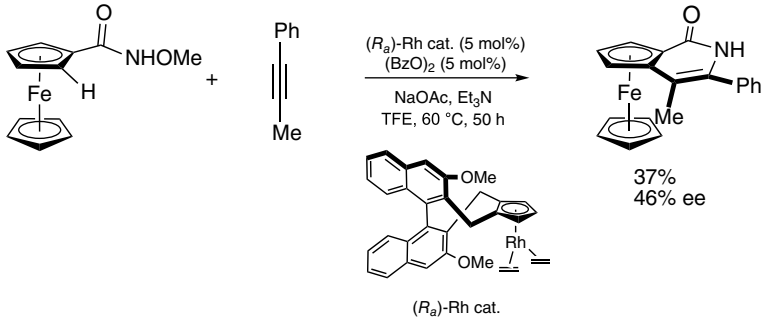

Scheme 20.29. C–H annulation of a carboxamide using an alkyne.

Intermolecular dehydrogenative annulation of *N*-ferrocenylformamide with internal alkynes was achieved by Ni-Al bimetallic catalysis using a chiral secondary phosphine oxide (SPO) as a chiral source [31]. The obtained planar chiral pyridinone-fused ferrocene was transformed into a pyridyl-fused ferrocene through reduction and acidic treatment (Scheme 20.30).

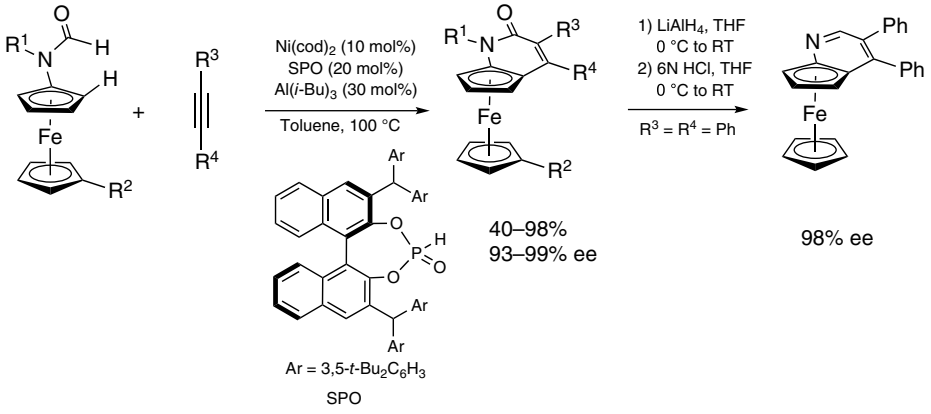

Scheme 20.30. C–H annulation of formamides using alkynes.

20.2.1.6. Au- and Pt-Catalyzed Cycloisomerizations An intramolecular hydroarylation of 2-ethylphenylferrocenes produced naphthalene-fused ferrocenes (Scheme 20.31). Cationic Au(I)- and dicationic Pt(II)-catalyzed reactions have been independently reported [32a, b]. When 2-(propargylamino)phenylferrocenes were subjected to the Pt(II)-catalyzed reaction, 7-*exo-dig*-selective cycloisomerization proceeded to give benzazepine-fused ferrocenes along with double-bond isomerization (Scheme 20.32) [32c].

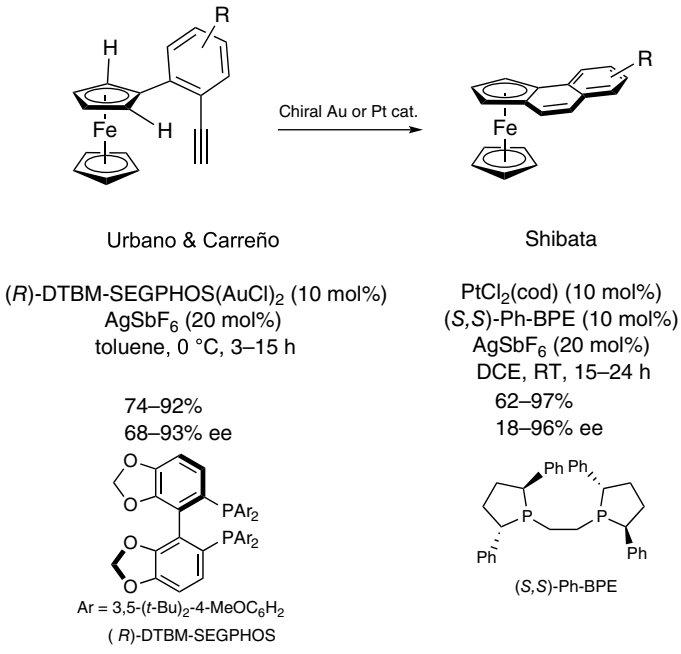

Scheme 20.31. Cycloisomerization of *ortho*-phenylene-tethered alkynes.

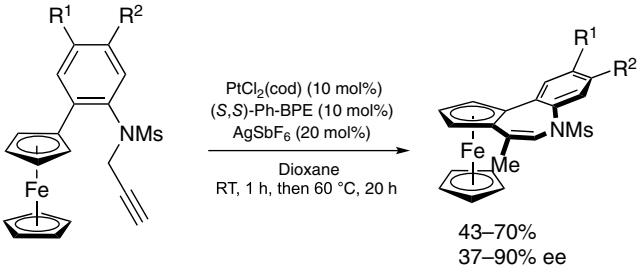

Scheme 20.32. Cycloisomerization of *ortho*-phenylene-tethered propargylamines. Source: [32c]/American Chemical Society.

20.2.2. Enantioselective Synthesis of Planar Chiral Arene-Chromium Complex

There are limited examples of catalytic and enantioselective syntheses of planar chiral arene-Cr complexes compared to those of ferrocenes. The main strategy for the enantioinduction is desymmetrization of disubstituted arene-complexes. An early example was Suzuki-Miyaura coupling of 1,2-dichlorobenzene complex using a Pd-planar chiral ferrocenyl catalyst, and mono-arylated product was obtained in moderate ee (Scheme 20.33) [33a]. Planar chiral cyclophane ligand has been found to be more effective for this transformation [33b]. The second arylation proceeded via kinetic resolution, which improved the ee of the mono-arylated product.

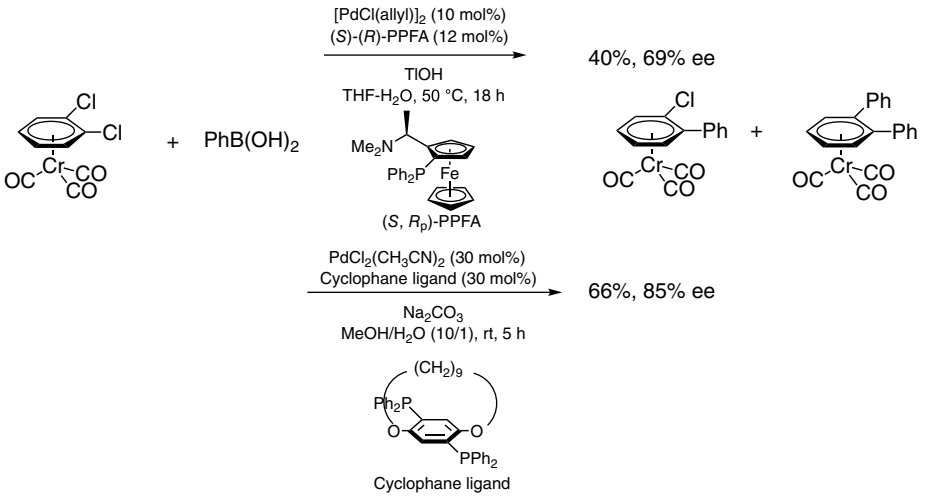

Scheme 20.33. Desymmetric Suzuki coupling of a dichloroarene chromium complex. Source: Based on [33a, b].

An intramolecular Heck reaction was also used for the enantioselective desymmetrization. A chlorobenzene complex with alkenyl substituents at the 2 and 6 positions was transformed into a monocyclized product in moderated ee (Scheme 20.34) [34].

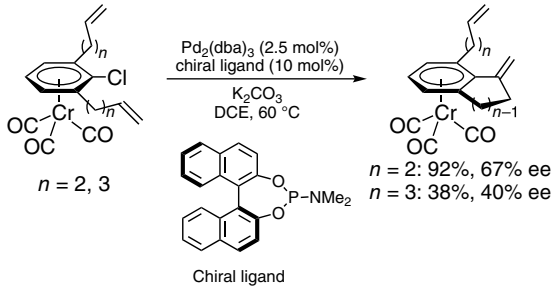

Scheme 20.34. Desymmetric intramolecular Heck reaction of 1,3-diallyl chromium complexes. Source: [34]/ ELSEVIER.

Highly enantioselective desymmetrization in the hydrogenolysis of $Cr(CO)_3$(5,8-dibromonaphthalene) complex using lithium borohydride and Suzuki-Miyaura coupling using various boronic acids was achieved in the presence of a Pd-BINOL-based phosphoramide catalyst (Scheme 20.35) [35a, b].

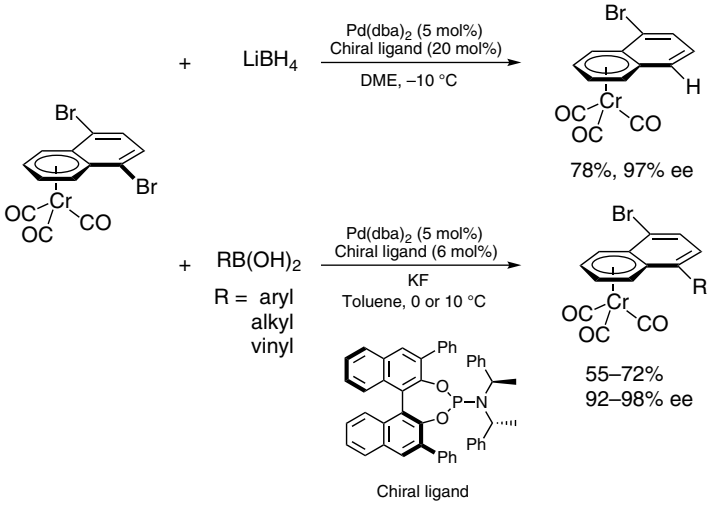

Scheme 20.35. Desymmetric reduction and Suzuki coupling of a 5,8-dibromonaphthalene chromium complex. Source: Based on [35a, b].

Chiral Mo-catalyzed olefin metathesis also induced planar chirality in the arene-Cr complex. One of isopropenyl groups on the arene moiety reacted with allylphosphine, which coordinated the metal center, to provide the corresponding bridged arene-Cr complex in high yields with excellent ee (Scheme 20.36) [36].

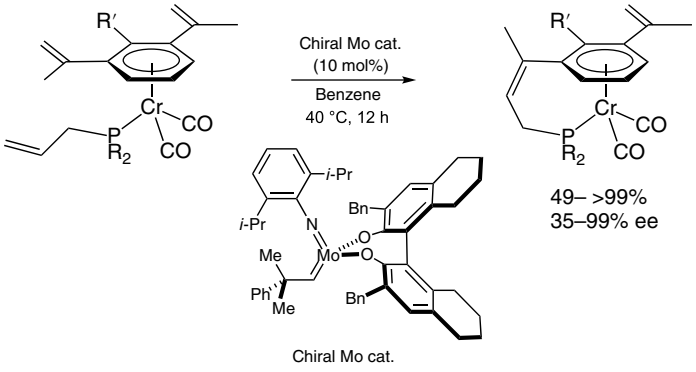

Scheme 20.36 Desymmetric intramolecular metathesis of 1,3-diisoproneyl chromium complexes. Source: [36]/John Wiley & Sons.

20.2.3. Enantioselective Synthesis of Planar Chiral Cyclophane

20.2.3.1. Rh-Catalyzed [2+2+2] Cycloaddition The enantioselective formation of a cyclophane ring system starting from *meta*- and *para*-disubstituted aromatic compounds is generally difficult, because the long tether moieties are flexible, and the construction of an asymmetric environment for high enantioinduction is difficult. Conversely, the construction of cyclophane skeleton along with benzannulation is a powerful strategy. In particular, Rh-catalyzed [2+2+2] cycloaddition of alkynes is a reliable protocol in this context due to the high catalytic activity of Rh(I)-BINAP derivatives for cyclotrimerization [37].

The first case of catalytic and enantioselective syntheses of cyclophane was achieved through the intramolecular [2+2+2] cycloaddition of triynes possessing etherate moieties [38]. *Meta*-cyclophanes were obtained in excellent ee, albeit in low yields (Scheme 20.37). The corresponding intermolecular reaction was also possible and the cyclotrimerization of 1,*n*-bis(methoxymethyl)-1,*n*-diynes with a bulky acetylene dicarboxylate gave planar chiral hexa-substituted cyclophanyl benzenes (Scheme 20.38) [39].

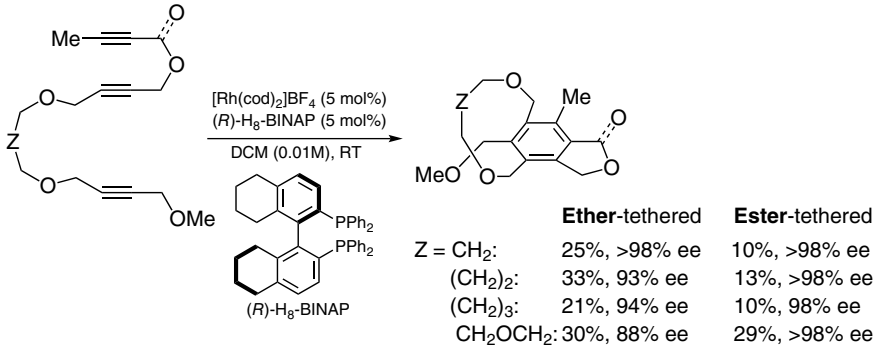

Scheme 20.37. Intramolecular cycloaddition of triynes for the synthesis of *meta*-cyclophanes. Source: [38]/American Chemical Society.

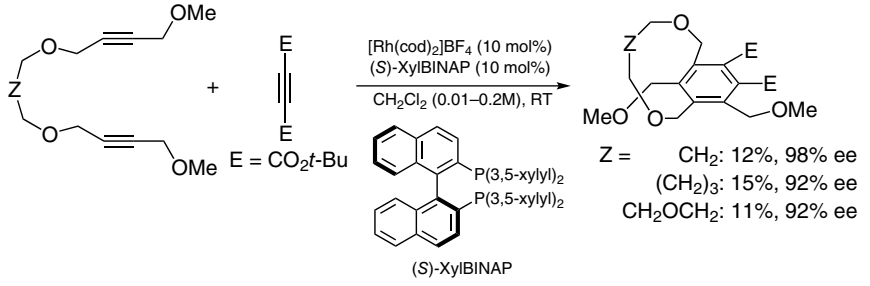

Scheme 20.38. Intermolecular cycloaddition of diynes for the synthesis of *meta*-cyclophanes. Source: [39]/ELSEVIER.

The intermolecular reaction of terminal 1,*n*-diynes with propiolate resulted in the selective formation of paracyclophanes (Scheme 20.39). However, the yield was low and the ee was reduced compared with the metacyclophane route [40]. In contrast, cyclic diynes possessing a nitrogen-tethered 1,6-diyne moiety were better substrates, and the intermolecular reaction with various terminal alkynes gave paracyclophanes in moderate to high yields along with high ee (Scheme 20.40) [41]. In this transformation, BINAP was inefficient and alkylene-tethered diphosphine was the choice of ligand.

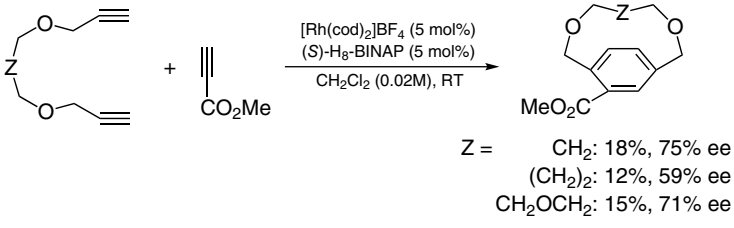

Scheme 20.39. Intermolecular cycloaddition of diynes for the synthesis of *para*-cyclophanes.

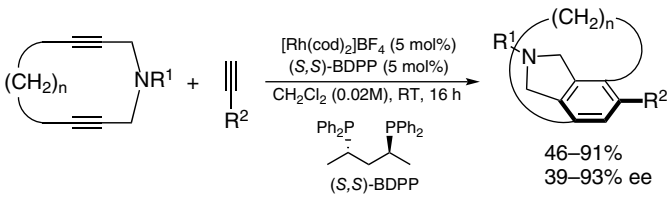

Scheme 20.40. Intermolecular cycloaddition of cyclic diynes for the synthesis of *para*-cyclophanes. Source: [41]/John Wiley & Sons.

This strategy was further upgraded to prepare complex planar chiral molecules. For example, an intramolecular reaction of biphenyl-tethered 1,7-diyne and alkene moiety of indene, which were connected with a long alkylene tether (*Z*), gave cycloadducts. Subsequent two-step oxidation and diastereoselective reduction of ketone provided planar chiral bent cyclophane based on the annulated *p*-terphenylene core (Scheme 20.41) [42].

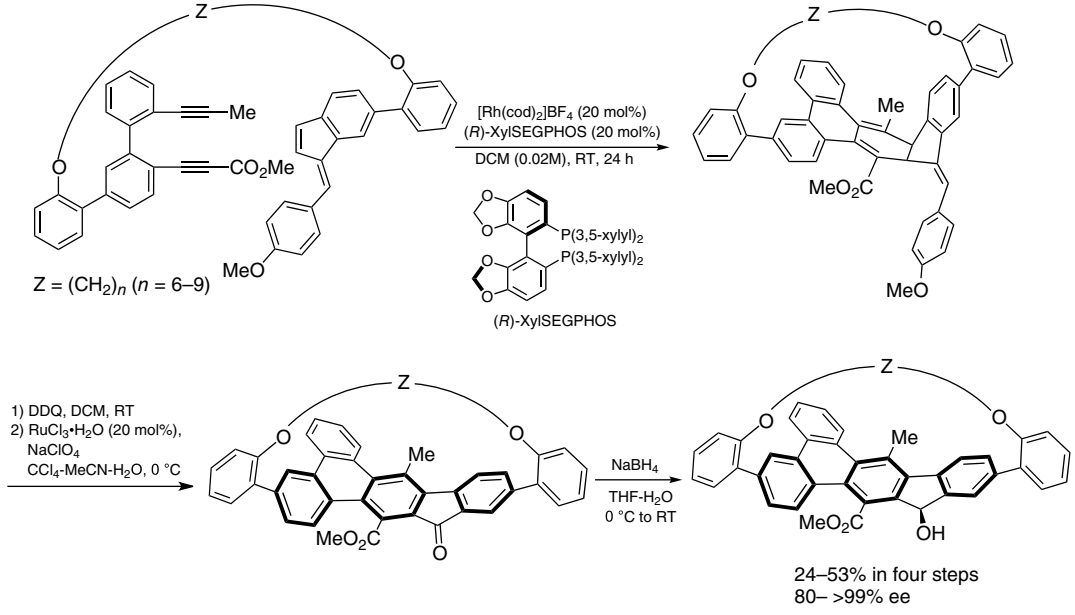

Scheme 20.41. Intramolecular cycloaddition for the construction of annulated *p*-terphenylene core. Source: [42]/John Wiley & Sons.

The consecutive intramolecular reaction of cyclic polyynes constructed with 2,5-bis(alkynyl)-1,4-bis(propargyloxy)benzene blocks was conducted under ambient conditions. As a result, planar chiral zigzag-type [8] to [12]cyclophenylene (CP) belts were prepared in good yield with high ee (Scheme 20.42). This is an elegant protocol for the asymmetric synthesis of chiral CP belts, which demonstrated characteristic chiroptical properties [43].

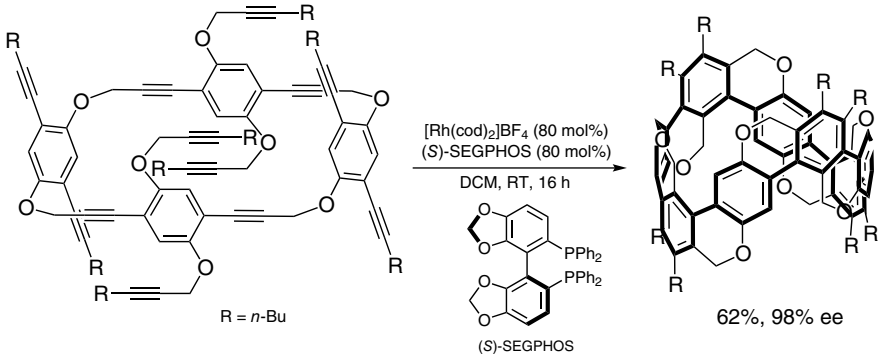

Scheme 20.42. Intramolecular cycloaddition for the construction of zigzag-type cyclophenylene belt.

When triynes, where 1,6-diyne and alkyne moieties were connected by a rigid aminophenol tether, were used as starting materials, intramolecular cycloaddition proceeded to give cyclophanes with a long ansa chain (n = up to 10) in good yield with high to excellent ee (Scheme 20.43) [44a]. This transformation can be used for the hetero[2+2+2] cycloaddition of diyne with nitrile, and planar chiral pyridinophanes possessing a longer ansa chain (n = up to 11) were prepared (Scheme 20.44) [44b].

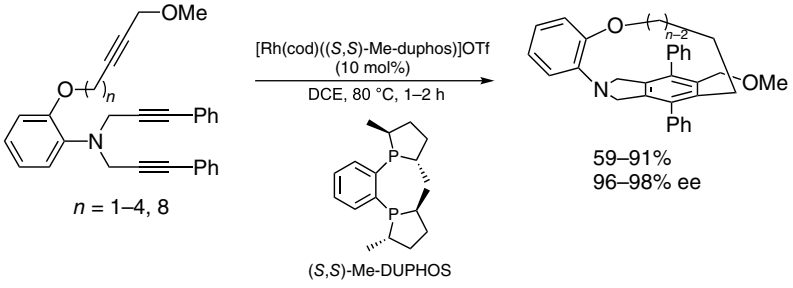

Scheme 20.43. Intramolecular cycloaddition of triynes for the synthesis of tripodal cyclophanes. Source: [44a]/American Chemical Society.

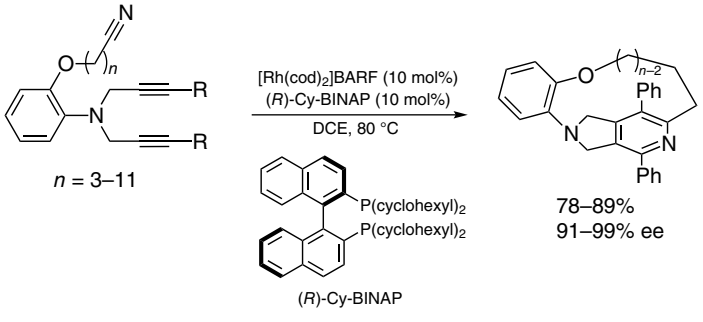

Scheme 20.44. Intramolecular cycloaddition of diyne-nitriles for the synthesis of tripodal azacyclophanes. Source: [44b]/ELSEVIER.

20.2.3.2. Other Protocols: Coupling and Ortho-Lithiation Consecutive inter- and intramolecular cross-couplings of *para*-disubstituted benzene derivatives are a facile access to constructing paracyclophane skeletons. However, the intramolecular reaction and its enantioinduction are generally difficult due to the flexibility of the ansa chain moiety. For example, Rh- and Pd-catalyzed couplings of 1,4-bis(bromomethyl)benzene derivatives with dithiols were reported under dilute conditions, but the yield and ee were low to moderate (Scheme 20.45) [45].

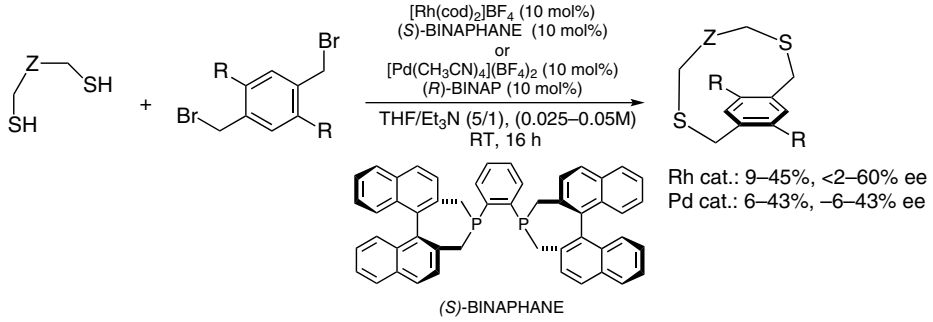

Scheme 20.45. Inter- and intramolecular cross-couplings of dibromides with dithiols. Source: Based on [45].

A different strategy for the asymmetric synthesis of planar chiral cyclophanes is the enantioselective introduction of substituent(*s*) to paracyclophane, whose ansa chain can flip at room temperature. When double Sonogashira couplings of achiral 2,5-diiodoparacyclophane with a flipping long ansa chain (*Z*) proceeded in the presence of a chiral Pd catalyst, chiral 2,5-bis(alkynyl)paracyclophanes could be prepared, where the ansa chain could not be flipped because of bulky alkynyl groups (Scheme 20.46) [46].

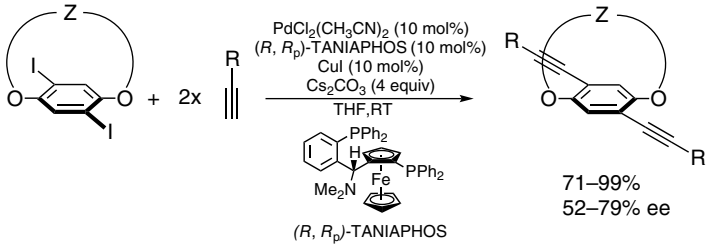

Scheme 20.46. Consecutive Sonogashira couplings of 2,5-diiodo-1,4-dixoa[*n*]paracyclophanes. Source: [46]/Royal Society of Chemistry.

This strategy was also effective for *ortho*-lithiation. Highly enantioselective *ortho*-lithiation and dilithiation of 1,*n*-dioxa[*n*]paracyclophanes were achieved with *sec*-butyllithium and a stoichiometric or catalytic amount of sparteine as a chiral source. When the aryllithiums were quenched by various electrophiles, such as iodine, iodomethane, and chlorodiphenylphosphine, planar chiral mono- and disubstituted paracyclophanes were obtained with good to excellent ee (Scheme 20.47) [47].

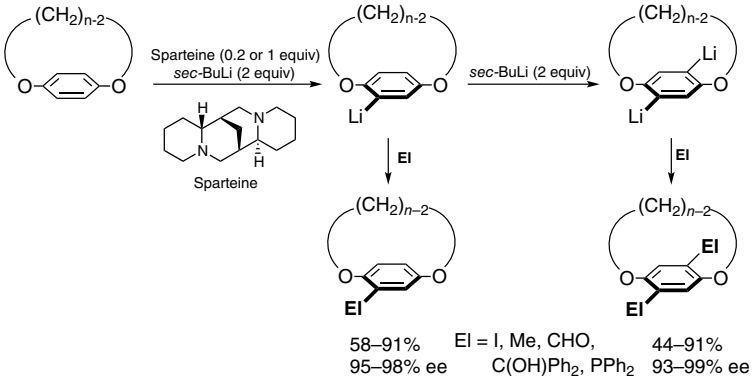

Scheme 20.47. Enantioselective lithiation of dioxa[*n*]paracyclophanes using a chiral diamine. Source: Based on [47].

20.2.4. Enantioselective Synthesis of Planar Chiral Cyclic *trans*-Alkenes

The use of allylic amines allowed for the enantioselective synthesis of planar chiral cyclic *trans*-alkenes. When an intramolecular S_N2 reaction of allylamine with allyl bromide was conducted, a nitrogen-containing nine-membered system possessing two alkene moieties was constructed. The presence of a stoichiometric amount of chiral lithium alkoxides derived from sugar derivatives achieved high enantioselectivity (80% ee). The reaction also proceeded in the presence of a chiral phase transfer catalyst; however, the ee of resulting cycloadduct was low (37% ee) (Scheme 20.48) [48].

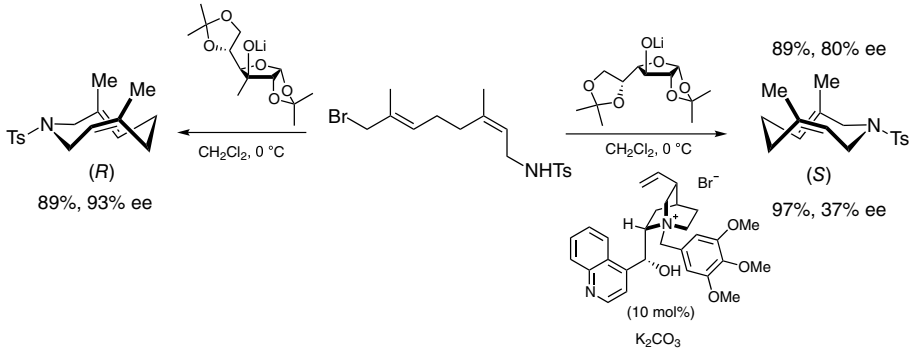

Scheme 20.48. Intramolecular S_N2 reaction for the synthesis of cyclic *trans*-alkenes. Source: [48]/American Chemical Society.

Pd-catalyzed intramolecular allylic or benzylic amination with allyl carbonate successfully proceeded by using an bis[2′-(diphenylphosphino)benzamido]-9,10-dihydro-9,10-ethanoanthracene (ANDEN-phenyl Trost ligand). The obtained cycloadducts were obtained in up to high yields with excellent ee (Scheme 20.49) [49].

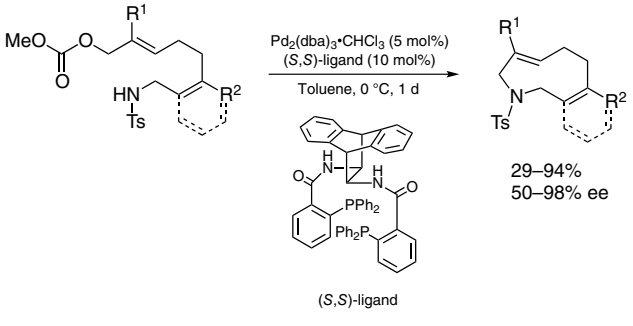

Scheme 20.49. Intramolecular allylic amination for the synthesis of cyclic *trans*-alkenes. Source: [49]/American Chemical Society.

20.3. ENANTIOSELECTIVE SYNTHESIS OF HELICALLY CHIRAL COMPOUNDS

The main topic of this section is the enantioselective synthesis of helically chiral helicenes, and it is divided into two sections dependent on the pattern for the generation of helical chirality. [2+2+2] Cycloaddition of triynes and cycloisomerization of arylalkynes were major catalytic protocols.

20.3.1. [2+2+2] Cycloaddition of Alkynes

20.3.1.1. Enantioselective Synthesis of Carbohelicene Derivatives The original synthesis of carbohelicene-like compounds, which have unaromatized ring in the helical skeleton, was conducted using a chiral Ni-catalyst. Intramolecular cyclotrimerization of triyne, where two alkynes are connected with 2,2′-disubstituted diarylethyne-tether, afforded a carbo[6]helicene-like compound in moderate ee (Scheme 20.50) [50].

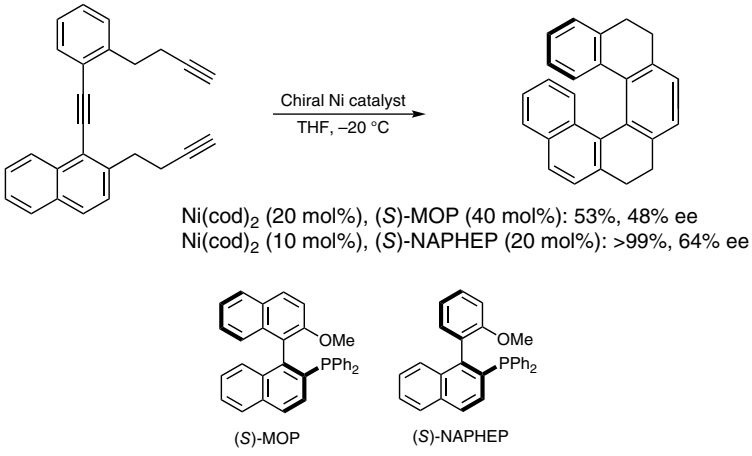

Scheme 20.50. Intramolecular cycloaddition of a triyne for the synthesis of a carbo[6]helicene-like compound. Source: Based on [50].

ortho-Phenylene- and 1,2-naphthylene-tethers were introduced in place of two ethylenes, and the intramolecular reaction afforded carbo[6]helicenes in one pot (Scheme 20.51) [51]. The resulting diaryl-substituted octa-cyclic compound was obtained in almost enantiomerically pure form following recrystallization.

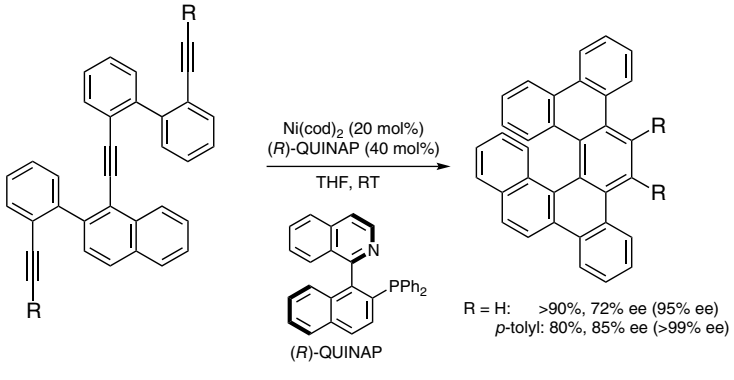

Scheme 20.51. Intramolecular cycloaddition of triynes for the synthesis of carbo[6]helicenes. Source: [51]/John Wiley & Sons.

In addition to the axially chiral phosphine ligands, a chiral *N*-heterocyclic carbene (NHC) ligand that had oxahelicene-like components was also effective, and dibenzocarbo[7]helicene was prepared from a terminal triyne in high ee (Scheme 20.52) [52].

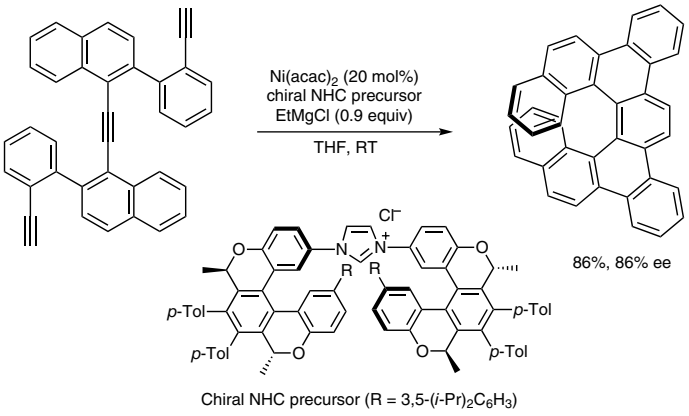

Scheme 20.52. Intramolecular cycloaddition of a triyne for the synthesis of a carbo[7]helicene. Source: [52]/Royal Society of Chemistry.

An analogous transformation was achieved by combining cationic Rh(I) catalyst with BINAP. Starting from disubstituted triynes, the corresponding carbo[7]helicenes were provided along with a small amount of S-shaped molecules (Scheme 20.53) [53]. Due to differences in the solubility of the enantiomerically pure and racemic forms, the ee of the first fraction was excellent and the second one was low.

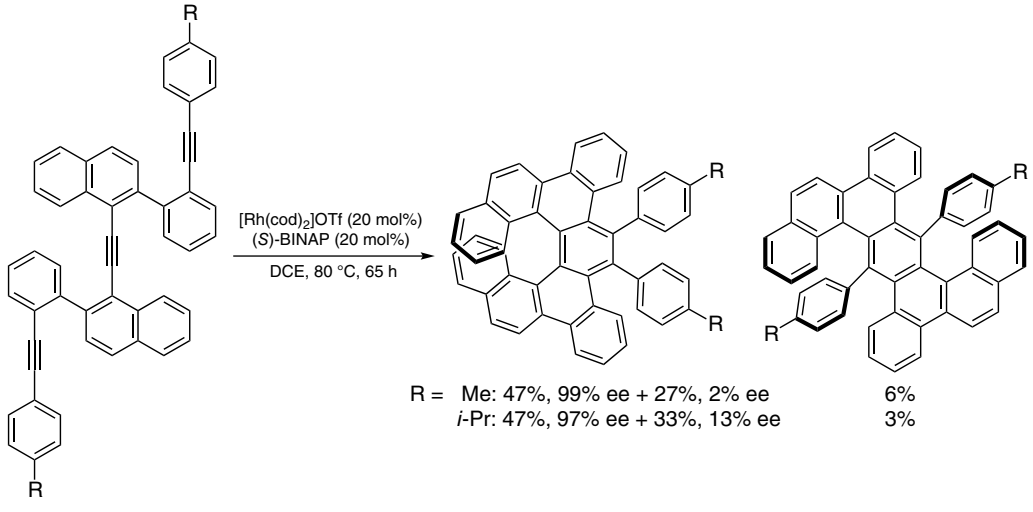

Scheme 20.53. Intramolecular cycloaddition of triynes for the synthesis of di-substituted carbo[7]helicenes. Source: [53]/John Wiley & Sons.

As an only example of intermolecular cycloaddition, a Pd-catalyzed reaction of two molecules of carbo[5]helicene-based benzyne and acetylene dicarboxylate was reported (Scheme 20.54) [54]. Triple helicenes containing three carbo[5]helicene moieties were prepared via dynamic kinetic resolution in good to excellent ee.

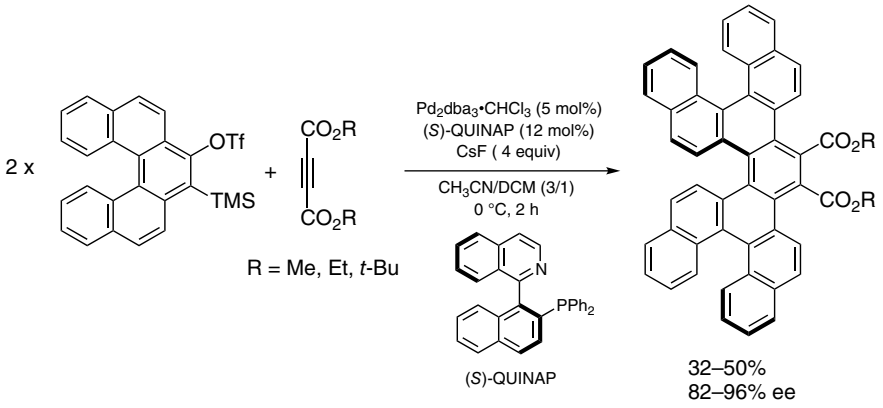

Scheme 20.54. Intermolecular cycloaddition of a benzyne precursor for the synthesis of triple carbohelicenes. Source: [54]/American Chemical Society.

20.3.1.2. Enantioselective Synthesis of Heterohelicene Derivatives Regarding the asymmetric synthesis of oxahelicene-like compounds, an aryloxylpropargyl moiety is a critical component in a polyyne system, and Rh-BINAP derivative catalysts stand unrivaled in this cyclotrimerization. For example, hexaynes with four phenoxylpropargyl moieties were transformed into oxa[9]- and [11]helicene-like compounds with four pyran cores in their helical structure (Scheme 20.55) [55].

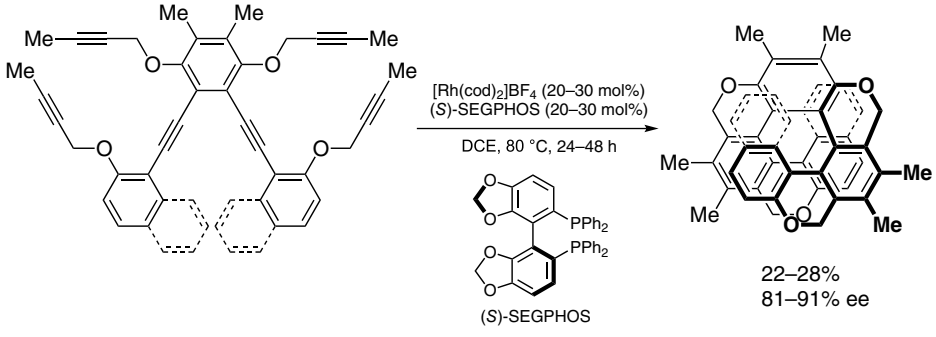

Scheme 20.55. Consecutive intramolecular cycloaddition of hexaynes for the synthesis of oxa[9]- and [11]helicene-like compounds. Source: [55]/John Wiley & Sons.

When 3,4-phenanthrenylene-tethered triynes were used, oxa[9]helicene-like compounds with two pyran cores in their helical structures were obtained in good to excellent ee (Scheme 20.56) [56].

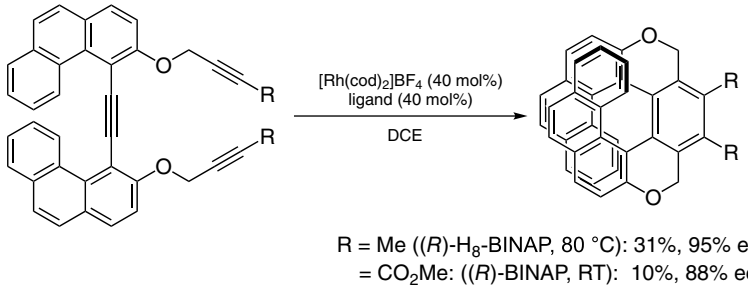

Scheme 20.56. Intramolecular cycloaddition of triynes for the synthesis of oxa[9]helicene-like compounds. Source: [56]/American Chemical Society.

A different type of hexayne, where four propargyloxy pendants were attached to its 1,4-bis(naphthalen-1-ylethynyl)benzene core, was subjected to an Rh-catalyzed reaction, resulting in S-shaped oxa[11]helicene-like compound in one pot. Although the *meso*-isomer was a major cycloadduct, the ee of the *dl* isomer reached 73% ee (Scheme 20.57) [57].

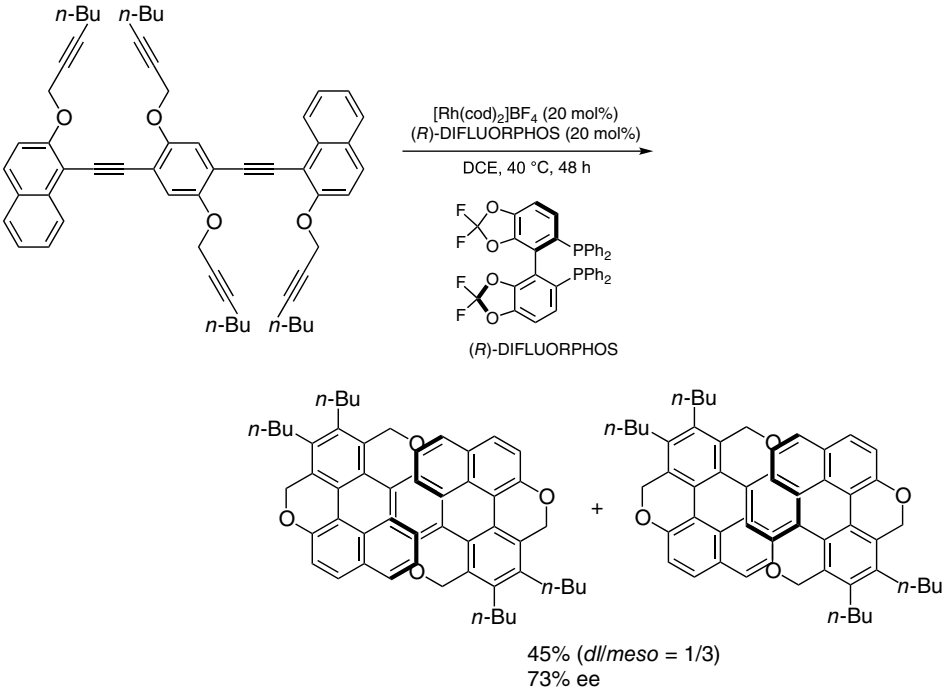

Scheme 20.57. Consecutive intramolecular cycloaddition of a hexayne for the synthesis of an oxa[11]helicene-like compound. Source: [57]/John Wiley & Sons.

Two sets of 2-(arylethynyl)phenyl) group were put in place of the two propargyloxy groups at the center of a benzene ring. The intramolecular reaction proceeded at room temperature with perfect diastereo- and enantioselectivities, and a configurationally stable S-shaped oxa[11]helicene-like compound was synthesized due to the fused benzene rings (Scheme 20.58) [58].

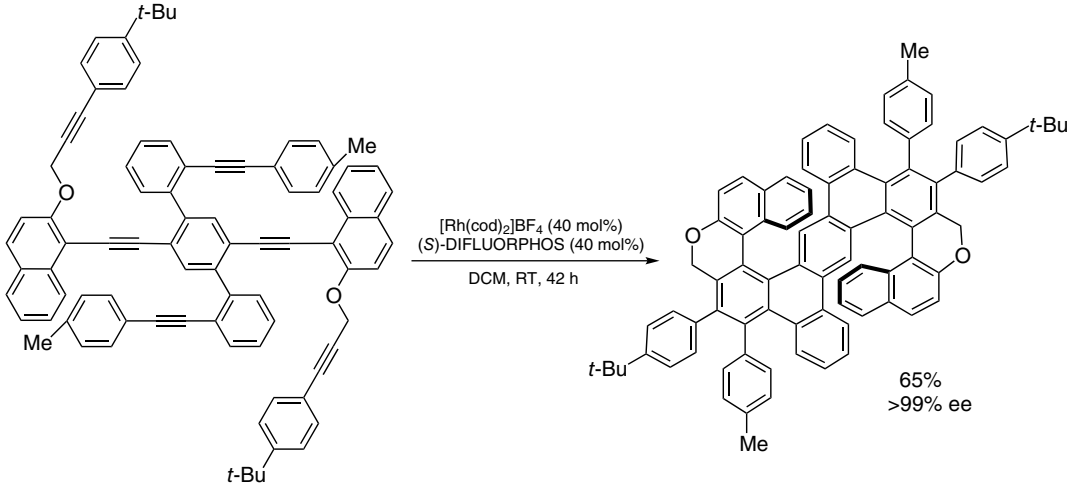

Scheme 20.58. Consecutive intramolecular cycloaddition of a hexayne for the synthesis of an S-shaped oxa[11]helicene-like compound. Source: [58] / John Wiley & Sons.

The following protocol is an elegant application of the asymmetric synthesis of belt- and Möbius-shaped cycloparaphenylenes. When a cyclic polyyne, consisting of five sets of 4-alkoxy-2,5-dialkynyl(propargyloxy)benzene, was subjected to an intramolecular reaction, a planar chiral cycloadduct was obtained after aluminum column chromatography. While the first eluate gave a product in moderate ee, it was excellent in the second eluate (Scheme 20.59) [59]. The authors speculated that the different enantiomeric excesses were derived from the different solubilities dependent on the ee, and that part of the product with high ee was solidified on the top of column and was not eluted in the first run.

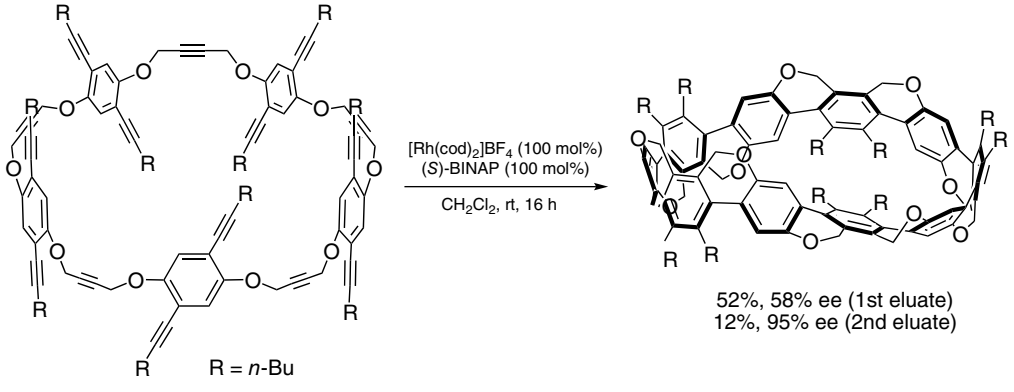

Scheme 20.59. Consecutive intramolecular cycloaddition of a polyne for the synthesis of a belt- and Möbius-shaped cycloparaphenylene. Source: [59]/American Chemical Society.

All examples listed above prepared oxahelicene-like compounds that possess pyran cores in their π-systems. Consecutive inter- and intramolecular reactions of tetraynes with a 1,4-diphenyl-1,3-diyne moiety and 1,4-diyne are a strategy for the construction of five-membered ring-containing helicenes. In this case, when dialkynyl ketone and dialkynylphosphinate were used as coupling partners, helically chiral heptacyclic compounds were obtained in moderate to high ee (Scheme 20.60) [60a, b]. A 1,2-naphthylene-tethered tetrayne was also converted into a phospha[9]helicene with two picene skeletons (Scheme 20.61) [60c].

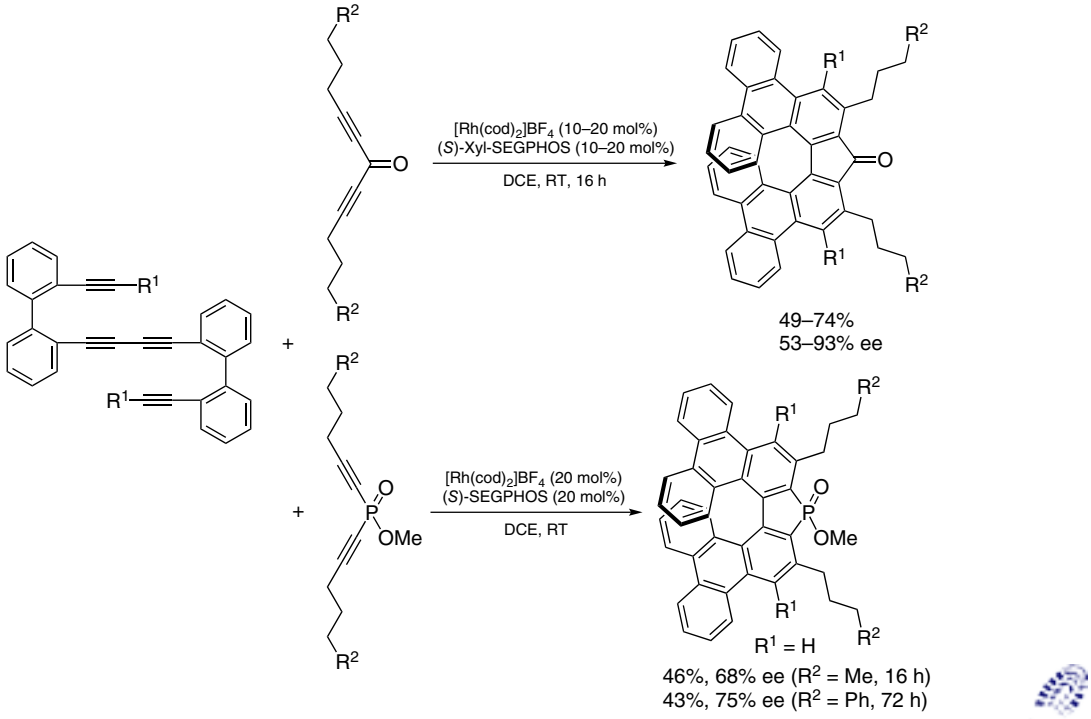

Scheme 20.60. Intermolecular cycloaddition of tetraynes with diynes for the synthesis of [7]helicenes. Source: Based on [60a, b].

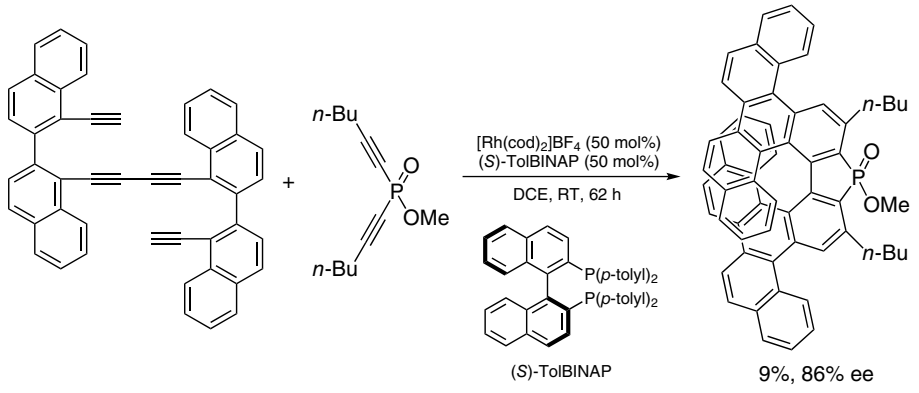

Scheme 20.61. Intermolecular cycloaddition of a tetrayne with a diyne for the synthesis of a phospha[9]helicene. Source: [60c]/ Royal Society of Chemistry.

This protocol could also be applied for the asymmetric synthesis of silahelicene. When dialkynylsilane was used as a 1,3-diyne, sila[7]helicene was synthesized in high ee but in low yield (Scheme 20.62) [61]. Notably, the product showed relative high CPL activity ($g_{lum} = -0.016$).

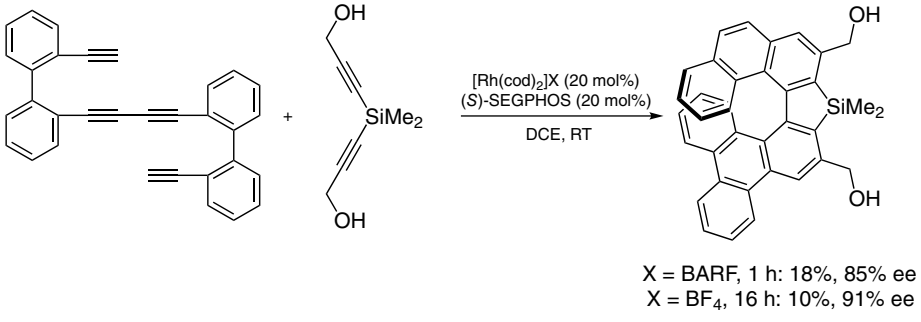

Scheme 20.62. Intermolecular cycloaddition of a hexayne with a diyne for the synthesis of a sila[7]helicene. Source: [61]/ John Wiley & Sons.

In the reaction of silyl-tethered tetraynes with *ortho*-phenylene- or 2,3-naphthylene-tethered 1,5-diyne, chiral Ir-catalyst was relevant, but a stoichiometric amount of Ni-complex was needed for the secondary intramolecular cycloadditions (Scheme 20.63) [62]. The resulting disila[7]helicenes were provided in high ee.

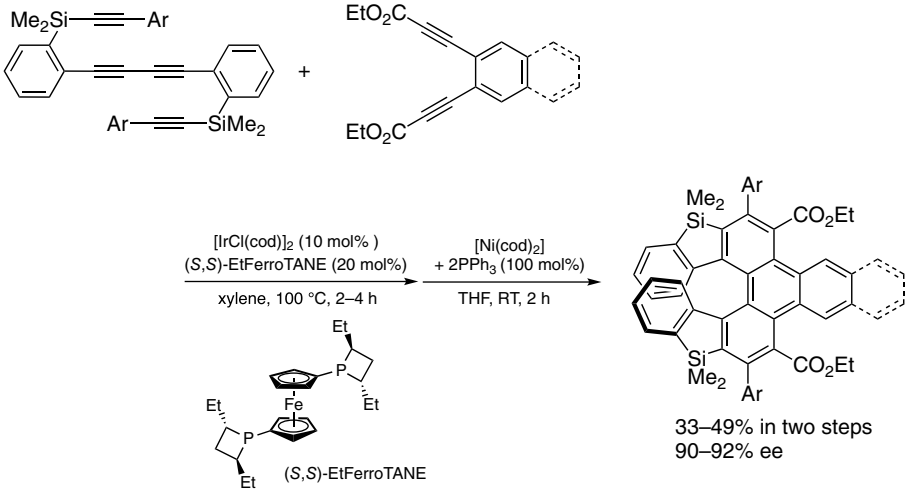

Scheme 20.63. Intermolecular cycloaddition of tetraynes with diynes for the synthesis of disila[7]helicenes. Source: [62]/ Royal Society of Chemistry.

20.3.2. Au(I)-Catalyzed Cycloisomerization of Arylalkynes

The Au(I)-catalyzed consecutive hydroarylation of arylalkynes is a powerful synthetic tool for the construction of helicene skeletons. The combination of a cationic Au(I) salt with BINAP derivatives can induce helical chirality. For example, amide- and 1,6-naphthylene-tethered tetraynes were transformed into S-shaped molecules and the ee of the *dl* isomer was almost perfect (Scheme 20.64) [63]. Subsequent deprotection and chlorination gave the corresponding double diazahelicene without any loss in ee. Additionally, when 2,7-naphthylene-tethered analogues were used, helicene-type compounds with two δ-lactam components were provided. This transformation also gave highly enantiomerically enriched diaza[10]helicenes (Scheme 20.65) [64].

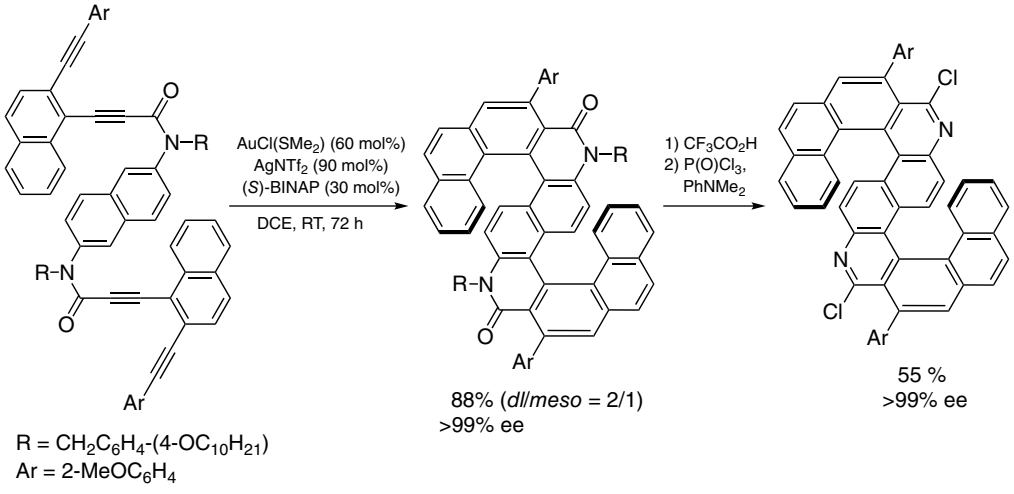

Scheme 20.64. Consecutive cycloisomerization of tetraynes for the preparation of S-shaped diaza[10]helicenes. Source: [63]/ American Chemical Society.

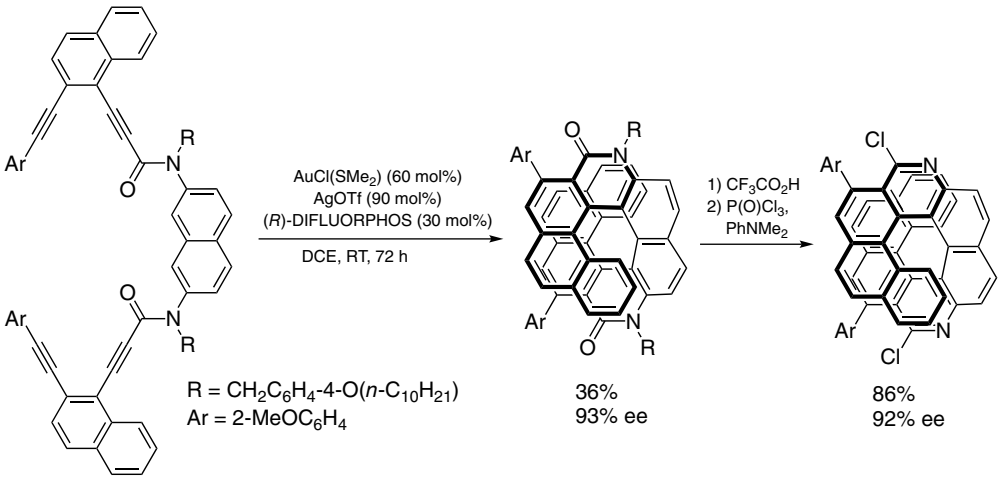

Scheme 20.65. Consecutive cycloisomerization of tetraynes for the preparation of diaza[10]helicenes. Source: [64]/John Wiley & Sons.

In place of an amide-tether, ketone-tether tetraynes were derived into carbohelicene-like cycloadducts that underwent methylation to give S-shaped carbo[10]helicene in two steps (Scheme 20.66) [65]. While the products were obtained as single diastereomers, the ee was moderate. Notably, they showed high CPL activity (g_{lum} = up to 2.7×10^{-3}).

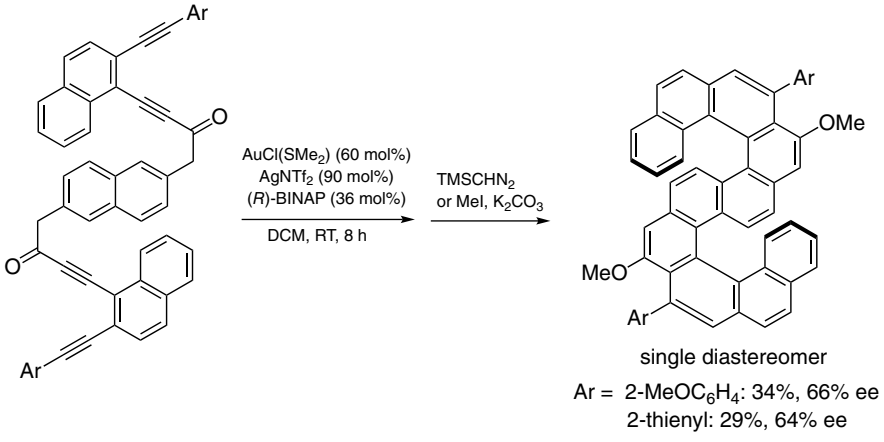

Scheme 20.66. Consecutive cycloisomerization of tetraynes for the preparation of S-shaped carbo[10]helicenes. Source: [65] / John Wiley & Sons.

A more direct approach to producing carbohelicene skeletons is via cycloisomerization of 2-alkynyl-1,1′-biphenyl. This transformation was achieved using a chiral cationic phosphinate ligand, which has a TADDOL-derived chiral moiety and an imidazolium unit. Consecutive cycloisomerization of 2,7-dialkynyl-1,8-diarylnaphthalene gave carbo[6]helicenes in high to excellent 6-*endo*/5-*exo* selectivity along with up to excellent enantioselectivity (Scheme 20.67) [66]. The present strong π-acceptor ligand can be finely tuned by the choice of aryl group and cationic part, and the use of 1,3-dimesityl-1,2,3-triazolium and 1,4-dimesityl-1,2,4-triazolium gave further better results [67].

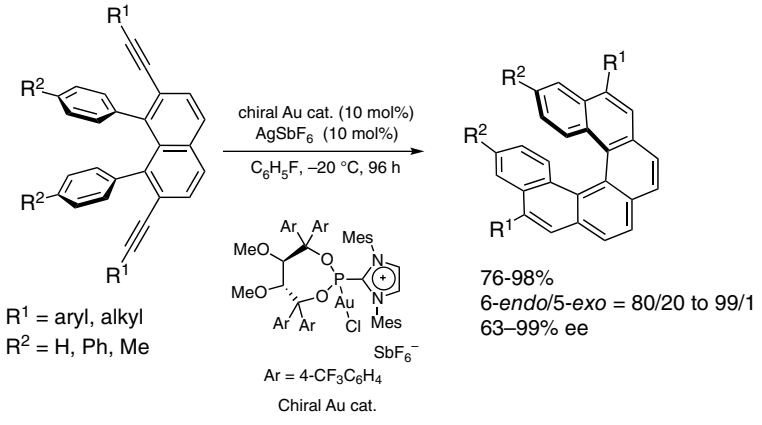

Scheme 20.67. Consecutive cycloisomerization of diynes for the synthesis of carbo[6]helicenes. Source: [66]/American Chemical Society.

An intramolecular reaction of 2-(2-alkynylphenyl)phenanthrene proceeded by using a cationic phosphinite ligand that had a trimesityl-1,2,3-triazolium unit, and helically chiral compounds were obtained in excellent ee (Scheme 20.68) [68]. This is the first example of enantioselective synthesis of 1,12-substituted carbo[4]helicene.

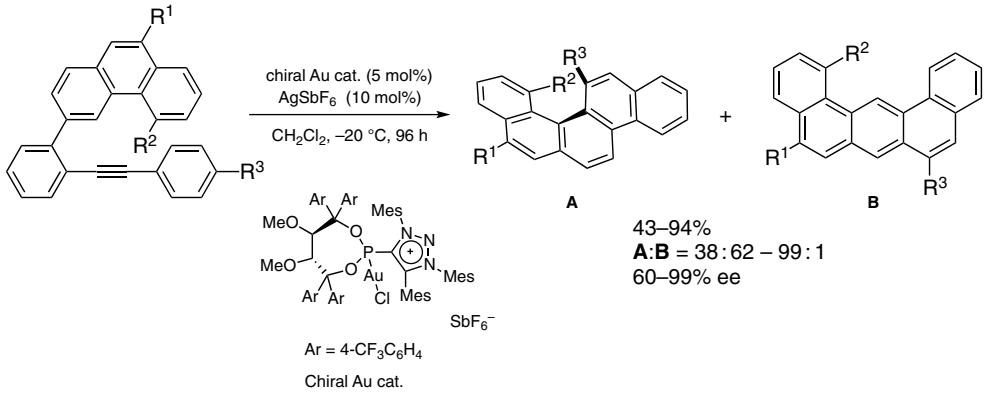

Scheme 20.68. Cycloisomerization of alkynes for the synthesis of disubstituted carbo[4]helicenes. Source: [68] / John Wiley & Sons.

The choice of chiral scaffold was important dependent on the substrate. BINOL-derived cationic phosphinate was effective in the highly enantioselective intramolecular reaction of 2-(2-alkynylphenyl) benzo[*c*]phenanthrenes, and 1-aryl-substituted carbon[5]helicenes were obtained in up to excellent ee (Scheme 20.69) [69].

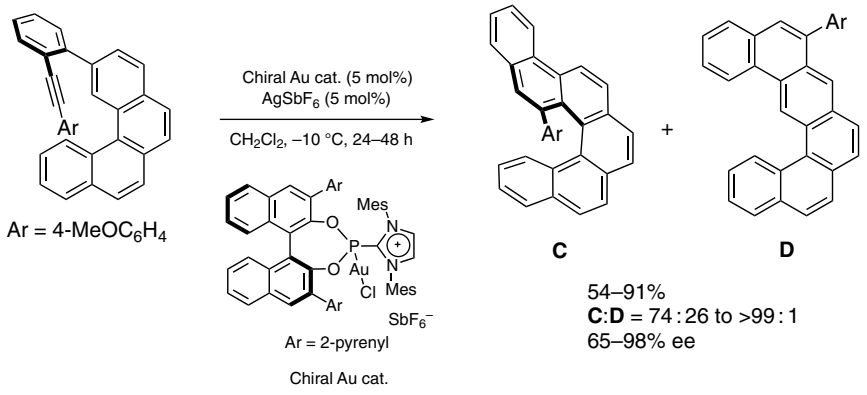

Scheme 20.69. Cycloisomerization of alkynes for the synthesis of substituted carbo[5]helicenes. Source: [69]/John Wiley & Sons.

As an exceptional example, an organocatalyzed cycloisomerization was reported. Consecutive cycloisomerization of 2,7-alkynyl-1,8-diarylnaphthalene using a bisquinine squaramide catalyst gave 5,12-bis(2-hydroxynaphthalen-1-yl)carbo[6]helicenes that possess both helical and axial chiralities (Scheme 20.70) [70]. Notably, excellent diastereo- and enantioselectivities were achieved in each entry. The reaction mechanism, which involved consecutive tautomerizations via vinylidene *ortho*-quinone methides (VQMs), was suggested according to the literature [71].

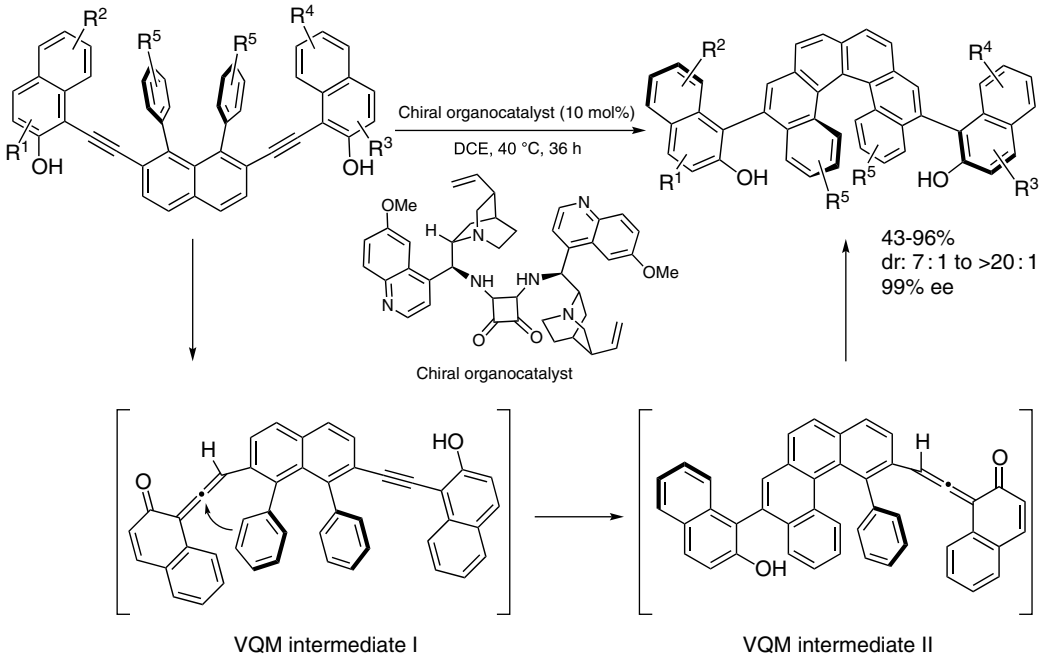

Scheme 20.70. Consecutive cycloisomerization of diynes for the synthesis of carbo[6]helicenes. Source: [70]/John Wiley & Sons.

20.3.3. Other Protocols

Fischer indole synthesis could also induce helical chirality. Intermolecular reaction of naphthalene- or phenanthrene-fused cyclohexanones with arylhydrazines gave aza[5]- to [7]helicene-like cycloadducts in up to high ee (Scheme 20.71) [72]. A SPINOL-derived phosphoric acid was effective, and the asymmetric synthesis of diaza[8]helicene-like compounds starting from 2,6-dihydrazinylnaphthalene was also conducted.

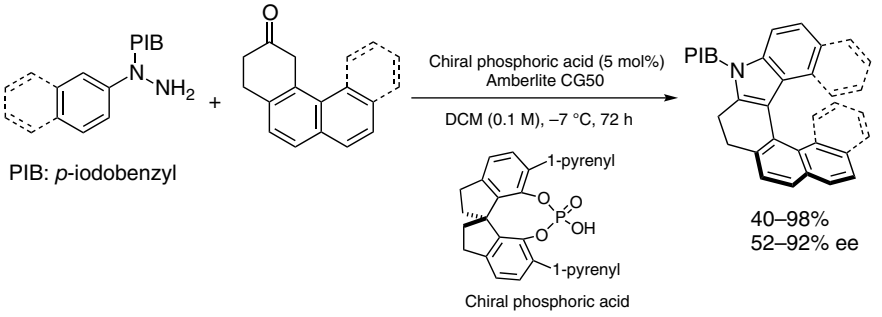

Scheme 20.71. Condensation of fused-cyclohexanones with arylhyrazines for the synthesis of azahelicene-like compounds. Source: [72]/John Wiley & Sons.

Transition-metal-catalyzed oxidative homo-coupling of arenols is an established protocol for the generation of axial chirality. A chiral V catalyst allowed for enantioselective coupling of benzo[*c*]phenanthren-2-ol derivatives along with formal dehydrative cyclization, and oxa[9]helicenes were prepared in one pot (Scheme 20.72) [73].

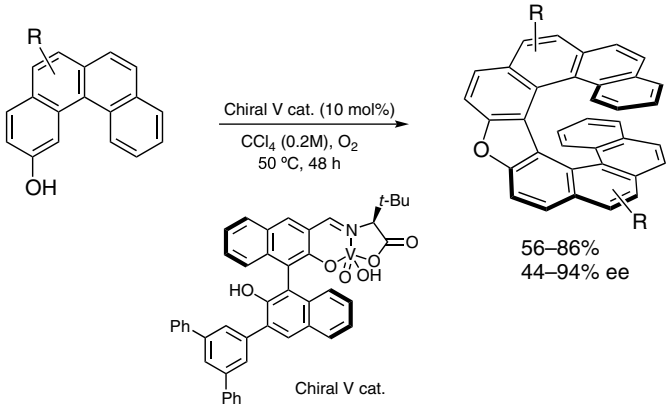

Scheme 20.72. Oxidative homo-coupling of arenols for the synthesis of oxa[9]helicenes. Source: [73]/American Chemical Society.

The Rh(III)-catalyzed C-H annulation of 1-aryl isoquinoline derivatives with alkynes provided azonia[5] to [7]helicenes (Scheme 20.73) [74]. The combination of a SPINOL-derived chiral Cp-Rh complex and amino acid-based imide was critical for highly enantioselective dynamic kinetic resolution.

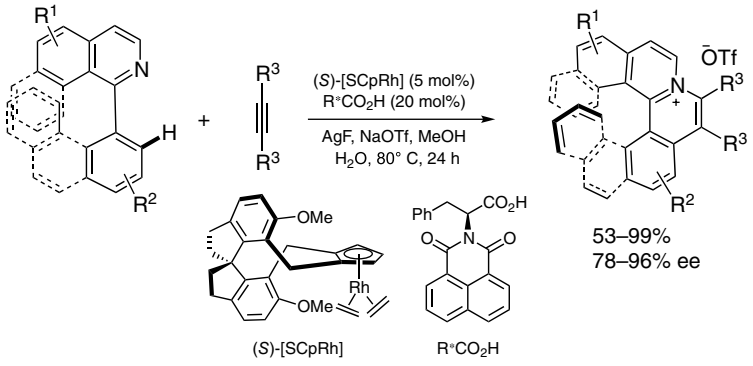

Scheme 20.73. C–H annulation of 1-arylisoquinolines with alkynes for the synthesis of azonia[5]- to [7]helicenes. Source: [74]/ American Chemical Society.

20.4. SUMMARY

This chapter listed various approaches to catalytic and enantioselective induction of planar and helical chiralities. For both approaches, cyclotrimerization of alkynes is a powerful and atom-economical synthetic tool. When the designed substrates were ready, which required several steps to be prepared in some cases, the desired enantioselective cycloaddition proceeded through the choice of chiral ligand. Cycloisomerization is also reliable for the construction of congested fused aromatic systems.

Carbo- and heterohelicenes attract much attention in material science due to their unique chiroptical properties. Therefore, the development of facile and comprehensive syntheses of helically chiral helicenes is still an outstanding issue and C-H activation appears to be a promising approach.

REFERENCES

1. (a) Lu, X.; Akasaka, T.; Nagase, S. *Chem. Commun.* **2011**, *47*, 5942–5957. (b) Wakahara, T.; Nikawa, H.; Kikuchi, T.; Nakahodo, T.; Rahman, G. A.; Tsuchiya, T.; Maeda, Y.; Akasaka, T.; Yoza, K.; Horn, E. *J. Am. Chem. Soc.* **2006**, *128*, 14228–14229. (c) Sawai, K.; Takano, Y.; Izquierdo, M.; Filippone, S.; Martín, N.; Slanina, Z.; Mizorogi, N.; Waelchli, M.; Tsuchiya, T.; Akasaka, T. *J. Am. Chem. Soc.* **2011**, *133*, 17746–17752. (d) Maroto, E. E.; Izquierdo, M.; Murata, M.; Filippone, S.; Komatsu, K.; Murata, Y.; Martín, N. *Chem. Commun.* **2014**, *50*, 740–742.
2. (a) Vedejs, E.; Jure, M. *Angew. Chem. Int. Ed.* **2005**, *44*, 3974–4001. (b) Kumar, R. R.; Kagan, H. B. *Adv. Syn. Catal.* **2010**, *352*, 231–242.
3. Recent reviews: (a) Gao, D.-W.; Gu, Q.; Zheng, C.; You, S.-L. *Acc. Chem. Res.* **2017**, *50*, 351–365. (b) Liu, C.-X.; Gu, Q.; You, S.-L. *Trends Chem.* **2020**, *2*, 737–749.
4. (a) Price, D.; Simpkins, N. S. *Tetrahedron Lett.* **1995**, *36*, 6135–6136. (b) Nishibayashi, Y.; Arikawa, Y.; Ohe, K.; Uemura, S. *J. Org. Chem.* **1996**, *61*, 1172–1174. (c) Tsukazaki, M.; Tinkl, M.; Roglans, A.; Chapell, B. J.; Taylor, N. J.; Snieckus, V. *J. Am. Chem. Soc.* **1996**, *118*, 3, 685–686. (d) Genet, C.; Canipa, S. J.; O'Brien, P.; Taylor, S. *J. Am. Chem. Soc.* **2006**, *128*, 9336–9337.
5. Siegel, S.; Schmalz, H.-G. *Angew. Chem. Int. Ed.* **1997**, *36*, 2456–2458.
6. Gao, D.-W.; Shi, Y.-C.; Gu, Q.; Zhao, Z.-L.; You, S.-L. *J. Am. Chem. Soc.* **2013**, *135*, 86–89.
7. Pi, C.; Li, Y.; Cui, X.-L.; Zhang, H.; Han, Y.-B.; Wu, Y.-J. *Chem. Sci.* **2013**, *4*, 2675–2679.
8. Shi, Y.-C.; Yang, R.-F.; Gao, D.-W.; You, S.-L. *Beil. J. Org. Chem.* **2013**, *9*, 1891–1896.
9. Pi, C.; Cui, X.-L.; Liu, X.-Y.; Guo, M. X.; Zhang, H.-Y.; Wu, Y.-J. *Org. Lett.* **2014**, *16*, 5164–5167.
10. Gao, D.-W.; Gu, Q.; You, S.-L. *J. Am. Chem. Soc.* **2016**, *138*, 2544–2547.
11. Cai, Z.-J.; Liu, C.-X.; Gu, Q.; Zheng, C.; You, S.-L. *Angew. Chem. Int. Ed.* **2019**, *58*, 2149–2153.
12. Xu, J.; Liu, Y.; Zhang, J.; Xu, X.; Jin, Z. *Chem. Commun.* **2018**, *54*, 689–692.
13. Huang, Y.; Pi, C.; Cui, X.; Wu, Y. *Adv. Synth. Catal.* **2000**, *362*, 1385–1390.
14. Shibata, T.; Shizuno, T. *Angew. Chem. Int. Ed.* **2014**, *53*, 5410–5413.
15. Lou, S.-J.; Zhuo, Q.; Nishiura, M.; Luo, G.; Hou, Z., *J. Am. Chem. Soc.* **2021**, *143*, 2470–2476.

16. Wang, S.-B.; Gu, Q.; You, S.-L. *Organometallics* **2017**, *36*, 4359–4362.
17. Liu, Y.-H.; Li, P.-X.; Yao, Q.-J.; Zhang, Z.-Z.; Huang, D.-J.; Le, M.-D.; Song, H.; Liu, L.; Shi, B.-F. *Org. Lett.* **2019**, *21*, 1895–1899.
18. Liu, L.; Song, H.; Liu, Y.-H.; Wu, L.-S.; Shi, B.-F. *ACS Catal.* **2020**, *10*, 7117–7122.
19. Liu, C.-X.; Cai, Z.-J.; Wang, Q.; Wu, Z.-J.; Gu, Q.; You, S.-L. *CCS Chem.* **2020**, *2*, 642–651.
20. Cai, Z.-J.; Liu, C.-X.; Wang, Q.; Gu, Q.; You, S.-L. *Nat. Commun.* **2019**, *10*, 1–8.
21. (a) Gao, D.-W.; Yin, Q.; Gu, Q.; You, S.-L. *J. Am. Chem. Soc.* **2014**, *136*, 4841–4844. (b) Deng, R.; Huang, Y.; Ma, X.; Li, G.; Zhu, R.; Wang, B.; Kang, Y.-B.; Gu, Z. *J. Am. Chem. Soc.* **2014**, *136*, 4472–4475.
22. Gao, D.-W.; Zheng, C.; Gu, Q.; You, S.-L. *Organometallics* **2015**, *34*, 4618–4625.
23. (a) Ma, X.; Gu, Z. *RSC Adv.* **2014**, *4*, 36241–36244. (b) Liu, L.; Zhang, A.-A.; Zhao, R.-J.; Li, F.; Meng, T.-J.; Ishida, N.; Murakami, M.; Zhao, W.-X. *Org. Lett.* **2014**, *16*, 5336–5338.
24. Liu, L.; Liu, H.; Zuo, Z.; Zhang, A.-A.; Li, Z.; Meng, T.; Wu, W.; Hua, Y.; Mao, G. *Chin. Chem. Lett.* **2020**, *32*, 239–242.
25. Xu, B.-B.; Ye, J.; Yuan, Y.; Duan, W.-L. *ACS Catal.* **2018**, *8*, 11735–11740.
26. Luo, S.; Xiong, Z.; Lu, Y.; Zhu, Q. *Org. Lett.* **2018**, *20*, 1837–1840.
27. Jia, L.; Liu, X.; Zhang, A.-A.; Wang, T.; Hua, Y.; Li, H.; Liu, L. *Chem. Commun.* **2020**, *56*, 1737–1740.
28. (a) Shibata, T.; Shizuno, T.; Sasaki, T. *Chem. Commun.* **2015**, *51*, 7802–7804. (b) Zhang, Q.-W.; An, K.; Liu, L.-C.; Yue, Y.; He, W. *Angew. Chem. Int. Ed.* **2015**, *54*, 6918–6921. (c) Murai, M.; Matsumoto, K.; Takeuchi, Y.; Takai, K. *Org. Lett.* **2015**, *17*, 3102–3105.
29. Zhao, W.-T.; Lu, Z.-Q.; Zheng, H.; Xue, X.-S.; Zhao, D. *ACS Catal.* **2018**, *8*, 7997–8005.
30. Wang, S.-B.; Zheng, J.; You, S.-L. *Organometallics* **2016**, *35*, 1420–1425.
31. Chen, H.; Wang, Y.-X.; Luan, Y.-X.; Ye, M. *Angew. Chem. Int. Ed.* **2020**, *59*, 9428–9432.
32. (a) Urbano, A.; Hernández-Torres, G.; del Hoyo, A. M.; Martínez-Carrión, A.; Carreño, M. C. *Chem. Commun.* **2016**, *52*, 6419–6422. (b) Shibata, T.; Uno, N.; Sasaki, T.; Kanyiva, K. S. *J. Org. Chem.* **2016**, *81*, 6266–6272. (c) Ito, M.; Okamura, M.; Kanyiva, K. S.; Shibata, T. *Organometallics* **2019**, *38*, 4029–4035.
33. (a) Uemura, M.; Nishimura, H.; Hayashi, T. *Tetrahedron Lett.* **1993**, *34*, 107–110. (b) Kanda, K.; Oshima, S.; Shizuno, T.; Hamanaka, R.; Fukai, M.; Shibata, T. *Heterocycles* **2014**, *88*, 1355–1370.
34. Kamikawa, K.; Harada, K.; Uemura, M. *Tetrahedron: Asymmetry* **2005**, *16*, 1419–1423.
35. (a) Kündig, P. E.; Chaudhuri, P. D.; House, D.; Bernardinelli, G. *Angew. Chem. Int. Ed.* **2006**, *45*, 1092–1095. (b) Urbaneja, X.; Mercier, A.; Besnard, C.; Kündig, E. P. *Chem. Commun.* **2011**, 3739–3741.
36. Kamikawa, K.; Arae, S.; Wu, W.-Y.; Nakamura, C.; Takahashi, T.; Ogasawara, M. *Chem. Eur. J.* **2015**, *21*, 4954–4957.
37. Tanaka, K. *Bull. Chem. Soc. Jpn.* **2018**, *91*, 187–194.
38. Tanaka, K.; Sagae, H.; Toyoda, K.; Noguchi, K.; Hirano, M. *J. Am. Chem. Soc.* **2007**, *129*, 1522–1523.
39. Tanaka, K.; Sagae, H.; Toyoda, K.; Hirano, M. *Tetrahedron* **2008**, *64*, 831–846.
40. Araki, T.; Hojo, D.; Noguchi, K.; Tanaka, K. *Synlett* **2011**, 539–542.
41. Araki, T.; Noguchi, K.; Tanaka, K. *Angew. Chem. Int. Ed.* **2013**, *52*, 5617–5621.
42. Aida, Y.; Nogami, J.; Sugiyama, H.; Uekusa, H.; Tanaka, K. *Chem. Eur. J.* **2020**, *26*, 12579–12588.
43. Nogami, J.; Tanaka, Y.; Sugiyama, H.; Uekusa, H.; Muranaka, A.; Uchiyama, M.; Tanaka, K. *J. Am. Chem. Soc.* **2020**, *142*, 9834–9842.
44. (a) Shibata, T.; Uchiyama, T.; Endo, K. *Org. Lett.* **2009**, *11*, 3906–3908. (b) Shibata, T.; Miyoshi, M.; Uchiyama, T.; Endo, K.; Miura, N.; Monde, K. *Tetrahedron* **2012**, *68*, 2679–2686.
45. (a) Tanaka, K.; Hori, T.; Osaka, T.; Noguchi, K.; Hirano, M. *Org. Lett.* **2007**, *9*, 4881–4884. (b) Hori, T.; Shibata, Y.; Tanaka, K. *Tetrahedron: Asymmetry* **2010**, *21*, 1303–1306.
46. Kanda, K.; Koike, T.; Endo, K.; Shibata, T. *Chem. Commun.* **2009**, 1870–1872.
47. (a) Kanda, K.; Endo, K.; Shibata, T. *Org. Lett.* **2010**, *12*, 1980–1983. (b) Kanda, K.; Hamanaka, R.; Endo, K.; Shibata, T. *Tetrahedron* **2012**, *68*, 1407–1416.
48. Tomooka, K.; Uehara, K.; Nishikawa, R.; Suzuki, M.; Igawa, K. *J. Am. Chem. Soc.* **2010**, *132*, 9232–9233.
49. Igawa, K.; Ichikawa, N.; Ano, Y.; Katanoda, K.; Ito, M.; Akiyama, T.; Tomooka, K. *J. Am. Chem. Soc.* **2015**, *137*, 7294–7297.
50. (a) Stará, I. G.; Starý, I.; Kollárović, A.; Teplý, F.; Vyskočil, S.; Šaman, D. *Tetrahedron Lett.* **1999**, *40*, 1993–1996. (b) Heller, B.; Hapke, M.; Fischer, C.; Andronova, A.; Starý, I.; Stará. I. G. *J. Organomet. Chem.* **2013**, *723*, 98–102.
51. Jančařík, A.; Rybáček, J.; Cocq, K.; Chocholoušová, J. V.; Vacek, J.; Pohl, R.; Bednárová, L.; Fiedler, P.; Císařová, I.; Stará, I. G.; Starý, I. *Angew. Chem. Int. Ed.* **2013**, *52*, 9970–9975.
52. Sánchez, I. G.; Šámal, M.; Nejedlý, J.; Karras, M.; Klívar, J.; Rybáček, J.; Budéšínský, M.; Bednárová, L.; Seidlerová, B.; Stará, I. G.; Starý, I. *Chem. Commun.* **2017**, *53*, 4370–4373.
53. Yamano, R.; Shibata, Y.; Tanaka, K. *Chem. Eur. J.* **2018**, *24*, 6364–6370.
54. Yubuta, A.; Hosokawa, T.; Gon, M.; Tanaka, K.; Chujo, Y.; Tsurusaki, A.; Kamikawa, K. *J. Am. Chem. Soc.* **2020**, *142*, 10025–10033.
55. Kimura, Y.; Fukawa, N.; Miyauchi, Y.; Noguchi, K.; Tanaka, K. *Angew. Chem. Int. Ed.* **2014**, *53*, 8480–8483.
56. Yamano, R.; Hara, J.; Murayama, K.; Sugiyama, H.; Teraoka, K.; Uekusa, H.; Kawauchi, S.;Shibata, Y.; Tanaka, K. *Org. Lett.* **2017**, *19*, 42–45.

57. Kimura, Y.; Shibata, Y.; Noguchi, K.; Tanaka, K. *Eur. J. Org. Chem.* **2019**, 1390–1396.
58. Kinoshita, S.; Yamano, R.; Shibata, Y.; Tanaka, Y.; Hanada, K.; Matsumoto, T.; Miyamoto, T.; Muranaka, A.; Uchiyama, M.; Tanaka, K. *Angew. Chem. Int. Ed.* **2020**, *59*, 11020–11027.
59. Nishigaki, S.; Shibata, Y.; Nakajima, A.; Okajima, H.; Masumoto, Y.; Osawa, T.; Muranaka, A.; Sugiyama, H.; Horikawa, A.; Uekusa, H.; Koshino, H.; Uchiyama, M.; Sakamoto, A.; Tanaka, K. *J. Am. Chem. Soc.* **2019**, *141*, 14955–14960.
60. (a) Tanaka, K.; Fukawa, N.; Suda, T.; Noguchi, K. *Angew. Chem. Int. Ed.* **2009**, *48*, 5470–5473. (b) Sawada, Y.; Furumi, S.; Takai, A.; Takeuchi, M.; Noguchi, K.; Tanaka, K. *J. Am. Chem. Soc.* **2012**, *134*, 4080–4083. (c) Nishigaki, S.; Murayama, K.; Shibata, Y.; Tanaka, K. *Mater. Chem. Front.* **2018**, *2*, 585–590.
61. Murayama, K.; Oike, Y.; Furumi, S.; Takeuchi, M.; Noguchi, K.; Tanaka, K. *Eur. J. Org. Chem.* **2015**, 1409–1414.
62. Shibata, T.; Uchiyama, T.; Yoshinami, Y.; Takayasu, S.; Tsuchikama, K.; Endo, K. *Chem. Commun.* **2012**, *48*, 1311–1313.
63. Nakamura, K.; Furumi, S.; Takeuchi, M.; Shibuya, T.; Tanaka, K. *J. Am. Chem. Soc.* **2014**, *136*, 5555–5558.
64. Tanaka, M.; Shibata, Y.; Nakamura, K.; Teraoka, K.; Uekusa, H.; Nakazono, K.; Takata, T.; Tanaka, K. *Chem. Eur. J.* **2016**, *22*, 9537–9541.
65. Satoh, M.; Shibata, Y.; Tanaka, K. *Chem. Eur. J.* **2018**, *24*, 5434–5438.
66. González-Fernández, E.; Nicholls, L. D. M.; Schaaf, L. D.; Farès, C.; Lehmann, C. W.; Alcarazo, M. *J. Am. Chem. Soc.* **2017**, *139*, 1428–1431.
67. Nicholls, L. D. M.; Marx, M.; Hartung, T.; González-Fernández, E.; Golz, C.; Alcarazo, M. *ACS Catal.* **2018**, *8*, 6079–6085.
68. Hartung, T.; Machleid, R.; Simon, M.; Golz, C.; Alcarazo, M. *Angew. Chem. Int. Ed.* **2020**, *59*, 5660–5664.
69. Redero, P.; Hartung, T.; Zhang, J.; Nicholls, L. D. M.; Zichen, G.; Simon, M.; Golz, C.; Alcarazo, M. *Angew. Chem. Int. Ed.* **2020**, *59*, 23527–23531.
70. Jia, S.; Li, S.; Liu, Y.; Qin, W.; Yan, H. *Angew. Chem. Int. Ed.* **2019**, *58*, 18496–18501.
71. Furusawa, M.; Arita, K.; Imahori, T.; Igawa, K.; Tomooka, K.; Irie, R. *Tetrahedron Lett.* **2013**, *54*, 7107–7110.
72. Kötzner, L.; Webber, M. J.; Martnez, A.; Fusco, C. D.; List, B. *Angew. Chem. Int. Ed.* **2014**, *53*, 5202–5205.
73. Sako, M.; Takeuchi, Y.; Tsujihara, T.; Kodera, J.; Kawano, T.; Takizawa, S.; Sasai, H. *J. Am. Chem. Soc.* **2016**, *138*, 11481–11484.
74. Wang, Q.; Zhang, W.-W.; Zheng, C.; Gu, Q.; You, S.-L. *J. Am. Chem. Soc.* **2020**, *143*, 114–120.

PART VIII

ASYMMETRIC POLYMERIZATION

21

ASYMMETRIC POLYMERIZATION

Jie Li and Xiao-Bing Lu
State Key Laboratory of Fine Chemicals, Dalian University of Technology, Dalian, China

21.1. INTRODUCTION

Chirality is a ubiquitous characteristic of living systems. Most naturally occurring macromolecules are optically active, and some of them possess highly sophisticated functionalities, such as selective recognition abilities, outstanding mechanical properties, supersensitive responses to external stimuli, and high catalytic activity under mild conditions. These functionalities arise from their unique chiral structural units and orderly arranged building blocks. In addition, the sequence and spatial arrangement of atoms or groups in a polymeric unit are critical to the material performance. Therefore, it is of great significance to achieve precise control of both the chirality and sequence of synthetic polymers to understand their chain structures, self-assembly, and selective recognition of biomolecules. Consequently, the development of efficient and practical methods for constructing enantiomerically enriched polymers has become a very important and attractive research field in both academia and industry [1–6].

Asymmetric polymerization, in which chirality is introduced to a polymer chain through repetitive, asymmetric reaction of prochiral monomer in the presence of a chiral reagent or catalyst, is one of the most challenging methods for synthesizing optically active polymers with configurational main-chain chirality. In terms of the reaction process, asymmetric polymerization can be classified into three categories: asymmetric synthesis polymerization of optically inactive prochiral monomers via enantioselective catalysis, enantiomer-selective polymerization of only one enantiopure isomer of the *racemic* monomers via a catalytic kinetic resolution, and helix-sense-selective polymerization mediated by an optically active initiator. In this chapter, we provide an overview of the most recent developments in asymmetric polymerization mediated by chiral catalysts or initiators that introduce chirality into the polymer main chain.

21.2. ENANTIOSELECTIVE POLYMERIZATION

21.2.1. Preparation of Optically Active Polyolefins

21.2.1.1. Polymerization of Vinyl Olefins In 1962, Natta and co-workers [7] facilitated the enantioselective polymerization of *racemic* monosubstituted vinyl olefins (**1**) using Ziegler–Natta catalysts to afford a mixture of two types of polymers: one predominantly originating from the

Catalytic Asymmetric Synthesis, Fourth Edition. Edited by Takahiko Akiyama and Iwao Ojima.

(*R*)-enantiomer and the other from the (*S*)-enantiomer (Scheme 21.1). The polymers with different steric structures were successfully separated by chromatographic methods. After that, optically active polyolefins resulting from the enantioselective polymerization of **2** and **3** using $TiCl_4$/Zn[(*S*)-2-methylbutyl]$_2$ and $TiCl_3$/Al[(*S*)-4-methylhexyl]$_3$ were documented [8]. Additionally, the enantioselective polymerization of vinyl ethers could be realized. In 1970, Chiellini reported the copolymerization of *racemic* 1-methylpropyl vinyl ether **4** with optically active vinyl ethers bearing an asymmetric carbon atom directly bonded to the oxygen atom. These copolymerizations proceeded through the stereospecific Al(O-*i*-C_3H_7)$_3$–H_2SO_4 heterogeneous catalytic system. The nonpolymerized **4** that was recovered was optically active, indicating that the process was stereoelective [9]. The polymerization of *racemic cis*-1-methylpropyl propenyl ether **5** with (–)-menthoxyaluminum dichloride in toluene at –78 °C provided chiral polymers with positive optical activity, and the residual monomers were converted by BF_3OEt_2 into a polymer having negative optical activity. However, no optical activity was observed in the polymers resulting from the polymerization of the *trans*-isomer (**6**) using the same catalyst [10].

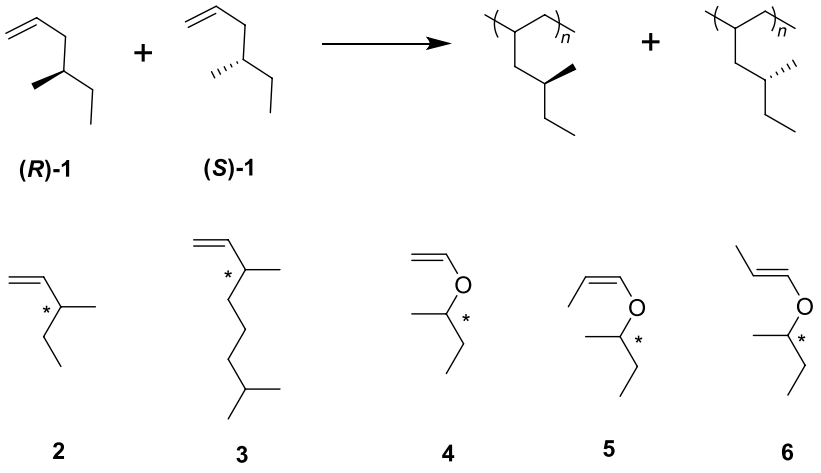

Scheme 21.1. Enantioselective polymerization of various *racemic* monosubstituted vinyl olefins.

Enantioselective polymerization of methacrylates such as compound **7** as a monomer was also achieved. In this process, the (*S*)-enantiomer was found to be preferentially polymerized in the presence of cyclohexyl Grignard reagents/(–)-sparteine (**Sp**) in toluene at –78 °C to afford an optically active polymer. The optical purity of the monomer, which was polymerized in the early stage of the polymerization, was greater than 90% and the optical purity of the unreacted monomer was nearly 100% at approximately 65% conversion [11–13]. Furthermore, the resultant polymers from the asymmetric polymerizations of compounds **8**, **9**, and **11–15**, mediated by Grignard reagent/(–)-**Sp** complexes, were highly isotactic [14–16].

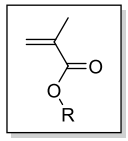

R =

7

8

9

10

11

12

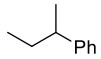

13

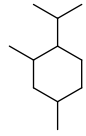

14

15

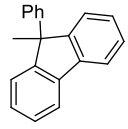

16

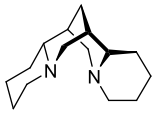

(–)-Sp

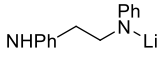

DPEDA-Li

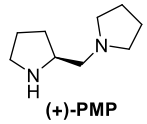

(+)-PMP

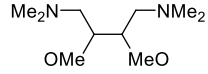

(+)-DDB

The anionic polymerization of **16** using *N,N′*-diphenylethylenediamine monolithium amide (**DPEDA-Li**) with (–)-**Sp**, (+)-1-(2-pyrrolidinylmethyl)pyrrolidine (**PMP**), and (+)-2,3-dimethoxy-1,4-bis (dimethylamino)butane (**DDB)** complexes could also be realized [17]. The resultant polymers exhibited optical rotations in the range of $[\alpha]_{365} = -54°$ to +119°, attributed to the chiral configurations of their main chains.

21.2.1.2. Polymerization of Diolefins The asymmetric anionic polymerization of substituted 1,3-dienes (**17**) (Scheme 21.2) mediated by (+)-2-methylbutyllithium or butyllithium/(–)-methyl ethyl ether gave polymers (**18**) with configurational main-chain chirality [18, 19]. Notably, the extent of chiral induction in the polymerization could be determined by analyzing the chiral diacid compounds (**19**) obtained from the ozonolysis of the polymers (**18**). In 1967, Natta et al. described the asymmetric synthesis polymerization of *trans*-1,3-pentadiene (**20**) upon λ-ray irradiation to afford optically active isotactic polymer **21** [20]. During this polymerization, the guest monomer molecule was included in the crystal lattice of the chiral host compound, perhydrotriphenylene (**22**). Additionally, the asymmetric inclusion polymerization of 1,3-dienes could also proceed in the presence of deoxycholic acid (**23**) [21, 22] and apocholic acid (**24**) [23, 24].

The cyclopolymerization of 1,5-hexadiene (**25**) yielded optically active poly(methylene-1,3-cyclopentane) (PMCP, **26**) (Scheme 21.3) with a molar optical rotation of $[\alpha]_{405}^{28} = -51.0°$ (c = 0.80, $CHCl_3$). This was accomplished using an optically active catalyst precursor, (*R,R*)-**27**, in the presence of excess methylaluminoxane (MAO) [25, 26]. The polymer microstructure could be interpreted by ^{13}C NMR at tetrad resolution. The enantioface selectivity for the cyclopolymerization of **25** in the presence of catalysts derived from (*R,R*)-**27** was 91% at 23 °C, indicating a highly isotactic microstructure. The polymerization proceeded exclusively via the cyclization mechanism, and the obtained polymer (**26**) was rich in *trans*-units (73%) with no plane of symmetry. This is the first enantioselective cyclopolymerization to produce a polymer with main-chain chirality. Optically active complexes **28** and **29**, which could be obtained by high-performance liquid chromatography (HPLC) with a chiral stationary phase, exhibited high enantioselectivity for the cyclopolymerization of **25** [27, 28].

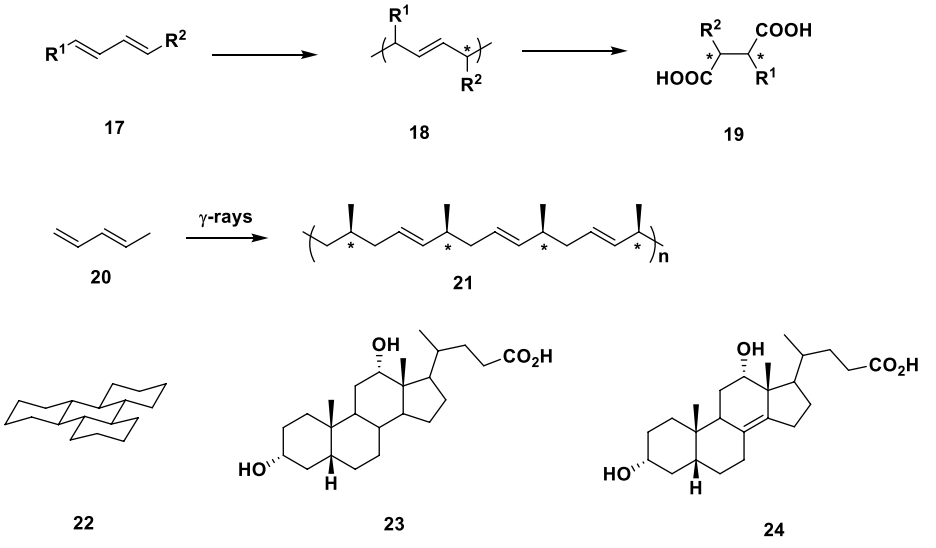

Scheme 21.2. Monomers and ligands used in asymmetric anionic polymerization of dienes.

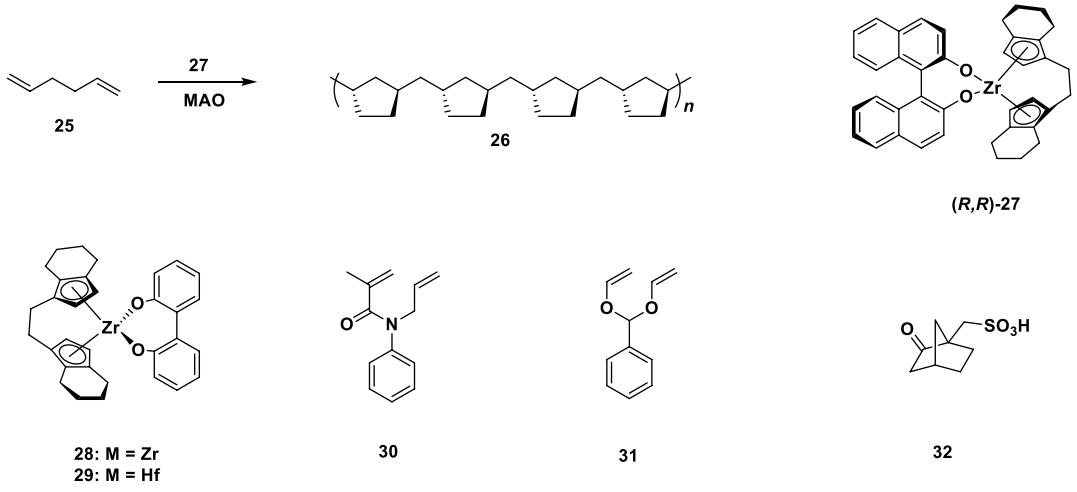

Scheme 21.3. Divinyl monomer and catalysts used in enantioselective cyclopolymerization.

Yokota et al. reported the enantioselective cyclopolymerization of divinyl monomer **30** using an initiating system consisting of chiral alkylsulfonic acid and a Lewis acid, providing optically active polymers with chiral cyclic units [29]. When the polymerization was carried out using $SnCl_4$/(–)-menthol, the resulting polymer exhibited optical activity ($[\alpha]_D = -5.6°$). The cationic cyclopolymerization of **31** using a $ZnCl_2$/10-camphorsulfonic acid (**32**) initiator system facilitated an optically active polymer with $[\alpha]_{435} = -17°$ [30].

21.2.1.3. Polymerization of Cyclic Olefins The asymmetric cationic polymerization of benzofuran **33** with $EtAlCl_2$ or $AlCl_3$ in the presence of chiral cocatalysts, such as (+)-*β*-phenylalanine, (+)-10-camphorsulfonic acid, tetramethylammonium 10-camphorsulfonate, (–)-brucine, ethoxytriethyltin, provided optically active polymers [31–36]. The specific rotation of the resultant polybenzofurans ranged from +10°

to +40°, depending on the polymerization conditions. Anionic polymerizations of achiral *N*-substituted maleimides (**34**) provided polymers with two possible types of structures [37]. Polymers with a *threo*-diisotactic structure are optically active, whereas those with a *threo*-disyndiotactic structure do not show any optical activity due to the equivalence of chiral stereogenic centers in their main chain.

Optically active polymers can be prepared by the asymmetric polymerization of achiral *N*-substituted maleimides using chiral **Sp**-based anionic initiators (Scheme 21.4), such as BuLi/(–)-**Sp** [38], BuLi-CuI/(–)-**Sp** [39], lithium (–)-menthoxide [40], lithium (*S*)-(+)-1-(2-pyrrolidinylmethyl)pyrrolidinylamide [40], BuLi/bisoxazolines (**35** and **36b**) [41–46], Et_2Zn/bisoxazolines [43–45, 47, 48], lithium oxazolidinylamide (**37**) [44, 49], and Co(II)-salen complexes [50–52] (**38**). ^{13}C NMR spectroscopy analysis showed that optically active poly(*N*-2-biphenylmaleimide) and poly(*N*-(2-phenoxy)-phenylmaleimide) mainly showed *threo*-diisotactic structures in their main chains [46]. The highest specific optical rotation ($[\alpha]_{435} = +762.3°$) was observed in the Et_2Zn/**36b**-mediated, asymmetric anionic homopolymerization of *N*-1-naphthylmaleimide in tetrahydrofuran at room temperature for 72 h [48].

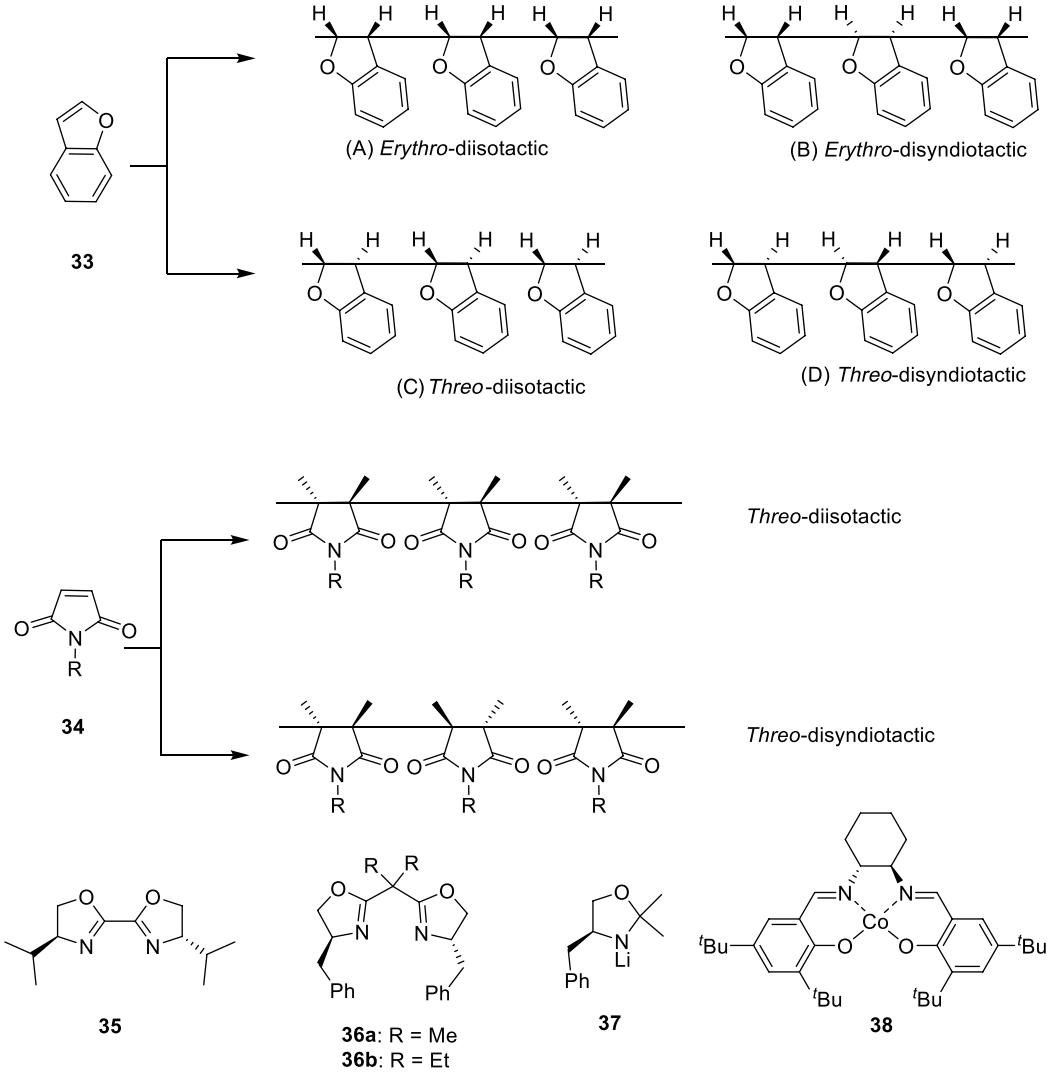

Scheme 21.4. Stereospecific polymerization of cyclic olefins, and employed ligands and catalysts.

21.2.2. Preparation of Chiral Polyketones from the Copolymerization of Olefins and CO

The copolymerization of carbon monoxide (CO) with olefins to polyketones (Scheme 21.5) represents a new, alternative route to low-cost thermal plastics with unique chemical and physical properties. A variety of chiral ligands in conjunction with metal ions have been employed in this asymmetric polymerization process.

Asymmetric alternating copolymerizations of propene with CO using palladium-(*S*)-BICHEP (**39**) complexes developed by Consiglio et al. produced polymers with essentially complete head-to-tail regioselectivity and high stereoselectivity (>93% diad unit content) [53–56]. However, the enantioselectivity was either low or not determined, with the exception of a few cases. In 1995, the highly enantioselective, alternating copolymerization of propene and CO by a $[Pd(MeCN)_4](BF_4)_2$ complex containing chiral ligand (*S,S*)-**40** was revealed by Takaya and co-workers [55]. Usually, both 1,4-ketone and spiroketal repeating units coexist in the backbone of α-olefin/CO copolymers. Notably, the interchange between the 1,4-keto and spiroketal units could be observed even in the absence of any metal catalyst. The degree of enantioselectivity in the formation of chiral, isotactic poly(1,4-ketone)s was found to be >90%, showing optical rotations of up to $[\alpha]_D = +22°$. Using this catalyst, the copolymerization of functionalized terminal alkenes with CO has also been investigated [57]. In 2000, a modified (*R*)(*Sp*)-JOSIPHOS system **41** was reported to show the highest catalytic activity (1797 g g(Pd)$^{-1}$ h^{-1}) for the copolymerization of propene/CO to give a polymer with complete regioselectivity (>99%), 97.5% of diad stereoregularity, and an optical rotation of $[\alpha]_D = -34.6$ [58]. Prior to this study, in 1995, Takaya and co-workers developed a chiral bidentate phosphine–phosphite ligand, BINAPHOS (**42**), for the asymmetric, alternating copolymerizations of monosubstituted ethenes and CO [59]. The palladium complex [Pd(Me)(MeCN)][B(3,5-$(CF_3)_2C_6H_3)_4$] was found to be a highly active catalyst that gave the alternating copolymer with a high molecular weight and high optical activity of $[\alpha]_D = +40°$.

In addition to propene, vinylarenes have also been applied in asymmetric copolymerizations with CO. In 1994, Brookhart et al. reported that a palladium complex of bisoxazoline ligand **43** enabled the enantioselective copolymerization of *p-tert*-butylstyrene with CO, affording polymers with isotacticities of over 98% and high optical activity ($[\alpha]_D = -536°$) [60, 61].

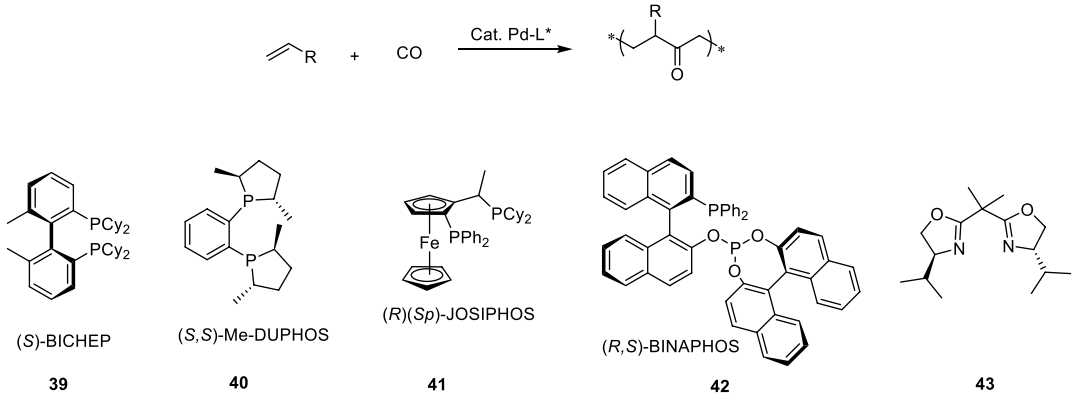

Scheme 21.5. Chiral ligands used in asymmetric alternating copolymerization of **α**-olefin with CO.

21.2.3. Enantioselective Epoxide Homopolymerizations and Copolymerizations

Owing to the stereogenic centers inherent to substituted epoxides, stereoselective epoxide polymerizations and copolymerizations for the synthesis of polymers with defined stereochemistry have gained tremendous attention in both industrial and academic laboratories for many years. In this section, we

present an overview of the recent advances in constructing epoxide-based chiral polymers through processes mediated by various well-defined catalysts.

21.2.3.1. Preparation of Chiral Polyethers via Enantioselective Epoxide Homopolymerization
Although the discovery of isotactic poly(propylene oxide) was as early as that of the widely used isotactic polypropylene, significant advances have been made in recent years – specifically, the development of bimetallic cobalt catalysts that allow for the extraordinarily fast production of isotactic polyethers with high levels of isotacticity via the kinetic resolution polymerization of terminal epoxides. Prior to this contribution, Coates and co-workers recently published an excellent review on stereoselective epoxide polymerization [62]. As a result, several representative examples are described herein to illustrate the most significant progress in the synthesis of isotactic polyethers.

In 1955, Pruitt and Baggett described that $FeCl_3$ could polymerize propylene oxide (PO) in diethyl ether at 80 °C to yield a brown solid, poly(propylene oxide) (PPO), after 88 h [63]. The resultant solid could be divided into amorphous and semi-crystalline materials using solvent fractionation. The crystallized white solid with a melting temperature (T_m) of 70 °C was later proved to have an isotactic microstructure. Following this study, a variety of metal-based catalysts, including Al [64–69], Zn [64, 70–75], Co [76–78], Ti [79, 80], and alkali-metal complexes [81–84], have been applied to this transformation. Among these catalysts, salenCo(III)X complexes are exceptional because of their high enantioselectivities and reaction rates for epoxide polymerization. In 2005, Coates et al. first reported a catalyst capable of polymerizing *rac*-PO to exclusively give regioregular isotactic poly(propylene oxide) (Scheme 21.6) [76]. The achiral catalyst (**44**) exhibited high activity and stereoselectivity for isospecific *rac*-PO polymerization, which resulted in isotactic PPO with an [*mm*] >99% and a high molecular weight (greater than 52 kDa). Based on the solid-state structure of salenCo(III)X complex **44**, which bears an axial methoxide group for the substitution of an acetate anion, a bimetallic mechanism was proposed to elucidate the nature of this enantioselective process [85]. The single-crystal X-ray diffraction analysis revealed that each metal ion was coordinated to a methanol molecule that was hydrogen-bonded to another methanol molecule, which was also hydrogen-bonded to the methoxide of an adjacent salenCo(III)OMe molecule. This arrangement induces an infinite coordination polymer with neighboring molecules related through pseudo-C2 symmetry, creating a chiral environment for the homopolymerization of PO where adjacent stacks exhibit mirror-image symmetry.

In 2008, the Coates group developed bimetallic complex **45**, which was the first catalyst capable of enantioselectively polymerizing a variety of monosubstituted terminal epoxides by combining them with an ionic cocatalyst salt, such as bis-(triphenylphosphine)iminium acetate ([PPN][OAc]) [77]. The chirality of the axial linker of the ligand, rather than that of the diamine backbone, was responsible for the chiral induction of this kinetic resolution polymerization process. The [*mm*] triad values of the resultant isotactic polyethers were typically higher than 95%, and in some cases they exceeded 98% with a selectivity factor (*s*-factor) in the range of 50–300 for a variety of monosubstituted epoxides. The Coates group then performed an in-depth mechanistic study that employed both theoretical and experimental methods [86]. From the results, it was believed that two *exo* active anionic ligands (chloride or carboxylate) and an *endo* polymer alkoxide were involved in the ring-opening of epoxides that were coordinated to adjacent metal centers. Specifically, it was the *endo* anion that initiated the polymerization and propagation of the polymer chain.

Inspired by these results, Coates et al. developed bimetallic chromium complexes **46** and **47** for the enantioselective polymerization of PO [87, 88]. More importantly, diol-, triol-, and polymeric-chain shuttling agents were used to obtain hydroxy-telechelic isotactic PPO with varying functionalities and structures, as well as controllable molecular weights with narrow distributions.

Since *meso*-epoxides possess two adjacent asymmetric carbon centers of opposite configurations, the attack of the *R*- or *S*-configuration center of a *meso*-epoxide induces the formation of an *–SS*- or *–RR*-configuration unit, respectively. Tsuruta and co-workers documented the synthesis of predominantly syndiotactic poly(cyclohexene oxide) catalyzed by zinc clusters containing six methoxy isopropyl groups in a chair-like structure [89]. In 1991, Sepulchre et al. reported the stereospecific polymerization of cyclohexene oxide (CHO) using diethylzinc modified with water and achiral or chiral alcohols [90].

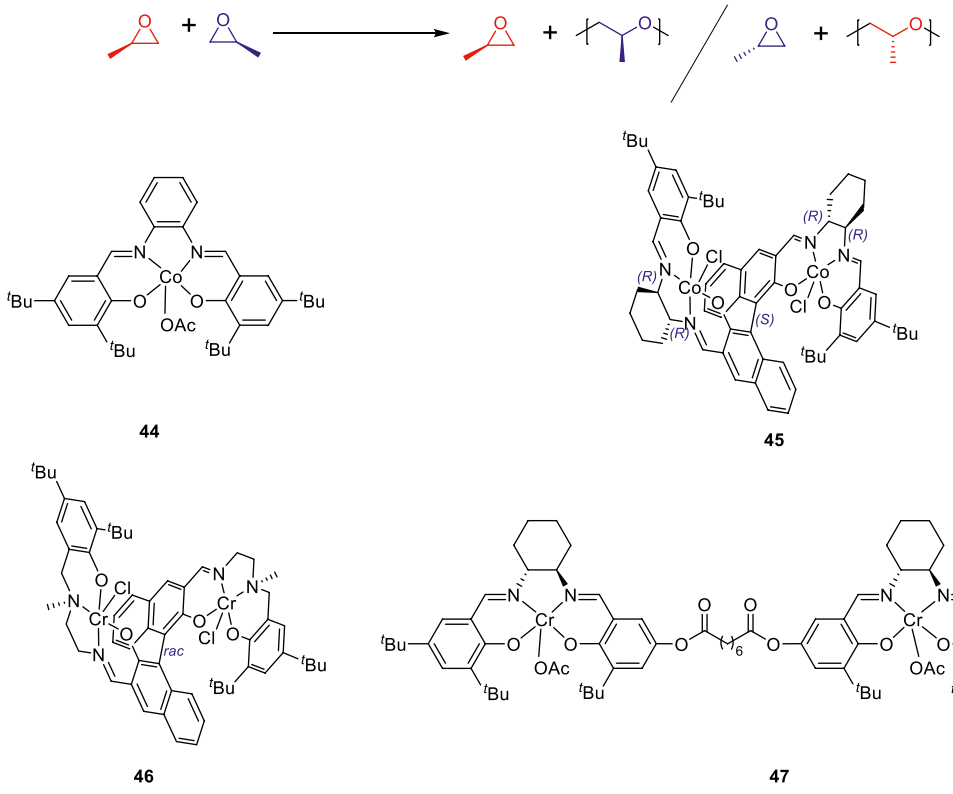

Scheme 21.6. Enantioselective resolution homopolymerization of propylene oxide, and used catalysts. Source: [76]/American Chemical Society.

Mediated by $ZnEt_2$/1-methoxy-2-propanol or $ZnEt_2$/(*1S,2R*)-ephedrine, a mixture of isotactic as well as syndiotactic poly(cyclohexene oxide)s could be formed. At least three different types of active sites were involved in the polymerization reaction.

21.2.3.2. Preparation of Chiral Polycarbonates Alternating copolymerizations of epoxides and CO_2 to give degradable polycarbonates represent a green process for the potential large-scale utilization of CO_2 as a safe and cheap C1 feedstock in chemical synthesis. In the late 1960s, Inoue et al. demonstrated this transformation for the first time [91, 92]. Subsequently, a number of highly alternating copolymers have been prepared via this strategy using various metal-based catalysts or organocatalysts. These atactic copolymers are typically amorphous, and most of them have low glass-transition temperatures. Introducing stereoregularity into the polymer chain is a promising approach for improving the thermal and mechanical properties of polymers.

21.2.3.2.1. Kinetic Resolution Copolymerization of racemic Epoxides with CO_2 Similar to the enantioselective polymerization of *rac*-epoxides, the major challenge in obtaining isotactic polycarbonates is the ring-opening of the terminal epoxides because the alkoxides have two areas to attack: either the methine or methylene carbon. In 2003, Coates and co-workers first reported the copolymerization of PO and CO_2 using (Salen)Co(III)OAc catalyst **48a**. The high selectivity of polymers over cyclic carbonates

TABLE 21.1. Binary catalyst systems based on chiral salenCo(III)X for *racemic* PO/CO_2 copolymerization.

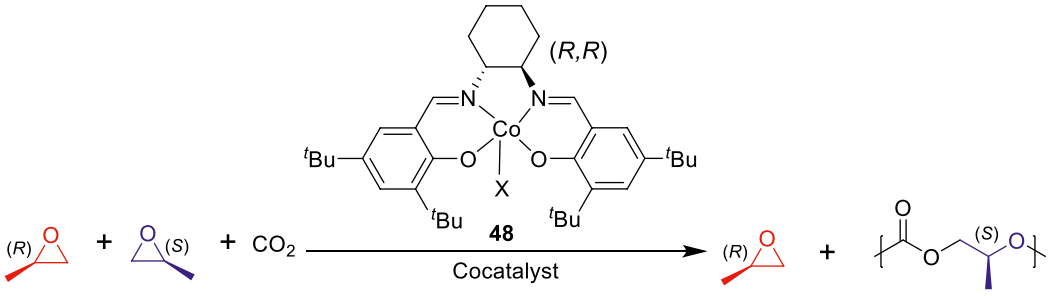

Catalyst	X	Cocatalyst	Temp.(°C)	k_{rel}
48a	OAc	—	25	2.8
48b	DNP	$^{n}Bu_4Cl$	25	3.4
48c	DNP	MTBD	0	6.2
48d	$O_2CC_6F_5$	PPNCl	–20	9.7
48e	OTs	DMAQ	22	5.4

OAc, acetate; DNP, 2,4-dinitrophenoxide; OTs, p-toluenesulfonate

and good regioselectivity (~80% head-to-tail linkages) were achieved when the process was performed at high catalyst loadings and CO_2 pressures (800 psi). Moreover, with *rac*-PO, the polymerization preferentially consumed (*S*)-PO over (*R*)-PO with a kinetic resolution coefficient (k_{rel}) value of 2.8. Thus, they proposed that the mechanism that occurs during polymerization to give the active alkoxide regiochemistry is the cobalt-catalyzed asymmetric ring-opening of aliphatic epoxides with benzoic acid, as explored by Jacobsen and co-workers [93].

Soonafter, Lu, and Wang designed a binary catalyst system based on chiral salenCo(III)/quaternary ammonium halide catalyst systems for the kinetic resolution of *racemic* terminal epoxides with CO_2 under mild conditions [94]. The axial X group of the catalyst and anion of the quaternary ammonium halide cocatalyst were proven to have significant effects on polymer/cyclic product selectivity. Enantiopure **48b**, in conjunction with $^{n}Bu_4NCl$, enabled iso-enriched poly(propylene carbonate) (PPC) with carbonate linkages of >99% and a low k_{rel} of less than 10. The effects of the diamine backbone and/or substituent groups of the salen ligand, the axial X group, and the cocatalyst (quaternary ammonium salts R_4NY, PPNY (Y = nucleophilic anion), *N*-methylimidazole, 7-methyl-1,5,7-triazabicyclo[4.4.0]dec-5-ene (MTBD)) on the activity, selectivity, and enantioselectivity for polycarbonate formation were investigated during the enantioselective resolution copolymerization of CO_2 with *racemic* PO [95]. They found that combining a bulky chiral salenCo(III)X bearing an axial X group with poor leaving ability and a bulky ionic ammonium salt (comprising a bulky cation and a nucleophilic anion with poor leaving ability) or a sterically hindered, strong organic base with low coordination ability was optimal for a binary catalyst system. In addition, when using MTBD as a cocatalyst, catalyst **48b** produced polycarbonates with relatively high enantioselectivity and a k_{rel} value of 6.2 (Table 21.1). Coates et al. almost simultaneously demonstrated a k_{rel} of 9.7 for the enchainment of (*S*)- over (*R*)-PO when the copolymerization was carried out at –20 °C and mediated by a **48c**/PPNCl catalyst system [85]. Nguyen and co-workers were able to achieve isotactic-enriched polycarbonates with a k_{rel} of 5.4 using *N,N*-dimethylaminoquinoline (DMAQ) with **48d** at room temperature [96].

In 2011, Lu et al. employed unsymmetric, multichiral cobalt-based complexes (**49**) bearing a chiral BINOL to catalyze the enantioselective copolymerization of CO_2 and *racemic* PO. This afforded perfectly regioregular PPC with >99% head-to-tail linkages and >99% carbonate linkages. Furthermore, the highest k_{rel} (24.3) for the enchainment of (*R*)-epoxide over (*S*)-epoxide was achieved at –20 °C [97].

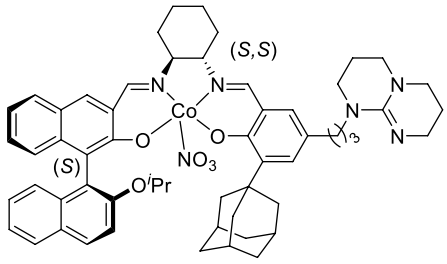

49

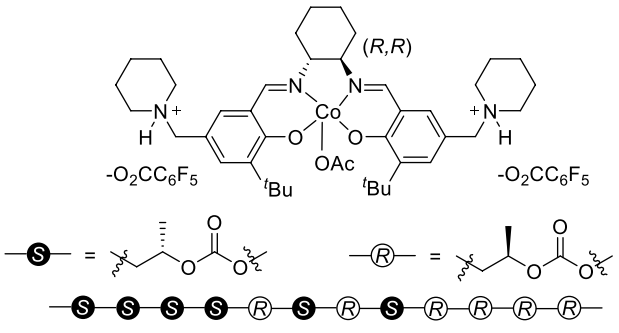

50

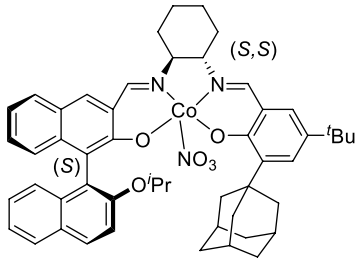

51

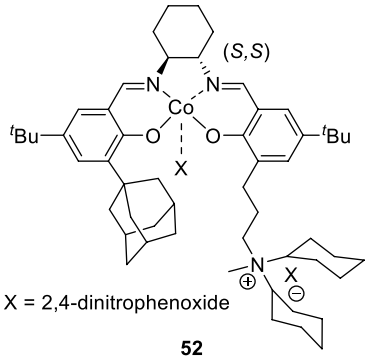

52

Interestingly, Nozaki et al. documented a salenCo(III) catalyst (**50**) with covalently attached piperidiniums for the preparation of stereogradient PPC [98]. The isotactic-enriched stereogradient PPC starts from an (*S*)-configuration-enriched PPC segment and ends with an (*R*)-enriched PPC block. Importantly, the resulting stereogradient PPCs were found to possess higher thermal decomposition temperatures than typical PPCs.

Kinetic resolution copolymerizations of CO_2 with other *racemic* terminal epoxides were also achieved by Lu et al. using enantiopure salenCo(III)-based catalysts. In combination with PPNCl, catalyst **49** mediated the enantioselective copolymerization of 1,2-butene oxide and 1,2-hexene oxide at 0 °C with k_{rel} values of 9.8 and 6.7, respectively [97]. Additionally, the kinetic resolution of styrene oxide with CO_2 was achieved by Lu et al. using **51**/[PPN][DNP] catalyst systems with a k_{rel} of 3.3 [99]. The kinetic resolution copolymerization of CO_2 with epichlorohydrin using a (salen)Co(III) complex (**52**) bearing a sterically hindered substituent group and a covalently tethered bulky ammonium salt exhibited a k_{rel} of 8.9 at –20 °C [100].

21.2.3.2.2. Asymmetric Polymerization of Meso-*Epoxides with CO_2* The opposite configurations of two asymmetric carbon centers inside *meso*-epoxides provide the opportunity to prepare isotactic (–*RR*– or –*SS*–) and syndiotactic (–*RR*–*SS*–) polycarbonates when they undergo enantioselective copolymerization with CO_2. The first example of the asymmetric copolymerization of CO_2 and CHO (Scheme 21.7) was documented by Nozaki et al. using an equimolar mixture of $ZnEt_2$ and (*S*)-α,α-diphenyl(pyrrolidin-2-yl) methanol as a chiral catalyst system, affording poly(cyclohexene carbonate) (PCHC) with 70% ee [101]. Subsequently, Coates and co-workers reported that using a well-defined, chiral, hybrid imine-oxazoline zinc complex (**53**) for the same reaction resulted in similar enantioselectivity but higher activity and a controllable molecular weight [102]. Inspired by the successful work of the kinetic resolution of terminal epoxides with CO_2 using salenCo(III)-based catalysts, in 2006, Lu et al. applied enantiopure **54** to the asymmetric copolymerization of CHO and CO_2 under mild conditions. Using equimolar PPNCl as the cocatalyst, isotactic-enriched PCHC with a low enantioselectivity of 38% ee was obtained when the

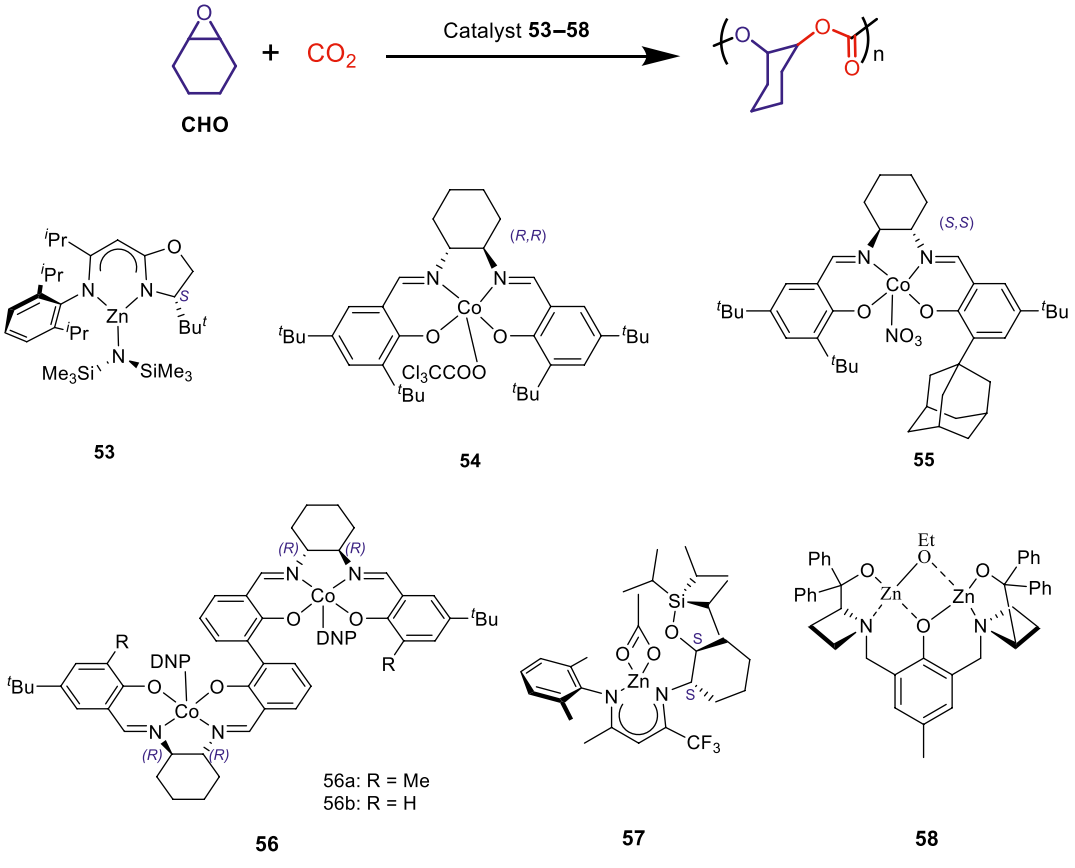

Scheme 21.7. Catalysts used in asymmetric copolymerization of *meso*-epoxides with CO_2.

copolymerization reaction was performed at 25 °C and 1.5 MPa of CO_2 pressure. Until 2012, a series of C1-symmetric catalysts that exhibited high stereoselectivity for the copolymerization of CHO with CO_2 were reported by Lu and co-workers. High enantioselectivity (84% ee) was observed at –25 °C using salenCo(III) complex **55** bearing a sterically bulky *ortho*-substituent on one side. Additionally, when the reaction was performed at –25 °C in a 1 : 3 mixture of CHO and (*S*)-2 methyltetrahydrofuran, which acts as a chiral induction agent, the highest selectivity (96% ee) was realized. Of importance, the resultant isotactic polycarbonate was the first semicrystalline CO_2-based polymer with a T_m of 216 °C.

Although catalyst **55** is highly enantioselective for CO_2/CHO copolymerization at –25 °C with enantiopure 2-methyltetrahydrofuran as a chiral induction agent, its catalytic activity of less than 3 h^{-1} (turnover frequency, mol of product (mol of catalyst h)$^{-1}$) was not satisfactory, and the molecular weight of the resultant polycarbonate was low. The most significant development in this area was reported in 2013 by Lu et al., who demonstrated a catalyst system comprising an enantiopure, biphenol-linked, dinuclear salenCo(III) DNP catalyst, (*R,R,R,R*)-**56**, and a nucleophilic cocatalyst, PPN–DNP (DNP = 2,4-dinitrophenoxide). This system provided the efficient and highly enantioselective copolymerization of CO_2/*meso*-epoxides to afford isotactic polycarbonates with enantioselectivities of up to 99% ee for the (*R,R*)-configuration [104]. The steric hindrance of the phenolate *ortho*-substituents strongly influenced the catalytic activity and product enantioselectivity. It was found that the bulky substituents on the aromatic rings were not the best choice in this study. Mediated by the dinuclear catalyst **56a**, isotactic PCHC exhibited a high T_m of 272.4 °C and a crystallization temperature (T_c) of 233.6 °C. An intramolecular bimetallic cooperation mechanism was proposed (Scheme 21.8) [103], in which the initiation is triggered by one of the two nucleophilic anions from the inside cleft of the bimetallic catalyst. The chain-growth step takes place between two cobalt ions and

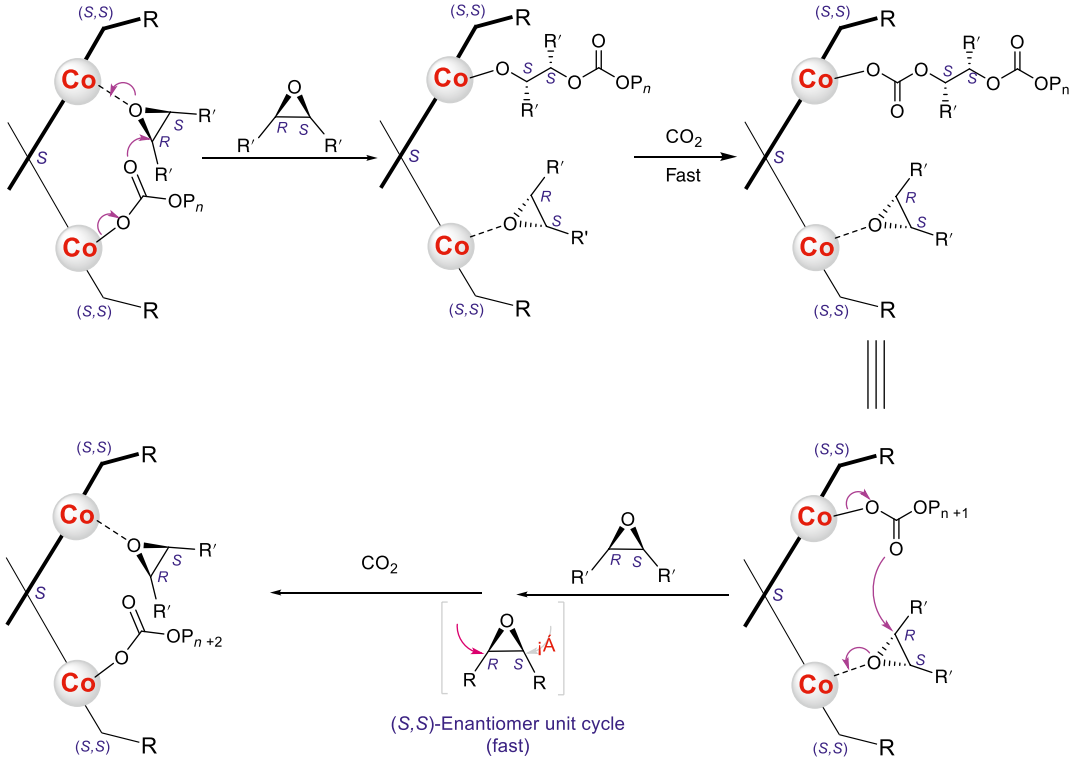

Scheme 21.8. Intramolecular bimetallic mechanism for enantioselective polymer chain growth from inside the cleft of dinuclear Co(III) catalyst. (Source: Reprinted with permission from Ref. [103]. Copyright 2014 The American Chemical Society.)

proceeds via the nucleophilic attack of the propagating carboxylate species at one metal center toward the epoxide bonded at the other metal center. Both the stereochemistry of the biphenol-linker and cyclohexyl diamine skeletons determine the enantiomeric preference of the asymmetric copolymerization.

Notably, the biphenol-linked dinuclear salenCo(III)DNP is a rare, chiral-privileged catalyst for copolymerizing CO_2 and various *meso*-epoxides, showing both high reactivity and enantioselectivity for producing the corresponding polycarbonates with more than 99% carbonate units and 99% ee. The reactivities are in the range of 120–1400 h^{-1} at ambient temperature, depending on the employed epoxides. A variety of highly isotactic polycarbonates were obtained, where most were crystalline and possessed T_m values of 179–257 °C. Interestingly, mixing the equivalent isotactic (*R*)- and (*S*)-polycarbonates from *meso*-epoxides exhibited a unique stereocomplexation with a significant improvement in thermal properties [103, 105, 106]. For example, isotactic (*R*)- and (*S*)-poly(cyclopentene carbonate) are typical amorphous polymeric materials. However, a new crystalline stereocomplex with a T_m of around 200 °C was afforded by mixing both enantiomers together. This proceeded via the formation of an interlocked ordered assembly between two polymers with opposite enantiomeric configurations. Meanwhile, novel, gradient polycarbonates were prepared via the **56**-mediated asymmetric terpolymerization of 3,4-epoxytetrahydrofuran, cyclopentene oxide, and CO_2, in which the decrement of one component and the increment of the other component occur sequentially from one chain end to the other [107]. The resultant terpolymers show perfectly isotactic structures and have unique crystalline-gradient natures, where their crystallinities continuously vary along their main chains. In addition to enantiopure dinuclear salenCo(III)X complexes, C1-symmetric *β*-diiminate zinc catalysts (**57**) designed by the Coates group and dinuclear zinc complex **58** bearing rigid azetidines reported by Wang and Chang et al. were demonstrated to be capable of yielding highly isotactic PCHC with up to 94% ee under mild conditions [108, 109].

21.2.3.3. Preparation of Chiral Poly(monothiocarbonate)s Sulfur-containing polymers are widely applicable owing to their facile degradation and biocompatibility, high refractive index for optical applications, and sorbent properties for wastewater treatment. Recently, Ren and Lu et al. first realized the enantioselective synthesis of highly stereoregular poly(monothiocarbonate)s with main-chain chirality through the asymmetric copolymerization of *meso*-epoxides and COS mediated by enantiopure biaryl-linked dinuclear Co(III) complexes (**59**) (Scheme 21.9) [110]. A binaphthol-linked, bimetallic complex with an (*R,R,R,R,R*)-configuration exhibited efficient enantioselectivity in mediating this asymmetric transformation, affording a variety of isotactic poly(monothiocarbonate)s with over 99% isotacticity. Moreover, the resultant chiral, sulfur-containing polymers have good optical properties with refractive indices of up to 1.56 and Abbe's numbers of up to 43.

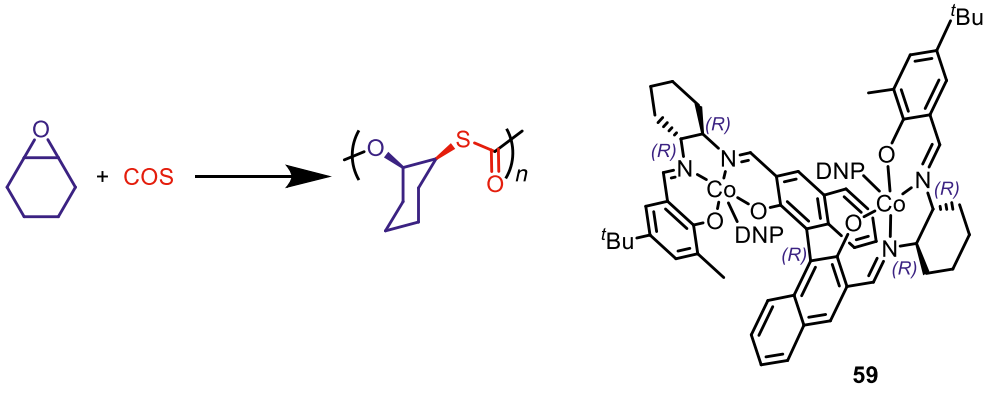

Scheme 21.9. Asymmetric copolymerization of cyclohexane epoxide with COS mediated by (*R,R,R,R,R*)-dinuclear cobalt complex. Source: [110]/Royal Society of Chemistry.

21.2.3.4. Preparation of Chiral Polyesters Aliphatic polyesters have garnered extensive interest from both academic and industrial scientists. Some of them can be recycled, composted, and incinerated with low environmental impact. In addition, polyesters used for medical purposes mainly originate from renewable, biomass-derived resources, such as lactide (LA). Alternating copolymerizations of epoxides and anhydrides provide a new route to degradable polyesters that can replace the step-growth condensation of diols and diesters at high temperatures (>250 °C) that is conventionally used for most polyester syntheses. In this section, we mainly focus on the synthesis of isotactic or syndiotactic polyesters with improved thermal properties, with a regard to the stereogenic centers inside lactones and epoxides. Given that there are numerous articles on this topic, we will only discuss a few novel studies on the asymmetric polymerization of *rac*-LA and *rac*-eight-membered cyclic diolide (DL), as well as the asymmetric copolymerization of epoxides with cyclic anhydrides to afford isotactic polyesters.

21.2.3.4.1. Enantioselective Polymerization of Lactides and Lactones The stereoselective polymerization of *rac*-LA is a robust method for the preparation of isotactic or syndiotactic polylactides (PLAs) (Scheme 21.10). Both enantiomorphic site-control and chain-end-control mechanisms were frequently observed in the formation of stereoregular PLAs. The site-control mechanism involves the chiral catalyst determining the incorporation of the monomer, while the chain-end-control mechanism involves the chirality of the growing polymer chain end affecting the selectivity of the next monomer insertion. Two parameters, P_m and P_r (P_m or P_r = probability of isotactic or syndiotactic enchainment determined by ^{1}H NMR spectroscopy, respectively), were used to evaluate the degree of stereoregularity of isotactic and syndiotactic PLA, respectively. P_m or P_r values of 0.50 indicated a completely atactic polyester. However, cases of P_m = 1.00 (P_r = 0) and P_r = 1.00 (P_m = 0) depict perfect isotactic or syndiotactic polymers, respectively [111].

The first report concerning the kinetic resolution polymerization of *rac*-LA to isotactic-enriched PLA was documented by Spassky et al. using (*R*)-salen binaphthyl-ligand aluminum methoxide catalyst **60**.

An *s*-factor of approximately 20 was demonstrated, in which the (*R*)-catalyst preferentially consumed D-LA over L-LA through the enantiomorphic site-control mechanism [112]. In 2002, Feijen et al. demonstrated that enantiopure (*R,R*)-salenAl(III)O^{i}Pr (**61**), based on Jacobsen's catalyst, polymerized L-LA significantly faster than D-LA with a k_{rel} of about 14 at 70 °C [113, 114], affording isotactic-enriched PLA (P_i = 0.92) with a controllable molecular weight and low polydispersity. Chen and Feijen et al. revealed that (*R,R*)-salanAl(III)OiPr (**62**) (salan, *N,N′*-disubstituted bis(aminophenoxide), a saturated version of Schiff-base salen ligand) could efficiently polymerize L-LA at a higher reaction rate than D-LA with a k_{rel} of 10.1 [115]. Chiral 2,2′-bipyrrolidine-based salanAl(III) complex **63**, developed by Kol et al., exhibited dramatic results when the effect of subtle ligand variations on its stereocontrol for the polymerization of *rac*-LA was evaluated [116]. The polymerization of *rac*-LA with (*R,R*)-**63a** at 50 °C gave isotactic-enriched PLA with P_m = 0.79, in which the consumption of L-LA was faster than that of D-LA through the same enantiomorphic site-control mechanism with a k_{rel} of 11.3. The polymerization of *rac*-LA with either (*R,R*)- or (*S,S*)-**63b** at 70 °C led to an almost atactic form of PLA with a slight heterotactic tendency of P_r = 0.64. Contrastingly, the *racemic* catalyst afforded PLA with almost perfect heterotacticity following an insertion/auto-inhibition/exchange mechanism.

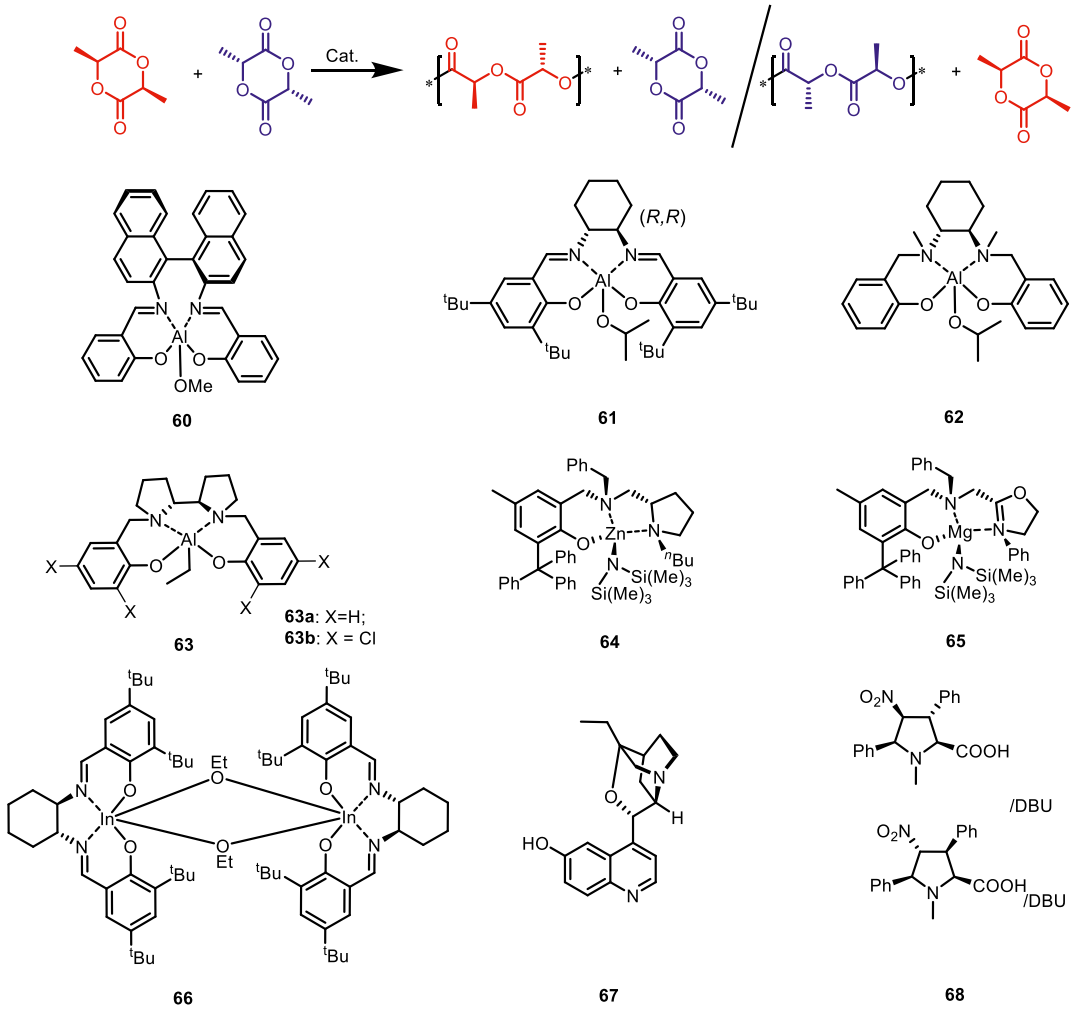

Scheme 21.10. Various catalysts involved in enantioselective polymerization of *racemic* lactides.

Aside from aluminum complexes, chiral aminophenolate zinc complex **64** [117] and oxazolinyl aminophenolate magnesium complex **65** [118], developed by Ma and co-workers, were also employed for the polymerization of *rac*-LA, affording isotactic-enriched PLA with P_m values of 0.84 and 0.78, respectively. In both cases, a nearly fourfold difference in the polymerization rate of D-LA over L-LA was observed, indicating an enantiomorphic site-control mechanism was occurring. In 2013, Mehrkhodavandi et al. described the first chiral indium salen catalyst (**66**) for asymmetric *rac*-LA polymerization [119]. Compared to those of aluminum complexes, a higher reaction rate and lower selectivity (5 vs. 14) were observed for the indium-based catalyst (**66**). The first example of an organocatalyst-mediated, stereoselective polymerization of *rac*-LA was reported by Chen and Miyake using a cinchona alkaloid, *β*-isocupreidine (ICD, a chinchona alkaloid derivative, **67**), consisting of both a chiral nucleophilic amine catalyst site and an electrophilic hydroxy moiety [120]. In this polymerization, L-LA was demonstrated to be preferentially polymerized by ICD and exhibited an *s*-factor of approximately 4.4 with the addition of 1 equiv. of BnOH. Recently, Cossio et al. discovered that amino-acid-based catalysts bearing multiple chiral centers were active for the efficient enantioselective polymerization of *rac*-LA, affording isotactic PLA with a P_m up to 0.96 when the conversion of *rac*-LA was 50% [121]. (2*S*,3*R*,4*S*,5*S*)-1-Methyl-4-nitro-3,5-diphenylpyrrolidine-2-carboxylic acid (*endo*-**68**) combined with 1,8-diazabicyclo[5.4.0]undec-7-ene (DBU) preferentially polymerized D-LA, whereas (*2S,3S,4R,5S*)-1-methyl-4-nitro-3,5-diphenylpyrrolidine-2-carboxylic acid (*exo*-**68**) preferred L-LA as the substrate. Both diastereoisomers were not only able to synthesize isotactic-enriched PLA with a P_m higher than 0.90 at room temperature, but also preferentially promoted the polymerization of one of the isomers (L or D) with respect to the other.

Poly(hydroxyalkanoate)s (PHAs) are aliphatic polyesters that are commercially implemented as biodegradable and/or biocompatible materials for biomedical, pharmaceutical, and packaging applications. In 2018, an elegant study contributed by Chen and co-workers reported that chiral salen-yttrium catalysts (**69**) could efficiently promote the kinetic resolution polymerization of *rac*-eight-membered cyclic DL to poly(3-hydroxybutyrate) (Scheme 21.11) with perfect isotacticity ([*mm*] > 99%) and low dispersity, as well as a high crystallinity, melting temperature (T_m = 175 °C), and molecular weight [122, 123]. Notably, with enantiomeric catalyst **69**, the kinetic resolution polymerization of *rac*-DL automatically stopped at 50% conversion. In this reaction, the (*R,R*)-catalyst preferentially polymerized (*R,R*)-DL to yield isotactic (*R,R*)-polyesters and the unreacted (*S,S*)-DL was retained with >99% ee.

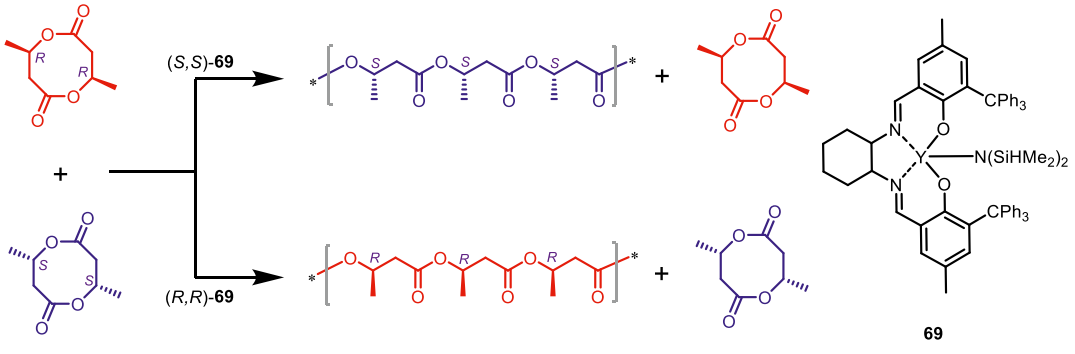

20

Scheme 21.11. Kinetic resolution polymerization of *racemic* eight-membered cyclic esters using chiral salen-yttrium complex.

Metal-catalyst/initiator- or enzyme-mediated enantioselective polymerizations of substituted *ε*-CL [124–127], *α*-alkyl-*β*-propiolactone (*β*-PL) [128–130], and *β*-butyrolactone (*β*-BL) [131, 132]

afforded biocompatible and biodegradable isotactic-enriched polyesters, but the k_{rel} values were relatively lower than those of similar polymerizations with *rac*-LA as the substrate.

21.2.3.4.2. Asymmetric Copolymerization of Epoxides and Cyclic Anhydrides The alternating copolymerization of epoxides with anhydrides is of great interest as a burgeoning route for preparing various degradable polyesters owing to the wide availability of both monomers [133, 134]. As described in Sections 2.3.1 and 2.3.2, the stereogenic centers inherent to substituted epoxides allow for the possibility of preparing stereoregular polymers with main-chain chirality through enantioselective polymerization. Using this strategy, Lu et al. realized the asymmetric copolymerization of *meso*-epoxides with cyclic anhydrides using enantiopure hydrogenated binaphthol-linked dinuclear Al(III) complexes (**70**) in conjunction with the nucleophilic cocatalyst PPNCl (Scheme 21.12). This catalyst system exhibited high activity and enantioselectivities of up to 99% ee under mild conditions [135, 136]. In particular, the steric hindrance of phenolate *ortho*-substituents was found to have an immense effect on the product enantioselectivity and catalyst activity. Neither small (methyl) nor bulky (trimethylsilyl (TMS)) groups were beneficial for this asymmetric copolymerization. Moreover, most of the resultant chiral polyesters were typical, semicrystalline materials with T_m values between 120 and 240 °C. Mixing selected isotactic (*R*)- and (*S*)-polyesters in a 1 : 1 mass ratio gave two crystalline stereocomplexes that exhibited enhanced thermal stability and new crystallization behavior compared to those of the parent, enantiopure polymers.

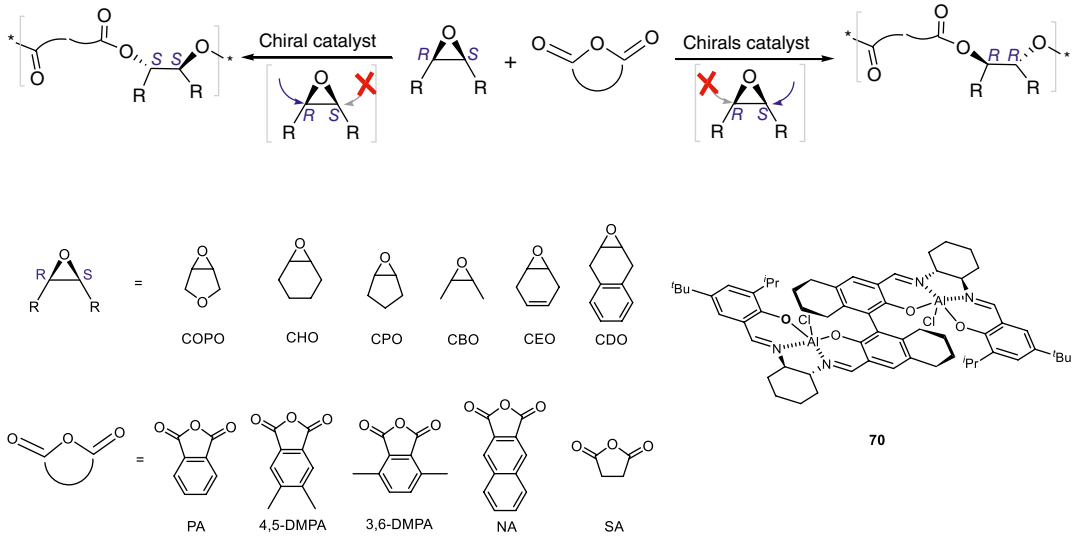

Scheme 21.12. Asymmetric copolymerization of various *meso*-epoxides with cyclic anhydrides mediated by enantiopure dinuclear aluminum complexes.

In terms of the enantioselective resolution copolymerization of *racemic* terminal epoxides with cyclic anhydrides, enantiopure dinuclear complexes **71** and **72** exhibited exceptional levels of enantioselectivity with a kinetic resolution coefficient exceeding 300 for various *racemic* epoxides (Scheme 21.13). They afforded highly isotactic copolymers (*s*-factors of more than 300) with completely alternating structures and low polydispersity indices [137]. The chiral induction of this kinetic resolution copolymerization process and the catalytic activation were influenced by the chirality of both the axial linker and the diamine backbones of the ligand. Moreover, most of the resultant isotactic polyesters were typical semicrystalline materials with T_m values ranging from 77 to 160 °C. In addition, macromolecular stereocomplexation occurred through an interlocked orderly assembly between two isotactic polyesters with opposite enantiomeric configurations [138].

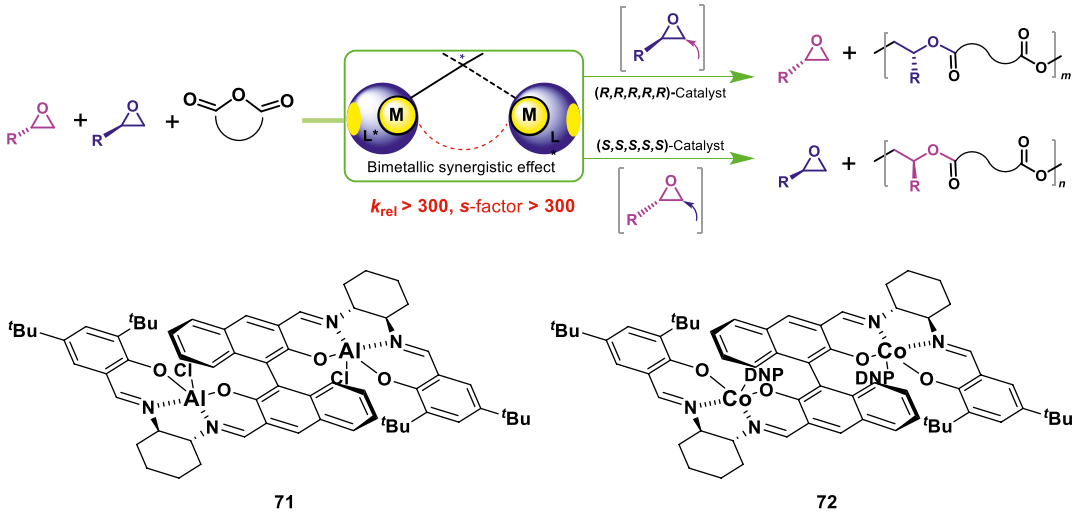

Scheme 21.13. Enantioselective resolution copolymerization of *racemic* terminal epoxides with cyclic anhydrides.

Recently, the enantioselective terpolymerization of *racemic* terminal epoxides, *meso*-epoxides, and anhydrides was achieved by Lu et al. using a chiral-privileged, dinuclear Al(III) catalyst system with multiple chirality. This system afforded optically active polyester terpolymers (>95 ee%) with either gradient or random distribution, as determined by the epoxides employed during their preparation [139]. In addition, the same group realized the enantioselective resolution copolymerization of *racemic cis*-internal epoxides and anhydrides to give optically active polyesters with two contiguous stereogenic centers, where the unreacted substrates were retrieved with good enantioselectivity [140]. Unexpected stereoconvergence was observed in this resolution copolymerization, where the *s*-factor for the enantioselective formation of the copolymer significantly exceeded the kinetic resolution coefficient based on the unreacted epoxide at various conversions.

21.2.4. Other Asymmetric Polymerization Reactions

21.2.4.1. Asymmetric Condensation Polymerization Chiral Lewis acids that mediate the enantioselective Diels–Alder polymerization of prochiral bisdienophiles with bisdienes enable the formation of optically active polymers with main-chain chirality [141]. In 1997, Ito et al. reported that the asymmetric polymerization of bismaleimide **73** with bisdiene **74** afforded optically active polymers (**75**) with $[\Phi]_D = +243°$ and $[\Phi]_{435} = +578°$ in the presence of BINOL-derived chiral aluminum catalyst **76** (Scheme 21.14) [142].

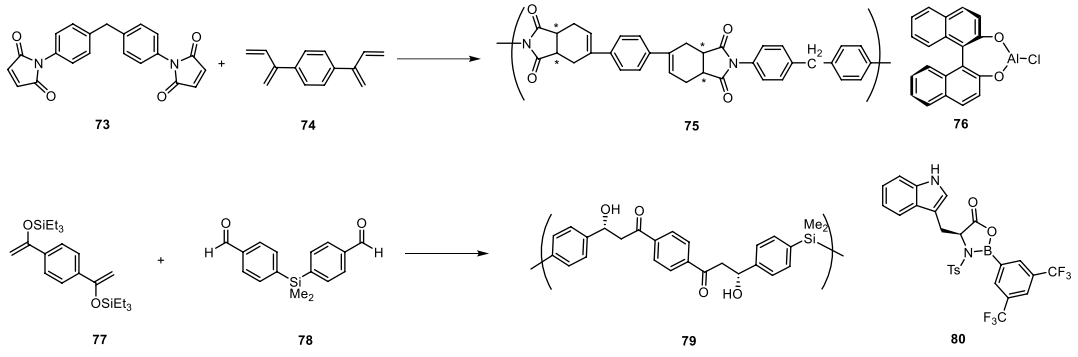

Scheme 21.14. Asymmetric condensation polymerization. Source: [142]/Royal Society of Chemistry.

In 2000, Itsuno et al. described the asymmetric allylation polymerization based on Sakurai–Hosomi allylation using a chiral (acyloxy)borane catalyst [143]. Dialdehyde **77** and bis(allylsilane) **78** showed excellent reactivity toward asymmetric polymerization to give polymer **79** in the presence of chiral oxazaborolidinone **80**. The resulting copolymer with a high molecular weight (48 200) exhibited a high molar optical rotation of $[\Phi]_{405}$ +1670° with approximately 95% ee in the main chain.

21.2.4.2. Oxidative-Coupling Polymerization The asymmetric oxidative-coupling polymerization of 2,3-dihudroxynaphthalenes (**81**) (Scheme 21.15) in the presence of CuCl/(*R*)-bisoxazoline (**82**) under O_2 afforded optically active poly(2,3-acetoxy-1,4-naphthalene) (**83**) with an enantioselectivity of approximately 40% ee [144]. Later, higher optical rotations of $[\alpha]_{405}$ –147° [145] and –223° [146] were achieved using disodium D-(–)-tartrate and vanadyl sulfate ($VOSO_4$) or $VO(stearate)_2$, respectively. It was estimated that the enantioselectivity of the resultant polymers was approximately 80%. SalenCo(II) complex **84** could also be used to facilitate the asymmetric oxidative coupling polymerization of dihydroxynaphthalene derivatives, producing a methanol-insoluble polymer with a specific rotation of $[\alpha]_D$ = +165° [147]. Additionally, the asymmetric oxidative-coupling polymerization of 2,2-binaphthyl derivatives was also investigated, which provided a variety of optically active polymers [148–151].

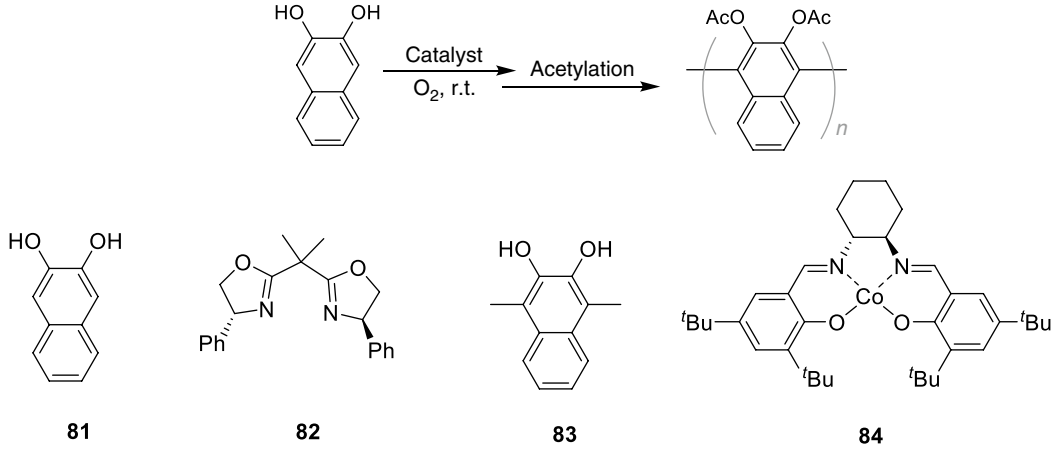

Scheme 21.15. Asymmetric oxidative-coupling polymerization of 2,3-dihudroxynaphthalenes.

21.3. HELIX-SENSE-SELECTIVE POLYMERIZATIONS

Research regarding chiral helical polymers has become a unique area in recent decades, as they possess outstanding properties owing to their specific helical configuration. Typically, chiral helical polymers are fabricated directly from chiral monomers. However, this method is hampered by a limited scope, high cost, and lack of accessibility of monomers. Helix-sense-selective polymerization is a popular approach for preparing chiral, helical polymers from achiral or prochiral monomers using chiral catalysts/initiators or external asymmetric field effects. These processes determine the helical structures based on the chiral substituents covalently bonded to the polymer backbone or noncovalent bonding interactions, the chirality of the chiral initiator or catalyst, or the chiral solvent, according to the "sergeants and soldiers" effect and the "majority rule." This intriguing phenomenon, being known as "chiral amplification" significantly associated with the origin of homochirality of living systems, is a unique process from which a small chiral bias is greatly enhanced via covalent or/and noncovalent interactions.

In terms of the difference in helix-inversion barriers, helix polymers can be classified into two categories: static and dynamic helical polymers. The former possess high helix-inversion barriers and are stable even in solution owing to the sufficiently large steric repulsion between their bulky side groups. Optically

active polymers with a helical structure have been produced from several types of monomers, such as olefins, acetylenes, acrylates, acrylamides, and isocyanides bearing bulky substituents. Previously, several comprehensive reviews have discussed the syntheses, structures, and functions of helical polymers in detail [4–6, 152]. Herein, we briefly describe the research focus on the synthesis of single-handed helical polyolefins and polyacetylenes using these strategies.

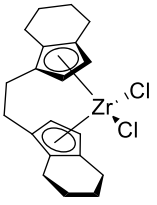

85

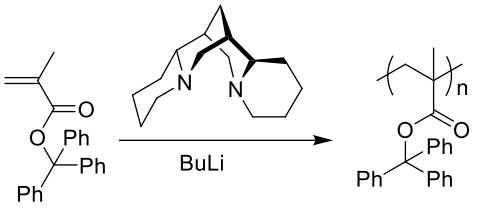

86

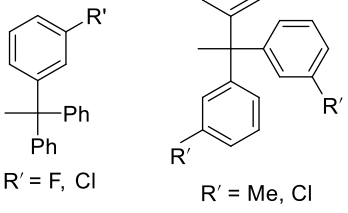

87 **88**

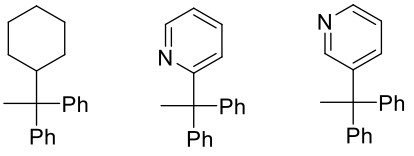

89 **90** **91**

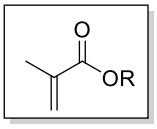

R =

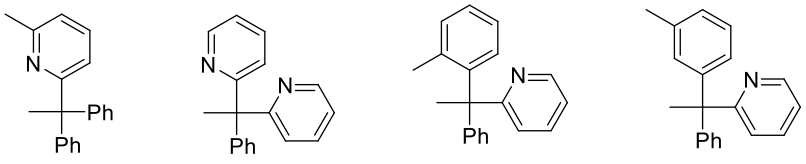

92 **93** **94** **95**

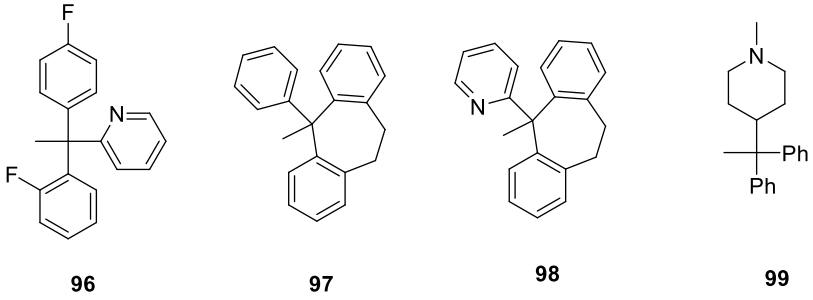

96 **97** **98** **99**

In 1986, Kaminsky reported that isotactic propylene and poly(1-butene), in the presence of zirconocene catalyst **85**, showed large optical rotations in suspension, which were attributed to their preferentially single-handed helical conformation in the solid state. However, it is worth mentioning that such a helical conformation disappears when the polymers are heated or completely dissolved [153].

The first example of an optically active vinyl polymer whose chirality arises not from stereogenic centers but exclusively from a single-handed helical conformation of the main chain was documented by Yuki and co-workers [154]. The anionic polymerization of triphenylmethyl methacrylate **86** using a BuLi/(–)-**Sp** complex obtained optically active, isotactic polymers with a preferential single-handed helix. The steric congestion of the bulky side groups of the resultant isotactic polymers is crucial for bringing about the single-handed helical conformation. If the triphenylmethyl group is removed from the polymer chain, the helical conformation is lost. Except for **86**, monomers **87** [155], **88** [155], **89** [156], **90** [157], **91** [158], **92** [159], **93** [160], **94** [161], **95** [162], **96** [163], **97** [164], **98** [165], and **99** [166] also gave single-handed helices.

The asymmetric polymerization of acrylates and acrylamides is more difficult than that of methacrylates. The helix-sense-selective polymerization of acrylates **100** [167] and **101** [168] mediated by (+)-l-(2-pyrrolidinylmethyl)pyrrolidine ((+)-**PMP**) and (+)-(2*S*,3*S*)-2,3-dimethoxy-l,4-bis(dimethylamino)butane ((+)-**DDB**) produced isotactic-enriched polymers with isotacticities between 61% and 70%, which were both sufficient for forming a single-handed helical conformation. The radical polymerizations of methacrylamides **102** [169], **103** [170], and **104** [171] were carried out in (–)-menthol as a solvent to afford optically active, highly isotactic helical polymers in good yields. Fluorenyllithium/(+)-**DDB** produced insoluble polymers with optical rotations of $[\alpha]_D$ +115° and 5.6° from **105** [172] and **106** [173], respectively, confirming the presence of single-handed helical polymers. The anionic polymerization of **107** [174] also produced optically active polymers. With respect to polymers having no stereogenic centers, their optical activity may arise from the helical chiral conformation of their main chain.

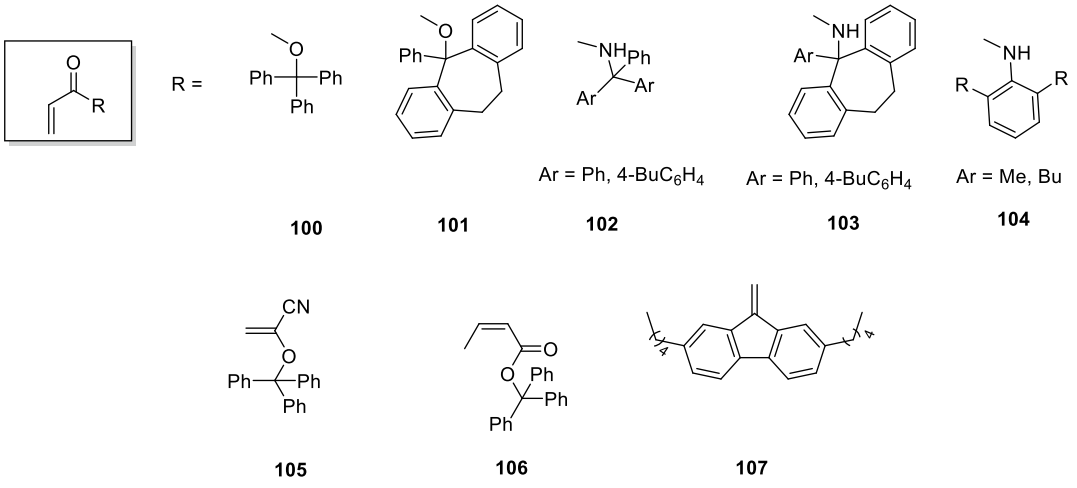

Akagi et al. described the synthesis of the helix-sense-selective polymerization of acetylene using Ti(OBu)/Et_3Al in chiral nematic liquid crystals resulting from chiral dopants, including **108** [175], **109** [176], and **110** [177]. The resultant helical polyacetylene films are hardly soluble and possess either a clockwise or counterclockwise structure, as determined by scanning electron microscope (SEM) analyses. In 2003, Aoki and co-workers described the first example of the helix-sense-selective polymerization of substituted acetylenes with stable chiral helicity in solution without the aid of other chiral substituents or other small molecules [178]. They constructed chiral helical polyacetylenes from an achiral acetylenic monomer using $[Rh(nbd)Cl]_2$ (nbd = 2,5-norbornadiene) as a catalyst and chiral *R*- or *S*-phenylethylamine (PEA) as a cocatalyst. Achiral acetylenic monomers bearing two hydroxymethyl groups and one alkyl group (**111**) underwent the helix-sense-selective polymerization process in this chiral catalytic system to give polyacetylenes with predominantly single-handed, helical structures. Moreover, the addition of copper(I) iodide (CuI) to the catalytic system improved the polymer yield [179].

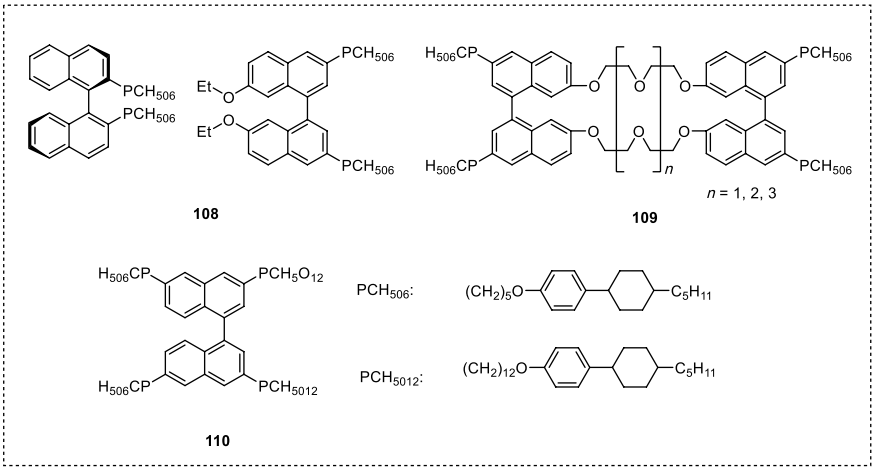

It is worthwhile noting here parenthetically that the self-assembly of small molecules through non-covalent interactions, such as hydrogen bonding, π–π stacking, ion-dipolar, and hydrophobic interactions, can also construct a multitude of structurally well-defined aggregates with supramolecular helicity [180]. For instance, Aida and co-workers described the self-assembly of amphiphilic hexa-*peri*-hexabenzocoronene having two dodecyl chains on one side and two triethylene glycol chains on the other into discrete nanotubes with helical structures [181]. The use of the amphiphilic hexa-*peri*-hexabenzocoronene bearing chiral side groups provided graphitic nanotubes with one-handed helical chirality [182].

21.4. SUMMARY AND OUTLOOK

This book chapter provides an overview of asymmetric polymerizations that create main-chain chirality, including enantiogenic polymerization, enantiomer-selective polymerization, and helix-sense-selective polymerization. Rather than providing a comprehensive overview of all the literature that has appeared over the decades, only typical examples of each class of asymmetric polymerization have been discussed. These examples emphasized the most recent developments in highly enantioselective epoxide polymerizations and copolymerizations that produce polyethers, polycarbonates, and polyesters. Despite being studied for several decades, asymmetric polymerization remains a fledgling field. A crucial problem in this field is the difficulty in determining the optical purity of the asymmetric centers of stereoregular polymers. Only limited types of polymers, such as 1,3-diene polymers, polycarbonates, and polyesters, can be directly determined through chiral gas chromatography or HPLC methods by their degradation into small molecules or derivatives. Another problem is the lack of chiral-privileged catalysts available for creating macromolecules with well-defined sequences and stereochemistry at each repeat unit.

Significant progress has been achieved in helix-sense-selective polymerization in recent decades, including the synthesis of various static and dynamic helical polymers. Their structures and functional applications have also been explored with respect to their use in chiral recognition, asymmetric catalysis, enantiomer separation, and chiral sensing. However, there are significant gaps in the knowledge of the structures and functions of artificial and natural helical polymers. The latter of these seem to gain their extraordinary functions from their hierarchically ordered assembly.

In comparison with helix-sense-selective polymerization, enantiogenic polymerization and enantiomer-selective polymerization have received relatively little attention, which is partially a consequence of the difficulty in creating macromolecules with well-defined sequences and chirality at each repeat unit. The discovery of bimetallic catalysts with multiple chirality for enantioselective epoxide polymerization and copolymerization is very significant. In recent years, many privileged chiral ligands have been developed for asymmetric catalysis in which various, chiral, small organic compounds are

synthesized [183]. Additionally, some of them are expected to be highly active and enantioselective in asymmetric polymerization.

Generally, the relative stereochemistry (the spatial arrangement of atoms or groups in a polymeric unit) of adjacent locations in the polymeric chains significantly affects the thermal or mechanical properties of a polymer. Therefore, precise control of both chirality and sequence has enabled the functional behavior of polymeric materials to be manipulated. The incorporation of stereochemically dynamic, switchable moieties can enable the switching between isomers with different crystallization properties [184], thus allowing control of the properties of the bulk material by external stimuli.

REFERENCES

1. Wulff, G. *Angew. Chem. Int. Ed.* **1989**, *28*, 21–37.
2. Okamoto, Y.; Yashima, E. *Prog. Polym. Sci.* **1990**, *15*, 263–298.
3. Okamoto, Y.; Nakano, T. *Chem. Rev.* **1994**, *94*, 349–372.
4. Yashima, E.; Maeda, K.; Lida, H.; Furusho, Y.; Nagai, K. *Chem. Rev.* **2009**, *109*, 6102–6211.
5. Liu, M.; Zhang, L.; Wang, T. *Chem. Rev.* **2015**, *115*, 7304–97.
6. Yashima, E.; Ousaka, N.; Taura, D.; Shimomura, K.; Ikai, T.; Maeda, K. *Chem. Rev.* **2016**, *116*, 13752–13990.
7. Pino, P.; Ciardelli, F.; Lorenzi, G. P.; Natta, G. *J. Am. Chem. Soc.* **1962**, *84*, 1487–1488.
8. Pino, P.; Ciardelli, F.; Lorenzi, G. P. *J. Am. Chem. Soc.* **1963**, *85*, 3888–3890.
9. Chiellini, E. *Macromolecules* **1970**, *3*, 527–533.
10. Higashimura, T.; Hirokawa, Y. *J. Polym. Sci., Part A: Polym. Chem.* **1977**, *15*, 1137–1143.
11. Okamoto, Y.; Ohta, K.; Yuki, H. *Chem. Let.* **1977**, *6*, 617–620.
12. Okamoto, Y.; Urakawa, K.; Ohta, K.; Yuki, H. *Macromolecules* **1978**, *11*, 719–723.
13. Okamoto, Y.; Ohta, K.; Yuki, H. *Macromolecules* **1978**, *11*, 724–727.
14. Okamoto, Y.; Gamaike, H.; Yuki, H., *Makromol. Chem.* **1981**, *182*, 2737–2746.
15. Okamoto, Y.; Urakawa, K.; Yuki, H. *J. Polym. Sci., Part A: Polym. Chem.* **1981**, *19*, 1385–1395.
16. Okamoto, Y.; Yashima, E.; Hatada, K.; Yuki, H.; Kageyama, H.; Miki, K.; Kasai, N. *J. Polym. Sci., Part A: Polym. Chem.* **1984**, *22*, 1831–1837.
17. Nakano, T.; Hidaka, Y.; Okamoto, Y. *Polym. J.* **1998**, *30*, 596–600.
18. Natta, G.; Farina, M.; Donati, M. *Makromol. Chem.* **1961**, *43*, 251–254.
19. Natta, G.; Porri, L.; Valenti, S. *Makromol. Chem.* **1963**, *67*, 225–228.
20. Farina, M.; Audisio, G.; Natta, G. *J. Am. Chem. Soc.* **1967**, *89*, 5071–5071.
21. Audisio, G.; Silvan, A. *J. Chem. Soc., Chem. Commun.* **1976**, 481–482.
22. Miyata, M.; Kitahara, Y.; Takemoto, K. *Polym. J.* **1981**, *13*, 111–113.
23. Miyata, M.; Kitahara, Y.; Takemoto, K. *Polym. Bull.* **1980**, *2*, 671–674.
24. Mijata, M.; Kitahara, Y.; Takemoto, K., *Makromol. Chem.* **1983**, *184*, 1771–1779.
25. Coates, G. W.; Waymouth, R. M. *J. Am. Chem. Soc.* **1991**, *113*, 6270–6271.
26. Coates, G. W.; Waymouth, R. M. *J. Am. Chem. Soc.* **1993**, *115*, 91–98.
27. Habaue, S.; Sakamoto, H.; Baraki, H.; Okamoto, Y. *Macromol. Rapid Commun.* **1997**, *18*, 707–713.
28. Habaue, S.; Sakamoto, H.; Okamoto, Y. *Polym. J.* **1997**, *29*, 384–386.
29. Haba, O.; Kakuchi, T.; Yokota, K. *Macromolecules* **1993**, *26*, 1782–1783.
30. Seno, M.; Kawamura, Y.; Sato, T. *Macromolecules* **1997**, *30*, 6417–6421.
31. Pino, P. Polymers. **1966**, *4*, 393–456.
32. Natta, G.; Farina, M.; Peraldo, M.; Bressan, G. *Makromol. Chem.* **1961**, *43*, 68–75.
33. Farina, M.; Bressan, G. *Makromol. Chem.* **1963**, *61*, 79–89.
34. Natta, G.; Farina, M. *Tetrahedron Lett.* **1963**, 703–709.
35. Takeda, Y.; Hayakawa, Y.; Fueno, T.; Furukawa, J. *Makromol. Chem.* **1965**, *83*, 234–243.
36. Hayakawa, Y.; Fueno, T.; Furukawa, J. *J. Polym. Sci., Part A: Polym. Chem.* **1967**, *5*, 2099–2109.
37. Cubbon, R. C. P. *Polymer* **1965**, *6*, 419–426.
38. Okamoto, Y.; Nakano, T.; Kobayashi, H.; Hatada, K. *Polym. Bull.* **1991**, *25*, 5–8.
39. Oishi, T.; Yamasaki, H.; Fujimoto, M. *Polym. J.* **1991**, *23*, 795–804.
40. Liu, W.; Chen, C.; Chen, Y.; Xi, F. *Polym. Bull.* **1997**, *38*, 509–514.
41. Onimura, K.; Tsutsumi, H.; Oishi, T. *Macromolecules* **1998**, *31*, 5971–5976.
42. Onimura, K.; Tsutsumi, H.; Oishi, T. *Polym. Bull.* **1997**, *39*, 437–444.
43. Oishi, T.; Onimura, K.; Isobe, Y.; Tsutsumi, H. *Chem. Lett.* **1999**, *28*, 673–674.
44. Oishi, T.; Onimura, K.; Isobe, Y.; Yanagihara, H. *J. Polym. Sci., Part A: Polym. Chem.* **2000**, *38*, 310–320.

45. Isobe, Y.; Onimura, K.; Tsutsumi, H.; Oishi, T. *J. Polym. Sci., Part A: Polym. Chem.* **2001**, *39*, 3556–3565.
46. Oishi, T.; Isobe, Y.; Onimura, K.; Tsutsumi, H. *Polym. J.* **2003**, *35*, 245–254.
47. Onimura, K.; Tsutsumi, H.; Oishi, T. *Chem. Lett.***1998**, *27*, 791–792.
48. Isobe, Y.; Onimura, K.; Tsutsumi, H.; Oishi, T. *Macromolecules* **2001**, *34*, 7617–7623.
49. Oishi, T.; Onimura, K.; Tanaka, K.; Tsutsumi, H. *J. Polym. Sci., Part A: Polym. Chem.* **1999**, *37*, 473–482.
50. Nakano, T.; Tamada, D.; Miyazaki, J.-I.; Kakiuchi, K. *Macromolecules* **2000**, *33*, 1489–1491.
51. Nakano, T.; Yade, T.; Okamoto, Y. *Macromolecules* **2003**, *36*, 3498–3504.
52. Lee, Y.-K.; Kitamura, S.; Onimura, K.; Tsutsumi, H.; Oishi, T. *J. Polym. Sci., Part A: Polym. Chem.* **2004**, *42*, 6157–6162.
53. Batistini, A.; Consiglio, G. *Organometallics* **1992**, *11*, 1766–1769.
54. Bronco, S.; Consiglio, G.; Hutter, R.; Batistini, A.; Suter, U. W. *Macromolecules* **1994**, *27*, 4436–4440.
55. Sperrle, M.; Consiglio, G. *J. Am. Chem. Soc.* **1995**, *117*, 12130–12136.
56. Bronco, S.; Consiglio, G. *Macromol. Chem. Phys.* **1996**, *197*, 355–365.
57. Kacker, S.; Jiang, Z.; Sen, A. *Macromolecules* **1996**, *29*, 5852–5858.
58. Gambs, C.; Chaloupka, S.; Consiglio, G.; Togni, A. *Angew. Chem. Int. Ed.* **2000**, *39*, 2486–2488.
59. Nozaki, K.; Sato, N.; Takaya, H. *J. Am. Chem. Soc.* **1995**, *117*, 9911–9912.
60. Brookhart, M.; Wagner, M. I.; Balavoine, G. G. A.; Haddou, H. A. *J. Am. Chem. Soc.* **1994**, *116*, 3641–3642.
61. Brookhart, M.; Wagner, M. I. *J. Am. Chem. Soc.* **1996**, *118*, 7219–7220.
62. Childers, M. I.; Longo, J. M.; Van Zee, N. J.; LaPointe, A. M.; Coates, G. W. *Chem. Rev.* **2014**, *114*, 8129–8152.
63. Pruitt, M. E.; Baggett, J. M. (to Dow Chemical Co.), U.S. Patent 2,706,181, filed June 6, 1952, issued April 12, 1955.
64. Takeda, N.; Inoue, S., *Makromol. Chem.* **1978**, *179*, 1377–1381.
65. Aida, T.; Inoue, S. *Macromolecules* **1981**, *14*, 1166–1169.
66. Kasperczyk, J.; Dworak, A.; Jedliński, Z., *Makromol. Chem., Rapid Commun.* **1981**, *2*, 663–666.
67. Aida, T.; Inoue, S. *Macromolecules* **1981**, *14*, 1162–1166.
68. Haubenstock, H.; Panchalingam, V.; Odian, G., *Makromol. Chem.* **1987**, *188*, 2789–2799.
69. Emig, N.; Nguyen, H.; Krautscheid, H.; Réau, R.; Cazaux, J.-B.; Bertrand, G. *Organometallics* **1998**, *17*, 3599–3608.
70. Furukawa, J.; Tsuruta, T.; Sakata, R.; Saegusa, T.; Kawasaki, A., *Makromol. Chem.* **1959**, *32*, 90–94.
71. Rabagliati, F. M.; Lopez-Carrasquero, F. *Eur. Polym. J.* **1985**, *21*, 1061–1065.
72. Rabagliati, F. M.; López, F., *Makromol. Chem., Rap. Commun.* **1985**, *6*, 141–144.
73. Huang, Y.; Gao, L.; Ding, M. *J. Polym. Sci., Part A: Polym. Chem.* **1999**, *37*, 4640–4645.
74. Oguni, N.; Fujita, T.; Tani, H. *Macromolecules* **1973**, *6*, 325–330.
75. Hasebe, Y.; Tsuruta, T., *Makromol. Chem.* **1988**, *189*, 1915–1926.
76. Peretti, K. L.; Ajiro, H.; Cohen, C. T.; Lobkovsky, E. B.; Coates, G. W. *J. Am. Chem. Soc.* **2005**, *127*, 11566–11567.
77. Hirahata, W.; Thomas, R. M.; Lobkovsky, E. B.; Coates, G. W. *J. Am. Chem. Soc.* **2008**, *130*, 17658–9.
78. Ajiro, H.; Peretti, K. L.; Lobkovsky, E. B.; Coates, G. W. *Dalton Trans.* **2009**, 8828–8830.
79. Colclough, R. O.; Gee, G.; Higginson, W. C. E.; Jackson, J. B.; Litt, M. *J. Polym. Sci.* **1959**, *34*, 171–179.
80. Osgan, M.; Price, C. C. *J. Polym. Sci.* **1959**, *34*, 153–156.
81. Krylov, O. V.; Livshits, V. S. *Tetrahedron Lett* **1965**, *6*, 1181–1185.
82. Tsuruta, T.; Inoue, S.; Yokota, Y., *Makromol. Chem.* **1967**, *103*, 164–174.
83. Price, C. C.; Carmelite, D. D. *J. Am. Chem. Soc.* **1966**, *88*, 4039–4044.
84. Price, C. C.; Fukutani, H. *J. Polym. Sci., Part A: Polym. Chem.* **1968**, *6*, 2653–2662.
85. Cohen, C. T.; Coates, G. W. *J. Polym. Sci., Part A: Polym. Chem.* **2006**, *44*, 5182–5191.
86. Ahmed, S. M.; Poater, A.; Childers, M. I.; Widger, P. C.; LaPointe, A. M.; Lobkovsky, E. B.; Coates, G. W.; Cavallo, L. *J. Am. Chem. Soc.* **2013**, *135*, 18901–18911.
87. Childers, M. I.; Vitek, A. K.; Morris, L. S.; Widger, P. C. B. *J. Am. Chem. Soc.* **2017**, *139*, 11048–11054.
88. Morris, L. S.; Childers, M. I.; Coates, G. W. *Angew. Chem. Int. Ed.* **2018**, *57*, 5731–5734.
89. Hasebe, Y.; Tsuruta, T., *Makromol. Chem.* **1987**, *188*, 1403–1414.
90. Sepulchre, M.; Kassamaly, A.; Spassky, N. *Makromol. Chem., Macromol. Symp.* **1991**, *42-43*, 489–500.
91. Inoue, S.; Koinuma, H.; Tsuruta, T. *J. Polym. Sci. Part B: Polym Lett.* **1969**, *7*, 287–292.
92. Inoue, S.; Koinuma, H.; Tsuruta, T., *Makromol. Chem.* **1969**, *130*, 210–220.
93. Tokunaga, M.; Larrow, J. F.; Kakiuchi, F.; Jacobsen, E. N. *Science* **1997**, *277*, 936–938.
94. Lu, X. B.; Wang, Y. *Angew. Chem. Int. Ed.* **2004**, *43*, 3574–3577.
95. Lu, X. B.; Shi, L.; Wang, Y. M.; Zhang, R.; Zhang, Y. J.; Peng, X. J.; Zhang, Z. C.; Li, B. *J. Am. Chem. Soc.* **2006**, *128*, 1664–1674.
96. Paddock, R. L.; Nguyen, S. T. *Macromolecules* **2005**, *38*, 6251–6253.
97. Ren, W.-M.; Liu, Y.; Wu, G.-P.; Liu, J.; Lu, X.-B. *J. Polym. Sci., Part A: Polym. Chem.* **2011**, *49*, 4894–4901.
98. Nakano, K.; Hashimoto, S.; Nakamura, M.; Kamada, T.; Nozaki, K. *Angew. Chem. Int. Ed.* **2011**, *50*, 4868–4871.
99. Wu, G.-P.; Wei, S.-H.; Ren, W.-M.; Lu, X.-B.; Li, B.; Zu, Y.-P.; Darensbourg, D. J. *Energ. Environ. Sci.* **2011**, *4*, 5084–5092.
100. Wu, G.-P.; Xu, P.-X.; Lu, X.-B.; Zu, Y.-P.; Wei, S.-H.; Ren, W.-M.; Darensbourg, D. J. *Macromolecules* **2013**, *46*, 2128–2133.
101. Nozaki, K.; Nakano, K.; Hiyama, T. *J. Am. Chem. Soc.* **1999**, *121*, 11008–11009.

102. Cheng, M.; Darling, N. A.; Lobkovsky, E. B.; Coates, G. W. *Chem. Commun.* **2000**, 2007–2008.
103. Liu, Y.; Ren, W.-M.; Liu, C.; Fu, S.; Wang, M.; He, K.-K.; Li, R.-R.; Zhang, R.; Lu, X.-B. *Macromolecules* **2014**, *47*, 7775–7788.
104. Liu, Y.; Ren, W. M.; Liu, J.; Lu, X. B. *Angew. Chem. Int. Ed.* **2013**, *52*, 11594–11598.
105. Liu, Y.; Wang, M.; Ren, W.-M.; He, K.-K.; Xu, Y.-C.; Liu, J.; Lu, X.-B. *Macromolecules* **2014**, *47*, 1269–1276.
106. Liu, Y.; Ren, W. M.; Wang, M.; Liu, C.; Lu, X. B. *Angew. Chem. Int. Ed.* **2015**, *54*, 2241–2244.
107. Liu, Y.; Ren, W. M.; He, K. K.; Lu, X. B. *Nat. Commun.* **2014**, *5*, 5687.
108. Ellis, W. C.; Jung, Y.; Mulzer, M.; Di Girolamo, R.; Lobkovsky, E. B.; Coates, G. W. *Chem. Sci.* **2014**, *5*, 4004–4011.
109. Hua, Y. Z.; Lu, L. J.; Huang, P. J.; Wei, D. H.; Tang, M. S.; Wang, M. C.; Chang, J. B. *Chem. Eur. J.* **2014**, 20, 12394–12398.
110. Yue, T.-J.; Ren, W. M.; Chen, L.; Gu, G.-G.; Liu, Y.; Lu, X. B. *Angew. Chem. Int. Ed.* **2018**, *57*, 12670–12674.
111. Stanford, M. J.; Dove, A. P. *Chem. Soc. Rev.* **2010**, *39*, 486–494.
112. Spassky, N.; Wisniewski, M.; Pluta, C.; Le Borgne, A. *Macromol. Chem. Phy.* **1996**, *197*, 2627–2637.
113. Zhong, Z.; Dijkstra, P. J.; Feijen, J. *Angew. Chem. Int. Ed.* **2002**, *43*, 4510–4513.
114. Zhong, Z.; Dijkstra, P. J.; Feijen, J. *J Am Chem Soc* **2003**, *125*, 11291–11298.
115. Du, H.; Velders, A. H.; Dijkstra, P. J.; Sun, J.; Zhong, Z.; Chen, X.; Feijen, J. *Chemistry* **2009**, *15*, 9836–9845.
116. Press, K.; Goldberg, I.; Kol, M. *Angew. Chem. Int. Ed.* **2015**, *54*, 14858–14861.
117. Wang, H.; Ma, H. *Chem. Commun.* **2013**, *49*, 8686–8688.
118. Hu, J.; Kan, C.; Wang, H.; Ma, H. *Macromolecules* **2018**, *51*, 5304–5312.
119. Aluthge, D. C.; Patrick, B. O.; Mehrkhodavandi, P. *Chem. Commun.* **2013**, *49*, 4295–4297.
120. Miyake, G. M.; Chen, E. Y. X. *Macromolecules* **2011**, *44*, 4116–4124.
121. Sanchez-Sanchez, A.; Rivilla, I.; Agirre, M.; Basterretxea, A.; Etxeberria, A.; Veloso, A.; Sardon, H.; Mecerreyes, D.; Cossio, F. P. *J. Am. Chem. Soc.* **2017**, *139*, 4805–4814.
122. Tang, X.; Chen, E. Y. *Nat. Commun.* **2018**, *9*, 2345.
123. Tang, X.; Westlie, A. H.; Watson, E. M.; Chen, E. Y. *Science* **2019**, *366*, 754–758.
124. Al-Azemi, T. F.; Kondaveti, L.; Bisht, K. S. *Macromolecules* **2002**, *35*, 3380–3386.
125. Peeters, J. W.; van Leeuwen, O.; Palmans, A. R. A.; Meijer, E. W. *Macromolecules* **2005**, *38*, 5587–5592.
126. van As, B. A. C.; van Buijtenen, J.; Heise, A.; Broxterman, Q. B.; Verzijl, G. K.; Palmans, A. R.; Meijer, E. W. *J. Am. Chem. Soc.* **2005**, *127*, 9964–9965.
127. Breteler, M. R. T.; Zhong, Z.; Dijkstra, P. J.; Palmans, A. R. A.; Peeters, J.; Feijen, J. *J. Polym. Sci., Part A: Polym. Chem.* **2007**, *45*, 429–436.
128. Spassky, N.; Leborgne, A.; Reix, M.; Prud'homme, R. E.; Bigdeli, E.; Lenz, R. W. *Macromolecules* **1978**, *11*, 716–719.
129. Leborgne, A.; Spassky, N.; Sigwalt, P. *Polym. Bull.* **1979**, *1*, 825–832.
130. Leborgne, A.; Grenier, D.; Prud'homme, R. E.; Spassky, N. *Eur. Polym. J.* **1981**, *17*, 1103–1106.
131. Xie, W.; Li, J.; Chen, D.; Wang, P. G. *Macromolecules* **1997**, *30*, 6997–6998.
132. Svirkin, Y. Y.; Xu, J.; Gross, R. A.; Kaplan, D. L.; Swift, G. *Macromolecules* **1996**, *29*, 4591–4597.
133. Longo, J. M.; Sanford, M. J.; Coates, G. W. *Chem. Rev.* **2016**, *116*, 15167–15197.
134. Paul, S.; Zhu, Y.; Romain, C.; Brooks, R.; Saini, P. K.; Williams, C. K. *Chem. Commun.* **2015**, *51*, 6459–6479.
135. Li, J.; Ren, B.-H.; Chen, S.-Y.; He, G.-H.; Liu, Y.; Ren, W.-M.; Zhou, H.; Lu, X.-B. *ACS Catal.* **2019**, *9*, 1915–1922.
136. Li, J.; Liu, Y.; Ren, W. M.; Lu, X. B. *J. Am. Chem. Soc.* **2016**, *138*, 11493–11496.
137. Li, J.; Ren, B. H.; Wan, Z. Q.; Chen, S. Y.; Liu, Y.; Ren, W. M.; Lu, X. B. *J. Am. Chem. Soc.* **2019**, *141*, 8937–8942.
138. Wan, Z. Q.; Longo, J. M.; Liang, L. X.; Chen, H. Y.; Hou, G. J.; Yang, S.; Zhang, W. P.; Coates, G. W.; Lu, X. B. *J. Am. Chem. Soc.* **2019**, *141*, 14780–14787.
139. Li, J.; Liu, Y.; Ren, W. M.; Lu, X. B. *Proc. Natl. Acad. Sci. USA.* **2020**, *117*, 15429–15436.
140. He, G.-H.; Ren, B. H.; Chen, S. Y.; Liu, Y.; Lu, X. B. *Angew. Chem. Int. Ed.* https://doi.org/10.1002/anie.202011259.
141. Itsuno, S. *Pro. Polym. Sci.* **2005**, *30*, 540–558.
142. Itsuno, S.; Shoichi, T.; Koichi, l. *Chem. Commun.* **1997**, 933–934.
143. Kumagai, T.; Itsuno, S. *Macromolecules* **2000**, *33*, 4995–4996.
144. Habaue, S.; Seko, T.; Okamoto, Y. *Macromolecules* **2003**, *36*, 2604–2608.
145. Habaue, S.; Murakami, S.; Higashimura, H. *J. Polym. Sci. Part A: Polym. Chem.* **2005**, *43*, 5872–5878.
146. Murakami, S.; Habaue, S.; Higashimura, H. *Polymer* **2007**, *48*, 6565–6570.
147. Habaue, S.; Aoyagi, H.; Murakami, S.; Higashimura, H. *Polym. Bull.* **2007**, *59*, 303–310.
148. Temma, T.; Takahashi, Y.; Yoshii, Y.; Habaue, S. *Polym. J.* **2007**, *39*, 524–530.
149. Temma, T.; Habaue, S. *J. Polym. Sci. Part A: Polym. Chem.* **2005**, *43*, 6287–6294.
150. Temma, T.; Hatano, B.; Habaue, S. *Polymer* **2006**, *47*, 1845–1851.
151. Xie, X.; Phuan, P. W.; Kozlowski, M. C. *Angew. Chem. Int. Ed.* **2003**, *42*, 2168–2170.
152. Nakano, T.; Okamoto, Y. *Chem. Rev*. **2001**, *101*, 4013–4038.
153. Kaminsky, W.; Külper, K.; Niedoba, S. *Makromol. Chem., Macromol. Symp.* **1986**, *3*, 377–387.
154. Okamoto, Y.; Suzuki, K.; Ohta, K.; Hatada, K.; Yuki, H. *J. Am. Chem. Soc.* **1979**, *101*, 4763–4765.
155. Okamoto, Y.; Yashima, E.; Ishikura, M.; Hatada, K. *Polym. J.* **1987**, *19*, 1183–1190.

156. Okamoto, Y.; Nakano, T.; Fukuoka, T.; Hatada, K. *Polym. Bull.* **1991**, *26*, 259–264.
157. Okamoto, Y.; Mohri, H.; Hatada, K. *Chem. Lett.* **1988**, *17*, 1879–1882.
158. Nakano, T.; Taniguchi, K.; Okamoto, Y. *Polym. J.* **1997**, *29*, 540–544.
159. Mohri, H.; Okamoto, Y.; Hatada, K. *Polym. J.* **1989**, *21*, 719–724.
160. Ren, C.; Chen, C.; Xi, F.; Nakano, T.; Okamoto, Y. J. *Polym. Sci. Part A*: *Polym. Chem.* **1993**, *31*, 2721–2728.
161. Yashima, E.; Okamoto, Y.; Hatada, K. *Macromolecules* **1988**, *21*, 854–855.
162. Okamoto, Y.; Nakano, T.; Asakura, T.; Mohri, H.; Hatada, K. *J. Polym. Sci. Part A: Polym. Chem.* **1991**, *29*, 287–289.
163. Wu, J.; Nakano T.; Okamato Y. *J. Polym. Sci. Part A: Polym. Chem.* **1998**, *36*, 2013–2019.
164. Nakano, T.; Matsuda, A.; Mori, M.; Okamoto, Y. *Polym. J.* **1996**, *28*, 330–336.
165. Nakano, T.; Satoh, Y.; Okamoto, Y. *Polym. J.* **1998**, *30*, 635–640.
166. Nakano, T.; Ueda, K.; Okamoto, Y. *J. Polym. Sci. Part A: Polym. Chem.* **2001**, *39*, 1610–1614.
167. Habaue, S.; Tanaka, T.; Okamoto, Y. *Macromolecules* **1995**, *28*, 5973–5974.
168. Tanaka, T.; Habaue, S.; Okamoto, Y. *Polym. J.* **1995**, *27*, 1202–1207.
169. Hoshikawa, N.; Hotta, Y.; Okamoto, Y. *J. Am. Chem. Soc.* **2003**, *125*, 12380–12381.
170. Amano, Y.; Okamoto, Y. *Polym. J.* **2005**, *37*, 629–632.
171. Azam, A. K. M. F.; Kamigaito, M.; Okamoto, Y. *J. Polym. Sci. Part A: Polym. Chem.* **2007**, *45*, 1304–1315.
172. Wulff, G.; Wu, Y. *Makromol. Chem.* **1990**, *191*, 2993–3003.
173. Ute, K.; Asada, T.; Nabeshima, Y.; Hatada, K. *Macromolecules* **1993**, *26*, 7086–7088.
174. Nakano, T.; Nakagawa, O.; Tsuji, M.; Tanikawa, M.; Yade, T.; Okamoto, Y. *Chem. Commun.* **2004**, 144–145.
175. Akagi, K.; Piao, G.; Kaneko, S.; Sakamaki, K.; Shirakawa, H.; Kyotani, M. *Science* **1998**, *282*, 1683–1686.
176. Akagi, K.; Guo, S.; Mori, T.; Goh, M.; Piao, G.; Kyotani, M. *J. Am. Chem. Soc.* **2005**, *127*, 14647–14654.
177. Goh, M.; Kyotani, M.; Akagi, K. *J. Am. Chem. Soc.* **2007**, *129*, 8519–8527.
178. Aoki, T.; Kaneko, T.; Maruyama, N.; Sumi, A.; Takahashi, M.; Sato, T.; Teraguchi, M. *J. Am. Chem. Soc.* **2003**, *125*, 6346–6347.
179. Katagiri, H.; Kaneko, T.; Teraguchi, M.; Aoki, T. *Chem. Lett.* **2008**, *37*, 390–391.
180. Pijper, D.; Feringa, B. L. *Soft Matter*, **2008**, *4*, 1349–1372.
181. Hill, J. P.; Jin, W.; Kosaka, A.; Fukushima, T.; Ichihara, H.; Shimomura, T.; Ito, K.; Hashizume, T.; Ishii, N.; Aida, T. *Science*, **2004**, *304*, 1481–1483.
182. Jin, W.; Fukushima, T.; Niki, M.; Kosaka, A.; Ishii, N.; Aida, T. *Proc. Natl. Acad. Sci. USA.* **2005**, *102*, 10801–10806.
183. *Privileged chiral ligands and catalysis*. Ed. Qi-Lin Zhou, WILEY-VCH Verlag GmbH & Co. KGaA, **2011**.
184. Wan, Z.-Q.; Ren, W.-M.; Yang, S.; Li, M.-R.; Gu, G.-G.; Lu, X.-B. *Angew. Chem. Int. Ed.*, **2019**, *58*, 17636–17640.

PART IX

ASYMMETRIC CATALYSIS IN CONTINUOUS-FLOW SYSTEM

22

CONTINUOUS-FLOW CHEMISTRY IN CATALYTIC ASYMMETRIC SYNTHESIS

Haruro Ishitani[2], Yuki Saito[1], and Shū Kobayashi[1,2]
[1]*Department of Chemistry, School of Science, The University of Tokyo, Tokyo, Japan*
[2]*Green & Sustainable Chemistry Social Cooperation Laboratory, Graduate School of Science, The University of Tokyo, Tokyo, Japan*

22.1. INTRODUCTION

Chemical reactions are generally conducted in a flask. This approach is familiar to us because fundamental chemical experimental education typically begins with such experiences in chemistry class. The reaction in a flask is termed a batch process in a more sophisticated chemical process such as chemical investigations in the laboratory. However, in more practical and advanced chemical processes, we notice that the process can be divided into two classes: batch process and flow process [1–9]. Flow manufacturing is an important technique that is used as a framework for the production of automobiles, electronic devices, steels, and foods. In chemical industries, the number of continuous-flow methods has gradually begun to increase, especially in fine chemical industries including the pharmaceutical industry [10]. Continuous-flow synthesis offers significant advantages over conventional batch synthesis in terms of efficiency, safety, and environmental compatibility. However, the production of fine chemicals such as active pharmaceutical ingredients (APIs), agrochemicals, electronic chemicals, and fragrances has mostly been carried out by repeating batch methods. In general, synthesis by flow methods seems to be more difficult than that by batch methods. It has generally been considered that synthesis by flow methods is primarily applicable for chemical products accessed through simple processes that are common in the petroleum industry, because controlling reactions to achieve a selective synthesis of the target molecules requires precise handling techniques and knowledge. Especially for API production, it has been believed that controlling stereocenters in molecules via bond-forming reactions is best achieved through the application of established reaction protocols. Since global requirements for innovation in human society represented by the Sustainable Development Goals of the United Nations, many fine chemical industries have turned their attention to continuous manufacturing [11]. To attain a more dominant role for continuous manufacturing in fine chemical industries including pharmaceuticals and agrochemicals, further development of catalytic stereoselective synthesis under continuous-flow conditions is necessary.

The idea of flow reactions for fine organic synthesis appeared in the early 1990s, when certain classes of polymer-supported reagents were developed [12–14]. Since then, after gaining considerable attention in continuous-flow chemistry during the past decades, many useful review papers have been published on this topic [1–9]. Therefore, this chapter summarizes reports on catalytic enantioselective flow reactions published since 2016, and the aim of this review is to provide an overview of the state-of-the-art in enantioselective flow catalysis.

Catalytic Asymmetric Synthesis, Fourth Edition. Edited by Takahiko Akiyama and Iwao Ojima.

22.2. OVERVIEW OF CATALYTIC PROCESSES IN FLOW ORGANIC SYNTHESIS

Continuous-flow systems in synthetic organic chemistry can be classified into four categories based on the styles of reactions carried out under flow conditions (Figure 22.1) [15].

Since this chapter focuses primarily on catalytic enantioselective systems and the first two types are both non-catalytic processes, Type III and IV flow reactions will be discussed in the following. Modern asymmetric synthesis of chiral compounds is heavily reliant upon enantioselective catalysis to improve efficiency. In this context, continuous-flow catalytic enantioselective reactions can be conducted by feeding homogeneous chiral catalysts with substrates. These processes are categorized as Type III continuous-flow reactions, and they can offer a straightforward approach for achieving catalytic enantioselective processes under flow. The practical benefits of using homogeneous catalysts for this process and the sustainability of product quality during the overall process are great advantages; however, quenching of catalytic reactions and processes to remove catalyst residues is unavoidable and inevitably requires interruption of the multistep flow reactions, thereby preventing the process from proceeding seamlessly. Moreover, advantages offered by applications of homogeneous catalytic reactions in batch systems may be limited in flow systems because the reaction rates of catalytic reactions are usually slow.

By contrast, the use of heterogeneous catalysts with column-type fixed-bed reactors (catalyst packed-bed reactors) can be categorized as Type IV flow reactions. Compared with the corresponding Type III catalytic flow reaction, Type IV system offers clear benefits. Advantages include the elimination of catalyst deactivation processes by undesirable interaction of products and avoidance of contamination of the reaction output by catalyst residues. From the viewpoint of construction of multistep sequential continuous-flow productions of high-value-added compounds, Type IV is thus ideal. Another important aspect in this context is the enhanced catalytic efficiency that can be achieved for Type IV catalytic flow reactions. The substrate/catalyst [S]/[C] ratio in a batch system changes along with the progress of a reaction. High [S]/[C] in the initial stage can be disadvantageous due to undesirable interaction between excess substrate and catalyst, and low [S]/[C] in the later stage reduces the frequency of contact between the two. Given the above considerations, most catalytic reactions in batch thus require long reaction times to run to completion. In Type IV catalytic flow reactions, reactants dissolved in a mobile phase are supplied to a packed-bed reactor, where a large amount of catalytic species exists. This is in clear contrast to the Type III flow with homogeneous catalysts as well as batch homogeneous/heterogeneous catalytic reactions, and generally leads to reduced reaction time to completion within the residence time on the column (Figure 22.2).

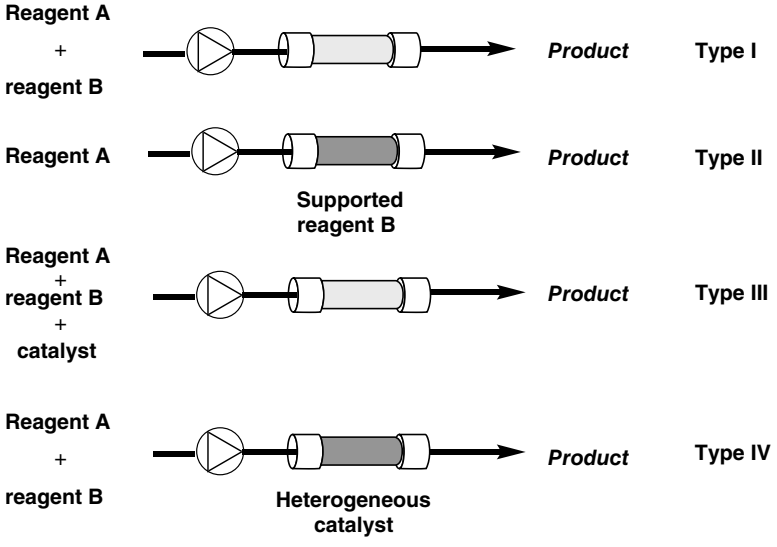

Figure 22.1. Classification of flow reactions in fine organic synthesis. Source: Based on [15].

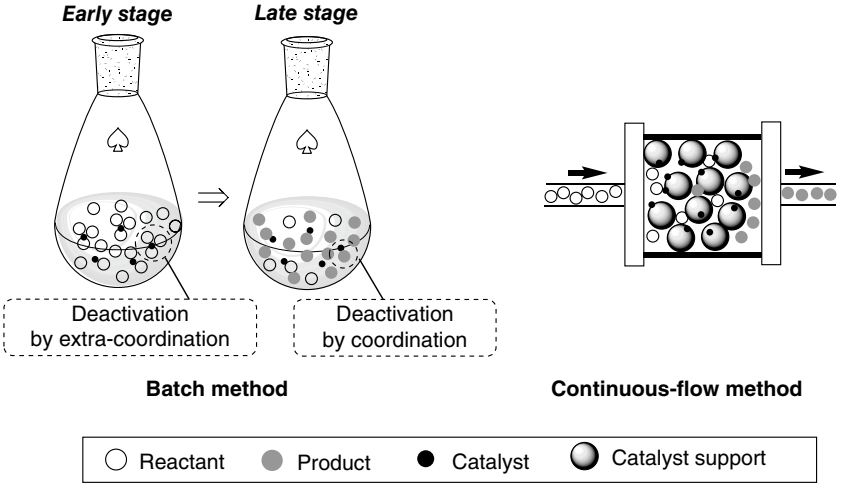

Figure 22.2. Batch method and continuous-flow method – from the viewpoint of catalyst.

Numerous studies have been conducted in the field of heterogeneous catalysis, including asymmetric catalysis, and many outstanding advances have been achieved. Regarding utilization of catalysis for fine organic synthesis in heterogeneous reactions, there remain a number of significant challenges to overcome to find more efficient, stable, and reliable methods, especially in continuous-flow systems. Highly active and stable heterogeneous chiral catalysts allow flow systems to be constructed that enable high productivity and long lifetime processes.

In the following sections, examples of catalytic flow processes will be described for Type III and IV reactions. More than 60 examples will be discussed; some of the results cited from the original literature are reevaluated using a parameter defined as [S]/[C] molar ratio per unit period (h). In this chapter, the ratio will be described as the substrate/catalyst molar ratio (SVmol) value, which corresponds to the amount of substance (or functional group; mole)-based space velocity – a contact mole ratio of [S]/[C] per unit period. This is because the yield in a flow reaction is considered a controllable outcome by changing the abovementioned SVmol, and the conditions required to attain the maximum yield or selectivity will not indicate the "optimal" conditions for reaction engineering, which is closely related to the catalytic flow chemistry. In addition to the fair evaluation of catalytic activity and process efficiency, the TOF value, corresponding to the value using SVmol × yield (before transferring to percentage), and the TON value, corresponding to the value using TOF × operation time which can maintain the yield constantly, will also be reevaluated where possible. Continuous-flow reactions that can be operated at high SVmol value produce the target product with high efficiency (productivity), and thus catalysts used under such reaction conditions will require high performances. The productivity can also be described in terms of space time yield (STY), which is defined as a weight of product produced in 1 hour divided by volume of a reactor ($g\,l^{-1}\,h^{-1}$).

22.3. ENANTIOSELECTIVE C–C BOND-FORMING REACTIONS THROUGH 1,4-ADDITION REACTIONS

Enantioselective 1,4-addition reactions of nucleophiles to electron-deficient olefins have been widely studied. Lewis/Brønsted acidic, organocatalytic, and transition-metal catalytic processes are all applied in asymmetric versions of this class of reaction. One of the most frequently applied reactions is the malonate addition to nitroolefins. A polymer-immobilized iminophosphorane/thiourea bifunctional catalyst **1** was introduced by Dixon et al. to facilitate a stereocontrolled 1,4-addition reaction of high pK_a malonate derivative **2** to nitrostyrene **3** (Figure 22.3) [16]. The continuous-flow conditions were set at $9.9\,h^{-1}$ of SVmol, and continuous running for 13 hours provided the product in 85% overall yield with 78% global enantiomeric excess (ee). The reported productivity was $7.14\,mmol_{prod}\,h^{-1}\,mmol_{cat}{}^{-1}$.

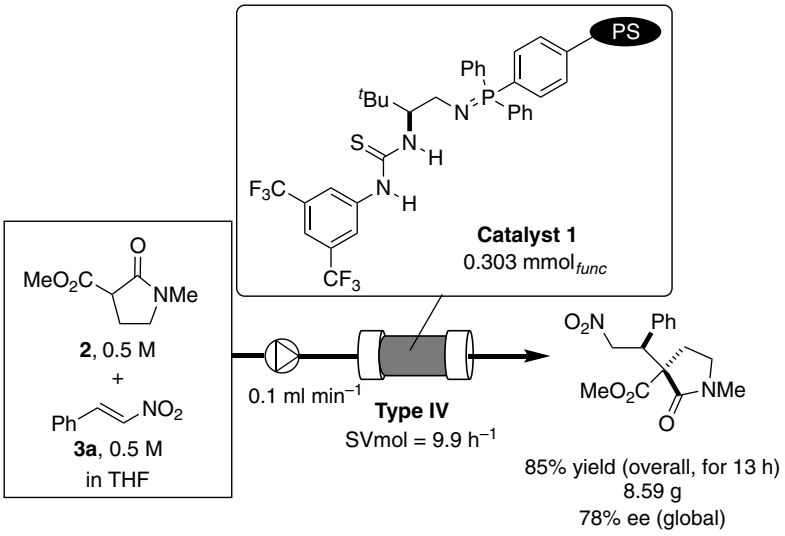

Figure 22.3. Type IV continuous-flow enantioselective 1,4-addition with polymer-supported bifunctional catalyst **1**. Source: [16]/Elsevier.

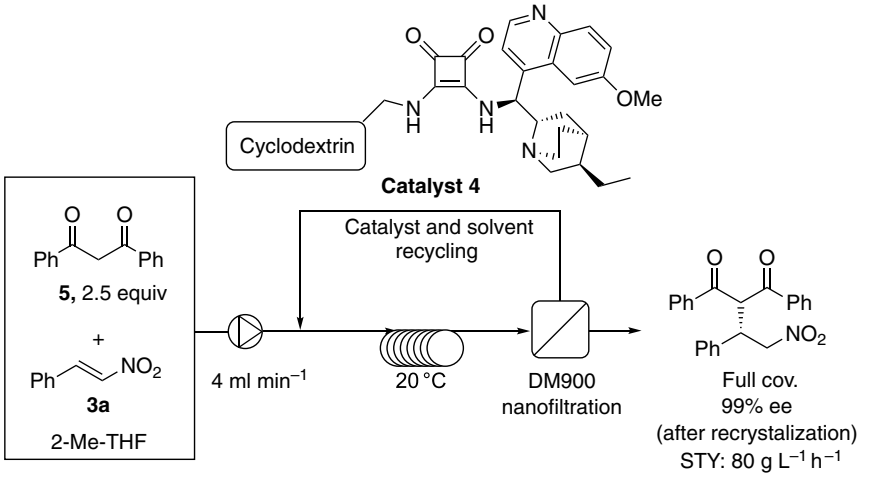

Figure 22.4 Type III continuous-flow enantioselective 1,4-addition and catalyst recycling. Source: [17]/Elsevier.

In 2019, Kupai and Szekely et al. developed enantioselective 1,4-addition of 1,3-diketones to nitroolefins with recyclable homogeneous H-bonding catalyst **4** under continuous-flow conditions (Figure 22.4) [17]. The squaramide was covalently attached to cyclodextrin, and the prepared catalyst **4** was flowed into a tube with substrates. The outlet was connected to an in-line membrane nano-filter system. The product was allowed to pass through the membrane and recrystallized in the permeance. By contrast, the catalyst **4** remained in solution and was reused by recycling along with the solvent. Continuous operation including reaction/catalyst recycling was successful for 24 hours.

These enantioselective 1,4-addition reactions to nitroolefins present an opportunity to develop efficient synthetic methods to access chiral nitrogen-containing value-added compounds. Kobayashi et al. applied their supported chiral calcium catalyst **6**, consisting of polymer-supported PyBOX ligand and calcium chloride, to continuous-flow enantioselective 1,4-addition of malonate to a nitrostyrene, and expanded to the sequential continuous-flow synthesis of chiral ropirlam, a drug molecule, in 2015 [18]. Similarly, in 2020,

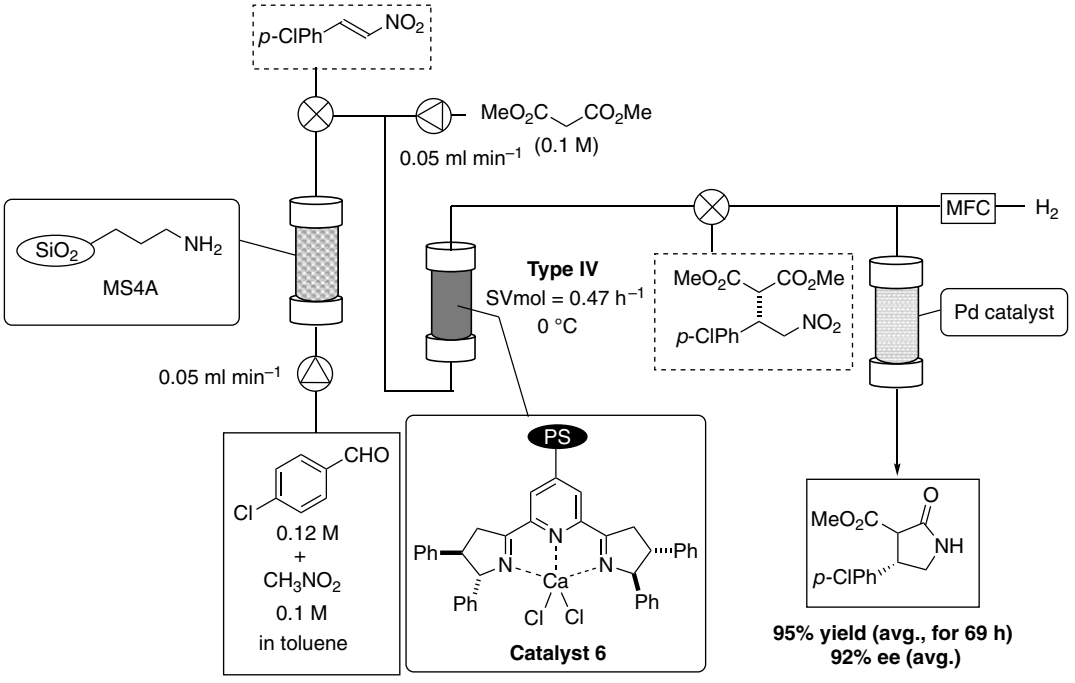

Figure 22.5 Sequential continuous-flow synthesis of the baclofen precursor. Source: [19]/John Wiley & Sons.

a sequential-flow synthesis of baclofen precursor with heterogeneous catalysts was reported (Figure 22.5) [19]. The key enantioselective 1,4-addition in baclofen synthesis was conducted with the packed-bed chiral calcium catalyst **6** at 0.47 h^{-1} SVmol, and gave the product in 93–96% yield with 92% ee over 69 hours operation. In this telescoped synthesis of APIs, all transformations were promoted by heterogeneous catalyses; thus, there was no requirement for quenching the reactions or for catalyst separation.

In 2019, the same group introduced the novel mesoporous silica/nickel–diamine composite **7** as a catalyst for heterogeneous enantioselective 1,4-addition reactions of malonate to aliphatic nitroolefin **3b** (Figure 22.6) [20]. The catalyst was prepared by simply mixing NiI_2, diamine ligand, and mesoporous silica. Detailed characterization of the composite indicated that a 1 : 1 complex of nickel–diamine, which is reported to be unstable in solution [21], was immobilized through Ni–O–Si bonds and stabilized by lattice oxygen on the silica wall. The flow reaction was conducted with 0.65 h^{-1} SVmol and connected with continuous-flow hydrogenation of the nitro group to the amino group, affording the corresponding lactam product **8**, as a precursor of pregabalin.

The polymer-bound nickel–diamine catalyst system was also used in malonate 1,4-addition reactions to nitroolefins (Figure 22.7) [22]. In that report, chiral diamine-bearing polymerizable styrene moiety was copolymerized with styrene and divinylbenzene (DVB) to prepare polymeric chiral ligand, and then the metal iodide was installed to give the heterogeneous chiral Ni catalyst **8**. The packed-bed reactor with the catalyst containing 0.1 mmol nickel was used under continuous-flow conditions at 1.5 h^{-1} SVmol, which was higher than that used in the previously discussed mesoporous silica system.

Not only immobilized chiral metal complexes but also immobilized chiral organocatalysts can provide an efficient approach for Type IV continuous-flow enantioselective 1,4-addition reactions. Pericás et al. have investigated this field extensively and demonstrated several examples to date [23]. As a recent example, a polystyrene-immobilized prolinol catalyst **9a** was employed for the synthesis of a key intermediate of GABAs under continuous-flow conditions. TBS-protected *cis*-4-hydroxy prolinol was immobilized on polystyrene by azide–alkyne cyclocondensation reaction, and the obtained catalyst was tested in a reaction using a neat mixture of reactants. Under the described conditions at 28 h^{-1} SVmol, the target product was obtained in high yields with high enantioselectivities on average, and a total of 7.22 g of the product

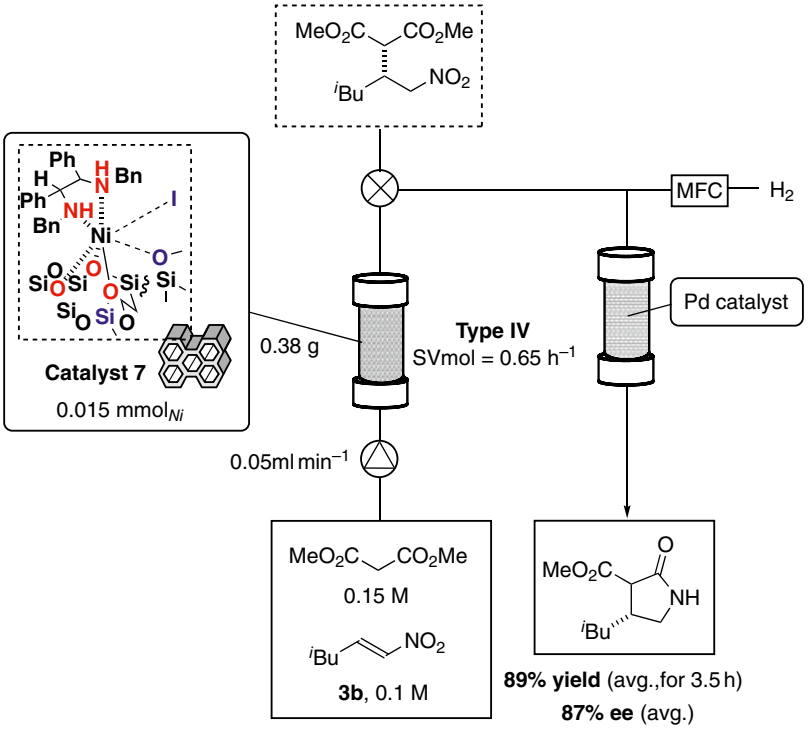

Figure 22.6. Mesoporous silica/Ni–diamine composite for continuous-flow synthesis of pregabalin precursor. Source: [20]/John Wiley & Sons.

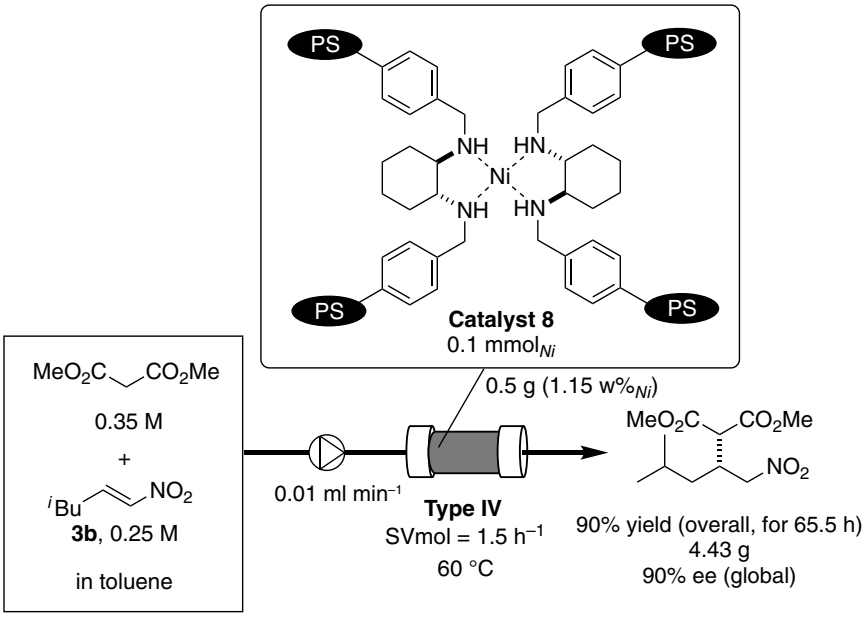

Figure 22.7. Polymer-bound nickel–diamine catalyst for continuous-flow 1,4-addition reaction. Source: [22]/John Wiley & Sons.

was obtained over 2.5 hours operation (Figure 22.8) [24]. The same group also utilized this enantioselective continuous-flow catalysis system for 1,4-addition of malonate to unsaturated aldehydes [25].

The same type of catalyst was also effective for 1,4-addition of aliphatic aldehydes to nitroolefins. A Wang resin-immobilized prolinol-type catalyst **9b** was introduced by Szcześniak et al. and utilized for the reaction under continuous-flow mode. The product was obtained in high yields with excellent enantioselectivity; however, deactivation of catalyst was observed after 9 hours for one substrate, and diastereoselectivity varied over time due to epimerization under the reaction conditions (Figure 22.9) [26].

The *cis*-4-hydroxy proline-type catalyst was further examined by Ochiai and Nishiyama et al. in 2020 (Figure 22.10) [27]. Copolymerization of proline-derived chiral monomer unit with styrene/DVB was adopted to gain chiral polymer catalyst **10** in that study, and 1,4-addition of aldehyde to nitroolefin, the same type of reaction investigated by Ayats' group, was again studied. The catalyst employed in the continuous-flow reaction at 6.0 h^{-1} SVmol showed excellent stereoselectivities for over 7 hours operation on average; however, deactivation began after the flow reaction started.

Pericàs' group chose chiral squaramide as a target H-bonding catalyst and evaluated its activity in 1,4-addition to functionalized nitrostyrenes such as **3c**, affording an oxygen-containing heterocyclic compound. A continuous-flow reaction was examined using an optimized catalyst **11** at 7.1 h^{-1} SVmol, and excellent activity and selectivity were maintained for over 4 hours operation (Figure 22.11) [28].

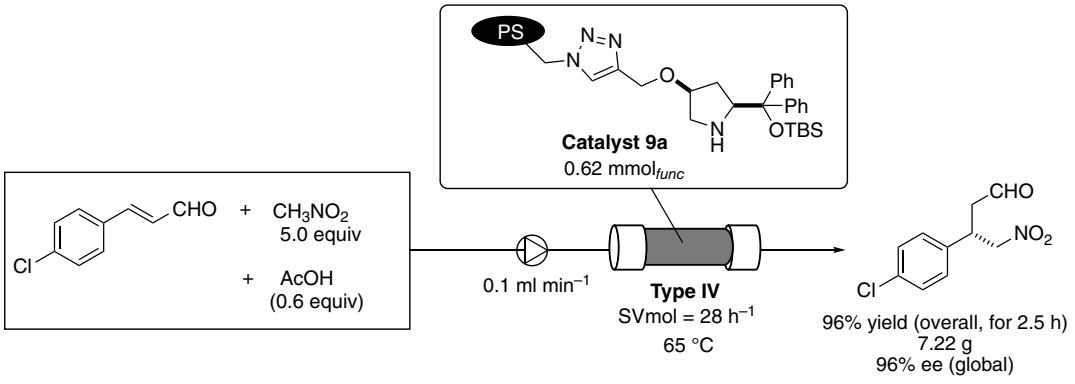

Figure 22.8. Immobilized organocatalytic continuous-flow 1,4-addition reaction. Source: [24]/American Chemical Society.

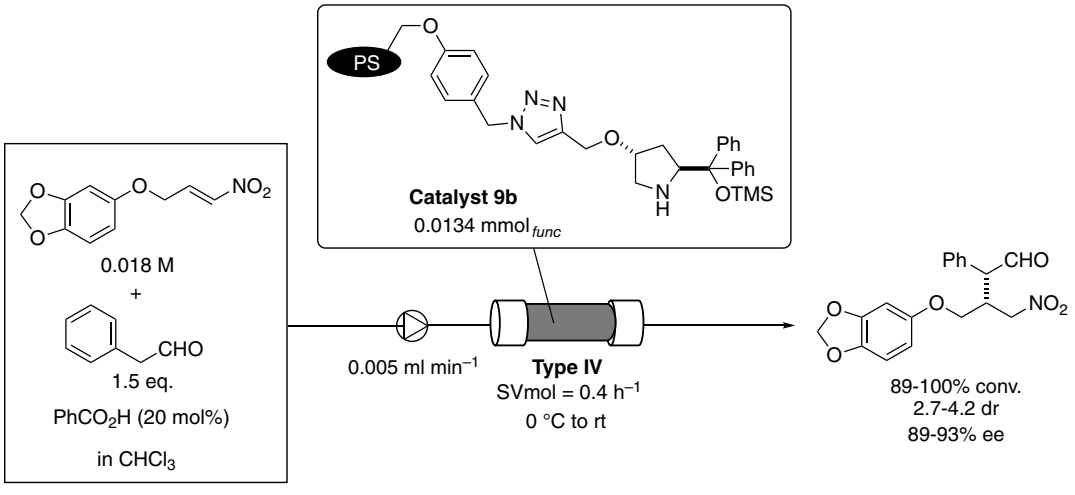

Figure 22.9. Continuous-flow enantioselective 1,4-addition reaction of aldehyde to nitroolefin (1). Source: [26]/John Wiley & Sons.

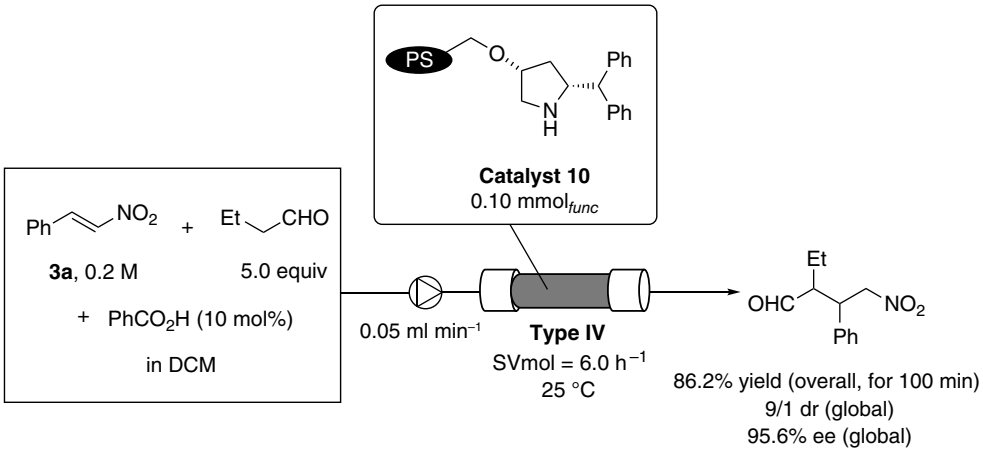

Figure 22.10. Continuous-flow enantioselective 1,4-addition reaction of aldehyde to nitroolefin (2). Source: [27]/American Chemical Society.

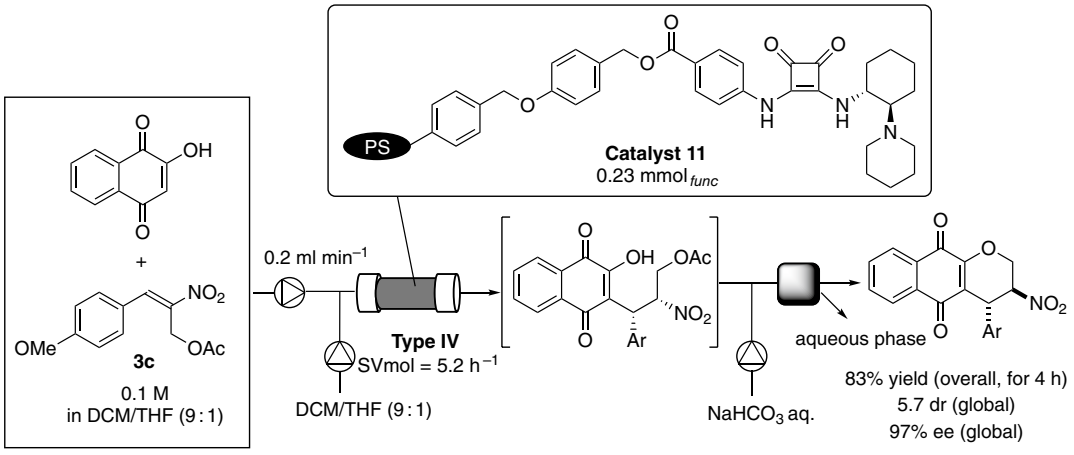

Figure 22.11. Hydroxyquinone 1,4-addition to nitrostyrene. Source: [28]/Royal Society of Chemistry.

Cyano groups in polyacrylonitrile can be used as anchors to immobilize functional catalytic sites. Tao, Wang, and Zhang et al. used their designer polyacrylonitrile fiber-bearing pyrrolidine moiety in continuous-flow organocatalytic enantioselective 1,4-addition of a ketone to a nitroolefin. The water/ethanol solution of cyclohexanone and *trans*-β-nitrostylene (0.05 M) was flowed at 0.028 ml min^{-1} into a packed-bed reactor containing 0.1 mmol of the catalytic moiety, which corresponds to 0.84 h^{-1} SVmol. The continuous reaction for 12 hours under these conditions, with a $substrate_{total}$/catalyst ratio of 10.1, gave the corresponding product in 68% overall yield with a *syn*/*anti* ratio of 97 : 3 and 99% global ee (Figure 22.12) [29]. The authors claimed the above yield was better than that obtained in the batch reaction with 10 mol% catalyst (63% in 24 hours).

In 2019, Ciogli et al. developed a silica-based bifunctional catalyst **13** including quinine and benzoic acid moieties (Figure 22.13) [30]. Addition of Brønsted acids often shows a co-catalytic effect in organocatalytic reactions including enamines and iminium intermediates; nevertheless, use of homogeneous acids sometimes inhibits the amine catalysis and requires additional purification steps. In that report, both the amine and the acid were separately immobilized on the same support, and this offered cooperative catalysis in a continuous-flow mode. The flow reaction of hydroxycumarin **14** with enone **15** to prepare an API warfarin was conducted at 0.1 h^{-1} SVmol, and 16 hours operation (TON = 1.6) gave the corresponding product in 97% overall yield with 78% global ee.

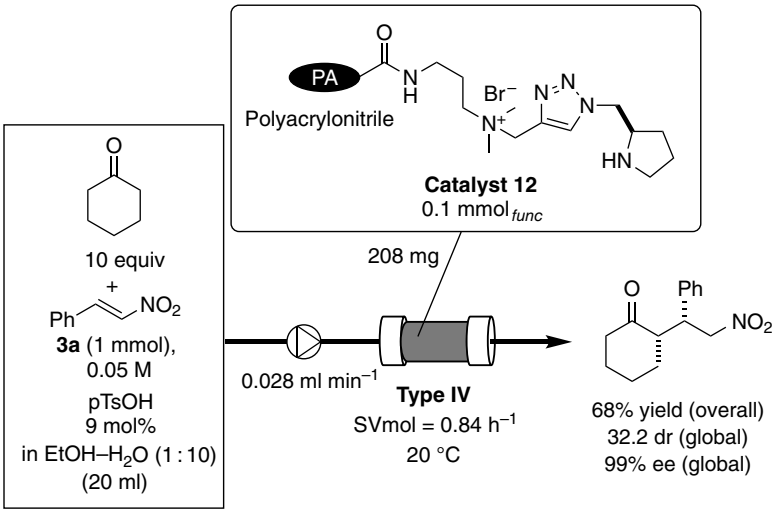

Figure 22.12. Continuous-flow 1,4-addition of ketone to nitroolefin. Source: [29]/Royal Society of Chemistry.

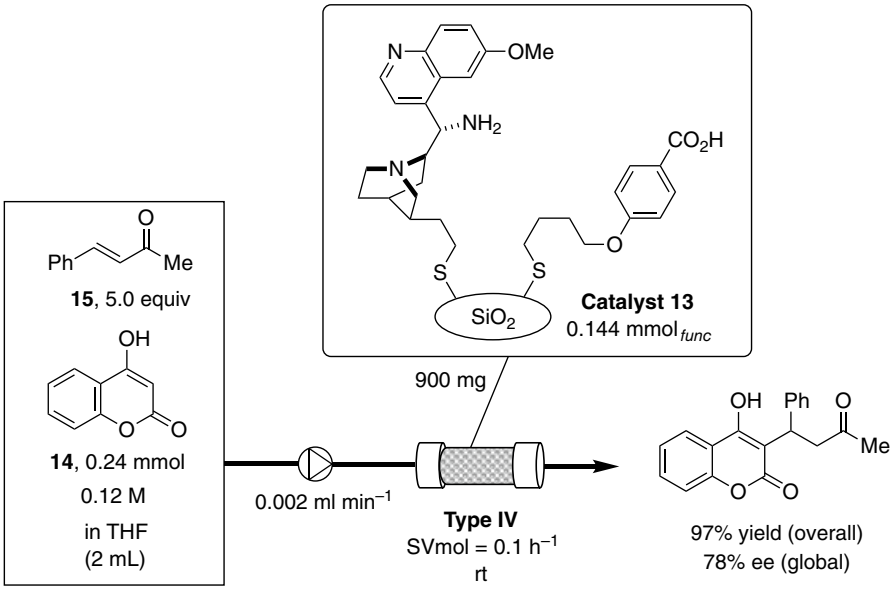

Figure 22.13. Quinine/benzoic acid bifunctional catalysis for enantioselective continuous-flow synthesis of hydroxycoumarin derivative. Source: [30]/John Wiley & Sons.

Chiral phosphoric acids (CPAs) are also considered powerful tools for enantioselective organocatalytic reactions. In 2017, Cui et al. developed a CPA-containing metal–organic framework (MOF) catalyst that was used in enantioselective 1,4-addition reactions of indole to electron-deficient olefins (Figure 22.14) [31]. MOFs have some attractive features such as well-defined and highly ordered nanopores and high surface area. Such systems can provide a promising platform for introducing heterogeneous chiral catalyst sites. In that work, the authors used a CPA-bearing isophthalic acid moiety (**L1**) and combined it with $MnCl_2$ to give a MOF with formula $[Mn_2{\cdot}\mathbf{L1}(H_2O)_2]$. Incorporation of a CF_3 group as a substituent of CPA enhanced the chemical stability of the material toward water, acid, and base as well as reactivity toward the target reaction, enantioselective 1,4-addition reaction of indole to a

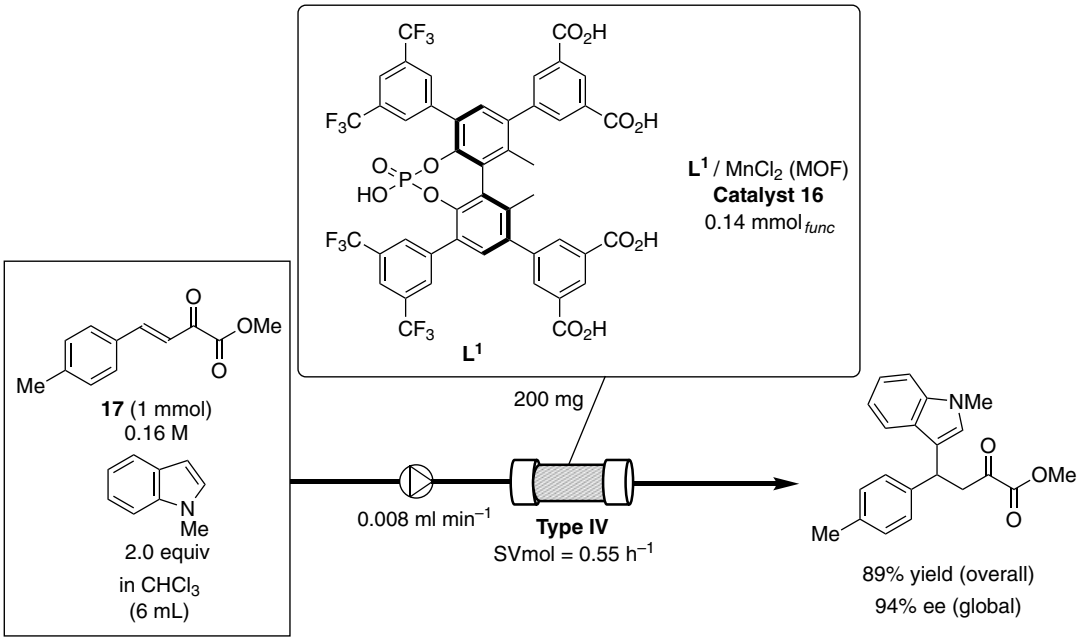

Figure 22.14. CPA-containing MOF-catalyzed enantioselective 1,4-addition of indole. Source: [31]/American Chemical Society.

β,γ-unsaturated-α-ketoester **17**. For the continuous-flow reaction, the authors adopted a packed-bed reactor containing 200 mg of the MOF catalyst **16**, which included 0.14 mmol of P atom, and 0.16 M solution of the ketoester, and flowed the solution at 0.5 ml h^{-1} (SVmol = 0.55 h^{-1}). The overall yield during 12 hours was 89%, and the global enantioselectivity of the product was 94% ee. The yields showed that slightly better reactivity of the catalyst was achieved in flow compared with that in batch.

Transition-metal-catalyzed 1,4-addition of aryl boronic acids to electron-deficient olefin is an effective tool to build C(sp^3)–aryl units. Several heterogeneous chiral catalysts have been developed and used under continuous-flow conditions. In 2018, Uozumi et al. developed an amphiphilic resin-supported chiral diene Rh complex (catalyst **18**) for enantioselective 1,4-addition of aryl boronic acids to enones in aqueous medium under continuous-flow conditions (Figure 22.15) [32]. The authors expected that the amphiphilicity of the resin would provide a suitable environment for the organic/aqueous biphasic system, and successfully validated their hypotheses in batch mode. The flow reaction was performed in water–ethanol mixed solvent to dissolve substrates. It was found that the addition of 1 equivalent of KOH improved the reactivity significantly, and the target product was obtained in 79% yield within 10 seconds residence time. Under the optimized flow conditions employed, 0.05 M substrate solution including **19**, 3 ml min^{-1} of flow rate, and 0.0625 mmol of Rh in the packed-bed reactor (SVmol = 144 h^{-1}), 12 hours continuous reaction gave the target product in 62% overall yield with 93% global ee (TON = 1073).

Kobayashi et al. immobilized a similar Rh complex on cross-linked polystyrene resin, which was generated by them, and used as a heterogeneous catalyst for continuous-flow 1,4-addition reactions of aryl boronic acids under biphasic medium. The authors adopted 2.4 h^{-1} SVmol conditions, under which the corresponding product was provided in 89% yield for 3–4 hours and with 99% ee on average [33]. The same group reported the use of a Rh/Ag bimetallic nanoparticle system for the same reaction. Although both nanoparticle and the Hayashi-type chiral diene were immobilized, the former is adsorbed on carbon black and the latter is incorporated within polystyrene substituted with triethoxysilane moieties; this transformed the system into a carbon black/siloxane-linked polystyrene hybrid. The flow reaction was tested at 5.6 h^{-1} SVmol, and the product was obtained in >90% yield and with 98% ee on average for over 17 hours operation (Figure 22.16) [34].

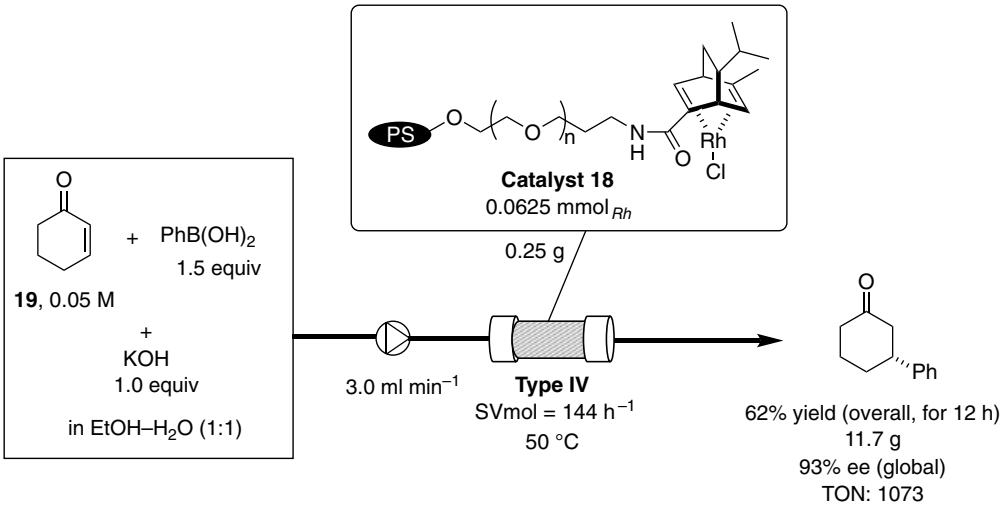

Figure 22.15. Amphiphilic resin-supported chiral diene Rh complex. Source: [32]/American Chemical Society.

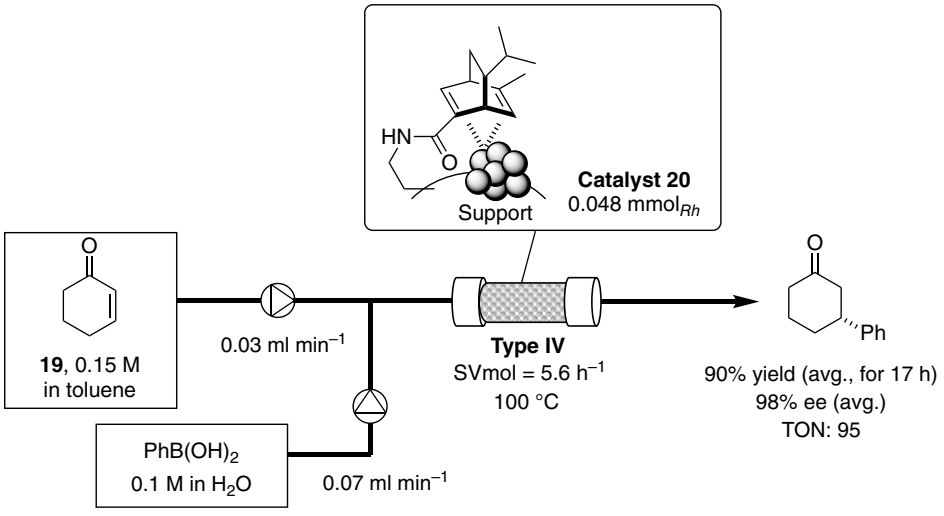

Figure 22.16. Ligand–Rh/Ag nanoparticle Co-immobilization system for continuous-flow aryl boronic acid 1,4-addition reaction. Source: [34]/Royal Society of Chemistry.

22.4. ENANTIOSELECTIVE C–C BOND-FORMING REACTIONS THROUGH 1,2-ADDITION REACTIONS

Nucleophilic addition reactions to C–O double bonds, including aldol and its related reactions, play important roles in synthetic organic chemistry, and enantioselective versions using heterogeneous catalyses have been investigated extensively. A recent demonstration of supported organocatalysis was reported by Pericàs' group, employing a chiral amine catalyst **21** for asymmetric Robinson annulation (intramolecular aldol reaction, Figure 22.17) [35]. Continuous-flow reaction using a catalyst was performed with a packed-bed reactor containing 0.56 mmol of catalyst **21** and 1.0 M DMF solution of the preformed meso triketone **22**. Although the flow rate of the reaction was appropriately changed to minimize the reduction in the performance of the catalyst, the conversion of the substrate decreased from 94

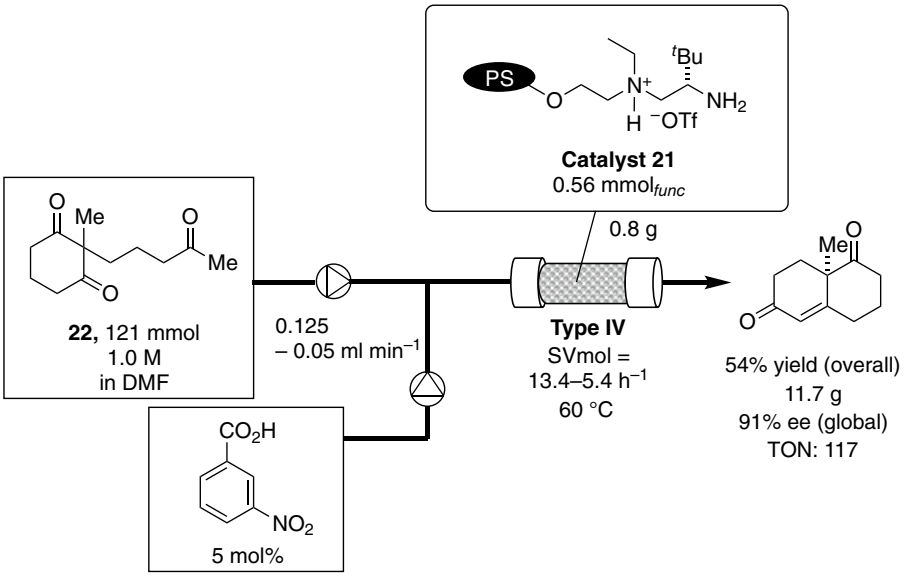

Figure 22.17. Asymmetric Robinson annulation. Source: [35]/American Chemical Society.

to 77% over 24hours operation. Based on the overall yield of the product, the TON was calculated to be 117; nevertheless, the enantioselectivity of each fraction was maintained at 92–91% ee.

Nakashima and Yamamoto used molecular proline tetrazole **23** directly in a packed-bed reactor with Celite, and examined aldol, Mannich, and *O*-nitroso aldol reactions using a solvent amount of a ketone. Choice of cosolvent was decisive, and a combination of EtOAc (10 vol%) and H_2O (3 mol%) allowed retention of the catalyst molecule to be compatible with its reactivity. A 0.1 M solution of aldehyde **24** in the appropriate solvent system was flowed into the reactor containing 270 mg of the catalyst molecule (1.94 mmol) at 0.1 ml min^{-1} flow rate (SVmol = 0.31 h^{-1}). The outcome of that work was evaluated using overall yield and global enantioselectivity after 9.9 mmol of the substrate supplement, which indicated a $substrate_{total}$/catalyst ratio of 5.1 (Figure 22.18) [36].

In 2019, Gröger et al. investigated a Type III asymmetric organocatalytic aldol reaction in aqueous medium under flow conditions (Figure 22.19) [37]. The greatest difficulty of such flow reactions is the solubility of the aldehyde in aqueous medium; thus, use of a buffer/2-propanol system was necessary. Detailed studies on the relationship between reactor size, flow rate, conversion, and ee indicated that fast flow with a large reactor gave better yield, even when the residence time was the same. Even under the optimized flow reaction conditions, however, the conversion and enantioselectivity were similar to those of the batch reaction.

In 2018, Harada et al. developed silica-immobilized H8-BINOL ligand for the enantioselective 1,2-addition of organo-Ti species to aldehydes (Figure 22.20) [38]. The prepared catalyst acted as an organocatalyst for enantioselective 1,2-addition of phenyl titanium species to aromatic aldehydes in a flow process. A 0.2 M solution stream of aldehyde at 2.5 ml h^{-1} flow rate was combined with a stream of excess organo-titanium solution and added into a pipette filled with the silica catalyst including 0.09 mmol of the BINOL unit (SVmol = 5.6 h^{-1}). This system gave the corresponding product in 72% overall yield in 17 hours of continuous run and 87% global ee.

In 2020, Andrés and Pedrosa et al. developed polystyrene-supported cinchona alkaloid-derived thiourea **28** as a catalyst for 1-naphthol addition to the C–N double bond in isatin derivative **29** (Figure 22.21) [39]. A post-immobilization strategy was adopted using thioisocyanate-functionalized polystyrene to achieve both immobilization and thiourea formation at the same time. The continuous-flow reaction was performed with 0.14 M solution of **29** (0.1 ml min^{-1}), a slight excess of 1-naphthol, and a packed-bed reactor containing 0.3 mmol of the catalytic moiety (SVmol = 2.8 h^{-1}). A run of 200 minutes continuous operation for substrate **29** resulted in 80% overall yield, which corresponds to 7.4 TON, and 88% global ee.

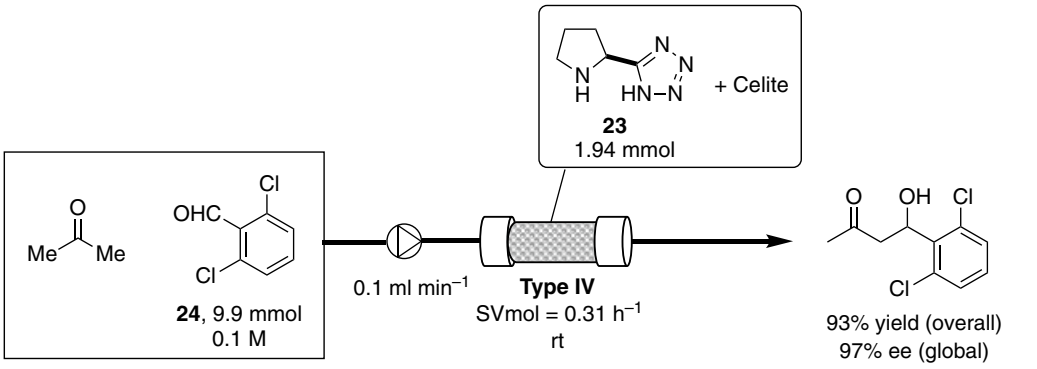

Figure 22.18. Continuous-flow Aldol reaction with a homogeneous catalyst-packed reactor. Source: [36]/John Wiley & Sons.

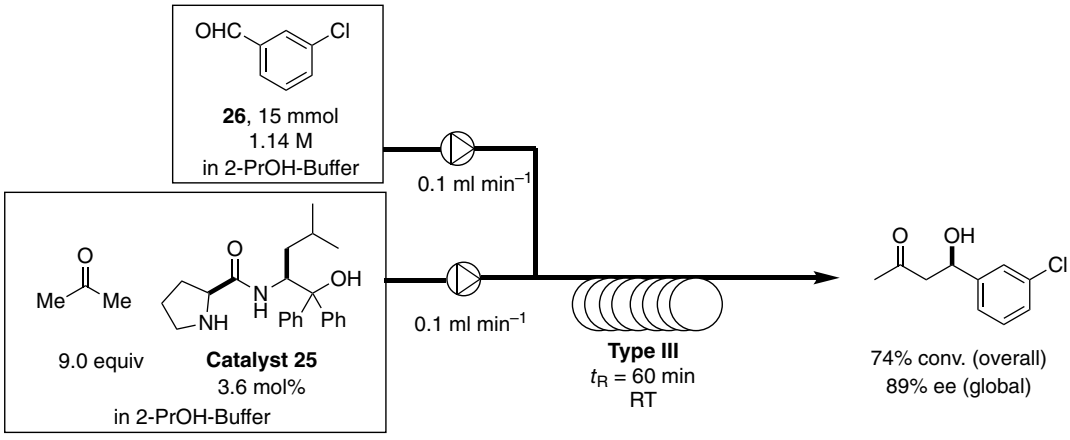

Figure 22.19. Asymmetric organocatalytic Aldol reaction (Type III) in hydrophilic medium. Source: [37]/Georg Thieme Verlag KG.

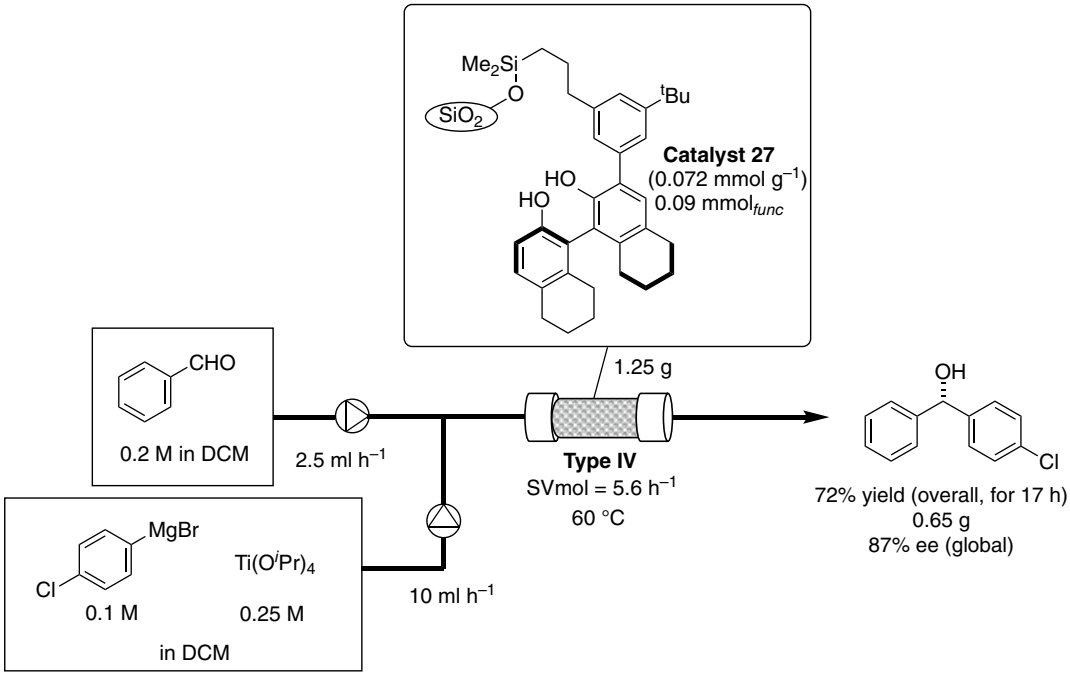

Figure 22.20. Silica-immobilized H8-BINOL as a catalyst for organo-titanium addition to aldehyde. Source: [38]/American Chemical Society.

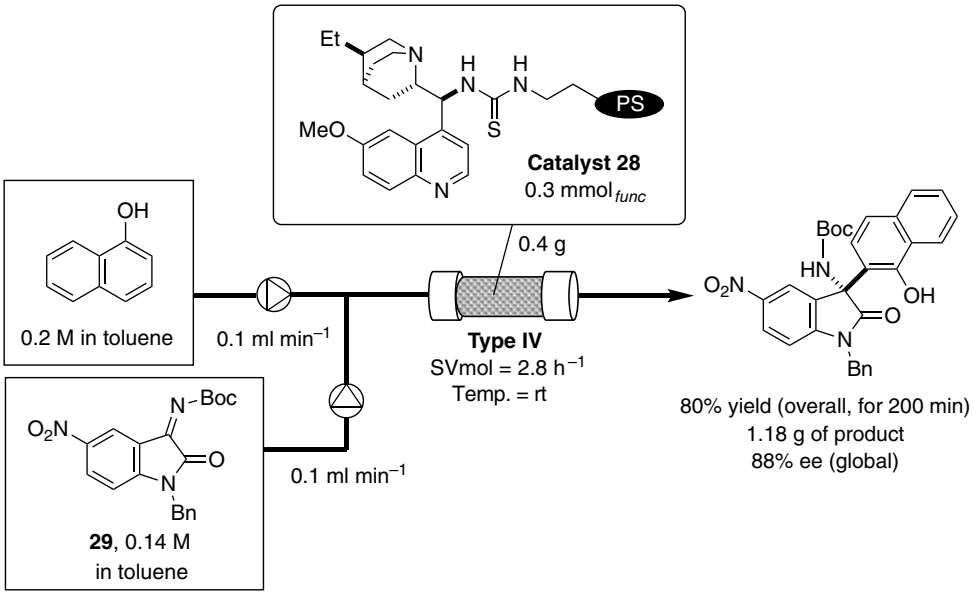

Figure 22.21. Polystyrene-supported cinchona alkaloid-derived thiourea catalysts. Source: [39]/John Wiley & Sons.

It is well known that carbon nanotubes and related materials exhibit many unique properties including adsorption of chemical substances. Wang and Lu et al. used porous carbon nanosheet (PCN) as a support for immobilization of chiral squaramide and used this in a Mannich-type reaction (Figure 22.22) [40]. 4-Aminobenzyl acrylate was used as an anchor for immobilization on the PCN surface, and polymerized with the squaramide monomer and DVB to give the polymer-coated PCN chiral catalyst **30**. For the continuous-flow reaction, 200 mg of the catalyst (6.5 wt% active site, 0.02 mmol) was used for the packed-bed reactor, and 0.06 M of the imine solution and 0.07 M of the nucleophile solution were flowed at 0.04 ml min^{-1} flow rate (SVmol = 7.2 h^{-1}). The outlet was pumped into the K_2CO_3 column with *N*-fluorobenzenesulfonimide solution to give the product. Continuous operation for 6 hours resulted in 91% overall yield with 88% global ee.

Shibasaki's group utilized this for immobilization of their rare-earth metal/alkali metal bimetallic insoluble catalyst composite **33** supported on multiwalled carbon nanotube (MWNT) and recently applied it to continuous-flow asymmetric Henry (nitro aldol) reaction of α-keto ester **34** with nitroalkanes. The conditions corresponding to 3.1 h^{-1} SVmol were applied in the reaction of **34** and nitroethane, and the flow reaction was maintained for 92 hours to give 92% overall yield (TON = 265), *anti*/*syn* ratio >97 : 3, and a global enantioselectivity of 97% ee (Figure 22.23) [41].

Self-supporting catalytically active sites are also occasionally found in the field of heterogeneous asymmetric catalysis. Ordered structure of MOF makes it possible to assemble functions of units toward systematical cooperation. In a recent contribution from Chen and Dong's group, a Lewis acid site, a chiral template moiety, and photothermal conversion species were combined into a copper-based covalent organic framework (catalyst **35**), which was used to catalyze an enantioselective Strecker-type three-component reaction of aldehyde **36**, amine **37**, and TMSCN (Figure 22.24) [42]. A 0.17 M acetonitrile solution of substrates was flowed onto a packed-bed reactor containing 100 mg of the MOF species corresponding to 0.11 mmol of copper over 8 hours (SVmol = 5.8 h^{-1}), and resulted in 90% overall yield and 93% global ee.

Enzymatic hydrocyanation reaction under continuous-flow conditions was also investigated and proved to be more effective than under the corresponding batch conditions. In that paper, 1 U of a specific enzyme was immobilized onto Celite by adsorption, and 150 mg of the composite was processed as the packed-bed reactor. Evaluating the results given in that paper using WHSV ($g_{PhCHO}/g_{Composite}$ h), more than 80% conversion was maintained with a range of 2.1 < WHSV (h^{-1}) < 10.6, and under the conditions of WHSV = 4.2 h^{-1}, the activity was maintained during 6–7 hours operation (Figure 22.25) [43].

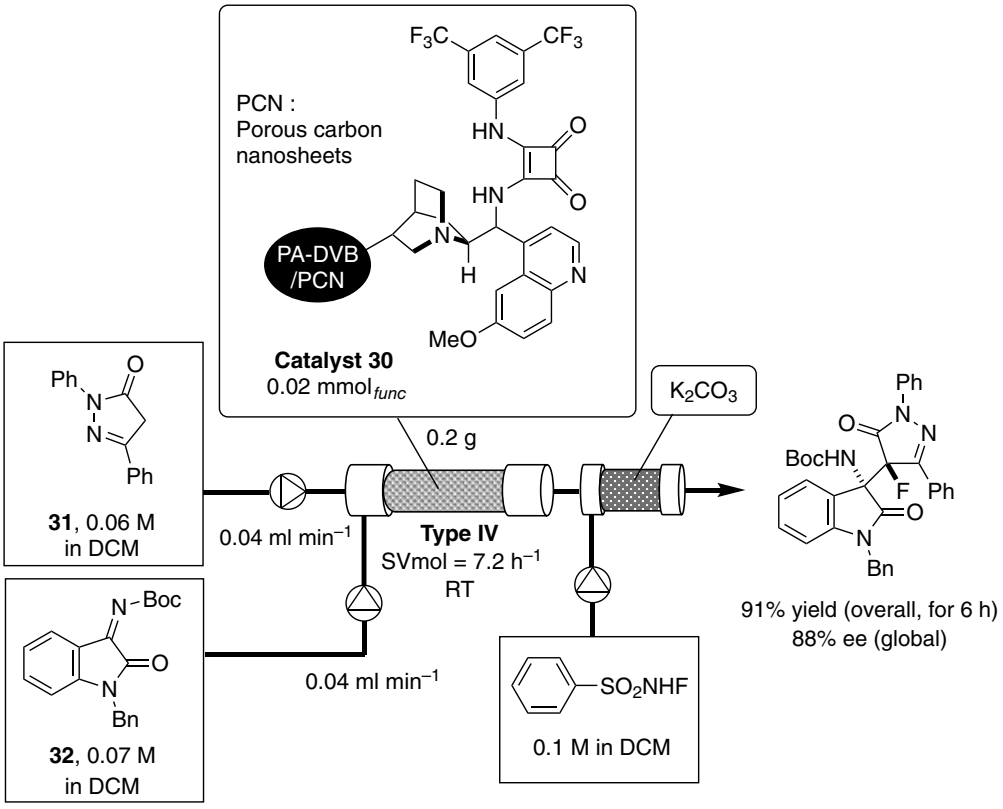

Figure 22.22. Porous carbon nanosheet/polymer hybrid-supported chiral squaramide for enantioselective Mannich-type reaction. Source: [40]/John Wiley & Sons.

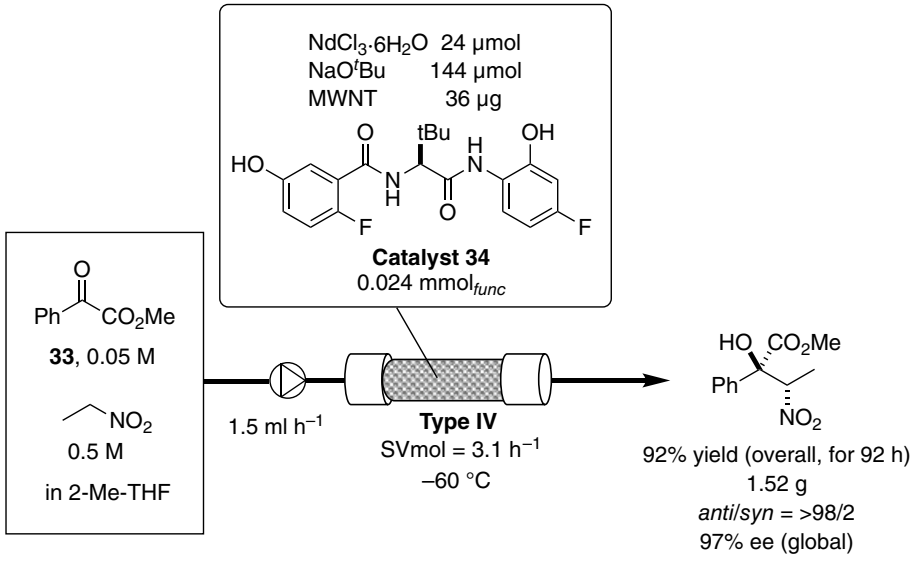

Figure 22.23. Continuous-flow enantioselective Henry reaction with Nd/Na heterobimetallic catalyst. Source: [41]/American Chemical Society.

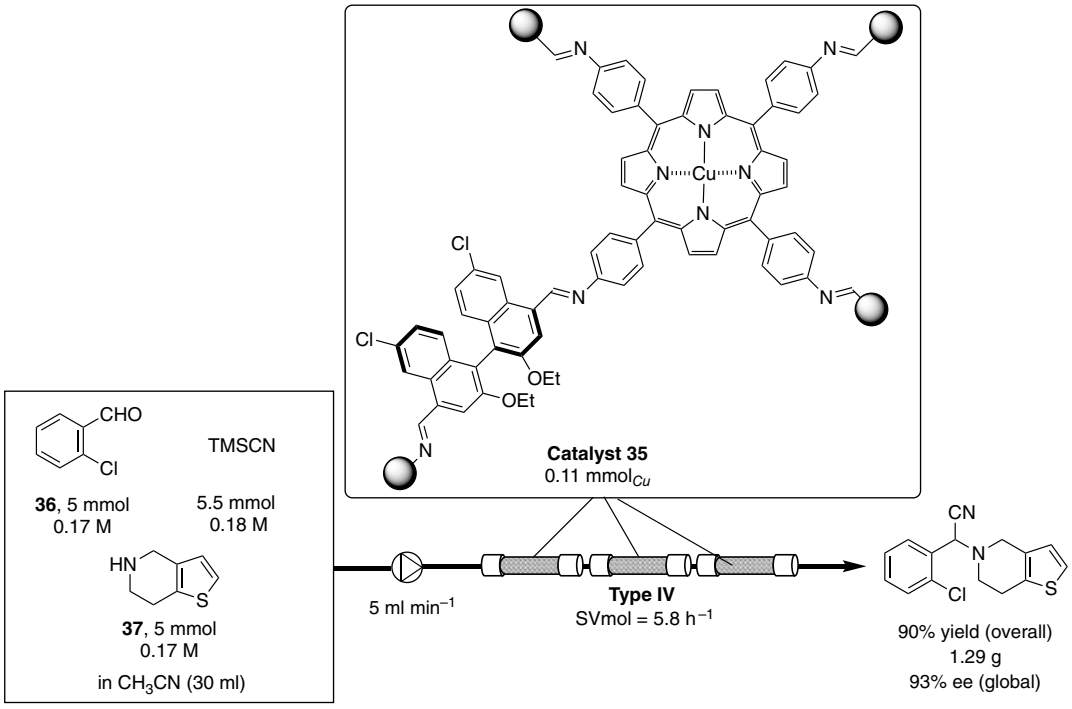

Figure 22.24. Continuous-flow enantioselective Strecker-type reaction with chiral MOF catalyst. Source: [42]/American Chemical Society.

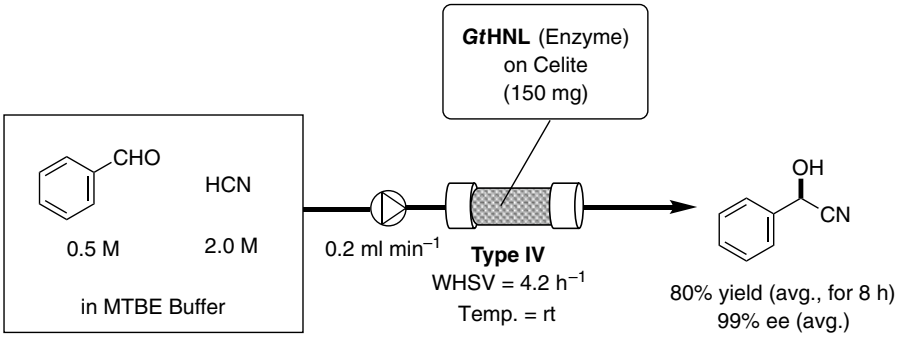

Figure 22.25. Continuous-flow hydrocyanation reaction with immobilized enzyme. Source: [43]/Royal Society of Chemistry.

Enantioselective Mannich reaction with heptanal and imine **39** was studied using a 500 nl microscale flow reactor with silica-immobilized secondary amine catalyst. The chip reactor containing the silica-immobilized catalyst **39** was integrated with a chiral HPLC column to enable in-line analysis of the crude mixture (Figure 22.26) [44].

One example of the asymmetric allylboration of aldehydes was reported in 2016 by Pericás' group, wherein immobilized CPA was used as a catalyst (Figure 22.27) [45]. CPA derived from BINOL was directly attached on a polystyrene matrix through copolymerization, and this was found to be highly active and selective under both batch and continuous-flow conditions. In continuous-flow experiments, 0.2 M aldehyde solution was flowed at 0.1 ml min^{-1} and combined with the allyborane stream to provide a packed-bed reactor containing 0.11 mmol of catalyst (SVmol = 10.9 h^{-1}). The system was maintained for over 28 hours to give the product in 92% overall yield (TON = 282) with 91% global ee.

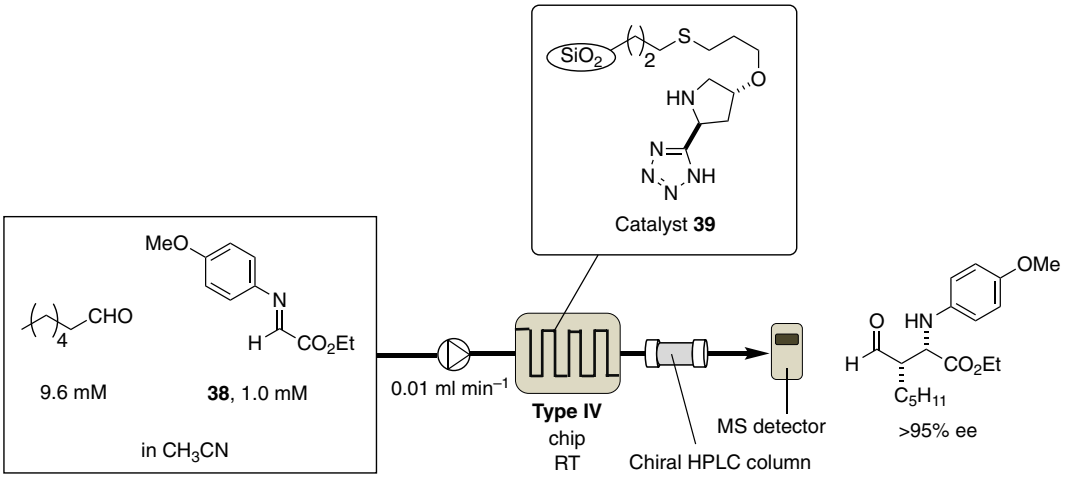

Figure 22.26. Type IV continuous-flow enantioselective Mannich reaction integrated with HPLC analysis. Source: [44]/John Wiley & Sons.

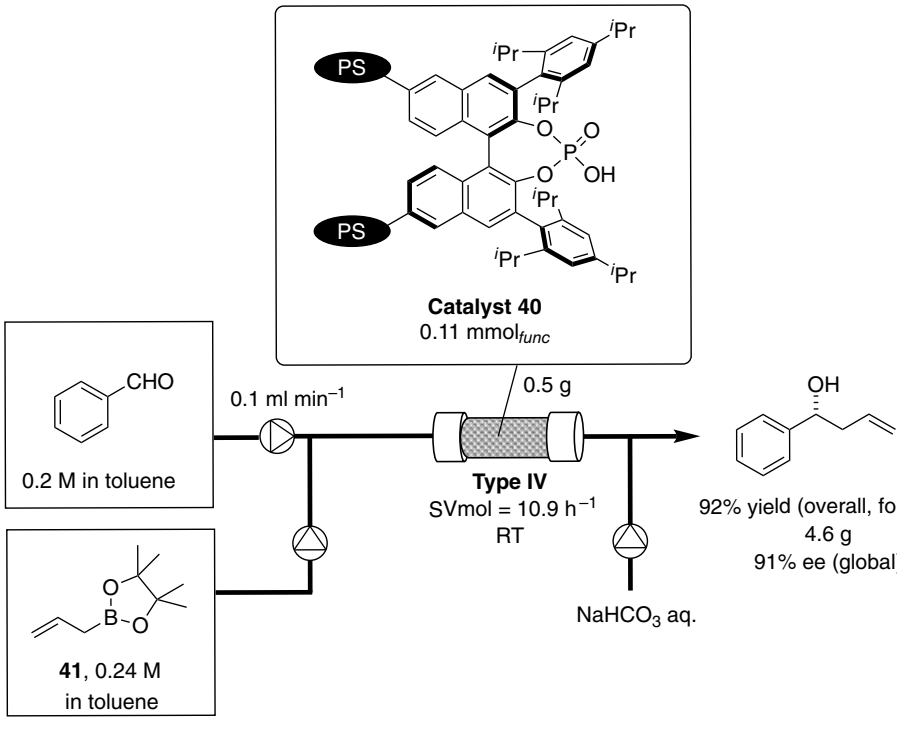

Figure 22.27. Continuous-flow asymmetric allylboration with polymer-supported CPA. Source: [45]/American Chemical Society.

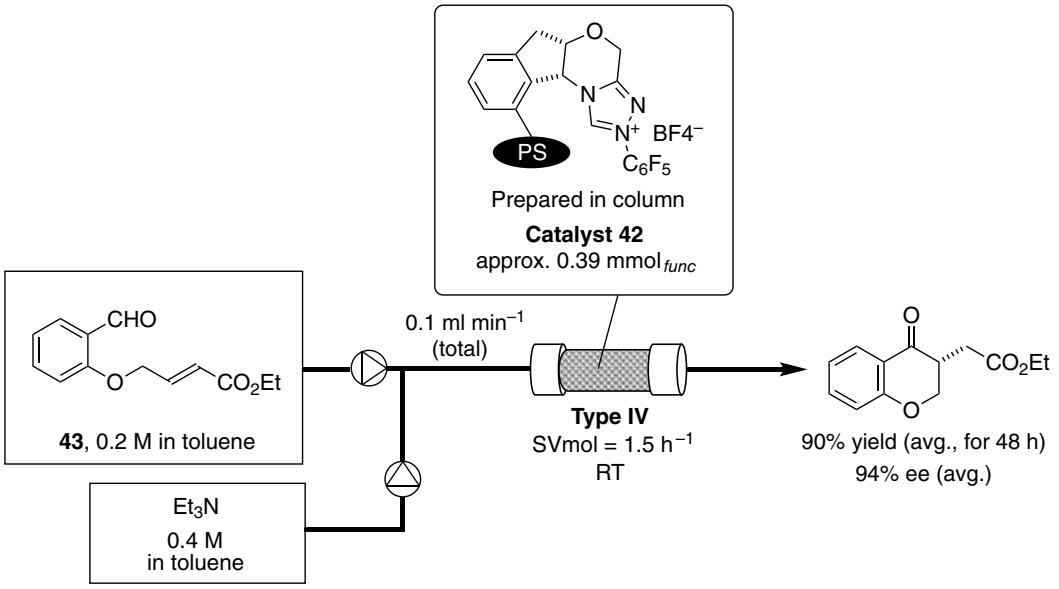

Figure 22.28. Chiral NHC catalysis under continuous-flow conditions. Source: [46]/American Chemical Society.

Asymmetric NHC catalysis provides a new and unconventional synthetic strategy to produce chiral molecules. Massi's group reported an example of asymmetric heterogeneous NHC catalysis under continuous-flow conditions in 2017 (Figure 22.28) [46]. The NHC catalyst **42** was prepared from indanol, fabricated in-column by copolymerization with styrene/DVB, and transformed into its BF_4 salt. The flow reaction was tested using 0.39 mmol of NHC in the packed-bed reactor with co-feeding of NEt_3 using 0.2 M solution of **43** at 0.1 ml min^{-1} total flow rate (SVmol = 1.5 h^{-1}). The system was maintained for over 48 hours to give the product in 90–95% conversion with 94% ee on average.

22.5. ENANTIOSELECTIVE C–C BOND FORMATION THROUGH CYCLOADDITION REACTIONS

Cycloaddition reactions are one of the most useful tools for constructing cyclic structures in organic synthesis. A recent contribution to organocatalytic Diels–Alder reaction along with Type IV continuous-flow chemistry was reported by de Finelli et al. The catalyst was a silica-immobilized imidazolidinone organocatalyst that was prepared by flow mode using commercial amino silica gel (stationary phase) and the catalyst precursor solution (mobile phase), despite a risk of nonuniformity of catalytic sites. Interestingly, the catalyst prepared in the flow mode exhibited superior stability over that made in the batch mode in a continuous-flow Diels–Alder reaction. A packed-bed reactor filled with 580 mg of the supported catalyst including 0.35 mmol of the catalytic functional group was treated with 0.24 M of the substrate solution at 0.0025 ml min^{-1} flow rate (SVmol = 0.1 h^{-1}). The system was maintained for 80 hours operation and afforded the product in 93% yield on average; however, the enantioselectivity for the corresponding *endo* adduct decreased from 89 to 62% ee (Figure 22.29) [47].

In 2019, Washio, Takizawa, and Sasai et al. combined flow chemistry and machine learning to identify the best reaction conditions for flow through multiparameter screening [48]. They employed Gaussian process regression (GPR), which is a kernel-based statistical learning algorithm. Their target reaction was the organocatalyzed Rauhut–Currier reaction of **47** and **48** and [3+2]-annulation sequence. Due to the high complexity of this domino reaction and various possible side reactions, the optimization under batch conditions resulted in only 20% yield but with high selectivity. For further improvement in yield, they employed machine learning under the Type III flow reaction conditions with catalyst **46**. By changing

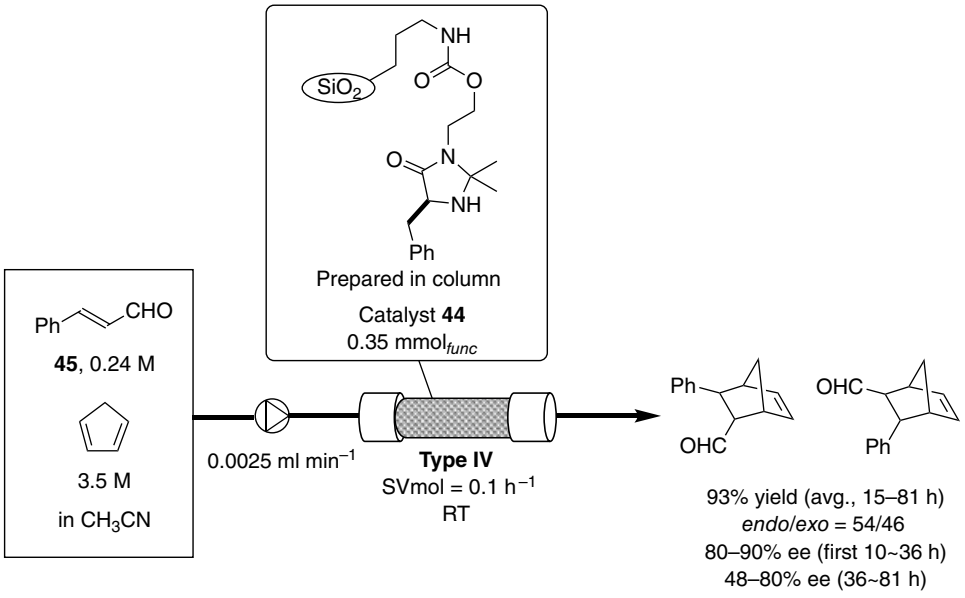

Figure 22.29. Continuous-flow enantioselective Diels–Alder reaction using immobilized organocatalyst. Source: [47]/John Wiley & Sons.

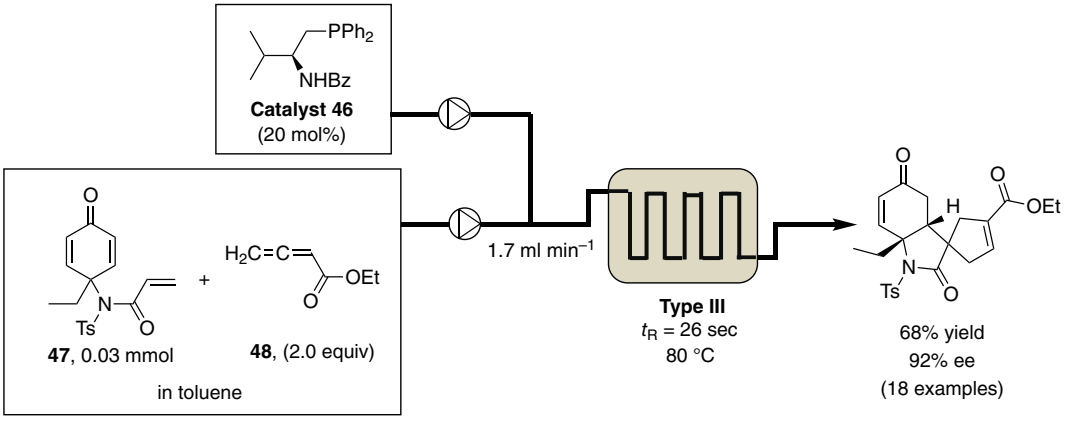

Figure 22.30. Optimization of Type III continuous-flow reaction with the assistance of machine learning.

the flow rate, reaction temperature, and stoichiometry of reagents as a result of machine learning, the yield could be improved to 76% with 94% ee (Figure 22.30).

Toste's group heterogenized anionic supramolecular compounds onto cationic polymer through ionic interaction. The monomer unit self-assembled to form polyanionic cage molecules by complexation with Ga^{3+}, and this encapsulated cationic substrate molecules and enhanced chemical transformations of the cationic substrates into neutral products via Prins and aza-Cope processes. The continuous-flow enantioselective reaction was performed with an enantiomerically enriched cage catalyst **49** (0.0055 mmol) in a packed-bed reactor, and a 3.0 mM aqueous solution of the substrate **50** was flowed at 3.0 ml h^{-1} flow rate, which corresponds to 1.6 h^{-1} SVmol, with an acetonitrile flow. Although the enantioselectivities of the product were below 60% ee, the catalytic activity was maintained for over 8 hours continuous operation (Figure 22.31) [49].

Organocatalytic cyclopropanation reactions of α,β-unsaturated aldehydes and 2-bromomalonates were investigated by Pericàs et al. In that study, the authors prepared beads- or monolith-type proline-based

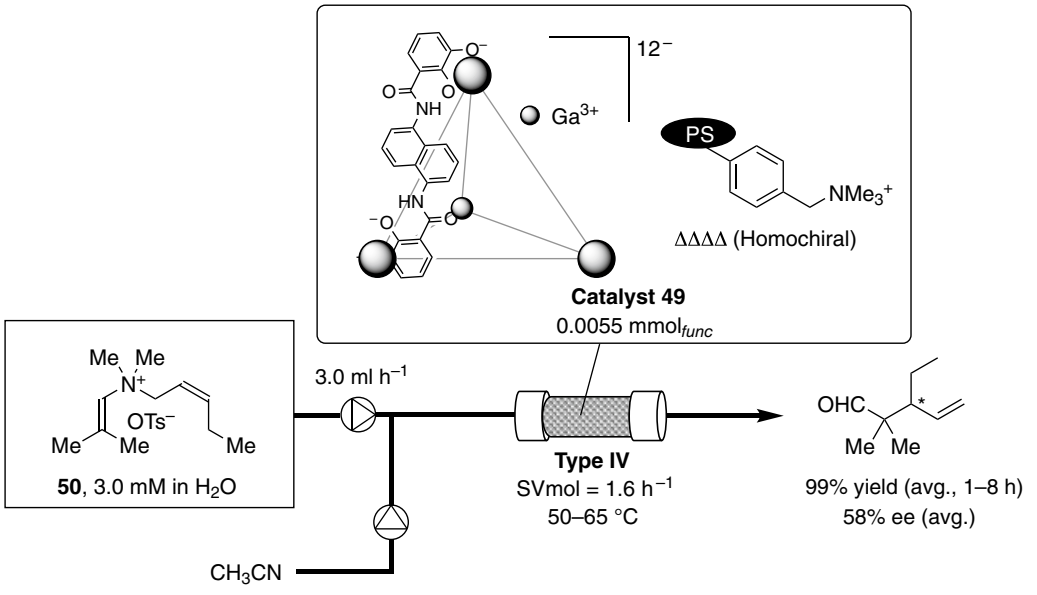

Figure 22.31. Homochiral cage catalyst for continuous-flow enantioselective aza-cope rearrangement. Source: [49]/American Chemical Society.

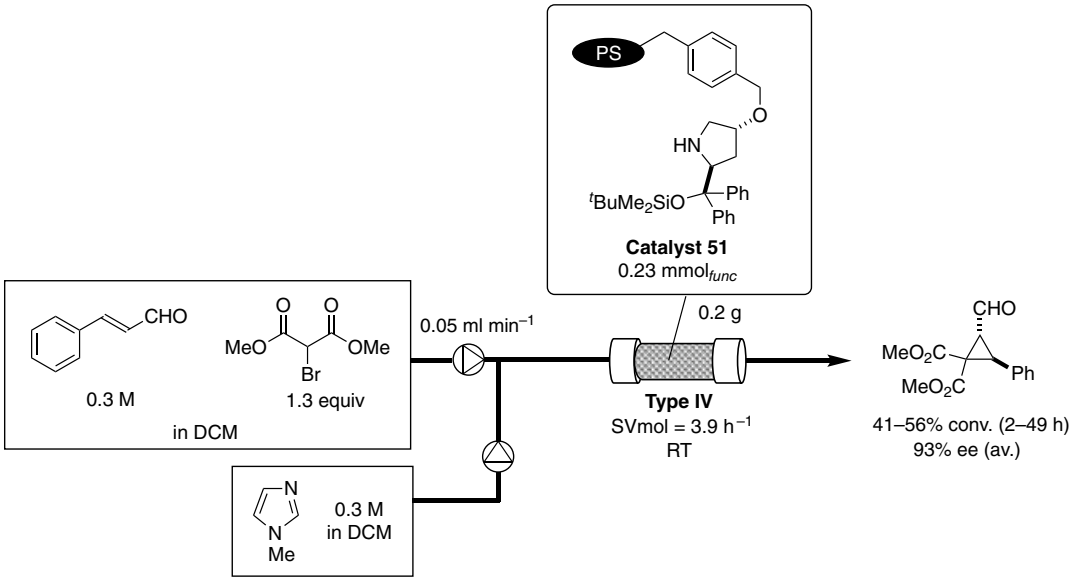

Figure 22.32. Anchor effects in organocatalytic enantioselective cyclopropanation. Source: [50]/American Chemical Society.

Hayashi–Jorgensen-type catalysts and evaluated them under continuous-flow conditions (Figure 22.32) [50]. As a general tendency, polymer beads-type catalysts gave higher yields than monolithic catalysts; moreover, they were evenly matched in enantioselectivity. For the continuous-flow reaction of cinnamaldehyde and 2-bromomalonate with catalyst **51** at 3.9 h^{-1} SVmol, moderate yields were maintained for over 47 hours with an average ee of 93%.

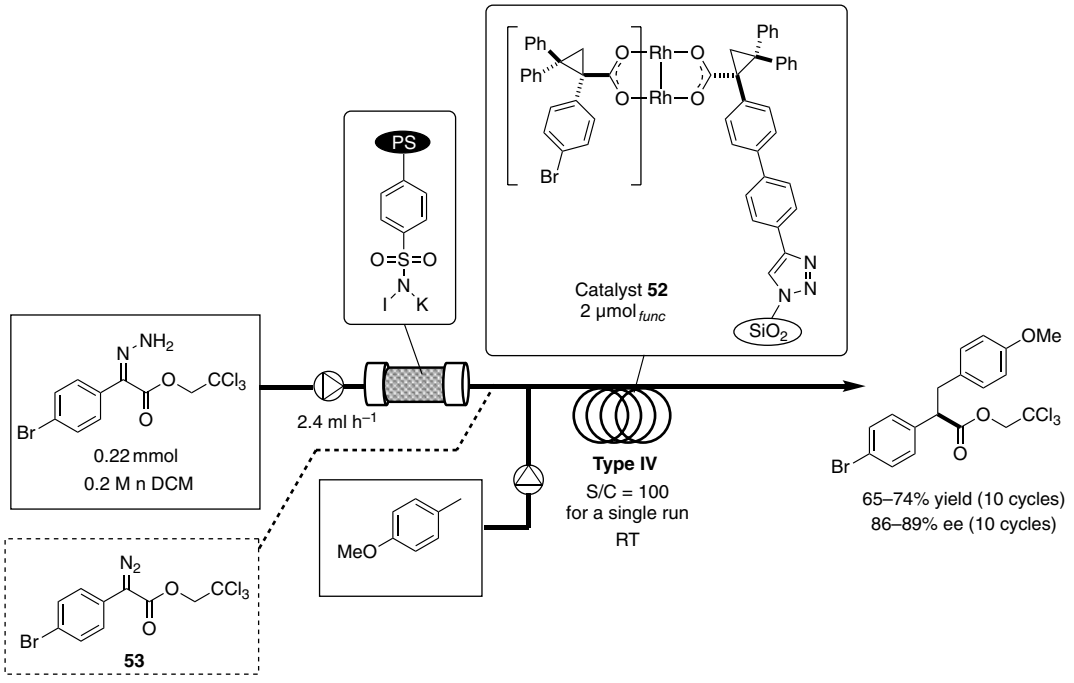

Figure 22.33. Continuous-flow enantioselective C–H insertion reaction with silica-immobilized Rh complex.

Metal-carbene-mediated C–C bond-forming reactions are one of the most useful classes of organic transformation reactions. In 2017, Beeler et al. reported a Type III continuous-flow asymmetric intermolecular Buchner ring expansion with a homogeneous chiral rhodium catalyst [51]. The flow reaction was performed by feeding ethyl diazoacetate, arene, and Rh catalyst in DCE into a tube reactor. Moderate yield with excellent enantioselectivity was observed for most of the substrates with 0.5 mol% of catalyst and 20 minutes residence time.

Silica-immobilized Rh dimer was developed by Davies and Jones et al. and Hatridge et al. for enantioselective C–H, O–H insertion reactions and cyclopropanation reactions, respectively, with diazo compounds [52, 53]. The aryl unit of chiral carboxylic acids was covalently immobilized onto silica via azide–alkyne cyclization. In the study conducted by Yoo et al. [52], a packed-bed reactor of polymer-supported oxidant was utilized prior to the chiral catalyst reactor for in-line generation of diazoesters. When a hollow-fiber flow reactor including chiral catalyst **52** was utilized in a small-scale C–H insertion reaction of 4-methoxytoluene with the diazoester **53** in which S/C = 100, the chiral reactor was repeatedly reused 10 times without significant loss of enantioselectivity (Figure 22.33).

In 2018, Maguire's group reported an intramolecular asymmetric C–H insertion reaction with heterogeneous Cu catalyst [54]. Immobilization of the catalytic copper species was achieved using tethered BOX, which was synthesized by copolymerization with styrene. Detailed comparison of homogeneous batch, heterogeneous batch, and heterogeneous flow conditions indicated that their heterogeneous catalysts did not offer an advantage over the homogeneous catalyst.

22.6. ENANTIOSELECTIVE C–C BOND-FORMING REACTIONS THROUGH HYDROFORMYLATION

The confined reaction space in flow reactors often provides suitable conditions for Type III flow reactions of gas–liquid systems. A Type III continuous-flow asymmetric hydroformylation was reported by Landis' group in 2016 (Figure 22.34) [55]. Besides an expected positive effect in gas–liquid mixing, a continuous-microflow

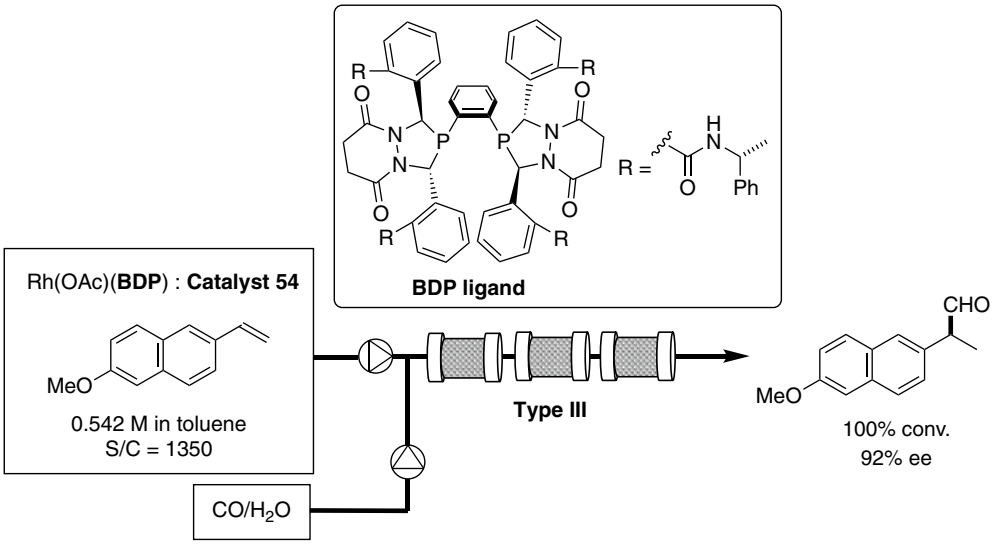

Figure 22.34. Type III continuous-flow asymmetric hydroformylation. Source: [55]/John Wiley & Sons.

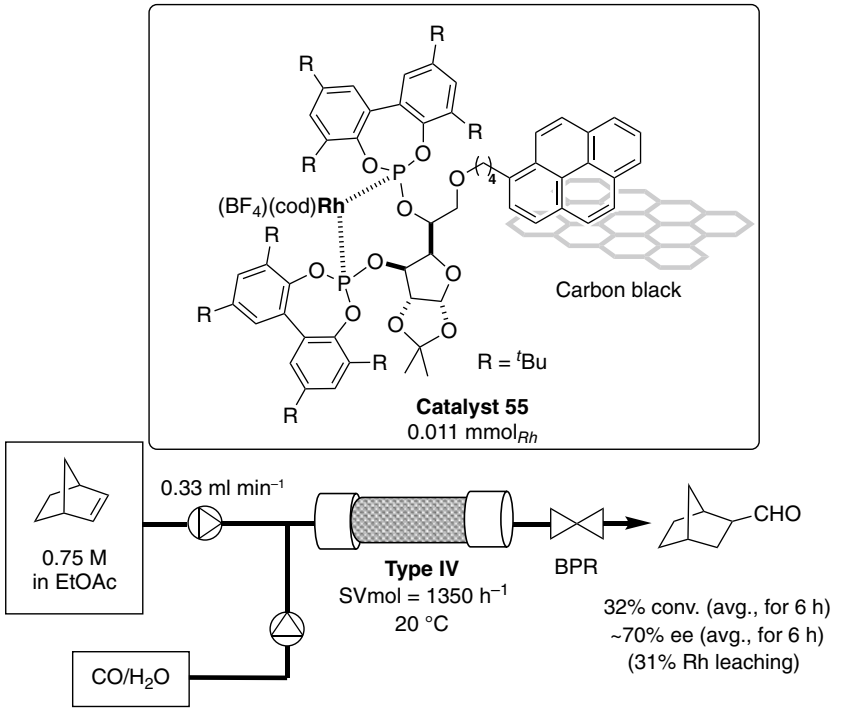

Figure 22.35. Heterogeneous Rh catalyst immobilized on carbon by π–π interaction. Source: [56]/John Wiley & Sons.

system can minimize operational difficulties associated with the toxicity of chemicals such as syngas in hydroformylation. The flow reaction was performed by feeding a toluene solution of 2-vinyl-6-methoxynaphthalene and Rh-diphosphine catalyst at S/C 1500 and syngas into a pipes-in-series reactor.

In 2019, Garcia-Suarez and Godard et al. reported a heterogeneous Rh catalyst system for enantioselective hydroformylation of norbornene (Figure 22.35) [56]. An immobilization mode adopted in that

work was π–π interaction between carbon black and the π system of the pyrene anchor in the tethered complex. The immobilized catalyst could work for several hours to afford the target product with moderate enantioselectivity; however, leaching of the rhodium from the packed-bed reactor was significant.

22.7. ENANTIOSELECTIVE C–X BOND-FORMING REACTIONS THROUGH OXIDATIVE PROCESSES

α-Amination of oxindole **57** was developed using thiourea-modified polymer **56** under continuous-flow conditions. Polymers of intrinsic microporosity were prepared by aromatic substitution of aryl fluoride with catechol, which was further functionalized to afford a polymer-supported bifunctional thiourea catalyst. The prepared catalyst was employed for an addition reaction of **57** with carbodiimide under continuous-flow conditions at 2.9 h^{-1} SVmol. The catalyst showed sustainable activity for 420 minutes to afford the target compound in 100% conversion with 74% ee on average (Figure 22.36) [57].

A similar type of amination was reported by Belder' group using a micro-flow reactor. Heterogeneous catalyst **9c** was prepared by on-chip photopolymerization of styrene monomers to build a monolith catalyst reactor. The prepared reactor was integrated with in-line HPLC/MS to enable in-line analysis. α-Amination of aldehyde with carbodiimide was performed under flow conditions. The target product was obtained with 50% ee (Figure 22.37) [58].

Wang and Xu et al. tried to develop an enantioselective H–F substitution reaction of activated C–H bonds in β-keto esters with electrophilic fluorinating agents and reported a Type IV continuous-flow system first (Figure 22.38)[59] and then a Type III flow system (Figure 22.39) [60]. While their motivation for "improvement" of their latter homogeneous version over the former immobilized heterogeneous system was to avoid synthetic difficulty associated with the immobilized catalyst, and indeed the latter system exhibited higher productivity (g h^{-1}) and STY (g h^{-1} l^{-1}), the advantage of the former can be clearly seen in catalyst performance. In the former heterogeneous continuous-flow system, 5.3 h^{-1} SVmol was adopted, and the system did not lose activity during 770 hours operation (TON = 4000).

In 2019, Meng et al. reported an enantioselective photooxygenation of 1,3-dicarbonyl compounds in a flow photoreactor (Figure 22.40) [61]. There are several challenges for scaling-up of photoreactions in

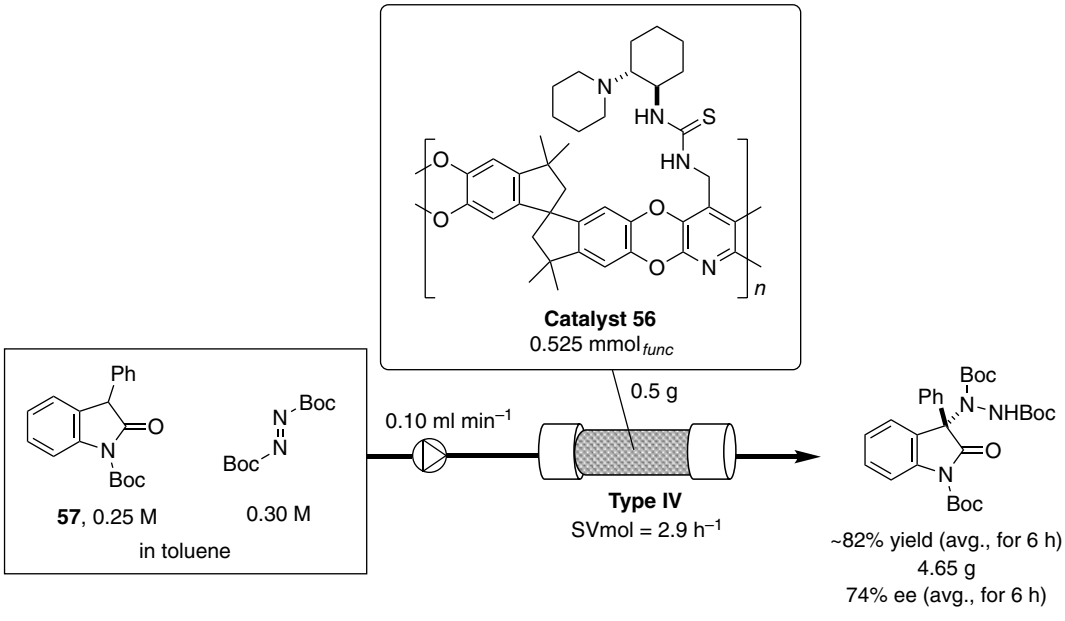

Figure 22.36. Continuous-flow enantioselective α-amination of oxindole. Source: [57]/Royal Society of Chemistry.

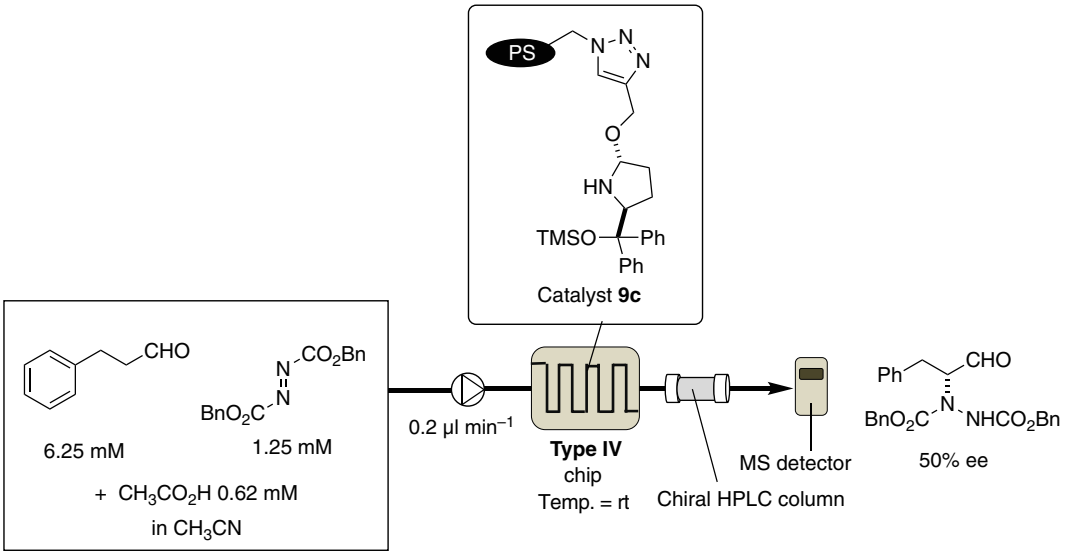

Figure 22.37. Photopolymerized chiral monolithic chip reactor for continuous-flow amination reaction. Source: [58]/Georg Thieme Verlag KG.

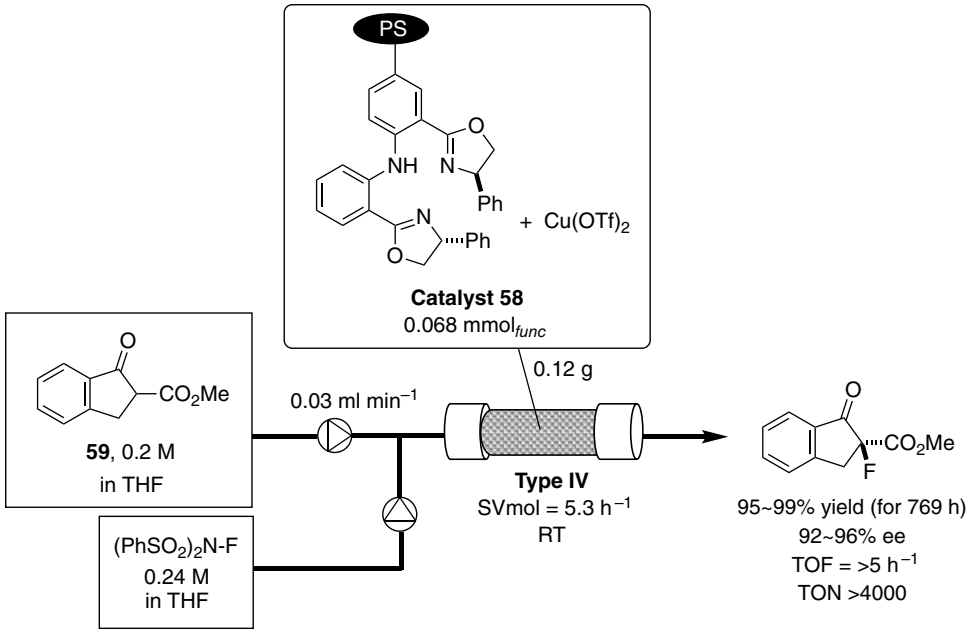

Figure 22.38. Type IV continuous-flow enantioselective electrophilic fluorination with heterogeneous Cu catalyst. Source: [59]/Royal Society of Chemistry.

batch reactions due to the attenuation effect of photon transport according to Bouguer–Lambert–Beer's law. Microflow photoreactors can solve this problem; however, most of the reported examples are limited to the synthesis of achiral compounds. The reported system consisted of a substrate/photocatalyst/phase transfer catalyst organic solution, aqueous basic solution, and oxygen, and offered a shorter (0.89 minute) reaction time while maintaining yields and enantioselectivities. Later they found that the phase-transfer

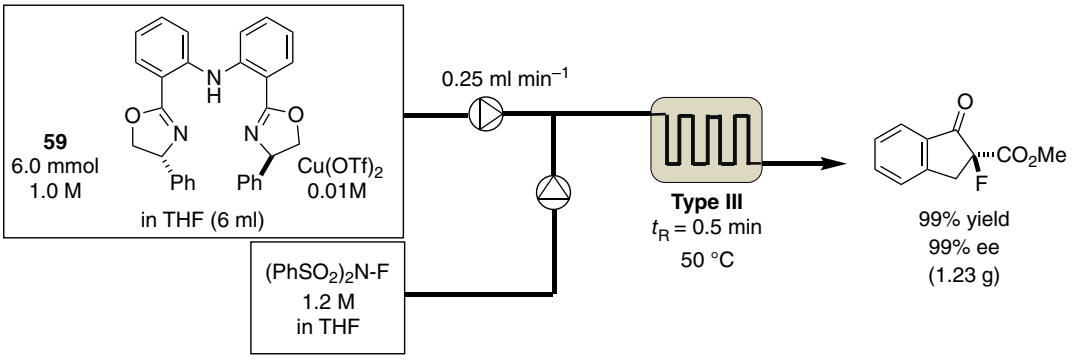

Figure 22.39. Type III continuous-flow enantioselective electrophilic fluorination. Source: [60]/Royal Society of Chemistry.

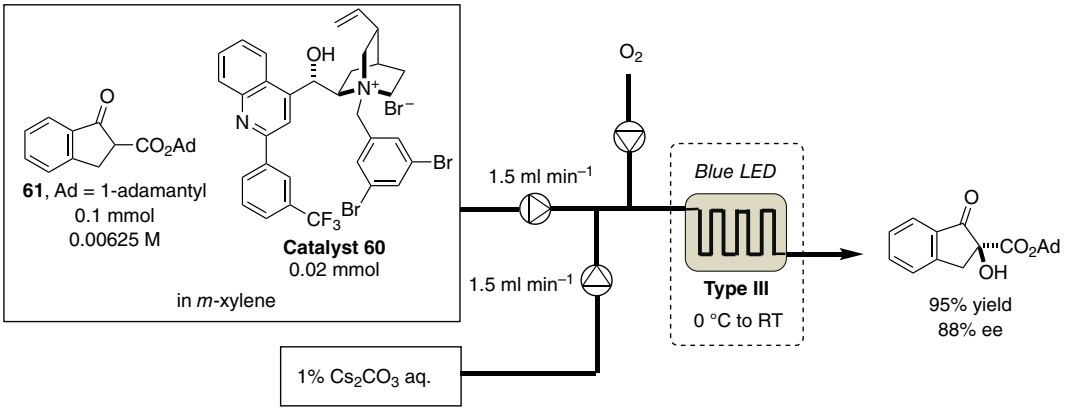

Figure 22.40. Type III continuous-flow enantioselective photooxygenation of 1,3-dicarbonyl compounds. Source: [61]/Royal Society of Chemistry.

catalyst employed possessed photocatalytic activity and the flow reaction could be performed in the absence of external addition of photocatalyst [62].

As an example of continuous-flow enantioselective C–O bond-formation reaction, Gao et al. reported a Type III continuous-flow electrochemical intermolecular lactonization of diketocarboxylic acid **61** with a chiral iodoarene reagent as a redox mediator **62**. Although the yield and the enantioselectivity of the target product were moderate, the micro-space of the flow reactor module allowed a lower concentration of electrolyte to be used (Figure 22.41) [63].

Another Type III continuous-flow enantioselective epoxidation with homogenous Fe(II) catalyst was reported in 2016. The design of the chiral ligand used in that work was inspired by porphyrin, and the corresponding epoxide was obtained in 88% yield and 90% ee under the continuous-flow mode with 2 minutes residence time. The authors claimed the time was shorter than that required in batch mode [64].

A Type III asymmetric sulfoxidation with chiral Mn(II) catalyst was also reported (Figure 22.42) [65]. A tetradentate porphyrin-like chiral ligand was used to prepare chiral catalyst **64**, and this was flowed with sulfide **65** and adamantane carboxylic acid. The reaction completed within 2 minutes residence time using only 0.35 mol% catalyst.

Esterification reaction does not include oxidative processes but is an important class of C–O bond-forming reaction, and sometimes can be seen as a kinetic resolution in asymmetric catalysis. A unique approach that was introduced recently is to use homogeneous catalysts such as enzymes and metal complexes in a packed-bed reactor as a heterogeneous catalyst. Yang's group developed a micro-droplet/silica crust system for this purpose; here, the ionic liquid droplet plays a key role in keeping the catalyst materials in the stationary phase [66, 67].

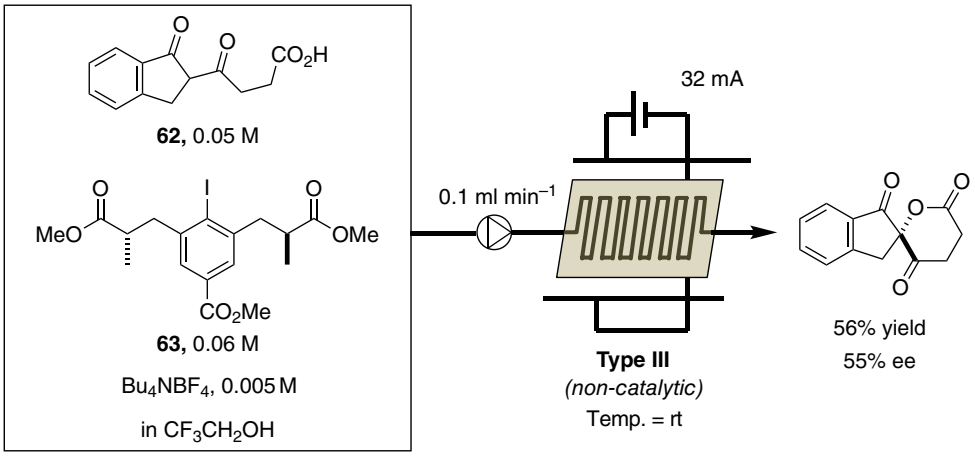

Figure 22.41. Continuous-flow enantioselective electrochemical process. Source: [63]/Georg Thieme Verlag KG.

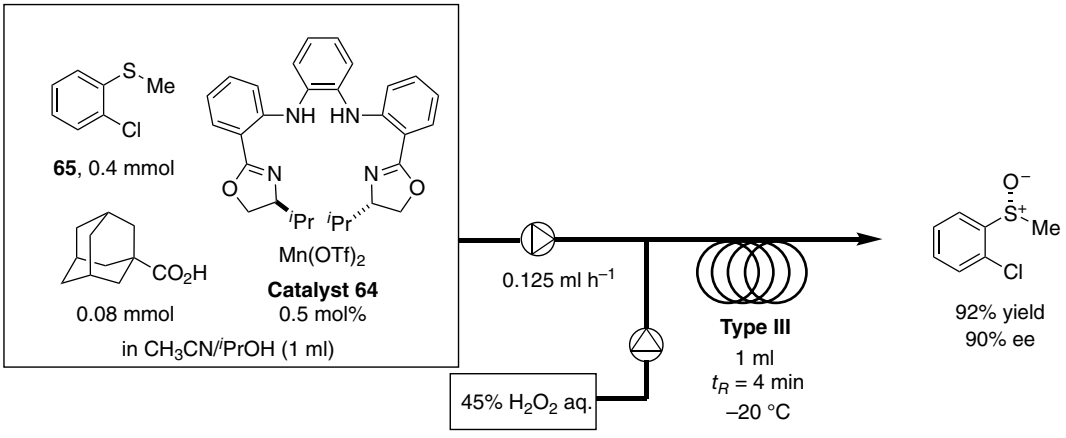

Figure 22.42. Type III continuous-flow enantioselective sulfoxidation. Source: [65]/John Wiley & Sons.

Pericàs et al. reported a continuous-flow kinetic resolution process for racemic secondary alchohol [68] and racemic BINOL monoacetate [69], respectively, using heterogeneous isothiourea catalysts (Figures 22.43 and 22.44). Different types of isothiourea catalysts **66** and **68** were introduced in this series of investigations; both of them were prepared through post-modification using azide-functionalized cross-linked polystyrene with alkyne-tethered isothiourea by copper-catalyzed azide–alkyne cyclization. In the latter case, the catalyst prepared was employed for the flow reaction at 3.2 h^{-1} SVmol. The catalyst showed good conversion with good selectivity factor ($s = 20$) in CH_2Cl_2 solvent, and both bis-acylated and remaining BINOL monoacetate were obtained in reasonable overall yields and with high enantioselectivity.

Several immobilized enzymes are commercially available and could be screened to attain high efficiency in kinetic resolution chemistry under continuous-flow conditions. In a report from Aguillón et al., a commercial lipase immobilized on acrylic resin was utilized for continuous-flow kinetic resolution of racemic secondary alcohol through acetylation with vinyl acetate [70]. In a recent report concerning the manufacturing of an intermediate of API, Kumaraguru and Ghosh et al. investigated a similar lipase-catalyzed kinetic resolution of racemic secondary alcohol through acetylation. In that report, the enzyme was directly packed into the reactor [71].

Desymmetrization of prochiral compounds to chiral compounds sometimes offers a useful route to give highly functional chiral compounds. Pericás et al. reported continuous-flow enantioselective

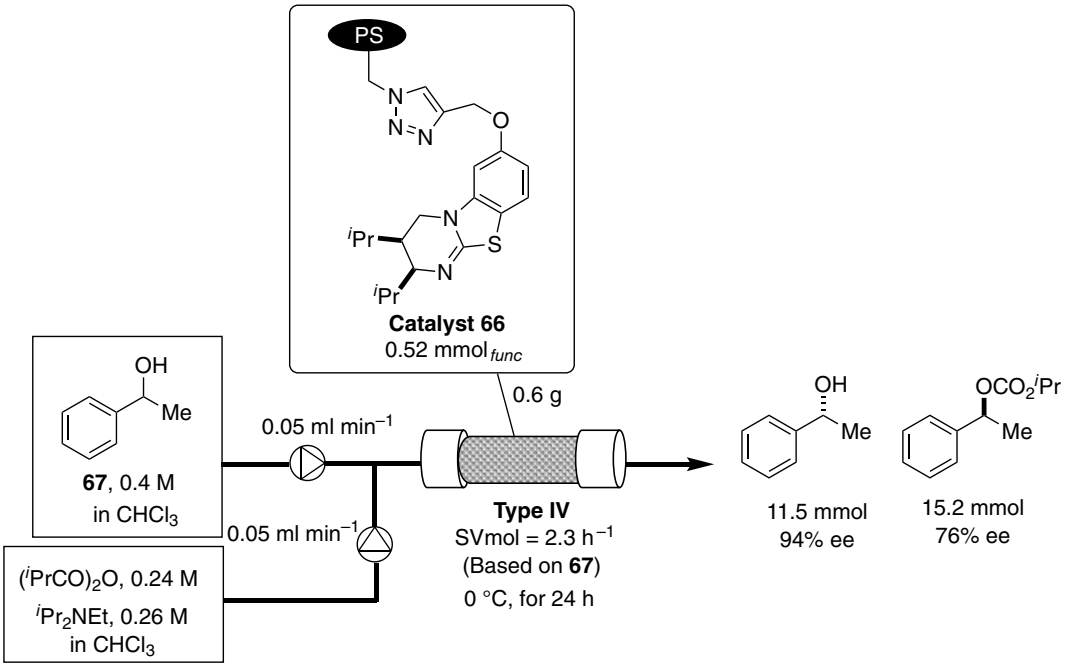

Figure 22.43. Continuous-flow kinetic resolution of racemic alcohol.

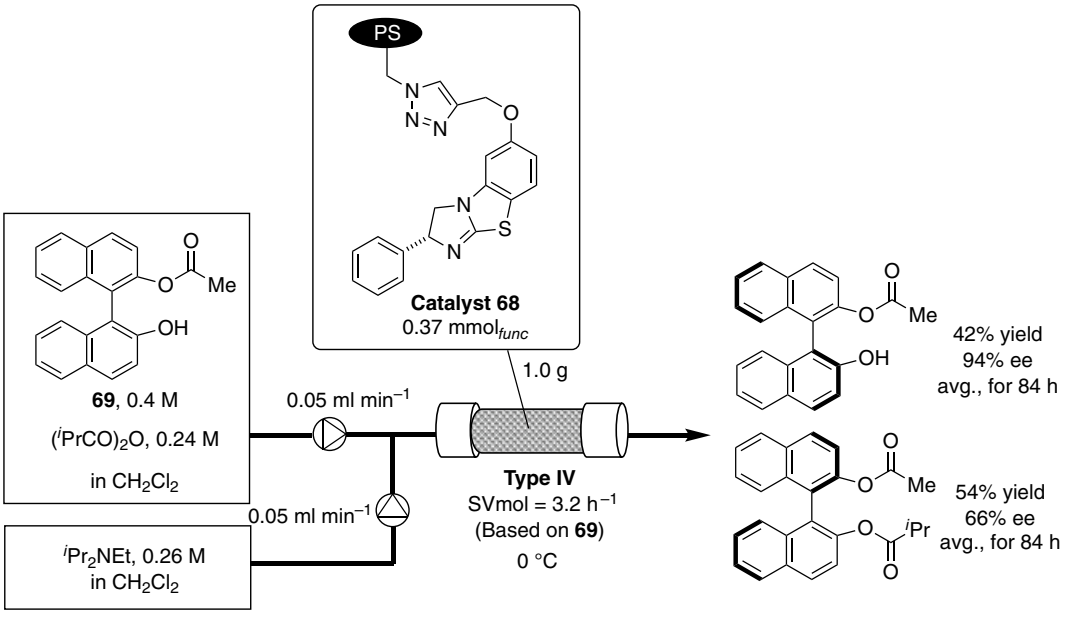

Figure 22.44. Supported isothiourea catalyst in continuous-flow kinetic resolution of BINOL monoacetate.

desymmetrization of oxetane compound **72** under Type IV continuous-flow conditions with immobilized organocatalyst (Figure 22.45) [72]. The organocatalyst adopted in that work originated in chiral 1,1′-spirodiindane-7,7′-diol (SPINOL) and immobilized it on a polystyrene backbone. A 0.1 M solution of **72** with a slight excess of thiol **71** was flowed at 0.5 ml min^{-1} into a packed-bed reactor including 0.34 mmol

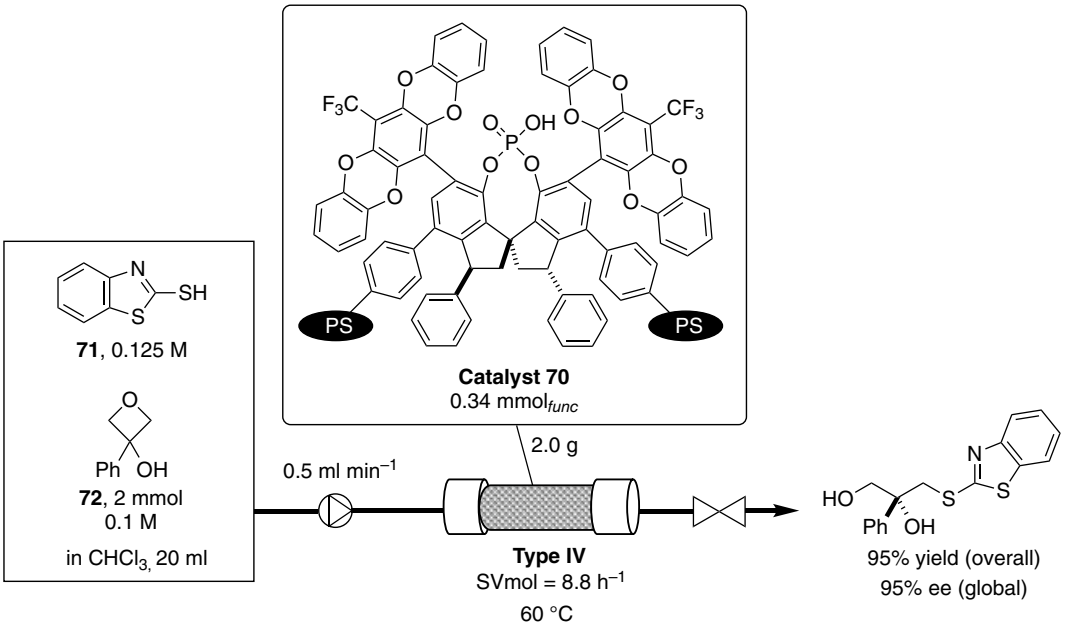

Figure 22.45. Continuous-flow desymmetrization with immobilized chiral SPINOL. Source: [72]/American Chemical Society.

unit of the immobilized catalyst **70** (SVmol = 8.8 h^{-1}). The authors demonstrated 17 kinds of substrate sets and showed high overall yields with high global enantioselectivities.

22.8. ENANTIOSELECTIVE REDUCTION OF DOUBLE BONDS THROUGH CONTINUOUS-FLOW SYSTEMS

Hydrogenation reactions of carbon–carbon or carbon–heteroatom double bonds are among the most important transformations for obtaining chiral organic compounds, and a relatively large volume of enantioselective hydrogenations under continuous-flow conditions including Type III and Type IV has been reported to date. Regarding chiral heterogeneous catalyst systems, chiral-modified Pt-heterogeneous catalysts are among the most extensively studied catalyst systems, and continuous-flow reactions with such modified heterogeneous catalysts have certainly dominated alternative homogeneous chiral catalysts over the past decade. Although many derivational investigations had been reported, in the following section a representative selection of some of the most recent work will be introduced.

In 2016, Degennaro and Luisi et al. reported a Corey–Bakshi–Shibata reduction in a microreactor with Type III under continuous-flow conditions (Figure 22.46) [73]. In-line monitoring of the reaction by IR allowed the progress of the reaction to be monitored, and it was found that a 10-minutes residence time with 8 mol% catalyst **73** provided the target product in acceptable yield and enantioselectivity.

Organocatalytic approaches are also applicable for continuous-flow enantioselective reduction. Benaglia et al. reported Type III continuous-flow thiourea **74** catalyzed enantioselective reduction of nitroenamine **75** to give chiral 2-nitro amines and 1,2-diamines (Figure 22.47) [74]. Although conversions of starting materials were moderate, high levels of enantioselectivities were obtained for several substrates, and the authors claimed higher STYs were achieved compared with batch conditions.

As a recent example of homogeneous transition-metal-catalyzed Type III continuous-flow enantioselective reduction of carbonyl compounds, Touge et al. (Takasago International Corporation) reported a continuous-flow asymmetric transfer hydrogenation involving dynamic kinetic resolution (Figure 22.48) [75]. The flow reaction was performed by feeding methyl 2-acetamido-3-oxooctadecanoate (**78**), HCO_2H, NEt_3,

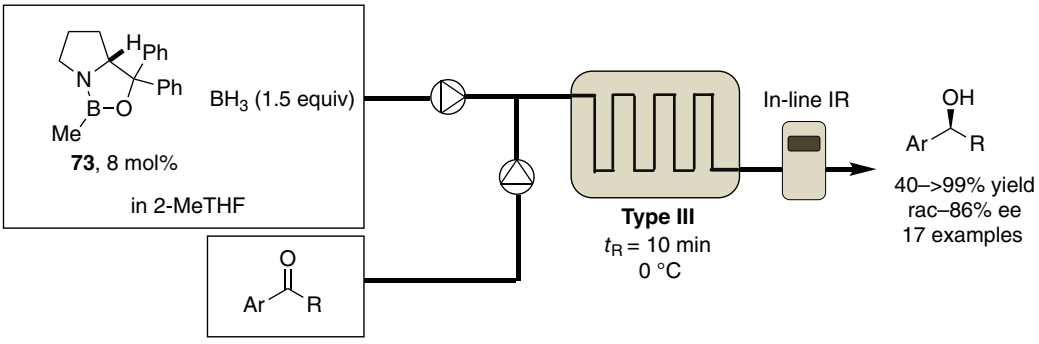

Figure 22.46. Type III Corey–Bakshi–Shibata reductions in a microreactor system. Source: [73]/Royal Society of Chemistry.

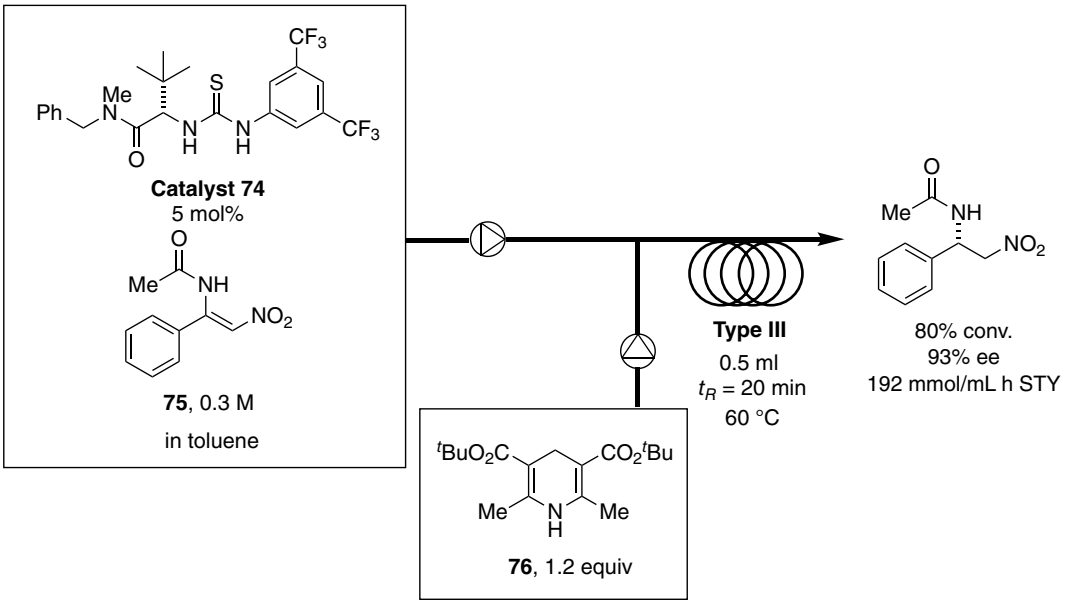

Figure 22.47. Type III organocatalytic enantioselective reductions of nitroenamines. Source: [74]/Royal Society of Chemistry.

and a ruthenium–diamine catalyst **77** in THF into a pipes-in-series reactor. The reaction in a 100-l reactor with 0.1 mol% catalyst **77** produced 77.4 kg of the product with 97% ee and 69% de. It should be emphasized that higher conversion was observed than obtained under batch conditions for the same reaction/residence time. The authors concluded that efficient removal of byproduct CO_2 might contribute to this improvement.

Polymer-tethering approaches have also been investigated by several groups. A polymer-supported chiral iridium catalyst **79** was studied by Blacker et al. for continuous-flow enantioselective Meerwein–Ponndorf–Verley-type reduction of ketones (Figure 22.49) [76]. It was found that ligands with a shorter spacer gave a longer lifetime for the catalyst than ligands with longer spacers, and the catalyst maintained a high level of conversion, 92–94% on average, for two days in reactions at 4.6 h^{-1} SVmol.

Kobayashi et al. reported a polymer-supported non-chiral iridium catalyst **80**/homogeneous CPA **82** system for the enantioselective asymmetric hydrogenation of imines or direct reductive amination (Figure 22.50) [77]. The system worked well for 50 hours to give the target amine derived from the imine **81** in high yields and with high enantioselectivities for the individual samples collected in the

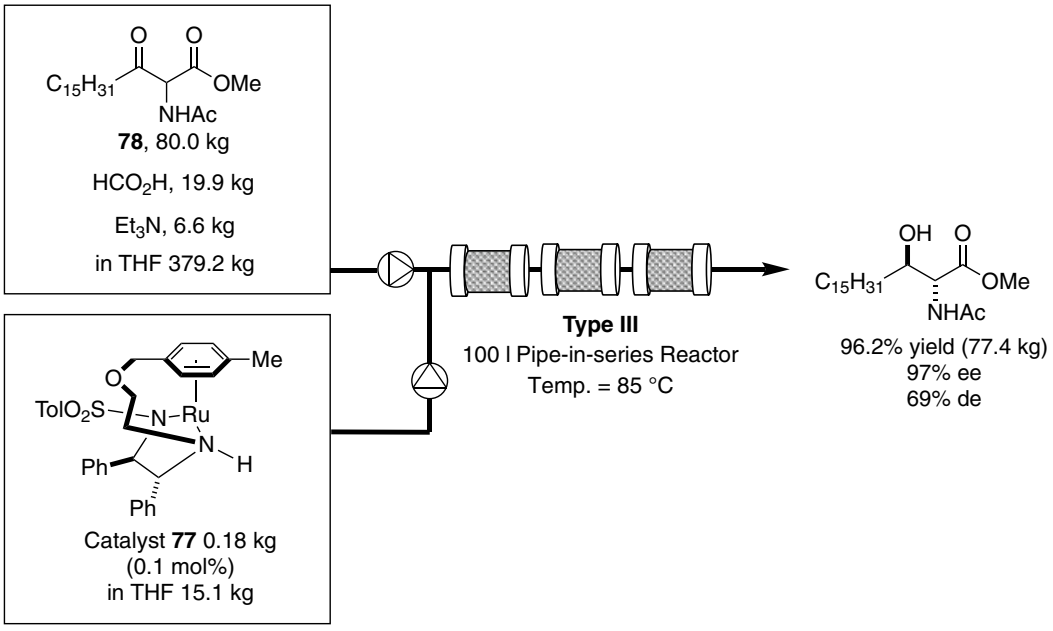

Figure 22.48. Type III continuous-flow asymmetric transfer hydrogenation involving dynamic kinetic resolution. Source: [75]/American Chemical Society.

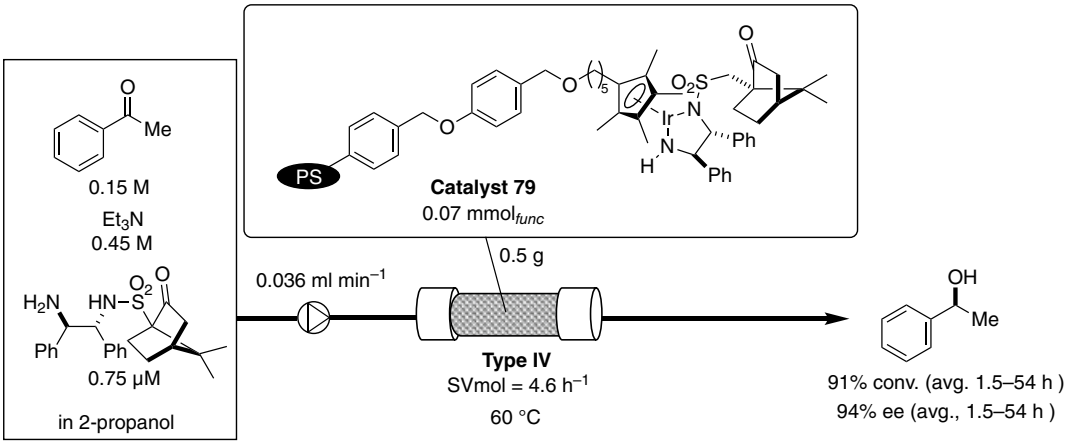

Figure 22.49. Continuous-flow enantioselective MPV-type reduction with supported chiral Ir catalyst. Source: [76]/John Wiley & Sons.

reaction at 3.3 h^{-1} SVmol. The catalyst could also be used for the enantioselective direct reductive amination of aliphatic ketones.

A polymer-supported organocatalyst was also used in Type IV continuous-flow enantioselective reduction as a chiral Lewis base catalyst. In 2017, Benaglia et al. introduced heterogeneous *N*-picolylimidazolidinines as a new class of chiral heterogeneous catalyst and used it in continuous-flow hydrosilylation of imines (Figure 22.51) [78]. A series of immobilized catalysts were first evaluated in batch mode, and a promising candidate was transferred to continuous-flow reaction consisting of 0.12 h^{-1} SVmol. Although activity was maintained for 7 hours operation (TON = 0.8), a decrease in the enantioselectivity was observed over time.

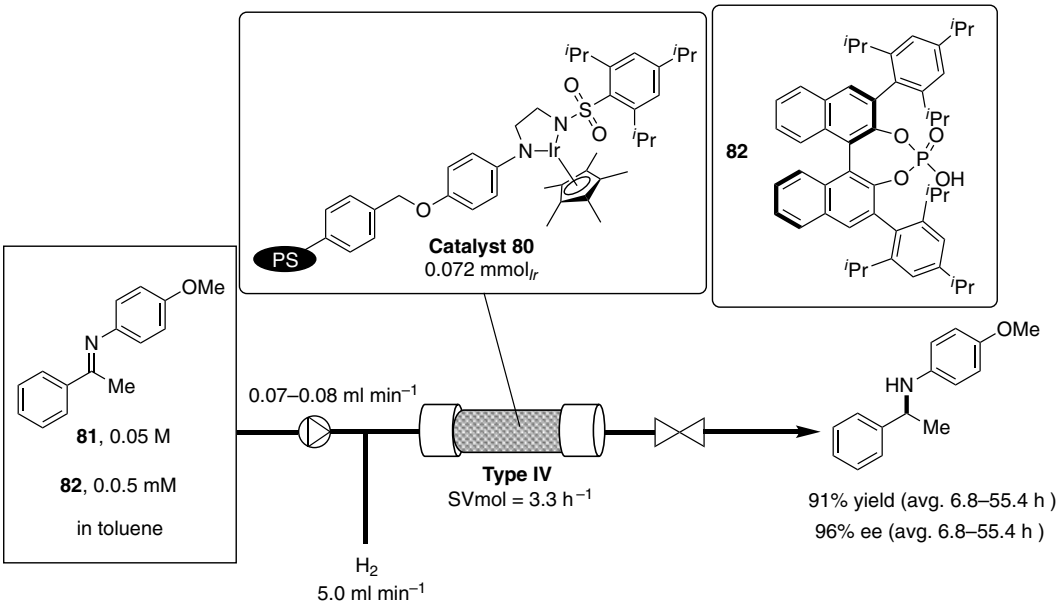

Figure 22.50. Enantioselective hydrogenation of imines using supported Ir/non-supported CPA system. Source: [77]/Springer Nature.

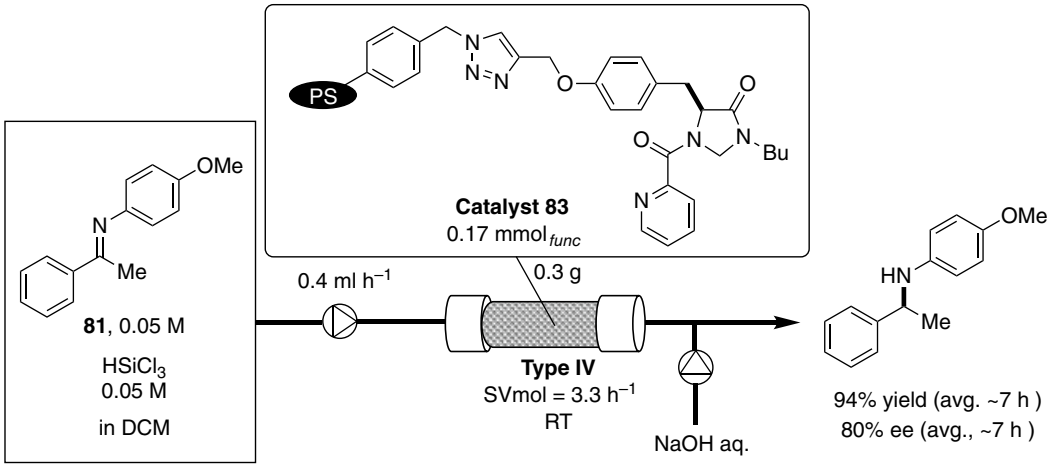

Figure 22.51. Continuous-flow organocatalytic enantioselective hydrosilylation of imines. Source: [78]/John Wiley & Sons.

As an unconventional immobilization technique, Leitner et al. have been investigating several methods that have been used in Type IV continuous-flow enantioselective hydrogenation reactions [79]. In their report of 2016, the so-called Augustine approach was used to immobilize cationic rhodium complexes on metal oxides, and these complexes were applied for continuous-flow enantioselective hydrogenation of enamide **85** to produce an API intermediate. According to the reported results, 470 h^{-1} SVmol was utilized for the catalyst system **84**, and high yields and high enantioselectivities were obtained from the individual samples collected; thus, the TON reached 7800 (Figure 22.52) [80].

In 2018, the same group investigated the use of supported ionic liquid phase (SILP)/supercritical CO_2 ($scCO_2$) chemistry for heterogeneous Type IV continuous-flow reactions. The SILP/molecular

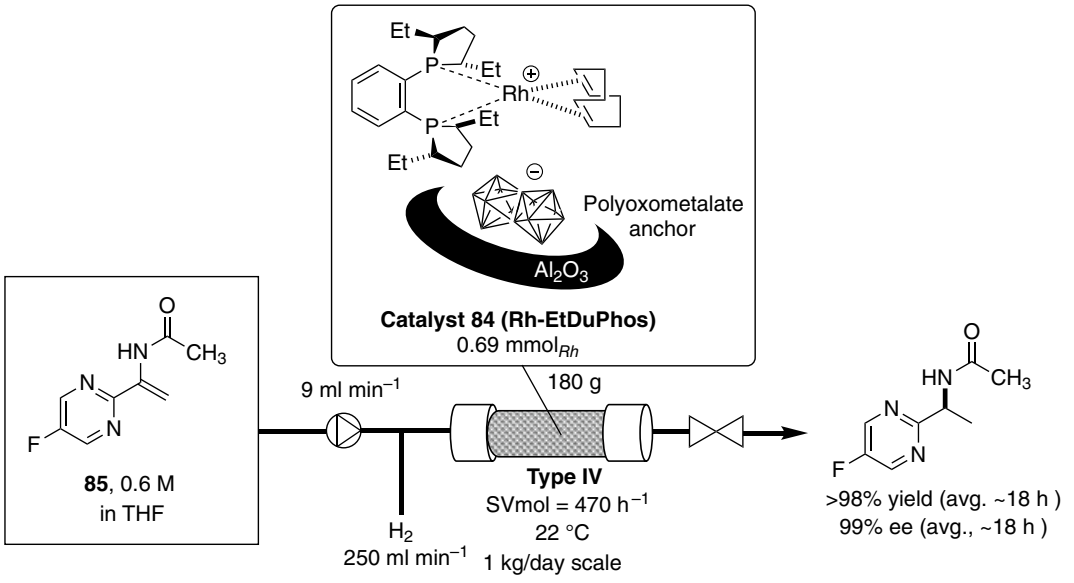

Figure 22.52. Supported rhodium-catalyzed Type IV continuous-flow enantioselective hydrogenation on enamide: Augustine approach. Source: [80]/American Chemical Society.

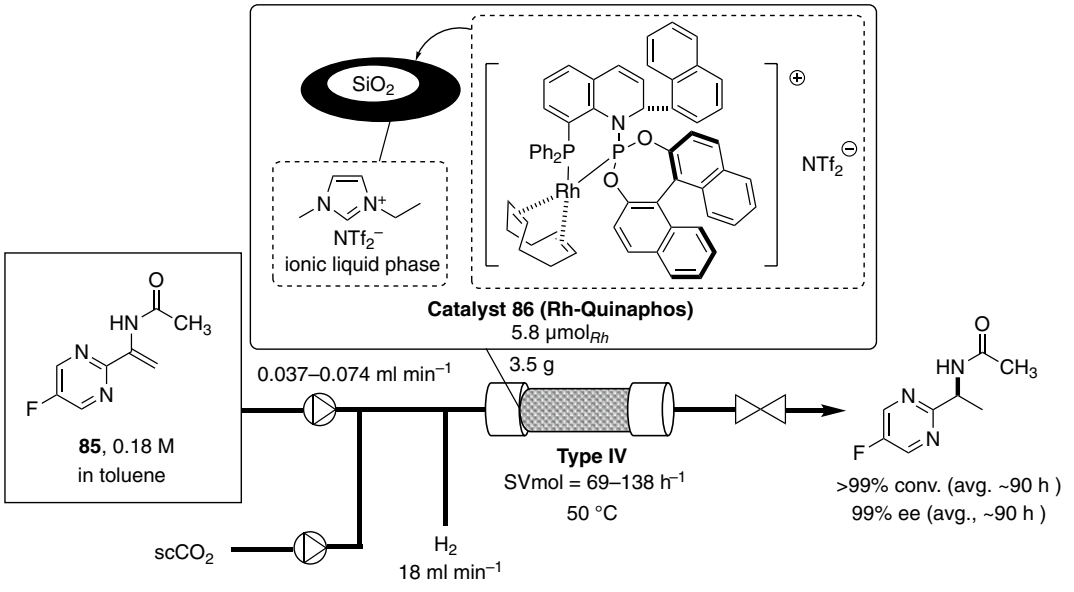

Figure 22.53. Supported rhodium-catalyzed Type IV continuous-flow enantioselective hydrogenation on enamide: SILP/ $scCO_2$ system. Source: [81]/American Chemical Society.

catalyst system consisted of SiO_2, [ethylmethylimidazolinium][NTf2], and Rh-Quinaphos (catalyst system **86**). Use of the cosolvent system was required to dissolve polar starting materials; thus, the authors called the global mobile phase *mod*CO_2. A high TON value of >13 000 was achieved without significant loss of enantioselectivities under conditions with 69–138 h^{-1} SVmol (Figure 22.53) [81].

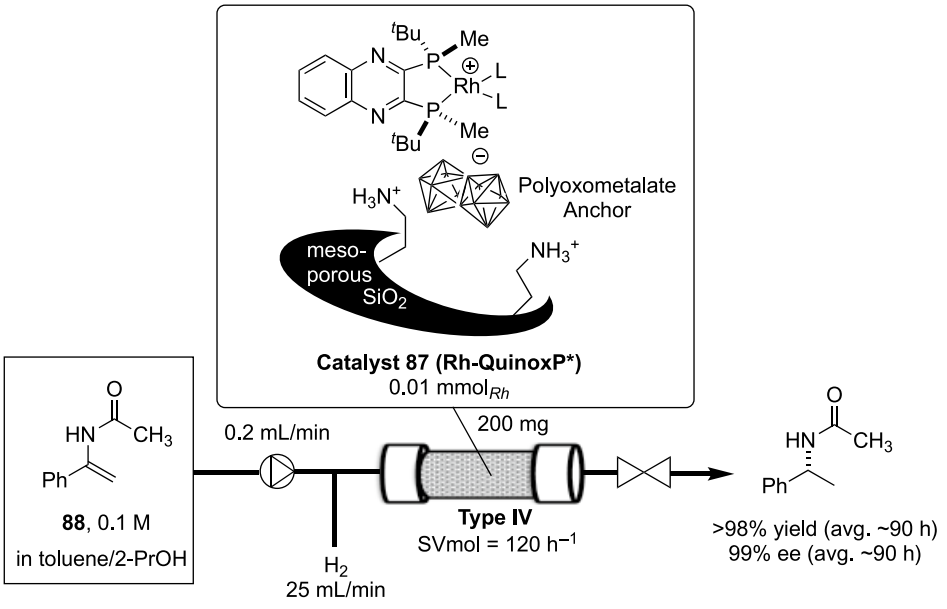

Figure 22.54. Modified Augustine approach for continuous-flow enantioselective hydrogenation of enamides. Source: [82]/ American Chemical Society.

Kobayashi et al. introduced a modified immobilization method with a cationic Rh complex using the Augustine approach. In contrast to the heteropoly acid/metal oxide non-covalent interaction in a conventional Augustine approach, the authors used amine-functionalized mesoporous silica, KIT-6, to anchor a cationic complex/heteropoly acid composite. Under conditions of 120 h^{-1} SVmol, high yields and enantioselectivities were attained from the individual samples collected during 90% operation, and the accumulated TON before decreased conversion was 10 800 (Figure 22.54) [82].

An example of assembling catalytic functions into a single heterogeneous material was demonstrated by Liu et al. using yolk–shell-mesostructured silica material **89**. The basic DABCO unit and chiral amino-sulfonamide unit were both mounted onto the shell part through a silane-coupling strategy and coupled with Ru precursor to add catalytic hydrogenation ability. A systematic 1,4-addition of aniline to enone and transfer hydrogenation with sodium formate was accomplished to give the desired 1,3-amino alcohol. Under continuous-flow conditions using 0.029 M enone solution (1.2 equiv. aniline and 10 equiv. formate) and a packed-bed reactor filled with 300 mg of the dual-functional catalyst containing 0.024 mmol of Ru, the flow reaction at 0.1 ml min^{-1} flow rate, corresponding to 7.3 h^{-1} SVmol, proceeded to afford the desired product in 91–99% yield with 94–95% ee during 4 hours operation (Figure 22.55) [83].

22.9. CONCLUSION AND OUTLOOK

Continuous-flow chemistry is a current key technology in the manufacturing of not only bulk or common chemicals but also fine and specialty chemicals. The approach will promote more convenient on-demand and on-site production as well as a more sustainable society. In line with the common key concept of this book, catalytic asymmetric synthesis, the applications of catalytic enantioselective continuous-flow reactions, especially with heterogeneous catalysts, will open the door to innovation in the future; however, compared with the progress achieved in conventional catalytic enantioselective processes in batch, catalytic enantioselective continuous-flow reactions remain limited. Some of the flow examples introduced in this chapter were recognized as slight modifications of the corresponding

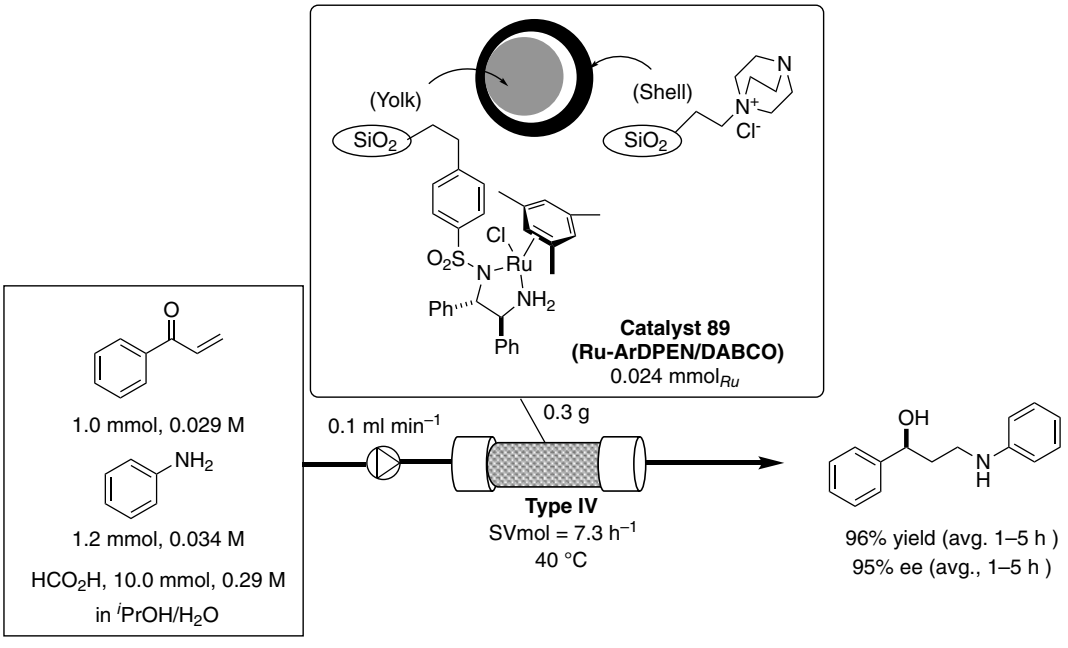

Figure 22.55. Assembling catalytic functions into single heterogeneous material for 1,4-addition of aniline to enone and asymmetric transfer hydrogenation. Source: [83]/John Wiley & Sons.

batch enantioselective reactions with slow addition of substrates. Furthermore, it is notable that there are only a few examples of continuous-flow enantioselective reactions with a high level of SVmol value and most of them are performed in a laboratory scale (up to several grams). Progress in this field will be highly dependent on the development of truly efficient heterogeneous chiral catalysts, and their application in continuous-flow modes. The overview from recent contributions in this field clearly indicates the importance of considering, designing, and developing chiral heterogeneous catalysts that are suitable for use as a stationary phase in packed-bed reactors under continuous-flow conditions from the initial stage of the investigation, not as an extension of fine batch investigations. As described in Section 22.2, Type IV continuous-flow asymmetric catalysis has clear advantages over continuous-flow asymmetric homogeneous catalysis (the Type III approach) as well as batch heterogeneous asymmetric catalysis. Therefore, it is desirable that all investigations in this field consider how to bring out the true potential of catalysis in the solid phase. We hope that this chapter will prove a touchstone for readers wishing to undertake innovative work on this new topic in catalytic asymmetric synthesis.

REFERENCES

1. X. Y. Mak, P. Laurino, P. H. Seeberger, *Beilstein J. Org. Chem.* **2009**, *5*, 19.
2. D. Webb, T. F. Jamison, *Chem. Sci.* **2010**, *1*, 675–680.
3. J. Wegner, S. Ceylan, A. Kirschning, *Chem. Commun.* **2011**, *47*, 4583–4592.
4. J. Wegner, S. Ceylan, A. Kirschning, *Adv. Synth. Catal.* **2012**, *354*, 17–57.
5. I. R. Baxendale, *J. Chem. Technol. Biotechnol.* **2013**, *88*, 519–552.
6. T. Tsubogo, T. Ishiwata, S. Kobayashi, *Angew. Chem. Int. Ed.* **2013**, *52*, 6590–6604.
7. D. Zhao, K. Ding, *ACS Catal.* **2013**, *3*, 928–944.
8. J. C. Pastre, D. L. Browne, S. V. Ley, *Chem. Soc. Rev.* **2013**, *42*, 8849.
9. R. Munirathinam, J. Huskens, W. Verboom, *Adv. Synth. Catal.* **2015**, *357*, 1093–1123.
10. A. Kirschning (Guest Editor), *Beilstein J. Org. Chem.* **2009**, *5*, 15.

11. S. Chatterjee, FDA perspective on continuous manufacturing, https://www.fda.gov/media/85366/download (accessed January 2012).
12. U. Kragl, C. Dreisbach, *Angew. Chem. Int. Ed.* **1996**, *35*, 642–644.
13. P. Hodge, D. W. L. Sung, P. W. Stratford, *J. Chem. Soc. Perkin Trans. 1* **1999**, 2335–2342.
14. Y. Orito, S. Imai, J. Nguyen-Gia-Hung, *J. Synth. Org. Chem. Jpn.* **1979**, *37*, 173–174.
15. S. Kobayashi, *Chem. Asian J.* **2016**, *11*, 425–436.
16. A. J. M. Farley, P. Jakubec, A. M. Goldys, D. J. Dixon, *Tetrahedron* **2018**, *74*, 5206–5212.
17. P. Kisszekelyi, A. Alammar, J. Kupai, P. Huszthy, J. Barabas, T. Holtzl, L. Szente, C. Bawn, R. Adams, G. Szekely, *J. Catal.* **2019**, *371*, 255–261.
18. T. Tsubogo, H. Oyamada, S. Kobayashi, *Nature* **2015**, *520*, 329–332.
19. H. Ishitani, Y. Furiya, S. Kobayashi, *Chem. Asian J.* **2020**, *15*, 1688–1691.
20. H. Ishitani, K. Kanai, W. J. Yoo, T. Yoshida, S. Kobayashi, *Angew. Chem. Int. Ed.* **2019**, *58*, 13313–13317.
21. D. A. Evans, S. Mito, D. Seidel, *J. Am. Chem. Soc.* **2007**, *129*, 11583–11592.
22. M. B. Buendia, S. Kegnæs, S. Kramer, *Adv. Synth. Catal.* **2020**, *362*, 5506–5512.
23. (a) C. Ayats, A. H. Henseler, M. A. Pericás, *ChemSusChem* **2012**, *5*, 320–325; (b) X. Fan, S. Sayalero, M. A. Pericàs, *Adv. Synth. Catal.* **2012**, *354*, 2971–2976; (c) R. Martín-Rapún, S. Sayalero, M. A. Pericàs, *Green Chem.* **2013**, *15*, 3295–3301; (d) C. Ayats, A. H. Henseler, E. Dibello, M. A. Pericás, *ACS Catal.* **2014**, *4*, 3027–3033.
24. S. B. Ötvös, P. Llanes, M. A. Pericàs, C. O. Kappe, *Org. Lett.* **2020**, *22*, 8122–8126.
25. S. B. Ötvös, M. A. Pericàs, C. O. Kappe, *Chem. Sci.* **2019**, *10*, 11141–11146.
26. P. Szcześniak, S. Buda, L. Lefevre, O. Staszewska-Krajewska, J. Mlynarski, *Eur. J. Org. Chem.* **2019**, 6973–6982.
27. H. Ochiai, A. Nishiyama, N. Haraguchi, S. Itsuno, *Org. Process Res. Dev.* **2020**, *24*, 2228–2233.
28. L. Osorio-Planes, C. Rodríguez-Escrich, M. A. Pericàs, *Catal. Sci. Technol.* **2016**, *6*, 4686–4689.
29. J. Du, B. Shuai, M. Tao, G. Wang, W. Zhang, *Green Chem.* **2016**, *18*, 2625–2631.
30. A. Ciogli, D. Capitani, N. Di Iorio, S. Crotti, G. Bencivenni, M. P. Donzello, C. Villani, *Eur. J. Org. Chem.* **2019**, 2020–2028.
31. X. Chen, H. Jiang, B. Hou, W. Gong, Y. Liu, Y. Cui, *J. Am. Chem. Soc.* **2017**, *139*, 13476–13482.
32. G. Shen, T. Osako, M. Nagaosa, Y. Uozumi, *J. Org. Chem.* **2018**, *83*, 7380–7387.
33. T. Kuremoto, T. Yasukawa, S. Kobayashi, *Adv. Synth. Catal.* **2019**, *361*, 3698–3703.
34. H. Min, H. Miyamura, T. Yasukawa, S. Kobayashi, *Chem. Sci.* **2019**, *10*, 7619–7626.
35. S. Canellas, C. Ayats, A. H. Henseler, M. A. Pericàs, *ACS Catal.* **2017**, *7*, 1383–1391.
36. E. Nakashima, H. Yamamoto, *Chem. Eur. J.* **2018**, *24*, 1076–1079.
37. L. Schober, S. Ratnam, Y. Yamashita, N. Adebar, M. Pieper, A. Berkessel, V. Hessel, H. Gröger, *Synthesis* **2019**, *51*, 1178–1184.
38. S. Watanabe, N. Nakaya, J. Akai, K. Kanaori, T. Harada, *Org. Lett.* **2018**, *20*, 2737–2740.
39. M. Rodríguez-Rodríguez, A. Maestro, J. M. Andrés, R. Pedrosa, *Adv. Synth. Catal.* **2020**, *362*, 2744–2754.
40. L. Zhao, X. Bao, Q. Hu, B. Wang, A. H. Lu, *ChemCatChem* **2018**, *10*, 1248–1252.
41. T. Karasawa, R. Oriez, N. Kumagai, M. Shibasaki, *J. Am. Chem. Soc.* **2018**, *140*, 12290–12295.
42. H.-C. Ma, G.-J. Chen, F. Huang, Y.-B. Dong, *J. Am. Chem. Soc.* **2020**, *142*, 12574–12578.
43. J. Coloma, Y. Guiavarc'h, P. L. Hagedoorn, U. Hanefeld, *Catal. Sci. Technol.* **2020**, *10*, 3613–3621.
44. R. Warias, A. Zaghi, J. J. Heiland, S. K. Piendl, K. Gilmore, P. H. Seeberger, A. Massi, D. Belder, *ChemCatChem* **2018**, *10*, 5382–5385.
45. L. Clot-Almenara, C. Rodríguez-Escrich, L. Osorio-Planes, M. A. Pericás, *ACS Catal.* **2016**, *6*, 7647–7651.
46. D. Ragno, G. Di Carmine, A. Brandolese, O. Bortolini, P. P. Giovannini, A. Massi, *ACS Catal.* **2017**, *7*, 6365–6375.
47. P. H. R. de Oliveira, B. M. Bruno, R. A. C. Leão, L. S. M. Miranda, R. A. S. San Gil, R. O. M. A. de Souza, F. G. Finelli, *ChemCatChem* **2019**, *11*, 5553–5561.
48. M. Kondo, H. D. P. Wathsala, M. Sako, Y. Hanatani, K. Ishikawa, S. Hara, T. Takaai, T. Washio, S. Takizawa, H. Sasai, *Chem. Commun.* **2020**, *56*, 1259–1262.
49. H. Miyamura, R. G. Bergman, K. N. Raymond, F. D. Toste, *J. Am. Chem. Soc.* **2020**, *142*, 19327–19338.
50. P. Llanes, C. Rodríguez-Escrich, S. Sayalero, M. A. Pericàs, *Org. Lett.* **2016**, *18*, 6292–6295.
51. G. S. Fleming, A. B. Beeler, *Org. Lett.* **2017**, *19*, 5268–5271.
52. C. J. Yoo, D. Rackl, W. Liu, C. B. Hoyt, B. Pimentel, R. P. Lively, H. M. L. Davies, C. W. Jones, *Angew. Chem. Int. Ed.* **2018**, *57*, 10923–10927.
53. T. A. Hatridge, W. Liu, C. J. Yoo, H. M. L. Davies, C. W. Jones, *Angew. Chem. Int. Ed.* **2020**, *59*, 19525–19531.
54. D. C. Crowley, D. Lynch, A. R. Maguire, *J. Org. Chem.* **2018**, *83*, 3794–3805.
55. M. L. Abrams, J. Y. Buser, J. R. Calvin, M. D. Johnson, B. R. Jones, G. Lambertus, C. R. Landis, J. R. Martinelli, S. A. May, A. D. McFarland, J. R. Stout, *Org. Process Res. Dev.* **2016**, *20*, 901–910.
56. A. Cunillera, C. Blanco, A. Gual, J. M. Marinkovic, E. J. Garcia-Suarez, A. Riisager, C. Claver, A. Ruiz, C. Godard, *ChemCatChem* **2019**, *11*, 2195–2205.
57. L. Martín, A. Maestro, J. M. Andrés, R. Pedrosa, *Org. Biomol. Chem.* **2020**, *18*, 9275–9283.

58. R. Warias, D. Ragno, A. Massi, D. Belder, *Chem. Eur. J.* **2020**, *26*, 13152–13156.
59. B. Wang, Y. Wang, Y. Jiang, M. Chu, S. Qi, W. Ju, D. Xu, *Org. Biomol. Chem.* **2018**, *16*, 7702–7710.
60. Y. F. Wang, Z. H. Jiang, M. M. Chu, S. S. Qi, H. Yin, H. Te Han, D. Q. Xu, *Org. Biomol. Chem.* **2020**, *18*, 4927–4931.
61. X. F. Tang, J. N. Zhao, Y. F. Wu, Z. H. Zheng, S. H. Feng, Z. Y. Yu, G. Z. Liu, Q. W. Meng, *Org. Biomol. Chem.* **2019**, *17*, 7938–7942.
62. X. F. Tang, J. N. Zhao, Y. F. Wu, S. H. Feng, F. Yang, Z. Y. Yu, Q. W. Meng, *Adv. Synth. Catal.* **2019**, *361*, 5245–5252.
63. W. C. Gao, Z. Y. Xiong, S. Pirhaghani, T. Wirth, *Synthesis* **2019**, *51*, 276–284.
64. W. Dai, Y. Mi, Y. Lv, S. Shang, G. Li, G. Chen, S. Gao, *Synthesis* **2016**, *48*, 2653–2658.
65. W. Dai, Y. Mi, Y. Lv, B. Chen, G. Li, G. Chen, S. Gao, *Adv. Synth. Catal.* **2016**, *358*, 667–671.
66. M. Zhang, R. Ettelaie, T. Yan, S. Zhang, F. Cheng, B. P. Binks, H. Yang, *J. Am. Chem. Soc.* **2017**, *139*, 17387–17396.
67. X. Zhang, Y. Hou, R. Ettelaie, R. Guan, M. Zhang, Y. Zhang, H. Yang, *J. Am. Chem. Soc.* **2019**, *141*, 5220–5230.
68. R. M. Neyyappadath, R. Chisholm, M. D. Greenhalgh, C. Rodríguez-Escrich, M. A. Pericàs, G. Hähner, A. D. Smith, *ACS Catal.* **2018**, *8*, 1067–1075.
69. J. Lai, R. M. Neyyappadath, A. D. Smith, M. A. Pericàs, *Adv. Synth. Catal.* **2020**, *362*, 1370–1377.
70. A. R. Aguillón, M. N. Avelar, L. E. Gotardo, S. P. de Souza, R. A. C. Leão, I. Itabaiana, L. S. M. Miranda, R. O. M. A. de Souza, *Mol. Catal.* **2019**, *467*, 128–134.
71. A. S. Krishna, S. Basetty, R. Nasam, S. L. Ralte, C. R. Reddy, G. Sudhakar, S. Pabbaraja, S. Chandrasekhar, P. S. Mainkar, T. Kumaraguru, S. Ghosh, *Org. Process Res. Dev.* **2020**, *24*, 2657–2664.
72. J. Lai, M. Fianchini, M. A. Pericás, *ACS Catal.* **2020**, *10*, 14971–14983.
73. S. De Angelis, M. De Renzo, C. Carlucci, L. Degennaro, R. Luisi, *Org. Biomol. Chem.* **2016**, *14*, 4304–4311.
74. M. Pirola, M. E. Compostella, L. Raimondi, A. Puglisi, M. Benaglia, *Synthesis* **2018**, *50*, 1430–1438.
75. T. Touge, M. Kuwana, Y. Komatsuki, S. Tanaka, H. Nara, K. Matsumura, N. Sayo, Y. Kashibuchi, T. Saito, *Org. Process Res. Dev.* **2019**, *23*, 452–461.
76. Y. Kawakami, A. Borissova, M. R. Chapman, G. Goltz, E. Koltsova, I. Mitrichev, A. J. Blacker, *Eur. J. Org. Chem.* **2019**, 7499–7505.
77. T. Yasukawa, R. Masuda, S. Kobayashi, *Nat. Catal.* **2019**, *2*, 1088–1092.
78. R. Porta, M. Benaglia, R. Annunziata, A. Puglisi, G. Celentano, *Adv. Synth. Catal.* **2017**, *359*, 2375–2382.
79. (a) U. Hintermair, T. Höfener, T. Pullmann, G. Franciò, W. Leitner, *ChemCatChem* **2010**, *2*, 150–154; (b) S. Wesselbaum, U. Hintermair, W. Leitner, *Angew. Chem. Int. Ed.* **2012**, *51*, 8585–8588; (c) J. Theuerkauf, G. Franciò, W. Leitner, *Adv. Synth. Catal.* **2013**, *355*, 209–219; (d) U. Hintermair, G. Franciò, W. Leitner, *Chem. Eur. J.* **2013**, *19*, 4538–4547; (e) Z. Zhang, G. Franciò, W. Leitner, *ChemCatChem* **2015**, *7*, 1961–1965.
80. Z. Amara, M. Poliakoff, R. Duque, D. Geier, G. Franciò, C. M. Gordon, R. E. Meadows, R. Woodward, W. Leitner, *Org. Process Res. Dev.* **2016**, *20*, 1321–1327.
81. D. Geier, P. Schmitz, J. Walkowiak, W. Leitner, G. Franciò, *ACS Catal.* **2018**, *8*, 3297–3303.
82. Y. Saito, S. Kobayashi, *J. Am. Chem. Soc.* **2020**, *142*, 16546–16551.
83. L. Wu, Y. Li, J. Meng, R. Jin, J. Lin, G. Liu, *ChemPlusChem* **2018**, *83*, 861–867.

INDEX

Catalytic Asymmetric Synthesis, Fourth Edition. Edited by Takahiko Akiyama and Iwao Ojima.